

BITUMINOUS MIXTURES & PAVEMENTS VI

PROCEEDINGS OF THE 6TH INTERNATIONAL CONFERENCE ON BITUMINOUS MIXTURES AND PAVEMENTS, THESSALONIKI, GREECE, 10–12 JUNE 2015

Bituminous Mixtures & Pavements VI

Editor

A.F. Nikolaides

Aristotle University of Thessaloniki (AUn), Greece



CRC Press

Taylor & Francis Group

Boca Raton London New York Leiden

CRC Press is an imprint of the
Taylor & Francis Group, an **informa** business

A BALKEMA BOOK

CRC Press/Balkema is an imprint of the Taylor & Francis Group, an informa business

© 2015 Taylor & Francis Group, London, UK

Typeset by MPS Limited, Chennai, India

Printed and bound in Great Britain by CPI Group (UK) Ltd, Croydon, CR0 4YY

All rights reserved. No part of this publication or the information contained herein may be reproduced, stored in a retrieval system, or transmitted in any form or by any means, electronic, mechanical, by photocopying, recording or otherwise, without written prior permission from the publishers.

Although all care is taken to ensure integrity and the quality of this publication and the information herein, no responsibility is assumed by the publishers nor the author for any damage to the property or persons as a result of operation or use of this publication and/or the information contained herein.

Published by: CRC Press/Balkema
P.O. Box 11320, 2301 EH Leiden, The Netherlands
e-mail: Pub.NL@taylorandfrancis.com
www.crcpress.com – www.taylorandfrancis.com

ISBN: 978-1-138-02866-1 (Hbk)

ISBN: 978-1-315-66816-1 (eBook PDF)

Table of contents

<i>Preface</i>	XI
<i>Organizing committee</i>	XIII
<i>Scientific committee</i>	XV
<i>Organizers</i>	XVII
<i>Bituminous binders, unbound materials</i>	
Statistical methods for evaluating associations between selected foamed bitumen parameters <i>A. Chomicz-Kowalska</i>	3
Double-edge-notched tension testing of asphalt cement for the control of cracking in flexible asphalt pavements <i>M. Paliukaite, M. Verigin & S.A.M. Hesp</i>	13
Viscoelastic continuum damage analysis of polymer modified asphalt in the cyclic semi-circular bending test <i>I.M. Lancaster & H.A. Khalid</i>	21
Assessment of linear and nonlinear viscoelastic responses of warm-mix asphalt binders <i>M. Sadeq, E. Masad, H. Al-Khalid & O. Sirin</i>	27
Hot stage processing of steel slag and the benefits for bituminous mixtures <i>I.G. Liapis & A. Chasiotis</i>	33
Permanent deformation of stabilized subgrade soils <i>J.M. Rasul, G.S. Ghataora & M.P.N. Burrow</i>	41
Study of mineral filler effect on asphalt mixtures properties <i>E. Remisova</i>	49
In situ service capability of tack coats <i>C. Raab & M.N. Partl</i>	55
Investigating rheological effects of WMA additives by means of a viscometer and a newly designed workability device <i>M. Ateş, S. Temel, P.H. Öz & H.J. Köroğlu</i>	61
Evaluation of predictive models for the rheological properties of paving asphalt binders <i>F.O. Martinez, S.M. Angelone & M. Cauhape Casaux</i>	65
Investigation of the rheological properties of asphalt binder modified with Sasobit <i>M. Hasaninia, M. Molayem, M. Ameri & R. Dourandish</i>	73
Investigation on the physical and rheological properties of acrylate-styrene-acrylonitrile polymer and nano aluminum oxide modified asphalt binders nano aluminum oxide modified asphalt binders <i>S.I. Albrka Ali, A. Ismail & N.I. Md. Yusoff</i>	81
Effect of polymer type on improving rheological parameters related to rutting resistance of asphalt binders <i>K. Al-Adham & H. Al-Abdul Wahhab</i>	89
Performance of polymer and crumb rubber modified asphalt binders subjected to high stresses in multiple stress creep recovery test <i>A.V. Kataware & D. Singh</i>	97

Fatigue performance characterization of warm-modified bituminous binders <i>D.M. Abd & H. Al-Khalid</i>	105
The performance of bitumen mastics with the addition of fly ash <i>A. Djurekovic & G. Mladenovic</i>	115
Statistical analysis of characteristics of slow breaking cationic emulsions used for cold waste asphalt recycling <i>D. Lepadatu & L. Judele</i>	123
Effect of polyphosphoric acid on high-temperature properties of bitumens from different crude sources <i>A.L. Faxina, T.F. Pamplona, F.P. Sobreiro & G.T.P. Fabbri</i>	127
 <i>Pavement design, construction and maintenance</i>	
Bridge deck asphalt plug joints: Problems and solutions <i>N. Ghafoori & M. Sharbaf</i>	135
Evaluation of triaxial geogrids for reduction of base thickness in flexible pavements <i>N. Ghafoori & M. Sharbaf</i>	141
A state of the art review into the use of geopolymer cement for road applications <i>A. Wilkinson, D. Woodward, B. Magee & S. Tretsiakova-McNally</i>	147
The state of pothole management in UK local authority <i>F. Saeed, S. Qamariatul, M. Rahman & A. Woodside</i>	153
Use of 3D modeling to assess pothole growth <i>G. McQuaid, P. Millar & D. Woodward</i>	161
Recent modifications to the 1993 AASHTO equations for forward-calculating subgrade and pavement moduli <i>M. Livneh</i>	167
Additional issues concerning recent modified 1993 AASHTO equations (AASHTOLIV) for analyzing measured deflection bowls <i>M. Livneh</i>	177
Evaluation of the AASHTO Pavement ME software for the control of thermal cracking <i>B.C. Ghimire & S.A.M. Hesp</i>	187
Appraisal of mechanistic-empirical pavement design guide for highways being implemented in the United States and complementary needs for pavement asset management <i>W. Uddin</i>	195
Lessons learned about successful flexible pavements <i>C.M. Chang, O. González & P. Krugler</i>	203
Comparison of clustering approaches on temperature zones for pavement design <i>A. Kumar & A.K. Swamy</i>	211
Effects of low vehicle speed on the service life time of asphalt pavements <i>A. Walther & I. Isailović</i>	221
Formulation of a thickness design equation for asphalt overlay using MEPDG program <i>V.P. Le, H.J. Lee, H.M. Park, J.M. Flores & S. Lee</i>	227
Why and when to consider alternate flexible and rigid pavement designs in a bidding process? <i>C.M. Chang, O. González & A. Wimsatt</i>	235
Structural rehabilitation with thinner layers <i>E. Jellema, M. Kowalczyk & W.C. Vonk</i>	243
 <i>Bituminous mixtures (hot, warm, and cold), specifications</i>	
The combined effects of aging and moisture conditioning on the indirect tensile strength, flow and fracture energy of warm mix asphalt <i>M.O. Hamzah, B. Golchin & J. Voskuilen</i>	255

Study of warm asphalt additives on bitumen binders and mixture properties <i>S.K. Nikolova & A.D. Nikolov</i>	265
Evaluation of fracture resistance of WMA mixes using semi-circular bending test <i>S.F. Chitragar & D. Singh</i>	271
Investigation on low temperature limiting criteria for asphalt mixture <i>A. Cannone Falchetto, K.H. Moon, M.P. Wistuba & M.O. Marasteanu</i>	277
Laboratory evaluation of clogging behavior of porous asphalt pavements <i>E. Lim, T.F. Fwa & K.H. Tan</i>	287
Determination of the scuffing resistance of porous asphalt using annex A of prTS 12697-50 (the ARTe) <i>M.M.J. Jacobs, R.C.M.A. van den Beemt & M.H.T. Frunt</i>	293
Investigating the packing condition of Porous Asphalt Mixture (PAM) using Discrete Element Method (DEM) <i>M.J. Chen & Y.D. Wong</i>	299
International use of rubberized asphalt open graded friction course <i>G.B. Way, K.E. Kaloush, K.P. Biligiri, J. Sousa, A. Pinto & R. Cao</i>	307
Fiber reinforced asphalt concrete: Performance tests and pavement design consideration <i>K.E. Kaloush, B.S. Underwood, W.A. Zeiada & J. Stempihar</i>	313
Development of durable structural asphalt mixtures for the UK trunk road network <i>I. Artamendi, B. Allen & P. Phillips</i>	319
Performance evaluation of HMAC asphalt concrete mixes <i>V. Haritonovs, J. Tihonovs & M. Zaumanis</i>	327
Asphalt concrete for very thin layers: Quality control data collected during construction and performance after eight years in service <i>A. Nikolaidis</i>	333
Fatigue characterisation of full-scale pavements using viscoelastic continuum damage approach for Qatar <i>H. Sadek, E. Masad, H. Al-Khalid & O. Sirin</i>	343
A new approach in fatigue testing and evaluation of hot mix asphalt using a dynamic shear rheometer <i>T.M. Ahmed & H. Al-Khalid</i>	351
Experimental evaluation of crack propagation in asphalt mixture based on photoelasticity <i>S. Büchler, A. Cannone Falchetto & M.P. Wistuba</i>	361
Measurement of flexural displacement and strain in bending test based on digital image analysis <i>H. Zhao, S. Gu, J. Ling & Y. Peng</i>	367
Investigation of asphalt recovery properties in fatigue test with single rest period <i>I. Isailovic, A. Cannone Falchetto & M.P. Wistuba</i>	373
Fatigue characterization of modified asphalt concretes by means of dissipated energy approaches <i>M. Pasetto & N. Baldo</i>	379
Development of a new aggregate-binder adhesion test method <i>A.H.A.A. Al-Haddad & H. Al-Khalid</i>	385
Evaluation of aging in asphalt cores at room temperature using low field nuclear magnetic resonance <i>I. Menapace, E. Masad, G. Papavassiliou & E. Kassem</i>	395
Influence of compaction method on stiffness performance of asphalt specimens <i>P. Georgiou, A. Loizos & A. Leventis</i>	401
Evaluation of rutting resistance of rubberized gap-graded asphalt mixtures <i>E. Santagata, O. Baglieri, M. Alam, M. Lanotte & P.P. Riviera</i>	407
Simulation of asphalt concrete plastic deformation behavior <i>A.T. Papagiannakis, H. Zelelew & E. Mahmoud</i>	413

Effect of interlayer bonding on pavement response under dynamic load in presence of asphalt concrete cross-anisotropy <i>M.U. Ahmed, R.A. Tarefder & A. Rahman</i>	421
Artificial neural network modelling of asphalt concrete's mechanical properties produced with using waste granite filler <i>H. Akbulut, C. Güreş, S. Çetin, M. Caner & A. Elmacı</i>	429
Asphalt mixtures improved by the use of nanotechnology <i>V.B. López, R.C. Barrasa, E.S. Caballero & C.M.-P. Montoliu</i>	435
Investigation of moisture susceptibility in hot-mix asphalt concrete <i>A. Rahim & T. Nguyen</i>	441
Investigation on binder-aggregate adhesivity using a nanotechnology chemically reactive silane additives based agent <i>D. Sybilski, M.P. Wistuba, W. Bankowski, S. Buechler & P. Heinrich</i>	447
Addressing durability of asphalt concrete by self-healing mechanism <i>R.C. Barrasa, V.B. López, C.M.-P. Montoliu, V.C. Ibáñez, F. Pedrajas & J. Santarén</i>	453
An experimental investigation on the influence of Hydrated Lime on asphalt mixtures (A case study in Iran) <i>N. Orouzadeh & H. Sabbagh</i>	463
Preliminary evaluation of the effects of lime on stone mastic asphalt mixtures workability <i>G. Betti, U. Pinori & A. Marradi</i>	469
Update on new and future CEN asphalt test methods <i>J.C. Nicholls & K. Lind</i>	479
Influence of sodium chloride and potassium formate as deicing agents on asphalt mixture durability <i>S. Anastasio, I. Hoff & C. Thodesen</i>	487
The effect of Montan waxes on the mechanical performance of an asphalt rubber mixture <i>A.M. Rodríguez-Alloza & J. Gallego</i>	493
Using tincal and colemanite wastes in bituminous hot mixtures as filler <i>C. Güreş & G.Ş. Selman</i>	499
Assessing temperature reduction potential of various additives on binder and asphalt mix level for mastic asphalt <i>B. Hofko, M. Dimitrov & M. Hospodka</i>	509
<i>Highway and pavement management systems, network operation systems</i>	
Network-level pavement life-cycle assessment tool <i>J. Cirilovic, G. Mladenovic & C.A. Queiroz</i>	519
Transport of oversize/overweight vehicles along the Egnatia motorway. Basic elements of a future permit fee policy <i>A. Kokkalis & P. Panetsos</i>	525
Pavement management: Data centric rules and uncertainty management in section classification by a fuzzy inference system <i>M. Mahmood, M. Rahman, S. Mathavan & L. Nolle</i>	533
<i>Pavement recycling, geosynthetics</i>	
First trial to design up to 50% recycled hot mix asphalt in Latvia <i>R. Izaks, V. Haritonovs & M. Zaumanis</i>	545
Influence of reclaimed asphalt content on asphalt mix characteristics doped by selected rejuvenators <i>P. Vacková & J. Valentin</i>	551
Mix design considerations for asphalt wearing courses with high reclaimed asphalt content <i>G.C. Falla, A. Blasl, R. Millow & D.L. Presti</i>	561

Stiffness and fatigue of AC20 recycled mixtures with 25% and 50% RAP <i>E. Manthos & A. Nikolaidis</i>	567
Effects of using reclaimed asphalt and/or lower temperature asphalt on availability of road network <i>J.C. Nicholls, M. Wayman, K. Mollenhauer, C. McNally, A. Tabaković, A. Varveri, S. Cassidy, R. Shahmohammadi & R. Taylor</i>	577
Influence of reclaimed asphalt content on the complex modulus of cement bitumen treated materials <i>C. Godenzoni, A. Graziani & M. Bocci</i>	589
Field validation of hot-recycled porous asphalt containing 20% RAP <i>F. Frigio, E. Pasquini & F. Canestrari</i>	597
Performance evaluation of hot recycled mixtures containing SBS modified binder <i>A. Stimilli, G. Ferrotti, D. Radicioni & F. Canestrari</i>	607
Moisture damage and low temperature cracking of bituminous mixtures made with recycled aggregates <i>M. Pasetto & N. Baldo</i>	617
Evaluation of laboratory and field warm mix asphalt mixtures with high contents of reclaimed asphalt pavement <i>T.A. Ahmed, H. Lee & C.M. Baek</i>	623
Environmental impact demonstrated by carbon footprint of cold recycling pavement technology <i>V. Snizek, J. Valentin & M. Engels</i>	629
Preliminary assessment on the use of scrap glass to produce asphalt mixtures <i>E. Manthos, G. Ridondelli, G. Betti & A. Marradi</i>	637
Polyester geogrids as asphalt reinforcement – a sustainable solution for pavement rehabilitation <i>F. Leite-Gembus & B. Thesseling</i>	645
Analysis over the use of reinforced flexible pavement with steel mesh in climbing lanes <i>A.F.B. Ressutte, R.M. Fortes, C.Y. Suzuki & J.B.R. da Silva</i>	653
 <i>Pavement assessment, surface characteristics</i>	
A simplified approach for the estimation of HMA dynamic modulus for in service pavements <i>K. Georgouli, M. Pomoni, B. Cliatt & A. Loizos</i>	661
Temperature correction of HMA moduli based on in situ pavement data <i>A. Loizos, V. Papavasiliou, C. Plati & C. Tsaimou</i>	671
Use of neural networks enhanced differential evolution for backcalculating asphalt concrete viscoelastic properties from falling weight deflectometer time series data <i>K. Gopalakrishnan, S. Kim, H. Ceylan & O. Kaya</i>	679
Accelerated pavement testing program with the mobile load simulator MLS10 – temperature analysis <i>B. Wacker</i>	687
State-of-the-art of Traffic Speed Deflectometer (TSD) <i>J.A. Krarup</i>	693
PELT based dynamic segmentation for network level pavement evaluation with 1 mm 3D data <i>Q. Li, K.C.P. Wang & G.W. Yang</i>	701
Measured pavement responses under falling/heavy weight deflectometer and heavy aircraft gear loadings <i>J.S. Gagnon & A. Larkin</i>	707
Modeling of pavement roughness performance using the LTPP database for southern region in the U.S. <i>Z.F.M. Jaafar, M. Ahlan & W. Uddin</i>	713

Road safety, road marking and street furniture

- Pavement skid resistance versus appropriate signage to tackle the visibility problem on motorway fast lanes along tight left curves 725
A. Kokkalis, A. Athanasopoulou & G. Kollaros
- Brighter and better all-weather road markings in Malaysia 731
M.H. Harun, N.S. Mohamad Noh & W.R. Wan Hanafi
- Safety audit using operating speeds V_{85} at rural road in Northern Greece 737
G. Mintsis, S. Basbas, C. Taxiltaris, N. Domoksis & K. Labropoulou
- The contribution of roundabouts to road safety: The case of 4 roundabouts in the municipality of Thermi Greece 745
D. Spanou, F. Kehagia & M. Pitsiava-Latinopoulou

Posters

- Assessment of generic pothole repair materials 759
J.C. Nicholls, K. Kubanek, C. Karcher, A. Hartmann, A. Adesiyun, A. Ipavec, J. Komacka & E. Nielsen
- Innovations for sustainable road infrastructure 767
F. Kehagia & K. Chondrosyros
- A multiple regression model for developing a RAP binder blending chart for stiffness prediction 775
S. Bressi, A.G. Dumont, A. Carter & N. Bueche
- Quality control in the construction of asphalt concrete pavement layers 785
B.G. Pecheny & A.D. Nikolov
- Asphalt bridge deck pavement behavior, the Egnatia experience 789
A. Kokkalis & P. Panetos
- Laboratory study of evaluating direct tensile properties of asphalt mixtures on reflective cracks 795
M. Khadem & R. Farahi
- Effects of bonus provisions on HMA superpave mixture specifications through pay factor analysis 801
S.S. Karimi, D.G. Goulias & C.W. Schwartz
- Evaluation parameters of impact sounding signals for interface condition assessment of concrete bridge decks 807
C.A. Rosales, H.J. Lee, J. Baek, W. Kim & J. Jeong
- Performance evaluation of Romanian modified bitumens using thermoplastic elastomer SBS 813
L. Judele & D. Lepadatu
- Plastic fines of road construction materials tested using the methylene blue method 819
A. Athanasopoulou, G. Kollaros & A. Kokkalis
- Stiffness and complex modulus of cold recycled mixes with different binder combinations 825
Z. Čížková, J. Suda, J. Valentin & O. Krpálek
- Maintenance strategy for the provincial road network of Xanthi, Greece 833
G. Kollaros, A. Kokkalis & A. Athanasopoulou
- Determining the allowable content of RAP in HMA using the blending charts and RAP mortar properties 841
C. Riccardi, P. Leandri & M. Losa
- Experience with designing and in-situ verification of cold emulsified mixes in the Czech Republic 849
J. Suda & J. Valentin
- Evaluation of applicability of residual products from solvent deasphalting process of heavy oil refining as a binder for asphalt pavement 859
S.D. Hwang, C.M. Baek, S.L. Yang & J.H. Im
- Author index 865

Preface

The papers contained in these Proceedings have been presented at the 6th International Conference ‘Bituminous Mixtures and Pavements’ that took place in Thessaloniki, Greece in June 2015. The number of papers finally accepted for publication and contained in this volume of Proceedings is one hundred thirteen (113).

The papers cover the recent developments worldwide in the areas of pavement materials, pavement design, construction and maintenance, recycling, surface characteristics and other related subjects in highway engineering.

Highway engineers are facing the challenge, not only to design and construct the pavements properly and economically but also to be sustainable and safe. This implies a thorough understanding of materials behaviour, their appropriate use in the continuously changing environment, and implementation of improved technologies and methodologies.

The distinguished Members of the Scientific Committee worked hard, with notable colleague zeal, providing invaluable work by reviewing the papers. I sincerely express my gratitude for their outstanding work.

The Organizing Committee, the heart of the Conference, worked with great enthusiasm in order to ensure the success of the Conference. My gratitude is also extended to every single one of them, personally.

Also, I would like to thank the Sponsors for their kind contribution that made the organization of this Conference possible at a low participation fee.

Finally, I thank the Authors for their high scientific level contribution, the Participants, from thirty five (35) countries, for attending the Conference, and in general all those who worked and contributed to the great success of this Conference.

Prof. A. F. Nikolaides, Editor,
Chairman of the Conference
Professor of Highway Engineering
Director of Highway Engineering Laboratory
Aristotle University of Thessaloniki, Greece

June 2015

Organizing committee

Chairman: Prof. Nikolaides A., *Aristotle University of Thessaloniki (ATh), Greece*

Members:

Woodward D., *Dr., Reader, University of Ulster, UK*

Uddin W., *Prof., University of Mississippi, USA*

Pyrgidis Chr., *Prof., ATh, Greece*

Kimoundris A., *Lecturer, ATh, Greece*

Kehagia F., *Assist. Prof., ATh, Greece*

Manthos E., *Lecturer, ATh, Greece*

Palantzas G., *Dr., ATh, Greece*

Scientific committee

Chairman: Woodside Alan, *OBE, Prof., University of Ulster, UK*

Vice-Chairman: Mouratidis Anastatios, *Prof., Aristotle University of Thessaloniki (AUTH), Greece*

Members:

Angelone Silvia, *Prof., University of Rosario, Argentina*
Bahia Hussain, *Prof., University of Wisconsin-Madison, USA*
Blab Roland, *Prof., Technical University of Vienna, Austria*
Burrow Michael, *Dr., Birmingham University, UK*
Canestrari Francesco, *Prof., Polytechnic University of Marche, Italy*
Ceylan Halil, *Prof., Iowa State University, USA*
Chang Carlos, *Assist. Prof., The University of Texas at El Paso, USA*
Collop Andy, *Prof., University of Leicester, UK*
Di Benetto Harve, *Prof., University of Lyon, ENTPE, France*
Eliou Nikolaos, *Prof. University of Thessaly, (UTH) Greece*
Evdorides Harris, *Dr., University of Birmingham, UK*
Ferreira Adelino, *University of Coimbra, Portugal*
Fortes Rita, *Prof., Presbyterian University Mackenzie, Brazil*
Fwa Tein Fang, *Prof., National University of Singapore, Singapore*
Goulias Dimitrios, *Assoc. Prof., University of Maryland, USA*
Grabowski Wojciech, *Prof., Poznan University, Poland*
Hunter Robert, *Dr., Hunter & Edgar, UK*
Kaloush Kamil Elias, *Assoc. Prof., Arizona State University, USA*
Khalid Hussain, *Dr., Liverpool University, UK*
Kokkalis Alexandros, *Assoc. Prof., Democretus University of Thace (DUTH), Greece*
Loizos Andreas, *Prof., National Technical University of Athens (NTUA), Greece*
Losa Massimo, *Prof., University of Pisa, Italy*
Martinez Fernando, *Prof., University of Rosario, Argentina*
Merighi Joao, *Prof., Presbyterian University Mackenzie, Brazil*
Mintsis George, *Prof., Aristotle University of Thessaloniki (AUTH), Greece*
Mohammad Louay, *Prof., Louisiana State University, USA*
Nicholls Cliff, *Dr., TRL, UK*
Nikolaides Athanassios, *Prof., Aristotle University of Thessaloniki (AUTH), Greece*
Othman Hamzah Meor, *Prof., Universiti Sains Malaysia, Malaysia*
Papagiannakis Athanasios, *Prof., University of Texas at San Antonio, USA*
Park Dae-Wook, *Prof., Kusan National University, Korea*
Pasetto Marco, *Prof., University of Padova, Italy*
Pratico Filippo, *Assoc. Prof., Mediterranean University of Reggio Calabria, Italy*
Puppala Anand, *Prof., University of Texas Arlington, USA*
Raab Christiane, *EMPA, Switzerland*
Santagata Ezio, *Prof., Politecnico di Torino, Italy*
Scarpas Athanasios, *Prof., Delft University of Technology, The Netherlands.*
Sengoz Burak, *Assoc. Prof., Dokuz Eylul University, Turkey*
Singh Dharamveer, *Assist. Prof., Indian Institute of Technology, Bombay, India*
Steyn Wynand JvdM, *Prof., University of Pretoria, South Africa*
Sybilsky Dariusz., *Prof., IBDM, Poland*
Tarefder Rafiqul, *Assoc. Prof., University of New Mexico, USA*
Uddin Waheed, *Prof., University of Mississippi, USA*
Wang Kelvin, *Prof., Oklahoma University, USA*
Woodward Dave, *Dr., Reader, University of Ulster, UK*

Organizers

Highway Engineering Laboratory, Department of Civil Engineering, Aristotle University of Thessaloniki (AUTH)
Built Environment Research Institute (BERI), University of Ulster, UK
Center for Advanced Infrastructure Technology (CAIT), University of Mississippi, USA

Supporting Institutions and Organizations

ASCE Transportation & Development Institute (ASCE T&DI), USA
Chartered Institution of Highways & Transportation (CIHT), UK
European Asphalt Pavement Association (EAPA)
Federal Aviation Administration (FAA)
International Society for Asphalt Pavements (ISAP)
Institute of Asphalt Technology (IAT)
Institution of Civil Engineers (ICE), UK
Transportation Research Board (TRB), USA
Transport Research Laboratory (TRL), UK

Sponsors

AEIFOROS METAL PROCESSING S.A.
AEGEAN MOTORWAYS S.A.
ESHA
BITUMIX S.A.
DEYKON A.T.E.
DYNATEST
GEOEDRASI L.T.D.
HELMA S.A.
HUESKER
KAISIDIS S.A.
KERIDIS WORKS S.A.
NETOIL S.A.

Bituminous binders, unbound materials

Statistical methods for evaluating associations between selected foamed bitumen parameters

A. Chomicz-Kowalska

ABSTRACT: The authors tested various bitumen intended for use in production of low temperature mineral-bitumen mixes with foamed binder. A few different binders were investigated, varying in hardness (from penetration grade PG 20 to PG 220) and type (neat, multigrade and FT synthetic wax modified). The evaluation covered the basic and rheological parameters of bitumen and characteristics of bitumen foam. After the first step in the analysis, which was to assess the parameters of bitumen before foaming, it was possible to distinguish three uniform groups of binders. The following step was to measure the characteristics of bitumen foam depending on foaming water content. The results helped evaluate the influence of the rheological parameters on the foaming ability of the bitumen. Mathematical models quantifying the relationships between parameters of foamed bitumen and the amount of foaming water were developed using statistical methods. The correlations were used to assign the binders for use in proper mineral-bitumen mix technologies according to valid recommendations.

1 INTRODUCTION

Hot mix asphalt mixtures (HMA), which are energy-consuming due to high production temperatures exceeding 150°C, are widely used in road construction. These temperatures result from heating the components of the mixture, aggregate and bitumen, to the temperature required to ensure proper bitumen viscosity and coating of the mineral material. HMA production-related high emissions of greenhouse gases have a strongly documented negative effect on the environment.

Solutions that considerably reduce production temperatures and thus limit the greenhouse effect (i.e. CO₂ emission to the atmosphere) include the application of such technologies as: WMA (Warm Mix Asphalt), HWMA (Half Warm Mix Asphalt) and CMA (Cold Mix Asphalt) (D'Angelo et al. 2008). In these technologies, proper grade bitumen with adequate additives (e.g. organic, chemical) have to be selected to obtain sufficiently low bitumen viscosity ensuring proper coating of aggregate particles and providing workability and compaction capacity of bituminous mixtures (Vaitkus & Cygas 2009).

More than ten years ago, warm mix asphalt (WMA) was introduced with production temperatures in the range 100°C–140°C (Perkins 2009). There are a few major types of WMA technologies: those that use water (small amounts of water are added into hot bitumen through a foaming nozzle with damp aggregates leading to the expansion of the binder phase and a reduction in the mix viscosity), hydrophilic material such as zeolite, and those that use additives to obtain the temperature reduction (organic additives such as

Fischer-Tropsch wax, montan waxes, fatty amides and chemical surface active additives, D'Angelo et al. 2008, Perkins 2009, Morea et al. 2012). Additive based techniques produce a decrease in bitumen viscosity when the mixing and placement temperatures are above the melting point of the wax, while the water based techniques reduce the surface tension of the binder without modifying, in theory, rheological properties (Morea et al. 2012).

Fischer-Tropsch (FT) wax significantly influences rheological properties of the bitumen by increasing its viscosity in the temperature range up to 100°C and increasing its softening point. At temperatures above 100°C, the viscosity is rapidly reduced thus the compaction temperature of the bituminous mixture can be lowered by about 20–30°C (D'Angelo et al. 2008).

As has been pointed out, the production and placing temperature of bituminous mixtures can also be reduced by modifying the technological process by the use of water in foaming. In 1956, Ladis H. Csanyi, Iowa State University, studied bituminous mixtures prepared with foamed asphalt in the cold technique of mixture production, CMA (Cold Mix Asphalt). In 1968, Mobil Oil in Australia, having acquired the patent rights, modified Csanyi's foam production method by replacing steam with cold water (Muthen 1999). Since that time, this process has been widely used and investigated by many researchers (Jenkins et al. 1999, 2000, Van De Ven et al. 2007, Ben & Jenkins 2014, Martinez-Arguelles et al. 2014). Jenkins et al. (1999) developed a new bituminous mixtures production process called HWMA (Half Warm Mix Asphalt) with foamed bitumen and temperatures below 100°C. Compared with WMA, the foaming

technology with the use of water does not need any chemical additives (Yu et al. 2013), but their addition is recommended when the bitumen has low foaming capacity.

The reduced production temperature technology allows raising the level of environmental protection through noticeably lower emissions of harmful substances from the traditional hot method and through the limited use of non-renewable energy in the process of bituminous mixtures manufacture. The application of HWMA with foamed bitumen to road paving brings environmental and economic benefits as compared to HMA (Van De Ven et al. 2007).

2 MATERIALS AND RESEARCH METHODOLOGY

2.1 Purpose of the research

The purpose of this laboratory study was to evaluate the properties of foamed bitumen produced with various binders, in terms of their suitability for use in the production of bituminous mixes intended for application to road pavement structural layers.

Physical and rheological properties of bitumen used in road construction vary widely depending on the chemistry of the crude oil source, methods used to refine it, composition and chemical and colloidal structure (Gaweł et al. 2001). Jenkins (2000) confirmed the influence of the factors listed above on the quality of the produced bituminous foam. Thus, each type of bitumen can be expected to behave differently. As the harder bitumen grades tend to clog the expansion chamber and the spray nozzle orifices, higher-grade bitumen types are preferred, where clogging is practically eliminated (Jenkins 2000).

Bissada (1987) and Abel (1978) found that soft bitumen grades (with lower viscosities) give better foaming properties and have higher expansion ratio and longer half-life than hard bitumen grades (with higher viscosities), ensuring better dispersion and coating of mineral material. Proper coating of aggregates is key to preventing defects and achieving long service life of pavements (Remisova 2004).

Different conclusions regarding decay parameters for two bitumen penetration grades (PG 60, PG 100) was reported by He and Wong (2006). At the same test conditions (bitumen temperature, air pressure, and water content), the harder binder had higher expansion ratios relative to the softer binder. It was also observed that half-life (*HL*) was longer for softer bitumen (PG 100). He and Wong (2006) concluded that the differences between viscosities of the bitumen types influenced the relationships they described.

Currently, most commonly used bitumen types for road construction purposes in Poland include 20/30, 35/50 and 50/70 PG neat bitumen (where e.g. 20/30 is a penetration range) and polymer modified bitumen: PmB 25/55-60 and PmB 45/80-55 (where 25/55 is the penetration range and 60 is the softening point) (Jaskuła & Judycki 2014, Radziszewski et al. 2014).

In 1999, multigrade bitumen developed in the mid-eighties by KSLA Shell (Sybilski & Mularczyk 1999) was introduced in Poland (Sybilski et al. 2000). The properties of those binders lie between those of a conventional penetration grade bitumen and those of a polymer-modified bitumen. Multigrade bitumens are manufactured in a special refining process of crude oil (Sybilski & Mularczyk 1999). According to Polish technical requirements included in *WT-2 (National Asphalt Pavements. Bituminous Mixes. Technical Requirements. 2014)*, the following multigrade bitumen types are allowed in Poland: MG 20/30-64/74, MG 35/50-59/69 and MG 50/70-54/64 (the grades are designated by the nominal penetration range followed by softening point range in compliance with *EN 13924-2*). The use of MG bitumen is growing in manufacturing of wearing courses, binding courses and bases due to their improved high and low temperature properties. Multigrade bitumens are graded according to the same penetration ranges at 25°C as road paving bitumen in *PN-EN 12591* and can be used as replacement.

2.2 Tested materials

The study covered 11 binder types, divided into three groups:

- Group A – road paving bitumen (neat): 35/50, 50/70, 70/100, 100/150, 160/220 that meet the requirements of Polish *PN-EN 12591*,
- Group B – special bitumen (multigrade): MG 20/30, MG 35/50, MG 50/70 according to *PN-EN 13924-2*,
- Group C – *FT* wax-modified bitumen: 50/70/1, 50/70/2, 50/70/3 (bitumen 50/70 with 1%, 2% and 3% *FT* modifier content, respectively).

The first group includes neat paving bitumen from one manufacturer with grades from PG 35 to PG 220. The second group, contains multigrade bitumen. The third group comprises modified bitumen produced with PG 50/70 binder (from Group A).

Although no additives are necessary for foaming with water, in order to show the applicability of the 50/70 bitumen for wider use (heavily trafficked pavements), *FT* synthetic wax was added 1%, 2% and 3% by weight to improve the bitumen foam parameters by lowering the viscosity of the bitumen at temperatures above 100°C (Silva et al. 2010). The presence of *FT* wax increases the stiffness of the binder, providing bituminous mixtures with better mechanical properties, higher resistance to permanent deformation in particular (Silva et al. 2010, Iwański et al. 2015).

2.3 Experimental program

The scope of the research related to determining the suitability of bitumen types for foaming technology in manufacturing of pavement structural materials was divided into two stages. First, rheological parameters before foaming were determined. Second, the

properties of the foam were measured at a varied content of foaming water (*FWC* – foaming water content). Mathematical models quantifying the relationships between parameters of the foamed bitumen and amount of foaming water were developed using statistical methods.

The significance of differences between the characteristics of the bituminous foam (for all the bitumen types) for *FWC* was evaluated using the one-way ANOVA. In addition, the results obtained for Group C bitumen, evaluated using the two-way ANOVA, were analysed to determine the significance of the influence of the change in the levels of the two parameters (*FWC*, *FT*).

The analysis of the results helped to find the relationships between the rheological parameters of the bitumen (before foaming) and the characteristics of the foam. After determining the optimal *FWC* level, the classification and suitability assessment were conducted in terms of the suitability of the binders for selected technologies used in road construction.

2.3.1 Bitumen properties

The following characteristics were determined in stage I of the study:

- penetration at 25°C (*PG*) acc. to *EN 1426*,
- softening point ($T_{R\&B}$) acc. to *EN 1427*,
- Fraass breaking point (T_{Fraass}) acc. to *EN 12593*,
- dynamic viscosity at 90°C and 135°C (η_{90} , η_{135}) acc. to *EN 13702-2*.

Other parameters evaluated included the penetration index (*PI*) and plasticity range (*PR*). Penetration index quantifies the binder temperature sensitivity and is an indicator for the dynamics of hardening/softening phenomena under temperature changes. *PI* is calculated based on the two most basic bitumen rheological parameters: the softening point and penetration, in accordance with the formula below, in compliance with *EN 12591*:

$$PI = \frac{20T_{R\&B} + 500 \log PG - 1952}{T_{R\&B} - 50 \log PG + 120} \quad (1)$$

Plasticity range, on the other hand, defines the temperature span in which the binder retains its visco-elastic properties and is computed according to equation (2) in compliance with *PN-EN 14023*:

$$PR = T_{R\&B} - T_{Fraass} \quad (2)$$

This parameter correlates well with the penetration index and for best effects the *PR* should exceed 60°C (Gaweł et al. 2001). Low values of both indices (*PI*, *PR*) suggest an increased temperature susceptibility of the binder.

2.3.2 Foamed bitumen properties

The physical characteristics of the bitumen foam were evaluated with the use of two empirical parameters: maximum expansion ratio (*ERM*) and half-life (*HL*) (Jenkins 2000). *ERM* is a measure of the bitumen foam

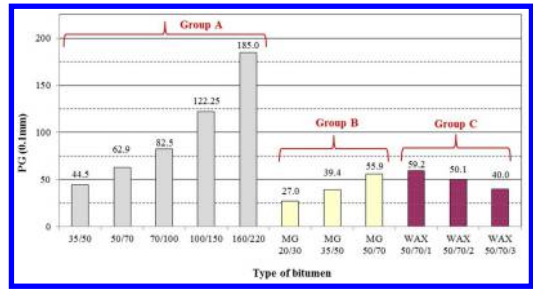


Figure 1. Summary of penetration measurement results at 25°C.

viscosity and therefore it is an estimate of how well the foam can be dispersed in the aggregates to create a uniform mineral-bitumen mix. Half-life indicates the foam stability and provides approximate information about the rate of foam decay (Muthen 1999). Those parameters are inversely proportional in terms of *FWC* – increase in *FWC* leads to an increase in *ERM* and decrease in *HL*, and vice versa (Jenkins et al. 2000).

The foam parameters (*ERM*, *HL*) of multigrade, modified (*FT wax*) and neat bitumens were evaluated during the second stage of the this study. The measurements were conducted under laboratory conditions using Wirtgen WLB 10S bitumen foaming plant, which is commonly used laboratory equipment. The tests were carried out with the following arrangements: water temperature: 20°C, water flow: 100 g/s, foaming time: 5 s, air pressure: 500 kPa, water pressure: 600 kPa. The temperatures of the bitumen were selected according to the experience gained by the authors (Iwański & Chomicz-Kowalska 2012a, 2012b, 2013, Iwański et al. 2015) and that of other researchers (Jenkins 2000, Martinez-Arguelles et al. 2014, He & Wong 2006) and were taken to be 170°C for the bitumen in Groups A and B, and 155°C for the bitumen in Group C.

The foaming water content ranged from 1.0% to 4.0% by mass of the binder, in 1.0% increments. The amounts of foaming water and foaming conditions were established based on the experience of the authors (Iwański & Chomicz-Kowalska 2012a, 2012b, 2013, Iwański et al. 2015) and other researchers (Martinez-Arguelles et al. 2014, He & Wong 2006, Xiao et al. 2011).

3 TESTS RESULTS AND ANALYSIS

3.1 Rheological properties of the bitumen

The first stage of the study was devoted to the evaluation of the rheological parameters of the bitumen. Figures 1 and 2 illustrate the results of penetration tests at 25°C (*PG*) and calculated penetration index values (*PI*). The remaining characteristics, softening point ($T_{R\&B}$), Fraass breaking point (T_{Fraass}), plasticity range (*PR*) and dynamic viscosity at 90°C (η_{90}) and 135°C (η_{135}) are summarized in Table 1.

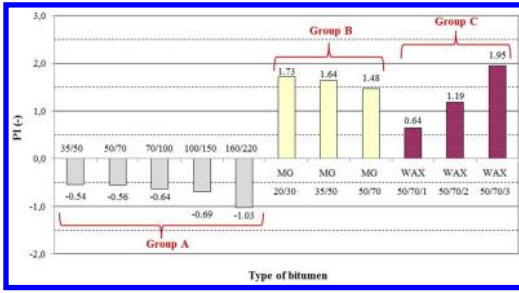


Figure 2. Summary of penetration indices.

Table 1. Bitumen properties.

Bitumen	$T_{R\&B}$ °C	T_{Fraass} °C	PR °C	η_{90} Pa·s	η_{135} Pa·s
35/50	53.9	-9.0	62.9	26.11	0.902
50/70	50.4	-9.4	59.8	14.43	0.506
70/100	47.4	-11.1	58.5	8.24	0.451
100/150	43.4	-13.4	56.8	4.53	0.286
160/220	38.6	-15.8	54.4	2.79	0.220
MG 20/30	72.2	-8.60	80.8	92.34	2.723
MG 35/50	66.5	-18.8	85.2	69.57	1.617
MG 50/70	60.8	-21.0	81.8	17.62	0.638
WAX 50/70/1	56.1	-14.2	70.3	15.31	0.590
WAX 50/70/2	60.8	-13.1	73.9	16.4	0.540
WAX 50/70/3	68.1	-12.3	80.4	17.3	0.500

Analysis of the results indicates that neat bitumen (Group A) met the requirements of *PN-EN 12591* and the multigrade bitumen (Group B), within the range of parameters assessed, conformed to *PN-EN 13924-2*. The binders from Group C were in accordance with the requirements of *PN-EN 14023* for PmB 45/80-55 (for WAX 50/70/1) and PmB 25/55-60 (for WAX 50/70/1 i WAX 50/70/2) in terms of *PG*, $T_{R\&B}$ and T_{Fraass} .

The properties of binders from Groups B and C were significantly different from the parameters of neat bitumen, in particular in terms of the softening point. As for the temperature of 60°C, which in Poland is regarded as the highest pavement temperature in summer and which is taken into account in the evaluation of bitumen permanent deformation resistance (wheel tracking test according to *WT-2* and *PN-EN 12697-22*), the softening point higher than that was obtained for bitumen 50/70 modified with the FT wax added in the amount exceeding 2.0% and for all multigrade bitumen types. This result indicates that the increase in the softening temperature obtained through the modification of bitumen 50/70 will reduce the susceptibility of bituminous mixtures to permanent deformation (rutting) (Silva et al. 2010, Iwański et al. 2014).

The evaluation of the mean values of dynamic viscosities for binders in Groups A and B recorded a drop at both temperatures with increasing penetration; opposite relationship was observed in FT wax-modified bitumen, where this parameter at a temperature of 135°C (η_{135}) decreased with decreasing

penetration due to higher amount of the modifier added.

Increased addition of FT wax affects the base binder by increasing its stiffness below 100°C (lower penetration at 25°C and dynamic viscosity at 90°C), with a drop in dynamic viscosity at 135°C, leading to the reduction in production temperatures. Modification of 50/70 bitumen with 3.0% FT wax resulted in obtaining a one grade harder binder (PG 35/50). Similar tests performed for bitumen 35/50 revealed (Silva et al. 2010, Iwański et al. 2014) that the addition of synthetic wax changed the grade of the bitumen (penetration-wise) from 35/50 to 20/30.

Penetration Index is another parameter that differentiates bitumen from Groups B and C from the neat bitumen in Group A. This parameter is used to assess deformation properties of binders. Binders used in road paving should have *PI* in the range from +2.0 to -2.0. Those with positive penetration indices are more suitable for road pavements as they maintain viscoelastic properties at low temperatures and at a short loading time (dynamic loading) and do not flow at high temperatures and long loading times (Radziszewski et al. 2011). Multigrade and FT wax-modified bitumen returned positive penetration indices, whereas the neat road paving bitumen types had negative values of *PI*. The investigated road paving bitumen were assigned to the sol-gel rheological type (*PI* from -2.0 to +2.0) (Gawęł et al. 2001). In Poland, eligible requirements are available only for multigrade bitumen, where in accordance with *PN-EN 13924-2*, *PI* should be +0.3 to +2.0 for all bitumen grades (multigrade: 20/30, 35/50 and 50/70). All binders in Group B satisfied these requirements.

It has to be noted that the plasticity range requirements specified in *PN-EN* standards refer only to polymer modified bitumen and the value of this parameter depends on the bitumen consistency at intermediate service temperatures (penetration at 25°C). The plasticity range should be $\geq 80^\circ\text{C}$ for polymer modified bitumen Class 3 (penetration 25–55 $\times 0.1$ mm), and $PR \geq 75^\circ\text{C}$ for Class 4 (penetration 45–80 $\times 0.1$ mm). From Table 1 it follows that only bitumen WAX 50/70/3 met the criterion ($PR = 80.4^\circ\text{C}$).

To compare the most commonly used bitumen in Poland, PG 35/50 and 50/70 and the corresponding multigrade bitumen, parameter *PR* was used, i.e. the temperature range in which the binder retains its viscoelastic properties. For MG 35/50, $PR = 85.2^\circ\text{C}$, and for MG 50/70, $PR = 81.8^\circ\text{C}$, which is 22.3°C and 22°C respectively more compared to neat bitumen. This indicates improved low and high temperature properties relative to paving bitumen, which translates into higher stiffness modules and higher resistance to rutting displayed by the bituminous mixtures made with those binders.

3.2 Influence of foaming water on bitumen foam characteristics

The basic parameter used to evaluate whether bituminous binders are suitable for foaming is the capability

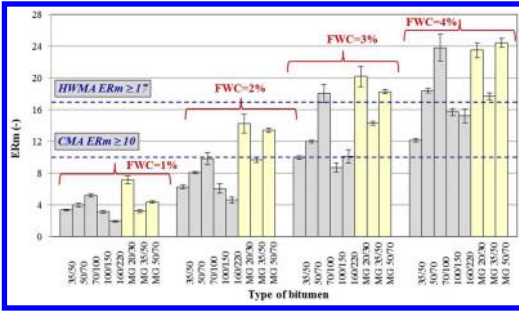


Figure 3. Summary of results from expansion ratio tests for bitumen from Groups A and B at varied level of *FWC* (error bars represent standard deviations).

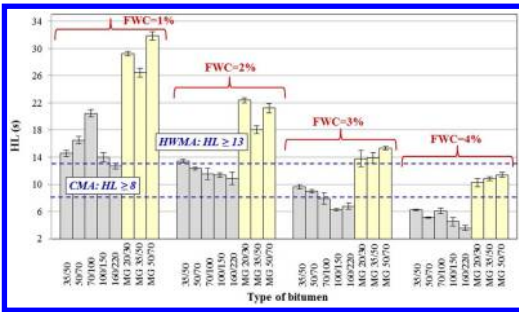


Figure 4. Summary of results from half-life tests for bitumen from Groups A and B at varied level of *FWC* (error bars represent standard deviations).

of producing the foam of required parameters. It is difficult to determine the foaming capability of binders or establish the optimal *FWC* when only basic rheological properties of bitumen are known.

As mentioned earlier, in the second stage of research, parameters *ERm* and *HL* were investigated. To correctly assess the foam properties, the characteristics of these parameters were measured four times varying the level of *FWC* (1%, 2%, 3%, 4%).

The second step in the analysis of the results resulted in determining the relationship between *ERm* and *HL* and changes in *FWC* levels. Obtained characteristics helped establish the optimal content of foaming water for each type of binders.

Figures 3 and 4 show mean values of expansion ratio and half-life, respectively, for the bitumen from Groups A and B versus the level of *FWC*.

The results indicate that the increase in the amount of water added during the foaming process (from 1% to 4%) had a clear effect on the parameters obtained for the investigated binders, increasing their expansion ratio values and lowering their half-life.

In Group A, the highest values of *ER* were reached by binder 70/100 and then binder 50/70, regardless of the amount of foaming water used. The lowest values were recorded for bitumen 35/50 at *FWC* = 4%, bitumen 100/150 at *FWC* = 3% and bitumen 160/220 at 1% and 2% content of *FWC*. In Group B, the least foaming binder was MG 35/50, with MG 20/30 having

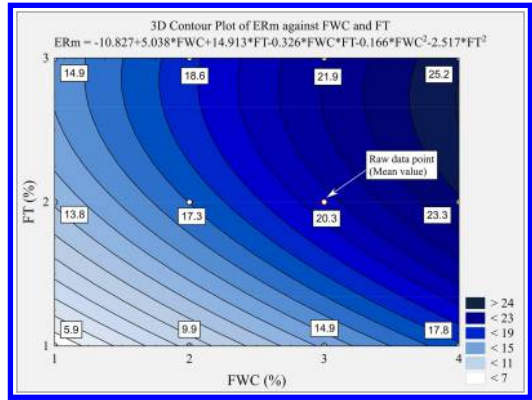


Figure 5. Dependence of *ERm* on changes in *FT* and *FWC* for bitumens from Group C ($R^2 = 0.989$).

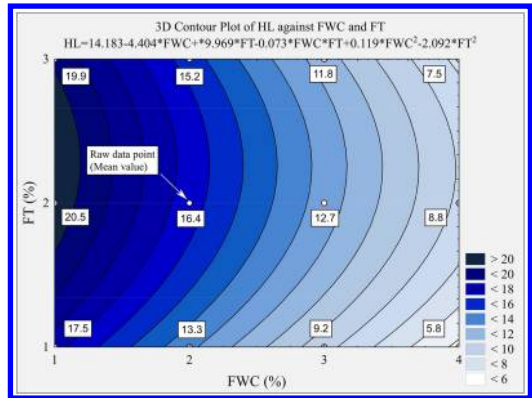


Figure 6. Dependence of *HL* on changes in *FT* and *FWC* for bitumen from Group C ($R^2 = 0.987$).

the best foaming capability at *FWC* from 1% to 3% and with MG 50/70 at *FWC* = 4%.

It has to be added that in terms of *HL*, for foamed bitumen manufactured on the basis of multigrade bitumen, longer *HL* were recorded compared with the foamed bitumen produced with neat base bitumen types.

The mathematical model was used to evaluate the impact of changes in *FWC* and *FT* wax content on the properties of bitumen in Group C. Based on the chosen optimization method (Montgomery 2001) it was assumed that for the case investigated, the following polynomial mathematical model of the second degree, expressed as (3), will be most adequate:

$$y = b_0 + b_1 \cdot x_1 + b_2 \cdot x_2 + b_3 \cdot x_1 \cdot x_2 + b_4 \cdot x_1^2 + b_5 \cdot x_2^2 \quad (3)$$

where x_1 = foaming water content (%); x_2 = *FT* wax content (%); $b_0 - b_5$ = values of model coefficients.

The graphical interpretation of the response surface of the expansion ratio and half-life changes relative to the synthetic wax content and foaming water amount for the bitumen in Group C is shown in Figures 5 and 6.

The increase in the amount of the modifier from 1% to 2% added to bitumen 50/70 brought a beneficial

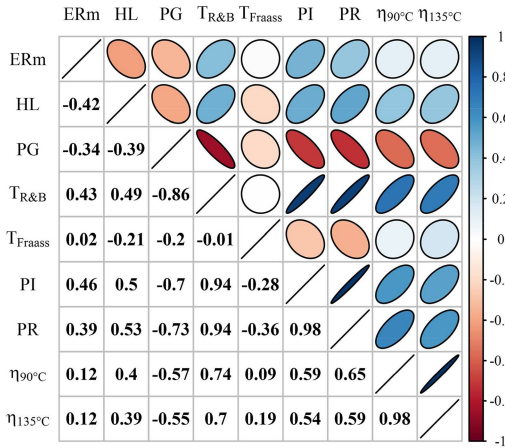


Figure 7. Correlation plot of the bitumen properties and the measured foaming parameters (bitumen in Groups A, B and C).

effect of increased expansion ratios and half-life. At 3% *FT* wax concentration, further increase in the value of *ERm* was recorded, but the half-life was shortened relative to bitumen 50/70+2%*FT*.

The obtained results confirm the observations made by other researchers that the binders with lower viscosity have better foaming capacities and allow limiting the amount of water added. The presence of 3% wax, however, negatively affected *HL* of the bitumen foam. Too low viscosity of the binder caused unstable bubbles to burst, leading to shortened half-life. This is because foam with lower viscosity and relatively low surface tension will be more likely to collapse prematurely before reaching its maximum volume (He and Wong, 2006).

The coefficients of determination for the developed functions in the form of second degree polynomials (Fig. 6, Fig. 7) were $R^2 > 0.98$, which indicate that the proposed models explain the variability in the results to the level higher than 98%.

Table 2 summarizes the results of significance assessment for the influence of *FWC* on the distribution of the investigated foamed bitumen parameters conducted using the one-way ANOVA. For the bitumen types grouped in Group C, the two-way ANOVA (Table 3) was used additionally to determine the significance of the influence of changes in the levels of *FWC* and *FT* and their interaction.

Analysis of variance (Table 2) revealed significant differences (p -value < 0.001) between the means of all the bitumen types, which indicates that *FWC* had significant influence on the changes in characteristics (*ERm*, *HL*) of the foamed bitumen.

The p -value (Table 3) obtained for statistic *F* for *FWC* and *TF* is much lower (p -value < 0.0001) than the assumed significance level ($\alpha = 0.05$), which means that these factors had a significant effect on changes in characteristics (*ERm*, *HL*) of the investigated foamed bitumen, except for their interaction (*FT*FWC*), where p -value = 0.49.

Table 2. Evaluation of significant influence (one-way ANOVA) of *FWC* on *ERm* and *HL* of foamed bitumen.

Bitumen	SS	df	MS	F	p-value
<i>Response: ERm</i>					
35/50	181.58	3	60.525	1263.13	<0.001
50/70	450.56	3	150.19	2465.54	<0.001
70/100	831.99	3	277.33	172.178	<0.001
100/150	345.57	3	115.19	377.937	<0.001
160/220	417.19	3	139.06	253.143	<0.001
MG 20/30	618.92	3	206.31	142.108	<0.001
MG 35/50	472.74	3	157.58	1254.36	<0.001
MG 50/70	863.14	3	287.71	1750.34	<0.001
WAX 50/70/1	336.33	3	112.11	1423.69	<0.001
WAX 50/70/2	200.18	3	66.728	326.710	<0.001
WAX 50/70/3	235.65	3	78.551	332.710	<0.001
<i>Response: HL</i>					
35/50	173.16	3	57.721	403.880	<0.001
50/70	281.52	3	93.840	706.200	<0.001
70/100	490.29	3	163.43	301.989	<0.001
100/150	232.65	3	77.551	355.876	<0.001
160/220	201.27	3	67.089	168.048	<0.001
MG 20/30	878.70	3	292.90	369.457	<0.001
MG 35/50	549.11	3	183.04	403.570	<0.001
MG 50/70	950.92	3	316.97	1085.21	<0.001
WAX 50/70/1	308.58	3	102.86	1338.00	<0.001
WAX 50/70/2	299.13	3	99.710	703.040	<0.001
WAX 50/70/3	332.06	3	110.69	177.751	<0.001

Table 3. Evaluation of significant influence (two-way ANOVA) of *FT* and *FWC* factors on *ERm* and *HL* in Group C.

Effect	SS	df	MS	F	p-value
<i>Response: ERm</i>					
<i>FT</i>	587.28	2	293.64	1697.06	<0.001
<i>FWC</i>	761.28	3	253.76	1466.57	<0.001
<i>FT*FWC</i>	10.890	6	1.8200	10.4900	<0.001
<i>Response: HL</i>					
<i>FT</i>	84.5220	2	42.2610	150.680	<0.001
<i>FWC</i>	938.215	3	312.738	1115.05	<0.001
<i>FT*FWC</i>	1.55300	6	0.25900	0.83000	0.4900

The measurement results for the foamed bitumen allowed determining in compliance with (Kim & Lee 2003) the optimal foaming water content for each of the binders. The mathematical models developed in the form of linear functions were used to determine the optimal *FWC* (Table 4).

The optimum *FWC* determined for the bitumen investigated ranged from 1.5% to 3.0%. For the bitumen grouped in Group A, optimum was determined at *FWC* = 2.5%, except the hardest bitumen (35/50), for which this value was 0.5% higher. All multigrade bitumen types had the same optimal foaming water content at the level of 3.0%. The *FT* wax modified bitumen, however, had different values of *FWC*. The increase in the amount of the modifier reduced the optimal *FWC*

Table 4. Properties of foamed bitumen at optimum *FWC*.

Group	Bitumen	FWC %	ERm –	HL s
Group A	35/50	3.0	10.0	9.6
	50/70	2.5	10.6	10.7
	70/100	2.5	14.2	11.5
	100/150	2.5	8.40	9.0
	160/220	2.5	8.0	8.5
Group B	MG 20/30	3.0	20.2	13.8
	MG 35/50	3.0	14.3	13.9
	MG 50/70	3.0	18.3	15.3
Group C	WAX 50/70/1	2.5	12.1	17.3
	WAX 50/70/2	2.0	17.3	16.4
	WAX 50/70/3	1.5	16.7	17.7

from 2.5% to 1.5%. This was due to the amount of the wax, where the binder viscosity at temperatures exceeding 100°C (before foaming) decreases with the increasing content of *FT* wax (Silva et al. 2010).

The results of the analyses indicate that bitumen viscosity influenced the value of the optimal amount of the foaming water, as for the binder with higher viscosity e.g., multigrade) greater (3%) *FWC* was required to obtain optimal characteristics of the bitumen foam.

No clear relationship, reported by other researchers, showing that softer binders had better foaming capacities was observed.

The parameters of foamed bitumen at the optimal *FWC* (Table 4) allowed the classification and assessment of suitability of the binders for selected technologies used in the road construction. The following criteria were adopted:

- $ERm \geq 10$ and $HL \geq 6s$ for the mixtures produced in cold system (CMA) according to *Wirtgen Cold Recycling Technology (2012)*, at aggregate temperatures ranging from 10°C to 25°C,
- $ERm \geq 8$ and $HL \geq 6s$ for the mixtures produced in cold system (CMA) according to *Wirtgen Cold Recycling Technology (2012)* at aggregate temperatures greater than 25°C,
- $ERm \geq 17$ and $HL \geq 13s$ for half-warm mixtures (HWMA) (Jenkins 2000).

Taking into account criteria adopted above, the only bitumen types that were not suitable for cold recycling (CMA) include bitumen in Group A: 100/150 and 160/220, for which higher aggregate temperatures need to be used (over 25°C). The poor foaming results of the softer binders (100/150 and 160/220) could be a result of too high initial bitumen temperature resulting in a strong decrease in bitumen viscosity. Too low bitumen viscosity could cause the bitumen foam bubbles to collapse prematurely, affecting both the maximum expansion ratio and half-life. For HWMA, only multigrade bitumen (MG 20/30 and MG 50/70) and 50/70 bitumen with 2% *FT* wax were recommended.

When selecting the type of foamed bitumen for the given type of the mixture, such factors as its intended use in structural layers, service requirements, traffic load and climatic issues have to be considered. These

mixtures can be produced at lower temperatures (e.g. HWMA with foamed bitumen) provided they meet the assumed requirements.

For example, in Poland, multigrade bitumen MG 20/30, being a very hard binder is used in binding courses and base courses of standard asphalt concrete and high stiffness modulus asphalt concretes. Medium hardness binder MG 50/70 is used in wearing courses and in binding and base courses in pavements subjected to lower traffic loads (Błazejowski et al. 2014).

The 50/70 binder, most popular in Poland, is recommended for modification with 2% *FT* wax (for greater traffic loads) to ensure the required mechanical parameters (resistance to permanent deformations) of the produced layer.

3.3 Assessment of relationships between selected parameters of bitumen

To determine how the investigated parameters are interrelated, the correlation analysis was performed. Normal distributions were found for all the parameters, therefore the Pearson correlation tests were chosen to evaluate interrelations between the pairs of the variables. The Pearson correlation coefficient (*r*) can take a range of values from +1 to -1 and describes the type (either positive or negative) and the strength of the linear relationship between two interval and/or ratio variables (Mason et al. 2003).

A correlation matrix was calculated for all the considered bitumen properties and foaming parameters (*ERm*, *HL*) to initially assess their relationships. A correlation plot visualizing this matrix is presented in Figure 7, where Pearson's correlation coefficients are shown in the lower portion of the plot and their graphical representations are given in the upper part. The colored ellipses represent strength and direction of the relationships. The analysis was carried out considering all of the previously mentioned bitumens and all foaming water content levels.

The inclusion of all levels of *FWC* in the calculations distorts the interpretation of the calculated correlation coefficients for the relationships between the foaming parameters and bitumen properties. Despite the fact that those calculated quantifications are weaker than found in reality, the results still show specific trends and validate them throughout the different foaming set ups. The correlation coefficients measuring the relationships between the properties of bitumens are undisturbed.

The analysis showed strong mutual correlations between the measured bitumen properties. This occurrence was probably caused by the fact that those characteristics, although measured under different conditions (various modes of loading, loading time, temperature), are related to the fundamental rheological properties of the bitumens. Additionally, *PI* and *PR* are calculated using Softening Point and Penetration values, resulting in a strong correlation with those parameters.

Table 5. Correlations for the pairs of variables.

Variable	PG	$T_{R\&B}$	T_{Fraass}	PI	PR	η_{90}	η_{135}
<i>FWC = 1.0%</i>							
ER	-0.45	0.55	0.19	0.60	0.45	0.01	-0.01
HL	-0.59	0.75	-0.39	0.77	0.83	0.63	0.62
<i>FWC = 2.0%</i>							
ER	-0.63	0.78	-0.03	0.84	0.73	0.25	0.24
HL	-0.63	0.84	-0.26	0.83	0.87	0.74	0.74
<i>FWC = 3.0%</i>							
ER	-0.59	0.74	-0.02	0.78	0.69	0.30	0.31
HL	-0.72	0.88	-0.35	0.90	0.94	0.63	0.58
<i>FWC = 4.0%</i>							
ER	-0.42	0.55	-0.01	0.64	0.55	0.15	0.17
HL	-0.70	0.84	-0.39	0.85	0.91	0.67	0.63

When looking at the relationships between the properties of the bitumens and their foamability (*ERm* and *HL*) some consistent trends are visible. A relatively strong negative correlation is observed between the foamability and penetration, meaning that bitumens with lower *PG* values produce higher quality foam. On the other hand, positive relationships were seen between the foamability and $T_{R\&B}$ (strong negative correlation with *PG*), *PI* and *PR*. Some positive relationships were observed between the measured dynamic viscosities and foaming properties, specifically bitumen foam Half-life times. Additionally, weak negative correlations were found between the T_{Fraass} and the foaming properties.

An additional analysis was carried out to avoid the confounding influence of the *FWC* variable on the calculation of the correlation coefficients. The correlations between the response variable (foamed bitumen properties: *ERm*, *HL*) and the explanatory variable (bitumen rheological properties: *PG*, $T_{R\&B}$, T_{Fraass} , *PI*, *PR*, η_{90} , η_{135}) this time were assessed for each level of *FWC* separately; results are presented in Table 5.

The computed results were in line with the previous findings (Fig. 7) and also the correlation coefficients from this analysis can be interpreted directly. The linear relationships between the foaming characteristics and bitumen properties were, in general stronger when considering the bitumen foam half-lives rather than *ERm*. A strong positive correlation was observed for the $T_{R\&B}$, *PI*, *TZP* and *PR*, and a negative relationship was seen for *PG*. Again, the dynamic viscosities were more strongly correlated with the bitumen foam *HL* than *ERm*. The relationships between foaming parameters and Fraass breaking point were mostly unrelated. The calculated relationships were more significant at *FWC* greater than 1%, which was caused by increased foaming variability and nonlinearities showing throughout the different bitumens when using the small amount of 1% *FWC*. The analysis outcomes show that in general, the most predictable foaming

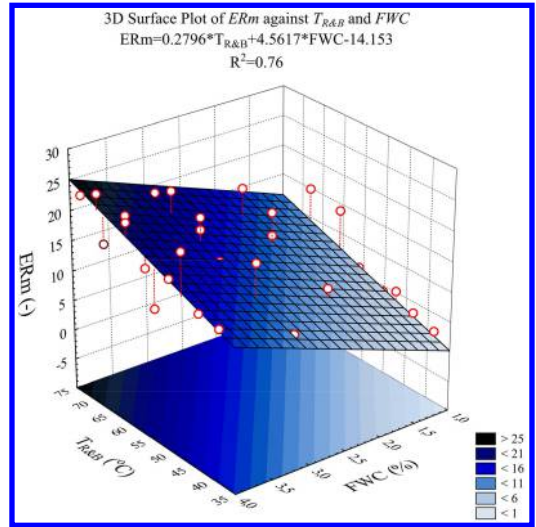


Figure 8. Response surface regression models for the dependent variable (*ERm*) vs. explanatory variables: $T_{R\&B}$ and *FWC*.

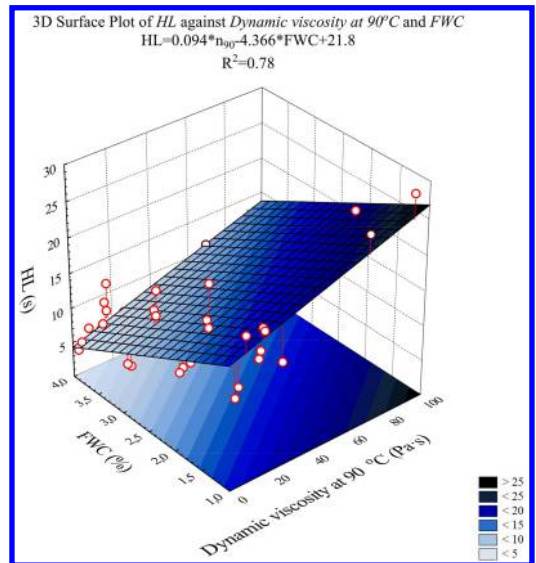


Figure 9. Response surface regression models for the dependent variable (*HL*) vs. explanatory variables: η_{90} and *FWC*.

results are obtained when using 2%–3% and even higher *FWCs*.

Figures 8 and 9 are a graphical representation of statistical models of the linear relationships between *ERm* and $T_{R\&B}$ as well as *HL* and η_{90} while taking into account the different *FWC*.

According to the calculated models, increase in *FWC* by 1% results, on average, in an increase of *ERm* by 4.56 and in decrease of foam half-life by 4.37 s. Similarly, an increase in softening point temperature

by 1°C results, on average in an increase of expansion ratio by 0.26. On the other hand, an increase in dynamic viscosity by 1 Pa·s results, on average, in an increase of half-life by 0.09 s.

4 CONCLUSIONS

On the basis of the rheological tests of the bitumen types and the assessment of the measured parameters of the foam produced from them, the following conclusions can be drawn:

- the amount of foaming water from was statistically significant in evaluation of foaming parameters, rising *FWC* increased the expansion ratios and decreased the half-life of bitumen foam;
- the optimal *FWC* for the investigated binders ranged from 1.5% to 3.0%; for neat bitumen, *FWC* = 2.5% (excl. the 35/50 binder, *FWC* = 3.0%), whereas for the *FT* wax modified bitumens, the optimal *FWC* fell from 2.5% to 1.5% with the increase in *FT* wax dosing (from 1.0% to 3.0%);
- the optimal amount of foaming water was affected by bitumen viscosity; the binders with higher viscosity at 135°C (multigrade bitumen) required higher *FWC* (3.0%) to obtain optimal characteristics of the foam, the higher *FWC* (3.0%);
- the multigrade bitumen types showed an excellent foaming capability, the highest expansion ratios and the longest half-life,
- among the neat bitumen types (Group A), at the optimal *FWC* = 2.5%, the best foamability was displayed by bitumen 70/100 and then bitumen 50/70, whereas the worst foamability characterized bitumens 100/150 and 160/220;
- foaming of soft binders (i.e. neat 100/150 and 160/220 pen) at standard temperatures resulted in decreased quality of bitumen foam, probably attributed the low viscosity of the bitumen;
- the application of the Fischer-Tropsch (*FT*) wax for the modification of bitumen 50/70 improved its foaming capability; the most beneficial properties of the foam were obtained with *FT* = 2.0% and *FWC* = 2.0% (*ERm* = 17.3, *HL* = 16.4 s);
- the modification of the neat bitumen 50/70 with the *FT* wax increased the range of its possible applications in foaming technologies, leading to harder binder and thus more rut resistant bituminous mix with better mechanical parameters;
- strong linear relationships were observed between the measured parameters of foamed bitumen (*ERm*, *HL*) and some of their rheological characteristics (before foaming).

The analyses and tests conducted in this study indicate that all the binders investigated in accordance with the assumed criteria could be used for the production of *CMA*, with a certain restraint in the case of bitumen 100/150 and 160/220, for which the temperature of the mineral material should be higher than 25°C.

For the *HWMA* production, only multigrade bitumen types (MG 20/30 and MG 50/70) as well as 2% *FT* wax modified bitumen 50/70 could be used.

ACKNOWLEDGEMENTS

The scientific research has been carried out as a part of the Project *Innovative recourses and effective methods of safety improvement and durability of buildings and transport infrastructure in the sustainable development* No POIG 01.01.02-10-106/09-01 financed by the European Union from the European Fund of Regional Development based on the Operational Program of the Innovative Economy.

REFERENCES

- Abel, F. 1978. *Foamed asphalt base stabilization*. 6th Annual Asphalt Paving Seminar, Colorado State University.
- Ben, MD., Jenkins, KJ. 2014. *Performance of cold recycling materials with foamed bitumen and increasing percentage of reclaimed asphalt pavement*. Road Materials and Pavement Design 15(2): 348–371. DOI:10.1080/14680629.2013.872051
- Bissada, AF. 1987. *Structural Response of Foamed-Asphalt-Sand Mixtures in Hot Environments*. Asphalt materials and mixtures 1115: 134–149. Transportation Research Record.
- Błażejowski, K., Olszacki, J. & Peciakowski, H. 2014. *Poradnik asfaltowy [Bitumen handbook]*. Orlen Asphalt Group.
- D'Angelo, J., Harm, E., Bartoszek, J., Baumgardner, G., Corrigan, M., Cowsert, J., Harman, T., Jamshidi, M., Jones, W., Newcomb, D., Prowell, B., Sines, R., Yeaton, B. 2008. *Warm-Mix Asphalt: European Practice*. FHWA Report No. FHWA-PL-08-007.
- Gawęł I, Kalabińska M, Piłat J. *Asfalty drogowe [Road bitumen]*. Warsaw, Poland: WKŁ; 2001, p. 255.
- He, G. & Wong, W. 2006. *Decay properties of foamed bitumens*. Construction and Building Materials 20: 866–877, DOI:10.1016/j.conbuildmat.2005.06.027
- Iwański, M. & Chomicz-Kowalska, A. 2012a. *Experimental study of water and frost resistance of foamed bitumen mixes in the cold recycling technology*. Proc. Euroasphalt & Eurobitume Congress 5 (P5EE-357).
- Iwański, M & Chomicz-Kowalska, A. 2012b. *Moisture and frost resistance of the recycled base rehabilitated with the foamed bitumen technology*. Archives of Civil Engineering 58(2): 185–198. DOI: 10.2478/v.10169-012-0011-2
- Iwański, M., & Chomicz-Kowalska, A. 2013. *Laboratory Study on mechanical Parameters of Foamed Bitumen Mixtures in the Cold Recycling Technology*. Procedia Engineering 57, 433–442 (2013), DOI:10.1016/j.proeng.2013.04.056.
- Iwański, M., Chomicz-Kowalska, A. & Maciejewski, K. 2015. *Application of synthetic wax for improvement of foamed bitumen parameters*. Construction and Building Materials 83: 62–69. DOI:10.1016/j.conbuildmat.2015.02.060
- Jaskuła, P & Judycki, J. 2014. *Durability of Asphalt Concrete Subjected to Deteriorating Effects of Water and Frost*. J. Perform. Constr. Facil. DOI:10.1061/(ASCE)CF.1943-5509.0000645, C4014004.

- Jenkins, KJ. 2000. *Mix Design Considerations for Cold and Half-Warm Bituminous Mixes with Emphasis on Foamed Bitumen*. PhD Dissertation, Department of Civil Engineering, Faculty of Engineering, University of Stellenbosch, Stellenbosch, South Africa.
- Jenkins, KJ., de Groot, JLA., Van de Ven, MFC. & Molenaar, AAA. 1999. *Half-warm Foamed Bitumen Treatment, A New Process*. Conference on Asphalt pavements for Southern Africa, Victoria Falls, Zimbabwe, 1999.
- Jenkins, KJ., Molenaar, AAA., de Groot, JLA. & Van de Ven, MFC. 2000. *Optimisation and Application of Foamed Bitumen in Road Building*. Doorwerth, Netherlands: Wegbouwkundige Werkdagen.
- Kim, Y. & Lee, DY. 2003. *Development of a mix design process for cold-in place rehabilitation using foamed asphalt*. Final report for TR-474 Phase 1. University of Iowa, USA.
- Komacka, J., Remisova, E., Liu G., Leegwater G. & Nielsen E. 2014. *Influence of reclaimed asphalt with polymer modified bitumen on properties of different asphalts for a wearing course*. Proc. ICTI 3, 179–185.
- Montgomery, DG. 2001. *Design and Analysis of Experiment*. John Wiley & Sons, 5th Edition.
- Martinez-Arguelles, G., Giustozzi, F., Crispino, M. & Flintsch, GW. 2014. *Investigating physical and rheological properties of foamed bitumen*. Construction and Building Materials 72: 423-433. DOI:10.1016/j.conbuildmat.2014.09.024
- Mason, RL., Gunst, RF. & Hess JL. 2003. *Statistical Design and Analysis of Experiments, With Applications to Engineering and Science*. John Wiley & Sons, 2nd Edition.
- Morea, F., Marozzi, R. & Castaño, G. 2012. *Rheological properties of asphalt binders with chemical tensoactive additives used in Warm Mix Asphalts (WMAs)*. Construction and Building Materials 29: 135–141. DOI:10.1016/j.conbuildmat.2011.10.010
- Muthen, KM. 1999. *Foamed asphalt mixes. Mix design procedure*. Contract Report CR 98/077, Pretoria, South Africa: SABITA Ltd & CSIR Transportek.
- Perkins, SW. 2009. *Synthesis of warm mix asphalt paving strategies for use in Montana highway construction*. FHWA Report No. FHWA/MT-09-009/8117-38.
- Radziszewski, P., Kowalski, K., Król, J., Sarnowski, M. & Piłat, J. 2014. *Quality assessment of bituminous binders based on the viscoelastic properties: polish experience*. Journal of Civil Engineering and Management 1(20): 111–120. DOI:10.3846/13923730.2013.843586
- Radziszewski, P., Piłat, J., Król, J., Kowalski, K. & Sarnowski, M. 2011. *Verification of requirements and methods for assessing viscoelastic properties of domestic neat and modified bitumens*. Warsaw University of Technology, Poland.
- Remisova, E. 2004. *Theory and measurements of bitumen binders adhesion to aggregate*. Komunikacie, 6(1): 58–63.
- Silva, HMRD., Oliveira, JRM., Peralta, J. & Zoorob, SE. 2010. *Optimization of warm mix asphalt using different blends of binders and synthetic paraffin wax contents*. Construction and Building Materials 24(9): 1621–1631. DOI:10.1016/j.conbuildmat.2010.02.030
- Sybilski, D. & Mularczyk, R. 1999. *Properties of asphalt concrete with multigrade bitumen*. V International Conference Durable and safe road pavements, Kielce, Poland.
- Sybilski, D., Mularczyk, R., Pałys, M., Kaczycka, J. 2000. *First application in Poland of Multigrade bitumen*. VI International Conference “Durable and safe road pavements”, Kielce, Poland.
- Vaitkus, A. & Cygas, D. 2009. *Analysis and evaluation of possibilities for the use of warm mix asphalt in Lithuania*. The Baltic Journal of Road and Bridge Engineering 4(2): 80–86. DOI: 10.3846/1822-427X.2009.4.80-86
- Van De Ven, MFC., Jenkins, KJ., Voskuilen, JLM. & Van Den Beemt, R. 2007. *Development of (half-) warm foamed bitumen mixes: State of the art*. International Journal of Pavement Engineering 8(2): 163–175, 2007. DOI: 10.1080/10298430601149635
- Xiao, F., Punith, VS., Putman, B. & Amirkhanin, SN. 2011. *Utilization of foaming technology in warm-mix asphalt mixtures containing moist aggregates*. Journal Materials and Civil Engineering 23(9): 1328–37.
- Yu, X., Wang, Y. & Luo Y. 2013. *Impacts of water content on rheological properties and performance-related behaviours of foamed warm-mix asphalt*. Construction and Building Materials 48: 203–209. DOI:10.1016/j.conbuildmat.2013.06.018.

Double-edge-notched tension testing of asphalt cement for the control of cracking in flexible asphalt pavements

M. Paliukaite, M. Verigin & S.A.M. Hesp

Department of Chemistry, Queen's University, Kingston, Ontario, Canada

ABSTRACT: The Superpave™ asphalt cement specification as implemented in much of North America sets an upper limit on the loss modulus ($G^*\sin\delta$) in an attempt to control fatigue cracking. However, soon after its implementation, $G^*\sin\delta$ was found to be deficient in that it lacks the ability to accurately correlate with fatigue performance in service. This is likely because $G^*\sin\delta$ reflects energy dissipation due to both detrimental damage and beneficial viscous flow processes in the linear viscoelastic regime, with only the former contributing to fatigue cracking. Our hypothesis has been that, within limits, cracking distress is inversely proportional to tensile failure strain in a thin fiber of asphalt cement as estimated by the critical crack tip opening displacement (CTOD). This paper compares CTOD values for a set of straight and modified asphalt cements with various rheological parameters. Large ranking differences are found and this is thought to relate to the base asphalt cement as well as the amount and type of modifiers present.

1 INTRODUCTION

Fatigue cracking is one of the main processes through which flexible asphalt pavements fail. It can be particularly prevalent in thinly designed roads that have aged, those that are heavily loaded or overloaded, and northerly climates where thermal stresses aggravate traffic induced damage (Andriescu et al. 2004, 2006, Hesp et al. 2009a, b). Numerous research efforts, of which many started long ago, have been conducted to understand this type of failure and to find the most appropriate test method(s) to control asphalt pavement fatigue life (for instance, see Saal & Pell 1960, Pell 1962, Kandhal 1977).

At various times over the past century, failure testing to control cracking of all origins has focused on ductility and force-ductility (e.g., Saal 1955, Clark 1956, Doyle 1958, Halstead 1963, Hveem et al. 1963, Serafin 1963, Abson & Burton 1964, Vallerga & Halstead 1971, Anderson & Wiley 1976, Kandhal 1977, Van Gooswilligen et al. 1989, others) and, more recently, double-edge-notched tension (DENT) protocols (e.g., Andriescu et al. 2004, 2006, Andriescu & Hesp 2009) to measure asphalt cement properties such as strain tolerance, strength and failure energies.

Rheological investigations have considered combinations of complex stiffness and phase angle at specific frequencies and temperatures or the shape of the entire master curve (Reese and Goodrich 1993, Anderson and Kennedy 1993, Reese 1997, Rowe et al. 2014, others).

Damage investigations have considered the micro-cracking processes that precede catastrophic failure in

so called time sweep and, more recently, linear amplitude sweep tests (LAS) (e.g., Saal & Pell 1959, Pell 1962, Phillips 1998, Smith & Hesp 2000, others).

Despite these numerous research studies over many years, a consensus on what type of properties need to be specified for the control of fatigue cracking distress is still lacking. One of the main reasons for why it is difficult to correlate binder test results obtained in the laboratory with field fatigue data is that in the real world there are potentially a very significant number of confounding factors.

Asphalt binders are often tested under non-equilibrium conditions (Traxler 1936, 1937, Brown et al. 1957, Brown & Sparks 1958, Blokker & van Hoorn 1959, Struik 1978, Fryazinov et al. 1979, Pechenyi & Kutznetsov 1990, Bahia & Anderson 1991, Claudy et al. 1992, El Hussein et al. 1998, Soenen et al. 2004, Zhao & Hesp 2006, Hesp et al. 2007, Kriz 2009, Schmets et al. 2010, Togunde & Hesp 2012, Ahmed et al. 2012, Judycki 2014, Hesp et al. 2014, others). Most modified and appropriately aged asphalt binders are thermorheologically complex in their behavior due to phase transitions that occur (polymer phase separation, wax crystallization, asphaltene precipitation, others). Chemical hardening through oxidation and volatilization and physical hardening through structuring and shrinkage, are known to vary widely between different asphalt cements. Some inferior quality materials can lose their low and intermediate temperature grades due to such processes within only a few years of service while others can retain satisfactory performance for many years (Reese and Goodrich 1993, Hesp et al. 2009a, b, Erskine et al. 2012).

Further, thermal stresses can contribute very significantly to fatigue cracking but this fact is rarely considered in laboratory studies (El Hussein et al. 1998, Hesp et al. 2000, Croll 2009). At very low temperatures the differential thermal contraction causes interfacial failure. The microcracks at the coarse aggregate interface allow water to enter the pavement surface, which upon freezing facilitates the start of fatigue distress.

Another reason for why there have been conflicting results is that some proposed test methods confound different damage mechanisms, such as interfacial failure in between parallel plates in a dynamic shear rheometer, microcracking, yielding, edge fracture (LAS test), or do their analyses under ill-defined shear rate regimes, such as in between parallel plates (LAS test), or within torsional cylinder flow rather than plane shear (4 mm parallel plate DSR test).

Add to the above the facts that design and construction practices and workmanship can vary widely and it is not difficult to understand why progress on the implementation of an effective fatigue grading test and associated acceptance criteria has been slow.

The authors are of the opinion that fatigue cracking in asphalt pavements is primarily dependent on the amount by which the thin asphalt cement fibers that bridge the coarse aggregate particles can stretch before they break. Thick pavements are less susceptible to fatigue because they deflect less compared to thin pavements. Old pavements crack more because oxidized binders are unable to stretch by much before failing. Asphalt binders that are modified with waxes, acids, bases, air blown residues, recycled asphalt-derived binder and other gelling additives, suffer from low strain tolerance and are therefore more prone to fatigue cracking. Binders at lower temperatures are stiffer and less strain tolerant and hence fatigue is more of a problem just around the freeze-thaw regime.

The objective of this study was to compare an approximate critical crack tip opening displacement as measured in the double-edge-notched tension test with a range of other properties that have been proposed for the control of fatigue distress. The loss modulus ($G^* \sin \delta$), the Glover-Rowe parameter ($G^* ((\cos \delta)^2 / \sin \delta)$), and the crossover temperature are compared with a limiting CTOD temperature for a range of straight and polymer modified asphalt cements. The CTOD is a failure mechanics property that reflects the strain tolerance of a very thin fiber of material in the ductile state under high constraint (such as in between two coarse aggregate particles). Hence, it provides a reasonable measure of the ability of a pavement to stretch before failure occurs, and as such the amount of cracking distress should be inversely proportional to CTOD.

2 BACKGROUND

2.1 Ductility methods

Kandhal (1977) provides a comprehensive background discussion on the low temperature ductility

of asphalt binders and shows how it relates to cracking performance of pavements around the United States. He confirmed that binders with low ductility at 4 and 15.6°C are likely to demonstrate poor pavement performance. Limits on ductility were proposed at 15.6°C (60°F) to predict loss of fines, raveling, thermal cracking and widespread cracking. When ductility fell below 10 cm due to age hardening, the loss of fines would be the first sign of distress. Below 8 cm, the road would start to ravel (coarse aggregate loss). Finally, below 5 cm, pavements started to crack, and below 3 cm the distress would be severe and surface conditions would be considered very poor. Kandhal's (1977) findings largely confirmed earlier studies that found similar limits on ductility relating to various types of distress (Clark 1956, Doyle 1958, Halstead 1963, Hveem et al. 1963, Serafin 1963, Abson & Burton 1964, and Vallerga & Halstead 1971). The author concludes that "Due to its empirical nature, it is not clearly understood what fundamental property is being measured by the ductility test. However, it is a desirable value indicating pavement performance."

Researchers at the Koninklijke/Shell Research Laboratory in Amsterdam included a low temperature ductility test on the asphalt cement in their Qualagon approach to asphalt binder grading (Van Gooswilligen et al. 1989). Their test temperature was adjusted according to the binder grade and the results obtained were found to be in line with the degree of binder homogeneity. Binders that suffer from low temperature phase separation (paraffinic demixing) were found to be particularly poor performers in the ductility test and in a number of other tests related to aging susceptibility (durability). The Shell researchers concluded that the low temperature ductility test was useful to discriminate binders that are of satisfactory quality from those that have "insufficient binding performance" (Van Gooswilligen et al. 1989).

2.2 Rheological methods

The Strategic Highway Research Program selected the binder loss modulus ($G^* \sin \delta$) for the control of fatigue cracking. It was argued that the energy dissipation during dynamic loading is reflective of the amount of damage sustained and that therefore it should represent fatigue life. It was further argued that typical ductility values are not realistic measures of how failure occurs during pavement cracking. While $G^* \sin \delta$ does show some correlation with fatigue performance, it is far from perfect (Andriescu et al. 2006, Gibson et al. 2012, Rowe et al. 2014, others). The fact that $G^* \sin \delta$ fails to accurately predict fatigue cracking is likely due to several factors. First, the loss modulus relates to the energy loss in sinusoidal loading and as such it reflects both energy dissipation due to detrimental damage and beneficial viscous flow mechanisms. Second, the loss modulus, similar to other rheological properties, is measured in the linear viscoelastic regime at very low strains. Fatigue cracking in a pavement is a high strain phenomenon and therefore a failure test would likely

be more appropriate. Reactive compressive stresses will favor asphalt cements that can stretch more rather than less before failing. Soon after the implementation of the Superpave specifications in the 1990s, it was shown by a number of research groups that $G^* \sin \delta$ fails to accurately correlate with fatigue in laboratory and full-scale accelerated loading tests (Andriescu 2006).

More recently, Glover et al. (2005) used a simple Maxwell model to derive a surrogate parameter for ductility, $G' / (\eta' / G')$, as they were motivated by the large number of reports discussed above that have demonstrated a good correlation between low temperature ductility and pavement cracking performance. The correlation between $G' / (\eta' / G')$ and ductility appeared to be very good below 10 cm for straight asphalt cements but no universal correlation was found for modified binders.

Rowe (2011) has shown that the above relationship can be expressed in a simplified form, $G^* ((\cos \delta)^2 / \sin \delta)$, casting it in a format with which most asphalt researchers are familiar through Superpave specifications. Rowe et al. (2014) was able to show that the above parameter is able to do better than $G^* \sin \delta$ in explaining premature raveling on airport runways in the Northeastern United States.

A question that remains to be answered though is whether a low strain rheological property can do better than high strain failure properties such as ductility or CTOD for all binders, including those that are polymer modified. Hence, the research discussed herein was started to investigate differences for a set of asphalt cements that are being evaluated in several Australian spray sealing trials (Choi and Urquhart 2014).

2.3 Double-edge-notched tension testing

The essential work of failure testing approach was first developed in Australia by researchers studying ductile failure in a variety of materials (Cotterell and Reddel 1977), and later extensively applied to polymers (Mai et al. 2000). The aim was to develop a simple test method, based on ideas first expressed by Broberg (1968), to determine the essential work of failure for thin specimens. The essential work reflects the energy used to separate two failure surfaces, separate from the plastic or non-essential work dissipated in areas away from the failure zone.

The essential work is identical to the J-integral for ductile failure (Mai and Cotterell 1986, Paton and Hashemi 1992, Chan and Williams 1994, Mai et al. 2000, others). J-integral values were inaccessible for thin specimens prior to the development of the essential work of failure analysis due to experimental difficulties (Andriescu 2006). Critical crack tip opening displacements were originally used to measure essential works of failure since the two are related in a simple manner as follows:

$$w_e = \text{CTOD} \times \sigma_{ty} \quad (1)$$

where w_e = the specific essential work required to separate two surfaces (J/m^2); CTOD = the critical crack

tip opening displacement (m); and σ_{ty} = the tensile yield stress (N/m^2).

However, Cotterell and Reddel (1977) had the ingenious insight to separate the essential from the non-essential work terms in a simple manner:

$$W_t = W_e + W_p \quad (2)$$

where W_t = the area under the force displacement curve (J); W_e = the total work required for the separation of the two surfaces; and W_p = the total work dissipated away from the failure zone.

Realizing that the essential term scales with the cross sectional area (LB), the plastic or non-essential term scales with a volume surrounding the ligament ($\beta L^2 B$), and that the plastic work vanishes for very small ligaments, Equation 2 can be rewritten in specific terms as follows:

$$W_t = W_e + W_p = LB \times w_e + \beta L^2 B \times w_p \quad (3)$$

$$w_t = W_t / LB = w_e + \beta w_p L \quad (4)$$

where w_t = the specific total work of failure (J/m^2); w_e = the specific essential work of failure (J/m^2); β = a factor that accounts for the shape of the plastic zone around the failure area; w_p = the specific plastic work of failure (J/m^3); L = the ligament length (distance between notches in DENT specimen) (m); and B = the specimen thickness (m).

Equation 4 shows that when the specific total work of failure is plotted versus L , a straight line is obtained with an intercept equal to the essential work of failure, w_e , and a slope equal to the plastic work term, βw_p . The β factor is equal to $\pi/4$ if the plastic zone is cylindrically shaped but different for diamond and ellipsoidal shapes (Andriescu 2006).

Equations 1 and 4 also provide the mechanistic basis for the application of CTOD in a performance-based asphalt cement specification. In an asphalt binder test, such as ductility or force-ductility, the plastic work can be very substantial, whereas in the mixture failure is highly localized and the essential work is therefore likely more important. We have chosen CTOD as the main property for acceptance since it is directly related to the essential work and it provides a measure of strain tolerance in the ductile state under high levels of constraint. As such, CTOD provides a measure of how much a thin binder fiber can stretch before it fails and should therefore be inversely proportional to the amount of distress. We consider the DENT CTOD an improved measure of ductility but of course the validation of that hypothesis requires extensive testing of asphalt cements from laboratory and field experiments.

Andriescu et al. (2004, 2006, 2009) has shown that the essential work of failure analysis is highly applicable to asphalt cement testing and that all conditions are valid to determine essential works of failure from tests on DENT specimens with various ligament lengths

between 5 and 25 mm. The essential work so determined is divided by the average net section stress in the specimen with the smallest ligament to calculate an approximate CTOD:

$$CTOD = w_e / \sigma_{nt,5 \text{ mm}} \quad (5)$$

where $\sigma_{nt,5mm}$ = the average net section peak stress for duplicate measurements with the 5 mm ligament specimen (N/m²).

This approximation was made for convenience in that it forgoes the need to do an additional test to measure the tensile yield stress in a dog bone shaped specimen. The validity of this has recently been discussed by Hesp et al. (2014).

The CTOD measurement has the advantage that it is a time-tested mechanistic property in failure mechanics used to design structures and materials against ductile failure. However, it still depends on appropriately conditioned samples from a laboratory aging protocol. It also depends on whether samples are cooled for sufficient periods of time prior to testing. However, with sufficient care, we believe that the application of CTOD for acceptance of asphalt cement can improve pavement quality over the current situation. For further background information and validation the reader is referred to Andriescu et al. (2004, 2006, 2009), Gibson et al. (2014), Hesp et al. (2009a, b, 2014).

3 EXPERIMENTAL

3.1 Materials

The materials used for this research were kindly provided by the Australian Road Research Board laboratories in Melbourne, Australia. The 8 samples have been used in two different spray sealing pavement trails in Australia that are currently being followed for performance (Choi and Urquhart 2014). Table 1 provides some pertinent information.

3.2 Procedures

Unaged asphalt cements were tested in a TA Instruments AR2000ex rheometer at 0.5–1.0% strain to determine their rheological properties such as complex modulus and phase angle.

The asphalt cements were also aged in the laboratory in a pressure aging vessel for a total of 72 hours each. A total of 15 g of asphalt cement was used in each pan and 12 of these were aged at once in order to produce enough material for further DSR and DENT testing. The aging temperature was kept constant at 100°C. These aging conditions were previously determined to produce materials with similar consistency to those obtained from existing Australian durability protocols (Choi and Urquhart 2014).

Aged asphalt cements were tested in the rheometer to determine the Superpave loss modulus, Glover-Rowe parameters and crossover temperatures for each

Table 1. Asphalt cements investigated.

Sample	Additive	HTPG	ITPG
A1	Straight	66.4	31.0
A2	Proprietary	66.4	24.8
A3	SBS	71.7	23.9
A4	Straight	64.9	26.8
A5	SBS	73.4	27.8
A6	SBS*	75.9	25.6
A7	SBS	78.5	27.8
A8	PBD	67.4	21.0

Note: Polymer contents ranged from 3–5% by weight of the asphalt cements. HTPG is the high temperature Superpave grade for the unaged asphalt cement. ITPG is the intermediate temperature Superpave grade for the 72 hour PAV-aged asphalt cement. Grades were determined according to AASHTO R29 (2010) protocols. SBS = styrene-butadiene-styrene copolymer. PBD = polybutadiene. *Sample A6 was a hybrid with both SBS and an unknown co-additive.

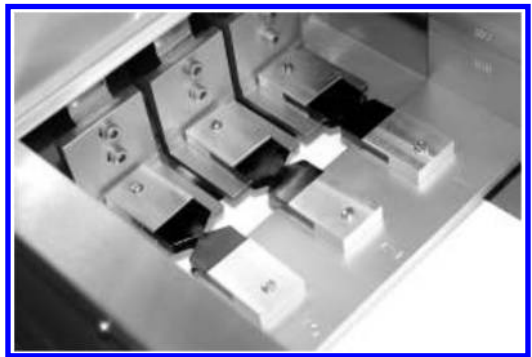


Figure 1. Double-edge-notched tension test specimens with 5, 10 and 15 mm ligaments just prior to testing. Note: The water was left out of the bath for image clarity.

PAV residue. Temperature sweeps between 35 and 5°C, at strains of 0.1%, were used for all experiments. Superpave loss moduli and crossover temperatures were determined at frequencies of 0.1 to 10 rad/s whereas the Glover-Rowe parameters were determined at 0.005 rad/s in a separate test.

The PAV residues were also tested in the double-edge-notched tension test according to the Ontario Ministry of Transportation laboratory standard LS-299 *Method of Test for Asphalt Cement's Resistance to Fatigue Fracture Using Double-Edge-Notched Tension Test (DENT)* (2007). In brief, samples were poured in silicone molds with aluminum end pieces for shear transfer of the force during the test. Notch depths varied to provide ligaments of 5, 10 and 15 mm. Sample thickness was kept constant at 10 mm. The samples were conditioned for 3 hours prior to testing in the water bath. Testing was done at a constant speed of 50 mm/min and temperatures ranging from 5 to 35°C. An image of three specimens prior to a test is provided in Figure 1.

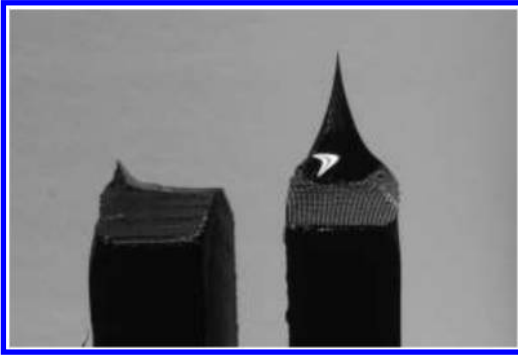


Figure 2. Images of samples that failed in the brittle-to-ductile transition zone (left) and ductile zone (right).



Figure 3. Images of polymer modified samples that failed through tearing.

The majority of the tests were conducted in the ductile state although on occasions it was possible to find samples that failed within the brittle-to-ductile transition zone with very low CTOD values. Figure 2 provides images of a brittle-to-ductile failure on the left and an entirely ductile failure on the right. Figure 3 provides images of some polymer modified samples that failed through what can best be described as a sudden tearing process at the end of stretching.

4 RESULTS AND DISCUSSION

Examples of typical raw data for two DENT tests are provided in Figure 4. The data processed according to Equation 4 are provided in Figure 5.

The replicate measurements show that the test is generally highly reproducible. Round robin evaluations conducted by the Ontario Ministry of Transportation, with 17 laboratories participating, have shown the coefficient of variation for the approximate CTOD obtained by this method to fall in the 10–15% range, which is as good as it gets for a failure test on a PAV residue (MTO 2014). Differences in CTOD between samples of equal Superpave grade but different modification technology can reach as high as several fold

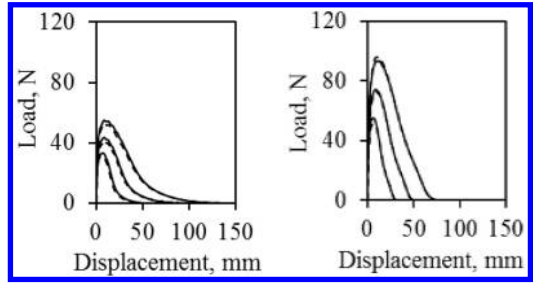


Figure 4. Representative force-displacement curves for two sets of DENT tests at 25°C (A2 (left) and A7 (right)). Dashed lines show replicate force-displacement curves.

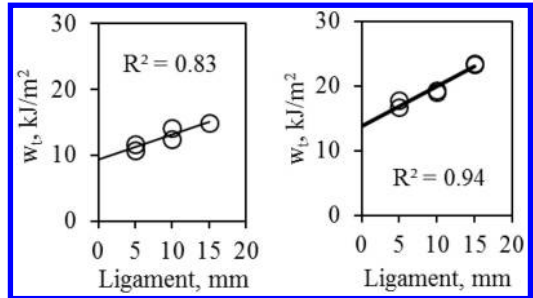


Figure 5. Linear regressions of total specific works of failure versus ligament lengths according to Equation 4 (A2 CTOD = 14.6 mm (left), A7 CTOD = 14.3 mm (right)).

(i.e., several hundred percent), suggesting that the testing error should be of little concern.

The individual traces for the three ligament length specimens look self-similar, indicating that the specimens go through the same sequence of events which is a crucial requirement to assure that the essential work of failure analysis is valid. Stretching, yielding, necking and/or tearing are the four possible mechanisms during failure.

A summary of all DENT and rheological results is provided in Table 2 where limiting temperatures are rounded to the nearest degree. Instead of the 5 MPa loss modulus temperature from the AASHTO M320 specification, the table lists the temperatures where $G^* \sin \delta$ reaches 10 MPa in order to bring the limits more in line with those obtained for the other parameters. While there appears to be some correlation between all parameters, a more close examination of the temperatures shows that there are also significant differences.

Difference between the Glover-Rowe limiting raveling and cracking temperatures seem to be only 2–4°C suggesting that a separation of the two is unnecessary.

The limiting $G^* \sin \delta$ temperatures for A4, A5 and A7 are 21°C while their limiting CTOD temperatures range from 17 to 25°C, which should lead to significant performance differences in service.

The data from Table 2 were obtained on residues that were aged for 72 hours at 100°C in the pressure aging vessel at 2.1 MPa. Since raveling and cracking

Table 2. Limiting temperatures for PAV residues.

Sample	$G^* \sin \delta$			CTOD mm	$T(G' = G'')$	
	10 MPa	180 kPa	450 kPa		0.1 rad/s	10 rad/s
A1	24	20	18	25	19	33
A2	19	16	13	16	12	26
A3	17	19	15	16	15	30
A4	21	17	14	19	12	26
A5	21	23	19	25	23	37
A6	19	21	18	19	20	35
A7	21	19	15	18	18	31
A8	15	15	11	16	13	27

Note: $T(G' = G'')$ = temperatures at which the loss modulus equals storage modulus or phase angle reaches 45° . The Glover-Rowe parameter $G^*((\cos \delta)^2 / \sin \delta)$ limit of 180 kPa is for the onset of raveling whereas at 450 kPa the pavement is expected to suffer from severe thermal cracking.

Table 3. Comparison between unaged and PAV-aged properties.

Sample	$T(\text{CTOD} = 10), 50 \text{ mm/min}$		$T(G' = G''), 10 \text{ rad/s}$	
	Unaged	PAV	Unaged	PAV
A1	6	25	9	33
A2	3	16	7	26
A3	5	16	3	30
A4	3	19	6	26
A5	5	25	4	37
A6	5	19	6	35
A7	9	18	9	31
A8	5	16	2	27

Note: $T(G' = G'')$ = temperatures at which loss modulus equals storage modulus or phase angle reaches 45° .

are cumulative forms of distress, properties of lesser aged residues should also be of importance. Table 3 provides a comparison between selected unaged and PAV-aged binder properties. This comparison shows that very substantial changes in performance are possible, stressing the need to assess performance-based properties at several levels of aging, since quality is obviously of little use if durability is lacking.

5 SUMMARY AND CONCLUSIONS

Given the results presented, the following summary and conclusions are offered:

- The asphalt cement loss modulus $G^* \sin \delta$ does not appear to correlate well with fatigue cracking in service. This is likely due to the fact that it reflects both damage and viscous flow mechanisms and that it is measured in the low strain, linear viscoelastic regime.

- The Glover-Rowe parameter $G^*((\cos \delta)^2 / \sin \delta)$ correlates well with ductility for unmodified asphalt cements of various oxidation levels. However, there appears to be no universal correlation when modified binders are included.
- The essential work of failure analysis provides an accurate way to measure ductile strain tolerance in the presence of severe constraint as in between two coarse aggregate particles.
- Different rankings for the fatigue grading of asphalt cements are obtained according to the CTOD compared to rheological properties such as loss modulus or Glover-Rowe parameter.
- Approximate CTOD values are in the 5–10 mm range before DENT specimens start to fail in a brittle fashion.
- The degree to which asphalt cements age in service appears to have an overriding influence on how the materials perform in terms of fatigue cracking. Hence, refinement of the pressure aging vessel protocol to better replicate aging in service would be a worthwhile endeavor.
- Assessment of durability by testing after various conditioning times in the PAV would allow for a better control of pavement cracking.

ACKNOWLEDGEMENTS

Special thanks goes out to Dr. Yong Choi of the Australian Road Research Board for providing the asphalt cement samples used for this study. Further, the Ontario Ministry of Transportation is gratefully acknowledged for financial support towards this research.

REFERENCES

- Abson, G. & Burton, C. 1964. In Bituminous Materials: Asphalts, Tars and Pitches. A.J. Hoiberg, Ed., Interscience Publishers, New York, Vol. 1, Chapter 5, 213–288.
- Ahmed, E.I., Hesp, S.A.M., Paul Samy, S.K., Rubab, S.D. & Warburton, G. 2012. Effect of warm mix additives and dispersants on asphalt rheological, aging, and failure properties. *Construction and Building Materials* 37: 493–498.
- Anderson, D.I. & Wiley, M.L. 1976. Force ductility – an asphalt performance indicator. *Proceedings, Association of Asphalt Paving Technologists* 45: 25–41.
- Anderson, D.A. & Kennedy, T.W. 1993. Development of SHRP binder specification. *Journal of the Association of Asphalt Paving Technologists* 62: 481–507.
- Andriescu, A., Hesp, S.A.M. & Youtcheff, J. S. 2004. Essential and plastic works of ductile fracture in asphalt binders. *Transportation Research Record: Journal of the Transportation Research Board* 1875(1): 1–7.
- Andriescu, A. 2006. *Essential Work of Fracture Approach to Fatigue Grading of Asphalt Binders*. Doctoral Dissertation, Queen's University, Kingston, Canada.
- Andriescu, A. & Hesp, S.A.M. 2009. Time-temperature superposition in rheology and ductile failure of asphalt binders. *International Journal of Pavement Engineering* 10(4): 229–240.

- Bahia, H.U. & Anderson, D.A. 1991. Isothermal low-temperature physical hardening of asphalt. *Proceedings, International Symposium, Chemistry of Bitumens 1*: 114–147, Rome, Italy.
- Blokker, P.C. & Van Hoorn, H. 1959. Durability of bitumen in theory and practice. *Proc. Fifth World Petroleum Congress*, Section VI, Paper 27: 417–432, New York, June 1–5.
- Broberg, K.B. 1968. Critical review of some theories in fracture mechanics. *International Journal of Fracture* 4: 11–19.
- Brown, A.B., Sparks, J.W. & Smith, F.M. 1957. Steric hardening of asphalts. *Proceedings, Association of Asphalt Paving Technologists* 26: 486–494.
- Brown, A.B. & Sparks, J.W. 1958. Viscoelastic properties of a penetration grade paving asphalt at winter temperatures. *Proceedings, Association of Asphalt Paving Technologists* 27: 35–51.
- Chan, W.Y.F. & Williams, J.G. 1994. Determination of the fracture toughness of polymeric films by the essential work method. *Polymer* 35(8): 1666–1672.
- Choi, Y. & Urquhart, R. 2014. *Post-ageing characterization of sprayed sealing binders. A laboratory study*. Austroads Technical Report AP-T270-14, Sydney, Australia.
- Clark, R.G. 1956. Asphalt Volatility and Weathering Tests. *Proceedings, Association of Asphalt Paving Technologists* 25: 417–431.
- Claudy, P., Letoffe, J., Rondelez, F., Germanaud, L., King, G. & Planche, J.-P. 1992. A new interpretation of time-dependent physical hardening in asphalt based on DSC and optical thermoanalysis. *Preprint Paper, American Chemical Society, Division of Fuel Chemistry* 37: 1408–1426.
- Cotterell, B. & Reddel, K. 1977. The essential work of plane stress ductile fracture. *International Journal of Fracture* 13(3): 267–277.
- Croll, J.G.A. 2009. Possible role of thermal ratcheting in alligator cracking of asphalt pavements. *International Journal of Pavement Engineering* 10(6): 447–453.
- Doyle, P.C. 1958. Cracking characteristics of asphalt cement. *Proceedings, Association of Asphalt Paving Technologists* 27: 581–597.
- El Hussein, H.M., Kim, K.W. & Ponniah, J. 1998. Asphalt concrete damage associated with extreme low temperatures. *Journal of Materials in Civil Engineering* 10(4): 269–274.
- Erskine, J., Hesp, S.A.M. & Kaveh, F. 2012. Another look at accelerated aging of asphalt cements in the pressure aging vessel. *Proceedings, Fifth Eurasphalt and Eurobitumen Congress*, Istanbul, Turkey, June 13–15.
- Fryazimov, V.V., Pechenyi, B.G. & Akhmetova, L.A. 1979. Interrelation of density, composition, and properties of asphalts. Translated from *Khimiya I Tekhnologiya Topliv I Masel* 9: 41–44.
- Gibson, N., Qi, X., Shenoy, A., Al-Khateeb, G., Kutay, M.E., Andriescu, A., Stuart, K., Youtcheff J.S. & Harman, T. 2012. *Performance Testing for Superpave and Structural Validation*. Report No. FHWA-HRT-11-045, Federal Highway Administration, U.S. Department of Transportation.
- Glover, C.J., Richard, R., Davison, R.R., Domke, C.H., Ruan, Y., Juristyarini, P., Knorr, D.B. & Jung, S. H. 2005. *Developing of a New Method for Assessing Asphalt Binder Durability with Field Validation*. Report No. FHWA/TX-05/1872-2. Texas Transportation Institute, Texas A&M University.
- Halstead, W.J. 1963. The relation of asphalt ductility to pavement performance. *Proceedings, Association of Asphalt Paving Technologists* 32: 247–270.
- Hesp, S.A.M., Terlouw, T. & Vonk, W.C. 2000. Low-temperature performance of SBS-modified asphalt. *Journal of the Association of Asphalt Paving Technologists* 69: 540–573.
- Hesp, S.A.M., Iliuta, S. & Shirokoff, J.W. 2007. Reversible aging in asphalt binders. *Energy & Fuels* 21(2): 1112–1121.
- Hesp, S.A.M., Genin, S.N., Scafe, D., Shurvell, H.F. & Subramani, S. 2009a. Five year performance review of a northern Ontario pavement trial. *Proceedings, Canadian Technical Asphalt Association* 54: 99–126.
- Hesp, S.A.M., Soleimani, A., Subramani, S., Marks, P., Philips, T., Smith, D. & Tam, K.K. 2009b. Asphalt pavement cracking: Analysis of extraordinary life cycle variability in Eastern and Northeastern Ontario. *International Journal of Pavement Engineering* 10(3): 209–227.
- Hesp, S.A.M., Johnson, K.A.N. & Andriescu, A. 2014. Double-edge-notched tension testing for the fatigue grading of straight and modified asphalt binders. *International Journal of Pavements* (In Press).
- Hveem, F.N., Zube, E. & Skok, J. 1963. Proposed new tests and specifications for paving grade asphalts. *Proceedings, Association of Asphalt Paving Technologists* 32: 271–327.
- Judycki, J. 2014. Influence of low-temperature physical hardening on stiffness and tensile strength of asphalt concrete and stone mastic asphalt. *Construction and Building Materials* 61: 191–199.
- Kandhal, P.S. 1977. Low temperature ductility of asphalt in relation to pavement performance. *American Society for Testing and Materials. Special Technical Publication* 628: 95–106.
- Kriz, P. 2009. *Glass Transition and Physical Hardening of Asphalt*. Doctoral Thesis, Department of Civil Engineering, University of Calgary, Calgary, Alberta, Canada.
- Mai, Y.-W., Wong, S.-C. & Chen, X.-H. 2000. Application of fracture mechanics for characterization of toughness of polymer blends. In: *Polymer Blends, Volume 2: Performance*. D.R. Paul & C.B. Bucknall, Eds., Wiley and Sons.
- Mai, Y.W. & Cotterell, B. 1986. On the essential work of ductile fracture in polymers. *International Journal of Fracture* 32, 105–125.
- Ministry of Transportation of Ontario, *LS-299 – Method of Test for Asphalt Cement’s Resistance to Fatigue Fracture Using Double-Edge-Notched Tension Test (DENT)*. Revision 23 to MTO Laboratory Testing Manual, 2007.
- Ministry of Transportation of Ontario. Round robin results for asphalt cement grading tests, 2014.
- Paton, C.A. & Hashemi, S. 1992. Plane-stress essential work of ductile fracture for polycarbonate. *Journal of Materials Science* 27: 2279–2290.
- Pechenyi, B.G. & Kuznetsov, O.I. 1990. Formation of equilibrium structures in bitumens. Translated from *Khimiya I Tekhnologiya Topliv I Masel* 7: 32–34.
- Pell, P.S. 1962. Fatigue characteristics of bitumen and bituminous mixes. *Proceedings, International Conference on Structural Design of Asphalt Pavements*, Ann Arbor.
- Phillips, M.C. 1998. Multi-step models for fatigue and healing, and binder properties involved in healing. *Proceedings, Eurobitume Workshop on Performance Related Properties for Bituminous Binders*, Luxembourg, Paper No. 115.
- Reese, R. & Goodrich, J.E. 1993. California Desert Test Road-A Step Closer to Performance Based Specifications.

- Journal of the Association of Asphalt Paving Technologists* 62: 247–313.
- Reese, R. 1997. Properties of aged asphalt binder related to asphalt concrete fatigue life. *Journal of the Association of Asphalt Paving Technologists* 66: 604–632.
- Rowe, G.M. 2011. Prepared discussion. *Journal of the Association of Asphalt Paving Technologists* 80: 649–662.
- Rowe, G.M., King, G. & Anderson, M. 2014. The influence of binder rheology on the cracking of asphalt mixes in airport and highway projects. *Journal of Testing and Evaluation* 42(5): 1–10.
- Saal, R.N.J. 1955. A study of the significance of the ductility test for bitumen. *Journal of Applied Chemistry* 5: 663–675.
- Saal, R.N.J. & Pell, P.S. 1960. Fatigue of bituminous road mixes. *Kolloid-Zeitschrift* 171(1): 61–71.
- Serafin, P.J. 1963. *Proceedings, Association of Asphalt Paving Technologists* 32: 341.
- Schmets, A., Kringos, N., Pauli, T., Redelius, P. & Scarpas, T. 2010. On the existence of wax-induced phase separation in bitumen. *International Journal of Pavement Engineering* 11(6): 555–563.
- Smith, B.J. & Hesp, S.A.M. 2000. Crack pinning in asphalt mastics and concrete: regular fatigue studies. *Transportation Research Record: Journal of the Transportation Research Board* 1728: 75–81
- Soenen, H., Ekblad, J., Lu, X. & Redelius, P. 2004. Isothermal hardening in bitumen and in asphalt mix. *Proceedings, Third Eurobitumen and Euraspalt Congress, Vienna, Paper 135*: 1–10.
- Struik, L.C.E. 1978. *Physical Aging in Amorphous Polymers and Other Materials*. Elsevier Scientific Publishing Company, Amsterdam, The Netherlands.
- Togunde, P. & Hesp, S. 2012. Physical hardening in asphalt mixtures. *International Journal of Pavement Research and Technology* 5(1): 46–53.
- Traxler R.N. & Schwyer H.E. 1936. Increase in viscosity of asphalts with time. *Proc. Thirty-Ninth Annual Meeting, American Society for Testing Materials* 36(II): 544–550, Atlantic City, New Jersey, United States.
- Traxler, R.N. & Coombs, C.E. 1937. Development of internal structure in asphalts with time. *Proc. Thirty-Ninth Annual Meeting, American Society for Testing Materials*, 37(II): 549–555, New York, United States.
- Vallerga, B.A. & Halstead, W.J. 1971. Effect of field aging on fundamental properties of paving asphalts. *Highway Research Record* 361: 71–92.
- Van Gooswilligen, G., de Bats, F.Th. & Harrison, T. 1989. Quality of paving grade bitumen – a practical approach in terms of functional tests. *Proceedings, Fourth Eurobitume Symposium* 290–297.
- Zhao, M.O. & Hesp, S.A.M. 2006. Performance grading of the Lamont, Alberta C-SHRP pavement trial binders. *International Journal of Pavement Engineering* 7(3): 199–211.

Viscoelastic continuum damage analysis of polymer modified asphalt in the cyclic semi-circular bending test

I.M. Lancaster & H.A. Khalid

University of Liverpool, Brodie Tower (Civil), Liverpool, UK

ABSTRACT: Notched semi-circular asphalt specimens were tested under cyclic loading at a range of applied loading levels and the damage growth modelled using the viscoelastic continuum damage theory (VECD). It was found that, as predicted by the theory, for each asphalt mixture, the pseudo-stiffness (C) versus damage (S) curves could be superimposed to form one unique curve. Both polymer modified and penetration grade bitumens were analysed in this study, and the effect of the level of polymer modification on the C versus S curves investigated. From these curves, the number of cycles to failure was predicted, and the improved damage resistance of the mixture due to increasing level of polymer in the binders demonstrated.

1 INTRODUCTION

Annual worldwide production of hot mix asphalt is approximately 1.5 billion tonnes, with Europe contributing around 300 million (EAPA 2014). Polymer modified bitumens are frequently used to enhance the performance of the asphalt pavement by improving the deformation and crack resistance. The fatigue performance of the pavement may also be improved by the addition of polymers. However, fully characterising the fatigue behaviour using the standard tests can be very time consuming.

The viscoelastic continuum damage (VECD) theory has developed over the past 30 years and has been applied to asphalt. When VECD is applied to the fatigue damage of asphalt it can significantly reduce the time required evaluating the material's fatigue performance.

In this paper the cyclic loading of a notched semi-circular bending specimen will be analysed using VECD, and the effect of polymer modification explored.

2 BACKGROUND AND THEORY

2.1 *Cyclic Semi-circular bending test*

The Semi-Circular Bending (SCB) geometry has proven to be particularly useful in areas where coring of specimens is common such as glaciology (Adamson et al. 1997), geology (Chang et al. 2002), and pavement analysis (Molenaar et al. 2002). For asphalt the geometry is particularly suitable for laboratory investigations as the standard asphalt compaction devices produce cylindrical specimens requiring minimal sawing before use in the SCB test. The notched SCB, as

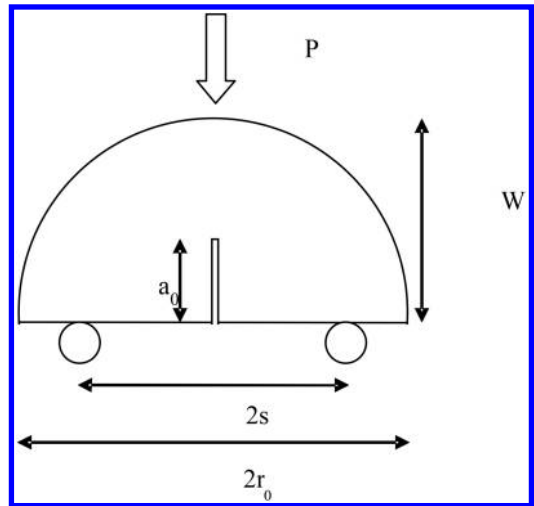


Figure 1. Schematic of the SCB geometry, where a_0 = notch depth; W = sample height; s = support span; r_0 = sample radius; P = applied load

shown in Figure 1, has been utilised by a number of authors to analyse the fracture and fatigue properties of asphalt (Hofman et al. 2003, Mohammad et al. 2004, Hassan & Khalid 2010, Huang et al. 2013, Abdo et al. 2013, Barman et al. 2014).

Huang et al. (2009) analysed the SCB geometry using finite element analysis and showed that the stiffness modulus, E , is

$$E = 1.977(e^{1.175s/r_0} - 1) \frac{P}{d} \quad (1)$$

where d is the vertical deflection at the middle point of the lower surface of the specimen.

For a specimen of thickness b , the horizontal stress σ_{hor} was also shown to be,

$$\sigma_{hor} = \frac{3Ps^2}{bd^2} \quad (2)$$

2.2 Viscoelastic Continuum Damage

Shapery (1984) developed the work potential theory and correspondence principles that form the basis of the VECD approach. Kim et al. (1997) applied this method to the fatigue analysis of asphalt, and was developed further by Kutay et al. (2008).

The time and temperature dependency of asphalt leads to its analysis being far from straightforward. Pseudovariables for stress and strain allow the time dependent viscoelastic problem to be simplified to a linearly elastic problem which is considerably easier to analyse. Damage within the material is then characterised by internal state variables. The stress may therefore be expressed as

$$\sigma = C\varepsilon^R \quad (3)$$

where σ = stress; C is the pseudostiffness; ε^R is the pseudostrain.

In the special case of cyclic testing with constant frequency

$$\varepsilon_N^R = |E^*|_{LVE} \varepsilon_0^N \quad (4)$$

where $|E^*|_{LVE}$ is the linear viscoelastic dynamic modulus of the undamaged material; ε_0^N is the peak strain in the N th cycle.

These equations may be combined and the pseudostiffness shown to be

$$C = \frac{\sigma_0^N}{|E^*|_{LVE} \varepsilon_0^N} = \frac{|E^*|_N}{|E^*|_{LVE}} \quad (5)$$

where $|E^*|_N$ is the dynamic modulus at the N th cycle

It is assumed that a single parameter for damage S can be used as the internal state variable. It is further assumed that the pseudostiffness is a function of that parameter and can therefore be written as $C(S)$, and that the damage evolution can be shown to be

$$S_{N+\Delta N} = S_N + \left(\frac{\Delta N}{f}\right)^{\frac{1}{1+\alpha}} \left(-\frac{I_0 R^2}{2} (C_{N+\Delta N} - C_N)\right)^{\frac{\alpha}{1+\alpha}} \quad (6)$$

where α is a material constant related to the rate of damage growth; I_0 is an initial stiffness parameter (assumed as equal to $|E^*|_{N=1}/|E^*|_{LVE}$); f is the test frequency.

For a stress controlled test where the fracture stress and the material's fracture energy are constant it is suggested that $\alpha = 1/m$ is the most appropriate relationship. The parameter m is slope of the log of the relaxation modulus versus log time.

Table 1. Binder formulations and empirical properties.

	I	II	III	IV
Polymer content	0	2.5	5	7.5
Needle penetration (25°C, 100 g, 5 s load) dmm	61	46	42	31
Softening Point °C	50.4	56.4	84.0	93.0
After RTFOT at 163°C				
Needle penetration (25°C, 100g, 5 s load) dmm	39	30	32	26
Softening Point °C	54.6	66.2	75.1	81
Change in mass %	-0.38	-0.36	-0.30	-0.28

3 MATERIALS AND SAMPLE PRODUCTION

3.1 Binders

A 50/70 penetration grade bitumen refined from a Venezuelan crude was used in this study, and designated as binder I. This was modified using a linear styrene-butadiene-styrene (SBS) copolymer at 2.5% weight for weight increments up to a total of 7.5% weight for weight, and these designated as binders II, III and IV. The modified binders were produced using a laboratory high shear mixer at 180°C, each with two hours of high shear mixing at 6000 rpm. The empirical properties before and after short term ageing by Rolling Thin Film Oven Testing (RTFOT) are shown in Table 1.

3.2 Asphalt mixture

A recipe mixture AC10 close surface course asphalt was produced using a UK limestone aggregate with the grading curve shown in Figure 2.

150 mm diameter by 120 mm high cores were produced by gyratory compaction to a target void content of 5.0%. Each core was sawn into two 50 mm thick slices, which were each sawn in half to produce semi-circular specimens. A 9 mm notch was cut in the centre of the base of the specimen perpendicular to the base to provide a known mode I crack initiation point.

4 EXPERIMENTAL RESULTS AND DISCUSSION

4.1 Cyclic SCB testing

Cyclic SCB testing was undertaken in a temperature controlled cabinet at 20°C, with each specimen conditioned for a minimum of four hours prior to testing. In all cases the span to diameter ratio was 0.8. As shown schematically in Figure 3 non-contact transducers were glued to the specimen to measure the vertical displacement of the specimen and the crack mouth

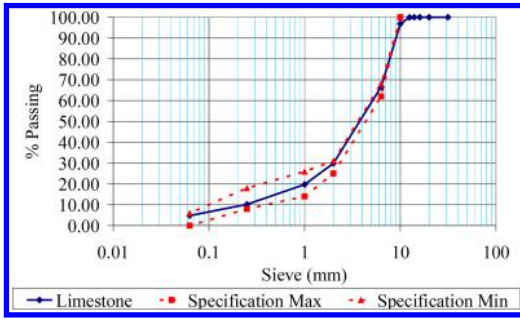


Figure 2. AC10 close surface course grading curve (PD6691).

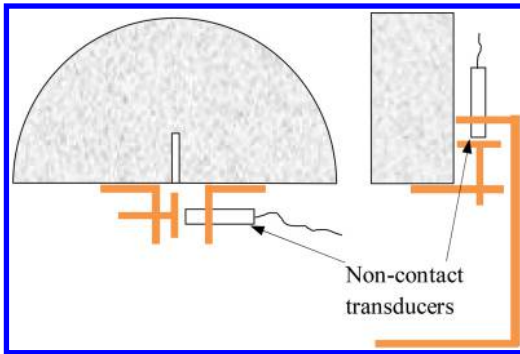


Figure 3. Front and side schematics of SCB specimen showing non-contact transducer placement.

Table 2. Horizontal stresses for 100,000 cycles to failure.

	I	II	III	IV
Horizontal stress for 100,000 cycles (Nmm^{-2})	0.156	0.245	0.333	0.368
R^2	0.956	0.975	0.986	0.983

opening displacement, and the applied force measured using a load cell.

The test was performed in controlled stress with a sinusoidal load applied to the top of the specimen at a frequency of 1.0 Hz. For each asphalt six tests were performed with two tests at applied loads of 0.5, 1.0 and 2.0 kN, and each test continued until catastrophic failure occurred which was at approximately 40% of the original modulus. Figure 4 shows a typical response of the vertical and crack mouth opening displacements (CMOD) during the course of the test, with the all the test results summarised graphically in Figure 5 as a classical Wöhler or S-N diagram.

A linear regression line of best fit was applied to the results and the correlation coefficient R^2 determined. From this line the horizontal stress required to produce one hundred thousand cycles to failure was then calculated and reported in Table 2.

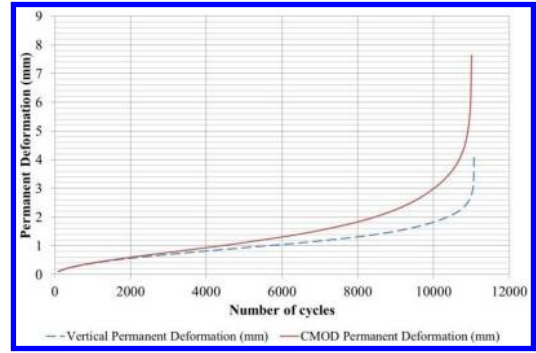


Figure 4. Typical evolution of vertical deformation and crack mouth opening displacement.

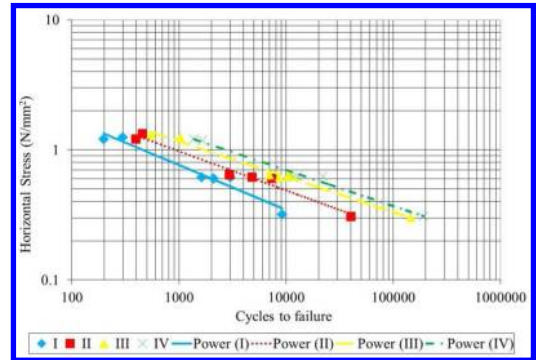


Figure 5. Summary of cyclic SCB testing.

As can be seen the increase in SBS content leads to a significant increase in the stress required to produce the same level of damage in the asphalt. At the 5.0% and 7.5% SBS contents, for a given stress level, the number of cycles to failure is approximately ten times that of the unmodified bitumen.

4.2 VECD fatigue life

The primary practical difficulty with traditional fatigue testing is the very long duration of the tests at low stress and strain levels which may lead to a full characterisation taking many weeks or even months to complete. This is both inconvenient and, particularly in a commercial environment, expensive. By using a VECD approach only the higher stress and strain level testing is required to produce the C-S data, from which the lower stress performance may be calculated.

4.2.1 Small samples used for determination of relaxation modulus

To obtain the asphalt's relaxation modulus, and hence α , small samples 14 mm × 50 mm were cored from a semi-circular specimen and tested on the dynamic shear rheometer (DSR). Sample holders were fabricated to hold the small samples in the DSR as shown in Figure 6, and the sample conditioned at 20°C prior to testing.



Figure 6. Small diameter core mounted on the rheometer.

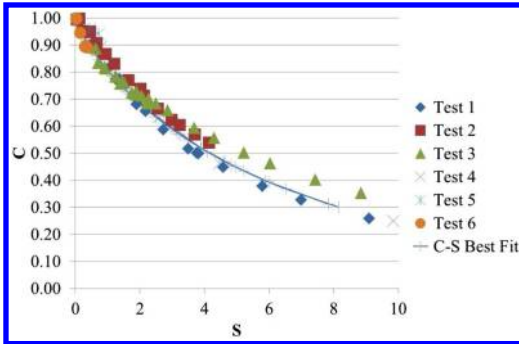


Figure 7. C-S curves for asphalt produced with binder III.

A frequency sweep test was carried out from 0.001 Hz to 100 Hz at a strain of 0.001% which was well within the linear viscoelastic region for the asphalts. This was then interconverted to a stress relaxation modulus and the parameter m determined. Further details of this testing and analysis can be found in a previous publication (Lancaster & Khalid 2013).

4.2.2 Application of VECD

Equations (5–7) were then used to generate the characteristic C-S curves for the four asphalts. As can be seen in Figure 7 for asphalt with binder III the results of all the tests collapse to form one unique C-S curve irrespective of the stress level.

The choice of curve to model C and S is arbitrary, although a number of possible models have been suggested by researchers (Lee et al. 2000, Christensen & Bonaquist 2005). In this study the model applied by Kutay et al. (2008) was used

$$C = \exp(C_1 S^{C_2}) \quad (7)$$

where C_1 and C_2 are regression coefficients.

As discussed earlier it is the low loading tests that consume take the vast majority of the testing time.

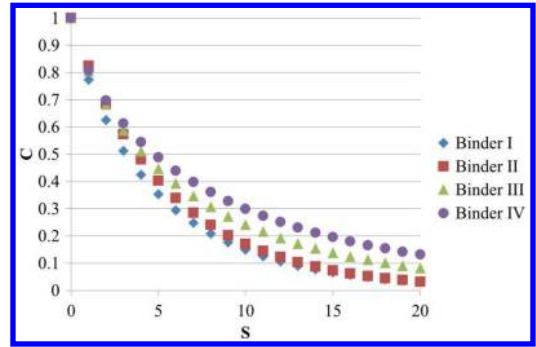


Figure 8. Best fit C-S curves.

Therefore the C-S curves were then recalculated using only the more rapid 1 kN and 2 kN peak to peak tests. To determine the best fit coefficients for C_1 and C_2 the solver function in Excel was used by reducing the absolute mean error between the C-S curve and the measured data to a minimum. A comparison of the best fit C-S for the four binders tested in this study can be seen in Figure 8.

As the polymer content increases the amount of internal damage that the material can accept for the same drop in modulus also increases, indicating an improved lifetime. Graphically this leads to a flattening of the C-S curve with increasing polymer content.

4.2.3 Predictions using VECD model data

Once the material's characteristic C-S damage behaviour curve known, it is possible to model additional laboratory tests. Underwood et al. (2006) demonstrated how, once C_1 and C_2 are known, the evolution of S may be calculated using,

$$S_{N+\Delta N} = S_N + \left(\frac{\Delta N}{f} \right) \left(-\frac{I \varepsilon^{R^2}}{2} \frac{\partial C}{\partial S} \right)^\alpha \quad (8)$$

Equation (7) may be differentiated to give

$$\frac{\partial C}{\partial S} = C_1 C_2 x^{C_2-1} \exp(C_1 S^{C_2}) \quad (9)$$

and equation (8) may then be iteratively solved.

An additional cyclic SCB test was undertaken on asphalt produced with binder I. This specimen had an initial modulus of 4058 MPa and was cyclically loaded at 0.5 kN peak to peak. Equations (1), (2), (4), (5), (8) and (9) were then used to predict the modulus evolution during the test as shown in Figure 9 below.

As can be seen there is good agreement between the measured data and the predicted values. To further validate the theory and results additional tests at alternative applied loads, frequencies and temperatures should be performed, but was beyond the scope of this study.

From the C-S data the loads necessary to produce a drop in modulus to 40% of the original value in 100,000 cycles were calculated for the four materials

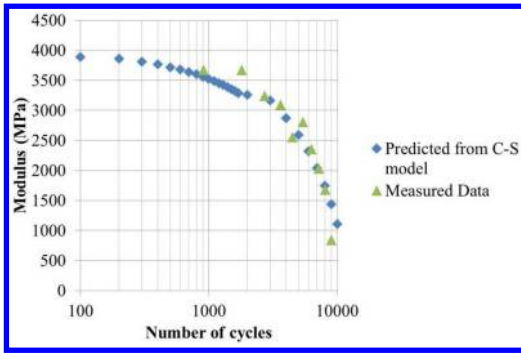


Figure 9. Predicted and measured SCB modulus for asphalt with binder I and 0.5 kN peak to peak cyclic

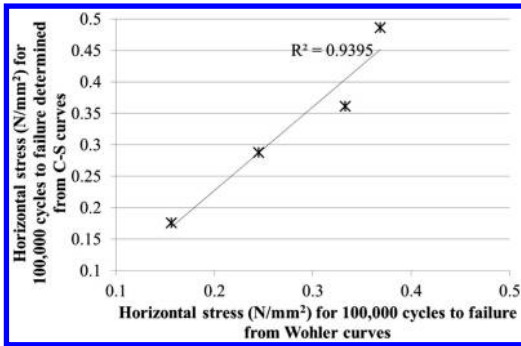


Figure 10. Correlation between Wohler and VECD predictions of stress for 100,000 cycles to failure.

tested. The correlation between these values and those determined previously from the Wohler diagrams was found to be very good as shown in Figure 10.

5 CONCLUSIONS

This paper has demonstrated the improved damage tolerance of asphalt with increasing binder polymer content in the notched cyclic SCB test. As the binder polymer content was raised, the number of cycles to failure for a given applied stress level increased significantly, with the number of cycles to failure in most highly modified asphalts being approximately ten times that of the unmodified asphalt.

Furthermore, VECD theory has been successfully applied to the SCB test to produce characteristic C-S curves for the materials. As the polymer content increased the C-S curve was seen to flatten. This can be interpreted as that the polymer modified binders produce asphalts that are able to maintain a higher proportion of their modulus for a given amount of internal damage.

The C-S curves were then successfully used to predict the stress required to produce a given number of cycles to failure. It was also demonstrated that the VECD approach could be used to predict behaviour under low-magnitude applied loads using the C-S

curves determined from high-magnitude load tests, thus saving considerable experimental time.

REFERENCES

- Abdo A.M.A., Jung S.J, and Baek S.I. 2013. Verification of testing parameters of semi-circle notched beam fatigue test. *Asian Journal of Civil Engineering*. 14(5): 643–654.
- Adamson R.M., Shapiro L.H. and Dempsey J.P. 1997. Core-based SCB fracture of aligned first-year sea ice. *Journal of Cold Regions Engineering*. 11(1): 30–44.
- Barman M., Ghabchi R., Singh D.V., Zaman M., Commuri S. and Hobson K. 2014. Evaluation of fatigue resistance of asphalt mixes using Four Point Beam Fatigue and Semi-Circular Bend test methods. *Computer Methods and Recent Advances in Geomechanics – Proceedings of the 14th International Conference of International Association for Computer Methods and Recent Advances in Geomechanics, IACMAG 2014*. 459–464
- Chang S-H, C-I Lee and S Jeon 2002. Measurement of rock fracture toughness under modes I and II and mixed-mode conditions by using disc-type specimens. *Engineering Geology* 66(1–2): 79–97.
- Christensen D.W. and Bonaquist R.F. 2005. Practical application of continuum damage theory to fatigue phenomena in asphalt concrete mixtures. *Journal of the Association of Asphalt Paving Technologists*. 74: 963–1002.
- EAPA 2014. Asphalt in Figures. European Asphalt Pavement Association, Brussels.
- Hassan M.M. and Khalid H.A. 2010. Fracture characteristics of asphalt mixtures containing incinerator bottom ash aggregate. *Transportation Research Record, Journal of the Transportation Research Board* 2180: 1–8.
- Hofman R., Oosterbaan B., Erkens S.M.J.G. and van der Kooij J. 2003. Semi-circular bending test to assess the resistance against crack growth. In *Proceedings of the Sixth RILEM Symposium on Performance Testing and Evaluation of Bituminous Materials*. Zurich, Switzerland, (Part I MN (ed)) RILEM: 257–263.
- Huang B., Shu X. and Zuo G. 2013. Using notched semi circular bending fatigue test to characterize fracture resistance of asphalt mixtures. *Engineering Fracture Mechanics* 109: 78–88.
- Huang L., Keming C. and Zeng M. 2009. Evaluation of semi-circular bending test for determining tensile strength and stiffness modulus of asphalt mixtures. *Journal of Testing and Evaluation* 37(2): 1–7.
- Lancaster I.M. and Khalid H. 2013. Viscoelastic characterisation of asphalt using small specimen sizes. *Proceedings of the 5th European Asphalt Technology Association Conference*. (Michael P. Wistuba ed(s)) *European Asphalt Technology Association. Technical University of Braunschweig, Braunschweig, Germany*, Paper no. 36.
- Lee H.J., Daniel J.S. and Kim, Y.R. 2000 Continuum damage mechanics-based fatigue model of asphalt concrete. *Journal of Materials in Civil Engineering*, 12(2): 105–112.
- Kim Y-R, Lee H.J., and Little D.N. 1997. Fatigue characterization of asphalt concrete using viscoelasticity and continuum damage theory. *Journal of the Association of Asphalt Paving Technologists*. 66: 520–569.
- Kutay E. Gibson N, and Youtcheff J 2008. Conventional and viscoelastic continuum damage (VECD)-based fatigue analysis of polymer modified asphalt pavements. *Journal of the Association of Asphalt Paving Technologists* 77: 395–434.

- Mohammad L.N., Wu Z. and Mull M.A. 2004. Characterization of fracture and fatigue resistance on recycled polymer-modified asphalt pavements *In Proceeding of the Fifth RILEM International Conference on Cracking in Pavements*, Limoges, France, 375–382.
- Molenaar A.A.A., Scarpas A., Liu X. and Erkens S.M.J.G. 2002. Semi-circular bending test; simple but useful? *Journal of the Association of Asphalt Paving Technologists*. 71: 794–815.
- Schapery R.A. 1984. Correspondence principles and a generalised J integral for large deformation and fracture analysis of viscoelastic media. *International Journal of Fracture*, 25: 195–223.
- Underwood B.S., Kim Y.R. and Guddati M.N. 2006 Characterization and performance prediction of ALF mixtures using a viscoelastoplastic continuum damage model. *Journal of the Association of Asphalt Paving Technologists*. 75: 577–636.

Assessment of linear and nonlinear viscoelastic responses of warm-mix asphalt binders

M. Sadeq

University of Liverpool, Liverpool, UK
Texas A&M University at Qatar, Doha, Qatar

E. Masad

Texas A&M University at Qatar, Doha, Qatar

H. Al-Khalid

University of Liverpool, Liverpool, UK

O. Sirin

Qatar University, Doha, Qatar

ABSTRACT: Warm-Mix Asphalt (WMA) technology is widely used in the paving industry due to its impact on reduction of asphalt mixing and compaction temperatures. Characterisation of WMA in the past had focused on evaluating the linear viscoelastic properties and associated Superpave specifications. In this study, evaluating the nonlinear viscoelastic responses of different WMA technologies is introduced. A comparison was made to show the difference in permanent deformation resistance of each binder type. Two WMA additives were tested after mixing them with modified and unmodified binders. The tests were conducted using a Dynamic Shear Rheometer to perform oscillatory and multiple stress creep recovery (MSCR) tests. Resistance to permanent deformation was evaluated using the rutting factor and irrecoverable creep compliance. The results showed that Sasobit stiffened the asphalt binder and increased its resistance against permanent deformation. On the other hand, Advera's effect was almost negligible on both binder types.

1 INTRODUCTION

Warm-Mix Asphalt (WMA) technology was introduced originally in some European countries in 1995 for the road construction industry. The ability of reducing asphalt's mixing and compaction temperature was the main motivation to implement WMA additives in asphalt production. Suppliers of additive producers claim that the compaction and mixing temperatures for WMA mixtures are 30°C less than the conventional hot mix asphalt (HMA). This reduction aided in minimizing the fuel consumption in asphalt factories and lowering smoke emissions during construction. With such improvements, paving practice became healthier and more facilitated. Several studies were introduced in the past years to evaluate the effect of using WMA additives with asphalt binders. The effect was investigated against all asphalt pavement distresses and their influence on pavement performance.

WMA technologies are manufactured in different forms, such as organic (wax), chemical, and foaming additives. Typically, WMA additives can be introduced in the mixing stage to reduce binder viscosity. The viscosity adjustment promotes enhanced binder coating

over the aggregates, thus improving the mixture workability and compaction at lower temperatures.

The characterisation of asphalt binders with WMA additives has focused on determining the Superpave parameters that are based on linear viscoelastic response. However, in the past few years, the Multiple Stress Creep Recovery (MSCR) test was introduced to assess the nonlinear viscoelastic response of asphalt binders. The test was performed for better evaluation of rutting resistance (Golalipour 2011; D'Angelo et al. 2007; Shirodkar et al. 2012). Many researchers used MSCR test to characterise the effect of mixing WMA additives with the asphalt binder (Arega et al. 2011; Zelelew et al. 2013; Adorjányi & Füleki 2011; Arega & Bhasin 2012). Studies showed that some WMA additives had demoted the rutting resistance of the asphalt pavement. Nevertheless, Sasobit, with the inclusion of wax, has improved the binder's stiffness and decreased the associated permanent strains.

In this study, the effect of WMA additives on binder properties has been investigated. Binders' linear viscoelastic properties were evaluated in the DSR using oscillatory test followed by the MSCR test to estimate their nonlinear properties.

Table 1. Properties of virgin asphalt binders.

Ageing Status	Test Properties	Results
Modified PG 76-22 Binder		
Unaged	viscosity at 135°C (Pa.s)	2.230
	$G^*/\sin(\delta)$ at 76°C (kPa)	1.812
RTFO aged	$G^*/\sin(\delta)$ at 76°C (kPa)	2.894
RTFO + PAV aged	$G^*.\sin(\delta)$ at 31°C (kPa)	1659
Unmodified 60/70 pen Binder		
Unaged	viscosity at 135°C (Pa.s)	0.483
	$G^*/\sin(\delta)$ at 64°C (kPa)	1.486
RTFO aged	$G^*/\sin(\delta)$ at 64°C (kPa)	2.527
RTFO + PAV aged	$G^*.\sin(\delta)$ at 25°C (kPa)	3759

2 OBJECTIVE OF THE STUDY

The main purpose of this study is to assess the rutting resistance of asphalt binders mixed with WMA additives. This aim was achieved by evaluating the linear viscoelastic properties and irrecoverable creep compliance of asphalt binders. The dynamic shear rheometer was used to perform the tests and determine the binder properties.

3 TESTING MATERIALS

Two asphalt binders were included in this study, modified PG 76-22 and unmodified 60/70 pen binders (PG 64-22). Both binders are currently used in the State of Qatar for pavement constructions (Sadek et al. 2013; Sadek et al. 2014). Details of virgin binder's properties were listed in Table 1. Asphalt binders were mixed with different WMA additives; Advera and Sasobit.

Advera is produced by PQ Corporation in the US as an aluminosilicate specialty zeolite free flowing white to grey powder as shown in Figure 1. Advera contains about 21% of entrapped water in its crystalline structure that starts to emit at temperature over 100°C (PQ Corporation 2014). In this study, 5% of Advera was mixed with both modified and unmodified binders for testing.

Sasobit was the second additive used in this study. It is a fine crystalline long chain aliphatic hydrocarbon which is manufactured by Sasol Wax in South Africa. Sasobit produced from natural gas using the Fisher Tropsch process of polymerization (Sasol Wax 2014). In this study, the 5-mm diameter prill was used as shown in Figure 2. As per supplier recommendations, Sasobit was added at a dosage rate of 2% of binder weight.

Both WMA additives acquired were listed in Table 2 for properties and dosage recommendations.

WMA additives were mixed in the lab with the asphalt binders using Silverson mechanical mixer after heating the binder at 160°C temperature. Mixing was performed for 10 minutes at a speed of 4000 rpm. Additives were added slowly and mixing was terminated when binder became homogenous.

Table 2. Properties of WMA additives used.

Property	Sasobit	Advera
Appearance	5-mm white prill	grey powder
Density (g/cm^3)	0.94	0.40–0.48
Water-solubility	Insoluble	Insoluble
Recommended Dosage*	0.8-4.0%	4.8–5.0%

* Dosages are based on binder's weight



Figure 1. Advera WMA additive acquired from PQ Corporation.

Since MSCR test was developed to evaluate the permanent deformation of short-term aged binder, WMA binders were aged using Rolling Thin Film Oven (RTFO) at 163°C for 85 minutes. Figure 2 shows the experimental matrix followed in this study. RTFO ageing was conducted to simulate the short-term ageing that would occur in mixing and compaction phases. The ageing was carried out by following AASHTO – T 240 (2009). Using the conventional temperature in short-term ageing was done to compare between HMA and WMA binders against permanent deformation at same short-term ageing conditions.

Dynamic Shear Rheometer (DSR) was adopted in this work to perform rheological testing on WMA binders. Three replicates of each binder type were tested using the 25 mm diameter plates' size. Samples were placed between the plates with 1-mm gap. The DSR used was from the TA Instrument (DHR-1 model) with Upper Heated Plate (UHP) system that assures heating the entire sample at the same temperature.

4 ANALYSIS METHODS

4.1 Linear viscoelastic analysis

The parameter ($G^*/\sin(\delta)$) is used in the Superpave system to assess the resistance to permanent deformation. The rutting parameter is related to the total dissipated energy during a loading cycle (Motamed & Bahia 2011). The oscillation stress/strain



Figure 2. Sasobit WMA additive acquired from Sasol Company.

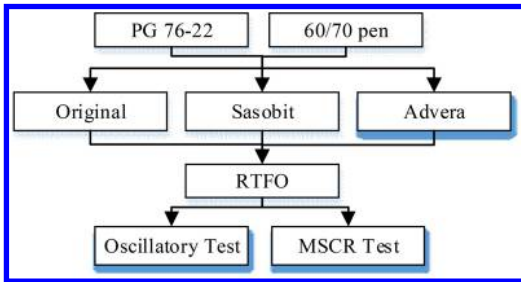


Figure 3. Experimental matrix.

test was performed according to AASHTO – T 315 (2009) in order to determine that parameter ($G^*/\sin \delta$). The DSR test was performed at 76°C for modified PG 76-22 binder and at 64°C for unmodified 60/70 pen binder (considered as PG 64).

4.2 Nonlinear viscoelastic analysis

New binder samples were also tested following the MSKR test protocol (AASHTO – TP 70 2009). The DSR was set to perform ten cycles of loading and unloading at two different stress levels, 100 Pa and 3200 Pa. In this test, the stress was applied on the sample for 1 second and then released for 9 seconds for relaxation.

The MSKR test results were used to calculate the average irrecoverable creep compliance (J_{nr}) as follows:

$$J_{nr}^n (\text{kPa}^{-1}) = \frac{\varepsilon_r^n - \varepsilon_0^n}{\text{Stress Level}} \quad (1)$$

where ε_0^n is the initial stain at the beginning of loading at 'n' cycle while ε_r^n is the strain value at the end of the unloading at 'n' cycle. Values of 'n' are from 1 to 10 for each stress level. Dividing the amount of irrecoverable strains over the stress level was meant to normalize the irrecoverable creep compliance value.

Table 3. Complex shear modulus (G^*) and phase angle (δ) for both asphalt binders tested with different WMA additives.

Additive Types	Parameters	PG 76-22	60/70 pen
Original (No WMA additive)	G^* (Pa)	2777	2524
	δ (°)	74	87
2% Sasobit	G^* (Pa)	3984	4006
	δ (°)	68	84
5% Advera	G^* (Pa)	3038	2802
	δ (°)	71	87

The normalization was presented by D'Angelo et al. (2007) to eliminate the effect of different stress levels in one test for better comparison between binders.

Similarly, percentage of recovery (R) is the average of measured recovery for 'n' number of cycles by using equation (2):

$$R_n (\%) = \frac{\varepsilon_c^n - \varepsilon_r^n}{\varepsilon_c^n - \varepsilon_0^n} \quad (2)$$

where ε_r^n is the value of strain at the end of loading at 'n' cycle.

Values of irrecoverable creep compliance (J_{nr}) and percentage of recovery was calculated for each cycle separately and then averaged at each stress level.

5 RESULTS AND DISCUSSION

5.1 Oscillatory Test

The results from the strain-controlled oscillation test were listed in Table 3. Results showed that the use of Sasobit has increased the complex modulus and decreased the phase angle of both asphalt binders. Having lower phase angle indicates that the asphalt binder became more elastic – less viscous – after mixing it with Sasobit. However, Advera influence on the binder is slight.

Complex modulus and phase angle were measured at low shear strain to get the linear viscoelastic properties of the asphalt binders. This test does not present the nonlinear behaviour of the binders that would affect its performance within asphalt mixtures. However, rutting factor given in Figure 4 indicated that adding 2% of Sasobit as WMA additive increased the potential of rutting resistance in the asphalt mixtures at early stages. On the other hand, Advera slightly affected the rutting resistance in both binder types.

5.2 MSKR Test

The irrecoverable creep compliance and percentage of recovery were calculated using the MSKR test results. Results in Figure 5 and Figure 6 were averaged for all cycles at each stress level. Data indicated that Sasobit and Advera have relatively slight effect on the percent of recovery and irrecoverable creep compliance (J_{nr}) on the modified PG 76-22 binder.

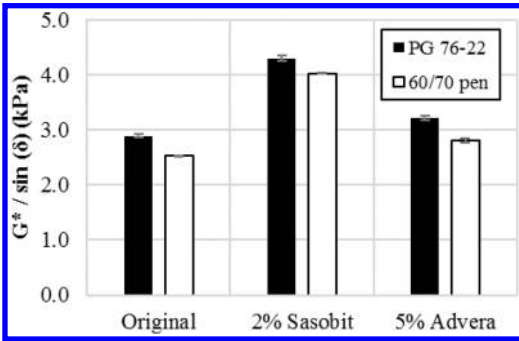


Figure 4. Rutting factor ($G^*/\sin(\delta)$) for RTFO aged modified PG 76-22 binder and unmodified 60/70 pen binder mixed with WMA additives.

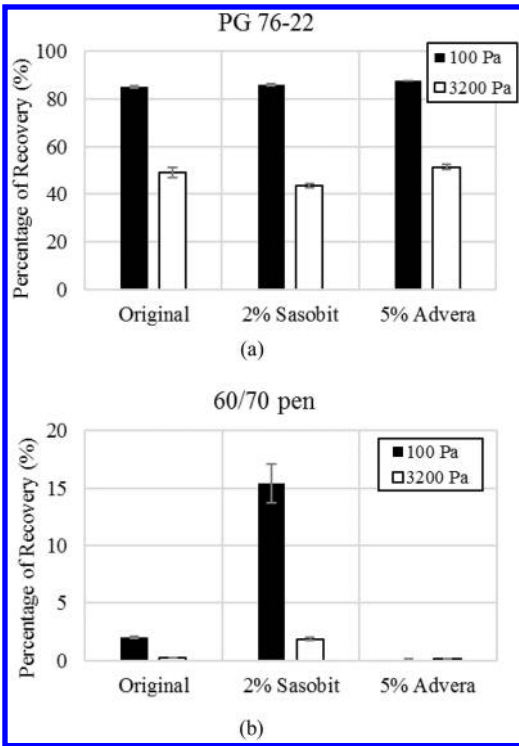


Figure 5. Percentage of recovery of both stress levels for (a) modified binder PG 76-22 (b) unmodified binder 60/70 pen with different WMA additives.

However, Sasobit increased the percentage of recovery and decreased the irrecoverable compliance for unmodified 60/70 pen binder. Although Advera showed very minimal effect on the recovery and J_{nr} for unmodified asphalt binders.

Testing results indicated that using Sasobit as WMA additive would help in lowering the mixing and compaction temperature of the modified asphalt binder, and would not affect the average permanent deformation of the binder. However, Sasobit showed relatively high influence on the unmodified asphalt binder in

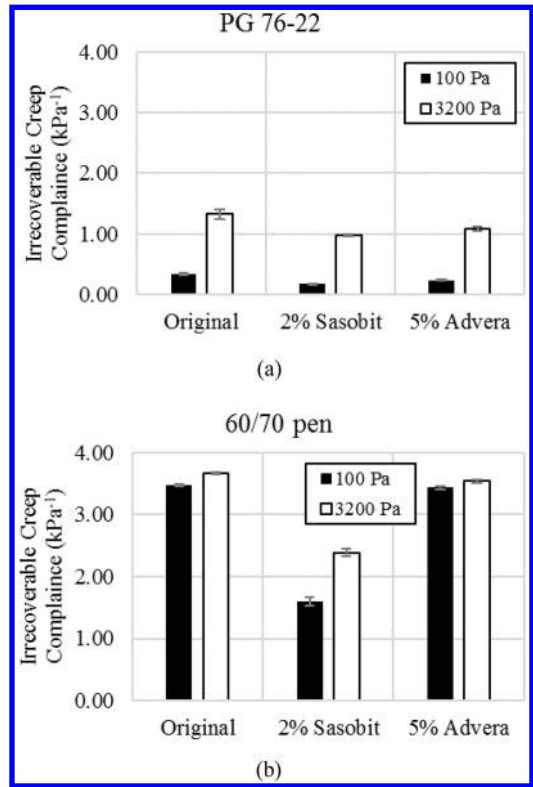


Figure 6. Irrecoverable creep compliance (J_{nr}) of both stress levels for (a) modified PG 76-22 binder and (b) unmodified 60/70 pen binder with different WMA additives.

increasing the percent of recovery. Sasobit would decrease the mixing and compaction temperature and at the same time increase the percentage of recovery and decrease J_{nr} at low and high stress levels.

Figure 7 and.

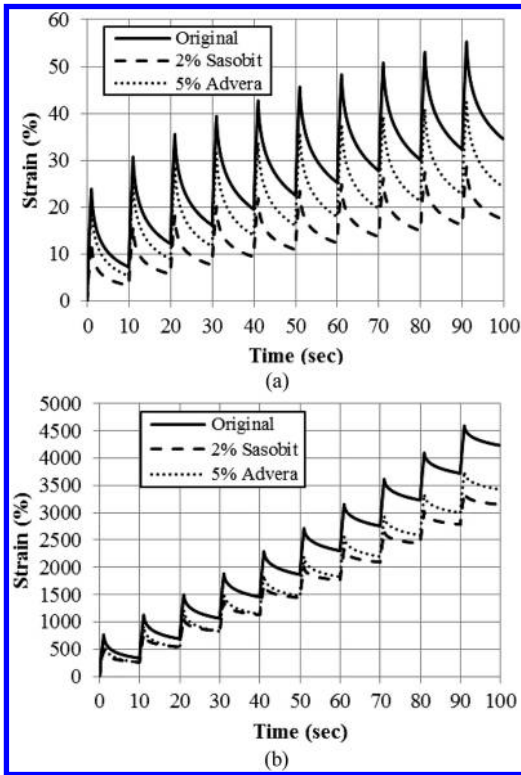


Figure 7. Ten cycles of MSCR test on modified PG 76-22 original binder, with 2% Sasobit, and with 5% Advera at (a) 0.1 kPa and (b) 3.2 kPa stress level.

to predict binders' resistance to permanent deformation. This factor depends on binder performance within the linear viscoelastic region. Alternately, Multiple Stress Creep Recovery (MSCR) test was developed to evaluate the asphalt binder at linear and nonlinear viscoelastic regions. The objective of this paper is to compare the resistance to permanent deformation of asphalt binders with and without WMA additives.

In this study, two WMA additives were mixed separately with modified and unmodified asphalt binders. Strain-controlled oscillation test was performed on each binder to estimate the linear viscoelastic properties in order to predict the rutting factor. DSR results showed that Sasobit stiffens the asphalt binder more than Advera. The latter showed a closer behaviour to the original binder. On the other hand, irrecoverable creep compliance (J_{ir}) results from MSCR test showed insignificant difference between WMA and HMA for the modified binder PG 76-22.

Reporting the average of normalized irrecoverable creep compliance would cloud up the effect of WMA additives on permanent deformation. The effect is best manifested in the accumulated permanent strain. Values of irrecoverable strain at the end of each cycle demonstrated the high influence of Sasobit on the performance of modified and unmodified asphalt binders.

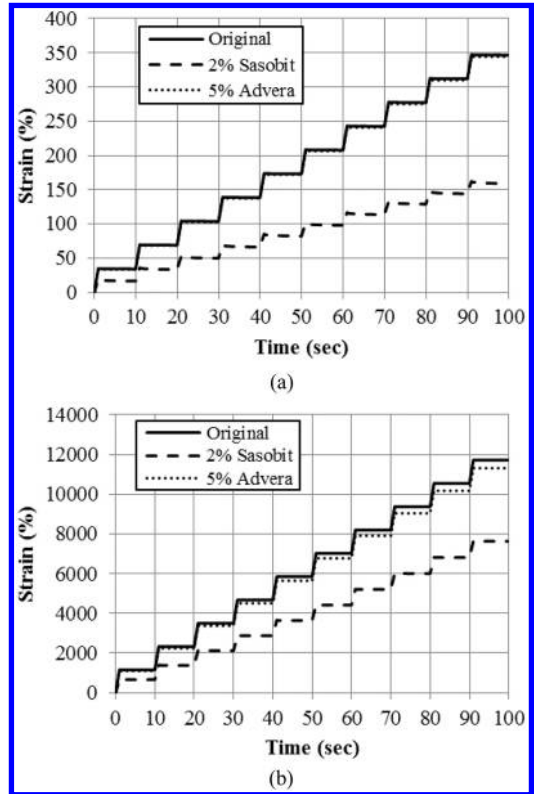


Figure 8. Ten cycles of MSCR test on unmodified 60/70 pen original binder, with 2% Sasobit, and with 5% Advera at (a) 0.1 kPa and (b) 3.2 kPa stress level.

ACKNOWLEDGMENT

This work was made possible by the NPRP award [NPRP 5-506-2-203] from the Qatar National Research Fund (a member of Qatar Foundation). The statements made herein are solely the responsibility of the authors.

REFERENCES

- AASHTO – T 240, 2009. Effect of Heat and Air on a Moving Film of Asphalt Binder (Rolling Thin-Film Oven Test). In American Association of State Highway and Transportation Officials.
- AASHTO – T 315, 2009. Determining the Rheological Properties of Asphalt Binder Using a Dynamic Shear Rheometer (DSR). In American Association of State Highway and Transportation Officials.
- AASHTO – TP 70, 2009. Multiple Stress Creep Recovery (MSCR) Test of Asphalt Binder Using a Dynamic Shear Rheometer (DSR). In American Association of State Highway and Transportation Officials.
- Adorjányi, K. & Füleki, P., 2011. Performance evaluation of bitumens at high temperature with multiple stress creep recovery test. *Hungarian journal of industrial chemistry veszprém*, 39(2), pp. 195–199.
- Arega, Z. et al., 2011. Influence of Warm-Mix Additives and Reduced Aging on the Rheology of Asphalt Binders with

- Different Natural Wax Contents. *Journal of Materials in Civil Engineering*, 23(10), pp. 1453–1459.
- Areaga, Z. & Bhasin, A., 2012. *Final Report: Binder Rheology and Performance in Warm Mix Asphalt*, Texas, USA: Texas Department of Transportation.
- D'Angelo, J. et al., 2007. Revision of the Superpave High Temperature Binder Specification: The Multiple Stress Creep Recovery Test (With Discussion). *Journal of the Association of Asphalt Paving Technologists*, 76, pp.123–162.
- Golalipour, A., 2011. *Modification of Multiple Stress Creep and Recovery Test Procedure and Usage in Specification*. University of Wisconsin – Madison.
- Motamed, A. & Bahia, H., 2011. Influence of test geometry, temperature, stress level, and loading duration on binder properties measured using DSR. *Journal of Materials in Civil Engineering*, (October), pp.1422–1432.
- PQ Corporation, 2014. Advera Warm mix asphalt. [Accessed May 18, 2014].
- Sadek, H. et al., 2013. Implementation of mechanistic-empirical pavement analysis in the State of Qatar. *International Journal of Pavement Engineering*, 15(6), pp. 495–511.
- Sadek, H. et al., 2014. Performance Evaluation of Full-Scale Sections of Asphalt Pavements in the State of Qatar. *Journal of Performance of Constructed Facilities*, p.04014123.
- Sasol Wax, 2014. Sasobit – Sasolwax US. [Accessed May 18, 2014].
- Shirodkar, P. et al., 2012. Characterization of creep and recovery curve of polymer modified binder. *Construction and Building Materials*, 34, pp. 504–511.
- Zezelew, H. et al., 2013. Laboratory evaluation of the mechanical properties of plant-produced warm-mix asphalt mixtures. *Road Materials and Pavement Design*, 14(1), pp. 49–70.

Hot stage processing of steel slag and the benefits for bituminous mixtures

I.G. Liapis & A. Chasiotis

AEIFOROS Metal Processing SA, Thessaloniki, Greece

ABSTRACT: When compared to natural aggregates for uses in the construction industry, slags have higher specific weight that acts as an economic deterrent. A method of altering the specific weight of EAFc slag by hot stage processing and mineral mixing, during steel production is presented. Measurements of specific weight are accompanied by XRD and XRF analysis and SEM spectral images for both unmodified and modified slag samples. The process is repeated for the most suitable mix in gas furnace and physical properties are examined. Unmodified and modified slags are then used in mix designs for the thin wearing course. The results show that addition of specific mineral can result in significant specific weight reduction of slag and, thus, the use of the modified slag in asphaltic concrete is proven economically beneficial. Alteration of the specific weight can result in tailoring slag properties for specific applications in the construction sector.

1 INTRODUCTION

Slags are recognised as a highly efficient, cost effective tool in the metal processing industry, by minimising heat losses, reducing metal oxidation through contact with air, removing metal impurities and protecting refractories and graphite electrodes. For the construction industry, the use of slags has been gaining ground over the last couple of decades (Motz & Geiseler 2001, Clifton et al. 1980).

Focusing on the case of electric arc furnace carbon steel (EAFc) slag the uses have significantly increased. According to Euroslag (2010), 22.3 million tonnes of EAF carbon steel slag were produced in European Union in 2010, 21% of which were stored prior to processing (interim storage) or final deposits. The remaining 79% was recycled through construction industry (Fig. 1).

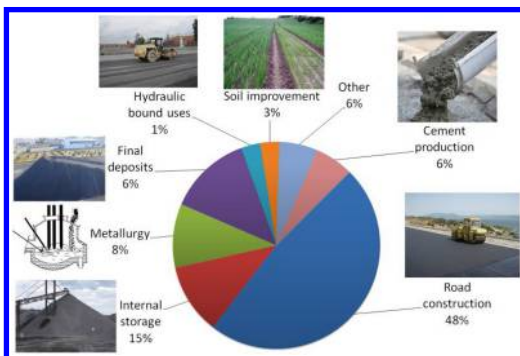


Figure 1. Applications of steel slag in EU (Euroslag 2010).

Road construction is the predominant field of application for slag aggregates, even though the percentage is decreasing compared to previous statistical data from Euroslag and bibliography (Geiseler 1996).

Steel slag recycling in Greece follows the same principles as the rest of the EU (Liapis & Likoudis 2012). The following figures show the uses of slag aggregates in terms of tonnage and turnover (Figs 2 and 3 respectively). The data were obtained from AEIFOROS SA.

The most common disadvantage among slags, Greek slags not being an exception, is the high specific

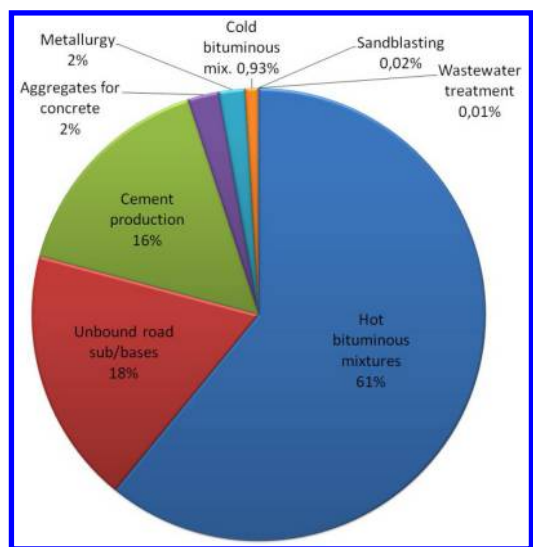


Figure 2. Slag recycling in Greece (in terms of tonnage).

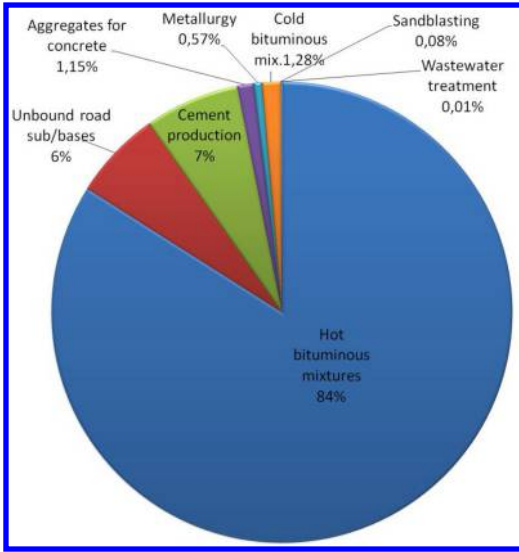


Figure 3. Slag recycling in Greece (in terms of turnover).

weight. This issue is strongly related to the commercial aspect of slag incorporation in constructional elements. The difference between the specific weight of natural aggregates and slag acts as an economic drawback in the use of slag in a wide range of applications. In Greece, the most common natural aggregate used for construction projects is limestone with specific weight of 2.6. Slags, in general, have specific weight between 3.2 and 3.6 (Maslehuddin et al. 2003) while Greek slags present specific weight closer to 3.2. In most constructional elements higher specific weight does not impose a threat to the physical and mechanical properties from an engineering point of view. Such constructional elements are unbound or hydraulically bound layers (Maslehuddin et al. 2003), bituminous mixtures (Liapis & Likoudis 2012) and cement concrete (Manso et al. 2006). Especially in the case of cement concrete applications where self-weight of the structure is important, use of higher specific weight aggregates is prohibitive, unless higher self-weight is considered at design stage.

In this article a new method of altering specific weight of EAFc slag is presented. The process is aiming at changing the physical properties of slag, focusing mainly at specific weight, when the slag is created inside the electric furnace. The method has minimal interference with the production process of steel, even by limited additions of specific minerals at high temperatures and subsequent appropriate cooling process (Kuo et al. 2008, Tossavainen et al. 2007). In this view five minerals are examined, namely perlite, ladle furnace slag, bauxite, diatomite and olivine. This paper presents the results of perlite mixing. The process falls within the scope of hot stage processing of metallurgical slags with the aim of tailoring slag properties to specific engineering applications (Engström et al. 2011, Durinck et al. 2008).



Figure 4. (a) High alumina crucible, (b) extraction of sample.

2 METHODS AND MATERIALS

2.1 Methods and experimental procedure

Aiming at the investigation of slag properties if slag was modified inside the furnace, it was considered necessary to examine the process at laboratory level prior to any full scale testing. At this initial stage a specific, as-produced slag sample was obtained, mechanically stirred and split in quantities of 40 g. For every 40.0 g subsample 4.0 g of a single mineral were added i.e. 10% per weight of slag. The mixed sample was then homogenised and melted from room temperature ($T_{ini} = 23^{\circ}\text{C}$) to final temperature $T_{fin} = 1550^{\circ}\text{C}$, with a temperature increase rate $\theta_{inc} = 30^{\circ}\text{C}/\text{min}$ in high-alumina, 50 ml-capacity crucibles (Fig. 4a) using electric resistance furnace (Fig. 4b). T_{fin} was maintained for a period of 300 s before extracting the crucible from the furnace. Subsequently, the mixed sample was water quenched in order to examine differences in phase formation. The process was repeated for all the minerals. Additionally, a slag sample was melted and water quenched without the addition of mineral and this was set as the control sample for the first part of the experiments. The procedure of mixing slag with minerals, melting and the following cooling idealised slag formation inside the furnace, where slag is created by the addition of foaming and reduction agents. At this initial part of the testing procedure five minerals were examined (Liapis & Papayianni 2015). In this paper the results of the most efficient mix, i.e. the mix with lower specific weight (slag-perlite) are presented.

The mixing ratio was set at 10 parts of slag to 1 part of mineral per weight. The mixing ratio was adopted due to constraints of chemical composition of slag in the furnace and specifically the basicity index B_2 as given by Equation 1 not to be lower than the value of 2 (Guo et al. 2006, Morales et al. 2001).

$$B_2 = \frac{\text{CaO}}{\text{SiO}_2} \quad (1)$$

where CaO and SiO_2 are concentrations of the respective oxides.

At the second stage of the experimental procedure, the process was repeated for the most suitable mix in a small industrial scale. Melting took place in a gas



Figure 5. (a) Gas furnace and (b) water quenching.

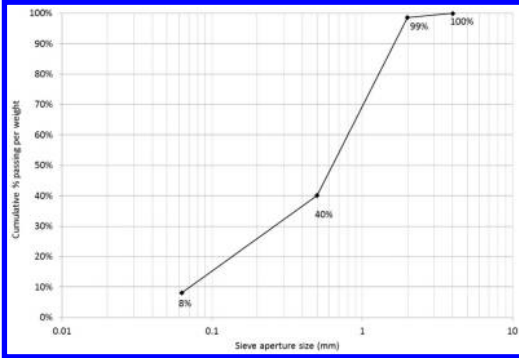


Figure 6. Grain size distribution of original slag sample.

furnace (Fig. 5a) and quenching in water baths (Fig. 5b). This, intermediate stage was necessary in order to determine the physical properties of the modified slag as well as to produce sufficient quantity of modified slag for the final investigation stage. The physical properties examined were flakiness and shape indices, Los Angeles coefficient, polished stone and aggregate abrasion value as well as volume stability for both modified and unmodified slag samples.

The final stage of the investigation included the design of bituminous mixtures according to the description in article ST6 of Greek Specifications concerning the thin wearing course. Samples were created for both modified and unmodified samples and the properties of the compacted mix examined.

2.2 Materials

For the first part of the experimental procedure a slag sample sized 0/2 mm was obtained. This slag sample, acting as reference for all laboratory testing, was produced in SIDENOR steel plant, Greece, using a 100 t electric furnace and following the normal production process of the steel plant with addition of lime as reduction agent, assisted by injection of graphite and air for foaming purposes. Upon tapping, slag was cooled by water spraying jets. It was subjected to crushing, de-ironing and sieving. The particle size distribution is shown in Figure 6.

The chemical composition of major oxides through X-ray fluorescence gave CaO 32.2%, FeO_x 30.5%, Al₂O₃ 14.7%, SiO₂ 11.4%, MnO 4.20%, MgO 3.10%,

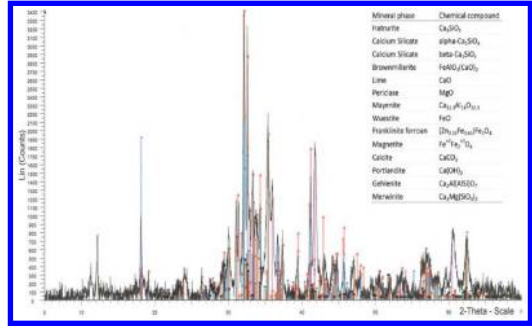


Figure 7. XRD on initial slag sample.

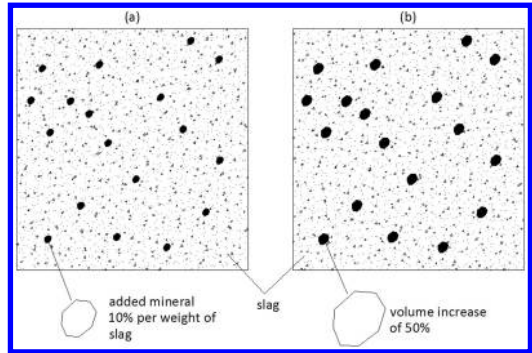


Figure 8. Principle in decreasing specific weight.

Cr₂O₃ 1.10% and TiO₂ 0.50% w/w. The X-ray diffraction pattern of the initial slag sample is shown in Figure 7.

For the purposes of the experiment, perlite 0/0,5 mm was used. Typical chemical was SiO₂ 76.0%, Al₂O₃ 14.1%, Na₂O 3.40%, K₂O 2.70%, CaO 1.20%, FeO_x 1.00 and MgO 0.20% w/w. The principle theory behind using perlite as additive mineral was the exploitation of expansion behaviour of perlite by making use of the prevailing high temperature inside the furnace. Perlite particles would be incorporated in the molten slag, heat transfer would lead to chemical decomposition and release of crystalline water of perlite resulting in the expansion of perlite grains (Fig. 8).

Additionally, the use of perlite would increase SiO₂ concentration in slag as suggested (Engström et al. 2011, Duchesne et al. 2010, Durinck et al. 2008, Kuo et al. 2008, Reichel et al. 2008) while contributing to the decrease of basicity index and viscosity of molten slag and, therefore, increase the foam index at the working temperatures (Stadler et al 2007, Morales et al. 2001).

3 RESULTS AND DISCUSSION

3.1 XRF, XRD, SEM analyses and specific weights

For the initial part of the experiment XRF, XRD, Scanning Electron Microscopy (SEM) spectral images analysis and specific weight measurements were performed to establish key characteristics of the water

Table 1. XRF analysis and basicity index.

Oxide/ index	EAFC slag	Slag after casting	Slag & perlite
CaO	32.2	30.5	32.2
FeO _x	30.5	29.9	28.4
Al ₂ O ₃	14.7	18.9	10.6
SiO ₂	11.4	10.1	16.4
MnO	4.20	4.30	4.20
MgO	3.10	3.00	3.50
Cr ₂ O ₃	1.10	1.00	1.00
TiO ₂	0.50	0.50	0.50
K ₂ O	0.10	0.20	0.40
ZnO	0.10	0.20	0.10
B ₂	2.83	3.02	1.96

quenched mix. X-ray fluorescence spectroscopy was performed using a Bruker S1 Turbo SD XRF spectrometer with 10 mm² SDD detector and typical resolution 145 eV at 100,000 cps by AEI FOROS SA. The results for a) the initial slag sample, b) the slag sample after casting without mineral mixing and c) the slag-perlite mix are shown in Table 1.

The results confirmed a) significant increase of SiO₂ content as expected by the addition of perlite and b) therefore significant decrease of the basicity index close to the value of 2. Increase in Al₂O₃ was attributed to the reduction/oxidation process by the interaction between slag and crucible vertical faces.

X-ray diffraction pattern analysis showed that the samples that were subjected to melting and subsequent water quenching presented significant increase in the background noise. X-ray diffraction analysis (XRD) was performed on pulverised material using a Bruker 3003 TT automatic diffractometer, with a nominal scanning step of 0.02°. Diffraction patterns were measured in a 2θ range of 10–90° using (Cu Kα) radiation of 50 kV and 30 mA at the Laboratory of Materials for Electrotechnics, Aristotle University of Thessaloniki. Mineralogy of slag phases was identified based on XRD patterns and chemical composition by Hellenic Cement Research Center (HCRC).

For the initial slag sample the following phases could be recognized: brownmillerite, calcite, clinoenstatite, gehlenite, johannsenite, larnite, magnesia/periclase, magnetite, quartz and wuestite. For slag after casting only 4 phases were recognised which were akermanite, enstatite, magnesia/periclase, zirconochromite. For the slag-perlite mix the recognised phases included akermanite, calcite, gandilite, larnite, maghemite and magnesiochromite.

The above listing of recognised phases emphasised the effect of cooling method on the phase formation mechanism. Rapid cooling increased glass content above 95%. At the same time, addition of Si-rich mineral enhanced the formation of silicious bonds (Kehagias et al. 2006)

For SEM micrographies JEOL scanning electron microscope with energy dispersive analysis was

Table 2. Specific weight.

Sample	EAFC slag	Slag after casting	Slag & perlite
Specific weight	3.286	3.231	2.989
% difference	1.70%	0.00%	−7.49%

Table 3. Physical properties of modified and unmodified slag samples.

Physical property	Spec.	Unmod. slag	Modified slag
Flakiness index	EN 933-3	5.34%	3.30%
Shape index	EN 933-4	7.30%	6.76%
MB _F value	EN 933-9	0.67	0.62
Sand equivalent	EN 933-8	73	77
LA coefficient	EN 1097-2	17.43%	17.80%
M _{DE}	EN 1097-1	8	8
ACV	EN 1097-2	13.2%	11.5%
Bulk density	EN 1097-3	1.653	1.575
Particle density	EN 1097-6	3.309	3.054
Water absorption	EN 1097-6	0.97	1.28
PSV	EN 1097-8	63	62
AAV	EN 1097-8	3.6	5.2
Health index	EN 1367-2	3.0	3.5

employed at the Physics department, Aristotle University of Thessaloniki. Figures 9a to c show typical SEM patterns of the three samples. SEM images were in agreement with XRD patterns, confirming higher degree of homogeneity in quenched samples and significant decrease in phase formations, similarly to the ones mentioned in literature (Mostafa et al. 2001). Homogeneity of microstructure was also a result of viscosity reduction at the molten state due to the addition of Si-rich mineral.

Specific weight measurements were performed on all samples. The addition of perlite resulted in 7.5% decrease of the specific weight compared to the control sample. The comparison of results between initial slag sample and the sample after casting showed that melting of slag without any additions of minerals caused reduction of specific weight by 1.7%, i.e. melting of slag decreased the percentage of impermeable air voids in slag grains.

3.2 Changes of physical properties

At the second stage of the experimental procedure slag-perlite mix was subjected to melting in a graphite crucible using gas furnace followed by water quenching in water baths. At this stage, all physical properties described in EN 13043 were determined for the resulting aggregates. For comparison purposes, physical properties of initial slag aggregates were also determined (Tab. 3).

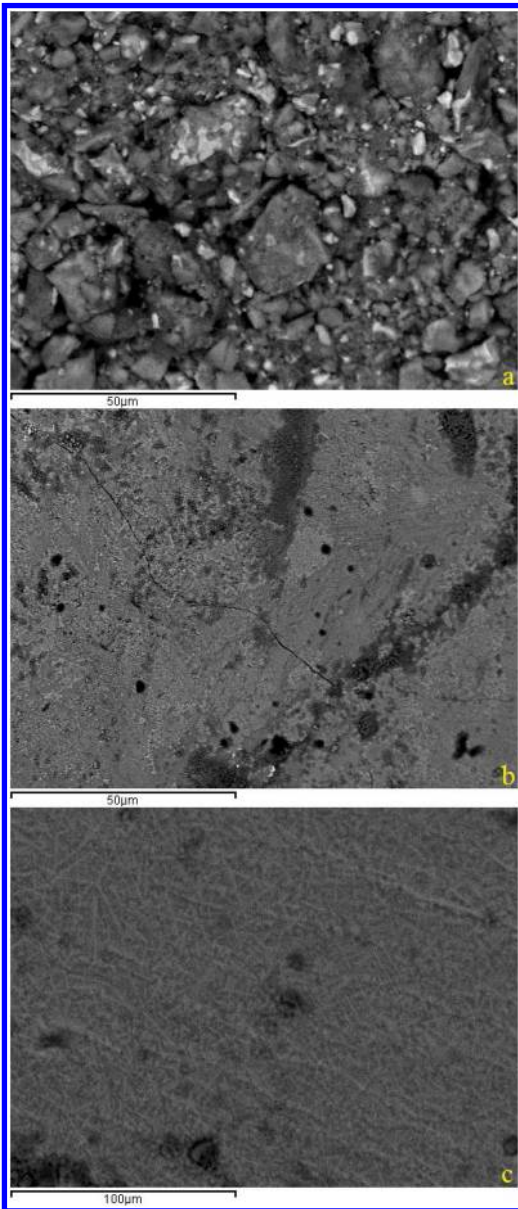


Figure 9. SEM of (a) initial slag sample, (b) slag after casting and (c) slag-perlite mix.

The results of the physical property testing showed that both slags present adequate characteristics that satisfy national specifications for wearing course applications. The comparison between the two slags highlighted the improvement of shape indices as described by shape and flakiness index due to water quenching. On the other hand, properties describing the durability of aggregates (M_{DE} , LA, PSV, AAV) showed marginal deterioration. This was attributed to the addition and subsequent expansion of perlite, mineral with low physical properties, which resulted in initiation of weak/stress concentration points in the

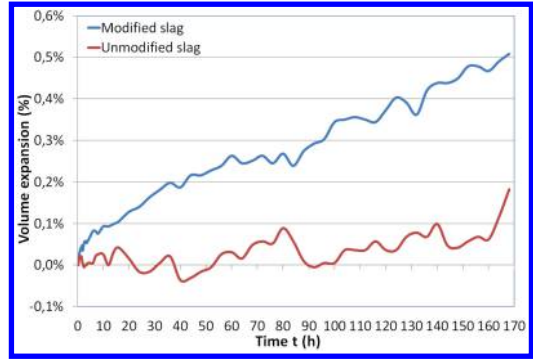


Figure 10. Volume stability test results.

grain frame. As expected, slag-perlite mix was 7.7% lighter compared to unmodified slag. At the same time, increased air voids added to the decrease of shape indices led to increase of water absorption.

Additionally, both modified and unmodified slag samples were subjected to steam test in order to obtain volume stability according to EN 1744-1, 19.3.

The results showed that modified slag presented volume expansion phenomena higher than unmodified slag sample (Fig. 10). The increase in volume expansion was attributed to the cooling process. As modified slag was water quenched, phase formation was interrupted, leading to increased free CaO and MgO content. During the steam test experiment CaO and MgO hydrated giving $\text{Ca}(\text{OH})_2$ and $\text{Mg}(\text{OH})_2$ and therefore leading to volume increase (Wang et al. 2010). It must be noted that, even though there was significant difference in volume expansion between the two samples, both values (0.18 and 0.51%) were low and the materials were classified in the lowest category ($V_{3,5}$ for volume expansion up to 3.5%) of EN specifications. As such, both materials could be used in the majority of applications including thin wearing course of asphaltic concrete.

3.3 Mix design of thin wearing course

As described previously, at the end of the intermediate stage, a new modified slag was produced presenting 7.5% lower specific weight while maintaining exceptional physical properties. At this final stage mix designs of asphaltic concrete were produced, complying with the specifications of ST6 of the Official body Technical Specification (Hellenic Ministry for the Environment, Physical Planning & Public Works).

For comparison purposes, two mix designs were produced; the first one with unmodified slag aggregates and the second entirely with modified slag. For the two mixes, both modified and unmodified slags were split into coarse aggregates sized 6,3/10 mm and fine aggregate sized 0/2 mm. Same amount of limestone filler was used in both mixes. Tables 4 (for unmodified) and 5 (for modified slag) present characteristics of the mixes.

Table 4. Characteristics of bituminous mix with unmodified slag.

Material	% in mix	WA (%)	Specific weight	Mass (kg)	Volume (m ³)
Binder	4.99	–	1.060	131	124
Air voids	–	–	–	–	96
Coarse agg.	75.1	1.16	3.268	1915	586
Fine agg.	19.9	1.50	3.167	492	155
Filler	5.0	1.15	2.263	88	39
Total agg.	100	–	3.198	2495	780
Total for mix	–	–	–	2626	1000

Table 5. Characteristics of bituminous mix with modified slag.

Material	% in mix	WA (%)	Specific weight	Mass (kg)	Volume (m ³)
Binder	5.25	–	1.060	129	121
Air voids	–	–	–	–	96
Coarse agg.	75.1	1.16	3.021	1775	588
Fine agg.	19.9	2.30	2.948	459	156
Filler	5.0	1.15	2.263	89	39
Total agg.	100	–	2.969	2323	783
Total for mix	–	–	–	2452	1000

Mix characteristics showed significant decrease of density of the compacted mix as 2626 kg/m³ for the mix with the unmodified slag aggregates was reduced to 2452 kg/m³ for the modified slag. The compacted mix with modified slag aggregates was 6,6% lighter than the one with unmodified slag.

3.4 Economic evaluation of slag modification in asphaltic concrete application

The economic evaluation is aiming at determination of the effects induced by hot stage processing of EAFc slag from an economic point of view in a specific time frame referenced as analytic horizon (Haddix et al. 2003). In this paragraph the economic benefits resulting from the modification of slag are compared to the economics of using unmodified slag aggregates in asphaltic concrete applications.

For a given volume of asphaltic concrete the cost of materials is given by the following equation.

$$TC_{mat} = TC_a + TC_{trans1} + TC_{proc} + TC_{trans2} + TC_{binder} \quad (2)$$

where TC_a = total cost of aggregates, TC_{trans1} = total cost of transportation between the factory producing slag and the asphalt plant, TC_{proc} = total cost of processing of aggregates in the asphalt plant for example drying, sieving, mixing with binder, not including cost of binder, TC_{trans2} = the total cost of transportation

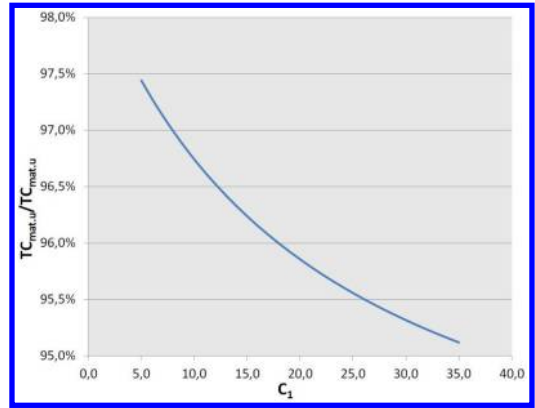


Figure 11. Total cost of raw materials for different values of C_1 .

between the asphalt plant and the working site and TC_{binder} = the total cost of binder.

The following equations (Eqns 3 to 8) can be applied

$$TC_a = m_a * C_a \quad (3)$$

$$TC_{trans1} = m_a * C_{trans1} \quad (4)$$

$$TC_{proc} = m_a * C_{proc} \quad (5)$$

$$TC_{trans2} = (m_a + m_{binder}) * C_{trans2} \quad (6)$$

$$TC_{binder} = m_{binder} * C_{binder} \quad (7)$$

$$m_a = \rho_a * V_a \quad (8)$$

where m_a = mass of aggregates, C_a = cost of aggregates per unit weight, C_{trans1} and C_{trans2} = cost of the two cases of transportation expressed per unit weight of the transported material, C_{proc} = the cost of processing per unit weight of aggregates, m_{binder} = mass of the binder and C_{binder} = the cost of binder per unit weight.

For the construction of $V_a = 1,00 \text{ m}^3$ of compacted mix and by substituting equations (3) to (8) into (2) and using the data from Tables 4 and 5, the ratio TC_{mat} for the modified slag ($TC_{mat.m}$) to TC_{mat} of unmodified slag ($TC_{mat.u}$) can be written as (eqn. 9)

$$\frac{TC_{mat.m}}{TC_{mat.u}} = \frac{\rho_a * m * C_1 + 0,129 * C_2}{\rho_{a.u} * C_1 + 0,131 * C_2} \quad (9)$$

where C_1 = sums of costs $C_a + C_{trans1} + C_{proc} + C_{trans2}$ and C_2 = sum of costs $C_{binder} + C_{trans2}$. C_1 and C_2 are common for modified and unmodified slags as are expressed in terms of cost per unit weight. By fixing the value of C_2 at 400, the ratio of equation 9 can be expressed for different values of C_1 (Fig. 11).

Typically, C_1 ranges between values of 15 and 25 and therefore the total cost of raw materials using modified slag aggregates is reduced between 3.8 and 4.5%

4 CONCLUSIONS

In this paper a process of hot stage processing of EAFc has been described, comprising mainly by mineral mixing, followed by water quenching of the molten slag. The aim was to investigate slag valorisation by modification of production process of steel, while making full use of high temperatures inside the furnace.

Summarising, it is proven that;

- During initial laboratory testing, results showed significant decrease of specific weight of modified slag compared to unmodified slag samples.
- Addition of 10% of perlite per weight of slag decreased specific weight of the mix by 7.5% compared to melted slag without any additions (control sample), this being primarily a result of volume expansion properties of perlite.
- XRF analysis showed that chemical composition was in accordance with the added mineral, in this case perlite
- XRD patterns showed significant increase of background noise in addition to broadening of the diffraction peaks, characteristic of high glass content and smaller crystalline size due to rapid cooling
- SEM captures confirm higher homogeneity of modified slag grains due to a) increase of SiO₂ and therefore reduction of basicity and viscosity of slag at molten state and b) rapid cooling through water quenching restricted phase formation
- During the small industrial scale production (second stage), sufficient quantity of modified slag was produced for laboratory testing of aggregates for the determination of physical properties. The comparison of results between modified and unmodified slag aggregates showed improvement in shape and flakiness indices and moderate deterioration of the physical properties describing durability characteristics (M_{DE} , LA, PSV and AAV).
- Volume stability results for the modified slag increased to 0.51 from 0.18% due to increased free CaO and MgO content. Even though the value of this physical property was increased, it was well below the lowest value described in EN 13043.
- At the final stage of the experimental procedure mix designs of asphaltic concrete for the thin wearing course were studied for both case of slag aggregates, modified and unmodified. The results confirm decrease of specific weight of the compacted mix by 6.6%.
- The economic benefit for the construction of thin wearing course with modified slag aggregates, for given value of binder cost and for a range of transportation and processing is determined between 3.8 and 4.5% compared to the cost with unmodified slag aggregates.

REFERENCES

Clifton, J.R., Brown, P.W., Frohnsdorff, G. 1980. Uses of waste materials and by-products in construction.

- Part II. Elsevier Scientific Publishing Company, 5(3): 217–228
- Duchesne, M.A., Macchi, A., Lu, D.Y., Hughes, R.W., McCalden, D., Anthony, E.J. 2010. Artificial neural network model to predict slag viscosity over a broad range of temperatures and slag compositions. *Fuel Processing Technology* 91 (8): 831–836
- Durinck, D., Engström, F., Arnout, S., Heulens, J., Jones, P.T., Bjorkman, B., Blanpain, B., Wollants, P. 2008. Hot stage processing of metallurgical slags. *Review. Resources, Conservation and Recycling* 52: 1121–1131
- Engström, F., Pontikes, Y., Geysen, D., Jones, P.T., Bjorkman, B., Blanpain, B. 2011. Review: hot stage engineering to improve slag valorisation options. In: *Proceedings of the 2nd International Slag Valorisation Symposium, Leuven, Belgium, 18–20 April 2011*. ACCO, 231–251
- Euroslag. 2010. Statistics 2010. Building Materials Institute. FEHs – Institut für Baustoff-Forschung e.V.
- Geiseler, J. 1996. Use of Steelworks slag in Europe. *Waste Management* 16 (1–3): 59–63
- Guo, M., Jones, P.T., Parada, S., Boydens, E., Dyck, J.V., Blanpain, B., Wollants, P. 2006. Degradation mechanisms of magnesia-chromite refractories by high-alumina stainless steel slags under vacuum conditions. *Journal of the European Ceramic Society* 26 (16): 3831–3843
- Haddix, A.C., Teutsch, S.M., Corso P.S.. 2003. *Prevention effectiveness – A guide to decision Analysis and Economic Evaluation*. 2nd ed. New York: Oxford University Press
- Hellenic Ministry for the Environment, Physical Planning & Public Works. ΣΤ-6. Ασφαλτόμιγμα για λεπτή αντιολισθηρή στρώση, Τεχνική Συγγραφή Υποχρεώσεων (Τ. Σ. Υ.) Έργων Οδοποιίας: 4–8.
- Kehagias, T. Komninou, P., Kavouras, P., Chrissafis K, Nouet, G., Karakostas, T. 2006. Crystal phase separation and microstructure of a thermally treated vitrified solid waste. *Journal of the European Ceramic Society* 26(7): 1141–1148
- Kuo, Y., Wang, J., Wang, C., Tsai, C.. 2008. Effect of water quenching and SiO₂ addition during vitrification of fly ash Part I: On the crystalline characteristics of slags. *Journal of Hazardous Materials* 152(3): 994–1001
- Liapis, I. & Likoudis, S. 2012. Use of electric arc furnace slag in thin skid-resistant surfacing. *Procedia – Social and Behavioral Sciences* 48: 907–918.
- Liapis, I. & Papayianni, I. 2015. Advances in chemical and physical properties of electric arc furnace carbon steel slag by hot stage processing and mineral mixing. *Journal of Hazardous Materials* 283: 89–97
- Luxan, M.P., Sotolongo, R., Dorrego, F., Herrero, E.. 2000. Characteristics of the slags produced in the fusion of scrap steel by electric arc furnace. *Cement and Concrete Research* 30(4): 517–519
- Manso, J., Polanco, J., Losanez, M., Gonzalez, J. 2006. Durability of concrete made with EAF slag as aggregate. *Cement & Concrete Composites* 28(6): 528–534
- Maslehuddin, M., Sharif, A.M., Shameem, M., Ibrahim, M., Barry, M.S. 2003. Comparison of properties of steel slag and crushed limestone aggregate concretes. *Construction and Building Materials* 17(2): 105–112
- Morales, R.D., Rodriguez-Hernandez, H., Conejo, A.N. 2001. A Mathematical Simulator for the EAF Steelmaking Process Using Direct Reduced Iron. *ISIJ International*, 41 (5): 426–436
- Mostafa, N.Y., El-Hemaly, S.A.S., Al-Wakeel, E.I., El-Korashy, S.A., Brown, P.W. 2001. Characterization and evaluation of the hydraulic activity of water-cooled slag and air cooled-slag. *Cement and Concrete Research* 31(6): 899–904

- Motz, H. & Geiseler, J. 2001. Products of steel slags an opportunity to save natural resources. *Waste Management* 21(3): 285–293
- Reichel, J., Rose, L., Kempken, J., Damazio, M.A., Carvalho, R.G., Loss, H.B., Pinto, E.M., Dutra, J.R., Karbowniczek, M. 2008. EAF-Foamy Slag in Stainless Steel Production New extremely efficient technology Easy to handle and cost-efficient. In: *9th European Electric Steelmaking Conference, Krakow, 19–21 May 2008*
- Stadler, S.A.C., Eksteen, J.J., Aldrich, C. 2007. An experimental investigation of foaming in acidic, high Fe_xO slags, *Minerals. Engineering* 20 (12): 1121–1128
- Tossavainen, M., Engström, F., Yang, Q., Menad, N., Lidstrom Larsson, M., Bjorkman, B. 2007. Characteristics of steel slag under different cooling conditions. *Waste Management* 27(10), 1335–1344
- Wang, G., Wang, Y., Ghao, Z. 2010. Use of steel slag as a granular material: Volume expansion prediction and usability criteria, *Journal of Hazardous Materials* 184(2): 555–560

Permanent deformation of stabilized subgrade soils

J.M. Rasul, G.S. Ghataora & M.P.N. Burrow

School of Civil Engineering, University of Birmingham, Birmingham, UK

ABSTRACT: Stabilization methods are often utilized to improve the performance of road pavement subgrades which are weak or whose performance is susceptible to small changes in moisture content. However, whilst a variety of performance models for natural materials have been developed and incorporated within road pavement design methodologies little research attention has been given to the characterization of similar performance models for stabilised subgrade soils. To address this, the research reported herein focuses on the permanent deformation characteristics and the development of associated models of performance for treated subgrade soils. The performance of three subgrade soils at varying moisture contents, each stabilised with lime and cement, is compared with those of naturally occurring soils. The results demonstrate an improvement in the performance of the stabilised material compared to their untreated natural state, albeit this improvement decreases with increased deviatoric stress. A statistical procedure is used to select the most appropriate models of material performance for the treated soils considered, by comparing the results of the permanent deformation with a number of performance models available in the literature. Thereafter the usefulness of the models for road pavement structural design is demonstrated via an analytical design procedure incorporating a finite element of the road pavement and the performance models.

1 INTRODUCTION

Analytical pavement design consists of two main processes. One is associated with development and characterization of numerical models to enable actual stresses and strains in layers of a road pavement to be determined. This requires the resilient modulus, Poisson's ratio and material density to be characterized and utilized within the model. The second process is associated with empirical studies to understand the number of load cycles to which the material within the pavement can undergo before failure as a function of stress and strain states. i.e. the development of so called performance models. The design is formulated by setting limits to these stresses and strains at critical locations within the theoretical model. Usually such limits are provided to prevent fatigue cracking and permanent deformation (rutting), (O'Flaherty, C. A., 2002).

For rutting it is usual to set a limit on the compressive strain at the top of the subgrade, whereas for fatigue cracking the limit is set to control the tensile strain beneath the bituminous layer. However each layer in a pavement structure contributes to the total surface rutting development. i.e. the rut is the sum of the permanent deformation of all layers of the pavement structure. As far as stabilized materials are concerned, pavement design standards such as that specified by AASHTO in its pavement design guide (AASHTO, 2002) specify that pavements with one or more stabilized layers should be designed for

fatigue cracking alone, but not for rutting (since it often assumed that permanent deformation is zero in these standards). However research by Wu et al. (2011) and others show that permanent deformation can occur in stabilized soils.

Several researchers modelled permanent deformation, a number of which related the permanent deformation to the number of load repetitions (Barksdale, 1972; Wolff and Visser, 1994), others linked it to the applied stresses (Duncan and Chang, 1970; Lentz and Baladi, 1981) and others (Li and Selig, 1996; Lekarp and Dawson, 1998; Puppala et al., 1999; Puppala et al., 2009) modified these models through introducing different soil properties such as moisture content and measures of strength. However, the literature associated with permanent deformation development in stabilized base and/or subgrade layers is limited (See Chittoori 2008 & 2012, Wu 2011).

This paper demonstrates the use of permanent deformation models in analytical pavement design procedures. From the review of the literature six models are selected and calibrated with permanent deformation test results and the suitability of these models for treated soils is assessed. The effect of moisture change on different types of subgrade soils is evaluated from permanent deformation test results and the improvements to subgrade soils with lime-cement stabilization are presented. The experimental procedure for permanent deformation of treated and untreated soils are described and a finite element

model was developed using ABAQUSTM software to analyze a hypothesized pavement section with different subgrade conditions.

2 MODEL DEVELOPMENT

The six models of material performance considered for further investigation are described below:

1) Veverka model (Lekarp and Dawson, 1998)

$$\varepsilon_{1,p} = a * \varepsilon_r * N^b \quad (1)$$

In which $\varepsilon_{1,p}$ is accumulated permanent strain, ε_r is the resilient strain, N is the number of load repetitions and a and b are regression parameters. This model relates the accumulated permanent deformation to the number of load repetitions and the resilient strain.

2) Khedr model (Lekarp and Dawson, 1998)

$$\frac{\varepsilon_{1,p}}{N} = A * N^{-m} \quad (2)$$

In which A and m are regression parameters

3) Sweere model (Lekarp and Dawson, 1998)

$$\varepsilon_{1,p} = a * N^b \quad (3)$$

4) Ullidtz model (Ullidtz et al., 1999)

$$\varepsilon_{pz} = AN^\alpha \left[\frac{\sigma_z}{P} \right]^\beta \quad (4)$$

where ε_{pz} : is the vertical plastic strain in micro strains at depth z , σ_z : is the vertical stress at depth z , P is a reference stress (atmosphere pressure) and A , α and β are constants.

5) Puppala model (Puppala et al., 2009)

$$\varepsilon_p = \alpha_1 N^{\alpha_2} \left(\frac{\sigma_{oct}}{\sigma_{atm}} \right)^{\alpha_3} \left(\frac{\tau_{oct}}{\sigma_{atm}} \right)^{\alpha_4} \quad (5)$$

where $\sigma_{oct} = (\sigma_1 + 2\sigma_3)/3$, $\tau_{oct} = (\sqrt{2}/3)(\sigma_1 - \sigma_3)$, σ_{atm} is the reference stress and $\alpha_1, \alpha_2, \alpha_3$ and α_4 are constants.

6) Li and Selig model (Li and Selig, 1996)

$$\varepsilon_{1,p} = a * \left(\frac{\sigma_d}{\sigma_s} \right)^m * N^b \quad (6)$$

where σ_d is the deviatoric stress; σ_s is the soil static stress and the other parameters are as previous.

In Li and Selig model, the effect of moisture change and material performance is taken into account through the soil static stress, Li and Selig list typical values of a , m and b for various soil types.

A single stress level can be used for calibration of the model and the calibrated model can be used for different expected stress levels in the pavement structural analysis. The model by Ullidtz uses the vertical stress and a reference stress at a certain depth for

the vertical permanent strain calculation, however the change in material quality cannot be accounted for if the calibrated model with a specified stress and material condition, for example moisture change, is used for different stress level and moisture contents. To overcome this, the resilient strain in Veverka's model can be substituted by the deviatoric stress resilient modulus ratio, [equation 7](#).

Li and Selig's model includes the moisture effect through the static strength of the material, here if the static strength, which is a property of the material, substituted by a mechanical property such as resilient modulus may give a better characterization of the permanent deformation of the subgrade material for treated and untreated cases, while the Li and Selig equation is applied to the untreated case only.

$$\varepsilon_{1,p} = a * \left(\frac{\sigma_d}{M_r} \right) * N^b \quad (7)$$

The vertical and radial stresses obtained from MLET analysis used to determine the deviatoric stress, or alternatively the resilient strain from the three layer system analysis directly can be substituted from [equation 8](#) (Huang, 2004).

$$\varepsilon_{radial} = \frac{1}{E} * (\sigma_z - \sigma_{radial}) \quad (8)$$

3 EXPERIMENTAL PROGRAMME

There is no standard specification procedure for a permanent deformation test for subgrade soils, therefore it was decided to use a process based on AASHTO T307 (AASHTO, 2003) and BS EN 13286-7 (BS, 2004). The stress levels specified to determine the resilient modulus of subgrade soils in AASHTO T307 together with the specified apparatus was used in combination with the procedure mentioned in BS EN 13286-7 for multi-stage permanent deformation were used.

The number of loading cycles was chosen to be 50000 cycles for single stage and 10000 cycles for each of the five stress combinations for multi-stage tests. The confining pressure was 27.6 kPa for all cases.

3.1 Soil types

Three types of soils were investigated in this research. Samples at three different moisture contents were prepared for stabilized and unstabilized subgrade soils, for this purpose proctor tests are carried out to determine MDD and OMC from which the moisture content at dry side and wet side of OMC are selected. The index test results of these are presented in the [table 1](#). These three soils are stabilized with 4% cement and 1.5% lime content.

3.2 Sample preparation

Samples were prepared by static compaction in 100 mm dia. and 200 mm height molds in five lifts, this method of compaction assures homogeneity of the prepared sample. Several researchers (Puppala *et al.*,

Table 1. Index properties of the soils.

	Soil type			Standard used
	A-4	A-6	A-7-5	
Liquid limit LL (%)	21	35	51	BS1377-2:1990 sections 4 and 5
Plastic limit PL (%)	14	21	31	
Plasticity Index PI (%)	6	14	20	
MDD(untreated) (g/cm ³)	1.938	1.925	1.480	BS1377-4:1990 section 3
OMC (untreated) (%)	11.0	12.0	20.0	
MDD(treated) (g/cm ³)	1.930	1.910	1.460	BS1924-2:1990 section 2
OMC (treated) (%)	12.5	12.5	24.0	

Table 2. Hypothesized pavement section properties.

Layer type	Thickness (mm)	Modulus of elasticity (MPa)	Poisson's ratio	Material property
Asphalt concrete	100	3000	0.3	Linear elastic
Base course	200	300	0.35	Linear elastic
Compacted subgrade	200	Variable	0.45	Linear elastic
Natural subgrade	–	Variable	0.45	Linear elastic

2009; Rout *et al.*, 2012; Mohammad and Saadeh, 2008) used a mold of 71 mm dia. to 142 mm in height. However samples of 100 mm dia. to 200 mm in height have been used by other researchers (Steven, 2005; Solanki *et al.*, 2010; Guo *et al.*, 2006).

4 FINITE ELEMENT MODELLING

A finite element model of road pavement was developed using ABAQUS, the model consists of four layers, see table 2 for the pavement section detail. Following a trial and error investigation to minimize boundary effects a model of 21.28 m by 3.8 m was selected, this corresponds to a depth of 140 times the loading radius and a horizontal extend of 25 times the loading radius. These radiuses correspond to those found by Kim *et al* (2009) of 140 to 20 times of the loading radius, respectively. A number of outputs from the model were compared with KENLAYER (Huang, 1993), a multilayer elastic model widely quoted in the literature. The results from comparison are given in table 3, from which it may be seen that both models are in reasonable agreement.

Table 3. Comparison of KENLAYER and ABAQUS.

Response	Position	ABAQUS			
		KENL AYER	12.16 × 3.8 (m)	15.2 × 3.8 (m)	21.28 × 3.8 (m)
Surface deflection (mm)	TopL1	1.186	1.119	1.141	1.185
Tensile strain (μ strain)	Bottom L1	−467	−468	−468	−469
E11	Top L2	−466	−466	−466	−467
Tensile stress (MPa)	Bottom L1	−2.54	−2.54	−2.54	−2.54
S11	Top L2	0.011	0.011	0.011	0.011
Compressive stress (MPa)	Bottom L2	0.080	0.080	0.080	0.080
S22	Top L3	0.080	0.080	0.080	0.080
Compressive stress (MPa)	Bottom L3	0.047	0.046	0.046	0.047
S22	Top L4	0.047	0.046	0.046	0.046
Compressive strain (μ strain)	Bottom L2	945	940	940	941
E22	Top L3	1480	1478	1478	1478
Compressive strain (μ strain)	Bottom L3	876	874	874	874
E22	Top L4	876	870	870	872

5 RESULTS AND DISCUSSION

Werkmeister *et al* (2001) proposed the shakedown concept for deformation characterization of unbound granular materials, see figure 1. They identified three ranges of material behavior. In range A the material is said to be in shakedown condition; the deformation is recoverable, in range B the material fails at a high number of load repetitions and in range C the material untimely fails. According to the shakedown concept soils A-4 and A-6, reach range C early in first 1000 cycles of load repetitions at 120%OMC, while soil A-7-5 resists permanent deformation well at this moisture content, see figures 2, 3 and 4. Figures 2 to 4 also demonstrate the sensitivity of sandy soils to moisture change.

Figure 5, 6 and 7 show the improvement to permanent deformation of the three types of soils.

However, the amount of the permanent deformation of treated soils depends on the type of the soil, stabilizer ratio and moisture content. From figure 8, it can be seen that soil A-7-5 undergoes permanent deformation of about three times the amount of the other two soils.

The behavior of the untreated subgrade soils with moisture increase, justifies the use of a method to

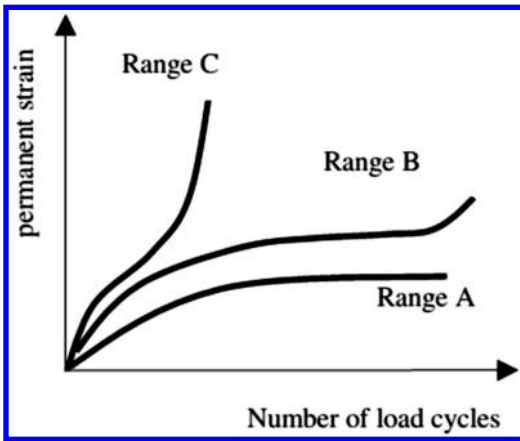


Figure 1. Indicative permanent strain behaviour (Werkmeister et al., 2001).

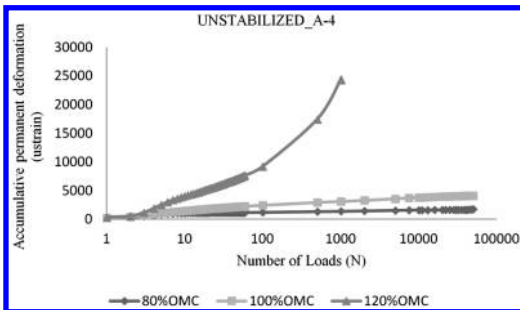


Figure 2. Permanent deformation behaviour of soil A-4 at different moisture contents.

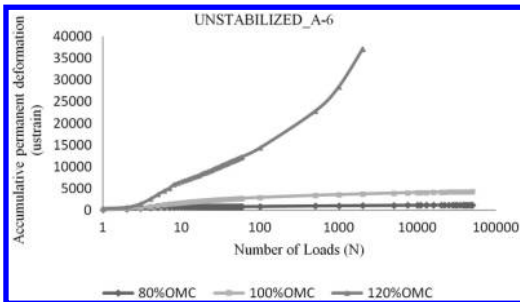


Figure 3. Permanent deformation behaviour of soil A-6 at different moisture contents.

improve the resistance capabilities to permanent deformation and failure of such soils. Li and Selig (1998) suggest two approaches to control the accumulation of permanent deformation on the top of the subgrade layer; one concerns the improvement of the subgrade by stabilization or modification, the other is to reduce the deviator stress by increasing the upper layer thicknesses. The shortcoming with the second approach may come from the fact that even by controlling the stress level, the subgrade layer could still be exposed to

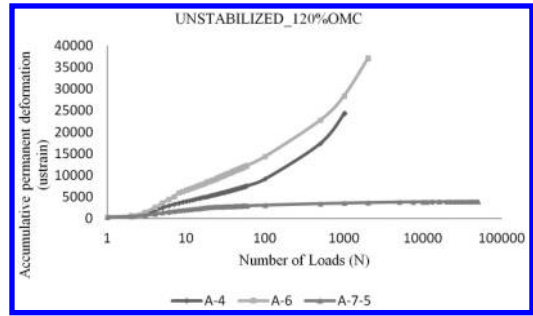


Figure 4. Permanent deformation behaviour of the three soils at 120%OMC.

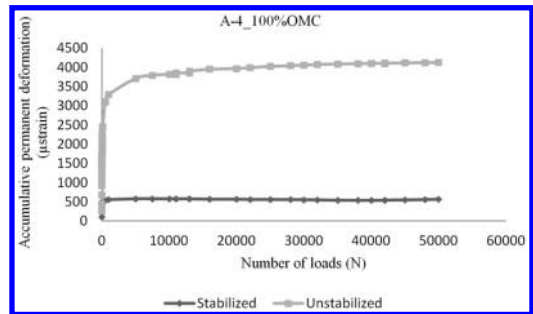


Figure 5. Permanent deformation resistance improvement of stabilized soil A-4.

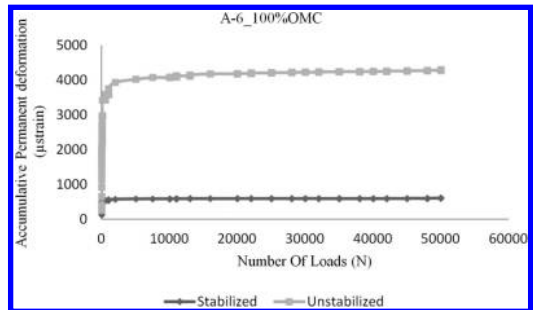


Figure 6. Permanent deformation resistance improvement of stabilized soil A-6.

moisture change and undergo high permanent deformations. Test results show this increase of moisture significantly affects the subgrade soil deformation. Therefore, in these circumstances the improvement of the soil with a stabilizer may be a superior solution for permanent deformation resistance.

The other factor that has been considered in preparing treated soils is the water content that cannot be controlled in the field easily. Three moisture contents were considered; 80%OMC, 100%OMC and 120%OMC. Figure 9 shows, for soil A-6 that the change in water content has a minor effect. Previous research on these soils show the same trend on resilient modulus value for soil A-6 (Rasul et al., 2013), while for soil A-4 the increase of moisture content from

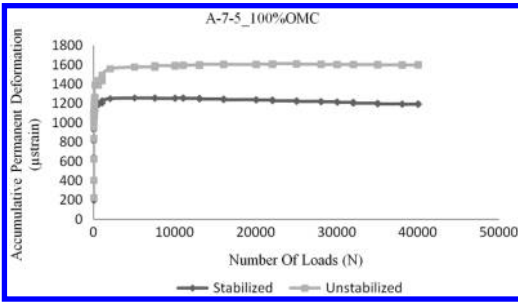


Figure 7. Permanent deformation resistance improvement of stabilized soil A-7-5.

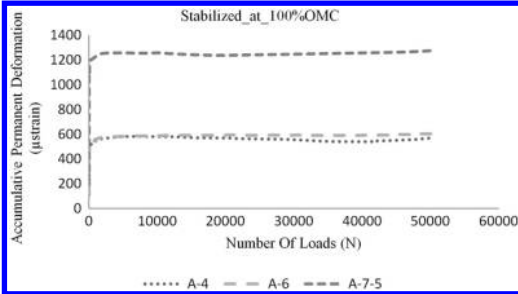


Figure 8. Permanent deformation comparison of the soils.

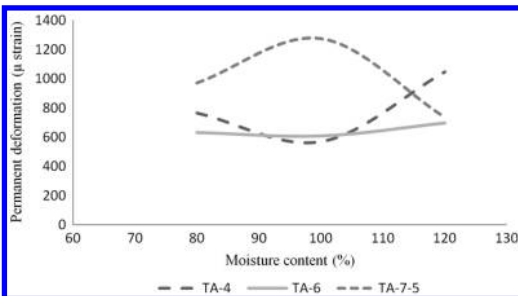


Figure 9. Comparison of effect of mixing water on permanent deformation.

dry side of the optimum moisture content to optimum and wet side accompanies with decrease in permanent deformation and beyond the optimum it increases rapidly, soil A-7-5 has different trend from both soils and experiences more permanent deformation with increase of moisture content and then decreases.

5.1 Model selection

Table 4 shows the results of the statistical analysis carried out to compare the suitability of the permanent deformation models for stabilized and unstabilized soils. As can be seen the coefficient of significance (R^2) for native soils is between 0.875 and 0.989 at optimum moisture content, irrespective of whether the model includes a measure of stress. These coefficients however for stabilized soils are low for models containing only the number of load repetitions and

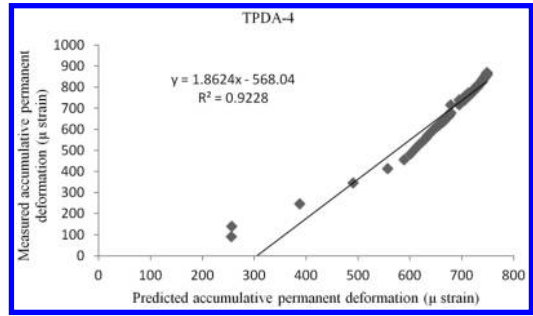


Figure 10. Comparison of measured to predicted permanent deformation for soil A-4.

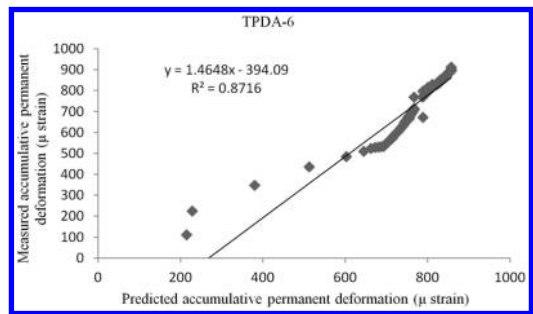


Figure 11. Comparison of measured to predicted permanent deformation for soil A-6.

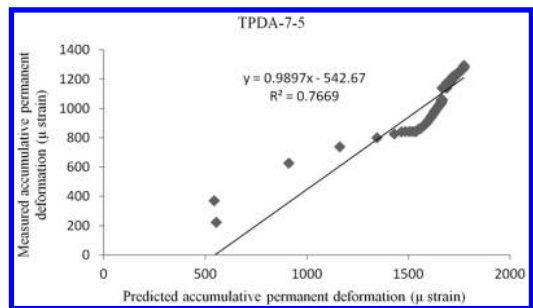


Figure 12. Comparison of measured to predicted permanent deformation for soil A-7-5.

vary between 0.475 and 0.773. However models containing the stress levels have higher coefficient of significance, ranging between 0.786 and 0.935. This highlights the significance of including the stress level in permanent deformation models.

The importance of introducing the stress level into the predictive permanent deformation equations is that the calibrated equation for a specified type of soil at an identified stress state can be used for permanent deformation prediction at different stress levels. This was validated by applying a deviatoric stress of 120 kPa to three types of soils at 100%OMC. As can be seen from the figures 10 through 12, there is good correlation between predicted and measured permanent deformation.

Table 4. Model parameters.

Soil type and moisture content	Veverka			Sweere			Puppala				
	a	b	R^2	a	b	R^2	α_1	α_2	α_3	α_4	R^2
A-4 (80%OMC) U	1.955	0.086	0.908	907.06	0.059	0.911	0.401	0.05	1.93	0.096	0.985
A-4 (100%OMC) U	1.825	0.168	0.908	1407.3	0.104	0.954	0.023	0.087	1.989	1.037	0.989
A-4 (120%OMC) U	1.240	0.440	0.969	1549.5	0.398	0.974	32.248	0.392	0.725	0.329	0.975
A-6 (80%OMC) U	1.055	0.076	0.945	670.45	0.060	0.912	0.135	0.05	2.35	-0.138	0.976
A-6 (100%OMC) U	1.843	0.107	0.938	1805.0	0.084	0.897	0.001	0.064	2.674	1.393	0.985
A-6 (120%OMC) U	2.031	0.341	0.965	3355.0	0.317	0.972	1405.1	0.313	-0.976	1.383	0.979
A-7-5 (80%OMC) U	1.233	0.035	0.861	920.79	0.032	0.712	8.91	0.021	0.907	0.366	0.941
A-7-5 (100%OMC) U	1.068	0.055	0.907	941.83	0.053	0.875	0.171	0.044	2.351	-0.112	0.966
A-7-5 (120%OMC) U	1.582	0.067	0.901	2145.5	0.060	0.799	0.508	0.043	1.094	1.266	0.953
A-4 (100%OMC) T	1.075	0.042	0.475	423.21	0.028	0.643	0.179	0.018	2.33	-0.343	0.797
A-6 (100%OMC) T	1.228	0.047	0.773	425.13	0.033	0.045	6.744	0.023	0.808	0.329	0.935
A-7-5 (100%OMC) T	2.205	0.038	0.623	988.53	0.023	0.571	0.067	0.01	2.887	-0.438	0.872
Continued											
Soil type and moisture content	Ullidtz				Khedr			Li and Selig			
	A	α	β	R^2	A	m	R^2	a	m	b	R^2
A-4 (80%OMC) U	1433.8	0.05	0.757	0.983	0.941	907.06	0.911	3259.4	0.757	0.05	0.983
A-4 (100%OMC) U	2974.9	0.098	1.418	0.993	0.896	1405.3	0.954	18668.	1.842	0.091	0.988
A-4 (120%OMC) U	2098.8	0.393	0.561	0.974	0.602	1549.4	0.974	9037.9	1.287	0.393	0.971
A-6 (80%OMC) U	1021.7	0.052	0.694	0.973	0.940	670.45	0.912	1949.4	0.694	0.052	0.973
A-6 (100%OMC) U	7597.1	0.067	2.572	0.981	0.916	1805.0	0.897	61873.	2.572	0.067	0.981
A-6 (120%OMC) U	5972.7	0.308	1.052	0.979	0.683	3355.0	0.972	7448.9	1.052	0.308	0.979
A-7-5 (80%OMC) U	1407.5	0.023	0.681	0.939	0.968	920.79	0.712	3047.9	0.681	0.024	0.939
A-7-5 (100%OMC) U	1447.8	0.044	0.706	0.961	0.947	941.83	0.875	2761.9	0.706	0.044	0.961
A-7-5 (120%OMC) U	5595.0	0.046	1.680	0.953	0.940	2145.5	0.799	17236.	1.68	0.046	0.953
A-4 (100%OMC) T	568.99	0.021	0.470	0.789	0.972	423.21	0.643				
A-6 (100%OMC) T	620.17	0.024	0.604	0.935	0.967	425.13	0.752				
A-7-5 (100%OMC) T	1414.7	0.014	0.567	0.858	0.977	988.53	0.571				

Most of the permanent deformation in a specified stress state develops in the first 100 cycles of the test. However the permanent deformation percentage of the 100 cycles to 50000 cycles, for example in this

research, is not identical for treated and untreated soils. The average percentage of accumulative permanent deformation at 100 cycles for treated soils is 83%, whereas it is 72% for untreated soils.

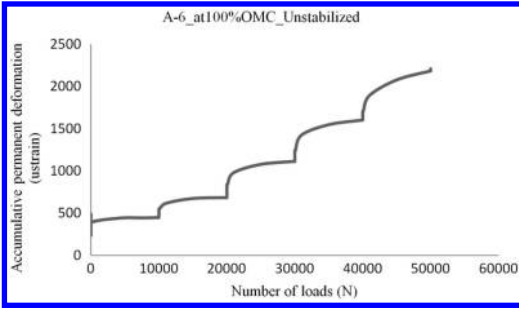


Figure 13. Multi-stage permanent deformation for native soil A-6.

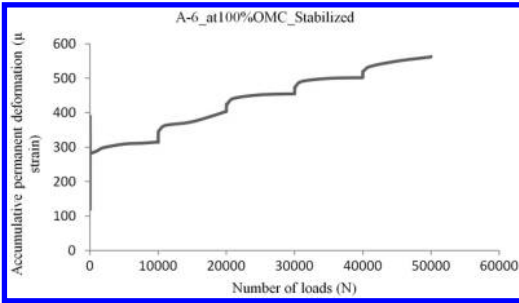


Figure 14. Multi-stage permanent deformation test for stabilized soil A-6.

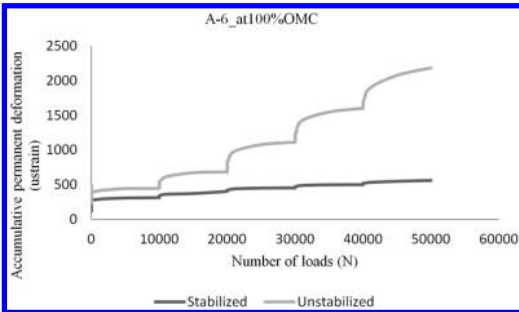


Figure 15. Comparison of permanent deformation development for Stabilized and unstabilized cases for soil A-6.

The effect of the stress level on the permanent deformation development can be ascertained by multi-stage permanent deformation tests for treated and untreated soils. Figures 13 through 15 are test results from multi-stage test for soil A-6 at 100%OMC, the increase of the accumulative permanent deformation can be noticed with increase in stress level.

6 ANALYSES OF HYPOTHESISED SECTION

A finite element model of a hypothetical pavement section was built to evaluate permanent deformation development. The pavement section's dimensions and properties are as those in table 2. The compacted subgrade layer's resilient modulus was varied as illustrated

Table 5. Model (equation 7) parameters..

Soil type and moisture content	α	b	R ²
A-4 (80%OMC) Untreated	1955.375	0.086	0.908
A-4 (100%OMC) Untreated	1707.794	0.171	0.992
A-4 (120%OMC) Untreated	1239.778	0.44	0.969
A-6 (80%OMC) Untreated	1055.233	0.076	0.945
A-6 (100%OMC) Untreated	1842.765	0.107	0.938
A-6 (120%OMC) Untreated	2030.604	0.341	0.965
A-7-5 (80%OMC) Untreated	1232.593	0.035	0.861
A-7-5 (100%OMC) Untreated	1068.274	0.055	0.907
A-7-5 (120%OMC) Untreated	1581.561	0.067	0.901
A-4 (100%OMC) Treated	1075.348	0.042	0.475
A-6 (100%OMC) Treated	1227.719	0.047	0.773
A-7-5 (100%OMC) Treated	2205.015	0.038	0.623

in table 6 and the resilient modulus values of the asphalt layer and the base layer were 3000 MPa and 300 MPa respectively. To quantify the contribution of the subgrade layer to total permanent deformation of the pavement section, the deviatoric computed stress from FEM and the material mechanical property represented by the resilient modulus from the laboratory tests were utilized in the model developed in section 3, equation 7. The calibrated model for each scenario at the deviatoric stress of 62.0 kPa was used for further analysis. Table 5 shows the calibrated model parameters for these three soils at different moisture contents of stabilised and unstabilized conditions. Using calibrated model for these cases the permanent deformation at 50000 cycles was determined for all these cases and tabulated in table 6.

As can be seen permanent deformation increases with increase in moisture content, for soils A-4 and A-6 these deformation is much higher than soil A-7-5 at 100%OMC and 120%OMC, indicating the sensitivity to moisture content of soils containing high proportion of silt and sand. However the stabilization improved the properties of soils A-4 and A-6 in higher rate than soil A-7-5 and they show a better resistance to permanent deformation.

7 CONCLUSION

- 1 Moisture change significantly affects the permanent deformation progression and development in subgrade soils, particularly sandy soils.
- 2 lime-cement stabilization improves the permanent deformation resistance of subgrade soils.

Table 6. Calculation of the permanent deformation from the model.

Soil type and moisture content	Mr	σ_d	σ_d/M_r	$\epsilon_{1,p}$
	(MPa)	(kPa)		
A-4 (80%OMC) U	185	133	0.719	3565
A-4 (100%OMC) U	157	126	0.803	8718
A-4 (120%OMC) U	66	84	1.273	184343
A-6 (80%OMC) U	120	113	0.942	2261
A-6 (100%OMC) U	82	94	1.146	6723
A-6 (120%OMC) U	44	67	1.523	123765
A-7-5 (80%OMC) U	88	98	1.114	2005
A-7-5 (100%OMC) U	74	89	1.203	2330
A-7-5 (120%OMC) U	49	71	1.449	4731
A-4 (100%OMC) T	233	143	0.614	1040
A-6 (100%OMC) T	214	115	0.537	1097
A-7-5 (100%OMC) T	168	105	0.625	2079

- Although the stabilization improves the resistance of the soil to permanent deformation, subgrade permanent deformation increases with the applied stress level.
- Equations of Permanent deformation that consider stress state in addition to the number of load repetitions are better able to predict permanent deformation. For example if they have been calibrated for a specified stress combination of an identified load, they can be used for different load levels.
- The equipment and procedures of AASHTO T307 and BS EN 13286-7 are found to be suitable for permanent deformation tests of untreated and treated subgrade soils albeit with some refinement.
- With one multi-stage permanent deformation test, the effect of different stress states and stress history can be quantified. The resilient modulus of the soil at a range of stress combinations can be determined correspondingly.
- The developed equation in this research can be used jointly with the finite element model to calculate the permanent deformation of unstabilized and stabilized subgrade layers. This will include the permanent deformation of these layers to total rut calculation developed on the surface of the road.

ACKNOWLEDGEMENTS

The authors would like to express their gratitude to the Kurdistan Regional Government (KRG) for

generously funding this work and the provision of laboratory facilities by School of Civil Engineering at the University of Birmingham to facilitate this research.

REFERENCES

- AASHTO (2003), AASHTO T 307-99 Standard method of test for determining the resilient modulus of soils and aggregate materials, American Association of State Highway and Transportation Officials, Washington, D.C.
- Barksdale, R. D. 1972. Laboratory evaluation of rutting in base course materials. In *Presented at the Third International Conference on the Structural Design of Asphalt Pavements, Grosvenor House, Park Lane, London, England, September. 11–15, 1972.* (Vol. 1, No. Proceeding).
- Chittoori, B., Puppala, A. J., Wejringsikul, T., Hoyos, L. R., & Le, M. 2012. Numerical Modeling of the Impact of Deteriorating Treated Subgrade Modulus due to Seasonal Changes on Pavement Performance.
- Duncan, J. M., & Chang, C. Y. 1970. Nonlinear analysis of stress and strain in soils. *Journal of the Soil Mechanics and Foundations Division*, 96(5), 1629–1653.
- Lekarp, F., & Dawson, A. 1998. Modeling permanent deformation behaviour of unbound granular materials. *Construction and Building Materials*, 12(1), 9–18.
- Lentz, R. W., & Baladi, G. Y. 1981. Constitutive equation for permanent strain of sand subjected to cyclic loading. *Transportation research record*, (810).
- Li, D., & Selig, E. T. 1996. Cumulative plastic deformation for fine-grained subgrade soils. *Journal of geotechnical engineering*, 122(12), 1006–1013.
- Mohammad, L., & Saadeh, S. 2008. Performance evaluation of stabilized base and subbase material. In *GeoCongress 2008 Conference*.
- O'Flaherty, C. A. (2002). Highways-The Location, Design, Construction, & Maintenance of Pavements.
- Puppala, A. J., Mohammad, L. N., & Allen, A. 1999. Permanent deformation characterization of subgrade soils from RLT test. *Journal of Materials in Civil Engineering*, 11(4), 274–282.
- Puppala, A. J., Saride, S., & Chomid, S. 2009. Experimental and modeling studies of permanent strains of subgrade soils. *Journal of geotechnical and geoenvironmental engineering*, 135(10), 1379–1389.
- Rasul, J.M., Burrow, M.P.N., Ghataora, G.S. 2014. The effect of wetting and drying on resilient modulus behaviour and pavement responses of lime-cement stabilised subgrade soils. In *Civil Engineering for Sustainability and Resilience International Conference, CESARE '14, Amman, Jordan, 24–27 April 2014*.
- Rout, R. K., Ruttanapormakul, P., Valluru, S., & Puppala, A. J. 2012. Resilient Moduli Behavior of Lime-Cement Treated Subgrade Soils. In *Geo Congress, ASCE* (pp. 1428–1437).
- Werkmeister, S., Dawson, A. R., & Wellner, F. 2001. Permanent deformation behavior of granular materials and the shakedown concept. *Transportation Research Record: Journal of the Transportation Research Board*, 1757(1), 75–81.
- Wolff, H., Visser, A. T., & Coulomb, M. 1994. Incorporating elasto-plasticity in granular layer pavement design. *Proceedings of the ICE-Transport*, 105(4), 259–272.
- Wu, Z., Chen, X., & Yang, X. 2011. Finite Element Simulation of Structural Performance on Flexible Pavements with Stabilized Base/Treated Subbase Materials under Accelerated Loading (No. FHWA/LA. 10/452). Louisiana Transportation Research Center.

Study of mineral filler effect on asphalt mixtures properties

E. Remisova

Faculty of Civil Engineering, University of Zilina, Slovakia

ABSTRACT: The mineral filler in asphalt mixture is an important component of the mixture as it plays an important role in stiffening and toughening an asphalt binder. In addition to affecting the mechanical properties of asphalts, mineral fillers are also important with respect to stripping or moisture damage. The paper presents mechanical properties of asphalt concrete AC 11 with paving grade bitumen 50/70 and polymer modified bitumen Sealoflex with two mineral limestone fillers according to empirical requirements. The produced and compacted mixtures were tested to determine voids characteristics (V_m , V_{FB}), water sensitivity (ITSR) and resistance to permanent deformation (WTS_{AIR} , PRD_{AIR}). The certain amount of filler in asphalt concrete was also substituted with hydrated lime. Laboratory research results support the benefit of adding hydrated lime to asphalt mixtures. Hydrated lime as an active mineral filler better moisture sensitivity and rutting resistance that contribute to extending the life cycle of asphalt pavement. The properties of the filler determine its interaction with bitumen and its contribution to the mixture's performance. The paper presents the positive effect of hydrated lime on affinity between bitumen and aggregate and the stiffening effect when it is mixed with bitumen.

1 INTRODUCTION

Asphalt mixtures properties depend on properties of mineral materials, nature and composition of bitumen binder and materials proportional ratio.

A bitumen binder covers and puts together aggregate particles to a mixture resistant to traffic and climatic conditions. A bitumen film thickness on mineral particles is varying from hundredths of a micron to several microns. The thickness of film depends on properties of mineral material (thinner for hydrophilic materials e.g. granite, quartz and thicker for the hydrophobic e.g. limestone), nature and composition of bitumen. The thickness increases with higher molecular weight and higher asymmetry of bituminous molecules (Grabowski and Wilanowicz, 2011).

Mineral filler in hot mix asphalt is an important component of mixture as it plays an important role in stiffening and toughening an asphalt binder. A mineral filler as active filler improves adhesion of bitumen to aggregate, dispersion of bitumen in a mixture, increases stiffness of mixture and accelerates curing of compacted mixture.

Mineral filler is defined as a portion of aggregate that is suspended in an asphalt binder without a particle-particle contact. This leads to the hypothesis that a mineral filler does not act as an aggregate or as a single component in a mixture but it acts as an integral component of mastic that is a true binder in a mixture. Mineral fillers in asphalts stiffen a mixture at the upper range of pavement temperatures with little stiffening at lower temperatures (Anderson, 1996).

In addition to affecting the mechanical properties of hot-mix asphalt, mineral fillers are also important with respect to stripping or moisture damage.

According to (Bahia and all, 2010) the important filler properties are geometry (size, shape, angularity and texture and fractional voids) and composition (a small number of chemical compounds that affect asphalt-filler interactions).

Filler content, surface area and surface absorption capacity affect optimal content of binder in a mixture. General limits of filler to binder mass ratio do not exist in current asphalt mix design procedures. From experiences in Slovak Republic, optimal ratio mass of filler to 1 mass unit of binder is from 1,5 to 1,75. Higher mass of filler in a mixture improves cohesion and internal stability of mixture and increases asphalt modulus. But high filler content can increase bitumen stiffness and therethrough influence workability of mixture. On the other side low filler content and high bitumen binder content can increase mixture sensitivity to rutting (Remišová, 2013).

The suitable filler is from natural limestone and dolomite rocks. Besides physical-mechanical properties of mixture it has positive effects on composite action between bitumen and aggregate. Fillers have different gradation parameters, geometry properties, specific surface, surface texture; air voids content and other physical-mechanical properties (Remišová, 2013).

(Grabowski and Wilanowicz, 2011) concluded that an addition of hydrated lime to fillers causes increasing finer particles content, specific surface and the Rigid

Table 1. Basic parameters of used bitumens.

Bitumen properties	CA 50/70	PmB Sealoflex
Penetration (0.1 mm)	58	71.5
Softening point (°C)	48.2	89
Penetration index	1.3	6.5
Viscosity at 60°C (mPa)	209000	342000
Viscosity at 130°C according EN 13302 (mPas)	1271	10042

Voids values as well as a decrease of volumetric mass concentration value.

When a hydrated lime is added to asphalts, it reacts with aggregate and strengthens bond between the bitumen and the aggregate interface. Lime reacts with highly polar molecules to inhibit the formation of water-soluble soaps that promote stripping. When those molecules react with lime, they form insoluble salts that no longer attract water (National Lime Association, 2006).

The ability of lime to improve the resistance of hot-mix asphalt mixtures to moisture damage, to reduce oxidative aging, to improve the mechanical properties and resistance to fatigue and rutting, is a reflection of its performance as active mineral filler and has led to observed improvements in the field performance of asphalt pavements (Little and Epps, 2001; National Lime Association, 2006).

2 EXPERIMENTAL

The main purpose of research was an assessment of mineral filler and hydrated lime influence on the basic properties of hot mix asphalt. The properties of mineral filler in mastics relating to stiffening effect of filler in mastic (delta ring and ball) are included in asphalts properties as water sensitivity ($ITSR$) and resistance to rutting (PRD_{AIR} , WTS_{AIR}). The asphalts properties were tested on the asphalt concrete AC 11 for wearing courses produced in laboratory conditions. The objective of research was to study performance of asphalts with different filler.

2.1 Materials

The tested materials included the coarse and fine aggregate, two limestone fillers and added hydrated lime in different portions by mass. One paving grade bitumen (CA 50/70) and polymer modified bitumen (PmB Sealoflex) were used in combination with one fine and coarse aggregate and different filler with the uniform bitumen content of mass 5,5 %. Properties of used bitumen binders are in Table 1.

Natural andesite with water absorption WA_{24} of 1.7% (fractions 4/8 and 8/11), resistance to fragmentation LA of 15.5% and shape index of 8.5% was used as coarse aggregate. Natural limestone, two limestone

Table 2. The particle size distribution of fillers.

	Gradation of fillers, passing in %				
	Sieve size (mm)				
	2	0.5	0.25	0.125	0.063
Filler Zirany	100	100	100	98.9	86.9
Filler Varin	100	100	99.9	91.9	77.7
Hydrated lime	100	100	100	99.5	82.3

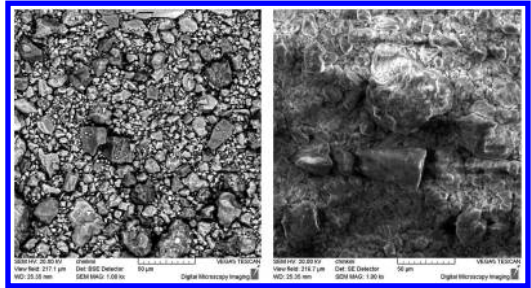


Figure 1. BSE and SE image of mineral filler from Varin.

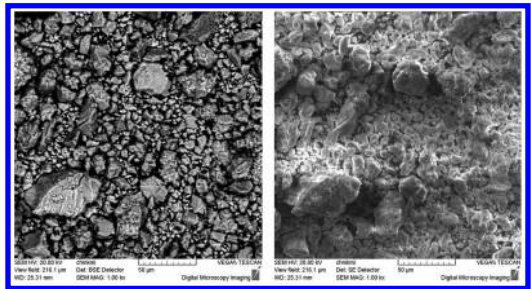


Figure 2. BSE and SE image of mineral filler Zirany.

fillers (Varin, Zirany) and hydrated lime was used as fine aggregate. Particle size distributions of tested fillers are in Table 2. Tested filler varied from passing 0.063 mm particles.

Between tested mineral fillers there aren't differences from chemical characterization point of view. However, the tested mixtures of asphalt concrete with the same aggregate, gradation and bitumen binder (the results in the next part of paper) show variety in mixture properties, mainly resistance to rutting, probably due to different mineral fillers. After that the high resolution images of fillers were used to study the angularity and shape properties of filler particles. Figure 1 and 2 illustrate images of tested mineral fillers using the electron microscope (Tesla Vega II) with high resolution imaging and backscattered electron detector BSE and secondary electron detector SE. No differences between fillers' angularity and shape were noticed from figures 1 and 2.

The stiffening effect of filler was tested using the delta ring and ball test according to EN 13179-1:2013.

Table 3. Stiffening effect of fillers.

	CA 70/100	Filler Zirany	Filler Varin	Filler Varin +1% HL	Filler Varin +2% HL
Softening point, in °C	45.4		54.7	55	58
$\Delta_{K\&G}$ with CA70/100	9	9.5	12.5		
		2–10	$\Delta_{K\&G8/16}$	$\Delta_{K\&G8/16}$	$\Delta_{K\&G8/16}$

Table 4. Affinity between used bitumen and coarse aggregate.

Affinity after 6/24 h rolling time, bitumen coverage in %		
	CA 50/70	PmB Sealoflex
Andesite	75/40	80/55
Andesite + 2% HL	85/70	–
Limestone	80/70	90/75
Limestone + 2% HL	95/90	–

The reached results are in Table 3. The effect on bitumen was demonstrated via increasing the softening point of bitumen/filler mastic consisting of 37.5% of filler and 62.5% of bitumen (in volume). The greatest increase of softening point was recorded using 2% of hydrated lime. The larger fractions of hydrated lime perform as a filler and increase the stiffness of bitumen and consequently of asphalts. The smaller fractions increase bitumen film thickness, enhance viscosity of bitumen and improve bitumen cohesion. The bitumen mastic coats the aggregate particles with a thicker film.

The hydrated lime effect on affinity between the bitumen and coarse aggregates influences the susceptibility of asphalts to stripping. Affinity between used bitumens (PGB 50/70 and PmB Sealoflex) and coarse aggregate was determined in accordance EN 12697-11:2012, the rolling bottle test, after 6 and 24 h rolling time (Table 4).

After bitumen and aggregate having been mixed, the process of interaction between aggregate and bitumen begins. These processes are determined by chemical and physical properties of aggregate and bitumen. Affinity between polymer modified bitumen and tested coarse aggregate was evaluated as sufficient. Polymers in bitumen contain polar groups that are more attractive and more absorbed of aggregate surface. From aggregate type point of view the aggregate contains mostly one dominant component and some minor mineral components. The limestone rocks consist of dominant component limestone, and silica, clay, micaous minerals as minor components. In term of affinity, the content of SiO_2 and Al_2O_3 in aggregate us the most important. The basic aggregate (limestone) with minor content of SiO_2 has good affinity to bitumen. The natural andesite (used as coarse aggregate in tested mixture), as neutral aggregate with SiO_2 content

Table 5. Aggregate gradations, bitumen content and volume characteristics of mixtures.

Sieve size, in mm	Gradation of tested mixtures Passing in %			
	AC 11 Zirany	AC 11 Varin	AC11 Varin +HL	
11.2	97	97	96	
8	76	76	80	
4	51	51	58	
2	29	29	37	
1	20	21	20	
0.5	15	16	15	
0.063	8.7	8.8	8.5	

Bitumen	50/70	Sealoflex PmB	50/70	Sealoflex PmB	50/70	50/70
Bitumen content (%)	5.5	5.5	5.5	5.5	5.5	5.5
Content of Hydrated lime (%)	–	–	–	–	1	2
Air voids content (%)	5.5	6.1	4.1	5.2	2.6	3.8
Void in mineral aggregate (%)	18.4	18.9	17.2	18	15.9	16.9
Void filled with binder (%)	70.4	67.7	75.9	71.5	83.6	77.7

of 57–61%, did not achieve adequate adhesion results (limit 70% for wearing course materials). The using 2% of hydrated lime improved affinity between materials to required level. The hydrated lime allows for the precipitation of calcium ions onto the aggregate surface, making it more favourable to bitumen binder. It can be observed mainly in the case of acid aggregate granodiorite.

2.2 Tested mixtures

Asphalt concretes AC 11 with similar aggregate gradation and the same bitumen content differed only in used mineral filler type and bitumen type (Table 5). Particle size distribution and volume properties are in Table 5 and Figure 3. The mixtures were produced in the laboratory according to EN 12697-35 + A1.

The mixtures with approximately same aggregate gradation and binder content would be comparable void characteristics. The maximum density of tested mixtures was in the range of 2.475–2.486 g.cm⁻³ following type of filler (Zirany, Varin, hydrated lime) and type of binder (PG or PmB). However greater differences were observed in bulk density of test specimens. These were subsequently expressed in differences in air voids content, void in aggregate and void filled with

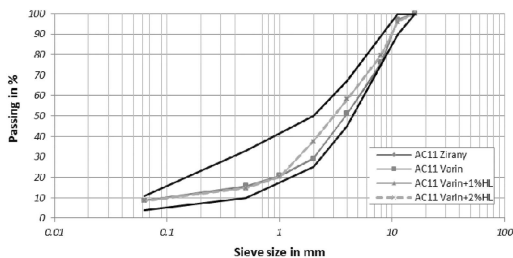


Figure 3. Aggregate gradation of tested mixtures with limits.

binder between mixtures. The mixtures with polymer modified bitumen show higher air voids content. The possibly reason could be in temperature during the test samples production.

3 TEST RESULTS

The following tests were performed on tested mixtures in order to assess the performance of the asphalts:

- water sensitivity test (*ITSR* values give information about durability with a respect to ingress of water);
- freeze-thaw resistance (low value of tensile strength indicate the potential for moisture damage);
- wheel tracking test (outputs of test provide an estimate of the resistance to rutting).

The water sensitivity tests were performed according to EN 12697-12:2008 method A on the base of indirect tensile strength of dry (ITS_{dry}) and wet (ITS_{wet}) cylindrical specimens. Determination of freeze-thaw resistance was performed according Slovak technical regulation TP 5/2010 (Lottman test; conditioning saturated samples by freezing at temperature $-18 \pm 3^\circ\text{C}$ for 16 h). The characteristics of resistance to permanent deformation (WTS_{AIR} and PRD_{AIR}) were determined in accordance with EN 12697-22 + A1:2007 using the small device, method B, in air, at the test temperature of 50°C .

The test results in Table 6 and Figure 4 show that the type of filler influences asphalt mixture properties. Although the water sensitivity of all tested asphalts expressed in ratio *ITSR* was similar (from 89% to 93%). There are the differences in strength of mixtures. The indirect tensile strength (dry and wet samples at 25°C) of mixture with the filler Varin and the polymer modified bitumen are higher than filler Zirany. The addition of hydrated lime to the mixture the strengths of mixture get raise. But in general, the strength was not improved. It means that the positive effect of hydrated lime addition on affinity between bitumen PGB 50/70 and andesite aggregate did not show total improvement of mixture water sensitivity expressed by the strengths ratio (*ITSR*).

The addition of hydrated lime to the mixture showed improvement of mixture resistance to water and freeze (conditioning saturated samples by freezing at temperature $-18 \pm 3^\circ\text{C}$ for 16 h). Added lime to asphalt

Table 6. The results of water sensitivity and wheel tracking of asphalts.

Mixture	AC 11 Zirany		AC 11 Varin		AC11 Varin + HL	
	Sealoflex 50/70	PMB	Sealoflex 50/70	PMB	50/70	2%
Bitumen Content of	–	–	–	–	1%	2%
Hydrated lime						
ITS_{dry} (MPa)	0.570	0.653	0.602	0.670	0.710	0.654
ITS_{wet} (MPa)	0.528	0.581	0.539	0.594	0.608	0.532
<i>ITSR</i> (%)	93	89	89.4	89	85.6	81.4
			(78)*		(77)*	(83)*
WTS_{AIR} (mm/1000 cycles)	0.06	0.03	0.13	0.02	0.12	0.09
PRD_{AIR} (%)	4.2	2.8	7.4	3.4	7.5	6.6

*Data in brackets are the value of *ITSR* after 1 freezing cycle (Lottman test)

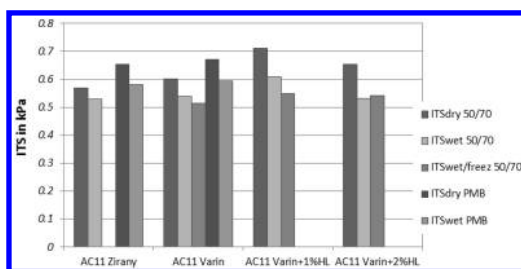


Figure 4. The indirect tensile strength of dry and wet samples and wet samples with one freezing cycle.

mixture strengthens the bond between aggregate and bitumen and reacts with highly polar molecules of bitumen. That stiffer and tougher bond better resists freezing water stresses. It could be assumed the wearing course durability in terms of resistance to failures caused by winter freeze-thaw cycles (raveling, potholes etc.) should be better.

Based on test result it can be stated the resistance of asphalt mixtures to permanent deformation is affected by bitumen type (Figure 5). The polymer modified bitumen with softening point of 89°C ensure sufficient wheel tracking resistance of mixture at the test temperature of 50°C . The mixture with filler Varin had worse results of deformation parameters using both tested bitumens. Markedly filler Varin affected properties of the asphalt mixture with PGB 50/70. The permanent deformation parameters were changed WTS_{AIR} (from 0.06 to 0.13 mm per 10^3 cycles) and PRD_{AIR} (from 4.2 to 7.4%). The test result of the mixture AC11 with the bitumen 50/70 and the filler Varin did not fulfill the Slovak requirements (WTS_{AIR} max 0.07 mm per 10^3 cycles and PRD_{AIR} max 5.0 %). The addition of hydrated lime caused the stiffening effect, the increase of bitumen softening point, the decrease of wheel tracking slope and proportional rut depth after 10000 load cycles.

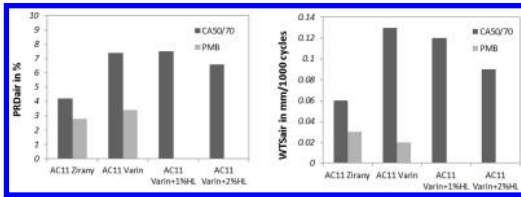


Figure 5. The wheel tracking test results of mixtures.

4 CONCLUSION

The mineral filler in an asphalt mixture affects the mixture's performances: filler influences the amount of asphalt content; filler affects workability during mixing and compaction, and final properties of asphalt mixtures.

The test results showed that the properties of the used filler determine its interaction with asphalt and its contribution to the mixture's performance. The water sensitivity of all tested asphalts expressed in ratio $ITSR$ was sufficient and similar (from 89% to 93%). The differences in strength of mixtures were noted. The bitumen-aggregate bond gets weakened in the presence of water. The results showed that the hydrated lime improves the asphalt resistance to water and freeze.

The resistance of asphalts to permanent deformation changed with filler type particularly when paving grade bitumen was used. The wheel tracking test parameters were changed approximately 50% level using filler Varin (with 77% passing to 0.063 mm); parameters WTS_{AIR} 0.13 mm per 10^3 cycles and PRD_{AIR} 7.4% compared with the mixture with filler Zirany (wheel-tracking slope 0.06 mm per 10^3 cycles and proportional rut depth after 10000 cycles 4.2%) The mixtures with the polymer modified bitumen proven sufficient wheel tracking resistance.

The adding of hydrated lime to the asphalt mixture the strengths of mixture get rise by reason of stiffening effect on bitumen. The softening point of bitumen and bitumen mastix increased and the wheel tracking slope and proportional rut depth after 10000 cycles of loaded wheel decreased. It is important to mention that the stiffening effect of hydrated lime on mixture can negatively influence the asphalt fatigue performance.

ACKNOWLEDGEMENTS

This paper was worked in as a part of solution of the project VEGA 1/0804/12 The influence of material composition of asphalt mixtures on characteristics of surface texture and emission.

REFERENCES

- Bahia, H.U. and all. 2010. Test Methods and Specification Criteria for Mineral Filler used in HMA, NCHRP Report for Project 9–45, final report, University of Wisconsin-Madison.
- Grabowski, W. and Wilanowicz, J. 2011. The specific surface of mineral fillers and their functional properties, 5th International Conference Bituminous Mixtures and Pavements Thessaloniki, Greece, 1–3 June 2011, ISBN 978-960-99922-0-6. pp. 246–255.
- Híreš M. 2014. Vplyv vápenného hydrátu na vlastnosti asfaltovej zmesi, diploma work, University of Zilina.
- Little, D.N., Epps, J.A. 2001. The Benefits of Hydrated Lime in Hot Mix Asphalt, Final report for National lime association.
- National Lime Association. 2006. Hydrated lime – a solution for high performance hot mix asphalt, fact sheet.
- Remišová E. 2013. Navrhovanie asfaltových zmesi pre netuhé vozovky, theses, University of Zilina.
- EN 13179-1:2013 Tests for filler aggregate used in bituminous mixtures. Part 1: Delta ring and ball test.
- EN 13302:2010 Bitumen and bituminous binders – Determination of dynamic viscosity of bituminous binder using a rotating spindle apparatus.
- EN 12697-11:2012 Bituminous mixtures. Test methods for hot mix asphalt.Part 11:Determination of the affinity between aggregate and bitumen.
- EN 12697-12:2008 Bituminous mixtures. Test methods for hot mix asphalt.Part 12: Determination of the water sensitivity of bituminous specimens.
- EN 12697-22 + A1:2007 Bituminous mixtures. Test methods for hot mix asphalt. Part 22: Wheel tracking.

In situ service capability of tack coats

C. Raab & M.N. Partl

Empa, Duebendorf, Switzerland

ABSTRACT: The use of tack or bond coats between different pavement layers is state of the art in most countries. Despite this fact, there are still some unanswered questions about best practice of application and additive and enduring effects of tack coats. The paper summarizes the results of an in situ evaluation of tack coats use and performance in Switzerland. In this research different parameters such as the influence of tack coat kind (polymer modified/non-polymer modified) and amount (application rate) of tack coat as well as the influence of time of application and the effect of application on milled surfaces were investigated. Further, an important point regarding the effectiveness of tack coats is the question of long term performance resp. the question after what time the bond will be optimal developed. Therefore, bonding properties determined directly after construction were compared to bonding properties determined after 2 months and bonding properties determined after trafficking. The results showed that the influence of short term curing and accelerated trafficking was not always visible but that the bonding properties clearly improved over a longer period of time.

1 INTRODUCTION

Tack or bond coats are commonly used between the different layers in a bituminous road construction (Kulkami, 2004; Raab & Partl, 2006). Especially in case of rehabilitation measures when parts of the pavement or damaged layers are replaced tack coats have to ensure the adhesion between the old and the new pavement parts thus providing a good functionality of the whole construction. Although the benefit of using tack coats is not debated (Hachiya et al., 1997; Mohammad, 2002; Recasens, et al., 2003; Canestrari, et al., 2005) it is not clear how much tack coats effectively contribute to the bonding properties. In most cases tack coats are applied empirically based on the practical experience of contractors and consultants. Parameters, such as type, surface characteristics and age of the underlying layer play an important role, although their influence is often neglected in reality. Generally there is also disagreement concerning tack coat rate and tack coat type (polymer modified versus non-polymer modified). Many investigations (West, 2005; Mohammad et al., 2002; Uzan, et al., 1978; Romanoschi & Metcalf, 2002) confirm that there is an optimum for the tack coat rate, depending on bitumen type, mixture and pavement properties, temperature as well as further parameters. On the contrary, in a more recent study Mohammad (Mohammad et al., 2009) could not find an optimal application rate. An interesting question is further the influence of time of application the tack coats and the development of bonding properties over time. Here, a laboratory study (Raab & Partl, 2009) could give first indications for a positive time effect, but long term investigations and investigations including real traffic are still missing.

2 OBJECTIVE

The paper summarizes the results of an in situ evaluation of tack coats use and performance in Switzerland. The objective of this study supported by the Swiss Road Administration ASTRA was the field evaluation of the short and long term bonding properties between the pavement layers regarding different tack coats types and application rates.

In order to determine the development of bonding properties over time they were measured directly after construction, 5 to 9 months after construction and after trafficking for two resp. three years.

Beside the evaluation of long term performance of bonding properties under real traffic conditions, an accelerated traffic simulator was used on two of the 10 evaluated test sites. Here, the bond values were evaluated 2 months after construction and after the application of 150'000 load cycles. On one test site the testing was done at two different positions.

3 TEST SITES

For the project 11 test sites were chosen. The pavement was either 2 or 3 layered. The surface layer material consisted either of asphalt concrete pavement (AC) or a so-called semi dense pavement layer AC SDA according to a Swiss Guideline (Swiss Guideline SNR 640426, 2012), both with a maximum aggregate size of 8 mm. The binder courses were either asphalt concrete (AC) or high modulus asphalt concrete (AC EME 1) with a hard binder (Swiss Standard SN 640340), again the maximum aggregate size was 22 mm for both type of pavements. Similarly, for the

Table 1. Pavement type of all test sites.

No.	Pavement type		
	layer 1	layer 2	layer 3
1	AC 8	AC T 22	–
2	AC 8	AC T 22	–
3	AC 8	milled, existing	–
4	AC SDA 8	AC EME 1	AC T 22
5	AC 8	AC EME 1	milled, existing
6	AC 8	AC EME 1	AC EME 2
7	AC 8	AC B 22	AC T 22
8	AC 8	AC B 22	AC T 22
9	AC 8	AC BT 22	milled, existing
10	AC 8	AC EME 1	milled, existing
11	AC SDA 8	AC EME 1	milled, existing

Table 2. Tack coat types and rates of all test sites.

No.	Tack coat type		Application rate g/m ²	
	Interface 1	Interface 2	Interface 1	Interface 2
1	HC	–	200	–
2	HCP	–	200	–
3	HC	–	300	–
4	HCP	–	250	350.
5	HCP	HCP	250	450
6	HCP	HCP	250	350
7	HCP	HCP	200	300
8	HC	HC	250	400
9	HCP	HCP	250	450
10	HCP	HCP	250	300
11	HCP	HCP	250	400

base layer either asphalt concrete (AC) or high modulus asphalt concrete with a hard binder (AC EME 2) according to the Swiss standard (Swiss Standard SN 640340) and a maximum aggregate size of 22 mm were used.

In order to evaluate the influence of a milled surface in some cases the tack coat and the overlay were applied on the milled surface of the existing pavement. Since tack coats in Switzerland normally consist of cationic bituminous emulsions (European Standard EN 13808, 2005), this kind of tack coat was chosen; they were either non polymer modified (HC) or polymer modified (HCP) emulsions. The evaluated test sites including pavement and tack coat type as well as tack coat application rates are shown in Tables 1 and 2.

4 TESTING

The interlayer bond properties between the different pavement layers were determined using the Leutner shear test (Leutner, 1978). Figure 1 shows the device. The test speed was 50 mm/min and all specimens were tested at a temperature of 20°C. Before testing all cores



Figure 1. Shear bond test device according to Leutner (Leutner, 1978).

having a diameter of 150 mm were conditioned in a temperature controlled chamber at 20°C.

For every test section at least 6 replicates (sometimes even up to 15) were used to determine the average shear force.

5 ACCELERATED TRAFFICKING

For accelerated pavement trafficking the Traffic Simulator MLS10 (Mobile Load Simulator) was used (Arraigada et al., 2012).

The MLS10 is a machine that simulates full-scale truck loading on pavements. The machine loads the pavement with unidirectional tire passings in a length of about 4.2 m, simulating the load of half an axle of a truck. The rolling speed of the tires can go up to 22 km/h, reproducing the passing of up to 6000 half axles per hour. A hydro-pneumatic suspension system allows setting the loads applied by the tires up to 65 kN, corresponding to a 130 kN axle load.

The MLS10 has a total weight of 32 t and essentially consist of a steel frame made of two large vertical iron plates connected through four robust tanks of about 2 m length and 1 m in diameter, thus creating a very stiff frame for the whole system. One of the tanks is used for water storage and the other three for diesel, each having 1300 liter capacity. This provides additional ballast and allows operating the on-board diesel engine of the machine for about 300 h without refueling. The engine is coupled with a generator that delivers the required power of 50 kW/h for a fully autonomous operation of the machine. Attached to the internal face of the frame plates are two pairs of guide rails that form a closed loop path, like a chain saw.

The tires for loading the pavement are mounted in four bogies, which are strong steel framed carriages

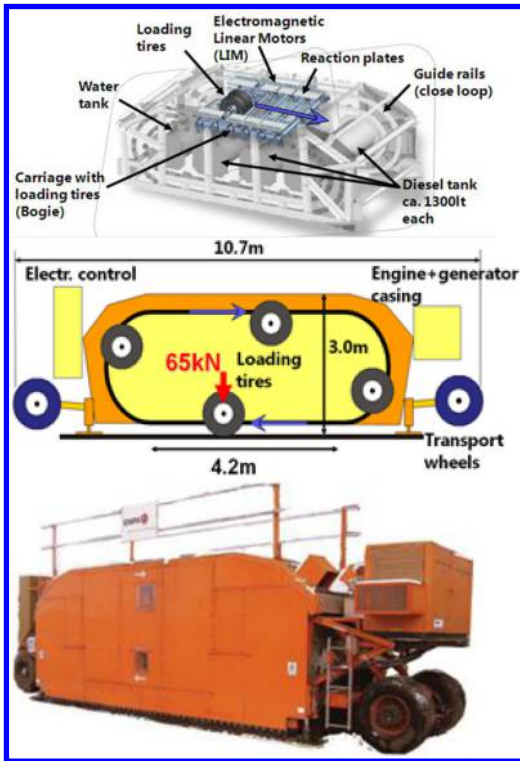


Figure 2. Frame and detail of one of the bogies; schema of the loading principle; view of the MLS10.

that are assembled to a chain rolling along the guide rails. The four bogies of the MLS10 have steel wheels that fit within the rails. The bogies are pulled contactless by 24 linear induction motors (LIM). The rails are built in such a way that the freely revolving tires touch down smoothly to the surface before loading the pavement along the trafficked path length.

The MLS10 is equipped with four transport wheels which can be raised and lowered hydraulically, thus lifting up the whole frame by about 1m and giving room for maintenance work, such as checking tire pressures and pavement sensors as well as measurements of profiles together with crack and damage inspection. The transport wheels allow maneuvering of the machine around the test site and driving the MLS10 to or off low bed trucks for long distance transport. The possibility of easily transporting the MLS10 on a flatbed truck makes it fully mobile. A detail of the frame and bulk view of the MLS10 is presented in Figure 2.

The MLS10 was in this case used for simulating traffic load in an accelerated way. Two motorway sites were chosen and on each test site 150'000 cycles were applied. The MLS10 was setup to apply 65 kN in each of the four bogies, using a super single tire configuration. This corresponds to half of a 130 kN axle load. The tire pressure was set to 10.5bar. The trafficking speed used for the tests was 22km/h. The load was channelized, i.e. no lateral wandering was applied.

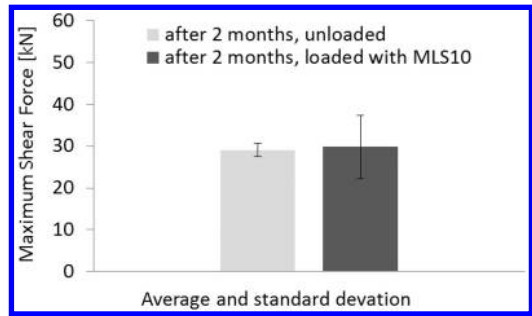


Figure 3. Shear forces for pavement type 6, AC8 on AC EME 1.

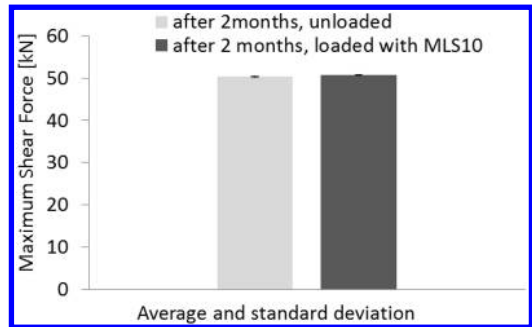


Figure 4. Shear forces for pavement type 6, AC EME 1 on AC EME 2.

6 ACCELERATED TESTING WITH MLS 10

Both test sections tested with accelerated traffic simulation had a three-layered pavement structure (motorway) according to type 6 with AC 8 for surface course on top of two high modulus asphalt concrete courses and type 10 with AC 8 surface and a high modulus asphalt concrete on top of the milled existing layer (see Figure 2). For type 10, two positions were tested.

Figures 3 to 6 show the results for the bond values (maximum shear force). From the Figures it is obvious that trafficking with the traffic load simulator MLS10 did not lead to a measurable increase of the bond forces. In case of the surface layer of both pavement types, the values after loading show quite a big scattering (high standard deviation), which indicates the potential of shear force increase due to MLS 10 loading.

Overall the bond forces are quite high from the beginning (requirement according to the Swiss standard is only 15 kN for surface course and 12 kN for the other layers). For the lower layers in Figure 4, the shear strength was around or even exceeded 50 kN, the measurable load of the machine, therefore an increase would not have been shown.

Further, it is worth mentioning, that all MLS10 loading took place at lower temperatures (0° to 5°C). This and the fact that a number of 150'000 cycles

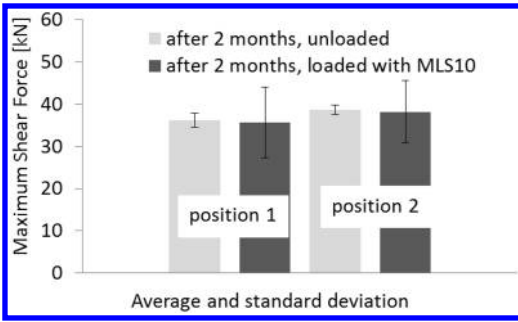


Figure 5. Shear forces for pavement type 10, AC8 on AC EME.

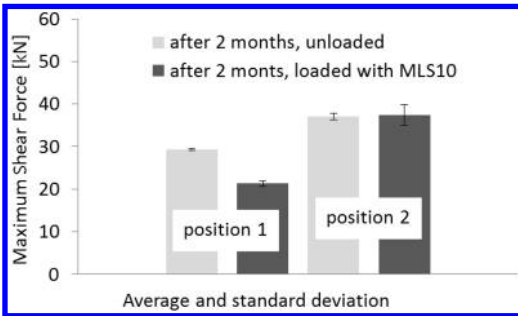


Figure 6. Shear forces for pavement type 10, AC EME on milled existing pavement.

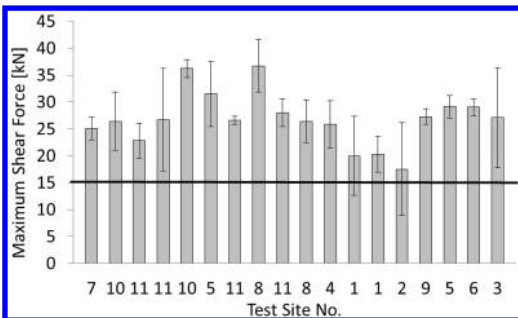


Figure 7. Maximum shear forces for the bond between surface and binder layer, solid line (15 kN) stands for the requirement according to Swiss standard for all investigated sites.

might not be enough for such a strong and stiff pavement structure (motorway) can explain the unexpected results.

7 RESULTS OF BOND TESTING

All test results for the bond testing (maximum shear force) directly after construction show for all the sites, all kind of pavement layers and for all types of tack coat very high values >20 kN (see Figures 7 and 8).

For all surface and binder courses the values are above the requirement from the Swiss standard (Swiss

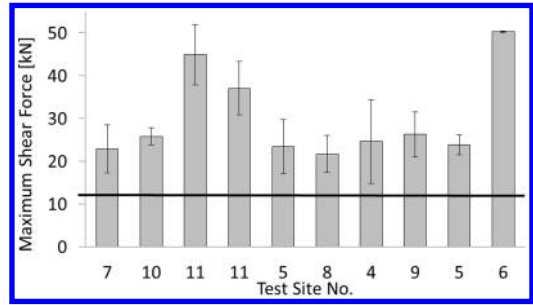


Figure 8. Maximum shear forces for the bond between binder and base layer, solid line (12 kN) stands for the requirement according to Swiss standard for all investigated sites.

Standard SN 640434, 2011) of 15 kN for a 150 mm diameter core and for the lower layers they are far above the required 12 kN.

The investigation shows that the cationic emulsions used in Switzerland seem to work very well.

In this investigation the average value of the maximum shear force does neither depend on the mixture type of the layer nor the type of tack coat (polymer modified versus non-polymer modified). Further, the application rate between 200 g/m^2 and 300 g/m^2 appears to have no influence on the measured maximum shear force, which also means that varying the applied amount according to surface roughness and the maximum aggregate size of the underlying layers seems to work well.

8 DEVELOPMENT FOR BOND OVER TIME

When looking at the development of the bond values over time as selectively depicted in Figures 9 and 10 for the three-layered pavement type 7, it becomes clear that shear bond values increase with time. The increase after 3 years (36 months) due to traffic compaction is in most cases smaller than the short term (after 5 resp. 9 months) increase due to curing and traffic compaction.

The Figures give the mean shear force – shear displacement curves for all determined bond values; the standard deviation is also depicted.

Figure 11 clearly shows the evolution of shear forces over time since the shear bond for this layer had been tested additionally 6 days after construction. As visible from the Figure there is a small, but noticeable increase of bond values after 6 days which can be contributed to the curing of the tack coat (cationic emulsion). The shear force increase over 3 years is about 50% or more than 10 kN for the bond between surface and binder course and about 25% or 6 kN for the bond between the lower layers.

Overall the greatest improvement of bonding properties can be determined after 5 resp. 9 months, although the bond values further increased due to traffic induced compaction as the measurements after 36 months show.

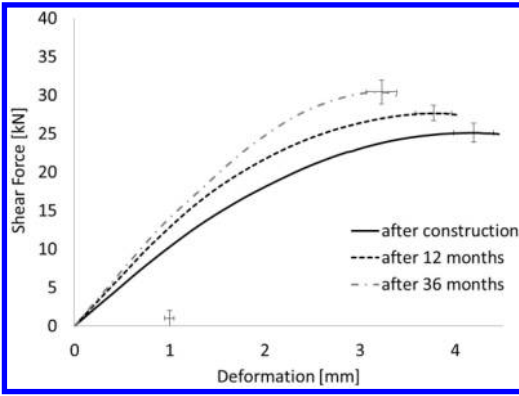


Figure 9. Shear force – displacement curves for surface and binder course of pavement type 7.

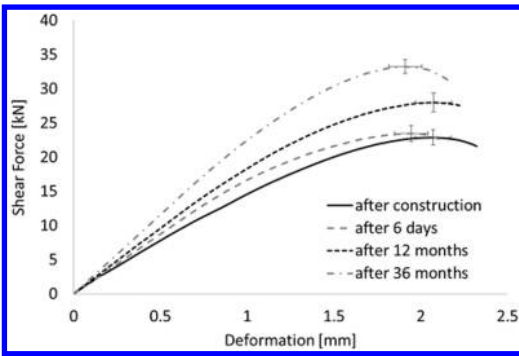


Figure 10. Shear force – displacement curves for binder and binder course (milled existing base course) of pavement type 7.

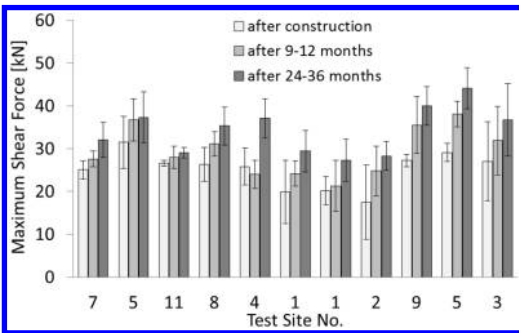


Figure 11. Maximum shear forces for the bond between surface and binder layer after construction, after 9 to 12 months and after 24 to 36 months for all investigated sites.

Additionally in Figures 12 and 13 the development of shear forces over time is given for all investigated layers and test sites. The Figures clearly show the increase of shear forces with time.

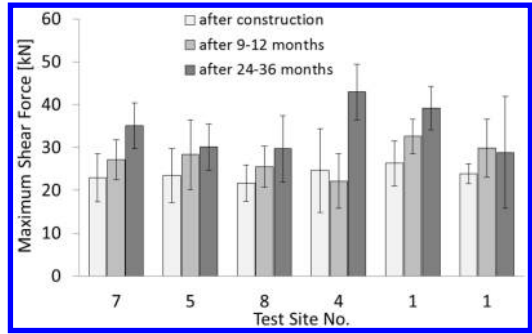


Figure 12. Maximum shear forces for the bond between binder and base layer after construction, after 9 to 12 months and after 24 to 36 months for all investigated sites.

9 CONCLUSIONS

Tack or bond coats are commonly used between the different layers in a bituminous road construction. In Switzerland they normally consist of cationic bituminous emulsions. A study investigating the short and long term behavior of tack coats looking at the bond values between pavement layers revealed the following:

- All test results for the bond testing at a test temperature of 20°C (maximum shear force) directly after construction show for all the sites, all kind of pavement layers and for all types of tack coat (polymer modified versus non-polymer modified) very high values.
- The shear forces are generally >20 kN while the requirements according to the Swiss Standard only demand 15 kN for the bond between surface and binder course and 12 kN for the bond between all other layers.
- The investigation shows that the cationic emulsions used in Switzerland seem to work very well.
- The average value of the maximum shear force at a test temperature of 20°C does neither depend on the mixture type of the layer nor the type of tack coat (polymer modified versus non-polymer modified). The application rates between 200 g/m² and 450 g/m² appear to have no influence on the amount of the maximum shear force, which also means that varying the applied amount according to surface roughness and the maximum aggregate size of the underlying layers as it is done in Switzerland seems to work well.
- Looking at the development of bond properties over time reveals a clear increase of shear forces due to curing and traffic compaction.
- The curing effect can already be seen when comparing test values directly after construction with values determined after 6 days.
- The greatest improvement of bonding properties can be generally determined after 5 resp. 9 months, although the bond values further increased due to traffic induced compaction as the measurements after 36 months show.

- Accelerated trafficking with the Mobile Traffic Simulator MLS10 did not lead to a measurable increase of the bond forces. Here it was found that the relative low test temperatures between 0°C and 5°C as well as the applied traffic load of 150'000 cycles was not enough for the strong and stiff motorway pavement constructions.

REFERENCES

- Arreigada, M., Partl, M.N., & Pugliesi, A. 2012. Initial Tests Results from the MLS10 Mobile Load Simulator in Switzerland, in *Advances in Pavement Design through Full-scale Accelerated Pavement Testing*, Davis, California – Jones, ISBN 978-0-415-62138-0, pp. 277–285.
- Canestrari, F., Ferrotti, G., Partl, M.N. & Santagata, F. 2005. Advanced Testing and Characterization of Interlayer Shear Resistance. *CD Proceedings of the 84th TRB Annual Meeting*, Washington DC, USA.
- European Standard EN 13808 2005. Bitumen and bituminous binders – Framework for specifying bituminous cationic emulsions European Committee for Standardisation, Brussels or Schweizer Norm SN 670205 NA, (2007): Bitumen und bitumenhaltige Bindemittel Rahmenwerk für die Spezifizierung kationischer bitumenhaltiger Emulsionen, Schweizerischer Verband der Straßen- und Verkehrsfachleute VSS, Zürich, (in German and French).
- Hachiya, Y. & Sato, K. 1997. Effect of tack coat on bonding characteristics at interface between asphalt concrete layers. In *Proceedings of 8th International Conference on Asphalt Pavements*, Seattle Washington, USA.
- Kulkarni, M. B. 2004. Effect of Tack and Prime Coats, and Baghouse Fines on Composite asphalt Pavements. PHD Thesis North Carolina State University, USA.
- Leutner, R. 1979. Untersuchungen des Schichtenverbunds beim bituminösen Oberbau. *Bitumen. Journal No 3*, 84–91, (in German).
- Mohammad, L. N., Raqib, M. A. & Huang, B. 2002. Influence of Asphalt Tack Coat Materials on the Interface Shear Strength. *Louisiana Transportation Research Center, Baton Rouge, LA, USA*.
- Mohammad, L. N., Bae, A. & Elseifi, M. 2009. Effect of Tack coat materials and application rate on the interface shear strength. In *Proceedings of 6th International Conference on Maintenance and Rehabilitation of Pavements and Technological Control Mairepav6*, 8–10th July in Torino, Italy, Vol II, pp 636–645.
- Raab, C. & Partl, M. N. 2006. Adhesion Testing of Rehabilitated Concrete Pavements. In *Proc.10th International Conference on Asphalt Pavements*, Paper No 79, Quebec, Canada.
- Raab, C. & Partl, M. N. 2009. Laboratory Study on Interlayer Bonding using Cationic Tack Coats. In *Proc. of 7th International RILEM Symposium ATCBM09 on Advanced Testing and Characterization of Bituminous Materials*, Volume 1, pp3...12, 27–29 May 2009 in Rhodes, Greece.
- Recasens, M., Jimenez P., Gonzalez, B., & Manuel J. 2003. Evaluation of the effect of tack coat s. LCB shear test. In *Proc. 6th RILEM Symposium PTEBM'03*, Zurich, Switzerland.
- Romanoschi, J. & Metcalf, J. B. 2002. The Characterization of Pavement Layer Interfaces. In *Proc. of the 9th International Conference on Asphalt Pavements*, Copenhagen, 2002.
- Swiss Standard SN 640430 Walzasphalt (Asphalt mixtures), Schweizerischer Verband der Straßen- und Verkehrsfachleute VSS, Zürich, 2012 (in German and French).
- Swiss Standard SN 640434 Prüfplan für Walzasphalt (Testing program for asphalt mixtures) Schweizerischer Verband der Straßen- und Verkehrsfachleute VSS, Zürich, 2011 (in German and French).
- Swiss Standard SN 670461: Bituminöses Mischgut, Bestimmung des Schichtenverbunds nach Leutner (Bituminous mixtures: Determination of Interlayer Bond using the Shear Test according to Leutner), Schweizerischer Verband der Straßen- und Verkehrsfachleute VSS, Zürich, 2000 (in German and French).
- Swiss Guideline SNR 640426 Semidichtes Mischgut und Deckschichten SDA, Festlegungen, Anforderungen, Konzeption und Ausführung (Semi dense mixtures for surface courses SDA, determination, requirements, concepts and realisation) Schweizerischer Verband der Straßen- und Verkehrsfachleute VSS, Zürich, 2012 (in German and French).
- West, R. C., Zhang, J. & Moore, J. 2005. Evaluation of bond strength between pavement layers. NCAT Report 05–08, National Center for Asphalt Technology, USA.
- Uzan, J., Livneh, M. & Eshed, Y. 1978. Investigation of adhesion properties between asphaltic-concrete layers, *Asphalt Paving Technology*, Vol.47.

Investigating rheological effects of WMA additives by means of a viscometer and a newly designed workability device

M. Ateş, S. Temel, P.H. Öz & H.J. Köroğlu

TÜBİTAK Marmara Research Center, Chemistry Institute, Gebze, Kocaeli, Turkey

ABSTRACT: The objective of this study is to analyze the effects of organic and inorganic warm mix asphalt additives on bitumen viscosity by ring and ball softening point device, rotational viscometer and workability device. Sasobit and Aspha-min are used as commercial organic and inorganic additives, respectively. Viscosity experiments are the first step of the laboratory stage, to determine the changes in bitumen characteristics caused by adding warm mix asphalt additives. Viscosity measurement is an appropriate method for organic and chemical additives as they can finely disperse and show their effect directly in bitumen. However, effects of inorganic additives on bitumen cannot be monitored by means of a viscometer. Due to this reason, a workability device was designed to measure the contribution of the additive to bitumen by measuring torque changes with adjustable temperature, time and mixing speed.

1 INTRODUCTION

Hot mix asphalt (HMA), is used as the primary paving material in the world, which consists of aggregate and asphalt binder which are heated and mixed together. The primary sources of emissions in an asphalt plant are the mixers, dryers and hot bins, which emit particulate matter, such as dust, smoke, exhaust vapor and other gaseous pollutants. Some other sources of emissions found at an asphalt plant are the storage silos, truck loading operations, binder storage tanks, conveyors, stockpiles etc.

In order to reduce the emissions from asphalt plants, the asphalt industry is constantly trying to reduce mixing and compaction temperatures of mixes, without significantly affecting their properties. The asphalt industry has been experimenting with warm and cold asphalt mixtures for decades to reduce energy requirements and for environmental benefits (Sutton 2002).

Warm mix asphalt (WMA) is an asphalt mixture which is mixed at temperatures lower than conventional hot mix asphalt. Typically, mixing temperatures of warm mix asphalt range from 100 to 140°C compared to mixing temperatures of 150 to 180°C for hot mix asphalt. Thus, warm mix asphalt has been gaining an increasing popularity in recent years. Rising energy prices, global warming and more stringent environmental regulations have resulted in an interest in warm mix asphalt technologies as a mean to decrease energy consumption and emissions associated with conventional hot mix asphalt production (Jones 2004).

European countries are already using warm asphalt technologies that allow reductions in mixing and compaction temperatures of about 20 to 55°C. The asphalt industry has developed several methods to reduce mixing and lay-down temperatures of asphalt mixtures. In principle, there are three major methods for the preparation of asphalt mixtures at low temperatures. These methods are based on foaming, water bearing agents and special bitumen additives.

The foaming process generally produces tiny steam bubbles inside the asphalt binder, which causes a volume increase, leading to increased wettability of the binder and lower high shear viscosities (Koenders et al. 2000).

The method with water bearing agents is based on the release of chemically bound water from the additives into the binder during the mixing process. Release of this water leads to a finely dispersed steam when it comes in contact with the heated aggregate and binder. The fine steam bubbles lead to micropores that improve the compaction properties of the binders.

The third method is based on adding special additives to the binder to reduce its viscosity. Such types of additives typically consist of paraffinic hydrocarbons. Paraffins are generally soluble in the asphalt binder in the temperature range of 80-120°C. When dissolved in binders, they lead to a significant reduction in viscosity.

In this study, the effects of organic (Sasobit) and inorganic (Aspha-min) warm mix asphalt additives on bitumen viscosity were investigated by employing a rotational viscometer and a newly developed workability device. The effects of the additives on the softening



Figure 1. Viscosity measurement preparation and test setup.

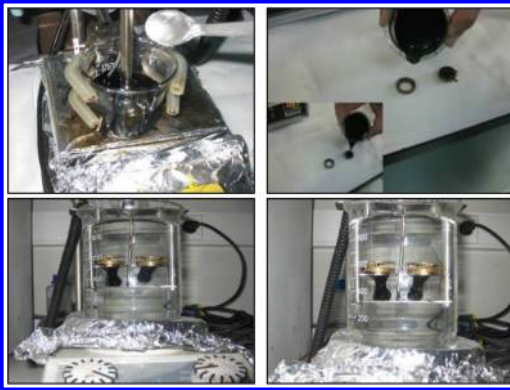


Figure 2. Ring and ball softening point preparation and test set-up.

point of bitumen were also examined for different ratios of additives.

2 EXPERIMENTAL

In the study, 50/70 TUPRAŞ bitumen was used as binder whereas Sasobit and Aspha-min were used as organic and inorganic additive, respectively. Viscosity measurements were performed by using the Brookfield (RVDV-II+P) viscometer device according to standard test method ASTM D4402 (2013). At given mixing temperature, mixing time and mixing speed, 70 g of bitumen and selected amounts of additives were mixed by using an appropriate agitator. After this mixing step, the blend was placed in a sample tube which was then transferred to the viscometer set at the desired measurement temperature. The viscosity measurement set-up is shown in Figure 1.

Ring and ball softening point measurements were performed according to TS EN 1427 and ASTM D36 standards (Fig. 2) (ASTM D36 2014) In the measurements, bitumen temperature was started at 5°C and increased with a 5°C/min rate until softening occurred.

Table 1. Workability device components.

Component	Remark
Paddle	Modified paddle blade
Motor	1.5kW power
Transducer	KTR GmbH
Bowl	6 liters
Heater and Thermometer	Electrical jacket (0–250°C)



Figure 3. Workability device.

Viscosity measurement is an appropriate method for organic and chemical additives as they can finely disperse and show their effect directly in bitumen. However, the effects of inorganic additives on bitumen cannot be monitored by means of a viscometer: due to this reason, a workability device was designed to measure the contribution of the additive to bitumen by measuring torque changes with adjustable temperature, time and mixing speed (Gudimettla et al., 2003; Bennert, 2009; Mogawer, 2008; Khalil et al., 2011).

The newly designed workability device consists of a mixer unit, a torque reader unit, a motor and a control panel (Table 1).

It was used to determine the effects of additives by mixing the aggregate, additive and bitumen at the same time (Fig. 3).

3 RESULTS AND DISCUSSION

3.1 Effect of additive amount

The effect of additive amount on bitumen viscosity was studied by preparing blends at a mixing rate of 800 rpm

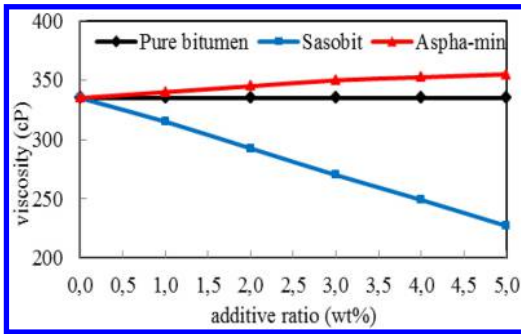


Figure 4. Viscosity results.

for 10 min. at 135°C. The additive amounts by weight of bitumen were in the range of 0–5 wt% and the results are shown in Figure 4. When 5 wt% organic additive was used, bitumen viscosity decreased by 32% compared to the viscosity of the bitumen without adding any additive.

According to a previous study (Wasiuddin 2007), usage of Sasobit in PG64-22 bitumen caused a decrease of viscosity. Viscosity of pure PG64-22 at 135°C was measured as 475cP. After addition of 2 wt% and 4 wt% Sasobit, bitumen viscosities were recorded as 335 and 317cP, respectively.

When 5 wt% of inorganic additive was added to the bitumen, viscosity increased by 8%. As the foaming and viscosity reduction properties of inorganic additive occur immediately after the adding process and the additives were mixed for 10 min before the sample was put into the viscometer, the additive effect could not be detected.

A few theoretical models have been presented for the determination of a particle suspension viscosity. Einstein presented a simple model for fluids with a low concentration of spherical particles as follows (Albert, 1906). This formula is valid for a very low particle volume fraction (Eq. 1):

$$\mu_r = \frac{\mu_{eff}}{\mu_{bf}} = 1 + \varepsilon\varphi \quad (1)$$

where φ = dispersed solid volume fraction in the liquid ($\varphi \cong 0.02$); ε = viscosity coefficient for very small solid particle (ε is 2.5 where solid concentration %1–10); μ = viscosity; r = relative; bf = blank fluid; eff = suspension.

When the experimental results and those from the Einstein model are compared to each other (Fig. 5), it can be seen that they perfectly fit. This proves that the viscosity reduction effect of an inorganic additive could not be detected by the viscometer and that additive behaves like a filler agent, and increases the viscosity after a period of time it is added to bitumen.

3.2 Ring and ball softening point

Softening point is defined as the temperature at which a bitumen sample can no longer support the weight

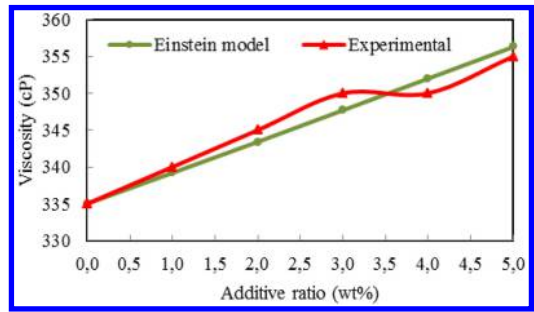


Figure 5. Comparison of Einstein model and experimental data.

Table 2. Ring and ball softening point results.

Additive ratio %	Asphalt additives	
	Aspha-min °C	Sasobit °C
3	45.0	45.0
5	49.0	72.0
6	49.5	92.0
7	50.0	93.0

of a 3.5 g steel ball. Basically, two horizontal disks of bitumen, cast in shouldered brass rings, are heated at a controlled rate in a liquid bath while each supports a steel ball. Softening point is reported as the mean of the temperatures at which the two disks soften enough to allow each ball, enveloped in bitumen, to fall for a distance of 25 mm.

Ring and ball softening point test is of one the criteria to define the stability of asphalt roads. Softening point is particularly important in extreme hot and cold climates. In warm climate regions, if softening point of bitumen is too low, the mixture in which it is included flows. On the contrary, in cold climate regions, if softening point of bitumen is too high, then asphalt mixtures may have cracking problems (Gandhi 2008).

For this purpose pure bitumen, organic additive-bitumen mixtures and inorganic additive-bitumen mixtures were prepared at 135°C 800 rpm with a mixing time of 10 min. Additives were used between 0–7wt% ratio and before the experiments blends were cooled down to 5°C and then heated with a 5°C/min rate. At the end of experiments two measurements were made and average results are shown in Table 2.

According to the results, pure bitumen softening point was measured as 45°C. After adding 7wt% inorganic additive, softening point of the bitumen-inorganic mixture was read as 50°C. When the same amount of organic additive was used, softening point was recorded as 93°C. There is a major difference between the softening points of these samples. High softening point of the organic additive-bitumen blend

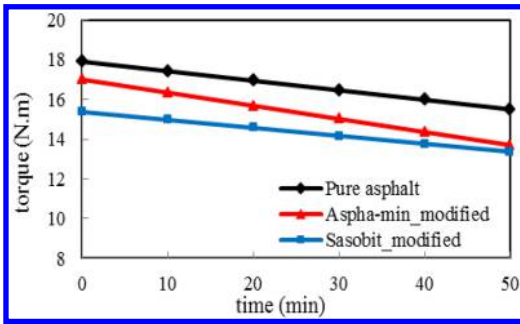


Figure 6. Workability results.

suggests it can be used in warm climate regions. However, for cold regions this property is not desired because of the fragile behavior of the organic additive-bitumen mixture. If the ratio of organic additive increases, brittleness of the bitumen mixture also increases in cold climate regions. On the other hand, the inorganic additive does not induce this fragility property. However, in this case more inorganic additive leads to a higher water susceptibility risk that can cause damage to asphalt.

3.3 Workability device

Inorganic additives reduce the viscosity of the bitumen immediately after they are mixed at 135°C. From the previously reported experiments it was concluded that the viscometer is not a suitable device to measure this viscosity change. Thus, a new workability device was designed to examine this change by mixing bitumen, additive and aggregate at the same time. In the experiments, 3 kg mixture blend consisting of 95 wt% aggregate, 4.7 wt% 50/70 TUPRAŞ bitumen and 0.3 wt% additive were mixed. Temperature was kept constant at 135°C for 50 min and the change in torque was measured. Torque measurements oscillated within a range and linear regression techniques were used to achieve data plotted in Figure 6.

Figure 6 proves that the viscosity reduction effect of the inorganic additive can easily be observed by means of the workability device. When compared to the pure asphalt sample, Aspha-min and Sasobit decreased the workability torques of asphalt mixtures. According to these results, Sasobit additive was more effective than Aspha-min. Sasobit has a capability to decrease the torque of the blend due to the structural similarities of bitumen and Sasobit. However, as discussed previously, the conditions of application area should also be taken into account to decide the kind of additive to use in an asphalt mixture.

4 CONCLUSIONS

The viscosity test is used as a primary method in the laboratory stage to define the behavior of warm mix

asphalt materials. Viscometer readings are useful particularly for organic and chemical additives which can easily disperse and are soluble in bituminous binders. Since inorganic additives behave differently and cause a viscosity reduction immediately after they are mixed with bitumen this effect cannot be detected by means of a viscometer. Inorganic additives cause foaming by releasing their crystalline water into bitumen. At 135°C, this process causes micro bubble forming that expands the volume of the mixture to supply a good coating of aggregate by bitumen. A workability device was designed to evaluate the effects of additives by mixing aggregate and bitumen at the same time. Studies showed that by this device torque change caused by inorganic additives can be easily measured.

ACKNOWLEDGEMENT

This research was supported by the TÜBİTAK KAMAG TARAL 1007 (Project No: 110G091) Project.

REFERENCES

- Albert, E. (1906). Eine neuebestimmung der molekül dimensionen: Ann. Phys. 19–289.
- ASTM D4402 (2013). Standard test method for viscosity determination of asphalt at elevated temperatures using a rotational viscometer.
- ASTM D36 (2014). Standard test method for softening point of bitumen (ring-and-ball apparatus).
- Bennert, T. (2009). Evaluation of workability and compactibility of warm mix asphalt. Rutgers University.
- Gandhi, T. (2008). Effects of warm asphalt additives on asphalt binder and mixtures properties; PhD. dissertation, Clemson University.
- Gudimetla, J.M. & Cooley, L.A. & Brown, E. R. (2003). Workability of hot mix asphalt; national center for asphalt technology report 03–03, Auburn.
- Jones, W. (2004). Warm mix asphalt-a state of art review; Australian Asphalt Pavement Association Advisory Note 17. KEW Victoria; Australia.
- Khalil, S. M. & Arshad, A. K. & AbdulRahman, M. Y. (2011). Development of workability measuring device for asphalt mixture using electronic transducer and temperature regulator, J. Basic. Appl. Sci. Res.1 (7) 721–726.
- Koenders, B.G., Stoker, D.A., Brown, P., Groot, P.C., Larsen, O., Hardy, D. & Wilms, K.P. (2000). Innovative Process in asphalt production and application to obtain lower operating temperatures; 2nd Eurasphalt & Eurobitumen Congress Spain; Barcelona.
- Mogawer, W.S. (2008). Evaluation of Incorporating evaluation of incorporating different dosages of Advera different dosages of Advera warm mix asphalt technology on HMA volumetric and workability on HMA volumetric and workability; Pavement Performance Prediction Symposium-Western Research Institute-July 18th, University of Massachusetts Dartmouth.
- Sutton, C.L. (2002). Hot mix blue smoke emissions Technical Paper T-143: Astec Industries, Inc.
- Wasiuddin, N.M. (2007). Effect of additives on surface free energy characteristics of aggregates and binders in hot mix asphalt; PhD. dissertation University of Oklahoma.

Evaluation of predictive models for the rheological properties of paving asphalt binders

F.O. Martinez, S.M. Angelone & M. Cauhape Casaux

School of Engineering, Road Laboratory, University of Rosario, Rosario, Argentina

ABSTRACT: In 1954, Van der Poel introduced the concept of bitumen stiffness modulus as a function of temperature and time of loading and a nomograph was proposed for estimating this rheological property based on empirical conventional results. Later, during the SHRP Program the Dynamic Shear Rheometer was adopted as a powerful instrument to characterize the physical properties of bituminous materials. This paper reviews the literature referring to models and procedures used to estimate or predict the rheological properties of asphalt binders based on routine conventional testing results and to evaluate these models using both graphical and goodness-of-fit statistical analysis methods using the information contained in a specially developed database.

1 INTRODUCTION

Pavement design is moving towards more mechanistic-based methodologies where the characterization of mechanical properties of paving materials plays a crucial role in the determination of pavement structure responses.

For the asphalt mixtures, the dynamic modulus E^* is the primary input material property. Among other factors, this dynamic modulus is highly dependent of the stiffness of the bitumen.

In 1954, Van der Poel introduced the concept of bitumen stiffness modulus as a function of temperature and loading time based on the simple concept of Young's modulus applied to viscoelastic materials (Van der Poel, 1954).

According to Van der Poel, the "stiffness modulus" of bitumen, S_{bit} , is defined as the ratio between stress and strain for given bitumen temperature and time of loading as:

$$S_{bit} = \left(\frac{\sigma}{\varepsilon} \right)_{t,T} \quad (1)$$

where σ = applied stress; ε = resulting strain; t = time of loading; T = bitumen temperature.

The term S_{bit} is now widely used among bitumen and asphalt technologists being an equivalent to the tensile modulus $E(t)$ for viscoelastic materials.

Based on the obtained results during 20 years of laboratory work, Van der Poel developed a nomograph for the estimation of the bitumen stiffness for a given condition of temperature and time of loading from results of conventional bitumen characterization tests like the Penetration at 25°C, Pen_{25} , and the Ring and Ball softening point $T_{R\&B}$ as input parameters.

According to Van der Poel, the accuracy of this nomograph is amply sufficient for engineering purposes and S_{bit} could be estimated at any temperature condition and time of loading within a factor of two (Bonnaure et al., 1977). Several researchers have also stated that the nomograph was developed for unmodified bitumens and not suitable to be used for polymer-modified bitumens (Read and Whiteoak, 2003; Anderson et al., 1994; Yussof et al., 2011).

Minor corrections to the original Van der Poel nomograph were introduced in 1966 and 1973 in order to take into account the observed inconsistencies for special cases and several asphalt binders (Heukelom, 1966; Heukelom 1973).

The mathematical functions used by Van der Poel in developing the nomograph were never described in any publication. However, Ullidtz has proposed the following approximation formula matching a limited portion of the nomograph (Ullidtz, 1979).

$$S_{bit} = (1.157 \times 10^{-7}) \cdot (t^{-0.368}) \cdot (e^{-PI}) \cdot (T_{R\&B} - T)^5 \quad (2)$$

where t = loading time in seconds; PI = Penetration Index; T = bitumen temperature in °C. The formula is restricted to t between 0.01 and 0.1 seconds, PI between -1.0 and $+1.0$ and $(T_{R\&B} - T)$ between 10°C and 70°C.

In 1998 the Shell International Oil Products developed a computerized version of the nomograph available as the commercial software BANDS 2.0 (Shell, 1998).

Viscosity is also a fundamental rheological property of asphalt binders. Viscosity is a measure of the resistance to flow of a liquid and is defined as the ratio

between an applied shear stress and the resulting rate of shear strain as:

$$\eta = \frac{\tau}{\left(\frac{d\gamma}{dt}\right)} \quad (3)$$

with η = viscosity; τ = shear stress; $(d\gamma/dt)$ = rate of shear strain γ .

The rotational viscometer test using the Brookfield rotational viscometer and the Thermosel system is presently considered the most practical test to determining the viscosity of bitumen. This device allows the testing of bitumen over a wide range of temperatures and rates of shear strain.

If the viscosity of the bitumen is measured at different temperatures, a relationship between testing temperature and viscosity can be formulated according to the ASTM A-VTS equation (ASTM, 2009) in the form of:

$$\log[\log(\eta)] = A + VTS \cdot \log(T) \quad (4)$$

where η = viscosity in cPois; T = bitumen temperature in °R; A = viscosity intercept parameter; VTS = Viscosity Temperature Susceptibility parameter.

Nowadays, the rheological properties of bitumen are usually determined using the Dynamic Shear Rheometer (DSR). In this equipment a sinusoidal oscillatory shear stress τ is applied to a thin disc of bitumen sandwiched between two parallel plates and the resulting shear strain γ is measured. The shear modulus G^* is calculated as:

$$G^* = \frac{\tau}{\gamma} \quad (5)$$

The measurements can be carried out at different frequencies and temperatures. Also the phase angle δ between stress and strains is determined.

The Dynamic Shear Rheometer (DSR) was adopted as a powerful instrument to characterize the rheological properties of bituminous materials over a wide range of temperatures and frequencies during the Strategic Highway Research Program SHRP (Anderson et al., 1994).

However, the DSR is a high cost equipment that is not available in many laboratories and thus it is necessary to have models or equations that could estimate the fundamental rheological properties of bituminous materials from more conventional testing results.

Bari and Witczak have developed a prediction procedure for the shear modulus G^* at a given temperature and frequency from the A-VTS relationship (Bari and Witczak, 2007).

At high temperatures or long loading times the asphalt binder behaves as a fluid while at low temperatures or short loading times it behaves as an elastic solid. In both cases, the asphalt binder could be considered as an incompressible body with the Poisson ratio

ν equal to 0.5 and hence, the following relationship holds:

$$Sbit = 2(1 + \nu) \cdot G^* = 3 \cdot G^* \quad (6)$$

In this paper, empirical and fundamental rheological properties of different bituminous binders were collected and compiled in a large database.

Based on the relationship formulated in Eq. 6, the first objective was to check the validity of the Van der Poel model comparing estimated and experimentally measured stiffness results of those binders.

The second objective of this work was to develop a predictive model of the stiffness of the bitumen using the same inputs as in the Van der Poel nomograph.

Finally, the third objective was to evaluate the relationships proposed by Bari and Witczak to estimate G^* from viscosity measurements.

In all cases, graphical and goodness of fit statistical analysis methods were used for the evaluation of the performance of the analyzed procedures.

2 MATERIALS AND METHODOLOGY

In this study, experimental results reported by Bari in his MSc. Thesis (Bari, 2001) and others obtained by the authors were considered totalizing 29 different asphalt binders, conventional and modified, with different aging conditions.

For all of them, the results of Penetration at 25 °C (Pen_{25}), Softening Point ($T_{R\&B}$), rotational viscosity at different temperatures, and shear modulus G^* and phase angle δ at different temperatures and frequencies were compiled in a large database containing more than 3000 rows. Table 1 presents the results of the conventional tests (Pen_{25} ; $T_{R\&B}$) and the A and VTS parameters of the A-VTS equation for these asphalt binders.

These results were used to evaluate the validity of the Van der Poel nomograph to estimate the stiffness of asphalt binders, to develop an estimation procedure of this rheological property from conventional test results and to evaluate the performance of the predictive model of G^* proposed by Bari and Witczak as it is described in the following section.

3 PROCEDURES AND RESULTS

3.1 Validity of the Van der Poel nomograph

From the experimental G^* results and based on the Eq. 6, the stiffness of the asphalt binders $Sbit_{calc}$ was calculated as $Sbit_{calc} = 3 \cdot G^*$ for all the asphalt binders, frequencies and temperatures included in the database.

Also, with the results of Pen_{25} , $T_{R\&B}$ and for the temperatures and frequencies used for the determination of G^* , the stiffness of the bitumen $Sbit$ was systematically calculated using the computerized version of the Van der Poel nomograph.

Table 1. Conventional properties of the considered asphalt binders.

Name	Type (*)	Pen ₂₅ (10 ⁻¹ mm)	T _{R&B} (°C)	A	VTS
C11	C	54.0	50.5	11.510	-3.8766
C12	C	22.3	64.0	11.006	-3.6749
C13	C	19.5	67.3	10.659	-3.5444
C14	C	39.0	51.5	10.631	-3.5518
C21	C	24.7	63.3	10.869	-3.6295
C22	C	13.7	76.0	10.013	-3.3005
C23	C	11.5	77.0	10.437	-3.4482
C24	C	18.2	63.8	10.642	-3.5420
N11	C	26.0	58.0	11.446	-3.8418
N12	C	7.0	70.0	11.298	-3.7671
N13	C	6.3	70.3	11.447	-3.8191
N14	C	15.8	59.8	11.754	-3.9475
P11	C	112.2	47.0	10.875	-3.6588
P12	C	30.0	58.0	10.732	-3.5827
P13	C	22.8	65.3	10.447	-3.4701
P14	C	66.2	51.3	10.763	-3.6076
P21	C	38.7	52.1	11.963	-4.0379
P22	C	11.8	63.3	11.892	-3.9918
P23	C	23.3	57.5	11.611	-3.9017
PG1	C	69.0	48.1	10.912	-3.6629
PG2	C	42.0	54.0	10.914	-3.6542
PG3	C	23.1	62.5	10.870	-3.6257
PG4	C	39.1	56.0	10.796	-3.6089
N21	M	45.8	84.5	8.497	-2.7675
N22	M	17.3	84.5	8.445	-2.7331
N23	M	14.0	84.0	8.742	-2.8412
N24	M	34.3	85.8	8.481	-2.7527
CA1	C	55.0	49.0	10.359	-3.4645
AM3	M	62.0	65.0	7.725	-2.5091
SB1	M	12.0	65.1	11.231	-3.7502
SB2	M	18.1	63.0	10.479	-3.4840
SB3	M	17.1	68.1	10.285	-3.4047
SB4	M	9.0	700	10.094	-3.3365

(*) C: Conventional; M: Modified.

Figure 1 shows the comparison between the calculated stiffness $Sb_{it_{calc}}$ and the stiffness Sb_{it} from the Van der Poel nomograph for the conventional asphalt binders in log-log space.

Figure 2 shows the same comparison for the modified asphalt binders. In these figures, the line of equality is shown. Also, according to the declared accuracy of the Van der Poel nomograph, other two lines within a factor of 2 are also presented. The visual evaluation of both figures shows that there is an excellent agreement between $Sb_{it_{calc}}$ and Sb_{it} for the conventional asphalt binders but this comparison is fair for the modified asphalt binders as it was expected.

To evaluate the performance of the comparisons, the correlation of these values was assessed using goodness of fit statistics according to subjective criteria proposed by Witczak (Witczak et al. 2002). The statistics include correlation coefficient R^2 , and the relationship Se/Sy (standard error of estimate values/standard deviation of measured values).

The resulting values are shown in Table 2. These results show that even though the Van der Poel nomograph was developed in the 50's with different crudes

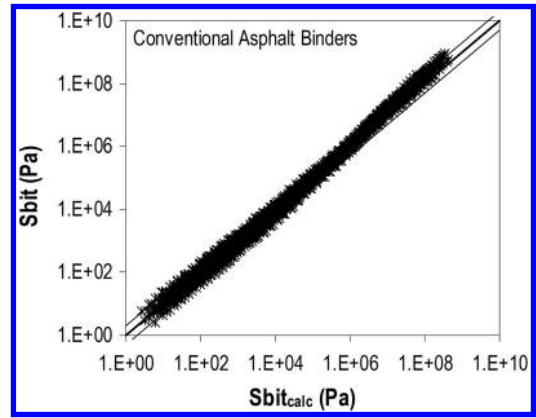


Figure 1. Comparison of $Sb_{it_{calc}}$ and Sb_{it} for the conventional asphalt binders.

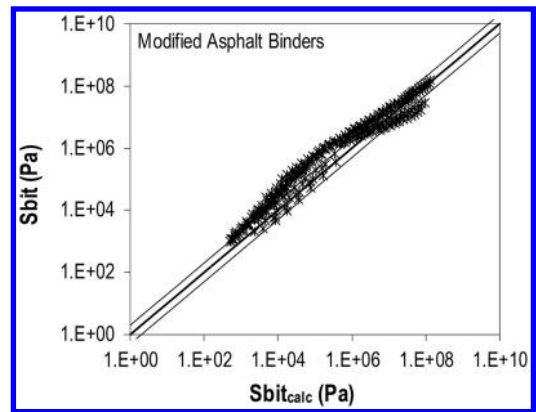


Figure 2. Comparison of $Sb_{it_{calc}}$ and Sb_{it} for the modified asphalt binders.

Table 2. Evaluation of the comparisons.

Asphalt Binders	R^2	Se/Sy	Evaluation
Conventional	0.995	0.072	Excellent
Modified	0.961	0.180	Excellent

and probably different production procedures, it continues to be valid for the estimation of the stiffness of asphalt binders with enough accuracy for practical purposes.

3.2 Development of an estimation procedure for the stiffness of asphalt binders.

As it was stated previously, the mathematical functions used by Van der Poel in developing his nomograph were never described in any publication.

Although the nomograph could be effectively used, it is inconvenient for analysis involving computers due to the lack of these mathematical expressions that could be programmed in a spreadsheet.

In order to save this inconvenient, an estimation model of the stiffness of asphalt binders was developed using the same inputs as in the original Van der Poel nomograph.

A nonlinear optimization procedure was applied using the Solver function included in the Microsoft Excel software minimizing the sum of the square errors between Sbit values resulting from the Van der Poel nomograph and those from the proposed model in the logarithmic space.

The resulting model is shown in Equations 7 to 11.

$$\ln(\text{Sbit}) = a_1 \cdot (T_{R\&B} - T)^2 + [a_2 \cdot \ln(f) + a_3] \cdot (T_{R\&B} - T) + [a_4 \cdot \ln(f) + a_5] \quad (7)$$

with:

$$a_1 = 6.148 \cdot 10^{-6} \cdot \text{PI}^2 - 1.800 \cdot 10^{-4} \cdot \text{PI} + 5.206 \cdot 10^{-4} \quad (8)$$

$$a_2 = 1.132 \cdot 10^{-4} \cdot \text{PI}^2 - 6.371 \cdot 10^{-4} \cdot \text{PI} - 4.448 \cdot 10^{-3} \quad (9)$$

$$a_4 = -3.452 \cdot 10^{-4} \cdot \text{PI}^2 - 3.456 \cdot 10^{-2} \cdot \text{PI} + 7.857 \cdot 10^{-1} \quad (10)$$

$$a_5 = 6.895 \cdot 10^{-4} \cdot \text{PI}^2 + 1.583 \cdot 10^{-2} \cdot \text{PI} + 8.595 \quad (11)$$

where a_1 to a_5 are equation coefficients; T = bitumen temperature in °C; f = frequency in Hz; PI = Penetration Index.

The Penetration Index PI (Pfeiffer & Van Doormaal, 1936) can be determined from the following equation:

$$\frac{20 - \text{PI}}{10 + \text{PI}} = 50 \cdot \left(\frac{\log 800 - \log \text{Pen}_{25}}{T_{R\&B} - 25} \right) \quad (12)$$

Figure 3 shows the comparison between Sbit values resulting from the Van der Poel nomograph and the Sbit estimated using the developed model in log-log space for the conventional asphalt binders. Figure 4 shows the same comparison for the modified asphalt binders.

The equation coefficients have been adjusted for to the results included in the database with PI between -1.3 to 4.7 , $(T_{R\&B} - T)$ between -68 to 71°C and frequency f between 0.16 to 16 Hz.

The visual evaluation shows that the estimation procedure is able to accurately estimate the stiffness of conventional and modified asphalt binders.

For the conventional asphalt binders, 98% of the estimated values are within the range defined by the factor of 2 used in the Van der Poel nomograph. For the modified asphalt binders, 100% of the estimated values are within the same range.

The performance of these estimations was evaluated according to the subjective criteria proposed by

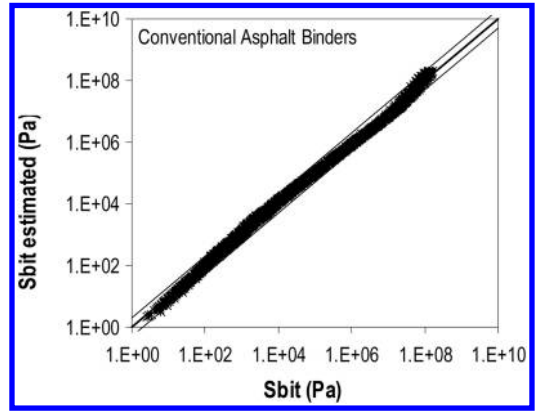


Figure 3. Comparison of Sbit values for the conventional asphalt binders.

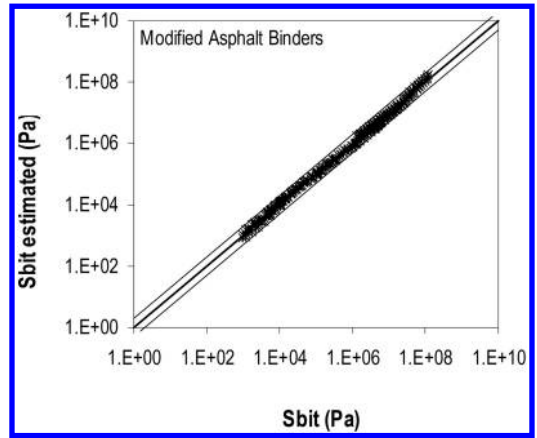


Figure 4. Comparison of Sbit values for the modified asphalt binders.

Table 3. Statistical evaluation of the estimation procedure.

Asphalt Binders	R ²	Se/Sy	Evaluation
Conventional	0.997	0.052	Excellent
Modified	0.998	0.045	Excellent

Witczak using goodness of fit statistics (in log-log space) as it is shown in Table 3.

Hence, the estimation procedure developed in this paper is able to accurately predict the stiffness of conventional and modified asphalt binders for practical purposes. The main advantage is that it is based on the results obtained with the conventional Penetration and Softening Point tests for different testing frequencies and bitumen temperatures.

3.3 Evaluation of the predictive model for δ and G^* proposed by Bari and Witczak.

Bari & Witczak (2007) have stated that the Guide for Mechanistic-Empirical Design of New and

Rehabilitated Pavements Structures developed under the NCHRP Project 1-37A uses viscosity as the principal asphalt binder input parameter. However, with the adoption of the performance grading system (PG) and the associated binder testing, complex shear modulus G^* data are becoming more available than the typical viscosity data. So, there is consensus among the pavement community that instead of viscosity, the complex shear modulus G^* should be the direct input parameter of the Design Guide.

Based on these statements, the authors developed a predictive model of the phase angle δ and the shear modulus G^* using the experimental information contained in a database for 33 different conventional and modified asphalt binders.

First a modified A-VTS relationship that reflects the effect of loading frequency on the binder viscosity is formulated as follows:

$$\log[\log(\eta_{f,T})] = A' + VTS' \cdot \log(T) \quad (13)$$

where $\eta_{f,T}$ = viscosity of the bitumen as a function of loading frequency f and temperature T in cPois; A' and VTS' = modified A and VTS parameters.

$$A' = 0.9699 \cdot f^{-0.0527} \times A \quad (14)$$

$$VTS' = 0.9668 \cdot f^{-0.0575} \times VTS \quad (15)$$

Second, the phase angle δ is obtained from the following equation:

$$\delta = 90 + (-7.3146 - 2.6162 \cdot VTS') \times \log(f \cdot \eta_{f,T}) + (0.1124 + 0.2029 \cdot VTS') \times [\log(f \cdot \eta_{f,T})]^2 \quad (16)$$

Finally, the complex shear modulus is predicted as:

$$G^* = 0.0051 \cdot f \cdot \eta_{f,T} \cdot (\sin \delta)^{7.1542 - 0.4929f + 0.0211f^2} \quad (17)$$

As the results reported by Bari in his MSc. Thesis were used in the development of the prediction model, the total database was depurated and only the experimental results obtained by the authors of this paper were considered for the evaluation of its performance. Few outlier points with measured phase angles greater than 90 degrees were also eliminated from the database.

Then, the equations (13) to (17) were systematically applied to the data contained in the reduced database and the estimated G^* values were compared with those results experimentally measured.

Figure 5 shows the comparison between measured and estimated phase angle values for all the asphalt binders (conventional and modified) while Figure 6 shows the same comparison for the G^* values using the model as it was proposed by Bari and Witczak.

For the phase angle, the data points are greatly scattered around the line of equality with a small correlation coefficient.

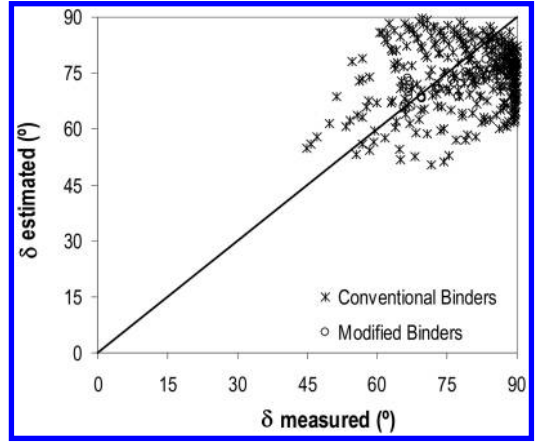


Figure 5. Comparison of measured and estimated δ values.

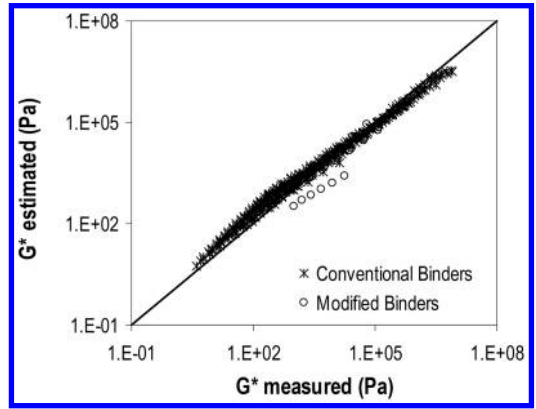


Figure 6. Comparison of measured and estimated G^* values.

However, the comparison for the G^* values is excellent with a very good correlation coefficient ($R^2 = 0.987$) and small Se/Sy ($Se/Sy = 0.100$).

These statistics are similar than those reported by Bari and Witczak in their study for 41 different asphalt binders.

It seems that the influence of the factor $(\sin \delta)$ on the final calculation of G^* is not very significant. Also, the factor $(\sin \delta)$ is within a narrow range between 0.4 and 1 for the measured values considered in this analysis.

Based on this observation, a simplified model is proposed for the estimation of G^* with the same functional form but where the factor $(\sin \delta)$ has been replaced by a constant C_2 as follow:

$$G^* = C_1 \cdot f \cdot \eta_{f,T} \cdot (C_2)^{C_3 + C_4 f + C_5 f^2} \quad (18)$$

with C_1 to C_4 : fitting parameters.

This model was optimized based on minimizing the sum of error squares from the logarithm of measured and estimated G^* values.

The resulting model is:

$$G^* = 0.0038 \cdot f \cdot \eta_{f,T} \cdot (0.9103)^{1.4817 - 0.5861f - 0.0270f^2} \quad (19)$$

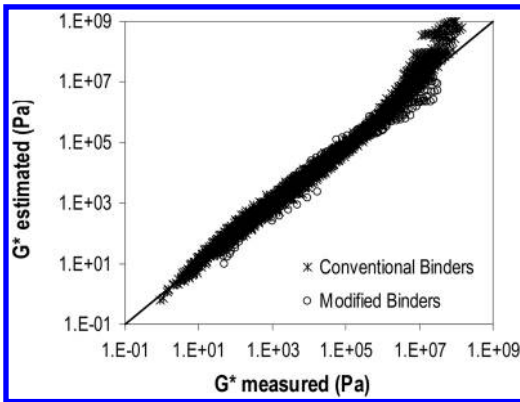


Figure 7. Comparison of measured and estimated G^* values with the simplified model.

Figure 7 shows the comparison between measured and estimated G^* values using the preceding model in the logarithmic space for the entire database.

The visual evaluation shows that the data points are well distributed along the line of equality with a small bias for the G^* values greater than 1.10^7 Pa.

The goodness of fit statistics are excellent with a correlation coefficient $R^2 = 0.982$ and $Se/Sy = 0.136$.

The main advantage of this simplified model is the estimation of G^* values without the need for estimating the phase angle δ .

The model is capable to predict G^* values with enough accuracy for conventional and modified asphalt binders and thus, the resulting estimations could be used as input in different predictive procedures of the dynamic modulus E^* of asphalt mixtures for the practical design of asphalt pavements based on mechanistic principles.

4 CONCLUSIONS

This paper has reviewed some models and procedures used to estimate the rheological properties of asphalt binders from routine conventional testing results and has evaluated these models using both graphical and goodness of fit statistical analysis.

Experimental results reported by Bari in his MSc. Thesis and others obtained by the authors describing the rheological properties of 29 different asphalt binders, conventional and modified, with different aging conditions were compiled in a large database.

The validity of the Van der Poel nomograph was evaluated assuming that the asphalt binder is an incompressible fluid with a valid theoretical relationship between S_{bit} and G^* .

The comparison of values of the stiffness of the asphalt binders calculated from the G^* measurements and those estimated with the Van der Poel nomograph is excellent.

It can be concluded that even though the Van der Poel nomograph was developed in the 50's with

different crudes and probably different production procedures, it continues to be valid for the estimation of the stiffness of asphalt binders with enough accuracy for practical purposes.

As the mathematical functions used by Van der Poel in developing his nomograph were never described in any publication, a mathematical model is proposed for the estimation of the stiffness of asphalt binders. This model, easily programmed in a spreadsheet, is suitable to estimate the stiffness of conventional and modified asphalt binders from the conventional Penetration and Softening Point tests results.

A model developed by Bari and Witczak to predict G^* values from viscosity measurements was also analyzed for a set of data. The comparison gives excellent goodness of fit statistics and with the same order of magnitude as those reported in the original study.

Finally, a simplified model is proposed for the prediction of G^* values without the need for estimating the phase angle δ .

It should be pointed out that these models were evaluated on an asphalt binder database available at the time this paper was prepared. As this is one of the objectives of an ongoing research project at the University of Rosario, other experimental results are being added to the database in order to verify or recalibrate the considered models to be included in a practical design procedure of asphalt pavements based on mechanistic principles.

REFERENCES

- American Society of Testing and Materials. 2009. D2493-01 Standard Viscosity-Temperature chart for asphalts. Volume 04.03.
- Anderson D. A, Christensen D. W., Bahia H. U., Dongré R., Sharma M. G. and Antle C. E. 1994. Binder characterization and evaluation, vol. 3: physical characterization. *Report SHRP-A-369*.
- Bari, J. 2001. Investigation of the rheological properties of typical asphalt binders used in Arizona. MSc. Thesis. Arizona State University.
- Bari, J. and Witczak, M. W. 2007. New predictive models for viscosity and complex shear modulus of asphalt binders: for use with mechanistic-empirical pavement design guide. *Transportation Research Record: Journal of the Transportation Research Board*, 2001: 9–19.
- Bonnaure F, Gest G, Gravois A, Uge P. 1977. A new method of predicting the stiffness of asphalt paving mixtures. *Proc Association of Asphalt Paving Technologists*, 46: 64–104.
- Heukelom W. 1966. Observations on the rheology and fracture of bitumens and asphalt mixes. *Proc Association of Asphalt Paving Technologists*. 36: 359–97.
- Heukelom, W. 1973. An improved method of characterizing asphaltic bitumens with the aid of their mechanical properties. *Proc Association of Asphalt Paving Technologists*. 42: 67–98.
- Pfeiffer, J. P. and van Doormaal. 1936. The rheological properties of asphaltic bitumen. *Journal of the Institute of Petroleum Technologists*. 22: 414.
- Read J, Whiteoak D. 2003. *The Shell bitumen handbook*. 5th ed. London. Thomas Telford Publishing.
- Shell International Oil Products. 1998. Bands2.
- Ullidtz, P. 1979. A fundamental method for the prediction of roughness, rutting and cracking in asphalt pavements.

- Proc Association of Asphalt Paving Technologists*. 48: 557–586.
- Van der Poel C. 1954. A general system describing the viscoelastic properties of bitumens and its relation to routine test data. *J. Appl. Chem.*; 4: 231–6.
- Witczak, M., Pellinen T. and El-Basyouny M. 2002. Pursuit of the simple performance test for asphalt concrete fracture/cracking. *Proc Association of Asphalt Paving Technologists*. 71: 767–778.
- Yusoff, N. I., Shaw, M. T. and Airey, G. D. 2011. Modelling the linear viscoelastic rheological properties of bituminous binders. *Construction and Building Materials* 25, 2171–2189.

Investigation of the rheological properties of asphalt binder modified with Sasobit

M. Hasaninia & M. Molayem

Department of Civil Engineering, Iran University of Science and Technology (IUST), Narmak, Tehran, Iran

M. Ameri

Center of Excellence of PMS, Safety and Transportation, IUST, Narmak, Tehran, Iran

R. Dourandish

Department of Civil Engineering, Payame Noor University, Shemiranat, Tehran, Iran

ABSTRACT: In order to reduce the creation of greenhouse gases in asphalt mixture production, many additives are used to lower the temperature of asphalt mixture production processes. Sasobit is a common additive that besides lowering the production temperature, can contribute to improving performance characteristics of the asphalt binder. The present study investigates the rheological properties of asphalt binders modified with Sasobit via frequency sweep, multiple stress creep and recovery, temperature sweep and viscosity tests. The Sasobit was added to the original binder at 1 and 2% by weight of binder. This additive increased the percentage of recovered strain (R_{diff}) of the binder and decreased the binder susceptibility against the shear stresses. The modified binders have lower phase angle (δ) and higher shear modulus (G^*) and viscosity at 60°C. However, the values of phase angle in modified binders have different trends in the frequency sweep test.

1 INTRODUCTION

One of the main factors that affect air pollutant is the road construction industry. In order to have environmentally friendly asphalt mixtures, it is necessary to lower the temperature at which asphalt mixtures are produced without any reduction in their performance characteristics and even improve the mechanical properties (Rubio et al., 2012).

There are different methods for warm mix asphalt production, among which utilizing Sasobit is one of the most common approaches. Sasobit is an artificial micro-crystalline wax, which has longer chains and different micro-structure than natural wax in asphalt. The lengths of dominant hydrocarbon chains are almost in the range of 40–115 Carbon atoms while the one in paraffin wax in natural asphalt is in the range of 22–45 Carbon atoms (Syroezhko et al., 2011).

Research shows that adding Sasobit to the asphalt binder increases the complex shear modulus of the binder at intermediate temperatures as well as the softening point and its maximum ductility force. Furthermore, it can reduce the penetration grade (Xiao et al., 2012a).

Binders modified with Sasobit are more resistant to rutting than the unmodified ones. Adding Sasobit increases the $G/Sin\delta$ $G/\sin\delta$ parameter and failure temperature. On the other hand, adding Sasobit causes decrease in phase angle and creep compliance of the original binder (Xiao et al., 2012a).

The performance at low temperature conditions of binders modified with Sasobit was investigated by Liu and Li (Liu and Li, 2012). They showed that by using Sasobit as a binder additive, the asphalt mixtures have lower resistance against low temperature cracking since the modified binders have higher stiffness and less physical hardening index (PHI).

In another study by Edwards et al. (Edwards et al., 2006), they demonstrated that warm mix asphalt mixtures containing Sasobit have higher resistance against rutting and higher dynamic modulus than ordinary hot mix asphalt mixtures.

The use of Sasobit in asphalt binders containing crumb rubber decreases the permanent deformation and penetration grade of the crumb rubber modified bitumen. It also increases the softening point and $G \times Sin\delta$ $G \times \sin\delta$ parameter of the crumb rubber modified binder. The amount of crumb rubber and its mesh structure as well as the amount of Sasobit added are the effective parameters on the foregoing performance characteristics of the modified asphalt binder (Akisetty et al., 2010).

Sasobit can improve the storage stability of crumb rubber in the binder, but it cannot stop the sedimentation at high temperatures (González et al., 2010).

Adding Sasobit to the polymer modified binders can contribute to increase in complex shear modulus and the fatigue parameter ($G \times Sin\delta$) ($G \times \sin\delta$) of the polymer modified binders (Jamshidi et al., 2013).

Sasobit increases the storage stability of the polymer modified binder. The results showed that, in the storage stability test, the difference between the upper and lower parts of softening point of the modified binder with 3 and 6% of Sasobit are 6.8 and 4.7% respectively. The difference between lower and upper parts of binders without Sasobit is 28% (Edwards et al., 2010).

There are few studies done on the properties of asphalt binders modified with Sasobit at high temperatures. In the present study, by using multiple stress creep and recovery test as well as time sweep, frequency sweep and viscosity tests, a more precise research has been carried out to investigate the performance characteristics of asphalt binders containing Sasobit. Utilizing various outputs of these tests, a more precise analysis of the performance of modified asphalt binders with Sasobit at higher temperatures can be performed.

2 PERFORMANCE MECHANISM OF SASOBIT

In general, the waxes are categorized as microcrystals, microcrystals and unshaped. They can also be categorized according to the production process into artificial, partially artificial and natural. Microcrystallines are composed of naphtha and isoparaphines (Edwards, 2005).

Sasobit is an artificial microcrystal wax which is different from the natural wax in bitumen. It has longer chain length and a finer crystalline structure. The length of dominant hydrocarbon chain in Sasobit is about 40–115 Carbon atoms while the length of Paraffin Carbon chain in asphalt is 22–45 Carbon atoms. This widespread hydrocarbon chain length promotes the performance characteristics of the binder and increases the performance temperature range of the modified binder (Syroezhko et al., 2011).

Reduction in viscosity to a desired level and consequently the reduction in mixing and compacting temperatures of asphalt mixtures are the results of having a more broad range in the hydrocarbon chain length of the Sasobit modified binders. Phisertrops paraffins are completely dissolved in binder at temperatures higher than 115C and constitute an isotropic dilution with asphalt binder and cause a decrease in the viscosity of the binder as far as they are in the liquid form. While cooling, the Phisertrops paraffins are grained and formed tiny crystals in asphalt binder and increase the stability and resistance against deformation of the binder (Syroezhko et al., 2011).

3 OBJECTIVE

The main objective of the present research is to compare the properties of ordinary asphalt binders with the ones modified with Sasobit. To this end, the fatigue and rutting performance of binders at intermediate and high temperatures were investigated by means of

Table 1. Properties of base binder.

Properties	Specification	Values
Density at 25 C (g/cm ³)	AASHTO T228	1.01
Penetration Index	AASHTO T49	60
Softening Point (C)	AASHTO T53	52
Viscosity at 120 C	AASHTO T201	1055
Viscosity at 135 C	AASHTO T201	361
Viscosity at 160 C	AASHTO T201	170
Ductility	AASHTO T51	>100

laboratory experiments including temperature sweep, multiple stress creep and recovery and frequency sweep tests. By calculating the recovered strain (R_{diff}), phase angle (δ), viscosity and Complex shear modulus (G) of the binder, an appropriate evaluation of the properties of Sasobit modified binders in comparison to the unmodified binders can be achieved.

4 MATERIALS AND SAMPLE PREPARATION

4.1 Raw materials

A 60/70 Penetration grade bitumen from the Pasargad company in Tehran, Iran was used as the base binder. The properties of this kind of binder are presented in table 1. The penetration grade of Sasobit in 25C is less than 0.1 mm. the melted Sasobit has a viscosity of 12mpois in 135C and it completely dissolves in binder at 115C so that it forms an isotropic solution with bitumen and in the liquid form it can decrease the viscosity of the binder (Hurley, 2006).

4.2 Mixing and sample preparation

A low shear mixer was used for mixing the Sasobit with binder. The Sasobit was added in the 1% and 2% by the weight of the original binder. All the binder samples were aged in the rolling thin-film oven (RTFO) after their mixing with Sasobit in order to represent a short term aging condition. In the RTFO process, the thin films of binders are subjected to heat and air circulation. An amount of 35 g of bitumen are put in six cylindrical glass bottles in a rotating carriage in an oven. The carriage rotates at a speed of 15 r/min at a temperature of 163C for 85 minutes while air is blown at an intensity of 4000 ml/min into the bottles.

5 EXPERIMENTAL PROGRAM

5.1 Multiple stress creep and recovery (MSCR)

This test has been used to measure the percent of recovered strain and unrecovered strain of asphalt binders. The elastic response of binder under the shear stresses can be calculated by this test methodology. The aged samples in the RTFO process are used in this test method. In order to conduct the MSCR test, the

Dynamic Shear Rheometer (DSR) is used. The binder sample is put under a 0.1 kPa shear stress for a 1 second duration followed by a 9 seconds rest period. This loading repeats for 10 cycles. Then after the completion of the first ten cycles, a similar procedure will be applied to the sample with a stress level of 3.2 kPa. According to ASTM D-7405-10a standard at each 0.1 sec interval the relevant output should be recorded (ASTM, 2010). The testing temperature is 60°C.

The value of strain at the end of each loading cycle (ε_1) can be obtained by the following relationship:

$$\varepsilon_1 = \varepsilon_c - \varepsilon_0 \quad (1)$$

In which ε_0 is the strain at the beginning of each cycle and ε_c is the strain value after the applied load at the end of first second.

By considering the nine seconds rest period, if the strain after this period is ε_r , then the total strain over the 10 second interval (ε_{10}) is:

$$\varepsilon_{10} = \varepsilon_r - \varepsilon_0 \quad (2)$$

For each 10 cycle of 0.1 kPa and 3.2 kPa shear stresses, the value of recovery percent can be calculated by:

$$\varepsilon_r (100, N) = \frac{(\varepsilon_1 - \varepsilon_{10}) * 100}{\varepsilon_1} \quad (3)$$

$$\varepsilon_r (3200, N) = \frac{(\varepsilon_1 - \varepsilon_{10}) * 100}{\varepsilon_1} \quad (4)$$

The average of recovery percent for each shear stress level is:

$$R_{100} = \frac{SUM(\varepsilon_r (100, N))}{10} \quad (5)$$

$$R_{3200} = \frac{SUM(\varepsilon_r (3200, N))}{10} \quad (6)$$

The difference of percent recovery between the two stress levels is achieved by the following relation:

$$R_{diff} = \frac{((R_{100} - R_{3200}) * 100)}{R_{100}} \quad (7)$$

The unrecovered percents in each cycle for the two shear stresses are:

$$j_{nr} (100 \cdot N) = \frac{\varepsilon_{10}}{100} \quad (8)$$

$$j_{nr} (3200 \cdot N) = \frac{\varepsilon_{10}}{3200} \quad (8)$$

The average unrecovered percent values for all ten cycles are:

$$j_{nr 100} = \frac{SUM(j_{nr} (100 \cdot N))}{10} \quad (9)$$

$$j_{nr 3200} = \frac{SUM(j_{nr} (3200 \cdot N))}{10} \quad (10)$$

And the percent difference between the two stress levels is:

$$j_{nr-diff} = \left(\frac{(j_{nr 3200} - j_{nr 100}) * 100}{j_{nr 100}} \right)$$

5.2 Temperature sweep test

In order to conduct the temperature sweep test the Dynamic Shear Rheometer (DSR) and a spindle with a diameter of 25 mm and 1 mm gap was used. The test is done in a temperature range of 25–80°C. During the test the loading frequency is kept at 1.59 Hz and the temperature is increased in 1°C increments in every minute. The complex shear modulus and the phase angle for each kind of binder will be measured (Biro et al., 2009).

5.3 Viscosity test

The viscosity of asphalt binder is a good indicator of its behavior at different temperatures, due to different performance characteristics of asphalt binder at different in service temperatures. Since the measurement of modified binder viscosity is done at 60°C, a spindle of 25mm in diameter and 1mm gap was used along with the DSR. Results of this test are presented as curves in terms of binder viscosity and the applied shear rates (Xiao et al., 2012b).

5.4 Frequency sweep test

In order to carry out the frequency sweep test, the DSR with a 25 mm diameter spindle is used. The applied strain is 0.1%. The phase angle and complex shear modulus for each frequency is the output of this testing methodology.

6 RESULTS AND DISCUSSION

6.1 Multiple stress creep and recovery (MSCR)

Different kinds of results can be achieved from the multiple stress creep and recovery test. The strain-time curve at a constant shear stress is one of useful results of the MSCR test. In this test the shear stresses of 100 Pa and 3200 Pa are applied to the modified and base binder specimens in ten cycles of loading and unloading. Results showed that binder modification with Sasobit had a considerable effect in reducing the strain. In the case of adding 2% of Sasobit the amount of strain had fallen from 1.8 to 0.5 under the shear stress of 100Pa. For the shear stress of 3200 Pa, the strain decreased from 60 to 30. This trend indicates the increase in binder resistance against applied stresses

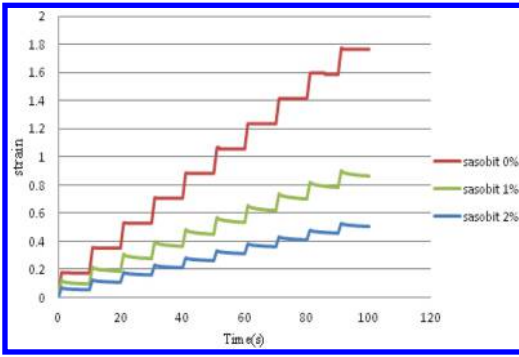


Figure 1. Strain versus time curve for a shear stress of 100 Pa.

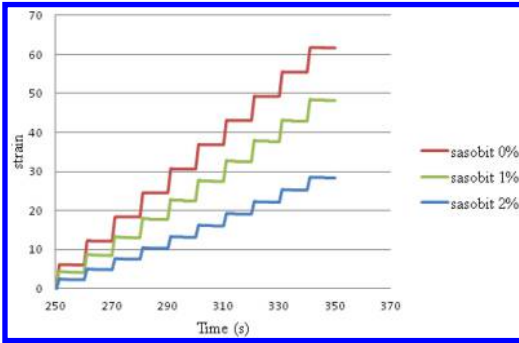


Figure 2. Strain versus time curve for a shear stress of 3200 Pa.

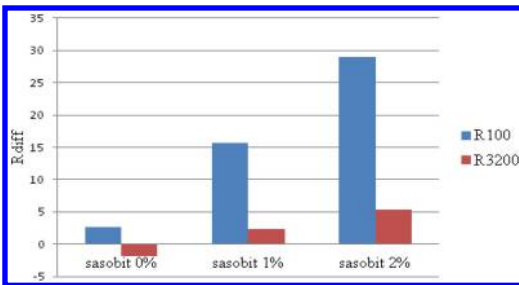


Figure 3. Recovery percent of the binders.

and reduction of binder's deformation after cyclic loading. The strain- time curves for the two loading rates are shown in Figures 1 and 2.

Another potential result from the MSCR test is the percent of recovered strain for the modified and unmodified asphalt binder. The more this percent is, the more elastic will be the response of the binder against the applied loads. In other words, increasing the percent of recovered strain, leads the binder to get more resistant against deformation. The result of the percent of recovered for the base binder and Sasobit modified binders are presented in Figure 3.

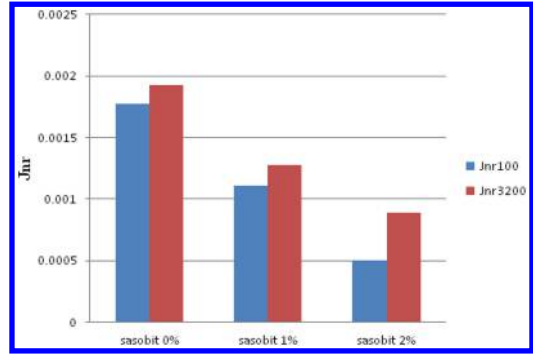


Figure 4. Percent of unrecovered for binders.

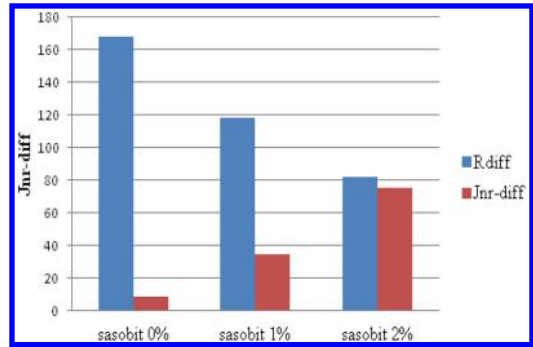


Figure 5. Difference in recovered and unrecovered.

From the results presented in Figure 3, it can be seen that for the case of 3200 Pa of shear load, the percent of recovery is negative in the unmodified binder. This means that under this loading condition the binder has no elastic response and all deformations take place in the plastic mode and there is no recoverable deformation. In this loading condition, adding 2% of Sasobit rises the recovered strain from -0.2% to 5% and for the 100 Pa loading, there is a considerable loading in the percent of recovered strain.

The unrecovered strain is another parameter which can be derived from the MSCR test. In contrast to the recovered percent, a lower value of unrecovered percent indicates higher resistance against deformation. The results of the unrecovered strain are presented in Figure 4.

Another result from the MSCR test is the difference between the percent of recovered or unrecovered in the two stress levels. According to results, the stress sensitivity of the binder to the applied stresses decreases by adding Sasobit. The results of this parameter for the unmodified binder and the two modified ones are illustrated in Figure 5.

Adding Sasobit causes a considerable reduction in the amount of difference between recovered and unrecovered of the modified asphalt binders. The addition of 2% of Sasobit reduces the difference of recovered from 167 to 80 and this difference for unrecovered case is 66 (i.e. from 9 to 75).

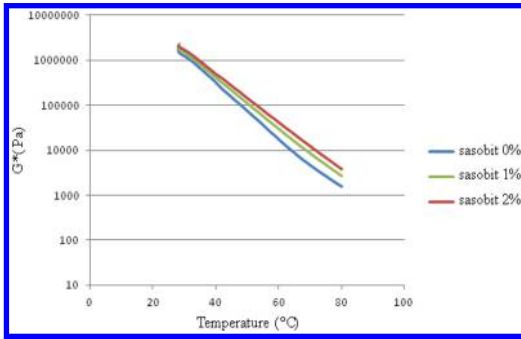


Figure 6. Temperature sweep test results for G^* .

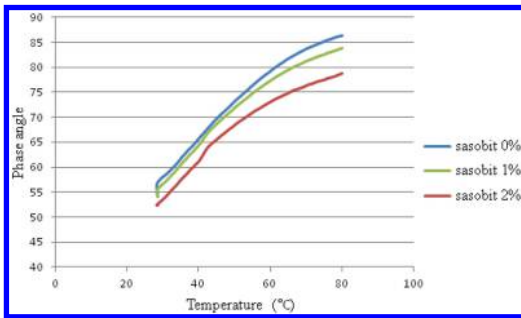


Figure 7. Temperature sweep test results for phase angle.

6.2 Temperature sweep test

The results of the temperature sweep test shows that adding Sasobit increases the complex shear modulus of the modified binders, while with increasing the temperature, the rate of changing of the complex shear modulus for both the modified and unmodified binders are the same. The value of increasing in complex shear modulus of modified binders in comparison to base binders is few at intermediate temperatures but it gets more as the temperature rises. The results of temperature sweep in terms of complex shear modulus (G^*) versus temperature are presented in Figure 6.

Results of temperature sweep for phase angle indicates that by increasing the temperature the phase angle of Sasobit modified binders decreases. This decrease is more at higher temperatures than intermediate temperatures. So using Sasobit as a binder modifier can improve the elastic properties of modified binders in the intermediate to high temperature range. The results of temperature sweep test for phase angle are presented in the Figure 7.

6.3 Viscosity test

The relationships between the shear rate with viscosity and shear stress for the base and modified binders at 60°C are illustrated in Figures 8 and 9 respectively. Since in base binder, the value of viscosity is independent of shear rates, it can be considered as a Newtonian fluid. On the other hand, for modified binders, by adding Sasobit, at the temperature of 60°C , the value

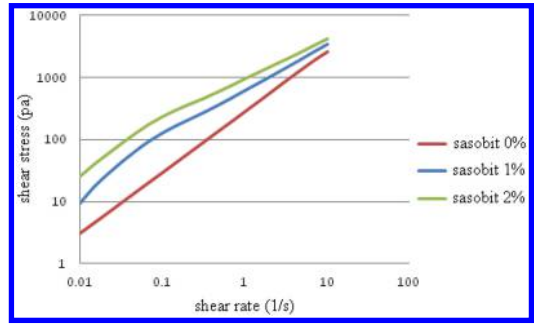


Figure 8. Viscosity versus shear rates at 60°C .

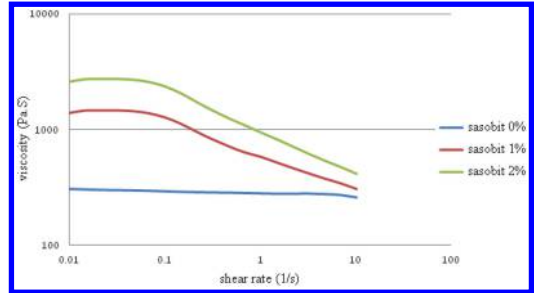


Figure 9. Shear versus shear rates (binder flow) at 60°C .

of viscosity is dependent on the shear rates. Increasing the shear rates cause decrease in the value of viscosity and in high shear rates, the viscosity of Sasobit modified binders are very close to the base binders. Adding Sasobit leads to increase the viscosity of modified binders at 60°C . The modified binders containing 2% of Sasobit has highest viscosity among others. Although it was reported that the value of viscosity of Sasobit modified binders is lower than base binders at higher temperatures in the range of $110\text{--}135^\circ\text{C}$ (Gandhi and Amirkhani, 2007), the present study shows an adverse effect at the temperature of 60°C . (Figure 8).

6.4 Frequency sweep test

The results of frequency sweep test in terms of phase angle and complex shear stress versus the value of frequency are shown in Figures 10 and 11 respectively. Results indicate that by adding Sasobit, the value of phase angle decrease at low frequencies. When frequency gets larger, the phase angles increases and eventually at high frequencies the modified binders have higher phase angles. For the complex shear stress, the frequency has no effect on the rate of change in complex shear stresses of all binders. However adding the Sasobit increases the complex shear stresses of the modified binders.

7 CONCLUSION

In this paper, the performance characteristics of binders modified with Sasobit were investigated by

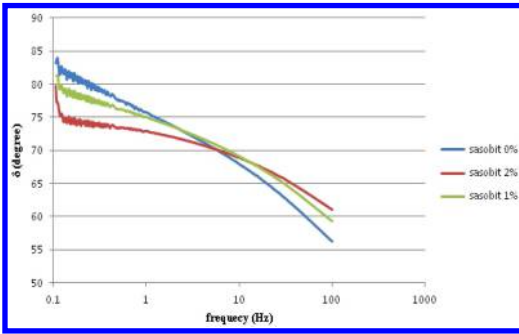


Figure 10. Phase angle in frequency sweep test.

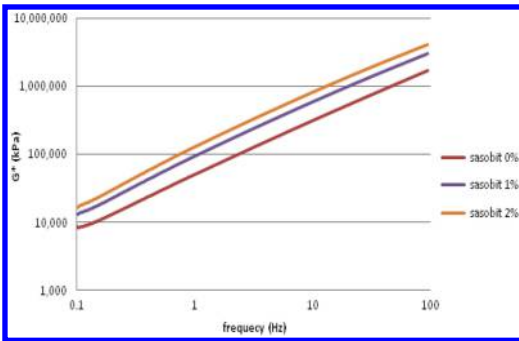


Figure 11. Complex shear stress in frequency sweep test.

means of laboratory experiments such as multiple stress and creep recovery test, temperature sweep test, viscosity and frequency sweep tests. The multiple stress and creep recovery test was used to assess the improvement of elastic and plastic response of modified and base binders against the applied stresses. Furthermore, by calculating the complex shear modulus, phase angle and viscosity which were obtained from temperature sweep, viscosity and frequency sweep tests, a more comprehensive knowledge about the behavior of base binder and Sasobit modified binder at higher performance temperatures can be obtained.

- 1) Adding Sasobit by 1 and 2% by weight of binder causes a considerable decrease in the accumulated of strains in the asphalt binder after 10 cycles of loading for the two stress levels of 100 and 3200 Pa. This means that under cyclic loading, the Sasobit modified binder undergoes less deformation.
- 2) Adding Sasobit by 1 and 2% by weight of binder increases the binder's percent of recovered strain R and decreases the percent of unrecovered strain j_{nr} of it. This phenomenon indicates a more elastic behavior of binder against applied loads which contributes to less deformation during loadings. The more difference between the values of recovered strain and unrecovered strain in modified binders is an indicator of decreasing the plastic deformation under higher loading amplitudes of the modified binders.

- 3) The MSCR test results showed that adding Sasobit can decrease the binder susceptibility against the shear stress.
- 4) The increase of complex shear modulus and decrease of phase angle of Sasobit modified asphalt binders compared to base binders in the temperature sweep test indicates that adding Sasobit can increase the resistance of modified asphalt binder against loading at high performance temperature and increases the elastic part of the material's behavior. The results of the temperature sweep test indicate that the amounts of increase in complex shear modulus and decrease in phase angle for modified binders is more at high performance temperatures (55–75°C) than intermediate performance temperatures. The values of complex shear modulus and phase angle for both modified and unmodified samples are close to each other at intermediate temperatures.
- 5) The results of the viscosity test showed that adding Sasobit increases the viscosity of the binder at intermediate temperature. Increasing the viscosity contributes to an increase in the stiffness of the binder, higher resistance against the penetration and increasing the resistance against rutting.
- 6) In the viscosity test, the base binder was a Newtonian fluid while by adding Sasobit, the behavior of the modified binder is dependent on the rate of shear stress and is no longer a Newtonian fluid.
- 7) By adding Sasobit, the complex shear modulus increased at different frequencies while the phase angle decreased at low frequencies and increased at high frequencies.

REFERENCES

- Akisetty, C. K., Lee, S.-J. & Amirhanian, S. N. 2010. Laboratory investigation of the influence of warm asphalt additives on long-term performance properties of CRM binders. *International Journal of Pavement Engineering*, 11, 153–160.
- ASTM 2010. Standard Test Method for Multiple Stress Creep and Recovery (MSCR) of Asphalt Binder Using a Dynamic Shear Rheometer. *MSCR D7405- 10a*.
- Biro, S., Gandhi, T. & Amirhanian, S. 2009. Midrange Temperature Rheological Properties of Warm Asphalt Binders. *Journal of Materials in Civil Engineering*, 21, 316–323.
- Edwards, Y. 2005. *Influence of waxes on bitumen and asphalt concrete mixture performance*. KTH Architecture and the built environment. PhD.
- Edwards, Y., Tasdemir, Y. & Butt, A. A. 2010. Energy saving and environmental friendly wax concept for polymer modified mastic asphalt. *Materials and Structures*, 43, 123–131.
- Edwards, Y., Tasdemir, Y. & Isacson, U. 2006. Influence of commercial waxes and polyphosphoric acid on bitumen and asphalt concrete performance at low and medium temperatures. *Materials and Structures*, 39, 725–737.
- Gandhi, T. S. & Amirhanian, S. N. Laboratory investigation of warm asphalt binder properties—a preliminary analysis. The fifth international conference on maintenance and rehabilitation of pavements and technological control (MAIREPAV5), Park City, Utah, USA, 2007. 475–480.

- González, V., Martínez-boza, F. J., Navarro, F. J., GALLEGOS, C., PEREZ-LEPE, A. & PáEZ, A. 2010. Thermo-mechanical properties of bitumen modified with crumb tire rubber and polymeric additives. *Fuel Processing Technology*, 91, 1033–1039.
- Hurley, G. C. 2006. *Evaluation of New Technologies for Use in Warm Mix Asphalt* Auburn, Alabama.
- Jamshidi, A., Hamzah, M. O. & You, Z. 2013. Performance of Warm Mix Asphalt containing Sasobit®: State-of-the-art. *Construction and Building Materials*, 38, 530–553.
- Liu, J. & Li, P. 2012. Low Temperature Performance of Sasobit-Modified Warm-Mix Asphalt. *Journal of Materials in Civil Engineering*, 24, 57–63.
- Rubio, M. C., Martínez, G., Baena, L. & Moreno, F. 2012. Warm mix asphalt: an overview. *Journal of Cleaner Production*, 24, 76–84.
- Syroezhko, A. M., Baranov, M. A., Ivanov, S. N. & Maidanova, N. V. 2011. Influence of natural additives and those synthesized by the Fischer-Tropsch method on the properties of petroleum bitumen and quality of floated asphalt. *Coke and Chemistry*, 54, 26–31.
- Xiao, F., Amirkhanian, S. & Zhang, R. 2012a. Influence of Short-Term Aging on Rheological Characteristics of Non-Foaming WMA Binders. *Journal of Performance of Constructed Facilities*, 26, 145–152.
- Xiao, F., Punith, V. S. & Amirkhanian, S. N. 2012b. Effects of non-foaming WMA additives on asphalt binders at high performance temperatures. *Fuel*, 94, 144–155.

Investigation on the physical and rheological properties of acrylate-styrene-acrylonitrile polymer and nano aluminum oxide modified asphalt binders nano aluminum oxide modified asphalt binders

Shaban Ismael Albrka Ali, Amiruddin Ismail & Nur Izzi Md. Yusoff

Sustainable Urban Transport Research Centre (SUTRA), Universiti Kebangsaan Malaysia UKM, Malaysia

ABSTRACT: This study investigates the physical and rheological properties of asphalt binder modified by acrylate-styrene-acrylonitrile (ASA) polymer and nano aluminum oxide (Al_2O_3). The tests implemented in the study were conventional tests, rotational viscosity, X-ray diffraction (XRD) and dynamic shear rheometer (DSR). The obtained results of conventional tests showed that the addition of both modifiers up to 5% increased the hardness of asphalt and reduced their temperature susceptibility. XRD results outcome approved new structural phases formed by using ASA polymer meanwhile structural of base binder had not changed by adding nano Al_2O_3 . The rheological property of modified binders enhanced at low temperatures and high temperatures, as the results of DSR test showed that the complex modulus and fail temperature were improved whereas the phase angle decreased slightly. Adding a different concentration of ASA and Al_2O_3 to base binder had significant effects of high temperatures rutting resistant and improved low temperature fatigue. Obviously the influence of nano Al_2O_3 on base asphalt binder was greater than modification of ASA polymer. **KEYWORDS:** modified asphalt binder, ASA polymer, nano Al_2O_3 , Physical and rheological properties and DSR.

1 INTRODUCTION

Recent roads need to show better performance under high traffic density and axle loading than in the past. The use of modified binders offers a promising way to improve asphalt binder and asphalt mixture (Selvavathi et al., 2002, Sikdar et al., 1999). In several cases, heavy traffic loading and severe weather conditions will result in serious functional damage of the asphalt-road surface (Ismail et al., 2012, Sun et al., 2006) regrettably, asphalt binder becomes fluid at higher temperatures and is stiff at lower temperatures, which can result rutting and cracking at high and low temperatures respectively. This temperature susceptibility limits its application. Hence, it is an essential to improve the performance of asphalt binder with the addition of various modifiers, such as rubber, polymer, and nanoparticles (Zhang et al., 2009, Huang, 2008, Fu et al., 2007). In recent years, polymeric materials and nanomaterial are commonly used as additives for modifying asphalt-road surfaces (Kumar et al., 2006, Sun et al., 2006), thereby mitigating numerous main causes of asphalt-pavement disasters that occurred over the last years (Wekumbura et al., 2007, Yildirim, 2007, Baghini et al., 2014, Al-Mansob et al., 2014). Moreover, the polymer and nanomaterial when they used as modifiers of asphalt should not lead to an extremely viscous at high temperatures or quiet toughness at low temperatures. Modifying

asphalt binder by polymers and nanomaterial can substantially improve the properties of asphalt binder which led to building of safer roads as well as the reduction of maintenance costs (Polacco et al., 2005, Pérez-Lepe et al., 2007). The polymers were used as modifiers of asphalt binder can be distributed into two categories, namely; elastomers which improve the elastic behavior of bitumen since they resist permanent deformation under tensile forces and recover their original shape after loading, plastomers operate to increase the viscosity and rigidity of bitumen by forming stiff network structures resisting deformation (Sengoz and Isikyakar, 2008, Chen and Huang, 2007, Casey et al., 2008). On the other hand, the commonly nanomaterial used in the modification of asphalt were known as nanoclay, nanosilica and carbon nanotube, testing of asphalt binder confirmed that the nanomaterial modified asphalt capable to increase the toughness and improve ageing resistances. Moreover, when small amounts of nanomaterial added to asphalt have significant influences on physical and rheological properties (Khattak et al., 2012, Paul and Robeson, 2008, Sinha Ray and Okamoto, 2003, Liu et al., 2009). In this paper, the main purpose is to investigate the physical and rheological properties of acrylate styrene acrylonitrile (ASA) and nano aluminum oxide (Al_2O_3) as modifiers of asphalt binder in terms of its conventional testes, viscosity, storage stability and rheological properties.

Table 1. Physical property of base binder, ASA and Al₂O₃.

Material	Properties	Value
Asphalt 60/70	Specific Gravity	1.03
	Penetration @ 25°C	70
	Softening point °C	47.0
	Viscosity @ 135°C	0.5
	Ductility cm	≥100
ASA	Size mm	2
	Specific Gravity	1.04–1.07
Al ₂ O ₃	Size, nm	13

2 MATERIALS AND METHODS

2.1 Materials and samples preparation

To prepare the modified asphalt binders, the following materials were used: (1) 60/70 penetration grade, base asphalt binder supplied from a factory in Port Klang, Malaysia; (2) acrylate styrene acrylonitrile (ASA) procured from Zibo Huaxing Additives Company china; (3) nano aluminum oxide (Al₂O₃) procured Shiji-azhuang Chanchiang Corporation in China. Table 1 shows the physical properties of the base asphalt binder and the modifiers. The mixes were prepared in the laboratory using Silverson high-shear mixer, nearly 250 grams of base binder heated up to become fluid, then different amounts of concentration of modifiers ASA and Al₂O₃ (3%, 5% and 7%) added by the mass of base binder under the speed of 5000 ramps and kept mixing for 90 minutes with consistent temperature nearby 170 ± 1°C, to produce homogenous mixes.

2.2 Physical properties

ASTM specifications implemented on conducting conventional tests; penetration, softening point and ductility to evaluate the changes of physical properties of ASA polymer and nano Al₂O₃ comparing with the base asphalt binder.

2.3 Viscosity

A rotational viscometer is normally used to determine the viscosity of the asphalt; the spindle 21 is lowered into bitumen approximately 10.5 g (±0.5 g) and rotated. Rotational viscosity is known as the degree of asphalt binder fluidity and is used to checked the ability of handling and pumping of unmodified and modified asphalt during mixing, compaction and storage (Al-Khateeb and Al-Akhras, 2011). Viscosity test is valid for unmodified and modified asphalt binders and in this paper the viscosity was investigated at the temperatures of 135°C, 155°C and 165°C.

2.4 High temperature storage stability

The storage stability of all binders was measured as follows. The samples were poured into aluminum-foil tubes; the tube with height of 16 cm and diameter of 3 cm. Therefore, the tubes were kept in an oven vertically for 48 hr. under a temperature of 163 ± 5°C. Then, the samples were divided into three equal parts

after cooled at room temperature. The upper and lower parts were used to estimate the storage stability of the ASA and Al₂O₃ determining the corresponding softening points. If the difference among the upper and the lower parts was more than 2.5°C, the materials were considered to be unstable. Meanwhile, if the softening points difference was lower than 2.5°C, the materials were considered to have great storage stability (Zhang et al., 2011, Al-Mansob et al., 2014).

2.5 X-ray diffraction (XRD)

XRD graphs in this study were achieved using a Bruker AXS, D8 Advance with wavelength 0.15406 nm the tests were conducted at room temperature for all binders.

2.6 Dynamic shear rheometer (DSR)

A dynamic shear rheometer (DSR) is used to describe the viscoelastic performance of asphalt at low, intermediate and high service temperatures. In this study, the rheological test was performed by using a Haake Rheostress 1 rheometer under the controlled-deformation conditions at temperatures varying between 10 and 75°C, and various frequencies between 1 rad/s (nearly 0.159 Hz) to 100 rad/s (nearly 15 Hz) using 25 mm and 8 mm diameter plates with 1 mm and 2 mm gaps respectively. Furthermore, the stress selected was adjusted to remain within the linear viscoelastic area for all the binders during the rheological testing (Yang et al., 2013). The failure temperatures are measured for all binders according to the Superpave specification for $G^*/\sin \delta$ values of less than 1.0 KPa in case of unaged asphalt. Moreover, the results of the complex shear modulus G^* and phase angle δ were used for the construction of master curves (Walubita et al., 2011).

3 RESULTS AND DISCUSSION

3.1 Effects of ASA and Al₂O₃ on physical properties of asphalt

The effect of several parentages of ASA polymer and nano Al₂O₃ on the physical properties of asphalt was investigated using conventional tests penetration, softening point, and ductility. As exhibited in Table 2, both modifiers show a remarkable reduction in penetration value as well as a great improvement in softening point. However, ASA polymer samples show an obvious reduction and improvement in penetration and softening point comparing with nano Al₂O₃ samples. The decrease in penetration and increase in softening points indicates an increase in hardness of the modified asphalt. Therefore, increasing the hardness of modified asphalt binders by polymer and nano leads to improved their temperature susceptibility (Airey, 2002). On the other hand, from Table 2 observed that the ductility of modified binders is gradually decreased with increasing ASA polymer or nano Al₂O₃

Table 2. Physical properties of unmodified and modified asphalt binders.

Percentage	ASA polymer contents (weight %)				Al ₂ O ₃ contents (Weight %)		
	0	3	5	7	3	5	7
Penetration, mm	70	48	22	36	28	25	38
Softening point°C	46	50	56	53	51	53	51
Ductility cm	>100	53	41	35	95	62	91

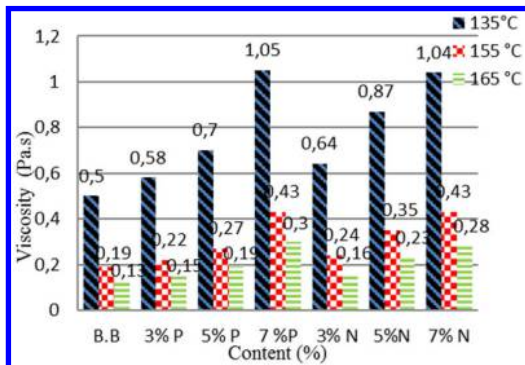


Figure 1. Dynamic Viscosity of base binder ASA and Al₂O₃ modified binders (B.B base asphalt, P = Polymer and N = Nano).

concentration up to 5%, which clarifies the rise in the stiffness of binders. In addition, the 7% for both modifiers show different behavior as the ductility value increase, but still stiffer than a base binder.

3.2 Dynamic viscosity

The dynamic viscosity is a measure of the flow characteristics of asphalt and can be used to verify that asphalt can be pumped and handled at a hot-mixing facility. It is also used to estimate the mixing and compaction temperatures of asphalt mixtures of base asphalt binder. In general, a higher viscosity results in higher mixing and compaction temperatures (Institute, 2007, Xiao et al., 2014). From Figure 1, it can be noted that increasing the test temperature lead to decrease the viscosity values immediately, regardless of the ASA polymer or nano Al₂O₃ concentration. Therefore, the modified asphalt with the highest ASA polymer concentration has the highest values of the viscosity than modifying binders with nano Al₂O₃ and base binders (B.B). Also, it is observed that the base binder has the lowest viscosity value.

3.3 Effects of ASA and Al₂O₃ on high temperature storage stability

The storage stability of modified asphalt binder has been recognized as an essential principle of manufacture and usage of the modified asphalt. Therefore, when the ASA polymer and nano Al₂O₃ modified

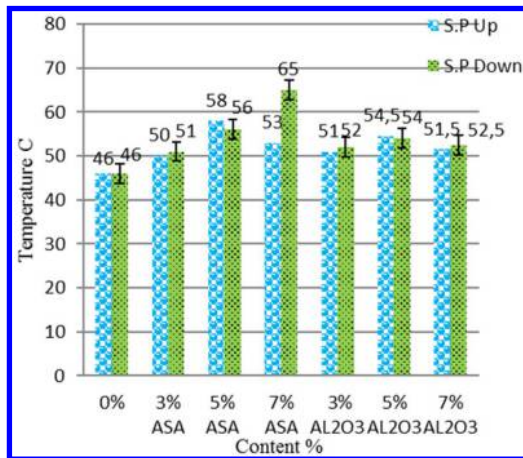


Figure 2. Storage stability evolutions of base asphalt, ASA and Al₂O₃ modified binders.

asphalt binder were kept under quiescent conditions at high temperature, ASA polymer and nano Al₂O₃ might progressively move up or down and finally a float or sedimentation could accrue, which may cause changes in properties between the up and the down parts of the tube mentioned above in Section 2.4 (Zhang et al., 2010, Wen et al., 2002). Figure 2 shows the results obtained from the softening point test. Furthermore, the differences among the up and down parts temperature of the ASA modified asphalt samples is less than 2.5°C for 5% and less of the ASA, but for 7% of ASA the temperature differences between the top and bottom are above the permitted values. Meanwhile, the differences between the top and bottom sections of the samples modified by Al₂O₃ are less than 1.5°C for whole binders. In general, the addition of ASA polymer and nano Al₂O₃ has significant effects as it increased the softening point. However, the storage stability of the nano Al₂O₃ modified asphalt is better than that of the ASA polymer modified asphalt, which specifies that the nano Al₂O₃ has better ability of dispersing and compatibility with asphalt than ASA polymer.

3.4 Structure of ASA polymer and nano Al₂O₃ modified asphalt

The XRD analysis was conducted to investigate the changes of structural characteristics of asphalt binder modified by ASA polymer and nano Al₂O₃. From Figure 3, show that the base asphalt binder was absolutely amorphous (non-crystalline) without any clearly defined peaks. In contrast, the ASA polymer has a semi-crystalline structure, as there are medium peaks around the angles of 45°C and 67°C. Furthermore, the modification of asphalt binder by using 3%, 5%, and 7% concentration of ASA polymer changes the phase of the two-component asphalt and of the ASA. A new broad reflection at a low angle centered nearly 23° with corresponding d spec parameter of 0.4 nm indicates a semi-crystalline phase of the ASA modified asphalt.

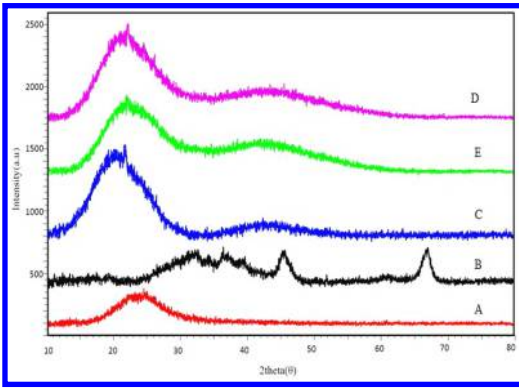


Figure 3. XRD patterns of base binder and ASA modified binders. (A) ASA Polymer, (B) base asphalt binder, (C) 3% ASA modified asphalt, (E) 5% ASA modified asphalt, (D) 7% ASA modified asphalt.

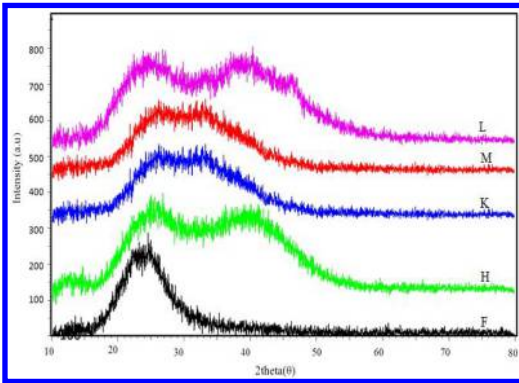


Figure 4. XRD patterns of base binder and Al_2O_3 modified binders. (F) Base asphalt binder, (H) Nano Al_2O_3 , (K) 3% Al_2O_3 modified asphalt, (M) 5% Al_2O_3 modified asphalt, (L) 7% Al_2O_3 modified asphalt.

Moreover, in order to measure the changes in the structure of the modified binders, the percentage of the crystalline phase was specified using dedicated software for both modifiers. It is recognized that increasing the concentration of the ASA polymer increases the percentage of the crystalline phase: at 3% of ASA, it was 2.72%, while at 5% of ASA; it has the highest value of 4.75%. In contrast, for 7% of ASA, a decrease in the amount of the crystalline phase is witnessed. Meanwhile, Figure 4 shows the results obtained of the base asphalt binder and nano Al_2O_3 modified asphalt binders. Furthermore, the nano Al_2O_3 is amorphous similar of base asphalt binder. Then, adding nano Al_2O_3 with different concentrations (3%, 5% and 7%) to the base asphalt, even it takes the same pattern of nano Al_2O_3 comparing with base asphalt binder, but the whole binders are still amorphous. That could mean the distribution of nano Al_2O_3 in the binders was random. However, the results approve that the ASA polymer has great effect on the structures of asphalt more than nano Al_2O_3 .

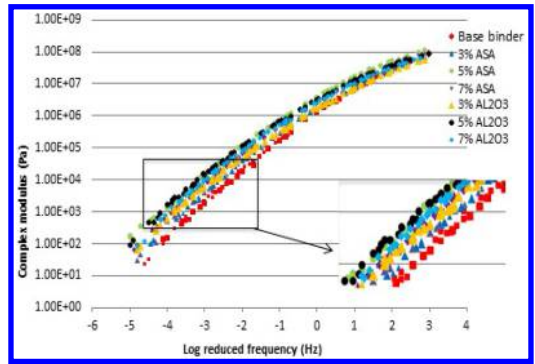


Figure 5. Complex modulus master curves of base binder, ASA modified binders and Al_2O_3 modified binders at the reference temperature of 25°C.

3.5 Influence of ASA and Al_2O_3 on rheological properties of asphalt

3.5.1 Rheological master curves

The master curves are generally constructed to analysis the behavior of material in a wide range of loading frequencies. Based on the time-temperature superposition principle the behavior of materials at a low frequency range can be theoretically transferred to represent the behavior of materials at a high temperature condition (Xiao et al., 2011, Cui et al., 2014). Thus, in the current case, the master curves were created at the reference temperature of 25°C then the data at all other temperatures are shifted horizontally with respect to time to create a single curve (Anderson et al., 1994, Cui et al., 2014). The G^* master curves of the base binder, the ASA modified binders and the Al_2O_3 modified asphalt binders. It is noted smooth curves of the G^* versus reduced frequency as present in Figure 5. Also, it is observed an increase in the G^* with the increasing of the reduced frequency.

Figure 5, show that the modified asphalt binders by ASA polymer and nano Al_2O_3 have higher G^* values than the base asphalt binder. This indicates that the addition of the ASA or Al_2O_3 to base asphalt binder had significant effects, which lead to increased G^* of modified asphalt. Particularly, with increase the concentration of both modifiers, up to 5% and less the G^* of asphalt binder also increased. In addition, the comparison of the master curve among the ASA polymer modifier revealed that the 5% had higher value of G^* compared with 3% and 7%. This is mostly due to the higher quantity of crystals contented in the 5% ASA. Meanwhile the modified asphalt binders by nano Al_2O_3 show a similar increase in G^* value, the modified binder with 5% has greater stiffness G^* value and 3% obtained the lowest value. Substantially, the evolution of both modifiers noted that the modified binders by nano Al_2O_3 have greater value of G^* comparing with modified binders by ASA polymer, which means nano Al_2O_3 has a greater resistance to deformation than ASA polymer. Therefore, if SBS, crumb rubber and nanoclay were used as modifiers of asphalt

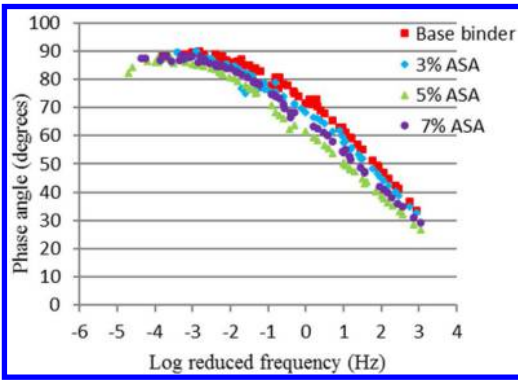


Figure 6. Phase angle master curves for base binder and ASA modified binders at the reference temperature of 25°C.

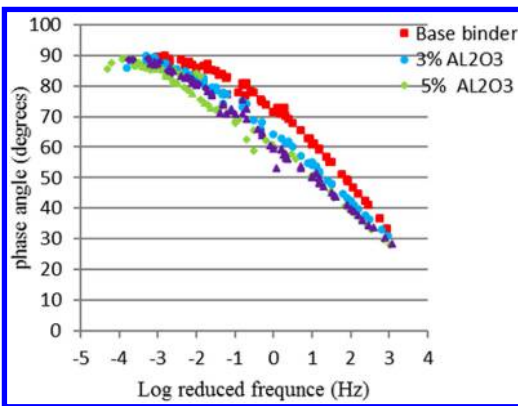


Figure 7. Phase angle master curves for base binder and Al_2O_3 modified binders at the reference temperature of 25°C.

binder, a comparable increase in G^* is realized (Yao et al., 2013, You et al., 2011, Kk et al., 2011).

The master curves of the phase angle of the base asphalt binder, ASA polymer modified binders and nano Al_2O_3 modified binders were showing in Figures 6 and 7. In general, the phase angle reduced with the increase of the reduced frequency for the control asphalt binder (Yang and You, 2015). Therefore, it is observed that all the modified binders have a lower value of phase angle than the base binder. Moreover, comparison among the modified binders by ASA polymer noted that the 5% ASA had the most significant effect on the asphalt phase angle, a slightly lower phase angle than the other, which means it has higher elastic recovery performance, whereas the same behavior observed with binders modified by nano Al_2O_3 , and 5% Al_2O_3 had the lower phase angle among the binders.

3.5.2 Fail temperatures

The temperature of $G^*/\sin \delta$ value is less than 1.0 KPa at 10 rad/s defined as the fail temperature of asphalt. Also, the fail temperature is often used to recognize the performance grade (PG) of asphalt (Xiao et al., 2014).

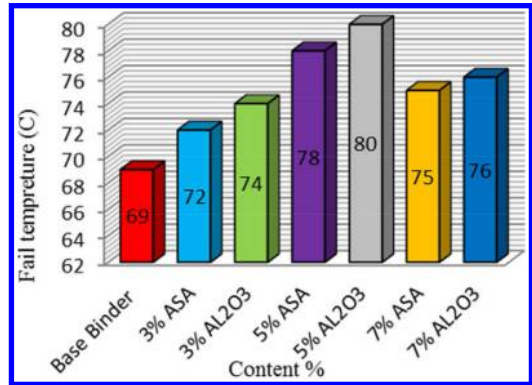


Figure 8. Fails temperatures of base asphalt binder, ASA modified binders and Al_2O_3 modified binders.

The results obtained from the DSR test is shown in Figure 8 and it is proved that the base asphalt binder had lowest fail temperature around 69°C than modified binders. Furthermore, the assessment of binders modified by ASA polymer show that 5% had higher value of failing temperature nearby 78°C, while the 3% and 7% have fail temperatures around 72°C and 75°C, respectively.

The modified binders by nano Al_2O_3 show the same behavior of polymer as the fail temperature increased with addition of nano, the fail temperatures noted in the concentration of nano 3%, 5% and 7% were around 74°C, 80°C and 76°C individually. Overall, the compressing between both modifiers proved that binders modified by nano Al_2O_3 have the highest value of the fail temperatures than those modified by ASA polymer. This is might due to the small size of nanoparticle, which assist it distributes more evenly than polymer in asphalt binder.

3.5.3 Fatigue parameter

The base asphalt binder and modified binders were determined according to Superpave performance principles. In Fatigue parameter, lower value of $G^* \cdot \sin \delta$ relates to greater resistance to fatigue cracking at low and intermediate temperatures (Tabatabaee and Tabatabaee, 2010). The Superpave specifications requirement at intermediate temperatures $G^* \cdot \sin \delta$ at 10 rad/s should be not greater than 5000 KPa for unaged condition. Figure 9 shows that $G^* \cdot \sin \delta$ value reduced as the concentration of modifiers increased. Moreover, modification of the base asphalt binder by ASA polymer improved the fatigue resistance up to 5%, whereas the modified binders by nano Al_2O_3 shows better improvement with notes that the lowest rate of $G^* \cdot \sin \delta$ was 5% Al_2O_3 .

3.6 Rutting parameter

Due to the physical properties of asphalt material, asphalt is more liable to rutting at high-service temperatures. $G^*/\sin \delta$ is used as a fundamental factor to describe the permanent deformation of an asphalt

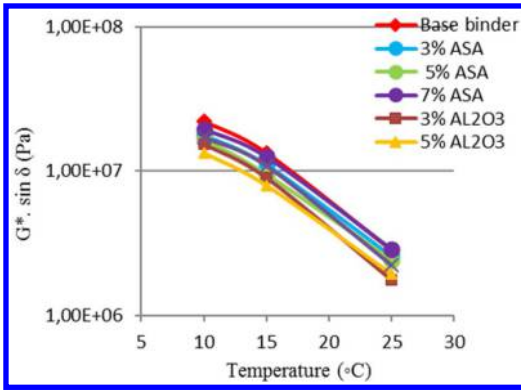


Figure 9. Effect of temperature on the fatigue-cracking parameter of base asphalt binder, ASA modified binders and Al_2O_3 modified binders.

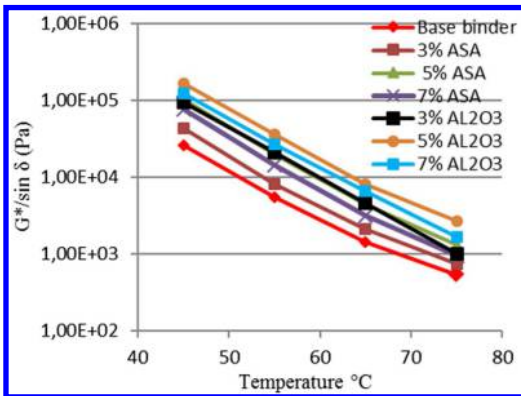


Figure 10. Effect of temperature on the rutting parameter of base asphalt binder, ASA modified binders and Al_2O_3 modified binders.

binder at a high performance temperature in Superpave specifications. Figure 10 show the graphs of rutting parameters values of base binder, ASA binders and Al_2O_3 modified binders at temperatures; namely 45, 55, 65 and 75°C under the constant loading frequency of 1.59 Hz or 10 rad/s. It is recognized that increases the $G^*/\sin \delta$ as the percentages of both modifiers increases up to 5%. Also, it is noted significantly that nano Al_2O_3 had higher $G^*/\sin \delta$ value compared with ASA polymer, which emphasizes that the addition of nano Al_2O_3 to base asphalt binder increased the rutting resistance higher than polymer. Generally, it can see that all modified binders have $G^*/\sin \delta$ values greater than 1.0 kPa at 70°C.

4 CONCLUSIONS

Based on the results and discussion the following conclusions were drawn.

- The results of conventional testing it were revealed that the addition of ASA and Al_2O_3 increased hardness of the modified binders and decreased their

temperature susceptibility. However, the enhancement was quite obvious on binders containing greater quantities of ASA polymer.

- The storage stability results shown that the nano Al_2O_3 has great storage stability comparing with ASA polymer which able to stored up 5% and less.
- X-ray diffraction results showed that the addition of the ASA polymer resulting additional interactions, which resulted in a change in the structure of the base asphalt binders, meanwhile the modification of asphalt by nano Al_2O_3 Remained at the similar structure.
- Master curves of all modified binders revealed that an increase in complex modulus value and decrease the phase angle compared with the base binder, which lead to enhanced elastic behavior of asphalt.
- It can be recognized that the addition of ASA and Al_2O_3 had great effects as improved the fail temperatures compared with the base asphalt binder.
- The results of the fatigue the rutting parameters, showed that the both modifiers were able to increase the resistance high temperatures rutting at and improved low temperatures fatigue.
- In general, the investigation of the conventional and rheological properties of ASA polymer and nano Al_2O_3 notes down that modification using nano Al_2O_3 had significant influence on asphalt binder greater than modification using ASA polymer. Also, the best concentration can be considered as the optimum content was 5% for both modifiers.

ACKNOWLEDGEMENTS

The authors would like to acknowledge the Sustainable Urban Transport Research Centre (SUTRA), Faculty of Engineering and Built Environment, Universiti Kebangsaan Malaysia (UKM) for providing research facilities and the Ministry of Science, Technology and Innovation (MOSTI), Malaysia for research funding through project 03-01-02-SF0999.

REFERENCES

- Airey, G. D. 2002. Rheological evaluation of ethylene vinyl acetate polymer modified bitumens. *Construction and Building Materials*, 16, 473–487.
- Al-Khateeb, G. G. & Al-Akhras, N. M. 2011. Properties of Portland cement-modified asphalt binder using Superpave tests. *Construction and Building Materials*, 25, 926–932.
- Al-Mansob, R. A., Ismail, A., Alduri, A. N., Azhari, C. H., Karim, M. R. & Yusoff, N. I. M. 2014a. Physical and rheological properties of epoxidized natural rubber modified bitumens. *Construction and Building Materials*, 63, 242–248.
- Al-Mansob, R. A., Ismail, A., Yusoff, N. I. M., Azhari, C. H., Karim, M. R., Alduri, A. & Baghini, M. S. 2014b. Rheological Characteristics of Epoxidized Natural Rubber Modified Bitumen. *Applied Mechanics and Materials*, 505, 174–179.
- Anderson, D. A., Christensen, D. W., Bahia, H. U., Dongre, R., Sharma, M., Antle, C. E. & Button, J. 1994.

- Binder characterization and evaluation, volume 3: Physical characterization. Strategic Highway Research Program, National Research Council, Washington, DC.
- Baghini, M. S., Ismail, A., Karim, M. R., Shokri, F. & Firoozi, A. A. 2014. Effect of styrene-butadiene copolymer latex on properties and durability of road base stabilized with Portland cement additive. *Construction and Building Materials*, 68, 740–749.
- Casey, D., McNally, C., Gibney, A. & Gilchrist, M. D. 2008. Development of a recycled polymer modified binder for use in stone mastic asphalt. *Resources, Conservation and Recycling*, 52, 1167–1174.
- Chen, J.-S. & Huang, C. 2007. Fundamental characterization of SBS-modified asphalt mixed with sulfur. *Journal of applied polymer science*, 103, 2817–2825.
- Cui, P., Wu, S., Li, F., Xiao, Y. & Zhang, H. 2014. Investigation on Using SBS and Active Carbon Filler to Reduce the VOC Emission from Bituminous Materials. *Materials*, 7, 6130–6143.
- Fu, H., Xie, L., Dou, D., Li, L., Yu, M. & Yao, S. 2007. Storage stability and compatibility of asphalt binder modified by SBS graft copolymer. *Construction and Building Materials*, 21, 1528–1533.
- Huang, S.-C. 2008. Rubber concentrations on rheology of aged asphalt binders. *Journal of Materials in Civil Engineering*, 20, 221–229.
- Institute, A. 2007. *The Asphalt Hand book*
- Ismail, A., Al-Mansob, R. A., Yusoff, B. M., Izz, N. & Karim, M. R. 2012. Effect Of Toluene As Disperser On The Bitumen Modified With Epoxidized Natural Rubber With Aging Simulation. *Australian Journal of Basic & Applied Sciences*, 6.
- Khattak, M. J., Khattab, A., Rizvi, H. R. & Zhang, P. 2012. The impact of carbon nano-fiber modification on asphalt binder rheology. *Construction and Building Materials*, 30, 257–264.
- Kök, B. V., Yilmaz, M. & Guler, M. 2011. Evaluation of high temperature performance of SBS+ Gilsonite modified binder. *Fuel*, 90, 3093–3099.
- Kumar, P., Chandra, S. & Bose, S. 2006. Strength characteristics of polymer modified mixes. *The International Journal of Pavement Engineering*, 7, 63–71.
- Liu, S., Cao, W., Fang, J. & Shang, S. 2009. Variance analysis and performance evaluation of different crumb rubber modified (CRM) asphalt. *Construction and Building Materials*, 23, 2701–2708.
- Paul, D. & Robeson, L. 2008. Polymer nanotechnology: nanocomposites. *Polymer*, 49, 3187–3204.
- Pérez-Lepe, A., Martínez-Boza, F. & Gallegos, C. 2007. High temperature stability of different polymer-modified bitumens: A rheological evaluation. *Journal of applied polymer science*, 103, 1166–1174.
- Polacco, G., Berlincioni, S., Biondi, D., Stastna, J. & Zanzotto, L. 2005. Asphalt modification with different polyethylene-based polymers. *European Polymer Journal*, 41, 2831–2844.
- Selvavathi, V., Sekar, V. A., Sriram, V. & Sairam, B. 2002. Modifications of bitumen by elastomer and reactive polymer—a comparative study. *Petroleum science and technology*, 20, 535–547.
- Sengoz, B. & Isikyakar, G. 2008. Analysis of styrene-butadiene-styrene polymer modified bitumen using fluorescent microscopy and conventional test methods. *Journal of Hazardous Materials*, 150, 424–432.
- Sikdar, P., Jain, S., Bose, S. & Kumar, P. Premature cracking of flexible pavements. *Journal of Indian Roads Congress*, 1999, 355–398.
- Sinha Ray, S. & Okamoto, M. 2003. Polymer/layered silicate nanocomposites: a review from preparation to processing. *Progress in polymer science*, 28, 1539–1641.
- Sun, D., Ye, F., Shi, F. & Lu, W. 2006. Storage stability of SBS-modified road asphalt: Preparation, morphology, and rheological properties. *Petroleum science and technology*, 24, 1067–1077.
- Tabatabaee, N. & Tabatabaee, H. A. 2010. Multiple Stress Creep and Recovery and Time Sweep Fatigue Tests. *Transportation Research Record: Journal of the Transportation Research Board*, 2180, 67–74.
- Walubita, L. F., Alvarez, A. E. & Simate, G. S. 2011. Evaluating and comparing different methods and models for generating relaxation modulus master-curves for asphalt mixes. *Construction and Building Materials*, 25, 2619–2626.
- Wekumbura, C., Stastna, J. & Zanzotto, L. 2007. Destruction and recovery of internal structure in polymer-modified asphalts. *Journal of materials in civil engineering*, 19, 227–232.
- Wen, G., Zhang, Y., Zhang, Y., Sun, K. & Fan, Y. 2002. Rheological characterization of storage-stable SBS-modified asphalts. *Polymer Testing*, 21, 295–302.
- Xiao, F., Amirkhanian, S., Wang, H. & Hao, P. 2014. Rheological property investigations for polymer and polyphosphoric acid modified asphalt binders at high temperatures. *Construction and Building Materials*, 64, 316–323.
- Xiao, Y., Van De Ven, M., Molenaar, A., Su, Z. & Zandvoort, F. 2011. Characteristics of two-component epoxy modified bitumen. *Materials and structures*, 44, 611–622.
- Yang, X., You, Z.-P. & Dai, Q.-L. 2013. Performance evaluation of asphalt binder modified by bio-oil generated from waste wood resources. *International Journal of Pavement Research and Technology*, 6, 431–439.
- Yang, X. & You, Z. 2015. High temperature performance evaluation of bio-oil modified asphalt binders using the DSR and MSCR tests. *Construction and Building Materials*, 76, 380–387.
- Yao, H., You, Z., Li, L., Goh S. W., Lee, C. H., Yap, Y. K. & Shi, X. 2013. Rheological properties and chemical analysis of nanoclay and carbon microfiber modified asphalt with Fourier transform infrared spectroscopy. *Construction and Building Materials*, 38, 327–337.
- Yildirim, Y. 2007. Polymer modified asphalt binders *Construction and Building Materials*, 21, 66–72.
- You, Z., Mills-Beale, J., Foley, J. M., Roy, S., Odegard, G. M., Dai, Q. & Goh, S. W. 2011. Nanoclay-modified asphalt materials: Preparation and characterization. *Construction and Building Materials*, 25, 1072–1078.
- Zhang, B., Xi, M., Zhang, D., Zhang, H. & Zhang, B. 2009. The effect of styrene-butadiene-rubber/montmorillonite modification on the characteristics and properties of asphalt. *Construction and Building Materials*, 23, 3112–3117.
- Zhang, F., Yu, J. & Han, J. 2011. Effects of thermal oxidative ageing on dynamic viscosity, TG/DTG, DTA and FTIR of SBS-and SBS/sulfur-modified asphalts. *Construction and Building Materials*, 25, 129–137.
- Zhang, F., Yu, J. & Wu, S. 2010. Effect of ageing on rheological properties of storage-stable SBS/sulfur-modified asphalts. *Journal of hazardous materials*, 182, 507–517.

Effect of polymer type on improving rheological parameters related to rutting resistance of asphalt binders

Khaleel Al-Adham & Hamad Al-Abdul Wahhab

Department of Civil Engineering, KFUPM, Saudi Arabia

ABSTRACT: Polymer additive should be sufficiently compatible with the asphalt and properly selected to improve rutting resistance of asphalt mix in a cost effective manner. At a given polymer content, the modified binders containing elastomers and plastomers differ widely in their rheological properties. The differences are more pronounced at higher temperatures up to 82°C. The main objective of this paper is to highlight the importance of selecting proper polymer type that would improve rutting resistance of modified asphalts by addressing the elastic and creep recovery. Each polymer has special characteristics which are used in asphalt modification. Four Arabian asphalts were modified with three types of plastomers and one type of elastomer with different concentrations (2–6%) from different sources. It was found that elastomers can increase the PG upper temperature by around 3°C more than Plastomers for the same amount of polymer and have higher tendency to increase the elastic recovery characteristics of asphalt binder by about 10% more than other types of polymers after Elastic Recovery (ER) and Multiple Stress Creep Recovery (MSCR) tests for PG 70, PG 76 and PG 82 binders. The relationship between ER and MSCR results indicated that elastomer modified asphalt binder with 30% MSCR recovery equal to 60% ER recovery while plastomer modified asphalts need to have at least 50% recovery.

Keywords: Arabian Asphalts, Polymer modified asphalts, Elastomers and Plastomers, Performance Grading, Elastic Recovery, Multiple Stress Creep Recovery.

1 INTRODUCTION

Roads in the Gulf Countries have been built to the best international standards, but they have shown early signs of distresses due to the harsh environment and traffic loading. Local asphalt pavement's temperature ranges between (–10°C) in the winter to (73°C) in the summer (Al-Abdul Wahhab et al., 1997, 1999). This has led to an increased demand to modify local asphalt binders to improve their performance to minimize cracking stress, which occurs at low temperatures, and permanent deformation, which occurs at high service temperatures.

Different methods have been used to upgrade the properties of asphalt binders. One of the most commonly used procedures is modification by addition of polymers (Becker et al., 2001). Use of polymers is the most convenient for asphalt modification for local contractors. Several polymer brands have been used locally.

Cost reduction of pavement maintenance and hence pavement lifetime extension overcomes the added cost of asphalt modification. While increasing pavement rutting resistance polymer modification can result in maintenance and rehabilitation cost reductions, additional cost savings and performance benefits can be realized where pavement rutting does not exist.

There are four major types of polymers that have been used to modify asphalt binders; Plastomers, Elastomers, reclaimed rubber and Fibers (Becker et al., 2001). Each of these groups has special characteristics which are used in asphalt modification. To improve rutting resistance of asphalt mix in a cost effective manner, it is required to select the proper polymer type which has the required tendency of recovering the deformation after applied stressed due to traffic loads. Many researchers studied different types of polymers to improve the performance of asphalt binders and mixes. These polymer modified asphalts have different characteristics such as Elasticity at high temperature (Isacsson, and Lu 1995), Rheology, compatibility, storage stability, low temperature properties and ageing (Lu and Isacsson, 2001), Viscosity (Isacsson et al. 2000), Elastic recovery (Stastna et al. 200; Yildirim 2007; Batten et al. 2011) and Creep recovery (Yildirim 2007; Batten et al. 201; Clopotel et al. 201; Peng et al. 201; Shirodkar et al. 2012; Wasage et al. 2011).

In this study, different methods were used to characterize the performance of asphalt binders against rutting at desert environment which may reach 82°C. Many researchers found that Performance Grading (PG) is not adequate to evaluate polymer modified asphalts due to deficiency in the elastic recovery evaluation of the modified binders; Elastic Recovery (ER)

and Multiple Stress Creep Recovery (MSCR) are used to achieve this requirement. (Masad et al., 2009).

Arabian asphalt binders were collected from all local asphalt producing refineries including Riyadh, Ras Tanura, Jeddah and Yanbu. Two different groups of polymers including elastomers and plastomers were used to improve the rutting resistance of Arabian asphalt binder. These asphalts were subjected to Performance Grading (PG) (AASHTO M320), Elastic Recovery (ER) (AASHTO T51) and Multiple Stress Creep Recovery (MSCR) (AASHTO TP 70-08). Binders were modified with 2%–6% of elastomeric polymers in addition to plastomeric ones to meet PG 70-16, PG 76-16 and PG 82-16.

2 OBJECTIVES

The main objective of this work is to compare the behavior of asphalt binder modified with Elastomers and Plastomers in terms of their resistance to rutting at high-service temperatures by evaluating their Performance Grading (PG), Elastic Recovery (ER) and Multiple Stress Creep Recovery (MSCR) characteristics.

3 MATERIALS

3.1 Asphalt binders

Asphalt cement samples were collected in from four asphalt producing refineries at Ras Tanura, Riyadh, Jeddah and Yanbu. These four refineries are selected in this study because they cover different temperature zones of the Kingdom of Saudi Arabia ranging from PG 64-10 to PG 82-10.

3.2 Polymers

Two types of polymers which are mostly used in local projects were selected to modify asphalt binders in this study. These polymer are divided into two subgroups in terms of their behavior; Plastomers (Polybilt and Titan) and Elastomers (SBS).

Elastomers are generally low modulus, flexible materials that can be stretched repeatedly to at least twice their original length at room temperature with an ability to return to their approximate original length when stress is released. The well-known materials with this property are thermoset rubbers, but many families of injection-moldable thermoplastic elastomers are replacing traditional rubbers. While plastomeric materials are usually unstable two phase systems, while elastomer modified bitumen can be stable two phase or even one phase (chemically bound) systems. When unstable systems are not sufficiently stirred, the polymer separates from the bitumen. This will result in non-homogenous bitumen with areas with high and low polymer content. When added to bitumen a compatible elastomer (like SBS) will absorb the oily fraction from the bitumen, which causes the polymer

to swell up to eight times its original volume. After some time, the swelled polymer starts to dissolve in the bitumen. This physical process takes time, at least several hours, and can be influenced by the production process and the use of additives. Plastomers (like Polybilt) melt at high temperature. When added to bitumen they appear as small droplets that are dispersed in the bitumen. The bigger the volume of the polymer in the bitumen, the more it will improve the properties of the bitumen.

4 SAMPLE PREPARATION AND TESTING

Neat asphalt was mixed properly with polymer; each polymer has specific mixing procedure. Asphalt is heated to specific temperature and the polymer is stirred in using shear mixing as simple propeller type blade, spun at 800 PRM. Once the asphalt reaches temperature and is uniform, Titan polymers were added gradually. Asphalt samples were treated with 2, 3, 4, 5, and 6% Titan polymers. The polymers were simply sprinkled on the asphalt surface and mixed for one hour. For Polybilt polymer the mixing was carried out at 165°C for a minimum of one hour, as the Polybilt needs a higher temperature to disperse than the Honeywell™ Titan.

When SBS polymers and their hybrid combinations were used, the mixing was carried out at 180-183°C with high shear mixing (around 5000 rpm) for a minimum of two hours. Samples were stored at around 145°C overnight in an oven to mature the SBS network. Samples were then heated in an oven at 180°C, and mixed for 15–20 min in the shear mixer at 180°C (at 800 rpm) before testing specimens can be prepared.

4.1 Flash point and viscosity

The Performance Grading (PG) system (AASHTO M320, ASTM D6373) was used to grade plain and modified asphalts. Dynamic viscosity (AASHTO TP48, ASTM 4402) was carried on the modified asphalt to determine asphalt workability, mixing and compaction temperatures based on viscosity. Flash point (AASHTO T48, ASTM 449), safety test, was also determined.

4.2 Rolling thin film oven (RTFO)

The RTFO test (AASHTO T-240, ASTM D 2872) was used to simulate the aging that takes place during the production and up to the first year life of the pavement. The base asphalt as well as modified asphalt was poured into cylindrical bottles.

35 grams of asphalt sample was poured in each cylindrical bottle. Then the bottles were placed horizontally in a convection oven, which was rotated at 163°C for 85 min. This process created a thin film of asphalt on the inside of the bottles. After the test the sample was collected for further tests. Dynamic Shear Rheometer (DSR) testing before and after RTFO

was done to investigate the short term aging effect of asphalt mixes.

4.3 *Dynamic shear rheometer (DSR)*

The dynamic temperature step measurements for the samples were performed in CSA II rheometer. All tests were carried out in a range of 64°C–82°C using a parallel plate set of diameter is 8 mm or 25 mm depending on the sample age. Strain in the linear viscoelastic range and frequency of 10 rad/s was used for all the tests (AASHTO T315, ASTM 7175). Sample is given the required time to reach the desired test temperature (within $\pm 0.1^\circ\text{C}$) then the DSR will automatically start holding period of 10 min. to allow the temperature to reach steady state plus 2 minutes was allowed before beginning measurements. Special software was used to calculate the dynamic shear viscosity, storage modulus and PG grading for all samples. Fresh asphalt and RTFO residue was run in DSR with plate diameter 25 mm. Asphalt samples were tested after PAV and became harder than that of fresh asphalt. Therefore, asphalt submersion cell with 8 mm diameter plate was used for PAV residue sample.

4.4 *Bending beam rheometer (BBR)*

The Bending Beam Rheometer (BBR) test (AASHTO T313, ASTM D6648) provides a measure of low temperature stiffness and relaxation properties of asphalt binders. These parameters give an indication of an asphalt binder's ability to resist low temperature cracking. The BBR is used in combination with the DTT to determine an asphalt binder's low temperature PG grade. As with other Superpave binder tests, the actual temperatures anticipated in the area where the asphalt binder will be placed, determine the test temperatures used. Because low temperature cracking is a phenomenon found mostly in older pavements, the test is run on the long-term aged residue from the PAV. The existing SHRP specification of performance grade system does not have criteria for durability and fatigue and also does not identify the performance characteristics of modified binders. Thus, many agencies look to other tests to identify elastomeric polymer modifiers, such as Elastic Recovery, Toughness and Tenacity (Masad et al. 2009).

4.5 *Elastic recovery utilizing the ductility bath*

The percentage of recoverable strain is used to evaluate the Elastic Recovery (ER) of polymer modified binders. This test is performed by utilizing the conventional ductility test (AASHTO T 51) at $25 \pm 0.5^\circ\text{C}$ (77°F) and with speed of 50 mm/min $\pm 5.0\%$. The sample is poured in the standard mold and then subjected to elongation at specified conditions to have a deformation value, and the distance to recover this deformation after 1 hour is recorded and the percent recoverable strain is calculated. The values of percent recovery were recorded for each combination of

polymer (type and amount) and asphalt source. To recommend a standard limit of ER test, (Masad et al. 2009; Batten et al. 2011) studied the elastic recovery of different modified asphalt-polymer combination and used a limit of 60% as percent recovery using this test, and found that all the acceptable samples should have more than this limit.

In this research, all the elastic recovery results were compared to the recommended limit of percent recovery (%R) mentioned in the previous studies. Since this limit had been used by many asphalt agencies and research centers around the world.

4.6 *Multiple stress creep recovery (MSCR) test*

This test method covers the determination of percent recovery and non-recoverable creep compliance (J_{nr}) of asphalt binders by means of the Multiple Stress Creep Recovery (MSCR) test. The MSCR test is conducted using the Dynamic Shear Rheometer (DSR) at a specified temperature. It is intended for use with RTFO residue. The percent recovery value is intended to provide a mean of determining the elastic response and stress dependence of polymer modified and unmodified asphalt binders. This test method is used to determine the presence of elastic response in an asphalt binder under shear creep and recovery at two stress levels at a specified temperature. For performance-graded (PG) asphalt binders, the specified temperature will typically be the PG high temperature from (AASHTO MP 19).

Asphalt binder is first conditioned using (AASHTO T 240, RTFO). A sample of the RTFO-conditioned asphalt is tested using (AASHTO T 315, DSR). The 25-mm parallel plate geometry is used with a 1-mm gap setting. The sample is tested in creep at two stress levels followed by recovery at each stress level. The stress levels used are 0.1 kPa and 3.2 kPa. The creep portion of the test lasts for 1 second, which is followed by a 9-second recovery. Ten creep and recovery cycles are tested at each stress level. Non-recoverable creep compliance (J_{nr}) has been shown to be an indicator of the resistance of an asphalt binder to permanent deformation under repeated load.

5 RESULTS AND ANALYSIS

5.1 *Superpave™ performance grading (PG)*

Tested samples have 2–6% of polymers, besides neat asphalt, of the binder weight for each type of polymer and tested at different temperatures starting from 64°C up to 82°C and different ageing conditions.

Change in temperature and ageing conditions affects significantly the visco-elastic behavior of the modified asphalt. If temperature increases, $G^*/\sin \delta$ will decrease due to reduction of viscosity and elasticity. Short term ageing conditions show higher values of $G^*/\sin \delta$ than fresh conditions for each polymer due to the increase in ageing and viscosity. Polymers of

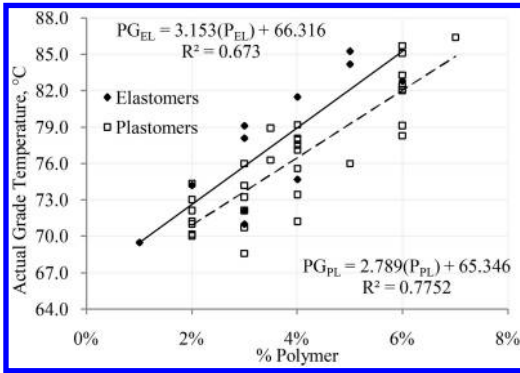


Figure 1. Effect of polymer type and amount on PG.

different types have remarkable influence in improving the elastic and viscous performance of the asphalt binder.

Figure 1 shows the comparison between elastomers and plastomers in improving the Performance Grade (PG) of asphalt binders. Elastomers can increase the PG upper temperature by around 3°C more than Plastomers for the same amount of polymer.

$$PG_{EL} = 3.4167(\%P_{EL}) + 64.499 \quad (1)$$

$$PG_{PL} = 2.9192(\%P_{PL}) + 64.45 \quad (2)$$

where PG_{EL} is the actual grade temperature of asphalt binder modified with an elastomer and P_{EL} is the percent of elastomer used.

Plastomers consist of entangled or branched macromolecules held together by intermolecular forces. In the solid state they deform permanently and do not recover after complete release of the force producing the deformation. This is because their macro-molecules are loose and can slip past each other on the application of pressure.

On the other hand, elastomers have unique properties because the macro-molecules are crosslinked by chemical bonds. The crosslinks prevent the long chain molecules from slipping past each other on the application of force from dissolving in solvents or melting by heating. The chain molecules of the crude rubber are joined by widely spaced crosslinks. After having been crosslinked, the soft plastic-like material exhibits a high degree of elastic recovery, loses its tackiness, becomes insoluble in solvents & infusible when heated and more resistant to deterioration caused by aging factors. Scrap or reject parts cannot be processed unless the crosslinks have been destroyed by chemical or mechanical processes.

5.2 Elastic recovery

The effect of polymers in improving the elastic recovery of Arabian asphalts that are modified with elastomers and plastomers was studied and shown in

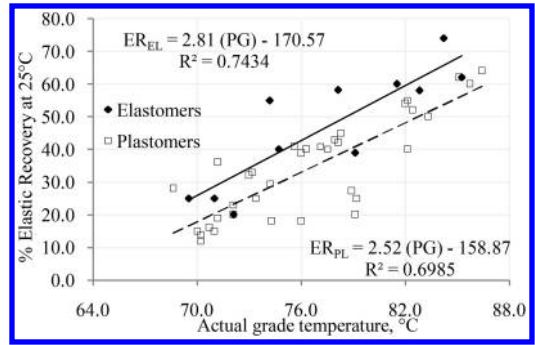


Figure 2. Relation between PG upper temperature and ER.

Figure 2. A good correlation was found between performance grade of the tested samples and percent recovery at 25°C.

The statistical model used to express the relation between the actual grade temperature and the percent recovery of asphalt samples modified with elastomers and plastomers are:

$$ER_{EL} = 2.81 PG - 170.57 \quad (3)$$

$$ER_{PL} = 2.52 PG - 158.87 \quad (4)$$

where: ER_{EL} is the % Elastic Recovery at 25°C of asphalt binder modified with elastomer.

The correlation between PG and ER is not affected by source of asphalt binder but it is highly affected by the type and amount of polymer used. Each asphalt-polymer combinations have been characterized by their performance against temperature and assigned a PG value. The generated models cover asphalt samples which are modified with elastomers and plastomers.

Elastomers have higher tendency to increase the recovery characteristics of asphalt binder by about 10% more than plastomers. This includes PG 70, PG 76 and PG 82 asphalts.

5.3 Multiple stress creep recovery

All samples in the experimental program have been tested using MSCR procedure that uses the DSR machine. The stress levels used are 0.1 kPa and 3.2 kPa. The creep portion of the test lasts for 1 second, which is followed by a 9-second recovery. Ten creep and recovery cycles were used at each stress level. The average values of the creep and recovery start and end points were determined to calculate the percent recoverable strain at the two stress levels in addition to the non-recoverable compliance J_{nr} . Figure 3 shows the relationship between actual grade temperatures, which was obtained from the PG system, and MSCR percent recovery test conducted at 64°C and 3.2 kPa stress level.

The result of this correlation shows a significance difference between elastomers and plastomer in terms of recovering the applied stresses. For asphalt binders

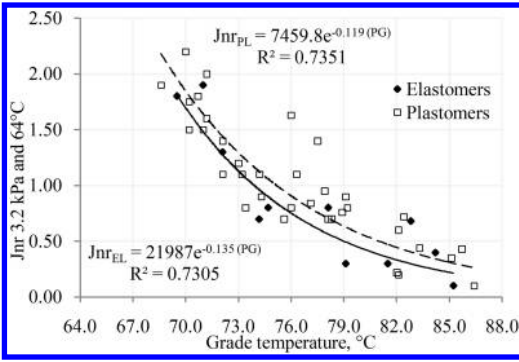


Figure 3. Relationship between PG and MSCR Jnr at 3.2 kPa stress level.

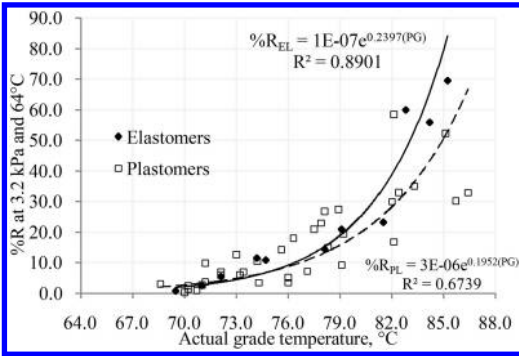


Figure 4. Relationship between PG and MSCR % recovery at 3.2 kPa stress level.

that have PG 82, with the increase of upper temperature, elastomers show higher value of percent recovery of about 10% and can be expressed by the following relations:

$$\%R_{EL,3.2} = 1E-07 e^{0.2397 (PG)} \quad (5)$$

$$\%R_{PL,3.2} = 3E-06e^{0.1952 (PG)} \quad (6)$$

Equations 5 and 6 are used to estimate the percent recovery of modified samples by an elastomer or a plastomer that have certain PG value. Equation 5 covers 11 samples of elastomeric asphalts with R^2 to 0.89 where Equation 6 covers 35 samples modified with plastomer with R^2 0.67.

Creep recovery of polymer modified asphalt binders when compared to elastic recovery, which evaluate the shear rate dependency of viscosity and elasticity, introduced an additional parameter of response time to the stress-dependency of both the elastic and viscous behavior of asphalt binders.

Figure 4 shows the other component of MSCR requirements, which is the non-recoverable compliance Jnr. Lower values of Jnr, are shown for the elastomer modified asphalts and hence higher traffic loads that can be withstand. These values of Jnr are presented in Equations 7 and 8.

$$Jnr_{EL,3.2} = 21987.8 e^{-0.135 (PG)} \quad (7)$$

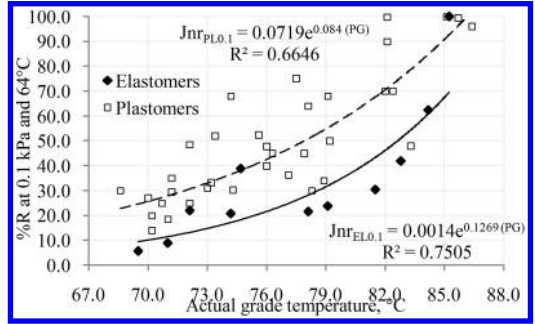


Figure 5. Relationship between PG upper temperature and MSCR% recovery at 0.1 kPa and 64°C.

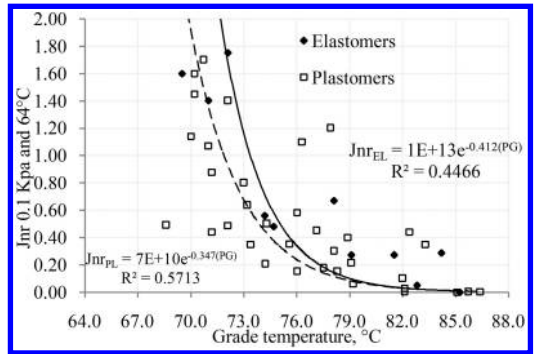


Figure 6. Relationship between PG and MSCR Jnr at 0.1 kPa stress level.

$$Jnr_{PL,3.2} = 7459.8 e^{-0.119 (PG)} \quad (8)$$

When low stress rates (i.e. 0.1 kPa) are applied, the molecules have plenty of time to creep out of their entanglement and flow slowly past each other. Molecules can maintain their minimum energy because any partial stretching of spring segments can be relaxed simultaneously with the general flow of the mass.

Figure 5 shows similar relationship between creep recovery of polymer modified asphalt binder at low stress level; 0.1 kPa. In this relationship, asphalt binders that are modified with plastomers have shown better performance in increasing the percent recovery of MSCR.

The results of slow rates of deformation polymer modified asphalts show a predominantly viscous flow behavior and normally elasticity does not become apparent. At 3.2 kPa stresses rates, an increasingly larger part of the deforming energy will be absorbed by an elastic intra- and intermolecular deformation while the mass is not given time enough for viscous flow. Figure 6 shows the results of Jnr compliance at low stress level of 0.1 kPa at certain performance temperature and type of polymer used in the modification of the asphalt binder. Equations 9 and 10 show the effect of polymer type on PG and Jnr values.

$$Jnr_{EL,0.1} = 1E+13e^{-0.412(PG)} \quad (9)$$

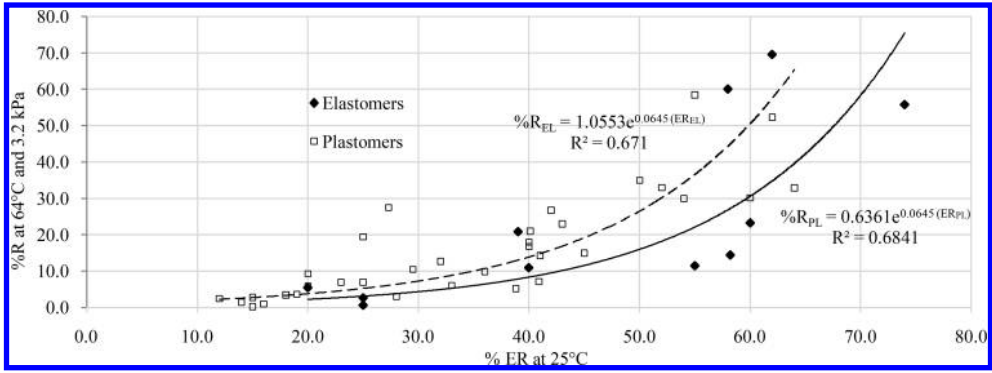


Figure 7. Relationship between %ER at 25°C and %R at 64°C and 3.2 kPa stress level.

$$\text{Jnr}_{\text{PL},0.1} = 7E+10e^{-0.347(\text{PG})} \quad (10)$$

Plastomers show better performance at low shear rates when compared to high rates, especially at lower PG temperatures.

5.4 Correlation between ER and MSCR

Figure 7 shows the correlation between Elastic Recovery ER at 25°C which has been used by many researches as rule of thumb and recommends a minimum value of 60% (Batten et al. 2011), and percent recovery of MSCR at 64°C and 3.2 kPa stress level. Equations 11 and 12 show the correlation model of percent recovery between the conventional elastic recovery and the creep recovery at certain service temperature.

$$\%R_{\text{EL}} = 0.636 e^{0.0645 (ER_{\text{EL}})} \quad (11)$$

$$\%R_{\text{PL}} = 1.055 e^{0.0645 (ER_{\text{PL}})} \quad (12)$$

The relationship shows that elastomer modified asphalt binder with 30% recovery equals to the 60% of ER test. While plastomer modified asphalts need to have at least 50% recovery.

6 CONCLUSIONS

Two polymer types were used to improve Arabian asphalts binders. Samples that have different combinations of asphalt source, polymer type and amount were tested for PG, ER and MSCR requirements.

Selecting the proper polymer type and amount would significantly improve certain characteristics of asphalt such as rutting resistance. Elastomers showed a remarkable behavior in improving rutting resistance compared to plastomer type. Elastomers can increase the PG upper temperature by up to 3°C more than Plastomers for the same amount of polymer. The correlation between PG and ER is not affected by source of asphalt binder but it is highly affected by the type and amount of polymer used. Each asphalt-polymer

combinations have been characterized by their performance against temperature. The generated models cover asphalt samples which are modified with elastomers. Elastomers have higher tendency to increase the recovery characteristics of asphalt binder by up to 10% more than plastomers. This includes PG 70, PG 76 and PG 82 asphalts.

The result of comparison shows a significance difference between elastomers and plastomer in terms of recovering the applied stresses. For asphalt binders that have PG 82 at desert environments which is the main target of this study, elastomers show higher value of percent recovery with about 10% and it, is exponentially increasing. The relationship between ER and MSCR percent recoveries shows that elastomer modified asphalt binder with 30% recovery correspond to the 60% of ER test. While plastomer modified asphalts need to have at least 50% recovery.

ACKNOWLEDGEMENTS

The authors would like to thank King Fahd University of Petroleum and Minerals in KSA for its finance support of this work and to Honeywell company for providing Titan polymers used in this study.

REFERENCES

- Al-Abdul Wahhab, H.I., I.A. Al-Dubabe, I.M. Asi and M.F. Ali (1997). Performance-Based Characterization of Arab Asphalt, *Building and Environment Journal*, v. 32, n. 2, pp. 1–9.
- Ali, M., H. Al-Abdul Wahhab, I. Asi and I. Al-Dubabe (1999). Characterization of Polymer Modified Gulf Asphalts, *Petroleum Science and Technology*, v. 17, n. 2, pp. 125–146.
- Batten, E., Mehta, Y., Nolan, A., Zorn, S., and Dahm, K. (2011). Correlation between PG Plus, Superpave PG Specifications, and Molecular Weight from GPC for Different Polymer Modified Binders. *Geo-Frontiers 2011*: pp. 4535–4543.
- Becker, Y., M.P. Méndez and Y. Rodríguez (2001). Polymer Modified Asphalt, *Vision Technologica*, v. 9, n. 1, pp. 39–40.

- Clopotel, C. S., Mahmoud E. and Bahia, H. U. (2011). Modification of the Elastic Recovery Test and its Relationship to Performance Related Properties of Modified Asphalt Binders, Presented at the *90th Annual Meeting of the Transportation Research Board*, Washington, D.C.
- Isacsson, U. and H. Zeng (1998). Low-Temperature Cracking of Polymer-Modified Asphalt, *Journal of Materials and Structures*, v. 31, pp. 58–63.
- Isacsson, U. and X. Lu (1995). Testing and Appraisal of Polymer Modified Road Bitumens – State of the Art, *Materials and Structures*, v. 28, pp. 139–159.
- Isacsson, Ulf and Lu, Xiaohu Royal (2000). Properties of Bitumens Modified with Elastomers and Plastomers. 2nd Eurasphalt & Eurobitume Congress Barcelona 2000 Institute of Technology Division of Highway Engineering SE – 100 44 Stockholm, Sweden.
- Lu, X. and U. Isacsson (2001). Modification of Road Bitumens with Thermoplastic, *Polymers, Polymer Testing*, v. 20, pp. 77–86.
- Masad, E., Huang, C.W., D'Angelo, J., Little, D., (2009). Characterization of asphalt binder resistance to permanent deformation based on nonlinear viscoelastic analysis of multiple stress creep recovery (MSCR) test. *Journal of the Association of Asphalt Paving Technologists (AAPT)* 78, 471–501.
- Peng, Y., Ruibo, R., Lizhi, W., and Xiaoning, Z. (2012) Characteristic Behavior of Asphalt with SBS and PE, *Sustainable Construction Materials*. pp. 421–429.
- Shenoy, A. (2004). High temperature performance grading of asphalts through a specification criterion that could capture field performance, *Journal of Transportation Engineering*, v. 130, n. 1, pp. 132–137.
- Shirodkar P., Mehta Y., Nolan A., Dahm K., Dusseau R., McCarthy L. (2012). Characterization of creep and recovery curve of polymer modified binder, *Construction and Building Materials*. v. 34. pp. 504–511.
- Stastna, J., L. Zanzotto and O.J. Vacin (2003). Viscosity Function in Polymer Modified Asphalt, *Journal of Colloid and Interface Science*, v. 259, n. 1, pp. 200–207.
- Wasage, T.L.J., Stastna J. and Zanzotto L. (2011). Rheological analysis of multistress creep and recovery (MSCR) test, *International Journal of Pavement Engineering*. v. 12, n. 6, pp. 561–568.
- Yildirim Y. (2007). Polymer modified asphalt binders, *Construction and Building Materials*, v. 21, n. 1, pp. 66–72.

Performance of polymer and crumb rubber modified asphalt binders subjected to high stresses in multiple stress creep recovery test

Aniket V. Kataware & Dharamveer Singh

Department of Civil Engineering, Indian Institute of Technology, Bombay, India

ABSTRACT: The present study was undertaken to evaluate performance of polymer and crumb rubber modified binders subjected to higher stress levels ranging from 0.1 kPa to 25.6 kPa at 76°C in Multiple Stress Creep Recovery test (MSCR). It was found that the elastic recovery of both the binders decreases with an increase in stress level. Both the binders show negligible elastic recovery at high stress levels. The polymer modified binder was found to be more elastic compared to crumb rubber modified binder. The rate of change of elastic recovery with stress level was higher for crumb rubber binder as compared to polymer modified binder, indicating that earlier is more stress sensitive. The J_{nr} value of polymer modified binder increases rapidly compared to crumb rubber binder with increase in stress level; this indicates crumb rubber binder is stiffer. Both the binders were found to be suitable for standard traffic loading at 3.2 kPa, however, their rank degraded when tested a high stress levels. This change in grading for PMB40 and CRMB 60 shows that high stress level will certainly help to better evaluate rutting properties and applicability of the binders. Overall, at tested temperature crumb rubber modified binder seems to be beneficial compared to polymer modified binder as far as high stresses are concerned.

1 INTRODUCTION

The majority of flexible pavements fail due to permanent deformation (rutting) in asphalt layers. Heavy vehicular load in combination with a high temperature are dominating factors to initiate rutting failure in a flexible pavement. Researchers have recommended using a stiffer binder on top layer of a flexible pavement so it can resist heavy traffic load. Recently FHWA has developed a new test called, multi stress creep recovery (MSCR) to better characterize a binder for rutting susceptibility. MSCR test is used to determine “non-recoverable creep compliance”, which is ratio of non-recoverable strain to applied stress. MSCR test simulates field loading condition therefore J_{nr} can be considered as rutting parameter (D’ Angelo, 2009). A higher value of percent recovery and a lower value of J_{nr} , indicate better rutting performance of a binder and vice-versa. Better correlation has been observed between J_{nr} and rutting performance of asphalt mixes in laboratory and field (D’ Angelo, 2009; Wasage et al., 2013; Tabatabaee N. and Tabatabaee H., 2010; Divya P. S. et al., 2013). The J_{nr} at 3.2 kPa obtained from MSCR test can be utilized to grade a binder in four different traffic categories in accordance with AASHTO MP 19. For example, a binder is appropriate for standard traffic (S), high traffic (H), very high traffic (V) and extreme traffic (E), if J_{nr} (kPa^{-1}) is in range of 2 to 4, 1 to 2, 1 to 0.5 and less than 0.5, respectively. It can

be seen that a desired value of J_{nr} decreases as traffic level increases.

Many researchers have reported that performance of modified binders significantly depends upon the magnitude of applied stress (Domingos & Faxina, 2013; Domingos & Faxina, 2014). Rutting occurs due to wheel load stresses in combination of high temperature. Due to heavy traffic in field, strains in binder are much more (100 times) than that of mix. Masadet. al. (2001) reported it to be 90 times and Koseet. al. (2000) reported as 500 times. D’ Angelo (2009) has reported better correlation between J_{nr} at 3.2 kPa. and rutting of pavement in field (Mississippi study). So, 3.2 kPa stress level is considered to be simulating field condition and therefore considered as standard stress level to determine J_{nr} (Tabatabaee N. & Tabatabaee H., 2010). However, the correlation was also observed between J_{nr} at high stress level (12.8 kPa. and 25.6 kPa.) and rutting of bituminous mix in laboratory (D’ Angelo, 2009; Wasage T. L. J. et al., 2013). It can be considered that the highest stress level, 3.2 kPa used in MSCR testing is significantly lower than what can be experienced in the field. Therefore current paper considers carrying out study on performance of modified binders for stress level up to 25.6 kPa. High stress could affect binder’s rheological properties such as J_{nr} , ER (Percent Elastic Recovery, %). Also it is helpful to see change in binder ranking and binder’s applicability for different site conditions.

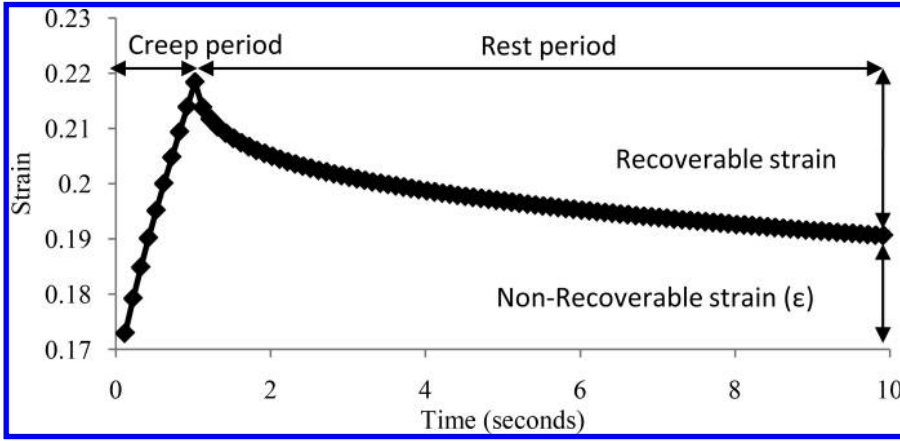


Figure 1. A Typical MSCR Test Curve.

2 OBJECTIVES

The primary objectives of the present study are to.

- Evaluate rutting performance of polymer and crumb rubber modified asphalt binders using multi stress creep recovery (MSCR) test at standard and high stress levels.
- Evaluate effects of high stress levels on percent elastic recovery of modified asphalt binders.
- Determine ranking of modified asphalt binders for different traffic levels under high stresses based on non-recoverable compliance parameters obtained from MSCR test.

3 OVERVIEW OF MULTIPLE STRESS CREEP RECOVERY (MSCR) TEST

The MSCR test is conducted in accordance with ASTM D7405. In this test, a binder sample is subjected to 1 second loading time followed by 9 second unloading time at stress level of 0.1 kPa and 3.2 kPa. At each stress level, 10 cycles are performed with no time lag and corresponding strain values are recorded. The MSCR curve with loading and unloading is as shown in Figure 1.

Strain values and applied stresses are being considered to evaluate different rheological parameters such as ER, J_{nr} , ER_{diff} , $J_{nr-diff}$, and binder grading (shown in Equation 1 to Equation 6) of the asphalt binders.

3.1 Percent recovery

For each of the ten cycles at a selected creep stress of σ , percent recovery, $e_r(\sigma, N)$, for $N = 1$ to 10 cycles:

$$e_r(\sigma, N) = \frac{(e_1 - e_{10}) * 100}{e_1} \quad (1)$$

where, e_0 = strain at time 0 sec,
 e_1 = strain at the end of 1 sec,
 e_{10} = strain at the end of 10 sec.

Average percent recovery at σ kPa: $ER\sigma$, for $N = 1$ to 10

$$ER\sigma = \frac{SUM(e_r(\sigma, N))}{10} \quad (2)$$

Percent difference in recovery between 0.1 kPa and σ kPa: ER_{diff}

$$ER_{diff} = \frac{((ER_{0.1} - ER\sigma) * 100)}{ER_{0.1}} \quad (3)$$

3.2 Non-recoverable creep compliance

For each of the ten cycles at a creep stress of σ kPa, the non-recoverable creep compliance, $J_{nr}(\sigma, N)$,

For $N = 1$ to 10 cycles:

$$J_{nr}(\sigma, N) = \frac{e_{10}}{\sigma_{100}} \quad (4)$$

Average non-recoverable creep compliance at σ kPa: for $N = 1$ to 10 cycles

$$J_{nr}\sigma = \frac{SUM(J_{nr}(\sigma, N))}{10} \quad (5)$$

Percent difference in non-recoverable creep compliance between 0.1 kPa and σ kPa:

$$J_{nr-diff} = \frac{((J_{nr}\sigma - J_{nr}0.1) * 100)}{J_{nr}0.1} \quad (6)$$

3.3 Binder gradation

Binder tested at high temperature performance grade can further graded in four categories as 'S', 'H', 'V' and 'E' if J_{nr} (kPa^{-1}) estimated at 3.2 kPa stress is in range of 2 to 4, 1 to 2, 1 to 0.5 and less than 0.5, respectively, in accordance with AASHTO MP 19 (Table 1).

Categorization has been made based on traffic level (ESALs) and load rate observed in field For

Table 1. AASHTO Designation: MP 19 for Binder Gradation (J_{nr} at 3.2 kPa).

Traffic level (ESALs) and Load Rate	Designation	Meaning	Recommended J_{nr} (kPa^{-1})
> 30 million and < 20 km/h	E	Extremely high traffic loading	0.0–0.5
> 30 million or < 20 km/h	V	Very high traffic loading	0.5–1.0
10–30 million or 20–70 km/h	H	High traffic loading	1.0–2.0
< 10 million and > 70 km/h	S	Standard traffic loading	2.0–4.0
–	*L	Low traffic loading	> 4.0

*Designated by author for discussion of results

example, a PG64-22 binder tested at 64°C will be graded as PG64E-22, for J_{nr} value in range of 0.0 to 0.05 kPa^{-1} will be considered suitable for extremely high traffic loading (i.e., ESALs > 30 million and Speed < 20 km/h). One more category as ‘L’ (for Low traffic) is being considered for explanation of results which corresponds to J_{nr} value more than 4.0 kPa. Binder with low value of J_{nr} is desired for extremely high traffic loading conditions, and vice versa. A binder with higher value of J_{nr} may exhibit higher permanent deformation behaviour. Usually, a higher percentage of modifiers are added to decrease percentage of J_{nr} and to make a binder more rut resistant.

4 MATERIALS COLLECTION

One polymer modified binder (PMB40) and one crumb rubber modified binder (CRMB60) were collected to carry out the study. As per IS 15462, for PMB 40 and CRMB 60 binder, 40 and 60 indicates penetration value and softening point value, respectively. Based upon information provide by manufacturer, CRMB60 binder was modified with crumb rubber gradation, 100% passing from number 30, and 80% passing from number 80 sieves. The basic tests such as penetration, softening point, ductility and viscosity were conducted in accordance with Indian Standards and results are reported as shown In Table 2. The binders were found to be acceptable as per IS standard. Higher temperature performance grades were observed as 82°C and 88°C for PMB 40 and CRMB 60 binders, respectively; indicating CRMB 60 is a stiffer binder compared to PMB 40.

4.1 Experimental plan and testing

The DSR instrument was utilized to perform MSCR test. The MSCR test is conducted at 76°C considering stress level ranging from 0.1 kPa to 25.6 kPa. Three replicates of each PMB 40 and CRMB 60 binders were tested. From strain obtained by MSCR test, different rheological parameters are determined such as percent recovery (ER, %), non recoverable creep compliance (J_{nr}), ER_{diff} , $J_{nr-diff}$. Also, at different stress levels, binder has been ranked based upon J_{nr} value.

5 RESULTS AND DISCUSSION

5.1 Effect of stress level on percent elastic recovery of asphalt binders

Percent elastic recovery (ER) indicates elastic nature of the binder and can be determined using Equation (2). A binder with high ER value is preferred to minimize rutting potential of a pavement. The Figure 2 shows a plot of ER (%) at 0.1 kPa, 3.2 kPa, 6.4 kPa, 12.8 kPa and 25.6 kPa stress levels, estimated at 76°C for PMB 40 and CRMB 60 binders.

The PMB 40 binder shows approximate ER of 79.6%, 22.7%, 12.8%, 4.8% and 0% at 0.1 kPa, 3.2 kPa, 6.4 kPa, 12.8 kPa and 25.6 kPa stress levels, respectively. Whereas CRMB 60 binder shows ER of 51.2%, 5.2%, 2.1%, 0.2% and 0.1% at 0.1 kPa, 3.2 kPa, 6.4 kPa, 12.8 kPa and 25.6 kPa stress levels, respectively. The PMB40 binder showed significantly high ER values compared to CRMB60. The presence of polymer network facilitates elastic nature to the PMB binder (Domingos & Faxina, 2013; Domingos & Faxina, 2014) whereas the CRMB60 binder showed less ER at all stress levels (Fig. 2). Both binders showed decrease in ER with an increase in stress level, as high stress level disturbs structure of the binder. At very high stress level (25.6 kPa) both binders showed zero ER.

Ratio of irrecoverable strain and stress is termed as non-recoverable creep compliance (J_{nr}) (Equation 4). As per AASHTO MP-19, J_{nr} at 3.2 kPa stress level is considered as indicative parameter of rutting potential of binder. Rutting occurs due to wheel load stresses in combination of high temperature. So, high temperature and wheel load together lead to high stresses. Therefore it can be considered that the highest stress level, 3.2 kPa used in MSCR testing is significantly lower than what can be experienced in the field. The Figure 3 show plot of average J_{nr} (kPa^{-1}) at 0.1 kPa, 3.2 kPa, 6.4 kPa, 12.8 kPa and 25.6 kPa stress level, estimated at 76°C for PMB 40 and CRMB 60 binders.

For PMB 40 binder, J_{nr} increased by 23%, 57% and 120% at stress level of 6.4 kPa, 12.8 kPa and 25.6 kPa, respectively as compared to 3.2 kPa. The increase in J_{nr} could be due to disturbance to polymer structure at higher stress level. For CRMB 60 binder, increase in stress level from 3.2 kPa to 6.4 kPa, 12.8 kPa and 25.6 kPa caused increased in J_{nr} by 29%,

Table 2. Basic Properties of Binders.

Tests	PMB 40		CRMB 60	
	Observed Value	Limit as per IS 15462	Observed Value	Limit as per IS 15462
Penetration(1/10) mm, Min	49	30–50	32	<50
Softening Point in °C, Min	61.8	60	60.7	60
Ductility in cm, Min	>100	–	20.4	–
Viscosity at 150°C, poise	7.1	3–9	12.8	3–9
PG grade as per ASTM D6373	PG 82-XX	PG 88-XX		

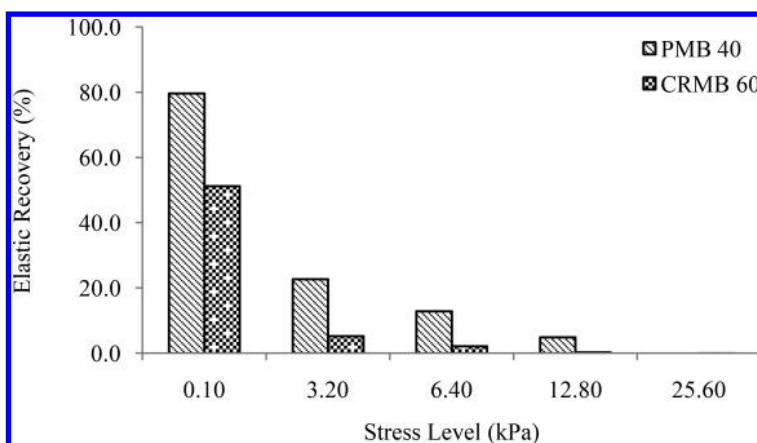


Figure 2. ER for PMB 40 and CRMB 60 at 76°C for different stress levels. Effect of stress level on non-recoverable creep compliance of asphalt binder.

70% and 130%, respectively. Overall, both binders showed increase in J_{nr} with an increase in stress level. Whereas, CRMB60 showed relatively lower J_{nr} value as compared to PMB 40, this is due to presence of crumb rubber particles which enhances stiffness of binder and exhibit resistance to stress level.

5.2 Relationship between percent elastic recovery and non-recoverable creep compliance of asphalt binder at different stress levels

The Figure 4 shows a plot between J_{nr} and ER for PMB40 and CRMB60 binders. Figure 4 indicates increase in J_{nr} with a decrease in ER. The ER is the highest for PMB 40 than CRMB60. The AASHTO TP70 provides a standard plot between J_{nr} and ER which can be used to identify presence of elastomeric polymer in binders. An asphalt binder is modified with an acceptable elastomeric polymer if it lies above the standard line on the graph and vice versa. At high stress level both binders showed different behavior (Fig. 4). The PMB 40 binder shows presence of elastomeric compound at 0.1 kPa and 3.2 kPa stress level, whereas for stress level of 6.4 kPa and higher, it shows absence (or breakage) of elastomeric compound, it clearly indicates that high stress level, PMB 40 binder behaves as a binder without elastomeric modification. Whereas CRMB 60 binder shows presence of elastomeric

compound only at 0.1 kPa and for stress levels 3.2 kPa and above, it shows absence of elastomeric compound, indicating at high stress level CRMB60 binder behaves like binder without elastomeric modification. The results indicate that PMB 40 behave considerably elastic in nature compared to CRMB60. The behavior of CRMB60 is expected as the crumb rubber particles increase stiffness of the binder but may not be elastic in nature as compared to polymer particles.

5.3 Effect of stress level on grading of asphalt binder

The both the binders were graded as per AASHTO MP 19 for all stress levels (Table1). The Figure 5 shows grading of PMB40 and CRMB60 at stress levels ranging from 0.1 kPa to 25.6 kPa.

The PMB40 binder is graded as ‘S’ at 3.2 kPa stress, whereas it was graded as ‘L’ for stress levels ranging from 6.4 kPa to 25.6 kPa. This decrement is due to failure of polymer structure of PMB40 at high stress level. A similar performance is observed in Figure 4, indicating performance equivalent to binder without elastomeric modifier. Therefore for sites where it is expected to have high stresses, PMB40 binder can be useful for low traffic condition instead of standard traffic condition.

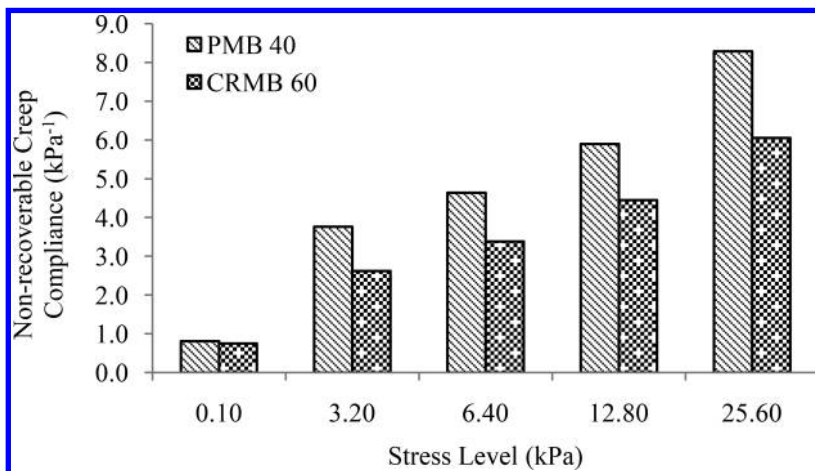


Figure 3. J_{nr} for PMB 40 and CRMB 60 at 76°C for different stress levels.

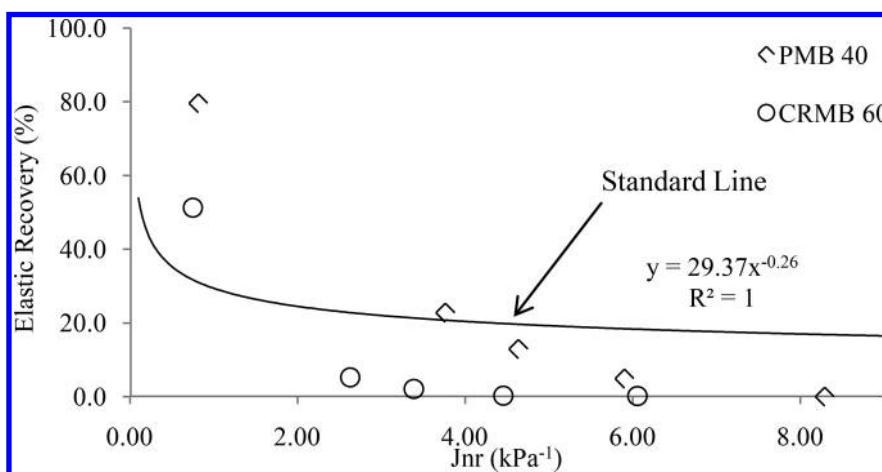


Figure 4. Plot between ER and J_{nr} for PMB 40 and CRMB 60.

The CRMB60 binder shows ‘S’ grading up to 6.4 kPa stress level and follows ‘L’ category at stress levels ranging from 12.8 kPa and 25.6 kPa. Crumb rubber modification induces more stiffness to the binder however; high stress level affects CRMB binder structure. Therefore at 12.8 kPa and 25.6 kPa stress levels, CRMB60 binder can be applicable for low traffic conditions. This change in grading for PMB40 and CRMB 40 indicates effect of high stress level on the binder’s performance and same need to be considered to characterize binder in better way.

Overall, both the binders showed decrement in grading with an increase in stress level. The PMB 40 is quite sensitive as compared to CRMB 60.

5.4 Effect of stress level on $J_{nr-diff}$ and ER_{diff} of asphalt binder

The $J_{nr-diff}$ indicates stress sensitive of a binder at unexpected heavy loading (Domingos & Faxina, 2013). The AASHTO MP 19 recommends that $J_{nr-diff}$ value for a

binder should not be more than 75%. The ER_{diff} and $J_{nr-diff}$ was estimated using Equation (3) and Equation (6) and Table 3 shows summary of ER_{diff} and $J_{nr-diff}$ for modified binders at different stress levels. The PMB 40 and CRMB 60 binders show $J_{nr-diff}$ more than 75% therefore fails to meet $J_{nr-diff}$ criterion as per AASHTO MP 19. Also it is observed that PMB40 binder more sensitive to stress than CRMB60. From ER_{diff} , it can be seen that both the binders show reduction in elasticity with an increase in stress level. The PMB 40 binder observed to show less reduction in ER at all stress levels except at 25.6 kPa stress, as compared to CRMB 60 binders.

6 CONCLUSIONS

The effects of high stress levels on rutting performance of polymer and crumb rubber modified binders were evaluated in this paper. It was observed that modified binders behave differently under high stresses. Based

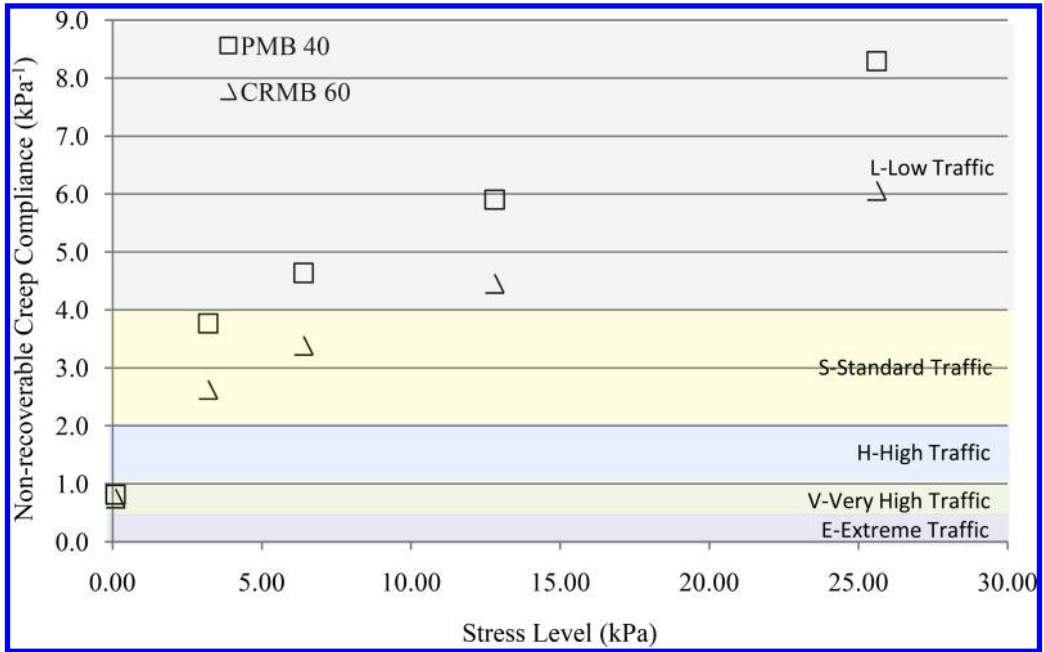


Figure 5. Grading of PMB 40 and CRMB 60 at 76°C for Different Stress Levels.

Table 3. ER_{diff} and $J_{nr-diff}$ for modified binders at different stress levels.

Stress Level (kPa)	PMB 40		CRMB 60	
	$J_{nr-diff}$ (%)	ER_{diff} (%)	$J_{nr-diff}$ (%)	ER_{diff} (%)
0.10	0.00	0.00	0.00	0.00
3.20	362.06	71.47	249.42	89.76
6.40	469.01	83.83	350.46	95.86
12.80	624.20	93.91	492.62	99.46
25.60	917.14	100.00	705.64	99.71

on the results and discussion above, the following conclusions can be drawn.

- The ER for both the binders decreases with an increase in stress level. The PMB 40 binder observed to have a better ER value than CRMB 60.
- The non-recoverable creep compliance (J_{nr}) increases with an increase in stress level for both the binders. The CRMB60 binder exhibits more rut resistant compared to PMB40; this may be due crumb rubber modification which facilitates stiffness to the binder.
- At 3.2 kPa stress level, the plot between ER and J_{nr} showed that PMB40 passes AASHTO MP 19 criterion, and showed it had sufficient amount of elastomeric polymer. The CRMB60 showed poor performance when compared with the standard value, and the results showed an absence of elastomeric behavior. At high stress level both the modified binders behave equivalent to a binder without elastomeric modification.

- Overall both binders showed degradation in ranking for different traffic conditions with increased stress level. This change in grading for PMB40 and CRMB 60 shows that high stress level will certainly help to better evaluate rutting properties and applicability of the binders.
- Based on $J_{nr-diff}$ and ER_{diff} , it was found that PMB 40 binder is more sensitive to stress as compared to CRMB 60.

REFERENCES

- Anderson, D.A. & Kennedy, T.W. 1993. Development of SHRP binder specification. *Journal of the Association of Asphalt Paving Technologies*, Vol. 62, 481–501.
- American Association of State Highway and Transportation Officials. 2013. *Standard specification for performance-graded asphalt binder, AASHTO designation: MP 19*.
- American Association of State Highway and Transportation Officials. 2013. *Multiple Stress Creep Recovery (MSCR)*

- Test of Asphalt Binder Using a Dynamic Shear Rheometer (DSR), AASHTO designation: TP 70.*
- American Society for Testing and Materials. 2010. *Multiple Stress Creep and Recovery (MSCR) of Asphalt Binder Using a Dynamic Shear Rheometer (DSR), ASTM designation: D 7405-10a.*
- ASTM D 7175. 2008. Standard Test Method for Determining the Rheological Properties of Asphalt Binder Using a Dynamic Shear Rheometer, *American Society for Testing and Materials*, United States.
- ASTM D 7405. 2010. Standard Test Method for Multiple Stress Creep and Recovery (MSCR) of Asphalt Binder Using a Dynamic Shear Rheometer, *American Society for Testing and Materials*, United States.
- Bouldin, M.G., Dongre, R., & D'Angelo, J. 2001. Proposed refinement of Superpave high-temperature specification parameter for performance-graded binders. *Transportation Research Record No. 1766*, Transportation Research Board of the National Academies, Washington, D.C. 40–47.
- D'Angelo, J. & Dongre, R. 2002. Superpave binder specifications and their performance relationship to modified binders. *Proceedings of Canadian Technical Asphalt Association*, No. XLVII. 91–103.
- D'Angelo, John. 2004. *Modified binders and superpave plus specifications. Superpave Technical Issues, Asphalt Institute.*
- D'Angelo, J. 2011. The Relationship of the MSCR Test to Rutting The Relationship of the MSCR Test to Rutting. *Road Materials and Pavement Design*, (January 2013), 37–41.
- D'Angelo, J., Kluttz, R., Dongre, R. N., Stephens, K., & Zanzotto, L. 2007. Revision of the Superpave High Temperature Binder Specification: The Multiple Stress Creep Recovery Test (With Discussion). *Journal of the Association of Asphalt Paving Technologists: From the Proceedings of the Technical Sessions.*
- Delgadillo, R., Bahia, H. U., & Lakes, R. 2012. "A nonlinear constitutive relationship for asphalt binders." *Materials and Structures*, 45(3), 457–473.
- Divya, P. S., Gideon, C. S., & Krishnan, J. M. 2012. Influence of the Type of Binder and Crumb Rubber on the Creep and Recovery of Crumb Rubber Modified Bitumen. American Society of Civil Engineers.
- Domingos, M. D. I., & Faxina, A. L. 2013. Rheological analysis of asphalt binders modified with Elvaloy®terpolymer and polyphosphoric acid on the multiple stress creep and recovery test. *Materials and Structures.*
- Domingos, M. D. I., & Faxina, A. L. 2014. Creep-Recovery Behavior of Asphalt Binders Modified with SBS and PPA. 04(April), 781–783.
- Kose, S., Guler, M., Bahia, H. U., & Masad, E. 2000. Distribution of Strains Within Hot-Mix Asphalt Binders: Applying Imaging and Finite-Element Techniques – Transportation Research Record: Journal of the Transportation Research Board – Volume 1728, Volume 1728/2000 Asphalt Binders 2000 - Transportation R. *Transportation Research Record: Journal of the Transportation Research Board*, 1728, 21–27.
- Masad, E., & Somadevan, N. 2002. Microstructural Finite-Element Analysis of Influence of Localized Strain Distribution on Asphalt Mix Properties. (October), 1105–1114.
- Tabatabaee, N., & Tabatabaee, H. A. 2010. Multiple Stress Creep and Recovery and Time Sweep Fatigue Tests. *Transportation Research Record: Journal of the Transportation Research Board*, 2180(-1), 67–74.
- Wasage, T. L. J., Stastna, J., & Zanzotto, L. 2011. Rheological analysis of multi-stress creep recovery (MSCR) test. *International Journal of Pavement Engineering*, 12(6), 561–568.

Fatigue performance characterization of warm-modified bituminous binders

D.M. Abd & H. Al-Khalid

School of Engineering, University of Liverpool, Liverpool, UK

ABSTRACT: This paper presents results of an investigation to evaluate the effect of Sasobit and Rediset WMX and LQ on the fatigue performance of bituminous binders. This study adopts a Time Sweep (TS) test method to study this phenomenon under controlled strain and stress modes using a Dynamic Shear Rheometer. Fatigue life is defined using the traditional approach based on number of cycles and reduction in initial stiffness. To accurately predict the fatigue life of unmodified and WMA-modified binders, the viscoelastic continuum damage (VECD) approach and Energy approach have been also adopted. It was found that WMA additives had a superior performance in terms of fatigue life. Results from the Energy and VECD approaches have been shown to correlate well with the traditional approach. VECD can be used to model the fatigue behaviour of WMA binders and predict the response of materials under different loading history.

1 INTRODUCTION

In recent years, pavement researchers have increasingly focused on reducing production and compaction temperatures to improve the environmental and economic impacts of hot mix asphalt (HMA) without adversely affecting workability, durability and performance of asphalt pavements. The introduction of new innovations and technologies in the form of warm mix asphalt (WMA), which is one of the main focuses of future pavement technology endeavours, will lead to substantial improvements in quality of life and economic prosperity. Warm mix signifies an asphalt mix that can be achieved practically at temperatures of around 30°C or cooler than the typical temperature used in HMA production. The reduction in the production temperature is allowed by the use of warm technologies such as organic additives, chemical additives and warm foaming to reduce the viscosity of the binder, which facilitates operating at lower temperatures.

Many studies have focused on the performance of warm asphalt mixtures, but only a few (Arega et al. 2011; Hanz, Mahmoud & Bahia 2011; Wasiuddin, Saltibus & Mohammad 2011; Xiao, Amirkhanian & Zhang 2011; Xiao, Punith & Amirkhanian 2012) are related specifically to the binder. Therefore, this study primarily focuses on fatigue performance characterization of warm-modified bituminous binders.

2 OBJECTIVE OF THE STUDY

This work aims to investigate the fatigue behaviour of warm additives, namely Sasobit and Rediset WMX

and LQ, in order to rank the modified bituminous binders in respect of their fatigue performance. In pursuit of this aim, the SHRP fatigue criterion for binders is questioned and a proposal is made to accurately predict the fatigue life of WMA binders based on the VECD concept.

3 EXPERIMENTAL METHODS

3.1 *Materials*

WMA additives Sasobit, Rediset WMX and Rediset LQ were incorporated into two binder grades in the study, namely 40/60 and 100/150 Pen, which are commonly used in the UK and are expected to have different fatigue life capacities. It is worth noting that, for the purpose of identifying fundamental fatigue performance of warm-modified bituminous binder, an original modified binder with no ageing effect was considered in this study. All warm additives were added at rates within the specified manufacturer tolerance. The recommended dosages of Sasobit, Rediset WMX and Rediset LQ which are adopted in this study are 2%, 2% and 0.5% by the weight of the bitumen respectively.

3.2 *Sample preparation*

The modified asphalt binders were prepared using the Silverson Shear mixer under controlled temperature, time and shear rate conditions. It has been reported and recommended that Sasobit and Rediset do not need a high shear rate for mixing, therefore the adopted shear rates for mixing and mixing time were 700 rpm and 5

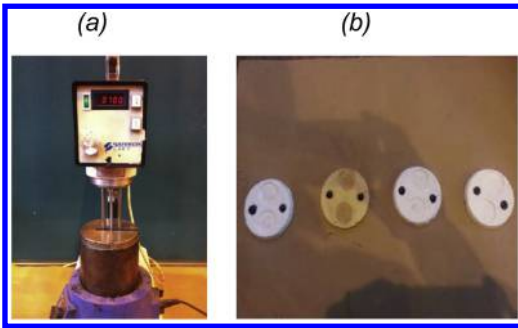


Figure 1. (a) Silverson Shear mixer (b) Silicon moulds.

minutes, respectively, as adopted by some researchers (Xiao, Punith & Amirkhanian 2012). In addition, the mixing temperature for both hard binder (40/60 Pen) and soft binder (100/150 Pen) was $150^{\circ}\text{C} \pm 5^{\circ}\text{C}$. The asphalt binder was preheated in an oven to the selected mixing temperature while, during mixing, the mixing temperature was maintained using an iso-mantle heater in order to keep a uniform temperature to achieve consistent mixing; and the container was also covered with an insulation mantel which was preheated to the required temperature, as can be seen in Figure 1-a. After mixing, modified bituminous binders were kept in the fridge at temperature below 10°C to avoid the effect of ageing. Prior to testing, virgin and modified binders were heated up using an oven maintained at 150°C but one should note that binders were just heated up for a certain time to soften them to prevent ageing and then they were stirred manually before being poured into a mould, as the received sample must be homogenized. Silicon moulds then used to prepare samples for amplitude sweep and fatigue tests, as seen in Figure 1-b. Both amplitude and fatigue tests were conducted with the 8 mm plate-plate set-up. All tests were conducted at a frequency of 10 Hz, using 2 mm gap settings and the test temperature was 20°C .

3.3 Mechanical testing

3.3.1 Determination of strain/stress amplitude

The stress or strain levels for the experimental work were chosen from the results of amplitude sweep stress and strain used in establishing the linear viscoelastic limits of the materials. According to the strategic Highway Research Program (SHRP), LVR is defined as a linear viscoelastic representation of the flow properties of the asphalt binder where the modulus is independent of stress or strain. The investigation can be performed by applying a varying (increasing) strain to the sample and observing the resulting stress or modulus (Anderson et al. 1994). It was defined that the LVR limit is the point at which the modulus decreased to 95% of the initial modulus (Anderson et al. 1994).

However, in order to shorten the testing time of fatigue test, a single stress level and a single strain level for 40–60 and 100–150 grades were chosen respectively above the LVR limit. Tests were conducted at

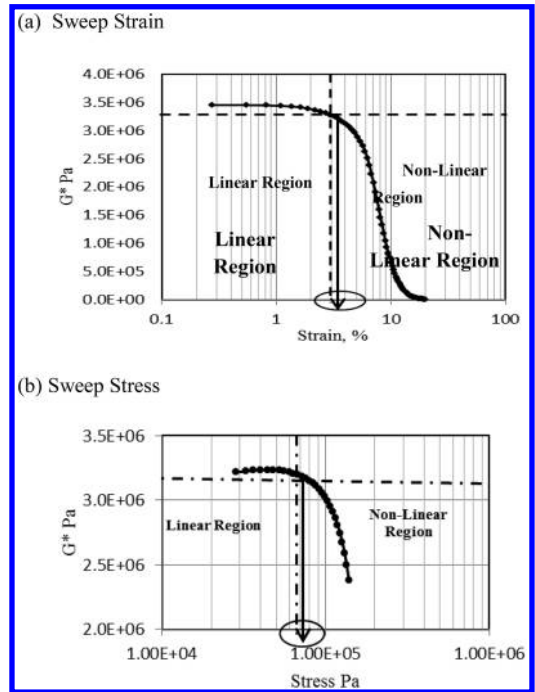


Figure 2. (a) Sweep strain (b) Sweep stress for 100–150 binder grade.

Table 1. Values of stress and strain used in fatigue tests.

Binder Grade	Strain Value	Stress Value
	%	Pa
40–60	3	2500000
100–150	3.5	100000

20°C and two replicates were performed for each condition. Figure 2 illustrates an example of sweep strain and stress for the 100–150 grade. It should be mentioned that sweep stress and strain were just conducted on virgin binders then the selected strain and stress values were implanted on all bitumen (virgin and modified) so that comparison could be made with the control binder. Table 1 summarized the selected controlled strain and stress values for both binder grades.

3.3.2 Fatigue tests

Asphalt binder plays a major role in determining the mechanical characteristics an asphalt mixture portrays in resisting distress. It has been reported that binder influences asphalt distress by approximately 40, 60 and 90% in terms of rutting, Fatigue and low temperature cracking respectively (Partl et al. 2013). In fact, Fatigue is one of the main types of asphalt pavement deterioration. In reality, fatigue life is defined as the number of standard axles passing until mechanical failure while, in the laboratory, it is defined as a

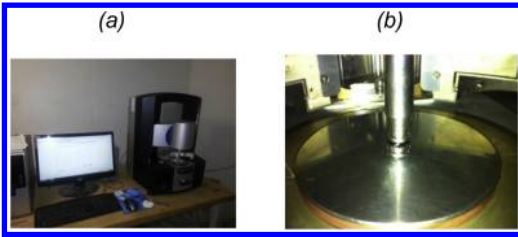


Figure 3. (a) Kinexus DSR (b) Loaded sample between plates.

number of stress or strain cycles to failure of a sample predicted by fatigue criteria.

In this study, fatigue tests were conducted in both controlled stress and strain using the Kinexus DSR (Figure 3). The Kinexus DSR, which was developed by the Malvern Instrument Company, has overcome the weaknesses of the previous generation of rheometers, and is associated with advances in shear and vertical (axial) testing in order to provide a rotational rheometer platform with unprecedented dual-action capabilities. Previous researchers recommended conducting fatigue test using DSR at relatively low temperature in order to minimize the edge effect of the sample as a heterogeneous flow (plastic flow) may accrue at high temperature. In fact, the sophisticated Kinexus DSR has the ability to overcome this issue because of machine capacity. This DSR incorporated a controlled hood temperature which keeps a uniform temperature during the test.

Many pavement engineers have questioned and investigated the fatigue performance of asphalt materials based on $|G^*| \cdot \sin \delta$ (Deacon et al. 1997; Tsai & Monismith 2005; Zhou et al. 2012). In fact, this approach lacks the ability to characterize the actual damage and deterioration of bituminous binder because it is measured under the conditions of relatively different from the rather complicated fatigue phenomenon which features many more cycles of loading and fatigue damage. Therefore, to address and investigate the real fatigue resistance of bituminous binder, this study adopts a Time Sweep (TS) test method to study this phenomenon under controlled strain and stress modes using a Dynamic Shear Rheometer. As mentioned previously, DSR time sweep was conducted with the 8 mm plate-plate set-up. All tests were conducted at a frequency of 10 Hz, using 2 mm gap settings and the test temperature was 20°C. It should also be noted that the fatigue test is carried out until complete failure occurs. In the fatigue test, at least two replicates were performed for each condition and the results presented in this study are the average of the replicates.

4 TRADITIONAL APPROACH

The traditional criterion which is the commonly used and acknowledged fatigue criterion of asphalt binder and a mixture is defined as a reduction in stiffness

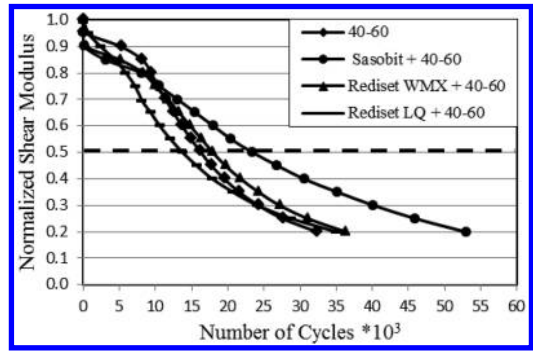


Figure 4. Number of cycles against normalized shear modulus at controlled strain mode for 40–60 grade modified with warm additives.

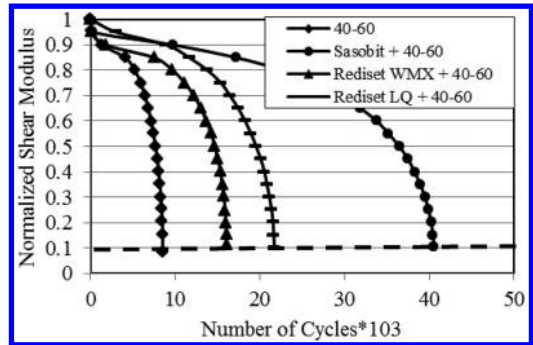


Figure 5. Number of cycles against normalized shear modulus at controlled stress mode for 40–60 grade modified with warm additives.

modulus of the material. Fatigue failure is defined as the number of cycles when the stiffness modulus decreases to 50% of its initial value (Hicks et al. 1993; Kim et al. 2003; Williams 1998); whereas, in the controlled stress mode, it is defined as a reduction of stiffness modulus of the sample to 10% of its initial value (Artamendi & Khalid 2005) or a complete fracture of the sample (Ghuzlan & Carpenter 2006). In this study, failure criteria of 50% reduction in stiffness modulus (strain mode) and reduction of stiffness modulus to 10% of initial value were adopted.

In all scenarios in Figures 4, 5, 7 and 8, Sasobit significantly increases the fatigue life of asphalt binder regardless of binder grade and test mode. This trend is not equivalent with other researchers, who reported that Sasobit has lower m-value which may negatively affect the fatigue life of bituminous binder. Therefore; direct fatigue test of bituminous binder and modified binder can accurately rank its performance rather than bending beam rheometer test of bituminous binder. Although rheological investigations indicate that Sasobit increases binder stiffness and slightly decreases phase angle, this does not mean it has lower fatigue life because, as mentioned previously, the interaction between Sasobit and asphalt binder is only physical but increase in binder stiffness is because it enlarges the

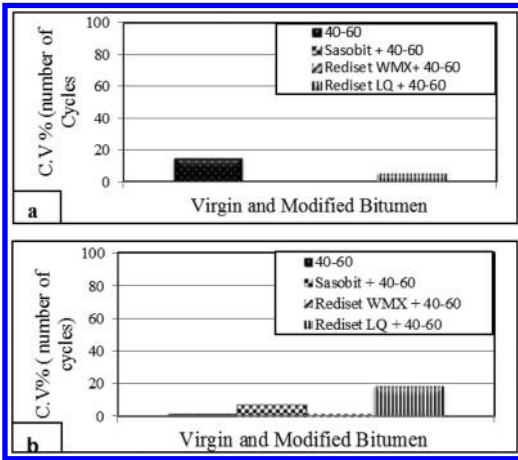


Figure 6. (a) Coefficient of variance (C.V) of number of cycles at 50% reduction in stiffness modulus (strain mode). (b) Coefficient of variance C.V of number of cycles to 10% reduction in stiffness modulus (stress mode).

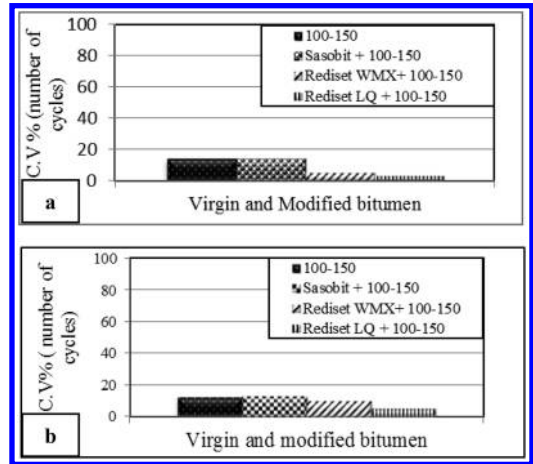


Figure 9. (a) Coefficient of variance (C.V) of number of cycles at 50% reduction in stiffness modulus (strain mode). (b) Coefficient of variance C.V of number of cycles to 10% reduction in stiffness modulus (stress mode).

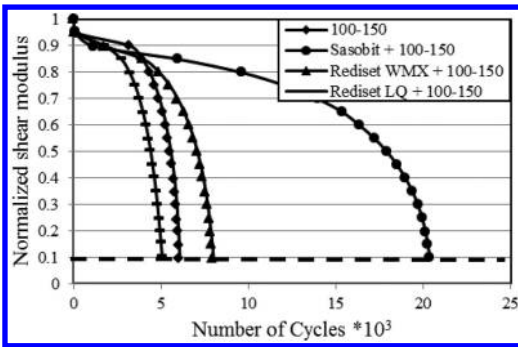


Figure 7. Number of cycles against normalized shear modulus at controlled strain mode for 100–150 grade modified with warm additives.

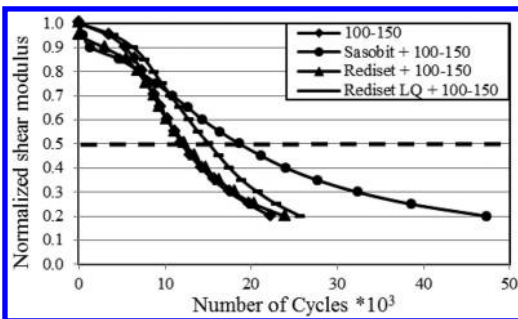


Figure 8. Number of cycles against normalized shear modulus at controlled stress mode for 100–150 grade modified with warm additives.

bee-like structures of bitumen (Menapace et al. 2014). In other words, Sasobit caused the catana phase and the peri phase to grow, which are assigned to asphaltenes and resins respectively, without adversely affecting the

ductility properties of bituminous binder. In fact, Sasobit leads to stiffening of the binder in a similar manner to fibre-reinforced materials.

Rediset WMX does not significantly improve the fatigue life of bituminous binder in terms of strain characterizations as seen in Figures 4 and 7 (controlled strain), in comparison with Sasobit; however, as illustrated in Figures 5 and 8, it could potentially improve the stress characteristics of asphalt binder. This, in fact, is because of the chemical structure of this additive. Rediset WMX is an organic chemical: it is carbon based with a paraffin wax and hydrocarbon wax concentration between 0–20%, which is thought to enhance the stress characterizations of bituminous asphalt.

Despite the superior performance of Sasobit and Rediset WMX, the trend of Rediset LQ was not clear.

The coefficient of variance on number of cycles at 50% reduction in stiffness modulus (strain mode) and at 10% reduction in stiffness modulus (stress mode) was also calculated. In all cases it can be said that it is acceptable as shown in Figures 6 and 9.

However, in the traditional approach, the performance is assessed on the number of cycles against the reduction in the stiffness modulus without taking into account other variables such as stress, strain, phase angle, etc. Therefore, within this study, Dissipated Energy Ratio (ER) and Viscoelastic Continuum Damage (VECD) were adopted which both are advanced criteria to assess the fatigue life of bituminous and asphalt mixtures.

5 ENERGY APPROACH

Once the load is applied to the material, the resulting stress will induce strain and the area under the strain-stress curve can be used to calculate the amount of

energy being input into the material. In perfect elastic materials, all the energy being input into the material is recovered during unloading. In contrast, for viscoelastic material, not all the applied energy could be recovered; therefore, in this case a retained part of energy is related to mechanical fatigue of the material and can therefore be interpreted as dissipated energy.

In this regard, Van Dijk proposed an approach related to the dissipated energy to characterize the fatigue performance of asphalt mixture (Van Dijk 1975).

Generally, in the fatigue process two stages are distinguished: initiation of micro-cracks and propagation of micro- and macro-cracks leading to specimen and material failure. In both stages some energy is dissipated during a single load cycle and can be calculated as explained in [equation 1](#):

$$W_n = \pi \cdot \sigma_n \cdot \varepsilon_n \cdot \sin \theta_n \quad (1)$$

where: n = cycle number; ε = strain amplitude; σ = stress amplitude; θ = phase angle.

Based on this concept and Van Dijk's work, Hopman proposed the use of an Energy Ratio to define the number of cycles (N_1) in a controlled strain mode to a point where cracks are considered to initiate (Hopman, Kunst & Pronk 1989) which is calculated as [equation 2](#):

$$R_i^e = \frac{n \cdot w_0}{w_i} \quad (2)$$

where

n = number of load cycles

w_0 = dissipated energy at the first cycle

w_i = dissipated energy at the i -cycle

However, in 1993, Rowe simplified the equation proposed by Hopman to identify the number of cycles (N_1) when cracks are conceded to initiate and more accurately it is a point where the micro-cracks coalesce to form a sharp crack (Rowe & Boulidin 2000).

In controlled strain mode, the equation of energy ratio can be written as following:

$$R_i^e = \frac{n}{E_i^*} \quad (3)$$

where R_i^e is Energy Ratio at controlled strain mode, E_i^* is the complex modulus at the i -cycle.

N_1 can be defined in this mode as the point at which the slope of the dissipated energy ratio as a function of load cycles diverts from a straight line, whereas; for the controlled stress mode, N_1 corresponds to the peak value when the Energy Ratio is plotted against number of load cycle and the simplified equation of calculation energy ratio as:

$$R_i^\sigma = n \cdot E_i^* \quad (4)$$

where E_i^* is the Energy Ratio at controlled stress mode.

Based on the Energy Ratio criterion to identify the performance of warm-modified bitumen, Sasobit

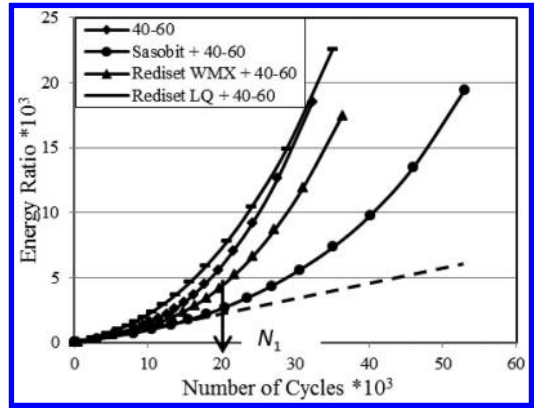


Figure 10. Number of cycles against energy ratio at controlled strain mode for 40–60 grade modified with warm additives.

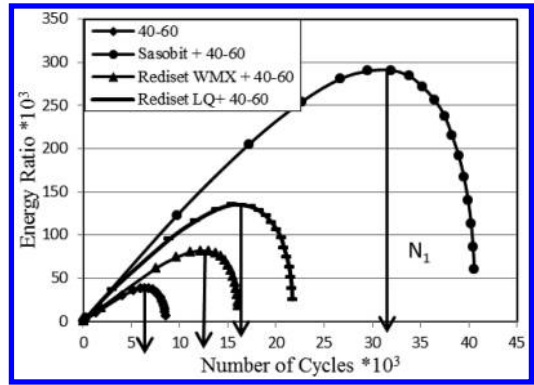


Figure 11. Number of cycles against energy ratio at controlled stress mode for 40–60 grade modified with warm additives.

also significantly improves the fatigue life of bitumen regardless of binder grade and fatigue test mode, as can be seen in [Figures 10-13](#). Examples of the N_1 have been given and also how it is calculated in [Figures](#).

Generally, the rank of all warm-modified bitumen in terms of fatigue performance was similar to what was reported using the Traditional Approach. And also although, it not shown, high correlations between the failure points in the Tradition Approach and Energy Approach in both strain and stress modes were found, [Figures 10–13](#).

6 VISCOELASTIC CONTINUUM DAMAGE APPROACH

In order to be able to accurately predict the fatigue performance of warm-modified bitumen, advanced mathematical models such as Viscoelastic Continuum Damage (VECD) offer a great potential for better understanding of fatigue cracking behavior (Kutay,

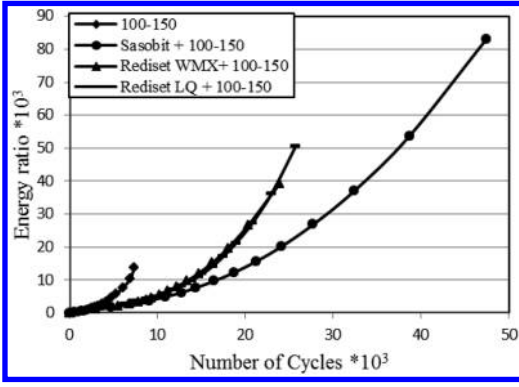


Figure 12. Number of cycles against energy ratio in controlled strain mode for 100–150 grade modified with warm additives.

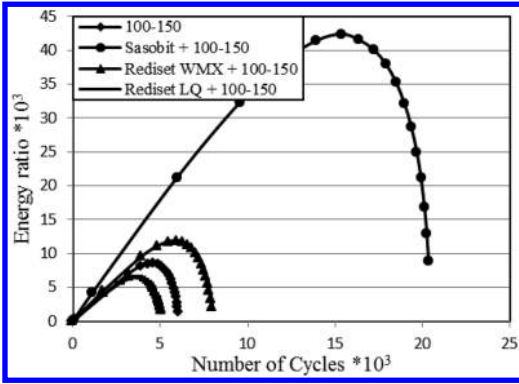


Figure 13. Number of cycles against energy ratio in controlled stress mode for 100–150 grade modified with warm additives.

Gibson & Youtcheff 2008a; Kutay, Gibson & Youtcheff 2008b) and also to model the fatigue behaviour of modified bitumen.

VECD has been successfully used by a number of researchers. Therefore, it would be a great to use this approach to rank the performance of warm-modified bitumen. Fatigue can be identified based on the curve of C - S . (C) is pseudostiffness which is defined as the loss of material stiffness, due to loss of material integrity caused by damage, while (S) is a single parameter which is used to quantify the damage growth (Kutay, Gibson & Youtcheff 2008a).

Damage parameter (S) is calculated as:

$$S_\varepsilon^{N+\Delta N} = S_\varepsilon^N + (\Delta N/f)^{\frac{1}{1+\alpha}} [-0.5I\varepsilon_N^R (C_{N+\Delta N} - C_N)]^{\frac{\alpha}{1+\alpha}} \quad (5)$$

$$S_\sigma^{N+\Delta N} = S_\sigma^N + (\Delta N/f)^{\frac{1}{1+\alpha}} \left[0.5 \frac{1}{I} \sigma_N^R \left(\frac{1}{C_{N+\Delta N}} - \frac{1}{C_N} \right) \right]^{\frac{\alpha}{1+\alpha}} \quad (6)$$

where ε^R is pseudostrain, σ^R is pseudostress, I is initial stiffness parameter, C is pseudostiffness, f is a constant frequency, S_ε is the damage parameter when ε^R is used in the analysis (strain mode), N is the damage parameter when σ^R is used (stress mode), N is the

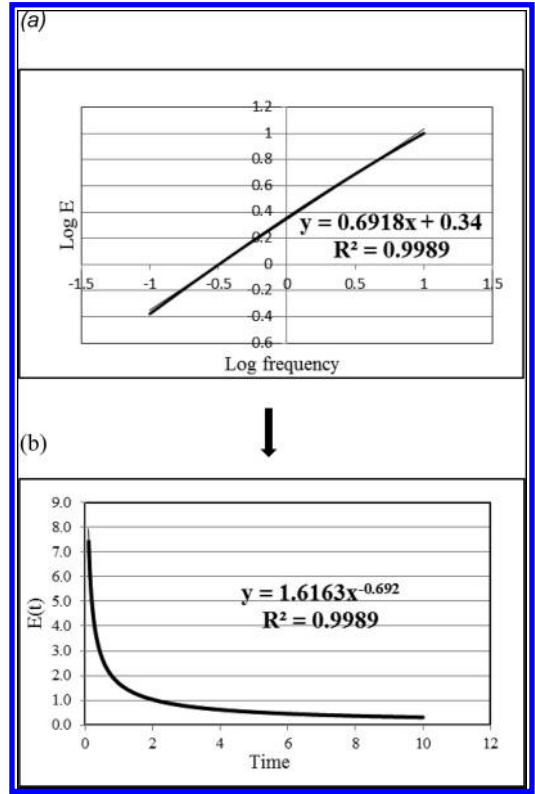


Figure 14. Example of conversion of the sweep frequency data to relaxation data (a) Sweep frequency data (b) Relaxation data.

number of cycles, α is a material constant related to the rate of damage.

α is calculated based on undamaged rheological properties using the slope of relaxation modulus (Hintz et al. 2011). Lee and Kim suggested that $\alpha = 1 + 1/m$ is more suitable for strain controlled tests, whereas $\alpha = 1/m$ is suitable for stress mode tests (Kutay, Gibson & Youtcheff 2008a; Lee & Kim 1998).

m is the maximum slope of the relaxation modulus plotted against time. In this study, it was difficult to run a relaxation test; therefore it was decided to use a method developed by Schapery and Park to convert sweep frequency test data to the relaxation data as can be seen in the Figure 14.

Where E is the stiffness modulus and $E(t)$ is the relaxation modulus. The sweep frequency (for each control and modified bitumen) was conducted within the linear region of material behaviour at 20°C.

As previously, data were analyzed based on the strain and stress modes; however according to VECD theory, a single damage characteristic curve behaviour of (C - S) should exist independent of loading frequency, temperature and mode of loading and (C - S) curves calculated at different temperatures and at different loading modes should collapse on a single curve (Kutay, Gibson & Youtcheff 2008a).

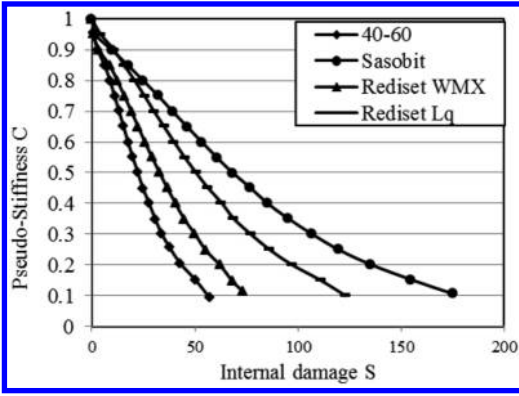


Figure 15. Pseudostress-based damage parameter of modified bitumen with 40–60 binder grade.

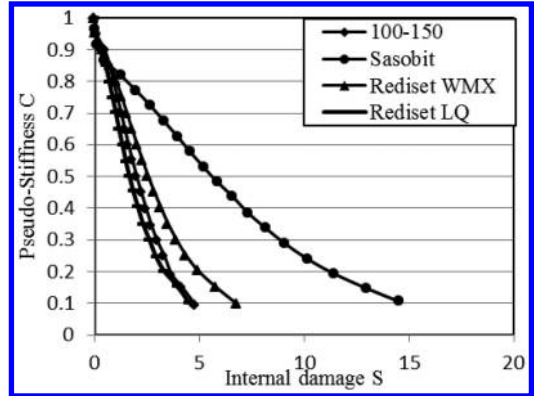


Figure 16. Pseudostress-based damage parameter of modified bitumen with 100–150 binder grade.

The characteristic curves of Figures 15–18 describe how the micro-cracks grow and propagate for particular bitumen. Sasobit significantly slows the degradation of the bitumen regardless of bitumen grade and fatigue mode because, as mentioned previously Sasobit increased the bitumen stiffness and acts as a fibre reinforcement to the material. Rediset WMX also delayed the deterioration and the development of micro-cracks. Rediset WMX, in fact, also acts as an adhesion promoter; therefore the performance of this additive should further increase the performance of warm asphalt mixture in terms of fatigue life. However, the trend performance of Rediset LQ is really unclear and needs to be further evaluated because, in the case of modifying the hard binder (40–60 pen) as is shown in Figure 15, Rediset LQ improves the stress characterization of bitumen, which is in agreement with (Hill et al. 2012) but this trend is inverse in the case of adopting the soft bitumen. This phenomenon may be because Rediset LQ slightly softens the bitumen and could improve the stress characterizations of hard material but a trend inverse with soft bitumen. A further investigation is needed of the behaviour of Rediset LQ in terms of warm asphalt mixture before a confident conclusion can be given.

It should be noted that the VECD approach is highly correlated with Traditional and Energy approaches as shown in Figures 19–22.

The main advantage of VECD approach is that it is based on a constitutive model and the characteristic curve can be utilized to model the fatigue behaviour of the material under any load history and temperature.

Once the damage characteristics of C-S curves were obtained, an exponential best-fit line was fitted to the curves in the following equation:

$$C = \exp(aS^b) \quad (7)$$

where a and b are constant parameters defining the best fit. Those parameters in table 2 could be further used to model the fatigue behaviour of warm modified bitumen and predict the response of the material to a given loading history.

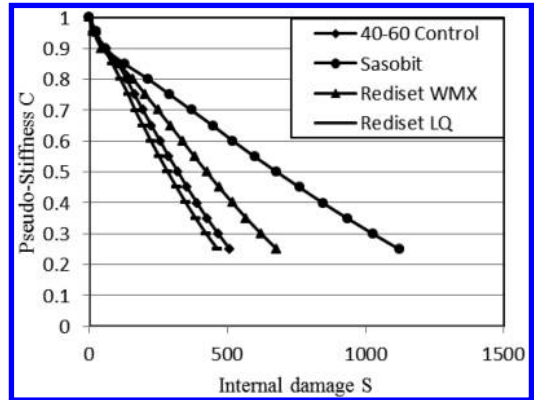


Figure 17. Pseudostrain-based damage parameter of modified bitumen with 40–60 binder grade.

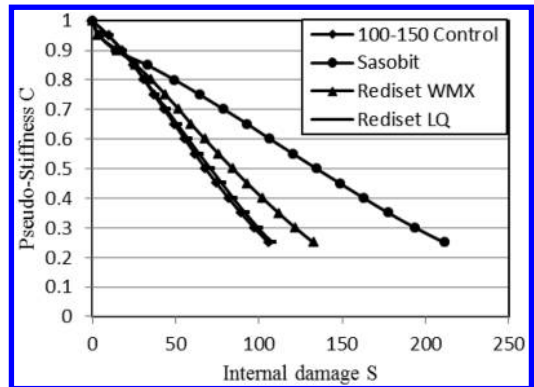


Figure 18. Pseudostrain-based damage parameter of modified bitumen with 100–150 binder grade.

7 SUMMARY AND CONCLUSIONS

This paper has investigated the fatigue performance of warm-modified bitumen adopting the Time Sweep (TS) test method to study this phenomenon under controlled strain and stress modes using a Dynamic Shear

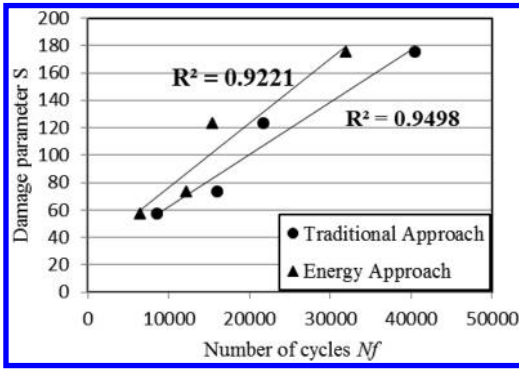


Figure 19. Comparison of damage parameter S (failure point) with 10% criteria and ER criteria of warm modified with 40–60 binder grade (stress mode).

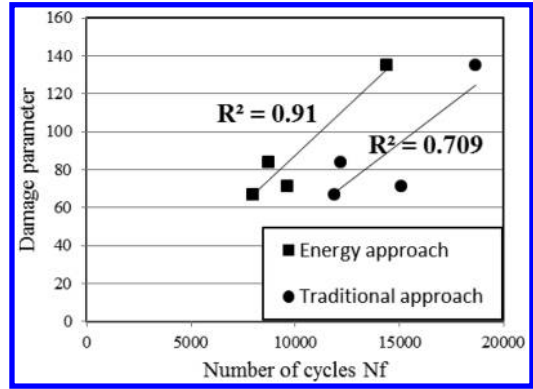


Figure 22. Comparison of damage parameter S (failure point) with 50% criteria and ER criteria of warm modified with 100–150 binder grade (strain mode).

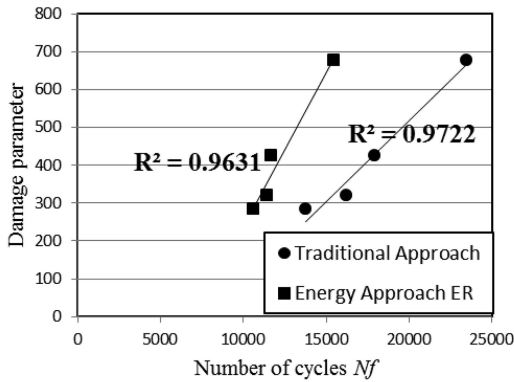


Figure 20. Comparison of damage parameter S (failure point) with 50% criteria and ER criteria of warm modified with 40–60 binder grade (strain mode).

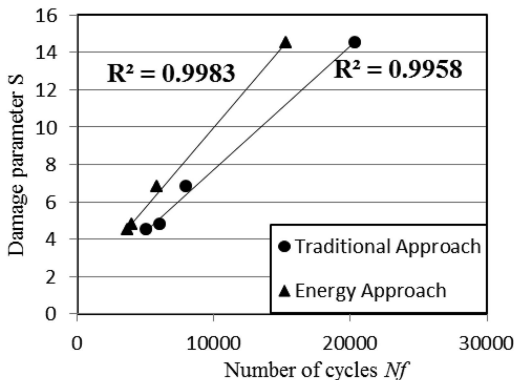


Figure 21. Comparison of damage parameter S (at failure point) with 10% criteria and ER criteria of warm modified with 100–150 binder grade (stress mode).

Rheometer (DSR). Based on the results presented, several conclusions can be drawn:

1. Sasobit significantly increases the fatigue life of asphalt binder regardless of binder grade and test

Table 2. α and exponential fit coefficient of damage characteristics curves of warm-modified bitumen.

Strain mode		α	a	b
40–	Control	2.45	–0.000470059	1.269063675
	Sasobit	2.60	–0.000423934	1.141816544
	Rediset WMX	2.47	–0.000434424	1.225063531
60	Rediset LQ	2.45	–0.000835248	1.194694844
	Control	2.28	–0.002140003	1.373177371
	Sasobit	2.39	–0.001609367	1.246417005
100–	Rediset WMX	2.35	–0.002378102	1.285505124
	Rediset LQ	2.37	–0.001801126	1.403693575
	Control	1.45	–0.013327043	1.273349534
40 - 60	Sasobit	1.60	–0.003952148	1.224752444
	Rediset WMX	1.47	–0.005861967	1.368248812
	Rediset LQ	1.45	–0.003906909	1.318899277
	Control	1.28	–0.260833807	1.400313291
	Sasobit	1.39	–0.09049833	1.192577159
150	Rediset WMX	1.35	–0.219457714	1.234338684
	Rediset LQ	1.37	–0.376271333	1.196674983

mode. In fact, Sasobit acts as fibre reinforcement to the bitumen. Previous studies showed that Sasobit increases the tendency towards cracking at low temperature. However, using the recommended dosage of Sasobit showed a superior performance in terms of resistance to fatigue cracking. This is confirmed using different criteria to rank the Sasobit-modified bitumen.

2. Despite the fact that the improved performance of Rediset WMX was not as significant as that of Sasobit, Rediset WMX also improves the fatigue life of bitumen.
3. The main advantage of the Energy Approach is its simplicity when used to investigate the fatigue behaviour of materials; however, it is not a constitutive model and cannot be applied to predict material's response under different loading histories.

4. The controversial point in this study is the performance of Rediset LQ. Further investigation is needed of the impact of Rediset LQ on the mechanical properties of warm asphalt mixtures before an accurate conclusion can be reached.

ACKNOWLEDGMENTS

The authors would like to acknowledge Naylor Chemicals and AkzoNobel for their assistance in providing the WMA additives and Nynas for supplying the straight-run binders.

REFERENCES

- Anderson, D.A., Christensen, D.W., Bahia, H.U., Dongre, R., Sharma, M., Antle, C.E. & Button, J. (1994) 'Binder characterization and evaluation, volume 3: Physical characterization', *Strategic Highway Research Program, National Research Council, Washington, DC*.
- Arega, Z., Bhasin, A., Motamed, A. & Turner, F. (2011) 'Influence of warm-mix additives and reduced aging on the rheology of asphalt binders with different natural wax contents', *Journal of Materials in Civil Engineering*, vol. 23, no. 10, pp. 1453–1459.
- Artamendi, I. & Khalid, H. (2005) 'Characterization of fatigue damage for paving asphaltic materials*', *Fatigue & fracture of engineering materials & structures*, vol. 28, no. 12, pp. 1113–1118.
- Deacon, J., Harvey, J., Tayebali, A. & Monismith, C. (1997) 'Influence of binder loss modulus on the fatigue performance of asphalt concrete pavements', *Journal of the Association of Asphalt Paving Technologists*, vol. 66, pp. 633–668.
- Ghuzlan, K.A. & Carpenter, S.H. (2006) 'Fatigue damage analysis in asphalt concrete mixtures using the dissipated energy approach', *Canadian Journal of Civil Engineering*, vol. 33, no. 7, pp. 890–901.
- Hanz, A., Mahmoud, E. & Bahia, H. (2011) 'Impacts of WMA production temperatures on binder aging and mixture flow number', *Journal of the Association of Asphalt Paving Technologists*, vol. 80.
- Hicks, R., Finn, F., Monismith, C. & Leahy, R. (1993) 'Validation of SHRP binder specification through mix testing (with discussion)', *Journal of the Association of Asphalt Paving Technologists*, vol. 62.
- Hill, B., Behnia, B., Hakimzadeh, S., Buttlar, W.G. & Reis, H. (2012) 'Evaluation of low-temperature cracking performance of warm-mix asphalt mixtures', *Transportation Research Record: Journal of the Transportation Research Board*, vol. 2294, no. 1, pp. 81–88.
- Hintz, C., Velasquez, R., Johnson, C. & Bahia, H. (2011) 'Modification and Validation of Linear Amplitude Sweep Test for Binder Fatigue Specification', *Transportation Research Record: Journal of the Transportation Research Board*, vol. 2207, no. 1, pp. 99–106.
- Hopman, P., Kunst, P. & Pronk, A. (1989) A renewed interpretation method for fatigue measurements, verification of miner's rule, *4th Eurobitume Symposium in Madrid*, vol. 1, p. 557–561.
- Kim, Y.-R., Little, D.N., Lytton, R.L., Kim, Y.-R., Little, D.N., Lytton, R.L., Kim, Y.-R., Little, D.N. & Lytton, R.L. (2003) 'Fatigue and Healing Characterization of Asphalt Mixtures', *Journal of Materials in Civil Engineering*, vol. 15, no. 1, p. 75.
- Kutay, M., Gibson, N. & Youtcheff, J. (2008a) *Use of pseudostress and pseudostrain concepts for characterization of asphalt fatigue tests*, CRC Press.
- Kutay, M.E., Gibson, N. & Youtcheff, J. (2008b) 'Conventional and Viscoelastic Continuum Damage (VECD)-Based Fatigue Analysis of Polymer Modified Asphalt Pavements (With Discussion)', *Journal of the Association of Asphalt Paving Technologists*, vol. 77.
- Lee, H.-J. & Kim, Y.R. (1998) 'Viscoelastic constitutive model for asphalt concrete under cyclic loading', *Journal of Engineering Mechanics*, vol. 124, no. 1, pp. 32–40.
- Menapace, I., Masad, E., Little, D., Kassem, E. & Bhasin, A. (2014) 'Microstructural, chemical and thermal analyses of Warm Mix Asphalt', *Sustainability, Eco-efficiency, and Conservation in Transportation Infrastructure Asset Management*, p. 157.
- Partl, M.N., Bahia, H.U., Canestrari, F., de la Roche, C., Di Benedetto, H., Piber, H. & Sybilski, D. (2013) 'Advances in Interlaboratory Testing and Evaluation of Bituminous Materials'.
- Rowe, G.M. & Bouldin, M.G. (2000) Improved techniques to evaluate the fatigue resistance of asphaltic mixtures, *2nd Eurasphalt & Eurobitume Congress Barcelona*, vol. 2000.
- Tsai, B.-W. & Monismith, C. (2005) 'Influence of Asphalt Binder Properties on the Fatigue Performance of Asphalt Concrete Pavements (With Discussion)', *Journal of the Association of Asphalt Paving Technologists*, vol. 74.
- Van Dijk, W. (1975) 'Practical fatigue characterization of bituminous mixes', *Journal of the Association of Asphalt Paving Technologists*, vol. 44, pp. 38–72.
- Wasiuddin, N., Saltibus, N. & Mohammad, L. (2011) Effects of a Wax-Based Warm Mix Additive on Cohesive Strengths of Asphalt Binders, *Proc., T&DI Congress 2011: Integrated Transportation and Development for a Better Tomorrow*.
- Williams, D.A. (1998) *Microdamage healing in asphalt concretes: relating binder composition and surface energy to healing rate*, Texas A&M University.
- Xiao, F., Amirkhanian, S.N. & Zhang, R. (2011) 'Influence of short-term aging on rheological characteristics of non-foaming WMA binders', *Journal of Performance of Constructed Facilities*, vol. 26, no. 2, pp. 145–152.
- Xiao, F., Punith, V. & Amirkhanian, S.N. (2012) 'Effects of non-foaming WMA additives on asphalt binders at high performance temperatures', *Fuel*, vol. 94, pp. 144–155.
- Zhou, F., Mogawer, W., Li, H., Andriescu, A. & Copeland, A. (2012) 'Evaluation of Fatigue Tests for Characterizing Asphalt Binders', *Journal of Materials in Civil Engineering*, vol. 25, no. 5, pp. 610–617.

The performance of bitumen mastics with the addition of fly ash

A. Djurekovic

Public Enterprise "Roads of Serbia", Serbia

G. Mladenovic

University of Belgrade, Faculty of Civil Engineering, Serbia

ABSTRACT: There are two potential uses of fly ash in asphalt mixtures: as a replacement of stone filler, or as a substitution for a certain percentage of bitumen. This paper focuses on the second option with the objective to investigate the interaction between fly ash and bitumen. Oscillatory tests were performed using a Dynamic Shear Rheometer (DSR) over a range of temperatures and frequencies, on original, short-term aged and long-term aged samples of fly ash-bitumen mastics. Additionally, testing using a Bending Beam Rheometer (BBR) was performed to assess resistance to low temperature cracking which is critical for modified bitumen with increased modulus. The addition of fly ash to bitumen improves the performance of the mastics and increases the viscosity and complex modulus at high temperatures and low frequencies, but has a negative effect on the resistance to cracking at low temperatures, thus increasing the low performance grade classification.

Keywords: Bitumen, Fly ash, Mastic, Complex modulus, Phase angle, Creep stiffness, Master curves

1 INTRODUCTION

Fly ash has been generated as a byproduct of coal combustion in thermal power plants. In Serbia, more than six million tons of fly ash are produced every year, mainly at the two power plants (PPs): TE Kolubara – Obrenovac and TE Kostolac. So far fly ash has been effectively used only for the production of cement and Portland-cement concrete. However, there is a potential for a much wider use of fly ash in road construction, in particular, for embankments and both unbound and bound sub-base and base layers. However, the application of fly ash in asphalt mixtures has been under-investigated.

On the other side, there are increasing demands for improved performance of asphalt pavements under higher traffic loading and harsher environmental conditions.

There are two potential uses of fly ash in the asphalt mixtures: as a replacement of the entire or a certain percentage of stone filler, or as a substitution for a certain percentage of bitumen. The use of fly ash in asphalt mixtures may be an attractive option because it may improve pavement performance and reduce the cost and environmental impact (Tapkin 2008).

Al-Suhaibani (1986) evaluated the use of fly ash as an asphalt extender in asphalt concrete mixtures. He studied the effect of the particle size of fly ash on the viscosity of bitumen, as well as the effect on air voids, density, and the mechanical properties of asphalt concrete. Medium sized fly ash has been used in the study (1 through 44 μ in size). The results indicated that the

addition of type F fly ash improves tensile strength, resistance to permanent deformation, and fatigue life. Furthermore, Al-Suhaibani & Tons (1991) studied the effect of the fly ash particle size, the aggregate gradation, and the binder content on the resilient modulus and rutting resistance of asphalt concrete mixes. They concluded that it is reasonable to replace up to 40 percent of the bitumen volume with medium fly ash for dry climates, while for moist climates the replacement should not exceed 30 percent.

Ali et al. (1996) studied the use of type F fly ash in asphalt concrete mixtures as a stiffening and void-filling material. The results indicated that the use of 2% of fly ash improves the resilient modulus of the mix at high and low temperatures and its stripping resistance.

Churchill & Amirkhani (1999) studied the effect of the use of fly ash on indirect tensile strength (ITS) under dry and wet conditioning as well as the tensile strength ratios (TSR) of asphalt concrete mixtures, using separate aggregate and fly ash sources. The study showed that the partial replacement of fine aggregate by 6–8% coal ash has a detrimental effect on the short-term ITS value. The results also suggested that the ash source did not have a substantial effect on ITS and TSR values.

Sharma et al. (2010) investigated the use of fly ash using different ratios of fly ash to bitumen in mastics and in asphalt mixtures. The fly ash to bitumen (FA/B) ratio ranged from 0.6 to 1.2. The authors found that an increase in the fly ash content improves the resistance to shear, while the phase angle decreases. They also

found that mastics become less susceptible to the FA/B ratio with an increase in temperature.

Sobolev et al. (2014) assessed the effect of fly ash on the rheological performance of bitumen and mastics using Dynamic Shear Rheometer (DSR). The study included two types of asphalt binder and both type C and type F fly ashes. A microstructural investigation of bitumen with fly ash using a scanning electron microscope (SEM) demonstrated a crack-arresting effect induced by fly ash particles at low temperatures. The investigation of the rheological performance of mastics with different fly ashes using DSR confirmed that fly ash can be used as a bitumen extender, replacing up to 15% of bitumen to improve its resistance to permanent deformation at high temperatures. The best improvement was achieved by adding 15% of fly ash type F or 30% of type C fly ash.

2 OBJECTIVES

The main objective of the present study is to investigate the potential use of fly ash, available in Serbia, in asphalt mixtures. Since the interaction between bitumen and fly ash needs to be characterized first, this paper focuses on the evaluation of the bitumen – fly ash mastics viscoelastic properties at high, intermediate, and low temperatures.

The previous work indicated that the stiffness of the bitumen-fly ash mastics increased compared to the stiffness of the original bitumen, resulting in the improved resistance to permanent deformation. This paper will focus on the long-term performance and investigate the stiffness and rheological parameters of the long-term aged samples at high, intermediate, and low temperatures.

3 THEORETICAL BACKGROUND

The complex behavior of bitumen and fine particle mastics is best described using dynamic loading. Testing can be performed either in stress or strain controlled modes. To better understand and model the properties of viscoelastic systems, the strain controlled mode is applied (SHRP A-370 1994). The range of frequencies and temperatures needs to be chosen in such a way to cover multiple scenarios of loading conditions. Parameters, such as complex modulus G^* , storage modulus G' , loss modulus G'' and phase angle, are generated during testing.

The Christensen-Anderson (CA) model (Christensen & Anderson, 1992) is used to construct bitumen/mastics master-curves. In the CA model, there are three primary rheological parameters: the glassy modulus (G_g), the crossover frequency (ω_c) and the rheological index (R), as shown in Figure 1. The complex modulus and phase angle are defined with equations (1) and (2):

$$|G^*(\omega)| = G_g \left[1 + \left(\frac{\omega_c}{\omega} \right)^{\frac{\log 2}{R}} \right]^{\frac{R}{\log 2}} \quad (1)$$

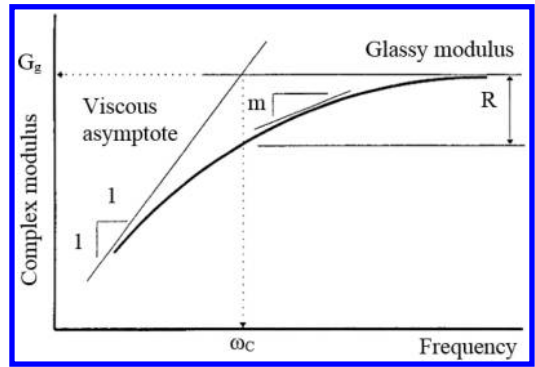


Figure 1. Illustration of the three CA model parameters (SHRP-A-367 1994).

$$\delta(\omega) = \frac{90}{1 + \left(\frac{\omega}{\omega_c} \right)^{\frac{\log 2}{R}}} \quad (2)$$

where G_g = the glassy modulus; ω_c = the crossover frequency (rad/s); and R = the rheological index.

The parameters ω_c and R have considerable physical meaning. The crossover frequency ω_c is defined as the frequency where the storage and loss moduli are equal, and the phase angle δ is equal to 45° . The rheological index R is the distance between the glassy modulus and the complex shear modulus at the crossover frequency and is considered a shape parameter for the master curve. The glassy modulus is the value that the complex modulus or storage modulus approaches at low temperatures and high frequencies. The value is typically close to 1 GPa in the shear loading for most bituminous binders (SHRP-A-367 1994).

To assess and calculate the model parameters, testing of the fundamental rheological properties using a dynamic shear rheometer (DSR) was performed. This testing using DSR enables the linear viscoelastic behavior of the mastics to be determined over a range of temperatures and time conditions associated with asphalt mixtures. In order to stay within the LVE (Linear-Visco-Elastic) limits, it is necessary to perform a number of oscillatory frequency sweeps over a broad range of constant temperatures with a small strain amplitude. The Time-Temperature Superposition principle (TTSP) is then used to analyze the individual data sets and create master-curves using statistical techniques of curve fitting and nonlinear regression.

4 METHODOLOGY

This work examines the rheological behavior of a series of bitumen mastics samples with varying percentages of fly ash content by weight.

4.1 Bitumen and mastics aging

The samples of bitumen and mastics were short-term aged in the RTFOT (Rolling thin film oven test) and long-term aged in the PAV (Pressure aging vessel) according to the SuperPAVE methodology (AASHTO R28 2013 & AASHTO T240-13 2013).

4.2 Frequency sweep testing

The DSR samples were prepared using the silicon molds. Two testing geometries were prepared: 25 mm and 8 mm. The range of temperatures for the DSR testing was chosen to be between 40°C and 5°C for 8 mm geometry, and between 40°C and 80°C for 25 mm geometry, with the overlapping temperature of 40°C (according to the EN 14770:2013) used for verification that the sample geometry did not affect the behavior of tested samples. The testing was conducted on twenty frequencies ranging between 0.1 Hz and 20 Hz.

The LVE limits were determined as proposed in the SHRP testing protocol (SHRP-A-370 1994). The testing was performed in the strain controlled mode, with strains of 1% and 0.5% for 25 mm and 8 mm geometries, respectively. This allowed for materials to stay in the LVE zone and avoid nonlinear behavior of the test samples.

The viscoelastic characteristics of the bitumen and mastics, based on the TTSP, were interpreted in the form of shifted master-curves at a reference temperature of 40°C.

4.3 Low temperature testing

To assess the low temperature performance after the long-term aging, bitumen beams were prepared according to the SuperPAVE procedure (AASHTO R 49-09 2013). Testing was conducted at three temperatures, between 0°C and -12°C, and on each of them the creep stiffness at 60 s (S_m) and the slope of the creep curve at 60 s (m-value) were determined.

5 MATERIALS

One unmodified bitumen and two types of fly ash were used in the testing program:

- Bitumen penetration grade 50/70, produced in the Refinery Pancevo, which corresponds to the performance grade bitumen PG 64-16;
- Two types of Fly ash: the FA1 from the PP Kolubara and the FA2 from the PP Kostolac.
- The chemical composition of the fly ash from the two PPs is presented in Table 1.

Both FA1 and FA2 have a similar chemical composition and can be classified as fly ash type F according to the ASTM C618-12a (2013). The slight differences in the Rigden voids and density could originate from variations in the exploitation process in the two PPs.

Table 1. Chemical composition of the fly ash samples (%).

Chemical	FA1	FA2
SiO ₂	50.21	56.38
Al ₂ O ₃	23.83	17.57
Fe ₂ O ₃	9.89	10.39
CaO	4.79	7.46
MgO	3.12	2.13
K ₂ O	0.44	0.57
Na ₂ O	0.35	0.38
TiO ₂	0.54	0.52
SO ₃	5.24	0.95
P ₂ O ₅	0.06	0.025

Three series of samples of mastics were prepared with each fly ash, containing 10%, 20%, and 30% of fly ash by mass in the mastics. The FA/B ratios for the three different concentrations were 0.11 (10/90), 0.25 (20/80) and 0.43 (30/70).

Before beginning the preparation of the mastics, both FA samples were sieved through the mesh sieve size 0.5 mm, in order to eliminate the coal residue particles that were present during the sampling and to better simulate the complex behavior that mastics with fly ash might exhibit. Figure 2 shows gradation curves for the two FA samples. The FA1 has a finer gradation, while the FA2 has a substantially coarser structure.

The physical characteristics of the FA1 and FA2, such as Rigden voids, specific gravity, fly ash volume (V_{fa}), and effective volume (V_e) in the mastics, are shown in Table 2. The V_{fa} and V_e were determined using the following relations developed by Heukelom (1965):

$$V_{fa} = \frac{\frac{m_{fa}}{\rho_{fa}}}{\frac{m_{fa}}{\rho_{fa}} + \frac{m_b}{\rho_b}} \quad (3)$$

$$V_e = \left| \frac{100}{(1 - S_R)} \right| V_{fa} \quad (4)$$

where m_f = mass of fly ash; m_b = mass of bitumen; ρ_{fa} = specific density of fly ash; ρ_b = specific density of bitumen; and S_R = Rigden voids.

6 RESULTS AND DISCUSSION

6.1 Complex modulus G^*

Based on the TTSP, the master-curves for the G^* at a reference temperature of 40°C for the unmodified bitumen and the bitumen-fly ash mastics have been developed and presented in Figure 3 (bitumen and FA1-mastics) and Figure 4 (bitumen and FA2-mastics).

Generated G^* master-curves are visually smooth and continuous because the unmodified bitumen and bitumen-fly ash mastics exhibit simple rheological

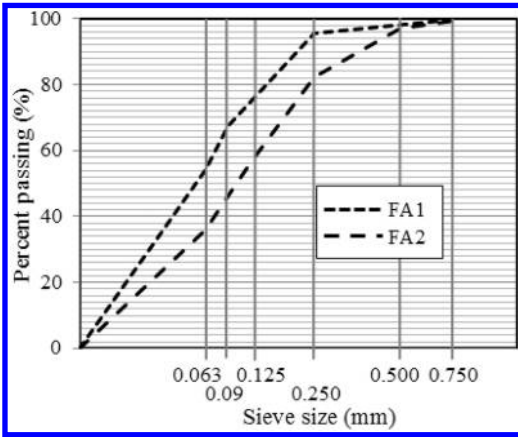


Figure 2. The gradation curves for fly ashes FA1 and FA2.

Table 2. The fly ash parameters and their volumetric participation in the mastics for three weight ratios.

Fly ash type	Specific gravity	Rigden voids	Weight by mass	V_{fa}	V_e
	(-)	(%)	(%)	(%)	(%)
FA1	1.977	53	10	5.4	11.4
			20	11.3	24.1
			30	18.0	38.2
FA2	2.028	46	10	5.2	9.7
			20	11.1	20.5
			30	17.6	32.6

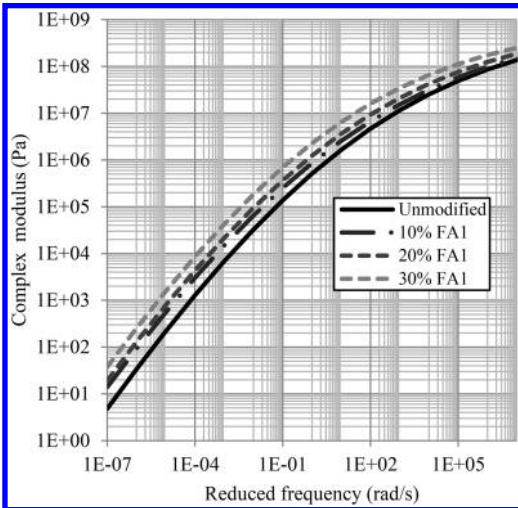


Figure 3. Master curves for bitumen and FA1-mastics.

behavior. Both sets of master-curves for FA-mastics are shifted vertically upwards compared to the master-curve for unmodified bitumen. However, the vertical shift is not completely linear for all mastics: for 30%

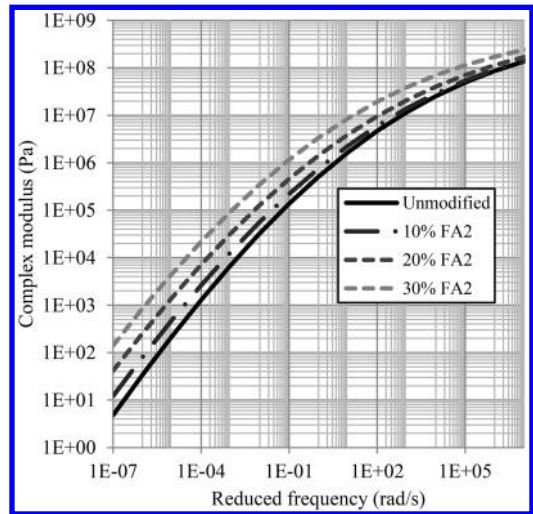


Figure 4. Master curves for bitumen and the FA2-mastics.

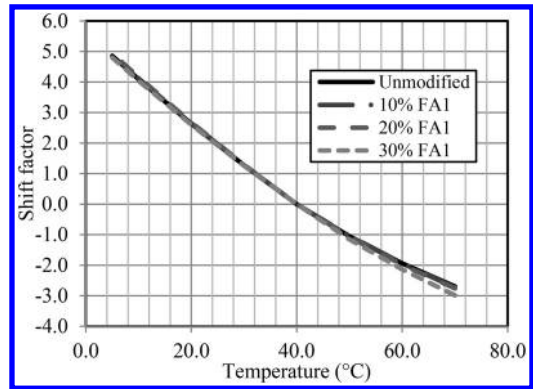


Figure 5. Shift factors for the unmodified bitumen and the FA1-mastics.

FA2-mastics, the higher shift is achieved, and the modulus value reaches 142 Pa at a high temperature, while for the corresponding FA1-mastics, this value is 38 Pa.

Master-curves for FA2-mastics show a higher increase in the G^* values at a high temperature and low frequency loading, indicating stronger fly ash influence. The FA1-mastics exhibit a somewhat lower increase in G^* values, and the curves translate vertically more equally. This comes from the FA1 having a finer gradation and higher Rigden voids, indicating that there is still more room for increasing the mass percentage of the fly ash FA1 in the mastics.

Shift factors for the two fly ash combinations are presented in Figures 5–6. The alignment of master-curves is fair and indicates simple rheological behavior.

6.2 G^* stiffening ratios

Figures 7–8 show stiffening ratios of the G^* for extreme combinations of temperature and loading

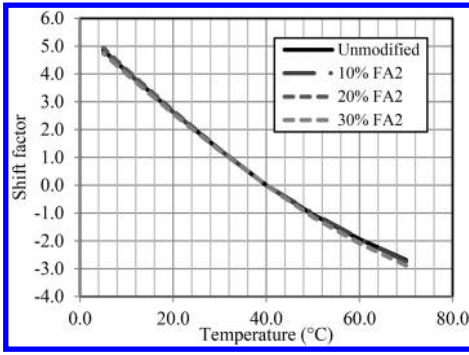


Figure 6. Shift factors for the unmodified bitumen and the FA2-mastics.

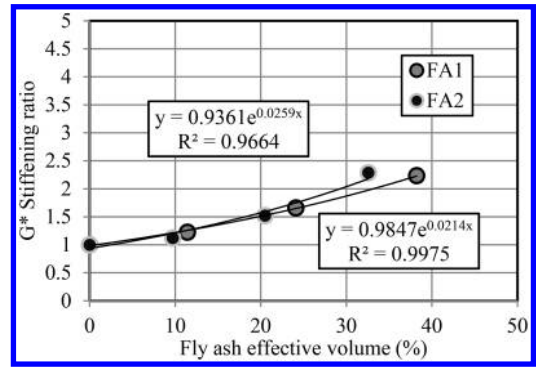


Figure 8. The G^* Stiffening ratios for low temperature and high frequency response.

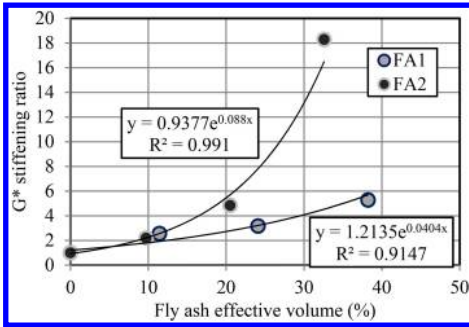


Figure 7. The G^* Stiffening ratios for high temperature and low frequency response.

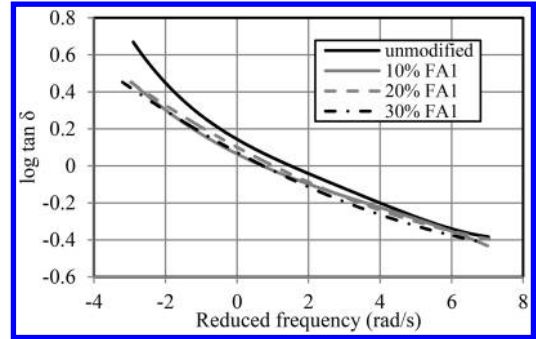


Figure 9. The loss tangent δ for the mastics with the FA1.

frequencies. For a high temperature and low frequency (Figure 7), the FA2-mastics show a much higher increase in the G^* stiffening ratio compared to the FA1-mastics, indicating stronger filling effect due to FA2 coarser gradation. The difference increases with the increase of the effective volume of fly ash in the mastics. For a low temperature and high frequency response, the stiffening ratios for both FA1 and FA2 are almost equal.

For low temperatures the stiffening effect is somewhat reduced, showing that fly ash is diluted in the bitumen suspension and the effect is similar to the mechanism that polymer modified bitumen exhibits during testing at intermediate and low temperatures.

The range of the stiffening ratio is between 1 and 18 for the FA2 and between 1 and 5.3 for the FA1 at low frequency (high temperature), while the stiffening ratios are between 1 and 2.3 for the FA2 and between 1 and 2.2 for the FA1 at high frequency (low temperature). The stiffening effect of the fly ash on the bitumen at higher temperatures is more pronounced than that at lower temperatures.

6.3 Loss tangent δ

The loss tangent is a dimensionless parameter which represents the ratio of energy lost to energy stored in a cyclic deformation: $\tan \delta = G' / G''$.

The loss tangent can also be thought of as an index of viscoelasticity. Values for phase angle δ can range from 0° for perfectly elastic solids to 90° for purely Newtonian liquids. The loss tangent values range between zero and infinity, the smaller values indicating a more elastic material response.

The loss tangent δ values are shown in Figures 9–10 for FA1 and FA2, respectively. For higher frequencies and lower temperatures, the experimental data revealed that the loss tangent decreased with increased content of the FA2. Thus, the mastics with the FA2 became more elastic (Figure 10). The loss tangent of the FA1 also decreased, but at a less steep rate in the glassy zone compared to that for the FA2-mastics. This observation is explained by the previous findings: the coarser gradation and the lower value for the Rigden voids create pronounced filling effect; thus, the behavior is characterized as more elastic. The FA1-mastics exhibit more viscous behavior compared to the FA2-mastics for the same FA/B mass ratio because of higher Rigden voids and the finer gradation of FA1 compared to FA2.

At medium frequencies, the value and the slope of the loss tangent decrease at the same ratio for the FA2 which indicates continuous elastic behavior. For low frequencies, the loss tangent gradually increases and eventually becomes inversely proportional to the frequency. Still, the increase is higher for the FA1,

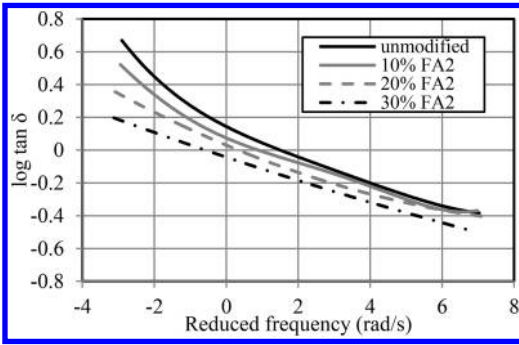


Figure 10. The loss tangent δ for the mastics with the FA2.

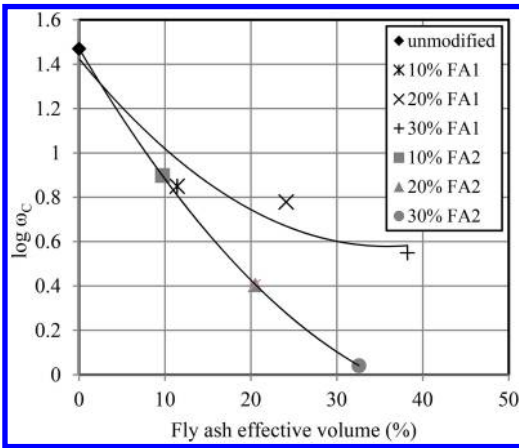


Figure 11. The effect of the fly ash content on the crossover frequency.

indicating behavior more similar to the unmodified bitumen sample.

6.4 Viscoelastic properties by CA model

Figure 11 shows a reduction in the crossover frequency (ω_c) with an increased filler effective volume. The change for FA1-mastics is less pronounced. The point where the viscous asymptote crosses the glassy modulus for the mastics with fly ash is lower than that for the unmodified bitumen. The crossover frequency indicates that the temperatures of viscoelastic solid-to-fluid transitions are different for the unmodified bitumen and mastics with fly ash. Therefore, the crossover frequencies for the FA2-mastics are much lower because of the increase in elastic response. The crossover frequency is being thought of as a hardness parameter, and consequently, the fly ash stiffening effect is more pronounced for the FA2-mastics compared to the FA1-mastics. Therefore, the FA2-mastics are much harder than the FA1-mastics.

Figure 12 shows a decrease in the rheological index R with an increasing FA effective volume. In general, the viscoelastic behavior of the FA2-mastics changes more slowly with time and temperature, followed by

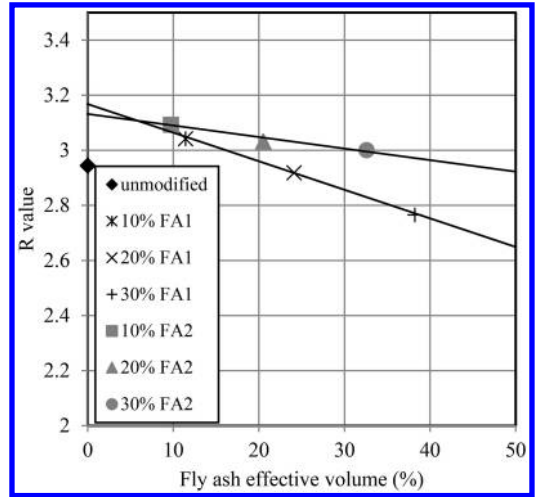


Figure 12. The effect of fly ash content on the R index.

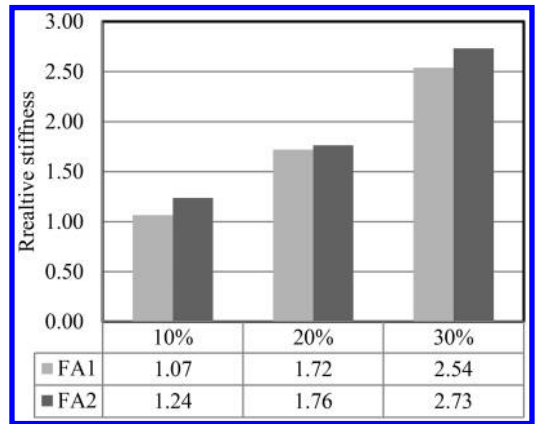


Figure 13. Change in relative stiffness at temperature of -6°C in respect to the fly ash content.

FA1-mastics and unmodified bitumen. According to the results obtained in this study, the rheological index R for the unmodified bitumen, FA1-mastics, and FA2-mastics range between 2.7 and 3.1. With higher values of the rheological index, the FA2-mastics show a slightly flatter master-curve and have an increased elastic behavior at the intermediate loading times and temperatures compared to the FA1-mastics.

6.5 Low temperature performance

The BBR (Bending Beam Rheometer) test (AASHTO T313-12 2012) was used to identify the change in the stiffness and m-value of the mastics compared to these of unmodified bitumen at low temperatures. Figure 13 shows the relative stiffness (S_r) values for specimens tested, generated by dividing the measured stiffness of FA-B specimens by the stiffness of the unmodified bitumen.

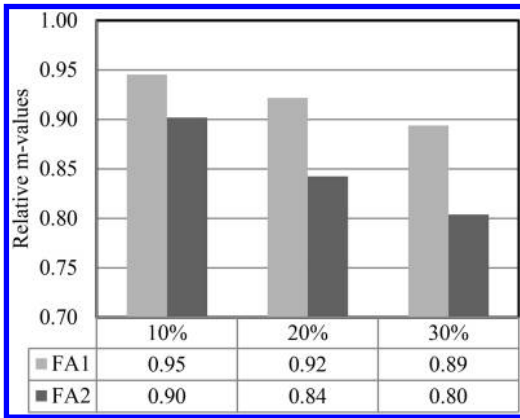


Figure 14. The change in the relative m-value at temperature of -6°C in respect to the fly ash content.

The values for the creep stiffness S_r show that there is a steady trend of increasing creep stiffness with the addition of the fly ash regardless of type. The increase is less pronounced for the FA1-mastics.

Figure 14 shows the relative m-values which represent the ability of the tested material to relax thermal stresses. This is an important characteristic which differentiates the two fly ash samples. The FA1-mastics show a lower decrease in the m-value, which indicates more viscous behavior at the low temperatures, compared to FA2-mastics that show a higher decrease in the m-value, which indicates less potential for the relaxation of thermal stresses, i.e. the material is less viscous. With a relatively higher decrease in the m-values, the FA2-mastics show less resistance to the low temperature thermal cracking at the same weight ratio levels and conditions, while the FA1-mastics show greater potential for use, having higher Rigden voids and the ability to distribute the bitumen more effectively between particles. These results show that the addition of the fly ash in the bitumen negatively affects the low temperature performance of mastics, thus increasing the low temperature performance grade of bitumen.

7 CONCLUSIONS

This paper described the characterization of the linear viscoelastic behavior of mastics with the two fly ashes available in Serbia, based on the rheological tests. The testing on bitumen and multiple combinations of bitumen and fly ash weight ratios were conducted on multiple temperatures and frequencies by use of the DSR. The CA model was used to characterize the LVE rheological behavior of the bitumen and mastics with fly ash. The following conclusions can be drawn from the test results and analyses:

- In terms of the master-curves of the G^* and phase angle, the FA2-mastics show the dominant effect of the fly ash filling effect. These filler particles

cause a hydrodynamic interaction which increases resistance during loading.

- The substantial stiffening effect has been noticed for the FA2-mastics according to the crossover frequency and G^* stiffening ratio.
- The stiffening effect is higher for FA2-mastics in relation to FA1-mastics due to the difference in the fly ash effective volume, as well as filling effect.
- The testing at low temperatures using the BBR testing showed an increase in the creep stiffness for both fly ash sample types by roughly the same ratio. However, the m-values for FA1 show a lesser decrease, indicating that it is less detrimental for mastics. The addition of the FA1 is less detrimental for mastics behavior at low temperatures compared to the FA2.

ACKNOWLEDGEMENTS

The work reported in this paper is a part of the investigation within the research project TR 36017 “Utilization of by-products and recycled waste materials in concrete composites in the scope of sustainable construction development in Serbia: investigation and environmental assessment of possible applications”, supported by the Ministry for Science and Technology, Republic of Serbia. This support is gratefully acknowledged.

REFERENCES

- AASHTO R28. 2013. *Practice for Accelerated Aging of Asphalt Binder Using a Pressurized Aging Vessel (PAV)*.
- AASHTO R 49-09. 2013. *Standard Practice for Determination of Low-Temperature Performance Grade (PG) of Asphalt Binders*.
- AASHTO T 240-13. 2013. *Standard Method of Test for Effect of Heat and Air on a Moving Film of Asphalt (Rolling Thin-Film Oven Test)*.
- AASHTO T 313-12. 2012. *Standard Method of Test for Determining the Flexural Creep Stiffness of Asphalt Binder Using the Bending Beam Rheometer (BBR)*.
- AASHTO T 315-12. 2012. *Standard Method of Test for Determining the Rheological Properties of Asphalt Binder Using a Dynamic Shear Rheometer (DSR)*.
- Airey, G.D., Rahimzadeh, G. & Collop, A.C. 2004. Linear rheological behaviour of bituminous paving materials. *J. Mater. Civ. Eng.*, 16(3): 212–220.
- Ali, N., Chan, J., Simms, S., Bushman, R. & Bergan, A. 1996. Mechanistic evaluation of fly ash asphalt concrete mixtures. *J. Mater. Civ. Eng.*, 8(1): 19–25.
- Al-Suhaibani 1986. *The use of fly ash as an asphalt extender*. PhD Thesis, Univ. of Michigan, University Microfilms International, Ann Arbor, MI.
- Al-Suhaibani A.R. & Tons, E.T. 1991. Properties of fly ash-extended asphalt concrete mixes. *Transportation Research Record*. Journal of Transportation Research Board, No. 1323: 123–133.
- Anderson, D.A. 1987. Guidelines for use of dust in hot-mix asphalt concrete mixtures. *Journal of the Association of Asphalt Paving Technologists*, 56, 492–516.
- ASTM C618-12a. 2013. *Standard Specification for Coal Fly Ash and Raw or Calcined Natural Pozzolan for Use in Concrete*.

- Chen, J.-S. & Peng, C.-H. 1998. Analyses of tensile failure properties of asphalt-mineral filler mastics. *Journal of Materials in Civil Engineering*, 10(4): 256–262.
- Christensen, D.W. & Anderson, D.A. 1992. Interpretation of dynamic mechanical test data for paving grade asphalt. *Journal of the Association of Asphalt Paving Technologists*, 61: 67–116.
- Churchill E.V. & Amirkhanian, S.N. 1999. Coal ash utilization in asphalt concrete mixtures. *J. Mater. Civ. Eng.*, 11(4): 295–301.
- EN 14770:2013. Bitumen and bituminous binders. Determination of complex shear modulus and phase angle. Dynamic Shear Rheometer (DSR).
- Faheem, A., Wen, H., Stephenson, L. and Bahia, H. 2008. Effect of Mineral Filler on Damage Resistance Characteristics of Asphalt binders. *Journal of the Association of Asphalt Paving Technologists*, 77: 885–908.
- Faheem, A. and Bahia, H. 2009. Conceptual Phenomenological Model for Interaction of Asphalt Binders with Mineral Fillers. *Journal of the Association of Asphalt Paving Technologists*, 78: 679–720.
- Heukelom, W. 1965. The Role of Filler in Bitumen Mixes. *Journal of the Association of Asphalt Paving Technologists*, 34: 396–429.
- Kim, Y.-R. and Little, D.N. 2004. Linear Viscoelastic Analysis of Asphalt Mastics. *Journal of Materials in Civil Engineering*, 16(2): 122–132.
- Rigden, P.J. 1947. The Use of Fillers in Bituminous Road Surfacing. A Study of Filler-Binder Systems in Relation to Filler Characteristics. *Journal Society of Chemical Industry*, 66: 299–309.
- SHRP-A-367 1994 *Binder Characterization and Evaluation Volume 1*.
- SHRP-A-370 1994 *Binder Characterization and Evaluation Volume 4: Test Methods*.
- SHRP-A-384 1994 *Aging: Binder Validation*.
- Sharma, V., Chandra, S., & Choudhary, R. 2010. Characterization of fly ash bituminous concrete mixes. *J. Mater. Civ. Eng.*, 22(12): 1209–1216.
- Sobolev, K., Flores Vivian, I., Saha, R., Wasiuddin, N.M., Saltibus, N.E. 2014. The effect of fly ash on the rheological properties of bituminous materials, *Fuel*, 116: 471–477.
- Soleymanni, R.H., Bahia, U.H. & Bergan A.T. 1999. Time-temperature dependency of blended and rejuvenated asphalt binders. *Journal of the Association of Asphalt Paving Technologists*, 68: 129–152.
- Tapkin S. 2008. Mechanical evaluation of asphalt-aggregate mixtures prepared with fly ash as a filler replacement, *Can J Civ Eng* 35: 27–40.
- Tunnicliff, D.G. 1967. Binding effects of mineral filler. *Journal of the Association of Asphalt Paving Technologies*, 36: 14–156.
- Yusoff, N.I.M., Shaw, M.T. & Airey, G.D. 2011. Modelling the linear viscoelastic rheological properties of bituminous binders. *Construction and Building Materials*, 25(5): 2171–2189.

Statistical analysis of characteristics of slow breaking cationic emulsions used for cold waste asphalt recycling

D. Lepadatu & L. Judele

Technical University “Gheorghe Asachi” Iasi, Romania
Faculty of Civil Engineering and Building Services

ABSTRACT: Bitumen emulsions could be presented as a dispersion of bitumen particles in water, stabilized with the addition of surfactants – surface active agents – or most commonly known as emulsifiers that allow the bitumen to be “diluted” in water. Cationic emulsions – the term cationic is derived from the migration of bitumen particles under an electric field, the droplets migrate toward the cathode (negative electrode), and hence the emulsion is called cationic. This imparts a positive charge to all the droplets. Since positive particles repel each other, all the droplets repel each other and remain as distinct bitumen drops in suspension. Statistical analysis of these complex chemical processes allows highlighting the influence of different parameters on these emulsions. This paper presents five cationic emulsions used as additives in cold waste asphalt recycling. Natural aggregates, cement and fly ash are added to the emulsion in order to improve the quality of the recycled mix.

1 INTRODUCTION

Bitumen emulsion is an area where technological progress is still being made to meet the requirements of pavement engineering. Although the anionic emulsions were developed first, they are currently less favored than the cationic emulsions, as cationic emulsions coat the aggregates more efficiently due to their positive load, having therefore better adhesion properties. The cationic emulsifying agent functions similarly to the anionic one; the negative portion of the head floats around in the water leaving a positively charged head. The cationic emulsion is both more favored and more widely used.

Asphalt emulsion has found wide applications in road construction and high-speed railways due to its advantages of low application temperature, good adhesion to aggregates, low cost, etc. It is usually used as a modifier or binder of cement-based materials to provide adequate flexibility or to be utilized as an adhesive and repair material (Fazhou et al. 2013). Bitumen emulsions are complicated and good chemistry is required to reach target desired emulsion properties (Bonakdar et al. 2001). A typical cationic emulsifying agent is shown below, together with a diagram showing the orientation of the agent at the bitumen-water interface and the positive charge imparted to each drop (Fig. 1). In a surface treatment, after the emulsion and the aggregate have been applied to the road surface, the emulsion should “break” leaving the asphalt cement holding the aggregate. The object of a surface treatment is to seal the road from moisture intrusion and provide a new skid resistant surface, while being opened to traffic as soon as possible and retaining the

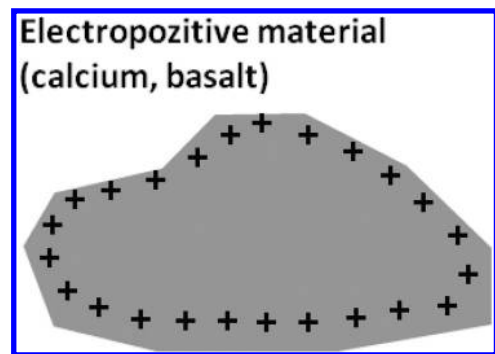


Figure 1. The influence of the material surfaces – electropositive material.

aggregate. At that point traffic may be allowed on the surface without loss of aggregate. The type of emulsion used has a large effect on the speed of the “break” of an emulsion (Salager et al. 2007).

Generally speaking, surfaces have a negative charge. The strength of this negative charge may be different from material to material (Fig. 2). Due to the chemical properties of the emulsions, they may react differently in specific weather and application conditions.

Because of this phenomenon, anionic and cationic emulsions break in different ways. In an application of cationic emulsion, positively charged drops of bitumen are applied to a negatively charged surface (Fig. 3).

The bitumen drops are immediately attracted to the surface and begin to break. The emulsion also loses water by evaporation. Thus the cationic emulsion has

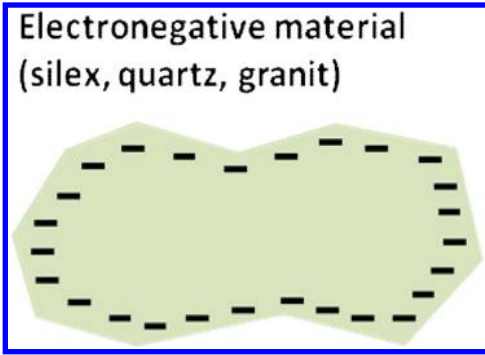


Figure 2. The influence of the material surfaces – electronegative material.

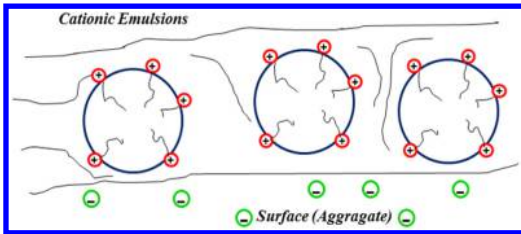


Figure 3. The orientation of the agent at the bitumen-water interface and the positive charge.

two breaking mechanisms at work and will break faster than a corresponding anionic emulsion.

Cationic bitumen emulsions tend to break through an electrochemical process and, therefore, weather conditions play a lesser role in the breaking rate of these types. Full curing of a cationic emulsion still requires the water to be lost through evaporation, absorption or “pushing out” by the action of rolling and traffic (Bourrel and Verzaro 1996).

Bitumen emulsions must remain stable so they can be transported, stored and handled. Ultimately, however, they must be made to separate or “break” so that the bitumen can coat aggregate particles or pavement surfaces.

Emulsions used in sprayed sealing work are required to break relatively quickly to prevent run-off of the emulsion and the possibility of rain damage. On the other hand, emulsions used in stabilization of soil must break relatively slowly to allow adequate mixing.

2 EXPERIMENTAL PROGRAM

2.1 Asphalt waste recycling

Asphalt waste recycling (Fig. 4) consists in using the material derived from milling the existing bituminous degraded road surfacing, with additions of emulsions and natural aggregates, and mixed together in a recycling machine. It uses material from the existing road

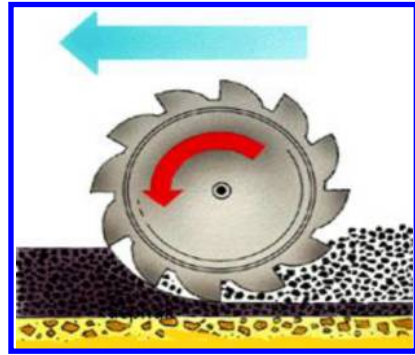


Figure 4. Asphalt waste recycling.

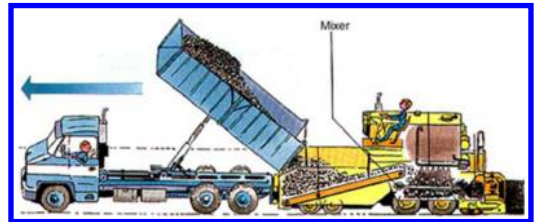


Figure 5. Conservation of natural aggregates resources by reusing milled material.



Figure 6. The asynchronous process.



Figure 7. The synchronous process.

structure with a minimum of input materials (aggregate production is reduced – figure 5). There is no need to use borrow pits and landfills. Layers resulting from recycling are thick, bound, homogeneous and have good cooperation with the layers immediately above and below. The foundation of the road is not in any

Table 1. The characteristics of cationic emulsions.

Technical specifications and performance classes of cationic bitumen emulsion type					
Emulsion type	E1	E2	E3	E4	E5
Breaking behavior	67	61	64	127	139
– breaking index with Sikaisol filler					
Bitumen Content	60.53	63.87	64.27	64.13	63.86
Adhesiveness (on andesite)	90	95	100	95	95
Viscosity:	22	44	40	29	36
– flow time, nozzle by 2 mm, 40°C					
Homogeneity	0.09	0.12	0.14	0.12	0.13
Sieve Residue test (on the 0.16 mm sieve)					
The tendency to settle (7 days of storage, 25°C)	3.11	2.11	3.41	3.91	2.86
Recovered bitumen					
Penetration 25°C	67	66	68	63	62
Softening point	48	48.4	56	53	47.6

way affected by the recycling of the superstructure. (Romanian Standard on “Cold pavement recycling” – march 1998).

2.2 Bituminous treatments

After the recycling operation, in which the existing material is used, the operation of the application of bituminous treatments usually follows. Usually they can be done in two ways:

1. The asynchronous process
2. The synchronous process

Before being used as addition in waste asphalt recycling and bituminous treatment as the basic ingredient, those five emulsions were subjected to laboratory analysis (Musteață 2010), obtaining the following results, which are summarized in Table 1. Then they are statistically analyzed in the next section.

3 RESULTS AND DISCUSSIONS

In figure 8 one can observe a significant growth for breaking behavior of E4 and E5 emulsions type with a relatively low viscosity, between 29 and 36. Meanwhile, for a very low viscosity 22 for E1 emulsion type we tear normal behavior compared to the other two samples where the viscosity is double, breaking behavior remains approximately on the same value (Fig. 9).

We observe subtle variations in bitumen content for emulsions E2-E5, while for E1 the value is the lowest (Fig. 10). In terms of adhesiveness, we can say that its values are good, all over 90 with a maximum for emulsions E3 and a minimum for E1 (Fig. 11).

Regarding the settling tendency, it ranges from 2.11 to 3.91; for other emulsions having closer values, from 2.80 to 3.40. Homogeneity has similar values for different categories of emulsions (0.12 and 0.14)

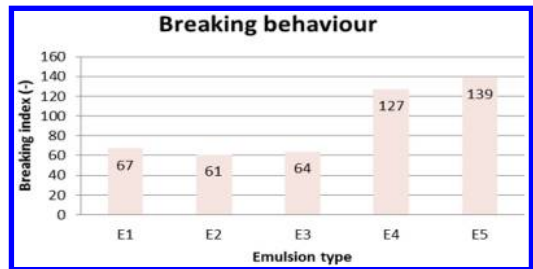


Figure 8. Breaking behavior of five cationic emulsions.

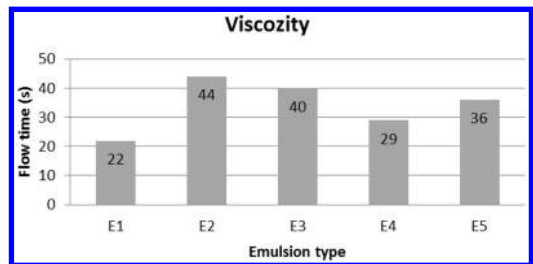


Figure 9. Viscosity of five cationic emulsions.

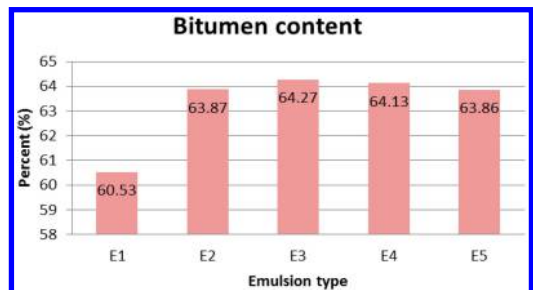


Figure 10. Bitumen content of five cationic emulsions.

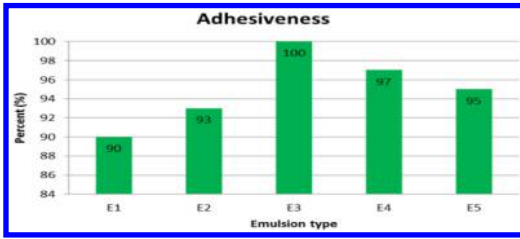


Figure 11. Adhesiveness of five cationic emulsions.

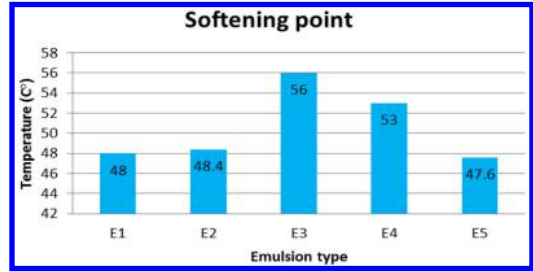


Figure 15. Softening point of five cationic emulsions.

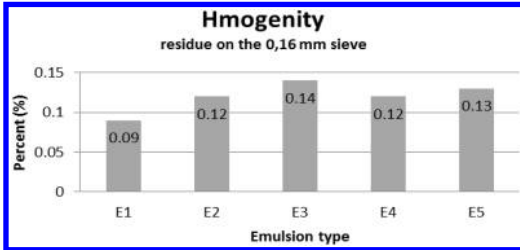


Figure 12. Homogeneity of five cationic emulsions.

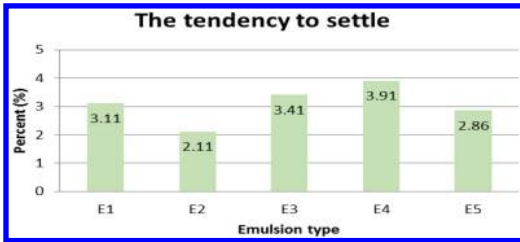


Figure 13. The tendency to settle of five cationic emulsions.

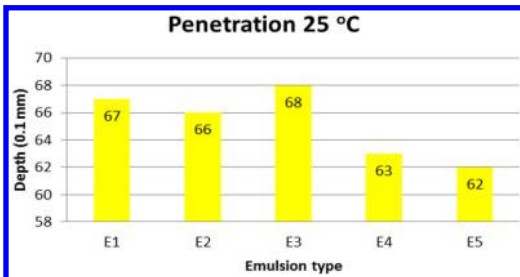


Figure 14. Penetration of five bitumens.

(Fig. 12). For E1 the value is 0.09, a higher variation than other types of emulsions.

Figure 14 shows the values of penetration and softening point for different recycled bitumens. Notice that for emulsion E3 there are maximum values for both characteristics, while for emulsion E1 there is a large increase in penetration correlated with a significant decrease in softening point (Fig. 15).

4 CONCLUSIONS

This paper presents five cationic emulsions used as additives in cold waste asphalt recycling and bituminous treatment. Laboratory results show that all of the analyzed characteristics successfully fall within the limits of applicable standards.

Most important, adhesiveness and breaking index with Sikaisol filler have very high values (this shows the behavior of emulsions when they reach the final mixtures). So there are very good chances that these emulsions will behave excellently when put into practice.

The five emulsions presented in this paper were used for researches on experimental design and behavior in time of cold rehabilitation works containing natural aggregates, cement, fly ash and slow rupture cationic bitumen emulsions covered in two cold road coatings or other asphalt layers.

It is our intention that in the period ahead to watch closely the development of waste asphalt recycling and bituminous treatments with those five analyzed emulsions. Our next step, after a while, is to carry out tests on the material put to work to assess the behavior of the studied emulsions.

REFERENCES

- Bonakdar, L., Philip, J., Bardusco, P., Petkov, J., Potti, J.J., Méléard, P. 2001, Rupturing of bitumen-in-water emulsions: experimental evidence for viscous sintering phenomena, *Colloids Surf. A: Physicochem. Eng. Aspects* 176: 185–194.
- Bourrel, M. and Verzaro F. 1996, Breaking mechanisms of asphalt emulsions for road construction, *L'Actualite Chimique* 42–48.
- Fazhou W., Yunpeng L., Shuguang H. 2013, Effect of early cement hydration on the chemical stability of asphalt emulsion, *Construction and Building Materials Journal*, 42: 146–151.
- Musteață M. 2010, Polchimic Laboratory of Giurgiu. *Research topics*.
- Regulatory 2004, “Norms on the implementation of bituminous layers very thin cold”, *Technical Regulation*.
- Salager J.L., Rondón M., Tolosa L., Pizzino A., Bullón J. 2007, Emulsion formulation engineering for the practitioner, in: *Encyclopedia of Surface and Colloid Science, second ed., Taylor & Francis, New York*.

Effect of polyphosphoric acid on high-temperature properties of bitumens from different crude sources

A.L. Faxina, T.F. Pamplona, F.P. Sobreiro & G.T.P. Fabbri

Department of Transports, Engineering School of Sao Carlos, University of Sao Paulo, Brazil

ABSTRACT: It is known that the mechanism of modification of bitumens with PPA depends strongly on the chemical composition of the base bitumen. In order to evaluate the impact of PPA on bitumens from different crude sources, three base 50/70 pen-grade bitumens with different performance grades (Reduc, Lubnor and Replan) were modified with five PPA proportions (0.0, 0.5, 1.0, 1.5 and 2.0%). The PG grading and the MSCR test were used to evaluate the effect of PPA concentration on bitumens. The high-temperature PG increased with increasing PPA proportion with different intensity depending on the base bitumen. It was observed an optimum PPA proportion for each base bitumen that leads to higher percent recoveries and lower non-recoverable compliances: 1.5% for Reduc, 1.0% for Lubnor and 2.0% for Replan. The set of rheological tests performed here showed to be an effective and practical tool to estimate the ideal PPA proportion for bitumen modification.

1 INTRODUCTION

The science of paving bitumens has been developed, since the beginning of the twentieth century, based on the use of pure bitumens and, later, on the incorporation of different modifiers, such as mineral filler, natural asphalts, aromatic oils, acids, polymers and recycled materials – such as crumb rubber from discarded tires and other polymer-based products. The main objective of the incorporation of modifiers into bitumens is to obtain a product that is more versatile and more resistant to environmental effects and excessive traffic loading.

The modification of bitumens with polyphosphoric acid (PPA) is not a new practice (Baumgardner et al. 2005, Martin & Baumgardner 2006). Bitumens have been modified with PPA since the seventieths, in an attempt to increase the viscosity without decreasing substantially the penetration and, consequently, to obtain bitumens that are less thermally susceptible (Baumgardner 2012) and more resistant to rutting without degrading their resistance to thermal cracking. Most recently, PPA has been used to widen the range of job temperature, i.e., the performance grade as per the Superpave (*Superior Performing Asphalt Pavements*) specification. According to Baumgardner et al. (2005), the addition of PPA can improve the rheological properties of bitumens at high temperatures, without affecting the performance grade (PG) at low temperatures.

It is known that the mechanism of modification with polyphosphoric acid depends strongly on the chemical characteristics of the base bitumen (Baumgardner et al. 2005; Baumgardner 2012) – this indicates that

the benefits obtained with the addition of PPA are not the same for all bitumens. Leite et al. (2004) observed that the addition of PPA to a vacuum residue led to a bitumen with characteristics superior to the original one and also indicated that the addition of 1.2% PPA to the vacuum residue with a PG 46-28 was enough to increase the high-temperature performance grade of the material (PG 58-22). Martin & Baumgardner (2006) evaluated the effect of different acid contents (0.0, 0.5 and 1.0%) on rubber-modified bitumen with 5% crumb rubber and pointed out that the addition of PPA increased the rotational viscosity at 135°C and the elastic recovery at 25°C, decreased the phase separation and increased or decreased the stiffness and the relaxation rate at low temperatures depending on the base bitumen.

D'Angelo (2012) evaluated the effect of different PPA contents on bitumens from different sources and observed that the bitumens behaved differently to PPA modification. The technical literature indicates that the addition of polyphosphoric acid has an impact substantially higher over the rheological properties of bitumens predominantly naftenic (Orange et al. 2004). The supposition that the polyphosphoric acid disperses the asphaltenes contributes to explain the higher level of intensity of PPA on naftenic bitumen, once these bitumens present a concentration of asphaltenes that is higher than those of aromatic nature.

The use of PPA has been defended by industries as a reducer of the polymer proportion in bitumen modification, apparently with economic motivations, once that the costs of acid incorporation is lower than the costs related to polymer incorporation in

bitumens. Some authors observed that the addition of a small amount of PPA in polymer-modified asphalt binders is able to reduce the proportion of polymer required to achieve an enhanced performance (Martin & Baumgardner, 2006, Faxina, 2011, Domingos et al. 2011, Arnold et al. 2012, Bernnet, et al. 2012). The reduction of polymer proportion makes the processing of the modified bitumen easier, reduces its viscosity, increases the workability of the bituminous mixture and increases the storage stability of the modified bitumen.

The polyphosphoric acid seems to be able to preserve some target characteristics of a bitumen modified with a certain amount of polymer even when this proportion is reduced. Bennert et al. (2012) observed that bituminous mixtures compounded with a bitumen modified with SBS (styrene-butadiene-styrene copolymer) + PPA and bituminous mixtures compounded only with SBS copolymer resulted in equivalent values of fatigue resistance. Equivalent resistances to permanent deformation were also observed for the same bituminous mixtures, although the results obtained from the MSCR (*multiple-stress creep and recovery*) test had indicated that the bitumen modified only with SBS presented higher resistance to permanent deformation. These authors (Bennert et al. 2012) also concluded that the tensile-strength relationship of the bituminous mixtures compounded with the bitumen modified with SBS and PPA is higher than that obtained for the bituminous mixtures compounded with the bitumen modified only with the SBS copolymer. This is an indication that the first bituminous mixtures presented a higher resistance to damage induced by water.

Based on the unique effects that the polyphosphoric acid has on bitumens with different chemical characteristics, this study aims to evaluate the effects of different proportions of PPA (0.0, 0.5, 1.0, 1.5 and 2.0%) on three bitumens, classified as 50/70 according to the penetration system, obtained from different sources. Oscillatory tests to determine the PG and the MSCR test were performed in order to compare the pure and the PPA-modified asphalt binders and also to evaluate the impact of PPA incorporation. The evaluation of the impact of the modification with PPA on bitumens from different sources on viscosity and fatigue resistance complements the analyses presented here and will be published opportunely.

2 MATERIALS AND TEST PROCEDURES

2.1 Materials

Three bitumens classified as 50/70 according to the penetration system were used to prepare the bitumens modified with PPA. The bitumens were supplied by three Petrobras Refineries (Brazil): Lubnor, Reduc and Replan. The PPA with commercial designation of Innovalt E200 was supplied by Innophos Inc. and the proportions used were 0.0, 0.5, 1.0, 1.5 and 2.0%.

2.2 Multiple stress creep and recovery test (MSCR)

The multiple-stress creep and recovery test is the substitute for the parameter $G^*/\sin \delta$ of the Superpave specification for control of permanent deformation. The MSCR test is performed in a dynamic-shear rheometer (DSR), using the plate-plate fixture of 25 mm in diameter and 1 mm in height, at the temperature correspondent to the performance grade of the pavement. This test is performed in controlled stress following the procedure ASTM D7405-08, where the sample is subjected to a constant stress during 1 second followed by a resting period under null loading per 9 seconds. The ASTM protocol specifies the application of 10 cycles of creep and recovery, without time intervals between them, only at the temperature of the PG of the pavement. However, in this study, the tests were run at 52, 58, 64, 70 and 76°C. During the first 10 cycles, a stress level of 0.1 kPa is applied and during the last 10 cycles a stress level of 3.2 kPa is applied. For each creep-recovery cycle, the following strains are registered: at the beginning of the creep period (ϵ_0) at 0 second, at the end of the creep period (ϵ_c) after 1 second and at the end of the recovery period (ϵ_r) after 9 seconds. Based on these strain values, the percent recovery (%R) and the non-recoverable compliance (J_{nr}) are calculated using equations 1 and 2, respectively.

$$\%R(\sigma, N) = \frac{[(\epsilon_c - \epsilon_0) - (\epsilon_r - \epsilon_0)]}{\epsilon_c - \epsilon_0} \cdot 100 \quad (1)$$

$$r \geq 0.7 \times \{a^2 + Hp \times [(Ep/Es)^{1/3}]^2\}^{0.5} \quad (2)$$

where $\%R(\sigma, N)$ is the percent recovery and $J_{nr}(\sigma, N)$ is the non-recoverable compliance at the stress level σ ($\sigma = 0.1$ or 3.2 kPa) for the n -th cycle of creep and recovery with n ranging from 1 to 10.

At each test temperature, the arithmetic average of the %R and J_{nr} values is obtained for 10 cycles at each stress level. Once that the non-recoverable compliance is the new parameter related to rutting obtained from the MSCR test, a new specification was developed (Table 1), based on limits for J_{nr} at different traffic levels (S, H, V and E), respectively designated as Standard, Heavy, Very heavy and Extremely heavy (D' Angelo 2010). The percent difference between the J_{nr} values at 0.1 and 3.2 kPa should not exceed 75%, in order to ensure that the bitumen is not excessively sensitive to abrupt variation of the stress level (Anderson et al. 2010, Asphalt Institute 2010a, b). Minimum values of percent recovery are also recommended and are shown in Table 2.

3 RESULTS AND FINDINGS

3.1 Effect of PPA content on the performance grade of bitumens

As indicated by literature, PPA proportions around 1.0 to 1.5% are enough to increase the performance grade

Table 1. Traffic level classification based on J_{nr} values according to the FHWA.

Condition	Property	Limit (kPa ⁻¹)	Traffic level	ESALs
Aged in the RTFO	J_{nr} at 3.2 kPa at the high-temperature performance grade of the pavement	4.0	Standard (S)	< 10 million
		2.0	Heavy (H)	> 10 million
		1.0	Very heavy (V)	> 30 million
		0.5	Extremely heavy (E)	> 100 million

Table 2. Percent recovery values recommended by the FHWA.

J_{nr} at 3.2 kPa (kPa ⁻¹)	R min (%)
1.01–2.0	30
0.51–1.0	35
0.251–0.50	45
0.125–0.25	50

Table 3. Amount of PPA needed to increase the PG at high temperatures.

Bitumen	PG 70	PG 76	PG 82	PG 88
Lubnor	0.00	0.35	1.05	1.45
Reduc	0.30	1.55	2.00	–
Replan	0.25	0.90	1.40	–

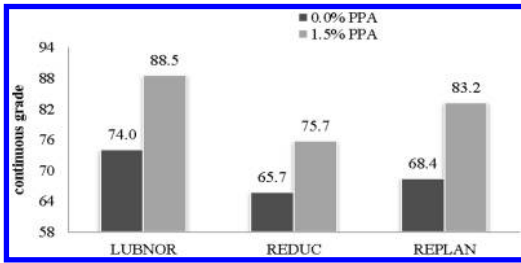


Figure 1. Continuous grades: base bitumens and bitumens + 1.5% of PPA.

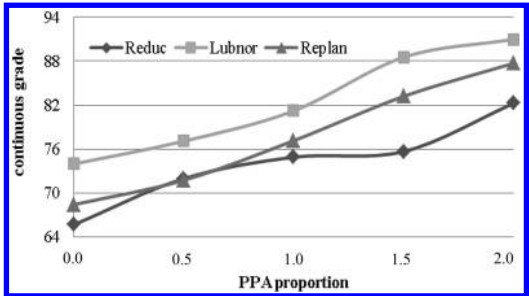


Figure 2. Continuous grade as a function of PPA proportion.

at high temperatures of a bitumen in one or two grades. In this sense, Figure 1 presents a comparison between the continuous grade of the bitumens modified with 1.5% PPA and the continuous grade of the base bitumen. The performance grade for these samples was obtained using the parameter $G/\sin \delta$ of the virgin samples, according to Table 3 from AASHTO M320-09. The addition of 1.5% of PPA was able to increase the PG of the Lubnor from 70 to 88 (3 levels) and the PG of the Replan from 64 to 82 (3 levels), while the PG of the Reduc increased from 64 to 70 (only one level). These results highlight how dependent of the chemical composition of the base bitumen the effect of PPA addition is. The Reduc resulted in the less sensitive to PPA addition for 1.5% of PPA. The Lubnor reached the highest PG, once the PG of the base bitumen is higher than the PG of the other two bitumens.

Figure 2 shows the continuous grade of the bitumens as a function of the PPA proportion. It is evident that some binders require a higher PPA proportion compared to others, in order to increase the PG in one, two or three levels. The Reduc and the Replan presented similar performance grades for low PPA proportions (0.5% for example). However, the Lubnor showed a more expressive increase of the PG with the increase of PPA proportion. It is also possible to

observe a linear sensitivity to the PPA addition mainly for the Replan and the Lubnor.

It is important to keep in mind that the performance grade of bitumens is only a classification criterion that is based on the stiffness level of the samples at the temperatures where permanent deformations occur. This criterion is useful to indicate that the modified bitumens are stiffer than the base bitumens, but it can not be used to classify or to rank different bitumens in terms of the resistance to permanent deformation. For that, the MSCR test should be performed in order to quantify the actual contribution that the PPA confers to the modified bitumens in terms of percent recovery and non-recoverable compliance.

3.2 Effects of PPA addition on the rheological properties of the MSCR test

One of main questions when one talks about PPA modification is if the level of modification provided by PPA is the same for all types of bitumen. The MSCR properties evaluated here will show that this is not true. Figures 3 and 4 present the percent recovery values of the pure and modified bitumens at 0.1 and 3.2 kPa, respectively. Figures 5 and 6 show the non-recoverable compliances of the pure and modified bitumens at 0.1 and 3.2 kPa, respectively. The

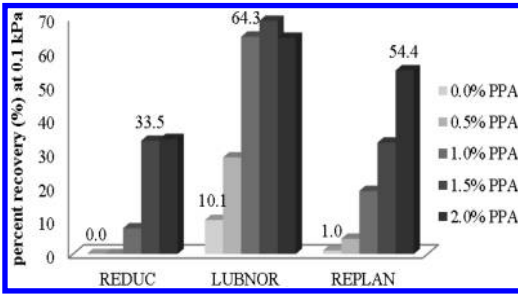


Figure 3. Percent recovery values of the pure and modified bitumens at 0.1 kPa.

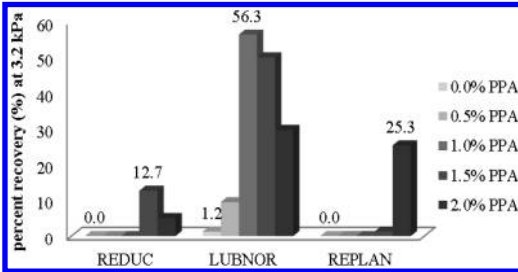


Figure 4. Percent recovery values of the pure and modified bitumens at 3.2 kPa.

first impression that arises looking at the results is that the effect of PPA addition is substantially different for both base bitumens. It is important to remind that the MSCR properties were obtained at the temperatures correspondent to the high PG of each bitumen, in such a way that the properties were obtained at an isomodus condition.

Based on the combination of the results of percent recovery and non-recoverable compliance, one can observe that there is an optimum PPA content for each bitumen. The optimum PPA content for the Reduc is 1.5% once that, in this proportion, the percent recovery values at 3.2 kPa were the highest and the non-recoverable compliance values at 0.1 and 3.2 kPa were the lowest. Although the percent recovery values for the Reduc for the PPA contents of 1.5 and 2.0% were equivalent at 0.1 kPa, the 3.2 kPa stress level is more relevant for the behavior of the material in terms of permanent deformation. For this reason, the results obtained at 3.2 kPa were adopted as reference. The lowest J_{nr} value indicates that the PPA content of 1.5% makes the Reduc more resistant to permanent deformation than the other PPA proportions.

The optimum PPA contents obtained for the Lubnor and the Replan are 1.0% and 2.0%, respectively. The optimum PPA content of the Lubnor was obtained adopting the same criteria related to the percent recovery used to obtain the optimum PPA content for the Reduc, once that the percent recovery at 0.1 kPa for the Lubnor with 1.5% PPA is slightly higher than the percent recovery of the Lubnor with 1.0% PPA. It would be a natural tendency to think that the addition of a PPA proportion above 2.0% could lead to better MSCR

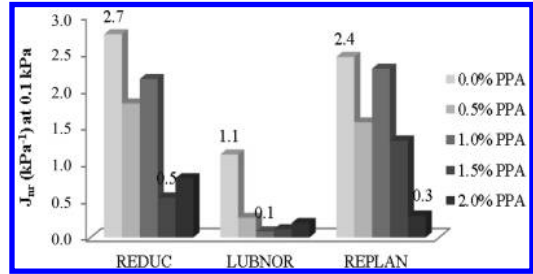


Figure 5. Non-recoverable compliance of the pure and modified bitumens at 0.1 kPa.

properties. However, one should keep in mind that the use of PPA contents higher than 2.0% are not recommendable to modify bitumen of 50/70 grade, once that high PPA proportions lead to excessive high viscosity values which may reduce the workability of the asphalt mixture.

The percent recovery at 0.1 kPa of the pure Reduc is 0.0%, but the addition of 1.5% of PPA increases this property in approximately three times. At this stress level, the percent recovery of the pure Lubnor is 10.1% and the addition of 1.0% of PPA increases this property six times. The addition of 2.0% of PPA increases the percent recovery of the pure Replan in approximately 54 times. At 3.2 kPa, the Lubnor is much more sensitive to PPA addition than the Reduc and the Replan. For the Reduc, the addition of 1.5% of PPA increases the percent recovery in 13 times in relation to the pure Reduc. For the Lubnor, the addition of the optimum PPA content increases the percent recovery in approximately 47 times and for the Replan this increase is of 25 times. One can conclude that the Lubnor is much more sensitive to PPA addition at the highest stress level, once that the pure Lubnor suffered the highest increase in percent recovery at 3.2 kPa even with a lower consumption of PPA.

For the Reduc, the addition of 1.5% of PPA reduced the non-recoverable compliance in 5 and 4 times at 0.1 and 3.2 kPa, respectively, in relation to the pure Reduc. For the Lubnor, the addition of the optimum PPA content reduced the J_{nr} values in 11 and 13 times at 0.1 and 3.2 kPa, respectively, and for the Replan this decrease was of 8 and 4 times, respectively. Again, one can conclude that the Lubnor is much more sensitive to PPA addition at both stress levels than the other pure bitumens, once that the addition of PPA at the optimum concentration for each bitumen led to a more expressive decrease in non-recoverable compliance even with a lower PPA consumption.

In order to ensure that the material will not be excessively sensitive to abrupt increases of the stress level, the relation $J_{nr,diff}$ between the J_{nr} values at 0.1 and 3.2 kPa was computed and the results are present in Table 4. As recommend by the literature [12–14], the values for $J_{nr,diff}$ should not exceed 75%. Data in Table 4 show that all the bitumen modified with PPA became more stress sensitive than the respective pure material.

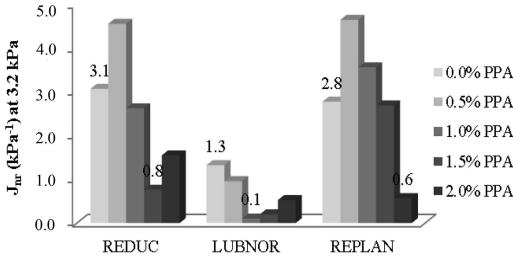


Figure 6. Non-recoverable compliance of the pure and modified bitumens at 3.2 kPa.

Table 4. $J_{nr,diff}$ values of bitumens at their optimum PPA contents.

Formulations	$J_{nr,diff}$ (%)
Reduc 0.0% PPA	12.02
Reduc 1.5% PPA	41.67
Lubnor 0.0% PPA	18.30
Lubnor 1.0% PPA	25.00
Replan 0.0% PPA	13.93
Replan 2.0% PPA	93.22

Table 5. Minimum PPA contents to obtain a maximum J_{nr} of 2 kPa^{-1} .

Bitumen	Temperature ($^{\circ}\text{C}$)		
	70	76	82
Reduc	1.15	1.50	1.95
Lubnor	0.00	0.25	–
Replan	0.90	1.20	1.60

This indicates that the PPA addition increases the sensitivity of the bitumen to abrupt changes in the stress level, which can be interpreted as a tendency to accumulate more rutting. However, taking into account the limit of 75% for $J_{nr,diff}$, the Replan with 2.0% of PPA is the only one that exceeds this limit. In practical terms, the addition of PPA increases the stress sensitivity of the pure bitumens, but this increase is not excessive for the Lubnor and the Reduc, allowing one to use these products with the addition of their respective optimum PPA contents. In terms of the best formulation, the Lubnor is the bitumen which showed the lowest $J_{nr,diff}$ values, resulting in the less stress-sensitive modified bitumens.

Table 5 presents the minimum PPA proportions required to achieve a maximum value of non-recoverable compliance of 2 kPa^{-1} at each test temperature. To obtain this maximum J_{nr} value using the Reduc, the high pavement temperature is 82°C and the PPA proportion is 1.95%. This analysis was not performed for the Reduc once that the formulations with low PPA proportions were not tested at higher temperatures. Using the Replan, the high pavement temperature is 88°C and the PPA content is 2.0%.

Table 6. Minimum PPA contents to obtain a minimum percent recovery of 30%.

Bitumen	Temperature ($^{\circ}\text{C}$)		
	70	76	82
Reduc	1.95	>2.00	>2.00
Lubnor	0.00	0.75	–
Replan	1.40	1.75	>2.00

Table 6 shows the minimum PPA contents needed to obtain a minimum percent recovery of 30% at each test temperature. To obtain this limit for percent recovery of the Reduc, the highest temperature would be 70°C and the PPA content would be 1.95%. At higher temperatures, PPA proportions higher than 2.0% should be used to obtain a minimum percent recovery of 30%. Using the Lubnor, the highest pavement temperature would be 88°C and the PPA proportion would be 2.0%. Using the Replan, the highest pavement temperature would be 76°C and the PPA content would be 1.75%.

4 CONCLUSIONS

This work intended to evaluate the effect of the addition of polyphosphoric acid to bitumens from different sources. The main conclusions are:

- The addition of PPA proportions ranging from 0.0 to 2.0% increased the high-temperature performance grade (PG) of the samples with different intensities, depending on the base bitumens; the bitumens from Replan showed to be the most sensitive to PPA modification, suffering an increase of the high-temperature PG with the lowest PPA consumption;
- To increase the high-temperature PG in one level, it was necessary to add 0.35% of PPA to the Lubnor (PG 70 to 76), 0.30% of PPA to the Reduc (64 to 70) and 0.25% of PPA to the Replan (64 to 70); to increase the high-temperature PG in two levels, it was necessary to add 1.05% of PPA to the Lubnor (PG 70 to 82), 1.55% of PPA to the Reduc (64 to 76) and 0.90% of PPA to the Replan (64 to 76); to increase the high-temperature PG in three levels, it was necessary to add 1.45% of PPA to the Lubnor (PG 70 to 88), 2.00% of PPA to the Reduc (64 to 82) and 1.40% of PPA to the Replan (64 to 82);
- In terms of the improvements provided by PPA addition, the Lubnor showed the highest increase of percent recovery and the highest reduction of non-recoverable compliance in comparison with the other two bitumens;
- All the modified bitumens at their respective optimum PPA contents resulted more stress-sensitive in comparison with the pure bitumens;
- Taking into account the upper limit of 75% for the parameter $J_{nr,diff}$, the Replan with 2.0% of PPA is the only bitumen that exceeds this limit;

although the PPA incorporation increases the stress-sensitivity of the bitumens, this increase is not excessive for the Lubnor and the Reduc, allowing one to use these bitumens modified with their respective optimum PPA contents; and

- The Lubnor is the bitumen less sensitive to abrupt variations on shear stress, once it presents the lowest $J_{nr,diff}$.

The results obtained here are useful to illustrate that bitumens from different sources do not behave similarly to PPA modification. The MSCR properties indicated that there is an optimum PPA content for each pure bitumen that provides a maximum percent recovery and a minimum non-recoverable compliance. These PPA contents are: 1.5% for the Reduc, 1.0% for the Lubnor and 2.0% for the Replan, although it is important to remark that the Replan at its optimum PPA content presented a stress sensitivity ($J_{nr,diff}$) superior to the recommended limit of 75%.

ACKNOWLEDGMENT

The first author acknowledges FAPESP (Sao Paulo State Research Funding Agency) for research funds (FAPESP process number 2006/55835-6) and the second author acknowledges CAPES (Brazilian National Research Funding Agency) for a masters scholarship.

REFERENCES

- Anderson, M., D'Angelo, J.A. & Walker, D. 2010. MSCR: a better tool for characterizing high temperature performance properties. *Asphalt* 25(2): 15–16, 18, 21–23.
- Arnold, T.S., Youtcheff, J. & Needham, S.P. 2012. Use of phosphoric as modifier for hot-Mix asphalt. *Transportation Research Circular* E-C160: 40–51.
- Asphalt Institute 2010a. Implementation of the multiple stress creep recovery test and specification. *Asphalt Institute Guidance Document*.
- Asphalt Institute 2010b. Guidance on the use of the MSCR test with the AASHTO M320 specification. *Asphalt Institute Guidance Document*.
- Baumgardner, G.L., Masson, J.-F., Hardee, J.R., Menapace, A.M. & Williams, A.G. 2005. Polyphosphoric acid modified asphalt: proposed mechanisms. *Association of Asphalt Paving Technologists* 74: 283–305.
- Baumgardner, G.L. 2012. Why and how of polyphosphoric acid modification – an industry perspective. *Transportation Research Circular* E-C160: 14–26.
- Bernnet, T. & Martin, J.V. 2012. Polyphosphoric acid in combination with styrene-butadiene-styrene block copolymer. *Transportation Research Circular* E-C160: 70–85.
- D'Angelo, J.A. 2010. The multiple stress creep recovery (MSCR) procedure. *Technical brief prepared by the United States Department of Transportation, Federal Highway Administration*.
- D'Angelo, J.A. 2012. Effect of polyphosphoric acid on asphalt binder properties. *Transportation Research Circular* E-C160: 27–39.
- Domingos, M.D.I., Pamplona, T.F., Faxina, A.L. & Gigante, A.C. 2011. Viscosidade rotacional de ligantes asfálticos modificados de mesmo grau de desempenho. *Panorama Nacional da Pesquisa em Transportes 2011*. ANPET, Belo Horizonte. [in portuguese].
- Faxina, A.L. 2011. Propriedades reológicas de ligantes asfálticos modificados virgens e envelhecidos a curto prazo. 17a. *Reunião Anual de Pavimento Urbana*. Porto Alegre. [in portuguese].
- Leite, L.F.M., Bittencourt, C.P. & Nascimento, L.A.H. 2004. Efeito do ácido polifosfórico no desempenho dos ligantes rodoviários. *Panorama Nacional da Pesquisa em Transportes 2004*. ANPET, Rio de Janeiro, v.1:n:40–51. [in portuguese].
- Martin, J.V. & Baumgardner, G. 2006. A new method to produce polymer modifier asphalt with crumb rubber and polyphosphoric acid: combining recycling and performance. *Asphalt Rubber 2006 Conference, Proceedings, 2006*. Palm Spring, California: 903–930.
- Orange, G., Dupuis, D. & Martin, J.V. 2004. Chemical modification of bitumen through polyphosphoric acid: properties-microstructure relationship. *3rd Eurobitume & Eurasphalt Congress*. Viena: 733–745.

Pavement design, construction and maintenance

Bridge deck asphalt plug joints: Problems and solutions

N. Ghafoori & M. Sharbaf
University of Nevada Las Vegas, USA

ABSTRACT: Asphalt Plug Joint (APJ), which serves as an expansion joint, is a flexible asphalt segment that spans between the bridge deck and abutment. As an expansion joint, it is required to allow bridge movement caused by expansion and contraction, to provide a smooth transition between the approach pavement and the bridge deck, to remain watertight and durable, and to keep debris entering the gap between the bridge deck and the abutment. In the United States, majority of state departments of transportation rely on manufacturers to design and construct Asphalt Plug Joints. Lack of available specifications/guidelines on type and quality of materials, proper joint geometry, effective compaction, suitable in-place temperature have contributed to premature failure of these expansion joints, resulting in uncomfortable and unsafe driving conditions and increasing maintenance costs. This paper describes the sources which can contribute to the premature failure of asphalt plug joints and offers appropriate mitigation solutions.

1 INTRODUCTION

The bridges are structures in permanent motion. The factors affecting the movement are traffic and seismic loads, wind, different type of impacts on the superstructure and expansion and contraction due to temperature variations. All these factors induce stresses into bridge decks and through bearings to piers and abutments. The joints are designed to accommodate these movements.

Over the lifetime of a bridge, the deck joints can be a source of many problems. During its service, without a proper design, installation and maintenance; the joints can deteriorate by leaking water and deicing chemicals towards the structural elements beneath the deck, and by losing their bond with the pavement and causing material distresses in the traffic lanes. The overall performance of the bridge can be drastically reduced and the repairing costs could be high. Therefore, to ensure performance of bridge superstructure, expansion joints should provide a smooth ride, a waterproof surface, and durable and stable at temperature cyclic variations. One of the most common bridge deck expansion joints is Asphalt Plug Joint (APJ).

There are multiple advantages in using asphalt plug joints. APJ construction is quick and simple to install in stages, easily repaired and maintained, and relatively inexpensive. It possesses waterproof properties and heals under traffic load and warm temperature. Asphalt plug joint is not as prone to snow plow damage and it can be cold milled when the road is resurfaced. Noise reduction can also be attributed to asphalt plug joints.

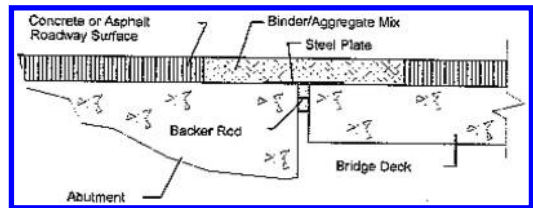


Figure 1. Abutment and bridge deck connection.

However, the use of APJ has some disadvantages as well. Notably, among them are: soft and pliable in hot temperatures promoting shoving and tracking, brittle/stiff in cold temperatures, very little accommodation for differential vertical placements, rutting with heaving in low volume traffic, and vulnerability to material distresses, such as delamination, spalling, raveling, debonding, aggregate polishing, and segregation and bleeding.

2 BACKGROUND

Asphalt plug joint, as shown in [Figure 1](#), connects an abutment with a bridge deck, making a smooth transition onto bridge surface. It allows for a bridge deck to expand or contract while at the same time keeping itself free of debris and water.

APJ is used for movements of maximum 50 mm (2 in). It consists of a polymer modified asphalt (PMA) with open-graded aggregates poured into a saw-cut “box” typically of 500 mm (20 in) wide and 50 mm

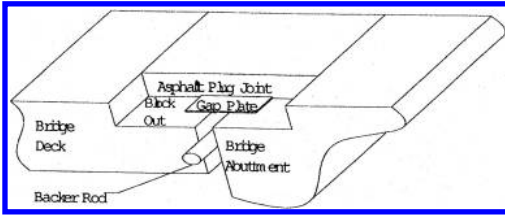


Figure 2. Typical APJ section.

(2 in) deep. Before placing the PMA, a backer rod is installed at the bottom of the joint and the space is filled with a closed cell polyethylene foam for waterproofing. A steel plate of typically 20 cm (8 in) wide is centered over the joint to prevent the binder to flow into the opening. The binders used for the joint are usually bitumen modified with plasticizers to obtain the desired flexibility. A typical APJ section is shown in Figure 2.

In the United States, researchers at the University of Wyoming performed extensive research regarding APJ material and developed design guidelines based on field observations, laboratory material tests, and analytical evaluations (Bramel et al. 1999).

In the beginning of 1990, when these types of joints started to be used, an evaluation of APJ was also carried out for the northeastern states of the United States. Fifteen years later, the authors published their results with respect to identifying the reasons for joint failure, the expected life span, material properties, and failures in installation and maintenance (Mogawer et al., 2004).

In comparison to the US, extensive studies have also been conducted in Europe and Australia. Australia developed a bridge design code AS-5100 for bearings and expansion joints (Velo & Oscar, 1996). United Kingdom adopted standards for installation of APJ joints through QC/QA practices. All principal manufacturers and installers, even though they have their own materials and techniques, adhered to these principles. The standard for APJ produced by the Bridge Joint Association was incorporated in the Design Manual for Roads and Bridges in UK. Also, it was specified that design of APJ should avert the need for excessive maintenance during its working life. Accent was put on following the manufacturer's instructions regarding joint installation and waterproofing the interface between expansion joint and bridge deck (Bridge Joint Association Standard, 2003).

In Switzerland, the first bridges with APJ were built in the 1980's. The Swiss Federal Roads Authority (ASTRA) together with industry representatives and laboratory testing experts developed guidelines regarding design, construction, maintenance and material testing after five years of gathering data and observing the performance of eighteen APJs. The findings led to the introduction of the ASTRA guidelines in 1996. The development and adoption of ASTRA guidelines was done in close coordination with the activities of a corresponding task group in Germany. The new guideline contained material requirements,

test procedures, instructions on quality management and construction (Partl et al., 2006).

Asphalt plug joints are used all over the US for new and rehabilitated bridges. Usually the contractors follow the manufacturers' recommendations and specifications. Each APJ component has a special design function that affects the overall performance of the joint. The backer rod prevents the binder to flow into the gap and the gap plate prevents the APJ mixture to be pushed into the expansion gap during traffic loads. The mixture has to be very resilient and resist at the contraction and extension of the bridge during temperature changes.

APJ systems, typically between 500 mm (20 in) wide and 70–160 mm (2.8–6.4 in) thick, are required to work within a temperature range from -25°C to $+45^{\circ}\text{C}$ and to sustain gap closings and openings from -12.5 mm to 25 mm (0.5–1 in). The APJ should accommodate vertical gap movements up to a maximum of 5 mm (0.2 in). The gap of the joint is covered by a sliding steel plate, which prevents the APJ material to be squeezed into the gap by traffic loads. Its width is typically 1060 mm (42.4 in).

Aggregates used in an APJ system should be graded, washed and drained crushed rock from the basalt, gabbro, granite, delerite and grit stone groups. The aggregate should be gap graded, having larger voids in mineral aggregate that allow larger asphalt content like 20%–40% by volume (Mogawer et al., 2004).

An ideal APJ material should have a modulus much lower than the pavement material and a nearly constant modulus of elasticity for the operating temperature range. Good range for an asphalt pavement is 1,300 to 4,500 MPa (218 to 653 ksi) at room temperature (Bramel et al., 1999).

The asphalt binder should be rubberized, polymer modified or shall comprise of a blend of bitumen with Styrene Butadiene Rubber (SBR). The tests on binder is usually performed by an independent testing facility and the testing should be performed before and during construction and as well as two and five years post construction (Bramel et al., 1999).

The block-out is typically between 500 mm (20 in) and 610 mm (24 in) wide and no thinner than 50 mm (2 in) spans between concrete and/or asphalt sections. The backer rod is usually placed to a minimum depth of 25–13 mm (1–0.5 in) (Bramel et al., 1999). The gap plate is made of aluminum, mild steel, and structural steel with or without corrosion protection. Usually the aluminum plates, which are more easily molded, are more suitable where the bottom of the block out cannot be leveled, or where the approach or trailing side has a weaker base than the concrete deck and a steel plate might displace the APJ material (Mogawer et al., 2004).

The size and shape of these gap plates can be from 6 mm (0.25 in) thick and 200 mm (8 in) wide with varying lengths. They are laid into the APJ binder and secured into the backer rod with nails. The gap plate role is to keep the binder/aggregate mix from extruding into the gap separating the abutment and bridge

deck. In addition, the caulking is used as a compressible material to fill the expansion joint gap in order to prevent the binder leaking away from the joint during the filling of the joint. It has to be heat resistant to withstand maximum safe heating temperature of the binder (Bridge Joint Association Standard, 2003).

The drainage must allow water at sub-surface level to be removed from the asphalt/waterproofing interface. The bridge deck requires discharge points at specified locations to allow the water to drain from the bridge deck into a designed drainage system (Mogawer et al., 2004).

3 PROBLEMS AND FAILURE MODELS

Typical failures in APJ are associated with improper design, material characteristics that lead to distresses in pavement, bad installation practice, and inadequate maintenance.

Critical failure modes usually occur when the expansion joint leaks or ride quality over the joint is poor. Leakage in the expansion joints may be due to tension cracks through the joint, debonding, or material spalling out of the block-out. Poor ride quality can occur due to rutting, material piling up due to compression, material flowing out of the block-out in the traffic lanes, and the track-out of the plug joint material by passing traffic (Mogawer et al., 2004). Material tests such as tensile strength, shear bonding strength, normal bonding strength, modulus of elasticity, and modulus of resilience are used to evaluate the failure modes. The temperature plays a crucial role in the performance of APJ therefore the tests are evaluated as functions of temperature to develop the ability of the material to resist to the service demands. Most authors agree that the APJ mixture acts “stiff” or “brittle” at colder temperatures and is “soft” or “pliable” at warm temperatures. A brief discussion over the source of problems and their associated failure modes is given below.

3.1 Design

Repair of deck joints is one of the most common and costly maintenance tasks usually occurring due to improper design loads, fatigue, movements, gap widths, joints sealants, drainage, mixture proportioning and, installation. Proper attention to each one of these design variables is essential to properly construct a lasting APJ and to minimize the cost of maintenance.

3.2 Material

APJ's failure usually begins when it becomes pervious, thus allowing water and deicing chemicals to enter and/or pass through the joint into the underlying superstructure. A combination of different effects and material distresses are the actual reason for the failure of the APJ system. Some of the distresses are described below.

- Debonding or separation is a material failure between APJ and adjacent pavement interface. This

is due to the glass transition temperature at which they become brittle, lose ductility, and crack; causing leaks and debonding.

- Cracking or splitting in tension is a material failure due to excessive stresses or strains induced by joint motion, material fatigue, and thermal stresses exceeding the materials capabilities at low temperatures. If they are not treated, the transverse and longitudinal cracks are avenues for water to enter into joints.
- Reflective cracking does not occur over the expansion gap because of the plate above, but rather at the edges of the plate where it develops cracks. Another reason for reflective crack occurrence is the continuous back and forth motion because APJ plate is not perfectly flat.
- Rutting is characterized by permanent deformation of pavement. It generally develops during the seasons, as channelized depressions in the wheel paths. Rutting can propagate more severe distresses like spalling that can result in joint failure. Another problem is the rideability issue that prevents a smooth transition, and steering that can accelerate rutting. In addition, rutting can increase due to increases in APJ skew angle.
- Raveling is a progressive separation of aggregate particles in a pavement from the surface downward or from the edges inward. Pavement has the rough and jagged appearance typical of surface erosion and in time can lead to more severe distresses that can cause joint to fail. Cold and warm weather can both influence in equal measure the raveling.
- Shoving/pushing is a form of plastic movement across pavement surface. It usually occurs in warm weather where asphalt touches a rigid object (plate) and is caused by traffic action combined with poor mix design, excessive moisture in the subgrade, or lack of aeration of liquid asphalt emulsions. The issue of skew angle is also a matter of pushing the material out of the joint due to traffic loading. Shoving/pushing will affect the ability of APJ to provide a smooth transition over the joint and may propagate other distresses that can lead to joint failure.
- Segregation is caused by a non-uniform distribution of coarse and fine aggregate components within asphalt mixture. It can lead to weakness areas that can later develop into severe distresses like debonding, rutting, and cracking.
- Bleeding is characterized as a film of asphalt binder on pavement surface. It usually creates a shiny, glass-like reflecting surface that can become sticky that when is wet exhibits loss of skidding. It is due to excessive asphalt binder in the mix and to low air void content. It prevents a smooth joint transition and may lead to further distresses.
- Polished aggregates are portions of aggregates extending above asphalt binder. Under repeated traffic loading, it decreases skid resistance of pavement. The process is faster if aggregates are susceptible to abrasion or subjected to excessive studded tire wear.

- Spalling is a condition when portions of APJ material are displaced from one or both sides of joint. It might be caused by a combination of the previous material distresses.
- Delamination is a condition when APJ becomes separated from the block-out. This type of distress is usually taking place in seal coats at the top of the asphalt layer, and is due to poor bonding. When plate moves is facilitating the occurring of delamination.
- Pot holes are due to fatigue cracking, localized disintegration or freeze-thaw cycles. When it is in the proximity of joint, it leads to plate exposure and water infiltration causing joint failure.
- Plate exposure/rusting is associated with joint debonding and presence of pot holes in different joint areas. In contact with water and environmental conditions plate starts to corrode and leads to joint failure.
- Use of aluminum components is not recommended, as they are easily damaged. Steel devices must be protected with a coating such as paint or galvanization. Joints should be designated for movements that are likely to occur. Sliding plate joints should not be used where vertical movements and rotations are probable (Partl et al., 2006).
- Minimum geometric considerations should be taken into account when selecting an APJ for use. One source recommended a joint depth of a minimum depth of 75 mm (3 in) and a maximum of 100 mm (4 in) while another stated a joint depth range from 70 mm (2.75 in) to 160 mm (6.25 in) (Mogawer et al., 2004).
- There is a minimum dimension for the APJ that is a wedge extending upward at 60° from the edge of the gap plate and debond. The fixed side of the plate must be secured with fasteners or APJ binder to force the joint motion into the preferred side (Bramel et al., 1999).

3.3 Installation

A bad installation practice has been proven in many cases to lead to APJ failures. Normally, contractors should follow the manufacturers' guidelines or manufacturers should install joints.

3.4 Maintenance

Many of the maintenance problems on bridges result from failed joints. Therefore, a proper maintenance done at the right time and at regular intervals extends the service life of the bridge and reduces the total lifecycle costs.

3.5 Quality control

Quality control during material production, installation process and construction are crucial for a durable functioning APJs.

4 SOLUTIONS

Based on the available information in literature and responses to a regarding design, construction and maintenance of asphalt plug joints, the following guidelines are offered. Most of the solutions presented herein are from US standards and state of the art practices used in US. Some of the recommendations are from UK design standards, and ASTRA design guidelines. It should be noted that geometric dimensions and limits, movement restrictions, general construction and maintenance practices are fairly common to all countries.

4.1 Design

- Joints details should be described and shown on the work plan. Drains should be placed uphill of the joint in the sidewalk or curb to prevent as much water as possible from reaching the joint (Purvis, 2003).
- The joint width must be sufficient to allow room for thermal expansion and contraction without letting the gap plate hit the abutting wearing course during this process. If the gap plate hits the wearing course on either side of the joint, the joint may fail and the wearing course may be damaged. Joint widths are typically no less than 500 mm (20 in) (Mogawer et al., 2004). Joint length and skew angle have to be carefully treated when using an APJ. A skew angle larger than 30° becomes prone to snowplow deterioration (Bramel et al., 1999).
- The joint movements should be limited to 1.9 cm (0.75 in) or less. The vertical movement should be restricted to 0.6 cm (0.25 in) or less, and joint gap should be limited to 5 cm (2 in). The joint width should be constrained to minimum of 40.6 cm (16 in) and maximum of 61 cm (24 in) (Bramel et al., 1999).
- The joint waterproofing must continue over its entire length just as the expansion gap of a bridge continues through any curb and sidewalk bridge. The waterproofing consists of sealant compatible with the substrate and tooled on the vertical and horizontal faces of the curb. If this sealant separates from the substrate the curb areas will leak and may cause damage to the underlying substructure, similar to leakage through the APJ (Partl et al., 2006).
- In UK, a typical APJ is required to be functional within a temperature range of -25°C (-13°F) to +45°C (+113°F) (Partl et al., 2006). In US, the seasonal temperatures vary greatly from north to south and within each state and they exceed the limits adopted for Europe (Partl et al., 2006; Bramel et al., 1999).
- Dynamic loading from traffic and end beam rotation can cause vertical movements (Mogawer et al., 2004). It is recommended using APJ in locations with less truck traffic and small bridge movement. An ADT of roughly 20,000 is said to provide a good

behavior of asphaltic plug joints in terms of traffic loads (Purvis, 2003).

- Asphalt plug joints are not recommended for airport and pedestrian bridges (slow moving or stationary traffic). It should not be installed where there is turning or breaking movements or in areas with high thermal shocks. APJs should be used when traffic is straight or when skew angle is less than 30° (Bramel et al., 1999).

4.2 Material

- The British APJ standard recommends that if the joint filling is mixed on site, the aggregate shall be delivered to the point of installation in pre-weighed sealed bags. The aggregate should be heated to avoid the increasing of the air voids in the mix but not too much as to exceed the installation temperature of the binder of 188°C–196°C (370°F–385°F), because at high temperature the adhesion between the binder and the aggregate might be compromised (Bridge Joint Association Standard, 2003). In most cases, the aggregates have 22 mm (0.87 in) maximum aggregate size (Malla et al., 2006).
- In UK, the APJ standard specifies that at the in-situ joint, the flashing should be used as a flexible membrane for waterproofing (Malla et al., 2006).
- The most recommended gap plate is stainless steel plate with a minimum thickness of 5 mm (0.2 in) and typically 200 mm (8 in) wide centered over the joint to prevent the binder to flow into the opening (Mogawer et al., 2004).
- Backer rod should be heat treated or highly resistant to heat for asphalt materials (Bramel et al., 1999).
- Spikes, a device used to keep the center of plate in line with the center of joint, should be placed 0.3 to 0.5 meters (1 to 1.5 feet) apart (Bramel et al., 1999).

4.3 Installation

- The removal of existing joint is done by dry saw cutting to an enough depth as to safely remove existing pavement by using jackhammer and hand tools. The empty gap created for future joint should be cleaned and dried with hot compressed air. The surface must be free of any debris, tanked and flooded with the APJ binder material. The new backer rod is installed and the gap plate shall span the expansion gap and should be fitted in a manner that the plate will be on a sound concrete support and nailed into place with locating pins. Afterward, the entire joint, including the vertical sides, must be tanked with APJ material again (Bramel et al., 1999).
- In Switzerland, ASTRA guidelines suggest that a typical installation procedure consists of pouring the binder in layers of 3 to 4 cm (1.2 to 1.6 in) at a temperature of 180°C (356°F) with an equal layer of hot stones added immediately. After the layer is cooled to about 80°C (176°F) another layer will be added until a height of 16 cm (6.3 in) is reached (Partl et al., 2006). The compaction can be done

with a 2-ton roller or with a vibratory plate compactor. The heated mix is placed in three lifts that each sandwich a filler coat of binder. The final coat is a coat of dry aggregate to help reduce binder track out and acts as an adhesive for the fine aggregate thus sealing the joint (Malla et al., 2006).

- Construction should be made during nominal temperatures at the time of placement. (Purvis, 2003).

4.4 Maintenance

- If the surfacing adjacent to a failed joint deteriorates, both joint and deteriorated surfacing should be replaced to improve ride quality and overall durability. Debris and gravel should be removed from surface to prevent damage to the seal. Joint seal should be repaired if any part is leaking because the water infiltration causes accelerated corrosion to integral parts of the structure and substructure (Mogawer et al., 2004).
- A proper APJ system should be bonded to sound concrete and joint seal has to match ambient temperatures. Joints should be installed after placing the overlay and has to be protected against unusual movement (Bramel et al., 1999).
- The skewed joints are prone to snowplow damage therefore they have to be protected. A failed joint should be entirely replaced since completely sealing the interface between existing and new joints is very difficult. Areas in the approach slab and deck that exhibit excessive vehicle wear should be repaired immediately to reduce impact loads on the joint (Malla et al., 2006).
- A specification regarding removal of asphalt plug joint should be developed (i.e., angle of hammer and hammer tip force).
- A manufacturer's representative should be present at the site during construction and maintenance.
- Contractor should be paid by cubic feet as opposed to linear feet.

4.5 Quality control

- The installer must provide a form after the installation is complete with the information pertaining to: bridge reference number and location, joint size and location on the deck, date of installation, and weather during installation, materials used, plate material and size, type of primer used, surface dressing, and use of debonding strip. Other pertinent information regarding the technical data of the joint system must be provided by the manufacturer (Partl et al., 2006).
- Contractors and inspectors should be made fully aware of materials, design, installation and removal of asphalt plug joint prescribed by public agencies.
- Quality aggregates and binder should be used. Specifications regarding aggregate type and gradation, asphalt type, binder to aggregate ratio, mixing time, deck condition at the time of placement, placing and deck temperature, compaction effort (type and

weight of steel roller, and number of passes), and cooling period should be established.

- Performance-based contract should be considered by public agencies (i.e. contractor should guarantee a minimum of eight through ten years of service life before replacement or major rehabilitation).

5 CONCLUSIONS

The results of a national survey amongst the US Departments of Transportation (DOTs) conducted by the authors revealed multiple distresses within the APJ conditions. Multiple sources are reported to contribute to the failure of APJs. Seventy three (73%) of the joints distresses was due to material failures, 55% of joint failure was attributed to improper design, 45% of the joint distresses had to do with poor installation, and 36% of the joint failures stemmed from inadequate maintenance.

While APJ is recognized as an effective expansion joint, it is not maintenance free and, thus, periodic replacement is required. Past experience has shown that asphalt plug joints can be low maintenance for about five years with an expected life of eight to ten years if properly designed and installed.

It is recommended that each public agency develops in-house specifications that include design, materials selection, mixing, placing, compacting, finishing and removal. A repair guideline should also be developed. Design parameters and material specifications should be verified through experimental programs.

ACKNOWLEDGEMENTS

This study was funded by a grant made possible by Nevada Department of Transportation (NDOT) under grant number P114-08-803. The authors extend their thanks to the US Departments of Transportation for their participation in a national survey.

REFERENCES

- Bramel, B.K., Puckett, J.A., Ksaibati, K., and Dolan, C.W. "Asphalt Plug Joints: Characterization and Specifications", Report FHWA-WY-99/03F, Wyoming Department of Transportation, University of Wyoming, May 1999, 118 pp.
- Bridge Joint Association Standard for Asphalt Plug Joints in UK, Document Ref: BJA/S2/APJ, 2003, 20 pp.
- Malla, Ramesh B., Shaw, Montgomery T., Shrestha, Matu R., Boob, Smita, "Sealing of Small Movement Bridge Expansion Joints", Prepared for the New England Transportation Consortium, NETCR-58, Project No. 02-6, 2006, 112 pp.
- Mogawer, Walaa S., Austerman, Alexander J., "Evaluation of Asphalt Expansion Joints", Prepared for the New England Transportation Consortium, 2004, 197 pp.
- Partl, M., N., Hean, S., Poulidakos L., "Asphalt Plug Joint Characterization and Performance Evaluation", EMPA Swiss Federal Laboratories for Materials Testing and Research, Switzerland, 2006, 14 pp.
- Purvis, R., "Bridge Deck Joint Performance." NCHRP Synthesis 319, Transportation Research Board, Washington, D. C., 2003, 58 pp.
- Velo, Oscar, Draft Australian Bridge Design Code AS-5100 Section 4 – Bearings and Expansion Joints. Trends in rehabilitation of deck joints and design developments of modular joints, 1996, 15 pp.

Evaluation of triaxial geogrids for reduction of base thickness in flexible pavements

Nader Ghafoori & Mohammadreza Sharbaf
University of Nevada Las Vegas, USA

ABSTRACT: An experimental program to assess performance of a triaxial geogrid-reinforced flexible pavement was carried out. Various laboratory tests were conducted using a steel cylindrical mold with dimensions of 1.8 m (6 ft) in diameter and 2.1 m (7 ft) in height. The studied reinforced and unreinforced (without geogrid) sections consisted of a locally-obtained subgrade with a minimum thickness of 1.5 m (5 ft) and an asphaltic surface course of 76 mm (3 in). The base thickness of both sections was kept constant at 406 mm (16 in). An hydraulic actuator provided 40 kN (9 kip) sinusoidal vertical load through a 305 mm (12 in) circular steel plate at a frequency of 0.77 Hz. The instrumentations include pressure cells, foil strain gauges, LVDT and a data acquisition system. A Triaxial type geogrid was placed in the mid-depth of aggregate base course. Performance of geogrid-reinforced section was compared with that of unreinforced section. Test results revealed that addition of geogrid reduced surface deflection. In addition, it decreased the vertical stresses experienced in base aggregate and subgrade layers.

1 INTRODUCTION

Geosynthetics have been successfully used for base reinforcement and subgrade improvement for unpaved and paved roads in the past several decades (Hass et al. 1988, Al-Qadi et al. 1994, Perkins 2002, Berg et al. 2000). They are available worldwide and their market is growing steadily because of their wide civil applications.

Geogrid is a major type of geosynthetics which could be used for soil reinforcement, separation, drainage and filtration (Giroud & Noiray 1981). Uniaxial, biaxial and triaxial geogrids are three common types of geogrid. Uniaxial and biaxial geogrids have tensile strength in one direction and two directions, respectively. Uniaxial geogrid is mainly used for reinforcing slopes, retaining walls, and embankments, whereas biaxial geogrid is commonly used for stabilizing roadways including unpaved roads, paved roads, and railroads (Dong et al. 2010). Triaxial geogrid has more stable grid structure (aperture) and it has a uniform tensile strength in all directions. Triaxial geogrid can provide improved performances compared to other types and more investigations are on-going regarding the benefits of application of triaxial-type geogrid (Giroud 2009).

Many studies have been carried out to investigate behavior of geogrid-reinforced paved roads. Das & shin (1994) revealed that the interface between the base and the subgrade is the most effective location of the geosynthetic for a weak subgrade improvement. At this

location the geosynthetic could provide full or partial separation, lateral restraint of the overlying granular material, and a tensioned membrane effect. Moreover, a decrease of shear stress at the geogrid-subgrade interface would decrease the anticipated vertical deformation (Perkins 1999). Murad Y. Abu-farsakh & Chen (10) reported that better performance is observed when geogrid layer is placed at the upper one-third of the base aggregate layer. Their results also demonstrated that the geogrid helps in redistributing the applied load to a wider area on top of the subgrade layer, thus resulting in a smaller accumulated permanent deformation in the subgrade. Dong et al. (2010) reported that biaxial geogrid, subjected to tension in different directions, can't provide uniform tensile strengths in all directions. The same author also reported that the biaxial geogrids have higher tensile strength and stiffness in their machine and cross-machine directions, but much lower strength and stiffness in other directions, especially in the 45° loading direction. Traffic loading is single-direction in highways but in parking lots and construction sites can have random directions. Since triangular aperture geogrid has a more stable grid structure, it provides nearly uniform properties in all directions and impressed performance as compared with uniaxial and biaxial geogrids (Dong et al. 2011, Watts & Jenner 2008, Dong et al. 2010, White et al. 2011). Qian et al. (2011) presented an experimental study on unreinforced and triangular aperture geogrid-reinforced bases. The experimental study revealed that triaxial geogrids reduced the permanent

deformation and vertical stress at the interface as compared with the unreinforced section. Moreover, the benefits are more considerable when a heavier-duty geogrid is used. They also reported that the stress distribution angle and the modulus ratio of base course to subgrade decreases with an increase of the load cycles (Qian et al. 2013). Giroud (2009) noted that the triangular structure for a geogrid could cause many probable benefits over biaxial structures. For example it can improve interlock, better stress transfer from soil to geogrid, and improve distribution of stresses within the geogrid structure.

This study investigated the performance of a triaxial geogrid-reinforced base aggregate layer under a 3 million cyclic loading. Two laboratory cyclic plate load tests were conducted on unreinforced and reinforced pavement sections constructed in a large cylindrical mold in order to assess the influence of triangular aperture geogrids on the reduction of surface deformations (rutting) and vertical stresses at the interface between the base and the subgrade. Moreover, foil strain gauges, installed on the ribs of geogrid, recorded the deformation of geogrid's ribs under cyclic loading. However, the amount of strains throughout 3 million repeated cycles were non detectable, indicating no vertical strain was experienced at the level where geogrid was placed within the base aggregate layer.

2 TEST SET-UP

A cylindrical mold with a diameter of 1.8 m (6 feet) and an height of 2.1 m (7 feet) was constructed to house the studied pavement sections. A hydraulic actuator, which had a force rating of 40 kN (9 kips) was attached between the two I-beams of the crosshead. A cyclic load was applied through a steel rod that fit into a concave-shaped hole on the loading plate that sat on the surface of the hot mix asphalt (HMA) surface layer. The loading plate was 305 mm (12 inches) in diameter. The applied load was kept constant at 40 kN (9 kips), which resulted in a loading pressure of 550 kPa (80 psi) and simulated dual tires under an equivalent 80-kN (18,000-lb) single-axle load. Figure 1 illustrates the test set-up. The load pulse, as shown in Figure 2, had a linear load increase from 2.2 kN (0.5 kips) to 40 kN (9 kips) in 0.3 s, followed by a 0.2-s period where the load was held constant at 40 kN (9 kips), followed by a linear load decrease to 2.2 kN (0.5 kips) over a 0.3-s period, followed by a 0.5-s resting period of 2.2 kN (0.5 kips) before the next loading cycle resumed. This load pulse, as shown in Figure 2, resulted in a frequency of 0.77 Hz.

For the purpose of this study, a triangular aperture geogrid made of polypropylene, as shown in Figure 3, was used. Its material and dimensional properties are given in Table 1.

The subgrade was a regular soil from a location in Southern Las Vegas, Nevada. It was classified as silty, clayey sand with gravel (SC-SM). It had a CBR of 8, R value of 20, Liquid Limit at 25 taps of 22, Plastic limit



Figure 1. Test setup and mold.

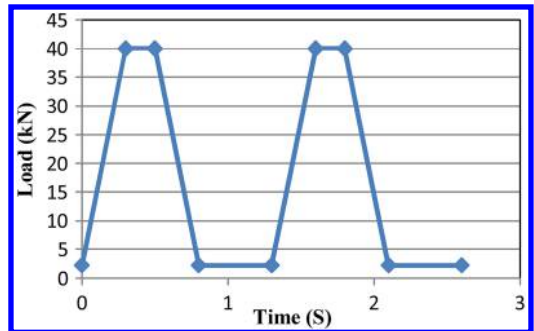


Figure 2. Loading details.

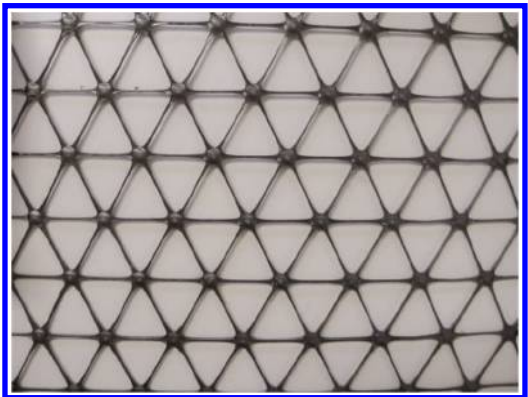


Figure 3. Triaxial aperture geogrid.

of 17, and plasticity index of 5. It had a maximum dry density of 2.03 gr/cm³ (126.9 pcf) corresponding to the optimum moisture content of 11.2% based on the Modified Proctor energy input as shown in Figure 4.

Table 1. Materials and dimension properties of geogrid.

Index Properties	Longitudinal	Diagonal	Transverse	General
Rib Pitch, mm (in)	33 (1.30)	33(1.30)	–	
Mid-rib Depth, mm (inch)		1.5 (0.06)	1.2 (0.05)	
Mid-rib Width, mm (inch)		0.6 (0.02)	0.7 (0.03)	
Rib shape				Rectangular
Aperture shape				Triangular
Structural integrity				
Junction efficiency, %				93
Aperture Stability, kg-cm/dg @ 5.0 kg-cm				3.0
Radial stiffness at low strain, Kn/m @ 0.5 % strain			200	
Radial stiffness at low strain, lb/ft @ 0.5% strain			15,075	
Durability				
Resistance to chemical degradation				100%
Resistance to ultra-violet light and weathering				100%

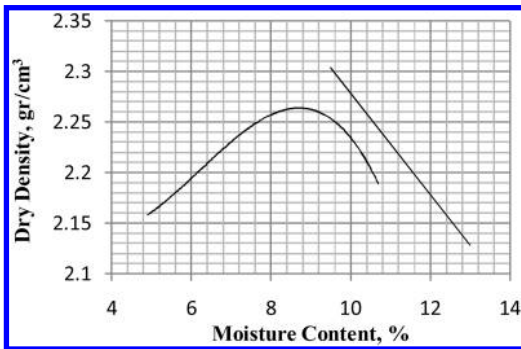


Figure 4. Modified proctor test results of subgrade layer.

Type II Class B road base aggregate, well-graded and commonly used in Nevada for paved roads, was used as the base material. The base course was classified as light gray, poorly graded gravel w/silt & sand (GP-GM). The maximum dry density of the base course was 2.265 gr/cm³ (141.4 pcf) which corresponded to the optimum moisture content of 8.7% based on the modified proctor compaction energy.

The instrumentation system included 4 earth pressure cells, a LVDT, and 6 foil strain gauges installed on the ribs of the geogrid. Three pressure cells were placed 5.1 cm (2 inches) below the interface between subgrade and base course at the distances of 0, 22.8 and 45.7 cm (0, 9 and 18 inches) away from the center of the mold as shown in Figure 5. The other pressure cell was placed 5.1 cm (2 inches) above the interface in the base course layer at the center of the mold. The displacement transducer was placed on top of the loading plate. The foil strain gauges were placed on two directions of the geogrid away from the center of the mold at 15.2 cm (6 inches) intervals as shown in Figure 5. All sensors were connected to a data acquisition system and the results were recorded throughout the repeated loading for up to 3 million cycles.

As for the construction of the two pavement sections, the silty clay subgrade was first placed and compacted in multiple lifts inside the steel mold. The



Figure 5. Installation of pressure cells.



Figure 6. Installation of geogrid and strain gauges.

loose thickness of each lift was 22.9 cm (9 inches) which resulted in a 12.7 cm (5 inches) thickness of compacted soil. The subgrade soil was compacted at a water content of 12.5% to the compaction level of 95% corresponding to Modified Proctor test.

The subgrade was prepared by using a tiller to mix the silty clay and water. Then, the silty clay was rake leveled and compacted using a vibratory rammer to a predetermined height to achieve the desired density. At the completion of subgrade preparation, the pressure cells were installed. To install pressure cells, holes of the same shape, but of a slightly larger size than that of the pressure cells, were excavated to a predetermined

depth with a hand trowel. Once, the bottom of each hole was flattened, the pressure cells were placed and leveled inside the holes, using a leveling device, before hole was backfilled and compacted with the same subgrade soil. The amount of soil needed to backfill was estimated by removing the amount of clay occupied by the pressure cell, which was calculated by multiplying the density of the soil by the approximate volume of the pressure cell from the soil excavated. Afterward, the base course layer was prepared by placing crushed limestone in two 25.4 cm (10 inches) loose lifts, mixed with desired water, and compacted to the final thickness of 40.6 cm (16 inches) resulting in an optimum density of 2.26 gr/cm³ (127 pcf) at the moisture content of 6.2%. The geogrid was installed at the center of base course layer between the two compacted lifts.

The HMA type 2C plant-mix aggregate with rap was prepared and delivered, as designated by Nevada Department of transportation from a local asphalt plant to the testing site. It had a bitumen ratio of 4.4 and sand equivalent of 60. Also the LA abrasion is equal to 24%. HMA was spread over the area of the test mold, rake-leveled, and immediately compacted to the predetermined height of 7.6 cm (3 inches) using a vibratory plate compactor at the level of 95% of optimum density of 2.604 Mg/m³ (162.5 lb/ft³).

3 RESULTS AND DISCUSSION

Tests were conducted on two different pavement sections, unreinforced and reinforced with a geogrid layer placed at the middle of its base layer. The results of the accelerated load tests, up to 3 million repeated loading, are graphically presented in Figure 7. As can be seen, the unreinforced section displayed a lower surface deflection up to 0.5 million strokes. There was no difference in surface deflection (rutting) between the two studied paving sections between 0.5 and 1.0 million cyclic loading. The reinforced section displayed lower surface deflections, as compared to that of the unreinforced section, reduction of 9, 12.4, 11, 9.6% at the repeated loading cycles of 1.5, 2, 2.5 and 3 million cycles, respectively.

The results of the vertical pressures, generated from the installed pressure cells in the unreinforced section are shown in Figure 8. Unfortunately, the pressure cell installed at the center point malfunctioned and unable to measure pressure at this location. Irrespective of the location of the pressure cells, the magnitude of vertical stresses remained steady throughout the 3 million cyclical loading. When comparing the central vertical pressure in the mid base aggregate layer with that obtained from the pressure cell installed at 22.8 cm (9 inches) off-center in the subgrade, a decrease of roughly 50% in vertical stress was experienced. The reduction in the vertical pressure was 88% when compared to that of 45.7 cm (18 inches) off-center pressure cell in the subgrade.

Figure 9 documents vertical stresses in geogrid-reinforced section. The stress at the center of base

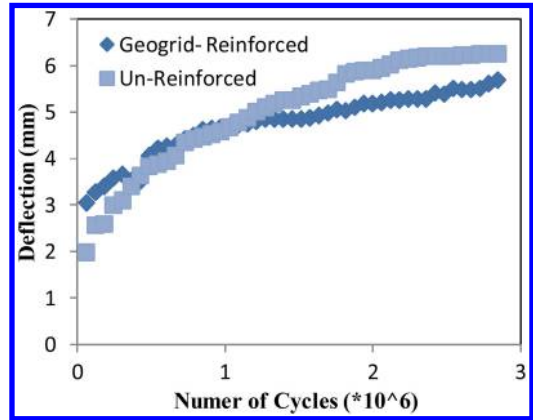


Figure 7. Surface deflection (rutting) of tests.

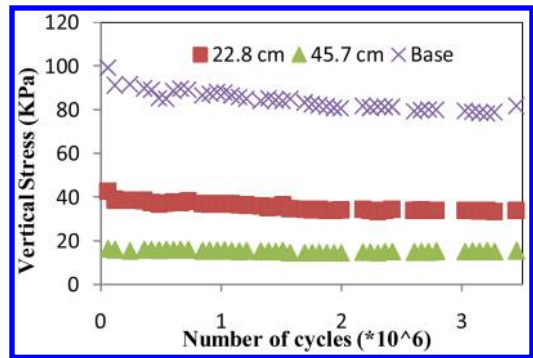


Figure 8. Vertical stresses of unreinforced-section.

layer is more than that of the subgrade. Also the pressure in center is more than the 22.8 cm (9 inches) offset and 22.8 cm (9 inches) offset is more than the 45.7 cm (18 inches). Moreover, the vertical stress has decreased in all locations at the first 0.5 million cycles. When comparing the central vertical stress in the mid base aggregate layer with that obtained from the pressure cell installed at center point in the subgrade, a decrease in the vertical stress of roughly 20% was experienced. The reduction in the vertical stress was 45% and 63% when compared to that of 22.8 cm (9 inches) and 45.7 cm (18 inches) off-center pressure cells in the subgrade.

The vertical stresses recorded at the center of base aggregate layer in both pavement sections are shown in Figure 10. The reduction of vertical stress was roughly 40% when triaxial geogrid was used.

A comparison of the vertical stress at the 22.8 cm (9 inches) off-center point of subgrade layer for both reinforced and unreinforced pavement sections are shown in Figure 11. As depicted, the triaxial geogrid-reinforced section experienced less vertical pressure, as compared to that of the unreinforced section, by an average of nearly 15%.

The Traffic Benefit Ratio (TBR) was used to evaluate the benefit of geogrid base reinforcement. TBR is defined as the number of load cycles carried by a

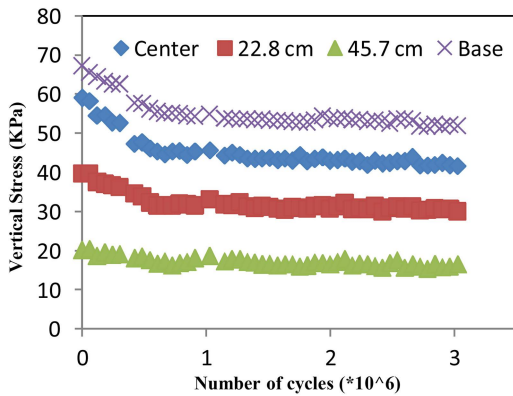


Figure 9. Vertical stresses of reinforced section.

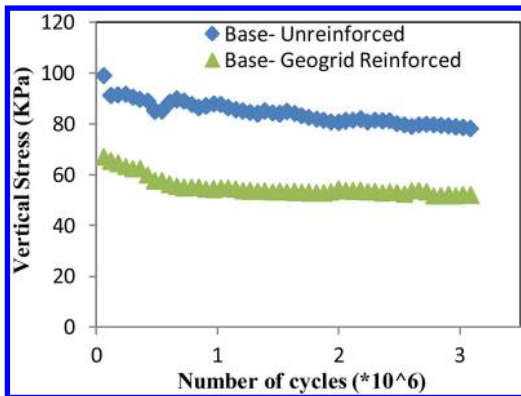


Figure 10. Center stress for both pavement sections.

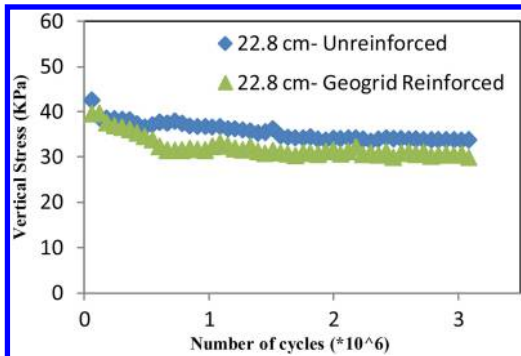


Figure 11. 22.8 cm stress for both sections.

reinforced section at a specific rut depth divided by that of an equivalent unreinforced section. The calculated TBRs are shown in Table 2. As can be seen, the geogrid-reinforced section produced larger TBRs than the unreinforced section in resisting the cycling strokes. Additionally, this ratio increased by increases in repeated loading (or rutting depth), indicating better performance can be expected when base aggregate layer is reinforced with a geogrid layer.

Table 2. Traffic benefit ratio.

Deflection (inch)	Unreinforced no. of cycles	Geogrid-reinforced number of cycles	Traffic Benefit Ratio (TBR)
0.19	1150000	1270000	1.104
0.20	1270000	1875000	1.476
0.21	1512000	2420000	1.6
0.22	1754000	2783000	1.587

4 CONCLUSIONS

- A smaller surface deflection (rutting) in geogrid-reinforced pavement was obtained when compared to that of equivalent unreinforced section.
- Use of geogrids in base aggregate layer resulted in 40% and 15% lower stresses at center of base aggregate and at 22.8 cm (9 inches) off-center point of subgrade layer, respectively.
- The highest TBR was recorded at the rutting depth of 5.3 mm (0.21 inch) which correspond to the repeated loading of 1.6 million cycles.

ACKNOWLEDGEMENT

This study was funded by a grant made possible by Nevada Department of Transportation (Grant No. P114-08-803). Thanks are extended to a number of manufacturers who donated materials.

REFERENCES

- Al-Qadi, I. L., Brandon, T. L., Valentine, R. J., Lacina, B. A., and Smith, T. E., 1994, Laboratory Evaluation of Geosynthetic Reinforced Pavement Sections, *Transportation Research Record. 1439, Transportation Research Board*, Washington, D.C.: pp. 25–31.
- Berg, R. R., Christopher, B. R., and Perkins, S. W., 2000, GMA White Paper II, *Geosynthetic Materials Association*, Roseville, MN: 100 p.
- Das, B. M., and Shin, E. C. 1994. Strip foundation on geogrid-reinforced clay: behavior under cyclic loading. *Geotext. Geomembr.*, 13(10): 657–666.
- Dong, Y.-L., Han, J., and Bai, X.-H. 2010. A numerical study on stress-strain responses of biaxial geogrids under tension at different directions. *Accepted for publication at ASCE G-I GeoFlorida Conference.*
- Dong, Y.-L., Han, J., and Bai, X.-H. 2010. Bearing capacities of geogrid-reinforced sand bases under static loading. *Proc., GeoShanghai Int. Conf. 2010, Ground Improvement and Geosynthetics*, Geotechnical Special Publication No. 207.
- Dong, Y.-L., Han, J., and Bai, X.-H. 2010. A numerical study on stress-strain responses of biaxial geogrids under tension at different directions. *Proc., GeoFlorida 2010: Advances in Analysis, Modeling & Design*, Geotechnical Special Publication No. 199, ASCE, Reston, VA: 2551–2560.
- Dong, Y.-L., Han, J., and Bai, X.-H. 2011. Numerical analysis of tensile behavior of geogrids with rectangular and triangular apertures. *Geotext. Geomembr.*, 29(2): 83–91.

- Giroud, J. P. 2009. An assessment of the use of geogrids in unpaved roads and unpaved areas. *Proc., Jubilee Symp. on Polymer Geogrid Reinforcement Conf.*, Tensar, Blackburn, UK.
- Giroud, J.P. and Noiray, L. 1981. Geotextile-reinforced unpaved road design. *J. Geotech. Eng.*, 107(9): 1233–1254.
- Hass, R., Walls, J., and Carroll, R. G., 1988, Geogrid Reinforcement of Granular Bases I Flexible Pavements, *Transportation Research Record. 1188, Transportation Research Board, National Research Council*, Washington, D.C.: 19–27.
- Murad Y. Abu-Farsakh and Qiming Chen, 2011, Evaluation of geogrid base reinforcement in flexible pavement using cyclic plate load testing, *International Journal of Pavement Engineering*, Vol. 12, No. 3: 275–288.
- Perkins, S. W. 1999. Geosynthetic reinforcement of flexible pavements: Laboratory based pavement test sections. *Rep. No. FHWA/MT-99/8106-1, Montana Dept. of Transportation*, Helena, MT, 140.
- Perkins, S.W., 2002, Evaluation of Geosynthetic Reinforced Flexible Pavement Systems Using Two Pavements Test Facilities, *Federal Highway Administration Report No. FHWA/MT-02- 008/20040*, Montana Department of Transportation Helena, MT, 120 p.
- Qian, Y., Han, J., Pokharel, S. K., and Parsons, R. L. 2011. Stress analysis on triangular aperture geogrid-reinforced bases over weak subgrade under cyclic loading—an experimental study. *Proc., 10th Int. Conf. on Low-Volume Roads, Transportation Research Board*, Washington, DC: 83–91.
- Watts, K., and Jenner, C. 2008. Large-scale laboratory assessment of geogrids to reinforce granular working platforms. *Proc., EuroGeo4: 4th European Geosynthetics Conf. (CD), N. Di on, ed., International Geosynthetics Society*.
- White, D. J., Vennapusa, P. K. R., Gieselman, H. H., Douglas, S. C., Zhang, J., and Wayne, M. H. 2011. In-ground dynamic stress measurements for geosynthetic reinforced subgrade/subbase. *Proc., GeoFrontiers 2011: Advances in Geotechnical Engineering, Geotechnical Special Publication No. 211*.
- Yu Qian, Jie Han, Sanat K. Pokharel and Robert L. Parsons, 2013, Performance of Triangular Aperture Geogrid-Reinforced Base Courses over Weak Subgrade under Cyclic Loading, *J. Mater. Civ. Eng.* 25: 1013–1021.

A state of the art review into the use of geopolymer cement for road applications

A. Wilkinson, D. Woodward, B. Magee & S. Tretsiakova-McNally

Ulster University, Built Environment Research Institute, Newtownabbey, Co. Antrim, Northern Ireland

ABSTRACT: This paper is a state of the art review of the use of geopolymer cement for road applications. Geopolymer cement is an alternative to Portland cement and is either naturally occurring rock-based or industrial by-product-based. Geopolymer cement has been around for at least the last 30 years. In recent years it has become an attractive potential alternative to Portland cement. The main reason for this renewed interest is the issue relating to the release of carbon dioxide into the atmosphere during the manufacture of Portland cement. It is estimated that 1 tonne of Portland cement produces approximately 1 tonne of CO₂ during its manufacture. The use of geopolymer cement can reduce this amount by as much as 90%. It is claimed that this will have a huge potential in reducing national targets in CO₂ emissions of many countries around the world. This state of the art review critically evaluates existing literature relating to these claims and focuses on the potential use of geopolymer concrete for road applications. In addition to environmental benefits, the existing literature suggests that geopolymer cement concrete has the potential to provide better mechanical properties than Portland cement concrete. Attractive properties include quicker compressive strength development, higher compressive and flexural strength, minimal shrinkage and resistance to chemical-attack and freeze-thaw cycles. The review will consider the different types of geopolymer cement, its properties and whether it can be used in road applications.

1 INTRODUCTION

A geopolymer is defined by the Geopolymer Institute (2014a) as an inorganic polymeric material which is formed through geopolymerisation. The term geopolymer cement refers to binders formed as a result of this geopolymerisation process (Saravanan et al, 2013). The mixture of this binder with aggregate and water forms geopolymer concrete. Although the term ‘geopolymer’ was first used in 1972 by Davidovits (2002), similar alkali-activated cements were mentioned in work by Glukhovskiy (1959). In current literature, an uncertainty remains with regards to the correct terminology, with alkali-activated cement often being referred to a geopolymer cement, and vice versa (Skvara, 2007). This is despite efforts to clarify the fundamental differences between the materials, by the Geopolymer Institute (2014b).

Geopolymer cement is regarded as an attractive alternative to ordinary Portland cement binders (Heath et al, 2013). This is due to the environmental benefits and performance properties of the material (Davidovits, 2013; Banah UK, 2014). Research into geopolymer cement and geopolymer cement concrete is ongoing, with various areas of research being considered. One area in which geopolymer cement can be applied is in road pavement applications.

This paper will critically review current knowledge of geopolymer cement. This will include basics of geopolymer chemistry, environmental benefits and

performance properties associated with geopolymer cement. In addition, current geopolymer cement and concrete applications will be reviewed, as well as current and potential road pavement applications.

2 GEOPOLYMER CHEMISTRY

2.1 *Materials*

Geopolymer cement typically consists of two components: an aluminosilicate material and a chemical activator. The aluminosilicate materials are divided into two main categories: industrial by-products and raw, rock-based materials (Davidovits 2013). The majority of research has considered the use of industrial by-products such as fly ash or blast furnace slag as potential precursor materials (Rangan, 2014; Duxson & Provis, 2008; Saravanan et al, 2013; Jayaranjan et al, 2014). Although Zeobond, an Australian geopolymer cement producer, use fly ash as an aluminosilicate constituent, (Zeobond, 2014), Heath et al (2013) argue that fly ash production in the UK is decreasing, reducing the potential for long term use of this source. In addition, consistency of fly ash properties cannot be guaranteed, due to the presence of contaminants such as calcium and iron. The presence of these impurities can impact upon properties such as strength, setting times, shrinkage and slump (Duxson et al, 2007). Therefore, fly ash is unlikely to be a key source

material for future geopolymer cement production in the UK.

Other precursor sources discussed by Davidovits (2013) are rock-based, raw materials, with high kaolinite contents. Although performance based research mostly focuses on the nature of fly ash geopolymer cement, Kuenzel et al (2014) and Cwirzen et al (2014) have studied variables which can impact upon the mechanical properties of kaolin-based geopolymer cement. Currently, Banah UK, a Northern Ireland based geopolymer cement producer, have selected locally sourced kaolinite as the aluminosilicate material for their cement. The kaolin is contained within lateritic clay, a waste material from Northern Irish basalt quarries (Banah UK, 2014).

The second component needed to produce geopolymer cement is a chemical activator which is generally used in the form of a mild alkaline reagent. This reagent is an aqueous silicate solution, containing silica and a metal alkali, with a molar ratio $\text{SiO}_2:\text{M}_2\text{O}$ greater than 1.65, where M is an alkali metal, either sodium (Na) or potassium (K) (Davidovits, 2008; Davidovits, 2013).

2.2 Geopolymerisation process

The Geopolymer Alliance (2014) identifies three main phases in the geopolymerisation process: dissolution, condensation and poly-condensation. Geopolymerisation is described by Al Bakri et al (2011) as the production of a geopolymeric material through inorganic poly-condensation. Several mechanisms of geopolymerisation are suggested in the literature (Davidovits, 2008; Khale & Chaudhary, 2007; Komnitsas & Zaharaki, 2007). Stages identified by the Geopolymer Alliance (2014) are described below.

The first phase of geopolymerisation is a dissolution of solid aluminosilicates. Upon mixing of the aluminosilicate material and a chemical activator, alkaline hydrolysis occurs. This produces aluminate and silicate ions, which could be considered as monomers (Duxson et al, 2006). A gel, or sol, is formed at this stage. At this gel phase, the second phase of geopolymerisation begins, when aluminium and silicone hydroxide fragments condense, producing a Si-O-Al bond and water (Hench, 1998; Geopolymer Alliance, 2014). This results in the formation of chains or networks, which may be represented in 2-dimensions by the following sequence examples: (-Si-O-Al-O-Si-O-) or (-Si-O-Al-O-Si-O-Si-O-), depending on the silica/alumina ratio (Davidovits, 1988).

The third stage of geopolymerisation is the poly-condensation of previously produced Si/Al-containing monomers at a temperature range between ambient and 90°C. The result is the formation of a rigid network or chain of silica and alumina tetrahedrals, all of which are joined by oxygen bridges.

This process has been studied since the late 1980's (Davidovits, 1988). More recent works by Xu & van Deventer (2000), Duxson et al (2006), Komnitsas & Zaharaki (2007) and ul Haq et al (2014) has studied and reviewed this process further. These studies, and the overall process, are widely accepted by geopolymer

experts throughout the literature. An alternative synthesis method for producing a lightweight foamed geopolymer has also been developed by Boke et al (2015). Coal fly ash and a sodium hydroxide (NaOH) solution were combined with a foaming agent, sodium hypochlorite (NaOCl). The addition of the NaOCl allowed for controlled foaming of the material when heated to a temperature of 90°C. The discovered synthesis method was able to maintain a stable state for 1 hour at ambient temperatures, prior to heat application. This provided suitable time for placement and moulding, eliminating the risk of premature foaming.

3 CO₂ EMISSIONS FROM CEMENT PRODUCTION

Sustainability and the environmental impact of products is increasingly becoming the focus of many organisations and governmental panels. A prime example of this is the Intergovernmental Panel on Climate Change report (2014). Minimising the carbon footprint of construction materials will play a key role in the UK meeting the target of reducing greenhouse gas emissions. The Climate Change Act (2008) has set a target of reducing greenhouse gas emissions by 80% by 2050, based on 1990 baseline levels. Therefore, the use of novel materials, such as geopolymer cement, may play a role in the solution to this problem.

3.1 Portland cement production

According to Benhelal et al (2013) the manufacture of Portland cement is responsible for approximately 5–7% of global CO₂ emissions. It was also suggested that for each tonne of cement produced, 900 kg of CO₂ would be emitted. While the World Business Council for Sustainable Development (2009) confirm continually decreasing emissions as cement production increases, it is clear that a change in direction is required. The two main causes of CO₂ production from cement production are fuel emissions from heating the kiln to 1450°C, and the decomposition of calcium carbonate in the kiln (Understanding Cement, 2012). This decomposition reaction accounts for around 65%, by mass, of the total emissions (Banah UK, 2014).

One way in which CO₂ emissions can be reduced is by replacing a percentage of cement in concrete with industry by-products, such as fly ash or silica fume. This provides an emissions reduction of 10–15%, (Davidovits, 2013). A review of potential energy savings and CO₂ reduction was also undertaken by Madloul et al (2011). Options such as alternative fuelling, dry kiln processes and waste heat recovery were recommended and supported by the review.

3.2 Geopolymer cement production

Geopolymer cement provides a more environmentally friendly alternative to conventional Portland cement. Depending on the source of aluminosilicate material, emissions can be up to 90% lower than Portland cement production (Davidovits, 2013). One of the

requirements for a geopolymer source material is an amorphous structure. Therefore, some materials will require more heat treatment than others, if any. As fly-ash is the result of an energy intensive process, an amorphous structure exists. This eliminates the need for kiln processing (Davidovits, 2013) Also, some slag sources require some heat treatment. McLellan et al (2011) claim that emissions from fly-ash based geopolymer concrete can be as low as 90 kg of CO₂ per tonne of cement produced. While this is currently the lowest possible emission level, fly-ash based geopolymer production is unlikely to exceed 250 kg of CO₂ per tonne of cement produced. This represents emissions between 70 and 90% less than ordinary Portland cement. McLellan et al (2011) and Davidovits (2013) also claim that slag based geopolymers can achieve emission reductions of between 70 and 80%.

As the raw materials used for geopolymer cement have not been subjected to high temperatures, calcination is required. A study of kaolin and metakaolin by Siddique (2008) states that a kiln temperature of 500–800°C is required to turn raw kaolin into metakaolin for geopolymer production. Despite this process, Banah UK (2014) claim that BanahCEM offers a reduction of CO₂ emissions by 80%, compared to Portland cement. This claim is supported by the Geopolymer Institute (2014c).

Therefore, based on the literature discussing Portland and geopolymer cement production, geopolymer cement presents an environmental alternative to conventional cement.

4 PERFORMANCE

4.1 Compressive and flexural strength

A key aspect of geopolymer cement concrete is its compressive and flexural strength. A Geopolymer Institute (2008) review of technical properties of geopolymer cement concrete published 90 MPa compressive strength and 10–15 MPa flexural strength at 28 days. Similar results are reported by Banah UK (2014), who achieved 28 day compressive strengths of up to 100 MPa. A further benefit highlighted during this study was that 80% of the 28 day strength was achieved at 7 days, much like ordinary Portland cement. A similar rate of strength development was also noted by Anuar et al (2011). As such, the potential final strength and strength development of geopolymer cement makes it a viable alternative to Portland cement for a wide range of applications.

Specialist geopolymer cements have also been developed. A fly-ash based, rapid-setting geopolymer cement was developed by Hawa et al (2013), for example. Compressive strengths of at least 60 MPa at 60 minutes, when cured at 80°C, were reported. This was followed by the development of ultra-high-performance geopolymer cement by Ambily et al (2014). This cement was based on a slag and silica fume mix. A 28 day compressive strength of 124 MPa was recorded. The addition of 3% (by mass) steel fibres yielded a 28 day compressive strength of 175 MPa.

The reason for this was tension transfer across the crack via the fibres, thereby increasing the load which could be placed on the specimens.

Based on published test results, geopolymer cement can potentially be used as an alternative to Portland cement in a variety of common applications. The potential to adapt and alter the cement/concrete is also available, providing solutions to more specific or specialist needs.

4.2 Other properties

Another important benefit of geopolymer cement is its resistance to acid and sulphate attack (Glasby et al, 2014), as well as freeze-thaw cycles (Abdulkareem et al, 2014). In terms of sulphate resistance, results from Douglas et al (1992) indicate that changes in the mechanical properties of geopolymer cement concrete specimens were minimal, after 120 days immersion in a 5% sodium sulphate solution. Further research has also indicated good resistance to acids, such as sulphuric acid and hydrogen chloride (Ariffin et al, 2013; Shi, 2003; Banah UK, 2014). In addition, Provis & van Deventer (2009), Davidovits (2013) and Abdulkareem et al (2014) discussed freeze-thaw properties. Mass loss of less than 0.1% and strength loss of 5% after 180 cycles was recorded by the Geopolymer Institute (2008).

Another property discussed in the literature is creep and shrinkage. In laboratory testing, drying shrinkage has been found to be minimal. Testing by the Geopolymer Institute (2008), Wallah (2010), Banah UK (2014) and Aurora Construction Materials (ACM) (2014) have all resulted in recorded shrinkage of less than 0.1%.

A particularly positive feature of geopolymer concrete is its durability. Laboratory testing discussed in the literature indicates a likely durability which exceeds Portland cement based concrete. The only way in which this can be accurately stated is by measuring the in-situ performance of geopolymer concrete. Therefore, due to the minimal field applications of geopolymer concrete, definite durability performance may take some time to determine.

Table 1 shows how geopolymer cement performs in comparison with geopolymer cement.

5 PAVEMENT APPLICATIONS

5.1 Current applications

Currently, the in-situ application of geopolymer cement and concrete is limited, especially in Europe. An early example of geopolymer cement concrete in use as a paving material is Pyrament (Davidovits, 2002). Introduced in 1988 by Lone Star Industries, Pyrament was marketed as blended cement (Geopolymer Institute, 2014d). A study, conducted in 1994 by Husbands et al examined the durability of the material, concluding that, despite its rapid setting times, the durability and performance levels would make it a suitable material for use by the US Army Corps

Table 1. Comparison of geopolymer cement with Portland cement.

Property	Portland cement	Geopolymer cement	Reference
Typical Setting Time	2.5 Hours	Up to 2.5 hours	Banah UK, 2014
Typical Compressive strength (28 Day)	<50 N/mm ²	<100 N/mm ² <68.7 N/mm ² 124 N/mm ² 90 N/mm ²	Banah UK, 2014 Ozyildirim, 1994 Ambily et al, 2014 Geopolymer Institute, 2008
Curing Time	1–2 Days	From 3 hours	Banah UK, 2014
Strength development	50% @ 3 Days 80% @ 7 Days	50% at 18 hours 80% at 7 days 48% at 24 Hours 52.08 N/mm ² at 24 h	Banah UK, 2014; Banah UK, 2014; Anuar et al, 2011 Ambily et al, 2014 Jayaseher et al, 2013
pH Tolerance	6.5–14	3.0–14	Banah UK, 2014
Mass Loss after 45 days in 5% HCl	>30%	<12%	Banah UK, 2014
Mass Loss in 10% HSO	>65%	<12% at 45 days 1.64% after 24 weeks	Banah UK, 2014 SureshThokchom & Ghosh, 2009
Resistant to Freeze-Thaw action	No	Yes 0.1% Mass loss after 180 cycles 0.5% Strength loss after 180 cycles	Banah UK, 2014 Geopolymer Institute, 2008 Geopolymer Institute, 2008
Typical Shrinkage on Curing	0.52–0.78 mm/m	0.02–0.06 mm/m <0.1%	Banah UK, 2014 Wallah, 2010; Geopolymer Institute, 2008; ACM, 2014
Explosive Failure in fire	Yes	No No	Banah, 2014 Pan et al, 2012
Flexural strength at 28 days		10–15 N/mm ² 6.6 N/mm ² 5 N/mm ²	Geopolymer Institute, 2008 Wagners, 2012 Vijai et al, 2012

of Engineering for paving projects. In addition, an investigation by the Virginian Transportation Research Council concluded that the performance of this material when used in highway repair applications was satisfactory. This investigation was conducted approximately 4 years after the placement of the material (Ozyildirim, 1994). Despite the apparent success and potential of this material, financial issues within the company ended production (McIntosh, 2012).

More recently, the Australian geopolymer cement and concrete producer, Zeobond, trialled the use of geopolymer concrete in a light pavement application (Aldred & Day, 2012). The use of geopolymer concrete has since expanded within Australia to use in precast walkway panels, in-situ footpaths and bicycle lanes. A visual examination by Andrews-Phaedonos (2014) stated that the concrete was showing satisfactory durability with no signs of stress or cracking apparent after between 3 and 4 years.

During this study by Andrews-Phaedonos, the use of geopolymer concrete as a paving material was supported by its inclusion in non-structural concrete specifications (van Deventer et al, 2013). The VicRoads Standard Specification (2013), section 703 – General Concrete Paving, acknowledged the possible use of geopolymer concrete as a paving material. Although the specifications are set to the same performance standards as conventional concrete, this may be a step towards the setting of geopolymer concrete standards.

In addition to applications in Australia, a study in Thailand by Hawa et al (2013) examined the potential use of geopolymer cement concrete as a material for rapid road repairs. The main issue with this study was the need for 80° curing temperatures. As a result, although laboratory testing yielded positive results, the curing requirements have meant that field testing has not been possible.

To date, recent research has been limited mostly to Asia and Australia, with precursor sources limited to industrial waste or by-products.

In terms of future developments, an aspect which may be considered by geopolymer cement manufacturers is the development of a one part cement, like Portland cement. Convincing the industry to adopt the use of a new material is a major challenge, as report by Egan (1998). Therefore, by simplifying the product to a single part may aid the adoption of geopolymer cement.

The potential use of rock-based geopolymer cement concrete for road applications is another area for future research. With concerns over the long-term availability of industrial by-products being evident throughout the literature, research into the use of rock-based geopolymer concrete for paving applications is necessary.

Finally, it is accepted throughout geopolymer research that the lack of homologated standards is harming the potential use of geopolymer concrete. Therefore, if geopolymer cement is to be widely included in specifications with its own standards,

rather than relying on Portland cement standards, set standards are required. The setting of geopolymer standards is an issue of vital importance to the future use of geopolymer cements.

6 SUMMARY

This paper reviewed the current and potential use of geopolymer concrete for road applications. It is suggested by the literature that, based on environmental and performance factors, geopolymer cement is a suitable alternative to Portland cement. One of the reasons for the lower CO₂ emissions from geopolymer cement production is the lack of calcium carbonate in the raw material. When kiln processed, calcium carbonate decomposition accounts for around 65% of Portland cement production emissions. This, combined with lower kiln temperatures, and thus lower emissions, can give geopolymer cement emissions up to 90% less than Portland cement. Despite the significant environmental benefit, the mechanical performance of the cement is not affected. Therefore, geopolymer cement can be used as an alternative to Portland cement in a wide variety of applications. Due to its resistance to various acid, sulphate and freeze-thaw attacks, it is also suited to a variety of applications where Portland cement is not adequate.

While geopolymer cement concrete paving applications are not yet common, laboratory testing and some field testing in Australia has indicated its potential use. This has also led to the inclusion of geopolymer cements in some Australian concrete paving specifications. Also, the potential for ambient curing, rapid setting geopolymer cement concrete may allow for the development of rapid repair solutions for pavements and highways.

One main concern with geopolymer concrete is the lack of homologated standards. Currently, geopolymer cement concrete is produced, placed, cured and tested using conventional concrete standards. Therefore, in order to expand the use of geopolymer cement concrete, standards specific to the material are required.

REFERENCES

Abdulkareem, O.A., Al Bakri, A.M.M., Kamarudin, H. and Khairul Nizar, I., 2014. Fire Resistance evaluation of lightweight geopolymer concrete system exposed to elevated temperatures of 100–800°C. *Key Engineering materials*, 594–595, pp. 427–432.

Al Bakri, A.M.M., Kamarudin, H., Bnhussain, M., Khairul Nizar, I., Rafiza, A.R and Izzat, A.M., 2011. Chemical reactions in the geopolymerisation process using fly ash-based geopolymer: A review. *Australian Journal of Basic and Applied Sciences*, 5(7), pp. 1199–1203.

Aldred, J. and Day, J., 2012. *Is geopolymer concrete a suitable alternative to traditional concrete?* CI-Premier, 37th Conference on Our World in Concrete & Structures. Singapore, 29–31 August 2012. Singapore: CI-Premier Conference Organisation.

Ambily, P.S., Ravisankar, K., Umarani, C., Dattatreya, J.K. and Iyer, N.R., 2014. Development of ultra-high-performance geopolymer concrete. *Magazine of Concrete Research*, 66(2), pp. 82–89.

Andrews-Phaedonos, F., 2014. *Specification and use of geopolymer concrete*. Melbourne: VicRoads.

Anuar, K.A., Ridzuan, A.R.M. and Ismail, S., 2011. Strength Characteristics of Geopolymer Concrete Containing Recycled Concrete Aggregate. *International Journal of Civil and Environmental Engineering*, 11(1), pp. 59–62.

Ariffin, M.A.M., Bhutta, M.A.R., Hussin, M.W., Mohd Tahir, M. and Aziah, N., 2013. Sulfuric acid resistance of blended ash geopolymer concrete. *Construction and Building Materials*, 43, pp. 80–86.

Aurora Construction Materials (ACM), 2014. *E-Crete: Engineering Properties and Case Studies*. [Pdf] Available at: http://www.acm.com.au/pdf/b69822_d3b9c3173f174bf59e9d3427892ab0c6.pdf [Accessed 23 January 2014].

Banah, U.K., 2014. *Introduction to Geopolymer Binders*. Ballyclare: Banah UK.

Benhelal, E., Zahedi, G., Shamsaei, E. and Bahadori, A., 2013. Global strategies and potentials to curb CO₂ emissions in cement industry. *Journal of cleaner production*, 51, pp. 142–161.

Boke, N., Birch, G.D., Nyale, S.M. and Petrik, L.F., 2015. New synthesis method for the production of coal fly ash-based foamed geopolymers. *Construction and Building Materials*, 75, pp. 189–199.

Climate Change Act 2008. (c.27). London: HSMO.

Cwirzen, A., Provis, J.L., Penttala, V. and Habermehl-Cwirzen, K., 2014. The effect of limestone on sodium hydroxide-activated metakaolin-based geopolymers. *Construction and Building Materials*, 66, pp. 53–62.

Davidovits, J., 1988. *Geopolymer Chemistry and Properties*. 1st International Conference on Geopolymer. Compiegne, France, 1–3 June 1988. Saint-Quentin: Geopolymer Institute.

Davidovits, J., 2002. 30 Years of Successes and Failures in Geopolymer Applications. Geopolymer Institute, *Geopolymer 2002 3rd International Conference*. Melbourne, Australia, 28–29 October 2002. Saint-Quentin: Geopolymer Institute.

Davidovits, J., 2008. *Geopolymer: Chemistry and Applications*. Saint-Quentin: Geopolymer Institute.

Davidovits, J., 2013. *Geopolymer Cement: A Review*. Geopolymer Institute: Saint Quentin.

Douglas, E., Bilodeau, A. and Malhotra, V.M., 1992. Properties and Durability of Alkali-Activated Slag Concrete. *Materials Journal*, 89(5), pp. 509–516.

Duxson, P., and Provis, J.L., 2008. Designing precursors for Geopolymer Cements. *Journal of the American Ceramic Society*, 91(12), pp. 3864–3869.

Duxson, P., Fernandez-Jimenez, A., Provis, J.L., Lukey, G.C., Palomo, A. and van Deventer, J.S.J., 2007. Geopolymer technology: The current state of the art. *Journal of Materials Science*, 42(9), pp. 291–2913.

Egan, J., 1998. *Rethinking Construction: Report of the Construction Task Force*. London: HMSO.

Federal Highway Administration, 2010. *Geopolymer Concrete*. Washington: FHWA.

Geopolymer Alliance, 2014. *The Geopolymerization Process*. [Online]. Available at: <http://www.geopolymers.com.au/science/geopolymerization>. [Accessed 9 December 2014].

Geopolymer Institute, 2014a. *What is a geopolymer? Introduction*. [Online] Available at: <http://www.geopolymer.org/science/introduction> [Accessed 21 September 2014].

Geopolymer Institute, 2014b. *Why Alkali-Activated materials are not geopolymers*. [Online] Available at <http://www.geopolymer.org/faq> [Accessed 22 September 2014].

Geopolymer Institute, 2014c. *Geopolymer cement for mitigation of Global Warming*. [Online] Available at: <http://www.geopolymer.org/applications/global-warming> [Accessed 22 September 2014].

- Geopolymer Institute, 2014d. *Geopolymer Cement*. [Online]. Available at: <http://www.geopolymer.org/applications/geopolymer-cement> [Accessed 11 December 2014].
- Geopolymer Institute. 2008. *Technical Data Sheet*, [online]. Available at: <http://www.geopolymer.org/science/technical-data-sheet> [Accessed 24 October 2014].
- Glasby, T., Day, J., Kemp, M. and Aldred, J., 2014. *Geopolymer Concrete for Durable Linings*. [Online] Available at: <http://www.tunneltalk.com/TunnelTECH-Jan2014> [Accessed 22 January 2015].
- Glukhovskiy, V.D., Gosstrojizdat Kiev, 1959. *Gruntosilikaty*. USSR, Patent 245 627 (1967), Patent 449894 (Patent Application 1958, granted 1974).
- Hawa, A., Tonnayopas, D., Prachasaree, W. and Taneerananon, P., 2013. Development and Performance Evaluation of Very High Early Strength Geopolymer for Rapid Road Repair. *Advances in Materials Science and Engineering*, 2013, pp. 1–9.
- Heath, A., Paine, K., Goodhew, S., Ramage, M. and Lawrence, M., 2013. The potential for using geopolymer concrete in the UK. *Proceedings of the Institute of Civil Engineers: Construction Materials*, 166(4), pp. 195–203.
- Hench, L.L., 1998. *Sol-Gel Silica. Properties, Processing and Technology Transfer*. New York: Noyes Publications.
- Husbands, T.B., Malone P.G. and Wakely, L.D., 1994. *Performance of concrete proportioned with Pyrament blended cement*. Technical Report CPAR-SL-94-2. US Army Engineer Waterways Experiment Station, Vicksburg, Mississippi.
- Intergovernmental Panel on Climate Change, 2014. *Climate Change 2014: Impacts, Adaption and Vulnerability*. Geneva: IPCC.
- Jayarajan, M.L.D., van Hullebusch, E.D. and Annachatre, A.P., 2014. Reuse options for coal fired power plant bottom ash and fly ash. *Reviews in Environmental Science and Bio/Technology*, 13(4), pp. 467–486.
- Jayaseher, C.A., Saravanan, G., Salahuddin, M. and Thirugnanasambandan, S., 2013. Development of Fly Ash based Geopolymer Precast Concrete Elements. *Asian Journal of Engineering*, 14(4), pp. 605–615.
- Komnitsas, K. and Zaharaki, D., 2007. Geopolymerisation: A review and prospects for the minerals industry. *Minerals Engineering*, 20, pp. 1261–1277.
- Krishnaraja, A.R., Sathishkumar, N.P., Sathish Kumar, T. and Dinesh Kumar, P., 2014. Mechanical behaviour of geopolymer concrete under ambient curing. *International Journal of Scientific Engineering and Technology*, 3(2), pp. 130–132.
- Kuenzel, C., Li, L., Vandeperre, L., Boccaccini, A.R. and Cheeseman, C.R., 2014. Influence of sand of the mechanical properties of metakaolin geopolymers. *Construction and Building Materials*, 66, pp. 442–446.
- Madlool, N.A., Saidur, R., Hossain, M.S. and Rahim, N.A., 2011. A critical review on energy use and savings in the cement industries. *Renewable and Sustainable Energy Reviews*, 15, pp. 2042–2060.
- McIntosh, A., 2012. *Geopolymer technology at work – Part 1: Pyrament blended cement*. [Online] Available at: <http://www.building-sustainability.com/?p=280> [Accessed 23 January 2015].
- McLellan, B.C., Williams, R.P., Lay, J., van Riessan, A. and Corder, G.D., 2011. Costs and carbon emissions for geopolymer pastes in comparison to ordinary Portland cement. *Journal of Cleaner Production*, 19, pp. 1080–1090.
- Nath, P. and Sarker, P., 2012. *Geopolymer concrete for ambient curing conditions*. The Australasian Structural Engineering Conference, Perth, Australia, 11–13 July 2012. Perth, Australia: Engineers Australia.
- Ozyildirim, C., 1994. A field investigation of concrete patches containing Pyrament blended cement. Virginia: Virginia Department of Transportation.
- Pan, Z., Sanjayana, J.G. and Kong, D.L.Y., 2012. Effect of aggregate size on spalling of geopolymer and Portland cement concretes subjected to elevated temperatures. *Construction and Building Materials*, 36, pp. 365–372.
- Provis, J.L. and van Deventer, J.S.J., 2009. *Geopolymers: Structures, Processing, Properties and Industrial Applications*. Cambridge: Woodhead Publishing.
- Rangan, B.V., 2010. *Fly Ash-based Geopolymer Concrete*. International Workshop on geopolymer Cement and Concrete. Mumbai, India, 7 December 2010. Mumbai, India: Allied Publishers Private Limited.
- Reed, M., Lokuge, W. and Karunasena, W., 2014. Fibre-reinforced geopolymer concrete for ambient curing for in-situ applications. *Journal of Materials Science*, 49(12), pp. 4297–4304.
- Saravanan, G., Jayaseher, A. and Kandasamy, S., 2013. Fly ash based geopolymer concrete – A state of the art review. *Journal of Engineering Science and Technology Review*, 6(1), pp. 25–32.
- Shi, C., 2003. Corrosion Resistance of alkali-activated Slag cement. *Advances in Cement Research*, 15(2), pp. 77–81.
- Siddique, B.C., Williams, R.P., Lay, J., van Riessan, A. and Corder, G.D., 2011. Costs and carbon emissions for geopolymer pastes in comparison to ordinary Portland cement. *Journal of Cleaner Production*, 19, pp. 1080–1090.
- Skvara, F., 2007. Alkali activated materials or geopolymers. *Ceramics-Silikaty*, 51(3), pp. 173–177.
- SureshThokchom, P.G. and Ghosh, S., 2009. Acid resistance of fly ash based geopolymer mortars. *International Journal of Recent Trends in Engineering*, 1(6), pp. 36–40.
- ul Haq, E., Padmanabhan, S.K. and Licciulli, A., 2014. Synthesis and characteristics of fly ash and bottom ash based geopolymers – A comparative study. *Ceramics International*, 40(2), pp. 2965–2971.
- Understanding Cement, 2012. *Clinker: reactions in the kiln*, [online]. Available at: <http://www.understanding-cement.com/reactions> [Accessed 8 December 2014].
- van Deventer, J.S.J., Brice, D.G., Bernal, S.A. and Provis, J.L., 2013. Development, standardization, and applications of alkali-activated concretes. *Geopolymer Binder Systems*, pp. 196–212.
- VicRoads Standard Specification, 2013. *Section 703 – General Concrete Paving*. Melbourne: VicRoads.
- Vijai, K., Kumutha, R. and Vishnuram, B.G., 2012. Effect of inclusion of steel fibres on the properties of geopolymer concrete composites. *Asian Journal of Civil Engineering*, 13(2), pp. 377–385.
- Wagners, 2012. *EFC: Earth Friendly Concrete*, [online] Available at: <http://www.wagnerscft.com.au/files/2613/4731/0397/Wagners-Earth-Friendly-Concrete.pdf> [Accessed 3 December 2014].
- Wallah, S.E., 2010. Creep behaviour of fly ash based geopolymer concrete. *Civil Engineering Dimension*, 12(2), pp. 73–78.
- World Business Council for Sustainable Development (WBCSD), 2009. *Cement Industry Energy and CO2 Performance – Getting the Numbers Right*. Geneva: WBCSD.
- Xu, H., and van Deventer, J.S.J., 2000. The geopolymerisation of aluminosilicate minerals. *International Journal of Mineral Processing*, 59, pp. 247–26.

The state of pothole management in UK local authority

Fauzia Saeed, Siti Qamariatul & Mujib Rahman

*Department of Mechanical, Aerospace and Civil Engineering,
Brunel University London, Uxbridge, UK*

Alan Woodside

Consulting Engineer, Lisburn, Northern Ireland

ABSTRACT: Road surface damage, particularly, potholes indicate an advance stage of deterioration. The rapid increase in the number of potholes in the UK road network is not only generating public concern, but also creating significant strain on maintenance budget. In this paper, results from a qualitative study focused on pothole management in local authority environment in the UK are presented. Local authorities in the UK are responsible for managing approximately 90% of the road network. The study involved developing an understanding on the current state of technical maturity of pothole repair, pothole management, including experts' opinion on future needs for research and development. In total, the response from eighty local authorities showed that despite good agreement on material selection, the definition of pothole together with the techniques for patch repair is widely variable resulting in inconsistent repair performance. Approximately 40% respondents indicated no record of repeat repair despite digital means of pothole recording either in a central database or in a localized system. It was found that approximately 87% respondents do not have a whole life cost model for patch repair. A strong opinion was expressed for further research and development on the repair process, overall management of the repair system and training to operatives.

Keywords: Local authority, Pothole management, Patch repair, Whole life cost.

1 FINANCIAL COST OF POTHOLE

Asphalt-surfaced roads account for 95% of the paved road network in the United Kingdom. Despite immense economic importance, there has been a deficiency of investment for decades to maintain and upgrade Britain's road network adequately. The lack of funding allied with repeated adverse weather and increasing traffic have created an alarming number of potholes, cracking, fretting and other types of deteriorations on aged asphalt roads.

In many cases, the presence of these distresses, particularly pothole, is the sign of advanced-stage of road deterioration (Wolters, 2003). These localised failed areas not only reduce ride quality, but also potentially create dangerous driving conditions. The situation has generated significant public dissatisfaction.

It is estimated by the Local Government Association (LGA) in UK that the repair bill for car damage by potholes could hit £1 billion in 2014. Another study by YouGov (2010) showed that businesses in England and Wales are suffering from poor road conditions with an incremental loss of £5 billion a year, which far outweighs the maintenance budget. The financial costs associated with potholes and deteriorating roads are not only limited to their repairs as they also affect road

users and the surrounding community. According to the ALARM survey 2013, the average cost to fill one pothole is £52, with a total of £99 million being spent in England. Various local authorities have given warnings regarding the increasing number of potholes, which could lead to the roads becoming unfit for purpose and eventually having to be closed down.

Due to the rapid increase in the number of potholes, and the funding deficit in road maintenance, it is hard to meet the demand for continuous maintenance on the pavements to meet road user expectations. Based on the ALARM report, in 2014/13, the total cost of pothole repairs was £106.7 million whereas in 2013/12 it was £112.7 million. However, despite reductions in pothole repair budgets in 2014, according to the ALARM Survey, there is an increase in investment in road infrastructure that will be available from April 2015.

The ALARM survey (2014) found that the expenditure figure includes an unexpected increase in the one-off "catch-up" cost, which targets how far the local road network is from being in reasonable condition. It is estimated that the expenditure cost in 2013 was £10.5 billion and in 2014 it has increased to £12 billion. Considering the importance of the problem, the Department of Transport have also created a challenge

fund of £200 million for additional pothole repair to put up investment upfront rather than wait for damage to occur.

Due to the current economic crisis, governments are implementing severe measures to identify ways to reduce road maintenance expenditure on potholes, and this will also be useful in formulating efficient future highway maintenance programmes. To examine how the financial cost of potholes can be reduced it is important to understand the current state of diagnostic techniques and repair practices in different local authorities, as UK local authorities maintain approximately 90% of the total road network.

2 PROBLEM STATEMENT

In an attempt to persuade the sector to work together and share best practice to ensure better road maintenance, the department of Transport in UK has developed a guidance document called Highway Maintenance Efficiency Programme (HMEP) in 2013. Although this guidance document covers general maintenance management of roads, pothole management still remains an area in highway maintenance management where significant subjectivity and variability exists in different local authorities. The variability can be found in defining and classifying potholes, material selections for pothole repair, diagnostic techniques to evaluate severity, and technical processes and standards used to carry out a durable repair.

It should be noted that managing local road networks is extremely challenging because of geography, road user characteristics, road types and maintenance practices and priorities involved. Hence it is likely that different local authorities will have different approaches to deal with pothole and patch repair aspects of road management. However, in order to have a consistent forecasting tool, it is important to minimise this variability, so that there are coherent practices, design standards and procurement methods to optimise the use of maintenance budgets.

The objective of this research is to develop an understanding on the present state of technical issues in tackling pothole problems, pothole recording, repair management processes, and need for research and development.

3 METHODOLOGY

Closed-ended questionnaire technique was adopted to carry out the research. Although this type of questionnaire does not allow expressing an alternative way of conveying views in writing, it gives an initial quantitative data, which can be used to create new theories and/or test existing hypotheses (Popper, 1959).

The survey was conducted between June and July 2014 using the Freedom of Information (FOI) request. The questionnaire is shown in Table 1. There are 13 questions to cover technical, management, and future need aspects. The advantages of using the FOI

Table 1. Questionnaire and response rate.

No	Question	Participants	Respondents	%Response
1	What is the usual thickness of a pothole in terms of depth?	80	73	91.25%
2	Do you operate a life cycle analysis (LCA) tool for pothole repair?	80	75	93.75%
3	What percentage of the recorded potholes was patched?	80	71	88.75%
4	Does the number of potholes in your network is growing annually?	80	77	96.25%
5	What is the percentage of repair that needs to be repaired again?	80	76	95%
6	Please state in percentage of annual maintenance budget that is assigned for repairing potholes	80	66	82.5%
7	Is there any availability of equipment to track the potholes in your region?	80	80	100%
8	What is the usual size of a patching of pothole?	80	75	93.75%
9	What materials are applied for pothole repair?	80	75	93.75%
10	What is the possible reason for the failure of pothole patch?	80	71	88.75%
11	Do you require more information on	80	74	92.5%
12	If additional funding was given, what would be the significance areas raised?	80	73	91.25%
13	What category of maintenance are you applying for pothole patching?	80	76	95%



Figure 1. Distribution of local authority participated in the study.

technique are that it is factually correct as well as cheaper compared to a telephone interview, and the actual response time of participants is fast, normally within 21 days (3).

The questionnaire was sent to approximately 80 local authorities across the United Kingdom. The local authorities were selected based on the geographic locations such as urban, semi-urban, and rural, the size of road networks and traffic level. The distributions of the survey respondent are shown in Figure 1. The red dots plotted on the map indicate the location of local authorities or organisations that responded to the survey. Out of 80, eight respondents shared their experience in terms of their opinions and understanding, which allows this survey to produce a comprehensive assessment. These eight respondents sent their answers in a word document via e-mail. Unfortunately, it was not possible to show all 80 respondents in Figure 1,

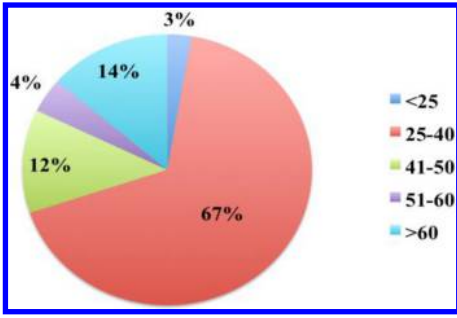


Figure 2. What is the usual thickness (mm) of a pothole in terms of depth?

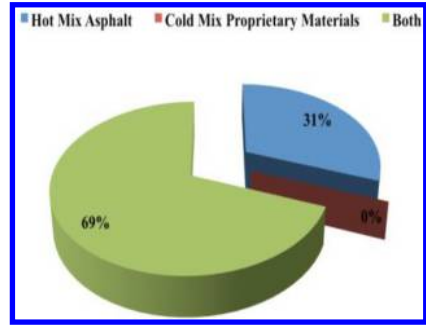


Figure 4. Material applied for patch repair.

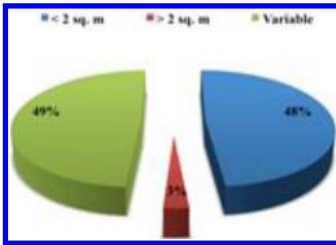


Figure 3. Typical size of patch repair.

because some of the organisations that responded did not specify details of their location. It should be noted that, as some of the answers were made through a word report and a few respondents answered the surveys partially, the response rate for individual questions was not 100%.

Despite that, the overall response rate for each question, as shown in Table 1, was more than 88%, which is considered sufficient to develop a good understanding on current state of pothole management in the UK.

4 RESULTS AND ANALYSIS

The questions and corresponding responses were grouped into three main categories covering technical, management, and future needs aspects. The results are discussed in the following sections.

4.1 Technical aspects

Question numbers 1, 8, 9 and 10 were used to evaluate the current state of technical practices involve in pothole diagnostic and repair process. The results are shown in Figures 2, 3, 4 and 5.

Figure 2 illustrates the typical depth of a localised depression on the road surface that authorities consider to be a pothole. It can be seen that 67% of respondents considered 25–40 mm is a typical depth, whereas 12% selected 40–50 mm and 14% considered greater than 60 mm to be a typical depth. It should be noted that according to the ADEPT report (ADEPT, 2010), a pothole is considered “shallow” when the depth is less than 25 mm and “deep” when depth is greater than 40 mm.

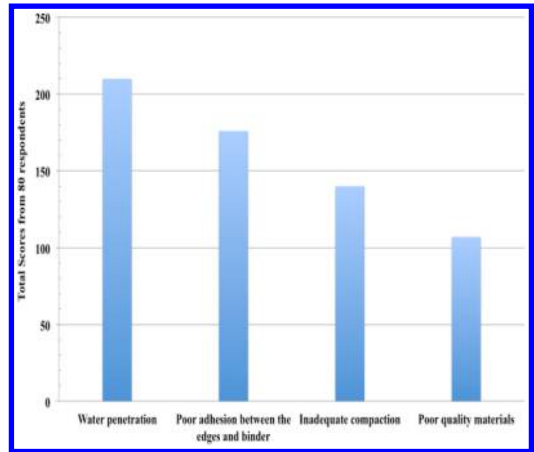


Figure 5. Total scores for the possible reasons for the failure of patch repair (1 = least likely reason, 4 = most likely reasons, score is a weighted calculation. Items ranked first are valued higher than the following ranks; the score is the sum of all weighted rank counts.)

Although the question did not specifically ask how councils separate deep and shallow potholes, the variability of responses suggests that there are discrepancies in pothole definition. In terms of typical area of patch repair, 48% of respondents (Figure 3) answered <math>< 2 \text{ m}^2</math>, while another 49% respondents said the extent of patch repair is variable. It is not clear why there is variability and what methods are utilised to define the extent of repair.

Figure 4 shows the materials used for pothole repair, where 69% answered both hot mix and proprietary cold mix, while approximately 24 local authorities (31% of respondents) used hot mix exclusively. It appears that many local authorities are moving towards permanent repair using hot mix material. In terms of patch repair failure (Figure 5), the majority of the respondents identified ‘Water penetration’ as the primary reason. The other major factors were identified as ‘Poor adhesion between the edges and binder’, ‘Inadequate compaction’ and the use of ‘Poor quality materials’. All of these factors are well known contributory elements in pavement deterioration and more

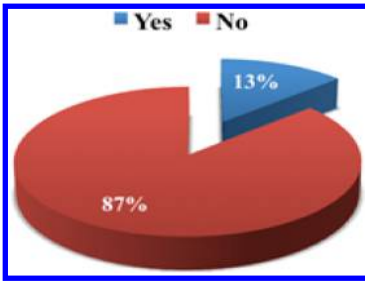


Figure 6. Do you operate a life cycle analysis (LCA) tool for pothole repair?

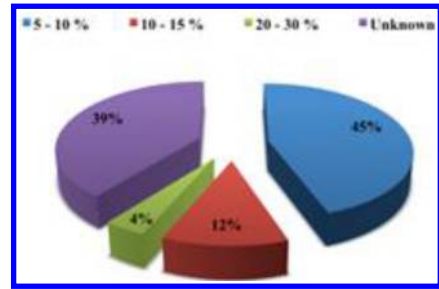


Figure 9. Percentage of repair that require repair again.

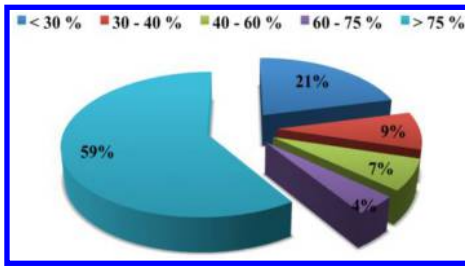


Figure 7. What percentage of the recorded potholes was patched?

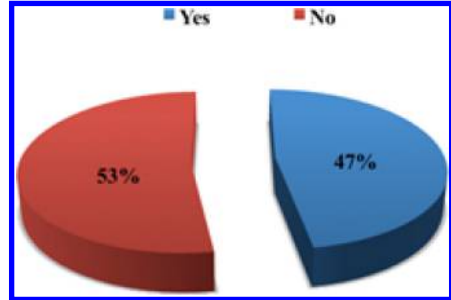


Figure 10. Is there any availability of equipment to track the potholes in your region?

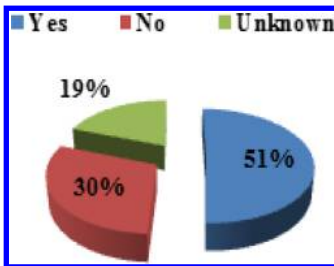


Figure 8. Does the number of potholes in your network is growing annually?

research and development is required in the context of patch repair.

4.2 Pothole and patch repair management

Management aspects of pothole recording, and repair management are examined in Questions 2, 3, 4 and 7 in Table 1. The results are shown in Figures 6 to 9.

As Life Cycle Assessment (LCA) is increasingly gaining importance in design and built projects, a question was asked whether local authorities are operating LCA in pothole maintenance activity. Figure 6 shows that overwhelmingly 87% answered no, while only 13% answered 'yes'. It will be useful to review LCA tools for those 13% respondents, to see whether the practice could be more widely implemented in other local authorities.

When asked what percentage of recorded potholes were repaired in the last year, as shown in Figure 7, 51% of respondents answered that 75% of reported

potholes were repaired, although a significant proportion (21%) said less than 30% of the reported potholes were repaired. This shows a clear maintenance backlog and the backlog is different in different local authorities.

As expected, 51% of respondents (Figure 8) answered that the number of potholes is increasing annually, while 19% said "do not know", but interestingly 30% reported that the number of potholes is going down in their network. A further in-depth investigation would be useful to evaluate the reasons for this pothole reduction, especially when there is evidence of maintenance backlogs. In a supplementary question, when asked what percentage of repairs are repeat repairs, the results as presented in Figure 9 show that 45% of respondents answered 5–10%, 12% said 10–15%, and 3% (three local authorities) answered that 20–30% require repeat repair, while a significant proportion 39% answered "Unknown". Clearly, there are variations in terms of pothole repair quality, recording and overall management. One of the respondents stated that when the government decreases the cost of highway maintenance, that has a direct impact on limiting services like road lighting, vegetation control and road cleaning and a decrease in the renewal and repair of highway resources including pathways, cycle tracks, bridges, carriageways, tunnels and borders (Gould, Parkman & Buckland, 2013).

In addition, as shown in Figure 10, 53% of respondents replied that there is no equipment available to track potholes, but 47% replied that there are means of recording potholes in their regions. When asked what types of maintenance they follow for pothole



Figure 11. What category of maintenance are you applying for pothole patching?

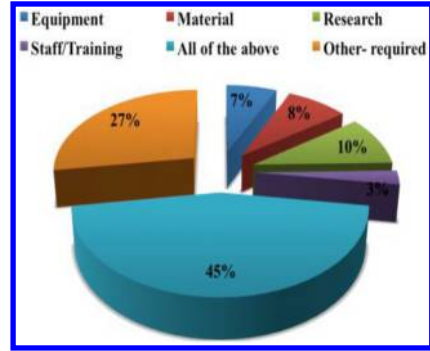


Figure 14. Do you require more information on pothole and patch repair related matter?

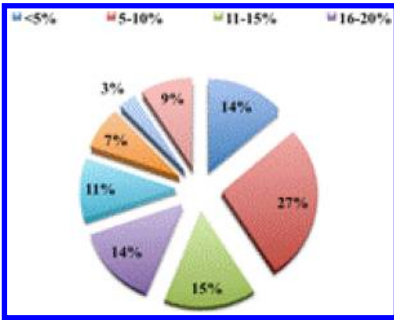


Figure 12. Please state in percentage of annual maintenance budget that is assigned for repairing potholes.



Figure 13. What category of maintenance are you applying for pothole patching?

patching, as illustrated in Figure 11, 59% of respondents answered ‘Reactive maintenance’, 25% chose ‘Planned maintenance’ and the remaining 16% of respondents picked ‘Routine maintenance’.

In order to evaluate dedicated funding allocation for patch repair, the percentage of annual maintenance spent on pothole repair, the priority of patch repair and records of additional costs due to repeat repair, results are gathered from the responses of Questions 6 and 13. The outcomes are presented in Figures 12 and 13.

Figure 12 shows that 27% of respondents replied that 5–10% of the annual maintenance budget is assigned for repairing potholes, while 14% of respondents answered that 16–20% of the maintenance

Comparison of different materials	24.3%	18
Development of new or innovative materials	46.0%	34
Development of alternative methods	37.8%	28
Improved maintenance (patching) management?	23.0%	17
Improves guidance, training and specifications	13.5%	10
Improved patching standards	14.9%	11
Mechanism of pothole formation	8.1%	6
Mechanism of pothole progression	9.5%	7
Prediction of pothole existence	23.0%	17
The way maintenance records are kept and what they contain	16.2%	12
other-required	31.1%	23
Total		74

Figure 15. If additional funding were given, what would be the significant areas to fund?

budget is spent on pothole repair. As shown in Figure 13, 59% of the budget is spent for pothole repair is “Reactive maintenance”, 25% is “Planned maintenance” and the rest with 16% selected as “Routine maintenance”. This variability will clearly influence the quality of repair and ultimately the cost of the repair process.

4.3 Future needs

The results are drawn from Questions 11 and 12 and the outcomes are presented in Figures 14 and 15.

According to Figure 14, 45% of respondents picked “All of the above” indicating that more investment is needed on repair material, repair equipment, research and training of operatives. A more specific answer could be found in Figure 15, where 46% of

respondents said improved material, 38% said alternative method of repair and 23% of respondents wish to have improved maintenance management and pothole prediction methods.

Other specific areas are improved guidance, training, understanding of pothole formation and better information management. All these areas require further research and development to optimise pothole repair cost.

5 FURTHER DISCUSSION

After analysing the questionnaire responses, a further in-depth assessment was carried out by examining eight respondents who shared their opinions and experience. Regarding formation of potholes, one participant stated that “the main factor is that most of the local road network is made up of evolved roads. Unlike engineered roads which were constructed after WW2 when carrying out structural maintenance only the top part of the pavement can be repaired which fails to address the main structural problem.” It was also added that the main factor that was important in preventative maintenance was intervening at the right time before they completely deteriorate.

Further comments were received concerning the factors delaying preventative maintenance and it was quoted that “there was not enough funding at the required level. With the current available resources it was difficult to balance resource allocation between the structural reactive maintenance and preventative maintenance.” It was also added “as almost all the money in highway maintenance came from the government, insufficient funding for highway maintenance had resulted in the backlog of repairs. This has had the significant effect of having fewer roads repaired and other roads which are not repaired deteriorate further which increases future repair costs”.

6 SUMMARY AND CONCLUSIONS

The research sample was collected from a closed-ended questionnaire survey; therefore the problem of wider economic cost to the community and country could be not identified. In addition, as local authorities manage different lengths and types of road networks, comparing the number of potholes repaired will not be an accurate comparison. However, based on this research the following points could be summarised.

- 75% respondent said with 25–50 mm as a typical depth of pothole, 3% said less than 25 mm as a pothole and 14% said greater than 60 mm is a pothole. Despite official guidance from ADEPT to define shallow and deep pothole, there appears to be still variances in defining the depth of localised surface damage as a pothole.
- Approximately 50% respondents said the size of patching is variable although 48% stated typical patch repair is less than 2 m². It is expected that

depending on the locations and network there will be degree variability in different LA. However, it is important to develop a consistent methodology to determine the extent of patch repair.

- 70% of the respondents stated hot mix asphalt (HMA) and propriety cold mix as a preferred material, although 31% respondents exclusively use hot mix as a preferred material. It shows that most local authorities are aware of hot mix asphalt material to use for permanent repair whilst cold mix asphalt is for temporary repair.
- As patching has become more expensive, and pressure to repair potholes to maintain roads in a safe and serviceable condition has increased, temporary repairs are often conducted. These temporary repairs are likely to cause repeat repairs.
- 87% participants do not operate life cycle analysis. It will be useful to review LCA tools for those 13% respondents who operate LCA, to consider whether the system could be more widely implemented in other local authorities.
- 60% of the respondents have the record for repeat repair, while 40% of the respondents do not have. It is likely that many LA are conducting large amount of repeat repair, which could be otherwise done permanent rehabilitation, saving substantial amount of repair cost. It is therefore important to implement a systematic recording system. A comprehensive and integrated system together with investment in technological development and life cycle analysis will optimum maintenance costs.
- In terms of maintenance management, 59.2% respondents answered reactive maintenance for pothole repair and 25% choose planned maintenance when applying pothole patching, whereas 11% use patching as routine, planned and reactive maintenance. Clearly, there are discrepancies in tackling pothole problem. It is important to develop a consistence framework for pothole management.
- Most local authorities have limited budget for pothole repair, ranging from 5% to 20%.
- Nearly 70% answered more research is needed together with staff training, better materials and equipment. The remaining 27% answered other information is needed, although specific areas were not mentioned. If additional funding is given, 46% of the respondents wanted to spend on improved repair equipment, better material, research to develop a durable repair and training to operatives.

It is apparent from this study that most local authorities do challenge pothole problems seriously despite significant variances in terms of definition, repair technique and material used. An initiative should be taken to minimise these differences.

Finally, climate change in the UK will lead to more unpredictable weather conditions, which will lead to more road damage and, consequently, an increase in repair costs. Therefore, it is important to invest in this aspect for a safe, efficient and reliable road network.

REFERENCES

- Adept. 2010. Potholes and Repair Techniques for Local Highways. Atkins.
- Burningham, S. & Stankevich, N. 2005. Why road maintenance is important and how to get it done, Transport Notes: Operational Guidance: Washington, DC.
- Department for Transport, 2014. Gearing up for efficient highway delivery and funding. London: Crown.
- Gould, E., Parkman, C., & Buckland, T. 2013. The Economics of Road Maintenance, London: ADEPT.
- Highways Agency. 2014. Potholes: reporting, damage claims and repairs. Available from: <<http://www.highways.gov.uk/our-road-network/land-property-and-compensation/claims-for-damage-caused-by-potholes/>> [Accessed on 15th November 2014]
- HMEP. 2014. Prevention and a better cure: Potholes review. London: Crown.
- HMEP. 2013. Potholes review: Prevention and a better cure. A follow-up report. London: Queen's Printer and Controller of Her Majesty's Stationery office.
- HMEP. 2012. Pothole Review: Prevention and a better cure. A follow-up report. London: Queen's Printer and Controller of Her Majesty's Stationery Office.
- HMEP. 2011. Potholes Review: Highways Maintenance Efficiency Programme. Progress Report. London: Queen's Printer and Controller of Her Majesty's Stationery office.
- Popper, K. The Logic of Scientific Discovery (1959), reprinted (2004) by Routledge, Taylor & Francis.
- The Annual Local Authority Road Maintenance (ALARM), survey 2011, AIA press and information office, HMPR limited, Buckingham court, London SW1E 6PE.
- University of Leeds. 2003. Treatment of Maintenance: Part of Toolkit for the Economic Evaluation of World Bank Transport Projects. Available from: <<http://www.its.leeds.ac.uk/projects/WBToolkit/Note8.htm>> [Accessed on 14th November 2014].
- Wilson, T.P. & Romine, A.R., 1999. Materials and procedures for repair of potholes in asphalt-surfaced pavement – Manual of practice, Illinois: Federal Highway Administration.

Use of 3D modeling to assess pothole growth

G. McQuaid, P. Millar & D. Woodward
Ulster University, Newtownabbey, Northern Ireland

ABSTRACT: This paper considers the use of 3D modeling to quantify the growth of pot holes. These are a common problem around the world and cause problems with the road user and those involved with its maintenance. Assessing the size of a pothole, or being able to understand their growth has not really been considered in the literature. 3D modeling techniques based on stereo photogrammetry were used to quantify 2d and 3d parameters of potholes. The experiment was carried out the laboratory. Roller compacted slabs were prepared and an artificial pothole created on its surface. This was photographed and a 3D model created. The artificial pothole was enlarged and the process repeated. At each stage the actual diameter, circumference and volume of the hole was determined. The 3D models were analyzed using DigitalSurf MountainsMap software. Good correlation was found between parameters from the 3d model and those measured. It is proposed that this method gives a simple and robust method to better understand potholes.

1 INTRODUCTION

A pothole is a localized road surface breakdown caused by factors including winter freeze-thaw weather conditions, moisture presence and inappropriate pavement construction. Last year over 1.7 million potholes were repaired in England at a cost of £90.9 million (ALARM, 2014). The carriageway maintenance backlog was approximately 12 years. The ALARM report concluded that research is required to make better use of funding. Although there has been work carried out into why they form and how they may be repaired relatively little research has considered how their physical parameters may be quantified and so better understood.

A pothole is a type of road surface texture. There are different scales of texture classified on wavelength i.e. microtexture, macrotexture, megatexture and surface roughness. These texture scales influence tyre-pavement interaction including skid resistance, surface drainage, surface noise and rolling resistance. Microtexture relates to the roughness of aggregate particles and contributes to skid resistance. Macrotexture relates to bulk removal of surface water, noise generation and rolling resistance. Pothole defects are referred to as examples of megatexture with wavelengths in the range of 50 mm to 500 mm.

Methods of texture measurement have been available for many years. For example, the PSV test for aggregate microtexture and the use of the volumetric patch technique for macrotexture. 2D laser technologies have been developed and used on devices such as TRACS for traffic-speed condition surveying. Research is now evaluating the use of 3D modeling and areal texture parameters to better understand road surface texture at its different wavelengths.

There are different techniques to create the 3D model e.g. using laser devices or stereo photogrammetry. Researchers such as Dondi et al (2010) and Sagiorgi (2012) have used laser devices to investigate change in surface texture roughness and potential collection of surface water. Although laser devices can produce good 3D models they tend to be quite slow and require expensive equipment. In contrast, stereo photogrammetry can use an ordinary SLR camera and the models are quite quick to produce.

A version of stereo photogrammetry, called close range photogrammetry (CRP) is used in this paper to produce 3D models of potholes for analysis. CRP has many potential applications in highway engineering for pavement surface texture investigation, monitoring and maintenance. Some of these applications have been developed by Millar (2012) and McQuaid (2015). For example, Millar and Woodward (2012) found good correlation with the volumetric patch technique derived Mean Texture Depth (MTD).

This paper summarizes an application of CPR which compared pothole data such as diameter, circumference, depth and volume determined from manual measurement of the actual pothole and from analysis of the pothole 3D model.

2 METHODOLOGY

The research methodology involved a number of stages. This included the application of the CRP method to make 3D models, the manufacture of potholes in the laboratory, manual measurement of pothole parameters and determining pothole parameters from the 3D models.



Figure 1. Calibrated steel framework of control points.

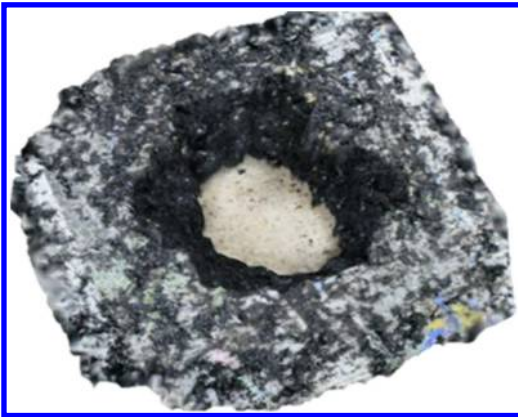


Figure 2. Example pothole TIN created and displayed in Zephyr.

2.1 Application of the CRP method

Triangular Irregular Network (TIN) 3D pothole models were made using 3DF Zephyr photogrammetric software. Zephyr requires multiple images to be captured of the pothole with at least 60% forward and 30% side overlap across the images. A Canon 6D EOS SLR camera with a 100 mm macro lens was used. The camera was handheld and used natural lighting conditions during image capture.

A steel framework of control reference points was used for scale. This is shown in Figure 1. The distances between individual control points were calibrated to two decimal places using a digital micrometer gauge. The use of this control framework allowed recovery of surface elevation and orientation for the created TIN. For the 3D capture of potholes in-situ, the use of a steel rule is sufficient. Following capture the images were imported into 3DFLOW 3DF Zephyr Pro photogrammetric software with relevant calibration documents. The use of filtering was minimized.

An example TIN of a pothole is shown in Figure 2, as displayed in Zephyr. The TIN file was then converted to a XYZ file format using MeshLab and exported to Digital Surf MountainsMap 7 spatial information

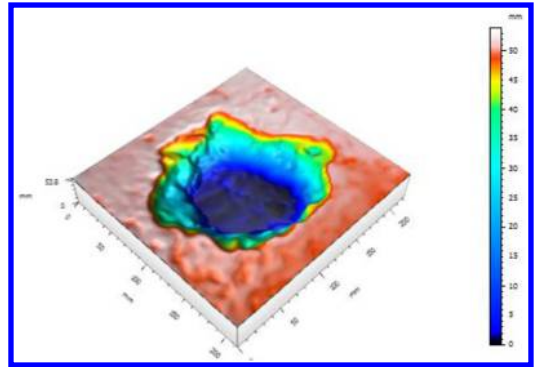


Figure 3. Color depth classified TIN of example pothole TIN displayed in MountainsMap.

software for analysis. The TIN mesh underwent initial operators to prepare the surface for analysis. This included leveling of the surface with respect to a least squared plane. An Area of Interest (AOI) was selected to remove redundant data from the TIN. Figure 3 shows a TIN that has been color depth classified in MountainsMap. The color depth classification is used to emphasize change in the z-axis elevation.

2.2 Assessment of a manufactured pothole

The laboratory 3D modeling experiments used potholes that were made in the laboratory. This used poorly compacted slabs of asphalt concrete made with 160/220 pen grade bitumen that were $275 \times 275 \times 40$ mm in size. They poorly compacted using a hand roller in the steel control framework as shown in Figure 1.

A 3D model of the AC specimen was made. A number of coarse aggregate particles were removed from the center of the specimen using a screwdriver to represent an embryonic pothole. A second 3D model was created of the specimen. The embryonic pothole was enlarged using a hammer and chisel and 3D models made at each stage of enlargement.

The secure positioning of the specimen in the control framework ensured consistent orientation of the captured TINs with time as the pothole got larger. Stage 0 refers to the original specimen surface. Stage 4 refers to the pothole at its maximum size. Figure 4 shows the TIN for the pothole at Stage 4.

Figure 5 presents a composite of pseudo color images for the manufactured potholes for Stages 0, 1, 2, 3 and 4 displayed in MountainsMap. Manual measurements were taken at each stage. Its diameter was recorded at three locations and an average calculated. A digital micrometer gauge was used to measure maximum depth.

A modified sand replacement method (BS 1377) was used to determine the volume of the pothole. A container of sand with a known weight was used to infill the pothole. The weight of sand not required was used to calculate the weight of the sand used. This



Figure 4. Laboratory manufactured pothole TIN at Stage 4, created and displayed in Zephyr.



Figure 6. Real in-situ pothole with steel rules for control purposes.

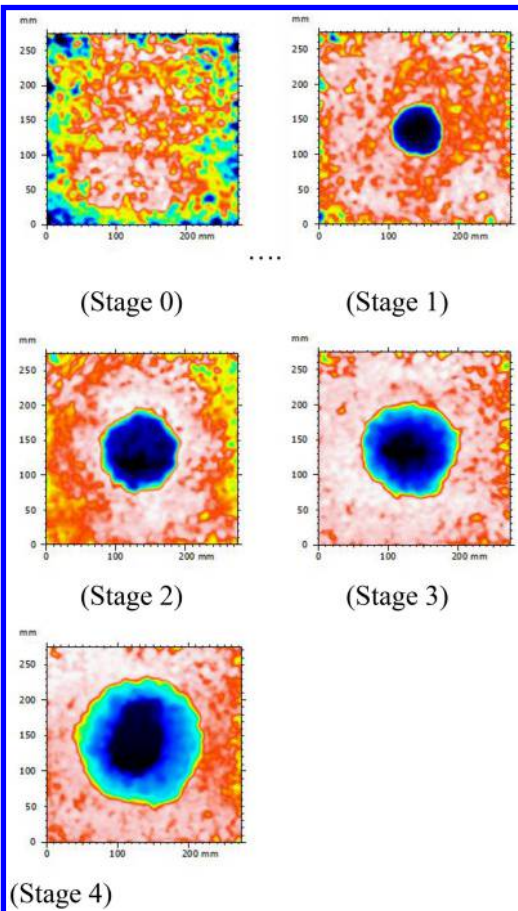


Figure 5. Comparison of 2D MountainsMap images for laboratory manufactured pothole at Stages 0, 1, 2, 3 and 4.

weight along with its corresponding density gave an approximate volume for the pothole. These manually recorded dimensions enabled comparisons to validate the dimensions obtained from MountainsMap analysis of the 3D model.

2.3 CRP assessment of a real pothole

The practicality of the CRP method was validated using real potholes. Figure 6 shows an example pothole. The two steel scale rules are used for control purposes. Images were taken using two devices i.e. the 20 mega-pixel Canon 6D SLR EOS camera used in the laboratory investigation and an Apple iPhone with 5 megapixel camera. Although the iPhone camera takes an image with less resolution these types of device are readily available and may offer better practicality for the user.

3 RESULTS

Many types of 2D and 3D surface texture parameter measurement, in accordance with BS EN ISO 25178-2 (2012), are possible using the MountainsMap software. For the purposes of this paper only a few of the possible methods were used. This included a volume of a hole or a peak study. This study allows the volume and maximum depth of a determined hole/peak to be calculated along with the surrounding redundant material. Figure 7 shows an example output of this study procedure. In this method, the user must select the edge of the pothole.

The distance measurement study was used to determine the diameter of the pothole for each TIN. Similar to the manual measurement, the diameter was recorded at three locations along the pothole TIN circumference and an average determined. Similar to the previous study this can also be subjective.

Table 1 presents the manually measured average diameter, maximum depth and volume data for Stages 1 to 4. Table 2 presents the same parameters measured from the corresponding TINs using MountainsMap. No measurements were recorded for the Stage 0 TIN as the pothole had not been formed.

The Abbott-Firestone curve (AFC) study was used to determine the volume of the void in the formed pothole. The AFC is a volume ratio based curve. An example AFC curve is shown in Figure 8.

The curve is divided into four volume parameters; volume of peak material (V_{mp}), volume of core

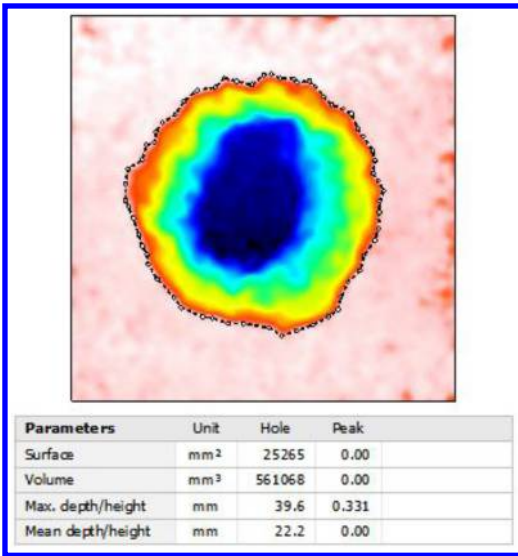


Figure 7. Volume of a hole or a peak study for Stage 4 pothole TIN.

Table 1. Manual measurements for the laboratory manufactured pothole.

Stage	Average Diameter (mm)	Maximum depth (mm)	Volume (mm ³)
0	—	—	—
1	35.67	10.00	5178
2	111.33	23.25	159142
3	130.00	31.00	234547
4	174.00	40.00	589482

Table 2. MountainsMap measurements for the laboratory manufactured pothole.

Stage	Average Diameter (mm)	Maximum depth (mm)	Volume (mm ³)
0	—	—	—
1	34.47	7.04	3373
2	111.33	23.20	129163
3	129.00	32.90	220071
4	173.00	39.60	561068

material (Vmc), volume of core voids (Vvc) and volume of valley voids (Vvv). The software adopts upper p (10%) and lower q (80%) default Areal Material Bearing Ratio (AMBR) limits. These are adjustable and allow investigation into how the surface texture of the pothole changes with depth.

The AFC Vvc value approximates the volume of the pothole. By adjusting the lower p and upper q AMBR limits, the void volume/loss of material can be determined. Figure 9 presents the change in Vvc with depth into the surface texture for all five stages

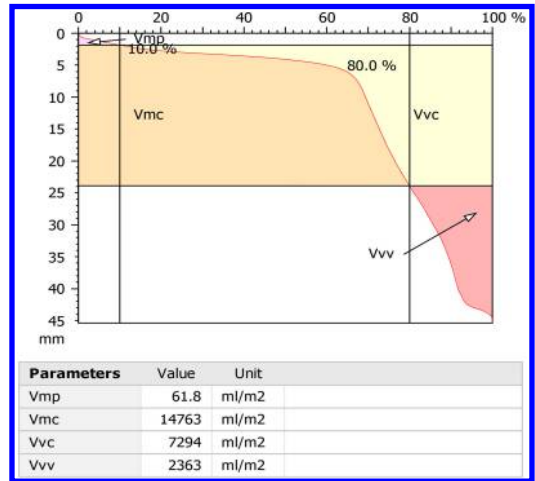


Figure 8. AFC for stage 4 pothole defect TIN displayed in MountainsMap.

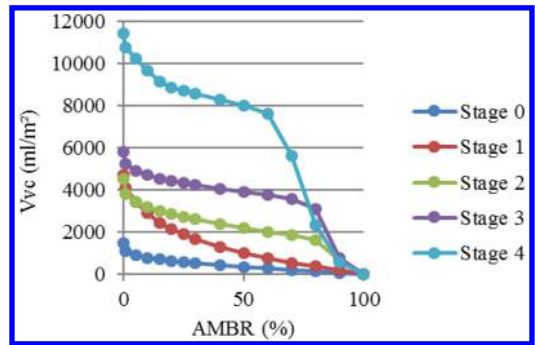


Figure 9. Vvc against AMBR for all five stages, derived from the AFC.

of the laboratory manufactured pothole. The prominent kink in the AFC plots shown in Figure 9 illustrate development of the pothole as it gets larger.

Single or multiple profiles can be extracted from the pothole TIN in MountainsMap. A step height calculation study can be carried out on the profile. An example is displayed in Figure 10. This study determines multiple steps across a profile and calculates parameters correspondingly. The step height calculation in Figure 10 reports a maximum depth of 38.9 mm for the pothole model. This compares with the compacted depth of 40 mm for the test specimen.

Figure 11 shows the real pothole example modeled in Zephyr using the images taken using the SLR camera. Table 3 compares the average diameter, maximum depth and volume for this pothole based on images for the SLR camera and the iPhone camera.

4 DISCUSSION

The data recorded manually was compared with that from the 3D models. Figure 12 plots the pothole

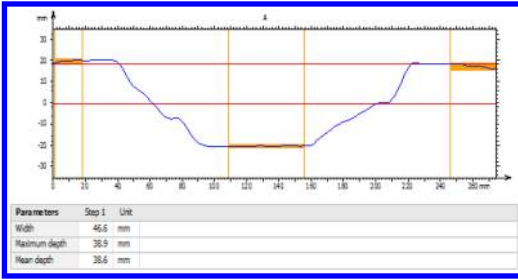


Figure 10. Step height calculation study for Stage 4 pothole TIN, in MountainsMap.



Figure 11. Real pothole TIN captured using Canon 6D camera device created and displayed in Zephyr.

Table 3. Real pothole measurements recorded using MountainsMap for both camera devices.

Camera	Average Diameter (mm)	Maximum depth (mm)	Volume (mm ³)
Canon 6D	217.00	63.00	1105122
iPhone	215.67	61.50	10919014

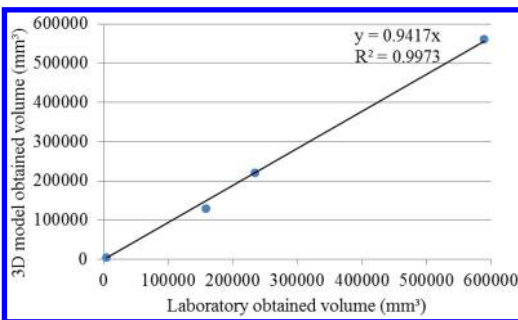


Figure 12. Comparison of pothole volume data for Stages 1, 2, 3 and 4.

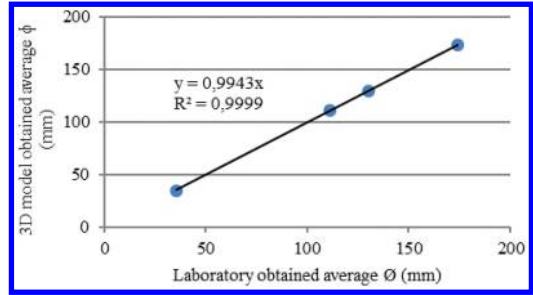


Figure 13. Comparison of pothole diameter data for Stages, 1, 2, 3 and 4.

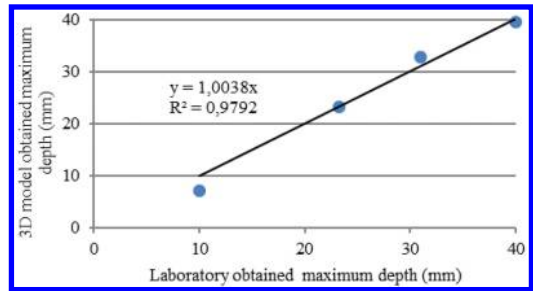


Figure 14. Comparison of pothole maximum depth data for Stages 1, 2, 3 and 4.

volume data from the volume of a hole or a peak study and the modified sand replacement test. This shows a linear relationship with a R^2 of 0.9973.

The plot shows a slight under-recovery for the 3D model data compared to the modified sand replacement method. This may be due to the difficulty of capturing texture at increasing depths into the surface. However, it is considered that this under-recovery is insignificant in relation to the scale of the texture being investigated. Figures 13 and 14 compare the MountainsMap TIN and manually measured average diameter and maximum depth data respectively.

Good correlations were found for both sets of data. For example, the slab thickness was 40 mm, the 3D model data in Table 2 showed the maximum depth of the pothole to 39.6 mm. The example step height calculation study presented in Figure 10 recorded a maximum depth of 38.8 mm. The variation in these recorded depths is insignificant in terms of the scale of the surface texture being investigated.

This agreement of different methods of measurement and analysis gives confidence in the use of 3D modeling. The good correlations between pothole volume, average diameter and maximum depth confirm the accurate recovery of surface texture with the use of the CRP method.

Figure 9 shows the AFC derived parameter V_{vc} plotted against the corresponding AMBR for each pothole stage. With the upper limit q maintained at 100%, the lower limit p was altered. When p is equal to 0% AMBR, maximum V_{vc} is found. At this point the limit

p is set at the top of the surface texture; therefore the full pothole falls within the core zone of the AFC profile.

Stage 4 recorded the highest V_{vc} , with Stage 0 demonstrating the smallest. The remainder of Figure 9 demonstrates how the volume of voids i.e. loss of material decreases with depth into the surface. Despite the expected relationship shown in Figure 9, Stage 1 and 2 do not fully agree with the trend at low AMBRs. At 0 to 10% AMBR, Stage 2 is expected to have a higher V_{vc} parameter, as its TIN represents an increased volume of a pothole. It was suspected that this initial variation at 0 to 10% AMBR is due to the presence of surface noise in the Stage 1 TIN.

With further consideration of the AFC, this did not appear to be the case. Therefore it was concluded that it was due to the way in which the pothole was made larger using the hammer and chisel. Between Stages 1 and 2 the pothole defect was increased horizontally and vertically. Between Stages 2 and 3 the pothole defect was predominantly increased vertically.

The real pothole had a more irregular shape compared to the one formed in the laboratory. Table 3 shows good comparison between the captured TINs for the SLR and iPhone devices. The lower resolution images of the iPhone had a minimum effect at the scale of texture being investigated.

5 CONCLUSION

The non-contact use of 3D modeling using Close Range Photogrammetry has been shown as an accurate method of analyzing manufactured potholes in a controlled laboratory environment. Strong linear relationships were found between diameter, circumference, depth and volume datasets. The AFC analysis demonstrated how volume changes with depth and with time.

The findings of the investigation show that 3D modelling using CRP offers a method to better understand real pothole. This new type of data can have a wide range of application from quantify pothole growth to optimising the maintenance of pothole defects of our road network within reduced budgets.

REFERENCES

- Asphalt Industry Alliance. 2014. Annual Local Authority Road Maintenance Survey. London.
- British Standards Institution. 1990. BS 1377-9: 1990 Methods of test for soils of civil engineering purposes – Part 9: In-situ tests, London.
- British Standards Institution. 2012. BS EN ISO 25178-2: 2012 Geometric product specifications (GPS) – Surface texture: Areal terms, definitions and surface texture parameters, London.
- Birch, J.S. 2006. Using 3DM Analyst Mine Mapping Suite for rock face characterization. In F. Tonon & J. Kottenstette (eds), *Laser and Photogrammetric Methods for Rock Face Characterization*.
- Chandler, H., Fryer, J. G. & Jack, A. 2005. Metric Capabilities of Low Cost Digital Cameras for Close Range Surface Measurement. *The Photogrammetric Record*, Vol. 20, No. 109: 2–26.
- Design Manual for Roads and Bridges. 2008. Volume 7, Pavement Maintenance Assessment, Section 3, Part 2.
- Dondi, G., Simone, A., Lantieri, C. & Vignali, V. 2010. Characterization of pavement surface texture using 3D Laser scanner technique. Proceedings of the 11th International Conference on Asphalt Pavement. August 1–6, Nagoya: Giappone.
- Flintsch, G.W., de Leon E., McGhee K. K., & Al-Quadi, Imad L. 2003. Pavement Surface Macrotexture Measurement and Application, Transportation Research Record, Journal of the Transportation Research Board, TRB, National Research Council, Washington D.C., Vol. 1860, pp. 201–209.
- McQuaid, G. 2015. Development of non-contact 3D measurement of areal pavement texture parameters. PhD Thesis, School of Built Environment, Ulster University.
- Millar, P. 2013. Non-Contact Evaluation of the Geometric Properties of Highway Surfacing Textures Using Close Range Photogrammetry. PhD Thesis, School of Built Environment, University of Ulster.
- Millar, P., Woodward, D. & McQuaid, G. 2012. Close up and Dirty, an Evaluation of the Character of Asphalt Surfacing in-situ Using Close Range Photogrammetry. MAIREPAV7, 7th International Conference on Maintenance and Rehabilitation of Pavements and Technological Control, Auckland, New Zealand, August 28–30.
- Sangiorgi, C., Bitelli, G., Lantieri, C., Irali, F. & Girardi, F. 2012. A study on texture and acoustic properties of cold laid microsurfacings. 5th International Congress of Sustainability of Road Infrastructure, Rome, Italy 29–31 October.

Recent modifications to the 1993 AASHTO equations for forward-calculating subgrade and pavement moduli

M. Livneh

Technion-Israel Institute of Technology, Department of Civil and Environmental Engineering, Haifa, Israel

ABSTRACT: Alternative methods of deriving layered elastic properties from pavement deflections consist of closed-form formulas to obtain the pavement structure and subgrade modulus directly. These calculation techniques, termed forwardcalculation, are used by several agencies around the world. Besides AASHTO 1993, which does not allow calculating subgrade and pavement resilient moduli in a fully direct manner, newer forward-calculation techniques include YONAPAVE and EVALIV. This paper suggests modified replacement equations, called AASHTOLIV, which like the old ones, still present basic deviations from the true elastic properties of the pavement structure and pavement subgrade. The suggested corrective equations take into account the influence of (a) errors induced in the forward-calculations as a result of correlative equations developed for the two-layer model and (b) depth to bedrock measured from the subgrade surface. The rate of depth to bedrock reveals a significant influence on forwardcalculated subgrade modulus and only a minor effect on forwardcalculated pavement modulus.

1 INTRODUCTION

Non-destructive testing (NDT) on pavements is having a significant impact on the design and evaluation of pavement systems. To determine the layer moduli of a pavement system, deflection measurements from NDT testing are performed. Commonly, these measurements utilize the Falling Weight Deflectometer (FWD) device, which applies an impact loading to the surface of the pavement. Sensors at the loading location and at fixed radii from the load center measure surface deflections. The resulting set of deflections is known as the deflection basin. Considerable background information on this method is provided in several existing studies; see, for example, Alavi et al. (2008).

Special computer programs can backcalculate a modulus profile for the pavement system from the peak values of the measured input force and the resulting deflection basin. These programs include (a) iterative elastic-layer backcalculation algorithms and (b) closed-form backcalculation algorithms (also known as direct-calculation algorithms or forward-calculation algorithms).

The closed-form backcalculation process differs from iterative backcalculation in that moduli estimates from the former are calculated directly from the load and the deflection data by means of closed-form equations rather than iteration. No seed-layer moduli or other stiffness properties are needed for

this closed-form method. In addition, several programs exist for this forwardcalculation procedure, such as the Wiseman-Greenstein program (Wiseman & Greenstein 1983), ROADHOG (Hall & Elliot 1992), DEFOD (Sides et al. 1992), the old AASHTO equations (AASHTO 1993, Baus & Jonson 1992), ROHDE (Rohde 1994), MDOT (Rada et al. 1997), Romanoschi-Metcalf (Romanoschi & Metcalf 1999), FDOT (Badu-Tweneboah et al. 2003), YONAPAVE (Hoffman 2003), FHWA (Stubstad et al. 2007), and the new EVALIV (Livneh 2010) program. All these programs offer quick, direct-calculation procedures that utilize a two-layer model for any given pavement structure. Thus, these programs require pavement-thickness input.

Various studies (Stubstad et al. 2006a, b, 2007) have demonstrated the usefulness of the forwardcalculation technique as a new approach to determine layered elastic moduli from in-situ load-deflection data. Their conclusion is that forwardcalculation presents several distinct advantages: (a) no assumption is needed for seed-layer moduli or other stiffness properties, thus the outputs of the forward-calculations are not dependent on any assumption; (b) a unique solution obtains for each load-deflection basin because the stiffnesses of the subgrade and the bound surface-course are not dependent on the other moduli within the pavement system; (c) forwardcalculation is easy to understand and relatively simple to perform; (d) forwardcalculation techniques produce considerably less scatter of

the data (for the same layer and test section) than do backcalculation techniques. Despite these advantages, the results obtained do not necessarily mean that forwardcalculation is superior to backcalculation.

Among the aforementioned forwardcalculation techniques, the old 1993 AASHTO is still in use by several agencies around the world, including the American FHWA (Federal Highway Administration) and the Israeli National Roads Company (formerly PWD). As the 1993 AASHTO equations do not allow calculating, in a fully direct manner, the subgrade and pavement resilient moduli, it becomes necessary to modify the existing forwardcalculating equations by replacing them with new ones, termed AASHTOLIV equations in the present paper. These new equations, like the old ones, inherit basic deviations from the true elastic properties of the pavement structure and the pavement subgrade. Thus, corrective factors are needed for AASHTOLIV to deal with these deviations. Given this background, the objectives of the present paper were formulated as follows:

- to present the old AASHTO equations together with their modification – i.e. the AASHTOLIV equations – for forward-calculation of the pavement and subgrade resilient moduli;
- to examine the accuracy of the AASHTOLIV equations and to develop corrective-factors in order make AASHTOLIV a legitimate, quick, and direct calculation method;
- to develop additional corrective-factor equations that take into account any given depth to bedrock measured from the pavement-subgrade interface;
- to demonstrate the use of the newly developed AASHTOLIV equations by presenting five forwardcalculation examples.

Finally, the issues of (a) how to fix the depth to bedrock as an input to the final corrected equations and (b) how to calculate the subgrade CBR value from the final AASHTOLIV forwardcalculated subgrade resilient modulus are discussed in an accompanying paper. Meanwhile, the sections to follow will detail the process of attaining this paper's four objectives and their associated conclusions.

2 MODIFYING THE OLD EQUATIONS

The 1993 AASHTO equations for calculating the subgrade resilient modulus and the pavement resilient modulus from the surface deflection basin measured by the FWD are as follows:

$$E_s = 0.24 \times P / (dr \times r) \quad (1)$$

$$r \geq 0.7 \times \{a^2 + Hp \times [(E_p/E_s)^{1/3}]^2\}^{0.5} \quad (2)$$

$$(E_s \times do) / (1.5 \times p \times a) = 1 / [1 + (Hp/a)^2 \times (E_p/E_s)^{2/3}]^{0.5} + \{[1 - 1 / (1 + (Hp/a)^2) \times 0.5] / (E_p/E_s)\} \quad (3)$$

where E_s denotes the subgrade resilient moduli, in MPa; P denotes the FWD dynamic load, in N; p denotes

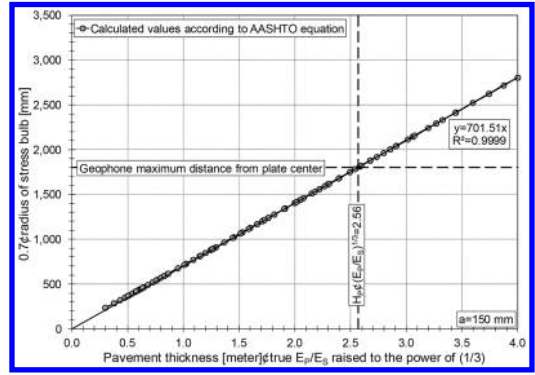


Figure 1. $0.7 \times$ radius of stress bulb versus true apparent structural number according to AASHTO equation (Eq. 2), for $a = 150$ mm.

the FWD dynamic pressure in MPa; a denotes the plate radius in mm; r denotes the radial distance (offset) from the plate center, where the deflection measurement is recorded, in mm; dr denotes the recorded deflection at a radial distance of r , in mm; do denotes the central recorded deflection in mm; E_p denotes the pavement resilient moduli, in MPa; H_p denotes the total pavement thickness in mm. Note: Equation 1 is derived from Boussinesq stress-distribution theory for a homogenous medium with a Poisson ratio of 0.5 and an applied concentrated load, and Equation 3 is derived from an approximate formulation of Burmister stress-distribution theory for a two-layer system.

In order to calculate E_s , the value of r to be inserted into Equation 1 should conform to that given by Equation 2. This latter equation calculates the radius of the stress bulb at the subgrade-pavement interface. As the maximum geophone distance from the center of the loading plate is, in the majority of cases, 1,800 mm, Figure 1, which is based on Equation 2, indicates that the implementation of Equation 1 for $H_p \times (E_p/E_s)^{1/3}$ values (termed in the present paper the apparent structural number for $a = 150$ mm) higher than 2.56 are not applicable. Thus, for these cases, the use of Equation 1 needs to be accompanied by a corrective expression as will be described in the next section. Note: H_p in the latter expression is given in meters.

At this juncture, it is worthwhile noting that the expression of the apparent structural number (i.e. $H_p \times (E_p/E_s)^{1/3}$) equals $1/0.550$ of the characteristic length as defined by Hogg (1938 & 1944) for a subgrade and pavement Poisson ratio of 0.5. The applicability of the Hogg model to pavement evaluation was discussed by Wiseman et al. (1977) and Hoffman (1997, 2003).

Following the above-mentioned findings, the suggested modified $E_{s_{uc}}$ equation is given by the following expression, where $E_{s_{uc}}$ denotes the forward-calculated AASHTOLIV subgrade modulus; i.e. the uncorrected equation:

$$E_{s_{uc}} = \min[0.24 \times P / (dr \times r)] \quad (4)$$

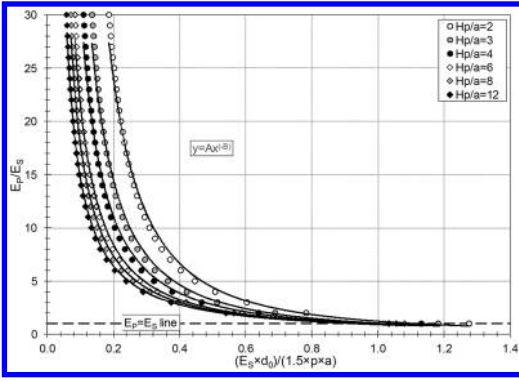


Figure 2. E_p/E_s versus normalized deflection – i.e. $E_s \times d_o / (1.5 \times p \times a)$ – according to AASHTO (Eq. 3) for various H_p/a values.

where r is equal to 900, 1,200, 1,500, and 1,800 mm; and d_r is the recorded deflections for each lateral distance, r . Again, the associated corrective expression for Equation 4 is developed in the next section

As for the E_p values, numerical calculations of Equation 3 lead to the relationships plotted in Figure 2. These curves enable obtaining E_p directly from the calculated E_s value (i.e. they are calculated from Equation 4) and the given H_p , a , and d_o data, whereas calculating E_p from Equation 3 (without Figure 2) needs the trial-and-error procedure.

The curves of Figure 2 can be formulized by mathematical equations with the aid of the regression technique. This operation is termed the curve fitting procedure. The following equations are then obtained for the purpose of calculating the pavement resilient modulus:

$$E_p/E_s = A \times [(E_s \times d_o) / (1.5 \times p \times a)]^B \quad (5)$$

$$A = -0.3447 \times [\log(H_p/a)]^3 + 0.8528 \times [\log(H_p/a)]^2 -$$

$$-0.5174 \times \log(H_p/a) + 0.8766 \quad (6)$$

$$B = -0.8883 \times [\log(H_p/a)]^3 + 2.8376 \times [\log(H_p/a)]^2 -$$

$$-3.6121 \times \log(H_p/a) + 2.9094 \quad (7)$$

where E_p , E_s , H_p , a , p and d_o denote the same variables given in Equations 1, 2 and 3; A and B denote curve-fitting coefficients as described in Equations 5 and 6, for which the coefficient of determination (R^2) is equal to 1.000 for both equations.

Finally, at this juncture, it is worthwhile noting that the R^2 values for the six curves of Figure 2 are also very high. They vary between 0.9923 and 0.9976.

3 CORRECTING MODIFIED EQUATIONS

In order to check the accuracy of the modified equations given in the previous section, simulated data for a surface deflection-basin were generated for various given data from a two-layer model with infinite

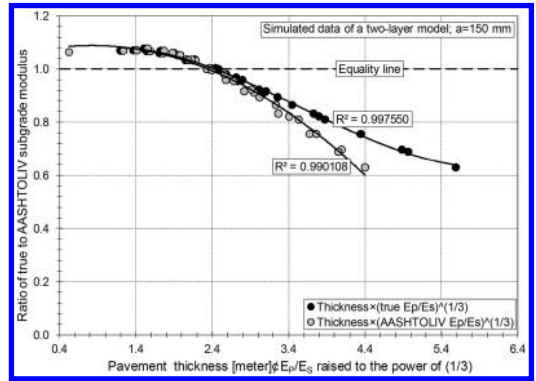


Figure 3. Ratio of true to AASHTOLIV (Eq. 4) subgrade modulus versus true and apparent AASHTOLIV structural numbers for all simulated two-layers structures with infinite depth to bedrock when $a = 150$ mm.

depth to bedrock. Surface deflection-basins can be calculated theoretically with the aid of the Burmister equations or with the Odemark-Ullidtz equations as formulated by Wiseman & Greenstein (1983). Such theoretical calculations were performed with the latter equations for the following given data: (a) subgrade and pavement Poisson ratio of 0.5, (b) subgrade modulus of 50 MPa, (c) ratio of pavement modulus to subgrade modulus from 5 to 30, (d) pavement thickness from 300 mm to 1,800 mm, (e) radius of loading plate of 150 mm, and (f) reference load of 9.5889 kN (i.e. reference pressure of 135.7 kPa). The outputs of these calculations were then used to calculate, for these given structures, the ratio of the true subgrade resilient modulus to that forwardcalculated by Equation 4 (which, along with Figure 3, the present paper terms the AASHTOLIV subgrade modulus).

For the current case (i.e., the case of $D/a = \infty$ where D is the depth to bedrock from pavement and subgrade interface and a is the radius of the loading plate), Figure 3 shows a variation of the subgrade modulus ratio with apparent AASHTOLIV structural number. This latter variation possesses a high R^2 value. It also shows ratio values higher than 1.0 (maximum 1.08) for apparent structural numbers lower than 2.40; i.e. similar to the borer value of 2.56 of Figure 1. The variation of the true apparent structural number clearly demonstrates the approximate nature of Equation 4. Thus, this equation needs to be multiplied by a correction factor (F_s) equal to the variation of the subgrade modulus ratio with the apparent AASHTOLIV structural number of Figure 3 for the $D/a = \infty$ curve. The use of the AASHTOLIV apparent structural number instead of the true apparent structural number stems from the fact the latter values are not those obtained from the AASHTOLIV forwardcalculations. According to Figure 3, the formulation of F_s is as follows:

$$F_s = -0.03815 \times [H_p \times (E_p/E_s)_{uc}^{1/3}]^2 + 0.06312 \times [H_p \times (E_p/E_s)_{uc}^{1/3}] + 1.0615 \quad (8)$$

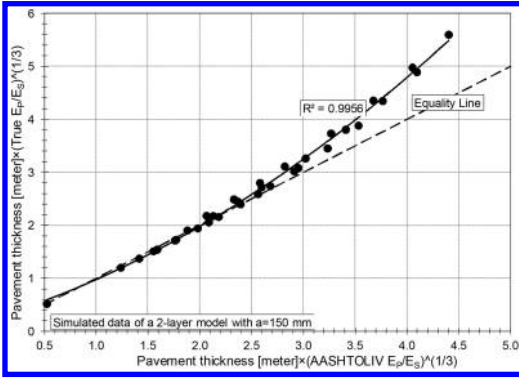


Figure 4. Corrected (true) apparent structural number versus AASHTOLIV (uncorrected) apparent structural number for all simulated two-layer structures with infinite depth to bedrock when $a = 150$ mm.

where F_s denotes the multiplier factor of Equation 4 to obtain corrected (true) E_s values for the case of infinite depth to bedrock; H_p denotes the total pavement thickness in meters; $(E_p/E_s)_{uc}$ denotes the forward-calculated E_p to E_s ratio by Equation 5 (i.e. the AASHTOLIV E_p/E_s).

As for the E_p values, Figure 4 depicts the variation of the corrected (true) apparent structural numbers with the AASHTOLIV (uncorrected) apparent structural numbers for the same simulated two-layer structures that possess infinite and definite depth to bedrock when $a = 150$. Again, for the $D/a = \infty$ case where D is the depth to bedrock and a is the radius of the loading plate, Figure 4 indicates that the R^2 value for this variation is also very high. To sum up, the formulation of this variation is as follows:

$$H_p \times (E_p/E_s)_c^{1/3} = 0.1350 \times [H_p \times (E_p/E_s)_{uc}^{1/3}]^2 + 0.5961 \times [H_p \times (E_p/E_s)_{uc}^{1/3}] + 0.2432 \quad (9)$$

where H_p denotes the pavement total thickness, in meters; $(E_p/E_s)_c$ denotes the corrected (true) E_p to E_s ratio; $(E_p/E_s)_{uc}$ denotes the forward-calculated E_p to E_s ratio by Equation 5 (i.e. the AASHTOLIV E_p/E_s).

To sum up, the corrected (true) E_s and the corrected (true) E_p (termed E_{s_c} and E_{p_c} , respectively) are the following:

$$E_{s_c} = F_s \times E_{s_{uc}} \quad (10)$$

$$E_{p_c} = (E_p/E_s)_c \times E_{s_c} \quad (11)$$

where $E_{s_{uc}}$ is calculated according to Equation 4; F_s is calculated according to Equation 8; and $(E_p/E_s)_c$ is calculated according to Equation 9.

Finally, it is worthwhile noting that the need for correcting the modified AASHTO equations in Section 2 stems from the two following facts: (a) some discrepancies exist between the calculated values (points) of Figure 2 and the calculated values of Equations 5, 6

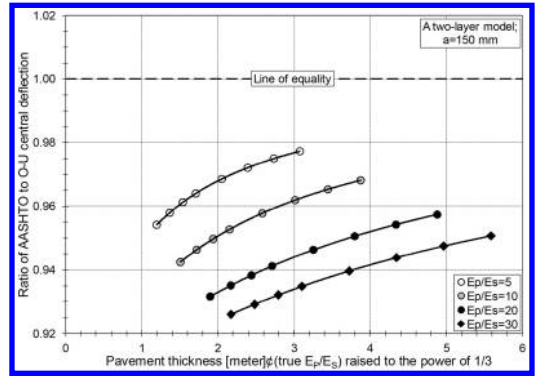


Figure 5. Ratio of AASHTO to O-U (Odemark-Ulitz) calculated central deflection versus the true apparent structural number for all simulated two-layer structures with infinite depth to bedrock when $a = 150$ mm.

and 7; (b) some discrepancies exist between the calculated central deflection (do) of the simulated data of H_p , E_s and E_p/E_s , (i.e. calculated according to the Odemark-Ulitz procedure) and those calculated by the AASHTO equation, (Eq. 3) for the same data. These latter discrepancies are shown in Figure 5 as the ratio of the two calculated central deflection (do). In addition, Figure 5 indicates that for a true apparent structural number exceeding the value of 1.0, the deflection ratio range is approximately 0.93–0.98.

4 CORRECTING FOR BEDROCK

Several researchers have found that the placement of a rigid layer within the subgrade exerts a considerable influence on backcalculated moduli. As has been pointed out: “Ignorance of rigid bottom considerations may lead to substantial errors in the predicted moduli of a pavement-subgrade system. The subgrade modulus may be significantly overreacted if a semi-infinite subgrade is falsely assumed, when actual bedrock exists at a shallow depth” (Uddin et al. 1986).

At this juncture, it should be noted that the U.S. Corps of Engineers recommend that a rigid layer be placed at 6 meters below the surface (Bush, 1980). In addition (according to Rohde & Scullion 1990), rigid layer depths from the pavement surface are commonly placed at depths of 2.5–3.5 meters in sandy subgrades or at 3.5–5.0 meters in sandy clay subgrades and 5.0–7.5 meters in clay subgrades. These depths may not involve in all cases a stiff layer underlying the subgrade, but they might serve as apparent depths caused by an increase in subgrade stiffness with depth. The more rapidly the subgrade increases in stiffness with depth, the shallower will be the rigid layer determined.

The ratio of the aforementioned bedrock modulus to subgrade modulus can be assigned the following values: 5, 10, 100 and 1,000 (Uzan 1998). The final

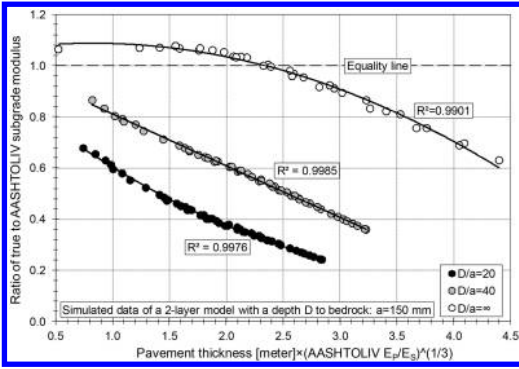


Figure 6. Ratio of true to AASHTOLIV (Eq. 4) subgrade modulus versus apparent AASHTOLIV structural numbers for all simulated two-layer structures with infinite and finite depths to bedrock when a modular ratio of bedrock to subgrade = 100.

ratio value is usually assigned by the user based on knowledge of the subsurface conditions; i.e. whether rock exists or not. In cases in which no outputs are seen in the vicinity of the pavement or no other information concerning the existence of a stiff layer is available, a ratio value of 5 is usually recommended.

In the same manner as seen in Section 3, simulated data from the surface deflection-basin are generated for various given data from a two-layer model with a definite depth to bedrock. Again, these surface deflection-basins were calculated with the aid of the Odemark-Ullidtz for the following given data: (a) subgrade and pavement Poisson ratio of 0.5, (b) subgrade modulus of 50 MPa, (c) ratio of bedrock modulus to subgrade modulus of 100, this being (according to Rode & Scullion 1990) a representative value for average conditions, (d) ratio of depth to bedrock from the pavement-subgrade interface D to the loading-plate radius a (i.e. D/a) of 20 and 40, (e) loading plate radius of 150 mm, (f) ratio of pavement modulus to subgrade modulus of from 6 to 48, (g) pavement thickness from 350 mm to 1,800 mm and (h) reference load of 9.5889 kN (i.e. reference pressure of 135.7 kPa).

The outputs of these calculations are then used to calculate for these given structures the ratio of the true subgrade resilient modulus to the forward-calculated moduli by means of Equation 4 (which, including Figure 3 and Figure 6, the present paper terms the AASHTOLIV subgrade modulus). Like Equations 5, 6 and 7, the data here obtained are given as a function of the apparent AASHTOLIV number in Figure 6. In the same manner, the outputs of the aforementioned simulated calculations are then used to calculate, for these given structures, the true apparent structural number.

The three correlative equations derived from the three curves of Figure 6 enable constructing the plot of the ratio of true to corrected AASHTOLIV (Eq. 10) subgrade modulus versus apparent

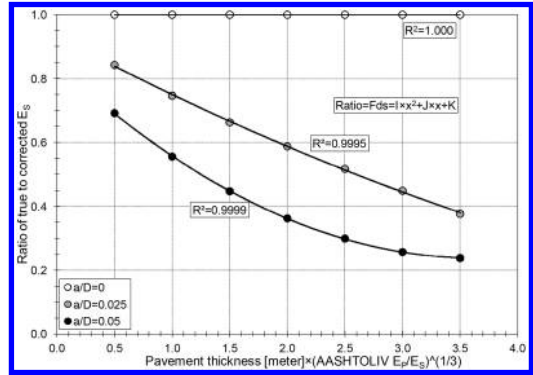


Figure 7. Ratio of true to corrected AASHTOLIV (Eq. 10) subgrade modulus versus apparent AASHTOLIV structural number for all simulated two-layer structures of Figure 6.

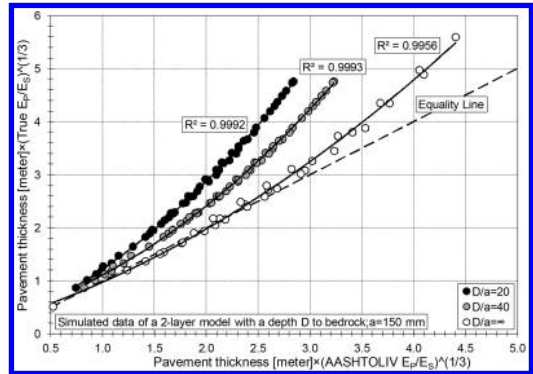


Figure 8. Corrected (true) apparent structural number versus apparent AASHTOLIV (uncorrected) structural number for all simulated two-layer structures with infinite and finite depths to bedrock when a modular ratio of bedrock to subgrade = 100.

AASHTOLIV structural number. This plot is shown in Figure 7.

In addition, for the aforementioned calculated data, Figure 8 depicts the variation of the corrected (true) apparent structural number with the AASHTOLIV (uncorrected) apparent structural number. For comparison purposes, Figure 6 includes the curve of Figure 3, and Figure 8 includes the curve of Figure 4, both for the case of infinite depth to bedrock.

In the same manner, the three correlative equations derived from the three curves of Figure 8 enable constructing the plot of the ratio of corrected (true) apparent structural number to apparent AASHTOLIV (uncorrected) structural number as a function of the latter structural number. This plot is shown in Figure 9.

Here again, the R^2 values of the two additional curves in Figure 6 and Figure 8 (i.e. for $D/a = 20$ and $D/a = 40$) almost approach the value of 1.0. In addition, the R^2 values of the two curves in Figure 7 and Figure 9 also almost approach the value of 1.0.

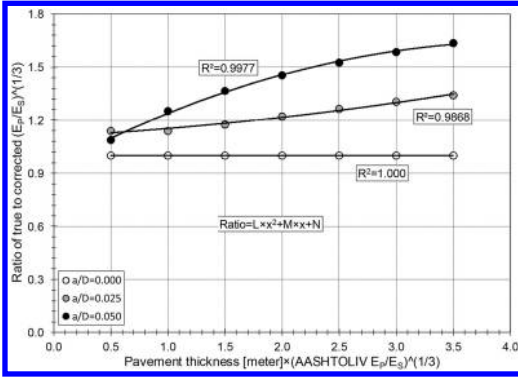


Figure 9. Ratio of true apparent structural number to corrected apparent AASHTOLIV structural number for all simulated two-layer structures of Figure 8.

Finally, by applying the curve-fitting technique, the data of Figure 7 lead to the following expressions:

$$Es_d = Fds \times Es_c \quad (12)$$

$$Fds = I \times [Hp \times (Ep/Es)_{uc}^{1/3}]^2 + J \times [Hp \times (Ep/Es)_{uc}^{1/3}] + K \quad (13)$$

$$I = 20.9497 \times (a/D)^2 - 0.1333 \times (a/D) \quad (14)$$

$$J = 40.1341 \times (a/D)^2 - 8.6734 \times (a/D) \quad (15)$$

$$K = -15.1365 \times (a/D)^2 - 2.3350 \times (a/D) + 1.0000 \quad (16)$$

where Fds denotes the multiplier factor (i.e. the ratio value of Figure 7) to obtain corrected (true) Es_d values for the case of a given depth to bedrock (from the pavement-subgrade interface) denoted by the ratio of D/a from the Es_c values of Equation 10; Hp denotes the total pavement thickness, in meters; $(Ep/Es)_{uc}$ denotes the forward-calculated Ep to Es ratio by Equation 5 (i.e. the AASHTOLIV Ep/Es); I , J and K denote the coefficient values of the correlative equations from the curves of Figure 7.

In the same manner, the data of Figure 9 leads to the following expressions:

$$Ep_d = Fdp \times Ep_c \quad (17)$$

$$Fdp = \{L \times [Hp \times (Ep/Es)_{uc}^{1/3}]^2 + M \times [Hp \times (Ep/Es)_{uc}^{1/3}] + N\}^3 \times Es_d / Es_c \quad (18)$$

$$L = -48.2608 \times (a/D)^2 + 1.5862 \times (a/D) \quad (19)$$

$$M = 217.3824 \times (a/D)^2 - 4.0296 \times (a/D) \quad (20)$$

$$N = -223.3608 \times (a/D)^2 + 9.9243 \times (a/D) + 1.0000 \quad (21)$$

where Fdp denotes the multiplier factor to obtain corrected (true) Ep_d values for the case of a given depth to bedrock (from the pavement-subgrade interface) denoted by the ratio of D/a from Ep_c values of Equation 11; Es_c denotes the corrected subgrade modulus for infinity depth to bedrock according to Equation 10; Es_d denotes the corrected resilient modulus for a given depth to bedrock denoted by the ratio of D/a according to Equation 12; L , M , and N denote the coefficient

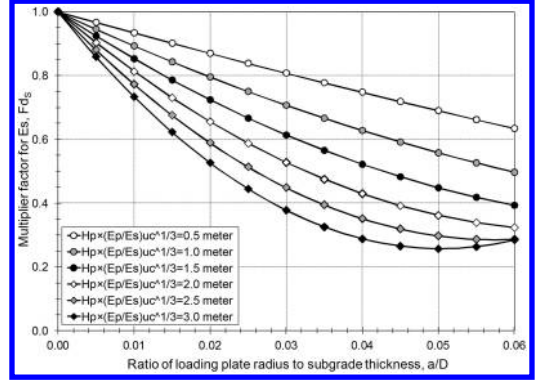


Figure 10. Graphical presentation of Equations 13–16; i.e. of the multiplier factor to adjust the corrected AASHTOLIV subgrade modulus for any given a/D value.

values of the correlative equations of the curves of Figure 9.

To sum up, Figure 10 shows a graphical presentation of Equations 13–16; i.e. the graphical presentation of the multiplier factor to adjust the corrected AASHTOLIV subgrade modulus for any given a/D value. This figure reveals the fact that use of Equations 13–16 should be limited to (a) a/D lower than 0.05 and (b) $Hp \times (Ep/Es)_{uc}^{1/3}$ lower than 3.0; i.e. only to data that do not range in the extrapolating region.

In the same manner, Figure 11 shows a graphical presentation of Equations 18–21; i.e. the graphical presentation of the multiplier factor multiplied by the ratio Es_c/Es_d (i.e. the value of $1/Fds$) to adjust the corrected AASHTOLIV pavement modulus for any given a/D value. In other words, in order to calculate the Fdp value, the Fds (Eq. 13) should be calculated first.

5 FORWARDCALCULATED EXAMPLES

In order to demonstrate the use of the new AASHTOLIV equations, including the effect of the existence of bedrock at a given depth from the subgrade surface, forwardcalculations were performed of deflections bowls measured at five given structures, four of them conventional (flexible) pavements and one all-asphalt pavement. Four of these structures (i.e. except for the conventional structure with a total thickness of 800 mm) were constructed at the same site (Ben Gurion International Airport) and possess a heavy clay subgrade. The remaining structure, which was constructed at a different site (Ovda Airport), possesses a hard silty subgrade.

These forwardcalculations include the finding of the subgrade and pavement resilient moduli for the two following cases: (a) the depth to bedrock from the subgrade surface is infinite, and (b) the depth to bedrock from the subgrade surface has a fixed value of $40 \times a = 6.0$ meters, with $a = 0.150$ meter, the radius of the lading plate. This fixed depth was chosen according to the recommendations outlined

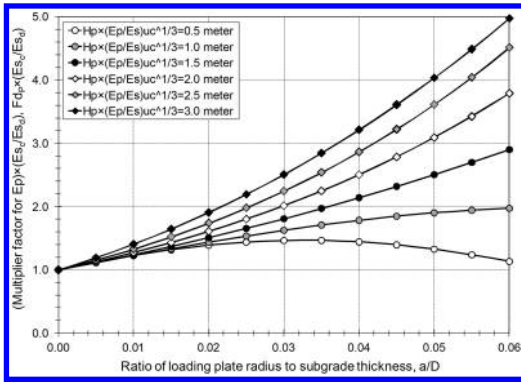


Figure 11. Graphical presentation of Equations 18–21; i.e. of the multiplier factor multiplied by the ratio E_s/E_s_d to adjust the corrected AASHTOLIV pavement modulus for any given a/D value.

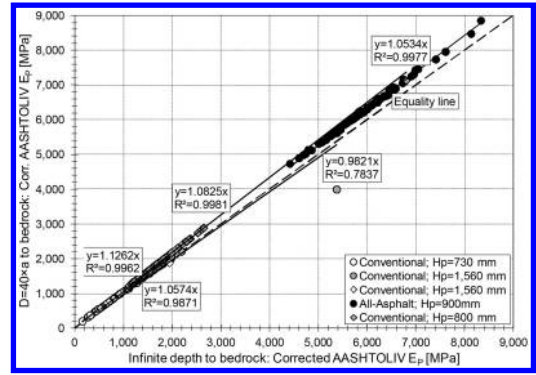


Figure 13. Corrected AASHTOLIV pavement modulus for infinite depth to bedrock versus corrected AASHTOLIV pavement modulus for 6.0 meter (i.e. $D/a = 40$) depth to bedrock for the five given structures.

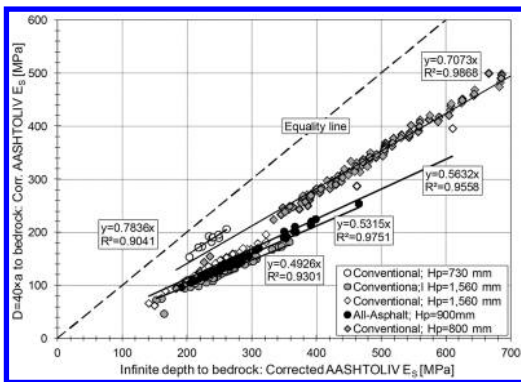


Figure 12. Corrected AASHTOLIV subgrade modulus for infinite depth to bedrock versus corrected AASHTOLIV subgrade modulus for a 6.0 meter (i.e. $D/a = 40$) depth to bedrock for the five given structures.

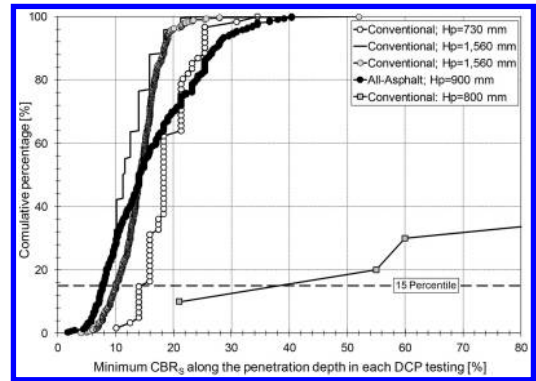


Figure 14. Cumulative distribution of the in-situ CBR values of the subgrade of the five given structures as measured by the DCP apparatus.

by Rohde and Scullion (1990) as described above in Section 4. Figure 12 depicts the AASHTOLIV forward-calculated data of the subgrade resilient moduli of the five structures for the two bedrock-depth cases. Similarly, Figure 13 depicts the AASHTOLIV forward-calculated data from these five structures for the two cases.

Figure 12 indicates that the corrected AASHTOLIV subgrade moduli calculated for a 6.0 meter depth to bedrock are much smaller than those calculated for infinite depth to bedrock. The ratio of these moduli ranges from 0.49 up to 0.78. The higher ratios are associated with smaller values of apparent structural numbers, while the lower ratios are associated with higher values of apparent structural numbers. This demonstrates, again, that the rate of depth to bedrock has a remarkable effect on the subgrade modulus output.

On the other hand, Figure 13 indicates that the corrected AASHTOLIV pavement moduli calculated for a 6.0 meter depth to bedrock do not differ substantially from those calculated for infinite depth to bedrock.

The ratio of these moduli ranges from 0.98 up to 1.13. Thus, the rate of depth to bedrock is demonstrated once again to have only minor effect on the pavement modulus output.

The strength values of the clayey subgrade of the four given structures at the Ben-Gurion International Airport site and the silty subgrade at the Ovda Airport site were measured in-situ by the Dynamic Cone Penetration (DCP) apparatus. The results obtained for these tests were converted to CBR values. Figure 14 shows the cumulative distribution of these CBR values for each given structure. Here it is important to note that the CBR values of this figure correspond to the minimum values detected along the penetration depth at each testing point.

Figure 14 indicates that the subgrade strength of a conventional structure having a total thickness of 730 mm is of a higher value than that associated with the subgrade of the three other structures for the same clayey subgrade of the Ben-Gurion International Airport site. The 15-percentile CBR value for the subgrade of this 730 mm structure equals 14.0%, and the three other 15-percentile CBR values range

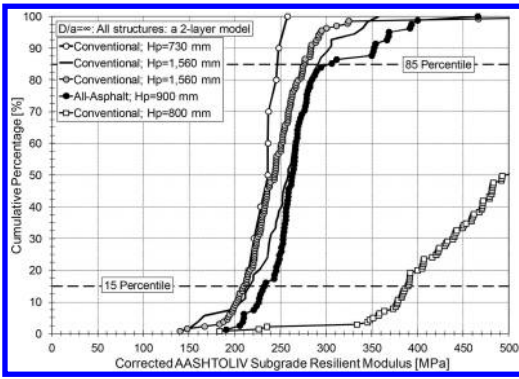


Figure 15. Cumulative distribution of the AASHTOLIV forwardcalculated subgrade moduli for infinite depth of bedrock for the five given structures.

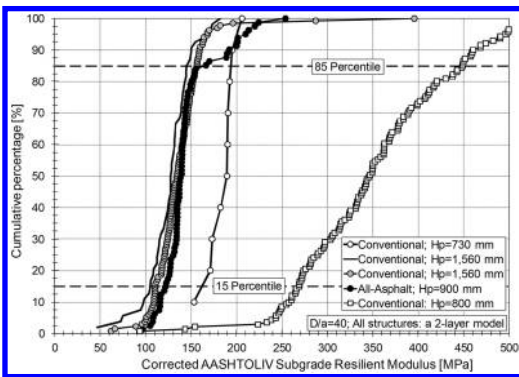


Figure 16. Cumulative distribution of the AASHTOLIV forwardcalculated subgrade moduli for 6.0 meter depth to bedrock for the five given structures.

from 7.8% up to 10.1%. For the hard silty subgrade of the OVDA Airport site with a conventional structure and a total thickness of 800 mm, its 15-percentile CBR value equals 38.0%. All these strength findings can be checked for compliance with the cumulative distributions of the forwardcalculated subgrade moduli. These distributions are given in Figure 15 for infinite depth to bedrock, and in Figure 16 for 6.0 meter depth (from the pavement-subgrade interface) to bedrock.

Figure 16 indicates that the cumulative distribution of the AASHTOLIV forwardcalculated subgrade moduli for the 6.0 meter depth to bedrock (from the pavement-subgrade interface) is in good compliance with that of the DCP-CBR distribution given in Figure 14, and better than that of Figure 15.

This compliance is well demonstrated in Figure 17, which shows the relationship between (a) the 15-percentile of the AASHTOLIV forward-calculated subgrade modulus for a 6.0 meter depth to bedrock and the 15-percentile of the DCP-CBR distribution of Figure 14 and (b) the 15-percentile of the AASHTOLIV forwardcalculated subgrade modulus for infinity depth to bedrock and the 15-percentile of the DCP-CBR distribution. Figure 17 utilizes the

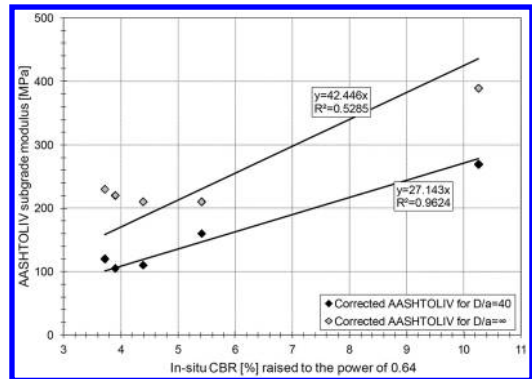


Figure 17. AASHTOLIV forwardcalculated subgrade modulus for 6.0 meter depth of bedrock and infinite depth of bedrock versus in-situ CBR values raised to the power of 0.64 for the 15-percentile values of Figures 14, 15 and 16.

E_S -CBR^{0.64} relationship as adapted from the TRL's equation (Powell et al. 1984). In this relationship, the E_S -CBR^{0.64} multiplier is 17.62.

Figure 17 indicates that the AASHTOLIV forwardcalculated subgrade modulus results for the 6.0 meter depth to bedrock modulus correlate very well with the DCP-CBR results ($R^2 = 0.96$), while the AASHTOLIV forwardcalculated subgrade modulus for infinity depth to bedrock correlate less with the same DCP-CBR results ($R^2 = 0.52$). In addition, the E_S -CBR^{0.64} multiplier in the first relationship is 27.14, or about 54% higher than the recommended TRL value of 17.62, but less than that associated with the multiplier value of 47.45 in the second relationship.

To sum-up, the forwardcalculated examples in this section clearly support the need to implement a given depth to bedrock in these calculations.

6 CONCLUSIONS

Findings from the current study on forwardcalculation of FWD deflection-basin measurements yield the following conclusions:

- The AASHTOLIV equations, based on the 1993 AASHTO two-layer model with infinite depth to bedrock, for calculating pavement and subgrade moduli require correction factors in order to minimize inherent errors.
- These correction factors are very much dependent on the apparent structural number obtained; i.e. the pavement thickness multiplied by the ratio of the AASHTOLIV pavement modulus to the AASHTOLIV subgrade modulus raised to the power of 1/3.
- The introduction of a rigid layer at a definite depth from the pavement-subgrade interface reduces substantially the aforementioned AASHTOLIV subgrade modulus and increases or sometimes reduces, both to a minor extent, the AASHTOLIV pavement modulus.

- The rates of the reduction or increase are again dependent on the apparent structural number obtained, together with the ratio of the depth to bedrock measured from the pavement-subgrade interface to the radius of the loading plate.
- The forward-calculated examples (a) support the need to implement a given depth to bedrock in these calculations, (b) comply better with the MEPDG relationship of $E_s\text{-CBR}^{0.64}$ for the case of a depth to bedrock (from the pavement-subgrade interface) of $D/a = 40$, and maybe even better for the case of D/a less than 40.

Finally, it follows from the above conclusions that knowledge of the ratio of the depth to bedrock measured from the pavement-subgrade interface to the radius of the loading plate is very crucial. The issue of how this depth to bedrock should be fixed as an input to the final corrected equations is discussed in an accompanying paper. The issue of how to calculate the subgrade CBR value from the final AASHTOLIV forward-calculated subgrade resilient modulus is also discussed in the accompanying paper.

ACKNOWLEDGMENT

The results presented in this paper were obtained in the course of engineering studies performed by the author for the Israeli Airport Authority. Thanks are therefore due this authority.

REFERENCES

AASHTO. 1993. *AASHTO Guide for Design of Pavement Structures 1993*. Washington, DC: American Association of State Highway and Transportation Officials.

Alavi, S., Lecates, J.F., Tavares M.P. & Sierra Transportation Engineers, Inc. 2008. *Falling Weight Deflectometer Usage*. NCHRP Synthesis 381, National Cooperative Highway Research Program, Synthesis of Highway Practice, Transportation Research Board, Washington, DC.

Badu-Tweneboah, K., Ruth, B.E. & Miley, W.G. 2003. Dynaflect Evaluation of layer moduli in Florida's flexible pavement systems. *Transportation Research Record* 1196: 96–107.

Baus, R. L. & Jonson, A.M. 1992. AASHTO direct structural capacity method error analysis. *Journal of Transportation Engineering* 118 (1): 20–32.

Bush, A.J. 1980. *Nondestructive Testing of Light Aircraft Pavements, Phase II, Development of Nondestructive Evaluation Methodology*. Report FHWA-RD-80-9-11. US Department of Transportation, Federal Highway Administration, McLean, VA.

Hall, K. D. & Elliot R. P. 1992. ROADHOG-A flexible pavement overlay design procedure. *Transportation Research Record* 1374: 9–15.

Hoffman, M.S. 1997. *Application of Elasticity Models for Evaluation of Flexible Pavements*. Thesis submitted in partial fulfillment of the M.Sc. Degree, Technion-Israel Institute of Technology, Haifa (in Hebrew).

Hoffman, M.S. 2003. Direct method for evaluating structural needs of flexible pavements with Falling-Weight Deflectometer deflections. *Transportation Research Record* 1860: 41–47.

Hogg, A.H.A. 1938. Equilibrium of a thin plate, symmetrically loaded, on an elastic foundation of infinite depth. *Philosophical Magazine* 25(168): 576–582.

Hogg, A.H.A. 1944. Equilibrium of a thin slab on an elastic foundation of finite depth. *Philosophical Magazine* 35 (243): 265–276.

Livneh, M. 2010. On the reliability of excluding thickness in forward-calculating pavement parameters. *Road Materials and Pavements Design* 11: 171–195.

Powell, W.D., Potter J.F., Mayhew, H.C., and Nunn, M.M. 1984. *The Structural Design of Bituminous Roads*. TRRL Laboratory Report 1132, Transportation and Road Research Laboratory, Wokingham, Berkshire, UK.

Rada, G.R., Shepher, K.L., Zeigler, T.D. & Smith, T.E. 1997. Montana's automated deflection analysis procedure. *Transportation Research Record* 1570: 151–162.

Rohde, G. T. 1994. Determining pavement structural number from FWD testing. *Transportation Research Record* 1448: 61–68.

Rohde, G.T. & Scullion, T. 1990. *MODULOS 4.0: Expansion and Validation of the Modulus Backcalculation System*. Report No. FHWA/TX-91/1123-3. Texas Department of Transportation, Austin, TX.

Romanoschi, S. & Metcalf, J. B. 1999. Simple approach to estimation of pavement structural capacity. *Transportation Research Record* 1652: 198–205.

Sidess, A., Bonjack, H. & Zoltan, G. 1992. Overlay design procedure for pavement maintenance management systems. *Transportation Research Record* 1374: 63–70.

Stubstad, R.N., Jiang, Y.J. & Lukanen, E.O. 2006a. *Guidelines for Review and Evaluation of Backcalculation Results*. Publication FHWA-HRT-06-152. US Department of Transportation, Federal Highway Administration, McLean, VA.

Stubstad, R.N., Jiang, Y.J. & Lukanen, E.O. 2007. Forward-calculation of pavement moduli with load-deflection data. *Transportation Research Record* 2005: 104–110.

Stubstad, R.N., Jiang, Y.J. & Lukanen, E.O. 2006b. *Review of the Long-Term Pavement Performance Backcalculation Results – Final Report*. Publication FHWA-HRT-05-150. McLean, Virginia: Office of Infrastructure Research and Development, Federal Highway Administration.

Uddin, W., Meyer, A.H. and Hudson, W.R. 1986. Rigid bottom considerations for nondestructive evaluation of pavements. *Transportation Research Record* 1070: 21–29.

Uzan, J. 1998. Estimation of subgrade thickness from deflection basin analysis. *Proceedings of 5th International Conference on the Bearing Capacity of Roads and Airfields, Trondheim, Norway*: 507–516.

Wiseman, G. and Greenstein, J. 1983. Comparison of methods of determining pavement parameters from deflection bowl measurement. *Proceedings of the Seventh Asian Regional Conference on Soil Mechanics and Foundation Engineering, Haifa, Israel*: 158–165.

Wiseman, G., Uzan, J., Hoffman, M.S., Ishai, I. & Livneh, M. 1977. Simple elastic models for pavement evaluation using measured deflection bowls. Ann Arbor, Michigan: *Proceedings of the Fourth International Conference on Structural Design of Asphalt Pavements*, Vol. II. Ann Arbor, Michigan: 416–426.

Additional issues concerning recent modified 1993 AASHTO equations (AASHTOLIV) for analyzing measured deflection bowls

M. Livneh

Department of Civil and Environmental Engineering, Technion-Israel Institute of Technology, Haifa, Israel

ABSTRACT: An accompanying paper developed modifications to the 1993 AASHTO equations for forward-calculating subgrade and pavement moduli, termed AASHTOLIV equations. It was shown through them that the rate of depth to bedrock has a significant influence on the forwardcalculated subgrade modulus and only a minor effect on the forwardcalculated pavement modulus. The present paper elaborates on the issue of how to fix the depth to bedrock as an input to the corrected final AASHTOLIV equations. The existing regression equations for predicting depth to bedrock lead in many cases to unrealistic results. In addition, the MODULUS 6 outputs, as was demonstrated, do not completely describe realistic results of a depth prediction to bedrock. These findings led to the recommendation of the use of the old method, in which a fixed depth is assigned as a function of the subgrade classification. The present paper also deals with the issue of how to calculate the subgrade CBR value from the corrected final AASHTOLIV forwardcalculated subgrade resilient modulus.

1 INTRODUCTION

In an accompanying paper (Livneh 2015), recent modifications to the 1993 AASHTO equations for forwardcalculating subgrade and pavement moduli were developed. Through these modified equations, which were termed the AASHTOLIV equations, it was shown that the rate of depth to bedrock has a significant influence on the forwardcalculated subgrade modulus and only a minor effect on the forwardcalculated pavement modulus. Thus, it seems only fitting, and perhaps even necessary, to elaborate on the issue of how to fix the depth to bedrock as an input to the corrected final AASHTOLIV equations.

It should be noted in this context that some sources around the world adopt fixed values for the rate of depth to bedrock (Bush 1980, Rohde & Scullion 1990), others use a predefined relationship between depth to bedrock and structure rigidity (Wiseman et al. 1977, Hoffman 2003), and still others use regression equations to predict the required depth (Rhode & Smith 1991). In addition to these methods, MODULUS 6 contains an inbuilt algorithm to predict the required depth. Thus, it is essential to examine all these methods in order to recommend the one to be implemented in the AASHTOLIV forwardcalculation.

Another issue dealt with in the present paper is the determination of the subgrade CBR value from the forwardcalculated subgrade resilient modulus. This calculation is necessary, as the Israeli Flex-Design method (Uzan 1966) for the flexible pavement design of inter-urban roads and the recent American FAARFIELD method (FAA 2009) for the flexible

pavement design of runways and taxiways still use the subgrade CBR value as a major input in both new pavement and overlay/reconstruction calculations. This CBR value is calculated from either the backcalculated or the forwardcalculated subgrade resilient modulus by using a pre-defined transformation equation specific to each method. Unfortunately, these equations lead to uncertain CBR results as was fully discussed by Livneh (2007). Thus, the present paper also deals with the issue of how to calculate the subgrade CBR value from the final AASHTOLIV forwardcalculated subgrade resilient modulus.

Given this background, the objectives of this study were formulated as follows:

- Presentation of some AASHTOLIV forward-calculated data together with some MODULUS 6 backcalculated data, both for the same measured deflection bowls, to demonstrate the effect of depth to bedrock on subgrades and pavement moduli and the interrelationship of these two methods.
- Description of various existing methods of predicting depth to bedrock and an examination of the outputs of these methods, including the inbuilt backcalculation contained in MODULUS 6.
- Making final suggestions (a) for predicting the depth to bedrock to be implemented in the AASHTOLIV equations and (b) for calculating subgrade CBR from the forwardcalculated AASHTOLIV subgrade resilient modulus.

The sections to follow will detail the process of attaining this paper's three objectives and their associated conclusions.

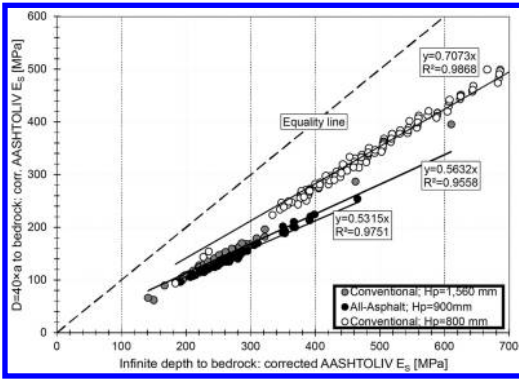


Figure 1. AASHTOLIV subgrade modulus for a 6.0 meter (i.e. $D/a = 40$) depth to bedrock versus AASHTOLIV subgrade modulus for infinite depth to bedrock for the three given pavement-structures (Livneh 2015).

2 EFFECT OF DEPTH BY AASHTOLIV

In order to demonstrate the effect of the existence of bedrock at a given depth from the subgrade surface, AASHTOLIV forwardcalculations were performed on deflection bowls measured at three given pavement-structures, two of them conventional (flexible) pavements and one of them all-asphaltic. Two of these pavement-structures, with a total thickness of 900 mm (all-asphaltic) and 1,560 mm (conventional), were constructed at the same site (Ben-Gurion International Airport), which possesses a heavy clay subgrade. The remaining structure, with a total thickness of 800 mm (conventional), was constructed at a different site (Ovda Airport) that possesses a hard-silty subgrade.

These forwardcalculations include the finding of the subgrade and pavement resilient moduli for the two following cases: (a) the depth D to bedrock from the subgrade surface is infinite and (b) the depth to bedrock from the subgrade surface has a fixed value of $40 \times a = 6.0$ meters, with a loading-plate radius (a) of 0.150 meter. Figure 1 depicts the AASHTOLIV forwardcalculated outputs of the subgrade resilient moduli of the three structures for the two bedrock-depth cases. Similarly, Figure 2 depicts the AASHTOLIV forwardcalculated outputs of the pavement resilient moduli of these three structures again for the two bedrock-depth cases.

Figure 1 indicates that the corrected AASHTOLIV subgrade moduli calculated for a 6.0 meter depth to bedrock (D), measured from the pavement-subgrade interface, are much smaller than those calculated for infinite depth to bedrock. The average ratio of these two moduli (i.e. the slope of the linear equation obtained from the zero intercept regression) ranges from 0.53 up to 0.71. The higher average ratio is associated with a smaller value of apparent structural number, while the lower average ratios are associated with higher values of apparent structural numbers, as defined by Equation 1:

$$SN_{ap} = Hp \times (E_p/E_s)^{1/3} \quad (1)$$

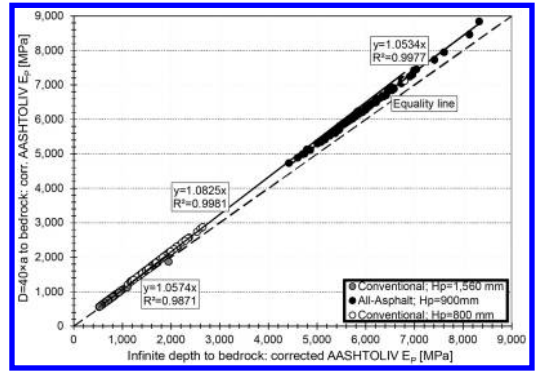


Figure 2. AASHTOLIV pavement modulus for a 6.0 meter (i.e. $D/a = 40$) depth to bedrock versus AASHTOLIV pavement modulus for infinite depth to bedrock for the three given pavement-structures (Livneh 2015).

where SN_{ap} denotes the apparent structural number, in meters; E_s denotes the subgrade modulus; E_p denotes the combined modulus of all pavement layers; and Hp denotes the total thickness of all pavement layers, in meters.

The findings of Figure 1 demonstrate, again, that the rate of depth to bedrock has a remarkable effect on the subgrade modulus output. Similar behavior of depth to bedrock is given by Rode & Smith (1991) and Uzan (1998). On the other hand, Figure 2 indicates that the corrected AASHTOLIV pavement moduli calculated for a 6.0 meter depth to bedrock (measured from the pavement-subgrade interface) do not differ substantially from those calculated for infinite depth to bedrock. The average ratio of these moduli ranges from 1.05 up to 1.08. Thus, the rate of depth to bedrock is demonstrated once again to have only minor effect on the pavement modulus output.

3 EFFECT OF DEPTH BY MODULUS

In addition to the AASHTOLIV outputs described in the previous section, it is also interesting to explore the effect of the existence of bedrock at a given depth from the subgrade surface with the aid of the MODULUS 6 program. This was done for the three given pavement-structures described in the previous section. As may be recalled, the MODULUS 6 program enables backcalculation of the required moduli for, inter alia, (a) the case of infinite depth to bedrock and (b) the case of backcalculated depth to bedrock (by the program), whereas the AASHTOLIV equations enable forwardcalculation of the moduli discussed only for a pre-defined depth to bedrock. Figure 3 depicts the MODULUS 6 backcalculated outputs of the subgrade resilient moduli of the three given structures for the two bedrock-depth cases. Similarly, Figure 4 depicts the MODULUS 6 backcalculated data of the pavement resilient moduli of these three structures, as well as for the same two bedrock-depth cases.

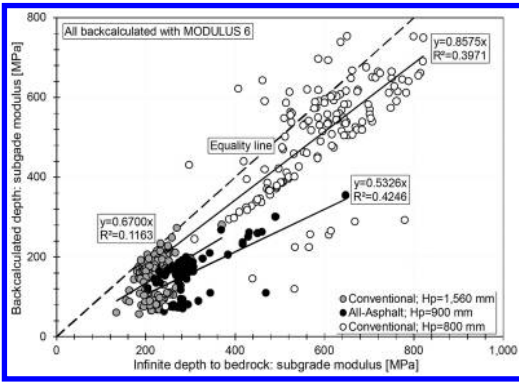


Figure 3. MODULUS 6 subgrade modulus for backcalculated depth to bedrock versus MODULUS 6 subgrade modulus for infinite depth to bedrock for the three given pavement-structures.

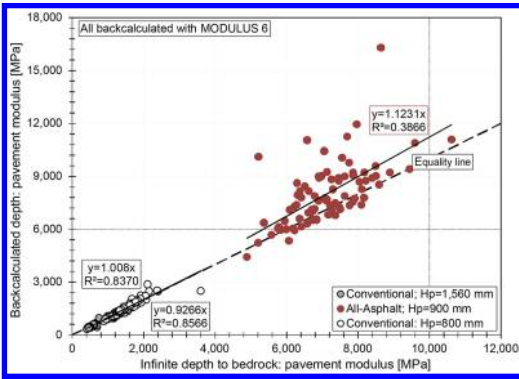


Figure 4. MODULUS 6 pavement modulus for backcalculated depth to bedrock versus MODULUS 6 pavement modulus for infinite depth to bedrock for the three given pavement-structures.

Here it should be added that in order to obtain the pavement modulus value from the asphalt layer and the granular layer moduli as backcalculated by MODULUS 6, use is made of Thenn de Barros (1966) relationship, defined by the following equation:

$$E_p = [(H_a \times E_a^{1/3} + H_g \times E_g^{1/3}) / H_p]^3 \quad (2)$$

where E_a denotes the asphalt-layer modulus; E_g denotes the granular-layer modulus; E_p denotes the combined modulus of all pavement layers; H_a denotes the total thickness of the asphalt layers; H_g denotes the total thickness of the granular layers; H_p denotes the total thickness of all pavement layers, i.e. the sum of H_a and H_g .

Figure 3 indicates that the MODULUS 6 subgrade moduli calculated for the backcalculated depth to bedrock (by the program) are again much smaller than those calculated for infinite depth to bedrock. The average ratio of these moduli (i.e. the slope of the linear equation obtained from the zero intercept regression) ranges from 0.53 up to 0.86. Again, the higher

average ratio is associated with a smaller value of the apparent structural number, while the lower average ratios are associated with higher values of the apparent structural numbers. This demonstrates, again, that the rate of depth to bedrock has a remarkable effect on the subgrade modulus output. It should be noted that the aforementioned average ratio values of Figure 3 are similar to those shown in Figure 1, but are associated with coefficients of determination (R^2) much lower than those given in Figure 1, especially for the Ovda Airport pavement-structure.

In contrast to Figure 3, Figure 4 indicates that the MODULUS 6 pavement moduli computed for the backcalculated depth to bedrock do not differ substantially from those calculated for infinite depth to bedrock. The average ratio of these moduli ranges from 0.93 up to 1.12. Thus, the rate of depth to bedrock is demonstrated once again to have only minor effect on the pavement modulus output. Furthermore, the average ratio values of Figure 4 are similar to those of Figure 2. In the present case, the all-asphalt pavement-structure at Ben-Gurion International Airport is associated with a coefficient of determination (R^2) lower than that given in Figure 2.

In this regard, it is also interesting to compare the subgrade modulus outputs of the AASHTOLIV equations with those of the MODULUS 6 program. Figures 5a and 5b show the relationship between the MODULUS 6 backcalculated subgrade modulus both for the infinite and backcalculated depth to bedrock and for the AASHTOLIV forwardcalculated subgrade modulus for infinite depth to bedrock. These calculated moduli refer to the aforementioned two pavement structures recently constructed at Ben Gurion International Airport. Figure 6 presents the same relationship for the pavement-structure constructed about thirty-five years ago at Ovda Airport.

These last three figures mentioned (i.e. Figures 5a, 5b and 6) demonstrate that for the case of infinite depth to bedrock, the average ratio of the two subgrade moduli (i.e. the slope of the linear equation obtained from the zero intercept regression as shown in the figures) ranges from 0.88 to 1.16. These ratio values are very much close to 1.0, indicating that the outputs of the two programs (i.e. MODULUS 6 and AASHTOLIV) are essentially close for the case of infinite depth to bedrock, a fact supporting the use of the AASHTOLIV equations given by Livneh (2015). Note: A direct comparison of the AASHTOLIV subgrade modulus for the case of a predefined depth to bedrock equal to $D = 40 \times a$ and the MODULUS 6 subgrade modulus for the case of backcalculated depth to bedrock is discussed further on in the present paper.

As for the relationship between the MODULUS 6 backcalculated subgrade modulus for the case of backcalculated depth to bedrock and the AASHTOLIV forwardcalculated subgrade modulus for the case of infinite depth to bedrock, the average ratio of these two subgrade moduli is 0.59 in Figures 5a and 5b, and 0.99 in Figure 6. Thus, the effect of the existence of a bedrock beneath the subgrade soil is remarkable in

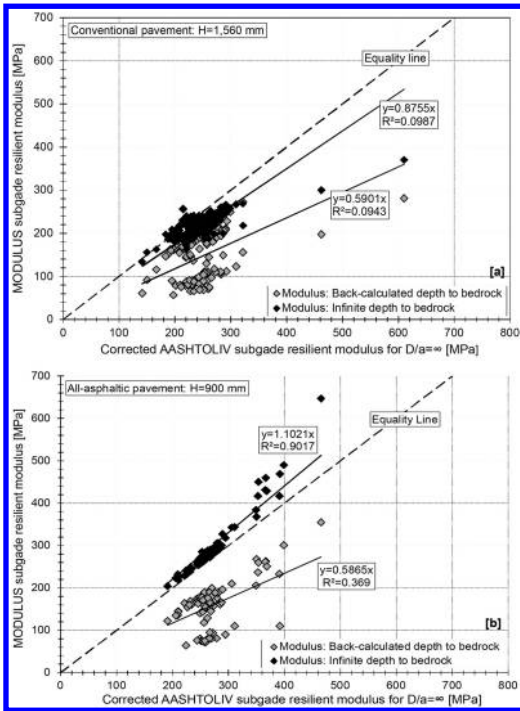


Figure 5. MODULUS 6 subgrade modulus for both infinite and backcalculated depth to bedrock (D) versus AASHTOLIV subgrade modulus for infinite depth to bedrock for the two given structures at Ben-Gurion International Airport.

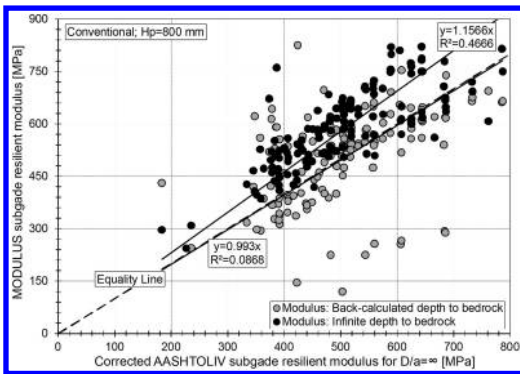


Figure 6. MODULUS 6 subgrade modulus for both infinite and backcalculated depth to bedrock (D) versus AASHTOLIV subgrade modulus for infinite depth to bedrock for the given structure of Ovda Airport.

the heavy clayey site on which Ben-Gurion International Airport is situated (Figures 5a and 5b), and only of very minor effect in the hard-silty subgrade characterizing the site of Ovda Airport. However, the scatter of the points shown in Figure 6 for the backcalculated depth to bedrock for the latter structure is noteworthy, for it makes the reliability of these results questionable. More details concerning these results are given in Figure 7.

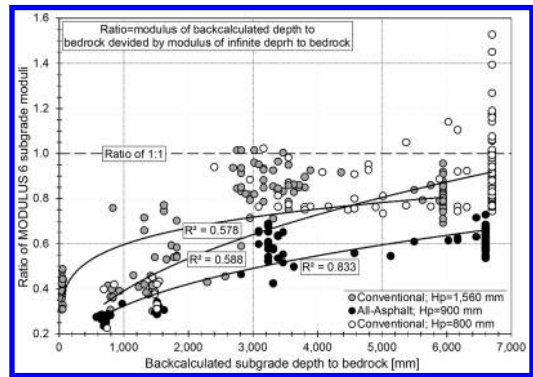


Figure 7. Ratio of backcalculated depth to bedrock (D) to infinite depth for MODULUS 6 backcalculated subgrade moduli versus backcalculated depth for the three given structures.

Figure 7 shows the influence of the MODULUS 6 backcalculated depth to bedrock on the ratio of the backcalculated subgrade resilient moduli. In the figure, this ratio is defined as the MODULUS 6 backcalculated subgrade modulus obtained for the backcalculated depth to bedrock divided by the same modulus obtained for the infinite depth. In general terms, this figure demonstrates the increase in the ratio of the backcalculated subgrade resilient moduli with the increase in the backcalculated depth. Obviously, for a backcalculated depth approaching infinity, these two types of backcalculations should yield the same results. However, for the structure of Ovda Airport, this ratio exceeds the value of 1.0 when D equals 5.5 meters and more, a fact that once again brings into question the reliability of these results. Additional discussion of these results is given further on in the present paper.

4 PRE-DEFINED DEPTH TO BEDROCK

As mentioned in several studies (see, for example, Rohde & Scullion 1990, Rohde & Smith 1991, Mahoney et al. 1993, Uzan 1998), in backward calculation or forward calculation of subgrade and pavement moduli, the depth of the underlying rigid bottom reflects either an existing rigid bottom (i.e. bedrock at a given depth) or an adjustment factor. The adjustment represents the fact that the measured deflection bowl has a finite horizontal extent, which may be due to the non-linear behavior of the pavement and subgrade materials. It does not necessarily mean that a rigid bottom really exists. In other words, these depths may not involve in all cases a stiff layer underlying the subgrade, but they might serve as apparent depths caused by an increase in subgrade stiffness with depth. The more rapidly the subgrade increases in stiffness with depth, the shallower will be the rigid layer determined.

Wiseman et al. (1977) suggested the use of $D/l_0 = 10$ for the Hogg model, where D denotes the

Table 1. D/lo values as a function of $H_p \times (E_p/E_s)^{1/3}$, based on Hoffman (2003).

Range of $H_p \times (E_p/E_s)^{1/3}$ [meter]	D/lo = D/ [$0.55 \times H_p \times (E_p/E_s)^{1/3}$]
$H_p \times (E_p/E_s)^{1/3} \geq 0.6$	5
$0.5 \leq H_p \times (E_p/E_s)^{1/3} < 0.6$	10
$0.4 \leq H_p \times (E_p/E_s)^{1/3} < 0.5$	20
$H_p \times (E_p/E_s)^{1/3} < 0.4$	40

depth to bedrock from the pavement-subgrade interface, and lo denotes the characteristic length of the system as defined by Hogg (1938 & 1944). The expression of lo (in meters) for a subgrade and pavement Poisson ratio of 0.5 is as follows:

$$l_o = 0.550 \times H_p \times (E_p/E_s)^{1/3} \quad (3)$$

where E_s denotes the subgrade resilient moduli, in MPa; E_p denotes the pavement resilient moduli, in MPa; H_p denotes the total pavement thickness, in meters.

The forwardcalculated [$H_p \times (E_p/E_s)^{1/3}$] AASHTOLIV value (termed also the apparent structural number, see Equation 1) should first be corrected before applying it into Equation 3. This is done with the following correction relationship taken from Livneh (2015):

$$H_p \times (E_p/E_s)^{1/3} = 0.1350 \times [H_p \times (E_p/E_s)_{uc}^{1/3}]^2 + 0.5961 \times [H_p \times (E_p/E_s)_{uc}^{1/3}] + 0.2432 \quad (4)$$

where [$H_p \times (E_p/E_s)_{uc}^{1/3}$] denotes the uncorrected apparent structural number as obtained directly from AASHTOLIV. Thus, for a corrected apparent structural number ranging from 0.5 to 3.5, the depth to bedrock from the pavement-subgrade interface (D) varies from 3 to 22 meters.

According to Hoffman (2003), the ratio of D/lo is not a fixed value but a function of the deflection-bowl shape defined by the area of the relative deflections; i.e. the ratio of the given measured deflection to the central deflection along the measurement line, starting at the loading center and ending at a radial offset of 900 mm. With the relationships given by Hoffman (2003), the aforementioned function of D/lo can be transformed to an equivalent function, depending on the apparent structural number variable. Table 1 displays the D/lo for defined ranges of $H_p \times (E_p/E_s)^{1/3}$.

Table 1 shows that for the most practical values of apparent structural numbers, the ratio of D/lo is half that of Wiseman et al. (1977); i.e. D/lo = 5, or D = 1.5 meters for $H_p \times (E_p/E_s)_{uc}^{1/3} = 0.5$ meter, and D = 11 meters for $H_p \times (E_p/E_s)_{uc}^{1/3} = 3.5$ meters.

In addition to the predefined depths, it should be added that the U.S. Corps of Engineers recommend that a rigid layer be placed at 6.0 meters below

the pavement surface; i.e. $B = D + H_p = 6.0$ meters (Bush, 1980). In addition, according to Rohde & Scullion (1990), rigid layer depths from the pavement surface are commonly placed at depths of 2.5–3.5 meters in sandy subgrades or at 3.5–5.0 meters in sandy clay subgrades and 5.0–7.5 meters in clay subgrades. As mentioned previously, these depths may not involve a stiff layer underlying the subgrade in all cases, but they might serve as apparent depths caused by an increase in subgrade stiffness with depth.

The ratio of the aforementioned bedrock modulus to subgrade modulus should also be assigned. According to Uzan (1998), the following values are utilized: 5, 10, 100 and 1,000. The final ratio value is usually assigned by the user, based on knowledge of the sub-surface conditions; i.e. whether rock exists or not. In cases in which no outputs are seen in the vicinity of the pavement or no other information concerning the existence of a stiff layer is available, a ratio value of 5 is usually recommended.

5 CALCULATED DEPTH TO BEDROCK

In contrast to the predefined depth values described in the previous section, it would appear that when Boussinesq equations are used for the homogenous case, the best results are obtained if a hard bottom is assumed to exist at a depth equal to the lateral extent of the measured deflection bowl (termed r_0), for which the anticipated deflection is zero. Thus, the assumption of a hard bottom at a finite depth related to the lateral extent of the measured deflection bowl, rather than at an arbitrary depth or at infinity, as is commonly assumed, yields more realistic pavement evaluation parameters for the given loads and method of measurement.

The use of r_0 alone to predict the depth to bedrock, however, does not lead to the required results, partly because of the existence of a layered system that is contrary to Boussinesq homogeneity. Corrective equations are therefore needed. To this end, Rohde & Smith (1991) developed four regression equations for estimating depth to a rigid layer using FWD data in the older version of MODULUS backcalculation program. They employed Boussinesq equations and the relationship between surface deflection and the inverse of radial offset to estimate the depth at which a zero deflection would occur together with FWD deflection basin parameters.

Thus, the aforementioned four regression equations, divided by a range of surface thicknesses, predict the depth to a rigid layer as a function of zero deflection point (r_0) and FWD deflection basin parameters, including Surface Curvature Index (SCI), Base Damage Index (BDI) and Base Curvature Index (BCI). These four equations were verified with field data. Later, Mahoney et al. (1993) evaluated these equations, developing a method adopted for use in the backcalculation program EVERCALC, used by the Washington State Department of

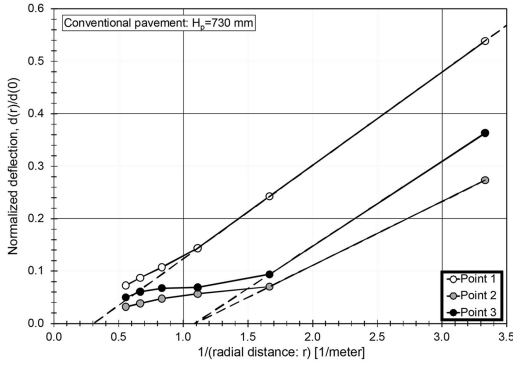


Figure 8. Example of deflection basins in normalized deflection-inverse radial space.

Transportation. The proposed four equations are as follows:

- (a) For pavements with asphalt surface layers less than 50 mm thick:

$$1/B=0.0362-0.3242 \times r_0+10.2717 \times r_0^2-23.6609 \times r_0^3-0.0037 \times BCI \quad (5)$$

- (b) For pavements with asphalt surfaces between 50 and 100 mm thick:

$$1/B=0.0065+0.1652 \times r_0+5.42898 \times r_0^2-11.0026 \times r_0^3-0.0004 \times BDI \quad (6)$$

- (c) For pavements with asphalt surfaces between 100 and 150 mm thick:

$$1/B=0.0413+0.9929 \times r_0-0.0012 \times SCI+0.0063 \times BDI-0.0778 \times \log(BCI) \quad (7)$$

- (d) For pavements with asphalt surfaces greater than 150 mm:

$$1/B=0.0409+0.5669 \times r_0+3.0137 \times r_0^2+0.0033 \times BDI-0.0665 \times \log(BCI) \quad (8)$$

where B denotes the depth to the top of the stiff layer, measured from the pavement surface, in feet (1 foot = 0.305 meter); r_0 denotes $1/r$ intercept by extrapolating the steepest section of the $1/r$ versus the deflection curve as shown in Figure 8, in $1/\text{feet}$ (1 foot = 0.305 meter); SCI denotes the Surface Curvature Index, equal to d_0-d_1 ; BDI denotes the Base Damage Index, equal to d_1-d_2 ; BCI denotes the Base Curvature Index, equal to d_2-d_3 ; d_i denotes the surface deflection in mill (1 mill = 24.5 μm), normalized to a 40 kN load at an offset i , in feet (1 foot = 0.305 meter).

After determining the apparent rigid layer for each FWD file is determined, Rohde & Scullion (1990) suggest that the average apparent rigid-layer depth for the listed sections be calculated by the following equations:

$$B_{av} = \frac{n}{\sum_{i=1}^n \frac{1}{B_i}} \quad (9)$$

Table 2. Depth to bedrock after Rohde and Scullion (1990).

Pavement	Hp [mm]	Ha [mm]	B_{av} [meter]	a/D
Conventional	1,560	220	14.8	0.011
All-Asphaltic	900	900	4.4	0.043
Conventional	800	150	1.7	0.171

$$D=B_{av}-H_p \quad (10)$$

where B_{av} denotes the average depth to an apparent rigid layer from the pavement surface, in feet (1 foot = 0.305 meter); B_i denotes the depth to the top of the stiff layer, measured from the pavement surface for the i th measured point, in feet (1 foot = 0.305 meter); n denotes the number of deflection bowls within one standard deviation of the mean $1/B_i$; D denotes the average depth to an apparent rigid layer, measured from the pavement subgrade interface, in feet; H_p denotes the total pavement thickness, in feet (1 foot = 0.305 meter).

Uzan (1998), on the other hand, claimed that the procedure based on the aforementioned four equations for estimating subgrade thickness was sensitive to deflection-measurement errors and may be inaccurate. He noted, in addition, that the calculated depth to rigid layer changes substantially when two of the four regression equations are used (i.e. using AC thickness corresponding to the transition from one equation to the other). This result, he argues, is an indication that the reliability of the four regression equations may not be accurate enough to predict depth to rigid layer.

As a result of these arguments, Uzan (1998) suggested a backcalculation procedure to predict depth to bedrock in the MODULUS 6 program. The procedure is based on a database of 21,840 cases that was calculated using, inter-alia, the spline interpolation technique. It is obvious that this method is not applicable with the AASHTOLIV equations. More details dealing with MODULUS 6 and AASHTOLIV results are given in the next section.

6 COMPARISON AND FINAL PROCEDURE

This section deals with a comparison of the calculated depth to bedrock as obtained from both Equations 5–10 and MODULUS 6 for the three given pavement-structures described previously. These depths were then compared with the predefined ones in order to suggest a final predictive procedure.

Using the four regression equations proposed in the previous section (i.e. Equations 5–8 for the measured deflection bowls of the given three pavement-structures leads to the results shown in Table 2. This table indicates that two entirely different rates of depth to bedrock were obtained at the Ben-Gurion International Airport: 14.8 meters for the conventional 1,560 mm thickness and 4.4 meters for the all-asphaltic

Table 3. Average depth to bedrock, including standard deviation and coefficient of variation derived from MODULUS 6.

Pavement	Hp [mm]	B [meter]		
		Average	St. Dev.	CoV [%]
Conventional	1,560	4.4	2.1	47.4
All-Asphaltic	900	2.1	2.3	110.2
Conventional	800	6.6	1.6	24.5

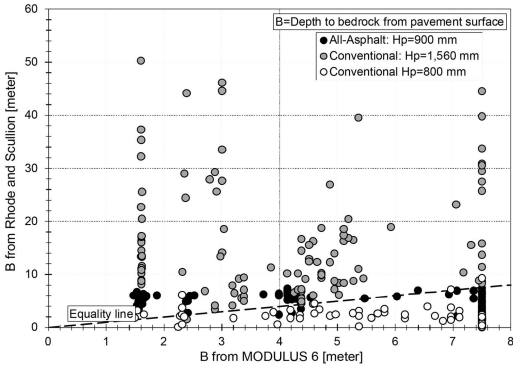


Figure 9. Calculated depth to bedrock derived from Equations 5–8 versus calculated depth to bedrock derived from MODULUS 6 for the three given structures.

900 mm thickness. In addition, the very shallow depth (1.7 meters) obtained for the Ovda Airport structure (with a conventional 800 mm thickness) seems to be unrealistic. These two findings make the use of Equations 5–10 for calculating depth to bedrock very questionable.

As for the MODULUS 6 outputs, the x-axis of Figure 7 shows the backcalculated depths for the three given pavement-structures. For the two pavement-structures at Ben-Gurion International Airport, the scatter of backcalculated depths is remarkable as may be seen in Table 3: the coefficients of variation are equal to 47.4% and 110.2%, respectively. Table 3 also shows that the average depth values are entirely different from those given in Table 2. A direct comparison of these values given in Figure 9 indicates that (a) no defined relationship exists and (b) the MODULUS 6 outputs, at least a major share of them, are also questionable.

A direct comparison of an AASHTOLIV subgrade modulus for the case of a predefined depth to bedrock equal to $D = 40 \times a$ and a MODULUS 6 subgrade modulus for the case of backcalculated depth to bedrock can be obtained from the average ratios (i.e. slope values) given in both Figure 1 and Figure 3. The ratio of these slope values denotes the average ratio of the AASHTOLIV to MODULUS 6 subgrade moduli at the specified depths. The values obtained are as follows: (a) $0.55/0.59 = 0.95$ for the conventional 1,560 mm structure, (b) $0.53/0.59 = 0.91$ for the all-asphaltic 900 mm structure, and (c) $0.71/0.99 = 0.71$

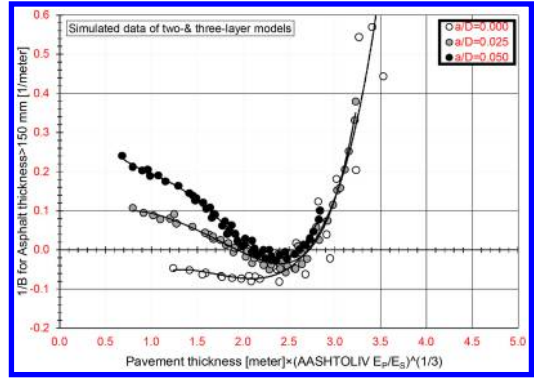


Figure 10. Calculated 1/depth to bedrock derived from Equations 8 versus calculated AASHTOLIV apparent structural number for two-layer simulated data, where a/D is equal to 0.00, 0.025 and 0.050.

Table 4. Average depth to bedrock (D) according to Hoffman (2003) and Wiseman et al. (1977) for the three given structures.

Pavement	Hp [mm]	SNap [m]	Average D [meter]	
			Hoffman	Wiseman et al
Conventional	1,560	2.28	6.3	12.5
All-Asphaltic	900	2.52	6.9	13.9
Conventional	800	1.23	3.4	6.8

Note: SNap denotes the corrected apparent structural number in meters; i.e. the value of $H_p \times (E_p/E_s)^{1/3}$ of Equation 4.

for the conventional 800 mm. These ratio values may indicate that they are directly connected with the average apparent structural number of these three structures; i.e. 2.25, 2.45 and 1.28 meters, respectively. This fact is compatible with the behavior of 1/B obtained from Equation 8 with the calculated AASHTOLIV apparent structural number for the two-layer simulated data, where a/D is equal to 0.00, 0.025 and 0.050, respectively. This behavior, plotted in Figure 10, point to the major impact of the apparent structural number on the results.

The pre-defined depth values (from the pavement-subgrade interface down to the bedrock; i.e. the D values) for the three given structures are given in Table 4. This table shows that the depth values obtained are not compatible with those of Table 2 and only partially compatible with those of Table 3.

The main conclusion derived from all the foregoing findings is that Equations 5–10, the relationships given by Hoffman (2003) and those by Wiseman et al. (1977), should not be used for calculating depth to bedrock. Instead, it is suggested that modified predefined values based on those given in Section 4 of Rohde & Scullion (1990) be implemented. The adopted depths from pavement to subgrade interface are these: 2.5 meters (i.e. $a/D = 0.060$) in sandy subgrades or 5.0 meters

(i.e. $a/D=0.030$) in sandy clay subgrades and 6.0 meters (i.e. $a/D=0.025$) meters in clay subgrades. A partial verification of the a/D value of 0.025 is given in the accompanying paper by Livneh (2015). Obviously, in cases in which in-situ geotechnical explorations indicate that a stiff layer actually exists at a certain depth from the ground's surface, this depth should be applied in the AASHTOLIV calculations.

7 FINAL CBR CONVERSION

Several pavement-design methods, among them the Israeli Flex-Design method for interurban roads (Uzan 1996) and the recent American FAARFIELD method for runways and taxiways (FAA 2009), still rely on the subgrade CBR value together with its equivalent resilient modulus. The latter is determined from the CBR value by a predefined correlative equation. The use of these two methods for overlay or reconstruction design involves a determination of the existing subgrade CBR value by various in-situ testing methods, including the Falling Weight Deflectometer (FWD). For that test, the subgrade CBR value is calculated from the FWD back-calculated or forwardcalculated subgrade resilient value.

However, use of the FWD involves, as previously stated, a serious lack of consistency in the interpretations made by various back- and forwardcalculation programs for the same field data (Zhou et al. 1989, Puppala 2008). Furthermore, the limitations of back- and forwardcalculations of stiffness parameters in the field when utilizing non-destructive test methods include poor agreement between interpreted moduli and the corresponding laboratory-measured or in-situ directly measured moduli. The reason for this inconsistency and lack of agreement stems partly from ignoring the depth to bedrock issue in various back- or forwardcalculations methods.

For example, the old AASHTO method (AASHTO 1993) recommended that E_s values backcalculated according to its method (see Equation 1 of Livneh 2015) be multiplied by a correction factor of $C_a = 0.33$ in the determination of SN for design purposes. The analyses described pertain to the fine-grained AASHTO Road Test site plus fine-grained soil from seven other projects. The old AASHTO method thus ignored the depth to bedrock issue; its suggested correction factor partly serves as compensation for the depth to bedrock issue. Furthermore, no attempt was made in the old AASHTO study to investigate the relationship between backcalculated and laboratory E_s values for granular subgrades.

In this context, it should be noted that a later research publication recommended a series of correction factors as a supplement to the old AASHTO design guide. Some of those correction factors are given in Table 5 (Von Quintus & Killingsworth 1997). In addition, some other ratios have been documented in the technical literature. In North Carolina, a comparison was conducted of subgrade soil resilient modulus

Table 5. Some old AASHTO modulus correction factors obtained from the LTPP study (Von Quintus & Killingsworth 1997).

Type of Structure above Subgrade	Correction Factor C_a	Coefficient of Variation [%]
Stabilized Subgrade	0.75	13
Full-Depth AC/PCC	0.52	37
Granular Base/Subbase	0.35	49

determined in the laboratory and backcalculation from three pavement sections (Ali & Khosla 1987). The correction factor C_a obtained varied from 0.18 to 2.44. In a Nottingham (England) study, a correction factor of 0.75 was found for a clayey subgrade (Tam & Brown 1989). The State of Washington (Mahoney & Pierce 1966, Newcomb 1987, Lee et al. 1988) showed that for local subgrades, the correction factor C_a ranged from 0.5 to 1.0 in the first reference, from 0.8 to 1.3 in the second reference, and from 0.4 and 1.3 in the third reference. For the LTPP study, the reported correction factor C_a ranged from 0.1 to 3.5 (Von Quintus & Killingsworth 1997). Furthermore, laboratory values were consistently higher (nearly two times) than the backcalculated values according to the study described in Chen et al. (1988). Finally, the correction factor C_a for subgrades in Michigan is, for design purposes, 1.0 (Dawson et al. 2009). In general, a detailed discussion of the differences between laboratory- and backcalculated measured resilient modulus can be found in Houston et al. (1992). This discussion also includes deviator stress effects.

An additional reference (Rahim & George 2003) shows that backcalculated moduli of the prepared subgrade (as tested by the FWD device directly on its surface) are in good agreement with laboratory values. Primarily because of confinement and overburden pressure, the backcalculated subgrade modulus based on deflection measurements of the finished pavement increases by approximately 40% and 100% for fine- and coarse-grained soil, respectively. In light of these results, Rahim & George (2003) conclude that the AASHTO factor of 0.33, computed from deflection measurements for adjusting backcalculated moduli, warrants further scrutiny and revision.

As mentioned before, all these inconsistent C_a values may result in part from ignoring the depth to bedrock issue in the associated back- or forwardcalculations methods. Thus, it may be concluded that when the depth to bedrock is included in these calculations, the value of C_a can be taken as 1.0. For this case, the suggestion is to convert the final AASHTO-LIV subgrade modulus into a CBR value by one of the following two equations:

$$CBR=Es/14 \quad (11)$$

$$CBR=(Es/25)^{1/0.64} \quad (12)$$

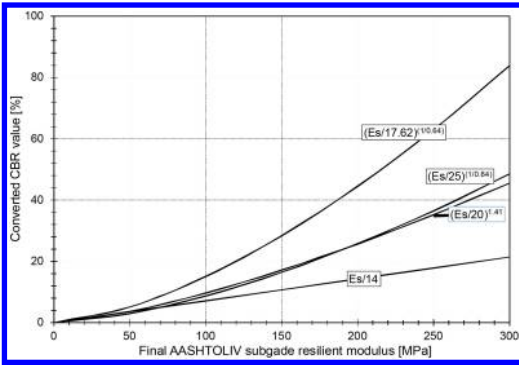


Figure 11. Converted CBR value versus final AASHTOLIV subgrade modulus according to (a) Flex-Design, (b) MEPDG, (c) modified MEPDG (i.e. replacing the denominator of 17.62 by 25) and (d) Equation 13.

where E_s denotes the final AASHTOLIV subgrade modulus, in MPa; CBR denotes the California Bearing Ratio, in percentage.

Equation 11 is taken from the Israeli Flex-Design program (Uzan 1966), and Equation 12 from the TRL's equation (Powell et al. 2004), its original denominator of 17.62 being replaced by the value of 25. This replacement is justified by cumulative field data, including that given in Livneh (2015), and leads to almost identical CBR results to those of Equation 11 in the region of E_s values equal 0 to 100 MPa (see Figure 11). In addition, it is suggested that the higher CBR value obtained from these two equations will be the final converted value.

Note that as shown in Figure 11, the relationship given in Equation 12 is very much similar to the one given in the following equation, which has been suggested for use in Israel (Livneh 2014):

$$CBR = (E_s/20)^{1.41} \quad (13)$$

Livneh (2014) also includes a detailed comparison of the various relationships found in the technical literature. Together with the above calculative procedure, it is very much recommended that the final E_s -CBR relationship in any rehabilitation design be assessed by conducting both FWD and in-situ CBR (DCP) tests on the existing pavements under consideration (Livneh 2000).

It should be noted that this recommendation is similar to the following (Monismith and Brown 1999): "As a part of this process, some procedures include the testing of materials in the laboratory to define their stiffness (modulus) characteristics, in particular, undisturbed subgrade specimens. Cores from the asphalt concrete and other treated layers may also be obtained. These results are important to insure that the moduli determined by back-calculation are reasonable. Relative to the core data, it must be recognized that the back-analysis provides values for the bulk

material while the cores provide spot values for the intact material."

8 CONCLUSIONS

Findings from the current study on (a) the depth to bedrock issue in forward calculation of FWD deflection-basin measurements and (b) the derivation of CBR from the forward-calculated subgrade modulus yield the following conclusions:

- The introduction of a rigid layer at a definite depth from the pavement-subgrade interface substantially reduces the AASHTOLIV subgrade modulus and increases or sometimes reduces, both to a minor extent, the AASHTOLIV pavement modulus. The same applies to the outputs of MODULUS 6.
- For the three case-studies described here, the outputs of the two programs (i.e. MODULUS 6 and AASHTOLIV) for the case of infinite depth to bedrock are essentially close, a fact that supports the use of the AASHTOLIV equations.
- A direct comparison of the AASHTOLIV subgrade modulus for the case of a predefined depth to bedrock equal to $D = 40 \times a$ and the MODULUS 6 subgrade modulus for the case of backcalculated depth to bedrock leads, for the given three case-studies, to close values when the apparent structural number is high, 2.25 meters and above.
- The MODULUS 6 backcalculated depths to bedrock yields, even for a given limited site, an unrealistic range of depth-values, some of them un-expectedly very much adjacent to the pavement-subgrade interface.
- The prediction of depth to bedrock with the aid of Rohde & Smith's (1991) four regression equations may lead again to unrealistic depth results.
- Applying a predefined depth to bedrock seems to be the most adequate alternative in the AASHTOLIV forward calculations; to this end, definite depth values stemming from the comparison of the available data given in the paper are suggested.
- When the AASHTOLIV equations are applied together with the suggested predefined depth to bedrock, the AASTHTO factor of 0.33 for adjusting backcalculated moduli, which was computed from deflection measurements, is replaced by the value of 1.0.

Finally, it follows from these conclusions that knowledge of the depth to bedrock is very crucial. When using the AASHTOLIV equations, then, it is essential to implement the suggested predefined depth values in the forward calculations. Obviously, in cases in which in-situ geotechnical explorations indicate that a stiff layer actually exists at a certain depth from the ground's surface, this depth should be applied in the AASHTOLIV calculations. Furthermore, the issue of how to calculate the subgrade CBR value from the final AASHTOLIV forward-calculated subgrade resilient modulus, discussed at the end of the present paper,

suggests that, where possible, the Es-CBR relationship in any rehabilitation design be assessed by conducting both FWD and in-situ CBR (DCP) tests on the pavements under consideration.

REFERENCES

- AASHTO. 1993. *AASHTO Guide for Design of Pavement Structures* 1993. Washington, DC: American Association of State Highway and Transportation Officials.
- Ali, N.A. and Khosla, N.P. 1987. Determination of layer moduli using a falling weight deflectometer. *Transportation Research Record* No.1117: 1–10.
- Chen, D.H., Bilyeu, J. and He, R. 1988. Comparison of resilient moduli between field and laboratory testing: A case study. *Proceedings of the 76th Annual Meeting of the Transportation Research Board*, Washington, DC.
- Dawson, T., Baladi, G.Y. and Haider, S.W. 2009. Back-calculation of resilient modulus of roadbed soils. *Proceedings of the Sixth International Conference on Maintenance and Rehabilitation of Pavements and Technological Control*, Torino, Italy.
- Federal Aviation Administration (FAA). 2009. *Airport Pavement Design and Evaluation*. Advisory Circular, AC 150/5320-6E.
- Hoffman, M.S. 2003. Direct method for evaluating structural needs of flexible pavements with Falling-Weight Deflectometer deflections. *Transportation Research Record* 1860: 41–47.
- Hogg, A.H.A. 1938. Equilibrium of a thin plate, symmetrically loaded, on an elastic foundation of infinite depth. *Philosophical Magazine* 25 (168): 576–582.
- Hogg, A.H.A. 1944. Equilibrium of a thin slab on an elastic foundation of finite depth. *Philosophical Magazine* 35 (243): 265–276.
- Houston, W.A., Mamlouk, M.S. and Perera, R.W.S. 1992. Laboratory versus nondestructive testing for pavement design. *ASCE Journal of Transportation Engineering*, 118 (2): 207–222.
- Lee, S.W., Mahoney, J.P. and Jackson, N.C. 1988. Verification backcalculation of pavement moduli. *Transportation Research Record* 1196: 85–96.
- Livneh, M. 2000. Small-scale dynamic devices for subgrade and granular layer characterization. *Proceedings of the 3rd Transportation Engineering Specialty Conference*, Canadian Society for Civil Engineering (CSCE), London, Ontario.
- Livneh, M. 2007. Uncertainty associated with pre-defined correlative expressions of various in-situ test outputs. *Proceedings of the 2007 Federal Aviation Administration (FAA) Technology Transfer Conference*, Atlantic City, NJ.
- Livneh, M. 2014. Uncertainty of backcalculated values in pavement overlay design when using the FWD device. *Proceedings of the 4th International Conference on Geotechnique, Construction Materials & Environment, (GEOMATE 2014)*, Brisbane, Australia.
- Livneh, M. 2015. Recent modifications to the 1993 AASHTO equations for forwardcalculating subgrade and pavement moduli. *Proceedings of the Sixth International Conference on Bituminous Mixtures and Pavements*, Thessaloniki, Greece.
- Mahoney, J.P. and Pierce, L.M. 1966. An examination of Washington state department of transportation transfer functions for mechanical-empirical AC overlay. *Transportation Research Record* 1539: 25–32.
- Mahoney, J.P., Winters, G.C., Jackson, N.C. and Pierce L.M. 1993. Some observations about backcalculations and use of a stiff layer condition. *Transportation Research Record* 1384: 8–14.
- Monismith, C.L. and Brown, S.F. 1999. Developments in the structural design and rehabilitation of asphalt pavements over three quarters of a century. *Journal of the Association of Asphalt Paving Technologists* 68A: 128–251.
- Newcomb, D.E. 1987. Comparison of field and laboratory estimated resilient moduli of pavement materials. *Journal of the Association of Asphalt Paving Technologists* 56: 91–106.
- Powell, W.D., Potter J.F., Mayhew, H.C., and Nunn, M.M. 1984. *The Structural Design of Bituminous Roads*. TRRL Laboratory Report 1132, Transportation and Road Research Laboratory, Wokingham, Berkshire, UK.
- Puppala, A.J. 2008. *Estimating Stiffness of Subgrade and Unbound Materials for Pavement Design*. NCHRP Synthesis 382. Washington, DC: Transportation Research Board.
- Rahim, A., and George, K. P. 2003. Falling weight deflectometer for estimating subgrade elastic moduli. *Journal of Transportation Engineering* 129(1): 100–107.
- Rohde, G.T. and Scullion, T. 1990. *MODULOS 4.0: Expansion and Validation of the Modulus Backcalculation System*. Report No. FHWA/TX-91/1123-3. Texas Department of Transportation, Austin, TX.
- Rohde, G.T. and Smith, R.E. 1991. *Determining Depth to Apparent Stiff Layer from FWD Data*. Research Report FHWA/TX-91-1159-1, Texas Department of Transportation, Austin, TX.
- Tam, W.S. and Brown, S.F. 1989. Back-analyzed elastic stiffness: Comparison between different evaluation procedures. *Nondestructive Testing of Pavements and Back-calculation of Moduli, ASTM STP 1026*, In A.J. Bush III and G.Y. Baladi, Eds., American Society for Testing and Materials, Philadelphia, pp. 189–200.
- Thenn de Barros, S., 1966. Deflection factor charts for two- and three-layer elastic systems. *Highway Research Record* 145: 83–108.
- Uzan, J. 1996. A pavement design and rehabilitation system. *Transportation Research Record* 1539: 110–115.
- Uzan, J. 1998. Estimation of subgrade thickness from deflection basin analysis. *Proceedings of 5th International Conference on the Bearing Capacity of Roads and Airfields*, Trondheim, Norway: 507–516.
- Von Quintus, H.L. and Killingsworth, B.H. 1997. *Design Pamphlet for the Determination of Design Subgrade in Support of the 1993 AASHTO Guide for the Design of Pavement Structures*. Report No. FHWA-RD-97-083, FHWA, Department of Transportation, Washington, DC.
- Von Quintus, H.L. and Killingsworth, B.M. 1988. Comparison of laboratory and in-situ determined elastic moduli. *Proceedings of the 76th Annual Meeting of the Transportation Research Board*, Washington, DC.
- Wiseman, G., Uzan, J., Hoffman, M.S., Ishai, I. & Livneh, M. 1977. Simple elastic models for pavement evaluation using measured deflection bowls. *Proceedings of the Fourth International Conference on Structural Design of Asphalt Pavements*, II. Ann Arbor, Michigan: 416–426.
- Zhou, H., Hicks, K.G. and Huddleston, I.J. 1989. Evaluation of the 1986 AASHTO overlay design method. *Transportation Research Record* 1215: 299–316.

Evaluation of the AASHTO Pavement ME software for the control of thermal cracking

B.C. Ghimire & S.A.M. Hesp

Department of Chemistry, Queen's University, Kingston, Ontario, Canada

ABSTRACT: An important part of the AASHTO Pavement ME software is used to predict low temperature cracking. Superpave™ grades for the asphalt cement can be used to provide rudimentary predictions of cracking. More accurate results can be obtained from indirect tensile test (IDT) data obtained for the asphalt mixture. This paper discusses cracking predictions for a number of pavements in Ontario, Canada. Superpave grades appeared to predict satisfactory performance but a majority of mixes failed early when IDT properties were used. This discrepancy is analyzed with tests on the recovered asphalt cements. It was found that the current aging protocols underestimate the degree of hardening that occurs during HMA production. This leads to an overestimation of a pavement's cracking performance when Superpave grades are used as input. Improving the asphalt cement aging and conditioning protocols, test methods and specifications, will go a long way towards rectifying this problem.

1 INTRODUCTION

Thermal cracking in northern climates remains a serious and ubiquitous form of distress, limiting the life cycles of most flexible pavements. This is in spite of long term research efforts to better understand and control this type of damage.

With the introduction in much of North America of the Superpave asphalt cement and mixture test methods and acceptance criteria in the mid to late 1990s, a flurry of publication and patent activity occurred describing developments to produce enhanced Superpave grade spans (XX-YY) through the use of a wide range of chemical modifications (for instance, see Kriech & Wissel 1989, Kamel & Miller 1991, De Filippis et al. 1995, Johnson and Juristovski 1995, Memom et al. 1995, Hayner 1999, Bonemazzi and Giavarini 1999, Collins and Jones 2000, Giavarini et al. 2000, Moore et al. 2000, Leclerc et al. 2002, Hagens et al. 2004, Villanueva et al. 2008, Hesp et al. 2009, Fee et al. 2010, Hesp and Shurvell 2010, Rubab et al. 2011, and others).

Today, asphalt cements are routinely modified to produce grades that are unavailable through straight distillation of common crude oils (Varadaraj et al. 2006, Kodrat et al. 2007). Grade spans over 86°C are typically modified with chemicals or polymers. Many of the methods are based on the formation of partially gelled structures in the asphalt binder. An increase in asphaltenes, or the addition of waxes, acids, bases, or other flocculants, can easily produce grade spans approaching or exceeding 100°C. However, what buyers of asphalt cement fail to recognize is that the low temperature performance can vary a great deal depending on the type of modification that is used. Hence,

they often end up paying more for less, as shown by premature and excessive thermal cracking distress after only several years of service (Yee et al. 2006, Hesp et al. 2009a, b, Hesp & Shurvell 2010, and others).

In addition to the proliferation of chemical modifiers based on the formation of gels, the wide introduction of recycling efforts in North America has added additional pressure on pavement life cycles. Recycled asphalt pavement (RAP) and recycled asphalt shingle (RAS) are now commonly promoted to replace a proportion of the virgin binder without any grade adjustment. Oxidized asphalt cements from RAP or RAS have the same effect as chemical modifiers used to gel the virgin material. This also leads to premature failures that could hardly be avoided when only the base asphalt cement is specified and no appropriate tests are conducted on the recovered asphalt cement and/or mixture.

It is the objective of our research program to investigate if accurate thermal cracking predictions can be obtained with the AASHTO Pavement ME software based on low temperature indirect tensile creep and strength data as obtained according to AASHTO method T322 *Determining the Creep Compliance and Strength of Hot Mix Asphalt (HMA) Using the Indirect Tensile Test Device*.

2 BACKGROUND ON THERMAL CRACKING

Thermal cracking in asphalt pavements has been studied for a long time (for instance, see van der Poel 1954, 1955, Heukelom 1966, McLeod 1972, Deme & Young 1987, and others). Failure in asphalt pavements at low temperatures is often a complex process and can

involve a number of different factors that lead to an increase in cracking severity with time. Low temperature cracks are often found transverse to the driving direction because this is how the bulk of the thermal strain energy is stored during cold periods in winter. The longitudinal direction is restrained whereas the transverse direction can often shrink enough to prevent longitudinal thermal cracks. In very old and/or severely aged pavements, the appearance of block type cracking indicates that the transverse shrinkage has become sufficient to also cause cracking in the longitudinal direction. However, these observations do not say much if anything about how and when each individual crack started. Evidence from thin yet conventionally designed pavement trials in northern Ontario and elsewhere suggests that the onset and severity of low temperature transverse and longitudinal cracking distress can be intricately linked to not only the binder's low temperature stiffness and relaxation ability but also its fatigue characteristics and moisture sensitivity, asphalt mixture design, traffic levels, structure of the pavement, paver-induced segregation, and subgrade characteristics (Deme & Young 1987, Robertson 1995, Deme 1996, Hesp 2009a, b).

Thermal cracking started to become a major problem in the 1950s and 1960s when increasing traffic loads made necessary the replacement of soft binders with harder ones in order to avoid excessive rutting. Several empirical methods (viscosity, penetration, ring and ball softening point) were used in an attempt to quantify the behavior of the binders. Based on such properties, van der Poel (1954, 1955) at the Shell Laboratory in Amsterdam developed a nomograph that he used in choosing asphalt binders for hot-mix construction. From this effort, he concluded that: "as all bitumens have approximately the same breaking strength, the Fraass temperature should be an equistiffness temperature, corresponding to a stiffness of roughly 10^8 N/m^2 at 11 sec."

Following his colleague's work, Heukelom (1966) conducted extensive studies that appeared to show a reasonable correlation between the stiffness of a binder and its failure behavior under various conditions. Heukelom's paper implied that the elongation at break, as measured in either tension or bending, at a specific loading time, was directly related to low temperature performance in the pavement. Heukelom also stated that the stiffness "can be regarded as the main parameter for fracture, and thus for the permissible deformation." Based on their work and other unpublished data, Krom & Dormon (1963) were the first to present a binder specification scheme that limits the binder stiffness at specific loading times and temperatures to control cracking due to traffic ($t = 10^{-2}$ s and low temperatures) and thermal stresses ($t = 10^4$ s and low temperatures).

One of the main shortcomings of the early work by van der Poel (1954, 1955) and Heukelom (1966) at Shell, as well as that of their followers such as McLeod (1972) in Canada, was that the properties such as penetration, viscosity and ring and ball softening

point, were measured at relatively high temperatures and then used to predict performance over the entire pavement time-temperature domain. In addition, the Shell researchers were very skillful at simplification and approximation. A close look at the comparisons made in the aforementioned papers reveals that the scatter for some of them was actually quite large. A point already observed by van der Poel himself when he stated that "the correlation is obvious, although the spread is large", in his discussion following the comparison of the difference between ring and ball softening point and Fraass temperature, $T_{R\&B} - T_{\text{Fraass}}$, and the penetration index, P.I. (van der Poel 1954). However, in those times the methods promoted by their effort were of practical importance since traffic levels were low and consequently tolerances were high.

The Superpave asphalt cement and mixture design method used a lot of the ideas of the above mentioned earlier researchers to develop methods for the prediction of thermal cracking distress. The asphalt binder specification method developed under the SHRP program, now known as AASHTO M320, employs a limit on binder creep stiffness and creep rate (AASHTO 2002). A thin asphalt beam is cooled for one hour at the grading temperature, after which it is loaded in three-point bending to measure the stiffness at 60 s, $S(60)$, and the slope of the creep curve, commonly known as the m-value, also at 60 s, $m(60)$. The binder specification sets an upper limit of 300 MPa on the stiffness and a lower limit of 0.3 on the m-value. If a binder passes these two criteria then it passes the grading test and it can be used in a particular climatic zone where the pavement surface temperature reaches 10°C below the grading temperature only once every 50 years.

While the philosophy behind the Superpave asphalt cement specification tests dates back to the aforementioned work by van der Poel (1954, 1955) and Heukelom (1966) at the Shell Laboratories, it is interesting to note that today nearly all asphalt cement low temperature grades are controlled by their m-value, reflecting the wide presence of gelling additives. A gel is defined in rheological terms as a material with an infinite viscosity (m-value equal to zero) and a stiffness approaching zero. These materials are of a high penetration index (PI) and retain thermal stresses rather than relax them. It was shown by McLeod (1972) that such binders show excessive cracking distress with a series of pavement trials constructed around Southwestern Ontario during the early 1960s. Besides showing divergent limiting stiffness and m-value temperatures, gel-type binders also have relatively low phase angles and ductility, high rheological indices (i.e., low curvature in their stiffness master curve), and they suffer from increased oxidative hardening (Rubab et al. 2011).

Work on pavement trials and problem contracts has shown that the current Superpave asphalt cement specification is deficient in that equal grades can show vastly different cracking performance and more than a few pavements crack in early life (Yee et al. 2006, Hesp et al. 2009a, b, Hesp & Shurvell 2010, and others).

Table 1. Pertinent contract information.

Contract	Highway	AADT	Grade
A	–	10,500	64-28
B	–	450	58-28
C	28	6,100	58-34
D	401	431,900	70-28
E	401	32,900	64-28
F	401	17,800	64-34
G	406	45,200	64-28
H	417	30,000	64-34

Note: Contracts A and B were placed on arterial and secondary roads within the City of Kingston. AADT = annual average daily traffic. Grades were determined according to AASHTO R29 (2010) protocols.

Hence, research is ongoing in an effort to improve our ability to predict and control pavement cracking. The approach discussed herein looks at low temperature mixture testing since it should deal with potential problems associated with the presence of RAP/RAS and overheating of the asphalt mixture during construction.

3 EXPERIMENTAL

3.1 Materials

Hot mix asphalt (HMA) samples were obtained from reconstruction contracts for the City of Kingston and from around the Province of Ontario. Samples were obtained directly from the paver and stored in cardboard boxes. Nearly all samples were processed within several weeks of collection.

The asphalt cements were extracted with toluene and toluene/ethanol solvent of reagent grade under a dry nitrogen gas blanket.

A list of pertinent contract information is provided in Table 1.

3.2 Procedures

The HMA samples were heated in their cardboard boxes within a forced convection oven. Boxes were placed in the oven at 120°C in late afternoon, processed in a bucket mixer around mid-morning the following day, and compacted at temperatures between 130 and 145°C in a gyratory compactor around 12 noon. Heating times and temperatures were kept constant for all mixes in order to provide similar degrees of short term oven aging.

Air voids were measured by weighing above and under water. All specimens used for testing were kept within a narrow air voids range of 4 to 6%.

The indirect tensile (IDT) creep and tensile strength properties were determined in a compression fixture mounted within an environmental chamber of a 100 kN MTS 810 servo-hydraulic test frame. Figure 1 provides a picture of the specimen within the IDT fixture just prior to testing.



Figure 1. Indirect tensile test fixture, specimen and extensometers just prior to testing.

Vertical and horizontal strains on both sides of the IDT specimens were measured with two sets of Epsilon model 3190 extensometers. Creep tests were conducted at 0, -10, -20 and -30°C, at loads varying from 1,000 to 8,000 N. Strength tests were conducted at -10 and -20°C at a loading rate of 12.5 mm/min. Creep strain values were plotted versus time for a minimum of three replicate tests and outliers were excluded from processing in the AASHTO Pavement ME software. All data processing followed AASHTO standard T322 *Determining the Creep Compliance and Strength of Hot Mix Asphalt (HMA) Using the Indirect Tensile Test Device*.

Creep strains at 1, 2, 5, 10, 20, 50 and 100 s at three temperatures were entered in the AASHTO Pavement ME software together with the indirect tensile strength at -10°C. The software program uses the creep strains to calculate creep compliance values that are fitted to a master curve (ARA 2004):

$$D(t) = D_0 + D_1 t^m \quad (1)$$

where:

$D(t)$ is the creep compliance (Pa^{-1}), and D_0 , D_1 and m are fitting constants.

The m -value from equation 1, the mixture stiffness E , and the undamaged mixture tensile strength σ_m from the IDT test are used by the software to calculate Paris law cracking parameters:

$$\Delta C = A \times \Delta K^n \quad (2)$$

where:

ΔC is the change in crack depth due to a cooling cycle, m ;

ΔK is the change in stress intensity factor due to a cooling cycle, $\text{N}\cdot\text{m}^{-3/2}$; and

A and n are the Paris law cracking parameters:

$$n = 0.8(1 + m^{-1}) \quad (3)$$

$$A = 10^{(\beta(4.389 - 2.52 \log(E\sigma_m^n)))} \quad (4)$$

The AASHTO Pavement ME software uses the Paris law together with local climate data to predict cracking in time following the TCMODEL algorithm (ARA 2004). Three levels of input are provided in the software. Level 1 uses actual laboratory IDT results at three temperatures for creep and one temperature for strength. Level 2 uses both creep and strength at a single temperature while level 3 input uses asphalt cement and mixture properties that provide estimates of the creep compliance instead of measured values (ARA 2004). In this investigation both level 1 and 3 input were used to obtain thermal cracking predictions.

After testing at low temperatures, the HMA was broken into smaller pieces and soaked in toluene overnight to extract the asphalt cement. After soaking, the aggregate was washed several more times with toluene followed by a 15/85 volume to volume mixture of absolute ethanol and toluene. Once nearly all the asphalt cement was removed from the aggregate, the solution was left to sediment overnight and the asphalt cement was recovered with a rotary evaporator under a blanket of dry nitrogen gas. The bulk of the solvent was removed under reduced pressure at a temperature between 50 and 70°C. Once no more solvent was visibly being distilled the temperature was raised to 160°C and the pressure reduced to below 50 mbar for an additional 2 hours to assure the complete removal of solvent. A nitrogen flow of 0.5 L/min was maintained to prevent further oxidative hardening during the recovery.

The recovered binders were used for testing in dynamic shear and bending beam rheometers (DSR and BBR) according to standard procedures (AASHTO T313 and T315 (2010)). Performance grades were determined according to AASHTO R29 (2010) protocols in order to compare the recovered grades to those provided with the mix designs.

4 RESULTS AND DISCUSSION

4.1 Asphalt mixture tests

Examples of the creep test results are provided in Figures 2–4. The load versus time graphs showed that the MTS 810 system was extremely accurate in terms of its ability to bring the load to the set point and to keep it there for the desired time. The time to reach the creep load was typically well below 1 s while the overshoot in load was kept below 1%.

A trimmed mean approach was used to obtain creep compliance averages to be used in the software. In this approach the highest and lowest values of the strain were discarded from each set of measurements before these were used in the software (AASHTO 2007).

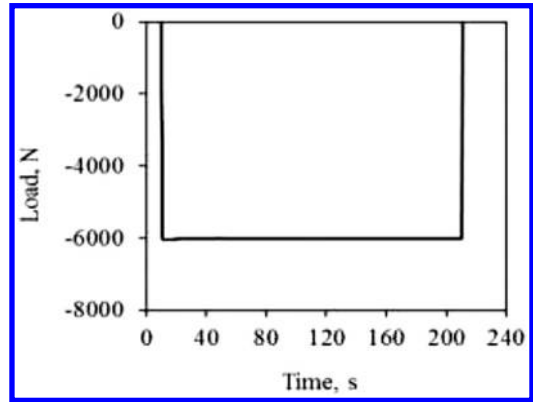


Figure 2. Creep load versus time graph at -30°C (loading time < 1 s and overshoot $< 1.0\%$).

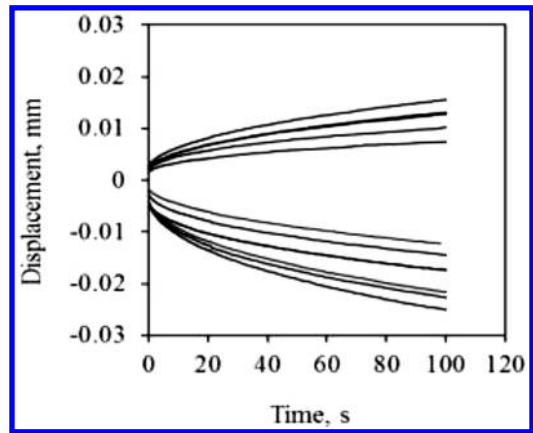


Figure 3. Set of horizontal and vertical IDT creep data obtained at 0°C (prior to trimming).

Creep data at each temperature were used to determine a master curve as shown in Figure 4. The shift factors were entered in an Excel spreadsheet and a visual observation was used to judge the quality of the data. Any obvious discontinuities in the master curve would indicate a problem with the raw creep data prompting a repeat of the testing.

The cracking predictions from the AASHTO Pavement ME software included the time to 190 m of cracks per kilometer of two lane road, which had been defined by the researchers that developed the software as an acceptable level of distress for a 15 year old road. The other output parameter was the total amount of cracking at the 15 year design life. Table 2 provides the predicted distress levels for the investigated pavements based on both their asphalt cement performance grade as given on the mix design sheet and the experimental IDT data.

The results show that there is quite a divergence between the predictions based on the PGAC grade and IDT data. This is most likely due to differences in asphalt cement aging during the production and reheating of the hot mix asphalt for compaction in the

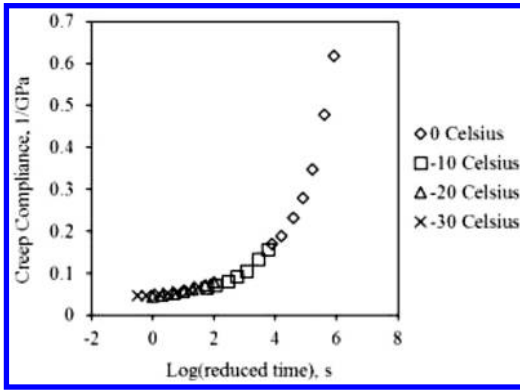


Figure 4. Creep compliance master curve (shifted to -20°C).

Table 2. AASHTO Pavement ME Output.

Contract	Years to 190 m/km		Cracking at 15 Years (m/km)	
	PGAC	IDT	PGAC	IDT
A	>15	>15	5.4	70
B	>15	>15	5.4	162
C	>15	2	5.2	377
D	>15	1	46.1	547
E	>15	1	47.1	544
F	>15	>15	46.1	74
G	>15	1	52.6	507
H	>15	2	5.0	398

Note: Contracts A and B are arterial and secondary roads within the City of Kingston. PGAC is AASHTO M320 performance grade as provided on the mix design.

laboratory. To further investigate the asphalt cements were extracted with toluene and toluene/ethanol mixtures and recovered for analysis of their rheological properties. The results of this investigation is discussed in the next section.

In addition to the regular IDT test with a conditioning period of between 1 and 4 hours at the test temperature, a number of contracts were investigated for their tendency to change performance after 72 hours of cold conditioning. It is well known that asphalt cements can physically harden during cold conditioning and that asphalt mixtures can show micro cracking due to the thermal shrinkage associated with the conditioning (Traxler 1936, 1937, Brown et al. 1957, Brown & Sparks 1958, Blokker & van Hoorn 1959, Struik 1978, Fryazinov et al. 1979, Pechenyi & Kutznetsov 1990, Bahia & Anderson 1991, Claudy et al. 1992, El Hussein et al. 1998, Soenen et al. 2004, Zhao & Hesp 2006, Hesp et al. 2007, Kriz 2009, Schmets et al. 2010, Togunde & Hesp 2012, Ahmed et al. 2012, Judycki 2014, Johnson & Hesp 2014, others). Hence, it was expected that this phenomenon should also have a bearing on the predictions from the AASHTO Pavement ME software.

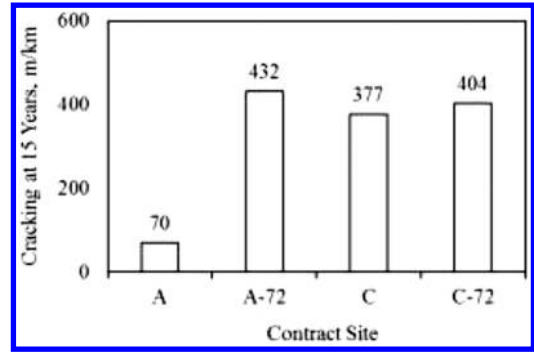


Figure 5. Effect of 72 hours of conditioning at -10°C on cracking predictions.

Figure 5 provides results for two mixes conditioned for either 1–4 hours at the test temperature or for 72 hours at -10°C followed by 1–4 hours at the test temperature. The data show that only a modest effect is seen for Contract A which reaches the 190 m threshold in 9 years after cold conditioning. This is likely due to the fact that its binder is of good quality. In contrast, the effect on the lesser quality binder from Contract C was not too significant, likely because it was already predicted to fail in early life after only 2 years of service and the software predicts a maximum amount of transverse cracking of only about 500 m/km. However, the nearly five-fold increase in cracking for Contract A due to 72 hours of cold conditioning is significant enough to warrant further investigation.

4.2 Asphalt binder tests

The asphalt binders as recovered were graded according to AASHTO R29 protocols (AASHTO 2010). Samples were also conditioned for an additional 72 hours in the BBR bath at cold temperatures and the grades were once again determined by pass and fail testing. The results of this investigation are provided in Table 3.

The findings of this investigation show that only Contracts A, B and E possessed recovered grades that are able to withstand the low temperature conditions encountered in the climatic zone for the contract location (as deduced from the grade given on the mix design). Samples C, D, F and H failed the low temperature grade requirements by anywhere from 1 to 6°C . After additional oxidative hardening in service, it is likely that the grade losses for Contracts C, D, F and H will result in early and excessive cracking distress. Samples E and G will also fare poorly while it is hoped that A and B will survive for at least 15 years without much distress.

Binders A and B were specified according to extended BBR and double-edge-notched tension protocols. They are limited to a 6°C grade loss over three days of conditioning at -18 and -8°C on their PAV residue. This has motivated asphalt sellers to produce materials that are significantly more resistant to oxidative and physical hardening. Whether the PAV

Table 3. Grades for recovered asphalt cements.

Contract	Superpave Grades		
	Mix Design	Recovered Grades	
		1 hr BBR, °C	72 h BBR, °C
A	64-28	83-32	83-30
B	58-28	74-31	74-30
C	58-34	72-32	72-30
D	70-28	96-21	96-21
E	64-28	82-30	82-29
F	64-34	79-33	79-33
G	64-28	—	—
H	64-34	76-30	76-30

Note: Asphalt cement for Contract F was not recovered.

aged residues for the recovered binders retain their favorable performance characteristics remains to be an issue worthy of further investigation.

Finally, the data from Table 3 also show that the RTFO aging protocol is not very good at replicating the high temperature grades. The recovered high temperature grades were anywhere from 12 to 26°C higher than the values obtained from DSR testing of the RTFO residue. Such differences are huge and might explain to some extent the poor performance of the mixes in terms of their low temperature creep properties. What lies at the heart of these big differences is unclear at this moment but they may indicate the presence of RAP (while none was disclosed on the mix design sheets), overheating of the mixes during production, or some till now unknown problem with the recovery process. However, we emphasize once more that great care was taken not to change the asphalt cement properties during the extraction and recovery processes under a nitrogen gas atmosphere.

5 CONCLUSIONS

Given the results and discussions provided herein, the following conclusions are given:

- The IDT test results show that 5 out of 6 regular Ontario paving contracts were seriously under-designed for thermal cracking.
- The premature and excessive cracking prediction is likely due to deficient laboratory aging protocols. Conditioning times in the RTFO, PAV and BBR prior to grading of the asphalt cement should be reassessed for their ability to replicate field aging.
- The recovered asphalt cements showed grade losses/deficits ranging from 1 to 7°C, which explains in large part the expected poor performance.

6 FURTHER WORK

Further work should focus on improving the laboratory aging protocols to more accurately reproduce what happens to the asphalt cement during production and

early life. Rolling thin film oven and pressure aging vessel methods were developed with a series of standard Strategic Highway Research Program Materials Reference Library (SHRP MRL) binders produced 30+ years ago. Asphalt binders have changed significantly since the 1980s and those changes have obviously resulted in more severe aging during production and in early life (Erskin et al. 2009, Hesp & Shurvell 2010, Rubab et al. 2011, Hesp & Shurvell 2012, Johnson & Hesp 2014).

Finally, there has also been a shift away from rather conventional thermal cracking with regularly spaced transverse cracks, to a more complete disintegration of the pavement structure (Hesp et al. 2009a). These types of failures point to physical hardening (differential shrinkage) weakening the interface followed by moisture ingress causing disintegration during spring thaw. This increased interfacial damage is likely due to the widespread introduction of waste engine oils, vegetable oils, and other detrimental additives in the asphalt cement supply (Hesp & Shurvell 2013). Hence, testing for moisture damage after freeze-thaw cycles would also help to mitigate both thermal and moisture induced distresses (El Hussein et al. 1998, Jaskula & Judycki 2014).

ACKNOWLEDGEMENTS

Special thanks goes out to Warren Lee and Seyed Tabib of the Ministry of Transportation of Ontario for their assistance with the collection of HMA samples and the processing of the IDT creep and strength data to produce thermal cracking predictions. Graeme Gillespie, Kelli-Anne Johnson, Phillip Maurer and David Sowah-Kuma are thanked for their help with sample preparation and the collection of experimental data. Financial support for this research through the Highway Infrastructure Innovations Funding Program of the Ministry of Transportation of Ontario is also gratefully acknowledged.

REFERENCES

- AASHTO T313, Standard Method of Test for Determining the Flexural Creep Stiffness of Asphalt Binder Using the Bending Beam Rheometer (BBR), AASHTO, 2010.
- AASHTO T315, Standard Method of Test for Determining the Rheological Properties of Asphalt Binder Using a Dynamic Shear Rheometer (DSR), AASHTO, 2010.
- AASHTO T322, Determining the Creep Compliance and Strength of Hot Mix Asphalt (HMA) using Indirect Tensile Test Device, AASHTO 2007.
- AASHTO M320, Standard Specification for Performance-Graded Asphalt Binder, AASHTO, 2009.
- AASHTO R29, Grading or Verifying the Performance Grade (PG) of an Asphalt Binder, AASHTO, 2010.
- Ahmed, E.I., Hesp, S.A.M., Paul Samy, S.K., Rubab, S.D. & Warburton, G. 2012. Effect of warm mix additives and dispersants on asphalt rheological, aging, and failure properties. *Construction and Building Materials* 37: 493–498.
- ARA, ERES Consultants Division. Guide for Mechanistic-Empirical Design of New and Rehabilitated Pavement

- Structures. Final Report 1-37A, Part 3. Design Analysis, National Cooperative Highway Research Program, Washington, D.C., March 2004.
- Bahia, H.U. & Anderson, D.A. 1991. Isothermal low-temperature physical hardening of asphalt. *Proc. Intern. Symp. Chemistry of Bitumens 1*: 114–147, Rome, Italy.
- Bonemazzi, F. & Giavarini, C. 1999. Shifting the bitumen structure from sol to gel. *Journal of Petroleum Science and Engineering 22*: 17–24.
- Blokker, P.C. & van Hoorn, H. 1959. Durability of bitumen in theory and practice. *Proc. Fifth World Petroleum Congress*, Section VI, Paper 27: 417–432, New York, June 1–5.
- Brown, A.B., Sparks, J.W., & Smith, F.M. 1957. Steric hardening of asphalts. *Proc. Association of Asphalt Paving Technologists 26*: 486–494.
- Brown, A.B. & Sparks, J.W. 1958. Viscoelastic properties of a penetration grade paving asphalt at winter temperatures. *Proc. Association of Asphalt Paving Technologists 27*: 35–51.
- Claudy, P., Letoffe, J., Rondelez, F., Germanaud, L., King, G. & Planche, J.-P. 1992. A new interpretation of time-dependent physical hardening in asphalt based on DSC and optical thermoanalysis. *Preprint Paper, American Chemical Society, Division of Fuel Chemistry 37*: 1408–1426.
- Collins, J.H. & Jones, G.R. 2000. Asphalt composition and method. United States Patent 6,074,469, June 13.
- Coombs, C.E. & Traxler, R.N. 1937. Rheological properties of asphalts. IV. Observations concerning the anomalous flow characteristics of air-blown asphalts. *Journal of Applied Physics 8*: 291–296.
- De Filippis, P., Giavarini, C. & Scarsella, M., 1995. Improving the ageing resistance of straight-run bitumens by addition of phosphorous compounds. *Fuel 74*(6): 836–841.
- Deme, I.J., & Young, F.D., Ste. Anne test road revisited twenty years later. *Proc. Canadian Technical Asphalt Association 32*: 254–283.
- El Hussein, H.M., Kim, K.W. & Ponniah, J. 1998. Asphalt concrete damage associated with extreme low temperatures. *Journal of Materials in Civil Engineering 10*(4): 269–274.
- Erskine, J., Hesp, S.A.M. & Kaveh, F. 2012. Another look at accelerated aging of asphalt cements in the pressure aging vessel. *Proc. Fifth Euraspphalt and Eurobitumen Congress*, Istanbul, Turkey, June 13–15.
- Fee, D., Maldonado, R., Reinke, G., Romagosa, H. 2010. Polyphosphoric acid modification of asphalt. *Transportation Research Record: Journal of the Transportation Research Board 2179*: 49–57.
- Fryazinov, V.V., Pechenyi, B.G. & Akhmetova, L.A. 1979. Interrelation of density, composition, and properties of asphalts. Translated from *Khimiya I Tekhnologiya Topliv I Masel 9*: 41–44.
- Giavarini, C., Mastrofini, D., Scarsella, M., Barre, L. & Espinat, D. 2000. Macrostructure and rheological properties of chemically modified residues and bitumens. *Energy and Fuels 14*: 495–502.
- Hagens, G., Manolis, S. & Vasiliu, G. 2004. Modified asphalt cement and process for preparing same. Canadian Patent 2,409,806, April 25.
- Hayner, R.E. 1999. Process for paving with asphalt containing mineral lubricating oil base stock. United States Patent 5,911,817, June 15.
- Hesp, S.A.M., Iliuta, S., & Shirokoff J.W. 2007. Reversible aging in asphalt binders. *Energy & Fuels 21*(2): 1112–1121.
- Hesp, S.A.M., Genin, S.N., Scafe, D., Shurvell, H.F. & Subramani, S. 2009a. Five year performance review of a northern Ontario pavement trial. *Proc. Canadian Technical Asphalt Association 54*: 99–126.
- Hesp, S.A.M., Soleimani, A., Subramani, S., Marks, P., Philips, T., Smith, D. & Tam K.K. 2009b. Asphalt pavement cracking: Analysis of extraordinary life cycle variability in Eastern and Northeastern Ontario. *International Journal of Pavement Engineering 10*(3): 209–227.
- Hesp, S.A.M. & Shurvell, H.F. 2010. X-ray fluorescence detection of waste engine oil residue in asphalt and its effect on cracking in service. *International Journal of Pavement Engineering 11*(6): 541–553.
- Hesp, S.A.M. & Shurvell, H.F. 2012. Waste engine oil residue in asphalt cement. *Proc. Seventh International Conference on Maintenance and Rehabilitation of Pavements and Technological Control*, MAIREPAV7, Auckland, New Zealand, August 28.
- Hesp, S.A.M. & Shurvell, H.F. 2013. Quality assurance testing of asphalt containing waste engine oil. *International Journal of Pavements* (in press).
- Heukelom, W. 1966. Observations on the rheology and fracture of bitumens and asphalt mixes. *Proc. Association of Asphalt Paving Technologists 35*: 3–48.
- Jaskula, P. & Judycki, J. 2014. Durability of asphalt concrete subjected to the deteriorating effects of water and frost. *Journal of Performance of Constructed Facilities* (in press).
- Johnson, K.-A. & Hesp, S.A.M. 2014. Effect of waste engine oil on the quality and durability of SHRP MRL binders. *Transportation Research Record: Journal of the Transportation Research Board* (in press).
- Johnson, R.A. & Juristovski, A.G. 1995. Physical properties of tall oil pitch modified asphalt cement binders, in Hardin JC (Ed), *Physical Properties of Asphalt Cement Binders*, STP 1241: 214–231, American Society of Testing and Materials, Philadelphia.
- Judycki, J. 2014. Influence of low-temperature physical hardening on stiffness and tensile strength of asphalt concrete and stone mastic asphalt. *Construction and Building Materials 61*: 191–199.
- Kamel, N.I. & Miller, L.J. 1991. Method for producing superior quality paving asphalt and product prepared therefrom. Canadian Patent 2,043,469, May 29.
- Kodrat, I., Sohn, D., & Hesp, S.A.M. 2007. Comparison of polyphosphoric acid modified asphalt binders with straight and polymer-modified materials. *Transportation Research Record: Journal of the Transportation Research Board 1998*: 47–55, Transportation Research Board of the National Academies, Washington, D.C.
- Krieche, A. & Wissel, H.L. 1989. Multigrade asphalt cement product and process. United States Patent 4,874,432, October 17.
- Kriz, P. 2009. *Glass Transition and Physical Hardening of Asphalt*. Doctoral Thesis, Department of Civil Engineering, University of Calgary, Calgary, Alberta, Canada.
- Krom, C.J. & Dormon, G.M. 1963. Performance requirements for road bitumens and their expression in specifications. *Proc. Sixth World Petroleum Congress*, Frankfurt/Main, June 19–26.
- Leclerc, G. & Paradis, M. 2002. Évaluation du PG 64-28 en vue de sélectionner ses usages au Québec. *Proc. Canadian Technical Asphalt Association 47*: 365–388.
- McLeod, N.W. 1972. A 4-year study of low temperature transverse pavement cracking on three Ontario test roads. *Proc. Association of Asphalt Paving Technologists 41*: 424–493.

- Memom, G.M., Boone, J.G. & Chollar, B.H. 1995. Furfural substitutes for chemical modification of asphalt, in Hardin JC (Ed), *Physical Properties of Asphalt Cement Binders*, STP 1241: 186–198, American Society of Testing and Materials, Philadelphia.
- Moore, H.F., Malone, D.P., Doolin, P.K. & Zalewski, D.J. 2000. Process for recovering lube oil base stocks from used motor oil formulations, asphalt blend compositions containing used motor oil bottoms from said process, and asphalt pavement compositions. United States Patent 6,068,759, May 30.
- Pechenyi, B.G. & Kuznetsov O.I. 1990. Formation of Equilibrium Structures in Bitumens. Translated from *Khimiya I Tekhnologiya Topliv I Masel* 7: 32–34.
- Robertson, W.D. 1995. Using the SHRP specification to select asphalt binders for low temperature service. *Proc. Canadian Technical Asphalt Association* 40: 170–195.
- Rubab, S., Burke, K., Wright, L., Hesp, S.A.M., Marks, P., Raymond, C. 2011. Effects of engine oil residues on asphalt cement quality. *Proc. Canadian Technical Asphalt Association* 56.
- Schmets, A., Kringos, N., Pauli, T., Redelius, P. & Scarpas, T. 2010. On the existence of wax-induced phase separation in bitumen. *International Journal of Pavement Engineering* 11(6): 555–563.
- Soenen, H., Ekblad, J., Lu, X. & Redelius, P. 2004. Isothermal hardening in bitumen and in asphalt mix. *Proc. Third Euro-bitumen and Eurasphalt Congress*, Vienna, Paper 135: 1–10.
- Struik, L.C.E. 1978. *Physical Aging in Amorphous Polymers and Other Materials*. Elsevier Scientific Publishing Company, Amsterdam, The Netherlands.
- Togunde, P. & Hesp, S. 2012. Physical hardening in asphalt mixtures. *International Journal of Pavement Research and Technology* 5(1): 46–53.
- Traxler R.N. & Schweyer H.E. 1936. Increase in viscosity of asphalts with time. *Proc. Thirty-Ninth Annual Meeting, American Society for Testing Materials* 36(II): 544–550, Atlantic City, New Jersey, United States.
- Traxler, R.N. & Coombs, C.E. 1937. Development of internal structure in asphalts with time. *Proc. Thirty-Ninth Annual Meeting, American Society for Testing Materials*, 37(II): 549–555, New York, United States.
- Van der Poel, C. 1954. A general system describing the viscoelastic properties of bitumens and their relation to routine test data. *Journal of Applied Chemistry* 4: 221–236.
- Van der Poel, C. 1955. Time and temperature effects on the deformation of asphaltic bitumens and bitumen mineral mixtures. *Journal of the Society of Plastic Engineers* 11: 47–53.
- Varadaraj, R., Moran, L.E. & Gale, M.J. 2006. High performance asphalt using alkyl aromatic sulfonic acid asphaltene dispersants. Canadian Patent 2,512,192, Issued on January 16.
- Villanueva, A., Ho, S. & Zanzotto, L. 2008. Asphalt modification with used lubricating oil. *Canadian Journal of Civil Engineering* 35: 148–157.
- Yee, P., Aida, B., Hesp, S.A.M., Marks, P. & Tam, K.K. 2006. Analysis of premature low temperature cracking in three Ontario, Canada, pavements. *Transportation Research Record: Journal of the Transportation Research Board* 1962: 44–51.
- Zhao, M.O. & Hesp, S.A.M. 2006. Performance grading of the Lamont, Alberta C-SHRP pavement trial binders. *International Journal of Pavement Engineering* 7(3): 199–211.

Appraisal of mechanistic-empirical pavement design guide for highways being implemented in the United States and complementary needs for pavement asset management

W. Uddin

Department of Civil Engineering, University of Mississippi, USA

ABSTRACT: Highway infrastructure network assets are imperative for passenger mobility and freight transport. The pavement part of a highway constitutes about 80 percent of its total construction and lifetime maintenance costs. The objective of this paper is to review pavement design evolution and show the equal importance of pavement asset management to sustain long-lasting highways. The post-2000 mechanistic-empirical pavement design presents a major departure from serviceability-performance concepts used in the previous highway pavement design methods of the American Association of Highway and Transportation Officials (AASHTO). The current method relates distresses to pavement performance prediction. Examples of asphalt pavement thickness designs using the 1993 AASHTO method with mechanistic-empirical methods are presented and compared. It is shown that safety, efficiency, and security of in-service highways do not depend only on accurate pavement thickness design and quality construction. This paper shows the continuing need of life-long pavement asset management for preserving safe and efficient highways.

1 INTRODUCTION

We live in a world of “global economy,” in which the global supply chain interconnects each country’s transportation hubs through import/export demand of agriculture commodities, manufacturing goods, and fossil fuels. Ships, air cargo, and land transport are used as freight carriers for most goods. As recently discussed in a National Academies report (NCFRP 2012a) U.S. companies collectively spend a trillion dollars a year on freight logistics. This is nearly 10% of the nation’s gross domestic product (GDP). The report states that considering about 80% of the population works and lives in cities and urban areas, 65% of goods originate or terminate in cities as per U.S. Department of Transportation (DOT) statistics based on a recent Commodity Flow Survey (NCFRP 2012b). The survey indicates that, on average, 42 tons of freight worth \$39,000 was delivered per person in the U.S. in 2007. About 4.5 million people or 3% of total employed work force in 2008 worked in transportation and warehouse industries (NCFRP 2012b). These statistics are indicative of the importance of the lifeline supply chain infrastructure to support our society and everyday life.

Roads represent the dominant mode of inland traffic in most countries and carry most of the passenger traffic and freight transport. The annual vehicle-mile-traveled (VMT) on highways has decreased over recent years in the United States. Overall, the 95.4% increase in VMT from 1980 to 2010 was observed with 2.97 trillion in 2010 (USDOT 2014). Heavy commercial

truck VMT increased to 9.7% of total 2010 VMT in the United States while trucks inventory was only 4.3% of total motor vehicle inventory for over 250 million vehicles. The average annual km driven by a truck is 42,566 km (26,604 mi), which is almost 2.24 times the distance traveled by a car. These statistics show that the highway pavements are stressed by commercial trucks more than ever and any pavement design method and performance modeling must include accurate traffic data and annual repetitions.

1.1 Objectives

The objectives of this paper are to (1) review the evolution of pavement thickness design methods from the start of the Interstate highway construction program in late 1950s to the post-2000 period, (2) discuss the variability in many design inputs and constructed pavement structure that significantly influence pavement performance but cannot be incorporated in the design process, and (3) show that longer lasting pavements can be guaranteed only by in-service monitoring as a part of the maintenance program and asset management.

Highway pavements are designed and constructed to:

- To provide a stable and smooth riding surface
- To support heavy moving loads without excessive deformation or damage to pavement
- To support traffic load repetitions during the design life without failure

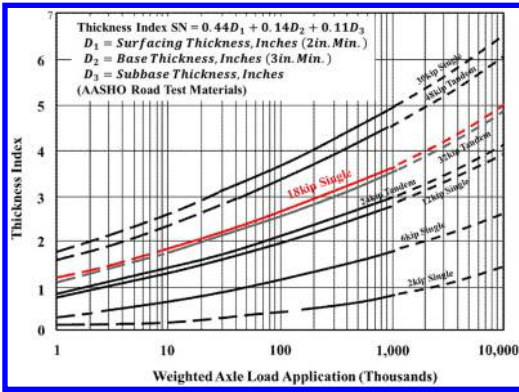


Figure 1. Traffic applications vs. pavement structure at the AASHTO road test (after AASHTO 1962).

1.2 Pavements are designed for trucks

Due to truck induced accelerated damage and failure of highways in the 1980's U.S. Congress authorized the Strategic Highway Research Program (SHRP) in 1987. This was a major pavement and asphalt research effort after the 1958–60 American Association of State Highway Officials (AASHTO) Road Test study of accelerated pavement testing in one location (Illinois). The mid-west state test site at Ottawa has harsh climate including spring-thaw season. Key lessons learned from the AASHTO Road Test, conducted at a cost of \$27 million (AASHTO 1962), include:

- Traffic load and number of repetitions were the most important factors, which affected performance and the damage was highly nonlinear. The thickness index represented pavement structure or Structural Number (SN), which was the basis of the original AASHTO and subsequent 1985 and 1993 AASHTO design guides for flexible pavements (AASHTO 1962, AASHTO 1993). As shown in Figure 1, for the 8,165 kg (18-kip) single axle load an asphalt pavement of thickness index 2 carried 20,000 Equivalent Single Axle Load (ESAL) applications but a 4 thickness index can carry 2 million ESALs to failure.
- A thickness index of 5.3 is required to carry the same 2 million applications of 13,609 kg (30 kip) ESAL (top curve in Figure 1).
- Pavement failure was based on the concept of serviceability-performance, and it was defined by the minimum acceptable present serviceability index (PSI). The following PSI model (Equation 1) was developed:

$$PSI = \int (Roughness, Cracking, Patching, Rutting) \quad (1)$$

- The ESAL applications are calculated by load equivalency factors based on SN values, which can be approximated by the 4th power law (Equation 2).

$$ESAL \text{ Factor} = \left(\frac{\text{Given Single Axle Load}}{\text{Standard 18 kip Axle Load}} \right)^4 \quad (2)$$

This ESAL factor defines the damage per application caused by a given vehicle load relative to the damage caused by the application of a standard 8,165 kg (18-kip) vehicle load.

- Using the 1993 AASHTO guide method, if nonlinear load damage of ESAL equivalency is not considered the pavement will fail prematurely, as shown in the following example (Uddin et al. 2013a). For 5 million ESALs if the designer expected primarily 8,165 kg axles then the thickness would be 20 cm surface. If the average trucks are actually overloaded to 10,886 kg per heavy axle then they will produce 15 million ESALs (three times as many) and require 25 cm surface.
- The AASHTO Road Test showed conclusively that the strength of base and subbase layers was important to the performance of pavements, in addition to the subgrade strength. In the 1985 and 1993 Guides, these layers were characterized by the resilient modulus properties instead of empirical parameters.
- The constructed asphalt layer and concrete layer at the AASHTO Road Test showed thickness variability, although the project followed strict material selection and construction quality controls. The asphalt layer thickness data of 1,384 tests showed that 7.7% of the data was below the design thickness values.
- A single subgrade and the environment.
- Evidence of interaction terms: load and materials, load and the environment, and load/material/environment.

On real projects the asphalt layer thickness variability is even more and it varies spatially; therefore, pavement distresses vary place to place leading to random failures.

1.3 1993 AASHTO design example

A parametric study was conducted to evaluate the variability of traffic and asphalt modulus on asphalt pavement thickness, based on the 1993 AASHTO asphalt pavement design equation. The detailed results are presented by Uddin & Jaafar (2013) for a given set of unbound layer material's resilient modulus values and thicknesses, two levels of asphalt resilient modulus, and six levels of cumulative traffic ESALs over 20 years of design. Figure 2 shows asphalt thickness values based on traffic volumes for both low and high asphalt modulus. Asphalt layer thickness increases at higher traffic levels. For low traffic levels, the thickness difference is not much. It can be seen that an asphalt layer with a low modulus requires 50% thickness at high traffic levels.

The range in asphalt thickness that increases due to 50% lower asphalt modulus is between 33% and 50% for traffic volumes 0.5 to 50 million ESALs (Uddin & Jaafar 2013). This implies that in summer months when the asphalt modulus value decreases by 50% or lower than the modulus in the reference month. A thicker asphalt layer is required in order for the pavement not to rut or have other excessive cracking

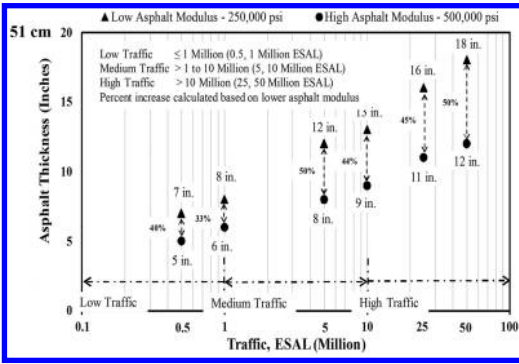


Figure 2. Effect of variations in ESALs and asphalt modulus on asphalt layer design thickness.

and roughness distresses on the pavement. This example illustrates that in the real world, pavement may fail earlier than the assumed design life for any or a combination of the following reasons:

- Underestimation of ESALs
- Spatial variability of layer modulus values
- Seasonal or temporal degradation of modulus values
- Variations in asphalt layer thickness, particularly less than design thickness

The 1993 AASHTO pavement design guide has the inherent limitation of the design equation based on a single subgrade and the environment. Additionally, the monthly seasonal variations are not simulated in temperature and moisture in sublayers, which result in modulus variations. Also, there is no mechanistic structural response parameter used to predict cracking or rutting distress on asphalt pavements.

2 EVOLUTION OF MECHANISTIC-EMPIRICAL DESIGN

2.1 SHRP – LTPP research

Due to truck induced accelerated damage of failure of highways in the 1980's the Congress authorized the Strategic Highway Research Program (SHRP) in 1987. This was a major pavement and asphalt research effort after the 1958–60 AASHTO Road Test. The SHRP's Long-Term Pavement Performance (LTPP) program included more than 1,000 pavement sections all across the U.S. and some in Canada. The \$50 million LTPP program was initially implemented during 1987–1992 and since then continued under follow up funding (FHWA 2015). The following LTPP objectives were established by SHRP:

- Evaluation of Existing Design Methods.
- Development of Improved Strategies and Design Procedures for Pavement Rehabilitation.
- Evaluation of Existing Design Methods.
- Development of Improved Strategies and Design Procedures for Pavement Rehabilitation.

- Determination of the Effects of: Loading, Environment, Material Properties and Variability, Construction Quality, Maintenance Levels on Pavement Distress and Performance.
- Determination of Specific Design Procedures to Improve Pavement Performance.
- Establishing a National Long-Term Pavement Database to Support these Objectives and Future Needs.

The author was involved at the outset in the early years as Materials Engineer in the SHRP-LTPP technical assistance team that developed and implemented data collection protocols of traffic, distress, and deflection, as well as field sampling and materials testing (LTPP 1989). This national effort collected initial sets of inventory, traffic, pavement condition, and materials property data. A key feature of the LTPP database design was to establish a special field “Construction Number” or CN to track any major maintenance and rehabilitation (M&R) treatment. The initial inventory data was assigned CN1, followed by CN2, CN3 etc. for subsequent major M&R. This allows the intervention effect of M&R with the CN as a dichotomous variable for developing improved prediction models of pavement performance and condition deterioration.

The most important accomplishment of LTPP was the compilation and maintenance of the national LTPP database, which is now available online by (FHWA 2014). The LTPP data collection and database updates have been continued at a cost of \$190 million from 1987 to 2007. The LTPP database was used to develop several pavement condition deterioration models for developing the latest mechanistic-empirical pavement design guide (MEPDG). This effort was undertaken by the National Cooperative Highway Research Program (NCHRP) through Project 1-37 and Project 1-37A, “Development of the 2002 Guide for the Design of New and Rehabilitated Pavement Structures” (NCHRP 2004). The MEPDG pilot implementation was supported by the USDOT's Federal Highway Administration (FHWA 2009).

2.2 MEPDG approach of pavement structural design

In an effort to develop and implement the next generation of pavement design methods for the 21st century, the U.S. DOT and AASHTO funded over \$60 million in the last 15 years to develop the MEPDG and associated special studies including the use of the LTPP and state asset management system (AMS) datasets. Pilot implementation has been done only in a couple of states. Another two million dollars or more is expected to cost to each state for the MEPDG's region-specific calibration efforts (MDOT 2013). Figure 3 shows the general framework of the MEPDG approach and extensive input data required to make one computation of design check for assumed thicknesses, material inputs, and traffic mix data.

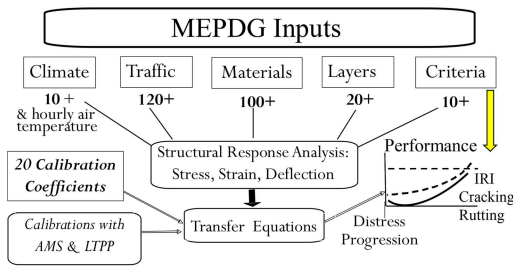


Figure 3. Framework of the MEPDG software.

Table 1. List of MEPDG models and inputs.

Pavement Condition Model	Number of Inputs (Examples)
1. IRI (called "smoothness")	11 (rut depth, cracking area, precipitation, Soil Plasticity Index.
2. Rutting in Asphalt	11 (traffic, asphalt thickness, plastic strain estimated from calculated elastic strain at asphalt mid-depth, resilient modulus and water contents of unbound layers)
3. Total Rutting (with rutting in unbound layers)	6 (asphalt layer thickness and tension modulus, average crack depth and standard deviation, stress intensity, fracture parameters)
4. Transverse Thermal Cracking	6 (load, temperature, tensile strain at bottom of asphalt, asphalt dynamic modulus and mx properties)
5. Fatigue Alligator Cracking	Note 1: Model
6. Top-Down Cracking (TDC)	Note 2: Field identification

Note 1: TDC models based on viscoelastic continuum damage model and asphalt-layer fracture mechanics (NCHRP 2010)

Note 2: No high speed nondestructive method in practice found in a recent Mississippi DOT research study (Uddin 2014).

The MEPDG approach is a major departure from the traditional 1993 and earlier AASHTO methods. Unlike only one performance model (based on PSI) used in traditional methods, the MEPDG method uses independent calculations of six condition deterioration parameters for comparison with the specified threshold criteria. The output includes the progression of each of these dependent condition variables and simply highlights which of these fails or passes over the design period. Table 1 lists the pavement condition deterioration models (FHWA 2009, MDOT 2013), which are incorporated in the MEPDG, the required number of inputs, and examples of detailed lab and field distress data for existing pavements in some cases. Overall, the MEPDG method analyzes adequacy of a pavement structure inputs for six failure modes with respect to the target criteria at a specified reliability level, such as 90%.

The use of some MEPDG terms defies the normal definitions that have prevailed historically in pavement

Table 2. MEPDG results of LTPP section analyzed for a student class problem (Uddin, unpubl.).

Pavement Distress Model	Target Maximum Distress Level Criteria	Predicted Distress Level at 90% Reliability
1. Terminal IRI	2.7 m/km (172 in/mile)	2.28 m/km (143.65 in/mile)
2. Rutting in Asphalt Layer Only	6.35 mm (0.25 in)	6.1 mm (0.24 in)
3. Total Rutting (in asphalt and all unbound layers)	19.1 mm (0.75 in)	11.94 mm (0.47 in)
4. Fatigue Alligator Cracking Area	25%	1.5%
5. Transverse Thermal Cracking	281 m/km (1,000 ft/mile)	5.1 m/km (27.17 ft/mile)
6. Top-Down Cracking	375 m/km (2,000 ft/mile)	69.2 m/km (369.08 ft/mile)

engineering, LTPP database definitions, and pavement asset management practices. Examples follow:

- "Smoothness" to describe the International Roughness Index (IRI)
- "Fatigue cracking" used to include both traditional bottom-up fatigue cracks, as well as top-down cracks.
- Recognize that top-down cracking is related to asphalt mix problems in thick pavements and may initiate from mid-depth (Taniguchi et al. 2009).

Recently, a class problem was solved to evaluate the thickness design for LTPP asphalt pavement section 28-3091 on U.S. Highway 46 in Mississippi using both the 1993 AASHTO and the MEPDG methods. The analysis used 20-year design truck traffic and other data from the LTPP database. The results showed that the thicknesses were adequate using both methods (Uddin, unpubl.). Table 2 shows the final outputs with the target maximum distress criteria associated with 90% reliability. Obviously, in this analysis rutting in the asphalt layer and IRI are the two most critical failure modes, which will occur soon after 20 years of design life. Most asphalt highway pavements reach the surface rutting and IRI target values within 15–16 years in Mississippi and, therefore, require maintenance due to safety concerns. Rutting in the wheelpaths can be filled with rainwater, which has great potential for hydroplaning incidents and needs timely maintenance.

Calibration of condition deterioration and performance models using the structural responses are required for empirical adjustments using field data collected in LTPP and region-specific condition data for all the above inputs. Calibration efforts are going on in 23 states including Mississippi (MDOT 2013).

The following concerns are offered related to the reliability and limitations of the MEPDG methodology for asphalt pavements.

- Related literature review shows that the distress deterioration models implemented in the AASHTO MEPDG did not consider condition deterioration progress affected by the confounding of pavement performance with the maintenance and rehabilitation intervention (as identified by CN in the LTPP database).
- Mechanistic equations can predict pavement structural response only for a known pavement structure, load, and layer material properties.
- In reality computational mechanics methods cannot analyze seasonal parameters or their interaction with loads.
- A big question that remains is how spatial variability of materials and thickness and seasonal variability of materials are accounted for in the MEPDG software.
- The author's attendance in MEPDG training session and software demonstration (MDOT 2013) do not provide the following outputs over the design life: 1) material modulus degradation curves of each layer with time, 2) time series plots of pavement temperature, freeze-thaw and monthly subgrade water content, and 3) monthly plots of structural responses needed for the IRI, cracking, and rutting progression predictions.
- Based on the author's class problems solved by students of a pavement course at the University of Mississippi (Uddin, unpubl.), the following observations are made for an asphalt highway pavement in Mississippi: 1) the thickness design originally based on the 1993 guide "passed" all MEPDG design criteria using the design modulus values. 2) For a lower subgrade modulus, the pavement failed the target value of top-down cracking early. 3) Should we build thicker asphalt layer to avoid any of the six failure modes when such problems can be corrected by timely maintenance.
- The above point refers to the need for life-cycle costs assessment and timely maintenance and rehabilitation treatment, which is not a part of the MEPDG methodology.
- The required MEPDG inputs are overwhelming because many of these inputs require lots of pavement section-specific field data and specialized laboratory testing.

All of these steps for the MEPDG implementation in state highway agencies will cause the design cost skyrocketing but perhaps it will provide good business for some consulting companies.

2.3 PADAP mechanistic-empirical software

A reliable pavement structural design method must take into account:

- Load Factors (traffic loads, load repetitions)
- Non-load factors (site environment, subgrade strength, other pavement layer materials)
- Interaction terms (load, environment, materials)
- Spatial and seasonal variability and layer material properties and subgrade soils

- Temporal variability of traffic history
- Spatial variability of asphalt layer thickness (construction quality, maintenance practice)

In a study for the Mississippi DOT, a diagnostic evaluation of several asphalt highway pavement sections showed signs of early failure because of excessive water in granular and lime-fly ash layers (Uddin 1999). This led to development of the PADAP mechanistic pavement design software.

The PADAP methodology corrects the back-calculated in situ pavement modulus values of unbound layers and soils for nonlinear behavior under any type of vehicular traffic by implementing the equivalent linear analysis method (Uddin 2007). The software includes the input of % coefficient of variability for each modulus that allows to reduce each design modulus value by one standard deviation (Figure 4). Annual climatological data are used to adjust the asphalt modulus for seasonal monthly temperature changes, and modulus values of unbound layers and subgrade are corrected for seasonal moisture changes from rainfall, as well as from spring-thaw simulations. This approach is used to calculate correct tensile strains in the asphalt layer and other responses for the design traffic load in every month of the year by using monthly adjusted modulus values. The resulting pavement responses can accurately estimate pavement distresses over design life using mechanistic-empirical equations of fatigue life and rutting life. Other distress deterioration equations for roughness and low-temperature thermal cracking are being implemented in the enhanced version.

The PADAP methodology predicts pavement damage for each class of vehicles in the traffic stream. The PADAP pavement design system provides a mechanistic methodology to pavement designers for modeling the effects of load, environment, and material properties. In-service environmental and load conditions are simulated for enhanced and realistic structural designs of pavement-subgrade systems. The variability in thickness and modulus leads to broad ranges of results from most mechanistic-empirical distress models.

The effects of the variability of layer modulus values are demonstrated by the analysis of data for an asphalt highway pavement section of US Highway 45 Alt in Northern Mississippi from the first implementation of the PADAP (Uddin 1999, 2007). Table 3 shows the layer thickness data and modulus data. Asphalt modulus varies with respect to summer and winter months due to temperature changes. The modulus values of unbound granular layers and subgrade varies with respect to monthly water content changes. The following observations are made related to computer simulations of monthly variations in modulus values and structural responses using the layered linear elastic analysis.

The modulus variations influence the predictions of the mechanistic-empirical pavement condition deterioration models.

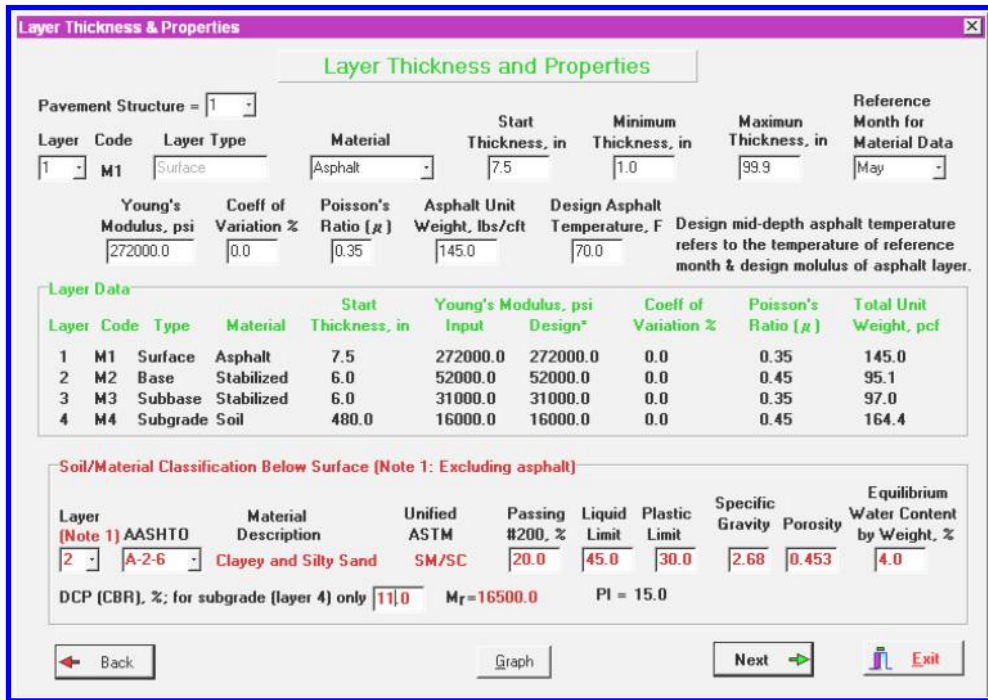


Figure 4. PADAP screen for layer data inputs.

Table 3. Modulus values of asphalt pavement.

Layer	Asphalt	Stabilized Base	Granular Subbase	Lime Treated Subgrade
	190.5 mm (7.5 in)	152 mm (6 in)	154 mm (6 in)	
Design modulus	272,000 (psi)	209,000 (psi)	50,000 (psi)	23,400 (psi)
	Young's Modulus (psi)			
Month	Seasonal Adjusted (Nonlinear – Layer 3, 4)			
1 to 12	Layer 1	Layer 2	Layer 3	Layer 4
Mean	285,930	194,384	24,726	13,228
Standard Deviation	185,923	9,991	5,003	1,284
+95%	404,061	200,732	27,950	14,043
-95%	167,799	188,036	21,547	12,412

- The mean monthly seasonal modulus is reduced by 38% compared to the design modulus.
- The mean nonlinear-corrected subgrade modulus is reduced by 43.5% due to monthly water content changes.
- Structural response using design modulus values are compared with lower 95% confidence level value with respect to the mean monthly modulus values:
 - Surface deflection increased by 25.1%
 - Tensile strain at the bottom of the asphalt layer increased by 11.3%

- Vertical stress in the middle of the base layer increased by 14.0%
- Vertical stress on the top of the subgrade increased by 19.9%
- Vertical strain on the top of the subgrade increased by 13.3%

- Any reduction in as-built asphalt layer thickness will increase the structural responses even more.

This example shows that if a design method uses one set of design modulus values without making appropriate nonlinear corrections and monthly seasonal adjustments then it is a significant limitation. This limitation affects the output accuracy of the AASHTO design and other mechanistic design methods.

3 PAVEMENT DESIGN CAN'T REPLACE ASSET MANAGEMENT

The bottom line is that calibrating and using the MEPDG guide will not avoid the needs for pavement asset management and maintenance programming activities. In fact the AMS database will complement the calibration effort and help for adapting new materials in future. A comprehensive cost and benefit analysis should be carried out to see the overall priorities of devoting funds to asset management vs. MEPDG calibration scope. Also, funds are required to handle the backlog of pavement rehabilitation and bridge repairs. Efficient use of the public fund is imperative in times of infrastructure funding crisis.

3.1 *The challenge of managing pavements*

Pavement design can't replace asset management and needs for timely maintenance and rehabilitation treatments. Early pavement failures are caused by errors in predicting traffic loads accurately, providing material properties, or using poor quality control and poor quality materials in the construction process. These factors result in inadequate pavement thickness and rough surface construction, which lead to early failures.

Incorporating new durable modified asphalt binders and sustainable asphalt materials such as warm mix asphalt is a major limitation in the MEPDG and other mechanistic-empirical pavement design methods. The asphalt mix properties used in different predictive equations are mostly based on tests and experience with neat asphalt binders. An illustration is the I-55 interstate asphalt highway project in Northern Mississippi where neat asphalt and eight other modified binders (polymer modified and rubber asphalt) were used. Test sections were constructed for the same thickness of the overlay layer for this research project (Uddin & Nanagiri 2002). The post construction monitoring showed that the neat control asphalt section rutted much earlier compared to the other sections paved with modified binders. The rutting models, developed from tests conducted for asphalt binder only, cannot make reliable predictions of rutting progression for paving mixes produced with modified binders.

3.2 *Assessing integrity and maintenance needs*

Field reality and pavement condition monitoring practice have always shown that pavements must be managed in the face of real world conditions and required performance in the field. Pavement design, no matter how "perfect", alone is not enough to provide safe and sustainable highways. The safety, efficiency, and security of in-service highways do not depend only on accurate pavement thickness design and quality construction. It is equally important to recognize the need of surface condition monitoring and structural integrity assessment on periodic basis for timely maintenance and rehabilitation treatment. Pavement asset management with application of life cycle assessment is imperative to achieve good quality maintained highways, as discussed thoroughly by Uddin et al. (2013b).

4 CONCLUSIONS

This paper presented an appraisal of post-2000 mechanistic-empirical pavement design methods using multicriteria condition attributes. Examples showed capabilities, listed limitations, and compared these with the traditional AASHTO asphalt pavement design method, which is based on the single performance attribute of serviceability.

A parametric study of asphalt thickness design indicated that it is important to have reliable values of design traffic applications and representative subgrade

resilient modulus. In practice there is a high level of uncertainty in traffic predictions and large spatial variability in subgrade soils. Seasonal variability of resilient modulus of unbound layers and subgrade soils affects thickness design. Ignoring these sources of variability often results in poor performance and early deterioration of pavements.

The required MEPDG inputs are overwhelming because many of these inputs require lots of pavement section-specific field data. However, unlike PADAP there is no spatial variability input for materials in the MEPDG method. These steps to implement the MEPDG software cause the design cost to skyrocket but may provide good business for some consulting companies. Equally important is the continuing need of life-long pavement asset management for providing safe, efficient, and sustainable highways to serve the society. Asset management database will provide complementary data for MEPDG calibrations and later verification when new materials are used for asphalt pavement construction.

It is recommended that each highway agency may carry out a comprehensive cost and benefit analysis to evaluate the overall priorities of devoting funds to asset management system activities vs. MEPDG calibration scope. Also, required funds should be allocated to handle the backlog of pavement rehabilitation and bridge repair programs. Prudent use of the public fund is imperative in times of infrastructure funding crisis.

REFERENCES

- AASHO. 1962. The AASHO Road Test: Report 5-Pavement Research. HRB Special Report 61-E, Highway Research Board, National Academy of Science, Washington, DC.
- AASHTO. 1993. AASHTO Design Guide for Pavement Structures. American Association of State Highway and Transportation Officials, Washington, DC.
- FHWA. 2015. About Long-Term Pavement Performance. Federal Highway Administration (FHWA), Research and Technology, January 20, 2015. <http://www.fhwa.dot.gov/research/tfhrc/programs/infrastructure/pavements/ltppt/> Accessed February 25, 2015
- FHWA. 2009. Guidelines for implementing NCHRP1-37A M-E Design procedures in Ohio: Volume 4 – MEPDG models validation and recalibration. Report FHWA/OH-2009/9D, Office of Research and Development, Ohio Department of Transportation and Federal Highway Administration.
- LTPP. 1989. SHRP-LTPP Guide for Laboratory Material Handling and Laboratory Testing, Version 1.0. Strategic Highway Research Program (SHRP), National Academy of Sciences, Washington, DC, August 1989.
- MDOT. 2013. Implementation of MEPDG in Mississippi – Draft Final Mississippi DOT Pavement ME Design User Input Guide. Report FHWA/MS-DOT-RD-013-170 Mississippi Department of Transportation, Jackson, Mississippi.
- NCFRP. 2012a. Guidebook for Understanding Urban Goods Movement. Report 14, National Cooperative Freight Research Program (NCFRP). Transportation Research Board, The National Academies, Washington, DC.

- NCFRP. 2012b. Preserving and Protecting Freight Infrastructure and Routes. Report 16, National Cooperative Freight Research Program. Transportation Research Board, The National Academies, Washington, DC.
- NCHRP. 2004. Mechanistic-Empirical Pavement Design Guide. NCHRP Project 137-A, National Cooperative Highway Research Program (NCHRP), Transportation Research Board, Washington, DC. <http://www.trb.org/mepdg/guide.htm> Accessed October 31, 2004
- NCHRP. 2010. Web-Only Document 162: Top-Down Cracking of Hot-Mix Asphalt Layers: Models for Initiation and Propagation. NCHRP Project 1-42A, National Cooperative Highway Research Program, Transportation Research Board, Washington, DC. http://onlinepubs.trb.org/onlinepubs/nchrp/nchrp_w162.pdf Accessed October 20, 2013
- Souliman, Mena I., Michael Mamlouk, Mohamed El-Basyouny, and Claudia E. Zapata. 2010. Calibration of the AASHTO MEPDG for Designing Flexible Pavements in Arizona Conditions. *IJP – International Journal of Pavements*, 9 (1-2-3): pp. 2–13.
- Taniguchi, S., I. Nishizaki, and A. Moriyoshi. 2009. Three-dimension diagnosis of pavement damage using CT scanner. *Proceedings, MAIRE PAVE6 Conference*, Torino, Italy, pp. 1 – 10.
- Uddin, W. unpubl. CE585-Highway Pavements. Course Lecture Notebook, University of Mississippi, Sept 2014.
- Uddin, W. 2014. An Overview of GPR Applications for Evaluation of Pavement Thickness and Cracking. *E-Proceedings, 15th International Conference on Ground Penetrating Radar (GPR 2014)*, Brussels, Belgium, June 30–July 4, 2014.
- Uddin, W. 2013 A Synthesis Study of Noncontact Nondestructive Evaluation of Top-down Cracking in Asphalt Pavements. Final Report FHWA/MS-DOT-RD-13-255, Research Study SS 255, The University of Mississippi for Mississippi Department of Transportation, Dec 2013.
- Uddin, W. 2007. A Methodology for Estimating Seasonal Nonlinear Modulus Values for Design and Evaluation of Asphalt Pavements. *Proceedings, 4th ICONFBMP, International Conference Bituminous Mixtures and Pavements*, Thessaloniki, Greece, April 19–20, 2007.
- Uddin, W. 1999. Improved Asphalt Thickness Design Procedures for New and Reconstructed Highway Pavements. Report FHWA/MS-DOT-RD-99-122, Final Report, State Study SS 122, Mississippi Department of Transportation.
- Uddin, W., Jaafar, Z. Fahmi M. 2013. Achieving sustainability without compromising long-term pavement performance for road infrastructure assets. *First IJP – International Journal of Pavements Conference Proceedings*, São Paulo, Brazil, December 9–10, 2013.
- Uddin, W., Hudson, W.R., Haas, R.. 2013a. Pavement Design or Pavement Management? Good Design Is Not Enough. *First IJP- International Journal of Pavements Conference Proceedings*, São Paulo, Brazil, December 9–10, 2013.
- Uddin, W., Hudson, W.R., Haas, R.. 2013b. *Public Infrastructure Asset Management*. McGraw-Hill, Inc., New York. ISBN 0071820116 ISBN-13: 978-0071820110
- Uddin, W. and Nanagiri, Yamini. 2002. Performance of Polymer-Modified Asphalt Overlays in Mississippi Based on Mechanistic Analysis and Field Evaluation. *IJP – International Journal of Pavements*, 1(1): 13–24.
- USDOT. 2014. National Transportation Statistics. U.S. Department of Transportation (US DOT), Washington DC, Updated July 2014. http://www.rita.dot.gov/bts/sites/rita.dot.gov/bts/files/publications/national_transportation_statistics/index.html Accessed November 10, 2014.

Lessons learned about successful flexible pavements

C.M. Chang & O. González

Department of Civil Engineering, The University of Texas at El Paso, Texas, USA

P. Krugler

Texas Transportation Institute, Texas, USA

ABSTRACT: Most of the time forensic investigation techniques are conducted to investigate the cause of pavement failures. These studies seek to learn valuable lessons to avoid the same mistakes in the future. Lessons learned about pavement performance are used to modify technical specifications to reduce the likelihood of failure. Relatively little, however, has historically been done to learn equally valuable information from pavements that have performed successfully. The high end of the performance spectrum presents equally promising opportunities to learn more about how pavements function, how they should be specified, and how they should be constructed. This paper describes the research study conducted for the Texas Department of Transportation (TxDOT) about successful flexible pavements and documented in the Final Report FHWA/TX-08/0-5472-1. The study included a definition of “successful pavements”, and a methodology to identify premium pavements. A database was developed with information collected for a group of pavement sections identified as successful. Pavement evaluation field and lab studies were conducted to gain insights into pavement characteristics resulting in superior performance.

1 DEFINITION OF SUCCESSFUL FLEXIBLE PAVEMENT PERFORMANCE

1.1 *Criteria to define a successful flexible pavement*

There is wide a range in the performance criteria to define a pavement as a successful. This wide range in performance criteria evidenced the difficulty in establishing a single set of parameters that reasonably identifies successful performance under the myriad of climatic, geographic, traffic, and local material factors. A list of potential factors to consider in the definition of successful flexible pavement performance was studied including:

- Age of the pavement section
- Drainage conditions
- Design service life
- Geographic location
- Maintenance history and treatment costs
- Material properties
- Pavement distresses
- Safety
- Serviceability (ride quality)
- Structural adequacy
- Subgrade conditions
- Traffic level (ADTs, ESALS)

Many of these factors are interrelated and not all of them needed to be explicitly included in the minimum criteria for defining successful performance.

For example, a section without distresses over its service life will more than likely be structurally adequate for the level of traffic and environmental factors acting upon the pavement structure. The level of maintenance expenditures which have been required to adequately maintain the pavement performance is certainly a factor to include in the criteria. This preliminary analysis lead to focusing on only key performance criteria that, together, capture virtually all the factors affecting pavement performance, either directly or indirectly.

Another important consideration in the criteria is the ease to apply them. From this perspective, the criteria bear upon measurable and objective parameters about pavement performance. Hence, and the following key factors are in the criteria.

Age of the Pavement: Age is a direct indicator of the length of time that the pavement has been exposed to environmental conditions. On less traveled rural roadways, age can become at least as definitive an indicator of superior performance as cumulative traffic loading. Another age-related aspect is that the determination of “successful” pavement performance is time-dependent. A pavement section may meet “successful” criteria in its early stage of life but later on rapidly deteriorate and no longer be described as successful (Krugler et al, 2007).

Cumulative Design Loading: The degree to which a pavement withstands traffic loading in comparison to its design loading is a most important indicator of successful performance. The definition criteria, therefore,

Table 1. TxDOT condition score classes.

Score	Range	Condition
90–100	A	Very Good
70–89	B	Good
50–69	C	Fair
35–49	D	Poor
1–34	F	Very Poor

Reference: Condition of Texas Pavements PMIS Annual Report, FY 2011–2014 (June 2014).

Table 2. TxDOT distress score classes.

Score	Range	Condition
90–100	A	Very Good
70–89	B	Good
50–69	C	Fair
35–49	D	Poor
1–34	F	Very Poor

Reference: Condition of Texas Pavements PMIS Annual Report, FY 2011–2014 (June 2014).

must be flexible enough to correctly evaluate a pavement which has already exceeded its service life, regardless of pavement age. A pavement in reasonable condition after surpassing design traffic loadings should be considered as successful.

Pavement Condition Score: The condition score provides a single descriptor of the overall pavement condition. This parameter combines ride quality and pavement distress characteristics of the pavement. Table 1 shows condition score classes used by TxDOT.

It is expected for a successful pavement to be in either very good or good condition, depending upon its stage of service life. The criteria for successful performance should also include the requirement for relatively low variability of condition scores within a successful pavement section. The maximum amount of variability allowed increases with increasing pavement age. Uniformity in performance is desirable and believed to be a strong indicator of quality in construction.

Although the condition score is a good overall indicator of performance, as it combines pavement distress and ride quality characteristics, this parameter alone would be inadequate to identify successfully performing pavements. The criteria in the definition of successful performance should also include independent distress score and ride quality factors.

Pavement Distress Score: The distress score reflects the degree of visible surface deterioration observed by pavement raters on an annual basis. Table 2 shows distress score classes defined by TxDOT.

Like the condition score, it is expected that a successful pavement be in either very good or good condition from a distress rating standpoint, depending on

Table 3. TxDOT ride score classes.

Score	Range	Condition
4.0–5.0	A	Very Good
3.0–3.9	B	Good
2.0–2.9	C	Fair
1.0–1.9	D	Poor
0.1–0.9	F	Very Poor

Reference: Condition of Texas Pavements PMIS Annual Report, FY 2011–2014 (June 2014).

Table 4. TxDOT traffic classes.

Score	Range	Condition
0–500	1	Low
501–10,000	2	Medium
Over 10,000	3	High

Reference: TxDOT Administrative Circular 5–92 (February 13, 1992).

the current age and stage of its service life. Relatively low variability is also a requirement.

Pavement Ride Score: The ride score expresses the ride quality on a scale from 0.1 (roughest) to 5.0 (smoothest). Table 3 shows descriptive ride score classes used by TxDOT.

As with other rating criteria, it is expected that a successful pavement be in either very good or good condition for ride quality, depending on the current age and stage of its service life. Relatively low variability is again a requirement.

Traffic Level: The traffic level is expressed in terms of average daily traffic for establishing traffic categories within the definition of successful performance. Table 4 shows TxDOT traffic.

Maintenance Expenditures: A pavement section in very good condition with a high condition score, high distress score, and high ride score may not actually perform in a successful manner if maintenance treatment costs over its service life are above the average maintenance costs in the area. It is possible that the high pavement scores are the result of excessive maintenance work that has been required. For this reason, pavement-related maintenance costs over a period of years are considered a crucial factor in the criteria for identifying successful flexible pavement sections.

1.2 What is a successful pavement performance?

“A successful flexible pavement is defined as a structure that has met performance expectations over its service life with only normally expected levels of maintenance for its age, materials utilized, traffic loads, and local conditions.” Using the criteria elements discussed before, a decision matrix was developed as a tool to identify successful pavements. The decision matrix is shown in Tables 5A, 5B, 5C, and

Table 5A. Decision matrix for identifying successful flexible pavements (0–7 years).

Parameter	ADT	Age of the pavement section	
		From 0 to 7 years	
		Minimum	Std. Dev.
Condition score	0 to 500	90	6
	501 to 10,000	90	8
	above 10,000	90	10
Distress score	1 to 500	92	6
	502 to 10,000	92	8
	above 10,001	92	10
Ride score	1 to 500	3.2	0.6
	503 to 10,000	3.6	0.7
	above 10,002	3.8	0.8
3-year average pavement maintenance expenditure	3 to 500	Below \$600/lane-mile	
	504 to 10,000	Below \$900/lane-mile	
	above 10,003	Below \$800/lane-mile	

Table 5B. Decision matrix for identifying successful flexible pavements (8–14 years).

Parameter	ADT	Age of the pavement section	
		From 8 to 14 years	
		Minimum	Std. Dev.
Condition score	0 to 500	85	6
	501 to 10,000	85	8
	above 10,000	85	10
Distress score	1 to 500	88	6
	502 to 10,000	88	8
	above 10,001	88	10
Ride score	1 to 500	3.0	0.6
	503 to 10,000	3.4	0.7
	above 10,002	3.8	0.8
3-year average pavement maintenance expenditure	3 to 500	Below \$600/lane-mile	
	504 to 10,000	Below \$900/lane-mile	
	above 10,003	Below \$800/lane-mile	

5D for the age of the pavement section of 0 to 7 years, 8 to 14 years, above 14 years, and beyond design life respectively (Krugler et al, 2007).

There are seven criteria in the decision matrix to assist in identifying a successful pavement section, as follows:

- annual maintenance expenditure average,
- minimum condition score average,
- standard deviation of condition scores,
- minimum distress score average,
- standard deviation of distress scores,

Table 5C. Decision matrix for identifying successful flexible pavements (above 14 years).

Parameter	ADT	Age of the pavement Section	
		above 14 years	
		Minimum	Std. Dev.
Condition score	0 to 500	80	6
	501 to 10,000	80	8
	above 10,000	80	10
Distress score	1 to 500	84	6
	502 to 10,000	84	8
	above 10,001	84	10
Ride score	1 to 500	2.8	0.6
	503 to 10,000	3.2	0.7
	above 10,002	3.4	0.8
3-year average pavement maintenance expenditure	3 to 500	Below \$600/lane-mile	
	504 to 10,000	Below \$900/lane-mile	
	above 10,003	Below \$800/lane-mile	

Table 5D. Decision Matrix for Identifying Successful Flexible Pavements (Beyond Design Life).

Parameter	ADT	Beyond Design Life	
		Minimum	Std. Dev.
		Condition score	0 to 500
501 to 10,000	70		3
above 10,000	70		10
Distress score	1 to 500	75	6
	502 to 10,000	75	8
	above 10,001	75	10
Ride score	1 to 500	2.5	0.6
	503 to 10,000	2.8	0.7
	above 10,002	3.0	0.8
3-year average pavement maintenance expenditure	3 to 500	Below \$600/lane-mile	
	504 to 10,000	Below \$900/lane-mile	
	above 10,003	Below \$800/lane-mile	

- minimum ride score average, and
- standard deviation of ride scores.

To determine if a pavement section meets the definition for successful performance, first calculate average values and standard deviations for the most recent condition, distress, and ride scores. Condition, distress, and ride scores are available from TxDOT's Pavement Management Information System (PMIS) database.

Determine the average annual pavement maintenance expenditure for the pavement section under consideration by averaging expenditure information for each of the segments of the pavement section. Calculate the three-year average maintenance expenditure for the pavement section (Krugler et al, 2007).

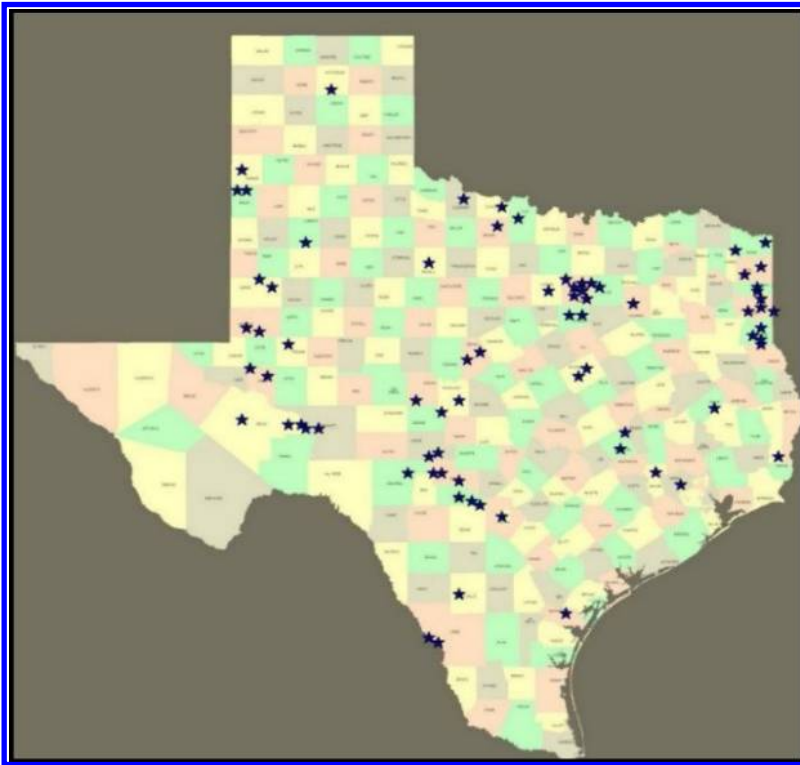


Figure 1. Geographic locations of nominated pavements (Krugler et al. 2007).

To be identified as a successful pavement, it is recommended that the pavement section be at least six years old and meet the maintenance expenditure criteria plus at least four of the other individual criteria listed in the decision matrix. If the section does not meet these requirements, but extenuating circumstances exist, engineering judgment should be used in determining if performance is considered successful.

2 IDENTIFYING SUCCESSFUL FLEXIBLE PAVEMENTS

Identification of particularly successful flexible pavements began by allowing the 25 geographically located TxDOT districts to nominate sections of pavement which in their opinions warranted the condition of being successful pavements.

A total of 75 nominations were received from 17 districts. Figure 1 shows locations of nominated pavements.

After receiving all nominations, visits to the pavement section site were scheduled. Pavement conditions were visually noted, photographed, and additional information was obtained. Unique subgrade conditions, unusual traffic considerations, and any unique aspects of construction and maintenance were discussed during these visits.

From the 75 nominations, 25 pavements were initially selected for field and lab tests to populate the database. A goal of the selection process was that the initially selected pavements include all commonly used types of flexible pavement structures and that these pavements would be distributed throughout the varied geographic and climatic regions of the state.

Other considerations in the selection process were that the list should include a variety of material types, pavement designs, and levels of traffic. Because of these non-performance related selection factors, and because the database could only include a limited number of pavements during the two-year research project, the selected pavements do not constitute an exclusive list of the best performing Texas flexible pavements. A number of the other nominated pavements provide equally impressive performances.

3 TESTING OF SUCCESSFUL FLEXIBLE PAVEMENT PERFORMANCE

Both in situ pavement testing and laboratory testing were performed in the 25 pavement sections. A one-mile length of a single lane of each pavement was selected for sampling and field testing. A number of nondestructive pavement tests were conducted on the selected pavements.

The pavement field tests included ground penetrating radar (GRP), falling weight deflectometer (FWD), and dynamic cone penetrometer (DCP). The objective of GPR testing was to investigate subsurface conditions and observe variations in layer thicknesses, if any. The objective of FWD testing on these sections was to evaluate pavement structural integrity and to measure the modulus of elasticity of the various pavement layers. The objective of DCP testing was to measure the in situ stiffness of flexible base and subgrade layers.

Core samples were obtained from asphalt mixture layers and other stabilized layers, and loose samples of flexible base layers and subgrade materials were taken by auger. Samples were obtained from two locations of each one-mile test length. These locations were generally 500 feet from each end of the section. For pavements including at least one asphalt concrete mixture layer, a total of ten 6-inch diameter cores were obtained; five from between the wheel paths and five from the outer wheel path.

3.1 Asphalt concrete mixture layer testing

The focus of testing asphalt concrete mixture layers was on aggregate gradation, asphalt binder content, aged asphalt binder penetration at 77°F, and the final percent air voids after years of traffic. These were selected for their importance to performance. The asphalt binder content, penetration, and air voids are a major factor in resistance to pavement cracking. The gradation is a major factor in resisting pavement deformation in the wheel paths. And the final percent air voids is a good indicator of the degree of protection that the surface layers are providing underlying moisture susceptible, unstabilized pavement layers.

3.2 Flexible base layer and subgrade testing

Flexible base materials were obtained from 17 pavement test sections. The remaining eight selected pavements either had underlying concrete pavement or did not have flexible base in the pavement structure. Sampling and testing of flexible base and subgrade focused on determining Atterberg limits, moisture content at time of sampling, and mineral type. In addition, the gradation of each flexible base sample was determined.

4 ANALYSES OF GROUPS OF SIMILAR PAVEMENT LAYER TYPES

Test results from groups of the similar pavement layer types were analyzed to provide recommendations for future specification performance as well as generally increase knowledge about desirable characteristics in flexible pavements. The evaluation methods also establish a framework for continued evaluations of specification requirements in the future, when additional pavement data sets should be available in the database.

4.1 Pavement air voids in all types of dense asphalt paving mixtures

The cored pavements for this project contained 30 different asphalt pavement layers designed to have optimally low air voids throughout their service lives. Of these, 7 were of unconfirmed mix type, although very likely dense-graded mixes; 17 were dense-graded mixes; 3 were CMHB mixes; 2 were SMA mixes; and there was 1 Superpave mix. Several interesting observations are made about the levels of air voids found in these successfully performing pavement layers after years of traffic compaction. Figure 2 shows the frequency distribution of pavement air void average values as found in the 30 dense asphalt pavement layers that were cored and tested. The data show an apparent skew toward the 3 to 4 percent air void levels. It is noteworthy that this has been the targeted design air void level in Texas for many decades. Historically, TxDOT had utilized a minimum asphalt requirement to assure adequate binder and film thickness in asphalt paving mixtures. Since about 1992, minimum requirements for Voids in the Mineral Aggregate (VMA) have indirectly established the minimum amounts of asphalt binder to include in asphalt paving mixtures. As older pavements tended to provide the best examples of particularly well-performing flexible pavements, most of the dense-graded pavement layers selected for evaluation were constructed prior to VMA specification requirements. However, the average asphalt contents found by extraction or ignition oven testing of pavement cores indicate that selected pavements generally had asphalt contents well above the minimum asphalt contents in specifications, thereby indicating generally higher VMAs as well.

4.2 Dense-graded asphalt paving mixtures

Construction inspection gradation test results were performed for two Type D and three Type C dense-graded asphalt pavements. The average job control gradations determined at the mix plants during production on these projects are shown on Figure 3 and Figure 4, which also display current specification upper and lower gradation requirements for these two mixture types

Similar gradation analyses were conducted for coarse-matrix high-binder paving mixtures, stone-matrix asphalt paving mixtures, surface treatments, and flexible bases. Since the specification requirements have changed over the years, it was observed that occasionally these average gradations were outside of current specification requirements.

Particular mention deserves the asphalt pavement containing tire rubber. Five of the selected 25 pavements included tire rubber in either a surface treatment or paving mixture. Three pavements included Type II crumb rubber blended into the surface treatment asphalt cement by the contractor and two pavements used AC-15-5TR in the underseal being placed below the new asphalt paving mixture layers. The single pavement mixture containing tire rubber was

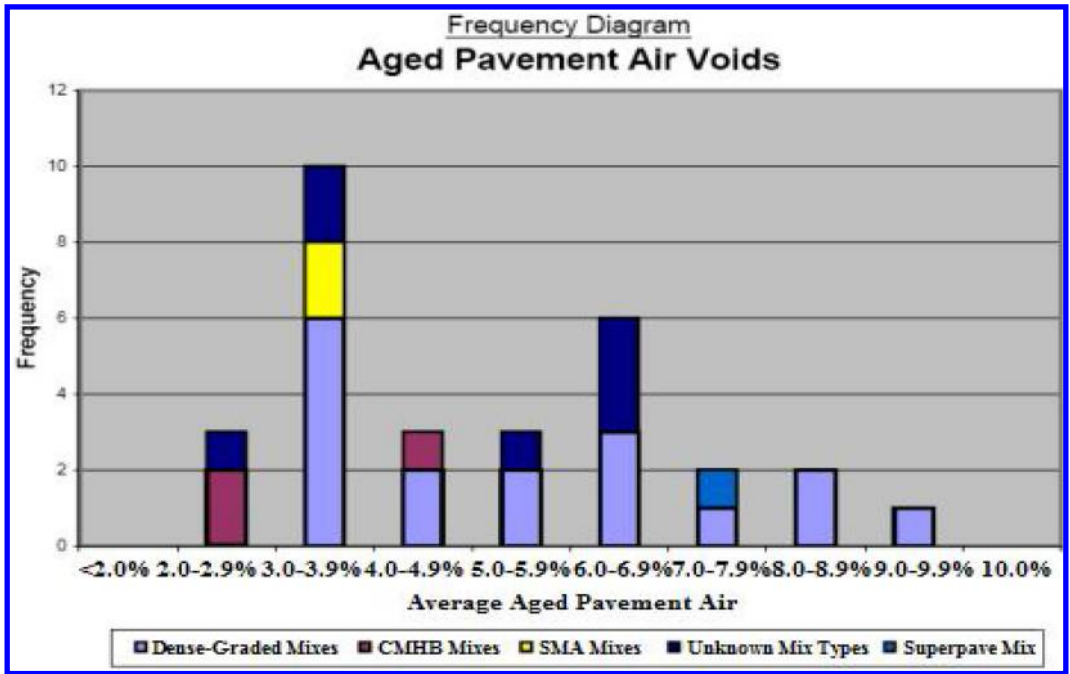


Figure 2. Frequency diagram of air voids in aged pavement layers – all asphalt concrete mix types (Krugler et al, 2007).

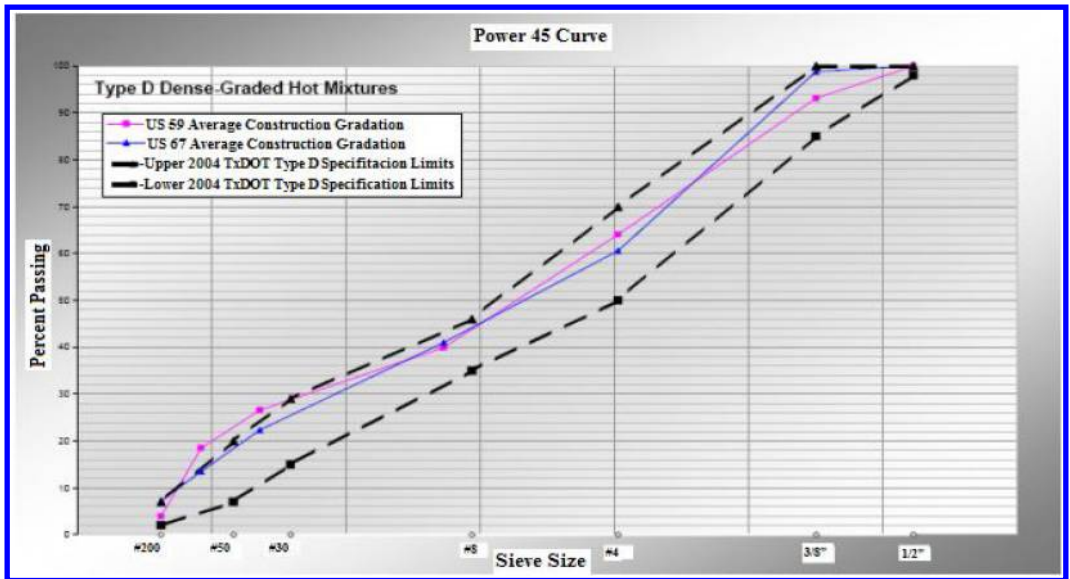


Figure 3. Power 45 average construction job control gradations–Type D mixes (Krugler et al, 2007).

a CMHB-F with Type II crumb rubber and it is one of the very best appearing pavement sections seen among all nominations, despite the fact that it was eight years old at the time of the evaluation and had not yet received any type of preventative maintenance.

5 LESSONS LEARNED: FINDINGS AND RECOMMENDATIONS

The criteria developed to identify successful pavements in Texas can be adapted by other Departments of Transportation using their own pavement condition

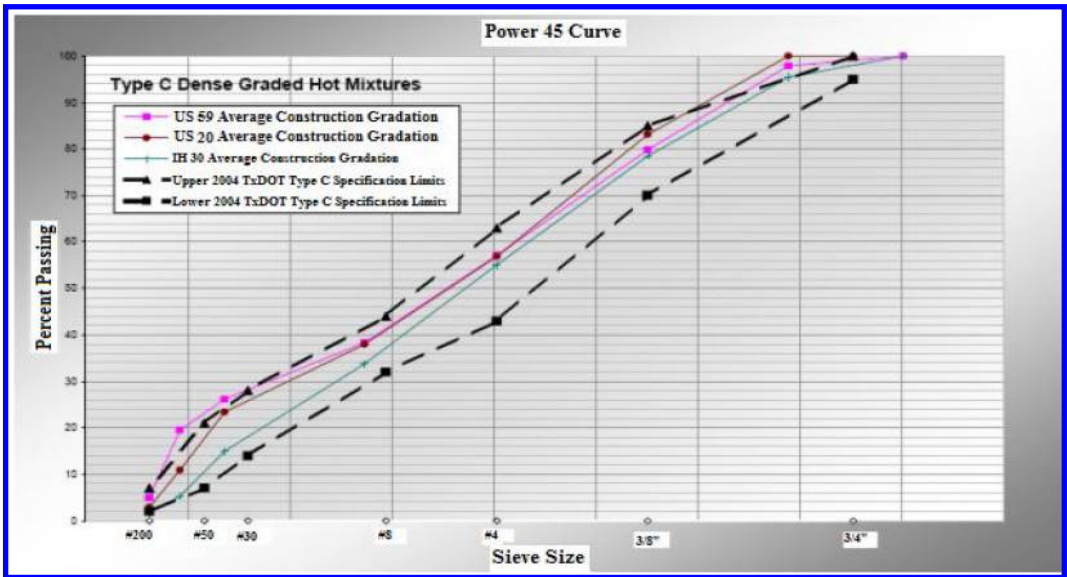


Figure 4. Power 45 average construction job control gradations–type C mixes (Krugler et al. 2007).

indexes and setting their own range for the decision matrix. While the success of each pavement appears to have somewhat differing factors involved, in general superior performance may be attributed to the combined result of good construction practice, high-quality materials, and timely maintenance.

In order to characterize each of these factors, and to establish the criteria for identifying successful flexible pavement sections in Texas, the rating methods used in PMIS offer the best and the most practical solutions for TxDOT.

The insight gained from the PMIS records led to the creation of a definition that requires compliance with a number of the selected performance criteria for a pavement’s performance to be considered successful. Also, engineering judgment is recognized in the definition as an important element in pavement performance evaluations.

Analysis of data in the PMIS, confirmed the superior pavement performance over time of the nominated sections by TxDOT engineers. Average condition scores, average distress scores, and ride scores comply with the decision matrix criteria. Pavement layer structure profiles with the GPR also show uniform profiles, and consistent with observations in the field and notes in history records regarding pavement performance.

Most of the back-calculated modulus values were within or above the range of expected typical values for the types of materials composing each layer. However, interpretation of back-calculated modulus values should consider the whole of the pavement structure rather than focusing on the individual values for each layer.

The VMA criteria in current specifications should be evaluated beyond that possible during this project, specifically to validate the current specification criteria or to support increased minimum values, should that be found appropriate for this most important mixture composition characteristic.

The maximum average annual pavement maintenance costs included in the definition vary by traffic level, with \$600 per lane-mile allowed for low traffic pavements, \$900 per lane-mile allowed for medium traffic pavements, and \$800 per lane-mile allowed for high traffic pavements. The selection of a lower allowable dollar rate for high traffic pavements compared to medium traffic pavements was based on demonstrated differences observed in PMIS maintenance cost records for nominated pavements.

The prototype system observed by the research team that integrates pavement evaluation video with GPR COLORPMAP data representations should be further developed, evaluated, and strongly considered for incorporation into the standard pavement evaluation testing protocol.

Pavement engineers should be encouraged to nominate, in a regular basis, flexible pavements that they find to be clearly performing beyond normal expectations.

ACKNOWLEDGEMENT

The authors would like to express their sincere appreciation to TxDOT for providing funding to conduct research project 0-5472 “A Database for Successful

Pavement Sections in Texas – Including Both Experimental and Non-Experimental Pavements”. This paper is based on the final report prepared under this research project.

REFERENCES

Krugler, P., Chang-Albitres, C., Scullion, T., and Chowdhury, A. (2007). “Analysis of Successful Flexible Pavement

Sections in Texas – Including Development of a Web Site and Database.” Final Report FHWA/TX-08/0-5472-1. Texas Department of Transportation (TxDOT), Austin, Texas.

Texas Department of Transportation (2014) “Condition of Texas Pavements.” *PMIS Annual Report FY 2011–2014*. Texas.

Texas Department of Transportation (1992) “TxDOT Administrative Circular 5–92, February 13, 1992” Texas.

Comparison of clustering approaches on temperature zones for pavement design

A. Kumar & A.K. Swamy

Department of Civil Engineering, Indian Institute of Technology Delhi, India

ABSTRACT: The asphalt pavement response depends on various factors including mixture properties, traffic and environmental characteristics. The selected grade of binder primarily depends on maximum and minimum pavement temperature expected in that particular region. In absence of actual pavement temperature data, air temperature data has been used as surrogate model. One such example is Superpave specifications for asphalt binder specifications. However, in other parts of world, availability of historical database is rare and network of weather stations are sparsely located. A map of homogeneous zones that experience similar temperature will facilitate binder selection for a given location. The temperature data collected by Indian meteorological department over past 63 years was used in this research. Using the above data, homogeneous air temperature regions were developed based on cluster analysis approach. This study compares homogeneous regions developed using unsupervised cluster analysis algorithms. Key issues with these clustering techniques are discussed in detail.

1 INTRODUCTION

It is a well-known fact that quantity of bitumen and binder characteristics has a major impact on the distress mechanisms occurring in a bituminous pavement. The three commonly occurring distress includes low temperature cracking, fatigue cracking and rutting. The binder content and quality significantly affect the above distress mechanisms. The extent to which they affect the distresses varies as per mix design(s), climatic conditions and operating conditions. Thereby, the choice of a binder for a particular region is of paramount importance for long term performance of the pavement. Due to viscoelastic nature, the behavior of bitumen binder is a function of the temperature it is subjected during its service life.

The Strategic Highway Research Program (SHRP) resulted in a new asphalt concrete mixture design methodology that considers expected pavement temperature while choosing binder to be used in mixture. The grade of binder is designated as Performance Grade (PG) that indicates the temperature range within which binder is expected to perform satisfactorily. The system makes use of the location specific maximum and minimum pavement temperatures which the binder can experience in its lifetime. For example, a binder grade of PG 64-22 implies that the binder must meet the necessary physical properties to a temperature of at least 64°C during summer and down to a minimum temperature of at least -22°C during winter. Further, this performance grading scheme considers unaged, short term aged and long term aged binder properties (Mirza et al. 2011). Due to practical issues with pavement temperature monitoring,

air temperature is used as surrogate. The Long Term Pavement Performance (LTPP) program formulated a Seasonal Monitoring Program (SMP) to document the response of pavements at a number of locations in the USA and Canada in different seasons. The dataset consisting of air and pavement temperature logs were used to develop regression models (Lukanen et al. 1998).

With expectation of better performance of pavements, Indian binder classification system moved from penetration grading system to viscosity grading system recently (IS 73:2006). But, this grading system still does not account for all expected field conditions. Current Indian specifications (IS 73:2006) regarding binder selection are too generalized regarding the choice of a binder. The broad climatic region classifications and traffic render the selection methodology lacking in robustness (Nivitha & Krishnan 2014). However, recently, as per the Indian Standard (IS 73:2013), it has been suggested that the choice of binder be done on the basis of the design maximum air temperature of the region where the binder is to be used. In order to relate current testing practice, and physical characteristics of binder with field conditions, homogeneous regions with similar air (or pavement) temperature needs to be specified. This helps field engineers to select binder is suitable for a particular region with little effort. The process of developing homogeneous sections using a robust methodology is the first step in this process. Cluster analysis approach has proved to provide reliable while developing zones experiencing similar temperature (Gerstengarbe et al. 1999, Kim et al. 2004). This research used cluster analysis approach to develop homogeneous zones based on 7-day average maximum and 1-day minimum

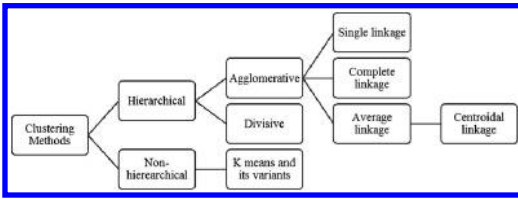


Figure 1. Classification of clustering algorithms.

air temperature for the Indian region. The goal of the present article is to compare different clustering approaches used in development of homogeneous temperature zones for its robustness and efficiency.

2 LITERATURE REVIEW

2.1 Basics of cluster analysis

Clustering is a mathematical tool used for classifying objects/attributes on the basis of similarities between their properties. The similarity between a pair of objects is calculated on the basis of a dissimilarity coefficient. For the same, Euclidean distance ‘ e ’ is used which is the distance between attributes for a pair of entities. For only two attributes, Euclidean distance turns out to be the linear distance between the two objects found using their coordinates on the plot (Papagiannakis et al. 2006). Clustering algorithms are basically divided into hierarchical and non-hierarchical as shown in Figure 1. Hierarchical algorithms form clusters in stages either by joining (agglomerative methods) or dividing existing clusters (divisive methods). On the other hand, non-hierarchical methods form all clusters at once to create a single level partition of data (Steinbach et al. 2000). Large data sets are easily processed by non-hierarchical methods and at a faster rate than the hierarchical methods.

However, non-hierarchical method requires specifying the number of clusters beforehand which by itself is variable. Determining the number of clusters is a challenging task and requires experience. Using statistical plots and measures, one can be aided in identifying the suitable number of clusters (Wang et al. 2007).

2.1.1 Hierarchical clustering

As mentioned previously, hierarchical clustering approach carries out either a merger of clusters (agglomerative) or a division of cluster (divisive) obtained in previous levels (Kim et al. 2004). This approach results in a nested order of partitions with a single cluster at the top followed by clusters at lower levels. The result of a hierarchical clustering can be displayed in the form of a dendrogram (Steinbach et al. 2000). Hierarchical methods begin with as many clusters as the data points and then form a dissimilarity matrix to finally compute the clusters. This process starts by grouping points with maximum similarity first, recalculation of the dissimilarity matrix to

obtain the relation of the newly formed cluster with the remaining entities (Gong and Richman 1995). The agglomerative hierarchical methods used in this study are discussed below:

2.1.1.1 Single Linkage (SL)

In single linkage analysis, the definition of a cluster is that it consists of a group of objects in which each member is similar to minimum one object in the same cluster than to any member of another cluster. This method tends to scatter the multidimensional space since it combines clusters by the shortest distance between them. Single objects tend to join an existing cluster rather than to act as the center of a new cluster making this clustering technique form poorly separated clusters (Gong and Richman 2005).

2.1.1.2 Complete Linkage (CL)

This clustering method works similar to the single linkage method but with a difference that the inter-cluster distance is found by the distance between the two data points, one from each cluster, that are at maximum distance apart. This ensures that all points in a cluster are within some maximum distance of each cluster. The multidimensional space gets “diluted” as with increasing size of a cluster, the updated distance between this cluster and other clusters or points becomes distant. Hence, the probability of a cluster getting a new entity becomes smaller. This method leads to highly separated compact groups (Gong and Richman 2005).

2.1.1.3 Centroidal Linkage (CL)

The centroidal linkage method is related to the average linkage between merged groups method. The distance between cluster ‘ k ’, formed by merger of clusters ‘ i ’ and ‘ j ’, and another cluster ‘ m ’ is given by:

$$d_{kms} = \frac{N_i}{N_i+N_j} d_{im} + \frac{N_j}{N_i+N_j} d_{jm} - \frac{N_i N_j}{N_i+N_j} d_{ij} \quad (1)$$

where ‘ d_{ij} ’ is the distance between object ‘ i ’ in cluster ‘ k ’ and entity ‘ j ’ in cluster ‘ m ’, likewise for d_{ij} s and N_i and N_j are the number of objects in cluster i and j , respectively. An object is joined to a cluster if it possesses an average degree of similarity with the current cluster members (Gong and Richman 2005).

2.1.2 Non hierarchical clustering

Nonhierarchical clustering consists of a constantly increasing ranking of cluster strengths as the groups progressively tend to be a part of larger clusters (Kim et al. 2004). The K means approach is described below.

2.1.2.1 K Means

The K means method is a widely used non-hierarchical method of clustering. K-means is founded on the notion that a center point can symbolize a cluster. The centroid is the mean or center point of a set of points. However, a centroid mostly does not coincide with an actual data point.

The basic algorithm involves selection of ‘K’ points as the initial seed points or centroids, assignment of all points to the closest centroid, recalculation of the centroid of each cluster and repetition of previous

two steps until there is no change in the centroids (Steinbach et al. 2000).

2.1.3 Affinity propagation

Affinity propagation accounts all data points simultaneously as possible “exemplars”, (serving as a typical example) which share real-valued “messages” among each other till a good, satisfactory quality of exemplars and corresponding clusters is achieved. Affinity propagation method requires a set of pairwise similarities between data points as input on the basis of which clusters are located. This is achieved by maximizing the total similarity between data points and their exemplars. Similarity can be stated in terms of a negative squared Euclidean distance for compatibility with other algorithms, or it can adopt higher quality application-specific models. The algorithm is somewhat similar to artificial neural networks (Dueck 2009).

2.2 Cluster analysis applications

Cluster analysis has been used in diverse areas for the purpose of classification. This includes biotechnology in analyzing gene expression data (Chen et al. 2002), climate classification (Gerstengarbe et al. 1999), classification of river yields (Isik et al. 2006), rainfall frequency analysis (Kim et al. 2004), pattern recognition, medicine, economics, finance and many more (Almeida et al. 2014). In the field of transportation engineering, cluster analysis has been used primarily in the grouping of variables used in the Mechanistic Empirical Pavement Design (MEPD). Wang et al. (2007) used cluster analysis approach to classify axle load distributions for MEPD and analysis. This study analyzed the spatial and temporal variations of load distributions by cluster analysis.

Wang et al. (2011) applied cluster analysis approach to identify loading patterns and estimation of full axle-load spectrum data using WIM (Weigh-in-Motion) data recorded in the state of Arkansas, USA. In another similar study, Liu and Harvey (2007) classified truck composition, volume, speed and axle load spectrum in the state of California, USA that are inputs for the MEPD.

Papagiannakis et al. (2006) applied hierarchical cluster analysis technique to identify groups of sites with decreasing similarities based on either the vehicle percentage by class or the percentage of axles by load interval. WIM data from the LTPP was used for this analysis. Regional traffic data obtained after the cluster analysis facilitated estimation of data for pavement design conditions with very few site-specific traffic details.

Yan et al. (2011) applied the cluster analysis method to model the traffic flow characteristics of port ships at the Tianjin port. The K-means algorithm was first used to form an initial region based in initial cluster centers and then optimized. It was further mentioned that the results of cluster analysis approach is affected by the choice of initial clusters.

Clustering is an unsupervised algorithm and there is no prior knowledge of the actual number of groups in the data. Thus, validation the cluster formed is required. Visualization of the data set is a vital aspect of verifying the results of any clustering algorithm. However, visualization of higher dimension data tends to be difficult for the user. Hence, the evaluation indices aid in choosing the optimal cluster number. Many research efforts are still in progress to zero-in on deciding the number of clusters best fitting a data along with evaluation of various clustering algorithms (Halkidi et al. 2002). Various indices have been proposed as indicators of cluster analysis quality. The indices just provide an indication of the partitioning quality. The domain experts need to subjectively choose the best method for their data (Halkidi et al. 2001).

Rossi et al. (2014) compared traditional and recent clustering methods and check upto what extent the accuracy of AADT values is affected by changing the input variables. The assessment and comparison of the clustering methods was done by comparing the values of mean absolute error in AADT values. Depending on the data sets and pattern of traffic, the results of clustering methods varied.

Steinbach et al. (2000) reported that hierarchical clustering is better clustering algorithm but it suffers from quadratic time complexity. On the contrary, K-means method and its variants possess a linear time complexity, but produce lower quality clusters. There are various quality indices and the relative ranking of different clustering algorithms can vary depending on the index used.

Gong and Richman (1995) compared various cluster techniques on precipitation data. They reported that the nonhierarchical methods were much better than the hierarchical methods. The nature of data determines the effectiveness of a particular algorithm. Iterating through different algorithms to explore the data and come to a meaningful result based on subjective judgment is the key to cluster analysis (Kim et al. 2004).

Wang et al. (2009) developed a visual cluster validation toolbox for use in MATLAB[®]. It is known as the CVAP (Cluster Validation Analysis Platform). The CVAP is an interactive toolbox which gives many validity indices, clustering algorithms and procedures. In addition, it provides an environment conducive for clustering, evaluation of results, find out the optimal Number of Clusters (NC) and compare various algorithms. It helps users to complete clustering in a quick and efficient way in order to attain robust clustering quality when there is no prior knowledge of the patterns in the input data set.

There are basically two types of indices for cluster validation, internal and external. The internal measures do not use external information to process the viability of a clustering structure. External validation indices have a-priori knowledge of the “true” cluster number hence are employed mostly for making a choice of the best clustering algorithm for that data set. Internal indices can be used for dual purpose-choosing the optimal algorithm and the best number of clusters

without prior cluster information (Liu et al. 2010). The internal indices which proved useful in comparing the clustering quality of algorithms in the present study were Silhouette and R-squared. However, other calculated internal indices were Calinski-Harbasz, Dunn, Homogeneity, Separation and Davies-Bouldin. The external indices calculated were Rand, Jaccard and Folkes-Mallows (FM) as discussed by Wang et al. (2009). On the whole, all the indices provided a basic idea of the clustering quality of the algorithms.

As mentioned previously, to choose binder for a given location, prior information regarding air temperature is required. Formation of homogenous zones experiencing similar air temperature is the first step towards achieving this end. Formation of these zones would facilitate later prediction of pavement temperatures using existing regression models with suitable correction factors. The present study involves a detailed analysis of the development of homogeneous zones based on 7 day average maximum and one day minimum temperatures for the Indian region. Various cluster analysis techniques such as the K means, hierarchical clustering (single, complete, centroidal) and the affinity propagation algorithm were used in developing these homogenous regions. The regions have been clustered for 99.73% reliability for 7-day maximum temperature and 1-day minimum air temperature.

3 DATA

The India Meteorological Department (IMD) maintains a network of about 550 well distributed surface weather stations where daily maximum and minimum temperature values are recorded (Srivastava et al. 2009). The same daily temperature data was obtained and used for analysis. The data set comprised of daily maximum and minimum temperatures for each day of the year for past 63 years (1951–2013). The raw data consisted of data arranged in 31×31 grid points for Latitudes, 7.5N, 8.5N ... 36.5, 37.5 (31 values) and Longitudes, 67.5E, 68.5E ... 96.5, 97.5 (31 values). The grid points were average of preceding and succeeding latitudes and longitudes (eg. 8.5N for average of 8N and 9N latitudes and likewise). The data accounted for leap years and the temperature was recorded in degree Celsius.

4 METHODOLOGY

The methodology adopted in this research consisted of four steps. In first step, data was filtered to remove observations outside area of interest. In second stage, data was processed to calculate average and standard deviation of 7-day average maximum and 1-day minimum temperature for all grid points. In next stage, homogeneous temperature zones were obtained by different clustering approaches. Homogeneous zones developed by different methodologies are compared in final stage. The flowchart of methodology used in the present work is presented in Figure 2. The

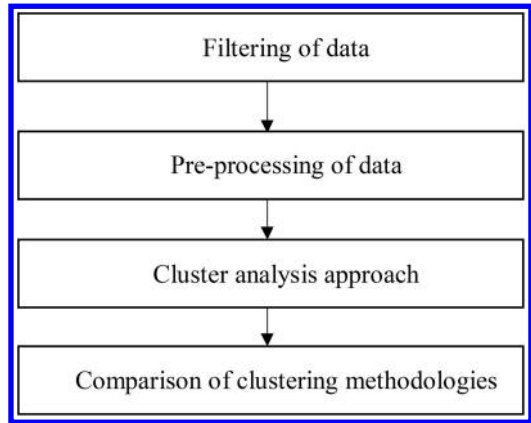


Figure 2. Methodology of analysis.

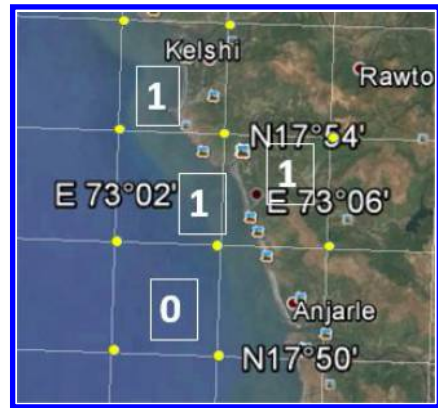


Figure 3. Filtering methodology.

detailed explanation of all the above steps is discussed in following subsections.

4.1 Filtering of data

Preliminary observation of temperature data indicated some absurd temperature values at certain grid points. When cross-referenced with Google™ earth, it was observed that these points were on the sea/land outside Indian political boundary. Due to absence of sensors, the temperature values at these grid points were interpolated. A methodology to filter the points on the land and sea was adopted. In this methodology, each grid point was mapped to a base matrix containing 31×31 elements. For each grid point, if more than one corner is located on land area within official boundary of India, corresponding base matrix element was assigned a numerical value of 1 and was considered for further analysis. On the other hand, if all corners were outside official boundary, then corresponding base matrix element was assigned numerical value of 0. Figure 3 below shows the methodology used for filtering the points on the land and sea.

After preliminary visual checking, a base matrix with zeros and ones was obtained. This matrix was

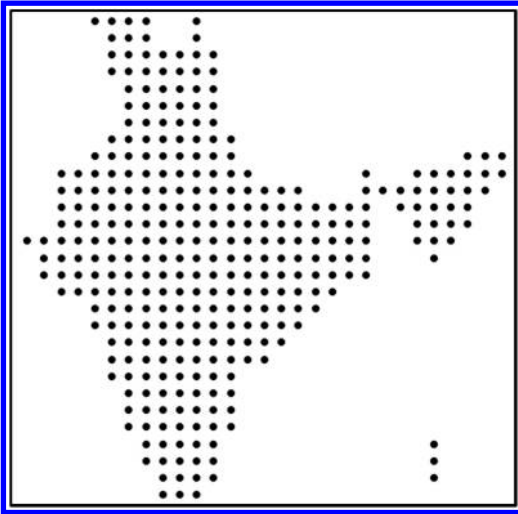


Figure 4. Maximum temperature grid points (329).

used as a filter to remove grid points of little/no interest.

4.2 Pre-processing of data

A MATLAB[®] code was written to compute 7-day average maximum and 1-day minimum temperature for a given year for all grid points. The recorded temperatures for each grid point were read by MATLAB[®] for all days in a given year. The 7 day average temperature was computed for a given year using moving average method. This process was repeated for all years during which temperatures were recorded. Thus, for a given grid point 63 values were computed. Similar exercise was repeated to obtain 1-day minimum temperature for a given grid point. The most recent 25 year averaged data was used for further analysis considering the Superpave specifications which takes into account at least 20 years of weather data for analysis as stated in the SHRP A-410 (Kennedy et al. 1994). Mean and standard deviation was computed using 7-day maximum and 1-day minimum temperature using data from immediate past 25 years. These values were stored in 4 matrices where each element was mapped to a combination of latitude and longitude. This process was repeated for all grid points. Finally, these 4 matrices (average 7-day maximum, standard deviation 7-day maximum, average 1-day minimum, standard deviation 1-day minimum), were multiplied by base matrix to eliminate grid point observations located outside the area of interest. Each matrix was identical to the map of India with grids holding temperature values. The final grid points created using QGIS[®] for 7 day average maximum temperature are shown below in Figure 4.

The above figure shows that the 329 filtered data points fit quite well with the Indian geographic map. These grid points hold the temperature values for

maximum of 7 day average temperature at 99.73% reliability which was calculated by:

$$Max\ temp = Mean + (3 \times SD) \quad (2)$$

Similarly, 357 minimum temperature data points holding minimum temperature values at 99.73% reliability are given by:

$$Min\ temp = Mean - (3 \times SD) \quad (3)$$

where SD stands for Standard Deviation.

4.3 Cluster analysis approach

The maximum of 7 day average temperature for all the 329 points were input in the CVAP toolbox as a '.txt' file and clustered using the algorithms as stated in section 2.1. The Euclidean distance measure was used in this stage. The range of clusters was limited between 8 and 15. This range came up by empirical calculations from the range of the maximum temperature which was from 16.32°C to 48.32°C (range being 32°C) and in order to divide into 4°C equal intervals, at least 8 clusters were needed. For each algorithm, the cluster membership was obtained for each data point. This stated the clusters to which each temperature data point belonged. The membership numbers varied depending on the algorithm. The same data point belonged to a different cluster for a different algorithm.

A map showing similar temperature zones was determined by mapping back the cluster membership obtained for a particular algorithm back to the grid format (31 × 31 grid of latitudes and longitudes). The zones were plotted in gray scale to identify the various zones visually.

4.4 Comparison of clustering methodologies

A temperature contour map was prepared using QGIS[®] software and the contour map layer was superimposed on the grid map obtained by cluster analysis. The number of contours was varied in an attempt to visually match the clustered zones with the contour regions. This was used for further interpretation and analysis of the clustering approaches. In addition, the validity indices were obtained for each clustering algorithm which were used for comparison.

Similar methodology was adopted for the analysis of the 1-day minimum temperature. In addition, the range of 1-day minimum temperature was -13.92°C to 19.58°C (range of temperature being around 34°C) and in order to divide into 4°C equal intervals, at least 8 clusters were needed. The range of clusters used here were also 8 to 15 chosen in a similar fashion as for maximum temperature.

5 RESULTS AND ANALYSIS

The results of cluster analysis are discussed below for maximum and minimum temperature data at 99.73% reliability level.

5.1 7-day average maximum temperature

After all the algorithms were run namely, K means, hierarchical single, hierarchical complete and hierarchical centroidal along with the affinity propagation algorithm, all the internal and external validity indices for each algorithm were tabulated for the cluster range of 8 to 15. Multiple clustering was chosen so that the number of iterations increases the clustering accuracy. The number of iterations for K means was kept as 10 since it gives the optimal result within 10 iterations. The optimal number of clusters was found to be different for all the range of clusters and the optimal clusters even varied with a particular index across various methods. Hence, initially the choice of a better clustering method turned out to be ambiguous as was also observed by Steinbach et al. (2000) and Chen et al. (2002). As suggested by Halkidi et al. (2002), visualization was resorted to make a judgment on the optimal number of clusters.

A plot showing comparison of various algorithms for the number of clusters (NC) ranging from 8 to 15 with respect to the validation indices of silhouette and R-squared available in CVAP was produced. The silhouette index is a measure of overall quality of the clusters and has been used to choose the optimal number of clusters by Wang et al. (2009). After choosing the optimal number of clusters from the plot, it was seen that Silhouette index was the highest (0.59051) for cluster size of 11 and for the K-means method. However, for the same, R^2 was highest with the value 1, which did not seem practical with cluster size of 8 for Hierarchical-Single method. The 8 clusters when visualized by mapping with temperature contours did not provide a good fit.

After lot of trial runs for each algorithm and for different number of clusters, the optimal number of clusters was found to be 11. Though this number was not predicted by indices in a few algorithms, the fitting to the contour map was found to be of good quality and the formation of no singleton clusters. Higher number of clusters resulted in very few points in one cluster thus making it unviable. The resulting clustered map was prepared for all the algorithms for optimal cluster level 11. The contour interval varies in each case in order to fit the data. It has been varied from 2.5°C to 4°C.

The CVAP toolbox provided the information that higher values of the external indices of Rand, Jaccard and FM indicate better clustering quality. Similarly, for the internal indices of Silhouette, Calinski-Harbasz, homogeneity, separation and R^2 , higher values denote better clustering quality and low values of the Davies-Bouldin index indicate a better clustering solution. It was observed that the optimal values for all indices varied across different algorithms. For example, the R-squared for hierarchical centroid method was the highest among all algorithms (0.999) whereas the external indices were highest for hierarchical single approach. But, the hierarchical single and centroidal approaches consisted of a singleton cluster and therefore these methods were discarded.

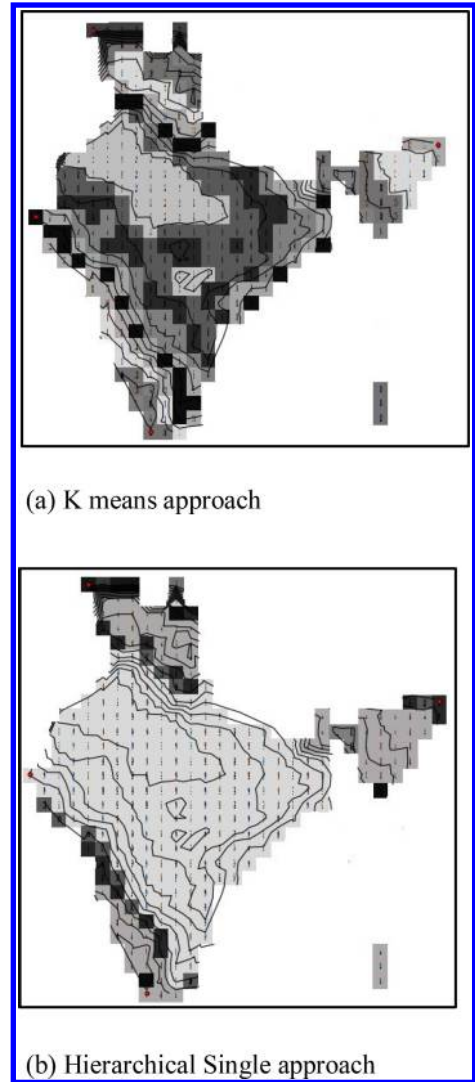
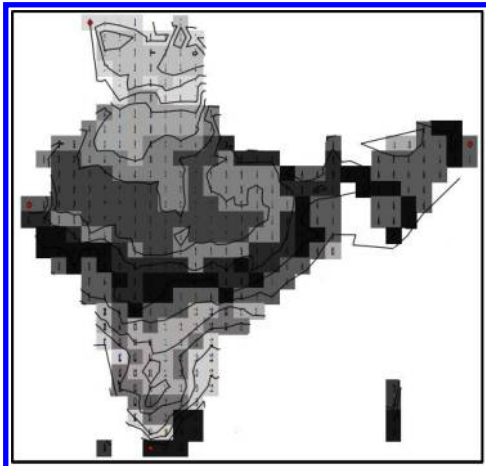
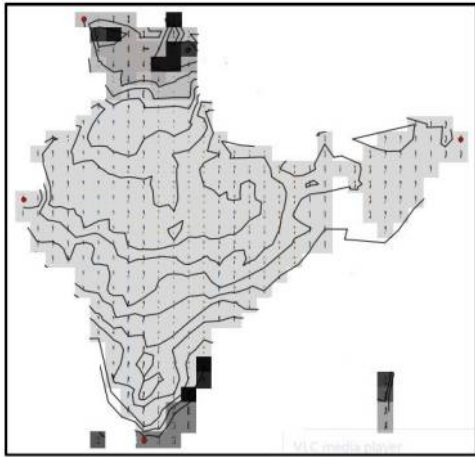


Figure 5. Seven day average Maximum temperature contour maps for various algorithms (a) K means and (b) Hierarchical Single.

For the final judgment, all the plots of the overlapped temperature contour layer and the clustered map layer was referred in order to check the fit of the clustering result. It was observed that the hierarchical-single approach provided a very poor fit as it created large clusters with no distinction of regional anomalies along with number of singleton clusters. The temperature had been shown to be uniform in the north-south direction which was an anomaly. With the K-means method, it was observed that it had a high R-squared value of 0.998 along with the highest silhouette index for the cluster size of 11. The silhouette index measuring the overall clustering quality has been used to choose the best clustering algorithm by Wang et al. (2009). Hence, the K-means was chosen to produce the best results. All the other approaches plotted the data



(a) Affinity Propagation algorithm.



(b) Hierarchical Single approach.

Figure 6. One day Minimum temperature contour maps for various algorithms (a) K means and (b) Hierarchical Single.

well but possessed drawbacks such as singleton clusters (hierarchical centroid and single) or non-optimal value of the silhouette index (hierarchical complete and affinity propagation). Figure 5(a) and Figure 5(b) below show the best fit by the K means method and the worst fit by the Hierarchical single method respectively. This does not coincide with the observation of Wu et al. (2010) and Steinbach et al. (2000) who stated that the hierarchical methods are better clustering methods over non-hierarchical methods.

Thus, on the whole evaluating the pros and cons the K means method proved to be better than the rest methods for clustering 7 day maximum temperature for the Indian region.

5.2 1 day minimum temperature

The comparison of various algorithms for the NC range 8 to 15 was performed. The results were compared with respect to the validation indices of Silhouette and R-squared available in CVAP. After choosing the optimal number of clusters from the algorithm comparison plot, the algorithms were compared with visual fit to the data. From the plot, it was seen that Silhouette index is highest (0.5851) for cluster size of 8 for the K-means method and for the affinity propagation algorithm, it stood at 0.5949. However, R^2 was highest (0.9962) for cluster size of 14 for the K-means method and with cluster size 8 for Hierarchical complete linkage method, it stood at 0.9963. However, 8 clusters when visualized by mapping with temperature contours did not provide a good fit. After several trial runs for each algorithm and for different number of clusters, the optimal number of clusters was found to be 14. In spite of the fact that this number was not predicted by indices in a few algorithms, superimposition of the contour map was found to provide reasonable clusters and no single member clusters were formed. The contour interval has been varied in each case in order to fit the data. It has been varied from 2.5°C to 4°C .

As stated before, the optimal values for all indices were different for each different algorithm. Taking R^2 into account, the best approach tends to be the K means and with respect to the optimal value of indices, the hierarchical single proves to be the better option. But, with R-square of 0.647, it is not at all preferred. This again does not correlate with the observation of Wu et al. (2010) and Steinbach et al. (2000) regarding the better performance of hierarchical methods over the non-hierarchical. For visual fit, the overlay maps were prepared and compared. It was inferred that as suggested by very low R-Square values for hierarchical-single linkage method, it provided a very poor fit similar to the case with maximum temperature. It created large clusters with no variation of temperature over long distances (north to south India) which does not hold true. The R-squared for K-means method is the highest among all algorithms (0.996). An important observation from the fitting provided by most algorithms was that a part of the Andaman and Nicobar islands have been shown to have similar minimum temperature to the Lakshadweep islands.

However, the affinity propagation algorithm produces the best results with well separated and compact clusters precisely mapped to the temperature contours correlated with the highest silhouette index of 0.561. The fitting provided by the hierarchical complete and centroidal linkage methods are comparable and similar. The K-means method has a lot of overlapping clusters making its score, less over the other methods (correlating with lowest homogeneity index of 0.015). There was a singleton cluster formed for the hierarchical centroid algorithm making it less attractive to choose as a clustering algorithm. The resulting clustered map prepared for the best (affinity propagation) and the worst algorithm (Hierarchical Single) for

optimal cluster level 14 is shown below in Figure 6(a) and Figure 6(b) respectively.

Affinity propagation algorithm proved to cluster the 1 day minimum air temperatures in the best possible way. On the whole it has been stated explicitly by Sturn et al. (2002) and also observed in this study that there is no single method that integrates clustering methods and visualization methods and helps comparing results produced by various clustering approaches.

6 CONCLUSIONS

The conclusions drawn from this study includes the comparison of cluster methodologies for developing homogenous temperature zones. It brings forward the pros and cons of each method and also provides scope for resorting to neural network techniques in order to achieve higher accuracy in results as was suggested by the affinity propagation algorithm, an elementary neural network technique in case of minimum temperature. Since, air temperature forms an integral part of the existing SHRP and LTPP models of predicting pavement temperature, the present study takes a closer look at the variation of air temperature within India. This would prove to be a meaningful input for development of pavement temperature contours using the homogeneous air temperature sections. Further it would lead to the selection of an optimal binder for regions experiencing similar temperature. In spite of involvement of subjective judgment, all the clustering approaches do provide an insight into the nature of temperature variation across the country. Thus, the cluster analysis approach has been successfully implemented to demarcate air temperature zones using 7-day average maximum air and 1-day minimum air temperatures using higher number of data points as used in earlier studies.

REFERENCES

Almeida R.M. S. F., Ramos N. M. M., Lurdes Simões M. and Freitas deVasco P.2014. Energy and water consumption variability in school buildings: review and application of clustering techniques. *Journal of Performance of Constructed Facilities*, in press.

Chen G., Jaradat S.A., Banerjee N., Tanaka T.S., Ko M.S.H. and Zhang M.Q. 2002. Evaluation and Comparison of Clustering Algorithms in Analyzing ES Cell Gene Expression Data. *Statistica Sinica* 12:241–262.

Dueck D. 2009. Affinity propagation: clustering data by passing messages. Ph.D. thesis University of Toronto, Canada.

Gerstengarbe F.W., Werner P. C. and Fraedrich K. 1999. Applying non-hierarchical cluster analysis algorithms to climate classification: some problems and their solution. *Theoretical and Applied Climatology* 64:143–150.

Ghuzlan K.A. and Al-Khateeb G.G. 2013. Selection and verification of performance grading for asphalt binders produced in Jordan. *International Journal of Pavement Engineering* 14(2):116–124.

Gong X. and Richman M.B. 1995. On the Application of Cluster Analysis to Growing Season Precipitation Data in North America East of the Rockies. *Journal of climate* 8: 897–931.

Halkidi M., Batistakis Y. and Vazirgiannis M. 2001. Cluster Validity Methods: Part I. *Journal of Intelligent Information Systems* 17:107–145.

Halkidi M., Batistakis Y. and Vazirgiannis M. 2002. Cluster Validity Methods: Part I. *SIG-MOD Record* 31: 40–45.

Indian Standard (IS) (2006). Paving Bitumen Specification (Third Revision). 73. New Delhi.

Indian Standard (IS) (2013). Paving Bitumen Specification (Fourth Revision). 73. New Delhi.

Isik S., Turan A. and Dogan E. 2006. Classification of river yields in turkey with cluster analysis. *Proc. World Environmental and Water Resources Congress, Omaha, 21–25 May, 2006*: 1–7. New York: American Society of Civil Engineers (ASCE).

Kennedy T.W., Huber G.A., Harrigan E.T., Cominsky, R.J., Hughes C.S., Quintus H.V. and Moulthrop J.S. 1994. *SHRP A-410 Superior Performing Asphalt Pavements (Superpave): The product of the SHRP Asphalt research program. Strategic Highway Research Program A-410*. Washington D.C.: National Academy of Sciences.

Kim K., Heo J., Nam W. and Shin E. 2004. Applicability of Various Clustering Techniques for Regional Frequency Analysis. *Proc. World Water Congress, Salt Lake City, 21 June-1 July, 2005*: 1–9. New York: American Society of Civil Engineers(ASCE).

Liu Y., Li Z., Xiong H., Gao X. and Wu J. 2010. Understanding of Internal Clustering Validation Measures. *Proc. IEEE International Conference on Data Mining, Sydney, 14–17 December, 2010*: 911–916. New Jersey: IEEE.

Lu Q. and Harvey J.T. 2007. Characterization of truck traffic in California for Mechanistic-Empirical Design. *Transportation Research Record* 1945: 61–72.

Lukanen E.O., Han C. and Skok E.L. 1998. Probabilistic Method of Asphalt Binder Selection Based on Pavement Temperature. *Transportation Research Record* 1609: 12–20.

Mirza M.W., Abbas Z. and Rizvi M.A. 2011. Temperature Zoning of Pakistan for Asphalt Mix Design. *Pak. J. Engg. & Appl. Sci.* 8(2011):49–60.

Nivitha M.R. and Krishnan J.M. 2014. Development of Pavement Temperature Contours for India. *Journal of the Institution of Engineers, India* 95(2): 83–90.

Papagiannakis A.T., Bracher M. and Jackson N.C. 2006. Utilizing clustering techniques in estimating traffic data input for pavement design. *Journal of Transportation Engineering* 132(11): 872–879.

Rendón E., Abundez I., Arizmendi A. and Quiroz E.M. 2011. Internal versus External cluster validation indexes. *International Journal of Computers and Communications* 5(1): 27–34.

Rossi R., Gastaldi M. and Gecchele G. 2014. Comparison of Clustering Methods for Road Group Identification in FHWA Traffic Monitoring Approach: Effects on AADT Estimates. *Journal of Transportation Engineering* 140(7), in press.

Srivastava A.K., Rajeevan M. and Kshirsagar S.R. 2009. Development of a high resolution daily gridded temperature data set (1969–2005) for the Indian region. *Atmospheric Science Letters* 10(4): 249–254.

Steinbach M., Karypis G. and Kumar V. 2000. A Comparison of Document Clustering Techniques. Technical Report #00-034. Dept. of Computer Science and Engineering. University of Minnesota, USA.

- Sturn A., Quackenbush J. and Trajanoski Z. 2002. Genesis: cluster analysis of microarray data. *Bioinformatic Applications Note* 18(1): 207–208.
- Wang K., Wang B. and Peng L. 2009. CVAP: Validation for Cluster Analyses. *Data Science Journal* 8: 88–93.
- Wang K.C.P., Li Q., Hall K.D., Nguyen V. and Xiao D.X. 2011. Development of Truck Loading Groups for the Mechanistic-Empirical Pavement Design Guide. *Journal of Transportation Engineering* 137(12): 855–862.
- Wang Y., Hancher D.E. and Mahboub K. 2007. Axle Load Distribution for Mechanistic-Empirical Pavement Design. *Journal of Transportation Engineering* 133(8): 469–479.
- Wu G., Liu S., Zhang Y. and Yan Q. 2010. Clustering Methods Evaluation As Well As Its Application to Waste Products Clustering Research. *Proc. International Conference of Logistics Engineering and Management, Chengdu, 8–10 October, 2010*: 2582–2587. New York: ASCE.
- Yan Z., Yan X., Huang M., Xie L. and Wang Z. 2011. Based on the Improved K – means Algorithm of Tianjin Port Traffic Flow Characteristic Analysis. *Proc. International Conference on Transportation Information and Safety (ICTIS), Wuhan, 29 June–2 July, 2011*: 1863–1870. New York.

Effects of low vehicle speed on the service life time of asphalt pavements

A. Walther & I. Isailović

Technische Universität Braunschweig, Department of Architecture, Civil Engineering and Environmental Sciences – Pavement Engineering Centre (ISBS), Braunschweig, Germany

ABSTRACT: The constant increase of traffic density in recent years, especially in the highest-level road system, leads to the significant axle-loading of the superstructure and inevitably affects the traffic quality. Additionally, maintenance projects for upgrading the bearing capacity of pavement layers lead to the further reduction in the road capacity. All this factors provoke a significant decrease in the average traffic speed. Using mechanistic pavement design procedure flexible pavements can be designed analytically. In addition to the asphalt stiffness, the fatigue resistance of the asphalt base course material serves as an input to the computation model. Both material parameters are gathered from laboratory testing using cyclic indirect tensile test (ITT). The standard procedure for fatigue testing implies cyclic sinusoidal loading till failure at the temperature of 20°C and frequency of 10 Hz. In order to simulate low traffic velocity, lower loading frequencies are implied. Finally the effects of reduced frequencies on fatigue resistance on the service life time of asphalt pavements are investigated.

1 TEMPERATURE- AND FREQUENCY DEPENDENT STIFFNESS MODULUS

The resulting strain of hot mix asphalt (HMA) in cyclic stress controlled tests largely depends on the stress amplitude and loading frequency. When HMA is loaded with higher frequencies in the elastic range, the resulting strain response is lower, compared to the same stress amplitude at lower frequency. Therefore, a uniform asphalt stiffness (amount of the complex dynamic modulus) is determined for different temperature-frequency combinations (Hürtgen, 2000).

According to the EN 12697-26 the stiffness ITT tests should be performed at at least four temperatures (−10°C, 0°C, 10°C and 20°C) and at different frequencies in range between 0.1 Hz and 10 Hz (see Table 1).

For the calculation of stiffness modulus in cyclic ITT test the following equation can be used:

$$E = \frac{\Delta F \cdot (0,274 + \mu)}{h \cdot \Delta u} \tag{1}$$

Table 1. Number of load cycles for multistage tests to determine the stiffness modulus in ITT test.

Loading frequency	Load cycle	Load cycles to determine stiffness modulus
10 Hz	110	98–102
5 Hz	100	93–97
1 Hz	20	13–17
0.1 Hz	10	3–7

where:

- E = stiffness modulus,
- ΔF = force amplitude,
- Δu = deformation amplitude,
- μ = Poisson’s ratio and
- h = specimen height.

Figure 1 shows the calculated stiffness moduli as stiffness modulus-frequency functions (the so-called isotherms) for one HMA AC 32 T S for base course.

For determination of the stiffness modulus master curve for one HMA with unmodified binder a shift factor α_T can be calculated using Equation 2.

$$\log \alpha_T = m \cdot \left(\frac{1}{T} - \frac{1}{T_0} \right) \tag{2}$$

where:

- T₀ = reference temperature,

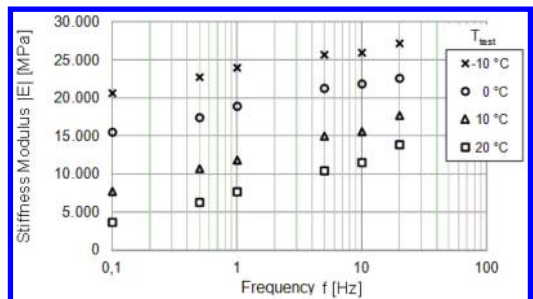


Figure 1. Determined isotherms for one AC 32 T S. Stiffness modulus at different test temperatures (−10°C, 0°C, 10°C and 20°C) and frequencies (0.1 Hz, 1 Hz, 5 Hz, 10 Hz).

Table 2. ITT test: temperature and frequency dependent stiffness moduli of an asphalt base course material AC 32 T S.

Frequency [Hz]	Test temperature [°C]			
	-10	0	10	20
0.1	20620	15496	7715	3666
0.5	22719	17407	10713	6265
1	23960	18905	11829	7659
5	25661	21248	14973	10433
10	25931	21825	15573	11506
20	27154	22563	17692	13843

Table 3. Parameters of master curve (sigmoid function) for AC 32 T S for a reference temperature of 20°C and a reference frequency of 10 Hz.

Parameter	w	y ₀	x ₀	z
	32587.06	1953.62	1.70	1.88

T = temperature for which the shift factor is to be determined and
 m = material constant (25000).

So each test frequency f can be referred to the corrected frequency f_R (Equation 3).

$$f_R = f \cdot \alpha_T \quad (3)$$

The stiffness master curve is to be approximated by an appropriate regression function, for example by means of the sigmoid function:

$$E = y_0 + \frac{w}{1 + e^{\left(\frac{\log(f_R) - x_0}{z}\right)}}, \quad (4)$$

where:

y₀ = intersection of function with ordinate,
 x₀ = intersection of function with abscissa,
 w, z = material parameters.

Table 2 shows an example of the temperature and frequency dependent stiffness moduli, which were determined by means of ITT on specimens of an asphalt base course material AC 32 T S.

Corresponding parameters of master curve (sigmoid function) determined by applying the least squares method for a reference temperature of 20°C and a reference frequency of 10 Hz are plotted in Table 3.

Figure 2 shows the obtained stiffness modulus master curve depending on the frequency and temperature for the considered mixture (AC 32 T S).

Applying the parameters of the master curve (Table 3) for further loading frequencies (0.1, 0.5, 1, 5, 10, and 20 Hz) results in the stiffness modulus distribution over the temperature (Figure 3). The determined isotherms from Figure 1 are also depicted for orientation purposes.

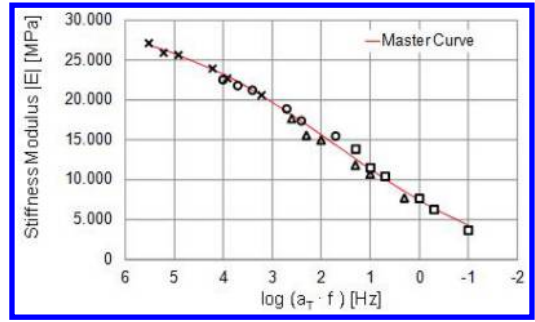


Figure 2. Stiffness modulus master curve for AC 32 T S.

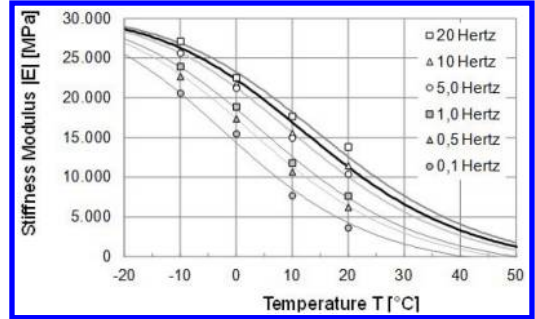


Figure 3. Temperature and frequency-dependent stiffness modulus functions for an asphalt base course material AC 32 T S gained using regression parameters of the master function specified in Table 3.

2 FREQUENCY DEPENDENT FATIGUE BEHAVIOR

In analogy to the stiffness modulus, the fatigue behavior of the HMA is also frequency dependent.

In ITT test a vertical acting compressive stress induces in the specimen a non-homogeneous stress state, where in the middle portion of the specimen a horizontal tensile stress is observed. This tensile horizontal stress leads primarily to the specimen failure.

For the evaluation of the number of loading repetitions at failure the Energy Ratio (ER) approach proposed by Rowe (2000) was used. ER is obtained by multiplying the stiffness modulus |E|_N and the corresponding number of load cycles N according to Equation 5.

$$ER_{(N)} = N \cdot |E|_N \quad (5)$$

By plotting ER versus the number of loading cycles, fatigue life is defined as the number of loading cycles for which ER achieves the maximum. The so-obtained point represents the transition between micro and macro cracking and is specified as N_{Macro}.

Figure 4 shows the typical evolution of the stiffness modulus and energy ratio in ITT test at two test frequencies (10 Hz and 5 Hz) at the same stress level (σ_o = 0.55 MPa) for the asphalt base course material AC 32 T S.

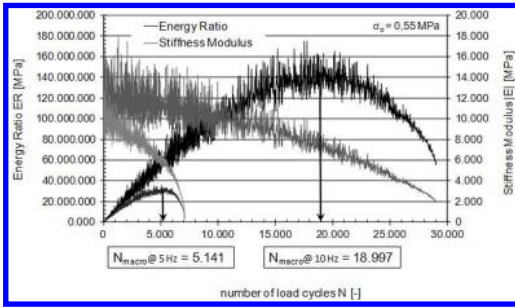


Figure 4. Evolution of the stiffness modulus and energy ratio in ITT test at two test frequencies (10 Hz and 5 Hz) at the same stress level ($\sigma_0 = 0.55$ MPa) for the asphalt base course material AC 32 T S.

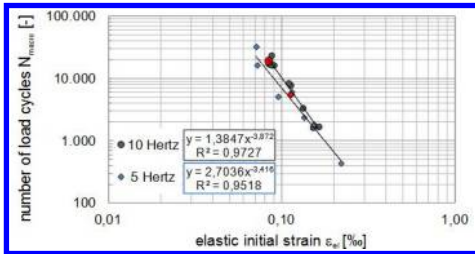


Figure 5. Frequency dependant fatigue functions for an asphalt base course material AC 32 T S.

For determination of the fatigue function at least nine single fatigue tests using three different stress amplitudes were carried out. Using calculated horizontal elastic initial strains ϵ_{el} and the corresponding number of load cycles N_{Macro} the fatigue function of the asphalt can be described as a power function (see Chapter 4). Figure 5 shows the resulting fatigue functions for AC 32 T S at two loading frequencies (10 Hz and 5 Hz).

3 LOADING FREQUENCIES IN THE PAVEMENT SUPERSTRUCTURE

The determination of the strain/stress frequencies which act in the pavements during traffic loading is a crucial task for pavement design procedure. Theoretically approaches were performed i.e. by Al-Quadi et al. (2008) and Losa & Di Natale (2012). The resulting strain frequency due to traffic in the pavement structure is significantly influenced by the traffic speed passing over and its thickness.

The Figure 6 shows the influence of the vehicle speed on the induced strain at the bottom of the HMA construction, containing 4 cm asphalt wearing course, 4 cm binder course and 10 cm base course (Mollenhauer et al., 2009). An analysis of the maximal strain values show that increasing vehicle speed results in decreasing strain, which corresponds to the increase in stiffness modulus of the HMA (see Chapter 1).

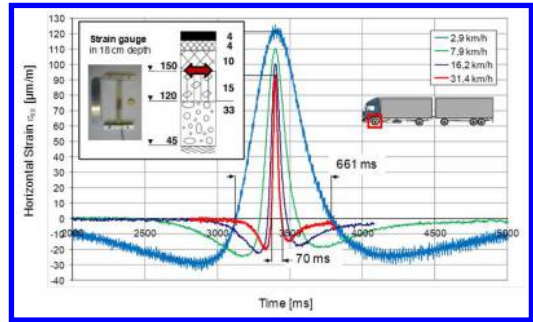


Figure 6. Induced strains at the bottom of the asphalt base course due to the variations of vehicle speed (Mollenhauer et al., 2009).

Table 4. Resulting strain frequencies at the bottom of asphalt base course as a function of the vehicle speed and the thickness of the asphalt pavement (Mollenhauer et al., 2009).

Asphalt thickness	Vehicle speed [km/h]			
	2.9	7.9	16.2	31.4
34 cm	0.5 Hz	1.2 Hz	2.2	3.9 Hz
22 cm	0.7 Hz	1.7 Hz	3.1 Hz	5.6 Hz
18 cm	0.8 Hz	1.9 Hz	3.9 Hz	7.1 Hz
14 cm	0.9 Hz	2.4 Hz	4.8 Hz	8.9 Hz

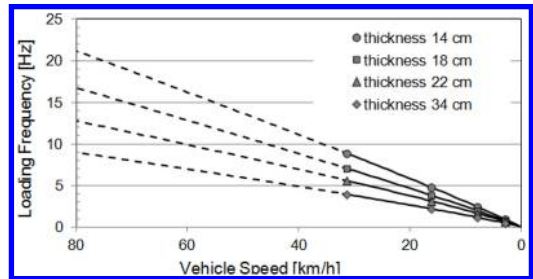


Figure 7. Resulting strain frequencies (measured and extrapolated) at the bottom of asphalt base course as a function of the vehicle speed and the thickness of the asphalt superstructure (Mollenhauer et al., 2009).

The thickness of the asphalt layers also shows a great influence on the induced strain frequency (see Table 4). With increasing thickness of the asphalt layers the induced strain frequency at the bottom of the asphalt base course decreases.

Extrapolating the values from Table 4 it is possible to get the strain frequencies for further vehicle speeds (Figure 7).

4 MECHANISTIC PAVEMENT DESIGN

Mechanistic pavement design is based on an iterative design approach. The model is composed of individual

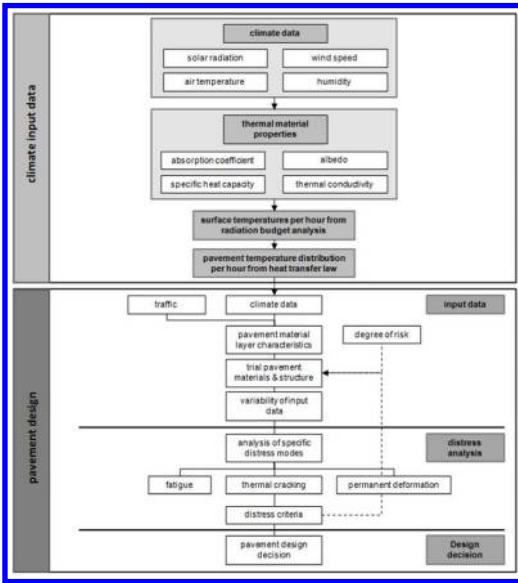


Figure 8. Flow chart of design approach used in this paper.

sub-models displaying climate and traffic input data, distress analysis, and design decision. For calculating pavement temperature distribution from climate input data every single hour of the design period is considered in the approach presented in this paper (Figure 8).

The mechanical analysis is based on a response model to calculate critical traffic-induced and/or temperature-induced stress. For this purpose, the pavement structure is represented by individual layers. Calculation of response is realized using the linear-elastic multi-layer theory according to Burmister (1943), where stresses and strains are calculated analytically for every point of the half space for defined initial and boundary conditions. Elastic layer properties are described in terms of stiffness modulus in function of temperature.

A distress model is used to relate critical stress to pavement deterioration. Horizontal tensile bending strains at the bottom of the asphalt layers are related to repetitions to cause fatigue cracking. This is found empirically from observation of pavement performance, and from linking critical stress limits with load repetitions that cause unacceptable pavement failure.

Asphalt fatigue properties are studied according to the European Standard for fatigue testing (EN 12697-24) using cyclic indirect tensile test. The numbers of load applications at fatigue failure N_{Makro} are obtained from the results of several fatigue tests at varying loading conditions. From the tests, a fatigue function (called Wöhler line) is found, which is drawn by executing a linear regression between N_{Makro} and the corresponding initial strain level ε , indicating the fatigue life duration in function of the applied load

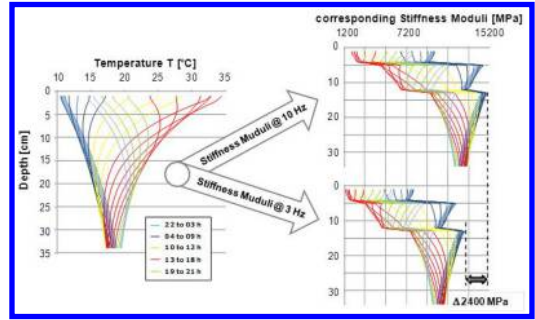


Figure 9. Hourly temperature distribution in the superstructure (left) with corresponding asphalt stiffness moduli determined by ITT at different frequencies (right) during a given day.

amplitude. As the Wöhler line can be expressed in the general form, with C_1 and C_2 as regression parameters,

$$N_f = C_1 \cdot \varepsilon^{C_2} \quad (6)$$

Analysis of fatigue evolution requires a cumulative damage hypothesis. This is realized by linear summation of cyclic ratios applying Miner's law (Miner, 1945; Monismith, 2004). The cumulative fatigue damage D due to load repetitions reads

$$D = \sum_{i=1}^n \frac{n_i}{N_{fi}} \leq 1, \quad (7)$$

where:

n_i = the number of actual traffic load application at strain/stress level i and

N_{fi} = the number of allowable traffic load application to failure at strain/stress level i .

Equation 6 allows predicting fatigue life in terms of the number of permissible load applications (due to traffic and thermal load cycles).

4.1 Superposition of load and temperature

To examine the impact on fatigue in the pavement structure due to low loading frequencies, a parametric study is carried out using mechanistic pavement design method. For this purpose a developed computer Software program is used (Walther, 2014). Here the temperature profile is converted into the superstructure on an hourly basis, using the energy balance at the road surface and the Fourier equation for heat conduction in the superstructure on an hourly basis (see, Walther & Wistuba, 2012). If the temperature distribution in the superstructure is known, the stiffness modulus of the asphalt layers in the structure can be assigned, since the frequency-dependent temperature stiffness function (master curve) of the asphalts are determined cyclic by indirect tensile test (Figure 9).

The hourly based temperature and stiffness moduli data are overlaid with the corresponding traffic data in a further step. As a result, executing elastic multi layer theory an hourly time variation curve of stress and strain in the superstructure is determined (Figure 10).

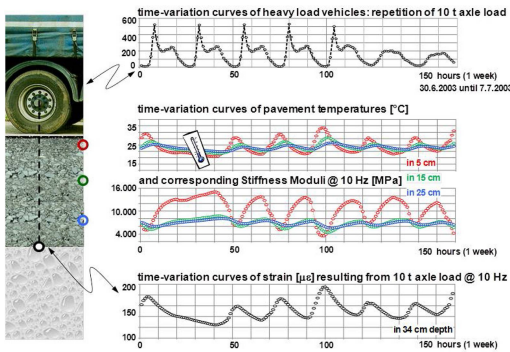


Figure 10. Time variation curves for temperature, traffic and the resulting strain at the bottom of the asphalt layer for a loading frequency of 10 Hz (Wistuba & Walther, 2013).

Table 5. Correlation between loading frequency and vehicle speed for an asphalt pavement structure exhibiting a thickness of 34 cm.

Frequency [Hz]	Vehicle speed [km/h]	Factor to 10 Hz
10	90	1.0
5	41	0.456
3	23	0.233

4.2 Input data

For the parametric study a standardised asphalt pavement structure according to German specification (RStO 12) is used exhibiting a thickness of 34 cm asphalt in total (4 cm wearing course, 12 cm binder course and 18 cm base course). Using the correlation between thickness of the superstructure and the loading frequency, the correspondent vehicle speeds are calculated (Table 5).

Table 6 shows the stiffness moduli of asphalt wearing- and binder course material in response to the loading frequency at different temperatures. The stiffness moduli for asphalt base course material (AC 32 T S) are presented in Table 2.

The loading frequency dependent fatigue function parameters of the asphalt base course are shown in Table 7; the resulting Equivalent Single Axle Loads (ESALs) at different loading frequencies are plotted in Table 8.

4.3 Results of mechanistic design procedure

The result of a mechanistic design procedure are calculated Miner sums (Equation 7), which are determined by the strains at the bottom of the asphalt base course and the present traffic load using material specific fatigue functions. Based on a static load of 50 kN, the resulting time variation curves of strains at the bottom of the asphalt course layer for a period of one month (July 2003) at three different loading frequencies (10, 5 and 3 Hz) are shown in Figure 11. As expected, different vehicle speeds lead to the different

Table 6. Stiffness moduli of asphalt wearing- and binder course material in response to loading frequency at different temperatures.

Temperature [°C]	Stiffness Moduli [MPa]			
	Wearing course		Binder course	
	10 Hz	3 Hz	10 Hz	3 Hz
-20	26123	25176	30483	29840
-10	22308	20515	27726	26273
0	16472	14137	22594	20187
10	10267	8190	15673	12949
15	7663	5914	12221	9694
20	5551	4151	9148	6969
35	1805	1199	3063	2007
50	360	115	525	90

Table 7. Fatigue functions of an asphalt base course material AC 32 T S for different loading frequencies at 20°C.

Parameter [-]	Loading frequency [Hz]		
	10	5	3
C ₁	1.3847	2.7036	5.1828
C ₂	-3.872	-3.416	-3.092
R ²	0.97	0.95	0.94

Table 8. Resulting equivalent single axle loads at different loading frequencies.

Parameter [-]	Loading frequency [Hz]		
	10	5	3
Heavy trucks per day	12465	5.679	3.186
ESALs [-]	141.43 mil.	64.44 mil.	36.15 mil.

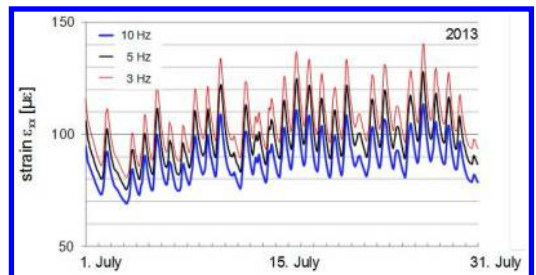


Figure 11. Resulting strain evolution at the bottom of an asphalt base course at 34 cm depth, taking into account different loading frequencies for duration of one month.

strain values in the pavement structure where a loading frequency of 10 Hz leads to the lowest strain values.

Effects on the Miner sum due to bonding characteristics between asphalt layers were studied in Walther & Wistuba (2013).

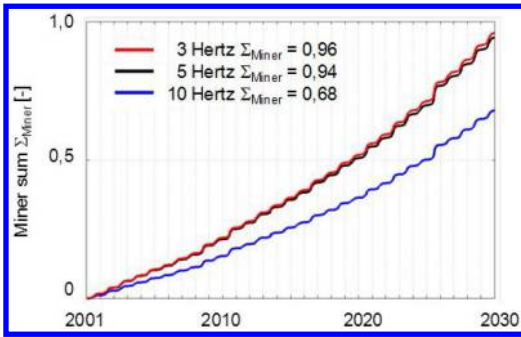


Figure 12. Resulting damage increments evolution over the life span due to different loading frequencies for an asphalt base course material AC 32 T S.

Figure 12 shows the damage evolution of the asphalt base course material considering different loading frequencies for a design period of 30 years. The lowest Miner sum (0.68) is calculated taking into account a loading frequency of 10 Hz. Decreasing the frequency to 5 Hz leads to a significant increase in the Miner sum from 0.68 to 0.94, whereas a further lowering of the loading frequency to 3 Hz exhibits only a minor impact on the damage.

5 CONCLUSIONS

Investigation on increase of fatigue damage in asphalt pavement structures due to different loading frequencies were performed in this paper. Functional correlations between vehicle speeds and resulting loading frequencies in asphalt pavement pavements were identified. In order to simulate the effect of various vehicle speed on the life span of asphalt pavements the mechanistic pavement design procedure for a design period of 30 years was conducted. For that purpose the stiffness tests at different test temperatures and frequencies and fatigue tests at different frequencies (10 Hz, 5 Hz and 3 Hz) were performed using cyclic indirect tensile test. The temperature-frequency stiffness functions, the fatigue functions, climate and traffic dates were considered.

It was found that different vehicle speeds lead to the different strain values in the pavements. With increased vehicle speed decreases the induced strain at the bottom of base course.

Vehicle speed of 90 km/h, which correspond to the loading frequency of 10 Hz for a 34 cm thick pavement induces the lowest strain value and thus leads to the highest fatigue life. On the other hand loading frequencies of 5 Hz and 3 Hz (corresponding vehicle speed of 20 to 40 km/h) show pretty similar results, leading to the quite reduction of fatigue life of the considered structure.

It has been demonstrated that vehicle speeds lower than 40 km/h have significant impact on the service life of asphalt pavements. In future these should be also considered in order to improve the accuracy of the calculated service life time.

REFERENCES

- Al-Qadi, I. L., M. A. Elseifi, P. J. Yoo, S. H. Dessouky, N. Gibson, T. P. Harman, J. A. D'Angelo, and K. Petros. 2008. Accuracy of Current Complex Modulus Selection Procedure from Vehicular Load Pulse: NCHRP Project 1-37A Mechanistic-Empirical Pavement Design Guide. In *Transportation Research Record: Journal of the Transportation Research Board*, No. 2087, Transportation Research Board of the National Academies, Washington, D.C., pp. 81–90.
- Burmister D. M. 1943. The General Theory of Stresses and Displacements in Layered Systems. *Journal of Applied Physics*.
- EN 12697-24. 2012. Bituminous mixtures – Test methods for hot mix asphalt – Part 24: Resistance to fatigue. *European Committee For Standardization*.
- Hopman, P., Kunst, P. & Pronk, A. 1989. A Renewed Interpretation Model for Fatigue Measurement. Verification of Miner's Rule. *4th Eurobitume Symposium, Vol. 1, Madrid, 4-6 October*, pp. 557–561, Spain.
- Hürtgen, H. 2000. Methoden zur Beschreibung der thermomechanischen Eigenschaften von Asphalt (Asphalt-Rheologie). *Schriftenreihe des Fachgebietes Konstruktiver Straßenbau im Institut für Verkehrswirtschaft, Straßenwesen und Städtebau der Universität Hannover, Heft 20*, Hannover.
- Losa, M. and Di Natale, A. 2012. Evaluation of Representative Loading Frequency for Linear Elastic Analysis of Asphalt Pavements. In *Transportation Research Record: Journal of the Transportation Research Board*, No. 2305, Transportation Research Board of the National Academies, Washington, D.C., pp. 150–161. DOI: 10.3141/2305-16.
- Miner M.A. 1945. Cumulative damage of fatigue, *Journal of Applied Mechanics*.
- Mollenhauer, K., Wistuba, M. & Rabe, R. 2009. Loading Frequency and Fatigue: In situ conditions & Impact on Test Results. *Proc., 2nd Workshop on Four Point Bending, 24.-25.09.2009, Minho*, Portugal, ISBN 978-972-8692-42-1.
- Monismith C.L. 2004. Evolution of long-lasting asphalt pavement design methodology: a perspective, *Lecture presented in June 2004 at Auburn University to the ISAP-sponsored International Symposium on Design and Construction of Long Lasting Asphalt Pavements*.
- Rowe, G.M. & Bouldin, M.G. 2000. Improved techniques to evaluate the fatigue resistance of asphaltic mixtures. *2nd Eurasphalt & Eurobitume Congress, Proc.0081.uk*, Barcelona.
- Walther, A. & Wistuba, M. 2012. Mechanistic Pavement Design Considering Bottom-Up And Top-Down-Cracking, *Proc., 7th RILEM Int. Conf. on Cracking in Pavements*, Delft.
- Walther, A. & Wistuba, M. 2013. Auswirkungen des Schichtenverbundes auf die theoretische Lebensdauer von Straßenbefestigungen aus Asphalt. *Straße und Autobahn*, 7, 501–507, Kirschbaum Verlag.
- Walther, A. 2014. Rechnerische Dimensionierung von Asphaltstraßen unter Berücksichtigung stündlicher Beanspruchungszustände. *Phd. Thesis, Institut für Straßenwesen*, TU Braunschweig.
- Wistuba, M. & Walther, A. 2013. Consideration of climate change in mechanistic pavement design. *Road Materials and Pavement Design*, Volume 14, Supplement 1: EATA 2013, Taylor & Francis.

Formulation of a thickness design equation for asphalt overlay using MEPDG program

Van Phuc Le & Hyun Jong Lee

Department of Civil and Environmental Engineering, Sejong University, South Korea

Hee Mun Park

Korea Institute Civil Engineering and Building Technology, South Korea

Julius Marvin Flores

Department of Civil and Environmental Engineering, Sejong University, South Korea

Sangyum Lee

Seoul Metropolitan Government, South Korea

ABSTRACT: This study developed an overlay design equation for flexible pavement in Seoul using the Mechanistic Empirical Pavement Design Guide (MEPDG) program. The total asphalt layer thickness was considered to be a function of the ratio of existing and new material's dynamic modulus, ratio of overlay and existing remaining Hot Mix Asphalt (HMA) thickness, and equivalent 80-kN (18kip) single-axle loads (ESAL). Multiple regression analysis was conducted using the synthetic database generated by the MEPDG program. The validation study showed that the asphalt overlay design equation is within reasonable range compared to the 1993 AASHTO Guide and BISAR 3.0 program. The overlay design equation was reduced into another equation that can predict new pavement thickness design. This new pavement thickness design equation also validates the accuracy and reliability of the overlay design equation.

1 INTRODUCTION

Structural overlay design for flexible pavements is mainly used to improve the structural capacity of the existing structure. The required thickness of the asphalt overlay must have sufficient structural capacity that can sustain further load application in a long span of time. Theoretically, overlay thickness must be estimated based on the actual conditions of the existing pavement however current methods practiced are empirical approaches, which are based on engineer's judgments only. Deflection approach is one empirical method wherein a larger pavement surface deflection implies weaker pavement and subgrade (AASHTO, 1993). Another empirical method is the effective thickness approach wherein the required thickness of asphalt overlay is the difference between the required new pavement thickness and existing effective pavement thickness (Huang, 2004). With the increasing demand for an alternative approach correlating theories and field pavement actual performance, mechanical-empirical (ME) approaches were established. In this approach, critical stresses and strains in the pavement are determined based on a mechanistic approach while the pavement damage effect

assumption is based on an empirical failure criterion (Huang, 2004).

Currently, the Mechanistic Empirical Pavement Design Guide (MEPDG) is the most powerful tool that uses ME approach in analyzing and designing pavement. It was developed to address the limitations of the 1993 AASHTO Guide, which used empirical approaches (MEPDG, 2004). In South Korea, current pavement design program is the Korean Pavement Design Guide (KPDG), which has the same principle with the MEPDG, however is limited to new pavement design only. There is a need to improve and develop new methods that considers both the mechanistic and empirical approach in designing asphalt overlays for an effective asphalt overlay thickness design in Seoul since current overlay thickness design methods are empirical approaches only.

In this study, asphalt overlay design equations were developed using the MEPDG program. The objective was to develop a mechanistic-empirical approach in designing asphalt overlay thickness for Seoul. This approach will provide adequate and economic asphalt overlay thickness design considering existing and new pavement material properties based on various traffic characteristics and subgrade condition. It can optimize

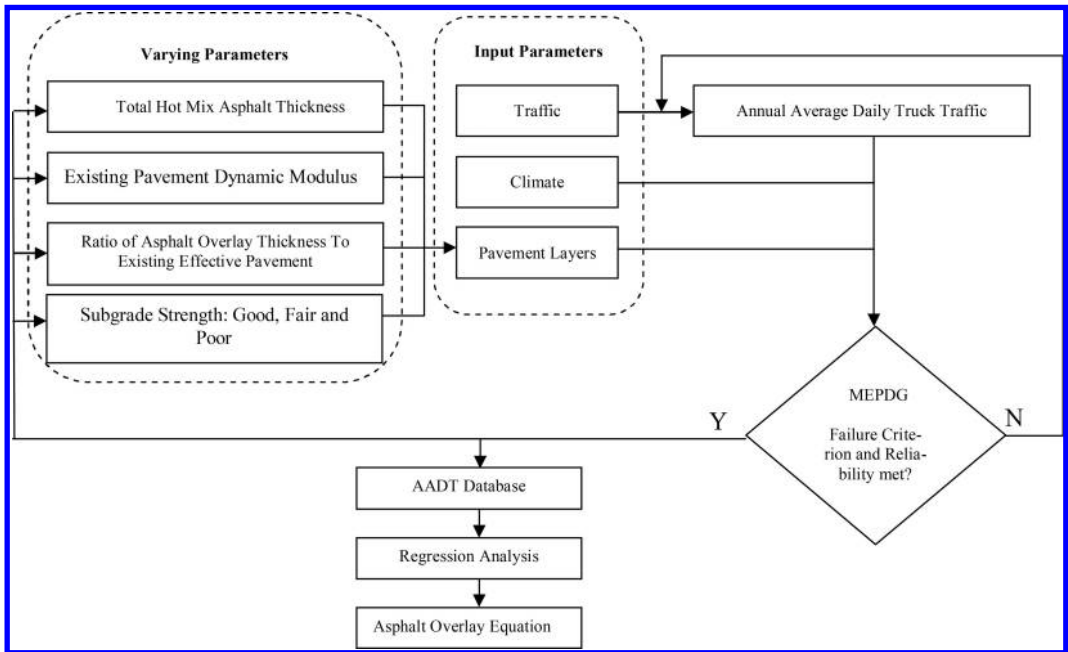


Figure 1. Schematic diagram of the analysis of the study.

the average pavement overlay life and reduce premature failure occurrence in the pavement. In developing the asphalt overlay design equation, material properties of each layer of the pavement, climate, and traffic characteristics of Seoul were considered.

2 DESIGN APPROACH

The new design mode of the MEPDG program was used as the main tool in this study since the overlay mode is more complex and has also its limitations. Permanent deformation always happen in the overlay mode of the MEPDG even thickness is increased (Wu et al. 2008).

The program has three main inputs: traffic, climate and pavement structure. Traffic adjustment factors, axle load distribution and general traffic inputs remains constant and are based on factual data from the Seoul Metropolitan Government, private engineering company, manual and online surveys. Likewise, climate remains constant and was determined by comparing Seoul's temperature to United States (US) weather stations in which is used in MEPDG.

In this study, the pavement was divided into four layers: subgrade, subbase, existing asphalt, and the asphalt overlay. The subgrade strength was characterized into three based on the surveyed data from laboratory and field tests (Falling Weight Deflectometer). Subbase layer strength of 180 MPa was used based on Seoul City's most common subbase strength. Moreover, using four (4) different dynamic modulus reduction of asphalt overlay material (10%, 20%, 30% and 50% reduction) simulated the existing pavement condition.

It was assumed that at 50% reduction, the pavement is severely damaged. In addition, by reviewing and collecting data from Seoul City's pavement management system database it was found that the minimum and maximum total pavement thickness used are 15 and 35 cm respectively. From these values, five (5) different total HMA thicknesses (35 cm, 30 cm, 25 cm, 20 cm, and 15 cm) were assumed to provide a wide range of data to be generated by considering current pavement thicknesses in Seoul. Different asphalt overlay ratios (2.0, 1.5, 1.0, 0.5, and 0.25) were analyzed to simulate all probable asphalt overlay scenarios (Le et al. 2015). The asphalt ratios assume the total thickness of the overlay material to the remaining thickness. A ratio of 2 means that the asphalt overlay thickness will be twice the thickness of the remaining thickness while a 0.5 ratio suggest that around 33% of the existing pavement will be removed. This can optimize the structural capacity of the pavement by assuming all probable milling scenarios in the field. These are the varying parameters of the study.

Figure 1 shows the schematic diagram done in the study. The initial input parameters are traffic, climate and pavement structure wherein all remains constant except for the assumptions said earlier.

3 DESIGN PARAMETERS

MEPDG program has three level inputs wherein input level 1 is the most complex however is the most accurate where actual traffic characteristic, $|E^*|$ (dynamic modulus) and dynamic shear modulus of binder are used. Level 2 is intermediate level, it does not require

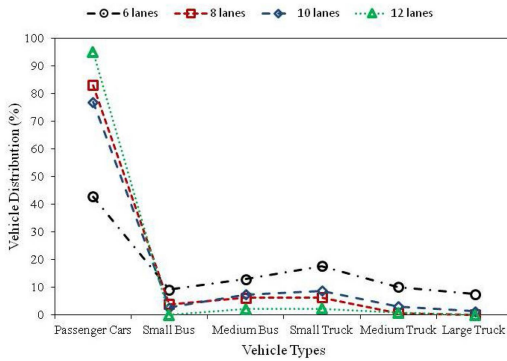


Figure 2. Vehicle distribution in Seoul City.

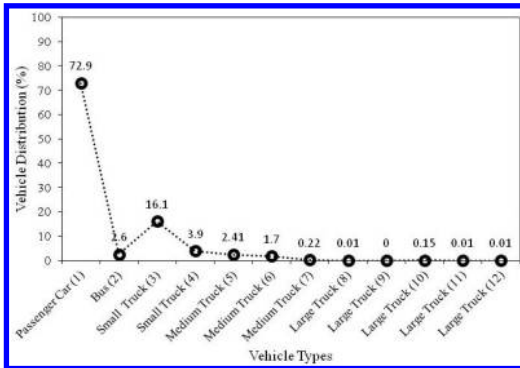


Figure 3. Vehicle distribution in Gyeonggido Province.

knowledge for all traffic parameters since it uses statewide traffic characteristics for axle load spectra. Laboratory test result of mixture to be used is only needed in this input level. Lastly Level 3 is the least complex input level since it only requires AADTT and truck percentages, while default values are used for the material property (MEPDG, 2004).

3.1 Traffic characterization

This study used input level 1 to consider actual traffic characteristics in Seoul such as truck traffic volume, truck traffic volume adjustment factors, axle load distribution factor, and other general traffic inputs. As shown in Figure 2, obtained vehicle distribution data in Seoul are composed of passenger cars, small and medium bus, and small, medium, large truck volumes. Based on Korean vehicle classification (KICT, 2009), medium and large trucks are sub classified into small classes. Using the Gyeonggido Province (nearby Seoul) local road data shown in Figure 3, distributions for medium and large trucks were determined.

Due to the small amount of medium truck (7) observed, it was considered as medium truck (6). Likewise, large truck classes 8, 9, 11 and 12 were considered as class 10 due to its small quantity. From the new Korean vehicle classification (KICT, 2009), class 4 is considered as medium truck. With this, classes 4,

Table 1. Vehicle class distribution.

KPDG Classification	2	4	5	6	10
MEPDG Classification	4	5	6	8	9
Vehicle Distribution, %	38.7	19.7	12.1	9.7	19.8

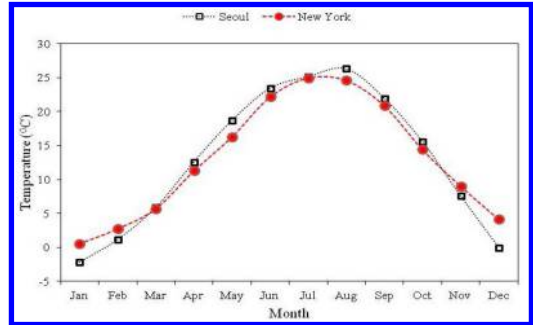


Figure 4. Comparison of Average temperature of Seoul and LaGuardia Airport, New York (Le et al. 2015).

5 and 6 are considered as medium truck classification while class 10 is considered as large truck. Using these assumptions, the final medium and large truck sub classifications were determined for the obtained Seoul City data. However, the MEPDG classifies vehicle types into thirteen (13) classes.

Passenger cars, small bus and small trucks were not included in this study due to its negligible effect on pavement damage. Comparing the axle configuration of both design guides, the final vehicle class distribution is shown in table 1. The final vehicle class distribution is composed of buses (4), medium trucks (5, 6 and 8) and large truck (9) (Le et al. 2015). This was used as input parameter in the MEPDG.

3.2 Climate characterization

MEPDG Program uses climate input in certain United States (US) weather stations only. Since this study used MEPDG as main tool for analysis, Seoul's climate was compared to twenty-two (22) cities in the US having almost same maximum and minimum temperature. Yearly temperature database of US weather stations were surveyed online. It was found that LaGuardia Airport in New York City has similar minimum and maximum temperatures with Seoul. The comparison of the average temperature of Seoul and La Guardia Airport in New York City is shown in Figure 4 (Le et al. 2015).

3.3 Materials characterization

3.3.1 Hot Mix Asphalt (HMA) overlay layer

Dynamic modulus value is an input parameter in the program however determining dynamic modulus of asphalt mixtures is time consuming and costly. This study used the Hirsch predictive model (Willis et al. 2009) to determine the dynamic modulus value of

Table 2. Average resilient modulus comparison between laboratory and field data.

Test	Average M_R (MPa)	Design M_R (MPa)
Laboratory	179	180
FWD	186	

* M_r = Resilient Modulus

the overlay material. The accuracy of the model was determined by comparing laboratory data of different mixtures to Hirsch model. The correlation coefficient was found to be 0.95 providing high reliability. Dense graded HMA mixtures were used as asphalt overlay material and its dynamic modulus was determined using Hirsch model.

3.3.2 Existing HMA layer

Four (4) different pavement conditions were evaluated in this study to simulate all possible pavement deterioration for rehabilitation. A reduction of 10%, 20%, 30% and 50% of the original dynamic modulus at 33Hz was calculated. Since this study utilizes Falling Weight Deflectometer (FWD) data to determine existing pavement condition; the FWD test speed of 0.03 second per hit was used as reference in estimating the reference frequency of the dynamic modulus reduction of the pavement. Dynamic modulus values were determined for 50%, 70%, 80% and 90% and were used as input parameter in the program. Existing HMA layer thickness is a varying parameter which is based on the HMA ratio to be used.

3.3.3 Subbase layer

Laboratory and field tests were conducted to survey and determine the most common subbase strength in Seoul. It was found that the average resilient modulus of subbase was 179 MPa and 186 MPa for the laboratory and FWD tests, respectively. Hence, this study used a design resilient modulus of 180 MPa as subbase strength as shown in table 2 (Le et al. 2015).

3.3.4 Subgrade layer

Subgrade classification was done in this study to consider the effect of subgrade strength to pavement performance. Subgrade strength classification from other countries were collated and compared and it was observed that subgrade can be characterized into three regions as shown in figure 5 (Müller, 2000, Cortèrèse et al. 1997, NYDOT and AAPA, 2002).

Laboratory and field tests were also conducted to further verify subgrade strength classification in Seoul. From the laboratory and field tests result, it was found that subgrade strength in Seoul can be classified as shown in table 3 and was used as input parameter in MEPDG (Le et al. 2015).

3.4 Failure criteria

Four (4) pavement distresses were evaluated in this study. Seoul City's standard failure criterion for top

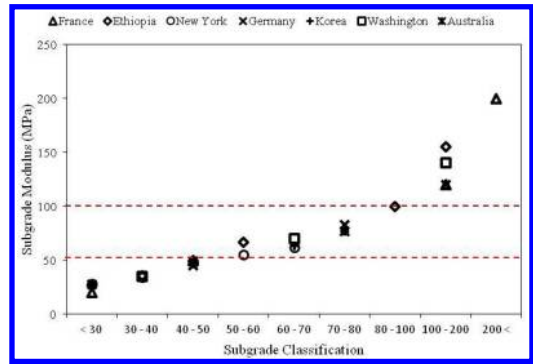


Figure 5. Subgrade strength classification of other countries.

Table 3. Subgrade strength classification (Le et al. 2015).

Type	Average M_R (MPa)	M_R (MPa)	Mean M_R (MPa)	Subgrade Strength
S1	127	$E \geq 100$	130	Good
S2	70	$50 < E < 100$	75	Fair
S3	41	$E \leq 50$	40	Poor

* M_r = Resilient Modulus

Table 4. Pavement distresses and limitations.

Pavement distress	Limit	Design Life (Years)
Top Down Cracking (m/km)	189.40	10
Bottom Up Cracking (%)	25	30
HMA Permanent Deformation (cm)	1.50	30
Total Permanent Deformation (cm)	1.91	30

*Distress limits from the Seoul Metropolitan Government standards.

down (TD) cracking, bottom up (BU) cracking, asphalt layer permanent deformation and total pavement deformation were used as shown in Table 4 (Le et al. 2015).

Overall structural capacity of asphalt pavements in Seoul is more than 30 years. However, after surveying asphalt pavements in Seoul, it was found that TD cracking occurs much earlier than BU cracking and permanent deformation. Using the MEPDG program in analyzing the generated database, it was observed that TD cracking also happens too early compared to BU cracking. Due to the direct traffic and temperature experienced on the surface of the pavement, TD cracking is not easy to control or predict. Therefore, an expected pavement design life of 30 years was used for BU cracking, total pavement and HMA deformation meanwhile a 10-year design life for TD cracking was used which is the typical overlay pavement design life in Seoul.

Table 5. Asphalt overlay design thickness equation coefficients.

Coefficient	Subgrade Condition		
	Good	Fair	Poor
a_1	0.32	-34.90	-80.50
a_2	-2.22	-0.01	-0.05
a_3	-5.12	30.12	74.16
b_1	-19.05	-1.03	2.70
b_2	-0.12	-0.02	-1.01
b_3	39.82	18.02	11.16
c_1	-0.01	-0.16	1.63
c_2	-4.95	-2.75	-0.66
c_3	0.43	0.87	-0.62
d_1	0.01	0.16	-1.94
d_2	-4.59	-2.65	-0.49
d_3	3.16	3.58	7.50

4 DEVELOPMENT OF ASPHALT OVERLAY DESIGN EQUATION

Annual Average Daily Truck Traffic was evaluated using the pavement distress limitations set. The condition was to meet all distress limitations and expected pavement life. From the evaluated AADTTs, a database was generated for each subgrade strength (good, fair and poor). All probable combinations (total HMA thickness, dynamic modulus ratios, and asphalt overlay ratios) were analyzed, a total of 300 data were generated where multiple regression analysis was applied. It was observed that there is a logarithmic relationship between AADTT and total HMA thickness and linear relationship between the dynamic modulus and asphalt overlay ratios. The general equation for asphalt overlay developed after the regression analysis is shown in equations (1.0-1.4).

$$\ln(W_{80}) = \frac{H_{AC\ total} \left\{ \left[A \left(\frac{|E^*|_{old}}{|E^*|_{new}} \right) + B \right] \right\}}{\left\{ \left[C \left(\frac{|E^*|_{old}}{|E^*|_{new}} \right) + D \right] \right\}} \quad (1.0)$$

$$A = a_1 \left(\frac{H_{AC\ new}}{H_{AC\ remain}} \right) a_2 + a_3 \quad (1.1)$$

$$B = b_1 \left(\frac{H_{AC\ new}}{H_{AC\ remain}} \right) b_2 + b_3 \quad (1.2)$$

$$C = c_1 \left(\frac{H_{AC\ new}}{H_{AC\ remain}} \right) c_2 + c_3 \quad (1.3)$$

$$D = d_1 \left(\frac{H_{AC\ new}}{H_{AC\ remain}} \right) d_2 + d_3 \quad (1.4)$$

where W_{80} = equivalent 80kN single axle load (in millions), $H_{AC\ total}$ = total AC thickness after overlay (cm) = $H_{AC\ new} + H_{AC\ remain}$, $H_{AC\ new}$ = asphalt overlay thickness, $H_{AC\ remain}$ = effective AC existing thickness after milling (cm), $|E^*|_{old}$ = dynamic modulus of existing pavement (MPa), $|E^*|_{new}$ = dynamic modulus of existing pavement (MPa), a, b, c and d = equation coefficients.

MATLAB program was used to generate the coefficients of the asphalt overlay equation for each subgrade

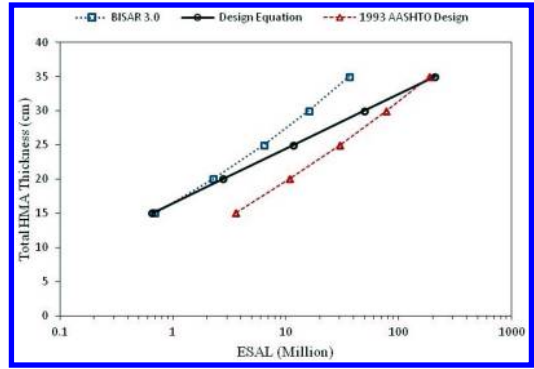


Figure 6. Comparison of the proposed asphalt overlay equation and other design methods (HMA ratio = 1, Existing pavement modulus of 70%).

Table 6. Parameters in the determining HMA thickness in Figure 6.

Layer	Thickness (cm)	Structural Layer Coefficient
Asphalt Overlay	7.5, 10, 12.5, 15, 17.5	0.44
Existing Asphalt Pavement	7.5, 10, 12.5, 15, 17.5	0.308
Subbase	30	0.13
Subgrade (Mr)	75 MPa (10869 psi)	

condition as shown in table 5. It was found that the equation has correlation coefficients of 0.97, 0.97 and 0.98 for good, fair, and poor subgrade condition, respectively. With the high correlation coefficient, the asphalt overlay equation can predict thicknesses for each subgrade type with high level of accuracy and reliability.

5 VALIDATION STUDY OF THE ASPHALT OVERLAY DESIGN EQUATION

Two different analyses were performed to validate the proposed asphalt overlay design equation. First, asphalt overlay thickness design equation is compared with 1993 AASHTO Design and BISAR 3.0 program. Figure 6 shows a sample asphalt overlay scenario wherein a 30% reduction of dynamic modulus and an HMA ratio of 1 is used. The predicted thickness by the proposed asphalt overlay equation is located between the thickness calculated by the 1993 AASHTO Design and BISAR 3.0 program. It can be concluded that the pavement thicknesses by the asphalt overlay equation is within reasonable range compared to the BISAR and AASHTO design measured thicknesses.

Table 6 shows the parameters used in calculating the ESALs for the given asphalt overlay scenario using the AASHTO equation and BISAR program.

Table 7. New asphalt pavement design thickness equation coefficients.

Coefficient	Subgrade condition		
	Good	Fair	Poor
<i>a</i>	3.5929	4.4502	6.8797
<i>b</i>	32.7200	48.1400	85.3200

Figure 7. Thickness comparison measured by MEPDG and the reduced equation.

Reduced equation for new pavement design was established and used as a second validation study. In considering new pavement design, existing HMA thickness is zero. Using the asphalt overlay thickness design equation; since the remaining HMA thickness is zero, the ratio of the new HMA and old thickness will approach infinity. This infinity values are raised to negative exponents in which will eventually be zero. The original asphalt overlay equation can then be reduced and be used in determining thickness of new pavement. The reduced original asphalt overlay design equation is shown by [equation \(2.0\)](#).

$$H_{AC-total} = a \ln(W_{80}) + b \quad (2.0)$$

where *a*, *b* = equation coefficients, W_{80} = equivalent 80-kN (18-kip) single-axle load (in millions)

Table 7 shows the coefficients of the new asphalt design thickness equation. To validate the accuracy and reliability of the reduced equation, thicknesses measured using MEPDG were also compared to the predicted thickness by the reduced equation as shown in [figure 7](#).

The high correlation coefficient suggests that the proposed overlay equation can predict thickness with high level of accuracy.

6 CONCLUSIONS

This study focused on the development of asphalt overlay design model in estimating asphalt overlay thickness using mechanistic-empirical approach. The MEPDG's new design mode was used as the main tool in analyzing and developing the asphalt overlay equation. Finding the optimum AADTT that satisfies the pavement distresses and limitations set in the MEPDG program generated a synthetic database that was used in the analysis. Total HMA thickness was considered to be a function of the new asphalt overlay material property, existing pavement condition, new asphalt overlay and existing pavement thickness and ESAL. The overlay design equation predicted thickness was compared to MEPDG design thickness and other design methods to validate its accuracy and reliability. The validation study showed that the predicted thickness by the asphalt overlay equation is within

reasonable range compared to the thicknesses measured by the AASHTO 1993 guide and the BISAR program. Meanwhile, the reduced equation can measure new design thickness which also validates the developed regression equation.

The asphalt overlay thickness design equation is a user-friendly mechanistic-empirical approach that engineers can use in estimating asphalt overlay thickness. Moreover, these equations provide adequate and economic thickness design considering the actual existing conditions of the pavement from traffic, climate and material property of urban roads.

ACKNOWLEDGEMENT

The authors would like to acknowledge the support from Development of Eco-friendly Pavements to Minimize Greenhouse Gas Emissions funded by Ministry of Land and Marine, and BK21 Plus Project: Disaster Prevention of Infrastructure.

REFERENCES

- AAPA, 2002. *Selection and Design of Flexible Pavements*. Australian Asphalt Pavement Association.
- AASHTO, 1993. *Guide for design of pavement structure*. American Association of State Highway and Transportation Officials.
- AI, 1983. *Asphalt overlays for highway and street rehabilitation, Manual Series No. 17*, Asphalt Institute.
- ARA, Inc., ERES Division, 2004. *Guide for mechanistic-empirical design of new and rehabilitated pavement structures*. Final Report, NCHRP Project 1-37A. Transportation Research Board of the National Academies, Washington, D.C.
- Christensen Jr, D.W., Pellinen, T., and Bonaquist, R.F., 2003. Hirsch model for estimating the modulus of asphalt concrete. *Journal of the Association of Asphalt Paving Technologists*; Vol. 72, 2033, p. 97–121.
- Cortèrèse, J.F., Goux, M.T., 1997. *Design Manual for Pavement Structures*. Paris: Laboratoire Central des Ponts et Chaussées.
- Guzina, B.B. and Osburn, R.H., 2002. *Effective Tool for Enhancing Elastostatic Pavement Diagnosis*. Transportation Research Record, 1806, 30–37.
- Huang, Y.H., 2004. *Pavement Analysis and Design*. 2nd ed. New Jersey: Prentice Hall.
- Korea Institute of Construction Technology (KICT), 2009. *Korea Pavement Research Program*. Ministry of Construction and Transportation.
- Le, V.P., Lee, H.J., Flores, J.M., Park, H.M., and Lee, S., 2015. *Development of a Regression Equation for Asphalt Overlay Design Based on Mechanistic-Empirical Approach*. International Journal of Pavement Engineering (under review).
- Li, J., Uhlmeier, J.S., Mahoney, J.P. and Muench, S.T., 2011. *Use of the 1993 AASHTO Guide, MEPDG and Historical Performance to Update the WSDOT Pavement Design Catalog*. State of Washington, Department of Transportation.
- Müller, K., 2000. *Directives for the Standardization of Pavement for Traffic Areas*. Roads Department, Ministry for Transport and Communications, Government of Malta.

- Nunn, M.E., Brown, A., Weston, D. and Nicholls, J. C., 1997. *Design of long-life flexible pavement for heavy traffic*. TRL report 250. Highways Agency.
- NYDOT, 2002. *Comprehensive Pavement Design Manual*. New York State Department of Transportation.
- Research and Development Division (RDD), 2003. RD/GN/042. *Guide Notes on Pavement Design for Carriageway Construction*
- Statistical Data [online]. Seoul Metropolitan Government. Available at: <http://english.seoul.go.kr/policy-information/traffic/major-traffic-statistics/> [Accessed 21 Jun 2014]
- Washington State Department of Transportation (WSDOT), 2011. *WSDOT Pavement Policy*. WSDOT, Olympia, WC.
- Willis, R., Timm, D., West, R., Powell, B., Robbins, M., Taylor, A., Smit, A., Tran, N., Heizman, M., Bianchini, A., 2009. *Phase II Ncat Test Track Findings*. National Center for Asphalt Technology, Auburn University
- Wu, Z., Chen, X., Gaspard, K., Zhang, Z., 2008. *Structural Overlay Design of Flexible Pavement by Nondestructive Test Methods in Louisiana*. Transportation Research Board Annual Meeting, 08-1704.
- Xu, B., Ranjithan, S.R. and Kim, Y.R., 2002a. *New condition assessment procedure for asphalt pavement layers using falling weight deflectometer deflections*. Journal of the Transportation Research Board, 1806, 57.69.

Why and when to consider alternate flexible and rigid pavement designs in a bidding process?

C.M. Chang & O. González

Department of Civil Engineering, The University of Texas at El Paso, Texas, USA

A. Wimsatt

Texas Transportation Institute, College Station, Texas, USA

ABSTRACT: Projects with alternate flexible and rigid pavement designs have been implemented by several transportation agencies in the United States to lower construction costs by attracting more contractors in the bidding process. The purpose of including alternate designs in the bidding process is to increase competitiveness and allow flexible and rigid pavement contractors to submit proposals. This paper describes the guidelines developed for the Texas Department of Transportation (TxDOT) to decide when alternate pavement designs should be considered in the bidding process. Results of a case study with a side-by-side comparison of pavement design and life-cycle costs are also presented.

1 WHY ALTERNATE FLEXIBLE AND RIGID PAVEMENT DESIGNS?

A number of studies have been conducted to develop methodologies to select the most adequate pavement type for a project. These methodologies are usually based on expected pavement performance and life cycle-cost analysis (LCCA). Due to the uncertainties in pavement performance over time and cost variability among contractors, there are a number of cases in which there is no a clear winner. A pavement alternate bid, with flexible and rigid equivalent pavement designs, is the answer to these cases. This paper presents a brief summary of the state-of-the-practice for pavement type selection and describes the methodology developed for the Texas Department of Transportation (TxDOT) to decide when to include alternate pavement designs in the bidding process.

1.1 *State of the practice for pavement type selection methodologies*

The Federal Highway Administration (FHWA), the American Concrete Pavement Association (ACPA), and the Asphalt Pavement Alliance (APA), have guidelines to assist in the selection of the pavement type. In 1998, the FHWA released an Interim Technical Bulletin with a procedure based on LCCA. This procedure is used for pavement type selection with the assistance of RealCost software (Walls et al. 1998). In 2002, ACPA published guidelines to compare pavement designs also using LCCA. Windows™ Pavement Analysis software (WinPAS™) and StreetPavement software were released by ACPA for this purpose.

In 2004, APA recommended the methodology developed in FHWA Demonstration Project 115 which compares life-cycle costs for flexible and rigid pavements (APA, 2004). In 2008, Clemson University reported that 94 percent of a total of 33 states and 2 Canadian provinces use the Present Value from LCCA to compare pavement alternatives (Rangaraju et al. 2008). From this study, it was also found that the major source of reference was the FHWA Life-cycle-Cost Analysis Interim Technical Bulletin (Walls et al. 1998). Nevertheless, differences in the application of LCCA methodology were due to different lengths in the analysis period (varying from 30 to 50 years), the timing of maintenance and rehabilitation interventions, salvage value estimates, and whether or not user costs were included in the analysis. It was also mentioned that RealCost software was the most popular tool to compare pavement designs using LCCA. The consensus was that including alternate flexible and rigid pavement designs in the bidding process results in the lowest construction costs without compromising pavement performance.

A number of Departments of Transportation (DOTs) around the United States have developed their own guidelines for pavement type selection. Table 1 shows a summary of methodologies developed by the California Department of Transportation (Caltrans), Colorado Department of Transportation (CDOT), Kentucky Transportation Cabinet (KYTC), Louisiana Department of Transportation and Development (LADOTD), Missouri Department of Transportation (MoDOT), Pennsylvania Department of Transportation (PennDOT), and Washington State Department of Transportation (WSDOT).

Table 1. Summary of pavement type selection methodologies for selected U.S. DOTs.

Caltrans (Velado, 2007)

- Develop pavement designs for 10, 20, and 40 years.
- Conduct life cycle cost analysis for the pavement design alternatives under study.
- Recommend a 4 percent discount rate. Use a deterministic approach.
- Consider delays or traffic diversions, vehicle operating and road accident cost.
- Use RealCost software.

CDOT (Demos, 2006)

- Recommend a 40 years analysis period.
- Incorporate LCCA in the selection process
- Use deterministic and probabilistic methods.
- A 4 percent discount rate is recommended for deterministic calculations.
- Salvage value is neglected for deterministic calculations.
- Present value is the economic indicator used to decide the pavement type.
- A 75 percent risk level is used in probabilistic analysis, and the discount and inflation rate varies.
- User costs estimates are based on the work area delays due to construction.

LADOTD (Temple, 1998)

- Use LCCA including initial construction and future rehabilitation costs, traffic control, and user costs for delays due to construction.
- If there is a difference of 20 percent in the LCCA, alternate pavement designs are included in the bidding documents.

MoDOT (MoDOT, 2004)

- Use LCCA in a period of 35 years.
- Compare pavement design alternatives using mechanistic methods.
- IRI (International Roughness Index) is recommended as the performance indicator.
- User costs are not considered in the pavement selection process.

MDOT (MDOT, 2004)

- Use LCCA with user costs based on “Construction Congestion Costs” from a study conducted by the University of Michigan.
- Recommends to use the process described in the FHWA SA-98-079 report.

PennDOT (Smith, 2005)

- Use LCCA in a period of 40 years.
- A 6 percent discount rate is recommended.
- Considers initial construction, future rehabilitation and maintenance costs, and user costs for delays due to construction.

WSDOT (MacDonald, 2005)

- Use LCCA in a period of 50 years for interstate highways or main roads; and 20 years for smaller arterials or major collectors.
- Consider initial construction, maintenance and rehabilitation costs, salvage value, and user costs.
- The present value is the economic indicator to compare pavement design alternatives.
- Use deterministic and probabilistic approaches.

2 ANALYSIS OF FLEXIBLE AND RIGID PAVEMENT DESIGNS USED BY THE TEXAS DEPARTMENT OF TRANSPORTATION

The pavement type finally selected is very sensitive to the parameters used in the design process and the criteria in the LCCA. To provide recommendations for alternate equivalent pavement designs, case studies were conducted to compare TxDOT flexible and rigid pavement designs. Four traffic levels, three environmental conditions, and two subgrade support conditions were considered in these case studies.

2.1 Case studies

Seven types of flexible pavement layer structures and three types of rigid pavement structures were included in the case studies. The design parameters used in the case studies are presented in Table 2.

Sensitivity analysis varying layer thicknesses and material properties was performed to investigate their impact in the pavement design. Table 3 shows the

flexible pavement layer structures for cases 1.A through 1.G.

Table 4 shows the rigid pavement layer structures for cases “2.A” through “2.C”. Each case was run for an effective modulus of subgrade reaction (k) of 285,103 t/m³ (10,300 pci) and 27,680 t/m³ (1,000 pci).

2.2 Results from the pavement design side by side comparison

Flexible Pavements:

1. For the thin Hot Mix Asphalt (HMA) layer structure results show a thickness range of 1.3 to 2.5 centimeters (1/2 to 1 inch) for a modulus of 4.5 GPa (650 ksi).
2. It is less expensive to build a pavement and place an overlay after 8 years than to build a pavement for a 15 or 30 year design life without an overlay.
3. A modulus of 4.5 GPa (650 ksi) is recommended for the asphalt layer when the HMA thickness layer is 20.3 centimeters (8 inches) or more. A modulus of 3.5 GPa (500 ksi) is recommended if the

Table 2. Overall pavement design parameters.

Parameters	Inputs
Length	30 years
Traffic Levels (18 KESALS)	<ul style="list-style-type: none"> • Very Low: 1 million • Low: 5 million • Intermediate: 15 million • High: 30 million
Environmental Condition	El Paso (ELP), Dallas (DAL), and San Antonio (SAT)
Subgrade Condition	Poor: 55 MPa (8 ksi); Good, 103.4 MPa (15 ksi)
Present Serviceability Index (PSI) Reliability	<ul style="list-style-type: none"> • Initial PSI 4.5, terminal PSI 2.5 • Initial PSI 4.0, terminal PSI 2.0 PSI of 4.2 was reset after an overlay for flexible pavements. <ul style="list-style-type: none"> • Flexible pavement: 95 percent • Rigid pavement: 95 and 99 percent
Maintenance and Rehabilitation	
<ul style="list-style-type: none"> • Flexible pavement: <ul style="list-style-type: none"> ○ Cases 1.A and 1.B: 15 and 30 years as the “minimum time interval for the first overlay”. ○ Cases C through F: 8, 15, and 30 years as the “minimum time interval to the first overlay”. ○ Case 1.G: For a ACP modulus of 3.45 GPa (500 ksi), 8 years and 15 years were the time intervals for the first overlay. When the ACP modulus was set to 4.5 GPa (650 ksi), no overlay was considered. • Rigid pavement: No major maintenance or rehabilitation 	

Table 3. Flexible pavement layer structures for sensitivity analysis.

Case	Material	Moduli Range		Thickness Range	
		GPa	ksi	m	in.
1.A	Hot Mix Asphalt	3.5 to 4.5	500 to 650	0.05	2
	Asphalt Stabilized Base	3.5 to 4.5	500 to 650	0.1 to 0.6	4 to 20
	Flexible Base	0.2 to 0.3	24 to 45	0.15 to 0.3	6 to 12
	Subgrade	0.05 to 0.1	8 to 15	6.1	240
1.B	Hot Mix Asphalt	3.5 to 4.5	500 to 650	0.05	2
	Asphalt Stabilized Base	3.5 to 4.5	500 to 650	0.15 to 0.4	6 to 16
	Flexible Base	0.2 to 0.3	24 to 45	0.15 to 0.5	6 to 20
	Subgrade	0.05 to 0.1	8 to 15	6.1	240
1.C	Hot Mix Asphalt	3.5 to 4.5	500 to 650	0.05 to 0.5	2 to 20
	Flexible Base	0.35	50	0.15	6
	Lime Treated Subgrade	0.25	35	0.2	8
	Subgrade	0.05 to 0.1	8 to 15	6.1	240
1.D	Hot Mix Asphalt	3.5 to 4.5	500 to 650	0.05 to 0.5	2 to 20
	Flexible Base	0.35	50	0.15	6
	Lime Treated Subgrade	0.25	35	0.45	18
	Subgrade	0.05 to 0.1	8 to 15	6.1	240
1.E	Hot Mix Asphalt	3.5 to 4.5	500 to 650	0.05 to 0.5	2 to 20
	Flexible Base	0.35	50	0.1 to 0.4	4 to 16
	Lime Treated Subgrade	0.25	35	0.2	8
	Subgrade	0.05 to 0.1	8 to 15	6.1	240
1.F	Hot Mix Asphalt	3.5 to 4.5	500 to 650	0.05 to 0.25	2 to 10
	Flexible Base	0.2 to 0.3	24 to 45	0.15 to 0.45	6 to 18
	Lime Treated Subgrade	0.25	35	0.45	18
	Subgrade	0.05 to 0.1	8 to 15	6.1	240
1.G	Hot Mix Asphalt	3.5 to 4.5	500 to 650	0.05 to 0.25	2 to 10
	Flexible Base	0.2 to 0.3	24 to 45	0.15 to 0.45	6 to 18
	Subgrade	0.05 to 0.1	8 to 15	6.1	240

HMA thickness layer is less than 20.3 centimeters (8 inches).

Rigid Pavements:

1. When the concrete slab thickness of sections with low k-values ($276.8 \text{ t/m}^3 - 10 \text{ pci}$) is compared

to sections with high k-values ($27,680 \text{ t/m}^3 - 1000 \text{ pci}$), the slab is about 7.6 centimeters (3 inches) thicker for low k-values and very low traffic. The slab thickness has an average of 12.7 and 20.3 centimeters (5 inches and 8 inches) for k values of $27,680 \text{ t/m}^3$ (1000 pci) and 276.8 t/m^3

(10 pci) respectively. The slab thickness of pavement sections with high k values was about 5 centimeters (2 inches) thinner than sections with low k values for low, intermediate, and high traffic levels. Pavement sections classified under these traffic levels had the following average thicknesses for high and low k value sections, respectively:

- a. Low traffic: 20 and 25 centimeters (8 and 10 inches).
 - b. Intermediate traffic: 25 and 30.5 centimeters (10 and 12 inches).
 - c. High traffic: 29.2 and 34.3 centimeters (11.5 and 13.5 inches)
2. A slab thickness increase from 1.3 centimeters (1/2 inch) for low traffic levels to about 2.5 centimeters (1 inch) for high traffic levels was observed when ESALs were increased by 58 percent. The low traffic level (1 million ESALs) resulted in a slab thickness of 17.8 centimeters (7 inches). A 58 percent increase in the traffic level (1.58 million ESALs) increases the slab thicknesses to 19 centimeters (7.5 inches). The high traffic level (30 million ESALs) the slab thicknesses was about 30.5 centimeters (12 inches).
 3. The most cost effective alternative was to place the concrete slab over 2.5 centimeters (1 inch) of HMA on top of 15.2 centimeters (6 inches) of a Cement Stabilized Base (CSB), and 20.3 centimeters (8 inches) of Lime Treated Subgrade (LTS).

The general conclusions for both pavement types are summarized as follows:

1. If the initial and terminal PSI values are changed, but the difference is the same, the thickness of the HMA layer in the flexible pavement structure is not greatly affected. In rigid pavements, changes in the PSI difference were found to be negligible for the slab thickness calculation. As a result, it is recommended an initial PSI of 4.5 and terminal PSI of 2.5 for flexible and rigid pavements when developing alternate pavement designs.
2. The influence of the environmental conditions represented by the El Paso, San Antonio and Dallas

districts in the layer thicknesses calculation was only observed for very low traffic (1 million ESALs).

2.3 Life-cycle cost analysis

LCCA was conducted for flexible pavement cases 1.B, 1.C, 1.3; and rigid pavement case 2.C. The LCCA procedure recommended by the FHWA was followed, and the main costs used as data inputs in the analysis were:

- Initial construction cost incurred by agencies to procure the pavement construction.
- Routine maintenance cost related to annual routine maintenance, which includes minor and spot work (e.g., pothole repair), and preventive maintenance, which includes periodic pavement work (e.g., crack seal and seal coat activities) (AASHTO, 1993).
- Salvage value at the end of the analysis period also called as residual value (AASHTO, 1993).
- User costs that belongs to two broad categories:
 - Vehicle Operating Costs (VOC), where the function of a VOC is: (a) to simulate the effects of the physical characteristics and condition (roughness) of a road on the operating speeds of various types of vehicles and on their consumption of resources (fuel, lubricants, tires), and (b) to determine their total operating cost.
 - User costs associated with work zone activities: These costs primarily include user delay costs resulting from lower operating speeds, stops, stop-and-go travel, and speed-change cycling.

Some other user costs, such as travel time, denial-of-use cost, discomfort cost, and accident cost, are also mentioned, but there is little evidence that they are considered by agencies in their LCCA.

Cash flow streams in the analysis period are converted to Net Present Worth (NPW) by using discount rates to compare the economic worth of the alternatives. NPW method involves all present and future costs converted to the present using a discount rate that depends on the agency policy, purpose of the analysis, risk level of the investment, and uncertainty of the cost

Table 4. Rigid pavement layer structures for sensitivity analysis.

Case	Material	28-day Modulus of Rupture		Thickness Range	
		MPa	psi	m	in.
2.A	Concrete Slab	4.3	620	0.1 to 0.4	4 to 15.3
	Hot Mix Asphalt	–	–	0.1	4
	Lime Treated Subgrade	–	–	0.2	8
2.B	Concrete Slab	4.3	620	0.1 to 0.4	4 to 15.3
	Hot Mix Asphalt	–	–	0.02	1
	Cement Treated Base	–	–	0.15	6
	Lime Treated Subgrade	–	–	0.2	8
2.C	Concrete Slab	4.3	620	0.1 to 0.4	4 to 15.3
	Hot Mix Asphalt	–	–	0.1	4
	Lime Treated Subgrade	–	–	0.45	18

estimate predictions. All costs are reduced to an equivalent single present cost for a fair comparison, all other things being equal (AASHTO, 1993).

An initial PSI of 4.5, terminal PSI of 2.5, and 95 percent level of confidence were used for the comparisons. A 4 percent discount rate was selected for the LCCA as recommended by previous studies (Rangaraju et al 2008).

The pavement layer structures for the LCCA were:

- Case 1.B (flexible):
 - Pavement Layer Structure: 5 centimeter (2 inch) HMA layer; 28 centimeter (11 inch) asphalt stabilized base; 15.2 centimeter (6 inch) flexible base; and a 6.3 centimeter (2.5 inch) overlay scheduled in year 16.
 - Materials Properties: HMA Modulus of 3.5 GPa (500 ksi)
- Case 1.C (flexible):
 - Pavement Layer Structure: 24 centimeter (9.5 inch) HMA layer; 15.2 centimeter (6 inch) flexible base; 20.3 centimeter (8 inch) lime treated subgrade; and a 6.3 centimeter (2.5 inch) overlay scheduled in years 9 and 20.
 - Materials Properties: HMA Modulus of 4.5 GPa (650 ksi).

- Case 1.E (flexible):
 - Pavement Layer Structure: 24 centimeter (9.5 inch) HMA layer; 10.1 centimeter (4 inch) flexible base; 20.3 centimeter (8 inch) lime treated subgrade; and a 6.3 centimeter (2.5 inch) overlay scheduled in year 9 and 19.
 - Materials Properties: HMA Modulus of 4.5 GPa (650 ksi).
- Case 2.C (rigid):
 - Pavement Layer Structure: 30.5 centimeter (12 inch) concrete slab; 2.5 centimeter (1 inch) HMA layer; 15.2 centimeter (6 inch) cement treated base; 20.3 centimeter (8 inch) lime treated subgrade.
 - Materials Properties: 4.3 MPa (620 psi) modulus of rupture for the concrete slab.

The pavement layer structure, initial construction and maintenance costs used in the LCCA were based in current TxDOT design practices and local project information. Unit material costs are shown in Table 5.

LCCA was performed with and without user costs (vehicle operating and time of delay costs associated with work zones). RealCost software was used to conduct the LCCA, and their models require as data inputs the design service life of the initial construction and future activities (e.g. overlays) for each pavement alternative (FHWA, 2004). A linear deterioration rate of the pavement service condition is adopted by RealCost. The parameters used in the LCCA are shown in Table 6.

Figure 1 shows the present value (\$/lane mile) for the LCCA without user costs. No overlays are considered in the rigid pavement alternative while all asphalt pavement designs have overlays. Differences in life-cycle costs of flexible pavement designs 1.B, 1.C, and 1.E when compared to rigid pavement design 2.C are 13 percent above, 2 percent below, and 2 percent above respectively. The impact of the layer structure and scheduled overlays on the present costs is also observed when comparing the flexible pavement alternatives. The flexible pavement structure for case 1.B with 28 cm (11 in.) of an asphalt stabilized base has higher life-cycle costs than a thicker asphalt

Table 5. Material costs used for flexible and rigid pavement designs (*).

Material	Cost
Hot Mix Asphalt	242–262 \$/m ³ (185–200 \$/cy)
Asphalt Stabilized Base	235 \$/m ³ (180 \$/cy)
Cement Stabilized Base	63 \$/m ³ (48 \$/cy)
Flexible Base	52 \$/m ³ (40 \$/cy)
Lime Treated Sub grade	26 \$/m ³ (20 \$/cy)
Concrete	54 \$/m ³ (45 \$/sy)**
	67 \$/m ³ (55 \$/sy)***

*based on data from <http://www.dot.state.tx.us/business/avgd.htm>

**for slabs 20.3 to 33 centimeters (8 to 13 inches) thick

***for slabs 35.5 to 38 centimeters (14 to 15 inches) thick

Table 6. Parameters used in the LCCA.

Traffic levels	<ul style="list-style-type: none"> • Very low traffic: 2,000 initial ADT; 3,590 maximum ADT • Low traffic: 10,000 initial ADT; 17,950 maximum ADT • Intermediate traffic: 20,000 initial ADT; 35,900 maximum ADT • High traffic: 55,000 initial ADT; 98,725 maximum ADT
Subgrade conditions	103.5 MPa (15 ksi) for flexible pavements
PSI	8,304 t/m ³ (300 pci) for rigid pavements
	Initial PSI: 4.5
	Terminal PSI: 2.5
Discount rate	4 percent
Analysis period	30 years
User costs	\$19.35 per vehicle hour*

*user costs were provided by TxDOT and represent the value of time in dollars per vehicle hour.

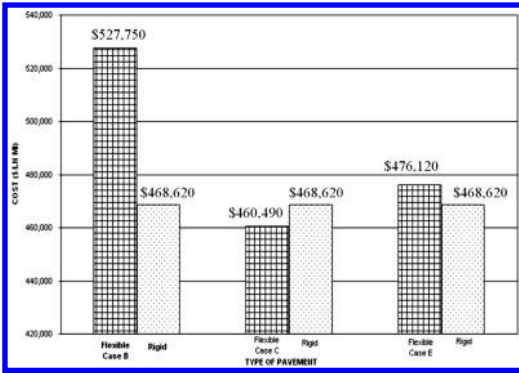


Figure 1. LCCA comparison for flexible and rigid pavement designs without user costs, 4 percent discount rate.

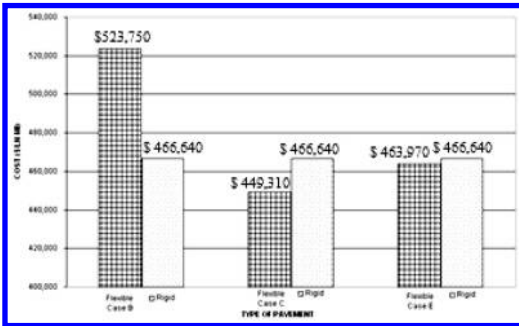


Figure 2. LCCA comparison for flexible and rigid pavement designs without user costs, 7 percent discount rate.

pavement on a lime stabilized subgrade and more frequent overlays as observed in cases 1.C and 1.E. It is also observed that the HMA thickness are the same for cases 1.C and 1.E, but the flexible base is 5 centimeters (2 inches) thicker in case 1.C and the time to place the next overlay is delayed 1 year resulting in \$15,000 of savings per lane mile.

LCCA was also conducted using a 7 percent discount rate. It is observed the influence of the discount rate in the results as shown in Figure 2. In this situation, case 1.E flexible pavement design has also lower life-cycle costs than the rigid pavement alternative. Life-cycle costs of flexible pavement designs 1.B, 1.C, and 1.E were 12 percent above, 4 percent below, and 1 percent below respectively than rigid pavement design 2.C. Overall, flexible pavement design 1.C has the lowest life-cycle costs when compared to the other alternatives.

In addition, four different traffic levels, based on Average Daily Traffic (ADT) level, were analyzed to study the effects of user costs in the total life-cycle cost.

- Very Low Traffic (1 million ESALs), Initial ADT: 2,000/Maximum ADT: 3,590.
- Low Traffic (5 million ESALs), Initial ADT: 10,000/Maximum ADT: 17,950.

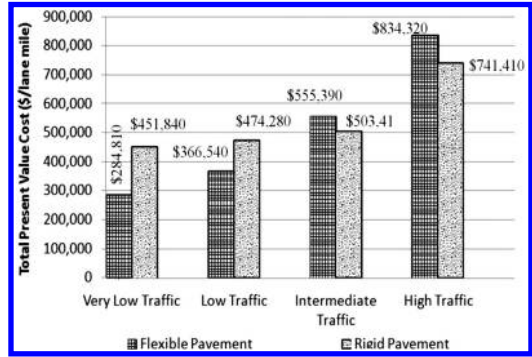


Figure 3. LCCA comparison including user costs.

- Intermediate Traffic (15 million ESALs), Initial ADT: 20,000/Maximum ADT: 35,900
- High Traffic (30 million ESALs), Initial ADT: 55,000/Maximum ADT: 98,725.

Results of LCCA, including user costs, are shown in Figure 3.

It is interesting to observe that LCCA, including user costs, show that life-cycle costs for rigid pavement were 37 percent and 23 percent higher than asphalt pavements for very low and low traffic respectively. However, life-cycle costs for rigid pavement were 10 percent and 13 percent lower than asphalt pavements for intermediate and high traffic respectively. These results reflect the influence of the traffic volume on life-cycle costs since user costs will increase when the average daily traffic increases.

A sensitivity analysis of the impact of work zone speed limit parameters on user costs was also conducted using RealCost. Work zone speed limit (mph), work zone length (miles), number of lanes opened during construction, work zone capacity (vphpl), queue dissipation capacity (vphpl), maximum queue length (miles), work zone duration (days), and work zone time were considered in this analysis. The life-cycle cost model in Real Cost does not consider congestion related emissions costs but agencies may include them in LCCA if calibrated models are available for their region. It was found that the most influential parameters impacting user costs were the number of lanes opened during construction, work zone capacity, work zone duration, and work time schedule.

3 WHEN TO CONSIDER ALTERNATE PAVEMENT DESIGNS?

A protocol of six steps was prepared for TxDOT to decide when a project is a good candidate for alternate pavement designs in the bidding process. Figure 4 shows the steps that are summarized as follows:

Step 1: The first step is to collect general project information: project name, region, county district, project size, and ESALs. The number of ESALs is the first criteria used to qualify a project for

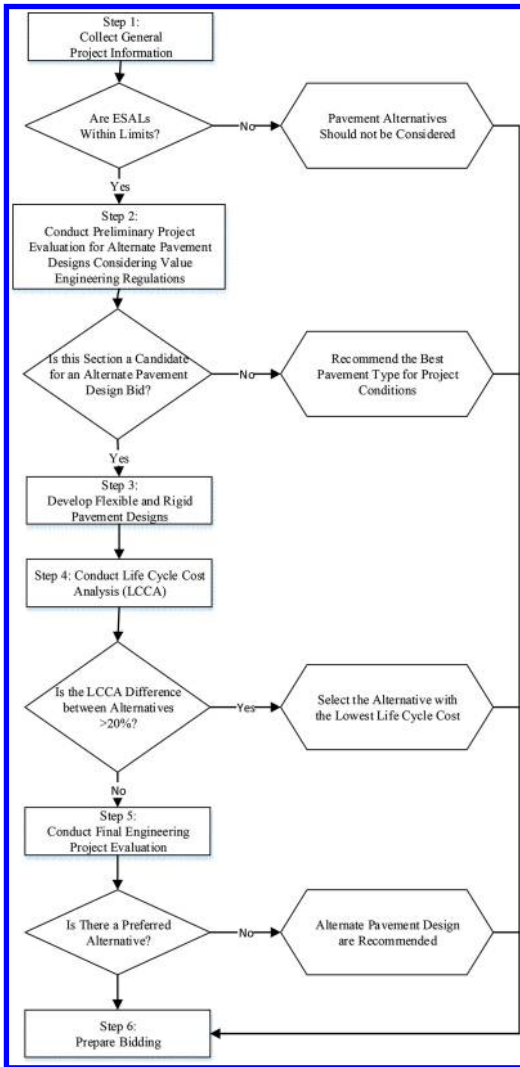


Figure 4. Flowchart to decide when to consider alternate pavement design in the bidding process.

pavement alternates. The limits of the ESALs are determined according to environmental conditions. Step 2: The second step is a preliminary project evaluation. A questionnaire is used to evaluate the project based on total lane miles, construction traffic control difficulties, number of bridge structures in the sector, number of driveways, estimated total project cost, underground utility issues, and subgrade condition. Value engineering regulations should be taken into account in this step for projects with an estimated total cost of \$50,000,000 or more. Value Engineering is defined by the US White House Office of Management and Budget as “an organized effort directed at analyzing the functions of systems, equipment, facilities, services, and supplies for the purpose of achieving the essential functions at the lowest life-cycle cost consistent

with required performance, reliability, quality, and safety” (OMB, 1993).

Steps 3 and 4: LCCA is conducted for the flexible and rigid pavement designs. If the life-cycle cost difference is greater than 20 percent, the alternative with the lowest life-cycle-cost is chosen. Otherwise, both designs are included in the bidding documents.

Step 5: A final project evaluation is performed before including the alternate equivalent pavement designs in the bidding documents.

Step 6: Bidding documents are prepared.

4 CONCLUDING REMARKS

Alternate pavement designs included in the bidding process attract more contractors; increasing competitiveness and as a result lowering construction costs without compromising pavement performance.

Guidelines are needed to decide when alternate pavement designs should be included in the bidding process. In order to effectively implement these guidelines, it is recommended: (a) to train the personnel involved in the pavement design process; (b) to maintain a database with updated construction and maintenance costs; and (c) to keep records of previous projects with information about typical sections, input design parameters, LCCA results, and project costs.

ACKNOWLEDGEMENT

The authors would like to express their sincere appreciation to TxDOT for providing funds to conduct research project 0-6085 “Considerations for Rigid vs. Flexible Pavement Designs When Allowed as Alternate Bids”.

REFERENCES

- AASHTO *Guide for Design of Pavement Structures*. 1993. American Association of State Highway & Transportation Officials (AASHTO), Washington D.C.
- Demos, G.P. 2006. *Life-Cycle Cost Analysis & Discount on Pavements for the Colorado Department of Transportation*. Report No. CDOT-2006-17, Colorado Department of Transportation (CDOT), Denver, Colorado.
- Federal Highway Administration. 1998. *Life-Cycle Cost Analysis in Pavement Design*, Interim Technical Bulletin (FHWA-SA-90-079) Washington D.C.
- Federal Highway Administration. 2004. *Life-Cycle Cost Analysis. Real Cost v. 2.1 User Manual*. Washington D.C.
- MacDonald, D. 2005. *Pavement Type Selection Protocol*. Washington State Department of Transportation (WSDOT), Olympia, Washington.
- Missouri Department of Transportation (MoDOT). 2004. *Pavement Design & Type Selection Process*. Jefferson City, Missouri.
- Office and Management and Budget (OMB). 1993. *Circular No. A-131*. Washington D. C.
- Pavement Type Selection Processes*. Asphalt Pavement Alliance, Lexington, Kentucky, 2004.

- Rangaraju, P.R., Amirkhanian, S., & Guven Z. 2008. *Life-Cycle Cost Analysis for Pavement Type Selection*. Clemson University & South Carolina Department of Transportation. Clemson, South Carolina.
- Smith, K.L., Stanley, M., Vandebossche, J., & Morian, D. 2005. *Pavement Life-Cycle Cost Analysis*. Pennsylvania Department of Transportation (PennDOT), Harrisburg, Pennsylvania.
- South Carolina Department of Transportation (SCDOT). 2007. *Pavement Type Selection Process – Memorandum*. Columbia, South Carolina.
- Temple, W.H., Zhang, Z., Lampert, J., & Zeringue K.M. 1998. *Agency Process for Alternate Design & Alternate Bid of Pavements*. Louisiana Department of Transportation & Development (LADOTD), Baton Rouge, Louisiana.
- Velado, M. 2007. *Life-Cycle Cost Analysis Procedures Manual*. California Department of Transportation (Caltrans), Sacramento, California.
- Walls, J. & Smith, M.R. 1998. *Life-Cycle Cost Analysis in Pavement Design – In Search of Better Investment Decisions. Interim Technical Bulletin*. U.S. Department of Transportation. Washington D.C.
- Wimsatt, A. J., Chang, C. M., Krugler, P. E., Scullion, T., Freeman, T. J., Valdovinos, M. B. 2009. *Considerations for Rigid vs. Flexible Pavement Designs When allowed as Alternate Bids: Technical Report*. Report No. FHWA/TX-09/0-6085-1, Texas Institute of Transportation (TTI), College State, Texas.

Structural rehabilitation with thinner layers

E. Jellema, M. Kowalczyk & W.C. Vonk

Kraton Polymers Research B.V., Amsterdam, The Netherlands

ABSTRACT: Traffic intensities and pavement loadings are ever increasing and therefore, more durable pavements are needed. Such a pavement should have improved rutting and cracking resistance, leading to a longer service life. By using SBS modified binders with relatively high polymer content it is possible to achieve this. We show that by using the Highly Modified Asphalt (HiMA) technology the fatigue resistance of the asphalt can be improved to the extent that asphalt pavement can be applied with reduced thickness. Potentially, the thickness reduction can more than compensate for the higher binder costs and still provide improved performance. We validated our laboratory experimental evidence in trials at the National Center for Asphalt Technology (NCAT, Auburn, Alabama). This paper reports an update on the performance of the NCAT test sections, which are a new pavement with reduced thickness and a structural rehabilitation. For both sections the HiMA technology was applied.

1 THEORETICAL BACKGROUND

1.1 *The effect of a polymer continuous phase*

Looking at the global asphalt pavement market, a significant share of the bituminous binders used is polymer modified. The most common polymer for modification is styrene-butadiene block-copolymer (SBS). SBS is used to decrease the damage that occurs under conditions of heavy traffic, but also in extreme climates.

SBS is an effective bitumen modifier, because both its aromatic and unsaturated aliphatic blocks have a strong interaction with bitumen components. Therefore, only a relatively low polymer concentration is needed to have a measurable effect on the bitumen properties.

When SBS is added to hot bitumen, it will completely dissolve and absorb up to ten times its own weight of the lighter components in the bitumen. Although it is possible to form a single phase system at the dissolving temperature (160–190°C), at lower temperatures there will always be two phases in the blend. By using fluorescence microscopy, these phases can be made visible: the polymer rich phase will light up and the asphaltene rich phase will appear dark.

Figure 1 shows a schematic representation of the addition of SBS to bitumen and the resulting phase morphologies. When a relatively low amount of SBS is used, e.g. 2.5%, the continuous phase in the blend will be asphaltene rich. At a moderate SBS concentration of 5%, the polymer rich phase and the asphaltene rich phase can appear as co-continuous phases in the blend. At an SBS concentration of 7.5%, the polymer rich phase is the continuous phase. So the higher the polymer concentration, the larger the polymer rich phase

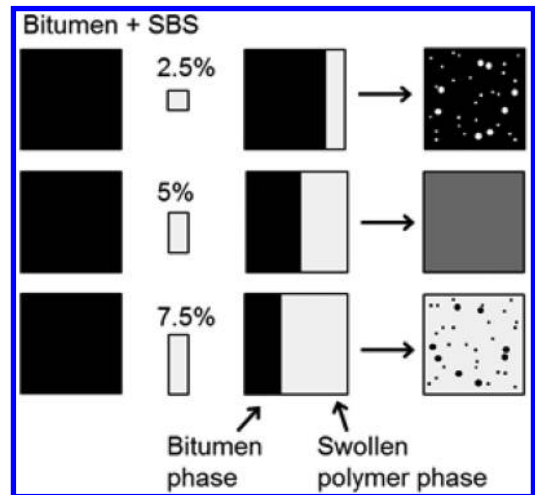


Figure 1. Schematic representation of phase morphologies of bituminous binder at different SBS concentrations.

will be and the smaller the asphaltene rich phase. If we assume that the binder properties are dominated by the continuous phase in the binder, we can expect a dramatic change in performance properties, going from an asphaltene rich continuous phase to a polymer rich continuous phase.

1.2 *Influence on asphalt mix properties*

To assess the influence of SBS modification on asphalt mix properties, the most relevant fail mechanisms will be considered: permanent deformation and cracking under the influence of fatigue or temperature.

Permanent deformation is the result of traffic load and the elastic response of the asphalt mix. The extent of the deformation depends on the initial deflection and the elastic recovery. In the previous section the existence of the polymer rich and the asphaltene rich phases in the binder was described. During an elastic recovery test, both phases will be deformed, but while the asphaltene rich phase will hardly show recovery, the polymer rich phase will have a strong tendency to regain its original shape. If the interaction/adhesion between the two phases is sufficient, even a small amount of SBS will improve the rut resistance of asphalt mixes and it will improve with every additional percentage of SBS.

The other fail mechanism, cracking, is defined as a two-step process: crack initiation and crack propagation. Cracks can be initiated by stress (thermal mechanism) or strain (traffic load) or a combination of the two. Crack initiation will obviously take place in the more rigid asphaltene rich phase of the two phase system. While crack initiation can function as a stress relief mechanism, crack propagation can lead to macro-cracks, which will decrease the structural integrity.

In a two phase system where the continuous phase is asphaltene rich, a crack can initiate and grow through the rigid material. When the crack meets the tougher polymer rich phase, it will not terminate, but grow around it. If we then consider a two-phase system in which the continuous phase is the tough polymer rich phase, a crack might initiate in the rigid asphaltene phase 'islands', but once it reaches the boundaries of this phase, the crack will either terminate or will be slowed down considerably by the tough polymer rich phase. At lower SBS concentrations there will be a positive effect, but the described phase inversion will have a major impact on the crack resistance, both thermal and fatigue cracking. Reducing cracking and crack propagation by using SBS modification has been described in the literature (Phillips 1999 & NCHRP 2010).

2 POLYMER DESIGN AND ASPHALT MIX RESEARCH

2.1 *Polymer continuous binder phase and workability*

In the previous section we have seen how a polymer continuous binder phase can influence binder and asphalt mix properties. To produce a bituminous binder with a polymer continuous phase, the SBS concentration needs to be preferably above 6%. With a standard SBS in a standard paving grade bitumen, the binder viscosity will be (too) high. To compensate for this, often softer bitumen grades are used, but this is not desirable, because their lower stiffness will result in significant deflections.

To solve this issue, we have developed a polymer which can be used to modify 40 pen bitumen

at a level of 7.5%, without workability issues. This polymer, the Kraton™ D0243, is smaller than standard SBS molecules and is more reactive towards bitumen, which makes this molecule also more compatible with bitumen.

2.2 *Asphalt mix fatigue testing and modeling*

Together with the Delft University of Technology, an extensive program was carried out in which highly modified asphalt mixes were compared with standard type mixes (Molenaar 2008, Scholten 2010 & Kluttz 2009). A selection of the results is briefly discussed here.

Conventional 4-point bending fatigue data were generated from tests on standard base course asphalt mix samples. For all samples a binder content of 4.6% on 100% of aggregate was used. The penetration value of the base bitumen was 40.

Figure 2 shows the results of fatigue tests on an unmodified asphalt mix and mixes with binders modified with 3, 6 and 7.5% of SBS. Looking at the maximum deflection to achieve 10^6 load cycles, we see improvement of about 155% for the binder with 7.5% compared to the unmodified bitumen: from about 50 to about 135 microstrain. Most likely, with a conventional SBS similar fatigue performance can be achieved at that concentration, but it would be (extremely) hard to meet the workability and compatibility criteria.

3-D Finite Element modeling (Scarpas 1997) was performed on the basis of fundamental material properties generated through the ACRE model (Erkens 2002). The modeling simulated the effect of traffic loading on structures with unmodified asphalt and the 7.5% modified asphalt (Fig. 3, Molenaar 2008). The design of the layers in the model is as follows:

- Unmodified: 15 m of subgrade, 30 cm of sub base and 25 cm of asphalt mix
- Highly modified: 15 m of subgrade, 30 cm of sub base and 15 cm of asphalt mix (in both cases the subgrade and sub base are the same and behave linear-elastically in the model)

This simulation shows that on the basis of the fundamental properties, a highly modified pavement applied at 60% of the thickness of unmodified asphalt, is expected to have less damage after the same number of load cycles. The model also showed the resistance to permanent deformation to have increased significantly, which is an obvious outcome at a polymer concentration of 7.5%.

The finite element modeling results indicate that a reduction of pavement thickness is possible by using highly modified asphalt. These data were obtained by using results of indirect tensile testing, uniaxial tensile testing and uniaxial compression testing.

Standard pavement design methods are in principle based on the (stiffness) modulus of the asphalt mix: the higher the modulus, the smaller the deflections and hence the lower the bottom up fatigue. So even when an asphalt mix is used with significantly better

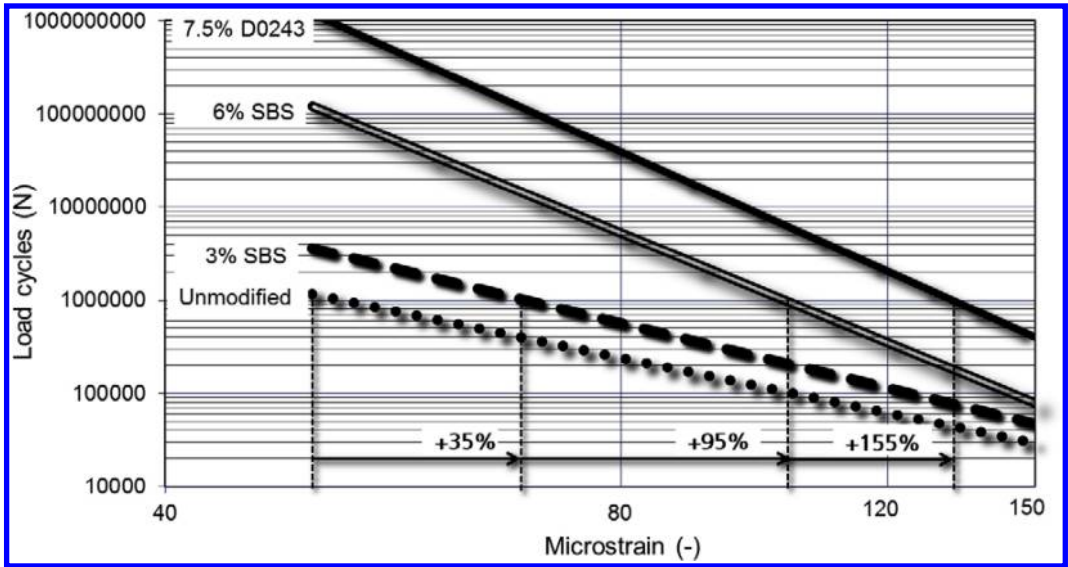


Figure 2. 4-point bending fatigue data, base course asphalt mix at 20°C and 8 Hz.

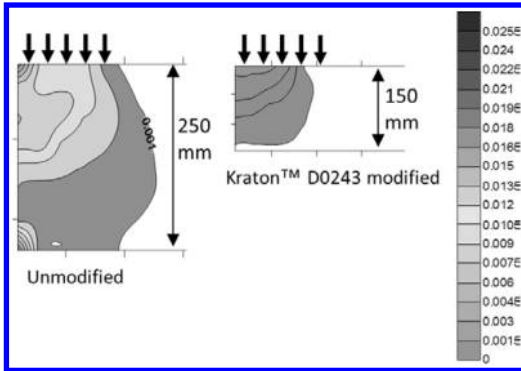


Figure 3. (Part of the) results of CAPA-3D finite element analysis showing damage in the two different structures with 25 cm of unmodified asphalt and 15 cm of highly modified asphalt.

fatigue resistance, but at the same asphalt modulus, the design method would still result in the same thickness. Fortunately, there are now design methods that allow fatigue criteria to be used and thus model calculations can be made. One design method, the Shell Pavement Design Method (SPDM), even allows the fatigue equation to be introduced. In the thickness design method the actual design strain is compared with the theoretical strain (maximum horizontal tensile strain at the bottom of the asphalt layer). Permanent deformation was also taken into account as the SPDM calculates also the vertical displacement at the top of the subgrade. Hence there are two criteria that can determine the pavement thickness in SPDM: rutting and fatigue. Using the data from the 4-point bending experiments (including the measured moduli) and varying the moduli of the subgrade and the sub base led to the results shown in Figure 4.

Figure 4 shows that even with relatively soft soils and not too strong sub bases, a significant thickness reduction can be achieved (-22%), which may, however, in the worst case not lead to sufficient cost compensation for the higher binder price. On the other hand, the other structures with thickness reductions from 34% to even 60% would more than compensate for the higher binder price and would result in lower costs up front. The cost reduction obviously stems from less asphalt and less energy and will also reduce the use of natural resources.

The finite element modeling and the pavement design method which makes use of the fatigue equation are two totally different methods to determine thickness reduction options, but they both lead to remarkably comparable results. This provides confidence for actual implementation of this concept of highly modified asphalt (HiMA), which is described in the next section.

3 HIGHLY MODIFIED ASPHALT IN PRACTICE

3.1 New pavement with reduced thickness

The NCAT test track is a 2.7 km long oval shaped track in Alabama, USA that is used to test new products and concepts of mix and pavement design (website: <http://www.pavetrack.com>). The track is trafficked with heavily loaded trucks. The loading is such that the asphalt test section is exposed to 10 million ESALs (Equivalent Single Axle Load) in a period of about two years, which would be equal to about 10 years of heavy traffic.

This is one of the best ways to simulate asphalt performance in practice. The trucks drive 16 hours per day, 5 days per week, have an axle load of 9.5 tons and drive at an average speed of 72 km/h. The NCAT test track

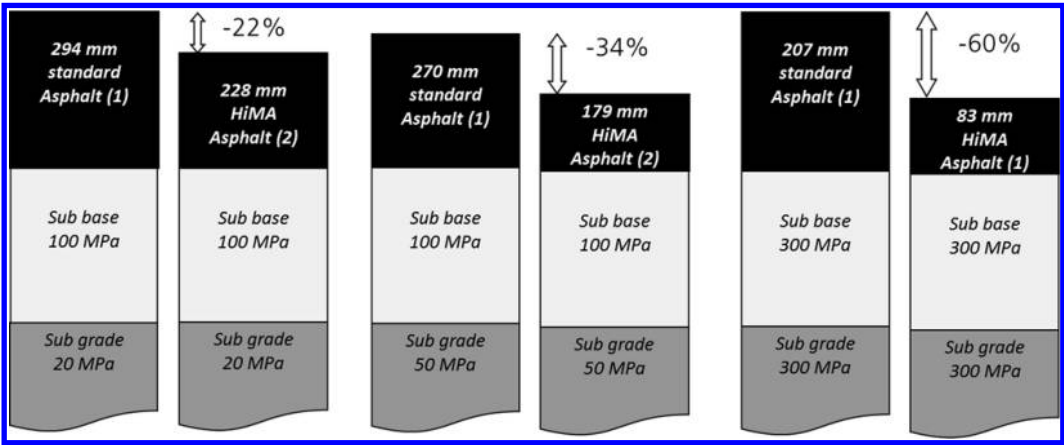


Figure 4. The potential asphalt pavement thickness reduction with different sub base and subgrade moduli (1: thickness determined by asphalt strain criterion; 2: thickness determined by subgrade strain criterion; HiMA = highly modified asphalt).

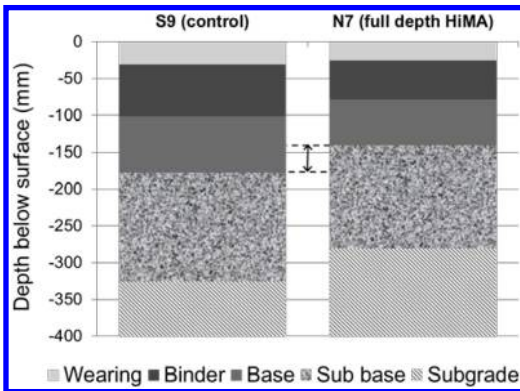


Figure 5. Pavement structure for the NCAT test sections S9 (control) and N7 (HiMA).

results are valued greatly in all of the United States and therefore the HiMA concept was tested there. The HiMA section was built in a set of relatively thin test sections that were designed to last at least one cycle (10 million ESALs) and show significant results after the test period. The control section S9, had a total asphalt bound thickness of 18 cm, while the HiMA section N7 was 14.5 cm thick (Fig. 5 & Table 1).

The HiMA section was thicker than aimed for, but the NCAT officials did not want to use thinner layers due to the used aggregate size and the fear of early failure, distorting the testing of the other sections. Except of the thickness, the mix design of the HiMA section is kept as close as possible to the mix design of the control section (Table 1). In the control section, standard PMBs were used in the wearing and the binder course. These had a PG of 76-22, with a binder based on 50/70 pen bitumen with about 3% of a standard SBS. The HiMA binder was based on the same bitumen, but with 7.5% of the specially designed SBS polymer.

Besides the actual trafficking of the section, extensive lab testing was carried out with the asphalt mix

used on the track, which is described in the various reports issued by NCAT (Timm 2012 & 2013). After the completion of the full testing period (10 million ESALs) there was no cracking in both constructions with a rut depth of 2 mm for the HiMA stretch and 7 mm for the control. Based on these results it was decided to enter into a second cycle of another 10 million ESALs. This cycle was completed after the summer of 2014.

At the time of writing of this paper, the amount of rutting and cracking in the sections is being determined and furthermore cycle forensic coring will be performed to determine the nature of the pavement damage. In this paper an update is given of the field performance of the sections.

After about 13 million ESALs, the first cracks appeared in the S9 control section (Fig. 6, top), while in the thinner HiMA section no cracks were visible. And after about 17.5 million ESALs, the first small cracks appeared in the N7 HiMA section, while the control section showed much more cracks (12% in the left wheel path, 21% in the right one and 9% for the total lane width, see Fig. 6). The S9 control section shows mostly typical fatigue cracking pattern in the wheel paths. At that point in time, the S9 control section underwent a resurfacing treatment due to damage that was too severe to be able to continue trucking. The N7 HiMA section showed only a few hairline cracks in the wheel path. These cracks appeared over the winter, but they have not grown beyond the width of the wheel path. At this moment it is not clear what has caused these cracks, but the cycle forensic coring likely will explain.

Figure 7 shows the average rut depth of both sections during the second trucking cycle. Overall, the rut depth for the thinner N7 HiMA section has been about 1/3 of the rut depth of the S9 control section. However, during the last half of the second trucking cycle the apparent rutting on the S9 control section has decreased, which brings the values closer to those of the N7 HiMA section. (The rut depth on

Table 1. Details on the mixes used in the test sections.

Layer Section	Wearing course		Binder course		Base course	
	HiMA	Control	HiMA	Control	HiMA	Control
Thickness (mm)	25	30	53	70	63	75
Nominal maximum aggregate size (mm)	9.5	9.5	19.0	19.0	19.0	19.0
SBS (%)	7.5	2.8	7.5	2.8	7.5	0.0
PG Grade	88-22	76-22	88-22	76-22	88-22	67-22
Bitumen (%)	6.3	6.1	4.6	4.4	4.6	4.7
Air voids (%)	6.3	6.9	7.3	7.2	7.2	7.4
Plant temperature (°C)	174	168	174	168	171	163
Compaction temperature (°C)	147	135	119	134	116	117
Asphalt mix price/ton (\$)	90	80	78	69	78	57

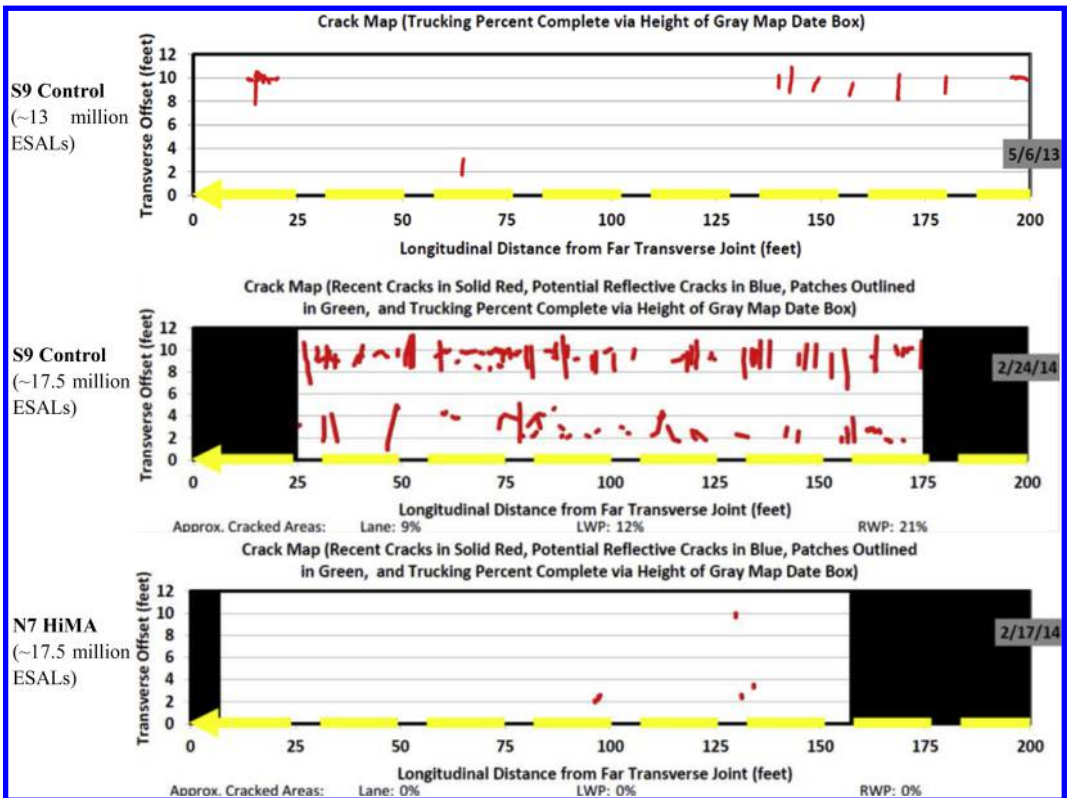


Figure 6. Crack maps for NCAT sections S9 and N7.

the N7 section has stayed more or less constant.) The graphs showing the roughness and unevenness (IRI value) values probably explain this behavior. At the moment the S9 rut depth starts to decrease, the IRI values increases dramatically. The roughness of the S9 surface is probably confounding the rutting measurement, especially considering that the deformations are still rather small. Furthermore, the resurfacing treatment of the S9 section after 17 million ESALs makes that the two sections cannot be compared after that moment. The IRI values of the N7 section have remained constant during the cycle.

3.2 HiMA for repair of a failed test track

The impressive results obtained with the 20% thinner N7 HiMA section, led to another opportunity in the NCAT research program. The N8, sponsored by the Oklahoma Department of Transportation (ODOT), was constructed in 2006 and after one research cycle (10 million ESALs) it needed to be repaired. This was done by performing a mill and inlay with paving fabrics in 2009. After only 3.5 million ESALs, the pavement had failed to such extent that rehabilitation was necessary and this was done with HiMA in 2010. The cross sections are shown in Figure 8 and are

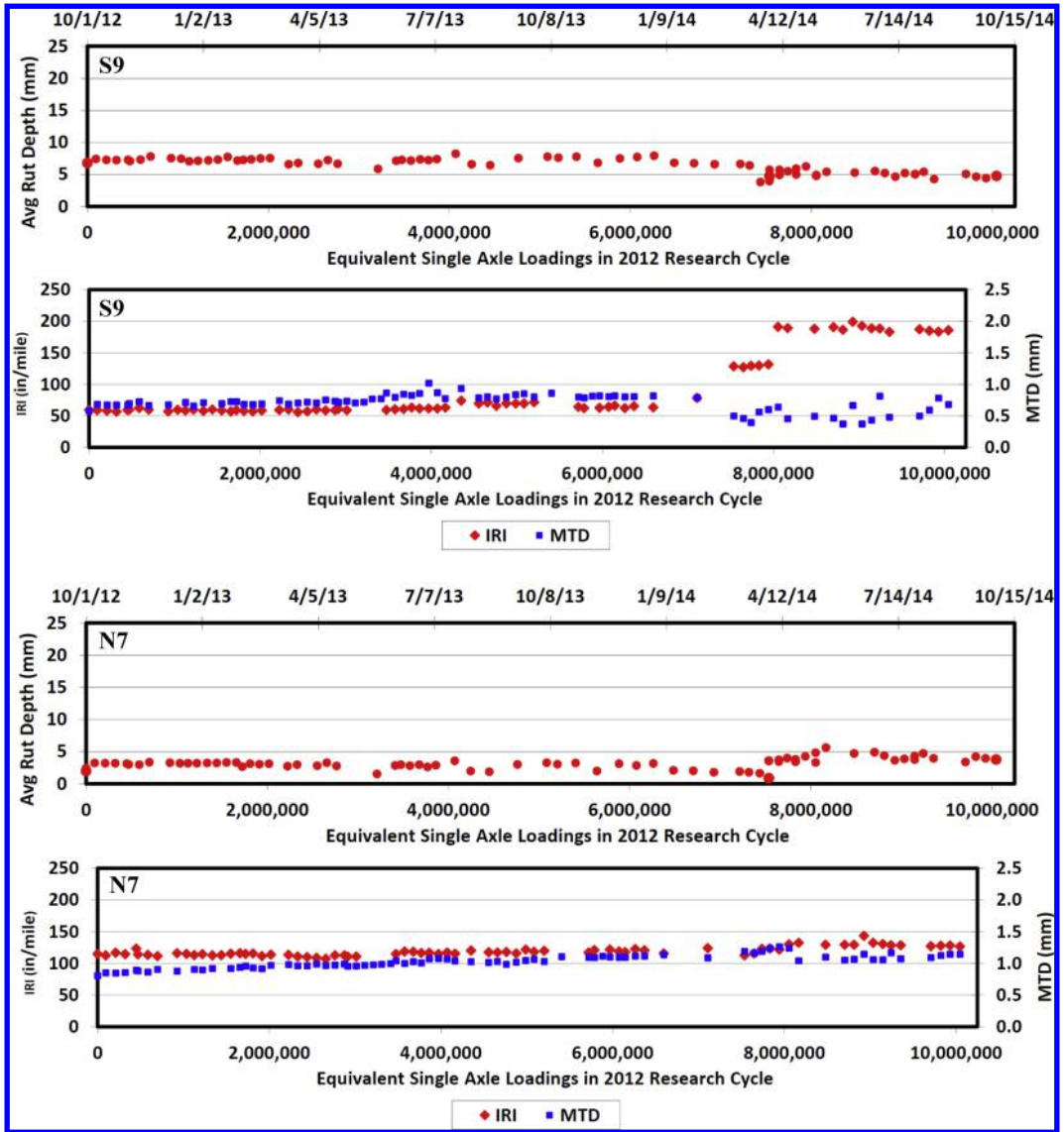


Figure 7. The average rut depth and IRI (International Roughness Index) and MTD (Mean Texture Depth) values for sections S9 (control, top graphs) and N7 (HiMA, bottom graphs) during the second trucking cycle.

described in more detail in the next sections. The pavements within this project were designed by ODOT's own design methods.

3.2.1 Original construction of N8

The original objective of the ODOT sections was the development of a perpetual pavement. The lifetime aimed at is 50 years and to save on costs, energy and material resources, the pavement should be as thin as possible. The N8 is the thinner one (25 cm of asphalt) of two test sections (the thicker one, with 35 cm of asphalt has performed well), both sponsored by the ODOT.

In Oklahoma, the subgrade materials are often soft and to take this into account, the soil under the two

sections was excavated to 1.2 m and replaced with soft subgrade. The top 20 cm were then replaced with the stiffer removed material to simulate lime stabilization (Fig. 8). The asphalt layer was 25 cm thick and consisted of a 5 cm thick rich bottom layer, 15 cm of dense Superpave mix and 5 cm of stone matrix asphalt (SMA) surface. The goal of N8 was to determine the pavement lifetime with this design. Information on the design, production and paving of the layers has been reported previously (Timm 2009a, b, Taylor 2009).

Near the end of the research cycle, after 7 million ESALs, roughness started to increase in section N8. The first cracks appeared after 8.3 million ESALs and rehabilitation was needed at the end of the trucking cycle, which was after 10 million ESALs.

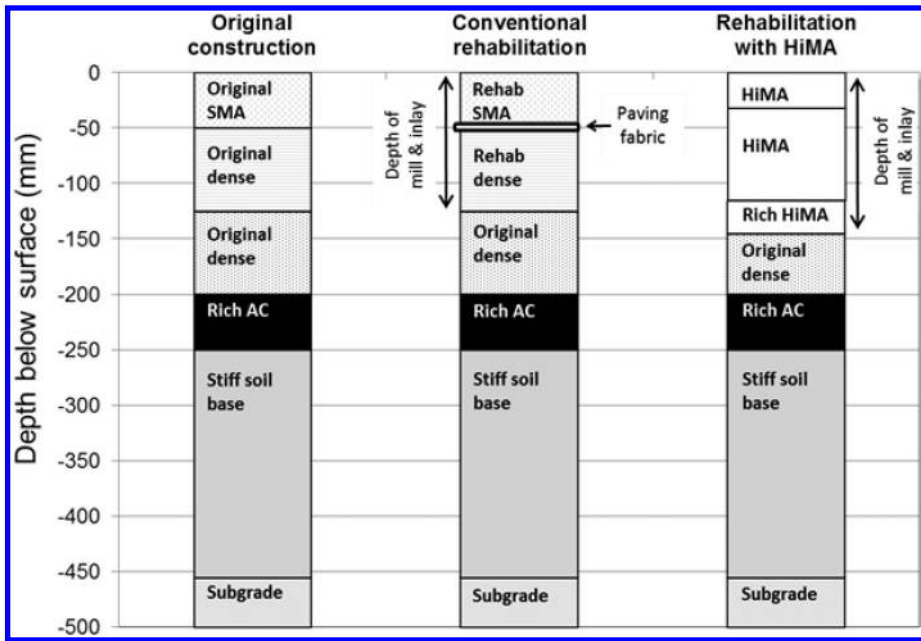


Figure 8. N8: Original construction and rehabilitation cross sections.

3.2.2 Conventional rehabilitation

When bottom up cracking occurs in flexible pavements, it is often best to remove the cracked pavement full depth and replace it. However, for economic and practical reasons it is more common to do a surface or structural mill and overlay. Such overlays can suffer from early failure by reflection cracks propagating to the surface (Pais 2000). Reflection cracking is mentioned as one of the main distresses in asphalt concrete overlays (Tsai 2010). Nevertheless, the motivating factors of a mill and overlay most of the time outweigh the performance challenges of frequent repair and user delay. Moreover, the lifetime of such overlays can significantly be improved by using polymer modified asphalt (Von Quintus 2007).

For the first N8 overlay, 12.5 cm was milled and replaced with an inlay, which is the standard practice of the ODOT. The inlay consisted of 7.5 cm of dense Superpave mix and 5 cm of SMA at the surface (Fig. 8). The mixes were the same as in the original pavement. A paving fabric was used between the two layers. The objective here was to determine the lifetime of this overlay design.

In the areas where the paving fabric was placed, it took longer before cracks appeared. However, after the cracks had formed, the pavement deteriorated faster in the areas with the fabric than without. Forensics revealed that the cracks extended down into the pavement and that rutting extended to the subgrade. Figure 9 shows such a severely distressed area. At that moment (after 3.5 million ESALs) the trucks could not drive over this section anymore and rehabilitation was needed again to be able to continue the research cycle. There was a need of a rehabilitation method that could

be executed relatively easy and would at least last for the remainder of the trucking cycle.

3.2.3 Rehabilitation with HiMA

The exceptional fatigue and rutting resistance of section N7 made HiMA the technology of choice to repair the severely distressed N8. This time 14.5 cm were removed and replaced with three lifts of HiMA (Fig. 8). The original proposal was to copy the mix designs of the N7 section with a 19 mm base and binder course and 9.5 mm wearing course (see Table 1). This design would provide maximum stiffness to minimize the potential for further subgrade rutting. However, the ODOT adjusted the designs somewhat; they proposed to use for the bottom lift a richer 9.5 mm mix (the same as the wearing course) to better mitigate reflective cracking from the remaining cracked bound pavement. The final design was to use the finer mix for the bottom layer in the same thickness as the wearing course. The thickness of the intermediate layer was increased in thickness to compensate for the thinner bottom layer.

After 4.2 million ESALs, which is already more than the conventional rehabilitation lasted, the average rut depth was approximately 1 mm and no cracks were visible. The visual state at that moment is shown in Figure 10. At the end of the testing period (5.3 million ESALs) the section was still in excellent condition. Therefore, the trafficking on the N8 section was continued in the next research cycle.

After approximately 15 million ESALs the first cracks had appeared. The average rut depth during the second 10 million ESALs trucking cycle is approximately 5 mm and does not increase significantly. The IRI value increased only slowly during the trucking



Figure 9. N8 pavement failure after conventional mill and inlay.

cycle, indicating that the rut depth determination is not influenced by large changes of the roughness of the surface, as was the case with the S9 section in paragraph 3.1.

A material cost comparison (net present value) of the different solutions for the N8 section shows that the costs of the original construction and a HiMA rehabilitation are 21% lower than making the original design followed by the standard rehabilitation method and then a HiMA rehabilitation. The material costs are the lowest when the original construction and rehabilitation are both constructed using HiMA mixes (material costs –24%).

The experience with the N8 has prompted the ODOT to apply HiMA for other repair projects (Powell 2013).

3.3 Global application of HiMA

Besides the successful NCAT testing there have been many commercial HiMA applications in for example Australia, the US, the Middle-East and Europe (including micro-surfacing and hot sprayed seals) and many others are being prepared (updates on HiMA applications can be found here: <http://www.pavewithkraton.com>). Some examples:

Port of Napier, New Zealand: heavily deformed section of the container terminal was structurally repaved

with a total thickness of 15 cm of asphalt mix: 10 cm of HiMA (40/50 + 7.5% SBS) in the base and 5 cm of standard PMB (5% SBS) in the wearing course. The base course was applied at 8°C in one layer and the crew indicated the mix to have ‘great workability’. Almost 2 years after the application there is no sign of any deficiency.

Parana Highway, Brazil: the old road surface based on a Cement Treated Base (CTB) with asphalt overlay showed severe rutting and cracking. The original rehabilitation design was to move away from the CTB and to get an overall asphalt bound layer of 27.5 cm. There the HiMA solution offered the 40% reduction opportunity (based on DARWIN ME calculations), which was then applied. The road carries very heavy traffic (32 million ESALS in 8 years) and till date the HiMA construction performs very well.

A21 highway near Cremona, Italy: in the summer of 2013 a HiMA binder (50/70 bitumen + 8% SBS) was successfully applied in 3 cm thick SMA and porous asphalt layers. The SMA reference section contains cellulose fiber, while the HiMA SMA is without fiber. Evaluation of cores taken from all trial sections showed significantly higher Marshall Stability and Indirect Tensile Strength values for the HiMA based asphalt compared to the reference material.

Istanbul, Turkey: the old surface of the road next to a highway had been overlaid several times. The last



Figure 10. HiMA rehabilitated section N8 after 4.2 million ESALs.

overlay, with an unmodified binder, showed severe rutting after only 6 months. The road was paved with a HiMA overlay of 10 cm consisting of 6 cm of binder course and 4 cm of wearing course. After 14 months, no rutting was observed.

4 CONCLUSIONS

This paper on highly modified asphalt has shown how polymer modification of bitumen can be used in a more efficient way than is done today. The simple solution is to increase the polymer level in such a way that a (sufficiently strong) polymer continuous network is formed, by which in particular the resistance to cracking makes a step change. This improved cracking resistance opens up the possibility to reduce the overall pavement thickness. However, as base course binders tend to be fairly hard, a new polymer was designed to cope with workability and compatibility issues. Lab evaluations and finite elements testing confirmed the theoretical considerations with such encouraging results that it was justified to invest significant resources into testing at NCAT. The results generated in the test sections in turn warranted the immediate commercialization of the product. The actual results obtained in trials and commercial applications have thus far confirmed the excellent results obtained in NCAT:

- Workability/compatibility with a wide range of bitumen grades appeared to be excellent
- Based on the data generated and the existing experience with traditional PMB, it is expected that the maintenance of HiMA sites will be at least as favourable as standard PMB sites
- None of the trials or commercial applications has shown any premature sign of failure

- HiMA has not only been proven in base and binder course applications, but appeared also successful in wearing courses
- HiMA has successfully been applied for full depth pavements as well as for rehabilitation of failed pavements
- Sections with as much as 40% overall asphalt pavement thickness reduction are performing well
- Using simple calculation tools one may expect the break-even point for making cheaper pavements at thickness reductions between 20 and 25%
- Based on the results generated today one may expect pavements to become cheaper by using more highly modified binders and still obtain improved performance

Some 30–35 years after the successful introduction of SBS into the paving industry, new polymer designs and their more effective use, will bring a new era of opportunities for making better and longer lasting infra-structure at lower costs.

Note: Our focus is mainly on initial costs, because often initial costs of longer lifetime pavements are higher than for conventional pavements, while in the case of HiMA we have proven the longer lifetime, which can be achieved at lower initial costs. Furthermore, since the HiMA concept is rather new, it is too early for a life cycle cost analysis.

REFERENCES

- Erkens, S.M.J.G. 2002. *Asphalt Concrete Response (ACRe), Determination, Modelling and Prediction, PhD. Thesis, Delft University of Technology, The Netherlands.*
- Kluttz, R.Q. et al. 2009. *Modified Base Courses for Reduced Pavement Thickness and Improved Longevity. Proceedings*

- of the International Conference on Perpetual Pavement, October, Columbus, OH.
- Molenaar, A.A.A. et al. 2008. *Advanced mechanical testing of polymer modified base course mixes, 4th Eurasphalt & Eurobitume congress, Copenhagen, Denmark.*
- NCHRP 2010. (Report 646) *Validating the fatigue endurance limit for hot mix asphalt.*
- Pais, J.C. et al. 2000. *Evaluation of Reflective Cracking Resistance in Bituminous Mixtures. Proceedings of the 4th International RILEM Conference, A.O. Abd El Halim, D.A. Taylor and El H.H. Mohamed, editors, RILEM Publications, p. 93–102.*
- Powell, R.B. 2013. In: *Asphalt Technology News, Fall 2013, Volume 25, Number 2, p. 1–2.*
- Phillips, M.C. 1999. *Multi-step models for fatigue and healing, and binder properties involved in healing; Eurobitume Workshop 99, Luxembourg.*
- Scarpas, A. et al. 1997. *Finite Element Simulation of Damage Development in Asphalt Concrete Pavements, 8th International Conference on Asphalt Concrete Pavements, Seattle, Washington, U.S.A.*
- Scholten, E.J. et al. 2010. *Build sustainable and economical pavements with a novel class of SBS polymers for bitumen modification, 5th Australian Road Engineering and Maintenance Conference, 16–17 March.*
- Taylor, A. J. et al. 2009. *Mechanistic Characterization of Resilient Moduli for Unbound Pavement Layer Materials. Report No. 09-06, National Center for Asphalt Technology, Auburn University.*
- Timm, D. et al. 2009a. *Strain Regimes Measured in Two Full-Scale Perpetual Pavements. Proceedings, International Conference on Perpetual Pavements, Columbus, Ohio.*
- Timm, D. et al. 2009b. *Design, Construction, and Instrumentation of the 2006 Test Track Structural Study. Report No. 09-01, National Center for Asphalt Technology, Auburn University.*
- Timm, D. et al. 2012. *Field and Laboratory Study of High Polymer Mixtures at the NCAT Test Track – Interim Report.*
- Timm, D. et al. 2013. *Field and Laboratory Study of High Polymer Mixtures at the NCAT Test Track: Final Report.*
- Tsai, F.-L. et al. 2010. *Prediction of Reflection Cracking in Hot-Mix Asphalt Overlays. Transportation Research Record No. 2155, Transportation Research Board of the National Academies, Washington, D.C., p. 43–54.*
- Von Quintus, H. L., J. et al. 2007. *Quantification of Effect of Polymer-Modified Asphalt on Flexible Pavement Performance. Transportation Research Record No. 2001, Transportation Research Board of the National Academies, Washington, D.C., p. 141–154.*

Publication disclaimer: We believe the information set forth above to be true and accurate, but any findings, recommendations or suggestions that may be made in the foregoing text are without any warranty or guarantee whatsoever, and shall establish no legal duty or responsibility on the part of the authors or any Kraton Polymers entity. Furthermore, nothing set forth above shall be construed as a recommendation to use any product in any specific application or in conflict with any existing patent rights. All Kraton Polymers entities expressly disclaim any and all liability for any damages or injuries arising out of any activities relating in any way to this publication or the information set forth herein.

Bituminous mixtures (hot, warm, and cold), specifications

The combined effects of aging and moisture conditioning on the indirect tensile strength, flow and fracture energy of warm mix asphalt

M.O. Hamzah

Universiti Sains Malaysia, Penang, Malaysia

B. Golchin

Department of Civil Engineering, Ahar Branch, Islamic Azad University, Ahar, Iran

J. Voskuilen

Ministry of Infrastructure and Environment, Major Projects and Maintenance, Utrecht, The Netherlands

ABSTRACT: In the last decade, some limited studies on the combined effects of aging and moisture conditioning for asphalt binders and asphalt mixtures have been carried out. This paper presents a new approach to evaluate the combined effects of these two parameters on the stiffness properties of Warm Mix Asphalt (WMA). Two asphalt binders, different compaction temperatures and a chemical warm asphalt additive named Rediset, were selected for fabrication of WMA samples. The combined effects of aging and moisture conditioning on the stiffness properties of asphalt mixtures were quantified from the indirect tensile strength (ITS) test. The effects of compaction temperatures and warm additive contents on the ITS, flow and fracture energy of WMA were investigated, as well. The test results showed that aging and moisture conditioning exerted opposing effects on the stiffness properties of WMA. Compaction temperature and test temperatures were identified as significant factors that affected the stiffness of WMA.

1 INTRODUCTION

From previous studies, aging process increases the stiffness of an asphalt mixture, while moisture damage exerts an opposing effect on mix stiffness. This subject matter has been the subject of investigation in a few literatures for hot mix asphalts (HMA). [Table 1](#) summarized the methodologies used to evaluate the effects of aging and moisture conditioning on the laboratory properties of asphalt binders and mixtures. In this paper, the stiffness properties of WMA incorporating a chemical warm additive subjected to moisture conditioning and aging were investigated in terms of indirect tensile strength (ITS) tests.

The first part of this study describes the combined effect of aging and moisture conditioning methods on the ITS of asphalt mixtures. The second part presents the results, analysis and discussions of the effects of compaction temperatures, warm additive contents and test temperatures on the ITS, flow and fracture energy of both WMA and HMA samples in unaged and dry condition. In the third part, the effects of continuous cycles of aging and moisture conditioning on the mechanical properties of WMA and HMA samples under indirect load are deliberated to determine the effect of test parameters on the performance of asphalt mixtures. These results can provide an initial informative data for prediction of the behaviour of WMA combined a chemical warm additive at a laboratory scale.

2 MATERIALS AND METHODS

2.1 *Materials*

Two asphalt binders, PG64 and PG76, were used in this study. PG64 was an unmodified conventional 80/100 penetration grade asphalt binder while PG76 was a polymer-modified 40/50 penetration grade asphalt binder. The rheological properties of these asphalt binders are presented in [Table 2](#). Crushed Granite aggregate supplied by Kuad Sdn. Bhd. was used as a local aggregate in this study. The median aggregate gradation was selected in accordance with JKR specifications for asphalt mixture type AC14 (JKR, 2008) as shown in [Table 3](#). The engineering properties of the aggregate are presented in [Table 4](#). Rediset was chosen as a chemical warm-mix asphalt additive to evaluate its effect on asphalt mixtures properties (see [Figure 1](#)). Rediset is a chemical warm-mix additive and is produced by Akzonobel (Hamzah et al. 2014).

2.2 *Test plan*

Test plan was conducted in three separate phase. In the first phase, ITS of asphalt mixtures fabricated with two different asphalt binders were investigated under aging and various type of moisture conditioning. A probable stiffness property of asphalt mixtures under combined effects of aging and moisture damage

Table 1. Studies on the combined effects of aging and moisture conditioning.

No.	Conditioning method	Test method
1	Water was used in the form of a vapor during the aging of asphalt binders in pressure aging vessels (PAV).	Chemical and rheological tests on the conditioned binders (Thomas 2002)
2	Asphalt mixtures saturated by vacuum and then aged in a humid environment for a period of up to one year.	Indirect tensile strength and flexural beam fatigue test (Lu & Harvey 2006)
3	Binders subjected to PAV aging and then subsequently submerged in a water bath for 4, 8, and 24 hours soak times.	Pull-off test for determining bond strength (Copeland et al. 2007)
4	Specimens were aged using long term aging process described in AASHTO R30. Then moisture susceptibility of unaged and long term aging specimen was investigated.	Indirect tensile strength of moist and dry asphalt mixtures (Xiao et al. 2011, Punith et al. 2012)
5	High pressure and high temperature were used to combine and speed up the aging and moisture damage of mixtures in presence of water (saturation ageing tensile stiffness method; SATS).	Stiffness modulus test under standard test conditions in the Nottingham Asphalt Tester (NAT) (Collop et al. 2007)
6	Modified SATS test according to EN 12697-45:2012 (Khan et al. 2013).	X-ray CT scanning, image analysis, dynamic shear rheometer test and stiffness modulus test (using NAT)

Table 2. Properties of asphalt binders.

Aging condition	Properties	Asphalt binder	
		PG64	PG76
Original binder	Viscosity at 135°C (Pa·s)	0.38	1.66
	Softening point (°C)	45	69
	Penetration (0.1 mm)	80	50
	Ductility (cm)	>100	90
	Flash point (°C)	331	344
	G*/sinδ at 64°C (Pa)	1653	–
	G*/sinδ at 76°C (Pa)	–	2374
Short-term aged binder (RTFO)	G*/sin δ at 64°C (Pa)	2442	–
	G*/sin δ at 76°C (Pa)	–	3968
Long-term aged binder (RTFO+PAV)	G*(sin δ) at 25°C (MPa)	2.58	5.41

Table 3. Aggregate gradation for AC14 wearing course according to Malaysians Public Works Department Specifications.

Sieve size (mm)	Percentage passing (Malaysian specification)
20	100
14	90–100
10	76–86
5	50–62
3.35	40–54
1.18	18–34
0.425	12–24
0.150	6–14
0.075	4–8

are shown in Figure 2. For this purpose, ITS of the following samples was determined:

- Unaged samples (designated as samples in cycle 0).
- Long-term aged samples (designated as samples after cycle 1).

Table 4. Engineering properties of granite aggregate.

Property	Test	
	Result	Test Method
Coarse aggregates bulk specific gravity	2.62	AASHTO T85
Absorption (%)	0.40	AASHTO T85
Fine aggregates bulk specific gravity	2.57	AASHTO T84
Absorption (%)	0.54	AASHTO T84
Fine aggregate angularity (%)	47.3	AASHTO T33 (Method A)
Course aggregate angularity (%)	49.5	AASHTO TP56 (Method A)
Flat and elongated (%)	23.3	BS 812-105
Los Angeles abrasion (%)	23.86	AASHTO T96
Aggregate crushing value (%)	19.25	BS 812-110



Figure 1. The form of warm additive.

- Long term aged samples after moisture conditioning of the samples in cycle 1 (designated as samples after cycle 2).

Following procedures were used for conditioning of the samples:

- Long-term oven aging of unaged samples at 85°C for 3 days.

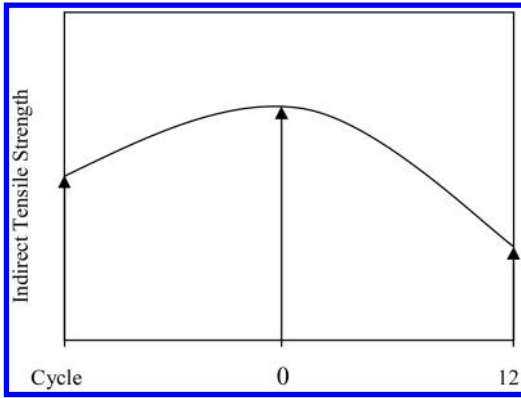


Figure 2. Probable combined effects of aging and moisture conditioning on the stiffness properties of asphalt mixtures.

- Using different type of moisture conditioning for conditioning of the long-term aged samples.
- Repeating the same long-term oven aging (at 85°C for 3 days) on moisture conditioned samples (or without moisture conditioned samples).

Following moisture conditionings were applied on the samples (see Figure 3):

- Vacuum saturation in distilled water for 30 minutes at room temperature and then submerging in distilled water for 24 hours at 60°C.
- Vacuum saturation in water mixed with sodium carbonate for 30 minutes at room temperature, freezing the samples in a refrigerator for 15 hours, and then submerging in water mixed with sodium carbonate for 24 hours at 60°C.
- Do nothing (These samples were introduced with name of 2 times aging samples).

In the second phase, the effects of compaction temperatures, warm additive contents and test temperatures on the ITS, flow and fracture energy of both WMA and HMA samples were investigated based on the experiment design presented in Figure 4.

In the third phase, one of the moisture induced damage from the first phase of the study was selected to condition HMA and WMA samples fabricated with different additive contents at various compaction temperatures. This process involved a series of vacuum, freeze and thaw on asphalt mixtures immersed in water mixed with sodium carbonate. In this phase, the effects of multiple aging and moisture conditioning on the stiffness properties of WMA were evaluated. Combination of aging and moisture conditioning was followed by a method mentioned in Table 5. Test parameters are warm additive content, compaction temperature, binder type and aging cycle while test outputs are the ITS, flow and fracture energy. All samples were fabricated with $7 \pm 0.5\%$ air voids. WMA and HMA samples fabricated with PGx asphalt binder, compacted at temperature y and tested at temperature z were designated as PGx-(TzWy) and PGx-(TzHy), respectively. For instance, PG64-(T15W140) is related



Figure 3. Moisture conditioning and long-term oven aging of samples.

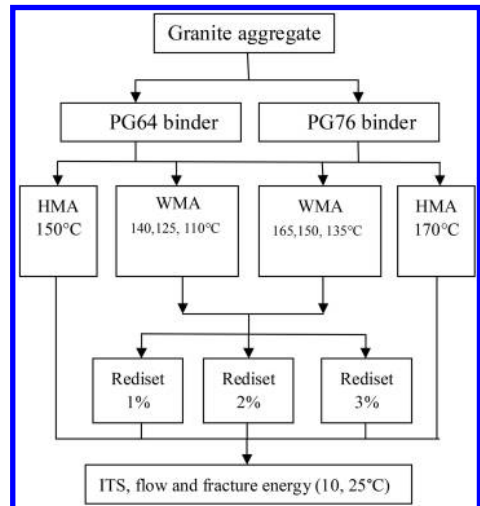


Figure 4. Experiment design for evaluation the effects of warm additive content and compaction temperature (second phase).

Table 5. Cycles of aging and moisture conditioning.

Number of cycle	Description of conditioning	Test results
Cycle 0	Unaged sample (no long-term aging and no moisture conditioning was occurred)	ITS ₀ , flow ₀ and fracture energy ₀
Cycle 1	Long-term aging of unaged samples	ITS ₁ , flow ₁ and fracture energy ₁
Cycle 2	Moisture conditioning + long-term aging of samples after cycle 1	ITS ₂ , flow ₂ and fracture energy ₂
Cycle 3	Moisture conditioning + long-term aging of samples after cycle 2	ITS ₃ , flow ₃ and fracture energy ₃

Table 6. Designations for asphalt mixtures.

Binder type	Test temperature	Mix type	Compaction temperature	Designation
PG64	25°C	HMA	150	T25H150
		WMA	110	T25W110
			125	T25W125
	15°C	HMA	150	T15H150
		WMA	110	T15W110
			125	T15W125
PG76	25°C	HMA	170	T25H170
		WMA	135	T25W135
			150	T25W150
	15°C	HMA	170	T15H170
		WMA	135	T15W135
			150	T15W135

to the WMA asphalt mixtures fabricated with PG64 asphalt binder compacted at 140°C and tested at 15°C. Also PG64-(T15W) refers to all WMA samples fabricated with PG64 asphalt binder and tested at 15°C. Further designations are introduced in Table 6.

2.3 Test procedure

The indirect tensile strength test was conducted on the conditioned and unconditioned samples. Before the test, the specimens were kept in an incubator at 15°C for 4 hours. After 4 hours, the specimens were tested by applying a vertical load and ITS vertical deformation was measured. The maximum failure load and its related flow (deformation in conjunction with ITS test) were recorded and the indirect tensile strength of the specimens was calculated using Equation 1.

$$ITS = (2000 \times F) / (\pi \times h \times d) \quad (1)$$

where

ITS = Indirect tensile strength (kPa)

F = Failure load (N)

h = Average height of specimen (mm)

d = Average diameter of specimen (mm)

The fracture energy was determined from the area under the load-deformation curve obtained in conjunction with ITS test. According to Xiao et al. (2013)

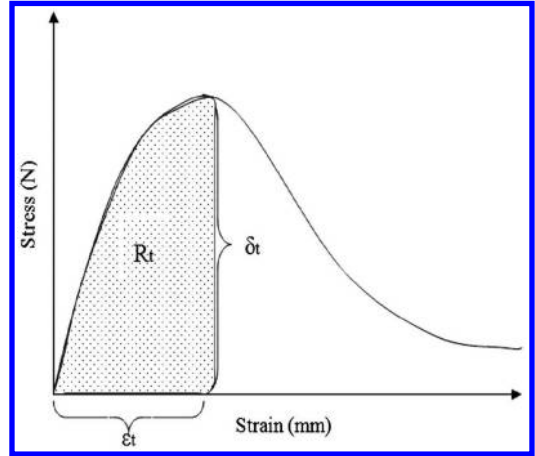


Figure 5. Curve of load versus deformation for demonstrating the fracture energy (Xiao et al. 2013).

fracture energy can be expressed as “the area under the load-deformation curve from the point of load application (starting from zero) to the maximum tensile stress” as shown in Figure 5.

For further investigation, unaged samples were tested at 15°C and 25°C to evaluate the interaction effects of test temperature with warm additive content and compaction temperature on the value of ITS, flow and fracture energy.

3 RESULTS AND DISCUSSIONS

3.1 Preliminary studies for the effects of moisture conditioning and aging

ITS test results of asphalt mixtures subjected to aging and moisture conditioning methods are presented in Figures 6 and 7. From the figures, aging increased the ITS of the asphalt mixtures, while the moisture conditioning reduced the ITS. The results showed that binder type and moisture conditioning state exhibit a noticeable effect on the ITS. For example, moisture conditioning using vacuum saturation and freeze-thaw exhibited the lowest ITS. Moisture conditioning slightly decreased the ITS of PG76 mixtures, while the same moisture conditioning exhibited remarkable effect on the ITS results of PG64 mixtures. It implies that PG64 asphalt mixtures are more prone to moisture susceptibility.

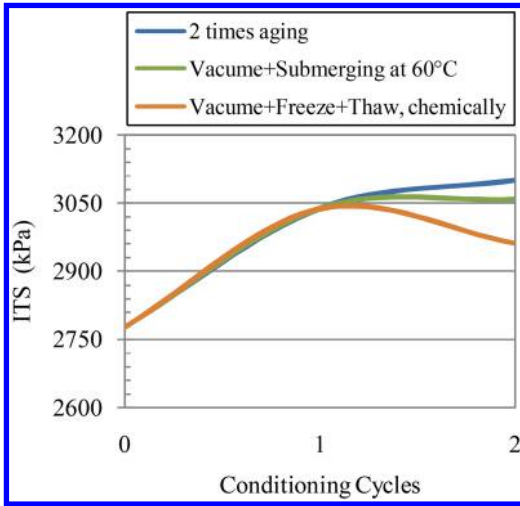


Figure 6. Effect of aging and moisture conditioning on the ITS of PG64 asphalt mixtures.

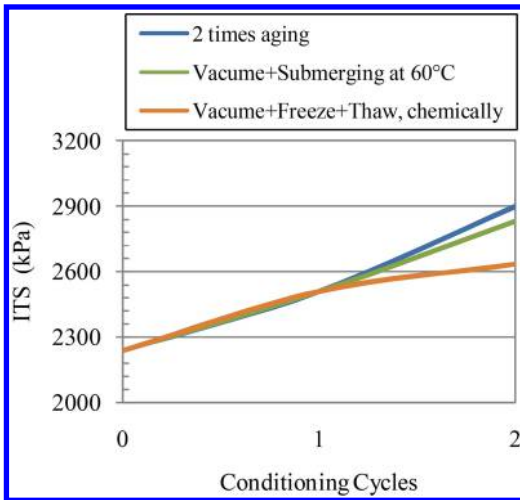


Figure 7. Effect of aging and moisture conditioning on the ITS of PG76 asphalt mixtures.

3.2 Mechanical properties of unaged WMA and HMA

The influences of warm additive content, compaction temperature and test temperature on the ITS are presented in Figure 8. The results indicated that there are obvious differences between the ITS of WMA samples prepared using different binder types and compacted at various temperatures. A limited effects of warm additive content on the ITS of unaged samples were observed. For instance, increasing the warm additive content from 1% to 3% for PG64-(T25W) exhibited very little increase in ITS. However, the ITS of WMA increase regardless of binder type, warm additive content and test temperatures. This can be due to the effects

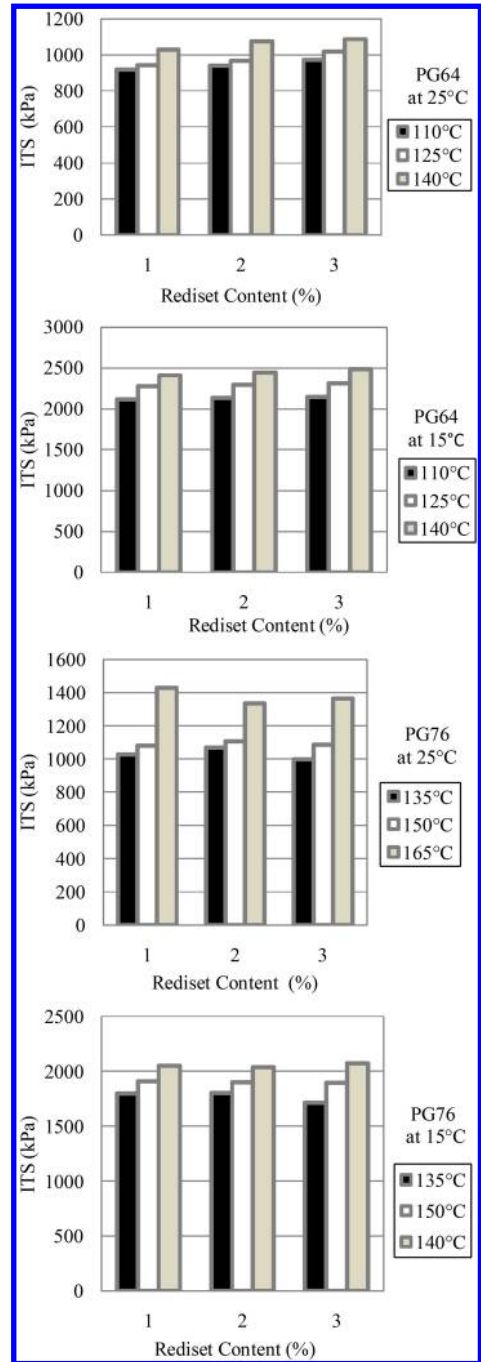


Figure 8. The effects of additive contents on the ITS of unaged asphalt mixtures.

of aging of the binders during mixtures fabrication. The use of polymer modified binder (PG76) showed that ITS of PG76-(T25W) was greater than the corresponding value of PG64-(T25W), while the ITS of PG76-(T15W) is lower than the corresponding value of PG64-(T15W).

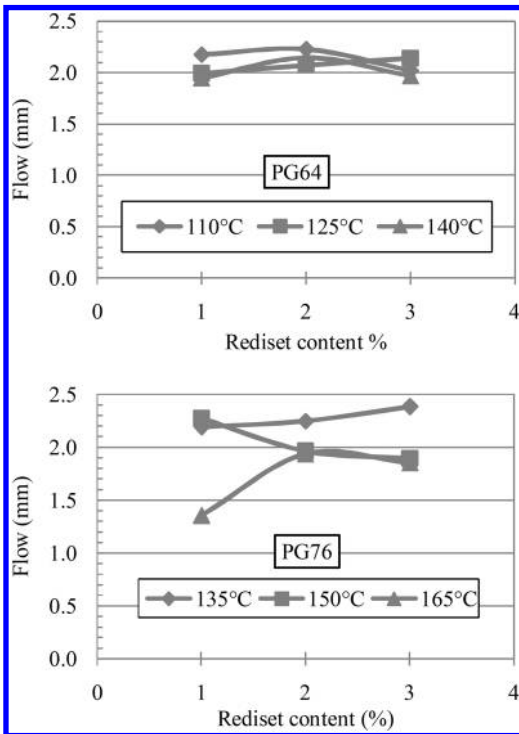


Figure 9. Fluctuation of the flow versus additive content at 25°C.

Figures 9 and 10 shows the influences of the additive content on the flow and fracture energy for WMA samples tested at 25°C. There appear to be no obvious trend on the effects of Additive content on the flow and fracture energy. The flow fluctuates between 1.9 mm to 2.2 mm and 1.4 mm to 2.4 mm for WMA fabricated with PG64 and PG76 binders, respectively. In addition, the fracture energy fluctuates between 11.3 J (joule) to 15.1 J and 11.6 J to 14.9 J for WMA prepared with PG64 and PG76 binders, respectively.

Mixture flows are comparable with each other when the effects of compaction and test temperature are investigated. For this purpose, Figure 11 presents the effects of compaction and test temperatures on the flow of WMA (average flow value of mixtures containing 1%, 2% and 3% additive) and HMA samples. The flow of HMA is less when compared to the corresponding value of WMA. This could be as a result of lower binders aging due to use of lower mixing and compaction temperatures of warm mixes. In most cases, the flow results of mixtures tested at 15°C are lower than those of mixtures at 25°C. This is because of higher brittleness of asphalt mixtures at lower temperatures. According to Xiao et al. (2013), the flow (resistance to deformation) can be related to mixture stiffness.

Similar to the flow test results, fracture energy are comparable with each other in terms of test temperatures and binder type. Figure 12 presents the overall effect of binder type, test temperature and additive

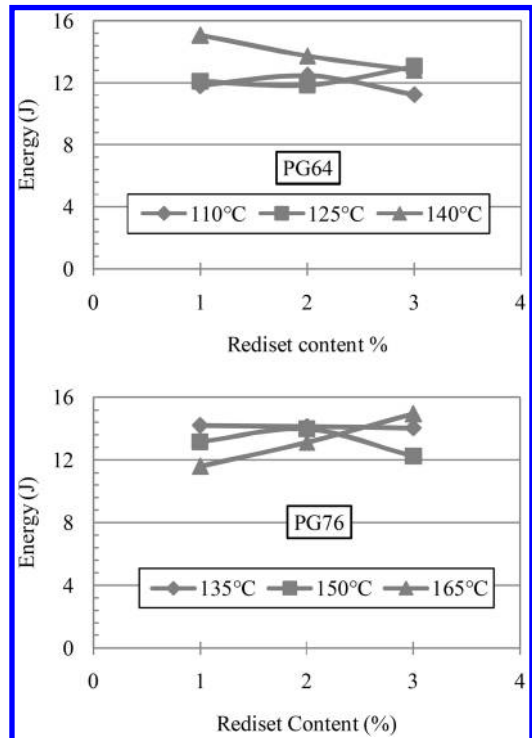


Figure 10. Fluctuation of the fracture energy versus warm additive content at 25°C.

content on the average fracture energy of WMA compacted at different temperatures. The results indicated that test temperature has significant effects on the fracture energy, while the effects of additive content on fracture energy is not significant. Among the different WMA scenarios illustrated in Figure 10, WMA prepared using PG64 binder with 1% additive and tested at 15°C exhibit the highest fracture energy.

3.3 Effects of warm additive contents and compaction temperatures on aged and moisture conditioned samples

Figures 13 and 14 respectively present the combined effects of aging and moisture conditioning on the ITS for PG64 and PG76. In general during the first cycle of conditioning, aging increases the ITS of both WMA and HMA samples, while during the second and third cycles of conditioning, moisture conditioning generally reduces the value of ITS. The ITS of HMA for both binders at different cycle of conditioning is high when compared to the corresponding values of WMA. Regardless of the effects of conditioning cycles, higher compaction temperature of WMA exhibit higher ITS when compared to the ITS of WMA compacted at lower temperatures. Higher warm additive content slightly increases the ITS of PG64-(W110), while higher amount of additive content slightly decreases the corresponding value of PG76-(W135). It implies that there may be an interaction between binder types

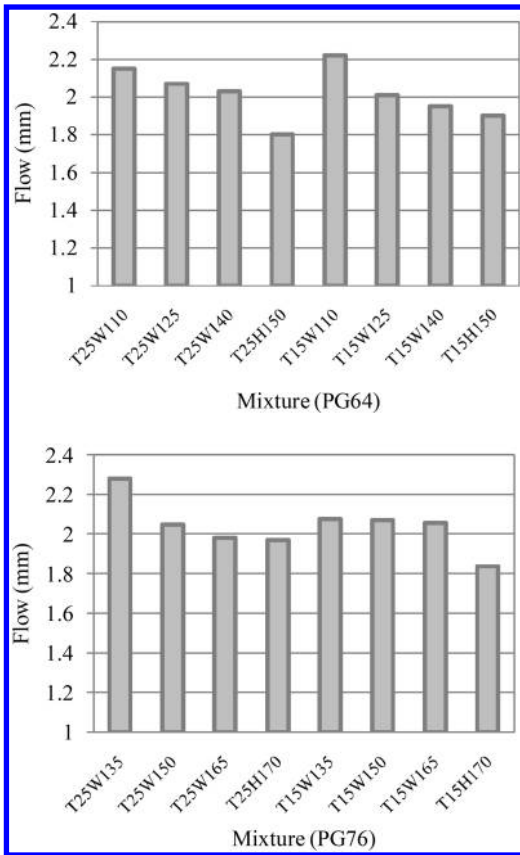


Figure 11. Effects of compaction and test temperature on the flow.

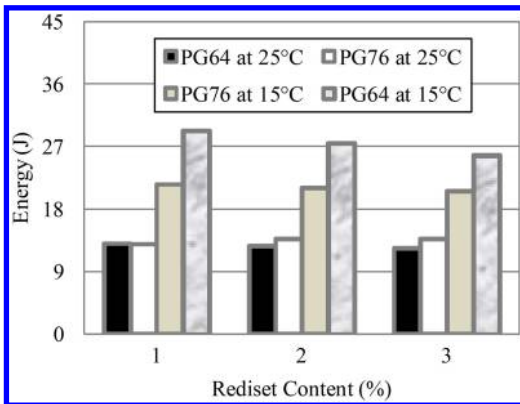


Figure 12. Effect of additive content and test temperature on the fracture energy.

and additive contents. Figure 15 shows the general trend of the effect of aging and moisture conditioning on the average ITS calculated from the ITS of all WMA and HMA samples at each cycle of conditioning. As can be seen, aging increases the ITS of samples

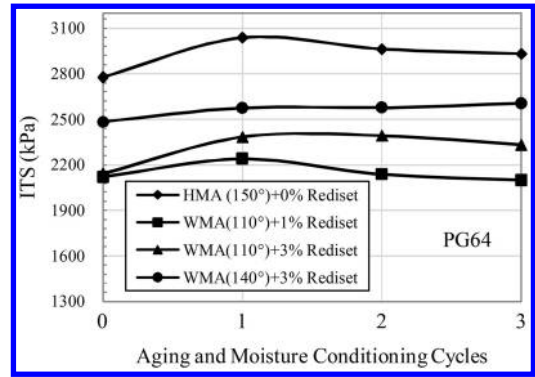


Figure 13. Combined effects of aging and moisture conditioning on the ITS of PG64 mixtures.

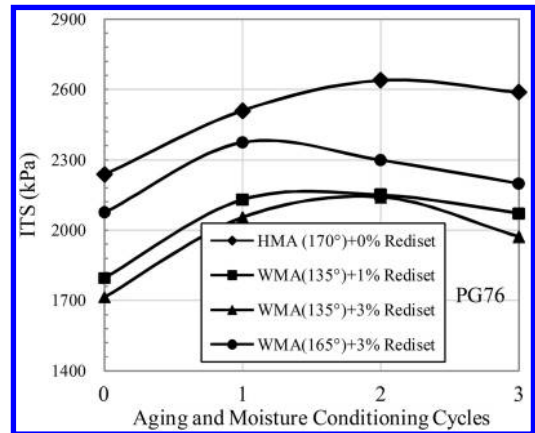


Figure 14. Combined effects of aging and moisture conditioning on the ITS of PG76 mixtures.

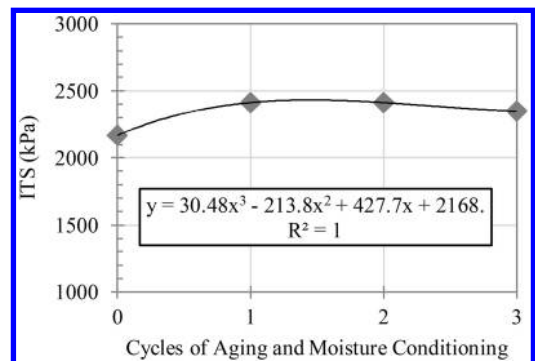


Figure 15. General trend of ITS in different cycles of aging and moisture conditioning.

at the first cycle of conditioning while moisture conditioning reduces the stiffness effect of aging during the second and third cycles of conditioning.

The combined effects of aging and moisture conditioning on flow for PG64 and PG76 mixtures are

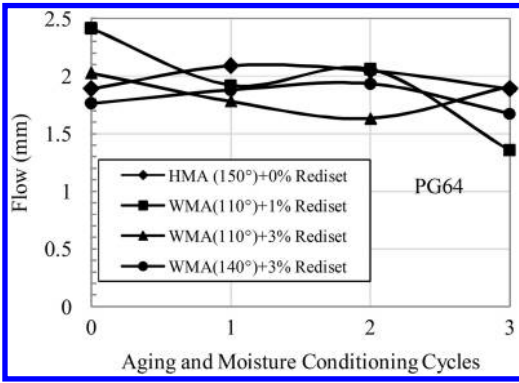


Figure 16. Combined effects of aging and moisture conditioning on the flow of PG64 mixtures.

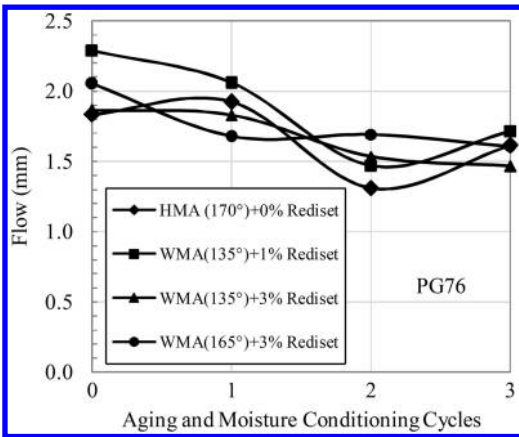


Figure 17. Combined effects of aging and moisture conditioning on the flow of PG76 mixtures.

presented in Figures 16 and 17, respectively. Although, Xiao et al. (2009) used the flow to evaluate the moisture susceptibility analysis of WMA (Xiao et al. 2009), noticeable trend was not observed for the effects of Rediset content as a warm additive on mixture flow during moisture conditioning and aging process. However, moisture conditioning and aging decreased the overall average flow of all WMA and HMA samples at different conditioning cycles as shown in Figure 18. The overall average flow for each cycle of conditioning is calculated using the average of the flow of all WMA and HMA samples at the same conditioning cycle.

Figures 19 and 20 show the combined effects of aging and moisture conditioning on the fracture energy of PG64 and PG76 mixtures, respectively. From the figures, the fracture energy of samples during the first conditioning cycle is higher than the corresponding values for other conditioning cycles. This occurred due to the higher fracture load that is used to break the aged samples. Regardless of the conditioning cycle and binder type, fracture energy of HMA mixtures is high when compared to that of WMA mixtures (except HMA prepared using PG76 at the end of the end of

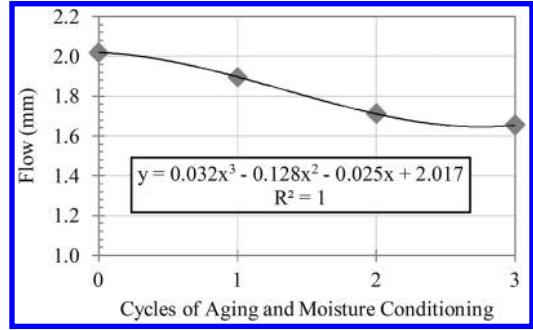


Figure 18. General trend of flow in different cycles of aging and moisture conditioning.

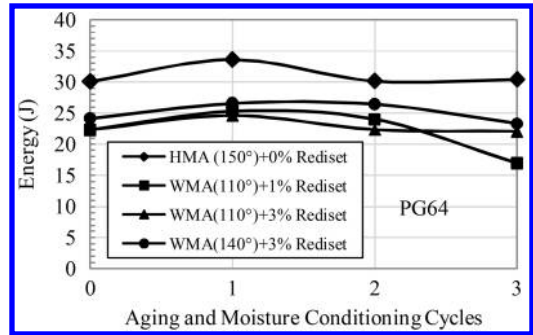


Figure 19. Combined effect of aging and moisture conditioning on the fracture energy of PG64 mixtures.

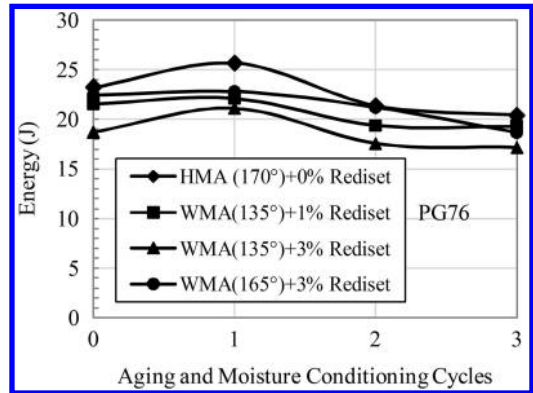


Figure 20. Combined effect of aging and moisture conditioning on the fracture energy of PG64 mixtures.

third conditioning cycle). Fracture energy decreases at end of cycle 2 and 3 due to the damages induced during moisture conditioning. Figure 21 shows the general effects of aging and moisture conditioning on the fracture energy. The maximum fracture energy is observed at the end of cycle one, while the minimum fracture energy is obtained at the end of cycle three. Relationship between fracture energy and ITS of all conditioned and unconditioned samples is illustrated in Figure 22. From the figure, fracture energy increases

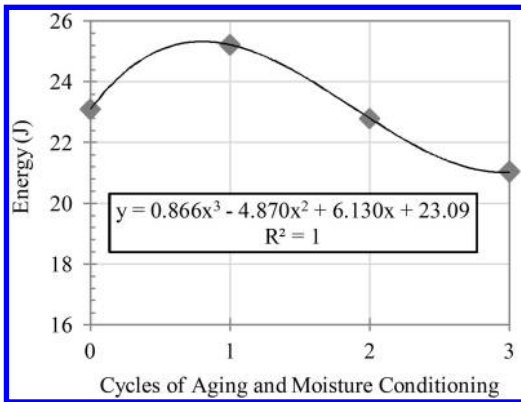


Figure 21. Trend of fracture energy in different cycles of aging and moisture conditioning.

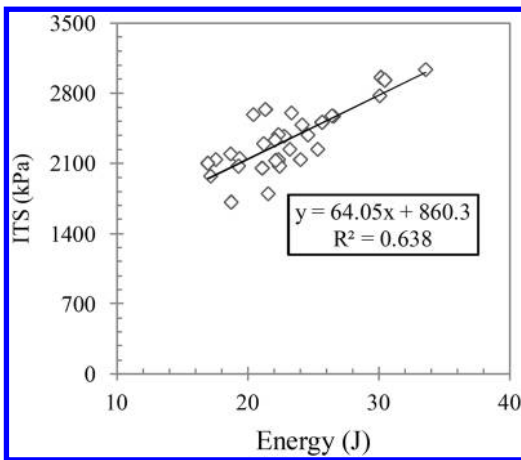


Figure 22. Fracture energy versus ITS in the process of multiple aging and moisture conditioning.

when ITS increases. A linear trend with low R-square is found between sample ITS and fracture energy.

4 CONCLUSIONS

From the results, it can be concluded that aging and moisture conditioning have opposing effects on the stiffness properties of WMA and HMA. Compaction and test temperatures were identified as significant factors that affect the stiffness of asphalt mixtures. Aging increased mix ITS, while moisture conditioning has the reverse effect. Type of moisture conditioning and also asphalt binder type exhibited significant effect on ITS. PG64 mixtures were identified as mixture that is more susceptible to moisture damage when compared to PG76 mixtures. The effects of conditioning using freeze and thaw were greater than other conditioning types without freezing and thawing. The ITS of WMA prepared at higher compaction

temperatures was greater than those fabricated at lower compaction temperatures. Also, the ITS of samples reduced when test temperature increased. No obvious trend was found for the effects of chemical warm additive on flow and fracture energy. The flow of WMA samples for both PG64 and PG76 mixtures decreased when compaction temperature increased. The combined effects of moisture conditioning and aging decreased the overall average flow of all WMA and HMA samples. Test temperature exhibited significant effects on fracture energy of both WMA and HMA. The fracture energy of the samples during the first cycle of conditioning was higher when compared to corresponding values of other conditioned cycles (aged and moisture conditioned samples).

Recently, response surface method (RSM) has been effectively used in asphalt binder and mixture studies as a statistical tool for design of experiments and developing regression models (Hamzah et al. 2013). Therefore, it is recommended to use RSM for evaluation of the combined effects of aging and moisture conditioning on the properties of asphalt mixtures.

ACKNOWLEDGMENTS

The authors would like to acknowledge the Malaysian Ministry of Higher Education that has funded this research project through the Exploratory Research Grant Scheme (ERGS) grant number 203.PAWAM.6730111. Many thanks are also due to the technicians of the Highway Engineering Laboratory at the Universiti Sains Malaysia for their kind assistance.

REFERENCES

- Collop, A. Choi, Y. & Airey, G. 2007. Effects of pressure and aging in SATS test. *Journal of Transportation Engineering* 133: 618–624.
- Copeland, A.R., Youtcheff, J. & Shenoy, A. 2007. Moisture sensitivity of modified asphalt binders: Factors influencing bond strength. *Transportation Research Record: Journal of the Transportation Research Board* 1998: 18–28.
- Jamshidi, A. 2013. Rheological properties of asphalt binders performance and sustainability of warm mixtures asphalt combined Sasobit. Phd thesis, Universiti Sains Malaysia.
- Hamzah, M.O. Golchin, B. & Tye, C.T. 2013. Determination of the optimum binder content of warm mix asphalt incorporating Rediset using response surface method. *Construction and Building Materials*, 47, 1328–1336.
- Hamzah, M.O. Golchin, B. Jamshidi, A. & Chailleux, E. (2014) Evaluation of Rediset for use in warm-mix asphalt: a review of the literatures. *International Journal of Pavement Engineering*, 1–23.
- JKR 2008. Standard Specifications for Road Works, Section 4: Flexible Pavements. Malaysia.
- Khan, R., Grenfell, J., Collop, A., Airey, G. & Gregory, H. 2013. Moisture damage in asphalt mixtures using the modified SATS test and image analysis. *Construction and Building Materials* 43: 165–173.

- Lu, Q. & Harvey, J.T. 2006. Long-term effectiveness of anti-stripping additives: Laboratory evaluation. *Transportation Research Record: Journal of the Transportation Research Board* 1970: 14–24.
- Punith, V. Xiao, F. Putman, B. & Amirkhanian, S.N. 2012. Effects of long-term aging on moisture sensitivity of foamed WMA mixtures containing moist aggregates. *Materials and Structures* 45: 251–264.
- Thomas, K.P. 2002. Impact of water during the laboratory aging of asphalt. *Road materials and pavement design* 3: 299–315.
- Xiao, F. Shivaprasad, P.V. & Amirkhanian, S.N. 2011. Low-Volume road WMA mixtures: moisture susceptibility of mixtures containing coal ash and roofing shingle with moist aggregate. *Journal of Materials in Civil Engineering* 24: 48–56.
- Xiao, F. Punith, V. Amirkhanian, S. & Thodesen, C. 2013. Improved resistance of long-term aged warm-mix asphalt to moisture damage containing moist aggregates. *Journal of Materials in Civil Engineering* 25: 913–922.

Study of warm asphalt additives on bitumen binders and mixture properties

S.K. Nikolova

Patconsult, Sofia, Bulgaria

A.D. Nikolov

Patpribor Construction Materials Testing Laboratory, Sofia, Bulgaria

ABSTRACT: A study was performed of asphalt mixtures produced with low temperature additives using two types of binders delivered from two different refineries. The rheological properties were tested of the binders with and without low temperature additives. It was observed that one of the low temperature additives Sasobit changes the rheological behaviour of the binder. The mechanical properties were tested of the asphalt mixtures produced with neat bitumen as well as bitumen with low temperature additives. The results show that the mechanical properties of the asphalt mixtures prepared with low temperature additives are comparable with those produced with neat bitumen, despite the fact that they were mixed and compacted at lower temperatures.

1 INTRODUCTION

The problem of the production and laying of asphalt mixtures at lower temperatures has been widely discussed in the world (Gonzales 2011, Newcomb 2011, Prowell 2011) as the energy resources necessary for production are limited and non renewable. It is also very important to significantly reduce carbon emissions in order to reduce the impact of greenhouse effect. In Bulgaria these technologies have not gained popularity that's why we have studied the influence of three organic additives for the production of warm asphalt with the most common bitumen and mineral materials in the country.

2 MATERIALS

Two main bitumen have been used

- No. A1 – blown bitumen grade 50/70 and
- No. A2 – distilled bitumen 70/100

Both meet the requirements of CEN EN 12591 Bitumen and bituminous binders.

The mixing of bitumen with additives is accomplished by mechanical stirring at 160°C using a laboratory propeller mixer at 150 rpm. Three additives are used –

- Sasobit – in the amount of 3% (B),
- Evotherm – respectively 0.4% (C) and
- Ceca Base – with 0.5% (D)

Asphalt mixtures were prepared in a laboratory mixer according to BDS EN 12697-35. It is equipped with a heater with a thermostatic control, which allows the maintenance of the required mixing temperature.

Compaction is carried out according to BDS EN 12697-30 at the appropriate temperature with 75 blows on each side.

3 TEST METHOD

- a) The neat bitumen and the binders with the additives for warm asphalt are tested according to BDS EN 12591;
- b) A dynamic viscosity in a temperature range of 80–170°C (BDS EN 13302);
- c) Complex modulus $G^*/\sin \delta$ (ASTM 7175-08) with Dynamic Shear Rheometer;
- d) The asphalt concrete mixes were tested according to BDS EN (13108-1/NA).

4 EXPERIMENTAL RESULTS

Table 1 and 2 show the test results of the properties according to the requirements of BDS EN 12591.

From the results it can be concluded that the additives Evotherm and Ceca Base do not substantially change the basic properties of bitumen, while Sasobit decreases the penetration and raises the softening temperature. Both bitumen have changed their grades and from 50–70 and 70–100, bitumen with this additive became 35–50 grade, as well as the softening point of both bitumen exceeds the requirements.

Differences in the additives influence is due to the differences in their nature. Sasobit has a direct influence on the characteristics of the bitumen, depending on the crystallization of the paraffin contained therein. Evotherm and Ceca Base are chemical additives and they influence the interaction between bitumen and

Table 1. Test results of blown bitumen, grade 50/70.

Characteristics	Test method	Binders			
		A1	A1B	A1C	A1D
Needle penetration 25°C, 0.1 mm	BDS EN 1426	59	40	58	57
Softening point, °C	BDS EN 1427	51.8	83.9	52.2	51.2
Breaking point, °C	BDS EN 12593	-11	-11	-12	-11
Change of mass, %	BDS EN 12607-1	0.5	0.15	0.22	0.18
Retained penetration after Rolling Thin Film Oven Test, %	BDS EN 12607-1	72.4	69.5	74.9	75.6

Table 2. Test results of distilled bitumen, grade 70/100.

Characteristics	Test method	Binders			
		A2	A2B	A2C	A2D
Needle penetration 25°C, 0.1 mm	BDS EN 1426	73	47	74	72
Softening point, °C	BDS EN 1427	48.3	82	49	48.5
Breaking point, °C	BDS EN 12593	-15	-14	-15	-15
Change of mass, %	BDS EN 12607-1	0.45	0.38	0.41	0.28
Retained penetration after Rolling Thin Film Oven Test, %	BDS EN 12607-1	68.9	71.3	70.5	72.3

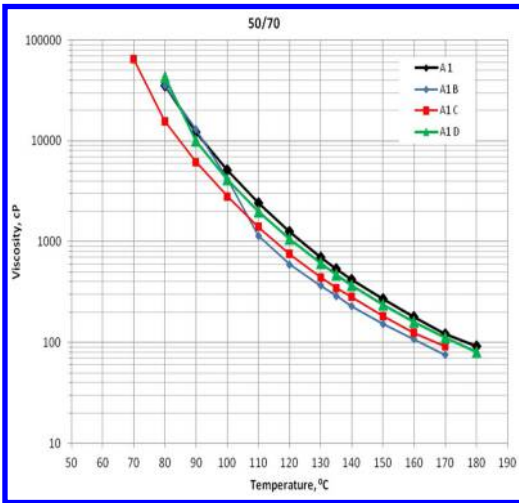


Figure 1. Binders viscosity dependence on the temperature of blown bitumen, grade 50/70.

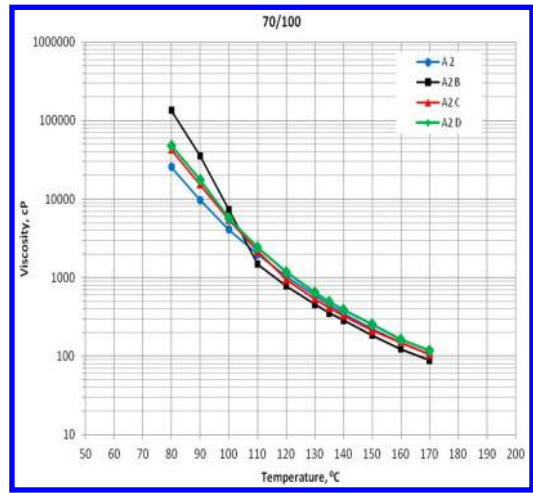


Figure 2. Binders viscosity dependence on the temperature of distilled bitumen, grade 70/100.

aggregates by improving chemical adhesion between them.

The determination of the optimum technological temperatures is performed by examining the temperature influence on the viscosity of the binders. The tests were carried out in the range from 80 to 160°C with rheoviscometer with rotating spindle according to BDS EN 13302. Test results for the temperature influence on viscosity are presented in Figures 1 and 2.

The test results of binders with additives Evotherm and Ceca Base showed no difference in viscosity compared to the neat bitumen in the tested interval of temperatures. It can be determined from Fig. 3 that bitumen containing 3% Sasobit reaches viscosity of

0.2 Pas, at temperature, which is with about 6°C less than the compared neat bitumen. As it is apparent from Tables 1 and 2 the bitumen with Sasobit changes its grade to 35/50. This is a prerequisite that the viscosity characteristics of this modified binder should be compared with the viscosity characteristics of a binder with grade 35/50. In that case the temperature difference between the temperatures at which both binders reach viscosity of 0.2 Pas will be much more.

The influence of additives on the warm asphalt over the complex modulus has been studied.

The tests were performed at 60°C in their linear viscoelastic area. The results are presented graphically in Figure 3.

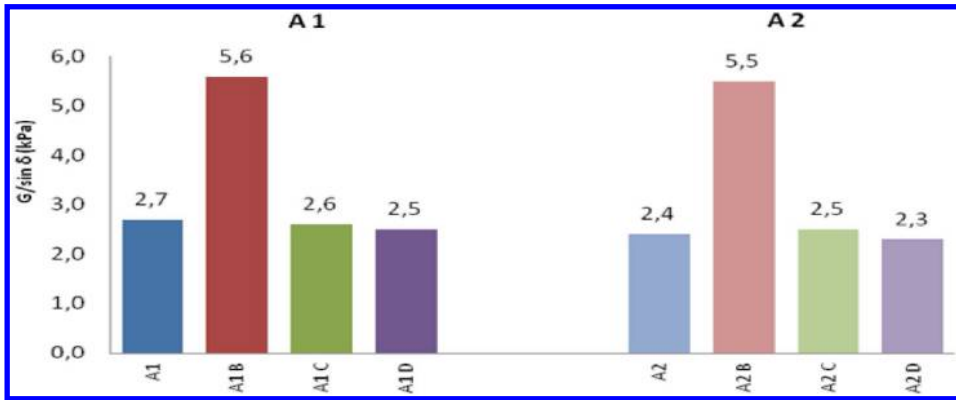


Figure 3. Complex modulus of binder with additives and without additives for warm asphalt.

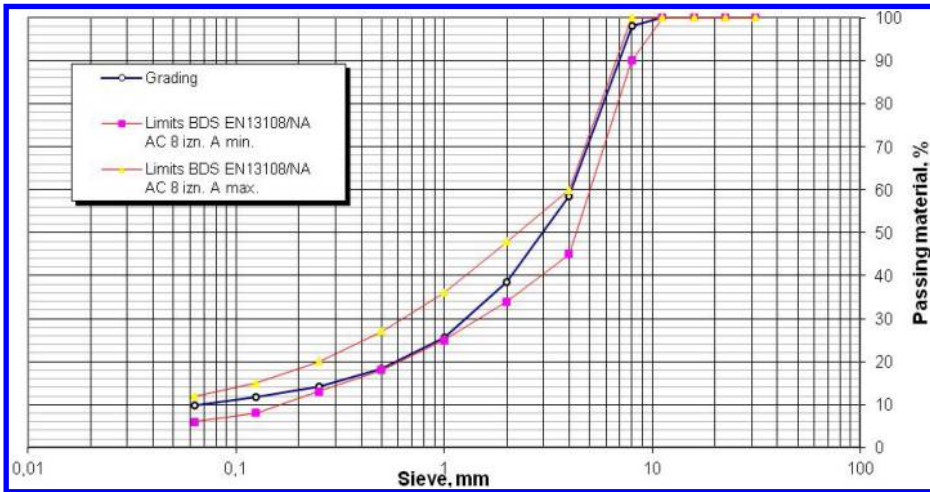


Figure 4. Sieving curve.

Table 3. Results from the tests of asphalt-concrete mixtures with additive Sasobit for warm asphalt compacted at different temperatures.

Characteristics	Test method	Asphalt mix with Bitumen A1 compacted at 150°C	Asphalt mix with SASOBIT, compacted at temperatures:		
			115°C	125°C	135°C
Maximum density, Mg/m ³	BDS EN 12697-5	2.465	2.467	2.464	2.467
Bulk density, Mg/m ³	BDS EN 12697-6	2.416	2.381	2.399	2.403
Voids in mineral aggregates, %	BDS EN 12697-8	14.6	15.9	15.1	15.1
Air voids, %	BDS EN 12697-8	2.0	3.5	2.6	2.6
Marshall stability, kN	BDS EN 12697-34	8.6	7.6	8.1	8.6
Flow, mm	BDS EN 12697-34	3	2.5	2	2.2
Water sensitivity, %	BDS EN 12697-12	95		96	

It is evident that Sasobit has influence on rheological behavior by increasing the value of $G^*/\sin\delta$ 1.8, while the other additives do not affect this indicator.

Test asphalt mixtures were prepared according to the following recipe:

- Mineral material, size 4/8 mm – 40%
- Mineral material, size 0/4 mm – 54%

- Mineral filler – 6%
- Content of binder – 5.5% to 100% mineral aggregate (5.2% to 100% of the mixture).

Asphalt mixtures with additives for warm asphalt have been compacted at 115°C, 125°C and 135°C, and the control sample with basic bitumen D1 has been compacted at 150°C.

Table 4. Results of asphalt mixture tests with additive Evotherm for warm asphalt compacted at different temperatures.

Characteristics	Test method	Asphalt mix with Bitumen A1 compacted at 150°C	Asphalt mix with EVOTHERM, compacted at temperatures:		
			115°C	125°C	135°C
Maximum density, Mg/m ³	BDS EN 12697-5	2.475	2.474	2.474	2.474
Bulk density, Mg/m ³	BDS EN 12697-6	2.416	2.374	2.376	2.413
Voids in mineral aggregates, %	BDS EN 12697-8	14.9	16.4	16.3	15.0
Air voids, %	BDS EN 12697-8	2.4	4.0	4.0	2.5
Marshall stability, kN	BDS EN 12697-34	8.6	6	7.5	8.5
Flow, mm	BDS EN 12697-34	3	3.1	2.9	3.1
Water sensitivity, %	BDS EN 12697-12	95		97	

Table 5. Results of asphalt mixture tests with the additive for warm asphalt Ceca Base compacted at different temperatures.

Characteristics	Test method	Asphalt mix with Bitumen A1 compacted at 150°C	Asphalt mix with CECABASE, compacted at temperatures:		
			115°C	125°C	135°C
Maximum density, Mg/m ³	BDS EN 12697-5	2.471	2.468	2.470	2.469
Bulk density, Mg/m ³	BDS EN 12697-6	2.416	2.385	2.402	2.407
Voids in mineral aggregates, %	BDS EN 12697-8	14.8	15.8	15.2	15.0
Air voids, %	BDS EN 12697-8	2.2	3.4	2.8	2.5
Marshall stability, kN	BDS EN 12697-34	8.8	6.5	6.9	7.5
Flow, mm	BDS EN 12697-34	3.1	2.7	2.9	3.0
Water sensitivity, %	BDS EN 12697-12	95		94	

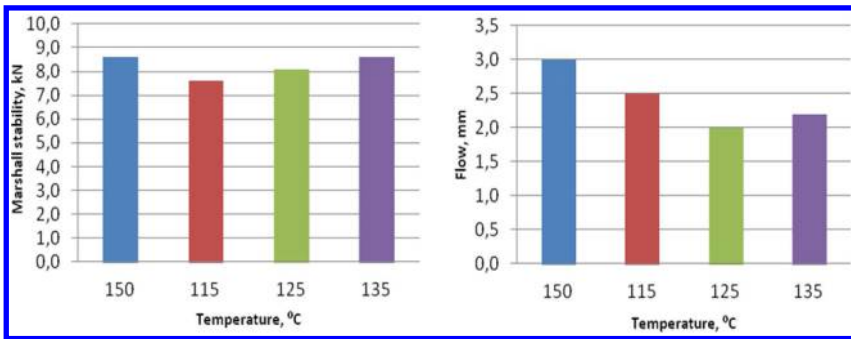


Figure 5. Dependence of Marshall stability and flow of asphalt mixtures with and without additive for warm asphalt Sasobit on temperature compaction.

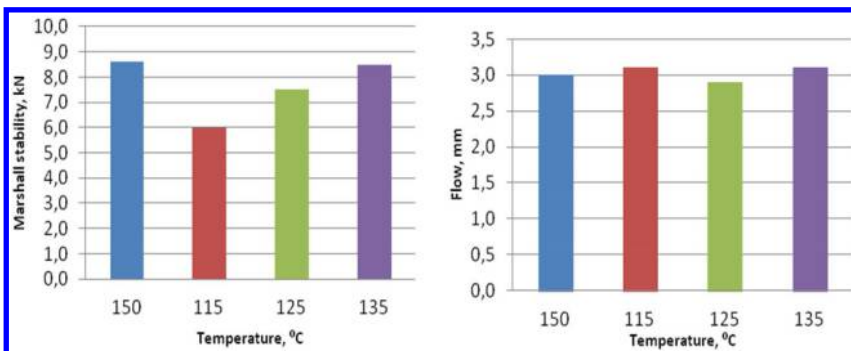


Figure 6. Dependence of Marshall stability and flow of asphalt mixtures with and without additive for warm asphalt Evotherm on temperature compaction.

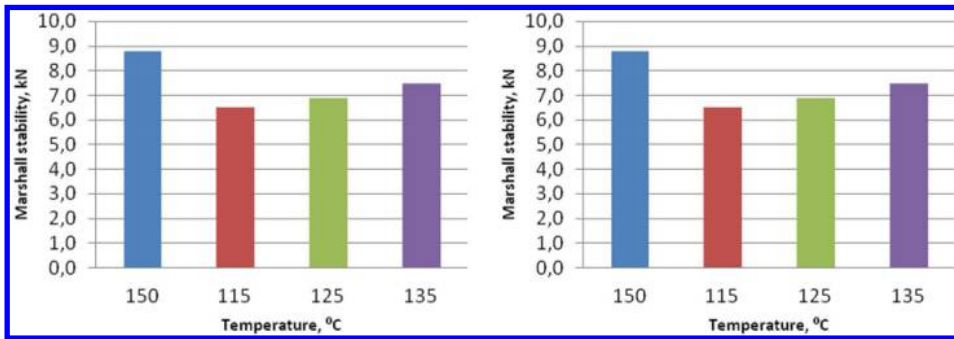


Figure 7. Dependence of Marshall stability and flow of asphalt mixtures with and without additive for warm asphalt Ceca Base on temperature compaction.

The results are presented in Tables 3, 4 and 5 and Fig. 5, 6 and 7.

5 CONCLUSIONS

Regardless of the technology of production of bitumen the additives for the production of warm asphalt reacted in the same manner.

From the three tested additives only Sasobit significantly changes the physico-chemical and rheological properties of bitumen, and bitumen modified with this additive changes to a harder grade bitumen.

The asphalt mixtures produced and compacted at lower temperatures with additives for warm asphalt show comparable physico-mechanical properties to asphalt mixtures produced and compacted at standard temperatures with neat bitumen.

REFERENCES

ASTM 7175-08 Standard Test Method for Determining the Rheological Properties of Asphalt Binder Using Dynamic Rheometer.
 BDS EN 1426 Bitumen and bituminous binders – Determination of needle penetration
 BDS EN 1427 Bitumen and bituminous binders – Determination of the softening point – Ring and Ball method.
 BDS EN 12591 Bitumen and bituminous binders – Specifications for paving grade bitumens
 BDS EN 12593 Bitumen and bituminous binders – Determination of the Fraass breaking point.

BDS EN 12607-1 Bitumen and bituminous binders – Determination of the resistance to hardening under the influence of heat and air – Part 1: RTFOT method.
 BDS EN 12697-5 Bituminous mixtures – Test methods for hot mix asphalt – Part 5: Determination of the maximum density.
 BDS EN 12697-6 Bituminous mixtures – Test methods for hot mix asphalt – Part 6: Determination of bulk density of bituminous specimens.
 BDS EN 12697-8 Bituminous mixtures – Test methods for hot mix asphalt – Part 8: Determination of void characteristics of bituminous specimens.
 BDS EN 12697-12 Bituminous mixtures – Test methods for hot mix asphalt – Part 12: Determination of the water sensitivity of bituminous specimens.
 BDS EN 12697-30 Bituminous mixtures – Test methods for hot mix asphalt – Part 30: Specimen preparation by impact compactor.
 BDS EN 12697-34 Bituminous mixtures – Test methods for hot mix asphalt – Part 34: Marshall test.
 BDS EN 12697-35 Bituminous mixtures – Test methods for hot mix asphalt – Part 35: Laboratory mixing.
 BDS EN 13302 Bitumen and bituminous binders – Determination of dynamic viscosity of bituminous binder using a rotating spindle apparatus.
 BDS EN 13108-1/NA Bituminous mixtures – Part 1: Asphalt concrete National Annex.
 Gonzales, J. A., Ligier, S., Grampre, L. (spring 2011). Warm Mix Asphalts with chemical additives, *EER N18*, 14–20.
 Newcomb D. (spring 2011). Warm Mix Asphalt. *European roads, Review, EER N18*, 4–5.
 Prowell B. D., Hurley G. C., Frank B. (2011). *Warm-Mix Asphalt: Best Practices, 2nd Edition, NAPA*.

Evaluation of fracture resistance of WMA mixes using semi-circular bending test

Srinivas F. Chitragar

Department of Civil Engineering, Basaveshwar Engineering College, Bagalkot, India

Dharamveer Singh

Department of Civil Engineering, Indian Institute of Technology, Bombay, India

ABSTRACT: The present study was undertaken to evaluate fracture resistance of Hot Mix Asphalt (HMA) and Warm Mix Asphalt (WMA) using Semi-Circular Bending (SCB) test. Two different WMA additives, one wax based (Sasobit®) and one chemical based (Evotherm®) were selected in this study. A dense graded asphalt mix with 19 mm nominal maximum aggregate size was designed in the laboratory using Marshall mix design method. The SCB samples of 150 mm diameter and 50 mm height with different notch depths: 20 mm, 25 mm and 32 mm were prepared in the laboratory with target air voids in range of $6.5 \pm 0.5\%$. The samples were tested by applying monotonic load at a rate of 0.5 mm/min at 35°C. The following parameters were estimated for each of the mixes: J-Integral or J_c , strain energy at failure, peak load at failure, and deformation at failure. It was found that the strain energy and peak load of all the mixes decrease with an increase in notch depth. The deformation at failure did not exhibit a clear trend with notch depth, it may be because of initiation of crack, which depends on aggregates geometry, mastic and orientation of the samples. The strain energy of WMA- Evotherm®(WMA-E) mix was found to be the highest followed by HMA and WMA- Sasobit®(WMA-S). The load at failure was found to be the highest for WMA-E and HMA mix, at 20 mm and 32 mm notch depths, compared to WMA- S mix. The deformation at failure was observed to be maximum for WMA- E. A large deformation at failure indicates a ductile behaviour of a mix. The J_c value for HMA, WMA- S and WMA- E mixes was found to be 0.21, 0.20, and 0.12 kJ/m², indicating that both HMA and WMA- S mixes performed equally good, whereas, WMA- E mix had a poor fracture resistance.

Keywords: warm mix, hot mix, semi circular bending, strain energy, Marshall mix design

1 INTRODUCTION

The use of warm mix asphalt (WMA) is gaining worldwide popularity in highway industry (Hurley and Prowell, 2006). The WMA additives (organic additives, chemical additives and foaming) can result in decrease in mixing and compaction temperatures of a mix, hence, saving in fuel consumption and less environmental pollution. It has been reported that WMA mixes perform equally good as compared to hot mix asphalt (HMA). However, there are still concerns on fatigue and fracture resistance of WMA mixes. Fracture of asphalt mixes can lead to premature failure of a pavement, and consequently a poor riding quality. Thus, it becomes essential to characterize fracture resistance of asphalt mixtures in laboratory during mix design stage (Ying et al., 2013). Several laboratory test methods namely, four point beam bending, indirect tensile test combined with dissipated creep strain energy (DCSE), disc shaped compact tension (DCT), Texas overlay tester (OT), direct tension based on viscoelastic continuum damage theory, and semicircular

bending (SCB), have been developed to evaluate fracture resistance asphalt mixes. The complexity of a test method, repeatability, reproducibility, and requirement of a skilled labour, time requirements are the major difficulties associated with each of the test. Among all available test methods, SCB is a fast, simple, reliable, and repeatable test, and does not require complicated set up. It was reported that critical energy release rate (J-integral or J_c) obtained from this test can be used as an indicator of resistance to fracture. A higher J-integral value indicates a stiffer mix, resulting in a better fracture resistance and vice versa.

The SCB test is preferred by many researchers due to ease in sample preparation, testing procedure, repeatability (Li et al., 2010; Huang et al., 2005; Mull et al., 2002; Wu et al., 2005; Xiang et al., 2010; Mostafa et al., 2012; Hao, et al., 2013) evaluated performance of asphalt mixes with different percentages of RAP using SCB test. It was reported that addition of RAP decreases failure load in SCB test, resulting in reduced strain energy and J-integral. The results show that addition of RAP with decrease fracture resistance of a mix.

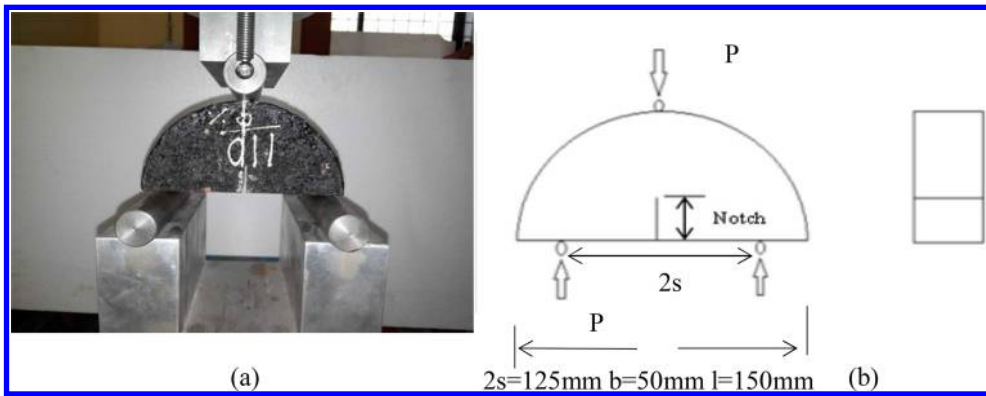


Figure 1. (a) Semi-circular bending test setup and (b) Schematic diagram of SCB test setup.

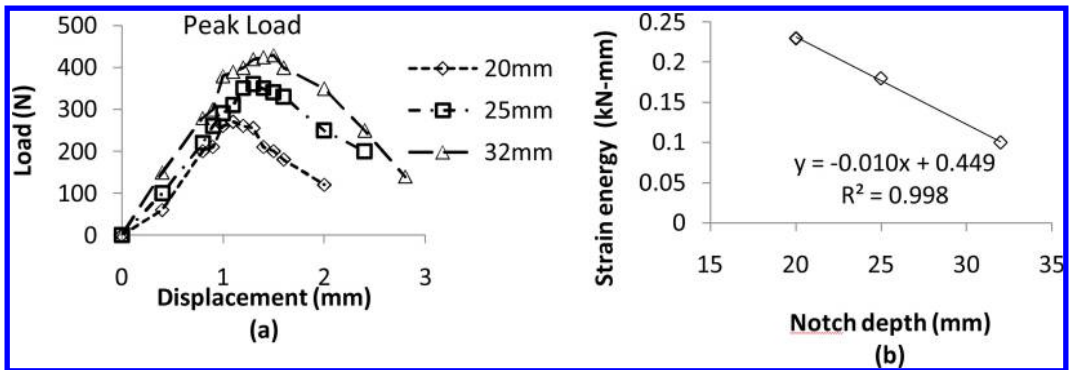


Figure 2. (a) Load vs vertical deformation graph and (b) Plot of notch depth and strain energy at failure.

Baoshan et al., (2005) used SCB and IDT test to evaluate fracture resistance of mixes with different percentages of RAP. The SCB tensile strength was approximately 3.8 times to the IDT strength. Overall, the literature review show that SCB can be a potential laboratory test to evaluate fracture resistance of asphalt mixes. It is a fast, simple, reliable, and repeatable test. However, limited attempts were found in the literature to assess the fatigue resistance of WMA mixes in the laboratory using SCB.

The present study was undertaken to evaluate fracture resistance of WMA mixes using Semi-circular bending test. Two WMA additives, one wax based (Sasobit®) and one chemical based (Evotherm®) were selected along with conventional HMA mixes were selected in this study.

2 OVERVIEW OF SEMI-CIRCULAR BENDING TEST

The SCB test is preferred by many researchers (Li et al., 2010; Huang et al., 2005; Mull et al., 2002; Wu et al., 2005; Xiang et al., 2010; Mostafa et al., 2012; Hao, et al., 2013) The Figure 1 (a) shows set up of SCB test, and its schematic is presented in Figure 1(b). A semi-circular sample is subjected to a load at a rate of

0.5 mm/min in a three point bending load configuration. The strain energy (U) to failure strain is estimated from load versus vertical deformation graph Figure 2 (a). A plot of notch depth and strain energy at failure is drawn, and slope of the line “ (du/da) ” is estimated as shown in Figure 2 (b). Thereafter, J_c is estimated from Equation (1).

The critical energy release rate (J-integral or J_c) obtained from this test can be used as an indicator of resistance to fracture. A higher J-integral value indicates a stiffer mix, resulting in a better fracture resistance and vice versa.

The J-Integral is then estimated using Eq. (1)

$$J_c = - \left(\frac{1}{b} \right) \left(\frac{dU}{da} \right) \quad (1)$$

where, J_c = critical value of J-Integral, kN/mm²,
 b = thickness of specimen, mm, a = notch depth, mm,
and U = strain energy, N-mm.

3 METHODOLOGY

The Figure 3 shows the methodology and experimental plan. The project started with materials collection, mix design, and performance evaluation of mixes in

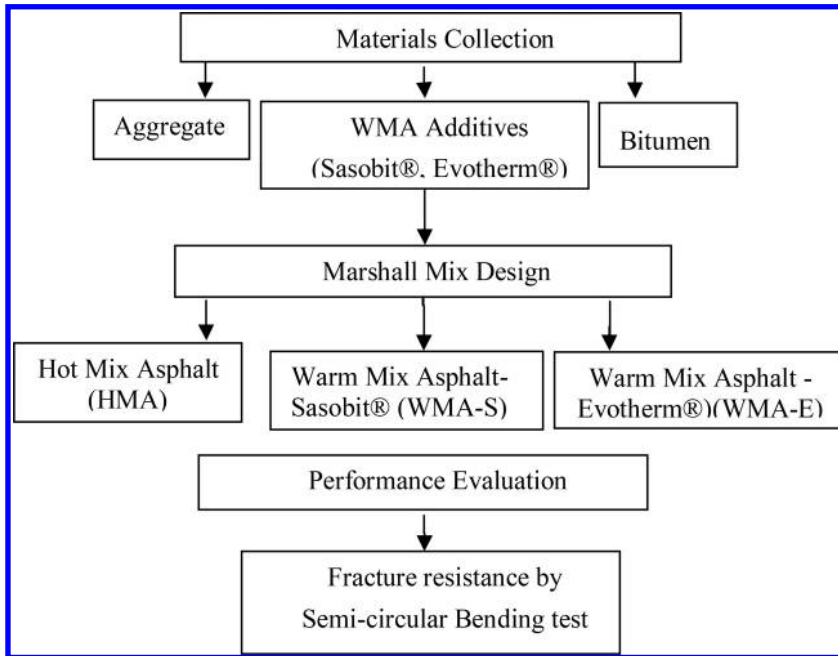


Figure 3. Flow chart of methodology.

laboratory. The detail discussion on each of the task is presented below.

3.1 Materials collection

The aggregates of different sizes: 20 mm and 10 mm down and stone dust were collected from J.M. Mhatre Infra Private Limited near Navi Mumbai. The aggregates were a basaltic rock with dark grey colour. The asphalt binder sample of viscosity grade (VG) was collected from Hindustan Colas Limited, Mumbai. The VG30 binder is generally used for construction of flexible pavements in India as per Indian Road Congress specification.

3.2 WMA additives

3.2.1 Sasobit®

Sasobit® is a long chain aliphatic hydrocarbon compound with chain lengths of 40–115 carbon atoms, derived from Fischer-Tropsch process. It reduces mixing and compaction temperature by 18–54°C (Gandhi and Amirkhani 2007; Hurley and Prowell 2005; Qin et al. 2014). Typically Sasobit® can be added at the rate of 1.5% to 2% by weight of asphalt (Gandhi and Amirkhani 2007; Hurley and Prowell 2005; Qin et al. 2014).

3.2.2 Evotherm®

Evotherm® is a product of MeadWestvaco Asphalt Innovations, Charleston, SC (Button et al., 2007). The product enhances the mix workability at lower temperatures (Prowell and Hurley, 2007), up to 56°C (Corrigan, 2011).

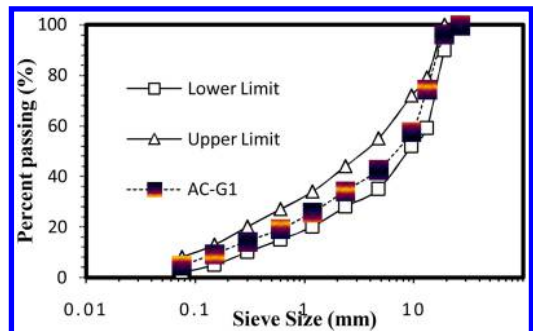


Figure 4. Gradation curve for AC.

3.2.3 Marshall mix design

In this study, asphalt concrete (AC) with nominal maximum aggregate size of 19 mm, and gradation shown in Figure 4 was designed (MoRTH 2013) using Marshall mix design.

First the HMA mix was designed (ASTM D6926). The mix samples were compacted with bitumen content in range of 4.5% to 6.5% of an interval of 0.5%. First, approximately 1200 gm of different sizes of aggregates and filler as an anti-stripping agent (lime) as per the blended design gradation were mixed and heated at the temperature 170–190°C. The required amount of bitumen was then heated at 150°C and mixed with aggregates. The Marshall samples of 100 mm diameter and 62.5 mm height were compacted with 75 blows on either side at compaction temperature ranging from 130–150°C. The Marshall samples were prepared at each of the bitumen content and their volumetric properties were determined.

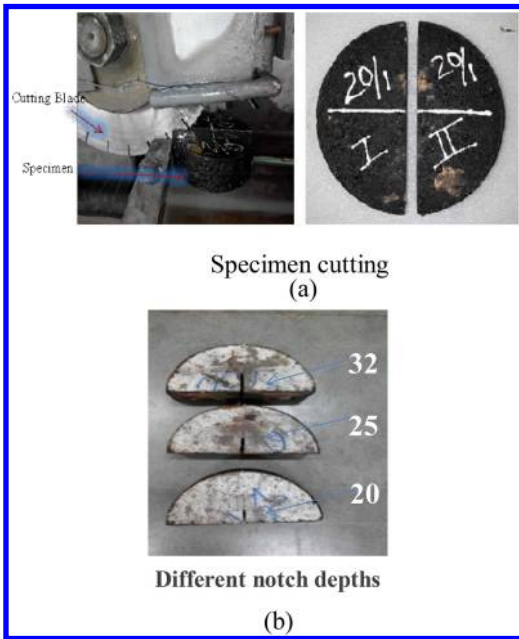


Figure 5. (a) Cutting of 150 mm circular specimen into two semicircle and (b) Different notch sizes of specimen.

The bitumen content of a mix was found by taking the average of bitumen content corresponding to maximum stability, maximum unit weight and 4% air voids and found to be 5.63%. The WMA mixes were prepared by addition 2% Sasobit® and 0.5% Evotherm®, keeping OBC percentage same as HMA mix. The only change was lower mixing and compaction temperatures for WMA mixes. The temperature for both WMA mixes was kept in range of 100–130°C.

3.2.4 SCB sample preparation and testing

The samples of 150 mm in diameter and 50 mm in height were compacted using Marshall Compactor machine with target air voids in range of $6.5 \pm 0.5\%$. Desired air voids was achieved by varying the number of blows by trial and error method.

The circular specimen of 150 mm in diameter was cut into two semi-circular halves as shown in Figure 5 (a). Three different notch depths: 20 mm, 25 mm and 32 mm with ± 1 mm to clearance and width 2 ± 0.5 mm were created in semi-circular samples shown in Figure 5 (b). The test was conducted by applying a load at a rate of 0.5 mm/min in a three point bending load configuration at 35°C.

4 RESULTS AND DISCUSSION

Figures 6 to 10 show variations of failure load, vertical deformation at failure and strain energy at failure, strain energy versus notch depth, and J_c for HMA, WMA with 2% Sasobit® (WMA-S) and, WMA with 0.5% Evotherm® (WMA-E) for 20 mm, 25 mm, and

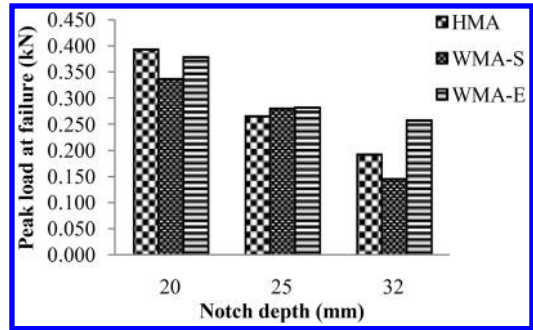


Figure 6. Load at failure for HMA and WMA mixes for different notch depths.

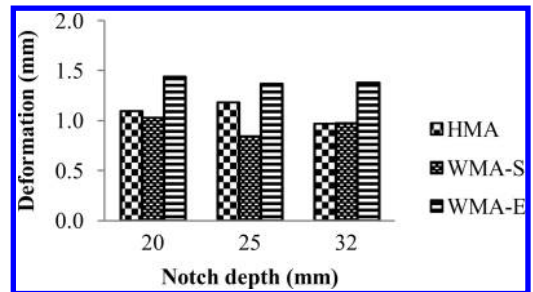


Figure 7. Vertical deformation at failure for HMA and WMA mixes for different notch depths.

32 mm notch depths, respectively, for target air voids in range of $6.5\% \pm 0.5\%$.

4.1 Load at failure

The Figure 6 shows variations of load at failure for HMA and WMA mixes, estimated at 20 mm, 25 mm and 32 mm notch depths. In general, it can be seen that the load at failure decreases with an increase in the notch depth for all types of mixes. The comparison of load at failure for different mixes depends on notch depth and type of a mix. No clear trend in peak load at failure was observed. For example, at 20 mm notch depth both HMA showed higher load at failure, while at 25 mm notch depth all the mixes shows almost same load at failure, and at 32 mm notch depth WMA-E showed maximum value. Overall, at 20 mm and 32 mm notch depths, WMA-E mix showed higher load at failure compared to WMA-S. However, it should be noted that variation in load at failure depends on aggregates orientation, geometry, and initiative of crack. Thus, the magnitude of load at failure may not be a right parameters to judge the strength potential of a mix.

4.2 Vertical deformation at failure

The Figure 7 shows variations of vertical deformation at failure for HMA, WMA-S and WMA-E mixes, estimated at 20 mm, 25 mm and 32 mm notch depths. Overall, vertical deformation for WMA-E mix was higher compare to HMA and WMA-S mix for all

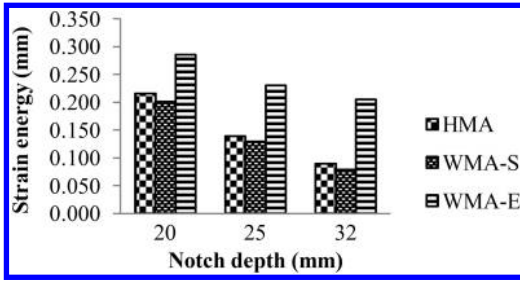


Figure 8. Variation of strain energy at failure for HMA and WMA mixes for different notch depths.

notch depths which shows mix with chemical additives bring ductile behavior in a mix. No trend was observed between notch depth and deformation at failure. The HMA and WMA-S mixes shows almost similar vertical deformation to failure at 20 mm and 32 mm notch depth, indicating that addition of Sasobit® did not result in any significant change in ductile behaviour of a mix. This was not expected, as addition of a wax based additive expected to impart ductile behaviour. On the contrary, at 25 mm notch depth, HMA shows high deformation compared to WMA-S mix. It is assumed that preparation of sample, distribution of aggregates and asphalt binder resulted in heterogeneous mixes, and hence crack initiates randomly for different types of notches and resulted in a different pattern for different mixes.

4.3 Comparison of strain energy at failure

The strain energy at failure was calculated from a graph plotted between load and vertical deformation. The area of curve up to peak load was calculated and reported as strain energy. The Figure 8 shows variations of strain energy at failures for HMA and WMA mixes, estimated at 20 mm, 25 mm and 32 mm notch depths. It can be seen that the strain energy at failure decreases with an increase in the notch depth for all types of mixes. At all the notch depths, it was found that the strain energy was high for WMA-E mix compared to HMA and WMA-S mixes. The strain energy remains almost similar for both HMA and WMA-S mixes for all notch depths indicating that HMA mix is equal to WMA-S mix.

The change in strain energy with notch depth for different types of mixes is also plotted in Figure 9. A straight line was fit to estimate slope of this line “(dU/da)” which was used further to estimate critical energy release rate, also called the critical value of J-Integral or J_c . The rate of decrease in strain energy is lower for WMA-E compared to HMA and WMA-S indicating that a mix with WMA-E fails gradually.

4.4 Critical energy release rate- J_c

The Figure 10 shows comparison of Critical Energy Release Rate- J_c for HMA, WMA-S and WMA-E mixes. It can be seen from this graph that J_c values for

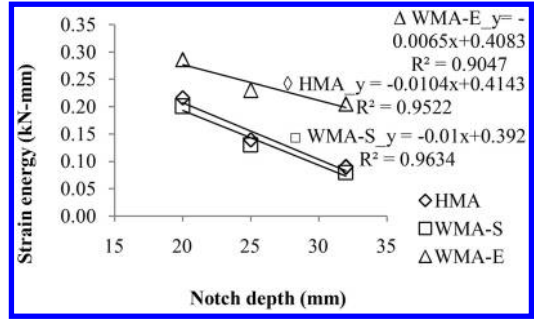


Figure 9. Change in strain energy at failure for HMA and WMA mixes for different notch depths.

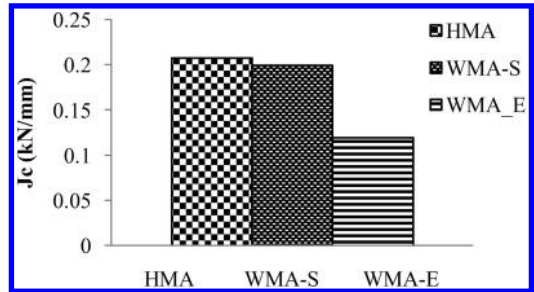


Figure 10. Comparison of critical energy release rate- J_c for HMA and WMA mixes.

HMA mix was the highest compared to WMA mixes. For example, J_c value for HMA, WMA- S and WMA-E mixes was found to be 0.21, 0.2, and 0.12 kJ/m², indicating that both HMA and WMA- S mix performed equally good, whereas, WMA- E mix had a poor fracture resistance. The results show that HMA mixes stronger and more fracture resistance compared to WMA mixes containing Evotherm®.

5 CONCLUSIONS

The present study evaluates fracture resistance property for HMA and WMA mixes with wax (Sasobit®, WMA-S) and chemical (Evotherm®, WMA-E) based additives using semi circular bending test. The following conclusions can be drawn based on the results and discussion presented above.

- The strain energy and peak load of all the mixes tested decreases with an increase in notch depth. However, deformation at failure did not exhibit a clear trend with change in notch depths.
- The strain energy of WMA- Evotherm®mixes was found to be highest followed by HMA and WMA-Sasobit®.
- The J_c value for HMA, WMA- Sasobit® and WMA-Evotherm® mixes was found to be 0.21, 0.2, and 0.12 kJ/m², indicating that both HMA and WMA-Sasobit® mixes performed equally good, whereas, WMA- Evotherm® mix had a poor fracture resistance.

ACKNOWLEDGEMENTS

The authors would like to thank undergraduate students for their help during experimental work and friends who helped and supported in all stages of this work.

REFERENCES

- ASTM D6926. "Standard Practice for Preparation of Bituminous Specimens Using Marshall Apparatus," ASTM International, West Conshohocken, PA, 2010,
- Baoshan Huang., Xiang Shu and Yongjing Tang. (2005). Comparison of Semi-Circular Bending and Indirect Tensile Strength Tests for HMA Mixtures. *Advances in Pavement Engineering*.
- Button, J. W., C. Estakhri, and A. Wimsatt. (2007). A Synthesis of Warm-Mix Asphalt. Publication FHWA/TX-07/0-5597-1, FHWA and Texas Department of Transportation.
- Corrigan, M. (2011). Warm Mix Asphalt Technologies and Research. Federal Highway Administration, <http://www.fhwa.dot.gov/pavement/asphalt/wma.cfm>. (Last accessed July 2012).
- Gandhi, T. S., and Amirghanian, S. N. (2007). Laboratory investigation of warm asphalt binder properties – a preliminary analysis. The fifth international conference on maintenance and rehabilitation of pavements and technological control (MAIREPAV5), Park City, Utah, USA, 475–80.
- Hao Ying., Mostafa A.E., Louay N.M., and Heshmat A.A. (2013). A Crack Propagation Model for Asphalt Mixtures Based on the Cyclic Semi-Circular Bending Test. 92nd Transportation Research Board Annual Meeting, Washington, D.C.
- Huang, B., Shu, X. and Tang, Y. (2005). Comparison of semi-Circular Bending and Indirect Tensile Strength Tests for HMA Mixtures, *Advances in Pavement Engineering*.
- Hurley, G. C., and Prowell, B. D. (2005). Evaluation of Sasobit® for Use in Warm Mix Asphalt.
- Hurley, G. C. and B. D. Prowell (2006). Evaluation of Evotherm® for Use in Warm Asphalt Mixes. NCAT Report No. 06-02, National Center for Asphalt Technology, Auburn, Alabama
- Hurley, G. C. and B. D. Prowell. (2006). Evaluation of Potential Processes for Use in Warm Mix Asphalt. *Journal of the Association of Asphalt Paving Technologists*, Vol. 75, Savannah, Georgia.
- Mohammad, L.N., Wu, Z. and Aglan, M.A. (2004). Characterization of Fracture and Fatigue Resistance on Recycled Polymer-Modified Asphalt Pavements, 6th Rilem Symposium PTEBM'03, Zurich, Switzerland, 375–387.
- MORTH. (2013). Specification for Road and Bridge works Fifth Revision Indian Road Congress.
- Mostafa A. Elseifi, Louay N. Mohammad, Hao Yang and Samuel cooper (2012). Modeling and Evaluation of the Cracking Resistance of asphalt Mixtures Using the Semi-Circular Bending Test at Intermediate Temperature. *Road Materials and Pavement Design*, Vol. 13, No. S1, pp. 124–139.
- Qin, Q., Farrar, M. J., Pauli, A. T., and Adams, J. J. (2014). Morphology, thermal analysis and rheology of Sasobit modified warm mix asphalt binders. *Fuel*, Elsevier Ltd, 115, 416–425.
- Prowell, B. D., and Hurley, G. C. (2007). Warm- Mix Asphalt: Best Practices, Quality Improvement Series 125, National Asphalt Pavement Association, Lanham, MD.
- Shu, X., Huang B. and Vukosavljevic, D. (2010). Evaluation of Cracking Resistance Asphalt Mixture using Semi-Circular Bending Test, GeoShanghai International Conference.
- Wu, Z., Mohammad, L.N., Wang, L.B., Mull, M.A. (2005). Fracture Resistance Characterization of Superpave Mixtures Using the Semi-Circular Bending Test. *Journal of ASTM International*, Vol. 2, No.3, 324–332.
- Ying, H., Mostafa, A.E., Louay, N.M. and Heshmat A.A. (2013). A Crack Propagation Model for Asphalt Mixtures Based on the Cyclic Semi-Circular Bending Test, Transportation Research Board Annual Meeting, Washington, D.C.

Investigation on low temperature limiting criteria for asphalt mixture

A. Cannone Falchetto

Technische Universität Braunschweig, Braunschweig, Germany

K.H. Moon

Samsung Corporation, Seoul, South Korea

M.P. Wistuba

Technische Universität Braunschweig, Braunschweig, Germany

M.O. Marasteanu

University of Minnesota, Minneapolis, USA

ABSTRACT: In this paper a new low temperature limit criteria for asphalt mixtures is investigated based on the current asphalt binder specification and on rheological modeling. Bending Beam Rheometer (BBR) tests are first performed on asphalt binders and asphalt mixtures and the ENTPE transformation is used to analyze the experimental data. Creep stiffness results measured on long term aged binder are used to predict the limiting asphalt mixture creep stiffness values which are then compared to results available in literature. The BBR creep values determined on short term aged asphalt binder are used to predict creep stiffness of the corresponding short term aged asphalt mixtures. Based on these results, a limit criterion for asphalt mixture stiffness is proposed. Due to large variations in the derived slopes of the mixture creep stiffness curves, a limiting value for the relaxation parameter, m -value, cannot be recommended at this stage.

1 INTRODUCTION

The development of the Performance Grade (PG) specifications (Anderson & Kennedy 1993) during the Strategic Highway Research Program (SHRP) at the beginning of the 1990's represents one of the most significant achievements in the area of asphalt paving materials characterization. The PG tests and analysis procedures are detailed in a number of AASHTO standards (AASHTO M320 2010, T313 2012, T315 2012) and are currently used to specify the asphalt binders for pavement applications; in addition, the PG system serves as basic tool to investigate the behavior of asphalt binders in many research studies. The success of the PG system is associated to the innovative application of fundamental concepts to asphalt binder material characterization and on the other hand to the reasonable level of complexity of the tests and analyses required as part of these specifications. However, this level of complexity is the result of a number of simplifying hypotheses. In the past years and more recently, these assumptions have been investigated by a number of researchers who proposed additional tests and analysis procedures to improve the material selection process depending on the specific use.

The development of the low temperature cracking criterion for asphalt binder was based on previous research conducted by Readshaw (Readshaw 1972)

who investigated the low temperature cracking resistance of pavements in British Columbia. Based on binder penetration index, on the corrected Ring & Ball softening point, and under a loading time of 2 hours in the Van der Poel's monograph, he concluded that asphalt binder having stiffness smaller than 2×10^8 N/m² (200 MPa) at the lowest temperature experienced are less prone to cracking. The SHRP research team based on additional information increased the limiting stiffness value to 300 MPa, and used the time-temperature superposition principle to reduce testing time by demonstrating that, in general, the binder stiffness at 60 seconds at $T_1^\circ\text{C}$ is approximately equal to the stiffness at 2 hours at $T_1-10^\circ\text{C}$ (Anderson & Kennedy 1993).

An additional parameter was introduced to control the rheological type of asphalt binders and to eliminate heavily blown asphalts, which in fact were associated with poor fatigue performance. This parameter, m -value, was selected as the slope at 60 seconds of the stiffness vs. time curve on a double logarithmic scale. The idea behind this criterion was that low m -value corresponded to slower relaxation of the thermal stresses which build up at low temperatures and that is very detrimental for material performance.

In the pioneering research performed in Canada in the 1960's very limited information are available on

mixture low temperature properties. The only significant reference can be identified in the paper by Burgess et al. (1971) and attached discussion by N. W. McLeod. Based on McLeod's research and analysis of data from St. Anne Test Road and from other pavements in Canada, a critical low temperature stiffness value at which transverse pavement cracking is likely to occur is 1,000,000 psi or 7 GPa; this value is twice as high as that previously proposed and was obtained for a paving mixture compacted to 3% air voids, Voids in the Mineral Aggregate (VMA) of 14.5%, and a loading time of 20,000 s (5.5hours).

2 OBJECTIVE AND RESEARCH APPROACH

In the past years, and more recently, a number of micro mechanicals (Hirsch 1962, Christensen et al. 2003) and analogical-based (Huet 1963, Di Benedetto et al. 2004, Cannone Falchetto et al. 2011) models were developed that allow predicting asphalt mixture properties from binder properties. One interesting application of these models is the possibility of determining the mixture creep stiffness that corresponds to current PG specification limit of asphalt binder: 300MPa. This can provide insight into the possibility of developing a similar criterion for asphalt mixture creep stiffness that can be used, for example, in quality control testing.

A critical challenge in conducting such an investigation is to reasonably match the aging conditions of asphalt binder and corresponding asphalt mixture. It is conventionally accepted that asphalt binder after Rolling Thin-Film Oven Test (RTFOT) (AASHTO T240 2013) matches the aging condition of short term aged mixture or loose mixture; therefore, the analysis performed in present research effort is based on RTFOT binder data and short term aged mixture data. In order to further compare the predicted mixture stiffness to the values proposed by McLeod (equal to 7 GPa) (Burgess et al. 1971), analysis and calculations were also conducted using data obtained on long term aged asphalt binder according to the Pressure Aging Vessel (PAV) (AASHTO R028 2012) procedure. The following steps provide a synthesis of the research approach followed:

1. Perform creep tests with the Bending Beam Rheometer (BBR) (AASHTO T313 2012) on a set of eight asphalt binders for both RTFOT and PAV aging conditions.
2. Conduct BBR creep tests on short term aged mixtures prepared with the set of binders in step 1 according to the procedure proposed by Marasteanu et al. (2009).
3. Calculate binder creep stiffness and *m*-value at 60 seconds, at the critical temperatures from the PAV binder creep testing data.
4. Apply the Ecole Nationale des Travaux Publics de l'Etat (ENTPE transformation) (Di Benedetto et al. 2004, Cannone Falchetto et al. 2011) to the PAV

- binder creep data to predict the long term aged mixture creep stiffness and to compare it to the value proposed by McLeod (7 GPa) (Burgess et al. 1971).
5. Determine the creep stiffness and *m*-value at 60 seconds, at the critical temperatures (obtained in step 3 for PAV binders), for the asphalt binders in RTFOT condition.
6. Use the ENTPE transformation with the RTFOT binder data from step 5 to predict short term aged mixture creep stiffness and *m*-value at the critical temperatures (obtained in step 3).
7. Compare the mixture values predicted in step 6 to the experimental mixture data obtained from BBR mixture testing (Marasteanu et al. 2009).

3 MATERIALS AND TESTING

Eight different asphalt binders and sixteen corresponding asphalt mixtures were prepared with two different types of aggregate: granite (GR) and limestone (LM). All the mixtures were prepared with the Superpave mix design procedure (SP-2) with air voids target of 4% and nominal maximum aggregate size (NMAS) of 12.5 mm. The optimum asphalt content, voids in the mineral aggregate (VMA), and voids filled with asphalt (VFA) for the granite aggregate source were 6.0%, 16.3%, and 75.9%, respectively. Analogously, the optimum asphalt content, VMA, and VFA for the limestone aggregate source were 6.9%, 16.2%, and 75.0%, respectively. Table 1 provides a summary of the asphalt binders used in this study for preparing the asphalt mixtures, while Figure 1 presents the sieve size curves. Additional information on the materials used can be found in different research efforts (Marasteanu et al. 2007, 2009, Cannone Falchetto et al. 2011).

All asphalt binders were short and long term aged according to RTFOT (AASHTO T240 2013) and PAV (AASHTO R028 2012) procedures and BBR creep tests (AASHTO T313 2012) were performed for both aging conditions at three different temperatures: low PG + 10°C, (low PG + 10)-6°C and (low PG + 10)-12°C. All asphalt mixtures were short term aged by conditioning the gyratory compacted samples for 2 hours at 135°C. Then BBR creep stiffness tests for asphalt mixture (Marasteanu et al.

Table 1. Asphalt binders.

Binder ID	Details	Code
B	PG58-34, modifier 1, Elvaloy	58-34 M1
C	PG58-34, modifier 2, SBS	58-34 M2
D	PG64-34, modifier 1, Elvaloy	64-34 M1
E	PG64-34, modifier 2, Black Max	64-34 M2
F	PG58-28, plain 1	58-28 U1
G	PG58-28, plain 2	58-28 U2
H	PG64-28, plain 1	64-28 U1
I	PG64-28, modifier 1, Elvaloy	64-28 M1

2009) were performed at three different temperatures, low PG + 10°C, (low PG + 10) + 12°C and (low PG + 10)-12°C. Two and five replicates were used per each testing condition for asphalt binder and asphalt mixture respectively. BBR mixture specimens were obtained through several cutting steps from gyratory compacted specimens (Marasteanu et al. 2009); Figure 2 provides a simple scheme of the preparation procedure.

In the case of BBR binder testing, the standard constant load of 100 g (980 ± 50 mN) was applied to the asphalt binder beams (102.0 ~ 125.0 mm × 12.7 ± 0.5 mm × 6.25 ± 0.5 mm) and maintained for 240 s. Asphalt mixture BBR creep tests were performed with the same BBR device used for asphalt binder testing. Asphalt mixture specimens present the same dimensions of the of the corresponding BBR binder beams; due to the higher material stiffness, a higher constant load of 4,000 mN, was used, and test duration extended to 1,000 s as proposed by Marasteanu et al. (2009). According to this testing procedure reliable and repeatable creep stiffness data can be obtained when at least three replicates are used (Marasteanu et al. 2009). In addition, it was also demonstrated, through digital image processing (DIP) and microstructural analysis that BBR mixture specimens are sufficiently large to be considered as representative of the material creep properties up to NMA equal to 19mm (Cannone Falchetto et al. 2012 and 2013, Moon et al. 2014a and 2014b).

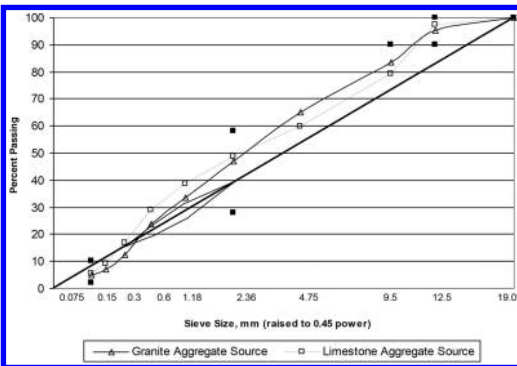


Figure 1. Gradation curve for HMA mix designs (Marasteanu et al., 2007).

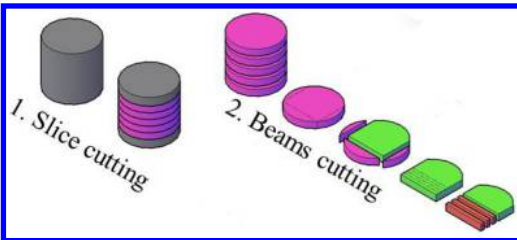


Figure 2. BBR mixture specimen: cutting sequence for sample preparation.

In both BBR creep tests methods (binder and mixture) the mid span deflection of the beam specimen, $\delta(t)$, was recorded for the entire duration of the test and the creep stiffness, $S(t)$, and m -value, $m(t)$, computed. Figure 3 present the testing setup.

The creep stiffness of asphalt binder and asphalt mixture was calculated according to Equation (1):

$$S(t) = \frac{\sigma}{\varepsilon(t)} = \frac{P \cdot l^3}{4 \cdot b \cdot h^3 \cdot \delta(t)} \quad (1)$$

where $S(t)$ = time dependent flexural creep stiffness (MPa); σ = maximum bending stress in the beam (MPa); $\varepsilon(t)$ = the time dependent bending strain in the beam (mm/mm); P = the constant load used (mN); l = length of specimen, (102.0 ~ 125.0 ± 1 mm); b = the width of specimen, (12.7 ± 0.5 mm); h = the height of specimen (6.25 ± 0.5 mm); $\delta(t)$ = deflection at the mid span of the beam (mm) and t = the time (s).

The m -value, which is the slope of log stiffness versus log time curve, was calculated as:

$$m(t) = \left| \frac{d \log S(t)}{d \log t} \right| \quad (2)$$

In addition, the critical cracking temperature of asphalt binder was obtained as the lowest temperature at which the following two conditions are met for long term aged binder: $S(t = 60 \text{ s}) \leq 300 \text{ MPa}$

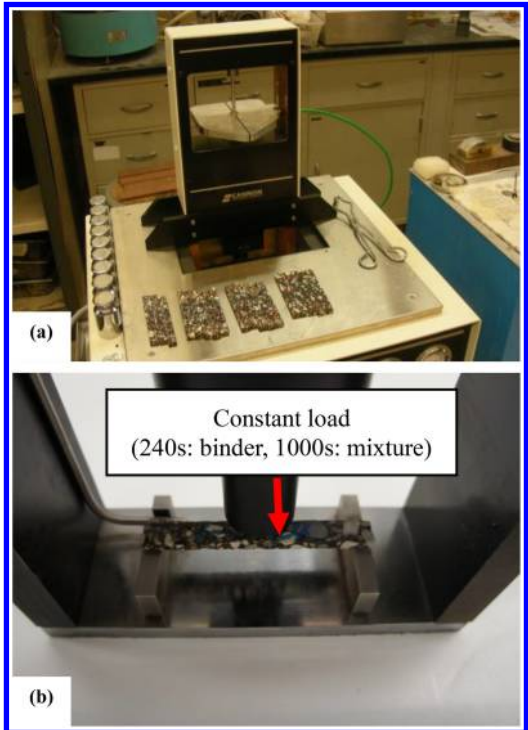


Figure 3. (a) BBR device and (b) BBR binder and mixture creep testing set up.

Table 2. Asphalt binders creep stiffness and m -value at 60 s at low PG + 10°C.

Binder ID	RTFOT aged		PAV aged	
	$S(60\text{ s})$, (MPa)	m -value	$S(60\text{ s})$, (MPa)	m -value
B	200	0.409	274	0.320
C	179	0.377	219	0.332
D	173	0.411	248	0.341
E	150	0.404	201	0.330
F	115	0.387	176	0.322
G	142	0.414	224	0.344
H	213	0.337	245	0.314
I	120	0.377	176	0.302

Table 3. Asphalt mixtures creep stiffness and m -value at 60 s low PG + 10°C.

Binder ID	Granite		Limestone	
	$S(60\text{ s})$, (MPa)	m -value	$S(60\text{ s})$, (MPa)	m -value
B	11226	0.122	8740	0.128
C	11114	0.132	9660	0.146
D	11353	0.151	9854	0.142
E	10633	0.152	8660	0.155
F	8641	0.144	8712	0.164
G	10648	0.173	11089	0.162
H	11927	0.152	11065	0.145
I	11883	0.157	8726	0.165

and $m(t = 60\text{ s}) \geq 0.300$ (AASHTO M320 2010, T313 2012).

Table 2 and Table 3 present the experimental results for asphalt binder and asphalt mixture at low PG + 10°C.

4 MODELING

In the past different micromechanical (Christensen et al. 2003) and analogical models (Huet 1963, Di Benedetto et al. 2004) were developed to investigate and describe the mechanical behavior of asphalt materials. The ENTPE transformation (Di Benedetto et al. 2004) represents a simple modeling solution to predict the properties of asphalt mixtures from the corresponding asphalt binder (forward problem) and vice-versa (inverse problem) when the transformation parameter is known. At low temperature the ENTPE transformation (Cannone Falchetto et al. 2011) presents the following expression for the prediction of creep stiffness $S(t)$:

$$S_m(t) = S_b(t10^{-\alpha}) \cdot (E_{\infty m} / E_{\infty b}) \quad (3)$$

$$\tau_m(T) = 10^\alpha \tau_b(T) \quad (4)$$

where $S_b(t)$ = asphalt binder creep stiffness (MPa); $S_m(t)$ = asphalt mixture creep stiffness (MPa);

Table 4. ENTPE transformation parameter, α .

ID	Binder Code	GR Mixture α	LM Mixture α
B	58-34 M1	3.17	3.09
C	58-34 M2		
D	64-34 M1		
E	64-34 M2		
F	58-28 U1	3.01	3.10
G	58-28 U2		
H	64-28 U1		
I	64-28 M1		

$E_{\infty b}$ = glassy modulus of binder (MPa); $E_{\infty m}$ = glassy modulus of mixture (MPa); t = time; α = transformation parameter; τ_b = asphalt binder characteristic time; τ_m = asphalt mixture characteristic time; T = temperature (°C).

Expression (4) is fundamental for relating the characteristic time of asphalt binder to the corresponding mixture. This expression is associated to different analogical models such as Huet (1963), 2S2P1D (Di Benedetto et al. 2004) and MCF (Cannone Falchetto and Moon 2015) models. However, when the transformation parameter, α , is known, Equation (3) can be directly applied to the experimental data, without the need of relying on any specific model.

The asphalt binders and mixtures used in this paper belongs to a set of materials investigated in a larger research efforts (Marasteanu et al. 2007, 2009, Cannone Falchetto et al. 2011) and, therefore, the parameters in Equation (3) are known. Table 4 provides the values of the transformation parameter, α , for the four sets of asphalt binders and mixtures into which the materials used can be subdivided, based on binder low PG grade and aggregate type (granite, GR, and limestone, LM). Additional details can be found elsewhere (Cannone Falchetto et al. 2011).

The transformation parameter α depends on aggregate type and on performance grade (PG) which is directly associated to the specific binder properties. Nevertheless, the same PG can be linked to different binder modifications: for example plain binders F, G and H have the same low PG of I and, hence, same α .

In order to obtain the value of creep stiffness at 20,000 s and to compare the predicted asphalt mixture creep stiffness to the experimental mixture creep stiffness, master curves were generated based on the Christensen, Anderson and Marasteanu (CAM) model (Marasteanu and Anderson 1999) expressed in terms of stiffness as:

$$S(t) = S_g \cdot \left[1 + (t_c / t)^\nu \right]^{-w/v} \quad (5)$$

where S_g = glassy creep stiffness asymptote (3 GPa for binder and 30 GPa for mixture); t_c = crossover time (s); and, ν and w = fitting parameters. The shift factor, a_T , was expressed as $a_T = 10^{C_1 + C_2 \cdot T}$ where C_1 and C_2 = fitting parameters and T = reference temperature (°C). The validity of using the same creep

Table 5. Mixture creep stiffness for PAV asphalt binder at $S_b(60s)$.

ID	Binder Code	T_{CR} (°C)	$S(60s)$, (MPa)		
			^f Binder (PAV)	Mixture (^a GR)	Mixture (^b LM)
B	58-34 M1	-24.4	300	11311	9793
C	58-34 M2	-26.4	300	11596	10041
D	64-34 M1	-25.6	300	11594	10040
E	64-34 M2	-27.0	300	11044	9562
F	58-28 U1	-22.7	300	11126	9633
G	58-28 U2	-20.6	300	11718	10147
H	64-28 U1	-20.0	300	11724	10153
I	64-28 M1	-23.7	300	12524	10849
^c μ				11580	10027
^d σ				486	402
^e CoV				3.9%	4.1%

^aGR: Granite, ^bLM: Limestone, ^c μ : Mean, ^d σ : Standard deviation; ^eCoV: Coefficient of Variation; ^f300 MPa: creep stiffness specification limit.

stiffness asymptote both for plain and modified asphalt binders was demonstrated in a previous work (Moon et al. 2013) and also successfully applied to other studies (Cannone Falchetto et al. 2012, Marasteanu et al. 2012).

5 INVESTIGATION OF THE LONG TERM AGED MIXTURE STIFFNESS FROM PAV BINDER STIFFNESS

In order to accomplish the first steps in the analysis the binder PAV data were used to predict the corresponding mixture creep stiffness based on the low temperature expression (Equation 3) of the ENTPE transformation (Di Benedetto et al. 2004, Cannone Falchetto et al. 2011). The results of predicted mixture $S_m(60s)$ are shown in Table 5.

The prediction of asphalt mixture creep stiffness at 20,000 s, $S_m(20,000s)$, obtained with the ENTPE transformation and the stiffness value of PAV asphalt binder at 20,000 s, $S_b(20,000s)$, at critical temperature, T_{CR} , were compared to the 7 GPa limit proposed by McLeod (Burgess et al. 1971). For this purpose, the CAM model (Marasteanu and Anderson 1999) was initially used to obtain the creep stiffness values at 20,000 s. First, master curve of asphalt binder creep stiffness were generated based on the experimental data of PAV aged binder. Then, based on the calculated critical cracking temperature, T_{CR} , (see Table 5 and 6), the value of shift factor, a_T , at T_{CR} was obtained.

Hence, by setting $t = 20,000s$ in Equation (5), $S_b(20,000s)$ of PAV aged binder at T_{CR} was determined. Finally, the $S_m(20,000s)$ for long term aged mixture was calculated from $S_b(20,000s)$ using the ENTPE transformation and finally compared to 7 GPa limit (Burgess et al. 1971). The schematic computation process for obtaining the binder creep stiffness

Table 6. Mixture creep stiffness for PAV asphalt binder at $S_b(20,000s)$.

ID	Binder Code	T_{CR} (°C)	$S(20,000s)$, (MPa)		
			Binder (PAV)	Mixture (GR)	Mixture (LM)
B	58-34 M1	-24.4	43	6236	5370
C	58-34 M2	-26.4	46	6282	5410
D	64-34 M1	-25.6	46	6387	5500
E	64-34 M2	-27.0	41	6547	5639
F	58-28 U1	-22.7	41	6548	5640
G	58-28 U2	-20.6	47	6617	5699
H	64-28 U1	-20.0	47	6620	5702
I	64-28 M1	-23.7	55	7072	6093
^c μ				46	6539
^d σ				4.5	261
^e CoV				9.9%	4.0%

^aGR: Granite, ^bLM: Limestone, ^c μ : Mean, ^d σ : Standard deviation; ^eCoV: Coefficient of Variation.

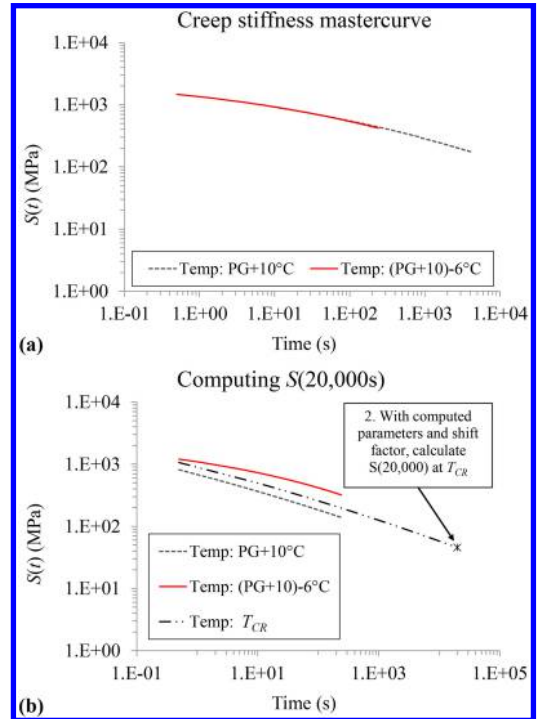


Figure 4. Computation process of PAV $S_b(20,000s)$ using CAM model.

at 20,000 s is shown in Figure 4 while the results of $S_b(20,000s)$ and $S_m(20,000s)$ are presented in Table 6.

Slightly different T_{CR} values were observed for binder having same PG (Table 5 and 6); this is most likely due to the different types of modifiers. By using the ENTPE transformation, the mixture creep stiffness, $S_m(60s)$, corresponding to the PAV binder low temperature limit criteria of 300 MPa was calculated: an average value of 11.6 GPa and 10.0 GPa

were obtained for granite and limestone mixtures, respectively, with small coefficient of variation (CoV).

An average value of $S_b(20,000\text{ s})$ equal to 46 MPa was determined for asphalt binder with a low CoV=9.9%. Finally, $S_m(20,000\text{ s})$ was obtained from the corresponding $S_b(20,000\text{ s})$. The average values of $S_m(20,000\text{ s})$ were 6.5 GPa and 5.6 GPa for granite and limestone mixtures, respectively (CoV = 4%).

This indicates that the average limiting stiffness values for the two types of mixtures are reasonably close to the 7 GPa limit originally proposed by McLeod (Burgess et al. 1971).

6 EVALUATION OF SHORT TERM AGED MIXTURE STIFFNESS FROM PAV AND RTFOT BINDER STIFFNESS

The creep stiffness of the RTFOT asphalt binder at the PAV binder critical temperature, T_{CR} , (see Table 5) has to be first determined in order to obtain the creep stiffness of short term aged asphalt mixture. Assuming a linear relation between $\log S(60\text{ s})$ and the test temperature for both PAV and RTFOT creep stiffness data, a corresponding RTFOT binder stiffness value at T_{CR} can be easily obtained, as shown in Figure 5.

The schematic computation process of RTFOT binder $S(60\text{ s})$ at the PAV binder critical temperature, T_{CR} , can be summarized as follow:

1. Determine the critical temperature, T_{CR} , from the experimental results of PAV binder $\text{Log}S(60\text{ s})$ using the current low temperature limit specification (steps 1–2 in Figure 5a and Table 5).
2. Obtain the value of $S(60\text{ s})$ for RTFOT asphalt binder based on T_{CR} , (step 3–4 in Figure 5b).

Although high values of the coefficient of determination, R^2 , were observed for most binders ($R^2 > 0.95$), CAM model (Marasteanu and Anderson 1999) was also used to validate the results since small deviations from the linear relation were found for some asphalt binders.

In order to obtain the RTFOT $S(60\text{ s})$ values at the PAV binder T_{CR} , a computation procedure similar to the one used in section 5 was selected. First, based on RTFOT binder creep stiffness experimental results, master curve was generated and the shift factor, a_T , at T_{CR} derived. Then, the RTFOT binder $S(60\text{ s})$ at PAV binder T_{CR} was calculated using CAM model and, compared to the results of RTFOT $S(60\text{ s})$ obtained using the simple regression method shown in Figure 5. Figure 6a shows the schematic procedure for obtaining RTFOT binder $S(60\text{ s})$ at PAV binder T_{CR} using CAM model, while the graphical comparison between regression and CAM model extrapolation of RTFOT binder $S(60\text{ s})$ are presented in Figure 6b (correlation coefficient, $\rho=0.989$). The computed results including the values of the coefficient of determination, R^2 , are presented in Table 7.

Then, simple regression RTFOT binder stiffness values, $S(60\text{ s})$, were used with the low temperature

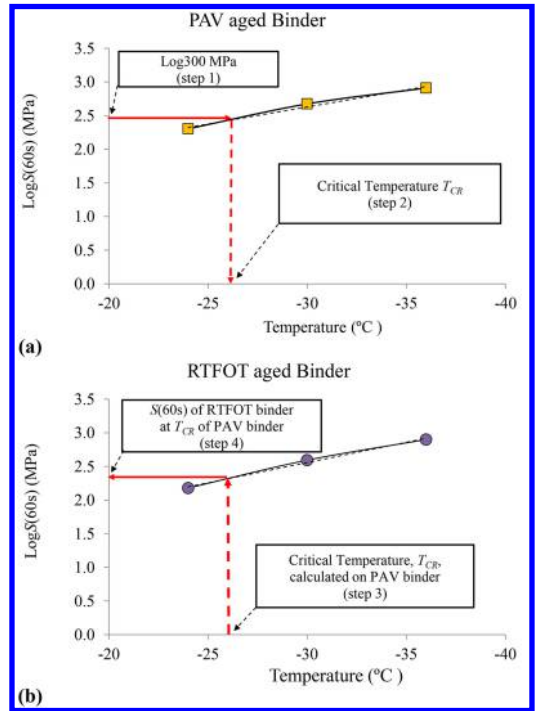


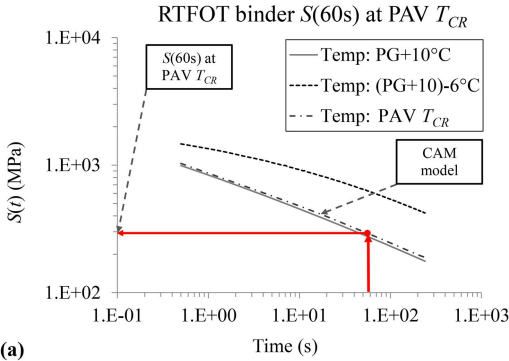
Figure 5. (a) PAV binder critical temperature, T_{CR} and (b) prediction of RTFOT binder $S(60\text{ s})$ at PAV binder T_{CR} .

Table 7. RTFOT binder $S(60\text{ s})$ at the corresponding binder PAV T_{CR} .

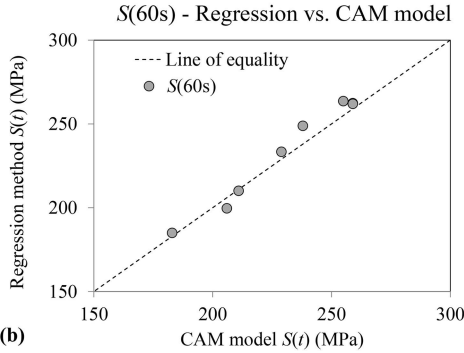
ID	Binder Code	RTFOT binder			
		$S(60\text{ s})$ at T_{CR} (MPa)	R^2 (%)	$S(60\text{ s})_{CAM}$ (MPa)	Diff. (%)
B	58-34 M1	211.0	98.33	210.0	0.5
C	58-34 M2	255.0	99.29	263.5	3.2
D	64-34 M1	229.0	99.98	233.3	1.8
E	64-34 M2	238.0	98.37	248.8	4.3
F	58-28 U1	206.0	98.22	199.6	3.2
G	58-28 U2	183.0	99.97	184.9	1.0
H	64-28 U1	259.0	99.97	262.3	1.3
I	64-28 M1	259.0	99.96	261.9	1.1

ENTPE transformation (Cannone Falchetto et al. 2011) to predict the mixture creep stiffness $S(60\text{ s})$ at the critical temperature, T_{CR} , obtained from the PAV binder creep stiffness experimental data.

The results are shown in Tables 8 and 9 and Figures 7. In addition, BBR mixture creep data were used with CAM model to obtain mixture $S(60\text{ s})$ at the same critical temperature, T_{CR} . The same calculation process previously used for RTFOT binder $S(60\text{ s})$ at PAV binder T_{CR} was followed. These results are also included in Tables 8 and 9 and Figures 7 to compare the $S(60\text{ s})$ values predicted through the ENTPE transformation with the experimentally obtained $S(60\text{ s})$.



(a)



(b)

Figure 6. (a) Computing process of RTFOT binder $S(60\text{ s})$ using CAM model and (b) comparison of RTFOT binder $S(60\text{ s})$ at T_{CR} of PAV binder based on regression and CAM model extrapolation.

Table 8. RTFOT binder $S(60\text{ s})$ at the corresponding binder PAV T_{CR} for Granite Mixtures.

ID	Binder Code	Aggregate Type	$S(60\text{ s})$ at T_{CR} , (MPa)			Diff (%)
			Binder (ENTPE)	Mixture (CAM)		
B	58-34 M1	GR	10593	11850	10.6	
C	58-34 M2	GR	11504	13430	14.3	
D	64-34 M1	GR	10897	10960	0.6	
E	64-34 M2	GR	11096	11910	6.8	
F	58-28 U1	GR	9781	11790	17.0	
G	58-28 U2	GR	10222	12190	16.1	
H	64-28 U1	GR	11366	13980	18.7	
I	64-28 M1	GR	11248	12720	11.6	
Average			10838	12354	12.0	
CoV (%)			5.5	7.9		

No significant differences were observed, except for three mixtures: F, G and H. The discrepancy between ENTPE predictions and CAM was as high as 20% when considering limestone mixtures. The average values of $S(60\text{ s})$ from ENTPE transformation prediction were 10.8 GPa and 9.5 GPa for granite and limestone mixtures, respectively, with small variations (CoV= 5.5% and 3.8% for the two mixture groups). Relatively limited differences of $S(60\text{ s})$ were observed

Table 9. RTFOT binder $S(60\text{ s})$ at the corresponding binder PAV T_{CR} for Limestone Mixtures.

ID	Binder Code	Aggregate Type	$S(60\text{ s})$ at T_{CR} , (MPa)			Diff (%)
			Binder (ENTPE)	Mixture (CAM)		
B	58-34 M1	LM	9158	9340	1.9	
C	58-34 M2	LM	9747	11280	13.6	
D	64-34 M1	LM	9424	10560	10.8	
E	64-34 M2	LM	9595	10800	11.2	
F	58-28 U1	LM	9310	11650	20.1	
G	58-28 U2	LM	9021	11230	19.7	
H	64-28 U1	LM	10045	12530	19.8	
I	64-28 M1	LM	9933	11640	14.7	
Average			9.529	11129	14.0	
CoV (%)			3.8	8.4		

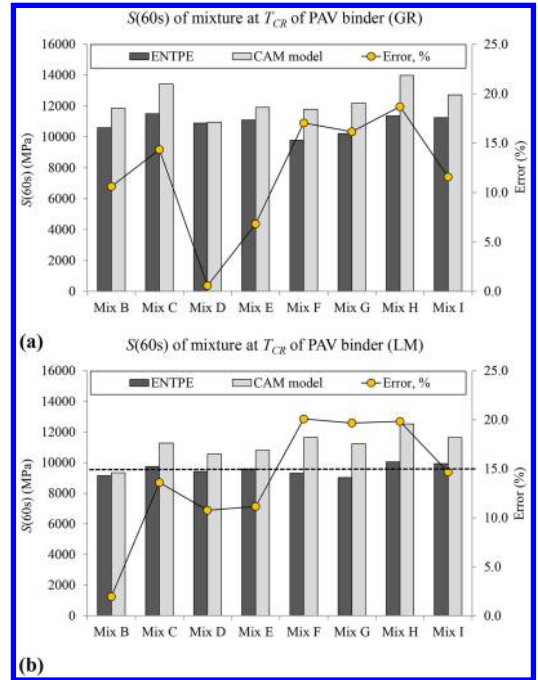


Figure 7. Short term aged mixture $S(60\text{ s})$ at PAV binder critical temperature: (a) granite mixtures and (b) limestone mixture.

between the average ENTPE transformation prediction and the average extrapolations obtained by the CAM model. This suggests that the creep stiffness of mixtures has similar values, both when predicted from the binder data using ENTPE transformation and when obtained by the CAM model on mixture experimental measurements. The results indicate that for short term aged asphalt mixtures, the 300 MPa limit imposed on PAV binders results in limiting values, $S(60\text{ s})$, for mixture in the range of 9.5 to 12.5 GPa.

Table 10. RTFOT binder $S(60\text{ s})$ at the corresponding binder PAV T_{CR} for Granite Mixtures.

ID	Binder Code	$S(60\text{ s})$ at T_{CR} , (MPa)			
		Aggregate Type	Binder (ENTPE)	Mixture (CAM)	Diff (%)
B	58-34 M1	GR	0.115	0.141	18.7
C	58-34 M2	GR	0.094	0.137	31.3
D	64-34 M1	GR	0.109	0.134	18.8
E	64-34 M2	GR	0.098	0.157	37.6
F	58-28 U1	GR	0.096	0.158	39.2
G	58-28 U2	GR	0.104	0.165	37.0
H	64-28 U1	GR	0.084	0.143	41.1
I	64-28 M1	GR	0.084	0.143	41.1
Average			0.098	0.147	33.1
CoV (%)			11.1	7.6	

Table 11. RTFOT binder $S(60\text{ s})$ at the corresponding binder PAV T_{CR} for Limestone Mixtures.

ID	Binder Code	$S(60\text{ s})$ at T_{CR} , (MPa)			
		Aggregate Type	Binder (ENTPE)	Mixture (CAM)	Diff (%)
B	58-34 M1	LM	0.116	0.154	24.9
C	58-34 M2	LM	0.096	0.143	32.8
D	64-34 M1	LM	0.110	0.139	21.0
E	64-34 M2	LM	0.100	0.175	42.9
F	58-28 U1	LM	0.097	0.147	34.0
G	58-28 U2	LM	0.105	0.148	29.1
H	64-28 U1	LM	0.085	0.135	36.8
I	64-28 M1	LM	0.085	0.132	35.4
Average			0.099	0.147	32.1
CoV (%)			10.9	9.2	

7 SHORT TERM AGED MIXTURE $M(60\text{ S})$ AT PAV BINDER T_{CR} FOR $M(60\text{ S}) = 0.300$

The ENTPE transformation and CAM model were also used to derive the $m(60\text{ s})$ of short term aged asphalt mixture at the corresponding T_{CR} for PAV binder. The results are shown in Tables 10 and 11 and in Figures 8.

Large differences were observed between the values of $m(60\text{ s})$ extrapolated through CAM model and the predictions obtained with ENTPE transformation. This is most likely due to fitting limitations experienced when the slope of the log stiffness is close to zero; hence, at the stage of the research, this makes the use of mixture m -value as a limiting parameter questionable.

8 SUMMARY AND CONCLUSIONS

In this paper, the possibility of developing low temperature limit criteria for asphalt mixture, analogous to that used for asphalt binder, was investigated. BBR creep tests were performed on eight asphalt binders

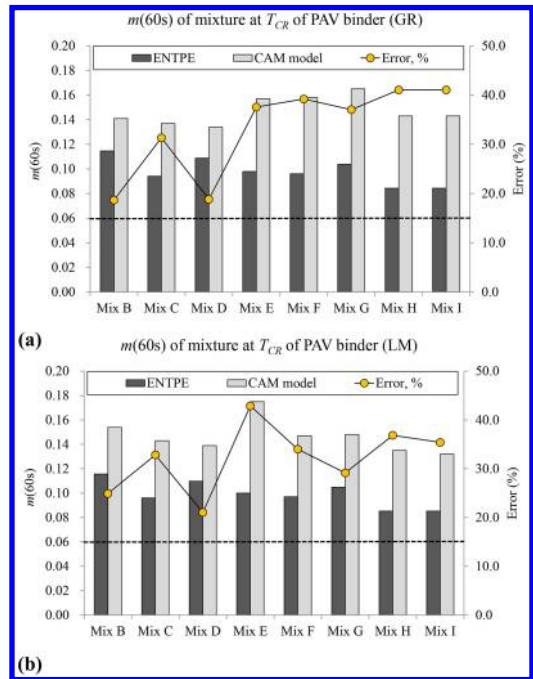


Figure 8. Short term aged mixture $m(60\text{ s})$ at PAV binder critical temperature: (a) granite mixtures and (b) limestone mixture.

and sixteen short term aged asphalt mixtures prepared with two different types of aggregate. The critical temperature of PAV aged asphalt binder was calculated and the limiting creep stiffness value of PAV binder data was then used to predict long term aged mixture stiffness through the ENTPE transformation. Then, the creep stiffness of PAV and RTFOT binders was used together with the ENTPE transformation to obtain the corresponding creep stiffness and m -value limits for short term aged asphalt mixtures at the binder critical temperature and finally compared to the mixture BBR experimental data. Based on the performed investigation, three main conclusions can be drawn:

1. At 20,000 s the predicted creep stiffness of long term aged asphalt mixtures is in the range of 5.6 ~ 6.5 GPa. These values are in reasonably good agreement with the value previously proposed by McLeod and equal to the 7.0 GPa.
2. The limiting creep stiffness at 60 seconds for short term aged mixtures, predicted from RTFOT binders creep stiffness data is comparable to that obtained from experimental BBR mixture creep stiffness. The values are in the range between 9.5 GPa and 12.5 GPa. These results consistently support the idea of using BBR creep tests on mixture as a routine method to discriminate mixtures that are too stiff and more prone to cracking. Additional research is needed to further validate and refine these findings.
3. The large variations observed in the relaxation parameter of asphalt mixture prevent the possibility

of defining a limiting criterion associated to $m(60\text{ s})$ at this time.

ACKNOWLEDGMENTS

This research was sponsored by Federal Highway Administration National Pooled Fund Study TPF 5(132). This support is gratefully acknowledged. The results and opinions presented are those of the authors and do not necessarily reflect those of the sponsoring agencies.

REFERENCES

- AASHTO M320-10-UL. 2010. Standard specification for Performance-Graded asphalt binder.
- AASHTO R028-12-UL. 2012. Standard practice for accelerated aging of asphalt binder using a Pressurized Aging Vessel (PAV).
- AASHTO T240-13-UL. 2013. Standard method of test for effect of heat and air on a moving film of asphalt binder (Rolling Thin-Film Oven Test).
- AASHTO T313-12-UL. 2012. Standard method of test for determining the flexural creep stiffness of asphalt binder using the Bending Beam Rheometer (BBR).
- AASHTO T315-12-UL. 2012. Standard method of test for determining the rheological properties of asphalt binder using a Dynamic Shear Rheometer (DSR).
- Anderson, D.A. & Kennedy, T. 1993. Development of SHRP binder specification. *Journal the Association of Asphalt Paving Technologists (AAPT)* 62: 481–507.
- Burgess R.A., Kopvillem O. & Young, F.D. 1971. St. Anne test road – relationship between predicted fracture temperatures and low temperature field performance. *Journal the Association of Asphalt Paving Technologists (AAPT)* 40: 148–193.
- Cannone Falchetto, A., Marasteanu, M.O. & Di Benedetto, H. 2011. Analogical based approach to forward and inverse problems for asphalt materials characterization at low temperatures. *Journal the Association of Asphalt Paving Technologists (AAPT)* 80: 549–581.
- Cannone Falchetto, A., Monteparà, A., Tebaldi, G. and Marasteanu, M. 2012. Microstructural and rheological investigation of asphalt mixtures containing recycled asphalt materials. *Construction and Building Materials* 35: 321–329.
- Cannone Falchetto, A., Monteparà, A., Tebaldi, G. and Marasteanu, M. 2013. Microstructural characterization of asphalt mixtures containing recycled asphalt materials. *Journal of Material in Civil Engineering (ASCE)* 25: 45–53.
- Cannone Falchetto, A. and Moon, K. H. 2015. Micromechanical – Analogical Modelling of Asphalt Binder and Asphalt Mixture Creep Stiffness Properties at Low Temperature. *Road Material and Pavement Design (RMPD)*, to be published.
- Christensen, D., Pellinen, T. & Bonaquist, R.F. 2003. Hirsch model for estimating the modulus of asphalt concrete. *Journal the Association of Asphalt Paving Technologists (AAPT)* 72: 97–121.
- Di Benedetto, H., Olard, F., Sauzéat, C. & Delaporte, B. 2004. Linear viscoelastic behavior of bituminous materials: from binders to mixtures. *Road Material and Pavement Design (RMPD)* 5(1): 163–202.
- Hirsch, T.J. 1962. Modulus of elasticity of concrete affected by elastic moduli of cement paste matrix and aggregate. *Journal of the American Concrete Institute* 59(3): 427–452.
- Huet, C. 1963. Etude par une méthode d'impédance du comportement viscoélastique des matériaux hydrocarbonés. *Thèse de doctorat d'ingénieur Faculté des Sciences de l'Université de Paris*.
- Marasteanu, M.O. & Anderson, D.A. 1999. Improved model for bitumen rheological characterization. Presented at *European Workshop on Performance-Related Properties for Bituminous Binders*, Luxembourg, Belgium.
- Marasteanu, M.O., Zofka, A., Turos, M., Li, X., Velasquez, R. & Li, X. 2007. National pooled fund study 776: investigations of low-temperature cracking in asphalt pavements. *Research report 2007-43*, Minnesota Department of Transportation (MN/DOT), Saint Paul.
- Marasteanu, M.O., Velasquez, R., Cannone Falchetto, A. & Zofka, A. 2009. Development of a simple test to determine the low temperature creep compliance of asphalt mixture, *IDEA Program Final Report NCHRP 133*, Transportation Research Board of the National Academies.
- Marasteanu, M.O. et al. 2012. Investigation of low temperature cracking in asphalt pavements, national pooled fund study phase II. *Research report 2007-43*, Minnesota Department of Transportation (MN/DOT), Saint Paul.
- Moon, K.H., Marasteanu, M.O. and Turos, M. 2013. Comparison of thermal stresses calculated from asphalt binder and asphalt mixture creep tests. *Journal of Material in Civil Engineering (ASCE)* 25: 1059–1067.
- Moon, K.H., Cannone Falchetto, A. and Hu, J.W. 2014a. Investigation of asphalt binder and asphalt mixture low temperature creep properties using semi mechanical and analogical models. *Construction and Building Materials* 53: 568–583.
- Moon, K.H., Cannone Falchetto, A. and Jeong, J.H. 2014b. Microstructural analysis of asphalt mixtures using digital image processing techniques. *Canadian Journal of Civil Engineering* 41(1): 74–86.
- Readshaw, E.E. 1972. Asphalt specifications in british columbia for low temperature performance, *Journal the Association of Asphalt Paving Technologists (AAPT)* 41: 562–581.

Laboratory evaluation of clogging behavior of porous asphalt pavements

Emiko Lim, T.F. Fwa & K.H. Tan

Centre for Transportation Research, National University of Singapore, Singapore

ABSTRACT: Porous asphalt has been used as surface wearing courses for road pavements to improve wet-weather driving safety, as well as to perform as a form of quiet pavement to reduce traffic noise. Both forms of benefits are derived from the presence of relatively high porosity in the porous pavement mixture. During operation, clogging of the porous layer may take place and this can seriously reduce the effective porosity of the porous mixture and impair the ability of the porous pavement to serve its intended functions. Therefore in the design of a porous asphalt pavement, it is important that its porosity, and hence drainage capacity, is retained sufficiently during operation to serve the intended functions throughout its service life. In this research, using permeability as the drainage capacity parameter, a laboratory study was performed to examine the drainage and clogging behaviors of different designs of porous asphalt mixtures used in Singapore, subject to the common clogging materials found in Singapore roads. Clogging was created by introducing the clogging materials in stages into the porous materials tested. A constant-head test was employed to determine the permeability of the porous materials at different stages of the clogging test. The relative clogging susceptibility of the different porous asphalt mixtures studied are compared by means of a coefficient of clogging potential.

1 INTRODUCTION

Porous asphalt pavements have been adopted in many parts of the world to improve wet-weather driving safety (Ferguson, 2005) and to serve as a form of quiet pavement to reduce traffic noise (Scholz & Grabowiecki, 2007). The former application relies on the high drainage capacity of the porous asphalt layer to drain away surface runoff on the pavement surface effectively from the tire-pavement contact area so that the wet-pavement skid resistance can be maintained at a sufficiently high value to ensure driving safety. In the latter application, the porous surface mixture works an effective noise absorption layer to cut down the reflected noise volume. For both applications, the benefits are derived from the high porosity present within the porous asphalt layer.

The effectiveness of a porous pavement is primarily governed by its porosity. Reductions in porosity of the porous surface layer caused by clogging can affect the performance of the porous pavement. Clogging of the porous surface layer is therefore a major durability concern of a porous pavement. Experiences with the use of porous asphalt pavement have found that permeability loss due to clogging is a major form of functional failure for porous asphalt pavements (EPA, 1999; Hamzah et al. 2013; Martin et al. 2014).

Clogging is a process that develops over time, due to the accumulation and deposition of sediments in the porous surface layer (Bouwer, 2002). This process decreases the porosity, permeability and hence effectiveness of a porous pavement.

Runoff carrying with it a large amount of suspended particles is known to be the main source that causes clogging of pore spaces in porous pavements during their life time (Nielsen, 2007; Siriwardene et al. 2007; Yong et al. 2008). Clogging may also occur due to the inorganic and organic particles from traffic activities and localized vegetation or dust that is often found on the roadway (Siriwardene et al. 2007).

According to Cooley (1999), sand particles and solid materials are pushed into the pores of the permeable pavement by the weight of the passing vehicles which may also crush them into a finer size distribution. These sand and solid particles can be brought into the pores by flowing water from a storm event too. It is possible that the vehicle weight may push materials into the pavement at the front part of the tire, and the back part of the tire may create a suction to remove some of the solids. Under certain conditions and depending on the type and size of solids, once in the pores, the clogging materials may become embedded and begin to accumulate, clogging the pores. When a significant percentage of the pores in the permeable pavement are clogged, the permeability of the pavement is reduced and water begins to pool on the pavement surface. This will defeat the purpose of having permeable pavements.

This paper reports a laboratory study conducted to analyze the permeability and clogging characteristics of porous asphalt mixtures as a function of mixture porosity. The experimental program considered four target porosity levels: 10%, 15%, 20% and 25%. These porosities were considered as they would cover the

likely range of porosity and permeability that a porous pavement material would go through in its entire useful service life.

The permeability coefficient was determined by means of a constant-head test and the clogging performance was determined by measuring the reductions in permeability coefficient as clogging developed.

2 METHODOLOGY OF STUDY

The laboratory experimental program made use of drop-hammer compacted specimens which were each 150 mm in diameter and 50 mm in thickness. The initial permeability coefficient of each test specimen was first determined before the clogging treatment began. Additional measurements of permeability coefficients were made at different stages of the clogging treatment. The following sub-sections describe the measuring method of permeability coefficients, the clogging materials, the clogging procedure, and the evaluation of the clogging potential of the porous asphalt materials tested.

2.1 Measurement of permeability coefficient

The determination of permeability coefficients of the test specimens were made using a constant-head permeameter developed at the National University of Singapore for the purpose of clogging test of porous asphalt specimens (Fwa et al., 2000). Figure 1 shows a schematic diagram of the constant-head test setup. A submersible pump provides constant inflow of water into the inlet cylinder such that a constant head of water can be maintained at the desired water head in the inlet cylinder. The flow of water can be controlled using valves. The flow rate of water is determined by measuring the volume of water collected from the inlet hose. In the present study, a constant hydraulic head of 41.5 cm was maintained throughout the test.

The test samples were sealed with waterproof thread tape to prevent side-flow of water and to enable only one-dimensional flow. Plasticine was used to seal off any leakage that would occur in the setup.

Since the flow within a porous asphalt specimen is non-laminar, the Darcy's flow equation for laminar flow is not applicable. Earlier studies by the authors have shown that the permeability coefficients for porous asphalt materials can be estimated from the following modified Darcy's equation (Fwa et al. 1998, 2002 and Tan et al. 2000),

$$v = k \cdot (i)^n \quad (1)$$

in which, $v = Q/tA$ (2)

$$i = H/L \quad (3)$$

where k = permeability coefficient in mm/s;
 i = hydraulic gradient;
 n = experimental coefficient;

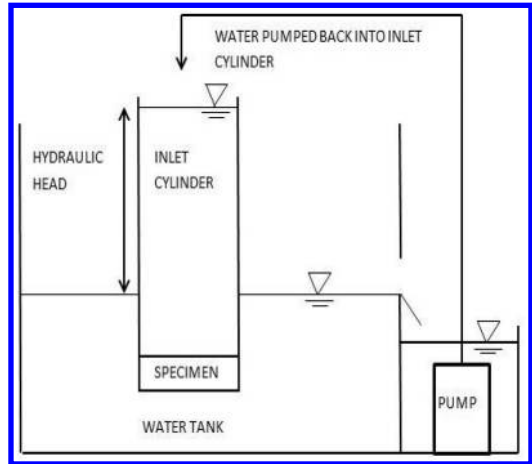


Figure 1. Schematic diagram of permeability and clogging test set-up.

L = thickness of specimen in mm;
 Q = amount of water collected in mm^3 ;
 t = test duration in seconds;
 A = cross-sectional area of specimen in mm^2 ;
 H = constant water head in mm.

It has been shown by the authors in their earlier works (Fwa et al., 1998, 2002; Tan et al., 2000) that for the mentioned test conditions, the value of n for porous asphalt materials can be taken as a constant of 0.7 without any errors of practical significance.

2.2 Measurement of clogging behavior

Different procedures have been used by past researchers to produce the effect of clogging. These procedures include using a flume test (Haselbach et al., 2006) and falling head permeameter (Deo et al., 2010; Joung et al., 2008). The clogging procedure adopted in this study is based on the work by Tan et al. (2000) using a constant head permeameter. This procedure was found to produce test results with good repeatability in terms of the deterioration trend of permeability caused by clogging.

2.3 Clogging materials

Table 1 shows the gradations of typical residual soils and construction sands commonly found on Singapore roads. Earlier studies by the authors (Fwa et al. 1998, 2002; Tan et al., 2000) found that of the various sizes of these clogging materials, the fines smaller than $75 \mu\text{m}$ had insignificant effects in inducing clogging as compared with the larger size materials. It was also found that sand with sizes between $600 \mu\text{m}$ and 1.18mm was the most detrimental in causing clogging of porous materials. Hence, the clogging sand with sizes between $600 \mu\text{m}$ and 1.18mm was used in the clogging procedure of the present study.

Table 1. Gradations of common clogging materials on Singapore roads.

Sand type	Medium – coarse sand	Fine – medium sand	Fine-coarse sand	Residual soil
Sieve Size	(% passing)	(% passing)	(% passing)	(% passing)
1.18 mm	100	–	100	100
600 um	50	100	70	94
420 um	25	50	58	90
300 um	–	25	42	84
150 um	–	–	20	72
75 um	–	–	–	58
63 um	–	–	–	48
45 um	–	–	–	38

2.4 Clogging procedure

To ensure that there is a sufficient number of data points for tracing the deterioration trend of permeability in the process of clogging, clogging materials were introduced in 10 stages so that ten intermediate permeability measurements were made before a test specimen was clogged. Trial clogging tests were conducted and it was found that applying 5.3 g (2000 g/m²) at each clogging cycle would achieve the aim of the clogging test. The clogging procedure is described below.

At each stage of the clogging treatment, 5.3 g of the clogging material was applied uniformly on the upper face of the cylindrical test specimen. The test specimen was attached in the holder at the lower end of the constant-head test cylinder, before the test cylinder was filled with water. Next, the valve at the lower end of the constant-head test cylinder was opened to allow water to flow through the test specimen under the constant head to bring the clogging materials into the test specimen. Before each addition of the clogging materials, permeability coefficient measurements were performed. The measurements were performed repeatedly at an interval of three minutes until the change in the measured permeability value was negligible.

At the end of each stage of clogging, besides taking the permeability measurement, the mass of clogging materials flushed out through the test specimen was also measured. The additional amount of clogging materials retained within the test specimen at the end of each stage of clogging treatment was obtained by deducting the flushed out amount from the amount of clogging material added.

Permeability measurements are taken for a total of 11 times, including the first measurement of the initial permeability before clogging and the subsequent 10 intermediate measurements in the entire process of clogging treatment. The entire test procedure, covering the clogging process and the permeability coefficient measurements took 2 to 2.5 hours per specimen.

2.5 Evaluation of clogging susceptibility of porous materials

The phenomenon of clogging of porous media has been a topic of active research. A main focus was to characterize the clogging potential of a porous material with respect to a given clogging material. In most cases, the relative clogging susceptibility of porous materials are evaluated by means of some forms of clogging coefficients or indices.

The Kozeny-Carmen's theoretical modelling of clogging has been used widely in the study of the clogging mechanisms of various porous media (Tan et al., 2003). Giroud (1996) used the Kozeny-Carmen equation as a reference for deriving the theoretical model for the reduction in the permeability of geotextiles due to soil clogging. Blazejeski and Sadzide (1997) also used the same equation to study the effect of decreasing porosity on sand permeability due to clogging. Wu and Huang (2000) derived a different theoretical equation based on the Kozeny-Carmen equation to study the effects of sediment clogging gravel beds. Tan et al. (2003) formulated a modified version of model developed by Wu & Huang (2000) for the clogging of permeable bases. The equation developed by Tan et al. (2003) is used in the present study to analyse the relative clogging susceptibility of the porous materials tested.

The Kozeny-Carmen model relates the permeability of a porous material to its porosity and tortuosity as shown below:

$$k = (\lambda \rho_w g / \eta_w) [n^3 / (1 - n)^2] (1 / s_v^2) \quad (4)$$

where k = permeability of porous medium (m/s);
 λ = shape factor function of tortuosity of medium;
 ρ_w = density of water (kg/m³);
 g = acceleration due to gravity (m/s²);
 η_w = viscosity of water (kg/m.s);
 n = porosity of permeable medium
 s_v = volumetric specific surface area of permeable medium
 $= 6/d_p$ for spherical particles (m⁻¹)
 $= 4/d_f$ for fibers (m⁻¹);
 d_p = mean particle diameter (m);
 d_f = fiber diameter (m).

The theoretical model formulation adopted by Tan et al. (2003) consists of a relationship between the initial permeability and the permeability at an intermediate stage of clogging of a porous material. This relationship is expressed as a function of its initial porosity, the amount of clogging materials deposited inside the porous material, and an empirical constant which can be considered as a factor that describes the relative permeability deterioration of the porous material during the clogging process. The clogging material retained within the specimen is represented the specific deposit which is defined as,

$$\sigma = V_c / V_T \quad (5)$$

where V_c is the volume of the clogging materials deposited within the porous specimen, and V_T is the

Table 2. Aggregate gradation and mix composition of porous asphalt mix designs studied.

Mix design	Porous asphalt PA-20	Porous asphalt PA-16	Porous asphalt PA-13
Sieve Size	(% passing)	(% passing)	(% passing)
20 mm	100	—	—
16 mm	95	100	—
13.2 mm	85	70	100
9.5 mm	72	59	85
4.75 mm	22	33	45
2.36 mm	18	22	30
1.18 mm	—	16	25
600 um	13	10	20
300 um	9	6	13
150 um	7	4	10
75 um	6	3	4
Asphalt Binder Content	% by Weight of Total Mix Min: 4.5 Max: 5.5	% by Weight of Total Mix Min: 4.5 Max: 5.5	% by Weight of Total Mix Min: 4.5 Max: 5.5

total volume of the porous specimen. V_c is calculated by dividing the mass of clogging material deposited in the test specimen by the density of clogging material.

By introducing an empirical numerical constant term known as the permeability deterioration factor α , Tan et al. (2003) applied the following relationship in the analysis of clogging behaviour of porous materials,

$$k = k_0(1 - n)^2/n^3 \{ (n - \alpha\sigma)^3 / [1 - (n - \alpha\sigma)]^2 \} \quad (6)$$

The permeability deterioration factor α is a positive value numerical constant. It is related to the rate of deterioration of permeability of porous material with respect to the amount of clogging material retained within it. A higher value of α implies a more rapid decrease in permeability for each unit amount of clogging material retained.

3 POROUS ASPHALT PAVEMENT MIXTURES STUDIED

The asphalt mixtures studied were the porous asphalt mixtures used in Singapore road construction. Table 2 shows the aggregate gradations and mix proportions of three open-graded/porous asphalt paving mix designs for pavement wearing course in Singapore: mix PA-13 with porosity ranging from 8 to 12%, mix PA-16 with porosity ranging from 15% to 20% and PA-20 with porosity from around 20% to more than 25%. Granite was used as the aggregate for the mixes. The asphalt binder used was a polymer modified binder of grade PG76-22. The porosity of each mix could be varied by adjusting the binder content within the allowable range of each mix design.

Table 3. Porosity and permeability coefficient values of test specimens.

Target porosity level	Porous asphalt	
	Actual specimen porosity (%)	Permeability coefficient (mm/s)
10%	8.82	2.50
	11.37	2.37
	10.78	2.18
15%	14.03	3.12
	16.23	4.72
	16.42	4.12
20%	18.54	8.67
	18.55	7.93
	21.64	7.67
25%	24.63	12.84
	23.82	11.74
	26.64	19.19

4 ANALYSIS OF TEST RESULTS

For each of the porous asphalt mixture, three specimens each were prepared for the following four target porosity levels: 10%, 15%, 20% and 25%. Each specimen was subjected to a permeability test to determine the initial permeability coefficient of the specimen. This was then followed by the clogging test to determine the deterioration trend of the specimen permeability as clogging developed. As explained earlier, at the end of each stage of addition of the clogging materials, the permeability of the test specimen was measured, and the additional amount of clogging materials retained inside the test specimen was determined.

4.1 Analysis of deterioration trend of permeability

Table 3 presents the porosity and initial permeability coefficient values of the porous asphalt test specimens. Plotted in Figure 2 are the clogging test results of the porous asphalt mixes studied. For each of the four permeability deterioration curves (i.e. one curve for each of the four target porosity levels studied), the range of measured permeability values at each of the 10 stages of the clogging process is also indicated for each stage.

The terminal stage is reached when the permeability deterioration curve begins to level off and there are negligible changes in the permeability coefficient values between successive clogging stages. It is seen from Figure 2 that the higher the initial porosity and permeability of the porous asphalt mixture, the longer it took to reach the terminal stage of clogging. However, in terms of the rate of deterioration of permeability with respect to the clogging process, a porous material with a higher initial porosity actually suffered a higher rate of deterioration.

4.2 Permeability deterioration factor

The rate of deterioration of permeability during the process of clogging can be represented by the

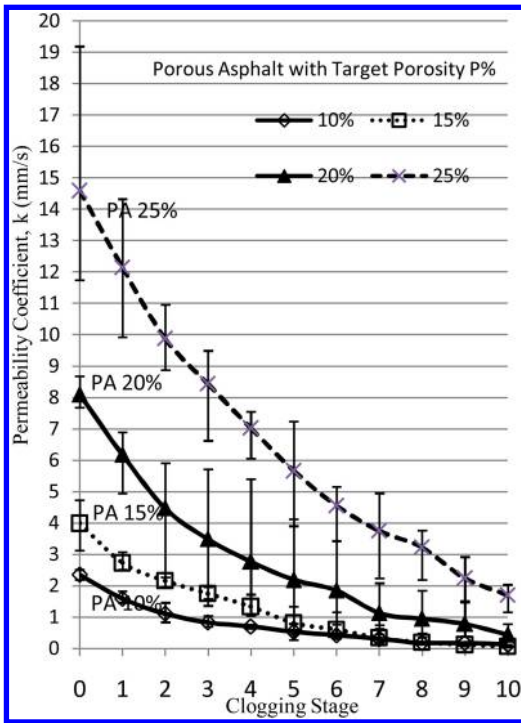


Figure 2. Results of clogging tests.

Table 4. Rates of increase of α with porosity.

Porous asphalt porosity (%)	Permeability deterioration factor α	Rate of increase of α per % rise in porosity
10	4.7	–
15	4.9	4.3%
20	5.2	6.1%
25	5.6	7.7%

permeability deterioration factor α . As explained earlier, a higher value of α implies a more rapid decrease in permeability. Table 4 tabulates the results of computed α values for the different porous asphalt materials tested in this study. These results are plotted in Figure 3.

From Table 4 and Figure 3, it can be noted that porous asphalt mixtures with higher initial porosity suffered higher degrees of clogging and higher rates of deterioration in their permeability. However, as can be seen from Figure 2, despite the higher rates of deterioration in permeability, a porous asphalt mixture with a higher initial porosity and permeability would always maintain a higher level of permeability compared to another porous asphalt mixture with a lower initial porosity and permeability. Hence, with respect to the level of permeability over the span of the service life of a porous asphalt pavement, it is always advantageous

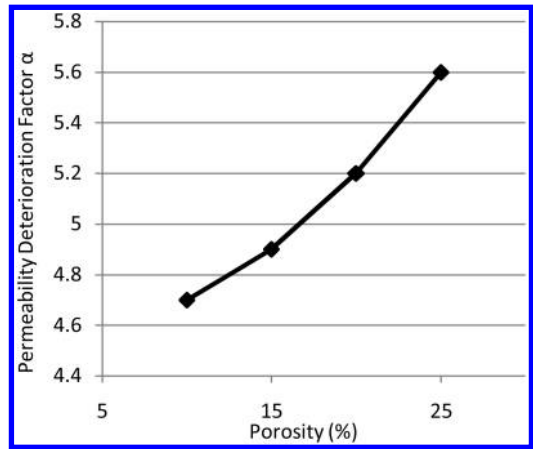


Figure 3. Variation of permeability deterioration factor α with porosity.

to have a porous asphalt mixture with a higher initial porosity and permeability.

The magnitudes of the permeability deterioration factor α are dependent on the properties of the porous asphalt mixtures and the properties of the clogging materials used. The properties of porous asphalt mixtures that would affect the α values include the initial porosity, the gradation of aggregates, and the type and grade of asphalt binder. As for the clogging materials, the type of materials and their gradation would have effects of the value of α .

5 SUMMARY AND CONCLUSIONS

This paper presents the results of a laboratory clogging study to analyse the clogging characteristics of porous asphalt mixtures used in Singapore. The study analyzed the permeability and clogging characteristics of the porous asphalt pavement mixtures at four levels of porosity values: 10%, 15%, 20% and 25%. The experimental setup of the clogging procedure adopted allowed the permeability coefficient of a test specimen to be measured at each stage of the clogging process, and enabled the permeability deterioration trend to be determined until the test specimen was close to being completely clogged when its permeability coefficient was reduced to a level of around 1 mm/s.

The permeability deterioration trends of the test specimens in the clogging process were characterized by a permeability deterioration factor α . A higher value of α implies a more rapid decrease in permeability. The α factor was found to be a function of the initial porosity of the porous asphalt mixtures tested. Although a porous asphalt mixture with a higher porosity tended to have a higher rate of permeability deterioration, it was still found to offer a higher permeability than a mixture with a lower porosity throughout the entire duration of the clogging test.

REFERENCES

- Blazejeski, R & Sadzide, M.B. 1997. Soil clogging phenomena in constructed wetlands with surface flow. *Water Sci. Technol* 35(5): 183–188.
- Bouwer, H. 2002. “Artificial recharge of groundwater: hydrogeology and engineering.” *Hydrogeology* 10(1): 121–142.
- Cooley Jr, Allen, 1999. Permeability of Superpave Mixtures: Evaluation of Field Permeameters *NCAT Report* No. 99–102.
- Deo, O, Sumannasooriya, M., & Neithalath. N. 2010. Permeability Reduction in Pervious Concretes Due to Clogging Experiments and Modeling, *Journal of Materials in Civil Engineering* 22(7): 741–751.
- EPA. 1999. *Preliminary data summary of urban storm water best management practices*. EPA Report EPA-821-R-99-012, U.S. Environmental Protection Agency, Office of Water, Washington D.C, USA.
- Ferguson, B.K. 2005. *Porous Pavements*. Boca Raton, Florida, CRC Press LLC.
- Fwa, T.F., Tan, S.A. & Chuai C. T. 1998. Permeability measurement of base materials using falling-head test apparatus. *Transportation Research Record* 1615: 94–99.
- Fwa, T.F., Tan S.A., & Guwe Y.K. 2002. Laboratory Evaluation of Clogging Potential of Porous Asphalt Mixtures. *Transportation Research Record* 1681: 43–49.
- Giroud, J.P. 1996. Granular filters and geotextile filters. *Proceedings Geofilter '96 Conf*, 565–680.
- Hamzah, M.O., Abdullah N.H., Voskuilen J.L.M. & Bochove G. 2013. Laboratory simulation of the clogging behaviour of single-layer and two-layer porous asphalt. *Road Materials and Pavement Design* 14(1): 107–125.
- Haselbach, L.V., Valavala, S., & Montes, F. 2006. Permeability Predictions for Sand Clogged Portland cement Pervious Concrete Pavement Systems. *Journal of Environmental Management*, 81: 42–49.
- Joung, Y. & Grasley, Z.C. 2008. *Evaluation and Optimization of Durable Pervious Concrete for Use in Urban Areas*. Southwest Region University Transportation Center, Texas Transportation Institute, February Research Rep. SWUTC, pp. 1–64.
- Martin, W.D., Putman, B.J. & Neptune A.I. 2014. Influence of aggregate gradation on clogging characteristics of porous asphalt mixtures. *Journal of Materials in Civil Engineering* 26(7): 04014026-1.
- Nielsen, C.B. 2007. Clogging of Porous Pavements – The Cleaning Experiment. Road Directorate, *Danish Road Institute*. www.roaddirectorate.dk.
- Scholz, M. & Grabowiecki, P. 2007. Review of permeable pavement system. *Building and Environment* 42(11): 3830–3836.
- Siriwardene, N.R., Deletic, A., & Fletcher, T.D., 2007 Clogging of stormwater gravel infiltration systems and filters: insights from a laboratory study. *Water Research* 41(7): 1433–1440.
- Tan, S.A., Fwa T.F., & Guwe Y.K. 2000. Laboratory Measurements and Analysis of Clogging Mechanism of Porous Asphalt Mixes. *Journal of Testing and Evaluation* 28(3): 207–216.
- Tan, S.A., Fwa, T.F., & Han, C.T. 2003. Clogging evaluation of permeable bases. *Journal of Transportation Engineering* 129(3): 309–315.
- Tan, S.A., Fwa, T.F., & Chuai C.T. 1999. Automatic Field permeameter for drainage properties of porous asphalt mixes. *Journal of Testing and Evaluation* 27(1): 57–62.
- Wu, F.C & Huang, H.T. 2000. Hydraulic resistance induced by deposition of sediment in porous medium. *Journal of Hydraulic Engineering* 126(7): 547–551.
- Yong, C.F., Deletic, A., Fletcher T.D., & Grace, M.R. 2008. The clogging behavior and treatment efficiency of a range of porous pavements. In: *11th International Conference on Urban Drainage*, Edinburgh, Scotland, UK.

Determination of the scuffing resistance of porous asphalt using annex A of prTS 12697-50 (the ARTe)

Maarten M.J. Jacobs, Rémy C.M.A. van den Beemt & Mark H.T. Frunt
BAM Infra Asfalt, Utrecht, The Netherlands

ABSTRACT: In the current version of prTS 12697-50, the Aachener Ravelling Tester (ARTe) is mentioned as one of the tests to determine the resistance to scuffing of an asphalt mixture. In the last 4 years, the ARTe has been used by BAM Infra Asfalt to characterise the scuffing resistance of porous asphalt mixes. In this research programme, the loss of aggregates due to ravelling has been determined using 3 procedures: visual inspection, loss of mass of the specimen and change in texture of the surface of the specimen. The change in surface texture of the slab has been determined using a laser scanning device with 2 lasers which are able to determine an accurate 3-D image of the surface.

In the test programme one type of a porous asphalt mixtures has been tested with a variation in bitumen content. From the test programme it is concluded that the ARTe is able to generate test results which comply to the behaviour of porous asphalt mixtures in practice: the less bitumen is used, the shorter the life span of a porous asphalt mixture will be. The test programme also indicates that material loss due to ravelling is determined more accurately using the laser scanner (change in texture) than using loss of mass.

In the paper the test programme, test devices (ARTe and laser scanner) and test results will be presented and discussed.

1 INTRODUCTION

Ravelling is the prevailing damage pattern of noise reducing asphalt layers like porous asphalt (PA) or thin noise reducing (TNR) asphalt layers. Ravelling is a process that develops rather quickly: for a long time the noise reducing asphalt layer will show no damage, but after reaching a critical boundary value the material loss will develop explosively. Under detrimental weather conditions a noise reducing surface layer will fail within one winter.

Often noise reducing asphalt layers are used in contracts with a long guarantee period. To be sure that the life span of a noise reducing layer will not cause problems during this period, a lot of research is carried out to optimize the life span (and so the ravelling resistance) of noise reducing asphalt layers. Although in practice the ravelling process is very complex, where properties like strength, flexibility, deflections and temperature stresses play an important role (Huurman (2012); Van de Ven (2012)), it is tried to simulate the ravelling process under lab conditions as good as it gets. In this way the revealing properties of asphalt mixtures can be optimized. One of the devices that are used in ravelling research is the ARTe, the Aachener Ravelling Tester.

The ARTe is one of the four devices that are mentioned in the European Technical Specification TS 12697-50 'Resistance to Scuffing'. This TS is the

precursor of a European standard (EN). The purpose of a TS is to get experiences with various test devices. After a few years these experiences are used to choose for the best performing test device. This device will be mentioned in the TS 12697-50.

In prTS 12697-50 three different methods are mentioned to describe the amount of ravelling:

- Based on differences noticed during the visual inspection of the tested surface before and after the test;
- Based on the weight difference of the specimen before and after the test;
- Based on the change of the surface texture before and after the test.

In this paper the experiences with the ARTe in the last two years are discussed. The configuration of the ARTe is optimized and an extensive test programme has been carried out with this device. Also the experiences with a surface scan device (SSD) will be discussed. With this SSD, the changes of the surface texture due to the ravelling of the test specimen in the ARTe can be measured objectively. It should be noticed that this SSD is not only applicable to measure stone loss due to ravelling, it also can be used to measure the texture or a change in texture of a pavement surface in practice or to scan cracked surfaces after crack propagation tests.

2 OPTIMISATION OF THE ARTE

Jacobs (2012) already described the ARTe comprehensively. The standard test procedure during a test with the ARTe can be summarized as:

- The standard surface area of the tested slab is 500 by 500 mm. Also slabs of 500 by 320 mm or 2 slabs each of 320 by 240 mm or 4 cores with a diameter of 150 mm can be tested in the ARTe;
- The thickness of the slabs can vary between 30 and 80 mm;
- The test temperature is $20 \pm 2^\circ\text{C}$;
- The temperature of the surface during the test should be lower than 25°C . To achieve this, the ratio between loading time and rest period is 1:1;
- The speed of the lateral moving table is $0,3 \pm 0,03$ m/s;
- The set of tyres rotates with a speed of 47 ± 1 rpm;
- The tyre pressure of the two tyres is 230 ± 10 kPa;
- The total mass of the set of tyres is 250 ± 5 kg;
- The used tyres are profiled with dimensions 165/75R14;
- In a standard test, the lateral moving table is moving 600 times vice versa.

With respect to the description Jacobs (2012) gave, two important changes have been implemented: one concerns the used tyres and one has to do with the test temperature and the temperature of the loaded surface during the test.

With respect to the tyres first it was the intention to use 2 smooth unprofiled PIARC-tyres. These tyres are also used to determine the skid resistance of road surfaces in accordance with CEN/TS 15901-9. It was assumed that these PIARC tyres should have a positive effect on the repeat- and reproducibility of the test over the years. Indeed the quality of the PIARC test tyres shall be constant over the years and these tyres will stay identical over the years with respect to rubber composition and hardness. However during the tests in the ARTe, the asphalt slabs show an extreme lubrication of the surface due to rubber from the PIARC-tyre. The rubber from the tyre was mixed with mastic from the asphalt slab and pushed into the air voids of the asphalt. This causes a substantial disturbance of the ravelling process. For this reason a standard profiled 165/75 R14 tyre is used in the ARTe.

The second important factor is the temperature of the slab during the test. Normally the test is performed in a temperature controlled room with a temperature of $20 \pm 2^\circ\text{C}$. Due to the large friction forces during the scuffing test, the temperature of the tyre and the slab increases substantially. This raise in temperature should be limited to avoid negative effects on the scuffing process in the ARTe. The temperature raise can be limited by using fans to cool the surface of the slab and the tyres. Also a rest period between the load repetitions is introduced. At the end a loading-rest period of 1:1 and forces cooling are used to keep the surface temperature of the slab below 25°C .

Table 1. PA mixture composition.

Mix	Code Ref.	A	B	C	D
Mixture composition (%m/m)					
Bitumen 70/100	5.1	3.7	4.2	4.7	5.5
Anti bleeding agent	0.2	0.14	0.16	0.18	0.22
Filler	5.3	3.8	4.3	4.8	5.7
Crushed sand	6.9	7.2	7.1	7.0	6.9
Aggregate 4/8	22.1	22.9	22.5	22.3	22.0
Aggregate 8/11	44.5	46.0	45.6	45.1	44.0
Aggregate 11/16	15.8	16.3	16.1	15.9	15.7
Grading (%m/m)					
Through C22,4	100.0	100.0	100.0	100.0	100.0
Through C16	98.4	98.4	98.4	98.4	98.4
Through C11,2	80.0	79.7	79.8	79.9	80.1
Through C8	40.0	39.0	39.3	39.6	40.4
Through C5,6	23.0	21.7	22.1	22.5	23.4
Through 2 mm	13.0	11.6	12.2	12.5	13.5
Through 500 μm	8.0	6.4	6.9	7.4	8.5
Through 63 μm	5.5	4.1	4.6	5.0	6.0
Mixture properties (kg/m^3)					
Maximum density	2494	2550	2530	2510	2478
Bulk density	1973	2016	2001	1985	1959
Air voids (%v/v)	20.9	21.0	20.9	20.9	20.9

Table 2. Bulk density of the tested slabs.

Mixture	Code Ref.	A	B	C	D
Bulk density (kg/m^3)					
Slab 1	1972	2013	2001	1984	1960
Slab 2	1972	2014	2003	1989	1963

3 VERIFICATION OF THE ARTE

After the optimisation of the test configuration, a verification test programme has been performed to find out whether the ARTe is able to predict the scuffing resistance in the right way. In a test programme a porous asphalt mixture with 5 different quantities of bitumen were tested. However, the composition and quality of the mastic for all the 5 mixtures is identical. So with changing the amount of bitumen, also the amount of filler is changed. It is expected that the amount of ravelling will increase with decrease of the amount of bitumen in the PA. In total 5 different PA mixtures are tested as shown in Table 1.

For each mixture 2 slabs are prepared. The measured bulk density of the slabs are presented in Table 2.

The obtained densities of the test slabs coincide very well with the desired densities. Before testing, all the

Table 3. Loss of mass during the scuffing test with the ARTe.

Mixture	Bitumen content (%m/m)				
	5.1	3.7	4.2	4.7	5.5
Mass loss halfway the test (grams)					
Slab 1	20	12	11	12	3
Slab 2	25	18	20	5	2
Average	22.5	15	15.5	8.5	2.5
Mass loss at the end of the test (grams)					
Slab 1	62	34	45	32	27
Slab 2	80	50	57	17	18
Average	71	42	51	24.5	22.5

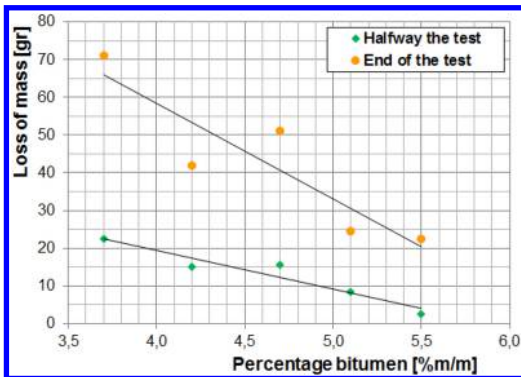


Figure 1. Material loss halfway and at the end of the scuffing test in the ARTe.

slabs are laboratory aged using the so-called Mandela ageing procedure: slabs on a perforated plate in an oven for 44 hours at 135°C (Van de Ven, 2012).

As already mentioned before, the resistance to scuffing is related to the loss of mass of the tested slab due to the disappearance of aggregate parts during the test. So the mass of the slabs before and after the test in the ARTe is measured. Also the loss of mass after half of the number of load repetitions is measured. In Table 3 and Figure 1 the data are presented.

From the test results, the following conclusions can be drawn:

1. The ravelling process does not pass linearly with time: halfway the test the material loss is about 30% of the material loss at the end of the scuffing test;
2. The results of the tests coincide pretty well with the expectations: the resistance to scuffing decreases (i.e. the material loss increases) as the amount of mastic in the PA slab decreases. However, the results are not consistent: some results (especially the slabs with 4.7% m/m bitumen) deviate from the trend. During the evaluation of the tests, it was found that for the slabs with 4.7% bitumen relatively much ravelling occurred close to the edges



Figure 2. Overall and detailed picture of the ATS.

of the slab. This damage, which is caused by the weakening of the material due to the preparation of the slabs during sawing and due to discontinuities of the sideways confinement of the slabs in the test device, causes an disturbance of the real ravelling process in the scuffing test.

To overcome the problems with material loss near the edges of the slabs, the ravelling damage is also determined using texture measurements. This will be discussed in the next paragraph.

4 DETERMINATION OF MATERIAL LOSS USING TEXTURE MEASUREMENTS

As already mentioned before, in the European technical standard prTS 12697-50 three possible ways are mentioned to determine the ravelling damage. One of the possibilities is to determine the change in texture of the surface of the slab due to stone loss in the scuffing test. To measure the material loss, BAM Infra Asphalt built an Asphalt Texture Scanner (ATS) which can measure the surface of a slab very accurately. By measuring the texture before and after the scuffing test, the difference between these two scans determines the amount of material loss during the scuffing test. In Figure 2 pictures of the ATS are given.

The ATS exists of a stiff frame where a rail and carriage is built in. On this carriage a camera and two lasers are mounted. The two lasers, one produces a green and the other a red laser line, are mounted

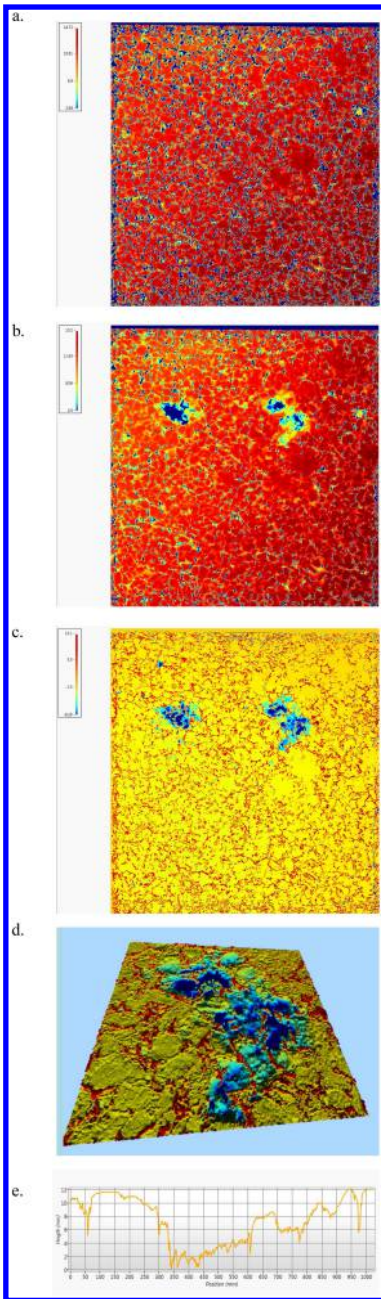


Figure 3. Results from the ATS measurements of a PA slab with 5.5% bitumen: (a) top view slab before the scuffing test, (b) top view slab after the scuffing test, (c) calculated difference before and after the test, (d) 3D picture of the material loss at the right side of the slab, (e) 2D picture of the material loss at the left side of the slab.

under different angles on the carriage. In the ATS the 2S Scanning Stereo Laser Triangulation (2DSSLT) is used. The advantage of this measuring technique is that occlusion, due to the invincibility of the surface caused by the fact that a laser beam cannot look around an

Table 4. Volume of the material loss due to the scuffing test.

Mixture	Bitumen content (%m/m)				
	5.1	3.7	4.2	4.7	5.5
	Volume of material loss (mm ³)				
Slab 1	49340	42200	51070	24860	21650
Slab 2	52680	45090	28470	35130	34940
Average	51010	43645	39770	29995	28295

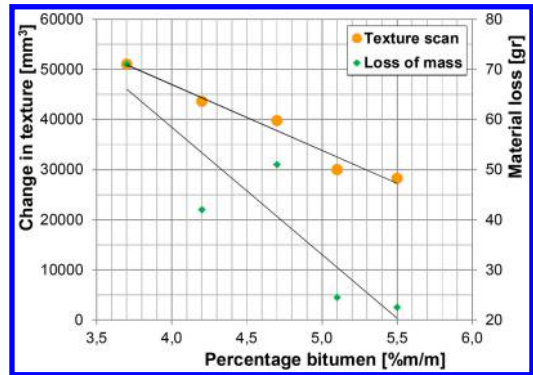


Figure 4. Change in texture volume and change in mass due to material loss in the scuffing test.

aggregate particle, in x- and y-direction can be eliminated. Besides that, the 2DSSLT-measuring device has the advantage that the measurements are very accurate without the necessity for an extreme large loading frame. The specifications of the ATS are:

- Maximum seize scanned surface: 400-400 mm;
- Accuracy in x-, y- and z-direction: 0.1 mm;
- Scanning speed at highest resolution: 50 minutes;
- Maximum measuring depth: 30 mm;
- Possibilities to make a 3D-scan of the measured surface. Also 2D scans are available to determine texture parameters (e.g. MPD);
- It is possible to compute the differences between two scans, e.g. between a scan performed before and after a scuffing test.

With the ATS it is possible to eliminate the ravelling near the edges of the slabs.

In the test programme all the slabs are measured in the ATS before and after the scuffing test with the ARTe. In Figure 3 some test results with the ATS are presented.

In Table 4 the material loss due to ravelling in the scuffing test is summarized. The data are calculated using a scanned surface of 400-400 mm and a accuracy of the measurements of 0.1 mm. The material loss is given in a volume of the missing aggregate parts.

In Figure 4 the results of the texture scans of the raveld surfaces are presented graphically. These scans cover a surface area of 400-400 mm. Also the loss of

mass of the slabs are given, based on a surface area of 500·500 mm.

From Figure 4 it is concluded that there is a more consistent view of the material loss in a scuffing test when the ravelling at the edges of the slabs is not taken into account in the seriousness of the ravelling.

5 CONCLUSIONS AND RECOMMENDATIONS

Based on the results of the research plan the following conclusions and recommendations can be formulated:

1. With the ARTe a ravelling process can be generated that meets the expectations and the behaviour in practice:
 - the more bitumen/mastic, the higher the resistance to ravelling;
 - the material loss increases exponential with the number of load repetitions.

At this moment it is not clear yet how the results of the laboratory measurements with the ARTe coincide with behaviour of PA mixtures in practice. With this respect, not only the scuffing device itself plays an important role but also the ageing procedure in the lab is very important;

2. In a scuffing test, the material loss near the edges of the specimen gives a nonexistent view of the actual resistance to ravelling of an asphalt mixture. Therefore, the material loss near the edges of the specimen/slab has to be eliminated from the test results;
3. By scanning only a part of the specimen, excluding the edges of the slab, the influence of undesired ravelling near the edges/discontinuities of the specimen can be removed from the test results.

REFERENCES

- Huurman M. *et al* (2012). LOT Winter damage theory: Validation and understanding of winter damage in porous asphalt. Paper O5EE-518 Eurasphalt & Eurobitume Congress, Istanbul.
- Jacobs M.M.J. *et al* (2012). Bepaling van de rafelings-eigenschappen van open asfaltmengsels met de ARTe (in Dutch). Paper CROW-Infradagen 2012, Ede, the Netherlands.
- Van de Ven M.F.C. *et al* (2012). Practical laboratory ageing method for porous asphalt. Paper A5EE-219 Eurasphalt & Eurobitume Congress, Istanbul.

Investigating the packing condition of Porous Asphalt Mixture (PAM) using Discrete Element Method (DEM)

M.J. Chen & Y.D. Wong

School of Civil and Environmental Engineering, Nanyang Technological University, Singapore

ABSTRACT: Packing condition is an important factor to asphalt mixture's mechanical performance. Porous Asphalt Mixture (PAM), with a characteristic feature of open-graded design, is beneficial for driving safety and environment. However, current gradation design methods are mostly based on dense gradations, and little research has been conducted in providing explicit and direct parameters to represent the packing condition in a mixture. In this study, six PAM gradations were designed and relevant parameters were obtained from both laboratory experiments and Discrete Element Method (DEM) simulation. Simulation results showed that the development of packing condition is not only related to the percentage of fines fraction, but also the proportions of particles within various size ranges, which corroborated with laboratory measurements. Hence DEM is an effective tool in analysing the packing condition in a mixture, and the findings should be a useful guide in PAM gradation design.

1 INTRODUCTION

As a kind of material used on surface layer of pavements, asphalt mixture is a three-phase material, generally being constituted of asphalt binder, mineral aggregates and air voids. Asphalt mixture's capability in bearing traffic loads and resisting deformation is mainly attributed to aggregate gradation, aggregate shape and surface texture, amount and type of asphalt binder, and compaction effort, among which aggregate gradation is the most unstructured factor and deserves more attention (Vavrik et al. 2002). In terms of Porous Asphalt Mixture (PAM), the most distinct feature is the open-graded design, namely coarse aggregates accounts dominantly in aggregate blend which are up to 70%~80% by mass (Rajib et al. 2000), resulting in the high content of air voids by volume, namely usually greater than 20%. Advantages from the high inter-connected air voids content of PAM material include mitigating aquaplaning, reducing splash and spray, enhancing skid resistance, lowering noise level, and generating cooling effect. (Fabb 1998; Khalid & Jimenez 1995), making it a suitable type of paving material for a tropical country like Singapore where temperature is high throughout the year and downpours occur frequently during two monsoon periods (namely northeast monsoon and southwest monsoon).

Given the high content of coarse aggregates in PAM, the aggregate packing is mostly created by the stone-to-stone skeleton formed by coarse aggregates (Hamzah & Cabrera 1996). However, most conventional methods of aggregate gradation design and associated packing theories are based on dense asphalt

mixture, such as Fuller's maximum density curve and Bailey method (Fuller & Thompson 1907; Vavrik et al. 2002). Meanwhile, desired packing condition achieved by selecting a proper value of Chosen Unit Wight (CUW) in Bailey method does not necessary lead to an adequate coarse aggregate structure (Shen & Yu 2011a; Sungho et al. 2009). Additionally, there is a tendency to shift the break point of PAM gradation further regarding gradation curve, aiming to improving PAM's stone-to-stone contact hence enhancing the strength and stability (Hasan et al. 2013).

On the other hand, conventional design method procedure is a trial-and-error process and substantial laboratory work and materials are involved. Therefore numerical simulation methods have been introduced in mixture design, wherein Finite Element Method (FEM) and Discrete Element Method (DEM) are the two general types. FEM is based on continuum theory and is available for dealing with the problems in relatively homogeneous objects (Cook et al. 2002). Due to its deficiency in solving the issue of slippage among aggregates in micro-mechanism, FEM is not suitable for simulating and analysing interlocking condition of compacted aggregates. In contrast, the characteristic capability of DEM is modelling particle-to-particle interaction can provide a good insight of the micro-mechanism in an assembly of particles, which is achieved by the alternate calculations between the equation of motion (namely Newton's second law) and force-displacement law (Cundall 1971; Cundall 1988). In terms of PAM, the main components are coarse aggregates and asphalt mastic (which is formed by asphalt binder, fine aggregates, and fillers),

thus it is more appropriate to regard PAM as a kind of discrete material and accordingly analyse the development of particle-to-particle interlocking within PAM material using DEM rather than FEM.

2 RESEARCH METHODOLOGY

2.1 PAM gradation design

Breaking sieve is an important factor in aggregate gradation, which is the sieve to differentiate coarse and fine fractions in an aggregate blend. Conventionally the size of breaking sieve is fixed as 4.75 mm (Rajib et al. 2000); and in Bailey method, it is selected as the one closest to $0.22 \times \text{NMAS}$ (nominal maximum aggregate size). In the case of PAM, higher air voids content is generally related to lower strength but better performance in permeability, which is controlled by having a lower proportion of fine aggregates. To ensure adequate performance in both aspects of strength and drainage, fine aggregates are suggested to be represented within the range of 15%–20% (Rajib et al. 2000). Based on existing PAM gradations proposed by various researchers (Boving et al. 2004; LTA, 2010; PennDOT, 2006), six PAM gradations were designed as given in Table 1, with the content of filler (aggregates of size smaller than 0.075 mm) set at 5%.

2.2 Laboratory experiments

2.2.1 Preparation of PAM specimens

Indonesian granite and asphalt graded as PG76 were used in this study as raw materials. Cylindrical PAM specimens were fabricated using gyratory compactor by 50 gyrations to simulate in-field compaction condition (AI 1996). In addition, given the weaker structure of PAM material as compared to conventional dense asphalt mixtures, ram pressure used in compaction was reduced to 300 kPa to avoid excessive aggregate breakage, rather than the ram pressure of 600 kPa suggested by AI (1996).

In terms of asphalt binder content, estimated binder content (EBC) was initially determined by aggregate surface area and thickness of asphalt film (AI 1997), and was subsequently adjusted according to draindown test and Cantabro test.

Draindown test and Cantabro test are widely used in PAM material to determine the upper limit and lower limit of binder content, respectively. Draindown test is conducted on loose asphalt mixture, and it is presented by the percentage of mastic loss as sample is heated in an oven at mixing temperature for one hour. Extreme draindown value generally happens in cases of overly-high content of asphalt binder or an inadequate amount of fines and fillers to form asphalt mastic, which may lead to bleeding and rutting; the recommended draindown value is lower than 0.3% by mass (Rajib et al. 2000). Cantabro test is used to evaluate PAM's resistance to abrasion, which is similar to Los Angeles (LA) abrasion test except that no steel ball is added in the

Table 1. Design of six gradations.

Sieve size mm	Passing percentage by mass					
	G1	G2	G3	G4	G5	G6
19	100	100	100	100	100	100
13.2	80	85	95	85	90	95
9.5	72	70	51	75	66	59
6.3	40	60	40	60	30	50
4.75	35	30	24	44	21	42
2.36	15	10	20	20	15	10
1.18	13	9	17	17	13	9
0.6	11	8	14	14	11	8
0.3	9	7	11	11	9	7
0.15	7	6	8	8	7	6
0.075	5	5	5	5	5	5

revolving drum chamber, and the PAM sample experiences 300 revolutions in the drum chamber at a speed of 30–33 rpm at 25°C. The result is denoted as abrasion loss value (ALV) and calculated as percentage weight loss after abrasion. The upper limit of abrasion loss value is recommended as 20% (Rajib et al. 2000). Meanwhile, it should be noticed that the asphalt temperature during Cantabro test are subject to change depending on the ambient temperature, influencing the sample's resistance to abrasion.

2.2.2 Volumetric measurements

As a kind of permeable material, air voids content is an important volumetric parameter for PAM, which is directly related to the essential function of drainage. Bulk density and theoretical maximum density (TMD) were respectively measured through geometry method and Rice test in the laboratory, so as to gain air voids content for each PAM design.

2.2.3 Performance tests

Performance in permeability is the basic function for PAM material, which is dependent on the amount and inter-connectivity of air voids. On the other hand, the increase in permeability or air voids content is generally at the cost of mixture's strength. In this study, permeameter suggested by Florida method was used to obtain coefficient of permeability (k) (Florida DOT 2004). Marshall stability was measured as well to assess samples' strength (ASTM 7 2006), and samples were conditioned in a water bath at 60°C for 30 minutes before loading.

2.3 Discrete Element Method (DEM) simulation approach

Particle Flow Code in 3 Dimensions (PFC3D), which is a kind of application software based on DEM (Itasca 2008), is utilised to simulate and analyse the packing condition in PAM groups in this study. PFC3D possesses the advantages in several aspects: (1) physical attributes measured in reality can be directly assigned to the elements in the model; (2) frictional behaviour

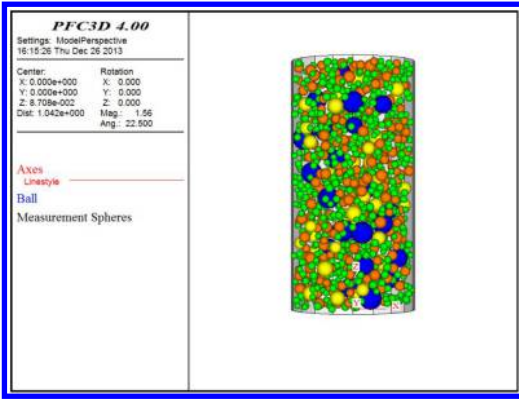


Figure 1. PAM model generated in PFC3D model.

among particles can be handled by setting proper slip and separation model; (3) particle-to-particle interaction can be explicitly described by contact-stiffness model; and (4) simulation parameters can be calculated along cycling (iteration) process.

The calculation process in PFC3D is a dynamic process, which is exerted on each particle and contact in each iteration, and the computation efficiency decreases with the incremental of contacts in a model (Liu & You 2011). The configuration of the PC applied for computation work in this study was: CPU of Core™ i7, RAM of 8.0 GB, and Operating System of 64-bit.

2.3.1 Generation of PAM model

In the PFC3D model, a cylindrical mould was established with radius of 50 mm and height of 200 mm. For each designed PAM (see Table 1), an assembly of particles according to designed PAM was generated in the mould with a total mass of 1,000 g. Herein, given particle-to-particle skeleton in PAM is mostly created by coarse aggregates, particles smaller than 2.36 mm were not created so as to guarantee adequate computational efficiency (see Figure 1). Particles in the model were represented by spheres and take into account the effects of irregular shape by setting proper friction coefficient across aggregate contacts.

Contact model selected in this study is Hertz model, which is suitable to describe contact behaviour among granular material without bonds, namely dominant loading condition is exclusively compressive stress and small strain (Itasca 2008). The mechanical and physical parameters set in the model were based on previous research on granite: elastic modulus and friction coefficient of the mould were 300 GPa and 0.0, respectively; shear modulus and Poisson ratio of the particles were 25 GPa and 0.2, respectively; and friction coefficient among particles were set at 0.5 to simulate the aggregate surface roughness and particle-to-particle sliding behaviour (Abbas et al. 2005; Kim & Buttlar 2009; Lu & McDowell 2007; Shen & Yu 2011b; You et al. 2008).

2.3.2 Compaction by magnification gravitation

Two compaction approaches are generally used in PFC3D to compact an assembly of particles, namely ‘applying gravitation method’ and ‘moving wall method’ (Itasca 2008). Due to the difficulty in determining the final height of assembly in ‘moving wall method’, herein PAM groups in PFC3D were compacted by applying gravitation.

A magnified gravitation method with magnification factor (MF) of 1,000 was used to quickly realise adequate interlocking condition for two considerations:

- The computation efficiency for a loose assembly to get compacted increases with the magnitude of applied gravitation, and meanwhile a MF value of 1,000 will not result in breakage within the models established for this study;
- ‘Applying gravitation method’ can be regarded as a process of consolidation and the pressure exerted on each particle is linearly proportionate to the total weight of particles above it. Hence, taking particles in the mid-height of the assembly as an average case, then the average pressure P can be obtained according to Equation 1 below, which equals to 625 kPa, which is very close to the recommended pressure of 600 kPa by AI (1996).

$$P = \frac{G}{A} = \frac{M_{half} \times g \times MF}{\pi \times R^2} \quad (1)$$

where M_{half} = half mass of the particles in PFC3D model, which equals to 0.5 kg; g = normal gravitation, namely 9.81 m/s²; and R = radius of the cylindrical mould, namely 0.05 m.

2.3.3 Simulation parameters

Four simulation parameters provided by PFC3D model were traced and recorded along the process of cycling, which are: (1) unbalanced force (UF), the mean value of out-of-balance force in assembly of particles; (2) contact force (CF), the mean value of normal force among effective contacts in PFC3D model, wherein effective contact means the contact with non-zero normal force; (3) porosity (n), the proportion of voids by volume; and (4) coordination number (C_n), the mean number of effective contacts around per particle. In addition, five measurement spheres were created at the bottom of the cylindrical mould in order to trace porosity and coordination number (see Figure 2).

3 RESULTS AND DISCUSSION

3.1 Experimental results

3.1.1 Determination of binder content

The selected binder contents for the six PAMs are given in Table 2. Binder contents for the PAMs were obtained based on aggregate surface area, and results from draindown test and Cantabro test were obtained to evaluate the feasibility of estimated binder content for the six PAMs. It can be found that binder

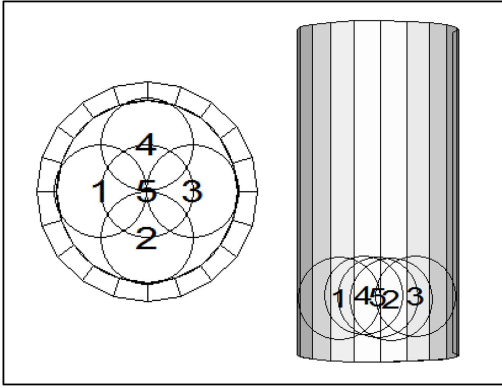


Figure 2. Top view (left) and side view (right) of measurement spheres.

Table 2. Determination of binder content.

Group	Binder content %	Draindown %	Abrasion loss value %
G1	4.3	0.00 (± 0.00)*	11.5 (± 1.9)
G2	3.8	0.00 (± 0.00)	23.3 (± 4.1)
	4.3	0.02 (± 0.01)	10.3 (± 3.7)
G3	4.7	0.02 (± 0.01)	9.5 (± 2.7)
G4	4.8	0.01 (± 0.01)	5.7 (± 2.2)
G5	4.2	0.00 (± 0.00)	15.6 (± 2.2)
G6	4.3	0.00 (± 0.00)	18.1 (± 5.3)

*value in parenthesis refers to standard deviation.

content was rational for almost all the PAMs except G2 due to the large abrasion loss value (ALV) from Cantabro test. Thus binder content was increased by 0.5% to achieve sufficient resistance to abrasion. It was also found that requirement for draindown test can be easily meet using PG76 asphalt at estimated binder content, and PAM's resistance to mechanical abrasion increased with asphalt binder content.

3.1.2 Volumetric parameters and performance of PAM groups

The results of volumetric measurements and performance tests (including permeability and Marshall stability) of the six PAM groups are given in Table 3 and Table 4, respectively. It was found that G1, G3, and G4 groups possessed relatively lower permeability and higher Marshall stability as compared with the other three PAM groups, which can be ascribed to the relatively lower air voids content in the former. With reference to the gradation design, the lower air voids content in G3 and G4 groups can be attributed to the higher proportion in fines fraction; the percentage of particles passing 2.36 mm sieve in the two PAM groups was 20% while that in the other groups was 15% or 10%. For G1 group, although the percentage of particles finer than 2.36 mm was 15%, which was the same as that in G5, the percentage of particles

Table 3. Volumetric parameters.

Group	Bulk density (g/cm^3)	Air voids content %
G1	2.02 (± 0.002)	16.5
G2	1.90 (± 0.001)	22.4
G3	2.05 (± 0.011)	16.0
G4	2.08 (± 0.005)	14.4
G5	1.96 (± 0.019)	24.3
G6	1.93 (± 0.001)	21.5

Table 4. Permeability and Marshall stability.

Group	Coefficient of permeability, k (cm/s)	Marshall stability (kN)
G1	0.13 (± 0.043)	7.6 (± 1.2)
G2	0.27 (± 0.005)	5.2 (± 0.2)
G3	0.07 (± 0.076)	8.6 (± 0.3)
G4	0.04 (± 0.012)	7.4 (± 0.8)
G5	0.21 (± 0.008)	5.5 (± 0.9)
G6	0.23 (± 0.052)	5.2 (± 0.7)

within 4.75 mm–2.36 mm was 20%, which was 6% higher than that in G5, thereby rendering the lower air voids content in G1 group. It was further found that, air voids content, as a relevant parameter to evaluate packing condition in PAM, is not only attributed to the percentage of fines fraction in terms of aggregate gradation, but also dependent on the proportions of particles in various size ranges.

3.2 DEM simulation results and discussion

In order to evaluate the development of packing condition within particle-to-particle framework, for each PAM group, four types of PFC3D models were established, which are Model(19.0-9.5), Model(19.0-6.3), Model(19.0-4.75), and Model(19.0-2.36), presenting the model constituting particles in the size ranges of 19.0 mm–9.5 mm, 19.0 mm–6.3 mm, 19.0 mm–4.75 mm, and 19.0 mm–2.36 mm, respectively. The proportions of the particles in each model were obtained according to the gradation design (see Table 1) while maintaining the total mass of particles as 1,000 g in each model.

3.2.1 Stability and equilibrium of compacted PAM groups

In PFC3D models, the stability and equilibrium of model should be evaluated in advance to ensure the rationality of later analysis based on simulation parameters. In terms of stability, it can be estimated via coordination number (Jiang et al. 2011). For the six PAM groups, the coordination number was all able to converge to an approximately constant value, indicating that the stability condition could be realised in the PAM groups along the process of compaction in

Table 5. UF/CF values of PAM groups in PFC3D models.

Group	Model (19.0-9.5)	Model (19.0-6.3)	Model (19.0-4.75)	Model (19.0-2.36)
G1	1.15E-12	8.93E-05	4.65E-05	1.48E-05
G2	5.38E-04	3.47E-05	1.30E-08	1.24E-05
G3	3.40E-04	2.77E-13	1.18E-04	2.71E-05
G4	2.23E-04	1.27E-04	1.10E-05	2.59E-05
G5	7.37E-04	4.51E-11	1.23E-04	1.32E-04
G6	1.39E-03	3.37E-04	1.47E-05	5.53E-04

Table 6. Porosity in PAM groups in PFC3D models.

Group	Model (19.0-9.5)	Model (19.0-6.3)	Model (19.0-4.75)	Model (19.0-2.36)
G1	42.8	42.0	41.1	38.1
G2	45.0	41.3	39.1	38.3
G3	43.3	42.7	39.9	41.7
G4	41.0	41.0	38.5	37.6
G5	41.4	42.3	42.6	39.9
G6	44.9	42.7	41.0	36.7

PFC3D model. Regarding equilibrium, it can be evaluated via the ratio of unbalanced force and contact force, namely UF/CF value. The UF/CF values for the six PAM groups in the final stage of cycling are given in Table 5, and it was found that all the UF/CF values were less than 0.001, being the upper limit suggested by Itasca (2008), which means all the six PAM groups achieved equilibrated condition upon compaction.

3.2.2 Porosity of PAM groups

Porosity, which is a simulation parameter that possesses similar meaning to voids content as measured in the laboratory, is an important parameter to describe aggregate interlocking.

Table 6 gives the resultant porosity in each type of PFC3D model for the six PAM groups. It was found that, for each PAM group, porosity generally decreases as finer particles are added in, indicating the process of packing development. This can be attributed to the fact that the void sizes are reduced due to the rearrangement of particles as finer particles are added in, and large and/or medium voids are partially filled by the finer particles as well.

3.2.3 Coordination number of PAM groups

Coordination number (CN) reflects the general situation of effective contacts around each particle, thus it is a significant parameter to describe particle-to-particle skeleton in an assembly of particles. For each PAM group, the coordination number within various size ranges in the four types of PFC3D model were recorded as shown in Table 7. For example, in Model(19.0-2.36), coordination number among 19.0mm–9.5mm particles is given as well, which

Table 7. Coordination number developed within various size ranges.

	Size range mm	Model (19.0-9.5)	Model (19.0-6.3)	Model (19.0-4.75)	Model (19.0-2.36)
G1	19.0-9.5	4.22	1.41	1.59	0.84
	19.0-6.3	4.33	3.83	2.55	
	19.0-4.75			4.33	2.75
	19.0-2.36				4.47
G2	19.0-9.5	4.12	2.77	1.53	0.93
	19.0-6.3		4.19	1.95	1.27
	19.0-4.75			4.45	2.98
	19.0-2.36				4.51
G3	19.0-9.5	4.26	3.31	2.45	2.32
	19.0-6.3	4.31	3.09	2.93	
	19.0-4.75			4.40	3.98
	19.0-2.36				4.38
G4	19.0-9.5	4.16	2.05	1.54	0.85
	19.0-6.3	4.27	2.60	1.66	
	19.0-4.75			4.43	2.57
	19.0-2.36				4.54
G5	19.0-9.5	4.16	2.01	1.44	1.11
	19.0-6.3	4.33	3.64	3.14	
	19.0-4.75			4.32	3.78
	19.0-2.36				4.34
G6	19.0-9.5	4.24	3.35	2.83	1.34
	19.0-6.3	4.32	3.48	1.74	
	19.0-4.75			4.34	2.11
	19.0-2.36				4.52

equals 0.84 for G1 group; this means that, as 19.0 mm–2.36 mm particles are generated and compacted for G1 group, the average effective contacts within 19.0 mm–9.5 mm particles is 0.84.

It should be noted that, in G8 group, the sharpest reduction in coordination number was upon the addition of 4.75 mm–2.36 mm particles as compared with other PAM groups, while the reduction generated by 9.5 mm–6.3 mm particles was smaller. This can be attributed to the other effect of finer particles on the interlocking condition in a mixture, namely the relative amount of finer particles. The volumetric proportion of particles within each size range in PFC3D model according to the gradation design is given in Table 8. With the various proportions of 4.75 mm–2.36 mm particles in the six PAM groups, the reduction of coordination number by percentage to the previous coarser PFC3D model within three size ranges (namely 19.0 mm–9.5 mm, 19.0 mm–6.3 mm, and 19.0 mm–4.75 mm) are given in Figure 3. It can be observed that, with the increasing volumetric percentage of finer particles (namely 4.75 mm–2.36 mm particles) being added, the coarser particles retained on different sieve sizes generally were being de-attached more severely. It can be explained that a high amount of fine particles can make the skeleton created by coarse particles to be disrupted and even make coarse particles to be dispersed amongst a mixture of fine particles without interlocking among coarse fraction, as that in fine-graded mixtures.

Table 8. Volumetric proportion of particles within each size range in PFC3D models.

Group	Size range, mm				
	19.0-13.2	13.2-9.5	9.5-6.3	6.3-4.75	4.75-2.36
G1	24.1	9.7	38.4	5.6	22.2
G2	17.4	17.4	11.6	32.2	21.4
G3	6.4	56.1	14.0	18.8	4.7
G4	19.5	13.0	19.5	19.2	28.8
G5	11.9	28.7	42.8	9.9	6.6
G6	5.8	41.5	10.3	8.5	33.9

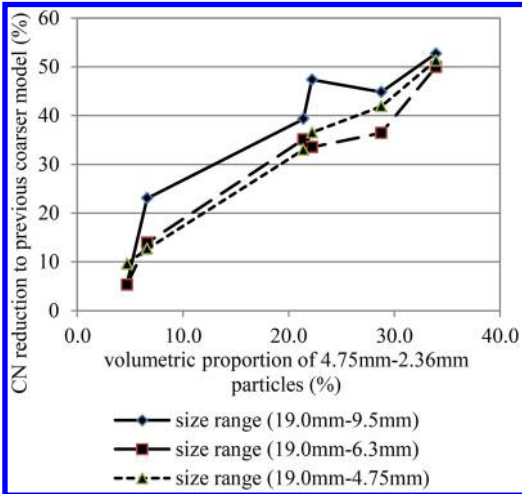


Figure 3. Coordination number reduction in various size range caused by the addition of 4.75 mm–2.36 mm particles.

Therefore, it can be concluded that the packing condition in PAMs is attributed to the size of finer fraction in terms of aggregate gradation, and the proportion of fine aggregates as well, which agrees with the findings of the air voids content of the six PAMs as measured in the laboratory.

4 CONCLUSIONS

This research was conducted to evaluate the packing condition within PAM material using DEM simulation. Six PAMs were designed, and relevant volumetric properties and performance parameters were obtained in the laboratory, and deep investigation in the development of particle-to-particle interlocking mechanism was conducted via PFC3D models.

According to the experimental results, performance in permeability for PAM material increases with air voids content, but it is at the expense of mixture strength, which agrees with the findings by previous researchers. On the other hand, air voids content is dependent on the amount of fine aggregates (those smaller than 2.36 mm), and the proportion of

aggregates in other size range as well (those within 4.75 mm–2.36 mm).

Four types of PFC3D models were established for the six PAM groups, which represented the assemblies composed of particles within different size ranges, namely 19.0 mm–9.5 mm, 19.0 mm–6.3 mm, 19.0 mm–4.75 mm, and 19.0 mm–2.36 mm. It was found that, for each PAM group, compacting condition is further enhanced as finer particles are added based on the observation of two simulation parameters, namely porosity and coordination number. Furthermore, according to the coordination number within various size ranges for each PAM group, it was found that the particle-to-particle skeleton created by coarser particles is affected by both size and amount of finer particles added in, which agrees with the finding of the air voids content as measured in the laboratory.

In addition, PAM's strength was assessed via Marshall stability herein, which however was a conventional index that cannot well reflect asphalt mixture's mechanical performance, and hence other property, such as resilient modulus, was suggested to be measured in further research to better evaluate mixture's strength. Meanwhile, asphalt binder content was determined through AI method, resulting in low asphalt content due to the low amount of fines in PAM. Hence, in case of PAMs used in normal roads, higher asphalt binder content will be required, and hydrated lime not more than 2% is also suggested as fillers for anti-stripping.

On the whole, the research has provided new insights into the development of packing condition in PAM material, and DEM is found to be an effective tool to evaluate the development of particle-to-particle interlocking among an assembly of particles with specific gradation design. The findings in this study can be a helpful guide in gradation design for PAM material.

REFERENCES

- Abbas, A., Papagiannakis, A.T., Masad, E., & Shenoy, A. 2005. A modelling asphalt mastic stiffness using discrete element analysis and micromechanics based models. *International Journal of Pavement Engineering* 6(2): 137–146.
- A.I. 1996. *Superpave mix design*. Lexington, KY : Asphalt Institute.
- AI. 1997. *Mix design methods for asphalt concrete and other hot-mix types*. Lexington, KY : Asphalt Institute.
- ASTM 2006. *Standard test method for marshall stability and flow of bituminous mixtures (D6927)*. Philadelphia, PA: American Society for Testing and Materials.
- Boving, T., Stolt, M., & Augenstern, J. 2004. *Investigation of the university of Rhode Island, Kingston, RI: porous pavement parking lot and its impact on subsurface water quality*. Zaca-tecas, Mexico: International Association of Hydrologists.
- Cook, R. D., Malkus, D. S., Plesha, M. E., & Witt, R. J. 2002. *Concepts and applications of finite element analysis*. New York, NY : Wiley.
- Cundall, P. A. 1971 A computer model for simulating progressive, large-scale movements in blocky rock systems.

- Paper presented at the International Symposium on Rock Mechanics*. Nancy, France.
- Cundall, P. A. 1988. Computer simulations of dense sphere assemblies micromechanics of granular materials, In M. Satake & J. T. Jenkins (eds). *Micromechanics of Granular Materials*: 113–123. Amsterdam: Elsevier Science Publishers B.V.
- Fabb, T. R. J. 1993. *The Case for the Use of Porous Asphalt in the UK*. Institute of Asphalt Technology.
- Florida DOT. 2004. *Florida Method of Test for Measurement of Water Permeability of Compacted Asphalt Paving Mixture (FM5-565)*. Florida: Department of Transportation.
- Fuller, W. B. & Thompson, S. E. 1907. The laws of proportioning concrete. *Journal of Transportation Division, American Society of Civil Engineering*, 59.
- Hamzah, M. O. & Cabrera, J. G. 1996. Aggregate grading design for porous asphalt, in *Performance and Durability of Bituminous Materials*: 10–22. London: E & FN Spon.
- Hasan, M. R. M., Yih, E. J., Hamzah, M. O. & Voskuilen, J. L. M. 2013. The effects of break point location and nominal maximum aggregate size on porous asphalt properties. *Construction and Building Materials* 44: 360–367.
- Itasca. 2008. *PFC3D Version 4.0*. Minneapolis, Minnesota: Itasca Consulting Group Inc.
- Jiang, Y. J., Ren, J. L., Xu, Y. S. & Li, D. 2011. Simulation method of mechanical properties of graded broken stone based on particle flow code. *Journal of Tongji University (Nature Science)* 39(5): 699–704.
- Khalid, H., & Jimenez, P. F. K. 1995. *Performance Assessment of Spanish and British Porous Asphalts Performance and Durability of Bituminous Materials*. London : Spon Press.
- Kim, H. & Buttlar, G. 2009. Discrete fracture modelling of asphalt concrete. *International Journal of Solids and Structures* 69: 2716–2723.
- Liu, Y. & You, Z. P. 2011. Accelerated discrete element modeling of asphalt-based materials with the frequency-temperature superposition principle. *Journal of Engineering Mechanics* 137(5): 355–365.
- LTA. 2010. *Engineering Group Materials & Workmanship Specification for Civil & Structural Works*. Singapore: Land Transport Authority.
- Lu, M. & McDowell, G. R. 2007. The importance of modelling ballast particle shape in the discrete element method. *Granular Matter* 9: 69–80.
- PennDOT. 2006. *Pennsylvania Stormwater Best Management Practices Manual*. Pennsylvania: the Department of Transportation.
- Rajib, B. M., Prithvi, S. K., Cooley, L. A., & Donald, E. W. 2000. *Design, Construction, and Performance of New-Generation Open-Graded Friction Courses (NCAT Report 00-01)*. National Center for Asphalt Technology.
- Shen, S. H. & Yu, H. N. 2011a. Characterize packing of aggregate particles for paving materials: particle size impact. *Construction and Building Materials* 25(3): 1362–1368.
- Shen, S. H. & Yu, H. N. 2011b. analysis gradation and packing for easy estimation of hot-mix-asphalt voids in mineral aggregate. *Journal of Materials in Civil Engineering* 23(5): 664–672.
- Sungho, K., Roque, R., Birgisson, B., & Guarin, A. 2009. Porosity of the dominant aggregate size range to evaluate coarse aggregate structure of asphalt mixtures. *Journal of Materials in Civil Engineering* 21(1): 32–39.
- Vavrik, W. R., Huber, G., Pine, W. J., Carpenter, S. H., & Bailey, R. 2002. *Bailey Method for Gradation Selection in HMA Mixture Design*. Transportation Research Record.
- You, Z. P., Adhikari, S., & Dai, Q. L. 2008. Three-dimensional discrete element models for asphalt mixtures. *Journal of Engineering Mechanics* 134(12): 1053–1062.

International use of rubberized asphalt open graded friction course

G.B. Way & K.E. Kaloush

Rubberized Asphalt Foundation, Arizona State University, USA

K.P. Biligiri

Indian Institute of Technology, Kharagpur, West Bengal, India

J. Sousa

Consulpav International, Walnut Creek, California, USA

A. Pinto

Rio de Janeiro State Highway Department, Brazil

R. Cao

Jiangsu Transportation Research Institute, Nanjing, China

ABSTRACT: The international use and technology of rubberized asphalt open graded friction course mixes has grown and expanded since it was first introduced in Arizona in the mid 1980's to its present use in not only the United States but also Portugal, Brazil and China. Rubberized asphalt open graded friction courses (RAFC) are placed as the top course wearing surface. Their function is multifaceted and includes providing a wet weather surface with very good friction properties (skid resistance), reduce reflective and fatigue type cracking, smooth riding surface in terms of the international roughness index and a surface that dampens the tire/pavement noise, and reducing emission rates of tire wear. RAFC's are composed of a high quality clean open grade aggregate. The binder content is typically in the range of 9 to 10 percent by weight of the aggregate and placed from 12.5 mm to 25 mm in thickness. The rubberize asphalt binder is composed of typically 80 percent asphalt (bitumen) and 20 percent recycled tire rubber. The objective of this paper is to review and summarize the use of RAFC's in various countries and to report on the technical research findings that have buoyed the use of this unique material.

1 INTRODUCTION

Open Graded Friction Courses (OGFC) began to be used in California and Arizona in the early 1950's (Morris & Scott 1973). The primary reason for using this material was to provide a surface with good skid resistance, good smooth ride and appearance. The original open graded mixtures consisted mostly of a single size 2.36 mm aggregate with approximately 5.5 to 6.5 percent paving grade asphalt. The resultant hot mix was mixed in a hot plant and placed with a laydown machine at a thickness of approximately 12.5 mm. From the 1950's to about 1985 these open graded hot mixes were placed on numerous pavements, however since they were open graded they were prone to mechanical raveling, [Figure 1](#).

In the 1970's the Federal Highway Administration suggested that states make greater use of open graded friction course mixes (FHWA 1974). Many states experimented with these mixes and found that they did not do well in areas with snow and ice and thus the use of such mixes virtually disappeared except in California and Arizona. In the 1980's Arizona began



Figure 1. Raveled open graded friction course without asphalt rubber binder.

to use open graded friction course with a type of rubberized asphalt called asphalt rubber (AR) binder. Asphalt rubber open graded friction courses (ARFC) are placed as the top course wearing surface. Their function is multifaceted and includes providing a wet weather surface with very good friction properties (skid resistance), reduce reflective and fatigue type cracking, smooth riding surface in terms of the international roughness index and a surface that dampens

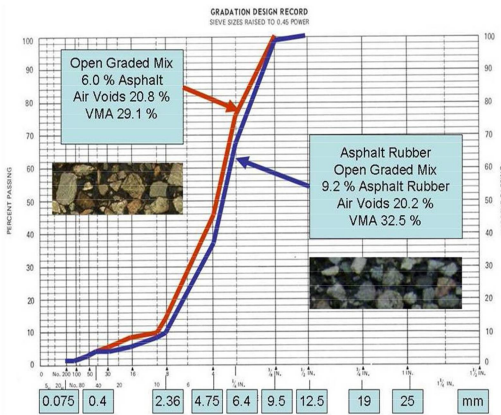


Figure 2. Open graded friction course gradation and binder content with paving grade asphalt or with asphalt rubber binder.

the tire/pavement noise, and reducing emission rates of tire wear. ARFC's are composed of a high quality clean open graded aggregate. The binder content is typically in the range of 9 to 10 percent by weight of the aggregate and they are typically placed from 12.5 mm to 25 mm in thickness. The asphalt rubber binder is composed of typically 80 percent asphalt (bitumen) and 20 percent recycled tire rubber. The objective of this paper is to review and summarize the use of ARFC's in various countries and to report on the technical research findings that have buoyed the use of this unique material. In addition the report contains some information about the ARFC's mechanical properties, noise properties and various performance measurements.

2 ASPHALTRUBBER OPEN GRADED FRICTION COURSE MIXES

Asphalt rubber began to be used as an asphalt modifier in the United States in the state of Arizona in the late 1960's. In 1978 it was patented by two asphalt supplier companies in Arizona (Heitzman 1992). In 1994 ASTM established two standards that define and specify AR (ASTM 2011a), (ASTM 2011b). The ASTM defines AR as a mixture of at least 15% ground tire rubber derived from scrap tires and 75% hot paving grade asphalt (bitumen). The Arizona Department of Transportation (ADOT) began using AR binder as a chip seal coat binder in the 1970's (Scofield 1989). Later in the 1980's the City of Phoenix, Arizona began using a hot mix with AR binder. They called this hot mix an AR gap graded mix (ARAC). Also in the 1980's the ADOT developed an open graded hot mix using AR as the binder (Way et al. 2012) and called this mix an AR open graded friction course (ARFC). Figure 2 shows the ARFC open graded gradation and binder content compared to a typical ARFC without asphalt rubber.

Table 1. AC and PCC pavements with associated sound intensity levels.

Location	Material	Additional Notes	SI Level (dBA)
AZ Marc 10	ARFC		96.6
AZ Marc 202	ARFC	Best Condition	97.4
CA SBd 40	RAC	High Binder	98.4
	(Type O)		
AZ Marc 10	P-ACFC		98.7
CA Sol 80	DGAC		101.7
CA Ker 58	PCC	New Broom	101.8
		(Longitudinal)	
AZ Marc 202	PCC	Longitudinal Tine	102.0
CA SM 84	Chip Seal	New	105.0
AZ Marc 202	PCC	New Transverse Tine	107.1
AZ Marc 202	PCC	New Random	109.2
		Transverse Tine	

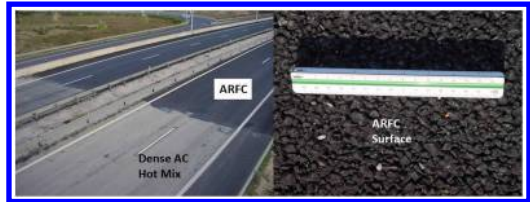


Figure 3. Portugal dense AC hot mix and asphalt rubber friction course surfaces.

As can be seen the ARFC has a much greater amount of binder which virtually eliminates the potential of the mix to ravel, it also reduces the incidence of reflective cracking while maintaining excellent macro-texture and skid resistance in wet weather (Zareh & Way 2009). It was also noticed that ARFC reduced the tire/pavement noise to such a degree that both City of Phoenix and ADOT conducted research studies to document the degree of tire/pavement noise reduction (Scofield 2003). This noise reduction was so significant that the ADOT covers all of its concrete pavements with ARFC to reduce noise, provide good skid resistance and a smooth ride (Gruner & Assaf 1990). A significant study conducted by both the California Department of Transportation (Caltrans) and ADOT (Donovan & Rymer 2003) compared the tire/pavement noise for various pavement surfaces and the ARFC was found to be the least noisy, as shown in Table 1.

3 ARFC IN PORTUGAL

Portugal began to use ARFC surfaces in about 2003 to provide a smooth riding surface, good wet weather skid resistance and less tire pavement noise Figure 3. It was reported that ARFC reduced the noise by 5–6 dBA when compared to a typical dense graded asphalt hot mix and 8–10 dBA when compared to a typical concrete surface (Ruivo 2004a) and (Ruivo 2004b).

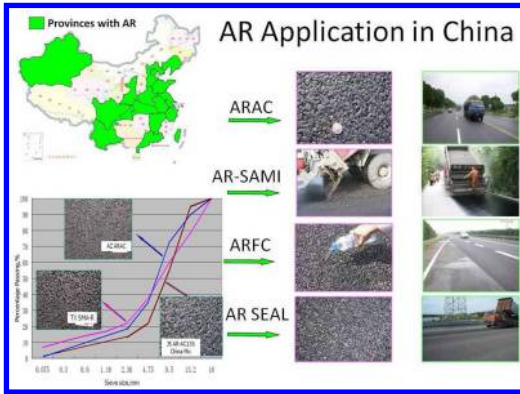


Figure 4. Use of ARFC and other AR materials in China.

4 ARFC IN CHINA

As China's economy has grown so has the number of scrap tires. In 2004 China produced about one hundred million scrap tires per year and by 2010 the amount had increased to 300 hundred million scrap tires per year. In the 1980's there had been some test trials of using scrap tire in a dry form in a dense graded hot mix. Later by 2004 experiments began on using both dry process and the wet process of asphalt rubber. From 2004 to 2007 many experimental test sections and test projects were constructed using AR as a chip seal coat interlayer referred to as a stress absorbing interlayer (SAMI). Also test sections of ARAC hot mixes were constructed; both the SAMI and ARAC test sections closely approximated the materials placed in both Arizona and California. From 2007 until now the use of AR in the wet process like that used in the US has grown, Figure 4. Implementation of AR as a hot mix or seal coat has reached over 20 China provinces (Cao 2012a). Additionally specifications and guidelines for AR are becoming more common in China (Tianjin 2006), (Jiangsu 2006) and (Beijing 2006). An International conference on AR was held in Nanjing, China in 2009 (Asphalt 2009).

Now that the use of AR is becoming more common in China attention has turned to measuring the tire/pavement noise of various pavement surfaces. Although the use of AR is still relatively new in China as well the measurement of tire/pavement noise is still relatively new in China; Jiangsu province in China measured the tire/pavement noise of various surfaces as previously done in Arizona and California. Table 2 represents the first effort within China to measure the tire/pavement noise using the OBSI method (Cao 2012b). As Figure 5 shows those pavement surfaces constructed with either ARFC or ARAC demonstrated very good tire/pavement noise reduction. It was reported that ARFC reduced the noise by 5–6 dBA when compared to a typical dense graded asphalt hot mix and 8–10 dBA when compared to a typical concrete surface.

The China ARFC surfaces are typically 25 mm in thickness with rubberized asphalt content ranging

Table 2. China OBSI noise measurements.

No.	Road	Surface Type	Binder Type	Tire-Pavement Noise (dBA)	Construction Date
1	Nanjing Ring G42	2.5cm ARFC13	Asphalt Rubber	96.0	2009 New Pvt
2	Shanghai Zhongnan	2.5cm OGFC13	Binder	98.2	2009 New Pvt
3	Ninghang G25	4cm ARAC13	Asphalt Rubber	98.8	2008
4	Ninghang G25	4cm SMA-13	SBS, PG70-22	98.9	2008
5	Haimen S336	4cm Sup-9.5	SBS, PG70-22	99.0	2005
6	Yantai G15	4.5cm SMA-13	SBS, PG70-22	99.2	2005
7	Haimen S336	2.5cm OGFC-9.5	SBS+fiber	99.4	2005
8	NingGao S55	2.5cm OGFC-13	Asphalt Rubber	99.5	2006
9	Nanjing Ring	4cm AC-13	Asphalt Rubber	99.6	2008
10	Haimen S336	4cm AC-13	PG64-22	99.6	2002
11	Yantai G15	4cm PA-13	High Viscosity Binder	99.6	2005
12	Shanghai Zhongnan	4cm SMA-13	SBS, PG70-22	99.7	2009 New Pvt
13	Ninghang G25	4cm PA-13	High Viscosity Binder	99.9	2007
14	Shanghai Huidong Road	4cm AC13	PG64-22	100.1	2001
15	Haimen	Concrete	Concrete	103.9	2002

*Note-All measurements in 2009



Figure 5. RJ 122 pavement before and after overlay placement with ARFC surface.

from 8–9 percent binder by weight of the mix. The Marshall stabilities range from 2.8 to 3.8 kN and the flow values from 30 to 36 (0.1 mm). The water permeability after construction was 1000 ml per minute by Chinese test (Cao et al. 2009).

5 ARFC IN BRAZIL

Brazil's first use of an Asphalt Rubber Open Graded Friction Course was commissioned by the DER-RJ Rio de Janeiro State Highway Department on a project on highway RJ-122 in the Rio de Janeiro province. The existing pavement was paved in the seventies; its surface became extensively cracked, making the riding unsafe and uncomfortable for the users Figures 5. Furthermore, the shoulders were lacking in many areas along the highway. The traffic volume is high and mainly of trucks. For those reasons, RJ-122 was chosen for applying this new field blend asphalt rubber technique (Pinto & Sousa 2012). The overlay project consisted of widening the roadway with a dense graded hot mix leveling and reshaping layer, followed by a 4.5 cm asphalt rubber gap graded structural layer and a 2.5 cm asphalt rubber open graded surfacing, Figure 6. The completed highway RJ-122 overlay pavement has structural and functional characteristics of the highest best quality ranking in the federal and state networks. In particular the skid resistance of 0.7 which is very good. The ride smoothness also was rated as very smooth riding.

The Brazilian ARFC surface is 25 mm in thickness with a rubberized asphalt content of 8.5 percent binder

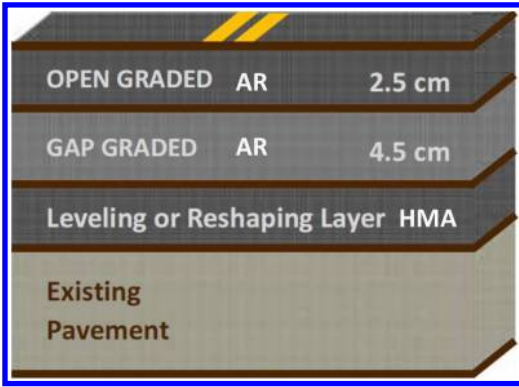


Figure 6. The new pavement structure, 2.5 cm of asphalt rubber open graded and 4.5 cm of asphalt rubber gap grade hot mix.

by weight of the mix. The gradation is substantially the same as the Arizona ARFC mix. The ARFC and supporting structure was evaluated in place by the use of a heavy vehicle simulator (HVS). The HVS applied a 15 ton dual tire load to the ARFC surface at a rate of 1000 wheel passages per hour. Approximately 150000 wheel loadings were applied to simulate long term wear (10–20 years) of very heavy traffic representing 2500000 ESALs of traffic loading.

The following test data results were obtained representing the before and after application of the cumulative loading. The Falling weight deflection of the center geophone went from 25 to 33, which is well below the accepted Brazilian criteria of failure of 64. Likewise there was no observed cracking at after the loading was completed. The permanent deformation (rut depth) was 3.7 mm after loading also below the Brazilian design failure criteria of 7 mm. The British pendulum test was 52 before loading began and 53 after loading, which is well above the Brazilian, design failure criteria of 47. The sand patch was 89 mm before loading and 90 after loading, which well within the Brazilian acceptance band of 0.6–1.2 mm.

6 ARFC MECHANICAL PROPERTIES

Arizona State University did extensive mechanical testing of ARFC mixes over the last 10 years (Kaloush et al. 2011). The testing included tests for the triaxial shear strength, dynamic modulus, permanent deformation, beam fatigue indirect tensile strength and creep; fracture and crack propagation; and moisture damage. Based on the asphalt rubber open graded (ARFC) laboratory test results from many studies, the following general observations about their mechanical properties were determined. Because the ARFC mixes have a very high air void content by design they have to be tested in a confined condition to obtain realistic dynamic modulus values. ARFC mixes typically are able to reduce the occurrence of reflective cracking

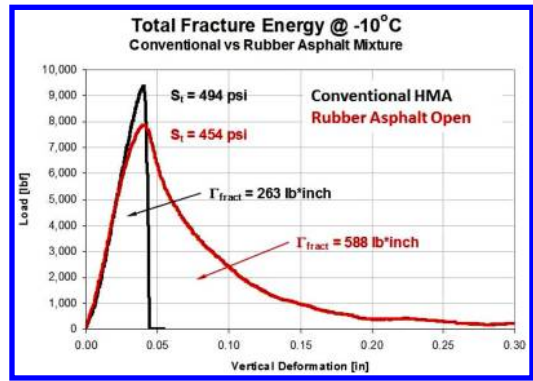


Figure 7. Greater total fracture energy with ARFC compared dense graded conventional HMA.

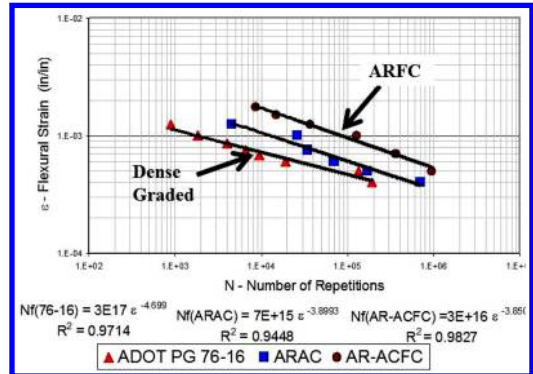


Figure 8. Greater fatigue cracking life with ARFC compared to dense graded conventional HMA.

and cracking in general. This crack reduction capability is substantiated by fracture test results, Figure 7 and beam fatigue test results, Figure 8. These test results show that ARFC mixes are better able to resist fracture and fatigue cracking. ARFC mixes are generally do not contribute to rutting since they are only placed 25 mm or less in thickness at the top of the pavement structure where shear stresses are very low. Likewise the single size stone gradation creates virtually only stone to stone contact also which reduces rutting.

7 CONCLUSIONS

The use of open graded friction course, ARFC, has grown from a few kilometers constructed in Arizona, California and Texas in the mid-1980s to thousands of kilometers in the US. These ARFC surfaces are durable, reduce cracking, provide a good skid resistant surface, smooth riding surface, are not prone to surface deformation (rutting), have good wear resistance and reduce the tire/pavement interface noise. The ARFC has been introduced into various countries such as Portugal, Brazil and China with good success. The use in Portugal in the 1990's to reduce noise, China in the 2000's to reduce noise and Brazil in the 2010's to

improve skid resistance and reduce reflective cracking. The use in these countries demonstrated and provided quantitative measures for the ARFC benefits. Studies in Arizona also showed that ARFC layers have service life more than 10 year, with good performance measures sustained at: IRI of 0.75 m/km, skid of 59 (measured at 100 km/hr) and noise levels maintained below 78 dB (Kaloush et al. 2011).

REFERENCES

- Asphalt Rubber 2009 Conference. (2009). Nanjing, China, ISBN: 978-988-18861-1-4, November 2–4.
- ASTM. (2011a) ASTM D8. Standard Terminology Relating to Materials for Roads and Pavements, American Society for Testing and Materials, ASTM International Standards Worldwide, Volume 04.03, Road and Paving Materials; Vehicle-Pavement Systems.
- ASTM. (2011b). ASTM D6114. Standard Specification for Asphalt-Rubber Binder, American Society for Testing and Materials, ASTM International Standards Worldwide, Volume 04.03, Road and Paving Materials; Vehicle-Pavement Systems.
- Beijing Highway Bureau. (2006). Design and Construction Guideline of Crumb Rubber Asphalt and Mixtures.
- Cao, Rongji, Bai Qi-feng and Qian Zhen-dong (2009) “Research on Mix Design Method and Application of Asphalt Rubber Open-graded Friction Course.” Proceedings AR2009, Nanjing, China, November 2–4, 2009, ISBN: 978-988-18681-1-4, pp 109–118.
- Cao, Rongji, (2012a) “Asphalt Rubber in China,” Rubber Pavements Association Meeting, Maui, Hawaii.
- Cao, Rongji. (2012b). email from Cao to George Way of China OBSI measurements, February.
- Donovan, P. and Bruce Rymer. (2003). Measurement of Tire Pavement Noise Sound Intensity Methodology. Proceedings AR2003 Conference, Brasilia, Brazil, December 1–4, ISBN: 85-903997-1-0, pp 399–412.
- FHWA. (1974). FHWA- RD 74-2 Technical Advisory on Friction Course.
- Gruner, J. R. and A. J. Assaf. (1990). Sound Level Survey”, Phoenix, Arizona, Western Technologies Inc.
- Heitzman, Michael A. (1992). “State of the Practice, Design and Construction of Asphalt Paving Materials with Crumb Rubber Modifier”, Federal Highway Administration, FHWA-SA-92-022.
- Jiangsu Expressway Construction Bureau. (2006). Construction Guide for Asphalt Rubber Pavement.
- Kaloush, Kamil, Maria Carolina Rodezno, Krishna Biligiri, George B. Way and Mark Belshe. (2011). Mechanistic-Empirical Pavement Design Guide Implementation and Preservation with Asphalt Rubber. Proceedings Southern African Transport Conference & Exhibition, Johannesburg, South Africa, July 12, 2011, pp 574–585.
- Morris, G.R. and Noel R. Scott (1973). Arizona’s Experience with Asphalt Concrete Friction Courses, 59th Annual Meeting AASHTO, Los Angeles, California, November.
- Pinto, Angelo and Jorge Sousa. (2012). The First Brazilian Experience with In Situ Field Blend Rubber Asphalt. Proceedings AR2012, Munich, Germany, October 23-26, 2012, ISBN: 978-989-20-3255-9, pp 633–650.
- Ruivoa, F. P. (2004). Noise Levels Generated by Two Pavement Surfaces (Conventional Old AC and AR-OGFC) on A8 – Portugal. Report for AutoEstradas do Atlântico: February.
- Ruivob, F. P. (2004). Noise Levels Generated by Two Pavement Surfaces (CRC and ARFC) on A8 – Portugal. AutoEstradas do Atlântico: February.
- Scotfield, L. A. (1989). The History, Development, and Performance of Asphalt-rubber at ADOT, Report Number AZ-SP-8902, ADOT, December.
- Scotfield, L. (2003). Development of Arizona’s Quiet Pavement Research Program, Asphalt rubber 2003 Proceedings, Brasilia, Brazil, December 1–4, 2003, ISBN 85-903997-1-0.
- Tianjin Construction Commission. (2006). Technical Specification of Waste Tire Rubber Powder Modified Asphalt Pavement In Tianjin.
- Way, George B., Kamil Kaloush and Krishna Propoorna Biligiri. (2012). Asphalt-Rubber Standard Practice Guide – An Overview. Proceedings Asphalt Rubber 2012, Munich, Germany, ISBN: 978-989-20-3255-9, October 23–26, 2012, pp 23–40.
- Zareh, Ali and George B. Way. (2009). Asphalt-Rubber 40 Years of Use in Arizona. Proceedings Asphalt Rubber 2009, Nanjing, China, ISBN: 978-988-18681-1-4, November 2–4, 2009, pp 25–45.

Fiber reinforced asphalt concrete: Performance tests and pavement design consideration

K.E. Kaloush & B.S. Underwood
Arizona State University, USA

W.A. Zeiada
University of Sharjah, UAE

J. Stempihar
Arizona Department of Transportation, USA

ABSTRACT: This paper highlights findings from several research studies on Fiber Reinforced Asphalt Concrete (FRAC) mixtures. The fibers are a blend of polypropylene and aramid fibers. The reinforcing strength contribution of fibers was evident in several mechanical tests. Flexural and fracture tests also indicated that the FRAC mixture is better able to resist the development and propagation of cracks when compared to the control mixture. The stiffness properties also showed that the FRAC mixture will provide better rutting and fatigue cracking resistance. Recommendations on the use of FRAC mixture moduli and/or structural layer coefficients in pavement design analysis are also discussed.

1 INTRODUCTION

Modifiers in Hot Mix Asphalt (HMA) have been used to mitigate both traffic and environmentally induced pavement distresses. These include modifiers for rutting resistance by increasing the stiffness of the asphalt binders, and reduce cracking by eliminating, delaying or inhibiting crack propagation. Other benefits is to reduce or lessen the drain down of the binder for certain mixtures. There are many types of modifiers and examples include: polymers (plastomers and elastomers), fillers, and fibers. Fibers have been used to improve the performance of asphalt mixtures against pavement distresses (Bueno et al. 2003, Lee et al. 2005). Early uses were in the 1960's with the use of asbestos and polyester; others over the years included polypropylene, glass, carbon, coconut, cellulose and very recently aramid (or Kevlar), in addition to more than thirty recycled waste fibers that have been and continue to be introduced into the market. Early research work in Arizona, USA looked into the benefits of using tire fibers with and without crumb rubber content.

There are several research studies reporting on experiments using synthetic fibers in asphalt concrete in the literature. Bueno et al studied the addition of randomly distributed synthetic fibers on the mechanical response of a cold-mixed, densely graded asphalt mixture using the Marshall test, as well as static and cyclic triaxial tests (Bueno et al. 2003). The results showed that the addition of fibers caused small variations in the

mixture's triaxial shear strength parameters. Lee et al evaluated the influence of recycled carpet fibers on the fatigue cracking resistance of asphalt concrete using fracture energy (Lee et al. 2005). It was found that the increase in fracture energy represents a potential for improving the asphalt mixture's fatigue life. A research study by Fitzgerald reported that the addition of carbon fibers to an asphalt mixture may have beneficial properties ranging from improved mechanical properties to reduced electrical resistance using the electric resistivity testing methodology (Fitzgerald 2000). Cleven subjected carbon fiber-reinforced asphalt mixtures to mechanical testing, which included diametral resilient modulus, repeated load permanent deformation, flexural beam fatigue tests and indirect tensile strength tests (Cleven 2000). The modified asphalt mixtures were observed to be stiffer, more resistant to permanent deformation, and had higher tensile strength at low temperatures. However, the carbon fiber modified samples showed no improvement in fatigue behavior as measured by the four point beam test or cold temperature creep compliance test. Jahromi and Khodai also investigated the characteristics and properties of the carbon fiber-reinforced asphalt mixtures through various laboratory tests (Jahromi & Khodai 2008). They reported that the addition of carbon fibers showed an increase in the mix's stability, decrease in flow value, and an increase in voids in the mix. They also found that the addition of fibers improved the fatigue life and permanent deformation of the mixtures.

Mahrez et al. utilized glass fibers in a Stone Mastic Asphalt (SMA) mixture. They found that the use of glass fiber in asphalt mixtures showed variable Marshall Stability results, and that the addition of glass fibers actually decreased the mixtures' stability and stiffness (Mahrez et al. 2003). In a different study, Mahrez & Karim used the wheel tracking test to characterize the creep and rutting resistance of glass fiber reinforced asphalt mixtures (Mahrez & Karim 2007). They reported that the inclusion of glass fibers resulted in higher resilient modulus, higher resistance to permanent strain and rutting. Putman and Amirkhani studied the feasibility of utilizing waste tire and carpet fibers in SMA mixtures (Putman & Amirkhani 2004). The study compared the performance of SMA mixtures containing waste tire and carpet fibers with mixes made with commonly used cellulose and other polyester fibers. No significant difference in permanent deformation or moisture susceptibility was found in mixtures containing waste fibers compared to cellulose or polyester. However, they reported that the tire, carpet, and polyester fibers significantly improved the toughness of the mixtures compared to the cellulose fibers.

Chowdhury et al evaluated two types of recycled tire fibers to determine whether they can be used in different types of asphalt mixtures as a replacement of the currently used cellulose or mineral fibers (Chowdhury et al. 2006). The researchers tested three different types of mixtures: SMA, Permeable Friction Course (PFC), and Coarse Mix High Binder (CMHB) mixtures with two different types of recycled tire fibers, one cellulose fiber, and a control mix with no fibers. The laboratory tests used to evaluate the mixtures were: drain-down, dynamic modulus, indirect tensile strength, and Hamburg wheel tracking tests. Mixtures containing tire fibers, in most cases, outperformed the mixtures containing cellulose fiber and mixtures with no fiber. The drain-down test results clearly revealed that the recycled tire fiber can be used in SMA and PFC mixtures as a replacement for cellulose fibers to prevent asphalt drain-down during construction. Wu et al examined the dynamic characteristics of three fiber-modified asphalt mixtures: cellulose, polyester and mineral fibers at dosages of 0.3%, 0.3%, and 0.4% respectively (Shaopeng et al. 2007). The experimental results showed that fiber-modified asphalt mixtures had higher dynamic modulus compared with the control mixture.

Since 2006, Arizona State University (ASU) has been engaged in a research program to evaluate the performance benefits of synthetic fibers. The fibers are a proprietary blend of collated fibrillated polypropylene and aramid providing a three dimensional reinforcement to the HMA. The polypropylene fibers are chemically inert, non-corrosive, and non-absorbent; whereas the aramid fibers have a high tensile strength, non-corrosive and have resistance to high temperatures. The physical characteristics of the fibers have been reported in other publications (Kaloush et al. 2010).

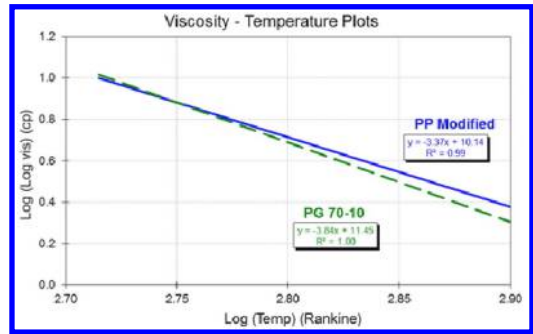


Figure 1. Viscosity-Temperature susceptibility of the polypropylene modified binder.

2 OBJECTIVE

The objective of this paper is to report on test results and findings regarding the performance of the Fiber Reinforced Asphalt Concrete (FRAC) mixtures at ASU. Advanced material characterization tests were conducted to assess FRAC performance on permanent deformation and cracking. Since the polypropylene fibers play a role in binder modification, conventional consistency binder tests are also run to assess the degree of binder properties modification at different temperatures.

3 BINDER CHARACTERISTICS

Figure 1 shows a comparison of typical viscosity-temperature susceptibility plots for a control PG 70-10 binder and one that is modified with polypropylene (PP) fibers at the rate of 0.5 kg per tonne of asphalt mixture (ASTM 1998). These plots were derived from conventional binder consistency tests including: penetration AASHTO T49-93, softening point AASHTO T53-92, and rotational viscosities at a range of temperatures AASHTO TP48. It is observed that the PP fibers improve the temperature susceptibility of the virgin binder especially at high temperatures. In fact, the small, or no-change, in viscosity at lower temperature is an advantage for the binder in keeping it on the softer side to resist thermal cracking.

4 RUTTING EVALUATION

One test to evaluate rutting of the asphalt mixture is by conducting the Flow Number (FN) test (Witczak et al. 2002). In this test, a repeated dynamic load is applied on cylindrical specimens for several thousand repetitions, and the cumulative permanent deformation, including the beginning of the tertiary stage (FN) as a function of the number of loading cycles over the test period is recorded. Figure 2 presents FN test results conducted at 54.4°C. The FN (inflection point in the axial strain slope) values of the FRAC mixture

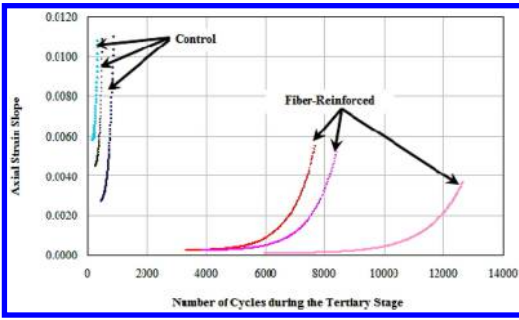


Figure 2. Flow number test results of asphalt mixtures.

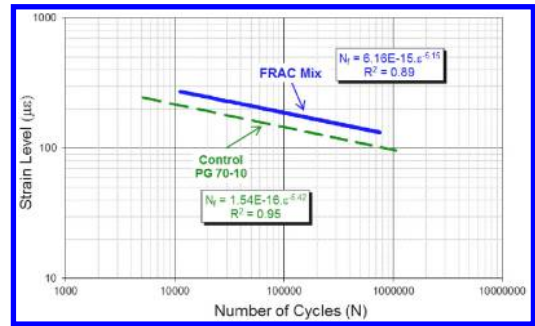


Figure 4. Comparison of control and FRAC mixtures at 21°C.

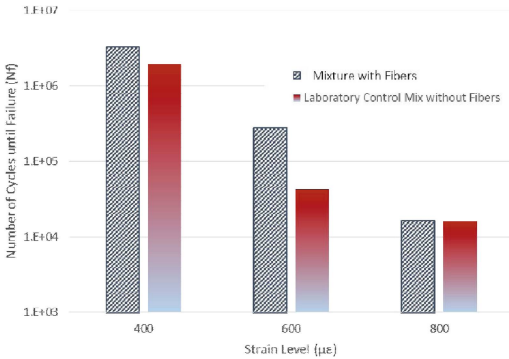


Figure 3. Fatigue life comparison at 4.4°C.

was found to be 10 to 15 times higher than the control mixture. It can be also observed that the control mix has higher strain slopes compared to the fiber-reinforced mixture. Lower values of strain slope during the tertiary stage means more energy is stored in the sample, and that the mix has higher potential to resist shear failure and further development of permanent deformation.

5 FATIGUE CRACKING EVALUATION

Four point bending fatigue tests are common laboratory tests according to AASHTO T321-03. Each beam is subjected to a different controlled strain rate at a range of temperatures. A 50% reduction in initial stiffness is used as the criteria to determine the number of cycles until failure (N_f). Initial stiffness is recorded as the stiffness of the beam at 50 loading cycles in accordance with SHRP M-009 (AASHTO 2006, AASHTO 2003, SHRP 1994). As an example, Figure 3 presents a fatigue comparison between the FRAC and control mixture at 4.4°C. The FRAC mixture shows performance improvement over the control mixture at 400 and 600 microstrain levels, 2 million versus 3.2 million cycles and 42,000 versus 280,000 cycles, respectively. At the 800 microstrain level, no difference in performance is observed. It is important to note that this comparison is valid since the initial

Table 1. Indirect tensile strength test results.

Mix	Temp. °C	Indirect Tensile Strength, kPa	Energy at Failure, J	Total Energy, J
FRAC	21.1	521	7.2	28.8
	10	1078	16.8	53.6
	0	1877	22.6	60.2
Control Mix	21.1	397	5.5	19.8
	10	952	8.3	37.2
	0	1786	19.8	50.6

stiffness of the beam samples for both mixtures analyzed was approximately 2,800 MPa. Another fatigue analysis for a different project is shown in Figure 4. It can be observed that the FRAC mixture has a higher fatigue life when compared with the control.

6 INDIRECT TENSILE STRENGTH TESTS

One commonly used parameter to evaluate asphalt mixtures is tensile strength which can be used to quantify the effects of moisture and to determine the fracture resistance of an asphalt mixture. Typically, the tensile strength can be accurately determined from an indirect tensile strength test (IDT) carried out in accordance with AASHTO TP9-02 (AASHTO 2002). The test is conducted by applying a constant rate of vertical deformation (2.0 in/min, 50.8 mm/min) until the specimen fails. Energy until failure and total fracture energy are also calculated as the area under the stress-strain plot. Table 1 shows typical IDT test results comparing FRAC and a control mixture. It is worth mentioning that the mixture used in this project was an open graded mix. The FRAC mixture shows higher indirect tensile strength, energy at fracture and total energy than the control mixture. Depending on the test temperature, the increase in tensile strength ranges from 5 to 31%; whereas the energy at fracture range is between 15 and 100%. The contribution of the fibers is evident in the post peak strength of the material as indicated by the total energy. This improvement ranges from 19 to 45%.



Figure 5. Flexural strength test set-up.

Although the specimen cracks, the fibers hold the specimen together which, in turn, requires more energy to completely fail the mixture. This is also demonstrated in the flexural strength test that follows.

7 FLEXURAL STRENGTH TEST

As mentioned above, fibers contribute to the improvement of the load carrying capacity after the formation of the first crack in the mix. This contribution by means of bridging cracks and pull-out can be noticed by looking at the post peak region of the mechanical response of mixes (load-deformation). Under tensile stress, fibers adsorb energy preventing a dramatic propagation of cracks. Flexural strength tests are conducted to evaluate residual strength and energy characteristics of the different mixtures as shown in Figure 5. Results of flexural strength tests performed on rectangular prismatic beams of conventional and FRAC asphalt mixtures are shown below. The flexural strength of the asphalt beams is defined as the flexural stress applied on the beam at the moment of failure. The following equation is used to assess the flexural strength (FS):

$$FS = \frac{3 \cdot F_{(peak)} \cdot L}{2 \cdot b \cdot d^2} \quad (1)$$

where,

$F_{(peak)}$ = peak load (lbs)

L = length of the support span (in)

b = width of the beam (in)

d = thickness of the beam (in)

As mentioned before, unlike conventional mixes, FRAC specimens do not break soon after initiation of the first crack. The fibers have the effect of increasing the work fracture which is referred to as toughness and is represented by the area under the load-deflection curve. In order to include the improvement in the material toughness imparted by the fibers the energy or work of fracture after the peak load should be included when estimating the residual strength. Banthia and Trottier presented a residual strength analysis approach on steel-fiber reinforced concrete that accounts for the toughness improvement imparted by the fibers

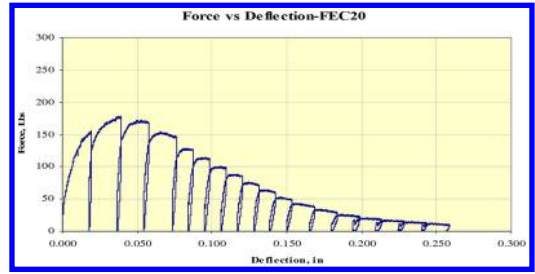


Figure 6. Typical load-deflection results for cyclic load test.

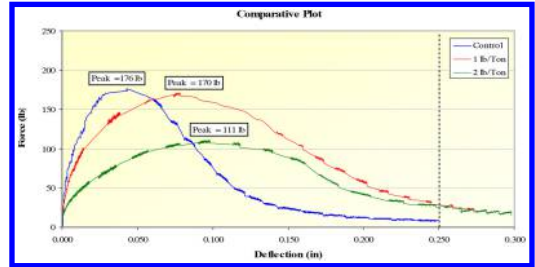


Figure 7. Comparison of control and FRAC mixtures in cyclic load tests.

(Trottier & Banthia 1994). The same approach is used to estimate the residual strength (RS) of asphalt mixes by using the following equation:

$$RS = \frac{E_{(post,0.25)} \cdot L}{(0.25 - \delta_{peak}) \cdot b \cdot d^2} \quad (2)$$

where,

$E_{(post,0.25)}$ = post peak energy up to 0.25 in displacement (lb-in)

δ_{peak} = deflection at the peak load (in)

L = length of the support span (in)

b = width of the beam (in)

d = thickness of the beam (in)

The arbitrary deflection value of 0.25 in for calculation of post peak energy is selected where every test reaches this point. Once the residual strength is estimated, it is added to the flexural strength for accounting for the improvement in toughness due to the use of fibers.

Figure 6 shows a typical load-deflection curve obtained from cyclic load test. Loading for both monotonic and cyclic load tests is controlled at a constant deflection rate of 0.025 in/min. For cyclic tests unloading is under load control at a rate of 10 lb/sec.

A comparison of load-displacement curves is presented in Figure 7, where a control, FRAC mix with 1 lb/ton (~0.5 kg/tonne) and 2 lbs/ton (~1 kg/tonne) are compared. The enhancement imparted by fibers in the post peak region is noticeable. The results also suggest that a dosage of 1 lb/ton (0.5 kg/tonne) provides optimum results for the condition of this test.

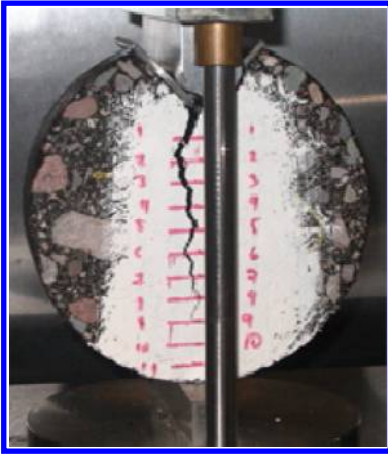


Figure 8. Typical C* fracture test setup.

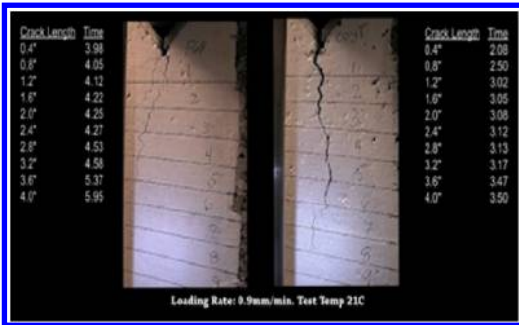


Figure 9. Crack length versus time comparison.

8 C* FRACTURE TESTS

A recent development of a C* Fracture Test for asphalt mixture was developed (Stempihar 2013). Specimens approximately 38-mm thick are cut from compacted gyratory specimens. A right-angle wedge is cut into the specimens to accommodate the loading device as shown in Figure 8. The tests can be conducted at a range of temperatures and loading rates. Once load and crack length versus time data are collected, results are analyzed and the C*-integral is plotted as a function of the crack growth rate. In addition, a simple visual observation and assessment of the crack length versus time for two different mixture types can be sufficient. In Figure 9, it is observed that the FRAC mixture sample (left) will take 5.95 minutes to reach a crack length of 100 mm (4 in) compared to a control mixture (right) that will take only 3.50 minutes to reach this crack length under the specified test conditions. What is also interesting is the severity of the crack after the test. The FRAC mixture's cracks are very tight compared to more open cracks or sample splits that are observed in control mixtures.

9 PAVEMENT DESIGN CONSIDERATION

The dynamic modulus testing program follows AASHTO TP 62-07. The improvement in modular ratio vary depending on test frequency and temperature, but an average modular value of 1.25 can be assumed for the FRAC mixture. It is the authors' experience that improvement of modular ratios in the range of 15 to 45% is possible, but they depend on the mixture quality under consideration for improvement. Lower quality asphalt mixtures would benefit from higher percentage improvement of the modular ratio; whereas high quality mixtures would see lower percentage improvement. These modified dynamic moduli can be used as input to determine the pavement performance using the AASHTO Mechanistic Empirical Pavement Design Guide, Pavement-ME (NCHRP 2004). Previous studies have shown that the performance of the FRAC mixture will be better in terms of rutting and fatigue cracking (Kaloush et al. 2010). Or an alternative design strategy would be to reduce the asphalt mixture layer thickness by 15 to 35%.

For AASHTO 1993 pavement design analysis with structural layer coefficient (a_1) consideration, the a_1 value for the fiber-reinforced mixture can be increased (by extrapolation) up to 0.5 (AASHTO 1993). Reminder that the layer coefficient is dependent on the resilient modulus value, which is highly correlated to the dynamic modulus property. In this approach, the analysis will also result in reduced thickness of the AC layer.

10 CONCLUDING REMARKS

The blend of polypropylene and aramid fibers used in improving the engineering properties of asphalt mixtures provide substantial benefits in reducing rutting, cracking and raveling potential. The reinforcing strength contribution of fibers was evident in several mechanical tests such as the indirect tensile test, especially when the energy until fracture and total fracture energy were compared to the control mixture. The flexural strength and C* fracture tests also indicated that the FRAC mixture is better able to resist the development and propagation of cracks when compared to the control mixture. The stiffness properties measured through the dynamic modulus and used for pavement performance prediction also indicated that the FRAC will provide better rutting and fatigue cracking resistance, or as an alternative design strategy reduce the asphalt mixture layer thickness. In either context, the use of fibers make them suitable candidate as a sustainable pavement material for asphalt concrete.

REFERENCES

AASHTO (1993) American Association of State Highway and Transportation officials, Guide for Design of Pavement Structures, Washington, DC.

- AASHTO Designation: T321-03 (2003). Determining the Fatigue Life of Compacted Hot-Mix Asphalt (HMA) Subjected to Repeated Flexural Bending.
- AASHTO TP9-02 (2002). Standard Test Method for Determining Creep Compliance and Strength of Hot Mix Asphalt (HMA) Using the Indirect Tensile Test Device (Draft Test Protocol). American Association of State Highway and Transportation Officials, Washington, D.C.
- ASTM D2493 (1998). Viscosity Temperature Chart for Asphalts. In Annual Book of ASTM Standards, pp230–234, Vol. 4.03.
- Bueno, B. S., Silva, W. R., Lima, D. C., Minete, E. (2003). Engineering Properties of Fiber Reinforced Cold Asphalt Mixes. Technical Note, Journal of Environmental Engineering, ASCE, Vol. 129, N. 10.
- Chowdhury, A., Button, J. W., and Bhasin, A. (2006). Fibers from Recycled Tire as Reinforcement in Hot Mix Asphalt, Texas Transportation Institute, Texas A & M University System, Report No. SWUTC/06/167453-1, April 2006.
- Cleven, M. A. (2000). Investigation of the Properties of Carbon Fiber Modified Asphalt Mixtures M. S. Thesis, Department of Chemical Engineering, Michigan Technological University.
- Fitzgerald, R. L. (2000). Novel Applications of Carbon Fiber for Hot Mix Asphalt Reinforcement and Carbon-Carbon Pre-forms, M. S. Thesis, Department of Chemical Engineering, Michigan Technological University.
- Jahromi, S. G., and Khodai, A. (2008). Carbon Fiber Reinforced Asphalt Concrete, The Arabian Journal for Science and Engineering, V. 33, No. 2B, October 2008, pp. 355–364.
- Kaloush, K.E., Biligiri, K. P., Zeiada, W. A., Rodezno, M. C. Reed, J. (2010). "Evaluation of Fiber-Reinforced Asphalt Mixtures Using Advanced Material Characterization Tests", Journal of Testing and Evaluation, ASTM International, Volume 38, No. 4.
- Lee, S. J., Rust, J. P., Hamouda, H., Kim, Y. R., Borden, R. H. (2005). Fatigue Cracking Resistance of Fiber-Reinforced Asphalt Concrete. Textile Research Journal, Vol. 75, N. 2, pp. 123–128.
- Mahrez, A., and Karim, M. R., (2007). Rutting Characteristics of Bituminous Mixes Reinforced with Glass Fiber, Proceedings of the Eastern Asia Society for Transportation Studies, Vol. 6.
- Mahrez, A., Karim, M. R., and Katman, H. A. (2003). Prospect of Using Glass Fiber Reinforced Bituminous Mixes, Journal of the Eastern Asia Society for Transportation Studies, Vol. 5.
- NCHRP 2004. Guide for Mechanistic-Empirical Design of New and Rehabilitated Pavement Structures. Final Report. National Research Council, Washington, D. C.
- Putman, B. J., and Amirkhani, S. N. (2004). Utilization of Waste Fibers in Stone Matrix Asphalt Mixtures, Journal of Resources, Conservation and Recycling, Recycled Materials in Highway Infrastructure, Volume 42, Issue 3, October 2004, pp. 265–274.
- Shaopeng, W., Qunshan, Y., Ning, L., and Hongbo, Y. (2007). Effects of Fibers on the Dynamic Properties of Asphalt Mixtures, Journal of Wuhan University of Technology-Materials Science Edition, China.
- SHRP Designation: M-009. Standard Method of Test for Determining the Fatigue Life of Compacted Bituminous Mixtures Subjected to Repeated Flexural Bending.
- SHRP-A-404. (1994). Fatigue Response of Asphalt-Aggregate Mixes. Asphalt Research Program, Institute Of Transportation Studies, University Of California, Berkeley. Strategic Highway Research Program, National Research Council, Washington, D.C.
- Stempihar, Jeff (2013). Development of the C* Fracture Test for Asphalt Concrete Mixtures. PhD Dissertation, Arizona State University.
- Trottier, J. F., and Banthia, N., (1994). Toughness Characterization of Steel Fiber Reinforced Concrete, Journal of Materials in Civil Engineering, Volume 6, No. 2, pp. 264–289.
- Witczak, M. W., Kaloush, K. E., Pellinen, T., El-Basyouny, M., & Von Quintus, H. (2002). Simple Performance Test for Superpave Mix Design. NCHRP Report 465. Transportation Research Board. National Research Council. Washington D.C.

Development of durable structural asphalt mixtures for the UK trunk road network

I. Artamendi, B. Allen & P. Phillips

Aggregate Industries, Hulland Ward, Derbyshire, UK

ABSTRACT: This study evaluates the properties of high modulus asphalt mixtures and assesses their potential for use as high quality structural layers on the UK trunk road network. High modulus mixtures, first developed in France and used now in the UK, are considered long life and durable structural materials. These mixtures are, however, susceptible to thermal damage, particularly under extreme weather conditions. In order to minimise the risk of thermal damage in high modulus mixtures, the use of softer binders has been investigated. Material properties evaluated included, workability, water sensitivity, deformation resistance, stiffness, and fatigue and fracture resistance. Analytical pavement design for a typical pavement structure incorporating these materials was also carried out. Design stiffness values were determined at the standard conditions for UK pavement design, i.e. 20°C and loading frequency of 5 Hz. Fatigue properties of the mixtures obtained experimentally using the four-point bending test were also incorporated in the analysis. It was found that the use of softer binders in high modulus mixtures have some of the benefits associated to these type of mixtures in terms of deformation and fatigue resistance. Also, pavement thickness can be considerably reduced when these mixtures are used instead of a conventional material. Alternatively, for a typical pavement thickness the used of these materials can extend the life of the pavement beyond that of a standard material.

1 INTRODUCTION

High modulus mixtures were first developed in France in the 1980s with the generic name of EME (Enrobé à Module Élevé) (Delorme et al. 2007). EME is described as a high modulus, long life asphalt complying with the European specifications for Asphalt Concrete (AC) (CEN, 2006a). There are two grades of EME in the French specifications: EME Class 1 and EME Class 2. The latter class has a significantly higher binder content, as defined by the richness modulus, and is generally now used in France and the UK.

Compared to traditional UK materials such as Dense Bitumen Macadam 50 pen binder (DBM50), EME2 has a higher binder content and lower air voids making it virtually impermeable and, therefore, more resistant to moisture damage. Furthermore, a fine aggregate grading results in a densely packed aggregate structure with good aggregate interlock. This, combine with a hard binder, gives the material superior deformation and fatigue resistance under heavy traffic conditions. High stiffness and fatigue resistance allows a reduction in pavement thickness.

French specifications for EME2 mixtures are based on richness modulus and on mixture requirements for air voids using the gyratory compactor, water sensitivity, wheel tracking, stiffness and fatigue (Delorme et al. 2007). In the UK, following trials of EME2 a specification for high modulus material for use in the base and binder course layers similar to the French EME2

and tailored to suit UK conditions was developed (Sanders & Nunn, 2005).

High modulus associated to EME2 mixtures, however, makes these materials susceptible to thermal damage, particularly under extreme temperature conditions. Thermal induced damage i.e. low temperature and thermal fatigue cracking, due to low temperatures and temperature variations, is directly related to brittleness of the binder at low temperatures. Furthermore, thermovolumetric changes occurring during cooling and heating periods are also responsible for the development of both macro and micro-cracks (Marasteanu, 2012).

In France, to limit thermal cracking, EME2 mixtures are primarily used in the lower layers (base course) where the material is less expose to low ambient temperatures and large temperature variations. Furthermore, care is taken to insulate the EME2 layers as soon as the installation is completed by covering them with the binder or surface course layers (Delorme et al. 2007).

In the UK, the bitumen specified in EME2 is typically 10/20 or 15/25 pen. Under severe winter conditions such as those experienced in 2010 and 2011, these materials can be susceptible to thermal damage. In order to minimize the risk of thermal induced damage in high modulus mixtures, the use of softer binders, 30/45 pen and 40/60 pen, has been investigated. Standard European test methods have been used to evaluate the properties of the mixtures including air voids,

Table 1. Grading and binder content.

Sieve size (mm)	AC 14 base/bin		AC 20 base/bin	
	%	Passing	%	Passing
31.5			100	(98–100)
20	100	(100)	99	(90–100)
14	96	(90–99)	84	(65–85)
6.3	53	(42–65)	47	(38–56)
2	29	(19–42)	30	(20–40)
0.250	15	(8–18)	11	(6–20)
0.063	8.2	(5.0–9.0)	6.0	(2.0–9.0)
Binder cont (%)	5.5	(5.3 min)	4.8	(4.2 min)

water sensitivity, deformation resistance, stiffness, and fatigue and fracture resistance.

Moreover, designed stiffness values were determined experimentally at the standard conditions used in the UK pavement design. Design stiffness and fatigue properties were then used for analytical pavement design using a multilayer, linear elastic pavement model for a typical UK pavement structure.

2 MATERIALS AND MIXTURES

Basalt aggregates and limestone filler were used to produce AC 14 base/bin mixtures with three penetration graded binders, 15/25, 30/45 and 40/60. The three mixtures had the same composition and grading but different pen grade bitumen. Binder content was 5.5% for all the mixtures. For comparison purposes, a standard AC 20 base/bin 40/60 mixture produce with granite aggregate was also used in the study. Binder content for this mixture was 4.8%. Grading and binder content complied with the specifications in the UK for AC 14 EME2 and AC 20 dense binder course mixture (BSI, 2010) and are given in Table 1.

Aggregates and bitumen were pre-heated in an oven to the target mixing temperature. Target laboratory mixing temperatures were 190, 185 and 170°C for mixtures produced with 15/25, 30/45 and 40/60 bitumen, respectively. Heated aggregates were mixed for 30 seconds in a mechanical mixer. Hot bitumen was then added to the aggregate blend and mixed for a further 2 ½ minutes. The mixtures were then compacted to slabs using a laboratory roller compactor.

3 TESTING

3.1 Gyrotory compaction

The gyrotory compactor was used to assess the workability of the mixtures. Proportioned aggregates blends and bitumen were mixed at the reference temperature and then compacted in 100 mm moulds. Three specimens per mixture were compacted. The load (stress) applied by the gyrotory compactor was 600 kPa, the angle was 1.25° and rotation speed was 30 rpm. Furthermore, the number of gyrations selected was 100. It should be noted that the same number of gyrations is

Table 2. Properties of the mixtures.

Property	AC 14 15/25	AC 14 30/45	AC 14 40/60	AC 20 40/60
Air voids @ 100 gyr (%)	5.2	5.2	5.1	5.0
ITSR (%)	79	90	82	85
Maximum rut depth, RD _{AIR} , (mm)	2.10	5.00	8.20	10.40
Proportional rut depth, PRD _{AIR} , (%)	4.1	9.8	16.1	20.2
Wheel tracking slope, WTS _{AIR} , (mm/10 ³ cycles)	0.07	0.16	0.30	0.44
Creep rate, f _c , (microstrain/cycle)	0.75	0.95	3.53	1.90
Stiffness modulus, ITSM @ 20°C and 124 ms, (MPa)	6536	4742	2770	5575
Stiffness modulus, 4PB @ 20°C and 8 Hz, (MPa)	11135	8486	6616	10691
Microstrain at 10 ⁶ cycles, ε ₆ , (µm/m)	154	94	93	75
Fracture toughness, SCB, K _{IC} , (N/mm ^{3/2})	29.2	31.6	28.5	27.4

used in the French method for EME2 mixtures 14 mm maximum nominal size. In order to determine air voids of gyrotory compacted specimens, the maximum densities of the mixtures were first determined.

Results showed that mean air voids at 100 gyrations for the AC 14 mixtures were 5.2% approximately and did not depend on the grade of the binder. Air voids at 100 gyrations for the AC 20 mixture was 5.0%. Moreover, all the mixtures showed air voids at 100 gyrations lower than the specified limit for 14 mm EME2 mixtures i.e. 6%, as shown in Table 2.

3.2 Water sensitivity

Resistance to moisture damage was evaluated by means of the water sensitivity test (CEN, 2008). Six cylindrical specimens 100 mm diameter cored from laboratory prepared slabs were used. A dry subset (3 specimens) was maintained at 20°C in a temperature controlled cabinet. A wet subset (3 specimens) was conditioned by applying a vacuum residual pressure of 6.7 kPa for 30 minutes followed by water conditioning at 40°C for a period of 70 h. Indirect tensile strength tests were then carried at 20°C and the Indirect Tensile Strength Ratio (ITSR) was then determined.

Results presented in Table 2 showed that ITSR values of the mixtures produced with the 30/45 pen bitumen were the highest followed by those produced with the 40/60 pen and the 15/25 pen. ITSR values for all the mixtures were above 70% which is the minimum value for EME2 mixtures in France. It should be noted, however, than the French method uses the Duriez test (Delorme et al. 2007) in which the compression strength ratio and not the indirect tensile strength ratio, is measured and specified.

Water sensitivity test results indicated good resistance to moisture damage for both the AC 14 and AC 20 mixtures. Furthermore, for the AC 14 mixtures binder grade did not have a large effect on water resistance which was mainly controlled by the volumetrics of the mixture, i.e. binder content and air void content. ITSR value for the AC 20 40/60 mixture, on the other hand, was similar to that of the AC 14 40/60 which might suggest good adhesion properties of both aggregates types. This might also reflect similar levels of air voids (~5%) for these two mixtures.

3.3 Resistance to deformation

3.3.1 Wheel tracking test

Wheel tracking tests were carried using a small size device, conditioning in air (CEN, 2003). Slabs $300 \times 300 \times 50 \text{ mm}^3$ were used. Two specimens per mixture were tested. The tests were performed at 60°C and the number of load cycles applied was 10,000. Maximum rut depth (RD_{AIR}), proportional rut depth (PRD_{AIR}) and wheel tracking slope (WTS_{AIR}) were then determined.

Wheel tracking test results presented in Table 2 showed that, as expected, resistance to permanent deformation increased as the penetration grade of the bitumen decreased. Results presented in Table 2 also showed that the AC 20 40/60 mixture was slightly less resistant to permanent deformation than the AC 14 with the same pen grade binder.

The French mixture design method uses the wheel tracking large size device for assessing the resistance to permanent deformation. For EME2 mixtures a maximum proportional rut depth of 7.5% is specified at 60°C and 30000 cycles. In this study, proportional rut depth values of the mixture with the 15/25 pen grade binder using the small size device (60°C and 10000 cycles) was below 7.5% whereas the mixtures with the softer grades were above this value.

3.3.2 Triaxial cyclic compression test

Resistance to permanent deformation was also evaluated using the triaxial cyclic compression test (CEN, 2005). In this test a cylindrical asphalt specimen is subjected to a confining pressure and a cyclic axial stress. The cumulative axial strains with number of cycles are then determined and presented in a creep curve. The creep rate (f_c) or rate of deformation is then calculated from the linear part of the creep curve.

Cylindrical specimens 100 mm diameter and 60 mm height core from slabs were used. A rubber socket was used to separate the specimen from the confining medium (air). Axial and confinement pressures were applied by a servo-pneumatic system. Two displacement transducers measured the vertical deformation of the specimen with number of load cycles. Test conditions applied were 40°C test temperature, 50 kPa confining stress and 200 kPa axial load pulse (peak-to-peak) (CEN, 2006b). The load pulse selected was 1 sec loading/1 sec unloading (block pulse) and the frequency was 0.5 Hz. Furthermore, maximum

number of load cycles applied to the specimen was 10000. Four specimens were tested per mixture.

The creep rate (f_c) was calculated by fitting a straight line through the linear part of the creep curve. Mean creep rate values determined as before are presented in Table 2. Results showed low creep rates for the AC 14 mixture produced with the 15/25 pen, indicating high resistance to permanent deformation. Creep rates also increased as the penetration grade of the bitumen increased. It was also found that creep rate for the AC 14 40/60 mixture was higher than that for the AC 20 40/60.

3.4 Stiffness

3.4.1 Indirect tensile stiffness test

Stiffness modulus was determined using the indirect tensile stiffness test (CEN, 2012a). Tests were carried out at 20°C and the loading time was 124 ms (CEN, 2006b). Cylindrical specimens 100 mm diameter and 50 mm height cored from slabs were used. Six specimens per mixture were tested.

Results presented in Table 2 showed that the stiffness of the AC 14 mixtures increased as the penetration grade of the binder decreased. It was also found that the stiffness of the AC 14 mixture produced with the 15/25 pen bitumen (6.5 GPa) was above the minimum value specified in the UK for EME2 mixtures i.e. 5.5 GPa (Sanders and Nunn, 2005). It should be noted that the specified value in the UK is for cores taken from trial sections and not for laboratory prepared specimens. Also, the stiffness of the AC 20 40/60 mixture was just above 5.5 GPa, thus, considerably higher than the AC 14 with the same pen grade.

3.4.2 Four-point bending stiffness test

Stiffness modulus was also determined using the four-point bending (4PB) stiffness test (CEN, 2012a). Beam specimens $400 \times 50 \times 50 \text{ mm}^3$ cut from slabs were used for testing. Five specimens per mixture were tested. Tests were carried out under controlled strain mode at a target strain of 100 microstrain. Test conditions selected were: temperature 20, 15 and 10°C and frequency 0.5, 1.0, 2.5, 5.0, 8.0 and 10.0 Hz. At each temperature and frequency the number of loading cycles applied was 100 and the stiffness of the specimen was defined as the stiffness at 100 cycles.

Stiffness values at the standard test condition for 4PB stiffness test, i.e. 20°C and 8 Hz (CEN, 2006b), are shown in Table 2. It can be seen that the stiffness of the AC 14 mixtures increased as the pen grade of the bitumen decreased. Also, the stiffness of the AC 20 40/60 mixture was markedly higher than that of the AC 14 with the same grade bitumen and just below that for the AC 14 15/25.

In France, stiffness tests are typically performed using the two-point bending (trapezoidal) test and the test conditions specified are 15°C and 10 Hz. For EME2 mixtures, the minimum stiffness value specified is 14000 MPa. Results from this study showed that the AC 14 mixture with the 15/25 bitumen had a

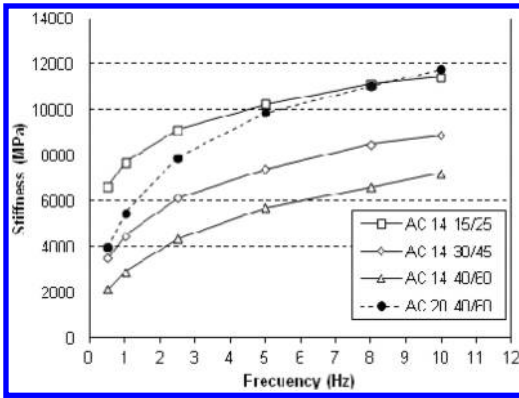


Figure 1. Stiffness values at 20°C from 4PB tests.

stiffness value of 14010 MPa at 10°C and 25 Hz using the 4PB test. This value was just above the minimum value specified for EME2 mixtures when the tests were carried out at the same conditions as those specified in France.

Stiffness test results at 20°C and at frequencies from 0.5 to 10 Hz are presented in Figure 1.

It can be seen that the stiffness increased as the loading frequency increased. Interestingly, the rate of increase in stiffness with frequency depended on the mixture type, i.e. AC 14 or AC 20, but not on the grade of the bitumen. Furthermore, this change in stiffness with frequency was more pronounced for the AC 20 mixture, particularly at low frequencies (see Fig. 1). This suggests that the AC 20 mixture is more susceptible to loading frequency and temperature than the AC 14 mixtures, particularly at low frequency and/or high temperature.

3.5 Fatigue resistance

Fatigue resistance was determined using the 4PB fatigue test (CEN, 2012b). Fatigue tests were performed at 20°C and 30 Hz (CEN, 2006b). Tests were carried out at different strain (microstrain) levels from 100 to 300 microstrain. Three strain levels were employed. At each strain level three specimens were tested.

Fatigue data was used to derive a relationship between the strain (ϵ) and the number of cycles to failure, defined as the number of cycles to 50% stiffness reduction (N_{50}). Strains and the corresponding fatigue lives were plotted on logarithmic scales, and a power equation was fitted through the experimental data in order to obtain a relationship between strain and fatigue life of the form $N_{50} = A(1/\epsilon)^b$, where A and b are regression constants.

Fatigue curves are shown in Figure 2. Regression constants A and b, and R^2 values are presented in Table 3. Fatigue resistance of AC mixtures is given by the microstrain at 10^6 cycles (ϵ_6) (CEN, 2006a). Microstrain at 10^6 cycles values (ϵ_6) were determined from the plots of the strain vs number of cycles to

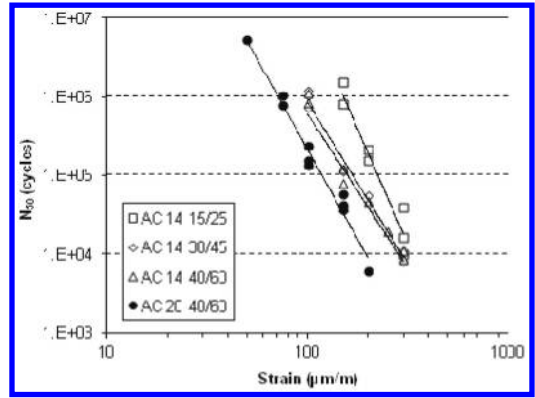


Figure 2. Fatigue lives.

Table 3. Fatigue regression constants and microstrain at 10^6 cycles.

Material	A	b	R^2	ϵ_6 microstrain
AC 14 15/25	5.80×10^{18}	5.86	0.94	154
AC 14 30/45	1.49×10^{14}	4.12	0.99	94
AC 14 40/60	4.15×10^{13}	3.92	0.91	93
AC 20 40/60	3.00×10^{14}	4.57	0.97	75

failure, and are shown in Table 3. The higher the ϵ_6 value the better the resistance to fatigue.

Results indicated better fatigue resistance of the AC 14 mixture with 15/25 pen bitumen compared to that with 30/45 and 40/60 pen bitumen, as seen by the ϵ_6 values. Differences between the fatigue resistance of the AC 14 mixtures with 30/45 and 40/60 pen bitumen were relatively small (see Table 3). Also, fatigue resistance of the AC 20 40/60 mixture was markedly lower than those for the AC 14 mixtures.

It should be noted that in France, fatigue testing is performed using the two-point bending (trapezoidal) test and the test conditions specified are 10°C and 25 Hz. For EME2 mixtures, the minimum ϵ_6 value specified is 130 microstrain.

3.5.1 Fracture resistance

Fracture resistance was evaluated by means of the semi-circular bending (SCB) test (CEN, 2010). In this test, a SCB specimen notched at the mid-point is loaded in a three point bending configuration. The maximum load (stress) sustained by the specimen and a geometric factor are then used to determine the fracture toughness (K_{Ic}). Fracture toughness is a measure of the resistance of a material to crack propagation.

SCB specimens were obtained by coring cylindrical specimens of 150 mm diameter (D) and 50 mm height (t) from slabs. These cylinders were cut perpendicular to the axis to obtain the semi-circular specimens, and then notched at the mid-point along the diameter in the direction of the load. Notch depth (a) was 10 mm and span (2s) was 120 mm. Tests were carried out at

Table 4. Design stiffness based on indirect tensile stiffness test at 20°C and 124 ms.

Material	Mean Stiffness MPa	STD MPa	Charac. Stiffness MPa	Design Stiffness MPa
AC 14 15/25	6536	359	6076	9213 (9000)
AC 14 30/45	4742	147	4553	7355 (7000)
AC 14 40/60	2770	85	2661	5047 (5000)
AC 20 40/60	5575	742	4625	7443 (7000)

a displacement rate of 5 mm/min and at a temperature of 0°C. Four SCB specimens per mixture were tested per mixture

Results presented in Table 2 showed that fracture toughness values of the AC 14 mixtures with different grade binder were in general very similar. Thus, for the test conditions used in the study, fracture toughness is primarily affected by the aggregate structure of the mixtures and the amount of binder. So, for mixtures with similar aggregate skeleton and with a relatively high amount of binder, binder grade had a limited effect on fracture toughness. Also, fracture toughness value for the AC 20 mixture was slightly lower than those for the AC 14 mixtures.

4 PAVEMENT DESIGN

4.1 Design stiffness

The UK analytical design method employs an effective in-service stiffness modulus that is measured at a frequency of 5 Hz and at a temperature of 20°C (DMRB, 2006). This effective in-service stiffness modulus is the stiffness attain by the material after approximately one to two years in service.

Design stiffness can be obtained by means of the indirect tensile stiffness test. Adjustments, however, have to be made to convert a loading time of 124 ms in the indirect tensile stiffness test to a design loading frequency of 5 Hz. Furthermore, material curing or ageing during the first year in-service also needs to be account for. Nunn (2008) defined the characteristic indirect stiffness modulus of an asphalt mixture as the stiffness value below which only 10% of all the samples tested are likely to fall. For an assumed normal distribution, this value is 1.28 standard deviations below the mean value. Then, the design stiffness (GPa) was calculated as follows, Design stiffness = 1.22 × Characteristic stiffness + 1.80.

Design stiffness values based on indirect tensile stiffness tests are presented in Table 4. These values were calculated using 6 laboratory prepared cylindrical specimens. For simplicity, the design stiffness values were rounded down to the nearest 1000 MPa (see values in brackets). These design stiffness represented the in-service stiffness after curing.

Design stiffness at the standard UK conditions of 20°C and 5 Hz can also be determined directly from four-point bending (4PB) stiffness tests carried out

Table 5. Design stiffness based on 4PB test at 20°C and 5 Hz.

Material	Mean Stiffness MPa	STD MPa	Charac. Stiffness MPa	Design Stiffness MPa
AC 14 15/25	10277	339	9843	9843 (9000)
AC 14 30/45	7407	39	7357	7357 (7000)
AC 14 40/60	5716	113	5571	5571 (5000)
AC 20 40/60	9903	227	9613	9613 (9000)

at the same conditions. Design stiffness values based on the 4PB tests are presented in Table 5. These values were calculated using 5 laboratory prepared beam specimens. Characteristic 4PB stiffness was calculated as before and the design stiffness was assumed to be the same as the characteristic stiffness. Thus, the effect of ageing or curing was not taken into account. Design stiffness values were rounded down to the nearest 1000 MPa (see values in brackets).

Design stiffness values presented in Tables 4 and 5 shows that for the AC 14 mixtures there is good agreement between the two proposed methods. For the AC 20 mixture, however, the design stiffness value based on the 4PB stiffness test was higher than that based on the standard approach.

Design stiffness values have been compared with those for standard materials, i.e. 8000 MPa for EME2 and 4700 MPa for DBM50 given in the UK pavement design manual HD26/06 (DMRB, 2006). It can be seen that design stiffness for AC 14 15/25 (9000 MPa) was slightly higher than that for EME2. Design stiffness for the AC 14 30/45 (7000 MPa) was between the EME2 and DBM 50 and the design stiffness for the AC 14 40/60 (5000 MPa) was similar to that for a DBM50. Also, the design stiffness values obtained for the AC 20 40/60 were well above that for a DBM50.

4.2 Analytical design

The UK design method for fully flexible pavements is based on a mechanistic-empirical method that uses a multi-layer, linear elastic response model. In the original work by Powell et al (1984) calculated horizontal tensile strains at the bottom of the asphalt base layer and vertical compressive strain at the top of the subgrade were used to predict the life of the pavement in terms of the cumulative number of 80 kN standard axels.

With the introduction of the foundation stiffness classes in pavement design (Nunn, 2004), the subgrade strain criterion became redundant. The current analytical design method relies on a single criterion that limits the strain at the underside of the base asphalt layer to a permissible level to achieve the require pavement life. The critical strain is that induced by a single standard wheel load (40 kN) represented by a circular area (0.151 m radius) with a uniform vertical stress.

Standard conditions for the design include linear elastic respond and full bond for all layers.

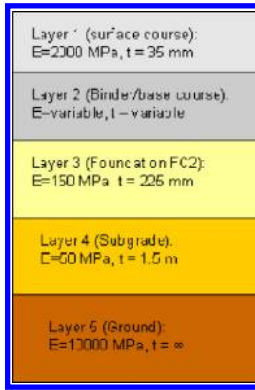


Figure 3. Pavement structure.

Calculations are carried out at an equivalent pavement temperature of 20°C and at an effective loading frequency of 5 Hz. Furthermore, the structural properties of the asphalt layers include a Poisson's ratio of 0.35 and the stiffness modulus measured at 20°C and 5 Hz.

In the current design method, the design life N , in msa, is given by Equation 1 (Nunn, 2004), as follows:

$$\frac{N}{10^6} = \left(\frac{\epsilon_r}{K_{Flex} \times K_{Safety} \times 201 \times 10^{-6}} \right)^{-4.16} \quad (1)$$

where:

ϵ_r = Calculated tensile strain at the underside of the asphalt layer

$$K_{Flex} = 1.089 \times E^{-0.172}$$

E = Design stiffness (GPa)

$K_{Safety} = 1$ (typical value)

A typical pavement model consisting of an asphalt surface course layer, an asphalt binder and base course layer, sub-base, sub-grade and the existing ground was used for analytical design (see Fig. 3). This pavement structure corresponds to a Foundation Class 2 (FC2) which is the standard UK foundation and is equivalent to 225 mm on Type 1 sub-base on a sub-grade with a CBR ratio of 5%. The surface layer was 35 mm thick and the stiffness was 2000 MPa. The design stiffness values of the binder and base course layers were determined from 4PB stiffness test and are given in Table 5. Layer thickness was variable. Stiffness of the sub-base was 150 MPa and the thickness 225 mm. The sub-grade was 1.5 m thick and the stiffness was 50 MPa. Finally, the ground was assumed to have a stiffness of 10000 MPa.

Critical strains induced by a standard wheel load were calculated using a linear elastic, multi-layer pavement model. Design curves for the proposed pavement structure and based on the tensile strains calculated at the underside of the base/binder asphalt layer were determined using Equation 1 and are presented in Figure 4.

It can be seen that for a given foundation class, the design curves depended solely on the design stiffness of the structural asphalt layers. Thus, for a given traffic,

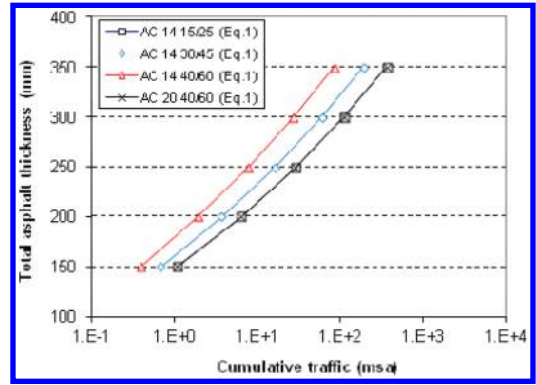


Figure 4. Design curves determined using Equation 1.

Table 6. Design asphalt thickness calculated using Equation 1.

Design Traffic (msa)	Design asphalt thickness (mm)					
	DBM 50	EME2	AC14 15/25	AC14 30/45	AC14 40/60	AC20 40/60
20	290	240	240	260	290	240
40	320	260	260	290	320	260
80	360	300	290	320	360	290

total asphalt thickness decreased as the design stiffness increased from 5000 MPa for the AC 14 40/60 to 9000 MPa for the AC 14 15/25. Also, the design curves for the AC 14 15/25 and AC 20 40/60 coincided as both mixtures had the same design stiffness (9000 MPa).

These design curves were used to determine total asphalt thickness for a given traffic density (msa). Design thickness for traffic densities of 20, 40 and 80 msa for two standard materials, DBM50 and EME2, given in HD/26 and for the mixtures used in the study are presented in Table 6. It can be seen that design asphalt thicknesses for AC 14 15/25 (and for AC 20 40/60) were the same as those for a standard EME2 for 20 and 40 msa. For 80 msa design thickness for the AC 14 15/25 was 10 mm less than that for the EME2. This reflected higher design stiffness of the AC 14 15/25 compared to the EME2. Also, design thicknesses for AC 14 40/60 were the same as those for the standard DBM50. Finally, design asphalt thicknesses for the AC 14 30/45 were between those for AC 14 15/25 and AC 14 40/60.

Alternatively, for a particular total asphalt thickness, design traffic life (msa) increases considerably for AC 14 15/25 and AC 30/45, in relation to the standard DBM50 material. Design lives for AC 14 40/60 are, on the other hand, the same as those for the standard DBM50 material.

4.3 Mixture fatigue considerations

The fatigue criterion used to calculate the design life of the pavement (Equation 1) is based on the

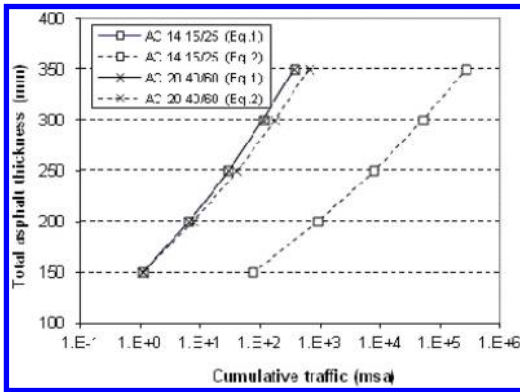


Figure 5. Design curves for AC 14 15/25 and AC 20 40/60 determined using Equation 1 and Equation 2.

fatigue characteristics of a DBM100 determined using a uniaxial fatigue test. In this test a controlled stress sinusoidal tension/compression stress loading at a frequency of 25 Hz and a temperature of 20°C was used. Furthermore, the same fatigue criterion was then used for mixtures with a similar binder volume produced with harder grade binders (e.g. DBM50).

The design criterion given by Equation 1 can be generalized to take into account the fatigue performance of different asphalt mixtures and also the different types of fatigue tests. If a new mixture is considered and its fatigue life measured using a different fatigue test, Equation 1 can be modified as follows (Nunn, 2004),

$$\frac{N}{10^6} = \left(\frac{\epsilon_r}{K_{Flex} \times K_{Safety} \times 201 \times 10^{-6} \times \frac{\epsilon_{6(New)}}{\epsilon_{6(DBM)}}} \right)^{-n} \quad (2)$$

where:

$\epsilon_{6(New)}$ = Strain at 10^6 cycles of the new mixture measured in the new fatigue test.

$\epsilon_{6(DBM)}$ = Strain at 10^6 cycles of the DBM mixture measured in a new fatigue test.

n = Exponent of the fatigue relationship for the new mixture determined from the new fatigue test. (Note: this criterion assumes that the exponent for the DBM mixture determined from the new method is the same as that determined with the original method i.e. -4.16).

In this work, fatigue properties were determined using the 4PB test. The strain at 10^6 cycles (ϵ_6) and the slope of the fatigue relationship (b) of the mixtures investigated are presented in Table 3. The regression constant “b” in Table 3 is the exponent of the fatigue relationship “n” in Equation 2. Also, the exponent of the AC 20 40/60 mixture determined with the 4PB fatigue, i.e. 4.57, is similar to the value determined for the reference DBM50 mixture using the original uniaxial tension/compression fatigue test method, i.e. 4.16.

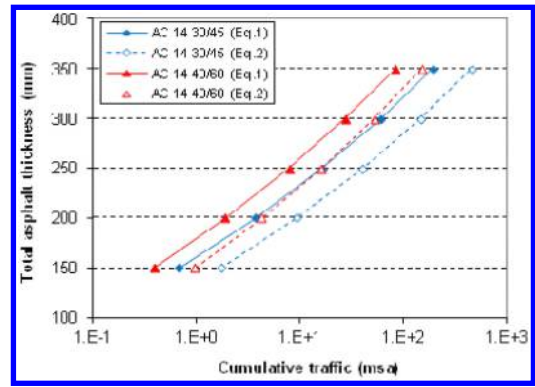


Figure 6. Design curves for AC 14 30/45 and AC 14 40/60 determined using Equation 1 and Equation 2.

Table 7. Design asphalt thickness calculated using Equation 2.

Design Traffic (msa)	Design asphalt thickness (mm)					
	DBM50	EME2	AC14 15/25	AC14 30/45	AC14 40/60	AC20 40/60
20	290	240	140	230	260	230
40	320	260	150	250	290	250
80	360	300	160	280	330	270

Design curves for the pavement model presented before (see Fig. 3) and calculated using Equation 2 are given in Figures 5 and 6. Figure 6 shows the design curves for AC 14 15/25 and AC 20 40/60. As shown before, the design curves for these two mixtures based on Equation 1 coincided as they only depended on the design stiffness (both mixtures had a design stiffness of 9000 MPa). However, when the fatigue properties are taken into account as in Equation 2, there is a large shift of the AC 14 15/25 design curve due to its enhanced fatigue properties compare to the reference mixture. Thus, higher ϵ_6 shifts the curves to the right whereas higher fatigue slope reduces the slope of the design curve.

Similarly, Figure 6 shows the design curves for AC 14 30/45 and AC 14 40/60 obtained using Equation 1 and Equation 2. It can be seen that improved fatigue properties in terms of ϵ_6 and fatigue slope (b), results in a reduction of pavement thickness for a given design traffic density (msa).

Design thickness for traffic densities of 20, 40 and 80 msa determined using Equation 2 are given in Table 7. Standard design thickness for DBM50 and EME2 are also included. It can be seen that when fatigue properties are included in the analysis, the design thicknesses for AC 14 15/25 are reduced considerably compared to the standard design thicknesses for EME2. Furthermore, the design thicknesses for AC 14 30/45 are also lower than those for the standard EME2. And the design thicknesses for AC 14 40/60 are also reduced in relation to the DBM50.

5 CONCLUSIONS

Based on the laboratory work carry the following conclusions can be drawn:

Gyratory compaction results indicated good mixture workability with air voids at 100 gyrations for AC 14 and AC 20 mixtures below 6%.

Resistance to water damage for the mixtures evaluated was considered adequate as seen by the retained strength values after water conditioning (ITSR > 70%).

Wheel tracking and cyclic compression tests showed that deformation resistance increased as the pen grade of the binder decreased. Also, for the two mixtures with the same pen grade binder results depended on the test method used.

Stiffness of the AC 14 mixture with the 15/25 bitumen was markedly higher than those with softer bitumens. High stiffness combine with hard bitumen may increase the risk of low temperature and thermal cracking, particularly under extreme temperature conditions. High stiffness was also obtained for the AC 20 40/60.

Fatigue resistance determined using the four-point bending fatigue test showed better fatigue resistance of the AC 14 mixture produced with the harder grade bitumen (15/25) compared to the softer ones (30/45 and 40/60). Differences between the fatigue performance of the 30/45 and 40/60 grade binders were relatively small. Fatigue resistance of the AC 20 40/60 mixture was the worst.

There were no significant differences between the fracture resistance of AC 14 mixtures produced with different penetration grade binders, as seen by fracture toughness values at 0°C. Fracture resistance of the AC 20 mixture was, on the other hand, marginally lower than those for the AC 14 mixtures.

The two methods employed to determine the design stiffness based on the indirect tensile stiffness and the four point bending tests showed good agreement particularly for the AC 14 mixtures. Design stiffness values used for analytical pavement design were based on laboratory stiffness values determined from 4PB test at 20°C and 5 Hz.

Design curves calculated using a multilayer, linear elastic pavement model for a standard UK foundation (Foundation Class 2) showed that the AC 14 15/25 and AC 14 30/45 gave a reduction in total asphalt thickness compared to a standard DBM50 material. Also, similar pavement thicknesses were obtained for AC 14 15/25 and a standard EME2.

When fatigue resistance was introduced in pavement design analysis, mixtures with better fatigue in relation to a standard material (i.e. DBM50) gave a considerable reduction in pavement thicknesses. Furthermore, for the same design stiffness, better

fatigue properties of the AC 14 15/25 compared to the AC 20 40/60 resulted in a considerable reduction of pavement thickness.

REFERENCES

- British Standard Institution (BSI), 2010. *Published Document PD6691. Guidance on the use of BS EN 13108 Bituminous mixtures – Material specifications.*
- Comité Européen de Normalisation (CEN), 2003. *EN 12697-22. Bituminous mixtures. Test methods for hot mix asphalt. Part 22: Wheel tracking.*
- Comité Européen de Normalisation (CEN), 2005. *EN 12697-25. Bituminous mixtures. Test methods for hot mix asphalt. Part 25: Cyclic compression test.*
- Comité Européen de Normalisation (CEN), 2006a. *EN 13108-1. Bituminous mixtures. Materials specifications. Part 1: Asphalt Concrete.*
- Comité Européen de Normalisation (CEN), 2006b. *EN 13108-20. Bituminous mixtures. Materials specifications. Part 20: Type testing.*
- Comité Européen de Normalisation (CEN), 2007. *EN 12697-31. Bituminous mixtures. Test methods for hot mix Asphalt. Part 31: Specimen preparation by gyratory compactor.*
- Comité Européen de Normalisation (CEN), 2008. *EN 12697-12. Bituminous mixtures. Test methods for hot mix asphalt. Part 12: Determination of water sensitivity of bituminous specimens.*
- Comité Européen de Normalisation (CEN), 2010. *EN 12697-44. Bituminous mixtures. Test methods for hot mix asphalt. Part 44: Crack propagation by semi-circular bending test.*
- Comité Européen de Normalisation (CEN), 2012a. *EN 12697-26. Bituminous mixtures. Test methods for hot mix asphalt. Part 26: Stiffness.*
- Comité Européen de Normalisation (CEN), 2012b. *EN 12697-24. Bituminous mixtures. Test methods for hot mix asphalt. Part 24: Resistance to fatigue.*
- Delorme, J.L., C. de la Roche and L. Wendling, L. 2007. *LPC Bituminous Mixtures Design Guide.* Laboratoire central des ponts et chaussées, DISTC – section Diffusion, Paris.
- Design Manual for Roads and Bridges (DMRB), 2006. *Volume 7 Pavement Design and Maintenance, Section 2 Pavement Design and Construction, Part 3: HD 26/06 Pavement design (DMRB 7.2.3).* London, The Stationary Office.
- Marasteanu, M. 2012. Investigation of Low Temperature Cracking in Asphalt Pavements, National Pooled Fund Study – Phase II. *Report MN/RC 2012-23*, Department of Civil Engineering, University of Minnesota, Minneapolis, Minnesota.
- Nunn, M. 2004. Development of a more versatile approach to flexible and flexible composite pavement design. *TRL Report TRL615*, Crowthorne, TRL Limited.
- Nunn, M. 2008. Relationship between ITSM of new material and design stiffness. *Unpublished Report.*
- Powell, W.D., J.F. Potter, H.C. Mayhew and M.E. Nunn. 1984. Design of bituminous roads. *Laboratory Report LR1132*, Crowthorne, TRL Limited.
- Sanders, P.J. and M. Nunn, 2005. The application of Enrobé à Module Élevé in flexible pavements. *TRL Report TRL636*, Crowthorne, TRL Limited.

Performance evaluation of HMAC asphalt concrete mixes

V. Haritonovs, J. Tihonovs & M. Zaumanis

Department of Roads and Bridges, The Institute of Transportation, Faculty of Civil Engineering, Riga Technical University, Riga, Latvia

ABSTRACT: Dolomite and gravel are the most available sedimentary rocks in the territory of Latvia. Utilization of local materials is one of the main aims of the road construction. However, according to Latvian Road Specifications dolomite and gravel cannot be used for average and high intensity roads because of its low quality (mainly, LA index). Therefore, mostly imported magmatic rocks (granite, diabase, gabbro, basalt) or imported dolomite are used which makes asphalt expensive. Hence there is a need to adapt High Modulus Asphalt Concrete (HMAC) technical solutions which allow application of local materials in long-life road pavements. The aim of the research is to develop a high performance asphalt concrete for base and binder courses using only locally available aggregates. The design of the asphalt includes a combination of empirical and performance based tests. Stiffness, resistance to rutting, fatigue and thermal cracking tests were carried out. High performance AC 16 base asphalt concrete was created using local dolomite and gravel aggregate with polymer modified (PMB 25/55-60) and hard grade (B20/30) bitumen. The paper also presents results of tests with the same type of asphalt concrete mixture, but using conventional bitumen (B70/100). The performance tests carried out showed that hard grade (B20/30) or polymer modified (PMB 25/55-60) bitumen with dolomite or gravel aggregates may be applied in High Modulus Asphalt Concrete for base and binder course.

1 INTRODUCTION

The main problem is the lack of high quality construction materials (components) in the Baltic states, most of which are imported (Vaitkus et al., 2012). In addition, the costs are influenced by considerable transportation distances and the increasing bitumen prices (Skrinskas, et al., 2010).

If the local material does not fulfill requirements, then one should seek the way for the improvement of its properties. If this is not possible, then one should seek the technological solution which will allow application of the weaker material (Sybilski D et al., 2010). One of a proper solution might be the use of dolomite as a component of High Modulus Asphalt Concrete (HMAC). Knowing that the binder courses, situated between 5 and 12 cm below the road surface, are subject to the highest stresses, high stiffness is probably the most important requirements for HMAC (Backer C et al., 2008.).

HMAC is a mixture of asphalt concrete designed for use in base and binder course of asphalt pavement. It has closed structure with comparatively large content of bitumen. This type of an asphalt mixture is designed not only by empirical properties but also by performance based properties (rut test, stiffness modulus and fatigue tests) (SPENS).

Hard road bitumen grades are applied, mainly 10/20, 15/25, 20/30 and polymer modified bitumen.

Hard bitumen assures the mixtures resistance to rutting. However large content of bitumen assure workability, fatigue durability and water resistance (Sybilski D et al., 2008).

France was also one of the first countries in which mechanistic asphalt pavement design was introduced into the general practice (AFNOR). In France, it is known under the acronym EME. In Poland, the acronym is AC WMS. Possible application of weaker mineral aggregate is one of the advantages of EME (in English HMAC). Application of High Modulus Asphalt Concrete allowed for saving on asphalt pavement's thickness thanks to higher stiffness modulus which reduce tension strains in asphalt base layer.

Standard road construction methods require an appropriate amount of high quality materials. That is why the researchers all over the world are searching for the road construction materials, which could allow usage of reduced amount of lower quality materials (Čygas et al., 2008; Elliott, 2009; Maupin and Diefenderfer, 2006).

The aim of the paper is to develop high performance asphalt concrete for base and binder courses with using only locally available aggregates – crushed dolomite and gravel. In order to achieve resistance to deformations at high ambient temperature hard grade (B20/30) and polymermodified bitumens (PMB 25/55-60) were used.

Table 1. Characteristics of aggregates.

Physical and mechanical properties	Gravel	Dolomite	Standard
	Results		
Los Angeles coefficient (LA), %	27	33	LVS EN 1097-2
Resistance to wear. Nordic test (A_N), %	–	21	LVS EN 1097-9
Flakiness Index (FI), %	4	5	LVS EN 933-3
Water absorption, %	1.4	2	LVS EN 1097-6
Grain density, Mg/m ³	2.76	2.80	LVS EN 1097-6
Fine content, %	0.4	1.0	LVS EN 933-1
Freeze/thawing (MS), %	7	7	LVS EN 1367-2

2 MATERIALS AND METHODS

The basic materials used in this study are fractionated crushed dolomite and gravel aggregate, unmodified hard grade bitumen B20/30 and SBS modified bitumen PMB 25/55-60 (B70/100 for reference mixture). Crushed dolomite aggregates were obtained from Pļaviņu DM Ltd. (Latvia), crushed gravel aggregates from Igate Ltd (Latvia) and bitumens (hard grade B20/30; unmodified B70/100 and modified PMB 25/55-60 from Grupa LOTOS S.A (Poland).

2.1 Properties of aggregates

The test results of dolomite and gravel main properties show very low flakiness index – 5 and 4, high frost resistance with average MS value of 7 and low fines content. However LA values for dolomite and gravel aggregates are low. These aggregates are suitable for use as a component of High Modulus Asphalt Concrete, where permitted LA value up to 40 (SPENS). The properties of dolomite aggregate are shown in Table 1.

The binder properties have been tested by means of conventional binder tests: needle penetration, softening point, aging and Fraas breaking point. The test results are listed in Table 2.

3 MIX DESIGN

In order to evaluate the influence of different mineral aggregates on HMAC physical and mechanical properties, several mixtures were designed, produced and tested on AC 16_{base/bin} asphalt concrete basis (HMAC-16).

Table 2. Typical characteristics of the bitumens.

Bitumen Parameter	PMB			Standard
	B 20/30	25/55-60	B70/100	
Penetration at 25°C, dmm	25.3	35.6	80.0	EN 1426
Softening point, °C	62.6	64.2	46.0	EN 1427
Fraas temperature, °C	–13.0	–17.0	–21.0	EN 12593
Kinematic viscosity, mm ² /s	1460	–	346	EN 12595
Dynamic viscosity, Pa·s	3277	–	160	EN 12596
Elastic recovery, %	–	>50	–	EN 13398
Ageing characteristics of bitumen under the influence of heat and air (RTFOT method)				
Loss in mass, %	–0.02	0.01	0.05	EN 12607-1
Retained penetration, %	75.9	72.1	76.0	EN 1426
Increase of a softening point, °C	6.9	7.9	5.4	EN 1427
Fraas breaking point after aging, °C	–11.0	–16.0	–17.0	EN 12593
Retained elastic recovery, %	–	>50	–	EN 13398

HMAC-16 asphalt concrete mixtures have been designed by using unconventional (bitumen – B20/30, PMB 25/55-66 and dolomite and gravel aggregates LA > 20) raw materials (Fig. 1). The basic idea of HMAC is to design a mix with hard grade bitumen at high binder content. (Rohde L. et al., 2008). The Marshall mix design procedure was used for the determination of the optimal bitumen content for the reference mixture, considering the mixture test results for Marshall stability and flow, as well as the volumetric values: air voids (V), voids in mineral aggregate (VMA) and voids filled with bitumen (VFB) Test specimens for Marshall Test were prepared in the laboratory by impact compactor according to EN 12697-30 with 2 × 50 blows of hammer 150°C temperature.

Table 3 shows all the designed and laboratory produced asphalt mixtures with different aggregates and bitumen.

Table 3. Types and components of HMAC mixes.

Bitumen	Aggregates	
	Gravel	Dolomite
PMB 25/55-60	HMAC 16 GR PMB	HMAC 16 D PMB
B 20/30	HMAC 16 GRB	HMAC 16 DB
B 70/100	HMAC 16 GR REF	HMAC 16 D REF

Following physical and mechanical characteristics of HMAC were determined:

- 1) Stiffness modulus, 10°C according to EN 12697-26 (4PB);
- 2) Resistance to rutting, 60°C and 10000 cycles, according to EN 12697-22;
- 3) Fatigue resistance 4PB-PR, 10°C and 10 Hz, according to 12697-24;
- 4) Asphalt concrete mixture density, according to EN 12697-5;
- 5) Asphalt concrete mixture bulk density, according to EN 12697-6;
- 6) Air voids content, according to EN 12697-8;
- 7) Stability and flow, 60°C, according to EN 12697-34 (samples were prepared by 2 × 50 blows).

3.1 Volumetric properties

Analysis of volumetric parameters of the different asphalt mixtures at different binder contents was performed. The quantity of bitumen for the HMAC was chosen in order to get air voids content in range from 2.0 % to 5.0 %. The results are presented in Tables 4 and 5. The binder content was optimized according to HMAC requirements developed in the SPENS programme (Sustainable Pavement for European New Member States).

3.2 Marshall test

Tables 6 and 7 contains Marshall test results at different binder contents and aggregate types for the mixtures that passed the requirement of having less than 5% air voids. The results show that HMAC mixtures have higher Marshall Stability compared to the reference mixture.

The Marshall stability of all the tested asphalt mixtures varied from 14.8 kN to 17.4 kN. The experiment showed that the highest Marshall stability is achieved with stiff bitumen 20/30.

4 PERFORMANCE EVALUATION

4.1 Wheel tracking test

A wheel tracking apparatus was used to simulate the effect of traffic and to measure the plastic deformations of the asphalt concrete samples. Tests were performed according to standard EN 12697-22 method B

Table 4. Volumetric properties of HMAC mixtures with dolomite aggregate.

Parameter	Mixtures		
	1. HMAC 16 D PMB	2. HMAC 16 D PMB	3. HMAC 16 D PMB
Bulk density, kg/m ³	2455	2457	2430
Maximum density, kg/m ³	2555	2551	2586
Voids content, %	3,9	3,7	6.0
VMA	17,8	18	18.3
VFB	78,2	79,6	67.2
Bitumen content, %	5,7	5,8	5.1

Parameter	Mixtures		
	1. HMAC 16 DB	2. HMAC 16 DB	1. HMAC 16 D REF
Bulk density, kg/m ³	2455	2457	2550
Maximum density, kg/m ³	2555	2551	2680
Voids content, %	3.9	3.7	4.8
VMA	17.8	18	17.6
VFB	78.2	79.6	72.4
Bitumen content, %	5.7	5.8	5.0

Table 5. Volumetric properties of HMAC mixtures with gravel aggregate.

Parameter	Mixtures		
	HMAC 16 GR PMB	HMAC 16 GRB	HMAC 16 GR REF
Bulk density, kg/m ³	2383	2367	2401
Maximum density, kg/m ³	2509	2492	2505
Voids content, %	4.9	4.9	4.2
VMA	17	17.7	17.6
VFB	70.8	71.9	75.4
Bitumen content, %	5.1	5.4	5.3

(wheel tracking test with small size device in air). This test method is designed to repeat the stress conditions observed in the field and therefore can be categorized as simulative. The resistance of asphalt mixture

Table 6. Marshall test results of HMAC mixtures with gravel aggregate.

Parameter	Mixtures		
	HMAC 16 GR PMB	HMAC 16 GRB	HMAC 16 GR REF
Bitumen content, %	5.1	5.4	5.3
Specimen height, mm	63.2	64.1	63.6
Stability at 60°C (kN)	14.8	17.4	10.2
Flow at 60°C (mm)	2.21	2.0	2.19

Table 7. Marshall test results of HMAC mixtures with dolomite aggregate.

Parameter	Mixtures		
	1. HMAC 16 D PMB	2. HMAC 16 D PMB	3. HMAC 16 D PMB
Bitumen content, %	5.7	5.8	5.1
Specimen height, mm	63.6	62.9	Not tested
Stability at 60°C (kN)	16.0	15.4	voids content
Flow at 60°C (mm)	3.8	5.9	>5%

Parameter	Mixtures		
	1. HMAC 16 DB	2. HMAC 16 DB	1. HMAC 16 D REF
Bitumen content, %	5.7	5.8	5.0
Specimen height, mm	64.2	64.0	63.3
Stability at 60°C (kN)	16.5	15.8	12.0
Flow at 60°C (mm)	2.8	3.4	4.2

to permanent deformation is assessed by measuring the rut depth and its increments caused by repetitive cycles (26.5 cycles per minute) under constant temperature at 60°C. The rut depths are monitored by means of two linear variable displacement transducers (LVDTs), which measure the vertical displacements of each of the two wheel axles independently as rutting progresses. The obtained results after 20 000 wheel passes demonstrate that the highest rut depth of 5.7 mm for the HMAC 16 DB mixture with 5.8% bitumen content. The reference mixture demonstrates similar result having 5.3 mm rut depth. HMAC 16 DB mixture having 5.7% bitumen content shows the highest rutting resistance 3.8 mm. The lowest rut depth was obtained in specimens with binder dolomite aggregate and PMB 25/55-60 and gravel aggregate and hard

Table 8. Wheel Tracking Test numerical values of HMAC mixtures with dolomite aggregate.

Parameter	Unit	Standard	Mixture		
			HMAC 16 D PMB	HMAC 16 D PMB	HMAC 16 DB
Bitumen content	%	EN 12697-1	5.7	5.8	5.7
Wheel tracking slope (WTS _{air})	mm/10 ³ cycles		0.04	0.04	0.14
Rut depth (RD _{air})	mm	EN 12697-22 B method	1.8	1.8	3.8
Proport. rut depth (PRD _{air})	%		3.6	3.6	7.6

Parameter	Unit	Standard	Mixture	
			HMAC 16 DB	HMAC 16 D REF
Bitumen content	%	EN 12697-1	5.8	5.0
Wheel tracking slope (WTS _{air})	mm/10 ³ cycles	B	0.22	0.20
Rut depth (RD _{air})	mm	EN 12697-22 method	5.7	5.3
Proport. rut depth (PRD _{air})	%		11.4	10.6

bitumen B20/30. Tables 8 and 9 summarizes the wheel tracking test results.

4.2 Fatigue

To determine the fatigue life of the prepared asphalt concrete mixes, a four point bending beam fatigue test was conducted. The test was run at 10°C, using 10 Hz frequency at 130 μm/m strain level. The beams were compacted in the laboratory using roller compactor. They were saw cut to the required dimensions of 50 mm width, 50 mm height and 400 mm length. The failure criterion used in the study is the traditional 50% reduction from initial stiffness. The obtained results indicate that HMAC mixtures have high resistance to fatigue, compared to the results of reference mixture made with conventional bitumen. HMAC mixes fatigue resistance corresponds to standard category ε6-130. HMAC mixes compliance with the SPENS requirements are given in Table 10.

Table 9. Wheel Tracking Test numerical values of HMAC mixtures with gravel aggregate.

Parameter	Unit	Standard	Mixture		
			HMAC 16 GR PMB	HMAC 16 GRB	HMAC 16 GR REF
Bitumen content	%	EN 12697-1	5.1	5.4	5.3
Wheel tracking slope (WTS _{air})	mm/10 ³ cycles		0.09	0.07	0.31
Rut depth (RD _{air})	mm	EN 12697-22 B method	3.3	2.5	8.3
Proport. rut depth (PRD _{air})	%		6.6	5.0	6.6

5 CONCLUSIONS

Use of relatively weak dolomite and gravel aggregates in High Modulus Asphalt Concrete was evaluated. This mixture was designed to have less than 5% air voids by using Marshall test method, and had high hard (B20/30) and polymer modified (PMB 25/55-60) bitumen. Testing was performed to compare this mix with AC16_{bin} reference mixture that was produced using conventional bitumen B70/100. Test results demonstrated that with optimum mix design HMAC mixture can provide high rut and fatigue resistance. However HMAC 16 DB mixtures with hard grade bitumen B20/30 and dolomite aggregate showed a little lower resistance to rutting. The reference mixture while having high rut resistance, proved that lower binder content results in shorter fatigue life.

The highest stiffness modulus is that of HMAC 16 DB (17900 MPa) and the lowest is that of HMAC 16 GRB (14300 MPa). In mixtures with stiff bitumen (20/30, PMB 25/55-60) the highest stiffness modulus were measured in asphalt concrete specimens with dolomite mineral aggregates.

Rut resistance and stiffness of reference mixtures doesn't meet SPEN project recommendations.

These results provide confidence that the weak Latvian dolomite and gravel may be applied in High Modulus Asphalt Concrete for base and binder courses. HMAC mixtures fulfill the HMAC asphalt concrete requirements in accordance with SPENS project recommendations (SPENS).

ACKNOWLEDGEMENTS

This work has been supported by the European Social Fund within the Project No.2013/0025/1DP/1.1.1.2.0/13/APIA/VIAA/019" New "Smart" Nanocomposite

Table 10. Compliance with SPENS requirements.

Parameter	Mixtures				Req.
	HMAC 16 D PMB	HMAC 16 D PMB	HMAC 16 DB	HMAC 16 DB	
Voids content, %	3.9	3.7	3.9	3.7	3.0–5.0
Rut resistance, mm/10 ³ cycles	0.04	0.04	0.14	0.22	0.03–0.25
Stiffness (10°C, 10 Hz), MPa	16700	16100	17100	17900	Smin 14000
Fatigue (10°C, 10 Hz, 130 μm/m)	ε6-130	ε6-130	ε6-130	ε6-130	ε6-130 (≤50%)
Water sensitivity, ITSR, %	100	100	98	94	ITSR 80

Parameter	Mixtures				Req.
	HMAC 16 GR PMB	HMAC 16 GRB	HMAC 16 D REF	HMAC 16 GR REF	
Voids content, %	4.9	4.9	4.8	4.2	3.0–5.0
Rut resistance, mm/10 ³ cycles	0.09	0.07	0.20	0.31	0.03–0.25
Stiffness (10°C, 10 Hz), MPa	15100	14300	9800	10200	Smin 14000
Fatigue (10°C, 10 Hz, 130 μm/m)	ε6-130	ε6-130	ε6-130	ε6-130	ε6-130 (≤50%)
Water sensitivity, ITSR, %	87	97	100	100	ITSR 80

Materials for Roads, Bridges, Buildings and Transport Vehicle".

REFERENCES

- AFNOR – Association Française de Normalisation. "Enrobés Hydrocarbonés: Couches d'assises: enrobés a module élevé (EME): NF P 98–140". Paris, 1999. (in Franch).
- Backer C., Visscher J., Glorie L., Vanelstraete A., Vansteenkiste S., Heleven L. (2008). A comparative high – modulus experiment in Belgium. In *Proceedings of Transport Research Arena Europe 2008 (TRA 2008)*

- International Conference*. 21–24 April 2008, Ljubljana, Slovenia.
- Čygas, D., Laurinavičius, A., Vaitkus, A., Perveneckas, Z., Motiejūnas, A.: Research of Asphalt Pavement Structures on Lithuanian Roads (I), *The Baltic Journal of Road and Bridge Engineering*, 3(2), pp. 77–83, 2008.
- Elliott, R.: Implementing High Modulus Asphalt Technology in The United Kingdom, *The International Seminar Maintenance Techniques to Improve Pavement Performance*, 10 p., 2009.
- Maupin, G. W., Diefenderfer, B. K.: *Design of High-Binder-High-Modulus Asphalt Mixture*, Final Report VTRC 07- R15, Virginia Transportation Research Council, 28 p., 2006.
- Rohde L., Ceratti J. A. P., Nñez P.V., Vitorello T. (2008). Using APT and Laboratory Testing to Evaluate the Performance of High Modulus Asphalt Concrete for Base Courses in Brazil. In *Proceedings of the Third International Conference on Accelerated Pavement Testing (APT '08.)*. 1–3 October, Madrid, Spain.
- Sivapatham P., Beckedahl H.J and Jannsen S. (2010) High Stable Asphalt for Heavy loaded Bus Test Lane Sections. In *Proceedings of the 11th International Conference on Asphalt Pavements ISAP 2010*. 1–6 August 2010, Nagoya, Aichi, Japan.
- Skrinskas, S., Gasiūnienė, V. E., Laurinavičius, A., Podagėlis, I.: Lithuanian Mineral Resources, Their Reserves and Possibilities for Their Usage in Road Building, *The Baltic Journal of Road and Bridge Engineering*, 5(4), pp. 218–228, 2010.
- Sustainable Pavements for European New Member States (SPENS) Document No. D8. [online]. [accessed on 10.10.2012.]. Available: <http://www.spens.fehrl.org>
- Sybilski D., Bankowski W., Krajewski M. (2010). High Modulus Asphalt Concrete with limestone aggregate, *International Journal of Pavement Research and Technology* (pp. 96–101), Vol. 3, No. 2.
- Sybilski D., Maliszewska D., Maliszewski M., Mularzuk R. (2008). Experience with High Modulus Asphalt Concrete in Warsaw street overlays. In *Proceedings of Transport Research Arena Europe 2008 (TRA 2008) International Conference*. 21–24 April 2008, Ljubljana, Slovenia.
- Vaitkus, A., Laurinavičius, A., Oginskas, R., Motiejūnas, A., Paliukaitė, M., Barvidienė, O.: The Road of Experimental Pavement Structures: Experience of Five Years Operation, *The Baltic Journal of Road and Bridge Engineering*, 7(3), pp. 220–227, 2012.

Asphalt concrete for very thin layers: Quality control data collected during construction and performance after eight years in service

A. Nikolaidis

Civil Engineering Department, Aristotle University of Thessaloniki, Greece

ABSTRACT: Asphalt Concrete for Very Thin Surfacing Layer (AC-VTSL) started to be used in Greece in the year 2005, after successful trial section laid in 2000 and monitored for five years. In 2006 the first major project was implemented where AC-VTSL was laid aiming at a thickness of 25 ± 3 mm over an area of approximately 2 million square meters of dual carriage motorway (approximate length 94 km). During the execution of asphalt works extensive quality control testing was carried out on polymer modified bitumen, properties of AC-VTSL, surface texture depth, tack coating, layer thickness, surface evenness, and constructional details (environmental temperatures, bituminous mix temperatures during laying, number of finishers used, etc). The paper presents construction details and evaluation of quality control results obtained assisted by statistical analysis. The final aim of this paper is to establish safe variation coefficients from targeted values after examining the performance of the very thin surface layer after a period of 10 years in use. This will be valuable information for National relevant specifications. The examination of the performance of the very thin surface layer is scheduled to take place in 2016, after ten years in service.

1 INTRODUCTION

Asphalt concrete for very thin (surfacing) layer (AC-VTL) was originally developed in France during 80s, called bétons bitumineux très minces. Due to its advantages in comparison to other alternative surfacing material, AC-VTL started to be used in many other European countries. In Greece, its first application started in 2005 after monitoring a trial section for four years.

The thickness of the very thin surface layer may vary from 20 mm to 30 mm, depending on the maximum nominal size of the aggregate mix. In the AC-VTL the aggregate particles are generally gap-graded to form a stone to stone contact and to provide an open surface texture (CEN EN 13108-2, 2006).

Due to thinner layer laid in comparison to other surfacing material (usually 40 mm to 50 mm) the amount of materials needed is less. This results in lower purchasing/construction cost, higher daily paving output, and economizing on hard aggregate resources.

The advantages of AC-VTL have led various countries to develop national specifications based on the French specification NF P 98-137 (1992). However, in May 2006 the relevant European standard EN 13108-2 (2008) was introduced.

In 2006 the first major application of AC-VTL was carried out on a Greek motorway known as Egnatia Odos, where nearly 2 million square meters were paved with this surfacing material. During the execution of asphalt works extensive quality control testing was carried out on polymer modified bitumen, properties of AC-VTL, surface texture depth, tack coating, layer

thickness, surface evenness, and constructional details (environmental temperatures, bituminous mix temperatures during laying, number of finishers used, etc).

2 SURFACE COURSES

Surface courses should have good and long lasting surface characteristics so as to provide good and long lasting skid resistance. In addition, it is of an advantage to have good draining and noise reducing ability.

The above becomes feasible with the use of hard and durable aggregates, provision of good surface texture, sufficient air voids and good and long lasting adhesion of bituminous binder on the aggregate particles used.

The materials most commonly used, worldwide, in surface courses are: asphalt concrete for very thin layer (AC-VTL), stone mastic asphalt (SMA), open graded asphalt mixture (OGAM), porous asphalt (PA), micro-surfacing (MS) and single or multiple surface dressing (SSD or MSD). More information regarding these materials can be found in bibliography (Nikolaidis 2014).

3 PROPERTIES AND ADVANTAGES OF THIN SURFACING

The properties and the advantages of AC-VTL are:

- a) They require lesser amount of material, hence lower cost and saving on the hard and durable aggregate natural resources. In Greece, the cost of AC-VTL is approximately 45% less than the cost of the alternative 40 mm open graded mix,

- b) Provide a pavement surface with very good surface characteristics,
- c) Provide a noise reducing surface,
- d) Provide a surface with draining ability, hence reduction of spray,
- e) The layer/mixture has good rutting resistance,
- f) Rapid construction can be achieved. In one of the projects executed in Greece a maximum daily output of 21.100 m² was achieved,
- g) Milling of the underlying layer in order not to raise the surface level, is not always necessary,
- h) It allows certain surface irregularities to be corrected.
- i) In case of renewal without recycling of the old very thin layer, smaller quantities of aggregate and bitumen material is wasted, and
- j) No modifications to conventional mixing plants are required to produce AC-VTL.

4 LARGE SCALE THIN SURFACING CONSTRUCTED IN 2006

During June to October 2006, a large scale project was completed along one of the major national motorways in Greece known as Egnatia Odos motorway, where AC-VTL was used as surfacing material. A total of 1,948,500 square meters of motorway surface was covered with AC-VTL surfacing material aiming to a layer thickness (25 ± 3) mm.

The above paved area resulted from 93.81 km length of two-lane dual carriageway by, on average, 10.4 m width, per direction. The asphalt works were carried out by two construction companies. One of the construction companies paved a surface of 1,275,000 m² of motorway (approximately 60.7 km length) and the other paved a surface of 673,500 m² (approximately 33.1 km length).

Analytically the total length and the length between junctions paved by the two construction companies, section A and section B, are as shown in Table 1. Table 1 also shows the average daily traffic volume and the percentage of commercial vehicles, from the year of construction until 2014.

4.1 Aggregate and bitumen used

The aggregate material used, in all cases, was diabas but the two companies used two different diabas quarries. The characteristic properties of the diabas aggregate, per quarry, are as shown in Table 2.

The bitumen used was SBS modified bitumen and the required properties are as shown in Table 3.

4.2 Target composition and properties of AC-VTL

The target aggregate mix compositions of the AC-VTL for the two aggregate sources used in the above project are as shown in Figure 1.

The characteristic properties of the AC-VTL as determined by two individual mix designs carried out

Table 1. Details of project sections.

Total length, km	Junction to junction	Length, km	ADT per direction
Section A 121.42 (WB = 60,69 EB = 60.73)	J1–J2, WB	8.44 km	6,100 (15%) ^(b)
	J2–J1, EB	8.44 km	
	J2–J3, WB	20.54 km	
	J3–J2, EB	20.50 km	
	J3–J4, WB	2.70 km	
	J4–J3, EB	2.70 km	
	J4–J5, WB	18.28 km	
	J5–J4, EB	18.20 km	
	J5–J6, WB	10.81 km	4,765
	J6–J5, EB	10.82 km	(19%) ^(b)
Section B 66,20 (WB = 33,1 EB = 33.1)	J6–J7, WB	12.22 km	3,900
	J7–J6, EB	12.32 km	(20%) ^(b)
	J7–J8, WB	20.80 km	
	J8–J7, EB	20.86 km	

(a) ADT = Average daily traffic; (b) Percentage of commercial vehicles (> 1500 kg).

Table 2. Characteristic properties of diabas aggregate used.

Property	Test method	Range of values	
		Quarry A	Quarry B
Polished stone value (PSV), %	CEN EN 1097-8	59–62	60–62
Aggregate abrasion value (AAV), %	CEN EN 1097-8	2.5–2.8	2.5–2.8
Resistance to fragmentation-LA coefficient, %	CEN EN 1097-2	10–11 (grading B)	13–14 (grading C)
Magnesium sulfate value, %	CEN EN 1367-2	1.0–1.5	1.5–2.0
Particle density, Mg/m ³	CEN 1097-6)	2.85	2.75
Water absorption, %	CEN EN 1097-6	1.2–1.3	0.9–1.0
Flakiness index, %	CEN EN 933-3	11.0–12.0	12.0–13.0
Methylene blue value, MB _F , g/kg	CEN EN 933-9	8.0–8.5	6.0–6.5
Sand equivalent, %	CEN EN 933-8	58–60	63–65

Table 3. Contractual requirements of SBS modified bitumen.

Characteristic property	Test method	Requirement
Penetration, at 25°C, dmm	CEN EN 1426	22–55
Softening point (SP), °C	CEN EN 1427	≥70
Elastic recovery, at 25°C, %	CEN EN 13398	≥70
Fraass point, °C	CEN EN 12593	≤-7
Storage stability, decrease in SP, °C	CEN EN 13399	≤5
<i>After hardening, CEN EN 12607-1</i>		
Retained penetration, %	CEN EN 1426	≥45
Increase in SP, °C	CEN EN 1427	≤10
Elastic recovery, at 25°C, %	CEN EN 13398	≥50

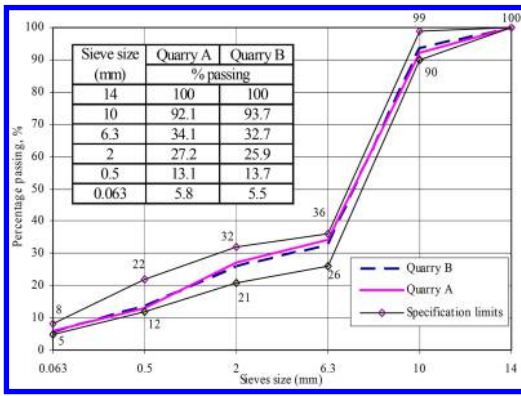


Figure 1. Target aggregate gradation mix compositions for quarry A & B.

Table 4. Characteristic properties of AC-VTL according to mix designs using aggregates from quarry A & B.

Characteristic property	AC-VTL	
	Quarry A	Quarry B
Optimum bitumen content, by weight of aggregate, %	5.50	5.70
Air voids, %, (CEN EN 13108-20)	13.0	11.6
Indirect tensile strength ratio (ITS), %, (CEN EN 12697-23)	93.4	94.2
Bulk density, kg/m ³ , (CEN EN 12697-29 (Procedure D))	2294	2254

using diabas aggregate from two different quarries are as shown in Table 4.

It is noted that the aggregate gradation limits and the mix design was carried out in accordance to the Greek standard TSY, Article ST 6 (2004) which complies with CEN EN 13108-2.

5 PRODUCTION, LAYING AND COMPACTION

The production, laying and compaction of AC-VTL was carried out in a similar manner to any other conventional asphalt concrete mix, paying special attention to the temperature of the mixture at all stages of handling. Some details on the production, laying and compaction of the AC-VTL are given below.

Production

The production of AC-VTL was carried out by two conventional asphalt concrete batch plants with capability of 1200 kg to 2000 kg per batch.

The mixing procedure was the same as in conventional asphalt concrete. The only difference was the higher mixing temperature, 170°C–175°C, due to incorporation of polymer modified bitumen.

Paving

Paving of the AC-VTL was carried out by wheel pavers. The screeds were variable up to 11 m and equipped with vibrating and propane gas heating devices. The tractor units possessed all automations for handling and automatic level and slope control devices.

The pavements over which the AC-VTL was laid were 1.5 to 5.0 years old. The pavement surface in most of its area had no surface defects. For about 9 km in total of the old pavement surface had developed premature rutting. Additionally, localized cracking was also present. Prior laying the AC-VTL all the previously mentioned defects corrected accordingly (mill and replace). The bituminous mix used for corrections was dense asphalt concrete with polymer modified bitumen with the same characteristics as for the AC-VTL.

Laying was carried out at the full width of the pavement, 10.7 m wide. Prior laying the AC-VTL bitumen emulsion was applied as tack coat. The spraying rate was required to vary from 250 g/m² to 400 g/m² of bitumen residue.

Compaction

Compaction of the AC-VTL, after preliminary compaction by the screed, was carried out by two or three 8 to 10 ton static steel-wheel rollers, applying 4 to 6 full passes. The environmental temperature throughout the asphalt works varied from 17°C to 34°C, without the presence of strong winds. The surface temperature of the layer after completion of the compaction, in all cases but one varied from 80°C to 123°C (the average surface pavement temperature after finishing the compaction was 102°C). In one location, only, the surface temperature after final compaction was found to be 74°C.

6 QUALITY CONTROL TESTING DURING EXECUTION OF WORKS

During execution of asphalt works extensive quality control tests were carried out concerning the following:

- Properties of polymer modified bitumen (PMB)
- Aggregate gradation, bitumen content and properties of AC-VTL
- Rate of tack coating
- Surface texture depth
- Layer thickness
- Environmental temperature
- Mixture temperature during laying and after completion of compaction, and
- Number of roller passes applied during compaction

6.1 Evaluation of results from properties of polymer modified bitumen (PMB)

In total one hundred fifty eight (158) samples of polymer modified bitumen (PMB) were taken. This resulted in one sample every 41 tons of PMB used.

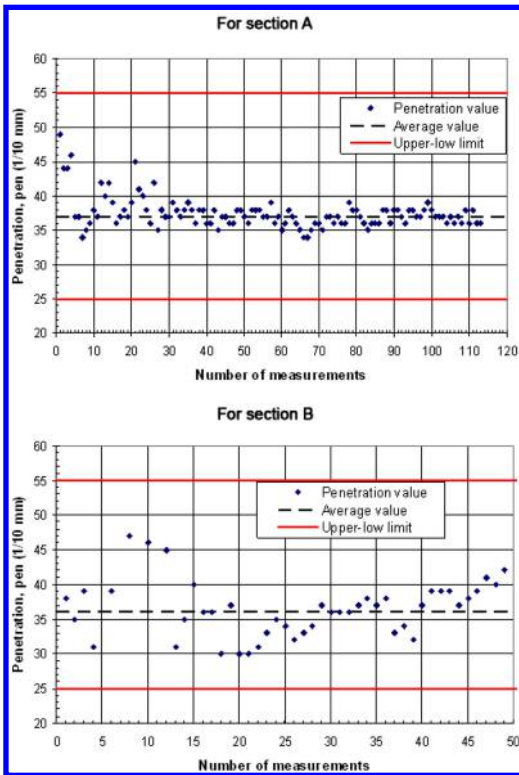


Figure 2. Penetration value results.

Based on the daily consumption of PMB, sampling was carried out once every day, in section A, and one every 1.3 days, in section B.

The results of penetration value of PMB, at 25°C, obtained are as shown in Figure 2. The average value was found to be 37, with standard deviation of 2.34, and in section B 36 and 3.17, respectively.

The results of softening point (Ring & Ball) value of PMB obtained are as shown in Figure 3. The average value was found to be 70°C, in both sections, and the standard deviation 2.19 and 4.68, in section A and B respectively.

The rest of the PMB characteristic properties found are as shown in Table 5.

6.2 Aggregate gradation, bitumen content and properties of AC-VTL

Sampling and frequency of sampling

In total one hundred six (106) samples of AC-VTL were taken, which results on average in one sample per 1000 ton of mixture produced, or one sample every 16,600 m² laid.

Based on the daily production/paving output in section A, one sample was taken every 1,470 tons of AC-VTL produced, or one sample every 24.350 m² laid, or one sample every 1.8 days.

Similarly, for section B, one sample was taken every 760 tons of AC-VTL produced, or one sample every 15,000 m² laid, or one sample every 1.25 days.

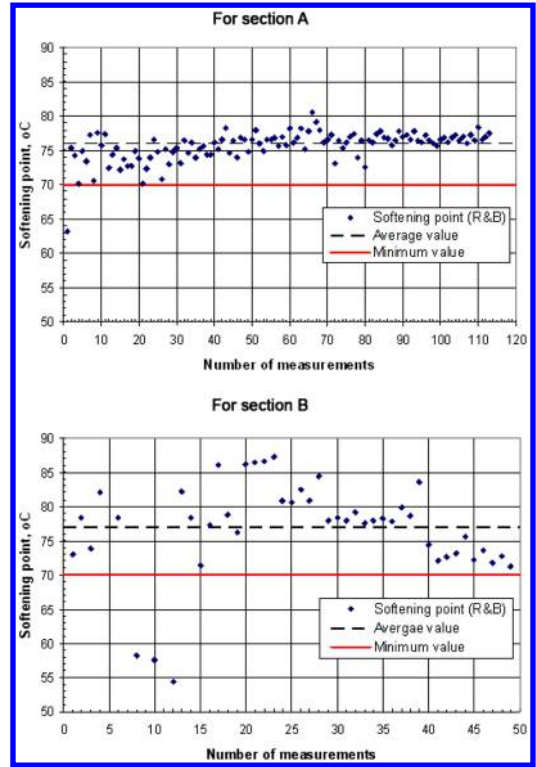


Figure 3. Softening point results.

Aggregate gradation

In section A from a total of 50 samples examined, the aggregate gradation in 32 samples was within the specified limit values and in 18 samples was outside the limits set for 6.3 mm sieve. It is noted that the average value of the gradation curve at sieve 6.3 mm was found to be slightly outside the specified limits.

Similarly, in section B from a total of 56 samples examined, the aggregate gradation in 45 samples was within the specified limit values and in 11 samples was outside the limits set for 6.3 mm sieve. As far as the average value of the gradation curve at 6.3 mm sieve it was found to be within the specified limits.

Bitumen content

In section A, from a total of 50 samples (sampling locations) examined, the bitumen content in 38 samples was found to be within the specified variation of $\pm 0.3\%$ with an average value of 5.39% by weight of aggregate (standard deviation = 0.176); in 10 samples the binder content was found to be less than the lower limit value, on average by -0.23% by weight of aggregate and in 2 samples more than the upper limit value by $+0.12\%$ by weight of aggregate.

Similarly, in section B from a total of 56 samples (sampling locations) examined, the bitumen content in 50 samples was found to be within the specified variation of $\pm 0.3\%$ with an average value of 5.73% by weight of aggregate (standard deviation = 0.192); in the rest 6 samples the binder content was found to be

Table 5. Characteristic properties of PMB.

Characteristic property	Average value Section		Min/Max value Section		Standard deviation Section	
	A	B	A	B	A	B
Elastic recovery, at 25°C, %	95.2	95.0	87.5/97.5	92.5/97.5	1.81	1.22
Fraass point, °C	-12.6	-13.0	-12.0/-13.5	-12.0/-13.0	0.55	0.45
Storage stability, decrease in SP, °C	2.3	3.0	1.7/2.9	0.5/4.7	0.47	1.32
<i>After hardening, CEN EN 12607-1</i>						
Retained penetration, %	87.2	87.0	81.0/91.7	85.7/89.7	2.83	1.45
Increase in SP, °C	3.5	3.0	2.4/4.2	2.0/5.0	0.57	1.11
Elastic recovery, at 25°C, %	84.0	87.0	75.0/87.5	85.0/87.5	4.51	1.16

on average more than the upper limit value by +0.16%, by weight of aggregate.

Air voids

In section A, from a total of 300 samples examined (50 sampling locations × 6 compacted specimens), the air voids in 216 laboratory compacted specimens was found to be within the specified variation based on the mix design (13.0 ± 1.25%) with an average value of 13.15% (standard deviation = 0.884); in 72 specimens the air voids was found to be less than the lower limit value, on average by -0.87% air voids and in 12 specimens more that the upper limit value on average by +1.05% air voids.

Similarly, in section B from a total of 336 samples examined (56 sampling locations × 6 compacted specimens), the air voids in 216 laboratory compacted specimens was found to be within the specified variation based on the mix design (11.6 ± 1.25%) with an average value of 11.66% (standard deviation = 0.675); in 24 specimens the air voids was found to be less than the lower limit value, on average by -0.50% air voids and in 60 specimens more that the upper limit value on average by +0.41% air voids.

Indirect tensile strength ratio

In section A, from a total of 150 samples examined (50 sampling locations × 3 specimens), the indirect tensile ratio in all cases was found to be greater than the minimum requirement (80%) with an average value of 87% (standard deviation = 3.263).

In section B, from a total of 168 samples examined (56 sampling locations × 3 specimens), the indirect tensile ration in all cases was found to be greater than the minimum requirement (80%) with an average value of 86% (standard deviation = 2.932).

Stiffness values

The indirect tensile stiffness modulus (IT-CY) of the AC-VTL measured at 20°C according to CEN EN 12697-26 on a large number of compacted specimens prepared from mixtures sampled from both sections was found to vary from 4580 to 5430 MPa. The standard deviation found was 542 MPa, which is considered to be high.

6.3 Rate of tack coating

In section A, from a total of 28 determinations the rate of tack coating in 27 cases was found to be within the recommended range (200 g/m² to 400 g/m² of binder residue) with an average value of 297 g/m² (standard deviation = 24.90). In one case only the rate of tack coating was found to be 132 g/m².

In section B, from a total of 16 determinations the rate of tack coating in 15 cases was found to be within the recommended range (200 g/m² to 400 g/m² of binder residue) with an average value of 291 g/m² (standard deviation = 20.15). In one case only the rate of tack coating was found to be 144 g/m².

6.4 Surface texture depth

The pavement surface macrotexture depth was carried out by a volumetric patch technique (sand patch method) according to CEN EN 13036-1.

In section A the measurements were carried out on average every 130 m length and in section B on average every 175 m length.

In section A, from a total of 939 surface macrotexture depth measurements in all, except two, cases the values obtained were greater then the minimum requirement of 0.8 mm. In two cases the values found to be 0.77 mm and 0.79 mm.

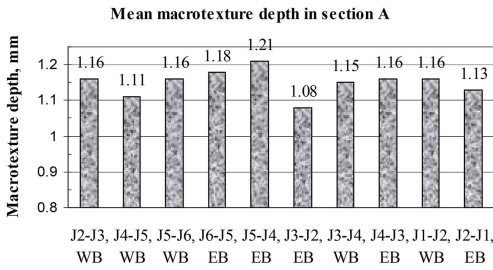
Figure 4 summarizes the results of mean surface macrotexture depths and standard deviations of results obtained in section A between major junctions, in the sequence of executing the asphalt works.

In section B, from a total of 379 surface macrotexture depth measurements in 368 cases the values obtained were greater then the minimum requirement of 0.8 mm. In eleven (11) cases the values found varied from 0.69 mm to 0.8 mm.

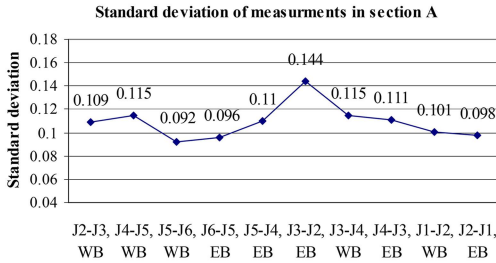
Figure 5 summarizes the mean results of surface macrotexture depths and standard deviation of results obtained in section B between major junctions, in the sequence of executing the asphalt works.

6.5 Layer thickness

The layer thickness was determined by extracting cores every, approximately, 250 m at random positions



(a) Mean macrotexture depth



(b) Standard deviation of results

Figure 4. Mean macrotexture depth in section A, between major junctions.

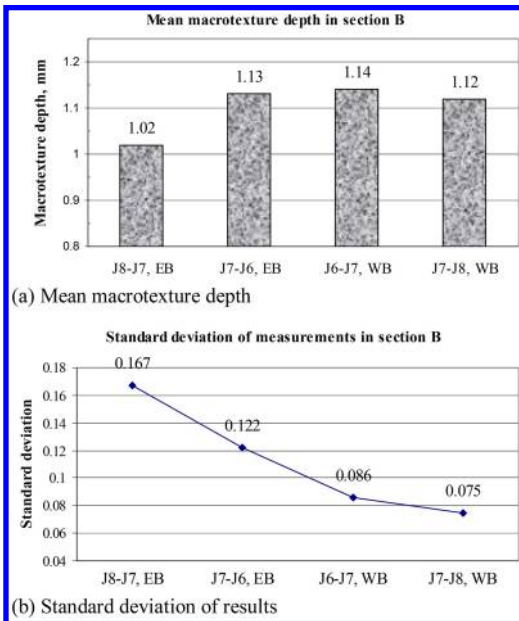


Figure 5. Mean macrotexture depth in section B, between major junctions.

across the width of the carriageway. The average thickness laid between junctions varied from 26 mm to 34 mm for section A, and from 29 mm to 30 mm for section B.

Summary of results together with the minimum and maximum values measured are shown in Table 6.

Table 6. Average thickness of AC-VTL laid.

Total length, km	Junction to Junction	Average thickness, mm (Min.-Max.)
Section A 121.42 (WB = 60.69 EB = 60.73)	J1 – J2	28 (23–35)
	J2 – J1	27 (22–33)
	J2 – J3	27 (20–45)
	J3 – J2	26 (20–40)
	J3 – J4	28 (25–34)
	J4 – J3	34 (29–40)
	J4 – J5	26 (23–41)
	J5 – J4	27 (24–37)
	J5 – J6	29 (23–40)
	J6 – J5	29 (24–38)
Section B 66.20 (WB = 33.1 EB = 33.1)	J6 – J7	30 (20–42)
	J7 – J6	29 (20–39)
	J7 – J8	30 (20–41)
	J8 – J7	29 (20–40)

6.6 Environmental temperature

The environmental air temperatures during the asphalt works in section A were varying between minimum 17°C to maximum 35°C. Similarly, the air temperatures during the asphalt works in section B were varying between minimum 25°C to maximum 35°C.

It is noted that air temperature measurements carried out daily during the morning, noon and early evening hours.

6.7 Mixture temperature during laying and after completion of compaction

The temperature of the AC-VTL was measured at the distinct stages: at the lorry (haulage truck) when arrived on site (TT), at the finisher (TF), and immediately after completion of compaction at the surface of the compacted layer (TCC).

For section A, the temperature of the mixture as arrived and measured at the lorry was on average 162°C (variation between minimum 148°C to maximum 168°C), the temperature at the finisher was on average 150°C (variation between minimum 135°C to maximum 159°C), and the surface temperature of the compacted layer, immediately after completion of compaction, was on average 104°C (variation between minimum 80°C to maximum 124°C).

Similarly for section B, the temperature of the mixture as arrived and measured at the lorry was on average 163°C (variation between minimum 150°C to maximum 168°C), the temperature at the finisher was on average 150°C (variation between minimum 140°C to maximum 159°C), and the surface temperature of the compacted layer, immediately after completion of compaction, was on average 102°C (variation between minimum 80°C to maximum 122°C).

6.8 Number of roller passes applied during compaction

The number of single roller passes applied during compaction, for section A, was varied from minimum 4 to



Figure 6. Compaction of AC-VTL (year 2006).



Figure 9. Surface details between junction 5 and 6, westbound 2014).



Figure 7. Resulted AC-VTL surface (year 2006).



Figure 10. Pavement after eight years in service between junction 6 and 7, westbound (year 2014).



Figure 8. Pavement after eight years in service between junction 5 and 6, westbound (year 2014).

maximum 8, depending on the environmental air temperature. Similarly, for section B, the number of single roller passes applied during compaction was varied from minimum 4 to maximum 6.

7 PRESENT CONDITION OF AC-VTL

In December 2014 a wind-screen survey for evaluation of the condition of the AC-VTL wearing course was

carried out. The survey was assisted by limited number of surface macrotexture measurements.

After more than eight years in service the condition of the wearing course was found to be very good.

In particular, no distresses caused by the failure of the AC-VTL wearing course were observed and the surface macrotexture depth was found to be greater than 0.8 mm.

Figures 6 and 7 show surface during construction and Figures 8 to 11 show surface after eight years of service.

8 CONCLUSIONS

From the quality control results obtained during execution of asphalt works the following conclusions are drawn:

1. All properties of polymer modified bitumen (PMB) used, apart from very few cases, were in accordance to the requirements. Only the softening point value in one sample in section A and in three samples in section B was lower than the required minimum of 70°C.



Figure 11. Surface details between junction 6 and 7, westbound 2014).



Figure 12. Pavement after eight years in service between junction 7 and 8, westbound (year 2014).



Figure 13. Surface details between junction 7 and 8, westbound 2014).

2. The overall average gradation curve of the aggregate mix in section A was found to be just outside the specified limits in 6.3 mm sieve, only. On the contrary the overall average gradation curve of the aggregate mix in section B was found to be within the specified limits. However, in 89% of the individual cases in section A the gradation of the aggregate mix was within the limits specified on each sieve; the corresponding value for section B was 80%.

3. The binder content (PMB) in the great majority of samples tested from section A and B was found to be within the acceptable range of variation ($\pm 0.3\%$) from the target value (76% of the samples from section A and 89% of the samples from section B). In few samples (24% of the samples tested) from section A, and fewer (11% of the samples tested) from section B the binder content was found to be outside the acceptable range of variation.
4. The air voids in the majority of samples tested from section A and B was found to be within the acceptable range of variation ($\pm 1.25\%$) from the target value (72% of the samples from section A and 64% of the samples from section B). In the rest of the samples the air voids were either lower or higher than the specified limits.
5. The indirect tensile strength ratio in all cases (samples from section A or B) was found to be higher than the lower specified limit of 80%.
6. The rate of tack coating in almost all cases (section A or B) was found to be within the recommended range of variation (3% of the measurements in section A and 6% in section B were found to be lower than the recommended low rate of tack coating)
7. The surface texture depth in almost all cases (section A or B) was found to be higher than the minimum required limit (0.2% of the measurements in section A and 3% in section B were found to be lower than the minimum required value of 0.8 mm).
8. The average layer thickness of AC-VTL was found to range between 26 mm to 34 mm, for section A, and between 29 mm to 30 mm, for section B. The minimum and maximum thicknesses laid in section A was found to be 20 mm and 45 mm, respectively, and in section B 20 mm and 42 mm, respectively.
9. The environmental air temperature during execution of asphalt works varied between 17°C to 35°C, for section A, and between 25°C to 35°C, for section B.
10. The lower temperature of the mixture arriving on site was 148°C for section A and 150°C for section B.
11. The lower temperature of the mixture in the finisher was 135°C for section A and 140°C for section B.
12. The lower surface temperature of the compacted layer was 80°C for section A and section B.
13. The number of roller single passes in all cases varied from 4 to 8 for section A and from 4 to 6 for section B.
14. The resulted surface immediately after construction was characterized as excellent.
15. Eight year after construction the pavement surface, judged by visual inspection, is considered to be very good.
16. The performance of the very thin surface layer is scheduled to be evaluated in details (texture depth, ravelling, bleeding, potholes, and slippage) in 2016, ten years after construction, subject to the agreement with the client.

Based on the performance of AC-VTL wearing course after eight years of service it can be concluded that when laid in accordance to requirements it can be considered as a long lasting attractive alternative material for wearing courses for the level of traffic volumes similar to the ones encountered.

REFERENCES

- CEN EN 933-3. 2012. *Tests for geometrical properties of aggregates. Part 3: Determination of particle shape – Flakiness index*. Brussels: CEN.
- CEN EN 933-8. 2012. *Tests for geometrical properties of aggregates. Part 8: Assessment of fines – Sand equivalent test*. Brussels: CEN.
- CEN EN 933-9. 2009. *Tests for geometrical properties of aggregates Part 9: Assessment of fines – Methylene blue test*. Brussels: CEN.
- CEN EN 1097-2. 2010. *Tests for mechanical and physical properties of aggregates – Part 2: Methods for the determination of resistance to fragmentation*. Brussels: CEN.
- CEN EN 1097-6. 2000. *Tests for mechanical and physical properties of aggregates – Part 6: Determination of particle density and water absorption*. Brussels: CEN.
- CEN EN 1097-8. 2009. *Tests for mechanical and physical properties of aggregates – Part 8: Determination of the polished stone value*. Brussels: CEN.
- CEN EN 1367-2. 2009. *Tests for thermal and weathering properties of aggregates – Part 2: Magnesium sulfate test*. Brussels: CEN.
- CEN EN 1426. 2007. *Bitumen and bituminous binders – Determination of needle penetration*. Brussels: CEN.
- CEN EN 1427. 2007. *Bitumen and bituminous binders – Determination of the softening point – Ring and Ball method*.
- CEN EN 12593. 2000. *Methods of test for petroleum and its products – BS 2000-80: Bitumen and bituminous binders – Determination of the Fraass breaking point*. Brussels: CEN.
- CEN EN 12697-23. 2003. *Bituminous mixtures – Test methods for hot mix asphalt – Part 23: Determination of the indirect tensile strength of bituminous specimens*. Brussels: CEN.
- CEN EN 12697-26. 2012. *Bituminous mixtures – Test methods for hot mix asphalt-Part 26: Stiffness*. Brussels: CEN.
- CEN EN 12967-29. 2002. *Bituminous mixtures – Test methods for hot mix asphalt – Part 29: Determination of the dimensions of a bituminous specimen*. Brussels: CEN.
- CEN EN 13036-1. 2001. *Road and airfield surface characteristics-Test methods-Part 1: Measurement of pavement surface macrotexture depth using a volumetric patch technique*. Brussels: CEN.
- CEN EN 13108-2:2006/AC. 2008. *Bituminous mixtures – Material specifications-Part 2: Asphalt concrete for very thin layers*. Brussels: CEN.
- CEN EN 13108-20. 2006. *Bituminous mixtures – Material specifications – Part 20: Type Testing*. Brussels: CEN.
- CEN EN 13398. 2003. *Methods of test for petroleum and its products – BS 2000-516: Bitumen and bituminous binders – Determination of the elastic recovery of modified bitumen*. Brussels: CEN.
- CEN EN 13399. 2003. *Methods of test for petroleum and its products – BS 2000-517: Bitumen and bituminous binders – Determination of storage stability of modified bitumen*
- NF P 98-137. 1992. *Couches de roulement: Béton bituminex très minches*. Paris, France: AFNOR.
- Nikolaides A. 2014. *Highway Engineering: Pavements, Materials and Control of quality*. Boca Raton, FL: CRC Press Taylor & Francis Group.
- TSY, Article ST 6. 2004. *Asphalt mix for thin antiskidding layer*. Athens: Ministry of Environment and Public Works.

Fatigue characterisation of full-scale pavements using viscoelastic continuum damage approach for Qatar

H. Sadek

University of Liverpool, Liverpool, UK
Qatar University, Doha, Qatar

E. Masad

Texas A&M University at Qatar, Doha, Qatar

H. Al-Khalid

University of Liverpool, Liverpool, UK

O. Sirin

Qatar University, Doha, Qatar

ABSTRACT: The population and economy in Qatar have been expanding significantly in the past six years. Accordingly, Qatar is encountering huge development in infrastructure. The existing mix design methods have been developed in the past to protect against rutting given the high temperatures in Qatar. However, these mixtures might be susceptible to fatigue damage. During the last three years, a comprehensive study was conducted for the evaluation of performance of full-scale trial sections. These sections involve the use of six different asphalt mixtures in the base course. The aim of this work is to conduct fatigue tests and to use the Viscoelastic Continuum Damage (VECD) approach in order to characterise the resistance of the sections against fatigue cracking. Results revealed that the use of VECD approach has major advantages; however, the uncertainty associated with fatigue tests as well as models and their parameters have substantial influence on the predicted fatigue life.

1 INTRODUCTION

In the past six years, the population and economy in the State of Qatar have been expanding significantly. Accordingly, Qatar is encountering huge development in infrastructure including the road network and highways. The existing mix design methods in Qatar have been developed in the past to protect against permanent deformation (rutting) given the high temperatures in Qatar. However, there is a concern that these asphalt mixtures might be vulnerable to fatigue damage especially that there is evidence of cracking and ravelling in some road sections in Qatar (Sadek *et al.* 2013).

Fatigue cracking is a major load-related distress that causes loss of asphalt pavement serviceability. It occurs when an asphalt mixture is subjected to repeated traffic loading (Artamendi and Khalid 2005, and Bhasin *et al.* 2009). Fatigue cracking can affect the ride quality significantly and can be a key factor for rehabilitation or replacement of an entire asphalt mixture (Kutay *et al.* 2009).

During the past three years, a comprehensive study was performed in order to assess the performance of full-scale trial road sections (Sadek *et al.* 2014b). These trial sections, which were constructed in 2010, involve the use of six different asphalt concrete mixtures in the base course. The general objective was to

investigate changes in the design method and the use of materials not currently permitted in Qatar Construction Specifications (QCS). One aspect of the study was to characterise the fatigue performance of cylindrical samples extracted from the trial sections by conducting the laboratory cyclic push-pull (tension and compression) fatigue test. This fatigue testing were performed using the Asphalt Mixture Performance Tester (AMPT) and associated software. The fatigue resistance was evaluated using the dissipated pseudo-strain energy (DPSE) and the crack growth index (R(N)) in a previous work (Sadek *et al.* 2014a). It was concluded that the R(N) method gives more reliable results and better indication of fatigue cracking resistance of field samples than the DPSE. In this paper, the Viscoelastic Continuum Damage (VECD) theory is implemented to characterise and compare the resistance of the trial sections against fatigue cracking. The analysis focused on comparing the fatigue life, N_f , of mixtures used in different sections.

2 OBJECTIVE OF THE STUDY

The main objective of this study is to evaluate the fatigue characteristics of different asphalt mixtures tested under a uniaxial cyclic fatigue test package on

the IPC Global Asphalt Mixture Performance Tester (AMPT). The VECD characterisation approach was implemented to characterise the resistance of the trial sections to fatigue damage and estimate their fatigue lives.

3 MATERIALS AND TESTING PROCEDURE

At the trial road location, six different pavement sections, about 150 m length each, were constructed as perpetual pavements in 2010 as a part of an access road to a sand processing plant in the south of Qatar. The location of the sections was selected due to its high traffic loading. From the opening day of the trial road in 2010, around 3600 heavy trucks are passing the trial road daily in both directions and 50% of them are fully loaded with washed and unwashed sand. The 20 years ESALs for this trial road was calculated to be 115 million.

The trial sections were designed to examine the effect of binder type, type of aggregate and mix design against different surface distresses and deteriorations under the same traffic condition. The layers and materials used in each trial section are demonstrated in Figure 1.

Section 4 is the control section that was designed following the standards of Qatar Construction Specifications (QCS-2010) which is basically the Marshall method. The Percentage Refusal Density (PRD) design method (BS EN 12697/32:2003, TRL 2002) was used in all other sections excluding the base course of section 5. The PRD test is used to obtain the design binder content at which the voids in mineral aggregate (VMA) at refusal density is only 3%. This requirement is supposed to ensure that no deformation will occur to reduce percentage air voids to lower than 3% in the field. This mix design comprises other criteria to accomplish durable asphalt mixture and field compaction.

Trial section 5 involved the use of a sulphur extended binder (Shell Thiopave) while section 6 included polymer-modified binder with an SBS modifier. The unmodified 60–70 Pen base binder was used to produce the modified binder. The aggregate used in the surface course for all trial sections was Gabbro that is imported from United Arab Emirates. This aggregate is an igneous rock that has been used in road construction for a long time in this region. A local aggregate in Qatar, Limestone, was used in the base course of trial section 3 to compare it with the performance of sections in which Gabbro was used.

In addition, for all sections, the same granular sub-base with limestone aggregate was used with an estimated design modulus of 450 MPa (TRL client reports C and D 2010). The subgrade is weathered limestone with a design modulus of 200 MPa (TRL client reports C and D 2010, Sadek *et al.* 2012 and 2014b). A day after paving, three pairs of field cores were extracted from each trial section and tested for compositional analysis and the results are summarised in Table 1.

Layers & Depth	Section 1	Section 2	Section 3A	Section 3B	Section 4	Section 5	Section 6
Surface course 50 mm	Marshall/PRD, 40-50 Pen, Gabbro	Marshall/PRD, 60-70 Pen, Gabbro	Marshall/PRD, 60-70 Pen, Gabbro	Marshall/QCS, 60-70 Pen, Gabbro	Marshall/QCS, 60-70 Pen, Gabbro	Marshall/PRD, PMB, Gabbro	Marshall/PRD, PMB, Gabbro
Upper base 135 mm	Marshall/PRD, 40-50 Pen, Gabbro	Marshall/PRD, 60-70 Pen, Gabbro	Marshall/PRD, 60-70 Pen, Limestone	Marshall/QCS, 60-70 Pen, Gabbro	Marshall/QCS, 60-70 Pen, Gabbro	Marshall/QCS, Shell Thiopave, Gabbro	Marshall/PRD, PMB, Gabbro
Lower base 135 mm							
Granular Sub-base 200 mm	(Crushed Limestone)						
Subgrade	Weathered Limestone						

Figure 1. Layers and materials' properties of all trial sections (TRL client report D 2010).

With the purpose of assessing the performance of the trial sections against fatigue cracking, fifteen specimens were extracted, cored and prepared from the base layer of all sections to standard size of 100 mm diameter and 150 mm height. Samples of trial section 3 were excluded from the testing and hence from the analysis due to their high segregation.

Table 1. Compositional analysis summary for all trial sections (TRL client report D 2010).

Section	Binder				Stability kN	Flow mm	Stiffness kN/mm ²
	content %	VIM %	VMA %	VFB %			
Surface course							
1	3.9	4.0	14.2	71.7	14.8	2.6	6.2
2 & 3A	3.8	4.9	14.3	69.1	14.7	2.6	5.7
3B & 4	3.8	5.3	14.8	64.4	13.4	2.7	5.2
5 & 6	3.8	4.7	14.1	68.5	14.4	2.5	5.8
Base course							
1	3.6	4.1	13.3	69.0	15.2	3.1	4.9
2	3.4	4.5	13.2	65.8	14.1	2.6	5.5
3A	4.4	4.2	14.2	71.2	11.5	2.9	4.0
& 3B							
4	3.5	4.8	13.7	64.9	14.1	2.6	5.4
5	3.9	NA	NA	NA	NA	NA	NA
6	3.5	4.2	13.2	67.9	15.2	2.6	5.9

The uniaxial push-pull fatigue test, one of the latest tests within the Simple Performance Test (SPT) suite, has a dynamic modulus ($|E^*|$) test built into it. The $|E^*|$ test is conducted as a fingerprint test for 50 cycles only at testing frequency and temperature being used for fatigue test. Then, a tension-compression cyclic loading is performed on the cylindrical specimens until termination criteria are met or the specimen fails.

In this study, a strain-controlled fatigue test was conducted at a temperature of 20°C and at loading frequency of 10 Hz. The test was performed twice with zero confinement using two strain amplitude levels for every specimen: (i) low strain amplitude ($55\mu\epsilon$) to determine material properties in the linear viscoelastic range, and (ii) high strain amplitude ($130\mu\epsilon$) to obtain the nonlinear viscoelastic material properties and prompt fatigue damage. Test data was collected every 10 cycles, and the termination criterion was to complete 200,000 cycles in both levels unless the specimen fails.

4 VISCOELASTIC CONTINUUM DAMAGE APPROACH

For the past decades, many studies were conducted to accurately characterise the fatigue resistance of asphalt pavements. However, the viscoelastic continuum damage (VECD) theory recently showed the ability to unify different temperatures, frequencies and loading modes or levels for analysis of fatigue characteristics of asphalt mixtures (Kutay *et al.* 2009). The VECD theory was essentially developed based on Schapery's viscoelastic constitutive theory (Schapery 1987) which attempts to describe the damage in a material on the macro-scale as a reduction in stiffness (Lee *et al.* 2000, Mbarki *et al.* 2012 and Underwood *et al.* 2012).

In the VECD approach, the fatigue performance can be assessed by the damage characteristic curve (C-versus-S curve). This curve relates the pseudostiffness modulus (or material integrity), C, to the amount of internal damage in a specimen, S. The pseudostiffness modulus is determined as follows:

$$C = \frac{\sigma_0^N}{\epsilon_N^R} = \frac{\sigma_0^N}{|E^*|_{LVE} \times \epsilon_0^N} = \frac{|E^*|_N}{|E^*|_{LVE}} \quad (1)$$

where σ_0^N is the stress amplitude, ϵ_N^R is the pseudostrain amplitude, ϵ_0^N is the applied strain amplitude, $|E^*|_N$ is the dynamic modulus measured in the Nth cycle and obtained from the test, and $|E^*|_{LVE}$ is the linear viscoelastic (undamaged) dynamic modulus. Equation (1) shows that the decrease in pseudostiffness corresponds to the decrease in the dynamic modulus. Consequently, when the fatigue test is conducted with a constant frequency, the 50% reduction in pseudostiffness (C) can be used as a failure criterion (AASHTO TP 8-64, Kutay *et al.* 2008).

Then, the amount of internal damage (S) at the peak of each cycle can be calculated as follows:

$$S_{N+\Delta N} = S_N + \left(\frac{\Delta N}{f}\right)^{\frac{1}{1+\alpha}} \left[-I \frac{[(\epsilon_N^R)^2]}{2} (C_{N+\Delta N} - C_N)\right]^{\frac{\alpha}{1+\alpha}} \quad (2)$$

where ΔN is the cycle increment, f is the constant frequency value and α is a material parameter representing the rate of damage growth and is calculated using the exponent of time, m , in the relaxation modulus-time power equation $[E(t) = E_\infty + E_c t^{-m}]$ derived by Schapery (1981) as $\alpha = 1/m$.

In addition, the value of I is the ratio of the initial dynamic modulus $|E^*|_N = 1$ and the linear viscoelastic dynamic modulus $|E^*|_{LVE}$ used to eliminate sample-to-sample variability.

Once the damage characteristic curve (C-versus-S curve) is obtained and plotted, the following equation can be used to fit it (Kutay *et al.* 2008):

$$C(S) = e^{aS^b} \quad (3)$$

where a and b are the fitting constants. In this study, the exponential equation (3) was used to fit the damage C-S curve and the fitting constants a and b are assumed to be 'universal parameters' representing the material behaviour against fatigue cracking. However, it was noticed that the uniaxial fatigue test conducted on the IPC Global Asphalt Mixture Performance Tester (AMPT) under strain-controlled mode was not 'truly' a strain-controlled test. The strain amplitude during the test was not constant and in most of the cases did not reach the required value. Therefore, a simulation approach was suggested by Kutay *et al.* (2008) in order to calculate the fatigue responses of any mixture under any specified strain amplitude.

The simulation is initialized with calculating the true pseudostrain (ϵ_T^R) value by multiplying the

required strain amplitude (ε_0) by the linear viscoelastic (undamaged) dynamic modulus ($|E^*|_{LVE}$). Then, at the first cycle interval (e.g. $N = 10$), the simulated internal damage parameter (S_N) $\cong 0$ assuming that there is no damage in the sample before testing and the dynamic modulus $|E^*|_N = |E^*|_{LVE}$. After that, the simulated internal damage value of the next cycle ($S_{N+\Delta N}$) is obtained using [equation 4](#):

$$S_{N+\Delta N} = S_N + \left(\frac{\Delta N}{f}\right)^{\frac{1}{\alpha}} \left[-I \frac{[(\varepsilon]_T^R)^2}{2} \frac{dC}{dS_N} \right]^{\alpha} \quad (4)$$

where dC/dS_N is a partial derivative of the fitting [equation \(3\)](#) which can be stated as:

$$\frac{dC}{dS_N} = a b S_N^{b-1} e^{a S^b} \quad (5)$$

Then, the simulated pseudostiffness for each cycle can be calculated as follows:

$$C_{N+\Delta N} = e^{a S_{N+\Delta N}^b} \quad (6)$$

As a result, the simulated damage characteristic curve (C-S simulated) is plotted to represent the fatigue behaviour of an asphalt mixture specimen under a specific strain amplitude. However, to be able to compare between different asphalt mixtures, the fatigue life (N_f) is estimated by a generalized VECD-based formulation derived in a study by Kutay *et al.* (2009). The N_f integration formulation is:

$$N_f = \int_{S_0}^{S_f} \left[-I \frac{[(\varepsilon]_T^R)^2}{2} \frac{dC}{dS_N} \right]^{-\alpha} f dS \quad (7)$$

Where S_0 is the initial damage value selected to minimize the initial stiffness reduction calculated in the simulated pseudostiffness values and to have as smooth reduction as possible and not a vertical discontinuity in the calculated C-S curve (Underwood *et al.* 2012). The S_f is the damage parameter value when the pseudostiffness (C) is equal to the preselected failure criteria (e.g. $C_f = 0.5$). The S_f value can be calculated as:

$$S_f = \left(\frac{\ln C_f}{a} \right)^{1/b} \quad (8)$$

The procedure discussed in this section in addition to the fatigue life (N_f) formulation were used in this study to estimate the number of cycles to fatigue failure for each asphalt mixture of the trial sections.

5 RESULTS AND DISCUSSION

5.1 Uniaxial cyclic fatigue test results

The uniaxial fatigue (push-pull) test was performed twice on each specimen using AMPT machine in a

Table 2. Average of material damage parameter (α) of the trial sections' mixtures.

Section	Slope m	$\alpha = 1/m$
1	0.235	4.2553
2	0.188	5.3191
4	0.181	5.5300
5	0.200	5.0000
6	0.189	5.2910

controlled-strain mode; first test was at strain amplitude (ε_0) of $55\mu\varepsilon$ and the second test was at ε_0 of $130\mu\varepsilon$. The original objective of conducting the test at low strain value was to obtain the linear viscoelastic (LVE) properties, e.g. dynamic modulus ($|E^*|_{LVE}$) and phase angle (δ_{LVE}). However, both strain levels were in effect high enough to surpass the LVE region and cause damage. Consequently, it was decided to analyse both tests independently and consider the dynamic modulus value from the first cycle interval ($N = 10$) in each test data as the $|E^*|_{LVE}$ used in the VECD approach. Therefore, the I value in [equations \(2\)](#) and [\(4\)](#) is equal to $|E^*|_{N=10}/|E^*|_{LVE} = 1$.

5.2 Linear viscoelastic characteristics of the trial sections

In order to perform the VECD analysis, two main inputs are required: the linear viscoelastic dynamic (undamaged) modulus ($|E^*|_{LVE}$) and the material damage parameter (α). The effect of α on the damage characteristic curve is significant and it was concluded in literature that using $\alpha = 1/m$ in strain-controlled or stress-controlled tests worked out best to represent the fatigue damage resistance of field samples (Kutay *et al.* 2008). [Table 2](#) shows the average material damage parameter (α) for each trial section calculated using the slope (m) of relaxation modulus-time power equation.

In addition, the average of the $|E^*|_{LVE}$ values of each trial section determined from the uniaxial fatigue tests is presented in [Figure 2](#).

According to the figures, the variability is very high among the samples of most of the trial sections in both tests. In addition, the average initial stiffness values of all samples in the second fatigue test are lower than those in the first test and do not follow the same trend. Consequently, this will surely affect the accuracy of the evaluation of fatigue resistance.

5.3 VECD analysis

The viscoelastic continuum damage analysis started with calculating the pseudostiffness modulus (C) and the internal damage (S) of each tested sample of the trial sections using [equations \(1\)](#) and [\(2\)](#). All calculations in this study were conducted using Matlab R2013a software package. [Figure 3](#) shows some examples of the C-S curves at both strain amplitudes' tests. It was noticed that there is non-convergence of C-S

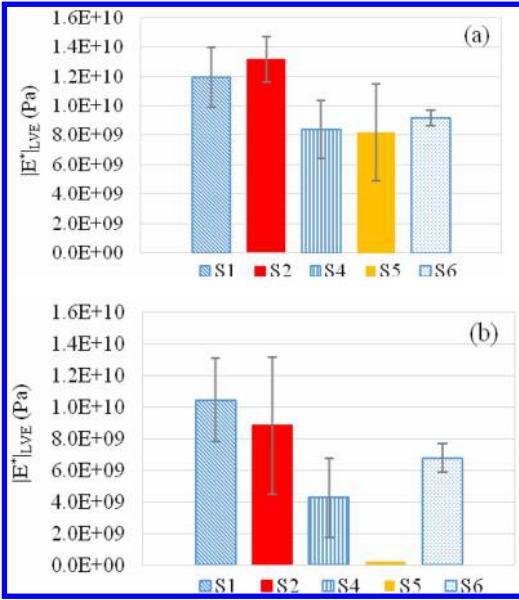


Figure 2. Average LVE dynamic modulus of all trial sections: (a) at strain level 1; (b) at strain level 2.

Table 3. Fitting parameters a and b for all samples of the trial Sections.

Section	Sample	$\varepsilon_0\text{-L}_1 = 55\mu\varepsilon$		$\varepsilon_0\text{-L}_2 = 130\mu\varepsilon$	
		a	b	a	b
1	1	-6.78E-05	0.9000	-4.40E-04	0.7572
	2	-6.05E-04	0.5159	-6.56E-05	0.7583
	3	-1.28E-04	0.6373	-2.87E-05	0.8642
2	1	-1.36E-06	1.2000	-1.00E-03	0.8228
	2	-1.00E-05	0.8852	-4.43E-05	0.8464
	3	-2.19E-04	0.6110	-4.88E-05	0.7751
4	1	-2.93E-05	0.9987	-1.00E-03	0.8304
	2	-1.00E-03	0.6886	-1.00E-03	0.7006
	3	-1.23E-06	1.2000	-1.14E-04	0.7868
5	1	-5.57E-04	0.8812	-1.00E-03	0.8957
	2	-4.60E-04	0.7399	SF*	SF*
6	1	-1.01E-05	1.1027	-4.53E-04	0.7618
	2	-9.74E-06	1.0469	-9.48E-05	0.8325
	3	-2.73E-04	0.6456	-1.22E-04	0.8022

*SF: Sample of this section failed after the first fatigue test.

curves of the same material and this can be attributed to the high variability among the field samples of most of the trial sections in both fatigue tests.

Each one of the C-S curves of all trial sections was fitted using the exponential equation (3) and the fitting universal constants, a and b , are summarized in Table 3.

As stated earlier, the conducted fatigue test was not truly a strain-controlled test. Therefore, a simulation using the required strain amplitude ($\varepsilon_0\text{-L}_1 = 55\mu\varepsilon$ and $\varepsilon_0\text{-L}_2 = 130\mu\varepsilon$) was implemented. The simulation starts with calculating the true pseudostrain (ε_T^R) value for each sample of the trial sections. Then, equations 4,

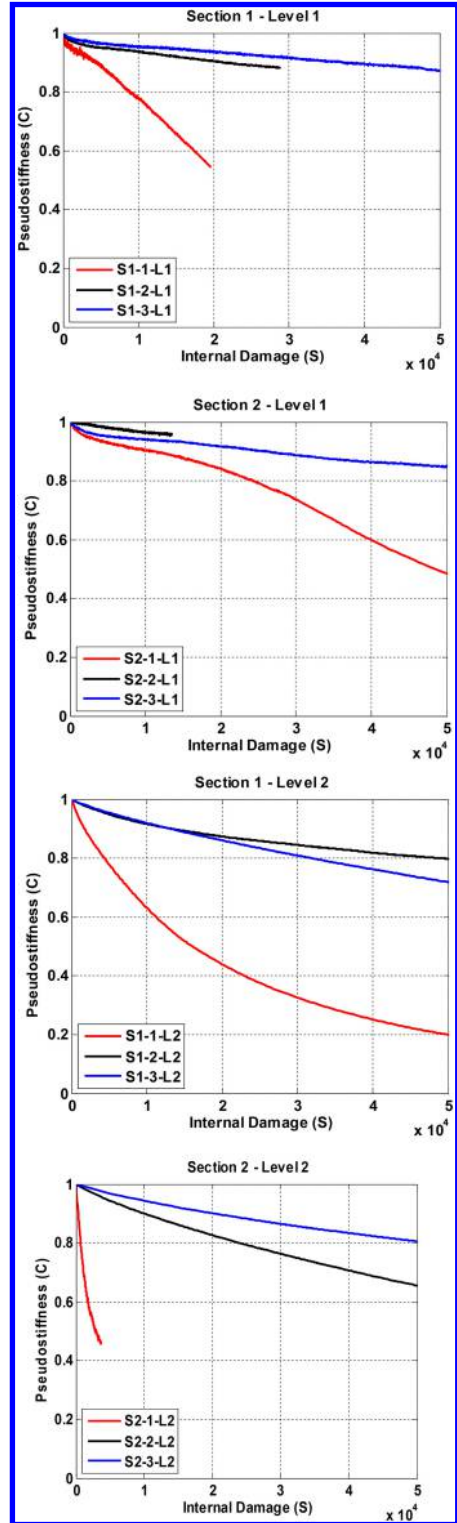


Figure 3. Damage characteristic curves for samples of trial sections 1 and 2 under strain amplitude L1 and L2.

5 and 6 were used to plot the simulated damage characteristic (C-S) curves as the examples shown in Figure 4. The value of S_0 for each sample was selected carefully to minimize the initial stiffness reduction calculated in the simulated pseudostiffness values. Accordingly, the S_0 value was not the same for all samples and sections as shown clearly in Figure 4.

Then, the fatigue resistance of each sample was assessed by comparing the number of cycles to failure (N_f) using equation (7). The failure criterion was selected to be 50% reduction in the pseudostiffness of the sample ($C_f = 0.5$). The calculated average N_f values are presented in Figure 5 for both fatigue tests.

5.3.1 Effect of binder

In order to evaluate the effect of using different binders, the average N_f value of trial sections 1, 2 and 6 and then sections 4 and 5 were compared. The results presented in Figure 5 manifested clearly that the effect of using different binders on fatigue life and resistance is significant.

Based on the analysis results of strain level 1 shown in Figure 5a, the trial section 2, with unmodified 60–70 Pen binder, and section 6, with polymer-modified binder (PMB), are performing almost the same against the fatigue cracking. However, section 1, with a stiff unmodified 40–50 Pen binder, has a higher N_f value (i.e., better performance). On the other hand, section 4, with unmodified 60–70 Pen binder, failed at a higher loading cycle than section 5, with Thiopave binder.

Figure 5b showed that section 2 is performing much better under the strain level 2 than sections 1 and 6. However, section 4, again, performed better than section 5 and failed at a higher N_f value. In general, the results show that the fatigue performance of each section changes with applied strain amplitude value and according to the initial dynamic modulus value (E^*_{LVE}). In addition, the standard error in each trial section is high and shows clearly the uncertainty in the results. Opposite to the results of this study, stiff mixtures with unmodified binder should have lower fatigue lives than those with modified binders.

5.3.2 Effect of mix design

The effect of using different asphalt mix design on the fatigue cracking resistance is assessed by comparing the average fatigue life (N_f) value of sections 2 (Marshall/PRD), and 4 (Marshall/QCS). Generally, the results displayed in Figure 5 revealed that the effect of using different mix designs on fatigue life is also significant.

The average fatigue life results of strain level 1 shown in Figure 5a indicate that the trial section 2, with PRD mix design, had almost double the fatigue life of section 4, with QCS mix design. Though, Figure 5b presented that trial section 4 has a higher N_f value compared to section 2 under the strain level 2. This is, again, shows a contradictory and emphasizes the importance of looking deeply on the fatigue model used and its parameters.

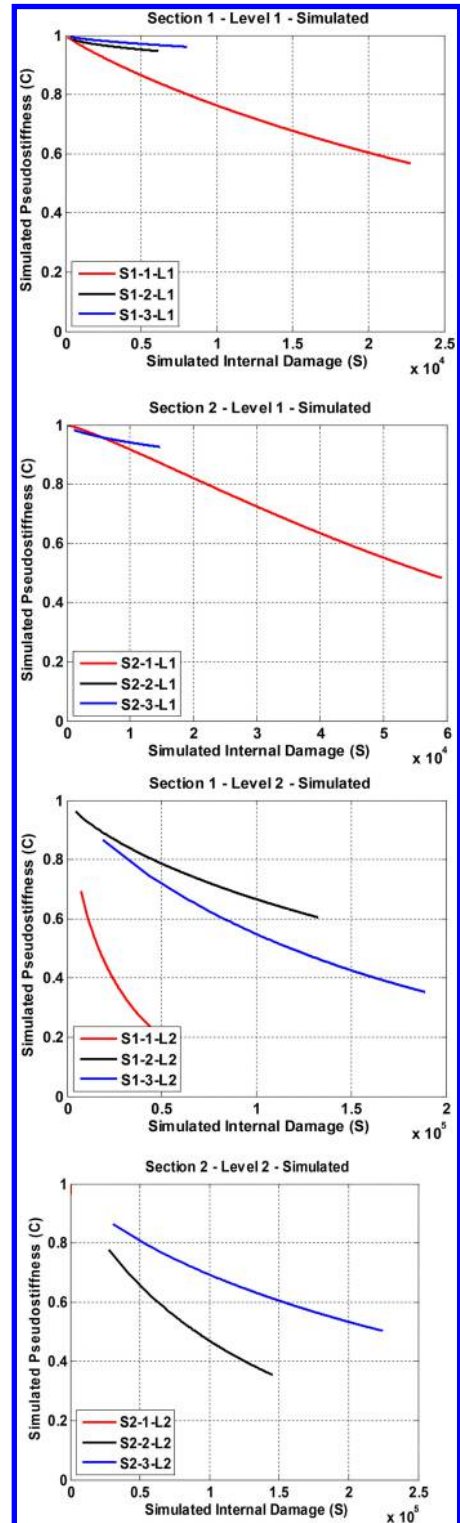


Figure 4. Simulated damage characteristic curves for samples of trial sections 1 and 2 under strain amplitude L1 and L2.

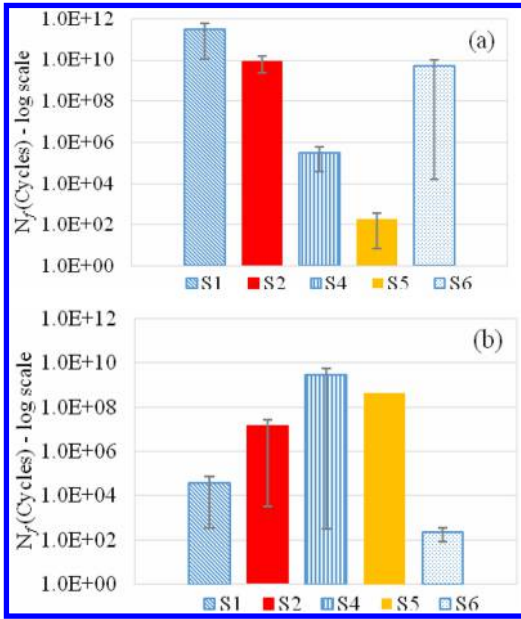


Figure 5. Comparison of average N_f results at $C_f = 0.5$ for all trial sections: (a) at strain level 1; (b) at strain level 2.

6 CONCLUSIONS

With the aim of evaluating the fatigue performance of different trial sections, a uniaxial cyclic fatigue test was conducted and the results were analysed using VECD approach. Comparisons were made between different field specimens at two different strain levels. The main findings of this study are outlined below.

- The effect of mix design and binder type is significant on the fatigue cracking resistance of asphalt pavements.
- The polymer-modified mixtures did not show improvement in the resistance to fatigue cracking while unmodified mixtures performed better against fatigue damage. This could be attributed to the design of these mixtures, which led to having all mixtures to have relatively low binder content.
- Mixtures of sections 1 and 2 had the highest fatigue lives in strain level 1 test while those in sections 4 and 5 had the highest fatigue lives in strain level 2 test.
- The strain amplitude value, initial dynamic modulus and selected initial internal damage have a significant effect on the fatigue performance of the mixture.
- The use of VECD approach has major advantages; however, the uncertainty associated with fatigue tests as well as models and their parameters have substantial influence on the predicted fatigue life.

More in-depth research that accounts for the high variability in estimating and predicting fatigue life is needed to better understand the behaviour of field mixtures against fatigue cracking.

ACKNOWLEDGMENTS

The work presented in this article was made possible by the financial support provided by Qatar National Research Fund (QNRF) through the National Priority Research Program project NPRP 4-789-2-293 to Texas A&M at Qatar. All statements are those of the authors and do not represent QNRF.

REFERENCES

- AASHTO Designation: TP 79-11. "Standard Method of Test for Determining the Dynamic Modulus and Flow Number for Hot Mix Asphalt (HMA) Using the Asphalt Mixture Performance Tester (AMPT)".
- AASHTO Designation: TP 08-64. "Method for determining the fatigue life of compacted hot-mix asphalt (HMA) subjected to repeated flexural bending." May 2002.
- Artamendi, I., and Khalid, H., 2005, "Characterization of fatigue damage for paving asphaltic materials". *Fatigue & Fracture of Engineering Materials & Structures*, 28, 1113–1118. DOI: 10.1111/j.1460-2695.2005.00949.x
- Bhasin, A. Castelo Branco, V.T.F. Masad, E. and Little, D.N., 2009, "Quantitative Comparison of Energy Methods to Characterize Fatigue in Asphalt Materials". *Journal of Materials in Civil Engineering*, 21(2), 83–92.
- BS EN 12697-32:2003. Bituminous mixtures. Test methods for hot mix asphalt. Laboratory compaction of bituminous mixtures by vibratory compactor.
- Kutay, M. E., Gibson, N., and Youtcheff, J., 2008, "Conventional and Viscoelastic Continuum Damage (VECD) Based Fatigue Analysis of Polymer Modified Asphalt Pavements". *Journal of Association of Asphalt Paving Technologists*, Vol. 77, 2008, pp. 395–434.
- Kutay, M. E., Gibson, N., Youtcheff, J., and Dongré, R., 2009, "Use of Small Samples to Predict Fatigue Lives of Field Cores: Newly Developed Formulation on Viscoelastic Continuum Damage Theory". *Transportation Research Record: Journal of the Transportation Research Board*, No. 2127, Transportation Research Board of the National Academies, Washington, D.C., pp. 90–97. DOI: 10.3141/2127-11.
- Lee, H. J., Daniel, J. S., and Kim, Y. R., 2000, "Continuum damage mechanics-based fatigue model of asphalt concrete". *Journal of Materials in Civil Engineering*, 12(2), 105–112.
- Masad, E., Kassem, E., and Little, D., 2011, "Characterization of Asphalt Pavement Materials in the State of Qatar: A Case Study". *International Journal of Road Materials and Pavement Design*, vol. 12, no. 4, 739–765.
- Mbarki, R., Kutay, M. E., Gibson, N., and Abbas, A. R., 2012 "Comparison between fatigue performance of horizontal cores from different asphalt pavement depths and laboratory specimens". *Road Materials and Pavement Design*, 13(3), 422–432, DOI: 10.1080/14680629.2012.685843
- Qatar Construction Specifications (QCS), 2010. The State of Qatar.
- Sadek, H., Masad, E., Sirin, O., Al-Khalid, H., and Little, D., 2012, "The Implementation of Mechanistic-Empirical Pavement Design Method to Evaluate Asphalt Pavement Design in Qatar". 5th Eurasphalt & Eurobitume Congress, Istanbul, 13–15th, June 2012.
- Sadek, H., Masad, E., Sirin, O., Al-Khalid, H., Sadek, M., and Little, D., 2013, "Implementation of Mechanistic-Empirical Pavement Analysis in the State of Qatar".

- International Journal of Pavement Engineering. 15(6), 495–511. DOI: 10.1061/(ASCE)CF.1943-5509.0000627.
- Sadek, H., Masad, E., Sirin, O., Al-Khalid, H., and Hassan, K., 2014a, “Characterization of Fatigue Resistance of Alternative Pavement Designs for the State of Qatar”. Proceeding of the 3rd International Conference on Transportation Infrastructure, 22–25th April 2014. Pisa, Italy.
- Sadek, H., Masad, E., Sirin, O., Al-Khalid, H., and Hassan, K., 2014b, “Performance Evaluation of Full-Scale Sections of Asphalt Pavements in the State of Qatar”. Journal of Performance of Constructed Facilities. Journal of Performance of Constructed Facilities (ASCE). DOI: 10.1061/(ASCE)CF.1943-5509.0000627.
- Schapery, R.A., 1981, “On Viscoelastic Deformation and Failure Behavior of Composite Materials with Distributed Flaws”. In *Advances in Aerospace Structures and Materials*, edited by S.S. Wang and W.J. Renton, 5–20 (American Society of Mechanical Engineers: New York, NY).
- Schapery, R.A., 1987, “Deformation and Fracture Characterization of Inelastic Composite Materials using Potentials”. *Polymer Engineering and Science*, Vol. 27, No. 1, 1987, pp. 63–76.
- TRL, 2002, *A guide to the design of hot mix asphalt in tropical and sub-tropical countries*. Overseas Road Note 19. TRL Limited.
- TRL Client Project Report 282, Phase C: Performance of Existing Pavement in Qatar, 2010.
- TRL Client Project Report 282, Phase D: Design of Site Trials, 2010.
- Underwood, B.S., Baek, C., and Kim, R., 2012, “Simplified Viscoelastic Continuum Damage Model as Platform for Asphalt Concrete Fatigue Analysis”. *Transportation Research Record: Journal of the Transportation Research Board*, No. 2296, Transportation Research Board of the National Academies, Washington, D.C., pp. 36–45. DOI: 10.3141/2296-04.

A new approach in fatigue testing and evaluation of hot mix asphalt using a dynamic shear rheometer

Taher M. Ahmed & Hussain A. Khalid

School of Engineering, University of Liverpool, UK

ABSTRACT: This paper describes a successful trial using a Dynamic Shear Rheometer (DSR) for fatigue testing of Hot Mix Asphalt (HMA) under controlled strain and stress test modes. A new fatigue index, FI^R , has been derived from the stress–pseudostrain hysteresis loop to be used in evaluating fatigue performance. Results have shown that there is a plateau region in the relationship of FI^R and normalised shear modulus, which can be used to evaluate fatigue performance. FI^R values were in agreement in terms of the ranking order with the results from other reliable approaches, such as the traditional and energy ratio approaches. In this work, limestone and granite aggregates were used with two binder grades: 40/60 and 160/220 to prepare four mixtures with two different gradations: gap-graded hot rolled asphalt and continuously graded dense bitumen macadam. The study demonstrated the suitability of the DSR for fatigue testing of full HMA. Also, limestone mixes were better fatigue performance than granite.

Keywords: Dynamic shear rheometer, fatigue index, pseudostrain energy, hot mix asphalt, strain and stress test modes

1 INTRODUCTION

Fatigue cracks represent one of the major distress forms in asphalt pavements. Cracks result in degradation of the pavement materials and eventually of the pavement structure. Many variables such as temperature, time of loading and material properties play a role in fatigue failure. Fatigue in asphalt is generally evaluated with repeated load tests on prepared samples either using a constant applied load (controlled stress), or using constant displacement (controlled strain). During fatigue life under repeated loading, materials exhibit three phases (Di Benedetto et al. 2004): phase I, or the adaptation phase, is characterised by a rapid decrease in stiffness due to heat generation and thixotropy (Carpender & Shen 2006, Ghuzlan & Carpenter 2006); phase II, or the quasi-stationary phase, is where the steady decrease in stiffness predominates fatigue life, and the degradation in the material is very slow over a number of load cycles; and phase III, or the failure phase, is where macro-cracks begin to develop and failure completely sets into the material at the end of this phase. Phases I and II are associated with crack initiation, while phase III is associated with crack propagation.

Traditionally, asphalt fatigue tests involve the manufacture of relatively large-size beams or cylinders, which are then conditioned and tested in flexure, tension–compression or diametrically to determine their fatigue properties. These tests may take a considerable amount of time to finish, thus rendering them

time-consuming and inefficient. At typical strain or stress levels adopted in a classical laboratory fatigue test, the duration can be anything from one day to several days (or even more), which ties up resources and leads to considerable delays in arriving at the required results.

In a move to rationalise test procedures and ensuing analyses for asphalt mixtures, a white paper by Christensen et al. (2009) advocated the standardisation of test and analysis protocols, which would lead to a significant reduction in material quantities and test duration; this protocol suggested fatigue testing and analysis based on a reduced cycle, simplified viscoelastic continuum damage (S-VECD) and damage mechanics analysis. In recent years, the Dynamic Shear Rheometer (DSR) has been used successfully as a technique in fatigue testing, but it was limited for use only with binder, mastic and fine aggregate mixture samples (Christensen et al. 2009, Kim et al. 2002, Kim & Little 2004, Huang et al. 2007, Masad et al. 2008, Tan et al. 2012, Woldekidan et al. 2013, Hintz & Bahia 2013).

In the literature, various approaches have been used as criteria to evaluate fatigue performance. The most common is called the traditional approach, in which fatigue failure is defined based on the mode of loading. For example, in the controlled strain mode, fatigue failure is defined as the number of cycles needed to reach 50% reduction in the initial stiffness modulus (Kim et al. 2003, Daniel et al. 2004, Artamendi & Khalid 2005), whereas in the controlled stress mode, failure

is defined either as the complete fracture of the sample (Ghuzlan & Carpenter 2006, Tayebali et al. 1992), or reduction in stiffness modulus of the sample to 10% of its initial value (Rowe 1993). The American Association of State Highway and Transportation Officials (AASHTO 2002) adopted the traditional approach in evaluating fatigue performance of asphalt pavements. (AASHTO 2002). The 50% reduction in stiffness modulus for the controlled strain mode predominantly falls within phase II, which is pragmatically considered as representative of the material's useful life. Mix's resistance to fatigue cracking, however, may continue until the second inflection point is reached, where phase III begins. This means that some data within phase II will be neglected because the test is stopped at 50% reduction, which may give misleading results by underestimating fatigue life. As this approach measures the number of cycles, the results always have high variability and data scatter; to minimise this effect, a large number of samples is required to obtain reliable results and this is time-consuming and expensive.

Applying a stress to a material creates a strain, and the area under the stress-strain curve represents the energy being put into the material. For elastic materials without any damage, the strain is recovered directly when the stress is removed and the stress-strain curve coincides, meaning the energy is recovered completely without losses. If the two curves for loading and unloading do not coincide, this indicates there is a difference between the amount of energy put into the material and the amount of energy recovered from the material, and this difference in energy loss is called dissipated energy. In this regard, an approach related to the dissipated energy concept was introduced by Van Dijk (1975, 1977) to characterise the fatigue performance of HMA. In Van Dijk's work, the fatigue criterion was defined as the point where the dissipated energy ratio (ER) begins to increase rapidly with number of cycles from the plateau value. ER was defined (Rowe 1993) as a function of the number of cycles and stiffness modulus for both strain and stress modes, as in Equations 1-3.

$$ER = \frac{n(\pi\sigma_o\varepsilon_o \sin \delta_o)}{(\pi\sigma_i\varepsilon_i \sin \delta_i)} \quad (1)$$

$$R_\sigma = nE_i^* \quad (2)$$

$$R_\varepsilon = \frac{n}{E_i^*} \quad (3)$$

where: n = cycle number; ε = strain amplitude; σ = stress amplitude; δ = phase angle; R_σ & R_ε = equivalent energy ratio for controlled stress and strain mode respectively; E^* = complex stiffness modulus; and 0, i = initial and i th cycle.

The criterion to define fatigue life in the stress mode is the number of cycles at the point when the ER reaches the peak point in the relationship of ER vs n , while in the strain mode it is defined as the point when the ER slope deviates from a straight line in the same relationship. The variation in results that is related to

number of cycles such as the traditional approach and ER is relatively high [8]; therefore to reduce the scatter in the results, more samples are required.

Another energy-related approach, referred to as dissipated pseudostrain energy (DPSE) (Masad et al. 2008, Bhasin et al. 2009) has been used in evaluating the fatigue performance of HMA. In this approach, real strain amplitude is converted to an equivalent pseudostrain to remove the viscoelastic contribution to dissipated energy. DPSE rate has been used to measure fatigue cracking resistance using a parameter called the crack growth index (Masad et al. 2008, Bhasin et al. 2009), which is based on Paris's law for crack growth and the J-integral. The results of the crack growth index were found to be consistent with field observations and independent of fatigue test mode (Bhasin et al. 2009). However, this technique used the so-called 'crack radius', which is practically impossible to measure because the crack always creates new surfaces with increase in the crack mouth opening displacement.

A further performance evaluation approach was based on Schapery's work on crack growth in viscoelastic media (Schapery 1984) and is called continuum damage mechanics (CDM). This approach was developed by Lee and Kim (Kim et al. 1997, Lee et al. 2000, Park et al. 1996) to characterise the damage in asphalt due to fatigue. The damage was quantified by a non-dimensional internal state variable (S), and this variable represents an indicator of the change in the pseudo-stiffness modulus (C). Fatigue is considered to have occurred when the pseudo-stiffness drops to 50% of the initial value. The C vs S curve represents a unique depiction of the deterioration of the material independent of test mode, temperature, frequency and other test variables. Although this approach requires somewhat complex calculations in addition to relaxation test parameters, it is versatile, can be used in mechanistic pavement design and enables reduction in number of fatigue samples tested.

In this work, a fatigue test approach using the DSR was introduced based on selecting a specified strain and stress amplitude. Also, a new index was derived based on the recovered and applied pseudostrain energy used in analysing the fatigue performance of HMA.

2 OBJECTIVES OF STUDY

This study aims at introducing a new index to evaluate the fatigue performance of asphalt mixtures tested using the DSR. The ability of the proposed fatigue index, FI^R , to rank mixtures in respect of their resistance to fatigue cracking is validated through comparison with established fatigue performance evaluation tools, namely the traditional and ER approaches discussed above. The validation process was facilitated through fatigue testing in the DSR of four asphalt mixtures including two aggregate gradations, namely gap-graded and continuous; two aggregates, limestone

and granite; and two binder grades, hard 40/60 and soft 160/220 Pen binders. The ranking efficiency of FIR for the mixtures tested has been demonstrated.

3 BACKGROUND AND THEORY

In fatigue tests using sinusoidal loading and unloading, two types of energy are produced: applied energy during loading and recovered energy during unloading. The difference between both energies is called the dissipated energy, which is equal to the hysteresis loop area (Ghuzlan & Carpenter 2006, Daniel et al. 2004). A sinusoidal wave was used in this work for fatigue testing to calculate the applied strain energy (ASE) and recovered strain energy (RSE). Figure 1 shows the typical sine wave of one-cycle loading for time loading t_0 to t_6 . Because the calculations are based on the DSR test, the time for one cycle is split into two parts: T_R (right direction of loading) and T_L (left direction of loading). Figure 2 is a stress-strain graph representing a typical hysteresis loop for a viscoelastic material. As shown in Figures 1 and 2, there are two intervals for loading t_0 to t_1 and t_3 to t_4 in T_R and T_L , respectively, as well as t_1 to t_3 and t_4 to t_6 , which are unloading periods in T_R and T_L , respectively. However, strain increases during unloading in periods t_1 to t_2 and t_4 to t_5 because of the viscoelastic behaviour of the material, this interval being the phase angle (δ). As shown in Figure 2, there are two parts to ASE: the first one, ASE_1 , is under the curve $t_0t_1t_2$, and the second part, ASE_2 , is above the curve $t_3t_4t_5$; while RSE_1 is the shaded area under the curve t_2t_3 and RSE_2 is the shaded area within the region t_5t_6 .

A useful technique to calculate ASE and RSE is to use the integration over the periods $[t_0, t_6]$ with the basic equation of the energy formula, as in Equation 4 (Larson 1999, Schapery 1990):

$$W = \int_{t_d}^{t_u} \tau(t) \frac{d\gamma(t)}{dt} dt \quad (4)$$

where W is the strain energy and $\tau(t)$ and $\gamma(t)$ are shear stress and strain, respectively. Equations 5 and 6 are the sinusoidal shear stress and strain functions.

$$\tau = \tau_0 \sin(\omega t) \quad (5)$$

$$\gamma = \gamma_0 \sin(\omega t - \delta) \quad (6)$$

where τ is shear stress; τ_0 is shear stress amplitude; γ is shear strain; γ_0 is shear strain amplitude; δ is phase angle; t is loading time and ω is angular frequency in rad/s.

To calculate the pseudostrain energy (PSE), the pseudostrain relationship in the formula below (Equation 7) has been used (Masad et al. 2008). The final formulations for applied pseudostrain energy and recovered pseudostrain energy are given in Equations 9 and 10 after integration processes using integration limits in Table 1.

$$\gamma^R = \frac{G_{Ive} \gamma_0}{G_R} \sin(\omega t - \delta_N + \delta_{Ive}) \quad (7)$$

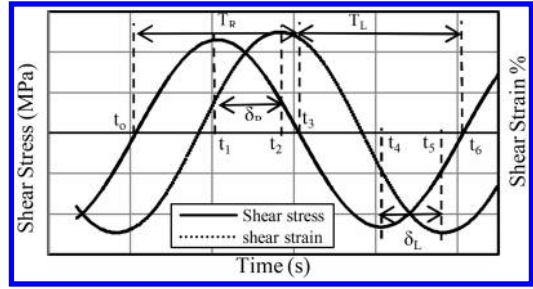


Figure 1. Typical one-cycle loading.

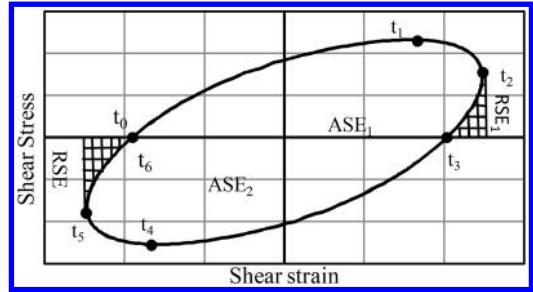


Figure 2. Typical hysteresis loop.

Table 1. Integration limits of the strain energy formula.

Energy	t_l	t_u	Period
ASE_1	0	$\frac{\pi}{2\omega} + \frac{\delta}{\omega}$	$[t_0, t_2]$
ASE_2	$\frac{\pi}{\omega}$	$\frac{3\pi}{2\omega} + \frac{\delta}{\omega}$	$[t_3, t_5]$
RSE_1	$\frac{\pi}{2\omega} + \frac{\delta}{\omega}$	$\frac{\pi}{\omega}$	$[t_2, t_3]$
RSE_2	$\frac{3\pi}{2\omega} + \frac{\delta}{\omega}$	$\frac{2\pi}{\omega}$	$[t_5, t_6]$

$$W = \int_{t_d}^{t_u} \tau(t) \frac{d\gamma^R(t)}{dt} dt \quad (8)$$

$$W_A^R = \frac{G_{Ive} \tau_0 \gamma_0}{G_R} \cos \delta - \delta_{Ive} 2 \sin 2\pi + 2\delta 2 + \sin 23\pi + 2\delta 2 + \sin \delta - \delta_{Ive} 4 2\pi + 4\delta - \sin \pi + 2\delta - \sin 3\pi + 2\delta \quad (9)$$

$$W_R^R = \frac{G_{Ive} \tau_0 \gamma_0}{G_R} \left[\frac{\sin(\delta - \delta_{Ive})}{4} (2\pi + 4\delta + \sin(\pi + 2\delta) + \sin(3\pi + 2\delta)) - \frac{\cos(\delta - \delta_{Ive})}{2} \left(\sin^2\left(\frac{\pi}{2} + \delta\right) + \sin^2\left(\frac{3\pi + 2\delta}{2}\right) \right) \right] \quad (10)$$

where γ^R = pseudostrain; G_{Ive}^* is dynamic modulus at linear viscoelastic; G_R is reference modulus; δ_N is phase angle; δ_{Ive} is phase angle at linear viscoelastic; W_A^R , W_R^R are applied and recovered pseudostrain energy.

4 EXPERIMENTAL WORK

The experimental work involved the preparation of 12 mm in diameter and 50 mm high cylindrical samples from HMA; and performing fatigue testing, which includes determining the appropriate strain and stress level to be used in the fatigue tests. Fatigue performance was evaluated using a fatigue index based on the pseudostrain energy. For verification of this index, two well-known approaches have been used to compare the results; these approaches are: the traditional approach and the ER approach.

5 MATERIALS AND MIX DESIGN

In this work, two kinds of mix: a hot rolled asphalt (HRA) and dense bitumen macadam (DBM) were prepared in the laboratory using two types of aggregate: limestone (L) and granite (G), with two binders: 40/60 and 160/220 penetration grades. The mixes were made according to British Standards recipes (BS 4987-1 2005, BS 597-1 2005, BS PD 6691 2010) and were denoted as DBM-G, DBM-L, HRA-G and HRA-L. Figures 3 and 4 show the particle size distribution of both mixes DBM and HRA, respectively. Steel moulds were used to prepare asphalt slabs (305 × 305 × 65 mm), which were compacted using a roller compactor (BS EN 12697-33 2003). The slabs were then cut into five beams (305 × 65 × 50 mm), two of which were discarded, and the remaining three were cored with an electric coring machine to obtain the cylindrical DSR samples. Table 2 shows the mix details.

6 PREPARATION OF DSR SAMPLES

In the literature, two techniques have been used to prepare DSR samples: Kim et al. (2002, 2003) prepared 15 g individual samples using a steel cylindrical mould 12 mm in diameter and 50 mm in height compacted by using a cylindrical rod at both ends. Zollinger (2005) prepared cylindrical samples 152 mm in diameter and 85 mm in height using the Superpave gyratory compactor (SGC) and then cored them to obtain small samples. Both techniques, however, have been used only with fine aggregate matrix (FAM) mixtures. In this study, full asphalt mixtures were produced whose properties are more representative than FAM mixtures of the material in the field. The number of DSR samples cored from each beam was 43–46. These samples were put in an oven for 24 h at 25°C to dry and kept in PVC tubes after coding, and then stored in a fridge at 10°C. Figure 5 shows DSR samples.

7 INSTRUMENTATION

In this work, a Kinexus-Pro DSR (Malvern) was used to test the cylindrical HMA. This was done after adding some modifications to the DSR to enable it to be tested. These modifications included design and manufacture

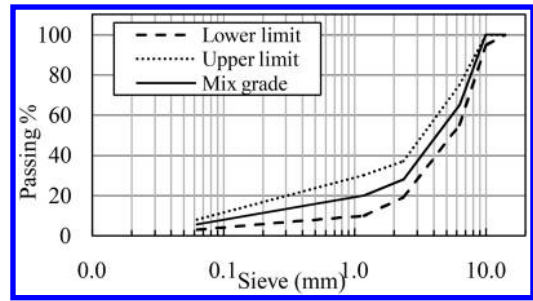


Figure 3. Grading curves of aggregate for DBM [28].

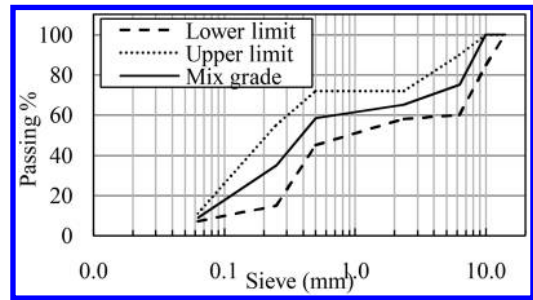


Figure 4. Grading curves of aggregate for HRA [28].

Table 2. Mix ID and material details.

Mix type	Type	Aggregate	
		Type	Apparent density (Mg/m ³)
DBM	Limestone		2.71
DBM	Granite		2.67
HRA	Limestone		2.71
HRA	Granite		2.67
Mix properties			
ID	G _{bulk} (Mg/m ³)	Air voids (%)	Binder grade
DBM-L	2.374	4.9	160/220
DBM-G	2.290	7.5	160/220
HRA-L	2.343	2.2	40/60
HRA-G	2.298	4.0	40/60

of end stubs and adjusting the fastening mechanism that was used to hold and set up samples in the proper position for testing. To control the sample temperature during testing, a temperature control unit (TCU) was designed and added to the DSR as an essential part. The full system is shown in Figure 6.

8 ANALYSIS OF VOLUMETRIC PROPERTIES

Scattering in the fatigue data is common; therefore, it is necessary to test a large number of samples to enhance the reliability of the results (Di Benedetto

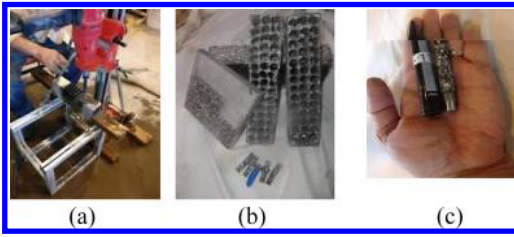


Figure 5. (a) Coring beam for obtaining DSR samples, (b) DSR samples and (c) sample ready for testing.

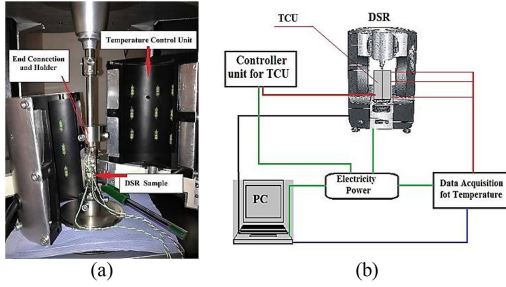


Figure 6. (a) The DSR apparatus assessors: and (b) schematic of system.

et al. 2004). In this study, an approach was used to select prepared samples for further use that would reduce the variability within the total number of samples prepared. This approach is based on measuring the sample's bulk density in according with the procedure in the British Standards (BS EN 12697-6 2004). The measured bulk density varied according to aggregate grading, shape, type and binder content, among other factors. The approach starts by finding the mode, 'M₀', of the measured sample's bulk density, i.e. the value with the highest frequency. This value, M₀, was used to calculate the standard deviation, σ , of the bulk density data using Equation 11. A range, R, was then calculated, using Equation 12, which is one σ value on either side of M₀. Thus, only those samples whose bulk density value fell within R were chosen for further use in the project. Table 3 summarises the values of bulk density and range limits for all the mixtures in the study and shown in Figure 7, together with the corresponding air voids.

$$\sigma = \sqrt{\frac{\sum_{i=1}^N (X_i - M_0)^2}{N}} \quad (11)$$

$$R = M_0 \pm \sigma \quad (12)$$

where σ is the standard deviation; M₀ is the mode value; X_i is a single bulk density measurement; N is the number of measurements and R is the range of bulk density of selected DSR samples.

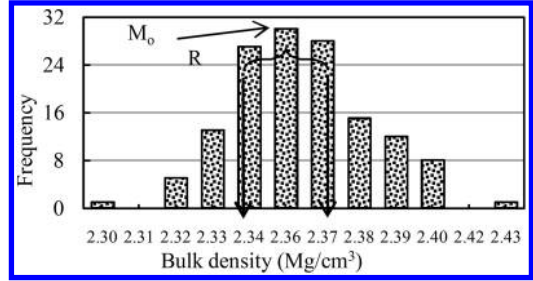


Figure 7. Typical bulk density histogram for HRA-L DSR samples.

Table 3. Bulk density and air void range of DSR samples.

Mix ID	Bulk density Mg/m ³			Air voids range (%)		
	Upper	Mode	Lower	$\sigma_{(M_0)}$	Upper	Lower
DBM-L	2.413	2.398	2.383	0.015	4.486	3.872
DBM-G	2.373	2.350	2.327	0.023	6.023	5.101
HRA-L	2.368	2.356	2.344	0.012	2.153	1.641
HRA-G	2.327	2.311	2.295	0.016	4.150	3.487

9 RESULTS AND DISCUSSIONS

9.1 Determination of strain and stress amplitudes

In the literature, different techniques have been applied. Kim et al. (2002, 2003) used amplitude sweep strain to find the maximum stress value that could be applied to the sample before causing damage. Masad et al. (2008) used high strain amplitude value 0.2% in fatigue testing for DSR samples prepared from fine aggregate matrix (FAM), and the stress corresponding to a 50% reduction of initial complex shear modulus (G^*) was used for fatigue testing in the stress test mode.

In this work, strain and stress amplitude for fatigue test was identified at the damage zone. To determine the strain amplitude in fatigue testing, sweep strain amplitude was used and performed for three samples, which were arbitrarily selected within the range R in Table 3; the changes in the slope of the strain–stress curve at each point were calculated using Equation 13.

$$\frac{\Delta\tau}{\Delta\gamma} = \frac{\tau_{i+1} - \tau_i}{\gamma_{i+1} - \gamma_i} \quad (13)$$

where τ_i and τ_{i+1} are shear stresses at shear strains γ_i and γ_{i+1} ; respectively.

At the instant when the slope changed from positive to negative, the value of the strain amplitude at the damaged region was identified, as shown in Figure 8. Table 4 details the strain range at starting damage and strain amplitude for fatigue testing. It is clear that the damage occurs earlier in DBM-G and the amplitude range (0.2–0.3%) is shorter than that of DBM-L (0.3–0.45%). This is possibly because air voids in DBM-G are higher than air voids in DBM-L, as detailed in Table 3. In HRA, the damaged regions for both granite and

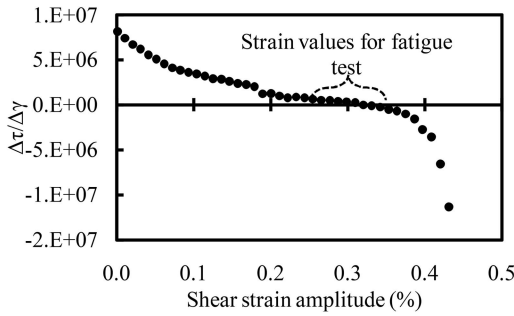


Figure 8. A typical sweep strain amplitude of HRA-L.

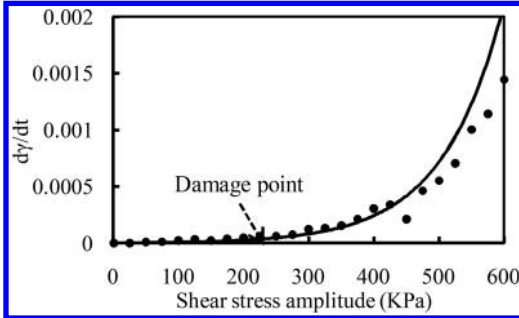


Figure 9. A typical stress amplitude sweep of HRA-L.

limestone were equal, perhaps because both mixes are homogenous.

Amplitude sweep stress test was performed on three DSR samples selected within the range R in Table 3. The strain response has been collected, and then strain response-time slopes were calculated for each stress value, which was applied to sample for several cycles. The strain response against time was plotted and fitted linearly for each stress amplitude value. The slopes of strain-time ($d\gamma/dt$) were evaluated from the fitted equations and also plotted against stress amplitude. At the instant when the slope ($d\gamma/dt$) increased dramatically, the stress amplitude was taken as stress value for fatigue test, as demonstrated in Figure 9.

It is noticeable that there is a marked increase in the strain response slopes which starts at definite shear stress value; this value can be defined at the point when there is divergence from the straight line in the relationship of strain response slope against shear stress amplitude, as demonstrated in Figure 9. This point is considered as start damage in materials, whereas it was about 150 KPa for DBM mixes and about 250 KPa and 400 KPa for HRA-L and HRA-G, respectively, as detailed in Table 4.

9.2 Fatigue analysis

9.2.1 Fatigue index

A new fatigue index (FI^R) was formulated based on the energy concept as a function of the ratio of pseudo-recovered energy to pseudo-applied energy (Eqn. 14). Logically, when W_R^R is equal to W_A^R , then

Table 4. Strain/stress amplitude test results.

Mix ID	Shear strain (%)		Shear stress at damage (KPa)
	at damage	for fatigue	
DBM-L	0.30–0.45	0.30	150
DBM-G	0.20–0.30	0.30	150
HRA-L	0.25–0.35	0.25	250
HRA-G	0.25–0.35	0.25	400

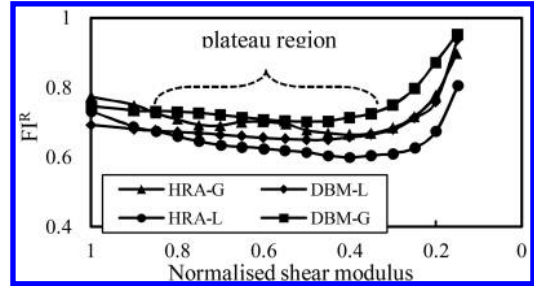


Figure 10. Fatigue index against normalised shear modulus for controlled strain test mode.

the fatigue index equals zero, which means no damage has occurred in the material. Otherwise, when the W_R^R is equal to zero, then the fatigue index equals one, which means that the sample is completely damaged. So, FI^R range is between one and zero.

$$FI^R = 1 - \frac{W_R^R}{W_A^R} \quad (14)$$

Firstly, five samples were selected within the range R to be tested for fatigue using the shear strain and stress values in Table 4. Figures 10 and 11 show the relationship of FI^R plotted against the normalised shear modulus for controlled strain and stress test mode, respectively. It is clear that there are plateau values for all mixes where the FI^R is barely constant between 0.85 to 0.35 of normalised shear modulus; and increases sharply after that, as shown in Figure 10.

This trend is similar to the one shown in the dissipated energy ratio approach (Daniel et al. 2004). In contrast, the plateau region (PR) in stress test mode is not as clear as in the strain mode, as shown in Figure 11; however, FI^R increased sharply beyond 0.2 of normalised shear modulus; this behaviour was found to be the same for the relationship of DER vs n (Ghuzlan & Carpenter 2006). The PR was defined between 0.85 and 0.2 of normalised shear modulus, and FI^R was calculated as average within PR.

Figures 10 and 11 demonstrate that the performance of HRA fatigue is higher than DBM (Brown 1995) and limestone is better than granite in both mixes tested in both modes.

9.2.2 Verification using other approaches

In this work, traditional approach (TA) (Kim et al. 2003, Daniel et al. 2004, AASHTO TP8-94 2002) and

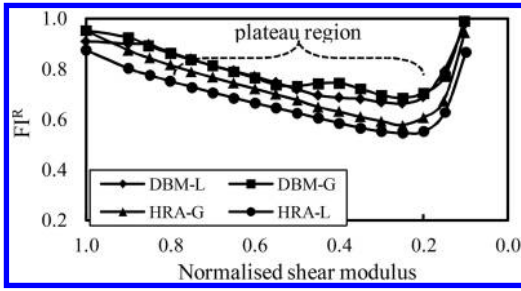


Figure 11. Fatigue index against normalised shear modulus for controlled stress test mode.

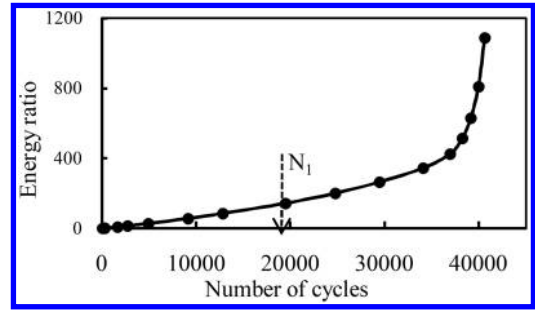


Figure 14. Energy ratio approach for HRA-L mixes tested in strain mode.

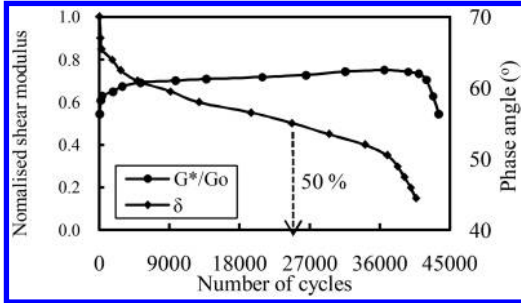


Figure 12. Traditional approach for HRA-L mix tested in strain mode.

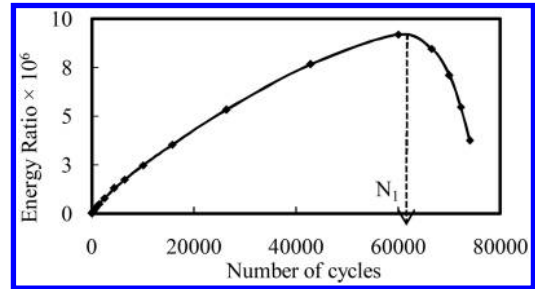


Figure 15. Energy ratio approach for HRA-L mix tested in stress mode.

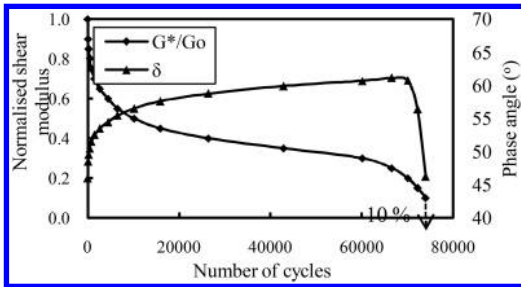


Figure 13. Traditional approach for HRA-L mix tested in stress mode.

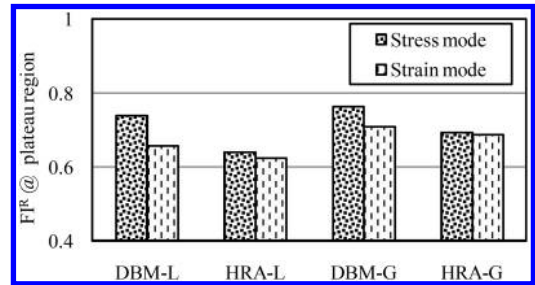


Figure 16. Fatigue performance of different mixes tested in strain and stress modes evaluated using FI^R approach.

energy ratio (ER) approach were used to verify FI^R . TA represents the changes in a material's modulus and phase angle against number of cycles, as presented in the typical examples given in Figures 12 and 13 for strain and stress test mode respectively.

The results of TA revealed that the phase angle begins to decrease quickly when the normalised shear modulus drops approximately below 0.35 and 0.2 for strain and stress test modes, respectively, as demonstrated in the typical examples given in Figures 12 and 13.

The energy ratio (ER) approach [16] was also used to study the validity of the FI^R parameter. Typical results for HRA-L are shown in Figures 14 & 15 for strain and stress test modes, respectively.

The outcomes of fatigue test using DSR and the analysed results are summarised in Figures 16–18 for all approaches: FI^R , TA and ER. It is clear that the

rank order is compatible in all approaches, as a number of cycles and fatigue index in both test modes where the performance of HRA fatigue is higher than DBM (Brown 1995) and limestone is better than granite, as shown in Figures 16 – 18. The main conclusion is that the TA and ER emphasise the feasibility of using the FI^R parameter to evaluate fatigue performance.

10 CONCLUSIONS

The following conclusions have been made based on the experimental results obtained in this study

1. An approach has been developed and used effectively to prepare full hot mix asphalt DSR samples of 12 mm in diameter and 50 mm in height. Also, a method for the statistical reliability of selecting

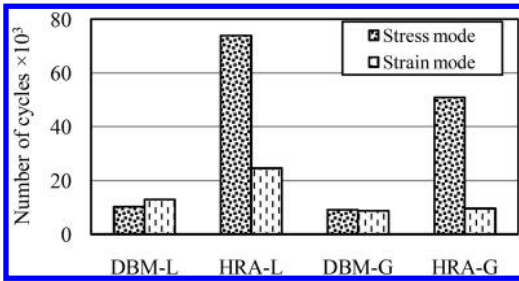


Figure 17. Fatigue performance of different mixes tested in strain and stress modes evaluated using TA approach.

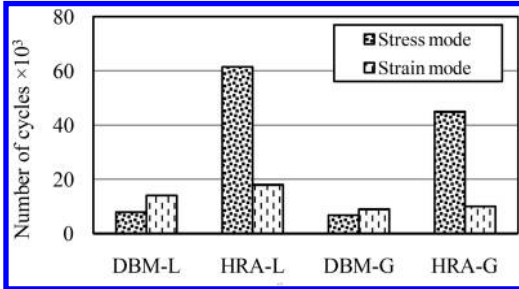


Figure 18. Fatigue performance of different mixes tested in strain and stress modes evaluated using ER approach.

DSR samples was proposed based on determining the mode and standard deviation of the samples' bulk density. The method ensures the availability of an adequate number of samples with minimum variability for any further testing and/or evaluation requirements in the project.

2. A simple method was devised to arrive at the strain and stress levels that should be adopted in conducting DSR fatigue tests.
3. A new fatigue index, FIR , was developed based on the concept of applied and recovered pseudo-strain energy to evaluate the fatigue performance of HMA. This index revealed an agreement with the results from other reliable approaches, namely the energy ratio and traditional approach.
4. This approach can only be used for aggregates up to 10 mm in size due to the limitations of the DSR capacity as maximum torque is 0.2 Nm. Although this may be an acknowledged shortcoming, with further development it should be possible to enhance the torque capacity of this device to enable testing materials containing aggregates larger than 10 mm.
5. The results confirmed that limestone gives a better fatigue performance for both HRA and DBM mixes than granite.
6. Future work aims to map out fatigue data obtained using a classical testing method, such as the two-point bend, to verify the suitability of the DSR technique in evaluating the laboratory fatigue performance of full asphalt mixtures.

ACKNOWLEDGEMENTS

The authors are grateful to several industrial organisations for the supply of materials used in this project. The authors also wish to acknowledge the financial support of the Iraqi government for the award of a research scholarship enabling this work to be conducted as part of a larger research project.

REFERENCES

- AASHTO, *Method for Determining the Fatigue Life of Compacted Hot Mix Asphalt (HMA) Subjected to Repeated Flexural Bending*, AASHTO TP8-94. 2002.
- Artamendi, I. and H. Khalid, *Characterization of fatigue damage for paving asphaltic materials*. *Fatigue & Fracture of Engineering Materials & Structures*, 2005. **28**(12): p. 1113–1118.
- Bhasin, Amit, Veronica T Castelo Branco, Eyad Masad, and Dallas N Little, *Quantitative comparison of energy methods to characterize fatigue in asphalt materials*. *Journal of Materials in Civil Engineering*, 2009. **21**(2): p. 83–92.
- Brown, S.F. *Practical test procedures for mechanical properties of bituminous materials*. in *Proceedings of the Institution of Civil Engineers: Transport*. 1995.
- BS 4987-1, *coated macadam (asphalt concrete) for roads and other paved areas*. 2005, British Standard Institution.
- BS 597-1, *Hot rolled asphalt for roads and other paved areas, in specification for constituent materials and asphalt mixtures*. 2005, British Standard Institution.
- BS PD 6691, *Guidance on the use of BS EN 13108 bituminous mixtures – material specifications*. 2010, British Standard Institution.
- BS EN 12697-6, *Bituminous mixtures-test methods for hot mix asphalt*. 2004, British Standard Institution.
- BS EN 12697-33, *Specimen prepared by roller compactor, in Bituminous mixtures-test methods for hot mix asphalt*. 2003, British Standard Institution.
- Carpenter, S. H. and S. Shen, *Dissipated Energy Approach to Study Hot-Mix Asphalt Healing in Fatigue*. *Transportation Research Record*, 2006. **1970**(1): p. 178–185.
- Christensen D., Richarded kim, Dallas Little, Eyad Masad, and Yong-Rak Kim, *practical approaches to continuum damage fatigue analysis*. 2009.
- Daniel, J.S., W. Bisirri, and Y.R. Kim, *Fatigue Evaluation of Asphalt Mixtures Using Dissipated Energy and Viscoelastic Continuum Damage Approaches*. *Journal of the Association of Asphalt Paving Technologists*, 2004. **73**: p. 557–583.
- Di Benedetto, H., C. De La Roche, H. Baaj, A. Pronk, and Robert. Lundström, *Fatigue of bituminous mixtures*. *Materials and Structures*, 2004. **37**(3): p. 202–216.
- Ghuzlan, K.A. and S.H. Carpenter, *Fatigue damage analysis in asphalt concrete mixtures using the dissipated energy approach*. *Canadian Journal of Civil Engineering*, 2006. **33**(7): p. 890–901.
- Hintz, C. and Bahia, H., *Simplification of Linear Amplitude Sweep Test and Specification Parameter*. *Transportation Research Record: Journal of the Transportation Research Board*, 2013. **2370**(1): p. 10–16.
- Huang, C.W., E. Masad, A.H. Muliana, and H. Bahia, *Nonlinearly viscoelastic analysis of asphalt mixes subjected to shear loading*. *Mechanics of Time-Dependent Materials*, 2007. **11**(2): p. 91–110.
- Kim, Y.R., H.J. Lee, and D.N. Little, *Fatigue Characterization of Asphalt Concrete Using Viscoelasticity and*

- Continuum Damage Theory (with Discussion)*. Journal of the Association of Asphalt Paving Technologists, 1997. **66**: p. 520–569.
- Kim, Y.R., D.N. Little, and R.L. Lytton, *Use of Dynamic Mechanical Analysis (DMA) to Evaluate the Fatigue and Healing Potential of Asphalt Binders in Sand Asphalt Mixtures*. Journal of the Association of Asphalt Paving Technologists, 2002. **71**: p. 176–205.
- Kim, Y.R., D. N. Little, and R. L. Lytton., *Fatigue and Healing Characterization of Asphalt Mixtures*. Journal of Materials in Civil Engineering, 2003. **15**(1): p. 75–83.
- Kim, Y.R. and D.N. Little, *Linear Viscoelastic Analysis of Asphalt Mastics*. Journal of Materials in Civil Engineering, 2004. **16**(2): p. 122–132.
- Larson, Ronald G., *The structure and rheology of complex fluids*. Vol. 2. 1999: Oxford university press New York.
- Lee, H.J., J.S. Daniel, and Y.R. Kim, *Continuum damage mechanics-based fatigue model of asphalt concrete*. Journal of Materials in Civil Engineering, 2000. **12**: p. 105–112.
- Malvern. <http://www.malvern.com/labeng/products/kinexus>
- Masad, E. , VTF. Castelo Branco, Dallas N. Little, and R. Lytton, *A unified method for the analysis of controlled-strain and controlled-stress fatigue testing*. International Journal of Pavement Engineering, 2008. **9**(4): p. 233–246.
- Park, S.W., Y.R. Kim, and R.A. Schapery, *A viscoelastic continuum damage model and its application to uniaxial behavior of asphalt concrete*. Mechanics of Materials, 1996. **24**: p. 14.
- Rowe, GM, *Performance of asphalt mixtures in the trapezoidal fatigue test*. Asphalt Paving Technology, 1993. **62**: p. 344–344.
- Schapery, RA, *Correspondence principles and a generalized J integral for large deformation and fracture analysis of viscoelastic media*. International Journal of Fracture, 1984. **25**(3): p. 195–223.
- Schapery, R.A., *A theory of mechanical behavior of elastic media with growing damage and other changes in structure*. Journal of the Mechanics and Physics of Solids, 1990. **38**(2): p. 215–253.
- Tan, Y., L. Shan, Y. Richard Kim, and B.S. Underwood, *Healing characteristics of asphalt binder*. Construction and Building Materials, 2012. **27**: p. 570–577.
- Tayebali, A. A., G. M. Rowe, and J. B. Sousa, *Fatigue Response of Asphalt-Aggregate Mixtures*. Association of Asphalt Paving Technologists-Proceedings, 1992. **61**: p. 333–360.
- Van Dijk and Visser, W., *Practical fatigue characterization of bituminous mixes*. Journal of the association of asphalt paving technologists, 1975. **44**: p. 38–72.
- Van Dijk and Visser, W. *Energy Approach to Fatigue for Pavement Design*. in *Association of Asphalt Paving Technologists Proc.* 1977.
- Woldekidan, MF, Huurman, M and Pronk, AC, *Linear and Nonlinear Viscoelastic Analysis of Bituminous Mortar*. Transportation Research Record: Journal of the Transportation Research Board, 2013. **2370**(1): p. 53–62.
- Zollinger, C.J., *Application of surface energy measurements to evaluate moisture susceptibility of asphalt and aggregates*. MSc Dissertation, 2005, Texas A&M University.

Experimental evaluation of crack propagation in asphalt mixture based on photoelasticity

S. Büchler, A. Cannone Falchetto & M.P. Wistuba

Technische Universität Braunschweig, Department of Architecture, Civil Engineering and Environmental Sciences – Pavement Engineering Centre (ISBS), Braunschweig, Germany

ABSTRACT: In this paper the deformation and crack propagation on the surface of asphalt mixture is investigated based on photoelasticity technique. The effectiveness of the photoelasticity measurements is evaluated with an experimental plan which includes six asphalt mixtures commonly used in Germany together with monotonic and fatigue tests on notched semi-circular bending specimens, under constant strain rate and cyclic loading, respectively. A digital camera capable of acquiring 30 images per second is used to record the deformation with different frame rates for monotonic and fatigue tests. During monotonic testing, minimal deformation on the specimen surface could be detected as load increased, while cracking occurred suddenly at peak load. A similar trend could be observed over a longer time for fatigue tests. Cracking occurred nearly at the end of the tests and needed an additional number of load cycles to reach complete failure.

1 INTRODUCTION

The multilayer theory for asphalt structures assumes that cracking occurs at the bottom layer due to bending associated to traffic load. Within this theoretical framework and under research project FE 09/0189/2011/ERB (Numerical simulation of crack propagation in flexible asphalt pavements as a result of traffic loads, Part II) a basic model was implemented and proposed by the “Institut für Straßenwesen” at RWTH Aachen to simulate the crack propagation in asphalt specimens.

Two testing procedures were implemented to verify and validate this newly developed model. The Technische Universität Braunschweig (ISBS) and the Technische Universität Dresden (ISSD), proposed two methods for obtaining an advanced visualization of crack propagation: one based on photoelasticity (ISBS) and a second one relying on photogrammetry (ISSD). This paper presents the results of study on the photoelasticity technique.

2 PHOTOELASTICITY: PRINCIPLES

Photoelasticity is not conventionally used to characterize asphalt materials; nevertheless this technique presents a significant potential for investigating the mechanical properties of asphalt mixture. The main principle of photoelasticity is based on the refraction of light rays passing a transparent material under load, while a polariscope is used to visualize stress patterns at the material surface. A polariscope consists of a

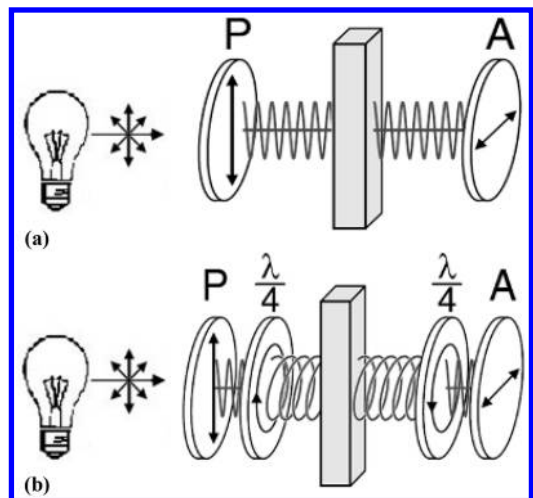


Figure 1. Photoelasticity schematic (a) plane polarized light and (b) circular polarized light.

light source and a transparent sample between two polarizing filters (Figure 1).

The light is converted by the polarizer P to plane polarized light. The light rays pass the unloaded and transparent material and hits the second polarizing filter A (analyzer). When the analyzer is rotated by 90° with respect to the polarizer, no light can pass through the analyzer and a black image can be observed. On the other hand, when a certain load is applied to a sample, a component of the light rays is refracted while the remaining can pass the analyzer and, eventually,

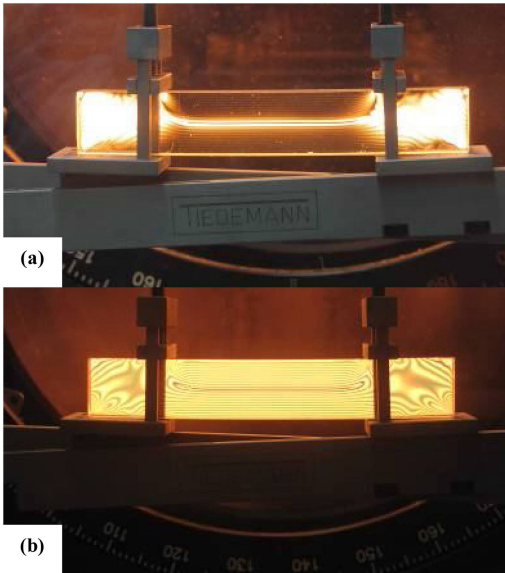


Figure 2. (a) Plane polarized light and (b) circular polarized light on the surface of a prismatic specimen.

a stress pattern consisting of isochromatics can be visualized.

Light rays which are randomly refracted by 90° to the polarizer, cannot be seen and, therefore, will appear as black areas. To prevent this phenomenon a quarter wave filter is placed before and after the sample to convert the plane polarized light into circular polarized light (see Figure 1). Figure 2 shows the difference between plane polarized light and circular polarized light.

Photoelasticity is not directly applicable to asphalt specimens since these are not transparent. The reflection method provides a simple solution to overcome this limitation (Figure 3).

The reflection method requires applying a photoelastic coating to the specimen surface. This coating is made of a transparent sheet of high-elongation material, such as rubber, with a thickness of 3 mm and a modulus of elasticity of 4 MPa. Depending on the specimen deformation the light rays are refracted by this coating layer which is glued to the specimen through a reflecting adhesive consisting of glue with reflecting particles having a small modulus of elasticity (7 MPa). Hence, even small deformations can be transferred to the photoelastic coating and can be visualized by the polariscope.

3 TEST METHODS

Three types of conventional asphalt mixtures used in Germany were selected for the experimental phase: a base layer AC 22 T S, a binder layer AC 16 B S and a surface layer AC 8 D S. Two different asphalt binder contents were used for each mix design; hence,

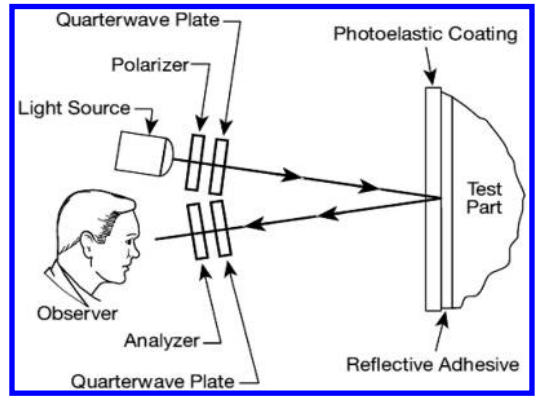


Figure 3. Principle of the reflection polariscope (Micro Measurement, 2011a, 2011b and 2011c).

Table 1. Asphalt mixtures and binder contents.

Mixture Type	Lower content [%]	Higher content [%]
AC 22 T S	4.1	4.6
AC 16 B S	4.5	5.0
AC 8 D S	6.2	6.7

six different asphalt mixtures were prepared in total (Table 1).

Specimens were prepared with a roller sector compactor according to EN 12697-33 (2013) capable of compacting asphalt mixture slabs as large as $50\text{ cm} \times 70\text{ cm}$. Specimen with a diameter of 150 mm and a thickness of 60 mm were cored out of the slabs and grinded on the front sides to obtain a smooth surface. Each core was then sawn in the middle and notched (width: 2 mm; depth: 10 mm). Finally a transparent layer of photoelastic material was used to coat each specimen.

3.1 Semi-circular monotonic bending test

Semi-circular bending tests were performed according to the European specifications (EN 12697-44 2010) (Figure 4).

Specimens were first conditioned for 4 hours at 5°C and then, tests were conducted at a constant temperature of 25°C . Deflection control (5 mm/min) was used to load the specimen. The stress at the tip of the notch was calculated according to EN 12697-44 (2010). Each test was filmed and recorded with 30 pictures per second frame rate for a maximum duration of 20s. Single picture-frame were then selected and used for interpreting the results.

3.2 Cyclic semi-circular bending test

Cyclic semi-circular bending tests were performed with samples and experimental design similar to those used for the monotonic semi-circular bending

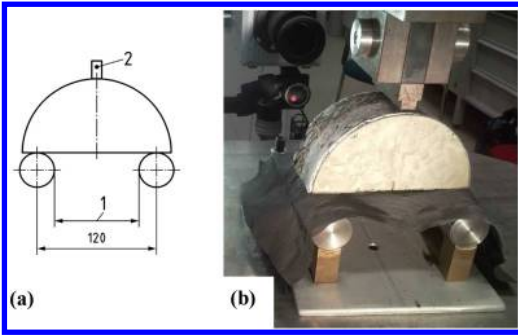


Figure 4. (a) Monotonic semi-circular bending test and (b) experimental setup with specimen coated with photoelastic material.

Table 2. Load amplitude as function of the stress at the tip of the notch.

	Binder content 1 [%]	Amplitude 1 [MPa]	Binder content 2 [%]	Amplitude 2 [MPa]
AC 22 T S	4.1	2.9	4.6	3.2
AC 16 B S	4.5	2.2	5.0	2.2
AC 8 D S	6.2	2.4	6.7	2.5

procedure. Based on the maximum load used for the monotonic tests, a cyclic sinusoidal load was applied to the specimen with a frequency of 10 Hz. (Table 2). The minimum stress level was fixed to 0.1 MPa.

The maximum duration of the tests was 28 minutes; in order to reasonably limit the number of photos recorded, an acquisition rate of 2 picture/frames per second was imposed.

4 VISUALIZATION

4.1 Monotonic semi-circular bending test

A visual comparison between a homogenous elastic specimen (plexiglass) and an asphalt specimen (AC 8 D S) is shown in Figure 5. An accumulation of isochromatics can be observed, for plexiglass, at the three points of the load application, which are connected by an area of a single isochromatic. At the tip of the notch a clear pattern can be also identified; this expands and propagate to the top of the specimen. Similar results obtained in previous research works confirm the present isochromatics trend (Ferber 1999, Backes 2009). On the other hand, only one accumulation of isochromatics could be observed on the asphalt specimen surface under the top loading point.

All tested specimen showed nearly no deformation (and hence stresses) up to the point of crack. Deformation (and stress) evolution are shown in Figure 6, while Figure 7 presents the crack propagation during a test for an AC 8 D S; the crack propagates from the tip of the notch and reaches the top of the specimen within half a second.

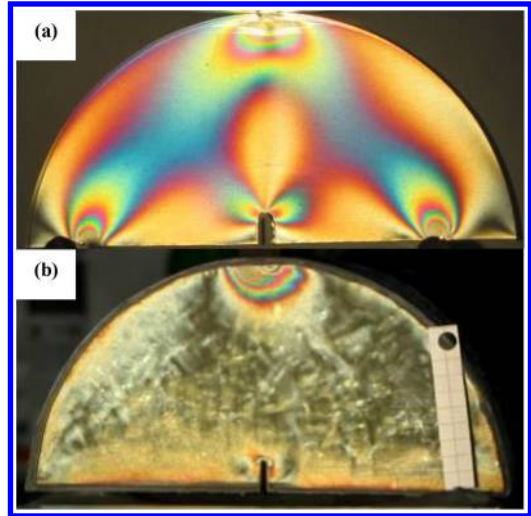


Figure 5. Visualization of (a) isochromatics in a homogeneous and elastic specimen and (b) nearly no isochromatics on an asphalt specimen AC 8 D S under loading.

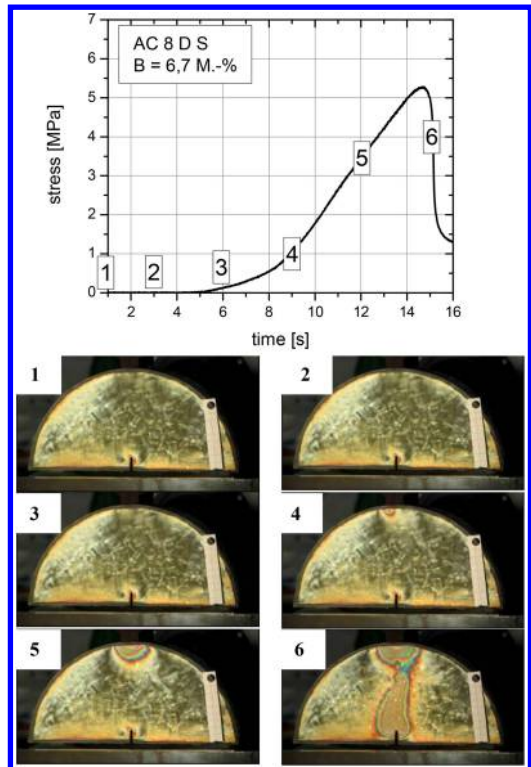


Figure 6. Deformation evolution in a monotonic bending test (AC 8 D S).

The propagation of the crack does not follow the ideal line of maximum stress, straight to the top of the specimen (see Figure 7); the single grains in the aggregate structure of the asphalt mixture deflected the crack pattern. At failure, the crack has reached the

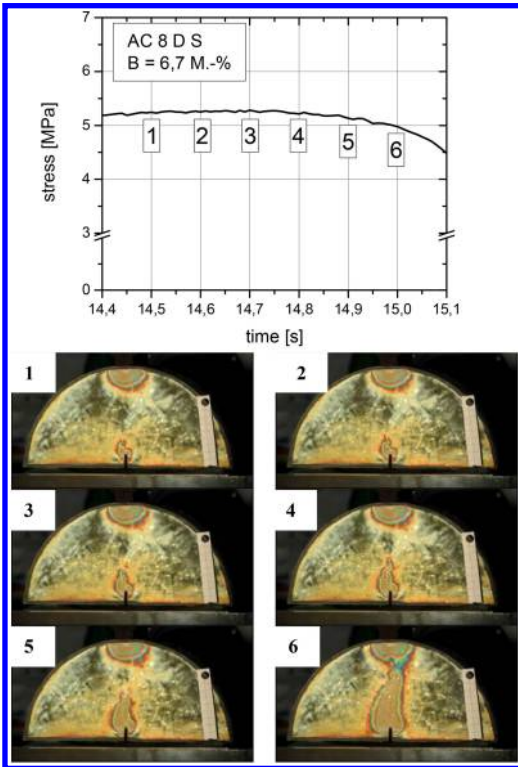


Figure 7. Crack propagation during a monotonic bending test (AC 8 D S).

top of the specimen which is entirely cracked; however, the photoelastic layers still hold the specimen together. Hence, the coating surface prevented the possibility of directly observing the exact cracking behind.

During the test, the crack appears very fast and suddenly, as if a quasibrittle failure occurred (Cannone Falchetto et al. 2014a and 2014b). The series of pictures obtained for each test indicate that the crack propagation is not linear. It initially appears with limited changes in the color pattern of the photoelastic coating and then increases exponentially. The selected asphalt binder content did not affect crack initiation and propagation. Asphalt mixtures AC 22 T S and AC 16 B S showed a similar behavior with respect to crack propagation; nevertheless, small differences associated to the crack path were observed due to the presence of larger aggregates which resulted in deviation of the crack path from the straight line. Figure 8 shows the difference during cracking for the three asphalt mixtures investigated.

4.2 Cyclic semi-circular bending test

The visualization of the cyclic tests resulted in pictures which are comparable to the monotonic tests. No strain or stress could be observed in the specimen up to 10% of the test duration. Then, small patterns of isochromatics appeared at the top of the specimen. The change in isochromatics increased very slowly till

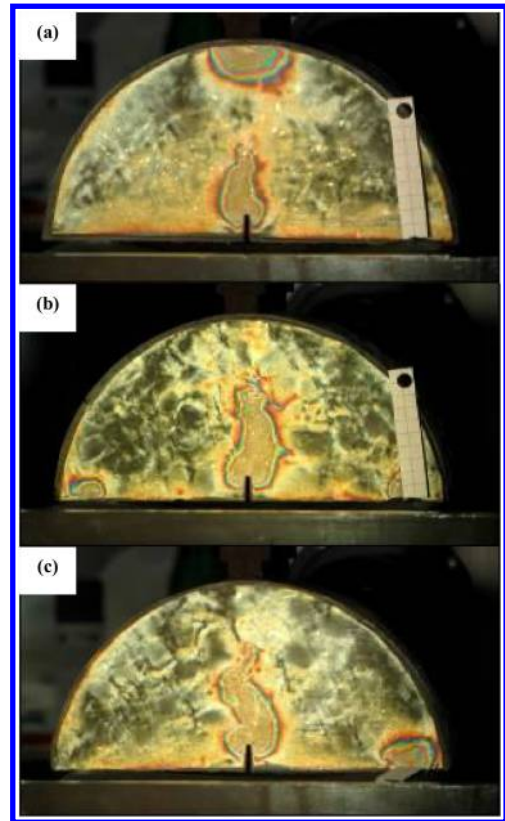


Figure 8. Crack line for asphalt mixtures (a) AC 8 D S, (b) AC 16 B S and (c) AC 22 T S.

80%–90% of the test duration. Then cracking occurred at the tip of the notch and propagated slowly (with respect to the monotonic tests) till the top of the specimen. Figure 9 shows an AC 8 D S after 258 load cycles without any significant strain. The crack starts consistently developing only after 12,900 load cycles and propagates through the specimen, showing a typical pattern observed in three-point bending tests. Finally, after 200 additional load cycles, the specimen failed.

As the crack was propagating a V-shaped isochromatic pattern appeared above the crack. In the middle of the specimen a strain less zone could be detected. In the monotonic tests this zone could also be identified, but its size is significantly smaller compared to what observed for cyclic loading. The specimens prepared with mixtures having larger aggregates (AC 16 B S and AC 22 T S) showed this patterns only partially. The location of the larger grains has a significant influence on the crack line (Figure 10). On the other hand, consistently V-shaped patterns were observed for the AC 8 D S mixture above the notch.

5 SUMMARY AND CONCLUSIONS

In this paper photoelasticity technique was used to visualize and evaluate deformation and crack

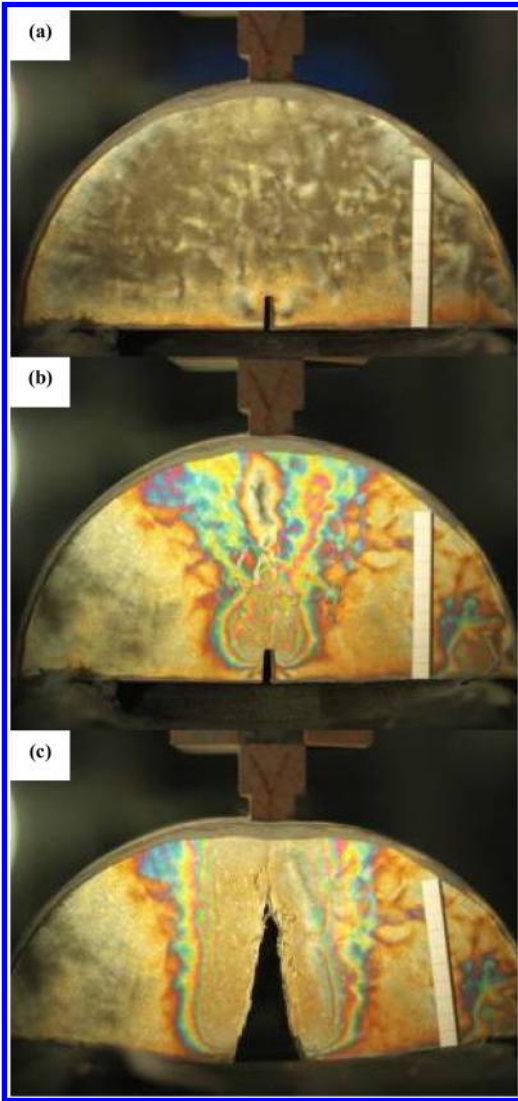


Figure 9. Cyclic semi-circular bending test: isochromatic patterns after 258 load cycles (left), after 12,900 load cycles (middle) and after 13,100 load cycles (right).

propagation in asphalt mixture. In order to visualize and observe strain patterns on the surface of asphalt mixture specimens a reflection polariscope was used. Monotonic and cyclic (fatigue) semi-circular bending tests were performed on notched specimens made with three asphalt mixtures commonly prepared in Germany. The deformation patterns were recorded through a digital camera capable of acquiring 30 images per second; for fatigue tests, pictures were taken every two seconds.

Very little deformation on the specimen surface could be visualized in monotonic tests as load increased. Cracking occurred suddenly as peak load was reached, suggesting a possible quasibrittle behavior. Analogous trend could be observed during fatigue

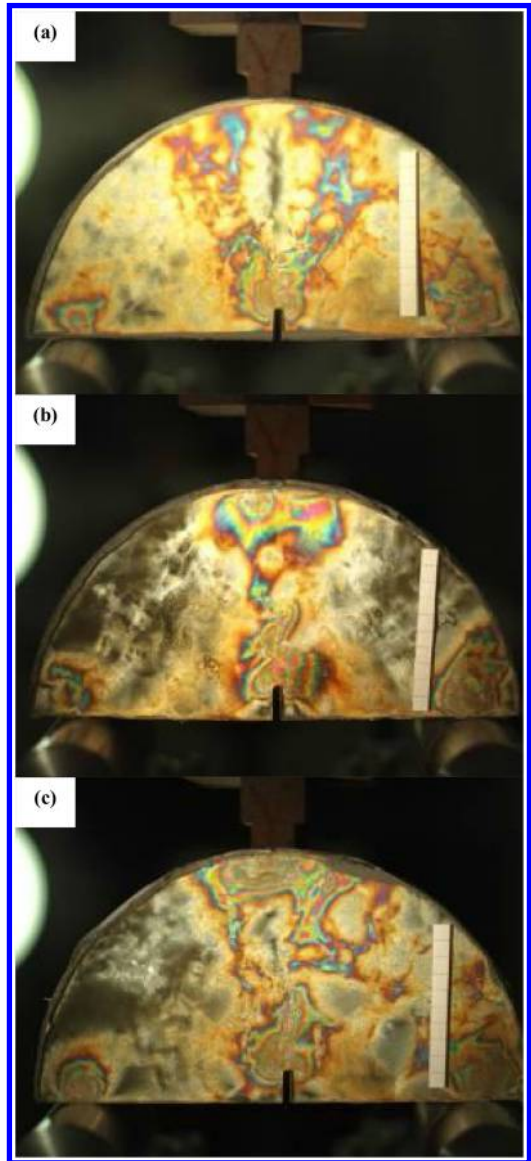


Figure 10. Patterns of isochromatic in a cyclic semi-circular bending test at ~90% of the test duration. AC 8 D S (left), AC 16 B S (middle) and AC 22 T S (right).

tests, although, over a longer time. First strain patterns developed after 10% of the test duration, while cracking occurred only at the end of the tests and needed an additional number of load cycles to reach complete failure.

The present findings provide solid support to the use of the proposed photoelasticity technique for visualizing the deformation on the surface of asphalt mixture specimen. Cracks can be detected and their propagation can be recorded for further analysis. Correlations with homogenous materials results and the link to stress calculation models are the objective of an ongoing research project.

ACKNOWLEDGMENTS

The authors would like to gratefully acknowledge the funding support of Federal Ministry of Transport, Building and Urban Development under the research grant FE 09/0189/2011/ERB “Numerische Simulation der Rissausbreitung in flexiblen Asphaltbefestigungen Infolge von Verkehrslasten, Teil II.

REFERENCES

- Backes, D. 2009. Experimentelle Spannungsanalyse – Spannungsoptik. *Engineering Competence Center, Hochschule für Technik und Wirtschaft des Saarlandes*, <ftp://ecc-s1.htw-saarland.de/Mitarbeiter/backes>.
- Cannone Falchetto, A., Marasteanu, M.O., Balmurugan, S. and Negulescu, I.I. 2014a. Investigation of Asphalt Mixture Strength at Low Temperatures with the Bending Beam Rheometer, *International Journal of Road Materials and Pavement Design* 14(1): 28–44.
- Cannone Falchetto, A., Le, J-L., Turos, M. and Marasteanu, M.O. 2014. Indirect Determination of Size Effect on Strength of Asphalt Mixtures at Low Temperatures, *Materials and Structures* 47: 157–169.
- EN 12697-33. 2013. Bituminous mixtures – Test methods for hot mix asphalt – Part 33: Specimen prepared by roller compactor.
- EN 12697-44. 2010. Bituminous mixtures – Test methods for hot mix asphalt – Part 44: Crack propagation by semi-circular bending test.
- Ferber, F. 1999. Numerische und experimentelle Untersuchungen rißbehafteter Strukturen, *Ha-bilitationsschrift, Universität Paderborn, Fachbereich Maschinentechnik*.
- Micro-Measurements 2011a. Introduction to Stress Analysis by the PhotoStress®Method, *Vishay Precision Group*, Raleigh, USA, www.vishaypg.com.
- Micro-Measurements 2011b. Photostress – A Brief Introduction – Pictorial Examples of Photo-Stress-Coated Parts – A Wide Selection of Industrial Case History Applications, *Vishay Precision Group*, Raleigh, USA, www.vishaypg.com.
- Micro-Measurements 2011c. LF/Z-2 Reflection Polariscopes Introduction Manual, *Vishay Precision Group*, Raleigh, USA.

Measurement of flexural displacement and strain in bending test based on digital image analysis

Hongduo Zhao, Songyuan Gu, Jianming Ling & Yizhou Peng

Tongji University, Key Laboratory of Road and Traffic Engineering of the Ministry of Education, Shanghai, P.R. China

ABSTRACT: Properties of pavement material are analyzed through the vertical load and displacement or strain in bending tests. The traditional displacement or strain results will be affected by the contact displacement between the beam and support, especially for asphalt mixture because of its viscous-elastic property. This paper presents a method for measuring the deflection and strain of the beam basing on digital image recognition technique. The measuring requirements are given including the image resolution, frames per second, accuracy of displacement etc. According to the requirements, a measurement system consisting of digital camera and image analysis software is developed. A standard procedure is established to capture the images of the beam with reference lines. Those images are analyzed to get the displacement of the key points. Then a method to calculate the flexural strain is developed. The measuring results are compared with traditional method carefully.

1 INTRODUCTION

Flexure experiments are widely used for evaluating the bending or fatigue characteristics of asphalt concrete. According to the standard test method of China (2011), deflection is most important parameter that affects flexure strain. In the three-points loading test flexural strain and load value can be calculated by equation (1) and (2):

$$\varepsilon = \frac{6hd}{L^2} \quad (1)$$

$$P = \frac{24d}{23dh^2} \times EI \quad (2)$$

where E = modulus of elasticity (MPa); I = moment of inertia (mm^4); P = the load value (kN); ε = the flexural strain; h = the beam's height (mm); L = span between the two supports (mm); and d = deflection (mm).

The methods are similar in Japan and United States (2011). However, the contact displacement between the beam and support or indenter (defined as asphalt mixture instrumentation compliance) will affect the deflection measurement like this:

- 1) If deflection is recorded by the machine through how long indenter moves down, then it will be mixed with asphalt mixture deformation from both indenter and supports.
- 2) If deflection is measured by displacement gauge attached on the beam underside, it is still affected by the deformation from the supports.

What's more, this method is based upon elasticity assumptions and ignores the asphalt viscoelastic

characteristics. So the flexural strain calculated this way involves deviation from real situation.

Can Wu (2014) explored the asphalt mixture instrumentation compliance by measuring both the indenter displacement and the beam underside displacement. He supposed that if there were no supports displacement, the two displacements would be the same. But the displacement at the beam underside was only 60–70% of the indenter displacement. The results showed that the asphalt mixture instrumentation compliance should not be ignored.

Yiqiu Tan (2009) developed a method for calculating the flexural strain at certain height in the four-points loading test. Span between the two supports, beam deflection and height of the measured points were related to the strain results. Theoretically it was identical with the tradition method for they all came from elastic mechanics. So the defects discussed above are not eliminated.

Leonardo Souza (2009) and Yongdi Ye (2011) tried to use strain films for actual strain measurement on beam surface. Though they got rid of the supports displacement influence, the craft of affixing the flakes could highly affect the result so the accuracy was hard to guarantee. Besides, strain flakes were pasted on the beams with epoxy glue so the collaborate deformation also affected the results. These uncertainties limited the application of this method.

With the development of digital image recognition technique, they are coming into use for deformation measurement. These non-contact methods achieve micron accuracy and have no defects like deformation uncoordinated. Zhupin Wang (2001) and Yongsheng Bi (2007) developed triaxial specimen deformation systems based on digital image measurement method.

In their study axial and radial measurement accuracy achieved 10^{-6} m. The local deformation in anywhere of the specimen could be studied as long as the images cover that place. These findings indicate that digital image recognition technique can be used as a promising non-contact method.

Xinjun Li (2010) also brought forward a method to build dynamic modulus master curve through digital image recognition technique. The asphalt mixture cylinder was wrapped in rubber membrane with grid for recognition. The contour of asphalt mixture cylinder was automatically captured and then macro strain was calculated. Sub-pixel accuracy is achieved through interpolating the gray change function, which helped to improve accuracy without expensive high definition cameras. According to the test outcomes, the contour and cracks could be clearly captured. The master curve had no obvious difference from the curve gained by Yanqing Zhao (2006) through the mechanic measurement. But the curve was smoother for more sampling points were gained compared to the traditional method.

Upon all these, this paper presents a technique for measuring the flexural displacement and strain based on digital image recognition. In this method the deformation process is recorded frame by frame. Then deflection or strain is calculated through image recognition results. Consequently the influence of asphalt mixture instrumentation compliance in strain measurement is discussed.

2 PRINCIPLE OF DIGITAL IMAGE RECOGNITION TECHNIQUE

Deformation of any continuous object can be regarded as points position change at edges. Points representing the edges are generally located in the positions where grey scale changes most dramatically in the image, so they can be identified through the first or second derivative of gray scale variation function. Then noise reduction is necessary to optimize the edge for better recognition, especially in the dynamic recognition process (2005). The most common ways are expansion algorithm and erosion algorithm. A simple expansion algorithm can be described as absorbing back ground points with nearly the same gray scale in the vicinity while the erosion algorithm is the opposite. Based on these algorithms, a clear edge and point location can be captured.

After obtaining the edges, the relationship between actual length and pixel numbers needs to be established, which is called calibration factor (C_f). The process can be described as follows: an object with known length (d_0) is placed on the asphalt mixture beam and the software analyzes how many pixels it contains (N_0). The calibration factor can be represented by equation (3):

$$C_f = \frac{d_0}{N_0} \quad (3)$$

Then the calibration can be used for calculating the length between any two points on the asphalt mixture beam by (4)

$$d = C_f \times N \quad (4)$$

where d = the real length of an object; N = pixels the object contains.

3 MEASURING REQUIREMENTS

There are two key parameters in the system that highly affects recognition results. They are sampling frequency and resolution.

Obviously if we enhance the sampling frequency, the deformation details will be better captured. However, more data will be involved in the analysis. So balance should be considered between efficiency and sampling frequency. According to the Nyquist' sampling theorem (2005) and engineering experience, sampling frequency should be eight times bigger than the loading frequency to get a clear wave shape. So the minimum requirement of sampling frequency can be calculated.

Resolution is another key parameter in the recognition process. Higher resolution helps to improve the accuracy. According to Bi's research (2007), camera of 640×480 resolution (at about 50 cm distance) is enough for the strain measurement. In his research each pixel represents 0.039 mm. When the sub-pixel recognition method is taken into consideration, the accuracy is no less than 0.01 mm. According to the traditional testing method, deflection is measured by dial indicator or linear variable differential transformer (LVDT) gauge. It is required by the standard that the accuracy should be no less than 0.01 mm. So the displacement measurement accuracy is also set as 0.01 mm in this study, which is no less than the traditional method. Resolution is set as 1293×783 in this study just to be sure. The accuracy will be tested again in the next section.

4 MEASUREMENT ACCURACY ANALYSIS

According to the image recognition method discussed above, the accuracy of flexural strain measurement derives from the absolute length testing accuracy and edge recognition accuracy. They are both examined in this section.

A high-accuracy manufactured steel plate is used for examining the absolute length accuracy. The diameter of the plate is 100 mm and the manufacture error is less than 0.01 mm, which means that any diameter's length stays between 99.99 mm to 100.01 mm. For the sake of recognition, the plate is blackened and placed on white background.

Two diameters in the plate are chosen randomly for building calibration and measuring each other. Diameter A is assumed to have a length of exactly 100 mm,

Table 1. Solution of diameter measurement.

Diameter A (mm)	Diameter B (mm)
100	99.9940
100.0075	100

Table 2. Solution of a certain line measurement.

Measure times	Length (mm)
1	65.4312
2	65.4335
3	65.4369
4	65.4351
5	65.4371
6	65.4390
standard deviation	0.002808

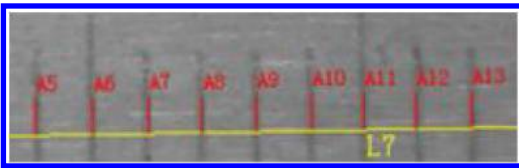


Figure 1. Identification of calipers' graduation.

then calibration is established to measure diameter B. Similarly diameter B is assumed to be exactly 100 mm long to test the length of diameter A. The conclusion of this process is shown in Table 1. Results show that deviations in the two tests are both less than 0.01 mm.

What's more, a line is drawn manually and measured six times. According to the error analysis principle (2006), the closer of the measurement for the same length in different times they are and the higher accuracy this method is. Results are shown in Table 2.

Deviation occurs in the 0.001 mm level in this test and the standard deviation is about 0.003 mm. Conclusion can be drawn that the absolute length accuracy matches the demands.

Except for the absolute length accuracy, the edge recognition accuracy also affects the results. The graduation of a slide caliper ruler is used to testify the recognizing ability. Just as it shown in Figure 1, every graduation is successfully recognized and marked. Theoretically the distance between two graduations is 1 mm and the specific measurement results are shown in Table 3.

The average value is 0.999 mm while the standard deviation is 0.0192 mm. Normality test is made and the result is corresponded to normal distribution with sig = 1. It's not logically to say how exact the lengths are but as they are quite reasonable, the conclusion that the edges are rightly distinguished can be drawn.

After the two kinds of accuracy are tested, the recognizing accuracy can meet the demands of flexural-tensile strain measurement.

Table 3. The identification results of calipers' graduation.

times	result (mm)	times	result (mm)
1	0.99337	11	1.02544
2	0.99169	12	1.02116
3	1.02301	13	0.97219
4	0.98573	14	1.02174
5	0.97757	15	1.02551
6	0.9875	16	0.99207
7	1.00625	17	0.98478
8	1.02521	18	0.98072
9	0.98406	19	1.0175
10	0.98859	20	0.97745

5 DEFLECTION AND STRAIN MEASUREMENT METHOD

Based on the image recognition technique introduced above, deflection and strain are all deduced through distance or locations of different points.

Deflection can be measured as follows. A point for recognition is drawn on the center near beam bottom. Then the location is recorded in every image. Deflection can be calculated through the vertical displacement of that point.

Strain measurement is much harder because as long as we use steel supports and indenters, the modulus difference between them will cause uncoordinated deformation. So it's more rational to develop a method with the asphalt mixture instrumentation compliance factor considered.

If coordinate system is built on the images and a line is drawn on the beam, coordinate changes of the points in the line can be captured before and after the deformation. According to the definition of strain, average strain in the line can be calculated by equation (4):

$$\varepsilon = \frac{l_1 - l_0}{l_0} \quad (5)$$

where ε = the flexural strain; l_0 = Original length of a certain line (pixels); and l_1 = length of the certain line after deformation (pixels).

The l_0 can be easily gained through image recognition by the start and end point coordinates. But when the loading process begins, the line will be deformed together with the beam into a curve, which makes it hard for detecting l_1 . The schematic is shown in Figure 2.

With the coordinates of different points, it's possible to fit the function of the curve. Then curve integral can be used to gain the actual length of the curve and then l_1 is calculated. The process can be described as follows.

Step 1: Draw a line on the beam just as it's shown in Figure 2 for strain measurement and then adjust the camera carefully until the line has a sharp edge. Camera will set up coordinates system itself in pixels.

Step 2: Choose 20–30 points in the line evenly and then record their coordinates through the image recognition software. It's assumed that they are $(x_1, y_1), (x_2, y_2) \dots (x_n, y_n)$. When the deflection data is needed

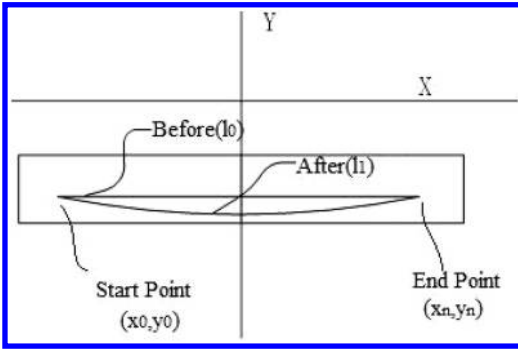


Figure 2. Schematic of the tested line before and after deformation.

in other tests, the line center vertical displacement can be used.

Step 3: Apply loads on the beam and record the new coordinates with the same abscissa but different ordinates. It's assumed that they are $(x_1, y'_1), (x_2, y'_2) \dots (x_n, y'_n)$. Factors like asphalt mixture instrumentation compliance and asphalt viscoelastic characteristic are all taken into consideration because where the line really lies is result of all influence factors. The coordinates are honest and true reflections of the beam deformation.

Step 4: Fit the $(x_1, y'_1), (x_2, y'_2) \dots (x_n, y'_n)$ into a curve like parabola or arc and acquire the curve function $f(x)$. Obviously $f(x)$ is continuous in the interval of (x_1, x_n) and has a continuous derivative function.

Step 5: According to curve integral equation, the length after deformation is achieved by equation (6):

$$l_1 = \int_{x_1}^{x_n} \sqrt{1 + f'(x)^2} dx \quad (6)$$

Then the average strain can be calculated by Equation (5).

No deflection data is used during the whole process and the influential factors including asphalt mixture instrumentation compliance and viscoelastic characteristics are contained in the curve function eventually. Besides this method has no relationship with any viscoelastic assumption. So this method is more promising than the traditional ones.

6 PREPARATION AND DEFLECTION MEASUREMENT

Preparation of flexural strain testing is as follows according to the above ideas. Beams are painted white using an acrylic graffiti spray gun to enhance contrast. As the paint layer is quite thin, the mechanical properties will not be affected. A black line, whose width is about 50 micron and length 10 centimeter, is drawn on the beam at the height to be measured. A camera is utilized for grasping the beam deformation from the beginning to the end. Then position change of the measured line is represented by two groups of coordinates.

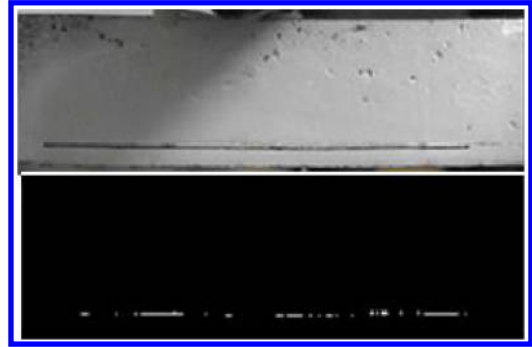


Figure 3. Comparison chart of before and after recognition.

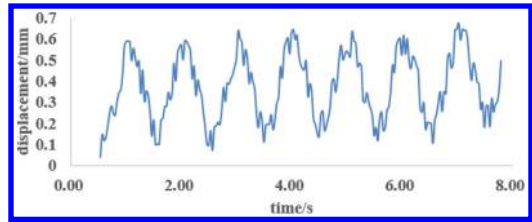


Figure 4. The dynamic deflection measurement results.

At last the curve is fitted to compute the length after deformation using MATLAB.

Figure 3 (the above one) shows a typical image captured by the camera, in which the black line for recognize can be clearly seen. The Figure 3 (the bottom one) presents the line for recognition after handled. Twenty points on the line and their coordinates are gained for further calculation as it's discussed above.

AC-13 beams are used for flexural strain measurement in the whole tests. The size is 250 mm × 30 mm × 35 mm. In the period of dynamic deflection measurement, sinusoidal load of 1 Hz is applied on the beams by the material testing system. A Camera with the ability to take 30 frames per second is used for image acquisition. According to the discussion before, the 30 Hz sampling frequency is enough for testing. The maximum force is 1.3 kN while the minimum force is 0 kN.

Points are drawn 0.5 cm above the beam bottom in the center for deflection measurement. Three abnormal points are deleted. The result is shown in Figure 4.

It can be clearly seen that deflection shows sinusoidal variation trend and the cycle is one second, which is the same as the loading cycle. The maximum deflection is 0.64 mm. Deflection peak in each cycle is slowly growing because of the creep deformation characteristics of asphalt mixture. As the distance measurement accuracy is carefully tested, the results can be seen as reliable.

7 FLEXURAL STRAIN MEASUREMENT

A six-step loading in displacement control mode is also applied on the beams for checking strain measurement.

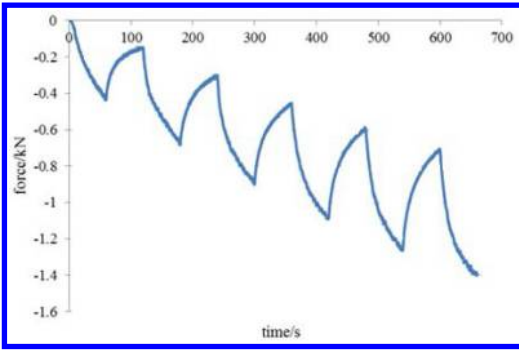


Figure 5. Force changing in the loading procession.

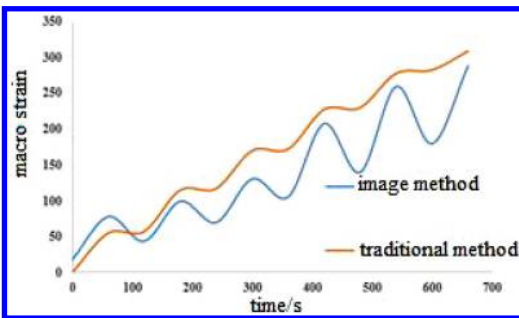


Figure 6. Strain changing trend by two methods.

In each step, the indenter moves 0.3 mm in one minute and then hold still for another minute. Image is taken every one minute when the loading step or the rest time ends. The force changing trend in the whole process is shown in Figure 5 and the strain changing trend calculated by the image recognition is presented in Figure 6. Strain is not starting from zero because of preloading. Deflection is kept in count by a dial indicator placed beneath the beam for calculating the strain by traditional method. The strain calculated by the traditional method is also shown in Figure 6 for comparison.

According to Equations (1) and (2) the load has a linear relationship with the deflection. However the force goes up when a loading step starts but quickly declines up to 40% when the deflection stays still, which is obviously contradicted to Equations (1) and (2). So it's safe to say that the traditional elastic mechanic method has significant deviation from the actual situation. In fact, it's the asphalt mixture instrumentation compliance and creep that cause this deviation. Creep needs no explanation but the asphalt mixture instrumentation compliance demands further discussion.

Firstly, it's necessary to prove the existence of asphalt mixture instrumentation compliance again. Creep can be defined as force declining while the deformation unchanged. But it can be seen clearly from Figure 6 that strain goes down with no deformation change. So creep cannot answer for the situation alone.

Secondly, the mechanism of asphalt mixture instrumentation compliance influence requires to be clarified. When the indenter stays unmoved, the deflection stops changing but the deformation doesn't. The indenter and supports pierce into the asphalt mixture beam in the surface and the beam's curvature goes down. In other word, when the supports displacement happens, the real deflection of the beam is not as high as observed. So that answers the reason of force and strain declining.

After the asphalt mixture instrumentation compliance is discussed, method proposed in this paper that taking it into consideration may reveal the reality better. According to Figure 6, strain calculated through image recognition goes down about 30% with the force when the indenter stays still. Besides, strain calculated through image recognition is about 20% less than the traditional method because the deflection is affected by the asphalt mixture instrumentation compliance in the traditional method.

8 CONCLUSION

According to the research done in this paper, the following conclusions can be drawn:

1. The method based on digital image processing technique can be used to measure the flexural displacement and strain in bending test. The algorithm developed for calculating strain through two groups of coordinates is reasonable.
2. Absolute length recognition accuracy is no less than 0.01mm, which meets the basic needs for measurement.
3. Deflection and strain changing behavior under different kinds of load is carefully studied through this image recognition system. Results indicate that the asphalt mixture instrumentation compliance influences the strain changing behavior greatly in the experiments. It also slackens the beam deformation so both the force and strain declines up to 70% and 30% in the experiment.

REFERENCES

- Can Wu. 2014. Construction Method of Pavement Condition Monitoring System. Shanghai. Tongji University School of Transportation Engineering, Master Degree Thesis.
- Johnson & Wichem. 2006. Applied Multivariate Statistical Analysis (5th Photocopy Edition), Beijing, China Statistics Press.
- Research Institute of Highway Ministry of Transport. Standard Test Methods of Bitumen and Bituminous Mixtures for Highway Engineering. Publication JTG E20-2011, Beijing: China Communications Press, 2011.
- Shih, FY Edupuganti. 2005. Decomposition of Arbitrary Gray-Scale Morphological Structuring Elements, London, England, Pattern Recognition, 38(12), P2323-2332.
- Souza, L.T., Souza, F.V., Castro, L.S. and Yongrak Kim. 2009. Experimental Testing and Finite Element Modeling to Evaluate the Effects of Aggregate Angularity

- on Bituminous Mixture Performance. In *Moisture Sensitivity of Asphalt Pavements*. CD-ROM. Transportation Research Board of the National Academies, Washington, D.C., pp. 2–9.
- Standard Method of Test for Determining the Fatigue Life of Compacted Hot-Mix Asphalt Subjected to Repeated Flexural Bending. Publication, AASHTO T321-03(TP8), AASHTO, 2011.
- Tao Su, Xi'an. 2006. *Real Time Signal Processing System Design*, Xidian University Press.
- Xinjun Li. 2010. *Dynamic Modulus Master Curve Builder System User's Guide*, Innovative Road and Transportation Technologies, LLC, pp. 1–12.
- Yiqiu Qin, Zejiao Dong, Gengliang Tian and Qingli Hu. 2009. *Evaluating Method of the Coordination Deformation between Asphalt Mixture and Fiber Bragg Grating Sensor*. Chongqing, China. *Journal of Civil, Architectural & Environmental Engineering*, 31 (4). pp. 100–104.
- Yongdi Ye. 2011. *Research on Fatigue Damage Performance of Asphalt Mixture by Bending Test*, Changsha, Changsha University of Science & Technology, Master Degree Thesis.
- Yongsheng Bi. 2007.12. *Research and Design of Plane Strain Apparatus in Soil Test*. Dalian University of Technology, Master Degree Thesis.
- Yanqing Zhao, Jian Wu, Jian Wen. 2006.8. *Determination and Analysis of Dynamic Modulus of Asphalt Mixture and Its Master Curve*. Beijing, China. *Highway*, 16 (8). pp. 163–167.
- Zhupin Wang. 2001.11. *Triaxial Test Based on Digital Image Processing and Utilize* Dalian University of Technology, Doctor Degree Thesis.

Investigation of asphalt recovery properties in fatigue test with single rest period

I. Isailovic, A. Cannone Falchetto & M.P. Wistuba

Technische Universität Braunschweig, Department of Architecture, Civil Engineering and Environmental Sciences – Pavement Engineering Centre (ISBS), Braunschweig, Germany

ABSTRACT: This paper presents an investigation on the recovery of mechanical properties of Hot Mix Asphalt (HMA) using dissipated energy approach. Different types asphalt mixture for surface course AC 11 D S were prepared in order to determine the influence of material aging, bitumen content, polymer modification and compaction energy on material ability to recover its initial characteristics. Recovery of material mechanical properties is observed during a single rest period, introduced into tension compression cyclic fatigue tests under stress control. The analysis of the experimental results reveals that there is a significant influence of the duration of rest period on recovery capability. A plateau phase is achieved when the duration of the rest period does not have any impact on asphalt recovery properties. Asphalt aging plays an important role in reducing the effects on material recovery. The degree of compaction used in this research seems to have no influence on material ability to restore its initial properties. Mixtures prepared with additionally 0.5% bitumen by mass show the best recovery characteristics compared to other variations. The newly defined Recovery Index introduced in this research effort represents a good and promising indicator for assessing the recovery properties of HMA. It can be successfully used for further pre-selection of pavement materials in order to achieve the optimal pavement lifespan.

1 INTRODUCTION

Understanding asphalt recovery property is critical for improving asphalt materials and pavement construction. This material characteristic can be observed when the pavement layers experience rest period between passages of two successive axles of the same or of different vehicles.

In order to limit tests duration, traditional laboratory methods for characterizing the fatigue life of hot mix asphalt (HMA) do not include rest periods in the testing procedure and, therefore, their influence on pavement life is neglected. Nevertheless, the current testing methods are not necessarily representative of the effective loading spectrum which a real pavement experiences.

When comparing the number of cycles required to achieve fatigue failure, obtained from conventional laboratory experiments, with the actual field measurements, a longer field fatigue life can be observed; hence, shift factors are conventionally used to match field observations to laboratory results (Carpenter and Shen, 2006). This means that rest periods allow a certain degree of recovery of material mechanical properties as a consequence of the relaxation of stresses (due to the material viscoelasticity) and healing of the micro cracks occurred in the asphalt mixture (Kim et al., 2006) while extending the durability of the pavement. This has been recognized by many

researchers and a considerable number of studies show significant impact of the rest phase on damage evolution in HMA structures (Little *et al.*, 1999, Carpenter and Shen, 2006, Kim *et al.*, 2006, Shen *et al.*, 2009).

The objective of this study is to experimentally evaluate the recovery capability of HMA having different mix design by introducing rest periods of various durations in the testing procedure. The analysis of the recovery properties is performed using the dissipated energy approach which is a fundamental analysis tool for observing the difference in material behavior during cyclic loading (Carpenter and Shen, 2006). In particular, it is expected that the findings can be used for selecting better pavement materials, since asphalt materials that has higher recovery ability accumulates less deformation and less damage in the asphalt layer (Luo, *et al.*, 2013).

2 EXPERIMENTAL STUDY

2.1 Test equipment and material composition

Strain field measurements on asphalt pavements have demonstrated that both tensile and compressive stress can be observed at the bottom of the HMA due to wheel loading (Wistuba and Perret, 2004). For this reason the use of the combined tension-compression test represents a reasonable configuration for the estimation

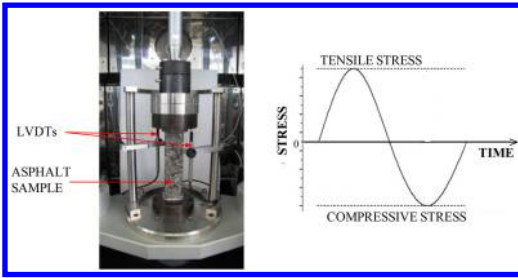


Figure 1. Testing machine (left) and the principle of tension-compression test (right).

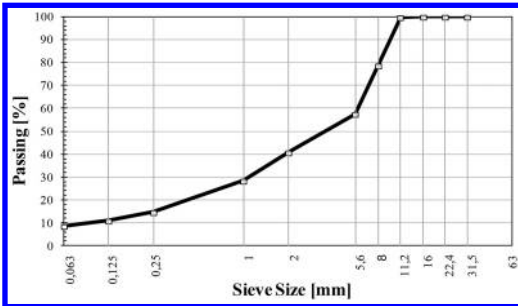


Figure 2. Aggregate gradation curve used to prepare HMA specimens.

of the fatigue life of HMA (Di Benedetto, 2013). In this research the uniaxial stress controlled tension – compression fatigue test is used. This test creates homogenous stress and strain fields in the middle portion of specimen. Figure 1 presents the test equipment used in the present study.

Fatigue – recovery tests were performed on a set of asphalt mixtures for surface course AC 11 D S. According to the German Technical Specifications these asphalt mixtures were prepared with maximum grain size of 11 mm with a bitumen with penetration grade 50/70 (DIN, 2013), and a polymer modified bitumen 25-55/55, in percentage of 5.9% by total mix weight. Figure 2 presents the aggregate gradation curve. The tested specimens had an air void of 2.5%.

Test specimens were cut from slabs of asphalt mixture ($50 \times 70 \times 4 \text{ cm}^3$) made with a Rolling Sector Compactor. Using standard compaction procedure it is possible to produce HMA slabs with the same mechanical characteristics compared to those in the field (Renken, 2000). The compactor uses a steel roller cylindrical sector to produce a kneading action and downward force to the specimen in both pre-compaction and main compaction phases (Wistuba, 2014). The pre-compaction is displacement controlled and simulates the compaction effort of paver, while the main compaction is force controlled and simulates the effective compaction by roller compactors in the field. Each phase consists of 12 roller passes. In addition, the following factors were modified in the

specimens' preparation and in the basic mix design, which includes plain 50/70 bitumen:

- Mixture long term aging using Brunswick Aging Procedure (final air voids content of 3.4% in the compacted mixture),
- Mixture preparation with additional 0.5% bitumen by weight (final air voids content of 1.0% in the compacted mixture),
- High slab compaction energy/effort of HMA (final air voids content of 2.2% in the compacted mixture), and
- Low slab compaction energy/effort of HMA (final air voids content of 2.6% in the compacted mixture).

Long-term mixture aging was simulated in the laboratory by exposing the loose mixture to hot air at the temperature of 80°C for 4 days (Büchler, *et al.*, 2009).

The low and high compaction degrees were achieved using different numbers of rolling repetitions during pre-compaction and the main compaction phases with the Rolling Sector Compactor as follows:

- 10 rolling repetitions for low compaction energy,
- 14 rolling repetitions for high compaction energy.

2.2 Description of the test and recovery index

A sinusoidal cyclic load in tension-compression configuration at the stress amplitude of 1.05 MPa was imposed to the prismatic specimens (specimen size $4 \times 4 \times 16 \text{ cm}^3$) in order to optimize test duration. A fixed frequency of 10 Hz and a temperature of 20°C were used during testing. Loading was applied until the material experienced a decay of the complex modulus down to 75% of its initial value ($|E_{100}^*|$), determined at 100th loading cycle (Phase 1, Figure 3). Then, a single rest period (RP) is applied in order to allow the specimen to recover (partly or completely) its initial mechanical characteristics; during the rest period specimen is stress-free. At the end of the rest period specimen is loaded with a new loading sequence (Phase 2, Figure 3) till failure. The following durations of the rest period were imposed: 500 s, 1000 s, 7500 s, 11000 s, 15000 s, 30000 s. The used testing procedure with one rest period does not simulate real loading conditions in the field; however, it provides the opportunity to better estimate the influence of the rest period on material recovery potential compared to procedures with rest periods after each cyclic repetition.

Conventionally, the absolute value of complex modulus is obtained from the axial stress and axial strain measurements according to Equation 1 (the calculation of the phase angle was also performed):

$$|E_n^*| = \frac{\sigma_{0n}}{\varepsilon_{0n}} \text{ [MPa]}, \quad (1)$$

where:

$\sigma_{0,n}$ = stress amplitude in cycle n [MPa],

$\varepsilon_{0,n}$ = strain amplitude in cycle n [-].

An approach based on dissipated energy was used to investigate the recovery properties of HMA. The

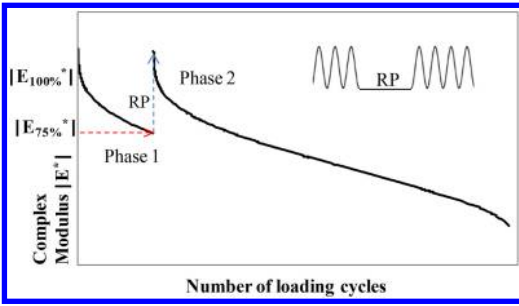


Figure 3. Test protocol used to characterize recovery capacity of HMA: loading phase 1 + rest period (RP) + loading phase 2.

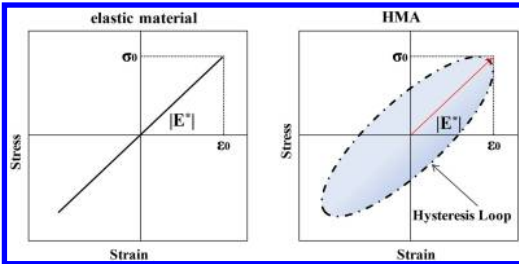


Figure 4. One loading cycle in strain-stress diagram for a perfectly elastic material (left), and for a viscoelastic material, such as hot mix asphalt (right).

energy dissipated within one loading cycle represents the difference between the energy provided to the material during the loading phase and the energy returned during unloading. Namely, if a material is perfectly elastic, the loading and unloading curves follow the same paths, meaning that all the energy is recovered or returned, without any energy dissipation (Figure 4 left). In case of viscoelastic material like HMA loading and unloading curves do not overlap, which indicates loss of energy within the material. Part of the energy is dissipated out of the system through external work, heat generation, or damage (Ghuzlan and Carpenter, 2000). The generated ellipse is called hysteresis loop and its area correspond to the energy dissipated in one loading-unloading cycle (Figure 4 right).

For the calculation of dissipated energy in one loading cycle the following equation can be used for linear viscoelastic material:

$$W_n = \pi \cdot \sigma_n \cdot \varepsilon_n \cdot \sin \phi_n \quad [\text{J/m}^3], \quad (2)$$

where:

W_n = dissipated energy in cycle n [J/m^3],

σ_n = stress amplitude in cycle n [MPa],

ε_n = strain amplitude in cycle n [%],

ϕ_n = phase angle in cycle n [$^\circ$].

The concept of dissipated energy has always been considered as effective in solving engineering problems, because it is based on material response. The mechanical behavior during cyclic loading is considered both in terms of strain and phase angle change

(in stress controlled test) during the material damage evolution. It is worth to mention that not all the dissipated energy in one loading cycle is responsible for material damage. Only a portion of the total energy that is dissipated is used for damaging the material (Ghuzlan and Carpenter, 2000).

The recovery properties of HMA in this research are determined through a Recovery Index (K) which represents the relative change in dissipated energy between the beginning of the first phase of the test (after 100 cycles) and the beginning of the second loading phase (after 100 cycles in the second phase) (Equation 3). By taking into consideration that dissipated energy in stress controlled fatigue test increases (as a consequence of permanent material deterioration), K can have negative values when the material mechanical properties are not completely recovered during the rest period. If, after the rest period, the material properties are the same as at the beginning of the tests, K will be equal to 0%.

$$K = \frac{W_1 - W_2}{W_1} \cdot 100 \quad [\%], \quad (3)$$

where:

K = Recovery Index [%],

W_1 = dissipated energy at 100th loading cycle in the first loading phase [J/m^3],

W_2 = dissipated energy at 100th loading cycle in the second loading phase [J/m^3].

Relative change in dissipated energy indicates the material capability of recovering its initial characteristics after the induced rest period. It is important to mention that this research does not explain the nature of material recovery and does not distinguish the effects behind this phenomenon. Relative recovery of the dissipated energy in rest period can be caused by material healing, thixotropy and temperature decrease in specimen (as a consequence of material heating during cyclic loading) (Di Benedetto, et al., 2011).

3 RESEARCH RESULTS AND ANALYSIS

The recovery properties of HMA, prepared with bitumen having penetration grade of 50/70, were evaluated under rest periods of different duration. All tests were performed at temperature $T = 20^\circ\text{C}$. The results are presented in Table 1 and Figure 5. The analysis reveals that the Recovery Index is highly dependent on the duration of the rest period, and it increases as the time for material recovery increases. Figure 5 reveals that beyond a certain rest period duration there is no influence on the recovery capacity of HMA and a plateau stage is reached. Most likely, the recovery mechanism during this time is completed and any additional duration of the rest period does not affect the recovery capacity of the material. For the HMA used in this research the plateau value is reached after approx. 14000 seconds.

In addition, Figure 5 shows that the Recovery Index reaches values which are over 0%. This implies that

Table 1. Recovery Index as a function of the rest period duration and mixture composition.

AC 11 D S with:	Rest period duration [s]	Recovery Index [%]
50/70	500	-17.04
	1000	-13.41
	7500	-0.57
	11000	0.18
	15000	4.43
	30000	2.98
25/55-55	1000	-14.23
50/70, aged		-20.91
50/70 with +0.5 M. -% Bin.		-7.39
50/70, high compaction		-11.73
50/70, low compaction		-12.18

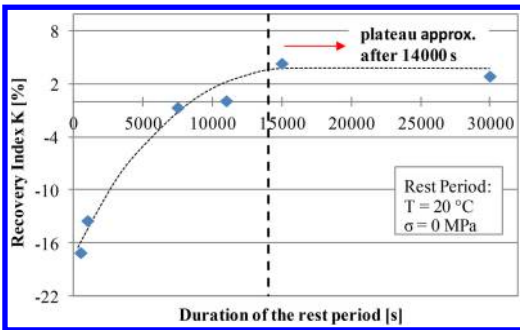


Figure 5. AC 11 D S with 50/70 bitumen; Recovery Index as function of rest period duration.

after the rest period specimen has better mechanical properties compared to them at the beginning of the test. This can be explained in the way, that during the tension-compression loading in the initial loading phase (Phase 1) some reengagement effects occurs in material, which induce slightly improvement of material characteristics. These material effects, overlapped with fully material recovery after certain rest period lead to the Recovery Indexes higher than 0%.

Analysis of the influence of material composition and specimen preparation on recovery properties of HMA is performed using one rest period of 1000 seconds. Material variations were made in terms of bitumen type and amount. Mixture long term aging was also considered. Results are presented in Table 1 and in Figure 6.

Material recovery is extremely dependent on aging. Aged samples show distinct lower ability to recover initial properties, which confirmed the theory from Little et al. (1999). Aging makes binder more brittle and more susceptible to fracture, as a consequence of higher asphaltene percentage.

Regard to bitumen type, mixture containing polymer modified bitumen 25/55-55, presents relatively small change in recovery behavior, which is also showed by the work of Kim and Roque (2006). This

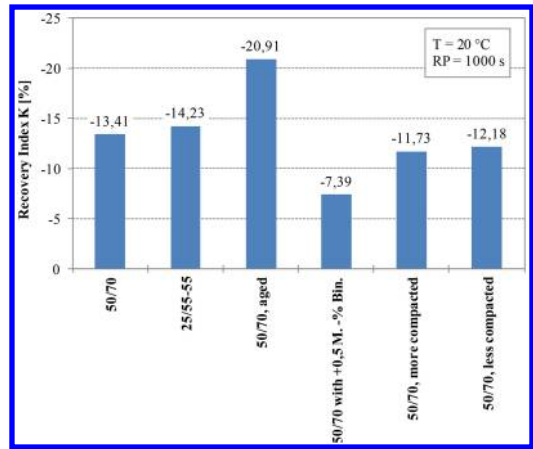


Figure 6. Recovery Index as a function of mixture composition after 1000 s rest period.

can be explained by the research performed by Little et al. (1999), who hypothesized that the polymer acts as a filler system that interrupts the ability of pure bitumen to reestablish contacts and to heal.

Specimens prepared with additional 0.5% bitumen by weight show the best recovery characteristics compared to others. This is most likely associated to a significant flow of bituminous mastic films that wet and partially close the initiated micro cracks.

The degree of compaction used in this investigation seems to have no significant influence on material ability to restore its initial properties. It is assumed that after the lowest number of rolling repetitions (a Rolling Sector Compactor was used in this research) the final HMA structure is reached, and it does not significantly change with application of additional two or four passes. Therefore, no change in HMA recovery properties is observed.

Small permanent deformation occurred due to the specific tension-compression cycling loading applied in a stress control. Average permanent deformation recovery in rest period from all the tests was 0.35%, which can be assumed as negligible to affect the material recovery properties. Hence, the effects of permanent deformation can be neglected.

The present research shows that Recovery Index can achieve 0%, meaning that, after rest period, a complete recover of HMA mechanical characteristics took place. Based on the recovery evaluation just at the beginning of second loading phase it is not possible to state that the material behavior after the rest period will follow the same trend as in the first phase. In order to verify this, one test with a nearly 0% Recovery Index was chosen (HMA with 50/70 bitumen with 7500 seconds rest period). The evolutions of complex modulus and dissipated energy over the number of loading cycles are presented in Figure 7.

It is shown that both parameters (complex modulus and dissipated energy) fully recover after the rest period. The superposition of the complex modulus and dissipated energy curves of Phase 1 and Phase 2

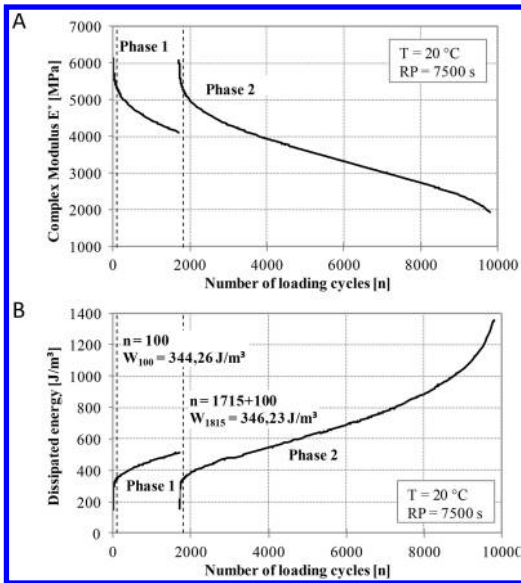


Figure 7. Recovery test on HMA with 50/70 bitumen and with 7500 s rest period. Evolution of complex modulus (A) and dissipated energy (B) over the number of loading cycles.

obtained by horizontal shifting Phase 2 to the beginning of the Phase 1 is presented in Figure 8. The plot clearly shows that the evolution of both values in Phase 2 correspond to the evolution in Phase 1, which provides solid evidence of the complete recover of hot mix asphalt properties in unloading phase. After the rest period the material behaves under loading like in undamaged conditions, and sustains nearly the same number of loading repetitions as in the first phase, until the same drop in complex modulus. This implies that the newly introduced Recovery Index can be used as a global indicator in evaluation of the recovery properties of HMA.

4 CONCLUSIONS AND COMMENDATIONS

In this research, a dissipated energy approach is applied to study the recovery properties of hot mix asphalt in fatigue stress controlled uniaxial tension-compression test with rest period. For addressing the material recovery ability, a newly proposed Recovery Index is used; this takes into account the dissipated energy at the beginning of the initial loading phase and at the beginning of the loading phase after the rest period. According to the analysis described in this paper, the following conclusions can be drawn:

- Material recovery is highly dependent on the duration of the rest period in a way that with the increase of rest period, the degree of recovery also increases.
- The impact of the rest period on recovery capacity of HMA is limited. After certain duration of the rest period there is hardly any influence on the

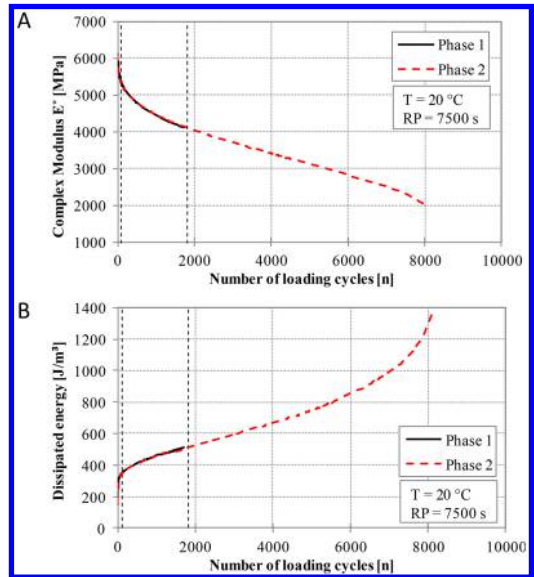


Figure 8. Recovery test on HMA with 50/70 bitumen and with 7500 s rest period. Superposition of complex modulus (A) and dissipated energy (B) curves of the Phase 1 and Phase 2 over the number of loading cycles.

material recovery and an asymptotic limit (plateau) is reached.

- Material recovery decreases with material aging, since binder is more brittle and more susceptible to fracture, as a consequence of higher asphaltene content.
- Polymer modified bitumen showed a relatively small change in recovery behavior compared to plain bitumen. More research and different polymer modifications need to be investigated in order to further support the findings on the influence of addition of polymers on material recovery.
- Specimens prepared with additional 0.5% bitumen by weight show the best recovery characteristics compared to others. This can be explained by higher flow processes of bituminous mastic film that positively influences closing of the initiated micro cracks.
- The degree of compaction used in this investigation seems to have no significant influence on material ability to restore its initial properties. It is assumed that after the lowest number of rolling repetitions in Rolling Sector Compactor, the final HMA structure is reached, and it does not change significantly with application of additional roller passes. Therefore, no change in HMA recovery properties is identified.
- The Recovery Index obtained based on dissipated energy calculation seems to be a good indicator for assessing the recovery properties of HMA. Although it considers just the first loading phase and beginning of the second one, it is showed that it predicts well the material behaviour in the rest of the second loading phase. Recovery Index can be successfully used for further pre-selection of pavement

materials in order to achieve the optimal pavement lifespan.

- More research on this field is needed in order to distinguish the effects that drive the material recovery during the rest period. Using tension – compression loading in stress controlled mode allows to have a test with negligible permanent deformation (similarly to strain controlled mode) and to exclude its influence on material recovery. In addition, temperature evaluation has to be recorded in order to isolate the temperature effects and to observe pure material recovery.

REFERENCES

- Büchler, S., Mollenhauer, K., Wistuba, M., and Renken, P. 2009. Aging of stone mastic asphalt and evaluation of cracking resistance. *Bearing Capacity of Roads, Railways and Airfields – Tutumluer & Al-Qadi (eds), Taylor & Francis Group, London*, ISBN 978-0-415-87199-0.
- Carpenter, S., and Shen, S. 2006. A Dissipated Energy Approach to Study HMA Healing in Fatigue. In *Transportation Research Record (TRR): Journal of the Transportation Research Board*, No 1970, pp.178–185.
- Daniel, S. and Bisirri, W. 2005. Characterizing Fatigue in Pavement Materials Using a Dissipated Energy Parameter. Proc., Geo-Frontiers Congress, Austin, Texas, United States, pp. 1–10.
- DIN Deutsches Institut für Normung. Bitumen and bituminous binders – Determination of needle penetration, German version prEN 1426:2013. Beuth Verlag Berlin, Germany, 2013.
- Di Benedetto, H., Nguyen, Q. T. and Sauzéat, C. 2011. Non-linearity, Heating, Fatigue and Thixotropy during Cyclic Loading of Asphalt Mixtures. *Journal of Road Materials and Pavement Design*, Vol. 12, pp. 129–158.
- Di Benedetto, H. 2013. Fatigue and other Phenomena during Cyclic Loading of Bituminous Materials. Keynote at EATA 2013, Braunschweig, Germany.
- Ghuzlan, A., and Carpenter, S. 2000. An Energy-Derived/Damage-Based Failure Criteria for fatigue Testing. CD-ROM. Transportation Research Board Meeting, Washington, D.C.
- Kim, B., and Roque, R. 2006. Evaluation of Healing Property of Asphalt Mixture. CD-ROM. Transportation Research Board Meeting, Washington, D.C.
- Little, D.N., Lytton, R. L., Williams, D. & Kim, Y. R. 1999. An analysis of the mechanism of microdamage healing based on the application of micromechanics first principles of fracture and healing. *Asphalt Paving Technology*, Chicago, pp. 501–537.
- Luo, X., Luo, R., and Lytton, L. 2013. Characterization of recovery properties of asphalt mixtures. *Construction and Building Materials* 48, pp. 610–621.
- Partl, M.N., Bahia, H.U., Canestrari, F., de la Roche, C., Di Benedetto, H., Piber, H., Sybilski, D. (Eds.). 2013. *Advances in Interlaboratory Testing and Evaluation of Bituminous Materials*. State-of-the-Art Report of the RILEM Technical Committee.
- Renken, P. 2000. Influence of Specimen Preparation onto the Mechanical Behavior of Asphalt Aggregate Mixtures. 2nd Eurasphalt & Eurobitumen Congress Barcelona.
- Shen, S., Chiu, H., and Huang, H. 2009. Fatigue and Healing in Asphalt Binders. CD-ROM. Transportation Research Board Meeting, Washington, D.C.
- Wistuba, M. & Perret, J. 2004. Comparative strain measurement in bituminous layers with the use of ALT. Proc., 2nd Int. Conf. on Accelerated Pavement Testing, Minneapolis, Minnesota, 25–29 September 2004.
- Wistuba, M. P. 2014. The German segmented steel roller compaction method – state-of-the-art report. *Int. Journal of Pavement Engineering*. Taylor and Francis, London.

Fatigue characterization of modified asphalt concretes by means of dissipated energy approaches

M. Pasetto

Department of Civil, Environmental and Architectural Engineering, University of Padua, Padua, Italy

N. Baldo

Chemistry, Physics and Environment Department, University of Udine, Udine, Italy

ABSTRACT: The results are discussed of a laboratory investigation on the fatigue response of asphalt concretes, evaluated by the four-point bending test. The experimental trial was performed on bituminous mixtures for base courses, made with both conventional and polymer modified bitumen. The mix design was based on gyratory tests and indirect tensile tests. The fatigue behaviour was evaluated for both stress and strain control mode, by means of the conventional approach, based on the reduction in the initial stiffness modulus, as well as using a dissipated energy method. The main goal of the research was to compare the fatigue resistance of the mixes considered, in light of the different approaches adopted in the study. Between the different approaches used for the fatigue data analysis, it has been verified a qualitative consistency in the mixtures ranking, independently from the control mode, with a higher fatigue resistance recorded for the polymer modified mixtures.

1 INTRODUCTION

On the basis of rational mechanistic principles, the performance characterization of a bituminous mixture is fundamental for the design of flexible pavements. At average operating temperatures, verification of the fatigue behaviour of the material is particularly important, with respect to repeated loading applications.

Laboratory fatigue tests can be conducted following many approaches. For example, the European EN 12697-24 Standard reports five separate Annexes, each of which describes a different test protocol: two-point bending test with trapezoid and prismatic samples (Annexes A and B); three- and four-point bending tests on prismatic beam specimens (C and D); repeated indirect tensile strength tests on cylindrical samples (E).

Although modern laboratory equipment allows the various tests to be conducted with stress and strain control, the Annexes of the EN 12697-24 Standard usually involve just one of the two methods of loading application. More precisely, Annexes B and E prescribe the stress control, while the others the strain control; only Annex D allows both of the loading modes (i.e. constant deflection or constant force).

Nevertheless, irrespective of the specifications of the Standard, the stress control tests are generally used for the fatigue study of thick pavements, while strain control tests are applied for flexible ones of the conventional type (Artamendi and Khalid 2005).

In the stress control procedure, since stress is maintained constant, with a consequent progressive

increase in the strain, the complete cracking of the sample is frequently reached at the end of the test. The failure condition is therefore clearly represented by the physical failure of the sample. However, there are other criteria of failure, for example associated to a 90% reduction of the initial stiffness modulus (van Dijk and Visser 1977), or with increasing strain, up to a value double that of the initial one.

Vice versa, in the strain control tests, strain is maintained constant and a progressive reduction in the stress is registered. Consequently, at a high number of cycles, since the stress will be reduced to a very low value, it is unlikely that an evident crack will be found in the sample, which will therefore not be completely broken. For this reason, within the road scientific community, the criterion of failure for the strain control tests is generally established as a 50% reduction of the initial stiffness (Tayebali et al. 1992), or initial stress.

The cited criteria of failure, although defined by consistent variations of the mechanical parameter considered (stiffness modulus, rather than stress or strain) with respect to the initial conditions of the sample, are purely arbitrary and do not fully represent the state of internal damage in the material.

To overcome this problem, Pronk (1997), for fatigue bending tests, introduced a rational criterion of failure, linked to the concept of dissipated energy, identifying the failure in correspondence to a number of loading cycles N_1 at which the micro-cracks coalesce, producing a macro-crack. N_1 therefore represents the triggering of that macro-crack, which then propagates in the material (Rowe 1993). In his approach, Pronk

Table 1. Physical and mechanical characteristics of the natural aggregates.

Physical ÷ mechanical properties	CL 0/5	CL 5/10	CL 10/15
Los Angeles coefficient [%] EN 1097-2	–	–	30
Equivalent in sand [%] EN 933-8	69	–	–
Shape Index [%] EN 933-4	7	5	5
Flakiness Index [%] EN 933-3	6	8	6
Particle density [Mg/m ³] EN 1097-6	2.75	2.78	2.79
Plasticity Index [–]	0	0	0
CEN ISO/TS 17892-12	–	–	–
Stripping in water (%) CNR 138/92	–	–	–

introduced an energy ratio R_n , defined as the ratio between the cumulative energy dissipated up to the n -th cycle and the energy dissipated at the n -th cycle.

In the strain control tests, the graphical representation of R_n with the varying of the number of cycles allows N_1 to be identified as the point at which R_n begins to show a non-linear trend. Vice versa, in the stress control tests, N_1 is identified as the peak point of R_n with the varying of the number of cycles. As already outlined by Artamendi and Khalid (2005), the accurate identification of N_1 appears to be more subjective in the strain control test method than in that with constant stress control.

In the present research the fatigue behaviour of bituminous mixtures for base courses was investigated by means of both the stress and the strain control four-point bending test (4PBT), interpreting the experimental data, as well as with the classic methodology based on a 50% reduction of the initial stiffness, also at the light of the approaches of Pronk (1997).

2 MATERIALS

2.1 Aggregates

Crushed limestone (CL) and filler have been used in the study. The aggregates derived from a quarry in northern Italy; they were available in three different fractions: 0/5, 5/10 and 10/15 mm. Table 1 reports the physico-mechanical properties of the aggregate fractions, whereas their grading curves are presented in Figure 1.

2.2 Binders

Three different bituminous binders were adopted in the laboratory investigation: a conventional bitumen (CB) and two bitumens modified with SBS (styrene-butadiene–styrene) polymers (PMB). The latter were named PMB 1 and PMB 2 and respectively characterized by a high and low polymer concentration, in order

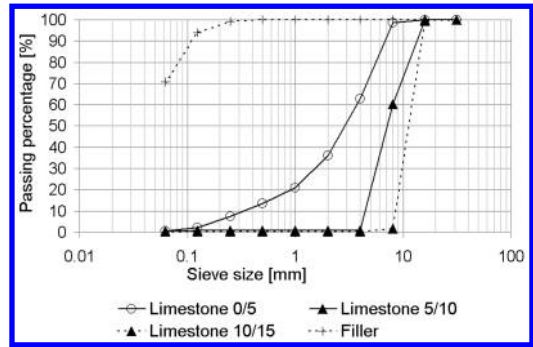


Figure 1. Aggregates grading curves.

Table 2. Bitumen characterization.

Properties	PMB 1	PMB 2	CB
Penetration (mm/10) EN 1426	23	46	69
Softening point (°C) EN1427	79	75	55
Ductility (cm) at 25°C CNR 44/74	>100	>100	>100
Fraass breaking point (°C) EN 12593	–13	–10	–8
Elastic Recovery (%) at 25°C EN 13398	>50	>50	>50

to evaluate its influence on the rheological behaviour of the asphalts. Table 2 reports the main physical properties of the three binders used in the experiment. The elastic recovery data are attested by the bitumen manufacturer. As it was expected, the hard modified bitumen, namely PMB 1, resulted largely superior with respect to the soft modified bitumen (PMB 2) and to the conventional binder, especially in terms of penetration. Both the polymer modified bitumens presented an improved softening point, with an increment of the softening temperature equal to 36% and 44% for PMB 1 and PMB 2 respectively. The ductility (evaluated by means of an Italian test) resulted adequate for all the binders.

3 MIXTURES

Three different high performance Asphalt Concretes for flexible pavement Base courses (BAC), were studied: BAC-1, BAC-2 and BAC-3. The PMB 1 binder was used for the BAC-1 mix, the PMB 2 one for BAC-2 and the conventional bitumen for BAC-3. The mixtures have different types of binder, but the same lithic skeleton.

3.1 Grading and composition of the mixes

The particle size distribution of the three BAC mixes was optimized by means of a trial and error procedure, with reference to the design grading envelope of

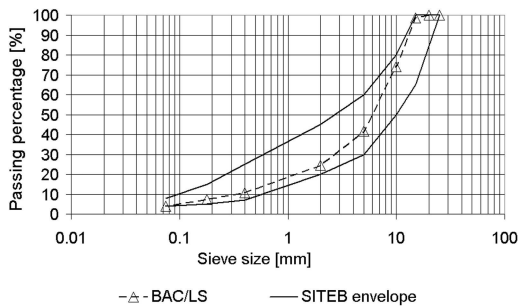


Figure 2. Design grading curve of the mixes.

SITEB (2000) for high performance asphalt concrete base courses, in order to identify a curve as close as possible to its centre, but compatible with the availability of the different aggregates in the sizes necessary to construct this ideal grading (Pasetto & Baldo 2013a, Pasetto & Baldo 2014a, Pasetto & Baldo 2014b). The aggregate skeleton of the mixtures resulted composed by the 55% of the finest limestone fraction 0/5, the 15% of the intermediate grading fraction 5/10 and 25% of the coarser one (10/15 mm), plus 5% of filler; the resulting grading curve is presented in Figure 2. The design grading curve is completely within the reference grading envelope (SITEB 2000) for base course asphalts with maximum aggregate size of 20 mm.

3.2 Optimization of the mixtures

The mix design procedure was based on the volumetric analysis of specimens prepared by gyratory compaction and the Indirect Tensile Strength (ITS) test at 25°C, on both dry and wet cylindrical samples, according to CIRS-Italian Ministry of Infrastructure Specifications (2001). Regarding the main gyratory test parameters, a speed of 30 gyrations/minute, a pressure of 600 kPa, an angle of rotation of 1.25° and a diameter of the mould of 150 mm, were used in the gyratory compaction.

For each of the 3 BAC mixes, different mixtures were analyzed, in which, having defined the type of bitumen, the amounts of binder were varied at intervals of 0.5% on the weight of the aggregate, in the range 4.0–5.5%. To support the phase of mix design, four gyratory specimens were produced for each mix.

The results of the mix design procedure are summarized in Table 3. The Tensile Strength Ratio (TSR) has been computed as the ratio between the indirect tensile strength of the specimens treated by means of 15 days of immersion in a thermostatic bath at 25°C (ITS_{wet}) and untreated (ITS_{dry}), respectively.

The Optimum Bitumen Content (OBC) was identified as that which satisfied the residual air voids (V_a) prerequisites in correspondence to three different gyration numbers. Moreover, the dry ITS and the TSR values of the mixtures prepared with the optimum bitumen content, should result higher than the minimum CIRS acceptance thresholds.

Table 3. Mix design results.

Property	BAC-1	BAC-2	BAC-3	CIRS requisites
V_a 10 revs (%)	12.72	12.64	12.25	10–14
V_a , 100 revs (%)	4.79	4.59	4.35	3–5
V_a 180 revs (%)	2.55	2.49	2.22	>2
Bulk density (g/cm ³)	2.560	2.566	2.572	–
ITS_{dry} (MPa)	1.12	0.98	0.73	>0.6
ITS_{wet} (MPa)	0.88	0.75	0.61	–
TSR (%)	79	77	83	>75

According to the data presented in Table 3, the Air Voids requisites prescribed by CIRS mix design procedure, at 10, 100 and 180 revs, were completely satisfied in correspondence of a total bitumen content equal to 4.75%, for all the mixes. At the optimum total bitumen content, both the dry ITS and the TSR values, resulted above the CIRS acceptance prerequisites for all the asphalt concretes examined. Hence all mixes produced in this study were acceptable for road construction according to the CIRS specification (CIRS 2001).

4 FATIGUE CHARACTERIZATION

The four-point bending fatigue tests were conducted using the protocol described in Annex D of the European EN 12697-24 Standard, for both stress and strain control mode, with a wave of sinusoidal loading without rest periods. The tests were all conducted at a temperature of 20°C and a frequency of 10 Hz. Three stress levels were used (0.75, 1.00 and 1.25 MPa), as well as three different strain levels (250, 275 and 300 $\mu\epsilon$). The beam specimens necessary for conducting the fatigue tests, with dimensions of 400 mm \times 50 mm \times 60 mm, were cut from 300 mm \times 400 mm \times 50 mm slabs produced by a laboratory compacting roller, in accordance with the EN 12697-33 Standard. The results of the fatigue tests were interpreted with two different approaches. In addition to the classical methodology based on a 50% reduction of the initial stiffness, the energy approach of Pronk (1997) was also applied.

4.1 Fatigue characterization based on the stiffness reduction approach

The classical fatigue curves, elaborated according to the applied stress (or strain) and number of cycles N_f , at which a 50% reduction of the initial stiffness is registered, are presented in Figures 3, 4, for the stress and the strain control test, respectively. The initial strain was evaluated at the 100th cycle (EN 12697-24, Annex D), since as generally recognized in the literature (Di Benedetto et al. 1996, Artamendi & Khalid 2005); this is the stage of the test when the material shows a stress-strain response that reliably represents

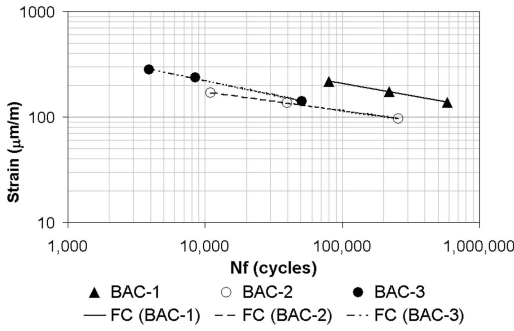


Figure 3. Fatigue life N_f versus initial strain for stress control test.

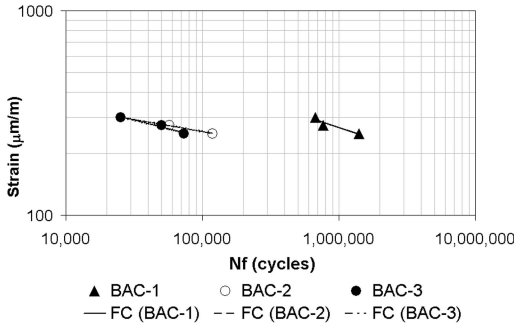


Figure 4. Fatigue life N_f versus initial strain for strain control test.

the initial conditions, without yet being significantly affected by damage phenomena. The regression analysis of the fatigue data was performed using a power law model of the type:

$$\varepsilon_0 = aN_f^{-b} \quad (1)$$

where a and b are regression coefficients depending on the type of material.

Tables 4, 5 report the regression coefficients and coefficient of determination R^2 for the stress and the strain control test, respectively. With reference to a fatigue resistance of 1,000,000 loading cycles (as indicated in Standard EN 12697–24, Annex D), and using Equation 1, it was possible to calculate the corresponding tensile strain ε (10^6), which was higher for the mixture with PMB 1, for both stress and strain control mode (Tables 4, 5). The ε (10^6) values evaluated by means of the stress control data, resulted quite different than those related to the strain control data

4.2 Fatigue characterization based on the energy ratio approach

Pronk's energy approach is based on the calculation of the energy ratio R_n , defined as the ratio between the cumulative energy dissipated up to the n -th cycle

Table 4. Fatigue curves – regression coefficients (N_f approach, stress control mode).

Mixture	a [$\mu\text{m}/\text{m}$]	b [–]	$\varepsilon(10^6)$ [$\mu\text{m}/\text{m}$]	R^2 [–]
BAC-1	2998.1	–0.232	122	0.9991
BAC-2	930.79	–0.182	75	0.9993
BAC-3	27398	–0.273	63	0.9965

Table 5. Fatigue curves – regression coefficients (N_f approach, strain control mode).

Mixture	a [$\mu\text{m}/\text{m}$]	b [–]	$\varepsilon(10^6)$ [$\mu\text{m}/\text{m}$]	R^2 [–]
BAC-1	5623.6	–0.220	269	0.8975
BAC-2	990.59	–0.118	194	0.9968
BAC-3	1607.70	–0.165	165	0.9637

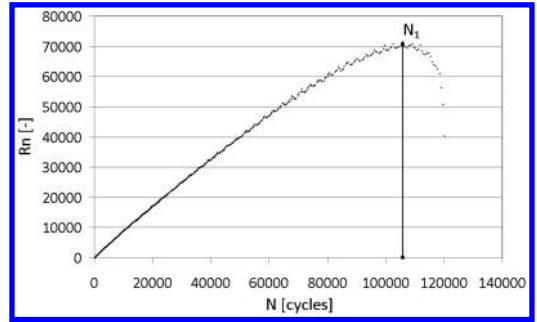


Figure 5. Determination of failure N_1 for mix BAC-1 at 1.25 MPa (stress control test).

and that dissipated at the n -th cycle, according to Equation 2:

$$R_n = \frac{\pi \sum_{i=0}^n \sigma_i \varepsilon_i \sin \phi_i}{\pi \sigma_n \varepsilon_n \sin \phi_n} \quad (2)$$

where σ is the stress, ε the strain, ϕ the phase angle, i the generic i -th cycle, n the n -th cycle. The study of the evolution of the energy ratio during the test allows the number of cycles N_1 to be determined in correspondence to which macro-cracks form.

An example of the determination of N_1 in the stress control mode, is presented in Figure 5, for the mix BAC-1: the peak value of the curve in the R_n - N plane, is clearly detectable.

Figure 6 instead, presents an example of the determination of N_1 using the strain control data for the mix BAC-1. It is possible that, with the varying of the number of cycles, the exact identification of the point in which R_n shows a non-linear trend depends, in practice, on the subjectivity of the researcher.

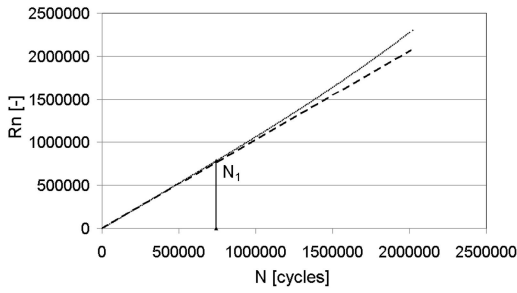


Figure 6. Determination of failure N_1 for mix BAC-1 at $250 \mu\text{m/m}$ (strain control test).

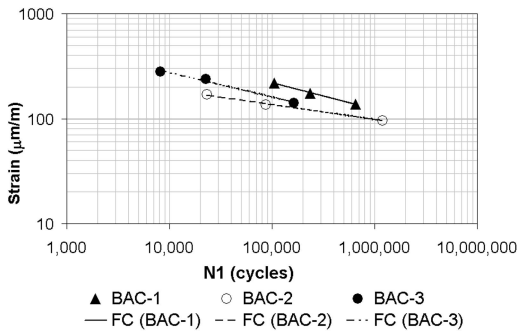


Figure 7. Fatigue life N_f versus initial strain for stress control test.

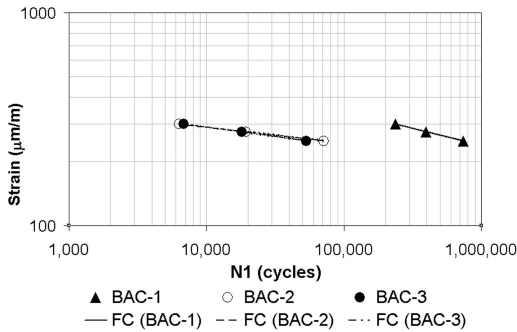


Figure 8. Fatigue life N_f versus initial strain for strain control test.

Figures 7, 8 present the fatigue curves in terms of N_1 and the initial strain value, for the various mixtures. Similarly to what was previously done for the classical fatigue curves, represented as a function of N_f , a power function, analogous to Equation 1, was also used in this case, substituting N_1 for N_f . Tables 6, 7 report the coefficients of regression and determination, as well as the value of $\varepsilon (10)^6$, for the stress and the strain control mode, respectively.

In order to allow a direct comparison between the fatigue rankings of the 3 mixtures, the $\varepsilon (10)^6$ values are reported in Table 8 for both the 50% and the dissipated energy criteria.

Table 6. Fatigue curves – regression coefficients (N_1 approach, stress control mode).

Mixture	a [$\mu\text{m/m}$]	b [-]	$\varepsilon(10^6)$ [$\mu\text{m/m}$]	R^2 [-]
BAC-1	4027.7	-0253	122	0.9972
BAC-2	709.21	-0143	98	0.9971
BAC-3	2393.4	-0235	93	0.9901

Table 7. Fatigue curves – regression coefficients (N_1 approach, strain control mode).

Mixture	a [$\mu\text{m/m}$]	b [-]	$\varepsilon(10^6)$ [$\mu\text{m/m}$]	R^2 [-]
BAC-1	2152.10	-0.159	239	0.9988
BAC-2	577.26	-0.075	205	0.9996
BAC-3	656.75	-0.089	192	0.9999

Table 8. Fatigue resistance comparison between the mixes in terms of $\varepsilon (10)^6$ values [$\mu\text{m/m}$].

Mixture	N_f , stress control	N_f , strain control	N_1 , stress control	N_1 , strain control
BAC-1	122	269	122	239
BAC-2	75	194	98	205
BAC-3	63	165	93	192

Although the comparative analysis of the $\varepsilon (10)^6$ values related to the different mixtures, using the conventional (N_f) as well as the Pronk (N_1) approach, leads to a similar ranking of the various materials (at least from a qualitative point of view), it can be observed that $\varepsilon (10)^6$ values determined from N_1 are different than those calculated with reference to N_f , for both the stress and strain control modes, as it has been already observed in previous studies (Pasetto & Baldo 2012a, Pasetto & Baldo 2012b, Pasetto & Baldo 2013b, Pasetto & Baldo 2014b). The interpretation in terms of N_1 allows the comparison between mixtures in the same damage conditions, corresponding to the formation of macro-cracks, and should be therefore considered more reliable and significant from a physical point of view (Rowe 1993).

5 CONCLUSIONS

The performance of bituminous mixtures for base courses, produced with conventional and polymer modified bitumen, was investigated in terms of fatigue life by means of 4PBAT tests, in a regime of stress as well as strain control; the results were interpreted using two different approaches.

With respect to the reference mixture, produced with conventional bitumen, the mixes made with polymer modified bitumen demonstrated a clearly higher fatigue resistance; in particular, the use of PMB 1 increased the fatigue life, expressed in terms of $\varepsilon (10)^6$, from 24% to 94%, in relation to the stress or strain control and the criterion of failure considered (N_i and N_f respectively).

The comparison between the mixtures conducted with the criteria N_f and N_i led to a similar quality evaluation, but the energy criterion showed a quantitatively different evaluation of the fatigue life than that of the classical approach, based on a 50% reduction of the initial stiffness.

The fatigue life evaluated by means of the stress control mode resulted, for each of the mixture studied, lower than that estimated with the strain control mode, for both the approaches considered in the study.

REFERENCES

- Artamendi, I. & Khalid, H. 2005. Characterization of fatigue damage for paving asphaltic materials. *Fatigue Fracture Engineering Material Structure* 28: 1113–1118.
- Di Benedetto, H., Ashayer Soltani, M.A. & Chaverot, P. 1996. Fatigue damage for bituminous mixtures: a pertinent approach. *Journal of Association of Asphalt Paving Technologists* 65: 142–158.
- Italian Ministry of Infrastructures and Transportation-CIRS. 2001. *Norme tecniche di tipo prestazionale per capitolati speciali d'appalto* (in Italian). Rome.
- Pasetto, M. & Baldo, N. 2012a. Fatigue Performance of Asphalt Concretes with RAP Aggregates and Steel Slags. In A. Scarpas, N. Kringos & I. A. L. Al-Qadi (ed.), *RILEM Bookseries* 4: 719–727; *Proc. 7th RILEM International Conference on Cracking in Pavements, Delft, 20–22 June 2012*. Springer Netherlands.
- Pasetto, M. & Baldo, N. 2012b. Fatigue Behavior Characterization of Bituminous Mixtures Made with Reclaimed Asphalt Pavement and Steel Slag. In A. D'Andrea & L. Moretti (ed.), *Procedia: Social & Behavioral Sciences* 53: 297–306; *Proc. SIIV-5th International Congress – Sustainability of Road Infrastructures 2012*. Amsterdam: Elsevier.
- Pasetto, M. & Baldo, N. 2013a. Resistance to permanent deformation of road and airport high performance asphalt concrete base courses. *Advanced Materials Research* 723: 494–502.
- Pasetto, M. & Baldo, N. 2013b. Fatigue Performance of Asphalt Concretes made with Steel Slags and Modified Bituminous Binders, *International Journal of Pavement Research and Technology* 6 (4): 294–303.
- Pasetto, M. & Baldo, N. 2014a. Influence of the Aggregate Skeleton Design Method on the Permanent Deformation Resistance of Stone Mastic Asphalt. *Materials Research Innovations* 18 (SUPPL. 3): S96–S101.
- Pasetto, M. & Baldo, N. 2014b. Fatigue performance and stiffness properties of Stone Mastic Asphalts with steel slag and coal ash. *Proc. 12th ISAP International Conference on Asphalt Pavements, Raleigh, 1–5 June 2014*.
- Pronk, A.C. 1997. Comparison of 2 and 4 point fatigue tests and healing in 4 point dynamic test based on the dissipated energy concept. *Proc. of the 8th International Conference on Asphalt Pavement, Seattle, 10–14 August 1997*.
- Rowe, G.M. 1993. Performance of asphalt mixtures in the trapezoidal fatigue test. *Journal of Association of Asphalt Paving Technologists* 62: 344–384.
- SITEB. 2000. *Capitolato d'appalto per pavimentazioni stradali con bitume modificato* (in Italian). Rome.
- Tayebali, A.A., Rowe, G.M. & Sousa, J.B. 1992. Fatigue response of asphalt-aggregate mixtures. *Journal of Association of Asphalt Paving Technologists* 61: 333–360.
- Van Dijk, W. & Visser, W. 1977. The energy approach to fatigue for pavement design. *Journal of Association of Asphalt Paving Technologists* 46: 1–40.

Development of a new aggregate-binder adhesion test method

A.H.A.A. Al-Haddad & H. Al-Khalid

School of Engineering, University of Liverpool, Liverpool, UK

ABSTRACT: Adhesion in asphalt mixtures can be defined as energy required to fracture the adhesive bond between binder and aggregate causing isolation from each other. The main objective of this study was to develop a simple, practical and reliable laboratory adhesion test method enabling direct measurement of the adhesive bond strength of binder-aggregate systems. The adhesion results were subjected to comparative analysis to determine the effect of various variables and parameters. Four binders: two conventional and the other two are their polymer modified varieties, and two types of aggregate, were used to arrive at standardised testing conditions. When the binder thickness increased, the failure transitioned from adhesive to cohesive accompanied by a decrease in the maximum tensile load at failure. Practical work of adhesion decreased with increased testing temperature but the largest decrease was due to moisture conditioning, which increased with increase in loading rate.

Keywords: Adhesion, Adhesive bond strength, Moisture damage, Practical work, Pull-off test.

1 INTRODUCTION

Adhesion can be defined as the molecular force of attraction in the area of contact between unlike bodies, e.g. adhesive and substrate, that acts to hold the bodies together. In the context of asphalt mixtures, adhesion may be used to refer to the amount of energy required to break the adhesive bond between bitumen and aggregates. By contrast, cohesion is the intermolecular force developed within the bitumen that holds the molecules of the bitumen, and is influenced by viscosity. Hence, adhesion failure between bitumen and aggregates can be considered as one of the main fundamental properties, which can be correlated with the quality, performance and serviceability of the flexible pavements. However, despite its significance, research is limited on mechanisms and processes of adhesion in asphalt mixtures, especially in connection with moisture damage.

Caro et al. (2008) explain relation between moisture damage and adhesion force through definition of moisture damage is submitted by Kiggundu and Roberts (1988) as 'the progressive functional deterioration of a pavement mixture by loss of the adhesive bond between the binder and the aggregate surface and/or loss of the cohesive resistance within the binder principally from the action of water'. The adhesive phenomenon involves thermodynamic, chemical, physical and mechanical components that need to be considered when modelling and characterising asphalt mixtures and pavements.

Bond strength is a critical parameter in evaluating a binder's ability to resist stripping. Adhesion between bitumen and aggregate is quantified by the

adhesive bond energy (Moraes et al. 2011). Therefore, a test method performed directly on the bitumen-aggregate system can effectively evaluate both cohesive and adhesive failure types, leading to a better understanding of the moisture sensitivity of asphalt mixtures.

An adhesion test method based on the pull-off (tension mode) presents a simple, practical and reliable approach in determining the adhesive bond strength of bitumen and aggregates, especially in respect of convenience in specimen preparation and testing. Also, adhesion test methods based on the pull-off (tension) mode can be applied to a wide range of substrates. The test can be used to quantify tensile adhesion strength and identify a failure mode, showing the weakest place in the tested system. However, the measured tensile strength is only the adhesion property at the time of testing, temperatures and environmental conditions. It remains a challenge to flexible pavement industries to develop an improved method for assessment of adhesion mechanisms.

2 ADHESION TEST METHODS

A variety of techniques based on the pull-off test have been adopted in evaluating binder-aggregate adhesion properties. Pneumatic Adhesion Tensile Testing Instrument (PATI) device was initially developed by the National Institute of Standards and Technology (NIST) to evaluate the adhesive bond strength of aggregates and bitumen in the presence of water or moisture. The modified version of the PATI device has been used by Kanitpong and Bahia (2003), Kanitpong and Bahia

(2004) and Kanitpong and Bahia (2005) in measuring the moisture-damage mechanisms based on the ASTM D4541 (Standard Test Method for Pull-Off Strength of Coating using Portable Adhesion Testers). A small asphalt sample is applied on a proper metal pull-stub that is pressed immediately onto a prepared aggregate surface to establish good bitumen-aggregate bond. A self-aligning piston and a reaction plate are screwed to the pull-stub and a pulling force is exerted using a pneumatic system. The pulling force is increased and failure occurs when the adhesive strength of the asphalt-aggregate system or the cohesive strength of the asphalt is reached. The control module records the failure force, which is converted into pull-off tensile strength (kPa) as a function of the bonding surface area.

Copeland (2007) modified the procedures for specimen preparation by introducing a device to allow for the compression of the specimens, and thus enabled a better controlling of the thickness of bitumen films. Canestrari et al. (2010) and Santagata et al. (2009) suggested a repeatable, reliable, and practical method for investigating the adhesion and cohesion properties of bitumen-aggregate systems based on the PATTI by using a modified version of the PATTI (the head of the pull-stub was improved with a 200 μm thick parametrical edge and eight cuts made along the edge allowed the excess asphalt binder to flow out as the stub was pressed on the aggregate surface. With these improvements the PATTI results became more reliable and the device became a practical tool to evaluate the adhesion/cohesion properties of the asphalt-aggregate system and the effects of moisture damage.

Research conducted at the University of Wisconsin-Madison (UWM) identified the PATTI, as an appropriate instrument for evaluating bond strength development in the newly developed Bitumen Bond Strength (BBS) test. (AASHTO TP-91, 2011) Recently developed at UWM in conjunction with the University of Ancona-Italy and the University of Stellenbosch-South Africa, the BBS test procedure has been used successfully to characterize moisture sensitivity and bond strength development in hot applied binders and bitumen emulsions, respectively (Miller 2010; Greyling et al. 2011; Greyling 2012).

A modified PATTI was developed to integrate the conventional measure of pressure with the additional measure of vertical displacement. The measurement of vertical displacement was used to estimate the deformation within the bitumen film and therefore the final strain at failure to estimated adhesion energy at failure (Merusi et al. 2013).

Merusi et al. (2013) tried to estimate the total work done by the external forces to separate the bitumen-aggregate interfaces. Energy-based criteria for adhesive/cohesive tensile failure were consequently established accounting for the elongation of the bitumen film. The interface bond energy and its stability upon moisture conditioning were then measured for different bitumen-aggregate systems.

A mechanistic design tool was developed at Delft University of Technology for Porous Asphalt Concrete called Lifetime Optimization Tool (LOT). The idealized adhesive zone represented by two stone columns glued by thin bitumen inter layer (a 6.7 mm diameter are used in DMA and DSR fatigue tests to give insight into adhesive zone fatigue behavior. Between two stone columns a 15 μm interface binder layer is assembled are placed in the same clamps in the rheometer during the DSR tests) was proved to be able to well explain the behavior of the region where the mortar meets the stone surface, i.e. the interface adhesion plus interfacial transition zone. Mo et al. (2011) and Mo (2010).

Kringos N. (2007) developed a computational tool for the fundamental analysis of combined mechanical and moisture induced damage of asphaltic mixes, which includes both physical and mechanical moisture damage inducing processes. Such a tool can greatly contribute to an improved material selection procedure and give insight into the various competing damage inducing processes within the asphalt mix. Lent et al. (2008); in order to quantification of the adhesion between bitumen and aggregates several experiments are conducted on bitumen-aggregate specimens. From the results of this research it is concluded that the treatments used for preparations of the stone samples for the laboratory experiments have influenced the surface characteristics of the stone samples.

Masad et al. (2010) and Howson (2011) presented a critical review of several studies in the areas of adhesives and polymers that demonstrate and explain the relationship between the ideal works of fracture or bond energy calculated based on surface free energy, and the practical work of fracture obtained from mechanical tests. These studies are very useful in understanding some mechanisms that govern the fracture behaviour of asphalt binders and asphalt mixtures, and to develop an experimental setup for conducting pull-off tests on asphalt binders that allow recording the force and displacement throughout the test. Masad et al. (2010) explained that practical work of fracture included all stored and dissipated components of energy (elastic, viscoelastic and plastic) that are associated with the deformation process.

3 OBJECTIVES OF THE STUDY

The main objectives of this study were to:

1. Establish the criteria and procedures for the proposed adhesion test method in terms of test setup and apparatus, specimen preparation, testing and data analysis; and
2. Evaluate different parameters (binder thickness, aggregate types, rate of applied load, test temperature and conditioning procedure) on the maximum tensile bond strength and tensile energy required to produce failure.

Table 1. Aggregate properties.

Composition	Agg. 1	Agg. 2
Petrological class	Sandstone	Tuff stone
SiO ₂ content (%)	62.72	51.21
Loss on Ignition (%)	3.1	9.3
Aggregate Abrasion Value (AAV)	4.4	4.61
Los Angeles Abrasion (LA)	12	14
Polished Stone Value (PSV)	63	68

4 METHODOLOGY

The experimental setup used by Masad et al. (2010) and Howson et al. (2012) developed in this research to measure the applied force and displacement of bitumen-aggregate samples with different film thicknesses. In summary, the force was recorded using servo hydraulic frame 5-kip (22.24 KN) load cell and displacement of the thin binder film was measured directly using Series IX Automated Materials Testing System ver 5.28 software, a high-resolution digital camera with image correlation software. The following factors were varied in testing each bitumen binder-aggregate combination (binder film thickness, deformation rate of loading, test temperature and condition procedures); in this study, specimens were subjected to dry conditioning at 10 and 20°C for 24 hrs before testing and, specimens were immersed in containers filled with water, before being placed in the conditioning cabinet for 24 hrs prior to testing at 20°C.

5 EXPERIMENTAL WORKS

5.1 Material; were included

5.1.1 Aggregates

Two types of aggregate which are suitable for use in surface layer of pavement Agg. 1 and Agg. 2 were selected; these materials were delivered in rocks of approximately 10 kg each. Analysis of mineral and chemical properties of selected aggregate and predicted relationship with water from chemical composition was conducted, as shown in Table 1.

The aggregate surface is always to some extent acidic and to some extent basic. Therefore a classification is made based on the silica (SiO₂) content of the aggregate to determine the dominance of acidic or basic properties. Majidzadeh & Brovold (1968). It can be seen from Table 1; Agg. 1 shows a higher SiO₂ content compared with Agg. 2, indicating that Agg. 1 is more acidic, or less basic than Agg. 2. Generally, a more acidic aggregate surface is more likely to strip than basic aggregates and thus increase the susceptibility to stripping. (Smith et al. 2001).

5.1.2 Binders

Four types of bitumen binder were selected for use in this study, as shown in Table 2.

Table 2. Binder types and symbols.

Binder Type	Penetration Grade	Symbol
Conventional	50	B1
	70	B2
Polymer Modified	50	B3
	70	B4

Table 3. Physical & rheological properties of binders

Test	Bitumen Binder Types			
	B1	B2	B3	B4
Penetration	41	65	44	77
Softening Point	53.8	47	63.4	54.4
Dynamic (absolute) viscosity	0.457	0.398	1.384	0.893
Complex Modulus (G*) *10 ⁷ @ 10°C and 10 Hz	3.23	4.13	1.50	1.87
Phase Angle (δ°)	37.38	39.15	42.49	46.99
Complex Modulus (G*) *10 ⁶ @ 10°C and 10 Hz	9.72	12.3	6.05	5.37
Phase Angle (δ°)	45.05	53.51	50.29	58.63
PI*	-0.5	-1.5	1.3	1

*(Read et al. 2003)

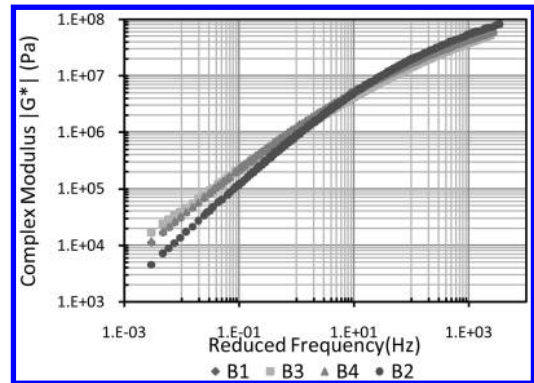


Figure 1. Master curves for the four binders used.

The physical and mechanical properties of the binders which are used are shown in the following Table 3. The complex shear moduli (G*) of the binders at different frequencies and temperatures were tested using DSR and their master curves at reference temperature 20°C were plotted, as shown in Figure 1.

5.2 Sample preparation

5.3 Aggregate stubs

Aggregate stubs were prepared by cutting the rock into sheet plate with uniform thickness (20–30 mm) by electrical sawing and coring with 12- mm diameter. Hence, large contact area will increase the probability

of the occurrence of cavitation. Therefore we chose a small contact area, in order to reduce the chance of cavitation. Both surfaces of the aggregate stubs were then polished (the polishing process included four stages using silicon carbide abrasive paper discs 180, 240, 600 and 1200 μm (MetPrep)) in order to obtain smooth and flat surfaces (relatively constant surface roughness in order to make zero gap by DSR). Dust from the sawing and drilling process and polishing powder was removed by cleaning the aggregate core samples (aggregate stubs) by immersion in distilled water, which was boiled for 15 min, and then drying with hot air. The aggregate stubs were marked by numbering both parts of pairs. The specific gravity of each aggregate type was calculated and the percentage of absorption for each pair of samples was determined. The finished aggregate stubs were placed in an oven for 12 hours at 160°C to remove all moisture from the stubs.

5.3.1 Bituminous binder

Bituminous binder samples were prepared between the two aggregate stainless steel holders using a Kinexus Pro+ rheometer (manufactured by Malvern Instrument Company, with a gap resolution of 0.1 μm). The aggregate stub stainless steel holders (some changes were made on the base and top plate parts of rheometer; these included manufacturing the end connections and the steel holder parts to fix the aggregate stubs in proper position). A stainless holder is shown in Figure 2.

After alignment of the stubs in the steel holders was checked, the aggregate sample was heated within the environmental cabinet, to remove water vapour and organic matter. A small drop of bitumen binder, heated to 140°C, was applied to the surface of the bottom aggregate stubs. The gap was reduced to the desired film thickness and the sample was allowed to cool for 15 minutes before the excess bitumen binder was removed by means of a heated knife. The prepared aggregate-binder sandwiches were conditioned for 24 hours at test temperature (10 or 20°C) to achieve full adhesive bond. After conditioning, the aggregate-binder sandwiches were moved to the testing chamber, which was maintained at a constant test temperature of 10 or 20°C.

5.3.2 Aggregate-binder sandwich

- A test aggregate-binder sandwich holder (steel for dry condition and aluminium for wet condition)



Figure 2. Aggregate steel holder and fixing device.

was manufactured in order to install the aggregate-binder, within the test machine as shown in Figure 2. The surfaces of holes for the fixing holders were cleaned of dust and previous gluing by hand with a chemical solution (white spirit solvent) in order to ensure cleanliness.

- The bottom and inside wells of the holes in both upper and bottom fixing steel holders were glued (Araldite 2012 for dry condition and Araldite 2021 for wet condition). The gluing period lasted for about half hour according to the company's specification in order to obtain a full connection
- The aggregate-binder sandwiches to rest horizontally by using a developed fixing device, as shown in Figure 2, while maintaining perfect alignment, in order to minimize any creep within the bitumen film induced by the weight of the upper steel holder Installed aggregate finger in fixing device for bottom part and late the upper part sliding slowly.

5.4 Testing and data acquisition systems

Testing of the aggregate-binder sandwich samples was performed using a servo hydraulic frame. The software controlled the operation of the testing machine and recorded force, loading rate, and displacement history. The entire testing apparatus was contained inside an environmental chamber that controlled the test temperature at 10 and 20°C. The stainless steel grips were custom designed to hold the sample holders. The upper grip was attached directly into the load cell, and the lower grip was attached to the floor of the testing chamber by means of a locking silicone-stainless steel joint. The locking silicone-stainless steel joint served the purpose of aligning the top and lower grips. A prepared aggregate-bitumen sample was inserted into the bottom grip, Figure 3, and locked in using a compression joint. The inside of the bottom grip was textured to provide a better hold and prevent the sample from moving during testing. The upper grip was lowered and attached to the sample through bearing force on a screw.

5.5 Analysis of failure mode

Types of failure (adhesive or cohesive failure) were determined based on the calculated percentage area of



Figure 3. Test setup for sample.

Table 4. Estimated binder thickness for adhesive failure.

Bitumen type	Estimated thickness (μm)		
	Mode of Failure		
	Adhesive Percentage area of adhesive $\geq 75\%$	Mixed 50%	Cohesive $\leq 25\%$
B1	16	47	78
B2	13	21.6	75
B3	11.6	21	70
B4	12	20.6	69

adhesive failure. Howson et al. (2010) and Howson (2011) used image analysis software ImageJ to calculate the grey intensity of the surface to estimate the total percentage area of adhesive failure was in the range of 5% to 45%, which is too low to be considered as sufficient for the occurrence of the adhesive mode of failure. In this study, adhesive mode of failure was characterised by the value of the total percentage area of adhesive failure of more than 75%, 25% for cohesive mode of failure and 50% for mixed mode of failure, as shown in Table 4 (BS EN ISO 4624:2003 and California Test 302; 2013). Immediately after completion of the test, the specimen was removed, and each aggregate sample holder was photographed using a camera (the resolution used was 8 megapixel digital camera, 3264 x 2448 pixels for 0.27*0.27 mm) in order to investigate the predominant type of failure (i.e. adhesive or cohesive). The percentage area of adhesive failure is a very important parameter to predict types of failure (adhesive or cohesive failure); calculations were determined via image processing of the top and bottom of each pair of aggregate stubs after failure.

The image analysis Paint.net 4.0v software was used to selected the circular image for the surface of the failure and then ImageJ 1.48v software was used to transfer circular colour image to gray scale and calculate the gray intensity of the failure surface by using program written in MatLab 14 e software to predicted the percentage area of adhesive failure (low gray intensity $\leq 50\%$). The gray level rises as more of the sample holder substrate becomes exposed, indicating more adhesive or less cohesive failure as shown in Figure 4. The adhesion contact area was then calculated from this equation:

$$A_a = P_a * A_T \quad (1)$$

where; A_a = the adhesive contact area, P_a = average percentage area of adhesive, and A_T = total contact area (113.143 mm²).

Best-fit curve has been plotted to determine the relationship between total percentage area of adhesive failure and various thicknesses of adhesive layer of bitumen, as illustrated in Figure 5.

The types of failure of either can be modelled as an S-shaped curve with respect to the thickness of

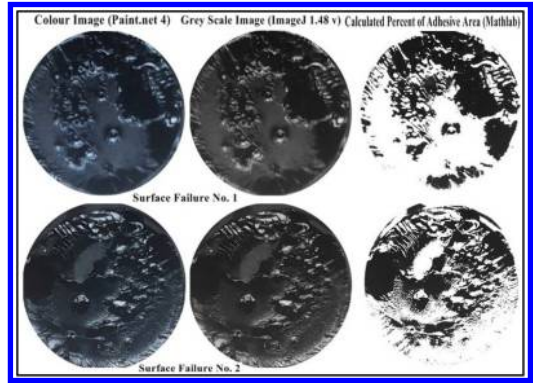


Figure 4. Example of image process.

the adhesive layer of bitumen. Hence, based on the specified bitumen and testing conditions, transition of the mode of failure of either adhesive or mixed cohesive and adhesive is expected to occur at the thickness shown in Table 4. It can be seen from Figure 5 that the transition of adhesive mode of failure for all asphalt binder types used is less than 16 μm for original bitumen binder and reduced to approximate 12 μm for modified as binder. Compared to the micromechanics analysis conducted by Lytton et al. (2005), transition of the mode of failure was expected to occur at a lower thickness of about 60 μm (0.060 mm).

6 RESULTS AND DISCUSSIONS

The experimental results obtained from the developed test setup for conducting pull-off test on asphalt binders with different variables (binder thickness, test temperature, aggregate types, test conditioning and rates of deformation) have been demonstrated.

6.1 Effect of binder thickness on the required energy to failure (practical energy)

The maximum applied load and displacement resulting from the direct tension test in four types of bitumen binder are shown in Figures 6 and 7 and Tables 5 and 6.

It can be observed that:

1. Increasing the thickness of the binder layer will increase the thickness of the cohesion layer and so increase the forces of cohesion between particles of bitumen, and these forces are weak, will decrease the amount of tensile strength required to failure and increase displacement as result reduced the amount of work required to failure (the amount of energy generated by applied load and stored in binder layer will be the largest forces that bind bitumen molecules and break these ties between particles). The stored energy in the bitumen layer will run on increase internal temperature and reduced viscosity and stiffness of the bitumen to resist increase in the deformation.

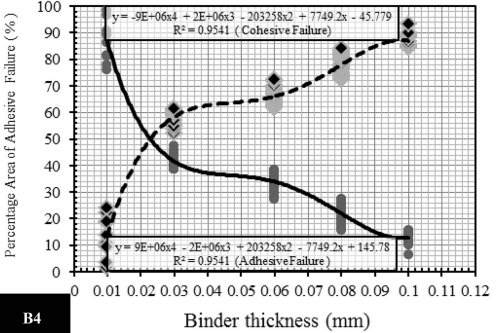
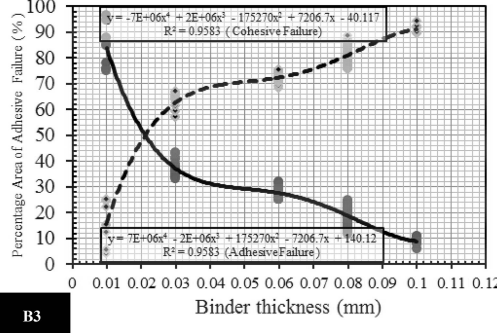
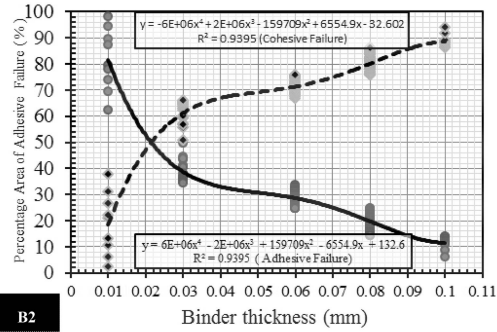
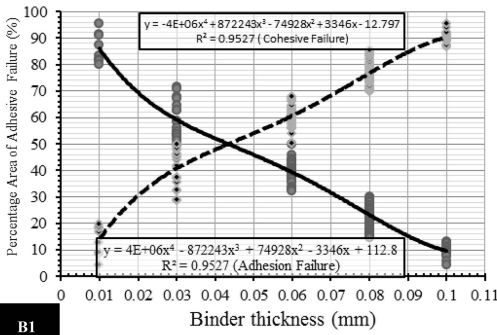


Figure 5. Total percentage area of adhesive failure and various thicknesses of adhesive layer of bitumen.

2. The reduction in max. tensile load applied to failure from thinnest to thicker binder thickness as shown in Table 7. It can be seen that the reduction ratio from 0.01 to 80 mm for B2 is smaller than other types.

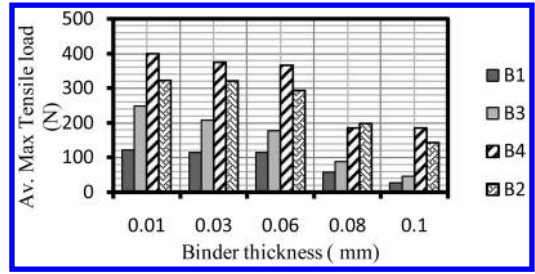


Figure 6. Av. Max. Tensile load at failure.

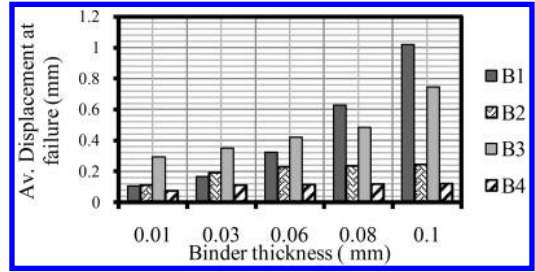


Figure 7. Displacement at failure point.

Table 5. Av. Max. Tensile load with standard deviation.

Binder Thickness (mm)	Av. Max Tensile load at failure, Lf (N)							
	B1		B2		B3		B4	
	Lf	σ	Lf	σ	Lf	σ	Lf	σ
0.01	122.52	3.19	321.78	9.21	207.73	1.95	400.17	1.74
0.03	115.70	5.81	320.32	4.74	249.03	8.27	375.47	3.77
0.06	115.34	1.53	293.95	8.68	178.12	1.94	365.51	4.04
0.08	58.12	1.57	198.03	5.60	88.59	2.25	184.61	7.48
0.10	27.34	1.25	142.41	2.20	46.11	3.11	185.31	9.35

Test condition (Agg. 2, Test temp. 10°C, dry condition and rate = 30 mm/min)

Table 6. Av. Displacement with standard deviation.

Binder Thickness (mm)	Av. Displacement at failure, Df (mm)							
	B1		B2		B3		B4	
	Lf	σ	Lf	σ	Lf	σ	Lf	σ
0.01	0.11	0.42	0.11	0.07	0.30	0.21	0.08	0.02
0.03	0.17	0.76	0.19	0.22	0.35	0.17	0.11	0.01
0.06	0.32	0.78	0.23	0.09	0.42	0.07	0.12	0.05
0.08	0.63	0.37	0.24	0.01	0.48	0.22	0.12	0.03
0.1	1.02	0.50	0.24	0.07	0.75	0.01	0.12	0.03

6.2 Practical work for fracture (failure energy)

Based on Harvey and Cebon (2005), the value of the tensile energy required to produce failure can be best described by the area under the curve of graph of tensile load versus pull-off displacement. The force and

Table 7. Reduction ratio in applied tensile load.

Binder thickness (mm)	Reduction in av. Max Tensile load at failure (%)			
	B1	B2	B3	B4
0.01	0.00	0.00	0.00	0.00
0.03	5.57	0.45	16.58	6.17
0.06	5.86	8.65	28.48	8.66
0.08	52.56	38.46	64.43	53.87
0.1	77.69	55.74	81.48	53.69

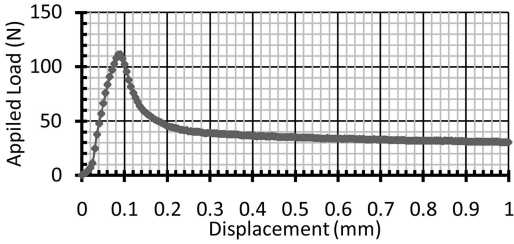


Figure 8. Load-displacement curve.

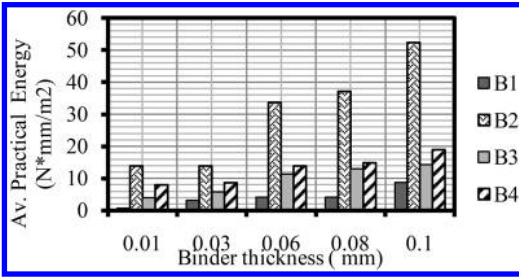


Figure 9. Effect of binder thickness on the Practical energy.

Table 8. Average and standard deviation of practical work of fracture.

Binder Thickness (mm)	Av. Practical Fracture Energy (N*mm/m ²)							
	B1		B2		B3		B4	
	Wp	σ	Wp	σ	Wp	σ	Wp	σ
0.01	0.61	0.15	13.83	3.40	3.91	0.54	7.89	1.02
0.03	3.18	2.60	13.91	5.51	5.72	2.62	8.64	1.35
0.06	4.03	4.43	33.69	6.59	11.28	3.40	13.87	1.65
0.08	4.07	5.46	37.12	8.73	13.02	5.17	14.90	2.62
0.10	8.77	7.91	52.44	9.38	14.31	8.42	18.88	11.05

displacement history data were combined. Microsoft Excel has been used to calculate the area under the curve of graph of tensile load versus pull-off displacement and to calculate the total practical work of fracture (Wp) as shown in Figure 8.

The results of practical work of fracture (failure energy) for the four types of binder with different binder thickness are presented in Figure 9 & Table 8.

Table 9. Effect of moisture conditions.

Binder Thickness (mm)	Av. Practical Energy (N*mm/m ²) in Dry Condition							
	B1		B2		B3		B4	
	Wp	σ	Wp	σ	Wp	σ	Wp	σ
0.01	17.28	2.39	4.45	3.62	22.38	1.44	37.16	2.58
0.03	31.07	2.21	13.79	2.85	25.47	5.02	38.41	1.88
0.06	42.95	1.05	19.64	0.56	38.56	1.77	46.42	1.84
Binder Thickness (mm)	Av. Practical Energy (N*mm/m ²) in Wet Condition							
	B1		B2		B3		B4	
	Wp	σ	Wp	σ	Wp	σ	Wp	σ
0.01	15.26	2.06	10.77	3.18	18.85	0.57	24.58	1.30
0.03	14.02	8.88	11.71	2.05	22.72	4.11	24.79	2.05
0.06	28.89	2.17	19.38	1.30	23.31	1.43	27.31	3.68

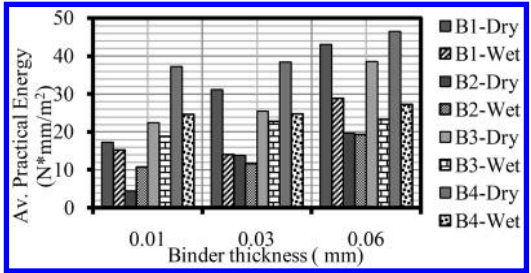


Figure 10. Effect of moisture conditions.

It can be seen from data in Table 8 and Figure 14 that the required energy to fracture increased with increasing binder thickness.

6.3 Effect of moisture conditions

Conditioning procedures (dry or wet); were found to have a deep effect on the test result. The bitumen-aggregate binder sandwiches were submerged in water for 24 hrs. All binder sandwiches were prepared with varied binder thickness (10, 30 and 60 μm) and were tested at 20°C with deformation rate of loading (30 mm/min). The results are tabulated in Table 9 and Figure 10.

When aggregate stubs were immersed in water (wet condition), the water penetrated the aggregate stubs and then worked to weaken the adhesion forces within the binder layer; thus, this will increase the distortion and reduce the tensile strength required to failure and so decrease the required work to failure.

It can be concluded from the summarized data of test results in Table 9 and Figure 11 that, work required to fracture of samples subjected to dry conditioning was higher compared to those subjected to wet conditioning.

6.4 Effect of change in deformation rate

Bitumen is a visco-elastic material and resistance of this material to the applied load depends on the cohesion force between binder particles and adhesion

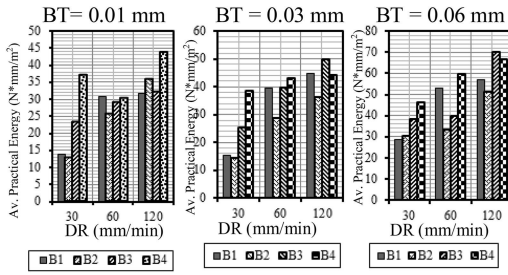


Figure 12. Effect of deformation rate on the failure energy.

Table 10. Effect of deformation rate.

Av. Practical Energy (N*mm/m ²) at 20°C								
Deformation Rate (DR) (mm/min)	B1		B2		B3		B4	
	Wp	σ	Wp	σ	Wp	σ	Wp	σ
Binder Thickness (0.01 mm)								
30	14.02	2.06	12.88	4.55	23.38	3.44	37.16	3.58
60	30.81	4.33	25.59	0.66	28.96	1.31	30.25	3.22
120	31.65	3.24	35.7	1.56	32.28	6.87	43.91	1.37
Binder Thickness (0.03 mm)								
30	15.26	2.88	14.44	0.87	25.47	5.02	38.41	4.88
60	39.56	5.77	28.72	4.87	39.52	2.58	43.22	2.58
120	44.8	3.1	36.36	0.87	49.73	1.17	44.23	1.3
Binder Thickness (0.06 mm)								
30	28.89	2.17	46.42	1.84	30.62	2.57	38.56	1.77
60	53.22	8.58	59.85	5.39	33.52	3.62	39.75	3.26
120	56.79	1.62	66.39	3.56	51.04	1.74	70.33	3.14

force between aggregate and binder; these forces need enough time to work together.

Increasing the deformation rates will not give enough time for the cohesion force between the binder molecules to work and assist in the tensile strength resistance (viscosity and stiffness of the binder need more time); so the resistance process will depend on the adhesion strength between the bitumen and aggregates, and this force will be great and require greater force to break it and thus will increase applied force and then increase the work required to failure. It can be concluded that, the practical work to failure increase with an increase in deformation rate of applied load, as shown from Figure 12 and Table 10.

6.5 Effect of testing temperature

The test temperature is a very important parameter affecting binder properties. Increasing the test temperature will decrease viscosity and stiffness of binder layer and increase deformation (displacement) and therefore reduce required tensile strength to failure and decrease the work required to failure. The results of practical work required to failure are summarised in Table 11 and Figure 13.

Table 11. Effect of test temperature on the Practical energy.

Binder Thickness (BT) (mm)	Av. Practical Energy (N*mm/m ²) at 10°C							
	B1		B2		B3		B4	
	Wp	σ	Wp	σ	Wp	σ	Wp	σ
0.01	14.02	2.06	5.42	5.50	15.38	4.44	37.16	2.58
0.03	15.26	8.88	12.66	4.46	25.47	5.02	38.41	4.88
0.06	28.89	2.17	14.61	2.51	38.56	1.77	46.42	1.84
0.08	31.20	3.64	15.98	1.34	50.32	1.65	51.32	4.86
0.1	33.22	4.25	31.47	1.67	54.15	2.12	54.26	5.16
Av. Fracture Energy (N*mm/m ²) at 20°C								
0.01	2.55	1.37	4.45	7.62	8.14	0.08	16.73	3.85
0.03	4.09	3.03	13.79	9.85	11.63	7.02	17.63	1.88
0.06	7.06	4.91	19.64	0.56	17.77	1.79	23.89	6.28
0.08	8.71	5.37	22.64	2.05	28.03	1.40	24.01	2.60
0.1	11.81	1.71	25.34	1.45	28.89	2.42	27.09	3.46

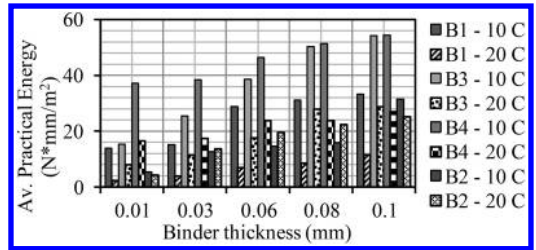


Figure 13. Comparison in fracture energy for four binders with different test temperatures.

When test temperature was increased the practical work (failure energy) required to cause failure reduced. This decrease was the result of a decrease in the failure load and/or a displacement at failure due to softening of bitumen binder and loss of its viscosity, as shown in the following figure and table.

6.6 Effect of aggregate type

Agg. 1 can be classified as a hydrophilic aggregate due to increasing the proportion of SiO₂ content compared with Agg. 2 (Smith et al. 2001). Thus it tends to strip more readily since water more easily replaces the bitumen film over each particle. It can be concluded the tensile bond strength value for Agg. 2 is higher than Agg. 1 as shown from Figure 14 and Table 12.

7 CONCLUSION

From the work presented on the proposed laboratory adhesion test, the following conclusion can be made:

- The experimental results showed that, as the thickness of the binder layer increased, the failure mode transitioned from adhesive to cohesive.
- Experimental data also showed that an increase in film thickness of the binder layer resulted in

Table 12. Effect of aggregate types on the Practical energy at dry condition ant 10°C.

Binder Thickness (mm)	Agg. Types	Av. Practical Energy (N*mm/m ²)							
		B1		B2		B3		B4	
		Wp	σ	Wp	σ	Wp	σ	Wp	σ
Deformation rate = 30 mm/min and test temp. 10°C									
0.01	Agg. 1	7.61	1.40	4.45	7.62	21.60	6.43	30.82	5.25
0.03		9.34	3.72	13.79	9.85	24.03	2.56	34.12	3.39
0.06		14.14	2.13	19.64	0.56	25.11	4.44	36.15	2.50
0.01	Agg 2	14.02	2.06	12.88	7.55	23.38	5.44	37.16	3.58
0.03		15.26	8.88	14.44	3.87	25.47	5.02	38.41	1.88
0.06		28.89	2.17	30.62	7.57	38.56	1.77	46.42	2.84
Deformation rate = 60 mm/min and test temp. 10°C									
0.01	Agg. 1	15.08	3.03	25.02	1.23	2.78	0.64	25.57	5.05
0.03		21.88	6.56	36.54	4.14	13.71	5.36	28.62	2.90
0.06		22.80	2.25	43.04	4.91	36.73	0.56	28.81	3.72
0.01	Agg. 2	30.81	4.33	30.25	3.22	25.59	0.66	28.96	1.31
0.03		39.56	5.77	43.22	2.58	28.72	4.87	39.52	2.58
0.06		53.22	8.58	59.85	4.39	33.52	3.62	39.75	3.26
Deformation rate = 120 mm/min and test temp. 10°C									
0.01	Agg. 1	9.95	6.00	2.22	0.23	29.11	2.54	38.32	3.62
0.03		13.40	3.69	12.65	1.44	34.61	5.39	38.78	5.76
0.06		26.23	1.03	44.74	0.56	36.27	4.94	52.83	1.53
0.01	Agg. 2	9.95	6.00	35.70	1.56	32.28	6.87	43.91	1.37
0.03		13.40	3.69	36.36	0.87	49.73	1.17	44.23	2.30
0.06		26.23	1.03	51.04	1.74	70.33	3.14	66.39	3.56

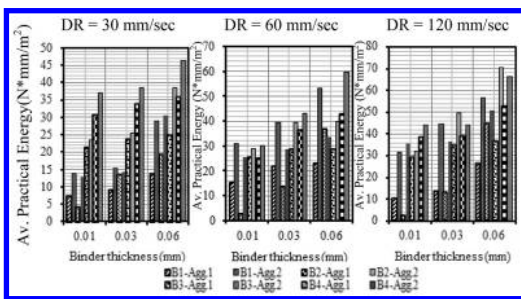


Figure 14. Effect of change aggregate types on the practical energy.

a decrease in the maximum tensile force at failure, an increase in the total displacement until failure, and an increase in the practical work of fracture.

- Mode of failure was found to change from adhesive to mixed cohesive and cohesive, and then expected to become fully cohesive as the thickness of adhesive layer of bitumen is continuously increased.
- Practical work (energy required to failure) of specimens subjected to dry conditioning was higher compared to the specimens subjected to wet conditioning (largest decrease in the practical work to

fracture was due to moisture conditioning in every test).

- The transition of adhesive mode of failure for all binder types used is less than 16 μm for original asphalt binder and reduced to approximate 12 μm for modified asphalt binder. Compared to the micromechanics analysis conducted by Lytton et al. (2005), transition of the mode of failure was expected to occur at a lower thickness of about 60 μm (0.060 mm).
- The cohesive mode of failure is characterised by the value of the total percentage area of adhesive failure of less than 75%. For the range greater than 75% of the total percentage area of adhesive failure, mode of failure can be classified as mixed cohesive and adhesive.
- Testing temperature and deformation rate both affected the measured practical work required to failure; when test temperature increased viscosity of binder decreased and then reduced ability to resist tensile bond strength and decreased required work to failure; and increasing the deformation rate increased the practical work for every binder and aggregate type.
- The aggregate substrate has a great effect on the tensile bond strength. Agg. 2 substrate performed in a superior manner to Agg. 1 in every test. It resulted in higher practical work to fracture with

changes in binder thickness, moisture conditioning and increased test temperature and rate of load is higher than Agg. 1. Agg. 1 required higher practical work to failure as compared to Agg. 2.

ACKNOWLEDGEMENTS

The authors would like to acknowledge Pavement Testing Services (PTS) for their assistance with some of the binder tests conducted.

REFERENCES

- Airey, G. D. & Choi, Y.-K. 2002. "State of the Art Report on Moisture Sensitivity Test Methods for Bituminous Pavement Materials". *Road Materials and Pavement Design*, Vol. 3, pp. 355–372.
- Canestrari, F., Cardone, F., Graziani, A., Santagata, F. A. & Bahia, H. U. 2010. "Adhesive and Cohesive Properties of Asphalt-Aggregate Systems Subjected to Moisture Damage". *Road Materials and Pavement Design*, Vol. 11, pp. 11–32.
- Caro, S., Masad, E., Bhasin, A. & Little, D. N. 2008a. Moisture susceptibility of asphalt mixtures, Part 1: mechanisms. *International Journal of Pavement Engineering*, 9, 81–98.
- Caro, S., Masad, E., Bhasin, A. & Little, D. N. 2008b. "Moisture Susceptibility of Asphalt Mixtures, Part 2: Characterisation and Modelling". *International Journal of Pavement Engineering*, Vol. 9, pp. 99–114.
- Copeland, A. R. 2007. "Influence of Moisture on Bond Strength of Asphalt-Aggregate Systems". PhD thesis, Vanderbilt University.
- Curtis, C. W., Lytton, R.L. & Brannan, C.J. 1992. "Influence of Aggregate Chemistry on the Adsorption and Desorption of Asphalt". *Transportation Research Record 1362, TRB*, National Research Council, Washington, D.C., pp. 1–9.
- Greyling, A. H. 2012a. "Development of a Standard Test Method for Determining the Bitumen Bond Strength of Emulsions-A South African Perspective". Stellenbosch University.
- Greyling, A. H. 2012b. "Development of a Standard Test Method for Determining the Bitumen Bond Strength of Emulsions-A South African Perspective". Stellenbosch University.
- Greyling, A. H. 2012. "Development of a Standard Test Method for Determining the Bitumen Bond Strength of Emulsions-A South African Perspective", MSc. Thesis Stellenbosch University.
- Harvey, J. & Cebon, D. 2005. "Fracture Tests on Bitumen Films". *Journal of materials in civil engineering*, Vol. 17, No. 1, pp. 99–106.
- Howson, J., Masad, E., Little, D. & Kassem, E. 2012. "Relationship Between Bond Energy and Total Work of Fracture for Asphalt Binder-Aggregate Systems". *Road Materials and Pavement Design*, Vol. 13, pp. 281–303.
- Howson, J. E. 2011. "Relationship Between Surface Free Energy and Total Work of Fracture of Asphalt Binder and Asphalt Binder-Aggregate Interfaces", PhD thesis Texas A&M University.
- Institution, B. S. BS EN 13302:2010. "Bitumen and Bituminous Binders. Determination of Dynamic Viscosity of Bituminous Binder using a Rotating Spindle Apparatus", British Standard Institution, London.
- Kantpong, K. & Bahia, H. 2005. "Relating Adhesion and Cohesion of Asphalts to the Effect of Moisture on Laboratory Performance of Asphalt Mixtures". *Transportation Research Record: Journal of the Transportation Research Board*, Vol. 1901, pp. 33–43.
- Kanitpong, K. & Bahia, H. U. 2003. "Role of Adhesion and Thin Film Tackiness of Asphalt Binders in Moisture Damage of HMA". Association of Asphalt Paving Technologists Technical Sessions, Lexington, Kentucky, USA.
- Kringos, N., Scarpas, A., Copeland, A. & Youtcheff, J. 2008a. "Modelling of Combined Physical-Mechanical Moisture-Induced Damage in Asphaltic Mixes Part 2: Moisture Susceptibility Parameters". *International Journal of Pavement Engineering*, Vol. 9, pp. 129–151.
- Kringos, N., Scarpas, T., Kasbergen, C. & Selvadurai, P. 2008b. "Modelling of Combined Physical-Mechanical Moisture-Induced Damage in Asphaltic Mixes, Part 1: Governing Processes and Formulations". *International Journal of Pavement Engineering*, Vol. 9, pp. 115–128.
- Lillte, D. N. & Jones, D. 2003. "Chemical and Mechanical Processes of Moisture Damage in Hot-Mix Asphalt Pavements". *Transportation Research Board National Seminar*, San Diego, CA, USA, pp. 37–70.
- Majidzadeh, K. & Brovold, F. N. 1968. "State of the Art: Effect of Water on Bitumen-Aggregate Mixtures", Special HRB Report 98, Highway Research Board, National Research Council.
- Masad, E. A., Howson, J. E., Bhasin, A., Caro, S. & Little, D. N. 2010. "Relationship of Ideal Work of Fracture to Practical Work of Fracture: Background and Experimental Results". *Journal of the Association of Asphalt Paving Technologists*, Vol. 79, pp. 81–118.
- Miller, T., Greyling, A., Bahia, H. & Jenkins, K. 2010. "Development of a Test Method for Determining Emulsion Bond Strength using the Bitumen Bond Strength (BBS) test: a South African Perspective". *International Sprayed Sealing Conference, 2nd*, Melbourne, Victoria, Australia.
- Mo, L., Huurman, M., Wu, S. & Molenaar, A. 2011. "Bitumen-Stone Adhesive Zone Damage Model for the Meso-Mechanical Mixture Design of Ravelling Resistant Porous Asphalt Concrete". *International Journal of Fatigue*, Vol. 33, pp. 1490–1503.
- Moraes, R., Velasquez, R. & Bahia, H.U. 2011. "Measuring the Effect of Moisture on Asphalt-Aggregate Bond with the Bitumen Bond Strength Test". *Transportation Research Record: Journal of the Transportation Research Board*, Vol. 2209, pp. 70–81.
- Read, J. & Whiteoak, D. 2003. "The Shell Bitumen Handbook", 5th edition, Thomas Telford Publishing.
- Santaga, F., Cardone, F., Canestrari, F. & Bahia, H. U. 2009. "Modified PATTI Test for the Characterization of Adhesion and Cohesion Properties of Asphalt Binders". 6th International Conference on Maintenance and Rehabilitation of Pavements and Technological Control (MAIREPAV6).
- Smith, M. R., Collis, L. & Fookes, P. 2001, "Aggregates: Sand, Gravel and Crushed Rock Aggregates for Construction Purposes", 3rd edition, Geology Special Publication No. 17. Geological Society of London.
- State of California, T.A.H.A. 2014. "Method of Test for Film Stripping", Test 302, Dept. of Transportation Division of Engg. Services.
- Van Lent, D., Molenaar, A. & Van De Ven, M. 2008. "Aggregate Characterisation in Relation to Bitumen-Aggregate Adhesion". MSc. thesis, Delft University of Technology.

Evaluation of aging in asphalt cores at room temperature using low field nuclear magnetic resonance

I. Menapace & E. Masad

Texas A&M University at Qatar, Doha, Qatar

G. Papavassiliou

Institute of Advanced Materials Physicochemical Properties Nanotechnology and Microsystems NCSR Demokritos, Attiki, Greece

E. Kassem

Texas A&M Transportation Institute, College Station, USA

ABSTRACT: In this paper, an innovative methodology that estimates the relative aging of asphalt cores is introduced. Asphalt concrete samples with different porosities (4, 7, and 10 percent) and aging conditions (unaged, 3-month, and 6-month aged) were investigated with Low Field Nuclear Magnetic Resonance (NMR) at room temperature. Unaged samples and samples with 4 percent air voids showed the highest amplitudes in the T_2 distributions, which correspond to the lowest viscosities, which imply a lower aging extent. The results were as expected, since oxidation reactions increase the viscosity and a higher percent air voids facilitates oxygen access. The advantage of the Low Field NMR analysis of aging compared to traditional methods is that it does not require binder extraction and is more accurate than analyses relying on mechanical measurements. Therefore, this method could be applied to assess aging of pavements throughout their life.

1 INTRODUCTION

Asphalt oxidation is a phenomenon that occurs in asphalt binders, leading to increase in stiffness, embrittlement and the progressive loss of resistance to fatigue cracking (Martin et al. 1990, Glover et al. 2009, Arega et al. 2013). Therefore, it is vital to develop methods that can evaluate the extent of aging of asphalt mixtures (Glover et al 2001, Glover et al. 2005). Some methods analyze the mechanical properties of asphalt concrete to evaluate aging (Mehrez et al. 2014, Poulidakos et al 2014), while others analyze the properties of asphalt binders extracted from asphalt cores (Farrar et al. 2006, Kim et al. 2006, Burr et al. 1993).

During asphalt mixing operations, asphalt loses volatile components and oxidizes (short-term aging), while when placed in the field a gradual oxidation occurs (long-term aging) (Airey 2003). Asphalt rheological properties including viscosity change with aging (Siddiqui & Ali 1999, Airey 2003, Prapaitrakul et al. 2009), and these changes are used to determine the aging extent of reclaimed asphalt pavement (Kim et al. 2006). In order to measure these rheological properties, binder must be extracted from the aged asphalt core, but this process is time consuming (Farrar et al 2006, Kim et al. 2006, Burr et al. 1993). The Dynamic Shear Rheometer (DSR) is used to measure the complex shear modulus G^* and phase angle, from

which the dynamic (shear) viscosity can be extrapolated. The rotational viscometer is used to directly measure viscosity at relatively high temperatures (i.e. mixing and compaction temperatures) (Farrar et al. 2006, Colbert & You 2012, Gandhi & Amirhanian 2008, Gandhi 2009). In this paper, the relative viscosity of the binders present in asphalt concrete samples, and consequently their relative aging extent, is estimated with Low Field Nuclear Magnetic Resonance. With this new methodology, binder extraction is not required. Moreover, the analysis can be performed at room temperature and directly on cores extracted from in-service asphalt pavements.

In Low Field Hydrogen (^1H) NMR, the relaxation times T_1 (spin-lattice, longitudinal) and T_2 (spin-spin, transverse) are related to petrophysical properties. There are three T_2 relaxation mechanisms for fluids in contact with solid surfaces: bulk relaxation, surface relaxation at the solid-fluid interface, and molecular diffusion in the internal magnetic field gradients. In oil/asphalt, bulk relaxation is dominant, which is inversely proportional to fluid viscosity, $T_{2\text{bulk}} \propto T/\mu$, where T is the absolute temperature and μ the viscosity (LaTorraca et al. 1999). The self-diffusion coefficient D also depends on viscosity (Freedman & Heaton 2004). Lighter oils are highly diffusive, with long T_1 and T_2 times, while as the viscosity increases, like in the case of asphalt, diffusion decreases, as well as

the T_1 and T_2 times (Coates et al. 1999). Short T_2 Spin Echo Decay (SED) may fall below the measurable NMR limit and may not be detected. In asphalt concrete samples, the hydrogen relative to the asphalt releases a signal in NMR, while the aggregates are not detected. Information about the sole binder can be therefore acquired. Since asphalt is composed by different compounds, in a T_2 measurement, the NMR signal decays with a distribution of T_2 values.

In Low Field NMR, the estimation of viscosity is usually performed with self-diffusion measurements. The high viscosity of asphalt implies that a high energy is required for the molecules to move, as many of them have high molecular weight, and contain ramifications and aromatic rings (Netzel & Turner 1989). Therefore, self-diffusion is at the measurable limits of NMR sensitivity. Only in a stable system at high temperatures, the self-diffusion coefficient of bitumen could be measured (Filippova et al. 2000), but at room temperature, lower diffusion values are expected and no reports were found with that information. The viscosity of heavy oil and asphalt was previously evaluated by means of Low Field NMR by Bryan et al. and other authors by using models for different viscosity ranges, which were derived experimentally (LaTorraca et al. 1999, Bryan et al. 2003, Bryan et al. 2005a, b, c, Bryan et al. 2006, Bryan et al. 2007, Bryan et al. 2008, LaTorraca et al. 1998, Mirotnich et al. 1999, Galford & Marschall 2000, Mirotnich et al. 2001, Hirasakia et al. 2003, Yang & Hirasaki 2008, Motta Cabrera et al. 2010). The mentioned studies showed a relation between the viscosity of asphalt and the T_2 and Relative Hydrogen Index (RHI) of the asphalt as measured by Low Field NMR. Although the exact viscosity value could not be measured with NMR, the order of magnitude could be estimated.

2 MATERIALS

Eighteen (18) cylindrical asphalt concrete samples, composed of limestone aggregates (nominal maximum aggregate size of 19.0 mm) and 4.4 percent of unmodified binder PG 67-22, were prepared using a Superpave gyratory compactor (SGC) (Mehrez et al. 2014). The samples were compacted such as the percent of air voids in the samples after coring and trimming were 4 ± 0.5 , 7 ± 0.5 , or 10 ± 0.5 percent. The final size of the samples was 5.08 cm in diameter by 5.08 cm in height.

The asphalt samples were aged in an environmental room at 60°C, which simulated several years of field aging exposure (Mehrez et al. 2014, Airey 2003). For each group with the same percent air voids (4, 7, and 10 percent), two samples (replicate 1 and 2) were not aged (0M), two samples were aged for 3 months (3M), and two samples were aged for 6 months (6M) in the environmental room. For example, 4%0M1 corresponds to 4 percent air voids, 0 months aging (unaged samples), and repetition number 1.

3 METHODS

3.1 Low field NMR

Aging of the asphalt concrete samples was investigated using a 2 MHz NMR Rock Core Analyzer by Magritek. The CPMG pulse sequence was applied for the T_2 measurements and 1000 echoes were recorded in order to acquire the spin-echo decay curves. The experimental parameters were set as follows: repetition time of 1 sec, pulse length of 20 μ s, 11.5 dB for $\pi/2$, and 5.5 dB for the π pulse.

The samples were analyzed at room temperature (23–24°C). The signal intensity is proportional to the number of resonating nuclei, which are proportional to the binder weight. Since the volume of the specimens is comparable, lower percent air voids samples have higher binder weight than higher percent air voids samples; thus, they have a stronger signal in NMR. Therefore, the background corrected SEDs were calibrated: the amplitudes were divided by the weight (in grams) of the binder present in the samples, which was estimated by weighing the samples and considering that the binder content is 4.4 percent of the sample weight. In this way, the signals are comparable, and the sole effect of the different viscosities was observed.

The calibrated NMR spin-echo decays were then converted to T_2 distributions with a Tikhonov regularization algorithm via error estimation in Matlab. Tikhonov's regularization is a method for inverting 1-D data by performing a Singular Value Decomposition Analysis and imposing a tuning parameter α , which acts as weight on the significant Singular Values (Day 2011, Mitchell et al. 2012). An algorithm with positive values constraint was used, which calculates α automatically.

4 RESULTS AND DISCUSSION

The 18 cylindrical samples with different air void percent and aging conditions were investigated with Low Field NMR at room temperature (23–24°C). Figure 1 displays the T_2 spin-echo decays (on the left) and the T_2 distributions obtained from the Tikhonov algorithm (on the right) of the 4 percent, 7 percent and 10 percent samples. For each percent air voids, three aging conditions are displayed, unaged (0M), 3-month-aged (3M) and 6-month aged (6M), with two replicates for each aging state. The area under the T_2 -distribution curve is proportional to the initial amplitude of the spin-echo train (Coates et al. 1999).

The signals are completely vanished after 1000 echoes, which correspond to 100 ms. It is clear that both fast and slow decaying components are present in the binder analyzed. Accordingly, the T_2 distributions show the presence of more than one component. The fast decaying component is represented by the main bell-shaped peak, with T_2 values around 0.18 ms. A couple of slower decaying components appear in the T_2 range 5 to 50 ms with lower amplitudes. In this

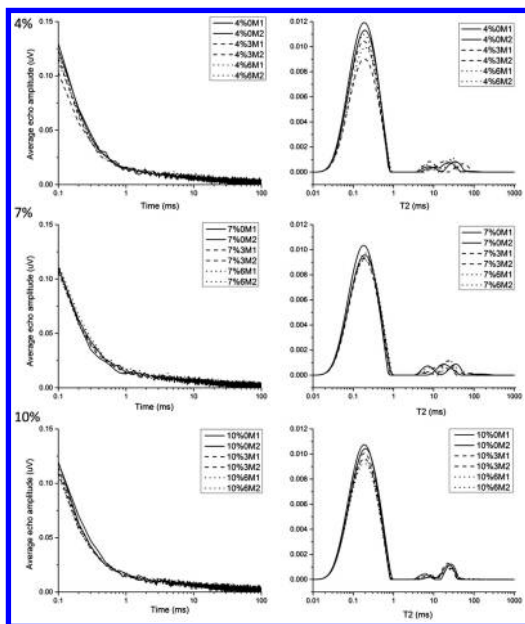


Figure 1. T_2 decays (left) and the T_2 distributions obtained from the Tikhonov algorithm (right) of the 4 percent, 7 percent and 10 percent air void samples.

study, only the main peak is considered, as the smaller peaks are insignificant.

The amplitudes of the main peaks relative to the different samples are slightly different. Considering the equation $RHI = AI_{\text{asphalt}}/AI_{\text{water}}$, where AI means amplitude index and $AI = \text{Amplitude}/\text{mass}$, an increase in amplitude implies an increase in the RHI value (Bryan et al. 2003). As oil/asphalt viscosity increases, the measurable NMR amplitude decreases, as well as the RHI. Therefore, RHI decreases with increasing fluid viscosity (Bryan et al. 2005b).

In the process of aging, viscosity increases due to the reaction of asphalt with oxygen, forming bigger molecules, which increase the steric hindrance, and the SARA fractions (asphaltenes, resins and saturates/aromatics) shift toward the preceding class, resulting in a more solid consistency (Siddiqui & Ali 1999, Airey 2003, Prapaitrakul et al. 2009, Mastrofini & Scarsella 2000). The solid components are no longer detectable with Low Field NMR, as they have faster decays compared to liquid compounds. Since the NMR does not detect decays shorter than 50 μs , the SEDs of the solid compounds do not contribute to the measurable signal. Both RHI and the T_2 values are related to the viscosity of the asphalt (Bryan et al. 2005). Besides the RHI decrease, with increasing viscosity, the T_2 should shift to shorter times. This shift is present in the samples that were cooled from a high temperature (70°C) to room temperature, and was less accentuated at lower temperatures (Menapace et al., submitted). However, the T_2 shift is not detectable in the T_2 distributions obtained at room temperature and all samples have similar T_2 values. Accordingly, Bryan

et al. (2005) stated that in very high viscosity oils, the viscosity is more dependent on RHI than T_2 , and developed an empirical equation that correlates viscosity only with RHI: $\ln(\mu) = 15.6282 - 8.0268 \cdot (\text{RHI})$. Although this is the most accurate equation available in the literature, it is not applicable to the samples analyzed in this study because of their high viscosity that is outside the range of the empirical equation. In another paper by the authors (Menapace et al., submitted), a more applicable empirical equation is proposed. Nevertheless, the form of the equation does not change, which means that $\ln(\mu)$ is proportional to $-RHI$. In this paper, only the qualitative changes in viscosity are considered. Therefore, if RHI (or the peak amplitude) decreases, the viscosity increases.

Since aged samples are supposed to have higher viscosity for a given percent air voids, they should present lower amplitude than the unaged samples. This trend can be observed in all three T_2 distribution graphs (Figure 1).

In the 4 percent air voids samples, both unaged replicates show stronger amplitudes in respect to aged samples. Nevertheless, a longer aging time does necessarily imply higher viscosity, as the lowest amplitude is observed for one of the 3-month aged replicates. If the average of the main peak values of the two replicates is considered, the 6-month aged samples show higher amplitude than the 3-month aged samples (Table 1).

In the 7 percent air voids samples, the highest intensity is observed for one of the unaged replicates. However, the second strongest amplitude is given by one of the 6-month aged replicates. If the average of the main peak values of both replicates is considered, the unaged samples show the highest amplitude, while the aged samples are not significantly different from each other, being the amplitude average of the 6-month aged samples slightly higher (Table 1). Therefore, also in this case, the unaged samples show the lowest viscosity but the aged samples do not show a trend in the viscosity as a function of the aging time.

In the 10 percent air voids samples, the two unaged samples show the strongest amplitude, the two 3-month aged samples show lower intensity than the unaged samples, and the 6-month aged samples show the lowest intensity. Therefore, the peak amplitude decreases as the aging time increases, which means that the viscosity increases with aging time, which is the expected trend. The trend is also clear from Table 1.

The T_2 decay and distributions were also compared for samples aged the same amount of time and differing in percent air voids. Figure 2 shows the T_2 SEDs (on the left) and the T_2 distributions obtained from the Tikhonov algorithm (on the right) of the unaged, 3-month aged and 6-month aged samples. For each aging state, three percent air voids are displayed (4 percent, 7 percent and 10 percent), with two replicates for each percent air void.

At a first glance it is clear that the 4 percent air voids samples show the highest amplitudes in each group of samples except in one replicate after 3 months aging. Therefore, the results are in line with the expected

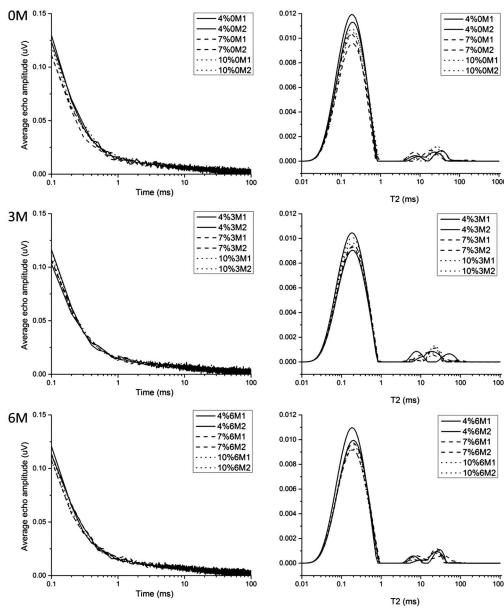


Figure 2. T_2 decays (left) and the T_2 distributions obtained from the Tikhonov algorithm (right) of the unaged, 3-month aged and 6-month aged samples.

trend. At a fixed aging time, it is expected that samples with higher percent air voids show higher aging extent due to higher accessibility of the binder by air.

Among the unaged samples with different percent air voids, the 4 percent samples show the highest intensity, which means their viscosity is lower; therefore, their aging extent is lower. However, the 7 percent samples show lower intensity than the 10 percent samples, which is the opposite of the expected trend (see Table 1). Unaged samples were not aged in the environmental room at 60°C and should not present differences depending on the percent air voids, as the effect of aging should not be present. Nevertheless, the unaged samples were stored in air at room temperature for over a year so they could present some extent of aging.

After 3 months of aging, one of the two 4 percent replicates shows very low amplitude (high viscosity), which is out of the trend. This replicate affects the average values of the amplitudes, resulting in higher intensity for 10 percent samples than for 4 percent (Table 1). The 7 percent samples still present the lowest intensity.

After 6 months of aging, the 4 percent samples show higher intensity (lower viscosity) compared to the 7 and 10 percent air void samples. In this case, the trend is respected, as the 10 percent samples show in average the lowest amplitude, corresponding to the highest viscosity (Table 1). However, 7 and 10 percent samples show similar amplitudes.

Table 1 shows for each sample the maximum peak value. It also shows the average values of groups of samples, such as that of two identical replicates or that

Table 1. Maximum peak values for each sample and average values with their relative standard deviations.

	4%	7%	10%	Average all (aging time)
0M1	1.19	1.03	1.08	
0M2	1.13	0.96	1.04	
Average 0M	1.16	1.00	1.06	1.07 ± 0.07
	±0.03	±0.04	±0.02	
3M1	1.05	0.94	1.01	
3M2	0.90	0.93	0.97	
Average 3M	0.98	0.94	0.99	0.97 ± 0.05
	±0.07	±0.01	±0.02	
6M1	0.99	0.92	0.96	
6M2	1.10	0.97	0.93	
Average 6M	1.05	0.95	0.94	0.98 ± 0.06
	±0.05	±0.03	±0.02	
Average all (% air voids)	1.06	0.96	1.00	
	±0.09	±0.04	±0.05	

relative to each percent air voids and aging condition, together with their relative standard deviations. Since the amplitude values are arbitrary, the values obtained from the T_2 distributions were multiplied by 100 for simplicity. The values highlight trends in the aging time and percent air voids.

Table 1 shows that in all cases the average of the two replicates for the unaged samples is higher than the aged samples. In 10 percent air void samples the amplitude decreases as the aging time increases, but in 4 and 7 percent air voids the amplitude is higher after 6 months aging than after 3 months aging. The table also shows that the amplitude of the 4 percent samples is highest for all aging times except 3 months aging, for which one replicate was out of the trend. Only after 6 months aging, the expected trend of decreasing amplitude (increasing viscosity) with increasing percent air voids is confirmed.

It is obvious from the data presented that the highest aging time and highest percent air voids are perfectly in line with the expected trends. With lower percent air voids and shorter aging times, this trend is mostly but not always respected. The fact that in 10 percent air voids samples the trend is respected could indicate that aging is more accentuated in that sample because of the higher amount of air voids, which facilitate the reactions of asphalt with oxygen. However, if we compare the average amplitude of all samples for each percent air voids in Table 1, the average amplitude of the 7 percent samples is lower than the 10 percent air void samples. This means that the 7 percent air void samples have, in average, higher viscosity than the 10 percent samples. From the data in Table 1, it appears that if aging time was long enough (6 months), samples with 10 percent air voids present slightly higher viscosity than samples with 7 percent air voids. However, if aging time was shorter (3 months) or no aging was performed in the environmental chamber, the 7 percent air voids samples were more affected by aging. It is possible that other mechanisms take place, which are related to other factors. For example, Terrel and Al-Swailmi

(1993) and Masad et al. (2006) introduced the concept of pessimum air void percentage and pessimum air void size, at which the moisture damage is maximum. Although the present samples were aged in a dry chamber, it is possible that aging may not follow a linear trend with respect to percent air voids. Moreover, when additional measurements were carried out with the NMR on the same samples heat treated at higher temperatures, the same trends were found (Menapace et al., submitted). Therefore, the inaccuracies in the trends are not to attribute to the NMR measurements, but to the samples themselves.

The results obtained with Low Field NMR confirm the ones previously obtained with mechanical tests (Mehrez et al. 2014). Nevertheless, while the above results show that the unaged 4 percent samples have lower viscosity than unaged 7 and 10 percent samples, mechanical tests showed that 4 percent samples had lower compliance than 7 and 10 percent samples. The discrepancy is attributed to the fact that compliance is affected by percent air voids as well as binder viscosity. Therefore, it is difficult to detect differences in aging of samples solely based on compliance. Thus, the direct measurement of binder viscosity in cores using Low Field NMR provides a more direct method to evaluate the effect of aging.

As previously mentioned, another paper by the authors (Menapace et al., submitted) presents the Low Field NMR results obtained on heat treated asphalt concrete samples as they cool down to room temperature. In the specified paper, where a larger data set was available and a stronger signal was obtained, due to the higher temperature and lower binder viscosity, the findings of the present paper were confirmed.

In summary, Low Field NMR was demonstrated to be a suitable methodology to assess the relative aging state of asphalt cores by evaluating their relative viscosities.

5 CONCLUSIONS

A new non-destructive methodology to evaluate the aging in asphalt cores is presented. The relative viscosity of the binder in asphalt concrete samples was estimated with Low Field NMR, at room temperature and without the need for binder extraction. Sample with different percent air voids and aging conditions were tested. Unaged samples and samples with the lowest percent air voids presented the lowest viscosities (low aging extent). The expected trend of increasing viscosity with increasing aging time was demonstrated for the 10 percent air void samples. In the 4 and 7 percent air voids samples, the viscosity of the aged samples was higher than that of unaged samples. However, there was no specific trend between aging duration (3 months or 6 months) and viscosity. Increasing viscosity was observed in samples with increasing percent air voids after 6 months aging, although the trend was not so clear for shorter aging conditions. Quantification of relative binder viscosity with this

approach was demonstrated to be more accurate than methods relying on the measurement of mechanical properties. Therefore, Low Field NMR is a promising method to assess aging of pavements throughout their life.

REFERENCES

- Airey, G.D. 2003. State of the Art Report on Ageing Test Methods for Bituminous Pavement Materials, *The International Journal of Pavement Engineering*, 4(3): 165–176
- Arega, Z. A., Bhasin, A. & De Kesel, T. 2013. Influence of extended aging on the properties of asphalt composites produced using hot and warm mix methods, *Construction and Building Materials*, 44: 168–174
- Bryan, J., Mirotchnik, K. & Kantzas, A. 2003. Viscosity Determination Of Heavy Oil And Bitumen Using NMR Relaxometry, *Journal of Canadian Petroleum Technology*, 42(7): 29–34
- Bryan, J., Kantzas, A. & Bellehumeur, C. 2005a. Oil-Viscosity Predictions From Low-Field NMR Measurements, *SPE Reservoir Evaluation & Engineering*
- Bryan, J., Moon, D. & Kantzas, A. 2005b. In Situ Viscosity of Oil Sands Using Low Field NMR, *Journal of Canadian Petroleum Technology*, 44(9): 23–30
- Bryan, J., Hum, F., Kantzas, A., MacPherson, R. & Hancsicsak, T. 2005c. In-Situ Viscosity Using Low Field NMR: A Field Case Study, *International Symposium of the Society of Core Analysts held in Toronto, Canada*
- Bryan, J., Mai, A., Hum, F. & Kantzas, A. 2006. Oil-And Water-Content Measurements In Bitumen Ore And Froth Samples Using Low-Field NMR, *SPE Reservoir Evaluation & Engineering*
- Bryan, J., Kantzas, A., Badry, R., Emmerson, J. & Hancsicsak, T. 2007. In Situ Viscosity of Heavy Oil: Core and Log Calibrations, *Journal of Canadian Petroleum Technology*, 46(11): 47–55
- Bryan, J., Kantzas, A. & Mai, A. 2008. Heavy Oil Reservoir Characterization Using Low Field NMR, *Back to Exploration – CSPG CSEG CWLS Convention*
- Burr, B.L., Glover, C. J., Davison, R. R. & Bullin, J. A. 1993. New Apparatus and Procedure for the Extraction and Recovery of Asphalt Binder from Pavement Mixtures, Asphalt Cement and Asphalt/Polymer Blends, *Transportation Research Record*, 1391, 20–29
- Coates, G. R., Xiao, L. & Prammer, M. G. 1999. NMR Logging Principles and Applications, Halliburton Energy Services, Houston
- Colbert, B. & You, Z. 2012. The properties of asphalt binder blended with variable quantities of recycled asphalt using short term and long term aging simulations, *Construction and Building Materials*, 26: 552–557
- Das, P.K., Kringos, N., Wallqvist, V. & Birgisson, B. 2013. Micromechanical Investigation Of Phase Separation In Bitumen By Combining Atomic Force Microscopy With Differential Scanning Calorimetry Results, *Road Materials and Pavement Design*, 14 (S1): 25–37
- Day, I. J. 2011. On the inversion of diffusion NMR data: Tikhonov regularization and optimal choice of the regularization parameter, *Journal of Magnetic Resonance*, 211: 178–185
- Farrar, M. J., Harnsberger, P. M., Thomas, K. P. & Wiser, W. 2006. Evaluation Of Oxidation In Asphalt Pavement Test Sections After Four Years Of Service, *Submitted for the International Conference on Perpetual Pavement*, September 13–15

- Filippova, A. G., Kirillova, L. G., Okhotina, N. A., Dvoyashkin, N. K., Filippov, A. V., Vol'fson, S. I., Liakumovich, A. G. & Samuilov, Ya. D. 2000. Viscosity of Polymer-Bitumen Binders, *Colloid Journal*, 62(6): 755–758. Translated from *Kolloidnyi Zhurnal*, 62(6): 832–836
- Freedman, R. & Heaton, N. 2004. Fluid Characterization using Nuclear Magnetic Resonance Logging, *Petrophysics*, 45(3): 241–250
- Galford, J. E. & Marschall, D. M. 2000. Combining NMR and Conventional Logs to Determine Fluid Volumes and Oil Viscosity in Heavy-Oil Reservoirs, paper SPE 63257, *SPE Annual Technical Conference and Exhibition, Dallas, Texas*
- Gandhi, T. & Amirhanian, S. 2008. Laboratory Simulation of Warm Mix Asphalt (WMA) Binder Aging Characteristics, Airfield and Highway Pavements: pp. 195-204, American Society of Civil Engineers, Conference proceedings, Bellevue, Washington, United States, October 15–18
- Gandhi, T., Akisetty, C. & Amirhanian, S. 2009. Laboratory evaluation of warm asphalt binder aging characteristics, *International Journal of Pavement Engineering*, 10(5): 353–359
- Glover, C. J., Davison, R. R., Domke, C. H., Ruan, Y., Juristyarini, P. & Knorr, D. B. 2001. Development of A New Method For Assessing Asphalt Binder Performance Durability, Report 1872-1, Project Number 0-1872
- Glover, C. J., Davison, R.R., Domke, C. H., Ruan, Y., Juristyarini, P. & Knorr, D. B. 2005. Development of New Method for Assessing Asphalt Binder Durability with Field Validation, Texas Transportation Institute, College Station, Texas
- Glover, C. J., Martin, A. E., Chowdhury, A., Han, R., Jin, X., Prapaitrakul, N. & Lawrence, J. 2009. Evaluation of Binder Aging and its Influence in Aging of Hot Mix Asphalt Concrete: Literature Review and Experimental Design, Report 0-6009-1, Project 0-6009
- Hirasakia, G. J., Lob, S.-W. & Zhang, Y. 2003. NMR properties of petroleum reservoir fluids, *Magnetic Resonance Imaging*, 21: 269–277
- Kim, K.W., Kim, K.A., Doh, Y.S. & Amirhanian, S. 2006. Estimation of RAP's binder viscosity using GPC without binder recovery, *Journal of Materials in Civil Engineering*, 18(4): 561–7
- Kleinberg, R. & Vinegar, H. 1996. NMR Properties of Reservoir Fluids, *The Log Analyst*, 37(6)
- LaTorraca, G.A., Dunn, K.J., Webber, P.R. & Carlson, R.M. 1998. Low-Field NMR Determinations Of The Properties Of Heavy Oils And Water-In-Oil Emulsions, *Magnetic Resonance Imaging*, 16(5/6): 659–662
- LaTorraca, G.A., Stonard, S.W., Webber, P.R., Carlson, R.M. & Dunn, K.J. 1999. Heavy Oil Viscosity Determination Using NMR Logs, *SPWLA 40th Annual Logging Symposium*
- Martin, K.L., Davison, R.R., Glover, C. J. & Bullin, J.A. 1990. Asphalt Aging in Texas Roads and Test Sections, Asphalt mix materials and mixtures, *Transportation Research Record*, 1269
- Masad, E., Castelblanco, A. & Birgisson, B. 2006. Effects of Air Void Size Distribution, Pore Pressure, and Bond Energy on Moisture Damage, *Journal of Testing and Evaluation*, 34(1)
- Mastrofini, D. & Scarsella, M. 2000. The Application of Rheology To The Evaluation Of Bitumen Ageing, *Fuel*, 79 1005–1015
- Mehrez, L., Kassem, E., Masad, E. & Little, D. 2014. Stochastic Identification of Linear-Viscoelastic Models of Aged and Unaged Asphalt Mixtures, *Journal of Materials in Civil Engineering*, 04014149
- Menapace, I., Masad, E., Papavassiliou, G., Kassem, E., 2015. Evaluation of Aging in Asphalt Cores Using Low Field Nuclear Magnetic Resonance, *submitted*
- Mirotnich, K.D., Allsopp, K., Kantzas, A., Curwen, D. & Badry, R. 1999. Low Field NMR-Tool for Bitumen Sands Characterization: A New Approach, paper SPE 56764, *SPE Annual Technical Conference and Exhibition, Houston, Texas*
- Mirotnich, K.D., Allsopp, K., Kantzas, A., Curwen, D. & Badry, R. 2001. Low-Field NMR Method for Bitumen Sands Characterization: A New Approach, *SPE Reservoir Evaluation & Engineering*
- Mitchell, J., Chandrasekera, T.C. & Gladden, L.F. 2012. Numerical estimation of relaxation and diffusion distributions in two dimensions, *Progress in Nuclear Magnetic Resonance Spectroscopy*, 62: 34–50
- Motta Cabrera, S.C., Bryan, J. & Kantzas, A. 2010. Estimation of Bitumen and Solids Content In Fine Tailings Using Low-Field NMR Technique, *Journal of Canadian Petroleum Technology*, 49(7): 8-19
- Netzel, D. A. & Turner, T. F. 1989. A Correlation of United States Tar Sand Bitumen Viscosities With NMR Spectroscopic Parameters, *Fuel Science and Technology International*
- Pauli, A.T., Grimes, R.W., Beemer, A.G., Turner, T.F., Branthaver, J.F. 2011. Morphology of Asphalts, Asphalt Fractions and Model Wax-Doped Asphalts Studied By Atomic Force Microscopy, *International Journal of Pavement Engineering*, 12(4): 291–309
- Poulikakos, L. D., dos Santos, S., Bueno, M., Kuentzel, S., Hugener, M. & Partl, M. N. 2014. Influence of short and long term aging on chemical, microstructural and macro-mechanical properties of recycled asphalt mixtures, *Construction and Building Materials*, 51: 414–423
- Prapaitrakul, N., Han, R., Jin, X. & Glover, C.J. 2009. A Transport Model of Asphalt Binder Oxidation in Pavements, *Road Materials and Pavement Design*, 10:sup1: 95–113
- Siddiqui, M.N. & Ali, M.F. 1999. Studies On The Aging Behavior Of The Arabian Asphalts, *Fuel*, 78: 1005–1015
- Straley, C., Rossini, D., Vinegar, H., Tutunjian, P. & Morriss, C. 1997. Core Analysis by Low Field NMR, *The Log Analyst*, 38(2)
- Terrel, R. L. & Al-Swailmi, S. 1993. Role of Pessimism Voids Concept in Understanding Moisture Damage to Asphalt Concrete Mixtures, *Transportation Research Record* 1386: 31–37
- Yang, Z. & Hirasaki, G. J. 2008. NMR measurement of bitumen at different temperatures, *Journal of Magnetic Resonance*, 192: 280–293

Influence of compaction method on stiffness performance of asphalt specimens

P. Georgiou, A. Loizos & A. Leventis

National Technical University of Athens, Laboratory of Pavement Engineering, Athens, Greece

ABSTRACT: Stiffness modulus of HMA is a fundamental material property, hence can be considered as a key element for the characterization of mix performance. Laboratory determination of stiffness modulus involves fabrication of asphalt specimens subjected to repeated loading. Over the years numerous laboratory compaction methods have been developed in an attempt to accurately simulate field conditions. Although has long been recognized and well documented from pavement engineers that the varying laboratory methods create volumetrically identical but mechanically different specimens, still no consensus has evolved as to which method is the best. In this paper the effect of three of the major laboratory compaction methods (namely, Marshall, gyratory and roller) and its factors on the indirect tensile stiffness of various asphalt mixtures is investigated. From the comparative analysis conclusions are derived as to which laboratory compaction method best emulates field compaction. More details and discussion are outlined in the paper.

1 INTRODUCTION

Stiffness modulus of HMA is a fundamental material property, hence can be considered as a key element for both the characterization of mix performance as well the analysis and rational design of flexible pavements. Laboratory determination of stiffness modulus involves fabrication of asphalt specimens subjected to repeated loading. Over the years numerous laboratory compaction methods have been developed in an attempt to accurately simulate the field conditions. Pavement engineers have long recognized and well documented that the varying laboratory compaction methods create volumetrically identical, but mechanically different specimens. This is due to the fact that the compaction method has a direct impact on the aggregate orientation and internal structure of the asphalt mixture (Tashman et al. 2002, Hunter et al. 2004, Iwama et al. 2007, Thyagarajan et al. 2010).

Multiple studies have attempted to assess the relationship between laboratory and field compaction methods and the resulting mechanical performance of the mixture. However, research in this area has reached conflicting conclusions and still no consensus has evolved as to which laboratory compaction method best resembles the field conditions. Researchers have speculated that the gyratory compactor produces specimens with mechanical properties closest to field cores (Von Quintus et al. 1991, Khan et al. 1998, Peterson et al. 2004). In contrast, other studies have shown that the laboratory roller compactor best emulates the mechanical performance of field cores (Sousa et al. 1991). More recent studies comparing the results of the indirect stiffness testing on specimens manufactured

from laboratory compaction methods have found that steel roller compacted specimens were of comparable stiffness to the site cores (Hartman et al. 2001, Airey et al. 2006, Hunter et al. 2009, Plati et al. 2014).

2 OBJECTIVES

The present study aims primarily to investigate the influence of the most commonly used laboratory compaction methods, namely Marshall, gyratory and roller, on the stiffness properties of various asphalt mixtures relative to field compaction performance, as shown graphically in [Figure 1](#). In addition, the effect of various compaction factors on the measured indirect tensile stiffness of laboratory compacted HMA specimens are also investigated, with the aim to gain more insight to the factors that affect HMA mechanical properties.

In order to accomplish these goals, a new construction project was monitored during both the paving and compaction processes of two asphalt mixtures, namely a dense- and open graded, which expected to exhibit different performance. More details about mix information and compaction pattern followed on site can be found elsewhere (Plati et al. 2014). During paving batches of plant produced mix samples were collected to be used for the laboratory compaction study, while after construction and prior to trafficking an adequate number of field cores were retrieved from characteristic pavement locations to be used as ground truth data for comparative analysis. Then, a comprehensive laboratory experimental study was performed, which comprised of fabrication of HMA specimens with

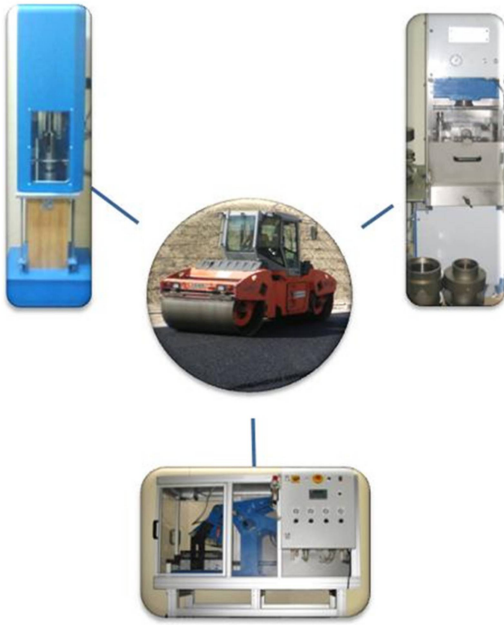


Figure 1. Scope of experimental study.

varying compaction methods and parameters and testing of air voids and stiffness modulus. The laboratory experimental data was analyzed to evaluate differences between methods and site compaction. The findings of the present study are highlighted in the following sections.

3 LABORATORY STUDY

3.1 Marshall compaction

The two asphalt mixtures were compacted using standard Marshall (impact) compaction, as described in EN 12697-30, at compaction energy level of 75 blows per side. Varying compaction temperatures were used to fabricate the asphalt mixture specimens, namely 135°C and 145°C for the dense graded mix and 140°C, 150°C and 160°C for the open graded mix to evaluate the impact of compaction temperature on stiffness modulus. Three replicates were fabricated at each temperature, which were subsequently subjected to volumetric and stiffness testing.

3.2 Gyratory compaction

Gyratory compaction of the two mixtures comprised a test matrix with various factors, namely internal gyration angle, temperature and specimen (initial) diameter, which are summarized in Table 1.

Three different values of internal gyration angle, which hereafter will be found as gyration angle or, simply, angle for sake of brevity, were selected; the gyration angle of 0.82° as suggested by the European Standard EN 12697-31, 1.16° according to the

Table 1. Factors and their level considered in the laboratory experiment.

Gyratory compaction	Dense graded	Open graded
Temperature (°C)	135, 145	140, 150, 160
Diameter (mm)	100, 150	
Gyration angle (°)	0.82, 1.16, 1.45	
Roller compaction	Dense graded	Open graded
Temperature (°C)	135, 145	140, 150, 160
Effort (passes)	35, 45, 55	45, 55, 65
Mode	S, V, SV, VS	

AASHTO T312 specification, and a higher value of 1.45° for which it was hypothesized to produce specimens with different performance.

Gyratory compaction was carried out at various temperatures, typical and higher ones, while the vertical pressure was held constant at standard 600 kPa, which is believed to approximate the contact pressures at which most of the compaction happens in the field (Delgadillo & Bahia 2008). In addition, the effect of different specimen geometry in terms of diameter (100 mm and 150 mm) was also investigated. A total of 36 specimens for both mixtures were fabricated. After compaction all specimens were trimmed, while the 150 mm diameter specimens were cored and 100 mm diameter specimens were obtained. Assessment of volumetric and stiffness properties for both groups of 100 mm diameter gyratory specimens, namely as compacted and cored, was followed.

3.3 Roller compaction

Roller compaction was performed with a steel segmented Roller Compactor, which provides a means of compacting slabs of asphaltic material in the laboratory under conditions which simulate in-situ compaction. According to EN 12697-33, three different approaches can be followed when using a smooth steel roller: a) compaction by a specified energy, b) compaction with controlled compaction energy and c) compaction to obtain compaction degree. For the current research study, the approach of compaction by specified energy was followed adjusting three compaction factors, namely the compaction mode, effort and temperature, which are summarized in Table 1.

The laboratory experiment was meant to mirror the four phases of field compaction; pre-compaction and the three main compaction phases. During the pre-compaction phase minimum compaction energy of 5 kN was applied in the asphalt mix in order to avoid bow effects and achieve a smooth surface in the compacted slab.

The main compaction phases simulated roller compaction in the field. Four modes of roller compaction (i.e. static (S), vibratory (V), static-vibratory (SV) and vibratory-static (SV)) were established including the pattern followed during field compaction, while varying the compaction effort (i.e. number of passes) and

temperature. The main compaction energy and vibration frequency (i.e. 10 kN and 40 Hz, respectively) reflected the operational characteristics of the steel wheel rollers used in the field compaction.

Taking into consideration the above operational principles multiple batches of the asphalt mixture were heated gently and placed in steel mould, moved beneath the roller and the compaction procedures were commenced. A total of 24 slabs were fabricated with regards to the dense graded mix and 36 slabs with regards to the open graded mix. After cooling of the slabs to room temperature, coring of four 100 mm diameter specimens was commenced from the top of each compacted slab. The cored specimens were trimmed to the flat ends (i.e. top and bottom) and their volumetric and stiffness properties were then evaluated.

3.4 Testing of mix specimens properties

Testing of mix specimens, both the laboratory and field compacted, included the determination of air voids content and stiffness modulus. Based on the bulk densities measured (EN 12697-6) and the maximum density (ρ_m) of each mixture the air voids contents (V_m) were calculated (EN 12697-8).

Stiffness testing was performed using the Indirect Tensile Stiffness Modulus (ITSM) test (EN 12697-26). This test consists of sinusoidal load pulses applied along the vertical diameter of specimen and characterized by the rise-time and transient horizontal deformation. A preliminary conditioning of ten load pulses is applied to bed the test specimen on the loading platens and to enable the equipment to adjust the load magnitude and duration in order to give the specified horizontal diametral deformation. Then, stiffness modulus is determined as the average modulus corresponding to five load pulses and the specimen is rotated through 90° about its horizontal axis. A further five load pulses are then applied and the resulting mean stiffness modulus is obtained. The stiffness modulus is then calculated as the average of these two mean values.

4 DATA ANALYSIS AND RESULTS

4.1 Air voids

The air void contents of all laboratory fabricated specimens of varying compaction methods and factors along with the field compacted specimens were calculated.

Figure 2 illustrates the compaction level achieved with respect to each compaction method covering the full spectrum of compaction factors considered. The box plot of air voids content data provides information about the center and spread of the compaction data. It is based on the median and interquartile range, which is believed to provide a realistic interpretation of the results. The ends of the vertical lines or whiskers indicate the minimum and maximum data values.

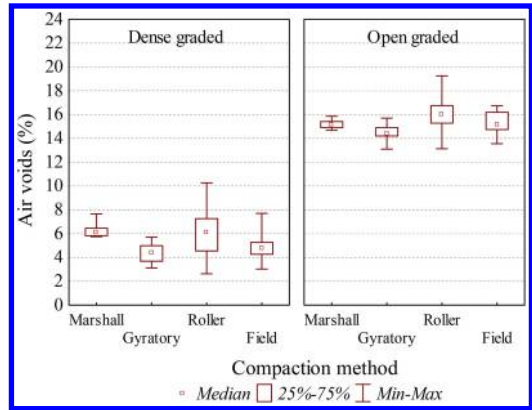


Figure 2. Air voids as a function of compaction method.

From Figure 2, variability of air voids content with respect to the dense graded mix is observed both between and within the various compaction methods. Increased variability is observed with respect to the roller compaction, relative to the other laboratory compaction methods, which can be attributed to the effect of compaction mode and effort. Compared to the field compaction variability, laboratory roller compaction method appears to show a similar performance hence indicating that the steel segmented roller compactor can simulate the in situ performance of field rollers. The median values for all compaction methods are generally close to the average and were calculated as 6.1%, 4.4%, 6.1% and 4.7% for the Marshall, gyrotory, roller and field compaction method.

In addition, less variability of air voids content is observed between and within the various compaction methods, which can be attributed to the smaller 12.5-mm nominal maximum aggregate size of the open- relative to the dense graded mix. Again, similar variability is observed between the roller and field compaction method. The median values were calculated as 15.2%, 14.4%, 16.0% and 15.1% for the Marshall, gyrotory, roller and field compaction method, respectively.

The above results, in general, indicate that the air void contents of the laboratory compacted specimens are comparable and approximated the air voids content of the field cores.

4.2 Stiffness

The stiffness performance of both laboratory and field compacted specimens was characterized using the ITSM test. Controlled deformation stiffness tests at a target deformation of 5 μm were performed at a test temperature of 20°C.

Figure 3 illustrates the stiffness modulus evolution with respect to compaction temperature for the specimens fabricated with the Marshall compaction.

From Figure 3, the general trend observed is a modulus increase as the compaction temperature does. In the dense graded mix, at 135°C the modulus has a

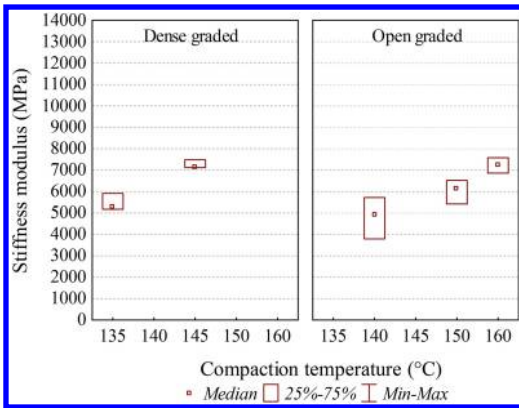


Figure 3. Stiffness of Marshall specimens as a function of compaction temperature.

median value close to 5300 MPa, whereas at 145°C the modulus reaches 7100 MPa. In the open graded mix, the modulus at 140°C has a median value close to 4900 MPa, while at 150 and 160°C values of 6100 and 7250 MPa were yielded.

The stiffness modulus evolution with respect to gyration angle, compaction temperature and (initial) diameter for the specimens prepared with gyratory compaction is illustrated in Figure 4.

The above results indicate that increasing the gyration angle from 0.82° to 1.16° a higher modulus is obtained, while a further increase from 1.16° to 1.45° reduces the modulus, as shown in Figure 4a. This trend appears to be more pronounced with respect to the dense graded mix; for the open graded mix, the gyration angle affects to a lesser extent the stiffness modulus.

The temperature effect was found to be mixture dependent, as shown in Figure 4b. Specifically, an increase in compaction temperature from 135°C to 145°C results in a decrease of modulus of the dense graded mix; a mean modulus decrease of the order of 14% was calculated. On the contrary, with respect to the open graded mix a mean modulus increase of the order of 17% is observed increasing the compaction temperature from 140 to 150°C, whereas a further increase in temperature does not affect significantly stiffness modulus.

In addition, it is interesting to note that coring 100 mm diameter from larger 150 mm specimen, a lower modulus is obtained with respect to as compacted 100 mm specimens. This effect is more pronounced with respect to the open graded mix, where a mean modulus decrease of the order of 29% is observed.

Figure 5 illustrates the stiffness modulus evolution with respect to compaction mode, temperature and effort (number of passes) for the specimens prepared with the roller compaction.

Figure 5a shows the influence of the compaction mode on the stiffness modulus for the full spectrum of temperature and roller compaction effort. The results

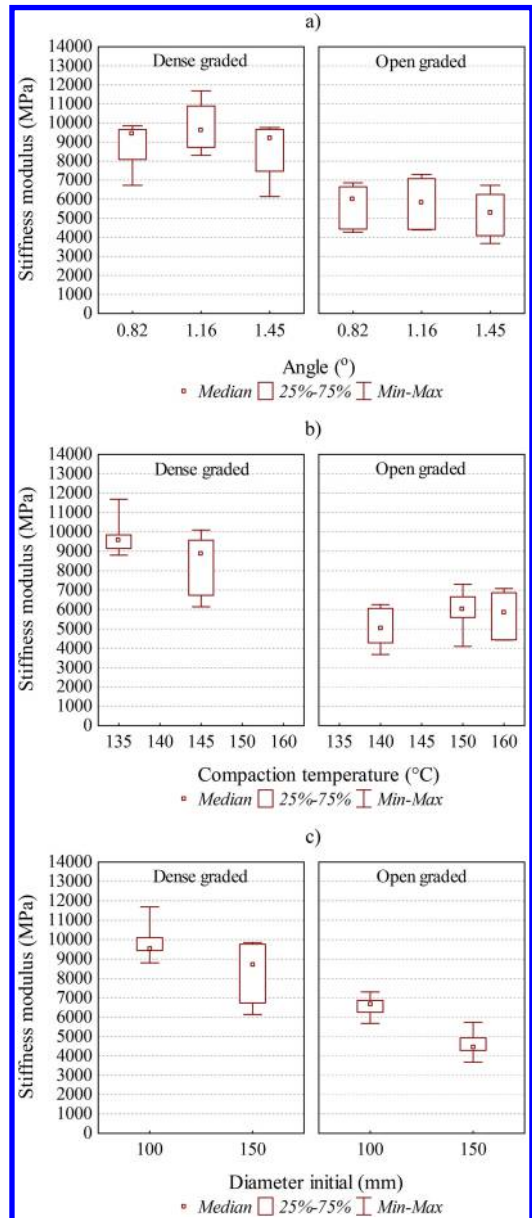


Figure 4. Stiffness of gyratory specimens as a function of a) gyration angle, b) compaction temperature and c) initial diameter.

from the dense graded mix indicate variability between the stiffness properties of the roller compacted specimens. However, for the open graded mix type it is pronounced that the laboratory compaction modes produce specimens with insignificant differences.

With respect to compaction temperature, the modulus increases significantly when passing from 135°C to 145°C in the dense graded mix, while the modulus of the open graded mix varies very little hence indicating that similar moduli can be obtained for a

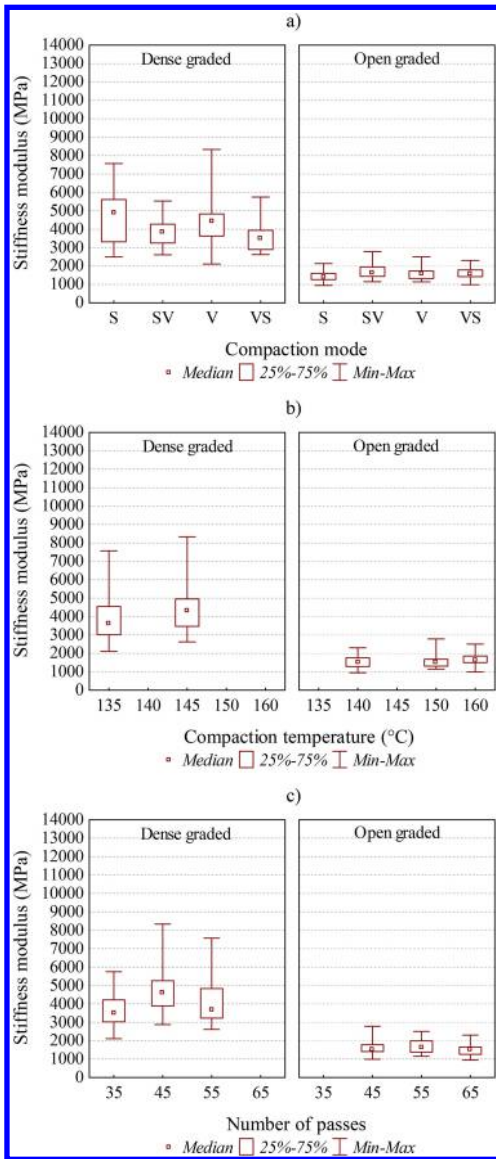


Figure 5. Stiffness of roller specimens as a function of a) compaction mode, b) compaction temperature and c) number of passes.

wide temperature range of compaction temperature (140–160°C), as shown in Figure 5b.

In addition, compaction effort (in terms of roller passes) seems to affect more the dense graded mix. Increasing the roller passes from 35 to 45 an increase in modulus of the order of 19% is observed, while additional passes reduces the modulus, possibly due to the reorientation and rearrangement of bitumen-coated aggregates. The compaction effort seems to marginally affect the modulus of the open graded mix.

Figure 6 summarizes the effect of each compaction method, including the field compaction, on the stiffness modulus. Field compaction seems to produce

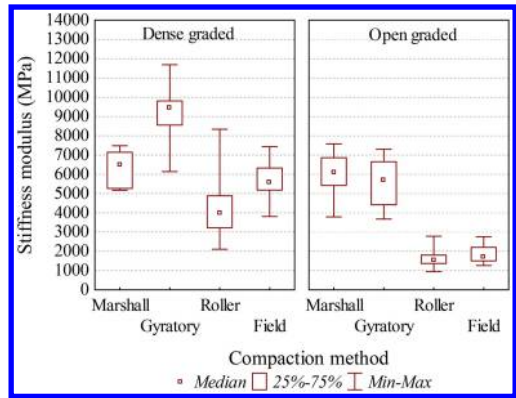


Figure 6. Effect of compaction methods on stiffness.

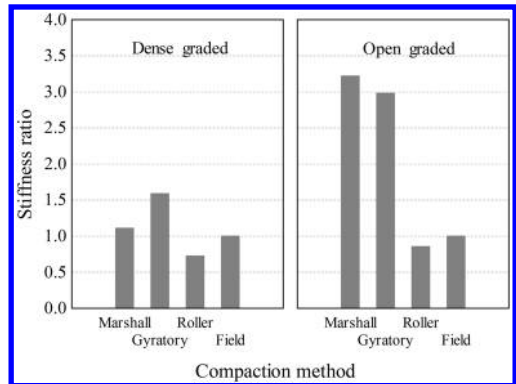


Figure 7. Stiffness ratio of laboratory compaction methods relative to field compaction.

specimens with relatively low variability in terms of the ITSM. Median values of 5600 and 1700 MPa were calculated for the dense and open graded mix, respectively.

Overall, the combined results for the two studied mixtures indicate that, in general, the mould-based compaction methods (Marshall and gyrotory) tend to produce specimens of higher stiffness than the roller compacted specimens, as shown in Figure 6. The gyrotory compacted specimens, with similar air void content to the field compacted specimens, as previously shown in Figure 2, have almost two fold the stiffness modulus of the field cores. It is also observed that, although the air voids of Marshall specimens are higher than the field cores, the modulus is higher, especially, for the open graded mix. On the contrary, the roller- and field compacted specimens are of comparable stiffness if the difference in air void content is accounted for (increased air voids for roller specimens).

In the light of the above, the stiffness ratio for each laboratory compaction method relative to field compaction was calculated. The mean stiffness was used for the analysis and the results in terms of the ITSM ratios (i.e. Marshall/field, gyrotory/field and roller/field) are presented in Figure 7.

In addition, considering the combined results from Figures 2–7 it is appreciated that some of the compaction factors investigated within each compaction method affect more significantly the stiffness performance of asphalt mixtures. For instance, with respect to gyratory compaction the (initial) diameter and compaction temperature were found to be the most important factors in affecting stiffness modulus. The compaction effort and temperature were found to affect mostly the stiffness modulus of roller compacted specimens.

5 CONCLUSIONS

This study has shown that the mould-based compaction methods (Marshall and gyratory) tend to produce specimens of higher stiffness than the roller specimens. This is more pronounced with respect to the open graded mix. In addition, the roller- and field compacted specimens are of comparable stiffness if the difference in air void content is accounted for (increased air voids for roller specimens).

Within each compaction method it is appreciated that some of the compaction parameters investigated affect more significantly the stiffness performance of asphalt mixtures. For instance, the compaction temperature along with (initial) diameter and compaction effort (number of passes) were found to be the most important factors in affecting the stiffness modulus of gyratory and roller compacted specimens, respectively.

The above findings may be considered as a preliminary guide in order to develop specifications for the specimen fabrication in the laboratory. Also, further research to evaluate the relationship between the mechanical performances of various asphalt mixtures with the internal structure characteristics from the application of different compaction methods is vital for the harmonization of laboratory compaction procedures towards better resembling the mechanical properties of field cores.

REFERENCES

AASHTO 2012. Preparing and Determining the Density of Hot-Mix Asphalt (HMA) Specimens by means of the Superpave Gyratory Compactor, AASHTO T312.

Airey, G.D., Collop, A.C., Zoorob, S.E. & Hunter, A.E. 2006. Comparison of field and laboratory compacted asphalt mixtures. *CD-Proceedings of the 10th International Conference on Asphalt Pavements; Québec, 12–17 August 2006*.

CEN, 2007. Bituminous mixtures – Test methods for hot mix asphalt – Part 6: Determination of bulk density of bituminous specimens, EN 12697-6.

CEN, 2007. Bituminous mixtures – Test methods for hot mix asphalt – Part 8: Determination of void characteristics of bituminous specimens, EN 12697-8.

CEN, 2007. Bituminous mixtures – Test methods for hot mix asphalt – Part 26: Stiffness, EN 12697-26.

CEN, 2007. Bituminous mixtures – Test methods for hot mix asphalt – Part 31: Specimen preparation by impact compactor, EN12697-30.

CEN, 2007. Bituminous mixtures – Test methods for hot mix asphalt – Part 31: Specimen preparation by gyratory compactor, EN12697-31.

CEN, 2007. Bituminous mixtures – Test methods for hot mix asphalt – Part 33: Specimen prepared by roller compactor EN 12697-33.

Delgadillo, R.A. & Bahia, H.U. 2008. Effects of Temperature and Pressure on Hot Mixed Asphalt Compaction: Field and Laboratory Study. *Journal of Materials in Civil Engineering* 20(6): 440–448.

Hartman, A.M., Gilchrist, M.D. & Walsh, G. 2001. Effect of mixture compaction on Indirect Tensile Stiffness and Fatigue. *Journal of Transportation Engineering* 127(5): 370–378.

Hunter, A.E., Airey, G.D. & Collop, A.C. 2004. Effect of asphalt mixture compaction on aggregate orientation and mechanical performance. *CD-Proceedings of the 8th Conference on Asphalt Pavements for Southern Africa (CAPSA '04); Sun City, 12–16 September 2004*.

Hunter, A.E., McGreavy, L. & Airey, G.D. 2009. Effect of compaction mode on the mechanical performance and variability of asphalt mixtures. *Journal of Transportation Engineering* 135(11): 839–851.

Iwama, M., Airey, G.D. & Hunter, A.E. 2007. Influence of asphalt mixture compaction method and specimen size on internal structure and mechanical properties. In Andreas Loizos, Tom Scarpas & Al-Qadi (eds), *Advanced Characterisation of Pavement and Soil Engineering Materials; Athens, 20–22 June 2007*. London: Taylor & Francis Group.

Khan, Z.A., Al-Abdul Wahab, H.I., Asi, I. & Ramadhan, R. 1998. Comparative study of asphalt concrete laboratory compaction methods to simulate field compaction. *Construction and Building Materials* 12: 373–384.

Peterson, R.L., Mahboub, K.C., Anderson, R.M., Masad, E. & Tashman, L. 2004. Comparing Superpave Gyratory Compactor data to field cores. *Journal of Materials in Civil Engineering* 16(1): 78–83.

Plati, C., Georgiou, P. & Loizos, A. 2014. Influence of different roller compaction modes on asphalt mix performance. *International Journal of Pavement Engineering*, DOI:10.1080/10298436.2014.925552, In Press.

Sousa, J.B., Deacon, J.A. & Monismith, C.L. 1991. Effect of laboratory compaction method on permanent deformation characteristics of asphalt-aggregate mixtures. *Journal of the Association of Asphalt Paving Technologists* 60: 533–585.

Tashman, L., Masad, E., D'Angelo, J., Bukowski, J. & Harman, T. 2002. X-ray Tomography to Characterize Air Void Distribution in Superpave Gyratory Compacted Specimens. *International Journal of Pavement Engineering* 3(1): 19–28.

Thyagarajan, S., Tashman, L., Masad, E. & Bayomy, F. 2010. The heterogeneity and mechanical response of hot mix asphalt laboratory specimens. *International Journal of Pavement Engineering* 11(2): 107–121.

Von Quintus, H.L., Hughes, C.S. & Scherocman, J.A. 1991. Asphalt-Aggregate Mixture Analysis System (AAMAS). *National Cooperative Highway Research Program Report* 338. Washington, D.C.: Transportation Research Board.

Evaluation of rutting resistance of rubberized gap-graded asphalt mixtures

E. Santagata, O. Baglieri, M. Alam, M. Lanotte & P.P. Riviera

Politecnico di Torino, Turin, Italy

ABSTRACT: The study described in this paper analyzed the rutting resistance of asphalt mixtures containing crumb rubber from end-of-life tires. Different rubberized gap-graded mixtures, both prepared in the laboratory and produced in a hot mix plant, were considered in the investigation. Moreover, a standard dense-graded mixture was used as a reference material. The experimental program included laboratory tests carried out on binders (Multiple Stress Creep Recovery tests) and on compacted mixtures (flow number and wheel tracking tests). In spite of the enhanced stiffness and elasticity of the binder phase, rubberized mixtures showed a lower rutting resistance than the traditional dense-graded mixture both in flow number and wheel-tracking tests. Such an occurrence was explained by referring to the limits of adopted testing protocols and improvements were suggested for future performance-based investigations.

1 INTRODUCTION

Use of crumb rubber derived from end-of-life tires in asphalt mixtures for road paving applications has been known since the 60's (McDonald, 1981). Since then, it has become popular worldwide due to the fact that it contributes to solve a serious waste management problem and to improve asphalt pavement performance (Santagata & Zanetti, 2012).

Crumb rubber can be incorporated into bitumen by means of the “wet” process (which leads to the production of “asphalt rubber”), or added in the hot mix plant in partial substitution of one or more aggregate fractions by means of the “dry” process (Heitzman, 1992; Epps et al., 1994; Caltrans, 2005). However, it is generally recognized that mixtures containing asphalt rubber generally exhibit a laboratory and field performance which is superior to that of “dry” mixtures (Amirkhanian, 2001; Caltrans, 2005; Way et al., 2012).

In the design and production of asphalt rubber mixtures, adoption of a gap-graded aggregate gradation is commonly recommended since it is assumed to provide sufficient void space to accommodate enough binder and to promote stone-to-stone contact (Caltrans, 2006; Liu et al., 2012). As a consequence of their internal structure and of the enhanced stiffness and elasticity of the binder phase, these mixtures are expected to yield limited permanent strains under repeated loading and may therefore be used for the formation of rut-resistant wearing courses (Lee et al., 2008; Hsu et al., 2011; Pasquini et al., 2011; Kaloush et al., 2012; Moreno et al., 2013).

In contrast with these expectations, in previous laboratory investigations performed by means of wheel tracking tests, the Authors found that in some cases rubberized gap-graded mixtures exhibited poor rutting resistance properties. Thus, further studies were

deemed necessary in order to determine whether such a reduced performance can derive from defects in mixture formulation or may be simply due to the ineffectiveness of adopted testing protocols.

Results reported in this paper were obtained in such a context, with the purpose of highlighting the effects of several composition-related factors on the permanent deformation response of gap-graded rubberized mixtures containing asphalt rubber.

Considered mixtures (prepared in the laboratory in controlled conditions and sampled from a hot mix plant) differed in terms of aggregate mineralogy and gradation, and binder dosage. Moreover, a standard dense-graded mixture containing conventional neat bitumen was also considered as a reference.

The experimental program included rheological tests carried out on binders and volumetric and mechanical tests carried out on compacted asphalt mixtures. On the basis of obtained results, rutting properties of the materials were critically analyzed and discussed. Furthermore, limits of the adopted testing protocols were highlighted and improvements were suggested for future performance-based investigations.

2 EXPERIMENTAL INVESTIGATION

2.1 *Materials*

Asphalt mixtures employed in the experimental investigation included two rubberized gap-graded mixtures and one reference dense-graded mixture.

Rubberized mixtures were produced with the same asphalt rubber (AR), a commercially available product containing a nominal amount of crumb rubber equal to 18% by weight of total binder, but different aggregate types, gradation and binder dosage.

Table 1. Composition of asphalt mixtures.

Mix code	Aggregate type	Aggregate gradation	Binder type	Binder dosage (%)
GG-L	Siliceous	GG	AR	8.0
GG-P	Basaltic	GG	AR	7.8
DG	Siliceous	DG	NB	5.5

The first one (GG-L) was manufactured in the laboratory by employing siliceous aggregates provided by a local contractor. Composition was defined according to technical specifications commonly adopted in Italy for rubberized gap-graded mixtures (ARI, 2013) with an optimum binder dosage of 8% by weight of dry aggregates. Reconstruction of target gradation was performed by subjecting aggregates to washed sieve separation and by thereafter combining single size fractions (all finer than 16 mm and retained on the 12.5, 8, 4, 2, 0.5, 0.18 and 0.063 mm sieves) in the needed quantities.

The second rubberized mixture (GG-P) was sampled from a hot mix plant which employed basaltic aggregates and the same asphalt rubber used in the laboratory-made blend. Its composition was determined by means of the ignition test (EN 12697-39, 2012), from which a binder content of 7.8% was obtained, and with sieve analysis of recovered aggregates (EN 933-2, 1995).

The dense-graded mixture (DG) was prepared in the laboratory with siliceous aggregates and neat 50/70 penetration grade bitumen (NB), which was employed with a dosage of 5.5%. Target aggregate gradation was defined according to Italian technical specifications for standard wearing courses (CIRS, 2001) and its reconstruction was made by following the same procedure adopted for mixture GG-L.

Composition and aggregate gradations of asphalt mixtures considered in the investigation are summarized in Table 1 and Figure 1.

2.2 Testing

The experimental program included laboratory tests carried out both on binders and mixtures.

Binders were evaluated by means of Multiple Stress Creep Recovery (MSCR) tests, performed with a dynamic shear rheometer in accordance to AASHTO TP 70-10 (2010). The MSCR test protocol consisted in applying 10 cycles of 1 s creep loading and 9 s recovery at two different stress levels (equal to 0.1 and 3.2 kPa). The 25 mm parallel plates geometry was employed for measurements with a 1.0 mm gap between the plates. Test temperature was set at 58°C, which corresponds to the high performance grade temperature commonly used in North-Central Italy.

Binders were tested in short-term aged conditions, simulated by means of the Rolling Thin Film Oven (RTFO) in accordance to AASHTO T 240 (2009).

Asphalt mixtures were subjected to preliminary characterization in order to assess their compaction properties by making use of the Gyrotory Shear

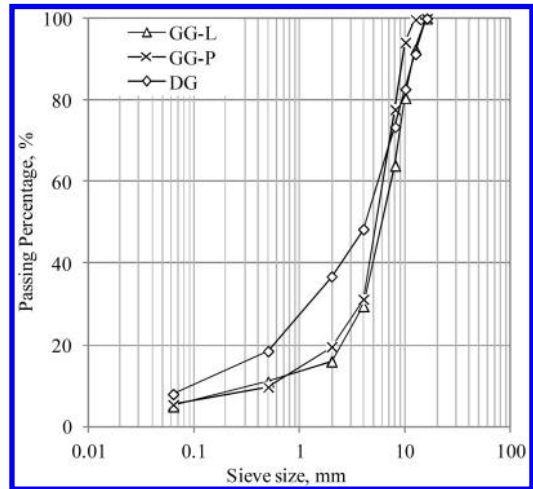


Figure 1. Aggregate size distribution of asphalt mixtures.

Compactor (GSC) (EN 12697-31, 2007). Cylindrical specimens (150 mm diameter) were prepared in the laboratory at a fixed number of gyrations, equal to 100, and at a compaction temperature of 175 and 150°C for rubberized mixtures and dense-graded mixture (DG), respectively. Densification curves of the materials were obtained by analyzing variation of sample height as a function of the number of gyrations recorded during the compaction process.

Flow number and wheel-tracking tests were used to determine resistance to permanent deformation of the mixtures.

Flow number tests were performed by means of the Asphalt Mixture Performance Tester (AMPT) in accordance to AASHTO TP 79 (2009). The adopted testing protocol consisted in applying repeated compressive stresses (equal to 600 kPa) to slender GSC specimens (100 mm diameter, 150 mm height) at a given temperature (equal to 58°C, chosen in accordance with the previously described MSCR tests). Cumulative permanent deformation developed in specimens was recorded as a function of loading cycles. GSC test specimens were obtained from larger ones (150 mm diameter, 170 mm) by following the instructions provided by AASHTO PP 60 (2011). In particular, over-height specimens were prepared by compacting the mass of mixture needed to reach target air voids content, which in this study was set equal to $6.8 \pm 0.5\%$. Cores with 100 mm diameter were then extracted from the center of the gyratory samples using a diamond coring stand and thereafter subjected to trimming by means of a masonry saw in order to obtain smooth and parallel end surfaces.

Volumetric properties of compacted mixtures (voids content, voids in mineral aggregates, voids filled with asphalt, according to EN 12697-8, 2003) were calculated based on the theoretical maximum density measured on loose blends with the pycnometer method according to EN 12697-5 (2009).

Table 2. Non-recoverable creep compliance values obtained from MSCR tests.

	AR	NB
$J_{nr0.1}$ (kPa ⁻¹)	0.748	0.013
$J_{nr3.2}$ (kPa ⁻¹)	0.814	0.008

Wheel tracking tests were performed by means of the Wheel Tracking Device (WTD) in accordance to EN 12697-22 (2007). Rectangular slabs were subjected to 30,000 passes of a loaded rubber wheel (700 N vertical load) at a single test temperature (set at 60°C). Rut depth produced by wheel loading was measured at regular intervals in 15 points distributed on the slab surface. Slabs (50 cm length, 18 cm width, 4 cm thickness) were prepared by means of a large-size roller compactor, operated according to EN 12697-33 (2007), at a geometric air voids content defined in order to reach an actual air voids content equal to that employed in GSC compaction (6.8±0.5%). In order to prevent the occurrence of internal thermal gradients which may bias experimental results, both AMPT specimens and WTD slabs were conditioned in an environmental chamber for 6 hours before testing.

Two replicates were performed for each material and test type, and average data were used in the analysis.

3 RESULTS AND DISCUSSION

3.1 MSCR tests

Experimental data retrieved from MSCR tests were analyzed in order to determine non-recoverable creep compliances ($J_{nr0.1}$ and $J_{nr3.2}$), given by the average non-recovered strains occurring in the 10 creep and recovery cycles divided by the corresponding applied stress. Obtained results are listed in Table 2.

As expected, asphalt rubber AR showed significantly lower non-recoverable creep compliance values than neat binder NB, revealing a higher anti-rutting potential due to the combined effects of higher stiffness and enhanced degree of elasticity.

For both binders, $J_{nr3.2}$ exceeded $J_{nr0.1}$, indicating a transition from linear to non-linear domain when passing from 0.1 to 3.2 kPa applied shear stress. However, the relative increase in non-recoverable creep compliance was higher in the case of binder AR, which proved to be characterized by a more pronounced non-linear behavior.

3.2 GSC compaction

From specimen height progressively recorded during GSC compaction, mixture densification curves were obtained by back-calculating percent compaction (C) values and by fitting them to the following relationship:

$$C = C_1 + k \cdot \log(N_g) \quad (1)$$

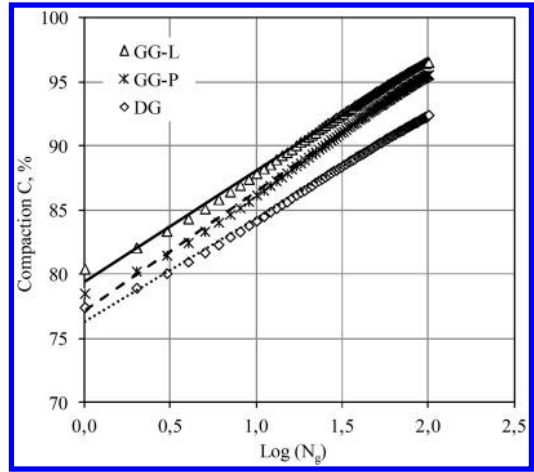


Figure 2. GSC compaction curves of asphalt mixtures.

Table 3. GSC compaction parameters of asphalt mixtures.

	GG-L	GG-P	DG
Self-compaction, C_1 (%)	79.4	77.2	76.3
Workability, k (-)	8.7	9.3	8.1

where C is compaction (%), C_1 is the self-compaction parameter corresponding to compaction at 1 gyration (%), k is the workability parameter, N_g is the number of progressive gyrations during the densification process.

Compaction curves and corresponding regression parameters are shown in Figure 2 and Table 3, respectively.

It was observed that rubberized mixtures exhibited higher self-compaction (C_1) and workability (k) values than those of the reference mixture. In particular, the gap in behavior appeared to be more pronounced when comparing mixtures GG-L and DG, the curves of which could be clearly distinguished from each other. Such a result is not fully coherent with expectations, since the use of AR was believed to increase resistance to compaction due to its high viscosity. Thus, it was inferred that the higher C_1 and k values of rubberized mixtures resulted from the combined effects of non-uniform aggregate skeleton (gap-graded) and high binder dosage, which overcame the counter effects of high binder viscosity.

3.3 Flow number tests

Typical results obtained from a flow number test are shown in Figure 3, where accumulated axial strains are plotted as a function of number of loading cycles. Three portions of the curve, corresponding to different stages of flow, can be clearly distinguished: a primary stage, in which rate of strain decreases as the number of loading cycles increases; a secondary stage, characterized by a rate of strain that remains

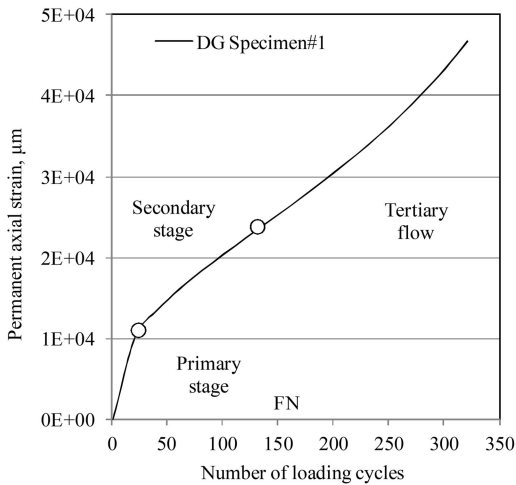


Figure 3. Typical results obtained from a flow number test (mixture DG).

almost constant with load repetitions; and a third stage (tertiary flow), in which strain rate rises dramatically, leading to failure.

The number of loading cycles corresponding to the point at which tertiary flow starts to take place is known as the flow number (FN) and is adopted for the evaluation of the anti-rutting potential of asphalt mixtures (NCHRP 9-33, 2011).

Franken's model recently introduced in AMPT data analysis (Biligiri et al., 2007; Dongrè et al., 2009) was used to calculate FN values, due to its effectiveness and consistency in fitting experimental data (Bonaquist, 2008). Obtained results are summarized in Table 4 which also contains the values of volumetric parameters (air voids, v , voids in mineral aggregate, VMA, and voids filled with asphalt, VFA) determined on test specimens.

Air voids of all the mixtures were very similar to each other and within acceptance limits. However, mixtures GG-L and GG-P were characterized by higher VMA and VFA values than mixture DG as a consequence of the gap-graded aggregate distribution and higher binder content.

Referring to FN values, a first observation was drawn by comparing the rubberized mixtures to each other. The use of tough basaltic stone aggregates in mixture GG-P was expected to produce enhanced rutting performance with respect to mixture GG-L, which is characterized by a very similar composition (aggregate gradation, binder type and binder content) but different aggregate mineralogy (siliceous). However, in contrast with expectations, the FN value of mixture GG-P was found to be slightly lower than that of GG-L, thus indicating a negligible influence on permanent deformation response produced by aggregate source.

Interpretation of results should also take into account the different conditions in which the two mixtures were manufactured (laboratory versus hot mix plant).

Table 4. Volumetric properties and FN values of asphalt mixtures.

	GG-L	GG-P	DG
v (%)	6.9	6.6	6.8
VMA (%)	22.1	22.9	20.0
VFA (%)	69.0	71.2	66.0
FN (–)	76	69	134

In fact, asphalt binders modified with crumb rubber are extremely sensitive to mixing time and temperature, due to different phenomena (swelling, devulcanization, depolymerisation) that may occur after long interaction periods and/or at high interaction temperatures (Abdelrahman and Carpenter, 1999). As a consequence, control of these factors appears to be crucial in order to obtain a final high-quality material.

Following the experience of previous research works (Santagata et al., 2012), a mixing time of 6 minutes and a mixing temperature of 190°C were adopted in this investigation for the preparation of the laboratory-made mixture. On the contrary, due to constraints that are inherent in the production process, a full control of mixing parameters could not be achieved in the hot mix plant, possibly resulting in the observed decay of material properties when passing from laboratory to full-scale conditions.

A second important consideration is related to the fact that both rubberized gap-graded mixtures showed significantly lower rutting resistance than reference mixture DG. In particular, the FN value obtained for the standard mixture was about 1.8–1.9 times those of mixtures containing asphalt rubber. This result is clearly in contrast with those obtained from MSCR tests discussed above. Contradiction between the response of binders and mixtures may be due in part to different mixture formulations (aggregate gradation and binder content) which result in different internal structures of bulk materials (Cooper et al., 1985; Monismith et al., 1985; Sousa et al., 1991). However, it may also be due to the ineffectiveness of testing protocols. For example, in their study conducted on gap-graded and open-graded asphalt rubber mixtures, Zeiada et al. (2011) found that dynamic modulus of these materials measured in triaxial testing configuration may be significantly affected by the level of lateral confinement imposed to the specimens.

In this study, the use of unconfined conditions in flow number tests, as recommended by AASHTO TP 79 (2009), probably led to an underestimate of actual performance of rubberized gap-graded mixtures. In particular, given the non-uniform aggregate size distribution of such type of materials, a lateral confinement may be necessary to better evaluate their rutting properties simulating the real conditions occurring in the field.

3.4 Wheel tracking tests

Results of wheel tracking tests were expressed in terms of proportional rut depth values (P_i) determined at

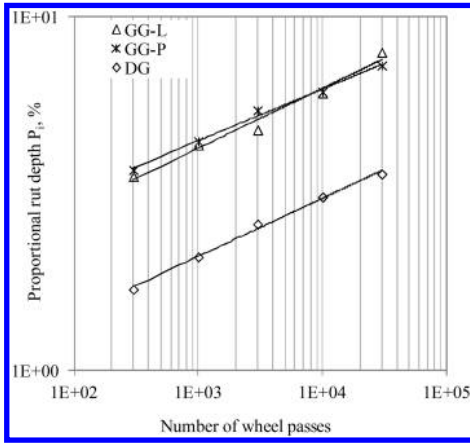


Figure 4. Wheel tracking curves of asphalt mixtures.

Table 5. Wheel tracking regression parameters of asphalt mixtures.

	GG-L	GG-P	DG
P_{100} (%)	2.9	3.2	1.4
β (-)	0.169	0.146	0.164

predefined loading intervals and thereafter fitted to the power law equation indicated below:

$$P_i = P_{100} \cdot \left(\frac{N}{100} \right)^\beta \quad (2)$$

where P_{100} and β are regression constants depending upon material characteristics and testing conditions.

P_{100} is the proportional rut depth after 100 loading cycles and provides a measure of the early response of the mixture under repeated loading, while β is related to the rate of strain accumulation exhibited throughout the test up to 30,000 cycles.

Comparative evaluation of the rutting performance of mixtures was based on the analysis of regression curves. Due to the fact that in the first part of the test permanent deformation response was characterized by a significant variability, fitting was performed by considering only data starting from the 300th loading cycle. Obtained curves and regression parameters are reported in Figure 4 and Table 5, respectively.

It was observed that curves corresponding to rubberized gap-graded mixtures were quite close to each other, whereas the curve corresponding to reference mixture DG was clearly different. In particular, mixture DG exhibited proportional rut depth values significantly lower than those of the other materials for any given number of wheel passes. This seemed to confirm the superior rutting performance of the traditional mixture with respect to the rubberized ones.

However, analysis of regression parameters revealed very similar results in terms of β values (especially

when comparing GG-L to DG), thus indicating a similar aptitude in accumulating permanent deformation under repeated loading. It was therefore concluded that the gap observed between the curves was mainly due to the difference in P_{100} values. This was explained by hypothesizing the occurrence of initial settlement phenomena under loading in the case of rubberized mixtures as a consequence of their gap-graded structure. Such a biasing effect should be taken into account when carrying out a performance-related comparison between mixtures of different type, possibly by focusing on permanent deformation rates rather than on proportional rut depth values.

4 CONCLUSIONS

In the study presented in this paper rutting properties of rubberized gap-graded mixtures were investigated and compared with those of a reference dense-graded mixture containing neat bitumen. The experimental program included rheological tests carried out on binders (asphalt rubber and neat bitumen) and volumetric and mechanical tests carried out on asphalt mixtures (gap-graded and dense-graded).

Analysis of obtained results revealed the existence of a substantial discordance between rutting performance of binders and that of corresponding mixtures.

In particular, while asphalt rubber showed significantly lower non-recoverable creep compliance values measured by means of MSCR tests with respect to neat binder, flow number and wheel tracking test results indicated a lower rutting resistance for rubberized mixtures as compared to that of the traditional dense-graded one.

Such a discrepancy was explained in terms of asphalt mix formulation, mainly related to the use of gap-graded aggregate size distributions and higher binder contents in rubberized mixtures. However, the possible ineffectiveness of adopted standard protocols was also highlighted.

More research is certainly needed to further investigate rutting properties of rubberized mixtures, by considering a wider array of binders, formulations and volumetric conditions. The use of alternative test protocols in addition to or in replacement of standard methods should also be explored. In particular, the use of repeated compressive loading in confined conditions is recommended for flow number tests, while the analysis of permanent strain rates from wheel tracking tests should be considered as an alternative to the simple assessment of proportional rut depth values.

ACKNOWLEDGEMENTS

The investigation described in this paper was carried out as part of the POLIPNEUS and TYREC4LIFE research projects, respectively funded by Ecopneus S.c.p.A. and by the European Commission.

REFERENCES

- AASHTO T 240. 2009. Effect of heat and air on a moving film of asphalt binder (Rolling Thin-Film Oven Test). American Association of State Highway Transportation Officials, Washington, DC.
- AASHTO TP 79. 2009. Standard method of test for determining the dynamic modulus and flow number for hot mix asphalt (HMA) using the asphalt mixture performance tester (AMPT). American Association of State Highway Transportation Officials, Washington, DC.
- AASHTO TP 70. 2010. Multiple stress creep recovery (MSCR) test of asphalt binder using dynamic shear rheometer (DSR). American Association of State Highway Transportation Officials, Washington, DC.
- AASHTO PP 60. 2011. Standard practice for preparation of cylindrical performance test specimens using the superpave gyratory compactor (SGC). American Association of State Highway Transportation Officials, Washington, DC.
- Abdelrahman, M.A. & Carpenter, S.H. 1999. Mechanism of interaction of asphalt cement with crumb rubber modifier, *Transportation Research Record* 1661: 106–113.
- Amirkhanian, S.N. 2001. *Utilization of crumb rubber in asphaltic concrete mixture – South Carolina experience*, Research report, Clemson University, Clemson, SC.
- ARI. 2013. *Asphalt rubber gap graded concrete mixture – Technical specification*, Asphalt Rubber Italia, Pistoia, Italy (in Italian).
- Biligiri, K. P., Kaloush, K.E., Mamlouk, M.S. & Witczak, M.W. 2007. Rational modeling of tertiary flow for asphalt mixtures, *Transportation Research Record* 2001: 63–72.
- Bonaquist, R. 2008. *Ruggedness testing of the dynamic modulus and flow number tests with the simple performance tester*, NCHRP Report 629, Transportation Research Board, National Research Council. Washington, DC.
- Caltrans. 2005. *Synthesis of Caltrans rubberized asphalt concrete projects*, State of California Department of Transportation, Sacramento, CA.
- Caltrans. 2006. *Asphalt rubber usage guide*, State of California Department of Transportation, Sacramento, CA.
- CIRS. 2001. *Performance-related technical specification for the construction and maintenance of road pavements*, Ancona, Italy (in Italian).
- Cooper, K.E., Brown, S.F. & Pooley, G.R. 1985. The design of aggregate gradings for asphalt base courses, *Journal of the Association of Asphalt Paving Technologists* 54: 324–346.
- Dongré, R., D'Angelo, J. & Copeland, A. 2009. Refinement of flow number as determined by asphalt mixture performance tester, *Transportation Research Record* 2127: 127–136.
- EN 933-2. 1995. Tests for geometrical properties of aggregates – Part 2: Determination of particle size distribution, European Committee for Standardization, Brussels, Belgium.
- EN 12697-5. 2009. Bituminous mixtures – Test methods for hot mix asphalt – Part 5: Determination of the maximum density, European Committee for Standardization, Brussels, Belgium.
- EN 12697-22. 2007. Bituminous mixtures – Test methods for hot mix asphalt – Part 22: Wheel tracking, European Committee for Standardization, Brussels, Belgium.
- EN 12697-31. 2007. Bituminous mixtures – Test methods for hot mix asphalt – Part 31: Specimen preparation by gyratory compactor, European Committee for Standardization, Brussels, Belgium.
- EN 12697-33. 2007. Bituminous mixtures – Test methods for hot mix asphalt – Part 33: Specimen prepared by roller compactor, European Committee for Standardization, Brussels, Belgium.
- EN 12697-39. 2012. Bituminous mixtures – Test methods for hot mix asphalt – Part 39: Binder content by ignition, European Committee for Standardization, Brussels, Belgium.
- Elliot, R.P., Ford, M.C., Ghanim, M. & Tu, Y.F. 1991. Effect of aggregate gradation variation on asphalt concrete mix properties, *Transportation Research Record* 1317: 52–60.
- Epps, J.A. 1994. *Uses of recycled rubber tyres in highways*, NCHRP Report 198 – Synthesis of Highway practice, Transportation Research Board, National Research Council, Washington, DC.
- Heitzman, M.A. 1992. *State of the practice – Design and construction of asphalt paving materials with crumb rubber modifier*, Report FHWA-SA-92-022, Washington, DC.
- Hsu, T., Chen, S. & Hung, K. 2011. Performance evaluation of asphalt rubber in porous asphalt-concrete mixtures, *Journal of Materials in Civil Engineering* 23(3): 342–349.
- Kaloush, K.E., Biligiri, K.P., Nordgren, T., Zeiada, W.A., Rodezno, M.C., Souliman, M.I., Reed, J.X. & Stempihar, J.J. 2012. Laboratory evaluation of asphalt-rubber gap graded mixture constructed on Stockholm Highway in Sweden. In *Proc. Asphalt Rubber Conference; Munich, Germany, 23–26 October 2012*.
- Lee, S.-J., Akisetty, C.K. & Amirkhanian, S.N. 2008. The effect of crumb rubber modifier (CRM) on the performance properties of rubberized binders in HMA pavements, *Construction and Building Materials* 22(7): 1368–1376.
- Liu, Y., Han, S., Zhang, Z. & Xu O. 2012. Design and evaluation of gap-graded asphalt rubber mixtures, *Materials and Design* 35: 873–877.
- McDonald, C.H. 1981. Recollections of early asphalt-rubber history. In *Proc. National seminar on asphalt-rubber; San Antonio, TX, USA, 27–29 October 1981*.
- Monismith, C.L., Epps, J.A. & Finn, F.N. 1985. Improved asphalt mix design, *Journal of the Association of Asphalt Paving Technologists* 54: 347–406.
- Moreno, F., Sol, M., Martín, J., Pérez, M. & Rubio, M.C. 2013. The effect of crumb rubber modifier on the resistance of asphalt mixes to plastic deformation, *Materials and Design* 47: 274–280.
- Way, G.B., Kaloush, K.E. & Biligiri, K.P. 2012. *Asphalt-rubber practice guide*, 2nd edition”, Rubber Pavement Association, Tempe, AZ.
- NCHRP 9-33. 2011. *A manual for design of hot mix asphalt with commentary*, Report 673, Transportation Research Board, National Research Council, Washington, DC.
- Pasquini, E., Canestrari, F., Cardone, F. & Santagata, F.A. 2011. Performance evaluation of gap graded asphalt rubber mixtures, *Construction and Building Materials* 25(4): 2014–2022.
- Santagata, E. & Zanetti, M.C. 2012. *The use of products from end-of-life tyres in road pavements*. Milan, Italy: Ecopneus (in Italian).
- Santagata, E., Riviera, P.P., Dalmazzo, D., Lanotte, M., Zanetti, M., Fiore, S. & Ruffino, B. 2012. Design and construction of a full-scale test section with asphalt rubber gap-graded wearing course mixture, In *Procedia: Social and behavioral sciences* 53: 524–534.
- Sousa J.B., Craus, J. & Monismith, C.L. 1991. *Summary report on permanent deformation in asphalt concrete*, SHRP A/IR-91-104, Strategic Highway Research Program, Washington, D.C.
- Zeiada, W.A.-E., Kaloush, K.E., Biligiri, K.P., Reed, J.X. & Stempihar, J.J. 2011. Significance of confined dynamic modulus laboratory testing: conventional, gap and open graded asphalt mixtures, *Transportation Research Record* 2210: 9–19.

Simulation of asphalt concrete plastic deformation behavior

A.T. Papagiannakis

Department of Civil and Environmental Engineering, University of Texas-San Antonio, San Antonio, TX, USA

H. Zelelew

Lucy Consulting Engineers, Washington, DC, USA

E. Mahmoud

Civil Engineering, University of Texas-Pan American, Edinburg, TX, USA

ABSTRACT: This paper presents Discrete Element Method (DEM) simulation results of the plastic deformation resistance of asphalt concretes subjected to the loading prescribed for the Asphalt Mixture Performance Test (AMPT). This consists of a repetitive vertical axial stress of 690 kPa for 0.1 sec followed by a rest period of 0.9 sec. Nine asphalt concretes were considered. These consisted of three mix designs, each prepared with three aggregate types and the same PG 76-22 binder. Their microstructure was captured by X-Ray tomography and processed to be input into DEM analysis. The viscoelastic properties of the asphalt mastics were obtained by fitting Burger models on frequency sweep DSR test data. The Flow Number (FN) values were obtained by fitting Francken models to the computed plastic deformation results. Plastic deformation resistance rankings for the nine mixtures were developed in terms of the simulated FN values. These rankings were in reasonable agreement with the plastic strain rankings obtained from uniaxial creep laboratory testing.

1 INTRODUCTION

Asphalt concrete (AC) mixtures are uniquely complex heterogeneous materials composed of air voids, mastic and aggregates. Mastics are blends of asphalt binder and fines, typically considered as particles passing sieve No. 200 (i.e., sizes finer than 0.075 mm). The distribution of these three phases and their interaction defines the mechanical properties of ACs and contributes significantly to their rutting resistance, load carrying capacity and durability. Pavement rutting consists of surface depressions along the wheel paths caused by the plastic deformation of the AC and the underlying granular layers. The AC plastic deformation properties are greatly influenced by the mastic rheology, aggregate properties, and the microstructure of mixture constituents.

The AC behavior is dominated by the interaction between mastics and distinct aggregate particles. The micromechanics-based Discrete Element Method (DEM) has been commonly used to simulate the large-strain behavior of granular materials such as ACs. The DEM technique is ideally suited to describe particle contact interaction (Cundall and Strack, 1979). The literature to date provides valuable insight into the modeling of the microstructure of ACs. Previous studies on modeling the AC mixture behavior using the micromechanical modeling approach include Shashidhar, 2000; Rothenburg *et al.*, 1992; Chang and

Meegoda, 1997; Buttlar and You, 2001; You and Buttlar, 2004; Abbas *et al.*, 2005; Collop *et al.*, 2006; and Zelelew 2008.

The objective of this paper is to simulate the cyclic Asphalt Mixture Performance Test (AMPT) as described in AASHTO TP 79-12, use the estimated Flow Number (FN) to compare the plastic deformation resistance of the 9 mixes and compare it to laboratory uniaxial creep data.

2 MATERIALS

Nine AC mixtures were considered in this study composed of 3 mixed designs and 3 aggregate types. The three mix designs were:

- A coarse-graded Coarse Matrix High Binder Type C (CMHB) mix,
- A gap-graded Porous Friction Course (PFC) mix, and,
- A fine-graded Superpave Type C (Superpave) mix.

The three aggregate types were:

- A hard limestone (HL)
- A granite (G) and,
- A soft limestone (SL)

Each of these nine mixtures was prepared with a PG 76-22 modified binder meeting Texas DOT

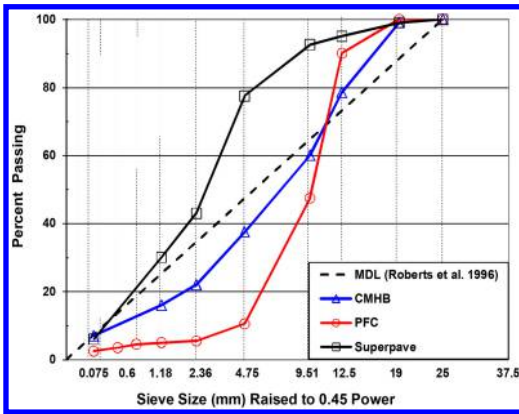


Figure 1. Aggregate gradations.

Table 1. Asphalt concrete mix design data.

	Mix Type		
	CMHB-C	Superpave-C	PFC
Aggregate	Hard Limestone		
Binder %	4.2	4.0	5.1
Air Voids at	7.3	7.4	19.5
VMA	12.7	12.7	27.2
VFA	70.2	68.5	26.4
Dust %	1.7	1.5	0.5
Aggregate	Granite		
Binder %	5.3	4.8	6.6
Air Voids at	6.9	6.9	19.6
VMA	13.7	13.2	27
VFA	69.7	69.9	25.8
Dust, %	1.3	1.3	0.4
Aggregate	Soft Limestone		
Binder %	5.8	5.2	7.1
Air Voids at	7.0	6.7	19.3
VMA	14.3	13.7	28
VFA	72.5	70.9	28.8
Dust, %	1.2	1.2	0.4

specifications. The aggregate gradations for each of the nine mix designs are shown in Figure 1 while the volumetric properties are presented in Table 1. Detailed mix design data and experimental test plan as well as numerical modelling of creep performance can be found elsewhere (Zeleeuw 2008).

3 X-RAY IMAGING

The AC performance test specimens were fabricated by coring the 150 mm diameter Superpave gyratory compacted (SGC) specimens to a diameter of 100 mm. The cored samples were also trimmed to a height of 150 mm. The X-ray CT scanning of AC performance

specimens was conducted by the Advanced Characterization of Infrastructure Materials Laboratory (ACIM) of the Texas Transportation Institute (TTI). Each of the three AC specimens was scanned perpendicular to their vertical axis at 1 mm distance interval to yield 150 2D image slices with an image resolution of 0.195 mm/pixel. Digital image processing techniques were then applied to effectively analyse the AC microstructure.

The X-ray CT images of the ACs were processed utilizing the Volumetric-based Thresholding Algorithm (VTA) developed by Zeleeuw and Papagiannakis (2011). The VTA algorithm provides a quantitative means of establishing a unique grayscale threshold for the boundaries between air-mastic and mastic-aggregate. Moreover, it allows visualizing the microstructure of these three phases in 2D and 3D. An example of the resulting 2D rectangular sections is shown in Figure 2. The white objects (grayscale = 255) in these figures represent mixture constituents. The watershed image segmentation technique was also utilized to separate the connected or/and overlapped aggregate particles.

4 ASPHALT MASTIC MODELING

The aggregate finer than 0.075 mm and binder proportions used in preparing the mastics were obtained from the volumetric properties of the AC mixtures. The PG 76-22 binder (RTFO-aged) was used to prepare the mastic specimens. Frequency sweep tests were conducted using a test temperature of 60°C using a wide range of frequencies (i.e., from 0.01 to 100 rad/sec). The Burger model consisting of a Maxwell and Kelvin-Voigt element coupled in series was used to describe mastic viscoelastic rheological models. Several researchers have implemented the Burger model to describe the viscoelastic behavior of mastics (Abbas *et al.*, 2005; Kim and Little, 2004; and Yu *et al.*, 2007). The Burger models were fitted to the frequency sweep test data by minimizing the squared differences between modeled and observed storage and loss shear moduli (Papagiannakis *et al.*, 2002; and Baumgaertel and Winter, 1989). The Burger model yielded a fairly good fit to the observed mastic behavior (R^2 of 0.75), although a higher number of Kelvin units would probably improve it. The constants of the Burger model for the mastics are shown in Tab 2. Additional strain amplitude testing was carried out to establish the limits of linear viscoelasticity. A value of 53% strain was selected as this limit beyond which the spring constants of the Maxwell and Kelvin models in Tab. 2 were set equal to zero.

5 FLOW NUMBER DATA

Recently, the use of the Flow Number (FN) obtained through the unconfined or confined AMPT has gained acceptance as a means of indexing the permanent deformation resistance of AC. The FN is defined as the number of load cycles corresponding to the minimum

Table 2. Burger Model Parameters; 60°C.

Mastic ID	Maxwell Element		Kelvin Element	
	E_M kPa	η_M kPa.sec	E_K kPa	η_K kPa.sec
CMHB-HL	225.0	45.5	13.1	10.6
PFC-HL	220.0	20.5	12.9	6.8
Sup.-HL	260.0	40.4	13.8	10.4
CMHB-G	200.0	30.5	9.7	6.3
PFC-G	90.0	10.5	8.9	3.3
Sup.-G	280.0	40.3	8.9	7.1
CMHB-SL	150.0	20.0	10.9	4.3
PFC-SL	80.0	7.4	7.6	3.2
Super.-SL	200.0	25.0	12.3	4.8

E_K η_K = spring, dashpot constants for Maxwell
 E_M η_M = spring and dashpot constants for Kelvin

rate of change of permanent axial strain (AASHTO TP 79). The AMPT involves applying a cyclic load for 0.1 second followed by a 0.9 second rest period. The number of load cycles and accumulated axial strains are continuously recorded by the AMPT built-in software. The AMPT FN test is terminated when either 10,000 load cycles are reached or when 50,000 micro-strain is accumulated (i.e., 5% strain), whichever occurs first. The FN is determined through the following steps (AASHTO TP 79):

- A curve is fitted to the plastic strain data using a *Francken* model that has the following form:

$$\epsilon_p = An^B + C(e^{Dn} - 1)$$

where, A , B , C and D are regression constants and n is the number of load cycles.

- Setting the second derivative of this model equal to zero gives the min. rate of change in plastic strain accumulation, which is defined as the FN.

As described next, the main issue with this method, is difficulty in establishing the minimum rate of strain change within the 10,000 load cycles of the test. Nevertheless, this method was shown to be preferable to the alternative methods described in AASHTO T79-12 FN (Ameri et al., 2014).

6 DEM SIMULATION OF AMPT

The study utilized the Particle Flow Code in two-dimensions (PFC^{2D}) version 3.1 software (Itasca, 2004). The methods described here can be readily extended to a three-dimensional DEM modeling approach, which should produce more accurate results. The first step in the DEM simulation process is to input the AC microstructure (shown in Figures 2a, 2b, and 2c) obtained as described above into the PFC^{2D} input module. The built-in *BALL* command generates particles and can assign mastic or aggregate attributes to them through their Cartesian coordinate locations identified from the processed images. An advantage of the PFC^{2D} is that it allows “clumping” similar adjacent

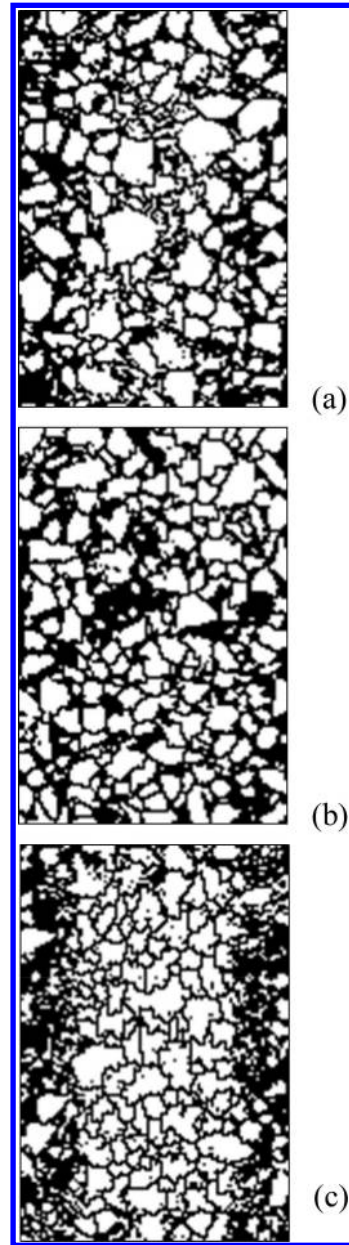


Figure 2. VTA processed AC images; (a) CMHB; (b) PFC and (c) Superpave.

particles together using the *FISH* clump function and thus, avoids force-displacement calculations between them.

Four rigid walls were defined as the boundary constraining the AC microstructural models. For the unconfined AMPT, the upper wall was used to load the AC model by specifying a wall velocity, while fixing the lower platen. The DEM simulation of the confined AMPT was conducted using a vertical axial deviator stress of 690 kPa and a confining pressure of 69 kPa. Before applying the wall velocity, a contact stress level

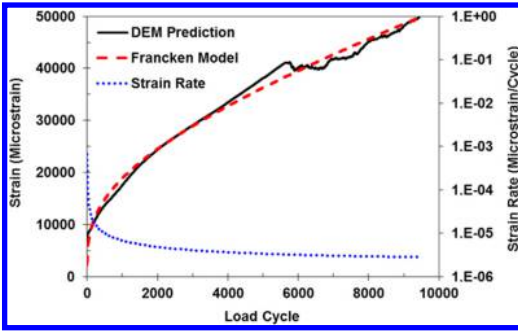


Figure 3. Strain vs. load cycles; CMHB-HL.

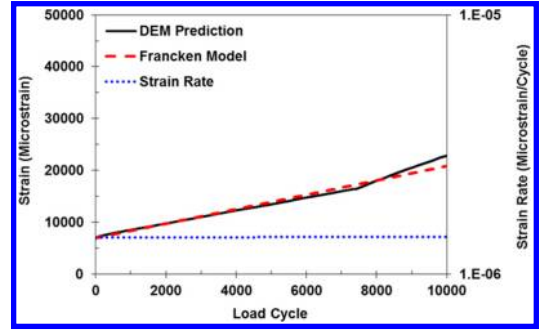


Figure 4. Strain vs. load cycles; PFC-HL.

of 35 kPa (i.e., 5% of the axial deviator stress) was used to obtain uniform initial stress distribution within the DEM specimen models. The AC model was loaded in a stress-controlled fashion by specifying the upper wall velocity. A numerical “servo-mechanism” implemented via the PFC^{2D} *FISH* function was devised to monitor the amount of stress generated by the displacement of the upper boundary. The stresses were computed by dividing the total force acting on the upper wall by the wall area.

Contact models describe the force-displacement interaction between particles. For the AC microstructure, the primary contacts include mastic-to-mastic, mastic-to-aggregate, and aggregate-to-aggregate. These interactions were defined using two contact models, namely a linear contact model (frictional law) and a linear viscoelastic model. The linear elastic contact model was used to define the aggregate-to-aggregate contacts. The DEM simulations included an aggregate-to-aggregate friction of 0.5 and the normal to shear stiffness ratio of 2.8. Previous studies showed that an elastic modulus value of 30 GPa is appropriate for aggregates (Abbas et al., 2005). In addition to this model, slippage in the aggregate-to-aggregate contact was allowed by means of the contact friction coefficient. The Burger model was used to describe the mastic-to-mastic and the mastic-to-aggregate contacts (Table 2). The elastic constants for the Burger model in the normal direction were obtained from those in the shear direction.

7 DEM SIMULATION RESULTS

The DEM simulations were performed using a time step of 0.05 seconds and were carried out over 10,000 loading cycles (or accumulated strain of 5%) to simulate the full length of the AMPT. The results were in the form of end of loading cycle vertical strain using a virtual gauge length of 100 mm centered at the mid-height of the sample. These strains were computed by tracking the vertical displacement of discrete elements located at the two ends of the virtual gauge on each side of a mixture model. The results of the DEM simulation were plotted as axial strain versus the number of load cycles. Figures 3 to 5 show the results for hard limestone mixtures, Figures 6 to 8 show the results for the

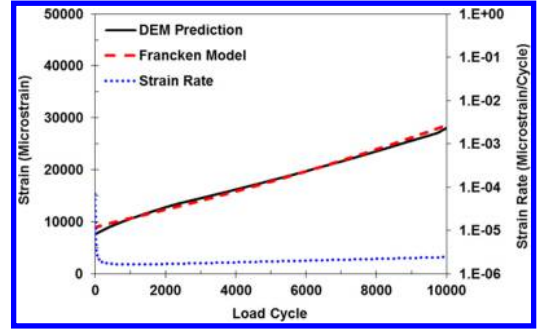


Figure 5. Strain vs. load cycles; Superpave-HL.

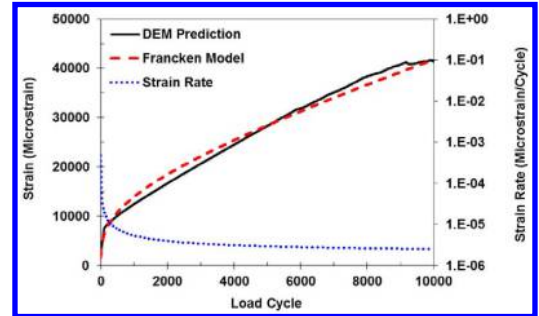


Figure 6. Strain vs. load cycles; CMHB-G.

granite aggregate mixtures and Figures 9 to 11 show the results for the soft limestone mixtures.

These figures allow the following observations to be made:

- All nine mixtures exhibited a steep increase in vertical strain in the first couple of hundred loading cycles.
- Some mixtures exhibited the anticipated increase in strain rate within the 10,000 load cycles (e.g., Figs. 4 and 6). Fitting the *Francken* model however, masked the minimum strain rate value suggesting a constant rate of axial strain accumulation up to 10,000 load cycles or to 5% strain accumulated. It is noted that the strain rate (dotted line) was plotted in log-scale.
- Some mixtures exhibited a decrease in strain rate at higher load cycles as a result of particle re-orientation (e.g., Figs. 3, 6 and 10).

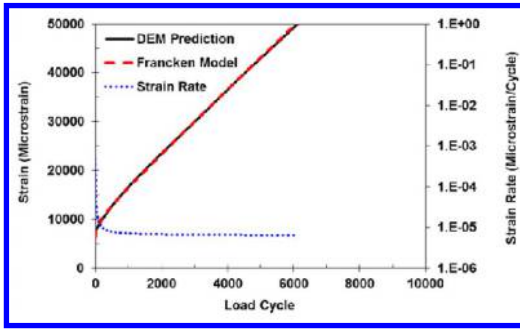


Figure 7. Strain vs. load cycles; PFC-G.

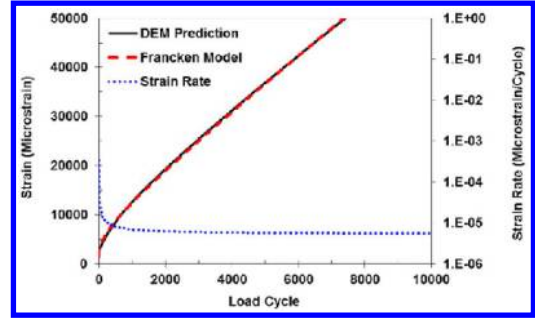


Figure 11. Strain vs. load cycles; Superpave-SL.

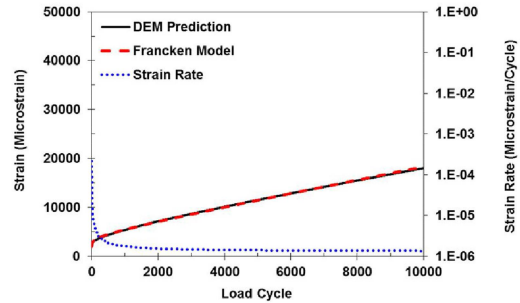


Figure 8. Strain vs. load cycles; Superpave-G.

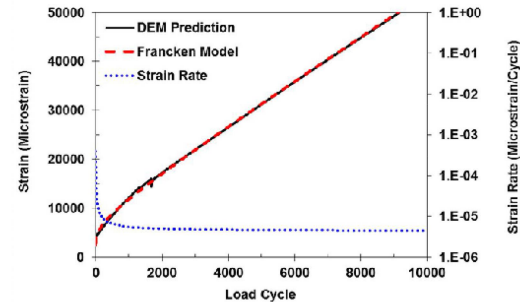


Figure 9. Strain vs. load cycles; CMHB-SL.

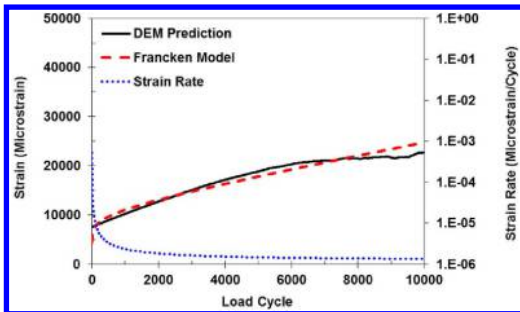


Figure 10. Strain vs. load cycles; PFC-SL.

Table 3. FN-related statistics from the DEM simulation

Mastic ID	FN	Strain at FN	Strain Rate at FN
CMHB-HL	9452	0.05	2.8×10^{-06}
PFC-HL	7410*	0.0164	1.4×10^{-06}
Sup.-HL	970/9725*	0.011/0.027*	$1.6/2.4 \times 10^{-06}$ *
CMHB-G	10000	0.042	2.5×10^{-06}
PFC-G	6134	0.05	6.5×10^{-06}
Sup.-G	10000	0.018	1.4×10^{-06}
CMHB-SL	9159	0.05	4.5×10^{-06}
PFC-SL	10000	0.025	1.3×10^{-06}
Sup.-SL	7416	0.05	5.6×10^{-06}

*min value obtained from raw strain data

raw data did and therefore the latter value was retained. Furthermore, the Superpave-HL mixture showed one minimum value by fitting the *Francken* model and another, much higher, by visually inspecting the raw strain data. In this case, both values were listed on [Table 3](#).

[Table 4](#) shows plastic deformation resistance rankings for the nine asphalt concrete mixtures simulated in terms of FN only, whereby the higher the FN value, the more plastic deformation resistant a mixture is. Accordingly, rankings were assigned letters, A for best, B for better, C for not as good and D for worst. [Table 4](#) retained the strain and strain rate information from [Table 3](#) to illustrate an important point. That is mixtures that rank the same in terms of FN value exhibit drastically different plastic strain levels at FN cycles. A case in point is the three mixtures that ranked as the best (i.e., ranked as A in [Table 4](#)). These three mixtures had drastically different strain levels at FN cycles:

- the Superpave-G mixture experienced strain of 0.018,
- the PFC-SL experienced strain of 0.025 and,
- the CMHB-G experienced strain of 0.042.

Similar observations can be made for other mixtures that rank in the same group in terms of FN alone.

Further analysis of the DEM simulation results reveals no clear trend between the strain level and the strain rate accumulation at FN cycles. For some of the

[Table 3](#) summarizes the calculated FN values, the strain level at FN and the rate of strain change at FN. It is noted that for the PFC-HL mix, the *Francken* model revealed no obvious minimum strain rate, while the

Table 4. Ranking mixtures in terms of FN only.

Mastic ID	Ranking	Strain at FN	Strain Rate at FN
CMHB-HL	B	0.05	2.8×10^{-06}
PFC-HL	C	0.0164	1.4×10^{-06}
Sup.-HL	B	0.027	2.4×10^{-06}
CMHB-G	A	0.042	2.5×10^{-06}
PFC-G	D	0.05	6.5×10^{-06}
Sup.-G	A	0.018	1.4×10^{-06}
CMHB-SL	B	0.05	4.5×10^{-06}
PFC-SL	A	0.025	1.3×10^{-06}
Sup.-SL	C	0.05	5.6×10^{-06}

mixtures the two values seem to be correlated. Consider for example the same three mixtures ranked as A above. The strain rate accumulation per cycle for the CMHB-G mixture is almost twice as large as that for the Superpave-G and PFC-SL mixtures. However, this is not always the case. Consider for example the mixtures ranked as B in Table 4. The strain rate accumulation per cycle for the CMHB-SL is twice as large as that for the CMHB-HL, although they exhibited the same strain rate at FN cycles.

Clearly, the FN value alone is not sufficient to characterize the plastic deformation resistance of asphalt concrete mixtures. Additional information on the amount of plastic strain and the rate of plastic strain accumulation is essential. Perhaps a tiered ranking system should be utilized, with rankings based on the number of FN cycles, followed by the accumulated plastic strain and the rate of plastic strain accumulation at FN cycles.

8 COMPARISON TO UNIAXIAL STATIC CREEP LABORATORY DATA

The results of the DEM simulation of cyclic loading were compared to laboratory data of uniaxial static creep obtained on the same asphalt concrete mixtures (Alvarado et al., 2007). These tests were conducted at the same temperature as the mastic testing (i.e., 60°C) but at a vertical stress level of 206 kPa, which is much lower than the 690 kPa used for the DEM simulations. The tests are typically run for 10000 sec (2.78 hrs).

Under static uniaxial creep, the logarithm of the creep compliance (i.e., strain divided by stress) versus the logarithm of loading time has a distinct shape. As shown in Figure 10, it is expected to be initially parabolic (primary zone) and then transitions to linear (secondary zone) to become nonlinear again (tertiary zone) past what is defined as the Flow Time (FT). The FT have been used as an index of the resistance of asphalt concretes to plastic deformation. A summary of the maximum strain values obtained from testing these nine asphalt concrete mixtures under uniaxial static creep is given in Table 5.

Table 5 includes rankings of the nine asphalt concrete mixtures tested in terms of the maximum strain

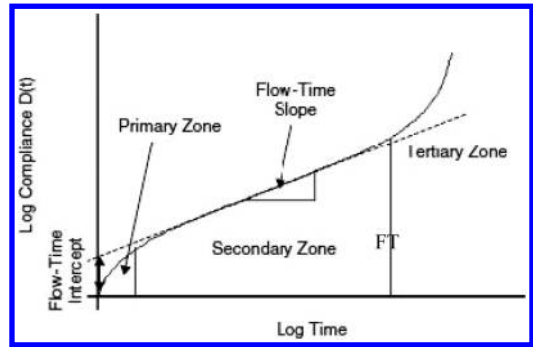


Figure 12. Characteristic uniaxial static creep test curve (Papagiannakis and Masad 2008).

Table 5. Results of uniaxial static creep laboratory tests.

Mastic ID	Max strain* at 10,000 sec	Ranking
CMHB-HL	0.0382	A
PFC-HL	0.00786	D
Sup.-HL	0.003175	A
CMHB-G	0.00486	B
PFC-G	0.00715	D
Sup.-G	0.00528	B
CMHB-SL	0.00675	C
PFC-SL	0.00732	D
Sup.-SL	0.00691	C

*Laboratory data from Alvarado et al. (2007).

exhibited at the end of the test. The lower the maximum strain observed the more resistant in plastic deformation the mix is. As a result, the letter A suggests the most resistant mix, B the less resistant mix and so on. It is noted that the strain levels are much lower than those obtained from the cyclic tests. This was anticipated given the much lower vertical stress applied in the laboratory tested samples. Comparing Tables 4 and 5 reveals no direct on-to-one matching of the rankings of these mixtures. For example only the PFC-G and Superpave-SL were ranked identically as D and C, respectively. Although the others did not quite match exactly, they were not further apart than one ranking level, (e.g., CMHB-HL ranked B using the simulated FN value, while it ranked as A with the laboratory uniaxial creep strain). This is not surprising, given the limitations pointed out earlier of using only FN to characterize plastic deformation resistance. The only exception was the mixture PFC-SL mixture that ranked as A using the FN value, while it ranked as D by the laboratory uniaxial creep strain measurement.

9 CONCLUSIONS

This paper presented a Discrete Element Method (DEM) approach for modeling the permanent deformation properties of asphalt concrete mixtures.

The DEM software package PFC^{2D} was used to simulate the AMPT with a focus on estimating the Flow Number (FN) as described in AASHTO 79-12. Nine AC mix designs were analyzed and their microstructure was captured using X-Ray computer tomography. The X-Ray images were processed through imaging techniques to translate pixels into elements of the asphalt concrete phases, namely air, asphalt mastic and aggregate.

The simulated strain versus number of loading cycle results were processed to determine the FN values. This was done by fitting a *Francken* model to the strain results and differentiating twice to establish the minimum strain rate. This approach had a number of challenges:

- In some cases, the *Francken* model masked the minimum plastic strain rate value.
- In most cases, the 10,000 load cycles were not sufficient to establish a minimum strain rate (i.e., the strain rate appeared to be constant up to the end of the test).
- In all cases, the FN value alone was not sufficient to rank the resistance of asphalt concretes to plastic deformation because mixtures with the same FN value exhibited drastically different plastic strains and plastic strain rates.

The DEM simulation results of these mixtures were compared to plastic strain results obtained on the same nine mixtures subjected to uniaxial static creep laboratory tests. The comparison was based on the ranking of the mixtures obtained by the two methods that is the simulated FN values versus the laboratory maximum plastic strain values.

Although it was possible to establish one-to-one matching of the ranking obtained by these two techniques for only 2 of the 9 mixtures, the remaining mixtures, with the exception of one, were not substantially different in ranking. It is recommended to utilize the amount of plastic strain and its rate accumulation in addition to the FN value to index the plastic deformation resistance of asphalt mixtures using the AMPT.

REFERENCES

- AASHTO TP 79-12, Standard method of test for determining the dynamic modulus and flow number for Hot Mix Asphalt (HMA) Using the Asphalt Mixture Performance Tester (AMPT), American Association of Highway and Transportation Officials (AASHTO), Washington D.C., January, 2012.
- Abbas A., Papagiannakis A.T., Masad E., and Shenoy A., "Modeling asphalt mastic stiffness using discrete element analysis and micromechanics-based models", *The International Journal of Pavement Engineering*, Vol. 6, No. 2, 2005, pp. 137–146.
- Alvarado, C et al., "Feasibility of Quantifying the Role of Aggregate Strength on Resistance to Load in HMA", Report No. TX FHWA/TX 06/0-5268-1, April 2007.
- Ameri, M. A.H. Sheikhmotevali and A.Fashipour, "Evaluation and Comparison of Flow Number Calculation Methods", *Journal of Road Materials and Pavement Design*, Vol. 15, Issue 1, 2014.
- Baumgaertel M., and Winter H.H., "Determination of discrete relaxation and retardation time spectra from dynamic mechanical data", *Rheological Acta*, Vol. 28, 1989, pp. 511–519.
- Buttler W.G., and You Z., "Discrete element modeling of asphalt concrete: a micro-fabric approach", *Transportation Research Record 1757*, Transportation Research Board, National Research Council, Washington, D.C., 2001, pp. 111–118.
- Chang K.G., and Meegoda J.N., "Micromechanical simulation of hot mix asphalt", *Journal of Engineering Mechanics*, Vol. 123, No. 5, 1997, pp. 495–503.
- Collop A.C., McDowell G.R., and Lee Y.W., "Modeling dilation in an idealized asphalt mixture using discrete element modeling", *Granular Matter*, Vol. 8, 2006, pp. 175–184.
- Cundall P.A. and Strack O.D., "Discrete numerical model for granular assemblies", *Geotechnique*, Vol. 29, No. 1, 1979, pp. 47–65.
- Itasca Consulting Group, "Particle flow code in two-dimensions (PFC2D) manual version 3.1", Itasca Consulting Group, MN, 2004.
- Kim Y., and Little D., "Linear viscoelastic analysis of asphalt mastics", *Journal of Materials in Civil Engineering*, Vol. 16, No. 2, 2004, pp. 122–132.
- Papagiannakis A.T., Abbas A., Masad E., "Micromechanical analysis of viscoelastic properties of asphalt concrete", *Transportation Research Record 1789*, Transportation Research Board, National Research Council, Washington, D.C., 2002, pp. 113–120.
- Papagiannakis A.T., and Masad, "Pavement Design and Materials", Wiley and Sons, Hoboken NJ, (2008) p. 153.
- Rothenburg L., Bogobowicz A., Haas R., Jung F.W., and Kennepohl G., "Micromechanical modelling of asphalt concrete in connection with pavement rutting problems", *Proceedings of the 7th International Conference on Asphalt Pavements*, 1992, pp. 230–245.
- Shashidhar N., Zhong X., Shenoy A.V., and Bastian E.J., "Investigating the role of aggregate structure in asphalt pavements", *8th Annual Symposium Proceedings on Aggregates, Asphalt Concrete, Base, and Fines*, Denver Co., 2000.
- You Z., and Buttler W.G., "Discrete element modeling to predict the modulus of asphalt concrete mixtures", *Journal of Materials in Civil Engineering*, Vol. 16, No. 2, 2004, pp. 140–146.
- Yu L., Shi-Feng R., and Guang-Hu X., "Discrete Element Simulation of Asphalt Mastics Based on Burgers Model", *Journal of Southwest Jiaotong University Journal of Southwest Butler University*, Vol. 1, No. 15, 2007, pp. 20–26.
- Zelelew H., "Simulation of the permanent deformation of asphalt concrete mixtures using discrete element method (DEM)", PhD Dissertation, Department of Civil and Environmental Engineering, Washington State University, Pullman, WA, 2008.
- Zelelew H., and Papagiannakis T., "A Volumetric thresholding algorithm for processing asphalt concrete X-Ray CT images", *International Journal of Pavement Engineering*, Vol. 12, No. 6, 2011, pp. 543–551.

Effect of interlayer bonding on pavement response under dynamic load in presence of asphalt concrete cross-anisotropy

M.U. Ahmed, R.A. Tarefder & A. Rahman

University of New Mexico, Albuquerque, New Mexico, USA

ABSTRACT: In this study, the effects of various interlayer bonding conditions on pavement strain behavior is evaluated considering dynamic loads, cross-anisotropy of Asphalt Concrete (AC), and pavement temperatures. A dynamic Finite Element Model (FEM) of an instrumented asphalt pavement section is developed in ABAQUS and cross-anisotropy of the AC layer is defined by the ratio of horizontal to vertical modulus (n -value). Field AC cores and granular aggregate base and subbase materials were collected during construction. Laboratory tests were conducted to determine the n -value and viscoelastic parameters of the AC. In addition, the resilient modulus test was conducted to determine the stress-dependency of the base and subbase course materials. These values and parameters are used as FEM model inputs through User-defined Material (UMAT) interface in the ABAQUS. For validation, model simulation was run Falling Weight Deflectometer (FWD) loading and model outputs were matched with FWD deflections. The validated model is further simulated by varying friction coefficient at the interface of two layers such as AC-AC, Base-Subbase, and Subbase-Subgrade respectively. The result shows that the variation in friction coefficient along the AC-AC layer interface affects the horizontal tensile strain at bottom of the AC layer higher compared to the other layer interfaces. The similar trend is observed in case of vertical strains in both AC and base layers. Effect of the AC-AC interlayer friction on strains during the summer is greater than that during the winter.

1 INTRODUCTION

A flexible pavement structure is constructed by compacting different layers of materials one above the other. Typically, stiffer material, such as Asphalt Concrete (AC), is placed on the top whereas the less stiff unbound materials, such as base, subbase, and subgrade, are placed at the bottom due to stress distribution caused by tire pressure. During the construction, different types of binder coats, such as tack coat, are used to enhance the bonding between different layers. This bonding may decrease with age. Considering fully-bonded condition for different layer interfaces may not produce accurate stress-strain during pavement analysis.

A number of researches have been performed on interlayer bonding (Nan and Tian 2009, Horak et al. 2009, Hariyadi et al. 2013, Jia et al. 2013). Some of these studies have concentrated on investigating interlayer bonding by laboratory testing and the rest has concentrated on investigating effect of interlayer bonding on pavement response considering isotropic material properties such as stiffness. It is known that the AC possesses cross-anisotropy, i.e., unequal vertical and horizontal stiffness (Masad et al. 2002, Wang et al. 2005, and Motola and Uzan 2007). Later, Ahmed et al. (2013) observed that the AC cross-anisotropy has significant effect on the pavement responses such as stress-strain.

Temperature is another important factor which affects the pavement responses since the AC stiffness is dependent on temperature (Diefenderfer 2002, and Appa 2003). Till today, the effect of interlayer bonding on pavement strains has not been studied in a combined platform of cross-anisotropic and temperature dependent AC stiffness under dynamic loading. Therefore, a study is initiated to perform to investigate the effect of interlayer bonding variation on strains in pavement layers combining the earlier mentioned factors at both high and low temperatures during the summer and winter respectively.

2 OBJECTIVES

Main goal of this study is to investigate the effect of interlayer layer bonding on pavement response such as horizontal and vertical strains. Specific objectives are to:

- Develop a dynamic FEM incorporating the cross-anisotropic and viscoelastic AC and stress-dependent unbound layers, such as base and subbase.
- Perform the FEM simulations at varying interlayer friction coefficients incorporating pavement temperatures during both summer and winter to determine strains in different layers of the instrumented pavement section.

3 DYNAMIC FINITE ELEMENT MODELING

3.1 Model Geometry

The geometry of the FEM is constructed based on an instrumented pavement section at mile post 141 (MP 141) on Interstate 40 (I-40) (see Figure 1(a)). It consists of four major layers: AC at the surface, aggregate layer at the base, Process-Place and Compacted (PPC) layer at the subbase, and a subgrade soil layer.

The AC layer consists of three lifts each with a thickness of 3.5 in. (88.9 mm). The PPC layer is prepared by processing (loosing) existing base and/or subgrade materials and then, compacting it in place. The thickness of the base is 6 in. (152.4 mm) and the subbase is 8 in. (203.2 mm). From Figure 1(a), it can be seen that horizontal asphalt strain gauges (HASGs) and vertical asphalt strain gauges (VASGs) were installed at the bottom and inside of the AC layer respectively. Earth pressure cells were installed at different depths to measure the vertical stress.

A quarter cube model is used for a 3D simulation (see Figure 1(b)). The depth and horizontal length of a model were selected as such there is no effect of stress near the boundary according to Duncan et al. (1968). Wave reflection by the boundary is one of the major concerns in a dynamic analysis. Dynamic amplification may occur due to this wave reflection that results from the insufficient distance to the boundary. Therefore, the final dimensions, i.e., length, width, and depth, of this entire model were selected to be 300 in. \times 300 in. \times 300 in. (7.62 m \times 7.62 m \times 7.62 m).

An 8-noded brick element (C3D8) is used for the mesh generation. It is a common practice to assign fine mesh near the loading region to capture the stress gradient and coarser mesh further from that region. The length of the smallest element is 0.6 in. (15 mm) based on the mesh sensitivity analysis according to Ahmed et al. (2013). An edge biased structure meshing pattern is used to obtain a smooth transition from fine mesh to coarse mesh. The bottom boundary is restrained to move along the three mutually orthogonal directions (see Figure 1(b)). Therefore, there will be no deflection in horizontal and vertical directions in this plane. Movements of the vertical boundaries are restrained only in the horizontal directions.

3.2 Material properties

Material properties, for different pavement layers, are determined through both field and laboratory testing. These are discussed in the following sections:

3.2.1 AC layer

Modulus of the field compacted AC core (E -value) was determined in the laboratory along vertical and horizontal directions to calculate the n -value. Relaxation modulus tests on AC core with two different loading modes were performed both axially and diametrically, i.e., indirect tensile testing (IDT) mode.

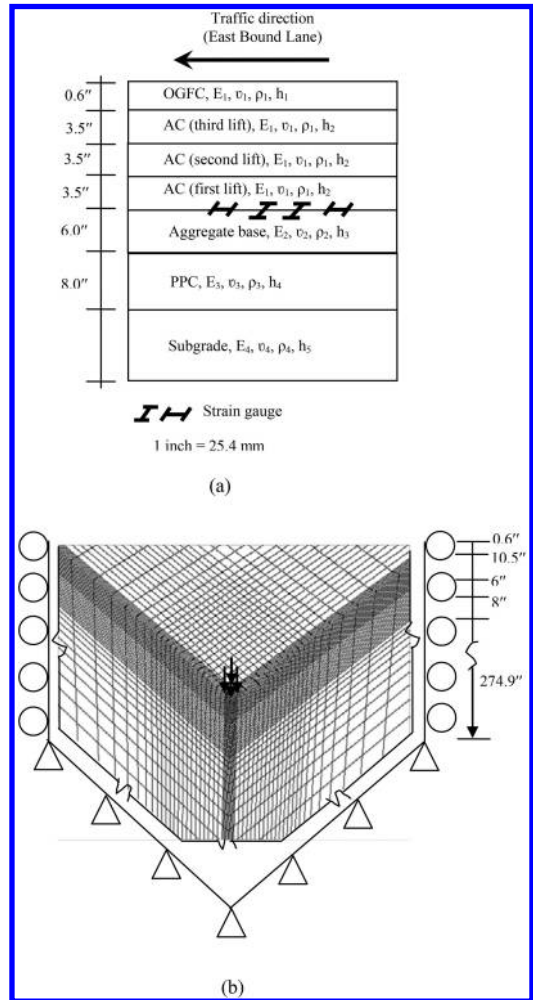
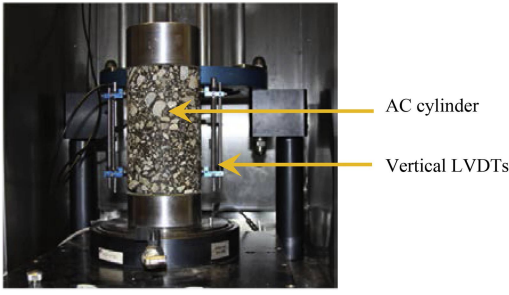


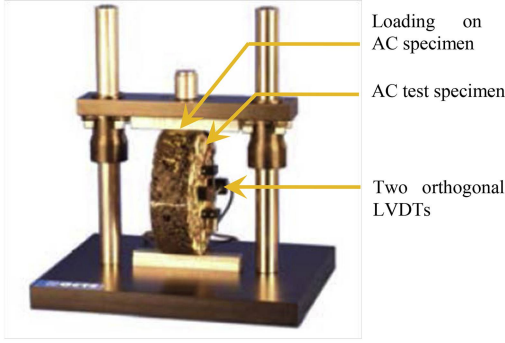
Figure 1. FEM development: (a) Pavement section, (b) Model geometry.

Figure 2(a) and (b) show the laboratory test setup. For determination of the degree of cross-anisotropy (n -value), strain-controlled test was conducted. A constant strain of 50 micro-strain was applied on the AC cylinder during the test. The vertical or axial stress due to this constant strain was measured. Ratio of the initial stress and constant strain is the vertical modulus or stiffness, E_v . The similar strain-controlled test was implemented during the IDT test to measure the strain which is transverse to the loading direction. Ratio of the initial indirect tensile stress and strain is the horizontal modulus or stiffness, E_h . Both of the uniaxial and IDT tests were conducted at the room temperature, i.e., 25°C. The degree of cross-anisotropy (n -value) is the ratio of the horizontal and vertical modulus. In this study, the n -value of the AC is 0.33.

The dynamic modulus test was also conducted on the field compacted AC core to determine the Prony series coefficients as required to assign the relaxation modulus variation to the AC layer in the dynamic



(a)



(b)

Figure 2. Laboratory testing for characterizing the AC: (a) Dynamic modulus, (b) Indirect tensile.

FEM. This test was conducted at different frequencies and temperatures according to the AASHTO TP 62-07 (2007) procedure. Considering the generalized Maxwell model, the variation of relaxation modulus is as follows:

$$E_v(t) = E_{0,v} \left[1 - \sum_{i=1}^m e_i \left(1 - e^{-t/\tau_i} \right) \right] \quad (1)$$

where $E_v(t)$ = vertical relaxation modulus at time t second (ksi), $E_{0,v}$ = instantaneous vertical modulus (ksi), e_i = Prony series coefficient, τ_i = relaxation time, and m = number of spring-dashpot. The instantaneous modulus ($E_{0,v}$) of the AC is 3074.16 ksi (21195.6 MPa) at 25°C. It is assumed that the Prony series coefficients for both vertical and horizontal modulus are the same except the instantaneous modulus. The horizontal instantaneous modulus ($E_{0,h}$) is the product of the vertical modulus and degree of cross-anisotropy (n -value), i.e., $E_{0,h} = n \times E_{0,v}$. Therefore, the generalized equation of the horizontal modulus is as follows:

$$E_h(t) = E_{0,h} \left[1 - \sum_{i=1}^m e_i \left(1 - e^{-t/\tau_i} \right) \right] \quad (2)$$

where $E_h(t)$ = vertical relaxation modulus at time t second (ksi), $E_{0,h}$ = instantaneous horizontal modulus (ksi), e_i = Prony series coefficient, τ_i = relaxation

Table 1. Prony series coefficient.

i	e_i	τ_i
1	0.2	1.1
2	0.2	4.7
3	0.15	9.75
4	0.15	100
5	0.1	250
6	0.1	470

Table 2. Backcalculated moduli of unbound layers.

Material	Density (pcf)	Poisson's ratio
Base	135	0.4
Subbase	120	0.4
Subgrade	110	0.45

Note¹: 1 pcf = 16.02 kg/m³

time, and m = number of spring-dashpot. Table 1 summarizes the Prony series coefficients.

These coefficients are also assumed to be same for the shear modulus except the instantaneous shear modulus. The equations of the instantaneous shear modulus are as follows:

$$G_{0,vh} = n' \times E_{0,v} \quad (3)$$

$$G_{0,hh} = \frac{E_{0,h}}{2(1 + \nu_{hh})} \quad (4)$$

where $G_{0,vh}$ = instantaneous shear modulus in vertical plane (ksi), $E_{0,v}$ = instantaneous vertical modulus (ksi), n' = conversion factor for shear modulus, $G_{0,hh}$ = instantaneous shear modulus in horizontal plane (ksi), $E_{0,h}$ = instantaneous horizontal modulus (ksi), and ν_{hh} = Poisson's ratio in horizontal plane. The value of n' -value is assigned equal to 0.38. The Poisson's ratio, ν_{hh} , of the AC is 0.3 as determined from the IDT test. A FORTRAN subroutine is developed to implement this cross-anisotropic viscoelastic model of the AC layer. This subroutine is integrated to the dynamic FEM in ABAQUS using the User Defined Material (UMAT) interface.

3.2.2 Unbound layers

Unbound layers, such as base, and subbase and subgrade, were assumed isotropic and stress-dependent in this study. The subgrade is assumed as isotropic and linear elastic. The subgrade modulus is predicted from the backcalculation of Falling Weight Deflectometer (FWD) deflection data using ELMOD, a backcalculation program and it is 25 ksi.

Laboratory resilient modulus is conducted on granular aggregates as collected from both base and subbase layers (see Figure 3).

Table 3 summarizes the parameters of the unbound layers which are used in the dynamic FEM model.

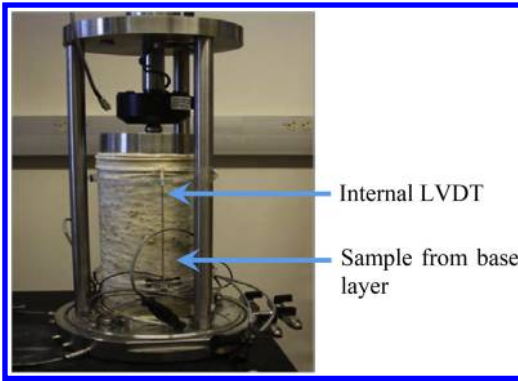


Figure 3. Resilient modulus test setup.

Table 3. Backcalculated moduli of unbound layers.

Layer	k_1	k_2	k_3
Base	5835	0.15	0.75
Subbase	13056	0.17	-0.02

The model is as below:

$$M_r = k_1 p_a \left(\frac{\theta}{p_a} \right)^{k_2} \left(\frac{\tau_{oct}}{p_a} + 1 \right)^{k_3} \quad (5)$$

where θ = bulk stress, τ_{oct} = octahedral shear stress, p_a = atmospheric pressure, and k_1, k_2, k_3 = regression coefficients that need to be determined from laboratory resilient modulus test.

4 TYPE OF LOADING

In this study, FWD test load data is used for model validation and wheel load is used to study pavement responses. The FWD test load is idealized by a circular area with 6 in. (150 mm) radius in FEM model. The target FWD test load is 9 kip (40.03 kN) which applies 79.6 psi (548.8 kPa) and duration of this load is 0.025 second.

Non-uniform vertical tire contact stresses are applied over the tire imprint area as the wheel load. Figure 4(a) shows the dimension of ribs of a single tire from the arrangement of a dual tire 275/80R22.5 as well as the distribution of vertical contact stress over the ribs based on the literatures [20]. There are about five ribs in this tire. The ribs are numbered according to the similar stress magnitudes. The non-uniform tire contact stress is applied on a quarter of this tire imprint area to generate a truck wheel load on the quarter cube model.

Figure 4(b) shows the loading duration of the single tire at 96.5 km/hr (60 mph). The loading duration for each of the ribs is assumed to be the same and the duration is 0.03 second. In addition, the peak stresses

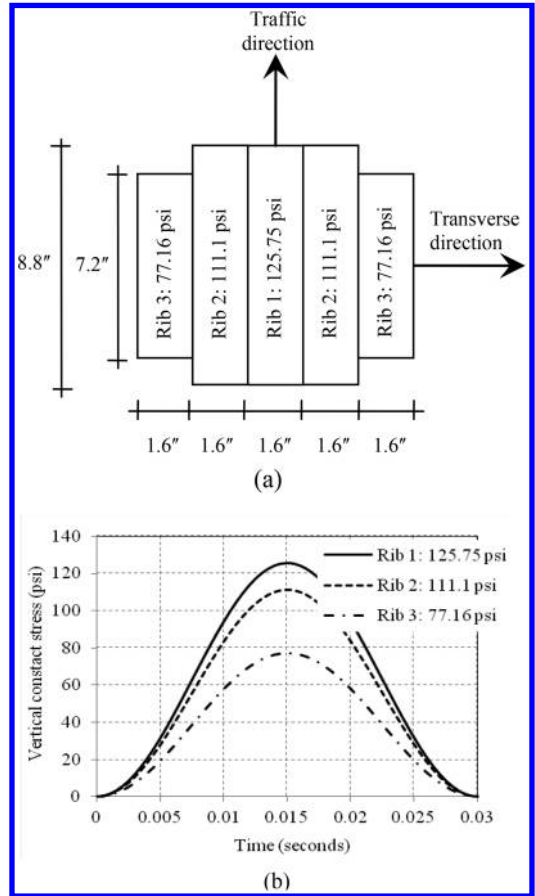


Figure 4. Tire contact stress: (a) Stress distribution over tire ribs, (b) Stress variation over time.

of the ribs are assumed to be attained at the same time, i.e., 0.015 second.

5 INTERLAYER BONDING

The layer interfaces are considered partially-bonded and coulomb friction law is used to model the contact between the interfaces. The friction coefficients required for this contact model are collected from the literatures in this study according to Romanoschi and Metcalf (2001). The friction coefficients along layer interfaces in AC are 0.7 and that along base-subbase as well as subbase-subgrade interfaces is 1.3. For the parametric study, friction coefficients of layer interfaces, such as AC-AC, Base-Subbase, and Subbase-Subgrade, are considered 0.1 and 1.0 respectively.

6 VALIDATION

The dynamic FEM is simulated under the FWD load considering pavement temperatures in both summer

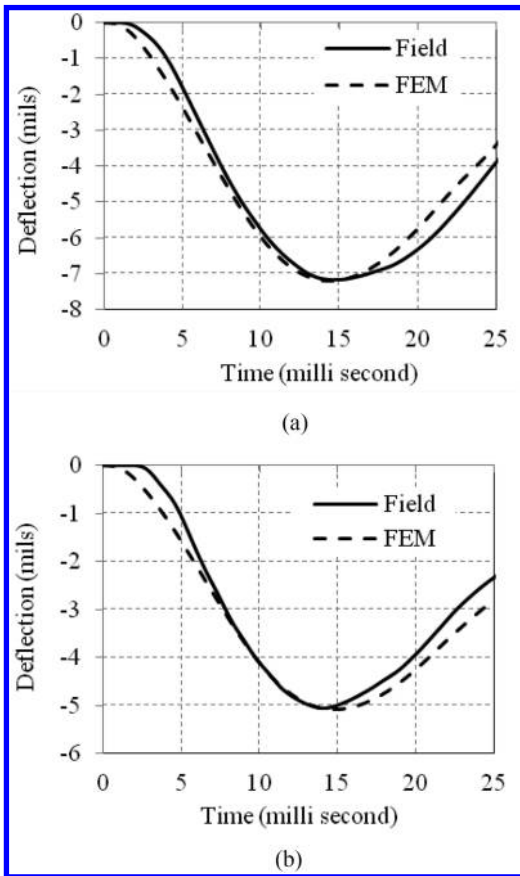


Figure 5. Comparison of time-deflection histories: (a) Summer, (b) Winter.

and winter. During summer, pavement surface and bottom temperatures were 35.1°C and 27.4°C respectively. Pavement surface and bottom temperatures were 4.1°C and 3.6°C respectively during winter. Figure 5(a) and (b) show the comparison between time-deflection histories at the loading point from field test and FEM simulation in both summer and winter respectively. In both of the cases, the Fem simulated time-deflection histories are close to the field measured time-deflection histories. Therefore, this model can be used for further parametric study to investigate the effect of interlayer bonding or friction on pavement responses.

7 DISCUSSION

The pavement responses, such as horizontal tensile strain and vertical strains in different layers, are determined at the bottom of the AC layer from the FEM simulations incorporating friction coefficients of 0.1 and 1.0 respectively. Simulations at two different frictional coefficients are repeated in both summer and winter to consider differential pavement temperatures.

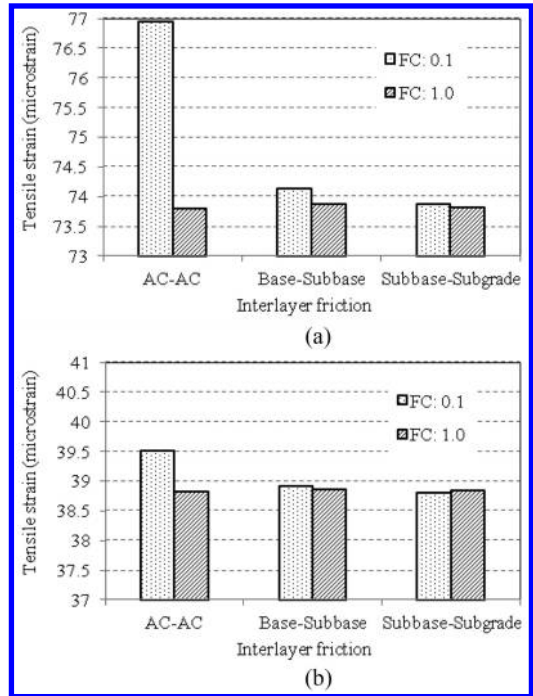


Figure 6. Horizontal tensile strain at bottom of the AC: (a) Summer, (b) Winter.

Figure 6 shows the effect of frictional coefficient variations on horizontal tensile strain at the bottom of the AC layer in both summer and winter. In Figure 6(a), the horizontal axis shows the identification of interlayer friction between different layers, such as AC-AC, base-subbase, and subbase-subgrade respectively. It is observed that the tensile strain frictional coefficient variation in AC-AC shows the highest strain difference, i.e., 3.75 microstrain, among all interlayer cases. Tensile strains are 77.0 and 73.75 microstrain at frictional coefficients of 0.1 and 1.0 respectively. However, this difference decreases in the winter (see Figure 6(b)). In winter, this strain difference is 0.75 microstrain. In both of the seasons, effect of interlayer friction in other unbound layers layer is very small.

The vertical strain in AC layer is also determined from the FEM simulations incorporating different interlayer frictional coefficients and temperatures in two different seasons. Figure 7(a) shows that the difference in vertical strain in the AC layer is 1.75 microstrain in summer which is the maximum among all the interlayer cases. In winter, this difference decreases to about 1.0 microstrain (see Figure 7(b)).

Figure 8 shows the effect of interlayer friction on vertical strain in base layer in both summer and winter. Figure 8(a) shows that the difference in vertical strain in the base layer is 3.0 microstrain in summer which is the maximum among all the interlayer cases. In winter, this difference decreases to about 2.25 microstrain (see Figure 8(b)). In summer, strain at frictional coefficient

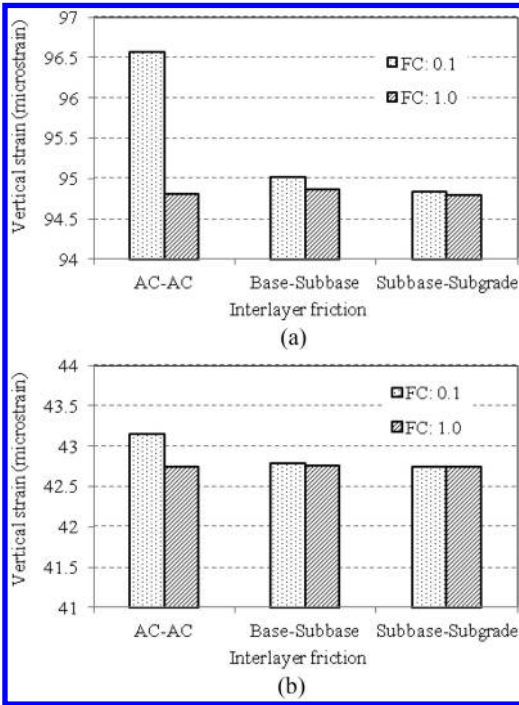


Figure 7. Vertical strain in the AC: (a) Summer, (b) Winter.

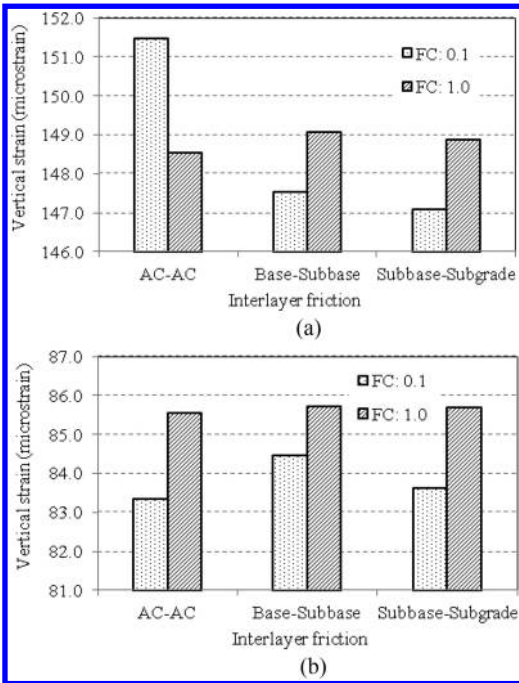


Figure 8. Vertical strain in the base: (a) Summer, (b) Winter.

of 0.1 is greater than that at frictional coefficient of 1.0; however, this trend of vertical strain is reversed.

In Figure 9(a), it is observed that base-subbase interlayer friction has greater effect on vertical strain the

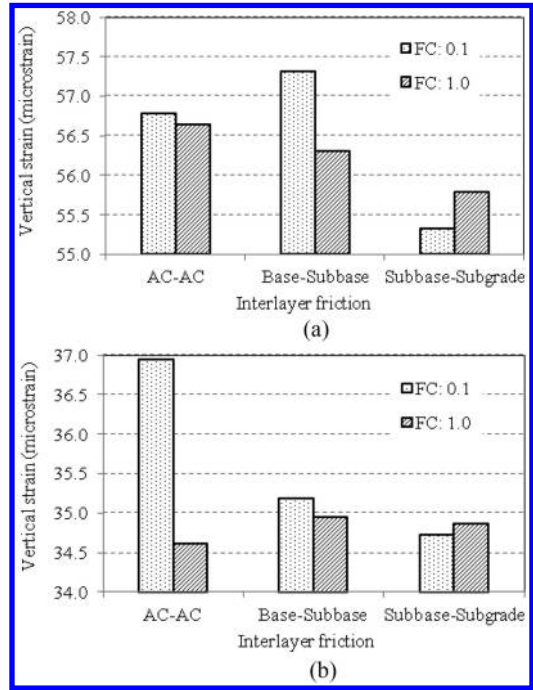


Figure 9. Vertical strain in the subbase: (a) Summer, (b) Winter.

subbase compared to other interlayer cases. However, the AC-AC interlayer friction has greater effect on vertical strain the subbase during winter which is similar to the previous trends (see Figure 9(b)).

Figure 10(a) shows that the effect of interlayer friction on vertical strain in subgrade is almost the same for all the cases. In addition, the strain difference is very small. During the winter, this effect decreases and the strain difference is very little (see Figure 10(b)).

8 CONCLUSIONS

The following conclusions are made based on the above discussions:

- Frictional coefficient variation in AC-AC interlayer has the highest impact on both horizontal tensile strain at the bottom of the AC layer as well as vertical strains in the AC and base layers.
- Effect of frictional coefficient variation on strains is higher in summer as compared to winter.
- Vertical strain in subgrade is almost insensitive to frictional coefficient variation in both summer and winter.

This study has not incorporated tire contact stress in horizontal direction which may have significant effect. In addition, relative motion along the layer interfaces has not been considered in the friction model. It is recommended to consider these issues in the future study.

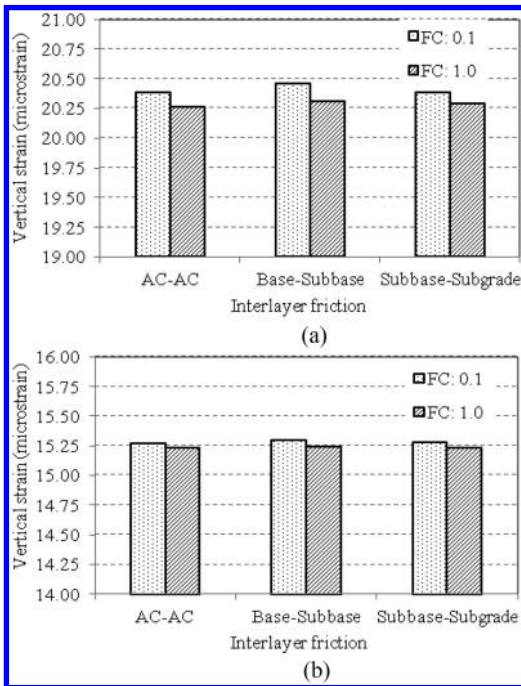


Figure 10. Vertical strain in the subgrade: (a) Summer, (b) Winter.

ACKNOWLEDGEMENT

The authors would like to acknowledge the Research Bureau, New Mexico Department of Transportation (NMDOT) for financial support to perform this study. Special thanks are extended to the NMDOT field exploration crew for field test and AC core collection from instrumented pavement section.

REFERENCES

AASHTO TP 62-07. 2007. Standard Method of Test for Determining Dynamic Modulus of Hot Mix Asphalt Concrete Mixtures. *AASHTO Provisional Standards*, Washington, D. C.

Ahmed M. U., Tarefder R. A., and Islam M. R. 2013. Effect of Cross-Anisotropy of Hot-Mix Asphalt Modulus on Falling Weight Deflections and Embedded Sensor Stress-Strain. In *Transportation Research Record: Journal of the Transportation Research Board*, No. 2369, pp. 20–29.

Appea A. K. 2003. *Validation of FWD Testing Results at the Virginia Smart Road: Theoretically and by Instrument Response*. Ph.D Dissertation, Virginia Polytechnic Institute and State University, Virginia, USA.

Diefenderfer B. K. 2002. *Moisture Content Determination and Temperature Profile Modeling of Flexible Pavement Structures*. Ph.D Dissertation, Virginia Polytechnic Institute and State University, Virginia, USA.

Duncan J. M., MonSmith C. L., and Wilson E. L. 1968. Finite Element Analyses of Pavements. In *Highway Research Record: Journal of Highway Research Board*, 228, pp. 18–23.

Hariyadi, E. S., Aurum, K. P., and Subagio, B. S. 2013. Theoretical Study of Bonding Condition at the Interface between Asphalt Pavement Layers. *Proceedings of the Eastern Asia Society for Transportation Studies*, Vol. 9.

Horak, E., Maina, J.W., Emery, S.J., and Walker, B. 2009. “Mechanistic Modeling of Potential Interlayer Slip at Base Sub-base Level.” *Proceedings of the 8th International Conference on the Bearing Capacity of Roads, Railways, and Airfields*, June 29–July 2, 2009, University of Illinois, Urbana Champaign.

Jia, X., Huang, B., and Li, L. 2013. A Simplified Approach Evaluating Interlayer Shear Resistance in Asphalt Pavement. *Proceedings of the 92nd Transportation Research Board (TRB)*, Washington, D.C.

Masad E., Tashman L., Somedavan N., and Little D. 2002. Micromechanics-Based Analysis of Stiffness Anisotropy in Asphalt Mixtures. *Journal of Materials in Civil Engineering, ASCE*, Vol. 14, No. 5, pp. 374–383.

Motola Y., and Uzan J. 2007. Anisotropy of Field-Compacted Asphalt Concrete Material. *Journal of Testing and Evaluation*, ASTM.

Nan, X. F., and Tian, Z. F. 2009. Experimental Research on Ultra Thin Friction Course Interlayer Bonding Strength.” *International Journal of Pavement Research and Technology (IJPRT)*, 2(4), 176–180.

Romanoschi S. A., and Metcalf J. B. 2001. Characterization of Asphalt Concrete Layer Interfaces, In *Transportation Research Record: Journal of Transportation Research Board*, 1778, pp. 132–139.

Wang L., Hoyos L. R., Wang J., Voyiadjis G., and Abadie C. 2005. Anisotropic Properties of Asphalt Concrete: Characterization and Implications for Pavement Design and Analysis. *Journal of Materials in Civil Engineering, ASCE*, Vol. 17, No. 5, pp. 535–543.

Artificial neural network modelling of asphalt concrete's mechanical properties produced with using waste granite filler

H. Akbulut, C. Gürer & S. Çetin

Afyon Kocatepe University, Engineering Faculty, Department of Civil Engineering, Afyonkarahisar, Turkey

M. Caner

Afyon Kocatepe University, Technology Faculty, Department of Civil Engineering, Afyonkarahisar, Turkey

A. Elmacı

Afyon Kocatepe University, Dazkırı Vocational High School, Dazkırı, Afyonkarahisar, Turkey

ABSTRACT: In this study, it was aimed to develop a model by means of Artificial Neural Network (ANN) in order to estimate Marshall stability of asphalt concrete produced with different amounts of waste granite mineral filler. In the scope of experimental test, asphalt design with Marshall method was performed using % 0, 2, 4, 6 and 8 mineral filler the amount by weight and measured Marshall stability value. Percentage of bitumen and mineral filler rates and unit volume weights of asphalt samples were used as input parameters and Marshall stability value was used output parameter for ANN model. Experimental data were divided randomly into three groups as training, validation and testing. In order to show the reliability of the model several ANN model results were given. The data which is experimentally obtained were compared the ANN model results and were found to be compatible with each other. Some error analysis results were presented for the accuracy of the proposed model.

1 INTRODUCTION

It is an important to use industrial waste for another production in terms of sustainability. This recycling issue supports the global economy. Flexible pavement construction is an important opportunity for the use of waste materials. Most waste materials can be recycled in pavement construction. Using waste materials in pavement construction may prevent unnecessary waste of limited budget resources and damage to the national economy (Çetin 2014).

Granite sludge can be thought as the waste matter and is obtained resulting from the purification of water that has been used to clean granite during cutting and polishing, consisting primarily of quartz. A considerable amount of waste comes out end of this process. Daily amount of this waste is about 70 ton in ÇİMSTONE factory (website 1 2014).

Mineral filler meeting the definition of an aggregate material is captured by sieves of 0.075 mm. The material which is finer than 0.075 mm does not meet the standard for being filler aggregate. Filler serves as a part of the mineral aggregate in bituminous hot mixtures, so the filler affects the load-carrying capacity and stability of the mix. Filler is used in bituminous hot mixtures to increase the ratio of fine aggregate, decrease the void ratio, and increase the ability of the mix to resist plastic deformation under high temperature conditions.

In our previous study mineral filler which was dried, milled and sieved using a No. 200 obtained from the granite sludge was used in bituminous hot mixtures as a filler material (Akbulut et al. 2012). Here filler ratios are used as 0%, 2%, 4%, 6% and 8% in the mix. A bituminous hot mixture design using the Marshall method was performed for the each of the different filler ratios and optimum bitumen ratios were determined.

ANN has been becoming increasingly popular in engineering applications for parameter estimation and modelling issues during the last decade. A numerous studies has been done in order to estimate Marshall stability value using neural network (Serin et al. 2011; Morova et al. 2012).

In this study, a neural network model is investigated to estimate Marshall stability of asphalt concrete using the results obtained from experimental study. While different amounts of waste granite mineral filler, bitumen value and unit volume weights were used as input parameters of the model, Marshall stability value was used as output. In order to verify accuracy of the model the results were compared with the experimental results.

2 ASPHALT CONCRETE MIX DESIGN AND EXPERIMENTAL STUDY

The Marshall mix design method and criteria were originally developed for airfield pavements, but were

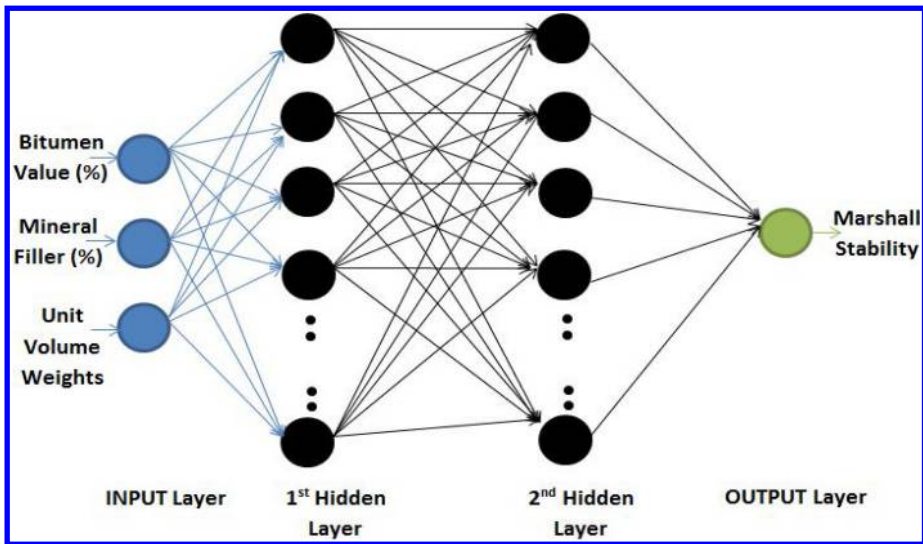


Figure 1. ANN model of Marshall stability prediction.

Table 1. Training parameters of the ANN model.

Network type	Feed forward network
Training function	Trainlm
Number of layer (input is excl.)	3
Number of neurons in layers (input is included)	3-x-x-1
Number of data train-validation-test	72-9-9
Ratios of train-validation-test	%80/%10/%10
Performance function	Mse
Maximum number of epochs	5000
Performance goal	0
Maximum validation failures	10
Training function	Trainlm

Table 2. Network performances as regression values for different neuron combinations for hidden layers.

No	Neuron numbers for hidden layers	“R” at training	“R” at test
1	25-7	0.99485	0.95288
2	25-7	0.98416	0.95865
3	25-7	0.98392	0.97046
4	23-8	0.98295	0.96028
5	22-9	0.97940	0.96349
6	22-9	0.99079	0.98786
7	21-10	0.99217	0.95867
8	19-11	0.99500	0.97458
9	18-12	0.98628	0.98373
10	17-11	0.99143	0.97996
11	10-10	0.97514	0.94833

later also adopted for use in highway pavements (Tosun, 2010).

For the purpose of designating the amount of asphalt mixture, “Marshall Method” commonly used is handled both in our country and the world (Chen & Richard 2003).

Stability is one of the most important properties of bituminous hot mixtures because of the dynamic loads from vehicles, long term static loads, stress caused by vehicle speeding and stopping, and shear effects or aggregate loss (Akbulut et al. 2011; Akbulut et al. 2012). Stability is the resistance to deformation of the hot mix bituminous pavement under heavy traffic. If pavement has low stability, higher deformation is expected (Akbulut et al. 2011). However, low or high stability values of bituminous hot mixture are undesirable because they may lead to different problems such as crack and rutting (website 3).

Recycled filler was added to the bituminous hot mixture in five different quantities so the bituminous hot mixture design could be tested using

the Marshall method on each filler combination independently. Bituminous hot mixture specimens were prepared according to the curve within the Turkish Highway Technical Specification (2006) wearing course specification limit gradation curves, and tests were scheduled for each 0.5% increment in bitumen content. Three bituminous hot mixture (BHM) specimens were prepared for each level of bitumen content. For all of the specimens, Marshall Stability-Flow tests were performed and the specimens’ weight, weight in water and surface dry-saturated to water were measured. The test results of Marshall Stability can be taken from (Akbulut et al. 2012).

3 ARTIFICIAL NEURAL NETWORKS

They are composed of an input layer, some hidden layers and an output layer. This network structure is called (multilayer perceptron) MLP as well (Iseri & Karlik

Table 3. Experimental data used for ANN model and ANN prediction results.

No	Filler (%)	Bitumen (%)	UVW	MS	ANN Output	% Error	No	Filler (%)	Bitumen (%)	UVW	MS	ANN Output	% Error
1	0	4.0	2.451	1541.6	1518.9	-1.47	46	4	5.5	2.542	1234.3	1204.4	-2.42
2	0	4.0	2.448	1487.7	1491.5	0.26	47	4	5.5	2.536	1151.5	1177.9	2.29
3	0	4.0	2.449	1433.9	1501.2	4.69	48	4	5.5	2.545	1196.8	1209.3	1.04
4	0	4.5	2.468	1050.6	1050.9	0.03	49	4	6.0	2.541	1252.6	1059.7	-15.40
5	0	4.5	2.483	1092.4	1081.9	-0.96	50	4	6.0	2.534	1129.7	1075.0	-4.85
6	0	4.5	2.474	1060.5	1033.7	-2.53	51	4	6.0	2.534	1019.0	1075.0	5.50
7	0	5.0	2.483	1106.9	1078.8	-2.54	52	4	6.5	2.519	1057.3	984.0	-6.93
8	0	5.0	2.479	1090.3	1079.2	-1.02	53	4	6.5	2.509	1005.3	1004.7	-0.06
9	0	5.0	2.466	1113.7	1089.4	-2.18	54	4	6.5	2.521	1027.2	975.3	-5.06
10	0	5.5	2.490	1158.2	1079.9	-6.76	55	6	4.0	2.553	1639.1	1603.9	-2.15
11	0	5.5	2.495	1062.3	1070.6	0.78	56	6	4.0	2.534	1569.6	1559.7	-0.63
12	0	5.5	2.505	1086.3	1053.0	-3.06	57	6	4.0	2.560	1576.9	1574.6	-0.14
13	0	6.0	2.516	1100.0	1071.3	-2.61	58	6	4.5	2.577	1529.8	1532.7	0.19
14	0	6.0	2.495	1000.8	1054.3	5.35	59	6	4.5	2.580	1556.3	1525.9	-1.96
15	0	6.0	2.499	1190.7	1114.9	-6.36	60	6	4.5	2.589	1512.3	1514.3	0.13
16	0	6.5	2.495	1140.4	1151.5	0.98	61	6	5.0	2.563	1233.2	1205.6	-2.24
17	0	6.5	2.511	1170.0	1151.8	-1.55	62	6	5.0	2.578	1229.7	1201.5	-2.30
18	0	6.5	2.512	1177.1	1145.9	-2.65	63	6	5.0	2.572	1137.3	1194.8	5.06
19	2	4.0	2.523	1193.6	1184.4	-0.77	64	6	5.5	2.542	1040.2	1026.8	-1.30
20	2	4.0	2.488	1138.3	1119.8	-1.62	65	6	5.5	2.540	1009.6	1025.4	1.57
21	2	4.0	2.514	1286.7	1278.7	-0.63	66	6	5.5	2.561	996.0	989.4	-0.66
22	2	4.5	2.529	1230.0	1206.8	-1.89	67	6	6.0	2.538	922.5	945.9	2.54
23	2	4.5	2.508	1221.0	1190.3	-2.51	68	6	6.0	2.542	913.4	933.9	2.24
24	2	4.5	2.491	1117.1	1075.2	-3.74	69	6	6.0	2.541	954.6	936.6	-1.89
25	2	5.0	2.521	1330.0	1286.8	-3.25	70	6	6.5	2.531	824.8	822.7	-0.25
26	2	5.0	2.519	1363.9	1309.4	-3.99	71	6	6.5	2.513	786.7	782.9	-0.48
27	2	5.0	2.523	1317.5	1267.6	-3.79	72	6	6.5	2.525	807.5	830.1	2.79
28	2	5.5	2.509	1225.0	1190.8	-2.80	73	8	4.0	2.540	1735.0	1730.8	-0.24
29	2	5.5	2.543	1132.2	1124.1	-0.72	74	8	4.0	2.550	1693.8	1693.2	-0.04
30	2	5.5	2.528	1165.6	1124.3	-3.54	75	8	4.0	2.548	1690.5	1702.9	0.73
31	2	6.0	2.539	1272.4	1228.2	-3.47	76	8	4.5	2.550	1276.4	1349.4	5.72
32	2	6.0	2.528	1184.1	1193.2	0.76	77	8	4.5	2.554	1315.5	1341.1	1.94
33	2	6.0	2.520	1150.7	1157.9	0.62	78	8	4.5	2.556	1362.2	1333.6	-2.10
34	2	6.5	2.502	1005.0	1006.6	0.16	79	8	5.0	2.542	1069.2	1079.1	0.93
35	2	6.5	2.518	954.5	999.1	4.68	80	8	5.0	2.544	1126.4	1081.9	-3.95
36	2	6.5	2.515	1056.7	1002.7	-5.11	81	8	5.0	2.542	1037.8	1078.7	3.94
37	4	4.0	2.557	1413.5	1415.9	0.17	82	8	5.5	2.536	999.1	927.1	-7.20
38	4	4.0	2.547	1478.1	1483.3	0.35	83	8	5.5	2.532	905.6	918.4	1.41
39	4	4.0	2.530	1469.4	1454.7	-1.00	84	8	5.5	2.537	863.2	929.0	7.62
40	4	4.5	2.523	1171.7	1167.9	-0.33	85	8	6.0	2.505	708.6	723.8	2.14
41	4	4.5	2.525	1195.7	1171.5	-2.03	86	8	6.0	2.514	700.0	746.4	6.63
42	4	4.5	2.543	1216.1	1217.3	0.10	87	8	6.0	2.520	739.5	749.0	1.29
43	4	5.0	2.530	1108.3	1125.1	1.51	88	8	6.5	2.508	708.6	703.5	-0.72
44	4	5.0	2.544	1199.5	1159.9	-3.30	89	8	6.5	2.511	685.8	695.2	1.37
45	4	5.0	2.549	1150.8	1171.1	1.76	90	8	6.5	2.514	658.5	683.8	3.84

2009). Each layer has a certain number of small individual and highly interconnected processing elements called neurons. Signals are passed through neurons over the connection weights. Each neuron receives multiple inputs from other neurons in proportion to their connection weights, and subjects them activation functions, and generates a single output signal which may be propagated to other neurons (Kurt et al. 2008). Thus neurons process these input data and feeds forward to the next layer.

To develop an ANN model, there must be three stages (Caner et al. 2011). Firstly, input and output data is chosen as vectors. There must be good relation

among these data. That is, output data must influenced by changing input variables. The number of neurons in the input and output layers is determined according to the number of input and output variable.

Secondly, the network is trained to predict an output based on input data in the training stage. Validation vectors are used to overcome overtraining problem in this stage. Some part of the whole training data is put aside for the purpose of validation and not used in training. During the training process validation error is calculated with training error after each training epoch. When the ANN begins to overtrain, the validation error will rise although the training error decreases. If the

validation error continuous rising for a specified number of epochs, the training process is stopped and the ANN parameters at the minimum validation error point are returned (Suzuki et al. 2000).

The Levenberg-Marquardt (LM) method is a modification of the classic Newton algorithm for finding the optimum solution to a minimization problem, and is often characterized as more stable and efficient than backpropagation (BP) algorithm, except that a larger memory space is needed. With the development of high speed computer technology, these shortcomings of the LM method are no longer the trouble. So LM network was adopted here to reduce the time of learning, and also to increase the rate of searching (Yuhong & Wenxin 2009).

During practical application, the number of hidden layers can be one or two. Number of neurons in the hidden layer/layers is mostly determined via trial and error method. But an estimating method is used in the study of (Kurt et al. 2008) for calculation the number of hidden layer. Determining of optimal number of hidden layer and the number of neurons in layer/layers are important structural problems of MLP.

Finally, the network is tested. Predicting output data are obtained via using input data that are not used for training stage. If experimentally obtained predicting data is existed, they are compared with one another.

If the results are not satisfactory network is re trained. If the test results are good enough training parameters is saved. At the end of testing stage, calculation different measures of error are used to show the effectiveness of the well trained network.

4 APPLICATION OF THE ANN ON THE EXPERIMENTAL DATA

The network structure which has two hidden layers is shown in Fig. 2. Three neurons (variables) which are bitumen value and mineral filler rates as percentage and unit volume weights are in the input layer. One neuron (variable) which is Marshall stability value is in the output layer.

Aim of the network is to predict Marshall stability value using data of input variables. To solve this problem; the network is trained by using Matlab codes. Percentages of data for training, validation and test stages are 80%, 10% and 10% respectively. The data for each set was chosen by using “dividrand function”.

Network performance was tested as choosing different neuron numbers for hidden layers. Using 11 a model which was given best regression between input and output was chosen (Table 1). Although the best combination of hidden layers was found as (22, 9), the other results were quite high. LM algorithm was used for all applications because its results are better than other algorithms for these applications. Two hidden layer was used because results of one hidden layer is not sufficient. Training parameters of the ANN were summarized in Table 2. Here number of validation

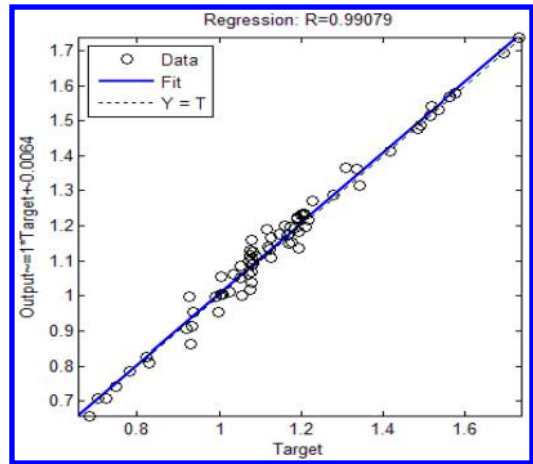


Figure 2. Linear regression results in training stage.

failure works usually as stopping criteria in network training stage.

In this study, all data sets used for ANN model, ANN output and its percentage errors were given in Table 3. The data was obtained from previous experimental test results (Akbulut et al. 2012). Total data consists of 90 samples which are divided as five different percentages of mineral filler.

The bitumen ratio varies between 4–6.5% with 0.5 increases. UVW indicates the unit volume weight of each sample. It is shown that percentage of prediction errors of ANN model varies almost between $\pm 5\%$.

5 RESULTS AND DISCUSSION

The ANN model which using LM algorithm is successfully applied to predict Marshall stability values. Best structure was chosen as (3,22,9,1) among the combinations in Table 2. Here the ANN structure has two hidden layers appears robust to variation of neuron numbers in hidden layers.

In order to understand correlation of the measured and estimated Marshall stability values in training and testing phase for proposed ANN were given in figures 3 and 4 respectively. It is shown from these results the model was good at Marshall stability prediction for both 72 training and 9 testing samples. Here, the dashed line is the perfect fit line where outputs and targets are equal to each other. The circles are the data points and colored line represents the best fit between outputs and targets. Here it is important to note that circles gather across the dashed line, so our outputs are not far from their targets. According to these results we can say that used MLP structure of ANN using three inputs is very well to predict Marshall stability values.

The error distributions of proposed ANN model against number of samples was given in figure 4. It is seen that most of the relative errors are between -5% and $+5\%$, and most of them smaller than 3%.

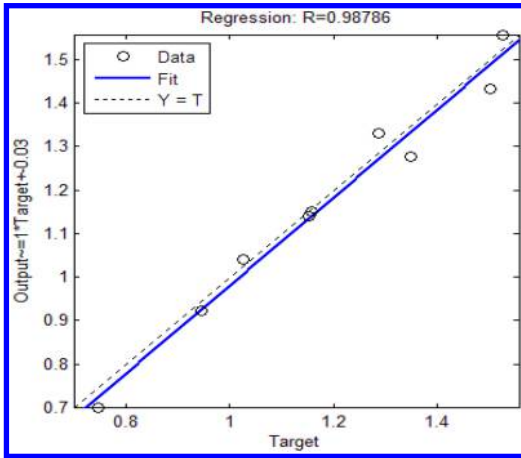


Figure 3. Linear regression results in test stage.

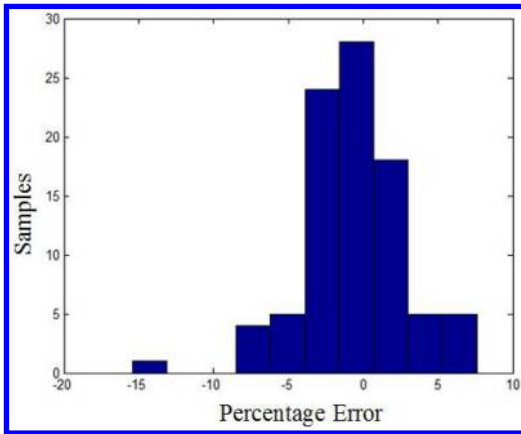


Figure 4. Error histogram of the ANN model vs. the number of samples.

REFERENCES

Akbulut H., Gürer C., Çetin S. 2011. Use of Volcanic Aggregates in Asphalt Pavement Mixes, *ICE Transport*, 164-TR2, 111-123

Akbulut H., Gürer C., Çetin S., Elmacı A. 2012. Investigation of using granite sludge as filler in bituminous hot mixtures. *Construction and Building Material* 36: 430-436

ASTM D70-09e1 2009. Standard Test Method for Density of Semi-Solid Bituminous Materials (Pycnometer Method), American Society for Testing and Materials, West Conshohocken, PA: USA.

ASTM C131-89 1992. Test method for resistance to degradation of small-size coarse aggregates by abrasion and impact in the Los Angeles machine, American Society for Testing and Materials, West Conshohocken, PA: USA.

ASTM D113-07 2007. Standard test method for ductility of bituminous materials, American Society for Testing and Materials, West Conshohocken, PA: USA.

ASTM D36/D36M-09 2009. Standard Test Method for Softening Point of Bitumen (Ring-And-Ball Apparatus), American Society for Testing and Materials, West Conshohocken, PA: USA.

ASTM D4402-06 2006. Standard test method for viscosity determination of asphalt at elevated temperatures using a rotational viscometer. American Society for Testing and Materials, West Conshohocken, PA, USA.

ASTM D6-95 2006. Standard test method for loss on heating of oil and asphaltic compounds, American Society for Testing and Materials, West Conshohocken, PA: USA.

ASTM D92-05a 2010. Standard Test Method for Flash and Fire Points by C Level and Open Cup Tester, American Society for Testing and Materials, West Conshohocken, PA: USA.

Çetin, S. 2014. Evaluation on the usability of structure steel fiber-reinforced bituminous hot mixtures. In M.A.J. Williams & H. Faure (eds), *Construction and Building Material* 64: 414-420.

Chen, W.F., Richard Liew, J.Y. 2003. *The Civil Engineering Handbook, New Directions in Civil Engineering*, CRC Press.

Iseri, A., Karlik, B. 2009. An artificial neural networks approach on automobile pricing. *Expert Systems with Applications* 36: 2155-2160.

Kurt, H., Atik, K., Ozkaymak, M., Recebli, Z. 2008. Thermal performance parameters estimation of hot box type solar cooker by using artificial neural network. *International Journal of Thermal Sciences* 47: 192-200.

Morova, N., Serin, S., Sargin, Ş., Terzi, S., Saltan, M., 2012, Modeling Marshall Stability of Light Asphalt Concretes Fabricated Using Expanded Clay Aggregate with Artificial Neural Networks, *Proceedings of International Symposium on Innovations in Intelligent Systems and Applications*, IEEE Conference Publications, doi: 10.1109/INISTA.2012.6246946.

Republic of Turkey, Ministry of Transport, General Directory of Highways (TCK). 2006. *Turkish State Highway Specifications*, Ankara: Turkey, 515-518.

Serin, S. Morova, N. Terzi, S. Sargin, Ş. 2011. Determining Amount of Bituminous Effects on Asphalt Concrete Strength with Artificial Intelligence and Statistical Analysis Methods, *Proceedings of International Symposium on Innovations in Intelligent Systems and Applications*, İstanbul. IEEE Xplore index. doi: 10.1109/INISTA.2011.5946139

Suzuki Y., Ovaska S., Furuhashi T., Roy R., Dote Y. 2000. *Soft Computing in Industrial Applications*. Springer-Verlag, London, UK.

Website 1 <http://www.cimstone.com.tr/>:2014.

Website 2 N. Tosun, "Bituminous Coatings Application Book", Date of Internet Access: 14.07.2010 http://www.armatmuhendislik.com/izolasyon_ve_yalitim/Bitumlu_kaplamlalar_uygulama_kitabi_Yazan_Necdet_Tosun.pdf

Website 2 Indiana Department of Transportation. Mix design. [http://www.in.gov/indot/files/Chapter_04\(4\).pdf](http://www.in.gov/indot/files/Chapter_04(4).pdf): 2014

Yuhong, Z., Wenxin, H. 2009. Application of artificial neural network to predict the friction factor of open channel flow. *Communications in Nonlinear Science and Numerical Simulation*, 14(5): 2373-2378.

Asphalt mixtures improved by the use of nanotechnology

V. Blanco López, R. Casado Barrasa, E. Sáez Caballero & C. Martín-Portugués Montoliu

Acciona Infraestructuras Technology Centre, Madrid, Spain

ABSTRACT: The last remarkable step forward in materials for roads infrastructures market was the development of Polymer Modified Binders (PMBs) during the 1970 decade. The use of polymers in pavements enhances their performance, although the ageing and hardening of the bituminous matrix are still to be solved. Further research is needed in order to develop new affordable and more durable asphalt materials that show less vulnerability to traffic loads and ageing, with the aim of increasing the lifetime of pavements. The main goal of this study is based on the use of nanotechnology to develop advanced high performance asphalt mixtures, suitable for the optimization of asphalt pavement sections and reduce the amount of natural resources used for road construction. The obtained result reveal that the use of nanomodified asphalt mixtures improves the mechanical properties, resistance to fatigue and aging compared to the traditional fragile asphalt mixtures allowing pavement section optimization.

1 INTRODUCTION

Road infrastructures are one of the pillars of the European economy. Around 50% of the goods transported across Europe are delivered by road; this sector also provides jobs to 5 million of employees and generates approximately 2% of European GDP (European Commission 2012). Another fact that makes roads one of the most important civil infrastructures is the citizen mobility, in which roads suppose more than 70% of civil transport in relation to its sector competitors: train, plane and boat (European Road Federation 2014).

Most of the European road network, including all trafficked roads and motorways, mainly consists in flexible pavement structures that throughout the years have taken an advantage, in terms of usage, in relation to rigid pavement designs. The flexible pavements consist of a structure divided in different layers so that traffic loads are distributed through the whole structure. The upper layers correspond to bituminous mixtures (split up in surface, binder and base courses), a sub-base layer is placed below asphalt layers (being possible the following construction solutions: graded-aggregate, soil-cement or gravel-cement) and a subgrade layer supporting the layers above (which depends on soil quality). The main construction materials used in this type of sections are bituminous binders and aggregates; the quality of these materials will depend on the layer and should meet the required technical specifications to provide good mechanical performance in order to prevent further degradation and failures (Kraemer & Albelda 2004, Huang 1993).

During its service life, flexible asphalt pavements are submitted to several degradation processes result of the combination of environmental conditions, oxidation and traffic loads. The typical pavement failures derived from pavement aging are reflection cracking and surface raveling; these problems will increase the expense of renovation and preservation and will reduce critical pavement parameters such as safety, performance and lifespan (ODOT 2010, FHWA 2003).

Asphalt binders are the main responsible in the problems above mentioned, considering that their degradation starts during the hot-mix process and will continue during its service life as result of oxidative ageing. Once paved, binders are continuously submitted to several degradation processes such as high-temperature rutting, low-thermal cracking and stress fatigue cracking that will compromise its performance along time (Lesueur 2009). These failures will be emphasized if unmodified asphalt binders are used instead of modified binders. Therefore, modification and reinforcement of asphalt binders is necessary (Zare-Shahabadi et al. 2010).

During the last 30 years, the main asphalt binder modification has been carried out by the addition of polymers, specially styrene-butadiene-styrene (SBS), which have enhanced asphalt binder service properties such as mechanical resistance, temperature susceptibility, adhesivity, and elasticity. However several problems are still unsolved such as the compatibility between polymer and binder, ultraviolet radiation (that produces the hardening of the asphalt) and oxidative ageing (Zhang et al. 2012, Polacco et al. 2008).

In order to address these limitations the addition of new modifiers should be studied in more detail.

The present study will demonstrate the advantages and improvements of using nanomaterials as asphalt modifiers.

2 BACKGROUND

Nanomaterials are being applied in a wide variety of industrial sectors such as: textile, packaging, automotive, biomedicine or telecommunications. Evidently, the materials related to the construction industry are being also experiencing the incorporation of nanomaterials. The use of nanomaterials in the construction industry related materials intends to change the properties of those matrixes in which are added, for instance, SiO₂ nanoparticles are incorporated to concrete in order to increase its self-compacting behaviour and improve its surface properties reducing the honeycomb effect (Larraza 2014). In transport infrastructure, and a number of promising developments exist that can potentially change the service life and life-cycle cost of transport infrastructure through the improvement of existing materials or the development of novel materials (Lee et al. 2010, Rana et al. 2009).

In the last few years, road construction bodies have adopted some requirements for the construction of durable asphalt pavements; these requirements are based in two principles: first, to extend the service life with minimum maintenance operations and; second, a sustainable construction reducing the consumption of natural resources and minimizing environmental impact. Considering these clauses, the main benefit that nanotechnology can provide to transportation engineering is in terms of materials improvement (Steyn 2008).

The main technical benefits in key properties of asphalt mixtures are listed below:

- Better stiffness modulus and rutting resistance: The addition of nanoparticles will increase asphalt mixture stiffness modulus, so that asphalt mixtures withstand higher loads preventing pavement cracking. A lower rutting parameter supposes higher plastic deformation resistance avoiding ruts failure (Yang & Tigheb 2013).
- Better Fatigue resistance: the material should perform under the applied regime of stresses and strains and withstand repeated flexural loads, both internally and externally, providing a long-term durability and service life (Yang & Tigheb 2013).
- Matrix stability: the nanomaterial should provide a good cohesion to stress and strain loads in order to keep the internal structure of the bituminous matrix intact and also provides a good adhesion between the aggregates, particles and the binder (Van de Ven et al. 2008).
- Improvements in thermo-oxidative aging resistance and UV radiation tolerance: rheology modification will lead to better resistance to temperature ageing and thermal sensitivity (Zhang et al. 2012).

Table 1. Grading curve of AC16-S.

Sieve mm	AC16-S % passing
32	100
22	100
16	95
8	67.5
4	42.5
2	31
0.5	16
0.25	11
0.063	5

Several studies and research projects have been carried out in the last few years in this field (Liu et al. 2010, Tao et al. 2009, Yu et al. 2009, Van de Ven et al. 2008, Beyene 2006), but most of them have focussed on binder modification and the evaluation of the enhanced properties in relation to unmodified binders. ACCIONA has continued the research carried out within the framework of the NANOFIR project “Application of nanotechnology in a new generation of pavements” a Spanish National Research and Development project. This study intends to go one step beyond of current works and demonstrate that the use of nanotechnology can report technical benefits in nanomodified asphalt mixtures and will prove that flexible pavement section using these mixtures could be optimized through a software simulation tool.

3 TESTS AND RESULTS

3.1 Study approach

The overall aim of this study is the demonstration of the enhanced properties of new asphalt mixtures that contains nanomaterials. The improvement of properties is provided by the addition of nanoclays and carbon black. The main objectives are described below:

- Development of different asphalt mixtures that contains different concentrations of nanoclays and carbon blacks. The mixing procedure will be either by dry and wet process.
- Characterization of the asphalt mixtures obtained using mechanical and dynamical testing procedures.
- Analysis of a typical pavement section with a simulation tool in order to optimize the structure and evaluate the new asphalt mixture performance.

The results obtained are shown in the following sections:

3.2 Study approach

In order to compare the performance of the different nanomaterials an AC16-S asphalt mixture (AM) was selected. The grading curve is presented in Table 1.



Figure 1. Asphalt binder modification laboratory plant.

Conventional 50/70 penetration grade bitumen was used in the investigation. The aggregates from different origins including limestone, silica, and porphyry were used to design the asphalt mixtures. Two different commercial organo-modified nanoclays (NC) with different particle size and properties were used in the investigation. Two different Carbon Black (CB) used for industrial applications were also selected for this study.

The software ALIZE-LCPC developed by IFST-TAR was used to simulate and optimize the pavement section performance.

3.3 Study approach

Test specimens were developed according to the standard UNE-EN 12697-30:2013 (Specimen preparation by impact compactor). Two different mixing procedures were carried out in order to introduce NC and CB into the asphalt mixtures to be compared with reference asphalt mixtures.

- Wet Process: In the wet process tests specimens were prepared by mixing the nanomodified bitumen aggregates. The nanomodified bitumens were obtained blending the bitumen and the nanomaterials using a high shear mixer device at 180°C during 30 minutes. The percentage of nanomaterials in asphalt binder varied from 4% to 8%.
- Dry Process: In the dry process test specimens were prepared by mixing the NC or CB together with the aggregates, prior the addition of the bitumen. The temperatures and mixing time were similar to reference AM. Different amounts of nanoclays and carbon black were added in range from 0.05% to 0.5%.

3.4 Study approach

In order to study the performance of nanomodified asphalt mixtures in comparison with reference mixtures, mechanical properties of asphalt mixtures were evaluated. The main asphalt mixture tests were performed following the European standards:

- UNE-EN 12697-6:2012. Determination of bulk density of bituminous specimens.



Figure 2. Wheel tracking test (left) and specimens after particle loss test.



Figure 3. Stiffness (left) and fatigue test (right).

- UNE-EN 12697-8:2003. Determination of void characteristics of bituminous specimens.
- UNE EN 12697-12:2009. Determination Water sensitivity test of the bitumen specimens.
- UNE-EN 12697-17:2006 Particle loss of porous asphalt specimen.
- UNE-EN 12697-22:2008+A1:2008. Wheel tracking.

In addition, the dynamic characterization of asphalt mixtures was carried out in order to analyse the performances of these new asphalt mixture in different flexible pavement sections. The following European regulations were applied:

- UNE-EN 12697-26:2012. Stiffness Modulus. Annex C: Indirect tensile strength.
- UNE-EN 12697-24:2013. Resistance to fatigue. Annex D: Four Point bending test.

During the development of the study different percentages of each nanomaterial were studied, varying from 0.05% to 0.5% (on total weight content) in case of dry process and; from 4% to 8% (on binder content) concerning the wet process.

Binder testing in the nanomodified bitumen's was carried out in previous studies according to the standards UNE-EN 12591 and UNE-EN14023, the obtained results showed an increase in softening point, penetration index, viscosity and better rheological properties.

After an initial characterization, tests results revealed that nanomodified asphalt mixtures using wet process were more promising than nanomodified asphalt mixtures obtained by dry process; therefore

Table 2. Characterization tests of AC16-S using wet process.

	Optimum Nano/B. content %	Binder content %	Voids content %	Density kg/m ³
REF	–	5.05	5.02	2268
NC-1	4.50	5.20	4.85	2315
NC-2	6.00	5.15	4.98	2294
CB-1	6.00	5.10	5.25	2321
CB-2	6.50	5.20	4.92	2348
Standard values	N/A*	>3.65%	4–6	N/A*

*Not applicable

Table 3. Characterization tests of AC16-S using wet process.

	Water sensitivity %	Wheel tracking 0.10 mm/10 ³ load cycles	Particle loss %
REF	92.2	0.081	12.3
NC-1	89.1	0.054	15.8
NC-2	88.2	0.035	17.5
CB-1	84.7	0.052	16.9
CB-2	85.3	0.038	18.7
Standard values	>85%	<0.01	<20%

it was decided to continue the study only with the samples obtained by wet process.

Wet process nanomodification results, including optimum percentages of nanomaterials on binder content (Nano/B) to fulfil the technical requirements, are shown in Tables 2 and 3.

All the obtained results fulfilled the Spanish specifications gathered in PG3 (MFG 2011). By comparing the results obtained with the reference sample it can be concluded that most properties are practically identical to reference values, excepting rutting resistance (wheel tracking) where the improvement was noticeable. Asphalt mixture density and binder content slightly increase when nanomaterial is added.

Dynamic tests, stiffness modulus and fatigue analyses were carried out on the reference and modified AC16-S asphalt mixtures. Stiffness tests were performed on cylindrical Marshall specimens of 101 mm diameter at 20°C. Fatigue tests were carried out on 50 × 50 × 400 mm specimens at 20°C and 30 Hz frequency. Both tests were performed in an IPC global machine.

Stiffness modulus results are expressed in terms of percentage, taking 0% as the reference value; so positive numbers will indicate an improvement in

Table 4. Stiffness Modulus test results.

	Stiffness %
REF	0
NC-1	+26.45
NC-2	+40.53
CB-1	+20.85
CB-2	+8.32

Table 5. Fatigue test results.

	Fatigue (%)
REF	0
NC-1	+18.1
NC-2	+33.02
CB-1	+14.28
CB-2	+3.27

properties in relation to the reference sample while negative numbers represent a decrease.

In case of the Fatigue parameter, the test results are linked with fatigue law equation (1):

$$N = K_1 \cdot \varepsilon^{K_2} \quad (1)$$

where N = load cycles until rupture; ε = deformation; K_1 and K_2 = fixed values that represent asphalt mixture fatigue performance, both values depend on the following parameters: stiffness modulus, binder content, binder viscosity, aggregates characteristics, voids content and pavement temperature.

The results are expressed in terms of percentage, taking 0% as the reference value, where 10⁶ load cycles (N) was chosen every case at their corresponding deformation (ε). Positive values show an increase while negative numbers represent a decrease.

After analyzing both dynamical test results, it can be said that the stiffness modulus and fatigue behavior of the modified asphalt mixtures are, in general, greater than those obtained for the reference asphalt mixtures. NC-2 showed the best improvement in both properties. A better fatigue behavior result indicates that the asphalt mixture will resist loads during a greater number of cycles which turn into a real pavement will suppose longer service life.

By taking into account the mechanical and dynamical tests results, it can be concluded that NC-2 (6%) added to an AC16-C asphalt mixture by using wet process, performs the best and will be suitable to use in pavement design.

3.5 Study approach

Once the nanomodified asphalt mixtures (n-AM) characterization was completed and the most suitable

nanomaterial was selected (NC-2 using wet process), the next step in this study was the evaluation of its performance into a flexible pavement section. The procedure carried out is based on the stress and strain comparison between different pavement sections by using the road software simulation tool LCPC-Alizé.

This software optimization is very useful in the countries where catalogue designs are being used. In countries where catalogue design is not implemented, the high performance properties of these nanomodified asphalt mixtures will allow to design analytically pavement sections with a reduction in its total thickness.

A typical asphalt pavement section 232 was selected according to the Spanish standard *Norma 6.1-IC* (catalogue of pavement sections for the design of pavement structures). In the chosen section, the following parameters have been considered:

- Average Annual Daily Traffic (AADT) between 800-2000 heavy vehicles.
- The section 132 is divided in 20 cm of bituminous mixtures separated in three layers (surface, binder, and base) and 20 cm of soil-cement as sub-base layer.
- Subgrade type E3 according to the Spanish standards.

Designed pavement section must comply with a value above the theoretical number equivalent of axles stipulated in road project; this number of theoretical equivalent axles is obtained according to the equation (2):

$$N = IMD_p \cdot CE \cdot \left[\frac{(1+c)^n}{c} \right] \cdot \gamma_s \quad (2)$$

where N = number of equivalent axles stipulated in the project (an equivalent axle corresponds to a 128 kN tandem axle); IMD_p = Average Annual Daily Traffic; CE = equivalence factor; n = pavement service life; γ_s = load increase coefficient; and c = annual accumulative growth.

In this case a bibliographic reference values have been chosen and the theoretical number of axles obtained was $N = 8.94 \cdot 10^6$ axles (Kraemer & Del Val 2004). Other criterion that determines if the pavement is designed correctly is coefficient K, represented in the equation (3). This coefficient correlated the theoretical axles and the axles that the designed pavement has. If the value of this coefficient is above of 1.0, the section is considered capable to undergo the loads until the end of its service life.

$$K = \frac{LOG(\text{section axles})}{LOG(\text{project theoretical axles})} > 1.0 \quad (3)$$

The enhanced dynamical properties given by the modified asphalt mixture will lead to pavement better performance. This performance will allow the optimization of the section by reducing the thickness of the asphalt layers without compromising their performance, properties and service-life. The results obtained after simulation were as given in Tables 6 to 8.

Table 6. Reference section results.

SECTION 132 REFERENCE			
Layer	Concept	Thickness (cm)	N (n° axles)
Surface course	BBTM11B	3	$1.98 \cdot 10^9$
Binder course	AC 22 S	7	$4.24 \cdot 10^9$
Base Course	AC 32 G	10	$7.30 \cdot 10^{10}$
Sub base	SC	20	$1.07 \cdot 10^7$
Subgrade	E3	Inf	$7.77 \cdot 10^8$
		N (n° axles)	$1.07 \cdot 10^7$
		Calculate K	1,011

Table 7. Reference section using n-MA results

SECTION 132 using n-MA			
Layer	Concept	Thickness (cm)	N (n° axles)
Surface course	BBTM11B	3	$6.65 \cdot 10^9$
Binder course	AC 22 S	7	$1.59 \cdot 10^{15}$
Base Course	n-AM	10	$1.53 \cdot 10^{10}$
Sub base	SC	20	$2.51 \cdot 10^7$
Subgrade	E3	Inf	$1.04 \cdot 10^9$
		N (n° axles)	$2.51 \cdot 10^7$
		Calculate K	1,065

Table 8. Optimized section results.

SECTION 132 OPTIMIZED			
Layer	Concept	Thickness (cm)	N (n° axles)
Surface course	BBTM11B	3	$4.64 \cdot 10^9$
Binder course	AC 22 S	7	$4.59 \cdot 10^{16}$
Base Course	n-AM	8	$1.64 \cdot 10^{10}$
Sub base	SC	20	$1.09 \cdot 10^7$
Subgrade	E3	Inf	$7.69 \cdot 10^8$
		N (n° axles)	$1.09 \cdot 10^7$
		Calculate K	1,012

Regarding the optimization results, it can be deduced that the three sections are rather oversized in relation to the theoretical number of axles stipulated, as well as the coefficient K which is above of 1.0 in all cases. As it shown in Table 8, it is possible to reduce the 20% of base course (2 cm of total section thickness) without compromising its performance.

4 CONCLUSIONS

The main conclusions of this study are presented below:

- Two different organo-modified nanoclays and two commercial carbon blacks were added to asphalt mixtures either by both wet and dry processes. After

- the initial results, it was decided to continue only with the nanomodified mixtures using wet process.
- An optimum percentage of each nanomaterial was selected taking into account the compliance of asphalt mixture standards.
 - The mechanical test results showed that nanomodified asphalt mixtures perform as well as reference asphalt mixtures fulfilling the required standards.
 - Most properties were similar to reference sample, excepting rutting resistance which showed a noticeable increase in comparison to reference values. Also slightly increase in binder content and asphalt mixture density was noted.
 - Dynamic test results, stiffness and fatigue, indicated that nanomodified asphalt mixtures have a significant increase in both parameters. An improved fatigue performance will ensure longer pavement service life.
 - NC-2 (6%) was selected to be used in pavement optimization.
 - Pavement optimization results through software Alizé-LCPC revealed that the use of nanomodified asphalt mixtures allows the reduction of 2 cm of the section chosen total thickness without compromising its performance due to the improvement in dynamical properties. In countries where a catalogue design is not being implemented, the high performance properties of the nanomodified asphalt mixtures will allow to reduce the pavement section total thickness by analytical design.

REFERENCES

- Beyene D. 2006. Effects of Nanoclay Modification on Rheology of Bitumen and on Performance of Asphalt Mixtures. M.Sc. Thesis. June 2006. TU Delf University.
- Cong P., Xu P. & Chen S. 2014. Effects of carbon black on the anti-aging, rheological and conductive properties of SBS/asphalt/carbon black composites. *Construction and Building Materials* 52 (2014) 306–313.
- Didier Lesueur. 2009. The colloidal structure of bitumen: Consequences on the rheology and on the mechanisms of bitumen modification. *Advances in Colloid and Interface Science* 145 (2009) 42–82.
- European Commission. 2012. Road transport: a change of gear. http://ec.europa.eu/transport/modes/road/doc/broch-road-transport_en.pdf
- European Road Federation. 2014. ERF: Position Paper for Maintaining and Improving Sustainable and Efficient Road Networks. http://www.irfnet.eu/images/Road-Asset-Management-for_web_site.pdf
- FHWA. 2003. Distress identification manual for the long-term pavement performance. US Department of Federal Highway Administration. Publication NO.FHWA-RD-03-031. June 2003.
- Huang, Y. H. 1993. *Pavement Analysis and Design*. Englewood Cliffs, N.J.: Prentice Hall. 1993.
- Kraemer C. & Albelda R. 2004. Evaluación técnico-económica de las secciones de firme de la Norma 6.1-IC. VI Congreso Nacional de Firmes 24–27 May 2004.
- Kraemer C. & Del Val M.A. 2004. *Ingeniería de las carreteras Vol I y II*. McGraw-Hill. 2004. ISBN 9788448139988.
- Larraza, I. 2014. Pan European Networks Horizon 2020 Projects Portal Issue 3. Pages 86-88. www.horizon2020.com
- Lee L., Mahendra S. & Alvarez P. 2010. Nanomaterials in the Construction Industry: A Review of Their Applications and Environmental Health and Safety Considerations. 2010 American Chemical Society. *ACS Nano* Vol 4, No 7.
- Liu G., Wu S., Van de Ven M., Molenaar A. & Besamusca J. 2010. Characterization of Organic Surfactant on Montmorillonite Nanoclay to be used in Bitumen. *Journal of Materials in Civil Engineering* Volume 22, Special issue: Asphalt and Modified Asphalt Materials.
- MFG 2011. Ministerio de Fomento del Gobierno de España. Dirección General de Carreteras. Pliego de Prescripciones Técnicas Generales para obras de carreteras y puentes (PG-3). Art 542 y Art 543. 2011.
- ODOT. 2010. Pavement distress survey manual. Oregon Department of transportation June 2010.
- Polacco G., Křížb P., Filippia S., Stastnab J., Biondia D. & Zanzottob L. 2008 Rheological Properties of Asphalt/SBS/Clay Blends. *European Polymer Journal* 44 (2008) 3512–3521.
- Rana A.K., Rana S.B., Kumari A., & Kiran V. 2009. Significance of Nanotechnology in Construction. *Engineering Int. J. of Recent Trends in Engineering and Technology*, Vol. 1, No. 4, Nov 2009.
- Steyn W. 2008. Research and application of nanotechnology in transportation. 27th Southern Africa Transport Conference (SATC 2008) 7–11 July 2008. Pretoria South Africa.
- Tao Y.Y., Yu J.Y., Li B. & Feng P.C. 2008 Effect of different montmorillonites on rheological properties of bitumen/clay nanocomposites. *J. Cent. South Univ. Technol.* (2008) 15(s1): 172–175.
- Van de Ven M., Molenaar A., Besamusca J. & Noordergraaf J. 2008. Nanotechnology for Binders of Asphalt Mixtures, Proceedings of the 4th euraspalt and eurobitume congress, Copenhagen, Denmark.
- Yang J. & Tigheb S. 2013. A Review of Advances of Nanotechnology in Asphalt Mixtures. *Procedia – Social and Behavioral Sciences* Volume 96, 6 November 2013, Pages 1269–1276.
- Yu, J.Y., Feng, P.C., Zhang, H.L. & Wu, S.P. (2009). Effect of organo-montmorillonite on aging properties of asphalt. *Construction and Building Materials*, 23, 2636–26.
- Zare-Shahabadi A., Shokuhfar A. & Ebrahimi-Nejad S. 2010. Preparation and rheological characterization of asphalt binders reinforced with layered silicate nanoparticles. *Construction and Building Materials*. Volume 24, Issue 7, July 2010, Pages 1239–1244.
- Zhang H., Yu J. & Wu S. 2012. Effect of montmorillonite organic modification on ultraviolet aging properties of SBS modified bitumen. *Construction and Building Materials* 27 (2012) 553–559.

Investigation of moisture susceptibility in hot-mix asphalt concrete

A. Rahim

California Polytechnic State University, San Luis Obispo, CA, USA

T. Nguyen

Pacific Gas & Electric, USA

ABSTRACT: The primary objective of this study was to evaluate moisture susceptibility on specimens prepared in the laboratory. Two liquid chemical-based and Hydrated Lime normally used in California were investigated. SuperPave mix design was employed and specimens of 4-inch diameter and 2.83-inch height were fabricated to test for moisture susceptibility employing Modified Lottman Test and Immersion Compression Test (ICT). For all the combinations tested in this study the Tensile Strength Ratio (TSR) ratio exceeded the 80 percent threshold. A peak amount of additive for both liquid additives and hydrated lime were observed for all agents tested in this study. Results from the ICT showed a retained compressive strength greater than the 75 percent threshold. However, the authors don't recommend its use as a tool to investigate moisture susceptibility in Hot Mix Asphalt (HMA) concrete. The two liquid antistripping proved to be cost effective as compared to hydrated lime additive investigated in this study.

1 LITERATURE REVIEW

A National Cooperative Highway Research Project (NCHRP), which was completed in 1991, presented a more comprehensive review of moisture damage problems (Hicks 1991). About 70 percent of the responding state and province departments of transportation in North America experienced moisture damage-related problems in their pavements. The major types of moisture damage related premature distresses included: rutting or permanent deformation in the wheel paths, bleeding in selected areas of the pavement, and alligator cracking with hundreds of millions of dollars are spent annually to rehabilitate and maintain such damage.

Although many factors contribute to the degradation of asphalt concrete pavements, moisture is a key element in the deterioration of the asphalt mixture. There are three mechanisms by which moisture can degrade the integrity of an asphalt concrete matrix: (a) loss of cohesion (strength) and stiffness of the binder film that may be due to several mechanisms; (b) failure of the adhesion (bond) between aggregate and the binder, and (c) degradation or fracture of individual aggregate particles when subjected to freezing. When the aggregate tends to have a preference for absorbing water, the binder is "stripped" away leading to premature pavement distress and ultimately to failure of the pavement (Terrel & Al-Swailmi 1994).

Stripping usually begins at the bottom of the Hot Mix Asphalt (HMA) layer, then travels upward. A typical situation is a gradual loss of strength over a

period of years, which causes rutting and shoving to develop in the wheel path. Stripping could be difficult to identify because surface indicators may take years to show. It is necessary to examine an HMA core to identify stripping. In some cases of stripping, HMA mix has lost so much adhesion between aggregate and the binder that a core cannot be removed in one piece (Kennedy et al. 1983 & Roberts et al. 1996).

When subject to moisture, water-sensitive pavements may suffer accelerated damage leading to a reduced pavement life. If asphalt pavement does suffer from water sensitivity, serious distresses may occur. As a result, the asphalt pavement reduces in performance and increases in maintenance costs. To alleviate or control this problem, various liquid or solid anti-stripping additives have been developed, which can be used to promote adhesion between the binder and aggregate. Anderson & Dukatz (1982) reviewed the effects of commercially available anti-stripping additives on the physical properties of the binder. Anderson & Dukatz's (1982) experimental studies of the physical and compositional properties of the binder with anti-stripping additives demonstrated that anti-stripping additives tend to soften the binder, reduce temperature susceptibility, and improve the aging characteristics of binder. Also, Anderson & Dukatz (1982) stated that the effect of an anti-stripping additive is binder specific.

Liquid anti-stripping agents and lime additives are among the most commonly used types of anti-stripping agents. However, if an additive is used when it is not needed or if it is used incorrectly, adverse affects may

Table 1. Specific gravity of coarse and fine aggregates.

Aggregate Type	Bulk Specific Gravity	Bulk Specific Gravity (SSD)	Apparent Specific Gravity	Absorption, %
Coarse	2.52	2.54	2.60	1.40
Fine	2.49	2.53	2.58	1.47

occur, including an increased economic cost and early maintenance and/or rehabilitation (Tunnick & Root 1984).

A variety of chemicals are being used to reduce the moisture sensitivity of hot-mix asphalt. The majority of chemicals presently used are alkyl amines and are sold under a variety of brand names. These chemicals are added directly to the binder either at the refinery or binder terminal, or at the contractor's facility during production of the mix. These types of chemical additives are generally referred to as "liquid antistripping agents or adhesion agents". Liquid antistripping agents are not only used in hot-mix asphalt but are commonly used in cold-applied, binder-bound patching materials and in the binders (Epps et al. 2003).

Hydrated lime, Portland cement, fly ash, flue dust, and polymers have been added to aggregates to provide resistance to moisture in hot-mix asphalt mixtures. Typically, these materials are added to the aggregate and mixed before the introduction of the binder in the hot-mix asphalt production process. In some cases, hydrated lime or Portland cement has been added in the drum mixing operation at the point of entry of the binder to the heated aggregate (Epps et al. 2003).

The objective of this research is to investigate the use of hydrated lime and other new liquid anti-stripping agents in mitigating moisture related problems in HMA constructed using two different aggregate types. An economical evaluation of the three agents used in the research will be conducted to evaluate their cost-effectiveness.

2 MATERIALS

2.1 Aggregate

Crushed stone aggregate commonly used on the Central Coast of California and supplied by Cal Portland was used in this research. Table 1 presents the specific gravity and absorption properties of the aggregate.

2.2 Binder

Binder Performance Grade 64-16 (PG 64-16) of 1.03 specific gravity was supplied by Oxnard refinery. The virgin binder was tested in the Dynamic Shear Rheometer (DSR) before and after being aged in Rolling Thin Film Oven (RTFO). The DSR test for unaged and aged binder was repeated after mixing with antistripping agents and the results are presented in Table 2.

Table 2. Dynamic Shear Rheometer test results.

Treatment	Additive content, %	Complex Modulus, Pa	Phase Angle, °	Shear Stress, Pa
Virgin Binder				
Control	0.0	2,047.25	88.09	193.00
Arr Maz CC	0.25	836.60	89.12	99.88
LOF-6500 ¹	0.50	467.10	88.80	56.79
	0.75	345.30	87.73	48.06
Arr Maz CC	0.25	674.20	89.02	83.03
XL-9000 ¹	0.50	347.40	89.20	41.60
	0.75	306.85	88.71	37.42
Lime ²	1.0	2,294.00	88.10	278.20
	1.5	3,505.00	87.90	424.70
	2.0	4,843.50	86.94	606.25
RTFO Aged Binder				
Control	0.0	2,775.00	86.18	323.60
Arr Maz CC	0.25	2,366.67	86.80	279.97
LOF-6500 ¹	0.50	2,235.33	87.02	266.20
	0.75	912.80	89.16	107.50
Arr Maz CC	0.25	2,622.67	86.51	313.60
LOF-6500 ¹	0.50	2,016.00	87.12	237.30
	0.75	728.10	88.76	88.16
Lime ²	1.0	3,981.50	85.33	478.45
	1.5	5,360.50	86.05	626.70
	2.0	11,850.00	83.71	1,478.50

¹Percentage of the weight of binder

²Percentage of aggregate weight

The rutting parameter ($G^*/\sin \delta$) values for the binder under different aging conditions and additive types are presented in Figures 1 and 2. As noticed in the figures liquid antistripping reduced $G^*/\sin \delta$ for the modified binder before and after aging in the RTFO. However, the opposite was the case for binder treated with hydrated lime. The rutting parameter ($G^*/\sin \delta$) increases by adding hydrated lime which means more resistance to rutting deformation.

2.3 Hot Mix Asphalt (HMA)

The design of HMA was conducted in accordance with the SuperPave mix design procedure. The design procedure began with aggregate selection, followed by a binder content selection. Four aggregate gradations (presented in Table 3) were considered for the study. The SuperPave mix design resulted in an optimum binder content of 6.0% with blend 4 as the design mix.

3 HMA TESTING AND RESULTS

Three different antistripping additives were investigated in this study. Two of which were chemical-based while the third was Hydrated Lime normally used in California. The two liquid antistripping agents used in this study included Arr Maz CC LOF-6500 and Arr Maz CC XL-9000 which were tested at 0.25%, 0.50%, and 0.75%. The Hydrated Lime was tested

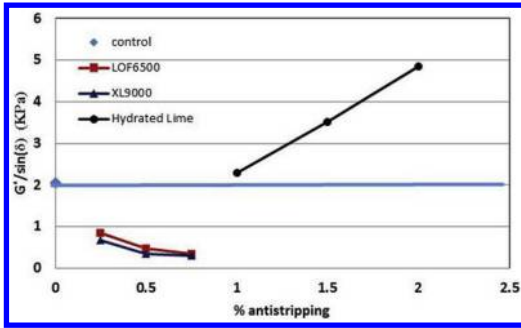


Figure 1. $G^*/\sin(\delta)$ for unaged binder mixed with different antistripping additives.

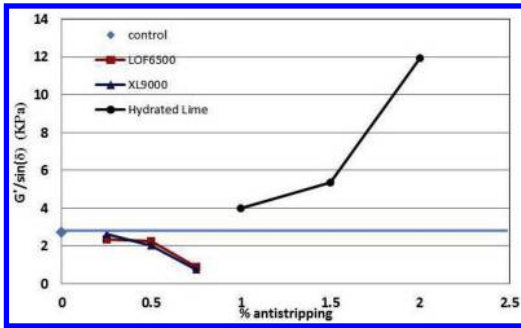


Figure 2. $G^*/\sin(\delta)$ for RTFO-aged binder mixed with different antistripping additives.

Table 3. Grain size distribution for different aggregate blends.

Sieve Size, mm	25	19	12.5	9.5	2.36	0.075
SuperPave Range	Percent Passing (%)					
	90–100	0–90	n/a ¹	n/a	19–45	1–7
Blend 1	7	22	19	28	21	3
Blend 2	6	17	13	36	24.8	3.2
Blend 3	2.5	7.5	12	46	28.5	3.5
Blend 4	2	4	7	50	33	4

¹Not Applicable

at 1.0%, 1.5%, and 2.0%. Six specimens were prepared per treatment combination and specimens were split into two sets; one set was sealed and placed in a water bath at room temperature (77° F) for two hours and the other set at 140° F for twenty-four hours. AASHTO T 283-03 was employed to evaluate the effect of water conditioning on the tensile strength of HMA. The tensile strengths of the conditioned specimens were then calculated and compared with those for the control (un-conditioned) specimens to determine the tensile strength ratio. Standard Test Method for Compressive Strength of Bituminous Mixtures (ASTMD 1074-96) was also conducted to evaluate the

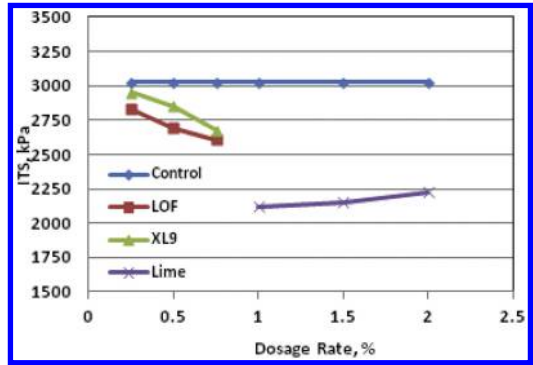


Figure 3. ITS for un-conditioned HMA treated with different antistripping additives.

effect of saturation and accelerated water conditioning of compacted HMA on compressive strength.

3.1 Indirect Tensile Test (ITS)

The tensile strengths for un-conditioned control HMA and HMA treated with three different antistripping additives are presented in Figure 3. It is noticed from Figure 3 that all treated HMA exhibited lower tensile strength than the control HMA when un-conditioned in water. The higher the percentage of liquid antistripping is, the lower the tensile strength for HMA. However, this trend was not clearly observed for HMA treated with hydrated lime. The behavior of mixes treated with hydrated lime needs explanation. It is believed that hydrated lime tends to increase the stiffness of the binder which would have adverse effect on the bond between the binder and aggregate particles at the un-conditioning state of the mix. In this case higher binder content would be needed to compensate for the impact of stiffened binder, an issue that was not investigated in this study. Figure 4 presents the tensile strength of all conditioned mixes treated with different antistripping agents compared to the control. From the figure, tensile strength of mixes treated with LOF-6500 expected to outperform mixes treated with XL-9000 and hydrated lime. Tensile strength for conditioned HMA treated with hydrated lime at rates of 1.5% and 2% exceeded that for control HMA. Also, a peak antistripping rate is evident for all mixes.

Tensile Strength Ratio (TSR) is normally used to present the results of the AASHTO T 283-03 test. This ratio is calculated as the ratio of the tensile strength for conditioned specimens and that for un-conditioned specimens and the minimum acceptable value is 80%. It can be seen in Figures 5 and 6 that all mixes treated with antistripping agents have exceeded the minimum TSR value of 80%. In Figure 5 it is noticed that XL-9000 produced the best TSR values for the liquid antistripping additives. However, by comparing Figures 5 and 6 it is noticed that HMA treated with hydrated lime performed the best in terms of TSR with a peak of 1.5% hydrated lime.

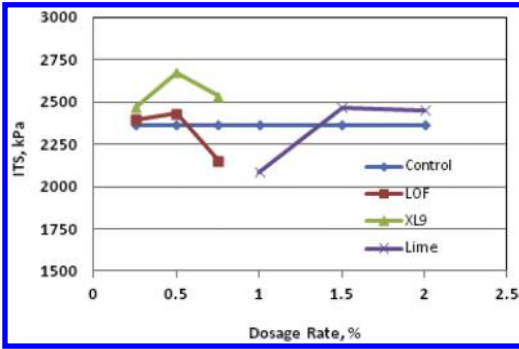


Figure 4. ITS for conditioned HMA treated with different antistripping additives.

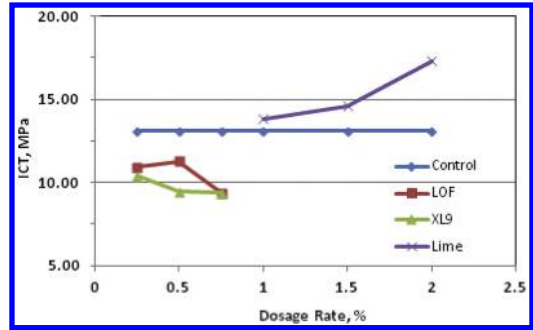


Figure 7. Compressive strength for conditioned HMA treated with different antistripping additives.

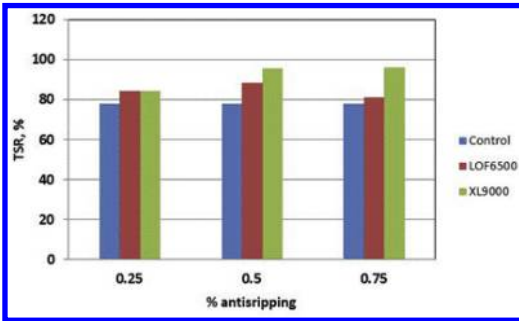


Figure 5. TSR for conditioned HMA treated with different antistripping additives.

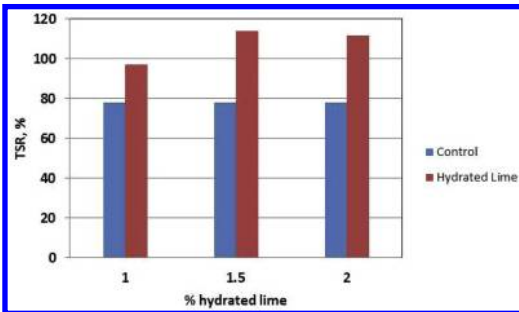


Figure 6. TSR for conditioned HMA treated with hydrated lime.

3.2 Immersion Compression Test (ICT)

Compressive strengths for all mix combinations tested in this study are presented in Figure 7. As noticed in the figure the compressive strength for HMA specimens treated with hydrated lime outperformed those for all other mixes.

Compressive Strength Ratio (CSR) is normally used to present the results for the ASTM D1075 test. This ratio is calculated as the ratio of the compressive strength for conditioned specimens and that for unconditioned specimens and the minimum acceptable value is 75%. It can be seen in Figures 8 and 9 that all treated specimens have exceeded the minimum CSR value of

75%. As the dosage rate increases the CSR decreases for mixes treated with both LOF-6500 and XL-9000. As noticed from the two figures HMA treated with 2% hydrated lime resulted in same CSR as that for HMA treated with 0.25% XL9000 antistripping.

Considering both TSR and CSR, an optimum hydrated lime content between 1.5% and 2.0% is proposed for the type of aggregate and binder used in this study. However, optimum contents between 0.25% and 0.50% for LOF-6500 and 0.25% to 0.75% for XL-9000 are proposed.

4 COST ANALYSIS

As important as the performance of these antistripping agents, cost also is another major concern and therefore, a brief cost analysis is conducted in this study. Arr Maz CC quoted LOF-6500 at \$1.60 per pound and XL-9000 at \$2.25 per pound. Per Lhoist North America (http://www.lhoist.us/Frame_Home.htm, Accessed in February 2011), the average cost of hydrated lime is about \$150 a ton, which comes out to be about \$0.08 a pound. For a one-ton HMA job, it would cost \$1.38 for LOF-6500 and \$1.94 for XL-9000, assuming a dosage rate of 0.50% of the total weight of the mix for the two liquid antistripping. For Hydrated Lime and assuming an optimum dosage rate of 1.5%, the cost of HL is \$2.40 per one ton of HMA. To account for the extra labor involved in HL handling and preparation, this unit cost is escalated to \$5.52. From the test results and the market price for the antistripping agents, it can be concluded that liquid antistripping would be the most cost effective among the three additives investigated in this study. However, the long-term performance of these agents has to be evaluated for more robust conclusion.

5 CONCLUSION

The study evaluated the moisture sensitivity performance of HMA treated with liquid antistripping agents and hydrated lime as compared to non-enhanced

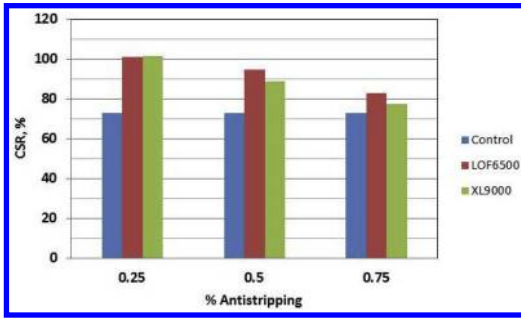


Figure 8. CSR for conditioned HMA treated with liquid antistripping.

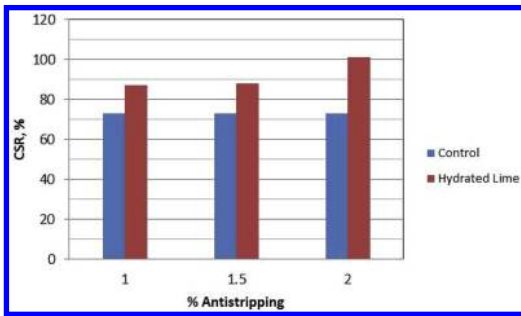


Figure 9. CSR for conditioned HMA treated with hydrated lime.

asphalt mixes. The following conclusions are drawn from the data collected and analyzed in this study:

- Adding hydrated lime to the mix is expected to increase the stiffness of the binder and consequently that for the HMA.
- According to the ITS results, for the un-conditioned specimens treated with liquid additives, the tensile strength decreased with an increase in additive amount. The opposite is true for hydrated lime-treated specimens.
- For tensile strength, a peak dosage rate is seen for both liquid additives and hydrated lime tested in this study (0.5%–0.75% for liquid antistripping and 1.5%–2.0% for hydrated lime).
- All treatment combinations had a Tensile Strength Ratio greater than the industry standard of 80%.

- The two liquid antistripping proved to be cost effective as compared to hydrated lime additive investigated in this study.
- All treatment combinations had a Compressive Strength Ratio greater than the industry standard of 75%.
- The Immersion-Compression Test has produced retained strengths close to 100 percent even when stripping is visually evident in the cores. According to Roberts et al. (1996) this makes the test not sensitive enough to measure damage induced by moisture because of the problem that developed by internal pore water pressure.

REFERENCES

- Anerson, D. and E. Dukatz, E. 1982. The Effect of Antistripping Additives on the Properties of Asphalt Cement. *Association of Asphalt Paving Technologists*, Vol. 51, pp. 298–317.
- Epps, J., Berger, E., Anagnos, J. N. 2003. Treatments – Moisture sensitivity of Asphalt Pavements. *National Seminar*, San Diego, CA.
- Hicks, R. G., 1991. Moisture Damage in Asphalt Concrete. *NCHRP Synthesis of Highway Practice 175*, Transportation Research Board, Washington, D.C.
http://www.lhoist.us/Frame_Home.htm, Accessed in February 2011.
- Kennedy, T., Roberts, F., and Lee, K. 1983. Evaluation of Moisture Effects on Asphalt Concrete Mixtures. *Transportation Research Record 911*. Washington D.C.: National Academy Press.
- Roberts, F., Kandhal, P., Brown, E., Lee, D., and Kennedy, T. 1996. Hot Mix Asphalt Materials, Mixture Design, and Construction. *2nd edition*. Lanham, Maryland: NAPA Education Foundation.
- Roberts, F. L., Kandhal, P. S., and Brown, E. R. 1996. Hot Mix Asphalt Materials, Mixture Design, and Construction. *NAPA Education Foundation*, Lanham, MD.
- Terrel, R. L., and Al-Swailmi, S. 1994. Water Sensitivity of Asphalt-Aggregate Mixes: Test Selection. *SHRP-A-403*, National Research Council, Washington, D.C.
- Tunnicliff, D. and Root, R. 1984. Use of Antistripping Additives in Asphaltic Concrete Mixtures. *NCHRP Report No. 274*. Washington D.C.: Transportation Research Board, National Research Council.

Investigation on binder-aggregate adhesivity using a nanotechnology chemically reactive silane additives based agent

Dariusz Sybilski

Road & Bridge Research Institute, Warsaw, Poland

Michael P. Wistuba

Technische Universität Braunschweig, Germany

Wojciech Bankowski

Road & Bridge Research Institute, Warsaw, Poland

Stephan Buechler

Technische Universität Braunschweig, Germany

Piotr Heinrich

Zydex, Warsaw, Poland

ABSTRACT: Bonding between bitumen and mineral aggregate is one of the most important prerequisites in asphalt pavement construction to ensure asphalt pavement durability. An adhesion agent based on nanotechnology, called ZycoTherm®, is reported to substantially improve coating of asphalt binder on aggregates, to ensure consistent and higher compaction and to eliminate stripping for making durable asphalt pavements over the service life. This paper presents results from laboratory testing of this product and critically discusses its effectiveness in comparison to a number of other adhesion agents widely used.

1 INTRODUCTION

Laboratory testing of application of ZycoTherm included two aspects: compaction properties of asphalt mixture completed in Technische Universität Braunschweig mbH, Germany, and adhesion of bituminous binder and mineral aggregates in Road and Bridge Research Institute, Poland. The task of the testing provided evaluation of improvement of both aspects with application of additive of ZycoTherm® (Sybilski 2014).

2 TESTING PLAN AND PRODUCTION OF THE ASPHALT TEST PLATES

For testing the compaction properties, an asphalt binding agent AC 16 B S as well as an asphalt concrete for asphalt surface layers AC 11 D S were produced in the laboratory of the TSW. One version each without the additive ZycoTherm® served as reference asphalt. From the asphalt mixture, the mixer and roller compactor was used to produce asphalt sample plates where the compaction temperature varies. An overview of the variants is represented in Table 1.

The compaction methods (load, number of rolls, etc.) stay the same with all compaction variants. Only the compaction temperature was varied. Four asphalt

Table 1. Overview for producing asphalt mixture variants.

Variant	Mixture type	Bitumen	Addition of ZycoTherm®	Compaction temperature, °C
1a	AC 16	50/70	No	135
1b	B S		Yes	135
1c			Yes	115
1d			Yes	95
2a	AC 16	25/55-55	No	145
2b	D S	A	Yes	145
2c			Yes	125
2d			Yes	105

sample plates of sizes $300 \times 260 \times 40 \text{ mm}^3$ (AC 11 D S) or $300 \times 260 \times 50 \text{ mm}^3$ (AC 16 B S) were produced for each variant.

2.1 Composition of the types of asphalt mixture

Both types of asphalt were mixed with compositions that are common in Germany. These can be obtained from the Table 2.

A gabbro and powdered limestone as well as bitumen from the stocks of the TSW were used for producing the asphalt sample plates. The stones were washed and oversize and undersize grain was removed

Table 2. Compositions of the type of asphalt applied.

Asphalt mixture		AC 16 B S	AC 11 D S
Bitumen		50/70	25/55-55 A
Bitumen content	M. %	4.3	6.0
Addition of Zyco Therm in Binder	M. %	0.10	0.15
Aggregate		Gabbro	Gabbro
> 16.0 mm	M. %	2.8	–
11.2–16.0 mm	M. %	18.5	0.5
8.0–12.0 mm	M. %	12.1	20.5
5.6–8.0 mm	M. %	12.8	10.8
2.0–5.6	M. %	15.2	23.3
0.063–2.0 mm	M. %	22.0	37.5
<0.063 mm	M. %	6.6	7.6



Figure 1. Cowles agitator (left) and mixer used (right) for the homogenisation of the bitumen ZycoTherm® mixture.

through a screen. A total of more than 500 kg of stones were prepared.

Additive ZycoTherm® was applied in 3 from 4 variants depending on the type of asphalt.

2.2 Adding ZycoTherm®

The addition of ZycoTherm® was carried out on the basis of the instructions “Mixing report with asphalt binding agent/Mixing report for asphalt mixtures” provided by the customer. A special mixer with a Cowles agitator for producing emulsions was used for this purpose, see Figure 1.

The additive ZycoTherm® was mixed together with the bitumen heated up to 160°C for at least 10 minutes. Then the resulting bitumen was added to the pre-heated stone in the mixer and the mixing process was started.

3 TESTING PROCEDURES

3.1 Degree of coating

During the 2 minute mixing process, all 8 asphalt variants were filmed and then the time for a specified percentage coating of the stones estimated. For evaluation, degrees of coating of 50%, 75%, 90% and 100% were selected.

Table 3. Estimated times for different degrees of coating during the mixing process.

Coating	Asphalt Variant							
	1a	1b	1c	1d	2a	2b	2c	2d
50%	25 s	15 s	19 s	19 s	37 s	22 s	30 s	30 s
75%	35 s	22 s	30 s	29 s	45 s	29 s	38 s	39 s
90%	50 s	32 s	40 s	43 s	55 s	42 s	44 s	46 s
100%	47 s	47 s	50 s	55 s	80 s	56 s	66 s	61 s

3.2 Power consumption

During the mixing process, the laboratory mixing device GZM 30+E from the company BPS Wennigsen used at TSW records the torque of the agitator and the mixing drum and converts this into a performance (W). The sum of the performance from the agitator and drum are specified in a diagram over a two minute mixing duration. As an alternative representation, the accumulated performance (energy, (Ws)) is represented in another diagram.

3.3 Compaction resistance

The compaction resistance T is determined on the basis of the change in thickness of the Marshall sample during the compaction procedure according to TP Asphalt StB, Part 10 B. On the basis of the reducing sample thickness, via the number of impacts, an exponential function can be determined whose parameter T permits a statement for the compaction. Small values for T refer to a material that is easy to compress whereas larger values to an asphalt that is difficult to compress.

3.4 Characteristic values of the asphalt test plates

After the production of the asphalt test plates with different compaction temperatures, the density by volume pb, SsD according to TP Asphalt StB, Part 6 is determined for each plate.

The raw density pm is determined on each mixed material TP Asphalt StB, Part 5 produced and thus, the void content V according to TP Asphalt StB, Part 8.

4 RESULTS

4.1 Degree of coating

The visually estimated times for different degrees of coating of the examined asphalt versions are represented in Table 3.

The mixing processes of both asphalt types show that the variant a (without ZycoTherm®) required a longer period for coating the stones compared with variants b, c, and d (with ZycoTherm®, with equal composition). Next to the times specified here, the influence can also be perceived subjectively during the mixing process.

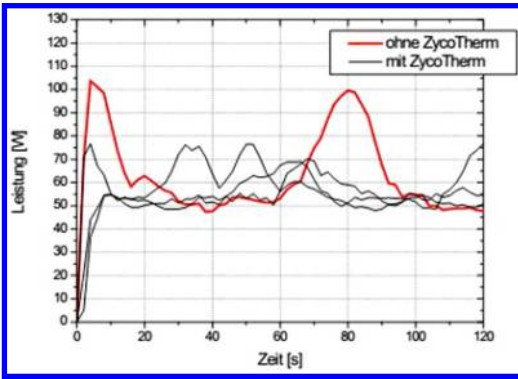


Figure 2. Recorded performances (W) during the mixing processes of the variants of the AC 16 B S.

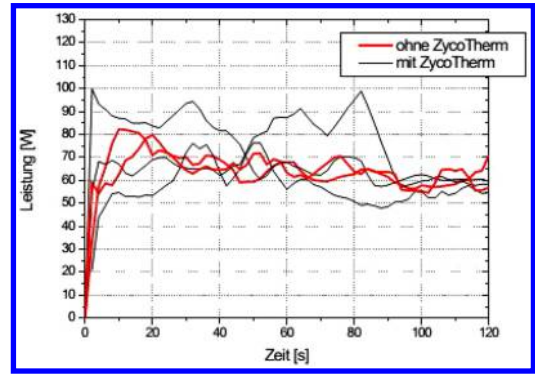


Figure 4. Recorded performances during the mixing processes of the variants of the AC 11 D S.

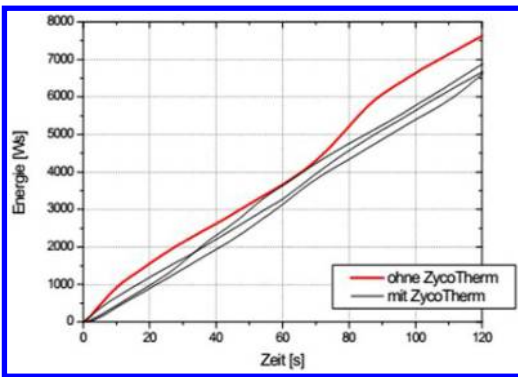


Figure 3. Recorded performances accumulated over time of the variants of the AC 16 B S.

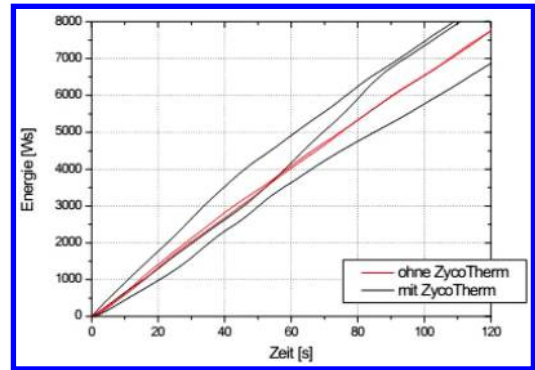


Figure 5. Recorded performances during the mixing processes accumulated over time of the variants of the AC 11 D S.

4.2 Power consumption, mixer

Figure 2 show the power consumption of the mixer in (W) over the time for the four variants of the AC 16 B S. The accumulated performances are represented on Figure 3 that leads to an improved overview.

Figure 4 shows the power consumption of the mixer over the time for the four variants of the AC 11 D S and Figure 5 the accumulated performances for AC 11 D S, analogue to AC 16 B S.

Whereas the representation of the performance for the mixing duration for both types of asphalt does not practically allow any statement, the accumulated performances for AC 16 B S have the tendency that the variants with Zycotherm® require less mixing performance. No tendency can be recognised for AC 11 D S.

4.3 Compaction resistance T

The compaction resistances for both types of asphalt with different compaction temperatures are specified in Table 4.

Despite different compaction temperatures, the compaction resistances show practically no differences. As a whole, the asphalt binding agent AC 16

Table 4. Compaction resistance T of the examined asphalt variants with different compaction temperatures.

Asphalt mixture	Variant	Compaction temperature, °C	Compaction force T , 21 Nm
AC 16 B S	1a	135	41.6
	1b	135	43.5
	1c	115	42.8
	1d	95	41.3
AC 11 D S	2a	145	37.3
	2b	145	34.2
	2c	125	36.5
	2d	105	36.5

B S is a little more difficult to compress compared with asphalt concrete AC 11 D.

4.4 Characteristic values of the asphalt test plates produced

The determined density by volume and void content per variant is specified as average value from the asphalt test plates produced here (Table 5). The raw density was determined only once per variant.

In addition, the raw densities for each type of asphalt are determined and thus, the average void content is calculated for each variant.

Depending on the type of asphalt, the raw density specifies an almost equal level as, except for the addition of ZycoTherm®, no changes were made in the composition.

The values determined for AC 11 D S were all within the critical range da of 0.025 g/cm³. For AC 16 B S, with a range of 0.029 g/cm³ the values are a little outside this permitted range but can be viewed as close to practice.

The void contents determined for the asphalt concrete AC 11 D S were all within the repeatability accuracy of r = 1.1 percent by volume and can be perceived as statically equal. However, the tendency of an increasing void content with reducing compaction temperature can be recognised.

For the asphalt binding agent AC 16 B S, the void content calculated with the average raw density is also

Table 5. Densities by volume, raw densities and void contents of the asphalt test plates produced at different compaction temperatures.

Asphalt mixture Variant	AC 16 B S				AC 11 D S			
	1a	1b	1c	1d	2a	2b	2c	2d
Compaction temperature, °C	135	135	115	95	145	145	125	105
Density, g/cm ³	2.511	2.508	2.506	2.513	2.508	2.500	2.491	2.483
Bulk density, g/cm ³	2.684	2.711	2.713	2.688	2.618	2.615	2.627	2.622
Void content, Vol. %	6.4	7.5	7.6	6.5	4.2	4.4	5.2	5.3
Average bulk density, g/cm ³	2.699				2.621			
Void content, Vol. %	7.0	7.1	7.2	6.9	4.3	4.6	5.0	5.3

Table 6. Overview for producing the asphalt mixture variants.

Variant	Mix type	Binder type	Addition of ZycoTherm®	Compac-tion Temp. °C	50% Coating achieved s	Compaction resistance 21 Nm	Void content Vol.-%
1a	AC 16 B S	50/70	No	135	25 s	41.6	7.0
1b			Yes	135	15 s	43.5	7.1
1c			Yes	115	19 s	42.8	7.2
1d			Yes	95	19 s	41.3	6.9
2a	AC 11 D S	25/55-55 A	No	145	37 s	37.3	4.3
2b			Yes	145	22 s	34.2	4.6
2c			Yes	125	30 s	36.5	5.0
2d			Yes	105	30 s	36.5	5.3

within the repeatability accuracy. If the raw density of the individual variants is applied, the repeatability accuracy is only just exceeded. Despite this range that is significant in some cases, with AC 16 B S no dependency of the compaction temperature can be recognised.

The compaction resistance does not show any difference for both asphalt types when adding ZycoTherm®, as documented in Table 6.

Table 7. Adhesion test results to Greywacke.

GREYWACKE	Plain				+0.15% ZYCOTHERM			
	6 h	24 h	48 h	72 h	6 h	24 h	48 h	72 h
8/11								
GREYWACKE 8/11 (50/70 B Spain)	75	45	35	25	80	60	55	50
GREYWACKE 8/11 (45/80-65 Spain)	85	60	35	25	80	65	55	55
GREYWACKE 8/11 (50/70 B Kuwait)	75	50	30	25	75	60	55	50

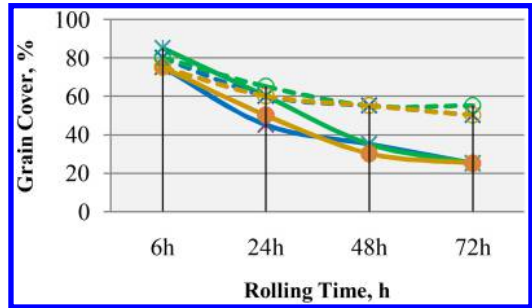


Figure 6. Adhesivity of binders to Greywacke without (continuous) or with (dash) ZYCOTHERM.

5 TESTING OF ZYCOTHERM FOR BINDER – AGGREGATE ADHESIVITY IMPROVEMENT

Binder-Adhesion property is one of the most important factor deciding on durability of road pavement (e.g. (Tarrer and Wagh 1991)).

Test results of binder – aggregates adhesivity with ZYCOTHERM addition have were performed according to rolling bottle test PN-EN 12697-11 (method A). Adhesion test with ZycoTherm® were performed on four aggregates: Greywacke, Limestone, Granite and Basalt. Two binders were used – plain bitumen 50/70 and PmB 45/80-65. Adhesion test was performed without and with 0,15% ZycoTherm® addition to binder. Test was performed by two operators. Presenting results are average of two operators. Tables 7–10 present the rolling bottle test results in 6, 24, 48, 72 hours.

Test results of binder – aggregates adhesivity with ZYCOTHERM addition performed according to rolling bottle test PN-EN 12697-11 (method A) proved that the adhesivity improvement with ZycoTherm® depends on the aggregate type. However, each of the component binder-aggregate prove the better property of the adhesion. Similar result have been proved in the ZycoTherm® application on the NCAT road test (Taylor and Willis 2011).

Table 8. Adhesion test results to Limestone.

LIMESTONE	Plain				+0.15% ZYCOTHERM			
	6 h	24 h	48 h	72 h	6 h	24 h	48 h	72 h
8/11								
LIMESTONE 8/11 (50/70 B Spain)	80	70	55	55	75	60	55	50
LIMESTONE 8/11 (45/80-65 Spain)	85	75	70	65	85	70	65	65
LIMESTONE 8/11 (50/70 B Kuwait)	80	75	55	55	75	65	55	45

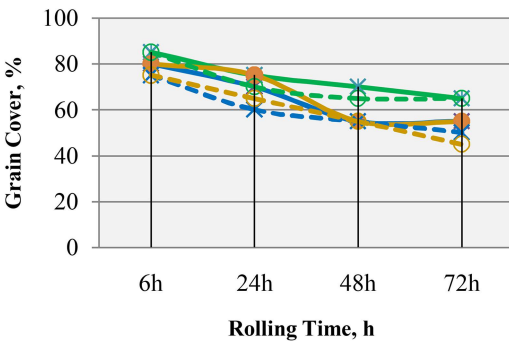


Figure 7. Adhesivity of binders to Limestone without (continait) or with (dash) ZYCOTHERM.

6 CONCLUSION

Goal of the examinations carried out here was to document the influence of the binding adhesion agent ZycoTherm® on the mixing process and to document the compaction properties of asphalt.

For this purpose, two types of asphalt that are common in Germany, an asphalt binding agent AC 16 B S with 50/70 and an asphalt concrete for asphalt surface layers AC 11 D S with 25/55-55 A, were mixed with and without ZycoTherm® and compressed at different temperatures. An overview of the variants produced is specified in table 6.

Table 9. Adhesion test results to Basalt.

BASALT	Plain				0.15% ZYCOTHERM			
	6 h	24 h	48 h	72 h	6 h	24 h	48 h	72 h
8/11								
BASALT 8/11 (50/70 B Spain)	65	30	20	20	65	40	30	30
BASALT 8/11 (45/80-65 Spain)	65	30	15	15	70	35	25	25
BASALT 8/11 (50/70 B Kuwait)	65	20	10	0	65	35	25	20

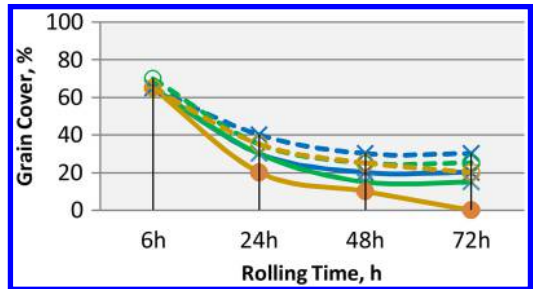


Figure 8. Adhesivity of binders to Basalt without (continuous) or with (dash) ZYCOTHERM.

Table 10. Adhesion test results to Granite.

GRANITE 8/11	Plain				0.15% ZYCOTHERM			
	6 h	24 h	48 h	72 h	6 h	24 h	48 h	72 h
GRANIT 8/11 (50/70 B Spain)	60	5	5	0	80	65	50	45
GRANIT 8/11 (45/80-65 Spain)	70	30	5	0	70	50	30	25
GRANIT 8/11 (50/70 B Kuwait)	65	20	10	0	75	55	40	35

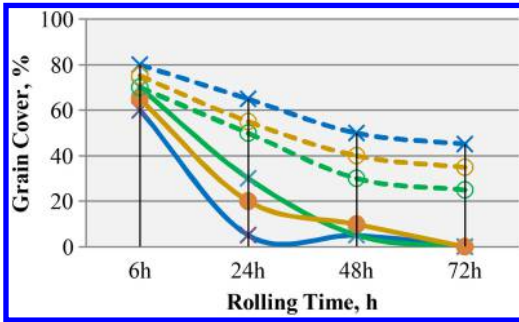


Figure 9. Adhesivity of binders to Granite without (continuous) or with (dash) ZYCOTHERM.

During the mixing processes, the power consumption of the laboratory mixer was recorded and the time that the degrees of coating of 50%, 75%, 90% and 100% were reached was noted. The times for reaching the degree of coating of 50% are specified in table 10. Therefore, the mixed material is coated quicker when Zycotherm® is added. On average, 20% less time is required. With regard to the mixing performance, for AC 16 B S a tendency was recognised that less performance was required when adding Zycotherm®.

The raw density of the asphalt mixture produced can be considered as equal for both types of asphalt.

The densities by volume of the roller compressed asphalt test plates only indicate small differences. The void content is specified as out coming result in table 6.

For AC 16 B S, no tendency could be specified with regard to the void content. The void contents are within a narrow range so that this can be considered as equal.

The void contents for AC 11 D S increase with reducing compaction temperature. This increase

however is not within the testing accuracy so that here, only one tendency can be specified, there is no statistical security. Deviations within these ranges can still be considered as close to practice.

As a summary, it can be stated that when adding Zycotherm® the time for coating the stones can reduce and with a significantly reduced compaction temperature an almost consistent void content can be achieved.

The test on binder – aggregate adhesion with addition of Zycotherm® proved improvement of asphalt – aggregate durability. Testing was performed on four aggregates and three bituminous binders – two plain bitumen and one polymer-modified bitumen. The test results showed variation of effectiveness of Zycotherm® depending on aggregate. It should be concluded that the improvement of adhesion property depends on the type of the aggregate. The percent of Zycotherm® addition should be decided depending on the mineral aggregates in asphalt mixture.

REFERENCES

- Sybilski D. et al.: Report on International interlaboratory binder-aggregate adhesion test in the frame of research works of RILEM Technical Committee SIB, IBDiM, PWS-619, 2014.
- Tarrer, A.R. and Wagh, V. (1991) The effect of the physical and chemical characterization of the aggregate on bonding, SHRP-A/UIR-91-507.
- Taylor A.J., Willis J. R.: Effects of NANOTAC additive on bond strength and moisture resistance of tack coats. NCAT, Final Report, November 2011.

Addressing durability of asphalt concrete by self-healing mechanism

R. Casado Barrasa, V. Blanco López & C. Martín-Portugués Montoliu

Acciona Infrastructures Technology Centre, Madrid, Spain

V. Contreras Ibáñez

Repsol Technology Centre, Madrid, Spain

F. Pedrajas

Laimat Soluciones Científico Técnicas S.L., Granada, Spain

J. Santarén

Tolsa SA., Madrid, Spain

ABSTRACT: Numerous methods are being employed for asphalt pavement preservation, but only the addition of rejuvenator partially recovers the original properties of the pavements by restoring the original asphaltenes/maltenes ratio. The main problem is that this type of treatment is superficial, only the first centimeters from the surface are affected. An innovation procedure to solve this problem is the addition of encapsulated rejuvenators into the asphalt mixes. Once the rejuvenator is released, it will be in contact with the bitumen around restoring the original properties of the binder and increasing the self-healing rate by closing the cracks or limiting its growth. In this paper two encapsulation methods developed by the authors are described. The autonomous repairing capability is also validated through a variety of comparative laboratory tests. Results from this study indicate that the self-healing chemistry developed has a high potential for its use in asphalt pavements by increasing its durability.

1 INTRODUCTION

Road transport is part of the lifeblood of the European economy and single market. It delivers goods across Europe fast, efficiently, flexibly and cheaply. About 44% of goods transported in the EU go by road and people also travel mainly by road, with private cars accounting for 73% of passenger traffic (European Commission 2013). It is also a vital economic sector in its own right, employing about 5 million people across the EU and generating close to 2% of its GDP (European Road Federation 2012). Therefore, it seems evident that in the next decades transport industry and the closely related construction sector should remain as dynamic and vigorous as possible.

It is also estimated that 90% of the 5.2M km of the Europe road network and 93% of the 4.1M km of US paved roads and highways are surfaced with asphalt mixes (EAPA 2012). This represents a huge amount of money and energy, from which a good part is for preservation and renovation of existing pavements. In fact, 50% of the annual construction budget is estimated to be spent on rehabilitation and repair of the existing pavements in Europe (Schlangen et al. 2013).

Environmental conditions combined with traffic loads contribute to premature deterioration

of asphalt concrete pavements, reducing their strength and durability over time. Actually, when several degradation processes occur, the stiffness of asphalt concrete increases while its relaxation capacity decreases, and as consequence the binder becomes more brittle causing the development of micro-cracks and in a near future the cracking on the interface between aggregates and binder occurs (Branthaver et al. 1993).

These pavement failures increase the expense of renovation and preservation of bituminous pavements and reduce critical parameters such as safety (Asphalt Institute 2013). Therefore structures that show higher durability and have longer “maintenance free” performance with low repair costs need to be investigated.

In order to prevent pavement distresses, numerous methods are being employed for asphalt pavement preservation, including the use of rejuvenator emulsions, fog seals and several different thin overlay technologies (Boyer 2000). Only the addition of rejuvenator partially recovers the original properties of the pavements by restoring the original asphaltenes/maltenes ratio to its original balance and reconstituting the binder’s chemical composition (Shen et al. 2007; Karlsson et al. 2006). The main problem is that once the rejuvenator is spread on the road surface to be effective it must penetrate into the

pavement not only in the first centimetres, so that the layers below could be equally damaged being the origin of future failures.

To address current limitations, embedded capsules containing asphalt rejuvenator are proposed as a promising technique to apply rejuvenator in asphalt mixes in an optimum and efficient way to compensate ageing of asphalt concrete.

2 BACKGROUND

The concept of self-healing materials is related to their inherent ability to partially reverse damage that might have occurred during its service life.

Cracking is one of the main distresses responsible for the service life reduction of asphalt pavement. On the contrary, self-healing is a process that reverses to cracking and increases the service life. The self-healing properties of asphalt materials present a new means to achieve reliable, durable, and sustainable asphalt pavements through maximizing the effect of microdamage recovery.

It is known that asphalt is a self-healing material by itself, but it only works if there is no traffic circulation. Also it has some limitations: it is a slow process at ambient temperature and non-effective if the cracks are significant (Qiu 2012; Garcia 2012).

The application of microcapsules containing rejuvenator derives from the success observed from some polymer self-healing materials. Encapsulation of active substances as adhesives or solvents is of particular interest for self-healing materials, coatings and many other construction applications (Garcia et al. 2010a; Blaiszka 2009).

The use of embedded capsules containing asphalt rejuvenator, as component of the asphalt mix, is a promising new technique to provide pavements self-healing properties that has been developed in the last few years. The main objective is to prevent ageing and oxidation of asphalt mixes in order to increase the lifespan of asphalt pavements and minimise rehabilitation works. Thus, the introduction of these materials into the asphalt mix would avoid operations associated with pavement recycling and could be a remarkable innovation.

Asphalt is a viscoelastic material where two phases can be considered: a phase "liquid" or volatile, composed by maltenes and a "solid" phase composed by asphaltenes. Theoretically, when a crack appears is closed by itself, but it would do it faster if the "liquid part" of bitumen increases. This process can be done by mixing with less dense oil, known as rejuvenator (Garcia et al. 2010b). Therefore, the inclusion of capsules that release rejuvenator will reduce cracking due to a more balanced maltenes/asphaltenes ratio.

Several methods of encapsulating asphalt rejuvenator in microcapsules have been developed in recent studies; some of the more successful were carried out by TUDelf University. These methods are different each other but all of them aim to obtain microcapsules with high thermal stability and high

mechanical strength able to withstand the high temperatures and mixing stress of the asphalt. Garcia, A. et al. (2010a and 2010c) reported a method to prepare rejuvenator capsules by using maltenes encapsulated in very porous sand and covered by a composite of resin and fine sand. Su, J.-F. et al. (2012 and 2013) have developed a method to synthesize microcapsules containing rejuvenator by in-situ polymerization using methanol-melanine-formaldehyde (MMF) prepolymer.

Based on the previous studies, ACCIONA in partnership with REPSOL, LAIMAT and TOLSA, has developed more advanced capsules with controlled release mechanism for increasing the self-healing ability of the asphalt mixes. This work was supported by CDTI, under the national Project CENIT.

3 METHODOLOGY

3.1 Study Approach

The overall aim of this study is the demonstration of the self-healing ability of asphalt mixes with embedded capsules containing rejuvenator in order to increase service life and prevent pavement distresses. Throughout the study, many factors have been evaluated from the encapsulation methods to its final self-healing evaluation.

The study has been divided in four main steps. In a first step, encapsulation methods for two different types of capsules (porous and polymeric) containing rejuvenator as healing agent were developed. Secondly, synthesised capsules were physically and chemically characterized. In a third step, the feasibility of the capsules incorporation into the asphalt mix together with the determination of their resistance to withstand the manufacturing process of asphalt mixes was deeply analysed. In the last step the mechanisms for the release of the rejuvenator and evaluation of the self-healing ability were studied.

3.2 Materials used in the investigation

Conventional binder, synthetic binder and rejuvenator, mainly composed of maltenes, were provided by Repsol.

Different materials for the formation of the capsule shell were used. Porous aggregate, specifically sepiolite, with different particle size varying from 38 μm up to 6 mm, were supplied by Tolsa. Commercial cellulosic (CE) and polymer (C) used for the formation of the polymeric shell, were provided by Laimat.

Aggregates from different origin: limestone, silica, porphyry and andesite, were used for the design of asphalt mixes.

4 TEST AND RESULTS

4.1 Encapsulation methods

In the present work two encapsulation methods developed by the authors are described. The first one, porous

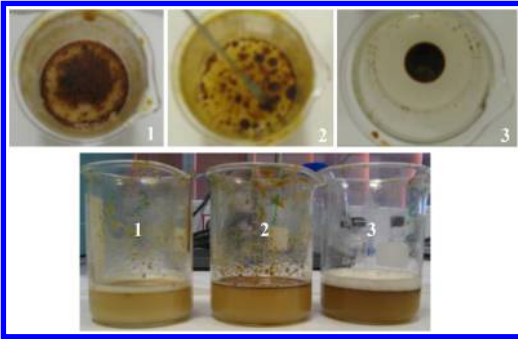


Figure 1. Influence of the emulsifier used.

aggregates with the rejuvenator embedded were prepared; the second one polymeric shell microcapsules containing the rejuvenator were synthesized.

4.1.1 Polymeric Shell

Different materials were selected for the formation of the microcapsule shell based on the required application. The encapsulating agents studied were: Cellulosic (CE) with high degradation temperatures (about 220°C), impact strength, flexible, tough and insoluble in aliphatic hydrocarbons and water, and; polymer (C) with thermal stability up to 200°C.

Emulsified and solvent evaporation for CE and C, respectively, were the encapsulation techniques selected taking into account the encapsulating material, the active substance, the functionality of the microcapsules in the matrix in which they are incorporated, the ratio encapsulant-active substance, the final properties of the microcapsules (size, density, dry solid, solid dispersion, ...), and the release mechanism (mechanical action, exposure to environmental influences, ...), etc.

The emulsifier was chosen using the HLB (Hydrophyle-Lipophyle Balance). After selecting the emulsifier suitable according to the active substance to be emulsified and the emulsion type to obtain: W/O or O/W or multi emulsion W/O/W, where rejuvenator microcapsules (O) are formed brown droplets into the encapsulant solution (W).

Some problems related to the drying process of the CE microencapsulation were observed. Therefore, C microencapsulation was selected as the most promising material for the formation of the shell achieving a content of rejuvenator of more than 80%. Further studies with microencapsulation C are shown in this section.

4.1.2 Porous aggregate

An impregnation method of rejuvenator in porous aggregates using sepiolites has been developed. This method consists of a vacuum impregnation process in which the rejuvenator penetrates into the sepiolite porous releasing the air of its internal structure. The method and impregnation system are described in Figure 2.

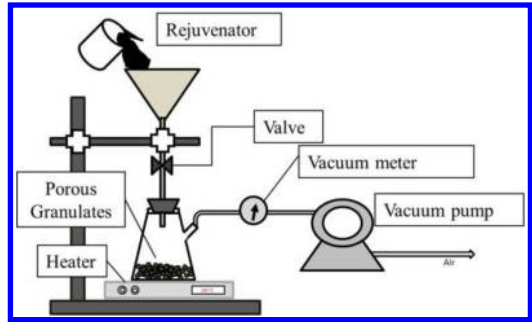


Figure 2. Impregnation method of rejuvenator in porous aggregate system.

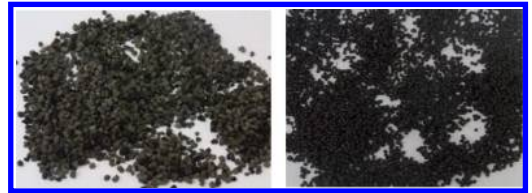


Figure 3. Physical aspect of the capsules synthesised: porous aggregates (left) and polymeric capsules (right).

Once the process finished, the excess rejuvenator was removed by filtration and was dried in an oven until all the rejuvenator in excess was released.

By using this method of preparation of the capsules, percentages of approximately 40% of rejuvenator were achieved.

4.2 Characterization tests

Characterization tests, both for polymeric and aggregate capsules, are described below.

4.2.1 Polymeric microcapsules

Polymeric capsules containing rejuvenator were characterised and compared with the reference or blank samples (empty capsules).

Particle size, morphology, thermal stability and mechanical strength of the capsules developed were the tests carried out.

Particle size and morphology was determined by optic microscopy. A slight increase in particle size in those containing rejuvenator (1–1.3 mm) compared to those empty (0.8–1 mm) was observed (Fig. 4).

Thermal stability was determined by Thermogravimetry Analysis (TGA) and Differential Scanning Calorimetry (DSC), (Fig. 5).

Results show that capsules are stable up to 220°C. Also, capsules filled with rejuvenator show slightly more thermal resistance.

In order to simulate the working temperatures of the asphalt mixes manufacture process the microcapsules were subjected to a heating slope of 5°C/min until 180°C in an air atmosphere, after that they were kept at the same temperature (isothermal) for 4 hours.

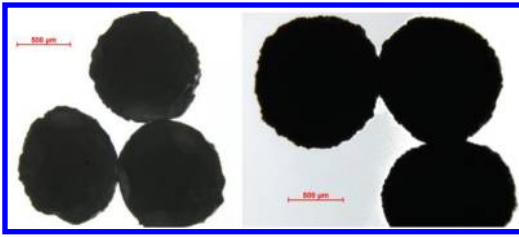


Figure 4. Optic microscopy 2x; empty capsules (left) and with rejuvenator (right).

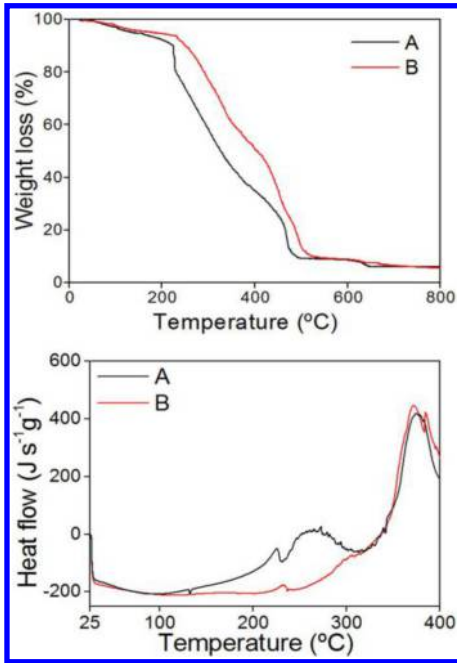


Figure 5. TGA (top) and DSC (bottom) for the capsules studied A) empty capsules & B) with rejuvenator.

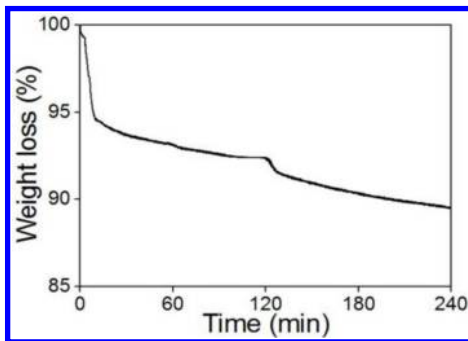


Figure 6. TGA Isotherm at 180°C 4 h.

Along the test a decrease of 10% in total mass was recorded, although when temperature was maintained for 4 h at 180°C, a 5% of mass loss was observed.

Compression tests have been performed on the capsules using an Infrared (IR) press in order to determine

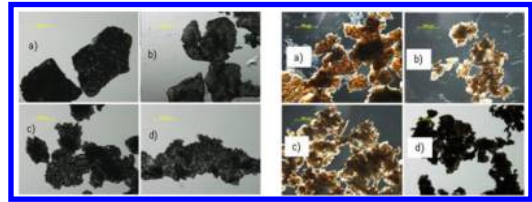


Figure 7. Optical microscopy of the shell of: empty capsules (left) and capsules with rejuvenator (right). Tons of load in an infrared press a) 2.5 t, b) 5 t, c) 10 t & d) 15 t.

Table 1. Adsorption capacity of rejuvenator into the sepiolite pores.

Sample	Impregnation %
Sepiolite A	42
Sepiolite B	40
Sepiolite C	45

the shell resistance. Loads from 2.5 to 15 tons were applied for 2 minutes. Visual inspections by using an optical microscopy were carried out.

According to Figure 7 empty microcapsules are slightly more resistance to compression compared to those containing rejuvenator. Also, at low loads capsules can be compressed without suffering any damage. As the load applied increased part of the rejuvenator is released; however even after applying 15 tons of loads some rejuvenator still remained.

Based on the temperature and shell resistance results, it can be concluded that the synthesized polymeric capsules withstand the high temperatures that are necessary for the manufacturing process of the asphalt mixes.

4.2.2 Porous aggregates

Several tests were carried to characterize the capsules based on porous aggregates developed. Maximum rejuvenator content and resistance to high temperature were the two main parameters evaluated.

Thermogravimetry tests were carried out in an oxygen atmosphere to quantify the percentage of rejuvenator that was adsorbed into the pores of the sepiolite. Sepiolites with different particle size were evaluated: sepiolite A – $\leq 4 \mu\text{m}$; sepiolite B – $600\text{--}250 \mu\text{m}$; sepiolite C – porous sand.

Following the same procedure than the performed for the polymeric capsules, but increasing the isothermal time, TGA at 180°C isothermal temperature for 72 hours was carried out in air atmosphere, in order to evaluate if they are feasible to withstand high production temperatures (Fig. 8). An approximately mass loss of 3% was observed, which could be linked to the presence of water.

Based on these results it can be concluded that the synthesized capsules resist the high temperatures required for the manufacturing process of the asphalt mixes.

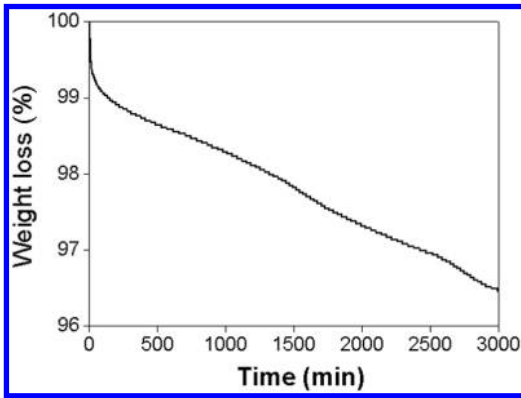


Figure 8. TGA Isotherm at 180°C 72 h.

4.3 Design and characterization of asphalt mixes

In this section the resistance of the capsules when incorporated into asphalt mixes was evaluated, as well as, their final properties in two types of asphalt mixes: very dense grades asphalt mixes and asphalt concrete AC16SurfS 50/70.

4.3.1 Very dense grade asphalt mixes

In order to evaluate the mechanical resistance of the capsules developed and to determine if the rejuvenator releases from the capsules during the manufacturing process of asphalt mix, mainly due to the mixing process with aggregates and the compaction, dense graded asphalt Marshall Specimens were prepared. Marshall specimens were produced according to the standard EN 12697-30 and compacted with 75 blows per face. The weight of the specimen was of 1200 g, where the 95% corresponded to 0/6 limestone aggregates and the 5% corresponded to synthetic binder. Also 1% w/w of capsules was added.

Synthetic binder is a light brown binder that allowed analysing visually the possible release of rejuvenator during the mixing and compaction process of the samples. Apparently, after the compaction process, it was observed that the capsules of the compacted faces that have been in contact with the Marshall hammer were slightly deformed; however no release of the rejuvenator was observed (Fig. 9).

In a second step, the specimens were broken by indirect tensile according to the standard EN 12697-23, that allowed evaluating them internally and therefore the condition of the capsules. After a visual inspection of the core of the specimens, no deformation was detected (Fig. 10).

Duplicate specimens were submitted to a cyclic compression test according to the standard EN 12697-25 and then broken by indirect tensile (EN 12697-23). The objective of this study was to evaluate the condition of the capsules in the core of the asphalt mixes when they were submitted to axial loads. The resultant fluency curves are shown in Figure 11.

No differences could be seen after the cyclic compression test between the specimens with capsules and



Figure 9. Very dense grade specimens: reference (left) and 1% capsules (right).



Figure 10. Core specimens after fracture by indirect tensile test.

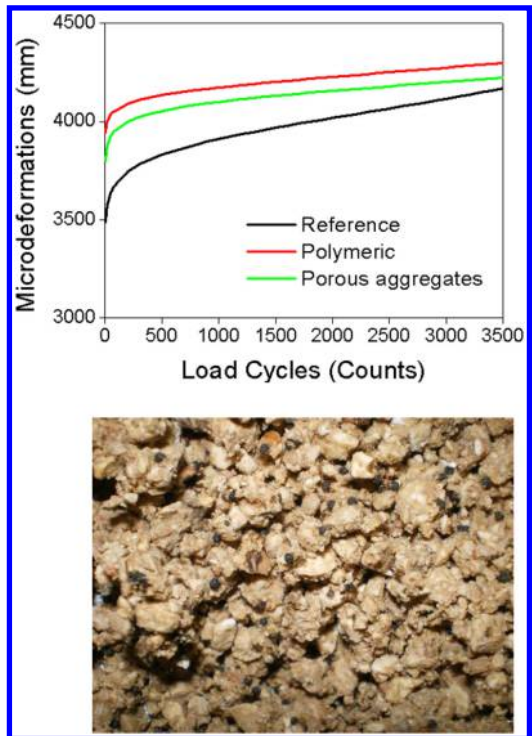


Figure 11. Fluency curves (top) and specimens submitted at a maximum load (bottom).

the reference samples. It can be concluded that all the capsules developed were designed to resist working conditions: high production temperatures (170–180°C), the mixing process with aggregates and the compaction process.

Table 2. Grading curve of the asphalt mix AC16SurfS 50/70.

Sieve mm	AC16 % passing
32	100
22	100
16	95
8	68
4	43
2	31
0.5	16
0.25	11
0.063	5

Table 3. Water sensitivity and stiffness modulus results.

Sample	Water sensitivity %	Stiffness (20°C, 5 Hz) MPa
Reference	93.3	6.398
Polymeric capsules	87.1	5.008
Porous aggregates	85.3	5.163

4.3.2 Asphalt concrete AC16SurfS 50/70

AC16SurfS was designed with limestone, silica and andesite aggregates. Their particle size composition is presented in Table 2. 4.9% of conventional bitumen 50/70 was used.

Capsules designed were added to the mix in 1% w/w. Marshall specimens were produced according to the standard EN 12697-30 and compacted with 75 blows per face or 50 blows per face depending on the test carried out.

The mechanical tests carried out were: determination of the water sensitivity (EN 12697-12) and stiffness modulus (EN 12697-26). Stiffness at 20°C and a frequency of 5 Hz was measured on circular specimens using IT-CY method (EN 12697-26:2012, Annex C). Results are shown in Table 3.

As it can be seen from Table 3, values of water sensitivity and stiffness modulus are slightly reduced by the addition of capsules to asphalt mixes. This reduction has no considerably effect in the final properties of the asphalt mixtures, as values of water sensitivity meets the minimum values of 85% required by the Spanish normative. Also, values in the range of 5000–7000 MPa are typical stiffness values for asphalt concrete mixtures.

4.4 Releasing tests and evaluation of the self-healing ability.

In this section different mechanisms for the release of the rejuvenator will be assessed. This particular study will aim at evaluating the self-healing ability of the

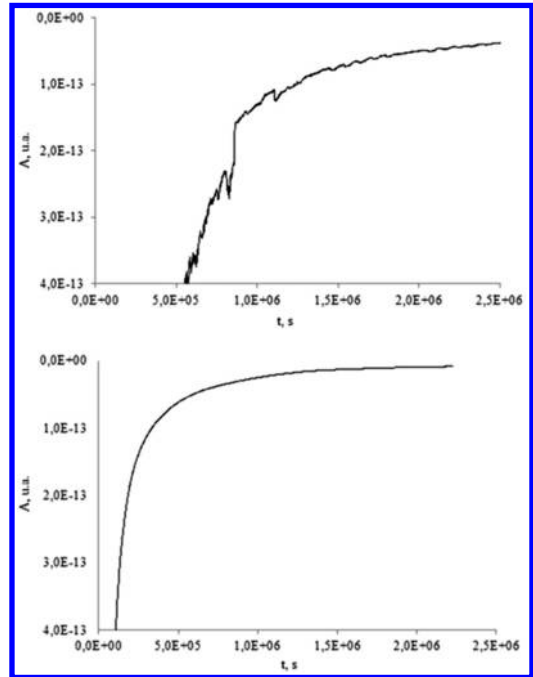


Figure 12. FTIR-ATR at 100°C for polymeric microcapsules (top) and porous aggregates (bottom).

capsules developed. To achieve this goal two main tests were carried out: diffusion and ageing tests.

4.4.1 Diffusion tests

Fourier Transform Infrared Spectroscopy by Attenuated Total Reflectance (FTIR-ATR) was used to monitor bitumen rejuvenator diffusion through the capsule shell. This test allows calculating the diffusion coefficient between the rejuvenator and bitumen through the shell of the capsule (Contreras et al. 2012).

The diffusion tests were carried out at a temperature of 100°C. Results are presented in Figure 12.

Results from these tests showed that the rejuvenator diffuses through the shell of the capsule in both porous aggregates and polymeric microcapsules. It should be noted that in the case of polymeric microcapsules the diffusion showed a very rapid initial step due to the remaining rejuvenator content over the shell, then it experienced a stabilization over the measured period of time (Fig. 12 top).

In order to minimize the short-term rejuvenator release and the initial diffusion rate of the polymeric microcapsules, a new synthesis of the polymeric shell may be necessary. The diffusion rate for the porous aggregates capsules showed a more homogeneous behaviour as it shown in Figure 12 bottom.

With these figures can be confirmed that the rejuvenator will be released in both mechanisms, making feasible later the self-healing effect

Table 4. Penetration and Ring&Ball results.

Sample	Penetration			Ring&Ball		
	dm			°C		
	UA	STA	LTA	UA	STA	LTA
1	59	34	17	50.4	56.2	67.8
2	208	116	58	38.6	43.4	51.8
3	77	48	32	50.6	56.1	62.0

Table 5. Penetration Index and Fraass Breaking point results.

Sample	Penetration Index			Fraass		
				°C		
	UA	STA	LTA	UA	STA	LTA
1	-0.7	-0.2	-0.2	-9	-10	-9
2	-0.5	-0.9	-0.4	-14	-12	-12
3	0	0.1	0.4	-9	-10	-10

4.4.2 Ageing tests

A procedure that simulates the short-term aging (occurring during storage, transport, laying and compaction of the mixture) and the long-term aging (oxidative process occurring during the service life of the road) were applied to the samples prepared, both at binder and asphalt mix level.

In a first step, conventional bitumen and bitumen mixed with filled capsules containing rejuvenator were exposed to a Short-Term Ageing test, RTFOT (EN 12607-1) and Long-Term Ageing test, RTFOT + PAV (EN 14769). Once the ageing tests were finished the basic properties of the binders, such as penetration, softening point, Fraass breaking point and SARA (saturates, aromatics, resins and asphaltenes) column chromatography, were analyzed.

The following tables show the results achieved, where samples 1, 2 and 3 correspond to 50/70 bitumen, 50/70 bitumen (80%) + Rejuvenator (20%) and 50/70 bitumen (78%) + Polymeric microcapsules (22%) respectively. Acronyms UA, STA and LTA correspond to Unaged, Short-Term Ageing and Long-Term Ageing.

Results from these tests show that the rejuvenator was released from both porous aggregates and microcapsules mostly during Long-Term Ageing. The penetration and Ring&Ball values showed common results after an ageing process (decrease of penetration grade and increasing of the softening point), while Fraass values remained mostly constant. The SARA analysis also validated these results as the original asphaltenes/maltenes ratio was partially restored, which shows that the binder's chemical composition was mostly recovered. With the sepiolites is difficult

Table 6. SARA column chromatography results.

Sample	Asphaltenes			Saturates		
	%			%		
	UA	STA	LTA	UA	STA	LTA
1	16.8	18.9	21.8	7.3	7.9	9.3
2	13.4	16.2	19.6	7.6	8.1	8.0
3	15.3	17.1	17.5	8.9	9.0	13.4

Table 7. SARA column chromatography results (cont.).

Sample	Napthenes/Aromatics			Polar/Aromatics		
	%			%		
	UA	STA	LTA	UA	STA	LTA
1	41.1	39.4	35.4	34.8	33.8	33.4
2	47.9	48.0	41.7	31.2	27.7	30.7
3	39.4	43.2	42.9	36.5	30.7	26.2

Table 8. Grading curve of the asphalt mix BBTM 11B.

Sieve mm	BBTM 11B % passing
32	100
22	100
16	100
8	97
4	66
2	24
0.5	17
0.25	11
0.063	5

to get any valid results due to their big influence on bitumen rheology.

In a second step, a discontinuous asphalt mix for very thin layers, named as BBTM 11B, was designed with porphyry and silica aggregates. 5% of polymer modified bitumen PMB 45-80/60 was used. Their particle size composition is presented in Table 8.

The total amount of capsules, both porous aggregates and polymeric microcapsules, added to the mix were an equivalent of adding 20% of rejuvenator in relation to the bitumen content. The ageing method proposed was the AASHTO R 30, which consisted on a combination of Short and Long-Term Ageing.

For Short-Term Ageing, the mix was prepared in a mixer and placed in a loose state on tray in a 25 mm thick layer. The tray was kept in a draft oven at 135°C for 4 hours and during that time the mix was mixed four times by hand. After that, the mix was compacted by using a gyratory compactor (EN 12697-31) with 200

Table 9. Water sensitivity and stiffness modulus results.

Sample	Water sensitivity %	Stiffness MPa
Reference	86.88	2736
Reference aged	98.18	3398
Porous aggregates	87.71	2646
Porous aggregates aged	92.76	2823
Polymeric microcapsules	94.60	584
Polymeric microcapsules aged	95.90	1018

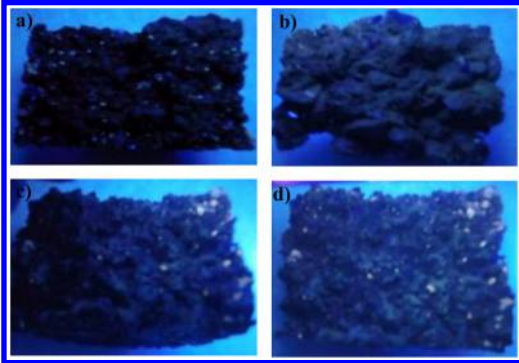


Figure 13. Specimens containing porous aggregates capsules under UV light. (a) reference unaged; (b) reference with rejuvenator; (c) capsules unaged; (d) capsules aged.

cycles. Short-term aged specimens were used later for Long-Term Ageing procedure. For Long-Term Ageing, the specimens were kept in a draft oven at 85°C for five days. After this process the specimens were cooled down for 16 hours. Reference samples (with no ageing process) were also produced in a gyratory compactor with 200 cycles for comparison. Water sensitivity (EN 12697-12) and stiffness modulus (EN 12697-26) tests were carried out in all the samples. Results are shown in Table 9.

From the above results it can be noted that stiffness results were very low for polymeric microcapsules due to the major part of rejuvenator has been released during mixing and compaction process.

It can be also concluded that mechanical properties in unaged samples were mainly conserved for porous aggregates specimens, while for Long-Term ageing procedure stiffness modulus decreased and water sensitivity increased, most probably due to the release of the rejuvenator.

These conclusions can be confirmed in Figure 13, where samples with porous aggregates capsules were broken by indirect tensile test and then examined under UV light in order to evaluate visually the release of rejuvenator. These specimens were compared with those produced with the same mix design (BBTM11B) but adding 20% of rejuvenator directly to the mix. It allowed identifying clearly the rejuvenator from the other components of the asphalt mix (see rejuvenator in green-brown color).

5 CONCLUSIONS

Main conclusions of the study are presented below:

- Embedded capsules containing asphalt rejuvenator are proposed as a promising technique to apply rejuvenator in asphalt mixes in an optimum and efficient way to compensate ageing of asphalt concrete.
- Two encapsulation methods – porous aggregate and polymeric capsule shell – were successfully developed and designed to withstand asphalt mixes working conditions: high production temperatures (170–180°C), the mixing process with aggregates and the compaction process.
- Percentages of impregnation of 40% for the porous aggregates capsules and more than 80% for the polymeric shell capsules were achieved.
- The incorporation of the capsules into the asphalt mixes has some influence on the final properties of the asphalt mixes, especially in terms of water sensitivity and stiffness modulus, which offer lower values than those for the reference samples. No further consequences can be attributed to this fact, as values obtained are within the expected values for this type of asphalt mixtures and meet the requirements for the Spanish specifications.
- According to the results the developed microcapsules can release their active agent by both ways: in response to a stimulus (such as mechanical damage or through a controlled released process) and by diffusion.
- Ageing tests confirm that the rejuvenator can be released when exposed to Long-Term Ageing.
- Bitumen rejuvenator diffusion tests show that the rejuvenator is released from the capsule shell along the time. Extrapolation to quantify the time is needed for the release of the rejuvenator when capsules are exposed to real conditions should be further studied.

ACKNOWLEDGMENTS

The authors acknowledge the financial support from the Centre for Industrial Technological Development (CDTI) of the Spanish Government within the program supporting the Strategic National Consortiums for Technical Investigation (CENIT) through the development of the TRAINER Project, “Development of a new technology for autonomous, intelligent self-healing of materials”.

REFERENCES

- Asphalt Institute. 2013. Asphalt Pavement Distress Summary www.asphaltinstitute.org.
- Blaiszka B.J. 2009. Microcapsules filled with reactive solutions for self-healing materials. *Polymer Volume 50, Issue 4*, 990–997.

- Branthaver, J.F., J.C. Petersen, R.E., J.J. Robertson, Duvall, S.S. Kim, P.M. Harnsberger, T. Mill, E.K. Ensley, F.A. Barbour, J.F. Schabron. 1993, Binder Characterization and Evaluation, Vol. 2: Chemistry, SHRP-A-368, National Research Council, Washington, DC, 1993.
- Boyer R.E. 2000. Asphalt rejuvenators: "Fact, or Fable", in: Transportation Systems 2000 (TS2K) Workshop, San Antonio, Texas.
- Contreras V., Lucio O., Pérez A., Quintero L.C. 2012. Estudio de la difusión de rejuvenecedor en betún por espectroscopia de infrarrojos. VII Jornada Nacional de ASEFMA. Mayo 2012.
- EAPA. 2012. Asphalt Figures 2012.
- European Commission. 2013. Road transport: a change of gear.
- European Road federation. 2012. European Road Statistics Annual Report 2012.
- García A., Schlangen E., van de Ven M., Sierra-Beltrán G. 2010a. Preparation of capsules containing rejuvenators for their use in asphalt concrete. *Journal of Hazardous Materials Volume 184, Issues 1–3*, 603–611.
- García A., Schlangen E., van den Ven M. 2010b. Two ways of closing cracks on asphalt concrete pavements: Microcapsules and Induction Heating. *Key Engineering Materials, Vols. 417–418*, 573–576.
- García A., Schlangen E., van den Ven M. 2010c. Properties of capsules containing rejuvenators for their use in asphalt concrete, *Fuel 90*, 583–591.
- García A. 2012. Self-healing of open cracks in asphalt mastic. *Fuel Volume 93*, Pages 264–272.
- Karlsson R, Isacsson U. 2006. Material-related aspects of asphalt recycling-state of the art. *J. Mater Civil Eng 2006;18(1):81e92*.
- Qiu J., 2012. PhD thesis is "Self Healing of Asphalt Mixes – Towards a better understanding of the mechanism". Tu Delf University 2012.
- Schlangen, E., Sangadji. S. 2013. Addressing Infrastructure Durability and Sustainability by Self Healing Mechanisms. Recent Advances in Self Healing Concrete and Asphalt. *Procedia Engineering Volume 54*, 39–57 The 2nd International Conference on Rehabilitation and Maintenance in Civil Engineering.
- Shen J., Amirkhania S., Aune Miller J. 2007. Effects of rejuvenating agents on superpave mixes containing reclaimed asphalt pavement. *J Mater Civ Eng; 19(5):376–84.1*
- Su, J.F., Schlangen E. 2012. Synthesis and physicochemical properties of high compact microcapsules containing rejuvenator applied in asphalt. *Original Research Article Chemical Engineering Journal, Volumes 198–199*, 289–300.
- Su, J.F., Qiu J., Schlangen E. 2013. Stability investigation of self-healing microcapsules containing rejuvenator for bitumen. *Original Research Article Polymer Degradation and Stability, Volume 98, Issue 6*, 1205–1215.

An experimental investigation on the influence of Hydrated Lime on asphalt mixtures (A case study in Iran)

N. Oroujzadeh

Institute of Chemical Technology, Iranian Research Organization for Science and Technology (IROST), Tehran, Iran

H. Sabbagh

Fouman Chimie Gostar Co., Tehran, Iran

ABSTRACT: Hydrated Lime (HL) has been known as an additive for asphalt mixture durability. It is observed to be the most effective additive when moisture damage becomes one of the most pressing pavement failure modes. Also the use of HL is a recognized way to decrease stripping phenomena on asphalt mixtures. In this research, we aimed to investigate the HL effect by performing laboratory tests on various aggregates and one percent of HL additive to figure out the changes in some principal HMA design factors. Test results have been used in one of the major high way construction projects in Iran (Zanjan-Tabriz highway (section 9)), with aggregates susceptible to premature stripping. Texas boiling water test (ASTM D3625) was used as a primary investigation of aggregate tendency to stripping and Lottman test (AASHTO T283) for examining the indirect tensile strength of asphalt mixtures. Evaluation of asphalt Mixture durability against moisture is done by TSR ratio, MRR and fatigue index. Results in our tests in a real project show the beneficial effects of HL on asphalt mixture durability and stripping Phenomena.

1 INTRODUCTION

The widespread use of asphalt mixtures in transportation system of many countries leads to high attention towards effective parameters and performance on flexible pavements. Studies have shown that selecting appropriate aggregate and other effective parameter results in increasing serviceability life of pavement and decreasing the cost of rehabilitations (Epps et al. 2001). Many researches have done to determine distress reasons and treatment and maintenance methods. Stripping is one of the main distresses that occur in hot mix asphalt pavements. Since stripping is caused by water, it is important to analyze how the asphalt to aggregate interaction changes in the presence of water (Little and Epps 2001). Although cohesion (the bonds between asphalt molecules) plays a part in moisture damage, the emphasis is more on the adhesion (the bonds between asphalt and aggregate) rather than cohesion. Active adhesion is the formation of bonds between asphalt and aggregate in presence of water. In other words, for asphalt to have active adhesion, it should have a higher affinity to the aggregate surface compared to water so that it can displace water from the aggregate surface (MS-4 2007). The standard definition of stripping is the breaking of the bond between asphalt and aggregate by the action of water (Akzo-Nobel Company). Several definitions for stripping have been presented that the definition “the decreasing of adhesion between asphalt cement and

mineral aggregate caused by partition of asphalt coating from aggregate surface in the presence of water” is the best that has been expressed by Hosla. It has been realized that Hydrated lime (HL) is an effective additive for asphalt mixture durability, when moisture damage becomes one of the most pressing pavement failure modes (Little and Epps 2001). In this research, we aimed to investigate the effects of hydrated lime on the strength, quality and composition of hot mix asphalt of Surface and Binder layers at severe humid weather conditions. Laboratory tests were done on various aggregates containing one percent of HL additive to figure out the changes in some principal HMA design factors. Test results have been used in one of the major high way construction projects in Iran (Zanjan-Tabriz highway (section 9)), with aggregates susceptible to premature stripping.

2 MATERIALS

2.1 Aggregates

Aggregates consist of inorganic polar compounds and differ widely in properties. Aggregates such as quartz, granite and sandstone have a high percent of silicon dioxide (SiO₂). The surfaces of these siliceous aggregates have silanol (SiOH) groups, which are weakly acidic. Aggregates such as marble and limestone have a high percent of calcium carbonate in them. Calcium

Table 1. The results of quality experiments on aggregates.

Experiment	Surface ASTM	Unit	Standard
Abrasion by Los Angeles in 500 rpm	C131	%	B/20
Materials weight decrease by sodium sulfate (salt cake)	C88	%	0.3–0.9
Percent of fracture in one front	D5821	%	98
Percent of fracture in two fronts	D5821	%	97
Flakiness	BS812	%	14
Sand	D2419	%	71
Equivalent The maximum size	D8	mm	19
Content of SiO ₂	–	%	62.3

carbonate is a base and this gives a weak basic character to its surface. Thus, the surface of aggregates can be either acidic or basic depending on the composition of the aggregates (MS-4 2007). Also, aggregates chemical composition, mineralogy, surface texture, porosity and shape can be effective on the adhesion quality of aggregate to asphalt thin film (Bagampadde et al. 2006, Masad et al. 2006). Aggregates used in asphalt mixture layers should absorb asphalt binder as well as possible so that aggregate particles hold each other and the mix become stable. Whatever the asphalt film adhere better to the aggregate particles, the pavement structure will be more stable and its stability and durability increases, so mineral aggregates play the main role in asphalt. In addition to the concern that dust weakens asphalt to aggregate bonds (adhesion), there is also concern that clay promotes the inclusion of water within the mixture, leading to weakened asphalt to asphalt bonds (cohesion). Plastic fines are another way to describe the clay present in an aggregate. The amount of plastic fines or clay can be inferred from the plasticity index (PI) (MS-4 2007).

In this case study, the crashed siliceous aggregates with the properties presented in Tables 1 and 2, have been used. With respect to utilization of these aggregate in Surface layer, Sieve test result are presented in Table 3.

2.2 Bitumen

Bitumen is a mixture of many organic compounds which are mostly hydrocarbons varying widely in structure and molecular weight (Morgan and Mulder 1995). It is oily nonpolar material in comparison to

Table 2. Aggregate properties value in project.

Test	Coarse Aggregate	Fine Aggregate	Filler	HL
Apparent Specific gravity, kg/cm ³	2.534	2.553	2.738	2.442
ASTM C128				
Water absorption, %	1.1	1.4	–	–
ASTM C127				

Table 3. Sieve test result.

Surface layer		
Seive size (mm)	Passing Percent	Accepted range
19	100	100
12.5	95	90–100
4.75	64	44–74
2.36	42	28–58
0.3	13	5–21
0.075	6.1	2–10

inorganic material such as aggregates. In addition to hydrocarbons, bitumen also contains certain amounts of polar organic compounds. Adhesion between bitumen and aggregate particles is a result of linkage between bitumen polar compounds and aggregates polar surface. Whereas bitumen is affected by the environment conditions, only the bitumen polarity is not adequate for good adhesion in the mixture (Robertson 2000). Also, high level of water can infiltrate in to the bitumen film and mainly change the bitumen rheological properties (Cheng et al. 2002). In this research project, the AC 85-100 bitumen of Tabriz refinery is used and its properties are presented in Table 4.

2.3 Filler

If it is inevitable to use aggregates susceptible to stripping, it is necessary to use anti-stripping agents in asphalt mixture to reduce the risk of stripping.

With respect to the severe humid weather conditions associated with this project (Tabriz-Zanjan freeway (section 9)), we had the two options: 1) treatment with liquid anti-stripping additive 2) treatment with active fillers such as hydrated lime, cement to decrease the risk of stripping damage in this project. So laboratory tests were necessary to indicate that the selected option will be beneficial for decreasing the risk of stripping. Liquid anti-stripping additives and lime are used generally. If it is not necessary to use these additives or if they use mistakenly, it may have negative effects on pavement performance. To obtain proper results, it's

Table 4. The properties of pure asphalt (Type of asphalt: 85–100 Tabriz petroleum).

Test	Standard	Result
Specific Gravity	ASTM D70	0.99
Loss of Weight	ASTM D1754	0.4%
Penetration	ASTM D5	90 dmm
Softening point	ASTM D36	49.0°C
Viscosity in 3 Temp. (cst)	ASTM D2170	(At 120°C) 1081 (At 120°C) 555 (At 120°C) 237
PI (Penetration index)		0.08
PVN (Pen. Viscosity number)		0.15

necessary to use actual bitumen and aggregate samples during laboratory tests. One of the most prevalent anti-stripping additives is hydrated lime that effectively decreases asphalt mixtures stripping susceptibility. Hydrated lime can improve aggregates surface chemical properties (Little and Epps 2001). Lime as a multipurpose additive in addition to reducing moisture susceptibility and its ability in controlling stripping, can decrease rutting and cracking and increase durability and strength against oxidation and aging (Little and Epps 2001).

The mechanism of lime is not well known. However lime addition for minimizing moisture susceptibility in asphalt mixtures is an accepted alternative. Lime is available in different forms which from hydrated lime (CaOH_2) and active lime (CaO) are effective for avoiding stripping of asphalt mixtures; nevertheless the first one is more prevalent. With respect to effectiveness and accessibility of hydrated lime, this material was used in Tabriz-Zanjan freeway project to prevent stripping of aggregates. The required amount of hydrated lime to decrease moisture susceptibility is equal to 1.0% of the dry aggregates weight. Adding hydrated lime to hot mix asphalt mixtures usually increases the optimum asphalt content by 0.1–0.3 percents.

3 EXPERIMENTAL TEST

Texas boiling water test (ASTM D3625) was used as a primary investigation of aggregate tendency to stripping and Lottman test (AASHTO T283) for examining the indirect tensile strength of asphalt mixtures. Then, Evaluation of asphalt Mixture durability against moisture is done by TSR (tensile strength ratio), MRR (modulus resilient ratio) and fatigue index.

3.1 Experimental test result

In this research, Marshall Specimens were prepared according to ASTM D1559 test method. Mixing and compaction temperatures for asphalt mixtures

Table 5. Compaction and mixing temperature.

Type of Layer	Mixing Range Temperature	Compaction Range Temperature	Compaction Effort in $7 \pm 1\%$ Voids
Surface	152–157°C	140–146°C	42 blows
Asphalt Institute Recommendations for viscosity	170 ± 20 centistokes	280 ± 30 centistokes	–

Table 6. Texas boiling test (ASTM D3625).

Layer Type	Result
Surface	Between 15 to 20%
Surface Modified	Between 5 to 10%

of Surface layer were determined using viscosity-temperature curves of bitumen as presented in Table 5.

Tests for evaluating bituminous mixtures are classified in two groups: test on loose (uncompacted) mix and test on compacted mix. Test on uncompacted asphalt mixtures are suitable for bitumen coated aggregates in presence of water. The main advantages of this test are simplicity, inexpensiveness. In this project, the boiling water test according to ASTM D3625 standard test method was used for evaluating the effects of hydrated lime on hot mix asphalt production process. In this test, loose mix is placed in boiling water for 10 minutes. Then visual observation is made of retained bitumen coating on the aggregate. The results of this test are presented in Table 6.

Evaluating compacted asphalt mixtures strength against moisture damage according to AASHTO T283 standard test method, is the most prevalent test method for determining hot mix asphalt moisture susceptibility. This test is a combination of Lottman, Tunnicliff and Root test methods and is similar to Lottman test method. Modified Lottman test procedure determines indirect tensile strength ratio, TSR. This is the ratio of the average tensile strength of the conditioned samples divided by the average tensile strength of the unconditioned samples. AASHTO T283 allows specimens that are compacted using Marshall Apparatus, California Kneading Compactor, Superpave Gyrotory Compactor, or U.S. Corps of Engineers Gyrotory Testing Machine. The minimum allowable tensile strength ratio is 0.7 (Roberts et al. 1996). Nevertheless, the proposed minimum ratio is considered as 0.8. The test results of Surface layer asphalt mixture either containing or not containing the lime are presented in Table 7.

For further assessment and evaluation of hydrated lime effects, the Marshall Stability test was performed according to ASTM D1075 (AASHTO T165) standard

Table 7. Test results of TSR value.

Layer		Surface		Surface Modified	
		Dry	Sat.	Dry	Sat.
Optimum bitumen %		5.4		5.5	
Situation		Dry	Sat.	Dry	Sat.
Lottman	Specific Weight	2177	2187	2198	2203
AASHTO T283	Void%	7.0	7.1	7.6	7.4
	Saturation %	66		62	
	ITS (kPa)	353	215	380	315
	TSR%	61		83	

Table 8. Test results of Marshall

Layer		Surface		Surface Modified	
		Dry	Sat.	Dry	Sat.
Situation		Dry	Sat.	Dry	Sat.
Marshal Result	Specific Weight (kg/m ³)	2249	2264	2263	2270
	Stability (kgN)	1238	941	1112	998
	Saturated/Dry Ratio	76		90	
	Flow (0.25 mm)	13.6	13.9	12.2	12.5
	Marshall Quotient (Q)	3.57	2.66	3.58	3.13

test method. Preparing and conditioning procedures for specimens are similar to immersed compression test, but the Marshall stability is determined instead of compressive strength in this test (Solaimanian et al. 2003). The test results of Surface layers asphalt mixture either containing (Surface Modified) or not containing the lime are presented in Table 8.

As it is obvious in Table 8, specific gravity of modified specimens for Surface is increased and Marshall Stability ratio is increased more than 20 percent compared to not modified mixtures. Also, with respect to the minimum allowable Marshall Stability and acceptable flow ranges in Iranian regulation, the “Q” parameter should be greater than 2.68. According to the data presented in table 8, the “Q” parameter after adjustment has an ascending trend.

To analyze accurately the effects of adding lime in order to improve performance properties of asphalt mixtures, performance tests using UTM (universal test machine) apparatus were performed (Roberts et al. 1996). Fatigue performance of asphalt mixtures was analyzed via performing indirect tensile fatigue tests to predict asphalt mixtures strength against cracking. This test was performed at three stress levels according to Table 9.

As it can be seen, increasing the stress level, increases the damages of pavement by fatigue mechanism, but the number of load repetition for fatigue destruction of asphalt pavements with hydrated

Table 9. Fatigue test result.

Stress (kPa)	Number of Load Repeation to Failure	
	Surface	Modified Surface
55623	27790	55623
22261	17658	22261
6103	2461	6103

Table 10. Resilient modulus ASTM D4123.

Layer Type	Height (mm)	Resilient Modulus (MPa)	Deformation (μm)
Surface	69.6	1011	12.1
Surface Modified	70.3	1652	10.6

Table 11. Rilient modulus ASTM D4123.

Layer type	Situation	Height (mm)	Resilient Modulus (MPa)		Deformation (μm)	MRR
			Surface	Modified		
Surface	Dry	72.3	1119	8.66	8.66	0.27
	Saturated	74.1	301	24.13		
Surface Modified	Dry	73.8	1988	7.45	7.45	0.51
	Saturated	74.0	1005	13.22		

lime is increased that lead to increasing in pavement serviceability life.

In order to survey the effects of lime addition on asphalt mixtures resilient modulus, indirect tensile test according to ASTM D4123 was performed on compacted specimens. This test was performed at 25 Celsius with a load amplitude of 200 N per centimeters of specimen height at a frequency of 0.5 Hz. The loading width and pulse width were 100 ms and 1000 ms, respectively. The results of this test are presented in Table 10.

As it can be seen in Table 10, the lime causes increase in resilient modulus and decrease in deformation of Surface layer asphalt mixtures.

Not only moisture damage is an independent distress, but also can lead to other early and premature distresses such as Thermal cracking, rutting, raveling, potholes and alligator cracking. Therefore, in order to assess the structural capacity and performance of pavement at project site moisture conditions, beside the TSR ratio, MRR was determined. This index is the ratio of saturated resilient modulus to dry resilient modulus which is related to the samples prepared by AASHTO 283 procedure. The minimum allowable resilient modulus ratio is 0.7 [2]. The laboratory test results of this ratio are presented in Table 11.

4 CONCLUSIONS

Following results are obtained from the study of hydrated lime addition effects in Surface layer asphalt mixture of Tabriz-Zanjan freeway (section 9) project:

1. According to Texas Boiling Water test results, hydrated lime addition resulted in stripping reduction.
2. According to Modified Lottman test results, hydrated lime addition resulted in increasing of indirect tensile strength (ITS) of lime modified mixtures. Also, TSR index was increased and its value for Surface layer asphalt mixture became more than 80%.
3. For further assessment and evaluation of hydrated lime effects, the Marshall Stability test was performed according to ASTM D1075 (AASHTO T165) standard test method. Marshall Stability ratio is increased more than 20 percent compared to not-modified mixtures and the “Q” parameter after lime treatment had an ascending trend.
4. Increasing hydrated lime content in hot mix asphalt production resulted in decline of moisture susceptibility and increase of strength.
5. To analyze accurately the effects of adding lime in order to improve performance properties of asphalt mixtures, performance tests using UTM apparatus were performed. Increasing the stress level, increased the damages of specimens by fatigue mechanism, but the number of load repetition for fatigue destruction of asphalt specimens with hydrated lime was increased that lead to increasing in pavement serviceability life.
6. The lime causes increase in resilient modulus and decrease in deformation of Surface layer asphalt mixtures
7. In order to assess the structural capacity and performance of pavements at project site moisture conditions, beside the TSR ratio, MRR ratio was determined. The results show that lime treatment increases MRR index.
8. With regard to the following [Table 12](#), we can see the variations in results of Surface layer asphalt mixture:

Table 12. Variation in results.

Layer	Texas boiling	TSR	Marshall Stability ratio	Q	Fatigue Resistance	MRR
Surface	↑	↑	↑	↑	↑	↑

REFERENCES

- Akzo – Nobel Company.
- Bagampadde U. Isacson U. and Kiggundu B.M., “Impact of Bitumen and Aggregate Composition on Stripping in Bituminous Mixtures” *Materials and Structures*, Vol. 39, 2006, pp. 303–315.
- Cheng, D., D.N. Little; R.L. Lytton, and J.C. Holtse, “Use of Surface Free Energy Properties of Asphalt – Aggregate System To Predict Damage Potential”, *Proceedings, Association of Asphalt Paving Technologists*, Vol. 71, 2002, pp. 59–88.
- Epps, J.; Sebaaly, Peter; Penaranda, Jorge; Maher, Michele; McCann, Martin; and Hand Adam. NCHRP 444: Compatibility of a Test for Moisture – Induced Damage with Superpave Volumetric Mix Design. Transportation Research Board, National Highway Research Council, Washington, D.C. 2000.
- Little, D.N. and Epps, J.A., “The Benefits of Hydrated Lime in Hot Mix Asphalt”, Report for National Lime Association, The Versatile Chemical, 2001.
- MS-24, 2007.
- Masad, E.C. Zolinger, R. Bulut, d.n. Little and R.L. Lytton, “Charaterization of HMA Moisture Damage Using Surface Energy and Fracture Properties”, *Asphalt Paving Technology: Association of Asphalt Technologists- Proceedings of the Technical Sessions*. 75, 2006.
- Morgan, P. and Mulder, A., “The Shell Bitumen Industrial Handbook”, Shell Bitumen, Surrey, United Kingdom, 1995.
- Robertson, R.E. Transportation Research Circular Number 499, “Chemical Properties of Asphalts and Their Effects on Pavement Performance”, Transportation Research Board, Washington, D.C. 2000.
- Roberts, F., P.Kandhal, E. Brown, D. Lee, and T. Kennedy, *Hot Mix Asphalt Materials, Mixture Design, and Construction* “2nd edition, Lanham, Maryland: NAPA Education Foundation, 1996.
- Solaimanian, M.J. Harvey, M. Tahmoressi and V. Tandon, “Test Methods to Predict Moisture Sensitivity of Hot-Mix Asphalt Pavements” *Moisture Sensitivity of Asphalt Pavements: A National Seminar*, San Diego, CA, Transportation Research Board, 2003.
- Sabbagh, H.M, P. Hayati, A. Kavussi “Evaluation of Hydrated Lime Effects on Asphalt Mixture Durability against Moisture: A Case Study in Iran” *5th Euroasphalt & Eurobitume Istanbul* 2012.

Preliminary evaluation of the effects of lime on stone mastic asphalt mixtures workability

G. Betti, U. Pinori & A. Marradi

Department of Civil and Industrial Engineering, University of Pisa, Italy

ABSTRACT: The main aim of the present research activity is to study the effect of lime in the prevention of binder drain down of SMA (Stone Mastic Asphalt) mixtures during the working process. Mixtures with high binder content are usually mixed with different types of fibers (cellulose fibers, glass fibers etc.), working as an additive able to prevent the binder drainage during production, transport and laying of mixtures. Hydrated lime is known to be more than just a moisture damage additive: it is to be considered an active filler able to create strong interactions between the aggregate and the bitumen. On the other hand, from a general point of view, filler markedly affect behavior of asphalt binder in HMA mixtures; typically, an increase in filler increase the optimum asphalt content, increase the density and increase the stability. Conversely, an excessive amount of filler in the mix could negatively increase the stiffness of the mix and the aggregate surface area thus reducing the asphalt film thickness. Hydrated Lime modifies the surface properties of the aggregate, allowing for the development of surface roughness more favorable to bitumen adhesion. This study address for evaluation of the effects of fiber replacement with lime for production of SMA mixtures; assessment will be mostly based on results of drainage tests. An optimization of the amount of lime to be added to the mix has been performed in order to reduce the binder drainage until values typically provided by the use of cellulose fibers. Moreover, volumetric and mechanical properties have been evaluated in order study the effect of lime on performances of optimized mixtures. Results appear to be promising regarding the possibility to replace cellulose fibers with hydrated lime.

1 OVERVIEW OF THE EFFECT OF LIME IN HOT MIX ASPHALT

Thanks to the intensive use that is being made in the last 40 years in the USA hydrated lime is known to be more of an additive against moisture damage, it is also considered an “active filler” that reduces the chemical aging of the bitumen and provide higher stiffness to high temperature compared to traditional filler (Lesuer et al. 2012).

Within the European area the use of lime seems to experience a significant expansion growing: results of different researches activities confirm the multiple benefits provided by the use of “filler mixed” as a solution to achieve high performance and long durable pavements (Little D. et al. 1999). These positives results led several European countries to introduce the hydrated lime in the standard specification of roads construction making the use of lime in asphalt mixtures mandatory.

The hydrated lime is mainly composed of calcium hydroxide $\text{Ca}(\text{OH})_2$, obtained by hydration of calcium oxide CaO known as “quicklime” (EN 459-1). For the purpose of asphalt mixtures production, the most widely used is the high-purity lime (CL 90 S in the EN 459-1 or ASTM C 1097 or Type I in AASHTO M 303).

Hydrated lime is generally provided in the form of white powder, with a dry absolute density ranging between $2.2\text{--}2.4\text{ g/cm}^3$, an apparent density of about $300\text{--}800\text{ kg/m}^3$ and a high level of porosity, close to 50%.

Because of its mineral origin and of its dustiness, the effect of using hydrated lime is generally compared with those provided by the traditional fillers; as a matter of fact the European standards for hot mixtures (EN 13108-1–13108-7) clearly state that “cement and hydrated lime are considered filler materials”. The EN standards mainly rank the properties of filler in terms of stiffening effect on the bitumen, particularly the voids in dry compacted filler (EN 1097-4 “Rigden air voids”) and the range of temperatures relative to the delta ring and ball test (EN 13179-1). For instance, while most of the limestone fillers have a value of Rigden voids of 30–34%, the hydrated lime has a value of 65–70%.

The addition of lime to asphalt mixtures can be provided in different manners: dry lime can be added in the mixer drum during the bitumen spreading or preliminarily added to the aggregates making them “marinate” for a few days.

Based on field experiences (Aschenbrener, T. et al, Collins, R. and Little, D.), the benefits provided by

the use of hydrated lime in terms of asphalt mixtures durability can be summarized as follow:

- increase the resistance to moisture-frost damages;
- increase the resistance of bitumen to the chemical aging;
- increase mechanical properties (stiffness, rutting resistance, fatigue resistance, thermal cracking resistance).

All those benefits led to assume (Lesueur et al. 2012) the use of 1–1.5% of lime (by the weight of dry aggregates) increases the durability of the mixture by 2–10 years, which generally corresponds to 10–50% of pavement life;

The reasons for such an increased durability is mainly due to the effects of the interaction of lime with both aggregates and bitumen (Lesueur et al. 2012):

- hydrated lime modifies the surface properties of aggregates, allowing for the development of surface composition and roughness more favorable to bitumen adhesion promoting a stronger adhesion with bitumen;
- hydrated lime allows the flocculation of any clay particle in the aggregates mix, preventing them from formation of a water-displaceable barrier between the bitumen and aggregates;
- bitumen modification which include a reduction of chemical aging and a physical effect due to its high porosity;
- bitumen recovered from filed cores containing hydrated lime shows a significantly lower viscosity. This is due to the reduction of the long term binder hardening as a results of oxidation process, improving the fatigue and thermal cracking resistance;

All the findings previously reported led to consider the hydrated lime a multifunctional additive able to improve the durability of asphalt mixtures, increase the mastic stiffness above room temperature and reduce brittleness at low temperature. Those properties appear to be extremely important for asphalt wearing courses due to their direct exposure to weather agents like rainfall frost and high temperature.

2 AIM OF THE RESERCH

The main aim of the research is to study the effect of hydrated lime (HL) on modifying the adhesion between aggregates and binder in SMA mixtures, mostly in terms of binder drain-down prevention during working process. Results have been compared with those obtained on the same type of mixtures made using cellulose fibers, assumed as the reference mixture. Totally 3 different recipes of SMA mixtures have been analyzed, with different amount of lime, in order to provide an optimization of mixtures behavior in terms of binder draindown. Mixture with fiber is still considered the reference mixture. The optimized SMA mixture has been further analyzed to study its volumetric and mechanical properties, comparing

results with those obtained on mixture made using fibers. The basic idea was to investigate if the use of lime can cause a negative change in the mixture performance with respect to those of mixture with fibers.

The primary aims of the present research activities can be summarized as follow:

- Evaluate the effects of fibers replacement with hydrated lime for production of SMA mixtures;
- Provide an optimization of the amount of lime to be added to the mix to prevent excessive binder drainage (let the mixtures behave like the ones produced using fibers);
- Compare volumetric and mechanical properties of mixture with lime with those of mixture with fibers.

In the next pages a description of the materials used is provided together with discussion on the results obtained.

3 MATERIALS AND METHOD

SMA mixtures are usually used as wearing course in order to provide additional benefits to the pavement structural and functional performances than traditional mixtures. Due to the high binder content and low amount of sand particles, it is usually mixed with different types of fibers (cellulose fibers, glass fibers, etc.) aiming to reduce the amount of binder drainage during production, transport and lying process. From a general point of view, the use of cellulose fibers allows the thickening of bitumen film around aggregates, increasing the mixture workability and durability. The typical amount of fibers commonly used for asphalt concrete production range between 0.3% and 0.5% by the weight of dry aggregates, depending on types of fibers and mixture characteristics.

Different SMA mixtures have been analyzed, both with fibers and different amount of lime, to evaluate the effect of fiber replacement with lime in terms of binder draining characteristics. Mixture with fiber is still considered the reference mixture.

All the tested mixtures are made with the same types of aggregates and amount of bitumen, having the following characteristics:

- Grade bitumen (pen 50–70 dmm);
- Quarried basaltic aggregates;
- High purity lime CL 90;
- Cellulose fibers ARBOCELL ZZ 8/1.

To overcome problems related to mixtures optimization in terms of aggregates distribution and amount of binder needed, a standard mixtures usually used for roadwork in Italy have been assumed. To confirm this assumption a comparison of studied mixtures particle size distribution have been made with the gradation band provided by the Italian Ministry of Transportation (Figure 2).

The amount of binder used is 5.5% (percentage on dry aggregates) and the total amount of filler in the



Figure 1. Picture of the materials used.

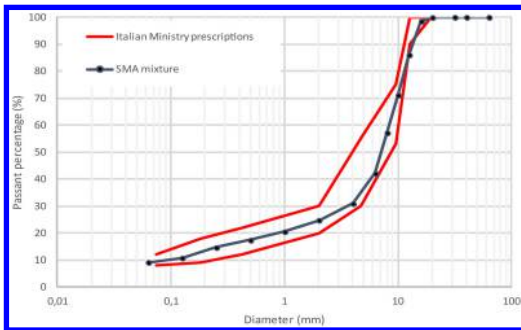


Figure 2. Grain size distribution of study mixture plotted together with the gradation band provided by the Italian Ministry of Transportation.

mix is 9.0%. Fibers are used at 0.3% on the weight of dry aggregates.

The addition of lime consisting in the replacement of part of the total amount of filler with lime. More deeply, mixtures with lime have been made replacing the 20% and 40% of the total amount of mineral filler with lime. The resulting frame of studied mixtures are reported in the subsequent Table 1 and Table 2.

A preliminary phase of the research involved the comparison of cellulose fibers and glass fibers in terms of binder drainage performances. Results obtained have suggested to proceed the research activity using only cellulose fibers and to consider SMA mixtures with cellulose fibers as the reference mixture. For this

Table 1. Coarse and fine aggregate in the mixtures.

Mix N°	Basalt 4/8 (%)	Basalt 8/12 (%)	Basalt 12/20 (%)	Basaltic sand (%)
1,2,3,4,5	19	32	20	20

Table 2. General frame of studied mixtures.

Mix N°	mineral filler (%)	cellulose fibers	glass/cellulose fibers	HL	bitumen (%)
1	9.0	0.3%	NO	NO	5.5
3	5.4	NO	NO	3.6 (40% of filler)	
4	7.2	NO	NO	1.8 (20% of filler)	
5	9.0	NO	NO	NO	



Figure 3. Mix N°1.



Figure 4. Mix N°3.

reasons, results from Mix N°2 (with glass fibers) 1 are not reported in the present paper.

Some pictures of the different mixtures analyzed are reported in Figure 3–6.



Figure 5. Mix N°4.



Figure 6. Mix N°5.

The aims of the research have been reached through a specific program of laboratory test. Firstly, the mixtures performances in terms of binder drainage have been evaluated by means of Schellenberg test, following prescriptions provided by UNI EN 12697-18 Standard Specification. Samples were prepared according to the UNI EN 12697-35; the use of a standard grade bitumen (pen 50–70 dmm) involve the need to heat the aggregates and binder to 150°C before proceeding to the mixing process.

The binder drainage test principle regards the amount of bitumen lost by drainage, after 1 hour at a temperature representative for the maximum temperature expected at the mixing plant; the percentage of bitumen lost can be calculated as the residue left on a beaker containing the mixture after it has been upturned. For standard grade bitumen test temperature is prescribed as the mixing temperature reported by UNI EN 12697-35 plus 25°C. After upturning, if the mass of the residue in the baker is higher than 0.5% of the original mixture mass, (and it is obviously not only drained binder, but mortar and/or aggregate particles), the remaining material must be washed with solvent over a 1 mm sieve, dried and the material on the sieve must be weighted to the nearest 0.1 g. For

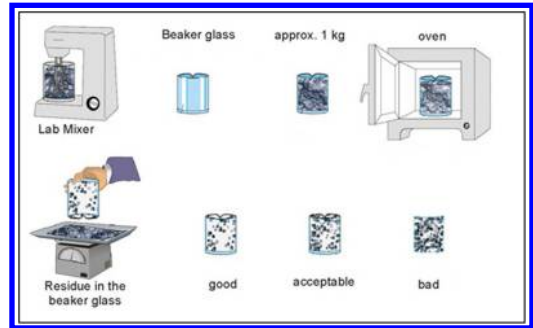


Figure 7. Schellenberg testing procedure.

each mixture, the drained materials D and, if applicable, the residue R over the 1 mm sieve, are calculated using the following equations:

$$D = 100 \cdot \frac{(W_3 - W_1 - W_4)}{(W_2 - W_1)} \quad (1)$$

$$R = 100 \cdot \frac{W_4}{(W_2 - W_1)} \quad (2)$$

where:

- D drained material, in percent (%);
- R residue on the sieve, in percent (%);
- W1 mass of the empty beaker, in grams (g);
- W2 mass of the beaker plus batch, in grams (g);
- W3 mass of the beaker plus retained material after upturning, in grams (g);
- W4 mass of the dried residue retained on the sieve, in grams (g)

A scheme of the Schellenberg testing procedure is reported in Figure 7.

According to literature, the amount of binder drained is recommended not to exceed a threshold value of 0.3%; from a practical point of view, mixtures with drainage values higher than 1% still exhibit a satisfactory behavior.

Once evaluated the mixtures performances in terms of binder drain down further tests have been carried in order to evaluate the effect of using lime on mixture workability and mechanical properties. Only the mixture showing the closer performance to the one of mixture with fiber were analyzed. More details about that will be provided during the discussion of the results obtained. It worth noting that, to completely characterize the mixtures behavior not only in terms of binder drainage, additional tests are needed to investigate any possible changes in the mixtures performances due the extensive use of lime as filler. The basic idea is to compare results obtained with those ones of a mixture made with cellulose fibers, considered as the reference mixture, to underline if any differences appears and if these can be considered positive or negative regarding the performances of the mixtures in terms of workability and mechanical properties.

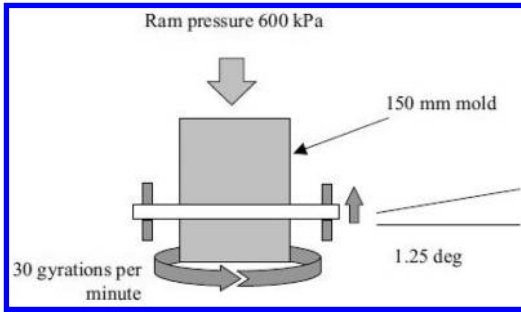


Figure 8. Gyratory compaction tests setting.

Mixtures workability mainly refers to the ability of the mixture to be worked and laid uniformly and the ability of the mixture to be properly compacted. Although in the practice both these aspects contribute to define the quality of asphalt layers, through laboratory tests is only possible to evaluate the second property, often reported as mixture compactability. This kind of property have been evaluated using data recorded during laboratory compaction by means of gyratory compaction. The compaction parameter were assumed to be as the one provided by the technical specifications actually used for road construction in Italy. A vertical pressure of 600 kPa was used with specimens 150 mm width. Compaction speed was set to 30 rotation/minute with a fix revolution angle of 1.25 degree (Figure 8) until reaching 130 rotation. Height of the specimen is recorded for each rotation. The compaction temperature was chose according to the UNI EN 12697-31 Standard Specification.

Knowing the weight of the specimen, the volumetric properties of the mixtures can be calculated for each rotation. Results obtained were also compared with requirement provided by the Italian Ministry of Transportation Technical Specification.

On the top of the specimen a Gyratory Load Plate Assembly (GLPA) was placed in order to evaluate the shear characteristics of the mixtures. The Gyratory Load Plate Assembly (GLPA) developed at the University of Wisconsin – Madison (Figure 9) is one of the most used equipment for the purpose of evaluating key compaction parameter. This device includes three load cells offset by 120° to dynamically measure the forces present during compaction and can be placed in the compaction mold. It offers insight into the gyratory shear properties of hot mix asphalt (HMA) as well as the load induced on the SGC itself during compaction. The resistance of the mix to the compactive effort that is being applied to the sample is measured as a means of determining how difficult a mix is to compact.

The load-cells allow measuring the variation of forces on top of the sample during gyration such that the position or eccentricity of the resultant force from the gyratory compactor can be determined in real time. The two dimensional distributions of the eccentricity of the resultant force can be used to calculate the effective moment required to overcome the internal



Figure 9. Gyratory load plate assembly.

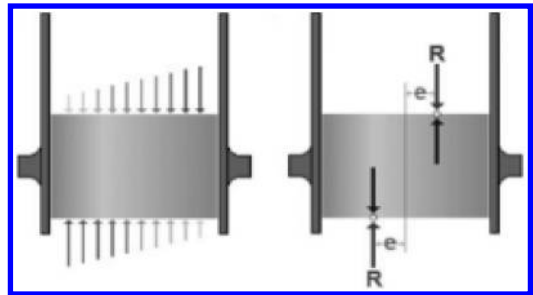


Figure 10. Distribution of compaction forces during compaction.

shear frictional resistance of mixtures when tilting the mold to conform to the 1.25 degree angle.

The data acquired from the GLPA can be interpreted in different ways. In the present study the SS (Shear Stress), one of the main outcomes of the GLPA, was used. Shear Stress can be considered a measure of the mixture resistance to compaction and can be calculated using following equation:

$$SS = \frac{R \cdot e}{A \cdot h} \quad (3)$$

where:

- SS Shear Strength [kN/m²];
- R load applied [kN];
- E load eccentricity [m²];
- A specimen's transversal section area [m²];
- H height of the specimen [m²].

To evaluate the mixtures mechanical properties indirect tensile strength, stiffness modulus tests and fatigue test have been carried out. Those tests were aimed to investigate any negative effects on mixtures mechanical properties related to the use of lime to replace a large part of mineral filler (as reported below, mixture 3 is made replacing 40% of the total filler with lime). Indeed, as reported in literature, an excessive amount of filler in the mixture could negatively increase the mastic stiffness and the aggregate specific surface thus reducing the asphalt film thickness.

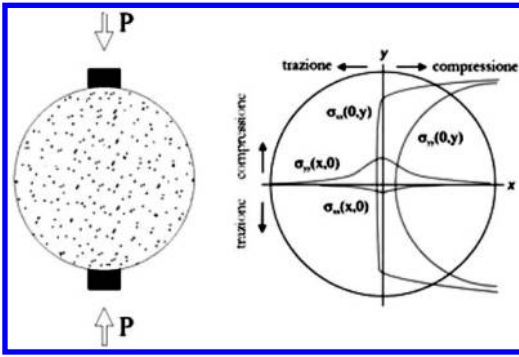


Figure 11. ITS breaking mechanism.

The indirect tensile tests is one the most common used for the mechanical characterization of a bituminous mixture. In this test a cylindrical specimen to be tested is brought to the specified test temperature, placed in the compression testing machine between the loading strips, and loaded diametrically along the direction of the cylinder axis with a constant speed of displacement until it breaks. The indirect tensile strength is the maximum tensile stress calculated from the peak load applied at break and the dimensions of the specimen.

In the present study ITS tests have been carried out following specification provided by the UNI EN 12697-23 standard. Test temperature was 25°C and specimen diameter was 150 mm.

The indirect tensile strength (ITS) is the maximum tensile stress experienced at break and can be calculated following equation hereinafter reported:

Where:

P maximum load applied to the specimen [N];

D diameter of specimen [mm];

h height of the specimen [mm].

Data recorded during the test can also be used to calculate the Indirect Tensile Coefficient (ITC), given by:

$$ITC = \frac{\pi D \cdot ITS}{2\varepsilon} \quad (5)$$

where ε is the vertical displacement [mm] at the breakage. This parameter measures the capability of the specimen deform itself before failure and is often considered an index of the mixture stiffness.

In the present study, specimens subjected to ITS test were previously compacted with 100 rotation to comply with the Italian technical specification.

The stiffness modulus S_m was introduced by the research SHRP (Strategic Highway Research Program) in order to have a mechanical parameter that can be easily determined and able to characterize the stiffness of the bituminous mixtures using a constitutive relation. This is the most common method for measuring stiffness modulus for HMA.



Figure 12. Specimen configuration under stiffness tests.

In this research, the stiffness modulus was evaluated following prescriptions provided by the standard UNI EN 12697-26 (Test methods for hot mix asphalt – Stiffness, Appendix C “Test applying indirect tension to cylindrical specimens IT-CY”), applying to the specimens a vertical loads and measuring the corresponding horizontal deformations.

Stiffness modulus of study mixtures was determined at a temperature of 20°C on cylindrical specimens previously compacted with 50 rotation in order to reach the design density.

Fatigue tests have been carried out on the same specimen used to perform stiffness modulus tests, following prescriptions provided by the UNI EN 12697-24 (Section E, IT-CY load configuration).

In fatigue tests, a cylindrical specimen is subjected to impulsive compressive loads with a sinusoidal wave shape. These loads develop a relatively uniform tensile stress which causes the breakage of the specimen by means of crack along the central part of the vertical diameter. The fatigue resistance is defined as the total number of load applications before the specimen breakage occurs.

Tests were undertaken at 20°C, applying three different load levels. During the test, the load and the horizontal deformation are continuously monitored and recorded at preselected intervals. When evident cracks appear on the vertical axis of the specimen, the test procedure can be concluded.

The material fatigue resistance is determined as the relationship between the logarithmic number of load applications and the initial horizontal deformation.

A complete discussion of the results obtained and their possible usefulness in the common practice is reported in the subsequent chapter.

4 RESULTS AND DISCUSSIONS

Results of Schellenberg tests carried out on the previous described SMA mixtures are reported in the subsequent table where $D_m(\%)$ is the percentage of binder drained during the test.

Table 3. Results of drainage test.

Mix N°	mineral filler (%)	cellulose fibers	HL	bitumen (%)	D _m (%)
1	9.0	YES	NO	5.5	0.06
3	5.4	NO	3.6 (40% of filler)		0.02
4	7.2	NO	1.8 (20% of filler)		0.17
5	9.0	NO	NO		0.39



Figure 13. Picture of the beaker after the test (Mix 1).

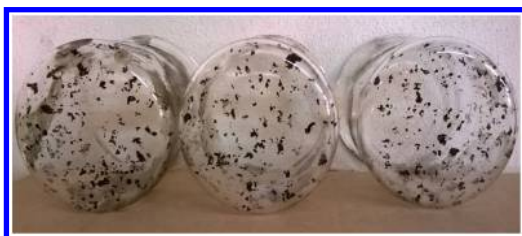


Figure 14. Picture of the beaker after the test (Mix 3)

Values of D_m(%) confirm that using lime, both replacing the 20% and the 40% of the total amount of filler, is possible to comply with the threshold value of 0.3%. Moreover, comparing the results obtained on mixtures with 40% of lime (Mix 3) and mixture with cellulose fibers (Mix 1) no significance differences appear. These results can be confirmed looking at the pictures taken at the end of the test on the bottom of the beaker.

In order to further evaluate the bitumen drainage behavior of SMA produced using HL, some characteristics were changed in the original mixtures and a new cycle of tests was performed. In particular, mixture 6 with 30% of lime was added and mixture 1 (→1*), 3 (→3*) and 5 (→5*) were modified by raising the amount of bitumen up to 6%, to underline the influence of the lime on binder drainage. This approach can be considered, from a general point of view, a sort of stress test regarding the drainage characteristics of SMA mixtures. For this reason, results obtained should be considered only for a relative comparison because they are obtained on non-optimized SMA mixtures.

Results reported in Table 3 underline that, with the same binder percentage, the mixture with 30% of lime shows an intermediate drainage between mixtures 3

Table 4. Results of drainage test.

Mix N°	mineral filler (%)	cellulose fibers	HL	bitumen (%)	D _m (%)
1*	9.0	YES	NO	6	0.07
3*	5.4	NO	3.6 (40% of filler)		0.09
5*	9.0	NO	NO		1.44
6	6.3	NO	2.7 (30% of filler)	5.5	0.12



Figure 15. Picture of the beaker after the test (Mix 3*).



Figure 16. Picture of the beaker after the test (Mix 5*).

(40% of lime) and 4 (20% of lime). Moreover, increasing the amount of binder used, in the mixture 1 the difference in terms of bitumen drainage is almost negligible, demonstrating the good quality of the fibers selected for the research.

The differences found analyzing results of mixture 3 and 3* appear to be more consistent. On the other side the result obtained with 6% bitumen is still far away from the 0.3% limit and next to 1%. It worth noting that the optimum binder content for the SMA mixture tested is about 5.5%.

Results of Schellenberg test underline that, fixing a threshold of D = 0.3%, there is substantially no difference in terms of binder drainage using cellulose fibers or substituting 40% of the total amount of filler with hydrated lime. Mixtures 1* and 3* were selected to be subject to further volumetric and mechanical tests in order to investigate additional effects related to the use of hydrated lime.

Firstly the volumetric properties of the mixtures were evaluated and compared with the technical specification provided by the Italian Ministry of Transportation.

Both mixtures comply with the technical specification provided by the Italian ministry of transportation. To evaluate the mixtures workability, the

Table 5. Results of volumetric tests.

Mixture 1*			
Rotations	VV (%)	Ministry technical specifications (%)	% GMM
10	13.6	8–12	87
50	6.0	2–4	94
130	2.9	≥2	97

Table 6. Results of volumetric tests.

Mixture 3*			
Rotations	VV (%)	Ministry technical specifications (%)	% GMM
10	12.9	8–12	87
50	5.3	2–4	95
130	2.0	≥2	98

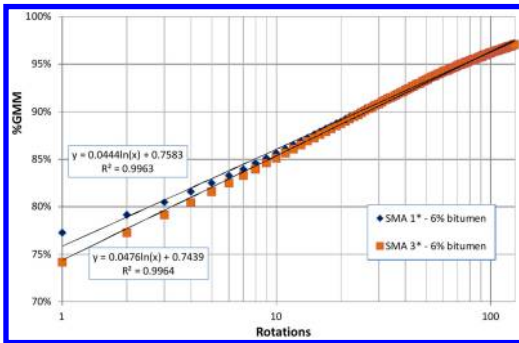


Figure 17. Trend of %Gmm of mixtures 1* and 3*.

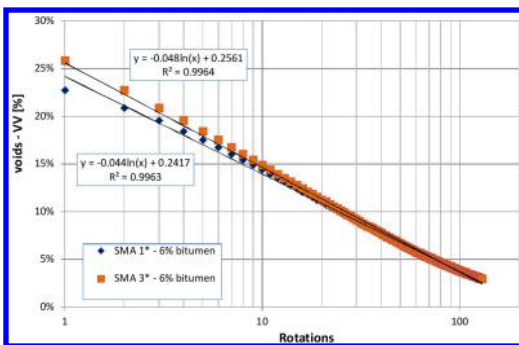


Figure 18. Trend of VV of mixtures 1* and 3*.

trend of %Gmm (percentage of maximum density) and air voids (VV) of the two mixtures were compared. Results are presented in Figure 17 & 18.

As an additional parameter to evaluate the mixtures workability, the Shear Strength were evaluated

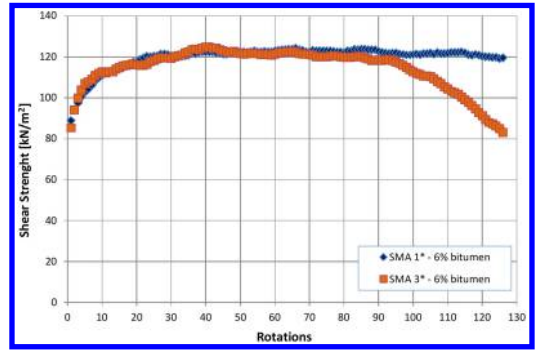


Figure 19. Trend of shear stress of mixtures 1* and 3* during compaction.

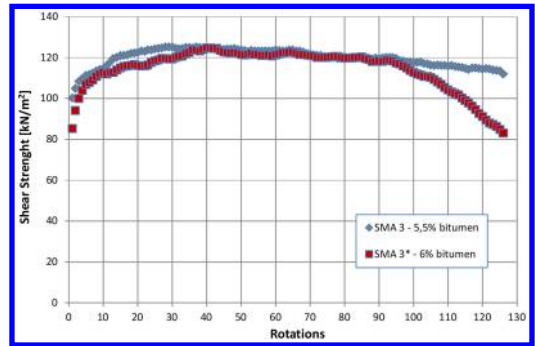


Figure 20. Comparison of Shear Strength trend for mixtures 3* (6% bitumen) and 3 (5.5% bitumen) during compaction.

during compaction by means of GLPA. A comparison between results obtained on mixture 1* and 3* is reported in Figure 19.

Results of volumetric tests appear to be similar for mixture with fibers and lime: in terms of workability no negative effects can be recognized in the substitution of fibers with lime, confirming the assessment based on the drainage tests. Regarding the shear resistance, mixture with fiber does not show a decrease in the value of Shear Strength while mixture with lime show a drop of shear resistance just after the N_{design} . This means that using fiber to prevent binder drainage is possible to have a sort of “safety margin” against the effect of excessive binder in the mix, even this condition appear to be, from a practical point of view, unrealistic. Repeating this kind of test on mixture 3 (with 5.5% of bitumen content) is possible to underline that no drop occur in the Shear Strength after N_{design} . This results confirm that this behavior is only due to the amount of binder in the mixtures.

To evaluate the mechanical properties of the mixtures an indirect tensile test were carried out. Results are reported in terms of Indirect Tensile Strength (ITS) and Coefficient of Indirect Tensile Strength (CTI) and compared with the technical specification provided by the Italian Ministry of Transportation.

Both mixtures gave the same results in terms of ITS, significantly higher than values prescribed by the

Table 7. Results of Indirect Tensile Strength tests – Mix 3*.

Mixture 1*			
Sample	ITS (MPa)	Average ITS (MPa)	Ministry Spec. (MPa)
1	0.8	0.8	>0.5
2	0.7		
3	0.8		

Sample	CTI (MPa)	Average CTI (MPa)	Ministry Spec. (MPa)
1	100	120	>45
2	140		
3	120		

Table 8. Results of Indirect Tensile Strength tests – Mix 3*.

Mixture 3*			
Sample	ITS (MPa)	Average ITS (MPa)	Ministry Spec. (MPa)
1	0.9	0.8	>0.5
2	0.7		
3	0.7		

Sample	CTI (MPa)	Average CTI (MPa)	Ministry Spec. (MPa)
1	160	139	>45
2	113		
3	145		

Ministry Specification. In terms of ITC, mixture with lime exhibited higher values than mixture with fibers even if the difference is small enough to be considered negligible. Results obtained allow to confirm that in terms of resistance to indirect tensile stress no negative effect can be recognized due to the use of lime.

Stiffness modulus tests and fatigue tests were carried out at 20°C on specimen compacted to N_{design} to evaluate the performance properties of the mixtures and their differences due to the substitution of fiber with lime. Results obtained are reported below where a comparison between mixtures with cellulose fibers and lime is performed.

Dynamic tests firstly underline the high performances of the analysed mixtures. Moreover no significant differences can be recognized between mixtures with cellulose fibers and those with lime, confirming that the mechanical properties of the mixtures are not negatively influenced by the replacement of 40% of filler with lime.

Table 9. Results of Stiffness Modulus Tests.

MIX	T°C	Sm (MPa)	Sm (MPa) diameter average	Sm (MPa) specimen average
1*	20	5268	5081	5107
		4894		
		5276	5133	
3*	20	4990		5091
		5111	5071	
		5030		
		5165	5112	
		5058		

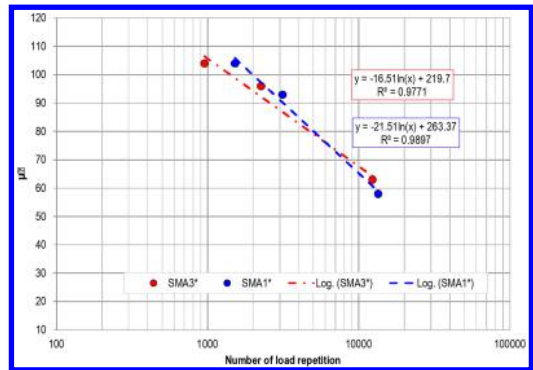


Figure 21. Results of fatigue test.

Results of fatigue tests are reported in Figure 21.

Study mixtures show equivalent fatigue resistance; however, the mixture with cellulose fibers seems to perform slightly better for higher deformation levels while mixture with lime exhibit a better performance for low level of deformation.

5 SUMMARY AND CONCLUSIONS

In the present study, the effects of cellulose fibers substitution with lime on binder drained by SMA (Stone Mastic Asphalt) mixtures has been evaluated. Experimental activity involved Schellenberg tests (to evaluate the amount of binder drained during transport, laying and compaction), workability tests, indirect tensile tests and dynamic behavior evaluation by means of stiffness modulus and fatigue resistance. Based on results obtained, the following conclusions can be underlined:

- Schellenberg tests allow confirming that in order to reduce the binder drainage under values commonly considered acceptable (0.3% of bitumen added to the mix) fibers results equivalent to hydrated lime, when 40% of the total amount of filler is replaced with hydrated lime;

- Workability of study mixtures is not adversely influenced by the replacement of fibers with lime. From a practical point of view, no negative effect is expected in asphalt layer, both during paving and compaction;
- Mixtures shear resistance, evaluated by means of GLPA recording system, also show no significant differences using lime instead of cellulose fibers until N_{design} is reached; when the number of gyratory rotation applied is over N_{design} , shear resistance with lime seems to decrease while SMA mixture with cellulose fiber does not show any significant variation. This behavior allow stating that, using fiber to prevent binder drainage is possible to have a sort of “safety margin” against the effect of excessive binder in the mix, even if this condition appear to be, from a practical point of view, unrealistic;
- ITS tests results largely exceed the threshold values provided by Italian Ministry of Transportation. No negative effect on ITS can be attributed to the use of lime instead of fibers;
- Dynamic tests have been carried out in order to evaluate the Stiffness Modulus and the fatigue resistance. In terms of Stiffness Modulus, study mixtures does not shows appreciable differences when lime is used. Resistance to repeated loading was found to be equivalent for mixture with fibers and lime.

Tests carried out within the present research activity allow stating that, in order to reduce the binder drain-down below acceptance threshold (0.3% of the amount of bitumen), mixtures with 40% of filler replaced with hydrated lime can be conveniently used in place of mixture containing cellulose fibers. The replacement of 40% of mixture filler with hydrated lime was found not to be detrimental for what concern workability, shear resistance and mechanical properties, when

mixtures with cellulose fibers are used as comparison reference.

Further tests are ongoing with the aim to confirm in the field the present results obtained through laboratory tests.

REFERENCES

- Aschenbrener, T. and Far, N. 1994, Influence of Compaction Temperature and Anti-Stripping Treatment on the Results from the Hamburg Wheel-Tracking Device, Report provided by the Colorado Department of Transportation, July 15, 1994.
- AASHTO T 305, Standard Method of Test for Determination of Draindown Characteristics in Uncompacted Asphalt Mixtures, *American Association of State and Highway Transportation Officials*, 2009.
- Collins, R. 1988, Status Report on the Use of Hydrated Lime in Asphaltic Conglomerate Mixtures in Georgia, Georgia DOT, Materials and Research.
- Lesueur D., Petit J., Ritter H.J., Increasing the Durability of Asphalt Mixtures by Hydrated Lime Addition: What Evidence?, *European Road Review*, vol. 20, pp. 48–55.
- Lesueur D, Le Petit J, Ritter HJ 2012, The mechanism of hydrated lime modification of asphalt mixtures: a state of the art review, *Road Materials and Pavement Design*, Vol. 14, pp. 1–16, 2012.
- Little D.N., Lesueur D. and Epps J. 1999. Effect of hydrated lime on the rheology, fracture and aging of bitumens and on the performance of asphalt mixtures, AIPCR/PIARC, *Use of modified bituminous binders, special bitumens and bitumen with additives in road pavements*.
- Little, D. N. 1994, Laboratory Testing Asphalt Mixtures Incorporating Crushed River Gravel Stockpile Treated with Lime Slurry prepared for Chemical Lime Corporation, Texas Transportation Institute.
- New Jersey Department of Transportation, Standard Specification for Road and Bridge Construction, 2007.

Update on new and future CEN asphalt test methods

J.C. Nicholls

TRL Limited, Wokingham, UK

K. Lind

Swedish Transport Administration, Borlänge, Sweden

ABSTRACT: EN 12697 is an extensive series of European norms for test methods and preparation procedures. Since the introduction of the harmonised asphalt specifications were published in 2006 (which required these test methods to be applied), several additional test methods have been published. These tests are crack propagation by semi-circular bending test, saturation ageing tensile stiffness (SATS) conditioning test, low temperature cracking and properties by uniaxial tension tests, determination of the ash content of natural asphalt and determination of friction after polishing. In addition, tests for interlayer bond strength, conditioning to address oxidative ageing, cohesion increase by spread ability-meter method (for cold mix asphalt), resistance to scuffing and surface shear strength test are being standardised. The paper will review these test methods in terms of why they are required, what options are covered by the draft, what the principal of the method and, for those still to be published, how far through the CEN system that the draft has reached.

1 INTRODUCTION

When the EN 13108 series of harmonised European specification and quality documents for asphalt were published in 2006, they were supported by the test methods in EN 12697. There were then 43 parts of EN 12697, which included procedures for sample preparation as well as actual test methods. The majority of the test methods are called up in one or more parts of EN 13108 whilst others covered properties on the road (e.g. EN 12697-40, in situ drainability [CEN, 2003a]) and pavement design purposes (e.g. EN 12697-36, thickness of a bituminous pavement [CEN, 2003b]).

Since then, some additional test parts have been added to the EN 12697 series whilst several of the existing parts have been updated. Furthermore, other properties have been identified and the associated test methods prepared. All the parts of EN 13108 are currently being revised to include the extension of CE marking for the additional test methods. Therefore, it is an opportune time to review the new test methods.

In addition, it has been agreed that the scope of EN 13108 is planned to explicitly include warm, half-warm and cold mix asphalts as well as hot mix asphalts. The revision will not go as far as bringing in this extension because all the necessary test methods and changes to existing EN 12697 part are not yet available. Nevertheless, some new parts are being prepared and the titles of future parts and revisions will exclude the term “for hot mix asphalt”.

Up to now, all the parts of EN 12697 have been published as full standards. Some of the new parts are being considered for publication as technical

specifications instead. A technical specification is effectively a draft standard that needs to be reviewed after three years for conversion to a full standard, continuation for a further three years or withdrawal.

This paper summarises the tests and the reason for producing the five parts published since 2006 together with a further five parts being prepared. Any revisions to parts existing in 2006 are not included.

2 RECENTLY PUBLISHED TESTS

2.1 *Determination of the ash content of natural asphalt*

An annex of EN 13108-4, hot rolled asphalt (CEN, 2006) is used to specify natural asphalt. However, the measurement of the ash content used a test method published by the Institute of Petroleum, which is not an international standard. Therefore that standard was converted into CEN standard EN 12697-47 (CEN, 2010a).

The method is for use in determining the ash content in natural asphalts (including lake asphalts), binders containing natural asphalts or bitumens. For the method to apply, any mineral matter in the binder has to be finely divided and cannot exceed 45% by mass.

The method involves gently heating a weighed sample of the natural asphalt in a silica crucible until fuming ceases. The sample is then ignited at $(650 \pm 50)^\circ\text{C}$ until free from carbon. The mass of ash is then calculated as a proportion by mass of the original sample.

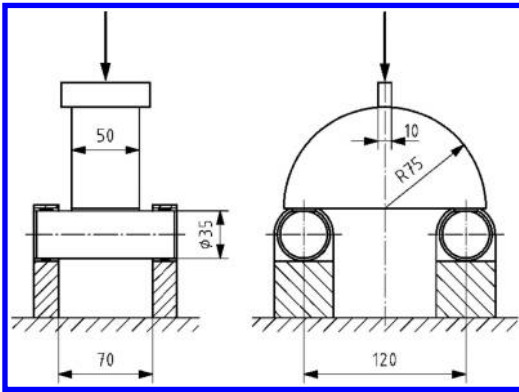


Figure 1. Example of the test frame and specimen for the SCB-test.

2.2 Crack propagation by semi-circular bending test

Fatigue has traditionally been monitored by EN 12697-24 (CEN, 2012), resistance to fatigue. However, there are two phases that measure the fatigue properties of a material, the crack initiation and crack propagation. EN 12697-24 tends to be associated with the former, so the semi-circular bending (SCB) test was standardised for the second phase of crack propagation as EN 12697-44 (CEN, 2010b).

The SCB test method determines the tensile strength or fracture toughness of an asphalt mixture. A half cylinder test piece with a centre crack is loaded in three-point bending in such a way that the middle of the base of the test piece is subjected to a tensile stress. During the test, the deformation increases at a constant rate of 5 mm/min. The corresponding load increases to a maximum value, F_{\max} , that is directly related to the fracture toughness of the test sample. In Figure 1, an example of the test frame and specimen is given.

The results of the test can be used to calculate:

- the maximum load that the material containing a notch (crack) can resist before failure, and
- when the presence of a notch is critical.

2.3 Saturation ageing tensile stiffness (SATS) conditioning test

The UK had a problem with water sensitivity of some base mixtures with consistent air voids contents and hard binder, in particular asphalt concrete mixtures with a binder content between 3.5% and 5.5%, air voids contents between 6% and 10% and 10/20 pen hard paving grade bitumen. The saturation ageing tensile stiffness (SATS) test was developed to assess the potential of mixtures for premature failure with these pore characteristics (Collop et al., 2007). The test was then converted into a European test method as EN 12697-45 (CEN, 2012b), although it is understood that the test has not been widely adopted outside the UK.

The SATS conditioning regime ages the specimens in the presence of water at a set pressure and temperature before a comparative test assesses the performance before and after conditioning. The comparative test is generally stiffness using indirect tension on cylindrical specimens to Annex C of EN 12697-26 (CEN, 2012), although other non-destructive test can also be used.

In the conditioning, nominally identical test specimens are subjected to moisture saturation by using a vacuum system. They are then transferred into a pressurised vessel partially filled with water, where they are subjected to a conditioning procedure by storage at 85°C temperature and 2.1 MPa pressure for 65 h. Most of the specimens are conditioned above the water line, but some are conditioned below.

The ratios of the stiffness, ϵ , measured before and after the conditioning on the individual specimens situated above the water are averaged to determine the sensitivity of the material to ageing and moisture. The average ratio is the SATS Durability Index of the mixture components when the comparative test is the indirect tensile stiffness modulus.

The test is intended to be used as a screening test for the assessment of a combination of aggregate, filler and additives in respect of the retained adhesion properties after simulated ageing in a moist atmosphere for lean/stiff base and binder course mixtures.

2.4 Low temperature cracking and properties by uniaxial tension tests

The bituminous binders in asphalt are highly temperature susceptible and there are large parts of Europe that experience freezing conditions, with low temperature cracking being a common mode of failure. However, there were no tests for the low temperature properties of asphalt so a suitable set of tests were standardised as EN 12697-46 (CEN, 2012d).

The series of uniaxial tension tests for characterising the resistance of an asphalt mixture against low temperature cracking are:

- the tensile strength in dependence of the temperature by uniaxial tension stress test (UTST);
- the minimum temperature that the asphalt can resist before failure by thermal stress restrained specimen test (TSRST);
- the tensile strength reserve in dependence of the temperature (by a combination of TSRST and UTST);
- the relaxation time by the relaxation test (RT);
- the creep curve to back calculate rheological parameters by tensile creep tests (TCT); and
- the fatigue resistance at low temperatures due to the combination of cryogenic and mechanical loads by uniaxial cyclic tension stress tests (UCTST).

In the UTST, a specimen is pulled with a constant strain rate at constant temperature until failure. Results of the UTST are the maximum stress (tensile

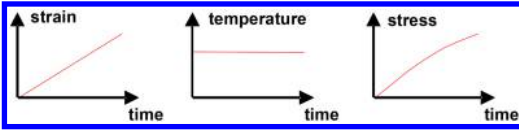


Figure 2. Test principle of UTST.

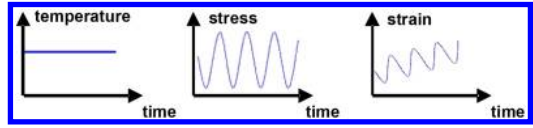


Figure 6. Test principle of UCTST.

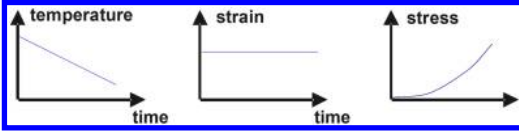


Figure 3. Test principle of TSRST.

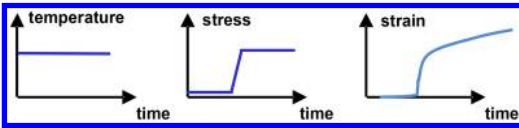


Figure 4. Test principle of TCT.

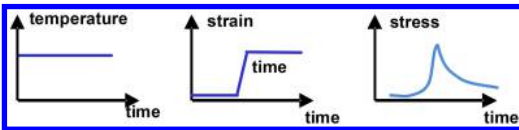


Figure 5. Test principle of RT.

strength) $\beta_i(T)$ and the corresponding tensile failure strain $\varepsilon_{\text{failure}}(T)$ at the test temperature T (Figure 2).

In the TSRST, a specimen, which length is held constant, is subjected to a temperature decrease with constant temperature rate. Due to the prohibited thermal shrinkage, cryogenic stress is built up in the specimen. The results are the progression of the cryogenic stress over the temperature $\sigma_{\text{mcry}}(T)$ and the failure stress $\sigma_{\text{cry, failure}}$ at the failure temperature T_{failure} (Figure 3).

In the TCT, the specimen is subjected to a constant tension stress σ at a constant temperature T . The progression of the strain ε is measured. After a given time, the stress is withdrawn. Rheological parameters describing the elastic and viscous properties of the asphalt can be determined by interpreting the strain measurements (Figure 4).

In the RT, the specimen is subjected to a spontaneous strain ε , which is held on constant level. The decrease of tension stress by relaxation over the testing time is monitored. The results are the time of relaxation t_{rel} and the remaining tension stress σ_{rem} after the test ended (Figure 5).

In the UCTST, a specimen is subjected to a cyclic tensile stress which is characterised by a sinusoidal stress to simulate the dynamic loading condition by traffic in combination with a constant stress, which symbolises the cryogenic stress. During the test, the strain response is monitored and the course of the stiffness is recorded until fatigue failure. Results of the tests are the number of applied load cycles until



Figure 7. FAP device.

failure N_{failure} and the number of load cycles until the conventional fatigue criterion is reached $N_{f/50}$ (Figure 6).

2.5 Determination of friction after polishing

The potential skid resistance of asphalt mixtures tend to be assessed by the micro-texture of the coarse aggregate, as measured by its polished stone value to EN 1097-8 (CEN, 2009), and the macro-texture of the surfacing, as measured by the patch test to EN 13036-1 (CEN, 2010c). However, the Wehner Schulze method was developed to determined the skid resistance of aggregates or asphalt mixtures directly, and this was standardised as the friction after polishing test in EN 12697-49 (CEN, 2014).

The test method determines the friction at 60 km/h after polishing during a fixed number of passes on surfaces of bituminous mixtures samples. These samples can be either produced in a laboratory or cores taken from the site.

The main piece of equipment is a device comprising a polishing station and a unit for measuring the friction (Figure 7). The polishing station, which is continuously supplied with a mixture of water and quartz powder, contains three polishing rollers that can be lowered and that move across the test surface at a predefined loading force.

In the friction measuring unit, a rotating measuring head is lowered onto the test surface while water is being added. The measuring head is fitted with three sliding blocks and can be declutched electronically. The moment generated by the contact between the rubber sliders and the surface is continuously measured and recorded until the measuring head comes to a standstill.

The friction force is calculated from the torque measurements and the friction coefficient. A graph of the friction coefficient μ is fitted on the measured points by a 6th order polynomial fitting. The mean value of the friction coefficient of the fitted graphs at 60 km/h is taken as the result. The test result FAP is the average calculated from at least two individual measurements.

3 NEW TESTS BEING DRAFTED

3.1 *Interlayer bond strength*

The bond between different layers is an important property for pavements but is not a property of just the layer being laid, so cannot be included in the asphalt specifications. However, it was agreed that a harmonised European test for this site property would be of benefit to the industry.

There cannot be a single test method for bond because there is more than one property. At the interaction of two rough horizontal surfaces, the resistance to a horizontal force will be considerable but there would be no resistance to lifting off the top layer; at the interaction of two smooth surfaces (say glass) with water present, the resistance to a horizontal force will be negligible but there would be considerable resistance to lifting off the top layer.

The draft, to be Part 48, gives three separate normative test methods, these being the torque bond test (TBT), shear bond test (SBT) and the tensile adhesion test (TAT). In addition, two further test methods are described in informative annexes, these being the compressed shear bond test (CSBT) and the cyclic compressed shear bond test (CCSBT). The five methods give different results because they measure different failure modes.

The TBT is suitable for testing the bond strength between pavement layers either on site or in a laboratory, and can be used to assess the capability of bond coats or tack coats. It assesses the resistance to the stresses generated primarily by traffic accelerating or braking, but also by thermal movements when the layers are of different materials (e.g. asphalt, micro-surfacing or cement concrete). The test can be carried out immediately after laying.

A core is carefully cut to below the layer interface but, if the test is undertaken on site, the core is not broken off. In a laboratory, the lower layer of the core has to be effectively secured. A steel plate is glued to the top road surface either in situ or the in the laboratory. A rotational horizontal force is then applied to the steel plate and the torque moment is measured. The

temperature will influence the test result so temperature conditioned specimens are tested in the laboratory whilst a correction factor is needed for in-situ tests.

The SBT is a laboratory test that assesses the resistance shear similarly to the TBT, but for horizontal shear stresses rather than torsional shear stresses. Again, the SBT can be used to assess the capability of bond coats or tack coats.

The thickness of the layer above the interface has to be greater than 20 mm and the layer(s) below the interface greater than 70 mm. Cylindrical test specimens are subjected to direct shear loading at controlled temperature with constant shear rate. The development of shear deformation and force is recorded and the maximum recorded shear stress is determined as shear strength at the interface between layers.

The TAT assesses the tensile bond strength between two road construction layers by determining the adhesion between a surface layer and the bottom layer, perpendicular to the plane of the specimen. The test is appropriate to thin surface layers where the mass of the surfacing may not be sufficient to hold it in place.

A test-plunger is glued on the incised and ground surface of the top layer and is pulled off with a suitable tension testing device at constant test temperature and strain rate. The maximum force related to the tension area is the adhesive tension strength.

The CSBT assesses shear behaviour of interlayers subjected to both horizontal and vertical traffic loads. A cylindrical specimen is subjected to direct shear loading whereas an axial load, normal to the interface, is applied to the specimen. The maximum shear stress at the interface between layers is determined.

The CCSBT assesses the interlayer bond stiffness at various temperatures, loading frequencies and normal stress levels. A cylindrical specimen is subjected to cyclic direct shear loading whereas an axial load, normal to the interface, is applied to the specimen. During the test, the temperature, frequency and normal stress are varied in several stages. As such, the complex shear stiffness as function of the test temperature, frequency and shear deformation amplitude at the interface between layers can be determined.

3.2 *Resistance to scuffing*

A mode of failure for asphalt that does not have a standardised test method is the resilience of surfacings to scuffing and other actions of traffic. In order to quantitatively assess this resilience requires a simulative test to scuff a sample. Four devices that have been developed for scuffing, so it has been decided to produce a draft for a Technical Specification, as Part 50, until the definitive method can be selected. However, a rational selection will require sufficient comparative studies with the four dedicated devices, which may be unlikely. It would be useful if another procedure could be developed using existing equipment.

Each of the devices are used for determining the resistance to scuffing of asphalt mixtures which are used in surface layers and are loaded with high shear



Figure 8. Example of ARTe device.

stresses in road or airfield pavement. These shear stresses occur in the contact area between tyre and pavement surface and can be caused by cornering of the vehicle. Due to these shear stresses, material loss will occur at the surface of these layers. The tests will normally be performed on asphalt layers with a high air voids content (e.g. porous asphalt), but can also be applied on other asphaltic mixtures. Test specimens used are either produced in a laboratory or cut from the pavement.

The four different devices are:

- The Aachener ravelling tester (ARTe)
- The Darmstadt scuffing device (DSD)
- The rotating surface abrasion test (RSAT)
- The Triboroute.

For the ARTe device (Figure 8), the slab is conditioned at $(20 \pm 2)^\circ\text{C}$ before mounting in the slab fixation box which, in turn, is mounted in the lateral moving table. During the test, the lateral moving table travels 600 times forwards and backwards over the slab. The slab is then removed from the slab fixation box and any loose material removed from the surface using a vacuum cleaner. The surface is inspected visually for any differences between the initial and end surface and the three dimensional texture of the slab surface measured.

For the DSD device (Figure 9), the asphalt specimens are photographed, weighed and then conditioned at $(40 \pm 1)^\circ\text{C}$ before being fixed in the device. The test tyre is lowered onto the specimen to applying $(1,000 \pm 10)\text{N}$ of pressure through the pneumatic pressure cylinder. When the targeted pressure is reached, the test starts. The tyre then moves over the table whilst any loose grains are vacuumed up or wiped off as required. After the test, another photograph is taken for visual comparison with the first photograph and the specimen is re-weighed.



Figure 9. Example of DSD device.



Figure 10. Example of RSAT device

For the RSAT device (Figure 10), the specimens are slabs of octagonal shape which are cured for at least 14 days before testing. A test specimen is mounted into the slab holder and then stored for a period of 14 to 18 hours at the test temperature, usually $(20 \pm 1)^\circ\text{C}$ but can be between $(-10 \pm 1)^\circ\text{C}$ and $(25 \pm 1)^\circ\text{C}$. A new wheel is used for each test with the specimen being preloaded using a minimum load of 20 kg for a period of at least 1 h and then the specimen is completely cleaned. The test lasts 24 h with 86 600 rotations in a relatively complex movement under a total wheel load of $(35.0 \pm 0.1)\text{kg}$. The test is stopped early if too much damage occurs on the specimen. During the test, any loose material is removed from the surface of the specimen using a vacuum cleaner and then separated between mineral aggregate and rubber in order to determine the aggregate loss during the test.

For the Triboroute device (Figure 11), the specimen is positioned on a rigid horizontal frame and the flatness and macro-texture of the upper surface is evaluated. The surface has to be free of any grease or other product capable of interfering with mechanical contact between the rubber pad and the target surface. For textures greater than 0.5 mm, the Triboroute is used in

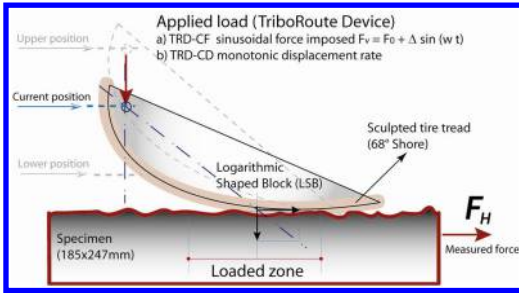


Figure 11. Schematic of Triboroute device.

controlled force whilst, for lower textures, it is used in controlled displacement rate. The specimen and fixation box are conditioned at the test temperature of $(20 \pm 2)^\circ\text{C}$ for at least 2 h. The test with controlled force comprises three phases of the pre-loading phase, the cyclic loading phase and the logarithmic shaped block (LSB) rising phase. The test with controlled displacement rate comprises two phases of the monotonic loading phase and the LSB rising phase.

3.3 Surface shear strength test

A variant of the TBT (Section 3.1) has been used (on airfield runways and taxiways) for slurry surfaces and other thin surfacings to assess their potential integrity. Therefore, the CEN Airfields group requested that the test method be standardised, which was agreed as Part 51. However, because of the limited experience with the test, it is proposed to issue it as a technical specification rather than a standard. The test measures the surface shear strength for airfield surface courses, which is regarded as a measure of the robustness of asphalt surface courses against shearing.

A plate is bonded to the surface course and rotated using a torque meter to determine the torsional strength of the top layer and, in the case of ultra-thin surface courses, the rotational shear strength between layers. The test can be carried out either in situ or in the laboratory cores which may be subjected to curing conditions. The in situ test is done without the necessity to core into the substrate. A curing procedure can be used to assess the effect of moisture in the development of surface shear strength with time.

The surface shear strength depends on the depth of the surface course together with the properties of the surface course material. The binder course material and any bonding agent applied between the two layers may have an influence on the test result for, in particular, ultra-thin surface course.

3.4 Conditioning to address oxidative ageing

The mandate for the asphalt specifications asks for requirements on durability but, because the properties of bitumen, and hence asphalt, will change with time, there is no assessment of that change. Part of the reason for the omission is that there is no accepted ageing

procedure that is applicable to all asphalts subject to all climatic conditions. Therefore, a draft is being prepared as Part 52, but again it is proposed to issue it as a technical specification rather than a standard.

The draft describes procedures for use on:

- loose asphalt for short-term ageing;
- loose asphalt for long-term ageing;
- compacted specimens with simple conditioning;
- compacted specimens with more complex conditioning.

The procedures are applicable to asphalt manufactured in the laboratory or in a mixing plant. The procedures on compacted specimens are applicable to specimens from laboratory production or cores taken from the field.

For the procedures on loose asphalt, the loose mixture is placed into a pan and conditioned within a heating cabinet with forced air ventilation for a specific duration at elevated temperature to accelerate ageing due to oxidation. Additionally pressure can be applied for further acceleration of conditioning. The procedure for long-term ageing has extended condition relative to the short-term ageing procedure.

For the simpler procedure on compacted specimens or cores from the field, the specimens are placed into a pan and conditioned within a heating cabinet with forced air ventilation for a specific duration at a specific temperature. For the more complex procedure on compacted specimens, the specimens are placed within a triaxial cell (comparable to triaxial cells used for permeability tests on soils) and a forced flow of gaseous oxidant agent (ozone enriched compressed air) through the specimen is used to condition the specimen for a specific duration at a specific temperature.

Material conditioned can then be used for further testing to assess the effect of oxidative ageing on the characteristics of the asphalt mixture and, hence, on their durability and recyclability. Alternatively, binder can be extracted from the conditioned mixture to assess the effect of oxidative ageing on binder characteristics taking into account potential effects of mineral aggregates on ageing.

3.5 Cohesion increase by spread ability-meter method

The move to explicitly include cold mix asphalt in the product standards requires tests to monitor some additional properties that are required. One of these is the workability of the mixture and how it changes with curing. A draft is proposed, to be Part 53, in which the property measured is the cohesion increase of a mixture under fixed temperature and hygrometry conditions, using a spreadability-meter (at least until a better name is found for the equipment).

The method was designed for cold mix asphalt mixtures, particularly emulsion mixtures, but can be used on other asphalt types apart from mastic asphalt. The mixtures, which have to have an upper aggregate size

not larger than 31.5 mm, can be either made up in a laboratory or be sampled from site.

For emulsion-based asphalts and other cold mix asphalt (those mixed and laid at temperatures below 60°C), the test method characterises the “pot-life” of the mixture, the time between mixing and compacting. This time depends on a number of parameters including the type and binder content of the emulsion, the type of aggregate and the type of grading curve. For other asphalt mixtures, the test method is intended to be of assistance to the designer for mixture design rather than as a type test.

The mixture is used to fill a mould and struck off with a straightedge before going into a climatic chamber or oven. The moulds are conditioned for a fixed time before being set in the workability-meter in which a piston applies a monitored shear force to the sample. The measurement of the resistance against the shear is measured on specimen after different conditioning times.

4 CONCLUSIONS

The tests that have been, and are being, added to the EN 12697 series will have different uses but will be of use to the industry. However, the new test methods that have not yet been published will not be available for being incorporated into the asphalt product standards until the five-year review after the one currently underway. The publication for the revised versions is currently scheduled for July 2016 with the final withdrawal of the existing standards for July 2017, but it is hoped to bring these dates forward.

ACKNOWLEDGEMENTS

The authors would like to thank the past and present members of CEN TC227/WG1/TG2 for their efforts in drafting the EN 21697 series of test methods.

REFERENCES

Collop, A., Y. Choi and G. Airey (2007). Effects of pressure and aging in SATS test. *Journal of Transportation Engineering* 133: 618–624.

Comité Européen de Normalisation (2003a). Bituminous mixtures – Test methods for hot mix asphalt – Part 36: Determination of the thickness of a bituminous pavement. *EN 12697-36:2003*. Most European standardisation institutions.

Comité Européen de Normalisation (2003b). Bituminous mixtures – Test methods for hot mix asphalt – Part 15: Determination of the segregation sensitivity. *EN 12697-15:2003*. Most European standardisation institutions.

Comité Européen de Normalisation (2006). Bituminous mixtures – Material specification – Part 4: Hot rolled asphalt. *EN 13108-4:2006*. Most European standardisation institutions.

Comité Européen de Normalisation (2009). Test for mechanical and physical properties of aggregates – Part 8: Determination of the polished stone value. *EN 1097-8:2009*. Most European standardisation institutions.

Comité Européen de Normalisation (2010a). Bituminous mixtures – Test methods for hot mix asphalt – Part 47: Determination of the ash content of natural asphalt. *EN 12697-47:2010*. Most European standardisation institutions.

Comité Européen de Normalisation (2010b). Bituminous mixtures – Test methods for hot mix asphalt – Part 44: Crack propagation by semi-circular bending test. *EN 12697-44:2010*. Most European standardisation institutions.

Comité Européen de Normalisation (2010c). Road and air-field surface characteristics – Test methods – Part 1: Measurement of pavement macro-texture depth using a volumetric patch technique. *EN 13036-1:2010*. Most European standardisation institutions.

Comité Européen de Normalisation (2012a). Bituminous mixtures – Test methods for hot mix asphalt – Part 24: Resistance to fatigue. *EN 12697-24:2012*. Most European standardisation institutions.

Comité Européen de Normalisation (2012b). Bituminous mixtures – Test methods for hot mix asphalt – Part 45: Saturation ageing tensile stiffness (SATS) conditioning test. *EN 12697-45:2012*. Most European standardisation institutions.

Comité Européen de Normalisation (2012c). Bituminous mixtures – Test methods for hot mix asphalt – Part 26: Stiffness. *EN 12697-26:2012*. Most European standardisation institutions.

Comité Européen de Normalisation (2012d). Bituminous mixtures – Test methods for hot mix asphalt – Part 46: Low temperature cracking and properties by uniaxial tension tests. *EN 12697-46:2012*. Most European standardisation institutions.

Comité Européen de Normalisation (2014). Bituminous mixtures – Test methods for hot mix asphalt – Part 49: Determination of friction after polishing. *EN 12697-49:2014*. Most European standardisation institutions.

Influence of sodium chloride and potassium formate as deicing agents on asphalt mixture durability

S. Anastasio, I. Hoff & C. Thodesen

Department of Civil and Transport Engineering, Norwegian University of Science and Technology, Trondheim, Norway

ABSTRACT: Abrasive resistance of four bituminous mixtures has been measured to evaluate the effects of sodium chloride and potassium formate on asphalt pavement durability. In both cases a correlation between the particle loss and the concentration of the deicer is found, the effects of potassium formate appear more consistent. Furthermore, alterations of the bitumen were measured evaluating the performance grade of the recovered binder. No significant correlation between particle loss and the critical temperatures of the extracted binders was found. However, a dependency of the extracted binder performance on the characteristics of the aggregates is suggested.

1 INTRODUCTION

Each year about 200,000 tons of salt are spread on the Norwegian road system in order to prevent and remove thin ice layers and/or to provide them with higher values of friction (Statens Vegvesen, 2011). Although its efficacy as anti-icing and deicing agent is undisputed, negative effects of deicing chemicals on the environment, built infrastructure and vehicles have in the last decade gained large attention (Hellstén et al., 2005; Fay and Shi, 2012).

pH-value, hygroscopic capacity and surface tension capacity of the chemical, and on the other hand on the air voids content, type of aggregate and adhesion properties of the mixture and its components are determinant in the choice of the chemical agent (Ekblad and Edwards, 2008). Currently, salts (mostly sodium chloride) and formates (generally potassium formate in northern Europe) are used as primary deicers on highway pavements and airport runways respectively since chloride based solutions are excluded from airfields in order to prevent corrosion of aircrafts and to a lesser degree, adverse environmental impacts (Farha et al., 2002). Moreover, the application of deicing chemicals on asphalt pavements, combined with freeze thaw cycles and high summer temperatures, has been identified as cause of premature deterioration of the pavement (Pan et al., 2008; Hassan et al., 2002; Alatyppö and Valtonen, 2007). During the cold season the effect of deicers consists primarily of an increment of ice pressure within the pores that can lead to loss of cohesion of the mixture and loss of aggregate material as observed at some airfields (Starck and Löfgren, 2007). Exposure to deicer has been found to cause hardening (Farha et al., 2002). However, this effect marginally affects mixtures conditioned at low

temperatures because of the slowdown of chemical reactions when the temperature decreases. A softening effect of freeze-thaw cycles on the bitumen should also be considered.

The present work aims to investigate the combined effects of deicing chemicals and freeze-thaw cycles on the cohesion of the asphalt concrete. The Cantabro test was selected to evaluate if chemical and thermal conditioning affects the abrasiveness of bituminous mixtures. Furthermore, in order to evaluate whether the abrasion rate of the mixture is related to chemical changes within the binder due to the thermal gradient or eventual chemical reactions, this research will include the PG-grading analysis on the extracted binder.

2 EXPERIMENTAL PROGRAM

2.1 *Materials*

For this study, four dense graded AC 11 mixtures with the same binder and filler, but different stone materials were designed according to the Norwegian specifications for asphalt concrete mixtures. Four types of aggregates, hereinafter named A, B, C and D, generally used as paving materials with a maximum size of 11 mm were chosen among quarries in the Trøndelag region in Norway.

In [Table 1](#) the content in percentage of the major minerals present, determined through an XRD analysis is shown. In order to collect a sample of material that represents the whole pallet, between 5–10 kg of stone aggregates underwent 1000 revolutions in the Los-Angeles (LA) drum, then 15 g of material were collected from the resulting fines (<0.125 mm) and sent to the laboratory for the analysis. Although this

Table 1. Mineralogical composition of the aggregates.

		A	B	C	D
Actinolite	[%]	–	40.6	–	–
Albite	[%]	18.3	18.1	35	30.4
Biotite	[%]	–	–	–	1.3
Calcite	[%]	0	4.4	0.4	16.3
Chlorite	[%]	–	–	–	16.1
Clinochlore	[%]	–	18.1	2.2	–
Epidote	[%]	–	11.8	–	–
Microcline	[%]	15.2	5.8	10.1	2.4
Muscovite	[%]	18.3	0	15.1	12.3
Quartz	[%]	48.2	1.2	37.2	21.3

Table 2. Deicing solutions included in the testing program.

Deicer	Concentration (%-by weight)
NaCl	25
NaCl	12.5
KCHO ₂	50
KCHO ₂	25
H ₂ O	100

method might give higher percentual content of weaker minerals, it provides an overview of the differences in terms of composition of the aggregates.

The mixture design was performed for each aggregate type using the Marshall and Gyrotory method according to the Norwegian specifications for dense graded AC 11 mixtures (Statens Vegvesen, 2014). A conventional 70/100 binder, widely used in Norway, was utilized, and a binder content of 6.0%, 5.1%, 5.7% and 5.8% respectively was determined.

2.2 Conditioning

The deicers selected for this investigation are sodium chloride (NaCl) and potassium formate (KCHO₂). Together with the reference samples stored in water, the testing program includes the deicing solutions given in Table 2. The samples, immersed in the solutions were subjected to eight freeze-thaw cycles. In order to simulate the cycles, an automated freezer was used. Opening and closing of the freezer were programmed in order to complete one cycle within 24 hours. The temperatures of the fluids were monitored during the process and reached values of –23 and +10°C. These temperatures are considered to be a good representation of the possible winter gradient.

2.3 Cantabro test

Although the Cantabro test is designed for open graded mixtures, it has been considered relevant in this project to use this test method also for dense graded mixtures. The combined action of freeze-thaw cycles and deicing

chemicals is supposed to affect the cohesion of the mixture causing loss of material. Since this test is used to evaluate the adhesion characteristics of an asphalt concrete sample, it has been considered suitable as an indicator of the deicer susceptibility.

Five samples per mixture and per conditioning were prepared and allowed to cure at room temperature for a minimum of 48 hours prior conditioning. The susceptibility of the asphalt mixtures was tested by storing the specimens in NaCl, CHKO₂ solutions and water. The samples were conditioned by exposing them to eight freeze-thaw cycles. Afterward, the Cantabro test (EN 12697-17) was performed at room temperature. The sample was then cleaned of loose particles and weighed.

The amount of damage experienced by each sample was quantified in terms of particle loss. The accumulated percentage of particle loss after 300 turns in the Los-Angeles drum was calculated as follows:

$$PL = 100 (W_1 - W_2) / W_1 \quad (1)$$

where W_1 = initial sample weight; and W_2 = final sample weight.

2.4 Extraction of the binder

After the conditioning in different deicing solutions, about 100 g of bitumen was extracted from each group of five samples following the procedure described in the EN 12697-1. Methylene chloride was used as solvent. This process and the solvent itself might have influenced the performance of the binder introducing discrepancies between the recovered and the original binder.

2.5 PG-grading of the bitumen

After the conditioning in different deicing solutions, the binder present in the samples was characterized using the ASTM (D6373 – 07) performance grading system, PG grading and compared to the original binder.

The procedure included the Dynamic Shear Rheometer (DSR) test, conducted on freshly extracted and short and long-term aged bitumen, and Bending Beam Rheometer (BBR) test, conducted on long-term aged bitumen.

3 ANALYSIS OF THE RESULTS

3.1 Cantabro test

The results of the first phase are shown in the following as average particle loss of five samples after eight freeze-thaw cycles. In Figure 1 the rate of particle loss, depending on the conditioning of the samples, are shown versus the concentration of the solutions of NaCl and KCHO₂. The rate of particle loss is expressed as ratio between the particle losses of the samples conditioned in deicers and subjected to freeze-thaw cycles

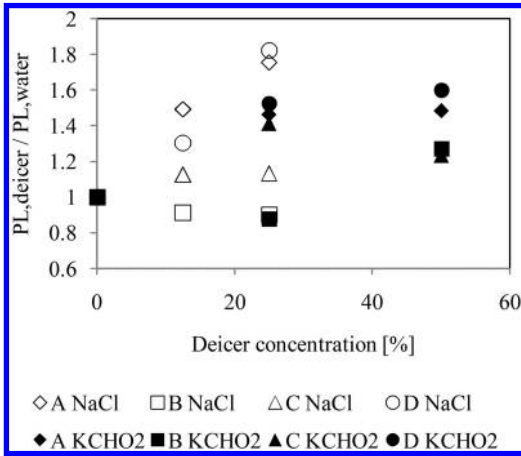


Figure 1. Rate of particle loss of asphalt concrete samples after eight days of conditioning in sodium chloride and potassium formate solutions. The ratio is calculated between samples exposed to deicers and samples conditioned in water.

($PL_{deicers}$) and of the samples stored in water (PL_{water}). Each value is the average particle loss of five samples. The 0% concentration indicates the control samples immersed in water.

The abrasion test showed a general increment of particle loss when the chemical concentration was increased. Compared to the samples immersed in water, larger differences are seen when NaCl is used. Moreover, similar results are measured when the half saturated concentrations are used (corresponding to 12.5 and 25% concentration of respectively NaCl and $KCHO_2$). A lower variation is generally observed in the C mixture while a significantly higher is visible in both A and D.

3.2 PG-grading

In order to evaluate if the increase of abrasiveness on the asphalt samples was due to a change in the physical properties of the binder, a PG binder grading analysis was conducted on the extracted material. The test was repeated twice for each material. The effect of the solvent used in the extraction should be considered in the results, however, the same technique was used for all the samples.

In Figure 2 the critical temperatures, evaluated with the DSR are reported and compared with the temperature measured for the control binder (not conditioned, dashed line). In terms of critical temperature each set of samples extracted from the same mixture shows a wide range of variation from the original binder depending on the conditioning. However, these changes in shear modulus are not ascribable to any trend dependent on the concentration or the nature of the deicers. Moreover, the figure shows a stiffening effect that highlighting the strong effect of the freeze-thaw cycles on the binder as observed by Farha et al. (2002).

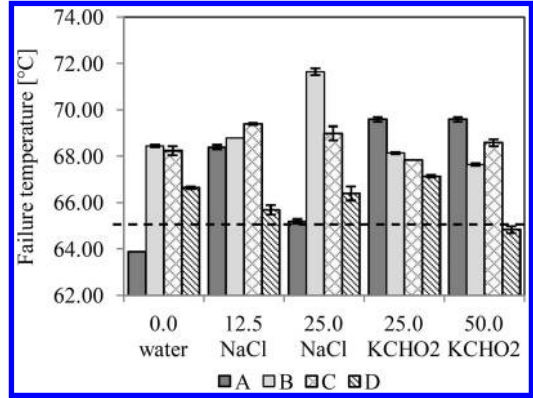


Figure 2. DSR: critical temperature of the extracted binders. The dashed line represents the critical temperature of the original binder. The error bars represent the minimum and maximum value per each set of two samples.

When the DSR test is carried out after the RTFO ageing of the binder, no significant differences are visible. However, the results tend to converge to constant values depending on the type of conditioning when the samples are tested at lower temperatures after PAV ageing (Figure 3). These constant values are anyway higher than the critical temperature scored by the original bitumen after ageing.

Except for the samples extracted from the sample A conditioned in water, the results from the BBR after the PAV aging process, as those from the DSR, appear uniform (Figure 4). As at higher temperature, a stiffening effect of the binder is noticeable. A higher deviation of the critical temperatures is measured between the two tests run per each material compared to the values recorded during the DSR test.

A particular behavior is observed for the samples belonging to the A mixture conditioned in water: a large softening of the binder is recorded at low temperatures compared to the other samples with the critical temperature reaching $-28.9^{\circ}C$ ($-17.5^{\circ}C$ was recorded for the original binder).

In order to evaluate if the overstated changes of the properties of the binder are related with the results from the Cantabro test, the rate of particle loss was compared to the critical temperatures recorded during the PG analysis. Figure 5 reports the values measured with the DSR test after extraction. Per each mixture the samples were grouped without differentiating between the chemical solutions. The black dot represents the critical temperature recorded testing the original binder and is related with the average particle loss of the dry samples.

The particle loss does not appear to be influenced by changes in the binder properties. However the figure suggests that the critical temperatures are grouped depending on the different mixture. Similar figures are obtained when the particle loss ratio is compared to the results from the other tests.

The same grouping is observable also when the same critical temperatures are compared with the

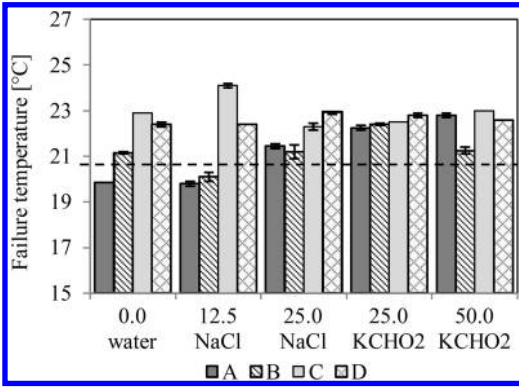


Figure 3. DSR: critical temperature of the binders after the PAV aging process. The dashed line represents the critical temperature of the original binder after the PAV aging process. The error bars represent the minimum and maximum value per each set of two samples.

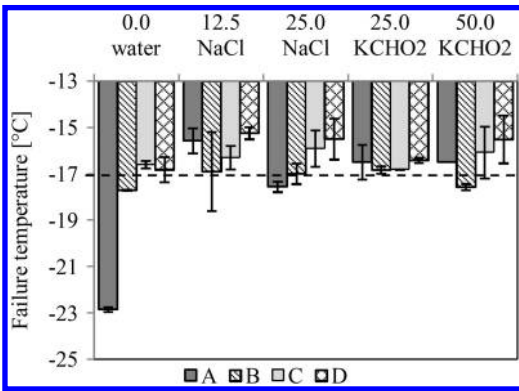


Figure 4. BBR: critical temperature of the binders after the PAV aging process. The dashed line represents the critical temperature of the original binder after the PAV aging process. The error bars represent the minimum and maximum value per each set of two samples, the values considered belongs to the same group of result as the nominal critical value (m-value or s-value).

minerals composing the aggregates but no particular trend depending on their content was visible. Figure 6 reports the data compared to the quartz content.

4 CONCLUSIONS

This paper presented a laboratory investigation of the effects of deicer chemicals and freeze-thaw cycles on asphalt concrete mixtures. Two commonly used chemicals (sodium chloride, NaCl, and potassium formate, KCHO₂) were used at different concentrations to provide an overview of the effects of deicing agents on asphalt performance. The Cantabro test, on samples exposed to deicers, confirmed the higher grade of deterioration observed in airports. In particular, the rate of particle loss due to exposure to deicing materials and freeze-thaw effects are heavily influenced by the

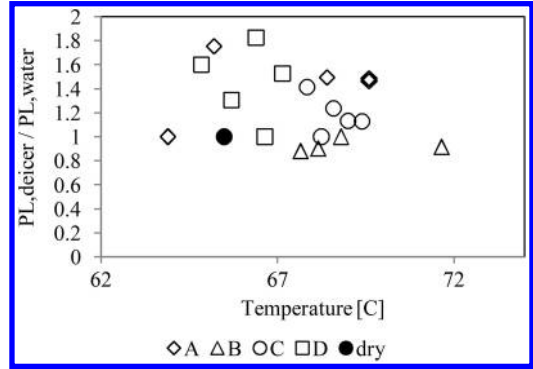


Figure 5. Particle loss of the samples compared with the critical temperature recorded after the DSR test on the extracted material. The black dot represents the failing temperature recorded testing the original binder.

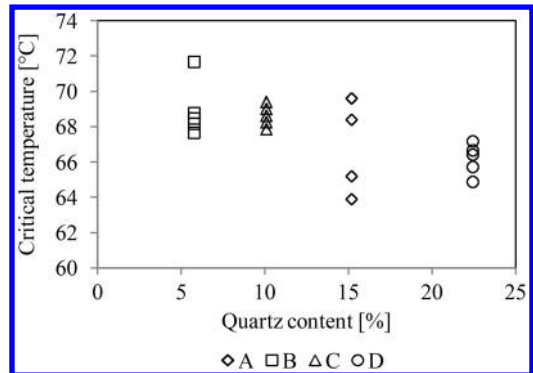


Figure 6. Critical temperature recorded on the DSR on the extracted materials compared with the quartz content of the aggregates contained in the mixture.

concentration and the nature of the deicer, increasing with increasing levels of saturation. Lower differences between the mixtures are observable for the samples conditioned in potassium formate.

Binder testing suggests a poor correlation between particle loss and the critical temperatures of the extracted binders at both high and low temperatures.

It is thus possible to conclude that, the propensity to abrasiveness of the pavements subjected to deicers at low temperatures is due to an increment of ice pressure within the pores, because of the higher volume occupied by the frozen solution of water and chemicals rather than to any chemical reaction. However, a stiffening effect on the binder has been measured. As previously indicated, this implies that the effect of freeze-thaw cycles is predominant at lower temperature and therefore, in order to evaluate more correctly the effects of deicers on the binder properties and then on the mixture performance, the test should be repeated after a storage at higher temperatures.

Moreover, the findings from this study suggest a relationship between binder performance after extraction, and the characteristics of the aggregates. Such an

outcome may imply a chemical interaction between the two materials results in a modification of the binder properties.

Further research will be conducted in order to understand how to minimize the loss of cohesion of asphalt mixture at low temperatures. More work is also necessary to investigate the interaction between aggregates and binder.

REFERENCES

- Alatypö, V. & Valtonen, J. 2007. Experiences on the effects of de-icing chemicals on bituminous airfield runways in Finland. *Federal Aviation Administration Worldwide Airport Technology Transfer Conference*. Atlantic City, New Jersey, USA.
- Ekblad, J. & Edwards, Y. 2008. Precision of method for determining resistance of bituminous mixtures to de-icing fluids. *Materials and Structures/Materiaux et Constructions*, 41(9), pp. 1551–1562.
- Farha, M., Hassan, Y., El Halim, A. A., Razaqpur, A., El-Desouky, A. & Mostafa, A. Effects of new deicing alternatives on airfield asphalt concrete pavements. *Federal Aviation Administration Technology Transfer Conference*, 2002.
- Fay, L. & Shi, X. 2012. Environmental impacts of chemicals for snow and ice control: State of the knowledge. *Water, Air, and Soil Pollution*, 223(5), pp. 2751–2770.
- Hassan, Y., Abd El Halim, A., Razaqpur, A., Bekheet, W. & Farha, M. 2002. Effects of Runway Deicers on Pavement Materials and Mixes: Comparison with Road Salt. *Journal of Transportation Engineering*, 128(4), pp. 385–391.
- Hellstén, P. P., Kivimäki, A. L., Miettinen, I. T., Mäkinen, R. P., Salminen, J. M. & Nystén, T. H. 2005. Degradation of potassium formate in the unsaturated zone of a sandy aquifer. *Journal of Environmental Quality*, 34(5), pp. 1665–1671.
- Pan, T., He, X. & Shi, X. Laboratory investigation of acetate-based deicing/anti-icing agents deteriorating airfield asphalt concrete. 2008. 773–793.
- Starck, P. & Löfgren, B. 2007. Influence of de-icing agents on the viscoelastic properties of asphalt mastics. *Journal of Materials Science*, 42(2), pp. 676–685.
- Statens Vegvesen. 2011. Mengderapportering vinteren 2010/2011.
- Statens Vegvesen. 2014. Håndbok N200 Vegbygging.

The effect of Montan waxes on the mechanical performance of an asphalt rubber mixture

A.M. Rodríguez-Alloza & J. Gallego

Department of Civil Engineering: Transport, Technical University of Madrid (UPM), Madrid, Spain

ABSTRACT: In recent years, Warm Mix Asphalt (WMA) has become an important new research topic in the field of pavement materials due to a growing concern over global warming. Though this technology is being incorporated to reduce energy consumption and greenhouse gases (GHG) emissions by lowering the manufacturing and compaction temperatures of asphalt mixtures without significantly affecting their mechanical properties, the influence of WMA additives on the properties of asphalt rubber mixtures has not yet been clearly identified. In this study the performance of the asphalt rubber (AR) mixtures with Montan waxes were evaluated and compared through several laboratory tests regarding their water sensitivity and resistance to permanent deformation and fatigue. The results of this study indicate that the waxes slightly worsened the water sensitivity but fulfilled the Spanish requirement, that the additives improved the resistance to permanent deformation and that only one of the waxes improved the fatigue life compared with the control mixture.

1 INTRODUCTION

1.1 Problem statement

Pavements containing crumb-rubber modified (CRM) binders save energy and natural resources by making use of waste products. Rubberized binders used in the construction of flexible pavements result in an improvement in resistance to rutting, fatigue and thermal cracking, they lower traffic noise and maintenance costs as well as contributing to prolonged pavement life (Huang B, Mohammad LN, Graves PS, Abadie C., 2002; Liang RY, 1996; Ruth BE, 1995; Shen J, Amirkhanian S, Lee S-J, 2005).

However, asphalts containing CRM binders (from now on will be referred as asphalt rubber (AR) mixtures) present one major drawback: the manufacturing temperature is higher. Usually, temperatures oscillate between 175°C and 180°C (CEDEX, 2007) as the rubber lends a greater viscosity to the binder and thus produces larger amounts of greenhouse gas (GHG) than conventional bituminous mixtures.

In the last few years, the WMA technology has been developed to reduce the manufacturing and compaction temperatures of asphalt mixtures. This technology offers a practical chance of decreasing energy consumption, greenhouse gases (GHG) emissions, fumes and odors from asphalt plants as well as to improve the working conditions at plants and paving sites (Hurley G, 2005). These benefits, combined with the effective reuse of a solid waste product, would make AR mixtures with WMA additives an excellent, environmentally-friendly material for road construction.

As the effect of WMA additives on the mechanical properties of rubberized mixtures has not yet been established in detail, this research study the level of mechanical performance of AR mixtures with two WMA additives (referred to hereafter as AR-WMA mixtures) as if these mixtures do not perform well, there will not be long-term energy savings or environmental benefits.

In this study, the performance of AR-WMA mixtures with two organic additives (Montan waxes) have been evaluated and compared in order to assess the effect of these additives when production/compaction temperatures are decreased through a series of laboratory tests that included the evaluation of water sensitivity, resistance to permanent deformation and resistance to fatigue.

2 MATERIALS

2.1 Virgin binder

The virgin binder used in this study is a 50/70 (50/70 10⁻¹ mm of penetration), which is widely used to produce asphalt mixes at conventional temperatures. Table 1 summarizes the basic specifications of the virgin binder.

Penetration grade was assessed according to EN 1426 (CEN, 2003), while the Softening Point was measured according to EN 1427 (CEN, 2007). The asphalt bitumen was also subjected to a fractionation analysis as specified in the NLT 373/94 standard (CEDEX, 1999).

Table 1. Specifications of the 50/70 bitumen.

Properties	Unit	Test results
Penetration (25°C)	0.1 mm	55.4
Softening point	°C	51.1
Composition	Unit	Test results
Asphaltenes	(%)	13.8
Saturates	(%)	9.7
Naphthene-aromatic	(%)	48.5
Aromatic-polar	(%)	28.0

Table 2. Gradation of crumb rubber.

Sieve (mm)	Accumulated (%)
2.000	100.0
1.500	100.0
1.000	100.0
0.500	94.1
0.250	23.7
0.125	3.7
0.063	0.4

Table 3. Thermogravimetric analysis of crumb rubber.

TGA	Rubber
Plasticizer + additives (%)	4.67
Polymer (rubber) (%)	57.41
Carbon black (%)	32.22
Ash (%)	6.02

2.2 Crumb rubber modifier

The crumb rubber modifier was manufactured by mechanical grinding at ambient temperature (50% from truck tires and 50% from car tires) and to ensure consistency only one batch of crumb rubber was used in this study. The gradation of the crumb rubber is provided in Table 2 and the thermogravimetric analysis in Table 3, both provided by the supplier.

Twenty percent was selected as the most appropriate amount of crumb rubber with respect to viscosity and workability (Hossain, Swartz, & Hoque, 1999), reflective cracking (Sousa, Pais, Saim, Way, & Stubstad, 2002) and cost efficiency (Wang & You, 2011).

2.3 WMA additives

The WMA additives selected for this study were two different Montan waxes. Additive 1 (A1) is a Montan wax which is produced by solvent extraction of lignite or brown coal. Additive 2 (A2) is a refined Montan wax blended with a fatty acid amide.

Table 4. Aggregates.

Aggregate	Size	%
Mylonite	8/11	20
Mylonite	4/8	48
Limestone	2/4	18
Limestone	0/2	13
Calcareous filler		1

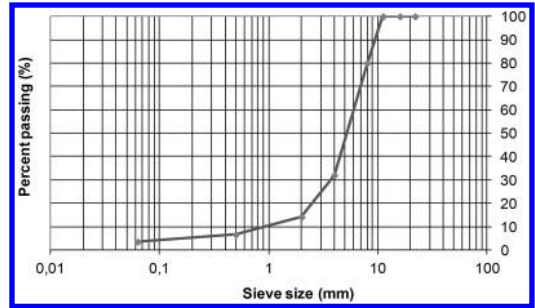


Figure 1. Grading curve of the AR mixture.

A 4% referred to the bitumen weight of each additive was added to the 20% CRM binder to produce the CRM binders with WMA additives.

2.4 Aggregates

The aggregates used to obtain the asphalt mixtures were milonite (a metamorphic rock), limestone and the calcareous filler. The different fractions of the sieves are reported in Table 4 and the dimensions of the sieves are conformed to the EN code regulations. To ensure consistency, the same aggregates were used throughout this study.

The grading curve can be observed in Figure 1.

2.5 Preparation of CRM binders containing WMA additives

An oil bath with a maximum temperature of 225°C, a mixer with a maximum velocity of 15,000 rpm, fitted with a propeller agitator and a one-liter metal container for mixing was used for the preparation of the binders.

The oil bath has a temperature probe which can be introduced into the mixing receptacle, allowing the temperature of the binder to be controlled with a precision of $\pm 1^\circ\text{C}$. A bitumen sample of 750 g was heated at 140°C and then placed in the oil bath. Additives were carefully added to the bitumen and the blends were subsequently mixed for 15 minutes at 4,000 rpm, ensuring that the additive was properly incorporated into the binder.

The blend was then heated to 185°C and the crumb rubber was added. The mixture was blended for 30 minutes at 2,000 rpm then for another 30 minutes at 900 rpm at a constant temperature of 185°C. Reheating and homogenization were carefully carried out

Table 5. Mixtures studied.

Mixture	Type	Rubber (%)	Additive (%)
AR	Control	20	0
AR + A1	AR-WMA	20	4
AR + A2	AR-WMA	20	4

at a controlled temperature in order to obtain reproducible results (Anderson, Marasteanu, Mahoney, & Stephens, 2000). Special attention was then paid to the thermal history and storage conditions of the test samples before testing (1 h at $25^{\circ}\text{C} \pm 0.5^{\circ}\text{C}$), because of their influence on rheological measurements (Soenen, Visscher, Vanelstraete, & Redelius, 2006).

2.6 Mixtures studied

In the present study, three bituminous mixtures were studied. The control mixture is an AR mixture which contains a 20% CRM binder while the other two were AR-WMA mixtures which contain a 20% CRM binder and 4% of additive. The mixtures selected for this study are listed in Table 5.

The selection of the production and compaction temperatures of the control mixture AR is based in previous studies that consider that the manufacturing temperature of this mixtures usually oscillate between 175°C and 180°C (CEDEX, 2007). On the other hand, the AR-WMA mixtures are evaluated and compared in order to assess the effect of the additives when working temperatures are decreased, specifically, -30 , -20 and -10°C .

The percentage of bitumen referred to the total weight of the dry aggregates chosen for the specimens was 9%. It must be noted that this is a higher percentage compared to conventional mixtures without rubber. The reason is that rubberized asphalt needs to be recovered by a bitumen film with a more relevant thickness.

3 TEST METHODS

3.1 Water sensitivity

The influence of water in the reduction of the WMA mixtures performance has been reported as one of the issues that need to be carefully controlled so the water sensitivity was determined according to EN 12697-12 standard (CEN, 2009). This test constitutes the assessment of the indirect tensile strength (ITS), carried out according to EN 12697-23 standard (CEN, 2004), of two identical groups of specimens conditioned in different environments: dry and wet with the application of vacuum.

All the specimens are subjected to the ITS test and the maximum strength is recorded. The ITS values are calculated in function of the geometrical dimensions of the specimens and the maximum strength. Finally,

the ratio (ITSR) between the average strength results of both groups of specimens (wet over dry) is evaluated in order to assess the water sensitivity of the mixture.

As the aggregate distribution chosen for this dissertation is a discontinuous one, in the Spanish context, the ITSR must be more than 90% (Ministerio de Fomento, 2014). It must also be taken into account that there are some differences between the minimum specified values for ITSR from one country to another.

3.2 Wheel-tracking test

In this study, the determination of the resistance to permanent deformation was carried out using the wheel-tracking test (WTT) according to EN 12697-22 standard (CEN, 2008) and the asphalt mixtures were compacted according to EN 12697-33:2006 standard (CEN, 2006).

The susceptibility of the control and AR-WMA mixtures to deform was assessed by measuring the rut depth (RD) formed by repeated passes of a loaded wheel at a temperature of 60°C . The main parameters obtained from this test are the Wheel Tracking Slope in air (WTS), calculated between the 5000th and the 10,000th cycles, and the Mean Proportional Rut Depth in air (PRD), according to the thickness of the specimen.

3.3 Resistance to fatigue

The fatigue cracking resistance of bituminous mixtures represents their ability to resist to the application of repetitive bending loads before failure. In this research, the fatigue resistance was determined using the four-point bending test procedure, according to the EN 12697-24 (CEN, 2013).

These tests were carried out at 20°C , at a frequency of 10 Hz and at eight different tensile strain levels, with one specimen tested for each strain level. The initial stiffness modulus of each tested specimen and the number of cycles that correspond to a 50% reduction of its initial value (failure criterion) was registered, thus obtaining the fatigue life of the specimen.

The control mixture was produced at 180°C and the AR-WMA mixtures were the ones produced at 160°C , 20°C below compared with the temperature of the control mixture. This decrease was considered to be representative to study the effect of the WMA additives considering the results of water sensitivity, stiffness modulus and resistance to permanent deformation of the present study.

4 RESULTS AND DISCUSSION

4.1 Water sensitivity

A summary of the results of the ITSR and the ITS values of the control and the AR-WMA mixtures can be seen are presented in Figure 2 and Figure 3.

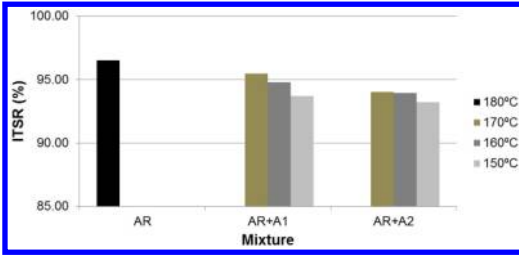


Figure 2. ITSR results of the studied mixtures.

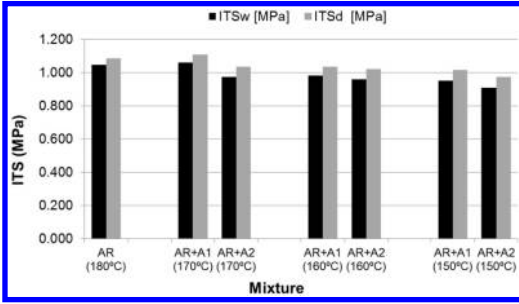


Figure 3. ITS results of the studied mixtures.

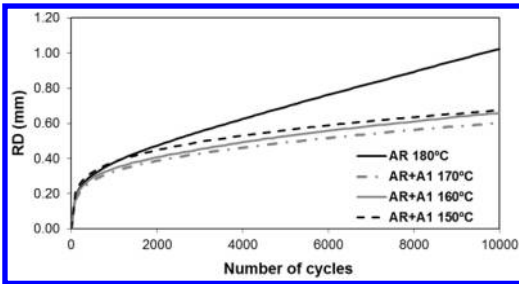


Figure 4. Evolution of RD of AR-WMA mixtures with A1.

It can be observed that for the AR-WMA mixtures with A1 and A2 the retained resistance was slightly less compared with the control mixture. However, these mixtures fulfill the water sensitivity a discontinuous mixture for a surface layer (90%). Besides, the ITS values for the dry and wet specimens were reduced as the compaction temperatures decreased. This effect might be associated with the increase of the percentage of air voids produced when the production/compaction temperatures were lower, which generated a further decrease in the resistance in the wet (ITS_w) and dry (ITS_d) specimens.

4.2 Resistance to permanent deformation

The evolution of the RD (mm) in air of the studied control and AR-WMA mixtures with the number of load cycles at 60°C is presented in Figure 4 and Figure 5. The RD and WTS values can be observed in Figure 6 and Figure 7.

According to the results it can be observed that for all the compaction temperatures the curves of

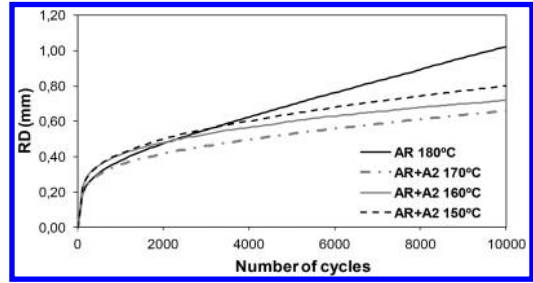


Figure 5. Evolution of RD of AR-WMA mixtures with A2.

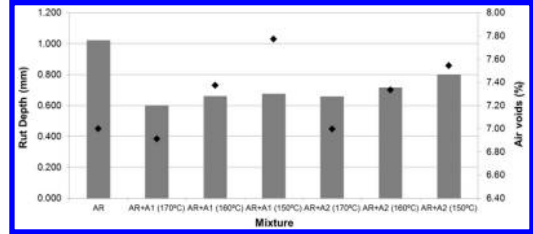


Figure 6. RD at 60°C.

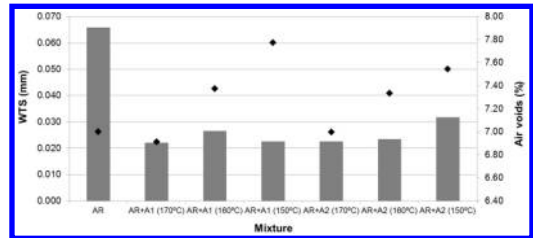


Figure 7. WTS at 60°C.

WMA mixtures are shifted on lower values, meaning that the addition of the waxes studied causes a reduction of the RD. Also, for the AR-WMA mixtures, as the compaction temperatures decreased, the RD increased slightly, never attaining the value of the control mixture.

All the WMA additives studied caused a reduction of RDs as a consequence of an increased global stiffness and the increase in the air voids content produced when the production/compaction temperatures were lower probably generated a further increase in the RDs of the AR-WMA mixtures studied. The WMA additive A1 led to a lower RD values than A2.

Besides, the WTS has been reduced to less than half, when compared to the control mixture. In the Spanish context, the WTS must be less than 0.07 (Ministerio de Fomento, 2014), which was fulfilled by all the mixtures. However, it appears that the air void content was not directly related to a certain value of WTS and these values are similar for each kind of mixture.

According to the results of the wheel-tracking tests, it can be stated that in terms of resistance to permanent deformation, the additives significantly improved the performance of the control mixture.

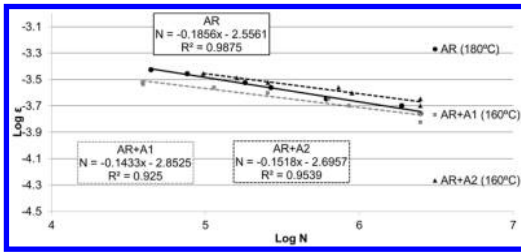


Figure 8. Fatigue performance of control and AR-WMA mixtures.

Table 6. Strain values of the control and AR-WMA mixtures.

Mixture	ϵ_6^*
AR	-3.6679
AR+A1	-3.7123
AR+A2	-3.6065

*Strain at 10^6 loadings

4.3 Resistance to fatigue

With the results obtained using the four-point bending test procedure, it was possible to determine the fatigue lines of the mixtures studied, which are presented in Figure 8.

It can be observed that for the mixture with A1 the fatigue resistance is shorter compared to the control mixture while for the mixtures containing A2 there was an improvement in the fatigue resistance.

Frequently, the fatigue life of the asphalt mixtures can be also compared with the strain value ϵ_6 which corresponds with 10^6 cycles. In Table 6 this values can be observed and compared.

Only the mixture with A1 has a higher strain value compared with the control mixture while the mixture with A2 has slightly lower value. This confirms that only the mixtures with A1 will have a shorter fatigue life.

5 CONCLUSIONS

In this study, the mechanical performance of AR mixtures with WMA additives (AR-WMA mixtures) were evaluated and compared with a control mixture regarding their water sensitivity and resistance to permanent deformation and fatigue. The WMA additives selected were two Montan waxes.

From these test results, the following conclusions were drawn.

The water sensitivity test results showed that the addition of the additives slightly reduced the retained resistance achieved and that the AR-WMA mixtures studied fulfilled the water sensitivity required by the Spanish standards for a surface layer and a discontinuous mixture (90%).

The loss of water resistance is due to the failure of the binder-aggregate interface and this often depends

on the chemical composition of the additive. It was also observed that as the production/compaction temperatures were lower, the retained resistance decreased due to an increase in the percentage of air voids.

Besides it was observed that the additives reduced the wheel-tracking slope (WTS) to less than half, when compared to the control mixture. Besides, as the compaction temperatures decreased, the mean rut depth (RD) slightly increased, probably due to the increase in the air voids content. The AR-WMA mixtures studied fulfilled the WTS required by the Spanish standards.

Also, the WMA additives were able to significantly improve the rutting resistance performance of the control mixture even though they were produced at much lower temperatures, confirming the efficiency of the WMA additive, even at low production/compaction temperatures.

Regarding to fatigue life, the mixture with A1 had a lower fatigue life while the mixture with A2 had a higher fatigue resistance. The strain values calculated is in keeping with these results.

Finally, it can be stated that additives studied improved the resistance to rutting and fulfilled the water sensitivity required by the Spanish standards for a surface layer and a discontinuous mixture. However, only one of the waxes improved the fatigue life of the control mixture.

REFERENCES

- Anderson, D., Marasteanu, M., Mahoney, J. and Stephens, J., 2000. Factors affecting the variability in the SHRP binders tests. Proceedings of the 79th Annual Meeting of the Transportation Research Board.
- CEDEX, 2007. Manual de Empleo de Caucho de NFU en Mezclas Bituminosas. Ministerio de Fomento, Ministerio de Medio Ambiente.
- CEDEX, 1999. Normas NLT. I, Ensayos de carreteras. NLT 373/94, fraccionamiento de los betunes asfálticos.
- CEDEX, 1992. NLT 349/90. Medida de módulos dinámicos de materiales para carreteras. Manual de Normas NLT. CEDEX, Madrid, 1992.
- CEN, 2013. EN 12697-24:2013. Bituminous mixtures – Test methods for hot mix asphalt – Part 24: Resistance to fatigue.
- CEN, 2009. EN 12697-12. Bituminous mixtures – Test methods for hot mix asphalt – Part 12: Determination of the water sensitivity of bituminous specimens.
- CEN, 2008. EN 12697-22:2008+A1:2008. Bituminous mixtures – Test methods for hot mix asphalt – Part 22: Wheel tracking.
- CEN, 2007. EN 1427:2007. Bitumen and bituminous binders – Determination of the softening point – Ring and Ball method.
- CEN, 2006. EN 12697-33:2006. Bituminous mixtures – Test methods for hot mix asphalt – Part 33: Specimen prepared by roller compactor.
- CEN, 2004. EN 12697-23:2004. Bituminous mixtures – Test methods for hot mix asphalt – Part 23: Determination of the indirect tensile strength of bituminous specimens.
- CEN, 2003. EN 1426. Bitumen and bituminous binders – Determination of needle penetration.
- Hossain, M., Swartz, S. and Hoque, E., 1999. Fracture and tensile characteristics of asphalt-rubber concrete.

- Journal of Materials in Civil Engineering, 11(4), pp. 287–294.
- Huang B., Mohammad L.N., Graves P.S., Abadie C., 2002. Louisiana experience with crumb rubber-modified hot-mix asphalt pavement. *Transport Res Rec: J Transport Res Board*, 1789:1–13.
- Hurley G.P.B., 2005. Evaluation of Sasobit® for Use in Warm Mix Asphalt. NCAT Report.
- Liang R.Y., L.S., 1996. Short-term and long-term aging behavior of rubber modified asphalt paving mixtures. *Transport Res Rec: J Transport Res Board*, 1530:11–7.
- Ministerio de Fomento, 2014. 543 Mezclas bituminosas para capas de rodadura. Mezclas drenantes y discontinuas. PG-3: Pliego de prescripciones tecnicas generales para obras de carreteras y puentes.
- Ruth B.E., R.R., 1995. Crumb rubber modifier (CRM) in asphalt pavements, *Proceedings of the transportation congress 1995*, pp. 768–85.
- Shen J., Amirkhanian S., Lee S.-J., 2005. Effects of rejuvenating agents on recycled aged rubber modified binders. *Int J Pavement Eng*, 6(4):273–9.
- Soenen, H., Visscher, J., De, Vanelstraete, A. and Redelius, P., 2006. Influence of thermal history on rheological properties of various bitumen. *Rheologica Acta*, 45(5), pp. 729–739.
- Sousa, J., Pais, J., Saim, R., Way, G. and Stubstad, R., 2002. Mechanistic-Empirical Overlay Design Method for Reflective Cracking. *Transportation Research Record: Journal of the Transportation Research Board*, 1809(-1), pp. 209–217.
- Wang, H. and You, Z., 2011. Intermediate temperature fatigue and low temperature cracking properties of rubber asphalt binder, 11th International Conference of Chinese Transportation Professionals: Towards Sustainable Transportation Systems, ICCTP 2011, August 14, 2011–August 17, 2011, American Society of Civil Engineers (ASCE), pp. 4121–4131.

Using tincal and colemanite wastes in bituminous hot mixtures as filler

C. Gürer

Department of Civil Engineering, Afyon Kocatepe University, Afyonkarahisar, Turkey

G.Ş. Selman

Graduate School of Natural and Applied Science, Afyon Kocatepe University, Afyonkarahisar, Turkey

ABSTRACT: Turkey has the largest boron reserves with respect to size, quality and diversity in the world. With the large quantity of boron production, some environmental problems were also occurred. The boron wastes have great potential to be used as secondary raw material. Therefore, the boron wastes can be used as filler in bituminous hot mixtures. In this study, bituminous hot mixture specimens were produced in accordance with the Marshall Design using wastes of colemanite (C) and tincal (T) as filler by a ratio of 7%. The test results were compared with specimen in which limestone filler added (L) by a ratio of 7%. The test results showed that specimens of (C) and (T) can be used in bituminous hot mixtures that behave as good as specimen (L). However, it was determined that bituminous hot mixture specimens of (T) series are better than specimens of (C) series.

1 INTRODUCTION

Turkey has the world's largest boron reserves (72.3%) and close to 600 000 tons/year of mine waste is disposed during the processing of boron in the mining industry (Öruç et al. 2004; Önal & Burat, 2008; Yenmez, 2009). If boron industry waste is discharged into lakes and seas, this would give damage to the aquatic environment; if polluted water is used in agricultural irrigation, the plants would suffer (Öruç et al. 2004; Önal & Burat 2008; Yenmez 2009; Libicki 1992; Nicholson 1995; Aşkın 1998; Rybicka 1998; Karadeniz 1996; Drew et al. 2002; De Rezende and De Carvalho 2003; Çetiner et al. 2006; Akbulut and Gürer 2007; Karaşahin and Terzi 2007). During the boron mining operations in the United States, taking measures to prevent damage to the environment is one of the most important precautions (Griffin 2003). If mining waste is used in an appropriate way problems and costs arising from the disposal of waste, pollution and devastation of the earth would be reduced. In addition, an economical gain can be obtained with new products comes from wastes, and pollution of ground and underground water can be prevented by these solutions (Rybicka 1996; Karadeniz 1996; De Rezende and De Carvalho 2003; Çetiner et al. 2006; Akbulut and Gürer 2007; Çetiner et al. 2006; Akbulut and Gürer 2007; Karaşahin and Terzi 2007). Çetiner et al. (2006) has reported that in Europe, especially towards 2000s, the accidents caused by mining waste disposal pools/dams resulted in serious environmental problems. Thus, the number of the researches focusing onto this subject has increased in recent years. All nations around the globe should follow

sustainable development methods, which require some goals to be set such as economic development, social development and environmental protection. Sustainable development consists of local and global efforts for basic human needs without destroying or degrading the natural environment (Griffin 2003). In this regard, the mining wastes should be recycled.

With the increasing human population, the need for civil infrastructures and raw materials is also increasing every passing day. Therefore, efficient use of available and other resources is crucial. Also boron and other mining wastes can be used as alternative aggregate raw material sources (Akbulut and Gürer 2007; Rafi et al. 2011; Selman 2013; Bäckström 2013). Although numerous studies associated with using boron wastes in construction industry exist in the literature (Demir and Orhan 2002; Kula et al 2002; Koyuncu and Güney 2003; Karacasu et al. 2004; Uğurlu et al. 2004; Kavas 2006; Ustabaş 2011), only limited number of the studies exists focusing on using boron wastes in bituminous hot mixtures (Selman 2013; Küçük-Sert and Küçük 2012; Terzi et al. 2013). Ustabaş (2011) has performed a study about wastes of colemanite and ulexite in Portland cement. Kavas (2006) reported that boron wastes can be used as fluxing agent in the production of red mud bricks. The use of clay containing boron waste becomes more common in the ceramic industry (Bentli et al. 2002; Emrullahoğlu and Emrullahoğlu 2002; Batar et al. 2007; Bayca et al. 2008). Demir and Orhan (2002) have obtained porous building blocks using pumice sand and borax waste. Karasu et al. (2002) have reported that boron waste can be used for the production of wall tile body as fluxing agent up to 10%. Uslu

Table 1. Rheological properties of bitumen.

Properties	Value	Standard
Source	Aliğa/Turkey	–
Penetration Grade	50/70	–
Penetration at 25°C	61	34
Specific gravity	1,039	35
Softening point (°C)	47	36
Loss on heating (%)	2.0	37
Flash point (°C)	290	38
Ductility (5 cm/dk)	> 100 cm	39
Viscosity at 135°C	0.409 Pa s	40
Viscosity at 165°C	0.106 Pa s	

and Arol (2004) have found that adding tailings up to 30% by weight has improved the quality of brick .95% of Turkey’s state road network consists from bituminous pavement (2014), so recycling aggregates from mining waste is not only economically important but also is environmental friendly. The aim of this study is investigating the mechanical properties of bituminous hot mixtures using tincal (T), colemanite waste (C) and limestone waste (L) as mineral filler. Thus, various tests were conducted to evaluate the properties of bituminous hot mixture. Based on these experimental results, the feasibility of using tincal and colemanite (T and C) wastes as mineral filler in bituminous hot mixtures was assessed comparing with control mixture using conventional limestone filler (L).

2 MATERIALS AND METHOD

2.1 Materials

In this study, limestone based aggregates and fillers were obtained from Afyonkarahisar region to be used. Colemanite and tincal wastes were taken from ETİBOR Emet and Kırka Borax Inc., which were used as waste filler aggregates. Colemanite wastes (C) were taken from coast of wastes pond and tincal wastes (T) were taken from the wastes of concentrator plant. These wastes were dried and milled and transformed into filler aggregates. Limestone coarse aggregates and traditional filler (L) derived from same sources are currently used in construction of pavements with bituminous hot mixture in Afyonkarahisar. 50/70 penetration bitumen was obtained from Aliğa Refinery that was used as binder. The rheological properties of the bitumen are given in Table 1.

2.2 Method

Testing procedure consists of two different phases including aggregate and bituminous hot mixture tests. In the first phase, the gradation analysis (ASTM C 136-84a 1992), specific gravity and water absorption (ASTM C127-88 1992; ASTM C 128-88 1992), Los Angeles abrasion (ASTM C 131-89 1992), freezing-thawing (TS EN 1097-2 1992), resistance loss after

freezing-thawing (TS EN 1097-2010) tests and chemical analysis on waste filler were performed.

Second phase includes following bituminous hot mixture tests: Marshall Stability-Flow (ASTM D 6927-06 2006), Mechanical Marshall Immersion (Whiteoak 1990), Marshall Stability after freezing-thawing cycle. Bituminous hot mixture designs for wearing layer were performed for three different fillers of specimens (L; T and C). Filler aggregates were used at a ratio of 7% in weight which ideally situated in the middle of the Turkish Highway Specification curve for each of the mixture series (L, T and C). Each series of bituminous hot mixtures were named after the code of filler specimens. Bituminous hot mixture briquettes specimens were produced in the ratio of 3.5; 4.0; 4.5; 5.0; 5.5; 6.0 percent in the laboratory according to the wearing layer curve of the specification. Three specimens were prepared for each rate of bitumen. Marshall Stability-Flow tests were performed and weights in water and air and surface dry-saturated were measured and stability versus bitumen %, bulk specific gravity versus bitumen %, void filled with bitumen versus bitumen %, void versus bitumen %, void in mineral aggregate versus bitumen% graphics were drawn respectively. Flow chart of the testing procedure was provided in Figure 1.

3 TEST RESULTS

3.1 Aggregate tests results

The mechanical and physical properties of aggregates, used in road pavement construction, and bituminous hot mixtures are extremely important, since they affect the performance. The tests results of aggregates were shown in Table 2. Apparently, according to the test results, the mechanical and physical properties of aggregates specimens are within the specification limits. The results of chemical analysis of T and C specimens were given in Table 3.

3.2 Bituminous hot mixture tests

3.2.1 Marshall stability-flow tests

Marshall Design tests were performed in order to determine the usability of tincal (T) and colemanite (C) waste as filler. The most important characteristic, expected from bituminous hot mixtures, is stability. Stability is defined as the strength of bituminous hot mixtures against various effects such as pressure, tension and shear force caused by traffic (Umar and Ağar 1994; Akbulut et al. 2012).

Bituminous hot mixtures used in wearing layers should provide at least 900 kg of stability value as specified by the Turkish Highway Technical Specification (2006). Maximum stability values of the T, C and L mixes correspond to optimum bitumen ratio was found as 1240; 1460 and 1480 kg respectively. The relationship between Marshall Stability and bitumen in percentage was shown in Figure 2.



Figure 1. Flow chart of the testing procedure.

Table 2. Physical and mechanical properties of aggregates.

Aggregate Test	Value	Limit	Standard
Los Angeles Abrasion Value (%)	22.4	<35	ASTM C 131-89 1992
Loss of Freezing-Thawing (%)	0.52	<12	TS EN 1097-2 1992
Loss of Resistance after Freezing-Thawing	29.6	–	TS EN 1097-2 1992
Coarse aggregate bulk specific gravity (>No:4)	2.683	–	ASTM C127-88 1992
Coarse aggregate apparent specific gravity (>No:4)	2.710	–	ASTM C127-88 1992
Fine aggregate bulk specific gravity (No:4 – No:200)	2.671	–	ASTM C128-88 1992
Fine aggregate apparent specific gravity (No:4 – No:200)	2.699	–	ASTM C128-88 1992
Filler aggregate apparent specific gravity (L)	2.738	–	ASTM C128-88 1992
Waste filler aggregate apparent specific gravity (T)	2.608	–	ASTM C128-88 1992
Waste filler aggregate apparent specific gravity (C)	2.562	–	ASTM C128-88 1992
Water absorption (%) (>No:4)	0.37	–	ASTM C128-88 1992
Water absorption (%) (No:4 – No:200)	0.65	–	ASTM C128-88 1992
Sieve Number (mm)		Passing (%)	Lower-Upper Limits
3/4 ¹¹ (19.0)		100	100
1/2 ¹¹ (12.5)		92.0	83–100
3/8 ¹¹ (9.5)		80.0	70–90
No:4 (4.75)		48.0	40–55
No:10 (2.00)		32.0	25–38
No:40 (0.42)		15.0	10–20
No:80 (0.180)		11.0	6–15
No:200 (0.074)		7.0	4–10

An increase in the density leads to better durability and stability properties. Therefore, density is considered to be another important physical property of the bituminous hot mixtures. The bulk

specific gravity values of the specimens of T, C and L series were obtained as 2.444, 2.453 and 2.452 gr/cm³ respectively. The values of T and C specimens are so close to L specimen. The relationship

Table 3. Chemical analysis results of T and C specimens.

Component	Boron waste (T) %	Component	Boron waste (C) %
CaO	11.78	CaO	13.59
SiO ₂	15.41	SiO ₂	24.77
Al ₂ O ₃	1.51	Al ₂ O ₃	7.11
Fe ₂ O ₃	0.43	Fe ₂ O ₃	3.22
MgO	13.62	MgO	6.27
Na ₂ O	7.92	Na ₂ O	0.16
K ₂ O	1.20	K ₂ O	2.76
P ₂ O ₆	0.02	Na ₂ O	0.16
TiO ₂	0.03	As ₂ O ₃	0.219
MnO	0.01	SrO	0.89
Cr ₂ O ₃	<0.002	SO ₄	0.34
B ₂ O ₃	>20000 ppm	B ₂ O ₃	22.46

between bulk specific gravity and bitumen is given in Figure 3.

Another important property for bituminous hot mixtures is void filled with bitumen (*VFB*). The property provides final bitumen film thickness around the aggregate grains and controls the properties of plasticity, durability and friction coefficients of bituminous hot mixtures (Akbulut and Güler 2007; Akbulut et al. 2012; Colorado Asp. Pav. Assoc. 2014). The binder film thickness between the aggregate and bitumen is vitally important in protecting the mixture from detrimental atmospheric effects, such as water, snow and etc. The percentage of *VFB* should be between 65–75% according to the TCK specifications. The relationship between *VFB* and bitumen in percentages is shown in Figure 4.

Another important parameter for bituminous hot mixtures is air voids content. Bituminous hot mixtures are designed based on unit weight and void ratio. Void ratio defined as percent of void volume at among aggregate particles coated by binder (Umar and Ađar 1994; Colorado Asp. Pav. Assoc. 2014). Upper and lower limits for void ratio were suggested in standards of many highway agencies (TCK 2006; Lavin 2003). According to the specifications of TCK the ratio of void should be between 3–5% in the bituminous hot mixtures used for wearing layer (TCK 2006). Void ratios corresponding to the optimum bitumen ratio for specimens of L, T and C series were found as 2.7; 3.2 and 2.5 respectively. The relationship between void and bitumen in percentage is given in Figure 5.

Voids in the mineral aggregate (*VMA*) are the air-void spaces that exist between the aggregate particles in a compacted bituminous hot mixture, including spaces filled with bitumen. Based on the fact that the thicker the bitumen film on the aggregate particles the more durable the mix, specific minimum requirements for *VMA* are specified in most specifications (Akbulut et al. 2012; Colorado Asp. Pav. Assoc. 2014). *VMA* values for L, T and C specimens with optimum bitumen ratios were found as 13.6%, 13.9% and 13.3% respectively. According to the Turkish Highway Technical Specification (2006), the minimum ratio of *VMA*

must be 14.0% in the wearing layers of bituminous hot mixtures. It was thought that if the filler ratio decreases, values of *VMA* meet the specification limits as stated by Akbulut et al. (2012). The relationship between void mineral aggregate and bitumen is shown in Figure 6 in percentage.

In the Marshall test, movement of the specimen during the fracture of specimen was measured and the measured value or amount of collapse is known as flow value (Umar and Ađar, 1994). The flow value indicates the behavior of bituminous mixtures under traffic and reflects their plasticity and flexibility properties (Whiteoak, 1990; Umar and Ađar, 1994; Akbulut et al., 2012; Asphalt Institute, 1989). The flow values of L, T and C specimens correspond to optimum bitumen ratio, which was determined as 3.0, 4.2, and 3.3 mm respectively. The relationship between Marshall Flow and bitumen is shown in Figure 7.

The Marshall quotient, also known as rigidity ratio, is defined as the ratio of the Marshall Stability to the Marshall Flow value of the bituminous hot mixture. The ratio was used for the estimation of stiffness modulus of bituminous mixtures (Whiteoak, 1990; Lavin, 2003). Çelik et al. (2007) have reported that specimens with high Marshall quotient are fractured with high displacement. The Marshall quotient values of L, T and C specimens for the optimum bitumen percent were found as follows: 4.9, 3.0, and 4.4 kN/mm respectively. The relationship between Marshall quotient and bitumen is given in Figure 8.

3.2.2 The test results of mechanical Marshall immersion

Principles of Marshall mechanical immersion test are based on measurement of change in the stability of compacted bituminous hot mixture specimens after immersed in water at 60°C. Understanding that ‘which mixture specimen is more resistant to the water effects’ is more feasible in this way (Whiteoak 1990). The test was performed for each series of specimens with optimum bitumen percent and loss of Marshall Stability calculated with equation (1).

$$\text{Loss of Marshall Stability} = \frac{S_2 - S_1}{S_1} \quad (1)$$

Specimens for immersing 24 and 48 hours in water bath at 60°C and Marshall Stability values (S_2) were also measured. Loss of Marshall Stability values were found by subtracting it from the highest Marshall Stability value (S_1). Loss of Marshall Stability values were obtained as in order of $C > T > L$ and $C > L > T$ after 24 and 48 hours of curing periods. Loss of Marshall Stability is given in Figure 9.

3.2.3 The effects of freeze-thaw cycle on bituminous hot mixture specimens

There are many factors that may affect the service life of road pavements such as freezing-thawing, raining, snowing etc. As a result of these effects, some losses in the mechanical properties of the bituminous

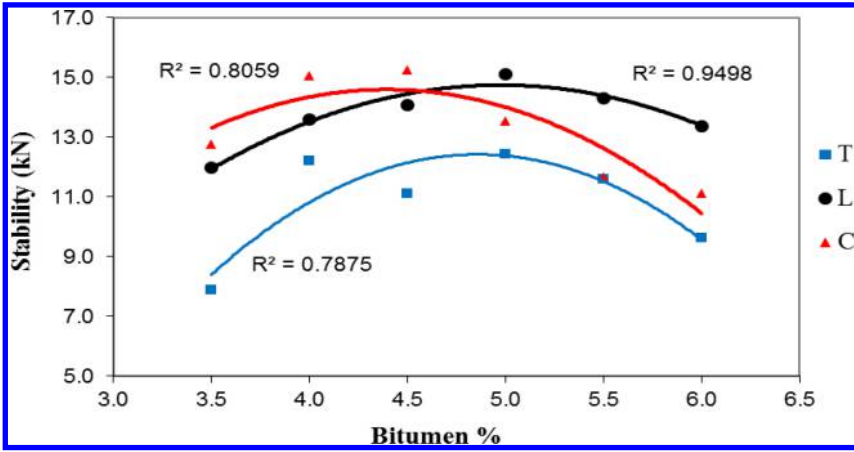


Figure 2. Relationship between Marshall stability and % bitumen.

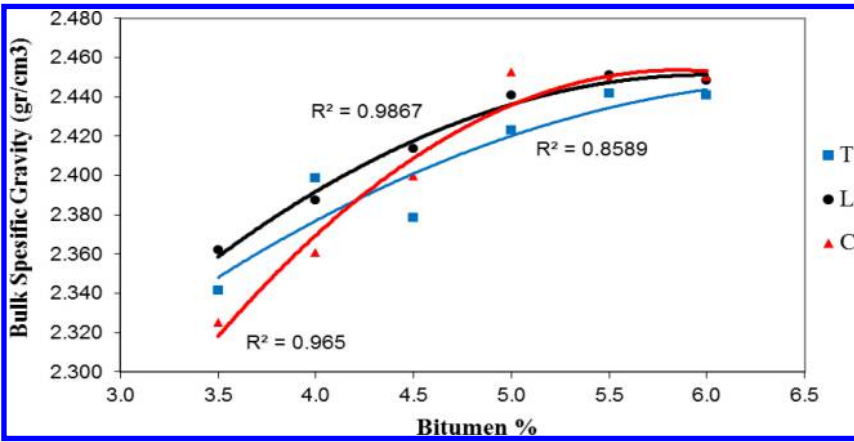


Figure 3. Relationship between bulk specific gravity and % bitumen.

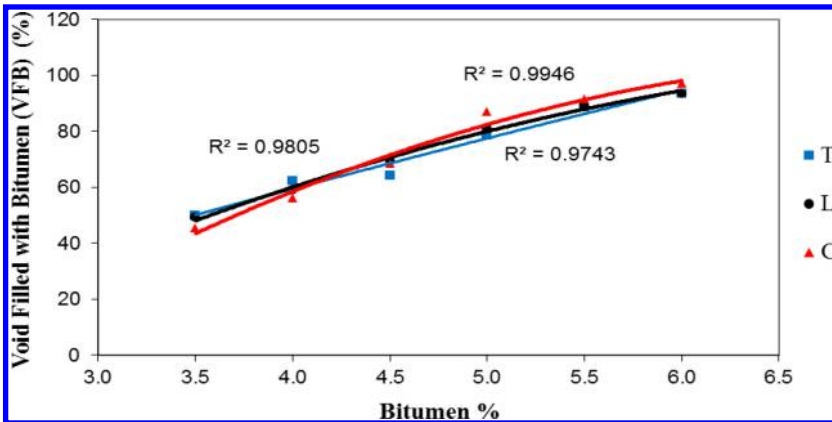


Figure 4. Relationship void filled with bitumen and bitumen %.

hot mixture pavement may occur. Numerous scientists reported that the amount of moisture damage was increased in bituminous hot mixture pavement with the increasing number of freeze-thaw cycles

(Hunter and Ksaibati 2002; Al-Qadi 2014). Therefore, the freezing-thawing test was performed as 5 cycles on compacted specimens produced at optimum bitumen percent stated by Hunter and Ksaibati (2002).

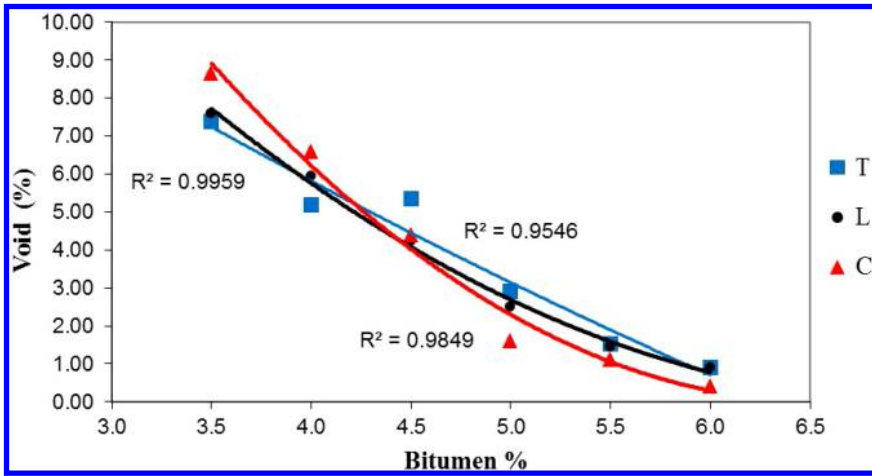


Figure 5. Relationship between void and % bitumen.

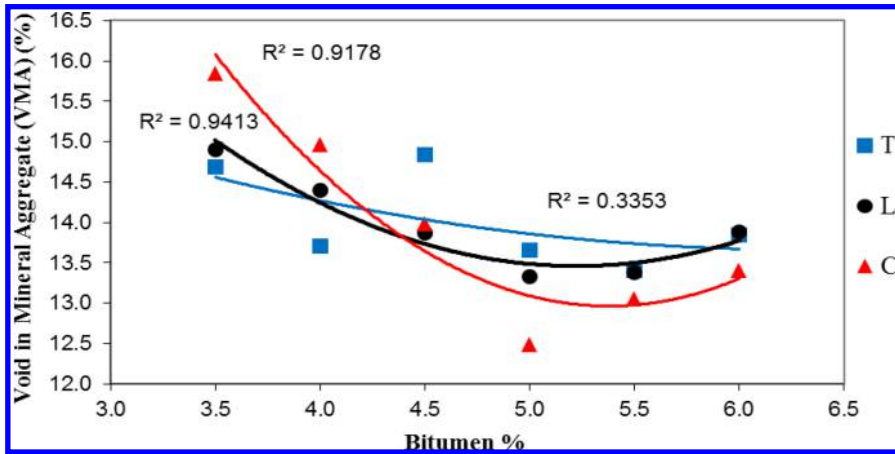


Figure 6. Relationship between void in mineral aggregate and % bitumen.

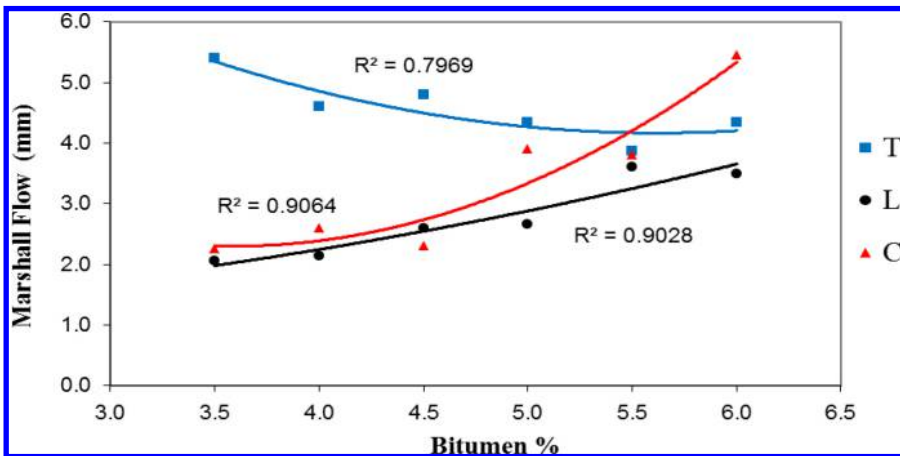


Figure 7. Relationship between Marshall Flow and % bitumen.

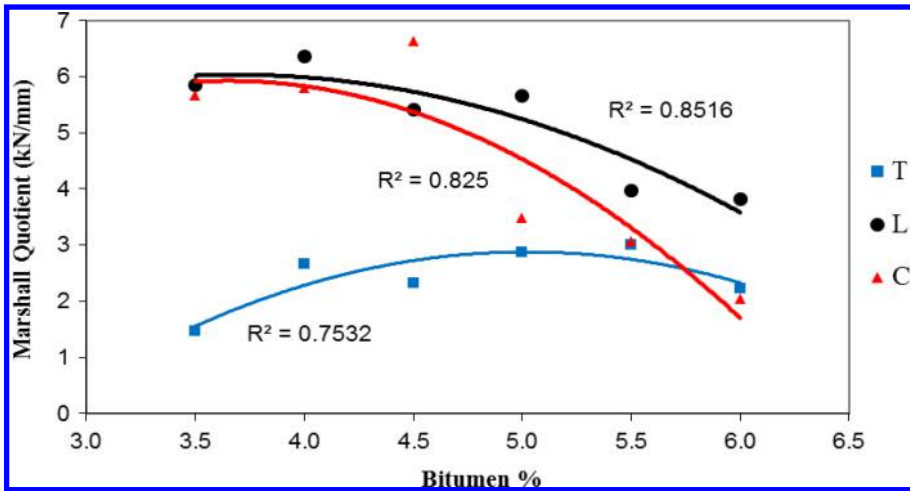


Figure 8. The relationship between Marshall quotient and % bitumen.

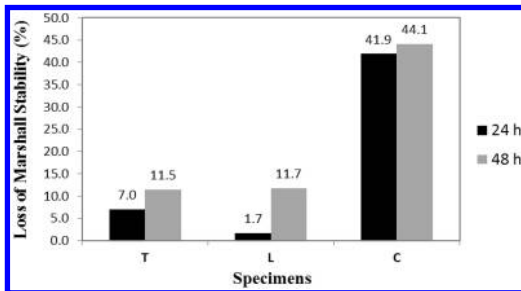


Figure 9. Loss of Marshall stability in percent.

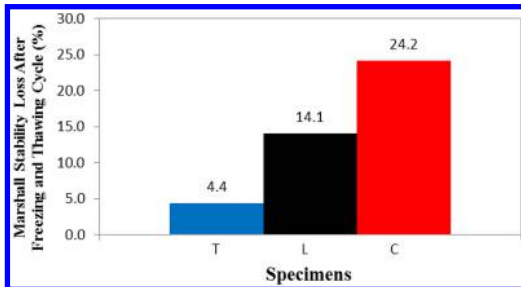


Figure 10. The loss of Marshall Stability after freezing-thawing cycle.

One cycle consist of freezing at -18°C for 16 hours and thawing at 60°C for 24 hours. According to the test results, the loss of Marshall Stability of specimens freezing-thawing cycle obtained as in order of $C > L > T$. After freezing-thawing cycle, the loss of Marshall Stability is given in Figure 10.

4 CONCLUSIONS

In order to determine the feasibility of the use of tincal and colemanite wastes in bituminous hot mixtures

as filler, aggregate and bituminous hot mixtures tests were carried out on the specimens. Based on the results of tests and analyses, the following conclusions and recommendations can be made.

Using tincal and colemanite waste as filler Marshall Design was performed for bituminous hot mixtures used in wearing layers and optimum bitumen ratios that were determined as 5.0–5.1 – 4.9% in weight for T; L and C specimens respectively. All ratios were found to be within the economical limits identified by the Turkish Highway Specifications (2006).

According to test results of Marshall Design, maximum values of Marshall Stability were obtained as in order of $L > C > T$ and all stability values were higher than specification limits. However, higher stability values are not a good feature. The flow results for C specimen were obtained as slightly greater than the specification limits. When the stability and flow results were considered together, it is expected that all of the specimens will exhibit good behavior under traffic.

Both T and C specimen's values of bulk specific gravity were obtained close to the traditional mixture specimen (L). Results of Marshall Stability are consistent with these values. Therefore, it is thought that specimens exhibit good permeability features. The amount of void in the C specimen was obtained as lower than others. Accordingly, C specimen may suffer from bleeding deterioration.

According to the specifications of most highway agencies, the ratio of VFB is required to be in the range of 70% to 85%. The VFB values of L, T and C specimens for the optimum bitumen percent were found as 82%, 75%, and 81% respectively. The VFB values of L, T and C specimens corresponding to the optimum bitumen percent were found as 13.6%, 13.9% and 13.3% that are close to the limit value (14%) of the specification. Therefore, it is thought that there are

better durability properties of T specimen than L and C specimens.

Based on the Marshall quotient calculations, it was expected that specimens of C and L series of behavior under traffic would be close to each other. However, the flexibility properties of the specimens of T series would be poorer than those of C and L series.

One of the important effects exposures to bituminous mixture is decreased in performance due to the stripping caused by water comes along with snow, rain, etc. Based on the test results of Marshall Mechanical immersion and freezing-thawing cycles, losses of Marshall Stability were obtained as in order of $C > T > L$. Test results show that, specimens of C series are more susceptible to moisture compared to the specimens of L and T series.

Road constructions have great potential for waste materials to be used. According to the results of the tests, it was thought that waste specimens of T and C can be used as filler for medium trafficked bituminous pavement; however, bituminous hot mixture contain T can exhibit better performance in the field than C specimens.

ACKNOWLEDGEMENTS

The authors wish to thank the Scientific Research Projects Coordination Department of Afyon Kocatepe University (Project Number: 14.MUH.06) for their financial support, Director of AKFALT (Afyonkarahisar Municipality Asphalt Laboratory) Kubilay AKIN; Responsible Engineer of AKFALT asphalt laboratory Faik KARAKOÇ; the asphalt laboratory assistants Ahmet İba and Balı Recep ENGİZ for their helps, KOLSAN Construction Inc. for providing aggregates, ETİBOR Emet and Kırka Borax Inc. for providing specimens of colemanite and tincal wastes.

REFERENCES

Akbulut, H., Güner, C. 2007. Use of aggregates produced from marble quarry waste in asphalt pavements. *Building & Environment*, 42(5): 1921–30.

Akbulut, H., Güner, C., Çetin, S., Elmacı, A. (2012). Investigation of using granite sludge as filler in bituminous hot mixtures, *Construction & Building Materials*, 36: 430–436.

Al-Qadi, I. L., Abuawad, I. M., Dhasmana, H., Coenen, A. R., Trepanier, J. S. 2014. Effects of various asphalt binder additives/modifiers on moisture-susceptible asphaltic mixtures. Research Report FHWA-ICT-14-004, Illinois Center for Transportation, IL, USA.

Asphalt Institute 1989. *The Asphalt Handbook*, Manuel series No:4 (MS-4), Edition, USA.

ASTM C136-84a 1992. Standard method for sieve analysis of fine and coarse aggregates. American Society for Testing and Materials, West Conshohocken, PA, USA.

ASTM C127-88 1992. Test method for specific gravity and adsorption of coarse aggregate. American Society for Testing and Materials, West Conshohocken, PA: USA.

ASTM C128-88 1992. Test method for specific gravity and adsorption of fine aggregate, American Society for Testing and Materials, West Conshohocken, PA: USA.

ASTM C131-89 1992. Test method for resistance to degradation of small-size coarse aggregates by abrasion and impact in the Los Angeles machine, American Society for Testing and Materials, West Conshohocken, PA: USA.

ASTM D5-06e1 2006. Standard Test Method for Penetration of Bituminous Materials, American Society for Testing and Materials, West Conshohocken, PA: USA.

ASTM D6-95 2006. Standard test method for loss on heating of oil and asphaltic compounds, American Society for Testing and Materials, West Conshohocken, PA: USA.

ASTM D4402-06 2006. Standard test method for viscosity determination of asphalt at elevated temperatures using a rotational viscometer. American Society for Testing and Materials, West Conshohocken, PA, USA.

ASTM D 6927-06 2006. Standard test method for marshall stability and flow of bituminous mixtures, American Society for Testing and Materials, West Conshohocken, PA: USA.

ASTM D113-07 2007. Standard test method for ductility of bituminous materials, American Society for Testing and Materials, West Conshohocken, PA: USA.

ASTM D70-09e1 2009. Standard Test Method for Density of Semi-Solid Bituminous Materials (Pycnometer Method), American Society for Testing and Materials, West Conshohocken, PA: USA.

ASTM D36/D36M-09 2009. Standard Test Method for Softening Point of Bitumen (Ring-And-Ball Apparatus), American Society for Testing and Materials, West Conshohocken, PA: USA.

ASTM D92-05a 2010. Standard Test Method for Flash and Fire Points by C Level and Open Cup Tester, American Society for Testing and Materials, West Conshohocken, PA: USA.

Aşkın, S. 1998. Evaluation of boron industry wastes. PhD Thesis, Celal Bayar University, Manisa, Turkey.

Bäckström, M. 2013. Compendium of mining and processing waste management technologies, Project: MIN-NOVATION Mining and mineral processing waste management innovation network, Baltic Sea Region Program, Orebro, Sweden.

Batar, T., Bayça, S., Solak, Ö., Sayın, E., Can, E., & Kahraman, B. 2007. Effects of boron ore and its tailings to the ceramic wall tile structure. In *Proceedings of 6th International Symposium on Raw Materials*, İzmir, Turkey, pp. 329–333.

Bayça, S.U., Batar, T., Sayın, E., Solak, O. & Kahraman, B. 2008. The influence of coal bottom ash and tincal (boron mineral) additions on the physical and microstructures of ceramic bodies. *Journal of Ceramic Processing Research*, 9(2), 118–122.

Bentli, T., Özdemir, O., Çelik, M. S. & Ediz, N. 2002. Boron tailings and evaluation strategies. In *Proceedings of 1st International Symposium on Boron, Kütahya/Turkey*, pp. 250–258.

Çelik, O. N., Yonar, F., & Ceylan, S. 2007. Filler effects on bituminous hot mixture performance. In *Proceedings of 7th National Congress on Transportation*, İstanbul, Turkey. pp 196–204.

Çetiner, E. G., Ünver, B., & Hindistan, M.A. 2006. Regulations related with mining wastes: European Community and Turkey. *Mining*, 45(1), 23–34 (in Turkish).

Colorado Asphalt Pavement Association. *Volumetrics in asphalt mixtures*: www.co-asphalt.com (July 1st, 2014).

Demir, İ. & Orhan, M. 2002. Using of boron waste in the production construction materials', In *Proceedings of*

- 1st International Symposium on Boron, Kütahya/Turkey, pp. 235–239.
- De Rezende, R. L. & De Carvalho, J. C. 2003. The use of quarry waste in pavement construction. *Resources Conservation & Recycling*, 39: 91–105.
- Drew, L. J., Langer, W H & Sachs, J. S. 2002. Natural aggregate mining. *Natural Resources Research*, 11(1): 19–28.
- Emrullahoğlu, Ö. F. & Emrullahoğlu, C.B. 2002. Effect of Etibor Kırka borax tailing addition on properties of floor tile body. In Proceedings of 1st International Symposium on Boron, Kütahya/Turkey, pp. 213–218.
- General Directorate of Highways of Turkish Republic (TCK), 2014:<http://www.kgm.gov.tr/Sayfalar/KGM/SiteTr/Kurumsal/YolAgi.aspx> (July 1, 2014).
- Griffin, T. S. 2003. Rio Tinto borax's initiative on sustainable development in mining operations. In Proceedings of The International Congress & Exhibition on Mining, Turkey, pp. 375–379.
- Hunter, E R, & Ksaibati, K. 2002. Evaluating moisture susceptibility of asphalt mixes, Report for United States Department of Transportation to the Mountain-Plains Consortium, University of Wyoming: Laramie: WY: USA.
- Karacasu, M., Koyuncu, H., Bakış, R., Taşpolat, L. T., & Yılmaz, G. 2004. The use of borax, sepiolite, zeolite, waste meerscham and contaminated river sediment in asphalt concrete mixtures. In Proceedings of 2nd International Symposium on Boron, Eskişehir: Turkey. 441–447.
- Karadeniz, M. 1996. Ore beneficiation plant waste – environmental impact – measures', General directorate of mineral research and exploration (MTA). Mining analysis and technologies (MAT) department. Ankara, Turkey.
- Karasu, B., Kaya, G., & Yurdakul, H. 2002. The effect of Etibor Kırka Borax Company's concentration and derivation wastes on the properties of wall tile bodies. In Proceedings of 1st International Symposium on Boron, Kütahya, Turkey, pp. 235–239.
- Karavaşin, M., & Terzi, S. 2007. Evaluation of marble waste dust in the mixture of asphaltic concrete. *Construction & Building Materials*, 21: 617–620.
- Kavas, T. 2006. Use of boron waste as a fluxing agent in production of red mud brick. *Building & Environment*, 41: 1779–1783.
- Koyuncu, H. & Güney, Y. 2003. Stabilization of borax wastes. Proceedings of 1st International Conference on Environmental Research and Assessment, Bucharest, Romania.
- Kula, İ., Erdoğan, Y., Olgun, A., Kalfa, O.M. & Sevinç, V. 2002. Effects of colemanite waste, coal bottom ash and fly ash on the properties of cement. Proceedings of 1st International Symposium on Boron, Kütahya: Turkey, pp. 202–206.
- Kütük-Sert, T. & Kütük, S. 2012. Physical and Marshall properties of borogypsum used as filler aggregate in asphalt concrete. *Journal of Materials in Civil Engineering*, 25(2): 266–273.
- Lavin, P. 2003. *Asphalt Pavements: A Practical Guide to Design, Production and Maintenance for Engineers and Architects*. 1st ed. Spon Press, Taylor & Francis Group.
- Libicki, J. 1992. Environmental facts of open quarry mining and social effects. Proceedings of 15th International Congress on World Mining, Madrid, Spain.
- Nicholson, D.T. 1995. The visual impact of quarrying. *Quarry Management*, 22 (7): 39–42.
- Oruç, F., Sabah, E., & Erkan, Z. E. 2004. Evaluation strategies of boron tailings according to sector. Proceedings of 2nd International Symposium on Boron, Eskişehir: Turkey, pp. 385–392.
- Önal, G. & Burat, G. 2008. Boron mining and processing in Turkey. *Gospodarka Surowcami Mineralnymi-Mineral Resources Management, The Journal of Polish Academy of Sciences*, 4/3: 24.
- Rafi, M. M., Qadir, A., Siddiqui, S.H. 2011. Experimental testing of hot mix asphalt mixture made of recycled aggregates. *Waste Management & Research*, 29(12): 1316–1326.
- Rybicka, E. H. 1996. Impact of mining and metallurgical industries on the environment in Poland. *Applied Geochemistry*, 11(1–2): 3–9.
- Selman, G. Ş. 2013. Using boron waste in construction industry. M.Sc. Seminar, Afyon Kocatepe University, Afyonkarahisar, Turkey.
- Terzi, S., Morova, N., Çolak, N., Serin, S., & Saltan, M. 2013. Using colemanite waste in asphalt concrete mixtures as filler. Proceedings of 10th National Congress on Transportation, İzmir Turkey.
- TS EN 1097-2. 2010. Tests for Mechanical and Physical Properties of Aggregates – Part 2: Methods for The Determination of Resistance to Fragmentation, Turkish Standard Institution, Ankara: Turkey.
- Republic of Turkey, Ministry of Transport, General Directorate of Highways (TCK). 2006. *Turkish State Highway Specifications*, Ankara: Turkey, 515–518.
- Uğurlu, A., Özdemir, M., Topçu, İ. B. 2004. Evaluation of boron containing clay wastes in cement. Proceedings of 2nd International Symposium on Boron, Eskişehir: Turkey, 405–411.
- Umar, F., Açar, E. 1994. *Asphalt Pavements*, 1st ed., Istanbul Technical University, Faculty of Construction Press, İstanbul: Turkey, pp. 138–165.
- United Nations General Assembly. 2005. World summit outcome, resolution A/60/1, adopted by the general assembly on 15 September 2005. retrieved 2014-02-17.
- Uslu, T., Arol, A. I. 2004. Use of boron waste as an additive in red bricks. *Waste Management*, 24: 217–220.
- Ustaş, İ. 2011. Investigating usability of colemanite and ulexite in cement, Proceedings of International Congress on Ready Concrete, İstanbul: Turkey, 367–375.
- Whiteoak, D. 1990. *The Shell Bitumen Handbook*. Shell Bitumen: England.
- Yenmez, N. 2009. The importance of boron minerals in Turkey as a strategic mine. *Istanbul University Journal of Geography*, 19: 59–94.

Assessing temperature reduction potential of various additives on binder and asphalt mix level for mastic asphalt

B. Hofko, M. Dimitrov & M. Hospodka

Vienna University of Technology, Institute of Transportation, Research Center for Road Engineering, Austria

ABSTRACT: In an ongoing study, the wax concentration in a polymer-modified binder is varied for different wax types to study their impact on binder viscosity by rotational viscometer (RV) tests. In addition, mastic asphalt (MA 11) was produced with different wax-modified binders in a lab mixer. The mixer is equipped with a dynamic torque sensor to derive the mixing-torque as a measure of workability during mixing. Thus, temperature reduction potential is studied on binder and mix level. As an alternative approach for temperature reduction of mastic asphalt, crushed aggregates were substituted by rounded aggregates.

It was found that amide wax has the highest potential for temperature reduction of mastic asphalt (-23 K at 4 wt.% related to binder mass). When substituting the 0/4 fraction by rounded aggregates, a reduction of 23 K can be realized, when substituting the 0/11 fraction, a reduction of 36 K is possible without use of waxes.

1 INTRODUCTION

Among the different asphalt mix types, mastic asphalt (German: Gussasphalt) holds a special position due to its composition, application and load transfer. The main components of mastic asphalt is filler with up to 40 wt.% (CEN, 2013) and bituminous binder with around 8 wt.% to 10 wt.%. Thus, about half of the mix is considered as mastic, the other half is taken up by coarse aggregates. Due to its composition with high binder and filler content, mastic asphalt is applied in the field without compaction, it is merely poured. Different from other asphalt mix types, mastic asphalt transfers load mainly by a stiff mastic and not by coarse aggregate interaction. In addition, the mix does not exhibit air voids. There is a wide range of applications for mastic asphalt as sealing and/or surface layer on bridges (Widyatmoko et al., 2005, Medani et al., 2007), as road surface layer for city centers where compaction would endanger historic buildings or as surface layers for walk and bike ways.

Since the mastic is responsible for load transfer, usually hard and in many cases polymer-modified binders are employed for mastic asphalt. To keep the mix pourable, the viscosity of the mastic and mix has to be low enough at the construction site. Thus, high temperatures of up to 250°C are necessary for mixing and paving. Since more than 70% of the total energy consumption for asphalt mix production are dedicated to the mixing plant (Canada, 2005), mastic asphalt is especially energy-intensive in production. Also, a number of reports show that workers health is increasingly affected when bitumen is handled at temperatures over 200°C (Hansen, 1991, Ruhl et al.,

2007, Kriech and Osborn, 2014). For these reasons, a temperature reduction in mastic asphalt is seen crucial for enhanced energy efficiency and a healthier work environment. The addition of waxes to bitumen is a state-of-the-art procedure to reduce the binder's viscosity above the waxes' drop points and reduce the mixing and paving temperature of asphalt mixes (Biro et al., 2009, Silva et al., 2010, Rubio et al., 2012, Wu and Zeng, 2012). Different types of waxes are available and employed with different effects on workability of the mix during production as well as on the performance of the mix in terms of resistance to permanent deformation at high temperatures and to cracking at low temperatures. Due to wax crystallization during cooling of the mix to ambient temperatures, waxes tend to increase the high temperature stability and decrease the low-temperature cracking resistance.

This paper compares the temperature reduction potential for a mastic asphalt mix with different wax-modified binders. In addition, an economic alternative to waxes for temperature reduction is investigated as well. Therefore, crushed aggregates are partly and completely substituted within the mastic asphalt. The investigations were carried out on two levels of observation, on the binder level and on the asphalt mix level.

2 MOTIVATION AND OBJECTIVES

Within a comprehensive research project, called <E>EMA ("High Efficiency Low Emission Mastic Asphalt"), optimized mastic asphalt mixtures are developed with regard to temperature reduction, mix

performance and economic efficiency. The following steps are taken by the project:

1. Bitumen is blended with different waxes and different wax concentrations to study the effect of the waxes and their concentration on the temperature reduction potential by rotational viscometer (RV) tests with temperature sweep.
2. Mastic asphalt is produced with bitumen modified with different waxes in a lab mixer. The lab mixer is equipped with a mixing torque measurement unit to assess workability of the mixes at different temperatures.
3. An alternative approach for temperature reduction is taken by substituting usually used crushed aggregates by rounded aggregates in the mix and the workability is analyzed as well.
4. Mastic asphalt slabs are produced in lab using the methods that show best potential for temperature reduction. The resistance to permanent deformation by uniaxial cyclic compression tests (UCCT) and to low-temperature cracking by thermal stress restrained specimen tests (TSRST) are assessed and results are compared to results from the reference mix.
5. Thus, an optimized mastic asphalt mixture can be recommended with a maximum temperature reduction potential while keeping the mix performance at a high level and keeping the material costs low.

This paper presents results of the first three research items.

3 MATERIALS

For the presented research a mastic asphalt with a maximum nominal aggregate size of 11 mm (MA 11) was used. The filler component is powdered limestone, the coarse fraction are totally crushed aggregates of porphyritic origin. The grading curve is shown in Figure 1. For the binder, an SBS-modified PmB 25/55-65 (PG 82-16) was used. The main characteristics of the binder are listed in Table 1.

The mix consists of 8.2 wt.% binder and shows a maximum density of 2.46 kg/m³ which is equivalent to the bulk density since no air voids are present in the mix.

Four waxes were employed to compare their temperature reduction potential, an amide wax (AW), a Fischer-Tropsch wax (FTW), a montan wax (MW) and a polyethylene wax (PEW).

As an alternative approach to lower the production temperature, the crushed aggregate was substituted partially and completely by rounded, calcitic aggregates, respectively. The filler component remained unchanged for each tested mix.

4 TEST METHODS AND TEST PROGRAM

Two test methods are applied to assess and compare the temperature reduction potential on binder level

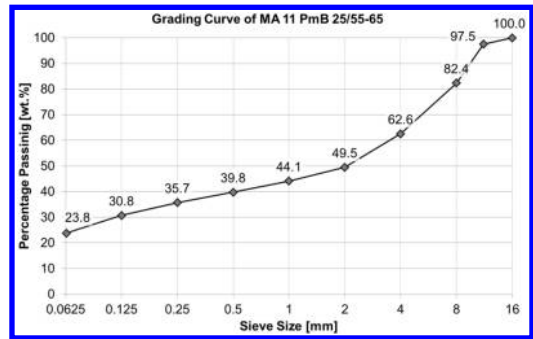


Figure 1. Grading curve.

Table 1. Main characteristics of the PmB 25/55-65.

Parameter	Value
Needle Penetration at 25°C	50 dmm
Softening Point Ring & Ball	77.6°C
Performance Grade	PG 82-16

as well as on asphalt mix level: (a) the rotational viscometer (RV) for bitumen testing and (b) measurement of mixing torque in a conventional lab mixer for asphalt mix production.

4.1 Rotational viscometer (Bitumen level)

The rotational viscometer (RV) is a test device to measure the dynamic viscosity of bituminous binders. Figure 2 shows the principle of the device: It consists of a coaxial system of cylinders, a static outer cylinder (1) and a rotating inner cylinder (2). The outer cylinder is filled with bitumen (4). The radius of the spindle R_1 used for this research is 16.6 mm, the radius of the outer cylinder R_2 19.0 mm.

The momentum that is needed to keep the spindle rotating with a constant speed of 20 rounds per minute (RPM) is directly related to the resistance of the spindle to rotation and is thus, a measure of the dynamic viscosity of the tested sample. The dynamic viscosity of bitumen obtained by RV is used to describe the workability of bitumen at mixing and production temperature (CEN, 2010).

4.1.1 Test program

As shown in Table 2, a comprehensive test program was carried out on the original binder (PmB), as well as on binder, modified with the different waxes at concentrations ranging from 2 wt.% to 30 wt.% based on bitumen mass.

To mix bitumen with the waxes, the following procedure was carried out for all samples:

- Bitumen, sealed in cans, was heated at 180°C for 4 hours within a thermal chamber

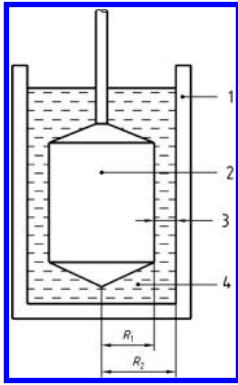


Figure 2. Principle of the RV (CEN, 2010).

Table 2. Test program for RV testing.

	0 wt.%	2 wt.%	4 wt.%	6 wt.%	10 wt.%	30 wt.%
PmB	3x					
AW		x	3x	x	x	x
FTW		x	x	x	x	x
MW		x	x	x		
PEW		x	x	x	x	

- The respective wax was also heated in a covered way at 180°C for 3 hours within a thermal chamber to melt it, which makes the mixing process easier.
- The preheated bitumen is placed on a heated sand bath and the pre-defined mass of melted wax is added to the bitumen while the bitumen is stirred by a mechanical mixing device for 20 min to ensure a homogeneous blend.
- After mixing, the samples are filled in the outer cylinders of the RV and are cooled down to room temperature. All samples rested for 24 h prior to RV testing.

For RV testing, the samples were heated in the device to 135°C and the dynamic viscosity was determined at 135°C, 140°C up to 250°C with temperature steps of 10 K. At each temperature a triple determination of the dynamic viscosity was obtained. For the original binder without wax modification and for the binder modified with 4 wt.% of AW, the RV was run on three separately mixed samples to check repeatability of the mixing process and of the test itself.

4.2 Mixing torque measurement (Mix level)

To assess the possible temperature reduction not only on bitumen level, but on larger scale, mixing-torque measurements with a temperature sweep were carried out on different mastic asphalt mix samples.

The device for these measurements is a standard compulsory lab mixer as shown in Figure 3. It consists of a rotating drum with a capacity of 30 l and a



Figure 3. Lab mixer with torque measurement device (Infratest).

Table 3. Test program for mixing-torque measurements on mastic asphalt MA 11.

	0/11	0/4	4/11	—
TC ^{*)}				
TR ^{**)}	—	4/11	0/4	0/11
PmB	3x	2x	2x	2x
PmB + 4 wt.% AW	2x			
PmB + 10 wt.% AW	2x			
PmB + 4 wt.% FTW	2x			
PmB + 4 wt.% PEW	2x			

*) TC = totally crushed aggregates

**) TR = totally rounded aggregates

reverse rotating mixer with variable speed from 25 to 60 RPM. The drum can be heated up to 250°C. In addition, a torque measurement device records the mixing torque in Nm necessary to rotate the mixer at a constant speed. The mixing torque is used as a measure for the workability of the mix.

4.2.1 Test program

Table 3 shows the test program carried out for mixing-torque measurements on the mastic asphalt mix (MA 11). As reference sample, the asphalt mix with the PmB was taken. In addition, mixes with 4 wt.% and 10 wt.% of AW and with 4 wt.% of FTW and PEW were tested. The mix design of these mixes consisted of 100% totally crushed aggregates (TC). As an alternative way to reduce the production temperature, an attempt was made by substituting a part of the totally crushed aggregates by totally rounded aggregates (TR). Thus, different mastic asphalt mixes with PmB and different aggregate geometries as shown in Table 3 were tested as well. For one mix the 0/4 fraction, for another mix the 4/11 fraction and for a third mix the complete 0/11 fraction was substituted by TR. It should be noted at this point, that the filler component was left unchanged and the grading curve of the mix was not altered either. For all mixes a triple or double replication of the mixing torque measurement on separate samples was run.

The standardized test procedure for obtaining the mixing torque at different temperatures is as follows:

- In case of PmB with wax modification, the wax-modified binder was produced according to the procedure listed in section 4.1.1 prior to asphalt mix production.
- Aggregates, binder and the lab mixer were preheated at 170°C. The aggregates were preheated for 5 hours; the binder and lab mixer for 3 hours.
- Fine and coarse aggregates were homogenized in the mixer for 30 sec, after that the binder was added and the mix was homogenized for a mixing time of 3 min at a mixing speed of 40 RPM. In all cases a constant asphalt mix mass of 22 kg was used for testing.
- After the initial mixing process, the actual mixing-torque measurements started at 170°C and 40 RPM for 300 sec. The sampling rate is 1 Hz. Subsequently, the mixer with the mix inside was heated to 190°C with intermediate mixing of 10 sec every 60 sec to ensure a homogeneous temperature distribution in the mix. When the set temperature was reached, another mixing-torque measurement started at 40 RPM for 300 sec. This procedure was continued every 20 K until 250°C were reached.

5 RESULTS AND DISCUSSION

5.1 Temperature reduction on bitumen level

RV tests were carried out according to the test program listed in Table 2. To present results of RV testing exemplarily, Figure 4 shows the dynamic viscosity vs. test temperature of the PmB and of the binder modified with different percentages of AW. Since the benchmark value for calculation of the temperature reduction on binder level is the dynamic viscosity of the PmB at 230°C, this value is marked in the diagram (77.2 mPa*s). As can be seen from the diagram in Figure 4, the viscosity of the binder is reduced with increasing wax concentration in the binder. The standard deviation for the PmB and the PmB with 4 wt.% of AW is implemented in the diagram as well but due to the small scattering of results it is not visible. The maximum standard deviation from three replicates is 3.5 mPa*s for the PmB and 6 mPa*s for the PmB with 4 wt.% of AW. This proves an excellent repeatability of the test itself, as well as a good repeatability of the mixing process of wax with the binder.

Figure 5 shows results of all tests in terms of dynamic viscosity at 230°C vs. wax concentration for all four wax types. The presented data are mean values given in a log-lin scale. In addition, a logarithmic function of the following form was employed to give an analytical link between wax concentration and dynamic viscosity:

$$\eta(wc) = a \cdot \ln(wc) + b \quad (1)$$

η dynamic viscosity [mPa*s]
 wc wax concentration [wt.%]
 a, b regression coefficients.

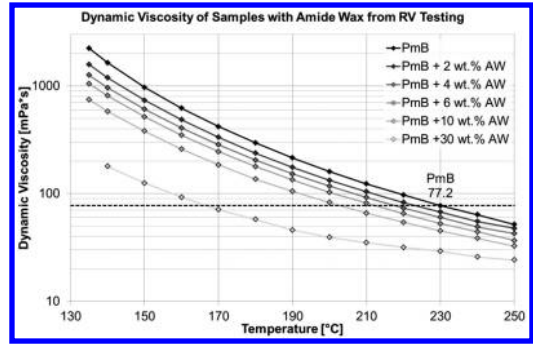


Figure 4. Dynamic viscosity vs. temperature for original binder (PmB) and AW modified PmB with different concentrations of wax.

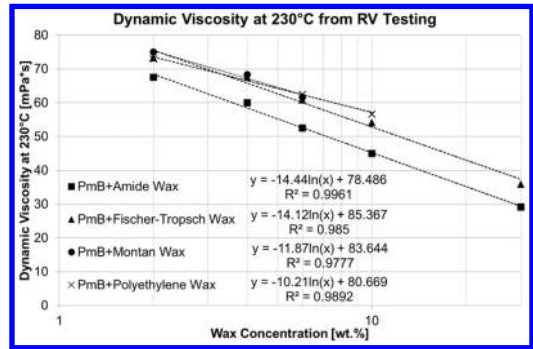


Figure 5. Dynamic viscosity at 230°C vs. wax concentration for all wax-modified binder samples.

Coefficient a describes the impact of wax concentration on the change in dynamic viscosity, coefficient b indicates the dynamic viscosity at a wax concentration of 1 wt.%. The lower the absolute value of b and the higher the absolute value of a , the higher is the viscosity reduction potential of the respective wax. In the presented case, the highest viscosity reduction occurs for AW, followed by FTW, MW and PEW. As visible from the diagram in Figure 5, AW seems to be a class of its own, since the combination of coefficients a and b is optimal. FTW and MW exhibit similar behavior, while the PEW shows the smallest incline a .

To determine the possible temperature reduction on bitumen level, results from the PmB were used as the reference sample. Since the production temperature of standard mastic asphalt is between 230°C and 250°C, the mean value of the dynamic viscosity of the PmB at 230°C was taken as the benchmark value (77.2 mPa*s). The equiviscous temperature at 77.2 mPa*s, i.e. the temperature where the same dynamic viscosity occurs, was derived from RV test data of all tested samples. For this, the dynamic viscosity between two measured data points was considered to have a linear trend. Results of this analysis are given in Figure 6. It shows the equiviscous temperature vs. wax concentrations for all tested samples. In addition,

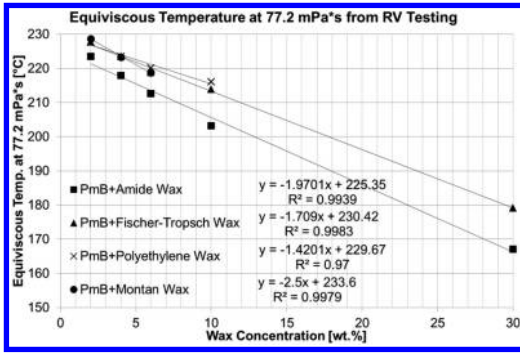


Figure 6. Equiviscous temperature at 77.2 mPa*s vs. wax concentration for all wax-modified binder samples.

a linear regression of the following kind was applied to the data:

$$T_{eq}(wc) = c * wc + d \quad (2)$$

T_{eq} equiviscous temperature [°C]
 wc wax concentration [wt.%]
 c, d regression coefficients.

Coefficient c gives the impact of the wax concentration on the temperature reduction, coefficient d gives the interception at 0 wt.% wax concentration. In theory, coefficient d should be 230°C for all samples, since this is the temperature at which the dynamic viscosity of 77.2 mPa*s of the original binder occurs. The actual values of d range from 225.4°C to 233.6°C. One explanation for this is the fact that the evolution of the dynamic viscosity between two temperatures with recorded data was considered linear when in fact it does not exhibit a linear behavior.

Similar to the results shown in Figure 5, the best temperature reduction potential occurs for the AW modified binder, followed by FTW, montan wax and PEW. If only the incline of the linear regression c was taken into consideration, MW would show the best behavior. This would be true for higher wax concentrations, but since the intercept d is the highest for MW, the higher incline does not get effective at low wax concentrations (below 10 wt.%) which are representative for use in construction practice, where economic considerations do not allow for higher concentrations than 4 wt.% of wax.

5.2 Temperature reduction on mix level

To assess the temperature reduction potential on mix level, mixing-torque measurements were carried out on the reference mix and wax-modified mixes, as well as on mixes with partial or complete substitution of crushed aggregates by rounded aggregates.

Figure 7 shows results for the tests with wax-modified mixes. The data points shown in the diagrams are mean values at those temperatures were more than 20 single mixing-torque measurements were recorded. The benchmark to assess the temperature reduction

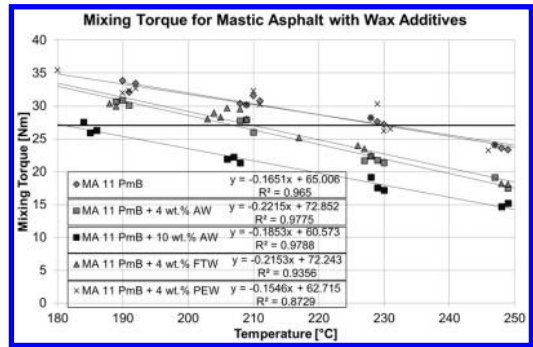


Figure 7. Mixing torque vs. temperature for the reference mix and the wax-modified mixes.

potential on mix level is the mixing torque of the reference mix (MA 11 PmB) at 230°C, which is analogue to the assessment on the binder level. For an analytical description of the link between mixing torque and temperature, a linear regression of the following kind was carried out:

$$M_{mix}(T) = g * T + h \quad (3)$$

M_{mix} mixing torque [Nm]
 T mixing temperature [°C]
 g, h regression coefficients.

Coefficient g indicates the temperature susceptibility of the mix regarding the mixing torque. A higher absolute value of g means a stronger decrease of the mixing torque with increasing temperature. Coefficient h gives the theoretical mixing torque at 0°C. A low coefficient h and a high absolute value of g are desired for a high potential of temperature reduction on mix level. From the coefficient values and a visual analysis of the mixes with 4 wt.% wax modification, AW and FTW show the best temperature reduction potential compared to the reference mix. AW shows a temperature susceptibility of -0.222 Nm/K, FWT of -0.215 Nm/K. PEW (-0.155 Nm/K) even shows a slightly worse behavior than the reference mix with -0.165 Nm/K. The mix with 10 wt.% of AW is a class of its own with clearly lower mixing torques, although the incline of the linear regression is smaller than for the 4 wt.% AW mix. Since the intercept with the y-axis at 0°C is much lower for the 10 wt.% mix (60.6 Nm) than for the 4 wt.% mix (72.9 Nm), the higher modified mix shows lower mixing torques than the lower modified mix.

Figure 8 includes data for the mixes where crushed aggregates were substituted by rounded aggregates. The diagram is analogue to Figure 7. The results indicate that the mixes with rounded aggregates behave similarly to the wax-modified mixes in terms of temperature reduction potential. All mixes with rounded aggregates show an incline of the linear regression between -0.221 Nm/K and -0.226 Nm/K. These values are similar to the 4 wt.% AW and FTW mixes.

In addition, the mixes with rounded aggregates where the 4/11 fraction and the complete 0/11 fraction

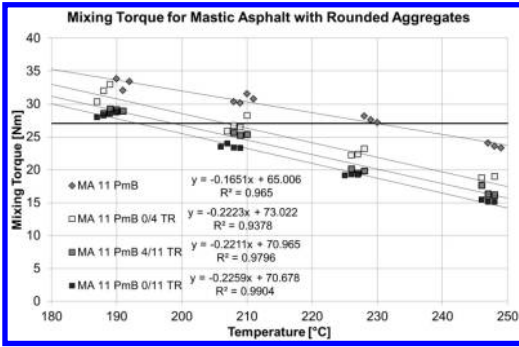


Figure 8. Mixing torque vs. temperature for the reference mix and mixes with partly and complete substitution of crushed aggregates by rounded aggregated.

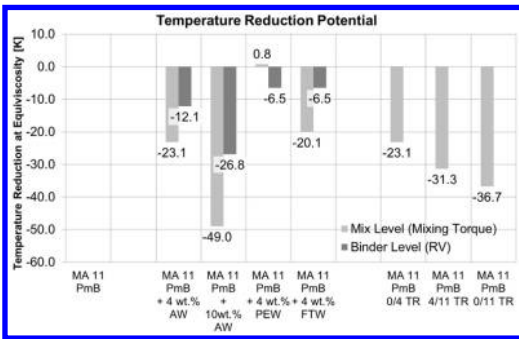


Figure 9. Comparison of temperature reduction derived from binder testing and mix testing.

was substituted exhibit smaller intercepts with the y-axis at 0°C (71.0 Nm and 70.7 Nm respectively) than the wax-modified mixes. Thus, these mixes show an even higher temperature reduction potential compared to wax-modified mixes.

5.3 Comparative Analysis

Figure 9 presents an overview of the temperature reduction potential of the tested products on binder and mix level. The reference for the calculated temperature reduction is the dynamic viscosity of the PmB at 230°C for the binder level and the mixing torque at 230°C of the MA 11 PmB for the mix level. The values given in 6 show the temperature difference at the same dynamic viscosity (77.2 mPa*s) and the same mixing torque (27.2 Nm) respectively for the different tested products.

Looking at the data for mixes with wax modification, it becomes obvious that the derived temperature reduction potential on binder level deviates strongly from the reduction potential on mix level. In case of AW and FTW, the results on binder level underestimate the temperature reduction potential. The difference between binder and mix level ranges from 13.6 K to 22.2 K. In case of PEW, the results on binder level overestimate the reduction potential by 7.3 K. The ranking

of the products (for 4 wt.% wax concentration) is the same for binder and mix level: PEW shows the lowest potential (a slight increase in temperature was measured on mix level), followed by FTW and AW.

Looking at the mixes with rounded aggregates instead of crushed aggregates, the reduction potential varies from -23.1 K to -36.7 K. The lowest reduction potential was obtained for the 0/4 TR, followed by 4/11 TR and 0/11 TR.

When results from wax-modified mixes and mixes with rounded aggregates are compared, it is obvious that the temperature reduction potential is equal or even higher for substitution of crushed aggregates. When only the 0/4 fraction is substituted, the temperature reduction is equal to 4 wt.% of AW, for substitution of the 4/11 and 0/11 fraction, the reduction is 8.2 K to 13.6 K higher than for wax-modified mixes.

6 SUMMARY AND OUTLOOK

Within <E>EMA (“High Efficiency Low Emission Mastic Asphalt”), a comprehensive research project, optimized mastic asphalt mixes with regard to maximum temperature reduction and high level of mix performance are developed. This paper contains results of investigations on the temperature reduction potential of different waxes on binder and asphalt mix level. In addition, an alternative approach for temperature reduction by substituting crushed aggregates partly or completely by rounded aggregates is analyzed as well.

To analyze the temperature reduction potential on binder level, an SBS-modified binder (PmB) with and without wax modification was tested in the rotational viscometer (RV) with temperature sweep at different wax concentrations. The temperature reduction potential on mix level was investigated by producing mastic asphalt with a maximum nominal aggregate size of 11 mm (MA 11) using PmB, as well as wax-modified binders. In addition, mixes with PmB and a partial or complete substitution of crushed aggregates with rounded aggregates were produced. The mixes were produced in a standard compulsory lab mixer that is equipped with a device to measure the necessary mixing torque at a constant mixing speed. The mixing-torque measurements were carried out with a temperature sweep from 170°C to 250°C.

To assess the temperature reduction potential, the binder viscosity at 230°C of the PmB was taken as a benchmark on binder level and the mixing torque at 230°C for the MA 11 PmB on mix level.

The following conclusions can be drawn from the results.

The evolution of the dynamic viscosity of the binder in RV vs. wax concentration can be fitted by a logarithmic function. The evolution of the equiviscous temperature vs. wax concentration can be described by a linear function. From RV tests on binder level, amide wax (AW) showed the highest reduction potential, followed by Fischer-Tropsch wax (FTW), montan wax (MW) and polyethylene wax (PEW).

The evolution of the mixing torque vs. temperature on mix level can be described by a linear function. The ranking of the waxes is the same as for the binder level. For PEW, no temperature reduction could be derived on mix level.

When the resulting temperature reduction on binder and mix level is compared, large differences between these two levels of observations were found. E.g. the temperature reduction of a 4 wt.% AW modified binder is 12.1 K on binder level and 23.1 K on mix level. The reduction potential is underestimated for AW, FTW and MW on binder level. For PEW, the reduction potential is overestimated on binder level. This shows that an assessment of the actual temperature reduction needs to be carried out on mix level if reliable values should be derived from testing.

Substitution of crushed aggregates by rounded aggregates has a high potential for temperature reduction in mastic asphalt. When the 0/4 fraction is substituted by rounded aggregates, 23.1 K temperature reduction is possible. This is an equal reduction compared to addition of 4 wt.% AW to the binder. When the 4/11 fraction is substituted, the production temperature can be reduced by 31.3 K, when the complete 0/11 fraction is substituted it can be reduced by 36.7 K. This shows that the use of rounded aggregates for mastic asphalt can be seen as an economic alternative for temperature reduction.

While crushed aggregates are necessary in other asphalt types to ensure a stable mix due to dominant intergranular contact of coarse aggregates and also to ensure a high friction value for surface layers, the situation is different for mastic asphalt. The dominant load transfer in mastic asphalt is a hard mastic with hardly any intergranular contact. Due to the binder excess in mastic asphalt, the surface has to be post processed by chip sealing with crushed aggregates after paving to realize a high friction value.

Tests on performance of the different mixes are currently running. The resistance to permanent deformation and to low-temperature cracking is investigated for the reference mix as well as for the wax-modified mixes and the mixes with rounded aggregates.

REFERENCES

- Biro, S., Gandhi, T. & Amirkhani, S. 2009. Midrange Temperature Rheological Properties of Warm Asphalt Binders. *Journal of Materials in Civil Engineering*, 21, 316–323.
- Canada, N. R. 2005. Road Rehabilitation Energy Reduction Guide for Canadian Road Builders. In: Conservation, C. I. P. F. E. (ed.).
- CEN 2010. EN 13302: Bitumen and bituminous binders – Determination of dynamic viscosity of bituminous binder using a rotating spindle apparatus. Brussels.
- CEN 2013. EN 13108-6: Bituminous mixtures – Material specifications – Part 6: Mastic Asphalt. Brussels.
- Hansen, E. S. 1991. Mortality of Mastic Asphalt Workers. *Scandinavian Journal of Work Environment & Health*, 17, 20–24.
- Kriech, A. J. & Osborn, L. V. 2014. Review and implications of IARC monograph 103 outcomes for the asphalt pavement industry. *Road Materials and Pavement Design*, 15, 406–419.
- Medani, T. O., Huurman, M., Liu, X. Y., Scarpas, A. & Molenaar, A. A. A. 2007. Describing the behaviour of two asphaltic surfacing materials for orthotropic steel deck bridges. *Advanced Characterisation of Pavement Soil Engineering Materials, Vols 1 and 2*, 1351–1368.
- Rubio, M. C., Martinez, G., Baena, L. & Moreno, F. 2012. Warm mix asphalt: an overview. *Journal of Cleaner Production*, 24, 76–84.
- Ruhl, R., Musanke, U., Kolmsee, K., Priess, R. & Breuer, D. 2007. Bitumen emissions on workplaces in Germany. *Journal of Occupational and Environmental Hygiene*, 4, 77–86.
- Silva, H. M. R. D., Oliveira, J. R. M., Peralta, J. & Zoorob, S. E. 2010. Optimization of warm mix asphalts using different blends of binders and synthetic paraffin wax contents. *Construction and Building Materials*, 24, 1621–1631.
- Widyatmoko, I., Elliott, R. C. & Read, J. M. 2005. Development of heavy-duty mastic asphalt bridge surfacing, incorporating Trinidad Lake Asphalt and polymer modified binders. *Road Materials and Pavement Design*, 6, 469–483.
- Wu, C. F. & Zeng, M. L. 2012. Effects of Additives for Warm Mix Asphalt on Performance Grades of Asphalt Binders. *Journal of Testing and Evaluation*, 40, 265–272.

*Highway and pavement management systems,
network operation systems*

Network-level pavement life-cycle assessment tool

J. Cirilovic

IMS Institute, Belgrade, Serbia

G. Mladenovic & C.A. Queiroz

University of Belgrade, Belgrade, Serbia

ABSTRACT: In addition to their attempt to keep overall maintenance costs low while keeping their road networks in the appropriate condition, road agencies are facing even more demanding challenges as they incorporate effects on global climate change and other environmental impacts into their decision-making process. Many studies and research initiatives have shown the impact of pavement condition on vehicle fuel consumption and maintenance costs, indicating that maintaining the pavement network at the lowest roughness level would lower fuel and parts consumption, which is beneficial for the environment. On the other hand, the more intensive pavement maintenance, which is required to keep roads as smooth as possible, is accompanied significant emissions and negative environmental impacts. The objective of this paper is to find an optimal maintenance plan at network level that minimizes the environmental impact during the entire pavement life-cycle, which includes both traffic and maintenance works.

1 INTRODUCTION

In addition to their need to keep overall maintenance costs low while keeping their road networks in the appropriate condition, road agencies are facing even more demanding challenges as they consider environmental impacts, including effects on global climate change, in their decision-making process.

Horvath and Hendrickson (1998) took into account both sustainable development and environmental impact when selecting a pavement type (either a rigid structure of reinforced concrete or a flexible construction of asphalt concrete). The LCA (Life Cycle Assessment) technique is considered the basic technique when it comes to assessing the environmental impact throughout the life cycle (Ekvall 2002) and has been applied to date by a number of researchers on numerous systems, including the highways (Park et al. 2003).

Zhang et al. (2008) integrated the costs related to environmental impact for pavement overlays into LCCA (Life Cycle Cost Analysis). In recent years, LCA has been applied to analysis of preventive maintenance (Giustozzi et al. 2012), winter maintenance (Fitch et al. 2013), and works that include recycling and use of milled asphalt (Santos et al. 2014).

Typically, the LCA is applied at the project level on roads and highways when there is specific project-related information available, while it has been far less frequently applied during the strategic analysis and decision-making processes at the road network level (Bryce et al. 2013).

The objective of the present study is to develop an optimal maintenance strategy and estimate the impact of different trigger levels on the overall CO₂ emissions on the Serbian state road network. However, within this paper, the methodology was applied to a virtual network containing five actual sections. Maintenance options included application of asphalt overlays in various thicknesses.

2 BACKGROUND AND PREVIOUS RESEARCH

Extensive research has been done in the past concerning the impact of traffic and pavement maintenance and operations on environment and climate change.

Many studies and research initiatives have modeled the impact of pavement conditions on vehicle fuel consumption and maintenance costs, indicating that maintaining the pavement network at the lowest roughness level would lower fuel and parts consumption, which is beneficial for the environment.

On the other hand, more intensive pavement maintenance is required to keep roads as smooth as possible, but that maintenance, which includes the production and placement of new pavement layers, and the related traffic congestion and diversions during maintenance works, is accompanied by extensive emissions and negative environmental impacts.

As a consequence of pavement surface deterioration, caused by traffic loading and aging, pavement roughness (typically expressed using International Roughness Index – IRI) increases, followed by certain reductions in vehicle operating speeds, then increased

fuel consumption and, finally, increased CO₂ emissions.

According to the model proposed by Yu and Lu (2013), every 1 m/km increase of the IRI leads to a 0.84 km/h decrease of the free flow average speed. Based also on this assumption, Yu et al. (2012) proposed calculating a fuel consumption factor (FCF) in order to describe the real fuel consumption of vehicles driving on the deteriorated pavements. FCF is a factor taking values greater than 1, and Yu et al. (2013) proposed two separate equations: one for passenger cars (Equation 1) and one for trucks (Equation 2).

$$FCF = 7.377 \times 10^{-3} \times IRI + 0.993 \quad (1)$$

$$FCF = 2.163 \times 10^{-3} \times IRI + 0.953 \quad (2)$$

Zhang et al. (2008) also used FCF, but used only one equation that also gives a simple linear relationship between IRI and FCF, as presented by Equation 3

$$FCF = 0.0667 \times IRI + 0.866 \quad (3)$$

Reger et al. (2014) considered that green-house gas (GHG) emissions are associated with the additional fuel consumption caused by roughness, also with separate consideration for passenger cars and trucks. The authors used the assumption that a change in fuel consumption is linear with respect to roughness, i.e. each additional unit of roughness (1 m/km), results in an increase of 1.05% in fuel consumption for cars and 0.725% for trucks.

3 METHODOLOGY

The overall Global Warming Potential (GWP), determined by CO₂ emission levels, was assessed during a period of time which included both maintenance activities on the pavement, i.e. hot-mix asphalt overlays in various thicknesses, and the usage phase.

GWP during maintenance activities was calculated as the sum of emissions resulting from (i) material production, (ii) transportation of materials from the asphalt plant to the job site and back to the asphalt plant, and (iii) laying down the asphalt.

CO₂ emissions during the usage phase were assessed through the HDM-4 model (Odoki and Kerali, 2000; The World Bank, 2011), while CO₂ emissions during the maintenance activities were calculated using the PaLATE software (Horvath, 2003).

As a case study and numerical example, the road database of the Public Enterprise, "Roads of Serbia," was used as a data source for the information about the network and sections, such as traffic levels, traffic composition, length of sections, their current condition, structural number, etc.

3.1 Mathematical model

In order to explore the relative difference between the usage phase and the production and placement

of a new asphalt layer (i.e. an overlay), the cumulative CO₂ emissions of both processes were calculated. The optimal solution ends to minimize the total GWP by achieving two objectives: (i) driving on the smoother asphalt pavement and (ii) prolonging the period between two maintenance activities which involves producing and placing the new asphalt layer, as shown by Equation 4.

$$GWP = \sum_{n=1}^{\infty} \left\{ \int_{t_{n-1}}^{t_n} CO_2^{usage}(s) \times dt + CO_2^{overlay}(w_n) \right\} \quad (4)$$

The main assumption was that the GWP in the usage phase is directly proportional to the current condition of the pavement (s), expressed through the International Roughness Index (IRI [m/km]), while the GWP of the maintenance treatment mainly depends on the thickness of the overlay (w_n [mm]).

3.2 Pavement deterioration model

The pavement deterioration model is based on the previous work of Tsunokawa and Schofer (1994), later adopted in many routines (Li and Madanat, 2002; Ouyang and Madanat, 2004; Ouyang and Madanat, 2006), which imply that road conditions follow a saw-tooth trajectory through time, meaning that pavement deteriorates to a point when maintenance treatment is applied, which is represented with instantaneous improvement in pavement condition.

Equation 5 presents the assumption that the deterioration rate depends only on the current condition of the pavement.

$$\frac{ds(t)}{dt} = F(s(t)) \quad (5)$$

The initial pavement condition is given by Equation 6.

$$s(0) = s_0 \quad (6)$$

The pavement deterioration model is formulated by Equation 7, as follows:

$$s_1 e^{f_1 t_n} = s_2 \quad (7)$$

After time t_n, the road deteriorates from condition s₁ to the condition s₂, while the factor f₁ is the deterioration factor, which should be calibrated in accordance to the specific climate and traffic conditions of the section.

3.3 Usage phase and corresponding CO₂ emission

The HDM-4 model was used for the calculation of CO₂ emissions during the usage phase. The model distinguishes between medium car and heavy truck emissions models. Based on data simulation, which included variations in only roughness parameter while maintaining constants of all the other road and vehicle parameters (such as geometrical characteristics of the road and mechanical properties of the vehicle), it

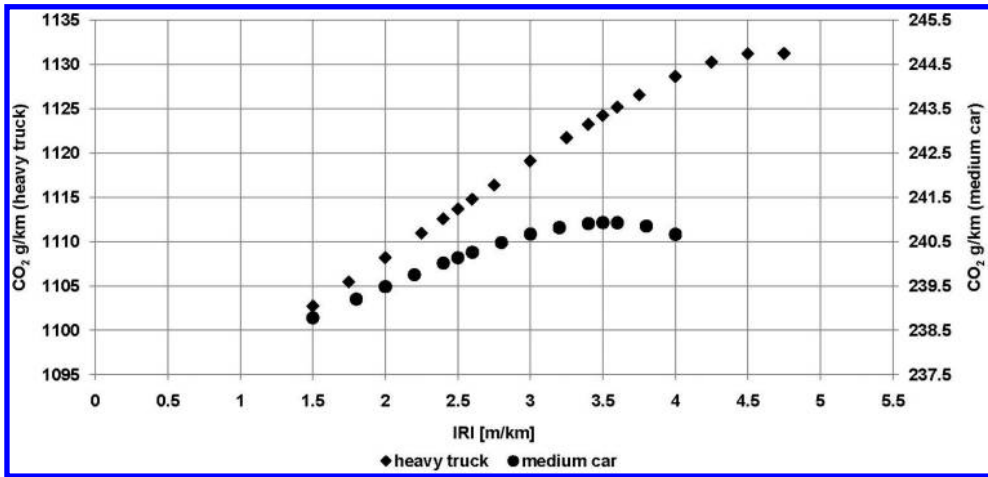


Figure 1. Change of CO₂ emission with roughness for heavy truck and medium car.

Table 1. Regression parameters for usage phase models.

parameter	model 1	model 2	model 3
	medium car	medium car	heavy truck
	$a + b \times IRI$ $+ c \times IRI^2$	$a + b \times IRI$	
a	234.7	237.9	1087.2
b	3.3	0.83998	10.5
c	-0.445	-	-
R ²	0.986	0.869	0.999
Significance	1.00E-08	4.24E-07	1.14E-20
SE estimate	-	0.26	0.27
SE a	0.33	-	-
SE b	0.24	-	-
SE c	0.04	-	-

Note: SE – standard error

was determined that there is close-to-linear relationship between roughness and CO₂ emissions for the range of conditions that most frequently occur on the real network (IRI lower than 4 m/km). However, both models (i.e. for medium cars and for heavy trucks) show nonlinear behavior for roughness greater than 4 m/km and greater than 5 m/km, for medium cars and heavy vehicles, respectively (Figure 1).

Table 1 shows the regression parameters for both medium car and heavy truck models.

Both the linear and non-linear regressions were explored for model development, based on the data obtained via data simulations using the HDM-4 model.

The linear model for medium cars has a coefficient of determination R² equal to 0.869. However, the non-linear regression model shows improved results compared to the linear regression model. The coefficient of determination R² equals 0.986 for the second-degree polynomial model. Therefore, the adopted relationship between CO₂ emissions during the usage phase

that is related to road condition expressed through the roughness index is given by Equation 8

$$CO_2 [g/km]^{passenger\ cars} = 234.7 + 3.3 \times IRI [m/km] - 0.4 \times (IRI [m/km])^2 \quad (8)$$

The linear model for heavy trucks has a coefficient of determination R² equal to 0.999 and was therefore used in the model (Equation 9).

$$CO_2 [g/km]^{heavy\ trucks} = 1087.2 + 10.5 \times IRI [m/km] \quad (9)$$

3.4 Maintenance phase pavement improvement model

The level of improvement depends on the intensity of the treatment, defined as the thickness of asphalt overlay w_n [mm], and the pavement condition prior to the treatment s_{2n} , as shown by Equation 10.

$$G(w_n, s_n) = s_{2n} - s_{1n} = g_1 \times \sqrt{w_n} + g_2 \times s_{2n} + g_3 \quad (10)$$

After the maintenance treatment, the pavement continues to deteriorate from s_{1i} to $s_{2(i+1)}$.

Equation 10 also shows that the reduction in roughness depends only on the maintenance treatment (overlay thickness) and the condition of the pavement before overlay. Calibration factors, g_i , are developed based on the Paterson bilinear model (Paterson 1990).

3.5 Maintenance phase and corresponding CO₂ emission

The maintenance phase actually involves three separate phases, i.e. (i) material production, (ii) material transportation, and (iii) processes. Within this paper, maintenance activities refer only to the application of overlays in various thicknesses, meaning that the two other phases of a life cycle, initial-construction and end-of-life, were not considered.

Input data included the volumetric composition of an asphalt mix (the ratio between bitumen and aggregate), transport distance, and equipment used for transportation and paving of asphalt mix.

A series of data records was generated using the PaLATE software, keeping all the parameters constant, except the overlay thickness (Figure 2).

Data records show a linear behavior; therefore, a linear regression equation was developed with the coefficient of determination R^2 being 0.999 (Equation 11).

$$CO_2[t/km]^{overlay} = 0.337 + 5.984 \times w[cm] \quad (11)$$

4 CASE STUDY

For the purpose of this analysis, five existing road sections from the main road network of Serbia were chosen for the application of the optimization model. These sections have substantially different

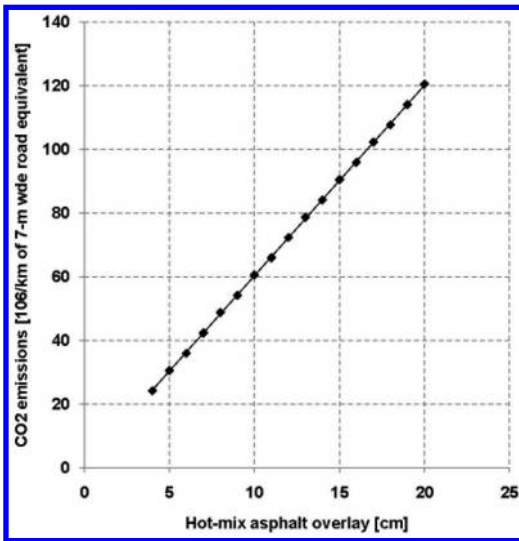


Figure 2. CO_2 emissions during maintenance phase.

traffic volumes ranging from AADT of 606 vehicles/day/year to AADT of 49230 vehicles/day/year and initial conditions ranging from $IRI = 2.01$ m/km to $IRI = 4.51$ m/km.

The optimization model is based on the genetic algorithms, and it gives an optimal solution in terms of minimizing the total CO_2 emissions during certain, previously defined, time frame. Several constraints were defined: (i) the analysis period was 30 years, (ii) the minimal time between two overlays is 4 years, (iii) the maximum time between two overlays is 12 years, and (iv) the condition after the intervention cannot be better than $IRI = 2.0$ m/km.

4.1 Results

Obtained results showed different maintenance thresholds depending on the traffic class of the road section (Figure 3).

For Section 1, which has very low traffic volume, the optimal solution dictates relatively rare and moderate overlays, keeping the section in poor condition. During the 30-year analysis period, the maximum value of the IRI is 6.35 m/km, and the optimal scenario involves application of overlays in thicknesses from 4.5 to 5.5 cm.

On the other hand, Section 5, which has a relatively high traffic level, demands more regular interventions on the pavement. The maximum value of the IRI is 4.25 m/km, and the optimal scenario involves application of overlays in thicknesses from 7.0 to 8.0 cm.

For Section 3, which has a moderate traffic volume, the maximum value of IRI is 4.33 m/km, and the optimal scenario suggests overlays in thicknesses from 4.5 to 6.0 cm. The other two sections, Section 2 and Section 4, show similar relationships, as shown in Figure 3.

The results show that with higher traffic volumes, the usage phase is more dominant than the maintenance phase. Therefore, in order to lower the overall emissions, overlays are needed more frequently than on the sections with low traffic.

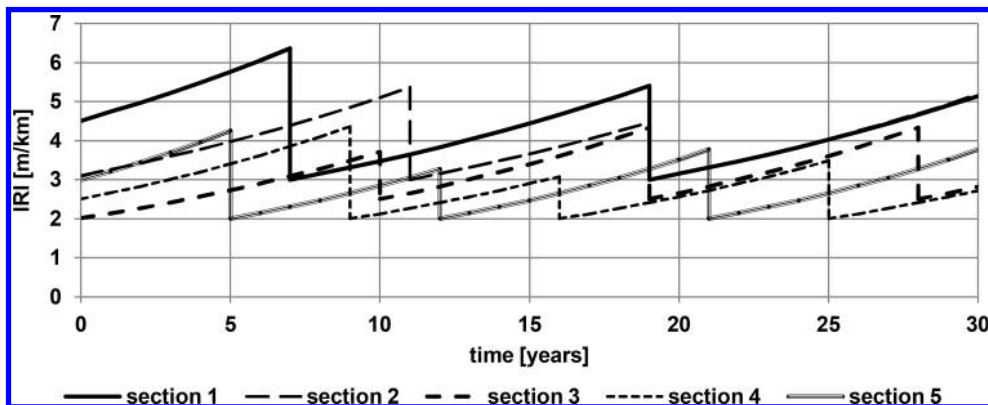


Figure 3. International Roughness Index for representative 5 sections during analyzed 30-year period.

5 CONCLUSIONS

This paper presented a methodology for finding an optimal pavement maintenance plan with minimal negative environmental impact. Maintenance options included the application of asphalt overlays in various thicknesses. CO₂ emissions during the usage phase were assessed through the HDM-4 model, while CO₂ emissions due to overlays were calculated using the PaLATE software. The numerical examples given for five actual sections of the Serbian road network showed a strong relationship between the frequency of asphalt overlays and traffic volumes.

The presented methodology can be used for wider analyses at network levels to optimize maintenance strategies regarding their environmental impact

REFERENCES

- Bryce, J., Katicha, S., Flintsch, G., Sivanewaran, N. & Santos, J. 2014. Probabilistic Lifecycle Assessment as a Network-Level Evaluation Tool for the Use and Maintenance Phases of Pavements. TRB 2014 Annual Meeting, paper no. 14-4639.
- Ekvall, T. 2002. Cleaner production tools: LCA and beyond. *Journal of Cleaner Production*, 10(5), 403–406.
- Fitch, M. G., Smith, J. & Clarens, A. 2003. Environmental Life-Cycle Assessment of Winter Maintenance Treatments for Roadways. *J. Transp. Eng.*, 139(2), 138–146.
- Giustozzi, F., Crispino, M. & Flintsch, G. 2012. Multi-attribute life cycle assessment of preventive maintenance treatments on road pavements for achieving environmental sustainability. *International Journal of Life Cycle Assessment*, 409–419.
- Horvath, A. & Hendrickson, C. 1998. Comparison of the Environmental Implications of Asphalt and Steel-Reinforced Concrete Pavements. Proceedings of the 1998 TRB Transportation Research Board Annual Meeting of National Academies, D.C. Washington, USA
- Horvath, A. 2003. A life cycle environmental and economic assessment of using recycled materials for asphalt pavements. Technical Report, University of California, Berkley, <http://www.uctc.net/papers/683.pdf>
- Li, Y. & Madanat, S. 2002. A steady state solution for the optimal pavement resurfacing problem. *Transportation Research Part A: Policy and Practice*, 36(6), 525–535.
- Ouyang, Y. & Madanat, S. 2004. Optimal scheduling of rehabilitation activities for multiple pavement facilities: exact and approximate solutions. *Transportation Research Part A: Policy and Practice*, 38(5), pp. 347–365.
- Ouyang, Y. & Madanat, S. 2006. An analytical solution for the finite-horizon pavement resurfacing planning problem. *Transportation Research Part B: Methodological*, 40(9), 767–778.
- Park, K., Hwang, Y., Seo, S. & Seo, H. 2003. Quantitative Assessment of Environmental Impacts on Life Cycle of Highways. *ASCE Journal of Construction Engineering and Management*, 25–31.
- Paterson, W. D. O. 1990. Quantifying the effectiveness of pavement maintenance and rehabilitation. In Proc., 6th REAAA Conf., Kuala Lumpur, Malaysia, p.14.
- Reger, D., Madanat, S. & Horvath, A. 2014. Economically and environmentally informed policy for road resurfacing: tradeoffs between costs and greenhouse gas emissions. Proceedings of 2014 Transportation Research Board Annual Meeting of National Academies, D.C. Washington, USA.
- Santos, J., Bryce, J., Flintsch, G., Ferreira, A. & Diefenderfer, B. 2014. A life cycle assessment of in-place recycling and conventional pavement construction and maintenance practices. *Structure and Infrastructure Engineering: Maintenance, Management, Life-Cycle Design and Performance*, DOI: 10.1080/15732479.2014.945095.
- Tsunokawa, K. & Schofer, J. L. 1994. Trend curve optimal control model for highway pavement maintenance: Case study and evaluation. *Transportation Research Part A: Policy and Practice*, 28 (2), 151–166.
- World Bank (2011). Road User Costs Knowledge System (RUCKS), <http://web.worldbank.org/WBSITE/EXTERNAL/TOPICS/EXTTRANSPORT/EXTROADSHIGHWAYS/0,,contentMDK:20483189~menuPK:1097394~pagePK:148956~piPK:216618~theSitePK:338661,00.html>
- Yu, B. & Lu, Q. 2012. Life cycle assessment of pavement: methodology and case study. *Transportation Research Part D: Transport and Environment*, 17 (5), 380–388.
- Yu, B., Lu, Q. & Xu, J. 2013. An improved pavement maintenance optimization methodology: Integrating LCA and LCCA. *Transportation Research Part A*, 55, 1–11.
- Zhang, H., Keoleian, G.A. & Lepech, M.D. 2008. An integrated life cycle assessment and life cycle analysis model for pavement overlay systems. *Life-Cycle Civil Engineering*, http://web.stanford.edu/~mlpech/pubs/ialcce_lcamodel.08.pdf

Transport of oversize/overweight vehicles along the Egnatia motorway. Basic elements of a future permit fee policy

A. Kokkalis

Department of Civil Engineering D.U.Th., Xanthi, Greece

P. Panetsos

Structures Inspection & Maintenance of Egnatia Odos AE, Thessaloniki, Greece

ABSTRACT: Every year, thousand of overweight/oversize vehicles transport indivisible heavy particles as energy generators or wind turbine propellers, along the Egnatia motorway. The slow pass of the overloaded trucks and overweight vehicles interrupt the motorway regular traffic conditions. More accidents and traffic jams are the consequences for the road users. Deterioration of pavement and bridge decks are the unfavorable effects on the motorway infrastructure. Procedures and engineering check methodologies for issuing permits of vehicles exceeding national weight/width/length/ height limits have been established and used by Egnatia Odos AE involving certain operational costs. Nowadays the toll cost for an oversize/overweight vehicle haulier to cross the Egnatia motorway is the same, 50€, as if it was doing so by a typical heavy good vehicle. This cost is considered unjustifiably low. An additional permit fee is proposed to be established for charging overweight/oversized vehicles for the various impacts and other consequences they may cause.

1 INTRODUCTION

1.1 *Overweight/Oversize vehicles*

Overweight/Oversize Vehicles (OOV), (Fig. 1) are defined as multi axle vehicles, usually composed both by a tractor and trailer(s), that carry heavy indivisible particles, as energy generators or wind turbine propellers. Their gross weight, their axle weight or their sizes (width, length, height) exceed the maximum legal values as defined by the Greek Presidential Act PD77/1998 in which the maximum length is set 18.75 m for a combination of tractor and trailer, the maximum width 2.60 m and the maximum height 4.00 m. The maximum weight of a combination of vehicles (tractor and trailer) is 44 tons. These values are in accordance with standard legal values set in Europe, USA, N Zealand and Australia (2014).

1.2 *Interruption of the OOV to the road users*

As the OOV carry heavy particles, they pass very slow, especially when crossing the consecutive uphill and downhill steep passages of Egnatia motorway. In combination with their width, when it is larger than 3.0 m and their length (with their escort vehicles), their slow passages cause traffic interruptions and delays, as well as accident prone traffic conditions. Also, during winter severe snowfalls, the articulated OOV may cause traffic closures as they are prone to sliding and overlap.



Figure 1. 24 axles overweight/oversize vehicle transporting energy generator over a bridge of Egnatia motorway.

1.3 *Effects of the OOV on the road infrastructure*

OOV may represent a significant additional deterioration and ageing factor for asphalt pavements. They can cause under certain conditions effects (stress/strain) on the bridge superstructures more unfavorable than the original bridge design code loading. These effects are even more severe on old deteriorated bridges which initial load capacity has been significantly reduced.

1.4 *Administrative effort for OOV transportation*

As OOV exceed the legal sizes/gross weights set by the Government, their passage along the Egnatia Motorway requires a permit. These permits are issued for hundreds of OOV by Egnatia Odos SA

OOV/Permit Discipline, following procedures and in some cases carrying out analytical engineering investigations. Patrolling of some of the OOV passages as well as temporary removal of overhead signs or safety barriers or supervision during crossing of specific bridges are also required.

2 OOV CHARGING POLICIES

2.1 *European practice*

The European Directive 2011/76 on the charging of heavy goods vehicle for the use of certain infrastructures denotes that the promotion of sustainable transport is a key element of the common European transport policy. It is known that the contribution of the transport sector to climate change and its negative impacts should be reduced, in particular congestion, which impedes mobility, and air and noise pollution, which create health and environmental damages. The objective of reducing the negative impacts of transport should be achieved in such a way as to avoid disproportionate obstacles to the freedom of movement in the interest of sound economic growth, the proper functioning of the internal market and territorial cohesion. Thus, user charges shall not discriminate on the grounds of the nationality of the haulier, the Member State, or the origin or the destination of the transport operation.

2.2 *Methods for charging for roads*

The principles of charging road users are that charges should be economically efficient, equitable, easy and cheap to collect and are not easily evaded (Yenny 2002).

2.2.1 *Taxes on vehicle fuel*

Taxes on vehicle fuel, that are most widely used, satisfy, to a certain extent, the above criteria. They are relatively inexpensive to collect, easy to administer and reasonably equitable, as they are proportionate to road use. Their main disadvantage is that they do not reflect the much higher damage done to roads by heavy vehicles. Although trucks consume more fuel per kilometer than cars and would therefore pay more fuel taxes per kilometer traveled, this is not in proportion to their higher impact on the roads. Therefore, fuel taxes need to be supplemented by additional charges on heavy vehicles. In Greece taxes on vehicle fuels imposed in last 5 years are already exhaustive and therefore no additional taxes of any type can be discussed. Furthermore in Greece and in Europe, in contradiction to USA, taxes on diesel would affect not only trucks but car drivers as well.

2.2.2 *Taxes on vehicle licenses*

They are common in most countries in the form of annual license fees (or two-year period, as in the United States, FHA, 2012). They are easy to collect, can differentiate between types of vehicle and reflect the costs

that each type causes to the roads. The main drawback is that they are not related to a distance-based practice. A truck used for only 50,000 km per year would pay the same as one traveling 200,000 km per year.

2.2.3 *Vehicle-distance traveled charges (or fees)*

Vehicle-distance travel fees are called direct user fees. They have been applied in some countries as in Norway, Sweden and New Zealand. The charges are administered through sealed hub odometers or other measuring devices. The problem is that such systems require a substantial initial outlay, sophisticated administration and are prone to evasion. Even in law-abiding New Zealand, the evasion is estimated at 10 to 20 percent. Some of these shortcomings can be avoided with modern charging systems, such as the ones now in use in Germany and Austria which are considered as a form of tolling.

2.2.4 *Tolls*

In the road transport sector, tolls calculated as distance-based charges for the use of infrastructure constitute a fair and efficient economic instrument to achieve a sustainable transport policy, since they relate directly to the use of infrastructure, which causes operational decay of the infrastructure, the environmental performance of vehicles and the place and time of use of vehicles and can therefore be set as a level which reflects the cost of pollution and congestion caused by the actual use of vehicles, without creating distortions to competition (ED 2011/76) and permitting the recovery of the infrastructure. The weighted average infrastructure charge may also include a return on capital based on market conditions. Actually, Member States may choose to recover only a percentage of those costs, to alleviate the fees asked.

Tolls are usually used for specific roads, bridges and tunnels and are therefore equitable, but they are a relatively expensive method of charging. They have significant capital costs (construction of toll plazas and tollbooth, controlled access) and operating costs (toll collection). Toll systems also reduce the economic benefits of the tolled facilities by minimizing entry and exit points, delaying traffic at tollbooths and diverting traffic to parallel roads with higher vehicle operating costs. The toll rate structure adopted in several countries is commonly based on the number of axles of trucks and buses. Several countries simply multiply the rate for a passenger car by the number of axles of a truck (or bus) to compute the toll rate for such vehicle.

In Greece and in Egnatia Motorway a typical escalation of toll rate structure under rule, as it is shown in Table 1, (i.e. 2.4€ for cars and 8.4€ for heavy vehicles), does not correspond to the damage heavy goods vehicles (HGV) cause to the infrastructure, which is much higher than the 8.4/2.4 proportion.

2.2.5 *Charges for non-standard and overweight vehicles*

The principle should be that these charges should compensate for the extra damage caused to the roads

Table 1. Toll rate structure for Egnatia motorway.

Vehicle Class	Toll fee	Class name	Class description
1	1.70€	Bicycles	
2	2.40€	Light trucks	Vehicles with or without trailer and up to 2.20 m high
3	6.00€	Trucks and buses	Vehicles with or without trailer, with two or three axles, and up to 2.20 m high
4	8.40€	Articulated buses and heavy trucks	Vehicles with or without trailer, with four or more axles, and higher than 2.20 m

by OOV. These charges in some countries reflect the costs imposed on the roads by these vehicles, as in Switzerland, in certain USA States and in Balkans, where the distances, in combination with the tonnage exceeding legal loads, are considered. In other cases, as in New Zealand, simply cover administrative costs (2014).

In Germany since January 2005 all trucks exceeding 12 tons gross weight pay between 0.09€ and 0.14€ per kilometer of road traveled on Germany's 12000 km motorway (Autobahn) network. The toll rate is calculated on the vehicle's environmental status (engine emission levels) and the number of axles.

The charges for OOV in Switzerland are calculated on the basis of the kilometers driven, the total permissible laden weight as well as the emission values of the towing vehicle (HVC Overview, 2013). For a vehicle or vehicle train with Euro 4, 5 engine and 100 tons weight, the permit fee for a 200 km route is calculated equal to $2.28 \times 100 \times 200 = 45600\text{ct}$ or ~ 450 euros.

Similar charges based on both mileage and tonnage are charged in Bulgaria, in Skopje and in other Balkan countries. In Denmark OOV moving on the Great Belt (~ 7 km bridge) heavier than 100 t and wider than 2,8 m have to follow a certain procedure to obtain a transport permission including a heavy and/or slowly moving load classification certificate. Interim threshold figures for the procedure are 350 t weight and 4.5 m width. For OOV wider than 4.5 m, passage must take place between 22:00 and 06:00 and the haulier must arrange himself for 2 escort vehicles behind the load. Night hours passage and single escorting is also required for those slow moving OOV under 45 km/h. The tolls range from $\sim 100\text{€}$ to $\sim 800\text{€}$.

OOV passage through Humberbridge, UK, wider than 3.5 m and heavier than 100 t have to pay additional 30£ plus toll and heavier than 150 t an additional fee by prior negotiation. OOV passage through Dartford tunnels either wider than 6 m or longer than 27 m or heavier than 150 t will be charged with 190£. OOV In north Yorkshire road infrastructure charges will be made for special services, including calculations

required to determine if the bridge or other structure is suitable to carry the abnormal load; and if any street furniture is required to be removed and replaced. OOV wider than 3.5 m and up to 150 t heavy are charged with 220£ for day hours and only 60£ during nighttime for passage along M6 motorway (HVC, 2013, Querioz, 2003, 2008).

Across Atlantic in certain US States exceptional hauling permits may be charged up to \$1000. The normal practice is to issue monthly or fixed time permits. For example, Washington DoT, vehicles or loads either over 14 ft wide or 125 ft long, one rear escort vehicle is required on multiple-lane highways and has to pay \$10 per trip. According to Pennsylvania DoT requires special insurance for OOV transport and charges \$76 for oversized trailers > 14 ft in width.

3 OOV PERMIT PROCEDURE AND OOV IMPLICATIONS

3.1 Administrative OOV permit issue procedure

All trucks, vehicle trains, self powered cranes that exceed 40tons (gross weight) or the maximum sizes set by the State Law (Act PD77/1998, Dimitropoulos, 2007) fill and submit a permit issue request to the OOV Permit Discipline of Egnatia Odos AE, the company that manages the operation, maintenance and exploitation of Egnatia Motorway. The company shall issue the permit in three working days, unless the vehicle weights more than 80 tons. In that case an engineering investigation of two levels is carried out as described in the next paragraph. On yearly base more than 5600 OOV permit requests are submitted and issued for Egnatia Motorway.

3.2 Bridge investigations for OOV weight more than 80 tons

In Egnatia motorway transport operators ask for permit for hundreds of OOV with gross weight exceeding 80 tons, as it is shown in statistics of Table 2, or the 5% of the total OOV passages.

For these extreme OOV two levels of analytical engineering assessment is followed in order to ensure that bridges along the permit route can safely bear the loads of the crossing overweight vehicles.

The objective of analytical bridge investigation is to support decision on whether an overweight load permit can be issued or not and if so, under what restrictions to guarantee serviceability and structural integrity of the bridge and structures of the motorway.

Permits for extra-legal loads can be issued for unrestricted or restricted travel. In general movement restrictions can concern the presence of other traffic, the vehicle speed and time of passage. Speed limits are sometime applied by transportation agencies and nominally justified by assuming that a higher speed may entail a higher dynamic response coefficient. The response also depends on other factors such as span length, road surface irregularity and deck stiffness

Table 2. Permits of OOV > 80 tons, in 2014.

Classification	Permits		Total Route Length km	Average Trip Length km
	%	(nbr)		
80–89.9	73.05	(225)	85,000	376
90–99.9	18.83	(58)	11,000	193
100–109.9	2.27	(7)	1,000	156
110–119.9	4.22	(13)	3,500	267
> 120	1.62	(5)	1,100	223
Total	–	(308)	101,600	

(Cantieni, 1983, Paulter *et al.*, 1992). In general there is no evidence that reducing speed reduces the dynamic response, and under certain conditions a lower speed causes higher stress on the bridge.

In principle, assessing a bridge to any of the OOV load models and travel conditions would require full formal re-evaluation of its capacity, carried out by a professional engineer. In practice, direct reassessment of the 1856 bridges and other structures, in the Egnatia motorway axis, is a very expensive task and in most cases unnecessary. To address the cost issue, the Egnatia approach is to estimate the capacity of the stock, using simplified and conservative approach first, then carrying out more detailed structural analysis only if a higher load rating is required. The assessment procedure includes two levels of refinement:

- Level 1. The assessment is based on the following principle: The bridge is rated for an overweight load if it is demonstrated, even conservatively, that the overweight load does not cause effects that are more severe than the original bridge design code loading. In practice the procedure aims to demonstrate that the new overweight load condition is not worse than the most critical load condition associated with the original design assumption or as-built situation, and therefore the overweight load does not reduce the original design safety level. It is believed that this principle protects against legal liabilities in the case of a failure, because, following this principle Egnatia Agency authorizes travel only of those vehicles whose effects are less than those expected under the design assumptions. The analysis is carried out assuming that the bridge was built exactly to the nominal design load (in other words, with no overstrength), thus the bridge is automatically rated for the overweight load if it can be demonstrated that the stresses it creates are everywhere lower than or equal to those considered at the design stage. For proceeding with this level simple single beam bridge models are used to calculate stress imposed by the OOV in comparison to the legal design load (e.g. 60/30 according to DIN standards). The comparison is carried out for the stress that results from the unfactored vehicle loads, targeting to check for the serviceability limit state (e.g. crack opening for pre-stressed superstructures). This type of analytical investigations can take up to a few working hours.

- Level 2. When a bridge is not sufficient from Level 1 assessment, the assessment proceeds to a higher level of refinement and is carried out by a professional engineer based on analysis of the available design documentation. In this level a three dimensional bridge superstructure model is constructed for the bridges of the permit route that do not pass level 1 check. Again a more accurate comparison between stresses induced by the OOV and the legal design load is carried out. If the legal design load stresses are not now exceeded then the OOV can get a permit with or without restrictions (e.g. permissive lane along the deck can be defined, crossing without traffic etc.). Based on the design documents and on the actual condition of the bridge, gained by detailed inspection, the capacity of the bridge can be calculated and compared to the stress demand of the OOV if after Level 2 checks the OOV overloads the bridge(s).

This type of analytical investigations can take 2 or more working days, depending on the number of critical bridges along the permit route. A conservative rule that often is applied is that no OOV that exceeds serviceability limits for pre-stressed concrete, causing temporary cracking opening in the tensile zone, get a permit issue. Even if cracks, in theory, would close after the OOV passage, as the pre-stressing tendons work in their elastic range, concrete tensile zone is always a brittle area and microcracks of the concrete cover can remain such as to let corrosive agents and water as chlorions, to insert in the mass of the concrete and to cause earlier dippasivation and initiation of corrosion of the bridge reinforcement. This type of deterioration will affect the durability of the concrete bridges and modify unfavorably the typical maintenance life cycle of the bridges, asking for rehabilitation costs.

If, as it is shown in Figure 2, the first superstructure repair is expected earlier than after 36 years from the time the bridge was set in operation, as a result of cracking induced by the OOV passages. Thus in terms of present value the cost of the bridge maintenance is increased and the funds for maintenance that are to be allocated will increase.

Cracking on some of the concrete superstructures has been already observed and recorded during detailed inspections of the bridges of the Egnatia Motorway. Most of them resulted from shrinkage or other effects but as are exposed to overloaded vehicle passages may widen and get worse (Fig. 3), extra OOV charges considering increase repair/rehabilitation budgets should be established as proposed in next paragraphs.

3.3 Heavy loads implications to pavements

Generally, axle loads showed a definite increase in time. Furthermore, considering the axle load frequency curve, there is a definite positive skewness pattern meaning that more axles are loaded at or over

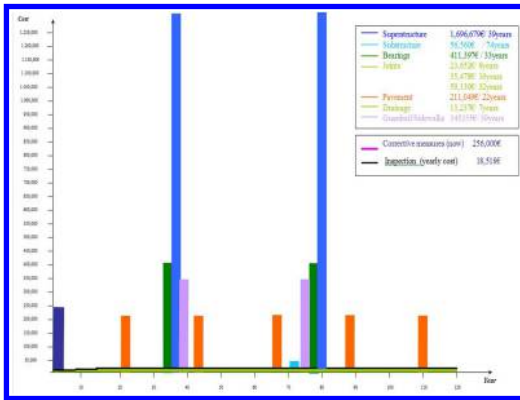


Figure 2. Typical bridge life cycle (120 years) costs.

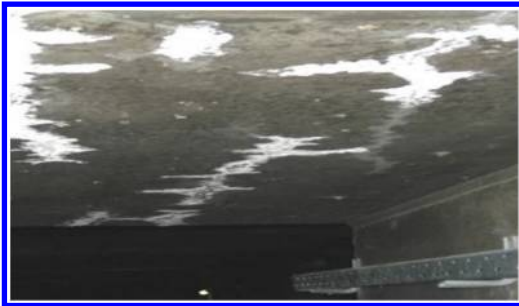


Figure 3. Hairline cracks at the soffit of the top boxbeam slab.

the legal load limit (Proios *et al.*, 2005, Mintsis *et al.*, 2007). Also, truck tire pressure is increasing year after year and this again results in more pavement distress (Attia & Ahmend, 2014). The typical pavement damage developed due to heavy loads is mainly rutting and fatigue cracks. Overall, the need for heavy maintenance and overlaying may be more frequent and costly. When considering equivalent standard axle loads (ESAL) of the overloaded HGV plus OOV to assess the additional damage caused to road pavements, it has been estimated that a high percentage of pavement damage did attributed to them. Overloaded HGV are illegal and their extra damage should be compensated by fining and other administrative measures. OOV are not illegal and their extra damage should be compensated by an appropriate pricing policy.

That additional damage and wear produced to Egnatia pavements due to that very heavy vehicles had been estimated to 35% by using the typical 4th power law and the 8.16 t standard axle load (Panetsos & Kokkalis, 2007). The specific procedure may overestimate the deterioration effect of very heavy vehicles. Furthermore, the volume of overloaded HGV is higher than OOV. Additionally, the great number of axles OOV platforms have, alleviate the stresses. It is expected that a small percentage of that 35% of extra deterioration may be attributed to OOV.

Hence, the pavement additional damage part referring to OOV has been re-estimated herein by applying

a modified COST 334 method (Glaeser, 2010, Glaeser & Ritzinger, 2012). This procedure concentrates on pavement rutting without overestimating the effect of very heavy axle loads. The following simplified formula has been used:

$$VDF = \Sigma(\text{single axle load}/10)^2 \quad (1)$$

where VDF: vehicle damage factor.

It has been found that only about a 2% of the extra pavement deterioration is attributed to OOV. This finally means that less than 0.5% of the total pavement damage may be attributed to OOV.

3.4 OOV motorway operational implications

Concerning motorway traffic, very wide OOV moving slowly along one or more traffic lanes, cause important delays to the rest of motorway users. The problem is alleviated permitting their move only during traffic off-peak hours. However, the length of the Egnatia motorway itself (675 km) and the lack of motorway service areas, practically necessitates that along certain sections of the motorway OOV moving during peak hours is inevitable. Hence the purpose is to avoid moving very wide loads along the central most heavily trafficked section of the motorway (around Thessaloniki area) during peak hours. Generally, that extra user costs from traffic delays imposed to the rest of the users should also be taken into consideration, when either OOV speed falls below the motorway lower speed limit of 50 km/h or the OOV width approaches that of a typical lane width of 3.5 m. Not only the very wide, but the very long OOV inhibit normal traffic as well.

As far as the dimensions is concerned, there may be used specific formulae or simply threshold values. For instance, in South Africa (2000) they use a rather complicated rule to evaluate this annoyance, based on the road usage factor (UF):

$$UF = 1,61757 \times 10^{-3} \times W^{4,7} + 7,5 \times 10^{-7} \times L^{5,6} \quad (2)$$

where W and L are the overall load width and length in meters and the applied rule for the usage factor is: UF < 0.54 no escort, UF ∈ [0.54, 0.94]: one own-escort required, UF ∈ (0.94, 2.73]: two own-escort required and UF > 2.73: one accredited-escort (either police or authority vehicle) and one own-escort required.

The above formula (as well as other similar ones) has been evaluated for Egnatia motorway. It introduces a degree of complication, in comparison with a simplified 'threshold-values' approach, and yields no actual benefit. Thus, a simple 'threshold-values' approach is proposed to be set, determining the threshold length to 22 m and the threshold width to 3 m.

OOV additional charges may also be justified on the grounds of increasing traffic accident potential. It is known that the greater the speed differences in a traffic stream, the higher the accident risks. It is

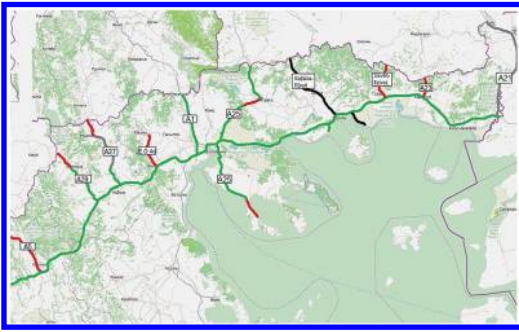


Figure 4. Egnatia motorway map and its transverse corridors.

fare those OOV greatly affecting the traffic flow, to compensate for that. Both the previously mentioned dimension threshold values and a moving speed lower than 50 km/h (lower speed limit for motorways) are proposed as limit values for extra charge for the delays and additional risks caused to other road users.

4 AN OOV PERMIT FEE CHARGING POLICY

4.1 Distance based charging component

Egnatia motorway is a 675 km long 2-lane dual motorway crossing the western and northern Greece (Fig. 4). Due to the very mountainous terrain crossed one can count across the motorway 1856 bridges and culverts, 155 of which are longer than 100 m. According to the relevant OOV data, there can be identified discrete travel patterns of OOV, which may be used to simplify the procedure: those OOV, who cross all the motorway, from Igoumenitsa to Kipi, those who entering from Scopia (Albania or Boulgaria) or from A1 motorway heading to the capital Athens and the reverse.

As it has been mentioned, OOV may do more damage to infrastructure and interfere more with routine traffic flow than vehicles with legal weight and dimensions (legal vehicles).

However, damage to infrastructure and interference with routine traffic is not similar to all sections of Egnatia motorway. The western very mountainous part has a very costly infrastructure, which may be deteriorated by OOV, whilst the central part (around Thessaloniki) has high traffic volumes, which, also, may be affected. It is considered fair to introduce a relevant compensation coefficient. For this purpose, the total length of the motorway has been divided approximately by 4. These 4 parts are not considered equivalent. A differentiation is proposed based on traffic volumes as well as on the mountainous of the terrain. The western section of the motorway (Igoumenitsa-Kozani) would account for 30% of the total fee, due to its very mountainous terrain, the central-western section (Kozani-Thessaloniki) for a 25%, justified on mountainous terrain and traffic volumes, the central-east section (Thessaloniki-Kavala) a 25% justified on traffic volumes and the eastern part of

the motorway (Kipi-Kavala) would have a lower percentage of 20%. Hence, the distance-based charges are propose to have the above relevant gravity factors.

4.2 A pricing proposal of OOV crossing Egnatia motorway

OOV may do more damage to infrastructure and interfere more with routine traffic flow than legal vehicles. For that reason, it is fare, a fee to be levied to compensate for the cost incurred through the use of public roads by OOV. A sound documentation of that additional charges should make up for the additional costs and nuisance caused. The funds would be used for maintenance and rehabilitation and would be charged on the basis of additional infrastructure deterioration/ageing risks, operational risks and delays, environmental impacts, need for escorting and man-hours spent for the administration and audits. Egnatia Odos AE receives, on average, 500 notifications per month for permitting transport of OOV along the motorway. Nowadays the toll cost of a transportation company to cross by its OOV the Egnatia motorway is the same, about 50€, as if it was doing so by a typical HGV, traveling along the total 675km of the motorway. This cost is considered very low and covers only the environmental and normal infrastructure deterioration costs.

Two basic classes of OOV have been previously outlined, on a weight and on a dimension basis. OOV less than 80 t and smaller than 22 m long or 3 m wide is proposed to be additionally charged with 50€ only for the typical permitting issue procedure. This means a base-fee of approximately 100€ for crossing the full length of the motorway covering the tolls plus the administrative cost.

For heavier OOV, which require a level-1 bridge structural assessment (§3.2), an additional engineering audit cost should be charged amounting to 50€, whilst for the most important level-2 bridge structural assessment that additional engineering investigation cost is proposed to amount to 200€.

Then, the case of compensation for the potential extra damage caused to the infrastructure, both pavements and bridges should be addressed. The additional cost to bridges, justified on reducing their design life, is a very important issue which should be dealt in a case-by-case basis, by relevant heavy charging, if not forbidding those passages. A motorway pavement 15-year heavy maintenance amounts approximately to 100 millions € and may come sooner due to additional heavy loads deterioration. However, as it has been mentioned, due to the great number of axes OOV platforms usually have, the proportion of deterioration attributed to OOV is not statistically different than other typical HGV. Thus, it is fare not to extra charge for that.

To justify probable traffic delays and accident risks is also a difficult issue, not because of the estimation and pricing of the lost traveler's time and additional fuel consumption or accident costs, but because there

is not a plausible way to return that extra charge directly to the affected users. However, it is fair those OOV affecting greatly the traffic flow, to compensate for that. A simplified variation of the formula used at South Africa (2000) is proposed for those OOV exceeding 22 m in length or 3m in width: the basic 50€ toll-fee is multiplied by a T-factor, where T:

$$T = W + L, \quad (3)$$

$$\text{whilst } W = (\text{width}/3\text{m})^4 \text{ and } L = (\text{length}/22\text{m})^4 \quad (4)$$

Following this approach, a very bulky OOV (i.e. 4 m wide and 30 m long) will have a $T = (4/3)^4 + (30/22)^4 = 3.16 + 3.46 = 6.62$.

Hence, the charge would be: $50 \times 6.62 = 331\text{€}$ for the full length of the motorway plus the 50€ for the administrative cost plus any potential cost for engineering audits. For the specific OOV, haulier escort vehicle is required to follow the platform with no extra cost. Whether there is involved Authority escort or Officers act as accredited escorts, this will be charged individually over and above the fee on a km and/or time basis. A fee of 1€/km seems a reasonable starting point.

Finally, if any temporary removal of overhead signs or safety barriers is required, this should be additionally charged on their real cost basis.

5 DISCUSSION AND CONCLUSIONS

The current global economic crisis is leading several countries as Greece to reduced vehicle utilization. As motorists try to reduce their driving miles and buy less fuel-consume vehicles, governments take in less money from fuels taxes. Therefore the funds available to the road sector are significantly less than the amount required to maintain the road network in a stable long-term condition, as well as to undertake justified rehabilitations. The road agencies should prepare an explicit long-term financing plan showing the size of the financing gap and suggesting how it might be bridged (Heggie & Vickers, 1998). Among other things the direct charges on OOV separately and in addition to the relatively low tolls that are charged for the moment along Egnatia motorway has to be examined.

Hence, a relevant documented pricing procedure has been proposed herein for OOV, taking into account:

- the typical tolls paid by HGV,
- the routine administrative cost,
- any possible engineering audit cost involved,
- compensation for the delays and risks caused to the rest of traffic,
- compensation for any specific deterioration induced to infrastructure and
- compensation for any official escort or works for tasks involved.

The purpose is to obtain a flexible, representative and not expensive permit fee policy.

It has also been concluded that particularly heavy OOV may cause measurable damages to bridge infrastructure in the form of reducing their expected design life. Furthermore, it has been concluded that because a typical OOV's platform involves many axles and wide and large tires, will not typically results in considerable damage to pavement infrastructure.

REFERENCES

- Attia, M. & Ahmend, M. 2014. Impact of vehicle class and tire pressure on pavement performance in MEPDG. *Int. Journal of Engineering Research and Applications*, Vol. 4, Issue 10, pp. 45–57.
- Cantieni, R. 1983. Dynamic load test on highway bridges in Switzerland. *EMPA Report No.211*. Swiss Federal Laboratories for Materials Testing and Research.
- Dimitropoulos, I., Vegiri, V. & Kazakos, S. 2007. Institutional framework of special transport at European and national level. *4th International Conf. Bituminous Mixtures and Pavements*, Thessaloniki, 19–20 April.
- Directive 2011/76/EU of the European Parliament on the charging of heavy goods vehicle for the use of certain infrastructures.
- Federal Highway Administration (FHWA) 2012. Oversize overweight load permits.
- Glaeser, K-P, 2010. Performance of articulated vehicles and road trains concerning road damage and load capacity. *11th Heavy Vehicle Transport Technology Conference*, Australia.
- Glaeser, K-P & Ritzinger, A. 2012. Comparison of the performance of heavy vehicles Results on the OECD study: moving freight with better trucks. *Transport Research Arena*, Paris.
- Greek Government 1998. Adjustment Greek legislature to the Directive 96/53/EC of July 25 1996 regarding the definition of the maximum permissive sizes and weights of the international transport vehicles. *Presidential Act PD77/1998*.
- HVC Swiss Federal Customs Administration 2013. Performance related heavy vehicle charge. HVC Overview.
- Main Roads Western Australia 2014. Special purposes vehicle standards operation conditions.
- Mintsis, G., Taxiltaris, C., Basbas, S., Filaktakis, A., Koutsoukos, K., Guy S. & Viskos, E., 2007. Temporal evolution of HGV traffic data along Egnatia motorway. *4th International Conf. Bituminous Mixtures and Pavements*, Thessaloniki, 19–20 April.
- Mintsis G., Basbas, S., Kokkalis, A. & Taxiltaris, C., 2011. Identification of overloaded heavy goods vehicles using vehicle speeds on uphill. *5th International Conf. Bituminous Mixtures and Pavements*, Thessaloniki, 1–3 June.
- NVF 2008. Road wear from heavy vehicles. *Report nr.08/2008*, Nordiska Vägtekniska Förbundet.
- NZ Transport Agency 2014. Road user charges administration fees review. New Zealand
- Panetos, P. & Kokkalis, A. 2007. Overloaded vehicle implications on road and bridge maintenance. *4th Int. Conf. Bituminous Mixtures and Pavements*, Thessaloniki, Greece, 19–20/4, 617–627.
- Paulter P., Chaallal O. & Proulx. J. 1992. Bridge dynamic and dynamic amplification factor – a review of analytical and experimental findings. *Canadian Journal of Civil Engineering*, No. 19, pp. 260–278.
- Proios, A., Mintsis, G., Taxiltaris, C., Basbas, S., Patonis P., & Filaktakis, A., 2005. The issue of the

- overloaded HGVs in the Greek national road network. *Proceedings of the 2nd Pan-Hellenic Conference on Highway*, Technical Chamber of Greece, Volos, Greece, 18–20 May.
- Queensland, Australia 2014. Heavy vehicle law national act. 12, September 2014.
- Querioz, C., 2003. A review of alternative road financing methods. *Europe Investment Bank Seminar*. Paris, France.
- Querioz, C., 2008. Road user charges. Current practices and perspectives in central and east Europe. *World Bank Transport paper no. 23*. Washington DC.
- South Africa Committee of State Authority 2000. Guidelines for granting of exemption permits for the conveyance of abnormal loads and for other events on public roads'. *TRH11, 7th edition*, Republic of South Africa, ISBN 1-868030-51-2.

Pavement management: Data centric rules and uncertainty management in section classification by a fuzzy inference system

M. Mahmood

Nottingham Trent University, Nottingham, UK

M. Rahman

Department of Civil Engineering, Brunel University, Uxbridge, UK

S. Mathavan

Visiting Research Fellow, Nottingham Trent University, Nottingham, UK

L. Nolle

Jade University of Applied Science, Jade Hochschule, Wilhelmshaven, Germany

ABSTRACT: Pavement section classification is one of the key elements of the decision-making process in a pavement management system. It helps to monitor the pavement conditions and assists in the optimization of maintenance and rehabilitation requirements. This paper presents a fuzzy inference system (FIS), with appropriate membership functions, for section classifications and for calculating the Pavement Condition Index (PCI). The FIS is a powerful tool to deal with the uncertainty and subjectivity involved in section classification. The input data of FIS were obtained from the Long-Term Pavement Performance (LTPP) database. The severity and extent of seven distress types, namely alligator cracking, block cracking, longitudinal and transverse cracking, patching, potholes, bleeding, and raveling, were used for fuzzy membership function and rule generation. The output fuzzified PCI was compared with the PCI calculated by Micro-PAVER. The result shows a correlation of approximately 76% between the two methods. A sensitivity analysis was carried out to evaluate the effect of each distress type on the classification model. It was found that within the tested sections, a pavement crack has the greatest influence on section classification compared to the other distress types.

1 INTRODUCTION

Generally, pavement performance is comprised of four key components: load bearing capacity, riding comfort, safety, and aesthetics. The objectives of pavement condition assessment are to monitor the pavement network conditions and to determine preservation needs, especially for preventative treatment and rehabilitation, in order to improve and/or maintain the performance (Shahin 2005, Hein & Watt 2005, Haas 2010, Sun & Gu 2011). The assessment of condition must be detailed, consistent, and efficient to optimize survey program and budget allocation.

Road pavement conditions can be characterized by different indicators in order to assess different aspects of pavement performance (Sun & Gu 2011). The widely used indicators are the Pavement Condition Index (PCI), the Present Serviceability Index (PSI), the Structural Index (SI), and the Foreign Object Damage (FOD) potential for airfield pavements. These indicators take account of surface distresses such as cracking, rutting, texture, profile, and potholes, together with structural condition indicators such as

pavement deflection and safety parameters such as skid resistance.

In recent years, machine based survey at traffic speed has become an integral part of routine condition assessment of pavement as this type of survey provides the technology to carry out repeatable, detail and fast collection of surface distresses. However, the analysis method requires improving in order to convert these vast sets of data into information in a most efficient way.

The use of artificial intelligence and soft computing techniques has gained popularity in the field of pavement engineering in recent decades due to the advances made in computational power. In this regard, the fast growing and easily accessible resources for technical computing allow the storage and management of large sets of data at low costs. The same processing capabilities have also made different automated data processing methods much more feasible than ever. These days, intelligent data analysis techniques, from artificial intelligence to soft computing, are used in pavement engineering for trend analysis, forecasting, classification, condition monitoring,

and even activities such as planning and scheduling. These vanguard methods not only provide very robust analysis procedures but are also adaptive and allow for situations that appear ambiguous to humans as well. Since real-life engineering decisions are made in uncertain environments that require a very high level of human expertise, which must also be consistent, the application of soft computing to these situations is an attractive option for practicing engineers. Consequently, this is the context in which intelligent techniques are considered for pavement performance evaluation and, thereby, management decisions.

A review of the literature shows that there are numerous researches in which intelligent decision-making has been applied to pavement condition estimation. In this regard, Eldin and Senouci used back-propagation neural networks for pavement condition rating of rigid pavements (Eldin & Senouci 1995). Terzi also developed a classification model based on the PSI for flexible pavements by using artificial neural networks (Terzi 2007).

A number of techniques based on fuzzy set theory have also been employed for pavement condition evaluation. Fuzzy analysis is an excellent tool for the evaluation of pavements, as it allows for approximate rather than fixed reasoning. Approximate reasoning has been shown to work better for situations where decision-making is inherently ambiguous. In this respect, Juang and Amir Khanian created a performance index called the Unified Pavement Distress Index (UPDI) based on fuzzy set theory for using in a priority-ranking model for the Pavement Management System (PMS) (Juang & Amir Khanian 1992). Shoukry et al. (1997) also created the universal pavement condition index, combining quantitative and qualitative data based on fuzzy sets. Fwa and Shanmugam proposed a distress rating scores procedure based on fuzzy logic theory for pavement condition rating and maintenance-needs assessment (Fwa & Shanmugam 1998). Furthermore, Bandara and Gunaratne proposed a new subjective pavement assessment methodology based on fuzzy set theory, considering predominant distress types, severity, and extent in flexible pavements (Bandara & Gunaratne 2001). Arliansyah et al. (2003) proposed a procedure based on fuzzy logic to calculate membership functions using linguistic terms based on expert opinion data for pavement condition assessment. Golroo and Tighe developed a comprehensive pavement condition assessment methodology by employing fuzzy set theory for Pervious Concrete Pavement Structures (PCPSs) (Golroo & Tighe 2009). In another research study, Liu and Sun employed forward Fuzzy Optimization Back-Propagation Neural Networks (FOBPNNs) for pavement performance assessment (Liu & Sun 2003). Koduru et al. (2010) presented a methodology for categorizing some pavement distresses based on an expert system and fuzzy logic to raise the consistency and reduce subjectivity. A recent study by Sun and Gu used the integrated Analytical Hierarchy Process (AHP) and fuzzy logic theory to develop a new approach to pavement condition assessment (Sun & Gu 2011).

2 RESEARCH OBJECTIVES

Pavement sections are normally classified based on their pavement condition index in order to categorize them as “good”, “moderate”, and “poor”. Conventionally, this has been done by comparing various pavement distress data against threshold values set out in the design standard. However, borderline values between two categories have a significant influence on subsequent pavement maintenance and rehabilitation decisions. Traditional crisp classification (i.e. exact reasoning) fails to address this issue.

In order to deal with these issues, previous researches, as reported earlier, used fuzzy logic together with a linear classification model, expert system, or artificial neural network to deal with uncertainty and subjectivity involved in the classification. However, expert systems require data training to cope with a given problem, which is time consuming. The aim of this study is to develop a simple and effective system that is able to deal with uncertain data. A novel Fuzzy Inference System (FIS) model has been developed in this study. Fuzzy membership functions are created for section classifications and then a fuzzy rule-base is developed for estimating the fuzzified PCI. The advantage of FIS is its ability to generate rules automatically from numerical data, although there is still flexibility to adjust any rule manually. This flexibility gives engineers more freedom to optimize the section classifications using one single system. In this sense, an FIS is more transparent than an artificial neural network.

The distress data used in this study were collected from the Long-Term Pavement Performance (LTPP) database (FHWA 2012). The results were compared with the PCI calculated by the software package MicroPAVER (U.S. Army Corps of Engineers 2012). MicroPAVER is industry standard software, widely used all over the world for pavement management. Some initial results from this research have been reported in an earlier paper by the present authors (Mahmood et al. 2013). The initial results were based on 71 pavement sections, which showed 56% correlation between the fuzzified PCI and the PCI values derived by MicroPAVER. This paper presents an extension of the initial work, where the number of sections has been increased to 291 in order to improve the performance of the model.

3 PAVEMENT CONDITION DATA AND INDEX

3.1 LTPP database

The LTPP database is one of the most comprehensive pavement databases in the world. This database was developed as part of the Strategic Highway Research Program (SHRP) (FHWA 2012). In LTPP, condition information from visual and/or automated pavement surveys is presented as numerical values assigned to each pavement section. These data comprise the performance requirements such as ride quality, roughness,

skidding resistance, and texture; distresses such as cracking, rutting, defects, patching, and edge deterioration; and structural conditions such as pavement life (Scott Wilson Pavement Engineering Ltd, unpublished internal report, 2005). In this research, seven of the most widely used distress types – alligator cracking, block cracking, longitudinal and transverse cracking, patching, potholes, bleeding, and raveling – and the distress quantities for each severity level – low, medium, and high – were used to develop the pavement classification model.

3.2 Pavement condition index (PCI)

The degree of pavement deterioration is a function of three main factors: distress type, severity, and distress quantity or density. The major issue is to use one single index that is capable of considering many of the potential combinations of all three factors for different distress types. To overcome this, the PCI was developed by the US Army Corps of Engineers to represent the pavement condition numerically in a range from 0 to 100, with 0 being the worst possible condition and 100 the best (Fwa 2006). The PCI procedure has been an ASTM standard since 1999 and is widely used for roads, airfields, and parking lots by many highway agencies worldwide. The PCI is estimated based on visual survey results in which distress types are identified along with their quantity and severity. Field verifications of the PCI inspection approach have shown that the PCI gives a good indication of structural integrity and operational conditions. Also, it is a valuable index to determine both the current condition and future performance under existing traffic, without the need for additional testing programs for roughness, skid resistance, and structural capacity (Shiyab 2007, Shahin & Walther 1990).

3.3 PCI calculation in PAVER system

MicroPAVER uses “deduct values” of PCI as a weighting factor to combine the effects of each particular distress type, severity level, and distress density on pavement conditions. The concept was originally proposed by Shahin and Walther (1990). Briefly, the calculation procedure is as follows:

- I. Identify distress types, severity levels, and quantities.
- II. Determine the density of each distress type for each severity level by using the following formulas:

(Distress is measured in square feet or metres)

$$Density\% = \frac{Distress\ Area}{Section\ Area} \times 100 \quad (1)$$

(Distress is measured in linear feet or metres)

$$Density\% = \frac{Distress\ Length}{Section\ Area} \times 100 \quad (2)$$

(Distress is measured by the number of potholes)

$$Density\% = \frac{Number\ of\ Potholes}{Section\ Area} \times 100 \quad (3)$$

- III. Determine the deduct value for each distress type from deduct value curves.
- IV. Reduce the number of deduct values from the maximum allowable number using Eq. (4).

$$m_i = 1 + (9/95)(100 - HDV_i) \quad (4)$$

where:

m_i = allowable number of deduct values.

HDV_i = highest individual deduct value for section i .

- V. Determine (q) the number of deduct values greater than two.
- VI. Calculate the total deduct value (TDV), which is the summation of all deduct values.
- VII. Determine the corrected deduct value (CDV) from a correction curve based on (TDV) and (q).
- VIII. Reduce to II the smallest individual deduct value that is greater than II.
- IX. Repeat steps V through VIII until q is equal to one.
- X. The maximum CDV is the largest CDV.
- XI. Calculate PCI by subtracting the maximum CDV from 100; $PCI = 100 - CDV_{max}$.

In the PAVER system, seven PCI ranges, as shown in Table 1, are used to classify pavement sections.

4 MODEL DEVELOPMENT IN FUZZY INFERENCE SYSTEM (FIS)

Generating membership functions and rules for FIS for high dimensional problems is challenging due to the sheer amount of data from which the parameters are tuned. This is called the *curse of dimensionality* (Naik 2004). To overcome this difficulty, the membership functions of inputs were established based on the k-means clustering and the rules were generated by Wang and Mendel’s method (Angelov & Buswell 2003, Naik 2004).

Three triangular membership functions were created for distress density, representing different severity levels (low, medium, and high) for each input. On the other hand, seven triangular membership functions were used for the output, “PCI”, to match the classification range with the PAVER system (as shown in Table 1). A custom built software application, FISPro (Fuzzy Inference System Professional) version 3.4, was then employed to design an FIS from the numerical data. This software is written in C++ with a graphical Java interface (Guillaume et al. 2010).

A brief overview of membership functions and rule generation methods is presented below.

4.1 Membership functions by k-means clustering

In fuzzy theory, fuzzy set A of universe X is defined by a function $\mu_A(x)$ called the membership function of the set A

$$\mu_A(x): X \rightarrow [0, 1]$$

Table 1. PCI range and pavement classification.

PCI range	Pavement classification
10–0	Failed
25–11	Very poor
40–26	Poor
55–41	Fair
70–56	Good
85–71	Very good
100–86	Excellent

where

$\mu_A(x) = 1$ if x is totally in A ; $\mu_A(x) = 0$ if x is not in A ; $0 < \mu_A(x) < 1$ if x is partly in A .

The degree of membership is represented by the membership function $\mu_A(x)$ for an element x of set A and ranges between 0 and 1. A membership function is a graphical representation which defines how each point in the variable space is mapped to the membership degree, that is, a value between 0 and 1. The graphical representation of a membership function can have different shapes such as triangular, trapezoidal, Gaussian, and so on (Negnevitsky 2002). The membership function is determined by expert knowledge or numerical data. Gaussian membership functions are usually better due to their smooth variation, but, on the other hand, require more data to be accurately trained as there are more parameters to be tuned.

As mentioned, whilst there are many methods available to generate membership functions from the numerical data, the k-means clustering algorithm was adopted as it was easy to implement and could be applied in a large data set. The basic concept of k-means clustering is to randomly select k initial cluster means, or centers. After many repetitions, these initial cluster means are updated in such a way that they represent the data clusters as well as possible (Dehzaangi et al. 2007). The steps taken to determine the membership functions are as follows:

- Initialize C_i by randomly choosing C points from among all the data points.
- Compute the membership matrix U , where the element u_{ij} is 1 if the j th data point x_j belongs to the group I and 0 otherwise.
- Compute the fitness function by the following equation. Stop if the fitness function value is lower than a certain threshold value.

$$J = \sum_{i=1}^c J_i = \sum_{i=1}^c \left(\sum_{k, X_k \in C_i} \|X_k - C_i\|^2 \right) \quad (5)$$

- Update the cluster centres C_i and calculate the new U matrix (Naik 2004).

4.2 Rule generation

FIS is one of the most popular methods used in classification problems. FIS is a method that interprets the values of an input vector and, based on user-defined rules, assigns values to the output vector. The advantages of this approach are knowledge

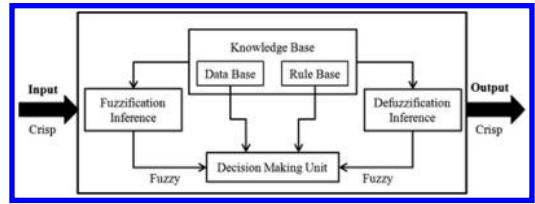


Figure 1. Fuzzy inference system structure (Jang 1993).

representation in the form of If–Then rules, the mechanism of reasoning in terms understandable by humans, the capacity to take linguistic information from human experts and combine it with numerical information, and the ability to approximate complicated nonlinear functions with simpler models (Negnevitsky 2002). Fuzzy inference systems are also known as fuzzy-rule-based systems, fuzzy models, or fuzzy associative memories (FAMs). The block diagram of a typical fuzzy inference system is shown in Fig. 1 (Jang 1993).

As mentioned earlier, for high dimensional problems, it is very difficult to generate every possible rule with respect to all antecedent combinations. The number of rules of a complete rule set can be calculated by using Eq. (6) (Angelov & Buswell 2003):

$$R = \prod_{i=1}^{n+1} m_i \quad (6)$$

where R is the number of rules; m is the number of membership functions for input i ; n is the number of inputs.

For example, the number of all possible rules in this study for seven input variables ($n = 7$) with three membership functions ($m = 3$) is $R = 3^{(7+1)} = 6561$ when all inputs participate in each rule.

The generation of rules in the classification model described in this work is difficult and complex as it maps seven inputs to one output. Nevertheless, the rules were generated based on Wang and Mendel’s method as it is simple, provides good performance, and can automatically generate rules from numerical data (Naik 2004). This method needs predefined fuzzy membership functions for each input and output. It can automatically generate rules from data. It starts by generating one rule for each data pair of the training set.

The i th pair one is written:

If x_1 is A_1^i and x_2 is $A_2^i \dots$ and x_p is A_p^i then y is C^i .

The fuzzy sets A_j^i are those for which the degree of match of x_j^i is maximum for each input variable j from pair i . The fuzzy set C^i is the one for which the degree of match of the observed output, y_i , is maximum (Guillaume et al. 2010).

A flow chart of the model development process is presented in figure 2.

5 RESULTS

One hundred and eighty flexible pavement sections were selected for building the fuzzy rules. The number

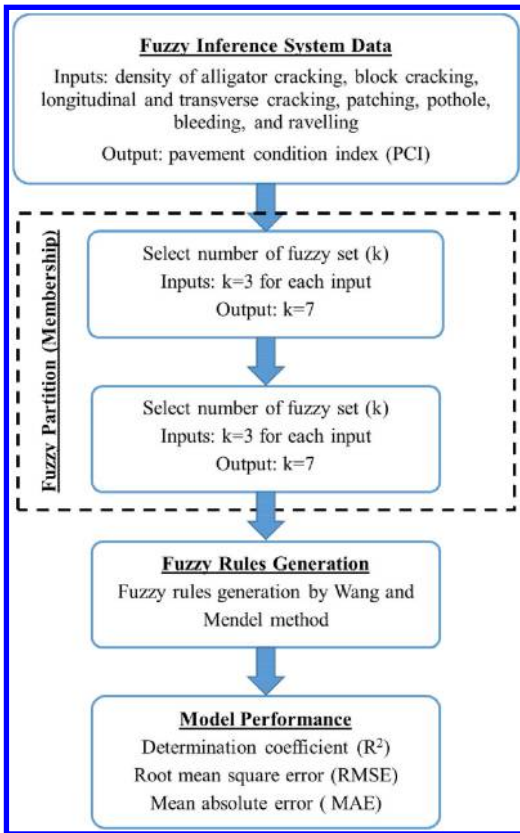


Figure 2. Model development flow chart.

of sections was then increased to 291 in order to further improve the accuracy of the model. For each section, seven types of distress (alligator cracking, block cracking, longitudinal and transverse cracking, patching, potholes, bleeding, and raveling), severity level, and extent of each section as defined in the LTP were used.

5.1 Membership function

Three triangular membership functions (low, medium, and high) were created for each input, while the seven triangular membership functions of PCI are created as shown in Figs. 3 to 10 for two data groups, where the x-axis represents the distress density for each input and PCI for output and the y-axis represents the membership function ranging from 0 to 1. It can be seen that, apart from the alligator cracks and potholes, the membership functions of the two data sets have no changes in the centre of clustering of input distresses and output PCI. However, the change in the centre of clustering of alligator cracking (Fig. 3) and potholes (Fig. 7) occurred because most distresses in the additional sections used in the second set (291 sections) had alligator cracking and potholes, resulting in modification in the membership function.

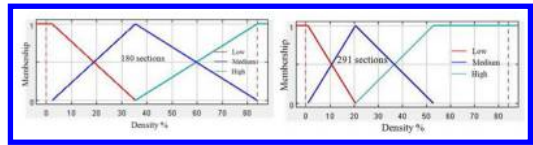


Figure 3. Membership functions for Alligator cracking.

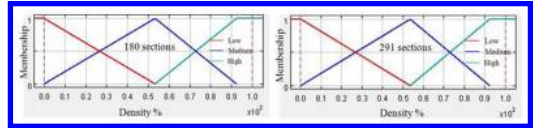


Figure 4. Membership functions for block cracking.

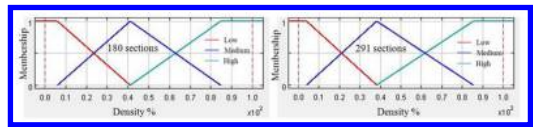


Figure 5. Membership functions for longitudinal & transverse cracking.

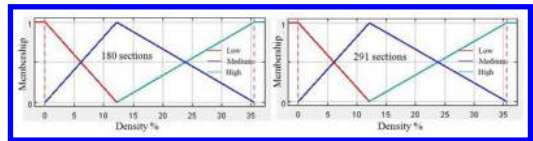


Figure 6. Membership functions for patching.

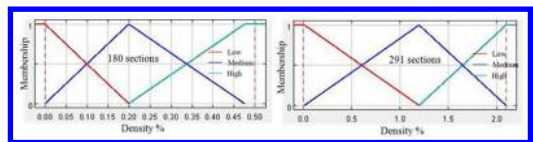


Figure 7. Membership functions for pothole.

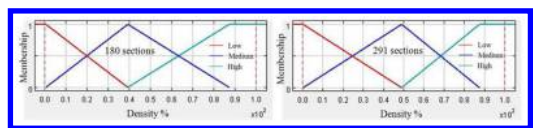


Figure 8. Membership functions for bleeding.

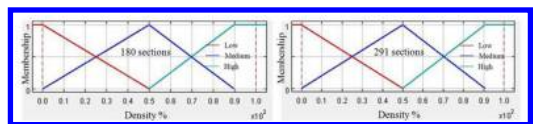


Figure 9. Membership functions for raveling.

5.2 Fuzzy rule generation

Tables 2 and 3 show the fuzzy rules of both data sets (180 and 291 sections). As the rules are dictated by the severity level of a data set, there are some differences between the two data sets, especially in the ‘poor’ category.

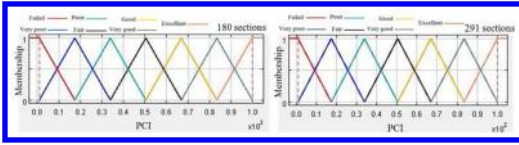


Figure 10. Membership functions for PCI.

Table 2. Fuzzy if then rules generated by 180 sections.

Rule No.	Distress type							Output rule - Then 'PCI' is ...
	Alligator Cracking	Block Cracking	Long & Trans. Cracking	Patching	Potholes	Bleeding	Ravelling	
1	High	Low	Low	Low	Low	Low	Low	Failed
2	Medium	Low	Medium	Low	Low	Medium	Low	Failed
3	Medium	Low	Low	Medium	Low	Low	Low	Failed
4	Medium	Medium	Low	Low	Low	Low	Low	Failed
5	Medium	Low	Medium	Low	Low	Low	Medium	Failed
6	Low	Low	Medium	Low	Low	Low	High	Failed
7	Medium	Low	Low	Low	Medium	Low	Low	Very poor
8	Low	High	Low	Low	High	Low	Low	Very poor
9	Medium	Low	Low	High	Low	Low	High	Very poor
10	Medium	Low	Medium	Low	Low	Low	Low	Poor
11	Medium	Low	Low	Low	High	Low	Low	Poor
12	Low	Low	Medium	Medium	Low	Low	Low	Poor
13	Low	Low	Medium	Low	High	Medium	High	Poor
14	Low	Low	High	Low	Low	High	Low	Fair
15	Low	Low	Medium	Low	Low	Low	Low	Fair
16	Medium	Low	Low	Low	Low	Low	Low	Fair
17	Low	Low	Low	Low	Medium	Medium	Medium	Fair
18	Low	Medium	High	Low	Low	Low	Low	Fair
19	Low	Low	Medium	Low	Low	Medium	Low	Fair
20	Low	Low	Medium	Low	Low	Low	Medium	Good
21	Low	Low	High	Low	Low	Low	Low	Good
22	Low	Low	Low	Low	Low	Low	Medium	Good
23	Low	High	Low	Low	Low	Low	Low	Good
24	Low	Low	Low	Medium	Low	Low	Low	Good
25	Low	Low	Low	Low	High	Low	Low	Very good
26	Low	Low	Low	Low	Low	Medium	Low	Very good
27	Low	Low	Low	Low	Low	Low	High	Very good
28	Low	Low	Low	Low	Low	Low	High	Very good
29	Low	Low	Low	Low	Low	Low	High	Very good
30	Low	Low	Low	Medium	Medium	Low	Low	Very good
31	Low	Low	Low	Low	Low	Low	Low	Excellent

These rules are used to calculate the PCI values for section classification. It is interesting to note that the number of rules only increases from 31 to 32, despite the addition of extra 110 sections. This indicates that the rules are largely dependent on the distress type and severity level rather than the number of sections.

5.3 Pavement Condition Index (PCI)

Figures 11a and 11b show the relation between the observed PCI and fuzzified PCI for both 180 and 291 sections. It can be seen that approximately 73.5% correlation was achieved for 180 sections, whereas the model accuracy improved to 76% with 291 sections. This means that the classification model improved as the number of sections increased, as more sections represent more possible variations of the distress type and severity, which helps the model to learn and create additional fuzzy rules.

Table 4 shows the coefficient of determination together with the root mean square error (RMSE) and Mean Absolute Error (MAE) to show the level of agreement of the PCI values in the two data sets calculated by two different methods. The performance of fuzzified PCI calculation improved by approximately 3% with 111 additional sections. It is expected that the level of accuracy will improve with further increases in the number of sections.

Table 3. Fuzzy if then rules generated by 291 sections.

Rule No.	Distress type							Output rule - Then 'PCI' is ...
	Alligator Cracking	Block Cracking	Long & Trans. Cracking	Patching	Potholes	Bleeding	Ravelling	
1	High	Low	Medium	Low	Low	Medium	Low	Failed
2	Medium	Low	High	Low	Low	Low	Low	Failed
3	Medium	Low	Low	Medium	Low	Low	Low	Failed
4	Medium	Medium	Low	Low	Low	Low	Low	Failed
5	High	Low	Medium	Low	Low	Low	Medium	Failed
6	High	Low	Low	High	Low	Low	High	Very poor
7	Low	Low	High	Low	Low	Low	High	Very poor
8	Low	Low	Medium	Low	Medium	Low	Low	Very poor
9	Low	Low	Medium	Low	Low	Low	High	Poor
10	High	Low	Medium	Low	Low	Low	Low	Poor
11	Low	Low	Medium	Medium	Low	Low	Low	Poor
12	Medium	Low	Medium	Low	Low	Low	Low	Poor
13	Low	Low	Medium	Low	Low	Medium	High	Poor
14	High	Low	Low	Low	Low	Low	Low	Poor
15	Low	Low	Low	Low	High	Low	Low	Poor
16	Low	Low	Medium	Low	Low	Low	Low	Poor
17	Medium	Low	Low	Low	Low	Low	Low	Poor
18	Low	Low	High	Low	Low	High	Low	Fair
19	Low	Medium	High	Low	Low	Low	Low	Fair
20	Low	Low	Medium	Low	Low	Medium	Low	Fair
21	Medium	Low	Low	Low	Low	Low	Medium	Fair
22	Medium	Low	Low	Low	High	Low	Low	Fair
23	High	Low	Low	Low	Low	Medium	Low	Fair
24	Low	Low	Low	Low	Low	Low	Low	Fair
25	Low	Low	Medium	Low	Low	Low	Medium	Good
26	Low	Low	Low	Low	Low	Low	Medium	Good
27	Low	High	Low	Low	Low	Low	Low	Good
28	Low	Low	Low	Low	Low	Low	High	Very good
29	Low	Low	Low	Low	Low	High	Low	Very good
30	Low	Low	Low	Medium	Low	Low	Low	Very good
31	Low	Low	Low	Low	Low	Low	Low	Very good
32	Low	Low	Low	Low	Low	Low	Low	Excellent

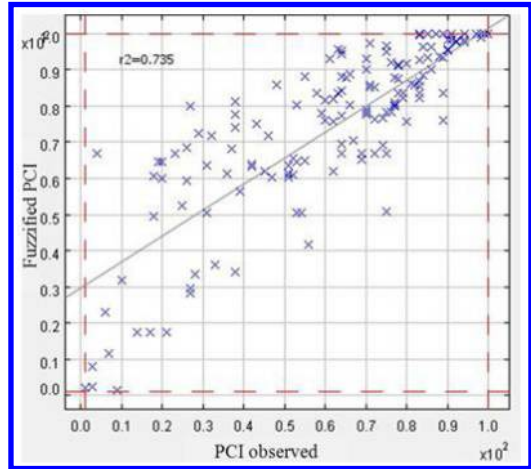


Figure 11a. The performance of a fuzzy inference system based PCI for 180 sections.

5.4 Error levels

To understand the level of error for each PCI category, the error levels are plotted for both data sets in Figs. 12a and 12b. The error level is the percentage difference between the fuzzified PCI (calculated by the fuzzy system) and the observed output (PCI calculated by PAVER software). It can be seen that the errors in the 'excellent' and 'very good' PCI classes are low compared to the 'medium' and 'worst' classes. This is because the proportion of the raw data used in this study was of either 'good' or 'excellent' quality. Moreover, the errors in the first data set are larger than those in the second data set because the distribution of raw data in a PCI category is better in the second set than in the first, as shown in Figs. 13a and 13b.

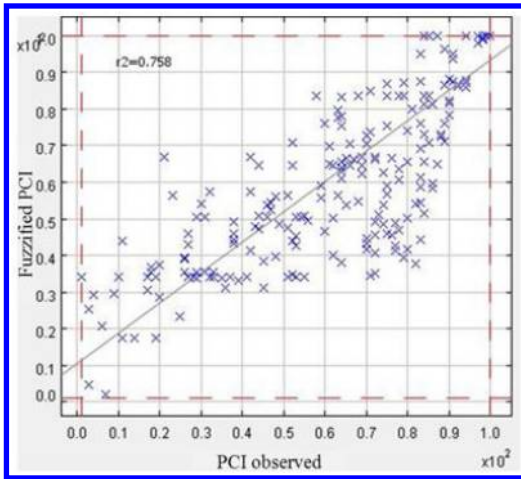


Figure 11b. The performance of a fuzzy inference system based PCI for 291 sections.

Table 4. The improvement of model performance with number of sections.

Number of sections	R ² (%)	RMSE	MAE
180	73.5	17.869	12.186
291	75.8	13.925	9.077

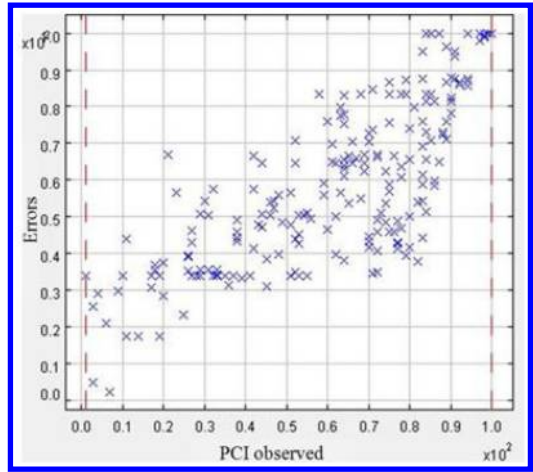


Figure 12b. Error levels in pavement classification system for 291 sections.

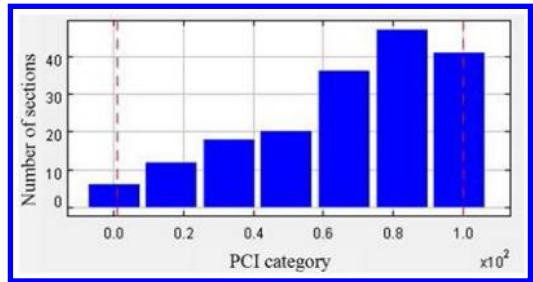


Figure 13a. Pavement distress data for each PCI category (180 sections).

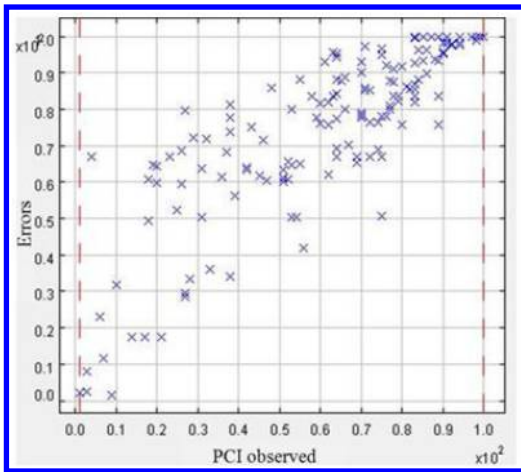


Figure 12a. Error levels in pavement classification system for 180 sections.

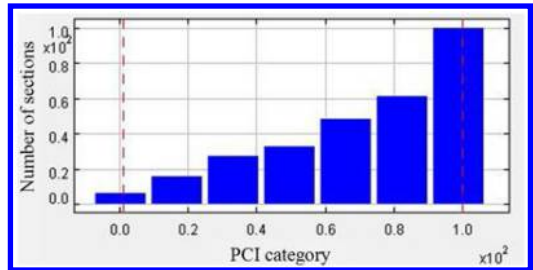


Figure 13b. Pavement distress data for each PCI category (291 sections).

5.5 Sensitivity of distress types

A sensitivity analysis was carried out to examine the effect of input variables on the efficiency of the fuzzy pavement classification system in the calculation of PCI. The analysis was conducted considering the following points:

- the effect of each input separately;

- the effect of all cracks (alligator, block, and longitudinal and transverse cracks);
- the effect of patching and potholes;
- the effect of bleeding and raveling.

The correlation between the fuzzified and conventional PCI calculations for each distress type and their level of influence on the PCI calculation are shown in Table 5. It can be seen from these figures that the determination coefficients for cracking, patching & potholes, and surface defects are 73, 4.7, and 6.4% respectively. It was found that for this given data set, the influence of alligator cracking is significantly

Table 5. Sensitivity level for each input variable.

Input variable	R ² (%)	Sensitivity level
Alligator cracks	56	High
Block cracks	2.8	Low
Longitudinal & transverse cracking	8	Low
Patching	4.3	Low
Pothole	0.6	Low
Bleeding	1.2	Low
Raveling	5.6	Low
All Cracks	73	High
Patching and pothole	4.7	Low
Bleeding and raveling	6.4	Low

higher than that of other types of distress. Therefore, the majority of the effect on PCI calculation comes from cracking, while patching, potholes, and surface defects have very little effect on the classification model.

6 SUMMARY AND CONCLUSIONS

A fuzzy inference system (FIS) was used to develop a fuzzified pavement condition index (PCI) for flexible pavement section classification. Compared to the conventional crisp (pass and fail) approach, this system has the potential to deal with uncertain and high-dimensional distress data.

Membership functions were developed for seven commonly used pavement distresses (alligator cracking, block cracking, longitudinal and transverse cracking, patching, potholes, bleeding, and raveling) extracted from two section data sets (180 sections, 291 sections) in the Long-Term Pavement Performance (LTPP) database. Triangular and semi-triangular shapes were used for the membership function for each distress type. These membership functions were then utilized in an FIS to generate rules for PCI-based section classifications.

The results showed an overall correlation of 76% between the fuzzified PCI and the PCI calculated by the commercial software MicroPAVER. This level of high correlation proves that the FIS-system-based PCI calculation has good potential in pavement section classification to optimize the influence of borderline values between two categories, which conventional crisp classification fails to address. The borderline values between two categories have a significant influence on the subsequent pavement maintenance and rehabilitation decision. Further research is underway to improve the model by considering more sections with different distress types. The sensitivity analysis showed that cracks have a significant influence on the fuzzified classification compared to the other distress types. Hence, it is possible to say that it is important to identify cracking severity during road condition assessments, as pavement management decisions

would be adversely affected by over- or under- estimation, resulting in erroneous prioritization and inefficient utilization of rehabilitation and maintenance funds.

As the proposed method deals with linguistic variables, pavement engineers will be able to easily understand and then realistically classify the sections, avoiding human judgments whilst utilizing numerical data of different pavement distresses to generate rules within a short period of time.

REFERENCES

- Angelov, P.P. & Buswell, R.A. 2003. Automatic generation of fuzzy rule-based models from data by genetic algorithms. *Information Sciences Journal* 150: 17–31.
- Arliansyah, J., Maruyama, T., & Takahashi, O. 2003. A Development of Fuzzy Pavement Condition Assessment. *Proc. JSCE*, 61(746): 275–285.
- Bandara, N. & Gunaratne, M. 2001. Current and Future Pavement Maintenance Prioritisation Based on Rapid Visual Condition Evaluation. *Journal of Transportation Engineering, ASCE* 127: 116–123.
- Dehzangi, O., Zolghadri, M. J., Taheri, S., and Fakhrahmad, S.M. 2007. Efficient fuzzy rule generation: A new approach using data mining principles and rule weighting. *Fourth International Conference on Fuzzy Systems and Knowledge Discovery (FSKD)*, IEEE, Haikou, 24–27 August 2007, 2: 134–139.
- Eldin, N. N. & Senouci, A. B. 1995. Use of neural networks for condition rating of jointed concrete pavements. *Advances in Engineering Software Journal* 23: 133–141.
- Fwa, T. F. 2006. *The handbook of highway engineering*. Boca Raton: Taylor & Francis Group.
- Fwa, T. F. & Shanmugam, R. 1998. Fuzzy Logic Technique for Pavement Condition Rating and Maintenance-Needs Assessment. *Fourth International Conference on Managing Pavements*, University of Pretoria, Durban, South Africa, 465–476.
- Golroo, A. & Tighe, S. L. 2009. Fuzzy set approach to condition assessments of novel sustainable pavements in the Canadian climate. *Canadian Journal of Civil Engineering* 36: 754–764.
- Guillaume, S., Charnomordic, B. & Lablee, J. 2010. FisPro 3.4 Manual. <http://www.inra.fr/mia/M/fispro/FisProEN.html>, 5 November 2012.
- Haas, R. 2010. Future Prospects for Pavement Management. *The 11th International Conference on Asphalt Pavement, International Society for Asphalt Pavements (ISAP)*, Nagoya, 1–6 August 2010, Aichi, Japan, 2026–2035.
- Hein, D. & Watt, D. 2005. Municipal Pavement Performance Prediction based on Pavement Condition Data. *Annual Conference of the Transportation Association of Canada*, Transportation Association of Canada, 18–21 September 2005, Calgary, Alberta.
- Jang, J. R. 1993. ANFIS: Adaptive-Network-Based Fuzzy Inference System. *IEEE Transactions on systems, MAN, and Cybernetic* 23(3): 665–685.
- Juang, C. H. & Amirhanian, S. N. 1992. Unified Pavement Distress Index for Managing Flexible Pavements. *Journal of Transportation Engineering, ASCE* 118: 686–699.
- Koduru, H. K., Xiao, F., Amirhanian, S. N. & Juang, C. H. 2010. Using Fuzzy Logic and Expert System Approaches in Evaluating Flexible Pavement Distress: Case Study. *Journal of Transportation Engineering, ASCE* 136: 149–157.

- Liu, Y., and Su, M. (2007). "Fuzzy optimization BP neural network model for pavement performance assessment". In: Grey Systems and Intelligent Services GSIS, IEEE International Conference, 1031–1034.
- Mahmood, M., Rahman, M., Nolle, L. & Mathavan, S. 2013. A fuzzy logic approach for pavement section classification. *International Journal of Pavement Research and Technology* 6(5): 620–626.
- Naik, V. C. 2004. *Fuzzy C-means clustering approach to design a warehouse layout*. M.S. thesis, University of South Florida, FL, USA.
- Negnevitsky, M. 2nd ed. 2002. *Artificial Intelligence: A guide to intelligent systems*. Essex: Pearson Education Limited.
- Shahin, M. Y. 2nd ed. 2005. *Pavement management for Airports, Roads, and Parking Lots*. New York: Springer.
- Shahin, M. Y., Welborn, W., Hammond, L., Kim, S., Meisel, R., Cerda, L. & Franzen, S. 2012. PAVERTM 6.5 User Manual. U.S. Army Corps of Engineers.
- Shahin, M.Y. & Walther, J.A. 1990. *Pavement Maintenance Management for Roads and Streets Using the PAVER System*. No. CERL-TR-M-90/05. Construction Engineering Research Lab (Army) Champaign IL, 40–54.
- Shiyab, A. M. 2007. *Optimum Use of the Flexible Pavement Condition Indictors in Pavement Management System*. Ph.D. Thesis, Curtin University of Technology, Australia.
- Shoukry, S. N., Martinelli, D. R. & Reigle, J. A. 1997. Universal Pavement Distress Evaluator Based on Fuzzy Sets. *Transportation research record* 1592: 180–186.
- Sun, L. & Gu, W. 2011. Pavement Condition Assessment Using Fuzzy Logic Theory and Analytic Hierarchy Process. *Journal of Transportation Engineering, ASCE* 137: 648–655.
- Terzi, S. 2007. Modelling the pavement serviceability ratio of flexible highway pavements by artificial neural networks. *Construction and Building Materials Journal* 21(3): 590–593.
- U.S. Department of Transportation, FHWA. 2012. Long-Term Pavement Performance LTPP. Standard Data Release 26.0 DVD.

Pavement recycling, geosynthetics

First trial to design up to 50% recycled hot mix asphalt in Latvia

R. Izaks, V. Haritonovs & M. Zaumanis

Riga Technical University, Riga, Latvia

ABSTRACT: Due to increasing cost of asphalt binder, significant economic savings can be realized using high content of Reclaimed Asphalt Pavement (RAP) in the production of new Hot Mix Asphalt (HMA). Moreover, this is an environmentally friendly alternative as it reduces the need for virgin materials. It has to be noted that in Latvia RAP is rarely used in production of HMA and this valuable material is mostly degraded for use in lower value applications. Three mixtures were designed, which were the combination of two different RAP sources and local dolomite aggregates. The RAP binder had significantly aged having penetration of around 38 mm, softening point of 56°C and Fraass temperature of -10°C. RAP was added at rates 30% and 50% for each RAP source. A softer binder grade (70/100 versus traditional 50/70) was added to compensate for the aged RAP binder. Hamburg wheel tracking test results demonstrated that all mixtures have high rutting resistance and fatigue test results using four point bending beam were similar to those of virgin mixture. This demonstrated that mixtures with high RAP content can be successfully designed to meet the local volumetric and performance-specification requirements.

1 INTRODUCTION

The history of asphalt pavement recycling dates back to the early 1900s. Recycling asphalt pavements first became popular in the U.S. in the 1970s during the oil embargo when the cost of crude oil skyrocketed. Today, the two primary factors that influence the use of reclaimed asphalt pavement (RAP) in asphalt pavements are economic savings and environmental benefits (Newcomb et al. 2007). RAP is a useful alternative to virgin materials because it reduces the use of virgin aggregate and the amount of virgin asphalt binder required in the production of hot mix asphalt (HMA) (Copeland 2011). For higher RAP content (above 25%), design and production takes extra effort, but the savings in using the higher RAP contents significantly outweigh the added costs. Blending to meet gradation and the appropriate binder grade in the final product are keys to successful mix design, production, and performance (Newcomb et al. 2007).

The most crucial characteristic of RAP material that affects the properties and performance of recycled mixtures is aging of its binder.

The methods for compensating for the aged, stiff binder and ensuring adequate pavement performance include the use of rejuvenating or softening additives, use of softer virgin binder grade and increase in total mixture binder content (Zaumanis 2014).

There is no consensus whether HMA which incorporates RAP performs any different compared to HMA without RAP. A number of researchers have pointed out that using RAP increased stiffness (Al-Rousan et al., 2008, McDaniel and Shah, 2002, Tabakovic

et al., 2010, Zaumanis 2014, Al-Qadi et al., 2012) while others have reported the opposite (Oliver, 2001, Widyatmoko, 2008). Also, at the time that some studies have revealed improving of fatigue resistance with using RAP (Oliver, 2001, Tabakovic et al., 2006, 2010, Widyatmoko, 2008), other studies have reported some degradation (Al-Rousan et al., 2008, McDaniel and Anderson, 2001, Zaumanis 2014, Al-Qadi et al., 2012).

2 OBJECTIVE

The objective of the research is to develop high content recycled mixtures using materials found in Latvia in order to meet the local volumetric and performance-specification requirements for medium and high traffic intensity roads of Latvia and to ensure performance of these mixtures similar to virgin asphalt.

3 MATERIALS AND METHODS

3.1 Aggregate

The aggregates used in this study were fractionated and crushed dolomite. Dolomite is one of the most available sedimentary rocks in the territory of Latvia. According to Latvian Road Specifications 2014, this dolomite can be used for medium and high traffic intensity roads in asphalt base and binder layers.

3.2 RAP materials

The first and most important step in design of recycled HMA is to determine the properties of RAP aggregate

Table 1. RAP aggregate gradation and bitumen content.

RAP source	A6 RAP	A7 RAP
Bitumen content, %	5.12	4.9
Sieve size, mm	passing, %	
22.4	100	100
16	100	99.4
11.2	96.4	92.4
8	89.3	57.1
5.6	81.9	34.4
4	74.7	26.1
2	63.8	21.7
1	52.8	19.3
0.5	41.3	17.4
0.25	29.4	14.9
0.125	20.2	12.5
0.063	16.2	11.1

and RAP binder. The basic required properties of RAP materials are binder viscosity, bitumen content and particle size distribution of aggregates.

Materials from two RAP sources were used in this research. Three mixtures were designed with RAP and one reference mixture using only virgin materials. RAP was added at a rate of 30% and 50% for each RAP source. It is important to note, that these percentages were selected based on the Latvian Road Specifications 2014, which define and specify the design requirements of recycled mixtures with RAP. 30% RAP is within the specified acceptable range while the mixture with 50% RAP is outside this range.

Two RAP sources were used. The first source of RAP (A7) was millings from a road rehabilitation project, where an upper layer of an existing pavement was removed. No crushing or screening was done for this material. The second source of RAP (A6) was millings from full-depth road reconstruction project, therefore the resulting RAP was a combination of different asphalt types. Prior to recycling this RAP was crushed and fractionated to size 0/11 mm. This was likely the reason for high dust content (16.2%).

The binder was extracted from both RAP sources according (EN 12697-1 clause B.1.2.) to determine the binder content and aggregate gradation in the RAP sources. The bitumen content is calculated by difference from the weight of extracted aggregates.

Table 1 shows the RAP gradation and the bitumen content for both RAP sources. With “A7” and “A6” representing the RAP source.

3.3 Virgin binder

Two types of new bitumen were used. Bitumen 50/70 was used to produce the reference mixture from virgin materials, while for all mixtures having RAP a softer grade bitumen (70/100) was added to compensate for the aged RAP binder and to ensure that the target binder grade is B50/70. The values of these virgin binder properties and requirements are shown in Table 2.

3.4 RAP binder properties

When using high percentages of RAP (>25%) one needs to know the properties of RAP binder (Kandhal *et al.* 1997). Therefore binder was recovered from both RAP sources by rotary evaporator according (EN 12697-3) to measure penetration, softening point, and Fraass breaking point. Table 2 demonstrates the physical properties of aged binder. Once the desired RAP percentage has been determined, the RAP binder and virgin binder should be combined and put through testing (if the RAP content exceeds 25 percent) to see that it conforms to the target binder grading requirement for the application (Newcomb *et al.* 2007). The penetration can be estimated using Equation 1:

$$a \lg pen_1 + b \lg pen_2 = (a + b) \lg pen_{mix} \quad (1)$$

where pen_{mix} is calculated penetration, pen_1 is penetration of RAP extracted binder, pen_2 is penetration of virgin binder, a and b is proportion of virgin (a) and aged (b) binder: $a + b = 1$.

Softening point temperature can be estimated using Equation 2:

$$T_{R\&Bmix} = a \times T_{R\&B1} + b \times T_{R\&B2} \quad (2)$$

where $T_{R\&Bmix}$ is calculated softening temperature, $T_{R\&B1}$ is softening temperature of RAP extracted binder, $T_{R\&B2}$ is softening temperature of virgin binder, a and b is proportion of virgin (a) and aged (a) binder: $a + b = 1$.

Fraass Breaking point of blended binder was determined in accordance with EN 12593. Table 3 demonstrates the properties of the combined binder at the demonstrated percentages. Target binder grade is B50/70.

3.5 Mix design

Aim of design of recycled HMA is to optimize RAP content and produce a mix with good performance fatigue, rutting, thermal resistance, and overall durability. Further, the mixture has to meet the required volumetric properties including air voids, voids in mineral aggregates (VMA), voids filled with asphalt (VFA), and dust proportion (Al-Qadi *et al.* 2007). Mixtures were designed using Marshall method, according to the Latvian Road Specifications 2014.

Marshall mix design procedure was used for the determination of the optimal bitumen content for the reference mixture AC-16 base/bin, considering the mixture test results for Marshall stability and flow, as well as the volumetric values: air voids (V), voids in mineral aggregate (VMA) and voids filled with bitumen (VFB).

All recycled asphalt mixtures were designed with optimal binder content. To calculate the minimal binder content of mixtures with RAP, it is necessary to know the combined aggregate bulk specific gravity. Calculating the combined bulk specific gravity

Table 2. Virgin and aged binder properties.

Property	Test method	Unit	Requirement	Requirement	Virgin binder values		Aged binder values	
			B50/70	B70/100	B50/70	B70/100	A6 RAP	A7 RAP
Penetration at 25°C	EN 1426	0.1 mm	50–70	70–100	64.5	86	38	55
Softening Point R&B	EN 1427	°C	46–54	43–51	47	46	59	50
Fraass Breaking point	EN 12593	°C	≤−8	≤−10	−17	−20.8	−9	−11

Table 3. Blended binder properties.

Property	Test method	Unit	Requirement	A6 RAP 30%	A7 RAP 30%	A7 RAP 50%
			B50/70	Percentage binder replacement, %		
Penetration at 25°C	EN 1426	0.1 mm	50–70	31,8%	36,5%	62,5%
Softening Point R&B	EN 1427	°C	46–54	66	73	65
Fraass Breaking point	EN 12593	°C	≤−8	50	47	49
				−16	−18	−16

requires knowing the bulk specific gravity of each aggregate component. The maximum theoretical specific gravity of the RAP was used to backcalculate the bulk specific gravity of the RAP aggregate. To estimate bulk specific gravity of the RAP aggregate Equation 3 and Equation 4 were used (Mc Daniel et al. 2001, Al-Qadi et al. 2012).

$$G_{se} = \frac{100 - P_b}{\frac{100}{G_{mm}} - \frac{P_b}{G_b}} \quad (3)$$

$$G_{sb} = \frac{G_{se}}{\left(\frac{P_{ba} G_{se}}{100 G_b} + 1 \right)} \quad (4)$$

where G_{mm} is theoretical maximum specific gravity, $G_{b(RAP)}$ is specific gravity of RAP binder, $P_{b(RAP)}$ the RAP binder content, G_{se} is effective specific gravity of aggregate, G_{sb} is bulk specific gravity of aggregate and P_{ba} are absorbed binder, percent by weight of aggregate. All recycled mixtures were designed with 4.1% binder content, the percentage binder replacement from RAP is shown in Table 4.

Test specimens for Marshall Test were prepared using impact compactor according to EN 12697-30 with 2×50 blows of hammer at 145°C temperature. Table 4 presents a summary of the properties of these five mixtures.

3.6 Methods

Four tests were chosen to assess the mechanical properties of the asphalt mixtures; the four point bending beam test was used to determine the fatigue resistance (EN 12697-24 Annex D) and stiffness modulus (EN 12697-26 Annex B), wheel tracking test was used to determine rutting resistance (EN 12697-22) and

Marshall test determine stability and flow according to (EN 12697-34).

3.6.1 Wheel tracking test

Tests were performed according to EN 12697-22 method B (wheel tracking test with small size device in air). Dimensions of wheel tracking test samples were of 305×305 mm and 50 mm high. The samples were compacted in the laboratory by using roller compactor.

Resistance to permanent deformation is assessed by the depth of the track and its increments caused by repetitive cycles (26.5 cycles per minute) under constant temperature (60°C). The rut depths are monitored by means of two linear variable displacement transducers (LVDTs), which measure the vertical displacements of each of the two wheel axles independently as rutting progresses (Haritonovs 2013).

3.6.2 Fatigue test

The test was run at 10°C, 10 Hz at 115 μm and 130 μm strain level. The beams were compacted in the laboratory by using roller compactor. They were saw cut to the required dimensions of 50 mm wide, 50 mm high and 400 mm long. The failure criterion used in the study is the traditional 50% reduction in initial stiffness.

3.6.3 Stiffness test

The test was carried out under the standard conditions of 50 μm target horizontal deformation, 10 Hz frequency, at 10°C test temperature. The beams were compacted in the laboratory by using roller compactor.

4 RESULTS AND DISCUSSION

4.1 Volumetric properties

Volumetric parameters of the different asphalt mixtures at different RAP contents were analyzed. The

Table 4. Summary of asphalt mixture properties.

Mix type	Binder	Asphalt content, %	Virgin asphalt content, %	Percentage binder replacement, %	Required value		
					AV, % 2.5–6.5	VMA, % ≥14	VFA, % ≤80
AC-16 base/bin	50/70	4.7	4.7	0.0	4.5	15.6	71.5
A6 RAP 30%	70/100	3.96	2.7	31.8	6.8	16.1	57.7
A7 RAP 30%	70/100	4.25	2.7	36.5	5.5	15.5	64.4
A7 RAP 50%	70/100	4.26	1.6	62.5	4.5	14.7	69.1

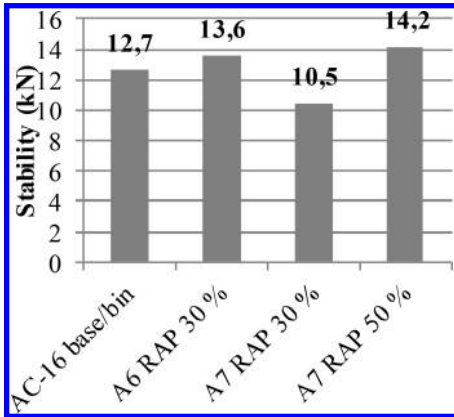


Figure 1. Marshall stability values.

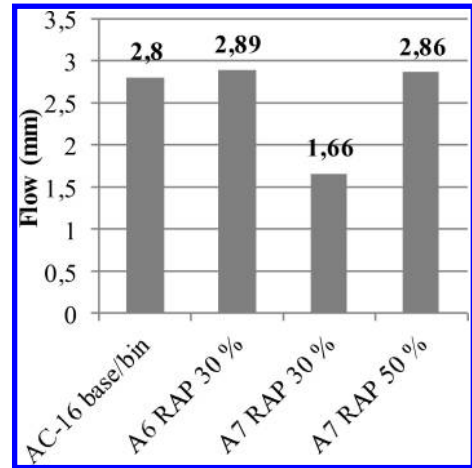


Figure 2. Marshall flow values.

volumetric result values: air voids (V), voids in mineral aggregate (VMA) and voids filled with bitumen (VFA) are presented in Table 4.

For the RAP mixtures, the VMA values decreasing with increase RAP percentage and the VFA values for all of the RAP mixtures are lower than the control mix. Table 4 indicates no significant difference between the air voids in references mix and recycled mixtures. Air voids significantly affect the rate of bitumen content in mixture. The A6 RAP 30% mixture with lowest bitumen content didn't meet the required value of air voids. Air voids decreasing in recycled mixtures with increase of RAP percentage, because increased the fine aggregate in mixture from RAP.

4.2 Marshall stability and flow test

All mixtures meet the minimum stability criteria of 10 kN for medium and high traffic intensity roads, and satisfy the VMA and VFA requirements. At the same time all mixtures meet Marshall flow criteria of 1–4 mm. The flow and stability values for all mixtures are presented in Figure 1–2. The results show that increasing the A7 RAP content in mixtures also increase Marshall stability and flow.

4.3 Wheel tracking test

Wheel tracking test is used to simulate the effect of traffic and to measure the deformation susceptibility

of asphalt samples. The obtained results demonstrate that the largest average rut depth of 3.4 mm and wheel tracking slope of 0.15 mm/1000 cycles appear for the AC-16 base/bin references mixture, the potential reason for this might be the highest bitumen content 4.7% for references mixture. A6 RAP 30% mixture with lowest bitumen content shows high resistance to permanent deformations, having an average rut depth value of 1.8 mm and wheel tracking slope of 0.04 mm/1000 cycles (Table 4). Figure 3 provides a summary of rut resistance properties of the test specimens.

Since wheel tracking test results were acceptable for recycled mixtures, it might be possible to redesign the mixture with increased binder content and as a result increase resistance to fatigue.

4.4 Fatigue test

To determine the fatigue life of the prepared asphalt concrete mixes, a four point bending beam test under controlled displacement was conducted. The obtained results indicate that mixture A7 RAP 50% showed far less resistance to fatigue, compared to results for references mixture made with virgin aggregates and mixtures made with RAP content of 30%.

The failure criterion, the traditional 50% reduction in initial stiffness A7 RAP 50% mixture reached to

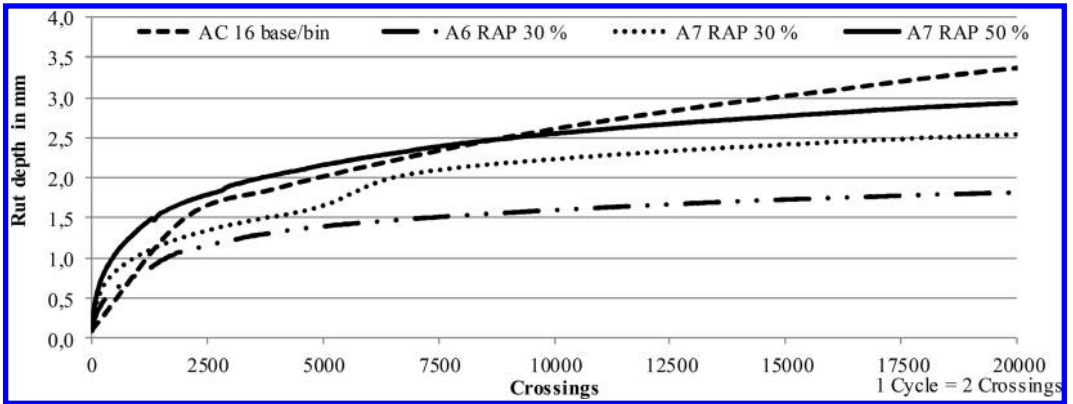


Figure 3. Wheel tracking test results.

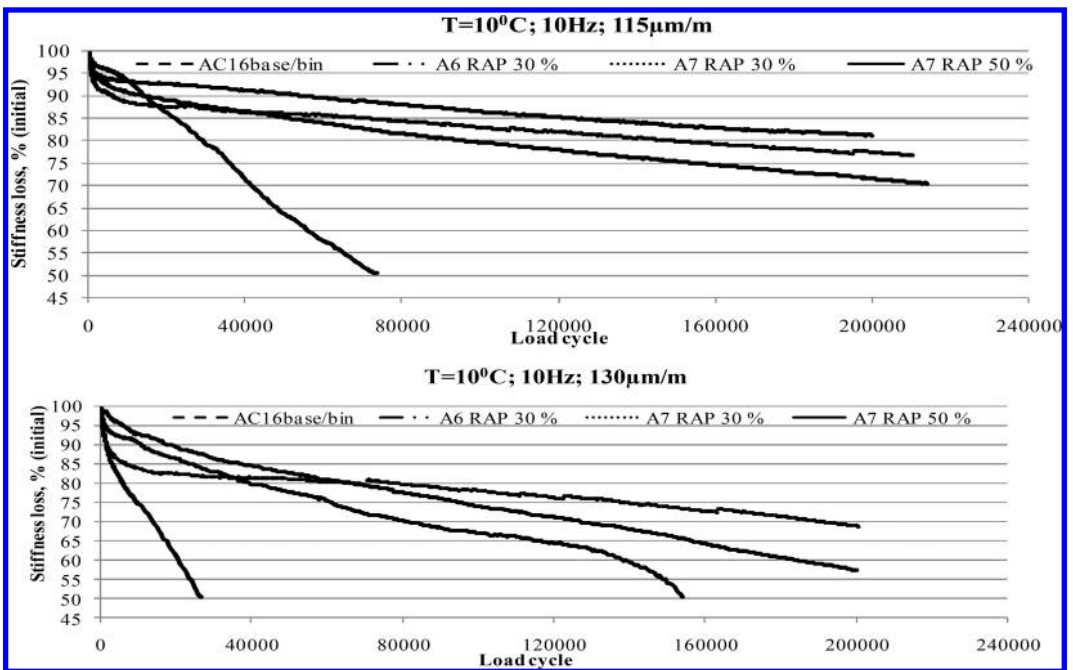


Figure 4. Fatigue test results.

73500 load cycle at 115 μm strain level and to 26500 load cycle at 130 μm strain level. Using higher virgin binder content in high RAP content mixes can compensate for the decrease in fatigue resistance. Figure 4 demonstrates stiffness curves.

4.5 Stiffness test

Mixtures containing RAP content of 30% for both RAP sources had lower stiffness than the reference mixture AC-16 base/bin B50/70, but these mixtures have similar resistance to rutting. With an increase in A7 RAP content, the stiffness of the mixture increases. The stiffness alone does not give the full picture

however, because the ductility or brittleness of the mixture will also affect its performance with respect to cracking.

The 50% RAP mixture contains a large part of aged asphalt binder, which is more brittle than virgin binder, therefore if interaction between the aged and virgin binder completely does not happen, the 50% RAP mixture to be more brittle than the references and 30% RAP mixtures, like in this research. A7 RAP 50% mixture were the similar stiffness result as references mix, but also less resistance to fatigue.

The combination of higher stiffness and more brittle behavior will likely result in a shorter fatigue life and a higher probability of thermal cracking occurring in the field.

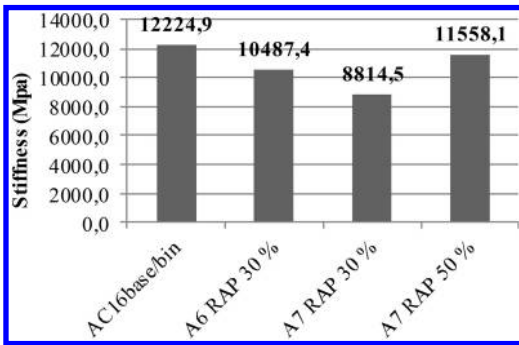


Figure 5. Stiffness test results.

Using small sizes of RAP aggregates leads to an increase in surface area, which in heating of the samples, results in liberating and bleeding more RAP binder into the mixing process. This in turn provides more interaction between the aged and virgin binders and is the likely cause of better virgin and aged binder blending. Figure 5 demonstrates stiffness modulus values.

5 CONCLUSIONS

The aim from the design process was to produce recycled mixes with similar properties to the reference mix AC16 base/bin (virgin mix made using bitumen B50/70). RAP has no significant effect on volumetric and mechanical properties of the recycled HMA in terms of Marshall stability and flow as well as rut resistance.

Test results also demonstrated that mixtures with RAP showed a little higher resistance to rutting compared to reference mixture, but all of them pass the Specification requirement $WTS_{AIR} < 0.3$ mm.

All recycled mixtures (except the A7 RAP 50%) compared to reference mixture showed similar fatigue resistance.

The use of RAP, especially high RAP content, in HMA decreased the fatigue resistance, probably due to the high percentage binder replacement which stiffens the asphalt mixture.

Based on the findings of this study it can be concluded that it is possible to design high-quality HMA with up to 50% RAP that meets the desired volumetric and performance requirements. There are no significant differences in mechanical properties (stiffness and fatigue behavior) between the recycled and virgin mixtures. Increasing the effective asphalt content of the recycled asphalt mixtures will help to increase the durability and fatigue resistance of the asphalt mixtures.

ACKNOWLEDGEMENTS

This work has been supported by the European Social Fund within the Project No.2013/0025/1DP/1.1.1.2.0/13/APIA/VIAA/019 “New ‘Smart’ Nanocomposite

Materials for Roads, Bridges, Buildings and Transport Vehicle”.

REFERENCES

- Al-Rousan, T., Asi, I., Al-Hattamleh, O. & Al-Qablan, H. 2008. Performance of Asphalt Mixes Containing RAP. *Jordan Journal of Civil Engineering* volume 2, No. 3.
- Al-Qadi, I.L., Elseifi, M. & Carpenter, S.H. 2007. Reclaimed Asphalt Pavement – A Literature Review. Series No. 07-001. Illinois Center for Transportation, University of Illinois.
- Al-Qadi, I.L., et al., 2012. Impact of high RAP contents on structural and performance properties of asphalt mixtures. Springfield: Illinois Center for Transportation, Report Number FHWA-ICT-12-002.
- Copeland, A., 2011. Reclaimed Asphalt Pavement in Asphalt Mixtures: State of the Practice. FHWA Report No.: FHWA-HRT-11-021.
- David E. Newcomb, E. Ray Brown, Jon A. Epps. 2007. Designing HMA Mixtures with High RAP Content. A Practical Guide. Quality Improvement Series 124. National Asphalt Pavement Association, Lanham, MD.
- Haritonovs V., Zaumanis M., Tihonovs J., Smirnovs J., 2013. Development of high performance asphalt concrete using low quality aggregates. *Civil Engineering’ 13 4th International Scientific Conference Proceedings*, Vol. 4 Jelgava, Latvia University of Agriculture, 2013, 371 pages, ISSN 2255-7776.
- Kandhal, P. S. & Foo, K. Y. 1997. Designing recycled hot mix asphalt mixtures using Superpave technology. ASTM Special Technical Publication, 1322, 101–117.
- McDaniel, R.S. and Anderson, R.M., 2001. Recommended use of reclaimed asphalt pavement in the Superpave mix design method: technician’s manual. West Lafayette, IN: North Central Superpave Center, Report Number NCHRP 452.
- McDaniel, R., Soleymani, H., and Shah, A. 2002. Use of Reclaimed Asphalt Pavement (RAP) Under Superpave Specifications: A Regional Pooled Fund Project, North Central Superpave Center, West Lafayette, IN.
- Oliver, J. W. H., 2001. “The Influence of the Binder in RAP on Recycled Asphalt Properties,” *International Journal of Road Materials and Pavement Design*, Vol. 2, No. 3, pp. 311–325.
- Tabakovic, A., Gibney, A., Gilchrist, M. & McNally, C. 2006. The influence of recycled asphalt pavement on 20mm binder course mix performance. University College Dublin
- Tabakovic, A., Gibney, A., McNally and Michael D. Gilchrist. 2010. Influence of Recycled Asphalt Pavement on Fatigue Performance of Asphalt Concrete Base Courses. DOI:10.1061/(ASCE)MT.1943-5533.0000093
- Widyatmoko, I. 2008. Mechanistic-empirical mixture design for hot mix asphalt pavement recycling. *Construction and Building Materials*, Vol. 22, Issue 2, pp. 77–87 doi:10.1016/j.conbuildmat.2006.05.041
- Zaumanis, M., Mallick, R.B. 2014. Review of very high-content reclaimed asphalt use in plant-produced pavement: state of the art. *International Journal of Pavement Engineering*, DOI: 10.1080/10298436.2014.893331

Influence of reclaimed asphalt content on asphalt mix characteristics doped by selected rejuvenators

P. Vacková & J. Valentin

*Department of Road Structures, Faculty of Civil Engineering,
Czech Technical University in Prague, Prague, Czech Republic*

ABSTRACT: The application of increased quantities of reclaimed material in asphalt mixes is a trend whose importance has been growing steadily in recent years. Along with this approach it is needed to find solutions in which reactivated bitumen in the Reclaimed Asphalt Pavement (RAP) will not have any negative impacts on mixture durability. The durability can be affected primarily by the rate of degradation of bitumen contained in the RAP. An important aspect is therefore the quantity of the reclaimed asphalt added to the asphalt mix. For the assessment of these effects in combination with selected types of rejuvenators and their influence on asphalt properties, asphalt concrete AC11 was selected as a suitable representative. Three levels of RAP in the AC mix were proposed: 20%; 35% and 50%. From the perspective of chemical additives, rejuvenators of a new product series developed by a Czech refinery, as well as existing Italian or German products were selected. Further Indian and U.S. additives were applied which are used mostly in the field of warm mix asphalt. Last but not least industrially produced binder for mixes with high RAP proportion was assessed as well. The additives were appropriately combined with the selected RAP contents. Various percentages of the additives were applied and different combinations created with varying quantities of additional new bituminous binder. The mixes were compared to one another according to the tests commonly applied in the Czech Republic (mainly moisture susceptibility, stiffness determination, rutting test and assessment of behaviour in low temperature range). The results of the conducted laboratory study are presented in this paper.

1 INTRODUCTION

Recent years have shown that the use of reclaimed asphalt material pavement (RAP) in road construction becomes a modern, advanced and unavoidable trend in most countries. Recycling of construction materials saves not only direct primary costs like purchasing raw materials but also facilitates savings of related costs like energy, material disposal and transport etc. Those factors are also connected to environment-friendly approaches, primarily in the case reducing the production of greenhouse gases. Material disposal can subsequently be reduced solely to waste or by-product materials which have no way of further utilisation – e.g. recycled material from asphalt pavements containing tar.

The bituminous binder in reclaimed material is usually considerably oxidised which means that it is stiffer and more brittle than common bituminous binders, (Mogawer 2012). If the asphalt mix uses higher percentages of RAP it can be expected that the resulting mix will be stiffer and less resistant to climate or traffic load changes. Thanks to the oxidised (aged) binder, the mix demonstrates increased stiffness which is also linked to higher resistance to permanent deformation. However the problem in this case is the resistance to fatigue and to frost cracking,

(Boriak 2013). These facts result in number of legislative restrictions towards the application of higher content of RAP in the mixes. Nevertheless, the negative properties can be reduced by suitable rejuvenators or additives. Following their development in the field of asphalt mixes, this direction improves the possibilities of using high contents of RAP and, in the future, facilitating the use of up to 100% reclaimed asphalt in new mix designs, (Zaumanis 2014c).

It is not known exactly how well the binder in reclaimed material is reactivated; therefore the optimum final quantity of binder in the mix is not known exactly and cannot be determined with absolute certainty. Not all of the binder in the reclaimed asphalt may be activated.

Nevertheless, oxidised bitumen in RAP can be reactivated by means of rejuvenators which influence the properties of the binder through its chemical properties. The addition of rejuvenators makes the binder usually softer and less brittle; a favourable proportion of the viscous and elastic behaviour of the material is renewed, (Terrel 1989). Some additives can also reduce the production temperature of asphalt mix and facilitate improved workability, (Zaumanis 2014a). Mixes with higher percentages of reclaimed material are usually stiffer and more difficult to work with. They require strict technological discipline during

compaction and require more compacting energy compared to mixes without RAP (Zaumanis 2014b). As noted by other findings, stiffer mixes tend to have poorer workability while the production temperature remains the same; therefore, additional increases of this temperature might be required, (Mogawer 2012).

Prior to selecting the appropriate rejuvenator, the resulting properties of the mix must be considered. Rejuvenators usually affect bitumen penetration and its softening point. The expected level of softening can be adjusted by the dosage of the additive, (Iterchmica 2014). Use of a higher quantity of additive usually results in a more significant effect on the properties. The manufacturers mostly recommend dosages according to existing nomographs based on the properties of the binder in the reclaimed asphalt and on the required final characteristics.

When a high content of RAP is applied to the mix, it is very important to know its input properties. The RAP material must be homogeneous which is best achieved when the pavement is cold milled by separate layers, through good quality records and documents of all maintenance interventions, documents for all existing pavement distresses and by proper storage of the RAP. The reclaimed asphalt should be re-crushed, re-sorted and stored in a way to eliminate climate impact.

2 MIX DESIGN AND USED VARIATIONS

Within the assessment of the effect of selected types of some available or developed rejuvenators on the behaviour of asphalt mixes with high content of RAP, asphalt mix AC11 for wearing course according to CSN EN 13108-1 was selected. In the mix 20%, 35% and 50% RAP of 0/11 mm grading was applied, whereas the reclaimed asphalt was obtained from various types of asphalt pavement structures. Therefore the material cannot be classified as homogeneous and it shows varying properties. The aggregate for the asphalt mix originates from Libodřice quarry (amphibolite).

From the perspective of the asphalt mix composition design, the RAP was first analysed by means of the extraction device to determine the quantity of soluble binder and the grading curve of aggregates contained in RAP. The grading curves of individual aggregate fractions and the grading curve of RAP, i.e. the purified reclaimed material, were used for the mix design. The grading curves of individual mixes were designed to be identical with the reference mix.

The extraction of bitumen from RAP revealed that the material contains on average 5.4% of binder. The designed content of the additional fresh bitumen assumed that all of the binder from the reclaimed asphalt will be activated. The reference AC11 mix was designed with the resulting quantity of 5.2% bitumen. The binder content was increased (or reduced) in some mix variations to allow observing the effect of this content or the used additives on the mix properties.

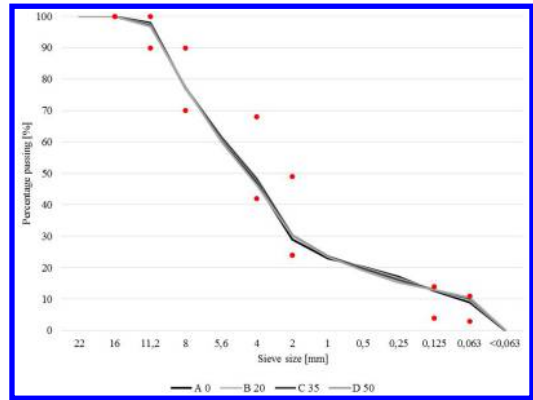


Figure 1. Grading curves of particular asphalt mixes.

Distilled bitumen 50/70 from two different refineries (Paramo and OMV) was used.

From the perspective of chemical additives, 3 rejuvenators from four different manufacturers, a nano-chemical additive (India – IND) and surface-active additives (U.S. – ET; Italy – IT; Germany – ST) were selected. Together with those additives, the impact of commercially manufactured binder (marked RE) which is intended for asphalt mixes with higher RAP content, was assessed as well.

The first of the rejuvenators used was the commercially available product (IT). Based on manufacturer's specifications, the additive helps to regenerate the binder in the reclaimed asphalt, facilitates good binder-aggregate adhesion and works as a high active antistripping agent. IT can be dosed into the bitumen or during production at the mixing plant straight to the asphalt mix. The commonly applied quantities range from 0.4 % to 0.6% per 10% of RAP in the mix. In the study, the used content ranged from 1.5% to 2% added directly to the asphalt mix, (Iterchmica 2014).

The second used rejuvenator was ST which, according to the product information, can regenerate aged bitumen in the reclaimed asphalt. It contains a group of chemicals which helps reactivating the aged binder properties, (StorImpex 2014).

Several versions of rejuvenators from a newly developed production by a Czech refinery were selected – Reju 161, Reju 182 and Reju 553. In the case of Reju 182, the rejuvenator is based on refined plant (rapeseed) oil. Reju 553 is made of mineral oil during vacuum oil distillation. All rejuvenators, once added to the mix, have an impact on bitumen penetration. The dosage of the additive depends on the required penetration improvement. According to the existing findings, aged binder is softened most by Reju 182; based on the available information, if 6% of the additive (related to bitumen) is used together with bitumen 20/30, the binder is softened up to 60 dmm, (Paramo 2014).

In case of IND additive it is supposed to improve workability of RAP in asphalt mixes and the adhesion. The additive is usually added to common asphalt

Table 1. Overview of tested asphalt mixes.

RAP	Mixture notation	Used bituminous binder	Content of added bitumen (%)	Virgin bitumen + RAP bitumen (%)	Dosage of the additive
0%	Referential – 50/70		5.2	5.2	–
20%	Referential – OMV 50/70				
	Referential – 20% RAP	OMV 50/70	4.1	5.2	–
	RE	RE binder	4.1	5.2	–
	RE (5.2%)	RE binder	5.2	6.3	–
	0.1% ZT	OMV 50/70 + 0.1% ZT	4.1	5.2	0.10% of added bitumen
	0.1% ZT (5.2%)	OMV 50/70 + 0.1% ZT	5.2	6.3	0.10% of added bitumen
35%	Referential – 35% RAP	OMV 50/70	3.3	5.2	–
	RE	RE binder	3.3	5.2	–
	0.1% ZT	OMV 50/70 + 0.1% ZT	3.3	5.2	0.10% of added bitumen
	0.15% ZT	OMV 50/70 + 0.15% ZT	3.3	5.2	0.15% of added bitumen
	Reju 553	OMV 50/70	3.3	5.2	6% of binder in RAP
	IT	OMV 50/70	3.3	5.2	1.4% of added bitumen
50%	Referential – 50% RAP	OMV 50/70	2.5	5.2	–
	Referential – 50% RAP – I	OMV 50/70	2.5	5.2	–
	Referential – 50% RAP – II	OMV 50/70	2.5	5.2	–
	RE	RE binder	2.5	5.2	–
	RE (3%)	RE binder	3.0	5.7	–
	ST	OMV 50/70	2.5	5.2	0.25% of asphalt mixture
	ET	OMV 50/70 + 0.5% ET	2.5	5.2	0.50% of added bitumen
	Reju 182	OMV 50/70	2.5	5.2	6% of binder in RAP
	Reju 553	OMV 50/70	2.5	5.2	6% of binder in RAP
	Reju 553 (4%)	OMV 50/70	2.5	5.2	4% of binder in RAP
	Reju 161	OMV 50/70	2.5	5.2	6% of binder in RAP
	IT (2%)	OMV 50/70	2.5	5.2	2% of added bitumen
	IT (1.5%)	OMV 50/70	2.5	5.2	1.5% of added bitumen
	IT	OMV 50/70	2.5	5.2	2% of added bitumen
	IT (4.9%)	OMV 50/70	2.3	4.9	2% of added bitumen

mixes and allows reduction of the mixing and compaction temperatures. It can also be used in extremes when the paving and compaction should be carried out under low outdoor temperatures (0–5°C) and the quality of the paved layers must still be guaranteed, (Zydex 2014).

Another applied additive was ET, which can be defined as a surface-active substance intended for warm asphalt mix production. The compaction temperature can be reduced by up to 30°C which may save over 20% energy. Mixing temperature reduction has a positive impact on emission generation as well. ET provides improved workability and adhesion of the bitumen. The intention was to use this effect in combination with an increased proportion of reclaimed asphalt in the mix, (MWV 2014).

The last used product was ready-to-use bituminous binder RE. Its chemical composition assists in rejuvenation of the aged binder in RAP and facilitates better homogenisation of the aged binder and RE, (Total 2014).

The particular versions of laboratory prepared asphalt mixes and contents of used additives are indicated in Table 1.

IND and ET additives were dosed straight into the bitumen, which was mixed sufficiently with the additive for 10–15 minutes at 150°C and then used in the asphalt mix. All rejuvenators were dosed straight into

the asphalt mix during its production. The additives were dosed in varying percentages to allow monitoring the effect of the rejuvenator on the resulting mix properties. Some mixes were prepared with lesser (or higher) contents of fresh bitumen added due to the same reason. The mixes with IT were prepared also in versions where the RAP was only heated to 110°C (in all other cases, the RAP heating temperature was set to 130°C).

From the perspective of asphalt mix preparation, the first stage involved mixing the aggregate fractions heated to 155–160°C; reclaimed material heated to the required temperature was added in stage two followed by the next step of adding bitumen and the selected additive. Filler was mixed in during the last stage. In the case of ST, the mix production was modified in compliance with the manufacturer’s recommendation. The additive was firstly mixed with heated RAP separately and then added to the mixer for further mixing with the aggregate and bitumen. The asphalt mixing temperature was always 155°C and compaction temperature for test specimens was 150°C.

The following characteristics were determined for the individual versions of AC11:

- bulk density and void contents;
- water susceptibility (mix durability determined by the ITRR value);

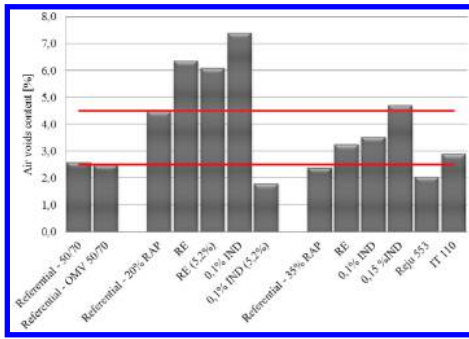


Figure 2a. Volumetric characteristics of asphalt mixes.

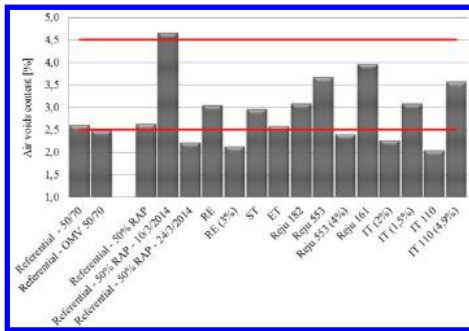


Figure 2b. Volumetric characteristics of asphalt mixes.

- stiffness modulus determined at 5°C, 15°C and 27°C;
- resistance to permanent deformation at 50°C;
- resistance to crack propagation in the low temperatures range tested on semi-cylindrical test specimens at 0°C and –10°C;
- low temperature characteristics, applying the tensile bending stress test at –5°C.

3 RESULTS OF THE EXPERIMENTAL TESTING AND DISCUSSION

The testing of particular mixes was divided into two steps. Stage one involved testing of Marshall test specimens and evaluation of asphalt mix maximum density. Test slabs were prepared in stage two with a height of 50 mm to allow their later use for tensile bending strength and relaxation tests. If the mix demonstrated poor results in stage one the testing of the mix was suspended. Experimental asphalt mixes were divided into 4 groups according to the RAP content: 0%, 20%, 35% and 50%. The mixes were compared within their groups and with the reference mix without RAP.

3.1 Voids content

Technical standard CSN EN 13108-1 defines the allowed range for void content for AC between 2.5 and 4.5%-vol. Although all mixes have identical grading

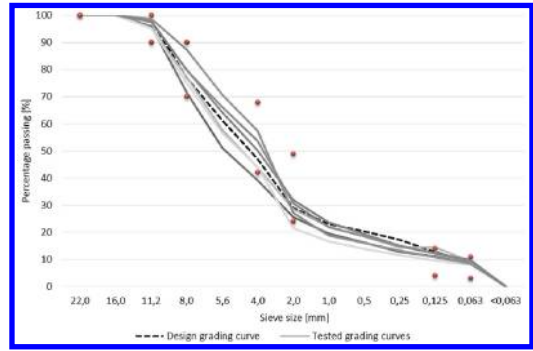


Figure 3. Grading curves of selected asphalt mixes.

curves and the test specimens of all mixes were compacted at same temperature, their void contents are dispersed within a range of 1.8–7.4%. A rather significant effect of RAP on the void content of the asphalt mix is obvious. In the case of using a larger quantity of heterogeneous reclaimed asphalt in a mix, identical grading curve cannot be guaranteed.

Experimental asphalt mixes were prepared in the defined groups using RAP 0/11 mm, which was obtained from the same location. Nevertheless, despite a large quantity of the reclaimed asphalt, which was reserved for the research, batches were taken one by one and, therefore, reclaimed asphalt with identical properties could not be ensured in each mix. On the other hand, it should be emphasised that despite repeated RAP grading analyses and binder extractions, homogeneity of reclaimed asphalt could not be guaranteed. Another reason is the fact that asphalt from different milled pavements is not stored separately by the RAP owners. At the same time, it is also true that pavements are milled by individual layers (selective cold milling) only exceptionally. The impact of heterogeneity of the RAP can then be observed in the grading curves of the laboratory mixes. Selected asphalt mixes were put in the extractor and analysed for their grading again. The actual grading curves are presented in Figure 3.

3.2 Stiffness modulus

Stiffness modules were determined in compliance with CSN EN 12697-26 using the IT-CY method (repeated indirect tensile stress on cylindrical specimens) at three temperatures (5°C, 15°C, 27°C). The range of stiffness modules obtained for $T = 15^\circ\text{C}$ spans from 6,500 to 11,500 MPa (mix with 35% RAP and IT even showed 14,000 MPa). In some cases, according to this characteristic, mixes fundamentally meet the requirements for HMAC which, in case of wearing courses paved in Central Europe, might lead to rather negative impact due to the shorter life-time at lower temperature. The stiffness modulus of a mix is linked not only to the stiffness of bitumen but also to the void content. Mixes with higher void contents tend to have less stiffness modules. The results present an interesting

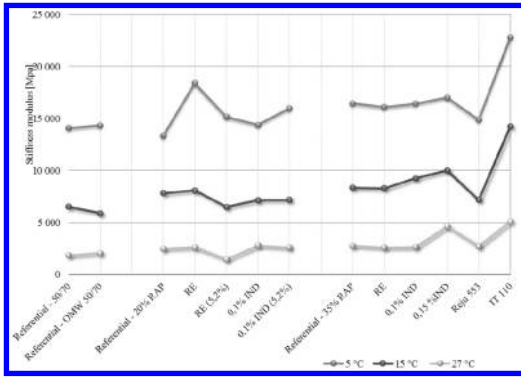


Figure 4a. Result of stiffness modulus testing.

finding concerning a lower thermal sensitivity when reclaimed asphalt was used, which might be caused by better coating of the aggregate particles by the bitumen film.

Asphalt mixes with 20% RAP have balanced stiffness values. The mix variation with RE binder reaches noticeably highest values at 5°C. Despite its high void content, the mix achieves almost the highest value in comparison to the other mix groups. When higher content of RE (mix D) is used, the stiffness values are lower; thermal susceptibility (the proportion of stiffness at 5°C and 27°C) is the lowest out of all designed mixes.

Mixes with 35% RAP demonstrate more or less even results for stiffness modulus under all temperatures. Asphalt mix with 0.15% ZT has a higher stiffness modulus at 5°C if compared to the mix with 0.10% of the same additive. This nevertheless resulted in a lower thermal susceptibility value. The mix with IT where RAP was heated only to 110°C has a stiffness exceeding all of the other mixes by several thousand MPa. The equivalent mix with 50% RAP also demonstrates high stiffness values; but still 20% lower though.

The values are quite unsteady for mixes with 50% RAP. The modulus varies in an interval of several thousand MPa. In this case, it is primarily the bitumen contained in the reclaimed asphalt that affects the stiffness of the mix. In general, this binder will always be aged and, therefore, stiffer. The RAP bitumen activity and softening effect of used rejuvenators have therefore direct impact on decreased stiffness of the aged binder. As is obvious from the results, mixes with ST and Reju recorded the lowest values. The additives act as real rejuvenators on the binder in the RAP; therefore, both stiffness modulus and strength characteristics decrease if compared to reference mixes with RAP.

The obviously highest values were demonstrated by mixes with ET and IT additives. Not only that these asphalt mixes have high stiffness values, they only show low thermal susceptibility, i.e. a much better resistance to temperature fluctuations. In mixes where IT additive was used (W and X), the effect of its content on the mix properties can be demonstrated. Mix W

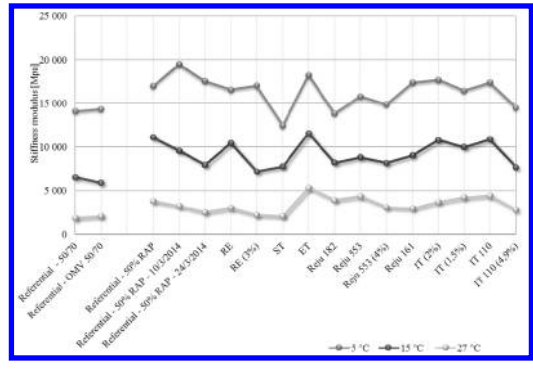


Figure 4b. Result of stiffness modulus testing.

contains 2% IT as recommended by the manufacturer and it is obvious that the mix performs better under lower temperatures. Mix X with 1.5% IT has a higher stiffness modulus at 27°C, thus demonstrating lower thermal susceptibility.

3.3 Moisture susceptibility (ITSR values)

Test specimens of each designed mix were tested in compliance with the method stipulated by CSN EN 12697-12 and a modified method according to AASHTO T283. Three groups of specimens were used: a) dry, b) water saturated with subsequent conditioning in a water bath at 40°C and c) water saturated specimens with a single freezing cycle. According to the results achieved, all of the mixes meet the threshold requirement of ITSR (EN) 70 % which is stipulated for the asphalt mix type by ČSN EN 13108-1. The indirect tensile strength values more or less identically copy the stiffness trend. In the Table 2 ITSR (EN) stays for the procedure according to CSN EN 12697-12 and ITSR (US) for the procedure according to AASHTO T283.

When the particular additives are applied to the bitumen or when the industrial binder RE is used, an increase in ITSR is obvious in comparison to dry specimens. With respect to the fact that this can be observed in the majority of the mixes, the measurements cannot be considered erroneous or incorrect, however baffling the positive effect of water on mix durability might be. It should be emphasised that all specimens from one asphalt mix used for the ITSR test were prepared at the same time with an identical grading curve.

Mixes with 20% RAP generally have lower indirect tensile strength values than the remaining groups. This could be caused by higher void contents or by softer resulting binder in the mix – most of the binder in the mix is virgin bitumen.

Mixes with 35% RAP have similar results like previous group. Although the strength values are slightly higher they are still well comparable. The lowest value was recorded for mix D where a higher content of RE bitumen was used. The highest values not only in this group but amongst all the other mixes, were reached by mix L where the RAP was only heated to 110°C. This result is confirmed by determined high stiffness

Table 2. Indirect tensile strength results and ITSR values.

RAP	Mixture	Indirect tensile strength (ITS)			ITSR (EN)	ITSR (US)
		R _{dry} (MPa)	R _{wet} (MPa)	R _{w+f} (MPa)		
0%	Referential 50/70	1.91	1.71	1.59	0.90	0.83
	Ref. – OMV50/70	1.67	1.68	1.80	1.01	1.08
	Referential – 20% RAP	1.62	1.45	1.41	0.89	0.86
	RE	1.77	1.63	1.48	0.92	0.84
20%	RE (5.2%)	1.40	1.45	1.42	1.04	1.02
	0.10% IND	1.56	1.67	1.50	1.07	0.96
	0.10% IND (5.2%)	1.84	1.76	1.57	0.96	0.85
	Referential – 35% RAP	2.09	1.99	1.94	0.95	0.93
	RE	2.16	1.77	1.88	0.82	0.87
	0.10% IND	2.53	2.52	2.01	1.00	0.80
35%	0.15% IND	1.94	2.18	2.16	1.12	1.11
	Reju 553	1.92	2.02	2.01	1.05	1.04
	IT 110	2.81	2.54	2.33	0.91	0.83
	Referential – 50% RAP	2.41	2.33	2.35	0.97	0.97
	Referential – 50% RAP – 10/3/2014	1.96	1.83	1.66	0.93	0.85
	Referential – 50% RAP – 24/3/2014	2.40	2.11	2.22	0.88	0.93
	RE	2.17	2.03	2.09	0.94	0.97
	RE (3%)	2.24	1.90	1.90	0.84	0.85
	ST	1.70	1.41	1.49	0.83	0.88
	ET	2.27	2.57	2.25	1.13	0.99
	Reju 182	1.69	1.75	1.73	1.03	1.02
	Reju 553	2.03	2.14	2.15	1.05	1.06
50%	Reju 553 (4%)	1.89	1.57	1.63	0.83	0.87
	Reju 161	1.85	1.87	1.78	1.01	0.96
	IT (2%)	2.33	2.51	2.10	1.08	0.90
	IT (1.5%)	2.08	2.26	2.44	1.09	1.17
	IT 110	2.37	2.48	2.33	1.05	0.98
	IT 110 (4.9%)	2.31	2.02	1.88	0.87	0.82

modules as well. The mix has good ITS characteristics even after exposure to water and frost, where the specimens showed higher ITS in comparison to the majority of dry specimens.

Asphalt mixes with 50% RAP demonstrate indirect tensile strengths which are fluctuating similarly to the stiffness modules. The lowest values are recorded by mixes with ST and Reju; this leads to a conclusion that both additives, if applied with RAP, have a negative effect on strength characteristics of the mix. Comparing mixes with different RAP content, mix options with 50% RAP demonstrate significantly higher ITS values for dry specimens.

3.4 Resistance to crack propagation

Resistance to crack propagation was tested according to CSN EN 12697-44. Semi-cylindrical test specimens of 100 mm diameter were tested at two selected temperatures: 0°C and -10°C.

For reference asphalt mixes without RAP the impact of the possible impact of used bitumen is visible. Two

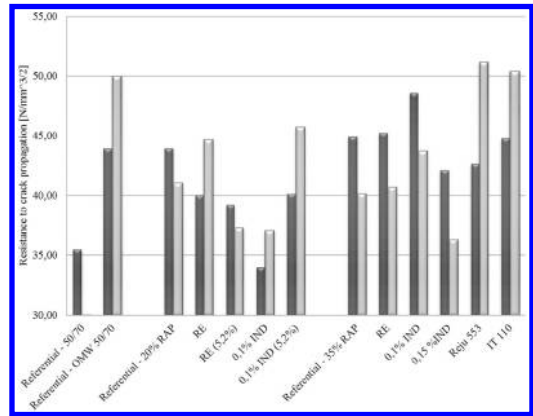


Figure 5a. Resistance to crack propagation.

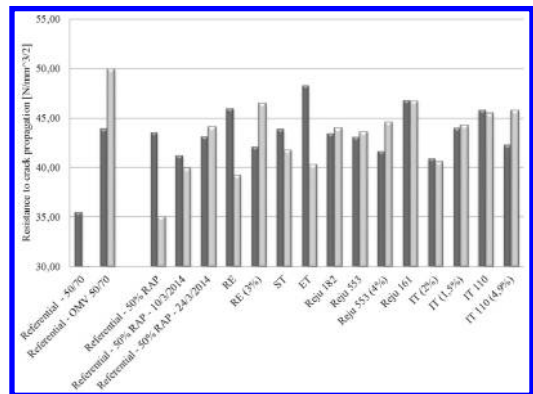


Figure 5b. Resistance to crack propagation.

different binders were applied to the reference mixes and their critical values differ from each other by almost $10 \text{ N/mm}^{3/2}$ (see Fig. 5a and 5b).

Asphalt mixes with ZT are especially worth to be compared with this test. The additive was used both in mixes with 20% and 35% RAP. When 20% reclaimed asphalt was used, it is obvious that the mixes perform better in terms of resistance to crack propagation at 0°C. For the mix with 35% RAP, the resistance to crack propagation behaves in the opposite manner – the specimens perform better at -10°C. When selected contents of ZT are compared, it is obvious that the increased quantity of the additive in the asphalt mix results in worsening of the resistance to crack propagation where not only the absolute values of fracture toughness but also the proportionate rate for both selected temperatures is lower. Such results correspond with the findings of other tests where a higher ZT content tends to improve mix properties at higher temperatures. Contrastingly, a higher content of ZT has a slightly “negative” effect with decreasing temperatures.

The asphalt mix options with IT show that higher content of the used additive applied in RAP heated

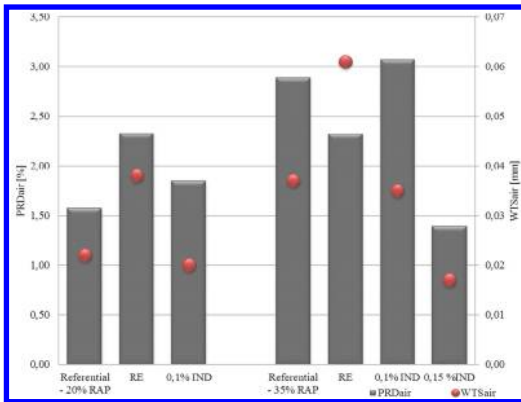


Figure 6a. Resistance to permanent deformation – mixes with 20% RAP.

at 130°C had rather negative influence. In contrast to that, if the heating temperature for reclaimed asphalt is reduced to 110°C an interesting improvement of the asphalt mix resistance to crack propagation has been observed. This finding indicates with respect to behaviour in low temperature range that this rejuvenator might be more active if lower RAP heating temperature is used.

Reference mixes with 50% of RAP from different sampling reach at 0°C similar values of fracture toughness. However the values vary distinctly when the test is taken at -10°C. In this case, the difference amounts up to 10 N/mm^{3/2}. As has been mentioned earlier, mixes were prepared with the same earmarked reclaimed asphalt stockpiled at the mixing plant and transported to the laboratory in batches what clearly demonstrate that it is impossible to ensure absolute homogeneity of RAP.

3.5 Resistance to permanent deformation (rutting)

First test conducted on the slabs was the rutting test. The slabs were tested at temperature of 50°C in a small test device with air bath. Rather than stiffness of the asphalt mix, the test of mix resistance against permanent deformation is related to its ability to withstand high number of repeated loading (accumulation of non-recoverable strain).

In case of mixes with 50% RAP, it is presumptive that the rut depth will be higher, particularly if rejuvenators have been applied. Mixes with higher RAP content are generally stiffer but their potential to relax is limited by the aged binder. Moreover, with respect to the existence of conglomerate particles of RAP which disintegrate during asphalt mixing due to the used temperature, the content of fine particles probably increases influencing the ability to resist permanent deformations, i.e. the asphalt mastic mass between the aggregate particles >4 mm increases and this can lead to gradual rutting due. As is obvious from the results, mixes that had good strength characteristics were more susceptible to rutting.

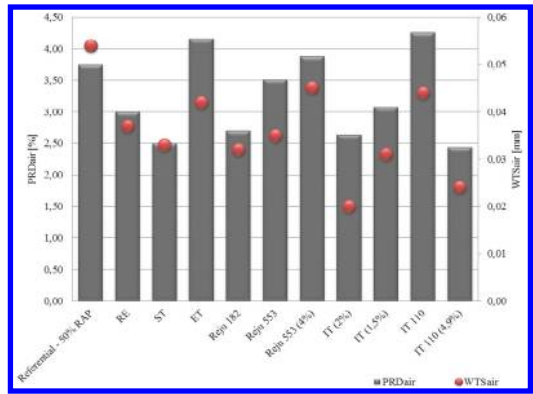


Figure 6b. Resistance to permanent deformation – mixes with 50% RAP.

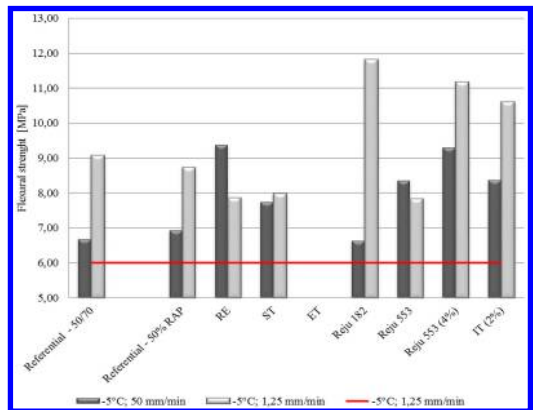


Figure 7a. 3-point bending test results – mixes with 20% RAP.

Asphalt mixes with ET or IT additives, where the RAP was only heated up to 110°C, have a slightly higher PRD values if compared to reference mix with 50% RAP. In contrast to that, mixes with IT and reclaimed asphalt heated to 130°C showed more positive results. Again, it can be observed that the heating temperature of RAP has an important impact on mix characteristics.

3.6 Flexural strength (3-point bending test)

Tensile bending (flexural) strength was tested in compliance with the procedure stipulated by TP151 for temperature of -5°C with two strain rates: 50 mm/min and 1.25 mm/min. The test was run on beams cut from the slabs after completion of the rutting test. In accordance with the technical specifications TP151, the results for the lower strain are determining. All of the tested mixes meet the minimum strength requirement of 6 MPa as stipulated so far only for HMAC mixes.

The reference mixes achieved the poorest results at higher strain rate, but on the other hand they reached the best results for 1.25 mm/min loading. This trend is obvious for each reference mix (although it does not

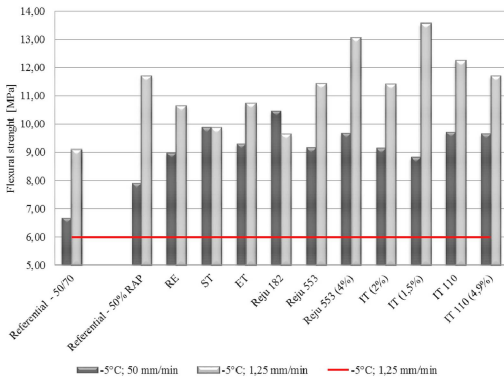


Figure 7b. 3-point bending test results – mixes with 50% RAP.

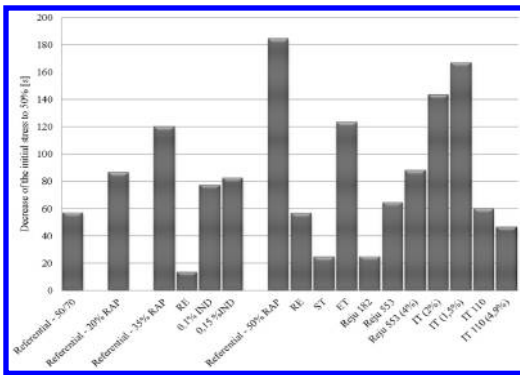


Figure 8. Decrease of the initial stress to 50%.

reach the highest values for mixes with 50% RAP, but it demonstrates very good strength results in comparison to the others).

It was supposed, that the results for the higher strain rate (50 mm/min) should be higher. Three mixes demonstrated for strength values opposite trend: mix with RE and 20% as well as 35% RAP and mix with Reju 182 and 50% RAP. The mix with ST also shows the same trend but the values for both strain rates were identical.

Asphalt mix with 35% RAP and 0.1% ZT in bituminous binder reached better values than the mix with 0.15% of the additive. This corresponds with the assumption that a lower content of the additive might improve low temperature behaviour. A similar trend can be observed for mixes with IT.

3.7 Relaxation test

Increased content of aged bitumen in mixes with RAP raise time necessary for the asphalt mix to relax after they have been loaded. As is obvious from the results (Fig. 8), the mixes without any additives, with varying proportions of reclaimed asphalt, relax significantly slowly (the difference between the basic reference mix and the mix with 50% RAP is more than triple).

Table 3. Mix valuation approach.

Point valuation	Relative ratio to the reference mix	Point valuation	Relative ratio to the reference mix
+1	0–10%	–1	0–(–10)%
+2	10–20%	–2	(–10)–(–20)%
+3	20–30%	–3	(–20)–(–30)%
+4	30–40%	–4	(–30)–(–40)%
+5	≥ 40%	–5	≤ (–40)%

Asphalt mixes with 35% RAP and ZT in both assessed options have a similar relaxation time while a higher content of the additive slightly reduces both regression parameters. The asphalt mix with RE demonstrates very fast relaxation, especially with 20% RAP content. Comparably good results have been reached also for mixes with ST and Reju 182.

Asphalt mixes with high strength characteristics have been discovered to relax significantly more slowly than mixes with lower strength properties. The results correspond with the stiffness values. The stiffer mixes have a slower relaxation.

Both mix options with IT where the RAP was heated to 110°C relax very well. The mix with the optimum percentage of bitumen and IT scores well both in the strength tests and in relaxation. In comparison to this circumstance, the course of relaxation and, particularly, the relaxation time achieved when RAP was heated to 130°C, is rather interesting. There is no specific explanation for this difference at the moment. This finding is obviously related to the used temperature; however it is unclear why. The mixes where RAP was heated to 130°C demonstrate an obvious impact of the higher content of used additive; application of additional 0.5% rejuvenator reduces the relaxation time by approximately 15%.

4 CONCLUSIONS

With increasing range of rehabilitation works, the amount of reclaimed asphalt and the need for depositing is raised. The reuse and recycling of such material should increase proportionately too. Such trend is important primarily from the environmental perspective where the utilisation of reclaimed asphalt not only reduces the exploitation of non-renewable resources but also lowers the consumption of energy and production of CO₂. The application of a higher RAP content in a mix should make the mix attractive from the economical perspective as well. Rejuvenation of the aged bitumen decreases the demand on virgin bitumen whose costs play major role in asphalt mix price.

The properties of asphalt mixes with higher content of reclaimed asphalt are undoubtedly mostly affected by the grading and quality of the RAP. Prior to using the RAP in a mix, it is necessary to take a sufficient number of reference samples to determine the

Table 4. Summary evaluation of the asphalt mixes.

RAP	Mixture	Void content	Stiffness modulus	Indirect tensile strength	ITSR	Crack propagation	Flexural strength	Σ
			15 °C	Rdry		0°C	1,25 mm/min	
0%	Referential- 50/70	ref	ref	ref	ref	ref	ref	-0,2
	Referential- OMV 50/70	0	1	2	2	3	0	
20%	Referential- 20% RAP	0	3	2	1	3	1	0,3
	RE	5	3	1	1	2	2	-0,3
	RE (5,2%)	5	4	3	2	2	-	-1,0
	0,1% IND	1	1	2	2	1	2	-1,2
	0,1% IND (5,2%)	5	2	1	1	2	-	-0,2
35%	Referential- 35% RAP	3	3	1	1	3	4	1,5
	RE	0	3	2	1	3	2	0,8
	0,1% IND	0	5	4	2	4	3	3,0
	0,15 %IND	3	5	3	2	2	2	1,7
	Reju 553	3	1	1	1	3	-	0,8
	IT 110	0	5	5	1	3	-	2,8
50%	Referential- 50% RAP	0	5	3	1	3	3	2,5
	Referential- 50% RAP - 10/3/2014	3	5	3	2	-	-	1,2
	Referential- 50% RAP - 24/3/2014	3	3	3	1	3	-	1,0
	RE	0	5	2	1	3	2	2,2
	RE (3%)	3	2	2	1	2	-	0,4
	ST	0	2	2	1	3	1	0,5
	ET	0	3	2	1	4	2	2,7
	Reju 182	0	3	2	2	3	1	1,2
	Reju 553	0	4	1	2	3	3	2,2
Reju 553 (4%)	3	3	1	1	2	5	0,8	
Reju 161	0	4	1	2	4	-	1,8	
IT (2%)	3	5	3	3	2	3	2,2	
IT (1,5%)	0	3	1	3	3	5	2,8	
IT 110	3	5	3	2	3	4	2,3	
IT 110 (4,9%)	0	2	3	1	2	3	1,5	

basic properties of RAP. With large-scale production, homogeneity of the reclaimed asphalt must be ensured to provide not only a similar grading curve but also similar binder content and properties. This can be achieved primarily by selective milling of pavement layers where the high quality wearing course is milled separately.

As shown by the presented results, the type and dosage of the used rejuvenator have a significant impact on the final properties. Asphalt mixes with high RAP content are generally stiff and show high strength values. However due to the aged binder content, these mixes are usually more brittle which means they are more susceptible to sudden changes, whether of the climate conditions or traffic loading.

With respect to the large number of tested mixes and performed tests, all mixes were evaluated together according to the selected parameters. They were compared to the reference mix without RAP and assessed with a simple scoring, which might be understood as arbitrary and subjective. Chosen assessment correlates to the percentage of improvement or deterioration in comparison to the reference mix. The void content was evaluated under different assumption. If the mix void content was within the allowed interval according to ČSN EN 13108-1, the mix scores 0. If void content differs by 0.5%, the mix scores (-3) points, exceeding the limiting value by >0.5% the mix scores (-5) points.

The evaluated tests were void content, stiffness at 15°C, indirect tensile strength, ITSR, fracture toughness at 0°C and flexural strength at the strain rate of

1.25 mm. The criterion weight for all the tests was 1. This is of course not fully correct, nevertheless the aim was to provide first simplified scoring of evaluated asphalt mixes. Since the tensile strength test was not performed for all test specimens the resulting scores were calculated as an average of the conducted tests.

Sample assessment:

If a mix outperformed the reference mix by 25% it scores (+3) points. If the mix performed 15% poorer it scores (-2) points.

Considerable differences in test results can be observed for the used rejuvenators. Therefore, it is important to realise what properties are required for the final mix before the rejuvenator is chosen. According to the evaluating criteria, mix with 35% RAP and 0.1% ZT scored the best. Contrastingly, the same mix with just 20% RAP had the poorest results of all the mixes tested. The reason might be the fact that the mix with 20% RAP had a void content almost about 3% higher. Good results were recorded also for the mix with ET. The application of the additive resulted in a significant improvement of strength characteristics; however such effect is rather undesirable in mixes with high RAP contents. Increased strength led to lower resistance to permanent deformation. In case of mixes with IT it is obvious that the effect of not only the additive dose but also the temperature of RAP heating is important. This effect is best visible in the results of resistance to permanent deformation and relaxation (see chapters 3.5 and 3.7). All mixes with IT generally scored very well. Although ST additive influenced a decrease in strength characteristics, mix scores well in

relaxation and resistance to permanent deformation. The binder in the mix is considerably softer than in other mixes. The newly developed Reju additives work on different bases and, therefore they must be considered separately. These rejuvenators achieve similar strength characteristics there are fundamental differences in resistance to permanent deformation, as well as in relaxation where Reju 182 performs significantly better.

The paper does not consider practical aspects if higher RAP content should be used. So far in many European countries asphalt producers are not equipped sufficiently to produce mixes with more than 25% RAP. In general the use of increased reclaimed asphalt content will be possible only in case that the asphalt mixing plants can either use drum-mix technology, double coated heating drum technology or installation of parallel drum has been made.

ACKNOWLEDGEMENT

This paper was prepared under the funding scheme of Competence centre program by the Technology Agency of the Czech Republic within the project Centre for effective and sustainable transport infrastructure (CESTI), project no. TE01020168.

REFERENCES

- Boriack, P., Katicha, S.W., Flintsch, G.W., 2013. A laboratory study on the effect of high RAP and high asphalt binder content on the performance of asphalt concrete
- ČSN EN 13108-1 – Bituminous mixtures – Material specifications – Part 1: Asphalt Concrete
- ČSN EN 12697-12 – Bituminous mixtures – Test methods for hot mix asphalt – Part 12: Determination of the water sensitivity of bituminous specimens
- ČSN EN 12697-22 – Bituminous mixtures – Test methods for hot mix asphalt – Part 22: Wheel tracking
- ČSN EN 12697-44 – Bituminous mixtures – Test methods for hot mix asphalt – Part 44: Crack propagation by semi-circular bending test
- Iterchimica, 2014. Technical data sheet, <http://greece.spanos-group.com/sites/default/files/products/downloads/iterlene-acf-1000.pdf>
- Mogawer, W., et al., 2012. Performance characteristics of plant-produced high RAP mixtures, *J Assoc. Asphalt Paving Technol*, Vol. 81, pp. 403–439.
- MWV, 2014. Technical data sheet. www.Evotherm.com
- Paramo, 2014. Technical data sheet.
- StorImpex, 2014. Technical data sheet.
- Technical specifications TP151, 2010. Specifications for High Modulus Asphalt Concrete. Ministry of Transportation, Czech Republic
- Terrel, R., Epps, J., 1989. Using additives and modifiers in hot-mix asphalt, *Quality Improvement Series (QIP 114A)*, NAPA, Lanham, MD
- Total, 2014. Technical data sheet. <http://www.total.co.at/bitumen/Strasenasphalten/regenis.html>
- Zaumakis, M., Mallick, R.B., Frank, R., 2014a. Evaluation of different recycling agents for restoring aged asphalt binder and performance of 100 % recycled asphalt. *Materials and Structures*. DOI: 10.1617/s11527-014-0332-5 <http://link.springer.com/10.1617/s11527-014-0332-5>
- Zaumanis, M., Mallick, R.B., Poulidakos, L., Frank, R., 2014b. Influence of six rejuvenators on the performance properties of Reclaimed Asphalt Pavement (RAP) binder and 100% recycled asphalt mixtures, *Construction and Building Materials*, Volume 71, pp. 538–550, ISSN 0950-0618, <http://dx.doi.org/10.1016/j.conbuildmat.2014.08.073>.
- Zaumanis, M., Mallick, R.B., Frank, R., 2014c. 100% Recycled hot mix asphalt: a review and analysis, *Resour Conserv Recyc* <http://dx.doi.org/10.1016/j.resconrec.2014.07.007>
- Zydex, 2014. Technical data sheet. <http://zycotherm.wordpress.com>

Mix design considerations for asphalt wearing courses with high reclaimed asphalt content

G. Canon Falla, A. Blasl & R. Millow

Institute for Pavement and Urban Engineering, Technische Universität Dresden, Germany

D. Lo Presti

Faculty of Engineering, University of Nottingham, UK

ABSTRACT: The amount of recycling of reclaimed asphalt (RA) in new asphalt pavements has grown up to the point that it is no longer simply an isolated green construction alternative but a common practice in almost all Europe. However, in general the share of recycling the RA in new asphalt courses is rather lower than it could be technically, especially in wearing layers. This paper presents the first results of a research on the feasibility of going toward 100% recycling of asphalt pavements into surface courses. The research is carried out within a two-year CEDR Transnational Road Research project, All Back 2Pave, coordinated by the Technische Universität Dresden in Germany together with two European university partners: University of Nottingham in the United Kingdom and University of Palermo in Italy. The main objective of the project is to establish, through laboratory test on binders and asphalt mixes, whether the use of high rates of RA is feasible in developing mixes with high level of durability. The paper focuses on one of the major challenges faced in the project: implementation of proper laboratory tests to characterize the RA and development of sound design practices to account the effect of the RA on the volumetric and mechanical properties of the final mix.

1 INTRODUCTION

Given today's societal concerns with environmental protection and sustainable development in a post-fossil fuel era, road authorities in Europe are working together to make the dismantling and end-of-life strategies of asphalt pavements more energy efficient. In this context, the amount of recycling of reclaimed asphalt (RA) in new asphalt pavements has grown to the point that it is no longer a simple green construction alternative but a common practice in almost all of Europe. In recent years, due to the rising cost of asphalt binder, new efforts have been made to increase the amount of RA used in asphalt pavement.

Several interdisciplinary research projects related to the usage of hot mix asphalts with RA have been carried-out in Europe during the last decades (DIRECT-MAT, 2011), (RE-ROAD, 2012). The outcomes of these projects showed that the durability of mixes with RA proved to be satisfactory. However, in general, the share of recycling of RA in new asphalt courses remains rather lower than it could be technically.

Highway authorities together with the asphalt paving industry worked together to develop new methods and design approaches to increase the share of recycling in pavement construction and rehabilitation. Economic and environmental benefits are the

driving forces behind research in asphalt pavement recycling. Economics benefits are mainly associated with the reduction of use of virgin materials (aggregates and binder). The environmental profit include reduced emission and energy consumption in the production and transportation of virgin materials as well as reduced demand of non-removable resources. Despite of these benefits, the amount of RA used in high volume roads in Europe is very limited, especially in surface layers. There is a common concern that the high quality requirements for wearing courses are not met if the major volumetric component of the mix comes from a recycled material. The background of this fear is the inherent heterogeneity of the RA, which properties depend in great extent on factors such as the technique used to reclaim the asphalt, the maintenance history of the road, the storage conditions, etc., which are not considered in standard mix design procedures.

On this context, this paper focus on giving an answer to the question: what are the limiting factors that determine the maximum amount of RA that can be used in the design of asphalt wearing courses?

The paper presents a design case that shows the results of laboratory tests that are used to determine the maximum RA content allowed on a target mixture of a typical wearing course of a high volume road in Germany.

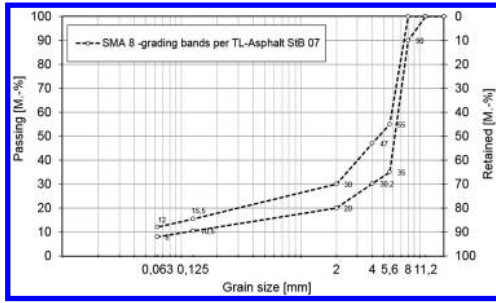


Figure 1. Grading bands of target mixture.

2 TARGET MIXTURE

The target mixture of this study is a Stone Mastic Asphalt (SMA) with a maximum grain size of 8mm (SMA 8) and the grading limits depicted in Figure 1.

The use of SMA in surface layers of heavy traffic roads is a common practice not only in Germany but also in all around Europe. The SMA as a surfacing material is widely used because of the even surface that can be obtained, which results in high driving comfort. SMA is characterized by a strong coarse aggregate skeleton that gives good resistance to permanent deformation and a high bitumen content (>6%) that provides enhanced resistance to fatigue. Polymer modified binders (PmB) are usually used in SMA to give greater deformation resistance and enhanced durability. The advantages in terms of longer life and improved performance make the SMA a cost effective alternative even its initial cost is around 20% higher than conventional asphalt concrete mixes.

The target mixture will be designed and produced according to the German regulatory environment for hot asphalt mixes with RA. There are three regulatory documents containing specifications at national level regarding the use of RA in Germany. The first, TL-Asphalt StB 07 (TL-Asphalt StB 07, 2007), is a document that contains general technical specifications for asphalt. It allows the use of RA in all types of asphalt mixes with the exception of porous asphalt. It also regulates the mix composition and the quality requirements for each type of mix. TL Asphalt-StB 07 is a general specification harmonized with the European norms. The second document, ZTV Asphalt-StB 07 (ZTV Asphalt-StB 07, 2007), is a contractual specification. In this document, the use of RA is excluded also from SMA mixes unless the bidder specifies otherwise. ZTV Asphalt-StB 07 deals with contractual issues applicable in Germany and it addresses the local concerns regarding the use of RA in SMA. Finally, the third document, TL AG-StB 09 (TL AG-StB 09, 2009) regulates specifications concerning the quality of RA itself.

3 SAMPLING AND COLLECTION OF MIX CONSTITUENTS

For the design of the target mixture the following constituent materials were sampled from the feedstock



Figure 2. Open air storage of RA at mixing plant.

of a mixing plant located in Gilching, near Munich, Germany:

- 1) Reclaimed asphalt: one source of RA was available at the mixing plant. The material records at the plant showed that the RA was made up of a bituminous surface originally designed as a SMA with a nominal grain size of 11 mm and a polymer modified bitumen. It is known that the RA was milled from the surface layer of a high volume road (highway A8) near Munich, Germany, however, the original mix design formulas and maintenance history of the RA were not available. The RA was stockpiled in open-air piles without fractionation (Figure 2). This may lead to an accelerated binder aging due to air exposure and oxidation. Furthermore, exposure to the environmental conditions will increase the moisture content in the RA resulting in high heat consumption and low thermal efficiency during mixing.
- 2) Coarse aggregates: Two sources of coarse aggregates of the fractions 8/11, 5.6/8 and 2/5.6.
- 3) Fine aggregates: One source of crushed fine aggregates (0.063–2).
- 4) Filler: One source of filler material with maximum grain size of 0.09 mm.
- 5) Fibres: One source of cellulose fibres. The function of the fibres is to avoid bitumen drain-down due to the high binder content and coarse aggregate skeleton of the SMA mix.
- 6) Virgin bitumen: a sample of the virgin bitumen was obtained from the bitumen tank of the mixing plant. The type of virgin bitumen was determined with a blending design study between the bitumen from the RA and different bitumen types. More details about the selection of the virgin bitumen are given in Section 6 herein.

4 MIXING PLANT CONSIDERATIONS

For mixes with high percentage of RA it is necessary to ensure that the binder of the RA is fully melted for blending with the newly added binder. It is known that blending is a function of mixing time, however,

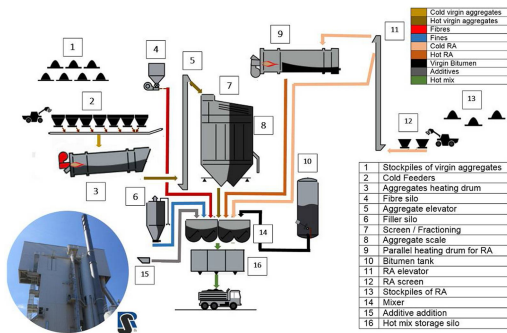


Figure 3. Scheme of mixing plant in Gilching, Richard Schulz Tiefbau GmbH & Co.

for mixes with high amount of RA increasing the mixing time is not sufficient to ensure proper commingling between virgin and RA binder. Therefore, mixing plants with special equipment such as batch plants with parallel drums, twin dryer drums or double barrel drums are a prerequisite in order to produce asphalt mixes with high shares of RA without impairing the material quality or exceeding the legal limits of emissions.

The plant in Gilching is a batch-type with a parallel drum (item 9 in Figure 3) to preheat the RA. Without the parallel drum the maximum RA that can be used in batch plants finds its limits at approx. 30% due to the very high temperature needed to transfer heat from the virgin aggregates to the RA. Even if the temperature and the associated emissions are not a problem, there are issues with excessive ageing of the binder from the RA due to contact with superheated aggregate particles.

5 CHARACTERIZATION OF RECLAIMED ASPHALT

The RA needs to be characterized before the actual mix design. This is because with ageing and oxidation some changes may occur in the mix: for the binder, this includes hardening and loss of ductility and for the aggregates, the gradation may change due to degradation caused by traffic loads and environmental conditions.

5.1 RA binder content

An automatic solvent extraction using trichloroethylene as solvent (per EN 12697-1) was used when determining the binder content in the RA. In the solvent extraction, the binder is extracted from the RA using a solvent in a centrifuge. The amount of bitumen in the RA is determined as the difference in mass before and after extraction. The results showed an average binder content of 4.8% in the RA.

Table 1. Test results on recovered bitumen from RA.

Lab (replicate)	Pen 1/10 mm	R&B °C	Fraass °C	Visc.@135°C mPa.s
UNOTT(1)	21	66.2	-8	1518
UNOTT(2)	21	65.8	-8	1518
UNOTT(3)	21	65.0	-8	1434
TUD(1)	-	66.8	-	-
TUD(2)	-	63.8	-	-
Mean	21	65.5	-8	1490

5.2 RA binder properties

The recovering of binder for further characterization was carried out separately at the laboratories of Technische Universität Dresden (TUD) and University of Nottingham (UNOTT). The method for separation and extraction was different at each lab:

- TUD: automatic solvent extraction using trichloroethylene as solvent per EN 12697-1 and 12697-3.
- UNOTT: Fractionating column by using DCM as solvent per EN 12694-4:2005

After recovering, a representative set of laboratory tests were performed to determine common bitumen quality indicators used in most European standards. In order to ensure reproducibility, the tests were performed on binders recovered from different random samples of RA (three at UNOTT and two at TUD). The results are reproduced in Table 1.

5.3 Properties of RA aggregates

Gradation: The gradation of the RA aggregates is one of the most important factors associated with the control of asphalt mixes with high RA content. At very high recycling rate, the gradation of the RA affects the overall performance of the final mix including stiffness, fatigue resistance, rutting and moisture damage. A sieve analysis (per DIN EN 12697-2) was conducted on two random samples of recovered aggregates to obtain the gradation (white-curve) of the RA. Figure 4 shows the mean gradation line of the RA together with the grading limits of a German SMA 11 mix. It is observed that the white-curve falls outside the original grading band and that the aggregates of the processed RA are finer and denser than the original ones. This is attributed to a strong mechanical degradation by milling and crushing. Let us recall that the particle size distribution of a recycled asphalt material may vary to some extent depending on the technique and equipment used to process the asphalt, and in this case, the RA was processed twice: initially it was milled from the road and afterwards it was crushed at the mixing plant.

Skid resistance: The aggregates ability to resist skidding is crucial when designing wearing course mixes. The Polished Stone Value (PSV) is a common evaluation method used for measuring skid resistance. Two skid test were performed to determine the PSV

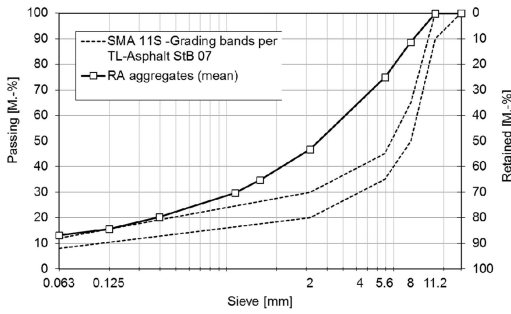


Figure 4. Grading of RA aggregates (white-curve).

of the RA aggregates. The tests showed that the RA aggregates have an average PSV value of 51, which means that the polishing characteristics of the RA aggregates are enough good to be used in SMA mixes for wearing courses of federal high volume roads (min. required PSV value of 51, acc. to TL Asphalt-StB 07).

6 SELECTION OF VIRGIN BITUMEN

The type of virgin bitumen that must be used in the mix depends on the properties of the bitumen in the RA and on the properties of the target binder. The target binder is the bitumen resulted from the mix between virgin and RA bitumen. In other words, the bitumen of the final mix.

The target binder selection was done based on traffic and loading requirements expected in wearing courses of high volume roads in Germany. According to the German bitumen specification, for a federal high volume road with a surface layer made of a SMA material, it is required to use a modified bitumen of the type 25/55-55. The contract specifications of this type of bitumen are presented in Table 2.

The German specifications only allow the adjustment of the RA bitumen properties by using a softer virgin bitumen of one grade above the target. The degree of adjustment depends on the ageing of the bitumen in the RA. In order to determine a suitable virgin bitumen, a comprehensive blend study was performed at the laboratory of UNOTT. The results showed that the properties of the bitumen from the RA do not differ much from the properties of the target binder. Therefore, it was decided to use as virgin binder a PmB 25/55-55 (i.e. the same type and grade as the target).

The properties of the recovered bitumen are plotted in the bitumen test data chart (BTDC) of Figure 3 together with the properties of the virgin bitumen. The BTDC is a useful system to visualize the temperature dependence of penetration index, softening point, Fraass breaking point and viscosity on one chart.

From the results in the chart it is deduced that the characteristics of both bitumens are very similar: the two regression lines are parallel and the line of the recovered bitumen is slightly shifted to the right, representing a relatively low hardening due to ageing.

Table 2. Contractual requirements for a PmB 25/55-55 (TL Bitumen-StB 07, 2007 [5]).

Attribute	Units	Specification	Requirements (PmB 25/55-55)
Pen @25°C	1/10 mm	EN 1426	25 to 55
R&B Temp	°C	EN 1427	≥55
Tensile ductility	J/cm ²	EN 13589	≥2@10°C
Flammable point	°C	EN ISO 2592	≥235
Fraass temp	°C	EN 12593	≤-10

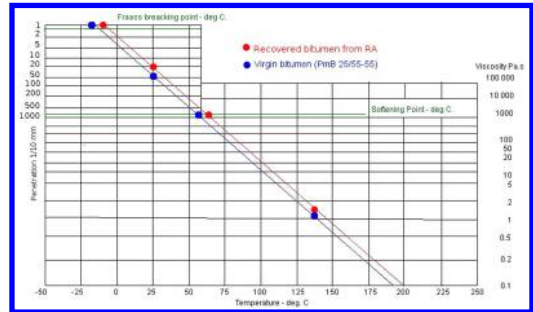


Figure 5. Bitumen test data chart of virgin binder and RA binder.

The two regression lines in the BTDC represent the two extreme cases of a blend between virgin and RA bitumens (i.e. 100% virgin bitumen for the blue line and 100% recovered bitumen for the red line).

7 MAXIMUM POSSIBLE RECLAIMED ASPHALT CONTENT

The maximum allowable percentage of RA that can be used is determined by adjusting the mix between recycled and virgin materials to the contractual specifications of the target binder (PmB 25/55-55) and to the grading limits of the target mix (SMA 8). Thus, the maximum possible RA content is taken as the minimum of those determined by the here called bitumen and grading approaches.

Bitumen approach: Very often, the recovered bitumen from the RA does not meet the requirements on the characteristics of the target bitumen due to excessive aging or hardening. In such case, a virgin binder, usually softer than the target, is added to bring the properties of the blend to the contractual stands. The virgin binder content to be added is calculated by the so-called blending design charts. Figure 6 shows the blending charts of the virgin and recovered bitumen. The charts correlate the Replaced Bitumen Content (RBC) with the empirical properties of the blend. By replaced bitumen content it should be understood the percentage of bitumen from the RA in the final blend. From the graphs it is observed that the maximum percentage of replaced bitumen that can be

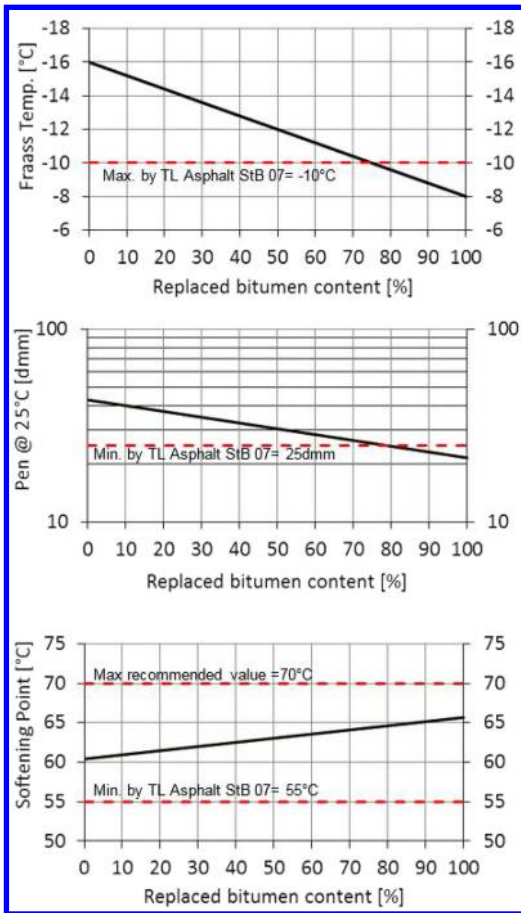


Figure 6. Traditional blending charts of empirical properties.

used in the final blend to comply with the specification requirements of a PmB 25/55-55 is around 72%, limited by the Fraass breaking point.

The charts in Figure 6 were developed assuming that 100% of the RA binder will mobilize and become active part of the binder in the new mix. However, in reality it is also possible that part of the RA bitumen remain non-active resulting in a partial blending scenario.

Considering the above, an extended version of the blending charts was created to account for the degree of blending between virgin and RA bitumen. The new charts, shown in Figures 7, 8 and 9, consider the amount of RA in the mix instead of the replaced bitumen content and they represent the most conservative case of the mix design, which corresponds to a mix with 7% of bitumen.

From the new charts, it is observed that there is no restriction on the amount of RA as regards contractual requirement of the bitumen (the max. RA content is capped to 97.8% by the binder content in the RA).

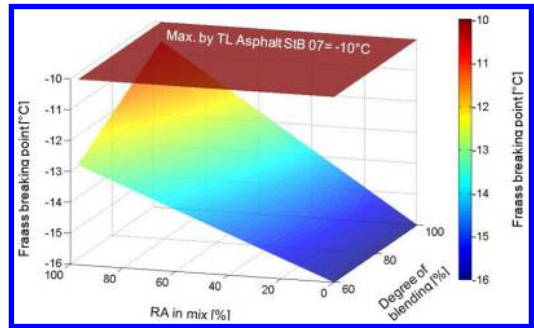


Figure 7. Extended blending chart of Fraass breaking temperature.

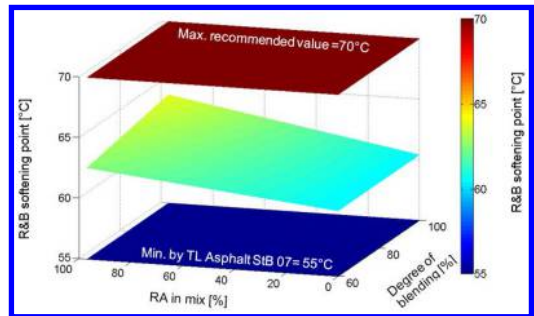


Figure 8. Extended blending chart of R&B softening point.

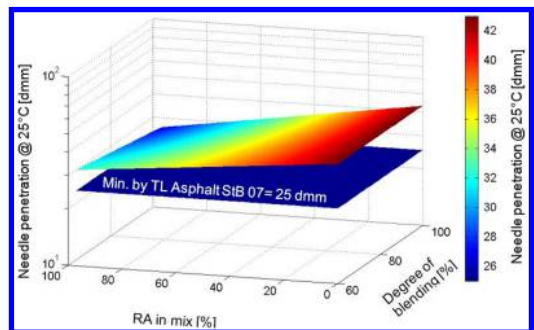


Figure 9. Extended blending chart of penetration index.

Grading approach: Since the grain size distribution of the RA does not meet the control points of the target mix (SMA 8S), it was necessary to add virgin aggregates in order to balance the grading. This was done by using an iterative algorithm that decreases the amount of RA and increases the amount of virgin aggregates. The results, shown in Figure 10, indicated that the maximum percentage of RA that can be used is 70%. Higher amounts of RA will result on mixes with grain size distribution outside the contractual limits. The grading of the mix with 70% RA is shown in Figure 11.

9 FURTHER INVESTIGATION PLANNED

This paper shows the first results of the AllBack2Pave project within work package No. 2. The AllBack2Pave project is a research initiative evaluating the feasibility of going toward 100% recycling of asphalt pavements into surface courses. The project consists of four technical work packages (WPs). In WP2, blend and mixture design will be performed. The aim of this WP is to achieve mix designs with acceptable volumetric and mechanical properties. The blend design will evaluate the addition of rejuvenating additives and warm-mix technologies. The plant production related aspects will be investigated in WP3. Factors such as fractionation and stockpiling of the RA in the mixing plant and quality control during the production process will be considered. WP4 is dedicated to the mechanical characterization of the asphalt mixes. The materials will be characterized in the lab in terms of stiffness, fatigue cracking behavior, rutting susceptibility, moisture damage resistance and permanent deformation behavior. WP5 aims to perform a sustainability assessment to determine the most cost and energy effective production process for asphalt surface mixes with high recycling rates. Find more information about AllBack2Pave and a complete list of participating institutions and associate partners on the project website <http://allback2pave.fehrl.org>.

% bitumen in mix: 7.00%					
Material	% in Mix	% in Mix Aggregates	% in Virgin Aggregates	% in Mix Bitumen	% in RAP
Crushed stone 8/11 (Gleichen)	0.00%	0.00%	0.00%	N/A	N/A
Crushed stone 8/11 (Treading)	0.00%	0.00%	0.00%	N/A	N/A
Crushed stone 5,6/8 (Gleichen)	13.05%	14.08%	50.00%	N/A	N/A
Crushed stone 5,6/8 (Treading)	13.05%	14.08%	50.00%	N/A	N/A
Crushed stone 2/5,6 (Gleichen)	0.00%	0.00%	0.00%	N/A	N/A
Crushed stone 2/5,6 (Treading)	0.00%	0.00%	0.00%	N/A	N/A
Sand 0/2	0.00%	0.00%	0.00%	N/A	N/A
Fines	0.00%	0.00%	0.00%	N/A	N/A
Fibres	0.30%	N/A	N/A	N/A	N/A
Bitumen 1	3.60%	N/A	N/A	51.40%	N/A
Additives	0.00%	N/A	N/A	0.00%	N/A
RA Aggregates	66.60%	71.84%	N/A	N/A	95.14%
RA Bitumen	3.40%	N/A	N/A	48.60%	4.86%
Sum	100.00%	100.00%	100.00%	100.00%	100.00%
SAP in mix	20.00%				

Figure 10. Composition of mix with maximum content of RA.

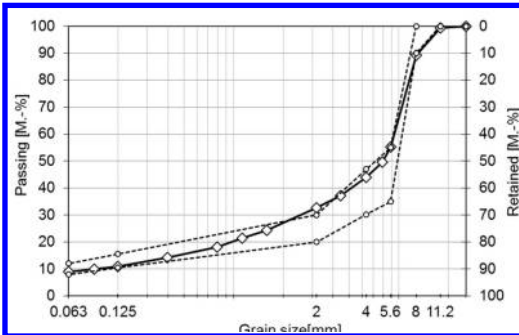


Figure 11. Gradation of mix with maximum content of RA.

8 CONCLUSIONS

The heterogeneity of the RA aggregates plays an important role when designing asphalt mixes for wearing courses where high quality aggregates with high resistance to wear/abrasion (polishing) are needed. Thus, properly milled (i.e. layer by layer) and stockpiled RA is a mandatory prerequisite in order to produce durable asphalt wearing courses with high content of RA. This is a major concern because in the majority of the cases the RA is produced and stockpiled by non-selective methods in which valuable high quality aggregates of wearing courses are milled/stockpiled together with lower quality materials of deeper layers. That means that the aggregates of the RA will automatically be downgraded losing economic value. One possible solution is to allow the use of high percentage of RA in wearing courses only if the RA material proceeds from the same location and layer where the new mix will be placed.

Because the major component of volume of asphalt mixes is made-up of aggregates, the performance of high RA content pavements is greatly influenced by the characteristics of the RA aggregates. Aiming towards 100% recycling, the distribution of particle sizes in the aggregates of the RA must have just the right density so that the final mix will contain the optimum amount of asphalt binder and air voids.

ACKNOWLEDGEMENTS

The research presented in this paper was carried out as part of the CEDR Transnational Road research Programme Call 2012. The funding for the research is provided by the national road administrations of Denmark, Finland, Germany, Ireland, Netherlands and Norway.

REFERENCES

- Direct-MAT. 2011. Dismantling and recycling techniques for road materials. Available at: <http://www.direct-mat.eu>
- RE-ROAD. 2012. End of life strategies of asphalt pavements. Available at: <http://re-road.fehrl.org>
- TL AG-StB 09. 2009. TL AG-StB 09: Technische Lieferbedingungen für Asphaltgranulat. Köln. FGSV Verlag GmbH.
- TL Asphalt-StB 07. 2007 Technische Lieferbedingungen für Asphaltmischgut für den Bau von Verkehrsflächenbefestigungen. Köln. FGSV Verlag GmbH.
- TL Bitumen-StB 07. 2007. Technische Lieferbedingungen für Straßenbitumen und gebrauchsfertige Polymermodifizierte Bitumen. Köln. FGSV Verlag GmbH.
- ZTV Asphalt-StB 07. 2007. Zusätzliche Technische Vertragsbedingungen und Richtlinien für den Bau von Verkehrsflächenbefestigungen aus Asphalt Forschungsgesellschaft für Straßen- und Verkehrswesen. Köln. FGSV Verlag GmbH.

Stiffness and fatigue of AC20 recycled mixtures with 25% and 50% RAP

E. Manthos & A. Nikolaides

Department of Civil Engineering, Aristotle University of Thessaloniki (AUTH), Thessaloniki, Greece

ABSTRACT: Nowadays there is an increasing concern for material conservation. In pavement engineering this concern was faced with the use of Reclaimed Asphalt (RA) or Reclaimed Asphalt Pavement (RAP) in new flexible pavement projects and/or rehabilitation projects. In this study five asphalt concrete (AC) mixtures were produced; a reference AC20-ref mixture with limestone aggregates and a 50/70 penetration grade bitumen, two recycled AC-20 mixtures containing 25% RAP and 50% RAP with 50/70 bitumen, and two recycled AC-20 mixtures containing 25% RAP and 50% RAP with 70/100 bitumen. The aggregate gradation in all mixtures was the same as well as their optimum binder content. The optimum binder content was derived from the mix design procedure of the reference mixture. The performance of all mixtures was determined in terms of their stiffness determined by applying indirect tension on cylindrical specimens (IT-CY) and fatigue resistance performance using indirect tensile test using cylindrical shaped specimens (ITT-CY). Results have shown that stiffness increases with the incorporation of RAP. The highest stiffness value was obtained when 50% RAP and 50/70 bitumen was used. As for the fatigue the performance of the mixtures vary depending on the RAP content and type of bitumen used. The AC mixture with 50% RAP and 70/100 bitumen showed the best fatigue performance of all mixtures tested (reference or recycled mixtures).

1 INTRODUCTION

With the dwindling supply of virgin materials, increasing production costs and shortage of landfill space to dispose of reclaimed materials, the use of recycled asphalt mixtures has become prevalent in the pavement industry. Recycled asphalts are produced from reclaimed asphalt pavement (RAP) with the addition of virgin materials (aggregates and bitumen). In order for the recycled asphalt to be ‘cost-effective, perform well, and be environmentally sound’ the Federal Highway Administration (FHWA) recommends the ‘use of recycled mixtures in the construction of highways to the maximum economical and practical extent possible with equal or improved performance’ (Copeland 2011). It is considered that the most economical use of RAP is in the intermediate and surface layers of flexible pavements because the less expensive binder of the reclaimed material (RAP) can replace a portion of the more expensive virgin binder (Copeland 2011). Waymen et al. (2012) investigated the benefits from using recycled asphalt versus warm mix asphalt (WMA) and demonstrated that even at low contents of RAP such as 15%, the recycling benefits outweigh those achieved by reducing temperature from 165 to 130°C.

In hot recycling the percentage of RAP usually used varies between 10% and 30%. According to several studies, recycled mixtures with the above contents of RAP perform similarly to conventional mixtures (Kandhal et al. 1995, McDaniel et al. 2000,

Widyatmoko 2008, McDaniel et al. 2002, Shah et al. 2007, Li et al. 2008). However, due to the shortage of raw materials and increased environmental awareness, in many countries, higher RAP contents have started to be used. As of 2011, more than 40 state agencies in US allow the use of more than 30% RAP (Copeland 2011). Apart from practical problems encountered during mixing, the use of high RAP content is also limited by the necessity of achieving comparative field performance of pavements constructed with conventional asphalts. An excellent review of very high-content RAP (>40%) use has been made by Zaumanis & Mallick (2015). According to their review there are issues that yet need to be addressed such as the development of a methodology to evaluate the blending of RAP and virgin binder in the laboratory and also the development of a fundamental test for evaluation of cracking resistance of asphalt mixes with high RAP contents.

Fatigue performance of recycled asphalts, especially when high RAP contents are incorporated, is of major concern. The general concept is that the aged stiff RAP binder typically increases stiffness of the recycled mixture (Al Qadi et al. 2012, West et al. 2013), can cause fatigue damage (Shah et al. 2007, Daniel et al. 2010), and low temperature brittleness (Terrel et al. 1992). McDaniel et al. (2000) concludes that at higher RAP contents, the indirect tensile test results and beam fatigue results showed increase in stiffness, which would lead in cracking if no adjustments in mix design were made. Bennert

and Dongre (2010) have reported that in high RAP contents the mix stiffness and consequently the magnitude of cracking will largely depend on the degree of blending between the virgin and RAP binders. West et al. (2013) has examined the use of recycled mixes with 55% RAP. The research showed that the recycled mixtures stiffness measured by dynamic modulus at different temperatures and frequencies increased by 25%–60% compared with virgin mixtures. Additionally the recycled mixtures fracture energy was examined. Virgin mixtures showed better results than the recycled mixtures. A study on long-term pavement performance (LTTP) for overlays of ~20 years and 30% RAP content by West et al. (2011) showed that fatigue, longitudinal and transverse cracking are the distresses that occur more often in RAP mixtures. The study however concluded that the pavements with recycled mixtures performed better than or equal to virgin pavements for majority of the cases.

Contrary to all the above, the studies by Al-Qadi et al. (2012) and McDaniel et al. (2012) showed increased fatigue life for mixtures containing 40% RAP or more compared with conventional mixtures. In these studies beam fatigue and Simplified Viscoelastic Continuum Damage (S-VECD) procedures were respectively used for evaluating fatigue performance. Similar beam fatigue results were obtained by Shu et al. (2008). West et al. (2012) developed relationships between laboratory results and test truck findings which suggest that mixtures with 50% RAP are expected to have better fatigue performance than the virgin control mix.

Another issue that researchers address is the water susceptibility of recycled mixtures. Water susceptibility of recycled mixtures is strongly connected with the water susceptibility of the reclaimed asphalt used. In general high content recycled asphalts are not susceptible to more stripping than conventional asphalts (Karlsson and Isacson 2006, Tran et al. 2012). Mogawer et al. (2012) has even reported increased moisture resistance of mixtures with high RAP content.

The resistance to plastic deformation which is related to the stiffness of high RAP content pavements is likely to be very good due to the presence of the aged RAP binder (McDaniel et al. 2000, Karlsson and Isacson 2006). Attention should be given when reduced binder grade or rejuvenators are applied. Carpenter and Wolosick (1980) and Noureldin and Wood (1987) showed that the rejuvenator or the virgin binder continues to penetrate (diffuse) in the aged binder film even after placement of the pavement. This phenomenon may lead to development of permanent deformation in early stages of pavement life until equilibrium is reached (Potter and Mercer 1997, Shah et al. 2007, Mogawer et al. 2012). West et al. (2013) suggest the evaluation of the recycled mixture's rutting resistance if a softer grade binder is used. Recycled mixtures paved at NCAT test track having 45% of RAP have showed excellent rutting performance, even when a softer binder grade was used (West et al. 2012). The

Table 1. Mixtures used in the study.

Mixture	Binder	Aggregates
AC20-ref	50/70	Limestone
AC20-25% RAP-50/70	50/70 + RAP binder	Limestone + RAP aggregates
AC20-50% RAP-70/100	70/100 + RAP binder	
AC20-25% RAP-50/70	50/70 + RAP binder	
AC20-50% RAP-70/100	70/100 + RAP binder	

same excellent performance was exhibited by plant produced mixtures with 40% RAP. Tran et al. (2012) have found no detrimental effect of the use of 12% rejuvenator (by RAP binder mass) on the performance of 50% laboratory produced RAP mixture.

Considering all the above the objective of this study was to evaluate and compare the stiffness and fatigue performance of recycled asphalt concrete mixtures with maximum aggregate size 20 mm (AC20) in the laboratory. The reclaimed asphalt (RAP) content of the recycled mixtures was 25% and 50%, so to see the effect of increasing RAP content in the recycled mix. Additionally two types of virgin binders were used in the recycled mixtures; a 50/70 penetration grade bitumen and a 70/100 penetration grade bitumen, so to see also the effect of the virgin binder type on the performance of the recycled mixes.

2 EXPERIMENTAL WORK

The experimental work of this study had two distinct phases.

The first phase included the design of an AC-20 mm mixture (reference mixture AC20-ref) with the Superpave mix design (Asphalt Institute 2001). The AC20-ref mixture was composed by limestone aggregates and 50/70 penetration bitumen. Optimum binder content and volumetric properties were determined for the latter. Additionally using the gradation and optimum binder content of the reference mixture, recycled mixtures containing 25% and 50% RAP were also designed so to have the same gradation and binder content with the reference mixture. In the recycled mixtures two types of virgin binders were used 50/70 and 70/100 penetration grade bitumen. Table 1 shows the five mixtures used in this study.

In the second phase of the study all mixtures were tested and compared in terms of stiffness and fatigue performance in order to determine the effect of RAP content and the effect of type of virgin binder used (50/70 or 70/100 penetration grade bitumen).

3 MATERIALS

3.1 RAP material

The RAP material used in this study came from a same source and had an aggregate maximum size of

Table 2. RAP aggregate gradation and binder properties.

RAP aggregate gradation	
Sieve size (mm)	Passing %
25	100.00
19	96.95
9.5	77.68
4.75	56.45
2.36	34.58
1.18	20.48
0.6	13.51
0.3	9.44
0.075	6.45
RAP bitumen properties	
RAP bitumen content	4.39% by RAP
Penetration (pen)	24
Softening point (°C)	66.8
Dynamic viscosity at 150°C (Pa.s)	0.955

Table 3. Virgin aggregates gradations.

Aggregate Sieve size (mm)	Passing %		
	A	B	C
25	100.00	100.00	100.00
19	94.79	100.00	100.00
9.5	63.86	99.50	99.73
4.75	0.66	53.88	95.64
2.36	0.54	11.90	79.07
1.18	0.51	5.34	48.36
0.6	0.50	4.04	31.29
0.3	0.48	3.49	21.12
0.075	0.45	2.60	14.15

19.0 mm. The extraction method (CEN EN 12697-1) was used to recover RAP aggregates and binder. The RAP bitumen content was found to be 4.39% per weight of RAP mix. RAP particle size distribution was determined on the 'clean' recovered aggregates. The recovered binder using rotary evaporator (CEN EN 12697-3) was tested in accordance with CEN EN 1426, CEN EN 1427 and CEN EN 13302, for determination of penetration, softening point and dynamic viscosity respectively. Table 2 shows the RAP aggregate gradation and RAP binder properties.

3.2 Limestone aggregates

The virgin aggregates used in this study were crushed limestone aggregates, all coming from the same quarry. The particle size distribution and characteristic properties of the limestone aggregates are shown in Tables 3 and 4.

3.3 Virgin binders

The virgin binders used in this study as already mentioned were 50/70 and 70/100 penetration grade bitumens. The penetration, softening point, penetration index and dynamic viscosity of the two bitumen types are shown in Table 5.

Table 4. Virgin aggregate characteristic properties.

Aggregate	Property			
	Particle density (kg/m ³)	Water absorption (%)	LA value (%)	Flakiness index (%)
A	2640	0.3	30	18.3
B	2618	0.5	–	21.7
C	2596	0.8	–	–

Table 5. Virgin binders characteristic properties.

Virgin binder	Property	Value
50/70	Penetration (pen)	68
	Softening point (°C)	48.5
	Penetration index	–0.9
	Dynamic viscosity (Pa.s) at 150°C (Pa.s)	0.280
	Dynamic viscosity (Pa.s) at 100°C (Pa.s)	2.3
70/100	Penetration (pen)	85
	Softening point (°C)	45.8
	Penetration index	–1.0
	Dynamic viscosity (Pa.s) at 150°C (Pa.s)	0.200
	Dynamic viscosity (Pa.s) at 100°C (Pa.s)	1.9

4 MIX DESIGN

4.1 AC20 reference mix

For the mix design of the reference mixture the Superpave mix design procedure as described in the Asphalt Institute SP-2 manual (Asphalt Institute 2001) was followed. Applying the above procedure the final aggregate gradation of the AC 20 reference mix was found to be as shown in Figure 1.

In order to determine the optimum bitumen content cylindrical specimens of 150 mm diameter were compacted using the gyratory compactor at three different bitumen contents. In each content two specimens were produced. Compaction was made at $N_{des} = 125$ gyrations. Following the procedure and criteria set by the Asphalt Institute SP-2 manual the optimum bitumen content was found to be 4.75% by weight of mix or 5% by weight of aggregates. The characteristic properties of the AC20-ref mixture properties at the optimum bitumen content (OBC) are shown in Table 6.

4.2 AC20 recycled mixtures

After aggregate gradation and optimum bitumen content were determined for the reference mixture, the recycled mixtures were designed so to have almost the same aggregate gradation and bitumen content as the reference mixture. Table 7 shows the gradations of the recycled mixtures with 25% and 50% RAP in comparison to the reference mixture gradation.

As it can be seen, Table 7, the maximum deference of percentage passing between reference and recycled mixtures is 2.3%.

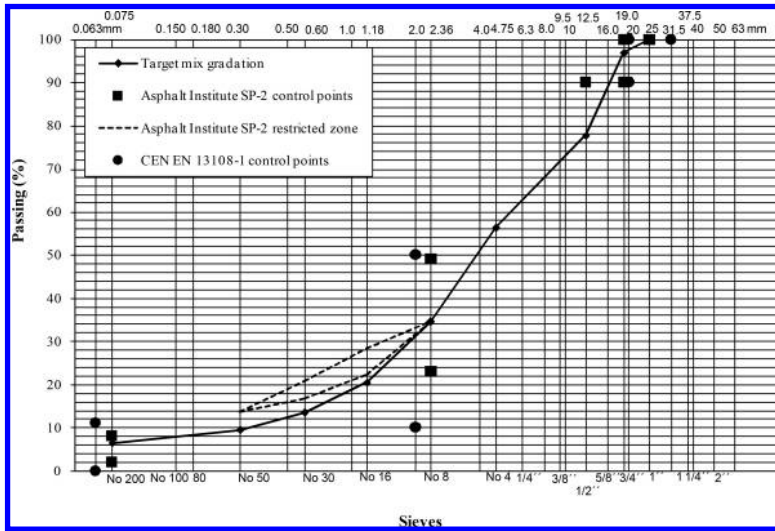


Figure 1. Mix design gradation.

Table 6. Characteristic properties at OBC.

Optimum Bitumen Content*	Bulk Specific Gravity (gr/cm ³)	Voids (%)	VMA (%)	VFA (%)	Stability (kN)	Flow (mm)
4.75	2.375	4.1	14.2	71.1	9.9	2.8

*by weight of mix

Table 7. Reference and recycled mixtures target aggregate gradations.

Sieve size (mm)	Passing %		
	Reference mix	Recycled mix with 25% RAP	Recycled mix with 50% RAP
25	100.00	100.00	100.00
19	96.95	95.95	96.65
9.5	77.68	78.47	77.92
4.75	56.45	55.47	54.18
2.36	34.58	33.57	32.77
1.18	20.48	20.85	21.39
0.6	13.51	14.39	15.38
0.3	9.44	10.38	11.38
0.075	6.45	6.76	7.11

All recycled mixtures produced with 4.75% bitumen content (OBC of the reference mix) taking into consideration the RAP binder content determined.

5 TESTING OF THE REFERENCE AND RECYCLED MIXTURES

For the reference and the recycled mixtures of this study 60 in total gyratory compacted cylindrical

Table 8. Aggregate gradations and binder content of recycled mixtures.

Sieves	Mixtures produced Percentage passing (%)				
	AC20- ref	AC20- 25%RAP- 50/70	AC20- 25%RAP- 70/100	AC20- 50%RAP- 50/70	AC20- 50%RAP- 70/100
25	100.0	100.0	100.00	100.00	100.00
19	95.62	93.48	93.15	93.11	94.31
9.5	75.81	76.87	76.22	79.20	78.30
4.75	55.42	53.23	54.11	52.64	53.62
2.36	33.22	32.41	33.12	31.91	31.88
1.18	19.48	20.80	20.80	21.59	21.23
0.6	12.89	14.51	14.42	15.62	15.42
0.3	9.11	10.41	9.25	11.55	11.42
0.075	6.36	6.79	6.77	7.17	7.12
Binder content (*) (%)	5.00	4.90	5.01	4.80	4.98

(*) by weight of aggregates

specimens (100 mm in diameter) were produced for stiffness and fatigue performance. After determining stiffness in accordance with CEN EN 12697-26 (2012) and fatigue performance in accordance with CEN EN 12697-24 (2012) some properties of the recycled mixtures were also determined. These properties were: aggregate gradations, properties of binder, and volumetric properties.

5.1 Aggregate gradations of reference and recycled mixtures

The aggregate gradations of the recycled mixtures, after extraction of the bitumen and sieve analysis, are as shown in Table 8.

Table 9. Measured properties of recovered bitumen.

Mixture	Property			Bitumen category CEN EN 12591
	Penetration (pen)	Softening point (°C)	Dynamic viscosity (Pa.s) 150°C	
AC20-ref	68	48.5	0.280	50/70
AC20-25% RAP-50/70	56	53.4	0.475	50/70
AC20-25% RAP-70/100	62	49.4	0.360	50/70
AC20-50% RAP-50/70	40	57.2	0.555	35/50
AC20-50% RAP-70/100	46	54.7	0.530	35/50

It is noted that the differences of all percentages passing are within the tolerance specified by CEN EN 13108-21 (2006) with respect to the mix design gradation curve. Additionally, all the bitumen contents are very close to the optimum bitumen content determined (maximum difference of 0.2%).

5.2 Properties of the recovered bitumen from reference and recycled mixtures

The binder properties of the recovered bitumen from the reference and recycled mixes are as shown in Table 9.

As it can be seen from Table 9 the incorporation of 50% RAP has hardened the bitumen by one category as specified by CEN EN 12591 (2009), regardless of the type of virgin bitumen added. The incorporation of 25% RAP had no affected on the category of the bitumen.

Penetration and softening point of recycled mixtures can be determined by two equations proposed by CEN EN 13108-1(2008) when the penetration and softening point of the virgin and RAP binder are known. These two equations proposed are as follows:

$$a \log Pen_1 + b \log Pen_2 = (a + b) \log Pen_{mix} \quad (1)$$

$$T_{R\&B\text{MIX}} = aT_{R\&B1} + bT_{R\&B2} \quad (2)$$

where Pen_1 is the penetration of the binder recovered from the reclaimed asphalt mix, Pen_2 is the penetration of the added binder, Pen_{mix} is the calculated penetration of the recycled mixture, $T_{R\&B1}$ is the softening point of the binder recovered from the reclaimed asphalt mix, $T_{R\&B2}$ is the softening point of the added binder and $T_{R\&B\text{MIX}}$ is the calculated softening point of the recycled mixture.

By implementing equation 1 and 2 for the recycled mixtures used in this study the resulting penetration and softening point values are shown in Table 10.

As it can be seen from Table 10, the theoretical determination of the penetration and softening point values are quite close to those measured.

Table 10. Determination of the penetration and softening points of the recycled mixtures.

Mixture	Bitumen Properties		Bitumen category CEN EN 12591
	Penetration (pen)	Softening point (°C)	
AC20-25% RAP-50/70	54	52.7	50/70
AC20-25% RAP-70/100	64	50.6	50/70
AC20-50% RAP-50/70	42	56.9	35/50
AC20-50% RAP-70/100	48	55.4	35/50

Table 11. Volumetric properties of reference and recycled mixtures produced.

Mixture	Mixture volumetric properties		
	Voids	VMA	VFA
AC20-ref	4.2	14.0	70.1
AC20-25% RAP-50/70	3.8	15.0	74.6
AC20-25% RAP-70/100	4.1	14.8	75.8
AC20-50% RAP-50/70	3.9	13.6	71.3
AC20-50% RAP-70/100	4.0	13.8	71.0

5.3 Volumetric properties of reference and recycled mixtures

The volumetric properties of all five AC mixtures tested are as shown in Table 11.

Comparing the values shown in Table 11 with those of the target mix, Table 6, it is obvious that the mixtures produced were very close to the target mixture.

6 STIFFNESS RESULTS

The determination of stiffness was carried out according to CEN EN 12697-26, Annex C, IT-CY at four temperatures: 0°C, 10°C, 20°C and 30°C. Additionally, stiffness was also measured at five different risetimes; 40 ms, 64 ms, 124 ms, 155 ms and 200 ms.

Figures 2, 3, 4 and 5 show the stiffness results per risetime for each testing temperature for the reference and recycled mixes.

As it can be seen from Figures 2 to 5, the stiffness, in all case, decreases as risetime increases, regardless to the testing temperature used.

In all cases recycled mixtures showed higher stiffness values than the reference mix. Additionally, mixtures' ranking with respect to their stiffness remains unchanged regardless of the testing temperature, at any level of risetime.

As for the effect of percentage of RAP to stiffness, the use of 50% RAP resulted in mixtures with the highest stiffness regardless of the type of virgin binder used, at any level of risetime.

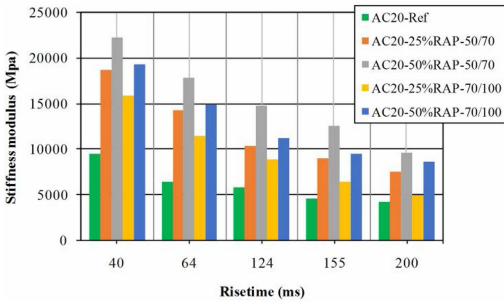


Figure 2. Stiffness values of mixtures at 0°C.

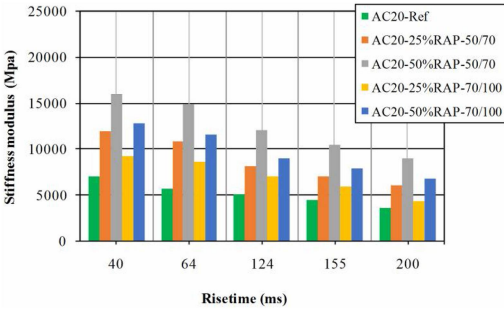


Figure 3. Stiffness values of mixtures at 10°C.

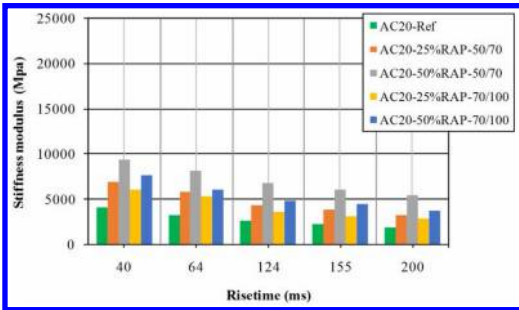


Figure 4. Stiffness values of mixtures at 20°C.

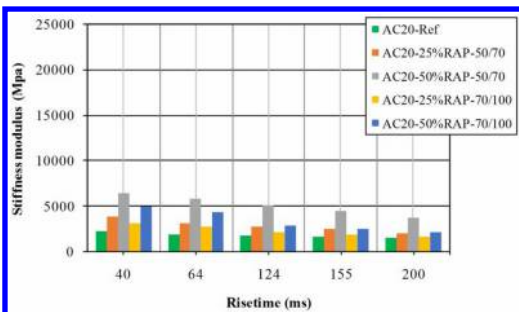


Figure 5. Stiffness values of mixtures at 30°C.

Table 12 shows the stiffness values at 20°C (most commonly testing temperature used) for all levels of risetime and AC mixtures used. As can be seen with the

Table 12. Stiffness values of mixes at 20°C.

Mixture	Stiffness (MPa)				
	40	64	124	155	200
AC20-ref	4183	3272	2624	2317	1893
AC20-25% RAP-50/70	6952	5828	4328	3853	3324
AC20-25% RAP-70/100	6117	5310	3666	3098	2907
AC20-50% RAP-50/70	9457	8178	6879	6070	5480
AC20-50% RAP-70/100	7673	6114	4847	4446	3774

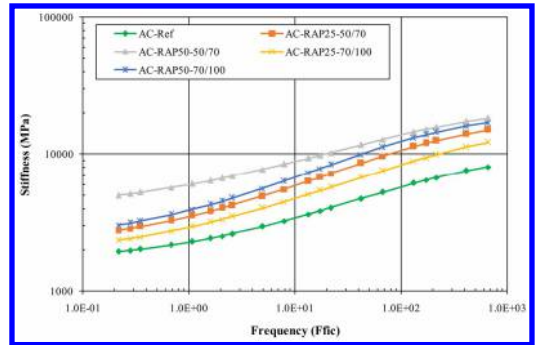


Figure 6. Stiffness master curves for the reference and recycled mixes.

addition of 50% RAP the stiffness increased by almost 100% or more, in comparison to the stiffness of the reference mix, regardless of risetime level chosen. As for the recycled mixtures with 25% RAP the stiffness increased by almost 50% or more. Needless to say that recycled mixtures with 50/70 virgin bitumen possess higher stiffness than recycled mixtures with 70/100 virgin bitumen, for the same RAP content.

6.1 Stiffness master curves

In order to better understand the behavior of the recycled mixtures stiffness master curves were also developed. The stiffness modulus of bituminous mixes obey the frequency temperature superposition which means that a master curve of the mixture's complex modulus can be constructed for a reference temperature from experimental data over a limited range of frequencies and temperatures (CEN EN 12697-26 2012). Thus, stiffness master curves can only be developed after complex modulus is determined.

Complex modulus can be defined as the relationship between stress and strain for a linear visco-elastic material submitted to a sinusoidal load wave form at time (t). In the IT-CY test procedure used a pulse load is applied to the specimen and the stiffness is determined with respect to risetime which is defined as the time necessary for the load to reach the peak

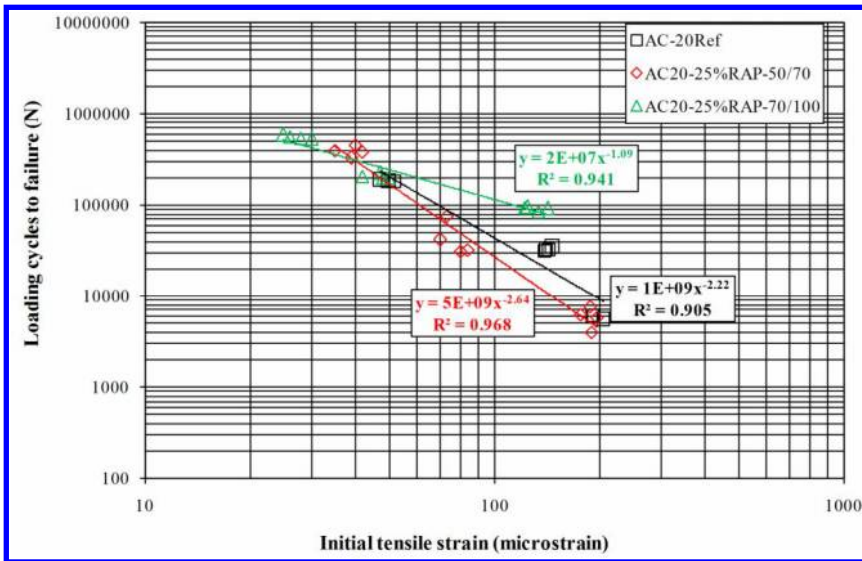


Figure 7. Fatigue lines of mixtures with 25% RAP.

value. In order to develop stiffness master curves using IT-CY results risetime (ms) should be converted to frequency (Hz). Additionally, in the case where risetime needs to be converted to frequency, the device used must also be taken into account (Nunn 1996). There are several studies in which master curves were developed with stiffness data determined by the IT-CY method (Pasetto & Baldo 2006, Losa 2007, Baldo et al. 2010, Pasetto & Baldo 2010, Pasetto & Baldo 2011, Pasetto & Baldo 2012).

All stiffness determinations of this study were carried out by using the Nottingham Asphalt Tester (NAT) device. In order to convert risetime to frequency the following relationship was used:

$$f = 1 / \pi t \quad (3)$$

where f is the frequency (Hz) and t is the risetime (ms).

For the development of the master curves all experimental stiffness data must be 'shifted' using a shift factor at a selected reference temperature. There are three different ways to determine the shift factor (Medani et al. 2004). In this study the shift factor was determined using the Arrhenius equation:

$$\log a_T = \log e \cdot \frac{\Delta H}{R} \left(\frac{1}{T} - \frac{1}{T_{ref}} \right) \quad (4)$$

where T is the experimental temperature (K), T_{ref} the reference temperature (K), ΔH is the activation energy (J/mol), R is the ideal gas constant = 8.314 J/(mol.K). After determining the shift factor mathematical models (polynomial or sigmoid models) are used in order to produce stiffness vs frequency equations.

After conversion of the experimental data at reference temperature 20°C and by using the sigmoid model

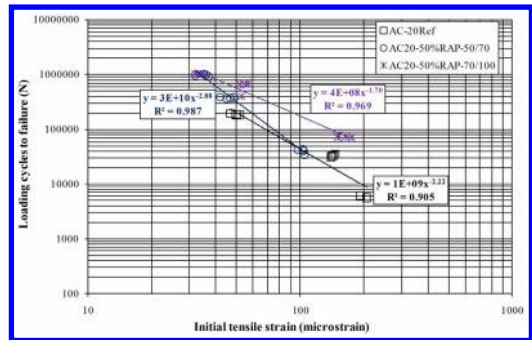


Figure 8. Fatigue lines of mixtures with 50% RAP.

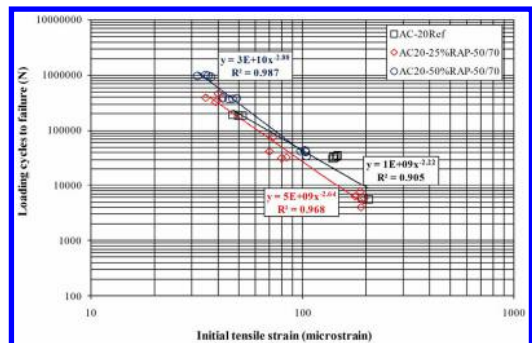


Figure 9. Fatigue lines of mixtures with 50/70 virgin binder.

the stiffness master curves of this study are plotted and are as shown in Figure 6.

The curves of Figure 6 verify that the effect of RAP content is dominant with respect to the stiffness of the mixtures tested.

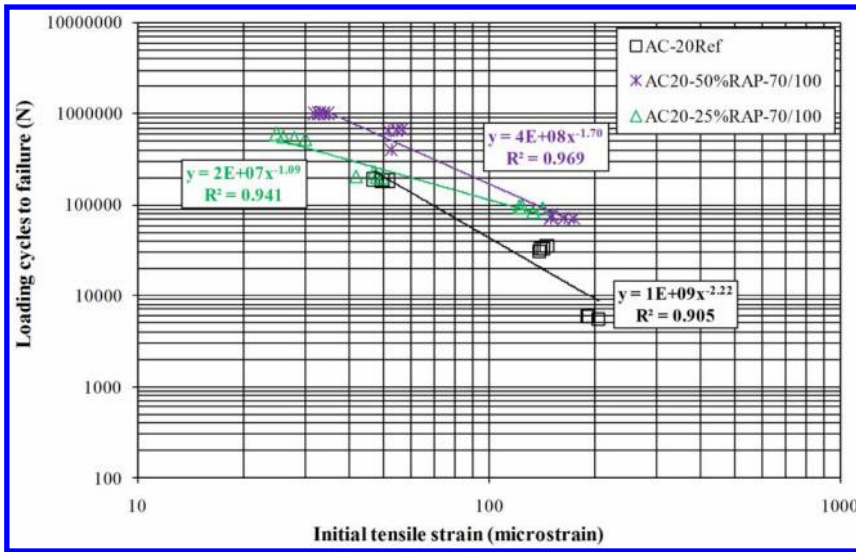


Figure 10. Fatigue lines of mixtures with 70/100 virgin binder.

7 FATIGUE RESULTS

Although requirements for asphalt concrete fatigue testing impose the use of two-point or four-point bending tests (CEN EN 13108-20 2006), the indirect tensile test was used in this study. The AC-20 cylindrical specimens were tested at three levels of stress using four specimens at each level. A repeated haversine load was applied with 0.1 sec loading time and 0.4 sec rest time. The test was conducted at 20°C. The fatigue data were analyzed by running a regression analysis to determine the fatigue relationship parameters in the following form:

$$N_f = k \times \left(\frac{1}{e_0} \right)^n \quad (5)$$

where N_f is the number of load applications, k and n are material constants and e_0 is the tensile strain in $\mu\epsilon$ at the center of the specimen.

Figures 7, 8, 9 and 10 show the results of the fatigue tests. Figures 7 and 8 show the effect of virgin binder type for the same RAP content on fatigue performance of the mixes, while Figures 9 and 10 show the effect of RAP content for the same virgin binder type in fatigue performance of the mixes.

As it can be seen from Figure 7 the fatigue performance of the reference mixture is slightly better to the AC-25%RAP-50/70. However, better fatigue performance to the reference mixture was resulted when 70/100 penetration grade bitumen was used.

When 50% RAP was used the best fatigue performance was obtained when 70/100 virgin bitumen was used, see Figure 8.

From Figures 7 and 8 it can be concluded that for the same RAP content (25% or 50%) the use of softer

virgin binder has improved the fatigue performance of the recycled mixtures.

Figure 9 shows that when 50/70 virgin bitumen was used the fatigue performance of the reference mixture seemed to be slightly more superior to recycled mixtures, certainly at strain levels greater than 100 microstrain.

Finally, Figure 10 shows that when 70/100 virgin bitumen is used both recycled mixtures gave better fatigue performance.

8 CONCLUSIONS

Based on the results obtained in this study the following conclusions can be drawn.

1. The incorporation of 25% RAP had no effect on the resulted bitumen category of the recycled mixtures compared to the bitumen category of the reference mix.
2. The incorporation of 50% RAP has resulted in hardening the bitumen of the recycled mixtures by one category compared to the bitumen category of the reference mix.
3. The values of penetration and softening point determined by the equations proposed by CEN EN 13108-1 were found to be very close to those measured in this study.
4. Stiffness of all mixtures decreased as risetime increased regardless of the testing temperature used.
5. Ranking of mixtures with respect to their stiffness remains unchanged regardless of the testing temperature at any level of risetime.
6. Recycled mixtures showed higher stiffness values than the reference mix.

7. The use of 50% RAP resulted in mixtures with the highest stiffness regardless of the type of virgin binder used (50/70 or 70/100), at any level of risetime.
8. At 20°C testing temperature the stiffness of the recycled mixtures with 50% RAP increased by 100% or more in comparison to the stiffness of the reference mix.
9. At 20°C testing temperature the stiffness of the recycled mixtures with 25% RAP increased by 50% or more in comparison to the stiffness of the reference mix.
10. Master curves have verified the dominant effect of the RAP content with respect to the stiffness of the mixtures.
11. For the same RAP content (25% or 50%) the use of softer virgin binder has improved the fatigue performance of the recycled mixtures.
12. When 50/70 virgin binder was used the reference mixture showed slightly superior fatigue performance than the recycled mixtures.
13. When 70/100 virgin binder was used both recycled mixtures showed better fatigue performance than the reference mixture.

As a general conclusion the use of RAP increases the stiffness of the resulted (recycled) mix which will cause reduction of required thickness or increase of design life.

However, the use of RAP may reduce fatigue performance of the resulted mix with respect to mixture without RAP if attention is not given to the selection of proper grade of virgin bitumen.

ACKNOWLEDGEMENT

The authors would like to thank the undergraduate students E. Alexandridou, A. Margariti and H. Tragaziki for their contribution to the laboratory work.

REFERENCES

Al Qadi I.L., Aurangzeb Q., Carpenter S.H., Pine W.J., Trepanier J. 2012. Impact of high RAP contents on structural and performance properties of asphalt mixtures. Illinois Center for Transportation, Report Number FHWA-ICT-12-002.

Asphalt Institute SP-2. 2001. Superpave mix design. *Superpave series No. 2 (SP-2)*. Lexington, USA: Asphalt Institute.

Baldo N., Dal Ben M., Pasetto M., Van de Ven M., Molenaar A. A. A.. 2010. Indirect Tensile Test for the Determination of the Stiffness and the Resilient Modulus of Asphalt Concretes: Experimental Analysis of the EN 12697-26 and the ASTM D 4123 Standards. Proceedings of the 11th International Conference on Asphalt Pavements, Nagoya, Japan.

Bennert, T. and Dongre, R., 2010. Backcalculation method to determine effective asphalt binder properties of recycled asphalt pavement mixtures. *Transportation Research Record: Journal of the Transportation Research Board*, 2179, 75–84.

Carpenter S., Wolosick J. 1980. Modifier influence in the characterization of hot-mix recycled materials. *Transport Res Rec: J Transport Res Board* 777: 15–22.

CEN EN 12591. 2009. *Bitumen and bituminous binders – Specifications for paving grade bitumens*. EN Standard. Brussels: CEN.

CEN EN 12697-1. 2005. *Bituminous mixtures – Test methods for hot mix asphalt – Part 1: Soluble binder content*. EN Standard. Brussels: CEN.

CEN EN 12697-3. 2005. *Bituminous mixtures – Test methods for hot mix asphalt – Part 3: Bitumen recovery: Rotary evaporator*. EN Standard. Brussels: CEN.

CEN EN 12697-24 +A1. 2012. *Bituminous mixtures – Test methods for hot mix asphalt – Part 24: Resistance to fatigue*. EN Standard Brussels: CEN.

CEN EN 12697-26. 2012. *Bituminous mixtures – Test methods for hot mix asphalt – Part 26: Stiffness*. EN Standard. Brussels: CEN.

CEN EN 1426. 2007. *Bitumen and bituminous binders – Determination of needle penetration*. EN Standard. Brussels: CEN.

CEN EN 1427. *Bitumen and bituminous binders – Determination of the softening point – Ring and Ball method*. EN Standard. Brussels: CEN.

CEN EN 13108-1:2006/AC. 2008. *Bituminous mixtures – Material specifications – Part 1: Asphalt Concrete*. EN Standard. Brussels: CEN.

CEN EN 13108-20. 2006. *Bituminous mixtures – Material specifications – Part 20: Type Testing*. EN Standard. Brussels: CEN.

CEN EN 13108-21. 2006. *Bituminous mixtures – Material specifications – Part 21: Factory Production Control*. EN Standard. Brussels: CEN.

CEN EN 13302. 2010. *Bitumen and bituminous binders – Determination of dynamic viscosity of bituminous binder using a rotating spindle apparatus*. EN Standard. Brussels: CEN.

Copeland, A. 2011. Reclaimed asphalt pavement in asphalt mixtures: state of practice. Research, Development and Technology Turner-Fairbank Highway Research Center, Report number FHWA-HRT-11-021.

Daniel, J., Pochily, J., and Boisvert, D. 2010. Can more reclaimed asphalt pavement be added? Study of extracted binder properties from plant produced mixtures with up to 25% reclaimed asphalt pavement. *Journal of the Association of Asphalt Paving Technologists*, 2180, 19–29.

Kandhal, PS, Rao, SS, Watson, DE, Young, B. 1995. Performance of recycled hot mix asphalt mixtures in state of Georgia. National Center for Asphalt Technology, NCAT Report 95-01.

Karlsson R., Isacsson R. 2006. Material-related aspects of asphalt of asphalt recycling state of the art. *Journal of Materials in Civil Engineering* 18 (1):81–92.

Li, X., Marasteanu, M., Williams, R., Clyne, T. 2008. Effect of RAP (proportion and type) and binder grade on the properties of asphalt mixtures. *Transport Res Rec: J Transport Res Board* 2051: 90–97.

Losa, M., Bacci, R., & Leandri, P. 2007. A New Step Towards Performance Based Specifications for Asphalt Pavements. In Proceedings of 4th SIIV International Congress. Palermo, Italy.

McDaniel, R., Soleymani, H., Anderson, R., Turner, P., Peterson R. 2000. Recommended use of reclaimed asphalt pavement in the superpave mix design method. NCHRP Web Document 30 (Project D9-12): Contractor's final report.

McDaniel, R., Soleymani, H., Shah, A. 2002. Recommended use of reclaimed asphalt pavement in the superpave mix

- design method: technician's manual. National cooperative Highway Research Program (NCHRP) Report 452. Transportation Research Board of the National Academies, Washington D.C.
- McDaniel R., Shah A., Huber G. 2012. Investigation of low- and high-temperature properties of plant-produced RAP mixtures. Research, Development and Technology Turner-Fairbank Highway Research Center, Report number FHWA-HRT-11-058.
- Medani, T.O., Huurman, M., and Molenaar, A. A. A. 2004. On the computation of master curves for bituminous mixes. Proceedings of the 3rd EuroBitume Congress. Vienna, Austria.
- Mogawer W., Bennert T., Daniel J. S., Bonaquist R., Austerman A., Booshehrian A. 2012. Performance characteristics of plant produced high RAP mixtures. *Road Materials and Pavement Design* 13 (1):183–208.
- Noureldin A.S., Wood L.E. 1987. Rejuvenator diffusion in binder film for hot-mix recycled asphalt pavement. *Transport Res Rec: J Transport Res Board* 1115: 51–61.
- Nunn M. E. 1996. The characterization of bituminous macadam by indirect tensile stiffness modulus. Crowthorne UK, TRL.
- Pasetto M., Baldo N. 2006. Critical Analysis of the EN 12697-26 Standard for the Determination of the Indirect Tensile Stiffness Modulus. Proceedings of the 10th International Conference on Asphalt Pavements, ISBN 978-2-550-49009-8, Québec City, Canada.
- Pasetto M., Baldo N. 2010. Experimental Evaluation of High Performance Base course and Road Base Asphalt Concrete with Electric Arc Furnace Steel Slags. *Journal of Hazardous Materials* 181 (1–3), p. 938–948.
- Pasetto M., Baldo N. 2011. Mix design and Performance Analysis of Asphalt Concretes with Electric Arc Furnace Slag. *Construction and Building Materials* 25 (8), p. 3458–3468.
- Pasetto M., Baldo N. 2012. Performance comparative analysis of Stone Mastic Asphalts with Electric Arc Furnace steel slag: a laboratory evaluation. *Materials and Structures* 45(3), p. 411–424.
- Potter J. & Mercer J. 1997. Full-scale performance trials and accelerating testing of hot-mix recycling in the UK. Paper presented at the eighth international conference on asphalt pavements, International Society for Asphalt Pavements, Seattle WA, 10-14 August 1997.
- Shah, A., McDaniel R., Huber G.A., Gallivan V. 2007. Investigation of properties of plant produced rap mixtures. *Transport Res Rec: J Transport Res Board* 1998: 103–111.
- Shu X., Huang B., Vukosavljevic D. 2008. Laboratory evaluation of fatigue characteristics of recycled asphalt mixture. *Constr Build Mater* 22 (7):1323–1330.
- Terrel, R., Joseph, P., and Fritchen, D. 1992. Five year experience of low temperature performance of recycled hot mix. Transportation Research Record: *Journal of the Transportation Research Board*, 1362, 56–65.
- Tran N.H., Taylor A., Willis R. 2012. Effect of rejuvenator on performance properties of HMA mixtures with high RAP and RAS contents. National Center for Asphalt Technology, NCAT Report 12-05.
- Waymen, M., et al. 2012. Life cycle assessment of reclaimed asphalt. European commission. WP3.2. Sponsored by European Commission, Grant SCP7-GA-2008-218747.
- West, R., et al. 2011. A comparison of virgin and recycled asphalt pavements using long-term pavement performance SPS-5 data. In: Transportation research board 90th annual meeting. Washington, DC: Transportation Research Board, Paper No. 22-3865.
- West R., Timm D., Willis R., Powell B., Tran N., Watson D., Sakhaeifar M., Brown R., Robbins M., Vargas-Nordbeck A., Leiva Villacorta F., Guo X., Nelson J. 2012. Phase IV NCAT pavement test track findings. National Center for Asphalt Technology, NCAT Report 12-10.
- West, R., Willis, J.R., and Marasteanu, M., 2013. Improved mix design, evaluation, and materials management practices for hot mix asphalt with high reclaimed asphalt pavement content. Auburn, AL: National Center for Asphalt Technology, Report Number NCHRP 752, Project Number 09-46.
- Widyatmoko, I. 2008. Mechanistic-empirical mixture design for hot mix asphalt pavement recycling. *Constr: Build Mater* 22 (2):77–87.
- Zaumanis, M., Mallick, R.B. 2015. Review of very high-content reclaimed asphalt use in plant-produced pavements: state of the art. *International Journal of Pavement Engineering*. Vol. 16, Issue 1, pp. 39–55.

Effects of using reclaimed asphalt and/or lower temperature asphalt on availability of road network

J.C. Nicholls & M. Wayman
TRL Limited, Wokingham, UK

K. Mollenhauer
Universität Kassel, Kassel, Germany

C. McNally & A. Tabaković
University College Dublin, Ireland

A. Varveri
Delft University of Technology, The Netherlands

S. Cassidy & R. Shahmohammadi
Lagan Asphalt, Dublin, Ireland

R. Taylor
Shell Bitumen, Manchester, UK

ABSTRACT: The use of reclaimed asphalt, secondary component materials and/or additives and lower temperature asphalt are being increasingly used in order to improve the sustainability of asphalt production. The use of reclaimed asphalt reduces the need for virgin materials whilst lower temperature asphalts have reduced CO₂ emissions, increased sustainability, improved working conditions for construction and maintenance crews, reduced noise level on the work sites, extended paving season and provided financial benefits from lower production and transport costs. However, there is uncertainty about the ageing and durability performance of these technologies because there is limited information available on their long-term performance. Changes in durability will affect the availability of the road network for highway authorities. CEDR commissioned a European project to assess these uncertainties. A site trial was commissioned on one of the Irelands busiest motorways (M3), comprising stone mastic asphalt mixtures containing varying proportions of the reclaimed asphalt with some using warm mix technology. The site has been monitored regularly over a full calendar year for the material performance. A suite of laboratory tests have been undertaken concentrating on the combined effect of ageing and moisture damage on the performance of asphalt mixtures on the site trial. The findings have been used to develop life-cycle analysis models to customise them for the effect of using alternative component materials on the availability of the network and their overall financial and environmental cost, both initial and whole-life. The costs identified are both direct (of the construction and maintenance) and indirect (on society in general, such as congestion). The paper describes the model and the assurance that can be given to the assumptions made within the model from the research findings. Comparative sensibility studies are included.

1 INTRODUCTION

1.1 Background

Reclaimed and secondary materials are being used evermore widely in the production of paving mixtures, primarily on the grounds of their reduced environmental impact. Similarly, hot mix asphalt [HMA] is starting to be replaced by lower temperature asphalts [LTA] (which can be subdivided into warm mix asphalt [WMA], half warm mix asphalt [HWMA] and cold mix asphalt [CMA]) in order to lower the temperatures at which the material is produced and placed

on the road. However, the assumption that their use will actually reduce the environmental impact in the longer term is rarely tested, even when that use has an adverse effect on the durability of the mixture. As a simple example, the use of 50% reclaimed asphalt (RA) will reduce the need for fresh aggregate by half, but this advantage will be wiped out if the durability is reduced by a third and the other aspects of construction would mean that such a use of RA had a negative effect on sustainability.

In order to allow the true benefits of lowering mixture temperatures or of using RA and secondary

component materials in pavement mixtures to be understood, a simple methodology to analyse the true cost, environmentally and financially, is required. For such a model to be precise, it will require reliable data about the durability of the pavement with different component materials, which currently is not readily available. In the absence of such data, estimates of the durability will be needed from material test results. However, such a model could still be used with even limited data in sensitivity analyses to understand what changes in durability will do to the effectiveness of the reputedly sustainable changes to construction techniques.

Some research had previously been undertaken on the durability of pavements constructed with RA, including the European Re-Road project, and the use of WMA, including the US Federal Highway Administration's International Technology Scanning Program study tour, but the data on both is limited. In Re-Road project, the in-service durability of surface asphalt courses prepared with considerably high rates of RA were evaluated by monitoring several existing trial sites. Some of the so-far elaborated results indicate that the addition of high amounts of RA in HMA may reduce the service lifetime compared to fully new materials (Kalman, 2011). During the Direct-Mat Project (www.direct-mat.eu), a data base was established containing details on road construction projects applying various kinds of recycling techniques. Although a high number of projects were gathered, generally the information on the actual long-term performance reached by the partly innovative recycling procedures is still missing. The incorporated literature review included several applications of RA in new HMA, but the comparable material performance is in terms of rutting and crack resistance. Nevertheless, some existing results did indicate a decreased resistance against fatigue, for mixtures containing high proportions of RA.

The problem with obtaining details of the life of materials is that those materials have to have been in service for longer than their expected service lives.

1.2 Project summary

This is the final report from the EARN project. The EARN project was designed to address the durability of road structures, layers and materials containing high proportions of reclaimed road materials. In order to model the availability of the road network and the consequences for maintenance needs, traffic congestion due to construction sites, relevant model parameters were identified from the durability of road materials and structures, influenced by mix design and material composition, conditions during road works (season, day/night, weather conditions) and environmental effects.

There is a need for engineers, particular the client's engineers, to understand the full implications of using RA and secondary materials. Whilst efforts to make highway construction more sustainable are laudable,

they must be effective over the longer-term and not be just reduced cost and/or environmental impact on the construction phase alone. If the use of such components in the mixtures does affect the serviceability or durability of the mixture, then any savings may be transitory.

The project built upon existing knowledge, supplemented by limited site and laboratory studies, to develop a specific model to look at this issue and to provide indicative values for use in the model. The available knowledge on the times required for construction and maintenance and on the relevant effects that determine the service lifetime of the different pavement layers have been reviewed. The site trial looked at mixtures with and without RA, but had to assess their durability from early-life properties. The laboratory trials concentrated on the combined effect of ageing and moisture damage on the performance of selected asphalt mixtures containing different proportions of RA. All three strands fed into life-cycle analysis models to customise them for the effect of using alternative component materials on the availability of the network and their overall financial and environmental cost.

2 EXISTING DATA

2.1 Durability

Asphalt pavement durability is a key factor in determining the performance of a pavement material and, as such, the pavement service life together with the pavement maintenance requirements during that service life. Therefore, it plays an important role regarding the environmental life-cycle of the road structure.

The durability of a pavement involves many relevant parameters that can be categorised as:

- The effects from traffic and weather as well as environmental and sub-base soil conditions.
- The parameters for unbound base layers, hydraulically bound base layers and bituminous bound base and finally surface layers.

A high number of parameters can affect the durability of road materials and the service lifetime of the pavement structure. The main aspects have been identified, of which five can be classified as related to environmental conditions, three traffic loading, two sub-base characteristics, four pavement type and structure, four unbound base layer, nine hydraulically bound base layer, eight bitumen stabilised base layer and ten asphalt layer.

However, many data sets are required to evaluate the effect of each parameter on the service lifetime of the pavement. Furthermore, the modelling of a pavement's service life is only possible if most of the parameters are known; otherwise, it is subjected to a wide range of uncertainty.

In addition, a list of asphalt additives and techniques for LTAs was established showing the high

Table 1. General service life assumptions for pavement management systems.

Road layer	Pavement material	Germany (FGSV, 2001)		Netherlands (IVON, 2012)		UK (SWEEP, 2013)	
		≥300 ESAL/day	<300 ESAL/day	Right hand lane	Full width	Surface life	Structural life
Surface asphalt layers	Asphalt concrete (AC)	12	18	12	18	8	–
	Very thin layer asphalt concrete (BBTM)	–	–	–	–	–	–
	Hot rolled asphalt (HRA)	–	–	–	–	–	–
	Stone mastic asphalt (SMA)	16	22	11	17	–	–
	Mastic asphalt (MA)	19	26	–	–	–	–
	Porous asphalt (PA)	–	–	10	18	–	–
Asphalt base layers	Asphalt concrete (binder layer)	26	30	–	–	–	20
	Asphalt concrete (base layer)	55	75	*	*	–	–
	Other base layers	–	–	–	–	–	–
	Hydraulically bound base layer	60	80	*	*	–	–
Rigid pavement	Unbound base layer	55	75	*	*	–	–
	Concrete surface layer	26	30	*	*	10	40
	Hydraulically bound base layer	55	70	*	*	–	–
	Asphalt concrete base layer	50	65	*	*	–	–
Maintenance materials	Unbound base layer	45	60	*	*	–	–
	Slurry surfacing	6	8	–	–	8	–
	Micro-surfacing	5	8	–	–	–	–
	Thin hot-mix asphalt layer on sealing	8	10	–	–	–	–

*Highway maintenance in the Netherlands aims at timely strengthening the asphalt base layers and (sub)bases and thus, never has to be replaced.

number of various techniques for reducing the energy consumption of asphalt paving works.

2.2 State of the art on durability of pavements

The current state of the art on the durability of pavements should be found in terms of the assumptions used to develop the pavement management system widely used to maintain road networks. The current assumptions for three countries are given in Table 1.

In order to improve the prediction quality for pavement management systems on project level (i.e. for specific road sites), results of laboratory performance tests can be introduced into PMS as demonstrated by Wistuba *et al.* (2013) during ERA-Net road project InteMat4PMS. This approach should improve the prediction quality and provide the link between laboratory-assessed road material properties and the predicted service life of the road structure built of the road materials (Figure 1). In InteMat4PMS, the approach was demonstrated for the fatigue resistance of asphalt base layer.

Therefore, the results of laboratory performance tests can be used for estimating the effect of road material composition on the service life of the road structure. This approach has been applied for the analysis of international research projects and additional literature regarding the effects on asphalt material performance of RA use or LTA mixtures.

2.3 Data review

Data from both literature and site were sought. The site data found was UK data on service lifetime of road

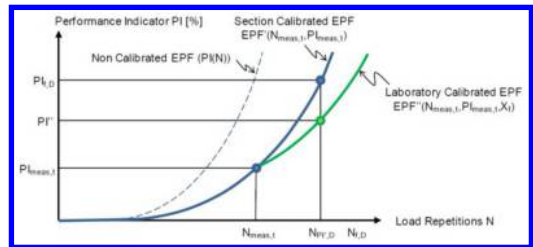


Figure 1. Calibration of performance indicator for PMS application based on laboratory material performance tests (Wistuba *et al.*, 2013).

structures (HAPMS), German data on asphalt material composition and pavement surface condition and the Dutch perpetual pavements study.

Some of the parameters that affect durability can be controlled by material and pavement engineering (e.g. mix design, raw material selection, and pavement design) while others are ancillary conditions which cannot be modified during road design and construction (e.g. weather conditions). Because of its effects on the frequency and extent of maintenance road works, the durability plays an important role on the environmental life-cycle performance of the road structure as well as on its life-cycle costs.

For evaluating additional effects on service lifetime yet not considered in life-cycle assessment (LCA) and life-cycle cost assessment (LCCA), European databases on structural and performance properties of the road network were assessed in detail. Unfortunately, due to lack of reliable structural data on road

network databases and the inhomogeneity of locality referencing with the detailed material databases, no conclusions could be drawn about the effect of including recycled materials or secondary materials on the service lifetime of the road structure.

What has been shown from international literature is that the use of RA in new HMA results in adequate material durability performance in most of the cases. However, some researchers have also identified reduced durability for mixtures containing RA. Altogether, the application of RA in new HMA exhibits additional procedures in mix design as well as asphalt mixture production on industrial scale. Because the sole number of production steps increases which individually affect the durability properties of the resulting asphalt mixture, the risk of reduced durability will increase in general. When all procedures were conducted in high quality conditions (as is usually the case in laboratory research as well as test section studies), no adverse durability effects were observed in most publications. Nevertheless, if there is any general adverse long-term performance, as indicated by database analysis in every-day paving industry, the higher risk will result in reduced durability for some of the projects. The increased use of various additives will further increase this development due to additional risks (e.g. incompatibilities to specific binders).

When considering the durability effect of asphalt mixture composition as well as the use of additives and or recycled materials, feasible laboratory conditioning procedures are needed in order to allow the estimation of long-term properties during mix design. Based on these results, durability effects can be implemented into LCA and LCCA in comparison to traditional asphalt mixtures with known durability properties.

For the effect of the construction season, paving during adverse weather conditions will slightly increase the risk for insufficient compaction and interlayer bonding. These independently occurring effects result in significant reductions of pavement and/or road material service lifetime. The reductions of -1.7% due to risk of insufficient compaction and 0.5% due to risk of insufficient interlayer bonding can be summed to produce a service life decrease of -2.2% for pavements constructed in winter months (October until January).

The splitting of larger construction sites into smaller patches, which may be necessary when using times of low traffic volume for conducting pavement maintenance works, incorporate the disadvantage of an increase in the number of joints. These areas of pavements often inhibit inadequate compaction properties and, therefore, a significantly decreased durability. Based on published research results, the effect of a reduced compaction degree on estimated service lifetime combined with the risk of inadequate joint design could be estimated to a reduced service lifetime of -14.4% .

More complete details of the effects of constituent materials, recycled and secondary sources materials and construction conditions on pavements durability

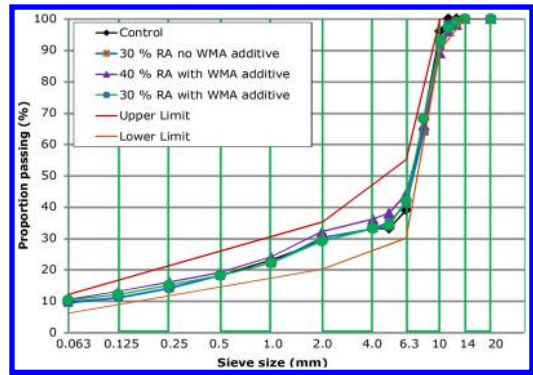


Figure 2. Particle size distribution.

derived from literature and site data review are given elsewhere (Mollenhauer *et al.*, 2014).

3 SITE TRIAL TO EVALUATE VARYING PROPORTIONS OF RECLAIMED ASPHALT

3.1 Design

The asphalt mixture investigated in this study was a 10 mm SMA typical of that used in Irish and European practice. The variations of the 10 mm SMA mixture are 0% RA as control; 30% RA and no additive; 40% RA and Cecabase RT 945 warm mix additive; and 30% RA and Cecabase RT 945 warm mix additive. The grading curves for these mixtures are presented in Figure 2, illustrating the good agreement between the control mixture grading and those of the mixtures containing RA. Using the control mixture grading as the guideline allowed the best particle distribution for the mix designs, and consequently the best mixture design as illustrated in Figure 2.

3.2 Construction

In collaboration with the Irish National Roads Authority, a section of the N3 national road was identified as a suitable road section for the site trial experiment. The site was located between Blanchardstown and Clonee Village, at the outskirts of the Dublin city. The GPS coordinates of the trial site are latitude $53^{\circ}24'19.35''$, longitude $-6^{\circ}24'30.55''$ to latitude $= 53^{\circ}24'6.43''$, longitude $= -6^{\circ}23'59.21''$. The section was chosen because the road section was due for resurfacing, it is close to the asphalt plant (c.60 km) and it is on a main commuter route into Dublin city with an average daily vehicle traffic count, one direction only, of 15 480 vehicles including HGV. Figure 3 illustrates a satellite image of the trial section and surrounding area. The road is a dual carriage way with three traffic lanes on each side (bus lane and two traffic lanes). The middle lane was chosen as the test lane because it will be subjected to the most trafficking, particularly from heavy goods vehicles. The traffic direction is towards Dublin city. Figure 4 shows



Figure 3. Satellite image of the trial road section.

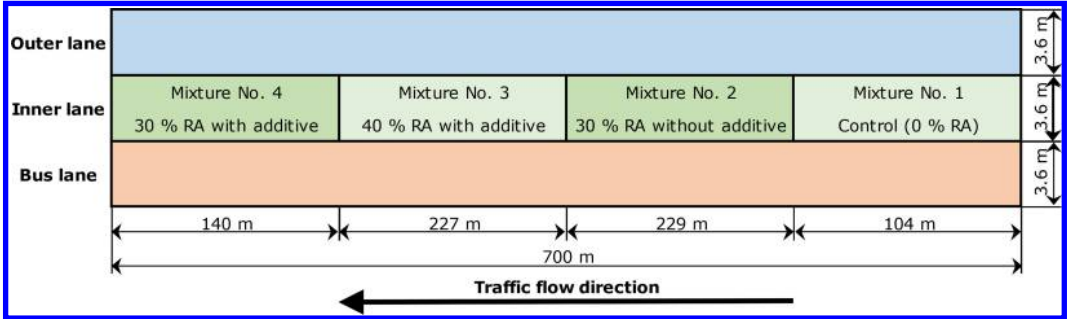


Figure 4. Schematic representation of the trail section.



Figure 5. Paving process of the trial section.

a schematic layout of the trial section. The site was split into four sections of varying lengths for the different mixtures.

To cover the trial section area, it was estimated that just over 230 tonnes of asphalt material was required. The work started with removal of the existing surface

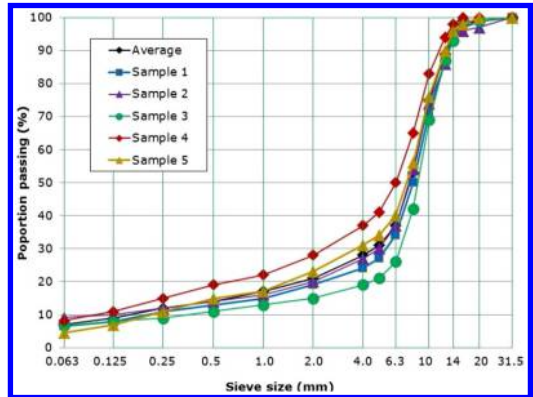


Figure 6. RA material grading after the binder removal.

course which was milled to a depth of 40 mm. An initial regulating course was then laid to a depth of 20 mm. The outer lane and bus lane (Figure 4) were resurfaced with a standard SMA, containing no RA or warm mix additive, to a depth of 40 mm. The test lane was resurfaced with the materials described above.

The paving process started with laying Section 1 (control mixture). The asphalt material was hauled from the plant to the site by truck and unloaded to the material transfer vehicle before it was sent to the paver. The purpose of the material transfer vehicle was to remix the material before sending it to the paver and laying it onto the road. Figure 5 shows the paving process. The paving process of the Section 1, passed as expected without any difficulties.

However, Section 2 proved to be more difficult because the mixture was cooling down rapidly with

Table 2. On-site work record of asphalt material.

Mix No.	RA content (%)	WMA additive	Load No.	Start Chainage (m)	End Chainage (m)	Discharge temp. (°C)	Rolling temp. (°C)	Weight (Tonnes)
1	0	No	1	0	104	150	134	30.00
2	30	No	2	104	155	115	105	17.20
			3	155	220	130	115	17.20
			4	220	333	150	130	28.90
			5	333	385	137	125	30.10
3	40	Yes	6	385	458	135	125	17.00
			7	458	560	134	128	28.80
			8	560	618	125	118	17.00
4	30	Yes	9	618	672	132	124	17.20
			10	672	700	136	128	28.65

Table 3. The quantity of the processed RA material by size.

Size (mm)	>16	16 to 12.5	12.5 to 6	<6
Quantity (T)	40	45	35	50
Proportion (%)	24	26	21	29

the consequential reduction in workability of the mixture. The paving of Sections 3 and 4 passed without much difficulty, highlighting the improved workability of the mixtures incorporating the warm mix additive, with up to 40% RA. The site work records are summarised in Table 3, giving section lengths, temperature and weight of each mixture.

The RA feedstock was supplied from a site on the M1 motorway in North County Dublin and was 14 mm porous asphalt derived from a single source. The material was milled and stored in a depot until required on this project. The total amount of RA material supplied was 170 tonnes. The quantity of the processed RA material by size is given in Table 3. The visual inspection revealed that the >16 mm material contained binder course material aggregate. Therefore, the >16 mm and <6 mm RA aggregate were screened out and not used for the trial asphalt mixtures.

The binder content in the RA was determined according to the EN 12697-39 (CEN, 2012a). Five samples of RA were taken and weighed. The samples were placed in the oven at 530°C for 30 min. Once the samples were cooled, they were weighed again and proportion of binder in the mixture calculated. The average binder content was 5.3%. Following the binder burn off procedure, the material particle size distribution was determined following EN 12697 2 (CEN, 2002). The RA material aggregate size distribution/grading is shown in Figure 6 and the binder contents were 5.2%, 5.4%, 4.8%, 5.7% and 5.4% with an average of 5.3%.

3.3 Monitoring

In order to assess the initial performance of the sections, the international roughness index (IRI), mean profile depth (MPD) and skid resistance by SCRIM were measured in accordance with ASTM

Table 4. In situ measurements of site performance.

Mixture No.	Test period	Mean IRI (m/km)	MPD (mm)	SCRIM Coeff.
1	0	1.24	0.86	–
2		0.98	0.76	–
3		1.07	0.68	–
4		1.38	0.77	–
1	6 months	1.21	0.62	0.50
2		1.11	0.61	0.47
3		1.15	0.55	0.44
4		1.58	0.73	0.46
1	12 months	1.29	0.77	0.49
2		1.11	0.64	0.48
3		1.16	0.53	0.45
4		1.44	0.70	0.46

E950/E950M (ASTM, 2009), EN ISO 13473-1 (ISO, 2004) and CEN/TS 15901-6 (CEN, 2009), respectively. The skid resistance measures are sideways force coefficient (SFC) and corrected SCRIM Coefficient (SC). Measurements were made initially (except for skid resistance) and then after 6 and 12 months with the results shown in Table 4.

The average IRI value for each section is <2 m/km which shows good ride quality of the pavement surface. The average MPD values are below 0.9 mm and above 0.4 mm, which indicates that the surfaces have suitable macro-texture depth for the type of the road (a National road) where the maximum speed limit is 100 km/h. The average SFC and SC value for each section is >0.3 which shows good friction quality of the pavement surface. These values reassure that MPD values are in safe levels and all sections have a good ride quality and are safe for road users.

The asphalt mixture material was also sampled from the paver for use in the laboratory evaluation of moisture damage and ageing (Section 4). In addition, a total of 108 cores (27 from each trial section) were taken 24 hours after the construction was completed.

Laboratory testing of the indirect tensile stiffness modulus (ITSM) in accordance with EN 12697-26 (CEN, 2012b) and the water sensitivity in accordance with EN 12697-12 (CEN, 2008) were undertaken in order to evaluate the material used on site. The tests

4 EXPERIMENTAL EVALUATION OF MOISTURE DAMAGE AND AGEING IN ASPHALT MIXTURES

4.1 Objective of laboratory testing

The objective of laboratory testing was to investigate the combined effect of ageing and moisture damage on the mechanical performance of selected asphalt mixtures containing various proportions of RA. For this study, site trials have been laid of mixtures both without and with RA from which cylindrical specimens were cored and utilised for laboratory testing. The coring procedure and the laboratory testing were carried out in two stages; in the first stage, field cores were taken 24 h after the construction of the trial section was completed and were evaluated for their propensity to moisture damage, while in the second stage asphalt cores were taken 12 months later and the same testing programme undertaken. In this manner, apart from the moisture damage susceptibility, the effect of ageing on the mechanical response of the selected mixtures was able to be evaluated.

4.2 Test protocol

A total of 27 cores were drilled from each section of the road trial. For each mixture, the specimens were divided into two subsets. The first subset was subjected to moisture conditioning, while the other subset was stored in a climate chamber in dry conditions at 20°C. In order to address the individual damage mechanisms associated with the two types of damage inducing processes, the moisture conditioning protocol applied is a combination of two different conditioning methods: (a) bath conditioning and (b) cyclic water pore pressure application. Cyclic pore pressure generation in the asphalt mixture is achieved by means of the moisture induced sensitivity tester (MIST). The MIST was designed as an accelerated conditioning device for the evaluation of the resistance of an asphalt mixture to stripping by simulating the high pressure fields which develop within an asphalt layer due to traffic loading.

MIST is a self-contained unit, Figure 8(a), which includes a hydraulic pump and a piston mechanism that is designed to cyclically apply pressure inside a sample chamber. The test involves placing a 100 mm or 150 mm diameter sample of 25 to 150 mm height inside the sample chamber, filling the chamber with water, closing the sample chamber lid, choosing the preferred conditioning settings and starting the test, Figure 8(b–d). The machine then automatically heats the sample to the desired temperature and starts cycling between zero and the selected pressure. Tests can be performed at different pressures and temperatures to replicate different traffic and environmental conditions. Furthermore, the user can specify the desired number of conditioning cycles.

In the applied protocol, the specimens were first subjected to moisture infiltration by placing them in a bath, filled with distilled water at an elevated conditioning temperature of 60°C, in order to facilitate the

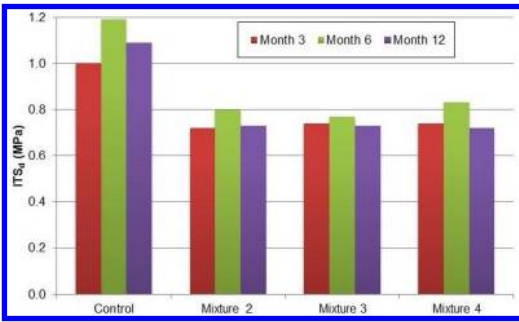


Figure 7a. ITS results after dry conditioning.

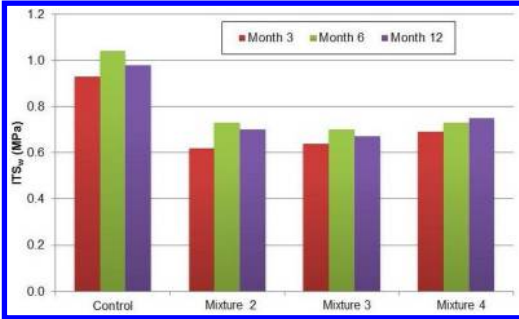


Figure 7b. ITS results after wet conditioning.

Table 5. ITSM test results.

Mixture No.	Stiffness (MPa) at time		
	3 months	6 months	12 months
1	1692.5	1703.2	1620.1
2	2295.3	2237.8	1789.6
3	2407.0	2322.5	2005.6
4	1898.4	2181.5	1629.9

were carried out soon after the trial was laid and then after 3 months, 6 months and 12 months of being in service and the results are given in Table 5 for ITSM and Figures 7(a) and (b) for indirect tensile strength (ITS).

The mixture stiffness values reduce between test months 3 and 12, with the control mixture having lowest reduction of 4.3% where the mixture containing 30% RA and no warm mix additive (Mixture 2) had the highest reduction of 22%. Mixtures 3 and 4 had stiffness reduction of 16.7% and 14.1% respectively.

The results show good resistance to the moisture damage with all mixtures achieving ITS ratio (ITSR) value about required 80%. An exception is the control mixture (Mixture 1) whose ITSR value dropped just below 80% (to 79.3%) at month 12. Results further show improvement in ITSR values in month 12 for Mixtures 2 and 4. This change is due to the improvement in material wet strength (ITS_w) for both materials.

More complete details of the site trials evaluating varying proportions of RA are given elsewhere (Tabaković *et al.*, 2014).



Figure 8. Moisture induced sensitivity tester.

Table 6. Testing matrix.

Type of conditioning	Mixture type	Week 0	Week 3	Week 6
Dry conditions	1	6	3	3
	2	6	3	3
	3	6	3	3
	4	6	3	3
Water bath	1	—	3	3
	2	—	3	3
	3	—	3	3
	4	—	3	3
Water bath & MIST	1	3*	3	3
	2	3*	3	3
	3	3*	3	3
	4	3*	3	3

*Only MIST conditioning was applied on the dry subset at week 0.

infiltration of water into the asphalt mixture and, consequently, accelerate the long-term degradation of the material properties. At fixed time intervals of three and six weeks, three specimens per mixture were removed from the bath, placed in a bath at 20°C for 2 h and then maintained in a climatic chamber at 20°C until tested for their strength using the indirect tension tester (ITT). An additional three samples per mixture were removed from the bath and further conditioned in the MIST device by applying 3500 cycles of pressure application at a temperature of 60°C and a pressure of 0.48 MPa. After MIST application, the samples were placed in a water bath, at 20°C for 2 h. After conditioning, the indirect tensile strength of each of the two subsets is determined in accordance with EN 12697-23 (CEN, 2003). Table 6 shows the number of specimens utilised for each type of conditioning level.

A total of six additional specimens per mixture were stored in a climate chamber at 20°C, after delivery.

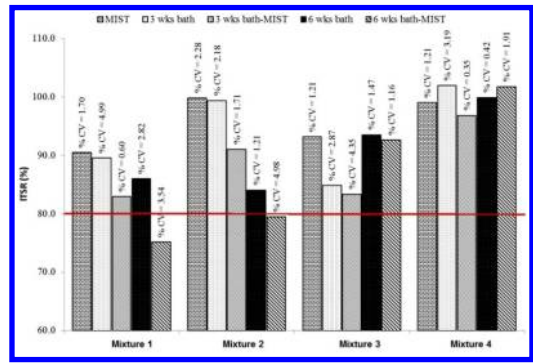


Figure 9a. Mean ITSR values for un-aged samples.

These dry specimens were kept in the chamber during the time of conditioning and were tested together with the conditioned specimens at each defined time interval. In this way, any differences in their strength due to age hardening effects were taken into account.

4.3 Laboratory tests without ageing

The laboratory tests carried out during the first phase of testing were on samples taken from site soon after laying in order to investigate the effect of RA on the moisture damage susceptibility of asphalt mixtures. Four variants of a typical SMA 10 mixture were prepared. The variations were 0% RA as control; 30% RA and no additive; 40% RA and warm mix additive; and 30% RA and warm mix additive. The Indirect Tensile Strength (ITS) to EN 12697-23 (CEN, 2003) and the Indirect Tensile Strength Ratio (ITSR) to EN 12697-12 (CEN, 2008) were used for the evaluation of moisture damage resistance of the mixtures.

The results showed that the inclusion of RA can affect the strength of the mixtures. ITS values were found to increase with increasing RA content in dry conditions, which can be explained by lower void content due to reduced compaction resistance. However, the rate of strength degradation due to moisture damage was found to be higher for the RA mixtures and increased RA content. The use of warm mix additive was shown to increase the resistance to moisture damage as shown by the MIST results, whereas the conventional test procedure according to EN 12697-12 (CEN, 2008) results in the contrary result. This first observation indicates the importance of the need for better understanding of moisture damage and its consideration in test procedures for durability assessment.

4.4 Laboratory tests including ageing

In the second stage, asphalt cores were collected from the field and tested for their indirect tensile strength under the same conditions. A comparison of the un-aged and aged are given in Figures 9(a) and (b) with the red horizontal line showing a threshold value below which an asphalt mixture is considered to be more susceptible to moisture damage.

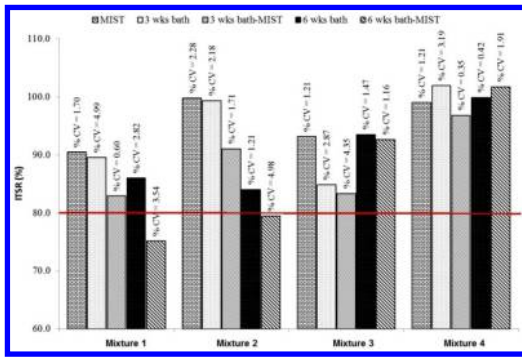


Figure 9b. Mean ITSR values for aged samples.

The results show that the inclusion of RA has an effect on mixture tensile strength. The ITS values were found to increase with increasing RA content. Also, the rate of strength degradation due to moisture damage was found to be lower for the RA mixtures compared to control mixtures. The use of warm mix additive was shown to increase the resistance to moisture damage induced both by bath conditioning alone and by combined bath-MIST conditioning.

The moisture conditioning protocol utilised for the characterisation of moisture susceptibility was found to quantify the effects of short- and long-term moisture damage to mixture degradation. The results showed that the inclusion of RA has an effect on mixture tensile strength with the ITS values increasing with increasing RA content. However, the change in RA content from 30% to 40% did not found to create major differences in the dry and wet ITS and ITSR values.

The rate of strength degradation due to moisture damage was found to be lower for the mixtures containing RA compared to the control mixture. The RA mixtures had a lower reduction in strength, before and after ageing, from the application of the various moisture conditioning protocols.

The TSR values of the RA mixtures, with and without WMA additive, were found to improve for the field aged mixtures. The results indicate that the asphalt mixtures underwent a curing process that lead to an increase in strength with time and enhanced their response to moisture damage. Therefore, it is recommended that ageing considerations are made when performance testing is necessary to validate the mix design with respect to moisture damage susceptibility.

The use of warm mix additive was found to increase the resistance to moisture damage induced both by bath and bath-MIST conditioning. A comparison between mixtures which had the same amount of RA and only differed with respect to the addition of WMA additive demonstrated the positive effect the WMA additive has on the moisture damage susceptibility characteristics of the mixtures.

More complete details of the experimental evaluation of moisture damage and ageing in asphalt mixtures are given elsewhere (Varveri *et al.*, 2014a; 2014b; 2014c).

5.1 Modelling approach and data sources

Carbon-footprinting (CF) and life-cycle costing (LCC) analyses have been conducted based on the EARN site trial of WMA together with a site trial of CMA for the CoRePaSol (Characterization of Advanced Cold-Recycled Bitumen Stabilized Pavement Solutions) project. Direct data collection at the trials and subsequent follow-up were the source of information on the key variables such as mix design recipes, energy consumption during production and cost of components, fuel and transport.

Other standard, reputable data sources were utilised to provide emissions factors for fuels, transport and embodied carbon values for constituent materials. The asphalt pavement embodied carbon tool (asPECT) v4.0 was used to conduct the CF analysis, and a bespoke model created to conduct the LCC analysis.

The 2014 update to asPECT included a facility to modify the standard UK emissions factors for when the tool is applied in another geographical region. The emissions factors for electricity, gas oil and diesel were therefore modified using those specific to Ireland (SEAI, 2012) and the 60:40 allocation of recycled content to recyclability benefits, employed by consensus to reflect the specific UK situation, was modified to 100:0 in favour of the recycled content method of allocation. Allocating benefits purely on the basis of only the recycled content will reward recycling in the current mixture at the present time.

Life cycle costs (LCC) are those directly associated with the planning, design, acquisition, disposal and support of an asset (NSW Treasury, 2004). Therefore, LCC incorporates the ongoing operating and maintenance costs rather than the traditional approach of just focusing on the initial capital cost. These costs are distributed over each stage of the assets lifetime, and, for the purpose of this analysis, have been allocated through the full life cycle. The LCC model developed estimates the overall direct and indirect life cycle costs of alternative asphalt mixtures over a 60 year investigation period for a 1 km lane length.

The total cost of one intervention is comprised of the individual costs incurred during each lifecycle stage (from material procurement to excavation and disposal). Depending on the lifetime and performance of the asset, there may be multiple interventions over the course of the 60 year investigation period. In this case, the model assumes that precisely the same intervention will be repeated and reapplies the original total cost as many times as is necessary.

When the lifetime of the asset exceeds the 60 year period (i.e. an intervention takes place at year 55 with a lifetime of 10 years, leaving 5 additional years of value), the model assumes the residual value using a linear rate of deterioration. This value is then subtracted from the total cost of that intervention in order to allow for an equitable comparison of treatments. The costs are then discounted back to the base year (year 0) of the analysis using a standard net present

Table 7. Calculated CO₂e footprints per tonne for the four mixtures used.

Component	Mixture 1	Mixture 2	Mixture 3	Mixture 4
Cradle-to-gate CO ₂ e footprint (kgCO ₂ e per t)	49.25	47.64	45.20	43.97
Cradle-to-site CO ₂ e footprint (kgCO ₂ e per t)	60.83	59.22	56.78	55.54
Total for the EARN trial installation (kgCO ₂ e) including regulating course and tack coat	18 784			

Table 8. Calculated CO₂e footprints for a 1 km single lane stretch over 60 years.

Cradle-to-grave CO ₂ e footprint for 1 km over 60 years (kgCO ₂ e), including tack coat	Mixture 1	Mixture 2	Mixture 3	Mixture 4
UK (8 year service life)	161 493	155 025	148 942	145 927
Germany (11 year service life)	117 118	112 413	107 990	105 794
Netherlands (16 year service life)	80 139	76 903	73 863	72 351

value (NPV) technique. This process is carried out for both direct and indirect costs for each mixture applying discount rates. It then compares the NPV for each of the asphalt mixtures to indicate which one delivers the most value for money.

Typically, a positive NPV value would indicate a positive investment, and vice versa. In the case of road interventions, where there are no revenues generated by the investment, thus all of the results will be negative. In this case, the highest value (closest to zero) demonstrates the most financially viable option.

5.2 Example for warm mix asphalt

The cradle-to-gate, cradle-to-site and total CO₂e footprints calculated for the works carried out at the trial site are presented in Table 7. The contribution of the different materials over a 60 year asset life is presented in Table 8, normalised to a 1 km stretch of single lane highway. Here the impact of variations on the service life is indicated, according to design lives specified for the UK, Germany and the Netherlands. The cost parameters were used to calculate cost in Euros per tonne for each of the four alternative materials and the net present value costs over the 60 year asset life as shown in Figures 10(a) to (d).

Clear savings are observed for the novel mix designs (Mixtures 2, 3 and 4) relative to the HMA control mixture (Mixture 1) in terms of both CO₂e and cost. The CO₂e savings range from between 3.3% to 10.7% cradle-to-gate and between 2.7% to 8.7% cradle-to-site on a per tonne basis. Mixtures 1 and 4 provide the most equitable basis for comparison between a HMA and LTA mixture containing RA. Comparing them, the savings associated with using the HMA would be 10.7% cradle-to-gate and 8.7% cradle-to-site respectively.

The total CO₂e footprint for the works as installed is calculated at 19.4 tonnes, including the four mixtures as surface course, the regulating course and the tack coats. If all 334 t of materials used on the works (in both the surface and regulating courses) were Mixture

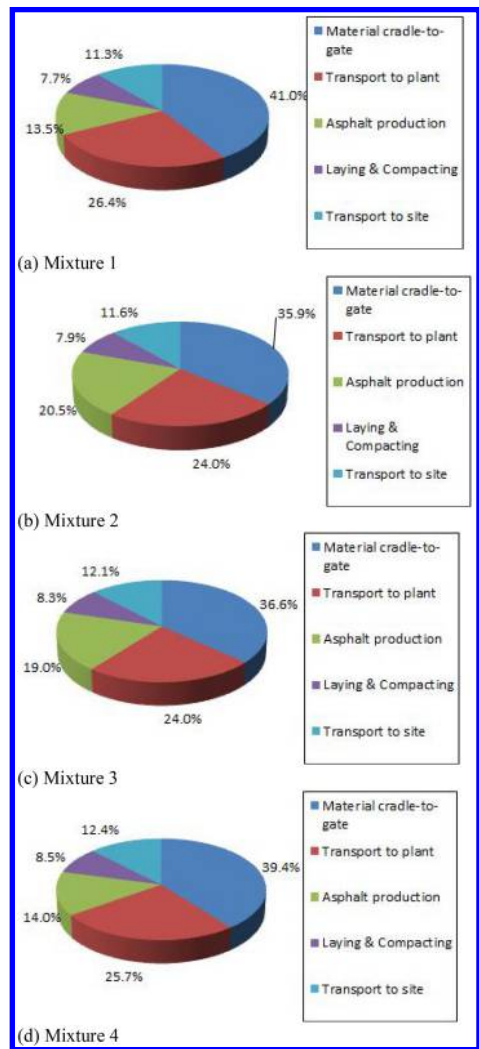


Figure 10. Contribution of the life cycle steps to the overall footprints cradle-to-site.

4, the total footprint would have been 17.8 t CO₂e, relative to 19.5 t for all HMA, a saving of 1.7 t CO₂e.

More complete details of the impact assessment modelling, together with a proposed decision model, are given elsewhere (Wayman *et al.*, 2014).

6 CONCLUSIONS

The principal findings from the EARN research project are:

- The use of LTA systems, RA, secondary by-products and/or binder additives can have an effect on the durability of flexible pavements, but that affect is not always adverse and may not be great.
- The effect of using lower temperature asphalt systems, reclaimed asphalt (RA), secondary by-products and/or binder additives can be modelled in the expected service life of mixtures.
- Data on the effect of each specific components and the extent to which they are incorporated into the mixture need to be collected in order to make the model more accurate.
- The MIST procedure is suitable for standardisation as procedure for asphalt in the EN 12697 series.

More detailed conclusions can be found in the published project deliverables.

ACKNOWLEDGEMENT

The research presented in this paper was carried out as part of the CEDR Transnational Road research Programme Call 2012. The funding for the research was provided by the national road administrations of Denmark, Finland, Germany, Ireland, Netherlands and Norway.

REFERENCES

American Society for Testing and Materials (2009). Standard test method for measuring the longitudinal profile of travelled surfaces with an accelerometer established inertial profiling reference. *ASTM E950/E950M*. West Conshohocken, PA: ASTM International.

Comité Européen de Normalisation (2002). Bituminous mixtures – Test methods for hot mix asphalt – Determination of particle size distribution. *EN 12697-2:2003*. Brussels: CEN.

Comité Européen de Normalisation (2003). Bituminous mixtures – Test methods for hot mix asphalt – Determination of the indirect tensile strength of bituminous specimens. *EN 12697-23:2003*. Brussels: CEN.

Comité Européen de Normalisation (2008). Bituminous mixtures – Test methods for hot mix asphalt – Determination of the water sensitivity of bituminous specimens. *EN 12697-12:2008*. Brussels: CEN.

Comité Européen de Normalisation (2009). Road and airfield surface characteristics – Procedure for determining the skid resistance of a pavement surface by measurement of the sideways force coefficient (SFCS): SCRIM. *CEN/TS 15901-6:2009*. Brussels: CEN.

Comité Européen de Normalisation (2012a). Bituminous mixtures – Test methods for hot mix asphalt – Binder content by ignition. *EN 12697-39:2012*. Brussels: CEN.

Comité Européen de Normalisation (2012b). Bituminous mixtures – Test methods for hot mix asphalt – Stiffness. *EN 12697-26:2012*. Brussels: CEN.

International Organization for Standardization (2004). Characterization of pavement texture by use of surface profiles – Determination of mean profile depth. *EN ISO 134731: 2004*. Geneva: ISO.

Kalman, B. (2012). How could we improve end of life strategies of asphalt pavements? FEHRL Road Research meeting, 18 October 2012, Brussels.

Mollenhauer, K., A. Ipavec, L. Gaspar, P. Marsac, K. Mirski, F. Batista, M. Antunes, C. McNally and R. Karlsson (2011). Synthesis of national and international documents on existing knowledge regarding the recycling of reclaimed road materials in asphalt. *DIRECT-MAT Deliverable D6; EC No. 218656*. www.transport-research.info/web/projects/project_details.cfm?id=38712.

Mollenhauer, K., C. Nicholls, A. Varveri, C. McNally, A. Gibney and A. Tabaković (2013). Service lifetime, suitable test methods for characterising and main parameters controlling durability of warm-mix asphalt containing RA. *EARN Milestone M2*. www.trl.co.uk/solutions/road-rail-infrastructure/sustainable-infrastructure/earn/.

Mollenhauer, K., C. Nicholls, A. Varveri, A. Tabaković, C. McNally and A. Gibney (2014). Effects of constituent materials, recycled and secondary sources materials and construction conditions on pavements durability derived from literature and site data review. *EARN deliverable D3*. www.trl.co.uk/solutions/road-rail-infrastructure/sustainable-infrastructure/earn/.

New South Wales Treasury (2004). Life cycle costing guidance. Available online at: www.treasury.nsw.gov.au/_data/assets/pdf_file/0005/5099/life_cycle_costings.pdf (accessed: December 2014).

Sustainable Energy Authority of Ireland (2012). Emissions factors. Available online at: www.seai.ie/Energy-Data-Portal/Emission_Factors/ (accessed: November 2014).

Tabaković, A., C. McNally, A. Gibney, S. Cassidy, R. Shahmohammadi, S. King and K. Gilbert (2014). Report of laboratory and site testing for site trials. *EARN deliverable D8*. www.trl.co.uk/solutions/road-rail-infrastructure/sustainable-infrastructure/earn/.

Varveri, A., S. Avgerinopoulos, A. Scarpas, C. Nicholls, K. Mollenhauer, C. McNally, A. Gibney and A. Tabaković (2014a). Report on the results of the laboratory tests for the RA mixtures without considering the effect of ageing. *EARN deliverable D2*. www.trl.co.uk/solutions/road-rail-infrastructure/sustainable-infrastructure/earn/.

Varveri, A., S. Avgerinopoulos, A. Scarpas, C. Nicholls, K. Mollenhauer, C. McNally, A. Gibney and A. Tabaković (2014b). Report on the results of laboratory tests for the RA mixtures after field ageing. *EARN deliverable D4*. www.trl.co.uk/solutions/road-rail-infrastructure/sustainable-infrastructure/earn/.

Varveri, A., S. Avgerinopoulos, A. Scarpas, C. Nicholls, K. Mollenhauer, C. McNally, A. Gibney and A. Tabaković (2014c). Laboratory study on moisture and ageing susceptibility characteristics of RA and WMA mixtures. *EARN deliverable D7*. www.trl.co.uk/solutions/road-rail-infrastructure/sustainable-infrastructure/earn/.

Wayman, M., D. Leal, S. Cassidy and R. Shahmohammadi (2014). Cost and CO₂e modelling of lower-temperature asphalt materials with recycled content, as used in site trials. *Combined EARN deliverable D5*

and D6. www.trl.co.uk/solutions/road-rail-infrastructure/sustainable-infrastructure/earn/.

Wistuba, M., A. Wenniger-Vycudil, G. Mladenovic, A. Alisov and J. Litzka (2013). Integration of

material-science based performance models into life-cycle-analysis processed in the frame of pavement management systems. *InteMat4PMS*. Braunschweig: University of Braunschweig.

Influence of reclaimed asphalt content on the complex modulus of cement bitumen treated materials

C. Godenzoni, A. Graziani & M. Bocci
Università Politecnica delle Marche, Italy

ABSTRACT: The objective of this study was to characterize the volumetric and stiffness properties of cold-recycled mixtures treated with bituminous emulsion and cement, produced using different reclaimed asphalt percentages (50%, 80% and 0%). In the first part of the experimental program, volumetric properties and compactability were analyzed using a gyratory compactor. In the second part, the complex modulus was measured by means of cyclic compression tests, on cylindrical specimens. A conventional frequency sweep procedure was followed in a range of service temperatures. The strain level was chosen focusing the attention on the linear domain. The experimental results showed that complex modulus was influenced by frequency and temperature similar to hot mix asphalt. In addition, the time-temperature superposition principle was verified only for the absolute value of the complex modulus but not for its phase angle. Results also showed the influence of bituminous and hydraulic mortars on the rheological response.

1 INTRODUCTION

The increasing use of reclaimed asphalt (RA) allows transportation agencies and contractors to make more efficient use of their resources. RA, produced from cold milling of existing pavements, is adopted as a component in new asphalt mixtures, replacing virgin aggregate (VA). However, the amount of RA used into asphalt mixture, affects its mechanical properties and durability.

Cold in-place recycling of bituminous pavements assumes fundamental importance both for economic and environmental reasons. RA is adopted in cold-recycled mixtures (CRM) where bitumen (either as emulsion or foam) and cement are used as binding agents. The composition of CRM can be extremely variable affecting their mechanical response. In particular, CRM properties vary depending on the proportions in which binders are mixed. If bitumen/cement ratio is greater than one and cement content is less than 1%, the bitumen is prevalently dispersed among the fine aggregate, creating non-continuous bonds within the coarse particles skeleton (Jenkins et al. 2007). As a consequence CRM show a behavior that is similar to that of granular materials i.e. high stress-dependency and failure by permanent deformation or shear stress (Asphalt Academy, 2009).

If the bitumen/cement ratio is less than one and cement content is greater than 1% (Grilli et al. 2012), the mixtures may be considered cement-bitumen treated materials (CBTM). Such mixtures generally exhibit asphalt-like properties i.e. time-temperature dependence and cumulative damage failure (Bocci et al. 2011, Stimilli et al. 2013, Thompson et al. 2009).

The objective of this study was to characterize the volumetric and stiffness properties of CBTM mixes, produced using different RA percentages (50%, 80% and 0%). To this aim, the influence of water content on the compactability of fresh mixes was first investigated, in order to determine the optimal moisture for compaction. Next, CBTM mixes with optimal moisture were compacted, cured and tested to measure the complex modulus E^* .

2 VOLUMETRIC PROPERTIES OF CBTM

The mechanical properties and the durability of cold-recycled mixtures are strictly related to their volumetric properties. Therefore, similar to hot mix asphalt (HMA), a thorough assessment of cold-mix volumetrics is essential, particularly in the compaction phase.

In Figure 1, the constituent materials of cold-recycled mixes produced using bituminous emulsion and cement, are stated both by mass and by volume. In the common practice, composition is specified by mass, whereas volume percentages must be calculated using the density of each material. In such a calculation, the aggregate component deserves a special attention. In fact, its composition is extremely variable because it may include RA, reclaimed aggregates from unbounded or cement-bounded layers and VA of various petrographic natures. Therefore, the average density ρ_A of the aggregate shall be calculated using the equation:

$$\rho_A = \frac{100}{\sum \frac{p_i}{\rho_i}} \quad (1)$$

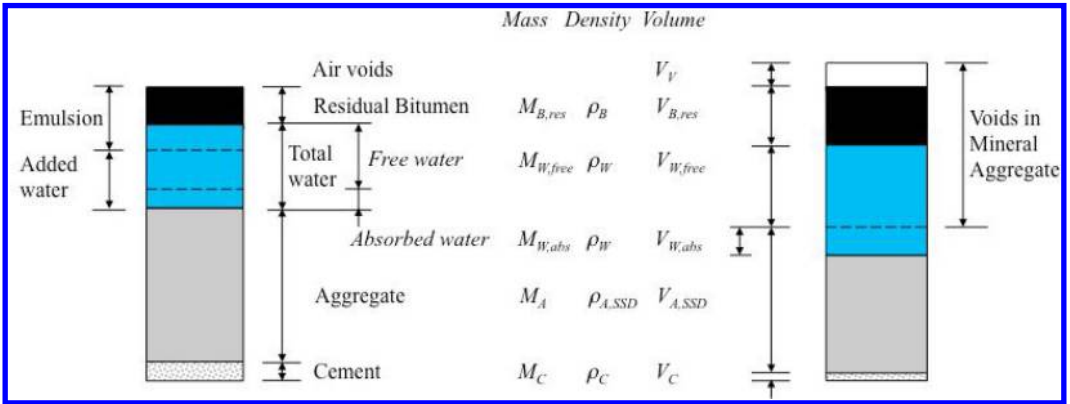


Figure 1. Constituent materials of cold-recycled mixes produced using bituminous emulsion and cement stated by mass and by volume.

where p_i represents the percentage by weight of each aggregate type and ρ_i is its density. In addition, the porosity of aggregate particles must be considered and hence the total water content of the mixture W_{tot} must be split into absorbed water W_{abs} and free water W_{free} i.e. the amount of water that actually enhances compactability by reducing internal friction. As a consequence, the saturated surface-dry density ρ_{SSD} of aggregate particles should be considered in the volumetric analysis.

In Figure 1, it is also shown that W_{tot} is the sum of the water coming from the emulsion W_{em} and additional water W_{add} added during mixing.

In the compaction phase of fresh mixtures the evolution of volumetric properties is often evaluated using the dry density ρ_d , i.e. the ratio of the total mass of solids to the total mixture volume:

$$\rho_d = \frac{M_S}{V_T} = \frac{M_A + M_C + M_{B,R}}{V_T} \quad (2)$$

where the symbols shown in Figure 1 have been used. In Equation 2, the mass of residual (fresh) bitumen from emulsion ($M_{B,res}$) is explicitly considered as part of the solids, whereas the mass of the aged binder is implicitly considered inside the aggregate mass M_A .

The use of ρ_d to evaluate compactability of CBTM mixes can be misleading when different mixture compositions need to be compared, typically for mix design. For example, comparing ρ_d of mixes having different fractions of RA and VA is not appropriate because particle densities may be considerably different. An approach based on volumetric properties, similar to HMA, appears more appropriate (Grilli et al. 2012).

Referring to the typical composition depicted in Figure 1, voids in the mineral aggregate (VMA) of a CBTM mix may be defined as:

$$VMA = \frac{V_V + V_{B,res} + V_{W,free}}{V_T} \cdot 100 \quad (3)$$

VMA is the volume percentage of space between solids particles (aggregate and cement); this space

includes: air voids, fresh bitumen and free water. VMA can be used to evaluate the degree of packing of the aggregate skeleton.

Similarly, the parameter voids in mixture V_m is the volume percentage occupied by air voids and water (i.e. the non-structural component of a cold-mix volume) and is defined as:

$$V_m = \frac{V_V + V_{W,free}}{V_T} \cdot 100 \quad (4)$$

From Equations 3 and 4 we observe that:

$$VMA = V_m + VB_{res} \quad (5)$$

where VB_{res} is the volume percentage of fresh bitumen. In addition, to evaluate the percentage of VMA occupied by water and fresh bitumen, the parameter voids filled with liquids VFL is defined as:

$$VFL = \frac{V_{B,res} + V_{W,free}}{V_V + V_{B,res} + V_{W,free}} \cdot 100 \quad (6)$$

VFL is particularly important in the compaction phase i.e. when fresh bitumen is still dispersed in small droplets inside free water. If VFL is less than 100%, the mixture contains air voids and hence is unsaturated. However, if an excessive compaction effort is applied, VFL may reach or exceed 100%. As a consequence, free water is squeezed out of the mixture together with a fraction of the dispersed fresh bitumen. Such an over-compaction clearly results in an undesirable and uneconomic change of mixture composition.

3 EXPERIMENTAL PROGRAM

Experimental activities carried out in the present study were divided into two phases. In the first phase, the influence of water content on the compactability of fresh CBTM mixes was investigated and the optimal water content for compaction was determined.

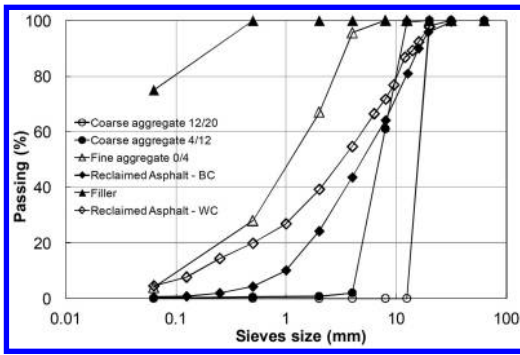


Figure 2. Grading curves of aggregates (by volume).

Table 1. Particle density and absorption of aggregates.

Designation ID	Particles Density ρ_a (Mg/m ³)	Water absorption WA ₂₄ (%)
40 RA 0/30	2.393	1.09
0/4 G _F 90	2.454	0.98
4/12 G _C 90/10	2.675	1.10
12/20 G _C 90/10	2.679	1.00
Filler	2.600	0.00

In the second phase, mixes with the optimal water content were compacted, cured and tested to measure the complex modulus E^* .

3.1 Materials and mixtures

Reclaimed asphalt, virgin aggregate, bituminous emulsion, Portland cement and water were used to prepare the CBTM mixes.

The RA was sampled from a cold in-place recycling jobsite, after milling of the aged asphalt surface layers (wearing and binder courses). Its average size distribution (“black curve”) obtained by wet sieving, is reported in Figure 2, together with the average size distribution of the extracted aggregate (“white curve”). The black curve is characterized by a continuous gradation, with a maximum dimension of 20 mm and a low content of fines, with respect to the white curve. This is typical of RA obtained from cold milling, because sand and filler form larger particles bounded by aged bitumen. The average bitumen content of RA was 4.5% by aggregate weight.

The VA was a crushed limestone; in particular, two coarse sizes (4/12, 12/20) one fine size, (0/4) and mineral filler, were employed in this study (Figure 2). Both RA and VA were also characterized in terms of particle density and absorption (Table 1).

A cationic slow-setting bituminous emulsion designated as C 60 B 6 (EN 13808) was selected in this research. The emulsion, specifically formulated for cold in-place recycling, ensures high mixing stability with cement (over-stabilized emulsion) and good workability during the compaction phase.

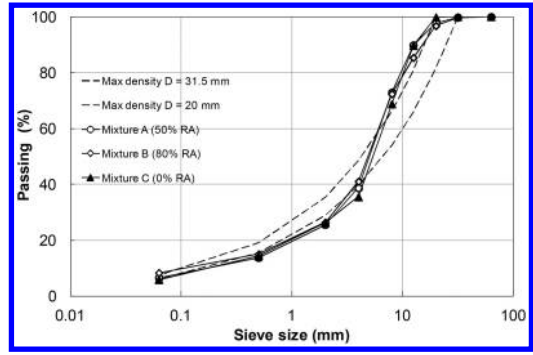


Figure 3. Grading curves of the tested mixes (by volume).

A Portland limestone cement type II/B-LL, strength class 32.5R (EN 197-1) was used. Its composition is a combination of clinker (65%–79%) and limestone dust (21%–35%).

Three mixtures with different RA content were analyzed in this study:

- Mix A: 50% RA, 50% VA;
- Mix B: 80% RA, 20% VA;
- Mix C: 0% RA, 100% VA.

Compositions similar to Mix A are often employed in cold in-place recycling projects, where bituminous layers are milled together with the underlying unbound or cement-bound foundation (Grilli et al. 2012, Bocci et al. 2014). In Mix B, the maximum RA content was used; the small fraction of fine aggregate was still necessary to meet gradation requirements, as specified below. Mix C was used as reference, to check the influence of RA on complex modulus.

For all mixes the emulsion content was 3.0%, by dry aggregate weight, corresponding to 1.8% of residual bitumen, whereas cement content was 2%, by dry aggregate weight.

Aggregate blends were adjusted using different VA sizes and dosages, in order to obtain the maximum density gradation described by the Fuller-type equation:

$$P_d = \left(\frac{d}{D} \right)^{0.45} \quad (7)$$

where P_d is the total passing the (square) sieve dimension d and D is the maximum size of the aggregate. It is highlighted that the gradation specified by equation 7 is by volume, whereas the mixture composition was specified by weight. Therefore, since RA and VA particles have different density, the gradation by volume was calculated. The grading curves of the mixtures are depicted in Figure 3, whereas the volumetric composition is summarized in Table 2, in terms of aggregate type (RA or VA) in the total aggregate and in the coarse or fine fractions. As it can be observed, the coarse fraction ($d > 4$ mm) of mixes A and B is mainly composed of RA (65.5% and 100%, respectively).

Table 2. Volumetric composition of the tested mixes.

Mixture ID (%)	Aggregate type	Fraction		
		Total (%)	Coarse (%)	Fine (%)
A (50%RA)	RA	52.7	65.5	34.0
	VA	45.7	34.5	66.0
B (80%RA)	RA	77.1	100.0	46.6
	VA	21.4	0.0	53.4
C (0%RA)	RA	0.0	0.0	0.0
	VA	98.3	100.0	100.0

3.2 Specimen preparation

Before mixing and compaction, VA and RA were oven-dried at 105°C and 40°C, respectively. The dry aggregate blend was initially mixed with a water amount corresponding to the absorption value (Table 1). To obtain homogeneous moisture, the wet aggregate blend was stored in a sealed plastic bag for 12 h, at room temperature. Afterwards, each blend was thoroughly mixed with a mechanical mixer for at least two minutes, gradually adding the remaining part of the mixing water, cement and emulsion, in this sequence. A visual evaluation was made to check for homogeneity and to verify that emulsion breaking had not taken place.

Immediately after mixing, specimens were compacted by means of a shear gyratory compactor (SGC) according to a standardized procedure (Bocci et al. 2011, Cardone et al. 2014, Grilli et al. 2012). In particular, the adopted protocol provided a 150 mm diameter mold, a constant pressure of 600 kPa, a gyration speed of 30 rpm and an angle of inclination of 1.25°.

In the first part of the experimental program, four total water contents ($W_{tot} = 3, 4, 5$ and 6% by dry aggregate weight) were selected to define the optimum water content of each mixture type. In this phase, about 4500 g of loose mixture were compacted with 180 revolutions. The compaction curves were analyzed using the volumetric approach described in Section 2.

In the second part of the experimental program, specimens for mechanical tests were prepared at the optimal water content. The mixture weight was adjusted to obtain specimens with height of 150mm and voids content $V_m = 10\%$. After compaction, specimens were cured for 7 days at 40°C and then cored to the diameter $D = 94$ mm. The curing temperature of 40°C was selected to obtain accelerated curing and to be sure that the definitive curing has been reached (Bocci et al. 2011).

3.3 Complex modulus testing

Uniaxial cyclic compression tests were performed using a servo-pneumatic testing equipment in control strain mode.

A sinusoidal (haversine) axial strain with 50 $\mu\epsilon$ amplitude (peak-to-peak) was applied at five frequencies (10, 3, 1, 0.3 and 0.1 Hz) and five temperatures (5, 15, 30, 40 and 55°C). The deformation was measured by means of two inductive transducers, fixed to



Figure 4. Cyclic compression test setup.

the lateral surface of the specimen 180° apart, with a measurement base of 70 mm (Figure 4). A total of 40 load cycles were applied at each frequency, and E^* was calculated as follows:

$$E^* = E_0 \exp(j\varphi) \quad (8a)$$

$$E_0 = \frac{\sigma_0}{\varepsilon_0} \quad (8b)$$

$$\phi = 2\pi f \Delta t \quad (8c)$$

where E_0 is the absolute value (norm) of the complex modulus, also called the stiffness (or dynamic) modulus, φ is the phase (or loss) angle, f is the test frequency (Hz), and j is the imaginary unit ($j^2 = -1$). The amplitude of the measured stress and strain signals (σ_0, ε_0) and the time lag Δt between the two signals were calculated performing a sinusoidal regression on the last ten loading cycles.

4 RESULTS AND ANALYSIS

4.1 Volumetric properties and optimal water content

In Figure 5, the SGC compaction curves obtained in the first part of the experimental program are reported. In particular, the percentage variation of the voids in mixture V_m and voids filled with liquids VFL are plotted as a function of the number of SGC gyrations. As it can be observed, for all mixtures and all water contents, V_m decreases and VFL increases. Results also showed that, increasing the RA content, mixture compactability improved. This is can be explained by the rounded shape and smooth surface texture of the reclaimed aggregate particles.

For a fixed number of gyration, an increase of water content produces a V_m decrease, indicating a reduction of the volume occupied by air voids and water. This is due to the larger water films that develop around the aggregate particles, which make it easier for them to be moved and reoriented into a denser configuration.

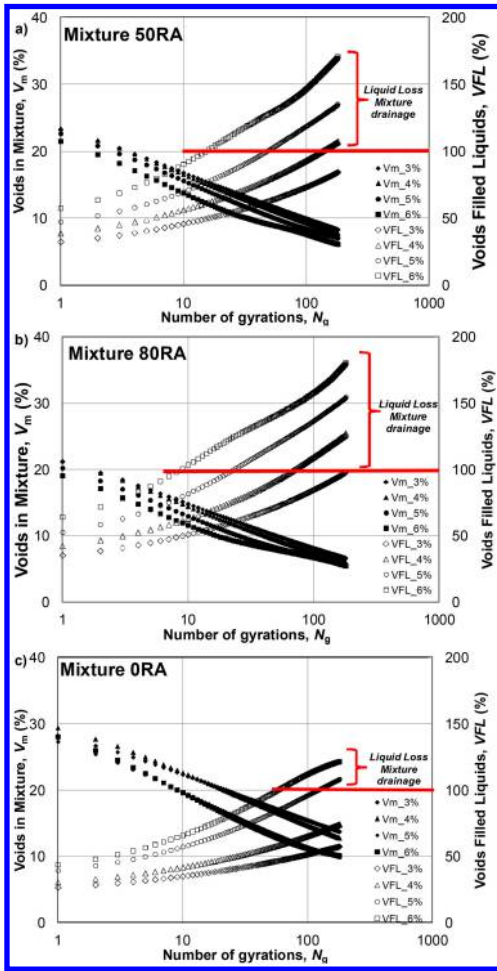


Figure 5. SGC compaction curves.

It can also be observed that, at higher water contents, the mixtures tends to reach saturation ($VFL = 100\%$) at lower number of gyrations. It is highlighted that values of $VFL > 100\%$ were calculated on the basis of the initial water content of the compacted samples. However, it can be hypothesized that further gyrations after saturation, caused liquids to be squeezed out of the mixture. This hypothesis was confirmed by visual observations of liquids draining from the top and the bottom of the mold, during the compaction process. Visual observations also suggested that the liquid lost was composed by water and fresh bitumen.

To highlight the importance of saturation, the final values of the dry density (i.e. after 180 gyrations) of all compacted specimens are reported in Figure 6, as a function of water content. In the same figure, for each mixture, the saturation curve is plotted. These curves are calculated using the equation (Lambe, 1979):

$$\rho_d = \frac{\rho_w \cdot S_r}{w + \frac{\rho_w \cdot S_r}{\rho_s}} \quad (9)$$

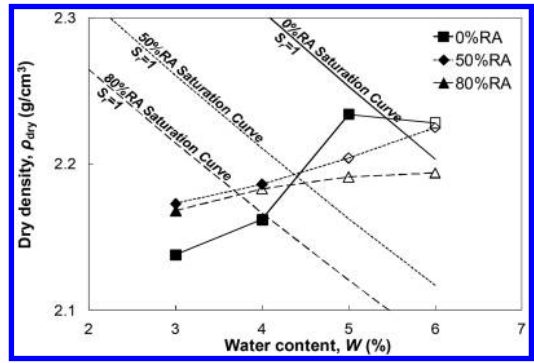


Figure 6. Dry density at 180 gyrations and saturation curves.

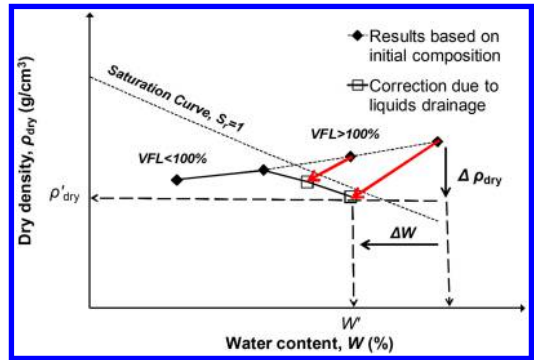


Figure 7. Dry density at 180 gyrations and saturation curves.

where ρ_w and ρ_s are the water density and the aggregate bulk density, respectively, w is the water content and S_r is the saturation degree, hypothesized equal to one ($S_r = 1$).

As previously observed, increasing water content leads to a voids reduction and hence to an increase of dry density. However, when $VFL > 100\%$, the dry density values plot to the right of the saturation curve, confirming that the initial water content is no more realistic. In these cases, the mixture composition should be corrected by fixing the limit condition $VFL = 100\%$. As shown in Figure 7, the correction brings to a reduction of both water content and dry density because both water and fresh bitumen drain from the specimens.

The compaction results were used to establish an optimal value of the total water content, based on the following criteria:

- W_{tot} should be high enough to enhance compaction, and
- W_{tot} should not lead to drainage of water and bitumen from the specimens.

According to these criteria, an optimal water content $W_{opt} = 4\%$ was chosen for mixtures A and B, whereas $W_{opt} = 5\%$ was chosen for mixture C.

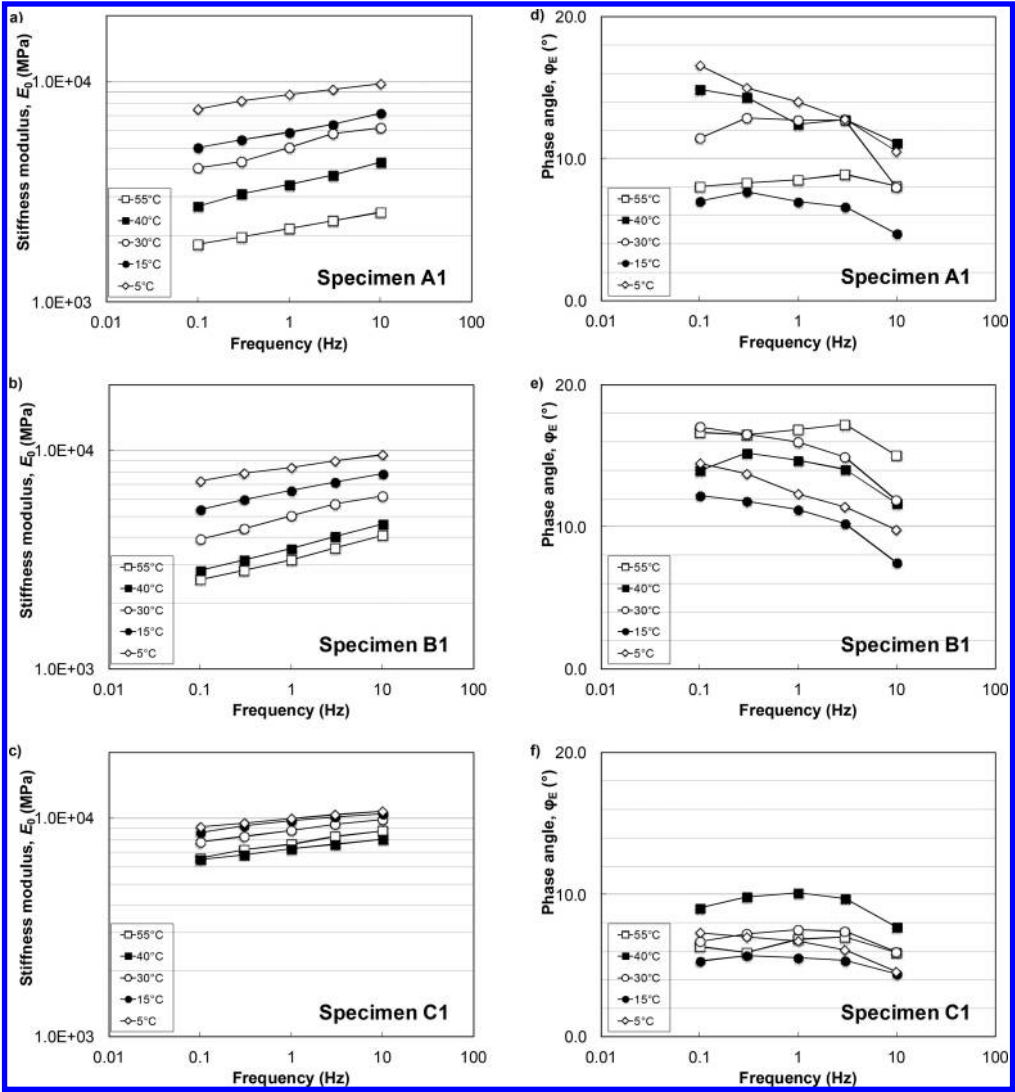


Figure 8. Isothermal curves of the stiffness modulus E_0 and phase angle φ on specimens A1, B1 and C1.

4.2 Complex modulus testing

The complex modulus E^* of the studied CBTM mixes, was measured after 7 days of curing at 40°C. The values of the stiffness modulus E_0 and phase angle φ measured on specimens A1, B1 and C1 are reported in Figure 8.

Isothermal curves at 5, 15, 30, 40 and 55°C showed an increase of E_0 with increasing test frequency and decreasing temperature (Figure 8a, b, c). The measured values ranged from 1840 MPa to 9800 MPa for specimen A1, from 2580 MPa to 9580 MPa for specimen B1 and from 6470 MPa to 10650 MPa for specimen C1.

Such an asphalt-like behavior (i.e. frequency-dependent and thermo-dependent) was particularly evident for mixes A (50%RA) and B (80%RA). In addition, different RA contents had a limited effect on the thermo-rheological response. The dependence on

Table 3. Shape parameters of the stiffness modulus master curves (reference temperature: $T_{ref} = 30^\circ\text{C}$).

Specimen ID	E_g MPa	E_e MPa	k	h	d	$\log \tau_0$
A1	13849	1443	0.14	0.30	2.22	-0.17
B1	17082	1993	0.12	0.42	2.68	-1.09
C1	12000	4500	0.18	0.45	1.35	1.12

temperature and frequency of mixture C (100%VA) was less marked.

The isothermal curves of the phase angle φ (Figure 8d, e, f) did not show a regular trend, suggesting that the viscous component of the thermo-rheological response is probably controlled by the interaction of diverse mechanical phenomena.

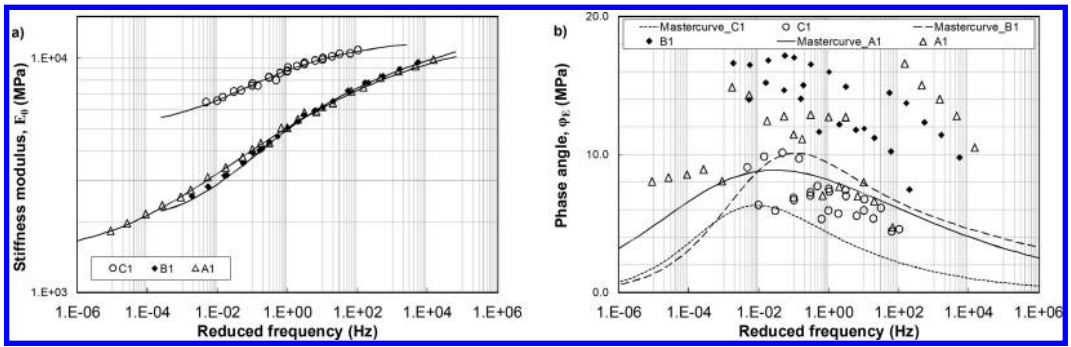


Figure 9. Master curves at 30°C of the stiffness modulus E_0 and phase angle φ .

To confirm similarities between the linear viscoelastic response of CBTM and HMA, validity of the time-temperature superposition principle (TTSP) was checked. To this aim the Huet-Sayegh rheological model was employed (Sayegh, 1967):

$$E^*(j\omega\tau) = E_e + \frac{E_g - E_e}{1 + \delta(j\omega\tau)^{-k} + (j\omega\tau)^{-h}}, \quad (10)$$

where $\omega = 2\pi f$ is the angular frequency, E_g and E_e are the glass and equilibrium moduli, respectively, τ is a characteristic time and δ , k , h are dimensionless model parameters. According to the TTSP, τ may be written as a function of the test temperature T as follows:

$$\tau(T) = a(T)\tau_{ref} \quad (11)$$

where $a(T)$ are the temperature shift factors used to describe the thermal dependence of E^* and τ_{ref} is the characteristic time at the reference temperature T_{ref} . In this study, the reference temperature selected for the master curves was $T_{ref} = 30^\circ\text{C}$.

The Huet-Sayegh model parameters and the temperature shift factors, calculated using a numerical optimization procedure, are summarized in Table 3.

Figure 9 shows the master curves of the stiffness modulus E_0 and phase angle φ , for the tested specimens. It is evident that a unique curve was obtained for E_0 , but not for φ . This indicates that the TTSP is verified for the stiffness modulus but not for the phase angle, confirming previous results on cold-recycled mixtures with similar cement/bitumen ratio (Cardone et al., 2014; Stimilli et al., 2012).

The larger dispersion of the E_0 values, which characterizes the master curves of mixes A and B (50%RA and 80%RA) with respect to mixture C (100%VA), highlighted the influence of RA content on the thermorheological response. In addition, it can be observed that the response of mixtures A and B is almost identical, whereas the response of mixture C is similar to that measured on cement-treated materials containing RA (Grilli et al., 2013). This suggests that the radical change produced by the addition of RA in CBTM mixes may not be explained only by the corresponding addition of aged binder.

A more representative explanation can be put forward considering the physical structure of CBTM

mixtures. This type of cold-recycled mixes can be represented as a skeleton of coarse aggregates bounded by bituminous and hydraulic mortars, formed by the finer aggregate particles. The coarse aggregate skeleton is formed by virgin aggregate and/or reclaimed aggregate (considered as “black rock”). The bituminous mortar is formed by the fresh bitumen, after emulsion breaking (Asphalt Academy, 2009), whereas the hydraulic mortar is formed by the hydrated cement.

In mixture C, where the skeleton is composed only by virgin aggregates, the hydraulic mortar brings to the formation of a cementitious structure similar to that of cement-treated materials. The bituminous mortar is enclosed in such a rigid structure, and its influence on the mechanical response is negligible (limited frequency and temperature dependence).

On the other hand, in mixtures A and B, the coarse aggregate is mainly composed by reclaimed asphalt. Consequently, the coarse particles, forming the skeleton of the mixture, are almost totally coated with aged bitumen; this hinders the formation of stable bonds with the hydraulic mortar. Therefore, the mechanical behavior of the mixture is controlled by the bituminous mortar, bringing to a clear dependence on temperature and frequency. This also explains the similarity between the response of mixes A and B, which contain nearly the same amount of “black rock” and bituminous mortar.

5 CONCLUSIONS

In the present study, the volumetric and thermorheological properties of cold-recycled mixtures, treated with 2% cement and 3.0% bituminous emulsion (corresponding to 1.8% fresh bitumen) were investigated. The influence of reclaimed asphalt content (0%, 50% and 80%) was evaluated.

The experimental results showed that an excessive compaction effort may cause free water to be squeezed out of the mixture together with a fraction of the dispersed fresh bitumen, modifying the initial composition of the mixtures. Therefore, the optimal water content was selected to guarantee densification and prevent liquid loss, during the compaction process.

Results also showed that, increasing reclaimed asphalt content, mixtures compactability improved, due to the shape and surface texture of the reclaimed aggregate.

The complex modulus values, highlighted that mixtures containing reclaimed asphalt exhibited an asphalt-like behavior (i.e. frequency-dependent and thermo-dependent), whereas the frequency- and thermo-dependence of the mixture containing only virgin aggregate was almost negligible.

For all reclaimed asphalt contents, validity of the time-temperature superposition principle was verified for the stiffness modulus but not for the phase angle.

Analysis of experimental results suggests that, in the mixture containing only virgin aggregate, the cementitious mortar (fine aggregate and cement) forms a rigid structure together with the coarse aggregate skeleton. This induces a mechanical behavior similar to that of cement treated materials. On the other hand, in mixtures containing reclaimed asphalt, the particles forming the coarse skeleton are almost totally coated with aged bitumen ("black rock"). This hinders the formation of stable bonds with the hydraulic mortar. In this case, the mechanical behavior is controlled by the bituminous mortar (fine aggregate and fresh bitumen), bringing to a clear dependence on temperature and frequency.

REFERENCES

- Asphalt Academy, 2009. Technical guideline (TG2): Bitumen stabilized materials (2nd ed.) *CSIR Built Environment, South Africa*, Pretoria: Asphalt Academy.
- Bocci, M., Grilli, A., Cardone, F. and Graziani A., 2011. A study on the mechanical behaviour of cement-bitumen treated materials. *International Journal of Construction and Building Materials*, 25 (2), 773–778.
- Bocci, M., Grilli, A., Cardone, F. and Ferrotti, G., 2014. Full depth reclamation for the rehabilitation of local roads: a case study. *International Journal of Pavement Engineering*, 15 (3), 191–201.
- Cardone, F., Grilli, A., Bocci, M. and Graziani A., 2014. Curing and temperature sensitivity of cement-bitumen treated materials, *International Journal of Pavement Engineering*, DOI:10.1080/10298436.2014.966710
- Grilli, A., Graziani, A. and Bocci, M., 2012. Compactability and Thermal Sensitivity of Cement-Bitumen Treated Materials. *Road Materials and Pavement Design*, 13 (4), 599–617.
- Grilli, A., Bocci, E. and Graziani A., 2013. Influence of reclaimed asphalt content on the mechanical behaviour of cement-treated mixtures. *Road Materials and Pavement Design*, 14 (3), 666–678.
- Jenkins, K.J., Long, F.M., & Ebels, L.J. 2007. Foamed bitumen mixes = shear performance? *International Journal of Pavement Engineering*, 8(2), 85–98.
- Lambe, W and R. V. Whitman (1969). *Soil Mechanics*. John Wiley.
- Sayegh G., 1967. Viscoelastic properties of bituminous mixtures. In: *Proceedings of the 2nd international conference on the structural design of asphalt pavements*. Ann Arbor, 1967
- Stimilli, A., Ferrotti, G., Graziani, A. and Canestrari, F., 2013. Performance evaluation of cold recycled mixture containing high percentage of reclaimed asphalt. *Road Materials and Pavement Design*, 14(sup.1), 149–161.
- Thompson MR, Garcia L, Carpenter SH, (2009) Cold in-place recycling and full-depth recycling with asphalt products (Report no. FHWA-ICT-09-036). *Illinois center for transportation*.

Field validation of hot-recycled porous asphalt containing 20% RAP

F. Frigio, E. Pasquini & F. Canestrari
Università Politecnica delle Marche, Ancona, Italy

ABSTRACT: The capability of reducing traffic noise and enhancing safety in wet conditions makes Porous Asphalt (PA) mixtures as one of the most common surface layers for road pavements. Thus, the use of Reclaimed Asphalt Pavement (RAP) in PA mixtures can lead to important economic and environmental benefits that should be strongly encouraged. However, most technical specifications do not allow such use of yet due to the inherent low durability and high air void content of PA mixtures. In this sense, reliable techniques allowing the use of RAP in PA mixtures are needed. In this research, the possible use of 20% of coarse fraction of RAP obtained from old PA surface layers in new PA mixtures was evaluated. A comprehensive laboratory and field study was carried out based on the construction of a full scale trial section. Results showed that recycled PA mixtures were able to outperform standard PA mixtures.

1 INTRODUCTION

Recycling of asphalt mixtures had become a priority goal for both administrations and producers due to the limited aggregate and binder supply and the increase of demand along with strict environmental regulations (De la Roche et al. 2013). The re-use of milled materials in new asphalt mixtures optimizes the use of natural resources and sustains the asphalt pavement industry since it allows considerable savings in materials, cost and energy. Thus, a technical support to evaluate any potential deterioration or improvement in performance compared with the mixtures currently used in road construction is necessary.

Nowadays, in many countries porous asphalt (PA) mixtures are extensively used as motorway surface layer due to their benefits in reducing traffic noise and improving safety during wet conditions (enhanced skid resistance and reduced spray and splash). On the other hand, porous asphalt mixtures are characterized by limited durability due to their high air void content that makes PA more susceptible to ravelling and water damage (Alvarez et al. 2011, Partl et al. 2010). As a consequence of their limited durability, maintenance processes in the motorway network are often performed on porous asphalt layers. Technical specifications adopted in many countries do not allow the use of any recycled materials in porous asphalt (PA) surface layers yet due to their inherent low durability. As a consequence, a huge amount of good quality milled material (mainly coming from old PA wearing courses) can be reused only in lower layers or must be disposed whereas, at the same time, a huge amount of natural resources needs to be used for new PA mixtures. In this sense, the re-use of reclaimed asphalt pavement (RAP) into PA should be strongly encouraged. As a matter of

fact, in recent years, considerable research concerning the use of RAP as substitute of natural aggregates in porous road surface layers has been conducted or is still on-going (Molenaar et al. 2011, Sung & Kim 2012; Fang et al. 2013).

2 OBJECTIVES

This study is part of a wider research project on hot recycling and discusses field investigations on PA mixtures including 20% RAP. A previous laboratory study suggested that 20% of selected coarse recycled aggregates would not compromise the durability of PA layers if adequate total binder content ($\geq 5.25\%$ by weight) is used (Frigio et al. 2015). This finding was attributed to the presence of still coated RAP aggregates that can better adhere to the virgin binder.

The promising results obtained on both durability and water resistance of laboratory recycled PA mixtures leads to further study on similar PA mixtures prepared in the asphalt plant during the construction of a real scale trial section along an in-service motorway (hereafter named field mixtures). In order to evaluate the durability and water susceptibility of the field mixtures, a comprehensive experimental program was carried out. The study focuses on the evaluation of durability issues as they are the main failure causes in PA (Hagos et al. 2007). In this sense, indirect tensile strength tests, particle loss (Cantabro) tests, semicircular bending (SCB) tests and repeated indirect tensile tests were carried out in both dry and wet condition to evaluate acceptability, durability, and water sensitivity of recycled mixtures. Moreover, compactability properties of the reference and the recycled PA mixtures

were compared. The construction of the trial section also allowed the field evaluation of the drainage properties of the studied materials.

3 EXPERIMENTAL PROGRAM

3.1 Materials

The aim of this study is to verify if the performance of standard PA mixtures (containing only virgin aggregates) can still be guaranteed if 20% of virgin aggregates are substituted with selected coarse RAP aggregates from old PA mixtures. In this sense, one reference PA mixture and two recycled PA mixtures prepared with 20% of RAP and different binder contents were investigated.

The reference mixture, hereafter named REF1_field, was a typical porous asphalt mixture prepared with virgin basaltic aggregates and a polymer (SBS) modified binder (5% by weight of the aggregates).

The recycled mixtures (hereafter named R20_5.25_field and R20_5.50_field) were prepared with 20% of RAP and two total binder contents (5.25% and 5.50% by the aggregates weight). RAP from milled PA surface layers were sieved so that only the 8/16 mm fraction was used in the recycled PA mixtures. The total binder content includes the virgin bitumen and the binder within the RAP which was equal to 4.0% by weight of RAP. Higher total binder contents were selected for the recycled PA mixtures to take into account that a part of the aged binder within the RAP acts as “black aggregate”.

The materials were taken from the field during the construction of a full-scale trial section as a part of an in-service motorway rehabilitation project. The mixtures were prepared at the asphalt plant according to the mix design previously developed in the laboratory (Frigio et al. 2015). Asphalt mixtures from the field were analyzed in the laboratory for determining the actual total binder content and aggregate grading curves. The materials prepared at the asphalt plant comply with acceptance requirements prescribed by Italian technical specification (ASPI 2013). Moreover, as shown in Table 1, all the aggregate grading curves strictly adhered to the composition requirements developed in the laboratory. It is also possible to notice that the recycled mixtures were characterized by almost the same grading curve (obtained after binder extraction from the produced PA mixtures) of the reference mixture without compromising volumetric properties and thus drainability.

3.2 Test program and methods

Materials taken from the asphalt plant were compacted in the laboratory using a gyratory compactor.

In order to study the compactability properties of the mixtures, the Compaction Energy Index (CEI) was evaluated. CEI was defined by Mahmoud & Bahia (2004) as the area under the gyratory compaction curve

Table 1. Field mixtures composition.

Sieve size (mm)	REF1_field Passing (%)		R20_5.25_field Passing (%)		R20_5.50_field Passing (%)	
	Design	Actual	Design	Actual	Design	Actual
20	100	100	100	100	100	100
14	91.5	88.3	93.5	91.1	93.5	91.8
10	41.3	46.9	45.9	45.9	45.9	52.8
6.3	23.9	23.8	23.4	25.0	23.4	25.1
2	15	14.3	13.6	15.0	13.6	15.3
0.5	9.1	10.0	8.9	10.7	8.9	8.9
0.25	7.5	8.0	7.3	8.4	7.3	7.2
0.063	5.3	5.7	4.8	5.3	4.8	5.1
Bitumen	5.00	4.91	5.25	5.22	5.50	5.39

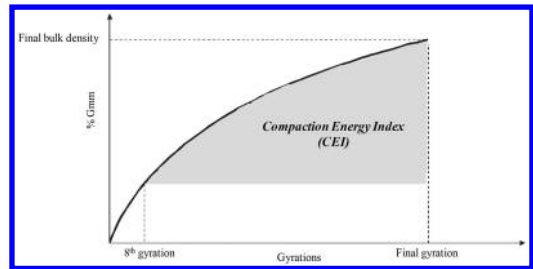


Figure 1. Compaction Energy Index results.

representing the work applied by the roller for compacting the mixture to the required density just before traffic opening (Fig. 1). In this sense, eight gyrations are generally selected to simulate the effort applied by the paver whereas, in the case of porous asphalt mixtures according to Goh & You (2012), CEI can be calculated from the whole compaction curve until a density of about 80% of the maximum specific gravity (G_{mm}) is reached. Asphalt mixtures with lower value of CEI are desired since they have better compaction properties (Mahmoud & Bahia 2004).

The mixtures were also evaluated in terms of mechanical properties and water sensitivity. In order to simulate water damage, specimens of each mixture were conditioned in air (dry) or in water (wet) at 40°C for a period of 72 h, as suggested by EN 12697-12 (Method A). Indirect tensile strength (ITS) tests, particle loss (Cantabro) tests and semi-circular bending (SCB) tests were carried out in both dry and wet conditions. Repeated indirect tensile tests were also performed in submerged condition with specimens fully immersed in water throughout tests in order to simulate real field conditions.

Finally, pavement drainability was measured in the field in order to evaluate if recycled PA surfaces are comparable to the reference PA surface and complies the technical specifications.

The overall experimental program is summarized in Table 2.

The indirect tensile tests were carried out at 25°C. According to the Italian technical specifications,

Table 2. Experimental program.

Type of test	Test condition	Test repetitions		
		REF1 _field	R20_5.25 _field	R20_5.50 _field
ITS	dry	4	4	4
	wet	4	4	4
Cantabro	dry	4	4	4
	wet	4	4	4
SCB	dry	4	4	4
	wet	4	4	4
Repeated indirect tensile	dry	3	3	3
	wet	3	3	3
	submerged	3	3	3
In situ drainability		6	6	6

(ASPI 2013) a diametrical line load is applied by imposing a constant deformation rate of 25 mm/min until the maximum failure strength (Indirect Tensile Strength ITS) is reached.

Cantabro tests were performed at 25°C in accordance with EN 12697-17. The Cantabro test consists in subjecting an asphalt concrete sample to 300 revolutions (30 revolutions/minute) inside the Los Angeles machine drum without any metal balls. The mass loss of the specimen at the end of the test gives a measure of the resistance to ravelling, by estimating the aggregate-binder bonding properties (Gubler et al. 2005).

Semi-circular bending tests (EN 12697-44) were carried out at 10°C. The experimental procedure consists in applying a three-point bending load to a half cylindrical specimen (cut from gyratory compacted samples with a diameter of 150 mm) having a central artificial notch. The test is conducted at a constant vertical deformation rate of 5 mm/min; load and vertical deformation are recorded continuously. Results are expressed in terms of fracture toughness and fracture energy (Mobasher et al. 1997; Li & Marasteanu 2010; Biligiri et al. 2012; Frigio et al. 2013).

Repeated indirect tensile tests were performed for the estimation of the fracture aptitude. According to the standard BS DD ABE, tests were carried out in controlled stress mode at a temperature of 20°C. In this test a load pulse along the vertical diameter of the test specimen with a peak load of 300 kPa is applied; the time for applying the load from zero to peak load (rise-time) is equal to 124 ms and the pulse repetition period (time between two consecutive load pulses) is equal to 1.5 seconds. The failure was defined when complete fracture of specimens was obtained. Tests were carried out under three different conditions: dry, wet condition (specimens kept in a water bath at 40°C for 72 h and tested in dry condition at 20°C) and submerged (specimens maintained in a water bath at 40°C for 72 h and tested at 20°C completely submerged in a water bath). For a reliable evaluation of the performance reduction due to water damage, the specimens of each mixture

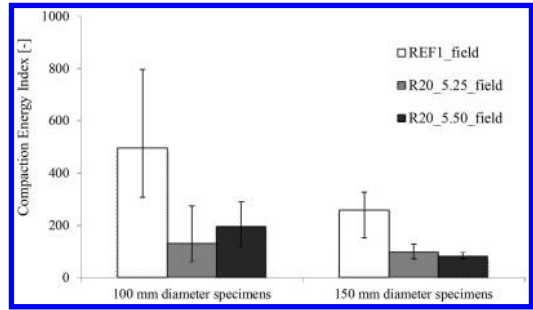


Figure 2. Compaction Energy Index results.

had been preliminarily divided into three classes characterized by homogeneous stiffness to be tested in the three different conditions.

Surface drainability was measured in the field using the outflow time test method according to the Italian technical specifications (ASPI 2013). The test consists in placing a cylindrical container of known volume, called permeameter, above the pavement before sealing the outer part of the pavement (out of the tested area) and the bottom of the permeameter in order to avoid any lateral leaking of water. Then, the permeameter is filled with water and the time of a fixed decrease of water volume (3.85 litres) is recorded. This time is governed by the water seepage through an annular area of the pavement layer under standardized hydraulic head conditions. In this study, a permeameter with an internal diameter of 140 mm and a maximum capacity of 6 litres water has been used. The drainage capability of the tested surface was expressed as the ratio between the known volume of water and the corresponding outflow time (l/min).

4 RESULTS AND ANALYSIS

4.1 Compactability

Compactability of reference and recycled PA mixtures was investigated by means of CEI values.

Results are obtained as the average of eight repetitions for 100 mm diameter specimens and as the average of four repetitions for 150 mm diameter specimens. Figure 2 shows the mean results for both reference and recycled PA mixtures along with the corresponding error bars reporting the minimum and the maximum value for each test condition.

Results show a significant decrease in CEI value for the recycled PA mixtures compared to the reference one, in case of both 100 mm and 150 mm diameter. Such outcome suggests that recycled PA mixtures can be compacted easily than the reference one and this can be attributed to the higher total binder content of the recycled mixtures. Moreover, the presence of pre-coated RAP aggregates tends to reduce the inter-granular friction helping the compaction of the recycled PA mixtures.

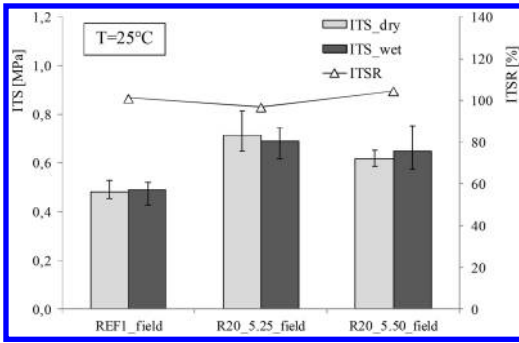


Figure 3. ITS mean test results.

4.2 ITS test

Indirect tensile test results in both dry and wet conditions are given in Figure 3 in terms of mean Indirect Tensile Strength (ITS) and Indirect Tensile Strength Ratio (ITSR) defined as:

$$ITSR = \frac{ITS_{wet}}{ITS_{dry}} * 100 \quad (1)$$

In Figure 3 the error bars representing the minimum and maximum values are also reported for each testing condition.

Results showed that all mixtures satisfied acceptance requirements prescribed in dry conditions by Italian technical specification (ASPI 2013) for PA mixtures in motorway pavements ($ITS \geq 0.40$ MPa). Moreover, the recycled porous asphalt mixtures provided higher performance than the reference mixture in both dry and wet conditions, confirming previous studies (Goh & You 2012, Frigio et al., 2013, Frigio et al., 2014).

In fact, the presence of still coated RAP aggregates allows better adhesion properties within the mixture improving performance under indirect tensile configuration tests.

As far as moisture susceptibility is concerned, results showed that recycled PA mixtures can perform as well as the reference one, demonstrating comparable water sensitivity characterized by high values of ITSR ($\approx 100\%$).

4.3 Cantabro test

Mean Cantabro test results for both dry and wet conditions are shown in Figure 4 in terms of particle loss percentage (the error bars indicate the minimum and the maximum value for each testing condition) along with the corresponding mean air void content. All studied mixtures demonstrated good performance in terms of ravelling in both dry and wet conditions as the results were consistent with international requirements for high traffic highways corresponds to a maximum of 20% and 35% loss in dry and wet conditions, respectively (Alvarez et al. 2010).

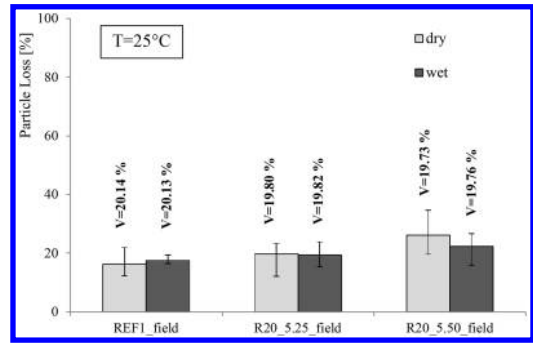


Figure 4. Cantabro mean test results.

Moreover, results measured on reference and recycled mixtures can be considered fully comparable and, thus, it can be asserted that the particle bonding of PA mixtures is not compromised due to the presence of RAP aggregates.

However, it is worth noting that the recycled PA mixture with higher total binder content (R20_5.50_field) exhibited slightly higher particle loss than the reference mixture in both dry and wet conditions, even if specimens were characterized by similar air void contents.

On the other hand, reference mixture experienced water damage (even if minor) whereas both recycled mixtures demonstrated the same performance even after the wet conditioning. According to previous study (Frigio et al. 2013), the presence of coated RAP aggregates tends to improve the aggregate-binder bonding, ensuring enhanced water resistance properties. Thus, as far as water sensitivity is concerned, the ability to preserve ravelling resistance after a wet conditioning is not affected by the presence of RAP aggregates in the mixture confirming the positive results obtained in the case of laboratory mixtures (Frigio et al. 2015).

4.4 Fracture properties – SCB test

Semi-circular bending (SCB) tests allowed the evaluation of the crack propagation aptitude in relation to the presence of recycled material in the PA.

During the test, the crack starts to propagate from the tip of the artificial notch where the concentration of the stresses is highest; then the crack tends to propagate in the direction of the applied load.

The results of this test allow the calculation of the maximum stress at failure σ_{max} (N/mm²), as defined in Eq. (2):

$$\sigma_{max} = \frac{4.263 * F_{max}}{D * t} \quad (2)$$

where F_{max} is the maximum force (N), D is the specimen diameter (mm), t is the specimen thickness (mm).

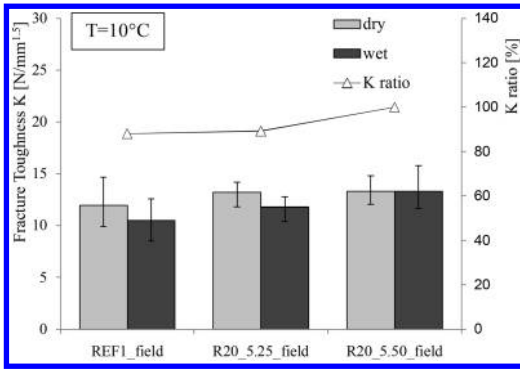


Figure 5. SCB mean test results in terms of fracture toughness.

According to EN 12697-44, the fracture toughness K ($\text{N}/\text{mm}^{1.5}$) was calculated as defined in Eq. (3):

$$K = \sigma_{\max} * f\left(\frac{a}{W}\right) \quad (3)$$

where a is the notch depth (mm), $f(a/W)$ is a geometric factor and W is the specimen height (mm).

The mean values of fracture toughness K for all the mixtures in both dry and wet conditions are shown in Figure 5 along with the water sensitivity parameter calculated as the ratio between K_{wet} and K_{dry} . Recycled mixtures showed slightly higher resistance to crack propagation than the reference mixture in both dry and wet condition, meaning that the presence of RAP aggregates tends to stiff the material. Moreover, the water sensitivity was found to be fully comparable between mixtures meaning that the presence of RAP does not affect the ability of PA mixtures to resist to water damage.

Furthermore, results were also analyzed in terms of total fracture energy G (Fig. 6), determined as the whole area under the load-displacement curve normalized with respect the area of ligament (Khalid and Monney 2009; Frigio et al. 2013). The parameter G (kJ/m^2) represents the work required to increase the fractured surface until complete failure, and it is calculated as defined in Eq. (4):

$$G = \frac{\int F * ds}{t * (W - a)} \quad (4)$$

where $\int F * ds$ is the area under the whole load-displacement curve.

The mean values of fracture energy G for all the mixtures in both dry and wet conditions are shown in Figure 7 along with the water sensitivity parameter calculated as the ratio between G_{wet} and G_{dry} . Recycled mixtures exhibited a decrease in fracture energy with respect to the reference one in both dry and wet condition, meaning that the presence of RAP leads to more brittle materials. The fracture energy for the recycled mixtures tends to increase with the binder content according to Biligiri et al. (2012). Similarly

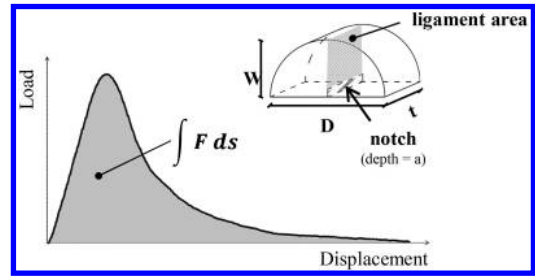


Figure 6. Fracture Energy.

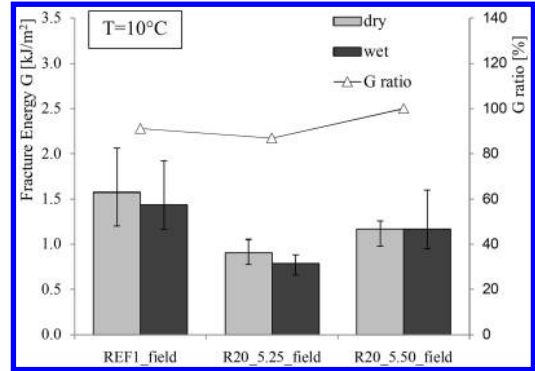


Figure 7. SCB mean test results in terms of fracture energy.

to the analysis of the fracture toughness, the water sensitivity in terms of fracture energy was taken into account through G_{ratio} parameter defined as the ratio between G_{wet} and G_{dry} . Both recycled PA mixtures showed similar water sensitivity with respect of the reference mixture.

4.5 Repeated indirect tensile test

Repeated indirect tensile tests were performed in order to investigate the water resistance of the mixtures similarly to what proposed by Kim and Coree (2005). It is well known that, in the field, asphalt pavements experience water damage only under repeated traffic loading and when they are saturated. Thus, in order to simulate closely real field condition, the specimens tested in submerged conditions were immersed in water throughout test: in this way the saturated sample is repeatedly loaded and water can inhaled into and exhaled from the sample at each load application (Poulikakos & Partl 2009).

The number of pulses at failure was taken into account for each specimen; the average data, along with error bars reporting the minimum and the maximum value obtained, are reported in Figure 8 for all the mixtures and testing conditions (i.e. dry conditioning and dry test, wet conditioning and dry test, wet conditioning and submerged test). First of all, it is interesting to notice that the water conditioning (both wet and submerged conditions) does not seem to significantly affect the performance of the PA mixtures.

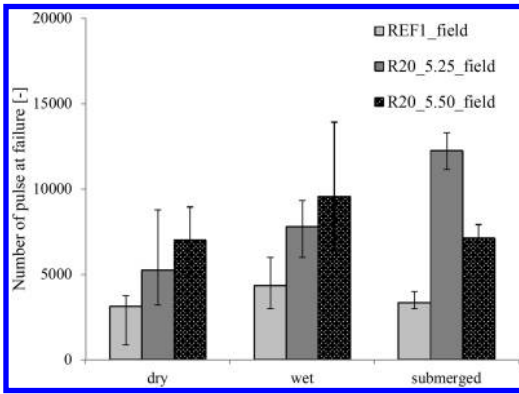


Figure 8. Repeated indirect tensile mean test results.

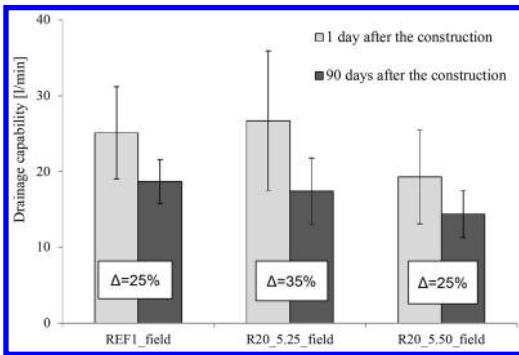


Figure 9. Drainability test results.

Both the recycled PA mixtures demonstrated to outperform the reference mixture for all tested conditions, meaning that the presence of RAP aggregates is able to improve the PA mixtures performance under repeated loading cycles. Moreover, the performance of recycled PA mixtures tends to improve as the total binder content increases, with the exception of the submerged condition case: the mixture R20_5.50_field showed a decrease in performance with respect of R20_5.25_field in submerged condition, still ensuring better results than the reference mixture.

4.6 Field drainability test

Drainage properties of the studied PA mixtures were evaluated in the field. The first measurements were taken 1 day after the construction of the full-scale trial section (before traffic opening) whereas the second measurements were taken 90 days after the construction in order to investigate the evolution in drainage performance.

Mean results in terms of drainage capability are given in Figure 9; each value is the average of six measurements spaced 50 meters apart. The percentage loss in drainage capability (Δ) due to post compaction and traffic loads is also given in Figure 9.

Results showed that all mixtures satisfied acceptance requirements prescribed by Italian technical specification (ASPI 2013) for PA mixtures in motorway pavements in terms of drainage capability measured within 14 days after the construction (drainage capability = $10 \div 25$ l/min). Moreover, only the recycled mixture with high total binder content (R20_5.50_field) showed a slight decrease in drainage capability with respect to the reference mixture both in terms of the measurements taken 1 day and 90 days after the construction.

As far as percentage loss is concerned, results were fully comparable for all mixtures demonstrating that the drainage evolution was not affected by the presence of RAP aggregates within PA mixtures and the results are within the limits even after 90 days.

4.7 Comparison with laboratory mixtures

As already specified, field mixtures were prepared according to the mix design defined in the laboratory during the previous phase of the research (Frigio et al. 2015). Thus, it is interesting to compare the performance of laboratory mixtures with those of the corresponding field mixtures. Main results are reported in Table 3 and Table 4.

It is interesting to notice that results were fully comparable, meaning that the laboratory research phase was representative of the real plant conditions and the selected mix design was accurate. Moreover, results showed that, generally, field mixtures were able to perform better than the corresponding laboratory ones, in both dry and wet conditions. In particular, results of repeated indirect tensile tests performed in dry, wet and submerged conditions are reported in Figure 10 for all laboratory and field mixtures. Field and laboratory reference mixtures showed comparable performance in all test conditions whereas significant differences in response can be observed for the recycled mixtures. In fact, both field recycled PA mixtures demonstrated enhanced performance with respect to the laboratory ones in all tested conditions. Analogous outcome can be noticed for the indirect tensile test results (ITS in Table 3 and 4), where both field recycled mixtures (R20_5.25_field and R20_5.50_field) showed better performance than the corresponding laboratory mixtures (R20_5.25_lab and R20_5.50_lab) whereas the field reference mixture (REF1_field) results even penalized with respect to the laboratory one (REF1_lab).

Those encouraging results suggest that the production of such delicate mixtures is possible even in large scale if an accurate mix design is performed.

4.8 Comparison among different field mixtures

Previous research studies concerning recycled porous asphalt mixtures were carried through both laboratory and field evaluations with the aim of investigate the effect of 15% of selected RAP from old PA surface layers on new PA mixtures (Frigio et al. 2013, Frigio

Table 3. Laboratory vs field mixes test results in dry condition.

Mixtures	ITS [MPa]	PL [%]	K [N/mm ^{1.5}]	G [kJ/m ²]
REF1_lab	0.58	36.26	10.22	1.42
R20_5.25_lab	0.56	28.04	10.33	0.95
R20_5.50_lab	0.53	22.20	14.51	0.88
REF1_field	0.48	16.33	11.92	1.57
R20_5.25_field	0.71	19.73	13.20	0.91
R20_5.50_field	0.62	26.16	13.29	1.17

Table 4. Laboratory vs field mixes test results in wet condition.

Mixtures	ITS [MPa]	PL [%]	K [N/mm ^{1.5}]	G [kJ/m ²]
REF1_lab	0.56	35.23	8.20	0.78
R20_5.25_lab	0.63	38.85	12.03	0.84
R20_5.50_lab	0.57	21.52	14.44	0.77
REF1_field	0.49	17.56	13.95	0.86
R20_5.25_field	0.69	19.39	10.50	1.43
R20_5.50_field	0.65	22.31	11.79	0.79

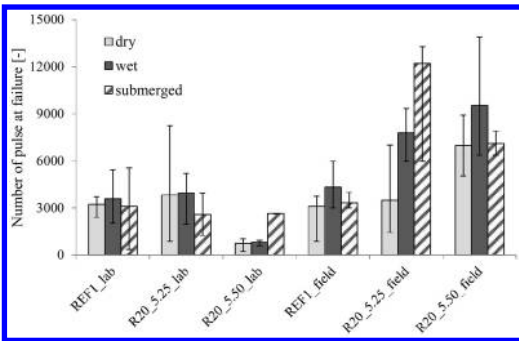


Figure 10. Repeated indirect tensile test results for laboratory and field mixes.

et al. 2014). Such investigations led to the mix design optimization of such recycled PA mixtures and the construction of a full-scale trial section.

Since the materials taken from asphalt plant during the construction of the previous and the present trial sections were subjected to the same experimental program, it is interesting to compare the performance of the two types of field mixtures including different amount of RAP (15% and 20%) and total binder contents. In particular, during the previous study three PA mixtures were prepared: one reference mixture including only virgin aggregates and 5.00% of binder content by aggregate weight (hereafter named REF2_field) and two PA mixtures including 15% of selected RAP aggregates and two total binder contents equal to 5.00% and 5.25% by aggregate weight (hereafter named R15_5.00_field and R15_5.25_field, respectively).

Table 5. Field mixes test results in dry condition.

Mixtures	ITS [MPa]	PL [%]	K [N/mm ^{1.5}]	G [kJ/m ²]
REF1_field	0.48	16.33	11.92	1.57
R20_5.25_field	0.71	19.73	13.20	0.91
R20_5.50_field	0.62	26.16	13.29	1.17
REF2_field	0.42	11.66	11.14	1.31
R15_5.00_field	0.44	21.32	12.87	1.25
R15_5.25_field	0.53	10.16	11.25	1.49

Table 6. Field mixes test results in wet condition.

Mixtures	ITS [MPa]	PL [%]	K [N/mm ^{1.5}]	G [kJ/m ²]
REF1_field	0.49	17.56	13.95	0.86
R20_5.25_field	0.69	19.39	10.50	1.43
R20_5.50_field	0.65	22.31	11.79	0.79
REF2_field	0.42	16.43	8.68	1.27
R15_5.00_field	0.44	19.29	12.04	1.33
R15_5.25_field	0.55	14.00	10.38	1.34

It is interesting to notice that, as the RAP content in the mixture increases, the optimum total binder content was found to increase as well since a larger amount of total binder is composed of aged binder within RAP whose prominent part acts as “black aggregate”.

Results of all field mixtures are reported in Table 5 and 6 as well as in Figure 11. The two types of field mixtures demonstrated comparable performance both in case of reference and recycled mixtures. In particular, field mixtures including 20% of RAP showed improved performance in terms of indirect tensile strength and repeated indirect tensile failure. Such outcome can be attributed to the higher presence of coated RAP aggregates that tends to improve adhesion properties within mixtures, as shown by previous results (Frigio et al. 2013).

Moreover, drainage capability measurements taken 1 day after the construction of both trial sections are given in Table 7. The results were found to be fully comparable and, in both cases, drainage properties exceeded the acceptance requirement prescribed by Italian technical specification (ASPI 2013) for PA mixtures in motorway pavements. All experimental results demonstrated that the partial substitution of virgin aggregates with different amount of selected RAP aggregates in PA mixtures is possible and guarantee improved performance with respect to the virgin PA mixture, if an accurate mix design is performed.

5 CONCLUSIONS

This paper presents an experimental study focused on the usability of selected reclaimed asphalt pavement (RAP) into porous asphalt (PA) mixtures. Only coarse RAP aggregates (8/16 mm) obtained by milling old PA

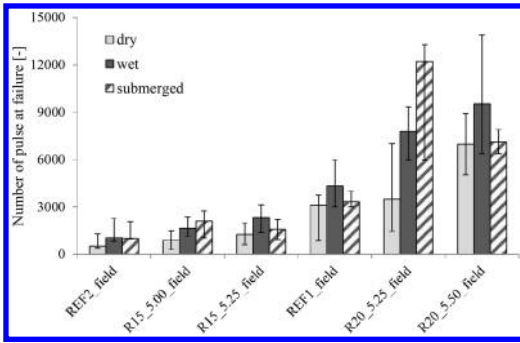


Figure 11. Repeated indirect tensile test results for field mixes.

Table 7. Drainability properties of field mixtures.

Mixtures	Drainage capability [l/min]
REF1_field	25
R20_5.25_field	27
R20_5.50_field	19
REF2_field	29
R15_5.00_field	31
R15_5.25_field	30

surface layers were used at a rate of 20% of the total aggregate weight.

In this sense, one reference mixture (without RAP) and two recycled mixtures prepared with different total binder contents (5.25% and 5.50% by aggregate weight) were investigated. All mixtures were prepared at the asphalt plant during the construction of a full-scale trial section along an in-service motorway in order to verify the performance of “real” mixtures. Such mixtures were prepared according to the laboratory mix design defined in a previous phase of the research and with the same materials.

A comprehensive laboratory experimental program for investigating acceptability, compactability, durability, fracture resistance and water sensitivity was carried out along with the in situ monitoring of drainage properties.

The following main conclusions can be drawn:

- recycled PA mixtures demonstrated better compactability properties than the reference mixture in terms of Compaction Energy Index;
- recycled mixtures were able to satisfy acceptance requirements typically prescribed by technical specification for PA mixtures in terms of indirect tensile strength (ITS);
- recycled PA mixtures provided higher performance in terms of ITS with respect to the reference mixture in both dry and wet conditions and similar water sensitivity (Indirect Tensile Strength Ratio – ITS_R);
- Cantabro test results showed that the presence of recycled aggregates does not sensibly affect the

resistance to ravelling (binder-aggregates bonding properties) and water susceptibility of the PA mixtures;

- recycled PA mixtures were characterized by similar or even enhanced crack resistance potential but lower fracture energy properties. Such effect on fracture energy tends to reduce as the binder content within recycled mixtures increases. Moreover the water sensitivity was found to be fully comparable between mixtures meaning that the presence of RAP does not affect the ability of PA mixtures to resist to water damage;
- results in terms of repeated indirect tensile tests showed that both recycled PA mixtures demonstrated to perform better than the reference mixture for all tested conditions;
- all mixtures satisfied acceptance requirements for PA mixtures in motorway pavements in terms of drainage capability. Moreover, the drainage evolution due to post compaction and traffic loads was not affected by the presence of RAP aggregates within PA mixtures.

In conclusion, the overall experimental results confirmed that including 20% of coarse recycled aggregates in porous asphalt mixtures does not compromise performance and durability of the PA layers if an adequate binder content is selected.

Moreover, the results were compared with those of previous research studies regarding laboratory PA mixtures including the same amount of RAP aggregates and total binder contents, demonstrating that the laboratory research phase was representative of the real plant conditions and the selected mix design was accurate. Generally, the field mixtures outperformed the corresponding laboratory ones, suggesting that the production of such delicate mixtures is possible even in large scale if an accurate mix design is performed.

Finally, the comparison with previous field PA mixtures including 15% of coarse RAP was carried out. The overall performance were found to be comparable; enhanced results obtained for field mixtures including 20% of RAP in terms of indirect tensile configuration tests suggested that the higher presence of coated RAP aggregates improves adhesion properties within mixtures, confirming previous studies.

ACKNOWLEDGEMENTS

This research was sponsored by Pavimental SpA. This support is greatly acknowledged. Data analysis and opinions are those of the authors and do not necessarily reflect those of the sponsoring agency.

REFERENCES

- Alvarez, A.E., Martin, A.E., Estakhri, C. & Izzo, R. 2010. Evaluation of durability tests for permeable friction course mixtures. *International Journal of Pavement Engineering* 11(1): 49–60.

- Alvarez, A.E., Martin, A.E. & Estakhri, C. 2011. A review of mix design and evaluation research for permeable friction course mixtures. *Construction and Building Materials* 25:1159–66.
- ASPI (Autostrade per l'Italia). 2013. Technical specifications for road pavements. Rome, Italy.
- Biligiri, K.P., Said, S. & Hakim, H. 2012. Asphalt mixtures' crack propagation assessment using semi-circular bending tests. *International Journal of Pavement Research and Technology* 5(4), 209–217.
- De La Roche, C., van de Ven, M., Planche, J.P., Ven den bergh, W., Grenfell, J., Gabet, T., Mouillett, V., Porot, L., Farcas, F. & Ruot, C. 2013. Hot Recycling of Bituminous Mixtures. *Advances in Interlaboratory Testing and Evaluation of Bituminous Materials RILEM State-of-the-Art Report*: 361–428.
- Fang, F.T., Chong, Y.C., Nyunt, T.T & Loi, S.S. 2013. Development of environmentally sustainable pavement mix. *International Journal of Pavement Research and Technology* 6 (4): 440–446.
- Frigio, F., Pasquini, E., Ferrotti, G. & Canestrari, F. 2013. Improved durability of recycled porous asphalt. *Construction and Building Materials* 48: 755–763.
- Frigio, F., Pasquini, E. & Canestrari, F. 2014a. Laboratory Study to Evaluate the Influence of Reclaimed Asphalt Content on Performance of Recycled Porous Asphalt. *Journal of Testing and Evaluation*. DOI:10.1520/JTE20140024
- Frigio, F., Pasquini, E., Parl, M.N. & Canestrari, F. 2014b. Use of Reclaimed Asphalt in Porous Asphalt Mixtures: Laboratory and Field Evaluations. *Journal of Materials in civil Engineering*. DOI:10.1061/(ASCE)MT.1943-5533.0001182
- Goh, S.W. & You, Z. 2012. Mechanical properties of porous asphalt pavement materials with warm mix asphalt and RAP. *Journal of Transportation Engineering* 133(1): 90–97.
- Gubler, R., Partl, M.N., Canestrari, F. & Grilli, A. 2005. Influence of water and temperature on mechanical properties of selected asphalt pavements. *Materials and Structure* 38(279), 523–532.
- Hagos, E.T., Molenaar, A.A.A. & Van de Ven, M.F.C. Voskuilen, J.L.M. 2007. Durability Related Investigation into Porous Asphalt. *International Conference on Advanced Characterisation of Pavement and Soil Engineering Materials*. Athens, 20–22 June 2007.
- Khalid, H. A. & Monney, O.K. 2009. Moisture damage potential of cold asphalt. *International Journal of Pavement Engineering* 10(5): 311–318.
- Kim, S. & Coree, B.J. 2005. Evaluation of Hot Mix Asphalt Moisture Sensitivity Using the Nottingham Asphalt Test Equipment. Final Report. *Center for Transportation Research and Education, Department of Civil, Construction, and Environmental Engineering*. Iowa State University.
- Li, X.J. & Marasteanu, M.O. 2010. Using semi-circular bending test to evaluate low temperature fracture resistance for asphalt concrete. *Experimental Mechanics* 50(7): 867–876.
- Mahmoud, A.F.F. & Bahia, H.U. 2004. Using the gyratory compactor to measure mechanical stability of asphalt mixtures. *Wisconsin Highway Research Program* 05-02.
- Mobasher, B., Mamlouk, M.S. & Lin, H.M. 1997. Evaluation of crack propagation properties of asphalt mixtures. *Journal of Transportation Engineering* 123 (5): 405–413.
- Molenaar, A.A.A., Mohajeri, M. & van de Ven, M.F.C. 2011. Design of Recycled Asphalt. *Proceeding of the APA's 14th International Flexible Pavement Conference*. Australia: Sydney.
- Partl, M.N., Pasquini, E., Canestrari, F. & Virgili, A. 2010. Analysis of water and thermal sensitivity of open graded asphalt rubber mixtures. *Construction and Building Materials* 24:283–91.
- Poulikakos, L.D. & Partl, M.N. 2009. Evaluation of moisture susceptibility of porous asphalt concrete using water submersion fatigue tests. *Construction and Building Materials* 25: 3475–3484.
- Sung, C.Y. & Kim, Y.I. 2012. Void Ratio and Durability Properties of Porous Polymer Concrete Using Recycled Aggregate with Binder Contents for Permeability Pavement. *Journal of Applied Polymer Science* 126: 338–348.

Performance evaluation of hot recycled mixtures containing SBS modified binder

A. Stimilli, G. Ferrotti, D. Radicioni & F. Canestrari

Università Politecnica delle Marche, Ancona, Italy

ABSTRACT: Over the last decades, Reclaimed Asphalt Pavement (RAP) has become one of the most recycled materials. Currently, RAP is mainly used for unbound layers, without exploiting the replacement of a portion of the more expensive virgin binder. Moreover, the increasing quantity of RAP which includes aged modified binders complicates material analysis. This paper presents a laboratory mechanical investigation on hot recycled mixtures prepared with RAP including aged Styrene-Butadiene-Styrene (SBS) modified binder. A reference mixture with 25% RAP and four mixtures with 40% RAP were investigated. Two total binder contents and two virgin SBS modified binders were used to produce mixtures with 40% RAP, which were designed using the Bailey method. Compactibility, stiffness properties, cracking and rutting resistance were evaluated on laboratory compacted specimens. Results suggest that amounts of RAP up to 40% are suitable for the production of new bituminous materials, when a specific and detailed mix design is performed.

1 INTRODUCTION

Over the last decades, the interest of agencies and contractors in adopting pavement recycling strategies has grown because of the constant rising of raw material and transport costs. In fact, replacing a portion of aggregate and virgin binder with Reclaimed Asphalt Pavement (RAP) leads to significant economic savings. In addition, important environmental benefits such as reduced pollution, lower demand for non-renewable resources and less landfill space for the disposal of milled materials can be achieved (West et al. 2013, Zaumanis & Mallick 2015).

Although the considerable advantages, some negative aspects (e.g. oxidation of reclaimed binder, variability in aggregate gradation, undefined degree of blending between virgin and aged binder) still discourage the use of high amount of RAP in new asphalt pavements.

Several studies (Apeageyi et al. 2011, West et al. 2009, Li et al. 2008) that investigated the effects of RAP on asphalt concrete in terms of mechanical performance showed that low RAP contents (up to 15%) have negligible effects on mechanical properties, whereas higher amounts of RAP could cause a marked decrease in performance (McDaniel et al. 2000). However, some researchers indicated that proper mix design and RAP material processing, as well as the use of softer virgin binders, can ensure high-quality and long lasting mixtures even with high RAP percentages (Aurangzeb et al. 2012, Tran et al. 2012, Al-Qadi et al. 2012, de la Roche et al. 2012). Another important factor, not deeply investigated so far in the

literature, is the use of increasing quantity of RAP which includes modified binder. The presence of aged polymers can significantly affect the interaction with the virgin binder and, consequently, the mechanical performance of the mixture (Stimilli et al. 2014). Therefore, this aspect further complicates the analysis and deserves more investigation. Recent studies on Porous Asphalt (PA) mixtures have shown promising results in terms of recycling of RAP containing SBS polymer modified binder (Frigio et al. 2013, Frigio et al. 2014).

Given this background, in this study a dense graded mixture including 25% of unfractionated RAP, currently employed as binder course of Italian motorways, was adopted as reference material in order to compare the mechanical performance of four mixtures produced with 40% of RAP. The latter were characterized by different total binder content (virgin binder and aged binder from RAP) and type of virgin binder (i.e. different level of polymer modification). Their aggregate grading curve was optimized by using the Bailey method (Vavrik et al. 2002) as a tool to achieve improved volumetric properties and aggregate gradation, even including high amount of reclaimed material.

Concurrently, in order to obtain a better control of the grading curve, two RAP fractions (coarse and fine) were employed in the production of 40% RAP mixtures. In all cases, the RAP contained aged Styrene-Butadiene-Styrene (SBS) polymer modified binder.

The main objective of this research investigation was to evaluate the effects caused by 40% RAP content

on the mechanical performance of hot recycled mixtures, analyzing the effects due to the use of different virgin polymer modified binders. For this purpose, a complete mechanical characterization was carried out on laboratory compacted specimens. The main properties of the mixtures related to the most common distresses underwent by asphalt binder courses were investigated with a wide set of performance-based tests. Moreover, an image analysis tool was adopted to evaluate the aggregate packing and its influence on the overall mixtures performance.

2 EXPERIMENTAL PROGRAM

Four dense graded mixtures containing high RAP percentages were investigated. All of them contain 40% of RAP, with the same virgin aggregate type and particle size distribution, but two different polymer modified binders (S and H) and two amounts of total binder (5.0% and 5.2% by aggregate weight).

Moreover, a fifth mix with 25% RAP and 4.8% of total binder content was studied as reference mixture (REF). The total binder contents considered for the mixtures containing 40% of RAP were higher than the 4.8% of the reference mixture as not all the aged binder coming from RAP takes part in the blending process (Frigio et al. 2014, Shirodkar et al. 2011, Oliver 2001). Therefore, as the RAP percentage increases, the amount of aged inactive binder (black aggregate) increases as well and must not be considered as effective for the mix.

Table 1 presents a summary of the overall experimental program.

First, the compactability properties were investigated through the calculation of the Compaction Energy Index (CEI) (Mahmoud & Bahia 2004), and the volumetric aggregate structure after compaction was characterized by performing a specifically calibrated image analysis.

Afterwards, a servo-pneumatic testing machine equipped with an environmental chamber was used to perform the following mechanical tests:

- cyclic uniaxial compression tests to measure the complex modulus (E^*) and the phase angle (δ) in accordance with AASHTO TP 79-09. Tests were run at five different temperatures (10, 20, 30, 40 and 50°C) by the application of sinusoidal load waves at six frequencies (0.1, 0.3, 1, 3, 10 and 20 Hz). Tests were carried out in controlled strain mode, setting $30\mu\epsilon$ as target strain level;
- Semi-Circular Bending (SCB) tests to evaluate the low temperature fracture resistance in accordance with EN 12697-44. Tests were run at a temperature of 10°C using a constant vertical deformation rate equal to 5 mm/min;
- cyclic triaxial compression tests to assess permanent deformation resistance, according to EN 12697-25. Tests were performed at a temperature of 40°C with a confining pressure of 50 kPa;

Table 1. Experimental program.

Test type	Number of replicates				
	REF	5.0%S	5.2%S	5.0%H	5.2%H
Semi Circular Bending (SCB) Permanent Deformation	4	4	4	4	4
Complex Modulus	2	2	2	2	2
Indirect Tensile Stiffness Modulus (ITSM)	6	6	6	6	6
Crack Initiation	6	6	6	6	6

- cyclic indirect tension tests for the assessment of the Indirect Tensile Stiffness Modulus (ITSM) according to EN 12697-26, and the subsequent estimation of the resistance to crack initiation (Read & Brown 1996). Tests were carried out at a temperature of 20°C in controlled-stress mode, with a rise time of 124 ms. Failure was established when the complete fracture of the specimen was obtained (BS DD ABE, 1997). A minimum of 3 stress levels for each mixture were applied.

3 MATERIALS AND SPECIMEN PREPARATION

3.1 Virgin aggregates and RAP

Three fractions of virgin crushed limestone aggregates (10/20 mm, 4/10 mm, 0/4 mm) were selected to produce all the mixtures.

RAP was milled from old pavements and processed by crushing and screening, in order to remove foreign matter and clumps.

For the reference mixture, 25% of unfractured RAP 0/16 was used following the current practice.

For the preparation of the 40% RAP mixtures, the unfractured RAP was divided in two fractions (0/8 mm and 8/16 mm), with the aim to reduce RAP variability and obtain more flexibility in meeting mix design requirements.

The aggregate size distributions of the three RAPs employed are reported in Figure 1. As far as the binder content is concerned, unfractured RAP is characterized by 4.9%, RAP 0/8 by 6.4% and RAP 8/16 by 5.0% of binder by aggregate weight.

3.2 Binders

Two polymer modified bitumens were used as virgin binder. They are coded Soft (S) and Hard (H) and are characterized, respectively, by 1.8% and 3.8% by the binder weight, of Styrene-Butadiene-Styrene (SBS) polymer. Binder H was selected because it is the same employed in the reference mixture and corresponds to

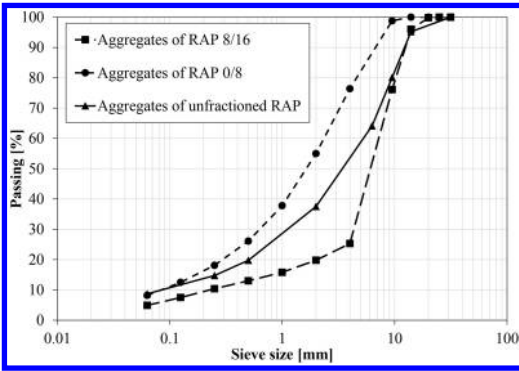


Figure 1. Particle size distribution of RAP aggregates.

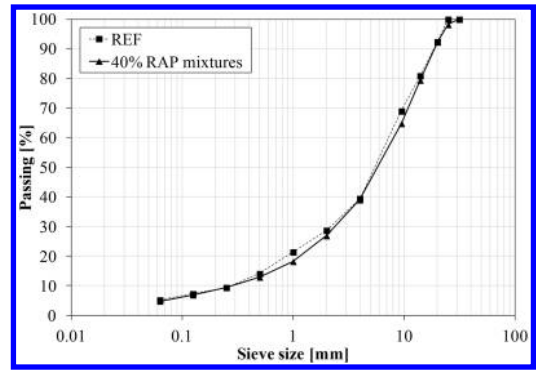


Figure 2. Mixture grading curves.

Table 2. Basic characteristics of the virgin binders.

Characteristic	Standard	Unit	Soft	Hard
SBS polymer content by weight	–	%	1.8	3.8
Penetration [25°C; 100 g; 5 s]	EN 1426	dmm	60	54
Ring and ball softening point	EN 1427	°C	66	71
Dynamic viscosity @ 135°C	ASTM D4402	Pa·s	1.24	1.24
Mass loss after RTFOT	EN 12607-1	%	0.08	0.05
Penetration after RTFOT	EN 1426	0.1 mm	37	27
Ring and ball softening point after RTFOT	EN 1427	°C	73	77

the original binder included in the RAP. At the same time, a softer binder was investigated to evaluate if a lower binder grade can be helpful to compensate the increase in stiffness due to higher amount of aged binder. The basic characteristics of the virgin binders are shown in Table 2.

3.3 Bituminous mixtures

The reference mixture with 25% RAP was prepared in accordance with the Italian specification for motorway binder courses, by using the Hard-modified bitumen (H) as virgin binder.

All the four mixtures containing 40% of RAP are characterized by the same grading curve that was designed using the Bailey method (Vavrik et al. 2002), in order to achieve an optimized aggregate packing. Figure 2 presents the grading curves of the five mixtures studied.

3.4 Specimen preparation

All the specimens tested were prepared in laboratory adopting a procedure aimed at simulating the in plant

production. Virgin aggregates and binder were pre-heated at 170°C and mixed with RAP (kept at ambient temperature) by means of a planetary equipment. The resulting mixtures were compacted at 160°C using the Superpave Gyratory Compactor (SGC) with a target air voids of 3.5% in order to obtain cylindrical specimens having a diameter $D = 150$ mm and a height $H = 170$ mm. Then, the specimens were cored and cut to get asphalt mixture samples with proper dimensions for each mechanical test.

4 RESULTS AND ANALYSIS

4.1 Compactability and aggregate packing

The Compaction Energy Index (CEI) was used to evaluate the compactability properties of each mixture. CEI was defined by Mahmoud & Bahia (2004) as the area under the densification curve representing the work required to achieve a target density during construction. Therefore, low values of CEI indicate mixtures with good compactability.

Figure 3 shows the CEI values calculated for each mixture as average of all the specimens ($D = 150$ mm; $H = 170$ mm) prepared for this study. It can be noted that the highest CEI value belongs to the reference mixture, hence indicating worst compactability aptitude, contrarily to what expected. In fact, the increase of RAP content could cause a reduction of mixture compactability due to the greater amount of stiff aged binder and the higher RAP variability. On the contrary, Figure 3 demonstrates that the optimization of the aggregate gradation using the Bailey method and the RAP fractioning in two sizes allow the potential negative effect of higher amount of RAP to be balanced.

As far as the comparison of the mixtures with 40% of RAP is concerned, as expected the increase of the total binder content led to a slight decrease in the CEI value regardless of the binder type. In fact, the higher the binder content, the higher its lubricity capability that helps to reach the optimum aggregate packing. Moreover, for both total binder contents (i.e. 5.0% and 5.2%) the CEI was lower when Soft binder was used.

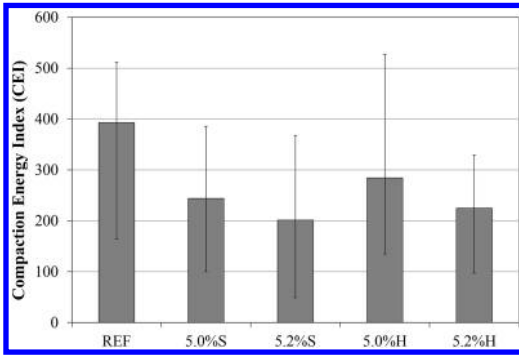


Figure 3. Compaction energy index.

Table 3. ANOVA: Influence of mixture type (REF, 5.0%S, 5.2%S, 5.0%H, 5.2%H) on the CEI value.

Mixture pairs	Significant?	p-value
REF vs. 5.0%S	No	0.096
REF vs. 5.2%S	Yes	0.024
REF vs. 5.0%H	No	0.198
REF vs. 5.2%H	Yes	0.036
5.0%S vs. 5.2%S	No	0.566
5.0%H vs. 5.2%H	No	0.388
5.0%S vs. 5.0%H	No	0.615
5.2%S vs. 5.2%H	No	0.695

Such a result can be explained considering the viscosity data of binder S and H presented in a previous study focused on the rheological characterization of the binder component (Stimilli et al. 2014). In particular, the viscosity analysis showed that binder S is characterized by lower viscosity than binder H at temperatures close to the mixing and compaction temperatures adopted in this study (i.e. 160 and 170°C). The lower the viscosity of the binder, the higher the workability of the corresponding asphalt mixture, as demonstrated by the CEI values.

Since the dimensions of the error bars in Figure 3 could generate doubts about the significance of CEI results, a one-way analysis of variance (one-way ANOVA) at 95% confidence level, was performed in order to check the statistical significance of the mixture type (REF, 5.0%S, 5.2%S, 5.0%H, 5.2%H) on the CEI value.

The ANOVA results are summarized in Table 3 in terms of the test outcome along with the relevant p-value. As supposed, experimental data show that there is no statistical difference between CEI values of different mixtures, for almost all pairs of mixes considered. Thus, the CEI results cannot be considered significant by alone but should be combined with other testing results.

For this reason, the compactability assessment was integrated by an image analysis of internal aggregate structure in order to correlate the aggregate packing with the mixture behavior. In fact, the aggregate grading and the particles connectivity have a significant impact on many aspects of mixtures performance when

the material is subjected to external loads. The image analysis represents a useful tool for interpreting test results, with particular attention focused on the impact of the aggregate skeleton built with the Bailey method.

The analysis was performed on 2-dimensional images of mixture section, processed through specific softwares (iPas 2 and MATLAB) (Sefidmazgi et al. 2012) that allow the calculation of two internal structure parameters: the total “aggregate proximity zone length” and the “aggregate-on-aggregate number of contact points”. As such parameters can be considered indicators of the aggregate packing level, the higher the proximity zone length and the number of contact points, the stronger the interlocking between aggregates. In particular, the software iPas converts Red Green and Blue (RGB) images into gray scale images where a significant difference in terms of colour intensity between the aggregate and the mastic can be easily detected in order to separate and quantify the phases of the material (i.e. air voids, aggregates, mastic). This separation can be performed using a threshold filtering: pixels with higher intensity are assumed to be aggregates, and pixels with lower intensity are assumed to be air voids and mastic (Sefidmazgi et al. 2012). At this point, gray scale images are finally converted into binary Black and White (BW) images (Fig. 4) which are implemented in MATLAB for microstructure analysis. Further details about the image analysis and the related parameters are available elsewhere (Sefidmazgi et al. 2012, Stimilli et al. under revision). A summary of the results, as average of 12 replicates, is provided in Figure 5.

Although mixtures designed with Bailey method have higher RAP content (40%), they showed proximity zone length and number of contact points comparable or even higher than the reference mixture (25% RAP). This suggests that a proper mix design and an accurate processing of RAP material (screened and fractioned in two sizes) provide the possibility to reach an optimum aggregate packing, overcoming the disadvantages caused by higher amount of RAP. Moreover, mixtures with binder S (low modified) were able to guarantee better aggregate packing for both binder contents in accordance with the compactability results (CEI) previously discussed, confirming that a softer binder provides improved workability. At the same time, the mixtures with lower binder percentage showed higher proximity zone length and number of contact points, with both virgin binder S and H. This observation demonstrates that with the same aggregate grading curve, although higher binder content ensures higher workability, less binder (5.0%) implies shorter distance between aggregates and, hence, an aggregate structure more packed, even keeping good compactability and workability properties.

4.2 Stiffness

The stiffness properties were evaluated in terms of complex modulus $|E^*|$ by performing cyclic uniaxial compression tests according to AASHTO TP 79-09.

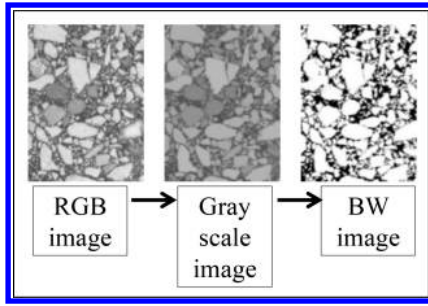


Figure 4. Image filtering steps.

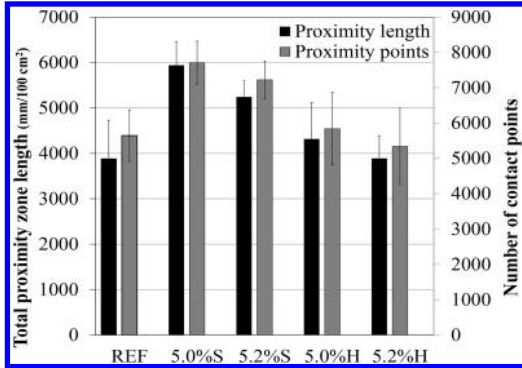


Figure 5. Image analysis results.

Test data are displayed in the Cole-Cole plane (Fig. 6) in terms of loss modulus (E_2) and storage modulus (E_1).

The impossibility of fitting the measured data with a continuous line demonstrates a non thermorheologically simple behavior of the materials, hence Time-Temperature Superimposition Principle was not considered valid. Such a tendency can be explained considering that both reclaimed and virgin binders are modified and these kinds of binders do not usually follow the Time-Temperature Superposition Principle (Di Benedetto et al. 2011), as also demonstrated by Stimilli et al. (2014).

As long as only the complex modulus norm is considered, the master curves reported in Figure 7 are obtained. A four-parameter sigmoidal function was adopted as analytical model for $|E^*|$ (Pellinen & Witczak 2002). The model optimization procedure was carried out allowing free variation of the shift factors.

Based on the master curves trends, it can be stated that the mixtures prepared with binder H were significantly stiffer than the others, within the temperature/frequency range investigated. In particular, comparing 40% RAP mixtures made with binder H (highly modified) and the reference mixture (prepared with the same type of binder H), it is possible to isolate the effect of higher quantity of RAP. As expected, the adding of a certain amount of RAP (i.e. 15%) caused a noticeable increment in the norm of the complex modulus regardless of the total binder content considered. On the contrary, using binder S (poorly modified) it is

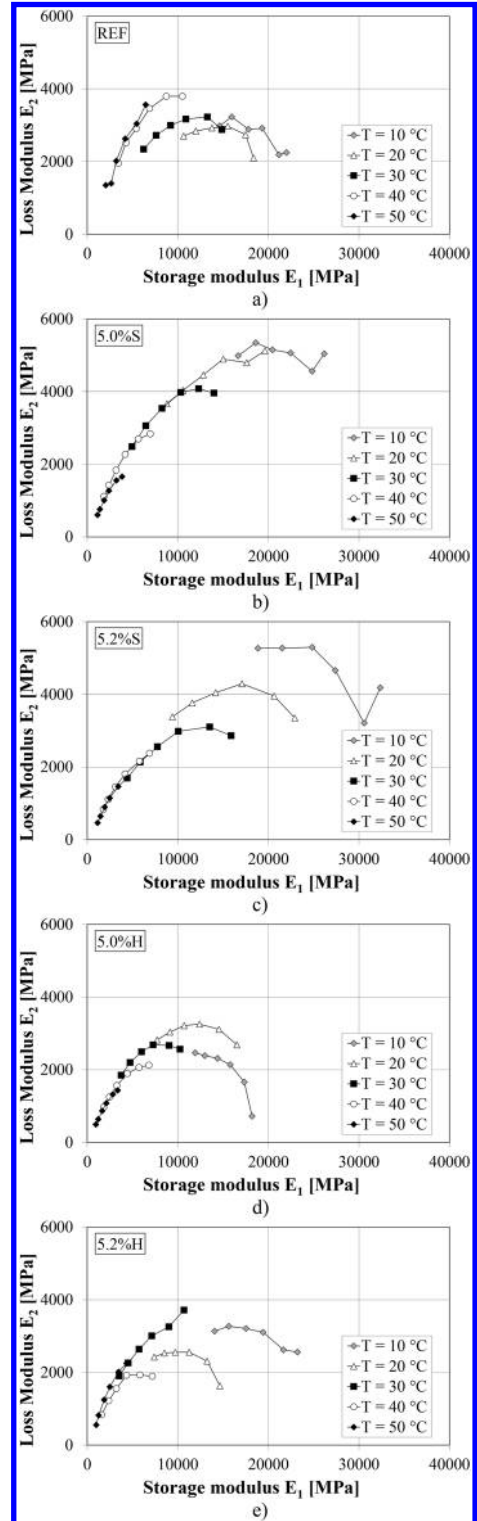


Figure 6. Complex modulus results in the Cole-Cole plane.

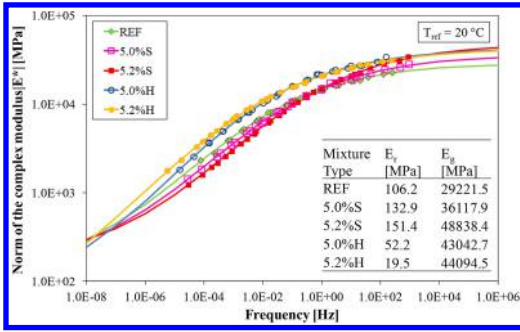


Figure 7. Master curves at 20°C within the temperature range investigated and values of the rubbery (E_r) and glassy (E_g) modulus.

possible to overcome the effects of higher quantity of RAP. In fact, the mixtures made with binder S showed complex modulus values close to the values recorded for the reference mixture.

Moreover, it is interesting to note that the reference mixture provided a significantly lower temperature susceptibility than the 40% RAP mixtures regardless of the type of binder used (S or H). This is demonstrated by the rate of the change in the complex modulus within the frequency range investigated, that is reflected in the values of the rubbery and glassy asymptotes (E_r and E_g respectively) found with the adopted master curve model (see the table in Fig. 7).

4.3 Semi Circular Bending (SCB) test

Semi-Circular Bending tests were performed according to EN 12697-44 to investigate the cracking propagation resistance at low temperature in terms of fracture toughness K and fracture energy G . The results, as average of four replicates, are presented in Figure 8.

All the mixtures with 40% of RAP had higher K values than the reference one. The same result can be noted analyzing the fracture energy G , with the exception of 5.2% H that had a value comparable with the reference mixture. Such a result suggests that the adding of a 15% RAP does not penalize the mixtures in terms of ductility and low modified binders can enhance the performance at low temperature. Again, the implementation of the Bailey method and the fractioning of RAP seem able to provide benefits in terms of performance, compensating the potential negative effect of high amount of RAP. In addition, the presence of SBS aged modified binders in the RAP aggregates can provide a further positive contribution to mitigate the stiffening effect of RAP, detrimental for the cracking aptitude of recycled mixtures. In fact, the aged polymer contained in the RAP binder is still able to provide a good elasticity even after the oxidation process underwent during the in service life (Stimilli et al. 2014).

Another aspect that can play a positive role for the development of good fracture properties is the

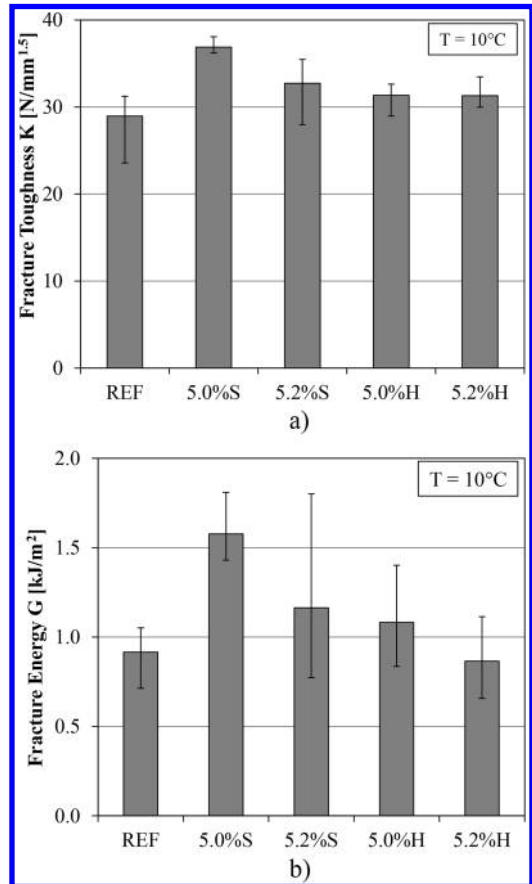


Figure 8. SCB mean test results.

improved adhesion between virgin binder and RAP aggregates. In fact, cracks propagate throughout the binder phase around aggregates: the higher the adhesion between the binder and the aggregates, the higher the cracking propagation resistance. In particular, RAP aggregates are coated by a thin film of binder that, even if aged, can be still partially reactivated providing a better interaction with the virgin binder, as shown by a specific study on this topic (Canestrari et al. 2014). Therefore, the improved adhesion expected in mixtures produced with higher amount of pre-coated aggregates (40% RAP) positively affects the overall fracture performance of the mixtures.

Moreover, as previously mentioned, fracture strength and fracture energy were higher in mixtures with binder S and decreased as the binder content increased. These findings can be attributed to the better aggregate packing achieved by mixtures produced with binder S and lower binder content (as shown by the image analysis results). Moreover, the data are consistent with the crack path length concept, strongly related to the image analysis parameters. The crack path length is referred as the path followed by the crack to propagate across the material (Stimilli et al.

2014 under revision): the higher the aggregate proximity zone length, the longer the crack path length and the higher the energy required to cause the failure, since the crack propagates throughout the binder phase around aggregates. In particular, mixtures made with binder S showed the highest proximity zone length. Moreover, in mixtures with lower binder content, the binder film that coats the aggregates is less thick, making the distance between aggregate smaller and the crack path length longer. This result is in accordance with the data presented in another study (Stimilli et al. under revision) where the low-temperature fracture mechanisms were analyzed through the Asphalt Thermal Cracking Analyzer (ATCA) on the same mixtures investigated in this paper and the same trend of the SCB results was detected.

4.4 Resistance to permanent deformation

The permanent deformation susceptibility was investigated through a cyclic triaxial compression test, which offers the best simulation of field conditions. As suggested by the EN 12697-25, the parameter f_c (creep rate) was used to compare the results and was calculated as the slope of the (quasi) linear part of the least square linear fit (Fig. 9). It represents the rate of the creep curve (cumulative axial strain vs. number of load application). Lower f_c values indicate a mixture less prone to accumulate permanent deformation. Therefore, the lower the f_c , the higher the rutting resistance of the mixture.

Average values of the parameter f_c are summarized in Figure 9. The reference mixture showed the highest f_c value. Again, considering that the aggregate skeleton is fundamental for the development of good rutting resistance, the optimization of the grading curve by means of the Bailey method and an accurate processing of RAP appear able to guarantee the development of a stronger and well structured aggregate packing less prone to deform under cyclic loading. In fact, the image analysis results showed that 40% RAP mixtures were characterized by similar or even improved aggregate packing compared to the reference mixture, despite the higher amount of RAP.

The best performance in terms of rutting resistance was recorded for 40% RAP mixtures prepared using binder H (highly modified), even with respect to the reference mixture, made with the same type of binder. In fact, the abovementioned aspect related to an improved aggregate packing combines with the effects of higher percentage of aged binder, which provides an increased stiffness in accordance to the stiffness analysis (Fig. 7).

At the same time, the 40% RAP mixtures made with binder S also showed improved rutting resistance compared to the reference mixture, although the presence of a softer binder that balanced the stiffening effect due to higher amount of RAP (Fig. 7). Such a result confirms the benefits achievable with the optimization of the aggregate grading curve. In fact, the image analysis and the compactability study showed that the

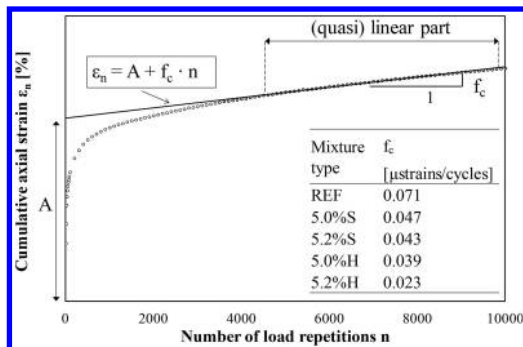


Figure 9. Schematic representation of the creep curve and the creep rates f_c , calculated for the mixtures studied.

mixtures with binder S provided the best performance in terms of aggregate packing.

As far as the 40% RAP mixtures are concerned, it is possible to note that the f_c is higher for lower binder content. This suggests that with an equal aggregate grading curve, the presence of higher quantity of binder makes the elastic capability provided by higher amount of polymer predominant, hence enhancing the possibility to recover part of the deformation accumulated during the loading phase.

Moreover, the mixtures with binder H performed significantly better than the ones prepared with binder S. As previously mentioned, such a result can be explained considering the higher stiffness measured for mixtures produced with binder H (Fig. 7) that is concurrently combined with the more pronounced elasticity provided by the chemical structure of the bituminous phase (binder H) characterized by higher amount of SBS polymer, with a consequent decrease in the tendency to accumulate permanent deformation.

4.5 Resistance to repeated loading

The resistance to repeated loading was evaluated through the cyclic indirect tension test (BS DD ABF 1997). Results are plotted in Figure 10 where the number of cycles to failure is reported as a function of the initial maximum horizontal strain (ϵ), determined using the maximum tensile stress developed at the centre of the specimen. Moreover, also the Indirect Tensile Stiffness Modulus (ITSM) previously measured according to EN 12697-26 are summarized in Figure 10. It is worth noting that the regression lines drawn in Figure 10 do not define real fatigue life but can be considered as an indicator of the crack initiation characteristics of the studied mixtures (resistance to early cracking).

It can be observed that all the 40% RAP mixtures were more resistant to repeated loading than the reference mixture. Such a result is quite surprising since higher amounts of RAP are expected to make the mixture more brittle due to the adding of aged stiffer materials. However, it supports the findings of the

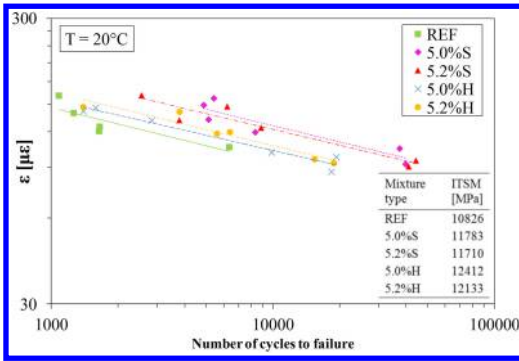


Figure 10. Strain vs. number of loading cycles relationships.

other mechanical tests demonstrating the importance of an adequate and accurate mix design to balance higher RAP content.

Additionally, it must be taken into account the improved adhesion between the virgin binder and the pre-coated RAP aggregates. In fact, as previously explained, it was shown with a specific study (Canestrari et al. 2014) that RAP aggregates can enhance the interaction with the virgin binder in terms of adhesion properties of the mixtures. The higher the adhesion between the binder and the aggregates, the higher the cracking propagation resistance.

Moreover, consistent results were achieved studying the fatigue properties of the only binder phase (Stimilli et al. 2014) where it was observed that the higher the reclaimed modified binder fraction in the bituminous blend, the higher the overall fatigue resistance.

No significant differences were detected among different binder contents. At the same time, the use of binder S (poorly modified) guaranteed an improvement in cracking resistance. The latter observation is in accordance with the SCB test results previously discussed, used to assess the low-temperature cracking resistance of the mixtures. Also in that case, the mixtures made with binder S were characterized by better performance in terms of cracking resistance than the mixtures made with binder H. Again, this behavior can be attributed to the better aggregate packing achieved by mixtures prepared with binder S (see the image analysis results) that guarantees a longer crack path length, hence requiring more energy or number of loading cycles to reach the same strain level (i.e. the failure condition). Moreover, it must be considered that the mixtures with binder S were characterized by lower stiffness values considering both the complex modulus (see Fig. 7) and the ITSM (see the table in Fig. 10). Lower stiffness values, keeping unaltered all the other variables (i.e. aggregate grading curve, amount of RAP, binder content), could imply a mixture less brittle and, consequently, a higher cracking resistance.

5 CONCLUSIONS

This paper discusses a laboratory study focused on the assessment of the mechanical properties of hot recycled mixtures prepared with high percentage of RAP including aged SBS modified binder. To this purpose, a comparison between a reference mixture with 25% of unfractionated RAP and four mixtures containing 40% of selected RAP was conducted. The mixtures with 40% of RAP were designed using the Bailey method and prepared with two different binder type S and H (low and high level of polymer modification respectively) and two total binder contents (5.0% and 5.2% by aggregate weight).

Based on the findings of this study, it can be concluded that the 40% RAP mixtures provide equal or even higher performance than the reference mixture, regardless of the parameters considered. In particular, the data measured through several mechanical tests carried out on laboratory compacted specimens led to draw the following observations:

- the mixtures designed using the Bailey method although containing higher amount of RAP, demonstrated higher workability than the reference mixture guaranteeing better compactibility and improved aggregate skeleton packing. In particular, the mixtures prepared with the low modified binder S showed a better behavior in terms of compactibility and aggregate packing. At the same time, a lower binder content seems able to provide an improved aggregate structure both for binder S and H;
- in terms of stiffness properties, all the studied mixtures did not show a thermo-rheologically simple behavior due to the presence of modified and aged binders. However, the master curves of the complex modulus norm can be used to compare results. They showed that the reference mixture had a lower temperature susceptibility than the mixtures with 40% of RAP, regardless of the binder type used (high or low modified). The 40% RAP mixtures made with the high modified binder H showed the highest complex modulus values within the temperature/frequency range investigated due to the stiffening effect of the aged binder contained in the RAP aggregates. On the contrary, the reference mixture and the 40% RAP mixtures made with the low modified binder S had comparable stiffness values. Such a result confirms that the use of a softer binder can help to mitigate the stiffening effect of increasing quantity of RAP;
- in terms of crack propagation resistance, mixtures designed with the Bailey method exhibited performance similar to the reference mixture. The use of the low modified binder S, as well as lower binder content, increased the mixture ductility and the energy required to cause the material failure. Therefore, it appears that higher quantity of RAP does not make the mixture more brittle. Such a finding is assumed as the result of the better aggregate skeleton built using the Bailey method, as well as the improved adhesion developed between

the pre-coated RAP aggregates and the virgin binder;

- all 40% RAP mixtures provided better performance to permanent deformation than the reference mixture. As expected, the mixtures with the high modified binder H showed the lowest susceptibility to permanent deformation;
- the reference mixture was characterized by lower repeated loading cracking resistance compared to the others mixtures. The binder content did not significantly affect the resistance to repeated loading, whereas a significant increase was observed using the low modified binder S.

On the basis of the above-mentioned findings, it can be concluded that the implementation of the Bailey method as a tool for optimizing the aggregate packing together with the fractioning of the RAP in two sizes, represent a useful and effective strategy to overcome the usage of high RAP content without compromising the mixture performance. Also, the improved adhesion between the virgin binder and the aggregate component provided by higher amount of pre-coated aggregates (40% RAP) positively affects the overall performance of the mixtures.

The use of the softer binder S seems able to guarantee a better interaction with high amounts of RAP in terms of mechanical performance and the reactivated portion of aged binder in the mixtures with 5.0% of total binder content appears adequate to optimize the mixture behavior.

Based on the promising results observed in this research, future works will include field applications in order to validate the laboratory results through the performance analysis of the same mixture produced in an asphalt plant.

ACKNOWLEDGEMENTS

This research was sponsored by Pavimental SpA. This support is greatly acknowledged. Data analysis and opinions are those of the authors and do not necessarily reflect those of the sponsoring agency.

REFERENCES

- Al-Qadi, I.L., Aurangzeb, Q., Carpenter, S. H., Pine, W. J. & Trepanier, J. 2012. Impact of High RAP Contents on Structural and Performance Properties of Asphalt Mixtures. *Report No. FHWA-JCT-12-002*, Springfield: Illinois Center for Transportation.
- Apeaygei, A., Diefenderfer, B. K. & Diefenderfer, S. D. 2011. Rutting Resistance of Asphalt Concrete Mixtures Containing Recycled Asphalt Pavement. *Transportation Research Record* 1840: 9–16.
- Aurangzeb, Q., Al-Qadi, I. L., Abuawad, I. M., Pine, W. J. & Trepanier, J. S. 2012. Achieving Desired Volumetrics and Performance for High Rap Mixtures. *Transportation Research Record* 2294: 34–42.
- Canestrari, F., Ferrotti, G., Cardone, F. & Stimilli, A. 2014. Innovative Testing Protocol for the Evaluation of Binder-Reclaimed Aggregate Bond Strength. *Transportation Research Record*, in press.
- de la Roche, C., Van de Ven, M., Planche, J.P., Van den Bergh, W., Grenfell, J., Gabet, T., Mouillet, V., Porot, L., Farcas, F. & Ruot, C. 2012. Hot Recycling of Bituminous Mixtures. In M.N. Partl, H.U. Bahia, F. Canestrari, C. de la Roche, H. Di Benedetto, H. Piber & D. Sybilski (eds) *State-of-the-Art-Reports 9: Advances in Interlaboratory Testing and Evaluation of Bituminous Materials*: 361–428. Berlin: Springer.
- Di Benedetto, H., Sauzeat, C., Bilodeau, K., Buannic, M., Mangiafico, S., Nguyen, Q. T., Pouget, S., Tapsoba, N. & Van Rompu, J. 2011. General overview of the time-temperature superposition principle validity for materials containing bituminous binder. *International Journal of Roads and Airports* 1 (1): 35–52.
- Frigio, F., Pasquini, E., Ferrotti, G. & Canestrari, F. 2013. Improved durability of recycled porous asphalt. *Construction and Building Materials* 48: 755–763.
- Frigio F., Pasquini, E. & Canestrari, F. 2014. Laboratory Study to Evaluate the Influence of Reclaimed Asphalt Content on Performance of Recycled Porous Asphalt. *Journal of Testing and Evaluation* 43 (6).
- Li, X., Marasteanu, M. O., Williams, R. C. & Clyne, T. R. 2008. Effect of Reclaimed Asphalt Pavement (Proportion and Type) and Binder Grade on Asphalt Mixtures. *Transportation Research Record* 2051: 90–97.
- Mahmoud, A. F. F., & Bahia, H. U. 2004. Using the gyratory compactor to measure mechanical stability of asphalt mixtures. *Wisconsin Highway Research Program* 05-02.
- McDaniel, R. S., Soleymani, H., Anderson, R. M., Turner, P. & Peterson, R. 2000. Recommended Use of Reclaimed Asphalt Pavement in the Superpave Mix Design Method. *NCHRP Project D9-12*.
- Oliver, J. W. H. 2001. The Influence of the Binder in RAP on Recycled Asphalt Properties. *Road Materials and Pavement Design* 2 (3): 311–325.
- Pellinen, T. K. & Witzczak, M. W. 2002. Stress Dependent Master Curve Construction for Dynamic (Complex) Modulus (with Discussion). *Journal of the Association of Asphalt Paving Technologists* 71: 281–309.
- Read, J.M. & Brown, S.F. 1996. Fatigue characterisation of bituminous mixtures using a simplified test method. In J.C. Cabrera & J.R. Dixon (eds), *Performance and durability of bituminous materials*: 161–173. E&FN Spon.
- Sefidmazgi N.R., Tashman, L. & Bahia, H.U. 2012. Internal Structure Characterization of Asphalt Mixtures for Rutting Performance Using Imaging Analysis. *Road Materials and Pavement Design* 13 (1): 21–37.
- Shirodkar, P., Mehta, Y., Nolan, A., Sonpal, K., Norton, A., Tomlinson, C., Dubois, E., Sullivan, P. & Sauber, R. 2011. Study of determine the degree of partial blending of reclaimed asphalt pavement (RAP) binder for high RAP hot mix asphalt. *Construction and Building Materials* 25: 150–155.
- Stimilli, A., Ferrotti, G., Conti, C., Tosi, G. & Canestrari F. 2014. Chemical and rheological analysis of modified bitumens blended with “artificial reclaimed bitumen”. *Construction and Building Materials* 63: 1–10.
- Stimilli, A., Canestrari, F., Teymourpour, P. & Bahia, H.U. Under revision. Low-Temperature Fracture Evaluation of Hot Recycled Mixtures through Asphalt Thermal Cracking Analyzer (ATCA).
- Tran, N. H., Taylor, A. & Willis, R. 2012. Effect of Rejuvenators on Performance Properties of HMA Mixtures with High RAP and RAS Contents. *NCAT Report No. 12-05*.
- Vavrik, W. R., Huber, G., Pine, W. J., Carpenter, S. H. & Bailey, R. 2002. Bailey Method for Gradation Selection in

- HMA Mixture Design. *Transportation Research Circular E-C044*.
- West, R., Kvasnak, A., Tran, N., Powell, B. & Turner, P. 2009. Testing of Moderate and High RAP Content Mixes: Laboratory and Accelerated Field Performance at the National Center for Asphalt Technology Test Track. *Transportation Research Record* 2126: 100–108.
- West, R., Willis, J. R. & Marasteanu, M. 2013. Improved Mix Design, Evaluation, and Materials Management Practices for Hot Mix Asphalt with High Reclaimed Asphalt Pavement Content. *NCHRP Report 752*.
- Zaumanis, M. & Mallick, R.B. 2015. Review of very high-content reclaimed asphalt use in plant-produced pavements: state of art. *International Journal of Pavement Engineering* 16 (1): 39–55.

Moisture damage and low temperature cracking of bituminous mixtures made with recycled aggregates

M. Pasetto

Department of Civil, Environmental and Architectural Engineering, University of Padua, Padua, Italy

N. Baldo

Chemistry, Physics and Environment Department, University of Udine, Udine, Italy

ABSTRACT: The paper presents the conclusions of an experimental evaluation of moisture damage and low temperature cracking behaviour of asphalt concretes, for road base courses, made with recycled aggregates, namely Reclaimed Asphalt Pavement (RAP) and steel slags, used at different proportions (up to 70% by weight of the aggregate), in partial substitution of limestone. The asphalt concretes were designed according to volumetric criteria, by means of the gyratory compactor. Indirect Tensile Tests were used in order to characterize the Stiffness and the Strength at failure of the mixes. The ageing effects have been investigated, performing the mechanical tests on the mixes under aged and unaged conditions. With respect to the control mixture, composed by a full natural aggregate skeleton, the asphalt concretes with recycled aggregates presented improved moisture damage, but a lower thermal cracking resistance, depending on the RAP and the steel slags contents, as well as on the ageing conditions

1 INTRODUCTION

Moisture damage, as well as thermal cracking at low temperatures, are relevant degradation phenomena that affect the durability and the service life of bituminous mixtures, used in road flexible pavements. The moisture damage resistance of a bituminous mixture is influenced by the content of bitumen and its adhesion to the grains of the lithic skeleton, as well as by the porosity of the asphalt concrete. Binder's rheological properties, especially the ductility, affect the low temperature cracking resistance of the mix.

The paper discusses the results of a laboratory testing concerning the moisture damage and the low temperature resistance of bituminous mixtures for road base courses, made with Electric Arc Furnace (EAF) steel slag and RAP aggregates.

2 MATERIALS

2.1 Aggregates

The artificial and recycled aggregates (EN 13043) considered in the study were what are known as marginal materials (Pasetto & Baldo 2012, Pasetto & Baldo 2013a, b, Pasetto & Baldo 2014); more specifically they are EAF steel slag and RAP aggregate. The marginal aggregates used in the study were supplied by different private companies in northern Italy, while the natural aggregate, namely crushed limestone (CL)

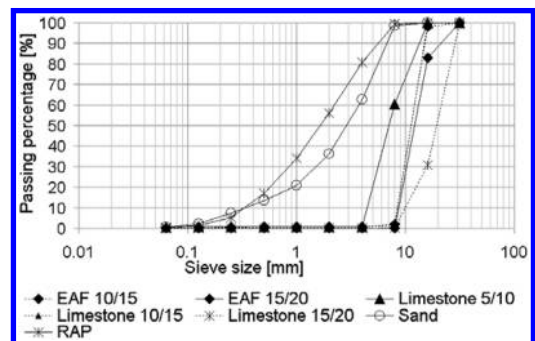


Figure 1. Aggregates grading curves.

and sand (NS), derived from a quarry in the same area. The grading curves of the aggregates reported in Figure 1, show that the 10/15 mm fractions of the EAF slag and limestone had an almost identical particle size distribution, while a relevant difference can be noticed between the 15/20 fractions: the first slag had a finer composition than the corresponding fraction of the limestone. The 5/10 mm fraction of the EAF slag presented an intermediate grading distribution. RAP and natural sand represent the fine aggregates.

Tables 1, 2 report the physical-mechanical properties of the recycled and natural aggregates, respectively.

Table 1. Physical and mechanical characteristics of the recycled aggregates.

Physical ÷ mechanical properties	EAF 10/15	EAF 15/20	RAP
Los Angeles coefficient [%] EN 1097-2	7	–	27
Sand Equivalent [%] EN 933-8	–	–	98
Shape Index [%] EN 933-4	8	3	10
Flakiness Index [%] EN 933-3	6	4	7
Particle density [Mg/m ³] EN 1097-6	3.87	3.74	2.36
Plasticity Index [–] CEN ISO/TS 17892-12	0	0	0

Table 2. Physical and mechanical characteristics of the natural aggregates.

Physical ÷ mechanical properties	NS	CL 5/10	CL 10/15	CL 15/20
Los Angeles coefficient [%] EN 1097-2			30	–
Equivalent in sand [%] EN 933-8	86	93	–	–
Shape Index [%] EN 933-4	–	9	2	4
Flakiness Index [%] EN 933-3	–	10	2	5
Particle density [Mg/m ³] EN 1097-6	2.81	2.44	2.72	2.78
Plasticity Index [–] CEN ISO/TS 17892-12	0	0	0	0

The Los Angeles test showed a good resistance of the EAF slag to abrasion and friction, with a LA coefficient lower than the acceptance requisites of SITEB – Italian Society of Bitumen Technologists Specifications (SITEB 2000), set at 25%. The Los Angeles coefficient of crushed limestone, as well as that of RAP aggregate, are higher than SITEB’s threshold, with differences of 20% and 8%, respectively. The mechanical resistance of the marginal aggregates is anyway higher than that of the natural ones.

The cleanliness, expressed in terms of Equivalent in Sand, resulted extremely good for all the aggregates and largely above the minimum SITEB threshold, fixed at 50%. Both the limestone and the marginal aggregates, namely EAF slag and RAP, presented satisfactory morphological properties, given that the Flakiness Index were consistently below the specification value, fixed by SITEB at 25%. All the marginal aggregates resulted as practically unaffected by the action of water, presenting non-determinable Atterberg Limits (Liquid Limit and Plastic Limit), as

Table 3. Major heavy metal content of EAF slags.

Element	IC [mg/kg]	TCLP leaching concentration	Limit leaching concentration – legal thresholds
Copper (Cu)	221.0	0.004 mg/l	0.05 mg/l
Cadmium (Cd)	<0.5	<1.0 µg/l	5 µg/l
Lead (Pb)	37.7	19.5 µg/l	50 µg/l
Zinc (Zn)	589.0	<0.001 mg/l	3 mg/l
Chromium	3534.0	32.7 µg/l	50 µg/l
Total (Cr)			
Nickel (Ni)	37.6	<3.0 µg/l	10 µg/l
Mercury (Hg)	<0.5	<1.0 µg/l	1 µg/l
Selenium (Se)	17.4	<5.0 µg/l	10 µg/l
Vanadium (V)	554.0	32.2 µg/l	250 µg/l
Arsenic (As)	5.5	<5.0 µg/l	50 µg/l
Beryllium (Be)	<0.5	<1.0 µg/l	10 µg/l

prescribed in the Italian technical regulations. The particle densities of the RAP aggregates are quite similar to those of the natural materials, but decidedly lower than those of the steel slags.

By Italian Law, the steel slags considered are “non-hazardous, special non-toxic and non-noxious” refuse; their pH resulted equal to 11.5. The chemical composition of the EAF slags has been analyzed with XRF (X-ray fluorescence); their toxicological characteristics were checked in terms of initial concentrations of heavy metals, measured with the ICP-AES methodology (Inductively Coupled Plasma – Atomic Emission Spectrometer), whilst their leaching was determined by the TCLP (Toxic Characteristic Leachability Procedure) given in Appendix A of Standard UNI 10802, following the method in Standard EN 12457-2.

The slags, in terms of oxides, contain a prevalence of FeO (30.4%) and CaO (27.7%), as well as SiO₂ (17.5%), MgO (6.6%) and Al₂O₃ (4.8%). The SiO₂/CaO ratio characterizes the EAF slag as a substantially alkaline aggregate and therefore suitable to guarantee the necessary adhesion with the weakly acid bitumen. With regard to the Initial Concentration (IC) of heavy metals (Table 3), the steel slags present higher contents of vanadium, zinc and chromium, the latter predominating over all the other metals; anyhow it is less than 0.4% of the total volume of slags.

The results in Table 3 demonstrate that, for the steel slag, the release of heavy metals by leaching is within the limits of the environmental regulations in force in Italy (Legislative Decree no. 152/2006). Therefore, given that the constituents of the mixtures do not present toxicological problems, it was considered unnecessary to proceed with leaching tests on asphalt specimens.

The steel slags investigated in the present research have been seasoned by the producer, exposing the material to the weather for a period of at least six months, during which the unbound fraction of calcium oxide was stabilized naturally and therefore they should not be subjected to a volumetric expansion.

However, a volumetric stability test on the EAF slags, according to the Standard EN 1744/1 part 15.3, has been performed and it showed a null expansion after the 168 hours suggested in the test protocol.

Lastly, neither the natural nor the artificial aggregates demonstrated any problems of affinity with the bitumen, with no stripping of the grains coated with binder after 24 hours of immersion in water at 25°C.

2.2 RAP binder and bitumen

Cold extraction (by centrifugation) of the bitumen of the RAP aggregate revealed a binder content of 4.12 % (EN 12697-1) on the weight of the mixture. The extracted bitumen showed a penetration of 15 dmm at 25°C (EN 1426) and a softening point, with the Ring & Ball Method, of 74°C (EN 1427); it is therefore a decidedly aged and particularly hard binder.

Even if, from a theoretical point of view, a softer binder should be used to compensate the hard RAP binder, a conventional bitumen (50/70 dmm pen) was used as virgin binder for all the mixtures in the experiments, according to the most common Italian road construction practices.

3 MIXTURES

Five mixes were designed with an integrated slag-RAP-limestone lithic matrix (S0R2, S0R4, S3R0, S3R2, S3R4) and one, used as control, with only natural aggregate (S0R0). Artificial and recycled aggregates were used up to 70% of the weight of the total aggregate. RAP aggregates were preheated at mixing temperature for 2 hours, before the mixing. The exposure of the RAP aggregates to such a high temperature and long period, will cause further aging of the RAP binder, but also a better blending between the virgin bitumen and the RAP binder. The virgin bitumen, RAP and the other aggregates (namely limestone and steel slags), have been mixed together in a heated lab mixer for one minute.

3.1 Grading and composition of the mixes

The particle size distribution of the mixes with artificial and recycled aggregates was optimized with reference to the design grading envelope of SITEB (SITEB 2000) for asphalt concrete base courses, in order to identify a curve as close as possible to its centre, but compatible with the availability of the different aggregates in the sizes necessary to construct this “ideal” grading. For the control mix (all natural) various amounts of marginal materials are substituted by limestone with an equivalent grading fraction. Table 4 reports the grading composition of the bituminous mixtures and proportions of the components, whereas the corresponding grading curves are presented in Figure 2.

The design grading curves (Fig. 2) are all within the reference grading envelope (SITEB 2000) for

Table 4. Aggregate type and particle size distribution of the mixtures.

Mix composition	Fraction [mm]	Quantity [%]					
		S0R0	S0R2	S0R4	S3R0	S3R2	S3R4
Crushed Limestone	5/10	25	15	12	29	21	14
	10/15	20	20	20	–	–	–
	15/20	12	12	11	–	–	–
Sand	0/2	40	30	13	38	26	12
RAP aggregate	0/10	–	20	40	–	20	40
EAF steel slag	10/15	–	–	–	10	18	18
Filler (additive)	15/20	–	–	–	20	12	12
	–	3	3	4	3	3	4

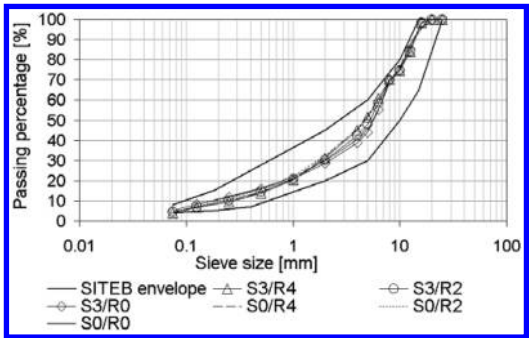


Figure 2. Design grading curve of the mixes.

base course asphalts with maximum aggregate size of 20 mm.

3.2 Optimization of the mixtures and moisture damage resistance

The volumetric mix design, according to CIRS-Italian Ministry of Infrastructure Specifications (CIRS 2001), based on the gyratory compaction procedure and the Indirect Tensile Strength (ITS) test at 25°C, on both dry and wet cylindrical samples, was used for the optimization of the bituminous mixtures. Regarding the main test parameters, a speed of 30 revs/minute, a pressure of 600 kPa, an angle of rotation of 1.25° and a diameter of the mould of 150 mm, were used in the gyratory compaction.

The Optimum Bitumen Content (OBC) for each mixture was determined in correspondence to the residual air voids content (Va) at 10, 100 and 180 revs, of 10–14%, 3–5% and over 2%, respectively (CIRS 2001). The binder content determined regards the virgin bitumen added to the granular mixtures; therefore, for the mixes containing RAP aggregate, the total bitumen content is given by the sum of the aged bitumen of the RAP and the OBC.

Table 5. Mix design results – OBC and air voids.

Mixes	OBC (%)	Va @ 10 revs (%)	Va @ 100 revs (%)	Va @ 180 revs (%)
S0R0	4.75	13.24	4.96	2.95
S0R2	3.90	13.09	4.89	2.89
S0R4	3.00	12.91	4.78	2.81
S3R0	4.85	12.20	4.27	2.48
S3R2	4.00	12.02	4.18	2.39
S3R4	3.10	11.88	4.03	2.27

The damage caused by the immersion in water is expressed by the Tensile Strength Ratio (TSR). It has been computed as the ratio between the indirect tensile strength of the specimens treated by means of 15 days of immersion in a thermostatic bath at 25°C (ITS_{wet}) and untreated (ITS_{dry}), respectively.

The Tensile Strength Ratio (TSR), a synthetic parameter representative of the moisture damage resistance, has been computed as the ratio between the indirect tensile strength of the specimens treated by means of 15 days of immersion in a thermostatic bath at 25°C (ITS_{wet}) and untreated (ITS_{dry}), respectively. The ITS_{dry} and the TSR values of the mixtures prepared with the optimum bitumen content should result higher than 0.6 MPa and 75%, respectively, in order to fulfill the CIRS acceptance requisites.

For each of the 6 asphalt concretes, different mixtures were analyzed, in which, having defined the type of aggregate and grading composition, the amounts of binder were varied at intervals of 0.25% on the weight of the aggregate. To support the phase of mix design, four gyratory specimens were produced for each mix. The results of the mix design procedure are summarized in Tables 5, 6 which detail for each material: OBC, Air Voids (Va) at 10, 100 and 180 revs, bulk density at 100 revs, ITS for dry and wet conditions.

The total bitumen content resulted to be within the typical range of base courses asphalt concretes, namely 4.5-5.5% by weight of the aggregates (SITEB 2000, CIRS 2001), for all the mixes. As it was expected, the greater the RAP content, the lower the virgin bitumen content that is necessary in order to optimize the mixture made with RAP aggregate.

The bulk density of the mixtures was obviously heavily affected by the integration of the EAF slags in the aggregate skeleton, given the high grain densities of the steel slag particles.

The Air Voids requisites prescribed by CIRS mix design procedure, at 10, 100 and 180 revs, were completely satisfied, for all the mixes. The ITS values in dry conditions, resulted largely above the CIRS acceptance requisite (at least more than double) for all the asphalt concretes, as well as the ITS on wet samples, always higher than the 75% of the correspondent ITS dry value (up to 92%, depending on the mix composition), so coming to the conclusion of the acceptability of these base courses asphalt concretes. The limit value of the TSR below which a bituminous mixture may

Table 6. Mix design results – Bulk density, ITS, TSR.

Mixes	Bulk density (g/cm ³)	ITS dry (MPa)	ITS wet (MPa)	TSR (%)
S0R0	2.410	1.62	1.35	83
S0R2	2.433	1.88	1.61	86
S0R4	2.469	2.35	2.06	88
S3R0	2.626	1.74	1.46	84
S3R2	2.661	1.90	1.73	91
S3R4	2.714	2.18	2.01	92

present problems of stripping, usually equal to 70% (Chiu & Lu 2007), has been largely overcome by all the asphalts, so demonstrating a satisfactory moisture damage resistance.

The mixes with marginal aggregates showed improved ITS values, with respect to the reference limestone-only asphalt concrete (S0R0), varying from 7% to 53%, depending on the dry/wet condition and on the mix composition; the mixture made with 30% EAF slag and 40% RAP (S3/R4) was characterized by the highest mechanical strength and moisture damage resistance. The rough texture of the steel slags, as well as the presence of a bitumen film on the RAP particles (aged binder), enable a strong adhesion between the new bitumen added to the mixes and the marginal aggregates grains, that allows, to the optimized asphalt concretes, to achieve higher mechanical strength and moisture damage resistance, with respect to the control mix (S0R0). Moreover, the greater the RAP content, the higher the ITS and TSR values.

3.3 Thermal cracking resistance

Materials damage can be expressed by strain energy density function, according to the following relation (Wu et al. 2007):

$$\frac{dW}{dV} = \int_0^{\epsilon_{ij}} \sigma_{ij} d\epsilon_{ij} \quad (1)$$

where σ_{ij} and ϵ_{ij} are stress and strain, respectively. In the indirect tensile test, the area under the stress–strain curve, computed for the peak stress and the correspondent peak strain, represents the critical value of dW/dV. The critical value of dW/dV at 0°C can be used to estimate the resistance to low temperature cracking (Wu et al. 2007). Some of the specimens were exposed to accelerated long-term ageing, by means of conditioning in an oven at 85°C for 5 days (Artamendi et al. 2009), in order to evaluate its effect on the low temperature properties of the mixtures.

The low temperature cracking test results, namely the peak strain and the critical value of dW/dV, determined for the indirect tensile tests performed at 0°C on the mixtures studied, are presented in Table 7.

The RAP asphalt concretes without steel slags were characterized by lower peak strain and critical values of dW/dV, with respect to the control mix S0R0

Table 7. Low temperature cracking test results.

Mixes	Peak strain [%]	Critical value of dW/dV [kJ/m ³]	Peak strain (post ageing) [%]	Critical value of dW/dV (post ageing) [kJ/m ³]
S0R0	1.00	34.95	0.67	27.66
S0R2	0.90	25.22	0.63	24.88
S0R4	0.83	24.88	0.50	18.23
S3R0	1.41	43.65	1.00	39.70
S3R2	1.31	40.52	0.94	33.62
S3R4	1.17	39.68	0.93	33.58

(dW/dV reduced up to 29%, depending on the RAP content), thus demonstrating a lower thermal cracking resistance, due to the stiffer behavior of the aged RAP binder (Behnia et al. 2011). The outlined trend is confirmed for the mixes in conditions of post-long term ageing, with greater differences of dW/dV, up to 34%.

However, the detrimental effect of the RAP, is much less pronounced for the mixes with steel slags. The reductions of dW/dV are no greater than 9% and 15%, for unaged and aged mixtures, respectively. Despite the aged condition of the RAP binder, the integration of the steel slags in the aggregate structure involved an improved ductility at low temperature and therefore a greater resistance to thermal cracking, probably due to the higher OBC of the mixtures containing EAF steel slags.

4 CONCLUSIONS

The paper discusses an experimental investigation concerning the moisture damage resistance and the low temperature response of asphalt concretes for road base courses, made with RAP and EAF steel slags.

Both the recycled aggregates studied have shown physical-mechanical characteristics substantially equivalent to those of natural stone aggregates usually used in transport infrastructure construction. Moreover, no hazardous leaching behavior was reported for the EAF steel slags.

The experimental results are extremely satisfactory for all the mixtures made with recycled aggregates, especially for those prepared with RAP, in terms of both acceptance requisites (Air Voids, ITS).

The mixes with RAP and steel slags were characterized by low water damage, thus demonstrating a good durability.

The thermal cracking resistance resulted lower for the asphalt concretes made with RAP, even if large benefits come from the integration of the EAF steel slags in the aggregate structures of the RAP mixes.

The post-long term ageing of the mixes leads to a further reduction of the low temperature cracking resistance, even if of a small amplitude.

Of the five mixes with marginal aggregates, S3R4, made with 30% EAF steel slags and 40% RAP, showed to be the best in all the laboratory tests.

There is a full agreement in the ranking of the mixes, between the different performance tests used in the investigation, namely moisture damage and low temperature cracking tests.

REFERENCES

- Artamendi, I., Allen, B. & Phillips, P. Influence of temperature and aging on laboratory fatigue performance of asphalt mixtures. *Proc. 7th International RILEM Symposium on Advanced Testing and Characterization of Bituminous Materials ATCBM09, Rhodes, May 2009.*
- Behnia, B., Dave, E.V., Ahmed, A., Buttlar, W.G. & Reis, H. 2011. Investigation of effects of the recycled asphalt pavement (RAP) amounts on low temperature cracking performance of asphalt mixtures using acoustic emissions (AE). *Transportation Research Board 90th Annual Meeting Compendium of Papers, Washington, D.C., 23–27 January 2011.*
- Chiu, C. & Lu, L. 2007. A laboratory study in stone matrix asphalt using ground tire rubber. *Construction and Building Materials* 21: 1027–1033.
- Italian Ministry of Infrastructures and Transportation-CIRS. 2001. *Norme tecniche di tipo prestazionale per capitolati speciali d'appalto* (in Italian). Rome.
- Pasetto, M. & Baldo, N. 2012. Fatigue Performance of Asphalt Concretes with RAP Aggregates and Steel Slags. *RILEM Bookseries, 7th RILEM International Conference on Cracking in Pavements 2012*, Volume 4: 719–727.
- Pasetto, M. & Baldo, N. 2013a. Resistance to permanent deformation of road and airport high performance asphalt concrete base courses. *Advanced Materials Research* 723: 494–502.
- Pasetto, M. & Baldo, N. 2013b. Fatigue Performance of Asphalt Concretes made with Steel Slags and Modified Bituminous Binders, *International Journal of Pavement Research and Technology* 6 (4): 294–303.
- Pasetto, M. & Baldo, N. 2014. Influence of the Aggregate Skeleton Design Method on the Permanent Deformation Resistance of Stone Mastic Asphalt. *Materials Research Innovations* 18 (SUPPL. 3): S96–S101.
- SITEB. 2000. *Capitolato d'appalto per pavimentazioni stradali con bitume modificato* (in Italian). Rome.
- Wu, S., Xue, Y., Ye, Q. & Chen, Y. 2007. Utilization of steel slag as an aggregate for stone mastic asphalt (SMA) mixtures, *Building and Environment* 42: 2580–2585.

Evaluation of laboratory and field warm mix asphalt mixtures with high contents of reclaimed asphalt pavement

T.A. Ahmed & H. Lee

University of Iowa, Iowa City, Iowa, USA

C.M. Baek

Korea Institute of Civil Engineering and Building Technology, Ilsan, Korea

ABSTRACT: Rutting and moisture-induced damage are considered two of the main distress that impact the performance of the asphalt mixtures. The main objective of this paper is to evaluate the moisture susceptibility of the Polyethylene (PE)-Wax based Warm Mix Asphalt (WMA) with high contents of reclaimed asphalt pavement (RAP) in comparison with Hot Mix Asphalt (HMA), both in the laboratory and the field. Based on the Hamburg Wheel-Track (HWT) test results, the moisture susceptibility of both HMA and WMA mixtures improved as the RAP amount was increased. Although WMA mixtures did not perform as well as HMA mixtures with RAP contents of 30%, 40% and 50%, it performed as well as HMA when the RAP content was increased to 75%. The specially designed WMA additive improved the moisture susceptibility of both laboratory and field WMA mixtures with high RAP contents. The average densities of the HMA and WMA test sections in Iowa were 94.3%, and 93.9%, respectively and those of the HMA, and WMA test sections in Ohio were 94.6%, and 95.2% respectively, all of which met the target density of 94%.

1 INTRODUCTION

Reclaimed Asphalt Pavement (RAP) has been used widely in the U.S. and is the world's most recycled product. The 2007 average national usage rate of RAP in HMA was estimated to be 12% and NAPA set a goal to double the national average RAP content from 12% to 24% in five years (NCAT 2010). A recent FHWA report stated that average RAP use is estimated at 12% in HMA and over half of the country uses less than 20 percent RAP in HMA (Copeland 2011). One of the most difficult aspects of designing a mix with high RAP content is to meet the volumetric mix design criteria due to a large amount of fine aggregate materials coming from the RAP materials (FHWA 2008). The Iowa DOT currently limits the maximum RAP use for the surface course to 15%. More than 15% RAP material can only be used when there is quality control sampling and testing of the RAP material; however, at least 70% of the total asphalt binder must be from a virgin source (Iowa DOT 2010). In addition, Iowa DOT requires a minimum asphalt film thickness (AFT) to ensure sufficient asphalt binder coating of the aggregate structure (Iowa DOT 2008). However, this AFT criterion also limits the RAP content due to the high dust content in the RAP materials.

Increased RAP contents also require changes in the performance grade of the virgin binder used because of the increased stiffness of the aged RAP binder.

The mixtures with a high RAP content (>20%) were found to be susceptible to low temperature cracking (McDaniel et al. 2000). It was recommended that up to 22% RAP can be added to the mixture without changing the low temperature grade of a -22 binder and up to 40% RAP can be added to a mixture as long as the virgin binder grade is one grade lower than the design binder grade (Beeson et al. 2010). In Iowa, if the amount of recycled binder from the RAP material exceeds 20% of the total asphalt binder, the designated virgin binder grade for the mix must be reduced by one temperature grade (Iowa DOT 2011).

The main objective of this research is to evaluate the rutting and moisture sensitivity of Warm Mix Asphalt (WMA) with varying contents of reclaimed asphalt pavement (RAP). First, the optimum fractionation sieve size was identified to isolate RAP materials within the stockpile that contained higher amounts of fine aggregate. Second, HMA and WMA (with a Polyethylene Wax-based additive) mix designs and Hamburg Wheel-Track (HWT) tests were performed with varying RAP contents accounting for a replacement of up to 75% of the total mixture's asphalt binder for a traffic level of 0.3 million ESALs. Finally, for field implementation under a traffic level of 10 million ESALs, HMA and WMA (with a specially designed PE Wax-based additive for a high RAP content) mix designs, HWT and Modified Lottman tests were performed on both laboratory and field mixtures.

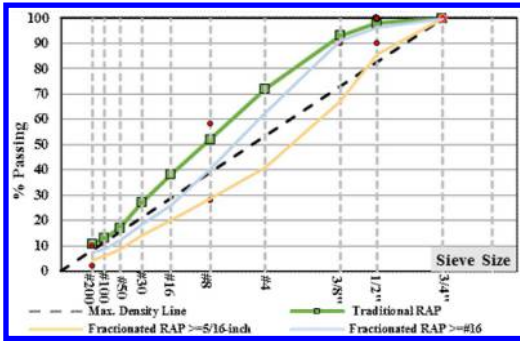


Figure 1. Aggregate gradation analysis.

2 RAP MATERIAL COMPOSITION ANALYSIS

In order to identify the optimum sieve size for fractionating RAP materials, a sieve-by-sieve analysis was performed on the recovered aggregates from the RAP materials retained on each sieve. The analysis showed significant variations in the asphalt content of the RAP materials retained on each sieve. It was concluded that the fractionation method was very effective in improving volumetric properties of the HMA mixture with a high RAP content (Shannon 2013). Figure 1 shows aggregate gradation analysis for the recovered aggregates from the traditional RAP (before fractionation) and the fractionated RAP materials retained on sieve sizes of No. 16 and 5/16-inch adopted for this study. The fractionated RAP materials contained less asphalt content than traditional RAP stockpile. Thus, in order to meet Superpave mix design requirements, it was necessary to fractionate the RAP materials.

3 EVALUATION OF LABORATORY MIXTURE

3.1 Materials

A Polyethylene (PE) wax-based WMA additive was used for this study which has a melting point of 100°C and crystallization point of 90°C. The selected PE wax-based WMA additive is positively charged to enhance the bonding of asphalt binder to aggregate surface and controls the crystallization process to make it less brittle at low temperature (Lee et al. 2013). Additionally, another form of the PE wax-based additive was specially designed to enhance the performance of the WMA mixtures with high RAP amounts by improving the rheological properties of the aged asphalt in the RAP materials.

The target performance grade for the laboratory mixtures was PG 64-22. However, PG 58-28 binder was used because Iowa DOT requires lowering the high temperature grade by one level for the mixtures with more than 20% RAP materials. Mixing and compaction temperatures used for mixtures with PG 58-28 binder were recommended by the supplier as 300°F (150°C) and 285°F (140°C), respectively. The target binder used for field mixtures was PG 70-22 and,

therefore, PG 64-28 binder was used. Mixing and compaction temperatures for mixtures with PG 64-28 binder were recommended as 311°F (155°C) and 293°F (145°C), respectively.

Limestone virgin aggregates along with varying amounts of fractionated RAP from I-80 rehabilitation project in Iowa were used for designing the mix with 1/2-inch nominal maximum size. The fractionated RAP materials after discarding RAP materials passing a No. 16 sieve were used with varying amounts of 30, 40, 50, and 75 % by binder replacement. For the field implementation, the fractionated RAP materials after discarding RAP materials passing a No. 5/16-inch sieve were used with the highest possible amount of 30% approved by Iowa DOT. With 30% fractionated RAP, the volumetric properties of the WMA mixture were satisfied.

3.2 Mix design

A total of ten mix designs were performed: four WMA mixes using PE wax-based additive with varying amounts of fractionated RAP materials of 30, 40, 50 and 75% by a binder replacement, one WMA mix using the specially designed PE wax-based additive with 30% RAP plus five corresponding HMA control mixes. Mixing and compaction temperatures were established based on the current Iowa DOT mix design requirements for HMA mixtures including RAP materials. WMA minimum mixing and compaction temperature can be determined using the aging index of the used asphalt binder without changing the performance grade (Bonaquist 2011).

The mixing and compaction temperatures for WMA mixtures with PE wax-based additive were determined to be 275°F (135°C) and 250°F (125°C), respectively and those for corresponding HMA mixtures were 300°F (150°C) and 285°F (140°C), respectively. Mixing and compaction temperatures for WMA mixture with the specially designed PE wax-based additive were determined as 285°F (140°C) and 266°F (130°C), respectively and those for the corresponding HMA mixture were 311°F (155°C) and 293°F (145°C), respectively.

3.3 Hamburg wheel-track test of laboratory mix

HMA loose mix was short-term aged for 4 hours at 135°C (275°F) followed by 2 hours at the compaction temperature. WMA loose mix was short-term aged for 2 hours at the compaction temperature followed by 16 hours at 60°C (140°F) (Bonaquist 2011). The rutting and moisture sensitivity evaluation of HMA and WMA mixtures was performed. Hamburg Wheel-Track (HWT) test is completed when the rut depth reaches 20 mm or until 20,000 passes are applied. HWT test results of WMA mixtures with PE wax-based additive and the corresponding HMA mixtures are plotted in Figure 2.

As can be seen from Figure 2, both HMA and WMA mixtures with 30% RAP by binder replacement didn't

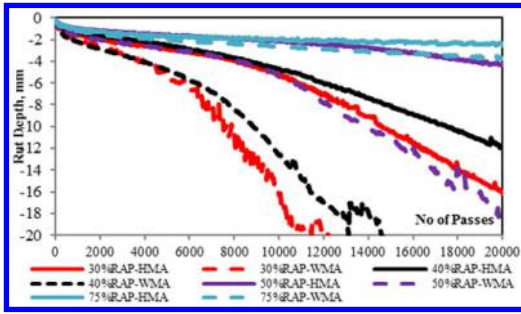


Figure 2. HWT test results of HMA and WMA mixtures at various percentages of RAP.

pass the HWT test with Stripping Inflection Point (SIP) values of 8,000 and 6,250, respectively. HMA mixtures with 40% RAP passed the test with the average maximum rut depth of 12.0 mm whereas WMA mixtures failed at 13,075 passes. The average SIP were 10,500 passes for HMA specimens and 6,875 passes for WMA specimens. Both HMA and WMA mixtures with 50% RAP by binder replacement passed the test with the average maximum rut depths of 4.2 mm and 18.5 mm, respectively. The average SIP values were 15,000 passes for HMA specimens and 10,750 passes for WMA specimens. Overall, the SIP values for both HMA and MA were significantly higher when the RAP amount was increased from 30% to 50%. Both HMA and WMA mixtures with 75% RAP by binder replacement passed the test with average SIP values greater than 20,000 passes and average maximum rut depths of 2.5 mm and 3.8 mm, respectively.

HWT test results of WMA mixtures with PE wax-based additive, WMA mixture with specially designed PE wax-based additive and the corresponding HMA mixtures are plotted in Figure 3. Both HMA and the specially designed WMA specimens with 30% RAP by binder replacement were tested again and the test results are plotted along with those of previous specimens with the same RAP contents in Figure 3. As can be seen from Figure 3, both HMA and specially designed WMA specimens passed the test with average maximum rut depths of 2.8 mm and 5.4 mm, respectively. The specially designed WMA mixtures for 30% RAP content exhibited a better performance than the regular WMA mixtures using PE wax-based additive with the same RAP content.

3.4 Modified Lottman test of laboratory mix

The specially designed WMA laboratory mixtures were tested using modified Lottman test. Figure 5 shows the indirect tensile strength (ITS) values with the numbers above the bars representing the average values and the whiskers representing the standard deviations. Overlapping of the standard deviations implies a similarity in the measured ITS values between the mixtures types. As can be seen from Figure 5, the specially designed WMA laboratory mixture exhibited a slightly lower conditioned ITS value than HMA

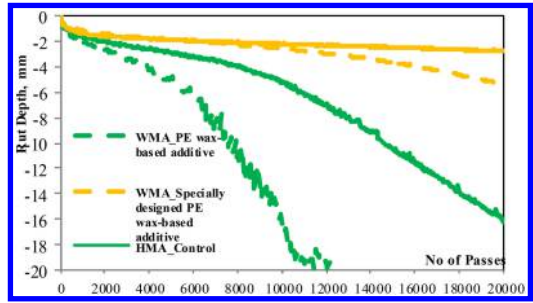


Figure 3. HWT test results of regular vs. special WMA with 30% RAP.

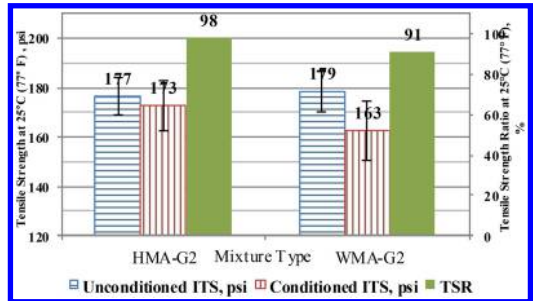


Figure 4. TSR test results of HMA and WMA.

mixture resulting in slightly lower Tensile Strength Ratio (TSR) value. Overall, both HMA and specially designed WMA mixtures met the minimum TSR requirement of 80%.

4 EVALUATION OF FIELD MIXTURE

The 0.5-mile long WMA test section was constructed in the evening of September 9, 2013 on the west bound section of Highway 6, Iowa City, Iowa. The 1.5-inch thick WMA surface layer was placed on top of 1.5-inch HMA intermediate layer. The mix was designed following Iowa DOT's Superpave mix design requirements for a high traffic level of 10 million ESALs. The mixtures used limestone virgin aggregate and 30% fractionated RAP by binder replacement (38% RAP by weight). WMA mix was prepared using a specially designed PE wax-based additive at a rate of 1.5% of asphalt content.

The target binder selected for asphalt mixtures with up to 20% RAP materials was PG70-22. Because Iowa DOT requires the binder grade to be lowered by one grade level for mixture with more than 20% RAP, PG 64-28 was used for building the test section. With an optimum asphalt content of 4.30%, HMA mixture was produced at 330°F (165°C) and WMA at 270°F (132°C). As shown in Figure 5a. and 5b., respectively, HMA mixtures produced significant amount of asphalt fume whereas WMA mixtures did not produced very little asphalt fume. To measure the field



Figure 5. Photos during construction of (a) HMA and (b) WMA.

densities, six cores were obtained from each test section. The target density was 94% and the average densities of the HMA and WMA test sections were 94.3%, and 93.9%, respectively.

The 1.0-mile long WMA test section was constructed on State Highway 158, Lancaster, Ohio in the evening of September 16, 2013. The WMA test section consisted of a 1.25-inch thick surface layer placed on top of 1.75-in WMA intermediate layer. The WMA mix was prepared using the regular PE wax-based additive at a rate of 1.5% of asphalt content. The mixtures were designed following Ohio DOT's Marshall mix design procedure. A blend of limestone and natural gravel aggregates were used along with 20% RAP materials by weight. The PG 70-22M binder was used for both HMA and WMA mixtures with an optimum asphalt content of 6.2%.

Overall, the WMA mixtures showed better workability during construction, which resulted in less compaction effort than HMA mixtures. The target field air voids during compaction was 6.0% and the nuclear gauge method was used to measure the mat densities during construction. Three cores were extracted and used to calibrate the nuclear gauge and four to six different locations per mile were selected to measure the densities of the surface layer. The average densities of the HMA, and WMA test sections were 94.6%, and 95.2% respectively.

4.1 Hamburg wheel-track test of field mix

HWT test results of HMA and WMA mixtures from Iowa and Ohio test sections are plotted in Figure 6. Both HMA and WMA mixtures from test sections passed the HWT test with average rut depths of 2.6 mm and 4.5 mm, respectively, from Iowa and 3.2 mm and 8.2 mm, respectively, from Ohio. The average SIP values were greater than 20,000 passes for all mixtures except for the WMA mixture from Ohio with an SIP value of 12,083 passes. Overall, all mixtures from Iowa and Ohio test sections exhibited an excellent rutting and moisture resistance. Particularly, specially designed WMA mixtures with high RAP contents

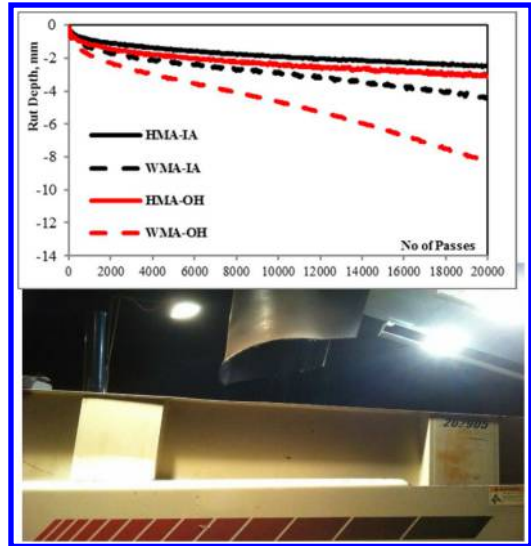


Figure 6. HWT test results of field mixtures of HMA and WMA.

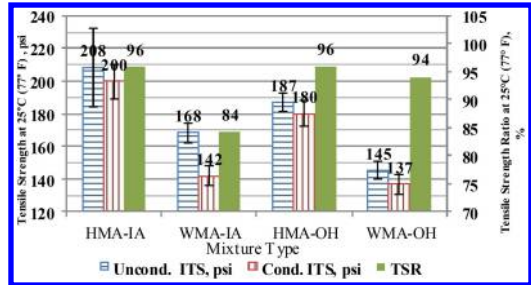


Figure 7. TSR test results of field mixtures of HMA and WMA.

applied in the Iowa test section exhibited an excellent performance.

4.2 Modified Lottman test of field mix

Figure 7 shows the indirect tensile strength (ITS) test results with the numbers above the bars representing the average values and the whiskers representing the standard deviation. WMA mixtures from Iowa exhibited lower ITS and Tensile Strength Ratio (TSR) values than HMA mixtures. However, TSR values of both HMA and WMA mixtures exceeded the minimum requirement of 80%. WMA mixtures from Ohio exhibited similar ITS values compared to HMA mixtures resulting in a similar TSR value. The TSR values of both HMA and WMA mixtures well exceeded the minimum requirement of 80%.

5 SUMMARY AND CONCLUSIONS

Based on Hamburg Wheel-Track (HWT) tests, it was found that RAP content had a significant impact on

the rutting and moisture susceptibility of both WMA and HMA mixtures. With RAP materials less than 50% by binder replacement, WMA mixture with PE wax-based additive did not perform as well as HMA mixtures. However, for 75% RAP materials, both WMA and HMA performed well with little or no rutting. Therefore, it can be concluded that high content of RAP materials improves the moisture susceptibility of both WMA and HMA mixtures. Based on modified Lottman tests, it was found that both HMA and WMA mixture with the specially designed PE wax-based additive exhibited an excellent resistance to moisture damage.

The test sections of WMA mixtures using the regular and the specially designed PE wax based additives were successfully constructed in Ohio and Iowa, respectively, and successfully met the field density requirements. WMA mixtures in these two test sections were found to be workable and easy to compact while producing less fume during construction. HMA and WMA field samples from the test sections successfully passed the HWT test and exhibited an excellent resistance to rutting and moisture damage.

The average densities of the HMA and WMA test sections in Iowa were 94.3%, and 93.9%, respectively and those of the HMA, and WMA test sections in Ohio were 94.6%, and 95.2% respectively, all of which met the target density of 94%. Based on the evaluation of both laboratory and field samples, it can be concluded that the specially designed PE wax-based WMA additive significantly improved the moisture susceptibility of the WMA mixtures with high RAP contents.

REFERENCES

- Beeson, M., Prather, M. & Huber, G. (2010). Characterization of Reclaimed Asphalt Pavement in Indiana: Changing INDOT Specification for RAP. In *Proc. 89th Annual TRB Meeting*, TRB, Washington, DC.
- Bonaquist, R. (2011). Mix Design Practices for Warm Mix. *Report No. NCHRP 691*, NCHRP, TRB.
- Copeland, A. (2011). Reclaimed Asphalt Pavement in Asphalt Mixtures: State of the Practice. *Report No. FHWA-HRT-11-021*. FHWA.
- FHWA (2008). User Guidelines for Waste and Byproduct Materials in Pavement Construction. *Report No. FHWA-RD-97-148*. FHWA.
- Iowa DOT (2010). Standard Specifications: Hot Mix Asphalt Mixtures. *Section 2303*. Iowa DOT.
- Iowa DOT (2011). Standard Specifications: Instructions for RAP in HMA Mixtures. *Materials I.M. 505*. Iowa DOT.
- Lee, H., Glueckert, T., Ahmed, T., Kim, Y., Baek, C. & Hwang, S. (2013). Laboratory Evaluation and Field Implementation of Polyethylene Wax-Based Warm Mix Asphalt Additive in USA. *International Journal of Pavement Research and Technology*, CSPE, Vol. 6 No. 5, pp. 547–553.
- McDaniel, R., Soleymani, H., Anderson, R., Turner, P. & Peterson, R. (2000). Recommended Use of Reclaimed Asphalt Pavement in the SuperPave Mix Design Method. *NCHRP Web Document 30*. TRB.
- NCAT (2010). Progress on Goal to Increase RAP Content. *Asphalt Technology News*. Vol. 22, No. 1. NCAT.
- Shannon, C., Lee, H., Tang, S., Williams, C. & Schram, S. (2013). Development of Optimum Fractionation Method for High-RAP Mixtures by Sieve-by-Sieve Analysis of RAP Materials. In *Proc. 92nd Annual TRB Meeting*, TRB, Washington, DC.

Environmental impact demonstrated by carbon footprint of cold recycling pavement technology

V. Snizek & J. Valentin

Czech Technical University in Prague, Czech Republic

M. Engels

Wirtgen GmbH, Germany

ABSTRACT: This paper presents detailed analysis of the cold recycling process with a focus on describing precisely the contribution to the reduction of CO₂, NO_x + HC emissions, CO and particle matters with respect to used machinery and the material processing. Impact is calculated from real selected job sites. The contribution caused of greenhouse gas emissions mainly by material production and machinery operation was studied as one of the objectives set within the European CoRePaSol project. Regarding the use of less traditional rehabilitation method of cold recycling, authors were also aware of potential differences within the life cycle of the newly reconstructed pavement. Exact data from machine measurements were ensured by the Wirtgen GmbH (producer of cold milling and recycler machinery) and the methodology was prepared by the Czech Technical University in Prague as a base for latter calculation tool combining traditional carbon footprint calculators with simple LCC approach (not included in this stage). This close cooperation allowed completion of the research with an objective result covering cold recycling technology done in-situ. It created ideal base for similar ongoing research on other alternative pavement rehabilitation technologies and their variants, as hot in-place asphalt recycling or in-plant recycling techniques. Final part of this paper concludes the total impact of CO₂ and other emissions and proofs, how minimally contribute used machines if compared to material production (bitumen and hydraulic binders) in terms of the total CO₂ production.

1 INTRODUCTION

Similarly to the duration of each construction process, even the renovation or construction of roads leads to formation of harmful substances, particularly in the form of air pollution emitted into the air. These substances occur in both the manufacture of primary construction materials (e.g. asphalt, hydraulic binder, aggregate) as well as during the processing of secondary materials (e.g. recycled asphalt material/RAP). Among another emission producers are building machines that provide handling, excavation, paving, spreading, compaction and other activities during the construction or demolition of an asphalt pavement. Influences of the above activities on the environment cannot be completely eliminated, but it is within the interests of the industry and the possibilities of the state to minimize these effects.

During the construction process, especially linear, which involves handling and processing of large amounts of materials, impact on the environment plays a key role. Influence of used construction machinery is also significant but not dominant. Therefore in total, it can be expected that thrift of the machines to the environment will be more apparent when using the

material less demanding methods such rehabilitation via cold recycling which is done in-situ.

In comparison with the traditional method of reconstruction or continuous repair of roads (mill & fill) only minimum amount of material logistically moves between mixing plant and the job site. The primary advantage of this technology lies in the incorporation of bituminous or hydraulic binders with the aim to improve the technical properties of the material and to build a new, high-quality road surface, directly on site, without any further transport.

2 GREENHOUSE GASES AND AIR POLLUTION

One of the main causes of unavoidable climate change on Earth is the increasing concentration of greenhouse gases in the atmosphere. These gases, most important of which are CO₂ (carbon dioxide), CH₄ (methane), N₂O (nitrous oxide), SF₆ (sulfur hexafluoride) and CFCs (chlorofluorocarbons) cause increasing temperature of the Earth's surface due to the so-called Greenhouse effect. Greenhouse gases are produced primarily in mining and energy production from fossil fuels,

industrial production, transport, waste management and agriculture.

In this context, we are talking about the so-called carbon footprint, which reflects the amount of released carbon dioxide and other greenhouse gases during the life cycle of a product or service into the air. Carbon footprint is further divided into direct/indirect and primary/secondary. On one hand, the primary carbon footprint arises immediately during the man-made activities and leads to release of greenhouse gases, e.g. driving a car, airplane flight, cooking, heating, electricity consumption. On the other hand, secondary carbon footprint indicates the amount of CO₂ released during the entire product life cycle. It includes emissions associated with the production, processing, preparation, transportation and disposal of the product, (Snizek et al. 2014b).

2.1 Carbon dioxide (CO₂)

It is an element in the atmosphere widely abundant, however its natural balance has been disrupted due to anthropogenic and its concentration in the atmosphere is still increasing. It is the main gas contributing to greenhouse effect and the subsequent warming of the planet. The combustion of carbonaceous fossil fuels - oil products, natural gas, coal, coke and fuels of biological origin (biomass, wood, biogas, biodiesel), (CENIA 2013).

2.2 Nitrogen oxides (NO_x)

It is also a biogenic element, but mainly from anthropogenic sources. The emergence of these oxides is associated mainly with the burning of refined fuels – gas, oil, gasoline and biomass. The primary sources of nitrogen oxide emissions, despite the use of catalysts in motor vehicle (55 %) are; industry, trade and settlements (22 %); services (22 %). Major anthropogenic sources are also chemical processes in industry, where the nitrogen oxides present.

Biological processes in soils are the natural source of nitrogen oxides. The presence of nitrogen oxides and sulfur oxides in the atmosphere causes acid rain and the consequent negative impact on vegetation, surface waters sources, buildings and the global ecosystem. Moreover, high concentration of NO₂ (nitrogen dioxide) is one of the factors causing photochemical smog in the form of ground-level ozone (CENIA 2013).

2.3 Hydrocarbons (HC)

Designation HC represents a group of volatile organic compounds – hydrocarbon. This is essentially fluorinated hydrocarbons (HFCs), hydrochlorofluorocarbons (HCFCs) and polycyclic aromatic hydrocarbons (PAHs). While the fluorocarbons are completely anthropogenic and are used as coolants in refrigerators, freezers and air conditioning, Hydrochlorofluorocarbons are also used as propellants in aerosols, foams blown during construction work, during packing goods

and are also included in some fire extinguishers. In contrast, polycyclic aromatic hydrocarbons are being produced during combustion of almost any carbonaceous fuels, petroleum processing and production of aluminium. For the majority of living organisms are toxic and carcinogenic. They are soluble in fats and oils, whereas only minimally in water, (CENIA 2013).

2.4 Carbon monoxide (CO)

Carbon monoxide is extremely poisonous and flammable gas, and is the main product of incomplete combustion of carbon-containing material. The Carbon monoxide cause can also be a design flaw or defect in the combustion system. The largest source of emissions in cities is the internal combustion engine (95% CO), especially in places of intensive traffic, particularly when idling. Other sources of emissions are combustion devices such as furnaces, boilers, stoves and cookers. CO participates in the formation of photochemical smog and after spontaneous conversion (36–110 days) to carbon dioxide is part of the greenhouse gases, (CENIA 2013).

2.5 PM – Particulate Matter

Atmospheric aerosol may be of natural or anthropogenic origin. It arises as a negative product of human activity. The most important anthropogenic sources are combustion processes in power plants, furnaces, welding and car engines. An example of a natural resource issues is a volcanic eruption, forest fires and dust on the wind. If this is the dust and particles that were taken from construction sites, eroded agricultural, mining and other areas, then this aerosol would also be anthropogenic. The size of entrained particles is related to the duration of their stay in the atmosphere before settling back to the surface (the smallest particles settle to a few weeks). Solid particles in the atmosphere scatter the solar radiation back into space, thus affecting the energy balance of the Earth, (CENIA 2013).

3 COMMON METHODS OF PAVEMENT REHABILITATION

Apart from the traditional method of pavement rehabilitation, nowadays, we are increasingly encountered with relatively new technology of road rehabilitation, especially in the form of recycling materials already incorporated. Recycling is done either directly at the construction site or in a mixing plant/centre, (Snizek et al. 2014a, Valentin 2009). If speaking about in-situ solutions mainly cold in-place or hot in-place recycling has to be mentioned. In both cases special machinery is used to disaggregate the existing pavement layer(s), add necessary new material or new binders, mix and repave. This process is usually done in one step with final compaction or grading and compaction of the in situ prepared mix. In the case of in-plant solutions the reclaimed material is added as aggregate substitute

Table 1. Traditional methods for reconstruction, (Snizek et al. 2014a).

- + Universally applicable
- + Can be also used for local roads within urban areas
- + Long-time experience
- + Relatively low demand for machinery within the implementation phase
- Intense for material resources – large number and demanding logistical movements
- In comparison to other solutions more expensive

Table 2. Traditional Method with > 20 % by mass of reclaimed asphalt material, (Snizek et al. 2014a).

- + Less expensive than the traditional method
- + Re-use of already used material
- + Relatively low demand for machinery in the implementation phase
- Currently, some countries have unresolved technical regulations (RAP is not allowed to be added to wearing courses or its share is significantly restricted)
- Very small proportion of mixing plants is able to process higher amount of RAP material into a mixture
- Increased investment in mixing plant equipment, if it is to process larger shares of RAP material
- Problem in obtaining recycled asphalt in a good quality (roads are not being milled separately by individual layers in the Czech Republic)

to cold or hot asphalt mix. Then ready-to-use asphalt mix is carried to construction site and paved by standardized machinery. Paved layer with an asphalt mix containing reclaimed material can be done as wearing course as ell. In case of in-situ cold recycling it is always to overlay the recycled structure by y thin top layer or at least by surface dressing.

Recycled materials are often underestimated, although their quality can be often higher than the quality of newly produced mixtures and materials. For this reason it is necessary to check and compare different possibilities of pavement rehabilitation, considering recycling as an option, which can safe costs and reduce environmental impacts.

3.1 Traditional methods (Mill & Fill)

Traditional method of rehabilitation is based on the milling of the old pavement layers by milling machine and paving of the new pavement layers one by one by asphalt paver. Traditionally, there are mainly virgin materials for new material production used. For some layers, there might be up to 20 % of RAP added as a widely applied standard. Of course present technological status allows use more or less up to 100 % RAP (see 3.2). This method is connected to large quantities of material transported from and to the job site.

Table 3. Cold in-place recycling, (Snizek et al. 2014a).

- + Energy gentlest method of reconstruction
- + Low time-consuming reconstruction
- + Small amount of material transported to the job site in comparison to the traditional method
- + Minimal need for new material
- Difficult to be used on streets with gullies and manhole covers
- Requires a special machinery (recyclers) for performing this technology

Table 4. Hot in-place recycling, (Snizek et al. 2014a).

- + Small amount of material being transported from and to the construction site in comparison with the traditional method
- + Minimal need for new material
- Higher energy demand
- Requires special equipment for heating and processing of the mixture
- Difficult to be used on streets or roads with gullies and manhole covers (municipal roads and streets)
- Limited depth of recycling

3.2 Traditional method with the addition of more than 20 % of the RAP (Mill & Fill with x % RAP)

Traditional method of rehabilitation is based on the milling of the old pavement layers by milling machine and paving of the new pavement layers one by one by asphalt paver. There are not only virgin materials for new mix production used but also high content of RAP added (20 % and more). Only specially equipped mixing plants can utilize such volumes of RAP. Additionally, the method is connected to large quantities of material transported from and to the job site.

3.3 Cold in-place recycling

Cold in-place recycling mainly as an in-situ road reconstruction technology presents a modern and environmental-friendly way of pavement rehabilitation mainly suitable mainly for asphalt pavements. This method is related to the small scale of material transported of and on the job site. However, newly recycled pavement needs to be covered by thin asphalt wearing course. Cold recycling method usually requires special machinery – recycler.

3.4 Hot in-place recycling

Hot in-place recycling presents a modern way of flexible pavement rehabilitation on the job site. However, this method is very energy demanding but on the other hand reducing the volume of material transported of and on the job site. Hot recycling has a limited usage also in recycling depth.

Table 5. Basic project data.

Type of road:	asphalt pavement (interurban)
Length	1,200 m
Width	4.75 m
Rehabilitation depth	150 mm

Table 6. The content of binders in mixtures.

Binders:	% by mass of the mixture added
Foamed bitumen	2.5
Bitumen emulsion	3.5
Water	3.0
Cement CEM II 32.5 R	1.0

Table 7. Basic data of materials (production).

Mix component	Density (t/m ³)	CO ₂ (kg/t)	Data source
Water	1.00	0.30	IVL
Cement 32.5 R	1.25	980	IVL
Bituminous emulsion (60%)	1.00	221	Eurobitume
Foamed bitumen	1.10	285	Eurobitume

Table 8. Basic data of fuel (production and consumption).

Substance	Density (t/m ³)	CO ₂ (kg/l)	Data source
Diesel – refining	0.84	0.26	Afteroilv
Diesel – consumption	0.84	2.66	Czech Ministry of Environment

4 WORKED EXAMPLE

Worked example described in this paper presents an asphalt pavement, which can be reconstructed by the technological option of cold recycling or through the use of standard recycling techniques. The aim of this part of the paper is to compare the amount of CO₂ produced in the later material production (hydraulic and bituminous binders) and CO₂ produced by the machinery during the road rehabilitation process.

In order to present the result a worked example was chosen with the following input parameters, (Chehovits 2012).

Individual technologies include various combinations of the following binders in a defined quantity.

It is considered that for certain conditions during the reconstruction, any of the following reconstruction techniques or cold recycling technology can be used.

Table 9. Technology of the road reconstruction.

1 CR – foamed bitumen, pre-spread cement
2 CR – foamed bitumen, cement slurry
3 CR – bitumen emulsion, pre-spread cement
4 CR – bitumen emulsion, cement slurry
5 CR – foamed bitumen
6 CR – bitumen emulsion
7 REC – pre-spread cement
8 REC – cement slurry
9 Pulverization

NOTE: CR = cold recycling, REC = recycling
Pulverization – should be understood as a very seldom-single used technique only applicable to roads with light traffic. This technique can be used in combination with other mentioned techniques together with pre-spread material (fines, aggregate). It is not a typical recycling technique.

Table 10. Average consumption of machines in the project (l/m²).

Construction machine	Fuel	Consumption (l/m ²)
Binding agent spreader	Diesel	0.0022
Water tanker	diesel	0.0046
Bitumen tanker	diesel	0.0052
Recycler (WR 240i)	diesel	0.0788
Padfoot compactor	diesel	0.0077
Vibratory compactor	diesel	0.0077
Grader	diesel	0.0109
Tandem roller	diesel	0.0077
Static roller	diesel	0.0070

*Fuel consumption is calculated on the basis of work done and the fuel consumption per working day (day snapshot).

Cold in-situ recycling is carried out by machines, comprising mainly of standard equipment used in construction processes (rollers, graders, cement spreader, water and asphalt tankers, etc.). Besides the standard construction machines, part of the set is also formed by special machines, mainly recyclers and cement slurry mixer. The assembly can also involve some specially equipped types of milling machines, which can replace the recycler for certain projects. The largest number of machines is needed for the implementation of road reconstruction in the case of cold recycling with foamed bitumen and pre-spread cement. The table below shows the average fuel consumption data corresponding with the construction machines, (Snizek et al 2012).

The amount of CO₂ produced per 1 m² of surface project is bound primarily to fuel consumption, in this case diesel. For the worked example values are summarized in Table 11.

The table below summarizes the total amount of CO₂ produced and consumed quantity of fuel for each machine within the worked example (cold-in place recycling with foamed bitumen and cement).

The recycler, as well as any other machine in the set can be replaced with another machine having the

Table 11. Average production of CO₂ by machines (t/m²).

Construction machine	CO ₂ (t/m ²)*
Binding agent spreader	6.502E-06
Water tanker	1.356E-05
Bitumen tanker	1.520E-05
Recycler (WR 240i)	2.302E-04
Padfoot compactor	2.276E-05
Vibratory compactor	2.276E-05
Grader	3.204E-05
Tandem roller	2.276E-05
Static roller	2.071E-05

*The calculation of CO₂ emissions is based on the work done and the amount of emissions per day snapshot, (Kawakani et al 2012, Chehovits 2012)

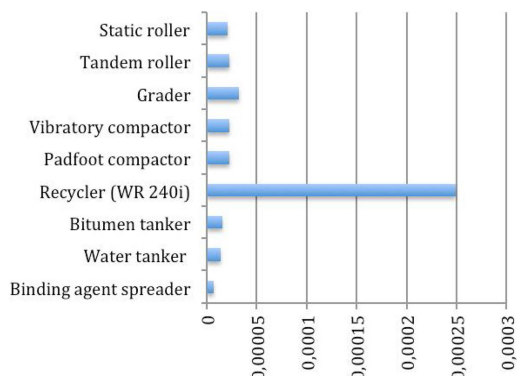


Figure 1. Average CO₂ production by machines (t/m²).

Table 12. Total CO₂ produced and consumed fuel on the worked example.

Construction machine	Consumption of fuel (l)*	Produced CO ₂ (t)
Binding agent spreader	12.69	0.0371
Water tanker	26.48	0.0773
Bitumen tanker	29.69	0.0867
Recycler (WR 240i)	449.37	1.3121
Padfoot compactor	44.44	0.1298
Vibratory compactor	44.44	0.1298
Grader	62.56	0.1827
Tandem roller	44.44	0.1298
Static roller	40.44	0.1181
Total	755	2.20

*Fuel consumption is calculated on the basis of work done and the fuel consumption per working day (day snapshot).

same capabilities. Following such modification, of course, the fuel consumption and CO₂ production varies. In order to maximise efficiency and workload on jobsite the machine specification should match the project specification. In the case of recyclers it is recommended to carefully choose their working width depending on the total project working width. The

Table 13. Alternative recyclers for the project

Construction machine	Consumption fuel (l)	Produced CO ₂ (t)
Recycler (WR 200, 3rd)	517.36	1.5107
Recycler (WR 200i, 4rd)	486.32	1.4201
Recycler (WR 2400, 1st)	396.15	1.1568
Recycler (WR 2500S, 2nd)	362.15	1.0575

Table 14. Average fuel consumption and CO₂ production of alternative recyclers.

Construction machine	Average fuel consumption (l/h)*	Average CO ₂ production (t/h)*
Recycler (WR 200, 3rd)	50	0.1511
Recycler (WR 200i, 4rd)	47	0.1420
Recycler (WR 2400, 1st)	67	0.2024
Recycler (WR 2500S, 2nd)	70	0.2115

*Fuel consumption is calculated on the basis of work done and the fuel consumption per working day (day snapshot).

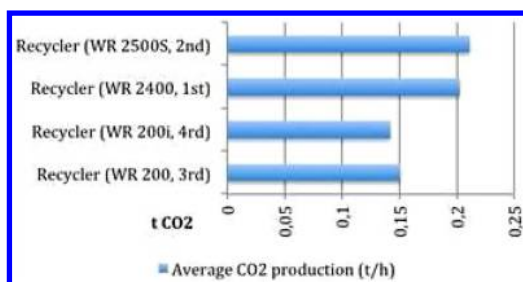


Figure 2. Average CO₂ production of alternative recyclers on project.

table below compares alternative recyclers for assembly machines, (Snizek et al 2012) and the consequence of an unfavourable choice.

Although the recycler WR 200i is the most environmental-friendly one from the four selected machines, it operates with narrow swath while the desired width of the recycled pavement is larger (see Table 14 and Figure. 2). Therefore, when comparing with other three machines the WR 200i and also WR 200 must execute 3 runs while the other two only 2 runs.

Despite the fact that construction machinery significantly contributes to the production of CO₂ during the road reconstruction, the largest producer of CO₂ is the industrial production of subsequently incorporated materials (hydraulic and bituminous binders in particular). Table 15 presents total CO₂ production during the production process for each incorporated material used in various combinations within the identified rehabilitation methods. Percentage of weight presents average content of material (binder or water) in the new

Table 15. Total production of CO₂ during the production of materials in the worked example (t/m²).

Construction machine	% weight in the mixture	CO ₂ (t)
1 Water	3.0	0.05
2 Cement CEM II 32.5 R	1.0	104.15
3 Cement slurry	4.0	127.07
4 Bit. emulsion (60%)	3.5	28.64
5 Foamed bitumen	2.5	36.94

Reference data sources: 1-IVL; 2-Athena & IVL; 3-Athena & IVL; 4-Eurobitume; 5-Eurobitume

Table 16. Technological variants focusing on CO₂ – Material and machines.

Technology of rehabilitation	CO ₂ (t) (kg/m ²)	Total CO ₂ (t)
1 CR – foamed bit., pre-spread cement	6.60	37.63
2 CR – foamed bit., cement slurry	6.53	37.24
3 CR – bit. emulsion, pre-spread cement	6.80	38.78
4 CR – bit. emulsion, cement slurry	6.82	38.87
5 CR – foamed bitumen	2.93	16.68
6 CR – bitumen emulsion	3.13	17.82
7 R – pre-spread cement	3.98	22.66
8 R – cement slurry	4.01	22.87
9 Pulverization	0.28	1.60

Data source: OptiRec software application (calculation based on data from machine producer and European emission standards)

cold recycled mixture. Values of CO₂ are calculated by the OptiRec software application based on inventories which are used within the calculation tool. Sources of unit reference numbers are show under the table.

The table below gives a general overview of available technological options with a focus on the production of CO₂ by machines and from material manufacturing. The table also includes the estimated quantity produced per m² of the project with the implemented technology.

The final part of this chapter is devoted to the proof of a minimum share of CO₂ production by construction machines involved in the road reconstruction. Following Table 16 and Figure 3 CO₂ emissions produced by the whole set of machines used for the technology are within 5-10 % of the total amount of CO₂ produced. The remaining major amount is produced during the production and processing of the incorporated material, (CENIA 2013).

5 CONCLUSION

It can be concluded that in the case of road reconstruction with one of the cold in-place recycling techniques 90-95 % of emissions are generated during the production process of used construction materials, mainly

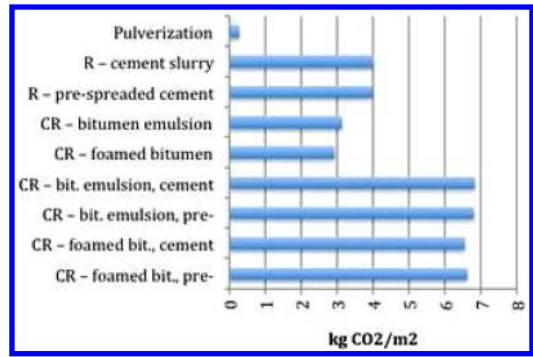


Figure 3. Overview of project's total CO₂/m² for each technology including material and machines.

Table 17. Technological variants and source of CO₂

Technology of rehabilitation	CO ₂ (t) material	CO ₂ (t) machines
1 CR – foamed bit., pre-spread cement	35.86	1.78
2 CR – foamed bit., cement slurry	35.69	1.55
3 CR – bit. emul., pre-spread cement	37.14	1.63
4 CR – bit. emul., cement slurry	36.97	1.90
5 CR – foamed bitumen	15.03	1.65
6 CR – bitumen emulsion	16.31	1.51
7 R – pre-spread cement	20.85	1.81
8 R – cement slurry	20.68	2.19
9 Pulverization	00.02	1.58

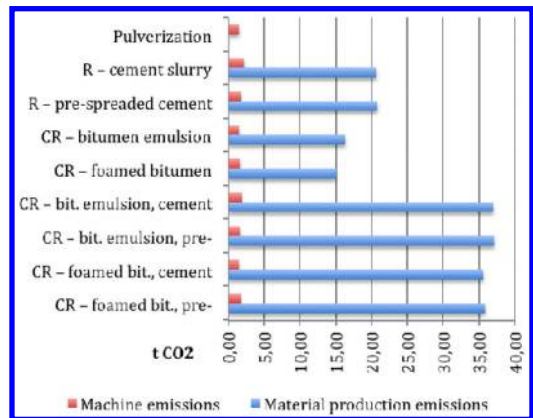


Figure 4. Technological variants and sources of CO₂.

the binders, where the crucial part of CO₂ is emitted. The influence of construction equipment used for road reconstruction remains in minority, reaching about 5-10 %.

The society should therefore seek primarily to eliminate just the emissions from the production and processing of building materials, and to maximize support for the use of once used and incorporated materials.

Recycled materials are often underestimated, although their quality can be often higher than the quality of newly produced mixtures and materials.

In this relation if going to answer the question of the impact of construction machinery on CO₂ emissions during cold recycling process as key emitter the recycler can be identified. Since cold-in place recycling runs complete recycling passage arrangement (up to 9 machines in some extremes), an important role is played by the recycler's working width in relation to the width of the reconstructed pavement. If possible, it is advisable to choose recycler with such working width that the number of crossovers during the road reconstruction is minimized and the grip of recyclers used to its maximum efficiency. In this way the emission and economic influences of the machinery will be minimized.

ACKNOWLEDGEMENT

This presentation has been supported by the research project Characterization of Advanced Cold-Recycled Bitumen Stabilized Pavement Solutions (CoRePaSol) carried out as part of the CEDR Transnational Road research Programme Call 2012. The funding for the research was provided by the national road administrations of Belgium (Flanders), Denmark, Finland, Germany, Ireland, Netherlands, Norway, Sweden and UK.

REFERENCES

- All calculations for this article were made by a software tool OptiRec v 6.38 (Dipl. Ing. Vaclav Snizek, CTU in Prague – Faculty of Civil Engineering).
- CENIA and Ministry of Environment of The Czech Republic (2013). Information about the substances reported to IPR, *web page*: <http://www.irz.cz/node/20>
- Chehovits & Galehouse (2012). Energy Usage and Greenhouse Gas Emissions of Pavement Preservation Processes for Asphalt Concrete Pavements, *National Centre for Pavement Preservation*, Okemos, Michigan, United States.
- Kawakami et al. (2012). Study on CO₂ Emissions of Pavement Recycling Methods, *1-6 Minamihara, Tsukuba-shi, Ibaraki, Japan*.
- Snizek et al. (2012). Roads, Related Constructions and Means of Their Management, *ISBN 978-80-01-04 996-9*, CTU in Prague.
- Snizek et al. (2014a). OptiRec - Instrument for the economical assessment of the road pavement reconstruction and recycling variants based on LCC, *ISBN 978-80-01-05446-8*, CTU in Prague.
- Snizek et al. (2014b). OptiRec - The Optimal Way of Road Structure Rehabilitation, *TRA 2014 – Transport Research Arena 2014*, Paris. 14.-17.04.2014
- Valentin (2009). Problems of Selected Performance Characteristics of Cold Recycling Mixes. *Ph.D. thesis*, CTU in Prague.

Preliminary assessment on the use of scrap glass to produce asphalt mixtures

E. Manthos

Aristotle University of Thessaloniki, Division of Transportation, Infrastructure and Regional Planning Engineering, Thessaloniki, Greece

G. Ridondelli, G. Betti & A. Marradi

University of Pisa, Department of Civil and Industrial Engineering, Pisa, Italy

ABSTRACT: Nowadays, increasing pressures to preserve natural aggregates and to minimize the amount of materials landfilled are forcing consideration of potential uses of waste materials in road construction and maintenance operations. This paper focus attention on possibility to use scrap glass as an aggregate in hot mix asphalt (namely “glassphalt”). The influence of glass on volumetric characteristics and resistance of HMA mixtures was analyzed through Marshall and gyratory compaction and indirect tensile tests. Glass is brittle, rich in silicon and have a smooth surface, so the key performance parameters of glassphalt concrete are resistance to raveling and to water damage: the bottle-rolling test, the Indirect Tensile Strength Ratio (ITSR) and the Cantabro test were used to evaluate them. Based on the results obtained it was possible to define the particularities of glassphalt concerning mix design and laboratory tests, as well as the effects induced in the mixture by different percentage of glass.

1 INTRODUCTION

The purpose of this investigation was to determine benefits and disadvantages obtained adding different percentages of scrap glass to asphalt mixtures, and to define the particularities of glassphalt concerning mix design and laboratory tests. This was done considering that when waste materials are used, the performance should be carefully evaluated using proper tests, to verify its compliance with appropriate technical specifications.

A binder course type mixture (AC-16) with glass in partial substitution (10% and 15%) of natural aggregates was designed and tested. Furthermore, an AC-12.5 containing 10% of glass was considered in order to evaluate the level of raveling of surface courses. A standard AC control mixture was tested to obtain reference characteristics for comparison.

Mix design was performed following the technical prescriptions mostly used in Italy for road construction.

1.1 Overview

The term “glassphalt” refers to an asphalt mixture where a percentage of natural aggregates is replaced by waste glass, previously subjected to cleaning and crushing. The use of this type of material provides benefits to the environment, as an alternative to disposal of

residues of mixed-color glass, which cannot be totally allocated to the production of new recycled packaging and becomes a surplus of waste.

The earlier experiences date back to the 1960's in the United States, where the use of high quantities of glass cullet (up to 40%) in asphalt concrete by Washington DOT resulted in rutting and stripping effects (AASHTO 2008). Following this, Washington DOT discontinued the use of glass aggregates, despite tighter specifications leading to the successful use of crushed glass as an aggregate in other states (Goldman 1987). In the decade 1975-1985 a significant experience in the field was undertaken in the city of Baltimore, Maryland (USA). From 1990 to 1995 the Department of Transportation of New York has used approximately 225,000 tons of glass to produce hot mix asphalt (FHWA 2008). In 1992, the Department of Transportation of New Jersey has promoted an incentive program which provided for the extra payment of one dollar per ton of asphalt containing percentages of broken glass between 5 and 10% (Halstestad 1993). In New York percentages up to 5% of glass reduced in the form of very fine sand continued to be implemented in the bituminous mixtures (CWC 1996-1).

Glass can be classified as a hydrophilic material having an acid behavior, which is due to the silicate (SiO_2) constituent. Hence using glass in asphalt mixtures can result in low bitumen absorption, causing inadequate adhesion or stripping especially for

wearing courses: this issue can be overcome using a lime based additive. Moreover, inappropriately crushed glass resulting in long and flat particles can also contribute to stripping.

Those problems were solved crushing glass to obtain particles <4.75 mm (NYS 2004). It was also found that limiting the size of glass cullet to the dimensions of fine aggregate in mixtures for surface courses improves skid resistance (Su and Chen, 2002) and reduces the risk of fragmentation during HMA production and compaction phases, avoiding variation to the design gradation curve and undesired loss of density of the final mix.

Two of the major beneficial properties of glassphalt are the thermal inertia and the light reflection or “sparkle effect”. Thermal inertia refers to the ability of glassphalt to keep heat longer than traditional mixtures and thus to facilitate paving in a longer period after production. Furthermore this allows transport over greater distances from the central plant to the paving site. The reflection and the “sparkle effect” refer to the glass capability to reflect light, which improves the nighttime visibility on the road (CWC 1996-1).

Furthermore, glassphalt mixtures appear to be easier to compact and allow a reduction of the amount of bitumen in the mix than standard mixtures.

Another major issue with the use of glass in asphalt mixtures was the percentage of residual impurities, including metals, plastics, wood and other debris: all relevant specifications recommend that this percentage should be below 2% by mass (CWC 1996-1).

2 BACKGROUND

Several researchers have studied and analyzed the use of crushed glass in asphalt mixtures. Larsen (1989) has reported that glassphalt has been successfully placed at least in 45 locations in the U.S and Canada between 1969 and 1988. Most of the locations were city streets, driveways and parking lots. Potential problems observed were the loss of adhesion between bitumen and glass; reduction of skid resistance especially with coarse particles; breakage of glass and subsequent raveling under studded tires; lack of adequate and consistent supply of glass; increased production cost (5 \$/Mg more than the conventional HMA mix in Connecticut USA at the time of the study). The report concluded that glassphalt should be used only as base course and that glass particles smaller than 9.5 mm should be used. It was also noted that hydrated lime should be added in glassphalt in order to prevent stripping.

In 1990 a Virginia state feasibility study was conducted by Hughes (1990) and a relevant report was issued. The report was based on laboratory evaluation and economic analysis of a Virginia surface HMA mix (12.5 mm maximum aggregate size), using two glass contents (5% and 15%). The glass used was continuously graded with maximum nominal size of 9.5 mm. The report concluded that the use of glass tends to

reduce the VMA (Voids in the Mineral Aggregate) and air voids in Marshall compacted specimens. Consequently the optimum bitumen content is also reduced. Neither the resilient modulus nor the indirect tensile strengths were adversely affected by the addition of up to 15% of glass, however some separation at the asphalt/glass interface was observed.

The Florida Department of Transportation (Murphy et al. 1991) tested three HMA mixtures to determine the effects of crushed glass: A control mix of 9.5 mm nominal maximum size, a 15% coarse glass mixture and a 15% fine glass mixture. The coarse glass mixture was the same as the control mixture except that 15 percent of the screenings were replaced with coarse crushed glass (100% passing the 9.5 mm sieve), while the fine glass mixture was the same as the control mixture except that 15 percent of the screenings were replaced with fine (100% passing the 4.75 mm sieve) crushed glass. AC-30 asphalt binder with and without antistripping agent was used to prepare Marshall specimens to be tested for tensile strength. The study showed that Marshall stability values decreased by 12–15% and dry indirect tensile strength decreased by 20% when 15% of the screenings were replaced with either coarse or fine glass. Tensile Strength Ratio values were 70%, 85% and 50% for control mix, coarse glass mix and fine glass mix respectively, either with or without an antistripping additive; it was found that adhesion promoters were unable to reduce the moisture damage.

Maupin (1998) considered two surface mixes that resulted prone to stripping on the basis of previous experiences. A chemical additive and hydrated lime were used as antistripping agents. Four levels of glass were used (ranging from 0% to 20%). The allowable Tensile Strength Ratio (TSR) of 0.85 and trends of wet strength curves were used to determine the maximum amount of glass that could be safely used. The TSR test did not indicate a significant negative effect when adding up to 12% glass. At 20% glass content, hydrated lime showed a significantly better effect than the chemical additive. The study recommends a maximum glass content of 15% to be used in asphalt concrete.

NCHRP report 435 (2013) gives a summary of glass cullet uses. It is mentioned that glassphalt has been used for over 30 years on country roads, highways, and even airport runways. As stated, lifetime, wear, slippage and cracking of glassphalt mixtures have proven to be comparable to conventional surface materials.

3 EXPERIMENTAL PROGRAM

The present research activity was primary aimed to assess the possibility of using crushed glass in partial substitution (10% and 15%) of natural aggregates for production of hot mix asphalt “glassphalt” for road pavement construction.

Mainly, a binder course type mixture (AC-16) was designed and tested. Furthermore, an AC-12.5 containing 10% of glass was considered in order to evaluate the level of raveling of surface courses.

Mix design was performed following the main technical prescriptions used in Italy for road construction (ASPI, ANAS, CIRS), to control aggregate characteristics, mix composition (bitumen and voids percentage) and performance (Marshall, volumetric and ITS values).

Mix design was referred to a standard AC control mixture (containing 0% of glass scrap). It is worth noting that the mixtures grain size distribution does not change as a result of substitution of natural aggregate with glass; this led to consider the volumetric and mechanical parameters of the mixture such as voids and strength depend only on physical and chemical characteristics of the glass (for the same bitumen content), and not on variation of particle size distribution and bitumen content.

Mix design volumetric method refers to three numbers of gyrations: N_i , N_d and N_m (where the subscripts i, d, m mean respectively initial, design and maximum). N_d describes the mixture state once the pavement has been built, while N_i and N_m are referred to compaction phase and long term behaviour (rutting) respectively. The Italian Technical Specifications considered in this study establish, for each AC type, N values that are referred to typical freeway and minor/major highway traffic levels and to national climate conditions:

$$\begin{aligned} N_i &= 10 \text{ (\%v} \approx 10\text{--}15\text{)}; \\ N_d &= 100\text{--}130 \text{ (\%v} \approx 3\text{--}6\text{)}; \\ N_m &= 180\text{--}220 \text{ (\%v} \geq 2\text{)}. \end{aligned}$$

Aggregates characteristics were evaluated by means of the following series of tests:

- petrographic analysis;
- flakiness index;
- particle density;
- Los Angeles coefficient;
- rolling bottle test.

The following tests were performed on AC mixtures:

- determination of Marshall parameters;
- determination of voids @ N_i - N_d - N_m gyrations of gyratory compactor;
- determination of Indirect Tensile Strength (ITS) and Indirect Tensile Strength Ratio (ITSR);
- Cantabro test (for AC-12.5 type).

The Marshall compacted specimens were compacted applying 75 blows on each side and their diameter was 100 mm. The specimens used for determining the voids at different number of gyrations were compacted at 180 gyrations and their diameter was 150 mm.

The specimens used to measure the ITS and ITSR values were compacted at 100 gyrations and had a diameter of 150 mm. The ITS test was carried out following UNI EN 12697-23 standard specification and the ITSR values were determined in accordance with UNI EN 12697-12. The test temperature was 20°C.

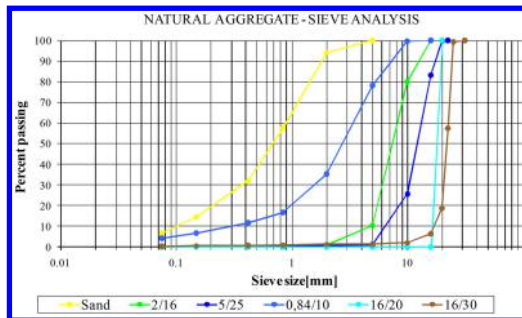


Figure 1. Aggregates size distribution.

4 MATERIALS

4.1 Aggregates

All aggregates used in this study were 100% crushed. The aggregate fractions used for all mixtures were: filler, sand, 2/16, 5/25, 0.84/10, 16/20 and 16/30.

Petrographic analysis showed that the sand and the fractions 5/25, 16/20, 16/30 were mainly composed by limestones and jaspers mildly metamorphosed; the 2/16 fraction was basaltic (it was used only for surface course) and the 0.84/10 fraction was obtained from gabbro partially metamorphosed into serpentinite. Filler consisted of a mixture of limestone and baghouse.

The Los Angeles values obtained were: 24% for 5/25, 16/20, 16/30 fractions, 23% for 0.84/10 fractions and 17% for the 2/16 fraction.

In order to make a direct comparison with the fragmentation resistance of the glass particles, coefficient of fragmentation (C_f) was evaluated for limestone 5/25 and basalt 2/16 fractions, resulting respectively 141 and 93. The coefficient of fragmentation (C_f) is a measure of aggregate fragmentation produced by a metal wheel rolling on the aggregate placed in a sort of rail. With respect to Los Angeles test, it is most suitable for smaller aggregate size, such as fine scrap glass: the Italian Standard CNR Fasc. 4/1953 requires an aggregate size of 4.7–9.52 mm for this test.

The flakiness index, evaluated only for 0.84/10 fraction and was found 8%.

Particle density with regard to the entire mix of fractions was found to be 2.70 g/cm³.

4.2 Glass

During experimental work it was observed that the gradation of glass scrap and the one of 0.84/10 fraction were very close. For this reason the substitution of natural aggregates with glass concerned only this fraction, with the aim of maintaining substantially the same “design curve” of the entire mixture of aggregates. The gradation of the glass fraction is showed in the following Figure 2.

Glass particle density was found to be 2.54 g/cm³ (UNI EN 1097-6) and flakiness index was found to be

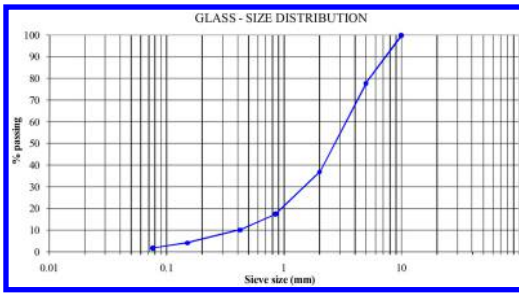


Figure 2. Glass gradation curve.

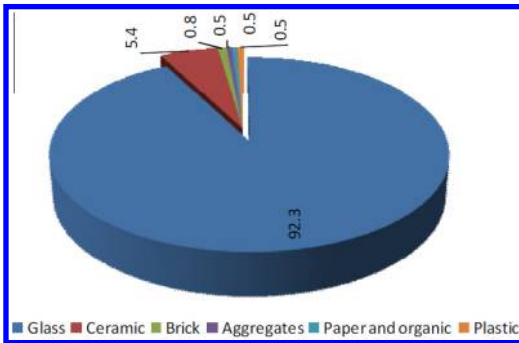


Figure 3. Percentages of undesirable materials in the glass scrap used in this study.

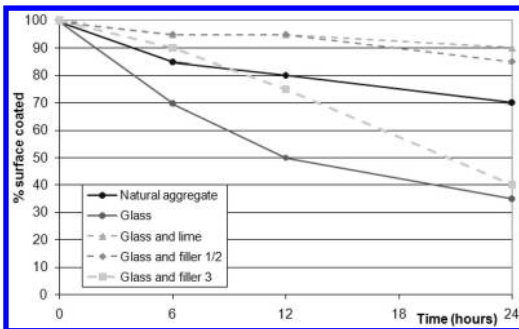


Figure 4. Coated surface (%) after 24 hours of rolling bottle test.

45%, much higher than the 8% of the 0.84/10 fraction of natural aggregates.

The Cf value is 203, considerably high if compared to natural aggregates (141 and 93 for limestone and basalt, respectively).

Although the presence of undesired materials can be quantified in 7.7% by mass of the total sample, the total amount of perishable materials, i.e. paper, plastic and organic, is 1%, which is certainly acceptable, considering the limit of the 2% (CWC, 1996). Figure 3 shows the % distribution of the undesirable materials in the glass used in this study.

4.3 Affinity between natural aggregates and glass with bitumen

The affinity between aggregate and bitumen was evaluated through the rolling bottle method described in UNI EN 12697-11. The test regarded the following samples (percentages are by mass of aggregate):

- natural aggregate + bitumen;
- glass particles + bitumen;
- glass particles + bitumen + 2% of filler type 1/2 (limestone and baghouse, used for AC mixtures in the present work);
- glass particles + bitumen + 2% of filler type 3 (low quality filler, undefined composition);
- glass particles + bitumen + 2% of lime.

Results and images of specimens after 24 hours of test are given below in Figures 4 and 5.

Without filler, the affinity glass-bitumen is below 40%, while for natural aggregates it is more than 70%. Furthermore, depending on type of filler (1/2, 3 or lime), the antistripping effect varies a lot. Thus it could be said that in the case of glass, filler is necessary to guarantee adhesion between bitumen and particles, and technical specifications about glassphalt should refer to affinity tests, to be performed mixing the glass particles and the filler. This is necessary to evaluate suitability of filler and the need of adding lime.

4.4 Bitumen

The binder used in this study was a 50/70 penetration grade bitumen with the following properties (Table 1).

4.5 Aggregate mixture gradation

The standard practice requires that the mixing/replacement of virgin material having density γ_n with a new material having density γ_v will be made considering “volume” instead of “mass” when γ_n and γ_v are significantly different. The volume can be considered as an indirect measure of the aggregate specific surface, which corresponds to a specific bitumen content. This relationship between volume and specific surface is much more pronounced as the difference between parameters such as shape and absorption of virgin aggregate particles and new aggregate particles is reduced. However, it is evident that the difference between the percentages by volume and by mass becomes negligible when the densities are next to one another and the quantities replaced are limited. In Figure 7 the difference between percentages by mass and by volume is given with respect to percentages by volume of substituted aggregate.

The ratio γ_n/γ_v for the materials used in this study (natural aggregates/glass) is approximately 1.07. As showed in Figure 7, for ratio 1.07 the difference between percentages by mass and by volume does not exceed 2%. Considering that 3% is normally the allowable tolerance for fine fractions in the production plant,

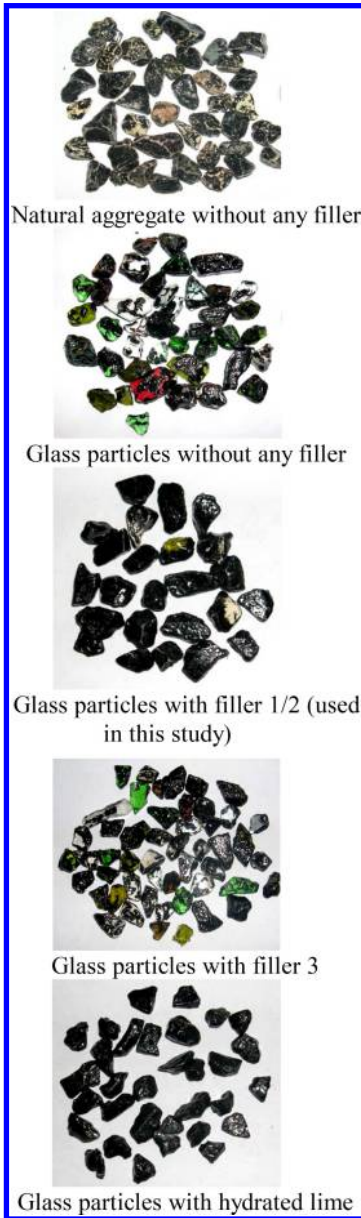


Figure 5. Images of coated surface of aggregates and glass used in this study.

it could be said that the substitution of natural aggregates with the glass particles in terms of mass rather than volume leads to negligible differences.

5 RESULTS AND DISCUSSION

5.1 Marshall and gyratory results

Tables 2, 3, and Figure 7 show the test results obtained for the AC-16 mix.

Table 1. Bitumen properties.

Property	Standard	Value
Penetration at 25°C (dmm)	UNI EN 1426	59
Softening point (° C)	UNI EN 1427	49.6
Penetration index	UNI EN 4163	-0.9
Fraas breaking point (° C)	UNI EN 12593	-8
Dynamic viscosity at 60°C (Pa·s)	UNI EN 12596	217
Kinematic viscosity at 135°C (mm ² /sec)	UNI EN 12595	378

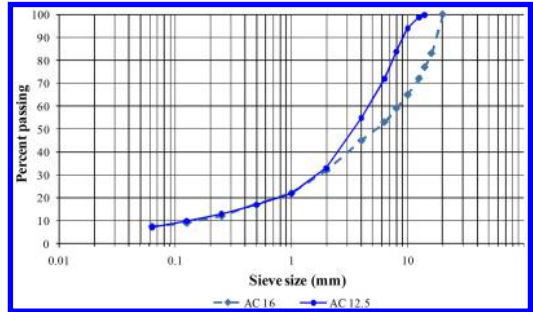


Figure 6. AC gradation curves.

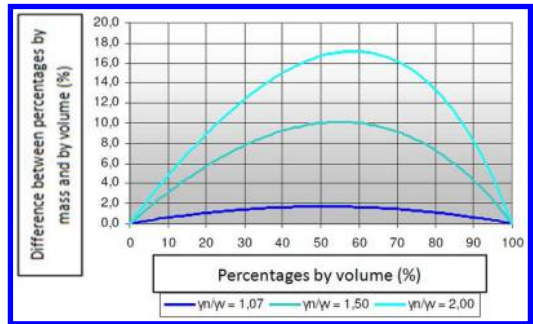


Figure 7. Variation of aggregate percentage calculated by mass or by volume.

Glassphalt AC-16 mixtures showed lower values for Marshall stability and flow. As more glass is incorporated in the mix the lower this values get. Voids have been reduced by 0.5% as 10% glass was incorporated in the mixture. For the 15% glassphalt mixture the voids have been reduced by 1.2%. In all cases mixtures fulfill the ANAS and CIRS Italian specifications.

Furthermore, by examining voids content at different gradation levels, voids showed the tendency to reduce as glass content was increased. Referring to UNI EN 12697-10 standard reference, the compaction level during gyratory compaction (that is $C = 100 - \%v$, where $\%v$ is the air void percentage in the mixture) can be written as follows:

$$C = C_1 + K \cdot \ln N, \quad (1)$$

Table 2. AC-16 Marshall and gyratory test results.

Properties	AC _R -16	AC _{G10%} -16	AC _{G15%} -16
Optimum bitumen content (%)	4.8	– (*)	– (*)
Marshall Stability (kN)	13.03	12.77	9.90
Marshall Quotient (kN/mm)	2.78	3.77	3.22
Marshall voids (%)	5.9	5.4	4.7
Voids @10gyr (%)	14.0	11.6	11.4
Voids @100gyr (%)	4.9	4.2	3.8
Voids @180gyr (%)	3.4	2.8	2.3

(*) Mix design was referred to ACR control mixture.

Table 3. National technical specifications.

Properties	ASPI	ANAS	CIRS
Optimum bitumen content (%)	4.5–6.0	4.5–5.5	4.5–5.5
Marshall Stability (kN)	≥10.00	≥9.00	≥10.00
Marshall Quotient (kN/mm)	≥2.50	>3.00	3.0–4.5
Marshall voids (%)	3–5	3–7	4–6
Voids @10gyr (%)	12–15	11–15	10–14
Voids @100gyr (%)	3–5	3–6	3–5
Voids @180gyr (%)	≥2	≥2	>2

Table 4. Compactability of AC-16 gyratory specimens.

Glass quantity (%)	K	C ₁	R ²
0	3.95	76.67	0.99
10	3.40	80.10	0.98
15	3.46	80.27	0.98

Where:

N is the gyrations number;

K is the workability;

C₁ is the compaction level for the first gyration and is generally referred to the mixtures self compactability.

Fitting accuracy of this model is good as far as R² is near to 1.

Looking to the results reported in Table 4 and Figure 8, the compaction level C is higher for glassphalt and the initial compactability C₁ is higher for higher glass contents; hence, glassphalt mixtures show a relevant tendency to be compacted easily, especially in the earlier stages of laying. This may be due to the lubricating effect of the smooth glass particles and to the higher quantity of “free” bitumen, resulting by the low adsorption of glass.

In all cases mixtures fulfill the ANAS and CIRS Italian specifications.

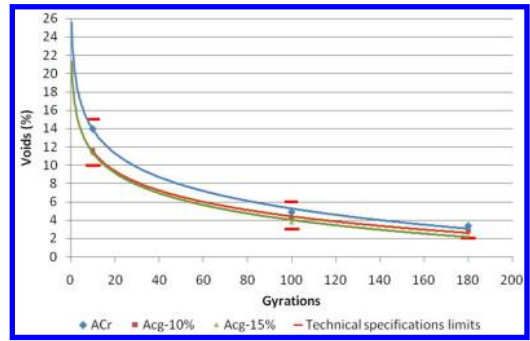


Figure 8. %voids vs. number of gyrations for AC-16.

Table 5. Indirect tensile strength and indirect tensile strength ratio results.

Mix	ITS MPa	ITSR %
ACR-16	1.38	88.7
ACG10%-16	1.34	84.7
ACG15%-16	1.41	78.8

5.2 Indirect Tensile Strength results

In the next Table the indirect tensile strength (ITS) and indirect tensile strength ratio (ITSR) results are reported.

ITS does not vary significantly with the incorporation of glass. On the contrary, ITSR values are reduced as glass content increases. Based on these results, the water sensitivity of the AC-16 mixture results affected by the glass content in the mixture. However, the value obtained is above the minimum value for base and binder course set by different national European authorities. This value is usually >70% (Setra 2008, HTS 2009). Moreover, the ASTM 4867 method, without the freeze-thaw cycle, initially used a 75% TSR minimum acceptance value; this was later increased to 85%. Lottman’s original recommendation of a minimum criterion of 70% was usually specified (Roberts, et al., 1996). A minimum TSR criterion of 80% was adopted for Superpave mix design AASHTO T 283 (AASHTO MP-2).

5.3 Cantabro Test

For the AC-12.5 the Cantabro test was also carried out. The Cantabro test (UNI EN 12697-17) was created with the intention of providing information on the behavior of bituminous mixtures in terms of cohesion, adhesiveness and resistance to traffic wear. The results are shown in Table 6.

The reference values for the loss in weight are given by literature mainly about porous asphalt: the recommendations establish maximum thresholds varying between 20% and 30% (CRR, 1997). The test showed

Table 6. Cantabro test results.

Glass quantity %	Specimen #	Weight loss %	Mean value %
0	1	10.2	10.2
0	2	10.7	
0	3	11.6	
0	4	8.8	
0	5	9.6	
10	1	10.1	10.4
10	2	9.6	
10	3	8.7	
10	4	11.9	
10	5	11.8	

that the mixture containing glass particles have no relevant problem of raveling and can withstand traffic abrasion as much as the reference mix.

6 CONCLUSIONS

Based on the results obtained in this study and with respect to the specific mixtures examined, the following conclusions can be reported.

Considering particle density of natural aggregates and glass, it could be assumed that the substitution of natural aggregates with the glass particles in terms of mass rather than volume leads to negligible differences.

Marshall voids showed a small reduction as 10% glass incorporated into the mixture. For the 15% glass mixture, voids are reduced by 1.2% (from 5.9% to 4.7%) but were still within the specified limits provided by Italian specifications.

Gyratory voids at 10 gyrations show a higher variation (2.6%: from 14.0% without glass to 11.4% with 15% of glass): results showed that the glassphalt mixture show a tendency to be more easily compacted, especially in the early stages of compaction. Hence it is strongly recommended that a gyratory compactor is used for the mix design of glassphalt mixtures.

Marshall stability showed lower values than those of the reference mixture but above the specified limits by technical specifications considered.

Indirect tensile strength does not vary significantly with the incorporation of glass. Indirect tensile strength ratio values are reduced as glass content is increased. All the glassphalt mixtures values obtained were above 70%.

Gyratory voids at 10 and 100 gyrations are significantly lower for the glassphalt mixture (compared to the reference mix), showing that glassphalt mix

can be compacted more easily. The reasons of this phenomenon are manifold. The glass, not absorbing bitumen, leaves it "free" in the mixture; this bitumen excess at first behaves as a lubricant reducing the energy required for compaction and then fills the intergranular spaces. Moreover, the smooth glass particles are more able to move around in the mixture, filling even the tightest spaces. Based on the assumption that the particle size of the reference mixture and the percentage of bitumen are well designed and that the voids percentages are the optimal ones, it is reasonable to expect that it is possible to reduce the quantity of bitumen due to the replacement of part of the natural aggregates with crushed glass.

For what concerns wearing course, the Cantabro test showed that the mixture containing glass particles have no relevant problem of raveling, and can withstand traffic abrasion as much as the reference mix.

REFERENCES

- CRR (Centre de Recherches Routières) 1997. *Code de bonne pratique pour la formulation des enrobés bitumineux*, Publication n. R 69/97.
- CWC (Clean Washington Center) 1996. *Best practice in glass recycling*. Washington.
- Goldman, A. L. 1987. Glassphalt to sparkle on Streets. *New York Times* (1857-Current file), July 6 1987, Prequest Historical Newspapers The New York Times: pp. 34.
- Halstestead, W. J. 1993. *Use of waste glass in highway construction*. Virginia Transportation Research Council, Virginia.
- FHWA 2008. *User guideline for waste and by-product materials in pavement constructions*. Publication n° FHWA-RD-97-148.
- Hughes, C.S. 1990. *Feasibility of Using Recycled Glass in Asphalt Mixes*. Virginia Transportation Research Council, Report No. VTRC 90-R3.
- Larsen, D.A. 1989. *Feasibility of Utilizing Waste Glass in Pavements*. Connecticut Department of Transportation, Report No. 343-21-89-6.
- Maupin, G. W. Jr. 1998. *Effect of glass concentration on stripping of glassphalt*. Virginia Transportation Research Council, Report No. VTRC 98-R30, March 1998.
- Murphy, K.H., R.C. West, and G.C. Page, 1991. *Evaluation of Crushed Glass in Asphalt Paving Mixtures*. Florida DOT Research Report No. FL/DOT/SMO/91-388.
- NYS (State of New York) Executive Department 2004. *Bituminous Concrete – Hot Mix Asphalt*. 08/10/04, Spec. No. 891.
- Roberts, F. L., Kandhal, P. S., Brown, E. R., Lee, D. & Kennedy, T. W. 1996. *Hot mix asphalt materials, mixture design and construction*. Lanham, Maryland, NAPA Education Foundation.
- Su, N. & Chen, J.S. 2002. Engineering properties of asphalt concrete made with recycled glass. *Resources, Conservation and Recycling* – n. 35: pp. 259–274.

Polyester geogrids as asphalt reinforcement – a sustainable solution for pavement rehabilitation

Fabiana Leite-Gembus & Bernd Thesseling
Huesker Syntethic GmbH, Gesher, Germany

ABSTRACT: The conventional method for rehabilitation of cracked concrete or asphalt pavements is the installation of new asphalt layers. But a new overlay does not make the cracks disappear; they are still present in the old asphalt layers. Because bituminous bound materials are unable to withstand the high tensile stresses that result from external forces like traffic and temperature variations, these cracks rapidly propagate into the new asphalt overlay. This phenomenon, known as reflective cracking, is one of the major problems associated with the use of asphaltic overlays. In order to tackle the problem of reflective cracking and to therefore prolong the service life of a pavement, a reinforcement grid made of high modulus polyester has proven to be a very effective solution. Geosynthetics as asphalt reinforcement have consistently shown outstanding results in addressing the issue of crack initiation and propagation, eliminating the damage caused by water intrusion that ultimately leads to the failure of the pavement structure. The increased pavement life achieved by the use of this technology not only prevents excessive disruption to traffic flow and local business, but it also demonstrates strong environmental and economic benefits. Through basic theory and practical experiences this paper will demonstrate the success and extended pavement life that can be achieved in both highway and airfield applications. Special attention is given to a comparison of Embodied Carbon Dioxide for different rehabilitation methods showing the sustainability of using polyester asphalt reinforcement to extend pavement life.

1 INTRODUCTION

Asphalt reinforcement has been used all over the world for many years to delay or even prevent the development of reflective cracks in asphalt layers. Using asphalt reinforcement can clearly extend the pavement life and therefore increase the maintenance intervals of rehabilitated asphalt pavements. This increase in pavement life does have the positive effect that not only the maintenance costs per year but also the amount of energy used for maintenance per year can be significantly reduced. Environmental and climatic protection is gaining an ever increasing importance, the road construction industry may therefore benefit from adopting these solutions in order to assist in tackling climate change.

Similarly the design of asphalt overlay and maintenance projects has to aim at reducing the overall embodied energy and thereby make them more sustainable. The need for sustainable designs and construction methods is now appearing more and more in corporate and social responsibility statements and could eventually become a criterion for the selection of construction methods.

2 CREATING AN ASPHALT REINFORCEMENT OVER ALMOST 40 YEARS

The idea of a reinforcing fabric for asphalt road construction first emerged in the early 1970s (Figure 1).



Figure 1. One of the first attempts to use a geogrid in asphalt pavement at the early 1970s.

The first experiences with geogrids were in the construction of earthworks and foundations, so the idea to use them in asphalt pavements was a logical next step.

The initial intention was that the embedded Geotextile layer was able to pick up the tensile stresses in the asphalt and prevent cracks from forming. However, it was soon realized that this principle did not work, but the product proved very useful at delaying the formation of reflection cracks in resurfaced roadways.

Even then polyester, abbreviated as PET, was a preferred raw material because of the compatibility of its mechanical properties with the behavior of asphalt. Since then many products made from different raw materials have been developed.

3 BASICS: REFLECTIVE CRACKING AND ASPHALT REINFORCEMENT

It is well known that cracks appear due to external forces, such as traffic loads and temperature variations. The temperature influence leads to the binder content in the asphalt becoming brittle; cracking starts at the top of a pavement and propagates down (top-down cracking). On the other hand, high stresses at the bottom of a pavement, from external dynamic loads, such as, traffic, lead to cracks that propagate from the bottom to the top of a pavement (bottom-up cracking).

A conventional rehabilitation of a cracked pavement involves milling off the existing top layer and installing a new asphalt course, but cracks are still present in the existing (old) asphalt layers. As a result of stress concentrations at the crack tips caused by external forces from traffic and natural temperature variations, the cracks will propagate rapidly to the top of the rehabilitated pavement.

Deteriorated concrete pavements are typically rehabilitated by installing new asphalt layers over the old concrete slabs. Temperature variations lead to a rapid crack propagation especially at the expansion joints to the top of the new asphalt overlay.

In order to delay the propagation of cracks into the new asphalt layers an asphalt reinforcement comprised of high tenacity polyester can be installed. The reinforcement increases the resistance of the overlay to high tensile stresses and distributes them over a larger area, thereby reducing the peak shear stresses at the edges of the cracks in the existing old pavement. The reinforcement also provides a normal load to the crack surfaces, thereby increasing the aggregate interlock (shear resistance) between both crack surfaces and thus increasing the resistance to reflective cracking.

High modulus polyester (PET) is a flexible raw material with a maximum tensile strain less than 12%. The coefficients of thermal expansion of polyester and asphalt (bitumen) are very similar. This leads to very small internal stresses between the PET fibers and the surrounding asphalt (similar to reinforced concrete). For this reason Polyester does not act as an extrinsic material in the asphalt package, however at this point

it should be mentioned that the aim of a PET-grid as asphalt reinforcement is not to reinforce asphalt in such a way as one reinforces concrete. The installation of a PET-grid as asphalt reinforcement improves the flexibility of the structure and avoids peak-loads over a cracked existing layer into the overlay and through this mechanism reflective cracking is delayed.

As found by De Bondt (De Bondt 1999) the bonding of the material to the surrounding asphalt plays a critical role in the performance of an asphalt reinforcement. If the reinforcement is not able to sufficiently adopt the high strains from the peak of a crack, the reinforcement cannot be effective. In his research, de Bondt determined an equivalent “bond stiffness” in reinforcement pull-out tests on asphalt cores taken from a trial road section. The equivalent bond stiffness of a bituminous coated PET-grid was found to be, by far, the best of all the commercial products investigated.

Furthermore, asphalt reinforcement must resist as much damage as possible from the stresses and strains applied during installation and overlaying / compaction of the asphalt. Very high forces can also be applied to the individual strands of the reinforcement by aggregate movement in the hot blacktop during compaction.

4 PRACTICAL EXPERIENCES

4.1 *Municipal Road Rosenstrasse, Ochtrup (Germany)*

The following project shall give an example of the successful use of asphalt reinforcement in roads. The project is located in the Northwest German town of Ochtrup. The road is a highly trafficked road. The majority of vehicles are trucks, because the road is one of the main connections to the nearby border of the Netherlands. Before rehabilitation, the road exhibited severe alligator cracking, longitudinal and transverse cracking in large scale. The original design called for milling, approximately 50 mm of the surface followed by installation of a new 50 mm asphalt surface course. Due to the problematic condition of the existing base, the expected lifetime of the new surface was only 2 years (Figure 2).

The more durable (but also much more expensive) solution would have been to remove the cracked binder and base course. An alternative to this solution was the installation of a Polyester Geogrid as asphalt reinforcement over the cracked binder course, where the thickness of the new wearing course would remain 50 mm. Therefore, the economical advantage had to be proven by a longer lifetime, which should be the main goal in most of these applications. The layers would have the same thickness, therefore the economical advantage results from the longer lifetime of the surface over the old cracked area.

After milling off the 50 mm surface course the asphalt reinforcement grid was installed, and covered



Figure 2. Surface after milling.

again with a 50 mm 0/11 AC asphalt layer. The whole project was finished in the summer of 1996.

4.1.1 Project update: June 2002

Six years after the repairs were carried out, the District's Chief Executive was asked for a condition report on the "Rosenstrasse". In his answer, he commented as follows: "I'm happy to inform you that the repairs have fully stood the test of time. The use of the asphalt reinforcement system under the 0/11 asphalt layer has meant that, to this day, no cracks have appeared in the asphalt-concrete surface. This method was chosen at the time to avoid the necessity of the additional work required for the binder and base course."

4.1.2 Project update: September 2009; Assessment by TÜV Rheinland

The TÜV Rheinland is a leader in independent assessment services. In 2009, the TÜV Rheinland was commissioned to document the cracking and assess the condition of "Rosenstrasse" along the portion of the road that was repaired in 1996.

The appraisal compared the current condition with the condition that existed before repairs were carried out. This comparison allowed conclusions to be drawn about the effectiveness of the asphalt reinforcement system for delaying the occurrence of cracks propagated from the lower asphalt layers.

On August 24th 2009, a visual inspection was done in accordance with Working Paper No. 9 (by the German FGSV; Research Association for Transportation in Germany). The TÜV used the image documentation of the construction measures used in May 1996 as the basis for its assessment. The District's Chief Executive responsible at that time provided additional necessary information.

4.1.3 Result

After 13 years of use, the cracking condition value (ZWRIS) for the section of the road repaired with the



Figure 3. Lateral crack at the edge.

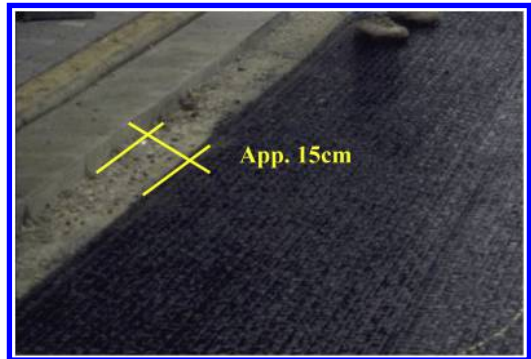


Figure 4. Fitted reinforcement (detail).

Polyester grid in 1996 was determined to be excellent. The visual inspection of the road surface revealed almost no damage with the exception of two areas. The damage in these areas, however, was due to subsequent repair work on the drainage system. A few lateral cracks were discovered at one point on the outer edge of the road. Small cracks along the road surface were also found at a few other points on the outer edges (Figure 3).

The photos documenting the condition of the site in 1996 (Figure 4) show that the distance between the reinforcement system and the road edge was always around 150–300 mm. TÜV Rheinland also confirmed: "The entire remaining road area is free of cracks."

The condition assessment by TÜV Rheinland revealed that the "Rosenstrasse" in the city of Ochtrup has, in spite of constant heavy traffic, remained in good condition to this day. The deployment of the asphalt reinforcement system to effect repairs has completely stood the test of time. This measure has shown that a Polyester asphalt reinforcement can keep the condition of rehabilitated roads at a high level over extended periods of time.

4.2 Salgado Filho Airport, Porto Alegre (Brazil)

In 2001 the existing access to an aircraft maintenance hangar (used by aircraft as large as the Boeing 777, with a weight over 250 tons) had to be resurfaced after more than 40 years of use. The existing pavement was made of 5.0×3.5 m concrete slabs, 250 mm thick. The slabs were resting on a layer of gravel.

The rehabilitation design involved the installation of an asphalt leveling layer first. In order to prevent the propagation of the expansion joints from the concrete slabs into the new surface, an asphalt reinforcement made of high modulus polyester was to be installed. A 50 mm asphalt surface course was installed on top of the polyester reinforcement.

Because it was not possible to block the access for an extended period of time, the rehabilitation work had to be finished in just one night. In order to stay within this very tight time frame, it was decided to only reinforce the heavily loaded inner portion of the pavement. The outer portions, which are not typically subjected to the heavy loading of aircraft traffic, were left unreinforced.

What initially was thought to be a purely practical solution developed into an ideal demonstration of the effectiveness of an asphalt reinforcement grid. By only reinforcing a portion of the pavement and leaving the remainder unreinforced, a direct side-by-side comparison of the performance of the reinforced and unreinforced sections was possible.

In October 2007, approximately 7 years after the rehabilitation, the first assessment of the pavement took place. At that time the designer, the technical manager of the airport, and an employee of the reinforcement manufacturer were present.

The expansion joints in the concrete beneath the unreinforced pavement areas had already propagated to the top of the surfacing. The vegetation, visible in the developed cracks, led to the conclusion that these cracks had existed for some time. In contrast, the PET-grid reinforced areas did not show any indications of cracking (Figures 5 and 6). Because the unreinforced section was not subjected to aircraft traffic, the propagation of the expansion joints in these areas can be conclusively attributed to the horizontal stresses that resulted from changes in temperature. The areas reinforced with the polyester grid were subjected to both temperature-induced and aircraft traffic-induced stresses.

For further details the reader is referred to a paper prepared by Monser and Montestruque (Monser et al. 2010).

5 EMBODIED ENERGY AND EMBODIED CO₂

5.1 Definitions

5.1.1 Embodied Energy (EE)

A vast field of research work is ongoing around the world to determine the embodied energy of individual products, services and construction materials. Treolar



Figure 5. Overview of the studied section: view from the dockyards to the terminal.



Figure 6. Joints of the concrete slabs reflect in the area where no reinforcement was used.

(1994) has provided the most well known definition that embodied energy is: “The quantity of energy required by all of the activities associated with a production process, including all activities upstream to the acquisition of natural resources and the share of energy used in making equipment and in other supporting functions i.e. direct energy plus indirect energy”.

Basically, this means all the input energy required to make a material, such as a clay brick. This includes the energy to extract the clay, transport it to the brickworks, mould the brick, fire it in the kiln, transport it to the building site and put the brick into place. It also includes all the indirect energy required, i.e., all the energy required to manufacture the equipment and materials needed to manufacture a brick, e.g. trucks, kilns, mining equipment, etc. All have a proportion of their energy invested in that single brick. The embodied energy is typically expressed in MJ/kg.

5.1.2 Embodied CO₂ (ECO₂)

Similarly the embodied CO₂ of a material is a calculated value of the quantity of CO₂ derived due to the extraction, processing and transportation of the material to the site based on the typical form of energy used. This value is expressed as the mass in kg of embodied CO₂ for 1 kg of material, shown as kg CO₂/kg (WRAP, 2010).

5.1.3 *Difference of Embodied Energy (EE) and Embodied CO₂ (ECO₂)*

The main difference is that two products with the same amount of EE can have a different amount of ECO₂ because the energy used for production may for example have been generated from coal fired power plants with high CO₂ output while for the other product mainly renewable energy sources may have been used. For example, two factories could manufacture the same product with the same technology and efficiency, resulting in the same EE per kilogram of product produced. The total CO₂ emitted by both, however, could vary widely dependent upon the source of energy consumed by the different factories.

5.1.4 *Sustainability*

Since the 1980's *sustainability* has been used in the sense of human sustainability on planet Earth and this has resulted in the most widely quoted definition of sustainability and sustainable development, that of the Brundtland Commission of the United Nations: "Sustainable development is development that meets the needs of the present without compromising the ability of future generations to meet their own needs" (United Nations – Brundtland Commission, 1987).

In the context of the construction industry this does mean that different construction techniques and designs for a specific project are compared for their ECO₂ as an indicator for their sustainability. As a matter of fact the ECO₂ is only one criterion beside social and economic considerations. However, the request for sustainability is now appearing more and more in corporate and social responsibility (CSR) statements on both the client's and contractor's side.

5.2 *Level of detail*

From the above definitions one can identify a certain variation of EE and ECO₂ for individual products being used on a specific construction site. For this technical comparison, however, a simplified approach has been chosen considering only the ECO₂ for the materials used on site without considering the individual transport distances and their installation. The authors of this paper appreciate that this comparison is not in line with the typical "cradle to gate" approaches used in this field, but it has been previously shown that the following comparison is sufficiently detailed to compare the two construction techniques without compromising on the accuracy of the results.

5.3 *Data source*

The ECO₂ values ("Carbon Footprint") used in the following chapters are taken from the latest ICE Inventory of Carbon & Energy V2.0 (Hammond, 2011). The University of Bath has created the ICE embodied energy & embodied carbon database which is the freely available. The aim of this work is to create an inventory of embodied energy and carbon coefficients for building materials. The data base is structured into

Table 1. Examples of embodied carbon dioxide (ECO₂) in construction materials*.

Material	kg ECO ₂ / kg of material	Note
Aggregate	0.0052	gravel or crushed rock
Aluminium	9.16	–
Asphalt	0.076	6% binder content
Bitumen	0.55	–
Cement	0.74	UK weighted average
Concrete 16/20	0.10	unreinforced
Reinforced	0.188	high strength
Concrete RC 40/50		applications/precast
PVC General	3.10	–
Polyester	1.93	derived from HDPE
Steel	1.46	average UK recycled content
Steel	2.89	Virgin steel

* Source: ICE Inventory of Carbon & Energy V2.0

34 main material groups e.g. Aggregates, Aluminium, Asphalt etc.

5.4 *Examples of embodied CO₂*

The amount of embodied carbon dioxide per kg of material can vary significantly as can be seen in Table 1. The more processing and energy that is required to achieve the final product the higher is the ECO₂.

Especially energy intensive processes like the production of cement are producing a high amount of CO₂. Cement manufacturing releases CO₂ in the atmosphere both directly when calcium carbonate is heated, producing lime and carbon dioxide, and also indirectly through the use of energy if its production involves the emission of CO₂.

6 COMPARISON OF EMBODIED ENERGY FOR REINFORCED AND UNREINFORCED ASPHALT OVERLAYS

The report "Sustainable Geosystems in Civil Engineering Applications" commissioned by the Waste and Resource Action Plan (WRAP, 2010) has analysed geosystems as alternatives to standard designs used by civil engineers. Parallel to geosystems for ground engineering the report has identified that "Reinforcement of the asphaltic or bound layers can increase the life of the surface layers, again by contributing to a strengthening of the bound layers. Such strengthening increases their ability to resist cyclic fatigue, thermal stresses during extremes of winter and summer temperatures, as well as increasing resistance to near-surface crack propagation." (WRAP, 2010). The report clearly identifies that asphalt reinforcements

can extend pavement life by limiting reflective cracking and thus providing more sustainable pavements as a consequence.

This paper aims to demonstrate the above referenced effect by comparing the ECO₂ based on the material consumption per year of lifetime of two construction techniques. One construction technique is the conventional rehabilitation of cracked overlays by milling and repaving, the second is a rehabilitation using PET asphalt reinforcement in the same process.

6.1 Basis for calculation

The example chosen for this comparison is a typical rehabilitation project with 5,000 m² of cracked

Table 2. Basis for calculation.

Project size	5,000 m ²
Asphalt thickness to be replaced	40 mm
Density of asphalt	2,500 kg/m ³ (compacted)
Bituminous emulsion (70%)	0.3 kg/m ² (unreinforced)
Bituminous emulsion (70%)	1.0 kg/m ² (reinforced)*
Asphalt reinforcement	0.3 kg/m ² (made of PET)
Improvement factor (reinforced to unreinforced asphalt)	3 (–)**
Design life (unreinforced):	4 years***

*Required amount of bituminous emulsion for HaTelit® asphalt reinforcement over milled surfaces acc. to manufacturer's recommendations.

**The improvement factor of 3 for the life time of reinforced asphalt as compared to unreinforced asphalt has been selected on the lower side of the potential range of 3 - 4 to account other potential failure mechanisms which make rehabilitation necessary but are not related with reflective cracking (Montestruque et al. 2004).

***The design life of the unreinforced asphalt overlay has been chosen as 4 years since a typical crack propagation rate of approx. 10 mm / year would result in cracks reaching the surface of the new overlay after 4 years. The crack propagation rate of approx. 10 mm / year is of course project specific and could vary.

wearing course to be replaced. Although the project size does not have any effect on the relative saving of ECO₂ it helps to give a better assessment for the saving potential.

6.2 Comparative calculation

A comparative calculation of the embodied CO₂ for reinforced and unreinforced asphalt overlays is presented on Table 3.

In the above comparison it can be seen that a conventional (unreinforced) rehabilitation method results in 7.72 kg embodied CO₂ per m² for the materials used. The alternative design using a PET asphalt reinforcement results in 8.57 kg embodied CO₂ per m² due to the additional asphalt reinforcement and a higher amount of bituminous emulsion. The comparison of the ECO₂ for the rehabilitation project then has to be put into relation with the design life. The design life for the unreinforced overlay is set to 4 years until first cracking is likely to have reached the surface again. The reinforced overlay on the other side would last at least 3 times longer, i.e. 12 years.

The result is a saving of 63% of ECO₂ per m² and year of design life for the reinforced overlay as compared to the unreinforced overlay. For a project of 5,000 m² to be repaved this would mean a total ECO₂ saving of 73,200 kg based on the significantly improved design life of 12 years.

7 CONCLUSIONS

Reflective cracking occurs in rehabilitated asphalt pavements. High tenacity Polyester as raw material is often chosen because of the high compatibility of its mechanical behaviour to the modulus of asphalt and its good behavior under dynamic loads. A bituminous coated Polyester asphalt reinforcement grid can show excellent results in delaying reflective cracking. This has been shown by numerous practical examples from the past several years.

Table 3. Comparative calculation of embodied carbon dioxide

	Material consumption (kg/m ²)	kg embodied CO ₂ per kg of material	embodied CO ₂ in kg/m ²	
			unreinforced	reinforced
Asphalt (~25 kg/cm)	100	0.076	7.60	7.60
Bituminous emulsion (70%, 0.3 kg/m ²)	0.21	0.55	0.12	–
Bituminous emulsion (70%, 1.0 kg/m ²)	0.70	0.55	–	0.39
Asphalt reinforcement	0.30	1.93	–	0.58
Total embodied CO ₂ for rehabilitation (kg/m ²)			7.72	8.57
Improvement factor (–)			1	3
Design life (improved)			4	12
Total embodied CO ₂ per year design life (kg/m ² /year)			1.93	0.71
ECO ₂ saving per m ² and year of Design life (%)				63
Total project CO ₂ saving (kg)				73.200

Using this information combined with the amount of embodied carbon dioxide (ECO₂) of construction materials used for a typical pavement rehabilitation project, a comparison has been made between a reinforced and an unreinforced solution. The comparison shows the significant savings of 63 % ECO₂ per year of design life of the reinforced as compared to the unreinforced overlay. This substantial saving is achieved by extending the pavement life and thus reducing the need for maintenance and the corresponding ECO₂.

Similarly to the saving of embodied carbon dioxide a significant cost saving per year of design life is achieved. This again shows that saving the environment and saving costs go very well hand in hand.

This paper has shown that asphalt reinforcement made of high modulus polyester does provide an efficient solution to save resources by extending pavement life and thus creating sustainable pavements.

REFERENCES

- De Bondt, A.H., (1999), *Anti-Reflective Cracking Design of (Reinforced) Asphaltic Overlays*, Ph.D.-thesis, Delft, Netherlands.
- Hammond, G.; Jones, C. (2011), "*ICE Inventory of Carbon and Energy V 2.0*", Sustainable Energy Research Team (SERT), Department of Mechanical Engineering, University of Bath, UK.
- Montestruque G.E., Rodrigues R.M., Nods M., Elsing A., (2004), Stop of reflective crack propagation with the use of PET geogrid as asphalt overlay reinforcement, *Proceedings of the Fifth International RILEM Conference*, Limoges, France.
- Monser C.A., Montestruque G.E., Silva A.E.F., (2010), Evaluation of an airport pavement after almost 8 years of overlay rehabilitation with a Polyester geogrid asphalt reinforcement, *Proceedings of the 9th International Conference on Geosynthetics*, Brazil.
- Treloar G.J. (1994), "*Embodied Energy Analysis of the Construction of Office Buildings*", Master of Architecture Thesis, Deakin University, Geelong, Australia.
- United Nations General Assembly (1987). "Report of the World Commission on Environment and Development: Our Common Future", Transmitted to the General Assembly as an Annex to document A/42/427 – *Development and International Co-operation: Environment; Our Common Future*.
- WRAP Waste and Resource Action Plan (2010), "*Sustainable Geosystems in Civil Engineering Applications*", UK.

Analysis over the use of reinforced flexible pavement with steel mesh in climbing lanes

A.F.B. Ressutte

São Paulo University, Department of Transportation Engineer, São Paulo, São Paulo, Brazil

R.M. Fortes

ERI – “Engineering and Research Institute” Pesquisas Ltda, São Paulo, São Paulo, Brazil
Amazonas Federal University – UFAM

C.Y. Suzuki

São Paulo University, Department of Transportation Engineer, São Paulo, São Paulo, Brazil

J.B.R. da Silva

IBTS (Brazilian Institute of Welded Screens), São Paulo, São Paulo, Brazil

ABSTRACT: The growth of the sugar alcohol sector in various regions of the São Paulo state, which has mostly one single lane highways, has motivated businessman in the industry to propose partnerships for the construction of climbing lanes, which would allow the transit of heavy vehicles to flow better in these highways. A review of the literature about steel mesh shows that the use of the same avoiding the appearance of cracks in the layers of asphalt layer, acting as a barrier against their spread keeping the uniform distribution of loads. The objective of this research was to develop this technology for construction and rehabilitation of climbing lanes in order to increase its service life through the use of steel mesh. For this, they were analyzed their performance, based on international best practices, using structural and functional evaluation tests in observing their behavior in a test section.

1 INTRODUCTION

In the late 1980s the Brazilian economy had a marked expansion, and this period was popularly known as “Brazilian miracle”. The demand for road transport infrastructure established strong investments both in the construction of new roads as improving and increasing the capacity of existing roads (Arakawa e Olio, 2006).

In order to improve the service level and reduce travel time and also the cost of operating vehicles and a safer trip can be deployed on the climbing lanes, which are auxiliary tracks built to the right side of the tread upwards specifically for heavy traffic.

The construction is justified when the length of the ramp causes a reduction of 15 km/h or more in speed of loaded vehicles according to AASHTO (1994). When a highway is affected on its level of service with a high traffic volume coupled with high percentage of heavy vehicles, the deployment of additional tracks in specific sections has shown that for cumulative number of equivalent standard axles (ESAs) is a viable option.

On the other hand, the growth of the sugar alcohol sector in various regions of the São Paulo state that has mostly one single lane highways, has motivated businessman in the industry to propose partnerships

for the construction of climbing lanes which would allow the release of heavy vehicles, however this type of solution turns out to be very costly to the state ultimately leading it to propose other solutions, especially for the construction of the pavement.

As examples of solutions that allow increasing the load bearing capacity applied to the pavement, one has to introduce the metal screen. The choice of the type to be adopted depends on the way that the pavement is compared to the level of structural and functional quality that is intended to reach. According to Fortes et al. (2011), the main causes of degradation of flexible pavements are the permanent deformation and the appearance of fatigue cracks because of the traffic.

The application of reinforcement in flexible pavements using the steel mesh was initiated in the countries of the north Europe around 1970. According to VTI (Swedish National Road and Transport Research Institute, 2003), after the application in some roads, the potential of the steel mesh was seen as reinforcement for pavements.

Thus, this technique brought the interest of organizations creating investigations as, for example, the project sponsored by the European Union called REFLEX (Reinforcement of Flexible Road Structures with Steel Fabrics you the Prolong Service Life). This

project showed interesting conclusions concerning the improvements by the introduction of the steel mesh as reinforcement, based on practical cases of roads in Sweden, Finland and Italy, helping to define guidelines to dimension and execution of reinforcement of pavements with the use of steel mesh.

2 METHODOLOGICAL ASPECTS

A bibliographical survey on national and international specific literature was accomplished presenting the condition of art on the subject. After this analysis, an inspection in the existing experimental section near Campo Limpo Paulista city was made. The conduction of the steel mesh was verified through functional evaluations of the experimental stretch, mapping of cracks, situation of the welded screen, and execution of diggings and also blocking for verifying the condition of the existing layers.

From this first experimental behavior diagnosis of the pavement executed with steel mesh, an analysis by the DER/SP (Department of Transportation of São Paulo) was taken while seeking new stretch where they could apply the steel mesh again but this time to recover additional tracks. We adopted the case study as a research strategy, aiming to apply the steel mesh on a highway that was already in the work in progress.

After analysis of DER/SP staff, it was decided to take advantage of the stretch ahead of the first experiment using steel mesh on Highway Edgard Máximo Zamboto – SP-354. It was then defined the km 68 for the test section, near the city of Campo Limpo Paulista. This section was chosen because of the construction of climbing lanes due to the high traffic of heavy vehicles had already been decided to be built.

3 REVIEW ABOUT STEEL MESH

The use of steel mesh as reinforcement of flexible pavements in general, according to Asphalt Academy (2008), aims to improve the roads giving the pavement a clear benefit for one or more structural features essentially increasing their lifetime use, so that there is an expenditure of less natural resources, as well as becoming more economic.

The application of steel mesh reinforcement is recommended on overlay of bituminous layers in order, essentially, to the control of differential settlements and increased pavement loading capacity according to (Heavy Vehicle Simulator) HVS – Nordic (1998). Investigation in Finland and Sweden has shown that reinforcement of flexible pavements with steel mesh is an economical construction technique to prevent the appearance of longitudinal cracks (Rathmayer et al., 2002).

3.1 *Reflex project*

The REFLEX project (Reinforcement of Flexible Road Structures with Steel Fabrics to Prolong

Service Life), funded by the European Union began in March 1999 and was conducted over a period of three years until February 2002. The main goal of the project was to develop a new methodology in construction and restoration of roads using steel mesh, to make the road infrastructure obtain an increase in its useful life, leading to a reduction in the use of natural resources, reducing the need for maintenance, reducing accidents and improving road traffic safety.

Research conducted in Finland and Sweden indicated that the enhancement of flexible pavements with steel mesh is a low-cost method to avoid longitudinal cracks according to Halonen et al. (2000). Field and laboratory testing still showed other applications in the construction and restoration of roads to give a better final performance as increased load capacity, preventing plastic deformation, avoiding cracks reflective etc.

3.2 *First application of steel mesh in SP-354*

In November 2012 was executed the first test section with the use of steel mesh near the city of Campo Limpo Paulista (Fortes et al., 2013a). The existing pavement rehabilitation project on the section of the SP-354 has a length of 400 m divided into 4 parts of 100 m.

Through this study, was investigated the performance of the steel mesh as anti-reflection method of cracks in asphalt pavements for new layers of recapping. It was observed that between screens and the edges reflection cracks occurred mainly in positions overlapping length of the meshes (amendment). In addition, these points the displacement of the belt was resulting in undulation thereof and with decreasing thickness of repaving, the surface presented pathologies that have evolved for potholes (Fortes et al., 2013b).

The best performance was in the subsection which was milled and had the fixing the steel mesh to the existing pavement and no overlap was performed. Thus is prevented from being moved and consequently prevents appearance of cracks. After 1 year of running this experimental subsection, in September 2014, it was observed that there was no evolution of defects that arose after the execution, in other words the cracking due to amendment of the screens, as can be seen in Figure 1 (a) and (b).

Also they were removed minor irregularities during milling even the pavement which resulted in a better screen settlement, avoiding the ripples that occur mainly due to the same irregularity and also while running the screen due to the movement of the construction equipments (Fortes et al., 2013c).

In general, it was observed that the construction using this new technology are in good condition and the pathologies that occurred was crack that emerged soon after the construction due to longitudinal seams and these defects have not been treated and have also suffered no evolution.



Figure 1. (a) Crack that appeared in March 1, 2013.



Figure 1. (b) The same crack in March 31, 2014.

4 NEW CASE STUDY IN CLIMBING LANE

At the end of October 2013 began the construction using reflex in deteriorated pavement in the climbing lane. The segment under study is located at km 68. In this local, the highway cross the city of Campo Limpo Paulista, where there is a break in the highway in the intersection to the urban area that accesses the city of Jarinu. The steel mesh was implanted on track towards Jarinu – Campo Limpo Paulista (track with heavier traffic).

The ground of the SP-354 has wavy features, with the presence of steep slopes reaching over 4.5% incline. In these passages, heavy vehicles inevitably lose speed in relation to passenger cars and therefore there is a greater demand for overtaking in these segments. Low-speed operation segments are, in general, those with greater need to implement additional tracks.

4.1 Existing road structure

The improvements that were made on Highway SP-354 consisted in the deployment of climbing lanes with a total width of 4.70 m platform, the width of 3.50 m intended for traffic of commercial vehicles and 1.20 m safety range. To evaluate the general condition of the pavement structure was performed functional survey of the segment comprising the additional track. The number N designed for the project period was 2,93E+07 (USACE) and 1,55E+07 (AASHTO).

It was found that after one year of construction of the additional track, the asphalt coating had patches,

Table 1. Structure of climbing lane pavement.

Layer	Thickness (mm)
Asphalt concrete	130
Graded crushed stone	200
Cracked rock	200

Table 2. Characteristics of the welded mesh Q138.

Steel	Diameter		Spacing		Dimensions	
	cm	inches	mm	inches	width (m)	length (m)
CA60	10	3.94"	0.32	0.13"	2.45	6

patch deterioration and shoving. In some segments located there was almost complete pavement distress with localized areas presenting local settlement, corrugations, ruttings and alligator cracks.

Through the geotechnical studies it was found that the subgrade soil types are LG ‘NG’ ON ‘and NS’ according to the classification of soils MCT (Miniature, Compacted, Tropical classification). Note that all geotechnical tests (CBR and expansion) of the subgrade soils were performed on soil samples molded in Energy Standard Proctor. Table 1 is the solution adopted for construction of climbing lane.

4.2 Study on welded mesh splices

These studies were oriented in “*Estudo do Comportamento de Estruturas de Concreto Armadas com Telas Soldadas: Ensaios sobre Emendas*”, published by the IBTS (Brazilian Institute of Mesh Welded), by the technical bulletin – 3rd edition – 1997 – IBTS “*Como projetar e construir estruturas de concreto com qualidade e produtividade*” – IBTS – Technical Information and ABNT NBR 16055 – concrete walls molded in locus for the construction of buildings – Requirements and Procedures. Their characteristics are given in Table 2.

The study aimed to define the splice procedure to be applied in the experimental section of the SP354, on the development of technology defined as Reflex (Reinforcement of Flexible Road Structures with Steel Fabrics to Prolong Service Life). The main objective was to complement the study for development of a new technology for the construction and rehabilitation/recovery highways, with the use of welded steel mesh in order to increase the life thereof, as well as allowing the reduction of use of natural resources.

A welded mesh panel covers a certain area on the reinforcement on the pavement, in order to perform the Reflex method, it is necessary to make an installation of welded mesh panels, so that the entire area is covered. When the distribution of the welded mesh on

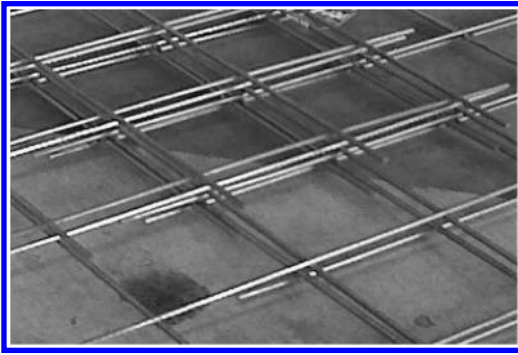


Figure 2. Detail of overlapping meshes.



Figure 4. 6 cm of thickness milling.



Figure 3. Pavement milling.

the pavement surface is held, so that the reinforcement becomes continuous throughout its length, it is necessary to splice the panels which are given by the overlap of meshes.

Splices of the longitudinal reinforcement must be tied with annealed wire, in the same plane. In the case of transversal splices, the spliced wires should also be in the same plane. Services of cutting and mooring shall be executed at the construction site. Figure 2 shows the lateral splices and the detail of the overlapping meshes. This overlapping must be avoided because it was observed that the pathologies (potholes) occurred in the coating, where the welded mesh was overlaid, resulting in a thickness of more than 3 wires.

4.3 Construction of test section in climbing lane

The experiment was held on 23.10.2013 in a local with a ramp slope of 3.6%. The main reason for mesh application in the climbing lane was that due to the new improvements made by the DER / SP in the SP-354 in 2012, part of the commercial vehicle traffic bordering highways as Anhanguera Highway (SP-330), was diverted causing an increase in requests in the pavement above the estimated project.

According to official data of the DER/SP, in 2012, there was an increase of 37% in the number of commercial vehicles passage (Table 3). Due to this new scenario, the pavement began to show high presence of potholes and alligator cracks.

Table 3. Evolution of traffic volume.

Year	Heavy Vehicle	
	Average Daily Traffic (ADT)	Growth Rate (%)
2008	1.501	–
2009	1.588	6
2010	1.690	6
2011	1.750	4
2012	2.393	37
2013	2.515	5
2014	2.584	3

Taking these data into consideration, it was decided the milling of the pavement and the application of the reflex technology (Figure 3). This option was adopted due to the first experiment conducted on the SP-354, which found the best performance in the section which was milled and applied the reflex. Milling was performed with 6 cm of thickness (Figure 4). We adopted a small change in the positioning of the mesh, as had been implemented in the first experiments, that is, the mesh placement with rails down and as a result, with the bars up, reversing the side.

This care occurred trying to reduce the thickness in placing screens, avoiding overlap. The coatings on the mend in the longitudinal direction was executed without overlapping any screen. In addition, there was an improvement in fixing them, going to use 5 mm steel bars, driven into the milled pavement (Figure 5). There was also careful to cut fabrics, in the corners, which occurred overlap of all screens, so there would overlap a maximum of two wires.

After the mesh fixations were applied binder layers and waterproof according to the rules of the DER/SP, besides the layer Hot Mix Asphalt (HMA) in thickness of 6 cm compacted.

4.4 Field measurements

In order to evaluate the structural behavior deflection evaluations were done with the use of



Figure 5. Detail of steel mesh.

Benkelman beam. These offset measurements were performed according to the Pavement Restoration Manual Asphalt DNIT (2006). The deflectometric measure did before the reflex application and after the restoration of the same was carried out. From the results it was observed that the structural behavior difference among portions with and without the mesh is still not significant. The tendency is that the difference grows with the age of the pavement using the reflex technology.

4.5 Structural assessment

The reinforcement design methods with steel mesh, in the bibliography, are based mainly on observation of experience works and laboratory testing. The use of numerical models appears as the appropriate means to the structural analysis of reinforced pavements using steel mesh according to Alves (2007). In this research we chose to make simplified structural analysis of the pavement test section with multiple layers with linear elastic behavior model. All calculations were performed using the Elsym-5 program.

The mechanical parameters of the material on different layers are described by their thickness, Young's modulus and Poisson's ratio, as soon as the calculation parameter, it is considered the layer with elastic modulus equivalent layer steel mesh (EL) where it can be determined according models REFLEX (2001). The equivalent modulus is given by Equation 1:

$$E_{El} = \frac{E_{steel} \cdot I_{steel} + E_{asphalt} \cdot I_{asphalt}}{I_{El}} \quad (1)$$

where E_{steel} = modulus of elasticity of the steel; I_{steel} = moment of inertia of steel; $E_{asphalt}$ = modulus of elasticity of the asphalt; $I_{asphalt}$ = moment of inertia of asphalt; E_{El} = modulus of elasticity of equivalent layer and I_{El} = moment of inertia of equivalent layer.

Using data from the steel mesh (Table 2) the cross section of steel bar has been converted into a square equivalent section. For a mesh with 10.0 cm spacing of

Table 4. Pavement structure adopted in the test section.

Layer	Thickness (mm)	Modulus of Elasticity (MPa)	Poisson (ν)
HMA	60	4,000	0.30
Steel Mesh	–	10,798	0.30
HMA	70	4,000	0.30
Graded crushed stone	200	300	0.35
Cracked rock	200	250	0.35
Subgrade	–	70	0.45

and a 4.2 mm of diameter, the equivalent layer elastic modulus was calculated as follows in Equation 2:

$$A = A_{\square} \Rightarrow \pi \cdot r^2 = a \cdot b \Rightarrow b = 3,30mm$$

$$E_{steel} \cdot \frac{3,3 \cdot 4,2^3}{12} + E_{asphalt} \cdot \frac{(100 - 3,30) \cdot 4,2^3}{12} = E_{El} \cdot \frac{100 \cdot 4,2^3}{12}$$

$$E_{El} = \frac{1}{100} \cdot (210000 \cdot 3,3 + E_{asfalto} \cdot 96,7) \quad (2)$$

The effect of reinforcement with steel mesh was analyzed for the typical structure of DER/SP flexible pavement design. The structure consists of a 13 cm of asphalt concrete, 20cm of graded crushed stone and 20 cm of cracked rock. The mechanical properties of all materials can be seen in Table 4.

Using the elasticity modulus of 4,000 MPa for asphalt concrete, as seen in Table 4, the elastic modulus equivalent to layer may be calculated according to the procedure described above (Equation 2), and then the modulus of elasticity was calculated with a value of 10,798 MPa.

To quantify the contribution of steel reinforcement to the early stages of a pavement's service life, a classical fatigue law was adopted in this study (Equation 3) where N = number of cycles for crack initiation; and ϵ_t = tensile strain at the bottom of the HMA layers. This equation, which was adopted by the Arizona Department of Transportation (ADOT), was calibrated by the fatigue behavior of 20 selected experimental sections. It should be noted that although there is a large variation among fatigue equations for HMA materials, the previous equation was used for relative comparison between reinforced and unreinforced cases (Elseifi et al., 2005).

$$N_{AASHTO} = 9.33 \times 10^{-7} e_t^{-3.84} \quad (3)$$

Compared with the year 2014, the data in Table 3 were used to calculate a new cumulative number of standard axle passes of 80 kN in the stretch with and without wire mesh and based on the design criteria to fatigue and specific deformation defined by the horizontal draw Dormon method (Equation 4), the N_{dim} values were calculated for both criteria assuming

Table 5. Admissible values.

Type of pavement	Number of standard axle 80 kN	
	USACE	AASHTO
Without Steel	5.35E + 07	1.34E + 07
With Steel		

Table 6. Mechanistic check

Pavement	Layer	Acting values		Admissible values	
		ϵ t (cm/cm)	ϵ v (cm/cm)	ϵ t (cm/cm)	ϵ v (cm/cm)
Without Steel	HMA	1.73E-04	–	3.75E-04	–
With Steel	Subgrade	–	3.12E-04	–	2.76E-04
Without Steel	HMA	2.10E-05	–	3.75E-04	–
With Steel	Subgrade	–	1.68E-04	–	2.76E-04

that the different pavements could support the same damage as seen in Table 5 and 6.

$$N_{USACE} = 6.067 \times 10^{-10} e_v^{-4.762} \quad (4)$$

It appears from the results obtained using the computer program Elsym-5 that the active values of horizontal tensile strain at the bottom fiber HMA layer ($=2.10 \times 10^{-5} \epsilon_{adm}$ and 1.73×10^{-4}) respectively to the sections with and without steel mesh are below the permissible values ($=3.75 \times 10^{-4} \epsilon_{adm}$), however the deformation analysis specifies compression vertical ϵ_v , the active value of the non-display option was higher than the permissible value. Therefore, the pavement structure using the scaled steel mesh according DER (2006), it was acceptable to serve the traffic in 2014.

5 CONCLUSION

The comparison of a highway traditionally built and the use of reflex technology was discussed in this paper, mainly the use of the mesh in the rehabilitation of flexible pavements for additional tracks. Thus it can be concluded that in general, the results have highlighted the structural behavior of the pavement.

From the construction point of view, the greatest difficulties were felt in fixing the wire mesh to the underlying bituminous layer, essential to prevent its movement or lifting during movement of work equipment. It is considered that the results achieved in this study were satisfactory.

It should be noted that the research is still in progress and that the problems of the amendments are being studied, since there is the willingness of manufacturers to provide the steel mesh in rolls which would facilitate

its implementation. For future studies it is suggested to develop more appropriate study the wire mesh in the presence of the pavement structure, for example, programs with use of the finite element method.

REFERENCES

- AASHTO (1994) *A Policy on Geometric Design of Highways and Streets*. American Association of State Highway and Transportation Officials, Washington, D.C.
- Alves, A. R. D. (2007) *Reforço de Misturas Betuminosas com Malhas de Aço*. Dissertação de Mestrado em Transportes, Instituto Superior Técnico, UTL.
- Arakawa, N. T.; Olio, A. L. D. (2006) *Terceira Faixa – Afunilamento Final*. Anais ao XXXVII Reunião Anual de Pavimentação, RAPv, Goiânia.
- DER – Departamento de Estradas de Rodagem de São Paulo (2006). *IP-DE-P00/001 Projeto de Pavimentação*. São Paulo, 53p.
- DNIT – Departamento Nacional de Infraestrutura de Transportes (2006). *DNIT IPR-720 Manual de Restauração de Pavimentos Asfálticos*. Rio de Janeiro, 246p.
- Elsiefi, M.; Al-Qadi, I. L. (2005). *Effectiveness of Steel Reinforcing Netting in Combating Fatigue Cracking in New Flexible Pavement Systems*. Journal of Transportation Engineering, ASCE, Vol. 131
- Fortes, R. M.; Ressutte, A. F. B. (2011) *Reflex ou Ari: Uma visão sobre a utilização de pavimento asfáltico reforçado com malha de aço (Reflexo or Ari: A view on the use of asphalt pavement reinforced with steel mesh)*. Trabalho apresentado ao V Congresso de Infraestrutura de Transportes, CONINFRA 2011, São Paulo.
- Fortes, R. M.; Ressutte, A. F. B.; da Silva, J. B. R.; Cahin, R.; Souza, C. L.; Vieira, V.; Barbosa Junior, A. S. B.; Bento, B. B. (2013a) *Estudo de desempenho sobre a utilização de pavimento asfáltico reforçado com tela de aço na SP354*. Trabalho apresentado ao VIII Congresso Brasileiro de Rodovias e Concessões, CBR&C, Santos.
- Fortes, R. M.; Ressutte, A. F. B.; da Silva, J. B. R.; Cahin, R.; Souza, C. L.; Vieira, V.; Barbosa Junior, A. S. B.; Bento, B. B. (2013b) *Estudo de desempenho sobre a utilização de pavimento asfáltico reforçado com tela de aço na SP354*. Trabalho apresentado ao XLII Reunião Anual de Pavimentação, RAPv, Gramado.
- Fortes, R. M.; Ressutte, A. F. B.; da Silva, J. B. R.; Cahin, R.; Souza, C. L.; Vieira, V.; Barbosa Junior, A. S. B.; Bento, B. B. (2013c) *Performance study over the use of reinforced flexible pavement with steel mesh at Brazilian Road*. Anais do I International Journal of Pavements Conference, IJPC, São Paulo, Brazil, December 9–10.
- Halonen, P.; Huhtala, M.; Pihlajamaki, J. (2000) *HVS-NORDIC, results from the first year in Finland – GS2-4*. Finland: Technical Research Centre of Finland (VTT).
- HVS-Nordic (1998) *Research Programme for full scale accelerated pavement testing in Finland and Sweden 1997-2003*, Linköping, 10 pp.
- Rathmayer, H. G.; Korkiala-Tanttu, L. (2002) *Steel Grids, an Efficient Way to Improve the Durability of the Pavement*. VTT – Technical Research Center of Finland, Building and Transport, Espoo, Finland.
- REFLEX Report T7:01 “Modelling of Flexible Pavement Reinforced by Steel Net”, 2001.
- VTI (Swedish National Road and Transport Research Institute) (2003). *VTI notat 30-2003. Stålarmering av Väg 600, Sundom*. Disponível em: <http://www.vti.se/templates/Page_11295.aspx>. Acesso em: 22 abr.

Pavement assessment, surface characteristics

A simplified approach for the estimation of HMA dynamic modulus for in service pavements

K. Georgouli, M. Pomoni, B. Cliatt & A. Loizos

*National Technical University of Athens (NTUA), School of Civil Engineering,
Laboratory of Pavement Engineering, Athens, Greece*

ABSTRACT: Structural condition and performance of an existing flexible pavement strongly depends on the in-situ properties of asphalt layers material. Non Destructive Testing (NDT) systems, such as Falling Weight Deflectometer (FWD), enable the assessment of the pavement structural condition. Hot Mix Asphalt (HMA) layers moduli can be estimated through backcalculation procedures. Since asphalt mix is a viscoelastic material, its behavior is expressed through the dynamic modulus (E^*), a key parameter which is determined, in case of an existing pavement, in the laboratory by testing cores extracted in the field. Given that, on the one hand coring is a destructive and time-consuming procedure and on the other that cores must be of a certain height in order to proceed with the laboratory testing, the need for estimating HMA E^* for in service pavements with NDT ensues. The present research is concentrated on the feasibility of backcalculation procedures to assess the E^* , by investigating the relation between the backcalculated in-situ moduli and the laboratory determined E^* . Towards this goal FWD testing was applied at several locations along a newly constructed pavement section, in order to estimate the asphalt layers modulus through backanalysis approach. Based on the backanalysis and laboratory results moduli were evaluated comparatively and the evaluation results seem promising in terms of estimating the E^* of in service pavements.

1 INTRODUCTION

Road authorities and highway agencies focus on preserving the pavement asset while maximizing the economic efficiency of the investment. From a structural standpoint this is translated into assessing the pavement structural condition. Pavement structural condition is strongly related with pavement behavior at every stage of its life. Shortly after the construction it provides information on the condition that was achieved during construction (quality control) and serves as important historical data. Periodical monitoring of the pavement structural condition is an integral part in order to establish management strategies.

Structural condition is related to the structural characteristics of the pavement as well as the mechanical characteristics of the layers individual mixes. Regarding flexible pavements, asphalt layers have a strong impact on the overall pavement performance, since it is mainly due to the mechanical characteristics of the asphalt base layer that the traffic loads are transferred to the subgrade significantly reduced. On this basis, stiffness modulus of asphalt mix layers forms an important parameter that determines on a great degree the performance of not only the asphalt layer but the pavement as well.

Non Destructive Testing (NDT) systems enable the assessment of the pavement structural condition

in a non destructive manner. Consequently, their implementation in pavement structural monitoring has gained popularity in current years.

Falling Weight Deflectometer (FWD) is commonly used by highway agencies to apply patterns of loading and record deflection data along the pavement. Current deflection analysis procedures utilize deflections, thicknesses and load levels as the input variables to solve for layer properties. This is an iterative process that compares calculated deflections with the measured deflections.

Backcalculation of pavement moduli has been an intensively researched subject for more than four decades. Many backcalculation methodologies exist employing different backcalculation procedures and algorithms (Andrei et al. 1999, Christensen et al. 2003, Bari & Witezak 2006, Obulareddy 2006, Birgisson et al. 2005). Classical backcalculation procedures include those that use the Odegaard – Boussinesq approach or in other words the Method of Equivalent Thickness (MET). The main problems any classical backcalculation procedure faces are convergence, accuracy, and the number of layers in the backcalculation program. On the other hand, genetic algorithms (GAs) can be used to backcalculate the pavement moduli by searching the entire search space of the objective function using guided random search techniques. The GAs are based on the Darwinian Theory

and are formulated on the mechanics of genetics and natural selection (Dongre et al. 2005, Tran & Hall 2005). The use of GAs in pavement engineering is relatively new and thus no thorough investigation has been carried out to address all aspects and challenges associated with the backcalculation procedure.

However, since asphalt mix is a viscoelastic material, the key-parameter for expressing and determining its stiffness is the dynamic modulus (E^*). E^* is a complex number which relates stress to strain for linear viscoelastic materials subjected to continuously applied sinusoidal loading in the frequency domain (Dougan et al., 2003). Therefore, it fully describes the strong influence of temperature (T) and loading time (t) (or frequency) on the hot mix asphalt (HMA) behavior, through the construction of the master curve. Determination of E^* in the laboratory requires advanced laboratory equipment.

In case of existing pavements, the dynamic modulus can be determined through laboratory testing on cores extracted from the field. However, this procedure is destructive and time consuming, as in many problems it is tedious to get all necessary data required for a dynamic analysis. Besides this, specimens must be of certain height in order to proceed with the laboratory testing.

Consequently, the need for estimating E^* in the field with NDT ensues. Since now, numerable studies have been conducted in order to estimate the in-situ stiffness through backcalculation procedures. The optimization models followed in this process (static or dynamic analysis) affect the final precision of the suggested solution. The majority of them are focused on the dynamic analysis frame, which is undeniably complex and computationally expensive (Varma et al. 2013, Levenberg 2012, Kutay et al. 2010, Ameri et al. 2009). On the other hand, static analysis techniques, although being simpler, seem to be practical and effective and their results are critically accepted.

In light of the above, the present study is concentrated on the development of a simplified approach for the estimation of the HMA modulus for in service pavements. Therefore, the feasibility of backcalculation procedures based on the static frame analysis to assess the E^* of the HMA layers, by investigating the relation between the backcalculated in-situ moduli ($E_{in-situ}$) and the laboratory determined (E^*_{lab}), is investigated.

For this purpose, NDT testing was performed at several locations of an existing pavement highway section. Then cores were taken at the exact positions that FWD testing was performed and were transferred to the laboratory in order for the E^* of the cores to be determined. Alongside, the in situ modulus of the asphalt layers was backcalculated using a classical backcalculation procedure (basin fitting) and the GAs procedure. A comprehensive comparative analysis on moduli is applied in order to investigate their relation and to evaluate the GAs procedure. It is noted, that the analysis is performed considering the composite moduli of the asphalt layers, since asphalt layers (and hence cores)

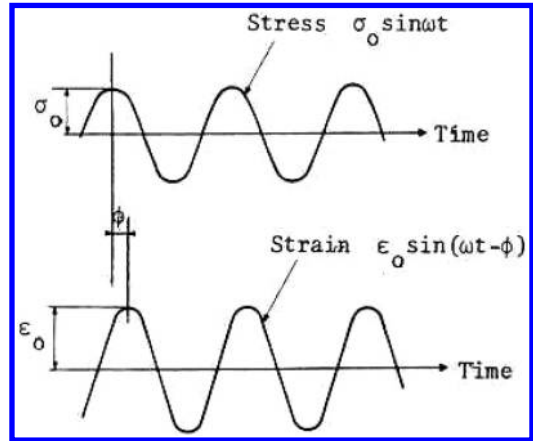


Figure 1. Phase Lag between Sinusoidal Stress and Induced Strain (Huang, 1993).

consist of asphalt base and wearing antiskid course as well.

The comparative evaluation of the aforementioned moduli aims to set a practical, but yet robust approach to estimate the HMA dynamic modulus in the field.

2 THEORITICAL BACKGROUND

2.1 Dynamic Modulus (E^*)

The ratio of the amplitude of the sinusoidal stress (at any given time, t), and angular load frequency (ω), $\sigma = \sigma_0 \sin(\omega t)$ to the amplitude of the sinusoidal strain $\epsilon = \epsilon_0 \sin(\omega t - \phi)$, at the same time and frequency, that results in a steady state response, is defined as the complex modulus (Witczak & Bari, 2004). In viscoelastic materials, the peak values of stress and strain do not appear simultaneously, and this phase lag is expressed through angle ϕ (Figure 1).

The complex dynamic modulus (E^*) can be mathematically expressed as follows:

$$E^* = \frac{\sigma}{\epsilon} = \frac{\sigma_0 \cdot e^{i \cdot \omega \cdot t}}{\epsilon_0 \cdot e^{i \cdot (\omega \cdot t - \phi)}} = \frac{\sigma_0 \cdot \sin(\omega \cdot t)}{\epsilon_0 \cdot \sin(\omega \cdot t - \phi)} \quad (1)$$

where, σ_0 = peak (maximum) stress; ϵ_0 = peak (maximum) strain; ϕ = phase angle, degrees; ω = angular velocity; t = time, seconds.

The dynamic modulus is defined as the absolute value of the complex modulus:

$$|E^*| = \frac{\sigma_0}{\epsilon_0} \quad (2)$$

To account for the influence of temperature and rate of loading the E^* can be determined from a master curve developed at any arbitrarily selected reference temperature. A master curve represents the

response of an asphalt mix at the selected reference temperature over a wide range of frequency or time. Master curves are constructed using the principle of time-temperature superposition. Data at various temperatures are shifted with respect to time until the curves merge into a single smooth function. The master curve of the moduli, as a function of time, formed in this manner describes the time dependency of material stiffness. The amount of shifting at each temperature required to form the master curve describes the temperature dependency of the material (Witczak and Bari, 2004 & Lundy et al., 2005). In general, the master curve can be mathematically modeled by a sigmoidal function described as:

$$\log|E^*| = \delta + \frac{\alpha}{1 + e^{-\beta + \gamma \cdot \log f_r}} \quad (3)$$

where, $|E^*|$ = Dynamic modulus (ksi); δ = minimum value of $|E^*|$; $\delta + \alpha$ = maximum value of $|E^*|$; β , γ = parameters describing the shape of the sigmoidal function; f_r = reduced frequency of loading at reference temperature; Hz:

The reduced frequency is related with the amount of shifting, expressed by the shift factor $a(T)$, by the following equation:

$$f_r = a(T) \cdot f \Leftrightarrow \log f_r = \log a(T) + \log f \quad (4)$$

where, $a(T)$ = shift factor as a function of temperature; f = frequency of loading at desired temperature, Hz; T = temperature of loading cycle, °F.

For precision, a second order polynomial relationship between the logarithm of the shift factor i.e. $\log a(T_i)$ (Equation 5) and the temperature in Fahrenheit degrees is used.

$$\log a(T) = a \cdot T_i^2 + b \cdot T_i + c \quad (5)$$

where, $a(T_i)$ = shift factor as a function of temperature T_i ; T_i = temperature of loading cycle, °F; a , b , c = coefficients of the second order polynomial.

From the aforementioned equations (1 to 5), it is feasible to determine E^* for any combination of temperature and loading time.

2.2 In-situ Modulus

One of the most common field tests used to evaluate the structural condition of a pavement is done with an FWD. This apparatus drops a circular load on the pavement structure that is representative of a heavy vehicle tire load (Goktepe et al. 2005). With the use of deflection sensors, the resulting deflection basin of the pavement surface can be measured. (Leiva-Villacorta 2012). Analysis of the deflection basin involves measurement of deflection at various distances from the load and selection of layer moduli such that the theoretical deflection basin matches the measured deflection values.

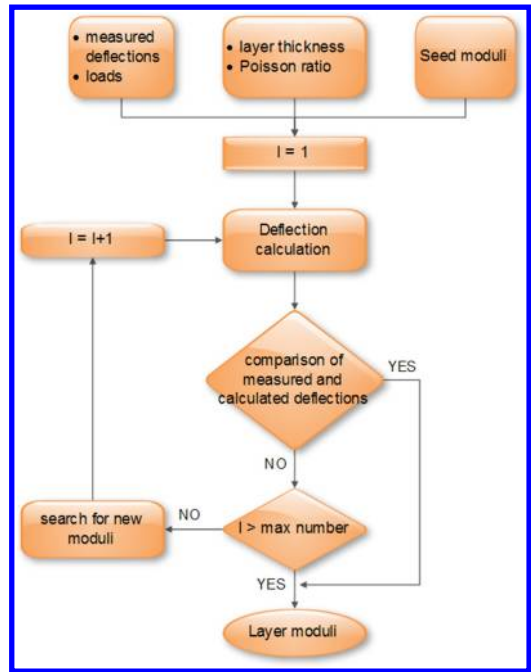


Figure 2. Flowchart of backcalculation procedure.

Developments in analytical techniques, coupled with improved deflection measurement capabilities, have resulted in several backcalculation techniques widely used in pavement evaluation. Backcalculation process consists of various analytical techniques that include iteration, database searching, closed-form solutions, and simultaneous equations, using non-linear regression equations developed from layered elastic analysis output data (Appea 2003). The iterative analysis procedure adjusts layer moduli, compares computed and measured deflections, and repeats the process until the theoretical and measured deflections reach an acceptable match. A schematic of the backcalculation procedure is shown in Figure 2.

Pavement response analysis (calculation of deflections) can be considered as either static or dynamic. Although the FWD test is intrinsically dynamic, the state-of-practice backcalculation techniques used to interpret the FWD records are primarily elastostatic based, partly because of the high computational cost of dynamic multilayered solutions. For engineering applications wherein simplicity is a virtue, elastostatic-based interpretation of the falling weight-induced force and deflection records remains the norm in estimation of the pavement's stiffness characteristics (Guzina & Osburn 2002).

Multi-layered elastic theory (MET) has been used extensively for the backcalculation process, because flexible pavement analyses have been mainly based on elastic theory. However, there are quasi-static methods such as WESLEA, Boussinesq-Odemark transformed section methods, nonlinear elastic viscoelastic, and finite element methods. Moreover, Genetic algorithms

(GA) as a robust and randomized search algorithm can be employed to optimize the search domain for backcalculation.

In the present investigation, the backcalculation procedure makes use of the static loading and it is performed in the framework of multiple elastic theory, a model which is based on Bussinesq's and Odemark's principles (Basin fit) (Dynatest 2002) and on genetic algorithms (GAs) which mimic the theory of evolution. These models seem to be efficient without being computationally wasteful.

2.2.1 Layered elastic backcalculation procedure

For a pavement structure the modulus of elasticity and Poisson's ratio for each layer are the material properties required for calculating the stresses, strains and deflections for analytical design and evaluation. It is usual to assume that pavement materials are linear elastic, homogeneous and isotropic. Most of the classical backcalculation procedures use Boussinesq's equations with Odemark's transformation of layered systems to semi-infinite half-space for backcalculation.

The basin fit methodology starts with a seed value for the stiffness modulus of each layer as an assuming parameter to start the procedure. Also, the collected data (thicknesses, temperatures and measured deflections) are set as input parameters. The theoretical deflection bowl for this pavement structure is calculated. The error between the measured deflections and calculated deflections is then assessed. The moduli in the structure are then increased/decreased by a small amount (typical 1%) and if the error in either of these deflection bowls is less than the original deflection bowl this is taken to be a better solution. This process is iterated until a minimum in error between the calculated and measured deflection bowls are found. Problems with this approach lay on the fact that several pavement structures (different combinations of layer stiffness) may result in the same deflection bowl and the process may output any one of these solutions. This can be overcome by specifying suitable limits for layer stiffness and seed values for the iterative process.

2.2.2 Genetic Algorithms backcalculation procedure

GAs are a family of adaptive techniques, devised by Holland (1975), used to solve optimization problems. GAs are inspired by biological evolution and are based on the principle, 'survival of the fittest'.

Conventional GAs have five operations (Goldberg 1989)—creation of population, evaluation, selection, crossover and mutation (Figure 3).

GAs work with a population of 'chromosomes of individuals', each representing a possible solution to the given problem. Each chromosome is assigned a 'fitness value' indicating how good a solution it is to the problem. The highly fit chromosomes are given opportunity to reproduce by cross breeding with other individuals in the population. This produces new chromosomes as 'offsprings', which share some features

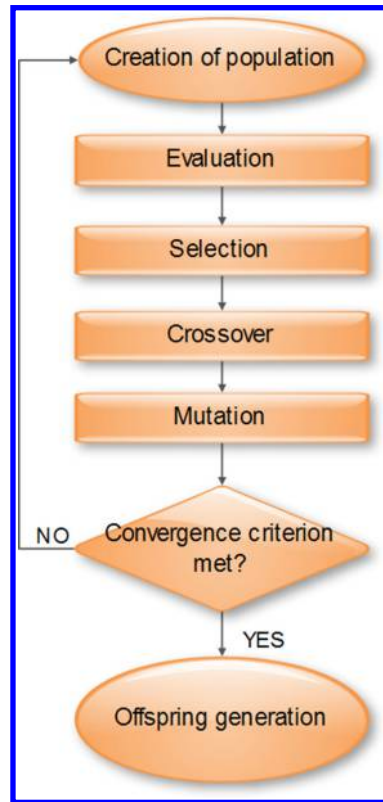


Figure 3. Flowchart of a genetic algorithm.

taken from each 'parent'. The least fit members of the population are less likely to get selected for reproduction, and so die out. A whole new population of possible solutions is thus produced by selecting the best individuals from the current generation, and mating them to produce a new set of chromosomes.

This new generation contains a higher proportion of the characteristics possessed by the good members of the previous generation. In this way, over many generations, good characteristics are spread throughout the population. By favoring the mating of the more fit individuals, the most promising areas of the search space are explored. If the GA has been designed well, the population will converge to an optimal solution to the problem. The global solution is possible only when the parameters are properly chosen. Improper selection of parameters can result in local minima.

3 DATA ACQUISITION

3.1 Test section

For the purpose of the present research study a highway flexible pavement section was selected. The typical pavement cross section is presented in Figure 4.

In terms of the material characteristics of the test section, the hot-mix asphalt (HMA) mixture of the antiskid wearing course corresponds to mix

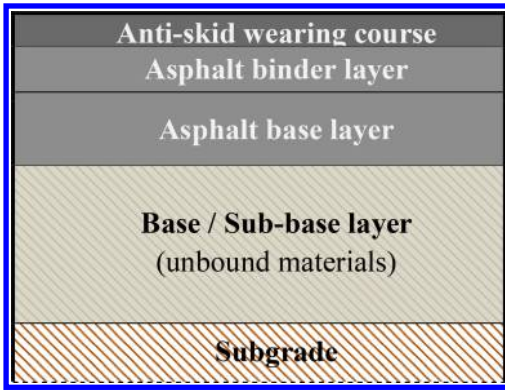


Figure 4. Cross section of the pavement under investigation.

Table 1. Composition of wearing course asphalt mixture.

Sieve size	Passing (%)
19 mm (3/4 in.)	100
12.5 mm (1/2 in.)	92
9.5 mm (3/8 in.)	69
4.75 mm (No. 4)	33
2.36 mm (No. 8)	21
1.18 mm (No. 16)	12
300 μm (No. 50)	5
75 μm (No. 75)	3.4

Table 2. Asphalt properties of wearing course HMA.

Test	Results
Penetration at 25°C (pen)	52
Softening point (°C)	72.8
Viscosity (MPa.s)	1170
Elastic recovery (%)	93

designation O-5, as defined in ASTM standards (D3515, 2009), with steel slag aggregate and an air void content of around 11%. The asphalt mixture was produced using an 80–100 asphalt penetration modified with SBS 4% and a binder content of 4.6% by mass of the mixture. Table 1 shows the HMA composition of the wearing course and Table 2 shows the asphalt properties.

Asphalt base and binder course consists of the same HMA mixture. The HMA mixture of the asphalt base course and binder course is a 19.0 mm nominal maximum aggregate size asphalt mixture with an air void content of 4.5%. The asphalt mixture was produced using a 50–70 grade asphalt penetration and 49.5°C softening point, with a binder content of 4.3% by mass of the mixture. The composition of the asphalt base course mixture is as follows (Table 3):

FWD measurements were performed at 20 locations along the selected pavement section. Then cores were

Table 3. Composition of asphalt base course.

Sieve size	Passing (%)
25 mm (1 in.)	100
19 mm (3/4 in.)	90.9
12.5 mm (1/2 in.)	71.3
4.75 mm (No. 4)	56.2
2 mm (No. 10)	38.5
0.42 mm (No. 40)	17.4
0.18 μm (No. 80)	12.9
75 μm (No. 200)	5.5

taken at the same locations and were transferred to the laboratory in order to determine the dynamic modulus.

3.2 *In-situ measurements*

The in situ data collection was performed using the NDT FWD and Ground Penetrating Radar (GPR) systems of the Laboratory of Pavement Engineering of NTUA. FWD was used for the conduction of the deflection basin tests, while GPR provided the thickness of the unbound base/subbase layer that serves as an input in the backcalculation procedure. The thickness of the asphalt layers was determined based on the cores that were extracted from the pavement.

The FWD system which was used for this investigation is vehicle-mounted and is equipped with a weight and nine velocity transducer sensors. In order to perform a test, the vehicle is brought to a stop and the loading plate (weight) is positioned over the desired location. The sensors are then lowered to the pavement surface and the weight is dropped. All given deflections are recorded by the nine sensors.

The diameter of the loading plate was 300 mm, the size of the falling weight applied was 50 kN and the generated stress was 700 kPa (Dynatest 2002). The nine deflection sensors were placed at a distance of 200 mm, 300 mm, 450 mm, 600 mm, 900 mm, 1200 mm, 1500 mm and 1800 mm from the center of the loading plate. Parallel to the deflection measurements, systematic measurements of the air temperature, pavement surface temperature and temperature within the asphalt layers were taken. The measurements of the air temperatures as well as the pavement surface temperature were recorded by the FWD system (use of infrared radiation etc), while temperature within the asphalt layers was taken through holes drilled in the pavement.

3.3 *Dynamic Modulus Testing*

Once the in situ measurements were completed, cores were taken at the same locations. The extracted cores from the field were transferred to the Laboratory of Pavement Engineering of NTUA, in order for the dynamic modulus (E^*) to be determined in the laboratory according to AASHTOT 342-11 (Figure 5).



Figure 5. E* laboratory determination.

A controlled sinusoidal (haversine) compressive loading was applied to each specimen for a range of loading frequencies and temperatures. Due to difficulties in obtaining reliable results at the temperature of -10°C and 54°C required for AASHTO T342-11, testing was conducted at six temperatures 4, 15, 20, 25, 37°C and six frequencies, 25, 10, 5, 1, 0.5 and 0.1 Hz. These difficulties have been also noted by other researchers (Bennert & Williams 2009). Each test specimen, individually instrumented with LVDT brackets, was tested for each of the 30 combinations of temperature and frequency loading starting with the lowest temperature and proceeding to the highest. Testing at a given temperature began with the highest frequency of loading and proceeded to the lowest. At the beginning of testing, the specimen was preconditioned with 200 cycles at 25 Hz. The applied loading was of a certain magnitude for each testing temperature so as to obtain axial strains between 50–150 microstrain.

It is noted that in the present study cores were not cut. So, samples consist of the asphalt base and wearing antiskid course as well. Consequently, the dynamic modulus that is determined in the laboratory is the ‘composite’ dynamic modulus of the asphalt layers.

The data results of the laboratory testing can be shifted with respect to the frequency of loading, in order to form the master curve at the selected reference temperature.

4 DATA ANALYSIS AND RESULTS

4.1 Data processing

Since a master curve represents the response of an asphalt mix at a selected reference temperature over

Table 4. Coefficients values for the master curve fit (α , β , γ , δ).

Specimen	α	β	γ	δ
A165	1.83414	-2.04848	0.48620	1.61902
A167	2.32441	-1.98129	0.49243	1.14393
A173	2.78710	-2.08511	0.43024	0.72077
A177	1.87337	-1.87873	0.50918	1.59236
A181	2.64713	-1.85387	0.41030	0.95163
A185	1.85933	-1.92819	0.66620	1.58762
A187	2.07239	-1.71467	0.60256	1.36756
A190	3.06472	-1.83910	0.40856	0.51255
A193	2.69696	-2.02513	0.46925	0.82718
A196	2.36451	-1.91401	0.47837	1.14160
K165	2.10186	-1.29266	0.53557	1.45813
K167	2.63203	-1.95371	0.40484	0.83294
K181	2.18960	-1.06660	0.52630	1.27253
K185.5	3.16070	-1.57499	0.35963	0.59851
K190	1.86363	-1.74393	0.59911	1.57963
K196	3.12381	-1.91070	0.40251	0.42242
D47	2.13385	-1.25788	0.51651	1.20194
D61	3.04396	-1.39463	0.36866	0.48036
D71	2.01714	-1.20384	0.50433	1.34671

a wide range of loading frequency (Christensen & Anderson 1992, Pellinen et al. 2002), the master curves of the 20 specimens were constructed considering as a reference temperature the one that was recorded during the FWD measurements. Temperature depending on the test location, ranged from 8.7 to 22.8°C .

A non-linear least square regression fitting procedure was performed in order to determine all the parameters for each sigmoidal function of Equation 3 (sigmoidal parameters: α , β , γ , δ) as well as those of equation 7 for the shift factor (polynomial parameters: a, b, c). Table 4 presents the coefficients of the sigmoidal function (δ , α , β , γ), while Table 5 presents the coefficients values for the shift factor.

The other contributing factor to dynamic modulus is the loading frequency. In order to determine the FWD frequency the time history was considered.

The form of pulse at all 20 locations suggested an imperfect sinusoidal load pulse. Imperfect sinusoidal load pulses can be approximated by trapezoidal pulse shapes, from which the block time pulse duration can be derived. Principally the ascent of the load pulse must be taken into account. The concluded FWD frequency (f_{FWD}) was 16.3 Hz. This is in accordance with international experience (Maher et al. 2005, Dynatest 2002).

Considering the parameters of Tables 4 and 5 and the frequency of the FWD testing, for each specimen the laboratory E* (E^*_{lab}) corresponding to the conditions of the in situ backcalculated modulus ($E_{in-situ}$) can be determined.

4.2 Comparative analysis

The in situ modulus was backcalculated using the basin fit (Dynatest 2002) and the genetic algorithms methodology (Pan et al. 2012).

Table 5. Coefficients values for the shift factor (α , b , c).

Specimen	a	b	c
A165	-0.000611	0.006202	1.168901
A167	-0.000163	-0.057483	3.202582
A173	-0.000250	-0.041369	2.586960
A177	-0.001047	0.067554	-0.830103
A181	0.000322	-0.125715	5.259701
A185	0.000208	-0.104872	5.360949
A187	-0.000092	-0.065450	4.058065
A190	-0.000261	-0.056333	4.028744
A193	-0.000039	-0.074773	4.319708
A196	0.000188	-0.117198	5.916197
K165	-0.000682	0.029616	1.129790
K167	-0.000765	0.025324	0.565647
K181	0.000113	-0.092551	6.158986
K185.5	-0.000484	-0.006486	1.832549
K190	-0.000225	-0.038396	2.922211
K196	-0.000506	-0.007160	2.207866
D47	-0.000174	-0.060099	4.802574
D61	-0.000080	-0.076323	5.449639
D71	-0.000299	-0.046081	4.532003

In both backcalculation methodologies, the closing match procedure needs innumerable iterations for approaching the measured deflection bowl. Errors between measured and calculated deflections can be minimized by the objective function of root-mean-square (RMS). It is used to control the convergence of the backcalculated deflections and to assess the acceptance or rejection of the final set of pavement moduli. The RMS is computed by:

$$RMS = \sqrt{\frac{1}{n} \cdot \sum_{i=1}^n \left(\frac{d_i^c - d_i^m}{d_i^m} \right)^2} \quad (6)$$

where, RMS is the root-mean-square error, n is the total number of the deflection measurement points, d_i^c is the backcalculated deflection at point i , and d_i^m is the measured deflection at point i . When the RMS value decreases, the accuracy of the backcalculated moduli is assumed to increase as the error between the measured and calculated deflections decreases.

Figure 6 shows the error between the measured deflections and calculated deflections, in terms of the RMS. The whole RMS spectrum is schematically illustrated in the form of boxplots.

The box itself contains the middle 50% of the data. The upper edge (hinge) of the box indicates the 75th percentile of the data set and the lower hinge indicates the 25th percentile. The range of the middle two quartiles is the inter-quartile range. The line in the box indicates the median value of the data. If the median line within the box is not equidistant from the hinges, then the data is skewed. The ends of the vertical lines or whiskers indicate the minimum and maximum data values, unless outliers are present in which case the whiskers extend to a maximum of 1.5 times the

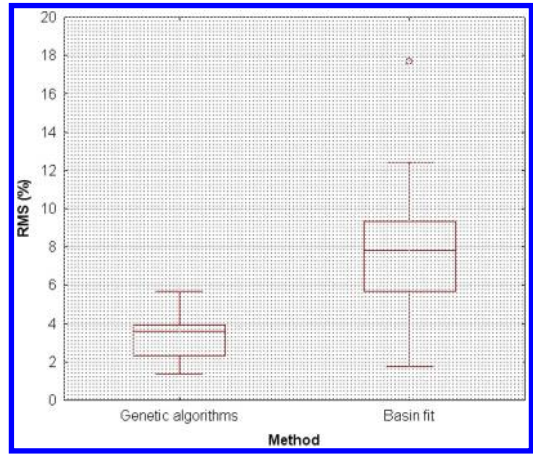


Figure 6. RMS of calculated deflections.

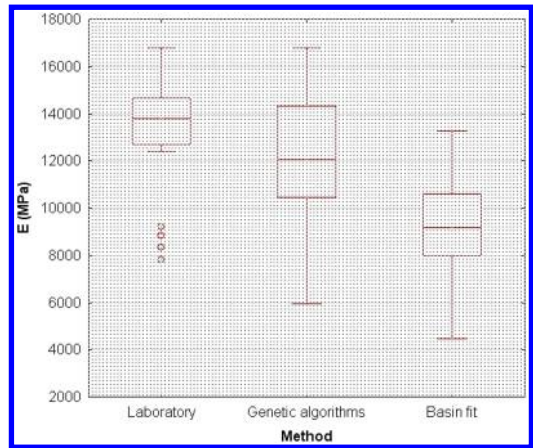


Figure 7. Asphalt modulus values.

inter-quartile range. The points outside the ends of the whiskers are outliers or suspected outliers.

The median RMS error for the genetic algorithms is found to be 3.6% and for the basin fit 7.8%. The lower RMS values in in case of GAs may be due to the fact that back-calculation based on genetic algorithms is carried out through many iterations.

Figure 7 presents the range of the modulus values determined in the laboratory (E_{lab}^*) and backcalculated with GAs (E_{ga}) and basin fit methodology (E_{br}).

E_{lab}^* values are in general higher than the backcalculated ones. This is in accordance to other studies on relevant research matter (Gedafa et al. 2010).

The E_{ga} values are closer to the E_{lab}^* values with the median value of E_{ga} being equal to 12052 MPa and the median value of the E_{lab}^* equal to 13794 MPa. The median value of the E_{br} is lower and equal to 9177 MPa. The position of the median line within the box implies that the data can be considered symmetrical (approximately). Also, the E_{ga} and E_{br} values have a greater range than the E_{lab}^* values. The percentage

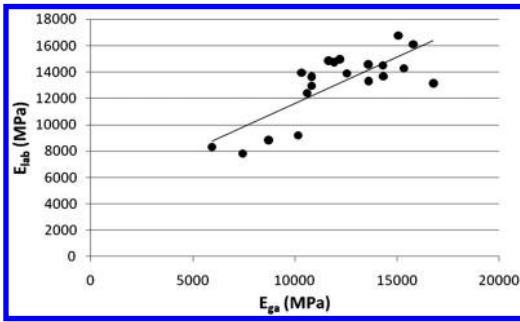


Figure 8. Correlation $E^*_{lab}-E_{ga}$.

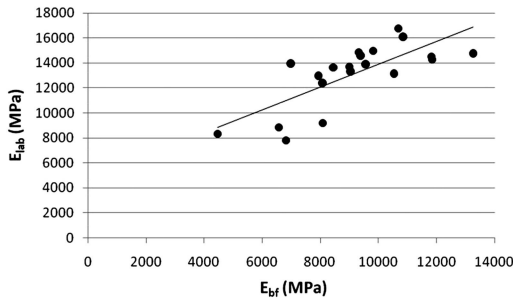


Figure 9. Correlation $E^*_{lab} - E_{bf}$.

Table 6. Constants of linear regression.

Regression	a	b	R ²
E^*_{lab} and E_{ga}	4611.8	0.7023	0.61
E^*_{lab} and E_{bf}	4760	0.9144	0.55

difference of the E_{ga} and E_{bf} values with regards to the E^*_{lab} values is 7.5% and 29.9%, respectively.

In order to investigate the development of a relation between the E^*_{lab} and $E_{in-situ}$, linear regression analysis was applied. The developed relationship is given by equation 7 while the related constants (a and b) as well as the correlation index (R^2) are included in Table 6. Figures 8 and 9 present the correlation between E^*_{lab} and E_{ga} and between E^*_{lab} and E_{bf} , respectively.

$$E^*_{lab} = a + b E_{in-situ} \quad (7)$$

The correlation in both cases can be characterized as good considering the R^2 value. However, in an attempt to further enable the comparison and the transition between the E^*_{lab} and the in situ moduli the ratio of these two data sets was determined. Figure 10 presents the ratio of E^*_{lab} values to the in situ backcalculated moduli.

In every case the median value of the ratios is greater than one meaning that the E^*_{lab} values are greater than the in situ backcalculated moduli. Ratio E^*_{lab}/E_{gen} is the one that approaches the most to one with a median

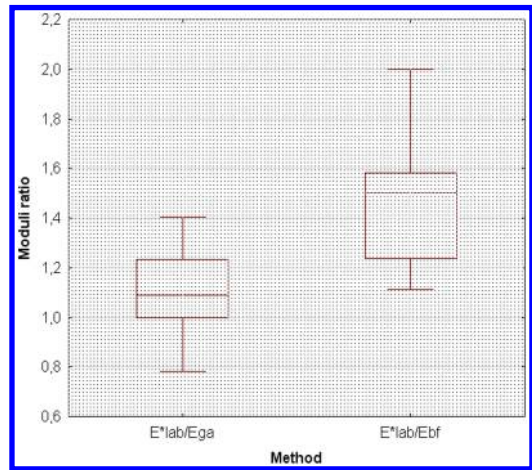


Figure 10. Boxplots of moduli ratio.

Table 7. Characteristic values of ratio $E^*_{lab}/E_{in-situ}$.

Characteristic values	E^*_{lab}/E_{ga}	E^*_{lab}/E_{bf}
Minimum value	0.78	1.11
Maximum value	1.40	2.00
Average	1.10	1.46
Standard deviation	0.16	0.23
Coefficient of variation (%)	14.5	16.2
Median	1.09	1.50

value of 1.09. Value of E^*_{lab}/E_{bf} ratio is 1.50. Table 7 presents the characteristic values of ratio $E^*_{lab}/E_{in-situ}$.

Ratio $E^*_{lab}/E_{in-situ}$ varies from 0.78 to 2.00. It is noted that according to relative study (Gedafa et al. 2010) the ratio ranged from 1.30 to 2.92.

The distribution of these ratios was also estimated. It was found that in every case the normal distribution can be adapted without significant bias, according to the Anderson-Darling test for goodness of fit.

The Anderson-Darling test is used to test if a sample of data came from a population with a specific distribution. It is a modification of the Kolmogorov-Smirnov (K-S) test and gives more weight to the tails than does the K-S test. The K-S test is distribution free in the sense that the critical values do not depend on the specific distribution being tested (note that this is true only for a fully specified distribution, i.e. the parameters are known). The Anderson-Darling test makes use of the specific distribution in calculating critical values. This has the advantage of allowing a more sensitive test and the disadvantage that critical values must be calculated for each distribution.

In Figures 11–12 the input values as well as the normal distribution curve, are presented for ratio E^*_{lab}/E_{ga} and E^*_{lab}/E_{bf} , respectively.

The statistics concerning the input and normal distribution as well as the results of the Anderson-Darling test for goodness of fit are presented in Tables 8–9.

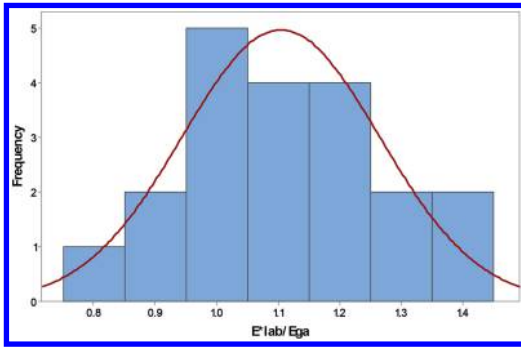


Figure 11. Distribution of ratio E^*_{lab}/E_{ga} .

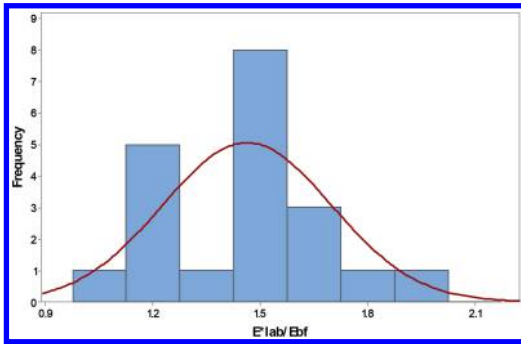


Figure 12. Distribution of the ratio E^*_{lab}/E_{bf} .

Table 8. Distribution statistics of E^*_{lab}/E_{ga} .

	Input distribution	Normal distribution
Mean	1.10	1.10
Median	1.07	1.10
Test value		Anderson-Darling 0.1885
Confidence		>0.15

Table 9. Distribution statistics of E^*_{lab}/E_{bf} .

	Input distribution	Normal distribution
Mean	1.46	1.46
Median	1.51	1.46
Test value		Anderson-Darling 0.4721
Confidence		>0.15

Based on the results of the Anderson-Darling test for goodness of fit, the normal distribution can be considered for the description of the data distribution. Therefore, the mean value can be considered as representative in order to quantify the ratio of E^*_{lab} to $E_{in-situ}$. The ratio is not uniquely specified but depends on the backcalculation methodology followed. As such, in case the genetic algorithms approach is followed the

weighted ratio of E^*_{lab} to the backcalculated modulus is 1.10. Accordingly, in case the basin fit methodology is followed the weighted ratio of E^*_{lab} to the backcalculated modulus is 1.46.

5 CONCLUSIONS

According to the findings of the present study the following conclusions can be drawn. In general, the laboratory determined HMA E^* values of the core specimens were higher than the in situ backcalculated modulus values regardless the considered backcalculation procedure. Only a limited number of data set values appeared an opposite trend.

Overall, the results presented in this study showed that the transition from laboratory determined dynamic modulus (E^*_{lab}) to backcalculated in situ modulus ($E_{in-situ}$) could be enabled, considering the ratio of E^*_{lab} to $E_{in-situ}$. For the present study, the weighted ratio in case the genetic algorithms approach is followed is 1.10, while in case the basin fit methodology is followed the ratio is modulated at 1.46. Given that backanalysis procedure with both methodologies was performed taking into account the same assumptions (thickness, Poisson ratio, linearity of the subgrade), it seems that the ratio of these two moduli is related to the backanalysis methodology followed.

It is noted that in the present research the composite dynamic modulus was studied, since core specimens were not cut at individual asphalt layers and as such the E^* laboratory determination was performed on the specimen of both asphalt base and wearing course.

The analysis results apply for the in subject matter pavement section and for the particular asphalt mix materials. Further investigation is needed by enriching the sample with other type material as well (additional type of bitumen, aggregates etc.), in order for the results to be considered as generic. It is believed that the proposed methodological frame is quite promising in terms of a simplified approach that enables the transition from dynamic laboratory modulus to in situ modulus.

REFERENCES

- AASHTO T342-11. 2001. Standard method of test for determining dynamic modulus of hot mix asphalt (HMA). American Association of State Highway and Transportation Officials, Washington.
- Alkasawneh, W. 2007. Backcalculation of pavement moduli using genetic algorithms. *Dissertation*. University of Akron, Ohio.
- Ameri, M., Yavari, N. & Scullion, T. 2009. Comparison of static and dynamic backcalculation of flexible pavement layers moduli using four software problems. *Asian journal of applied sciences* 2: 197–210.
- Andrei, D., Witzczak, M.W. & Mirza, W. 1999. Appendix CC-4: Development of a revised model for the dynamic (complex) modulus of asphalt mixtures. *Development of the 2002 Guide for the Design of New and Rehabilitated Pavement Structures*. Final Document: NCHRP 1-37A.
- Appea, A.K. 2003. Validation of FWD testing results at the Virginia smart road: theoretically and by instrument

- responses. *Dissertation*. Faculty of the Virginia Polytechnic Institute and State University, Blacksburg, Virginia.
- Bari, J. & Witczak, M.V. 2006. Development of a new revised version of the Witczak E* predictive model for hot mix asphalt mixtures. *Journal of the Association of Asphalt Paving Technologists* 75: 381–423.
- Bennert, T. & Williams, S.G. 2009. Precision of AASHTO TP62-07 for Use in Mechanistic – Empirical Pavement Design Guide for Flexible Pavements. In *Transportation Research Record: Journal of the Transportation Research Board, No. 2127, Transportation Research Board of the National Academies, Washington, D.C.*: 115–126.
- Birgisson, B., Sholar, G. & Roque, R. 2005. Evaluation of a predicted dynamic modulus for Florida mixture. In *Transportation Research Record: Journal of the Transportation Research Board, No. 1929, Transportation Research Board of the National Academies, Washington, D.C.*: 200–207.
- Christensen, D.W., Pellinen, T.K. & Bonaquist, R.F. 2003. Hirsch model for estimating the modulus of asphalt concrete. *Journal of the Association of Asphalt Paving Technologists* 72: 97–121.
- Christensen, D.W. & Anderson, D.A. 1992. Interpretation of dynamic mechanical test data for paving grade asphalt cements. *Journal of the Association of Asphalt Paving Technologists* 61: 67–116.
- Dongre, R., Myers, L., D'Angelo, J., Paugh, C. & Gudimetlla, J. 2005. Field evaluation of Witczak and Hirsch models for predicting dynamic modulus of Hot-Mix Asphalt. *Journal of the Association of Asphalt Paving Technologists* 74: 381–442.
- Dougan, C., Stephens, J., Mahoney, J. & Hansen, G. 2003. E*-dynamic modulus test protocol – problems and solutions. The Connecticut Department of Transportation in Cooperation with the U.S. Department of Transportation, Federal Highway Administration.
- Dynatest 2002. Evaluation of layer modulus and overlay design (ELMOD), User manual.
- Gedafa, D., Hossain, M., Romanoschi, S. & Gisi, A. 2010. Comparison of moduli of Kansas superpave asphalt mixes. Kansas Department of Transportation, Material & Research Center: Kansas.
- Goktepe, S., Agar, E. & Lav, A.H. 2006. Advances in backcalculating the mechanical properties of flexible pavements. *Advances in Engineering Software* 37: 421–431.
- Goldberg, D.E. 1989. Genetic algorithms in search, optimization and machine learning. Reading (MA): Addison-Wesley.
- Guzina, B.B. & Osburn, R.H. 2002. An effective tool for enhancing the static backcalculation of pavement moduli. Submitted to committee A2B05, at 81st Annual Meeting of Transportation Research Board, Washington, D.C.
- Highways Department 2009. Guidance notes on backcalculation of layer moduli and estimation of residual life using Falling Weight Deflectometer test data, *Research & Development Division*.
- Holland, J.H. 1975. Adaptation in natural and artificial systems. Ann Arbor, MI: The University of Michigan Press.
- Huang, Y. 1993. Pavement analysis and design. 1st Edition, Prentice Hall, Upper River Saddle, New Jersey.
- International journal for numerical and analytical methods in geomechanics *Faculty of Civil and Environmental Engineering, Technion – Israel Institute of Technology, Technion City, Haifa 32000*
- Kutay, E., Chatti, K. & Lei, L. 2010. Backcalculation of dynamic modulus (E^*) master curve from FWD surface deflections. TRB Committee AFD80, 89th Annual Meeting, 10–14 January 2010, Washington.
- Leiva-Villacorta, F. 2012. Advanced computing techniques in structural evaluation of flexible pavements using the Falling Weight Deflectometer. A dissertation submitted to the Graduate Faculty of Auburn University Auburn, Alabama.
- Levenberg, E. 2012. Inverse analysis of viscoelastic pavement properties using data from embedded instrumentation. *International journal for numerical and analytical methods in Geomechanics* 37 (9): 1016–1033.
- Lundy, J., Sandoval-Gil, J., Brickman, A. & Patterson, B. 2005. Asphalt mix characterization using dynamic modulus and APA testing. Oregon Department of Transportation Research Unit and Federal Highway Administration.
- Maher, A., Gucunski, N. & Bennert, T. 2005. Implementation of Mechanistic Pavement Design: field and laboratory implementation. Center for Advanced Infrastructure & Transportation (CAIT) Rutgers, The State University Piscataway.
- Obulareddy, S. 2006. Fundamental characterization of Louisiana HMA mixtures for the 2002 Mechanistic-Empirical Design Guide. *Master's Thesis*. Louisiana State University.
- Pan, E., Sangghaleh, A., Molavi, A., Zhao, Y. & Yi, P. 2012. An efficient and accurate genetic algorithm for backcalculation of flexible pavement layer moduli. Department of Civil Engineering, The University of Akron, Ohio.
- Pellinen, T.K., Witczak, M.W. & Bonaquist, R.F. 2002. Asphalt mix master curve construction using sigmoidal fitting function with non-linear least squares optimization. Proceedings of the Pavement Mechanics Symposium at the 15th ASCE Engineering Mechanics Conference (EM2002). Columbia University, New York, NY.
- Robbins, M.M. 2009. An Investigation into dynamic modulus of hot mix asphalt and its contributing factors. *Thesis*. Auburn University, Auburn, Alabama.
- Tran, N.H. & Hall, K.D. 2005. Evaluating the predictive equation in determining dynamic moduli of typical asphalt mixtures used in Arkansas. *Journal of the Association of Asphalt Paving Technologists* 74: 1–17.
- Varma, A.B., Kutay, M.E. & Chatti, K. 2013. Data requirements from Falling Weight Deflectometer tests for accurate backcalculation of dynamic modulus master curve of asphalt pavements. *Airfield and highway pavements 2013, Sustainable and efficient pavements ASCE 2013*: 445–455.
- Witczak, M. & Bari, J. 2004. Development of a master curve (E^*) database for lime modified asphaltic mixtures. Department of Civil and Environmental Engineering, Arizona State of University, Tempe, Arizona.

Temperature correction of HMA moduli based on in situ pavement data

A. Loizos, V. Papavasiliou, C. Plati & C. Tsaimou

National Technical University of Athens, Athens, Greece

ABSTRACT: Rational pavement management requires estimation of HMA moduli from in situ data for detailed structural evaluation of in service pavements. Considering that the HMA moduli are strongly influenced by temperature during the survey, a correction to a reference temperature is needed. Therefore the choice of the temperature correction equation is a critical impact factor in terms of selection of a reasonable pavement rehabilitation strategy. In order to investigate whether the use of in situ pavement data would improve correction effectiveness of HMA moduli, a road experiment was conducted. Field data was utilized for development of two temperature correction equations, which were then implemented for temperature correction of backcalculated moduli. Furthermore, related algorithms from the international experience were also utilized for comparative purposes. The overall analysis showed that temperature correction based on backanalysis of in situ data is quite promising. The related findings and results are displayed and discussed thoroughly.

1 BACKGROUND AND OBJECTIVES

Determination of Hot Mix Asphalt (HMA) moduli is critical for an in depth evaluation of an in service pavement. Maintenance, rehabilitation and redesign strategies require in situ HMA moduli information in order to make important decisions through a profound analysis.

Laboratory tests or in-situ measurements can provide information about HMA moduli. Yet, it is well known that the modulus of asphalt layers is strongly influenced by temperature variations and this correlation explains the fact that HMA moduli for the same pavement vary in accordance with the temperature registered within the body of the asphalt layers. For this reason temperature dependence of HMA moduli has been intensively studied by several researchers over the years, resulting in the development of multiple unique algorithms for temperature correction of HMA moduli to a reference temperature.

Some of the aforementioned algorithms require complicated and rather difficult to determine laboratory values (e.g. Fernando et al. 2001 and Park & Kim 1997), while others require only backcalculated moduli and temperature data, but their implementation is questionable for other asphalt mixes. In addition, previous research (Plati et al. 2014) showed that the implementation of existing algorithms may lead to non reliable results and uncertainties as far as temperature correction is concerned.

It is suggested (Hakim et al. 2002) that ideally FWD testing should be performed at various temperatures, in order to develop an algorithm for the temperature sensitivity of HMA moduli for each site under investigation. Therefore it is worthwhile examining whether

the development of an equation based on in situ data would improve correction process for an in service pavement.

For the above reasons the present research focuses on the development of temperature correction equations and examines their applicability and performance on a specific test pavement. The importance of the suggested correction procedures is the use of not complicated laboratory data that is time consuming and in some cases difficult to perform. For the purpose of this investigation a road experiment was conducted. Non Destructive Testing (NDT) methods were utilized for in situ data collection along a test pavement. Two approaches were considered for the development of the temperature correction equation: a) use of moduli estimated from laboratory testing on cores at different temperatures and b) use of backcalculated moduli values at different HMA temperatures during the survey. The two developed equations were utilized for correction of HMA backcalculated moduli at reference temperature (20°C). Furthermore temperature correction was performed utilizing existing algorithms from the international literature. The HMA moduli corrected with the two developed equations and the existing algorithms as well were examined and analyzed through statistical processes. The paper outlines the related considerations and results, highlighting the importance of the value of using in situ data for pavement assessment.

2 ROAD EXPERIMENT

For the purposes of the present research a road experiment was conducted on an un-trafficked test pavement



Figure 1. In situ road data collection.

Table 1. Measured temperatures at mid-depth of HMA layers.

Minimum Measurement	Maximum Measurement	°C	°C
(A)-(Reference)		19.2	20.1
(B)		24.1	25.9
(C)		26.9	28.0
(D)		31.9	32.5

(traffic only during construction), based on Non-Destructive Testing (NDT) including Falling Weight Deflectometer (FWD) and Ground Penetrating Radar (GPR) (Fig. 1). The length of the test pavement is 1600 m and it consists of 2 lanes per direction.

The experiment consisted of four FWD measurement sets into one period. During the FWD measurements, the mid-depth temperature of the HMA layers was recorded and presented in Table 1.

Along the pavement measurements were conducted at 27 points. Three measurement points were chosen in accordance with the extracted HMA cores for the development of temperature correction equation. These three test points were excluded from the overall analysis and comparison.

GPR data was calibrated utilizing extracted cores in order to determine pavement layer thicknesses (Loizos & Plati 2007). According to GPR analysis the HMA thickness was ranged between 10.5 and 14 cm. Figure 2 shows the cross section of the test pavement (typical flexible pavement). In-situ data, i.e. thicknesses and FWD deflections were used for the backanalysis of HMA moduli with ELMOD software (ELMOD4 training manual).

Moreover, for the same test pavement 5 sample cores were extracted for laboratory testing (Fig.3). Each core was cut in three specimens according to each individual asphalt layer. These cores were tested in laboratory and the Indirect Tensile Stiffness Modulus (ITSM) of the asphalt mixes was estimated at 6 different temperatures, i.e. 10, 15, 20, 25, and 30°C.

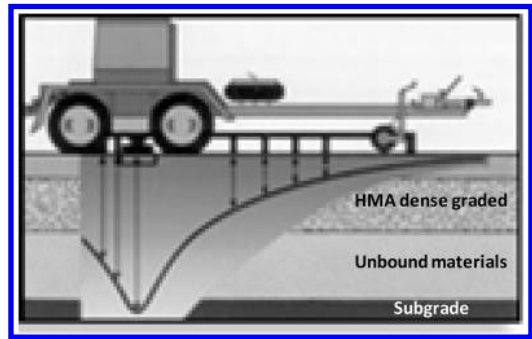


Figure 2. Cross section of the test pavement.

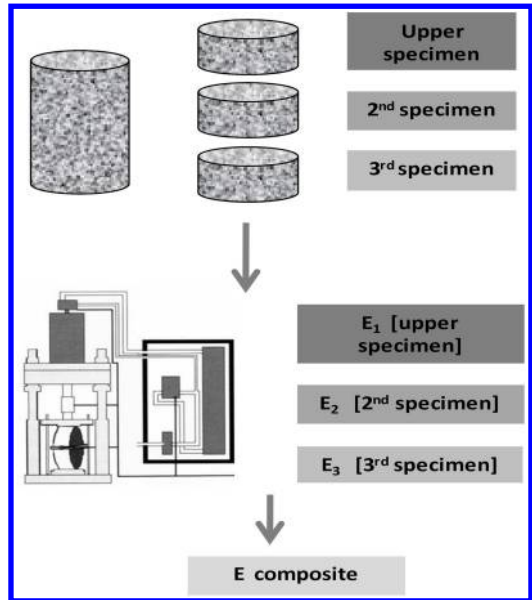


Figure 3. Laboratory testing of cores.

The ITSM values of the three specimens of each core were used for the estimation of one composite modulus (SHRP 1993).

HMA laboratory and backcalculated moduli were utilized for the development of two temperature correction equations as described below.

As one of the most commonly used reference temperatures is this of 20°C, the developed equations concern temperature correction at 20°C.

Further to the above, FWD data from different measurement periods were used for comparison purposes. Two of the measurements were conducted before the period concerning the development of the equations, while the third measurement was conducted after the aforementioned period. The relative data concerning these three measurements are presented more analytically in section 4. These measurements are used for the evaluation of the developed equations for temperature correction.

Table 2. Laboratory moduli at 10, 15, 20, 25 and 30°C.

Temperature °C	Moduli MPa
10	10,578
15	9177
20	6239
25	4176
30	2603

Table 3. Backcalculated moduli.

Temperature °C	Moduli Mpa
19.7	9719
25.1	7221
27.5	6121
32.2	4641

3 EQUATIONS FOR TEMPERATURE CORRECTION

3.1 Equation resulted from laboratory testing

The first developed equation for the temperature correction of the HMA moduli is based on laboratory testing of the extracted cores from the test pavement. The average laboratory moduli for every testing temperature are presented in Table 2.

Using modulus data shown at Table 2 the following equation (1) derived:

$$E_{20}^{Lab} = E_T e^{0.071(T - 20)} \quad (1)$$

where E_{20} = HMA corrected modulus at 20°C (MPa); and E_T = HMA backcalculated modulus at measured temperature T (°C) (MPa).

3.2 Equation resulted from backanalysis data

The second temperature correction equation is developed utilizing backanalysis results. The average backcalculated moduli from the three points chosen for the development are shown at the Table 3 in relation to the average of the four different measured temperatures.

Using moduli shown at Table 3 the following equation (2) derived:

$$E_{20}^{FWD} = E_T e^{0.060(T - 20)} \quad (2)$$

where E_{20} = HMA corrected modulus at 20°C (MPa); and E_T = HMA backcalculated modulus at measured temperature T (°C) (MPa).

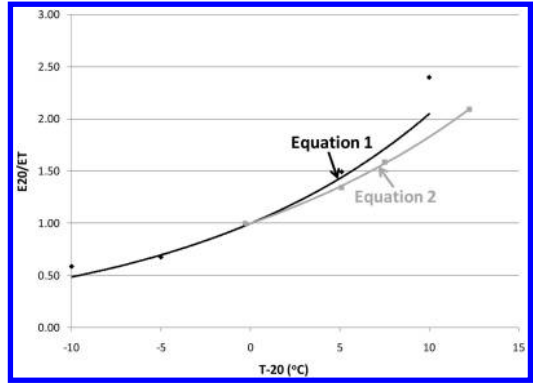


Figure 4. Laboratory and backanalysis equations for temperature correction of HMA moduli.

3.3 Comparison of developed equations

Figure 4 demonstrates the comparison of the two developed equations. It can be seen that there are differences between the two equations. Specifically, the laboratory equation seems to be more sensitive to temperature variations than the backanalysis one. Both equation have a high correlation coefficient ($R^2 = 0.952$ for the laboratory equation and $R^2 = 0.998$ for the backanalysis equation).

4 TEMPERATURE CORRECTION OF BACKCALCULATED MODULI

Both HMA moduli of the aforementioned measurements of the same period and HMA moduli of the three different measurement periods were corrected at 20°C. The evaluation of the two developed equations is performed based on the comparison between corrected and reference moduli. HMA backcalculated moduli of FWD measurement corresponding to temperature approximately equal to 20°C (Table 1, measurement A) are considered to be equal to the reference ones.

As far as the measurements of the same period are concerned, HMA backcalculated moduli of periods B (25.1°C), C (27.5°C) and D (32.2°C) are corrected to 20°C with both laboratory and backanalysis equations. The results are shown at Figures 5a and b respectively.

Moreover statistical analysis based on the paired t-test was performed. In particular, this test determined whether the corrected and the reference modulus differ from each other in a significant way. The test was applied between measurements A-B, A-C and A-D (where A is the reference measurement). According to the statistical analysis results, for the laboratory equation for all the measurements the differences between corrected and reference moduli are significant. However the differences between corrected and reference moduli using backanalysis equation are not significant. The above results are summarized in Table 4, where “S” represents significant differences and “NS” not significant differences.

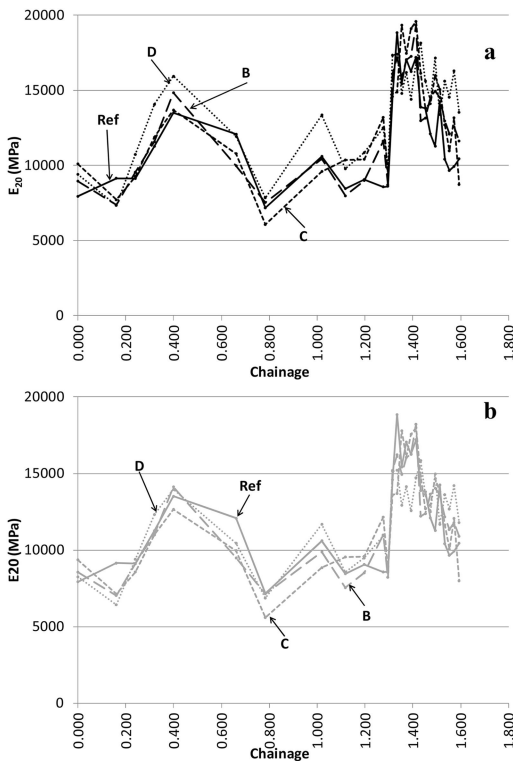


Figure 5a, b. HMA corrected moduli from laboratory (5a) and backanalysis (5b) equation for measurements B, C and D.

Table 4. T-test for corrected and reference moduli at 20°C.

Measurement	T-test	
	Laboratory	Backanalysis
Ref-B	S	NS
Ref-C	S	NS
Ref-D	S	NS

Furthermore, Root Mean Square Percentage Error (RMSPE) values were calculated for corrected and reference moduli at $T_{ref} = 20^{\circ}\text{C}$. RMSPE was used in order to determine the percentage difference between corrected and reference values. Table 5 summarizes RMSPE values for both equations. Temperature in the parenthesis represents the average value of each period.

As shown at Table 5 backanalysis equation corresponds to smaller RMSPE values than the laboratory one. Furthermore measurement D with the maximum measured temperature has also the maximum RMSPE value.

Comparison with the reference values was also performed with the three different periods where three more FWD measurements at the same test pavement were conducted, herein referred as measurement I,

Table 5. RMSPE for corrected and reference moduli at 20°C.

Measurement	RMSPE %	
	Laboratory	Backanalysis
B (25.2°C)	15.2	12.7
C (27.5°C)	20.3	16.4
D (32.3°C)	27.6	18.6

Table 6. Measured temperatures at mid-depth of HMA layers for measurements I, II and III.

Measurement	Minimum °C	Maximum °C
(I)	13.1	13.8
(II)	21.3	22.1
(III)	23.1	23.9

measurement II and measurement III. The recorded mid-depth temperatures are shown at Table 6.

Figures 6a and b illustrate the correction results based on laboratory and backanalysis equations respectively.

Moreover according to t-test results, for both equations concerning measurement I the differences between corrected and reference moduli are significant. Yet, t-test for measurements II and III shows that the differences between corrected moduli and the reference ones for both equations are not significant (Table 7). On the contrary to the results from Table 4 there is an indication that laboratory equation can be quite promising for measurements II and III. However this may be due to the fact that the temperature for these two measurements is close enough to the reference one. Further investigation is needed.

Table 8 summarizes RMSPE values for both equations, laboratory and backanalysis ones. Temperature in the parenthesis represents the average value of each period.

Table 8 confirms the results from Table 5, i.e. backanalysis equation corresponds to smaller RMSPE values than the laboratory one. Furthermore measurement I with the minimum measured temperature has the maximum RMSPE value for both equations. This fact may be attributed to the lack of low temperature measurements at the same period utilized for the development of the backanalysis equation, as well as to the difference from the reference. This result is based only on one measurement and potentially more measurements at low temperatures are needed in order to justify the results.

Moreover, comparing Tables 5 and 8, it is noticed that RMSE values are larger for measurements concerning the same period utilized for the development of correction equations than for measurements from

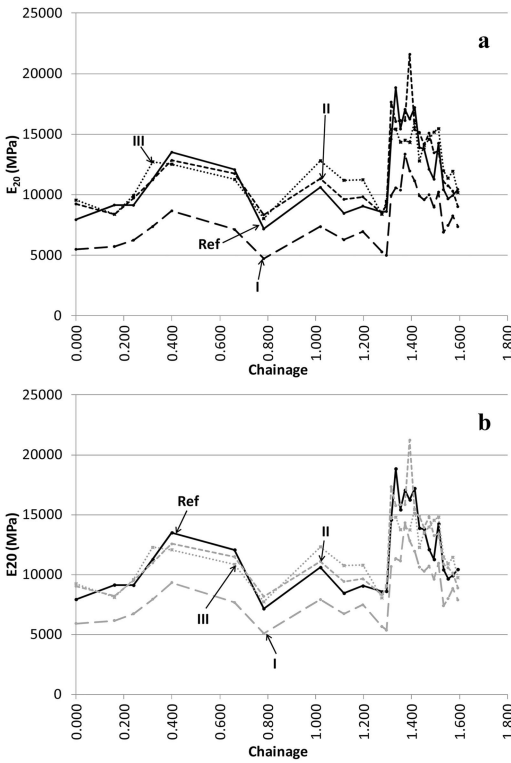


Figure 6a, b. HMA corrected moduli from laboratory (6a) and backanalysis (6b) equation for measurements I, II and III.

Table 7. T-test for corrected and reference moduli at 20°C.

T-test		
Measurement	Laboratory	Backanalysis
Ref-I	S	S
Ref-II	NS	NS
Ref-III	NS	NS

different periods. This fact needs more investigation as the influence of climatic conditions and time interval considering an un-trafficked pavement appears to be significant.

Figure 7 shows the influence of temperature variation on the correction of HMA moduli. In this figure RMSE (%) values were plotted versus measured temperatures.

It can be seen that increase in the difference between measured and reference temperature results in higher RMSE value. This is more noticeable for the laboratory equation which seems to have a greater tendency of RMSE increase with respect to temperature deviation from the reference value (20°C). Moreover there is an indication that for the same difference from the reference temperature (measurements C and I) RMSE value is higher for the lower temperature (measurement I).

Table 8. RMSPE for corrected and reference moduli at 20°C.

Measurement	RMSPE %	
	Laboratory	Backanalysis
I (13.5°C)	31.4	26.5
II (21.7°C)	12.8	11.9
III (23.7°C)	15.7	13.9

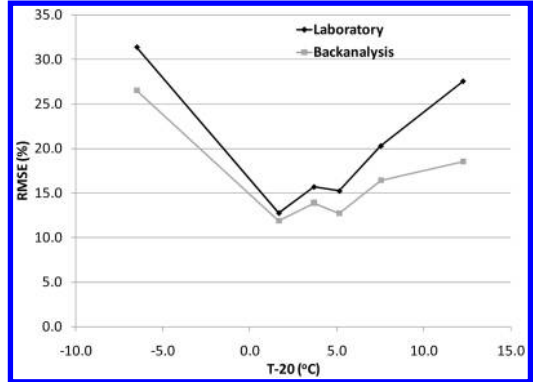


Figure 7. RMSE vs temperature variation.

Table 9. Temperature correction algorithms.

No.	Algorithm
1.	Ullidtz (1987)
2.	Jung (1990)
3.	Johnson and Baus(1992)
4 a,b,c	Baltzer and Jansen (1994)
5.	Kim et al. (1995)
6.	Ali and Lopez (1996)
7.	Braun Intertec (1996)
8.	Chen et al. (2000)
9.	Lukanen et al. (2000)
10.	Noureldin (2005)
11.	English Highways (2008)
12.	ELMOD

5 TEMPERATURE CORRECTION WITH EXISTING ALGORITHMS

Temperature correction of HMA backcalculated moduli was also performed based on the international experience and practice. Plenty of algorithms have been developed through years. However for the needs of present research the algorithms that require only temperature data and are based only on a reference temperature of 20°C or on any user-specified reference temperature were implemented. Table 9 shows the algorithms used in this investigation with chronological order.

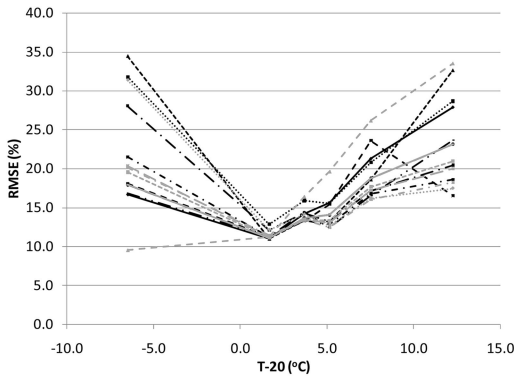


Figure 8. RMSE vs temperature variation for existing algorithms.

Table 10. RMSPE for corrected and reference moduli at 20°C.

Measurement	RMSPE %		
	min	max	average
B (25.2°C)	12.4	19.6	14.1
C (27.5°C)	16.1	26.2	19.0
D (32.3°C)	16.5	33.5	23.2
I (13.5°C)	9.6	34.5	21.8
II (21.7°C)	11.0	12.9	11.4
III (23.7°C)	13.3	16.4	14.1

Figure 8 displays the RMSE (%) in relation to measured temperatures for the different algorithms, indicatively. It can be seen that there are deviations between algorithms concerning the RMSE, sometimes high enough.

Figure 8 also shows that the curves from temperature correction with existing algorithms do not always have the same trend with the curve from correction with the developed equations. In some cases RMSE does not increase with the increase of the difference between reference and measured temperature.

Table 10 displays the minimum, maximum and average values of RMSE (%) resulting from the implementation of existing algorithms for all measured temperatures, i.e. for the three measurements of the first period referred as measurements B, C and D and for the three more measurements of three different periods referred as measurements I, II and III.

It is noticed that temperature correction based on the existing algorithms may approach the reference values quite enough. Especially the minimum RMSE in some temperatures is lower than the ones with the developed backanalysis equation (Tables 5, 8, 10). However this may be coincidental and therefore the engineer cannot be sure which algorithm results in more accurate corrected moduli, unless there are data at the reference temperature from the survey.

Table 11a. RMSPE for corrected and reference moduli at 20°C (continue).

Measurement	RMSPE %						
	1	2	3	4a	4b	4c	5
B (25.2°C)	15.7	15.6	13.2	15.4	12.9	14.1	13.2
C (27.5°C)	21.6	20.8	18.6	23.6	16.8	18.8	17.2
D (32.3°C)	27.9	28.7	32.7	16.5	18.6	23.2	20.5
I (13.5°C)	16.7	31.8	24.5	18.1	21.5	18.0	28.1
II (21.7°C)	11.0	12.9	11.0	11.2	11.3	11.1	12.1
III (23.7°C)	14.3	15.9	13.4	13.3	13.4	13.7	14.4

Table 11b. RMSPE for corrected and reference moduli at 20°C.

Measurement	RMSPE %						
	6	7	8	9	10	11	12
B (25.2°C)	12.4	14.1	12.7	13.4	19.6	12.5	13.1
C (27.5°C)	16.6	18.8	16.2	17.7	26.2	16.1	17.2
D (32.3°C)	23.7	23.2	17.5	21.0	33.5	18.3	20.0
I (13.5°C)	16.8	18.0	31.4	19.6	9.6	20.2	20.4
II (21.7°C)	11.2	11.1	12.1	11.2	11.2	11.4	11.2
III (23.7°C)	14.4	13.7	14.1	13.5	16.4	13.4	13.4

Tables 11a, b present analytically the RMSE values shown at Figure 8.

It seems that RMSE for the same algorithm differ from temperature to temperature and in some cases the variation is quite high. For example algorithm 10 correspond to a rather low RMSE value for measurement I, while in measurement D the RMSE value is a considerably higher. On the contrary, as far as backanalysis equation is concerned, RMSE range is around the same for all measured temperatures except the low one of 13.5°C.

The research analysis has shown that results from the existing algorithms should be evaluated and utilized with caution. Therefore it may useful to develop an equation based on in situ data for assessing algorithms results.

6 CONCLUSIONS

The present research highlights the importance of temperature correction of HMA moduli as an impact factor of multiple functions in terms of a detailed structural pavement evaluation. For this reason two in situ temperature correction equations were developed based on laboratory testing and backanalysis results. From the implementation of the equations in field the following additional aspects can be discussed:

Based on the road experiment it seems that the equation developed from backanalysis data approaches better the reference values than the equation from laboratory data.

In addition, it is noticed that the equation based on laboratory data is more sensitive to temperature variations than the one based on backanalysis data.

More in detail, notwithstanding the limited low temperature data, for both equations there are higher discrepancies for correction of HMA moduli from lower temperature than correction from higher temperature.

There is also an indication that for both equations the deviations from the reference values are higher for the measurements conducted at different periods than the one utilized for the development of the equations. This may be due to the influence of climatic conditions on HMA mixes.

Moreover, as far as the specific road experiment is concerned, it seems that the proposed equation based on backanalysis data has consistency in the deviation from the reference values against existing international algorithms. This fact is considered to be a critical issue for the temperature correction of HMA moduli. The equation resulted from in situ data appears to be more promising.

In general, it could be stated that, if possible, it is worthwhile to develop an in situ equation for the temperature correction of HMA moduli, since this issue affects the structural pavement evaluation which may further have a significant impact on decision strategies.

Further investigation is needed in order to investigate whether developed backanalysis equations can be extended to other pavements, with the same or similar characteristics. Moreover it is important to examine the influence of time on the development of equations for temperature correction of HMA moduli.

REFERENCES

Ali, H. A. & Lopez, A. 1996. Statistical Analyses of Temperature and Moisture Effects on Pavement Structural Properties Based on Seasonal Monitoring Data, *Transportation Research Board*, National Research Council 1540: 48–55. Washington, DC.

Baltzer, S. & Jansen, J. M. 1994. Temperature Correction of Asphalt-Moduli for FWD Measurements, *Fourth International Conference on the Bearing Capacity of Roads and Airfields*. Minneapolis: 753–768.

Chen, D., Bilyeu, J. Lin H. H. & Murphy M. 2000. Temperature Correction on Falling Weight Deflectometer Measurements, *Transportation Research Record*, Transportation Research Board 1716: 30–39. Washington, DC. ELMOD4. Training Course Manual.

English Highways Agency. 2008. Design Manual for Roads and Bridges, No HD 29/08, The Stationery Office, 7(3), Part 2.

Fernando, E.G., Liu, W. and Ryu, D. 2001. *Development of a Procedure for Temperature Correction of Backcalculated AC Modulus*. Federal Highway Administration/Texas Transportation Institute Report 1863-1. Texas: Texas Transportation Institute.

Hakim, B. A., Brown, S. F. & Armitage, R. J. 2002. Pavement evaluation and strengthening design: Sixteen years experience. *Ninth International Conference on Asphalt Pavements, Copenhagen, 17–22 August 2002*. 2 (Paper 3.1.1.).

Johnson, A. M. & Baus, R. L. 1992. Alternative Method for Temperature Correction of Backcalculated Equivalent Pavement Moduli, *Transportation Research Record*, National Research Council 1355: 75–81. Washington, DC.

Jung, F. W. 1990. *Interpretation of Deflection Basin for Real-World Materials in Flexible Pavements*. Research Report RR-242. Ontario: Ontario Ministry of Transportation, Research and Development Branch.

Kim, Y. R., Hibbs, B. O. & Lee, Y. C. Temperature Correction of Deflections and Backcalculated Moduli, *Transportation Research Record*, National Research Council 1473: 55–62. Washington, DC.

Loizos, A. & Plati, C. 2007. Accuracy of pavement thickness estimation using different ground penetrating radar analysis approaches. *NDT & E International Journal* 40(2): 147–157.

Lukanen, E. 1996. *Temperature Adjustment for Backcalculated Asphalt Moduli*. Facsimile Memorandum received from Braun Intertec Corporation.

Lukanen, E. O., Stubstad, R. N. & Briggs, R. 2000. *Temperature Predictions and Adjustment Factors for Asphalt Pavement*. Publication No. FHWA-RD-98 085, USA: US Department of Transportation, Federal Highway Administration.

Noureldin, S., Zhu, K., Harris, D. A. & Li, S. 2005. *Non-Destructive Estimation of Pavement Thickness, Structural Number and Subgrade Resilience along INDOT Highways*. Publication FHWA/IN/ JTRP-2004/35, West Lafayette, Indiana: Joint Transportation Research Program, Indiana Department of Transportation and Purdue University.

SHRP. 1993. *SHRP's Layer Moduli Backcalculation Procedure*. SHRP-P-655, National Research Council Washington, DC.

Park, S. & Kim, Y.R. 1997. Temperature Correction of Backcalculated Moduli and Deflections Using Linear Viscoelasticity and Time-Temperature Superposition. *Transportation Research Board*, National Research Council 1570: 108–117. Washington, DC.

Plati, C., Papavasiliou, V., Loizos, A. & Tsaimou C. 2014. Implementation of algorithms of asphalt moduli temperature correction. *Proceedings of the 12th international conference on asphalt pavements, Raleigh, North Carolina, 1–5 June 2014*.

Ullidtz, P. 1987. *Pavement Analysis*. Amsterdam: Elsevier.

Use of neural networks enhanced differential evolution for backcalculating asphalt concrete viscoelastic properties from falling weight deflectometer time series data

K. Gopalakrishnan, S. Kim, H. Ceylan & O. Kaya

Iowa State University, Department of Civil, Construction and Environmental Engineering, Ames, IA, USA

ABSTRACT: The new AASHTO pavement design guide of Pavement ME Design recommends the use of Asphalt Concrete (AC) dynamic modulus, $|E^*|$, as a design parameter for flexible pavements. This study investigated the feasibility of employing Neural Networks (NNs) as well as nature-inspired meta-heuristics to backcalculate AC $|E^*|$ master curve coefficients based on enhanced single-drop FWD data from full-depth asphalt pavements. The overall approach involved first generating a synthetic database of AC $|E^*|$ master curve (input) – FWD time series data (output) scenarios for a variety of pavement layer thicknesses and pavement temperatures using a computationally-efficient layered viscoelastic forward analysis tool. The use of a NN forward analysis surrogate model within the framework of a hybrid global optimization scheme, referred to as VENNDE (ViscoElastic-Neural Network-Differential Evolution) yielded satisfactory predictions of the AC dynamic/relaxation modulus master curve as well as subgrade modulus and is therefore recommended for future investigations.

1 INTRODUCTION

The new American Association of State Highway and Transportation Officials (AASHTO) pavement design guide (Mechanistic-Empirical Pavement Design Guide (MEPDG)) and the associated software (AASHTOWare Pavement ME Design, formerly known as DARwin ME) employs the principle of master curve based on time-temperature superposition principles to characterize visco-elasto-plastic properties of asphalt/bituminous materials. The Asphalt Concrete (AC) dynamic modulus ($|E^*|$) is one of the most sensitive inputs in the design of AC pavements using Pavement ME Design (Schwartz et al. 2013). Its master curve be constructed from multiple values of measured dynamic modulus at different temperature and frequency conditions in the laboratory.

The AC $|E^*|$ master curve is constructed using frequency (or time)-temperature superposition concepts represented by shift factors. The combined effects of temperature and loading rate can be represented in the form of a master curve relating $|E^*|$ to a reduced frequency (f_r) or a reduced time (t_r) by a sigmoidal function. Depending on which parameters (i.e., reduced frequency (f_r) or reduced time (t_r)) was utilized in the construction of $|E^*|$ master curve, various sigmoidal function equations for $|E^*|$ master curve have been reported in the literature (Pellinen et al. 2004, Schwartz 2005, Witczak 2005, Kutay et al. 2011). In this paper, the sigmoidal function equation utilizing reduced frequency (f_r) is defined as dynamic modulus

$|E^*|$ master curve equation while the sigmoidal function equation utilizing reduced time (t_r) is defined as relaxation modulus $E(t)$ master curve equation.

The dynamic modulus $|E^*|$ master curve equation utilizing reduced frequency (f_r) in this study is described as:

$$\text{Log } |E^*| = C_1 + \frac{C_2}{1 + e^{-(C_3 - C_4 \log(f_r))}} \quad (1)$$

where f_r = reduced frequency of loading at reference temperature; C_1 = minimum value of $|E^*|$; $C_1 + C_2$ = maximum value of $|E^*|$; C_3 and C_4 = parameters describing the shape of the sigmoidal function.

The function parameters C_1 and C_2 will in general depend on the aggregate gradation and mixture volumetric properties while the parameters C_3 and C_4 will depend primarily on the characteristics of the asphalt binder (Schwartz 2005). The reduced frequency (f_r) can be shown in the following form:

$$f_r = (f) a_T(T) \quad (2)$$

where f = frequency of loading at desired temperature; T = temperature of interest; $a_T(T)$ = shift factor as a function of temperature.

The equations widely used to express the temperature-shift factor of $a_T(T)$ include the Williams-Landel-Ferry equations, the Arrhenius equations and second-order polynomial equations (Pellinen et al.

2004, Witczak 2005, Kutay et al. 2011, Varma et al. 2013b). The shift factor utilized in this study is logarithm of the shift factor computed by using a second order polynomial (Kutay et al. 2011, Varma et al. 2013b) described as:

$$\text{Log}(a_T(T)) = a_1(T^2 - T_{ref}^2) + a_2(T - T_{ref}) \quad (3)$$

where T_{ref} = Reference temperature, 19°C (or 66.2°F); a_1 and a_2 = the shift factor polynomial coefficients.

The values for C_1 , C_2 , C_3 , C_4 and $a_T(T)$ coefficients of the master curve are all simultaneously determined from laboratory test data using nonlinear optimization techniques, e.g., Solver function in Excel software. According to the theory of viscoelasticity, $|E^*|$ and $E(t)$ can be converted from one to another through numerical inter-conversion procedures Park & Schapery(1999). The relaxation modulus $E(t)$ utilizing reduced time (t_r) is described as:

$$\text{Log}(E(t)) = c_1 + \frac{c_2}{1 + e^{-(c_3 - c_4 \log(t_r))}} \quad (4)$$

where t_r = reduced time at reference temperature;

c_1 , c_2 , c_3 , and c_4 = the relaxation modulus $E(t)$ coefficients

Highway agencies, faced with the challenge of implementing the MEPDG/Pavement ME Design, are looking to field testing as a possibility for characterizing the required pavement material properties for use in new design. The laboratory testing requirements are extensive, and the idea of obtaining default regional properties for specific materials and structures in the field is attractive.

Falling Weight Deflectometer (FWD) testing has become the predominant method for characterizing in-situ material properties for design of rehabilitated pavements. The state-of-the-practice in FWD analysis involves static back-calculation of pavement layer moduli, although FWD measurements capture the entire time history of deflections under dynamic loading conditions. If the damaged $|E^*|$ master curve of the asphalt concrete (AC) in an in-service pavement can be derived from the time histories of routinely collected FWD deflection data, it would not only save lab time and resources, but it could also lead to a more accurate prediction of the pavement's remaining service life.

2 OBJECTIVES AND SCOPE

The main objective of this work is to derive AC $|E^*|$ or $E(t)$ master curve from single-drop FWD time-history data. In the case of static backcalculation of AC layer modulus from FWD peak-deflection data either through the optimization or Neural Networks (NN) approach, a forward model (Finite Element [FE] or Layered Elastic Analysis [LEA] based) is necessary. Similarly, in the case of backcalculation of AC $|E^*|$ master curve from FWD time-history data, a viscoelastic or dynamic forward model is necessary. In this

study, a computationally efficient layered viscoelastic forward model, developed by researchers at the Michigan State University (Kutay et al. 2011), was utilized. This study only focused on full-depth AC pavements as a first step to isolate potential backcalculation issues that are only related to the $|E^*|$ master curve of the AC layer. Owing to the successful use of the NN approach in the static backcalculation of the pavement layer properties from FWD data by the authors (Ceylan et al. 2007, Ceylan et al. 2013), the first series of experiments focused on using the NN approach for backcalculation of AC viscoelastic properties. But, when the NN approach, as implemented in this study, failed to give satisfactory predictions, an evolutionary optimization approach, referred to as Differential Evolution (SCE), was utilized in conjunction with a surrogate NN forward model.

3 NEURAL NETWORKS VISCOELASTIC BACKCALCULATION APPROACH

The overall goal of the NN based viscoelastic backcalculation approach is to use the FWD deflection-time histories to backcalculate AC $E(t)$ master curve coefficients. First, a computationally efficient layered viscoelastic (VE) forward analysis algorithm (Kutay et al. 2011) was employed to generate a database of AC master curve-dynamic deflection case scenarios for a variety of pavement layer thicknesses and pavement temperatures. This VE forward analysis program attempts to simulate more realistic FWD test conditions with respect to the existence of a non-uniform temperature profile across the depth of the AC layer (Varma et al. 2013a). This enables usage of a single FWD drop to characterize the VE properties and the time-temperature shifting to get the AC relaxation modulus master curve ($E(t)$) which can subsequently be converted to provide the $|E^*|$ master curve.

3.1 Development of synthetic database

The VE forward analysis program outputs pavement surface deflection-time histories based on the following inputs: FWD stress-time history, AC $E(t)$ master curve coefficients and shift factors, pavement temperature, pavement layer thicknesses and Poisson's ratios, and unbound layer moduli. The FWD stress-time history for a standard 9-kip loading was used. For full-depth AC analysis, the inputs were reduced to AC $E(t)$ master curve coefficients (c_1 , c_2 , c_3 , and c_4) and shift factors (a_1 and a_2), pavement temperature (T_{ac}), AC layer thickness (H_{ac}), subgrade layer modulus (E_{sub}), AC Poisson's ratio (μ_{ac}) and subgrade Poisson's ratio (μ_{sub}). A comprehensive synthetic database consisting of 10,000 datasets were generated through batch simulations of the VE forward analysis program by randomly varying the inputs within the min-max ranges summarized in Table 1.

Some anomalies were discovered in the outputs extracted from the results of 10,000 VE forward

Table 1. Summary of input ranges used in the generation of 10,000 VE forward analysis scenarios for NN based viscoelastic backcalculation.

Parameter	Min Value	Max Value
Pavement temperature (T_{ac})	0 deg-C (32 deg-F)	45 deg-C (113 deg-F)
AC layer thickness (H_{ac}):	12.5 cm (5 in.)	114 (45 in.)
Subgrade modulus (E_{sub}):	34.5 MPa (5,000 psi)	138 MPa (20,000 psi)
AC Poisson's ratio (μ_{ac}):	0.3 (constant)	
Subgrade Poisson's ratio (μ_{sub}):	0.4 (constant)	
c_1	0.045	2.155
c_2	1.8	4.4
c_3	-0.523	1.025
c_4	-0.845	-0.38
a_1	-5.380×10^{-4}	1.136×10^{-3}
a_2	-1.598×10^{-1}	-0.770×10^{-1}

analysis simulations. It was discovered that the E(t) curves generated by considering the upper and lower limits of c_1 , c_2 , c_3 , and c_4 based on MSU E(t) database of 100+ HMA mixtures can result in master curves well outside the database. This can lead to unexpectedly high deflection magnitudes, unreasonable deflection time-histories and sometimes negative deflections (see Figure 1 which displays only the left-half of the deflection-time history data for deflections measured at 0-, 200-, and 300-mm from the load plate center). To overcome these issues, it was decided to include only those scenarios in the database where the sum of E(t) sigmoid coefficients c_1 and c_2 was within certain limits. After imposing the limits on the sum of sigmoid coefficients, $c_1 + c_2$, and eliminating unreasonable deflection-time histories, the processed database was utilized in NN inverse modeling.

3.2 Neural networks inverse modeling and analysis

Literature review (Dougherty 1995, TR Circular 1999, Adeli 2001, Flintsch 2003, Gopalakrishnan et al. 2010) suggests that NNs and other soft computing techniques like fuzzy mathematical programming and evolutionary computing (including genetic algorithms) are increasingly used instead of the traditional methods in civil and transportation applications. They have become standard data fitting tools especially for problems that are too complex, poorly understood, or resource intensive to tackle using more traditional numerical and/or statistical techniques. The ability to 'learn' the mapping between inputs and outputs is one of the main advantages that make the NNs so attractive. Efficient learning algorithms have been developed and proposed to determine the weights of the network, according to the data of the computational task to be performed. A recent review of NN applications in

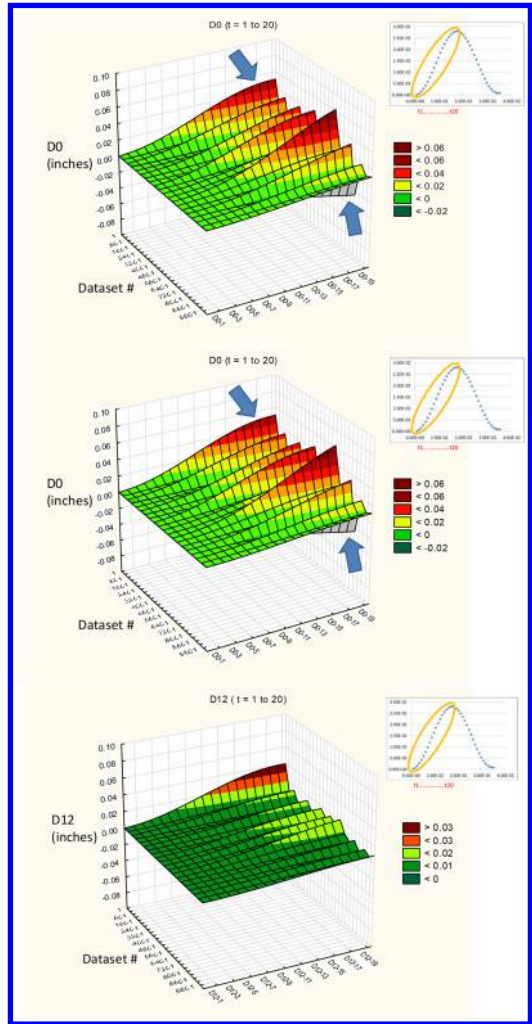


Figure 1. Deflection-time history (from time interval 1 to 20) outputs from 10,000 VE forward analysis simulations: D1 (top); D2 (middle); D3 (bottom).

pavement engineering was presented by Ceylan et al. (2014).

The NNs in this study were designed, trained, validated and tested using the MATLAB Neural Network toolbox (Beale et al. 2011). All of the NNs were conventional two-layer (1 hidden layer and 1 output layer) feed-forward networks. Sigmoid transfer functions were used for all hidden layer neurons while linear transfer functions were employed for the output neurons. Training was accomplished using the Levenberg-Marquardt (LM) backpropagation algorithm, a second-order numerical optimization technique that combines the advantages of Gauss-Newton and steepest descent algorithms. The hidden neurons were varied (25, 30, 45, and 60) to determine the best-performance NN architecture. Separate NN models were developed for each of the four E(t) master curve coefficients, c_1 , c_2 , c_3 and c_4 . Seventy percent of the

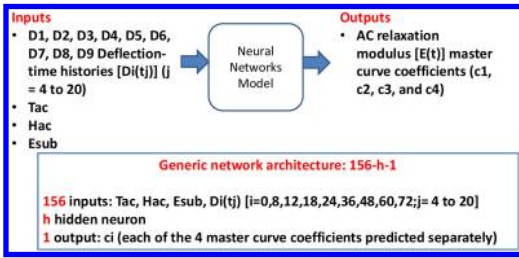


Figure 2. Inputs, outputs and generic network architecture details for the NN inverse mapping models considering pre-peak FWD time-history data (scenario #1)

processed synthetic datasets were used for training, 15% were used for validation (to halt training when generalization stops improving), and 15% were used for independent testing of the trained model.

Two sets of analyses were carried out to investigate if NNs can predict AC $E(t)$ master curve coefficients from all the deflection sensors of the standard FWD configuration: D1, D2, D3, D4, D5, D6, D7, D8, and D9 which represent deflections from a distance of 0-, 200-, 300-, 450-, 600-, 900-, 1200-, 1500-, and 1800-mm, respectively, from the center of the FWD load plate. These analyses included: scenario #1 – using only partial (pre-peak) pulse deflection-time history data; scenario #2 – using full pulse deflection-time history data. Scenario #1 was considered in light of the indications from the reported literature as well as correspondence with the FWD manufacturers that the latter portions of the FWD deflection-time history curve typically includes noise and integration errors (Kutay et al. 2011). For the sake of illustration, the NN inputs and outputs, and the generic architectural details for the NN inverse mapping models (for scenario 1) are illustrated in Figure 2.

3.3 Results and discussion

The training performance (Mean Squared Errors [MSEs]) and correlation coefficients (R) of best-performance NN architectures in predicting $E(t)$ master curve coefficients, $c_1, c_2, c_3,$ and $c_4,$ from D1, D2, D3, D4, D5, D6, D7, D8, and D9 pre-peak deflection-time history data (scenario #1) are summarized in Table 3. While 25 or 30 hidden neurons were deemed sufficient to achieve best-performance models for three of the $E(t)$ master curve coefficients ($c_1, c_2,$ and c_3), 60 hidden neurons were required to predict c_4 with reasonable prediction accuracy. Similarly, the training performance (MSEs) and R-values of best-performance NN architectures in predicting $E(t)$ master curve coefficients from full pulse deflection-time history data (scenario #2) are summarized in Table 2. The NN prediction accuracies for all four $E(t)$ master curve coefficients ($c_1, c_2, c_3,$ and c_4) have improved further when considering the full pulse deflection-time history data as opposed to considering only pre-peak deflection-time history data.

Table 2. Performance summary of NN backcalculation models in predicting $E(t)$ master curve coefficients ($c_1, c_2, c_3,$ and c_4) from pre-peak FWD deflection-time history data (scenario #1)

Output	NN Arch.	# Epochs	Training Perf. (MSE)	Gradient	Training R	Validation R	Testing R	All R
c_1	156-30-1	75	0.169	0.248	0.733	0.656	0.673	0.713
c_2	156-25-1	50	0.170	0.417	0.817	0.776	0.789	0.807
c_3	156-25-1	44	0.065	0.171	0.758	0.674	0.648	0.727
c_4	156-60-1	150	0.009	0.090	0.709	0.518	0.516	0.655

Table 3. Performance summary of NN backcalculation models in predicting $E(t)$ master curve coefficients ($c_1, c_2, c_3,$ and c_4) from full pulse FWD deflection-time history data (scenario #2)

Output	NN Arch.	# Epochs	Training Perf. (MSE)	Gradient	Training R	Validation R	Testing R	All R
c_1	332-25-1	33	0.115	0.129	0.815	0.731	0.714	0.788
c_2	332-25-1	32	0.145	4.210	0.825	0.800	0.782	0.815
c_3	332-30-1	33	0.047	0.646	0.820	0.712	0.572	0.765
c_4	332-30-1	160	0.004	0.007	0.861	0.718	0.645	0.797

These results demonstrate the potential of NNs to predict the $E(t)$ master curve coefficients from single-drop FWD deflection-time history data. However, the current prediction accuracies are not sufficient enough to recommend these models for practical implementation. It should be noted that this study only focused on a simple and straightforward implementation of feedforward Multi-Layer Perceptron (MLP) NNs. It is possible that more sophisticated NN implementations could provide improved predictions.

4 VENNDE: VISCOELASTIC-NEURAL NETWORKS-DIFFERENTIAL EVOLUTION BACKCALCULATION APPROACH

In the traditional static backcalculation approach involving iterative optimization, a forward pavement analysis model is used to compute theoretical deflections under the applied load and the given pavement structure using assumed pavement layer moduli. These theoretical deflections are then compared with measured deflections and the assumed moduli are then adjusted in an iterative procedure until theoretical and measured deflection basins match acceptably well. The moduli derived in this way are considered representative of the pavement response to load, and can be used to calculate stresses or strains in the pavement structure for analysis purposes. This is an iterative method of solving the inverse problem, and will not have a unique solution for most cases. Apart from the fact that the backcalculated moduli solutions are highly sensitive to the measured deflections, the solutions typically require searching of a multimodal nonlinear space formed by the variables, where traditional numerical approaches do not operate well Liu & Han (2003). Several previous studies, including the ones by the authors, have successfully demonstrated the usefulness of evolutionary optimization techniques (starting

with Genetic Algorithms [GAs]) in achieving accurate, faster, and near-global backcalculation solutions.

Recently, (Varma et al. 2013b) proposed the use of GA based optimization scheme in combination with a VE forward solver to backcalculate AC E(t) master curve coefficients and shift factors as well as unbound layer moduli based on FWD deflection-time history data. In this study, the Differential Evolution (DE) algorithm is used owing to its success in achieving accurate results and fast convergence in the static backcalculation of pavement layer properties from FWD data. In addition, a trained NN based surrogate VE forward analysis model is employed in place of the actual VE forward calculations during the backcalculation process. Since thousands of forward analysis runs are executed during the optimization process with the goal of minimizing the error between the computed and actual deflection time histories, the use of a surrogate NN based VE forward analysis model significantly reduced the total computational time and resources during the backcalculation. The overall backcalculation approach, referred to as VENNDE (ViscoElastic Neural Networks-Differential Evolution backcalculation approach) and pronounced as ‘vendy’, is depicted in Figure 3.

4.1 Development of surrogate forward NN module

The surrogate forward NN module is an important component of the VENNDE as it significantly reduces the computational time required for VE forward calculation of deflection-time histories for each of the individuals in the generation while DE explores the multi-modal search space for optimal solutions. The comprehensive synthetic database developed during the first phase of this research (described in Section 3.1) was used to train the surrogate forward NN module to map the non-linear relation between input pavement layer properties (AC layer thickness, AC mid-depth temperature, AC E(t) master curve coefficients and shift factors, subgrade layer modulus and Poisson’s ratios of AC layer and subgrade) and output deflection-time histories.

Based on a parametric sensitivity analysis, a conventional two-layer (1 hidden layer with 25 neurons and 1 output layer) feed-forward network was deemed sufficient for forward modeling. Sigmoid transfer functions were used for all hidden layer neurons while linear transfer functions were employed for the output neurons. Training was accomplished using the LM backpropagation algorithm implemented in the MATLAB NN Toolbox. Separate NN models were developed for each of the deflections (9 sensor locations and 40 time intervals). Except for the first three time intervals, deflection-time histories at all other time intervals were predicted by NN with very high accuracy (R-values greater than 0.98). It was decided not to use the deflection information for the first three time intervals during the DE error minimization search process. The computed deflection-time histories are

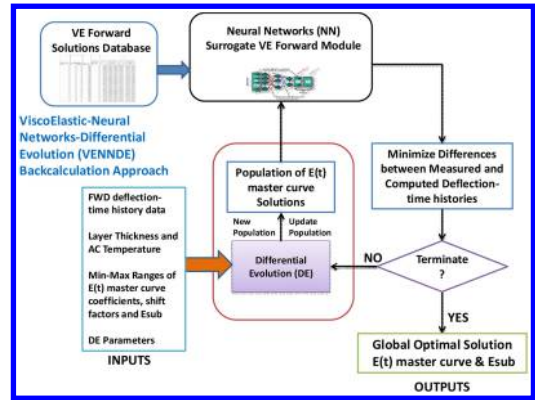


Figure 3. Overall operational flow schematic of VENNDE: a viscoelastic-neural networks-differential evolution backcalculation approach

passed on to the DE module during fitness evaluation which is described in the next section.

4.2 Neural networks-differential evolution optimization

DE is a simple and efficient heuristic for global optimization over continuous spaces. Storn & Price (1995) proposed DE as a new heuristic approach that has the ability to handle non-differentiable, nonlinear, and multimodal cost functions, lends itself very well to parallel computation, has few control variables to steer the minimization, and has good convergence properties. It has been demonstrated through several benchmark optimization problems that DE converges faster and with more certainty than many other acclaimed global optimization methods.

Owing to its simplicity and advantages over other optimization methods, DE has been successfully applied in different fields for solving complex, nonlinear, non-differentiable, and non-convex optimization problems such as inwater distribution system optimization (Zheng et al. 2013), electrical power distribution (Coelho et al. 2014), traffic signal control (Bi et al. 2014), structural system identification Yildiz(2013), etc. In these applications, either the classical version of the DE or the hybrid version (i.e., DE in combination with other evolutionary algorithms or enhancement of DE operators) has been employed. This paper is the first of its kind to apply DE in the backcalculation of AC viscoelastic properties from FWD time history data.

A brief description of the DE algorithm is as follows. A fixed number of vectors, within a population of potential solutions in an n-dimensional search space, are randomly initialized (*initialization*), and then evolved over time to explore the search space to locate the objective function minima. At each iteration, new vectors are generated by the combination of vectors randomly chosen from the current population (*mutation*). The produced vectors are then mixed with a predetermined target vector (*recombination*)

and a trial vector is produced. For the next generation, the trial vector is accepted if, and only if, it yields a reduction in the cost function value (*selection*). The population size (NP), scaling factor (F), and crossover control constant (CR) are the three important control variables in the DE algorithm. For the current study, optimal values of NP, F, and CR were chosen as 10, 0.85, and 0.9, respectively, based on preliminary parametric sensitivity analysis results. The VENDEE framework was implemented in the MATLAB environment by adapting the DE code presented by (Price et al. 2005).

Backcalculation of AC viscoelastic properties from FWD deflection-time history data can be treated as a global optimization problem where the objective is to determine the unknown AC viscoelastic properties as well as unbound layer moduli by minimizing the differences between measured and computed deflection time histories. Although the objective function or error minimization function can be defined in a number of ways, a simple objective function representing sum of the squared differences between measured and computed deflection-time histories as shown in Eq. 1 was selected for this study:

$$\text{Minimize } f = \sum_{k=1}^m 1000 \sum_{i=1}^n (D_i^k - d_i^k)^2 \quad (5)$$

where f is the objective (error) function to be minimized; m is the number of FWD deflection sensors; D_i^k is the FWD deflection at sensor k ; d_i^k is the deflection computed by the VE forward analysis model (or the NN surrogate module) at sensor k ; n is the total number of deflection data points (time intervals) recorded by a sensor. The search space for VENDEE was defined by the bounds on the variables shown in Table 1. A hypothetical case study with the following pavement properties was carried out to evaluate the performance of the proposed VENDEE backcalculation approach: $H_{ac} = 20$ cm (8 in.); $\mu_{ac} = 0.3$; $E_{sub} = 80$ MPa (11,590 psi); $\mu_{sub} = 0.4$; $c_1 = 1.433$; $c_2 = 2.233$; $c_3 = -0.262$; $c_4 = -0.7687$; $a_1 = -4.6 \times 10^{-4}$; $a_2 = -1.41 \times 10^{-1}$.

4.3 Results and discussion

In the DE search process, at iteration 1, a population of specified solution vectors is randomly initialized within the bounds of the search space. Through successive iterations, the solution vectors are evolved to find optimal solutions through the mutation, crossover, and selection operation procedures of DE strategy. In Figure 4, Cost of the system Vs iterations during the VENDEE backcalculation process, the cost of the system (objective function value of the best member of the population) is plotted against iterations for the hypothetical case study. The cost decreases with successive iterations as the DE algorithm finds new child generations with lower cost. The case study took about 140 seconds (2.3 minutes) using a typical 64-bit Windows based Desktop computer to achieve convergence. It

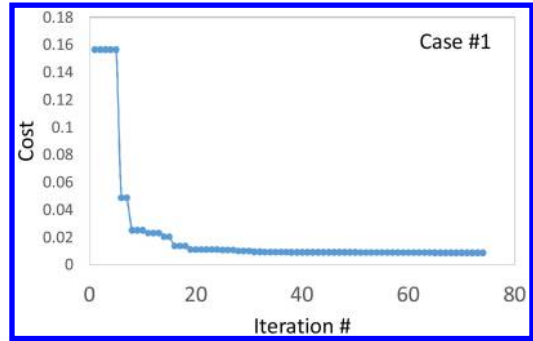


Figure 4. Cost of the system Vs iterations during the VENDEE backcalculation process.

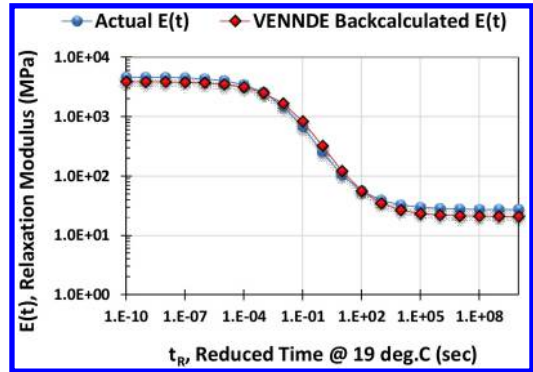


Figure 5. Comparison of actual and VENNDE backcalculated $E(t)$ master curves for the hypothetical case study.

is seen from Figure 4, Cost of the system Vs iterations during the VENDEE backcalculation process that VENNDE is able to locate near-global minima in about 25 iterations after which there is not significant decrease in cost.

Comparison of the actual and VENNDE backcalculated AC $E(t)$ master curves in Figure 5 indicate that VENNDE was able to successfully backcalculate the AC viscoelastic properties from deflection-time history data although there is still some room for improvement. More case studies, especially using field data, need to be carried out to substantiate these findings. Similarly, the VENNDE backcalculated subgrade moduli, 82.5 MPa (11,960 psi) is also very close to the actual subgrade moduli, 80 MPa (11,590 psi).

5 SUMMARY OF FINDINGS AND RECOMMENDATIONS

5.1 Findings

- This study demonstrated that NNs are capable of predicting the $E(t)$ master curve coefficients from single-drop FWD deflection-time history data. However, the current prediction accuracies are not sufficient enough to recommend these models for practical implementation.

- A NN-based surrogate forward VE model was successfully developed based on a synthetic database of viscoelastic solutions generated by batch runs of forward VE model. Except for the first three time intervals, deflection-time histories at all other time intervals were predicted by NN with very high accuracy (R-values greater than 0.98).
- A hypothetical case study was carried out to evaluate the performance of the proposed VENNDE (ViscoElastic-Neural Networks-Differential Evolution) backcalculation approach. The case study took about 140 seconds (2.3 minutes) using a typical 64-bit Windows based Desktop computer to achieve convergence to near-global optimal solutions.
- Comparison of the actual and VENNDE backcalculated AC E(t) master curves indicated that VENNDE was able to successfully backcalculate the AC viscoelastic properties from deflection-time history data although there is still some room for improvement. More case studies, especially using field data, need to be carried out to substantiate these findings.
- The VENNDE was also able to successfully backcalculate unbound layer (subgrade) moduli, from deflection-time history data.

5.2 Recommendations

- This study only focused on a simple and straightforward implementation of feedforward Multi-Layer Perceptron (MLP) NNs for the backcalculation of AC E(t) master curve from FWD time history data. It is possible that more sophisticated NN implementations could result in more accurate inverse mapping models.
- One approach to improve the prediction accuracy of the proposed backcalculation approach is to hybridize the DE stochastic search optimization with a local search optimizer such as Nelder-Mead simplex method, viz., use the near-global optimal solution predicted by DE optimization as a seed solution to the local search optimizer.

ACKNOWLEDGMENTS

The authors would like to thank the Iowa Highway Research Board (IHRB) and the Iowa Department of Transportation (DOT) for sponsoring this research in part. The project technical advisory committee (TAC) members from the Iowa DOT, including Dr. Scott Schram, Messrs. Chris Brakke, Ben Behnami, and Jason Omundson are gratefully acknowledged for their guidance, support, and direction throughout the research. The authors would like to extend their sincerest appreciation to Profs. Emin Kutay and Karim Chatti and Mr. Sudhir Varma at Michigan State University (MSU) for their timely technical support and detailed discussions on viscoelastic forward analysis and dynamic backcalculation.

The contents of this paper reflect the views of the authors who are responsible for the facts and accuracy of the data presented within. The contents do not

necessarily reflect the official views and policies of the IHRB and ISU. This paper does not constitute a standard, specification, or regulation.

REFERENCES

- Adeli, H. 2001. Neural networks in civil engineering: 1989–2000. *Computer-Aided Civil and Infrastructure Engineering* 16: 126–142.
- Beale, M.H., Hagan, M.T. & Demuth, H.B. 2011. *Neural Network Toolbox™ User's Guide*. Natick, MA: MathWorks, Inc.
- Bi, Y., Srinivasan, D., Lu, X., Sun, Z. & Zeng, W. 2014. Type-2 fuzzy multi-intersection traffic signal control with differential evolution optimization. *Expert Systems with Applications* 41(16): 7338–7349.
- Ceylan, H., Gopalakrishnan, K. & Guclu, A. 2007. Nonlinear Pavement Analysis Using Artificial Neural Network Based Stress Dependent Models. *Journal of the Transportation Research Board, Transportation Research Record* 2005: 86–94.
- Ceylan, H., Gopalakrishnan, K., & Kim, S. 2013. Improving the Accuracy and Usability of Iowa Falling Weight Deflectometer Data. In *Trans Project 11–415*, Institute for Transportation, Iowa State University.
- Ceylan, H., Bayrak, M. B., & Gopalakrishnan, K. 2014. Neural Networks Applications in Pavement Engineering: A Recent Survey. *International Journal of Pavement Research & Technology* 7(6): 434–444.
- Coelho, L., Bora, T. & Mariani, V. 2014. Differential evolution based on truncated Lévy-type flights and population diversity measure to solve economic load dispatch problems. *International Journal of Electrical Power & Energy Systems* 57: 178–188.
- Dougherty, M. 1995. A review of neural networks applied to transport. *Transportation Research, Part C* 3(4): 247–260.
- Flintsch, G.W. 2003. Soft computing applications in pavement and infrastructure management: state-of-the-art. CD-ROM, *Proceedings of the 82nd Annual Meeting of the Transportation Research Board, Washington, D.C., 12–16 January 2003*: National Research Council.
- Gopalakrishnan, K., Ceylan, H., & Attoh-Okine, N. (Eds.) 2010. *Intelligent and Soft Computing in Infrastructure Systems Engineering: Recent Advances*. Studies in Computational Intelligence (SCI) Series, Springer-Verlag, Inc., Berlin, Germany.
- Kutay, E., Chatti, K. & Lei, L. 2011. Backcalculation of Dynamic Modulus Mastercurve from Falling Weight Deflectometer Surface Deflections. *Transportation Research Record: Journal of the Transportation Research Board* 2227: 87–96.
- Liu, G.R. & Han, X. 2003. *Computational inverse techniques in nondestructive evaluation*. Boca Raton: CRC Press.
- Park, S.W. & Schapery, R.A. 1999. Methods of Interconversion Between Linear Viscoelastic Material Functions, Part I: A Numerical Method Based on Prony Series. *International Journal of Solids and Structures* 36: 1653–1675.
- Pellinen, T., Witczak, M. & Bonaquist, R. 2003. Asphalt Mix Master Curve Construction Using Sigmoidal Fitting Function with Non-Linear Least Squares Optimization. *Recent Advances in Materials Characterization and Modeling of Pavement Systems*. ASCE: 83–101.
- Price K, Storn RM & Lampinen JA 2005. *Differential evolution: a practical approach to global optimization*. Berlin: Springer.

- Schwartz, C.W. 2005. Evaluation of the Witzczak dynamic modulus prediction model. *CD-ROM, Presented at 84th Annual Transportation Research Board Meeting, Transportation Research Board*. Washington, D.C.
- Schwartz, C. W., Li, R., Ceylan, H., Kim, S., & Gopalakrishnan, K. 2013. *Global Sensitivity Analysis of Mechanistic-Empirical Performance Predictions of Flexible Pavements*. *Transportation Research Record: Journal of Transportation Research Board* 2368: 12–23.
- Storn, R& Price, K. 1995. *Differential Evolution – A Simple and Efficient Adaptive Scheme for Global Optimization over Continuous Spaces*. Technical Rep. No. TR-95-012 Berkeley CA: International Computer Science Institute Transportation Research (TR) Circular 1999. *Transportation Research Circular No. E-C012 – Use of Artificial Neural Networks in Geomechanical and Pavement Systems*. Transportation Research Circular, Prepared by A2K05 (3) Subcommittee on Neural Nets and Other Computational Intelligence–Based Modeling Systems. Washington, D.C.: Transportation Research Board, National Research Council.
- Varma, S., Kutay, M.E. & Chatti, K. 2013a. Data Requirements from Falling Weight Deflectometer Tests for Accurate Backcalculation of Dynamic Modulus Master curve of Asphalt Pavements”. *2013 Airfield & Highway Pavement Conference*, Los Angeles, California: 1–11.
- Varma, S., Kutay, E., & Levenberg, E. 2013b. Viscoelastic Genetic Algorithm for Inverse Analysis of Asphalt Layer Properties from Falling Weight Deflections. *Transportation Research Record: Journal of the Transportation Research Board* 2369: 38–46.
- Yildiz, A.R. 2013. Comparison of evolutionary-based optimization algorithms for structural design optimization. *Engineering Applications of Artificial Intelligence* 26(1): 327–333.
- Witzczak, M.W. 2005. *Simple performance tests: Summary of Recommended Methods and Database*. National Cooperative Highway Research Program Report 547, Transportation Research Board, Washington, D.C.
- Zheng, F., Zecchin, A.C. & Simpson, A.R. 2013. Self-Adaptive Differential Evolution Algorithm Applied to Water Distribution System Optimization. *J. Comput. Civ. Eng.* 27(2): 148–158.

Accelerated pavement testing program with the mobile load simulator MLS10 – temperature analysis

B. Wacker

Federal Highway Research Institute, Bergisch Gladbach, Germany

ABSTRACT: The German Federal Highway Research Institute (BAST) is using the Mobile Load Simulator MLS10 for accelerated pavement testing since 2013. During the first attempts to evaluate structural changes, it has been noticed that the temperature within the MLS10 and of the experimental infrastructure itself increased. To describe these characteristics, a test program for temperature analysis with temperature sensors and an infrared-camera was developed. During this test phase a standardized as well as a modified setup of the MLS10 was used. The results of these experiments can be used to improve further test programs in the future, especially for the adaptation of experimental parameters.

1 INTRODUCTION

Due to its central position in Europe, Germany's federal motorway network is one of the most important networks to cope the commercial transport on the continent. The evaluation of the existing infrastructure will be one of the main topics during the next years in order to use the available budget for maintenance accurately and efficiently. Therefore, it is necessary to assess possible damages and to examine their effects on the construction. The German Federal Highway Research Institute (BAST) uses the Mobile Load Simulator MLS10 for accelerated pavement testing on different constructions since April 2013. Besides non-destructive methods, sensors are applied to measure structural effects as well as variations in temperature inside, below, and beside the Mobile Load Simulator MLS10.

During first attempts to evaluate structural changes with the MLS10, it has been noticed that the temperature within the MLS10 and of the experimental infrastructure itself increased. To describe these characteristics, a test program for temperature analysis with temperature sensors and an infrared-camera was developed. During this test phase a standardized as well as a modified setup of the MLS10 was used. The temperature variations were constantly observed and measured throughout the loading phase but also during the cooling phase. The latter took place with two different modes.

The results of these experiments can be used to improve further test programs in the future, especially for the adaptation of experimental parameters. Furthermore, detailed information about the temperature level inside the MLS10 is relevant for all users of MLS Test Systems and other accelerated pavement facilities.

2 ACCELERATED PAVEMENT TESTING

Accelerated Pavement Testing (APT) is the setup of wheel loads to special constructed or in service pavements. Under controlled and accelerated conditions, the pavement response and performance can be observed in a short period of time (Saeed & Hall (2003)). APT is important to develop new strategies to analyze pavement structure and innovative materials. Elaborate laboratory tests and full scale APT should be done before testing innovative materials under real road conditions. Information about the response and performance of the pavement has been provided with non-destructive tests before, during, and after the testing. In most of the cases during the test program continuous measurements with sensors were necessary.

Below-mentioned APT facilities for different experimental tests will be described. The first part gives an overview of facilities worldwide, the second part presents the Mobile Load Simulator MLS10 at BAST, and the third part shows the infrastructure at BAST.

2.1 *Facilities worldwide*

Wynand (2012) characterizes different types of APT facilities. The different types can be described with the shape of the test section (straight line or in a circle), the position of the facility (fixed or mobile), and with the type of loading (rolling wheel or hydraulic actor impulse).

Fixed facilities are for example circular test tracks (in- and outdoor) and impulse actors (indoor). The infrastructure of the circular test track is fixed at one location and cannot be moved to somewhere else. The moving of impulse actors together with the entire infrastructure to another spot is very complex and



Figure 1. Mobile Load Simulator MLS10 at BAST.

expensive. There are different impacts to note for using these facilities. The impulse actors create constant impulses like hammer blows; they are not directly comparable to a rolling wheel. By using the circular test track the impact of shearing forces are important to consider during the evaluation.

Wynand (2012) gives examples for mobile facilities like the Accelerated Loading Facility (Mobile-ALF) and the Heavy Vehicle Simulator (HVS). Both facilities are using uni-directional or bi-directional loading setups with a rolling wheel. During the uni-directional loading the acceleration factor will slow down and with the bi-directional loading the reality is not pictured right. The facilities are not closed up to the side and to the top, so the wind and weather conditions are able to influence the test sections. In addition to these full scale facilities, there is the MMLS3 (Model Mobile Load Simulator 3). In Raab & Partl (2014) the functional information are summarized and the 1 : 3 scale machine is described.

2.2 Mobile Load Simulator MLS10

Since the mid of the 19th century visions of a realistic full scale accelerated pavement test facility were persecuted. The first idea by BAST in cooperation with MAN in 1955 was a fixed APT unit in a test hall with 20 loading wheels and a speed of 15–60 km/h. This first idea has never been implemented, but the basic concept influenced the following decades.

The Mobile Load Simulator MLS10 is one of the concepts who followed this first idea. In comparison to the first vision it is mobile and smaller. The dimension of the 40 t machine is 12.5 m in length, 3.3 m in width, and 3.5 m in height. With the use of the MLS10 it is possible to get the most uni-directional, straight loading setups to the test section so far. After the development and construction phase in South Africa, the first tests with the prototype were carried out in Mozambique and Switzerland in 2006 (EMPA, (2009)). The results provided new input for the development of next generation machines. In August 2012 the MLS10 arrived at the Federal Highway Research Institute (BAST) in Germany (Figure 1). With the final certification the test operation was started in April 2013.



Figure 2. One of four Bogie inside the MLS10 (LMT Products (Pty) Ltd).

To be able to react to special experimental situations (e.g. change the position for measurements) the Mobile Load Simulator MLS10 uses transport wheels at the front and the back. For long distances it is necessary to use a heavy load truck to transport the MLS10 to the next location. It is possible to operate the MLS10 with high-voltage current or with diesel generator. However, high-voltage current is preferred in order to reduce the pollution and the noise at test sides.

To operate the Mobile Load Simulator MLS10, it is necessary to lift up the transport wheels and lower the machine onto the four corner jacks. Thereby, one of the loading wheels inside the MLS10 is set down to the test section. During the test program, only one of the four loading wheels is on the ground at a time. All wheels are moving with the same distance to each other in a closed chain through the machine. To hold the loading wheels, four Bogies are placed inside the MLS10 (Figure 2). It is possible to use the MLS10 with different configurations. First of all, the loading wheels can be changed between twin and super single tires. Secondary, there is an option to adjust the load between 40 and 75 kN. That is possible by using a hydraulic system (gas-oil mixture) for every Bogie. The standard adjustment at BAST is 50 kN with a tire pressure of 8.5 bar. Using this load it is possible to operate the MLS10 with a maximum speed of 22 km/h. That means about 6.000 uni-directional loading cycles per hour. All impacts are applied to a 3.5 m long test section in the middle of the MLS10.

Each Bogie (Figure 2) owns six axes with steel wheels at the sides. These steel wheels lead the Bogie through the machine. With 24 linear motors the MLS10 is moving the four Bogies. Reaction plates at every Bogie are installed to connect it to the linear motor.

For special research questions lateral movement with the Mobile Load Simulator MLS10 is possible. To realize a lateral movement of about 500 mm in each direction it is possible to create shearing forces and simulate the tracking.

To reduce the noise during the operation time, the MLS10 is covered and closed up. On top of the machine there are four ventilator systems installed to create an air exchange during and after the loading time.

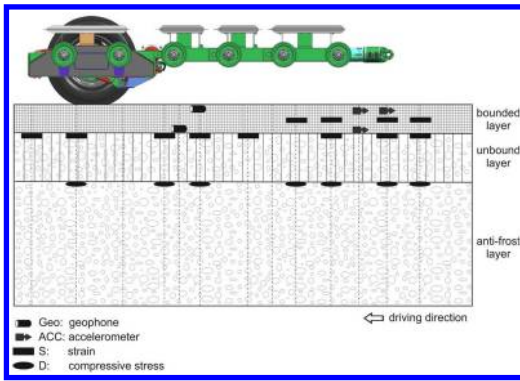


Figure 3. Test track with sensors.

2.3 Test track at BAST

The BAST is using several test halls with asphalt and concrete test sections. One test hall is provided for the asphalt pavement test track. The entire test hall is independent of climate changes so that the research can be focused at the influence of loading conditions. Rabe (2004) designed a full scale road construction inside concrete sag (38.0 m in length, 7.5 m in width and up to 3.5 m in depth). At the moment the hall includes eight German standard constructions with embedded sensors in different layers. These constructions are loaded with accelerated pavement testing equipment. Therefore, test programs with various loading and measurement periods are developed.

It is important to have a well-engineered instrument setup with sensors and data-logging equipment. This setup is used for different questions. The main question is about the structural behavior and the second question is about the monitoring of the accelerated pavement equipment. Triggered by the loading signals, it is possible to see changes at the peaks of the signals for each sensor. These changes can be analyzed and evaluated to get an overview. If just one peak differs from the other three, it could be an indication for a different loading situation at one of the loading wheels. In that case, an inspection is necessary to adjust the loading again.

For the first test with the Mobile Load Simulator MLS10, a destroyed test section was rebuilt with a lot of embedded sensors to define the influence of the machine (Scherkenbach (2013)). For this, pressure and strain sensors in different layers were used (Figure 3). The most important sensors are the pressure sensors on top of the frost blanket gravel and the strain sensors at the bottom of the asphalt. In order to recognize the signals and the construction method, sensors in other positions were installed as well.

In addition to the constantly measured data during the accelerated pavement test, the sensors can be used for non-destructive test methods as well. To get the most useful data, a wide open measurement program is necessary. That includes the sensor data, non-destructive tests during, and destructive test at

the end of the loading period. Relevant for the non-destructive tests are Falling Weight Deflectometer (FWD), Ground Penetration Radar (GPR), transverse evenness, and visual observations. Beside the regular evaluation of the FWD data, the sensors are able to measure the loading coming out of these tests as well. Due to this possibility, it is technologically feasible to analyze the changing of the surface and the structure itself at a time. In Wacker et al. (2014) it can be seen that the loading and temperature effect are important factors to the collected data.

Relevant data, like temperature and loading times, have to be collected and stored to use them during the evaluation process.

3 TEMPERATURE ANALYSIS

In the following chapters the background of the temperature analysis and the experimental setup are explained.

3.1 Results of previous research programs

The first experimental results with the Mobile Load Simulator MLS10 have been very important for further research programs. Wacker et al. (2014) used first results to evaluate structural changes and to optimize the use of non-destructive methods during the regular operation of the MLS10. The main focus of the first experiment was on the behavior of the APT-facility. There are some questions to the functional impacts and the service of the MLS10.

On the one hand, the strain and pressure sensors collected an increase of the peaks during a loading day. The influences on the whole test setup will be evaluated in the future.

On the other hand, integrated sensors detected a temperature increase of about 6–8 K per loading day (8 h). The sensors are located approx. 6 cm under the road surface. After detecting this change, a data logging system was placed inside the MLS10 at different positions: on the surface and 90 cm above the surface. At each position the temperature increase was detected. This will influence most of the data collected. The data logging system showed first an abrupt rising of the temperature and then a slower rising during the loading phase. At the end of the loading phase the temperature dropped a little bit and reduced constantly. At the moment the Mobile Load Simulator MLS10 was lifted up for inspection the temperature dropped abruptly.

To get more information about the temperature behavior during the loading and cooling down phase, the following research program was developed.

3.2 Temperature research program and setup

The program was constructed to show the differences between a standard and modified setup of the Mobile Load Simulator MLS10 during the loading and cooling down phase. The standard setup with a closed up

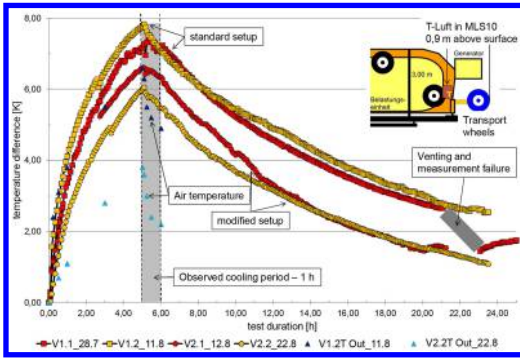


Figure 4. Air temperature inside MLS10.

system is the regular use. For the modified setup the lateral insulation on both sides of the MLS10 was pushed upwards to create a gap. On the basis of this procedure a better air exchange and slower temperature rising was expected.

For this research program, the indoor asphalt test track was used. Each loading phase was finished after 5 h and the cooling down phase was observed in detail for one hour. During the cooling down phase, two different modes were applied. At a first mode the MLS10 was left on the four corner jacks. At a second mode the machine was lifted up immediately after the loading phase.

In addition to the sensors inside the test track, two temperature sensors at the surface were installed to detect the differences between the rolling track and non-rolling track. One temperature sensor on the right hand side in the back of the MLS10, approx. 90 cm above the surface, measured the air temperature inside the machine.

An infrared camera was installed at different places inside the MLS10 to visualize the change of the temperature. To observe the linear motor, the camera was installed in the middle of the MLS10. With other positions, the loading wheels were observed from the front and the back. During the observation of the loading wheels, it was possible to analyze the asphalt surface temperature as well.

To measure the temperature inside the test hall and close to the MLS10, an air thermometer was used. This thermometer was located on a table in a distance of one meter to the MLS10.

3.3 Interpretation of the test results

At a first step the data were used to analyze the difference between the temperature at the beginning of the loading phase and the following measured temperatures.

The air temperature inside the Mobile Load Simulator MLS10 was measured on the right hand side in the back of the MLS10. In addition, the air thermometer at the outside of the MLS10 was analyzed as well. To eliminate the factor of different start temperatures, the temperature differences were monitored. The minimal increase of 5.4 K was observed with the modified setup

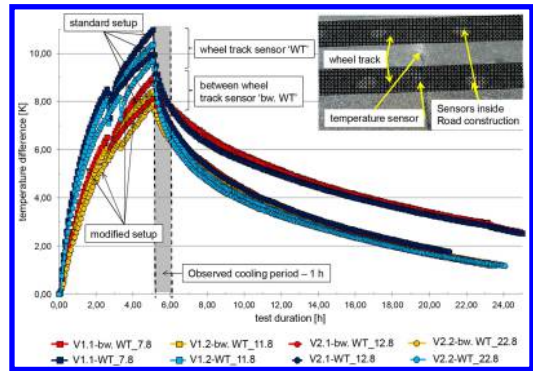


Figure 5. Asphalt surface temperature.

and the maximum increase of 7.8 K with the standard setup. The differences in air temperature between the setups, however, were not as much as expected.

Figure 4 shows an example of temperature changes during one measuring day of each setup and mode. In total, the standard setup of the MLS10 produces a steeper increase than the modified setup. During the cooling down phase of the mode in which the MLS10 was lifted up immediately after the loading shows a faster cooling rate (approx. 0.6 K/1st hour) than the other mode (approx. 0.3 K/1st hour). The outside temperature, close to the MLS10, dropped around 1.65 K/1st hour.

The asphalt surface temperature was measured at two different locations, inside the rolling track and between the twin tires. To eliminate the factor of different start temperatures, the temperature differences were monitored. These temperature differences show that the temperature inside the rolling track increases on an average of 10.1 K and the sensor between the twin tires increases on an average of 8.2 K over all setups and modes during the loading days.

The same characteristics of the temperature change between the standard and modified setup can be taken for the asphalt surface in Figure 5. Noticeable is the fact that the cooling rate inside and outside the rolling track is equal over the last 18 h of the cooling period. During the first hour after the loading period the temperatures were reducing separately from each other. Inside the wheel track the temperature dropped approx. 3.0 K and between the twin tires approx. 1.3 K.

The asphalt temperature was measured in different layers inside the structure. The first sensor is based in 6.5 cm and the second one in 12.0 cm below the surface. The temperature of the sensor closer to the surface increased with an average of 5.6 K. The maximum was reached 20 min. after the loading period has stopped. The temperature data of the bottom sensor had an average maximum difference of 1.3 K 6–7 h after the loading period has stopped, see Figure 6. Because of the asphalt, the effect of short events above the surface is not that big on these sensors and the data look very homogenous. Neither the modified setup nor the standard setup has any influence on the

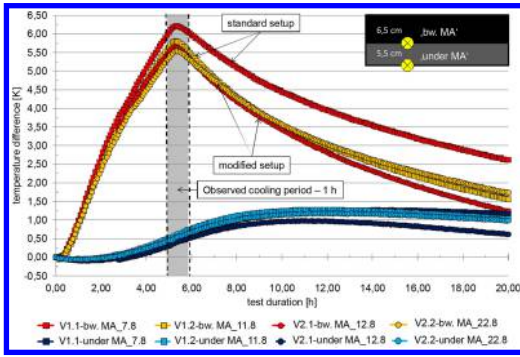


Figure 6. Asphalt structure temperature.

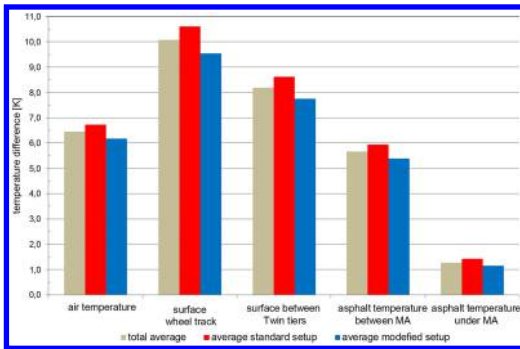


Figure 7. Average values of each sensor position.

asphalt temperature. But the behavior of the higher asphalt layer is interesting for further measurements. With these results it is possible to coordinate the best measurement time, to get equal properties of the construction, especially when examine asphalt pavements.

In Summary it is helpful to take a look at the average data of the sensor. Therefore, the overall average value and the average value of each setup, standard or modified, were determined. Figure 7 shows that the highest average temperature difference is measured at the surface inside the wheel tracks. Between the twin tires the second highest difference was measured while the third highest change occurred at the air temperature inside the MLS10. All in all the standard setup showed higher temperatures than the modified setup. During the cooling period it looks like the same and the temperature at the surface get the main change. On the basis of these results the influence of the Mobile Load Simulator MLS10 on the test track was evaluated and can be attended during the next test programs.

The next paragraphs describe the infrared pictures. Three camera positions are relevant:

- view to the linear motors,
- view to the loading wheels from the front and the back
- view to the asphalt surface from the front and the back.

A trend of the temperature changes can be identified with the pictures, but it is very difficult to get an

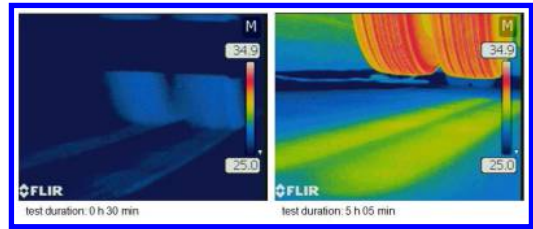


Figure 8. Infrared pictures; beginning & end of loading period.

accurate value with just one scale during the whole loading day. For the evaluation eight points of time are relevant. That includes five points of time for the loading period and three for the cooling down phase. Figure 8 shows one picture after five minutes of loading and one picture after five hours of loading and five minutes after starting the cooling down phase. Each position was monitored just ones with every setup and mode.

Based on the infrared pictures of the view from the front to the loading wheels, the wheels are 8 K warmer after the loading period. There were recognizable differences between the standard and modified setup. It was not possible to detect the differences with the view from the back. From that position all setups were nearly equal and the wheels were approx. 9 K warmer in comparison to the start temperature. That could be influenced by the return of the loading wheels from the top of the machine.

To analyze the surface temperature, the same infrared pictures were used as for the loading wheels. These pictures did not show the same temperature rising as the sensor data did (difference of approx. 3 K). The data are nearly constant if the camera is directed from the back, from the front there are differences between each setup and mode. During the first hour after loading the temperature reduction was similar to the sensor data with approx. 3.5–4.0 K.

To describe the situation at the linear motors it is important to know that there are two linear motors together on each position with a small gap in between. For the evaluation, the upper one has been observed separately from the lower one. The upper one was warmer, on average 3 K, than the lower one. During the loading period of five hours the upper linear motor heated up with an average of 18 K and the lower one with 15 K. Because of this heating the 24 linear motors are relevant factors for the temperature changing inside the MLS10. It is not possible to see a relevant connection between the standard and modified setup. The modified setup is getting warmer than the standard setup. Neither the temperature data coming from the sensor data nor the originating idea of the modified setup do support this statement.

4 CONCLUSIONS

The evaluation and conclusion will focus on the sensor data because they are more detailed and provide more

information over the whole heating process. With the infrared pictures the behavior and characteristics of the asphalt surface, the loading wheels and the linear motors could be visualized but they are not that constant as sensor data. To get more information out of the infrared pictures it is necessary to change the test setup, to have more possibilities to do adjustments at the camera continuously during the loading period.

With this research further adjustments for next test setups are provided. For example, it is necessary to detect the right moment to do the non-destructive measurements to get the most significant characteristics. The highest temperature was measured on the surface inside the wheel track five minutes after the loading period. Inside the asphalt pavement, 6 cm below the surface, the highest temperature has been measured 20 minutes after the loading period. It could be useful to start the measurement approx. 15 minutes after loading to respect the whole temperature range from the beginning and the end of loading.

The trend of sensor data has shown that the standard setup was warmer at all positions than the modified setup. The biggest influence of the different setups has been detected on the surface. Due to the different of approx. 1.1 K in the wheel track between the standard and modified setup it could be useful to do further research at these topic. To get more input about the constant behavior of this difference it is necessary to observe this during the next tests. If the behavior is constant it could be possible to calculate the surface temperature out of the air temperature during tests with

the MLS10. In addition, it could be useful to observe all sensors over a long loading time on one day. Therefore, it is possible to find a maximum temperature rising during loading with the Mobile Load Simulator MLS10.

REFERENCES

- EMPA. 2009. Pilot-study for the evaluation of a Mobile Full-Scale Accelerated Pavement Testing Equipment, ASTRA Bundesamt für Straßen CHLMT Products (Pty) Ltd. 2013 User Manual and Raab, C. & Partl Dr., M.N. 2014. http://www.empa.ch/plugin/template/empa/*/36639, release order date 22nd November 2014.
- Rabe, R. 2004. Bau einer instrumentierten Modellstraße in Asphaltbauweise zur messtechnischen Erfassung der Beanspruchungssituation im Straßenbau, BAST Project 03342.
- Saeed, A. & Hall Jr., J.W. 2003. NCHRP Report 512: Accelerated Pavement Testing: Data Guidelines. Washington D.C.:Transportation Research Board: 59pp.
- Scherkenbach, M. 2013. Sensortestfeld – Analyse neuer und alter Sensoren, BAST Project 10000.
- Wacker, B. & Scherkenbach, M. & Rabe, R. & Golkowski, G. 2014. Belastungseinrichtung Mobile Load Simulator MLS10 und Sensorik zur Beanspruchungsdetektion im ersten gemeinsamen Versuchsbetrieb, BAST Project 13000.
- Wynand Jvd M, S. 2012. NCHRP Synthesis 433: Significant Findings from Full-Scale Accelerated Pavement Testing. Washington D.C. Transportation Research Board.

State-of-the-art of Traffic Speed Deflectometer (TSD)

J.A. Krarup

Greenwood Engineering, Denmark

ABSTRACT: Huge savings in pavement maintenance budgets can be achieved through high-resolution and detailed pavement structural condition data. Rolling Wheel Deflectometer (RWD) and Traffic Speed Deflectometer (TSD) introduce the possibility of continuous strength assessment throughout the investigated network at traffic speed. In this case no traffic interference occurs. This paper reviews TSD principle and capability, technical details, repeatability and verification from accessible results. Specific attention is given to dynamic pavement response features measured by the TSD.

1 MEASURING SYSTEM

1.1 Introduction to TSD

The Greenwood Traffic Speed Deflectometer is the first non-contact device that measures pavement surface velocity when the surface deflects as response to a rolling wheel load. The TSD has become commercial available and TSDs are now delivered in Denmark, UK, Italy, Poland, South Africa, Australia, China, and USA.

At network level most TSD users generate 10 m average values for bearing capacity indices. Even 5 m average values are reported with only minor signal noise. Data are collected at traffic speed eliminating traffic control and eliminating traffic safety problems for operators and traffic. The continuous data allows for pin-pointing of exceptional pavement features. Most TSDs are equipped with subsystems for roughness/texture profiling, digital imaging, GPS, and some with crack detection and ground penetrating radar (GPR). Combined TSD and GPR data are used in Australia, Italy and Finland. Using data presentation overlaid onto digital maps pavement engineers can locate and evaluate pavement problems directly without using (or in combination with) complex pavement management systems.

TSD is the equipment that can contribute to fewer, faster, more sustainable and better planned maintenance interventions.

Localizing weak spots at an early stage makes it possible to do shorter and focused early preventive maintenance and by that reduce traffic delays, then saving resources.

The ROADEX project reported calculations on a low volume northern European road network that demonstrates the effect of limiting repair and maintenance actions using short interval condition data. For example ROADEX Report IV “Benefits and Savings” (2012) estimates that by designing and planning repair

and maintenance using 10 m instead of 100 m intervals corresponds to a saving of 35%.

1.2 Context for TSD

Besides climate and traffic prognoses the Mechanistic Empirical Pavement Design Guide (MEPDG) procedure includes a number of elements:

1. Pavement model (layer thicknesses and material properties)
2. Load model (stationary plate or dynamic rolling wheel load, contact stress distribution)
3. Response model (calculation of surface deflections, stresses and strains at points of interest)
4. Response Criteria (acceptable damage, fatigue)

When MEPDG is used for design of maintenance interventions to an existing pavement it is important to assess the structural condition of the existing pavement. This can be done by applying a known load to the pavement and simultaneously measure the surface deflection. Various deflectometers have been developed to do this. With data describing the pavement model and the load, the response model can compute deflection basins. By iteration the properties in the pavement model can be adjusted until an acceptable coincidence between the calculated deflection basin and the measured deflection basin is achieved. The pavement model for the existing pavement can be used as basis for calculating the effect and benefit of a number of alternative and relevant maintenance actions until a solution that satisfies the demand for added structural life time is found.

1.3 TSD principle

1.3.1 Load

The TSD technology is clever because it can be installed in a vehicle with standard truck properties.

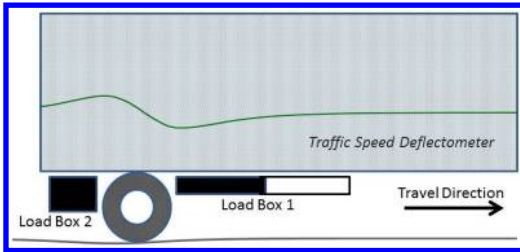


Figure 1. TSD load boxes.

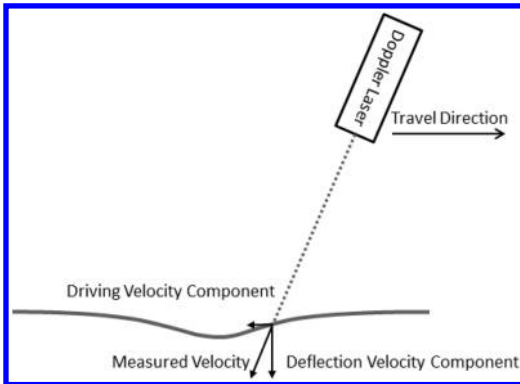


Figure 2. Illustration of two velocity components picked up by the TSD doppler lasers.

The truck has a semi-trailer with a single axle that allows the load to be an authentic rolling wheel load with characteristics similar to most of the traffic loads occurring on road pavements. The load can be set to be very close to for example a 10-ton axle load as used in many pavement design procedures. By adjusting the dead load in the two load boxes on the trailer the static axle load can be selected to relevant levels of axle loads matching the design load, see Figure 1.

On any common parking site the load boxes can be detached or attached to the TSD trailer with the help of a hydraulic system. This feature allows selecting of load level without adjustment of dead load in the boxes.

As the TSD follows traffic the nature of the load will be dynamic and realistic. The load variation from a TSD along the road will fit into the real load pattern that is distressing a road pavement in general, similar dynamics, and similar load level and load duration. In cases where a single roughness element, for instance a bridge joint, creates a concentrated bump impact, then TSD will act (load and measure) accordingly.

The dynamic load variation is monitored by two different systems: by accelerometers and by strain gauges mounted directly on the load axle and read with high frequency.

Lately other strain-gauges are mounted on a TSD to monitor the horizontal force in the driving direction, this can be used for investigation of energy consumption and rolling resistance; data have not yet been published.

1.3.2 Non-contact deflection measurement

Distance measuring lasers have been used in other deflectometer applications; they can use triangulation or time-of-flight to determine the distance to the reflecting object. In a deflectometer the distance measuring lasers requires that both the unloaded and the loaded surface shape are measured, and then the difference calculated assuming that the values were measured at the same spot both times.

With the TSD it is the pavement surface velocity that is measured. The lasers are Doppler lasers and not distance measuring lasers. Doppler lasers detect the change in the light properties when the emitted light is reflected. This eliminates the need for finding the same spot on the pavement for the comparison between loaded and un-loaded situation.

TSD as a system has existed for more than 10 years and there are continuous updates to new and better sensors and features improving TSD performance and data processing.

The TSD Doppler lasers measure the relative velocity between sensor and the reflecting surface. This value represents the velocity in direction of the light beam, and contains a component of velocity in the driving direction and a component in the direction of deflection as shown in Figure 2. The driving velocity is typical orders of magnitude larger than the deflection velocity. Normal traffic speed can for example be 20 m/s, where a typical deflection velocity can be 1 mm/s. Extraction of the deflection velocity requires advanced algorithms that are present in the TSD software package.

1.3.3 Pavement deflection

As response to the TSD axle load, the pavement surface is deformed. The deviations from the unloaded surface establish the pavement surface deflection basin.

If pavement materials had no mass and were homogenous, isotropic, and perfect elastic, then the deflection basin would be symmetrical before and after loading.

As real pavement materials have mass, and are not perfect elastic then the deflection basin is influenced by inertia and even by visco-elastic properties of the bituminous materials, and maybe other effects. The deflection basin becomes asymmetrical and there is a deflection delay, defined as the time or distance between the maximum load and the maximum deflection as shown in Figure 3. Some of these phenomena are seen in FWD plots of time series shown in Gurd (1995).

When the deflection delay is shifted when comparing to deflection basins measured by stationary equipment, then a very close fit is seen in most cases.

1.3.4 TSD history and background

Since the comprehensive American full-scale road tests after the 1950s several deflectometers have been developed. Many of them as one-of-a-kind and only few of them are commercial available.

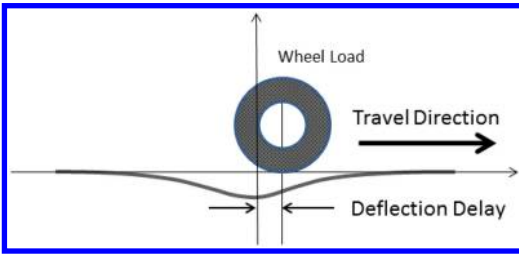


Figure 3. Deflection delay.

Table 1. Commercial available deflectometers.

Device Year of early version	Stationary/ Rolling	Report Interval	Pro- ductiv- ity	Traffic Safety
Name, Year	–	M	km/d	–
Benkelman 1950s	Stationary	Variable	30	Low
Lacroix 1960s	Slow	Discrete	50	Low
FWD. 1970s	Stationary	Variable	50	Low
Curviameter. 1970s	Rolling 18km/h	Continuous	50	Med.
TSD. 1990s	Rolling Traffic speed.	Continuous	300	High

The TSD was invented in the 1990s by Leif Grønsvov, Greenwood Engineering, Denmark. Years before Leifs father, Niels Grønsvov, who during most of his professional career held a position as head of the equipment garage belonging to the Danish Road Institute, had developed an advanced one-of-a-kind second Lacroix deflectometer based on same principles as the Lacroix Deflectograph.

When the Danish Road Directorate from a traffic safety point of view decided to go for traffic speed devices, then Leif Grønsvov elaborated on his idea of using Doppler lasers and measure deflections while travelling at traffic speeds.

The first TSD was delivered to the Danish Road Directorate, and later another first-generation TSD was delivered to Highways Agency in UK.

At of writing this TSD number 9 is being manufactured. An overview of commercial available deflectometers is given in Table 1.

2 DEFLECTION DATA IN PAVEMENT ENGINEERING

As introduced above MEPDG includes measured deflections to establish a characterization of the structural condition of a road pavement. Based on this characterization selection of the optimal rehabilitation action can be decided. With existing Falling Weight

Deflectometer technology it became common to back-calculate E-moduli for the layers in the pavement model. Several back-calculation software packages were developed around the world. One important thing regarding Falling Weight Devices is that the loading plate creates an axial symmetrical response distribution in the pavement. This allows for relatively simple computational solutions, but it is different from the true response distribution created by a rolling axle load.

Even given some differences experience from Australia shows good results when using TSD output to establish deflection basins as input to traditional back-calculation methods described by Muller & Roberts (2012). Various other approaches are described by Zofka (2013).

Over the years researchers and pavement engineers have developed interpretations of FWD deflection basins without using elastic layer theory. One example is the Area Under the Pavement Profile, AUPP, that establish a strong relationship to the horizontal strain at the bottom of the asphalt layer, Thompson (1998). Another strong relationship is demonstrated by Gurp (1995) between the difference between center deflection and deflection 300 mm from the load center, often named the Structural Curvature Index, SCI300.

2.1 New deflection basin characteristics

Another possibility with TSD is that the detailed and authentic deflection basin can be analyzed for asymmetrical characteristics and reveal pavement properties that support finding the optimal decision for preventive maintenance.

The state-of-the-art TSD is configured with most sensors measuring deflections at positions in front of the wheel load, and then two or three sensors located to measure deflections after the wheel load. This new sensor configuration allows for a better localization of the maximum deflection and for the asymmetry between the deflections in front of the load and the deflections after the load.

The deflection delay, the deflection bowl curvature, and the distance between points of inflection (maximum slope of deflection) are examples of such characteristics that could possibly be used as indicators of for instance de-bonding and/or oxidation of bitumen.

2.2 Back-calculation using deflection velocities

The Doppler laser output is relative velocity, measured in the direction of the light beam. With known driving velocity of the TSD the vertical surface deflection velocity can be found, and also the slope of the deflection basin at sensor positions can be exported as output. With a dynamic response model back-calculation can be made matching measured and calculated deflection velocities or deflection slopes.

Moving into dynamic interpretation of pavement characteristics turns the back-calculation focus away

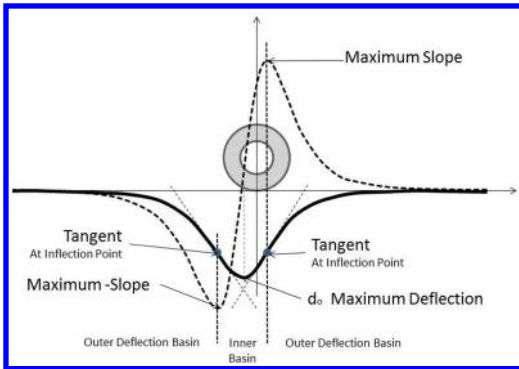


Figure 4. Deflection basin characteristics.

from the maximum deflection that is a distance, and onto the maximum deflection velocity that better describes dynamics of the pavement deflection.

It is more informative to know how long and how fast a certain element has moved, than to know only how long it has moved.

The raw TSD report includes both the vertical pavement velocity and the slope of the deflection. Maximum slopes (positive and negative) indicate the positions where the maximum vertical deflections occur, at the inflection points of the deflection basin as shown in Figure 4.

From the Technical University in Darmstadt Germany Bald & Nguyen (2014) presented an “Evaluation of Load Carrying Capacity of Asphalt Superstructures from Deflection Measurements” where the deflection basin is separated into an inner part of the deflection basin with upwards curvature and the outer parts with downward curvature. The Westergaard radius is indicating the inflection points where the deflection basin slopes have positive and negative maximum. Following this concept the analysis finds the “thickness of the stress distributing layer” and points at locations where layer de-bonding occur.

2.3 Verification

The TSD user in South Africa, SANRAL, has reported from an extensive acceptance testing on a comprehensively instrumented test sites that the TSD measures real pavement behavior even at speeds as low as 2.5 km/h, Kannemeyer (2014).

During comparison between TSD and FWD over a day’s measurement data revealed a significant difference between the two systems during the day. From data analysis it was concluded that the TSD measured correct where the FWD had a significant temperature dependent influence from the rubber buffers. Kannemeyer stated: “Although FWD has been around for some time, cannot be used as *true* reference for accepting TSD measurements”.

In the US Federal Highway Administration (FHWA) conducted measurements at the MnRoad pavement test facility. FHWA used geophones and accelerometers built into the pavement surface.

Even though FHWA cannot obtain the same accuracy and precision as SANRAL as they did not have the same precise positioning of the wheel loads during the experiment as they did in the South African verification trials, the FHWA contractor do give promising statements for the TSD. The FHWA report is expected in Spring 2015.

3 ON-THE-ROAD TESTS

3.1 First generation TSD tests

TRL was assigned by Highways Agency, HA, in the UK to introduce the TSD to network level scanning of pavement structural condition. After a few years of testing, network level campaigns were introduced where TRL contracted with operator teams to cover relevant parts of the HA network. For decades HA and TRL operated more than a dozen slow moving Lacroix Deflectographs.

The TSD was taken into operation in order to substitute the deflectographs and eliminate the traffic safety issues and to continue the time series of relative deflection from the deflectographs. The UK TSD has a limited number of Doppler lasers that are sufficient to measure and report the relative deflection, but not sufficient for deflection basin interpretation.

In 2010 the Australian ARRB leased the Danish TSD and measured 18,000 km for examination, validation and demonstration. Methods for network analysis were developed and standard TSD procedures are applied in Australian road authorities, see Warren (2014).

In Germany Bundesanstalt für Strassenwesen, BAST, have had pilot measurements made several times, see Jansen (2014).

3.2 Second generation TSD tests

The two first-generation TSDs were designed and manufactured for installation in a freight container. The perspective at that time was to make it possible to ship the container with the TSD equipment.

In all TSDs the Doppler sensors are mounted inside a stiff beam made of steel plates, see Krarup (2012). The open steel profile beam with sensors is often called the measuring beam or the sensor beam.

The technical specifications from the third customer required to have the TSD system built into a custom made semi-trailer with cable channels and no visible cables. Greenwood introduced the current mechanical system holding the sensor beam. This system allows the sensor beam to be rolled on rails in the floor and repositioned at various positions with respect to the wheel load.

Since the third TSD it has been possible to position the sensor beam so that some sensors could measure behind the wheel load. It also allowed the sensor beam to be positioned in the middle between the trailer axle and the tractor axle where deflections are minimal when both loads are removed from the trailer. This

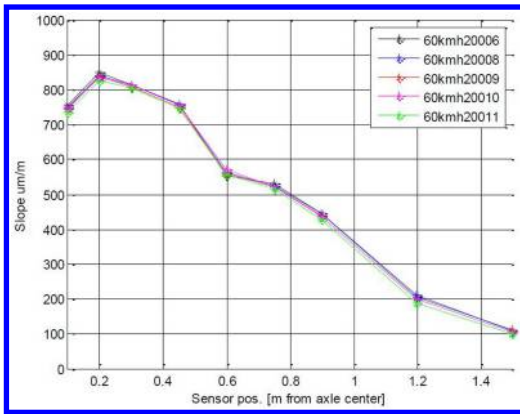


Figure 5. Average deflection slope ($\mu\text{m/m}$) at each doppler sensor position.

can be very helpful for diagnosis purposes. During travel and measurements the sensor beam is absolutely firmly locked to the rails in the floor of the semi-trailer.

3.3 Factory inspection tests

Prior to shipping a new TSD a comprehensive factory inspection program is conducted to assure that each component and subsystem works as expected. Each vital sensor is verified in the lab before it is installed and connected to the TSD system.

For instance the subsystem for load monitoring strain gauge system, this subsystem has to be calibrated with various static loads on plate scales and then tested with dynamic loading. Another test is long term test to test for signal drift. An alternative dynamic load monitoring subsystem includes a vertical accelerometer. Signals from both systems are recorded and synchronized for comparison as acceptance test.

Not only sensor and data collection systems have to be inspected and tested. Power supply, energy storage, and climate control are crucial for optimal and successful operation of a TSD.

In general most tests are made both stationary and on-the-road on selected test sections with various pavement characteristics. Some sections are smooth and some rough, some are heavy-duty motorway pavements and some are thin local road pavements.

The example selected is a local road. Figure 5 shows the repeatability for SCI300 along five runs at 60 km/h on a 1000-m long test section. When runs are compared with Pearson correlation coefficients between samples, then correlation coefficients are found for each pair in the interval 0,9995 to 0,9999. Same section and data are used in Figure 6 that shows average values of the deflection slope from each sensor position.

At the factory inspection test only the driver's skills to keep the truck at 60 km/h and on the same line for repeated runs was applied. No markings or laser guide lines were used. Still Figure 6 shows the graphs inside a band approximately 20 micrometer wide.

4 OPERATION

In daily use the operation of the TSD truck and data collection system requires a truck driver and a TSD operator. A number of calibrations have to be conducted with regular intervals to assure correct signals from the sensors involved in the TSD system.

Data collection is recommended to be made at speeds above approximately 40 km/h to keep the pavement response in the frequency domain where visco-elastic properties are not significant.

As mentioned earlier data collection is also successful even at much lower speeds, but at low speeds the data interpretation and modelling becomes much more complex and the influence of speed becomes significant.

In research projects a TSD with sensors positioned both in front and behind of the load will be able to measure the full asymmetric deflection basin. Data from measurements made at lower speeds will include the visco-elastic effects that will be seen as deflection basin asymmetry as the visco-elastic effect is significant behind but not in front of the wheel load.

Experience shows that a daily production of 200–300 km of data is realistic. As the Doppler lasers are optical sensors, it is not possible to operate during rain or on wet pavements.

For TSD data measured on flexible pavements there are many tools available for pavement analysis. For rigid pavements TSD there are not a similar variety of pavement analysis procedures.

Data measured on rigid pavements reveal clear response to joints, cracks and faulting, but no research has established models to support this analysis and validate the features in the data.

For rigid pavements and even normal concrete bridges there are active proposals applying for research project funding.

5 CALIBRATION

5.1 Distance calibration

Almost all data collection electronics and computers are working in time domain with a time frequency as reference. Almost all road infrastructure related information is referenced to distance (or coordinates).

For most road condition measuring systems, the Distance Measuring Instrument, DMI, is used to get equidistant pulses that can be used for reorganizing collected data from time domain into distance domain.

The DMI in a TSD is an optical rotary encoder that provides the same number of electronic pulses for each revolution of the wheel axle where it is attached. Calibration of the encoder is to find the scale factor that relates a number of encoder pulses to a "true" distance on the road.

The TSD user decides how accurate a scale factor is required. High accuracy can be obtained using a photocell to detect markings, like reflective tape, defining start and stop of a "true" distance on the road.

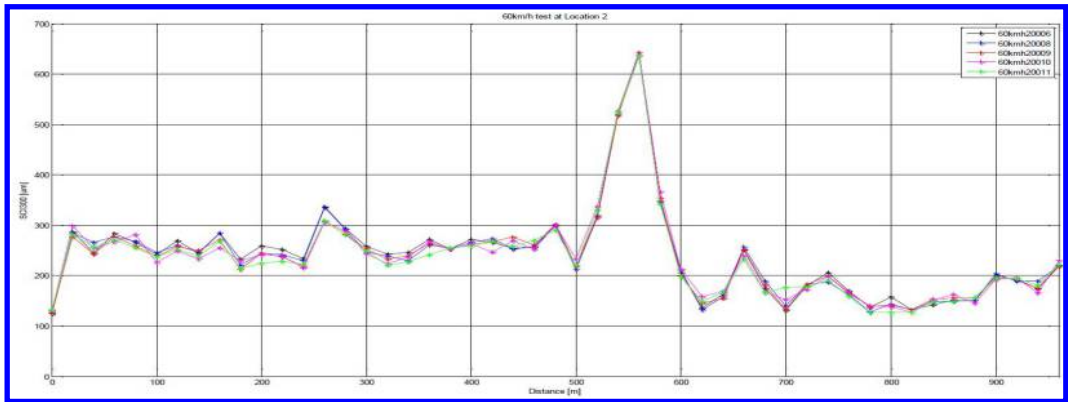


Figure 6. 1000-m local road with cracks between 500 m and 600 m. Five repeated TSD runs at 60 km/h. The Y-axis maximum is 700 m. The five graphs show 20-m average values of Structural Curvature Index SCI300 (μm).

If repetitions are required then markings and photocell is the way to get high repeatability.

During distance calibration all other requirements for minimum speed are suspended as it does not matter what other sensors measure during distance calibration.

As the data storage is controlled by pulses from the DMI it is very important to have a good DMI scale factor at all times, and it does not take very long time to do a distance calibration.

5.2 Inertial sensors

Scale factor recalibration of accelerometers and gyroscopes is a task for the sensor manufacturer only. Verification of the inertial sensors can be made at service of the TSD. Offsets due to mechanical mounting has to be dealt with, and TSD operators are trained to do offset calibration and conduct check of functionality of inertial sensors, procedures can be done at any level parking area.

5.3 Profiler calibration

The TSD has an inertial profiler as an integrated sub-system. The minimum configuration is one triangulation laser and one accelerometer. Test of functionality is easy and not very time consuming, and can be done frequently.

At TSD service the triangulation laser can be verified and diagnosed, but if it needs recalibration it has to be done by the supplier only. The particular triangulation laser brand generally performs well for more than 15 years without recalibration.

5.4 Doppler lasers

The Doppler laser in a TSD is based on basic photonic characteristics of laser light and optical elements. No ruler or velocity measuring instrument can be used for recalibration in the field or at service.

During service at Greenwood Engineering the sensor can be verified in a laboratory setup including features that expose the Doppler laser for vibrations,

temperature variations or dust/moisture between the laser and the moving object that reflects the laser light to the sensor. In the setup relevant TSD travel velocities and typical pavement surface characteristics can be applied.

Recalibration can be made by the sensor supplier only.

5.5 TSD system

A calibration procedure that takes one to two hours to perform is the way to calibrate sensor offsets and prepare the system for measurements. A calibration file is stored and system calibration values are often valid for weeks.

In case the TSD is moved to a different climatic region or has been exposed to mechanical alterations, then the system calibration should be repeated. Most users conduct calibration before and after projects or campaigns.

6 CONCLUSIONS

The TSD is the most accurate and safe deflectometer to operate on a highway network.

TSD is the authentic experiment for structural evaluation of pavement condition. It is the experiment that a falling weight deflectometer tries to simulate.

Both for network level and project level the TSD delivers reliable data.

The load is an authentic semi-trailer axle load and can be selected for various load levels by combining and arranging the load boxes.

Measured TSD data contains more information than other traditional systems and makes it possible to develop new interpretations and analyses.

The continuous output from the TSD can be used in future pavement maintenance planning systems with more flexibility in length of sections for repair.

TSD output can avoid expensive maintenance actions previously based on functional distress data only.

It is expected that when pavement material researchers discover the capability of the TSD they will start to develop more relationships between results from the laboratory and data from a TSD. This development will create new and better pavement performance indicators.

TSD can be the basis for development of future and better pavement design procedures.

With the new pulling force monitoring system TSD data can be used to direct heavy commercial traffic to the least energy consuming routes, and by that contribute to CO₂ reduction.

In the future the TSD concept and technology can be developed for applications for rigid pavements, airports runways, and railroads.

REFERENCES

- Bald, J.S. & Nguyen.A-D. 2014. Evaluation of Load-Carrying Capacity of Asphalt Superstructures from Deflection measurements. *Presentation at Transport Research Arena TRA, Paris 2014*.
- Gurp C.A.P.M. 1995. Characterization of Seasonal Influences on Asphalt Pavements with the use of Falling Weight Deflectometers. *Proefschrift PhD thesis, Technische Universiteit Delft 1995. Delft*.
- Jansen D. 2014. Evaluation of the TSD in Germany. *Presentation at Pavement Evaluation 2014. Blacksburg, Virginia, USA*.
- Kannemeyer L. et al. 2014. Verification of Traffic Speed Deflectometer measurements using Instrumented Pavements in South Africa. *Presentation at Pavement Evaluation 2014. Blacksburg, Virginia, USA*.
- Krarup J. 2012. Traffic Speed Deflectometer TSD. *Presentation at FWDUG 2012. Sacramento, California, USA*.
- Muller W. & Roberts J. 2012. Revised approach to assessing traffic speed deflectometer data and field validation of deflection bowl predictions. *Intern. Journal of Pavement Engineering*, 2013 Vol. 14, Nos. 3–4, pp. 388–402. Taylor & Francis.
- ROADDEX 2012. Benefits & Savings (2012). *Publications*, www.roadex.org.
- Thompson M. 1998. The AUPP Algorithms. *Personal note from Professor Emeritus Marshall R. Thompson, Uni.of Illinois, Urbana, Illinois, USA*.
- Warren G. 2014. Combining pavement data collection methodologies using the TSD as a platform. *Presentation at TRIMM (Tomorrows Road Infrastructure Monitoring Methods) conference, 2014 Brussels*.
- Zofka A. et al. 2014. Alternative Approach for Interpreting Traffic Speed Deflectometer Results. *Paper presented at TRB annual meeting 2014 Washington DC, USA*.

PELT based dynamic segmentation for network level pavement evaluation with 1 mm 3D data

Q. Li, K.C.P. Wang & G.W. Yang

School of Civil and Environmental Engineering, Oklahoma State University, Stillwater, OK, USA

ABSTRACT: With the development of 3D laser imaging technology, the latest iteration of PaveVision3D Ultra technology can obtain 1 mm resolution data at full-lane coverage in three dimensions at highway speed. With extensive amount of 1 mm 3D data from rapid network level survey, how to use such big data for pavement management and maintenance practices remains a challenge. Traditionally, highway routes are broken into predefined segments of fixed lengths for pavement evaluation, which can present problems in data redundancy and limitations to provide recommendations for project prioritization. In this paper, the Pruned Exact Linear Time (PELT) method is implemented to dynamically segment pavement sections into uniform subsections with consistent condition states. The PELT is based on optimal partitioning algorithm with a pruning step to reduce the computational cost, while not affect the exactness of the resulting segmentation. Pavement roughness, cracking, rutting, and predicted hydroplaning speed for safety analysis are calculated from the 1mm 3D data collected on a test site. PELT is applied to identify change points and determine homogeneous segments based on the calculated performance indicators. The dynamic segmentation process can assist DOT effectively using the available 1 mm 3D pavement surface condition data to optimize pavement management decision-making.

1 INTRODUCTION

Segmenting pavement network into homogenous sections is important for road maintenance scheduling and management systems. Three types of segmentation approaches are used by highway agencies: fixed-length segments, variable-length segments, and dynamic segmentation. Fixed-length static method breaks highway routes into pre-defined lengths (such as every 0.1 miles) and are insensitive to changes in pavement attributes, which can result in significant data redundancy and problems to provide recommendations for project prioritization (Thomas 2003). Variable-length static method, on-the-other-hand, can break pavement into any length, but may be too sensitive to attribute changes and result in a large number of fine segments within a highway network (Thomas 2003). A well-known example of this method is the cumulative difference approach (CDA) proposed by AASHTO (AASHTO 1986).

Dynamic segmentation (DS) can accommodate the integration of both fixed and variable-length methods and provide more flexible data management. Two classical DS algorithms: binary segmentation and neighborhood segmentation, are widely used to estimate the locations of multiple change points of a data set. Binary segmentation (Scott and Knott 1974) first identifies a single change point for the entire data, and the procedure is repeated for the split data sets until no change points are found in any parts of the data.

The binary segmentation search method is computationally efficient with an $O(n \log n)$ calculation complexity. However this method does not search the entire solution space and is an approximate algorithm (Killick et al. 2012). The neighborhood segmentation algorithm (Auger and Lawrence 1989) minimizes the objective using a dynamic programming technique to obtain the optimal segmentation change points. Whilst this algorithm is exact (Killick et al. 2012), the computational complexity is $O(mn^2)$ where m is the maximum number of change points, which is considerably higher than that of binary segmentation.

In recent years, the advance of laser and sensor technology changed the landscape of collecting pavement surface data. An innovative 3D laser imaging system, PaveVision3D Ultra (3D Ultra for short), is capable of automatically acquiring 3D laser imaging intensity and range data from pavement surface and reconstruct the 3D virtual pavement surface at 1 mm resolution at 60 mph (Wang 2011). With extensive amount of 1 mm 3D data for rapid network pavement survey, the number of possible solutions to the multiple change point problem (computation complexity) increases exponentially. As a result, the existing traditional methods are unable to fulfill automated dynamic segmentation for network level evaluation with balanced computation cost and data accuracy.

In this paper, the newly developed Pruned Exact Linear Time (PELT) method (Killick et al. 2012) is implemented to dynamically segment pavement

sections into uniform subsections using 1 mm 3D pavement surface data. Similar to the neighborhood segmentation method, the PELT algorithm conducts an exact search but is significantly more computationally efficient. By removing solution paths that are known not to lead to optimality (called as “prune” process), the PELT method achieves the computation complexity to $O(n)$ level. Pavement IRI, rutting, fatigue cracking, and predicted hydroplaning speed are calculated from the 1 mm 3D data collected on a test site using the 3D Ultra technology. Subsequently, PELT method is applied to segment the case study pavement into homogenous sections, which can be further used by decision makers for project prioritization and maintenance scheduling.

2 PAVEVISION3D ULTRA DATA ACQUISITION SYSTEM

The PaveVision3D laser imaging system has been evolved into a sophisticated system to conduct full lane data collection on roadways at highway speed up to 60 mph (about 100 km/h) (Wang 2011). The resolution of surface texture data in the vertical direction is about 0.3 mm and in the longitudinal direction is approximately 1 mm at data collection speed of 60 mph. 3D Ultra is able to acquire both 3D laser imaging intensity and range data from pavement surface through two separate sets of sensors. Recently, two 3D high resolution digital accelerometers have been installed on the system, which allows to be capable of reporting compensated pavement surface profile and generating roughness indices. The collected data are saved by image frames with the dimension of 2,048 mm in length and 4,096 mm in width. In summary, the 1 mm 3D pavement surface data can be used for:

- Comprehensive evaluation of surface distresses: automatic and interactive cracking detection and classification based on various cracking protocols;
- Profiling: transverse for rutting and longitudinal for roughness (Boeing Bump Index and IRI);
- Safety analysis including macro-texture in term of mean profile depth (MPD) and mean texture depth (MTD), hydroplaning prediction, and grooving identification and evaluation;
- Roadway geometry including horizontal curve, longitudinal grade and cross slope.

3 PELT METHOD BASED DYNAMIC SEGMENTATION

3.1 The PELT methodology

Assuming an ordered sequence of data, $y_1:n = (y_1, \dots, y_n)$ has m change points with their positions at $\tau = (\tau_1, \dots, \tau_m)$. Consequently the m change points split the data into $m + 1$ segments, with the i th segment containing $y_{(\tau_{i-1}+1):\tau_i}$. The objective to identify

Table 1. Pseudo-code for the PELT method (Killick et al. 2012).

Input:	A time series of the form, (y_1, y_2, \dots, y_n) where $y_i \in \mathbb{R}$. A measure of fit $C(\cdot)$ dependent on the data. A penalty β which does not depend on the number or location of changepoints. A constant K that satisfies equation.
Initialize:	Let $n =$ length of time series and set $F(0) = -\beta$, $cp(0) = 0$, $R_1 =$ (Officials)
Iterate:	For $\tau^* = 1, \dots, n$
	1. Calculate $F(\tau^*) = \min_{\tau \in R_{\tau^*}} [F(\tau) + C(y_{(\tau+1):\tau^*}) + \beta]$
	2. Let $\tau^1 = \arg\{\min_{\tau \in R_{\tau^*}} [F(\tau) + C(y_{(\tau+1):\tau^*}) + \beta]\}$
	3. Set $cp(\tau^*) = [cp(\tau^1), \tau^1]$
	4. Set $R_{\tau^*+1} = \{\tau \in R_{\tau^*} \cup \{\tau^*\} : F(\tau) + C(y_{(\tau+1):\tau^*}) + K \leq F(\tau^*)\}$
Output:	The change points recorded in $cp(n)$.

multiple changepoints can be formulated to minimize (Killick et al., 2012):

$$\sum_{i=1}^{m+1} [C(y_{(\tau_{i-1}+1):\tau_i})] + \beta_f(m) \quad (1)$$

where C is the cost function and $\beta_f(m)$ is the penalty to guard against over fitting. The PELT method considers the data sequentially and searches the solution space exhaustively. Computational efficiency is achieved by removing solution paths that are known not to lead to optimality. The assumptions and theorems which allow removal of solution paths are explained further in Killick et al. (2011). Pseudo-code for the PELT method is given in Table 1.

3.2 Test site

The test site for this paper is a 6.2 mile long flexible pavement on Interstate 40 west of Russellville Arkansas. Extensive cracking is observed on the pavement surface, especially in the right wheelpath. The 1 mm 3D pavement surface data are collected using the 3D Ultra technology. Pavement roughness, cracking, rutting, and hydroplaning speed are calculated for each image frame, which are subsequently used to obtain homogenous pavement segments based on the PELT method.

3.3 International Roughness Index (IRI) analysis

Two digital high accuracy accelerometers are mounted inside the 3D road surface sensors to provide the inertial reference information. The measured pavement longitudinal road profiles are obtained by combining the height information with the inertial reference data. Filtering algorithms are applied to remove unwanted data for IRI calculation. IRI values in the left and right wheelpaths and the average IRI are calculated in inches per mile for each image frame.

The PELT segmentation results for average IRI are presented in Figure 1. The change points locate at miles

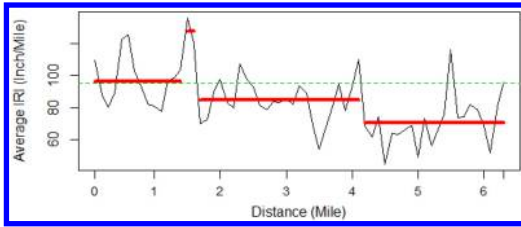


Figure 1. Average IRI segmentation results.

1.4, 1.6 and 4.1. The beginning 1.4 miles (22.5% of the total length) of pavement has “moderate” roughness condition if 95 inch/mile is set as the IRI threshold between “good” and “moderate” conditions. Generally speaking, the roughness of this test section is in “good” condition.

3.4 Fatigue cracking analysis

The AASHTO Designation PP67-10 (AASHTO 2013a) *Quantifying Cracks in Asphalt Pavement Surfaces from Collected Images Utilizing Automated Methods* outlines the procedures for quantifying cracking distress at network level. In PP67-10, 30 cracking related values are measured and reported considering 3 cracking types (longitudinal, transverse, and pattern cracking), 2 attributes (cracking length and cracking width), and 5 traffic zones (3 in non-wheelpath and 2 in wheelpath). In order to produce manageable results, only fatigue cracking is studied in this paper, which is estimated from pattern cracking in both wheelpaths and reported as the percentage of the wheelpath areas.

The PELT segmentation results for fatigue cracking are presented in Figure 2. The change points of fatigue cracking in both left and right wheelpaths are located at exactly the same mile posts (miles 1.5, 2.3, 2.4 and 6.1), which indicates that the test pavement site has consistent cracking distributions in both wheelpaths. However, the left wheelpath has much less amount of cracks than the right wheelpath, whose data are shown in Figure 2. Assuming pavement with less than 5% of fatigue cracking in wheelpath areas is in “good” condition, while pavement with more than 25% fatigue cracking in “poor” condition, the first 1.5 miles of the pavement are classified to have “moderate” fatigue distress problems. It is observed that pavements at mile 2.3 and mile 6.1 have more than 25% of wheelpath areas with fatigue cracking. Further investigation of these two spots shows that severely spalled interconnected fatigue cracks have formed a complete pattern, as illustrated in Figure 3.

3.5 Rutting analysis

Rutting is defined as the permanent traffic-associated deformation within pavement layers. The recently provisional approved AASHTO Designation PP69-10 (2013b) *Standard Practice for Determining Pavement*

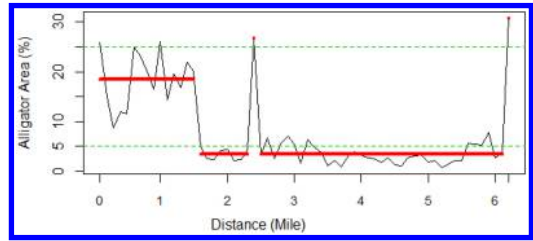


Figure 2. RWP alligator cracking segmentation results.

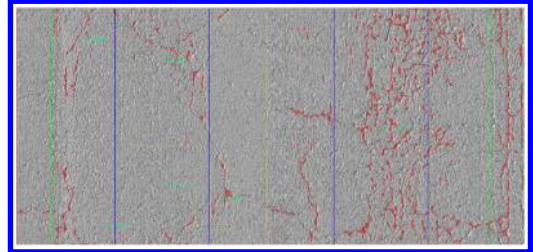


Figure 3. Example crack map at mile 2.3.

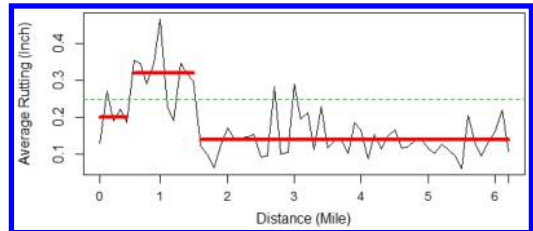


Figure 4. Average rutting segmentation results.

Deformation Parameters and Cross Slope from Collected Transverse Profiles has been implemented into the 3D Ultra system for rutting characterization and cross slope measurements. Rutting in the left and right wheelpaths and the average rutting are calculated in inches for each image frame.

The PELT segmentation results for rutting are presented in Figure 4. The change points of average rutting are located at mile 0.5 and mile 1.5. Assuming pavement with less than 0.25 inches of rutting is in “good” condition and pavement with rutting greater than 0.75 inches in “poor” condition, only pavement segment from mile 0.5 to mile 1.0 has “moderate” rutting problems while the rest of the section has minor rutting. No segment is classified to be in “poor” condition for rutting.

3.6 Hydroplaning analysis

During high intensity rainfall events, hydroplaning will likely occur and affect driving safety. Hydroplaning is dependent on surface texture properties, flow path slope, flow path length, rainfall intensity, and pavement surface type. PAVDRN model has been widely used to estimate hydroplaning speed (HPS) (Anderson et al. 1998). It uses a one-dimensional

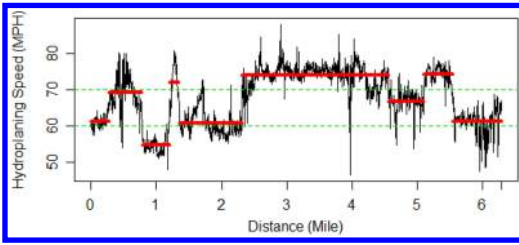


Figure 5. Hydroplaning speed segmentation results.

steady state form of the kinematic wave equation (Equation 2) to calculate the water film depth (WFD). Flow path length and flow path slope can be obtained by Equations 3 and 4. The program also uses a condensation of formulas (Equations 5 and 6) to determine a relationship between velocity at which hydroplaning initiates and WFD (Anderson et al. 1998).

$$WFD = \left[\frac{nL_f I}{36.1S_f^{0.5}} \right]^{0.6} - MTD \quad (2)$$

$$S_f = (S_l^2 + S_c^2)^{1/2} \quad (3)$$

$$L_f = W \frac{S_f}{S_c} \quad (4)$$

$$HPS = 26.04WFD^{-0.259} \quad (WFD < 0.095in) \quad (5)$$

$$HPS = 3.09A \quad (WFD \geq 0.095in \text{ or } 2.4mm) \quad (6)$$

where MTD : Mean Texture Depth (in); L_f : Flow path length (in); S_f : Flow path slope (mm/mm); S_l : Longitudinal grade; S_c : Cross slope; I : $(i - f)$ = Excess rainfall rate (in/hr); i : Rainfall intensity (in/hr); f : Infiltration rate or permeability of pavement (in/hr); n : Manning's roughness coefficient. In this study, the MTD is substituted by Estimated MTD ($EMTD$) derived from the simulated sand patch based volumetric measuring method using 1 mm 3D surface data continuously collected at highway speed (Luo et al. 2014). Cross slope and longitudinal grade data are acquired with an Inertial Measurement Unit (IMU) system. The rainfall precipitation data are obtained from NOAA'S National Water Service (NOAA 2014).

The PELT segmentation results for predicted hydroplaning speed are presented in Figure 5. The change points are located at miles 0.3, 0.8, 1.2, 1.3, 2.3, 4.6, 5.1 and 5.5. The posting speed limit for this pavement is 70 mph. Five pavement segments: 0–0.3, 0.8–1.2, 1.3–2.3, 4.6–5.1 and 5.5–6.2 may be subjected to potential hydroplaning if road users are driving above the speed limit. The predicted hydroplaning speed for segment 0.8–1.2 is around 55 mph.

3.7 Discussions

The change points for the four indicators are combined in Figure 6. The segments derived from the PELT method are marked in three colors: green for segments

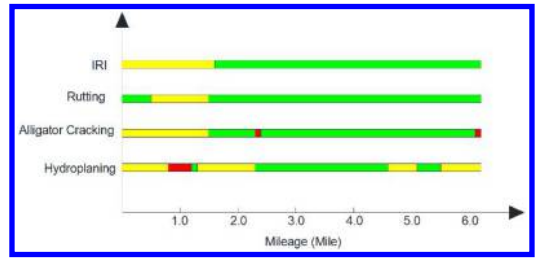


Figure 6. Aggregated dynamic segmentation results.

in “good” condition, yellow for “moderate” condition, and red for “poor” condition. It can be seen that the pavement section in the beginning demonstrates worse condition than that in the rest of the section. Even though the pavement in the second half is considered to be in “good” condition according to IRI and rutting values, some segments have experienced “moderate” to “poor” conditions if it is evaluated based on fatigue cracking and predicted hydroplaning speed. In other words, no roughness and rutting issues are found on the pavement, while hydroplaning related safety hazardous may be presented at several locations. The dynamic segmentation results can assist DOT decision makers to evaluate pavement performance in a comprehensive manner from various perspectives.

4 CONCLUSIONS

The newly developed 3D Ultra data acquisition system can obtain 1 mm resolution pavement surface data at full-lane coverage in three dimensions at highway speed. Aiming to evaluate network level pavement performance for project prioritization using extensive 1 mm 3D data, the PELT method is implemented to dynamically segment pavement sections into uniform subsections. Pavement IRI, rutting, cracking, and predicted hydroplaning speed are calculated from the 1 mm 3D data. PELT is subsequently applied to identify change points and determine the dynamic segments based on the calculated performance indicators. Comparing to the traditional method based on predefined segments with fixed lengths, the PELT method can reduce data redundancy and is able to provide recommendations for maintenance scheduling. The PELT dynamic segmentation process can assist DOT effectively using the available 1 mm 3D pavement surface condition data to optimize pavement management decision-making.

REFERENCES

- AASHTO. *Guide for Design of Pavement Structures*. Technical Report, Washington, D.C., 1986.
- AASHTO. *Quantifying cracks in asphalt pavement surfaces from collected images utilizing automated methods*. AASHTO Designation PP67-10. Washington, D.C., 2013a.

- AASHTO. *Standard Practice for Determining Pavement Deformation Parameters and Cross Slope from Collected Transverse Profiles*. AASHTO Designation: R69-10. Washington, D.C., 2013b.
- Anderson David A. & R. Scott Huebaer, Joseph R. Reed, John C. Wamer, and John J. Henry. *Improved Surface Drainage of Pavements*. Final Report NCHRP Web Doc 16, Washington D. C., 1998.
- Auger, I. E. & Lawrence, C. E. Algorithms for the optimal identification of segment neighborhoods. *Bulletin of Mathematical Biology*, 51 (1), 1989, pp. 39–54.
- Killick, R., Fearnhead, P. & Eckley, I. A. Optimal detection of changepoints with a linear computational cost. *JASA*, 107(500), 2012, pp. 1590–1598.
- Luo Wenting et al. Surface Drainage Evaluation for Rigid Pavements Using IMU and 1 mm 3D Texture Data. In *Transportation Research Record: Journal of the Transportation Research Board* (In Press), TRB, National Research Council, Washington, D.C., 2014.
- NOAA. Precipitation Frequency Data Server (PFDS). National Water Service, Hydrometeorological Design Studies Center. <http://dipper.nws.noaa.gov/hdsc/pfds/>, Accessed on July 2014.
- Scott, A. J. & Knott, M. A cluster analysis method for grouping means in the analysis of variance. *Biometrics*, 30(3), 1974, pp. 507–512.
- Thomas Fridtjof. Statistical Approach to Road Segmentation. *Journal of Transportation Engineering*, Vol. 129, No. 3, 2003, pp. 300–308.
- Wang Kelvin C. P. Elements of Automated Survey of Pavements and a 3D Methodology. *Journal of Modern Transportation*, Volume 19, Number 1, 2011, pp. 51–57.

Measured pavement responses under falling/heavy weight deflectometer and heavy aircraft gear loadings

Jeffrey S. Gagnon & Albert Larkin

FAA Airport Technology R&D Branch, William J. Hughes Technical Center, Atlantic City Int'l Airport, NJ, USA

ABSTRACT: A Falling/Heavy Weight Deflectometer (F/HWD) applies a load impulse to the pavement surface which is supposed to simulate the dynamic short term loading of a moving wheel load. The deflection basin measured is then used to calculate in-situ pavement strengths. In reality, how well does the F/HWD simulate the moving load of an aircraft? The FAA Airport Technology R&D Branch held a F/HWD round-up in May 2010 inside the National Airport Pavement Test Facility (NAPTF) located at the William J. Hughes Technical Center in Atlantic City International Airport, NJ. Inside the NAPTF, specially constructed rigid and flexible pavement test sections of typical airfield cross sections were instrumented and tested. The flexible pavement structure was a 127-mm asphalt surface, 127-mm asphalt base, 305-mm crushed stone subbase on a silty-clay subgrade with a 7 to 8 CBR. Soil pressure cells were placed at the interfaces of the surface, base, subbase and subgrade materials. Strain gages were also installed within the pavement structure. The instruments were monitored to measure the pavement responses caused by various loadings of the F/HWDs at 40-kN, 55-kN, 73-kN, 110-kN and 160-kN. Pavement responses were also be measured under full scale loading tests performed by the National Airport Testing Vehicle single wheel module at the same load levels as the F/HWDs. This paper will summarize the comparison of the measured pavement response values between different F/HWDs loads and the heavy aircraft loading of the single wheel module.

1 INTRODUCTION

In October and November of 2010 and April of 2011, the Federal Aviation Administration (FAA) hosted a Falling/Heavy Weight Deflectometer (F/HWD) Round-Up in the National Airport Pavement Test Facility (NAPTF) at the William J. Hughes Technical Center in Atlantic City, NJ. Over a period of five months, seven pieces of F/HWD equipment performed tests on the pavement. [Table 1](#) summarizes the equipment and dates on which the tests were performed.

The main objectives of this paper are:

1. Present details of F/HWD Round Up at FAA's NAPTF.
2. Present Pressure Cell readings (stresses) at different depths within a flexible pavement structure under different loading conditions.
3. Compare measured stresses between the F/HWD equipment and the full scale static and dynamic loading tests.

2 F/HWD TEST PAVEMENT

The project required the development of a controlled test pavement within the NAPTF facility. The Round-Up included a rigid and a flexible pavement section each 18 meters (60 ft) long by 4.6 meters (15 ft) wide.

Table 1. F/HWD roundup participants.

Participants	Test Date
FAA KUAB HWD	10-7-2010
ARA Dynatest HWD	10-19-2010
JILS HWD	10-19-2010
ERI KUAB FWD	10-20-2010
PaveTesting FWD	10-20-2010
Carl Bro HWD	11-04-2010
ERDC Dynatest HWD	04-20-2011

Construction began in December 2009 and was completed in May 2010. The concrete section consists of four (4) 4.6 m by 4.6 m slabs. The pavement was constructed in the east end of the facility over a high strength subgrade (CBR 25-30). The layout of the test pavement is shown below in [Figure 1](#).

2.1 Pavement structure

The pavement structure was constructed over a high strength subgrade as shown in [Figure 2](#). The high strength subgrade was excavated to allow for the placement of a medium strength subgrade (CBR 5-7). The highstrength subgrade was replaced for two reasons. The first was that the pavement cross-section designed

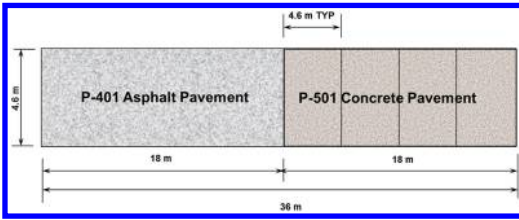


Figure 1. Test pavement layout.

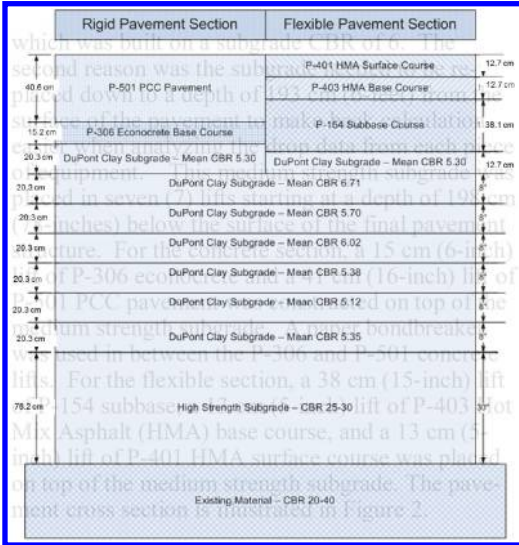


Figure 2. Pavement cross section.

was a typical airport pavement cross section built at the Atlantic City International Airport which was built on a subgrade CBR of 6. The second reason was the subgrade needed to be replaced down to a depth of 193 cm (6-feet) from the surface of the pavement to make back calculation easier when analyzing the drop data from each piece of equipment. This medium strength subgrade was placed in seven (7) lifts starting at a depth of 198 cm (78-inches) below the surface of the final pavement structure. For the concrete section, a 15 cm (6-inch) lift of P-306 econocrete and a 41 cm (16-inch) lift of P-501 PCC pavement was constructed on top of the medium strength subgrade. A paper bondbreaker was used in between the P-306 and P-501 concrete lifts. For the flexible section, a 38 cm (15-inch) lift of P-154 subbase, a 13 cm (5-inch) lift of P-403 Hot Mix Asphalt (HMA) base course, and a 13 cm (5-inch) lift of P-401 HMA surface course was placed on top of the medium strength subgrade. The pavement cross section is illustrated in Figure 2.

2.2 Pavement instrumentation

The test pavement was instrumented with twenty-six strain gages installed in eleven separate locations throughout the pavement structure. Nine strain gage locations are in the concrete pavement with 2 strain



Figure 3. Installation of a pressure cell at PC-1.

gages at each location. The other two strain gage locations are in the flexible pavement with 4 strain gages at each location. Two temperature trees consisting of three thermistors at three different vertical locations were also installed in each pavement type. Finally, nine pressure cells and two multi-depth deflectometers were installed in the flexible pavement.

2.2.1 Strain gages

The strain gages in the concrete pavement were placed with two sensors at each location. One sensor was placed 2.54 cm (1") below the surface of the P-501 and the other was placed 2.54 cm (1") above the bottom interface of the P-501. Within the flexible pavement, two locations consist of four strain gages. Gages were placed at 1.27, 11.43, 13.97 and 24.13 cm (0.5", 4.5", 5.5", and 9.5") below the surface of the P-401 HMA surface course.

2.2.2 Multi-depth deflectometers (MDD)

Two MDD's were embedded within the flexible pavement structure. The MDD's were designed to measure pavement deflections at seven depth locations within the pavement. The sensors used for this project acquire data at 11.43 cm (4.5"), 24.13 cm (9.5"), 40.64 cm (16"), 57.15 cm (22.5"), 127 cm (50"), and 196.85 cm (77.5") below the asphalt surface.

2.2.3 Pressure cells

Pressure cells were embedded at two locations in the flexible pavement and there no pressure cells installed in the concrete pavement section. The two locations coincided with the drop locations. One location consisted of six pressure cells acquiring data at the following depth locations: 11.43 cm (4.5"), 24.13 cm (9.5"), 34.29 cm (13.5"), 44.45 cm (17.5"), 54.61 cm (21.5"), and 57.15 cm (22.5") below the asphalt surface. The other location consisted of three pressure cells acquiring data at 11.43 cm (4.5"), 24.13 cm (9.5"), and 69.69 cm (23.5") below the asphalt surface. Figure 3 shows a pressure cell installation at the top of the subgrade lift.

2.2.4 Temperature sensors

Temperature sensors were placed in two locations, one within the concrete pavement and the other within the flexible pavement. Each location consisted of three sensors collecting data at varying depths. The concrete temperature data was collected at 1.27 cm (0.5"), 11.43 cm (4.5"), and 20.32 cm (8") below the surface of the P-501 PCC. The flexible data was collected at 1.27 cm (0.5"), 7.62 cm (3"), and 11.43 cm (4.5") below the surface of the P-401 HMA course.

3 F/HWD TESTING PLAN

A standardized test pattern and recommended test loads were provided to each participant during the testing process. The original participants came during the months of October and November of 2010 with a late participant completing their testing in April of 2011. The FAA HWD equipment performed multiple test runs both before and after the other participants completed their testing.

3.1 Drop locations

A test plan using a total of 33 test locations was developed. Testing on the concrete pavement consists of drop locations as follows: directly over strain gage locations, center of slabs, corner of slabs, and along center of joints. For the flexible pavement, drop locations are either directly on or near the various sensors embedded within the pavement. The drop locations are shown in Figure 4.

3.2 Testing cycles

Testing locations were not enough to define the testing plan. Other factors were involved in developing the test plan and led to the development of two cycles for testing of both concrete and flexible pavement sections. The intent of Cycle 1 was to collect a baseline of data at each test location. Understanding that the data for a given drop location could change based on the direction of testing, it was determined to specify testing directions and to utilize two testing directions. As such, Cycle 1 requires testing at each drop location traveling first from west to east and then from east to west. The number of drops for Cycle 1 totaled 66. The intent of Cycle 2 was to investigate repeatability of test results. As such, a small sample of the first drop locations was chosen to be repeated in both test direction. The number of drops for Cycle 2 totaled 22.

3.3 Testing load levels

At each test location, participants performed a seating drop and three test drops for both concrete and asphalt pavement sections. The load levels for testing were dependent upon the type of equipment being used. For FWD testing, the three test load level drops were 40 kN (9,000 lb.), 55 kN (12,000 lb.), and 73 kN

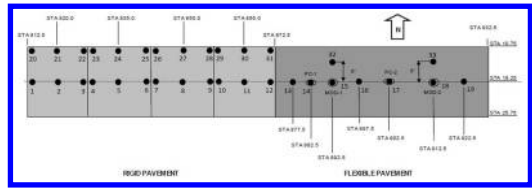


Figure 4. F/HWD drop locations.

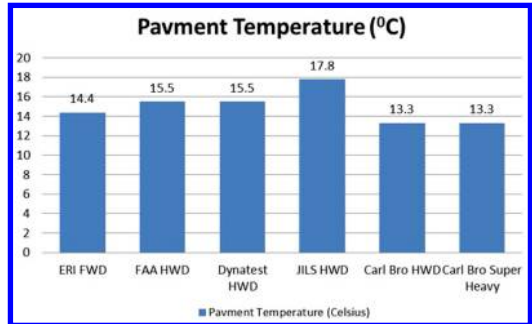


Figure 5. Pavement surface temperature.

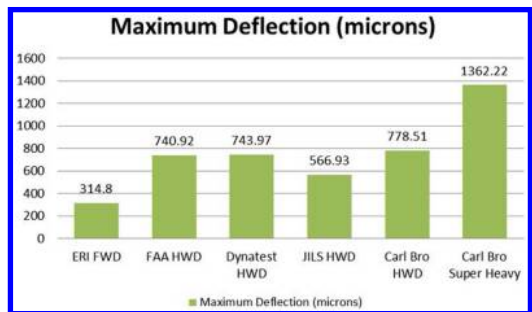


Figure 6. Average maximum deflection (D0).

(16,000 lb.) For HWD testing, the three test load level drops were 55 kN (12,000 lb.), 110 kN (24,000 lb.), and 160 kN (36,000 lb.) The physical setup of any particular equipment dictated what testing load levels could achieve during the testing. Equipment capable of testing at either testing level only tested at one. There was one exception which was the Carl-Bro HWD which could test up to 312 kN (70,000 lb.) and was considered a Super Heavy Weight (SHWD).

3.4 F/HWD testing results

Figures 5, 6, and 7 summarize the results of the tests performed by each piece of equipment on the asphalt pavement sections only. Figure 5 summarizes the pavement surface temperature at time of testing. As shown in the Figure 5 pavement temperatures ranged from a low of 13.3°C to a high of 17.8°C so the deflections and stress results should not have been affected too much by the pavement temperature at the time of testing for comparison.

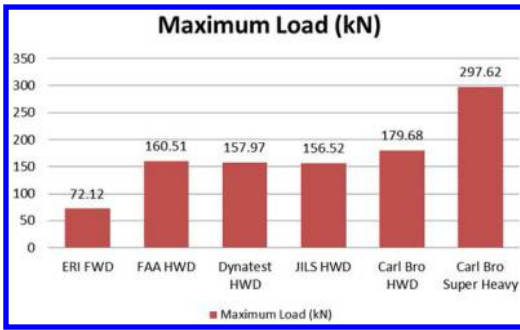


Figure 7. Average maximum load.

Table 2. PC-1 readings for F/HWD testing.

Sensor Location Below Surface (cm)	PC-1 Sensor (Avg Measurements) (kN/m ²)					
	ERI FWD	FAA HWD	Dynatest HWD	JILS HWD	Carl Bro HWD	Carl Bro Super Heavy
11.43	Noise					
24.13	45.61	53.99	91.66	105.05	149.81	185.77
26.67	14.49	13.00	28.06	30.16	33.63	36.95
40.64	Bad Calibration Factor					
54.61	13.25	14.39	25.59	26.98	26.06	28.20
57.15	13.32	15.21	25.37	26.05	26.96	28.75

Figure 6 summarizes the average maximum deflection (D0) under the highest average load for all of the asphalt deflection basins. As noted the deflections ranged from 314.8 microns under a 72.12 kN load to a high of 1,362.22 microns under a 297.62 kN load.

Figure 7 summarizes the average maximum loads recorded by each piece of equipment on the asphalt pavement sections only. The average maximum loads ranged from a low of 72.12 kN for the ERI FWD to a high 297.62 kN for the Carl Bro SHWD.

4 PRESSURE CELL READINGS UNDER F/HWD LOADS

Pressure cell readings were recorded at differing depths within the asphalt pavement sections as noted in paragraph 2.2.3. Table 2 and Figure 8 summarize the average recorded gage readings for the Pressure Cell 1 (PC-1) location under F/HWD loading at the highest loading rate, 73 kN for FWD, 160 kN for HWD and 312 kN for the SHWD. For the F/HWD testing the pressure cell at 11 cm (4.5") below the surface did not properly record the results as noted in Table 2 as noise. Also throughout the testing it appeared the pressure cell at the PC-1 location 41 cm (16") below the surface had a bad calibration factor.

Table 3 and Figure 9 summarize the average recorded gage readings for the Pressure Cell 2 (PC-2) location under F/HWD loading.

5 FULL SCALE TESTING

Full scale testing was performed using the National Airport Testing Vehicle (NAPTV) in both static mode at two different load levels of 6,818 kg (15,000 lb.)

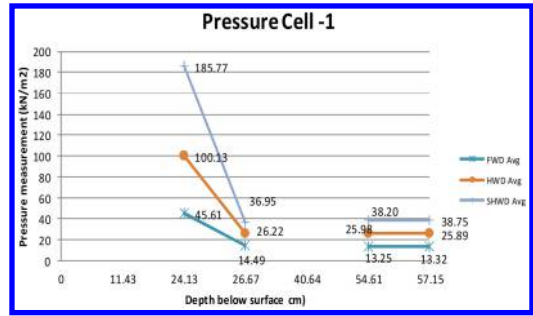


Figure 8. Pressure cell 1 readings.

Table 3. PC-2 reading for F/HWD testing.

Sensor Location Below Surface	PC-2 Sensor (Avg Measurements) (kN/m ²)					
	ERI FWD	FAA HWD	Dynatest HWD	JILS HWD	Carl Bro HWD	Carl Bro Super Heavy
11.43	179.20	250.40	425.84	273.24	253.98	648.84
24.13	47.42	50.12	92.65	88.02	56.47	105.66
54.61	11.18	11.88	20.97	21.02	13.96	26.86

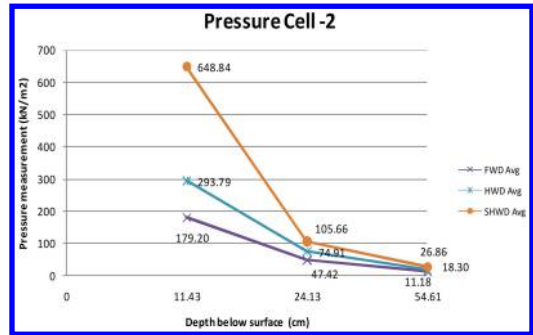


Figure 9. Pressure cell 2 readings.

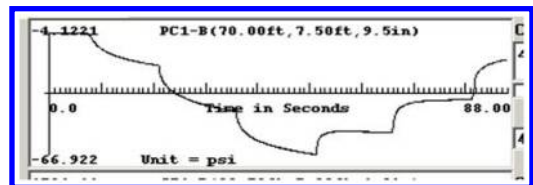


Figure 10. Static load test with no rest period.

and 15,909 kg (35,000 lb.) and slow rolling mode at 15,909 kg (35,000 lb.). The static testing at 6,818 kg (15,000 lb.) was performed with a step increase of 2,272 kg (5,000 lb.) with no rest periods in between steps as shown in Figure 10. The 15,909 kg (35,000 lb.) static test was also performed in a step increase starting at 2,272 kg (5,000 lb.) and increasing up to 15,909 kg (35,000 lb.) with a 50 second release or rest period in between load increases as shown in Figure 11.

Dynamic loading or slow rolling tests were performed in both directions of east to west and then west to east at 15,909 kg (35,000 lbs) and at two different speeds of 0.25 ft/sec and 0.5 ft/sec. Each direction was recorded in one file as shown in Figures 12 and 13.

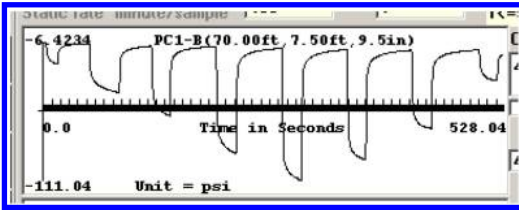


Figure 11. Static load test with rest period.

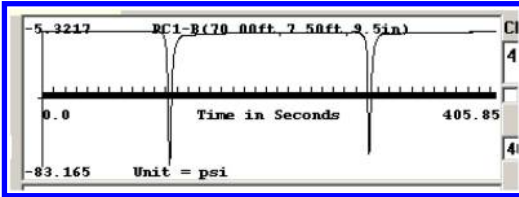


Figure 12. Dynamic loading at 0.25 ft/sec.

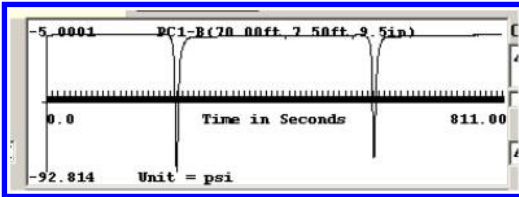


Figure 13. Dynamic loading at 0.5 ft/sec.

Table 4. Gage reading for full scale testing.

Sensor Location Below Surface (cm)	PC-1 Sensor (kN/m ²)		PC-2 Sensor (kN/m ²)	
	0.5 ft/s	.25 ft/s	0.5 ft/s	.25 ft/s
Description	E-W/W-E	E-W/W-E	E-W/W-E	E-W/W-E
11.43	1309.9121	1270.26585	1267.27	1295.35
24.13	536.71	605.38	582.90	627.07
26.67	313.79	359.16		
40.64	Bad Calibration Factor			
54.61	122.18	122.87	0	0
57.15	127.49	126.18		

6 PRESSURE CELL READINGS FULL SCALE TESTING

Table 4 below summarizes the average recorded gage reading for the dynamic testing performed at both the PC-1 and PC-2 locations and at both speeds of 0.5 ft/sec and 0.25 ft/sec. The stress level recorded range from a high of 1,310 kN/m² at 11.43 cm below to surface at the interface of the P-401 surface and base course to a low of 122 kN/m² at 54.6 cm below the surface in the P-154 subbase course.

7 SUMMARY

Figures 14 and 15 summarize the comparison between the stresses measured under full scale static and

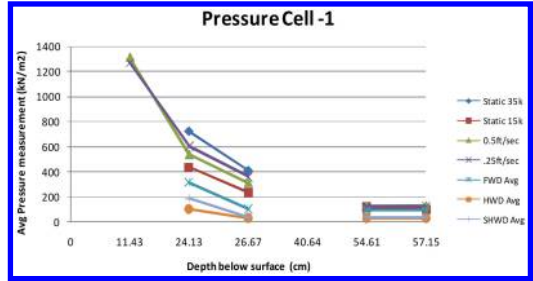


Figure 14. Pressure cell 1 measured stresses.

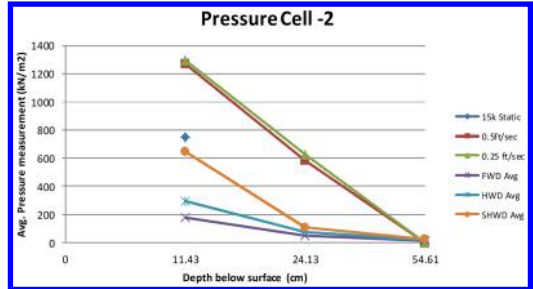


Figure 15. Pressure cell 2 measured stresses.

dynamic loading and measured under F/HWD testing equipment for only the asphalt pavement section. There is only one reading for the 15k static load in Figure 15 due to the failure of the pressure cell recordings at a depth of 24.13 and 54.61 cm.

In both figures the stresses induced by full scale testing whether static or dynamic are greater than those induced by any of the F/HWD testing equipment. It is clear that none of the F/HWD testing equipment can achieve a state of stress in the pavement layers that full scale testing can achieve.

8 CONCLUSIONS

By evaluating the full scale test results, it illustrates that the longer and the heavier a load stays in one place the higher the stress levels in each layer, i.e. the 59,909 kg static load induces the highest stress with the 0.25 ft/sec full scale test inducing the second highest stress levels.

Possible reasons for the F/HWD testing equipment being unable to achieve a state of stress in the pavement layers that full scale testing are:

- The F/HWD equipment have been designed to simulate the load pulse of a vehicle traveling at highway speeds and their shorter load pulse duration do not model the load pulse of a slow rolling aircraft gear.
- The footprint of the F/HWD load is a 30.5 cm diameter circle encompassing approximately 730 cm² while the full scale loading foot print is more rectangular or elliptical in shape and covers an area of approximately 1,300 cm².

ACKNOWLEDGMENTS

The work described in this paper was supported by the FAA Airport Technology Research and Development Branch, ANG-E26, United States of America, Dr. Michel Hovan, Manager. The contents of this paper

reflect the views of the authors, who are responsible for the facts and accuracy of the data presented within. The contents do not necessarily reflect the official views and policies of the FAA, USA. The paper does not constitute a standard, specification, or regulation.

Modeling of pavement roughness performance using the LTPP database for southern region in the U.S.

Z.F. Mohamed Jaafar & M. Ahlan

Department of Civil Engineering, The University of Mississippi, USA

W. Uddin

Center for Advance Infrastructure Technology (CAIT), The University of Mississippi, University, USA

ABSTRACT: The objective of this study is to develop a model to predict the pavement roughness deterioration. The focus is on 34 asphalt pavement test sections with bound base included in the General Pavement Study (GPS) 2 of the Long-Term Pavement Performance (LTPP) database for the southern region of the United States. The enhanced linear regression equation developed in this study with Pearson's Correlation R of 0.498 includes initial International Roughness Index (IRI), pavement age, equivalent single axle load (ESAL) traffic, and design structural number, as well as a dichotomous variable for construction number. The validation results of the prediction had an average difference of -1.6% compared to the mean measured IRI value on 7 test sections. In contrast, AASHTO Mechanistic-Empirical Pavement Design Guide (MEPDG) method gave an average difference of 4.2% . Hence, the IRI predictions from the MEPDG will underestimate number of years to reach the acceptable target IRI value.

1 INTRODUCTION

1.1 *Background on pavement condition*

Historically, pavement longitudinal roughness has been an important component of serviceability-performance concept used in the development 1960–1993 American Association of State Highway and Transportation (AASHTO) pavement design procedures. Currently, roughness (or smoothness called in the post-2000 MEPDG guide) is measured on annual basis by many highway agencies as a part of the highway pavement management system. The IRI prediction model is used for life cycle assessment of pavement design alternatives. Therefore, the IRI was selected as an important pavement condition attribute in this study.

1.2 *Objective and scope*

The primary objective of this study is to develop an enhanced pavement roughness deterioration model incorporates initial International Roughness Index (IRI₀), pavement age, cumulative ESAL traffic, and Structural Number (SN) as the independent variables. This study focuses only on GPS 2 sections in southern climatic region of the LTPP study as part of the Strategic Highway Research Program (SHRP).

Pavement sections include asphalt layer overlaid and compacted over a bound base. The LTPP data of 34 sections were compiled and analyzed using the Statistical Package for the Social Sciences Software (www.ibm.com/us/en/).

2 REVIEW OF RELEVANT LITERATURE

2.1 *The world bank and other studies in Brazil*

Many researchers reported different approaches to model and predict International Roughness Index (IRI) in future years. Paterson (1987) developed and implemented the performance models in the Highway Design and Maintenance Standards Model (HDM-III). The empirical data used to predict surface roughness were based on initial roughness IRI₀, modified SN, cumulative ESAL traffic, and pavement age since construction, rehabilitation or reconstruction. The reported R value is 0.866. In addition, a correlation between roughness and quarter-car index (QI) was developed, where IRI is equal to QI/13.

In 1989, a new model was developed to predict the progression of roughness over pavement life (Paterson 1989). It was developed based on field data in the Brazil-United Nations Development Program (UNDP) road cost study and includes structural,

surface distresses and environmental-age-condition factors, respectively. The new model predicted the increase of roughness over time and incorporated modified SN, thickness of crack layer, area of cracking (%), and changes in ESAL per lane. In addition, increase in rut depth, increase in area of surface patching, pavement age, and road surface anomalies such as potholes were also considered as other contributing factors. The model had R value of 0.768. The researcher concluded that the development of road roughness involved a few stages which occurred through multiple mechanisms. The road surfaces degraded over time due to traffic loading, exaggerated by weak pavement strength and exposure to the environment condition over the years (Paterson 1989).

Cardoso & Macron (1998) reported several pavement performance models as a function of the pavement age or the number of standard axle load application. Data from the road network of the State of Santa Catarina in Brazil were used and the models were implemented in the Pavement Management System (PMS). Five different models were established including the models to predict QI based on age and cumulative ESAL, respectively. The model predicted QI for three different regions according to subgrade layer types and the R values ranged from 0.332 to 0.831. The predicted results overestimate when compared to previous Brazilian studies by Queiroz (1981).

Soncim & Fernandes (2010) developed performance models, which included pavement age, traffic volume, and rainfall intensity. An ANOVA was performed from the data collected in 2009 from road roughness surveys on a 650 km road network in the State of Bahia, Brazil. The model was verified using field data and compared to other roughness prediction models. The results showed a reasonable correlation between observed and predicted values with R equal to 0.83. All the above models from Brazil showed that ESAL and IRI_0 are the major predictors.

2.2 MEPDG regression equation for IRI

The Mechanical-Empirical Pavement Design Guide, MEPDG, was developed under the National Cooperative Highway Research Program (NCHRP) and implemented by the Federal Highway Administration (FHWA 2009). However, it is observed that no traffic variable is included in the following MEPDG's IRI final regression equation formulation (Equation 1).

$$IRI = f(IRI_0, RD, TC, FC_{Total}, PRECIP, Age, FI, PI, FSAND, SILT, CLAY) \quad (1)$$

where,

IRI_0 = Initial IRI after construction, in./mile

RD = Average rut depth, in.

FC_{Total} = Area of fatigue cracking (combined alligator, longitudinal, and reflection cracking in the wheel path)

TC = Length of transverse cracks, ft/mile

PRECIP = Mean annual precipitation, in.

Age = Pavement age, years

PI = Subgrade soil plasticity index

FI = Mean annual freezing index, °F-Days

FSAND = Fine sand particles in subgrade (%)

SILT = Silt particles in subgrade (%)

CLAY = Clay size particles in subgrade (%)

In general, a total of 11 input parameters are required to predict future IRI using the MEPDG final regression equation. The pavement age, precipitation, freezing index, plasticity index, and composition of sand, silt, and clay in subgrade layer were used to calculate site factor (SF) which is one of the required independent variable. This regression equation was reportedly developed using the LTPP data. The LTPP database also includes cumulative ESAL traffic and construction number (CN). However, the MEPDG equation does not have traffic and construction number. The CN identifies any major maintenance, repair, and rehabilitation activity. The IRI regression formulation does not include traffic variable and the CN factor.

The functional form of the MEPDG for regression as shown in Equation 1 is similar to the AASHO road test equation for present serviceability index (PSI) in term of roughness, cracking, and patching terms (AASHTO 1993). All other terms in the equation are trying to include the effects of site soil and environmental conditions. But the AASHO equation is related to the ESAL application. In the MEPDG method, IRI for a single year is predicted based on initial IRI and surface distresses but no term is used for the effect of traffic repetition on roughness. To understand the consequences, two sets of computations were made using 1995 IRI data for LTPP test section 28-3085 in Mississippi. First run using all terms including pavement distress data. In the second run zero value was given to distress data assuming that there is no traffic. The results of predicted IRI are presented as follows:

- Measured IRI = 2.137 m/km
- MEPDG predicted IRI (using cracking and rut depth data from LTPP) = 2.2 m/km (3% difference with respect to measured IRI)
- MEPDG predicted IRI (assuming no traffic, no cracking, no rut depth) = 1.806 m/km (-15.5% difference with respect to measured IRI)

Considering pavement distress data, the MEPDG equation overestimated IRI by 3% but if the distress is ignored, than the equation gives lower IRI by 15.5% compared to the measured value. That implies that if there is no traffic on the road at all then the roughness is reduced. This is the limitation of the MEPDG. It further shows, that missing traffic attribute is a major limitation because cracking distress can happen due to only environmental stress without any traffic on the road.

3 LTPP DATA COLLECTION

The GPS 2 data were collected for all 34 test sections from the online LTPP InfoPave database (www.infopave.com). The statewide distribution of the

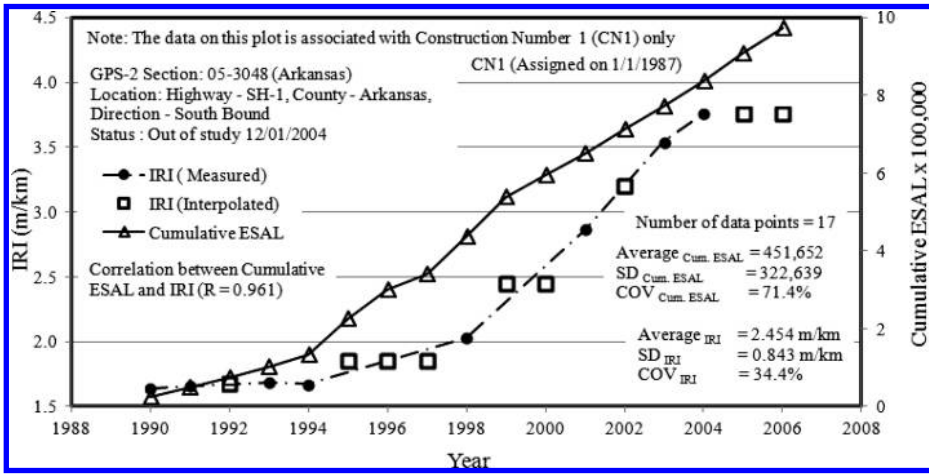


Figure 1. IRI and cumulative ESAL traffic data for GPS 2 test section in Arkansas.

LTPP sections follows: Alabama (5), Arkansas (4), Florida (4), Georgia (6), Louisiana (1), and Mississippi (14). The IRI regression equations, developed in this study, are based on the data sets from 1990 to 2006. The developed regression equations are verified using measured data sets from 2007, 2010, and 2011 for test sections in Mississippi, and test sections in Florida and Georgia are verified using 2009 data.

3.1 Dependent variable IRI

The dependent variable of the regression equation is average yearly IRI in meter per kilometer (m/km). In the LTPP database, the IRI for both left and right wheel paths are measured with at least 5 runs for each section. These IRI values are averaged and the mean values from multiple runs are calculated. The processed IRI data show that about 60% of the data are missing from the database. The following approach is used to interpolate the missing data:

- If the missing IRI data are before the first measured data, they are given the same values as the measured data for the following year.
- Same IRI as the last measured data are assumed if the missing data appear after the final year of measured IRI.
- If data is missing between two measured data points than the average of these two data points is assigned.

Figure 1 shows the measured and interpolated IRI values, as well cumulative ESAL for a single test section 05-3048 in Arkansas. Total 17 data points are included in the plot. The IRI value in 1992 was interpolated by incorporating mean IRI values between 1991 and 1993. The IRI values for 1995 to 1997 are the average interpolated values between 1994 and 1998. The IRI values for 2005 and 2006 are assumed identical to IRI in 2004. A similar approach was used to interpolate missing IRI values for other test sections. The ESAL plots show cumulative values of the total annual

ESAL. A strong correlation between yearly IRI and cumulative ESAL is observed with R equal to 0.961.

3.2 Independent variables

Four independent variables are considered to develop the regression equation in this study. They are IRI_0 , pavement age (year), pavement structure SN, and cumulative ESAL traffic application.

- The IRI_0 is the IRI measured in 1990. It is important to include IRI_0 in the regression equation since this value describes the road surface condition at the beginning of the analysis period.
- The age attribute was chosen since it reflects the impacts of season and the environment. The pavement age is calculated by subtracting the initial construction year from the IRI measurement year (1990 to 2006). If the road was constructed in 1985, the corresponding age is 5 years (1990–1985), which explains that the pavement is exposed to traffic loads and the environmental condition for five years.
- Another important input is the pavement SN that is used in the 1993 AASHTO and earlier guides (AASHTO 1993). The SN represents the overall structure constructed to sustain the traffic loads. The 1993 SN equation considers structural layer coefficients, layer thicknesses, and base and sub-base drainage coefficients. Higher SN exhibits stronger pavement and better load carrying capacity to ensure smooth road surfaces over the service life.
- The final variable selected is cumulative ESAL traffic application. About 26% of traffic data are missing from the LTPP database, and the default estimated ESAL data in the LTPP database are not accurate. Thus, the missing ESALs are interpolated based on the average annual rate of growth (AARG). Figure 1 shows the example of cumulative ESAL plotted for LTPP test section 05-3048 in Arkansas.

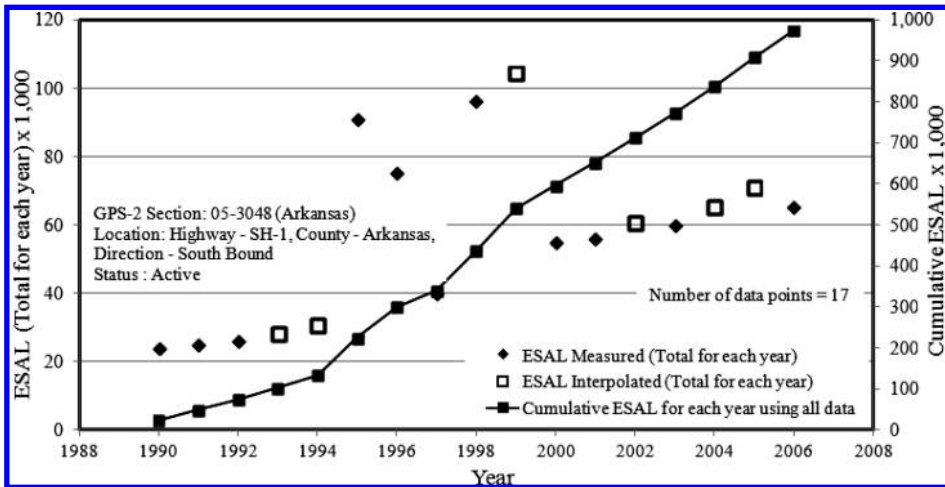


Figure 2. Annual ESAL and cumulative ESAL traffic data for GPS 2 test section in Arkansas.

4 METHODOLOGIES FOR IRI MODELING

The following steps were implemented in this study:

- 1) The IRI, SN, ESALs, CN, and construction dates data were downloaded from the LTPP database and saved to the model database folder for all 34 test sections.
- 2) The IRI_0 data were determined from the downloaded data sets. The IRI_0 refer to the IRI at the beginning of the analysis period (1990).
- 3) The average yearly IRI values from left and right wheel path from different runs were averaged for each year. The steps were repeated for data of all years depend on the availability of the data. The missing data were interpolated as discussed in Figure 1. For all 34 test sections, the following statistics are related to the measured and interpolated IRI_0 values. These statistics were computed from test sections with IRI_0 less than 2 m/km, except for test section 05-2042 at US 82 highway in Ashley County, Arkansas.
 - Number of test sections = 34
 - Average $IRI_0 = 1.071$ m/km
 - Standard Deviation (SD) = 0.440 m/km
 - Coefficient of Variation (COV) = 41.1%

- 4) The measured ESAL values were determined from the database. The missing values were estimated using AARG, which were determined by averaging growth rate before and after average years. The average year is 8.5, obtained by dividing 17 (number of years from 1990 to 2006) by 2. The ESAL values for the missing data were determined using Equation 2.

$$ESAL_{s_y} = ESAL_{s_{(y-1)}} \times (1 + AARG) \quad (2)$$

where, y is the year of the measured or interpolated IRI. The latest ESAL depends on the ESAL of the preceding year multiplied with the AARG.

- 5) The statistical analysis was carried out to determine any significant correlation between variables selected in the regression equation as shown in Table 1. Example of yearly IRI vs. age plot is shown in Figure 3.

Figure 3 shows a positive correlation between yearly IRI and age. A total of 578 data points were included (17 years \times 34 test stations). The data collected from the LTPP database show a large variability in yearly IRI data. The Pearson's R, mean, SD, and COV for IRI data shown are associated with the combined measured and interpolated data.

- The yearly IRI ranged from 0.594 m/km to 4.048 m/km. The mean of yearly IRI is 1.2426 m/km. In addition, SD and COV are 0.6 m/km, and 48.3%, respectively.
- The pavement age ranged from 0 to 34 years. Test section 05-3058 in Arkansas was assigned with zero age since the IRI profiling was carried out in the same year when road first opened to traffic. The mean age for the selected test sections is 16 years, while the SD and COV are both 7 years and 43.4%, respectively. A positive correlation between yearly IRI and age was observed with Pearson's R equal to 0.228. This implies that IRI increases with age.
- The correlation between yearly IRI and cumulative ESAL traffic was also analyzed. The calculated mean is 3,154,314. The SD is 6,487,700 resulted in

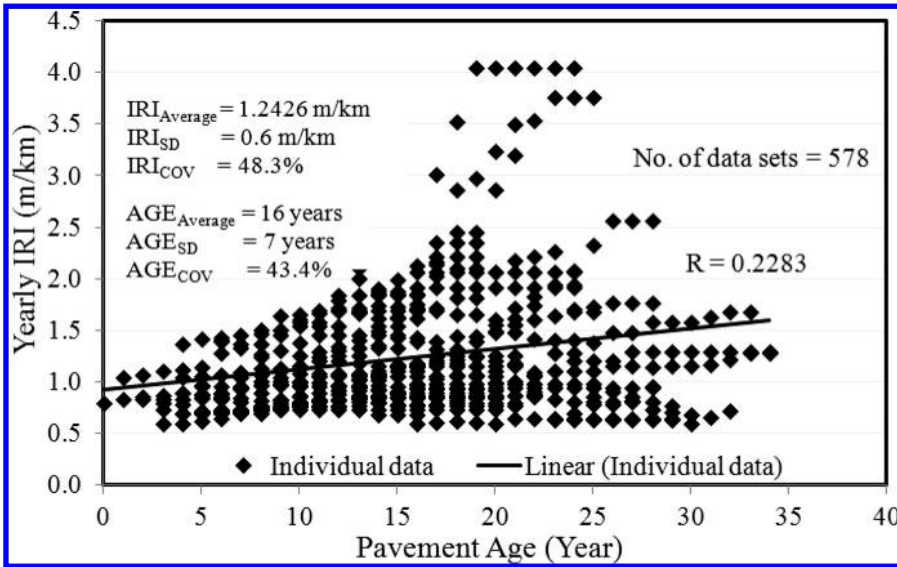


Figure 3. Correlation between yearly IRI and pavement age.

COV equivalent to 205.7%. The R value between cumulative ESAL traffic and yearly IRI is -0.192 . In general, cumulative ESAL traffic shows a larger variation compared to yearly IRI data.

- The average SN recorded in the analysis is 4.8 with COV approximately 27%. The SN ranged from 1.4 to 7.9. Continuous traffic flow over the years affected IRI and structural capacity. There is a moderate negative correlation between yearly IRI and SN ($R = -0.305$). This implies that IRI relatively higher for weaker pavement structure.
- On the other hand, R value is less than 0.1 between SN and age. Therefore, there is no significant correlation between SN and age.
- The IRI_0 has an average value of 1.071 m/km. The SD and COV are 0.4336 m/km and 40.5%, respectively. The correlation between the yearly IRI and IRI_0 was observed with R value of 0.397.

Table 1 summarizes the correlations between each variable. It can be seen that all independent variables (IRI_0 , Age, SN, and Cumulative ESAL) show statistically significant correlations with dependent variable (yearly IRI). All variables have statistically significant correlations except for SN and age with p-value more than 0.05. There is some variation in each variable, depicted by COV less than 50%. The exception is cumulative ESAL, which has a COV of about 206% indicating large variation in traffic volume in the data. Higher variations in the data sets will give a better final regression equation. The formulation of the linear regression equation follows:

$$IRI_{iy} = f(IRI_{0i}, SN_i, Age_{iy}, Cum. ESAL_{iy}) \quad (3)$$

where i = LTPP section number, and y = year of data
 IRI_y = IRI at given year
 IRI_{0i} = Initial IRI for section i (1990)

SN_i = Structural number for section i at initial year (1990)

Age_{iy} = Pavement age for section corresponding to IRI year, y and

$Cum. ESAL_{iy}$ = Cumulative ESAL for section i (1990 to 2006).

- 6) Equation 4 shows the developed regression equation. The R value for this preliminary regression equation is 0.481.

$$IRI_y = 0.997 + 0.404(IRI_0) - 0.074(SN) + 0.013(Age) - 1.309 \times 10^{-7}(Cum. ESAL) \quad (4)$$

This preliminary regression equation does not include CN, which could be a contributing factor to IRI progression. The CN identify changes in the pavement structure caused by major maintenance or rehabilitation treatments events. When a test section first entered the LTPP program, CN1 was assigned. The subsequent maintenance or rehabilitation changed the section's construction number to CN2, CN3, etc.

5 ENHANCED IRI MODELING

Due to the availability of CN data, further analysis was conducted to visualize CN impacts on yearly IRI. Figure 1 as shown in data collection section, describes the IRI time series data for a single test section. The CN for this section remains as original CN1. Figure 1 also shows that, the IRI consistently increased every year.

In general, most of the test sections have more than one CN value. Only 12 test sections included in this study were at CN1. The remaining 22 test sections have more than one CN values. Only test section 28-2807 located at SH6, in Lafayette County, Mississippi recorded CN1 to CN4. As an illustration,

Table 1. Correlation between each variable used in FZ regression equation development.

		CN 1 to CN 4				
CN = Construction Number		Yearly IRI (m/km)	Initial IRI, IRI ₀ (m/km)	Pavement Age (Year)	Structural Number, SN	Cumulative ESALs
Pearson Correlation	Yearly IRI (m/km)	1.000	.397	.228	-.305	-.192
	Initial IRI, IRI ₀ (m/km)	.397	1.000	.291	-.279	-.094
	Pavement Age (Year)	.228	.291	1.000	-.046	.305
	Structural Number, SN	-.305	-.279	-.460	1.000	.380
	Cumulative ESALs	-.192	-.094	.305	.380	1.000
Sig. (2-tailed), α = 0.05	Yearly IRI (m/km)		.000	.000	.000	.000
	Initial IRI, IRI ₀ (m/km)	.000		.000	.000	.023
	Pavement Age (Year)	.000	.000		.269	.000
	Structural Number, SN	.000	.000	.269		.000
	Cumulative ESALs	.000	.023	.000	.000	
	Number of sample, N			578		
	Sample mean, \bar{x}	1.243	1.071	16.0	4.8	3,154,314
	Standard deviation, SD	0.600	0.434	7.0	1.3	6,487,700
	Coefficient of variation, COV (%)	48.3%	40.5%	43.8%	27.2%	205.7%

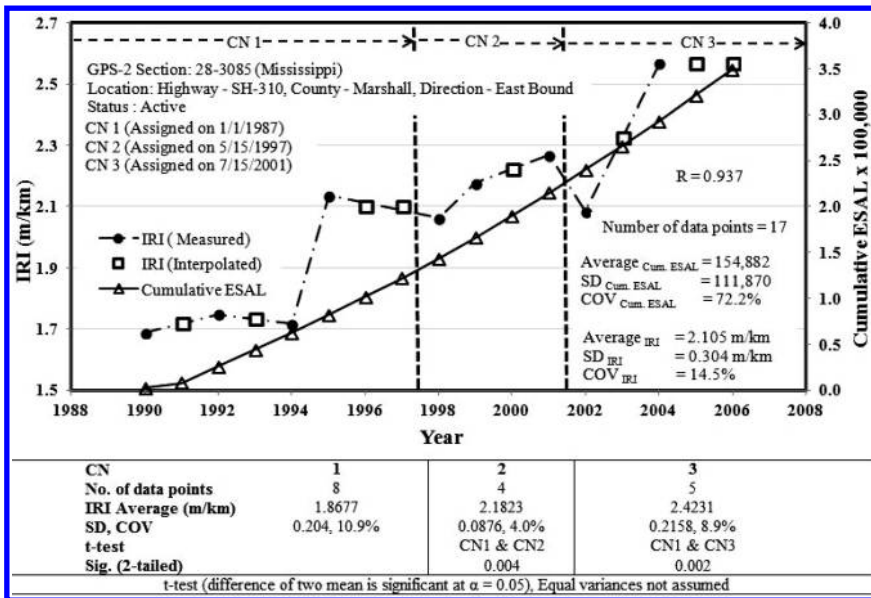


Figure 4. IRI and cumulative ESAL traffic data for GPS 2 test section in Arkansas.

Figure 4 shows different CN values for section 28-3085, located at SH-310, in Marshall County, Mississippi. This test section has three construction number (CN1, CN2, CN3), which were assigned in 1987, 1997, and 2001.

Figure 4 also shows IRI and cumulative ESAL time series plot. The vertical lines describe the year of each CN value. A strong correlation between yearly IRI and cumulative ESAL was observed with R value equal to 0.937. It is observed that IRI values at each subsequent CN decreased sharply as seen in CN2 and CN3 years and then increase again until the subsequent maintenance and rehabilitation year.

5.1 Enhanced regression equation

An enhanced regression is developed including CN as dichotomous (dummy) variable as shown in Equation 5. The Pearson's R for the enhanced regression equation is 0.498.

$$IRI_y = 0.990 + 0.3637(IRI_0) - 0.074(SN) + 0.013(Age) - 1.734 \times 10^{-8}(Cum. ESAL) + 0.154(CND) \quad (5)$$

All input variables are described previously in Equation 3, except CND. The CND refers to the dichotomous variable to identify construction number. For

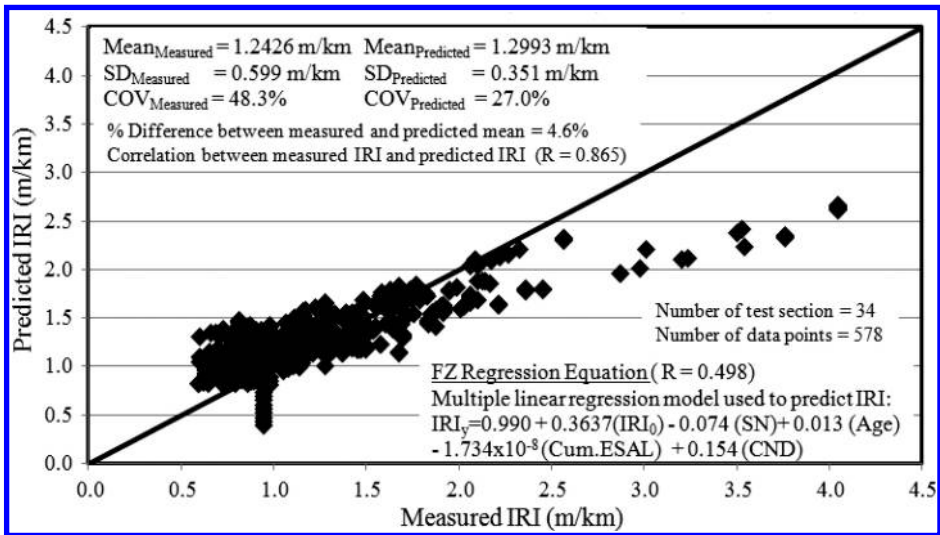


Figure 5. Measured and predicted IRI values using all data sets (1990–2006).

test section with CN1 only, the associated CND is 0. For test sections with more than one CN values, the corresponding CND is 1. Without CN, the R value for the linear regression is 0.481, but when CND is introduced, the R value improved to 0.498. It is very important to include the dichotomous variable to consider the effect of CN related changes in the pavement structure. This statement is supported by an independent sample t-test shown in Figure 4 table. The t-test compares whether there are statistically significant differences between the mean of yearly IRI between CN1 with respect to CN2 mean and CN1 mean with CN3 mean. The results show that p-values are less than alpha value 0.05 for both pairs. This confirms that the mean IRI values for CN2 and CN3 are statistically significant, compared to the mean IRI of data sets within CN1 period. This concept of using CN in regression was not discussed in the MEPDG model development and implementation (FHWA 2009). Figure 5 shows predicted and measured IRI values for all 578 data points associated with 34 LTPP's GPS 2 test sections. All data points shown are used to establish the linear regression equation. The correlation between measured and predicted IRI is 0.865. The difference between the mean of for predicted and measured IRI is 4.6%. The regression equation fits the data very well.

5.2 Model verification

The enhanced regression equation was verified using the measured data sets for years beyond 2006, which is 2007, 2010, and 2011. Table 2 summarizes the statistics for the measured and predicted IRI. State code number 12 refers to Florida, while 13 and 28 codes refer to Georgia and Mississippi, respectively. The IRI values for all test sections are verified for a single year except those years for test section 28-3087 in Mississippi. In these data sets, all test sections in Mississippi

are still active and have most recent year's data available (www.ltpsrco.com/Sections/agsMS.php).

Only test section 28-3083 has CN1, while other test sections have greater CN value. Thus, all sections will have CND equal to 1 except 0 for test section 28-3083. The measured and predicted data were plotted for all 7 test sections, as shown in Figure 6. The correlation between measured and predicted IRI is 0.94. The difference between the mean of for predicted and measured IRI is -1.6%. The regression equation works very well for GPS 2 test sections in the southern states.

5.3 Comparison of enhanced regression equation with AASHTO MEPDG equation

A comparison is made using the enhanced regression equation and the MEPDG equation (FHWA 2009, MDOT 2013). A total of 10 data sets were identified from 1990 to 1995. The data for 11 independent variables required by the MEPDG are limited to only old data sets because of the following reasons:

- Missing rut depth data for recent years
- Missing distress data (fatigue cracking and transverse cracking) for recent years
- Missing plasticity index (PI) data for most of the test sections

Among all the missing data, the most critical data not available for later years is the rut depth data. Table 3 shows summary data for comparison using the MEPDG IRI equation and the enhanced FZ regression equation. The measured and predicted IRI values are plotted in Figure 7.

Table 3 shows that the MEPDG predictions are relatively poor for nine out of 10 of data sets compared to the FZ regression equation's prediction. The Pearson's R value of FZ regression equation is 0.874 which is higher than the R value of 0.819 for prediction by the MEPDG regression equation.

Table 2. Verification of enhanced regression equation using future year's data sets.

State_ Code	SHRP_ ID	Year	CN	IRI (m/km)		% Difference	IRI ₀ (m/km)	Cumulative ESAL	Age (Year)	SN	CND	
				Measured	Predicted							
12	4096	2009	2	1.3463	1.6527	22.8%	0.5986	387,690	35	5.8	1	
12	4100	2009	2	0.7698	1.4130	83.6%	0.6864	1,049,836	33	5.7	1	
13	4420	2009	2	1.3757	1.6089	16.9%	1.3905	2,011,565	25	4.4	1	
28	3083	2011	1	2.0130	1.9907	-1.1%	1.4611	717,419	33	2.0	0	
28	3087	2007	2	2.7144	2.0860	-23.2%	1.0034	1,294,642	25	4.7	1	
28	3087	2010	2	2.7006	2.1139	-21.7%	1.0034	1,641,815	28	4.7	1	
28	3085	2011	3	2.7350	2.4513	-10.4%	1.6880	740,616	33	1.4	1	
28	3090	2011	2	1.8534	1.9440	4.9%	1.2099	845,464	37	4.6	1	
N							8					
Average (\bar{x})				1.9385	1.9076	-1.6%	1.1302	1,086,131	31	4.2		
SD (s)				0.7429	0.3332	-55.2%	0.3792	536,000	5	1.6		
CV (s/ \bar{x})				38.3%	17.5%	-54.4%	33.6%	49.3%	14.6%	38.7%		
95%		Upper limit		2.4533	2.1385	% difference is based on measured data and $\alpha = 0.05$						
		lower limit		1.4237	1.6767	95% CI = $\bar{x} \pm 1.96*(s/\sqrt{n})$						

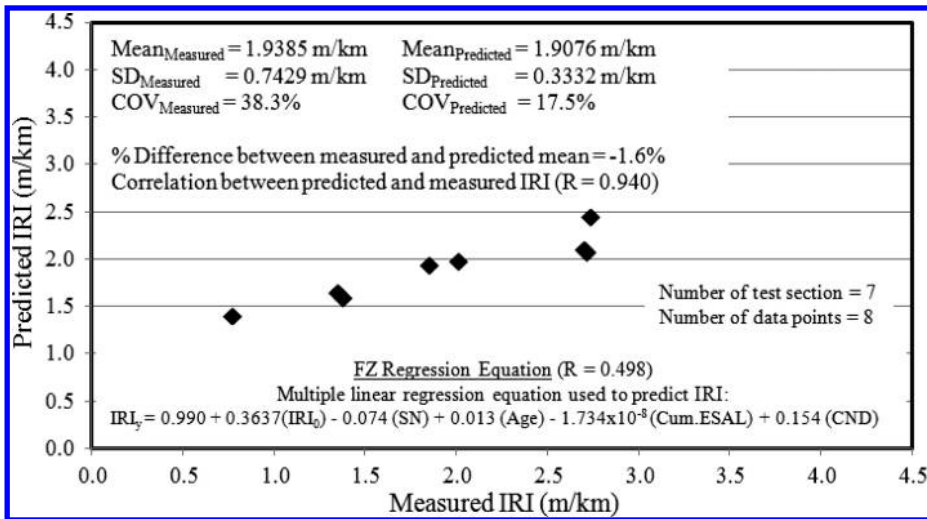


Figure 6. Measured and predicted IRI using enhanced regression equation.

As a consequence, the higher the IRI predictions from the MEPDG indicate lesser number of years to reach acceptable target IRI value, as compared to the enhanced FZ regression equation's predictions. This implies that the MEPDG predictions lead to underestimate pavement life.

The mean IRI by the MEPDG regression predictions shows 23.1% difference compared to the mean measured IRI value. This difference is significantly higher than the 5.5% difference of the enhanced equation prediction with the mean measured IRI value. Therefore, the enhanced regression equation developed and validated in this study is acceptable.

6 CONCLUSION AND RECOMMENDATION

The LTPP database provides important and useful data for pavement performance modeling studies. The performance models reviewed from Brazil are not applicable for road systems in the U.S since the LTPP database are based on high quality and thicker pavements in the National Highway System (NHS). The analysis of 34 test sections in the U.S southern region was model to develop the regression equation in this study. The enhanced equation had better R value of 0.498. The verification results of the enhanced equation predictions for seven test sections have an average

Table 3. Data used to predict IRI and compare the MEPDG and enhanced regression equation.

No.	State	State Code	SHRP ID	Year	IRI (m/km)				
					Measured	MEPDG Regression Equation	% Difference	FZ Regression Equation	% Difference
1	AL	1	1019	1995	1.510	1.913	26.7%	1.402	-7.2%
2	AL	1	4125	1990	0.952	1.433	50.6%	1.264	32.8%
3	AL	1	4125	1994	1.098	1.448	31.9%	1.355	23.4%
4	AL	1	4125	1995	1.104	1.524	38.1%	1.367	23.8%
5	GA	13	4119	1992	0.977	1.215	24.3%	0.821	-16.0%
6	MS	28	1016	1993	1.051	1.145	9.0%	1.083	3.0%
7	MS	28	2807	1995	1.186	1.740	46.7%	1.262	6.4%
8	MS	28	3083	1995	1.713	1.579	-7.8%	1.685	-1.7%
9	MS	28	3085	1995	2.137	2.200	3.0%	1.883	-11.9%
10	MS	28	3090	1995	1.425	1.549	8.7%	1.452	1.9%
Average					1.125	1.488	23.1%	1.222	5.5%
Standard Deviation (SD)					0.187	0.271		0.206	
Coefficient of Variation (COV)					16.6%	18.2%		16.9%	
Pearson's R (Predicted vs Measured)						R = 0.8193		R = 0.8737	

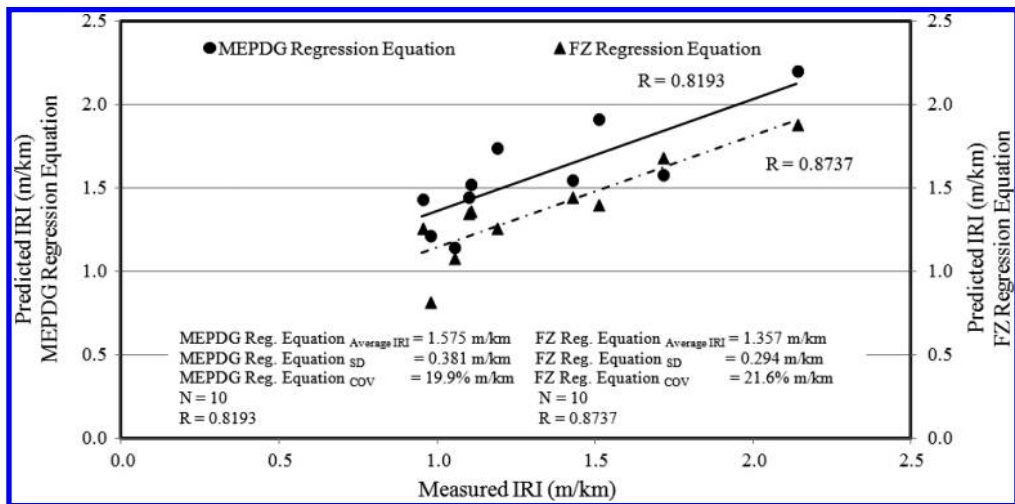


Figure 7. Comparison between measured and predicted IRI using the MEPDG and FZ regression equations.

difference of -1.6% compared to the mean measured IRI value. For a second data set, the MEPDG regression equation predictions showed relatively higher, 23.1%, which is about 4 times difference compare to the mean IRI value, 5.5% difference of the enhanced equation predictions.

The MEPDG regression equation was developed using the LTPP data which had 11 input variables. However the MEPDG model did not consider effect of CN and cumulative ESAL traffic. This is probably the primary reason the MEPDG equation overestimated the IRI values. It is recommended to implement the enhanced regression equation and calibrate if necessary for other environmental regions of the U.S and abroad.

ACKNOWLEDGMENTS

The research was conducted at the Center of Advance Infrastructure Technology (CAIT) at the University of Mississippi. The senior author appreciates the funding support for his PhD studies provided by Universiti Sains Malaysia and Ministry of Education Malaysia (MOE).

REFERENCES

AASHTO. 1993. AASHTO design guide for guide for pavement structures. American Association of the State Highway and Transportation Officials, Washington, DC.

- Cardoso, S.H. & Macron, A.F. 1998. Pavement performance models for the State of Santa Carina, Brazil. In *4th International Conference on Managing Pavement*: 568–582. Durban, South Africa.
- FHWA. 2009. Guidelines for implementing NCHRP1-37A M-E Design procedures in Ohio: Volume 4 – MEPDG models validation and recalibration. Federal Highway Administration, U.S Department of Transportation, Washington, DC.
- MDOT. 2013. Implementation of MEPDG in Mississippi-Draft Final Mississippi DOT Pavement ME Design User Guide. Report FHWA/MS-DOT-RD-013-170 Mississippi Department of Transportation, Jackson, Mississippi.
- Paterson, W.D.O. 1987. Road deterioration and maintenance effects: Models for planning and management. John Hopkins University Press for World Bank. Baltimore, MD.
- Paterson, W.D.O. 1989. A transferable causal model for predicting roughness progression in flexible pavements: 70–84. In *Transportation Research Record* 1215, TRB National Research Council, Washington, DC.
- Queiroz, C.A.V. 1981. Performance prediction models for pavement management in Brazil. Ph.D Dissertation. The University of Texas at Austin.
- Soncim, S.P. & Fernandes, J.L. 2012. Roughness performance model for surface treated asphalt highways. *IJP- International Journal of Pavements*, 11(1-2-3): pp. 93–102.
- Wen, H. & Chen.C. 2007. Factors affecting initial roughness of concrete pavement. In *Journal of Performance of Constructed Facilities*, 21 (6): pp. 459–464.

Road safety, road marking and street furniture

Pavement skid resistance versus appropriate signage to tackle the visibility problem on motorway fast lanes along tight left curves

A. Kokkalis, A. Athanasopoulou & G. Kollaros
Department of Civil Engineering D.U.Th., Xanthi, Greece

ABSTRACT: Obstructed visibility is rather common at tight left downgrade curves along motorway fast lanes in mountainous terrain. The problem is due to the safety barriers in motorway medians which obscure visibility to stopping sight distance for the typical obstacle. Stopping sight distance should be provided for V_{85} along any motorway section. However, a usual combination of the minimum acceptable radius for the horizontal curves, together with the maximum allowable downgrades, results to provided visibility to low obstacles corresponding to as much as 50 km/h lower than V_{85} vehicle speeds. To overcome the problem either a troublesome shift of the barrier to the inside of the curve should be made or excessively anti-skid fast lane pavements should be provided. Also, certain Design Guidelines accept significant relaxations to the values of vehicle speeds to stop safely ahead of low objects. In this paper the upper limits of anti-skid properties of motorway pavements are first evaluated. The gap between required values and the possibly achieved ones is identified. Hence, complementary vertical signage would be necessary to warn drivers. An evaluation of that signage is made, whether it should inform the drivers how much they have to reduce their speed under wet pavement conditions, or what other behaviour have to adopt. The paper advocates that a non-passing signage is the best along these motorways subsections.

1 THE VISIBILITY ISSUE ALONG MOTORWAY FAST LANES

Roads crossing mountainous terrain usually have to follow the lowest acceptable design parameters for the selected design speed (V_e), i.e. minimum radii and maximum gradient, or the cost will sharply raised due to increased earthworks and costly engineering works. Highway engineers know by experience that when they design a motorway crossing mountainous terrain they have to tackle the keen visibility deficiency along the fast lanes. As a matter of fact, long bridge parapets and safety barriers on a motorway central reserve area along left curves may obscure visibility to stopping sight distance to the typical low height object. The problem becomes keener in downgrades which increase safe stopping distance.

New Jersey barriers (NJ) are the typical safety barriers on Greek motorways central reserves. A (short) NJ has an average typical height of 0.83 m. Considering the vision line for the typical eye height of 1.06 m (OMOE, 2002), the visibility to the vehicle ahead is unobstructed over the safety barrier. However, what would be the case if a large object fell from the leading vehicle or drifted or rolled and seated on the fast lane? According to Table 10-4 of (OMOE 2002), the basic obstacle height for $V_{85} = 120$ km/h is 0.35 m, where V_{85} is the 85th higher percentile speed. That size of obstacles should be early visible by a driver moving that fast either to avoid them or brake before them and should not be hidden by the central reserve motorway

barrier. Highway Design Guidelines, in general, propose for motorways combinations of horizontal curves and gradients with inadequate visibility to safe stopping along fast lanes. Along mountainous terrain it is almost inevitable to use tight horizontal curves (R). Obviously, the term ‘tight’ is relevant. By that term we mean any radius used corresponding to the design speed (V_e) or ($V_e + 10$) km/h of the motorway. Thus for class A roads and $V_e = 100$ km/h, any curve with $R < 600$ m is considered as tight.

The motorway visibility problem can be outlined (Kokkalis, 2011) by the typical horizontal layout geometry of the problem (Fig. 1). The various assumptions related to distances, widths and positions are presented there. Considering a typical left hard shoulder width of 0.975 m, the vision line and the typical profile of a NJ barrier it is calculated that a typical value for ‘a’ equals to 1.15 m. Thus, the distance of the eye to the NJ side wall equals to:

$$a+b = 1,15+1,75 = 2,9m \quad (1)$$

Resolving the problem (for $R = 600$ m), we have that the critical sight distance equals to:

$$Ssd=2\sqrt{[(600+2.9)^2-600^2]}=118m \quad (2)$$

In any place along a road-lane, the available sight distance should be at least the required total stopping distance (ssd). Ssd depends on vehicle velocity, usually V_{85} , road gradient and friction values between

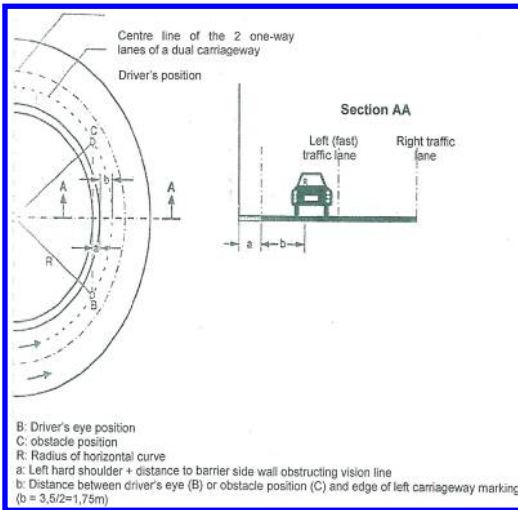


Figure 1. Geometric model to calculate critical visibility length (BC line) along left turns in dual carriageways.

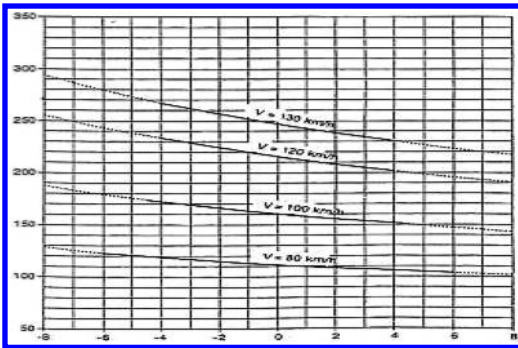


Figure 2. Required visibility length for safe stopping S_h or ssd, (OMOE, 2002).

the tyre end the pavement. Obviously, at downgrades more distance is required for a vehicle to stop safely, since gravity adds to vehicle inertia. In mountainous terrain, it is most probable that the maximum acceptable values for road gradient will be commonly used. For $V_e = 100 \text{ km/h}$, this maximum acceptable gradient equals to $s = 6\%$. This downgrade slope adds considerably to the required ssd. Figure 2 (OMOE, 2002) outlines the required visibility lengths for safe stopping. According to that and for a downgrade $s = 6\%$ ssd amounts to 240 m. This is twice as much as the available 118 m calculated in (2).

Hence, the problem of insufficient visibility to obstacles along motorway fast lanes is keen. Even in flat road sections, along tight left horizontal curves the ssd amounts to 215 m (Fig. 2), far greater than the available.

The geometric key to resolve the problem is to increase $(a+b)$ distance (Fig. 1). This requires the bothersome and safely ambiguous shift of the NJ barrier to the inside of the circular curve.

To resolve the problem in the most adverse (but not infrequent) combination of data ($R = 480 \text{ m}$ for $V_e = 100 \text{ km/h}$ & $s = 6\%$), we have:

$$240/2 = \sqrt{[480 + (a+b)]^2 - 480^2} \rightarrow (a+b) = 14,8 \text{ m} \quad (3)$$

which means many meters shift of the NJ barrier to the inside of the curve.

2 WAYS TO TACKLE THE MOTORWAY VISIBILITY ISSUE

2.1 Shifting the central motorway barrier

As mentioned, adequate visibility could be obtained if the NJ barrier would be shifted to the inside of the curve. Considering eq. (1), this means that a $14,8 - 2,9 = 12 \text{ m}$ shift is required (Fig. 1). In similar visibility problems at the slow lanes of a mountainous road, (along right tight curves in cuts), it is common practice to extend earthworks and level the slopes for unobstructed sight line. This action results to correspondingly wider construction limits and, usually, considerably deeper cuts and greater amount of earthworks, all acceptable to achieve safe drive. Apart from the above, considering to apply that widening along a motorway central reserve exhibits certain design difficulties: the additional pavement width should be kept without trafficking, usually through zebra delineation or banking, a practice which may induce unsafe driving practices. Actually, along Egnatia motorway this practice has been applied in only one case with controversial results. Hence, tackling the problem by shifting the NJ barrier to the inside part of the turn is not a good practice.

2.2 Adopting relaxations plus signage

The simplest way Road Design Guidelines in various countries, tackle the problem is to consider the required visibility for V_e , instead of, for V_{85} . For the data of the problem outlined above, this assumption decreases the required visibility length from 240 m to 180 m. A 5.4 m shift to the inside of the turn is still required for the NJ barrier. The problem is seriously alleviated but not resolved.

Cypriot road geometric design standards (2002), tackle the problem by adopting further relaxations. According to them, a relaxation may be adopted where the strict application of design standards would lead to disproportionately high costs. A relaxation means the adoption of design figures for certain design parameters referring to a one or more steps lower V_e . It should be mentioned herein, that the steps for V_e are not the typical 10 km/h, but the consecutive values V_e takes are: 120, 100, 85, 70, 60 and 50 km/h. The relaxation for the required minimum stopping sight distance to the typical 0.26 m object height may be extended to two V_e steps, on the condition that the required (for V_e) sight distance above the safety

Table 1. Vision deficit to low objects along tight left downgrade fast lane motorway curves for V_{85} .

V_e (km/h)	Min. R (m)	Max. Down-grade (%)	Available vision (m)	$V_{85} =$ $V_e + 20$ or 30 (km/h)	Ssd/ Ssd (m)	Ssd/ Available vision
80	280	7	81	110	210	2.6
90	370	7	93	120	250	2.7
100	480	6	106	120	240	2.3
110	600	5	118	130	270	2.3

barrier to the 1.05 m object height (representing the stop lights of the front vehicle) is available. This means that for a $V_e = 100$ km/h, ssd to low obstacles should be provided for 70 km/h, instead for the strictly required V_{85} speed of ~ 120 km/h. According to Table 3.5 of the Cypriot road geometric design standards (2002), the 'two step below desirable minimum' stopping sight distance is, for $V_e = 100$ km/h, only 120 m. This is actually the value which the horizontal layout of the problem (Fig. 1, eq. (2)) provides. It seems that the Cypriot Standards resolve the problem and no further action is required. Actually, after a parametric study of the problem, it has been concluded that the Cypriot Standards resolve the problem in its generalized form: the typical horizontal layout of the visibility problem at left curves (Fig. 1) with the minimum required R for a specific V_e , always provide the required visibility to stop ahead of a low obstacle for a two-step, 30 km/h, V_e -relaxation, on the assumption that the downgrade slope is not too near to the highest permissible. Hence adopting convenient relaxations is a convenient way to radically resolve the issue. Obviously relevant speed limit signage is necessary. The relaxation-adoption route may have a sound fiscal documentation but, undoubtedly, leaves serious engineering issues half-answered.

2.3 The insurmountable friction deficit

Generally, sufficient pavement skid resistance should be regarded as one of the most important safety practice when considering motorway safety. The necessary sight distance for safe stopping would be radically reduced if the values of pavement friction would be high. Highway Guidelines (OMOE, 2002), require adequate visibility for safe stopping to be provided for V_{85} . For normal friction values, the Guidelines adopt the key parameters which are outlined in Table 1. It should be commented that the adopted friction values are conservative, to make up for these cases where old tyres run on polished wet pavements. The adoption of an adverse combination of parameters is normal practice in engineering safety issues.

In Table 1 the visibility deficit problem is presented for $V_e = 80, 90, 100$ and 110 km/h, the typical design speed range for motorways in mountainous terrain. The minimum horizontal radius as well as the maximum permitted gradient has been considered. Vision lines have been calculated according to equation (2).

Stopping sight distances (ssd), have been taken from Figure 2. The appropriate operation speed is for V_{85} . According to the Highway Guidelines (OMOE, 2002), for motorways there is a rough relationship between V_e and V_{85} :

$$\begin{aligned} V_{85} &= (V_e + 30)\text{km/h, when } V_e < 100\text{km/h and} \\ V_{85} &= (V_e + 20)\text{km/h, when } V_e \geq 100\text{km/h} \end{aligned} \quad (4)$$

From Table 1 it appears that for V_{85} the required vision length to a low obstacle is, for all cases, more than two times the available ones. Even if considering V_{70} , (approximately equal to $(V_e + 10)$, Kokkalis *et al.*, 2011) the ratio ssd/available vision line had values around 1.8 (Kokkalis, 2011). The question arises, what would be the target pavement friction values which would reduce safe stopping to the available vision line?

The mathematics behind the calculated ssd values need to be outlined. Relevant curves have been derived connecting tangential friction factors (f) with speeds (Kokkalis & Panagouli, 1998). The shape of all these curves is similar. Data correlations result in a similar polynomial equation of the type:

$$f = \text{constant term} - a_1(V) + a_2(V^2) \quad (5)$$

where a_1 is approximately $\sim 3a_2$

Because there is a great variety of data (tyres, pavement surfaces and conditions) and highway engineers have to cater and provide adequate safety for adverse conditions, the (lowest pavement friction) 85th to 95th percentile distribution curves are adopted. Thus, the actual friction values are higher along the 85% to 95% of the total number of road sections. According to Lamn *et al.* (1999), a new evaluation data background (for Germany), yields for skid resistance the equation:

$$f = 0,708 - 0,721(V/100) + 0,241(V/100)^2 \quad (6)$$

where the variable V (speed) is given in km/h.

Also, based on multi-nation data an overall regression equation has been developed (Lamn *et al.*, 1999):

$$f = 0,59 - 0,485(V_e/100) + 0,151(V_e/100)^2 \quad (7)$$

The coefficient of determination (R^2) of the equation equals to 0.731 and the standard error of estimate to 0.044.

The standard method used to measure skid resistance is a test vehicle driven with constant speed. An additional ‘measurement wheel’ is carried which is braked on wet pavement conditions and the force is measured in relation to the weight. SCRIM vehicle, the Stuttgarter tribometer (SRM) and the Swedish skidometer are typical equipment used. The equation (6) has been derived on measurements taken by SRM.

The friction quality of Greek pavements is, as expected, considerably poorer. It is estimated that approximately 20% of wet pavements in Greece could be covered by using the overall regression equation (7). Actually, pavements in national or provincial roads in Greece are very slippery. This is due to the fact that limestone aggregates are used and resurfacing works rarely take place. However, if we restrict only to motorway pavements, where anti-skid surfacing is the rule, a similar equation may not come short. Furthermore, the same fact that we restrict only to motorway pavements, where higher quality control standards apply, would result in a tighter percentile distribution curve, which may permit the use of a shifted equation yielding slightly higher friction values: higher constant term due to harsh micro-texture and even a slightly gentler reduction of f-values with speed, due to maintained macro-texture. Also, the good drainage conditions, usually established on motorway pavements, ensures that rainfall water is promptly run off the pavement surface, thus the water film is not thick enough to cause a sharp drop in friction with higher vehicle speeds, permits a polynomial curve of milder slope (like the one measured in USA pavements (Lamm *et al.*, 1999), to be adopted.

In this effort the mathematics involved are outlined below (Kokkalis, 2011).

Ssd comprises of two terms, the reaction distance (S_1) and the braking distance (S_2). Following the basic equation from physics, we have:

$$S_1 = Vt_r / 3.6 \quad (8)$$

$$S_2 = \int_0^v V / f(V) + (s / 100) + (D / M) dV \quad (9)$$

where, t_r is driver perception-reaction time, $f(V)$ is equation (7), s is grade (%), (+ for upgrade and – for downgrade), D is vehicle aerodynamic drag force and M is vehicle mass in kg.

Equations (8) & (9) have been applied to the lines of Table 1. The following assumptions have been made:

- The shape of the polynomial equation (5) remains the same,
- The polynomial equation may have a higher constant term (friction for almost zero speed),
- The operational speed used is V_{85} ,
- Overtaking is a maneuver requiring higher driver alert (even in motorways) than the average design value of 2 seconds for perception-reaction time (for category A roads) considered in equation (7).

Perception and reaction time is taken to 1.5 sec, still conservative for an overtaking maneuver.

By equating the available vision line to the required ssd, the unknown was set the constant of equation (7). The result is that the constant term should take values as high as 1 to fulfill equality.

How realistic could be to accept such high initial friction values, to secure that the available vision line to low obstacles without any barrier shift to the internal of the curve is adequate for safe stopping? The highest values for the constant term of the regression equations (6), (7) are around 0,8 and they refer only to circuit pavements. Hence, it seems that this route, to tackle the insufficient visibility along tight downgrade left motorway curves by providing very high friction pavements along the fast lanes has not even a theoretical resolution.

2.4 Considering friction values in dry and wet pavement conditions plus signage

It is known that most dry pavements provide adequate skid resistance but in wet pavements conditions skid resistance values drop considerably: the water film should be expelled to permit tyre-pavement adhesion to develop. As mentioned, the higher the vehicle speed, the less time is available for that contact to be made. Thus, available friction drops with speed. The German road design standards (RAA, 2008) actually follows a similar approach, justified on available tyre-pavement friction values on dry and wet surfaces. On the condition that the required sight distance above the safety barrier to the 1.05 m object height is available, appropriate vertical signage is recommended, so that drivers reduce vehicle speed only under wet pavement conditions, when the available friction is lower. The height of the central reserve barrier should be at most 0,90 m and no planting or anti-glaring fences are recommended along tight left turns, because they obstruct vision lines. Thus, ahead of a tight left turn a composite speed limit sign is recommended, permitting V_{85} speed at dry pavement condition, for example 120 km/h, and restricting the permissible speed to 80 or even 70 km/h at wet pavement conditions. A depiction of this sign (Fig. 3) is presented at page 3/14 of the Appendix III at the Volume 6 (on motorway vertical signage), (OMOE, 2002).

2.5 Evaluating signage alternatives

Considering that only via appropriate signage the keen visibility deficit issue along motorway fast lane tight left downgrade curves can be resolved, the question arises, which is the appropriate sign to effectively and judiciously warn drivers?

Posting the relevant K-12 sign (Fig. 4), in combination with a speed limit sign is out of the question for motorways, because, as a rule, they do have anti-skid pavements.

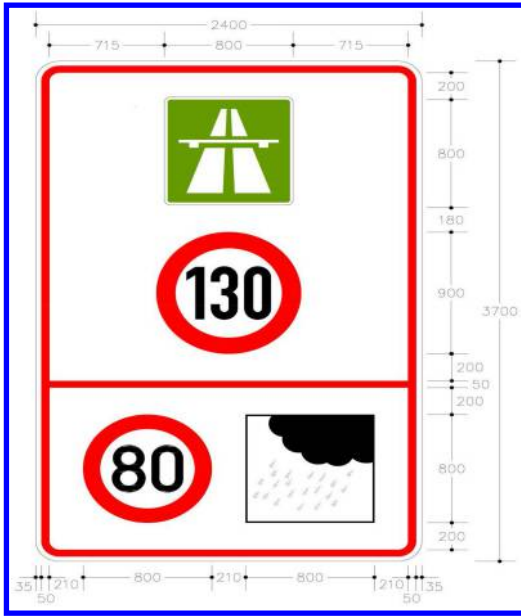


Figure 3. A motorway sign prompting drivers to radically reduce their speed in wet pavement conditions.



Figure 4. K-12 sign declaring slippery road.

Figure 3 sign is efficient and almost impressive but also implies that a defect exists at the motorway when raining. On the other hand, a simple P-32 speed limit (Fig. 5) is insufficient. Drivers generally ignore speed limits considering them as arbitrary and extra-conservative.

The Π-67 Greek Highway Code sign may be an appropriate solution, if it declares lower speed for the fast lane. However, is it proper to reversely differentiate speed limits and impose lower speed to the fast lane (i.e. 80 km/h for the fast lane and 100 km/h for the slow lane)? This is contrary to Highway Code principles. Many drivers may think that an abnormal sign like this is an error, though some others may be impressed and become suspicious and watchful.

In Figure 6 a different approach is outlined. The K-25 sign is preferred, which warns for hazards other than all the previous K-1 to K-24 Highway Code signs highlight (among which is the Fig. 4, K-12 sign). This is true because it is actually the visibility problem and not the slippery pavement problem which urges for reduced speed. On the same pole a P-30 no overtaking sign should exist. Drivers along mountainous

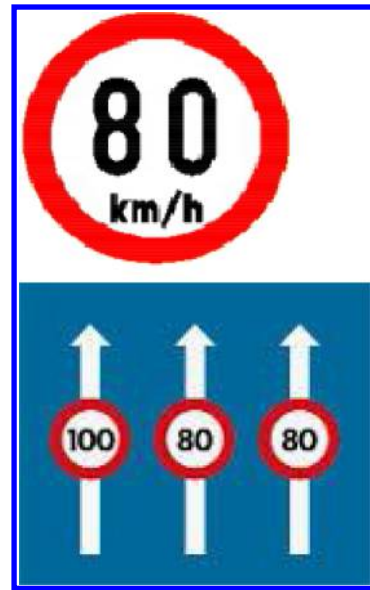


Figure 5. A P-32 speed limit sign and a Π-67 typical lane speed limit sign.

motorways are familiar with P-30 sign (actually with the similar P-31 sign), which is typically valid inside tunnels. Both these signs do not declare any infrastructure fault, but the suspension of the usual overtaking manoeuvre along that motorways subsection due to temporary safety issues. Below the pole with both K-25 and P-30 signs, it is recommended to exist a tag declaring the length of the motorway along which the overtaking prohibition is valid. This length refers only to the central section of the tight horizontal curve along which the visibility is insufficient and is normally in the order of only a few hundred meters and will make the warning more acceptable. Generally, in motorways, the fast lanes are used either when traffic volumes are high or during an overtaking manoeuvre. In high traffic volumes speeds are low and no visibility deficit to low height objects arises. In the second case, if an accident occurs during the overtaking manoeuvre, due to the existence of an obstacle on the fast lane, liability issues are clearer, it is the driver who violated the traffic sign to be blamed for, without any cumbersome and dubious procedure, i.e. to find out the operating speed of the vehicle.

3 DISCUSSION AND CONCLUSIONS

Safety barriers along tight left horizontal downgrade curves usually obscure visibility to stopping sight distance to the typical low object, although the appropriate sight distance to the stop lights of leading vehicles is maintained above the barrier. Considerable shift of the barrier to the inside of the curve is a drastic, but a non-preferred action involving serious



Figure 6. K-25 and P-30 signs.

implications. The adoption of relaxations and appropriate speed limit signage, which drastically restricts speeds in wet pavement conditions, are controversial practices.

From Table 1 it appears that for V_{85} , for the maximum permitted downgrades, the available vision length to a low obstacle is less than half the required for safe stopping. Friction need to take unrealistically high initial values (around 1) to achieve stopping ahead of a low obstacle. Although sufficient friction supply should be regarded as the most important safety practice when considering motorway safety, such high friction values is practically impossible to be achieved.

The German Guidelines (RAA, 2008) proposes (Fig. 3) a markedly reduced speed in wet pavement conditions. In this paper the sign combination of Figure 6 is considered as the right proposal to overcome motorway fast lanes visibility problems: the K-25 sign of the Highway Code warns for other than the known hazards, together with a P-30 no overtaking sign. Actually, to exist a hazardous obstacle along motorways fast

lanes is a rare and specific event, which is covered by K-25 sign. As far as P-30 sign is concerned, on the one hand it directly averts moving along the fast lane and, on the other hand, drivers moving along mountainous motorways are familiar with it. This combination of signs does not imply any pavement defect but only suspends the overtaking manoeuvre for a few hundred meters along tight downgrade left curves.

REFERENCES

- Kokkalis A., Anti-skid pavements to secure safe stopping before obstacles on motorway fast lanes along tight horizontal curves, *5th Int. Conf. Bituminous mixtures and Pavements*, Thessaloniki, Greece, 1–3 June 2011.
- Kokkalis A., G. Mintsis, C. Taxiltaris, S. Basbas and J. Dimitropoulos, Conclusions drawn by operational velocities measurements and speed limits enforcement in motorways, *Proceedings of the 3rd Pan-Hellenic Highways Conference*, to be held in Patra, Greece, November 2011.
- Kokkalis A., Prediction of skid resistance from texture measurements, *Proc. Institution of Civil Engineers, journal of Transport*, No. 129, May 1998, pp. 85–93.
- Kokkalis A. and O. Panagouli, Fractal evaluation of pavement skid resistance variations I & II: surface wear and surface wetting?, *Journal of Chaos, Solitons & Fractals*, Elsevier Science Ltd., Vol. 9, No. 11, 1998, pp. 1875–1899.
- Lamn R., B. Psarianos and T. Mailaender, Highway Design and Traffic Engineering Handbook, *McGraw-Hill*, New York, ISBN 10 0070382956, 1999.
- OMOE, Ministry of Public Works, *Guidelines for the Design of Roadworks*, (Greek acronym: OMOE), 7 Volumes, Greece, 2002.
- RAA, German Road and Transportation Research Association, *Richtlinien für die Anlage von Autobahn, R1 RAA*, ISBN 978-3-939715-51-1, 2008.

Brighter and better all-weather road markings in Malaysia

Mohd Hizam Harun & Nur Syaza Mohamad Noh

Public Works Department, Malaysia

Wan Radhiah Wan Hanafi

Roadcare (M) Sdn. Bhd.

ABSTRACT: Road markings are essential in providing delineation to the road users. They should be visible especially under poor lighting. The most critical time is at night when it rains. Malaysia have started using all-weather thermoplastic as road marking materials since 2010 which incorporate special reflective elements which are capable in giving relatively high retro-reflection even though when they are submerged in thin film of water. However, it was observed that the brightness of this more costly road marking material at some locations does not last long. So, what could have gone wrong? This paper highlights some good and bad practices in laying the road markings which result in satisfactory and poor performances respectively. Correlations between the brightness and durability of the road markings with the various procedures of heating and laying the thermoplastic powder, different qualities of the powder, inter-mix and drop-on reflective elements, different techniques in incorporating drop-on reflective elements, variation in the heating and laying temperatures, and the conditions of the road surface during laying, are discussed. These findings will be used to improve the standard specification for brighter and longer lasting road markings.

1 INTRODUCTION

Thermoplastic road markings will appear bright and glowing after installation. The ability to reflect light from vehicles' headlamps at night could help motorists to see the road markings clearly, and thus feel safe and comfortable. However, when it rains, conventional glass beads could not reflect light effectively when submerged in thin film of water on the road surface, resulting in the road markings appear dull and difficult to see. Consequently, all-weather thermoplastic (AWT) road markings have been introduced and included in the new specification of Public Works Department (PWD) Standard Specification for Road Works JKR/SPJ/2012 Section 6: Road Furniture, Sub-Section 6.3: Road Markings (2012), hereinafter referred to as SPJ. Malaysia is the first country in Southeast Asia that uses the AWT road markings, its inception in October 2010. Befitting the tag 'all-weather', the road markings could be clearly visible in all weather conditions, especially at night and when it rains. Fish (1996) defines all-weather road markings as markings that are visible at night under dry conditions and also under rainy conditions up to 0.25 inches per hour of rainfall.

However, there are complaints that the AWT road markings are not able to last long. This would cause discontent among the road authorities as the price of AWT road markings is three times more expensive than the ordinary thermoplastic road lines. So what could have gone wrong?



Figure 1. All-weather thermoplastic road markings.

2 AWT ROAD MARKINGS

AWT road markings comprise of high performance thermoplastic powder, inter-mix reflective beads and drop-on beads. The performance of the AWT road markings depends on three parameters, namely.

1. Materials.
2. Applicator machines.
3. Workers.

2.1 Materials

2.1.1 Material specifications

As specified in clause 6.3.2 of the SPJ, thermoplastic materials (i.e. the white or yellow powder) shall comply with BS EN 1871 (2000). High performance thermoplastic powder which complies with BS EN 1871 and certified by recognised agencies should always be used; materials of inferior quality will not hold the drop-on beads firmly even though the beads are properly embedded during application. If the white thermoplastic powder change its colour to grayish or yellowish if overheated, that is a clear indication of inferior quality thermoplastic material that should be immediately rejected from sites. Substantial different in cost (~35%) between the superior (RM2,700/ton) and inferior (RM2,000/ton) product may encourage the contractor to use the cheaper product if enforcement is lacking. Materials without certification should not be accepted.

2.1.2 Reflective beads

The thermoplastic material should contain inter-mix reflective beads, and these beads should comply with BS EN 1424 (1998). In addition, during application on to the road surface, drop-on reflective beads are dropped (usually by gravity) shortly after the heated thermoplastic material is spread, and these beads should comply with BS EN 1423 (1998). Both BS EN 1424 and 1423 refer to glass beads, with a minimum value of refractive index (ability to refract light in water) of 1.5.

Other types of reflective material such as micro-crystalline ceramic beads have higher refractive index of 2.4. The ability of ceramic beads to reflect light towards the source of the light (i.e. retro-reflection). In the context of road lines, it is the ability of the beads to reflect light towards vehicles' driver) is said to be similar to diamonds. For normal glass beads, the refractive index is relative low (usually about 1.5), but there are high performance glass beads with refractive index of 1.9. Beads of inferior quality will not be able to reflect light towards the vehicles' drivers, or reflect the light towards many other directions (diffuse reflection). During the day and when it does not rain, normal glass beads are sufficient, but at night or when it gets dark, especially when it rains, the superiority of ceramic beads will be more pronounced. Ceramic beads are said to be seven times brighter than glass beads.

The quantity of inter-mix beads is not specified in the SPJ. It is recommended that it should be not less than 10% by weight of the thermoplastic powder with at least 3% ceramic beads. For drop-on beads, the quantity is specified of not less than 400 g/m². However, the proportion of each type of beads is not specified. It is recommended that the drop-on beads should contain at least 30% of micro-crystalline ceramic beads (refractive index >2.4) with the remaining composition consists of 70% high performance glass beads (refractive index >1.9).



Figure 2. Glass beads.

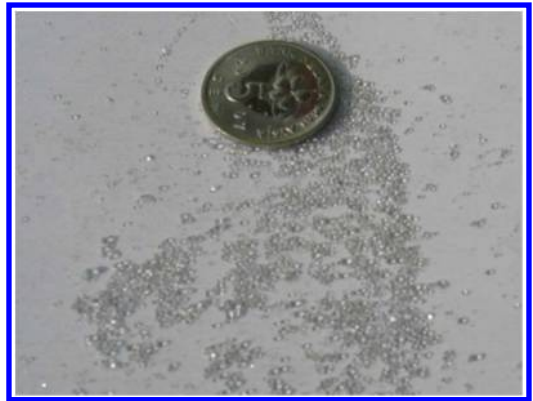


Figure 3. Micro-crystalline ceramic beads.



Figure 4. Comparison of size between glass beads and micro-crystalline ceramic beads.

2.1.3 Performance specifications

SPJ clause 6.3.2 stipulates that the performance of the thermoplastic road line material shall comply with BS

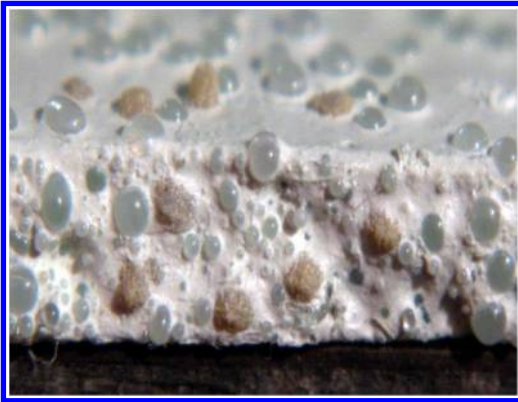


Figure 5. Inter-mix micro-crystalline ceramic beads and glass beads inside road markings.

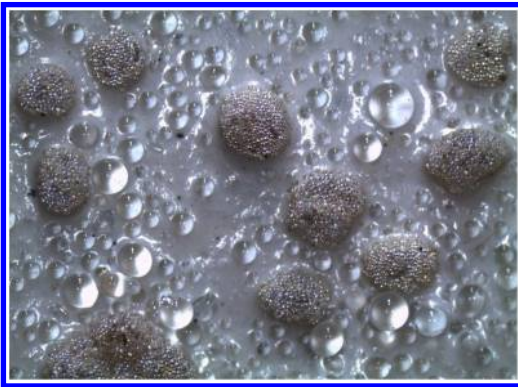


Figure 6. Drop-on micro-crystalline ceramic beads and glass beads on road markings.

EN 1436 (2007). Among other things, the BS EN 1436 specifies:

1. Luminance factor β in dry condition not less than 0.60.
2. Luminance coefficient under diffuse illumination Q_d not less than 160 $\text{mcd/m}^2/\text{lux}$.
(Note: If the luminance factor β can be achieved, Q_d does not need to be evaluated, and vice versa).
3. Coefficient of retro-reflected luminance R_L in dry condition (ASTM-E1710) not less than 300 $\text{mcd/m}^2/\text{lux}$.
4. Coefficient of retro-reflected luminance R_L in wet condition (ASTM, E2177-11) not less than 75 $\text{mcd/m}^2/\text{lux}$.

(Note: Q_d measures the brightness of the road markings in day light illumination and street light, while R_L measures retro-reflection when lighted by vehicles' headlamp.

The SPJ specifies that the R_L shall be not less than 300 $\text{mcd/m}^2/\text{lux}$ (dry condition) and not less than 75 $\text{mcd/m}^2/\text{lux}$ (wet condition) within 7 days after



Figure 7. Retro-reflectometer.

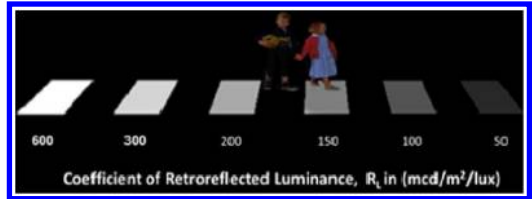


Figure 8. Coefficient of retro-reflected luminance.

the road markings are laid. However, after acquiring more knowledge on good and bad practices in laying road lines, the Superintendent Officer is encouraged to request the contractor to carry out the testing on the 6th or 7th day to allow any loose drop-on beads, if there is any, to detach prior to testing. Consequently, the requirement on the R_L will be reviewed and changed accordingly. It has been suggested that the requirement for the test to be carried out 'within 7 days' be changed to 'within 10–20 days' while the minimum value of R_L remain unchanged.

In the opinion of the European Union Road Federation, ERF (2013), a good road markings are those with performance level under dry conditions not less than 150 $\text{mcd/m}^2/\text{lux}$, whereas for wet conditions, the minimum performance level should be 35 $\text{mcd/m}^2/\text{lux}$. Apart from this, Fish (1996) stated that most research has come to a conclusion that a minimum acceptable level of retro-reflectivity is around 100 to 120 $\text{mcd/m}^2/\text{lux}$.

Asdrubali et al (2013) observed that while the only performance parameter considered was R_L , at urban level the reflection in daylight condition Q_d is equally (or more) important.

2.2 Applicator machines

2.2.1 Drop facility for beads

If a mixture of glass beads and micro-crystalline ceramic beads is used as a drop-on reflective element, the applicator machine should be equipped with a double-drop facility with two units of dispenser. The larger ceramic beads (typically 1.1–1.3 mm) should be



Figure 9. Applicator machine with double-drop facility.



Figure 11. Embedment of drop-on beads.



Figure 10. Applicator machine with single-drop facility.



Figure 12. The optimum thickness is 2.0–2.5 mm.

dropped first, followed by the smaller glass beads (usually 0.7–0.8 mm). If the smaller glass beads fall first, it would impede the larger ceramic beads from filling up the space in between the smaller beads, and this can lead to the larger beads from being easily detached from the road markings by the passing traffic. Similarly, the larger ceramic beads would be loosely embedded into the road markings if both types of bead drop simultaneously from a single-drop facility with one unit of dispenser.

2.2.2 Height of spreader shoe

The height of the spreader shoe above the road surface should not be too high. It is recommended that the height should be 40–50 mm. If it is higher, there is a possibility that up to 10% of the drop-on beads will be blown away before they reach the road markings by the wind or passing traffics. It should not be too close because the drop-on beads will not satisfactorily embed into the road markings. The target is to get the beads embedded into the road markings layer by about 50–60%.

A study elsewhere has shown that high retro-reflectivity could be achieved if the degree of sinking

of glass beads is between 55 and 60 % of their diameter. A sinking degree less than 50% weakens their resistance to tyres, while a sinking degree higher than 60% limits the retro-reflection properties (ERF, 2013).

2.2.3 Speed of application

The applicator machine should not be pushed too fast as some of the relatively light glass beads or ceramic beads will be blown by the wind.

2.3 Workers

2.3.1 Laying thickness

The optimum thickness of the overlaid thermoplastic powder is typically 2.0–2.5 mm. If thinner, the drop-on beads would not stick firmly to the road markings. If thicker, most of the drop-on beads would sink into the road markings.

2.3.2 Road surface condition

Prior to the application of the road markings, the surface of the road should be clean and dry. Surface which is dirty, sandy and wet would cause the road markings to easily peel off.



Figure 13. The mixing temperature should be as recommended by the material's supplier.

After rain, it is advisable to wait for at least 12 hours for the moisture on the road surface to dry. The formation of small holes (pinholes) on the road markings indicates that the road surface has not adequately dried when the road markings are installed. It is also recommended that road markings are installed not less than 72 hours after paving works to let the bitumen sufficiently harden.

2.3.3 Overheating

If the thermoplastic material is inadvertently overheated above the recommended mixing temperature, the viscosity during application, and thus the embedment of the drop-on beads, will be affected even though the material is allowed to cool down.

2.3.4 Mixing and laying temperatures

The mixing temperature of the thermoplastic material should be as recommended by the supplier. Usually the temperature is 200–220°C. However, if the road markings are installed in the evening when the temperature is a bit cooler, or in cooler highlands, the mixing temperature should be increased up to 230–240°C. Laying temperature (the temperature of the thermoplastic material as it flows out from the spreader shoe) should be similar to the mixing temperature. If applied at cooler temperatures, the drop-on beads would not stick firmly while if the temperature is higher, the drop-on beads would sink. While the R_L could be achieved when the test is carried out within seven days, the loosely attached drop-on beads would eventually detach from the road markings by passing traffics. In contrast, the R_L could not be achieved when a lot of drop-on beads sink into the road markings if the laying temperature is too hot. The applicator team should be equipped with hand-held contactless thermometers to rapidly check the temperatures.

3 FUTURE WORKS

The rate of degradation of the road markings varies with traffic intensity. However, this is still unknown.

Consequently, the SPJ presently only specify the initial minimum coefficient of retro-reflected luminance R_L of 300 and 75 mcd/m²/lux, in dry and wet conditions respectively, which are to be achieved within seven days after laying the road markings. The performance of the AWT road markings, which will be installed transversely to expedite the degradation, will be periodically monitored before the requirements of R_L after, say, six and/or 12 months are incorporated into the SPJ.

4 CONCLUSION

For countries like Malaysia, being located in the region with tropical climate and experiencing frequent heavy rainfall, it is envisaged that it is imperative to have all-weather thermoplastic road markings for the safety and comfort of the road users. Some good practices which are based on experience have been highlighted which need to be adhered to in order to consistently produce high quality road markings. Nonetheless, further studies need to be carried out to ensure that the road markings are not only visible at all times, but also durable.

REFERENCES

- Asdrubali Francesco, Cinzia Buratti, Elisa Moretti, Francesco D' Alessandro and Samuele Schiavoni. Assessment of the performance of road markings in urban areas: The outcomes of the CIVITAS RENAISSANCE Project. CIRIAF, Interuniversity Centre of Research on Pollution by Physical Agent, University of Perugia, Italy. The Open Transportation Journal, 2013.
- ASTM International. Standard test method for measurement of retro-reflective pavement marking materials with CEN-prescribed geometry using a portable retro-reflectometer. E1710 – 11.
- ASTM International. Standard test method for measuring the coefficient of retro-reflected luminance of pavement markings in a standard condition of wetness. E2177 – 11.
- British Standards Institution. Road marking materials – Physical properties. BS EN 1871: 2000.
- British Standards Institution. Road marking materials – Premix glass beads. BS EN 1424: 1998.
- British Standards Institution. Road marking materials – Drop on materials – glass beads, antiskid aggregates and mixtures of the two. BS EN 1423: 1998.
- British Standards Institution. Road marking materials – Road marking performance for road users. BS EN 1436: 2007 +A1: 2008.
- European Union Road Federation. Marking the way towards a safer future. An ERF position paper on how road markings can make our road safer.
- Fish, Joseph K. Evaluation of all-weather pavement markings: Report on two years of progress. Semisequicentennial Transportation Conference Proceedings, Iowa State University, Ames, Iowa. May 1996.
- Public Works Department, Malaysia. Standard specification for road works, Section 6: Road furniture – Sub-section 6.3: Road markings. JKR/SPJ/2012-S6.

Safety audit using operating speeds V_{85} at rural road in Northern Greece

G. Mintsis, S. Basbas, C. Taxiltaris, N. Domoktsis & K. Labropoulou

Faculty of Rural & Surveying Engineering, Aristotle University of Thessaloniki, Thessaloniki, Greece

ABSTRACT: Before the introduction of the new Guidelines for the Design of the Road Network (National Road Design Standards) in the early 2010, road design in Greece was lacking of a clear methodology to secure continuity in driving performance. This paper describes the research carried out in order to study the safety level provided by older designs. For that, the Safety Criteria introduced by the new Guidelines were tested in road sections of the rural network of Northern Greece.

1 INTRODUCTION

For more than forty (40) years road design in Greece was guided by principles and rules set in the beginning of 1960 decade adopted in the National Road Design Standards. One of the most important principles of that Manual was the distinction between tangents as curves as far as the operational role of an alignment element is concern. The dynamic element of vehicle-driver system was taken into account only when curves were to be examined. Tangents were considered simply as the connecting links between curves. This led to alignments that in many cases forced drivers to develop driving profiles characterized from sudden changes in speed therefore highly demanding of continuing attention and concentration. The new Greek Design Standards (OMOE), that were recently introduced, introduced the principle of harmony and continuity in driving profile by recognizing tangents as being alignment elements that affect and in a way when combined harmonically with curves do not create a highly demanding environment in terms of ability and continuously paid attention.

The principle of harmonic design is implemented of a set of rules that concern geometry and operation most important of which are the safety criteria I, II and III.

However the majority of road link in Greece have been designed and built before the introduction of the new Design Standards (OMOE) and obviously do not offer the driving environment envisaged by OMOE.

This paper tries to answer a question raised many times as to what extent order designs and constructions fulfill the operation and safety requirements set by the new Standards (OMOE) and whether the implementation of the Safety Criteria exercise could assist authorities in defining road alignment elements that need to change in geometry and so combined together with other existing road elements to create

an infrastructure that secures safe and comfortable driving.

Three (3) road sections of different category of the rural primary and secondary road network of the Prefecture of Serres in Northern Greece were used to be examined under the above presented concept.

2 STUDY AREA

Prefecture of Serres was defined as the study area and specific road sections of the primary and the secondary rural road network were selected for the collection of the data required. For the final selection of the road sections surveyed the existing data base of EGNATIA ODOS S.A. was used that was created from data collected from different Road Safety Improvement Studies developed by this Organisation. In all 18 road sections of the rural road network were examined with lengths ranging from 2.3 km to 25.3 km. Finally, three of those roads sections were selected and studied in terms of geometry and operation. The selection methodology is described below.

3 METHODOLOGY – SELECTION OF ROAD SECTIONS

The following criteria were defined and used for the selection of the three (3) road sections of the rural network of the Prefecture of Serres.

1. The road sections had to belong to the prevailing road categories of the Prefectures road network auditing to the current National Road Design Standards (OMOE-ΛΚΟΔ).
2. To have reasonable length.
3. To show small width variations along their entire length.

Table 1. Road sections considered in the study.

Road code	Road section	Length m	Lane width m	Road group	Road category	Design speed km/h
EO*-O2	Boundaries of Prefecture of Thessaloniki – Strimonas River Old Bridge	10,210	4.00	A	AIV	80
EΠO**-10	Kala Dendra – Heraklia	20,684	3.40	A	AIII	80
EO-59	Amfipolis – Mesoraxi Junction	24,084	4.25	A	AII	90

*EO: National Road

**EΠO: Regional Road

For the application of the first criterion (a.) the 18 initially considered road sections were classified in road categories according to the road classification system introduced by the National Road Design Standards. All road sections belong to Road Group A as being sections of the rural network of the Prefecture of Serres. In addition to that and by the use of the EGNATIA ODOS S.A. data base the road sections were also classified ranked according to their operational character and an operational ranking was attributed to each sections. The combination of the above described grouping and ranking resulted to the categorization of the sections to road categories from AII to AIV.

The final three (3) road sections used in the study were selected when the other two selection criteria (band c) were also considered. Table 1 shows the specific road sections and their basic characteristics where their exacted location in the entire road network is presented in Figure 1.

Speed data collection and safely analysis were performed at specific road sub-sections that were selected out of the three study road sections selected with the use of the methodology described above. For that a detailed analysis of the geometry of the three road sections was performed that led to the identification of a series of road sub sections selected for study which also were grouped in the following four groups.

Group 1: Road sections with low gradient ($\leq 5\%$) and low bendiness (comfortable values of the horizontal curvature).

Group 2: Road sections with low gradient ($\leq 5\%$) and limited bendiness (limited horizontal curvature).

Group 3: Road sections with high gradient ($> 5\%$) and low bendiness (comfortable values of the horizontal curvature).

Group 4: Road sections with high gradient ($> 5\%$) and limited bendiness (limited horizontal curvature).

All road sections considered are aligned at a plain terrain. The classification criteria to the above four groups were quantified according to the provisions made by the Design Standards for the calculation of the operating speed (V_{85}) for signal carriageways and the definition of the limited (allowed) values of the radius of the horizontal curvature in a flat terrain for design speed of 80 km/h and 90 km/h.

In particular the grouping of the sub-sections according to bending criterion to low and limited

bendiness was performed by the use of the limited value of curve radius increased by two (2). Thus sub-sections with road curve radius smaller than 500 m for design speed (V_c) 80 km/h and 660 m for design speed (V_c) 90 km/h were grouped in groups 2 and 4. All other sub-sections were placed in groups 1 and 3.

Additional criteria for the selection of the road subsections were defined as:

- existence of reasonable length to allow valuable results,
- existence of both tangents and curves in the horizontal alignment,
- longitudinal profile with slopes of about the same magnitude.

Exception to the above third rule constitute the selected sub-sections of the road section “Amfipolis – Mesoraxi” where in one of the two finally selected sub-sections both steepness criteria ($> 5\%$ and $\leq 5\%$) have been applied.

The application of the above described methodology led to the final selection of the road sub-sections where the speed data were collected. Altogether twelve (12) sub-sections were identified and studied along the three (3) road sections. The alignment characteristics of the road sub-sections are given in the Table 2.

4 DATA COLLECTION

Site visits and inspections of the road sub-sections revealed that there were inconsistencies among the horizontal alignments provided by EGNATIA ODOS S.A. and the physical layout of the particular sub-sections. Therefore, site alignment surveys were conducted with the use of GPS device. The so collected survey data were input in the road design software ANADELTA and the required alignment element values were calculated. Superelevation measurements were made on site with the use of appropriate survey instruments.

Vehicle speed data were collected at carefully pre-decided location in each of the study road sub-sections with the use of radar speed meter. Additional care was given in order not to influence drivers' behaviour if they had seen the observer. Therefore the observer remained sitted in the vehicle that was carefully placed

Table 2. Selected road sub-sections for speed measurements.

Road section	Length m	Gradient %	Alignment m		Alignment elements		
			Low bendiness	Limited bendiness	Independent tangents	Dependent tangents	Horizontal curves
Boundaries of Prefecture of Thessaloniki – Strimonas River Old Bridge	10,210	≤5%	2,205	–	2	–	1
		≤5%	2,648	–	3	1	3
		≤5%	–	1,045	2	–	1
Kala Dendra – Heraklia	20,684	≤5%	–	1,430	1	1	2
		≤5%	–	963	1	3	4
		≤5%	,846	–	2	1	3
		≤5%	,863	–	2	1	4
		≤5%	,968	–	1	1	3
Amfipolis – Mesoraxi Junction	24,084	≤5% & > 5%	2,046	–	3	–	3
		≤5% & > 5%	1,423	–	3	–	5
		≤5%	2,695	–	2	–	1
		≤5%	1,792	–	2	–	2
		≤5%	1,792	–	2	–	2
Total	54,978		15,486	3,438	24	8	32

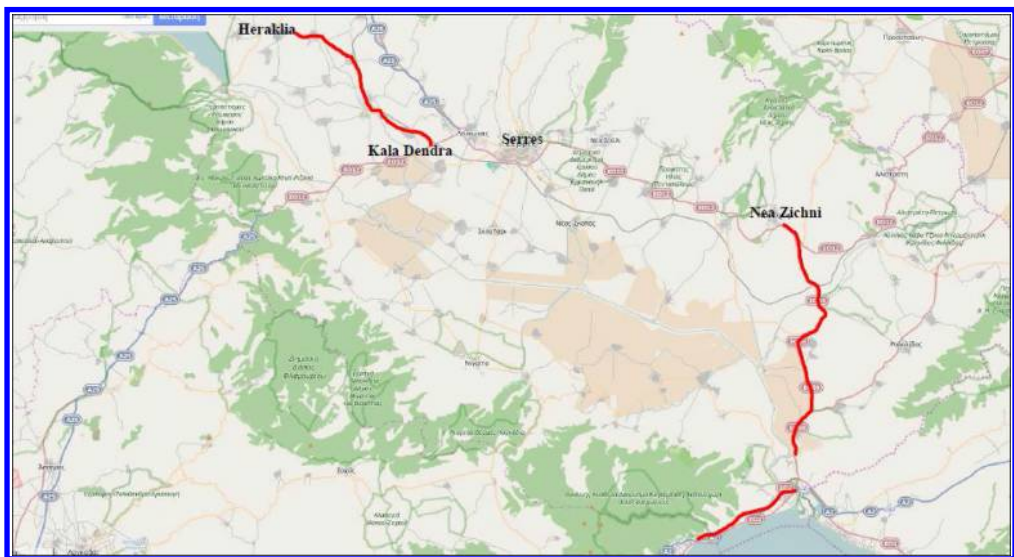


Figure 1. Selected road sub-sections for speed measurements (Source: ©Contribution by OpenStreetMap).

by the side of the road. A sampling limit of 100 vehicles per data collection period was imposed in order for the analysis to produce scientifically sound results.

5 DATA ANALYSIS – RESULTS

The aim of the analysis was tri-fold.

1. To produce values for different speed statistical parameters that allow the recognition of the speeding behaviour of drivers at the particular road sub-sections and their variations along sub-sections. Emphasis was given in the calculation of the operating speed (V_{85}) of the different elements (30 tangents and 32 curves) of the twelve (12) sub-sections.

2. To apply the three (3) distinctive safety criteria adopted in the Road Design Standards (OMOE-X).
3. To examine the existing speed limits on the basis of the adopted speed behaviour from the road users.

In all speeds were measured at 64 road elements (tangents and curves) as it is shown in Table 2. Mean speed, standard deviation and operating speed (V_{85}) were calculated for each of the 64 different elements of the road alignment.

Typical examples for the distribution of mean speed and standard deviation values are given in Figures 2 and 3 accordingly for the road section Amfipolis – Mesoraxi Junction.

Operating speed (V_{85}) values also calculated as shown in Table 3 for the different alignment elements of the same road section.

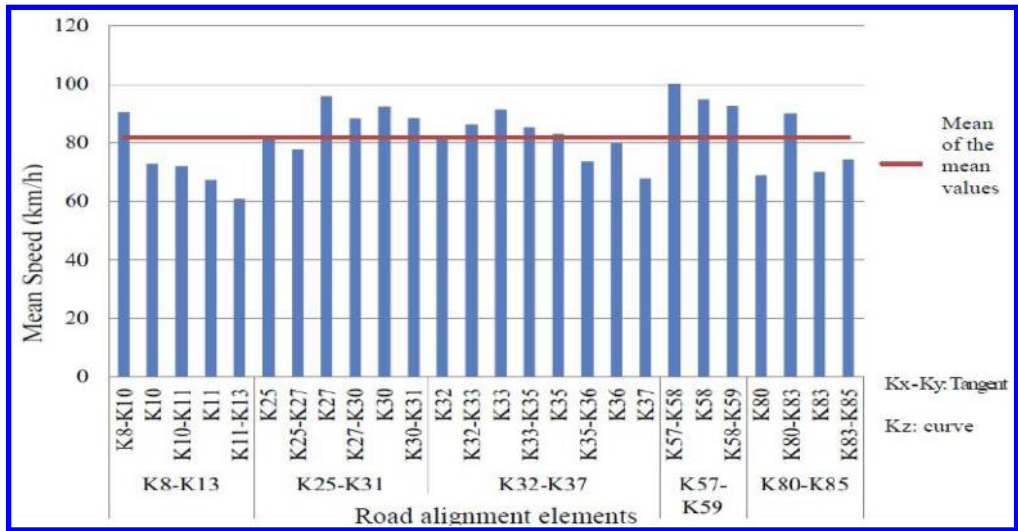


Figure 2. Distribution of mean speed values along the Amfipolis–Masoraxi Junction road section.

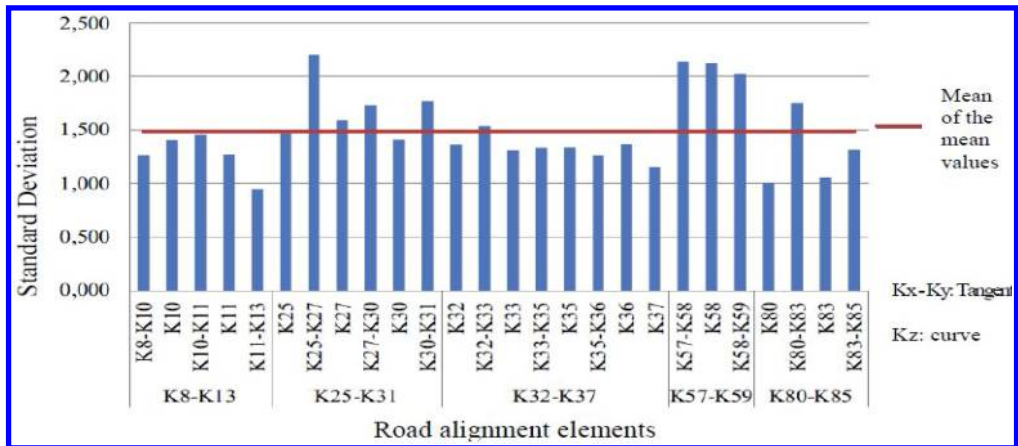


Figure 3. Distribution of standard deviation values along the Amfipolis–Masoraxi Junction road section.

Table 3. Operating speed for road alignment elements along Amfipolis–Mesoraxi Junction road section.

Amfipolis–Mesoraxi Junction									
Road alignment elements									
K8-K13		K25-K31		K32-37		K57-K59		K80-K85	
Elements*	V ₈₅ km/h	Elements*	V ₈₅ km/h	Elements*	V ₈₅ km/h	Elements*	V ₈₅ km/h	Elements*	V ₈₅ km/h
K8-K10	101	K25	96	K32	95	K57-K58	119	K80	77
K10	89	K25-K27	95	K32-K33	100	K58	113	K80-K83	105
K10-K11	87	K27	112	K33	104	K58-K59	112	K83	78
K11	80	K27-K30	103	K33-K35	99			K83-K85	87
K11-K13	69	K30	104	K35	97				
		K30-K31	106	K35-K36	86				
				K36	94				
				K37	81				

*Kx-Ky: tangent, Kz: curve

Table 4. Safety criteria values/acceptance level for the road section boundaries of the prefecture of Thessaloniki–Strimonas River Old Bridge.

Subsection	Alignment element	V_{85}	Criterion I	Acceptance level	Criterion II	Acceptance level	Criterion III	Acceptance level
K6-K10	K6-K7	106	26	not accepted				
	K7	96	16	moderate	10	good	0.01	good
	K7-K10	108	28	not accepted	12	moderate		
K16-K22	K16-K17	94	14	moderate				
	K17	85	5	good	9	good	-0.15	not accepted
	K17-K19	81	1	good	4	good		
	K19	87	7	good	6	good	0.03	moderate
	K19-K21	99	19	moderate	12	moderate		
	K21	97	17	moderate	2	good	0.01	good
	K21-K22	106	26	not accepted	9	good		
K32-K35	K32-K34	84	4	good				
	K34	60	20	moderate	24	not accepted	0.12	not accepted
	K34-K35	73	7	good	13	moderate		

Table 5. Safety criteria values/acceptance level for the road section Kala Dendra – Heraklia.

Subsection	Alignment element	V_{85}	Criterion I	Acceptance level	Criterion II	Acceptance level	Criterion III	Acceptance level
K30-K35	K30	75	5	good			0.00	good
	K30-K34	79	1	good	4	good		
	K34	69	11	moderate	10	good	-0.12	not accepted
	K34-K35	87	7	good	18	moderate		
K55-K59	K55	69	11	moderate			-0.20	not accepted
	K55-K56	78	2	good	9	good		
	K56	74	6	good	4	good	-0.16	not accepted
	K56-K57	80	0	good	6	good		
	K57	73	7	good	7	good	-0.29	not accepted
	K57-K58	78	2	good	5	good		
	K58	82	2	good	4	good	-0.12	not accepted
	K58-K59	82	2	good	0	good		
K75-K78	K75	90	10	good			-0.10	not accepted
	K75-K76	87	7	good	3	good		
	K76	82	2	good	5	good	-0.13	not accepted
	K76-K77	80	0	good	2	good		
	K77	58	22	not accepted	22	not accepted	-0.24	not accepted
	K77-K78	71	9	good	13	moderate		
K96-K100	K96	75	5	good			-0.18	not accepted
	K96-K97	84	4	good	9	good		
	K97	73	7	good	11	moderate	-0.21	not accepted
	K97-K98	69	11	moderate	4	good		
	K98	64	16	moderate	5	good	-0.02	moderate
	K98-K100	79	1	good	15	moderate		
	K100	77	3	good	2	good	-0.09	not accepted

The level of service in terms of safety and operation provided by the road sections studied were examined by the use of the safety criteria adopted in the National Road Design Standards. The scope of this exercise was not only to access the level of safety and operation level provided by the road sections, but mainly to examine the level of compliance of old road designs to the safety control procedures introduced in the Design Standards.

In particular, three (3) safety criteria examine the deviation between design (design Speed – V_e) and operation (operational speed – V_{85}) with the use of Safety Criterion I ($V_e - V_{85}$), the existence of harmonic driving profile along the road with the use of Safety Criterion II ($V_{85i} - V_{85i+1}$) and the safe and comfortable driving around road curves with the use of Safety Criterion III ($f_{exist.} - f_{demand.}$). A common ranking is used in all three safety criteria

Table 6. Safety criteria values/acceptance level for the road section Amfipolis–Mesoraxi Junction.

Subsection	Alignment element	V_{85}	Criterion I	Acceptance level	Criterion II	Acceptance level	Criterion III	Acceptance level
K8-K13	K8-K10	101	11	moderate				
	K10	89	1	good	12	moderate	-0.06	not accepted
	K10-K11	87	3	good	2	good		
	K11	80	10	good	7	good	-0.02	moderate
K25-K31	K13	69	21	not accepted	11	moderate	-0.01	moderate
	K25	96	6	good			-0.10	not accepted
	K25-K27	95	5	good	1	good		
	K27	112	22	not accepted	17	moderate	-0.11	not accepted
	K27-K30	103	13	moderate	9	good		
	K30	104	14	moderate	1	good	-0.09	not accepted
K32-K37	K30-K31	106	16	moderate	2	good		
	K32	95	5	good			-0.13	not accepted
	K32-K33	100	10	good	5	good		
	K33	104	14	moderate	4	good	-0.10	not accepted
	K33-K35	99	9	good	5	good		
	K35	97	7	good	2	good	-0.12	not accepted
	K35-K36	86	4	good	11	moderate		
	K36	94	4	good	8	good	-0.09	not accepted
K57-K59	K37	81	9	good	13	moderate	-0.02	moderate
	K57-K58	119	29	not accepted				
	K58	113	23	not accepted	6	good	-0.30	not accepted
	K58-K59	112	22	not accepted	1	good		
K80-K85	K80	77	13	moderate			0.03	good
	K80-K83	105	15	moderate	28	not accepted		
	K83	78	12	moderate	27	not accepted	-0.23	not accepted
	K83-K85	87	3	good	9	good		

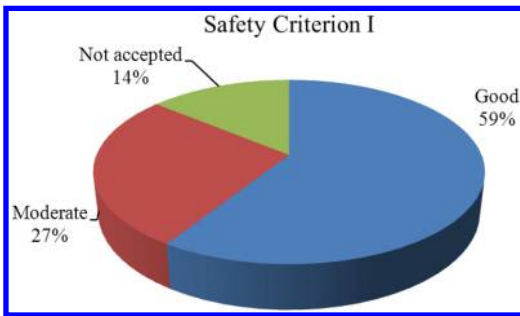


Figure 4. Acceptance level of the Safety Criterion I for all road elements.

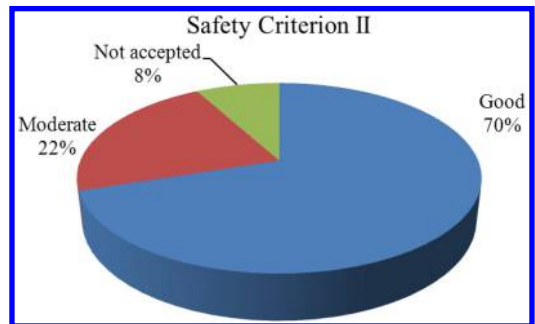


Figure 5. Acceptance level of the Safety Criterion II for all road elements.

expressed as “good”, “moderate” and “not acceptable” case.

The above mentioned procedure was applied in all twelve (12) sub-sections using data defined (V_e), calculated (V_{85}), measured (superelevation) and accepted (f – Design Standards) and the values of the three safety criteria were calculated for all the different alignment elements of the three road sections.

The results of this exercise for the three road sections are presented in Tables 4, 5 and 6 for the respective road sections.

Figures 4, 5 and 6 present the results for the three distinctive safety criteria for all 64 road alignment elements where considered together.

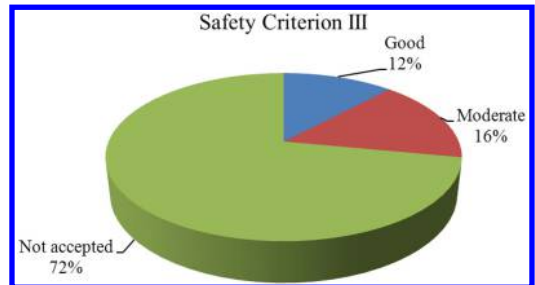


Figure 6. Acceptance level of the Safety Criterion III for all road elements.

In the final stage of the analysis the speed limits prevailing for the particular road sections according to the Greek Road Traffic Code were compared with statistical values of vehicle speed such as V_{75} and V_{85} that consider to express driving attitude to safe driving along the specific road sections.

The cumulative distribution of vehicle speed values was produced for selected alignment elements of the road sections and compared to the prevailing speed limits.

In all but three cases 75th percentile of speed (V_{75}) exceeded speed limit by 6% to 25%. All the same the 85th percentile of speed (V_{85}) exceeded speed limit in all two cases from 16% to 35%. These findings raise a question to whether the imposed speed limits are, in most cases, too conservative and also if a reconsideration of the limits should be put under discussion.

6 CONCLUSIONS

The question set to be answered by this research work was whether old road designs in Greece offer to drivers safety and comfort and therefore harmony in driving profiles in the way that new National Design Standards (OMOE) consider harmonic driving along roads. To answer this question driving behavior as expressed by speed profiles was measured and studied at three road sections of the rural primary and secondary road network in the Prefecture of Serres in Northern Greece.

In all 64 alignment elements were examined separately and combined. They belong to three (3) distinctive road sections categorized as roads of AII, AIII and AIV category respectively. With the use of speed and geometry data measured and calculated the three (3) safety criteria I, II and III introduced by the new Standards (OMOE) where applied at twelve (12) road sub-sections to examine whether there were consistency in speed variation between design and operation, along the different alignment elements and also where curves could have been driven safely and comfortably with given speeds.

The analysis showed that there was a rather good relation between alignment and safety checks when criteria I ($V_e - V_{85}$) and II ($V_{85i} - V_{85i+1}$) were applied. Out of all cases 59% of the elements satisfied the Criterion I requirement of “good” and 27% as “moderate”. All the same the respective percentile values for Criterion II were 70% and 22%. However the results were quite contrary when Safety Criterion III was examined and 72% elements (curves) were found to be “not accepted” and only 12% to be accepted (“good”).

Once more it was found that curves and their high value of curvature is the weak point of the old road design in Greece and need to be look after. On the other hand it is interesting to note that as far as compliance between design and operation is concerned the findings are much better and even more when continuity and harmony in driving profile is examined.

Finally the results showed that there is degree of conservatism in the definition and establishment of the legal speed limits. Discrepancies even of 35% were observed between speed limits and operating speed V_{85} .

REFERENCES

- Domoktsis, N. & Labropoulou K. 2014. *The use of operational speed in Road Safety*. Diploma Thesis, Faculty of Rural & Surveying Engineering, Aristotle University of Thessaloniki, Thessaloniki.
- Kokkalis A., Mintsis G., Taxiltaris, C., Basbas, S. & Dimitropoulos I. 2012. *Conclusions from operational speed counts for the imposition of speed limits in motorway segments*. Proc. of the 3rd Pan-Hellenic Highway Engineering Conference, 9–10 February 2012, Athens.
- Ministry of Infrastructure, Transport and Network. 2005. *Guidelines for the Design of the Road Network (National Road Design Standards) – OMOE*, Athens.
- Touliatos, P., Evaggelidis, D., Lyberopoulos, G., Vaniotou, M. & Anagnostopoulou, A. 2009. *Speed counts analysis and utilization of results in the determination of speed limits*, Proc. of the 4th Pan-Hellenic Greek Road Safety Conference, 5–6 November 2009, Athens.

The contribution of roundabouts to road safety: The case of 4 roundabouts in the municipality of Thermi Greece

D. Spanou, F. Kehagia & M. Pitsiava-Latinopoulou

Department of Civil Engineering, Aristotle University of Thessaloniki, Thessaloniki, Greece

ABSTRACT: Roundabouts are circular intersections with specific design and traffic control features, offering improved road safety, operational efficiency and level of service. Compared to other types of intersections, roundabout installation is strongly promoted as an effective safety intersection treatment, mainly because the potential conflict points between vehicles, pedestrians and other prone users are limited and speeds into and through the intersections are decreased. According to statistical studies relating to fatal accidents and injuries, roundabouts are proved to be safer in low or moderate traffic capacity conditions. The main objective of this paper is to examine the safety aspects of roundabouts, focusing on the effectiveness of roundabouts in reducing intersection crash frequency and severity, discussing crash and accident statistics based on international data resources and presenting the case of 4 roundabouts in the municipality of Thermi, Greece.

1 INTRODUCTION

Roundabouts are designed in such a way so as to effectively control the traffic flow at intersections without the use of stop signs or traffic signals. In recent years researchers have shown particular interest on the benefits of roundabouts, which constitute basic elements in both urban and rural traffic networks. Improvements in capacity and road safety are included in these benefits and make roundabouts an effective measure for improving the overall traffic conditions. The main attributes contributing to these benefits are the reduction of conflict points and the prevailing lower speed levels in comparison to other types of at-grade conventional intersections. However the improved safety of roundabouts is related to their geometric design, which determines their efficiency and operation level.

This paper examines the main features and advantages that roundabouts offer, as an alternative to other types of conventional intersections. At the same time, the basic geometric design features are described, with special reference to their contribution to the level of road safety that roundabouts offer to all their users. Towards this direction the paper presents and analyses accident statistics in roundabouts from various countries relating them with the type of road users and highlights their benefits on road safety providing the findings from before and after case studies, concerning the reduction in the number of accidents after the conversion of traditional intersections into roundabouts. Moreover towards this purpose, the results of a case study concerning the benefits derived from the conversion of a number of junctions of other type to roundabouts in the municipality of Thermi of the Prefecture of Thessaloniki are given.

2 BASIC ELEMENTS OF ROUNDABOUTS

2.1 Definition

Roundabouts are circular intersections with specific design and traffic control features. Basic elements of these intersections are the counterclockwise circulation around a central island (for right-hand traffic countries, like Greece), yield control of all entering traffic to all oncoming circulation already moving into the roundabout, channelized approaches and appropriate geometric curvature, ensuring the desired speed into the circulatory roadway.

2.2 Key features

For a better understanding of the following sections the basic components of a roundabout design are shown in [Figure 1](#), such as:

- Intersection approaches
- Central island (9)
- Splitter islands (3)
- Circulatory roadway (8)
- Apron (10)
- Entrance line (5)
- Lane use horizontal markings (4)
- Outer borderline of the circulatory roadway (6)
- Accessible pedestrian crossings (2)
- Pedestrian refuge on splitter islands (1)
- Bicycle treatments
- Landscaping buffer (7)
- Road lighting pole (A)
- Sidewalk (B)
- Regulatory sign of circular path (C)
- Exit sign (D)
- Yield control sign (E)



Figure 1. Key roundabout features (MITN, General Secretariat of Public Works, Directorate of Road Work Studies, 2011)

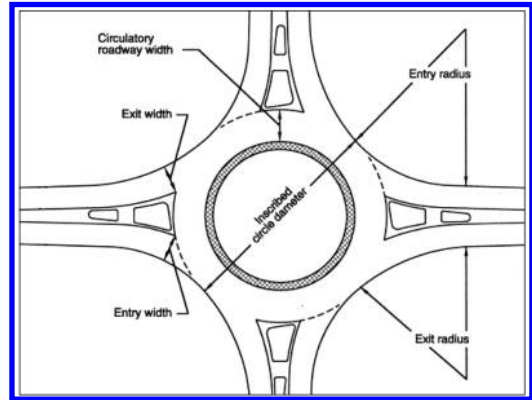


Figure 2. Key roundabout geometric dimensions (Federal Highway Administration, 2000)

2.3 Roundabout categories

Depending on the size and number of approach lanes, roundabouts are divided into three main categories:

- Mini-roundabouts
- Single-lane roundabouts
- Multilane roundabouts

Taking into account the external environment of the roundabout, namely, depending on whether a roundabout is constructed in urban, rural or suburban area, there is a further differentiation in the following subcategories:

- Mini-roundabouts
- Urban compact roundabouts
- Urban single-lane roundabouts
- Urban double-lane roundabouts
- Rural single-lane roundabouts
- Rural double-lane roundabouts

Generally, urban roundabouts are characterized by smaller inscribed circle diameter, due to spatial constraints. Moreover, special attention should be given to the choice of the geometric characteristics of the roundabouts according to its location securing thus the safety of vulnerable users i.e. pedestrians and cyclists. More specifically in rural areas approach speeds are higher and therefore great importance should be given on adequate visibility and section detail issues. Generally it could be said that, keeping the external environment constant, roundabouts with the same number of lanes tend to show similarities in specific design elements.

3 GEOMETRIC DESIGN OF ROUNDABOUTS

Roundabouts require specific geometric design and show some peculiarities in their operation. The general idea of their design is based on the reduction of conflict points of traffic and of prevailing speeds. Roundabouts' main characteristics are the curved entries and exits to ensure low speeds, the giving way to the already moving within the roundabout traffic, the

deflection of traffic when entering the roundabout, the traffic circulation around the central island, the existence of splitter islands along the approaches and the pedestrian traffic only through the appropriate crossing locations.

The basic principles that should govern the geometric design of each roundabout category are:

- Adequate traffic deflection to ensure low entry speeds and consistent speeds within the roundabout.
- Proper alignment of the approaches, in order to avoid exiting-circulating conflicts.
- Appropriate number of lanes to achieve the desired traffic capacity.
- Smooth channelization aimed at comfortable driving.
- Adequate accommodation for the design vehicle.
- Design to meet the needs of pedestrians and cyclists.
- Adequate visibility, for driver recognition of the existence of the roundabout and the conflicting traffic.

The main design elements relating to roundabouts are listed below and are shown in the following figure (Fig. 2):

- Inscribed circle diameter
- Circulatory roadway width
- Entry width
- Exit width
- Entry radius
- Exit radius

In countries where roundabouts are constructed and used mainly for reasons of road safety and protection of vulnerable users, there are no guidelines for design elements that increase traffic capacity and roundabouts are constructed much smaller compared to those of other countries. The opposite occurs in countries in which the priority is given to increased traffic capacity, where roundabouts are having less compact form.

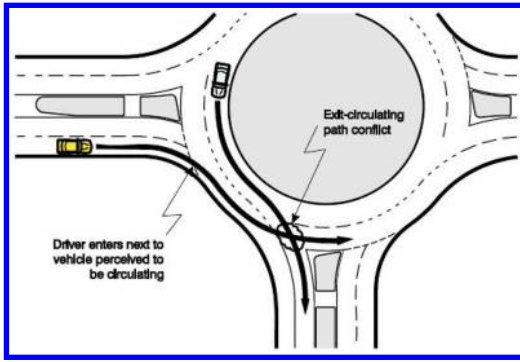


Figure 3. Vehicle conflict point on exit because of wrong lane selection of the moving vehicle into the roundabout (National Cooperative Highway Research Program, 2010).

4 ROAD SAFETY AT ROUNDABOUTS

4.1 General

The level of safety provided by a roundabout is mainly related to its particular design characteristics. In specific, their design converts all traffic movements into right turns minimizing thus potential conflicts (Fig. 4). The reduction of conflicts due to the physical geometric characteristics of roundabouts has proved to be more effective in comparison with the expected, but not certain, driver's obedience to the traffic regulations (Fig. 3). A second key advantage that is achieved by the operation of a roundabout and ensured by the appropriate geometry is speed management, which provides multiple benefits for users, regarding the safety factor such as:

- Reduction of the frequency and severity of collisions for vehicles, pedestrians and cyclists as well as for other vulnerable groups (elderly, children, people with disabilities, etc.).
- Provision of more time for drivers approaching the intersection and consequently better visibility in order to adjust their speed and carefully enter the roundabout (particularly at the intersections of urban with rural roads, where speed limits are different).
- Insurance of safer penetration of incoming circulation into the roundabout.
- Provision of more time to all users so that they could identify and correct any traffic behavior faults, which is very crucial especially for new users.

4.2 Statistics referring to the impact of roundabouts on road safety

Numerous "before and after" studies are internationally undertaken, in order to investigate the positive impacts on road safety derived from the conversion of a conventional intersection to a roundabout.

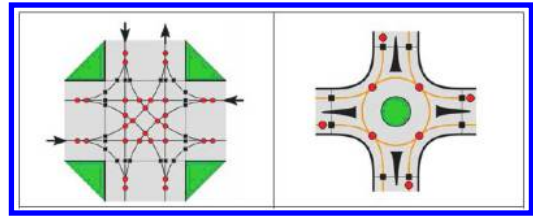


Figure 4. Vehicle and vehicle-pedestrian conflict points in a crossing junction and roundabout respectively (4 approaches) (MITN – General Secretariat of Public Works – Directorate of Road Work Studies, 2011).

Table 1. Mean crash reductions in various countries after the construction of roundabouts.

Country	Mean reduction (%)	
	All crashes	Injury crashes
United States	37	51
United Kingdom	–	25–39
Germany	36	–
France	–	57–78
Australia	41–61	45–87

*Source: Robinson et al., 2000.

The results of a study by Robinson et al. (2000) given in Table 1 reveal significant reductions in accidents after the conversion of conventional intersections to roundabouts in various countries. Specifically, the reduction for the United States rose to 51%, for the United Kingdom ranged between 25–39%, for France between 57–78% and for Australia between 45–87%. In addition the same study for single-lane roundabouts resulted in a reduction of 73% in the number of accidents involving injuries, while in multi-lane roundabouts, the accidents involving injuries have been decreased by 31%. Also Ogden (1996) demonstrated that the construction of roundabouts can reduce accidents by 60–80% in high-speed intersections and by 50–80% in low-speed intersections. Later, Elvik (2003) found slightly smaller road safety improvement rates, in cases of roundabouts which replaced signalized intersections instead of intersections regulated only with STOP and give way signs (i.e. reductions of 59% and 46% instead of 64% and 53% for fatal and serious accidents respectively).

Finally, a 2004 study in the UK showed that out of a total of 207,400 road accidents involving injuries, the 18,000 (8.7%) occurred at roundabouts with the rate of fatal accidents at roundabouts being 0.35%, while at other crossings 0.88% (The Highways Agency, Transport Scotland, Welsh Assembly Government, The Department For Regional Development Northern Ireland, 2007).

However, the statistics that have emerged from these studies do not show the same level of road safety

Table 2. British crash rates for pedestrians at roundabouts and signalized intersections.

Intersection type	Pedestrian crashes per million trips
Mini-roundabout	0.31
Conventional roundabout	0.45
Flared roundabout	0.33
Signals	0.67

*Source: Federal Highway Administration, 2000.

improvements for the various countries. This is likely due to the existing differences from country to country:

- In traffic volumes.
- In the design of the various geometric and operational elements (operation of only single-lane roundabouts in some countries).
- In the definition of accidents occurred at intersections as each country defines different distance, over which an accident is not considered to be associated with the specific intersection.
- In the definition of accidents involving injuries and more specifically in the definition of death due to accident as this varies among countries depending on the period in which death occurs (just on the spot or some days after staying in hospital).
- In cultural differences which influences driving behavior.

In any case, the comparison of statistics should be made for roundabouts with similar geometric and operating characteristics, taking into account as well any existing differences. In this way, wrong assessments are avoided and correct and reliable conclusions can be made, in order to proceed with the appropriate measures that should be taken towards the improvement of road safety at roundabouts.

Regarding the impact of roundabouts on vulnerable users' safety, the survey results are not so clear. Schoon & van Minnen (1993) reported that the reduction in the number of accidents involving cyclists at roundabouts reaches 30%, well below 47%, which represent the overall road safety improvement rate that roundabouts induced. On the other hand, the same survey indicated that roundabouts reduce the number of accidents involving at least one pedestrian by 89%. Hydén & Várhelyi (2000) also demonstrated reductions of 60% and 80% in the number of accidents involving cyclists and pedestrians respectively. Brüde & Larsson (2000) found that the rate of reduction for vulnerable users is highly related with the roundabout category. More specifically for accidents involving cyclists they found reductions of the order 21% at single-lane roundabouts and 112% for multi-lane roundabouts, while the respective reductions for accidents involving pedestrians were 79% and 12% for the two roundabout categories. Stone et al. (2002) showed an even lower reduction percentage in accidents involving pedestrians, of around 7%.

Table 3. Crash percentage per type of user at roundabouts and conventional intersections in 15 towns in western France.

User category	Other crossings (%)	Roundabouts (%)
Pedestrians	6.3	5.6
Bicycles	3.7	7.3
Mopeds	11.7	16.9
Motor cycles	7.4	4.8
Cars	65.7	61.2
Utility vehicles	2.0	0.6
Heavy goods vehicles	2.0	3.0
Bus/coach	0.8	0.6
Miscellaneous	0.4	0.0
Total	100.0	100.0

*Source: Federal Highway Administration, 2000.

In addition a survey conducted in Great Britain found that accident rates involving pedestrians are much higher at signalized intersections than roundabouts (Table 2).

However a French survey in 15 cities concerning the comparison of accident distribution per user category, between roundabouts and the rest conventional intersections showed that accidents involving bicycles and mopeds constitute almost the one quarter of the total accident percentage occurring at the roundabouts, while the respective value for the rest of intersections is around 15% (Table 3). The above result shows that nevertheless the overall reduction of accidents involving vulnerable road users at roundabouts they continue to remain significantly high, a fact that should be treated properly.

4.3 Distribution of accidents by accident type in relation to geometric design elements

The main accident types that occur in a roundabout are:

- Single-vehicle accidents, mainly due to crashes towards fixed objects and elements of the roundabout.
- Other accidents between vehicles, including collisions between vehicles already moving into the roundabout, collisions between vehicles which are already moving into the roundabout and those exiting the roundabout, collisions between vehicles leaving and vehicles entering the roundabout, collisions at the entrance and exit etc.
- Accidents involving pedestrians and other vulnerable users, when one of them is hit by a passing vehicle.
- Accidents between the incoming and already moving into the roundabout traffic.
- Accidents during approach (e.g. due to lane changing and path overlapping when approaching the roundabout).

Table 4 gives the accident distribution by accident type, for various countries.

Table 4. Percentage of accidents by accident type at roundabouts in various countries.

Country	Single-vehicle accidents (%)	Approaching accidents (%)	Entering-circulating accidents (%)	Other vehicle accidents (%)	Pedestrian accidents (%)
United Kingdom	30	25	20	18	6
Germany	28	17	30	–	–
France	28	7	37	15	10
Australia	18	22	51	9	9

*Source: Kennedy, 2007.

**Values for Germany and Australia refer to accidents that caused only property damage.

The accident distribution by accident type depends on the roundabout category i.e. small roundabouts with small diameter of the central island have many more accidents between incoming and already moving into the roundabout traffic, while double-lane roundabouts have more single-vehicle accidents and accidents during the approach to the roundabout. The most important geometric elements affecting accidents and are related directly or indirectly to their incidence are:

- The curve of the entry path. By increasing this curve and thereby the deflection of the vehicle path when entering (reduction of the entrance path radius), accidents between incoming and already moving into the roundabout traffic are being reduced, while accidents at the entry and single-vehicle accidents are increasing.
- The entry width. The larger the entry width, the greater effect it has on the increase of accidents between incoming and already moving into the roundabout traffic, while reducing the accidents at the entry.
- The ratio of the inscribed circle diameter to the diameter of the central island. Great value of this ratio leads to greater chances of accidents due to large traffic width within the circulatory roadway.
- The angle between the centerlines of two successive approaches. A wide angle reduces the necessary vehicle path deflection and thereby increases the risk of an accident, both at the entrance and at the exit.
- The approach width relative to the entry width, as this indicates the level of widening and therefore the possibility of an accident due to collisions with adjacent vehicles.
- The visibility to the left. Increased visibility at the entrance and to the left leads to increased entry speed and eventually causes more single-vehicle accidents, but also accidents between incoming and already moving into the roundabout traffic.

4.4 Accident frequency and severity

Kennedy (2007) tried to summarize, from a number of surveys that took place in various countries, the average accident frequency values at roundabouts-expressed in accidents per year. The results of this

Table 5. Accident frequency and severity at roundabouts in different countries.

Country	No. of roundabouts in study	Accident frequency (accidents per year)	Accident severity (% fatal and serious)
United States	11	1.5	–
United Kingdom	1162	1.77	7
France	27000	0.05	–
Australia	290	0.6	–

*Source: Kennedy, 2007.

study are given in Table 5 and they are based on the sample of roundabouts selected for the surveys referring to four-arm roundabouts with single-lane circulatory roadway. Specifically it was found that in the United States the frequency was 1.5 accidents per year for a small number of roundabouts (11) and with reference to the year 1998. In the UK, a 2007 survey gave a frequency of 1.77 accidents per year, while accident severity, expressed as the percentage of fatal and serious accidents of total accidents, was 7%. In France it was found a frequency of 0.05 accidents per year, based on data of a 2005 survey for about 27,000 roundabouts, while in Australia a frequency of 0.6 accidents per year for a sample of 290 roundabouts, according to a research undertaken in 1998.

According to surveys and as expected, the frequency of accidents at roundabouts increases with the number of approaches and the number of lanes, due to the increased traffic flow and hence the increase of conflict points for both cases. Table 6 presents the results of a survey conducted in 2004 in Great Britain, on the frequency and severity of accidents, for a sample of 1162 roundabouts and for a five-year period, depending on the number of approaches and lanes.

Here it should be pointed out that accident rate-defined as accidents per 100 million vehicles traveling through the roundabout- is a more representative indicator for comparisons between sites but its estimation depends on the availability of traffic flow data, which is not feasible in most cases. Thus, the table below (Table 7) provides values of the accident rate for the countries studied so far, where data acquisition was feasible. The values given refer to single-lane

Table 6. Average accident frequency and severity at UK roundabouts by number of arms, for the period 1999 to 2003.

No. of arms	No. of sites	Accident frequency (accidents/year)			Accident severity (% fatal and serious)
		Single cway roads	Double cway roads	Grade separated junctions	
3	326	0.63	1.28	0.79	9.3
4	649	1.08	2.65	1.79	7.1
5	157	1.72	3.80	3.66	7.1
6	30	2.11	4.62	5.95	5.2
All	1162	1.00	2.60	1.87	7.2

*Source: The Highways Agency, Transport Scotland, Welsh Assembly Government, The Department For Regional Development Northern Ireland, 2007.

Table 7. Accident rates at roundabouts in different countries.

Country	No. of roundabouts	Accident rate (accidents per 100 million vehicles)	Mean total vehicle inflow (vehicles per day)
United States	11	8	–
United Kingdom	44	36	28000
Germany	–	53–162	5000–25000
France	179	4.5	–
Australia	–	4–8	–

*Source: Kennedy, 2007.

roundabouts, except for the United Kingdom, where they refer to larger roundabouts. In the United States, the accident rate is 8% for a sample of just 11 roundabouts, based on data for the year 2003 and in the United Kingdom it appears to be quite high, reaching 36%, based on a 2007 survey referring to a sample of 44 roundabouts with traffic flows ranging between 10,000 and 50,000 vehicles per day, with an average value of 28,000 vehicles. In Germany the accident rate ranges between 53 and 162 according to data from a research undertaken in 2005, a value too high which is due to the inclusion of only property damage accidents. The average accident rate in 179 urban roundabouts in France according to data of a 1991 research is only 4.5%, while in Australia it ranges between 4 and 8 accidents per 100 million vehicles, also including only property damage accidents, based on a 1993 survey.

5 CASE STUDY: FOUR AT GRADE ROUNDABOUTS – MUNICIPALITY OF THERMI

In this case study the design elements of four roundabouts in the Municipality of Thermi are described



Figure 5. Municipality of Thermi, Thessaloniki Prefecture, Region of Central Macedonia, Greece (<http://el.wikipedia.org/>)



Figure 6. Roundabouts position (<https://maps.google.gr/>)

in relation to the benefits derived for the area on the topic of road safety and traffic capacity. Municipality of Thermi is located on the southeast side of the city of Thessaloniki, Greece and north to the airport “Macedonia” and according to the National Statistics Office, in 2001 its population was 11,412.

The Municipality had the highest population growth in the decade 1991–2001. This increase is due to the decentralization that took place during this decade as a large part of the population moved to the suburbs of the city of Thessaloniki. The road network of the settlement of Thermi is radial with Paramana square at its center, being crossed by 11 roads.

According to the police statements the conversion from a junction of other type to roundabout resulted to an enhanced effect on safety for all examined junctions. This positive effect, which varies from junction to junction according to its design elements, is mainly due to the reduced speed and the increased awareness aiming to deflect from ahead path. Additionally, before and after remarks show that roundabouts’ application genuinely improved the level of service and the functionality of the intersections by increasing the circulatory capability.



Figure 7. Intersection before the construction of the roundabout (<https://maps.google.gr/>).

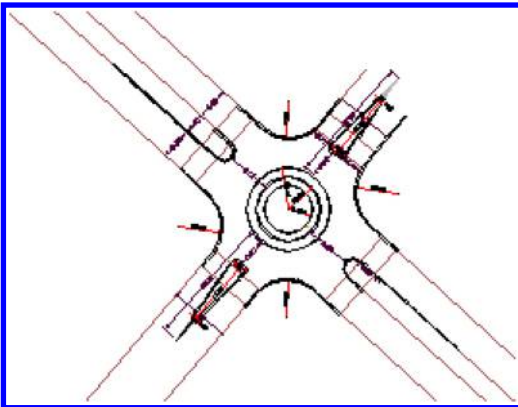


Figure 8. Roundabout design (Directorate of Technical Services, Municipality of Thermi, Thessaloniki, Greece).



Figure 9. Intersection during the construction of the roundabout (Directorate of Technical Services, Municipality of Thermi, Thessaloniki, Greece).

5.1 *Ap. Kougiami Street – P. Tsaldari Street intersection*

Road safety interventions that have taken place in the municipality of Thermi include the construction of



Figure 10. Intersection before the construction of the roundabout (<http://gis.ktimanet.gr/wms/ktbasemap/default.aspx>).

a roundabout at the site where Ap. Kougiami street (1) intersects with P. Tsaldari street (2), in July 2014, replacing a non-signalized intersection. The main reason for the construction of the roundabout under consideration was the emergence of severe accidents involving pedestrians at this site, although it is sparsely populated.

The intersection was converted into a single-lane roundabout with one lane of traffic in each direction per approach. The inscribed circle diameter is 26 m and the central island' diameter is 16.8 m resulting to the circulatory roadway width of 4.6 m. For the Ap. Kougiami street splitter islands were also constructed, while remained the existing islands on the P. Tsaldari street.

5.2 *Charilaou – Thermi Street/Ap. Kougiami Street intersection*

This at-grade roundabout was constructed in early 2014, on the provincial road of Charilaou – Thermi (1), at the position of the intersection with the Kougiami street (2) in the expanding urban plan of the settlement of Thermi.

The provincial road of Charilaou – Thermi connects the settlement of Thermi with a non-residential area where the prevailing operational speeds are high with at the same time a significant presence of pedestrians. Also, it is worth mentioning the increase in traffic volumes in this site due to the attraction of the area for business as well as residential purposes.

Thus the construction of this roundabout in the place of a previously signalized intersection emerged as necessary aiming to slow down the observed high speeds and consequently to avoid accident occurrence as well as to facilitate the traffic from and to the settlement of Panorama through a new non-signalized street.

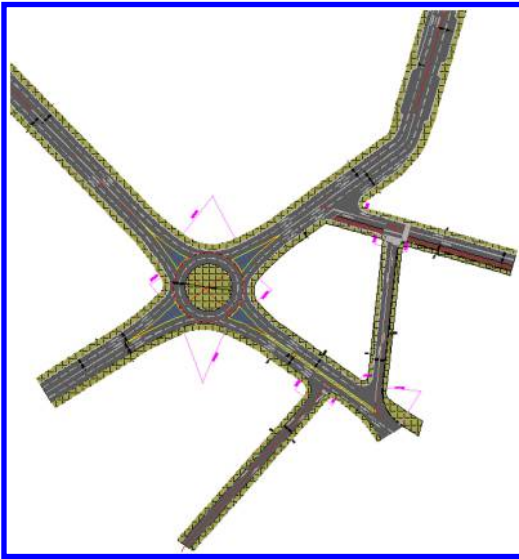


Figure 11. Roundabout design (Directorate of Technical Services, Municipality of Thermi, Thessaloniki, Greece).



Figure 13. Intersection before the construction of the roundabout (<http://gis.ktimanet.gr/wms/ktbasemap/default.aspx>).



Figure 12. Intersection during the construction of the roundabout (<https://maps.google.gr/>).

The construction included a double-lane roundabout with two lanes of traffic in each direction per approach and for the circulatory roadway. The intersection point of the roadways corresponds to chainage 0 + 887.66 on the main road (Route Thessaloniki – Thermi) and to chainage 0 + 962.24 for the perpendicular street. The content between the axes angle is $\hat{\alpha} = 91.211 \text{ grad}$. The inscribed circle diameter is 36m, and the central island has a diameter of 24 m. As a result, the circulatory roadway width is 6 m in order to achieve simultaneous circulation of traffic in two lanes and avoid delays at the entries and exits. All four splitter islands are kerbed so as to avoid their use from traffic.

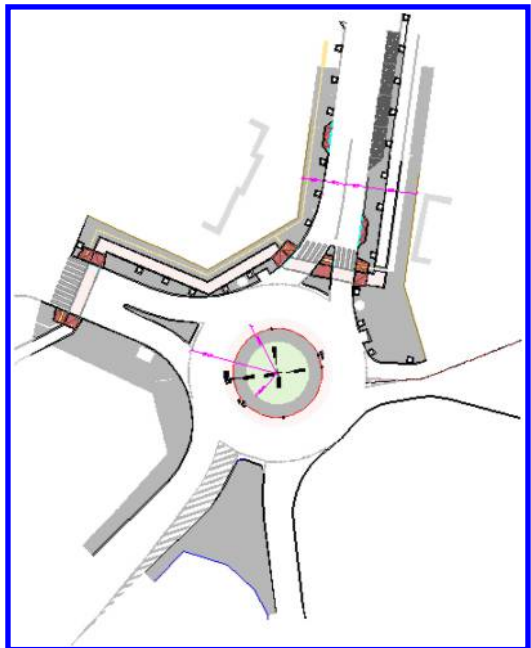


Figure 14. Roundabout design (Directorate of Technical Services, Municipality of Thermi, Thessaloniki, Greece).

5.3 B. Tavaki Street/Sot. Petroula Street intersection

B. Tavaki street (1) constitutes the entrance to the settlement of Thermi for vehicles entering the Thessaloniki – Polygyros highway through its intersection with the Sot. Petroula street (2). Thus, this intersection



Figure 15. Intersection after the construction of the roundabout (<https://maps.google.gr/>)



Figure 17. Intersection after the construction of the roundabout (<https://maps.google.gr/>).



Figure 16. Intersection before the construction of the roundabout (<http://gis.ktimanet.gr/wms/ktbasemap/default.aspx>).



Figure 18. Photo looking north-east along El. Venizelou street (<https://maps.google.gr/>).

is characterized by the high speed of entering vehicles in the settlement. In addition conflict points were observed due to the drivers' violation of the prohibited left turns to Sot. Petroula street during their entry to the settlement.

For this reason, in August 2012 a roundabout was constructed, in the place of a previous, insufficient to regulate the traffic, triangular island with two triangular splitter islands at the entrances of B. Tavaki and Sot. Petroula street aiming to achieve the reduction of conflict points between traffic flows and increase pedestrian safety.

The roundabout constructed is a single-lane roundabout with one lane of traffic in each direction for

the two main approaches and one for the circulatory roadway. The inscribed circle diameter is 28 m and the central island has a diameter of 17 m. As a result, the circulatory roadway width is 5.5 m. For the two main approaches splitter islands were also constructed.

5.4 *Capetan Chapsa Street – El. Venizelou Street intersection*

The Capetan Chapsa (1) (continuation of the Charilaou – Thermi street into the settlement) – El. Venizelou (2) intersection was problematic in terms of road safety, since it was a non-signalized site with high pedestrian use, where eight approaches ended with only two one-way streets. For this reason, the chosen solution was a single-lane roundabout construction, completed in 2012, aiming to improve traffic capacity and increase pedestrian safety. However, the roundabout was poorly designed with the centerlines of the approaches not intersecting in its center and with the absence of pedestrian crossings in all its approaches.

Roundabouts are often a standard solution when it comes to the conversion or the original design of an intersection, in both urban and rural environment. The attitude of the public is favorable towards them, as both drivers and pedestrians benefit from the minimization of delays, even at peak hours, as opposed to signalized intersections. This improved level of service reflects the contribution of roundabouts to the increase of traffic capacity and to the general functional benefits.

Technically, the geometry of roundabouts aims to reduce speeds, contributing thereby to a higher safety level, which is considered to be the most important advantage roundabouts offer. Examples include the reduction of the number of accidents and in many cases the limitation of their seriousness only to property damage. Crash reductions resulting from conversion of conventional intersections to modern roundabouts can be attributed primarily to two factors: reduced traffic speeds and elimination of specific types of motor vehicle conflicts that frequently occur at angular intersections. These conflicts include left turns against opposing/oncoming traffic, front-to-rear conflicts (often involving the lead vehicle stopping or preparing to stop for a traffic signal or stop sign), and right-angle conflicts at traffic signals and stop signs.

The adaption of roundabouts in the landscape and their potential aesthetic treatment are also considered to be positive elements, because a smooth continuation of the current situation is maintained, without elements that do not match and do not belong to their wider installation environment being observed. Another benefit that favors the environment is the reduction of the energy consumed by vehicles and the gases emitted, due to the smoother flow of traffic, with fewer accelerations and decelerations, since absolute stops of the vehicles are avoided.

The data collected for the case study in the Municipality of Thermi showed a general safety and traffic capacity benefit from converting conventional intersections, either from stop sign or traffic signal control, to modern roundabouts. It was pointed out that the construction of the four roundabouts improved significantly road safety at these junctions, eliminating conflict points between traffic flows and ensuring their safer use by drivers and pedestrians.

However, the construction of roundabouts is not a panacea. Like any transportation project, so the installation of roundabouts has drawbacks and causes, where appropriate, negative effects (large space requirements, expropriations of significant resources, increased construction cost, etc.). Often, indeed, signaling an intersection outweighs the construction of a roundabout, depending on the circumstances, the users that will be served and the objectives set for any treatment. For this reason, caution and care on the part of engineers is required, to fully understand the needs and constraints of the area and take the right decision, to meet the drivers' and pedestrians' needs and avoid blind construction of improper treatments.

- Brabander, B., Nuyts E. & L. Vereeck 2005. Road safety effects of roundabouts in Flanders. *Journal of Safety Research* 36: 289–296.
- Brabander, B. & L. Vereeck 2006. Safety effects of roundabouts in Flanders: Signal type, speed limits and vulnerable road users. *Accident Analysis and Prevention* 39 (2007): 591–599.
- Brilon, W. 2011. Roundabouts: A State of the Art in Germany. Paper presented at the 3rd International TRB-roundabout Conference. Carmel, Indiana.
- Brüde, U. & Larsson, J. 2000. What roundabout design provides the highest possible safety? *Nordic Road Transport Res.* 2, 17–21.
- Directorate of Technical Services, Department of Transportation, Traffic, Hydraulic and Reclamation Projects, Municipality of Thermi 2013. Project study: “Road safety interventions on Ap. Kougiami Street of the settlement of Thermi”, No. of Study: 41/2013. Thessaloniki, Greece.
- Directorate of Technical Services and Environment, Department of Technical Works and Urban Planning Applications 2010. Project: “Paving regeneration on V. Tavaki and D. Karaoli Streets of the municipality of Thermi”, No. of Study: 97/2010. Thessaloniki, Greece.
- Efraimides E. & Iordanopoulos P. 2008. Thesis: “Evaluation of implementing Traffic Calming Measures in urban areas: The case of Thermi”. Thessaloniki, Greece.
- Elvik, R. 2003. Effects on road safety of converting intersections to roundabouts. Review of evidence from Non-U.S. studies. *Transportation Research Record* 1847, paper 03–2106.
- Federal Highway Administration 2000. *Roundabouts: An Informational Guide*. U.S. Department of Transportation. Publication No. FHWA-RD-00-067.
- Hydén, C. & Várhelyi, A. 2000. *The effects on safety time consumption and environment of large scale use of roundabouts in an urban area: a case study*. *Accid. Anal. Prev.* 32 (1), 11–23.
- Institute of Transportation Engineers 2008. *Enhancing Intersection Safety Through Roundabouts: An ITE Informational Report*. Publication No. IR-127. Washington, D.C.
- Insurance Institute for Highway Safety 2000. *Crash Reductions Following Installation of Roundabouts in the United States*.
- Kennedy, J. 2007. *International comparison of roundabout design guidelines*. Published Project Report PPR206.
- Ministry of Infrastructure, Transport and Networks (MITN), General Secretariat of Public Works, Directorate of Road Work Studies 2011. *Road Work Studies Instructions*, Volume 10, Part 2: *Roundabouts* (RWSI). Consultant: NAMA Consulting Engineers & Planners SA (Project).
- National Cooperative Highway Research Program 1998. *Modern Roundabout Practice in the United States*. NCHRP Synthesis 264. A Synthesis of Highway Practice. Georges Jacquemart, P.E., AICP, Buckhurst Fish & Jacquemart Inc., Transportation Research Board – National Research Council. Washington, D.C.
- National Cooperative Highway Research Program 2010. *Roundabouts: An Informational Guide*. Second Edition. NCHRP Report 672. U.S. Department of Transportation, Federal Highway Administration (FHWA). Washington, D.C.
- Ogden, K. W. 1996. *Safer roads: A guide to road safety engineering*. Monash University: Institute of Transport Studies.
- Robinson, B. W. et al. 2000. *Roundabouts: An informational guide*. Washington: U.S. Department of Transportation.

- Federal Highway Administration. Report FHWA-RD-00-067.
- Schoon, C. & van Minnen, J. 1993. *Ongevallen op rotondes II: tweede onderzoek naar de onveiligheid van rotondes vooral voor fietsers en bromfietsers*. Stichting Wetenschappelijk Onderzoek Verkeersveiligheid (SWOV), rapport R-93-16. Leidschendam.
- Spanou, D. 2014. Thesis: “*Roundabouts: Geometric design, Adaption in landscape and Road Safety – Case study in the city of Kavala*”. Aristotle University of Thessaloniki. Faculty of Engineering. Department of Civil Engineering.
- Postgraduate Specialization Programme “Environmental Protection and Sustainable Development”. Thessaloniki, Greece.
- Stone, J.R., Chae, K. & Pillalamarri, S. 2002. *The effects of roundabouts on pedestrian safety*. Southeastern Transportation Center, working paper. Tennessee.
- The Highways Agency, Transport Scotland, Welsh Assembly Government, The Department For Regional Development Northern Ireland 2007. *Design Manual for Roads and Bridges: Geometric Design of Roundabouts*. Volume 6: Road Geometry, Section 2: Junctions, Part 3. TD 16/07.

Posters

Assessment of generic pothole repair materials

J.C. Nicholls

TRL Limited, Wokingham, UK

K. Kubanek

TPA GmbH, Stuttgart, Germany

C. Karcher

EAPA, Brussels, Belgium

A. Hartmann

University of Twente, The Netherlands

A. Adesiyun

FEHRL, Brussels, Belgium

A. Ipavec

Slovenian National Building & Civil Engineering Institute

J. Komacka

University of Zilina, Slovakia

E. Nielsen

Danish Road Directorate, Copenhagen, Denmark

ABSTRACT: Potholes are a major problem for road authorities. There are many causes of potholes, with cold damp conditions being considered the main cause in colder climates whilst countries nearer the equator also have extensive potholes. Currently, there is no pan-European, or even national, assessment method for assessing the suitability of potential repair materials. A European ERA-Net project was set up to look at permanent pothole repairs. The project team developed a definition and selected suitable test methods based, as far as possible, on European norms following an extensive questionnaire. The project team also reviewed some national trials, carried out laboratory tests on proprietary repair materials (hot asphalt, cold asphalt and resin-based varieties) and undertook life cycle cost analyses for different scenarios. From the findings, guidelines have been produced to select a repair technique and/or material with a durability corresponding to the estimated lifetime of the existing pavement. The paper briefly reviews the research findings and then explains the guidelines for assessing pothole repair materials. However, the project team does understand that the cleaning out of the pothole and the application of the repair are also major influences on the durability of any repair.

1 INTRODUCTION

1.1 *Project*

All European countries are faced with the problem of potholes (Figure 1) and how to repair them. The immense economic loss due to the damage, the repair of potholes with materials that are only good on a short-term basis and, most importantly, the increasing numbers of crashes with resulting injuries and even deaths caused by potholes requires an improvement in the methods and techniques and road agencies need methodologies to deal with these problems. Many

approaches just deal with repair methods which are durable only on a short-term base and are, therefore, not cost-effective. Therefore, road agencies need durable construction and maintenance methods for the repair of damage which occurs after hard winters due to repeated frost-thaw cycles and other mechanisms.

The POTHOLE project, on which this report is based, was set up to address the need of road agencies for durable construction and maintenance methods for the repair of damage which occur after hard winters due to repeated frost-thaw cycles.



Figure 1. Examples of potholes.

The detailed results and conclusions are given the Work Package Reports (Nicholls, 2011; Ipavec, 2012; Rosenberg, 2012; Komačka and Remišová, 2012; Hartmann, 2013; Kubanek, 2013a) together with a set of guidelines for pothole repairs (Kubanek, 2013b),

1.2 Questionnaire

A questionnaire was circulated asking about the definition(s) of “pothole” used around Europe (Nicholls, 2011). The questions covered definitions, properties required and associated test methods and trials of pothole repair materials. The results were extensive but inconclusive (Figure 2).

1.3 Definition of the term “pothole”

The following definition was developed from the responses which did not conflict with other existing definitions (Nicholls, 2011):

“a local deterioration of the pavement surface in which the material breaks down in a relatively short time and is lost causing a steep depression”

More detail is given in the following notes:

1. Generally, potholes require rapid remedial action to maintain the safety of road users.
2. Potholes will also need to be reinstated to maintain the functional requirements and comfort, but the time-constraints on rectification for these requirements will not be as immediate.



Figure 2. Number of responses to the questionnaire from the countries of Europe.

3. Potholes will typically have a depth of at least 30 mm and an area equivalent to a diameter between 100 mm and 1 m with the values for a specific situation depending on several factors including the traffic speed and intensity, the type of vehicle (particularly the presence of bicycles and pedestrians) and the climate.
4. Potholes can grow once they have emerged, but generally stop growing after a certain time. However, other potholes can appear close to an existing one.
5. Potholes can occur due to several mechanisms (such as fracture, attrition and seasonal conditions).

2 EXISTING STANDARDS, TECHNIQUES, MATERIALS AND EXPERIENCE WITH THEM ON THE EUROPEAN MARKET

2.1 General

In a review of current specification documents, almost no requirements for material properties were found. There were some test methods listed in a few standards or technical specifications but no values were given as the requirements needed (only some broad limits for particle size distribution of aggregate grading).

The size of the aggregate used for repair material depends on the depth of the pothole to be repaired. In most cases, repair materials contain aggregates which have a maximum aggregate particle size not more than about 10 mm or 11 mm (depending on set of sieve sizes used). The aggregate grading has a great effect on the performance of an asphalt mixture, with dense-graded asphalt mixture supposedly performing well at warm and hot temperatures whilst open-graded asphalt mixtures are required for satisfactory workability at freezing temperatures.

2.2 Materials

The main types of material found to be used for pothole repair (Ipavec, 2012) are:

- bitumen-based cold-mix materials (cold-mix asphalt CMA)
- bitumen-based hot-mix materials (hot-mix asphalt HMA)
- cement-based materials
- synthetic binders, although these are not widely used.

Cold-mix asphalt mixtures are mostly used for temporary repairs but, with proper installation, they can be more durable. The major limitation for these materials is that they cannot normally be compacted to the same level as hot-mix asphalt mixtures. The advantages include short application time and applicability in harsh winter conditions. The binder can be either cutback bitumen or bitumen emulsion. Cutback bitumen can be difficult to work at low temperatures and often require some warm-up time in the sun before use whilst bitumen emulsion can have a relatively short time to break and cure, so slow-setting emulsions are required.

Hot-mix asphalt mixtures present a more durable solution which is easy to install and to compact and provides more effective bonding with the existing asphalt pavement. Attention must be paid to the required mixture temperature for compaction, with hot-box equipment being needed to maintain the temperature for multiple small repairs. There are two generic types of hot mix asphalt:

- Matrix dominated mixtures (such as hot rolled asphalt and mastic asphalt) with higher bitumen content and lower permeability that are easy to compact and have good durability but the surface is often quite smooth, requiring chippings to provide better skid resistance.
- Aggregate dominated mixtures (such as asphalt concrete and stone mastic asphalt) with lower bitumen content and higher permeability that require higher compaction energy and have shorter durability.

Cement-based materials need to be fast-setting or rapid-hardening cement-based materials that are intended for rapid pavement repair. However, because any repaired patch deflection under the traffic needs to be similar to that of the surrounding pavement, repairs using strongly cement-based materials are not recommended.

2.3 Techniques

Pothole repair techniques include temporary repairs that are used in emergency circumstances when a pothole represents a potential hazard for safety and rideability or in harsh winter conditions when there is no alternative solution and when a defect should be repaired immediately or in a short time. The methods include throw-and-go (no preparation or cleaning of

the pothole and compaction by traffic only; usable in harsh winter conditions and with a high rate of application, but the worst durability; normally cold-mix-asphalt), throw-and-roll (no preparation or cleaning of the pothole and compaction by the tyres of the maintenance crew truck; usable in harsh winter conditions and with a high rate of application; normally cold-mix asphalt), edge seal method (similar to throw-and-roll but with a ribbon of bituminous tack material on top of the patch edge) and spray-injection patching (placing heated bitumen emulsion and virgin aggregate simultaneously into a pothole with no compaction).

Semi-permanent procedure (using hot or cold-mix asphalt) involve removing water and debris from the pothole, forming the vertical edges to the pothole, placing the mixture into the hole and then compacting it using vibratory plate compactors, drum vibratory rollers or tamper. An option for smaller potholes is leave out the edge straightening, but this omission could have the effect of shorter durability.

Permanent or more durable repair involve preparation including edge formation (by saw cutting), cleaning the excavation with the removal of all debris, loose material and water (drying), the application of bond coat to base (bottom) and sides, infilling the pothole with asphalt material (mostly hot-mix, also cold-mix asphalt or cement-based material is used) and then compaction with vibrating plates, drum vibratory rollers or tamper.

The proper preparation of potholes is essential for a good repair. No matter how good quality and durable the material that is used for pothole infilling is, it will not perform well and not last long enough if it is applied in inappropriate circumstances. The prepared patch area (normally rectangular shape) must include the whole area affected by the pothole and any associated distress in surroundings. The cut edges should be clean and neat. All unsound and debonded material should be removed. A good bond is needed, usually with a cationic emulsion, which must be evenly applied. Every type of infill material should be fully compacted. Finally, blinding with some coarse sand over the emulsion ensures that the bitumen does not stick to vehicle tyres. For deeper potholes (more than 40 mm), the asphalt should be installed in multiple layers (each compacted separately).

3 EXPERIENCE FROM TRIAL SECTIONS

The issued questionnaire was later supplemented with a secondary one which focused on experience gained by dedicated trial sections for the durability of various pothole repair materials. Three countries reported systematic trial sections (Rosenberg, 2012).

- Denmark – at Tuelso, two series installed in 2008 and 2009 of 19 materials (Figure 3).
- Slovenia – at Ljubljana one series installed in 1999 of six materials and in 2012 a series of ten materials at two locations (Novo Mesto and Nova Gorica).



Figure 3. Trial of pothole repair options in Tuelso.

Table 1. Estimated durability of 25 generic pothole repair materials.

Durability	Repair materials based on			
	Hot bitumen	Cold bitumen	Cement	Synthetic binder
<1 year	DK	DK, SL	DK × 3	DK × 3
1-2 years	DK	DK, UK × 3	DK	DK
>2 years– 3 years	–	DK × 2	–	DK × 2
>3 years	–	–	–	–

where DK = Repair material tested in Trial Tuelso, Denmark
 SL = Repair material tested in Trial Ljubljana, Slovenia
 UK = Repair material tested in Trial HAPAS, United Kingdom

- United Kingdom – HAPAS scheme of four repair materials at individual sites.

In 2012 a total of 25 different repair materials had been surveyed for periods ranging from one to 12 years covering four generic types of materials:

- Hot applied bituminous materials (four materials).
- Cold applied bituminous materials (ten materials).
- Cementitious materials (four materials).
- Synthetic binders (seven materials; resins of acrylate, epoxy or polyurethane and two materials).

Detailed description of conditions at the trial sites, selection criteria and other accessible material data can be found in (Rosenberg, 2012). From the various trial sections the generic types could be evaluated according to their estimated durability and divided into four age groups (Table 1).

The result from this evaluation is as follow:

- a. The same conditions (traffic and climate) and evaluation methods are not used for the different trial sites and, therefore, it is difficult to determine the actual durability of the various repair materials. It is, therefore, important to develop a common evaluation system that uniquely determines when damage is being assessed to have a negative effect on the functional properties of the repair.

- b. If the assessment system is to be applicable throughout Europe, it will be necessary to define categories of durability with reference to the different climate zones and different traffic classes.
- c. It has not been possible to classify the different generic types in durability categories based on the evaluation of the trial sites because, within each generic type of material, great variation exists in the estimated durability for each repair material.
- d. It appears that each generic type of repair material has an associated set of typical damage mechanisms. Therefore, it may be necessary to rank the importance of each laboratory test differently for each generic type of repair material.
- e. It appears that some of the generic types of repair materials have limitations on their application, such as size of the pothole and the temperature during application.
- f. It is suggested that the durability of pothole repair materials are categories as follows:
 - Category I: Durability less than 1 year (short-term durability)
 - Category II: Durability between 1–3 years (medium-term durability)
 - Category III: Durability more than 3 years (long-term durability)

4 TEST PROGRAMME

4.1 Required tests and evaluation methods for use in the laboratory and in situ

The tests and evaluation methods identified as currently used to select pothole repair materials and techniques were reviewed from the questionnaire responses. It appears that pothole repair materials and techniques need to be assessed by a certification procedure prior to use because the size of works makes compliance checking impractical. The principal requirements of the materials that need to be assessed in order to ensure durability and the associated test methods are (Nicholls, 2011):

1. Standard properties for surfacing materials, where the principal properties are:
 - 1.1 Deformation resistance by wheel-tracking to EN 12697-22 (CEN, 2003a) or cyclic compression to EN 12697-25 (CEN, 2005).
 - 1.2 Texture depth to EN 13036-1 (CEN, 2010).
 - 1.3 Air voids content to EN 12697-5 (CEN, 2009), -6 (CEN, 2012a) and -8 (CEN, 2003b).
 - 1.4 Water sensitivity to EN 12697-11 (CEN, 2012b).
 - 1.5 Binder affinity to EN 12697-12 (CEN, 2008).
2. Compactibility in adverse conditions to EN 12697-10 (CEN, 2001) but at a low temperature.
3. Setting/curing time needed prior to traffic, which will depend on the material type but possibly a test such as a development of the steel ball depression test (an adaptation of an existing non-CEN test).



Figure 4. Slovakian cold asphalt specimens.

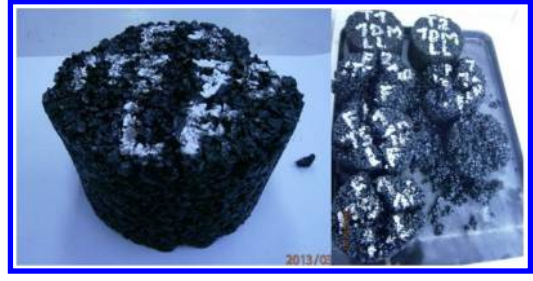


Figure 5. Cold asphalt specimens from Germany after ITS testing.

4. Sensitivity to conditions using repeated tests for different temperatures and humidities and/or freeze/thaw cycles (an adaptation of an existing non-asphalt test).
5. Adhesion (including the use of tack/bond coat) to the tensile option of the draft for prEN 12697-48, interlayer bond strength.
6. Recyclability (but only as a consideration at this stage) from a desk-top chemical evaluation/data sheet.

4.2 Laboratory tests

4.2.1 Materials tested

Three types of materials (hot asphalts, cold asphalts and synthetic-binder mixtures) were selected from the myriad available for laboratory tests (Komačka and Remišová, 2012). The hot asphalts chosen as a benchmark for comparison with the cold asphalts and the synthetic-binder materials were an asphalt concrete, AC 11, and a soft asphalt, SA 8. The later was chosen because, although currently only used in Scandinavia, soft asphalts do have properties that would be useful in pothole repair materials.

4.2.2 Cold asphalts

Fourteen cold asphalts currently available in the European market were tested (Figures 4 and 5). Tests of particle size distribution, binder content and air voids content were used to select one cold asphalt from each country involved in the testing (Germany, Slovakia, Slovenia and the United Kingdom) for further investigation in terms of compactibility, indirect tensile test, water sensitivity and sensitivity to freeze-thaw cycle) on specimens prepared and tested at two temperatures (5°C and 20°C).

The tests used were similar to those normally used for hot mix asphalt in order to allow for direct comparisons to be made.

The results of the tests demonstrated the following:

- Only a few of the cold asphalts have more than one aggregate fraction and continuous particle size distribution; one or two fractions of aggregate predominate in most of the tested cold asphalts.
- The cold asphalts with unsuitable aggregate gradations have high air voids contents that may negatively influence their performance.

- No cold asphalt with an air voids content lower than 10% was found.
- Some of the cold asphalts contain binders that do not become hard after application of the material; the mixtures stay soft, and they have little or no resistance to loading (and some of them even disintegrated spontaneously).
- Intensity of compaction is critical to cold asphalt performance as it is to how mix asphalt; low compaction decreases the values of the performance parameters and shortens the service life.
- Cold asphalts differ with regard to compactibility; the differences between the compaction curves prove that mixture composition (aggregate gradation and binder) is more important than the compaction temperature (which is low) with the viscosity of the binders in the tested cold asphalts not changing significantly in the temperature range from 5°C to 20°C.
- The type of cold asphalt, the temperature conditions and the cure time influence the indirect tensile strength of the cold asphalts.
- The highest indirect tensile strength values of cold asphalts were found for the compaction and conditioning temperatures of (20 ± 1)°C and the lowest for (5 ± 1)°C, as would be expected.
- Differences in the indirect tensile strength among the cold asphalts can be high (double or more) and depend on the temperature conditions before and after application; better results are achieved at elevated compaction and curing temperatures (20°C).
- Cure time is a positive factor because the values for indirect tensile strength increase over time; the amount of change depends on the temperature conditions and can be significant (up to 50%).
- Only one of the tested cold asphalts was water resistant in all the tested scenarios of compacting and conditioning temperatures; the others had little or no resistance to the influence of water. (The test samples were soft or disintegrated before or during testing.)
- Only one of the tested cold asphalts proved resistant to freeze-thaw cycles; the others have little or no resistance. (The test samples were soft or disintegrated before or during testing.)

- Taking into account all the ways of comparing compactibility and indirect tensile strength (dry, wet, freeze-thaw), compactibility could be removed from the list of relevant properties that should be tested for cold asphalts.

4.2.3 Analysis of results

The following findings emerged from the comparison of the test results for the cold and hot asphalts:

- A large difference exists only in the first stage of compaction; thereafter, the ratio of the changes in height increases slowly. The increase means that the change in height of the compacted cold-asphalt specimens is faster.
- The total changes in height of all the tested cold asphalts were higher than for SA 8; two of the cold asphalts had a greater change in height and two had lower when compared with AC 11.
- Only one cold asphalt had values from the indirect tensile, water sensitivity and sensitivity to freeze-thaw cycle tests that were close to the hot asphalt values; even this material is comparable only with SA 8 with the soft 250/330 bitumen. The other tested cold asphalts were significantly weaker than the hot asphalts.

Taking into account the findings mentioned above, it seems useful to determine some requirements for the components of cold asphalts and the parameters of the final mixture. These could include: a minimum number of aggregate fractions that should be used in a mixture; limitations on the particle size distribution (minimums and maximums passing through defined sieves); a required air voids content; binder properties; and required values for the results of the selected tests.

Different approaches could be used to apply the requirements above. All of the requirements could be accepted, or only some of them could be used. Moreover, various formulations of the requirements for each parameter are possible. Numbers, limits, and descriptive requirements are suitable. One of the possible sets of requirements was recommended by the consortium as follows:

- The maximum nominal size of the aggregate used in a mixture should be in the range of 4 mm to 10 mm.
- The air voids content of a cold asphalt should be as low as practicable so that it is as similar to the original surrounding material as possible.
- The indirect tensile strength (ITS) of a cold asphalt, as determined according to EN 12697-23 (CEN, 2003c), should be at least 20% of the ITS for a hot asphalt. The ITS requirement should be evaluated for cold-asphalt specimens with the temperature before compaction being +5°C, the compaction of the specimens being by an impact compactor according to EN 129697-30 (CEN, 2012c) the storage and conditioning of the specimens before testing being +5°C and the test temperature being +5°C.

4.2.4 Synthetic binders

New knowledge about synthetic-binder materials has been gained. Two materials with different compositions and synthetic binders were tested. From experience and the test results, the following can be concluded:

- The workability time of the synthetic-binder mixtures is very short, so the mixture must be prepared and compacted within a few minutes.
- It is recommended to prepare at one time only the quantity of a mixture that is needed for one pothole.
- The workability of the mixtures is lower and shorter at elevated temperatures (20°C).
- Both the tested materials had comparable strength values regardless of differences in the material composition.
- The temperature conditions before and after compaction of the specimens had only a small influence on the indirect tensile strength.
- Both materials are resistant to water and frost.
- Approximately the same values of indirect tensile strength were found at test temperatures of 5°C and 25°C; it seems that the stiffness of the tested synthetic-binder mixtures is independent of temperature.
- The tested synthetic-binder materials had higher indirect tensile strength than the tested hot asphalts.

5 WHOLE-LIFE CYCLE COSTS AND BENEFITS

Typically, potholes appear towards the end of the service life of an asphalt pavement and pothole repair aims to ensure the asphalt pavement achieves its planned service life. Potholes can be repaired with different materials and different techniques which influence the survival rate of the pothole patching. For road agencies, the challenge is to decide on the most cost-effective set of repair activities for the remaining service life of the asphalt pavement. A tool that can facilitate road agencies in their decision making is life-cycle cost-benefit analysis (LCCBA).

Potholes can be repaired with a number of different materials using several different techniques. It was not feasible to address all the potential combinations in LCCBA. The combinations that were considered are depicted in Table 2 (Hartmann, 2013). A special case is milling and resurfacing which is not used to repair single potholes but to renew the entire section where potholes occur. It will allow the determination of the moment when patching is no longer cost-effective and renewing the entire section is the better alternative.

In order to schedule pothole repair, an agency needs to know when and how many potholes are likely to occur within the remaining life time of the asphalt section. Predicting the occurrence and progression of potholes is, however, a challenging task, because a number of factors need to be considered such as road design, asphalt age, traffic intensity, and weather conditions. Due to the difficulties of addressing every

Table 2. Repair alternatives.

Repair alternative	Repair material	Repair technique
1a	Cold-mix asphalt	Unprepared fill-and-roll
1b	Cold-mix asphalt	Prepared fill-and-roll
2a	Synthetic binder	Prepared fill-and-roll
3a	Hot-mix asphalt	Unprepared fill-and-roll
3b	Hot-mix asphalt	Prepared fill-and-compaction
3c	Hot-mix asphalt	Milling and resurfacing section

Table 3. Pothole scenarios.

Scenario	1	2	3	4
Top asphalt layer depth	50 mm	30 mm	30 mm	50 mm
Remaining service life	6 years	3 years	6 years	3 years
Traffic intensity	High	High	Low	Low
Amount of precipitation	High	Low	Low	High

Traffic intensity: High = 50×10^6 axles/year
 Low = 10×10^6 axles/year
 Precipitation: High = 100 mm/month
 Low = 25 mm/month

possible contextual situation, it is proposed that four scenarios varying on four factors are selected: thickness of top asphalt layer, remaining service life, traffic intensity, and amount of precipitation (Table 3). It is believed that these scenarios cover typical but also contrasting repair situations.

For each scenario, it is assumed that, on a standard 1 km of road, one pothole appeared at the start of the first analysis year. In Scenarios 1 and 2, a high number of additional potholes appear annually which increases over the remaining service life of the asphalt section. In Scenarios 3 and 4, only one additional pothole appears each year. The total number of potholes to be repaired depends on the patching survival which, in turn, is influenced by repair material and technique. It becomes apparent that the total number of potholes to be repaired in one year can increase if the survival rate of the already repaired potholes is less than the remaining service life. The four scenarios suggest that an agency has to repair potholes every year of the remaining service life. However, the scenarios do not show when the repair will take place or, in other words, how long a pothole exists from its occurrence until its repair. For an agency, it can be cost-effective to wait before a pothole is repaired (except for emergency repairs). From a user perspective, a period with unpatched potholes means a period of higher risks of accidents, longer travel time and higher vehicle operation costs; the more potholes there are, the higher the impact is on users and the higher the user costs are. Two response times are distinguished: immediate repair and

deferred repair. Twelve repair strategies were analysed which combine repair alternative and response time.

After running LCCBA, the following conclusions can be drawn:

1. In all four scenarios, the agency costs for the immediate repair are higher than for the deferred repair, because traffic management costs can be reduced through the bundling of pothole repairs. On the other hand, user costs for deferred repair are higher than for immediate repair, because the existence of potholes for a longer period increases vehicle operation costs, travel time and accident risk.
2. In all four scenarios immediate repair strategies are preferable compared to deferred repair strategies. Although deferred repair strategies have lower agency costs, the user costs increase drastically and, thus, the total costs. Even for scenarios 3 and 4 with lower traffic intensity, the user costs are considerably higher compared to the agency costs.
3. In all four scenarios, the unprepared patching of potholes with cold-mix asphalt (alternative 1a) incurs the highest costs compared to other patching strategies. The low patching survival of this strategy increases the total number of potholes to be repaired.
4. In all four scenarios, the repair alternatives 1b, 2a, 3a and 3b show very similar costs. Although these strategies have different patching survival rates and repair costs, the longer patching survival and higher costs of one strategy is outweighed by the shorter patching survival and lower costs of another strategy.
5. In scenario 1 and 2, a deferred resurfacing of the road section is more cost-effective than a deferred patching of potholes. The high traffic intensity of both scenarios leads to high user costs which favour the resurfacing option.
6. In scenario 3 and 4, deferred patching of potholes is more cost-effective than a deferred resurfacing of the road section. The low traffic intensity of both scenarios reduces the user costs which favour the patching option.

6 CONCLUSIONS

The POTHOLE project has identified that the problem of pothole is a current topic in all European countries, but still there is no uniform definition, for which one has been provided. More importantly, a lot of approaches for the repair of pothole which do not ensure durability are very common throughout Europe. Therefore, a list of test methods were developed which can help to ensure the use of quality material in the future. Based upon the study of European techniques, a compilation of different materials and procedures has been made and developed further, taking the analysing of existing trial sites into account, categories which show an estimated durability if certain materials and procedures are combined.

Detailed results and conclusions are given the final report (Kubanek, 2013a) as well as the more detailed reports of the different work packages

The results of different strategies for pothole repair were shown in a Life Cycle Cost Benefit Analysis. Guidelines for pothole repairs (Kubanek, 2013b) have been developed based upon all the results of the project can now be easily used by stakeholders that are facing the question which material and procedures should be used for what purpose.

ACKNOWLEDGEMENTS

The POTHOLE project was a European research project within the scope of the Joint Research Programme “ERA-Net Road” funded by Belgium, Germany, Denmark, Finland, France, Netherlands, Norway, Sweden, Slovenia and the United Kingdom represented by the Austrian Research Promotion Agency (FFG). The study was completed in September 2013 having been undertaken by institutions from seven countries (Germany, Belgium, Denmark, Netherlands, Slovakia, Slovenia and the United Kingdom).

REFERENCES

- Comité Européen de Normalisation. 200. Bituminous mixtures – Test methods for hot mix asphalt – Part 10: Compactibility. EN 12697-10:2001. Most European standardisation institutions.
- Comité Européen de Normalisation. 2003a. Bituminous mixtures – Test methods for hot mix asphalt – Part 22: Wheel tracking. EN 12697-22:2003. Most European standardisation institutions.
- Comité Européen de Normalisation. 2003b. Bituminous mixtures – Test methods for hot mix asphalt – Part 8: Determination of voids characteristics of bituminous specimen. EN 12697-8:2003. Most European standardisation institutions.
- Comité Européen de Normalisation. 2003c. Bituminous mixtures – Test methods for hot mix asphalt – Part 23: Determination of the indirect tensile strength of bituminous specimens. EN 12697-23:2003. Most European standardisation institutions.
- Comité Européen de Normalisation. 2005. Bituminous mixtures – Test methods for hot mix asphalt – Part 25: Cyclic compression. EN 12697-25: 2005. Most European standardisation institutions.
- Comité Européen de Normalisation. 2008. Bituminous mixtures – Test methods for hot mix asphalt – Part 12: Determination of the water sensitivity of bituminous specimens. EN 12697-12:2008. Most European standardisation institutions.
- Comité Européen de Normalisation. 2009. Bituminous mixtures – Test methods for hot mix asphalt – Part 5: Determination of the maximum density. EN 12697-5:2009. Most European standardisation institutions.
- Comité Européen de Normalisation. 2010. Road and air-field surface characteristics – Test methods – Part 1: Measurement of pavement macro-texture depth using a volumetric patch technique. EN 13036-1:2010. Most European standardisation institutions.
- Comité Européen de Normalisation. 2012a. Bituminous mixtures – Test methods for hot mix asphalt – Part 6: Determination of bulk density of bituminous specimens. EN 12697-6:2012. Most European standardisation institutions.
- Comité Européen de Normalisation. 2012b. Bituminous mixtures – Test methods for hot mix asphalt – Part 11: Determination of the affinity between aggregate and bitumen. EN 12697-11:2012. Most European standardisation institutions.
- Comité Européen de Normalisation. 2012c. Bituminous mixtures – Test methods for hot mix asphalt – Part 30: Specimen preparation by impact compactor. EN 12697-30:2012. Most European standardisation institutions.
- Hartmann, A. 2013. Life-cycle cost-benefit analysis. Deliverable D6 of ERA-Net project POTHOLE. Brussels: FEHRL. www.fehrl.org/?m=32&id_directory=70201.
- Komačka, J, and E Remišová. 2012. Comparison of the performance of common and new materials for repairs of potholes. Deliverable D5 of ERA-Net project POTHOLE. Brussels: FEHRL. www.fehrl.org/?m=32&id_directory=7020.
- Kubanek, K. 2013a. Permanent pothole repairs: Final report. Deliverable D7 of ERA-Net project POTHOLE. Brussels: FEHRL. www.fehrl.org/?m=32&id_directory=7022.
- Kubanek, K. 2013b. Guidelines for pothole repairs. Annex to Deliverable D7 of ERA-Net project POTHOLE. Brussels: FEHRL. www.fehrl.org/?m=32&id_directory=7022.
- Ipavec, A. 2012. Study of existing standards, techniques, materials and experience with them on the European market. Deliverable D3 of ERA-Net project POTHOLE. Brussels: FEHRL. www.fehrl.org/?m=32&id_directory=7018.
- Nicholls, J.C. 2011. Definition of potholes and test methods for materials used in their repair. Deliverable D1 and D2 of ERA-Net project POTHOLE. Brussels: FEHRL. www.fehrl.org/?m=32&id_directory=7016.
- Rosenberg, J. 2012. Evaluation of techniques and materials from existing trial sites in Europe. Deliverable D4 of ERA-Net project POTHOLE. Brussels: FEHRL. http://www.fehrl.org/?m=32&id_directory=7019.

Innovations for sustainable road infrastructure

F. Kehagia

Civil Engineering Department of AUTH, Greece

K. Chondrosyros

Civil Engineer

ABSTRACT: During the 20th century, the development of highway infrastructure provides safe, fast and easy driving. The integration of new technological achievements is at benefit of passengers, drivers and vehicles: high-quality materials, safety devices, intelligent transportation systems, electronic information. However, in the context of the 21st century, persistent challenges have to be faced: the increase in demand for road transport services, the consumption of large quantities of resources and energy, adverse climatic conditions, new road maintenance practices. The main question is how road highway infrastructure meets and handles the challenging future. Innovative practices in design, construction and maintenance of road infrastructure are implemented worldwide in order to reduce the reliance on virgin building materials and to reduce the impact of climate change through the reduction in CO₂ emissions. The main objective of this paper is to present some of these innovative practices that provide a sustainable and environment-friendly infrastructure.

1 INTRODUCTION

It is undoubtful that quality of life has improved by transportation system providing opportunities for travel or transfer goods from one place to another. Economic growth and increased personal wealth contributed to a considerable surge in demand for mobility in the past decade, especially in rapidly emerging countries. However, nowadays, the construction of road network impose a burden on societies of increasing signs of environmental stress, notably in the form of poor air quality, excessive noise and traffic congestion and significant habitat segmentation. Environmental protection, mitigation and sustainability are words that have become parts of our lives (Dulac et al, 2012).

In the context of the 21st century, the need of green or sustainable roads and a balance between socio-economic development and respect for the environment has been set. Persistent challenges have to be faced: the increase in demand for road transport services, the consumption of large quantities of resources and energy, adverse climatic conditions, new road maintenance practices. The main question is how road highway infrastructure meets and handles the challenging future (Kunz, 2012). A holistic approach which would cover the different aspects of road construction, operation and maintenance, road energy and environment is necessary.

In order to face these road challenges, new innovations practices have been developed worldwide,

based on application-oriented research, in design, construction and maintenance of road infrastructure and implemented. The main objective of this paper is to present some of these innovative practices that provide a sustainable and environment-friendly road infrastructure.

2 GREEN HIGHWAYS

2.1 Sustainable roads

The concept of sustainability has been gained increased interest as potential solution for many global, regional and local problems facing society in the late twenty years. The general meaning of the sustainability refers to the viability of natural resources and ecosystem over time and to the maintenance of human living standards and economic development. For the engineer, creating sustainable systems involves making decisions based on many dimensions: technology, ecology, economics, using tools in order to support them, as life cycle assessment, environmentally conscious design, industrial ecology (Carpenter, 1995).

In 1994, the Organization for Economic-Cooperation and Development (OECD) defined *sustainable transport* as “transportation that does not endanger public health or ecosystems and meets mobility needs consistent with (a) use of renewable resources at below their rates of regeneration

and (b) use of non-renewable resources at below the rates of development of renewable substitutes”. The European Road Federation (ERF) has defined the concept of *sustainable roads* as: “effectively and efficiently planned, designed, built, operated, upgraded and preserved roads by means of integrated policies respecting the environment and still providing the expected socio-economic services in terms of mobility and safety”.

Road construction has a negative impact on surrounding ecosystems and overall environmental quality. Today, the need for a straightforward method of integrating sustainable road practices into a common standard is crucial. Sustainable or green roads include sustainable practices than modern construction techniques as the use of recycled materials, ecosystem management, energy reduction, increasing the water quality of storm water runoff, reducing air pollution and maximizing overall societal benefits. The consideration of economical, ecological and social aspects in the life cycle of road infrastructure is a prerequisite to ensure the mobility in the long term.

2.2 Sustainability rating systems

The need to be able to quantify sustainability for highways has been suggested by various agencies. The main reason was the lack of adequate information of decision makers to make informed decisions and trade-offs on sustainable techniques on road infrastructure. A rating system will prove beneficial in the design and construction of new surface road system assessing and classifying how sustainable or “green” infrastructure projects are. Moreover, it is used in the upgrade and reformation of existing road systems. Many methodologies and rating systems have been developed. Among them, is the *Envision rating system*, a broad-based infrastructure rating system, developed by the Institute for Sustainable Infrastructure, the *Greenroads rating system*, developed by the Greenroads Foundation, a transportation-specific rating system and *INVEST*, the Infrastructure Voluntary Evaluation Sustainability Tool, developed by the Federal Highway Administration (FHWA), also a transportation-specific rating system. Green highway classifications will help transportation decision and planning makers to have a more clear understanding of techniques and incentives for maximizing sustainable efforts.

3 CHALLENGES AND INNOVATIONS

3.1 The challenges of road infrastructure

The road sector, today, faces huge challenges, including ambitious demands such as better, quicker and less expensive production, construction and maintenance: (Kunz), (Mouratidis)

- There is a current and future need to absorb the increasing flow of vehicles by means of the existing

infrastructure. The increase in demand for road transport services will not keep pace only with the construction of new road links. Over the period 2000–2020, forecasts expect a 35% increase of passenger transport and even a 70% increase of the transport.

- Fossil fuel resources are getting increasingly scarce. Through an increasing use of alternative materials with a recycling management, the dependence of natural resources can be reduced.
- The energy consumption for planning, construction and operation will be minimized and renewable energy may be provided.
- Roads will be subject to greater climatic stress in the future (extreme climate events, such as flood, heavy snow). Highways must be designed in a way to confront adverse climate, and also be adequately equipped to protect passengers and vehicles.

3.2 New innovations in road design

According to the European Commission’s project “New Construction Concepts (NR2C)”, the road infrastructure of future has to represent four dominant characteristics: reliable (for optimizing the availability of infrastructure), environment friendly (for reducing the environment impact), safe and smart (for optimizing flows of traffic) and human (for harmonizing infrastructure with the human dimensions).

Lots of technologies and innovations are developed in private and public research centers. This strategy aiming at sustainability would conserve existing resources, generate less waste and emissions, abolish barriers that prevent the use of alternative materials and reduce energy consumption. Some of these innovations practice, as in the main concept of road design or as only in pavement design, are presented.

3.2.1 The Forever Open Road

The “Forever Open Road” concept is under a research program of the Forum of European Highway Research Laboratories (FEHRL) which adopts a holistic approach for the new generation road.

It is a road that is adaptable, automated and climate change resilient and can be applied whether motorway, rural or urban. The adaptable road will be based on a prefabricated/modular system. It will adapt to increasing travel volumes and to changes in demand for public transport, cycling and walking. It will power vehicles, harvest solar energy, measure its own performance and even repair itself. The automated road will incorporate a fully integrated information, monitoring and control system, communicating between road users, vehicles and operators. It will support a cooperative vehicle-road system that will manage travel demand and traffic movements. It will measure, report and respond to its own condition, providing instant information on weather, incidents and travel information. The resilient road will adapt itself to the impacts of extreme weather conditions and climate change. The road will monitor flooding, snow,

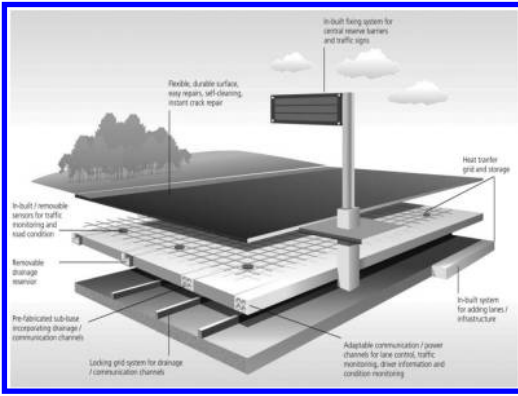


Figure 1. The Forever Open Road.



Figure 3. Solar Road.



Figure 2. Solar Arch.

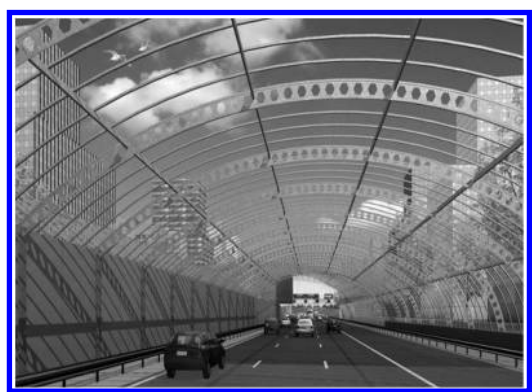


Figure 4. Sustainable Highway.

ice, wind and temperature change, and mitigate their impacts through integrated storm drainage, automatic heating and cooling, and will be linked to the integrated information system for travelers and operators.

3.2.2 Solar Arch

The “Solar Arch” by industrial designer Tyson Steele (USA) is a concept covering for rural roads that can generate renewable solar energy for off-grid highway lightning. The Solar Arch can also supplement electricity demands in neighboring areas. Apart from generating renewable energy the Solar Arch can also reduce icing in winter and keep the roads cool in summer. The arch design is in compliance with AASHTO standards for US interstate bridges and passageways. Variations of the design include a longer version with lined troughs on each side so topsoil can be packed into the outer supports, increasing its insulation properties and reducing its visibility in naturally pristine areas.

3.2.3 Solar Roadways

The “Solar Roadways” project is being developed by Solar Roadways in Idaho, USA. The concept of this project is the possibility of the installation of solar panels that could be installed on a wide range of surfaces

(roads, pavements, playgrounds). The panels also contain LED lights for traffic signs, lane marking, as well as heating elements which are useful in winter conditions as they have the ability to melt ice and snow. Solar Roadways could also be used to charge electric vehicles, and future technology could even allow for charging while driving. The generation of electricity from the road panels would over time cover the construction cost, whilst if deployed widely, would provide a decentralized electricity grid system. The solar panels need to be wired up, so that errors can be easily detected and repaired.

3.2.4 The Sustainable Highway

The “Sustainable Highway” concept offers an integrated solution to motorway emission and noise problems. It consists of a motorway canopy made of cold-bendable laminated glass. The air is cleansed of fine particulates using electrostatic filtering while the nitrogen oxide emitted by the vehicles is disposed by adsorption. Solar cells incorporated into the glass produce clean energy. The excess heat that accumulates in the summer is stored in the groundwater and used to heat the asphalt in the winter. This still leaves plenty



Figure 5. Road Solar Collector pipe system.

of heat for such purposes as domestic heating. Furthermore, bio-fuel can be produced under the canopy, creating a conversion of carbon dioxide into oxygen (Vakar & Snijder).

3.2.5 Road Solar Collector

Black roads can be used to collect solar heat in summer. The temperature on a black road in full sunshine will often be 15°C higher than the air temperature in the shade. This temperature can be collected by water circulating through an array of pipes embedded in the surface of the road, allowing continuous collection of heat on hot summer days: generating on site renewable energy. Heat is in plentiful supply in summer, but is urgently demanded in winter for space heating. This time gap between supply and demand calls for Seasonal Thermal Energy Storage. The gap can readily be bridged by using a thermal bank: the heat from the road can be transferred down to a thermal bank in the ground. This can be achieved using thermoactive foundations or boreholes and will increase the natural temperature of the ground (around 10°C at a depth below six meters in northern Europe) up to 30°C. The ground receives heat slowly. Once heat is absorbed by the ground it will only make away very slowly. The thermal bank can maintain its warmth through to the winter when it can be readily extracted by a suitably adapted ground source heat pump. The work in the last years has focused on minimizing the depth of the pipes in the road without compromising the structural stability of the road.

3.2.6 Hypar-nature-Wildlife Crossing

The “Hypar-nature” design concept combines design, ecology, and engineering into a solution that is both cost effective and elegantly simple. The hypar-nature bridging system is inspired by the demands of ecological engineering. The design distills the adjacent landscapes and habitats, condenses and amplifies multiple landscape bands across the structure, and then extends these bands into habitat corridors that provide connections for a larger cross-section of species. The bridging system consists of precast modules that serve as abutment, beam, and deck. This single element



Figure 6. Hypar-nature wild crossings.

is the key to cost effectiveness, speed of construction, and modularity. Two modules are joined at the midspan acting as three-hinged arch, eliminating the need for a center pier. No on site concrete work is required. Instead the hyparnature modules are optimized for being efficient to transport, erect, combine, and recombine as needed. The same modules, oriented differently, can also incorporate bicycle paths separated from traffic and the wildlife crossing above (Kociolek, 2011).

3.2.7 Smart Highway

Smart Highway is interactive and sustainable road of tomorrow by designer Daan Roosegaarde and Heijmans Infrastructure. Current designs include Glowing Lines, glow in the dark lining absorbs energy during the day and glows in the dark. The lining emits light for as long as ten hours providing a safe and sustainable alternative to conventional lightning of dark roads. The first pilot of Glowing Lines has been realized at N329 in Oss, the Netherlands, and will be further launched international. New designs include more features like Dynamic Paint (temperature-controlled marking lights up and becomes transparent again, depending on temperature. The marking warns road users when the road deck can be slippery), Interactive Light (controlled by sensors: it only turns on when traffic approaches. It is a sustainable and cost-saving alternative to continuous lightning, Electric Priority Lane (induction charging offer electric cars the possibility to charge themselves while driving), Dynamic Lines (road deck markings can be flexibly adjusted, to show a continuous line or dotted line providing dynamic traffic control, adjustable depending on the situation) and Wind Light (the wind generated by passing cars activates small windmills along the road. The windmills generate energy, which is used to light up the lamps in the windmills).

3.2.8 Wind Turbine Bridge

Using the space between a viaduct, the installation of 26 wind turbines could produce 36 million kilowatt hours of electricity per year. Additionally, the roadway across the bridge would be densely lined with solar



Figure 7. The Glowing Lines feature of Smart Highway.



Figure 9. Modieslab.



Figure 8. Wind Turbine Bridge.

cells coated in clear plastic, producing another 11.2 million kilowatt hours. The entire viaduct itself would be turned into a promenade and park. Solar powered greenhouses would be installed along the bridge, creating an ultra fresh farmer's market. The entire structure repurposes abandoned structures, producing 40 million kilowatt hours of electricity (that is enough to power 15000 homes).

3.3 Innovations in pavements

3.3.1 Modieslab

Modieslab is a revolutionary new road surface. It is a prefabricated road slab manufactured from concrete elements, constructed from two different open layers of concrete on a further supporting layer of concrete, designed to be anchored to piled foundations. The system consists of concrete elements, which are constructed from two different open layers of concrete on a supporting layer of concrete. Water run-off channels help rainwater to be quickly discharged. Furthermore these channels also give the road surface self-cleaning

properties. Modieslab also offers opportunities for small features like detection and signaling. An optional piping system in the construction layer keeps the road surface cool in the summer and warm in the winter. Thus, the surface itself actually manages to remove a lot of snow and ice, which helps to prevent damage to the road surface caused by salting. Modieslab is characterized by high noise reduction, circa 6 db, and low rolling resistance, which results in considerably lower emissions of CO₂ NO_x and fine particles. Since this time, three trials have taken place, most recently a 100 metre test lane on the A12 motorway near Utrecht, involving a full-scale motorway set up under intensive traffic conditions.

3.3.2 Greener roads through new mixing and compaction technologies

Lowering the maximum temperature of the asphalt during production and mixing allows a reduction of fuel consumption at the mixing plants, since less energy is needed to heat the minerals and the bitumen. The second advantage of lower temperatures is the significant decrease of asphalt smoke that construction workers are exposed to. The Ammann Compaction Expert (CAE) enables the operator of a roller to choose the optimal vibration mode on the road construction site. Very fast compaction is achieved. Over-compaction is prevented and in addition, the energy consumption of the machine itself is minimized. Intelligent compaction with high-tech measurement and control equipment therefore is a key enabling technology for the wider application of lower temperature asphalt. Compaction machines can be controlled using GPS positioning technology. Real time displays of machines' current positions, compaction work done, and positions where additional compaction is necessary allow use of the machines to be planned. The combination of intelligent compaction modes, positioning technology and on-machine displays allow the new low temperature asphalts to be applied on road construction sites (IRF 2009).



Figure 10. Rollpave.

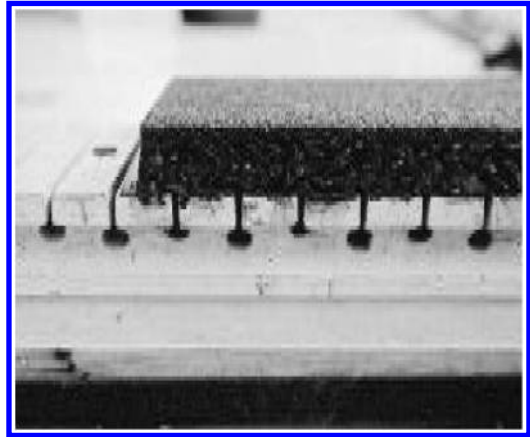


Figure 11. Rollpave.

3.3.3 Road on a roll – Rollpave

The Rollpave concept has also been developed from the Dutch ‘Road to the Future’ Innovation programme, and is a prefabricated asphalt mat, approximately 30 mm thick, that is laid on top of an existing pavement with sufficient structural strength to carry the design traffic. The design allows for repairs to be carried out 50% faster than conventional methods, whilst providing a low noise surface course, comparable to a 2-layer porous asphalt; this is reported to give noise reductions of circa 6 dBA from conventional dense asphalt layers (Kehagia, Manthos, 2014).

3.3.4 Ecotechnic Road Systems

Ecotechnic Road Systems is a modular concept of mitigating solutions concerning an appropriate combination of low noise pavement and anti-noise barrier subsystems. “Euphonic pavement” composite multi-layer consists of double porous layer, a micro porous asphalt wearing course (20 mm, 0–5 mm basaltic) and porous asphalt base course (40 mm, 0–25 mm limestone), connected by neck to a layer with a Helmholtz resonators system in either the third or fourth layer. The Helmholtz resonators are designed to absorb noise over the range 100 to 250 Hz. Compared to the reference pavement, these pavements typically are 2 to 4 dB better from 80 to 250 Hz, 8 to 14 dB better from 315 to 800 Hz, and 2 to 6 dB better from 800 to 5,000 Hz. The main remedial measures of the acoustic control/abatement solution designed and implemented for the city of Genoa, in the framework of the NR2C project (Kehagia, Manthos, 2014).

3.3.5 Intelligent road infrastructure

A promising approach for future road construction is based on a surface which is manufactured in a production plant and can be unrolled on a conventional base. The top layer is called car-pad. The industrial fabrication of the car-pad enables the integration of sensors inside the top layer of the road. Integrated wireless sensor nodes allow to measure passing vehicles and different ambient road conditions like temperature or moisture. Each passing vehicle generates structure-borne sound which propagate through the top layer

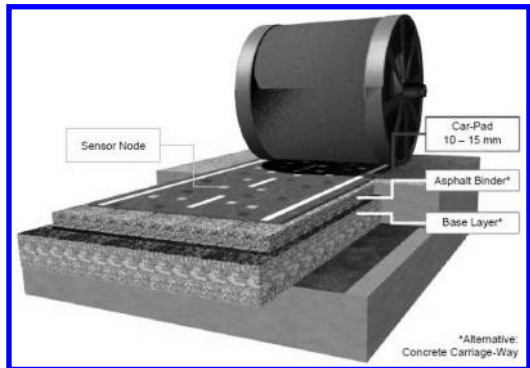


Figure 12. Structure of “intelligent” road.

of road and can be detected by an accelerometer. Accelerometers have very small dimensions, are cheap and can easily be integrated inside a sensor node. After preprocessing, the data are transmitted to small base stations mounted in beacons at the side of the road. These base stations combine the information of the different sensor nodes to a more global view of the traffic flow at this part of the road. The base stations transmit this information to a central traffic management center and to the passing cars. Due to the very dense sensor network not only the traffic flow but also local events like accidents or other dangerous situations like cars in blind spots can be detected and road users can be warned. Since the information is determined by the infrastructure and not by a car based system, the system will even work if most users are not equipped with a vehicle on board unit. To participate from warning signal no special hardware is needed. The on board unit can be integrated into the navigation system (Wunderlich et al. 2011).

3.3.6 Nanomaterials in asphalt pavements

In pavement engineering research, nanotechnology is used as a form of new material, device, and system at

the molecular level. In recent years, some researchers have started to work on the improvement of asphalt materials with nanomaterials in asphalt cement and emulsions. A small percent of nanomaterials may significantly improve the performance of asphalt materials. In some research work, it was found that 2% of nanoclay in the asphalt binder may increase the shear complex moduli by as much as 184%. This indicates that rutting resistance of such asphalt is likely improved. Furthermore polymer modified nanoclay (PMN) in the asphalt decreases the viscosity of the modified asphalt binders, which may have potential benefit in warm mix asphalt application. The addition of PMN in the control asphalt binder increases the recovery ability of asphalt binder. Researchers have also used nanotubes, nanosilica, and other nanomaterials to modify asphalt materials (Zhanping, 2013).

4 CONCLUSION

The highway of the future will be a real freeway, non-dependent on energy and free of environmental burden. Adaptable to weather conditions and able to manage on-road incidents, the freeway of the new generation will be constantly free and suitably open to traffic. Highly innovative and application-oriented research is needed in order today problems of transport of road infrastructure be minimized. Existing processes and products of basic research, (sensor technology, risk management, simulation methods or the use of innovative construction materials and structures), should be transferred promptly in a solution-oriented way into practice. The overall challenge for road of future is to provide convincing ideas to handle effectively all these issues. Lots of technologies are already available in private and public research centers. The high cost of these constructions is offset by minimizing the environmental and social impacts proving a positive net present value. However, a holistic approach is necessary, which would cover the different aspects of road construction, operation and maintenance taking into account a cost-benefit analysis in all stages.

REFERENCES

- Carpenter, S. 1995. When are technologies sustainable?. PHIL & TECH 1:1&2 Fall
- Dulac J., etal, 2012. Global travel growth, estimated future needs for road infrastructure and impacts on energy demands and carbon emissions: an analysis. Routes-Roads, No. 357, pp. 27–33
- ERF. 2009. Sustainable roads and optimal mobility. Discussion Paper. Brussels
- FEHRL, 2008. NR2C, New Road Construction Concepts FOREVER OPEN ROAD, <http://www.foreveropenroad.eu/>
- IRF. 2007. Sustainable roads. Discussion Paper
- IRF. 2009. Innovative Practices for Greener Roads
- Kehagia F., 2009. The implementation of sustainability in highway project *International Journal of Sustainable Development and Planning*, Vol. 4, No. 1, pp. 1–9
- Kehagia F., Manthos E., 2014, Fresenius Environmental Bulletin, Vol. 23, No. 11a, pp. 2803–2808
- Kociolek A., 2011. “Hypar-nature”-A precast concrete design for wildlife, *ASPIRE*, Fall 2011
- Kunz, 2012. The next generation of roads in France and in Germany. Routes-Roads No 355, pp. 27–35
- MODIESLAB, http://www.modieslab.nl/userfiles/ModieSlab_brochure_UK.pdf
- Mouratidis A., Kehagia F., 2014 On the Track of Road Evolution. *Journal of Infrastructure Development* 6(1) pp. 1–15
- ROAD SOLAR COLLECTOR, <http://www.e-hub.org/road-solar-collector.html>
- SMART HIGHWAY, <http://www.smarthighway.net/>
- SOLAR ARCH, <http://www.ecofriend.com/solar-arch-scalable-tunnel-generates-solar-energy-insulates-roads.html>
- SOLAR ROADWAYS, http://ec.europa.eu/environment/european_green_capital/smart-streets/
- Vakar L., Snijder, Sustainable Highway for Environmentally Constrained Urbanized Areas
- Zhanping You, 2013. Nanomaterials in Asphalt Pavements, *International Journal of Pavement & Technology*, Vol. 6, Issue 3
- Wind Turbine Bridge, <http://www.gizmag.com/solar-wind-bridge-concept/17771/>
- Wunderlich et al. 2011. Intelligent Road Infrastructure-A Concept Study, 5th International Conference on Sensor Technologies and Applications

A multiple regression model for developing a RAP binder blending chart for stiffness prediction

S. Bressi & A.G. Dumont

Traffic Facilities Laboratory (LAVOC), Ecole Polytechnique Federale de Lausanne (EPFL), Lausanne, Switzerland

Alan Carter

Department of Construction Engineering, École de Technologie Supérieure (ETS), Montreal, Canada

Nicolas Bueche

Nibuxs Sàrl, Ecublens, Switzerland

ABSTRACT: The increase in the use of Reclaimed Asphalt Pavement (RAP) makes it necessary to focus on the interaction between the old and the virgin binders represented by the so-called blending chart. Different types of linear binder blending chart are currently available to predict the characteristics of the final blend. This study constitutes part of a wider research campaign whose aim it is to provide prediction models for the rheological properties of RAP, taking into account a selection of variables that cause its heterogeneity. The objective of this paper is to provide a multiple regression model at medium and high temperatures for the prediction of the complex modulus and phase angle of binder blends. The models consider more than one variable at the same time: the type of virgin and aged binders, the percentage of aged binder, the loading frequency and the temperature. Thus, within a specific validity range based on the extreme values defined by the experimental domain, it is possible to predict the rheological properties of the binder blends, and to carry out a sensitivity analysis on the effects of each parameter.

1 INTRODUCTION AND OBJECTIVES

Recycled Asphalt Pavement is commonly used for the rehabilitation and new construction of roads. The increasing quantity of recycled materials and diminishing availability of virgin aggregates pose the problem of how to raise the amount of RAP in asphalt mixes without compromising performance. Guidelines have been developed since the seventies and eighties (NCHRP 1978, Epps et al. 1980) and have been subjected to several reviews over the years. Certain differences can be encountered in the evolution of the use of RAP among different countries. For example after a survey carried out in 2007 (NCDOT) among 50 States in the US and Canada, the usage rate of RAP was estimated to be 12% but with wide oscillations. On the other hand in Europe the strategies are divergent among EU member States. In the North of Europe RAP is used in higher quantities than in the South (Kalman et al. 2013).

Even if RAP is nowadays commonly used, it is not possible to claim a complete understanding of the chemical and physical phenomena involved during the fabrication process of a new mix containing a high percentage of RAP. One of the most important aspects

in this context is the study of the interaction between the old and the new binders and the blend behaviour. This is proved by the many efforts made in recent studies in this direction (Shirodkar et al. 2010, Nahar et al. 2012, Booshehrian 2013). In recent years the viscoelastic characteristics of the old and virgin bitumen were computed (Al Qadi et al. 2007, Swiertz et al. 2011), and a new calibration of the parameters for the 2S2P1D model was defined for certain types of blends (Mangiafico et al. 2014). Also in this specific research domain there are many different methods available to determine the characteristics of a blend. In Europe for example the method is based on the penetration and softening point of the RAP and virgin binder (EN 13108-8:2005), while in the US the blending models take into consideration the initial rheological characteristics of the binders as described by the NCHRP Report 452 (2001). Both blending charts are represented by a straight line that expresses linearity with the variation of RAP binder in the blend.

This paper aims to provide additional information concerning the rheological characteristics of the blends using several percentages of artificially aged binder and different types of virgin unmodified binder. A nonlinear multiple regression model was developed

for the blend stiffness prediction at medium and high temperatures considering several variables at the same time: the complex modulus of the virgin and aged binders, the loading frequency, the testing temperature and the percentage of aged binder in the blend. A sensitivity analysis was carried out to understand which factors have the strongest influence on the results.

2 MATERIALS AND RESEARCH PLAN

Two types of unmodified virgin bitumen were used with different penetration grades:

- 50/70 (penetration grade at 25°C of 56 10⁻¹ mm)
- 70/100 (penetration grade at 25°C of 82 10⁻¹ mm)

The master curves of the complex modulus and phase angle (Figure 1) were firstly computed testing the *frequency sweep* (21 frequencies tested from 0.16 to 16.7 Hz) with the Dynamic Shear Rheometer (DSR) (Anderson 1994) and using the Time-Temperature Superposition (TTS) principle (Ferry 1980) with a reference temperature of 20°C.

Both binders were subsequently artificially aged to simulate the long-term ageing RTFOT+PAV (ASTM D6521). The characteristics of the binders obtained after artificial ageing are summarised in Table 1.

In this way the RAP binder originating from RAP material was reproduced in the laboratory. The two virgin and two aged binders were mixed together by hand for 1 minute to compose different blend combinations characterized by different percentages of aged binder (Table 2) according to the following steps:

- The virgin binders 50/70 and 70/100 were heated at 136°C and 133°C respectively for one hour;

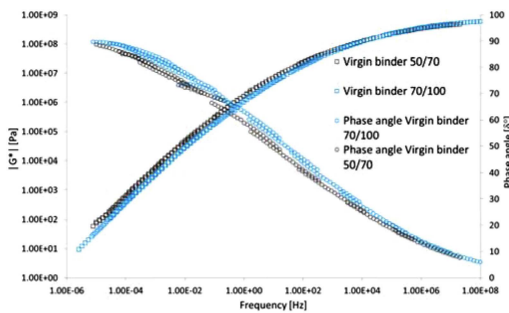


Figure 1. Master curves of complex modulus and phase angle of virgin binders 50/70 and 70/100 (T_{ref} = 20°C).

Table 1. Characteristics of the two artificially aged binders.

	70/100 (RTFOT + PAV)	50/70 (RTFOT + PAV)
Penetration @ 25°C	26	19
R&B (Temp. °C)	62	58
IP [EN 12591]	-0.05	-1.34

- The aged binder (RTFOT+PAV) was heated at 135°C for one hour (Poulikakos et al. 2013).

All the blends were then subjected to short-term RTFOT ageing (ASTM D 2872) in order to simulate a new asphalt production. The steps are summarised in Figure 2.

Finally the bitumen obtained from each combination was poured into the mould for DSR testing. Shear strains or stresses were applied to test specimens in the DSR by mounting the test specimens between parallel plates. All the tests were conducted in the previously determined Linear Viscoelastic Region (LVR),

Table 2. Summary of sample combinations.

Number of combination	Type of virgin binder	Type of aged binder	Content of aged binder
1	50/70	50/70	0%
2	50/70	50/70	10%
3	50/70	50/70	20%
4	50/70	50/70	40%
5	50/70	50/70	50%
6	50/70	50/70	70%
7	50/70	50/70	80%
8	70/100	70/100	0%
9	70/100	70/100	10%
10	70/100	70/100	20%
11	70/100	70/100	40%
12	70/100	70/100	50%
13	70/100	70/100	70%
14	70/100	70/100	80%
15	50/70	70/100	10%
16	50/70	70/100	50%
17	50/70	70/100	70%
18	50/70	70/100	80%
19	70/100	50/70	10%
20	70/100	50/70	50%
21	70/100	50/70	70%
22	70/100	50/70	80%

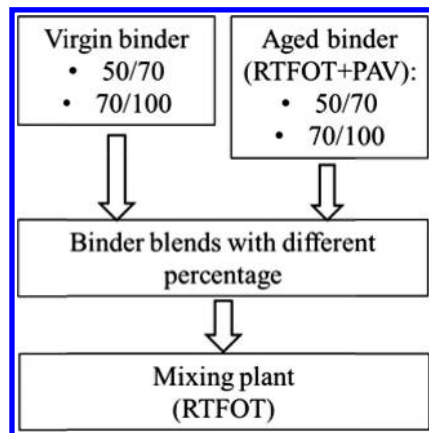


Figure 2. Schematic representation of sample creation.

see Figure 3. Indeed, before conducting complex modulus tests, it was necessary to carry out a *stress sweep* at the test temperature in order to establish the limit of the linear viscoelastic region of the behaviour of the binder. The LVR limit was defined as the point where the storage modulus (G') decreased to 95% of its initial value as prescribed by SHRP specifications (Anderson et al. 1994).

Subsequently, several frequency sweeps (21 frequencies tested from 0.16 to 16.7 Hz) were conducted at 30, 40, 50 and 60°C measuring the complex modulus and phase angle. Medium and high temperatures were selected since binders are generally more sensitive to blending at these temperatures than at low temperatures (Kandhal et al. 1997).

3 METHODOLOGY

3.1 Modelling

Multiple regression is a statistical technique (Mickey et al. 2009) that allows the development of models that take into account several variables, where the objective is to explain the behaviour of one dependent variable (in this case the complex modulus or the phase angle) as a function of several independent variables (i.e. stiffness of virgin binder, stiffness and percentage of aged binder in the blend and loading frequency). To calculate the coefficients of the models in order to carry out the sensitivity analysis and predict the final stiffness of the blend, it is possible to apply the least square fit algorithm expressed in Equations 1–2 in matrix form.

$$\beta = (X'X)^{-1} \cdot X'y \tag{1}$$

The matrix and vectors of the system are defined:

$$y = \begin{bmatrix} y_1 \\ y_2 \\ \vdots \\ y_n \end{bmatrix}; X = \begin{bmatrix} 1 & x_{11} & x_{12} & \dots & x_{1k} \\ 1 & x_{21} & x_{22} & \dots & x_{2k} \\ \vdots & \vdots & \vdots & \dots & \vdots \\ 1 & x_{n1} & x_{n2} & \dots & x_{nk} \end{bmatrix}; \beta = \begin{bmatrix} \beta_0 \\ \beta_1 \\ \beta_2 \\ \vdots \\ \beta_k \end{bmatrix} \tag{2}$$

where:

y = vector ($n \times 1$) of the observations on the dependent variable (i.e. measurements of complex modulus or phase angle)

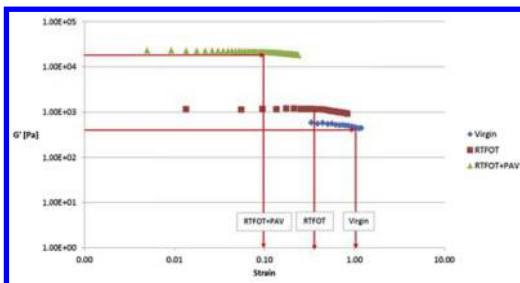


Figure 3. Stress sweep at 50°C with different aging levels of bitumen 70/100.

X = model matrix ($n \times (k + 1)$)

β = vector ($(k + 1) \times 1$) of unknown coefficients of the model.

A multiple regression model was developed for every testing temperature. These models allowed not only observing of the evolution of the importance of the parameters involved, as the temperature increases, but also the prediction of the complex modulus and phasing angle once the initial parameters were set.

The variables considered were:

- x_1 = complex modulus of the virgin binder
- x_2 = complex modulus of the aged binder
- x_3 = percentage of the aged binder in the blend
- x_4 = loading frequency.

3.2 Goodness of fit

Different criteria were applied to verify the goodness of fit of the models proposed:

- Coefficient of determination (R^2) that in this case expresses the variability of all the regressors
- Analysis of variance (ANOVA) (Bilal et al. 2011).

It was important to verify the goodness of fit of the models since a priori it is not possible to define the model that fits the data more accurately (linear, linear with interaction, second degree model etc.).

3.3 Sensitivity analysis

As stated above, the computation of the coefficients of the models is fundamental for carrying out a sensitivity analysis evaluating the effect that each parameter has on the final result. The coefficients of the model show the sensitivity of the related parameters as an average value over the entire domain of validity – the higher the coefficient, the greater the importance of the related parameter. For the purpose of the sensitivity analysis the relative effects were calculated using Equation 3:

$$\beta_r = \frac{\beta_i}{\beta_0} \tag{3}$$

A sensitivity analysis was carried out on the complex modulus and phase angle, taking into account the parameters mentioned above (stiffness of virgin and aged binder, percentage of aged binder and load frequency) and their interactions.

4 RESULTS

4.1 Modelling results

The values of the complex modulus and phase angle at each testing temperature for each blend were extrapolated for each frequency tested (21 points) from the frequency sweep conducted with DSR. An example is shown in Table 3.

As can be seen from Table 3 adding small quantities of RAP bitumen does not significantly change the

Table 3. Results of $|G^*|$ for all blends at 50°C and 1 Hz.

Number of combination	Type of virgin binder	Type of aged binder	Content of aged binder	Complex modulus $ G^* $ [Pa]	Phase angle (δ) [°]
1	50/70	50/70	0%	19 104	76.1
2	50/70	50/70	10%	20 520	76.2
3	50/70	50/70	20%	21 706	71
4	50/70	50/70	40%	51 582	69.3
5	50/70	50/70	50%	58 907	65
6	50/70	50/70	70%	102 800	63.6
7	50/70	50/70	80%	115 520	63.3
8	70/100	70/100	0%	7 009	84.6
9	70/100	70/100	10%	8 533	80.2
10	70/100	70/100	20%	10 964	81.5
11	70/100	70/100	40%	20 291	79.3
12	70/100	70/100	50%	23 770	76.4
13	70/100	70/100	70%	32 306	74
14	70/100	70/100	80%	55 398	72.1
15	50/70	70/100	10%	17 267	82.1
16	50/70	70/100	50%	26 933	66.4
17	50/70	70/100	70%	-	-
18	50/70	70/100	80%	61 539	63.2
19	70/100	50/70	10%	14 380	73.3
20	70/100	50/70	50%	32 207	73.5
21	70/100	50/70	70%	98 642	63.7
22	70/100	50/70	80%	-	-

complex modulus of the blend. Indeed, up to 20% RAP bitumen content (combinations 1-2-3 and 8-9-10) the stiffness of the blend does not exhibit any significant changes. For the phase angle, small oscillations occur up till 10% of RAP binder in the blend, after which the angle starts to drop more rapidly.

After testing all the possible models fitting the data, a second-degree model with interactions was chosen since it showed the highest goodness of fit. All the stiffness prediction models were developed applying the least square fit technique with multiple variables.

These can be divided into several sections: the constant factor term (a_0), four main factor terms ($a_1 = |G^*|$ of the virgin binder, $a_2 = |G^*|$ of the aged binder, $a_3 =$ percentage of aged binder, $a_4 =$ frequency), six two-way factor interaction terms (a_{12} , a_{13} , a_{23} , a_{14} , a_{24} , a_{34}), three three-way factors (a_{123} , a_{124} , a_{234}), one four-way factor (a_{1234}) and two second-degree factor terms (a_{33} , a_{44}).

The values of all the coefficients at every testing temperature are summarised in Table 4 and 5.

The results of R^2 and ANOVA for the type of model chosen are shown in Table 6 for the complex modulus and in Table 7 for the phase angle.

For all the models at every temperature the ANOVA table shows p-values <0.05 and R^2 in every case is higher than 0.9; the developed models thus accurately fit the real data set.

After having carried out the calculation of the relative effects with Equation 3, it was possible to determine which parameters most influence the result summing all the contributions given by the main

Table 4. Coefficients of models for complex modulus prediction.

Coefficients	30°C	40°C	50°C	60°C
a_0	2 426 798	731 198	190 651	29 220
a_1	-217 312	-134 328	-24 684	-10 707
a_2	-31 930	-52 840	-41 047	-16 905
a_3	524 911	303 162	144 309	18 359
a_4	1 155 825	480 596	142 377	7 528
a_{12}	58 044	76 673	-5 465	13 917
a_{13}	10 500	-73 404	-18 626	-11 401
a_{14}	-143 738	-89 364	-14 778	-6 380
a_{23}	-16 432	-982	-11 071	-7 164
a_{24}	30 131	-41 788	-38 839	-19 015
a_{34}	28 507	212 570	128 702	16 243
a_{123}	132 491	98 814	-18 095	20 024
a_{124}	10 327	54 427	-7 694	17 390
a_{134}	-11 968	-50 611	-15 577	-15 416
a_{1234}	125 693	72 505	-27 134	18 009
a_{33}	127 833	67 197	6 756	1 206
a_{44}	-756 757	-204 564	-34 473	-15 894

Table 5. Coefficients of models for phase angle prediction.

Coefficients	30°C	40°C	50°C	60°C
a_0	34.75	52.41	65.45	75.12
a_1	3.65	2.10	2.09	1.66
a_2	1.69	1.44	1.90	3.38
a_3	-8.08	-7.61	-7.06	-4.56
a_4	-8.53	-6.34	-4.88	-0.34
a_{12}	-0.43	0.06	0.31	-0.91
a_{13}	-1.00	-0.59	0.21	-3.04
a_{14}	1.59	-1.82	-0.68	-1.45
a_{23}	-1.43	-0.21	-0.13	2.58
a_{24}	1.92	0.29	-0.82	3.49
a_{34}	1.69	-2.52	1.10	-2.19
a_{123}	-1.07	-1.33	2.40	-1.25
a_{124}	1.55	-0.97	-1.13	-1.94
a_{134}	-1.03	-2.01	0.09	-1.39
a_{1234}	1.39	1.32	0.24	0.85
a_{33}	-0.24	3.59	3.24	1.32
a_{44}	10.30	2.52	0.33	6.08

effects and the interaction terms related to corresponding main effect. This was particularly important at high temperatures (50 and 60°C) because the interaction terms were not negligible and it would not be possible to determine the importance of a parameter only looking at the main effect. The fact that the interactions between the main effects increase as the temperature increases (Table 4 and 5), means that the non-linear components in the model, that describes the physical phenomena occurring, increase. Note that, in this case of multiple regression, the nonlinearities are developed in 5 dimensions (four independent variables and one dependent variable). An example of calculation of the measure of importance, i.e. the sum of every contribution related to a parameter (main effect and

Table 6. ANOVA table and R² for second-degree model at every temperature for complex modulus.

	SS ¹	df ¹	MS ¹	F ¹	P ¹	R ²
30°C						
2° degree	5.1E+14	17	3.0E+13	3.0E+02	2.7E-144	0.96
Residual	2.3E+13	226	1.0E+11			
Total	5.3E+14	243				
40°C						
2° degree	5.5E+13	17	3.2E+12	2.3E+02	2.3E-138	0.94
Residual	3.3E+12	239	1.4E+10			
Total	5.8E+13	256				
50°C						
2° degree	4.6E+12	17	2.7E+11	1.7E+02	6.1E-144	0.91
Residual	4.7E+11	300	1.6E+09			
Total	5.1E+12	317				
60°C						
2° degree	1.9E+11	17	1.1E+10	2.6E+02	1.8E-151	0.95
Residual	1.1E+10	256	4.2E+07			
Total	2.0E+11	273				

¹SS: Sum of the squares; df: degree of freedom; MS: Mean squares; F-statistic; p-value, R² = coefficient of determination

Table 7. ANOVA table and R² for second-degree model at every temperature for phase angle.

	SS ¹	df ¹	MS ¹	F ¹	P ¹	R ²
30°C						
2° degree	5.9E+05	17	3.5E+04	7.4E+02	1.4E-187	0.98
Residual	1.1E+04	226	4.7E+01			
Total	6.0E+05	243				
40°C						
2° degree	9.5E+05	17	5.6E+04	3.6E+02	1.9E-159	0.96
Residual	3.7E+04	239	1.6E+02			
Total	9.9E+05	256				
50°C						
2° degree	1.7E+06	17	9.7E+04	1.1E+03	3.1E-265	0.98
Residual	2.7E+04	310	8.9E+01			
Total	1.7E+06	327				
60°C						
2° degree	1.8E+06	17	1.0E+05	1.6E+02	8.9E-125	0.91
Residual	1.7E+05	256	6.7E+02			
Total	2.0E+06	273				

¹SS: Sum of the squares; df: degree of freedom; MS: Mean squares; F-statistic; p-value, R² = coefficient of determination

interactions) (Saltelli et al. 2004) for the effect a₁ is given by the Equation 4.

$$\begin{aligned}
 \text{Measure of importance of } a_1 & \\
 &= a_1 + a_{12} + a_{13} + a_{14} + a_{123} \\
 &\quad + a_{124} + a_{134} + a_{1234} \quad (4)
 \end{aligned}$$

The results regarding the measure of importance for the complex modulus are shown in Figures 4-5-6-7 and for the phase angle in Figures 8-9-10-11.

From a comparison of Figures 4-5-6-7 and Table 4 it is possible to draw certain conclusions regarding the complex modulus:

- The general trend showed that the importance of each parameter increases as the temperature rises. This confirms that in the high temperature domain

binders are generally more sensitive to blending than in the low temperature domain (Kandhal et al. 1997). When the temperature of 60°C is exceeded all the effects showed similar importance.

- The effect of the stiffness of the virgin binder (a₁) is, as expected, negative, (Table 4) which means that the lower the complex modulus of the virgin binder, the lower the complex modulus of the blend will be.
- The same trend was observed for the stiffness of the aged binder (a₂); the effect is negative. It is possible to state that the stiffness of the virgin binder is more relevant than the stiffness of the aged binder for 30 and 40°C, for 50°C and 60°C they become similar.
- The percentage of the aged binder (a₃) and the loading frequency (a₄) are the most important factors until 50°C. As the temperature rises, both effects

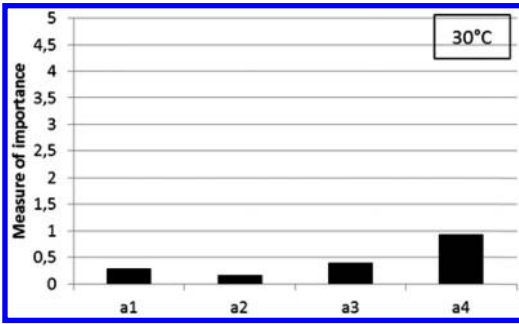


Figure 4. Relative effects on $|G^*|$ blend results at 30°C (a1 = type of virgin binder, a2 = type of aged binder, a3 = % of aged binder, a4 = load frequency).

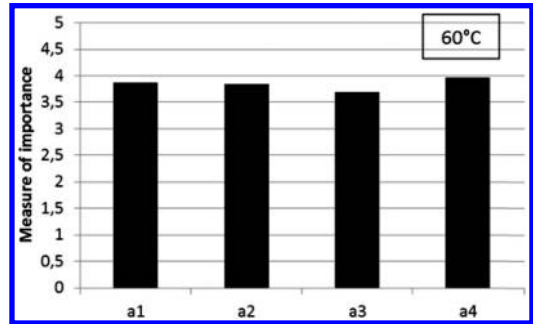


Figure 7. Relative effects on $|G^*|$ blend results at 60°C (a1 = type of virgin binder, a2 = type of aged binder, a3 = % of aged binder, a4 = load frequency).

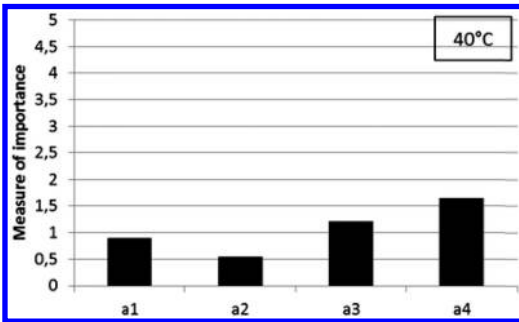


Figure 5. Relative effects on $|G^*|$ blend results at 40°C (a1 = type of virgin binder, a2 = type of aged binder, a3 = % of aged binder, a4 = load frequency).

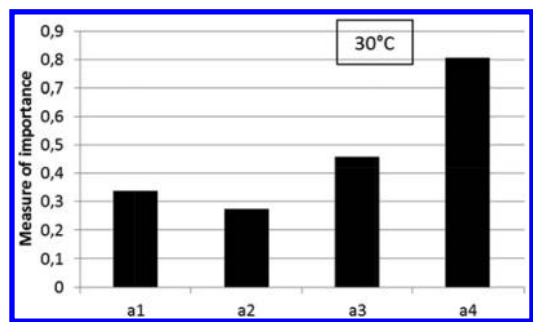


Figure 8. Relative effects on phase angle results at 30°C (a1 = type of virgin binder, a2 = type of aged binder, a3 = % of aged binder, a4 = load frequency).

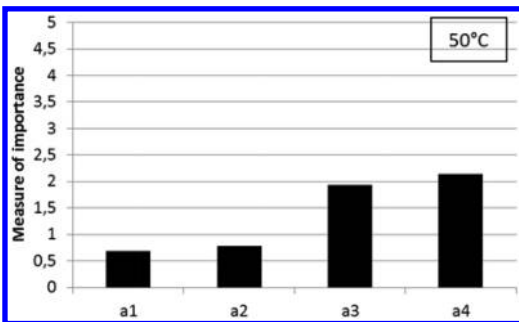


Figure 6. Relative effects on $|G^*|$ blend results at 50°C (a1 = type of virgin binder, a2 = type of aged binder, a3 = % of aged binder, a4 = load frequency).

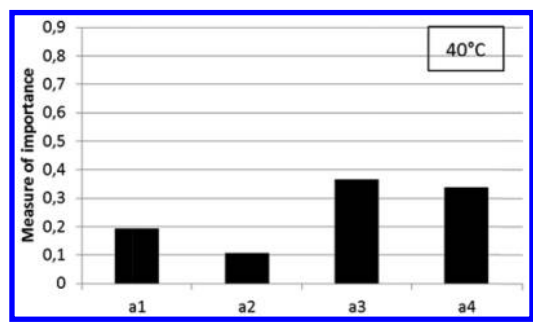


Figure 9. Relative effects on phase angle results at 40°C (a1 = type of virgin binder, a2 = type of aged binder, a3 = % of aged binder, a4 = load frequency).

increase. This is particularly evident for the effect of the percentage of aged binder that increases considerably as the temperature changes until the effect becomes as important as that of the load frequency at 50°C.

From a comparison of Figures 8-9-10-11 and Table 5, it is possible to draw certain conclusions regarding the phase angle:

- The general trend showed that the importance of each parameter decreases as the temperature rises. When the temperature of 60°C is exceeded all the

effects showed similar importance slightly higher than that at 50°C.

- The effects of the stiffness of the virgin and aged bitumen are positive (Table 5), which means that if the stiffness of both increases the phase angle also slightly increases.
- The percentage of the aged bitumen and the load frequency have the strongest impact on the phase angle, meaning that if the amount of RAP binder in the blend or the loading frequency increases, the phase angle decreases significantly. The loss modulus (G'') will become predominant in relation to the

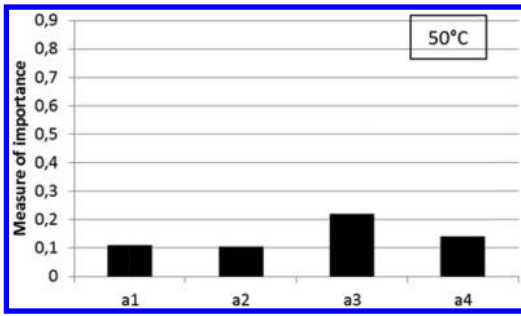


Figure 10. Relative effects on phase angle results at 50°C (a1 = type of virgin binder, a2 = type of aged binder, a3 = % of aged binder, a4 = load frequency).

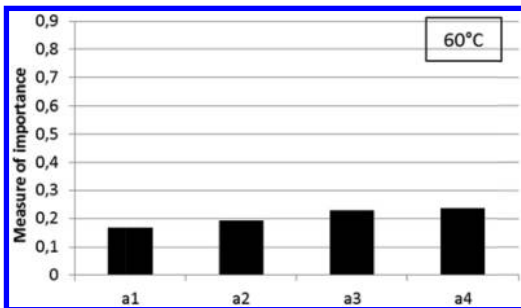


Figure 11. Relative effects on phase angle results at 60°C (a1 = type of virgin binder, a2 = type of aged binder, a3 = % of aged binder, a4 = load frequency).

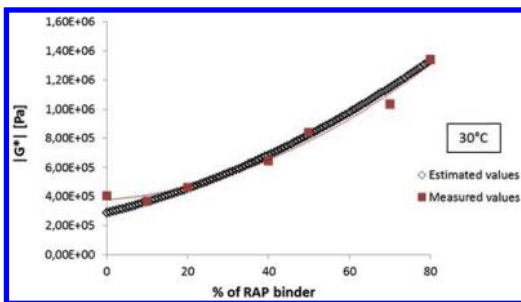


Figure 12. Example of $|G^*|$ prediction model for 70/100 blend at 30°C at 1 Hz.

storage modulus (G''), indicating a greater hardening of the blend as the quantity of RAP binder or the load frequency increases. Moreover at 40; 50 and 60°C the percentage of RAP binder has an effect comparable to or higher than that of the frequency, which indicates the comparative significance of this parameter.

Summarising after the results of the sensitivity analysis, it is possible to assert that the complex modulus and phase angle of the blend are influenced more by the amount of RAP bitumen than by its rheology at medium and high temperatures (with the only exception for the complex modulus at 60°C where all the parameters show similar significance). This represents

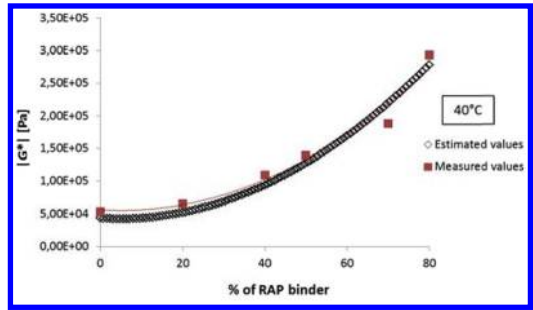


Figure 13. Example of $|G^*|$ prediction model for 70/100 blend at 40°C at 1 Hz.

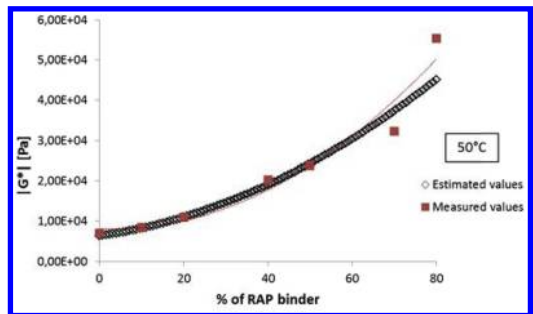


Figure 14. Example of $|G^*|$ prediction model for 70/100 blend at 50°C at 1 Hz.

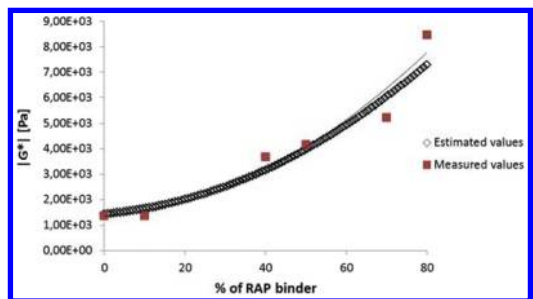


Figure 15. Example of $|G^*|$ prediction model for 70/100 blend at 60°C at 1 Hz.

a remarkable conclusion since it is more difficult to control the characteristics of the RAP binder during the mix production than to control the amount of RAP. The same assertion is valid if a comparison is made between the effects of virgin and aged binder properties. The rheological characteristics of the virgin binder have greater significance than those of the aged binder at 30 and 40°C. The scenario changes when the temperature of 50°C is exceeded, as then the effect of the RAP binder becomes comparable to or higher than that of the stiffness of the virgin binder.

By calibrating the second-degree model at every testing temperature with the coefficients in Tables 4 and 5 it is possible to predict the final complex modulus and phase angle.

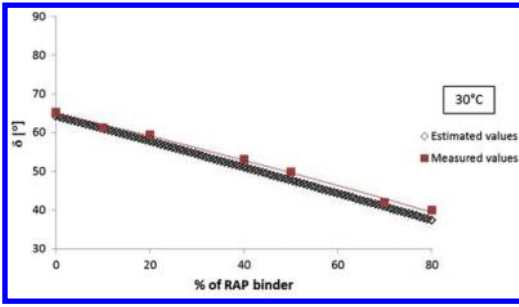


Figure 16. Example of δ prediction model for 70/100 blend at 30°C at 1 Hz.

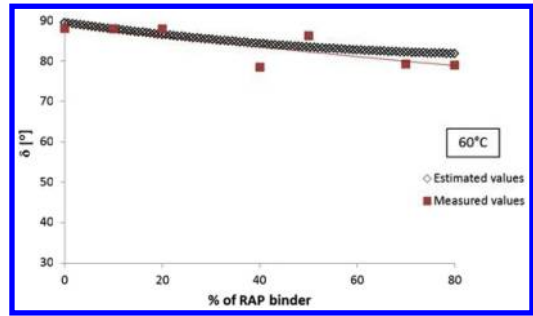


Figure 19. Example of δ prediction model for 70/100 blend at 60°C at 1 Hz.

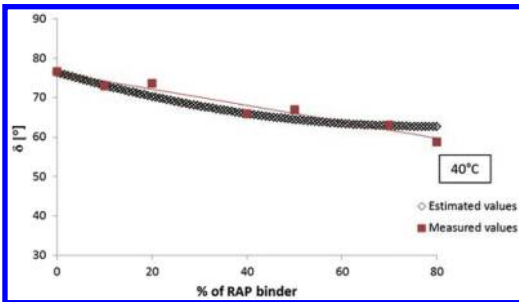


Figure 17. Example of δ prediction model for 70/100 blend at 40°C at 1 Hz.

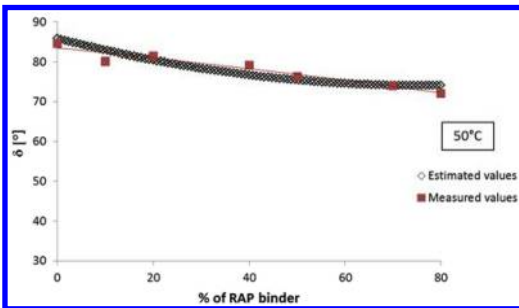


Figure 18. Example of δ prediction model for 70/100 blend at 50°C at 1 Hz.

A 2D graphical representation, where only the percentage of RAP binder is varied and the other parameters are kept constant (70/100 virgin binder, 70/100 RAP binder and load frequency equal to 1 Hz) is provided in Figures 12-13-14-15 for the complex modulus and in Figures 16-17-18-19 for the phase angle.

Regarding the complex modulus prediction (Figures 12-13-14-15), with the exception of the case at 30°C where the curve is represented by an almost straight line, for higher temperatures (40, 50, 60°C) the relationship is not linear. The curves show an upward facing concavity and in those cases with a small quantity of RAP binder in the blend the complex modulus does not vary significantly. The same trend was observed for all the blend combinations tested. In

the case of the phase angle, an almost linear behaviour was observed at 30°C. As expected based on the sensitivity analysis results, the impact of the percentage of RAP binder is stronger at 30 and 40°C; indeed the decrease of the phase angle is more evident at these temperatures, while it becomes negligible at 60°C.

5 CONCLUSIONS

The present study proposes a methodological approach to develop a non-linear binder blending chart to predict the complex modulus and phase angle, taking into account more than one parameter at a time. After having defined the parameters involved – the stiffness of the virgin binder, the stiffness of the aged binder, the percentage of aged binder in the blend and the loading frequency – several combinations were tested with DSR. Multiple regression analysis and other statistical tools were applied to define the most suitable model and test the goodness of fit.

A second-degree equation with interaction was chosen to express the blending model and was calibrated at every testing temperature (30, 40, 50 and 60°C). With respect to the cases analysed and the validity domain of each parameter, from the comparison between the importance of the effects (i.e. sensitivity analysis) it is possible to draw the following conclusions:

- Small quantities of RAP binder (up to 10–20%) do not have any meaningful impact on the rheology of the blend.
- As the temperature increases, all the effects become more significant (i.e. higher absolute values). This confirms that in the high temperature domain binders are generally more sensitive to blending than in the low temperature domain (Kandhal et al. 1997).
- The stiffness of the virgin binder (a_1) will have a stronger influence on the final modulus of the blend than the stiffness of the aged binder (a_2) at medium temperatures (30 and 40°C). This represents an advantage because the rheology of the new binder is less variable than the rheology of the RAP binder (Bressi et al. 2015). Nevertheless since this does not apply at 50°C and 60°C (a_2 becomes comparable

to or higher than a_1), the rheological characteristics of the aged binder cannot be neglected at high temperatures.

- The amount of aged binder in the blend and the loading frequency (a_3 and a_4) have the greatest effect (with the only exception for the complex modulus at 60°C where a_3 is slightly lower than the others effects). The complex modulus of the blend is more influenced by the amount of RAP binder than by the rheological characteristics of the RAP binder. This is another positive result as far as production is concerned, since once the degree of blending is determined; it is easier to control the amount of RAP in the mix than the rheological characteristics of its binder.
- Different models (i.e. one for every testing temperature) were developed in order to predict the stiffness of the final binder blend, considering different input parameters at the same time. This constitutes a new blending chart developed on the basis of the rheology characteristics and not only the penetration grade and softening point as the current European method proposes.

Further work will be carried out to extend the validity domain of the models, testing other types of bitumen, and for the validation of the present models. Since the models developed showed high non-linearities at high temperatures (50 and 60°C) further tests are required at 70°C and 80°C for a better understanding of the physical phenomena occurring.

REFERENCES

Al-Qadi I., Elseifi M., Carpenter S.H. 2007. Reclaimed Asphalt Pavement-A literature review. (Research Report FHWA-ICT-07-001). Illinois Center of transportation.

ASTM, ASTM D6521 2008. Standard practice for accelerated aging of asphalt binder using a pressurized aging vessel (PAV). West Conshohocken. PA: American Society Testing & materials.

ASTM: ASTM D2872: Standard Test Method for Effect of Heat and Air on a Moving Film of Asphalt (Rolling Thin-Film Oven Test).

Anderson, D.A. 1994. 'Binder Characterization, Vol. 3: Physical Properties', SHRP-A-369, Strategic Highways Research Program, Nat. Research Council, Washington, D.C.

Bilal M. Ayyub and Mc Cuen R. 2011. Probability, Statistics and Reliability for engineers and scientists (Third edition). A Chapman & Hall book. Taylor and Francis Group.

Booshehrian A., Mogawer W. S. and Bonaquist R. 2013. How to construct an asphalt binder master curve and assess the degree of blending between RAP and virgin binders. Journal of Materials in Civil Engineering, pp. 1813–1821.

Bressi S., Carter A., Bueche N., Dumont A. G. 2015. Impact of different ageing levels on binder rheology. International Journal of Pavement Engineering, pages 1–11. DOI:10.1080/10298436.2014.993197

EN 13108-8: 2005. Bituminous Mixtures. Materials Specifications. Part 8: Reclaimed Asphalt.

Epps, J.A., Little, D.N., Holmgreen, R.J., and Terrel, R.L. 1980. Guidelines for Recycling Pavement Materials, NCHRP Report No. 224, Transportation Research Board, Washington, DC.

Ferry, J. D. 1980. Viscoelastic properties of polymers (3rd edition) New York, NY: John Wiley & Sons.

Kalman B. et al. 2013. Re-Road-Summary Report. End of life strategies of asphalt pavements. Re-Road.

Kandhal P., Foo K.Y. 1997. Designing recycled hot mixture asphalt mixtures using superpave technology. NCAT Report no. 96-5 p. 7–22.

Mangiafico S., Di Benedetto H., Sauzéat C., Olard F, Pouget S., Planque L. 2014. New method to obtain viscoelastic properties of bitumen blends from pure and reclaimed asphalt pavement binder constituents. Road materials and pavement design.

McDaniel, R., and R. M. Anderson. NCHRP Report 452 2001. Recommended Use of Reclaimed Asphalt Pavement in the Superpave Mixture Design Method: Technician Manual. TRB, National Research Council, Washington, D.C.

Mickey R., Dunn O. J., Clark V. A. 2009. Applied statistics. Analysis of Variance and Regression (Third edition). Wiley series.

Nahar S.N. et al. 2012. First observation of the blending zone morphology at the interface of reclaimed asphalt binder and virgin bitumen. Transportation Research Board.

National Cooperative Highway Research Program. 1978. NCHRP Program Synthesis of Highway Practice No. 54: Recycling Materials for Highways, Transportation Research Board, Washington DC.

Poulikakos L. D., Dos Santos S., Bueno M., Kuentzel, S. Hugener, M. Partl M.N. 2013. Influence of short and long term aging on chemical, microstructural and macro-mechanical properties of recycled asphalt mixtures. Construction and Building Materials.

Saltelli, A., S. Tarantola, F. Campolongo, and M. Ratto (2004). Sensitivity Analysis in Practice. John Wiley & Sons, Chichester, United Kingdom.

Shirodkar, Mehta, Nolan, Sonpal, Norton, Tomlinson, Sauber, DuBois. 2010. A Study to Determine the Degree of Partial Blending of Reclaimed Asphalt Pavement (RAP) Binder for High RAP Hot Mix Asphalt. Transportation Research Board.

Swiertz D., Mahmoud E, Bahia H.U. 2011. Estimating the effect of recycled asphalt pavements and asphalt shingles on fresh binder, low-temperature properties without extraction and recovery. Transportation Research Record: Journal of the Transportation Research Board, 2208, 48–55.

Quality control in the construction of asphalt concrete pavement layers

B.G. Pecheny

State Technical University of Belgorod, Belgorod, Russia

A.D. Nikolov

Patpribor Construction Materials Testing Laboratory, Sofia, Bulgaria

ABSTRACT: In asphalt concrete mixes main structure-forming role is played by the crushed mineral aggregate. With those mixes, in the course of compaction internal friction appears between the grains forming lattice of stone aggregate, which when quickly compacted results in aggregates wedging and in some cases, leads to their crushing. When asphalt mixes prepared from coarse aggregates are compacted at high speed, the bitumen film in the contact area between the grains is squeezed and its thickness decreases. This leads to coming together and crushing of the mineral aggregates and fraction lattice because the friction force at the points of contact considerably exceeds the shearing force of the remaining parts in the mix.

Keywords: asphalt concrete layer; compaction coefficient; mineral aggregates crushing; properties of asphalt mixture; quality control; preparation of samples using reheated asphalt mixture.

1 INTRODUCTION

Laboratory test specimen of hot asphalt mixes with coarse aggregates content over 50% of the total mass are prepared according to GOST 12801-98 by applying force for 3 minutes achieving pressure of 40 MPa. This pressure is achieved within 5 to 10 seconds. Achieving the necessary pressure of 40 MPa within 5–10 seconds is as required according to the compaction standard passes through an inertia stage. It occurs especially when simultaneously compacting three specimens with diameter of 71.4 mm (area $3 \times 40 = 120 \text{ cm}^2$) or one cylindrical specimen with diameter of 101.0 mm (area 80 cm^2). In a short period the compacting force reaches 48 t in the first case, and 32 t in the second case. Of course this model of laboratory compaction of asphalt mixes does not correspond to the real process of laying and compacting of the asphalt mix.

For the purposes of this study asphalt test specimens were prepared, compacted by three methods: according to GOST, a combined method with preliminary vibration and the Marshal method.

The asphalt mix properties were examined depending on the time for achieving the compacting pressure of 40 MPa. Asphalt laboratory specimen compaction by various methods, as well as pavement asphalt concrete compaction, is followed by crushing of mineral aggregate in a mixture, which affects the quality indicators and their convergence. These effects also appear in the definition of such an important figure as the compaction coefficient of asphalt concrete in a pavement.

2 GOAL OF RESEARCH

Tests were performed to determine:

- Dispersion coefficient (variation coefficient of strength determination at 50°C at various modes of specimens compaction);
- Fragmentation of aggregates following compaction and subsequent extraction;
- Compressive strength at 20°C and 50°C;
- Average bulk density (compaction coefficient).

3 TEST RESULTS

The blending was performed in a laboratory mixer. Asphalt mixes were prepared with grading type A, B, C, D and E according to GOST (9128-2009) from limestone and crushed gravel, activated mineral filler and bitumen grade BND 60/90. The samples were compacted at 40 MPa, while the times to achieve that load were 10, 25, 40 and 60 seconds. There were compacted 7 test specimen of each grading at every time to reach loading of 40 MPa. The temperature of mixing was $150^\circ\text{C} \pm 5^\circ\text{C}$ as per to GOST 12801-98, and mixing was performed for 90 seconds. Compaction was carried out at the same temperature.

The results from the determination of dispersion coefficient (variation coefficient) and compressive strength at 50°C are shown in Fig. 1.

It can be seen from Fig. 1 that the dispersion of results from the testing of compressive strength

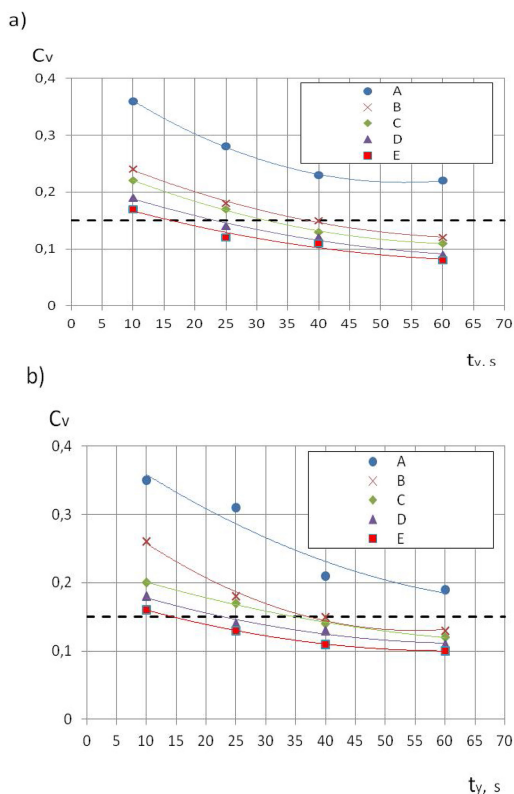


Figure 1. Dependence of the variation coefficient C_v of compressive strength at 50°C of asphalt test specimens on the time for achievement of compacting pressure: a) with limestone, b) with crushed gravel.

at 50°C with grading type A, as expected, is considerable at different times for achieving maximum pressure of 40 MPa. The variation coefficient significantly exceeds the limit values of 0.16–0.20 in accordance with GOST 9128-2009. The optimal time for reaching the maximum pressure for compaction of 40 MPa for asphalt mixes prepared from limestone with type B grading is no less than 35 s, for type C – no less than 30 s, for type D – no less than 25 s, and for type E – no less than 15 s. For asphalt mixes prepared from crushed gravel the time for reaching maximum pressure is within 10 s.

Determination of mineral aggregates fragmentation in asphalt mixes type A and B upon standard compaction in accordance with GOST 12801-98 at compression of 40 MPa and compaction in accordance with EN 12697-30 by the method of Marshal is given in Table 1.

There are considerable differences in the fragmentation values of aggregates for the two methods of compaction as can be seen. In the first place, attention should be paid to the fragmentation decrease in the case where maximum compaction force of 40 MPa is achieved in 40 seconds, and not in 10 seconds.

Table 1. Fragmentation of crushed aggregate in asphalt concrete specimens depending on the method of compaction.

Method of compaction of asphalt concrete specimens	Fragmentation of crushed mineral aggregate, % at its content in the mix		
	25	45	65
Compression of press (plate) 40 MPa			
For 10 s	16*/14/12	19/16/16	26/22/19
For 40 s	10/10/8	15/12/11	20/16/15
Combined vibration for 3 min and compression at 20 KPa 3 min	8/6/4	10/9/8	15/12/12
Marshal compaction			
50 blows	4/3/3	5/4/3	6/5/5
75 blows	5/5/5	6/5/5	7/6/6

*Fillers: limestone/granite/crushed gravel

Fragmentation of mineral aggregates in asphalt mixes is considerably decreased when the combined method of compaction according to GOST 12801-98 and the drop weight impact testing method according to EN 12697-30 were used.

Asphalt concrete test specimens were prepared with bitumen grade BND 60/90 with crushed aggregate and grading type A, B, C, D and E according to GOST 12801-98, as well as according to Marshal, and compacted by 75 blows. Upon determining the average compression density at 20°C, the test specimens were decompacted, new test specimens were prepared and the same characteristics were determined. As seen from Table 2, the average density and compressive strength at 20°C of the test specimens prepared for a second time are higher than those of the originally prepared test specimens. The average density of test specimens prepared for a second time according to GOST 12801-98 are by 1.7–1.9% higher than those originally prepared, and by 0.7–0.8% higher than those prepared according to Marshal.

Fragmentation of the crushed aggregate upon compaction of asphalt concrete mixes is not taken into account when determining such important characteristics as the coefficient of compaction Q , characterizing the degree (level) of asphalt concrete compaction in the pavement. Q is determined based on the ratio between the average density at 20°C of samples with non-damaged structure of asphalt concrete taken from the asphalt layer, and the average density of test specimen of the same sample prepared in a laboratory (GOST 12801-98, point. 26, EN 13108-20, point C.4). The preparation of laboratory test specimens at the relevant temperature causes bitumen ageing, while compaction causes fragmentation of mineral material, which changes the physical and mechanical properties

Table 2. Physical and mechanical properties of asphalt concrete test specimens prepared under laboratory conditions then decompacted and prepared for a second time.

Asphalt concrete test specimen with grading	Average density, kg/m ³		Compressive strength at 20°C, MPa	
	Compacted	Again Compacted	Compacted	Again Compacted
Type A	2380*	2426	4.6	6.0
	2410	2430	5.0	6.0
Type B	2390	2432	4.9	7.1
	2420	2438	5.2	7.3
Type C	2396	2440	5.3	7.9
	2424	2446	5.8	8.0
Type D	2408	2450	5.5	8.3
	2429	2453	6.1	8.8
Type E	2416	2458	6.2	9.4
	2437	2462	7.0	9.4

*Numerator: properties of asphalt test specimens compacted in laboratory conditions, decompacted and compacted again according to GOST 12801-98; Denominator: properties of test specimens compacted in accordance with the Marshal method.

of test specimens prepared again as compared to the original ones. In Clause 6.1.1 of GOST 12801-98 and 1, EN 13108-20 it is stated that a second preparation of laboratory test specimens is not allowed.

4 PROPOSED METHODOLOGY CHANGES

It is obvious that a change should be made in the methodology for determining the coefficient of compaction of asphalt concrete in the asphalt layers. The following methodology for determination of the compaction coefficient of asphalt layers is proposed. At the start of asphalt layers construction, works of laying and compaction of asphalt concrete mix are carried out on a reference section in the presence of representatives of the control laboratory and according to specified regulations. After 24 hours a sample is taken from the asphalt layer and the average density at 20°C is determined. This value of the asphalt concrete average density P_e will serve as reference value for each section of the asphalt layer that is executed. Thus the compaction coefficient Q is determined by the ratio between the average density of the test specimens from the section under control P_k and the average density of the test specimens taken from the layer on the reference section P_e .

$$Q = P_k/P_e. \quad (1)$$

It is proposed that the quality control and homogeneity of asphalt mixes delivered to the site for laying should be carried out by comparing the average density of test specimens prepared by the Marshal method, delivered for placing on the reference section and the average density of the test specimens prepared from mix delivered to the section under control.

Samples from the asphalt concrete mix delivered to the site are taken from the truck. The preparation of test specimen from the asphalt concrete mix intended for

the reference section by the Marshal method is carried out through a different number of blows – 75, 65, 55, 45. The average volume density is determined after 24 hours at 20°C P_e .

The number of blows required to achieve the average density value P_e is determined from the correlation average volume density – number of blows N_e .

The subsequent control over the construction of asphalt layers is exercised through the characteristic average density P_{ma} of the Marshal test specimens from the asphalt mix delivered to the controlled section at number of blows equal to N_e , and the average density of samples taken from the reference section P_e . The quality of the mix delivered to the site can be evaluated though the value of density of asphalt concrete samples from the controlled section P_{ma} and the value of this property of samples from the reference section P_e . The comparison between the density of the sample from the controlled section P_k and P_e , allows determination of the asphalt concrete quality at the end of the day.

Thus the methodology allows control over the quality of asphalt mix delivered to the construction site, as well as the quality of laying and compaction of asphalt concrete in the pavement.

5 CONCLUSIONS

1. It has been established that when preparing asphalt concrete test specimens according to GOST 12801-98 in the course of reaching compaction pressure up to 40 MPa within 5–10 s, fragmentation of the mineral aggregates takes place. This leads to considerable dispersion of the results for the tested samples. It is proposed that the time of reaching compacting pressure up to 40 MPa should be fixed at no less than 40 s, which increases the convergence of the results for the tested specimen.

2. The limitation of the method of determining the coefficient of compaction of asphalt concrete in the asphalt layers has been shown, since when preparing test specimens for a second time, a fragmentation of the mineral aggregate and ageing of the bitumen is taking place, which considerably changes the structure and properties of the specimens prepared for a second time. It has been proposed that the coefficient of compaction should be determined by the correlation between the average density of samples taken from the controlled section asphalt layer and the average density of samples taken from the asphalt layer on the reference section executed at the start of construction works in accordance with the regulations.
3. Method of quality control of asphalt mixes delivered to the site for laying is proposed.

REFERENCES

- ASTM D 6926-10. Standard Practice for Preparation of Bituminous Specimens Using Marshall Apparatus. Designation D5581-96 (Reproved 2001) Standard Test Method for Resistance to Plastic Flow of Bituminous Mixtures Using Marshall Apparatus (6 inch-Diameter Specimen).
- EN 12697-30:2004+A1:2007(E). Bituminous mixtures. – Test methods for hot mix asphalt – Part 30: Specimen preparation by impact compactor.
- EN 13108-2 0:2006. Bituminous mixtures – Material specifications – Part 20: Type Testing.
- GOST 12801-98. Materials on the basis of organic binders for road and airfield construction. Test method.
- GOST 9128-2009. Asphaltic concrete mixtures for roads, aerodromes and asphaltic concrete. Specifications.

Asphalt bridge deck pavement behavior, the Egnatia experience

A. Kokkalis

Department of Civil Engineering D.U.Th., Xanthi, Greece

P. Panetsos

Structural Maintenance of Egnatia Odos S.A., Thessaloniki, Greece

ABSTRACT: Egnatia Odos is a 675 km motorway crossing a particularly mountainous terrain. A great number of bridges have been constructed along its route. The standard construction bridge deck pavement practice is to lay 2X5cm asphalt over a bituminized waterproofing membrane. Few variations have been applied to this practice. Most Egnatia bridge pavements have been trafficked for 5 to 15 years carrying 1 to more than 10 million Standard Axles, whilst they have been exposed to a variety of adverse weather conditions. The mountainous of the terrain implies that the bridge geometry comprises many tight curves and steep slopes (for motorway standards). This means that there is a high need for consecutive braking for heavy vehicles along downgrade bridges. Also centrifugal forces develop along bridge horizontal turns. Thus, high horizontal shear strains apply to the bridge pavements and may cause a variety of wear and pavement damages. That wear has been observed as pot holes, shoveling, raveling or other type of shear failure, mostly appearing to downgrade decks in comparison to their twin upgrade decks of a bridge as well as to bridge decks in comparison to their adjacent embankments. In this paper an attempt is made to present and classify the extended experience concerning waterproofing and pavement surfacing behavior of decks which has been gathered by Egnatia during 15 years of operation, together with a scientific documentation of the observed damages and decay.

1 BRIDGES CONSTRUCTED AND SUPERVISED BY EGNATIA ODOS SA

Egnatia Odos SA is the Greek company responsible for the construction and operation of Egnatia motorway and the Pan-European corridors in Greek territory (Figure 1). Egnatia is a 675 km long 2-lane dual motorway crossing the western and northern Greece.

It is also a collector route for the Balkan and south-eastern European transport system. Pan-European Corridors IV (Berlin – Sofia – Thessaloniki), IX (Helsinki – Alexandroupolis) and X (Vienna – Belgrade – Thessaloniki) all end at Egnatia Motorway.



Figure 1. Egnatia motorway map and its transverse Pan-European corridors.

Those entire Pan-European transverse corridors total 350 km in Greek territory and are known as vertical axes.

Most of those 1,000 km of motorways cross a mountainous terrain. The diverse terrain together with frequently imposed strict environmental conditions, led to the construction of a great number of bridges (instead of high embankments) summing a total length of 50 km. Travelling along Egnatia motorway and its vertical axes, one can count more than 2,000 bridges, 200 of which are longer than 100 m. Deck structures are all twin split carriageway bridges, in accordance with the practice followed in the construction of German highways. Actually 3% of the motorways length runs over bridges, the construction cost of which corresponds to about 10% of the total motorways cost. The overall construction cost of the Egnatia motorway and its vertical corridors amounted approximately to 10b€.

2 WATERPROOFING AND PAVING PRACTICE AT EGNATIA BRIDGES

Reinforcing steel (rebar) in bridges is particularly susceptible to corrosion. Because of the porous nature of concrete, moisture and winter road treatment chemicals can seep into the concrete, reaching the rebar

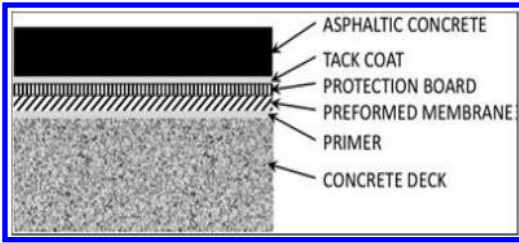


Figure 2. Typical components of concrete deck waterproofing.



Figure 3. Laying waterproofing membranes over a concrete bridge.

within. Exposed to these corrosive elements, the rebar will begin to develop rust corrosion products that are 2–10 times more voluminous than the original steel pieces (Park *et al.*, 2008, Kepler *et al.*, 2000). As these corrosion products continue to build, stress on the surrounding concrete increases until the surface begins to crack and spall. This would affect the pavement and could weaken and compromise the stability of the bridge structure. Thus, a practice to inhibit water ingress is imperative.

Winter motorway deicing is a common practice in the mountains of northern Greece. The exposure of the decks to deicers is a primary cause of corrosion-related distress. The service life of a deck is dependent on the exposure conditions, the concrete permeability, the concrete cover, and the type of reinforcing steel. The life-cycle of typical motorway bridge extends to 100 years and rebar corrosion is, probably, the most important factor diminishing bridge life. Stipulating the risk of future corrosion is necessary so that the best repair or preventive strategy can be implemented.

In deicing environments, asphalt pavement overlays should not be placed directly on the deck concrete without a membrane, as the asphalt pavement may be cracked and hold chloride-laden water against the concrete surface and cause accelerated corrosion and deterioration that is difficult to identify until serious problems develop. Waterproofing systems are designed to keep water off the bridge deck upper surface. Various types of waterproofing membranes are the most common type of bridge deck protection, whilst deck membranes are applied to protect the underlying deck, they require a traffic bearing surface to protect the membrane itself from damage (Fig. 2). Obviously, the long-term performance of membrane systems is strongly affected by the integrity of the asphalt overlay.

Outlining the typical Egnatia waterproofing practice, the concrete deck surface must be at least two weeks old before starting relevant works. The membrane is then installed on the bridge deck by first preparing the deck surface which must be sound, dry, clean and free of protrusions and rough edges. Abrasive blasting may be used to remove any contamination, avoiding the use of water to clean the deck, as the surface must be dry before the primer is applied.

The surface may also be cleaned with brooms, vacuum, or compressed air to remove any loose material and dust before applying the membrane system. Common practice is to first apply a primer coat over the deck to enhance the bond between the concrete deck and the membrane. Typically, the membrane is provided in roll form and is installed by merely rolling out the membrane in strips, as suggested in Figure 3. The membrane may be cut to fit as necessary to insure that it is coextensive with the deck surface. The placement of preformed membranes should begin on the low point of the deck and provide adequate lap between adjacent strips. This permits water to drain without accumulating against the seams. The width of the horizontal overlaps should be at least 20 cm and that of the longitudinal overlaps should be at least 10 cm. Once a course of the membrane has been laid out and fitted in place, it is heated to a temperature of approximately 100°C to form a tight integument which is highly waterproof and tightly secured to the deck. While the membrane is still in this heated condition, it is pressed down, preferably by means of a hand roller to insure that all air bubbles are rolled out from between the deck and the membrane before the material has cooled. When installing the membrane, ambient temperature preferably should be at least 10°C, in order to allow the membrane to be properly heated and to retain heat long enough for the membrane to be rolled to remove air bubbles.

Then, a minimum and maximum time should be specified between membrane application and the first layer of the asphalt overlay placement. The minimum time allows for the membrane to cure properly and depends on the manufacturer's recommendations. The maximum time reduces the length of time that the membrane is exposed to potential damage. Normal values range from 1 to 5 days. A tack coat is then used to enhance the bond between the membrane and the overlay to come.

Membranes may include liquid applied acrylics, urethanes, neoprenes, vinyls, rubberized asphalts, silicones and preformed membranes such as rubberized asphalts, neoprenes and butyl rubbers, hypalons,

vinyls, and ethylene propylene rubbers. The usual type of waterproofing membranes along Egnatia bridge decks are hot applied rubberized or bituminized asphalt membranes according to AASHTO (2010). In few cases (Kristallopigi, Metsovit and Grevenitikos bridges), an acrylic membrane has also been applied.

In Europe using waterproofing membranes for bridge decks moisture protection is the most common practice. However, it should be mentioned that in many US States hot-dip galvanized rebar is used to eliminate the risk of spalling, because the zinc corrosion products are less voluminous and migrate away from the bar into the matrix of the concrete. The migration alleviates the potential for increased pressure, thus eliminating the risk of spalling (NCHRP, 2008 & 2012).

Bridge deck pavements are extensively used both to protect the bridge deck against moisture and to provide good ride quality and skid resistance. According to OSMEO (2002) an asphalt 5 cm course is put directly on the tack coat above the waterproofing membrane and is normally an A260 asphalt base course layer. In case the waterproofing membrane is susceptible to damages by the overlaid coarser aggregates of the base course, a 20 mm thick sand asphalt protective layer is recommended to be placed. The temperature of the asphalt should not exceed 170°C degrees at pouring. During compacting the temperature should not exceed 150 degrees. Only vehicles involved with the asphalt courses is permitted to the bridge deck area, since it is contractor's responsibility not to damage the membrane. Then, over the base layer, a 5 cm A265 wearing course is laid. Finally it is laid the typical for motorways 2.5 cm antiskid layer. Overall a 12–13 cm of asphalt layers cover and protect the waterproofing membrane of the bridge decks. This thickness is the typical thickness of protective pavement layers at concrete bridge decks in most countries all over the world.

3 DISTRESSES AND DAMAGES AT WATERPROOFING STRUCTURES AT EGNATIA BRIDGES

Most Egnatia and vertical axes bridge pavements have been trafficked for 5 to 15 years. Traffic volumes vary considerably along motorway sections, been heavier in the proximity of Thessaloniki central Egnatia area. Actually, along the motorways one can meet a bridge having carried light traffic (almost one million Standard Axles (SA)) and another one having carried more than ten millions SA. Obviously, the number of SA been carried has a direct effect on the distresses and damages induced to the overlay waterproofing structure of the bridge decks. However, even in bridge decks trafficked only by two millions SA, a number of (premature) failures has been observed.

A typical bridge in a mountainous terrain is usually exposed to a variety of adverse weather conditions. Deck winter temperatures are ~1°C lower than the



Figure 4. Pot holes and raveling appeared at a downgrade bridge deck in Egnatia motorway.



Figure 5. Pot holes appeared at a bridge deck in Egnatia motorway.

surrounding surfaces. Deck moisture exposure too, especially over rivers and ravines, is markedly greater. Hence, water freezing and thawing cycles are more severe in deck pavements.

Also, the mountainous of the terrain implies that the road alignment, hence the bridge alignment as well, comprises many tight curves and steep gradients (for motorway standards). This practically means that there is a high need for consecutive braking for heavy vehicles along downgrade bridges. Plus, high centrifugal forces develop along bridges at tight horizontal curves (as tight horizontal curves are determined the minimum ones corresponding to the design speed V_e or even to $(V_e + 10)$ km/h). Thus, high horizontal shear strains apply and upset bridge pavements. Also, as seen in Figure 1, the structure of the (relatively thinner compared with the adjacent pavements) deck pavements include a potential slippage surface (membrane). The bond strength between the waterproofing membrane and the concrete deck or the overlay has always been a matter of research (FHWA, 2001, Nicholls *et al.*, 2007). High horizontal stresses in combination with the adverse weather may cause a variety of wear and pavement damages such as cracking, pot holes, shoveling, raveling (Fig. 4 & 5) or other types of shear failure.

Such the deterioration reduces service life of the bridge system and increases repair and rehabilitation costs. It worth's mentioning that these damages are systematically more extended and severe at downgrade

decks in comparison to their twin upgrade deck of the bridge. The only sound explanation should be the additional effect of the horizontal braking forces of the heavy good vehicles along downgrades. Also, that pavement wear appears in greater frequency and severity along bridges than to adjacent similar embankment sections.

Although several types of defects have been observed within waterproofing systems, the four predominant ones are:

- lack of adhesion between the waterproofing membrane and the concrete deck,
- lack of adhesion between the waterproofing membrane and the asphalt surface,
- moisture penetration through the membrane and
- pot holes, raveling and similar local failures in the overlay pavement generally appearing more frequently than the adjacent pavements.

The typical degradation mechanism is the accumulation of water above the membrane in the bottom portion of the asphaltic concrete. This phenomenon combined with freezing and thawing cycles and repeated hydraulic pressure from traffic, weakens both the asphalt layers as well as the bond between the asphaltic concrete and the membrane (NCHRP, 2012). Hence, damages to the asphalt overlay itself, both induce membrane deterioration and been worsen by that deterioration.

Fatigue cracking is also a primary mode of distress in bridge deck pavements and directly affects the durability of the asphalt overlay and the whole waterproofing structure. Fatigue cracking, in conjunction with moisture ingress, typically reduces the stiffness of the asphalt mixture and the adhesive bond between the asphalt layer and the bridge deck. Several studies have been conducted to assess the fatigue cracking potential of mixtures in bridge deck pavements (Park *et al.*, 2008). As mentioned, moisture been trapped within the deck or in the inner face between the deck and the membrane may expand when froze, causing the asphalt to lift and crack. Air blistering underneath the membrane has also a similar result. Blistering will also result in puncturing of the membrane by the coarse aggregates of the base course. Hence, the waterproofing structure will experience maintenance problems resulting to water leakage passing through the asphalt into the concrete deck. If the highway has been salted, the leaks can result in rapid rusting of reinforcement rods, deck plates and other ferrous metal parts.

Many attempts have been made to solve the bridge deck waterproofing problem but none of these has been entirely successful from the standpoints of effectiveness, cost, ease of installation and durability. Various coatings have been employed but have not provided a durable, fully waterproofed layer over the entire surface and for a long period of time. Various sheet materials have also been utilized but these have been difficult to install and have not bonded well to the deck and also frequently form air pockets when entrained moisture becomes heated during

warm periods (Nicholls *et al.*, 2007). Generally, waterproofing bituminized membranes protected by asphalt overlays were found to be quite efficient and particularly cost-effective in preventing salt intrusion into the underlying deck. When properly constructed, they can prevent salt infiltration, but their service life depended on the rate at which the membrane deteriorated. In any case, after 15 years of service, membranes are expected to have been deteriorated and exhaust their design life as a result of ageing and traffic fatigue.

4 DISCUSSION AND CONCLUSIONS

As mentioned, Egnatia Odos SA has gathered extended experience in using asphalt pavements and bituminized membranes to waterproof bridge decks. This accumulative experience is summarized below. That experience is generally in accordance with the similar one gathered by other Highway Agencies. An extended presentation of the issue is made by NCHRP (2008 & 2012). More specifically, the combined experience shows that asphalt concrete overlays with a waterproofing bituminized membrane have, more or less, the advantages of:

- low cost,
- track record of successful previous installations,
- familiarity with the product and the method,
- desired service life,
- ease of installation,
- speed of installation,
- availability,
- improved rideability of the surface,
- staged construction possibilities and
- compatibility with asphalt temperatures.

and the disadvantages of:

- certain installation or other problems resulting in water getting trapped underneath the membrane,
- voids under the membrane and membrane blistering resulting in punctured waterproofing membranes,
- early moisture penetration through the membrane,
- lack of adhesion between the waterproofing membrane and the concrete deck and horizontal shear failure at the membrane,
- spalling and deterioration of concrete deck below the membrane,
- difficulty of removal,
- underlying deck cannot be seen or inspected and effectiveness of membrane is unknown,
- necessity for lane closure during maintenance and
- shoving of the membrane over time.

In NCHRP (2008 & 2012) it is also mentioned certain remarkable observations. For instance, grading of the aggregate for pavement directly over the membrane should be sized for minimal potential for puncture and proper use of the membrane primer and tack coat. Engineers should be careful to select the membrane types appropriate for the deck condition (for example, not using sheet membranes on rough surfaces). Also,

It may be preferable to use three inches (7.5 cm) for the top overlay course, so that the membrane will not be damaged when milling and resurfacing the top wearing course. Generally, waterproofing membranes are not expected to last much longer than the asphalt wearing surface. However, one resurfacing of the asphalt overlay should be always taken into account. To achieve this, the initial asphalt thickness has either to be sufficient to allow the top surface to be milled without damaging the membrane, or the milling depth should be shallower.

At Egnatia Odos SA bridge decks, the waterproofing structure lifespan has not, as a rule, been reached yet. As mentioned, the first trafficked bridge decks along Egnatia motorway are 15 years old. Extensive research in US (NCHRP, 2008 & 2012) determine the expected lifespan of the membrane-overlay system in 12–19 years, on average 15 years, when installed on new bridge decks and anywhere between 6 and 19 years when installed on existing bridge decks. It should be mentioned that the three Egnatia motorway bridge decks previously mentioned, with the more expensive acrylic waterproofing membranes have, overall, displayed a better performance and expected to live longer than similar ones with the bituminized membranes.

As far as the cost is concerned, a typical bituminized fabric has been cost about 10€/m² whilst the acrylic membrane cost reached 40€/m². Taking into account both the asphalt concrete overlay and the bituminized membrane, the mean installed waterproofing structure cost amounts about 50€/m². It should be mentioned that, in a relevant evaluation study, Kepler *et al.*, (2000) compared the life cycle costs of 33 different corrosion protection systems and concluded that the use of hot rubberized asphalt membrane was the second-lowest cost strategy. However, spending for the membrane itself 40€/m², instead of 10€/m² (acrylic ones instead of bituminized ones) may mean a fourfold cost for that specific item, a 70% increase in cost for the whole waterproofing structure (membrane-overlay pavement), but, actually, only an approximately 2–3% increase for the total cost of the bridge.

REFERENCES

- AASHTO 2010. Bridge construction specifications. 3rd edition, *AASHTO*, Washington D. C.
- FHWA 2001. Long term pavement performance. Test method for determining the creep compliance, resilient modulus and strength of asphalt material using the indirect tensile test device. *FHWA* Version 1.1, LTPP Test Protocol.
- Kepler, J. L., D. Darwin & C. E. Locke 2000. Evaluation of corrosion protection methods for reinforced concrete highway structures. SM Report No. 58, *University of Kansas Center for Research*, Lawrence, 222p.
- NCHRP 2008. Guidelines for selection of bridge deck overlays, sealers and treatments. Project 20-07, Task 234, *Transportation Research Board*.
- NCHRP, 2012. Waterproofing membranes for concrete bridge decks. *Transportation Research Board Synthesis* 425.
- Nicholls, J. C., R. W. Jordan, K. E. Hassan, J. T. Williams & A. S. M. Badr 2007. Asphalt surfacing to bridge decks. 4th *International Conf. Bituminous Mixtures and Pavements*, Thessaloniki, 19–20 April, Greece.
- OSMEO (Greek acronym for Guidelines for the Design of Transportation Works), 2002. *Greek Ministry of Public Works*, 3rd edition, 1st Volume, Greece.
- Park H. M., J. Y. Choi, H. L. Lee & E. Young. 2008. Performance evaluation of a high durability asphalt binder and a high durability asphalt mixture for bridge deck pavements. *Construction Technology*, Elsevier Ltd.
- Zimmerman, J.M., Olson, S.A., & Schultz, A. E. 2007. Determining economic strategies for repair and replacement of low slump overlays of bridge decks. Minneapolis, *Minnesota Department of Transportation*, MN/RC-2007-14.

Laboratory study of evaluating direct tensile properties of asphalt mixtures on reflective cracks

Mahmood Khadem

M.Sc of Road and Transportation in Civil Engineering, CEO of Rahbord Taradod Pars Consulting Engineering, Tehran, Iran

Ronak Farahi

M.Sc of Urban Management in Faculty of Management, University of Tehran, Tehran, Iran

ABSTRACT: One of the most important problems in pavements rehabilitation is detecting of reflective cracks when paved new HMA overlay paved on old pavement. Studies represent the complexity of the problem and the fact that these kinds of cracks are a variable and complex phenomenon. Usually, this failure spread from the lower layers to the overlay and it may cause from wheels loads stresses, stresses due to temperature gradient, volume variation of lower layers or all three combination. After the studying on reflective cracks mechanism it demonstrated that tensile stress due to wheel loads passage is one of the main factors that causing these cracks. So in this experimental research, the performance of different flexible asphalt mixture to increase tensile strength of mixtures has been evaluated, and then we evaluated the tensile strength of variable sample against on reflective cracks comparative, which due to decrease the tensile strength of mixture. Four type of Asphalt including sulfuric, mastic, recycled rubber and geosynthetic reinforced has been studied. Analysis shows that the samples of mixture have different affect on increasing tensile strength in asphalt mixtures. In this research we prepared mastic, sulfuric (with 50%) and geogrid reinforced increased tensile strength has been observed compared to other sample; moreover we evaluated the effect of loading rate on increasing the tensile strength.

Keywords: reflective crack, geosynthetic

1 INTRODUCTION

One of the most important problems in using overlay in pavement rehabilitation is the reflection of crack after application. It is one of the most concerning factors for pavement maintenance engineers and clients. Studies show that it is a complex and variable phenomenon. It spreads from the base and subbase (minority) and old and fails HMA (majority) to the overlay and can be caused by wheel load stresses, stresses due to temperature gradient and both at the same time. When the overlay stress equals to the tensile strength, failure happens. Increasing traffic loads, adverse weather conditions and not allocating credit for improvement at the specified time in order to maintain the roads are the main reasons of this problem. It causes to be vulnerable for asphalt during the whole service life. These factors lead to the reduction of the useful lifetime of asphalt overlay or increasing the cost of maintenance or both simultaneously.

Cracks in overlays happen when the layer could not sustain against shear and tensile strength than accrue the movement. This stress is concentrated on the cracks in the old layer. Its phenomenon leads to reflective cracks (Bhutta, 1998).

Generally, based on earlier studies and widespread researches on the factors causing the development and spreading of cracks in pavement layers, these three factors are introduced as the main causes:

Weather condition and thermal stress: consecutive heating and cooling of pavement layers during the day, month and year, and different thermal conductivity coefficients of the layers due to their diverse materials cause dissimilar deformations and thus lead to the advance of tensile stresses and cracking in layers and spreading the crack in the pavement.

Traffic loads: Passage of traffic loads cause different stresses in the layers that cause fatigue due to both the frequency of traffic passage and increasing of tensile and shear stresses in the pavement. Furthermore, the main reason of spreading the cracks of the aged pavement to the overlay is the traffic loads.

Settling of the lower layers: Improper conditions in applying the pavement, inadequate compression of the layers, different modulus of resilience of the layers proportional to weather conditions and also the stability of loading conditions cause vertical settlement in base layers and even the bed soil. And this in repetition causes the development and spreading

Table 1. Bitumen properties.

Properties	Penetration at 25 C, 1/10 mm	Softening point, C	Loss of Weight	PI	PVN
Standard	ASTM-D5	ASTM-D36	ASTM-D1754	ASTM-D6	-
Test Value	64	48	0.1	-0.35	-0.90

of the cracking due to elimination of upper layer support.

The mechanism of cracks' growth in overlays depends on the characteristics of the contact area between the overlays and old layer (Scrapas, 1996). The group of researchers in Delf university in the Netherlands has studied on using finite element methods to evaluate how the crack growth and what is the initiation of its in overlays. Also, they evaluate the effect of interlock contacts with CAPA 3D software (Scrapas, 1996).

After we search a lot about the history of the test that prepares a condition which confronts asphalt samples to direct tensile force we could not find the machine, because the entire standard test evaluated the indirect tensile stress in asphalt sample. In real projects the tensile stress happens as tensile due to bending of sample such as ITS and, On the other hand, analyzing the direct stress is important to asphalt mixture although it has not been analyzed before.

The widespread use of asphalt mixtures on the transportation system in many countries led to high attention touts effective parameters and performance of flexible pavements. As the result, selecting appropriate aggregate and other effective parameter results in the increasing serviceability life of pavement and decreasing the cost of rehabilitations (Bhutta, 1998).

2 EXPERIMENTAL TEST

In this study different asphalt specimens have been prepared and investigated, in order to analyze their tensile strength. Specimens Including sulfuric asphalt with 30%, 40% and 50% sulfur as the percentage of bitumen, mastic asphalt, polymer asphalt with recycled rubber, reinforced asphalt with geosynthetic materials and simple asphalt.

2.1 Bitumen properties

Asphalt bitumen 60/70 commonly used in the region was selected for this research. The bitumen properties were evaluated by laboratory tests, which are demonstrated in the Table 1.

2.2 Aggregate

Aggregate is the major structural framework of asphalt mixture to absorb and control different stresses on pavement. In our project, we have done our tests on

Table 2. Aggregate properties value in the project.

Experiment	Test Value for retained sieve 4.75 mm	Test Value for passing sieve 4.75 mm	Standard No.
Fractured Percent	95-98	-	ASTM-D5821
LA	19	-	ASTM-D131
PI	-	N.P	ASTM-D4318
SE	-	63	ASTM-D2419
Loss weight	6.4	8.3	ASTM-C88
Flakiness	-	22	BS 812

Table 3. Aggregate properties value in the project.

Properties	Test Value	Standard
Retained Sieve 4.75 (mm)		
Specific gravity	2.547	ASTM-C28
Apparent Specific gravity, kg/cm ³	2.669	ASTM-C28
Water absorption, %	1.78	ASTM-C27
Passing Sieve 4.75 (mm)		
Specific gravity	2.424	ASTM-C28
Apparent Specific gravity, kg/cm ³	2.639	ASTM-C28
Water absorption, %	3.35	ASTM-C27
Passing Sieve 0.075 (mm)		
Apparent Specific gravity, kg/cm ³	2.607	ASTM-C28

Table 4. Sieve test result.

Sieve	Size (mm)	Passing (%)	Retained (%)
3/4	19	100	0
1/2	12.5	95	5
4	4.75	59	41
8	2.36	43	57
50	0.3	14	86
200	0.075	6	94

crushed aggregate with a nominal size of 19mm. This aggregate is brought from the local region of the projection in order to simulate the real technical experience (Table 2). In Table 3 you can find technical parameters of this aggregate and in Table 4 its sieve size of gradation.

According to our target it's necessary to use same aggregate and bitumen in addition the gradations of all samples are similar. On the other hand, we have made mastic asphalt mixtures with some different properties. In fact, because of the time limitation of the study, we could not find new aggregate gradation, so we used (S.J) model with gradation (Table 5).

2.3 Experimental test

In this research, we have compared the asphalt mixture parameters together in specific test and condition to receive the correct results, So we tried to observe made samples with specific aggregate, bitumen and

Table 5. Sieve test result.

Sieve	Size (mm)	Passing (%)	Retained (%)
3/8	19	100	0
4	4.75	59	41
8	2.36	43	57
16	1.18	44.8	11.5
30	0.6	36.8	8
50	0.3	14	86
100	0.15	27.2	3.8
200	0.075	6	94



Figure 1. Geotextile photo.



Figure 2. Geogrid photo.

some percentages of it (Or near it). We prepared 3 samples from different types of asphalt mixtures (simple mixture, reinforced mixture by Geo-textile figure and, 2 Geo-grid figure 1 sulphuric mixture with (30%–40%–50%) sulphur as the percent weight of bitumen, and modified mixture with CRM (with gilsonite and rubber) and mastic mixture (with S.J. gradation). With optimum bitumen, although the mastic samples had different percentages of bitumen because of the gradation format. We used Geosynthetic panels which made of polymeric materials, defined by ASTM. The materials in soil, rocks and soil materials, that are associated with some of the project engineering is used.

2.3.1 Marshal test

It is obvious that the optimum bitumen content is highly dependent on the type of asphalt mixtures, such as mastic asphalt. The optimum bitumen content was defined by Marshall Stability curves, specific gravity, air voids (%), Marshall Flow curves and VMA (%) according to the Asphalt Institute manual. In this study, three Marshall Specimens for each gradation were prepared in the laboratory condition, according to ASTM D1559-76 assuming high traffic volume

Table 6. Marshall results.

Properties	Value
Optimum binder content (%)	6
Marshall stability (kgf) (defining the optimum binder content)	1050
Specific gravity (gr/cm^3) (defining the optimum binder content)	2.252
Air voids (%) (Defining the optimum binder content)	4
Marshall flow (mm) (controlling the optimum binder content)	12
Voids in mineral aggregates (%) (controlling the optimum binder content)	15



Figure 3. Asphalt mixture sample.

area. Afterwards, the air voids, voids in mineral aggregate (VMA), Marshall Stability, Marshall Flow and resilient modulus were evaluated. Table 6 shows the summary of Marshall Test results for simple sample.

Marshal method was used to prepare the specimens with $150 \times 70 \times 50$ mm cubic containers. The only difference was that in Marshal Method, a cylindrical specimen is used but in this study, cubic specimens are equipped and a square-shaped foot hammer was used instead of disk-shaped foot Marshal Hammer. This hammer was designed and prepared specifically for this lab experiment. Hence, the energy obtained from drop of this hammer is the same as Marshal Hammer.

According to our purpose in this research we focused on comparing the strength of direct tensile of different samples, although there are indirect tensile strength standard devices. The device used in this experiment is basically for polymer engineering for rubber and polymeric samples. After some alterations on device according our research purposes, we made some alteration on the device. This device has two major segments:

a) Mechanical segment: The important parts of this segment are the following:

1. Opening and closing jaws in order to hold the specimen and loading.
2. Fixed jaws that the opening, closing jaws are settled on them.



Figure 4. Tensile test machines.

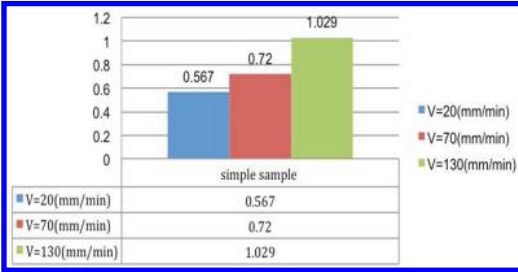


Figure 5. Average tensile strength of a simple sample.

3. Loading sensors that are connected to computers and the jaws.
 4. Other embedded mechanical parts.
- b) The available software for the computations is pre-installed on the attached loading method.

2.3.2 Loading

The device loading is a single-axle tension with a software controlled rate ranging between 0 and 1000 mm/min. Loadings were applied to the specimens with three different rates of 20 mm/min, 70 mm/min and 130 mm/min which simulates vehicles' low, average and high speed. The second rate (70 mm/min) is somehow near the loading rate in Marshal Test.

As mentioned before, the equipments and software of the test, are based on the direct tension test with non-standard machine that we don't have any specification of its and test. In this study, we focused on comparison of modified sample that was commonly in use in project with simple sample to analyze the strength of different sample against tensile force Figure 5. The comparative results of analysis based on the tension test on the specimens are in the following charts due to comparative research, we calculated tensile strengths of different samples on simple sample so, the rate of this portion is in Figure 6, Figure 7. In these charts and table, we divide the parameter by loading speed according the test procedure to evaluate the effects of load speed on sample strength.

As mentioned before, the equipments and software of the test, are based on the direct tensile. In this study, we focused on the comparison of modified sample that are commonly in use in project with simple sample to

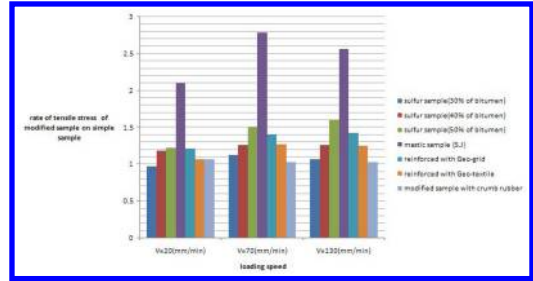


Figure 6. The stress rate of modified sample on simple sample.

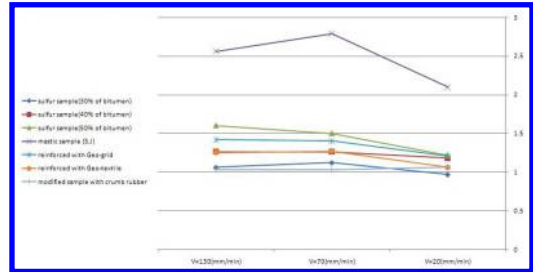


Figure 7. The stress rate of modified sample on simple sample.

analyze the strength of different samples against tensile force. The comparative results of analysis based on the tension test on the specimens are in the following charts.

2.4 Analysis of the results

Practically, the Mastic asphalt showed 2.5 times tensile strength in comparison to sample asphalt and was better than other samples. So it is the best type of asphalt for the overlay. According to the specimens' results, it showed exceptionally effective resistance to reflective cracks and if it's manufacturing and applying a condition (such as the bitumen percentage and the environmental parameter) is provided, mastic asphalt overlays should have a very extensive lifetime.

Geo-grids and Geo-textile are obtaining an increasing application in the road industry. Therefore, based on this study, if suitable cohesion, adherence and control of these materials with asphalt are considered, they can be significant methods to control reflective cracks in overlays. It increases up to 40% of strength of tension, which its fiber can absorb. So if these methods were used in real projects with better supervision, they would postpone cracks.

The result shows that the performance of Geo-grid against tensile stress is 20% better than Geo-textile. This variation shows that the cohesion between asphalt mixture and fiber is an effective parameter to absorb stress, so it's very important to control it.

Sulfur as an extra product of refineries mixed with bitumen in asphalt design would lead to increasing the

tensile strength of the specimen up to 50% of simple sample, alongside improving bitumen and asphalt. If the percentage of sulfur increases, it can be a better reaction against stress the result shows that 40% sulfur can increase tensile strength 1.3 of simple samples and 50% sulfur 1.5times, therefore in order to control the cracks, 40% and 50% samples are more suitable than 30%. Beside observe the safety, security and environmental issues it would offer higher strength compared to ordinary asphalt.

On the other side, recycled rubber as a polymeric material in the bitumen, didn't show significant difference in tensile strength of the simple sample and so, application of this material in overlays is not recommended however it's very difficult to prepare Homogeneous mix between bitumen and polymer. It's except that CRM couldn't improve tensile parameter the same as pressure condition.

Another result shows that the rate of the loadings were effective on samples strengthen. The rate of loading is simulated to the vehicle speeds, then if it increases from 20 mm/min to 70 mm/min in all samples the rate of stress were increased with extraordinary like slopes. On the other hand the difference depends on the performance of asphalt mixture against loading. It demonstrated that under increasing the rate of loading the elastic parameter has a more important role than viscose parameter in the asphalt mixture. On low speed 20 mm/min can simulate to the place such as stopping place.

3 CONCLUSIONS

According to the nature of reflective cracks and related numerous damages, one of the best methods for preventing this, is to renew the overlays that could deferment the time of renewed cracking. Consequently, other options for the mix design of asphalt samples were studied in this experiment.

Based on the procedure of the researches, following results were obtained:

- Increasing the loading rate, increased tensile stress of the specimens with different extent and this could be due to asphalt samples behavior that in higher loading rates, the elastic characteristics will dominate comparing to viscous characteristics.
- In reinforced samples, increasing the loading rate, increased tensile stress, which is due to insufficient time for detaching of reinforcing layer of the asphalt mixture will improve the efficiency of the sample.
- The net tensile stresses of specimens were determined in a non-standard test condition in order to select a suitable overlay, all the advantages and disadvantages should be considered. In short, based on this study, mastic asphalt with higher strength and better technical characteristics is the best option for the overlays in order to resist reflective cracking.

REFERENCES

- Bhutta, S.A, 1998, "Mechanistic-Empirical Pavement Design Procedure For Geosynthetically Stabilized Flexible Pavements", Department of Civil Engineering Virginia Polytechnic Institute and State University Blacksburg, VA-24060.
- Cleveland, G.S., Button, J.W., and Lytton, R.L., "Geosynthetics in Flexible and Rigid Pavement Overlay Systems to Reduce Reflection Cracking", Sponsored by the Texas Department of Transportation In Cooperation with the U.S. Department of Transportation Federal Highway Administration. October, 2002.
- Francken, L. and Verstraeten, J., "Interlaboratory test program. Part II, Repeated loading tests", Draft Report, RILEM TC 152-PBM, 1994.
- Scrapas, A., De Bondet, A.H. Molenaar, A.A.A., and Gaarkeuken, G., (1996) "Finite Elements Modelling of Cracking in pavement", Proc. of 3rd RILEM Conference, pp. 82.
- Sida, M., "Mastic asphalt for pavement Surfacing", TRB Annual Meeting, (2003).

Effects of bonus provisions on HMA superpave mixture specifications through pay factor analysis

S.S. Karimi, D.G. Goulias & C.W. Schwartz

Department of Civil and Environmental Engineering, University of Maryland, College Park, MD, USA

ABSTRACT: With the use of Superpave mix design methodology highway agencies have been developing and/or adopting specifications for Hot Mix Asphalt (HMA). In an effort to further promote improvements in mixture quality and performance these acceptance specifications are further modified to include bonus provisions. After addressing (i) the differences in HMA mixture properties in plant versus behind the paver, and (ii) assessing the risks associated with the acceptance of Superpave mixtures to both the agency and contractor, it was equally important to (iii) evaluate the effects of a bonus provision incorporated into the HMA acceptance specification in regards to pay factors. The pay factor study was based on simulation analysis using the population characteristics of dense graded Superpave mixtures and the bonus provisions of the revised specification. The study examined the impact of the current HMA production quality on the composite mixture percent within specification limits (CMPWSL) and mixture pay factor (MF) and assessed the impact of alternative specification tolerances. Comparatively to the no-bonus provision, the pay factors generated from the revised specification provided higher incentives for higher quality HMA mixtures and increased pay deduction for lower quality.

1 INTRODUCTION

With the use of Superpave mix design highway agencies have experienced a reduction in binder content for asphalt mixtures that may lead to premature failure due to difficulties in compaction and thus lower density and higher permeability, and lower film thickness around the aggregate particles (NCHRP Project 9-33). Maryland's State Highway Administration (MSHA) concern with the lower asphalt levels in Superpave mixes have lead efforts through the HMA Pay Factor Team to explore strategies to increase the asphalt content in Superpave mixes. The first analysis of the study had as objective to examine HMA mixture properties at the plant and behind the paver by comparing quality control (QC) and quality assurance (QA) data (Karimi et al., 2012). The next objective of the study was the development of Operating Characteristic (OC) curves in order to quantify risks to both agency and contractor (Karimi et al., 2014). The analysis presented in this manuscript has the objective of assessing the impact of a bonus pay factor provision incorporated into a revised acceptance specification.

2 POPULATION CHARACTERISTICS OF DENSE GRADED MIXTURES

In these analyses, only dense graded HMA mixtures were considered due to the large amount of data available in the Maryland SHA database since this represent

Table 1. Population characteristics for dense graded mixtures.

Property	Delta Mean*	Std. Dev.
0.075	0.992	1.20
2.36	-0.192	3.88
4.75	0.066	5.60
AC	-0.002	0.31

*Deviations from the target values.

the more common mixture used in the state. In the simulation analyses the population characteristics of the four mixture parameters considered for acceptance were used. These include asphalt content and percent passing the 0.075, 2.36, and 4.75 mm sieves (Table 1) and reflect the values obtained from the quality assurance data. The correlations between these mixture parameters were considered as well, Table 2. Based on the population characteristic of these mixture properties and their correlations simulation analysis were run for producing the Composite Mixture Percent within Specification Limits (CMPWSL) and calculating the expected mix pay factor (MF).

3 COMPOSITE MIXTURE PWSL AND SPECIFICATION TOLERANCES

HMA acceptance specifications typically include more than just the AC since the influence of the

Table 2. Correlations between mix parameters for dense graded mixtures.

Property	0.075	2.36	4.75	AC
0.075	1	0.338	0.208	0.242
2.36	0.338	1	0.562	0.261
4.75	0.208	0.562	1	0.305
AC	0.242	0.261	0.305	1

Table 3. Original specification tolerances.

Property	Original Tolerances	Revised Tolerances
0.075 mm	±2%	±2%
2.36 mm	±5%	±5%
4.75 mm	±5%	±7%
AC	±0.5%	±0.5%

aggregate properties have an important role in the volumetric characteristics of Superpave mixtures and their performance (NCHRP Project 9-33). In Maryland the following four mixture properties are used for determining mixture acceptance and pay factors: aggregate percent passing 0.075 mm; aggregate percent passing 2.36 mm; aggregate percent passing 4.75 mm; asphalt content (AC). The specifications define a lot as a maximum of 6,000 tons and a subplot as a maximum of 1,000 tons of production. A minimum of one set of quality acceptance tests and one set of QC tests are required for each subplot, where each set of tests consists of measurements of the above mixture properties. Contractors often opt to perform more than the minimum number of QC tests, either on plant samples or on supplementary samples obtained from behind the paver. The tolerances from the target values for the specification properties with the no bonus are shown in Table 3. With the revision of the HMA specification to include a bonus provision, the tolerance of the 4.75 mm sieve was also modified, Table 3, reflecting an increase in aggregate production variability due to the crushing operations at the quarries.

The aforementioned tolerances are used in calculating the Percent within Specification Limits (PWSL) of each property which feeds into the CMPWSL calculation, Equation 1. CMPWSL is then used in calculating the MF. The Composite Mixture PWSL (CMPWSL) is calculated by:

$$CMPWSL = [f_1 PWSL_1 + f_2 PWSL_2 + f_3 PWSL_3 + f_4 PWSL_4] / \Sigma f \quad (1)$$

where: PWSL1 = asphalt content; PWSL2 = aggregate passing 4.75 mm/#4 sieve; PWSL3 = aggregate passing 2.36 mm/#8 sieve; PWSL4 = aggregate passing 0.075 mm/#200 sieve; and the f_i are the relative weights of, f_1 = asphalt content = 62; f_2 = aggregate passing 4.75 mm/#4 sieve = 7; f_3 = aggregate passing 2.36 mm/#8 sieve = 7; f_4 = aggregate passing 0.075 mm/#200 sieve = 24.

4 PAY FACTOR PROVISIONS

The pay factor equation without the bonus provision is shown in equation 2. This pay factor sets a cap of 100% payment for lots that have a CMPWSL of above 90%.

$$\begin{cases} MF = 0.55 + 0.5CMPWSL \\ \text{if } CMPWSL \geq 90\% \text{ } MF = 1 \\ \text{if } CMPWSL < 40\% \text{ } MF = 0 \end{cases} \quad (2)$$

The population characteristics for each mix parameter were thus used to evaluate the CMPWSL and MF at the long run. This was achieved by running several thousands of simulation runs reflecting simulated lots and sublots with population characteristics as those observed for these dense graded Superpave mixtures. The results are shown in Figure 1. It can be observed that under pay equation 1 with a maximum cap (i.e., max 100% pay for $\geq 90\%$ CMPWSL), the contractor over the long run can never achieve a pay factor of 100% even when producing at or above 90 CMPWSL. Ultimately, such observations led the agency to the conclusion that a revised pay equation was needed that more fairly assigns payments to contractors when achieving 90% CMPWSL. In most specifications a 90% CMPWSL is used to assign 100% MF, since this reflects the Acceptable Quality Level (AQL). This AQL value represents the minimum quality level for fully acceptable material (TRB Circular, 2002). When quality is based on Percent Within Specification Limits (PWSL), the AQL is the PWSL value for which the material is considered fully acceptable. A 90% PWSL is commonly used for AQL of HMA. The developed acceptance plans should in this case be designed so that AQL material will receive an expected pay (EP) of 100 percent (Burati et al., 2006). Furthermore, to provide incentives for higher material quality a bonus provision is often considered into the acceptance specification. The above considerations led to the adoption of a new pay factor provision, equation 3, in which the contractor can achieve up to a 5% incentive if CMPWSL exceeds 90%.

$$\begin{cases} MF = 0.55 + 0.5CMPWSL \\ \text{if } CMPWSL < 40\% \text{ } MF = 0 \end{cases} \quad (3)$$

As in the previous case, the population characteristics for each mix parameter were used to evaluate the CMPWSL and MF at the long run using simulation analyses. The results are shown in Figure 1. It can be observed that with the bonus provision the contractor at the long term can now achieve on the average a pay factor of 100% when producing at 90 CMPWSL.

5 EFFECTS OF MIXTURE PROPERTIES & SPECIFICATION TOLERANCES ON CMPSWL AND MF

5.1 Reduction in asphalt content variability

The goal of this analysis was to examine how a reduction in AC variability will affect the average MF while

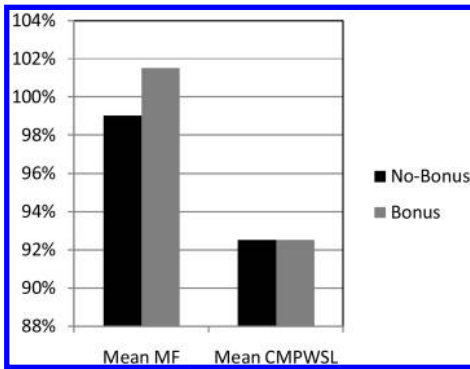


Figure 1. CMPWSL and MF for dense graded superpave mixtures.

holding the variability of all other parameters (percent passing 0.075, 2.36 and 4.75 mm) constant at the population characteristics.

Asphalt content was judged to be the most critical parameter since: (i) current dense graded SUPERPAVE mixtures in the state experience a lower AC content; (ii) it significantly affects mixture compaction and performance, as is reflected in the relative weight of this parameter in equation 1; and (iii) represent the mixture component with the highest cost and thus the primary mixture parameter of potential interest in attempting to reduce HMA production cost. In this analysis the standard deviation of AC was set at 75%, 50% and 25% of the population, Figure 2. As it can be seen from this figure, a contractor that is able to produce an HMA mixture with 75% lower variability (0.25 SD/SD_{pop}) than the current QA population variability can increase MF from 99.7% to about 101.2%. Furthermore, the bonus provision incentivizes the contractor to reduce its production variability by approximately 50%. This is evident by the fact that the difference between the two pay factor equations at $\frac{SD}{SD_{pop}} = 1$ is only 0.7% but increases to 1.6% at $\frac{SD}{SD_{pop}} = 0.5$ and remains unchanged after that. Past studies have shown that such reduction in variability is attained by good contractors with rigorous quality control, while smaller inexperienced contractors may experience challenges in achieving so (Karimi et al., 2014).

5.2 Modifying specification tolerances

The effects of changing specification limits (tolerances) on the average MF were also examined by using both pay factor provisions. In both specification versions, the tolerance for AC is $\pm 0.5\%$. All other tolerances were kept constant and the AC tolerance was changed. The results are shown in Table 4 and Figure 3. As it can be seen, a change in the tolerance of AC content of about 20% will result in a change of 4% CMPWSL and 1.4 versus 1.6% in MF for the no-bonus versus the bonus specification.

Similarly, the effect of changing the 0.075 mm percent passing specification tolerance was examined.

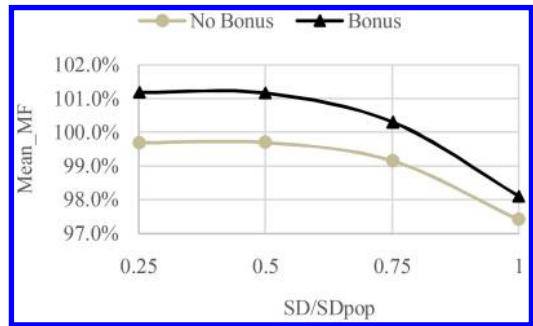


Figure 2. Effect of reduction in asphalt content variability on MF.

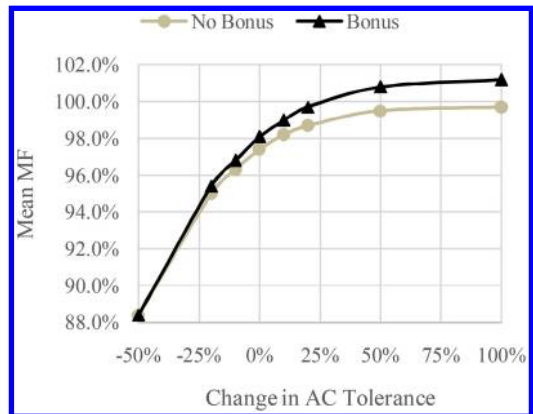


Figure 3. Effects of change in percent AC specification tolerance on MF.

The current specification suggests a tolerance of $\pm 2\%$. The results are shown in Table 5 and Figure 4. A change in the tolerance of 0.075 mm percent passing specification tolerance of about 20% will result in a change of 2.3% CMPWSL and 0.7% versus 1.0% in MF for the no-bonus versus the bonus specification.

Similarly, the effect of changing the 2.36 percent passing specification tolerance was also examined. The current specifications suggest a tolerance of $\pm 5\%$. The results are shown in Table 6 and Figure 5. As it can be seen, a change in the tolerance of 2.36 mm percent passing specification tolerance of about 20% will result in a change of 0.7% CMPWSL and 0.07% versus 0.22% in MF for the no-bonus versus the bonus specification.

Finally, the effect of changing the 4.75 mm percent passing specification tolerance was examined. However, for this property the tolerance in the revised specification was modified by the agency producing thus a different CMPWSL for each case, Table 7. As it was mentioned previously, the original specification with the no-bonus provision had a tolerance of $\pm 5\%$ while the revised one with the bonus provision had a tolerance of $\pm 7\%$. The results are shown in Table 7 and Figure 6. As expected, the mean CMPWSL for the more strict tolerance ($\pm 5\%$) is lower than in the case with a wider tolerance ($\pm 7\%$) for this mixture

Table 4. Effect of AC tolerance on CMPSWL and MF.

AC Tolerance	% Change	Mean CM	% Change CM
1	100	92.4	7
0.75	50	91.6	6
0.6	20	89.4	4
0.55	10	88.0	2
0.5	0	86.2	0
0.45	-10	83.6	-3
0.4	-20	80.7	-6
0.25	-50	66.9	-22

No-Bonus			Bonus	
AC Tolerance	Mean MF	% Change MF	Mean MF	% Change MF
1	99.7	2.4	101.2	3.1
0.75	99.5	2.1	100.8	2.7
0.6	98.7	1.4	99.7	1.6
0.55	98.2	0.0	99.0	0.9
0.5	97.4	0.0	98.1	0.0
0.45	96.3	-1.1	96.8	-1.3
0.4	95.0	-2.4	95.4	-2.8
0.25	88.4	-9.3	88.4	-10.0

Note: CM is CMPSWL.

Table 5. Effect of 0.075 mm tolerance on CMPSWL and MF.

0.075 mm Tolerance	% Change	Mean CM	% Change CM
4	100	90.9	5.6
3	50	89.8	4.4
2.4	20	88	2.3
2.2	10	87.3	1.5
2	0	86.1	0.0
1.8	-10	84.8	-1.5
1.6	-20	83.4	-3.1
1	-50	78.0	-9.3

No-Bonus			Bonus	
AC Tolerance	Mean MF	% Change MF	Mean MF	% Change MF
4	98.8	1.5	100.4	2.4
3	98.5	1.2	99.9	1.9
2.4	98.1	0.7	99.1	1.0
2.2	97.8	0.5	98.6	0.5
2	97.4	0.0	98.0	0.0
1.8	96.9	-0.5	97.5	-0.6
1.6	96.4	-1.0	96.7	-1.4
1	94.0	-3.5	94.0	-4.1

Note: CM is CMPSWL.

property. As it can be seen, a change in the tolerance of 4.75 mm percent passing specification tolerance of about 20% will result in a change of 0.1% versus 0.2% in MF for original versus the revised specification.

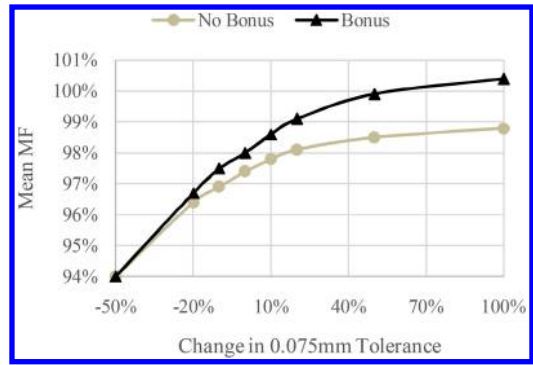


Figure 4. Effects of change in 0.075 mm specification tolerance on MF.

Table 6. Effect of 2.36 mm tolerance on CMPWSL and MF.

2.36 mm Tolerance	% Change	Mean CM	% Change CM
10	100	87.5	1.76%
7.5	50	87	1.13%
6	20	86.6	0.71%
5.5	10	86.4	0.49%
5	0	86	0.00%
4.5	-10	85.7	-0.28%
4	-20	85.4	-0.65%
2.5	-50	83.9	-2.45%

No-Bonus			Bonus	
AC Tolerance	Mean MF	% Change MF	Mean MF	% Change MF
4	97.9	0.40	98.7	0.57
3	97.7	0.20	98.5	0.41
2.4	97.6	0.07	98.3	0.22
2.2	97.5	0.02	98.2	0.03
2	97.4	0.00	98.0	0.00
1.8	97.3	-0.21	97.8	-0.29
1.6	97.2	-0.32	97.6	-0.49
1	96.6	-0.90	96.9	-1.21

Note: CM is CMPSWL.

Overall, the simulation analysis results indicate that the change in AC content tolerance has the most significant effect on MF reflecting the heavy weight of the AC content in calculating the CMPWSL, Equation 1. It can also be observed that with the bonus provision of the revised specification a MF above 100% is achievable with small reductions in AC variability. Also, it was observed that across all tolerance adjustments the MF change in the bonus pay equation is more pronounced than in the case of no-bonus provision, both in terms of higher and lower quality material.

This result indicates that any further adjustments in mixture property tolerances of the revised specification with the bonus provision may further promote higher quality HMA mixtures and discourage lower quality materials since these are associated with higher monetary incentives and penalties respectively.

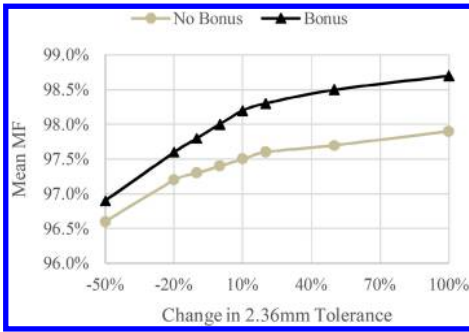


Figure 5. Effects of change in 2.36 mm specification tolerance on MF.

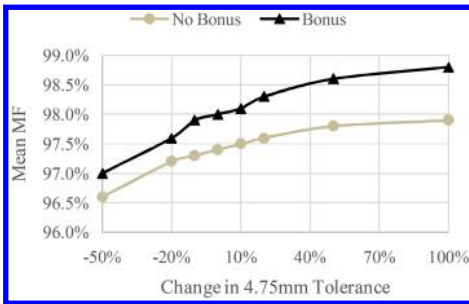


Figure 6. Effects of change in 4.75 mm specification tolerance on MF.

Finally, as it was pointed out previously that under the specification with no-bonus provision contractors were never able to achieve 100% payment even if the agency increases the tolerance by 100%.

6 CONCLUSIONS

The analysis of this study lead to the following conclusions:

1. The simulation analyses have shown that, i) a contractor with tight control over the variability of mixture production can significantly reduce the AC content and still receive a reasonable pay factor, ii) due to the high weight of the AC content in the final composite pay factor equation, the effects of changing AC tolerances has a more pronounced impact on the pay factor than any other mixture property, iii) the revised specifications with the bonus provision have provided higher pay factor values. The average PF under the new specification is very close to 1.00, over the long run, for material meeting or exceeding the AQL;
2. Based on the historical variability of HMA production, the maximum achievable Composite Mix Percent Within Specification Limits (CMPSWL) for dense graded mixtures is 92.5%. The corresponding average mix pay factor (PF) at this quality level is equal to 99% and 101.5% for the no-bonus and bonus pay factor provisions, over the long run;

Table 7. Effect of 4.75 mm tolerance on CMPWSL and MF.

4.75 mm Tolerance ¹	% Change	Mean CM ¹	% Change CM ¹
14.0/10.0	100	87.5/86.9	1.7/2.0
10.5/7.5	50	87.1/86.4	1.3/1.5
8.4/6.0	20	86.6/86.0	0.8/1.0
7.7/5.5	10	86.4/85.7	0.4/0.6
7.0/5.0	0	86.1/85.1	0.0/0.0
6.3/4.5	-10	85.8/84.7	-0.3/-0.5
5.6/4.0	-20	85.4/84.3	-0.6/-0.9
3.5/2.5	-50	83.9/83.4	-2.5/-2.0

4.75 mm Tolerance ¹	No-Bonus		Bonus	
	Mean MF	% Change MF	Mean MF	% Change MF
4	97.9	0.0	98.8	1.0
3	97.8	0.3	98.6	0.5
2.4	97.6	0.1	98.3	0.2
2.2	97.5	0.0	98.1	0.0
2	97.4	0.0	98.0	0.0
1.8	97.3	-0.2	97.9	-0.2
1.6	97.2	-0.3	97.6	-0.5
1	96.6	-1.0	97.0	-1.0

Note: ¹ Revised /Original specification; CM is CMPSWL.

3. Across all tolerance adjustments the MF change in the bonus pay equation is more pronounced than in the case of no-bonus provision, both in terms of higher and lower quality material.

The analysis and methodology used in this study could be used elsewhere in helping adjusting pay schedules for accepting higher quality materials and modifying specification tolerances based on CMPWSL and MF.

REFERENCES

- Burati J. 2006. "Evaluating Specification Limits," Transportation Research Record No. 1946, pp. 92-98, Transportation Research Board of the National Academies, Washington, D.C.
- Burati J., Weed R. 2006. "Accuracy and Precision of Typical Quality Measures," Transportation Research Record No. 1946, pp. 82-91, Transportation Research Board of the National Academies, Washington, D.C.
- Karimi S., Goulias, D., Schwartz, C. 2012. "Evaluation of Superpave HMA Mixture Properties at the Plant versus Behind the Paver: Statistical Comparison of QC and QA data. ASCE Transportation Engineering Journal, 138 (7), 924-932.
- Karimi S., Goulias, D., Schwartz, C. 2014. "Risk and Expected Pay Factor Analysis for Assessing Gap and Dense-graded Superpave Mixture Specifications." International Journal of Pavement Engineering, 16(1), 2015. (Published on-line, 13 May 2014).
- NCHRP. 2010. "Project 9-33: A Mix Design Manual for Hot Mix Asphalt." Report 673. Transportation Research Board, Washington D.C.
- TRB, 2002. "Circular E-C037: Glossary of Highway Quality Assurance Terms." Washington DC.

Evaluation parameters of impact sounding signals for interface condition assessment of concrete bridge decks

Cristina Amor Rosales & Hyun Jong Lee

Department of Civil & Environmental Engineering, Sejong University, Republic of Korea

Jongeun Baek

Korea Institute of Civil Engineering and Building Technology, Republic of Korea

Wonjae Kim & Jaehoon Jeong

Department of Civil & Environmental Engineering, Sejong University, Republic of Korea

ABSTRACT: An impact sounding method is used to detect damages of materials subjectively based on sound characteristics such as intensity. This paper proposed an objective approach to distinguish between damaged and undamaged interface of pavement systems by analyzing impact signal and its frequency spectra. Two parameters, skewness and β -parameter were proposed to quantify the level of damage. The skewness value and β -parameter of the frequency spectra of bonded interface is less than 1.5 and less than 2.0 respectively. On the other hand, the unbonded interface frequency spectra have skewness value and β -parameter of greater 1.5 and greater than 5.0 respectively. Using the proposed evaluation parameters, levels of interface damages of concrete bridge deck pavement could be identified in the field.

Keywords: Impact Sounding, Interface Damage, Concrete Bridge Deck Pavement, Non-Destructive Testing, Frequency Analysis

1 INTRODUCTION

The interface layer of concrete bridge deck is one of the most vulnerable sections in pavement system (Pouteau et al., 2008; Mehta et al., 2007). Surface distresses, commonly cracking and tearing, mostly start with the deterioration in the pavement interface layer (Kim et al., 2013; Chabot et al., 2013). This interface deterioration or delamination, have two types: stripping and layer debonding. Stripping happens when adhesion between asphalt binder and aggregate is weakened and moisture infiltration worsens the condition. Debonding occurs due to improper tack between asphalt layers or asphalt overlay and concrete pavement. These material issues cannot be determined by visual inspection of the pavement, especially at the early stages of problem therefore non-destructive techniques such as impact echo, ground penetrating radar, and sounding methods have been introduced to determine the condition of composite pavement.

In the recent Strategic Highway Research Program (Heitzman et al., 2013), non-destructive tests (NDT) such as ground penetrating radar (GPR) and impact echo (IE) were evaluated. As several studies were conducted to determine the effectiveness of GPR, including the individual studies of various states in determining interface condition on pavement system,

GPR method still display weaknesses on determining shallow debonding, interface debonding where moisture is present and detailed boundaries of damaged area when collection speed is increased (Gregoire & Van Geem, 2013; Kryszynski & Sudyka, 2012; Halabe et al., 2007; Al-Qadi & Lahouar, 2004). Impact echo method, on the other hand, focuses on delamination of concrete and reinforcement rather than on interface layer (Gucunski et al., 2008, Medina & Garrido, 2007; Gassman & Tawhed, 2004, Tawhed & Gassman, 2002; Sansalone & Streett, 1997; Sansalone & Carino, 1989). In addition, the equipment used requires direct contact to surface leading to a slower speed and stationary data acquisition. Both NDT tests also demonstrate complexity and time-consuming data analysis, indifference on the exact severity of damage and only provide assistance in accurately locating the damages.

Since GPR and impact echo test methods have disadvantages and requires an in-depth training in order to represent the clearly the damages caused by deteriorated interface layer, traditional tests such as coring and impact sounding test are still performed. Impact sounding test is one of the non-destructive methods used in determining the road condition. Hammer hitting and chain dragging are the common and widely used methods since they are economical and provide

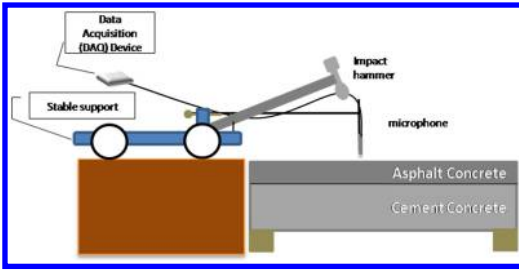


Figure 1. Impact sounding test set-up (Rosales et al, 2015).

fast result. Determining the damages using hammer hitting or chain dragging is assessed by using human ear and how the person differentiate the sound. In fact, ASTM Standard 4580 or known as the sounding method for detecting pavement deterioration do not provide exact values as reference for deterioration (ASTM, 2012). Consequently, the human factor makes this method subjective and qualitative in approach.

Several studies attempted to quantify impact sounding test by proposing different post-analysis method (Lu et al., 2013; Zhang et al., 2011; Suda et al., 2004; Henderson et al., 1999) by analyzing the time waveform, the frequency spectra and the time-frequency domain spectra of impact sound data at sensitive ranges. Even with accurate results obtained from these studies, the frequency range used in this study was out of the human perception range and their analysis techniques were too complicated to be applied in practice. Also, these studies focus on reinforcement rather than on debonding and deterioration of pavements. Therefore, a faster and more scientific way to measure interface condition using impact sounding method is suggested. In this study, parameters of impact sound frequency spectra were established and used to identify the interface layer condition.

2 IMPACT SOUNDING TEST

2.1 Impact sounding equipment set-up

The impact sounding test setup is presented in figure 1. A commercially available hammer (612 grams, 21.5 mm spherical hammer head) was connected to a stable stand and allowed to have a free fall impact on the surface of the pavement system. A pressure field microphone with a preamplifier (model PCB 378B11) was placed 5 mm above and 50 mm away from the hitting point to receive the impact sound signals. The microphone is then connected to National Instruments DAQ (DAQ model 9234) and the signals are sampled at 12800 Hz. A simple data acquisition and analysis program based on Lab View 2013 software was developed.

2.2 Impact sounding test analysis

Impact sound is a transient signal which has short duration and wide broadband spectrum (Randall,

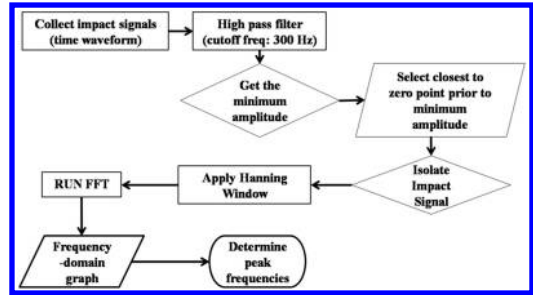


Figure 2. Process algorithm for frequency spectra conversion.



Figure 3. Slab specimen configuration (Rosales et al, 2015).

1987). This wide broadband spectrum is obtained by converting the time waveform signals of impact sound to frequency spectra using Fast Fourier Transform (FFT) technique. Figure 2 presents the conversion algorithm of time waveform to frequency spectra used in this study. Collected impact sound signals were filtered using high pass with cutoff frequency of 300 Hz. The 10 millisecond length impact signal was isolated manually by selecting the closest zero-amplitude point prior to the minimum amplitude. This signal is isolated and Hanning window is applied prior to FFT conversion. The resulting frequency spectra displayed narrow frequency peaks which give distinct pattern and shape for different interface condition.

3 LABORATORY TEST

3.1 Preparation of slab specimen

Three PCC slab specimens 60 cm long, 60 cm wide and 20 cm thick were prepared for the study as shown in figure 3. Two PCC slabs had single and double steel reinforcement in the middle of the slab and one PCC slab had no reinforcement. The slabs were overlaid with a 5-cm-thick AC layer. Tack coat was applied prior to placement of AC layer for better bonding. To simulate a completely debonded interlayer condition, the concrete surface of the PCC slab with single reinforcement was covered with plastic tape before pouring of asphalt mixtures. After one week, the plastic tape was carefully detached from the PCC slab and the AC layer was placed right before the test to keep the interlayer debonded.

3.2 Impact sounding test for slab specimen

Impact sounding test was conducted on the center and edged sections of the slab specimens. Impact sounding time waveform and frequency spectra of the three slabs is presented in figure 4. It is observed from

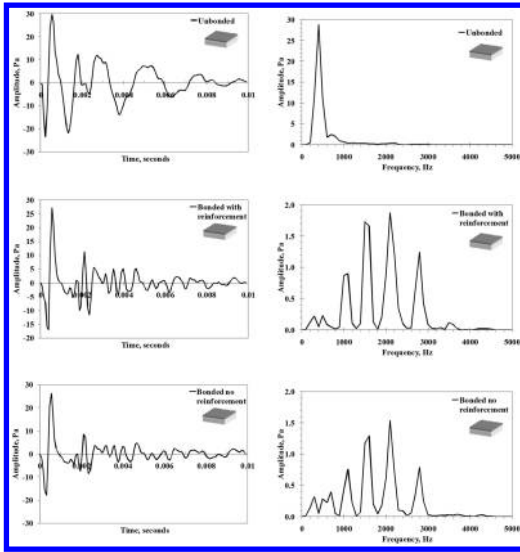


Figure 4. Time waveform and frequency spectra of slab specimen.

these graphs that there is a significant difference in the time waveform and frequency spectra of unbonded and bonded interface slab specimen. However, no significant difference is observed between bonded slabs with reinforcement and without reinforcement. For that reason, reinforcement configuration will not affect the interface condition assessment of concrete bridge deck.

4 EVALUATION PARAMETERS FOR INTERFACE CONDITION ASSESSMENT

Preliminary laboratory experiment showed that the frequency spectra of different interface layer condition showed the following distinct characteristics:

1. The pattern and shape of frequency spectra is significantly different between unbonded and bonded interface.
2. Impact sound of unbonded interface layer showed higher amplitude level compared with bonded interface.

From these obtained findings and different patterns, evaluation parameters were extracted in the frequency spectra to identify the bonding condition of the interface.

It was observed in the laboratory data that the frequency spectra of the unbonded interface tend to skew to the right whereas bonded interface layer skew to the center, similar to normal distribution. Thus, using skewness value, it can quantitatively describes the shape of the frequency spectra as the peaks forms bell-shaped pattern to the right, center or left of the frequency spectra depending on the bonding condition.

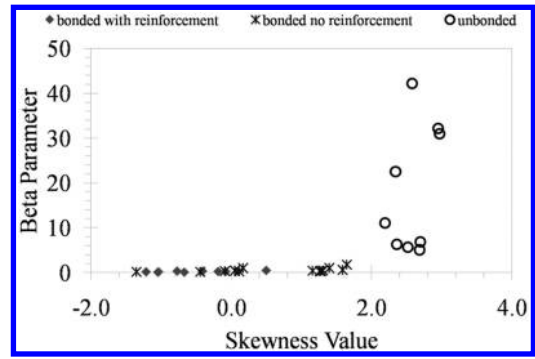


Figure 5. Matrix comparison for evaluation parameters of laboratory specimen.

The equation of skewness, based on statistics references (Beckman, 1973; Cohen, 1966; Collins, 1957) is:

$$\text{skewness} = \frac{\sum_{i=1}^n (X_i - \bar{X})^3}{(N-1)\sigma^3} \quad (1)$$

where X_i is the amplitude data of i th frequency, \bar{X} is the mean, σ is the standard deviation and N is the number of data points. In this study, to compute the skewness the frequency spectra, the data points considered are those from frequency values with dominant peaks.

On the other hand, it also observed that on unbonded interface, the frequency spectra amplitude is concentrated on frequencies less than 1000 Hz. Consequently, another parameter can be used wherein the ratio of the average amplitude of peak frequencies below 1000 Hz and above 1000 Hz is computed. This parameter named Beta (β)-parameter for this study is written in equation as:

$$\beta = \frac{\text{Ave. Amplitude of frequencies below 1000 Hz}}{\text{Ave. Amplitude of frequencies above 1000 Hz}} \quad (2)$$

Similar with skewness value, β -parameter is computed using the peak frequencies dominant in the frequency spectra.

These two parameters are plotted in a graph as shown figure 5. In this figure, it is observed that the skewness value of unbonded specimen is always greater than 1.5 whereas bonded slabs have skewness value less than 1.5. β -parameter, on the other hand, showed that unbonded specimen have values as high as 43.0 and as low as 5.0 compared with the consistent value of bonded specimen whose β -parameter is always less than 2.0. Since these two parameters display mutually exclusive space in the quadrant, these optimum values for skewness value and β -parameters are used as parametric condition in determining bonded section and unbonded section in the field data.

The decision values for the evaluation parameters selected from the laboratory test result. In table 1, the optimum skewness and β -parameter values for level of deterioration is presented.

Table 1. Matrix comparison for assessment of interface condition.

Level of Deterioration	Skewness Value	β -Parameter
Minor Deterioration	<1.5	<2.0
Intermediate Deterioration	Does not satisfies both parameter	
Major Deterioration	>1.5	>5.0

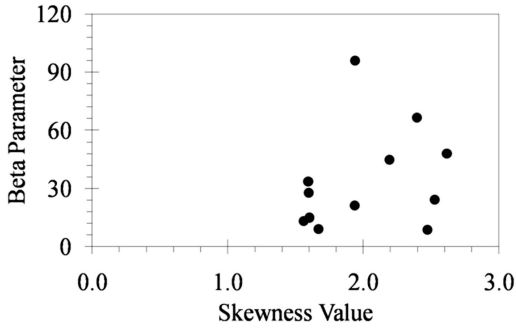


Figure 6. Matrix comparison for evaluation parameters of heaved section in the field.

5 FIELD VALIDATION

Impact sounding test was performed in Yanggok Bridge in Jeollabukdo, South Korea. A bridge underwent total replacement of AC layer which made possible to investigate the interlayer surface of concrete bridge deck. Initial inspection was performed and six sections were selected according to its varying surface condition. Impact sounding test was conducted every 30 cm of the width of the concrete bridge starting from point closest to the concrete barrier.

Initial field test was performed in the bridge where heaved surface is observed. Matrix comparison graph shown in figure 6 was plotted and it showed that the points at heaved section of the concrete bridge deck display similar results with laboratory test for unbonded specimen. Accordingly, skewness value and β -parameter can provide promising result in quantifying impact sounding signals to assess interface condition in the field.

A total of 90 data points in the concrete bridge deck were evaluated using impact sounding test, visual inspection and deterioration depth. There were three levels considered: minor deterioration, intermediate deterioration, and major deterioration. Of these three levels, most data points show intermediate deterioration as exposed concrete aggregates and deterioration depth of 5–15 mm was observed. In general, the bridge condition has intermediate damages on the interface where there are sections with exposed aggregates of concrete deck as presented in table 2.

Figure 7 presents the mapped result of the inspection based on the surface condition and on deterioration depth measured after removal of old AC layer.

Table 2. Summarized point assessment per level of interface damage.

Level of Interface Damage	Number of Points Assessed per Level		
	Sounding test	Visual Inspection	Deterioration Depth After Milling
Minor	30	15	18
Intermediate	56	60	67
Unbonded	4	15	5
Total Points		90	90

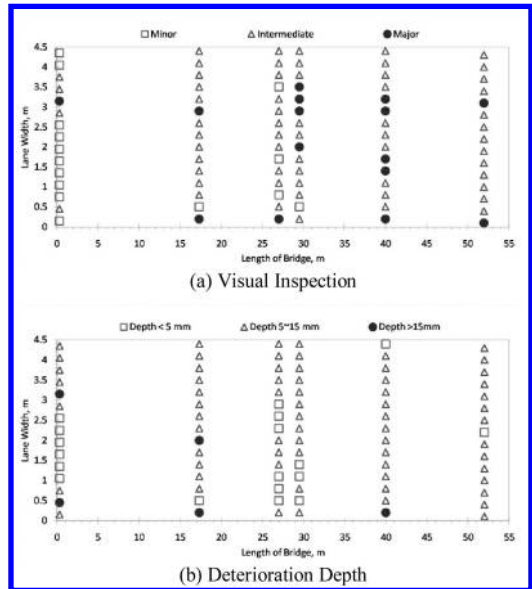


Figure 7. Interface condition assessment of bridge deck by (a) visual inspection (b) deterioration depth after milling.

This result showed that the sections near the wheel path and near concrete barrier have major interface damage. Points near the barrier, where road elevation is lowest also indicate major interface damages.

In table 3, more than 55% of assessed points using impact sounding test conform to visual inspection and deterioration depth assessment of interface condition. Similarly, more than 65% of intermediate deterioration detected by impact sounding conforms to other test.

Figure 8 showed the mapped interface condition assessment of the concrete bridge deck using impact sounding test. Impact sounding test identified four points in the concrete bridge deck with major interface deterioration. Though there is a low percentage matched between sounding test and deterioration depth after milling evaluation, it is observed that the location of the major interface damage between these two evaluation methods is close. As the deterioration depth is measured after milling, there is a possible discrepancy of identifying the exact location of the point

Table 3. Comparison of results of different methods of interface condition assessment method.

Level of Interface Damage	Visual Inspection	Deterioration Depth After Milling
Matched Points with Sounding Test		
Minor	8	8
Intermediate	40	45
Major	3	1
Total Matched Points	51	54
Percentage Matched with Sounding Test		
Minor	53.3	44.4
Intermediate	66.7	67.2
Major	20.0	20.0
Overall percentage	56.7	60.0

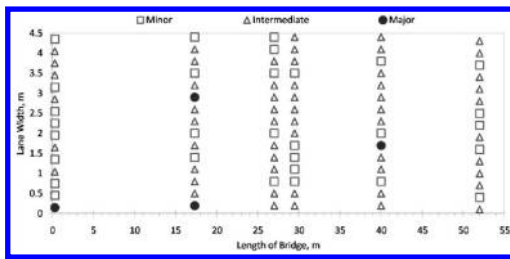


Figure 8. Interface condition assessment of bridge deck by im-pact sounding test.

where sounding test is conducted Additional field validation is being performed to improve the proposed method.

Generally, impact sounding test evaluated the concrete bridge as intermediately damaged on the interface. This assessment coincides with the assessment using visual inspection. Thus, the evaluation parameters used in impact sounding assessment demonstrate a promising method.

6 CONCLUSION

This study presents the quantitative interpretation of impact sounding frequency spectra for interface condition assessment of concrete bridge deck. Laboratory impact sounding test result shows that there is a significant difference in the amplitude, the shape and the peak pattern of the frequency spectra of bonded and unbonded interface of slab specimen. Consequently, skewness value and beta-parameter are proposed as evaluation parameters to quantify the significant differences observed in the frequency spectra. Evaluation parameters are used in the analysis of field data and results show comparable quantitative assessment of interface condition with visual inspection. Hence, the proposed skewness value and beta-parameter of

the impact sounding frequency spectra can be useful to determine different level of assessing interface condition. Additional field validation of proposed evaluation parameters is underway.

ACKNOWLEDGMENT

The authors would like to acknowledge the support from Sejong University Research Fund, Development of Eco-friendly Pavements to Minimize Greenhouse Gas Emissions funded by Ministry of Land and Marine, BK21 Plus Project: Disaster Prevention of Infrastructure.

REFERENCES

- Al-Qadi, I.L. & Lahouar, S. 2004. Ground penetrating radar: State of the practice for pavement assessment. *Materials Evaluation*, 62: 759–763.
- ASTM 2012. ASTM D4580/D4580M-12: Standard practice for measuring delamination in concrete bridge decks by sounding. *ASTM Volume 04.03 Road and Paving Materials; Vehicle Pavement Systems*. West Conshohocken, PA: ASTM International.
- Beckman, R. J. 1973. Introductory engineering statistics, 2nd Edition – Guttman, I, Wilks, S.S. and Hunter, S. *Journal of the American Statistical Association*, 68: 247–247.
- Chabot, A., Hun, M. & Hammoum, F. 2013. Mechanical analysis of a mixed mode debonding test for “composite” pavements. *Construction and Building Materials*, 40: 1076–1087.
- Cohen, A.C. 1966. *Statistics and Experimental Design in Engineering and Physical Sciences*. Technometrics, vol.8.
- Collins, D.N. 1957. The engineering applications of statistics. *Journal of the American Statistical Association*, 52: 366–366.
- Gassman, S. L. & Tawhed, W. F. 2004. Nondestructive assessment of damage in concrete bridge decks. *Journal of Performance of Constructed Facilities*, 18: 220–231.
- Gregoire, C. & Van Geem, C. Year. Use of radar in road investigation BRRC experience. *7th International Workshop on Advanced Ground Penetrating Radar (IWAGPR)*, 2–5 July 2013. 1–6.
- Gucunski, N., Slabaugh, G., Wang, Z., Fang, T. & Maher, A. 2008. Impact echo data from bridge deck testing: visualization and interpretation. *Journal of the Transportation Research Board*, 2050: 111–121.
- Halabe, U. B., Hing, C. L., Klinkhachorn, P. & Gangarao, H. V. S. 2007. Subsurface defect detection in FRP bridge decks using ground penetrating radar. *AIP Conference Proceedings*, 894: 1443–1452.
- Heitzman, M., K. Maser, N.H. Tran, R., Brown, H. Bell, S. Holland, H. Ceylan, K. Belli, & D. Hiltunen 2013. *Nondestructive testing to identify delaminations between HMA layers*. 500 Fifth St. NW, Washington, D.C. 20001: Transportation Research Record.
- Henderson, M. E., Dion, G. N. & Costley, R. D. 1999. Acoustic inspection of concrete bridge decks. *SPIE’s International Symposium on Nondestructive Evaluation Techniques for Aging Infrastructure & Manufacturing*. 219–227.
- Kim, T. W., Baek, J., Lee, H. J. & Lee, S. Y. 2013. Effect of pavement design parameters on the behaviour of orthotropic steel bridge deck pavements under traffic

- loading. *International Journal of Pavement Engineering*, 15: 471–482.
- Krysinski, L. & Sudyka, J. 2012. Typology of reflections in the assessment of the interlayer bonding condition of the bituminous pavement by the use of an impulse high-frequency ground-penetrating radar. *Nondestructive Testing and Evaluation*, 27: 219–227.
- Lu, Y., Zhang, Y., Cao, Y., Mc Daniel, J. & Wang, M. 2013. A Mobile Acoustic Subsurface Sensing (MASS) system for rapid roadway assessment. *Sensors*, 13: 5881–5896.
- Medina, R. & Garrido, M. 2007. Improving impact-echo method by using cross-spectral density. *Journal of Sound and Vibration*, 304: 769–778.
- Mehta, Y. 2007. Evaluation of interlayer bonding in hma pavements *Wisconsin Highway Research Program*.
- Pouteau, B., Balay, J. M., Chabot, A. & Larrard, F. D. 2008. FABAC accelerated loading test of bond between cement overlay and asphalt layers. *Pavement Cracking*. CRC Press.
- Randall, R. B. 1987. *Frequency analysis*, Brüel & Kjaer.
- Rosales, C.A., Baek, J., Lee H.J. & Kim, W.J. 2015. Analysis of Impact Sounding Signals to Determine the Interface Bonding Condition of Concrete Bridge Deck Pavement. *International Journal Pavement Engineering (IJPE)*. (under review)
- Sansalone, M. & Carino, N. J. 1989. Detecting delamination in concrete slabs with and without overlays using impact echo method. *ACI Materials Journal*, 86.
- Sansalone, M. & Streett, W.B. 1997. *Impact-echo: non-destructive evaluation of concrete and masonry*, Bullbrier Press.
- Suda, T., Tabata, A., Kawakami, J. & Suzuki, T. 2004. Development of an impact sound diagnosis system for tunnel concrete lining. *Proceedings of the 30th ITA-AITES World Tunnel Congress Singapore, 22–27 May 2004*, 19: 328–9.
- Tawhed, W. F. & Gassman, S. L. 2002. Damage assessment of concrete bridge decks using impact-echo method. *ACI Materials Journal*, 99: 273–281.
- Zhang, G., Harichandran, R. & Ramuhalli, P. 2011. Application of noise cancelling and damage detection algorithms in NDE of concrete bridge decks using impact signals. *Journal of Nondestructive Evaluation*, 30: 259–272.

Performance evaluation of Romanian modified bitumens using thermoplastic elastomer SBS

L. Judele & D. Lepadatu

Faculty of Civil Engineering and Building Services,
Technical University "Gheorghe Asachi" Iasi, Romania

ABSTRACT: The performance of the products and processes used in road service is sometimes limited. In order to improve one or more of their features, polymers can be added, increasing the resistance of the asphalt to permanent deformation at high road temperatures, without adversely affecting the properties of the bitumen or asphalt at other temperatures, reducing the Fraass breaking point temperature and improving the flexibility of the asphalt. The polymers are organic, inorganic or mixed macromolecular substances. Building materials are especially organic or mixed polymers because during manufacturing they pass through a plastic phase, which facilitates their processing. In the present paper five bitumens commonly used in Romania to manufacture asphalt-polymer binder have been used. The copolymer adopted for this study is an SBS copolymer and it is routinely used for bitumen modification. Bitumens determinations have been made in laboratory before and after the modification, comparing the results and drawings conclusions. The use of modified bitumens offers a solution to reducing the frequency of maintenance works required at particular locations and provides a much longer service life for maintenance treatments at difficult sites.

1 INTRODUCTION

The performance of the products and processes used in road service is sometimes limited. Polymers can be added to improve it, thus modifying, according to the usage, one or more of the following characteristics:

- *Thermal susceptibility* – characterizes the consistency variation in relation to the temperature. Usually the modification aims at reducing this susceptibility, broadening the range that separates cracking at low temperatures from softening at high temperatures.
- *Cohesion* – is defined as being the energy necessary to break the binder coating. It varies depending on the temperature, going through a maximum point. The aim of the modification is to increase the maximum cohesion and/or cohesion range, thus achieving satisfactory consistency across the whole range of working temperatures.
- *Elasticity* – materials and binders strain under the influence of traffic and temperature variations. Elasticity represents the capacity to endure this deformation in a reversible way, without breaking.
- *Fatigue resistance* – under the effect of the traffic, the materials are repeatedly under stress and wear out their resistance capital. The change targets the increase of this capital, especially for low temperatures.

The Polymers are macromolecular substances, of organic, inorganic or mixed nature. In building materials industry, the organic or mixed polymers are especially used since, during the manufacturing process they undergo a plastic phase, making their processing easier. In the case of the materials made of polymers used in constructions, it is not the plasticity that is the fundamental feature, but their elasticity, flexibility and rigidity, according to their field of application.

The modification of bitumens requires a sum of quite complex, sometimes simultaneous processes that can be summarized as follows: after a first stage which always consists in dispersing the polymer in the basic binder, the modification takes place either:

- Through partial or total dissolution of the polymer;
- Through a swelling of the polymer that adsorbs a fraction of the basic binder;
- Through a chemical reaction between the polymer and the basic binder, usually under the influence of a catalyst (a phenomenon sometimes called grafting) (Champion-Lapalu et al. 2000).

One of the most important modifiers in the styrenic block copolymers is styrene-butadiene-styrene (SBS) block copolymer. The structure of SBS copolymers consists of SBS three block chains, having two phase morphology of spherical glassy polystyrene block domains within a matrix of rubber polybutadiene (Bulatovic et al. 2012).

Table 1. Characteristics of the bitumens used.

Bitumens	A	B	C	D	E	F	G
Penetration at 25°C (1/10 mm)	119	112	79	162	133	113	191
Ball-and-ring softening point (°C)	43	41	46	40	41	42	39
Fraass breaking point (°C)	-15	-8	-12	-16	-10	-9	-15
Plasticity interval (°C)	58	49	58	56	51	51	54
Asphaltene content (%)	6.1	3.4	10.7	14.5	6.8	7.5	≤3
Colloidal instability index (I _c)*	0.20	0.08	0.23	0.36	0.16	0.15	<0.1

*I_c = according to the generic composition determined with IATROSCAN.

S.B.S.s are polymers made of three successive sequences:

(Poly)styrene (Poly)butadiene (Poly)styrene
 S B S

There are more types that differ from one another through:

- Their linear or star shape;
- Gram-molecular weight;
- Styrene and butadiene percentages.

As far as their structure is concerned, the SBSs are thermoplastic elastomers: their behavior depends on the temperature (Culture 2000). Below a threshold close to 100°C, they are like elastic bodies: they can undergo important deformations without breaking, in an almost irreversible way, down to very low temperatures. Over 100°C, their behavior is like that of a liquid whose viscosity decreases while temperature rises. The shift from elastic body behavior to that of a viscous liquid is reversible through a single change in temperature.

1.1 Manufacturing SBS bitumens

The SBS bitumens are manufactured by hot-mixing the polymer with the bituminous base in controlled temperature conditions (Readand D. Whiteoak 2003). To satisfy the numerous applications of the SBS bitumens, the formulae must be adjusted according to needs. They differ in terms of:

- The choice of polymers and their dosage;
- The origin and consistency of the basic bituminous binder;
- The nature and dosage in prospective additives: adhesion additives, plasticizers, flux oils, resins etc.

Similar to EVA bitumens, the SBS bitumens present two phases at working temperatures: the bitumen phase and the polymer phase. For little content of polymer, the bitumen forms the continuous phase. When the SBS content increases, there is an inversion that leads to the occurrence of a continuous phase of polymer where the bitumen is dispersed. This transition is accompanied by an important change of the binder properties. These binders are usually manufactured in fixed installations, then stored and transported

to the location where they are used. They can be manufactured in mobile installations, too.

2 EXPERIMENTAL PROGRAM

Seven bitumens commonly used in Romania were used to make the bitumen-polymer binders, their characteristics are to be found in table 1 (Musteata 2010). Although they differ as regard the asphaltene content, their generic composition and most likely the nature of the crude-oil (raw material) of origin, they are all bitumens that are compatible with polymers, meaning that, by mixing them with these polymers, we get products that appear to be homogenous at visual examination and whose properties correspond to the intended use.

The copolymer chosen for this study is used to modify bitumens. It is a SBS copolymer with molecular weight of around 100,000 with a styrene content of 25%.

Starting from these bitumens, bitumen-polymer binders were developed in the following operating way: the polymer is introduced as powder into a reactor that contains bitumen previously brought to the desired temperature; the mixing is done mechanically for 3 h at 170°C. The results after 5% additions in the polymer mass, a percentage that is found in asphalt binders, are shown in table 2.

The modified binders that result from this type of fabrication and whose properties proved to be fit for road building are two-phase binders (on optical microscopy scale): one of the phases consists in swollen copolymer and bitumen oils (the polymer phase) and the other in residual bitumen (the bitumen phase).

Immediately after manufacturing, the following characteristics were identified:

- The ball-and-ring softening point;
- The Fraass breaking point;
- Penetration at 25°C;
- Asphaltene content;
- The colloidal instability index (I_c).

We dealt with the plasticity interval in a classic way (the softening point – Fraass breaking point) to highlight the variation of the thermal susceptibility in relation to the initial bitumens, so grading the change brought by SBS.

Table 2. Manufacturing characteristics of the modified binders with 5% SBS copolymer.

Modified binders	A ₅	B ₅	C ₅	D ₅	E ₅	F ₅	G ₅
Penetration at 25°C (1/10 mm)	82	87	59	75	82	75	135
Ball-and-ring softening point (°C)	88	62	87	80	83	83	80
Fraass breaking point (°C)	-12	-9	-10	-18	-8	-13	-17
Plasticity interval (°C)	100	71	98	91	98	96	97

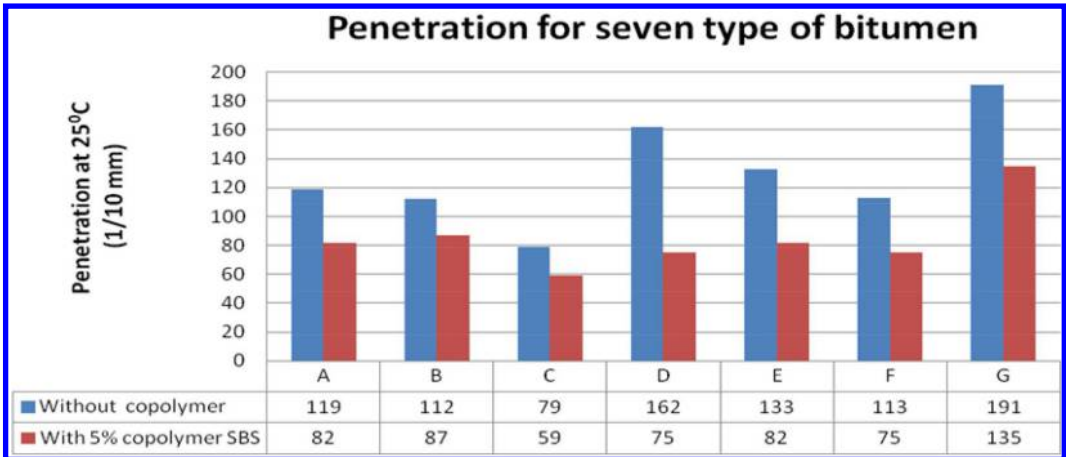


Figure 1. Penetration for seven types of bitumen.

The purpose of modifying the bitumens with 5% SBS is that of determining the way in which the addition of polymer improves their properties in order to subsequently improve the characteristics of the asphalt mixtures they will be part of.

3 RESULTS AND DISCUSSIONS

For six out of seven modified binders, there was a rise of the softening point (around 40°C); for one of them it was only 20°C. There were not any significant variations of the Fraass breaking point (+4 to -20°C). For all these binders the plasticity interval is widened only by raising the softening point; this is an important feature to know from the point of view of the changes of the binders by polymer additions, since it can be linked to the other characteristics under study.

Bitumens display an elastic recovery, specific to the properties of the elastomers, but, under the influence of the polymer, it varies depending on the bitumen types. For the same curves at -10°C, we also notice differences between them as regarding the breaking point.

4 STATISTICAL ANALYSIS

The diagram below shows that the penetration at 25° has the lowest value for the type C bitumen and the highest value for the G type bitumen, as well as an

overall decreasing trend for all types of bitumen when introducing the copolymer (Fig. 1).

The introduction of the polymer into the composition of the bitumens triggers a significant raise of the softening point, (doubling its value, except for the B type which has a slightly lower value). For the bitumens of the A and C types, the increase is more than double (Fig. 2).

The plasticity interval keeps the same increase amount (roughly doubling the initial values) when introducing the copolymer, with the same exception for the B type bitumen which presents a lower increase value (Fig. 3).

To highlight the advantages of introducing the copolymer into the bitumen composition, a global analysis of these characteristics was tried, as shown in the table 3.

Thus, we can notice that there are percentage decreases of the penetration values with a maximum of 54% for the D type bitumen with the copolymer comparing to the normal one. Significant increases of the softening point values at the introduction of the copolymer are observed for the bitumens of types A, E and G, with a maximum of 51%, while for the plasticity interval, the maximum increase value is 48% for the E type bitumen (Fig. 4).

5 CONCLUSIONS

For all these modified binders we noticed great reproducibility of characteristics such as the softening point

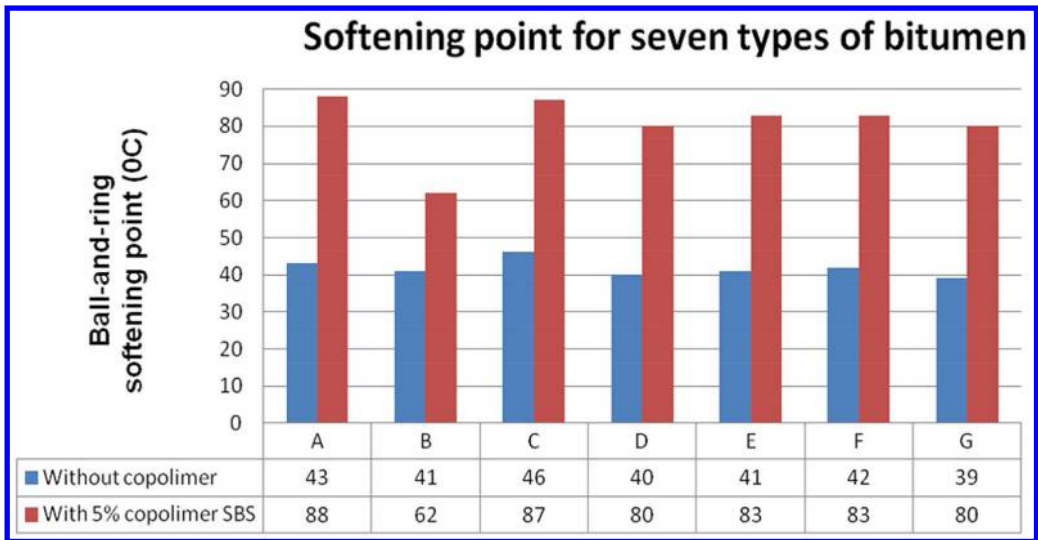


Figure 2. Softening point for seven types of bitumen.

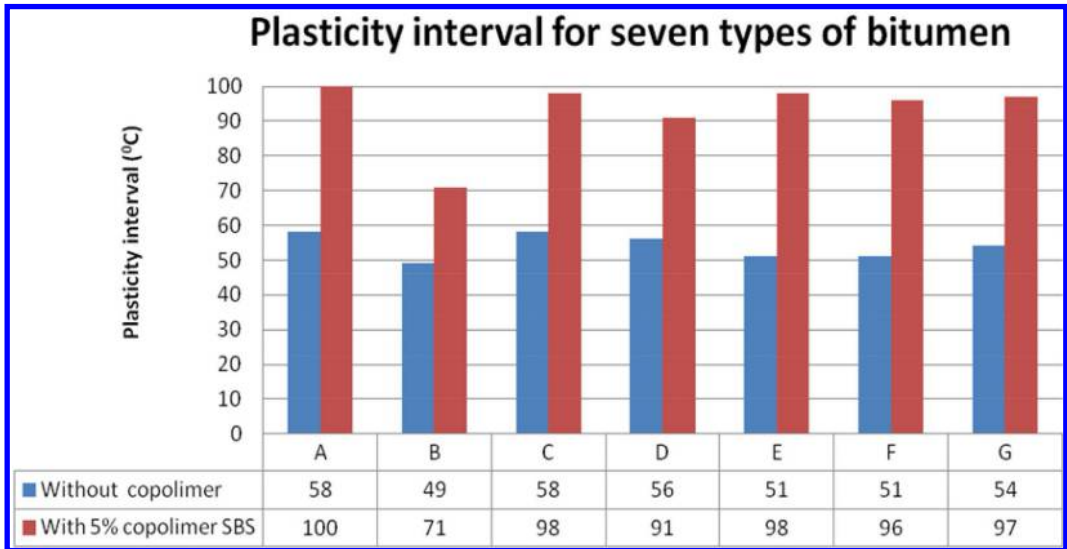


Figure 3. The plasticity interval for seven types of bitumen.

Table 3. Properties variations for bitumens with 5% SBS copolymer.

Bitumens with 5% SBS copolymer	A	B	C	D	E	F	G
Penetration	-0.31	-0.22	-0.25	-0.54	-0.38	-0.34	-0.29
Plasticity interval	0.42	0.31	0.41	0.38	0.48	0.47	0.44
Ball-and-ring softening point (°C)	0.51	0.34	0.47	0.50	0.51	0.49	0.51

and the Fraass breaking point, mechanical properties and micro-morphology and, most notably, they are always closely connected. In conclusion, we can assert that these binders modified by adding 5% SBS have overall, on manufacturing, interesting properties

(increased plasticity interval, improvement of the mechanical properties). These are reproducible for the given operating conditions, but, in terms of micro-morphology, they are easily influenced by the nature of the initial bitumen. The first conclusion is based

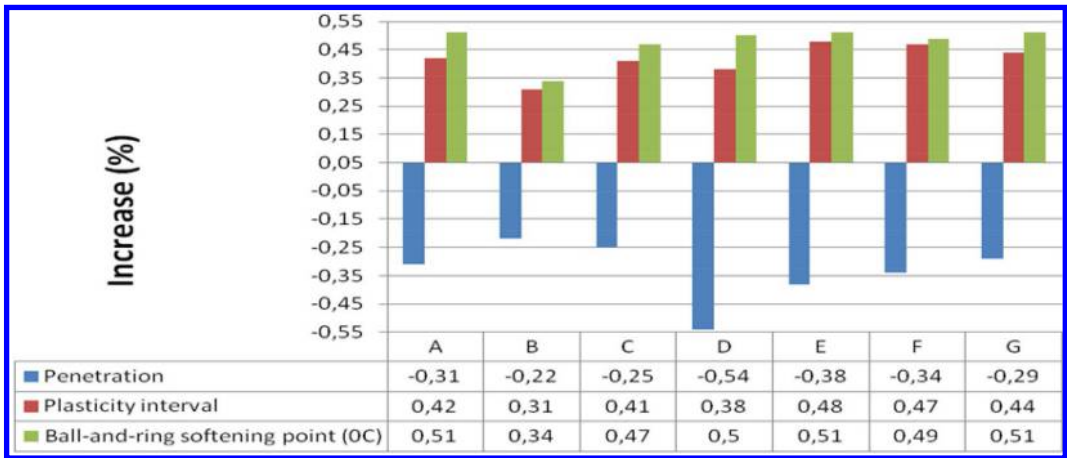


Figure 4. Characteristics variation of the seven types of bitumen.

on the nature of the initial bitumen when modified by adding polymer: on manufacturing, it greatly determines the micro-morphology of the binder, observed through optical microscopy, as well as the working properties such as the softening point and the Fraass breaking point, the penetration and the mechanical properties; but it also greatly influences the future stability of these modified binders. The other conclusion draws attention on the testing procedures regarding the type of the modified binders and on the analysis of the results. The tests used in this study are commonly used by the manufacturers of modified binders and by laboratories. The fact that the results depend greatly on the preservation conditions of the samples and on the preparation of the test specimens, raises the issue of their significance; not a single test result will be able to be used viably unless it is explicitly associated to the operating conditions and confronted with the working (especially thermal) conditions of the binder.

REFERENCES

- Bulatovic V. O., Rek V. and Markovic K. J. 2012, Polymer modified bitumen, *Materials Research Innovations*, 16(1).
- Champion-Lapalu L., Planche, J.P., Martin, D., Anderson, J.F. Gerard 2000, Low-temperature rheological and fracture properties of polymer-modified bitumens, *Euroasphalt & Eurobitume Congress, Barcelona*.
- Culture Bitume 2000, Les bitumes modifies SBS, No.2.
- Musteață M. 2010, Polchimic Laboratory of Giurgiu. *Research topics*.
- Readand J., Whiteoak D. 2003, The Shell Bitumen Handbook, *Thomas Telford Publishing*.
- Vasiljevic-Shikaleska A., Popovska-Pavlovska, F.S., Cimmino, D., Duraccio, C. Silvestre 2010, Viscoelastic Properties and Morphological Characteristics of Polymer-Modified Bitumen Blends, *Journal of Applied Polymer Science*, 118 (3): 1320–1330.

Plastic fines of road construction materials tested using the methylene blue method

A. Athanasopoulou, G. Kollaros & A. Kokkalis
Democritus University of Thrace, Greece

ABSTRACT: In order to identify the nature of the fines in natural soils, various methods can be employed. Using laboratory procedures, soil samples from Xanthi Prefecture have been examined and characterised. The results were correlated in order to check the soils' suitability as foundation materials for pavements of roadways passing through areas where such soil types are abundant. For the soils tested, no good correlation has been found between the MBV and the other properties determined through the laboratory testing. The main reason for such behaviour is the lack of adequate swelling clay minerals content. The methylene blue test could supplement the sand equivalent and Atterberg limits tests, since with these the existence of clay-size grains is determined, but not the existence of active clayey minerals as well.

1 INTRODUCTION

In highway construction works, "fines" is a general term being used to describe particles passing the 0.063, 0.074 or 0.08 mm sieve. Some types of fines can significantly affect the stiffness and freezing-thawing behaviour of unbound and hydraulically bound layers even if they are present in small amounts, whilst other types are considered to be relatively inert and have almost no effect on pavement performance. In order to identify the nature of the fines, various methods can be employed: sand equivalent, Atterberg limits test, Enslin–Neff water absorption, X-ray diffractometry, methylene blue, carbonate content determination, and soil suction measurements (Petkovšek et al. 2010).

In order to place a material within classification reference frames or to compare it with standards, road material assessment is commonly made employing specific grading fractions. The fine and sand fractions, along with the maximum grain size, D_{max} , are determinant in inferring the use potential of road materials. For the classification procedure, other characteristics are introduced, such as cleanliness, expressed using the Sand Equivalent, SE, and Methylene Blue Value, MBV.

In performing the Methylene Blue test quantities of a standard aqueous solution of methylene blue (MB) dye are added to a sample of dry fine aggregate passing the No. 200 (0.075 mm) sieve until adsorption of the dye ceases. The MB solution is titrated stepwise in 0.5 ml increments from the burette into a continually stirred fine aggregate suspension. After each addition of MB solution and stirring for one minute, a small drop of the aggregate suspension is removed with a glass rod and placed on a filter paper. Initially, a well-defined circle of MB-stained dust is formed and

is surrounded with an outer ring of clear water. Successive additions of MB solution are repeated until the end point is reached when the ring of clear water turns light blue. The MBV of a specific fine aggregate fraction is reported as milligrams of methylene blue per gram of the material tested.

Kandhal's et al. (1998) experimental results led to the recommendation of the methylene blue test over the sand equivalent test, because the former is best related to stripping in Hot Mix Asphalt. On the other hand, researchers (Woodward et al. 2002) pointed out that the MB test is rock type specific and its application to rock types other than basalt can be a problem.

The cation exchange capacity, specific surface area, swell potential and mineral content of clay deposits and soils are commonly estimated using the methylene blue adsorption test method (Abayazeed & El-Hinnawi 2011, Yukselen & Kaya, 2008). Traditionally, the characterisation of clays has been made using time-consuming physical and chemical methods, which require costly equipment. Adsorption of methylene blue by clays in various applications is a quick and cheap method for the estimation of cation exchange capacity and surface area (ASTM 2003, AASHTO T 330-07 2011). The methylene blue dye adsorption test has been included in the European Standards for the determination of harmful fines in aggregates suitable for mortars and concrete (CEN 1999, Yool et al. 1998).

2 METHYLENE BLUE AND CLAYS

Methylene blue (3,7-bis dimethylaminophenazotium chloride) is a thiazine (cationic) dye most commonly used for dyeing cotton, wool, and silk. The chemical structure of MB (basic blue 9, C.I.

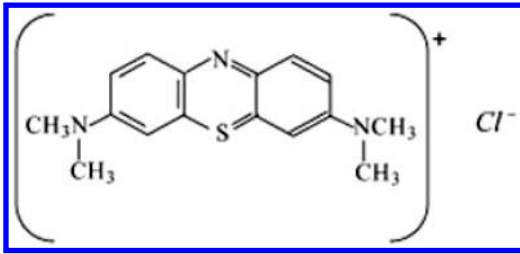


Figure 1. Chemical structure of methylene blue.

52015; chemical formula, $C_{16}H_{18}ClN_3S \cdot 3H_2O$; molar mass $373.90 \text{ g mol}^{-1}$), is shown in Figure 1. This structure presents decentralized positive charge on the organic framework, which could play a major role in keeping the species on the surface of the clay. Methylene blue is a cationic dye and absorbs (maximum visible absorbance at a wavelength of 664 nm) on a variety of solids, such as kaolinite (Tehrani-Bagha et al. 2011), montmorillonite (Almeida et al. 2009, Cottet et al. 2014), palygorskite (Al-Futaisi et al. 2007, Chen et al. 2011), sepiolite (Al-Futaisi et al. 2007, Doğan et al. 2007), diatomaceous earth (Shawabkeh & Tutunji 2003, Al-Ghouti 2003), activated carbons (Rodriguez et al. 2009), and even wastes of phosphorous rocks (Malash & El-Khaiary 2010).

Clay particles are formed in a multi-layer manner. Swelling of clay can be attributed to the presence of free cations in the interlayer space. These cations lead to the absorption of water molecules behaving as dipoles and chemical balance is achieved due to the presence of negatively charged clay materials. The term diffuse double layer refers to the charged surface and the distributed charge around the particles. The distance between layers has a role in the swelling behaviour of clays. If there is a small distance between the layers, then there is no swelling because the attractive forces among the layers are strong enough to outfight the absorption of water. If the distance between the layers is substantial, the interlayer bonds are weak and water is absorbed in the interlayer. The absorption continues until the bonds fail and swelling occurs as the clay particles are separated and rearranged. Factors, such as the density of the surface charge, the type and the valence of the cations, the concentration of the electrolytes and the dielectric constant also play a role in the swelling of clays, magnifying or decreasing the major mechanisms previously mentioned (Nikolaides et al. 2007).

Swelling depends on the type of clay mineral. The minerals of the smectite group are considered to be swelling. The group's major representative is montmorillonite. Illite, margarite, and pyrophyllite are clay minerals that can be classified as non-swelling. Hang & Brindley (1970) used different measurements to investigate montmorillonite, kaolinite, and illite. They found that methylene blue absorption could be used for the assessment of both the surface areas and exchange capacities of clay minerals. They also gave the projected area of the MB molecule 130 \AA^2 . The MB

molecule can be regarded approximately as a rectangular volume of dimensions $17.0 \times 7.6 \times 3.25 \text{ \AA}$.

The activity of the fine clayey particles present in soil materials can be determined either by their plasticity index or by their methylene blue value. The swell potential of clays has been determined using the methylene blue method. Çokça (2002) investigated the relationship between the MB value, initial soil suction and swell percentage of expansive soil samples. Chiappone et al. (2004) reported the results of MB tests used to identify the presence of relatively high activity clay minerals in soils and compared two methylene blue tests methods, AFNOR and ASTM. Yukselen & Kaya (2008) in an effort to estimate the suitability of the methylene blue test for determining the cation exchange capacity, surface area, and swell potential of clayey soils, compared the results of the methylene blue test using a spot test and titration method, the BET-N2 adsorption method and swell index determination. Pentrák et al. (2012) found that the MB spectra better reflected the changes in layer charge of acid treated clay minerals with non-swelling layers than the cation exchange capacity values.

2.1 Mechanisms of MB adsorption on swelling clays

Four reactions have been accounted when methylene blue came in contact with clays (Cenens & Schoonheydt 1998): (a) ion exchange, (b) dimerization, (c) trimerization, and (d) protonation. However, the relative amounts of these four forms of MB depend not only on the loading, but also on the type of both clay and exchangeable cation. Protonation of methylene blue should not be considered as a reaction with clays, but with water only. Monomers at low loading levels dominate the adsorption of MB on laponite (Schoonheydt & Heughebaert 1992), while with the increase of the loading level dimers and trimers are formed.

One of the most important soil properties that can be related to its physical or chemical behaviour is specific surface area. Soil adsorbs or desorbs nutrients or pollutants based on its specific surface area.

Surface area measurements correlate well with soil characteristics due to their capability of integrating the properties of soils, providing at the same time a more direct evaluation of the physical and mineralogical properties. Consequently, surface area classes could result in groupings that have a narrower range of physical properties than groups based on mineral species. The surface area measured by water-vapour (H_2O), or ethylene glycol monoethyl ether (EGME) methods represents the total specific surface area, whereas only external surfaces can be determined by the nitrogen (N_2) adsorption method. Thus, samples containing considerable amounts of expansible layer-silicates can be characterised in a vary limited extend.

Dye molecules have also been used for determining both the "electropositive" and "electronegative"

Table 1. Properties of the soils tested.

Property	Value range
Natural moisture (%)	1.53–7.90
Percent passing No. 200 sieve (%)	8–23
Liquid Limit, LL (%)	23–33
Plastic limit, PL (%)	10.3–22.8
Plasticity Index, PI (%)	0.7–24.0
Linear Shrinkage, LS (%)	0.00–8.63
Specific gravity	2.59–2.73
Free swell	10.67–56.67
Methylene Blue Value, MBV (mg/g)	4.00–24.83

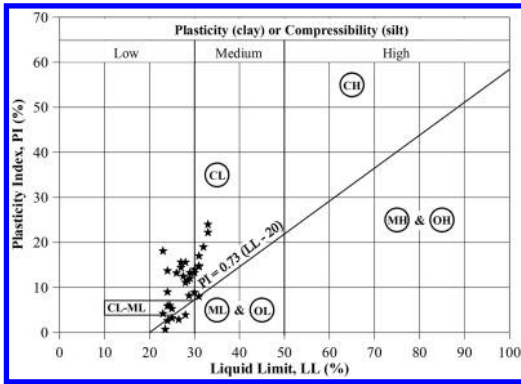


Figure 2. Soils' classification according to the Unified Soil Classification System.

surface area of soils and clays. The cationic dye methylene blue (3,7-bis dimethylaminophenazinium chloride) has also been used as a sorbate for determining the surface area of clay materials.

3 LABORATORY TESTING

Clay soil samples from 46 different sites in Xanthi area, Northern Greece, had been collected and brought to the laboratory where they air-dried. The material properties ranged into the limits shown in Table 1. The grain size distribution of the soil samples revealed that most of them had a high clay-content (material with grain diameter lower than $2\ \mu$). Atterberg limits tests have shown high Plasticity Index (PI) values that exceeded or were equal to 15 for 7 of the soil samples, reaching up to a 24 value. For twelve of the samples, it was not possible to determine PI.

In Figure 2 (Unified System for fine-grained soils) the soil samples are represented by points having as coordinates the liquid limit and the plasticity index. The samples tested fall in a relatively narrow vertical band. According to the USCS, the soil samples could be characterized as clays of medium and low plasticity (in a percentage of about 87%, as CL). If classified according to AASHTO classification system (Fig. 3)

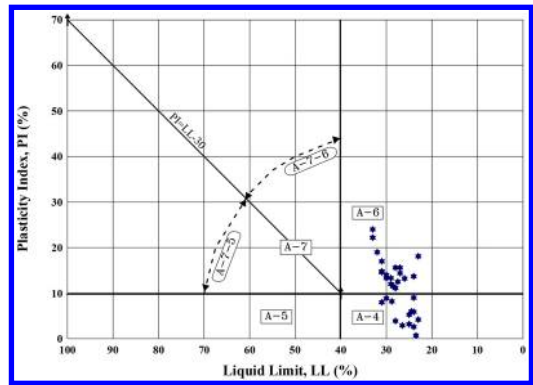


Figure 3. Soils' classification according to the AASHTO Classification System.

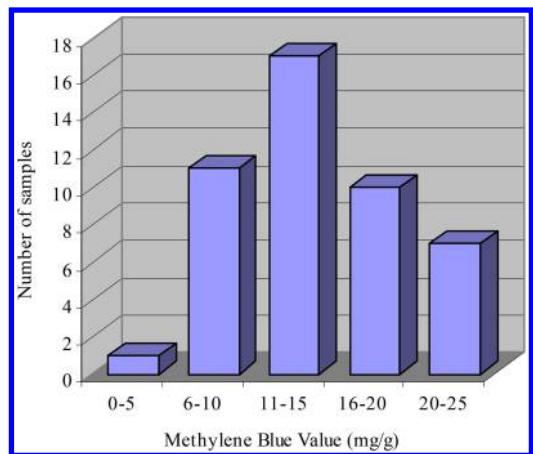


Figure 4. Distribution of soil samples according to their MBV.

soils are characterized as belonging to A-6 and A-4 groups.

The samples were also tested for their specific gravity, Linear Shrinkage (LS), and Free Swell (FS) characteristics and the fraction passing the No. 200 sieve was subjected to methylene blue test using the titration method (AFNOR, 1998). The values obtained ranged to scales shown in Table 1.

On the completion of the laboratory test programme, an attempt was made to correlate the properties, through which is possible to check the suitability of soil materials that will be used in pavement layers. The MBV ranged between 4.00 and 24.83 mg/g. Their distribution is given as a histogram in Figure 4.

During the statistical treatment, the attention has been focused mainly to properties arising from the test for the determination of the argillaceous components in soils with the methylene blue method. The choice of those quantities is easily justified by the

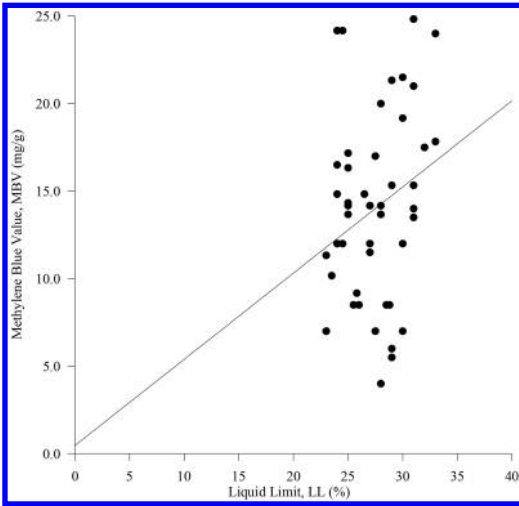


Figure 5. Variation of methylene blue value with the liquid limit of the soils tested.

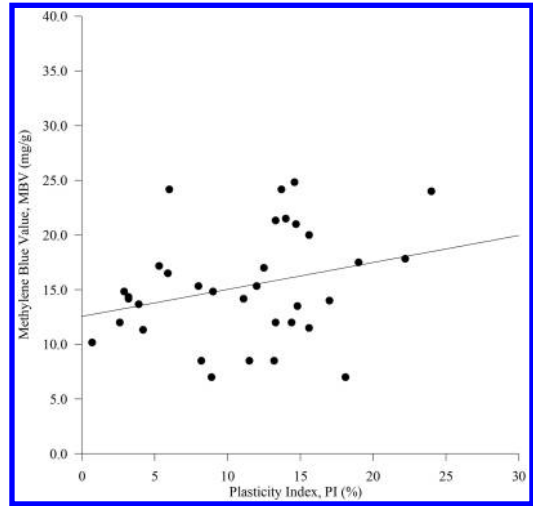


Figure 7. Variation of methylene blue value with the plasticity index of the soils tested.

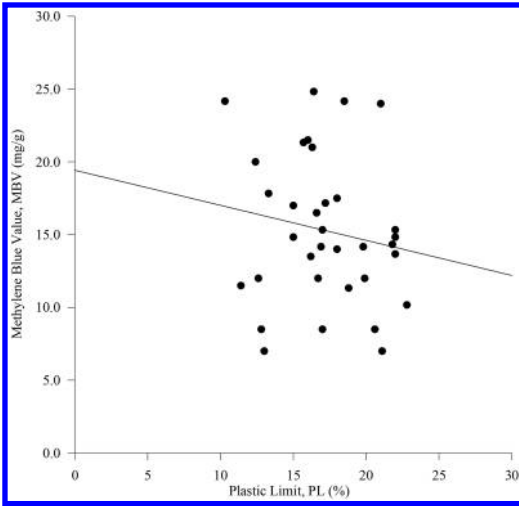


Figure 6. Variation of methylene blue value with the plastic limit of the soils tested.

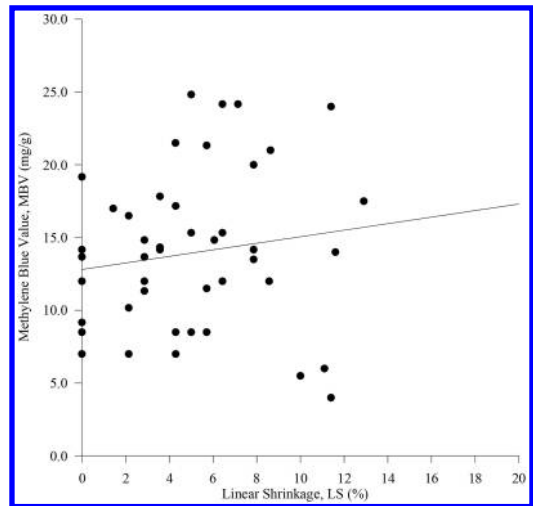


Figure 8. Variation of methylene blue value with the linear shrinkage of the soils tested.

high percentages of fine grained material in the samples and the relatively high swelling grades they are expected to be displayed in the field, constituting a source of risks for the integrity and longevity of pavement structures. The regression of all magnitudes with MBV are shown in Figures 5 to 9, along with the linear fit line.

For the correlation of the different values, data from all 46 soil samples have been used, with the exception of the Plastic Limit and the Plasticity Index, where the values of non-plastic soils have not been taken into account.

The equations that resulted from the linear regression analyses with the methylene blue value as the

independent variable are:

$$MBV = 0.4924728469 \times LL + 0.4643202011 \quad (1)$$

$$MBV = -0.2407061155 \times PL + 19.41930712 \quad (2)$$

$$MBV = 0.2466972014 \times PI + 12.55158335 \quad (3)$$

$$MBV = 0.2249811108 \times LS + 12.8028983 \quad (4)$$

$$MBV = 0.0732482259 \times FS + 11.82321632 \quad (5)$$

4 CONCLUSIONS

Most of the soils sampled in different sites of Xanthi's broader region are favourable and adequate to be used

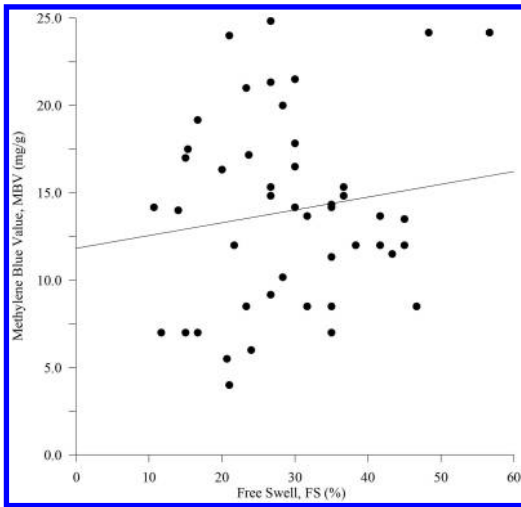


Figure 9. Variation of methylene blue value with the free swell of the soils tested.

as subgrade in road construction works, since they have low plasticity.

If a new classification system is devised, it could be possible for soils having homogenous engineering properties to differentiate in categories. These groups which will be based on the argillaceous phase activity, that is, on methylene blue value, in combination with the Atterberg limits values. Both test procedures are easily performed.

For the soils tested, no good correlation has been found between the MBV and the other properties determined through the laboratory testing. The main reason for such behaviour is the lack of adequate swelling clay minerals content. The MB test could supplement Atterberg limits tests, since with these the existence of clay-size grains is determined, but not the existence of active clayey minerals as well.

REFERENCES

AASHTO (American Association of State Highway and Transportation Officials) 2011. The qualitative detection of harmful clays of the smectite group in aggregates using methylene blue AASHTO Designation: T 330-07.

Abayazeed, S.D. & El-Hinnawi, E. 2011. Characterization of Egyptian smectitic clay deposits by methylene blue adsorption. *American J. of Applied Sciences* 8(12): 1282–1286.

AFNOR (Association française de Normalization) 1998. Mesure de la capacité d'adsorption de bleu de méthylène d'un sol ou d'un matériau rocheux. Détermination de la valeur de bleu de méthylène d'un sol ou d'un matériau rocheux par l'essai à la tache Norme Française NF P 94-068, pp. 68–94.

Al-Futaisi, A., Jamrah, A. & Al-Hanai, R. 2007. Aspects of cationic dye molecule adsorption to palygorskite. *Desalination* 214: 327–342.

Al-Ghouti, M.A., Khraisheh, M.A.M., Allen, S.J. & Ahmad, M.N. 2003. The removal of dyes from textile wastewater: a

study of the physical characteristics and adsorption mechanisms of diatomaceous earth *Journal of Environmental Management* 69: 229–238.

Almeida, C.A.P., Debacher, N.A., Downs, A.J., Cottet, L. & Mello, C.A.D. 2009. Removal of methylene blue from colored effluents by adsorption on montmorillonite clay *Journal of Colloid Interface Science* 332: 46–53.

ASTM (American Society of Testing and Materials) 2003. *Annual Book of ASTM Standards Volume 04.03 Road and Paving Materials; Vehicle-Pavement Systems*. West Conshohocken, PA. ASTM International.

CEN (Comité Européen de Normalisation), 1999. EN 933-9 standard, Tests for geometrical properties of aggregates. Part 9: Assessment of fines. Methylene blue test.

Cenens, J., & Schoonheydt, R.A. 1998. Visible spectroscopy of methylene blue on hectorite, laponite b, and barasym in aqueous suspension. *Clays and Clay Minerals* 36: 214–224.

Chen, H., Zhano, J., Zhong, A. & Jin, Y. 2011. Removal capacity and adsorption mechanism of heat-treated palygorskite clay for methylene blue. *Chemical Engineering Journal* 174: 143–150.

Chiappone, A., Marello, S., Scavia C. & Setti, M. 2004. Clay mineral characterization through the methylene blue test: Comparison with other experimental techniques and applications of the method. *Canadian Geotechnical Journal* 41: 1168–1178.

Çokça, E. 2002. Relationship between methylene blue value, initial soil suction and swell percent of expansive soils. *Turkish Journal of Engineering and Environmental Science* 26:521–529.

Cottet, L., Almeida, C.A.P., Naidek, N., Viante, M.F., Lopes, M.C. & Debacher, N.A. 2014. Adsorption characteristics of montmorillonite clay modified with iron oxide with respect to methylene blue in aqueous media. *Applied Clay Science* 95: 25–31.

Doğan, M., Özdemir, Y. & Alkan M. 2007. Adsorption kinetics and mechanism of cationic methyl violet and methylene blue dyes onto sepiolite. *Dyes and Pigments* 75: 701–713.

Hang, P.T. & Brindley, G.W. 1970. Methylene blue adsorption by clay minerals. Determination of surface areas and cation exchange capacities (clay-organic studies XVIII). *Clays and Clay Minerals* 18: 203–212.

Kandhal, P.S., Lynn, C.Y. & Parker, Jr., F. 1998. *Tests for plastic fines in aggregates related to stripping in asphalt paving mixtures*. NCAT Report No. 98-3. Auburn, AL. National Center for Asphalt Technology.

Malash, G.F. & El-Khaiary, M.I. 2010. Methylene blue adsorption by the waste of Abu-Tartour phosphate rock *Journal of Colloid Interface Science* 348: 537–545.

Nikolaides, A., Manthos, E. & Sarafidou, M. 2007. Sand equivalent and methylene blue value of aggregates for highway engineering. *Foundations of Civil and Environmental Engineering* 10: 111–121.

Pentrák, M., Czimerová, A., Madejová, J. & Komadel, P. 2012. Changes in layer charge of clay minerals upon acid treatment as obtained from their interactions with methylene blue. *Applied Clay Science* 55: 100–107.

Petkovšek, A., Maček, M., Pavšič, P. & Bohar, F. 2010. Fines characterization through the methylene blue and sand equivalent test: comparison with other experimental techniques and application of criteria to the aggregate quality assessment. *Bull Eng Geol Environ* 69: 561–574.

Rodriguez, A., Garcia, J., Ovejero, G., Mestanza, M. 2009. Adsorption of anionic and cationic dyes on activated carbon from aqueous solutions: equilibrium and kinetics. *J. Hazard. Mater.* 172: 1311–1320.

- Schoonheydt, R.A. & Heughebaert, L. 1992. Clay adsorbed dyes: methylene blue on laponite. *Clay Miner.* 27: 91–100.
- Shawabkeh, R.A. & Tutunji, M.F. 2003. Experimental study and modeling of basic dye sorption by diatomaceous clay. *Applied Clay Science* 24: 111–120.
- Tehrani-Bagha, A.R., Nikkar, H., Mahmoodi, N.M., Markazi, M. & Menger, F.M. 2011. The sorption of cationic dyes onto kaolin: kinetic, isotherm and thermodynamic studies. *Desalination* 266: 274–280.
- Woodward, D., Woodside, A. & Jellie, J. 2002. *Clay in Rocks*. Society of Chemical Industry (SCI) Lecture Paper Series. England, Society of Chemical Industry.
- Yool, A.I.G., Lees, T.P. & Fried, A. 1998. Improvements to the methylene blue dye test for harmful clay in aggregates for concrete and mortar. *Cement and Concrete Research*, 28(10): 1417–1428.
- Yukselen, Y. & Kaya, A. 2008. Suitability of the methylene blue test for surface area, cation exchange capacity and swell potential determination of clayey soils. *Engineering Geology* 102: 38–45.

Stiffness and complex modulus of cold recycled mixes with different binder combinations

Z. Čížková, J. Suda, J. Valentin & O. Krpálek

Department of Road Structures, Czech Technical University, Prague, Czech Republic

ABSTRACT: Standard design for cold recycled asphalt mixes specifies the use of bituminous emulsions, foamed bitumen or hydraulic binders (cement, lime etc.). In Central European countries, often the combination of cement and bituminous binder is used as the most preferable solution because of increased bearing capacity which can be provided by the final structural layer similarly to cement stabilized materials. For this reason it is expected that strength properties as well as stiffness are improved, nevertheless the strain-related behaviour explained usually by stiffness modulus, resilient modulus or complex modulus is not largely assessed. During the experimental study, cold recycled mixtures with bituminous emulsion and foamed bitumen have been designed. In both cases the same reclaimed asphalt material was used. The mixes were then produced also with 1% and 3% cement by mass of the cold recycled mix. For all mixes, stiffness was assessed by the repeated indirect tensile stress test (IT-CY) evaluating different curing periods. It has been found that the stiffness values are raised depending on the duration of curing. Further it was clearly confirmed and demonstrated that increase is strongly subject to the content of cement in the cold recycled mix. In parallel the evaluated mix design options were compared to the trends which have been found for results of indirect tensile strength (ITS) test. Since the main objective of this paper is to compare stiffness and dynamic complex modulus, testing has been done for selected mixes using the four-point beam test (4PB-PR). The focus was oriented on possible correlations and comparability of values gained by these two tests characterizing the strain behaviour of the material. It was further expected to get some verification of suitability for 4PB-PR since being a more advanced test providing broader information about the material behaviour.

1 INTRODUCTION

Cold recycled asphalt mixes are a multiphase system made from several components. Some of them have complicated internal structure and show increased thermal susceptibility. In fact, reclaimed asphalt pavement (RAP) consists of irregularly shaped aggregate, bituminous binder (usually of unknown origin and range of its ageing) and air voids. Despite the complex structure, the material behaviour can be described by application of known theory of viscoelasticity (Collop 1995, Ferry 1980, Tschoegl 1989, Underwood 2011).

One of the determining characteristics of bituminous materials, and thus also cold recycled asphalt mixes, is that they have time-dependent behaviour, which can be observed especially when deformation (strain) behaviour is determined. When these mixes are subjected to a very small loading, then it results in a combination of elastic, delayed elastic and viscous behaviour. In the range of low temperatures and high loading frequencies these mixes behave like elastic material in a solid phase with almost fully reversible response. At elevated temperatures and low stress frequency behaviour of these mixes is similar to viscous liquids with irreversible response. In the range of moderate temperatures and for the whole given frequency

range, asphalt mixes exhibit viscoelastic behaviour, or more precisely delayed response combined with viscous flow.

Rheological performance-based measurements, which result in characterization tools like complex (master) curves, depict the behaviour of the cold recycled mix in the most complex way and provide information about functionalities e.g. between the complex dynamical modulus and stress duration and frequency of loading. The value of the complex modulus and the slope of the master curve can be considered as valuable information for prediction of mentioned functional properties of cold recycled asphalt mixes. This is the reason why it is recommended to perform assessment of pavement structures by applying preferably time-demanding and more difficult but simultaneously more complex performance-based tests. One of the methods, which can be considered for the assessment of deformation behaviour, is four point beam bending test (4PB-PR). With this test it is possible to get values of complex dynamic modulus for given temperatures and stress frequencies (Zou 2010).

Another simple performance-based test which is also suitable for characterising the ability of a mix to resist the effects of loading is determination of the stiffness modulus usually by the repeated indirect

Table 1. Evaluated experimental mix designs.

Mix	Bituminous emulsion (% by mass)	Foamed bitumen	Cement
BCSM-BE	3.5%	–	3.0%
BCSM-BE (ref 1)	3.5%	–	1.5%
BCSM-BE (ref 2)	3.5%	–	1.0%
BSM-BE	3.5%	–	–
BCSM-BE (ref 3)	2.5%	–	1.0%
BCSM-FB	–	4.5%	3.0%
BCSM-FB (ref 1)	–	4.5%	1.0%
BSM-FB	–	4.5%	–

tensile stress test (IT-CY). Both tests are not required for the cold recycled mixes in many countries, where cold recycling is regularly used. Therefore the testing procedures were assumed from relevant European standard for hot asphalt mixes (ČSN EN 12697-26).

The main objective of this paper is a detailed investigation of the cold recycled mix behaviour by applying these performance-based tests. Findings from these tests were compared to the results of the indirect tensile strength test (ITS), which is usually required for declaring the quality of cold recycled mixes in most countries because of its simplicity. The output of this test is, nevertheless, just one empiric value for a given temperature, frequency and time of specimen curing.

2 MATERIALS

For experimental evaluation of stiffness modulus and dynamic complex modulus different types of cold recycled mixes were designed representing possible options of used binders and their combinations. Table 1 summarizes the material composition of designed cold recycled mixes in terms of used binders with emphasis on mixtures, where either bituminous emulsion or foamed bitumen is used in combination with hydraulic binder (cement).

Within the cold recycled mix assessment it is differentiated which of the two binder types is dominant in the mix. Basic set for the laboratory evaluation consists of four mixtures, namely BCSM-BE (mixture containing 3% of cement in combination with bituminous emulsion), BSM (mixture containing only bituminous emulsion), BCSM-FB (mix containing 3% of cement and foamed bitumen) and BSM-FB (mixture containing only foamed bitumen). For these four basic mixtures the complex modulus at various temperatures and frequencies was tested as well. For the determination of the stiffness modulus by IT-CY this set was completed by four other cold recycled mixtures with different content of bituminous and/or hydraulic binder. In fact more cold recycled mix options have been tested including evaluating potential and impact of fly-ash or lime.



Figure 1a and 1b. Measuring device 4PB-PR and IT-CY test in Nottingham Asphalt Tester.

All designed mixes contained the same type of screened RAP with 0/22 mm grading; cement CEM II/B 32.5 and bituminous emulsion C60B8 were used. For the production of foamed bitumen standard bitumen 70/100 according to EN 12591 was applied. When preparing the foamed bitumen 3.8% of water was added. The amount was determined in accordance with the procedure which is recommended for cold recycling technology by (Wirtgen Manual 2012). Foamed bitumen was injected in the mix at the temperature of 170°C by means of the Wirtgen WLB10S laboratory equipment. The mix as such was mixed using a twin-shaft compulsory mixing unit Wirtgen WLM 30.

The optimal moisture content of the cold recycled mix for the composition specified in the Table 1 was determined according to (ČSN EN 13286-2).

3 METHODOLOGY

3.1 Determination of stiffness modulus by the IT-CY method

The bearing capacity of a pavement layer is usually characterized by stiffness or modulus of elasticity. Stiffness modulus is defined as a ratio of material stress and strain and it characterizes its ability to resist the effects of loading. Higher stiffness value means that the material is more resilient to traffic loading than the material with a lower value. It usually means that better resistance to permanent deformations can be expected by the mixes with higher stiffness, on the contrary it is more difficult to find a straight relation to fatigue life.

Stiffness modulus was determined according to repeated indirect tensile stress test (IT-CY) in compliance with (ČSN EN 12697-26). It is a non-destructive performance-based test with good reproducibility and repeatability, during which e.g. the Nottingham Asphalt Tester (Fig. 1b) device loads the test specimen by a vertical pulse characterized by the force (P), which causes horizontal deformation (Δ). Effects of

the vertical force are transferred to the horizontal – perpendicular – direction by the Poisson ratio (μ), which is dependent on the type of material as well as on the specimen temperature. That is because the ratio of the perpendicular axial deformation or the ratio of orthogonal axial force varies at different temperatures. Stiffness modulus characterizes short term rheological behaviour of asphalt mix taking into account deformations lasting only for tens or hundreds of milliseconds.

The cylindrical specimens of 150 ± 1 mm diameter were prepared by putting the cold recycled mix in cylindrical moulds and compacting by the static pressure of 5.0 MPa. For all test specimens firstly basic volumetric properties, as well as the indirect tensile strength according to (TP 208) and stiffness modulus at 15°C according to (ČSN EN 12697-26) were determined. Specimens were tested after 7, 14 and 28 days. All cold recycled mixes were stored for one day at 90–100% relative humidity and temperature of $(20 \pm 2)^\circ\text{C}$. Further the specimens were stored at laboratory conditions with 40–70% relative humidity and temperature of $(20 \pm 2)^\circ\text{C}$ for the rest of their curing time.

3.2 Measurement of complex modulus 4PB-PR

Measurement of complex modulus was performed according to EN 12697-26. This standard prescribes that a beam specimen with smooth surface and entire edges is clamped by clips in the test equipment in four points (4PB-PR). All clamps should allow free rotation and shift in the longitudinal direction. The outer clamps should be firm, to defend vertical movements. Inner clamps deduce vertical cyclic loading. The evaluation of the test results is based on Euler-Bernoulli theory.

4PB-PR is a simple test, which can be characterized by a simple mechanistic theory, whereas gained results are important values applicable to the pavement design purposes. Nevertheless such conclusion cannot be fully applied for several reasons which are further summarized. The respective testing is influenced by factors, which introduce to the testing methodology errors or deviations which influence the overall result. These conditions are not attended by the testing methodology in any manner. It is the only question if it is possible to avoid them.

Firstly, the testing beam has to be locked in by the clamps. Such clamping locally constitutes stress and deformation which is introduced to the beam material. This extra stress and deformation can represent fatigue damage or local non-linear effects not included in the calculation of complex modulus.

Secondly, it is not possible to design 4PB-PR apparatus, which would except friction, allow at the same time free displacement and will not deteriorate during the life-time. Such deformations related to the apparatus might influence the test results.

Thirdly, shear forces act on the test beam in the area between the outer and inner clamps. These forces are

causing additional testing beam deformation, whereas such deformations are not taken into account in the used test methodology. Forces related to the shearing strain in this area equal $F/2$, i.e. the half of applied total loading.

Fourthly, clamps limit the possibility of displacement in cross-section. This leads according to our experience to ineligibile deformations of the testing beam in the areas close to the clamps and this is not in accordance with the deflection theory.

Fifth factor influencing the test results is the specimen shape factor, which can be defined as a function of shape and test specimen dimensions. Similarly weight factor should be considered as well. This can be defined as a function of beam weight and apparatus weight, which by its inertial force influences acting force. The magnitude of measurement error or inaccuracy is dependent on the shear modulus and Poisson's ratio related to the tested material. These two factors are included in the calculation of complex modulus (Huurman 2012).

Dynamic complex modulus was determined by the 4PB-PR test method (Fig. 1a) in the temperature range from -20 to $+27^\circ\text{C}$ and frequency from 0.1 to 40 Hz by the controlled deformation of 50 microstrain. These frequencies correspond to the real pavement loading caused by vehicles passing with different speed in the aforesaid temperature range.

Testing slabs were produced by segment compactor and after their curing as specified further the slabs were cut to required shape of beam specimens according to (EN 12697-26). Respective curing of testing specimens was as follows:

- Cold recycled mixes stabilized by cement and bituminous emulsion or foamed bitumen were firstly stored two days at 90–100% relative humidity and temperature of $(20 \pm 2)^\circ\text{C}$. Further the test slabs were stored in dust free area of the laboratory at 40–70% relative humidity for additional 26 days at the same temperature.
- Cold recycled mixes stabilized by bituminous emulsion or foamed bitumen were stored for 1 day at 90–100% humidity and temperature of $(20 \pm 2)^\circ\text{C}$. Further the test slabs were conditioned at $(50 \pm 2)^\circ\text{C}$ in a climatic chamber for additional 4 days. The test specimens were then stored at 40–70% humidity and the temperature of $(20 \pm 2)^\circ\text{C}$ for 14 days after this accelerated curing.

4 RESULTS FOR STIFFNESS AND ITS TESTING OF COLD RECYCLED MIXES

Figures 2 and 3 show successive increase in both determined characteristics during the first 28 days of test specimens curing. At the same time the extent of characteristic increment in relation to the added hydraulic binder is illustrated.

In general it is possible to state, that time-dependent increase of stiffness modulus does very well

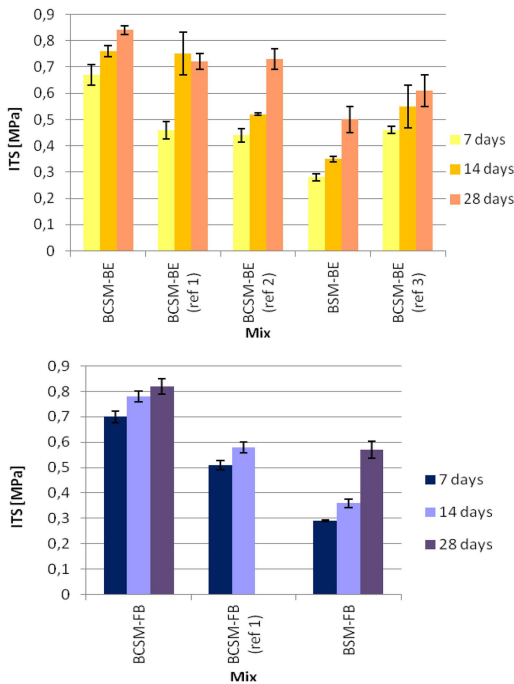


Figure 2a and 2b. ITS values – mixes with bituminous emulsion/ITS values – mixes with foamed bitumen.

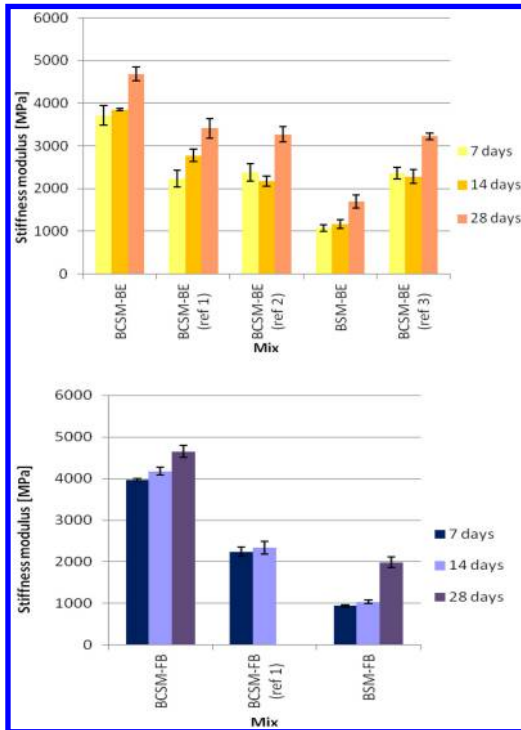


Figure 3a and 3b. Stiffness modulus – mixes with bituminous emulsion/Stiffness modulus – mixes with foamed bitumen.

Table 2. Time influence on ITS and stiffness modulus values.

Indirect tensile strength [MPa]						
	BSM-BE		BCSM-BE(ref 2)		BCSM-BE	
7 days	0.28	100%	0.44	100%	0.67	100%
14 days	0.35	25%	0.52	18%	0.76	13%
28 days	0.50	79%	0.73	66%	0.84	25%
	BSM-FB		BCSM-FB (ref 1)		BCSM-FB	
7 days	0.29	100%	0.51	100%	0.70	100%
14 days	0.36	24%	0.58	14%	0.78	11%
28 days	0.57	97%	–	–	0.82	17%

Stiffness modulus [MPa]						
	BSM-BE		BCSM-BE (ref 2)		BCSM-BE	
7 days	1076	100%	2380	100%	3717	100%
14 days	1164	8%	2177	–9%	3852	4%
28 days	1695	58%	3274	38%	4687	26%
	BSM-FB		BCSM-FB (ref 1)		BCSM-FB	
7 days	941	100%	2240	100%	3971	100%
14 days	1036	10%	2331	4%	4175	5%
28 days	1988	111%	–	–	4652	17%

correspond with indirect tensile strength values. From the point of view of both characteristics it is nevertheless possible to observe a difference if mixes with diverse content of cement are compared.

As can be induced from the Table 2 increase of both characteristics is always faster for mixes with higher cement content. The table summarized selected values of ITS and stiffness for mixes with same bituminous binder content and 0%, 1% and 3% cement. If comparing the assessed curing period between 7 and 28 days it can be stated that for mixes with higher content of hydraulic binders faster increase in strength properties is visible within the first 7 days. For the rest of the evaluated curing period the strength increase is rather slow. On the contrary for mixes containing only bituminous binder a very slow strength enhancement can be observed and even between the 14 and 28 days of curing there is still significant increase of the strength values.

From the presented stiffness and ITS results following conclusions can be made. There is an important difference in values determined after 7 days specimens curing for cold recycled mixes with cement and without cement. This difference then gradually decreases as can be seen in Table 3. Further, it is possible to show, that the use of cement has more positive influence on stiffness values than on indirect tensile strength values. Such finding does very well correlate with values gained also for other assessments done within the project CoRePaSol.

5 RESULTS FOR 4PB-PR TESTING OF COLD RECYCLED MIXES

Results of dynamic resilient modulus determined by dynamic loading using 4PB-PR test method are

Table 3. Influence of cement content on ITS and stiffness.

Indirect tensile strength [MPa]						
	7 days		14 days		28 days	
BSM-BE	0.28	100%	0.35	100%	0.50	100%
BSCM-BE (ref 2)	0.44	57%	0.52	49%	0.73	46%
1% cement						
BSCM-BE	0.67	139%	0.76	117%	0.84	68%
3% cement						
BSM-FB	0.29	100%	0.36	100%	0.57	100%
BSCM-FB (ref 1)	0.51	76%	0.58	61%	–	–
1% cement						
BSCM-FB	0.70	141%	0.78	117%	0.82	44%
3% cement						
Stiffness modulus [MPa]						
BSM-BE	1076	100%	1164	100%	1695	100%
BSCM-BE (ref 2)	2380	121%	2177	87%	3274	93%
1% cement						
BSCM-BE	3717	245%	3852	231%	4687	177%
BSM-FB	941	100%	1036	100%	1988	100%
BSCM-FB (ref 1)	2240	138%	2331	125%	–	–
1% cement						
BSCM-FB	3971	322%	4175	303%	4652	134%

summarized in the Table 4. The shown values are always determined as an average from last 10 measured values (complex dynamic modulus, loss angle) at different temperatures and for different frequencies. These results were used for decomposing the complex modulus to its real and imaginary part. These decomposed values are necessary, because they are used as input data in IRIS Rheo-Hub software. This calculation software (or any similar available on the market) allows successively to calculate and adjust the so called master curves.

The master curves were designed by using time-temperature superposition principle with relevant shift in horizontal and vertical plane. Shift factors were used to determine the temperature dependence of rheological behaviour and extension of time-frequency range at given reference temperature.

For the description of the shift factor in horizontal plane Williams-Landel-Ferry equation with C1 and C2 parameters was used. For the description of the shift in vertical plane a polynomial equation is preferred (Dealy 1999, Ferry 1980). The parameters of the vertical and horizontal shift are listed in the Table 5. All calculations were made in the IRIS Rheo-Hub software tool. The reference temperature for master curve determination was set at 20°C.

As generally known, temperature and time have dramatic influence on viscoelastic response of bituminous binders and asphalt mixes. This is the reason why viscoelastic properties are usually determined in wide spectrum of temperatures and/or stress levels. Behaviour of an asphalt mix or bitumen depends on

the temperature as well as frequency and duration of repeated loading. If these variables are in a range, where the material behaviour is defined as viscoelastic and it is possible to characterize the material as temperature-rheologically “simple”, then it is possible to express the effect of time (frequency) and temperature by time-temperature superposition. Material characteristics given as a time-dependent function or frequency-dependent function (such as results of dynamic testing, or material spectrum measured at different temperatures), can be shifted along axes for creating various master curves (Ferry 1980). The master curves of the researched cold recycled asphalt mixes with different binders (bitumen, cement, or their combination) are given in figures 4a and 4b.

When analyzing the master curves from the right to the left, it is evident, that in the field of the lowest tested temperatures and highest frequencies, the material has tendency to behave almost elastically. The transition from viscoelastic to elastic behaviour is evident from the last determined values in the decreasing imaginary part of the master curves. The real part of the master curve is increasing proportionally to the raising frequency. At the same time the first derivation is decreasing and is reaching almost zero level for the last couple of values. This phenomenon correlates very well with the transition of the material properties to the elastic area, where equilibrium modulus is reached (Kim 2008, Ferry 1980). From the loss angle change it is clear, that cold recycled asphalt mixes are thermo-mechanically sensitive materials (Tschoegl 1989). Comparing assessed mixes in terms of used binders, the influence of cement is evident in enhanced elastic properties at high temperatures and low frequencies. At the same time thermal susceptibility is decreased if cement is used. This fact is evident from comparing the elastic modulus curves, where the slope of elastic curve is more gradual for mixes with cement (less difference between the lowest and the highest determined modulus).

The difference between foamed bitumen and bituminous emulsion is apparent especially in the elastic modulus master curve. The variation might be partly caused also by different residual binder content. The binder itself will not play a role since for foamed bitumen and the bituminous emulsion 70/100 bitumen was used. The applicability of the test for cold recycled mix assessment seems however to be complex, because the correct preparation of unpaired beam specimens came repeatedly up with certain problems. The clear reason is the brittle character of these stabilized materials. This leads to low reproducibility of the results as well.

First problem related to cold recycled asphalt mixes and 4PB-PR testing appeared already during demoulding of the test slabs. Because the material is more brittle, it is necessary to secure sufficient separation between the steel bottom plate of the mould and the compacted material. Even if the separation is made properly, sometimes the whole slab can be broken during demoulding. Another problem occurred when beam specimens were cut from the slabs to get the

Table 4. Dynamic complex modulus and phase angle values (4PB-PR test method).

Testing temp. (°C)	Frequency (Hz)	BCSM-BE		BCSM-FB		BSM-BE		BSM-FB	
		E* (MPa)	δ (-)	E* (MPa)	δ (-)	E* (MPa)	δ (-)	E* (MPa)	Δ (-)
0	50	5 930	0.00	6 459	0.00	6 211	0.00	7 543	0.00
	30	5 482	0.00	6 162	0.03	5 619	0.52	7 509	0.00
	20	5 100	1.05	5 782	0.59	5 137	3.74	7 050	0.92
	10	4 745	4.65	5 482	3.45	4 761	7.00	6 570	4.79
	8	4 589	5.45	5 385	4.53	4 651	8.25	6 453	5.54
	5	4 472	7.00	5 149	5.80	4 396	9.82	6 095	7.25
	2	4 195	8.29	4 941	7.57	3 972	12.33	5 599	9.20
	1	4 012	9.24	4 702	8.39	3 627	13.83	5 249	10.82
	0.5	3 721	9.37	4 461	9.09	3 309	14.23	4 833	11.52
	10	50	4 620	0.03	5 669	0.10	4 495	5.80	5 222
30		4 210	3.03	5 203	1.22	3 960	5.78	4 723	5.43
20		3 729	4.08	4 582	3.87	3 503	8.95	4 156	7.35
10		3 482	7.13	4 152	6.76	3 164	12.24	3 651	11.97
8		3 403	8.12	4 066	7.63	3 053	13.05	3 565	12.96
5		3 243	9.38	3 851	9.29	2 855	14.88	3 261	14.90
2		3 314	11.32	3 551	11.23	2 515	16.98	2 794	17.20
1		2 844	11.56	3 247	12.28	2 298	18.21	2 438	19.10
0.5		2 614	11.87	2 842	12.82	1 981	18.81	2 037	20.91
20		50	3 870	0.00	2 852	12.69	2 829	6.44	3 892
	30	3 441	4.20	2 411	14.71	2 605	11.95	3 416	9.93
	20	2 955	4.85	2 039	26.11	1 983	14.86	2 827	13.29
	10	2 631	8.92	1 946	14.57	1 693	19.41	2 432	17.10
	8	2 550	10.10	1 955	15.97	1 637	20.28	2 343	18.06
	5	2 413	11.42	2 421	13.33	1 500	22.37	2 157	20.18
	2	2 178	13.47	2 174	13.58	1 239	24.15	1 780	22.87
	1	2 001	13.95	2 181	16.28	1 062	25.18	1 565	23.78
	0.5	1 704	12.89	2 078	16.60	809	23.67	1 241	24.40
	30	50	3 053	6.66	3 168	3.61	1 925	17.01	2 398
30		2 701	9.26	2 732	6.87	1 566	20.79	2 107	16.65
20		2 115	8.88	2 207	9.27	1 120	22.72	1 537	19.33
10		1 872	12.08	1 967	14.35	910	23.81	1 260	23.35
8		1 852	12.23	1 889	15.31	879	24.43	1 211	24.67
5		1 769	13.55	1 784	16.51	820	25.55	1 085	26.39
2		1 554	15.26	1 524	18.19	654	25.36	859	27.31
1		1 455	15.31	1 367	18.58	581	23.97	735	27.58
0.5		1 271	15.96	1 150	17.67	452	26.01	568	26.74

Table 5. Parameters of horizontal and vertical shift within the time-temperature superposition.

Mix		BCSM-BE	BCSM-FB	BSM-BE	BSM-FB
T _{ref}	[°C]	20			
T _{min}	[°C]	0			
T _{max}	[°C]	30			
Fit of horizontal shift aT [K]	C1	100	100	100	100
	C2	1458.3	1215.5	1249.9	1016.7
Fit of vertical shift bT [-]	a ₀	1.07	1.01	9.89E-01	9.94E-01
	a ₁	1.1E-02	1.00E-02	2.52E-02	6.5E-03
	a ₂	-2.4E-05	3.50E-05	2.96E-04	-5.7E-04

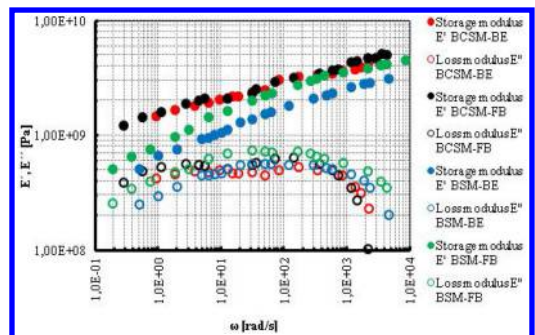


Figure 4a. Master curves of cold recycling mixes – E', E''.

necessary test specimens. During the cutting the material has tendency to brake off edges of the beams (figure 5). This finding is not unique. The same was found out in the past within several studies and master

student projects at the CTU in Prague, as well as during fatigue experiments on cold recycled asphalt mixes made e.g. at the University College in Dublin.

To compare the methodology of stiffness modulus testing by IT-CY and the dynamic modulus gained by

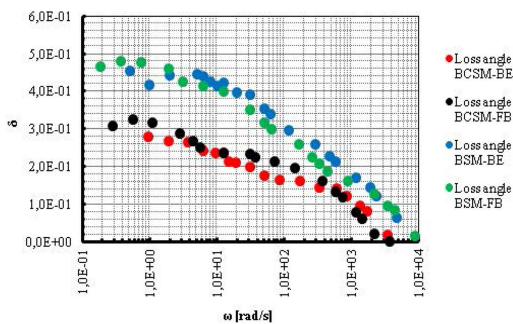


Figure 4b. Master curves of cold recycling mixes – Loss angle.



Figure 5. Damaged beam specimens (BCSM-BE, BCSM-FB, BSM-BE, BSM-FB) – before testing.

Table 6. Stiffness modulus determined by IT-CY method.

Mix	Stiffness modulus (IT-CY) (MPa) @ 15°C
BCSM-BE	4 287
BCSM-FB	4 652
BSM-BE	1 745
BSM-FB	2 254

4PB-PR test, selected values of IT-CY stiffness modulus are shown in the Table 6. The comparison itself is a challenging and ambiguous because of different method of test specimen manufacturing (segment compactor for 4PB-PR vs. hydraulic press for IT-CY) as well as the principles of loading. However, the results show some trend or as the case may be it is possible to make some assumptions on the gained findings. Stiffness of cold recycled mixes with cement correlate more with the results of complex dynamic modulus at higher frequencies of loading (30–50 Hz), while the mixes with only bituminous binders have stiffness according to IT-CY more similar to lower frequencies (2–5 Hz) of 4PB-PR testing. The given comparison is just approximate due to the fact, that complex dynamic modulus were determined at temperatures of 10°C and 20°C, while the stiffness test is according to the standard procedure in the Czech Republic done at 15°C.

6 CONCLUSIONS

Results presented mainly for determination of stiffness on cold recycled mixes represent only a small part of a more complex study done within the CoRePaSol project, where also other optional designs of this type of stabilized material were tested and compared, e.g. with various bituminous binders for foam production, with different types of reclaimed materials including recyclable concrete or unbound base layer material. Additionally stiffness values are available even for cold recycled mix options with multiple recycled asphalt, which was laboratory aged, re-crushed and re-used in a new cold recycled mix.

In general it can be stated that stiffness modulus determination by using IT-CY test method is a suitable procedure for cold recycled mix assessment and can be always done in parallel to indirect tensile strength test. This destructive test is so far used more often when characterizing cold recycled mixes. Stiffness determination is required in smaller number of countries using cold recycling techniques. It is therefore possible to recommend use both test methods – IT-CY and ITS test. Results from both these tests complement each other very well. Additionally stiffness determination has so far better shown the curing time dependency as well. On the other hand, if comparing ITS and stiffness for mix design with increasing cement content, stiffness modulus seems to be less sensitive to cement

content in the mix, if comparing results to cold recycled mixes with same RAP but only bituminous binder content. This is valid mainly for results gained after more than 14 days curing when the difference becomes very small.

On the other hand, complex modulus was assessed only by 4PB-PR test procedure. It was known that, in the past, doubts were raised about suitability of the test especially because of test specimen preparation. It was proven by the research study within CoRePaSol project that the test would provide more data and most probably could better explain the behaviour of the tested material. Nevertheless, reproducibility of the test seems to be very low mainly influenced by the quality of gained test specimens. Solving initial problems of demoulding $30 \times 40 \times 5$ cm test slabs it was then usually very problematic to properly cut test beams. Gained test specimens showed always some damages like loss of aggregate particles or impaired edges, which immediately influence the test results. Despite these facts, it was possible to get data for a selected temperature and frequency interval and even plot master curves. Nevertheless, the variation of measured values is much higher than in case of IT-CY stiffness modulus test.

Simple comparison of IT-CY and 4PB-PR was done to evaluate whether there is any correlation between IT-CY stiffness and complex modulus at some frequency, ideally concurrent for all tested cold recycled mix designs. As was discussed within [chapter 3](#), such correlation was not found, only presumptions can be made for cold recycled mixes with or without cement.

From the practical point of view and expectations of the National Road Authorities as defined within the CoRePaSol project, if the 4PB-PR test would be required for cold recycled mix characterization, it could be performed only by a limited number of laboratories requiring suitable test apparatus and expecting more time demanding procedure for test specimen preparation.

ACKNOWLEDGEMENT

This paper is an outcome of the research project “Characterization of Advanced Cold-Recycled Bitumen Stabilized Pavement Solutions (CoRePaSol)”

carried out as part of the CEDR Transnational Road Research Programme. The project was funded by the National Road Administrations of Belgium (Flanders), Denmark, Finland, Germany, Ireland, Netherlands, Norway, Sweden and UK.

REFERENCES

- Collop, A.C., Cebon, D.; Hardy, M.S.A., 1995. Viscoelastic Approach to Rutting in Flexible Pavements. *Journal of Transportation Engineering* 121 (1) (January): 82–93., doi:10.1061/(ASCE)0733-947X(1995)121:1(82).
- Czech Ministry of Transportation: Technical specification TP 208, 2009. Recyklace konstrukčních vrstev netuhých vozovek za studena, Ministerstvo dopravy, odbor silniční infrastruktury, Praha.
- ČSN EN 12697-26, 2012. Bituminous Mixtures – Test Methods for Hot Mix Asphalt – Part 26: Stiffness. Czech Office for Standards, Metrology and Testing.
- ČSN EN 13286-2, 2011. Nestmelené směsi a směsi stmelené hydraulickými pojivy – Část 2: Zkušební metody pro stanovení laboratorní srovnávací objemové hmotnosti a vlhkosti – Proctorova zkouška, ÚNMZ.
- Dealy, J.M., Wissbrun, K.F., 1999. *Melt Rheology and Its Role in Plastics Processing: Theory and Applications*. Springer.
- Ferry, J.D., 1980. *Viscoelastic Properties of Polymers*. 3rd edition, Wiley.
- Huurman M., Pronk A. C., 2012. A detailed FEM simulation of a 4-point bending test device. Vol. 2012, p. 1–12. ISBN 978-0-415-64331-3.
- Kim, Y., 2008. *Modeling of asphalt concrete*. 1st edition, McGraw Hill Professional.
- Tschoegl, N.W., 1989. *The Phenomenological Theory of Linear Viscoelastic Behavior: An Introduction*. Springer-Verlag.
- Underwood, B.S., Taeyoung Yun, Kim, Y.R., 2011. Experimental Investigations of the Viscoelastic and Damage Behaviors of Hot-Mix Asphalt in Compression. *Journal of Materials in Civil Engineering* 23 (4) (April): 459–466, doi:10.1061/(ASCE)MT.1943-5533.0000197.
- Wirtgen: *Wirtgen Cold Recycling Technology*, 2012. Manual, Wirtgen GmbH, first edition, Windhagen, Germany.
- Zou, G., Zhang, X., Xu, J. Chi, F., 2010. Morphology of Asphalt Mixture Rheological Master Curves. *Journal of Materials in Civil Engineering* 22 (8): 806–810, doi:10.1061/(ASCE)MT.1943-5533.0000024.

Maintenance strategy for the provincial road network of Xanthi, Greece

G. Kollaros, A. Kokkalis & A. Athanasopoulou

Democritus University of Thrace, Greece

ABSTRACT: Pavements during their lifecycle degrade depending on traffic loading, climate and time. For an effective management of road pavements, the selection of the right maintenance strategy at the right time is of paramount importance. The suitable maintenance strategy will be influenced by the type, severity, and extent of the pavement surface distresses and its structural condition. Proper decision about the right treatment also depends on the extent or frequency of distress occurrence. Problem spots on the provincial road network of Xanthi Territory have been located and possible causes were investigated. Following an extended survey and data collection from official agencies, in-situ measurements and photographic imprinting of the most important damages, pavement maintenance methods and rehabilitation techniques were studied. The proposals on maintenance and restoration are focused on the amelioration of the roadway, the prolongation of the service life and on safe traffic in a tolerable cost framework.

1 INTRODUCTION

A number of reasons have set off road maintenance as an essential activity. First, it preserves the road in a safe condition as it has originally been constructed. Second, it protects adjacent resources and user safety. Third, through maintenance operations, a convenient and efficient travel is provided along the route, while the user costs are decreased. Finally, equipment like electricity cables, gas pipelines, water pipes, and telephone lines often need to be included in highway's maintenance programme.

While roads have to be maintained in a safe condition, maintenance operations must also be carried out safely. Properly maintained highways support local and national economies since they ensure that freight and people can move safely and efficiently. In urban places, most of the daily trips to school, shopping centres, sanitary institutions, or to spots of leisure like parks, cinemas, and restaurants depend on the availability of a well maintained road network.

Despite its importance, it's a usual phenomenon for maintenance to be neglected or improperly performed. This leads to accelerated deterioration of the road structure and finally to premature failure from both vehicle loading and climatic impacts.

Pavement maintenance consists of a structured investigation and intervention programme to safeguard the structure of the road and to ensure an optimized economic performance of the facility.

Apart from subjective factors like politics, users can determine the most cost-effective treatment organizing pavement management systems. Factors taken into

consideration when a selection is made include (Gao et al. 2012, Labi & Sinha 2005):

- type and expected life of the existing pavement
- roadway use and level of traffic
- traffic loading
- type and extent of distress
- surface friction
- crack condition
- climate and environmental factors
- cost of treatment
- available budget
- availability of qualified staff and contractors
- availability of quality materials
- time of year of placement
- facility downtime
- pavement noise

Because road networks are extensively used by both private and commercial users, the costs of delay on congested roads can be considerable. The delay costs can be significantly higher if the congestion due to large traffic volumes is added to the disruption by maintenance works

Common causes of flexible pavement deterioration are the action of traffic and climate. These actions result in structural deterioration and surface faults. Structural deterioration typically includes (Oliver 2007): (a) deformation of the pavement surface due to traffic loading; (b) loss of surface texture, reducing skidding resistance; (c) polishing of the stone in the surfacing, which also reduces skidding resistance; (d) oxidation of the binder, resulting in surface deterioration and cracking; and (e) fatigue strain

development in the foundation, leading to structural deterioration. The precise identification of a defect and its cause is very important due to similarities often found between the visual appearances of pavements with quite different damages.

2 FUTURE DIRECTIONS OF ROAD MAINTENANCE

The process of pavement deterioration is complex, since it involves the structural damage caused by different types of pavement distress. Deterioration is the result of the interaction between materials, traffic, and climate over time. The alteration of pavement performance over time is signified by deterioration (Rouse & Chiu 2009). Performance could be defined as the ability of the road to satisfy the demands of traffic and environment over its design life. Due to the inherent complexity of the pavement deterioration process, the expected conditions could be best predicted using deterioration models (Mubarak 2009) or performance models (Fwa et al. 2000).

An indicator of future success of the road maintenance plans could be good quality information about the road conditions ‘an essential prerequisite for sound decision-making about the need for road maintenance’ and the type of treatment that is subsequently applied.

The decision making process has to recognise and incorporate long-term environmental costs and benefits of pavement management units if the goal is to have road networks at a sustainable state (Theodorakopoulos 2002). Pellecuer et al. (2014) have presented an assessment of life cycle environmental benefits of pavement maintenance and discusses their incorporation in pavement management systems.

The condition of a road network can be rated based on off-pavement inspections that are made over the same sections as for the pavement defects. In such a case, particular features, which can be on the pavement or off of it, are inspected against a common referencing system. Then the results could be directly compared in order to ensure the efficient operation of the whole roadway.

Features other than the pavement itself that have significant importance and must normally be included in maintenance schedules are characterised by their structural and statutory importance, their role in meeting environmental needs, the way they improve the road’s appearance, and by their provision of services to users, both cyclists and pedestrians (Elhadidy et al. 2014). Of course some features may fit into more than one category.

3 FEATURES THAT MEET ENVIRONMENTAL NEEDS

From a road maintenance aspect, the following environments need to be considered: (1) the living world within the road-influenced space (wildlife habitat); (2) persons using the roadway; (3) persons living

or working adjacent to a road; (4) people indirectly affected by road activities. A major role in road maintenance is played by external influences. Maybe the most successful road maintenance will be that which is noticed least in terms of its impacts on the road user, the environment, and those living and working close to the carriageway.

The range of ground conditions crossed by roads is very wide. The behaviour differs from site to site as well as the emissions from them. Maintenance predictions are easier on undisturbed ground. Consequently, in various cases road maintenance issues and influences can extend below and beyond the carriageway width.

Roadways can affect wildlife and ecological systems. Such effects include loss of wildlife habitat, fragmentation, mortality, and increased competition. Within a roadway’s zone, the wildlife must be the subject of special maintenance provisions (wildlife crossings, culverts and habitat restoration).

Roadways have to be reasonably free of litter which is dropped by users or is blown from elsewhere. When the accumulated quantities have reached a given level, they must be removed.

Debris and detritus need to be collected separately from litter, since their size is often large presenting a hazard for the public using the road.

Since detritus is usually composed of silt, it can block drains and service ducts. Detritus it is normally swept away or otherwise removed within a maintenance operation.

The aesthetic appearance of a highway is particularly important when efforts are made to minimise the impact on a given landscape. Horticultural provisions can screen the road and its traffic from nearby homes of residents, reduce noise, as well as enhance the appearance of a road.

In order for trees, bushes, flowers, and other plant species to achieve desired landscaping effects, they all need to be well established (if new) and managed. The spread of pests onto roadside land must be prevented. The control of pests on a regular basis must adopt methods that will not cause problems, as with the use of toxic substances.

Moreover, considerable effort is being devoted in comparison with the past, for the noise reduction on the pavements. The maintenance requirements have to accommodate the constantly increasing traffic loads on pavements and make them produce even less noise at the same time. Care must be given with the application of chip sealing, since in such a case traffic noise will increase.

4 TYPES OF MAINTENANCE TREATMENTS

Various cracking deterioration prediction models are available, such as the PAVENET-R model; the Austroads model; the Brazilian model; the KLW (Ker Lee Wu) fatigue cracking prediction model; the Indian model, and models incorporated in the HDM-4 system which continues being developed (Ferreira et al.

2012). These models have been developed in the period 1994–2010. The more recently designed model (Ausroads) can also predict roughness and rutting of sealed granular pavements.

Cracking maintenance treatments include sealing (clean and seal, rout and seal, or saw and seal), crack filling (usually for more worn pavements), full depth repair, fog sealing (application of diluted emulsion as a temporary measure), seal coat, double chip seal (two successive seal coats), slurry seal (when the primary problem is the surface oxidation and hardening), microsurfacing or polymer-modified slurry seal, thin hot-mix overlays, and pothole patching.

The materials are required to be cheap and meet criteria for strength, resistance to deformation, skidding resistance, impermeability, low noise and spray generation. In Table 1, cracking and other distresses in flexible pavements are listed along with remedial actions and predictions for preventive maintenance measures.

In asphalt pavements, rutting is a major form of pavement distress, occurring because of plastic deformation of both the asphalt and the lower layers of the pavement. Theoretically, it is possible for rutting deformation to continue under traffic loading up to a stage of structural failure. In practice, long before reaching this stage, maintenance treatment or rehabilitation of the rutted pavement would have to be performed to restore pavement surface condition.

5 THE PROVINCIAL ROAD NETWORK OF XANTHI

The main routes comprising the provincial road network in Xanthi area, are two in the West-East direction, one originating from Xanthi and moving South and one with a North Western orientation. The first two connect Xanthi with Komotini, the capitals of two adjacent Territories, Xanthi and Rhodopi. They are characterized by two sites in the mid-distance, namely Iasmos and Porto Lagos. The third axis connects the cities of Xanthi and Drama with an intermediate destination the town of Stavroupolis having an elevation of 110 metres. The last axis joins Xanthi with the historical town of Abdera. There are no concrete roads in Xanthi's provincial road network.

Rouse & Chiu (2009) have described a local road maintenance strategic framework, where the recognised needs of pavements distressed by traffic, environment and geology are going to be faced by actions of periodic (resealing or rehabilitation) and routine maintenance. This mix of maintenance activities will target to objectives like lower costs, and increased quantity and quality. The goals in such a maintenance model will be effectiveness (combination of quality and quantity aspects), economy (combination of lower total expenditures and higher quality) and efficiency (combination of lower cost and higher quantity) (Hanna et al. 1993). For the condition of Xanthi's road network, the mission will be to maintain

Table 1. Distresses in flexible pavements; prediction for preventive maintenance treatments.

Category of distress	Type of distress	Potential actions
Surface defects	Rutting	Ruts are filled with micro surfacing or strip chip seal, then a thin cold mix surface or chip seal is laid
	– Densification of pavement	Preventive maintenance cannot repair problem
	– Unstable asphalt concrete	Sand seal, chip seal, micro-surfacing
	Bleeding	Fog seal, thin cold treatment, chip seal, thin hot mix overlay
	Raveling	Unstable pavement, not a candidate for preventive maintenance
Cracking	Shoving	Thin cold treatment, chip seal, thin hot mix overlay
	Polished aggregate	Not a candidate for preventive maintenance
	Fatigue cracking	Thin cold treatment, chip seal, thin hot mix overlay
	Block cracking (low to moderate)	Crack treatment
	Edge cracking	Crack treatment
Patching and potholes	Longitudinal cracking	Crack treatment
	Reflection cracking	Crack treatment
	Transverse cracking	Crack treatment
	Patch/Patch deterioration	Extensively patched pavements are not good candidates for preventive maintenance
	Potholes	Pothole pavements are not good candidates for preventive maintenance

a safe and efficient provincial network throughout its lifetime.

Data were collected for the condition of pavements in all routes comprising the provincial road network in Xanthi area. The in-situ survey was accompanied by photographing and video recording. The main defects noticed on the network are categorized and shown in Tables 2, 3 and 4. In these tables the probable causes are depicted and some remedial measures are described. As the amounts of data increase, the introduction of new technologies could better service the information collection process. Technologies already in use include laser systems, ground penetrating radar, image-recognition systems, and electronics. Smart roads, which use sensors within road components to feed real-time information regarding their condition and performance is a new concept.

Table 2. Wear in the road, causes, proposed solutions – Cracking.






	Causes	Maintenance- Rehabilitation
Longitudinal cracks on the road axis and sides		
	Pavement cracking due to reduced subgrade bearing capacity in conjunction with reduced thickness of asphalt layers and base.	In most cases the sealing – filling of cracks of this type is the most appropriate maintenance treatment.
9.6 km Xanthi - Iasmos road		
Alligator cracking		
	Reduced subgrade bearing capacity Full fatigue of the pavement because of repeated loadings of the traffic volume combined with the existence of weak subgrade or reduced thickness of the underlying layers.	A. Local appearances For the radical restoration of alligator cracks (if they are caused by reduced subgrade bearing capacity): (i) completely remove all asphalt layers, the unbound aggregates layers, and part of the subgrade (ii) proper measures for lowering the water table and (iii) reconstruct the layers with new appropriate materials B. Extended cracking When the alligator type cracks are due to the fatigue of the pavement, the only remedy is to restore the upper layer with an added asphalt layer with its depth dependent on the pavements condition, removing or not the existing cracked layer.
30.5 km Xanthi - Iasmos road		
Transverse cracking		
	Shrinkage of pavement's surface due to low temperatures Defective work during construction Cracking of underlying layers, such as cement treated layers of crushed material.	Removal and replacement of the destroyed pavement with the addition of new material
15.4 km Xanthi – Stavroupoli road		
Slippage cracks		
	Slipping of the traffic layer on the underlying layer due to poor cohesion. The poor coherence is due to absence of adhesive coating or to inadequate adhesive coating or to the existing water, soil, and lubricants in the interlayer space	Removal of the pavement around the crack up to the point of good cohesion and filling with hot asphalt mix. Before filling, the surface must be thoroughly cleaned and sprayed with a cationic emulsion adhesive coating
23.6 km Komotini-Iasmos		
Shrinkage cracks		
	Shrinkage of asphalt mix or of road base and subbase materials. If the surface layer has a small thickness, then the cause is shrinkage of the subgrade.	Depending on the size of the cracks, the maintenance can be made using cold asphalt mix, added asphalt layer or replacement of the asphalt concrete.
12.0 km Komotini – Iasmos		

Table 3. Wear in the road, causes, proposed solutions – Deformations.





	Causes	Maintenance- Rehabilitation
<p>Rutting, local settlements and heaves, transverse folds</p>  <p>3.7 km Xanthi – Porto Lagos road</p>	<p>a) poor compaction of all layers, b) subgrade settlement, c) low asphalt mix stability, d) resilient asphalt mix behaviour.</p>	<p>Deformation maintenance could include from a simple filling with hot or cold asphalt mix to complete removal of the assaulted area and its replacement with new materials.</p>

Table 4. Wear in the road, causes, proposed solutions. – Disintegrations.

<p>Material detachment – Potholes</p>  <p>21.9 km Xanthi - Iasmos road</p>	<p>a) Usage of non-clean aggregates, b) Usage of aggregates having a tendency to decompose, c) lack of binder material in the asphalt mix, d) reduced traffic layer, e) local failure during layer construction, mainly the base, f) poor road drainage.</p> <p>Potholes could be created due to deterioration of aggregate detachment from the pavement's surface. Decisive element for the appearance of such damages on the road is the low bearing capacity of the pavement which is due to inadequate thickness of crushed stone base and probably to its defective construction.</p>	<p>Cleaning of the areas from loose materials and filling of depressions with suitable hot or cold asphalt mix or when the pavement's condition is much deteriorated the option of additional asphalt layer is also examined.</p>
<p>Material detachment – Removal of surfacing material</p>  <p>1.0 km Xanthi - Abdera</p>	<p>Reduced asphalt layer thickness Local failure during the construction stage Use of aggregates tending to decompose</p>	<p>Cut in a way that sound material exists on the sides. Thorough cleaning, spraying with cationic emulsion filling with appropriate cold or hot asphalt mix.</p>
<p>Surface polishing</p>  <p>2.9 km Xanthi – Stavroupoli road</p>	<p>a) polished surface aggregates b) asphalt emersion on the surface of the pavement or c) coarse aggregate immersion.</p>	<p>Maintenance of the surface layer and restoration of its anti-skidding capacity with: a) laying of new asphalt surface layer made of appropriate asphalt mix and hard aggregates, b) laying of a porous pavement, c) chip sealing method, d) asphalt coating in single or double layer, e) surface scraping using a special milling machine</p>

6 CONCLUSIONS AND COMMENTS

Ideally, a pavement management programme for a road network would maintain all sections at high levels of service and efficient structural conditions, while at the same time would require only minimum use of resources at a low cost. Such a management programme has also to impact the environment as little as possible and ensure safety to traffic operations, as well as to minimise the disruption of various social activities and the inconvenience of community actions. It is obvious that there are conflicts among these requirements. Therefore, the decision process in programming of pavement maintenance activities must involve a multi-parametric consideration that could address the different competing requirements.

The evaluation of the provincial road network of Xanthi has led to the localisation of certain problems requiring special caution and their confrontation could be characterised as necessary and urgent.

In the majority of sections, the morphology and the functional character of the roads do not justify superior geometric characteristics. However, with regard to the structure of the roads, there is a serious demand for maintenance interventions and damage restoration.

In the roads as a whole, cracking appears in the traffic lanes, parallel, transversely, and on their axes. The pavement cracks constitute the more often and serious failure form noted, while crack types vary widely.

The pavement decomposition is the second in seriousness and frequency order problem that occurs across the Xanthi's provincial road network. This decomposition mainly appears as detachment of aggregates from the pavement's surface, material detachment in slab form, and potholes. Decisive element for the appearance of such damage in the roads constitutes the low bearing capacity of the pavements that is owed to small thickness and a likely defective construction of the crashed stone base course.

Pavement surface distortions or deformations are intense in a number of points in all provincial routes. Their size and frequency increase the road's venturousness, since the speed of the moving vehicles is high for the geometric characteristics that generally prevail in the provincial road network of Xanthi, because the traffic volumes that transverse the network are low. Hence, the maintenance of the provincial road network is considered indispensable for the drivers' safety and comfort. Main failure forms falling into the category of deformations are rutting, local settlements and heaves, as well as transverse folding. Frequently, what appears as failure is loss of the surface dressing and not serious damage to the surface course. The more experience and knowledge has been gained of road construction materials and highway surfaces, the better the judgement, taking into account the available funds for maintenance.

Finally, in numerous sites across the road network polishing phenomena appear on the pavement's surface. Such conditions are mainly owed to the polish of surface aggregates, to the emergence of asphalt on

the pavement's surface, or to the immersion of coarse grained aggregates. The slipperiness is directly associated to traffic accidents. So, special care must be given to the restoration of the anti-skidding capacity of the surface.

The survey on the road axes comprising the provincial network has shown that damages could be mainly attributed to the inadequacy of pavement structure which is composed on both the excessively small thickness of the road base, and the poor quality and reduced thicknesses of the asphalt base and traffic layer. These structural weaknesses, combined with the vehicle loads, have caused serious damages to the asphalt pavements.

Referring to the road network as a whole, it could be stated that the pavements are not in tolerable condition, so as to permit the traffic to move relatively safely and comfortably.

Maintenance and strengthening interventions on the pavements are considered essential in the present phase, so as to avoid further evolution of the existing damages that are possible to lead to a total destruction of the pavement. It is estimated that these interventions will lengthen the road's life and, in combination with improvements in the vertical and horizontal alignment (road widening, bypass of built-up areas, construction of shoulders and guidance lanes) will improve the traffic conditions and will increase the volume capacity and road's safety.

Although the total thickness of the pavements remains small with respect to the transferred loads and their expected increase with course of time, the perfect construction of the reinforcement will improve the functional characteristics of the network.

In order to integrate the survey of failures and lay out a complete restoration programme for the provincial road network of Xanthi, geological sections need to be made, laboratory tests on the granular and asphalt materials, roughness checks implication of destructive and non-destructive methods using precise instruments, experimental research and on site observations to estimate the capability to use new, of better quality, as well as recycled materials. The objective of such extensive work will be to develop a general prediction model for Xanthi's road network and expand it to the entire Greek territory.

Environmental issues generally do not arise across the roadways network. The knowledge and experience gained by individuals performing maintenance operations is probably the most helpful tool for any maintenance programme. Future road planning and maintenance execution needs could benefit by knowledgeable and experienced engineers.

REFERENCES

- Elhadidy, A.A., Elbeltagi, E.E. & Ammar, M.A. 2014. Optimum analysis of pavement maintenance using multi-objective genetic algorithms. *Housing and Building National Research Center HBRC Journal*, (in press): 7 p.

- Ferreira, A., Micaelo, R. & Souza, R. 2012. Cracking models for use in pavement maintenance management. *A. Scarpas et al. (Eds.), 7th RILEM International Conference on Cracking in Pavements* 429–439.
- Fwa, T.F., Chan, W.T. & Hoque, K.Z. 2000. Multiobjective optimization for pavement maintenance programming. *ASCE Journal of Transportation Engineering* 126: 367–374
- Gao, L., Xie, C., Zhang, Z. & Waller, S. 2012 Network-level road pavement maintenance and rehabilitation scheduling for optimal performance improvement and budget utilization *Comput.-Aided Civ. Infrastruct. Eng.* 27: 278–287.
- Hanna, P.B., Hanna, A.S. & Papagiannakis, T.A. 1993. Knowledge-based advisory system for flexible pavement routine maintenance *Canadian Journal of Civil Engineering* 20(1): 154–163.
- Labi, S. & Sinha, K.C. 2005. Life-cycle evaluation of flexible pavement preventive maintenance. *Journal of Transportation Engineering of ASCE* 131: 744–751.
- Mubaraki, M. 2009. Predicting pavement condition deterioration for the Saudi inter-urban road network. *GeoHunan International Conference 2009 Material Design, Construction, Maintenance, and Testing of Pavements, Geotechnical Special Publication No. 193*: 56–61.
- Oliver, J.E. 2007. Basic road maintenance operations. (in O’Flaherty, C.A. *Highways. The Location, Design, Construction & Maintenance of Pavements*, 4th Edition, Ch. 17 Basic road maintenance operations) pp. 452–478.
- Pellecuer, L., Assaf, G.J. & St-Jacques M. 2014. Life cycle environmental benefits of pavement surface maintenance. *Canadian Journal of Civil Engineering* 41: 695–702.
- Rouse, P. & Chiu, T. 2009. Towards optimal life cycle management in a road maintenance setting using DEA. *European Journal of Operational Research* 196: 672–681.
- Theodorakopoulos, D.D., Chassiakos, A.P., Manariotis, I.D. & Patarias, P. 2002. A decision support system for highway pavement management in Greece, *Proceedings of the 7th International Conference on Applications of Advanced Technologies in Transportation*, K.C.P. Wang, S. Madanat, S. Nambisan and G. Spring, eds., ASCE, Boston, 553–560.

Determining the allowable content of RAP in HMA using the blending charts and RAP mortar properties

C. Riccardi, P. Leandri & M. Losa

University of Pisa, Pisa, Italy

ABSTRACT: A method to determine the allowable percentage of RAP that can be added in a Hot Mixture Asphalt (HMA) is presented. It is based on a new approach used to determine rheological properties of the RAP binder that overcomes the limitations of the RAP binder extraction and recovery method. From DSR frequency sweep tests carried out on mortars composed of RAP and fresh binder, the master curves of the complex modulus and of the phase angle of the RAP binder can be back-calculated by using the Modified Nielsen model and the Voigt model. The PG grade of the RAP binder can be calculated from the master curves, and used as input in the two approaches reported in the NCHRP 452 to calculate the allowable content of RAP in Superpave mixtures. The method is very effective in determining the allowable content of RAP binder in HMA.

1 INTRODUCTION

The use of reclaimed asphalt pavement (RAP) in Hot-Mix Asphalt (HMA) mixtures has increased in recent years. When the residual service life of asphalt pavements is approaching the end (Losa et al. 2008), the materials composing the structure still retain considerable value. The extensive use of RAP as a component in new HMA pavements, more than a cost saving option, represents an environmentally positive method of recycling. Experience has shown that properly designed HMA containing high RAP percentages can be used effectively even in high performance surface layers (Leandri et al. 2012). In order to stimulate the use of RAP materials in the construction of new HMA, the Federal Highway Administration developed guidelines for the use of RAP in the Superpave method as described in NCHRP 452 (McDaniel and Anderson, 2001). These guidelines reflect the fact that the effect of aged binder from RAP on the performance properties of the virgin binder depends upon the level of RAP in the HMA. When the level is low, the effect is minimal, and the RAP is likened to a “black rock” that influences the mix volumetric and performance through its aggregate gradation and properties. As the level of RAP in the HMA increases, the black rock analogy breaks down; the aged binder blends with the virgin material in sufficient quantity to significantly affect its performance properties.

Therefore, low amounts of RAP, typically 10 to 20 percent, can be used without characterization of its recovered binder properties; there is not enough of the old, hardened RAP present to significantly change the properties of the asphalt binder, and the RAP may be solely accounted for as a component of the

aggregate. When RAP is added in amounts greater than 20 percent, the characterisation of the RAP binder is recommended, along with the use of blending charts to determine what performance grade of virgin asphalt binder should be used in the mix design. In the NCHRP 452 recovery and testing of RAP binder is recommended, but research studies (Stroup-Gardiner & Nelson 2000; Ma & Zhang 2008; Ma & Huang 2008) consistently showed that this method is not accurate because it alters the binder properties and, after solvent extraction, part of the RAP binder remains on the aggregate, sometimes to a considerable extent. Binder hardening is another often-cited result of the solvent extraction (Kondrath 2009; Burr et al. 1991). SHRP research demonstrated that hardening appears to occur with all commonly used solvents, even using low temperature extraction processes (Stroup-Gardiner & Nelson 2000). After the binder is extracted, it must be recovered from the solvent solution for characterization. Concerns when using a particular recovery method include the presence of residual solvent after recovery as well as the aging of the binder depending on temperature and how labor intensive the method is. Researches indicated that even 0.5% residual solvent could cause a 50% decrease in viscosity (Peterson et al. 2000).

In the light of these considerations, a new approach to determine the mechanical properties and the PG grade of the RAP binder, avoiding the extraction and recovery method, was proposed recently (Leandri et al. 2015). In this paper, in order to determine the allowable percentage of RAP in HMA, the PG grade of the RAP binder is estimated by the latter method, and the results are used in the two blending approaches reported in the NCHRP 452. In the first approach (designated Method

A in NCHRP 452), the percentage of RAP that will be used in an asphalt mixture is known, and the appropriate virgin asphalt binder grade for blending needs to be determined. In the second approach (designated Method B in NCHRP 452), the maximum percentage of RAP that can be used in an asphalt mixture, while still using the same virgin asphalt binder grade, needs to be determined.

2 BACKGROUND

The approach used in this study to estimate the PG grade of the RAP binder, is based on the evaluation of rheological properties of two different mortars composed of fresh binder and RAP material passing #100 sieve:

- the Selected RAP (SRAP) mortar, composed by the selected RAP material passing the #100 sieve and fresh binder;
- The Burned Selected RAP (BSRAP) mortar, composed of the resulting aggregates, after the SRAP was burned in the ignition oven, and the fresh binder.

The #100 sieve is selected to assure the reasonableness of the test procedure considering that the DSR gap should be at least ten times bigger than the maximum aggregate particle size (Liao et al. 2013) otherwise a larger aggregate size could cause reliability problems of DSR measurements.

The BSRAP is tested for determining the aggregate size gradation and the maximum volumetric packing fraction ϕ , which denotes the contribution of volume filling to stiffening; this parameter is determined by using the Rigden Voids apparatus, according to the European standard UNI EN 1097-4.

The complex modulus of the bituminous matrix, composed of the fresh and RAP binder, is back calculated from the shear stress tests carried out with the Dynamic Shear Rheometer (DSR) on BSRAP and SRAP mortar.

The results of tests performed on the BSRAP mortar, are used to calculate the parameters of the Modified Nielsen model (Leandri et al. 2015), which takes into account of the variation of frequency and temperature:

$$\left(\frac{G_m^*}{G_b^*}\right)_M = \frac{1+A \cdot B \cdot V_p}{1-B \cdot \psi \cdot V_p} - (a \cdot \ln(f) - b)V_p^c \quad (1)$$

where G_m^* is the complex modulus of the mortar (aggregate particles and bitumen); G_b^* is the complex modulus of the bitumen; V_p is the volume fraction of aggregate particles.

A is a constant that is equal to:

$$A = K_E - 1 \quad (2)$$

where K_E is the generalized Einstein coefficient that is an indicator of the physical chemical contribution

to stiffening; it represents the stiffening rate of composites as a function of particles addition, and by this way it includes in the equation an interaction factor between particles and suspension.

This parameter is determined, from the equation (1), by non-linear curve fitting of the measured stiffening ratio versus the volume fraction V_p at frequency equal to 20 Hz, and it is found to vary with temperature (T) according to the following equation:

$$K_E = \alpha e^{\beta T} \quad (3)$$

where α and β are two regression coefficient.

B accounts for the relative moduli of particles and bitumen phases and it is equal to:

$$B = \frac{G_p^*/G_b^*-1}{G_p^*/G_b^*+A} \quad (4)$$

where G_p^* is the modulus of particles.

The constant B tends to 1 for very large G_p^*/G_b^* ratios, like the values obtained in this study where aggregate particles are much stiffer than the bitumen.

The coefficient ψ is given by the equation (5):

$$\psi = 1 + \frac{1-\phi}{\phi^2} V_p \quad (5)$$

where ϕ is the maximum volumetric packing fraction. It is the maximum amount of particles that can be added to the matrix without the appearance of air voids; it denotes the volume-filling contribution to stiffening and it can be determined by using the Rigden voids apparatus. It is calculated as the ratio between the true and the apparent volume of the particles and it is equal to 0.63.

The coefficients a , b and c in equation (1), can be determined by a regression fitting method, considering all the data at different V_p and different temperatures. The method to determining all the parameters are explained in detail elsewhere (Leandri et al. 2015).

By considering the aggregate particles are the same in both the BSRAP and the SRAP mortars, we can assume the stiffening ratio $(G_m^*/G_b^*)_M$ is the same in both the mortars; consequently, we can calculate the complex modulus of the bitumen compound (G_b^*), composed by the H, the S and the SRAP binder, by using the same coefficients of the Modified Nielsen Model determined for the BSRAP mortar.

Once the complex modulus of the bitumen compound is estimated, it has been demonstrated that the complex modulus of the RAP binder can be calculated by using the Voigt model, according to the equation (6):

$$G_2^* = \frac{G_C^* - G_1^* V_1}{V_2} \quad (6)$$

where G_1^* , G_2^* and G_C^* are the complex moduli of the fresh binder, of the RAP binder, and of the blend of the fresh and RAP binder respectively; V_1 and V_2 are the percentages of the fresh and of the RAP binder.

3 BLENDED CHARTS

If the critical temperatures of the recovered RAP binder are known, the two blending approaches described in the NCHRP 452 may be used. In one approach (designated Method A), the percentage of RAP that will be used in an asphalt mixture is known, and the appropriate virgin asphalt binder grade for blending needs to be determined. In the second approach (designated Method B), the maximum percentage of RAP that can be used in an asphalt mixture while still using the same virgin asphalt binder grade needs to be determined. The desired binder grade for a mixture is determined based on the climate and traffic level for the particular project where the mixture will be used. Usually, the specifying agency determines what the binder grade should be and specifies that in the contract documents. When RAP is used, however, the virgin binder grade may need to be changed (i.e., softened) to account for the addition of the old, hardened RAP binder. Because it is usually the mix designer who determines how much RAP to use in the mix, the designer may need to determine what that virgin binder grade should be.

3.1 Method A: Blending at a known RAP percentage (Virgin Binder Grade unknown)

If the final blended binder grade, percentage of RAP, and RAP binder properties are known, then the properties of an appropriate virgin asphalt binder grade can be determined using the equation (7) reported in the NCHRP 452.

$$T_{Virgin} = \frac{T_{Blend} - (\%RAP \times T_{RAP})}{(1 - \%RAP)} \quad (7)$$

where T_{Virgin} = critical temperature of the virgin asphalt binder; T_{Blend} = critical temperature of the blended asphalt binder (final desired); %RAP = percentage of RAP expressed as a decimal (i.e., 0.30 for 30 percent); and T_{RAP} = critical temperature of RAP binder.

3.2 Method B: Blending at a known Virgin Binder Grade (RAP percentage unknown)

There may be cases in which a particular virgin binder in a RAP mixture should be used. The binder grade may be fixed based on economics and availability or on the specifications for a given project. In these cases, the percentage of RAP that could be used with a specific virgin binder grade and that still meet the final blended binder properties have to be found. Therefore, if the final blended binder grade, virgin asphalt binder grade, and RAP binder properties are known, then the appropriate amount of RAP to use can be determined using the equation (8) reported in the NCHRP 452:

$$\%RAP = \frac{T_{Blend} - T_{Virgin}}{T_{RAP} - T_{Virgin}} \quad (8)$$

where T_{Virgin} = critical temperature of the virgin asphalt binder; T_{Blend} = critical temperature of the blended asphalt binder (final desired); %RAP = percentage of RAP expressed as a decimal (i.e., 0.30 for 30 percent); and T_{RAP} = critical temperature of RAP binder.

4 TEST RESULTS

4.1 Materials

One RAP material source was used in this study along with a two components fresh binder: a Hard (H) and a soft (S) binder. The H binder is a 35/50 Penetration Grade, with the characteristics reported in Table 1. The S binder is characterized by a kinetic viscosity of 8000 mm²/s at 60°C and, due to its low consistence, the bitumen cannot be characterized by using traditional tests, like penetration, softening point and so on. The S bitumen mixed with the RAP binder, acts as a rejuvenator of the aged binder, whereas the H binder acts as virgin binder, added to obtain the design Asphalt Content (AC) of the mixture. The characteristics of binders are reported in Table 1.

The relevant properties of the SRAP and the BSRAP are reported in Table 2.

Totally 18 mixes were composed considering three different volume percentages of the SRAP and the BSRAP (20%, 40%, 60%), and three different percentage combinations of the H and S bitumens (90%H+10%S, 80%H+20%S, 70%H+30%S); the RAP binder contents in the SRAP mortars with V_p = 20%, V_p = 40% and V_p = 60% are equal to 6%, 16% and 36% respectively.

The Asphalt Content (AC) of the SRAP is determined by using the Soxhlet extractor.

Specimens were prepared by mixing the particles and the binder at 140°C for two hours in order to allow the diffusion process, as demonstrated recently (Yousefi et al. 2014). In order to have the same ageing

Table 1. Properties of the Hard bitumen.

Hard Bitumen	
Penetration (dmm)	41.4
Softening Point (°C)	52.2
Viscosity@100°C (Pa s)	4.98
Viscosity@150°C (Pa s)	0.266
Pen Grade	35/50
Kinetic viscosity@135°C (mm ² /s)	370

Table 2. Properties of the SRAP and BSRAP.

Mortar	Asphalt Content %	Passing to 0.15 mm %	Maximum Volumetric Packing Fraction Φ
SRAP	9.89	100	–
BSRAP	0	100	0.63

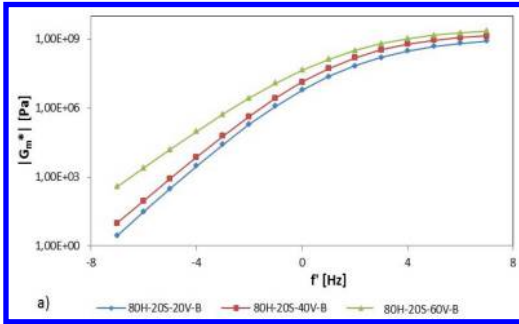


Figure 1. Complex modulus Master Curves of BSRAP mortars at different Vp and at a constant percentage of the S and H bi-tumen at reference temperature $T = 20^{\circ}\text{C}$.

Table 3. Parameters of the modified Nielsen model.

Mortar	70H+30S + BSRAP	80H+20S + BSRAP	90H+10S + BSRAP
a	1.48	1.30	1.14
b	4.46	4.06	3.41
c	1.68	1.20	1.20
α	4.57	4.57	4.57
β	0.017	0.017	0.017
Φ	0.63	0.63	0.63

of the binders, the BSRAP mortars are prepared in the same way.

Then we subjected all the mortars to RTFO and PAV aging.

All the mortars are tested by using the DSR at five temperatures: 0° , 10° , 20° , 30° , 40°C ; frequency sweep tests from 0.2 Hz to 20 Hz, with a constant strain rate of 0.05%, in the classical plate-plate (8 mm) configuration, and with a 2 mm gap, are used to determine the master curves of the complex modulus (G_m^*) and of the phase angle (δ) in the Linear Viscoelastic Range (LVE). The strain level is chosen by Amplitude sweep tests and the optimal conditioning time of the mortars, at different temperatures, is chosen as the time over which the complex modulus is no longer growing. Therefore the conditioning times at 0° , 10° , 20° , 30° , 40°C are 50', 40', 30', 20' and 10' respectively. The same tests are also performed on the fresh binder compound in order to determine the complex modulus (G_b^*) and the phase angle master curve.

4.2 Results

Some examples of the complex modulus master curves resulting from DSR tests on mortars are reported in Figure 1.

The results of rheological tests on BSRAP, are used to calculate the parameters of the Modified Nielsen Model (1), according to the procedure described above, which are summarized in Table 3.

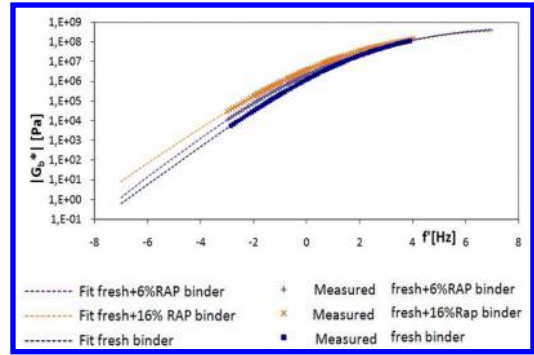


Figure 2. Complex Modulus of the blend and the fresh binder (70H+30S) versus reduced frequency.

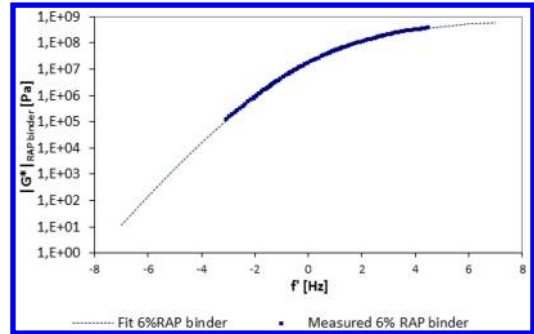


Figure 3. Master curve of the complex modulus of the RAP binder.

Considering that the aggregate particles are the same in both the BSRAP and the SRAP mortars, we can assume that the stiffening ratio $(G_m^*/G_b^*)_M$ is the same in both the mortars; therefore, by using for the SRAP mortar the same coefficients of the Modified Nielsen Model estimated for the BSRAP mortar, we can calculate the complex modulus master curves of the bituminous matrix G_b^* composed by the fresh binder and the RAP binder. The results are reported in Figure 2 for two percentages (6% and 16%) only that are considered the more representative.

The complex modulus of the RAP binder calculated by using the equation (6) is reported on the master curve in Figure 3.

5 ESTIMATING THE PG GRADE OF THE RAP BINDER

The PG grade of the compounds of the H and S binders, reported in Table 4, are determined by using the DSR and the BBR apparatus in accordance to the Superpave specification (AASHTO MP1).

The PG grade of the RAP binder is calculated by using the master curves of the complex modulus and the phase angle determined on the SRAP mortars.

Experimental results have shown that the phase angle is slightly affected by the RAP binder, therefore

Table 4. PG grade of the compound of the Hard and Soft binder.

Compound	PG
70H+30S	58-22
80H+20S	64-16
90H+10S	64-16

Table 5. Parameters of the complex modulus Master Curve of the 70H+30S+6%RAP binder.

G_e^* (Pa)	0
G_g^* (Pa)	7.00E+08
f_c (Hz)	0.678
k	0.195
m_e	1.100

Table 6. Parameters of the phase angle Master Curve of the 70H+30S+6%RAP binder.

δ_m	f_d	R_d	m_d
80.95	8.23E-06	16.90	9.36

the master curve of the phase angle of the bituminous matrix composed by the fresh and the RAP binder could be used; in the same way, according to studies by Christensen (1969) and Hashin (1970), the phase angle of composite materials is theoretically equal to that of the matrix material, thus we can use the phase angle master curve of the SRAP mortar even for the compound of the fresh and RAP binder.

5.1 High temperature PG grade

In order to determine the higher temperature of the PG grade, the parameters $G^*/\sin \delta$ at 10 rad/s is calculated by using the following procedure.

We consider the master curve of the RAP binder determined on the unaged mortars. The parameters are reported in Table 5 for the complex modulus and in Table 6 for the phase angle.

The equation of the complex modulus master curve (9) follows the model reported in the NCHRP Report 459 (Bahia et al., 2001):

$$G^* = G_e^* + \frac{G_g^* - G_e^*}{[1 + (f_c/f')^k]^{m_e/k}} \quad (9)$$

where $G_e^* = G^* (f \rightarrow 0)$ is the equilibrium complex modulus, $G_e^* = 0$ for binders; $G_g^* = G^* (f \rightarrow \infty)$ is the glass transition complex modulus; k and m_e are two dimensionless shape parameters; f_c is the location parameter with dimensions of frequency, where the G_g^* and m_e asymptotes intercept; f_c^* is the frequency where the G_e^* and m_e asymptotes intercept given by (10):

$$f_c^* = f_c \left(\frac{G_e^*}{G_g^*} \right)^{1/m_e} \quad (10)$$

Table 7. Parameters to determine $G^*/\sin \delta$.

T [°C]	$\log a_T$	f' [Hz]	G^* [Pa]	δ [°]	$G^*/\sin \delta$ [Pa]
68	-4.80	2.48×10^{-5}	4465	80.65	4525
76	-5.37	6.72×10^{-6}	1239	80.94	1255
80	-5.64	3.64×10^{-6}	671.3	80.79	680.1

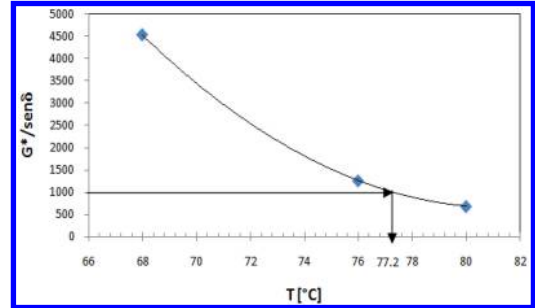


Figure 4. $G^*/\sin \delta$ versus Temperature.

f' is the reduced frequency, function of both temperature and strain.

The equation of the phase angle master curve (11) follows the model reported in the NCHRP Report 459 (2001):

$$\delta = 90I - (90I - \delta_m) \left\{ 1 + \left[\frac{\log(f_d / f')}{R_d} \right]^2 \right\}^{-m_d/2} \quad (11)$$

where

$$I = \begin{cases} 0 & \text{if } f' > f_d \\ 1 & \text{if } f' \leq f_d \end{cases} \text{ for binders}$$

The well-known Williams-Landel-Ferry (WLF) formulation is used in the model to express the temperature-shift factor a_T .

$$\log \frac{a_T(T)}{a_T(T_0)} = - \frac{c_1(T - T_0)}{c_2 + (T - T_0)} \quad (12)$$

where T_0 is the reference temperature equals to 20°C, c_1 and c_2 are equal to 18.41 and 135.8 respectively.

First of all the temperature shift factor is determined for three different temperatures: 68°C, 76°C, 80°C (Table 7).

Then the reduced frequency that corresponds to 10 rad/s (1.59 Hz) is calculated and, by using the equations (9) and (11), the complex modulus and the phase angle at 1.59 Hz and at the three different temperatures are calculated; therefore the values of the parameter $G^*/\sin \delta$ are calculated and reported in Table 7.

A relationship of the parameters $G^*/\sin \delta$ versus temperature can be determined, as reported in Figure 4, and the temperature corresponding to the limit value $G^*/\sin \delta > 1000$ Pa is determined. By using data

Table 8. Parameters of the inter-conversion DSR-BBR.

	Temperature °C		
	-6	-12	-18
ω (rad/s)	2.78	9.72	129.62
$\log a_t$	1.45	1.45	1.45
f' (Hz)	12.47	43.62	581.37
G^* (Pa)	1.02×10^8	1.62×10^8	4.8×10^8
δ	45.01	40.71	32.47
$S(60)$ (Pa)	2.61×10^8	5.11×10^8	8.66×10^8
$m(60)$	18.02	8.31	4.03

reported in Table 7, the High temperature PG grade of the RAP binder is 76, which is confirmed from the results of tests on RTFOT aged binders too.

5.2 Low temperature PG grade

In order to determine the Low temperature PG grade the data from the RTFO and PAV mortars are used.

Since DSR frequency sweep tests are performed, the well-known inter-conversion method is applied for converting temperature shear properties to low temperature creep properties (SHRP 369-A). The DSR test conditions that correspond to a user defined BBR loading time and temperature are defined based on the relationship provided in equation (13):

$$T_d = \left[\frac{1}{273+T_s} - \frac{2.303 \times R \times \log(t_s \times \omega)}{250000} \right]^{-1} - 273 \quad (13)$$

where T_d is the test Temperature (°C) for dynamic testing at frequency ω , in the case in exam we can fix 10°C, considering the limitation of DSR for testing mortars at lower temperatures; T_s is the specified temperature (°C) for creep testing (we can fix three different temperatures: -6, -12, -18°C); R is the ideal gas constant, 8.31 J°K-mol; t_s is the specified creep loading time (60 s), ω is the dynamic testing frequency (rad/s).

Therefore solving equation (13), the corresponding DSR test conditions were found: the DSR testing temperature is 10°C and the corresponding frequencies ω are reported in Table 8.

Using the equation of the master curve of the complex modulus and of the phase angle calculated from the data of the RTFO + PAV aged BSRAP and SRAP mortars, G^* and δ can be calculated at the corresponding reduced frequency as reported in Table 8.

Therefore the BBR parameters $S(60)$ and $m(60)$ can be estimated by using the shear properties of the complex modulus and phase angle through application of equation (14) for the stiffness and (15) for m -value.

$$S(t) \approx \frac{3G^*(\omega)}{[1+0.2 \sin(2\delta)]} \quad (14)$$

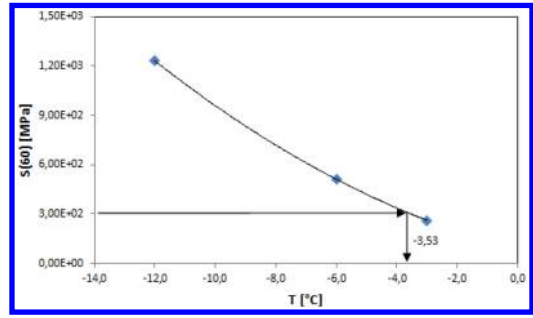


Figure 5. $S(60)$ versus Temperature.

where $S(t)$ is the creep stiffness at time t (Pa); $G^*(\omega)$ is the complex modulus at frequency ω (Pa); δ is the phase angle at frequency ω ,

$$m = \frac{d(\log G^*)}{d(\log \omega)} \quad (15)$$

where m is the slope of G^* vs frequency plot at a given frequency; δ is the phase angle; G^* is the complex modulus; ω is the frequency (rad/s).

All the parameters are summarized in Table 10. Interpolating the $S(60)$ found for the three different temperatures, the low temperature performance grade corresponding to the limit of 300 MPa could be determined. As reported in Figure 5 the BBR test temperature is -3.53°C that corresponds to -13.53°C, therefore the low temperature PG grade is equals to -10.

Therefore the PG grade of the RAP binder is equal to 76-10.

6 HOW TO USE THE BLENDED CHARTS

6.1 Method A: Blending at a known RAP percentage (Virgin Binder Grade unknown)

If the final blended binder grade, the percentage of RAP and RAP binder properties are known, then the properties of an appropriate virgin asphalt binder grade can be determined by using the equation (7) reported in the NCHRP 452.

Using the equation (7) for the high, intermediate, and low critical temperatures separately, the properties of the virgin asphalt binder needed to satisfy the assumptions can be determined.

For example let's assume that the specifying agency requires a blended binder grade of PG 64-22 or better, the RAP percentage in the mixture is 30 percent, and the RAP properties are as indicated in Table 9.

Through equation (7) the estimated critical temperatures of the virgin binder, reported in Table 10, are determined.

As indicated in Table 10, the minimum high temperature grade of the virgin asphalt binder should be 58.3°C to satisfy the requirements of the blended grade

Table 9. RAP binder properties.

Aging	Property	Critical Temperature (°C)	
ORIGINAL	G*/sin δ	High	77.2
PAV	G* sin δ	Intermediate	28
	S-value	Low	-3.53
	PG	76-10	

Table 10. Estimated critical temperatures of the virgin binder.

Aging	Property	Critical Temperature (°C)	
ORIGINAL	G*/sin δ	High	58.34
PAV	G* sin δ	Intermediate	23.71
	S-value	Low	-15.63
	PG	64-28	

(PG 64-22) by using the RAP in Table 9 at 30 percent. This means that a PG 64-xx grade would be needed to ensure that the minimum required value of 58.3°C would be achieved. Moreover the minimum low-temperature grade of the virgin asphalt binder should be -25.63°C as reported in Table 10 (-15.63°C -10°C factor in AASHTO MP1) to satisfy the requirements of the blended grade (PG 64-22) using the RAP in Table 9 at 30 percent. This means that a PG xx-28 grade would be needed to ensure that the minimum required value of -15.63°C would be achieved. To meet the intermediate temperature grade (G* sin δ), the virgin asphalt binder would need to have a critical intermediate temperature no higher than 23.7°C. Because the maximum critical intermediate temperature for a PG 64-28 binder is 22°C, the selected binder should easily meet all blended binder requirements.

6.2 Method B: Blending at a known Virgin Binder Grade (RAP percentage unknown)

If the percentage of RAP that could be used with a specific virgin binder grade and that still meet the final blended binder properties have to be found, the equation (8) reported in the NCHRP 452 could be used.

For example let's suppose that the specifying agency requires a blended binder grade of PG 64-22 or better, the virgin binder grade is a PG 58-22, with the properties summarised in Table 11, and the RAP is a PG 76-10 with the characteristics summarised in Table 9.

Using equation (8) for the high, intermediate, and low critical temperatures separately, the percentage of RAP needed to satisfy the assumptions can be determined.

As indicated in Table 12, a percentage of RAP between 24 percent and 58 percent would satisfy all the requirements of the blended grade (PG 64-22) using

Table 11. Properties of the virgin binder (70H+30S).

Aging	Property	Critical Temperature (°C)	
ORIGINAL	G*/sin δ	High	59.65
PAV	G* sin δ	Intermediate	17.01
	S-value	Low	-11.75
	PG	58-22	

Table 12. Estimated percentage of RAP to achieve final blended grade.

Aging	Property	Temperature	%RAP to achieve	
			PG 64-22	PG 70-28
ORIGINAL	G*/sin δ	High	24.8	58.9
PAV	G* sin δ	Intermediate	72.7	
	S-value	Low	62.2	75.75

the RAP and virgin asphalt binders in Table 9 and in Table 10.

7 CONCLUSION

In the present study a method to determine the allowable percentage of RAP that could be added in a mixture without considering rutting, fatigue and thermal cracking resistance is presented. It is based on a new approach, proposed recently, to determine rheological properties of the RAP binder that overcomes the limitations of the extraction and recovery method. From DSR frequency sweep tests carried out on mortars composed of RAP and fresh binder, the master curves of the complex modulus and of the phase angle of the RAP binder can be back-calculated by using the Modified Nielsen model and the Voigt model, by this way avoiding the extraction and recovery method to characterize the properties of the RAP binder.

Once the master curves are known, the PG grade of the RAP binder can be calculated and used as input in the two approaches reported in the NCHRP 452 to calculate the allowable content of RAP in Superpave mixtures. It's possible to determine the PG grade of the virgin binder to be used in order to obtain a certain PG of the blended mixtures, if the percentage and the PG of the RAP binder is known, or to determine the percentage of RAP that could be added in a mixture knowing the PG of the virgin binders, of the RAP binder and of the final blend.

The examples described in the paper show the application of the method confirming that it's very effective in overcoming the limitations reported in literature on the use of the extraction and recovery method to determine the properties of the RAP binder and the related allowable content of RAP in HMA.

REFERENCES

- AASHTO MP1. 2000. Performance Graded Binder Specification.
- Bahia, H.U., Hanson D.I., Zeng, M., Zhai, H., Khatri, M.A., Anderson, R.M. 2001. Characterization of Modified Asphalt Binders in Superpave Mix Design. NCHRP Report 459. *National Academy Press Washington, D.C.*
- Burr, B., and Davison R., Jemison H., Glover C., Bullin, J. 1991. Asphalt Hardening in Extraction Solvents. In *Transportation Research Record: Journal of the Transportation Research Board* – Volume 1323/1991, pp. 70–76.
- Christensen, R.M. 1969. Viscoelastic properties of heterogeneous media. *J. Mech. Phys. Solids*, 17, 23–41.
- Hashin, Z. 1970. Complex moduli of viscoelastic composites. General theory and application to particulate composites. *Int. J. Solids Struct.*, 6, 539–552.
- Kondrath, E. 2009. Reclaimed Asphalt Pavement in Hot Mix Asphalt. *New Jersey Department of Transportation.*
- Liao, M.C., Airey G., and Chen J.S. 2013. Mechanical Properties of Filler-Asphalt Mastics. *International Journal of Pavement Research and Technology* Vol. 6, No. 5.
- Losa, M., Bacci, R., Leandri, P. 2008. A statistical model for prediction of critical strains in Pavements from deflection measurements. *International Journal of Road Materials and Pavement Design*, EATA08 Volume 9 special issue, ISSN 1468-0629, pp. 373–396.
- Leandri, P., Cuciniello, G., Losa, M. 2012. Study of sustainable high performance bituminous mixtures. *5th SIV International Congress – Sustainability of Road Infrastructures, Procedia – Social and Behavioral Sciences* 53 (2012), ISSN 1877-0428, doi 10.1016/j.sbspro.2012.09.900, pp. 495–503.
- Leandri, P., Riccardi, C., Losa, M. 2015. A new approach to estimating rheological properties of the rap binder at intermediate temperatures. *International Journal of Road Materials and Pavement Design*, DOI: 10.1080/14680629.2015.1029695.
- Ma, T., and Huang, X. 2008. Recycling law of aged asphalt based on composite theory of material. In *Journal of Southeast University*, Volume 38(3), pp. 520–524.
- Ma, T., and Zhang, D.Y. 2008. Research on influence and modification of extraction and recovery experiments for SBS modified asphalt. In *Journal of Southeast University*, Volume 40(5), pp. 511–523.
- McDaniel, R.S. and Anderson, R.M. 2001. Recommended use of reclaimed asphalt pavement in the superpave mix design method: technician’s manual. NCHRP Report 452, *National Cooperative Highway Research Program.*
- Peterson, R., and Soleymani H., Anderson, R., McDaniel, R. 2000. Recovery and Testing of RAP Binders from Recycled Asphalt Pavements. *Proceedings of Association of Asphalt Paving Technologies*, pp. 72–91.
- Soleymani, H.R., and Bahia, H.U. 1999. Blending charts based on performance-graded asphalt binder specification. In *Transportation Research Record: Journal of the Transportation Research Board* – Volume 1661, pp. 7–14.
- Stroup-Gardiner, M., and Nelson, J. 2000. Use of Normal Propyl Bromide Solvents for Extraction and Recovery of Asphalt Cements. *NCAT.*
- Yousefi Rad, F., Roohi Sefidmazgi, N., Bahia, H.U. 2014. Application of Diffusion Mechanism to Study Degree of Blending Between Fresh and RAP Binder in Dynamic Shear Rheometer. *Accepted for Publication in the Transportation Research Record: Journal of the Transportation Research Board*, Vol. TRB.
- SHRP 369-A. 1994. Binder Characterization and Evaluation. Vol. 3: Physical characterization.

Experience with designing and in-situ verification of cold emulsified mixes in the Czech Republic

J. Suda & J. Valentin

Department of Road Structures, Czech Technical University, Prague, Czech Republic

ABSTRACT: The presented paper summarizes results of experimental research done by the Czech Technical University in Prague in the field of developing design method and further assessment of designed and tested cold emulsified asphalt mixes. The objective of this research was to monitor and evaluate selected physical and mechanical properties of the mixes as well as performance-based tests, such as stiffness and rutting resistance, in relation to the methodology of specimens' preparation. Nevertheless the real behaviour of a mix in a pavement structure cannot be fully and exactly cut up by laboratory tests; therefore, to gain additional experimental data, more than 1.8 km long trial section was prepared. The aim of the project was to verify on a suitable road section within the road network in the Czech Republic cold emulsified mix technology as a part of a standard pavement structure. For this pavement original structure and dimensions were known, as well as its overall technical condition and real traffic loading. Therefore, it is possible for the near future to monitor the behaviour of this technology under real traffic and climatic conditions. The selected rural road was of low traffic category. Because of its bad service condition and necessary reconstruction, the base layer was firstly cold recycled in-situ. Aggregates for the emulsified mixes were taken from a local quarry and the used emulsion was designed exactly for this type of aggregates. Used emulsifier and its content were optimized with respect to final mix quality and good workability. Trial job site was divided in six sections with five different pavement structure compositions, which should check the designed cold emulsified mixes in wearing and binder courses. The analysis of laboratory results, and in-situ monitoring, and their possible relations are presented in the paper.

1 INTRODUCTION

Emulsified asphalt mixes represent a rather novel technology in the Czech Republic. In general, cold emulsified mixes are a composite material which contains crushed aggregates or normal sand with corresponding grading as well as optimal content of bituminous emulsion and water. These components are mainly processed at normal atmospheric temperatures. Cold emulsified mixes are known e.g. in France as grave emulsions. Specific properties of these mixes so far allow their use on roads where lower traffic intensities and lower amount of heavy loaded vehicles is expected. Benefits to use these mixes on this part of road infrastructure prevail.

Their importance is increasing in relation to the development of bituminous emulsions, which constitute an essential element of this technology. In general, the mixes provide benefits particularly from the environmental perspective; they allow reducing energy requirements and lower CO₂ generation during production in comparison to hot asphalt technologies. Together with the possibility of in-situ mix preparation and paving on a small scale using common machinery, the technology becomes suitable for construction or rehabilitating primarily lower-category

road infrastructure (Thanaya 2007). Generally, their application can be recommended to stabilized base layers for traffic loading classes II to VI according to the classification used in the Czech Republic or in Germany, to binder course for classes III to VI and to wearing course for classes IV to VI (TP 170, ČSN 73 6114). Another advantage can be seen in the possibility of paving even under slightly worsened or difficult weather conditions since windy and wet environment does not restrict paving of the mix at all. However, emulsified asphalt mixes are considered unequal to hot asphalt mixes, particularly due to the need for a higher compacting power necessary to overcome the higher friction among the aggregate particles which, objectively, results in a higher void content. Imperfect coating of the individual particles by bituminous binder, which further affects particularly the moisture susceptibility of the mix can be seen as another distinctive disadvantage. Another, equally important perspective is the character of binder adhesion to the aggregate. Here, the correct bituminous emulsion design must be emphasized and the properties of the aggregate considered (Grünner 2007). Within the implied character of the standard binder applied, emulsified asphalt mixes are a thermo-mechanically sensitive multi-phase system (Suda 2013). The most critical issues in case of

the emulsion-based technology are the mix properties within the process of emulsion destabilization, or during the emulsion consolidation and curing. The curing time can range from 2 to 24 months depending on weather conditions (Thanaya 2009, Gaudefroy 2009).

2 PILOT TRIAL SECTION

A pilot job site, 1.8 km long, was completed on Highway III/44441 between Hraničné Petrovice and Moravský Beroun (east part of the Czech Republic) in July 2014. The trial section focused on the issues of using and verifying the new emulsified asphalt mix technology. The project intended to verify the technology of emulsified asphalt mixes, cold mixed and paved, in-situ and in variants for both the wearing and binder courses, applying for some of the mixes 30% reclaimed asphalt pavement (RAP). The project also included in-situ cold recycling of a base layer with standard application of bituminous emulsion and cement. The initial pavement structure originates from the 1960s when the road was built on the basis of penetration macadam technology, followed by repairs by covering either by numerous thin emulsified coatings or asphalt layers of varying composition. Therefore, the coatings of such pavements cannot be recycled in a manner that would ensure recovery of the original function; they can only be recycled by in-depth cold recycling technology according to (TP 208) with the intention of obtaining a good quality and homogeneous base layer. A new asphalt mix had to be laid on the base layer; the pilot application of cold emulsified asphalt mixes was in this case an option. The trial section was selected to suit the purpose of verifying one of the possible environmental friendly and cost effective rehabilitation methods for lower-category roads.

The project aimed to complete a suitable job site with the application of emulsified asphalt mix during repair of the selected existing pavement which would verify the application of emulsified asphalt mixes designed and manufactured according to the intended technical specification “Cold asphalt mixes” in the Czech Republic. The general aim was to verify both the practical viability of the technology and the functionality of the pavement completed which is a necessary precondition for the subsequent development of any new technology not only in Czech Republic. Highway III/44441, km 3.492 to km 5.320 with a length of 1,815 m was chosen as a suitable trial section. The road itself is a class III road with annual average daily traffic of 184 vehicles in total and informative traffic breakdown to 80% passenger cars and 20% heavy loaded vehicles and tractors in total. For the completion as such, the trial section was divided into 6 subsections, approx. 300 m long each with 5 different designs being verified and a reference section. Composition of the pavement sections is indicated in Table 1.

Table 1. Pavement structure composition for the trial section.

Sub-section No. 1	
RS 0/32 CA (in-situ); 150 mm; TP 208	w = 4.5 m
PS-E; ČSN 73 6129	
EAC 16; 50 mm	w = 4.3 m
PS-E; ČSN 73 6129	
EAC 11; 40 mm	w = 4.2 m
Sub-section No. 2	
RS 0/32 CA (in-situ); 150 mm; TP 208	w = 4.5 m
PS-E; ČSN 73 6129	
EAC 16; 80 mm;	w = 4.2 m
Emulsion surface dressing; ČSN 73 6129	w = 4.2 m
Sub-section No. 3	
RS 0/32 CA (in-situ); 150 mm; TP 208	w = 4.5 m
PS-E; ČSN 73 6129	
EAC 16; 80 mm;	w = 4.2 m
Emulsion surface dressing; ČSN 73 6129	w = 4.2 m
Sub-section No. 4	
RS 0/32 CA (in-situ); 150 mm; TP 208	w = 4.5 m
PS-E; ČSN 73 6129	
EAC 16 + 30% RAP; 50 mm	w = 4.3 m
PS-E; ČSN 73 6129	
EAC 11 + 30% RAP; 40 mm	w = 4.2 m
Sub-section No. 5	
RS 0/32 CA (in-situ); 150 mm; TP 208	w = 4.5 m
PS-E; ČSN 73 6129	
EAC 16 + 30% RAP; 80 mm;	w = 4.2 m
Emulsion surface dressing; ČSN 73 6129	w = 4.2 m
Sub-section No. 6 (reference)	
RS 0/32 CA (in-situ); 150 mm; TP 208	w = 4.5 m
PS-E; ČSN 73 6129	
ACL 16; 50 mm; ČSN EN 13108-1	w = 4.3 m
PS-E; ČSN 73 6129	
ACO 11; 40 mm; ČSN EN 13108-1	w = 4.2 m

Note: RS 0/32 CA – cold recycled base layer with use of cement and bituminous emulsion; PS-E – emulsion tack coat; EAC – emulsified cold asphalt concrete; ACL = asphalt concrete for binder courses; ACO = asphalt concrete for wearing courses.

3 MATERIALS AND DESIGN METHODOLOGY FOR EMULSIFIED ASPHALT MIXES

The design of emulsified asphalt mixes per se was carried out at the Faculty for Civil Engineering, CTU in Prague. The aggregate for the emulsified asphalt mixes was obtained from local sources in the region of the job site, or from nearby quarries Bílčice (basalt) and Valšov (graywacke). The aggregate is most appropriate for use primarily in road construction; these are traditional quarries that produce good quality crushed aggregate. The aggregate properties are indicated in Table 2. Sorted RAP of grading 0/11 mm with residual binder contents of 6.3% by mass was also added to selected mixes (30%). In cooperation with the MeadWestVaco Europe s.p.r.l. European research centre and the Austrian emulsion manufacturer, Vialit Asphalt GmbH & Co. KG, a suitable type of emulsion was prepared and adjusted to this type of mix with respect

Table 2. Aggregate characterization.

Aggregate properties	Maximum density (Mg.m ⁻³)	Shape index (SI) (%)	Grading	
			Fine (G _A /G _F) (-)	Coarse (G _C) (-)
HDK Bílčice 8/16	3 074	13	-	90/15
HDK Bílčice 8/11	3 067	21	-	90/15
HDK Bílčice 4/8	3 061	16	-	90/15
SDK Valšov 0/4	2 828	-	85	-

Table 3. Bituminous emulsion characterization.

Property	C60B7	
Particle polarity	(-)	positive
pH value	-	2.2
Bitumen content	(%)	62
Dyn. viscosity @ 25°C, shear rate 1 s ⁻¹	(mPa.s)	45
Residuum (sieve 0.5 mm) after 7 days storage	(%)	1.0

to the used aggregates. Slow-breaking cationic emulsion (C60B7) was applied. The emulsion parameters are indicated in Table 3 and it was prepared with standard 70/100 bitumen, continuous phase (water) with HCl and 1.2% of emulsifier, Indulin GE7.

There is currently no global “generally accepted” design method for cold asphalt mixes. It is possible to use findings of the American approach as formulated in the Cold Mix Design Manual or national technical regulations applied in France (NF). Besides, with respect to the lack of uniformity in laboratory methods and evaluation thereof, particularly in the early curing stages, it is difficult to create reliable correlations between experimental results described in literature sources by various experts and specialist teams. From the regulatory point of view emulsified asphalt mixes are currently in a preliminary stage of standardization. The design per se follows the technical conditions based on the aforementioned approaches. The essence of the design methodology is depicted in Figure 1.

The mixes were processed in the laboratory with the intention of reproducing mixing in a mobile mixing plant as much as possible. The laboratory mixes were produced in batches using a twin-shaft mixer Wirtgen WLM 30. The individual mixes were mixed in the “One Step” manner at 18–25°C. The mixing aimed to coat the aggregate grains with the binder as well as possible while avoiding over-mixing, thus destroying the bitumen film. Czech technical preliminary specifications for cold emulsified mixes stipulate cylindrical test specimens with 150.0 ± 1.0 mm diameter and 200–300 mm height. Nevertheless, test specimens of 101.60 ± 0.1 mm diameter and 63.5 ± 2.5 mm were selected as more appropriate for the purposes of design and experimental research.

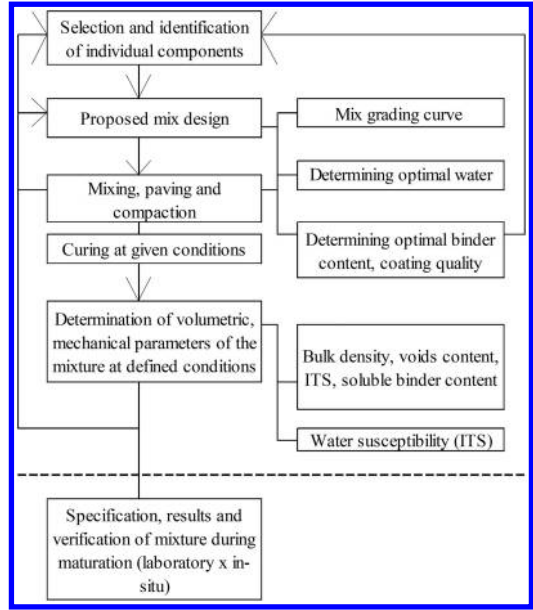


Figure 1. Principles of the cold emulsified asphalt mix design methodology.

Table 4. Requirements on empirical properties of cold emulsified asphalt mixes.

Characteristic	Requirement	
Maximum particle size <i>D</i>	11 mm	16 mm
Moisture*	-3% to +2%	
Laboratory set reference density and optimum moisture content	to be declared	
Minimum indirect tensile strength <i>R_{ITS}</i> after 7 days @ 15°C	0.30 MPa	
Moisture susceptibility (7 days air + 7 days saturated curing)	70% of <i>R_{ITS}</i>	
Voids content (%)	Wearing course	5.0–12.0
	Binder course	
	Base course	
Minimum content of soluble bitumen (% by mass)	Wearing course	5.6
	Binder course	-
	Base course	4.1

*Recommended maximum deviation from the declared value.

The test specimens were compacted by static pressure of 5.0 MPa by pressing the pistons from both sides with permitted release of excess water. The test specimens were left in the moulds under (20 ± 2)°C for (24 ± 6) hours. The curing conditions included air curing under 20 ± 2°C with 40–70% humidity for 7 days and also combined curing in water with 7 days air and 7 days water saturated.

The requirements stipulated in Table 4 for empirical properties of an emulsified asphalt mix define the determination of the optimum mix water content, comparative bulk densities of the compacted mixes, void contents, minimum contents of soluble binder, indirect

Table 5. Characteristics of designed cold emulsified asphalt mixes.

Mix characteristic	Standard	Symbol	Unit	EAC 11 + EAC 11	30% RAP	EAC 16	EAC 16 + 30% RAP
Soluble bitumen content	ČSN EN 12697-1	B _{min}	% by mass	6.1	6.2	5.4	6.6
Maximum density	ČSN EN 12697-5+A1	ρ _{mv}	kg/m ³	2 536	2 540	2 573	2 590
Bulk density	ČSN EN 12697-6+A1	ρ _{b,dim}	kg/m ³	2 287	2 329	2 268	2 369
Voids content (specimen)	ČSN EN 12697-8	V _m	% vol.	9.8	8.3	11.9	8.5
Indirect tensile strength ratio	ČSN EN 12697-12	ITSR	%	73	77	71	71
Indirect tensile strength @15°C	ČSN EN 12697-23	ITS _d	MPa	0.53	0.43	0.43	0.42
Indirect tensile strength @15°C	ČSN EN 12697-23	ITS _w	MPa	0.39	0.36	0.3	0.3
Stiffness modulus @15°C after 7 days air curing	ČSN EN 12697-26	IT-CY	MPa	1 880	1 440	1 396	1 285
Stiffness modulus @15°C after 7 days air curing and 7 days saturated		IT-CY	MPa	800	920	895	887
Stiffness modulus ratio @15°C		ITMR	%	43	64	57	69
Moisture	ČSN EN 13286-2	w	%	5.65	5.3	5.35	5.4
Density according Proctor modified	ČSN EN 13286-2	ρ _{b,dry}	kg/m ³	2 195	2 077	2 077	2 080
Flexural strength @-5°C	TP151		MPa	0.51	1.39	0.50	0.77
Resistance to crack propagation (fractural toughness) @0°C	ČSN EN 12697-44	Kic,i	N/mm ^{3/2}	26.47	25.54	18.31	25.28
Resistance to crack propagation (fractural toughness) @-10°C	ČSN EN 12697-44	Kic,i	N/mm ^{3/2}	21.54	22.59	22.22	27.62

tensile strength after 7 days air curing and moisture susceptibility parameter.

Within the trial section job site, four types of emulsified asphalt mixes were designed: EAC11; EAC11 + 30% RAP, EAC16 and EAC16 + 30% RAP. The grading composition in individual mixes is indicated in chart 1. The particular empirical, mechanical and deformation parameters of the designed emulsified asphalt mixes are shown in Table 5. Tensile bending strength and resistance to crack propagation were also determined for the mixes designed using the semi-cylindrical specimens after 28 days' curing.



Figure 2. Wirtgen KMA 200 mixing plant.

4 FINDINGS FROM MIXING, PAVING AND COMPACTION

The actual expert monitoring during the job site completion of the trial section provided by the Faculty of Civil Engineering, CTU in Prague was divided into two days. The first monitoring was scheduled to include the participation of a French expert in the field of emulsifier application and bituminous emulsion production. From the perspective of cold emulsified asphalt mix production and upon the previous recommendation, a mobile mixing plant (Wirtgen KMA 200 see Figure 2) with a conveyor belt attached to transfer the asphalt mix was secured. The mixer, including the operator, was provided on the basis of a subcontract. The emulsified asphalt mix was prepared in the contractor's production premises. Bituminous emulsion was dosed by a pump from the tank trucks on site. In contrast to the original plan, the aggregate was dry

pre-mixed in a standard hot-mix plant. This was due to the fact that the production of cold emulsified asphalt mixes, as a standard, utilizes machinery that allows dosing at least three aggregate fractions separately. However, the KMA 200 mobile mixing plant only allows separate dosing of the reclaimed asphalt and the dry aggregate mix in the hopper at the same time. This meant that e.g. coarse aggregate could not be separated from fine particles and sequential mixing of the binder with aggregate and the mixing water was not possible. Due to that, the dry aggregate mix was prepared at the contractor's mixing plant. Unfortunately, because of the conditions of a standard mixing plant, this method involved the undesired effect of preheating, or in other words, the pre-production at the mixing plant did not allow dosing and pre-mixing the aggregate without heating it in the drying drum (filters were

blocked by fine particles). Hot aggregate prepared in this manner was subsequently dosed into the double shaft mixer. It is only logical that the pre-heated aggregate pre-mix was transported to the KMA unit and, subsequently, dosed straight in the mixer with a direct impact on the humidity properties and, particularly, on the change of emulsion breaking. The method with hot (approx. 100–120°C) aggregate can be declared absolutely inappropriate as there is increased water evaporation and, primarily, a significantly accelerated breaking of the bituminous emulsion which caused a deterioration in the coating of particularly larger aggregate particles and, practically, is likely to cause increased moisture susceptibility of the mix. Moreover, the mix prepared in this manner also contradicted the design parameters of the mix.

The verification production for the purposes of determining the necessary quantity of mixing water commenced without issues. The mix compacted well and showed visual characteristics of continuously coated material. Nonetheless, in the course of emulsion breaking and consolidation during the completion of the first sub-section, it became obvious that the compacted mix as such had minimal adhesion. Based on this finding, dosage of individual components was checked. It was discovered that the mixing plant only doses a part of the required binder quantity. Any further paving was suspended to determine the reason. The original belief that the low temperature of the emulsion (approx. 30°C) was at fault was refuted. It should be emphasized that the type of used emulsion, similarly to the cold recycling technologies, can only be additionally heated to a maximum of 40°C. Such emulsions are commonly used in a range of 20–35°C.

The real cause was discovered to be the lack of technical preparation of the production plant. The subcontractor failed to perform due maintenance and the emulsion pump and dosage system held a large quantity of sediments from preceding production. This resulted in clogging of the dosing jets and probably also affected the insufficient function of the pump. The problem was solved in roughly two days by necessary technical intervention.

The mix was paved and pre-compacted by VÖGELE SUPER 1803-2 asphalt paver within the entire pavement width. The compacting set consisted of two steel-drum rollers, the former being BW 154 AD (11 t) and the latter BW 120 AD (2.5 t). From the point of view of compacting as such (see Figure 4), the following compaction method should have been applied: at least 4–6 passes by a steel-drum roller without vibration (to prevent tearing of the mix). Even higher numbers of passes are generally recommended to ensure the best wedging of the aggregate particles. About one hour later, several passes of a rubber-coated roller to smooth the mix was recommended; this is the latest point for a visual check of compaction quality (compact surface with no mix tears or minor transverse cracks). One or two passes by a lighter steel drum roller can be applied to conclude the series.



Figure 3. Examples of produced mix, including a test sample (mix from KMA 200) – example of aggregate coating quality.

The recommended method was not applied for the compaction – a light steel-drum roller was not even present on the day of the first site meeting. The first (crucial) compaction stage followed the recommendations and specifications straight on site, involved a maximum number of passes by medium-weight or heavy steel-drum rollers (without vibration). However, the same rollers were used for the subsequent smoothing after 60 minutes which means the surface was not smoothed as necessary and the minor transverse crack or local “defects” in the completed layer were not prevented (see Figure 4).

In relation to the above mentioned, it is also not obvious (and the information has not been provided) whether the formula for dry aggregate mixing (for both EAC16 and EAC11) was modified – the aggregate grading curves for all four mixes differed according to the valid type test protocols. No verification could be made during the first day of site monitoring; the results of analyses conducted by the contractor’s laboratory were not handed over. The impression obtained during the second site inspection was of the pre-mixed aggregate being stored on the same piles without distinguishing if it is for EAC11 or EAC16 mix, although both mixes were made during the day. There should be information on the actual situation during production itself and the actual materials used. The water and emulsion doses remained different for each mix which affects the resulting parameters. It would be ideal to have taken samples and extractions of all four mixes. Within the framework of the problems that occurred during mixing, CTU only had the opportunity to source



Figure 4. Compaction of cold emulsified asphalt mix layer/Appearance of compacted layer (transverse surface cracks which should be “smoothed” by suitable roller).

a few specimens of the binder course mix which were subsequently analyzed (see Table 6).

5 INSPECTION AND ASSESSMENT OF THE FINISHED TRIAL SECTION

The first inspection of the finished trial section was done about two months after paving. The inspection consisted of a visual check of the individual sub-sections and a set of tests on core samples.

The following faults were discovered within the framework of the visual inspection. Wearing course of section no. 1 shows porous structure, or there is an obvious loss of large particles from the wearing

Table 6. Results of control testing done during trial section realization.

Mix		Section	Section
		No. 5 (EAC 16 + 30% RAP)	No. 3 (EAC 16)
Residual binder content	[%]	6.0	5.8
Maximum density	[g/cm ³]	2.520	2.653
Bulk density	[g/cm ³]	2.257	2.242
Voids content	[%]	10.2	14.4
ITS [MPa] – air curing	7 days	0.41	0.33
	14 days	0.54	0.37
ITS decrease	[%]	61.1	56.1
Stiffness modulus [MPa] – air curing	7 days	1550	990
	14 days	1640	1480
ITMR	[%]	38.6	48.7



Figure 5. Sub-section No. 1 – material loss in the wearing course.

course in a number of spots along the entire length of the segment (see Figure 5). The loss of mass from the surface was caused already during the compaction when large particles from the mix stick on the steel-drum of the roller. Deterioration can be therefore expected during the winter seasons due to weather conditions or chemical treatment. It will be accompanied by short transverse cracks which, again, have been caused during compaction as such. Unfortunately, this fault caused by errors during completion itself can have a negative impact on the perception of the emulsified asphalt mix technology as such. Sections no. 2, 3 and 5 received a single surface dressing

Table 7. Results of control analyses of mixes from cored specimens – volumetric properties.

Mix		Section	Section	Section	Section
		No. 1 EAC 11	No. 1 EAC 16	No. 3 EAC 16	No. 5 EAC 16 + 30% RAP
Layer thickness	[mm]	55	30	65	77
Residual binder content	[%]	6.2	3.4	4.9	6.0
Fine particles	[%]	13.1	15.9	9.9	13.8
Bulk SSD density	[g/cm ³]	2.224	2.214	2.388	2.262
dimensions	[g/cm ³]	2.164	–	2.327	2.258
Maximum density	[g/cm ³]	2.537	2.608	2.668	2.535
Voids content	[%]	14.7	–	12.8	10.2

Table 8. Results of control analyses of EAC mixes from cored specimens – strength properties.

Mix		Section	Section	Section	Section
		No. 1 EAC 11	No. 1 EAC 16	No. 3 EAC 16	No. 5 EAC 16 + 30% RAP
Indirect tensile strength	[MPa]	0.37	not defined	0.44	0.57
Stiffness modulus	[MPa]	960	–	1080	1340
Thermal susceptibility	[–]	4.9	–	9.1	6.4
Fractural toughness (0°C)	[N/mm ^{3/2}]	7.5	–	9.1	13.5
Fractural toughness (–10°C)	[N/mm ^{3/2}]	12.3	–	18.5	18.4

according to (ČSN 736129). Here, the damage in the surface dressing is obvious already in local spots with a loss of aggregate due to either an unsuitable type of crushed aggregates, insufficient cleaning of the surface or the application of unwashed aggregate and, probably, inappropriate type of emulsion, or its poor quality. Another shortcoming is the overlapping of the emulsion coating between the lanes, particularly in section no. 3. This is a breach of the existing technical specifications which rightly emphasize method of linking up the coating. In section no. 4, the pavement structure composition was modified due to technological reasons, i.e. the layer of EAC11 + 30% RAP was replaced by AC 11 mix. This and the reference section showed no visual damage. From the point of view of pavement deformation due to traffic load, no problems are visible in any of the sections completed.

A set of tests on cored specimens was performed for the subsection. The tests can be divided into tests of emulsified asphalt mixes and tests of the finished layers (see Tables 7, 8).

Four core specimens were taken from subsection 1, 3, 5. It is obvious that the required thickness of layers

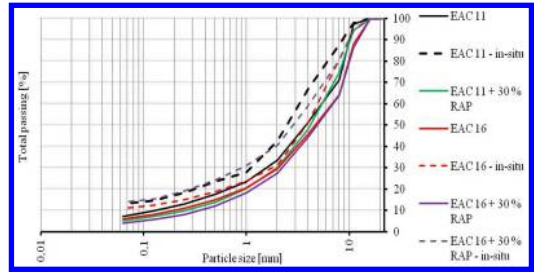


Figure 6. grading curves for EAC mixes.

was not always fulfilled within the individual subsections. According to the cored specimens extracted in some spots, very little thicknesses were discovered even in the binder course. This does not pose a fundamental problem based on the essence of cold emulsified asphalt mix as such because of its advantage and applicability in cases of evening out various levels in the pavement cross section. From the point of view of overall pavement structure, this finding can be considered a fault in the completion per se which might consequentially affect the general functionality of the pavement.

As is obvious from the analysis of cored specimens, the paved layers are not thick enough in some cases. The ascertained content of fine particles is absolutely sufficient to create enough mastic to bind the mix itself. On the other hand, such an increase in comparison to the design (see Figure 6) will increase specific surface and thus the necessary quantity of bituminous emulsion. The content of residual bituminous binder as determined is absolutely insufficient in the case of EAC16 mix from section no. 1. For section no. 3, it amounts to the threshold value. Penetration of 57 mm⁻¹ and softening point of 49.6°C were determined for the extracted binder (originally 70/100) from the cored specimens. Such hardening of the binder has probably been caused by binder oxidation due to a relatively high voids content which boosts up impact of the air on the bitumen (Serfass 2011).

The results of voids contents determined for the cored specimens, similarly to the results presented in table 7, document higher values achieved during the paving and compaction of the individual EAC mix types within the subsections. Again, it should be stated that in comparison to the type test protocols, the voids contents are about 20% higher. In the case of subsection no. 1, the voids content determination could not be verified with respect to the problems associated with the dimension approximation of the extracted core specimens for mix EAC16. The same applies to the indirect tensile strength and stiffness modulus values presented in table 8. The strength characteristics indicated for mixes EAC16 have an increasing trend when compared to the results given in table 6 which proves the gradual consolidation of the layer as such. This finding is in full compliance with the expectations stipulated for this type of mix.

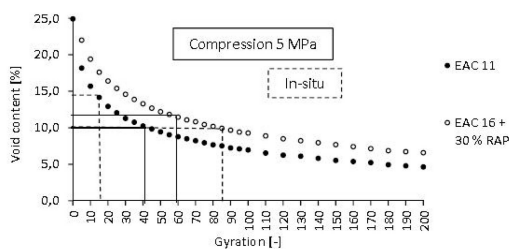


Figure 7. Comparison of compaction methods (static pressure vs. gyratory compactor).

6 EXPERIMENTAL TESTING OF EMULSIFIED ASPHALT MIXES

The effort towards obtaining knowledge of the cold emulsified asphalt mix behavior and properties is important not only from the perspective of optimal mix design but also with respect to predicting its behavior and eliminating the possible failures during the pavement structure life cycle. Mix EAC 11 was pinpointed for subsequent testing that observed selected volumetric, deformation and functional parameters.

One of the specific problems within the framework of cold emulsified asphalt mixes is determining the correlation between laboratory and in situ compaction. Some sources mention compaction of cold emulsified mixes in the laboratory by impact compactor (Thanaya 2009), hydraulic press or gyrator. Gyratory compaction (SUPERPAVE Gyratory Compactor Troxler 4140) was selected for comparison with the static pressure method. Based on the methods applied in France, the voids content achieved during the paving corresponds with gyrator compaction under 60 revolutions and static pressure of 600 kPa. According to the French methodology (NF P 98-139, Serfass 2000, Harman 2001) the gyrator revolution count is also stipulated based on the layer thickness and mix type regardless of the traffic load. The value of 60 revolutions applied by the gyrator corresponds with the layer thickness of 5–10 cm. The laboratory design of cold asphalt mixes assumes the voids content in the mix under 60 revolutions in the gyrator within the range of 5–12%-vol. and, at the same time, under 10 revolutions in the gyrator, the voids content must exceed 12% in compliance with the requirements of the standard (XP P98-121); this value represents the qualitative parameter of compaction upon paving. Figure 7 and Table 9 summarize a comparison of the aforementioned compacting machinery and the resulting volumetric, mechanical and deformation parameters of selected emulsified mixes. In the case of the gyrator, the comparison follows the rules of (NF P 98-139). It should be mentioned that the compaction results achieved in situ are not quite relevant for the purposes of comparison with respect to the aforementioned problems in completion, namely the differences between the designed mix and the

Table 9. Comparison of selected characteristics for EAC11 mix for different compaction methods.

EAC 11	Gyrator 60 rev./ 600 kPa	Hydraulic press 5.0 MPa	Hydraulic press vs. gyrator (%)
Bulk density ($\text{kg}\cdot\text{m}^{-3}$)	2231	2211	99.1
Voids content (%)	8.8	10.1	114.8
Indirect tensile strength – 7 days air curing (MPa)	0.61	0.53	86.9
Indirect tensile strength – 14 days curing (7a + 7w) (MPa)	0.53	0.39	73.6
Stiffness modulus – 7 days air curing (MPa)	1727	1880	108.9
Stiffness modulus – 14 days curing (7a + 7w) (MPa)	1199	800	66.7

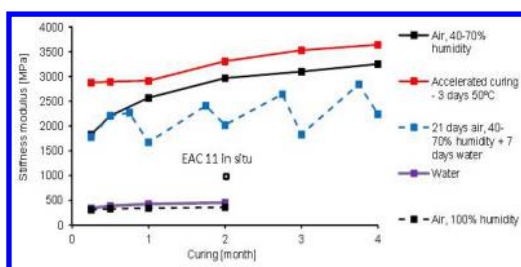


Figure 8. Curing conditions impact; mix EAC11.

mix actually completed in-situ (Lesueur 2000, Serfass 2011).

Another important issue that affects the resulting properties of cold emulsified asphalt mixes is the influence of the curing conditions. The laboratory testing involved some research of the effect of curing conditions on the EAC 11 mixes. Figure 8 shows five curing methods of test specimens; the first method follows the standardized conditions, i.e. air curing at the temperature of $(20 \pm 2)^\circ\text{C}$ and 40–70% humidity. The second method involves 100% humidity since production at the temperature of $(20 \pm 2)^\circ\text{C}$. The third method observed the influence of accelerated curing where the specimen cured under standard conditions for 4 days after production and, subsequently, was put in a dryer at $(50 \pm 2)^\circ\text{C}$ for three days. The fourth option involved curing of specimens immersed in water immediately after production and the fifth is a combination of cyclic air curing for 21 days under $(20 \pm 2)^\circ\text{C}$ and 40–70% humidity and, then, saturated water curing for 7 days.

Cold asphalt mixes are a multi-phase system of many components some of which also have a complex internal structure characterized by high thermal sensitivity. Basically, these are the components of irregular aggregate grains with slightly higher binder content and a small proportion of the volume filled by

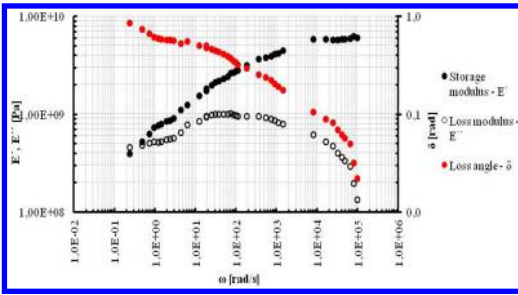


Figure 9. Master curves for EAC 11 (28 days curing).

air voids. Despite its complex structure, the material behavior can be described by means of the visco-elasticity theory (Collop 1995; Ferry 1980; Tschoegl 1989; Underwood 2011; Zou 2010). One of the linear visco-elastic parameters is the complex modulus. Dynamic complex modules were measured by the 4PB-PR method according to (ČSN EN 12697-26) in the -20°C to $+27^{\circ}\text{C}$ temperature range and under the frequency of 0.1 Hz to 40 Hz after 28 days of air curing. The master curves (see Figure 9) were compiled by the time-temperature superposition method through shifts in both the horizontal and the vertical level to determine the thermal dependence of the material's rheological behavior and to extend the time and frequency range under the relevant temperature within the IRIS Rheo-Hub. The Williams-Landel-Ferry equation with parameters $C_1 = 100.00$, $C_2 = 1070.08$ was used to describe the horizontal shift while a polynomial function with parameters $a_0 = 0.964$, $a_1 = 1.553\text{E}-02$, $a_2 = 1.537\text{E}-04$ described the vertical shift (Ferry 1980; Dealy and Wissbrun 1999). Analyzing the master curves from right to left, it is obvious that the material tends to behave in an almost elastic manner in the lowest temperature range and highest frequency range. The shift from visco-elastic to elastic behavior is clearly visible in the values measured within the dropping imaginary part of the complex curve. With increasing frequency, the real part of the complex curve gradually increases while its derivation decreases and, in the last values, almost touches 0. This phenomenon correlates with the shift of material properties towards the elastic field and with reaching the modulus equilibrium point, (Ferry 1980; Kim 2008). As is obvious from the phase angle change, the cold-compacted asphalt mixes are highly thermos-mechanically sensitive materials in comparison to hot-compacted asphalt mixes.

With respect to permanent deformation standard rutting test was conducted in a small test device under 60°C according to (ČSN EN 12697-22). The test specimen was loaded by 10,000 cycles with a roll frequency of 0.44 Hz. The results achieved are not too reproducible (see Figure 10) since considerable deformation and damage to the test specimens occurred. The next stage should be a discussion on whether the test conditions really correspond with the actual conditions of

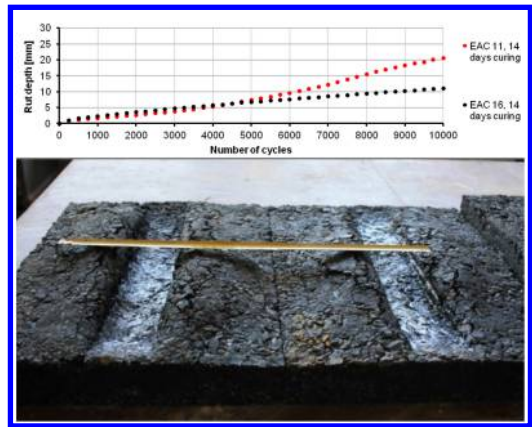


Figure 10. Results of rutting test for EAC mixes.

use within the framework of pavement structure life when cold asphalt mixes are applied, or whether there is another factor involved. The fact does not restrict the options for exploiting the mixes in road construction because, based on French findings (Lesseur 2000), e.g. the rutting tests usually delivered poorer laboratory results, i.e. they never corresponded with reality in the pavement. So far, cold mixes have always behaved better in-situ throughout their life.

7 CONCLUSION

This paper described the individual stages of a pilot cold asphalt mix project, which intended to verify the viability of the emulsified asphalt mix technology in the Czech Republic. The project was required to verify the design methodology and acquire initial experience with the mix production and subsequent completion in-situ for the purposes of compilation of the "Cold Asphalt Mixes" technical specifications. Based on the presented results, it can be stated that the project has been successfully finished; the findings obtained will be utilized not only in the specifications but also in the building of arguments from the point of view of recommendations for the contractors. The project faced a number of problems, of a technical nature in particular, particularly general lack of good preparation on the part of the contractor. Nevertheless experiences which can be derived from the practical problems identified at the pilot project are important with respect to future applications of this technology.

ACKNOWLEDGEMENTS

This paper was prepared under the funding scheme of Competence centre program by the Technology Agency of the Czech Republic within the project Centre for effective and sustainable transport infrastructure (CESTI), project no. TE01020168.

REFERENCES

- Collop, A. C., D. Cebon, and M. S. A. Hardy. 1995. "Viscoelastic Approach to Rutting in Flexible Pavements." *Journal of Transportation Engineering* 121 (1) (January): 82–93. doi:10.1061/(ASCE)0733-947X(1995)121:1(82).
- ČSN EN 12697-22 + A1, 2005. *Asfaltové směsi – Zkušební metody pro asfaltové směsi za horka – Část 22: Zkouška pojiždění kolem*.
- ČSN EN 12697-26, 2012. *Bituminous Mixtures – Test Methods for Hot Mix Asphalt – Part 26: Stiffness*. Czech Office for Standards, Metrology and Testing.
- ČSN 73 6114, 1995. *Vozovky pozemních komunikací – Základní ustanovení pro navrhování*, Czech Office for Standards, Metrology and Testing.
- ČSN 736129, 2006. *Stavba vozovek – Postřikové technologie*, Czech Office for Standards, Metrology and Testing.
- Dealy, J. M., and K. F. Wissbrun. 1999. *Melt Rheology and Its Role in Plastics Processing: Theory and Applications*. Springer.
- Ferry, John D. 1980. *Viscoelastic Properties of Polymers*. 3rd ed. Wiley.
- Gaudefroy V., Wendling L., Odie L., Fabre J. C. 2008. In: *Laboratory characterization of cold mix treated with bitumen emulsion*, In: *Proceedings of the 4th Eurasphalt and Eurobitume congress*, s. 1–11.
- Grünner, K. 2007. *Asfaltové emulze při výstavbě a údržbě cest*, C.S. Bitunova, pages 152, ISSN: 978-80-969771-5-4
- Harman, T., Bukowski, J., Moutier, F., Huber, G. 2001. *The History and Future Challenges of Gyrotory Compaction 1939–2001*.
- Kim, Y. 2008. *Modeling of asphalt concrete*. 1st ed. McGraw Hill Professional.
- Lesueur, D. 2000. *Predicting the in-place compacity of cold mixes*, 2nd Eurasphalt & Eurobitume Congress Barcelona.
- NF P 98-139, 1994. *Enrobés hydrocarbonés, Couches de roulement: bétons bitumineux á froid*, ISSN 0335-3931.
- Serfass, J.-P., Carbonneau, X., Delfosse, F., Triquigneaux, J.-P. 2010–2011. *Comportement et méthodologie d'évaluation – Enrobés á l'emulsion, fruits d'une federation de competences*, RGRA.
- Suda, J., Valentin, J., Žák, J., Šedina, J., Miláčková, K. 2013. *Experience with experimental designs and performance assessment of cold asphalt mixtures – New type of pavement structure in the Czech Republic*, *Research and Applications in Structural Engineering, SEMC 2013*, pp. 1795–1799.
- Thanaya N. A. 2007. In: *Rewiew and Recommendation of Cold Asphalt Emulsion Mixtures Design*, In: *Civil Engineering Dimension*, s. 49–56.
- Thanaya I. N. A., Zoorob S. E. 2009. In: *A Laboratory Study on Cold-Mix, Cold-lay Emulsion Mixtures*, In: *Proceedings of the Institution of Civil Engineers*, s. 47–55.
- TP170, 2009. *Navrhování vozovek pozemních komunikací*, MD – OSI.
- TP 208, 2009. *Recyklace konstrukčních vrstev netuhých vozovek za studena*, MD – OSI.
- Tschoegl, Nicholas W. 1989. *The Phenomenological Theory of Linear Viscoelastic Behavior: An Introduction*. Springer-Verlag.
- Underwood, B. Shane, Taeyoung Yun, and Y. Richard Kim. 2011. "Experimental Investigations of the Viscoelastic and Damage Behaviors of Hot-Mix Asphalt in Compression." *Journal of Materials in Civil Engineering* 23 (4) (April): 459–466. doi:10.1061/(ASCE)MT.1943-5533.0000197.
- XP P98-121, 2005. *Assises de chaussées, Graves.émulsion*, ISSN 0335-39312005.
- Zou, G., X. Zhang, J. Xu, and F. Chi. 2010. "Morphology of Asphalt Mixture Rheological Master Curves." *Journal of Materials in Civil Engineering* 22 (8): 806–810. doi:10.1061/(ASCE)MT.1943-5533.0000024.

Evaluation of applicability of residual products from solvent deasphalting process of heavy oil refining as a binder for asphalt pavement

S.D. Hwang, C.M. Baek, S.L. Yang & J.H. Im

Korea Institute of Civil Engineering and Building Technology (KICT), Goyang-Si, Gyeonggi-Do, South Korea

ABSTRACT: One of the refining process using heavy oil sources is the solvent deasphalting process (SDA). The SDA extracts most of oil components and thus, the residual products from such process contain more asphaltene compared to the conventional asphalt binder for the road pavement. In this study, the chemical and physical properties of the residual products (SDA pitch) have been investigated in order to evaluate the applicability as a binder for the asphalt pavement. For the chemical property of the SDA pitch, the composition of SARA (Saturate, Aromatic, Resin, Asphaltene), the elementary composition, and the functional group are analyzed. For the physical property of the SDA pitch, the basic material property tests for the conventional asphalt binder, such as penetration test, softening point test, flash point test, ductility test, and rotational viscometer test, are performed. The rheological properties of the SDA pitch are also investigated using the dynamic shear rheometer (DSR).

Keywords: Pitch, Solvent Deasphalting Process, SARA Analysis, Asphalt Binder

1 INTRODUCTION

Global oil prices have been increased dramatically since 2007 and the price of asphalt has risen by approximately double in the price 10 years ago. Also, the current demand for the fuel is outpacing the supply of traditional crude oil sources. Thus, it is necessary to develop asphalt alternation materials and new construction methods for pavement maintenance. Recently, the petroleum industry have put a great effort both to extract more valuable products like fuel from heavy oil sources such as Canadian oil sands and Venezuelan heavy oils and to utilize low price heavy oil fractions into refining process (Nu 2007).

As the oil becomes heavier type, new oil refining technologies should be developed because conventional technologies may not meet the demand for oil and petrochemical products. Advanced countries such as US, Canada, etc. are currently underway to secure the oil refinement technologies and develop new refinement technology for the light oil by using heavy oil (Nu 2007). Currently, Korea government is trying to obtain the oil blocks of extra heavy oil, which is low price and lots of deposit amount, and develop new refinement technologies for the light oil to produce high quality synthetic oil and high value chemical materials.

However, as the upgrading process for heavy oil fractions is enhanced, it is not easy to use residues from the upgrading process such as bitumen, asphaltene, and pitch used for construction materials. Asphalt used as construction materials is employed for the purpose of asphalt binder, waterproof, and etc. thus the

asphalt should perform with sufficient workability and durability. With reference to the upgrading process for heavy oil fractions, many researches have been conducted for a process of solvent extraction by local refinery companies (Yang 2014). These researches lead to production of low quality asphalt binder because oil are extracted from crude oil as much as possible. Since the residues from the upgrading process for heavy oil fractions have insufficient oil component, which is major component to provide asphalt functionality, they could not be used as asphalt binder without modifications.

In this study, the chemical and physical properties of the residual products, named SDA pitch, have been investigated in order to evaluate the applicability as a binder for the asphalt pavement.

2 SOLVENT DEASPHALTING PROCESS (SDA)

Oil sand generally consists of bitumen (15–20%), inorganic materials (sand, clay, and mineral, 70–75%), and water (3–5%). Its original reserves is similar to the amount of typical light crude oil that is approximately 2.3 trillion barrel (Hwang et al. 2008). Extra-heavy oil fractions represented by oil sand bitumen and extra-heavy oil are applied into refining progress as a synthetic crude oil (SCO) form, which is produced by upgrading process (full upgrading or partial upgrading) instead of application into refining progress directly because its description is poor when comparing with light crude oil (Nho et al. 2011).



Figure 4. Result of SARA analysis.

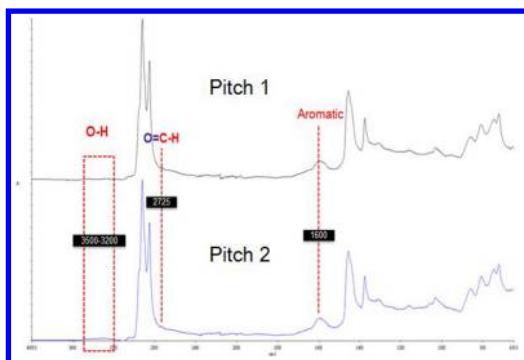


Figure 5. FT-IR spectra of two types of pitch.

components except asphaltene. However, the pitch has all the components of SARA.

In terms of contents ratio, aromatic is more than 50% and resin and asphaltene are about 20% for both pitch 1 and 2. Saturate contents are 3.1% and 1.3% for pitch 1 and pitch 2 respectively. Thus, extraction rate of pitch 1 is better than that of pitch 2.

Saturate content of pitch 1 and pitch 2 are lower than conventional asphalt binders (in this case PG 58-22 and PG 64-22). However, total chemical composition does not greatly differ from conventional asphalt binders.

3.2 SARA analysis by FT-IR

Fourier transform infrared spectroscopy (FT-IR) is one of most important analytical tools for characterization of crude oil fractions. FT-IR is typically used to determine functional groups in the fractions of crude oils (Ali et al., 1989 and Rudzinski et al., 2000). FT-IR spectra are run on a Spectroscopy Spectrum 100 (Perkinelmer Inc.) at 4 cm^{-1} resolution. In order to develop the spectra of samples, attenuated total reflection (ATR) is used in the range between $4,000\text{ cm}^{-1}$ and 650 cm^{-1} . Figure 5 show the FT-IR spectra of pitch 1 and pitch 2.

From Figure 5, similar to the results of SARA analysis by TLC-FID, there is no great difference between pitch 1 and pitch 2.

The strong peak at around 2900 cm^{-1} is vibrational mode of aliphatic C-H and the medium peak at about 1370 cm^{-1} is bending mode of aliphatic C-H thus, peaks of saturate are observed in that range. Also, the peak at 1600 cm^{-1} indicates stretching peak of aromatic functional group. Consequently, saturate and aromatic functional groups are presented mainly in the FT-IR spectra.

The weak peak at about 1700 cm^{-1} is carbonyl functional group produced by oxidation of truncated asphaltene or resin components. Another weak peak at 1700 cm^{-1} is C-H stretching peak of aldehyde occurred by oxidation effect.

There is a difference between pitch 1 and pitch 2 in broad band (from 3500 cm^{-1} to 3200 cm^{-1}). The difference is H-bonded hydroxyl group peaks and relatively strong peak is observed in the spectrum of pitch 2. Based on this observation, it can be concluded that oxidation level of pitch 2 is higher than that of pitch 1.

3.3 SARA analysis by NMR

Nuclear magnetic resonance (NMR) is not common technique for characterizing crude oils, however, some studies mentions that NMR can be used for the API gravity of the petroleum samples (Trejo et al. 2004).

In this study, dissolved pitch with CDCl_3 is analyzed by 400 MHz NMR (400MR-DD2, Agilent) and ^1H -NMR and ^{13}C -NMR are measured by 256 and 5000 cycles respectively.

Figure 6 shows ^1H -NMR and ^{13}C -NMR spectra of two types of pitch.

In Figure 6 (a) and (b), the spectra of pitch 1 and pitch 2 show almost similar behavior but there is difference slightly in contents of saturate and oxidized functional group. Physical property of pitch 2 may change because it shows more oxidized functional group. From Figure 6 (c) and (d), it can be seen that pitch 1 and pitch 2 are almost same in contents.

4 PHYSICAL PROPERTIES OF PITCH

In order to evaluate physical properties of the SDA pitch, the basic material property tests, such as penetration test, softening test, flash point test, and ductility test are conducted. Also, PG grade of the SDA pitch is determined by short-term aging, long-term aging, DSR (dynamic shear rheometer) test, and BBR (bending beam rheometer) test.

4.1 Basic material property tests

Figure 7 shows the results of basic material property tests.

Based on the test results in Figure 7, the SDA pitch shows decreased flexibility and increased stiffness when comparing with conventional asphalt binder (PG 64-22). The penetration test cannot be performed with all two types of pitch due to their too high stiffness. Especially, pitch 2 shows five times lower penetration

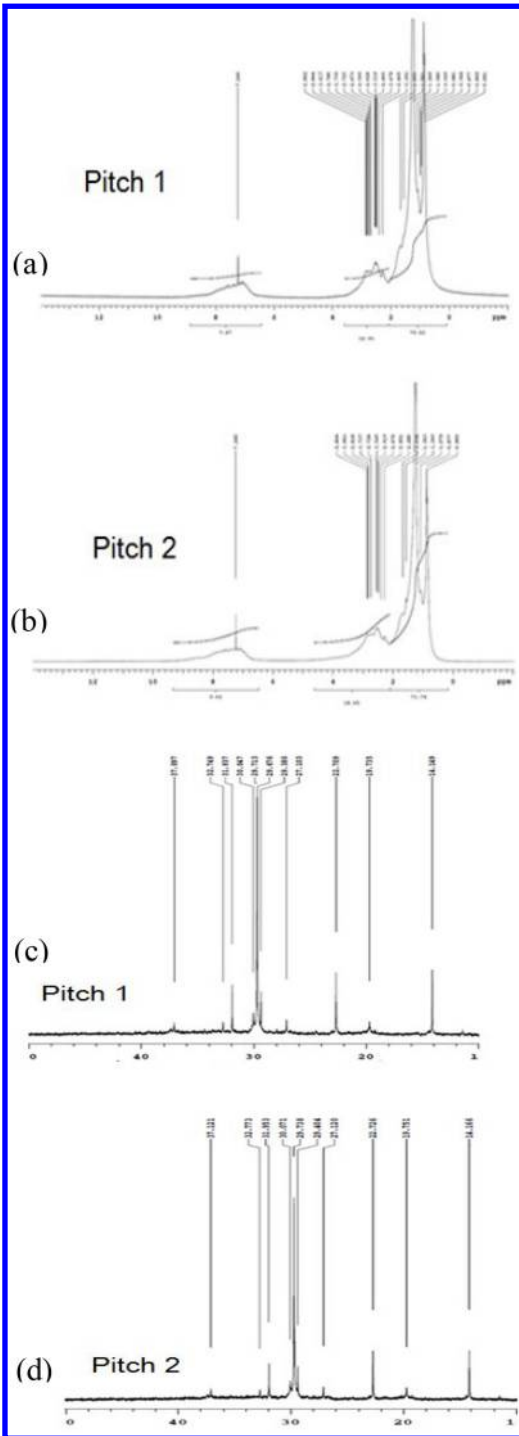


Figure 6. Results of analysis for: (a) pitch 1 ^1H -NMR and (b) ^{13}C -NMR.

value than pitch 1 and 10 times lower penetration value than control asphalt binder. The rotational viscosity test, also, cannot be conducted with the SDA pitch because of too high viscosity property. Thus, it is hard

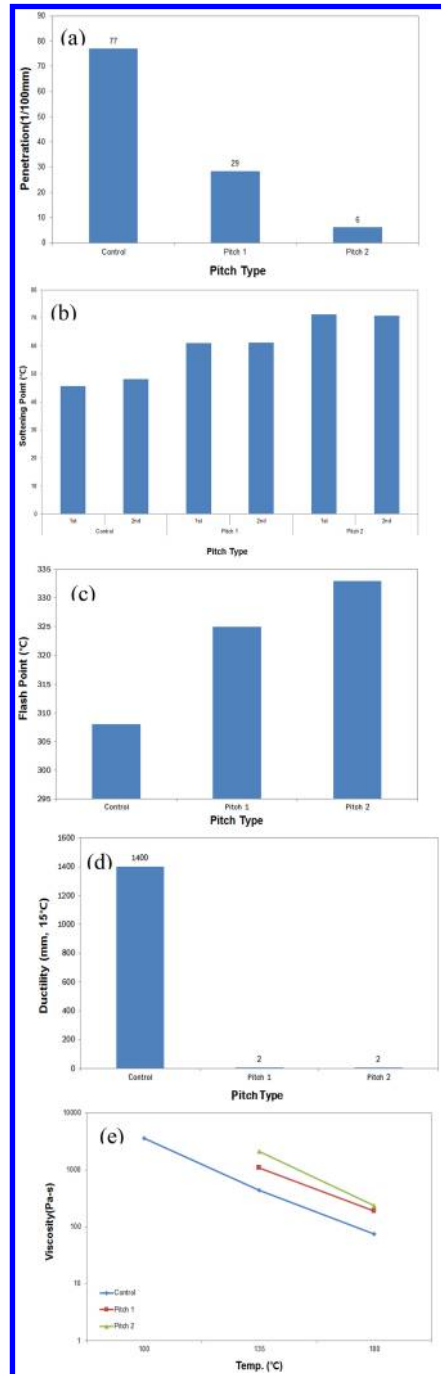


Figure 7. Results of basic material property tests: (a) penetration test, (b) ring and ball test, (c) flash point test, (d) ductility test, and (e) rotational viscosity test.

to deform or process the SDA pitch. The ductility of the SDA pitch is 2 mm because the test is finished right after starting. For the flash point test, all two types of pitch meet the safety criteria (over 240°C).

Table 1. Result of performance grade.

Test Type	Temp.	Control	Pitch 1	Pitch 2
Rotational	135°	435	1075	2125
Viscosity, cP	180°	75	340	235
Original DSR	52°			
G*/sin δ	58°	2.325	30.214	60.245
≥1.0 kPa	64°	1.100	12.113	29.221
	70°	0.552	4.501	18.118
	76°		2.107	7.771
	82°		1.021	3.468
	88°		0.512	1.636
	94°			0.810
RTFO DSR	52°			
G*/sin δ	58°	7.566	35.446	61.882
≥2.2 kPa	64°	3.417	18.218	30.274
	70°	1.630	6.731	18.324
	76°		3.188	8.912
	82°		1.587	3.949
	88°		0.824	1.872
	94°			0.929
BBR	Stiffness	92	N	N
	(<300 MPa)	(-12°)		
	M-value	0.322	N	N
	(>0.3)	(-12°)		
Performanc grade		64-22	76	82

These material properties of the SDA pitch may lead to good resistance to permanent deformation and poor resistance to cracking. Therefore, the SDA pitch may not be suitable to be used in asphalt pavement.

4.2 PG grade of pitch

Table 1 presents the results of performance grade tests.

From the test results (Table 1 and Figure 8), the SDA pitch shows higher high temperature grade than the control asphalt binder. The high temperature grades of pitch 1 and pitch 2 are increased to 76°C (1 step) and 82°C (2 steps), respectively. The low temperature grade cannot be determined because the BBR specimen was damaged at 0°C before bending is arisen.

Moreover, the difference of G*/sin δ after RTFO-aging is the biggest in conventional asphalt binder and the smallest in pitch 2. Since the SDA pitch contains more oxidized functional group, aging effect may not work much on the SDA pitch. In details, during the SDA process some of saturate contents are changed to resin due to forming hydroxyl group (-OH) by oxidation.

Based on the results, the physical property of pitch is changed greatly depending on saturate contents and low saturate contents lead to brittle behavior property. Therefore, the SDA pitch may show better resistance for permanent deformation and less resistance for cracking than typical asphalt binders. This observation is very similar to the results of basic material properties of the SDA pitch.

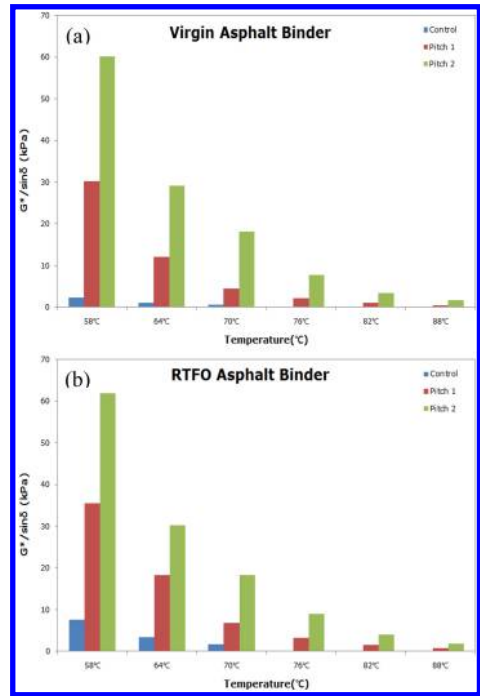


Figure 8. DSR test results: (a) before and (b) after RTFO.

5 CONCLUSIONS AND RECOMMENDATIONS

In this study, the chemical and physical properties of the residual products, named SDA pitch, have been investigated in order to evaluate the applicability as a binder for the asphalt pavement. Based on the analysis, the following conclusions are drawn to support the applicability of SDA pitch.

- According to the basic material property tests results, the SDA pitch is too hard and brittle due to very high viscosity.
- Based on the PG grade test, the SDA pitch shows brittle property at low temperature. Especially, since the BBR test cannot be performed at low temperature due to specimen's damage, the SDA pitch may be vulnerable to cracking at low temperature.
- However, the SDA pitch shows better resistance for permanent deformation than typical asphalt binders, so it could be used as modifier and special asphalt binder alternation material.
- The SDA pitch still includes all the SARA components similar to the conventional asphalt binder and thus, with the appropriate modifiers or additives to soften the SDA pitch, it could be used as a binder for the asphalt pavement.

ACKNOWLEDGEMENTS

The authors would like to acknowledge the financial support from the Ministry of Science, ICT and Future Planning under research project Development

of Upgrading Package Process Technology for Production of Synthetic Crude Oil and Chemical Materials from Low Price Heavy Oil Fractions.

REFERENCES

- Ali, M.F., Bukhari, A. and Hasan, U.M. 1989. Structural Characterization of Arabian Heavy Oil Residue. *Fuel Science and Technology International* 7 (8): 1179–1208.
- Hwang, S.Y., Woo, C.S., and Kang, K.H. 2008. Extraction and Vacuum Distillation Characteristics of Oil Sand Bitumen Using Solvent. *Applied Chemical Engineering* 12 (2): 361–364.
- Kwon, E.H., Lee, E.M., Kim, M.Y., Chang, H.S., Guahk, Y.T., Kim, K.H., and Nho, N.S. 2014. The Rheological Behaviors and Non-Newtonian Characteristics of Maltenes Made by SDA Method from Oil Sands Bitumen. *Applied Chemical Engineering* 25 (2): 209–214.
- Lee, J.M., Shin, S., Ahn, S., Chun, J.H., Lee, K.B., Mun, S., Jeon, S.G., Na, J.G., and Nho, N.S. 2014. Separation of Solvent and Deasphalted Oil for Solvent Deasphalting Process. *Fuel Processing Technology* 119: 204–210.
- No, N.S., et al. 2011. Development of Next-Generation Integrated Upgrading Process for Extra-Heavy Oil Fractions. Daejeon: Korea Institute of Energy Research.
- Nu, N. 2007. Refining Alberta's Energy Advantage: An Unprecedented Investment Opportunity. Alberta Employment, Immigration and Industry.
- Rana, M.S., Samano, V., Ancheyta, J., and Diaz, J.A.I. 2006. A Review of Recent Advances on Process Technologies for Upgrading of Heavy Oils and Residua. *Fuel* 86 (9): 1216–1231.
- Rudzinski, W.E., Aminabhavi, T.M., Sassman, S., and Watkins, L.M. 2000. Isolation and Characterization of the Saturate and Aromatic Fractions of a Maya Crude Oil. *Energy Fuels* 14 (4): 839–844.
- Trejo, F., Centeno, G., and Ancheyta, J. 2004. Precipitation, Fractionation and Characterization of Asphaltenes from Heavy and Light Crude Oils. *Fuel* 83 (16) 2169–2175.
- Yang, S.L. 2014. Evaluation of Applicability of Heavy Oil Upgrading By-Product (Pitch) as a Pavement Paving Material. *International Journal of Highway Engineering* 16 (5): 9–18.

Author index

- Abd, D.M. 105
Adesiyun, A. 759
Ahlan, M. 713
Ahmed, M.U. 421
Ahmed, T.A. 623
Ahmed, T.M. 351
Akbulut, H. 429
Al-Abdul Wahhab, H. 89
Al-Adham, K. 89
Al-Haddad, A.H.A.A. 385
Al-Khalid, H. 27, 105, 343, 351, 385
Alam, M. 407
Albrka Ali, S.I. 81
Allen, B. 319
Ameri, M. 73
Anastasio, S. 487
Angelone, S.M. 65
Artamendi, I. 319
Ateş, M. 61
Athanasopoulou, A. 725, 819, 833
- Baek, C.M. 623, 859
Baek, J. 807
Baglieri, O. 407
Baldo, N. 379, 617
Bankowski, W. 447
Barrasa, R.C. 435, 453
Basbas, S. 737
Betti, G. 469, 637
Biligiri, K.P. 307
Blasl, A. 561
Bocci, M. 589
Bressi, S. 775
Büchler, S. 361
Bueche, N. 775
Buechler, S. 447
Burrow, M.P.N. 41
- Caballero, E.S. 435
Caner, M. 429
Canestrari, F. 597, 607
Cannone Falchetto, A. 277, 361, 373
Cao, R. 307
Carter, A. 775
Cassidy, S. 577
Cauhape Casaux, M. 65
Çetin, S. 429
Ceylan, H. 679
Chang, C.M. 203, 235
Chasiotis, A. 33
- Chen, M.J. 299
Chitragar, S.F. 271
Chomicz-Kowalska, A. 3
Chondrosyros, K. 767
Ćirilovic, J. 519
Čížková, Z. 825
Cliatt, B. 661
- da Silva, J.B.R. 653
Dimitrov, M. 509
Djurekovic, A. 115
Domoksis, N. 737
Dourandish, R. 73
Dumont, A.G. 775
- Elmacı, A. 429
Engels, M. 629
- Fabrizi, G.T.P. 127
Falla, G.C. 561
Farahi, R. 795
Faxina, A.L. 127
Ferrotti, G. 607
Flores, J.M. 227
Fortes, R.M. 653
Frigio, F. 597
Fruent, M.H.T. 293
Fwa, T.F. 287
- Gagnon, J.S. 707
Gallego, J. 493
Georgiou, P. 401
Georgouli, K. 661
Ghafoori, N. 135, 141
Ghataora, G.S. 41
Ghimire, B.C. 187
Godenzoni, C. 589
Golchin, B. 255
González, O. 203, 235
Gopalakrishnan, K. 679
Goulias, D.G. 801
Graziani, A. 589
Gu, S. 367
Gürer, C. 429, 499
- Hamzah, M.O. 255
Haritonovs, V. 327, 545
Hartmann, A. 759
Harun, M.H. 731
Hasaninia, M. 73
Heinrich, P. 447
Hesp, S.A.M. 13, 187
- Hoff, I. 487
Hofko, B. 509
Hospodka, M. 509
Hwang, S.D. 859
- Ibáñez, V.C. 453
Im, J.H. 859
Ipavec, A. 759
Isailovic, I. 373
Isailović, I. 221
Ismail, A. 81
Izaks, R. 545
- Jaafar, Z.F.M. 713
Jacobs, M.M.J. 293
Jellema, E. 243
Jeong, J. 807
Judele, L. 123, 813
- Kaloush, K.E. 307, 313
Karcher, C. 759
Karimi, S.S. 801
Kassem, E. 395
Kataware, A.V. 97
Kaya, O. 679
Kehagia, F. 745, 767
Khadem, M. 795
Khalid, H.A. 21
Kim, S. 679
Kim, W. 807
Kokkalis, A. 525, 725, 789, 819, 833
Kollaros, G. 725, 819, 833
Komacka, J. 759
Köroğlu, H.J. 61
Kowalczyk, M. 243
Krarup, J.A. 693
Krpálek, O. 825
Krugler, P. 203
Kubanek, K. 759
Kumar, A. 211
- Labropoulou, K. 737
Lancaster, I.M. 21
Lanotte, M. 407
Larkin, A. 707
Le, V.P. 227
Leandri, P. 841
Lee, H. 623
Lee, H.J. 227, 807
Lee, S. 227
Leite-Gembus, F. 645
Lepadatu, D. 123, 813

- Leventis, A. 401
 Li, Q. 701
 Liapis, I.G. 33
 Lim, E. 287
 Lind, K. 479
 Ling, J. 367
 Livneh, M. 167, 177
 Loizos, A. 401, 661, 671
 López, V.B. 435, 453
 Losa, M. 841
- Magee, B. 147
 Mahmood, M. 533
 Mahmoud, E. 413
 Manthos, E. 567, 637
 Marasteanu, M.O. 277
 Marradi, A. 469, 637
 Martinez, F.O. 65
 Masad, E. 27, 343, 395
 Mathavan, S. 533
 McNally, C. 577
 McQuaid, G. 161
 Menapace, I. 395
 Millar, P. 161
 Millow, R. 561
 Mintsis, G. 737
 Mladenovic, G. 115, 519
 Mohamad Noh, N.S. 731
 Molayem, M. 73
 Mollenhauer, K. 577
 Montoliu, C.M.-P. 435, 453
 Moon, K.H. 277
- Nguyen, T. 441
 Nicholls, J.C. 479, 577, 759
 Nielsen, E. 759
 Nikolaides, A. 333, 567
 Nikolov, A.D. 265, 785
 Nikolova, S.K. 265
 Nolle, L. 533
- Orouzadeh, N. 463
 Öz, P.H. 61
- Paliukaite, M. 13
 Pamplona, T.F. 127
 Panetsos, P. 525, 789
 Papagiannakis, A.T. 413
 Papavasiliou, V. 671
 Papavassiliou, G. 395
- Park, H.M. 227
 Partl, M.N. 55
 Pasetto, M. 379, 617
 Pasquini, E. 597
 Pecheny, B.G. 785
 Pedrajas, F. 453
 Peng, Y. 367
 Phillips, P. 319
 Pinori, U. 469
 Pinto, A. 307
 Pitsiava-Latinopoulou, M. 745
 Plati, C. 671
 Pomoni, M. 661
 Presti, D.L. 561
- Qamariatul, S. 153
 Queiroz, C.A. 519
- Raab, C. 55
 Radicioni, D. 607
 Rahim, A. 441
 Rahman, A. 421
 Rahman, M. 153, 533
 Rasul, J.M. 41
 Remisova, E. 49
 Ressutte, A.F.B. 653
 Riccardi, C. 841
 Ridondelli, G. 637
 Riviera, P.P. 407
 Rodríguez-Alloza, A.M. 493
 Rosales, C.A. 807
- Sabbagh, H. 463
 Sadek, H. 343
 Sadeq, M. 27
 Saeed, F. 153
 Santagata, E. 407
 Santarén, J. 453
 Schwartz, C.W. 801
 Selman, G.Ş. 499
 Shahmohammadie, R. 577
 Sharbaf, M. 135, 141
 Singh, D. 97, 271
 Sirin, O. 27, 343
 Snizek, V. 629
 Sobreiro, F.P. 127
 Sousa, J. 307
 Spanou, D. 745
 Stempihar, J. 313
 Stimilli, A. 607
- Suda, J. 825, 849
 Suzuki, C.Y. 653
 Swamy, A.K. 211
 Sybilski, D. 447
- Tabaković, A. 577
 Tan, K.H. 287
 Tarefder, R.A. 421
 Taxiltaris, C. 737
 Taylor, R. 577
 Temel, S. 61
 Thesseling, B. 645
 Thodesen, C. 487
 Tihonovs, J. 327
 Tretsiakova-McNally, S. 147
 Tsaimou, C. 671
- Uddin, W. 195, 713
 Underwood, B.S. 313
- Vacková, P. 551
 Valentin, J. 551, 629, 825, 849
 van den Beemt, R.C.M.A. 293
 Varveri, A. 577
 Verigin, M. 13
 Vonk, W.C. 243
 Voskuilen, J. 255
- Wacker, B. 687
 Walther, A. 221
 Wan Hanafi, W.R. 731
 Wang, K.C.P. 701
 Way, G.B. 307
 Wayman, M. 577
 Wilkinson, A. 147
 Wimsatt, A. 235
 Wistuba, M.P. 277, 361, 373, 447
 Wong, Y.D. 299
 Woodside, A. 153
 Woodward, D. 147, 161
- Yang, G.W. 701
 Yang, S.L. 859
 Yusoff, N.I. Md. 81
- Zaumanis, M. 327, 545
 Zeiada, W.A. 313
 Zelelew, H. 413
 Zhao, H. 367